SANDIA REPORT

SAND91—0893/1 • UC—721
Unlimited Release
Printed December 1991

SAND91-0893/1
0002
UNCLASSIFIED

12/91
570P STAC

Preliminary Comparison with 40 CFR Part 191, Subpart B for the Waste Isolation Pilot Plant, December 1991

Volume 1: Methodology and Results

WIPP Performance Assessment Division

Prepared by
Sandia National Laboratories
Albuquerque, New Mexico 87185 and Livermore, California 94550
for the United States Department of Energy
under Contract DE-AC04-76DP00789

Issued by Sandia National Laboratories, operated for the United States Department of Energy by Sandia Corporation.

Available to DOE and DOE contractors from
Office of Scientific and Technical Information
PO Box 62
Oak Ridge, TN 37831

Prices available from (615) 576-8401, FTS 626-8401

Available to the public from
National Technical Information Service
US Department of Commerce
5285 Port Royal Rd
Springfield, VA 22161

NTIS price codes
Printed copy: A22
Microfiche copy: A01

SAND91-0893/1
Unlimited Release
Printed December 1991

Distribution
Category UC-721

PRELIMINARY COMPARISON WITH 40 CFR PART 191, SUBPART B FOR THE WASTE ISOLATION PILOT PLANT, DECEMBER 1991

VOLUME 1: METHODOLOGY AND RESULTS

WIPP Performance Assessment Division
Sandia National Laboratories
Albuquerque, New Mexico 87185

ABSTRACT

Before disposing of transuranic radioactive wastes at the Waste Isolation Pilot Plant (WIPP), the United States Department of Energy must have a reasonable expectation that the WIPP will comply with the quantitative requirements of Subpart B of the United States Environmental Protection Agency's (EPA) Standard, *Environmental Radiation Protection Standards for Management and Disposal of Spent Nuclear Fuel, High-Level and Transuranic Radioactive Wastes*. Sandia National Laboratories, through iterative performance assessments of the WIPP disposal system, is conducting an evaluation of the long-term performance of the WIPP that includes analyses for the Containment Requirements and the Individual Protection Requirements of Subpart B of the Standard. Recognizing that unequivocal proof of compliance with the Standard is not possible because of the substantial uncertainties in predicting future human actions or natural events, the EPA expects compliance to be determined on the basis of specified quantitative analyses and informed, qualitative judgment. Performance assessments of the WIPP will provide as detailed and thorough a basis as practical for the quantitative aspects of that decision.

The 1991 preliminary performance assessment is a snapshot of a system that will continue to evolve until a final compliance evaluation can be made. Results of the 1991 iteration of performance assessment are preliminary and are not suitable for final compliance evaluations because portions of the modeling system and data base are incomplete, conceptual model uncertainties are not fully included, final scenario probabilities remain to be determined, and the level of confidence in the results remains to be established. In addition, the final version of the EPA Standard, parts of which were remanded to the EPA in 1987 for further consideration, has not been promulgated. Results of the 1991 preliminary performance assessment do not indicate potential violations of Subpart B of the Standard and support the conclusion based on previous analyses, including the 1990 preliminary performance assessment, that reasonable confidence exists that compliance with Subpart B of the Standard can be achieved.

ACKNOWLEDGMENTS

The WIPP Performance Assessment Division is comprised of both Sandia and contractor employees working as a team to produce these annual preliminary comparisons with EPA regulations, assessments of overall long-term safety of the repository, and interim technical guidance to the program. The on-site team, affiliations, and contributions to the 1991 performance assessment are listed in alphabetical order:

Performance Assessment Division

Name	Affil.	Primary Author of Doc: Sect.	Major Code	Area of Responsibility
R. Anderson	SNL			Division Manager
B. Baker	TEC	V.2:§6.4		SEC02D, Hydrology, Office Manager
J. Bean	UNM	V.2:§4.2.1		BRAGFLO & BOASTII, 2-Phase Flow
J. Berglund	UNM	V.2:Ch.7 Editor V.2	CUTTINGS	Task Ldr., Undisturbed Repository, Cuttings/Cavings/ Engr. Mech.
W. Beyeler	SAI	V.2:§5.3; 6.1;6.3	PANEL GARFIELD	Geostatistics, Analytical Models, CAMCON Systems Codes
K. Brinster	SAI			Geohydrology, Conceptual Models
R. Blaine	ECO			SEC02D & CAMCON Systems Codes
T. Blaine	EPE			Drilling Technology, Exposure Pathways Data
J. Garner	API	V.2:§5.3	PANEL	Source Term, Sens. Anal.
A. Gilkey	UNM			CAMCON Systems Codes
L. Gomez	SNL			Task Ldr., Safety Assessments
M. Gruebel	TRI	V.1:Ch.1,2, 8,9,10		EPA Regulations
R. Guzowski	SAI	V.1:Ch.4		Geology, Scenario Construction
J. Helton	ASU	V.1:Ch.3,4 V.2:Ch.2,3	CCDFPERM	Task Ldr., Uncert./Sens. Anal., Probability Models
H. Iuzzolino	GC	Editor V.3	CCDFPERM	LHS & CAMCON System Codes
R. Klett	SNL			EPA Regulations
P. Knupp	ECO			STAFF2D & SECOTR, Comp. Fluid Dyn.
C. Leigh	SNL		GENII-S	Exposure Pathways
M. Marietta	SNL	Editor (Set)		Dep. Div. Manager, Tech. Coord.
G. de Marsily	UP	V.2:§6.2		Task Ldr., Geostatistics
R. McCurley	UNM	V.2:§4.2.3		SUTRA & CAMCON System Codes
A. Peterson	SNL	Editor V.3		Task Ldr., Inventory
J. Rath	UNM	V.2:§4.2.3		SUTRA, Engr. Mech.
R. Rechard	SNL	Editor V.2 & V.3		Task Ldr., CAMCON, QA, Ref. Data
P. Roache	ECO	V.2:§6.4	SECO	Task Ldr., Comp. Fluid Dyn.
D. Rudeen	UNM	V.2:§4.2.2; 6.5		STAFF2D, Transport
J. Sandha	SAI	Editor V.3		INGRES, PA Data Base
J. Schreiber	SAI	V.2:§4.2.1; 5.2.5 Editor V.3		BRAGFLO & BOASTII, 2-Phase Flow

P. Swift	TRI	V.1:Ch.5,11		Task Ldr., Geology, Climate Var.
M. Tierney	SNL	Editor V.3		Task Ldr., CDF Constr., Probability Models
K. Trauth	SNL			Task Ldr., Expert Panels
P. Vaughn	API	V.2:§5.1; 5.2;5.2.5; App.A	BRAGFLO	Task Ldr., 2-Phase Flow & Waste Panel Chemistry
J. Wormeck	ECO			Comp. Fluid Dyn. & Thermodyn.

The foundation of the annual WIPP performance assessment is the underlying data set and understanding of the important processes in the engineered and natural barrier systems. The SNL Nuclear Waste Technology Department is the primary source of these data and understanding. Assistance with the waste inventory comes from WEC and its contractors. We gratefully acknowledge the support of our departmental and project colleagues. Some individuals have worked closely with the performance assessment team, and we wish to acknowledge their contributions individually:

J. Ball	ReS	Computer System Manager
H. Batchelder	WEC	CH & RH Inventories
R. Beauheim	SNL	Natural Barrier System, Hydrologic Parameters
B. Butcher	SNL	Engineered Barrier System, Unmodified Waste-Form Parameters, Disposal Room Systems Parameters
L. Brush	SNL	Engineered Barrier System, Source Term (Solubility) and Gas Generation Parameters
L. Clements	ReS	Computer System Support
T. Corbet	SNL	Natural Barrier System, Geologic & Hydrologic Parameters, Conceptual Models
P. Davies	SNL	Natural Barrier System, Hydrologic & Transport Parameters, & 2-Phase Flow Mechanistic Modeling
P. Drez	IT	CH & RH Inventories
E. Gorham	SNL	Natural Barrier System, Fluid Flow & Transport Parameters
S. Howarth	SNL	Natural Barrier System, Hydrologic Parameters
R. Kehrman	WEC	CH & RH Waste Characterization
R. Lincoln	SNL	Project Integration
F. Mendenhall	SNL	Engineered Barrier System, Unmodified Waste Form Parameters, Waste Panel Closure (Expansion)
D. Munson	SNL	Reference Stratigraphy, Constitutive Models, Physical & Mechanical Parameters
E. Nowak	SNL	Shaft/Panel Seal Design, Seal Material Properties, Reliability
J. Orona	ReS	Computer System Support
J. Tillerson	SNL	Repository Isolation Systems Parameters
S. Webb	SNL	2-Phase Flow Sensitivity Analysis & Benchmarking

API = Applied Physics Incorporated
ASU = Arizona State University
ECO = Ecodynamics Research Associates
EPE = Epoch Engineering
GC = Geo-Centers Incorporated
IT = International Technology
ReS = ReSpec
SAI = Scientific Applications International Corporation
SNL = Sandia National Laboratories
TEC = Technadyne Engineering Consultants
TRI = Tech Reps, Inc.
UNM = Univ. of New Mexico/New Mexico Engineering Research Institute
UP = University of Paris
WEC = Westinghouse Electric Corporation

Peer Review

Internal/Sandia

T. Corbet
D. Gallegos
M. LaVenue
S. Hora

Management/Sandia

W. Weart
T. Hunter

PA Peer Review Panel

R. Heath, Chairman	University of Washington
R. Budnitz	Future Resources Associates, Inc.
T. Cotton	JK Research Associates, Inc.
J. Mann	University of Illinois
T. Pigford	University of California, Berkeley
F. Schwartz	Ohio State University

Department of Energy

R. Becker
J. Rhoderick

Expert Panels

Futures

M. Baram	Boston University
W. Bell	Yale University
G. Benford	University of California, Irvine
D. Chapman	The World Bank, Cornell University
B. Cohen	University of Pittsburgh
V. Ferkiss	Georgetown University
T. Glickman	Resources for the Future
T. Gordon	Futures Group
C. Kirkwood	Arizona State University
H. Otway	Joint Research Center (Ispra), Los Alamos National Laboratory
M. Pasqualetti	Arizona State University
D. Reicher	Natural Resources Defense Council
N. Rosenberg	Resources for the Future
M. Singer	The Potomac Organization
T. Taylor	Consultant
M. Vinovski	University of Michigan

Source Term

C. Bruton	Lawrence Livermore National Laboratory
I-Ming Chou	U.S. Geological Survey
D. Hobart	Los Alamos National Laboratory
F. Millero	University of Miami

Retardation

R. Dosch	Sandia National Laboratories
C. Novak	Sandia National Laboratories
M. Siegel	Sandia National Laboratories

Geostatistics Expert Group

G. de Marsily, Chairman	U. of Paris
R. Bras	Massachusetts Inst. of Tech.
J. Carrera	U. Politechnica de Cataluña
G. Dagan	Tel Aviv U.
A. Galli	Ecole des Mines de Paris
A. Gutjahr	New Mexico Tech.
D. McLaughlin	Massachusetts Inst. of Tech.
S. Neuman	U. of Arizona
Y. Rubin	U. of California, Berkeley

Report Preparation (TRI)

Editors:

Volume 1: M. Gruebel (text); S. Laundre-Woerner (illustrations)
Volume 2: D. Scott (text); D. Marchand (illustrations)
Volume 3: J. Chapman (text); D. Pulliam (illustrations)

D. Rivard, D. Miera, T. Allen, and the Word Processing Department
R. Rohac, R. Andree, and the Illustration and Computer Graphics Departments
S. Tullar and the Production Department

J. Stikar (compilation of PA Peer Review Panel comments)

PREFACE

The Waste Isolation Pilot Plant (WIPP) is planned as the first mined geologic repository for transuranic (TRU) wastes generated by defense programs of the United States Department of Energy (DOE). Assessing compliance with the long-term performance criteria of Subpart B of the United States Environmental Protection Agency's (EPA) Standard, *Environmental Radiation Protection Standards for the Management and Disposal of Spent Nuclear Fuel, High-Level and Transuranic Radioactive Wastes* (40 CFR Part 191), is a cornerstone for the DOE's successful implementation of a TRU-waste disposal system.

This report (the *1991 Preliminary Comparison*) is a preliminary version of the planned document, *Comparison with 40 CFR Part 191, Subpart B for the Waste Isolation Pilot Plant* (the *Comparison*). The *1991 Preliminary Comparison* is the second in a series of annual "Performance Analysis and DOE Documentation" reports shown in the timing for performance assessment in the 1991 DOE report *Strategy for the Waste Isolation Pilot Plant Test Phase* (DOE/EM/48063-2). The Test Phase schedule and projected budget may change; if so, the schedule for the performance-assessment reports will also change. Where data and models are available, the text is a preview of the final report scheduled for 1996 (DOE/EM/48063-2). This report is a preview of the final *Comparison* only to the extent that the Standard, when repromulgated, is the same as the vacated 1985 Standard. This report treats the vacated Subpart B of the Standard as if it were still effective, because the DOE and the State of New Mexico have agreed that compliance evaluation will continue on that basis until a new Subpart B is promulgated. The approach to the Standard and the resultant methodology reported here do not reflect the EPA's efforts to develop a new Subpart B.

The *1991 Preliminary Comparison* is based on last year's reports: the *Preliminary Comparison with 40 CFR Part 191, Subpart B for the Waste Isolation Pilot Plant, December 1990* (SAND90-2347), *Data Used in Preliminary Performance Assessment of the Waste Isolation Pilot Plant (1990)* (SAND89-2408), and *Sensitivity Analysis Techniques and Results for Performance Assessment at the Waste Isolation Pilot Plant* (SAND90-7103). The *1991 Preliminary Comparison* consists of four volumes. Volumes 2 (Probability and Consequence Modeling) and 3 (Reference Data) will be published in December 1991 with this volume (Methodology and Results). Volume 4 (Uncertainty and Sensitivity Analyses) will be published in March 1992.

Performance assessment is a dynamic process that relies on iterative simulations using techniques developed and data collected as work progresses. Neither the data base nor the models are fixed at this stage, and all aspects

of the compliance-assessment system are subject to review as new information becomes available. Much of the modeling system described in this report will not change as the work progresses. Some of it will change, however, as problems are resolved and new models and data are incorporated into the system for use in subsequent simulations.

Vertical change bars in the right margins of Volume 1 of the *1991 Preliminary Comparison* indicate changes from the text published in the single-volume *1990 Preliminary Comparison*. Chapters 3 through 7 and Chapters 10 and 11 of the 1991 report, however, have been substantially revised or rewritten since the 1990 version and do not contain change bars. Chapters 3, 4, and 5 have been revised to reflect additions to the methodology and data used in evaluating the WIPP. Chapters 6 and 7 contain the results of the 1991 preliminary performance-assessment calculations. Chapters 10 and 11 discuss the 1991 results and summarize the status of the work to be completed to develop an adequate basis for evaluating compliance with Subpart B of the Standard.

Volumes 2, 3, and 4 do not contain change bars. Volume 2 is a compilation of essentially new material or material that was presented in a briefer form in 1990. Volume 3 is based on *Data Used in Preliminary Performance Assessment of the Waste Isolation Pilot Plant (1990)*, SAND89-2408, but contains numerous additions and refinements to the reference data base. Volume 4 reports the results of the uncertainty and sensitivity analyses for the 1991 calculations. Sensitivity analyses identify aspects of the modeling system that have the greatest potential to affect performance, thereby helping guide ongoing research. Because new data or new interpretations of existing data may change the conceptual models and/or the ranges and distributions of parameters throughout the life of the WIPP Project, sensitivity analyses are also iterative. Volume 4 is substantially revised and rewritten compared to the previous year's report, *Sensitivity Analysis Techniques and Results for Performance Assessment at the Waste Isolation Pilot Plant*, SAND90-7103.

Continuous publication of performance-assessment results as each new change is made is not feasible. As will be the case in subsequent *Preliminary Comparison* reports, results presented here reflect the improvements made during the previous year. The process is dynamic, however, and both the results and the description of the system are in part already out of date. In addition, data used in the 1991 performance assessment were accepted through July 1, 1991. This report presents a snapshot of a system that will continue to evolve until the final *Comparison* is complete.

The final *Comparison*, which will provide both quantitative and qualitative input to the determination of WIPP compliance with 40 CFR Part 191, Subpart B, will be without precedent as a completed performance evaluation for this type

of geologic repository. Therefore, careful planning is required to assure that the final *Comparison* will be adequate to support the determination of compliance. Coordination among the performance-assessment team at Sandia National Laboratories; the DOE WIPP Project Site Office (Carlsbad, New Mexico), WIPP Project Integration Office (Albuquerque, New Mexico), and Headquarters; the WIPP Panel of the National Research Council's Board on Radioactive Waste Management; the New Mexico Environment Department; the Environmental Evaluation Group; and the EPA is extremely important prior to preparation of the final *Comparison*. The draft of the final *Comparison* will be extensively reviewed prior to final publication. Responding to comments and revising the report will be necessary before the report can be published.

The 1991 DOE report *Strategy for the Waste Isolation Pilot Plant Test Phase* (DOE/EM/48063-2) outlines possible procedures that may be followed prior to the final determination of WIPP compliance. The DOE's decision process for the WIPP will involve all the activities necessary to document compliance with the applicable regulations, to complete the necessary institutional interactions, and to prepare a summary statement and recommendation for the Secretary of Energy upon which a final determination of compliance can be based. Additional documentation other than that required for compliance with Subpart B of 40 CFR Part 191 will be needed for the Resource Conservation and Recovery Act (RCRA), the National Environmental Policy Act (NEPA), and applicable Federal and State regulations. All of these documents will be reviewed by the cognizant DOE organizations whose concurrence is needed. The purpose of the review is to ensure that the analysis and documentation are adequate and appropriate to support the determination of compliance, to obtain the necessary permits and approvals, and to comply with DOE orders.

Once the process of documentation and review (both internal and external) has been completed, the DOE will prepare an internal summary report for the Secretary of Energy. This report will include a recommendation as to whether waste disposal at the WIPP should begin. Given a determination of compliance with the applicable regulations, a favorable record of decision on a new supplemental environmental impact statement, and a favorable readiness review, the Secretary will decide whether the WIPP should begin receiving TRU waste for permanent disposal. If land-withdrawal legislation mandates or the DOE signs with another agency a memorandum of understanding that provides for an independent certification of the DOE's compliance determination, the decision process will be amended.

This *1991 Preliminary Comparison* provides an opportunity for interested parties to monitor the WIPP performance assessment and give constructive input for future annual iterations and the final *Comparison*.

CONTENTS

FIGURES

TABLES

EXECUTIVE SUMMARY

The Waste Isolation Pilot Plant (WIPP) near Carlsbad, New Mexico, is a research and development project of the United States Department of Energy (DOE). The WIPP is designed to be the first mined geologic repository to demonstrate the safe disposal of transuranic (TRU) radioactive wastes generated by DOE defense programs since 1970. Before disposing of radioactive waste at the WIPP, the DOE must have a reasonable expectation that the WIPP will comply with the quantitative requirements of Subpart B of the United States Environmental Protection Agency's (EPA) *Environmental Radiation Protection Standards for Management and Disposal of Spent Nuclear Fuel, High-Level and Transuranic Radioactive Wastes* (40 CFR Part 191, U.S. EPA, 1985), referred to in this report as the Standard. Comparing the long-term performance of the WIPP disposal system with the quantitative requirements of the Standard will help determine whether the disposal system will provide safe disposal of radionuclides.

Performance assessment as defined for the Containment Requirements of Subpart B of the Standard means an analysis that identifies the processes and events that might affect the disposal system, examines the effects of these processes and events on the performance of the disposal system, and estimates the cumulative releases of radionuclides, considering the associated uncertainties, caused by all significant processes and events (§ 191.12(q)). As used in this report, performance assessment includes analyses for predicting doses as well as the definition in the Standard, because the methodology developed for predicting releases for the Containment Requirements can be used for predicting doses for the Individual Protection Requirements.

Recognizing that unequivocal proof of compliance with the Standard is not possible because of the substantial uncertainties in predicting future human actions or natural events, the EPA expects compliance to be determined on the basis of specified quantitative analyses and informed, qualitative judgment. Performance assessments of the WIPP will provide as detailed and thorough a basis as practical for the quantitative aspects of that decision. Performance assessments will provide quantitative, probabilistic analyses of disposal-system performance for comparison with the regulatory limits. However, the three quantitative requirements in Subpart B specify that the disposal system design must provide a reasonable expectation that the various quantitative tests can be met. Specifically, the qualitative nature of the EPA's approach is established in the Containment Requirements of the Standard: what is required is a reasonable expectation, on the basis of the record before the DOE, that compliance with the Containment Requirements will be achieved.

Sandia National Laboratories (SNL), as the scientific program manager for the WIPP, is responsible for developing an understanding of the processes and systems that affect long-term isolation of wastes in the WIPP and applying that understanding to evaluation of the long-term WIPP performance and compliance with the Standard. SNL defines and implements experiments both in the laboratory and at the WIPP, develops and applies models to interpret the experimental data, and develops and applies performance-assessment models. This report summarizes SNL's late-1991 understanding of the WIPP Project's ability to quantitatively evaluate compliance with the long-term performance requirements set by Subpart B of the Standard. It documents one in a series of annual iterations of performance assessment: each iteration builds on the previous year's work until a final, defensible compliance evaluation can be made. Results of this preliminary performance assessment should not be formally compared to the requirements of the Standard to determine whether the WIPP disposal system complies with Subpart B. The disposal system is not adequately characterized, and necessary models, computer programs, and data bases are incomplete. Furthermore, Subpart B of the Standard was vacated in 1987 by a Federal Court of Appeals and remanded to the EPA for reconsideration.

Instead of presenting a formal compliance evaluation, this report examines the adequacy of the available information for producing a comprehensive comparison to the Containment Requirements and the Individual Protection Requirements of the 1985 Standard, in keeping with the Consultation and Cooperation Agreement (as modified) between the DOE and the State of New Mexico. Defensibility of the compliance evaluation ultimately will be determined in part by qualitative judgment, on the basis of the record before the DOE, regarding reasonable expectations of compliance, assuming that concept is retained by the EPA in repromulgating Subpart B.

Adequate documentation and independent peer review are essential parts of a performance assessment, without which informed judgments of the suitability of the WIPP as a waste repository are not possible. An extensive effort is being devoted to documenting and peer reviewing the WIPP performance assessment and the supporting research, including techniques, models, data, and analyses.

Compliance-Assessment Overview

A performance assessment must determine the events that can occur, the likelihood of these events, and the consequences of these events. The WIPP performance assessment is, in effect, a risk assessment. Risk can be represented as a set of ordered triples. The first element in each triple describes things that may happen to the disposal system in the future (i.e.,

the scenarios). The second element in each triple describes how likely these things are to happen (i.e., scenario probability). The third element in each triple describes the consequences of the occurrences associated with the first element (i.e., EPA normalized releases of radionuclides to the accessible environment).

An infinite number of possible 10,000-year histories of the WIPP exist. These possible histories are grouped into summary scenarios for probability assignment and consequence analysis. To increase resolution in the evaluation, the summary scenarios involving human intrusion into the repository are further decomposed into computational scenarios. For the 1991 performance assessment, computational scenarios are distinguished by the time and number of intrusions, whether or not a brine reservoir is encountered below the waste, and the activity level of waste intersected. Probabilities are based on the assumption that intrusion boreholes are random in time and space (Poisson process) with a rate constant that is sampled as an uncertain parameter in the 1991 calculations.

The models used in the WIPP performance assessment exist at four different levels. Conceptual models characterize the understanding of the system. An adequate conceptual model is essential both for the development of the possible 10,000-year histories for the WIPP and for the division of these possible histories into the summary scenarios. Mathematical models are developed to represent the processes of the conceptual model. The mathematical models are predictive in the sense that, given known properties of the system and possible perturbations to the system, they project the response of the system conditional on modeling assumptions made during development. Numerical models are developed to provide approximations to the solutions of the mathematical models. Computer models implement the numerical models and actually predict the consequences of the occurrences associated with the scenarios.

As uncertainties will always exist in the results of a performance assessment, the impact of these uncertainties must be characterized and displayed. Thus, sensitivity and uncertainty analyses are an important part of a performance assessment. Sensitivity analysis determines the importance of specific components or subsystems to the results of the consequence analyses. Uncertainty analysis determines how imprecise knowledge about the disposal system affects confidence in the results of the consequence analysis. Uncertainty in the results of the risk analysis may result from the completeness of the occurrences considered, the aggregation of the occurrences into scenarios for analysis, the selection of models (at all four levels above) and imprecisely known parameters for use in the models, and stochastic variation in future occurrences.

Many techniques are available for uncertainty and sensitivity analysis. The WIPP performance assessment uses Monte Carlo analysis techniques. A Monte Carlo analysis involves five steps: selection of variable ranges and distributions; generation of a sample from the parameter value distributions; propagation of the sample through the analysis; analysis of the uncertainty in results caused by variability in the sampled parameters; and sensitivity analyses to identify those parameters for which variability in the sampled value had the greatest effect on the results.

No single summary measure can adequately display all the information produced in a performance assessment. Thus, decisions on the acceptability of the WIPP should be based on a careful consideration of all available information rather than on a single summary measure. Complementary cumulative distribution functions (CCDFs) are used to display information on scenario probability and consequence. Uncertainty resulting from imprecisely known parameter values results in a family of CCDFs. Conceptual model uncertainty has not yet been adequately addressed in any performance assessment but could be included through the set of imprecisely known variables or by separate performance assessments for each alternative conceptual model. This will be addressed in future annual performance assessments. Variability in the family of CCDFs can be displayed by showing the entire family or by showing the mean and selected quantile curves. For human-intrusion scenarios of WIPP performance, CCDFs will be compared to the limits set in the Containment Requirements of the Standard.

Results

As previously indicated, compliance with the Containment Requirements will be evaluated using a family of CCDF curves that graph exceedance probability versus cumulative radionuclide releases for all significant scenarios. All results are preliminary and are not suitable for final compliance evaluations because portions of the modeling system and data base are incomplete, conceptual model uncertainties are not fully included, final scenario probabilities remain to be determined, the final version of the EPA Standard has not been promulgated, and the level of confidence in the results remains to be established. Uncertainty analyses required to establish the level of confidence in results will be included in future performance assessments as advances permit quantification of uncertainties in the modeling system and the data base.

Simulations of undisturbed performance indicate zero releases to the accessible environment in the 10,000 years of regulatory concern for the Containment Requirements. Because no releases are estimated to occur in the 10,000-year regulatory period for undisturbed performance, the base-case

summary scenario is not analyzed, but it is included in CCDF construction through its estimated probability and zero consequences.

For the 1991 performance assessment, the factors used to define the computational scenarios are time and number of intrusions, whether or not a brine reservoir is encountered below the waste, and activity level of the waste intersected. Drilling intrusions are assumed to follow a Poisson process. The rate constant is an imprecisely known variable with the upper bound defined by the EPA Standard as 30 boreholes/km^2/10,000 years and lower bound of zero. For this performance assessment, the regulatory time interval of 10,000 years is divided into five disjoint time intervals of 2000 years each, with intrusion occurring at the midpoints of these intervals (at 1000, 3000, 5000, 7000, and 9000 years). An uncertain area fraction of the waste panels is assumed to be underlain by a pressurized brine reservoir in the Castile Formation. Four activity levels for CH waste and one activity level for RH waste are defined and their distributions sampled to represent variability in the activity level of waste penetrated by a drilling intrusion.

For the 1991 performance assessment, 45 imprecisely known parameters were sampled for use in consequence modeling for the Monte Carlo simulations of repository performance. For each of these 45 parameters, a range and distribution was subjectively assigned based on available data. These parameters specify physical, chemical, and hydrologic properties of the geologic and engineered barriers. Parameters for climatic variability and future drilling intrusions are also included.

Important differences between the 1990 and 1991 Monte Carlo analyses are the inclusion in the 1991 modeling of a two-phase (brine and gas) flow computer code that allows examining effects of waste-generated gas in uncertainty and sensitivity analyses, the addition of parameters related to dual porosity (both chemical and physical retardation) in the Culebra, the use of a set of conditional simulations for transmissivity in the Culebra instead of the simple zonal approach of the 1990 performance assessment, and the inclusion of a preliminary analysis of potential effects of climatic variability on flow in the Culebra. Distributions for parameter values for radionuclide solubility in repository brine and radionuclide retardation in the Culebra were based on judgment from expert panels.

Latin hypercube sampling is used to incorporate parameter uncertainty into the performance assessment. A Latin hypercube sample of size 60 was generated from the set of 45 variables. After the sample was generated, each element of the sample was propagated through the system of computer codes used for analysis of human-intrusion scenarios. Each sample was used in the

calculation of both cuttings/cavings and subsurface groundwater releases for intrusion times of 1000, 3000, 5000, 7000, and 9000 years. Two types of intrusions were examined: those involving penetration of one or more boreholes to or through a waste-filled room or drift in a panel without intersecting pressurized brine below, and those involving penetration of exactly two boreholes to or through a waste-filled room or drift in a panel, with one borehole also intersecting a pressurized brine reservoir below. Consequences of intrusions involving penetration of one or more boreholes through a waste-filled room or drift in a panel and into a pressurized brine reservoir were found to be similar to and bounded by the second type of intrusions.

Except for a few low-probability releases, cuttings/cavings dominate the CCDFs for total releases. Based on the performance-assessment data base and present understanding of the WIPP disposal system, the summary CCDF curves showing exceedance probability versus total cumulative normalized releases to the accessible environment resulting from both groundwater transport in the subsurface and releases at the surface during drilling are the preferred choice for preliminary comparison with the Containment Requirements. These preliminary summary curves were generated including the effects of waste-generated gas, dual-porosity transport in the Culebra, and a preliminary estimate of changes in recharge caused by climatic variability, and are considered to be the most realistic choice for an informal comparison with the Containment Requirements. Informal comparison of these preliminary results with the Containment Requirements indicates that, for the assumed models, parameter values, and scenario probabilities, summary CCDFs (mean and median curves) lie an order of magnitude or more below the regulatory limits.

Conclusions

Conclusions that can be drawn for each of the requirements in the 1985 Standard are:

- **Containment Requirements**. As previously noted, results presented in this report are preliminary and are not suitable for evaluating compliance with the Containment Requirements of the Standard. As explained in more detail in Chapter 11, portions of the modeling system and the data base are incomplete, conceptual model uncertainties are not fully included, final scenario probabilities remain to be estimated, and the level of confidence in the results has not been established. In addition, the Standard has not been repromulgated since its 1987 remand.

  Informal comparison of these preliminary results with the Containment Requirements indicates that, for the assumed models, parameter values, and

scenario probabilities, summary CCDFs (mean and median curves) lie an order of magnitude or more below the regulatory limits.

- **Assurance Requirements**. Plans for implementing the first two Assurance Requirements (Active Institutional Controls and Monitoring) are preliminary. The design for passive institutional controls is currently being considered by an expert panel. Implementation of passive institutional controls can occur only after their design has been selected. Barrier design is an integral part of the SNL research effort. The WIPP Project has satisfied the natural resources requirement and has published a summary report to that effect. The EPA stated in the Standard that current plans for mined geologic repositories meet the waste removal requirement without additional design.

- **Individual Protection Requirements**. Previous and current evaluations of undisturbed performance at the WIPP have indicated that no releases to the accessible environment will occur within 10,000 years. Dose predictions are therefore not expected to be required for the 1000-year period specified by the Individual Protection Requirements. However, as with the Containment Requirements, formal comparison to the Standard cannot be prepared until the bases of the compliance-assessment system are judged adequate.

- **Groundwater Protection Requirements**. Studies have determined that no groundwater near the WIPP meets the criteria for "special source of ground water" as specified in the Standard. Based on the 1985 Standard, the Groundwater Protection Requirements are not relevant to the WIPP disposal system. No further action should be necessary.

1. INTRODUCTION

[NOTE: The text of Chapter 1 is followed by a synopsis that summarizes essential information, beginning on page 1-29.]

Before disposing of radioactive waste at the Waste Isolation Pilot Plant (WIPP), the United States Department of Energy (DOE) must have a reasonable expectation that the WIPP will comply with the quantitative requirements of Subpart B of the United States Environmental Protection Agency's (EPA) *Environmental Radiation Protection Standards for Management and Disposal of Spent Nuclear Fuel, High-Level and Transuranic Radioactive Wastes* (40 CFR Part 191; U.S. EPA, 1985), referred to herein as the Standard (included as Appendix A of this volume). Comparing the long-term performance of the WIPP disposal system with the quantitative requirements of the Standard will help determine whether the disposal system will provide safe disposal of radionuclides. This report is a preliminary version of the planned *Comparison with 40 CFR, Part 191, Subpart B, for the Waste Isolation Pilot Plant*. The planned scope of that document includes the final report for the performance assessment of the WIPP disposal system and relevant data for determining whether to proceed with disposal at the WIPP.

1.1 40 CFR Part 191, The Standard (1985)

The Standard promulgated in 1985 by the EPA is divided into two subparts (Figure 1-1). Subpart A applies to a disposal facility prior to decommissioning and limits annual radiation doses from waste management and storage operations to members of the public in the general environment. Subpart B applies after decommissioning and limits probabilities of cumulative releases of radionuclides to the accessible environment for 10,000 years. Subpart B also limits both radiation doses to members of the public in the accessible environment and radioactive contamination of certain sources of groundwater within or near the controlled area for 1,000 years after disposal. Appendix A of the Standard specifies how to determine release limits, and Appendix B of the Standard provides nonmandatory guidance for implementing Subpart B. The *Compliance Strategy* (U.S. DOE, 1989a) discusses the WIPP interpretation of various terms and definitions contained in the 1985 Standard.

The concept of "site" is integral to limits established by Subparts A and B for releases of waste from the repository, both during operation and after closure. "Site" is used differently in the two subparts; the meaning of

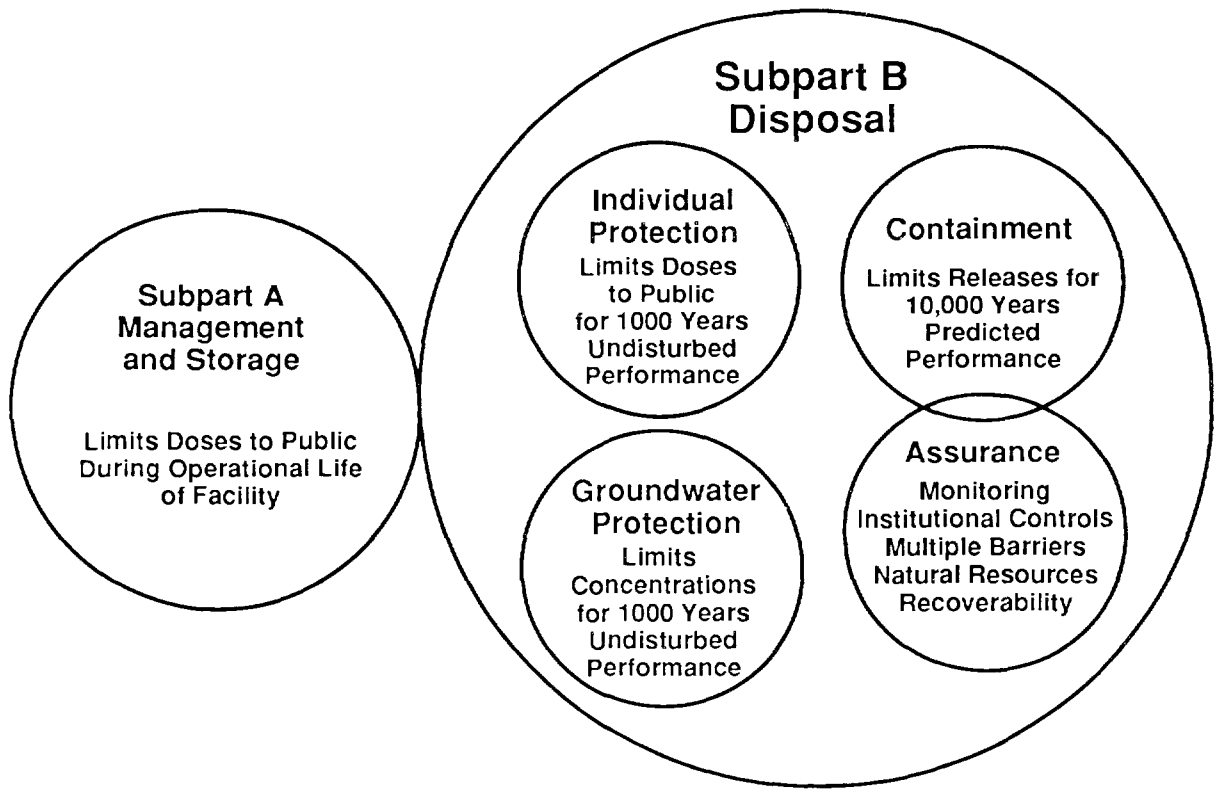

Figure 1-1. Graphical Representation of 40 CFR Part 191 Environmental Standards for Management and Disposal of Spent Fuel, High-Level, and Transuranic Waste (after U.S. DOE, 1989a).

"site" at the WIPP for each subpart is discussed and defined below in the appropriate section. The definitions of "general environment," "controlled area," and "accessible environment," which are also important in assessing compliance with the Standard, depend on the definition of "site." "Site" has also been used generically for many years by the waste-management community (e.g., in the phrases "site characterization" or "site specific"); few uses of the word correspond to either of the EPA's usages (Bertram-Howery and Hunter, 1989a; also see U.S. DOE, 1989a).

1.1.1 STATUS OF THE STANDARD

Subpart B of the Standard was vacated and remanded to the EPA by the United States Court of Appeals for the First Circuit in July 1987. The Court found that the EPA had neither reconciled the Individual Protection Requirements with Part C of the Safe Drinking Water Act nor explained the divergence between the two sets of criteria; furthermore, the EPA had not explained the basis for the 1,000-year design criterion in the Individual Protection Requirements. The Court also found that the Groundwater Protection Requirements were promulgated without proper notice and comment. Working Draft 3, a proposed revison of the Standard, was prepared for discussion within the EPA in April 1991. A repromulgated Standard is not expected before mid-1993. The Second Modification to the Consultation and Cooperation Agreement (U.S. DOE and State of New Mexico, 1981, as modified) commits the WIPP Project to proceed with compliance planning with the Standard as first promulgated until such time as a revised Standard becomes available. Therefore, this report discusses the Standard as first promulgated. Compliance plans for the WIPP will be revised as necessary in response to any changes in the Standard resulting from the repromulgation.

1.1.2 SUBPART A

Subpart A limits the radiation doses that may be received by members of the public in the general environment as a result of management and storage of transuranic (TRU) wastes at DOE disposal facilities not regulated by the Nuclear Regulatory Commission (NRC). Subpart A requires that "the combined annual dose equivalent to any member of the public in the general environment resulting from discharges of radioactive material and direct radiation from such management and storage shall not exceed 25 millirems to the whole body and 75 millirems to any critical organ" (§ 191.03(b)). The general environment is the "total terrestrial, atmospheric, and aquatic environments outside sites within which any activity, operation, or process associated with the management and storage of...radioactive waste is conducted" (§ 191.02(o)). The site as defined for Subpart A is "an area contained within the boundary of a location under the effective control of persons

possessing or using ... radioactive waste that are involved in any activity, operation, or process covered by this Subpart" (§ 191.02(n)).

"Site" for the purposes of Subpart A at the WIPP is the secured-area boundary shown in Figure 1-2. This area will be under the effective control of the security force at the WIPP, and only authorized persons will be allowed within the boundary (U.S. DOE, 1989a). In addition, the DOE will gain control over the sixteen-section (16 mi^2) area within the proposed land-withdrawal boundary; this boundary is referred to in the agreement with New Mexico and in the WIPP *Final Safety Analysis Report* (FSAR) (U.S. DOE, 1990a) as the "WIPP site boundary." This control will prohibit habitation within the boundary. Consequently, for the purposes of assessing operational doses to nearby residents, the assumption can be made that no one lives closer than the latter boundary (Bertram-Howery and Hunter, 1989a). The boundary indicated as "WIPP" on illustrations in this volume is the boundary of the proposed land-withdrawal area.

The DOE compliance approach to the Standard is described in the WIPP *Compliance Strategy* (U.S. DOE, 1989a; also see Bertram-Howery and Hunter, 1989a and U.S. DOE, 1990b). Compliance with Subpart B is the topic of this report; therefore, Subpart A will not be discussed further. Discussions contained in this report elaborate on the DOE's published strategy (U.S. DOE, 1989a; U.S. DOE, 1990b) for evaluating compliance with the remanded Subpart B. These discussions provide the regulatory framework for the methodology employed.

1.1.3 SUBPART B

In evaluating compliance with Subpart B, the WIPP Project intends to follow to the extent possible the guidance found in Appendix B of the Standard (U.S. DOE, 1989a). The application of Subpart B to the WIPP is discussed in detail in Chapter 2. The Containment Requirements (§ 191.13(a)) necessitate probabilistically predicting cumulative releases for 10,000 years. The Individual Protection Requirements (§ 191.15) set limits on annual doses for 1,000 years. The Assurance Requirements (§ 191.14) complement the Containment Requirements. The Groundwater Protection Requirements (§ 191.16) limit radionuclide concentrations in specific groundwater sources for 1,000 years. Some necessary definitions and interpretations are given below.

Controlled Area

The controlled area as defined in Subpart B of the Standard is

> (l) A surface location, to be identified by passive institutional controls, that encompasses no more than 100 square kilometers and

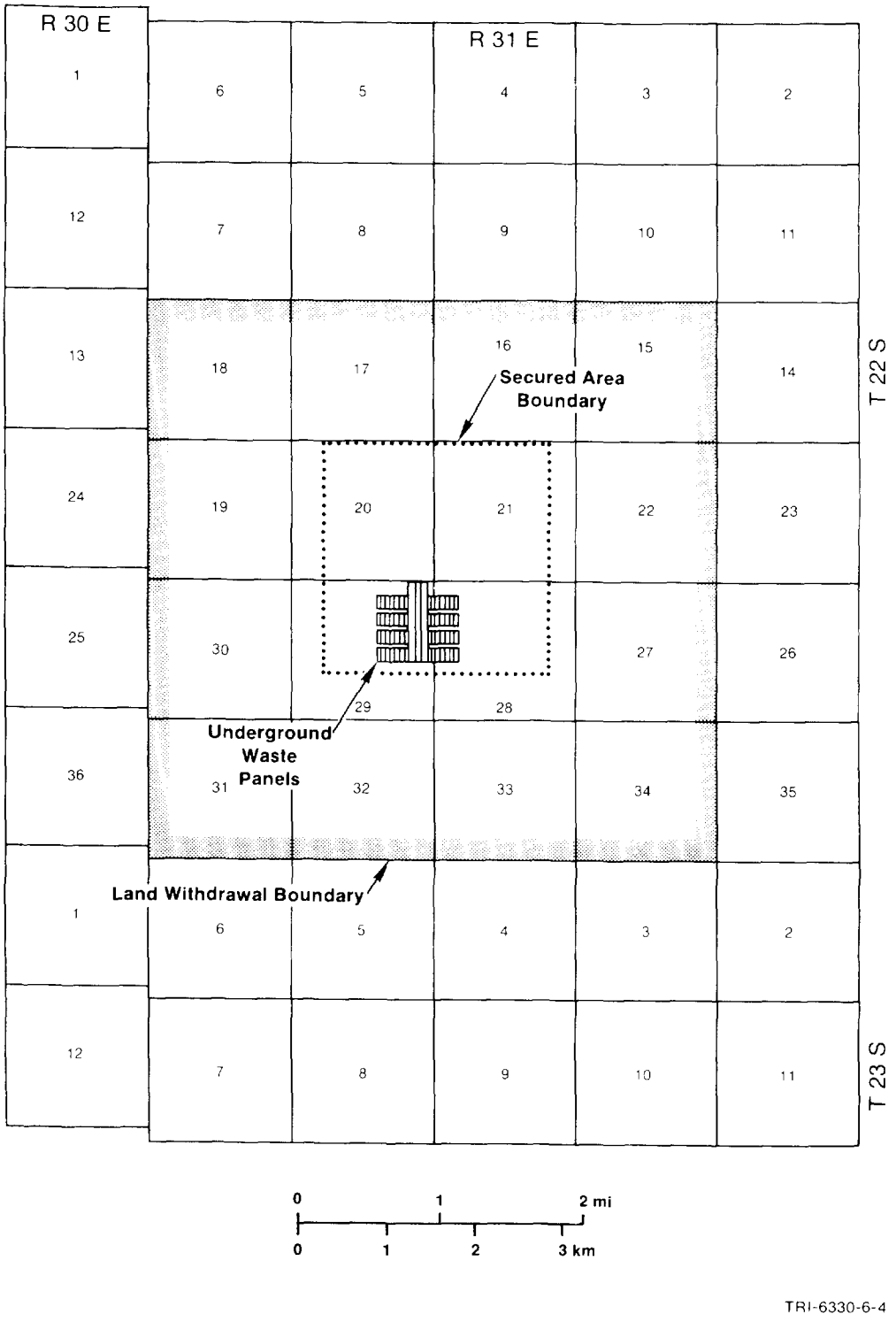

Figure 1-2. Position of the WIPP Waste Panels Relative to WIPP Boundaries and Surveyed Section Lines (U.S. DOE, 1989a).

> extends horizontally no more than five kilometers in any direction from the outer boundary of the original location of the radioactive wastes in a disposal system; and (2) the subsurface underlying such a surface location (§ 191.12(g)).

The controlled area is limited to the lithosphere and the surface within no more than 5 km (3 mi) from the outer boundary of the WIPP waste-emplacement panels. The boundary of this maximum-allowable controlled area does not coincide with the secured area boundary (Figure 1-2) or with the boundary proposed in legislation pending before Congress for the WIPP land withdrawal (Figure 1-3). The accessible environment is "...(1) the atmosphere; (2) land surfaces; (3) surface waters; (4) oceans; and (5) all of the lithosphere that is beyond the controlled area" (§ 191.12(k)). According to this definition, the surface of the controlled area is in the accessible environment; the underlying subsurface of the controlled area is not part of the accessible environment (Figure 1-3). Any radionuclides that reached the surface would be subject to the limits, as would any that reached the lithosphere outside the subsurface portion of the controlled area.

The term "disposal site" is used frequently in Subpart B and in Appendix B of the Standard. The "site" for the purposes of Subpart A and the "disposal site" for the purposes of Subpart B are not the same. For the purposes of the WIPP strategy for compliance with Subpart B, the disposal site and the controlled area are the same (U.S. DOE, 1989a). The Standard defines "disposal system" to mean any combination of engineered and natural barriers that isolate the radioactive waste after disposal. For the WIPP, the disposal system is the combination of the repository/shaft system and the geologic and hydrologic systems of the controlled area (Figure 1-3). The repository/shaft system, as defined, includes the WIPP underground workings and all emplaced materials and the altered zones within the Salado Formation and overlying units resulting from construction of the underground workings.

The surface of the controlled area is to be identified by passive institutional controls, which include permanent markers placed at a disposal site, along with records, government ownership, and other methods of preserving knowledge about the disposal system. The disposal site is to be designated by permanent markers and other passive institutional controls to indicate the dangers of the wastes and their location (§ 191.12(e); § 191.12(g)).

"Reasonable Expectation" of Compliance

The EPA discusses the overall approach of the Standard in a preamble to the regulations. The three quantitative requirements in Subpart B specify that the disposal system design must provide a "reasonable expectation" that their

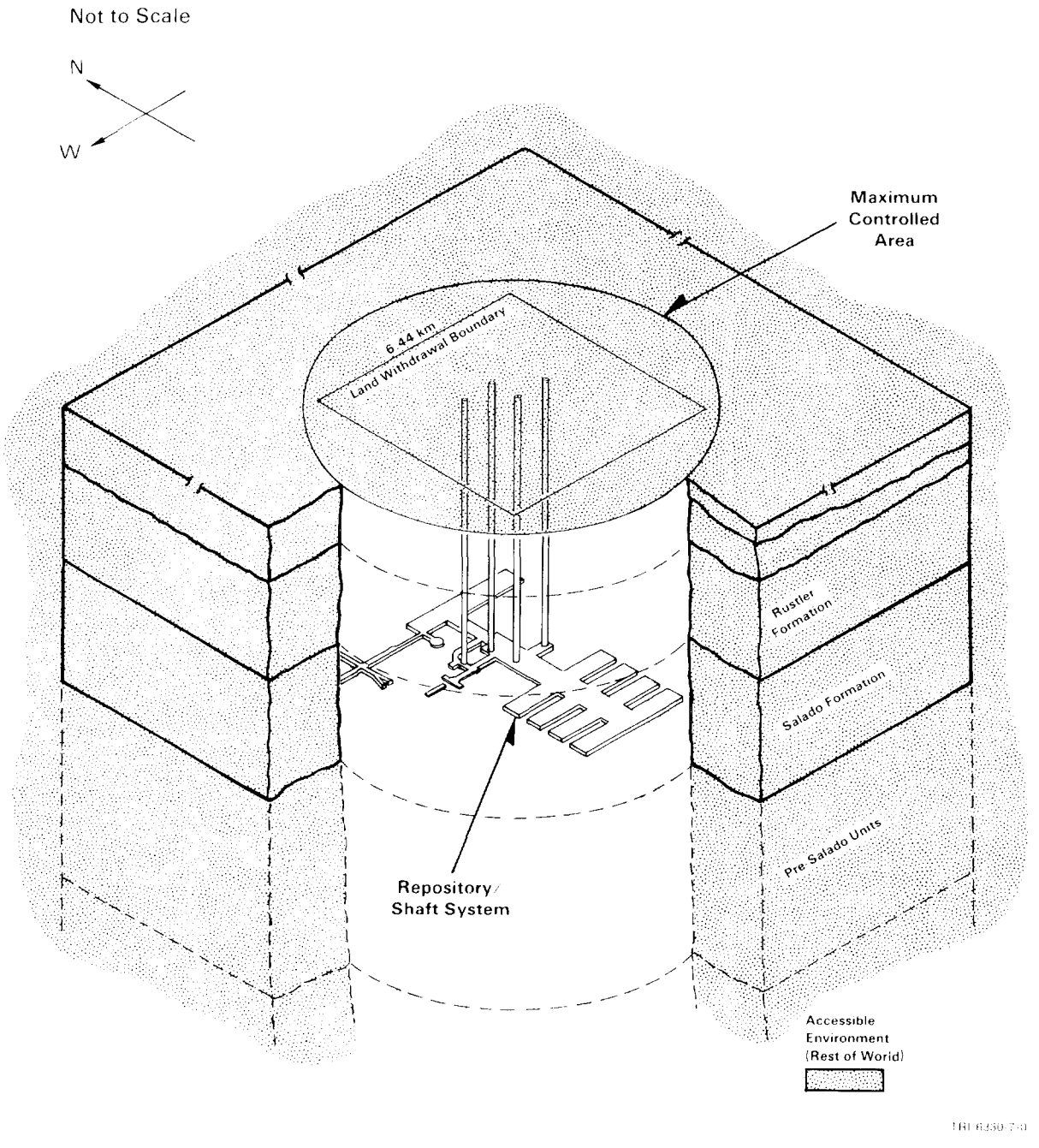

Figure 1-3. Artist's Concept Showing the Two Components of the WIPP Disposal System: Controlled Area and Repository/Shaft System. The repository/shaft system scale is exaggerated. The proposed land-withdrawal boundary is shown at the same scale as the maximum extent of the controlled area (Bertram-Howery and Hunter, 1989b).

various quantitative tests can be met. In the preamble, the EPA states that this test of qualitative judgment is meant to "acknowledge the unique considerations likely to be encountered upon implementation of these disposal standards" (U.S. EPA, 1985, p. 38071). The Standard "clearly indicates that comprehensive performance assessments, including estimates of the probabilities of various potential releases whenever meaningful estimates are practicable, are needed to determine compliance with the containment requirements" (U.S. EPA, 1985, p. 38076). These requirements "emphasize that unequivocal proof of compliance is neither expected nor required because of the substantial uncertainties inherent in such long-term projections. Instead, the appropriate test is a reasonable expectation of compliance based upon practically obtainable information and analysis" (ibid.). The EPA states that the Standard requires "very stringent isolation while allowing the [DOE] adequate flexibility to handle specific uncertainties that may be encountered" (U.S. EPA, 1985, p. 38077).

In the preamble to the Standard, the EPA states that it clearly intends qualitative considerations to have equal importance with quantitative analyses in determining compliance with Subpart B (U.S. EPA, 1985, p. 38066). The EPA states that "the numerical standards chosen for Subpart B, by themselves, do not provide either an adequate context for environmental protection or a sufficient basis to foster public confidence..." (U.S. EPA, 1985, p. 38079). The EPA also states that "factors such as [food chains, ways of life, and the size and geographical distributions of populations] cannot be usefully predicted over [10,000 years]....The results of these analyses should not be considered a reliable projection of the 'real' or absolute number of health effects resulting from compliance with the disposal standards" (U.S. EPA, 1985, p. 38082).

The EPA's assumptions regarding performance assessments and uncertainties are incorporated in Appendix B of the Standard, which the EPA intends the implementing agencies to follow. The EPA intends these assumptions to "discourage overly restrictive or inappropriate implementation" of the requirements (U.S. EPA, 1985, p. 38077). The guidance in Appendix B to the Standard indicates that "compliance should be based upon the projections that the [DOE] believe[s] are more realistic. Furthermore,...the quantitative calculations needed may have to be supplemented by reasonable qualitative judgments in order to appropriately determine compliance with the disposal standards" (U.S. EPA, 1985, p. 38076). In particular, Appendix B states:

> The [EPA] believes that the [DOE] must determine compliance with §§ 191.13, 191.15, and 191.16 of Subpart B by evaluating long-term predictions of disposal system performance. Determining compliance with § 191.13 will also involve predicting the likelihood of events and

> processes that may disturb the disposal system. In making these various predictions, it will be appropriate for the [DOE] to make use of rather complex computational models, analytical theories, and prevalent expert judgment relevant to the numerical predictions. Substantial uncertainties are likely to be encountered in making these predictions. In fact, sole reliance on these numerical predictions to determine compliance may not be appropriate; the [DOE] may choose to supplement such predictions with qualitative judgments as well.

The qualitative section of the Containment Requirements (§ 191.13(b)) states:

> Performance assessments need not provide complete assurance that the requirements of 191.13(a) will be met. Because of the long time period involved and the nature of the events and processes of interest, there will inevitably be substantial uncertainties in projecting disposal system performance. Proof of the future performance of a disposal system is not to be had in the ordinary sense of the word in situations that deal with much shorter time frames. Instead, what is required is a reasonable expectation, on the basis of the record before the [DOE], that compliance with 191.13(a) will be achieved.

The EPA stated in the preamble to the Standard that the agency recognized that too many uncertainties exist in projecting the behavior of natural and engineered components for 10,000 years and that too many opportunities for errors in calculations or judgments are possible for the numerical requirements to be the sole basis for determining the acceptability of a disposal system. Qualitative Assurance Requirements were included in the Standard to ensure that "cautious steps are taken to reduce the problems caused by these uncertainties." These qualitative Assurance Requirements are "an essential complement to the quantitative containment requirements" (U.S. EPA, 1985, p. 38079). Each qualitative requirement was chosen to compensate for some aspect of the inherent uncertainty in projecting the future performance of a disposal system. The Assurance Requirements begin by declaring that compliance with their provisions will "provide the confidence needed for long-term compliance with the requirements of 191.13" (§ 191.14).

Determining compliance with Subpart B depends on the estimated overall probability distribution of cumulative releases and on the estimated annual doses; however, it also depends on the strength of the assurance strategies (U.S. DOE, 1987, currently in revision) that will be implemented and on the qualitative judgment of the DOE and its analysts. The preceding discussion demonstrates the EPA's recognition of the difficulties involved in predicting the future and in quantifying the outcomes of future events. The EPA clearly expects the DOE to understand the uncertainties in the disposal system's behavior to the extent practical, while recognizing that substantial uncertainties will nevertheless remain.

1.2 Application of Additional Regulations to the WIPP

In addition to 40 CFR Part 191, the Resource Conservation and Recovery Act (RCRA) and the National Environmental Policy Act (NEPA) are considered in an overall evaluation of the WIPP as a repository for TRU wastes. This report does not provide an evaluation of the WIPP in regard to these additional regulations. However, the two regulations are briefly discussed as part of the overview of the WIPP.

1.2.1 RCRA

The Resource Conservation and Recovery Act (RCRA) was enacted in 1976 to provide management of hazardous waste. In July 1990 the EPA authorized the State of New Mexico to apply the RCRA regulations to facilities in the state that managed radioactive mixed waste. In March 1989 the DOE had petitioned the EPA for a "no migration" determination for the WIPP Test Phase. The DOE submitted models to demonstrate, to a reasonable degree of certainty, that the emplaced waste would not migrate from the disposal unit during the WIPP Test Phase. The EPA issued a conditional "no migration" determination, for the WIPP Test Phase only, in November 1990. Strategies are currently being developed for RCRA compliance after the Test Phase is completed.

1.2.2 NEPA

The National Environmental Policy Act (NEPA) (42 USC 4321 et seq.) of 1969 requires all agencies of the Federal Government to prepare a detailed statement on the environmental impacts of proposed "major Federal actions significantly affecting the quality of the human environment." In compliance with NEPA, the DOE has published the *Draft Environmental Impact Statement, Management of Commercially Generated Radioactive Waste* (U.S. DOE, 1979), the *Final Environmental Impact Statement: Waste Isolation Pilot Plant* (FEIS) (U.S. DOE, 1980a), and the *Final Supplement Environmental Impact Statement, Waste Isolation Pilot Plant* (FSEIS) (U.S. DOE, 1990c). An additional supplemental environmental impact statement is planned prior to permanent disposal at the WIPP (U.S. DOE, 1991a).

1.3 Organization of the Comparison

The organization of this report and of the final *Comparison*, which will evolve from this report, is based on the requirements of the Standard. Within the format of the requirements, the report is organized according to the methodology developed by the performance-assessment team to implement the guidance found in Appendix B to the Standard. This level of organization

reflects the program elements described in the DOE management plan for the Test Phase (U.S. DOE, 1990b).

The *1991 Preliminary Comparison* report is organized into four volumes. Volume 1 (this volume) contains the methodology and results for the 1991 preliminary performance assessment. Volume 2 describes the consequence and probability models used and contains the 1991 computational data base. Volume 3 is the 1991 reference data base. Volume 4 contains techniques and results of the uncertainty and sensitivity analyses for the 1991 performance assessment. Volumes 2 and 3 are published concurrently with Volume 1 (this volume); Volume 4 will be published 3 months after Volumes 1 through 3. The results presented in Volume 4 will be used to guide subsequent performance assessments.

Because this report is a preliminary version of the final report, many sections are preliminary or incomplete. In Volume 1 (this volume), brief descriptions of the Standard and the WIPP Project are provided in Chapter 1. Chapter 2 discusses application of Subpart B of the Standard to the WIPP disposal system. Chapter 3 provides an overview of the compliance-assessment methodology for the WIPP Project. Chapter 4 identifies and describes the scenarios being used in the compliance assessment. Chapter 5 describes the components of the compliance-assessment system. Chapter 6 presents the results of the second preliminary performance assessment relative to the Containment Requirements (§ 191.13) of the Standard. Chapter 7 describes results relative to the Individual Protection Requirements (§ 191.15) of the Standard. Chapter 8 describes plans for implementing the Assurance Requirements (§ 191.14) of the Standard. Chapter 9 discusses the relevance of the Groundwater Protection Requirements (§ 191.16) of the Standard to the WIPP. Chapter 10 considers the adequacy of the computational bases for the assessment. Chapter 11 identifies the status of the work necessary for the final performance assessment.

Appendix A contains the full text of the Standard, as promulgated by the EPA in 1985. Appendix B contains comments from the New Mexico Environment Department (NMED) and the Environmental Evaluation Group (EEG) on the *Preliminary Comparison with 40 CFR Part 191, Subpart B for the Waste Isolation Plant, December 1990* (SAND90-2347), and the performance-assessment team's responses to those comments.

The final *Comparison* will be reviewed extensively. The planned organization of the final *Comparison* includes an appendix similar to Appendix B of this report that will present official comments from reviewers outside the DOE and responses to those comments from the performance-assessment team, analogous to the comment-response section typically provided in decision-basis documents. This appendix (B) will appear in each *Preliminary Comparison*.

This report focuses on Subpart B of 40 CFR Part 191. Compliance with other regulatory requirements and analyses for other purposes, such as safety assessments, are discussed in separate documents. The methodology described here is also used for safety assessments.

1.4 Description of the WIPP Project

This section presents the mission of the WIPP Project and identifies the participants in the Project, then briefly describes the physical setting, the repository/shaft system, and the waste.

1.4.1 MISSION

Congress authorized the WIPP in 1979 (Public Law 96-164, 1979) as a research and development facility. The WIPP is designed as a full-scale pilot plant to demonstrate the safe management, storage, and disposal of TRU defense waste. The WIPP performance assessment will help the DOE determine whether the WIPP will isolate wastes from the accessible environment sufficiently well to satisfy the disposal requirements in Subpart B of the Standard. Predictions with respect to compliance with Subpart B of the Standard will provide input to the decision on whether the WIPP will become a disposal facility. That decision is expected upon completion of the performance assessment. The DOE will apply Subpart A of the Standard to the WIPP beginning with the first receipt of TRU waste for the Test Phase (U.S. DOE, 1989a). "Disposal," as defined in the Standard, will occur when the mined repository is sealed and decommissioned.

1.4.2 PARTICIPANTS

The DOE is the implementing agency, as defined in the Standard, for the WIPP Project. The WIPP Project is managed by the DOE WIPP Project Integration Office (Albuquerque, New Mexico) through the DOE WIPP Project Site Office in Carlsbad, New Mexico. The WIPP Project Site Office is assisted by two prime contractors: Westinghouse Electric Corporation (WEC) and Sandia National Laboratories (SNL). The operating contractor is responsible for all facility operations at the WIPP and is also responsible for compliance with Subpart A and with the Assurance Requirements of Subpart B of the Standard. WEC is the management and operating contractor during the Test Phase. SNL, as the scientific program manager for the WIPP, is responsible for developing an understanding of the processes and systems that affect long-term isolation of wastes in the WIPP and applying that understanding to evaluate the long-term WIPP performance and compliance with the Standard. SNL defines and implements experiments both in the laboratory and at the WIPP, develops and

applies models to interpret the experimental data, and develops and applies performance-assessment models (U.S. DOE, 1991b).

The DOE and the State of New Mexico have had an Agreement for Consultation and Cooperation since 1981 (U.S. DOE and State of New Mexico, 1981). This agreement ensures that the State, through the New Mexico Environment Department (NMED), has an active part in assuring that public safety issues are fully addressed. In addition, review of the WIPP Project is provided by the National Research Council's Board of Radioactive Waste Management (BRWM) WIPP Panel, the Advisory Committee on Nuclear Facility Safety, and the Defense Nuclear Facilities Safety Board. The EPA maintains a dialog with the WIPP Project concerning the *Preliminary Comparison* reports. The WIPP also receives close public scrutiny. Finally, the National Defense Authorization Act, Fiscal Year 1989 (Public Law 100-456) assigned the Environmental Evaluation Group (EEG) to the New Mexico Institute of Mining and Technology, with the responsibility for independent technical evaluation of the WIPP with regard to the protection of public health and safety and the protection of the environment.

1.4.3 PHYSICAL SETTING

The characteristics of the WIPP are described in detail in the FEIS (U.S. DOE, 1980a), Lappin et al. (1989), the WIPP *Final Safety Analysis Report* (FSAR) (U.S. DOE, 1990a), the FSEIS (U.S. DOE, 1990c), Brinster (1991), and Beauheim et al. (1991). Additional detailed discussion in the *1991 Preliminary Comparison* is in Chapter 5 of this volume and in Volume 2. The WIPP (Figure 1-4) is in southeastern New Mexico, about 42 km (26 mi) east of Carlsbad, the nearest major population center (pop. 25,000 in the 1990 U.S. census). The area surrounding the WIPP has a small population density. Two smaller communities, Loving (pop. 1,500) and Malaga (pop. 150), are about 33 km (20 mi) to the southwest. Less than 30 permanent residents live within a 16-km (10-mi) radius. The nearest residents live about 5.6 km (3.5 mi) south of the WIPP surface facility (U.S. DOE, 1990a).

The surface of the land within the proposed land-withdrawal boundary has been leased for cattle grazing. At present, none of the ranches within ten miles use well water for human consumption because the water contains large concentrations of total dissolved solids. Drinking water for the WIPP is supplied by pipeline from wells about 30 mi (48 km) north of the area (U.S. DOE, 1990a).

Potash, oil, and gas are the only known important mineral resources. The volumes and locations of these resources are estimated in the FEIS for the

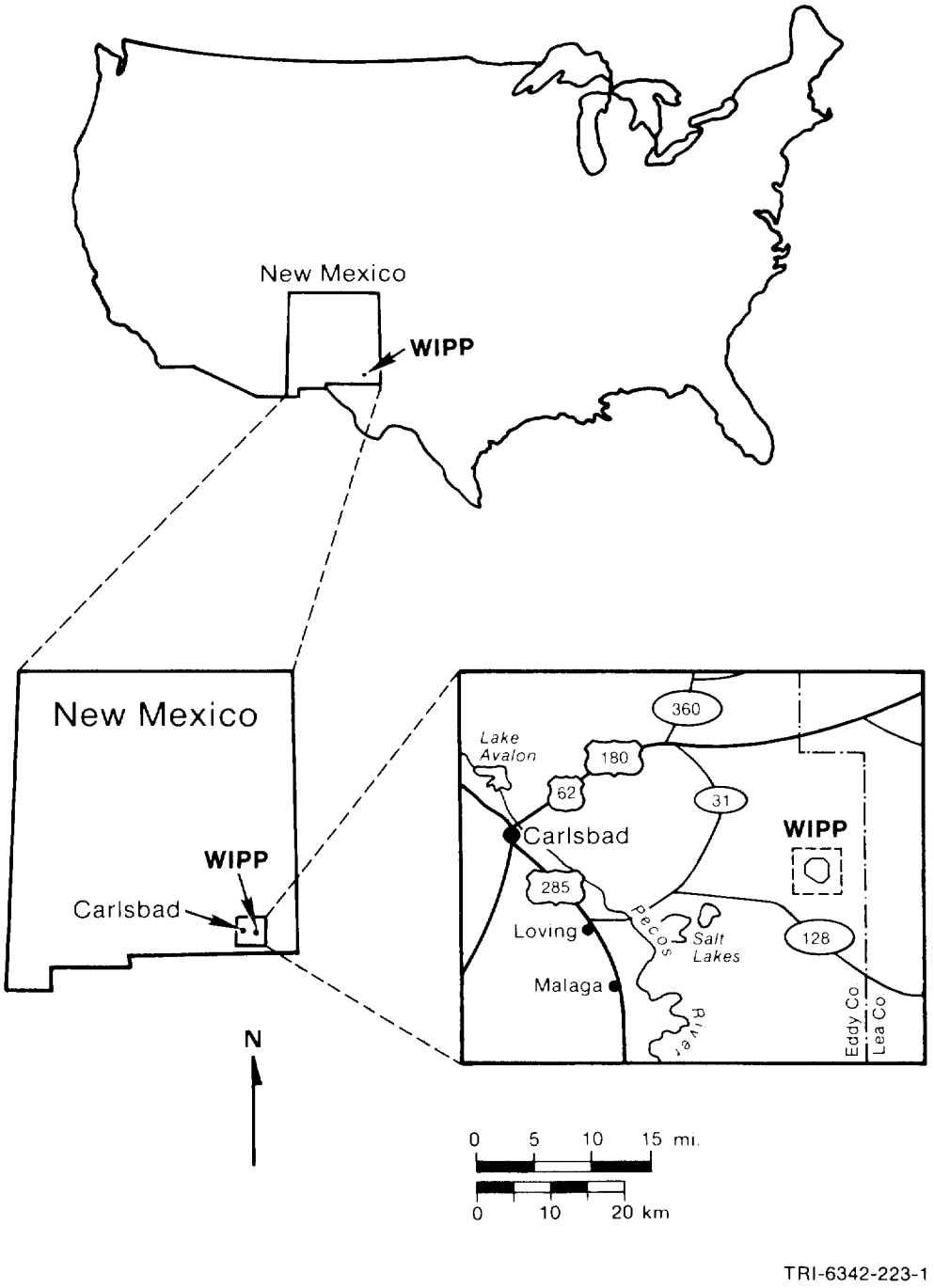

Figure 1-4. WIPP Location Map (after Bertram-Howery and Hunter, 1989a).

WIPP (U.S. DOE, 1980a). The surrounding area is used primarily for grazing, potash mining, and hydrocarbon exploration and production.

About 56 oil and gas wells are within a radius of 16 km (10 mi); the wells generally tap Pennsylvanian strata, about 4,200 m (14,000 ft) deep. The nearest well is about 3 km (2 mi) to the south-southwest of the waste panels. The surface location of the well, which is capable of producing gas, is outside the proposed land-withdrawal boundary, but the borehole is slanted to withdraw gas from rocks within the boundary. Except for this well, resource extraction is not allowed within the proposed land-withdrawal boundary.

Three potash mines and two associated chemical processing plants are between 8 and 16 km (5 and 10 mi) away. Potash mining is possible within a radius of 3 to 8 km (2 to 5 mi) (U.S. DOE, 1990a). The potash zone is about 137 m (450 ft) thick and is encountered about 457 m (1,500 ft) below the surface (Figure 1-5).

The WIPP is in the Delaware Basin between the high plains of West Texas and the Guadalupe Mountains of southeastern New Mexico. Prominent topographic features in the area are Los Medaños ("The Dunes"), Nash Draw, Laguna Grande de la Sal, and the Pecos River (Figures 1-6 and 1-7).

Los Medaños is a region of gently rolling sand dunes that slopes upward to the northeast from Livingston Ridge on the eastern boundary of Nash Draw to a low ridge called "The Divide." The WIPP is in Los Medaños.

Nash Draw, 8 km (5 mi) west of the WIPP, is a broad, shallow topographic depression with no external surface drainage. Nash Draw extends northeast about 35 km (22 mi) from the Pecos River east of Loving, New Mexico, to the Maroon Cliffs area. This feature is bounded on the east by Livingston Ridge and on the west by Quahada Ridge.

Laguna Grande de la Sal, about 9.5 km (6 mi) west-southwest of the WIPP, is a large playa about 3.2 km (2 mi) wide and 4.8 km (3 mi) long formed by coalesced collapse sinks that were created by dissolution of evaporite deposits. In the geologic past, a relatively permanent, saline lake occupied the playa. In recent history, however, the lake has undergone numerous cycles of filling and evaporation in response to wet and arid seasons, and effluent from the potash and oil and gas industries has enlarged the lake. The lake contains fine sand, clay, and evaporite deposits (Bachman, 1974).

The Pecos River, the principal surface-water feature in southeastern New Mexico, flows southeastward, draining into the Rio Grande in western Texas. At its closest point, the river is about 20 km (12 mi) southwest of the WIPP.

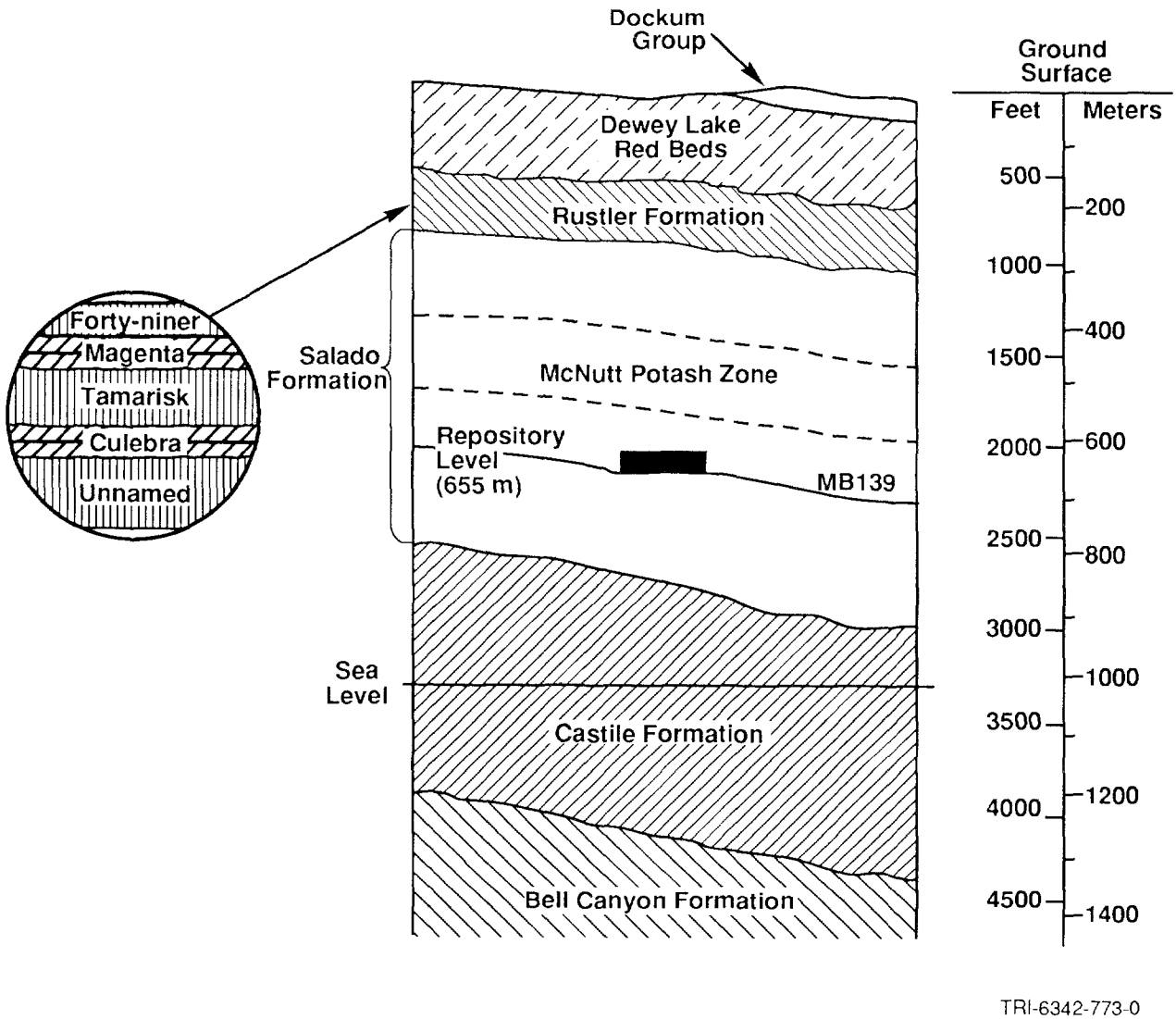

Figure 1-5. Generalized WIPP Stratigraphy (modified from Lappin, 1988).

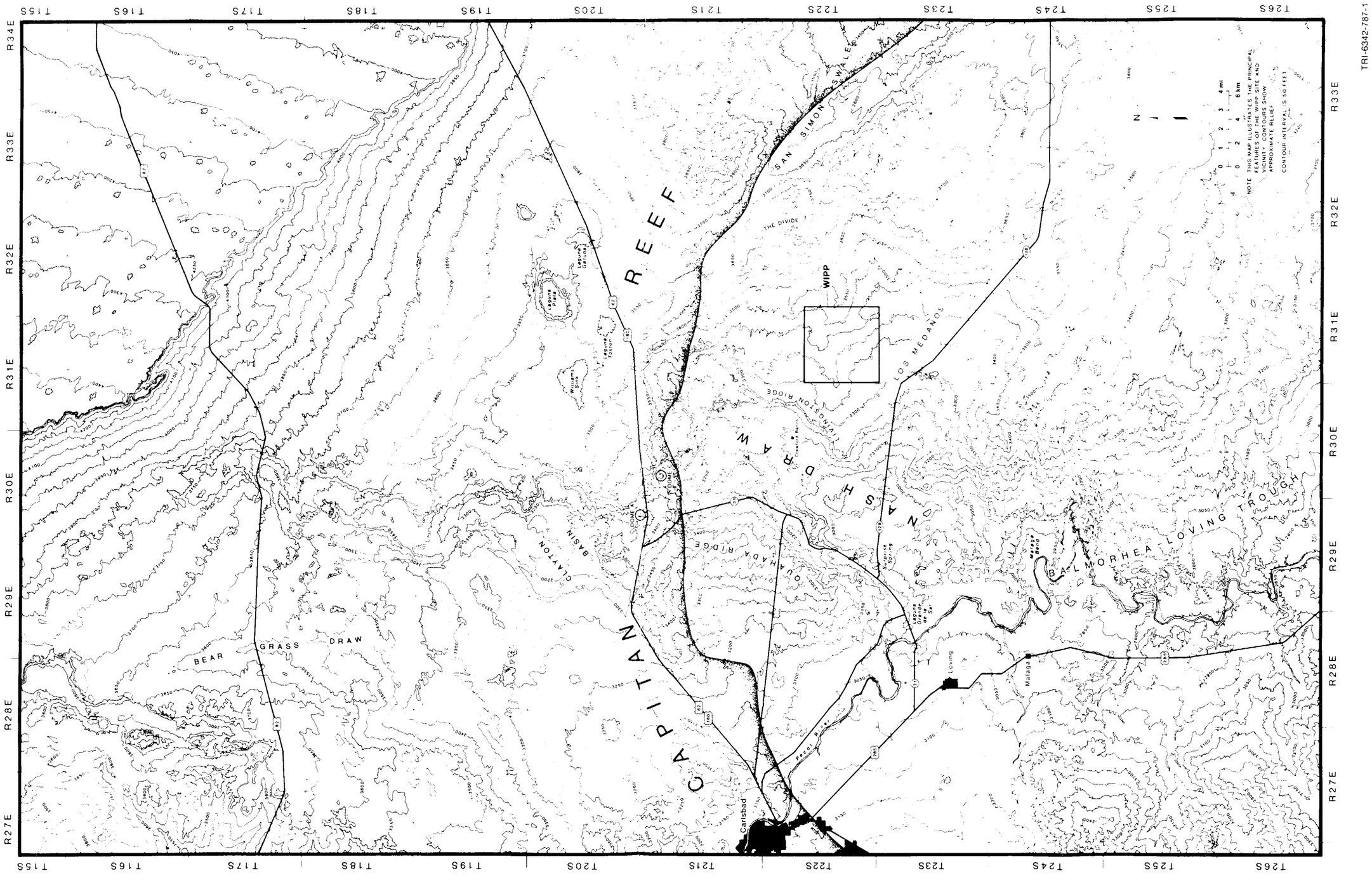

TRI-6342-787-1

Figure 1-6. Topographic Map of the WIPP Area (Bertram-Howery et al., 1990).

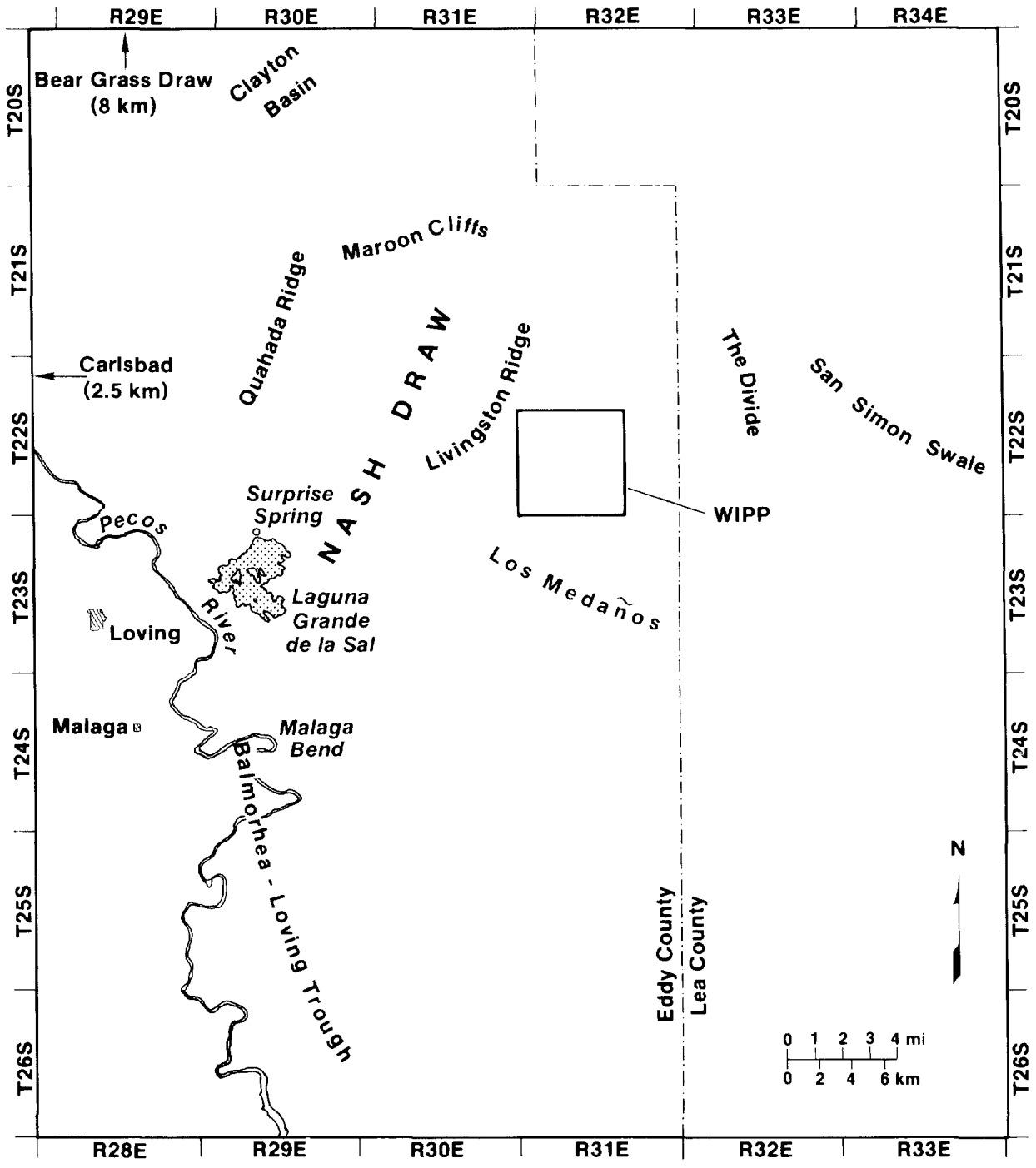

Figure 1-7. Map of the WIPP Area, Showing Physiographic Features (Bertram-Howery et al., 1990).

Surface drainage from the WIPP does not reach the river or its ephemeral tributaries.

Geologic History of the Delaware Basin

The Delaware Basin, an elongated, geologic depression, extends from just north of Carlsbad, New Mexico, into Texas west of Fort Stockton (Figure 1-8). The basin covers over 33,000 km^2 (12,750 mi^2) and is filled to depths as great as 7,300 m (24,000 ft) with sedimentary rocks (Hills, 1984).

Geologic history of the Delaware Basin is contained in Powers et al. (1978a,b); Cheeseman (1978); Williamson (1978); Hiss (1975); Hills (1984); Harms and Williamson (1988); and Ward et al. (1986). A broad, low depression formed about 450 to 500 million years ago during the Ordovician Period as transgressing seas deposited clastic and carbonate sediments. After a long period of accumulation and subsidence, the depression separated into the Delaware and Midland Basins when the area now called the Central Basin Platform uplifted during the Pennsylvanian Period, about 300 million years ago.

Rock units representing the Permian System through the Quaternary System are shown in Table 1-1. During the Early and mid-Permian, the Delaware Basin subsided more rapidly, and a sequence of clastic rocks rimmed by reef limestone formed. The thickest of the reef deposits, the Capitan Limestone, is buried north and east of the WIPP but is exposed at the surface in the Guadalupe Mountains to the west (Figure 1-8). Evaporite deposits of the Castile Formation and the Salado Formation, which hosts the WIPP, filled the basin during the Late Permian and extended over the reef margins. Evaporites, carbonates, and clastic rocks of the Rustler Formation and the Dewey Lake Red Beds were deposited above the Salado Formation before the end of the Permian Period.

Beginning with the Triassic Period and continuing to the present, the geologic record for the area is marked by long periods of nondeposition and erosion. Those formations that are present are either relatively thin or discontinuous and are not included in the performance assessment of the WIPP. Near the repository, the older, Permian-Period deposits below the Dewey Lake Red Beds were not affected by erosional processes during the past 250 million years (Lappin, 1988).

Minimal tectonic activity has occurred in the region since the Permian Period (Hayes, 1964; Williamson, 1978; Hills, 1984; Section 5.1.1-Regional Geology in Chapter 5 of this volume). Faulting during the late Tertiary Period formed the Guadalupe and Delaware Mountains along the western edge of the basin. The most recent igneous activity in the area was during the mid-

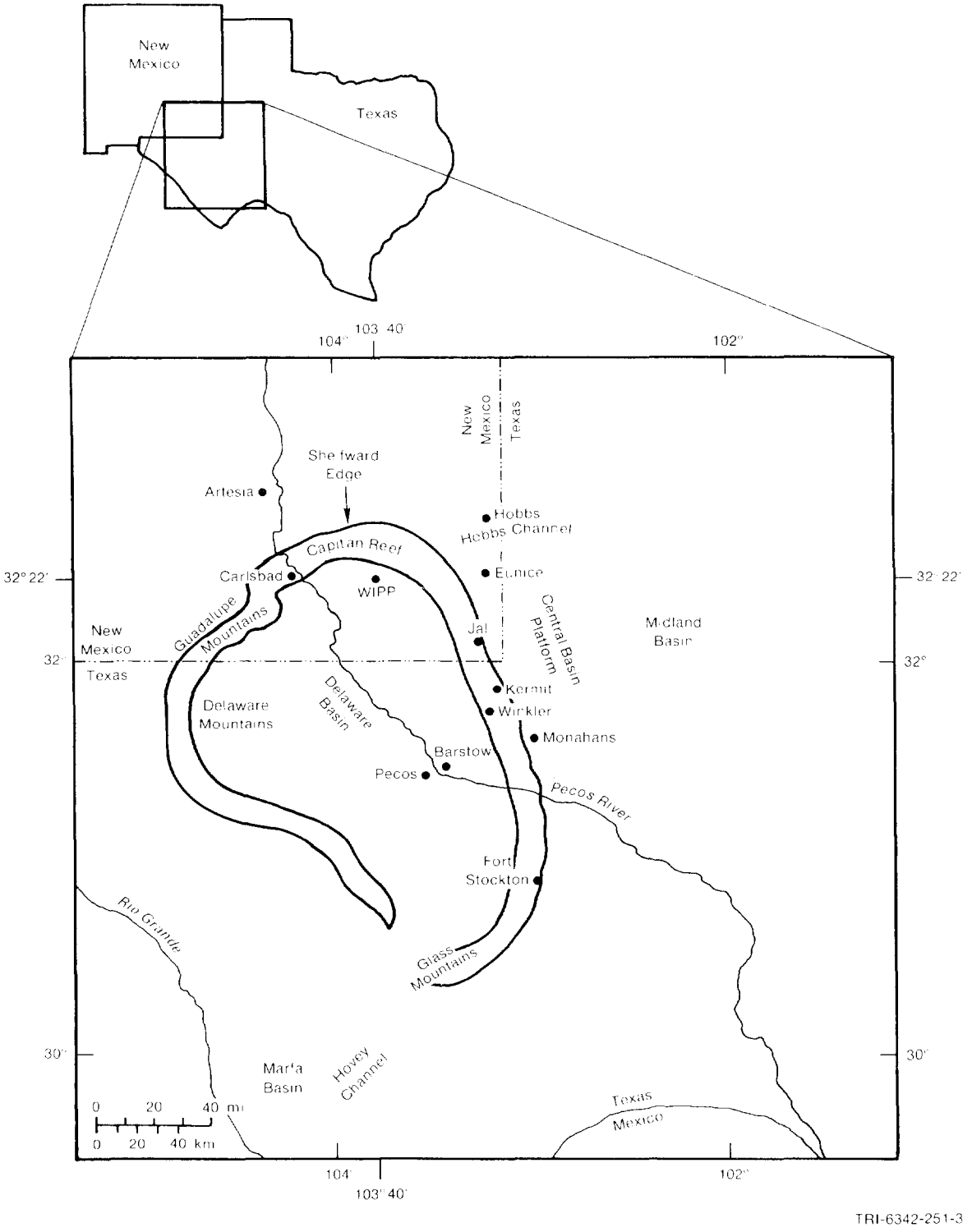

Figure 1-8. Location of the WIPP in the Delaware Basin (modified from Richey et al., 1985).

TABLE 1-1. MAJOR STRATIGRAPHIC DIVISIONS, SOUTHEASTERN NEW MEXICO

Erathem	System	Series	Formation	Age Estimate (yr)
Cenozoic	Quaternary	Holocene	Windblown sand	
		Pleistocene	Mescalero caliche	~500,000
			Gatuña Formation	~600,000±
	Tertiary	Pliocene	Ogallala Formation	5.5 million
		Miocene		24 million
		Oligocene	Absent Southeastern New Mexico	
		Eocene		
		Paleocene		66 million
Mesozoic	Cretaceous	Upper (Late)	Absent Southeastern New Mexico	
		Lower (Early)	Detritus preserved	144 million
	Jurassic		Absent Southeastern New Mexico	208 million
	Triassic	Upper (Late)	Dockum Group	
		Lower (Early)	Absent Southeastern New Mexico	245 million
Paleozoic	Permian, Upper (Late)	Ochoan	Dewey Lake Red Beds, Rustler Formation, Salado Formation, Castile Formation	
	Permian, Upper (Late)	Guadalupian	Capitan Limestone and Bell Canyon Formation	
	Permian, Lower (Early)	Leonardian, Wolfcampian	Bone Springs, Wolfcamp	286 million

Source: Modified from Bachman, 1987

Tertiary Period about 35 million years ago and is evidenced by a dike 16 km (10 mi) northwest of the WIPP (Powers et al., 1978a,b). Major volcanic activity last occurred over 1 billion years ago during Precambrian time (Powers et al., 1978a,b). None of these processes affected the Salado Formation at the WIPP.

Stratigraphy and Geohydrology

The Bell Canyon Formation of the Delaware Mountain Group is the deepest hydrostratigraphic unit being considered in the performance assessment

(Figure 1-5). Understanding fluid flow in the Bell Canyon is necessary because oil and gas drilling into deeper Pennsylvanian strata could penetrate the WIPP and saturated sandstones of the Bell Canyon Formation.

The Castile Formation near the WIPP consists of anhydrite and lesser amounts of halite. The Castile Formation is of interest because it contains discontinuous reservoirs of pressurized brine that could affect repository performance if penetrated by an exploratory borehole. Except where brine reservoirs are present, permeability of the Castile Formation is extremely low, and rates of groundwater flow are too low to affect the disposal system within the next 10,000 years.

The 250-million-year-old Salado Formation is about 600 m (2,000 ft) thick and consists of three informal members:

a lower member, mostly halite with lesser amounts of anhydrite, polyhalite, and glauberite, with some layers of fine clastic material. The unit is 296 to 354 m (960 ft to 1160 ft) thick, and the WIPP repository is located within it, 655 m (2,150 ft) below the land surface (Jones, 1978). Marker Bed 139 (MB139), an anhydritic bed about 1 m in thickness that is a potential pathway for radionuclide transport to the repository shafts, also occurs in this unit, about 1 m or less below the repository (Lappin, 1988).

a middle member, the McNutt Potash Zone, a reddish-orange and brown halite with deposits of sylvite and langbeinite from which potassium salts are mined (Jones, 1978).

an upper member, a reddish-orange to brown halite interbedded with polyhalite, anhydrite, and sandstone (Jones, 1978).

These lithologic layers are nearly horizontal at the WIPP, with a regional dip of less than one degree. The Salado Formation is intact in the WIPP area, and groundwater flow within it is extremely slow because primary porosity and open fractures are lacking in the highly plastic salt (Mercer, 1983). The formation may be saturated throughout the WIPP area, but low effective porosity allows for very little groundwater movement. The Salado Formation is discussed in more detail in Section 5.1.2-Stratigraphy in Chapter 5 of this volume.

The Rustler-Salado contact residuum, a transmissive, saturated zone of dissolution residue, occurs above the halite of the Salado Formation in and near Nash Draw. Brine in the Rustler-Salado contact residuum becomes more concentrated as it moves toward the southwest and is nearly saturated with salt in the lower region of Nash Draw near the Pecos River.

The Rustler Formation, the youngest unit of the Late Permian evaporite sequence, includes units that provide potential pathways for radionuclide migration away from the WIPP. Five units of the Rustler, in ascending order, have been described (Vine, 1963; Mercer, 1983):

the unnamed lower member, composed mostly of fine-grained, silty sandstones and siltstones interbedded with anhydrite west of the WIPP but with increasing amounts of halite to the east.

the Culebra Dolomite Member, a microcrystalline, grayish dolomite or dolomitic limestone with solution cavities containing some gypsum and anhydrite filling.

the Tamarisk Member, composed of anhydrite interbedded with thin layers of claystone and siltstone, with some halite just east of the WIPP.

the Magenta Dolomite Member, a very-fine-grained, greenish-gray dolomite with reddish-purple layers.

the Forty-niner Member, consisting of anhydrite interbedded with a layer of siltstone, with halite present east of the WIPP.

Most groundwater flow in the Rustler Formation occurs in the Culebra Dolomite and Magenta Dolomite Members. The intervening units (the unnamed lower member, the Tamarisk Member, and the Forty-niner Member) are considered aquitards because of their low permeability throughout the area.

Groundwater flow in the Culebra Dolomite Member near the WIPP is apparently north to south (see "Potentiometric Surfaces" in Section 5.1.8-Confined Hydrostratigraphic Units in Chapter 5 of this volume). Recharge is apparently from the north, possibly at Bear Grass Draw where the Rustler Formation is near the surface and at Clayton Basin where karst activity has disrupted the Culebra Dolomite (Mercer, 1983). Discharge is to the west-southwest either into the Pecos River at Malaga Bend (Hale et al., 1954; Hale and Clebsch, 1958; Havens and Wilkens, 1979; Mercer, 1983), into Cenozoic alluvium in the Balmorhea-Loving Trough, which is a series of coalesced, lens-shaped solution troughs formed by an ancestral Pecos River, or into both (Brinster, 1991). Culebra Dolomite Member water contains large concentrations of total dissolved solids (Haug et al., 1987; LaVenue et al., 1988).

Small amounts of water can be produced from the Magenta Dolomite Member from a thin, silty dolomite, along bedding planes of rock units, and along fractures (Mercer, 1983). The unit is present at and near the WIPP but is absent because of erosion in the southern part of Nash Draw. Regionally, flow direction is similar to flow in the Culebra Dolomite Member and is either toward Malaga Bend or more directly southward to the Balmorhea-Loving

Trough. Near the WIPP, flow is locally from east to west, perpendicular to flow in the Culebra.

Rock units younger than the Rustler Formation are believed to be unsaturated throughout most of the WIPP area. However, saturation of these units could occur as a result of climatic changes or breaching a pressurized brine reservoir. Overlying the Rustler Formation are the youngest Permian rocks, the Dewey Lake Red Beds. The Dewey Lake Red Beds consist of alternating layers of reddish-brown, fine-grained sandstones and siltstones cemented with calcite and gypsum (Vine, 1963). Drilling has identified only a few localized zones of relatively high permeability (Mercer, 1983; Beauheim, 1987a). Three wells in the WIPP area produce only small amounts of water from the Dewey Lake Red Beds for livestock (Cooper and Glanzman, 1971).

The Dewey Lake Red Beds are unconformably overlain east of the WIPP by Triassic rocks of the undifferentiated Dockum Group (Figure 1-7). The lower Dockum is composed of poorly sorted, angular, coarse-grained to conglomeratic, thickly bedded material interfingering with shales. The Dockum Group is the chief source of water for domestic and livestock use in eastern Eddy County away from the WIPP and in western Lea County (Nicholson and Clebsch, 1961; Richey et al., 1985). Recharge to the Triassic rocks is mainly from downward flow from overlying alluvium.

A long depositional hiatus occurred from Triassic time to the late Tertiary Period (Table 1-1). No rocks represent the Jurassic or Cretaceous Periods east of the Pecos River near the WIPP. The Tertiary Period is represented by a very thin Ogallala Formation remnant present only at The Divide west of San Simon Swale. The Quaternary Period is represented by the Gatuña Formation, which occurs as discontinuous stream deposits in channels and depressions (Bachman, 1980, 1984; Mercer, 1983); the informally named Mescalero caliche; and localized accumulations of alluvium and dune sands.

1.4.4 REPOSITORY/SHAFT SYSTEM

The WIPP repository is about 655 m (2,150 ft) below the land surface in the bedded salt of the Salado Formation. Present plans call for mining eight panels of seven rooms (Figure 1-9). As each panel is filled with waste, the next panel will be mined. Before the repository is closed permanently, each panel will be backfilled and sealed, waste will be placed in the drifts between the panels and backfilled, comprising two additional panel volumes, and access ways will be sealed off from the shafts. Because the WIPP is a research and development facility, an extensive experimental area is also in use and under construction north of the waste-disposal area (U.S. DOE, 1990b). Additional information on the repository design is in Chapter 5 of this volume.

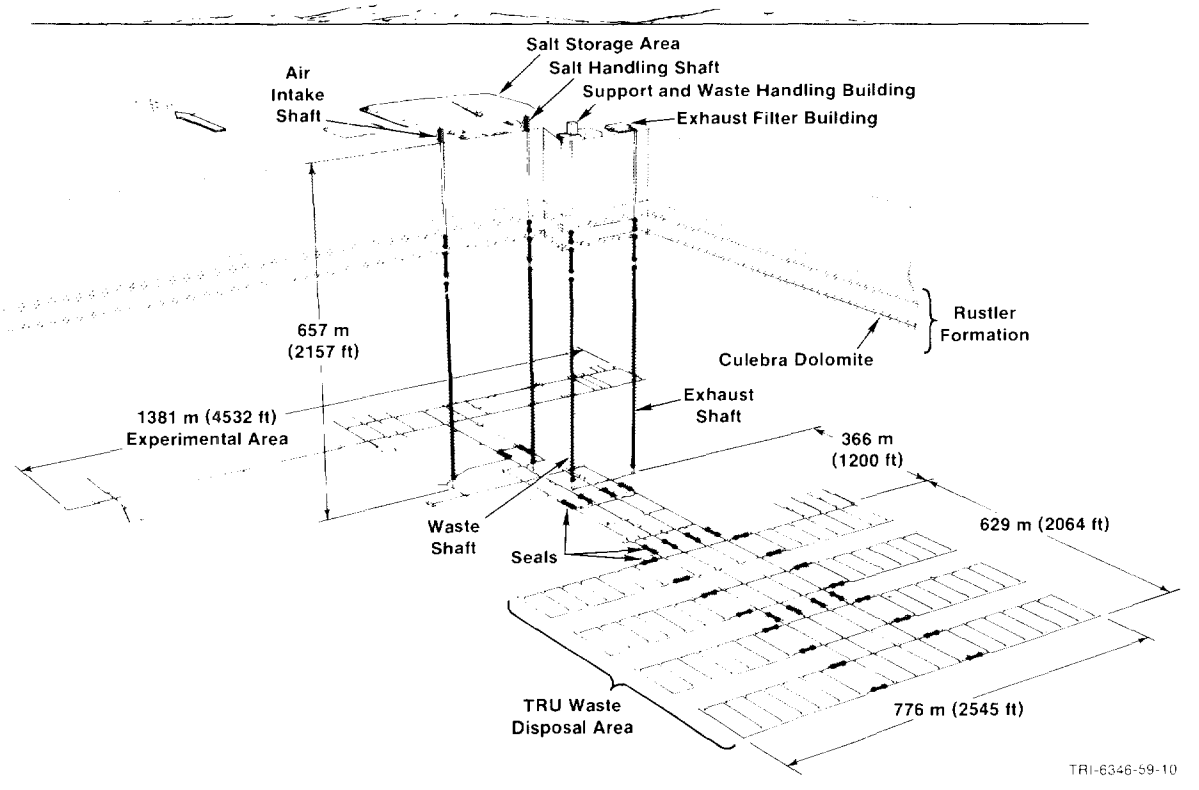

Figure 1-9. Proposed WIPP Repository, Showing Both TRU-Waste Disposal Areas and Experimental Areas (after Waste Management Technology Dept., 1987).

1.4.5 WASTE

The TRU waste for which WIPP is designed is defense-program waste generated by United States government activities since 1970. The waste consists of laboratory and production trash such as glassware, metal pipes, solvents, disposable laboratory clothing, cleaning rags, and solidified sludges. Along with other contaminants, the trash is contaminated by alpha-emitting transuranic (TRU) elements with atomic numbers greater than 92 (uranium), half-lives greater than 20 years, and curie contents greater than 100 nCi/g. Additional contaminants include other radionuclides of uranium and several contaminants with half-lives less than 20 years. Approximately 60 percent of the waste may be co-contaminated with waste considered hazardous under the Resource Conservation and Recovery Act (RCRA). The waste scheduled for disposal at the WIPP is described in more detail in Volume 3 of this report.

In accordance with DOE Order 5820.2A (U.S. DOE, 1980b), heads of DOE Field Organizations can determine that other alpha-contaminated wastes, peculiar to a specific waste-generator site, must be managed as TRU wastes. The WIPP Waste Acceptance Criteria (WAC) determine which TRU wastes will be accepted for emplacement at the WIPP. The most recent draft of the WAC report is currently being prepared (WIPP-DOE-69-Rev. 4), and much of the WAC data used in this report are from the Revision 4 draft. Data used in this report from the draft WAC are not expected to change in the published version. Under current plans, most TRU waste generated since 1970 will be disposed of at the WIPP; a small amount will be disposed of at other DOE facilities. Inventories of the waste to be disposed of at the WIPP are in Volume 3, Chapter 3 of this report.

Waste Form

Alpha-emitting TRU waste, although dangerous if inhaled or ingested, is not hazardous externally and can be safely handled if confined in a sealed container. Most of the waste, therefore, can be contact handled (CH) because the external dose rate (200 mrem/h or less) permits people to handle properly sealed drums and boxes without any special shielding. The only containers that can currently be shipped to the WIPP in a TRUPACT-II (NuPac, 1989) truck-transport container are 55-gallon steel drums, metal standard waste boxes (SWBs), 55-gallon drums packed in an SWB, and an experimental bin overpacked in an SWB (U.S. DOE, 1990c). Additional information on waste containers is in Volume 3, Chapter 3 of this report.

A small portion of the waste volume must be remotely handled (RH); that is, the surface dose rate exceeds 200 mrem/h so that the waste canisters must be packaged for handling and transportation in specially shielded casks. The

surface dose rate of RH-TRU canisters cannot exceed 1,000 rem/h; however, no more than 5 percent of the canisters can exceed 100 rem/h. RH-TRU waste in canisters will be emplaced in holes drilled into the walls of the rooms (U.S. DOE, 1990a).

The WIPP's current design capacity for all radionuclides is 6.2×10^6 ft^3 (approximately 175,000 m^3) containing about 16,000,000 Ci of CH-TRU waste and no more than 5,100,000 Ci of RH-TRU waste. The total curies of RH-TRU waste is limited by the First Modification to the Consultation and Cooperation Agreement (U.S. DOE and State of New Mexico, 1981). The complex analyses for evaluating compliance with Subpart B of the Standard require knowledge of the waste inventory. Therefore, all analyses will be based on current projections of a design volume inventory, estimated at about 532,500 drums and 33,500 boxes of CH-TRU waste. The wastes are classified as retrievably stored or newly generated (future generated). If approved, ten defense facilities eventually will ship TRU waste directly to the WIPP: Idaho National Engineering Laboratory, Rocky Flats Plant, Hanford Reservation, Savannah River Site, Los Alamos National Laboratory, Oak Ridge National Laboratory, Nevada Test Site, Argonne National Laboratory-East, Lawrence Livermore National Laboratory, and Mound Laboratory (U.S. DOE, 1990c). Additional information on inventory estimates is in Volume 3 of this report.

A hazardous constituent of CH-TRU waste is lead that is present as incidental shielding, glovebox parts, and linings of gloves and aprons (U.S. DOE, 1990b). Trace quantities of mercury, barium, chromium, and nickel have also been reported. A significant quantity of aluminum is also identified in CH-TRU waste. An estimate of the quantity of metals and combustibles is discussed in Volume 3 of this report. Sludges contain a solidifier (such as cement), absorbent materials, inorganic compounds, complexing agents, and organic compounds including oils, solvents, alcohols, emulsifiers, surfactants, and detergents. The WAC waste-form requirements designate that the waste material shall be immobilized if greater than 1% by weight is particulate material less than 10 microns in diameter or if greater than 15% by weight is particulate material less than 200 microns in diameter. Only residual liquids in well-drained containers in quantities less than approximately 1% of the container's volume are allowed. Radionuclides in pyrophoric form are limited to less than 1% by weight of the external container, and no explosives or compressed gases are allowed. A list of CH-TRU waste forms identified as also containing trace quantities of hazardous chemical constituents is in Volume 3, Chapter 3 of this report. These hazardous materials are not regulated under 40 CFR Part 191 but are regulated separately by the EPA and New Mexico under the Resource Conservation and Recovery Act (RCRA). Many of these chemicals, if present in significant quantities, could affect the ability of radionuclides to migrate

out of the repository by influencing rates of degradation of the organics, microbial activity, and gas generation. The effects of these processes are being studied.

Radionuclide Inventory

The radionuclide composition of CH-TRU waste varies depending upon the facility and process that generated the waste. The existing RH-TRU waste contains a wide range of radionuclides. An estimate of the CH- and RH-TRU radionuclide inventories is in Volume 3 of this report.

The fissile material content in equivalent grams of plutonium-239 allowed by the WAC for CH-TRU waste is a maximum of 200 g for a 55-gallon drum and 5 g/ft^3 up to 350 g for boxes. An RH-TRU waste package shall not exceed 600 g.

Subpart B of the Standard sets release limits in curies for isotopes of americium, carbon, cesium, iodine, neptunium, plutonium, radium, strontium, technetium, thorium, tin, and uranium, as well as for certain other radionuclides (Appendix A of this volume). Although the initial WIPP inventory contains little or none of some of the listed nuclides, they will be produced as a result of radioactive decay and must be accounted for in the compliance evaluation; moreover, for compliance with the Individual Protection Requirements, any radionuclides not listed in Subpart B must be accounted for if those radionuclides could contribute to doses.

Possible Modifications to Waste Form

If ongoing research does not establish sufficient confidence in acceptable performance or indicates a potential for unacceptable performance, modifications to the waste form or backfill could be required. SNL has conducted preliminary research on possible modifications (Butcher, 1990). The Engineered Alternatives Task Force (EATF), assembled by WEC, identified specific alternatives, ranked alternatives according to specific feasibility criteria, and recommended further research (WEC, 1990; U.S. DOE, 1990d). The DOE will make decisions about testing and, if necessary, implementing alternatives based on the recommendations of the EATF and performance-assessment considerations provided by SNL.

Chapter 1–Synopsis

Purpose of This Report

Before disposing of transuranic (TRU) radioactive waste at the Waste Isolation Pilot Plant (WIPP), the United States Department of Energy (DOE) must have a

reasonable expectation that the WIPP will comply with pertinent regulations. This report considers the regulations promulgated by the Environmental Protection Agency (EPA) as 40 CFR Part 191 (the Standard).

Regulatory compliance will be determined by establishing a reasonable expectation that long-term performance of the WIPP disposal system will meet the requirements of the Standard.

This 1991 report contains the second preliminary assessment of predicted long-term performance of the WIPP but does not yet provide a definitive assessment of compliance.

The Standard

The 1985 Standard is composed of two subparts and two appendixes. The full text of the Standard is in Appendix A of this report.

The U.S. Court of Appeals has vacated Subpart B of the Standard and remanded it to the EPA for clarification.

The WIPP Project has agreed to continue evaluating compliance with the original Standard until a revised Standard is available.

A repromulgated Standard is not expected before 1993.

Subpart A

> applies to a disposal facility prior to decommissioning and contains the standards for management and storage of TRU wastes,
>
> sets limits on the amount of radiation from waste management and storage operations that is acceptable for members of the public outside the waste disposal facility.

This report does not discuss the approach chosen for assessing compliance with Subpart A.

Subpart B

> applies to a disposal facility after it is decommissioned and contains the standards for disposal of TRU wastes,
>
> sets probabilistic limits on cumulative releases of radionuclides to the accessible environment for 10,000 years after disposal (Containment Requirements),

defines qualitative means of increasing confidence in containment (Assurance Requirements),

sets limits on the amount of radiation that is acceptable for members of the public in the accessible environment within or near the specified controlled area for 1,000 years after disposal (Individual Protection Requirements),

sets limits on the acceptable amount of radioactive contamination of certain sources of groundwater within or near the controlled area for 1,000 years after disposal (Groundwater Protection Requirements).

This report discusses the approach for evaluating compliance with Subpart B.

Appendix A specifies how to determine release limits.

Appendix B provides nonmandatory guidance for implementing Subpart B.

A "Reasonable Expectation" of Compliance

Because of the uncertainties in long-term projections, the EPA does not expect absolute proof of the future performance of the disposal system.

The three quantitative requirements in Subpart B of the Standard specify that the disposal system shall be designed to provide a "reasonable expectation" that their quantitative tests can be met.

The EPA intends the qualitative Assurance Requirements to compensate for uncertainties in projecting future performance of the disposal system over 10,000 years.

Application of Additional Regulations to the WIPP

Resource Conservation and Recovery Act (RCRA)

The EPA has issued a conditional "no migration" determination for the WIPP Test Phase. The EPA determined that the DOE had demonstrated, to a reasonable degree of certainty, that hazardous constituents will not migrate from the disposal unit during the Test Phase.

National Environmental Policy Act (NEPA)

The DOE has issued environmental impact statements (EIS) evaluating the effects that disposal of

radioactive wastes at the WIPP would have on the quality of the environment.

The Purpose of the WIPP Project

The WIPP is a full-scale pilot plant for demonstrating the safe management, storage, and disposal of defense-generated, radioactive, transuranic waste.

The long-term performance of the WIPP is being predicted to assess whether the WIPP will isolate wastes from the accessible environment sufficiently well to satisfy the disposal requirements in Subpart B of the Standard.

Upon completion of the performance assessment, the decision will be made on whether the WIPP will become a permenent disposal facility. The DOE will apply Subpart A of the Standard to the WIPP beginning with the first receipt of radionuclides for the Test Phase.

Participants in the WIPP Project

The DOE has overall responsibility for implementing the WIPP Project.

Westinghouse Electric Corporation (WEC) is the management and operating contractor (MOC) during the Test Phase. The MOC is responsible for operations once the decision is made to permanently emplace waste at the WIPP.

Sandia National Laboratories (SNL) provides scientific investigations for evaluating compliance with the long-term performance criteria in Subpart B of the Standard.

New Mexico and the DOE have an agreement for consultation and cooperation for the WIPP.

The Board of Radionuclide Waste Management (BRWM) of the National Research Council, the Advisory Committee on Nuclear Facility Safety, and the Defense Nuclear Facilities Safety Board review the WIPP Project.

The U.S. Congress assigned the Environmental Evaluation Group (EEG) the responsibility of independent technical evaluation of the WIPP.

Physical Setting

The WIPP is in southeastern New Mexico, about 42 km (26 mi) east of Carlsbad, the nearest major population center (pop. 25,000).

Less than 30 permanent residents live within a 16-km (10-mi) radius of the WIPP; the nearest residents live about 5.6 km (3.5 mi) south of the WIPP surface facility.

The quality of well water has always been poor; drinking water for the WIPP is supplied by pipeline.

Potash, oil, and gas are the only known important mineral resources in the area. Subject to valid existing rights, resource extraction is not allowed within the proposed land-withdrawal boundaries.

The WIPP is in the Delaware Basin in an area of gently rolling sand dunes known as Los Medaños.

Minimal tectonic activity has occurred in the region during the past 250 million years. Faulting about 3.5 to 1 million years ago formed the Guadalupe and Delaware Mountains along the western edge of the basin.

The most recent igneous activity in the area was about 35 million years ago; major volcanic activity last occurred over 1 billion years ago. None of these processes affected the Salado Formation at the WIPP.

The Bell Canyon Formation, deposited more than 250 million years ago, is about 600 m (2,000 ft) below the WIPP repository. Exploratory drilling into this formation for oil and gas could penetrate the WIPP.

The Castile Formation, the formation below the rock unit hosting the WIPP, contains discontinuous reservoirs of pressurized brine that could affect repository performance if breached by an exploratory borehole.

The Salado Formation, the bedded salt that hosts the WIPP, has slow groundwater movement because the salt lacks primary porosity and open fractures.

Several rock units above the Salado Formation could provide pathways for radionuclide migration away from the WIPP:

- The Rustler-Salado contact residuum, above the salt of the Salado Formation, contains brine.

- Groundwater flow in the Rustler Formation, above the residuum, is most rapid in the Culebra and Magenta Dolomite Members. Water in the Culebra Dolomite contains high concentrations of total dissolved solids; recharge is apparently an uncertain distance north of the WIPP, and discharge is to the west-southwest.

Units younger than the Rustler Formation are currently unsaturated throughout most of the WIPP area. However,

	climatic changes or breaching a pressurized reservoir could cause saturation in the future.
The WIPP Repository/Shaft System	The WIPP repository is about 655 m (2,150 ft) below the land surface in salt that is 600 m (2,000 ft) thick. Groundwater movement in the bedded salt is extremely slow; the repository has remained dry while it is ventilated, but slow seepage of brine does occur. The WIPP underground workings are composed of four shafts connected to a single underground disposal level. The shafts will be sealed upon decommissioning of the WIPP. The WIPP repository is designed with eight panels (groups) of seven rooms each. As each panel is filled with waste, the next panel will be mined.
Radionuclides Accepted at the WIPP	The TRU waste for which the WIPP is designed is defense-program waste generated by U.S. government activities since 1970. A projected inventory shows that the contaminated waste will typically be composed of laboratory and production trash, including glassware, metal pipes, solvents, disposable laboratory clothing, cleaning rags, and solidified sludges. Approximately 60 percent of the waste may be co-contaminated with waste considered hazardous under the Resource Conservation and Recovery Act (RCRA). Most of the waste has external dose rates so low that people can handle properly sealed drums and boxes without any special shielding. A small portion of the waste has a higher external dose rate and must be remotely handled. Waste canisters will be packaged for handling and transportation in specially shielded casks. For disposal at the WIPP, both contact-handled and remotely handled waste must comply with the WIPP *Waste Acceptance Criteria*.

2. APPLICATION OF SUBPART B TO THE WIPP

[NOTE: The text of Chapter 2 is followed by a synopsis that summarizes essential information, beginning on page 2-16.]

Subpart B of the Standard applies at the WIPP to probabilities of cumulative releases of radionuclides into the accessible environment (§ 191.13) and to annual radiation doses received by members of the public in the accessible environment (§ 191.15) as a result of TRU waste disposal. Actions and procedures are required (§ 191.14) for increasing confidence that the probabilistic release limits will be met at the WIPP. Radioactive contamination of certain sources of groundwater (§ 191.16) in the vicinity of the WIPP disposal system from such TRU wastes would also be regulated, if any of these sources of groundwater were found to be present (U.S. DOE, 1989a). Each of the four requirements of Subpart B and their evaluation by the WIPP Project is discussed in this chapter. The full text of the Standard is reproduced as Appendix A of this volume.

Appendix B to the Standard is EPA's guidance to the implementing agency (in this case, the DOE). In the supplementary information published with the Standard in the *Federal Register* (U.S. EPA, 1985, p. 38069), the EPA stated that it intends the guidance to be followed:

> ...Appendix B...describes certain analytical approaches and assumptions through which the [EPA] intends the various long-term numerical standards of Subpart B to be applied. This guidance is particularly important because there are no precedents for the implementation of such long-term environmental standards, which will require consideration of extensive analytical projections of disposal system performance.

The EPA based Appendix B on analytical assumptions it used to develop the technical basis for the numerical disposal standards. Thus, the EPA "believes it is important that the assumptions used by the [DOE] are compatible with those used by the EPA in developing this rule. Otherwise, implementation of the disposal standards may have effects quite different than those anticipated by EPA" (U.S. EPA, 1985, p. 38074). The DOE compliance approach to the Standard is described in the WIPP *Compliance Strategy* (U.S. DOE, 1989a; also see U.S. DOE, 1990b).

The WIPP compliance assessment for Subpart B is based on four concepts. First, a performance assessment must determine the events that can occur, the likelihood of these events, and the consequences of these events.

Determining the possible events is commonly referred to as scenario development. In general, each combination of events and processes (scenario) is composed of phenomena that could occur at the WIPP. Similarly, evaluating the likelihood of events happening determines probabilities for these scenarios. These probabilities characterize the likelihood that individual scenarios will occur at the WIPP. Determining consequences requires calculating cumulative radionuclide releases or possibly human radiation exposures for individual scenarios. In most cases, such calculations require complex computer models.

Second, as uncertainties will always exist in the results of a performance assessment, the impacts and magnitudes of these uncertainties must be characterized and displayed. Thus, uncertainty analysis and sensitivity analysis are important parts of a performance assessment. Uncertainty analysis characterizes the uncertainty in analysis results that derive from uncertainty in the information on which the analysis is based. Sensitivity analysis attempts to determine the impact that specific information has on the final outcome of an analysis.

Third, no single summary measure can adequately display all the information produced in a performance assessment. Thus, decisions on the acceptability of the WIPP, or any other complex system, must be based on a careful consideration of all available information rather than on a single summary measure. To facilitate informed decisions as to whether "reasonable expectations" exist for the WIPP to comply with Subpart B, the WIPP performance assessment will generate and present results of detailed analyses. Consideration of these results must also include any available qualitative information as prescribed in § 191.13(b).

Fourth, adequate documentation is an essential part of a performance assessment. Obtaining independent peer review and successfully communicating with interested parties requires careful documentation. An extensive effort, therefore, is being devoted to documenting and peer reviewing the WIPP performance assessment and the supporting research, including techniques, models, data, and analyses. Without adequate documentation, informed judgments on the suitability of the WIPP as a waste repository are not possible.

The EPA requirements for radionuclide containment and individual radiation protection drive the performance assessment. Chapter 2 documents the assumptions and interpretations of the Standard used in the performance assessment.

2.1 Containment Requirements

The primary objective of Subpart B is to isolate most of the waste from the accessible environment by limiting probabilities of long-term releases (U.S. EPA, 1985, p. 38070). This objective is reflected in § 191.13, the Containment Requirements.

2.1.1 PERFORMANCE ASSESSMENT

Quantitatively evaluating compliance with 191.13(a) requires a performance assessment, which has specific meaning within the Standard:

> "Performance Assessment" means an analysis that: (1) identifies the processes and events that might affect the disposal system; (2) examines the effects of these processes and events on the performance of the disposal system; and (3) estimates the cumulative releases of radionuclides, considering the associated uncertainties, caused by all significant processes and events. These estimates shall be incorporated into an overall probability distribution of cumulative release to the extent practicable (§ 191.12(q)).

The assessment as defined must provide a reasonable expectation that releases resulting from all significant processes and events that may affect the disposal system for 10,000 years after disposal have (1) a likelihood of less than one chance in ten of exceeding quantities calculated as specified in Appendix A of the rule; and (2) a likelihood of less than one chance in 1,000 of exceeding ten times the specified quantities (§191.13(a)). Numerical limits have been placed not on the predicted cumulative radionuclide releases, but rather on the probability that cumulative releases will exceed quantities calculated as prescribed.

The term "performance assessment" has come to refer to the prediction of all long-term performance, because the performance-assessment methodology, with minor modifications, can also be used to assess compliance with the 1,000-year undisturbed performance for the Individual Protection Requirements. Henceforth, this report will refer to the assessment of compliance with both §191.13(a) of the Containment Requirements and the Individual Protection Requirements as the "performance assessment."

Qualitatively evaluating compliance (§191.13(b)) requires informed judgment by the DOE as to whether the disposal system can reasonably be expected to provide the protection required by §191.13(a). Thus, instead of relying on the performance assessment to prove that future performance of the disposal system will comply, the DOE must examine the numerical predictions from the perspective of the entire record, and judge whether a reasonable expectation exists on that basis.

For the WIPP performance assessment, the disposal system consists of the underground repository, shafts, and the engineered and natural barriers of the disposal site. The engineered barriers are backfill in rooms; seals in drifts and panel entries; backfill and seals in shafts; and plugs in boreholes. Engineered modifications to the repository design could include making the waste a barrier. Natural barriers are the subsurface geologic and hydrologic features within the controlled area that inhibit release and migration of hazardous materials. Barriers are not limited to the examples given in the Standard's definition, nor are those examples mandatory for the WIPP. As recommended by the EPA in Appendix B, "...reasonable projections for the protection expected from all of the engineered and natural barriers...will be considered." No portion will be disregarded, unless that portion of the system makes "negligible contribution to the overall isolation provided" by the WIPP (U.S. DOE, 1989a).

2.1.2 HUMAN INTRUSION

In the Second Modification to the Consultation and Cooperation Agreement, the DOE agreed to prohibit further subsurface mining, drilling, slant drilling under the withdrawal area, or resource exploration unrelated to the WIPP Project on the sixteen square miles to be withdrawn under DOE control. The Standard clearly limits reliance on future institutional control in that "performance assessments...shall not consider any contributions from active institutional controls for more than 100 years after disposal" (§ 191.14(a)). The Standard further requires that "disposal sites shall be designated by the most permanent markers, records, and other passive institutional controls practicable to indicate the dangers of the wastes and their location" (§ 191.14(c)). Analysis of the probability of human intrusion into the repository may include the effectiveness of passive institutional controls over a 9,900-year period because such controls could substantially reduce the probability of intrusion and improve predicted repository performance (Bertram-Howery and Swift, 1990).

Determining compliance with the Standard requires performance assessments that include the probabilities and consequences of disruptive events. The most significant event to affect a disposal system within a salt formation will probably be human intrusion. The EPA noted that salt formations are easy to mine and are often associated with economic resources. Typical examples of human intrusion include but are not limited to exploratory drilling for any reason, mining, or construction of other facilities for reasons unrelated to the repository. The possibility of inadvertent human intrusion into repositories in salt formations because of resource evaluation must be considered, and the use of passive institutional controls to deter

such intrusion should be "taken into account" in performance assessments (U.S. EPA, 1985, p. 38080).

The EPA gives specific guidance in Appendix B of the Standard for considering inadvertent human intrusion. The EPA believes that only realistic possibilities for human intrusion that may be mitigated by design, site selection, and passive institutional controls need be considered. Additionally, the EPA assumes that passive institutional controls should "...reduce the chance of inadvertent intrusion compared to the likelihood if no markers and records were in place." Exploring for subsurface resources requires extensive and organized effort. Because of this effort, information from passive institutional controls is likely to reach resource explorers and deter intrusion into the disposal system (U.S. EPA, 1985, p. 38080). In particular, as long as passive institutional controls "endure and are understood," the guidance states they can be assumed to deter systematic or persistent exploitation of the disposal site, and, furthermore, can reduce the likelihood of inadvertent, intermittent human intrusion. The EPA assumes that exploratory drilling for resources is the most severe intrusion that must be considered (U.S. EPA, 1985). Mining for resources need not be considered within the controlled area (Hunter, 1989).

Effects of the site, design, and passive institutional controls can be used in judging the likelihood and consequences of inadvertent drilling intrusion. The EPA suggests in Appendix B of the Standard that intruders will soon detect or be warned of the incompatibility of their activities with the disposal site by their own exploratory procedures or by passive institutional controls (U.S. EPA, 1985).

Three assumptions relative to human intrusion have been made by the WIPP performance-assessment team:

> No human intrusion of the repository will occur during the period of active institutional controls. Credit for active institutional controls can be taken for no more than 100 years after decommissioning (§ 191.14(a)). The performance assessment will assume active control for the first 100 years.
>
> While passive institutional controls are effective, no advertent resource exploration or exploitation will occur inside the controlled area, but reasonable, site-specific exploitation outside the controlled area may occur. The period of effective passive control will be factored into the performance assessment as soon as specifications for passive controls are developed.
>
> The number of exploratory boreholes assumed to be drilled inside the controlled area through inadvertent human intrusion is to be based on

> site-specific information and, as specified in Appendix B of the Standard (U.S. EPA, 1985, p. 38089), need not exceed 30 boreholes/km^2 (0.4 mi^2) per 10,000 years. No more severe scenarios for human intrusion inside the controlled area need be considered. While passive institutional controls endure, the drilling rate assumed for inadvertent human intrusion will be significantly reduced, although the likelihood cannot be eliminated.

Given the approach chosen by the EPA for defining the disposal standards, repository performance must be predicted probabilistically to quantitatively evaluate compliance. Determining the probability of intrusion poses questions that cannot be answered by numerical modeling or experimentation. Projecting future drilling activity requires knowledge about complex variables such as economic demand for natural resources, institutional control over the site, public awareness of radiation hazards, and changes in exploration technology. Extrapolating present trends 10,000 years into the future requires expert judgment. All approaches to assessing drilling probability presently being considered by SNL will include expert judgment.

2.1.3 RELEASE LIMITS

Appendix A to the Standard establishes release limits for all regulated radionuclides. Table 1 in that appendix gives the limit for cumulative releases to the accessible environment for 10,000 years after disposal for each radionuclide per unit of waste. Note 1(e) to Table 1 defines the unit of waste as an amount of TRU wastes containing one million curies of alpha-emitting transuranic radionuclides with half-lives greater than 20 years. Note 2(b) describes how to develop release limits for a TRU-waste disposal system by determining the waste unit factor, which is the inventory (in curies) of transuranic alpha-emitting radionuclides in the waste with half-lives greater than 20 years divided by one million curies, where transuranic is defined as radionuclides with atomic weights greater than 92 (uranium). Consequently, as currently defined in the Standard, all transuranic radioactivity in the waste cannot be included when calculating the waste unit factor. For the WIPP, 1.186 x 10^7 curies of the radioactivity design total of 1.814 x 10^7 curies comes from transuranic alpha-emitting radionuclides with half-lives greater than 20 years. This number is based on the design radionuclide inventories by waste generator for contact-handled (CH) and remotely handled (RH) waste (Volume 3, Chapter 3 of this report). Regardless of the waste unit, WIPP calculations have assumed that all nuclides in the design radionuclide inventories for CH- and RH-waste are regulated and must be included in the release calculations. Therefore, the release limits used by the WIPP are somewhat reduced and are more restrictive.

Note 6 of Table 1 in the Standard's Appendix A describes the manner in which the release limits are to be used to determine compliance with § 191.13(a): for each radionuclide released, the ratio of the cumulative release to the total release limit for that radionuclide must be determined; ratios for all radionuclides released are then summed for comparison to the requirements of § 191.13(a). Thus, the quantity of a radionuclide that may be safely released depends on the quantities of all other nuclides projected to be released but cannot exceed its own release limit. The summed normalized release cannot exceed 1 for probabilities greater than 0.1, and cannot exceed 10 for probabilities greater than 0.001 but less than 0.1 (§ 191.13(a)). Potential releases estimated to have probabilities less than 0.001 are not limited (§ 191.13(a)). Calculation methods for summed normalized releases are described in more detail in Volume 3, Chapter 3 of this report.

2.1.4 UNCERTAINTIES

The EPA recognized that "[s]tandards must be implemented in the design phase for these disposal systems because active surveillance cannot be relied upon ..." over the very long time of interest. The EPA also recognized that "standards must accommodate large uncertainties, including uncertainties in our current knowledge about disposal system behavior and the inherent uncertainties regarding the distant future" (U.S. EPA, 1985, p. 38070).

Performance assessment requires considering numerous uncertainties in the projected performance of the disposal system. The WIPP Project will use the interpretation of the EPA requirement for uncertainty analysis developed in previous work at SNL for high-level waste disposal (Chapter 3 of this volume; Cranwell et al., 1990; Pepping et al., 1983; Hunter et al., 1986; Cranwell et al., 1987; Campbell and Cranwell, 1988; Rechard, 1989). The EPA has explicitly recognized that performance assessments will contain uncertainties and that many of these uncertainties cannot be eliminated. For the WIPP, uncertainties will be parameter uncertainties, that is, uncertainties about the numerical values in or resulting from data, uncertainties in the conceptual model and its mathematical representation, and scenario uncertainty. The WIPP Project will use expert judgment for parameters or models identified by sensitivity analyses as being important to WIPP performance assessment and for which significant uncertainty exists in the data sets and conceptual models. Thus far, conditional on existing data sets and conceptual models, these parameters include radionuclide solubility, geochemical retardation of radionuclides in the Culebra Dolomite above the repository, dual porosity, permeabilities related to the repository room and its contents, and human-intrusion borehole properties. Data from expert panels quantifying radionuclide concentrations in brines in WIPP waste panels and radionuclide retardation in the Culebra Dolomite are being compiled.

Additional expert panels are planned to quantify other parameters and thus address the uncertainty in using those important data sets and associated conceptual models.

In addition, WIPP performance assessment must also include the potential for human intrusion and the effectiveness of passive institutional controls to deter such intrusion. Including these factors in the WIPP performance assessment requires using expert judgment. An expert panel has already identified future societies' possible technical capabilities, needs, and levels of intelligence. An additional panel is currently developing a marker methodology to maximize both information that could be communicated to future generations and marker lifetimes. Another expert panel may develop strategies concerning barriers to intrusion-by-drilling.

One type of uncertainty that cannot be completely resolved is the validity of various models for predicting disposal system behavior 10,000 years into the future. Although models will be validated (checked for correctness) to the extent possible, expert judgment will be relied upon where validation is not possible. Uncertainties arising from the numerical solutions of a mathematical model are resolved in the process of verifying computer programs. Completeness in scenario development or screening is most appropriately addressed through peer review and probability assignment (U.S. DOE, 1990b).

The WIPP Project will assess and reduce uncertainty to the extent practicable using a variety of techniques (Table 2-1). The techniques in Table 2-1 are typically applied iteratively. The first iteration can include rather crude assumptions leading to preliminary results that help focus these techniques in subsequent iterations. In this manner, the resources required to implement the techniques in Table 2-1 can be directed at the areas of the WIPP performance assessment where the benefits of reducing uncertainty would be the greatest.

The necessity of considering uncertainty in estimated behavior, performance, and cumulative releases is recognized in the Standard in § 191.12(p), § 191.12(q)(3), § 191.13(b), and in Appendix B (U.S. EPA, 1985). Parameter uncertainty is mentioned only in one paragraph in Appendix B, although parameter uncertainty is a major contributor to the other areas of uncertainty. Model uncertainty and scenario uncertainty are not mentioned at all, yet they could be even more important sources of uncertainty than the parameters. Although uncertainties must be addressed, no guidance is provided in the Standard as to how this is to be accomplished.

TABLE 2-1. TECHNIQUES FOR ASSESSING OR REDUCING UNCERTAINTY IN THE WIPP PERFORMANCE ASSESSMENT

Type of Uncertainty	Technique for Assessing or Reducing Uncertainty
Scenarios (Completeness, Logic, and Probabilities)	Expert Judgment and Peer Review Quality Assurance
Conceptual Models	Expert Judgment and Peer Review Sensitivity Analysis Uncertainty Analysis Quality Assurance
Computer Models	Expert Judgment and Peer Review Verification and Validation* Sensitivity Analysis Quality Assurance
Parameter Values and Variability	Expert Judgment and Peer Review Data-Collection Programs Sampling Techniques Sensitivity Analysis Uncertainty Analysis Quality Assurance

*to the extent possible
Source: Bertram-Howery and Hunter, 1989b

2.1.5 COMPLIANCE ASSESSMENT

The Standard assumes that the results of the performance assessment for § 191.13(a) will be incorporated into an overall probability distribution of cumulative release to the extent practicable. In Appendix B, the EPA assumes that, whenever practicable, results can be assembled into a single complementary cumulative distribution function (CCDF) that indicates the probability of exceeding various levels of summed normalized cumulative releases (Figure 2-1).

Descriptions of a procedure for performance assessment based on the construction of a CCDF are available (Cranwell et al., 1990; Pepping et al., 1983; Hunter et al., 1986; Cranwell et al., 1987; Campbell and Cranwell, 1988; and Rechard, 1989). The construction of CCDFs follows from the development of scenario probabilities and the calculation of scenario consequences. Further, the effects of different types of uncertainties can be shown by constructing families of CCDFs and then reducing each family to a

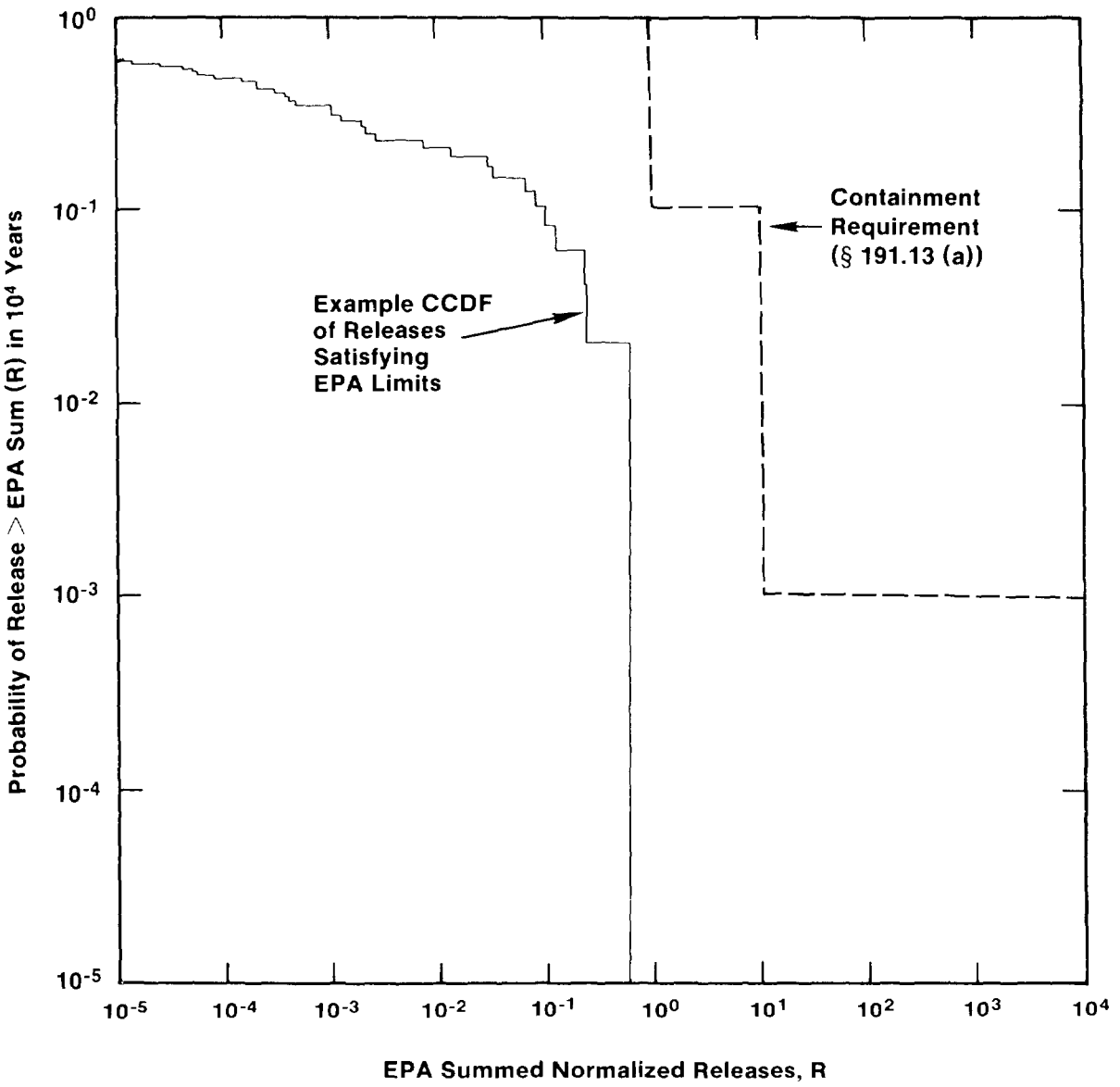

TRI-6342-192-1

Figure 2-1. Hypothetical CCDF Illustrating Compliance with the Containment Requirements (after Marietta et al., 1989).

single CCDF. The construction of families of CCDFs and the single CCDF is described in Chapter 3 of this volume.

The EPA assumes that a single CCDF will incorporate all uncertainty, and if this single distribution function meets the requirement of § 191.13(a), then a disposal system can be considered to be in compliance with the Containment Requirements (U.S. EPA, 1985). Thus, EPA assumes that satisfying the numeric requirements is sufficient to demonstrate compliance with § 191.13(a) but not mandatory. A basis for concluding that a system provides good isolation can include qualitative judgment as well as quantitative results and thus does not totally depend upon the calculated CCDF. The Containment Requirements (§ 191.13(a)) state that, based upon performance assessment, releases shall have probabilities not exceeding specified limits. Noncompliance is implied if the single CCDF suggested by the EPA exceeds the limits; however, § 191.13(b) states that performance assessments need not provide complete assurance that the requirements in § 191.13(a) will be met and that the determination should be "on the basis of the record before the [DOE]." Given the discussions on use of qualitative judgment in Appendix B, this means the entire record, including qualitative judgments. The guidance states that

> it will be appropriate for the [DOE] to make use of rather complex computational models, analytical theories, and prevalent expert judgment relevant to the numerical predictions.... In fact, sole reliance on these numerical predictions to determine compliance may not be appropriate; the [DOE] may choose to supplement such predictions with qualitative judgments as well (U.S. EPA, 1985, p. 38088).

The likelihood that excess releases will occur must be considered in the qualitative decision about a "reasonable expectation" of compliance, but is not necessarily the deciding factor (Bertram-Howery and Swift, 1990).

At present, single-scenario CCDF curves are used extensively in performance-assessment sensitivity analysis for comparing various intermediate results in the modeling process. Such CCDF curves do not establish compliance or noncompliance, but they convey vital information about how changes in selected model parameters may influence performance and compliance (Bertram-Howery and Swift, 1990).

No "final" CCDF curves yet exist. Because probabilities for specific scenarios and many parameter-value distribution functions are still undetermined (see Chapters 4 and 5 of this volume), all CCDF curves presented in Chapter 6 of this volume are preliminary. Although the compliance limits are routinely included on all plots as reference points, the currently available curves cannot be used to judge compliance with the Containment

Requirements because the curves reflect an incomplete modeling system (Volume 2 of this report) and incomplete data (Volume 3 of this report) and because the Standard has not been repromulgated.

2.1.6 MODIFYING THE REQUIREMENTS

The EPA acknowledged that implementation of the Containment Requirements might require modifying those standards in the future. This implementation

> ...will require collection of a great deal of data during site characterization, resolution of the inevitable uncertainties in such information, and adaptation of this information into probabilistic risk assessments. Although [EPA] is currently confident that this will be successfully accomplished, such projections over thousands of years to determine compliance with an environmental regulation are unprecedented. If--after substantial experience with these analyses is acquired--disposal systems that clearly provide good isolation cannot reasonably be shown to comply with the containment requirements, the [EPA] would consider whether modifications to Subpart B were appropriate.
>
> Another situation that might lead to suggested revisions would be if additional information were developed regarding the disposal of certain wastes that appeared to make it inappropriate to retain generally applicable standards addressing all of the wastes covered by this rule (U.S. EPA, 1985, p. 38074).

In discussing the regulatory impacts of the Standard (U.S. EPA, 1985, p. 38083), the EPA acknowledged that no impact analysis had been performed for TRU wastes. The EPA evaluated the costs of the various engineering controls potentially needed for repositories for commercially generated spent fuel or high-level waste to meet different levels of protection for the Containment Requirements and concluded additional precautions beyond those already planned were unnecessary. No such analysis was performed prior to promulgation of the Standard for the only TRU-defense-waste repository, the WIPP. An impact study was recently initiated for TRU-waste repositories, but findings are not yet available.

2.2 Assurance Requirements

The EPA included Assurance Requirements (§ 191.14) in the 1985 Standard to provide confidence the agency believed is needed for long-term compliance with the Containment Requirements by disposal systems not regulated by the NRC. These requirements are designed to complement the Containment Requirements because of the uncertainties involved in predicting long-term performance of disposal systems (U.S. EPA, 1985, p. 38072).

The Assurance Requirements include six provisions: active institutional controls; monitoring after decommissioning to detect performance deviations; passive institutional controls; different types of barriers encompassing both engineered and natural barriers; avoidance of sites where a reasonable expectation of future resource exploration exists, unless favorable disposal characteristics compensate; and the possibility of removal of wastes for a reasonable period of time. Each Assurance Requirement applies to some aspect of uncertainty about long-term containment. Limiting reliance on active institutional controls to 100 years will reduce reliance on future generations to maintain surveillance. Carefully planned monitoring will mitigate against unexpectedly poor system performance going undetected. Markers and records will reduce the chances of systematic and inadvertent intrusion. Multiple barriers, both engineered and natural, will reduce the risk should one type of barrier not perform as expected. Considering future resource potential and demonstrating that the favorable characteristics of the disposal site compensate for the likelihood of disturbance will add to the confidence that the Containment Requirements can be met for the WIPP. A selected disposal system that permits possible future recovery of most of the wastes for a reasonable period of time after disposal will allow future generations the option of relocating the wastes should new developments warrant such recovery (U.S. DOE, 1990b). In promulgating the Standard, the EPA stated that "[t]he intent of this provision was not to make recovery of waste easy or cheap, but merely possible...because the [EPA] believes that future generations should have options to correct any mistakes that this generation might unintentionally make" (U.S. EPA, 1985, p. 38082). The EPA also stated that "any current concept for a mined geologic repository meets this requirement without any additional procedures or design features" (ibid.).

2.3 Individual Protection Requirements

The Individual Protection Requirements (§ 191.15) of the Standard require predicting potential doses to humans resulting from releases to the accessible environment for undisturbed performance during the first 1,000 years after decommissioning of the repository, in the event that performance assessments predict such releases. Although challenges to this requirement contributed to the remand of Subpart B to the EPA, the WIPP Project cannot assume that the requirement will change when the Standard is repromulgated.

The methodology developed for assessing compliance with the Containment Requirements can be used to estimate doses as specified by the Individual Protection Requirements. One of the products of scenario development for the Containment Requirements is a scenario for undisturbed conditions. The

undisturbed performance of the repository is its design-basis behavior and reasonable variations in that behavior resulting from uncertainties in natural barriers and in designing systems and components to function for 10,000 years. Undisturbed performance for the WIPP is understood to mean that uncertainties in such repository features as engineered barriers (backfill, seals, and plugs) must be specifically included in the analysis of the predicted behavior (U.S. DOE, 1990b).

> "Undisturbed performance" means predicted behavior of a disposal system, including consideration of the uncertainties in predicted behavior, if the disposal system is not disrupted by human intrusion or the occurrence of unlikely natural events (§ 191.12(p)).

Human intrusion means any human activity other than those directly related to repository characterization, construction, operation, or monitoring. The effects of intrusion are specifically excluded for the undisturbed performance analysis (U.S. DOE, 1989a).

Unlikely natural events at the WIPP are those events and processes that have not occurred in the past at a sufficient rate to affect the Salado Formation at the repository horizon within the controlled area and potentially cause the release of radionuclides. Only the presence of groundwater has significantly affected the Salado near the WIPP at the repository horizon for the past several million years. Therefore, the WIPP Project will model only groundwater flow and the effects of the repository as the undisturbed performance (U.S. DOE, 1989a). Because of the relative stability of the natural systems within the region of the WIPP disposal system, all naturally occurring events and processes that are expected to occur are part of the base-case scenario and are assumed to represent undisturbed performance (Marietta et al., 1989).

The EPA assumes in Appendix B of the Standard that compliance with § 191.15 "can be determined based upon best estimate predictions" rather than a CCDF. Thus, according to the EPA, when uncertainties are considered, only the mean or median of the appropriate distributions, whichever is greater, need fall below the limits (U.S. EPA, 1985, p. 38088).

The Individual Protection Requirements state that "the annual dose equivalent from the disposal system to any member of the public in the accessible environment" shall not exceed "25 millirems to the whole body or 75 millirems to any critical organ" (§ 191.15). These requirements apply to undisturbed performance of the disposal system, considering all potential release and dose pathways for 1,000 years after disposal. A specifically stated requirement is that modeled individuals be assumed to consume 2 ℓ (0.5 gal)

per day of drinking water from a significant source of groundwater, which is specifically defined in the Standard.

> "Significant source of ground water" ... means: (1) An aquifer that: (i) Is saturated with water having less than 10,000 milligrams per liter of total dissolved solids; (ii) is within 2,500 feet of the land surface; (iii) has a transmissivity greater than 200 gallons per day per foot, provided that any formation or part of a formation included within the source of groundwater has a hydraulic conductivity greater than 2 gallons per day per square foot ...; and (iv) is capable of continuously yielding at least 10,000 gallons per day to a pumped or flowing well for a period of at least a year; or (2) an aquifer that provides the primary source of water for a community water system as of [November 18, 1985] (§ 191.12 (n)).

No water-bearing unit at the WIPP meets the first definition of significant source of groundwater at tested locations within the proposed land withdrawal area. At most well locations, water-bearing units meet neither requirement (i) nor (iii): total dissolved solids exceed 10,000 mg/ℓ and transmissivity is less than 200 gallons per day per foot (26.8 ft^2/day or 2.9 x 10^{-5} m^2/s) (Lappin et al., 1989; Brinster, 1991). Outside the land withdrawal area, however, portions of the Culebra Dolomite Member do meet the requirements of the first definition. The WIPP Project will assume that any portion of an aquifer that meets the first definition is a significant source of groundwater and will examine communication between nonqualifying and qualifying portions. No community water system is being supplied by any aquifer near the WIPP; therefore, no aquifer meets the second definition of significant source of groundwater (U.S. DOE, 1989a).

The Dewey Lake Red Beds are saturated only in some areas. Based on current evaluations, neither the Magenta Dolomite Member nor the Culebra Dolomite Member of the Rustler Formation (Figure 1-5) appears to meet the entire definition of a significant source of groundwater. Aquifers below the Salado Formation are more than 762 m (2,500 ft) below the land surface at the WIPP. The nearest aquifer that meets the first definition of a significant source of groundwater over its entire extent is the alluvial and valley-fill aquifer along the Pecos River. Communication between this aquifer and any other aquifers in the vicinity of the WIPP will be evaluated (U.S. DOE, 1989a). Studies will include reviewing and assessing regional and WIPP drilling records and borehole histories for pertinent hydrologic information (U.S. DOE, 1990b).

No releases from the repository/shaft system are expected to occur within 1,000 years (Lappin et al., 1989; Marietta et al., 1989; Chapter 7 of this volume); therefore, dose predictions for undisturbed performance could be

unnecessary. To date, analyses of undisturbed conditions suggest successful long-term isolation of the waste.

2.4 Groundwater Protection Requirements

Special sources of groundwater are protected from contamination at levels greater than certain limits by the Groundwater Protection Requirements (§ 191.16). There are no special sources of groundwater as defined in § 191.16 at the WIPP; therefore, the requirement to analyze radionuclide concentrations in such groundwater is not relevant to the WIPP (see Chapter 9 of this volume).

Chapter 2-Synopsis

WIPP Compliance Assessment

The WIPP compliance assessment is based on four ideas:

A performance assessment must determine the events that can occur (scenario development), the likelihood of those events, and the consequences of those events.

The impact of uncertainties must be characterized and displayed because uncertainties will always exist in the results of a performance assessment.

No single summary measure can adequately display all the information produced in a performance assessment. Decisions on the acceptability of the WIPP must be based on a careful consideration of all available information, including qualitative information not in the calculations.

Adequate documentation and independent peer review are essential parts of the performance assessment and supporting research.

Containment Requirements

The primary objective of the Containment Requirements of the Standard is to ensure isolation of the radionuclides from the accessible environment by limiting the probability of long-term releases.

Performance Assessment

Subpart B of the Standard defines "performance assessment" as an analysis that

identifies the processes and events that might affect the disposal system,

examines the effects of these processes and events on the performance of the disposal system,

estimates the cumulative releases of radionuclides, considering the associated uncertainties, caused by all significant processes and events.

Disposal systems are to be designed to provide a reasonable expectation, based on performance assessments, that cumulative releases for 10,000 years after disposal from all significant processes and events that may affect the disposal system have

a likelihood of less than one chance in ten of exceeding quantities specified in Appendix A of the Standard,

a likelihood of less than one chance in 1,000 of exceeding ten times the quantities specified in Appendix A of the Standard.

This report refers to the assessment of compliance with both the Containment Requirements and the Individual Protection Requirements as the "WIPP performance assessment."

Probability of Human Intrusion

Performance assessments must consider the probability of human intrusion into the repository within the 9,900-year period after active institutional controls, such as post-operational monitoring, maintaining fences and buildings, and guarding the facility, are assumed to end.

Typical examples of human intrusion include but are not limited to exploratory drilling, mining, or construction of other facilities for reasons unrelated to the repository.

The EPA assumes that exploratory drilling for resources is the most severe intrusion that must be considered.

Performance assessments may consider the effectiveness of passive institutional controls such as permanent markers and records to indicate the dangers of the wastes and their location.

Three assumptions relative to human intrusion at the WIPP have been made by the performance-assessment team:

No human intrusion into the repository will occur during the period of active institutional controls. Credit for active institutional controls can be taken only for 100 years after decommissioning.

While passive institutional controls are effective, no advertent resource exploration or exploitation will occur inside the controlled area, but reasonable, site-specific exploitation outside the controlled area may occur and should be considered in the performance assessment.

No more than 30 exploratory boreholes/km^2 (0.4 mi^2) will be assumed drilled inside the controlled area through inadvertent human intrusion in the 10,000 years of regulatory interest. While passive institutional controls endure, the rate for exploratory drilling may be significantly reduced, although the likelihood cannot be eliminated.

Release Limits

Appendix A to the Standard establishes release limits for all regulated radionuclides, based on a calculated "waste unit factor" that considers alpha-emitting radionuclides with atomic weights greater than 92 (uranium) with half-lives greater than 20 years. Consequently, all TRU waste scheduled for disposal in the WIPP cannot be included when calculating the waste-unit factor.

To determine compliance with § 191.13(a), for each radionuclide released, the ratio of the cumulative release to the total release limit for that radionuclide must be determined. Ratios for all radionuclides released are then summed for comparison to the requirements.

Uncertainties

For the WIPP, uncertainties in parameters, scenarios, and mathematical, conceptual, and computer models are significant considerations.

The WIPP Project will reduce uncertainty to the extent practicable using a variety of techniques that are typically applied iteratively.

Expert judgment will be used for parameters that have significant uncertainty in data sets.

Expert judgment will also be used to include the potential for human intrusion and the effectiveness of passive institutional controls to deter such intrusion.

Models will be validated (checked for correctness) to the extent possible. Expert judgment must be relied upon where validation is not possible.

Compliance Assessment

The EPA suggests that, whenever practicable, the results of the performance assessment be assembled into a single complementary cumulative distribution function (CCDF).

A CCDF is a graphical method of showing the probability of exceeding various levels of cumulative release.

According to the EPA guidance, if the CCDF shows that releases have probabilities that do not exceed specified limits, then a disposal system can be considered to be in compliance with the Containment Requirements.

The CCDF could show that some releases have probabilities that exceed the specified limits; EPA guidance states that compliance should be determined from all information assembled by the DOE, including qualitative judgments.

The likelihood that excess releases will occur must be considered in a qualitative decision about a "reasonable expectation" of compliance but is not necessarily the deciding factor.

No "final" CCDF curves yet exist. Because probabilities for specific scenarios and many parameter-value distribution functions are still undetermined, all CCDF curves presented in this report are preliminary.

Modifying the Requirements

The Containment Requirements could be modified by the EPA if

- complete analyses showed that disposal systems that clearly demonstrated good isolation could not reasonably comply with the requirements,

additional information indicated that the general requirements were too restrictive or not adequate for certain types of waste.

Assurance Requirements

Each Assurance Requirement applies to some aspect of uncertainty about the future relative to long-term containment by

limiting reliance on active institutional controls to 100 years to reduce reliance on future generations to maintain surveillance,

monitoring to mitigate against unexpectedly poor system performance going undetected,

using markers and records to reduce the chances of systematic and inadvertent intrusion,

including multiple barriers, both manmade and natural, to reduce the risk should one type of barrier not perform as expected,

avoiding areas with natural resource potential, unless the favorable characteristics of the area as a disposal site outweigh the possible problems associated with inadvertent human intrusion of the repository,

selecting a disposal system that permits possible future recovery of most of the wastes for a reasonable period of time after disposal, so that future generations have the option of relocating the wastes should new developments warrant such recovery.

Individual Protection Requirements

The Individual Protection Requirements apply only to undisturbed performance and require predicting potential annual doses to humans resulting from releases to the accessible environment during the first 1,000 years after decommissioning of the repository, if performance assessments predict such releases.

The EPA assumes that compliance can be determined based upon "best estimate" predictions rather than a CCDF.

One of the requirements is that individuals be assumed to consume 2 ℓ (0.5 gal) per day of drinking water from a significant source of groundwater. The WIPP Project has concluded that:

	No water-bearing unit at the WIPP met the EPA's first definition of significant source of groundwater everywhere prior to construction of the WIPP (or currently). The WIPP Project will assume that any portion of a water-bearing unit that meets the definition is a significant source of groundwater. No community water system is currently being supplied by any aquifer near the WIPP; therefore, no aquifer meets the second definition of significant source of groundwater. The nearest aquifer that meets the definition of significant source of groundwater over its entire extent is along the Pecos River. Communication between this aquifer and any other aquifers in the vicinity of the WIPP will be evaluated. No releases from the undisturbed repository/shaft system are expected to occur within 1,000 years; therefore, dose predictions for undisturbed performance may be unnecessary.
Groundwater Protection Requirements	Special sources of groundwater are protected from contamination at levels greater than certain limits. No special sources of groundwater are present at the WIPP; therefore, the requirement to predict concentrations of radionuclides in such groundwater is not relevant.

3. PERFORMANCE-ASSESSMENT OVERVIEW

Jon C. Helton[1]

[NOTE: The text of Chapter 3 is followed by a synopsis that summarizes essential information, beginning on page 3-85.]

The design and implementation of a performance assessment is greatly facilitated by a clear conceptual model for the performance assessment itself. The purpose of this chapter is to present such a model and then to indicate how the individual parts of the WIPP performance assessment fit into this model. The WIPP performance assessment is, in effect, a risk assessment. As a result, a conceptual model that has been used for risk assessments for nuclear power plants and other complex systems is also appropriate for the WIPP performance assessment.

3.1 Conceptual Model for WIPP Performance Assessment

3.1.1 RISK

Risk is often defined as consequence times probability or consequence times frequency. However, this definition neither captures the nature of risk as perceived by most individuals nor provides much conceptual guidance on how risk calculations should be performed. Simply put, people are more likely to perceive risk in terms of what can go wrong, how likely things are to go wrong, and what are the consequences of things going wrong. The latter description provides a structure on which both the representation and calculation of risk can be based.

In recognition of this, Kaplan and Garrick (1981) have proposed a representation for risk based on sets of ordered triples. Specifically, they propose that risk be represented by a set R of the form

$$R = \{(S_i, pS_i, \mathbf{cS}_i), i=1, \ldots, nS\}, \quad (3\text{-}1)$$

where

S_i = a set of similar occurrences,

pS_i = probability that an occurrence in the set S_i will take place,

---

[1] Arizona State University, Tempe, Arizona

$\mathbf{cS}_i$ = a vector of consequences associated with S_i,

nS = number of sets selected for consideration,

and the sets S_i have no occurrences in common (i.e., the S_i are disjoint sets). This representation formally decomposes risk into what can happen (the S_i), how likely things are to happen (the pS_i), and the consequences for each set of occurrences (the $\mathbf{cS}_i$). The S_i are typically referred to as "scenarios" in radioactive waste disposal. Similarly, the pS_i are scenario probabilities, and the vector $\mathbf{cS}_i$ contains environmental releases for individual isotopes, the normalized EPA release summed over all isotopes, and possibly other information associated with scenario S_i. The set R in Equation 3-1 will be used as the conceptual model for the WIPP performance assessment.

Although the representation in Equation 3-1 provides a natural conceptual way to view risk, the set R by itself can be difficult to examine. For this reason, the risk results in R are often summarized with complementary cumulative distribution functions (CCDFs). These functions provide a display of the information contained in the probabilities pS_i and the consequences $\mathbf{cS}_i$. With the assumption that a particular consequence result cS in the vector $\mathbf{cS}$ has been ordered so that $cS_i \le cS_{i+1}$ for i=1, ..., nS, the CCDF for this consequence result is the function F defined by

F(x) = probability that cS exceeds a specific consequence value x

$$= \sum_{j=i}^{nS} pS_j, \qquad (3\text{-}2)$$

where i is the smallest integer such that $cS_i > x$. As illustrated in Figure 3-1, F is a step function that represents the probabilities that consequence values on the abscissa will be exceeded. Thus, "exceedance probability curve" is an alternate name for a CCDF that is more suggestive of the information that it displays. To avoid a broken appearance, CCDFs are often plotted in the form shown in Figure 3-2, which is the same as Figure 3-1 except that vertical lines have been added at the discontinuities.

The steps in the CCDFs shown in Figure 3-1 and Figure 3-2 result from the discretization of all possible occurrences into the sets S_1, ..., S_{nS}. Unless the underlying processes are inherently disjoint, the use of more sets S_i will tend to reduce the size of these steps and, in the limit, will lead to a smooth curve. Thus, Equation 3-2 really defines an estimated CCDF. Better estimates can be obtained by using more sets S_i and also by improving the estimates for pS_i and $\mathbf{cS}_i$. However, various constraints, including

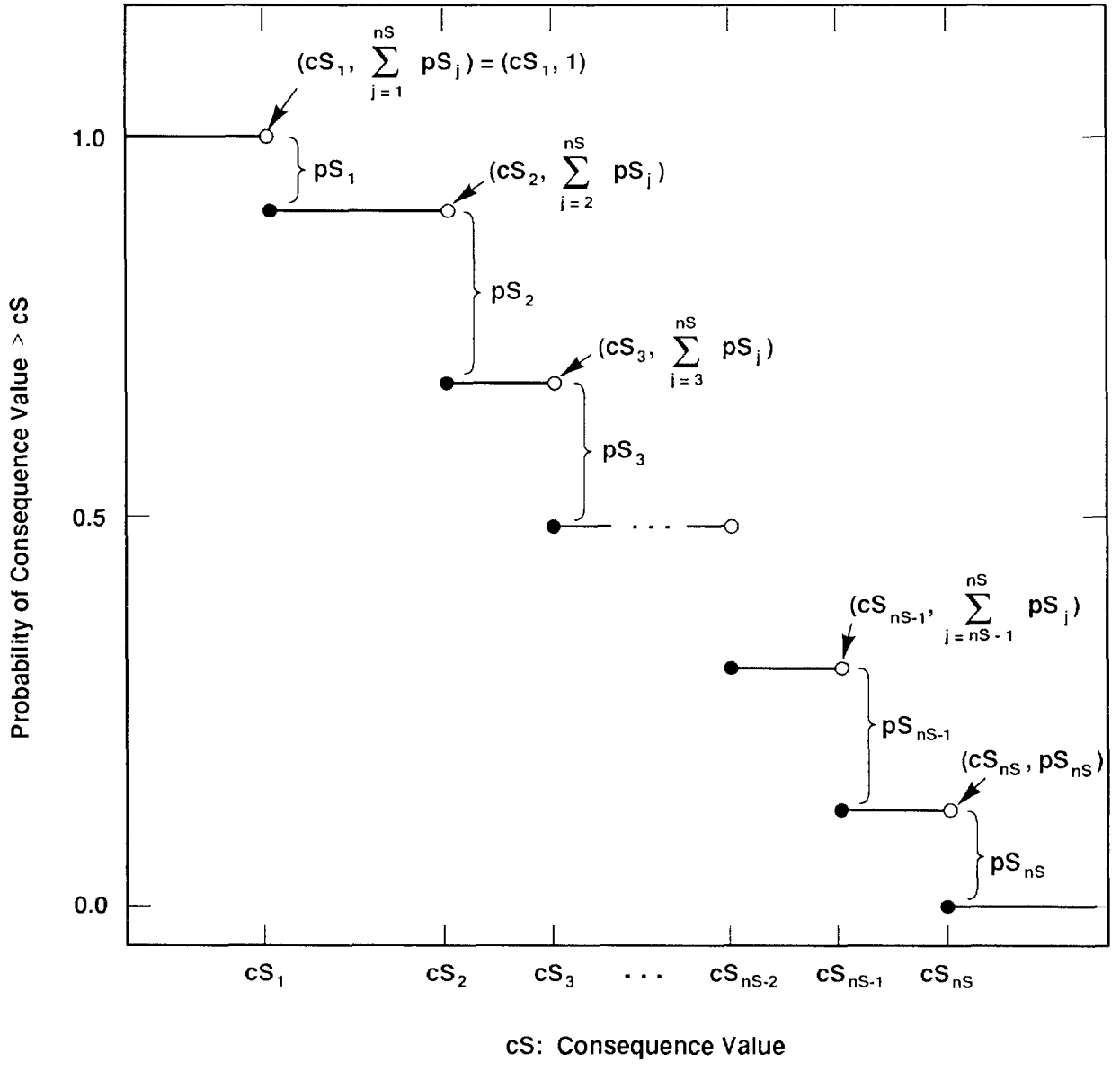

TRI-6342-730-5

Figure 3-1. Estimated CCDF for Consequence Result cS (Helton et al., 1991). The open and solid circles at the discontinuities indicate the points included on (solid circles) and excluded from (open circles) the CCDF.

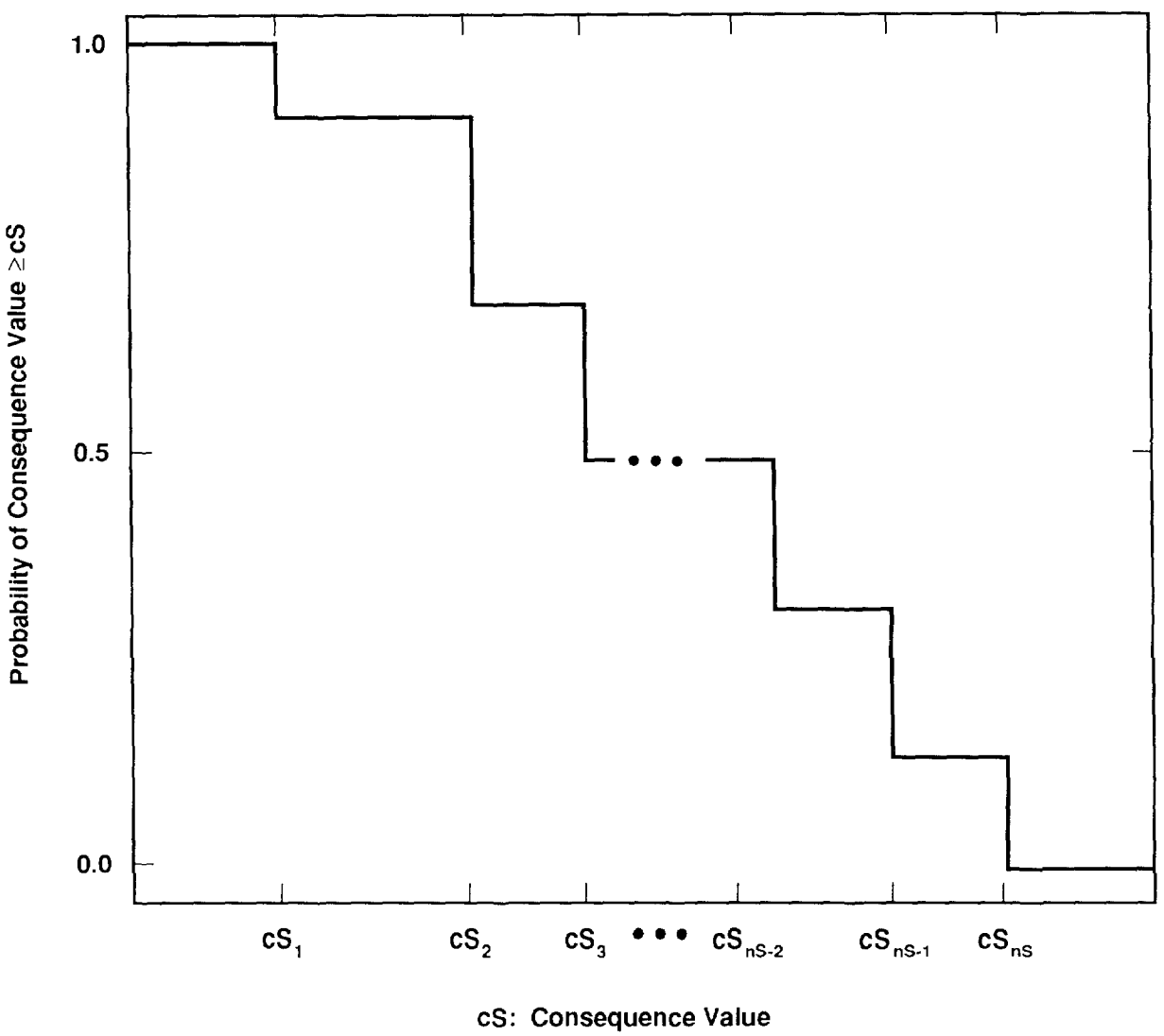

Figure 3-2. Estimated CCDF for Consequence Result cS Including Vertical Lines at the Discontinuities (Helton et al., 1991). This figure is the same as Figure 3-1 except for the addition of the vertical lines at the discontinuities.

available information and computational cost, will always limit how far such efforts can be carried. The consequence result of greatest interest in the WIPP performance assessment is the EPA sum of normalized radionuclide releases to the accessible environment. This sum is one of many predicted quantities (e.g., travel time, dose to humans, ...) that could be the variable on the abscissa in Figures 3-1 and 3-2. However, the normalized release is special in that the Standard places restrictions on certain points on its CCDF. As discussed in Chapter 2 and illustrated in Figure 3-3, the probabilities of exceeding 1 and 10 are required to be less than 0.1 and 0.001, respectively. The CCDF in Figure 3-3 is drawn as a smooth curve, which is the limiting case for a large number of scenarios S_i. If the number of scenarios S_i is small, then the CCDF for the normalized sum will resemble the step functions shown in Figures 3-1 and 3-2, although smoothing procedures can be used to develop continuous approximations to these curves. Additional discussion of the CCDF for normalized releases is given in Section 3.1.4-Risk and the EPA Limits.

3.1.2 UNCERTAINTY IN RISK

A number of factors affect the uncertainty in risk results, including completeness, aggregation, model selection, imprecisely known variables, and stochastic variation. The risk representation in Equation 3-1 provides a convenient structure in which to discuss these uncertainties.

Completeness refers to the extent that a performance assessment includes all possible occurrences for the system under consideration. In terms of the risk representation in Equation 3-1, completeness deals with whether or not all possible occurrences are included in the union of the sets S_i (i.e., in $\cup_i S_i$). Aggregation refers to the division of the possible occurrences into the sets S_i and thus relates to the logic used in the construction of the sets S_i. Resolution is lost if the S_i are defined too coarsely (e.g., nS is too small) or in some other inappropriate manner. Model selection refers to the actual choice of the models for use in a risk assessment. Appropriate model choice is sometimes unclear and can affect both pS_i and $\mathbf{cS}_i$. Similarly, once the models for use have been selected, imprecisely known variables required by these models can affect both pS_i and $\mathbf{cS}_i$. Due to the complex nature of risk assessments, model selection and imprecisely known variables can also affect the definition of the S_i. Stochastic variation is represented by the probabilities pS_i, which are functions of the many factors that affect the occurrence of the individual sets S_i. The CCDFs in Figures 3-1 and 3-2 display the effects of stochastic uncertainty. Even if the probabilities for the individual S_i were known with complete certainty, the ultimate result of a risk assessment would still be CCDFs of the form shown in Figures 3-1 and 3-2.

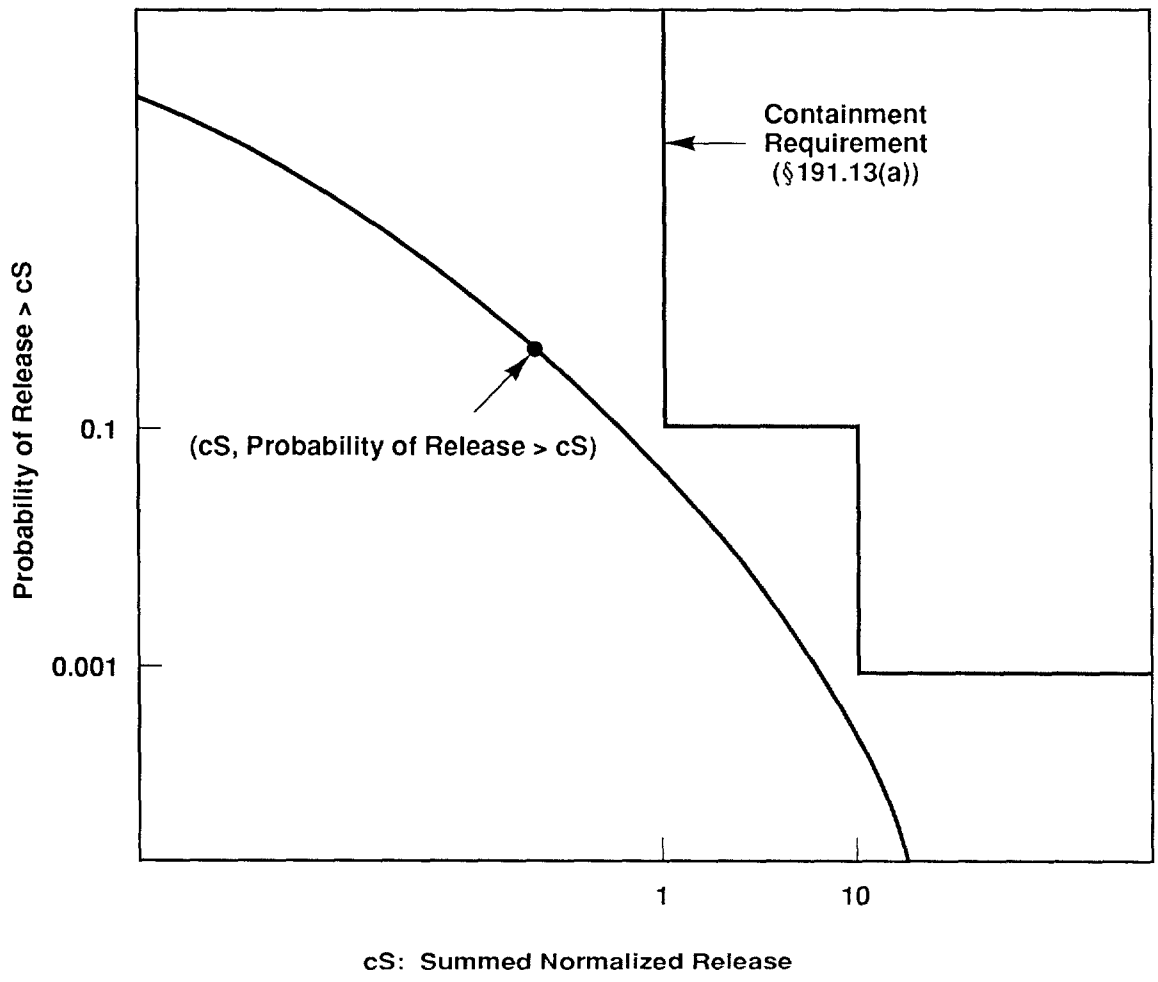

Figure 3-3. Illustration of Hypothetical CCDF for Summed Normalized Release for Containment Requirements (§ 191.13(a)). For a limited number of scenarios, the CCDF will look like the step functions shown in Figures 3-1 and 3-2.

The calculation of risk begins with the determination of the sets S_i. Once these sets are determined, their probabilities pS_i and associated consequences $\mathbf{cS}_i$ must be determined. In practice, development of the S_i is a complex and iterative process that must take into account the procedures required to determine the probabilities pS_i and the consequences $\mathbf{cS}_i$. Typically, the overall process is organized so that pS_i and $\mathbf{cS}_i$ will be calculated by various models whose exact configuration will depend on S_i and which will also require a number of imprecisely known variables. It is also possible that imprecisely known variables could affect the definition of the S_i.

These imprecisely known variables can be represented by a vector

$$\mathbf{x} = [x_1, x_2, \ldots, x_{nV}], \tag{3-3}$$

where each x_j is an imprecisely known input required in the analysis and nV is the total number of such inputs. In concept, the individual x_j could be almost anything, including vectors or functions required by an analysis and indices pertaining to the use of several alternative models. However, an overall analysis, including uncertainty and sensitivity studies is more likely to be successful if the risk representation in Equation 3-1 has been developed so that each x_j is a real-valued quantity for which the overall analysis requires a single value, but it is not known with preciseness what this value should be. With the preceding ideas in mind, the representation for risk in Equation 3-1 can be restated as a function of $\mathbf{x}$:

$$R(\mathbf{x}) = \{(S_i(\mathbf{x}), pS_i(\mathbf{x}), \mathbf{cS}_i(\mathbf{x})), i=1, \ldots, nS(\mathbf{x})\}. \tag{3-4}$$

As $\mathbf{x}$ changes, so will $R(\mathbf{x})$ and all summary measures that can be derived from $R(\mathbf{x})$. Thus, rather than a single CCDF for each consequence value contained in the vector $\mathbf{cS}$ shown in Equation 3-1, a distribution of CCDFs results from the possible values that $\mathbf{x}$ can take on.

The individual variables x_j in $\mathbf{x}$ can relate to different types of uncertainty. Individual variables might relate to completeness uncertainty (e.g., the value for a cutoff used to drop low-probability occurrences from the analysis), aggregation uncertainty (e.g., a bound on the value for nS), model uncertainty (e.g., a 0-1 variable that indicates which of two alternative models should be used), variable uncertainty (e.g., a solubility limit or a retardation for a specific isotope), or stochastic uncertainty (e.g., a variable that helps define the probabilities for the individual S_i).

3.1.3 CHARACTERIZATION OF UNCERTAINTY IN RISK

If the inputs to a performance assessment as represented by the vector **x** in Equation 3-3 are uncertain, then so are the results of the assessment. Characterization of the uncertainty in the results of a performance assessment requires characterization of the uncertainty in **x**. Once the uncertainty in **x** has been characterized, then Monte Carlo techniques can be used to characterize the uncertainty in the risk results.

The outcome of characterizing the uncertainty in **x** is a sequence of probability distributions

$$D_1, D_2, \ldots, D_{nV}, \tag{3-5}$$

where D_j is the distribution developed for the variable x_j, $j=1, 2, \ldots, nV$, contained in **x**. The definition of these distributions may also be accompanied by the specification of correlations and various restrictions that further define the possible relations among the x_j. These distributions and other restrictions probabilistically characterize where the appropriate input to use in the performance assessment might fall given that the analysis is structured so that only one value can be used for each variable under consideration. In most cases, each D_j will be a subjective distribution that is developed from available information through a suitable review process and serves to assemble information from many sources into a form appropriate for use in an integrated analysis. However, it is possible that the D_j may be obtained by classical statistical techniques for some variables.

Once the distributions in Equation 3-5 have been developed, Monte Carlo techniques can be used to determine the uncertainty in $R(\mathbf{x})$ from the uncertainty in **x**. First, a sample

$$\mathbf{x}_k = [x_{k1}, x_{k2}, \ldots, x_{k,nV}], \; k=1, \ldots, nK, \tag{3-6}$$

is generated according to the specified distributions and restrictions, where nK is the size of the sample. The performance assessment is then performed for each sample element $\mathbf{x}_k$, which yields a sequence of risk results of the form

$$R(\mathbf{x}_k) = \{(S_i(\mathbf{x}_k), pS_i(\mathbf{x}_k), \mathbf{cS}_i(\mathbf{x}_k)), \; i=1, \ldots, nS(\mathbf{x}_k)\} \tag{3-7}$$

for k=1, ..., nK. Each set $R(\mathbf{x}_k)$ is the result of one complete performance assessment performed with a set of inputs (i.e., $\mathbf{x}_k$) that the review process producing the distributions in Equation 3-5 concluded was possible. Further, associated with each risk result $R(\mathbf{x}_k)$ in Equation 3-7 is a probability or weight[1] that can be used in making probabilistic statements about the distribution of $R(\mathbf{x})$.

In most performance assessments, CCDFs are the results of greatest interest. For a particular consequence result, a CCDF will be produced for each set $R(\mathbf{x}_k)$ of results shown in Equation 3-5. This yields a distribution of CCDFs of the form shown in Figure 3-4.

Although Figure 3-4 provides a complete summary of the distribution of CCDFs obtained for a particular consequence result by propagating the sample shown in Equation 3-6 through a performance assessment, the figure is hard to read. A less crowded summary can be obtained by plotting the mean value and selected percentile values of the exceedance probabilities shown on the ordinate for each consequence value on the abscissa. For example, the mean plus the 5th, 50th (i.e., median), and 95th percentile values might be used. The mean and percentile values can be obtained from the exceedance probabilities associated with the individual consequence values and the weights or "probabilities" associated with the individual sample elements.[1] The determination of the mean and percentile values for cS = 1 is illustrated in Figure 3-5. If the mean and percentile values associated with individual consequence values are connected, a summary plot of the form shown in Figure 3-6 is obtained. Due to their construction, the percentile curves hold pointwise above the abscissa, and thus, do not define percentile bounds for the distribution of $R(\mathbf{x})$, which is a distribution of functions. However, the mean curve is an estimate for the expected value of this distribution of functions.

The question is often asked: "What is the uncertainty in the results of this performance assessment?" The answer depends on exactly what result of the performance assessment is of concern. In particular, the question is often directed at either (1) the total range of risk outcomes that results from imprecisely known inputs required in the assessment or (2) the uncertainty in quantities that are derived from averaging over the outcomes derived from these inputs.

---

[1] In random or Latin hypercube sampling, this weight is the reciprocal of the sample size (i.e., 1/nK) and can be used in estimating means, cumulative distribution functions, and other statistical properties. This weight is often referred to as the probability for each observation (i.e., sample element $\mathbf{x}_k$). However, this is not technically correct. If continuous distributions are involved, the actual probability of each observation is zero.

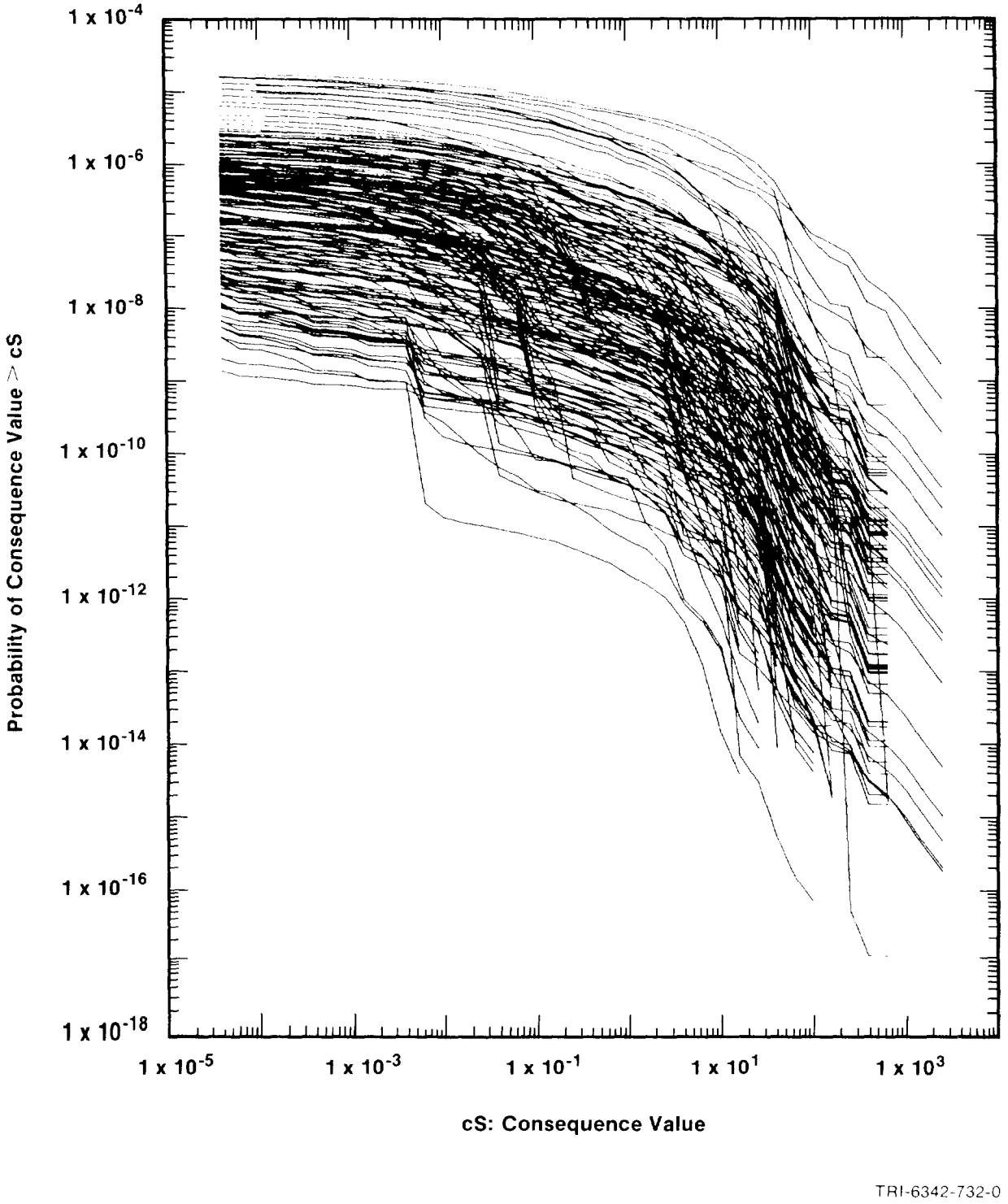

Figure 3-4. Example Distribution of CCDFs Obtained by Sampling Imprecisely Known Variables (after Breeding et al., 1990).

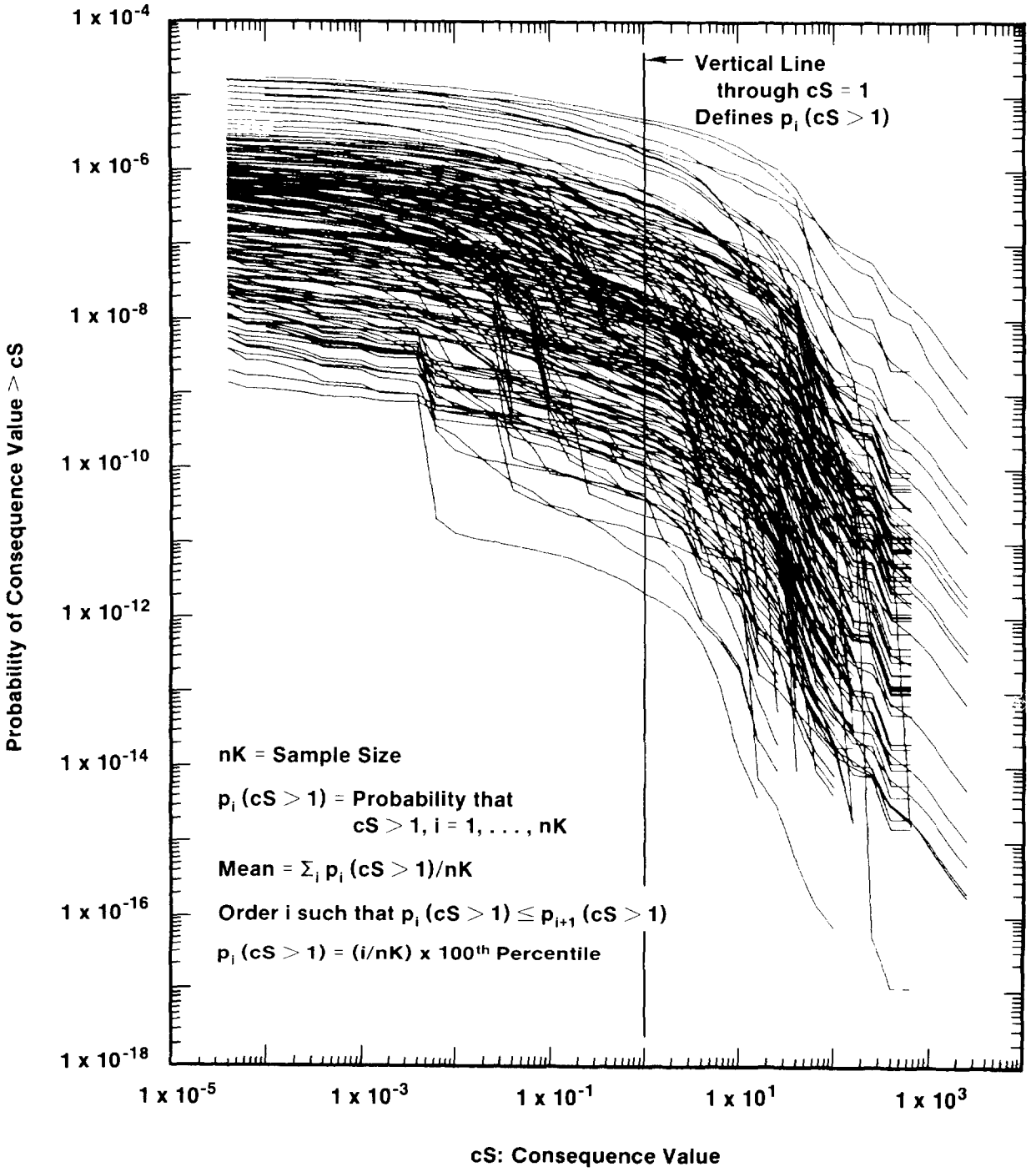

Figure 3-5. Example Determination of Mean and Percentile Values for cS = 1 in Figure 3-4.

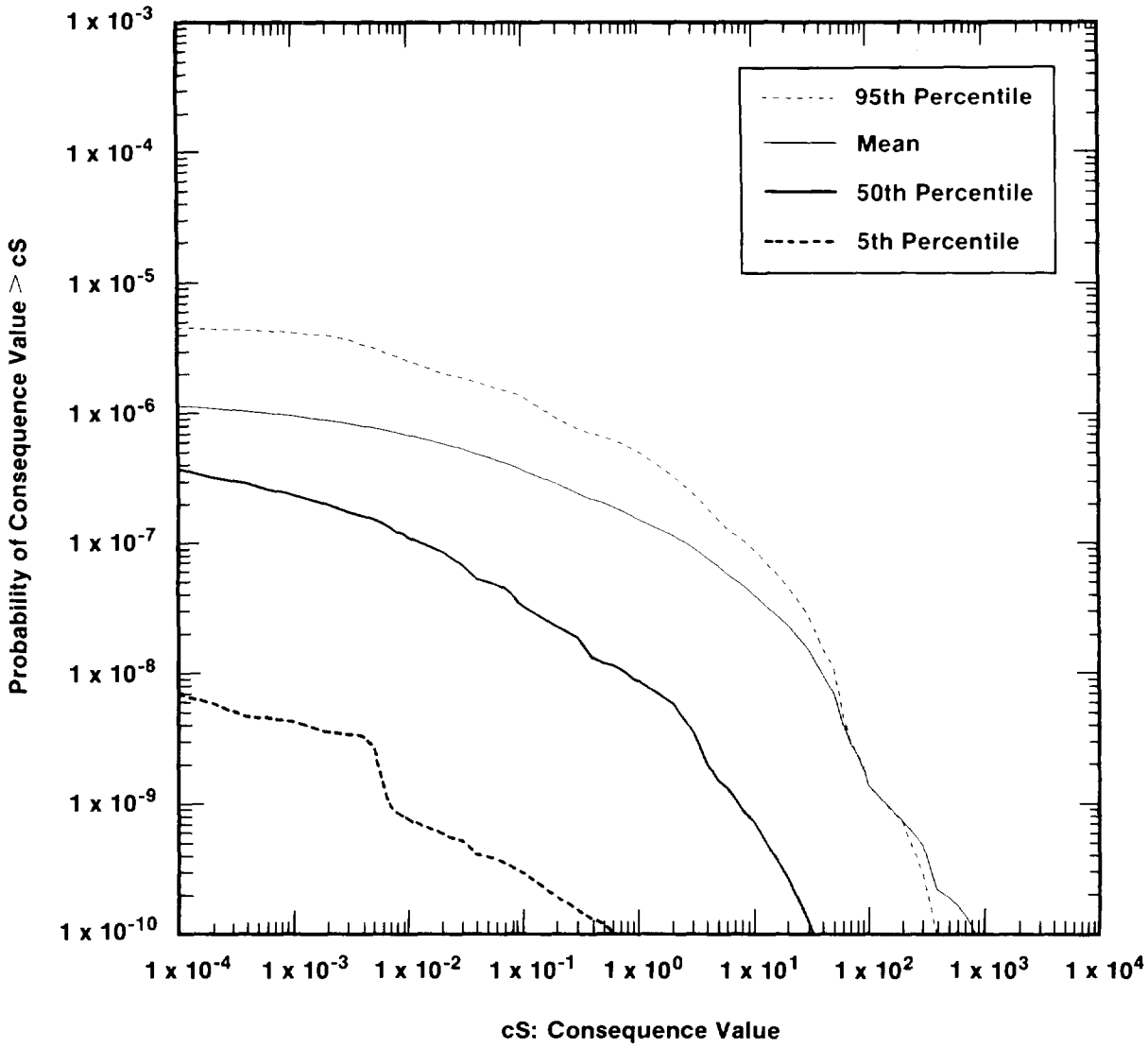

Figure 3-6. Example Summary Curves Derived from an Estimated Distribution of CCDFs (after Breeding et al., 1990). The curves in this figure were obtained by calculating the mean and the indicated percentiles for each consequence value on the abscissa in Figure 3-4 as shown in Figure 3-5. The 95th percentile curve crosses the mean curve due to the highly skewed distributions for exceedance probability. This skewness also results in the mean curve being above the median (i.e., 50th percentile) curve.

The answer to questions of the first type is provided by results of the form shown in Figure 3-4, which displays an estimated distribution for CCDFs conditional on the distributions and models being used in the analysis. The mean and percentile curves in Figure 3-6 summarize the distribution in Figure 3-4. The percentile curves in Figure 3-6 also provide a way to place confidence limits on the risk results in Figure 3-4. For example, the probability is 0.9 that the exceedance probability for a specific consequence value falls between the 5th and 95th percentile values. However, this result is approximate since the percentile values are estimates derived from the sampling procedures and are conditional on the assumed input distributions.

Questions of the second type relate to the uncertainty in estimated means. If a distribution of CCDFs is under consideration, then the "mean" is a mean CCDF of the type shown in Figure 3-6. Because most real-world analyses are very complex, assigning confidence intervals to estimated means by traditional parametric procedures is typically not possible. Replicating the analysis with independently generated samples and then estimating confidence intervals for means from the results of these replications is possible. When three or more replications are used, the t-test (Iman and Conover, 1983) can be used to assign confidence intervals with a procedure suggested by Iman (1981). When only two replications are used, the closeness of the estimated means and possibly other population parameters can indicate the confidence that can be placed in the estimates for these quantities. The results of a comparison of this latter type for the curves in Figure 3-6 are shown in Figure 3-7.

Uncertainty in risk results due to imprecisely known variables and uncertainty in estimates for means and other statistical summaries that result from imprecisely known variables can be displayed in a single plot as shown in Figure 3-8. For figures of this type, the confidence interval for the family of CCDFs would probably be obtained by a sampling-based approach as illustrated in conjunction with Figure 3-6. As indicated earlier, this produces confidence intervals that hold pointwise along the abscissa. Similarly, the mean curve would be obtained by averaging over the same curves that gave rise to the preceding confidence intervals. The confidence intervals for the mean would have to be derived by replicated sampling or some other appropriate statistical procedure.

The point of greatest confusion involving the risk representation in Equation 3-1 is probably the distinction between the uncertainty that gives rise to a single CCDF and the uncertainty that gives rise to a distribution

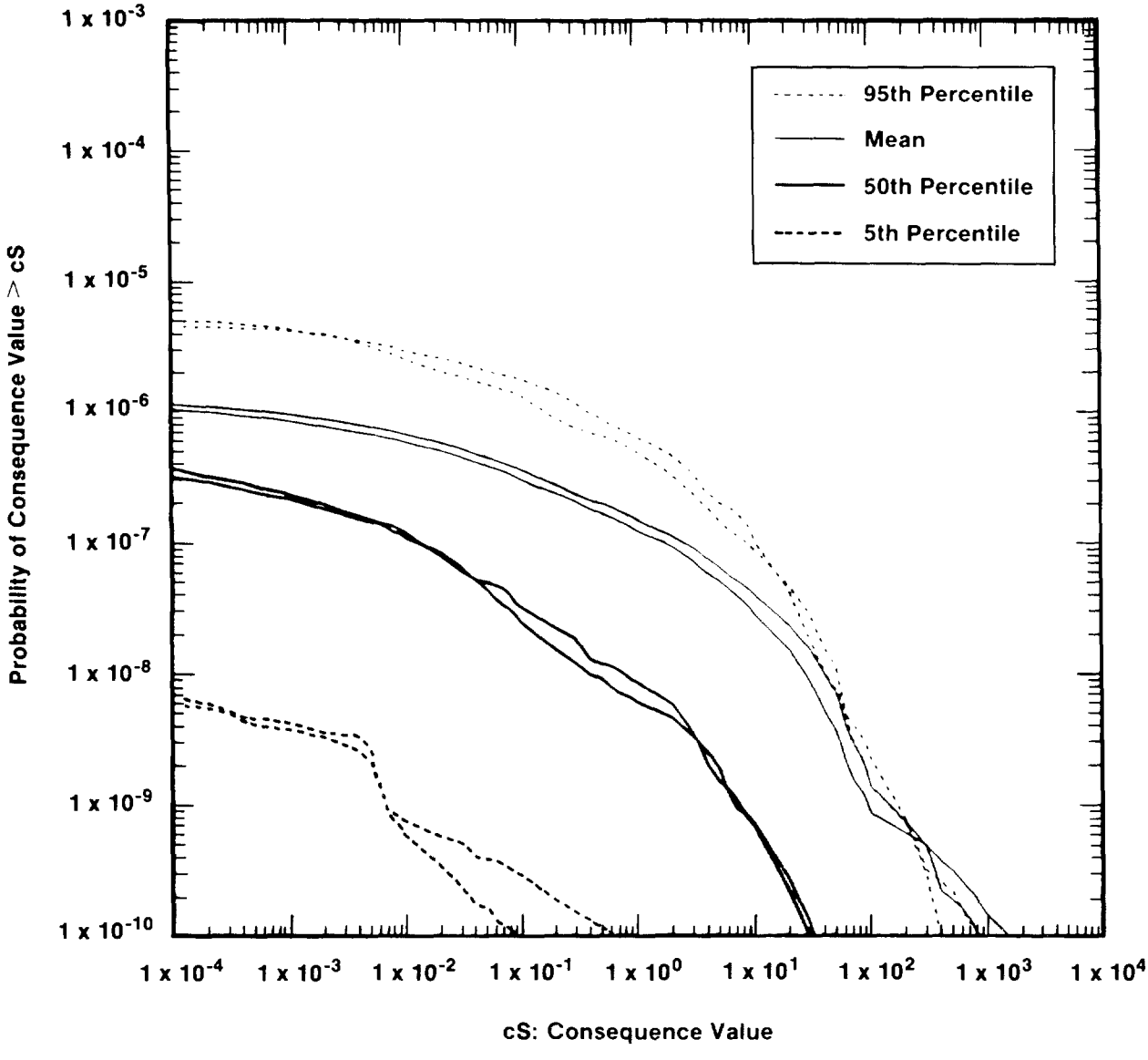

Figure 3-7. Example of Mean and Percentile Curves Obtained with Two Independently Generated Samples for the Results Shown in Figure 3-4 (after Breeding et al., 1990; additional discussion is provided in Iman and Helton, 1991). The two samples have the same number of elements and differ only in the random seed used in their generation.

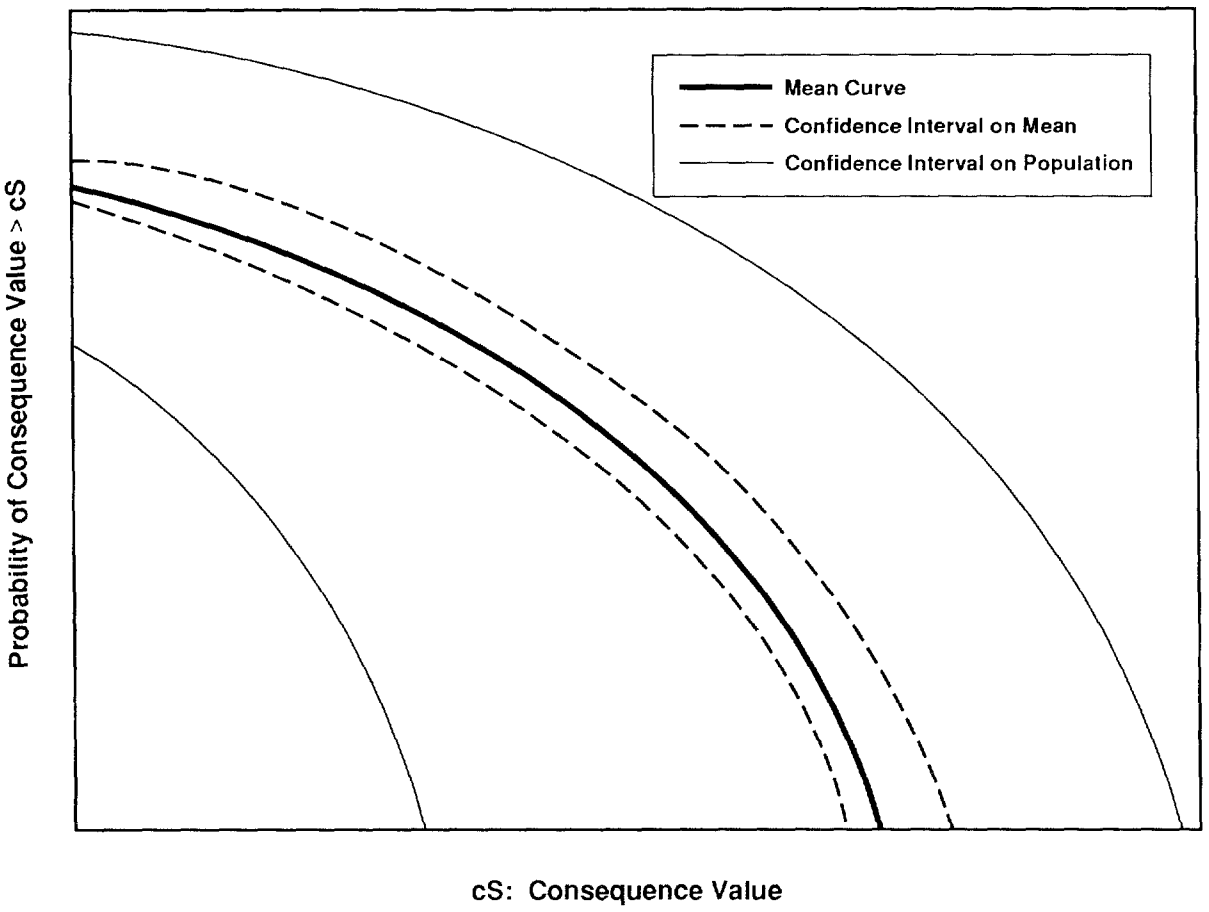

Figure 3-8. Example Confidence Bands for CCDFs (Helton et al., 1991).

of CCDFs. A single CCDF arises from the fact that a number of different occurrences have a real possibility of taking place. This type of uncertainty is referred to as stochastic variation in this report. A distribution of CCDFs arises from the fact that fixed, but unknown, quantities are needed in the estimation of a CCDF. The development of distributions that characterize what the values for these fixed quantities might be leads to a distribution of CCDFs. In essence, a performance assessment can be viewed as a very complex function that estimates a CCDF. Since there is uncertainty in the values of some of the input variables operated on by this function, there will also be uncertainty in the output variable produced by this function, where this output variable is a CCDF.

Both Kaplan and Garrick (1981) and a recent report by the International Atomic Energy Agency (IAEA) (1989) have been very careful to make a distinction between these two types of uncertainty. Specifically, Kaplan and Garrick distinguish between probabilities derived from frequencies and probabilities that characterize degrees of belief. Probabilities derived from frequencies correspond to the probabilities pS_i in Equation 3-1 while probabilities that characterize degrees of belief (i.e., subjective probabilities) correspond to the distributions indicated in Equation 3-5. The IAEA report distinguishes between what it calls Type A uncertainty and Type B uncertainty. The IAEA report defines Type A uncertainty to be stochastic variation; as such, this uncertainty corresponds to the frequency-based probability of Kaplan and Garrick and the pS_i of Equation 3-1. Type B uncertainty is defined to be uncertainty that is due to lack of knowledge about fixed quantities; thus, this uncertainty corresponds to the subjective probability of Kaplan and Garrick and the distributions indicated in Equation 3-5. This distinction has also been made by other authors, including Vesely and Rasmusen (1984), Paté-Cornell (1986) and Parry (1988).

As an example, the WIPP performance assessment includes subjective uncertainty in quantities such as solubility limits, retardation factors, and flow fields. Stochastic uncertainty enters into the analysis through the assumption that future exploratory drilling will be random in time and space (i.e., follow a Poisson process). However, the rate constant λ in the definition of this Poisson process is assumed to be imprecisely known. Thus, there is subjective uncertainty in a quantity used to characterize stochastic uncertainty.

A recent reassessment of the risk from commercial nuclear power plants performed by the U.S. Nuclear Regulatory Commission (U.S. NRC, 1990) has been very careful to preserve the distinction between these two types of uncertainty and provides an example of a very complex analysis in which a significant effort was made to properly incorporate and represent these two different types of uncertainty. Many of the results used for illustration in

this chapter are adapted from that study. A similarly careful effort to represent uncertainty in performance assessment for radioactive waste disposal will greatly facilitate the performance and presentation of analyses intended to assess compliance with the EPA release limits.

3.1.4 RISK AND THE EPA LIMITS

As discussed in Chapter 2 of this volume, the EPA has promulgated the following standard for the long-term performance of geologic repositories for high-level and transuranic (TRU) wastes (1985):

> 191.13 Containment requirements.
>
> (a) Disposal systems for spent nuclear fuel or high-level or transuranic radioactive wastes shall be designed to provide a reasonable expectation, based on performance assessments, that the cumulative releases of radionuclides to the accessible environment for 10,000 years after disposal from all significant processes and events that may affect the disposal system shall:
> (1) Have a likelihood of less than one chance in 10 of exceeding the quantities calculated according to Table 1 (Appendix A); and
> (2) Have a likelihood of less than one chance in 1,000 of exceeding ten times the quantities calculated according to Table 1 (Appendix A).

The term "accessible environment" means: "(1) The atmosphere; (2) land surfaces; (3) surface waters; (4) oceans; and (5) all of the lithosphere that is beyond the controlled area" (U.S. EPA, 1985, 191.12(k)). Further, "controlled area" means: "(1) A surface location, to be identified by passive institutional controls, that encompasses no more than 100 square kilometers and extends horizontally no more than five kilometers in any direction from the outer boundary of the original location of the radioactive wastes in a disposal system; and (2) the subsurface underlying such a surface location" (U.S. EPA, 1985, 191.12(g)). The preceding requirements refer to Table 1 (Appendix A). This table is reproduced here as Table 3-1.

For a release to the accessible environment that involves a mix of radionuclides, the limits in Table 3-1 are used to define a normalized release for comparison with the release limits. Specifically, the normalized release for TRU waste is defined by

$$nR = \sum_i \left(Q_i/L_i\right) \left[1 \times 10^6 \text{ Ci/C}\right] \qquad (3\text{-}8)$$

TABLE 3-1. RELEASE LIMITS FOR THE CONTAINMENT REQUIREMENTS (U.S. EPA, 1985, Appendix A, Table 1)

Radionuclide	Release limit L_i per 1000 MTHM* or other unit of waste (curies)
Americium-241 or -243	100
Carbon 14	100
Cesium-135 or -137	1,000
Iodine-129	100
Neptunium-237	100
Plutonium-238, -239, -240, or -242	100
Radium-226	100
Strontium-90	1,000
Technetium-99	10,000
Thorium-230 or -232	10
Tin-126	1,000
Uranium-233, -234, -235, -236 or -238	100
Any other alpha-emitting radionuclide with a half-life greater than 20 years	100
Any other radionuclide with a half-life greater than 20 years that does not emit alpha particles	1,000

* Metric tons of heavy metal exposed to a burnup between 25,000 megawatt-days per metric ton of heavy metal (MWd/MTHM) and 40,000 MWd/MTHM.

where

Q_i = cumulative release (Ci) of radionuclide i to the accessible environment during the 10,000-yr period following closure of the repository,

L_i = the release limit (Ci) for radionuclide i given in Table 3-1,

and

C = amount of TRU waste (Ci) emplaced in the repository.

For the 1991 WIPP performance assessment, $C = 11.87 \times 10^6$ Ci.

In addition to the previously stated Containment Requirements, the EPA expressly identifies the need to consider the impact of uncertainties in calculations performed to show compliance with these requirements. Specifically, the following statement is made:

> ...whenever practicable, the implementing agency will assemble all of the results of the performance assessments to determine compliance with [section] 191.13 into a "complementary cumulative distribution function" that indicates the probability of exceeding various levels of cumulative release. When the uncertainties in parameters are considered in a performance assessment, the effects of the uncertainties considered can be incorporated into a single such distribution function for each disposal system considered. The Agency assumes that a disposal system can be considered to be in compliance with [section] 191.13 if this single distribution function meets the requirements of [section] 191.13(a) (U.S. EPA, 1985, p. 38088).

The representation for risk in Equation 3-1 provides a conceptual basis for the calculation of the "complementary cumulative distribution function" for normalized releases specified in the EPA standard. Further, this representation provides a structure that can be used for both the incorporation of uncertainties and the representation of the effects of uncertainties.

With respect to the EPA Containment Requirements (§ 191.13(a)), the sets S_i, $i = 1, \ldots, nS$, appearing in Equation 3-1 are simply the scenarios selected for consideration. Ultimately, these scenarios S_i derive from the significant "processes" and "events" referred to in the Standard. These scenarios S_i will always be sets of similar occurrences because any process or event when examined carefully will have many variations. The pS_i are the probabilities for the S_i. Thus, each pS_i is the total probability for all occurrences contained in S_i. Finally, $\mathbf{cS}_i$ is a vector of consequences associated with S_i. Thus, $\mathbf{cS}_i$ is likely to contain the releases to the accessible environment for the individual radionuclides under consideration as well as the associated normalized release. In practice, the total amount of information contained in $\mathbf{cS}_i$ is likely to be quite large.

The preceding ideas are now illustrated with a hypothetical example involving $nS=8$ scenarios $S_1, S_2, \ldots, S_8$. If the probabilities pS_i and consequences $\mathbf{cS}_i$ associated with the S_i were known with certainty, then a single CCDF of the form shown in Figure 3-1 could be constructed for comparison with the EPA release limits. Unfortunately, neither the pS_i nor the $\mathbf{cS}_i$ are likely to be

known with certainty. When this is incorporated into the representation in Equation 3-1, the set R can be expressed as

$$R(\mathbf{x}) = \{(S_i, pS_i(\mathbf{x}), \mathbf{cS}_i(\mathbf{x})), i = 1, \ldots, nS = 8\}, \quad (3\text{-}9)$$

where $\mathbf{x}$ represents a vector of imprecisely known variables required in the estimation of the pS_i and the $\mathbf{cS}_i$. For this example, the S_i are assumed to be fixed and thus are not represented as functions of $\mathbf{x}$ as is done for the more general case shown in Equation 3-4. The effect of uncertainties in $\mathbf{x}$ can be investigated by generating a random or Latin hypercube sample (McKay et al., 1979) from the variables contained in $\mathbf{x}$. This creates a sequence of sets $R(\mathbf{x})$ of the form

$$R(\mathbf{x}_k) = \{(S_i, pS_i(\mathbf{x}_k), \mathbf{cS}_i(\mathbf{x}_k)), i = 1, \ldots, nS = 8\} \quad (3\text{-}10)$$

for k = 1, ..., nK, where $\mathbf{x}_k$ is the value for $\mathbf{x}$ in sample element k and nK is the number of elements in the sample.

As previously illustrated in Figure 3-1, a CCDF can be constructed for each sample element and each consequence measure contained in $\mathbf{cS}$. Figure 3-9 shows what the resultant distribution of CCDFs for the normalized EPA release might look like. Each curve in this figure is a CCDF that would be the appropriate choice for comparison against the EPA requirements if $\mathbf{x}_k$ contained the correct variable values for use in determining the pS_i and $\mathbf{cS}_i$. The distribution of CCDFs in Figure 3-9 reflects the distributions assigned to the sampled variables in $\mathbf{x}$. Actually, what is shown is an approximation to the true distribution of CCDFs, conditional on the assumptions of this analysis. This approximation was obtained with a sample of size nK=40, so 40 CCDFs are displayed, one for each sample element. In general, a larger sample would produce a better approximation but would not alter the fact that the distribution of CCDFs was conditional on the assumptions of the analysis.

Figure 3-9 is rather cluttered and hard to interpret. As discussed in conjunction with Figure 3-6, mean and percentile curves can be used to summarize the family of CCDFs in Figure 3-9. The outcome of this construction is shown in Figure 3-10, which shows the resultant mean curve and the 90th, 50th (median), and 10th percentile curves. The mean curve has generally been proposed for showing compliance with § 191.13(a) (e.g., Cranwell et al., 1990; Cranwell et al., 1987; Hunter et al., 1986).

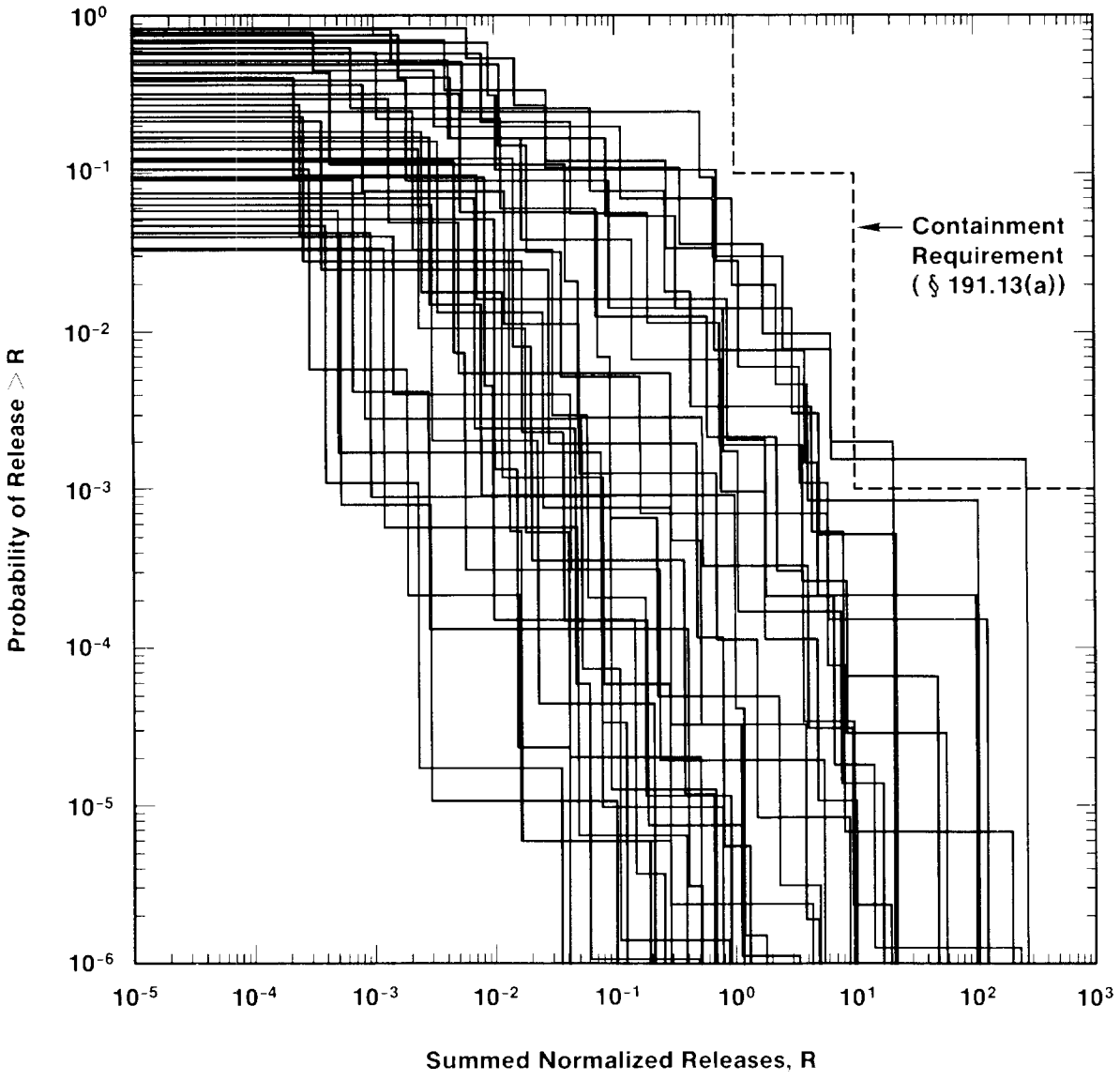

TRI-6342-1299-0

Figure 3-9. Hypothetical Distribution of CCDFs for Comparison with the Containment Requirements (§ 191.13(a)).

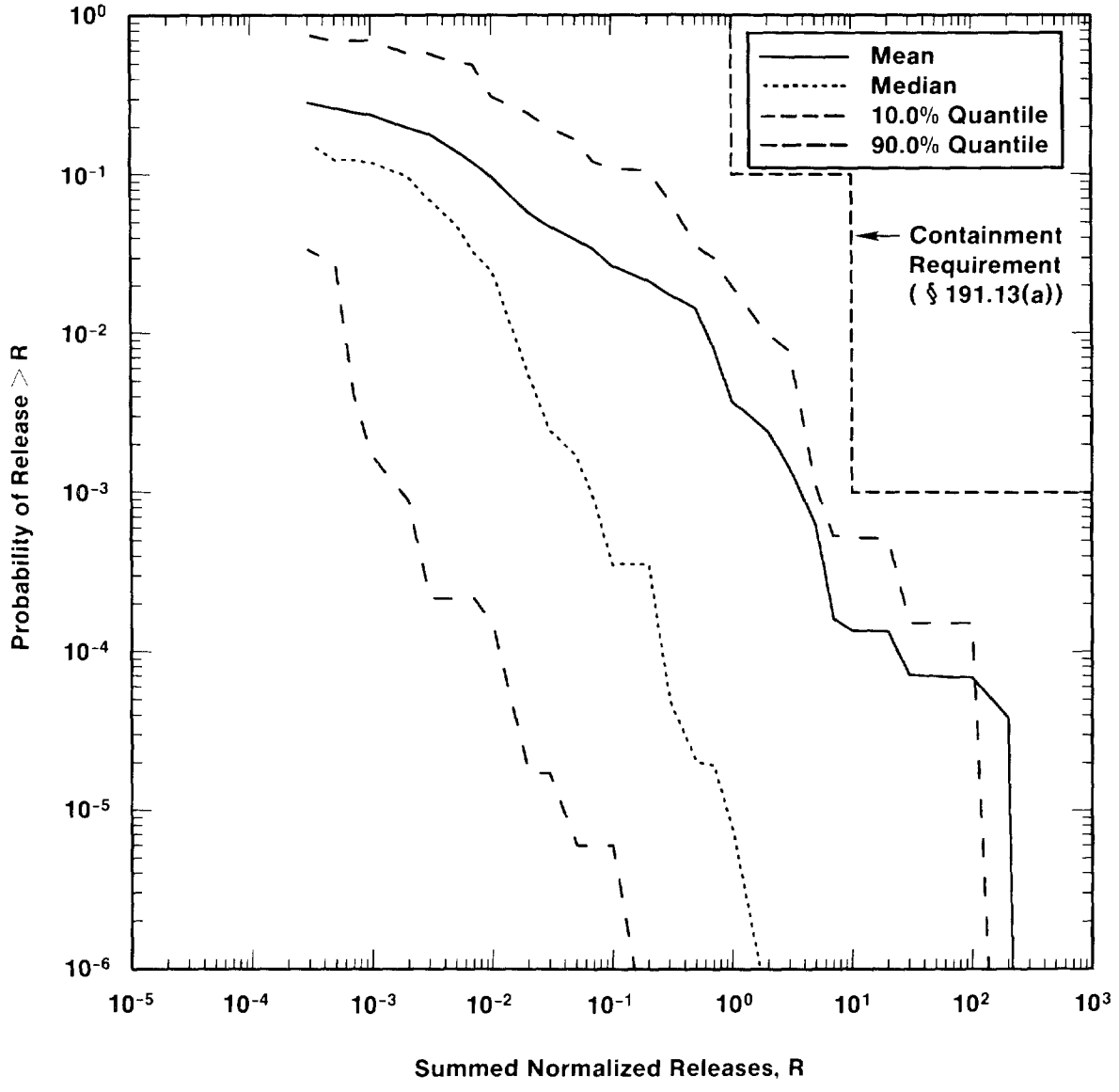

Figure 3-10. Mean and Percentile Curves for the Example Distribution of CCDFs Shown in Figure 3-9.

Now that Figures 3-9 and 3-10 have been introduced, the nature of the EPA's probability limits can be elaborated. Specifically, § 191.13(a) requires that the probability of exceeding a summed normalized release of 1 shall be less than 0.1 and that the probability of exceeding a summed normalized release of 10 shall be less than 0.001. Because quantities required in a performance assessment are uncertain, the probabilities of exceeding these release limits can never be known with certainty. However, by placing distributions on imprecisely known quantities, distributions for these probabilities can be obtained. To the extent that the distributions assumed for the original variables are subjective, so also will be the distributions for these probabilities.

In the example, an estimated distribution of probabilities at which a normalized release of 1 will be exceeded can be obtained by drawing a vertical line through 1 on the abscissa in Figure 3-9. This line will cross the 40 CCDFs generated in this example to yield a distribution of 40 exceedance probabilities. A similar construction can be performed for a normalized release of 10. Means (actually, estimates for the expected value of the true distribution, conditional on the assumptions of the analysis) for these two distributions can be obtained by summing the 40 observed values and then dividing by 40. The result of this calculation at 1, 10, and other points on the abscissa appears as the mean curve in Figure 3-10.

The EPA suggests in the guidance in Appendix B that, whenever practicable, the results of a performance assessment should be assembled into a CCDF. This is entirely consistent with the representation of risk given in Equation 3-1. The EPA further suggests that, when uncertainties in parameters are considered, the effects of these uncertainties can be incorporated into a single CCDF. Calculating a mean CCDF as shown in Figure 3-10 is one way to obtain a single CCDF. However, there are other ways in which a single CCDF can be obtained. For example, a median or 90th percentile curve as shown in Figure 3-10 could be used. However, whenever a distribution of curves is reduced to a single curve, information on uncertainty is lost.

Replicated sampling can characterize the uncertainty in an estimated mean CCDF or other summary curve. However, representing the uncertainty in an estimated value in this way is quite different from displaying the variability or uncertainty in the population from which the estimate is derived (Figure 3-9). For example, the uncertainty in the estimated mean curve in Figure 3-10 is less than the variability in the population of CCDFs that was averaged to obtain this mean.

Preliminary analyses for § 191.13(a) have typically assumed that the individual scenario probabilities are known with certainty and that the only

uncertainties in the analysis relate to the manner in which the summed normalized release required for comparison with the EPA Standard is calculated. As an example, Figure 3-11 shows the family of CCDFs that results when the same sample used to construct the CCDFs in Figure 3-9 is used but the individual scenario probabilities are fixed. In this case, the values for the pS_i do not change from sample element to sample element, but the values for $\mathbf{cS}_i$ do. This results in a very simple structure for the CCDFs in which the step heights for all CCDFs are the same. Mean and percentile curves can be constructed from these CCDFs as before and are shown in Figure 3-12. The hypothetical results on which Figures 3-9 and 3-11 are based were constructed so that the normalized release for scenario S_{i+1} is greater than the normalized release for scenario S_i for each sample element. The step heights associated with the individual scenarios in Figure 3-11 would still be the same if this ordering did not exist, but there would be a more complex mixing of step heights.

Another approach to constructing a CCDF for comparison with the EPA Standard is based on initially constructing a conditional CCDF for each scenario and then vertically averaging these conditional CCDFs with the probabilities of the individual scenarios as weights. This approach is described in Cranwell et al. (1987; also see Cranwell et al., 1990; Hunter et al., 1986) and has been extensively used in calculating CCDFs for comparison with § 191.13(a). Figure 3-13 gives a schematic representation for this construction approach. This approach is applicable to situations in which the scenario probabilities are known and, in this case, yields the same mean CCDF as shown in Figure 3-12.

3.1.5 PROBABILITY AND RISK

A brief discussion of how the concepts associated with a formal development of probability relate to the definition of risk in Equation 3-1 is now given. The intent is to emphasize the ideas involved rather than mathematical rigor. A more detailed development of the mathematical basis of probability can be found in numerous texts on probability theory (e.g., Feller, 1971; Ash, 1972). In addition, several excellent discussions of different conceptual interpretations of probability are also available (Barnett, 1982; Weatherford, 1982; Apostolakis, 1990). A familiarity with the basic ideas in the mathematical development of probability greatly facilitates an understanding of scenario development.

A formal development of probability is based on the use of sets. The first of these sets is called the sample space, which is the set of all possible outcomes associated with the particular process or situation under consideration. In the literature on probability, these individual outcomes are referred to as elementary events. As an example, performance assessment

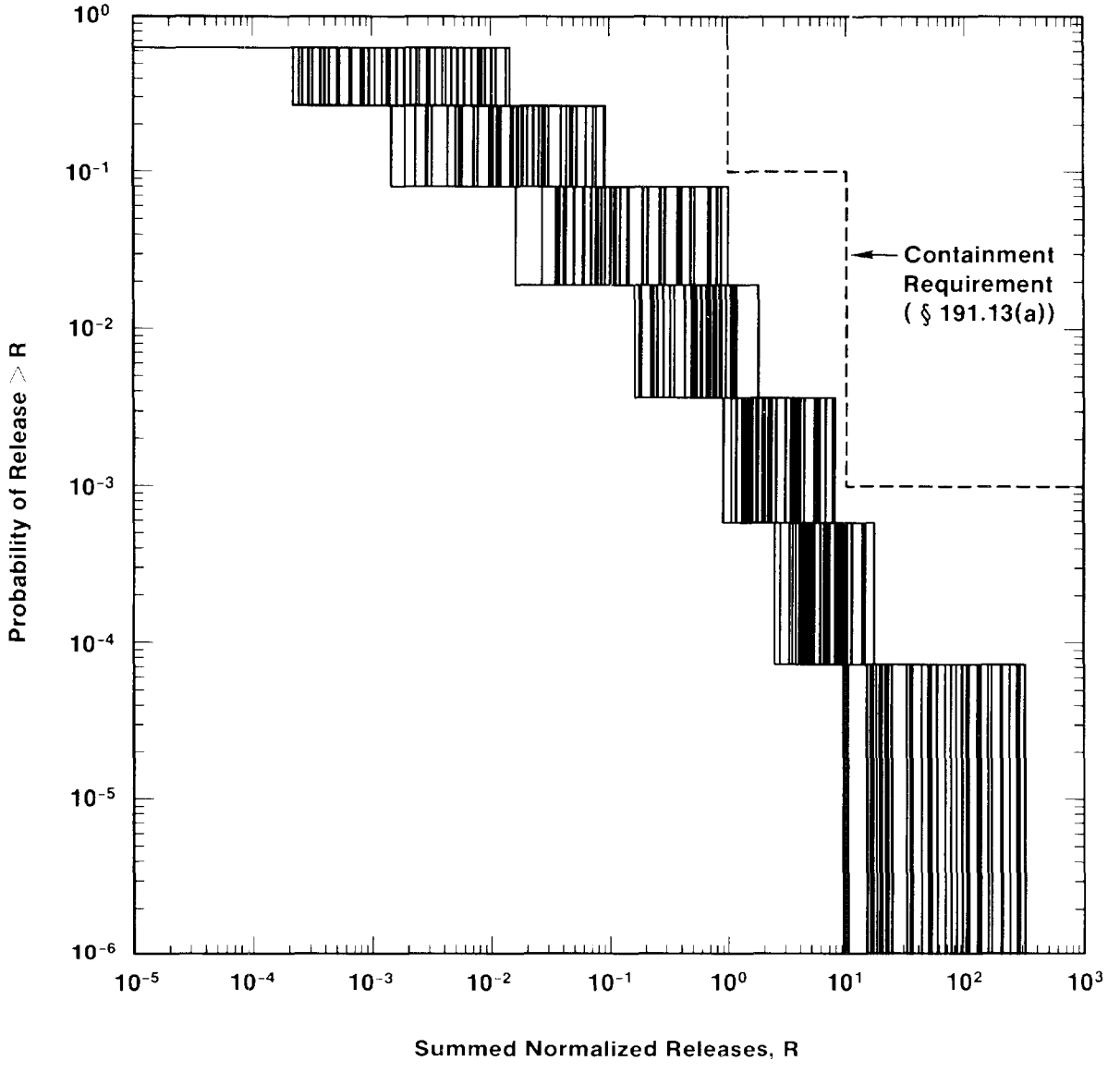

TRI-6342-1502-0

Figure 3-11. Hypothetical Distribution of CCDFs Generated for Comparison with the Containment Requirements in Which the Scenario Probabilities Are the Same for All Sample Elements.

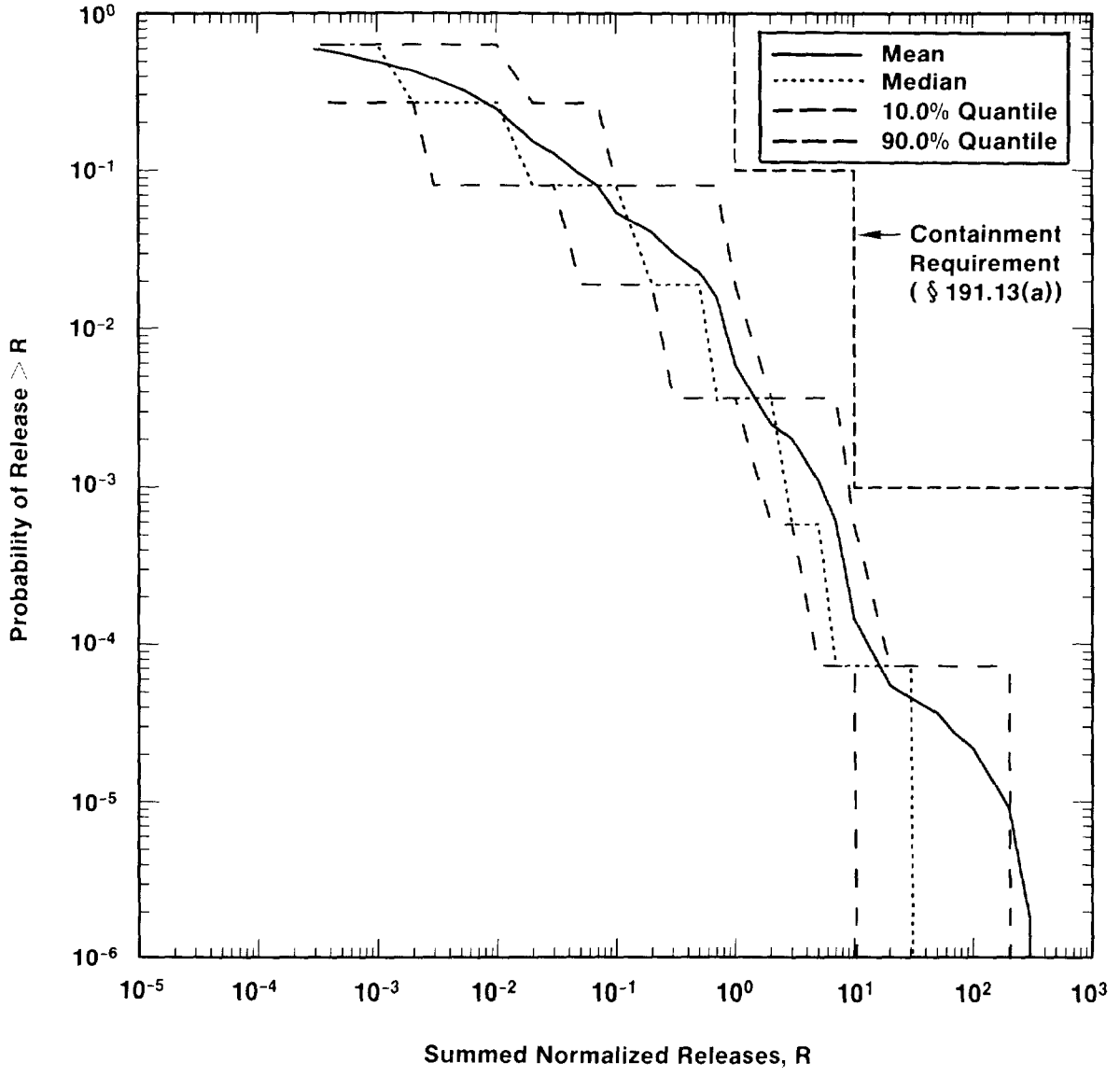

Figure 3-12. Mean and Percentile Curves for the Example Distribution of CCDFs Shown in Figure 3-11.

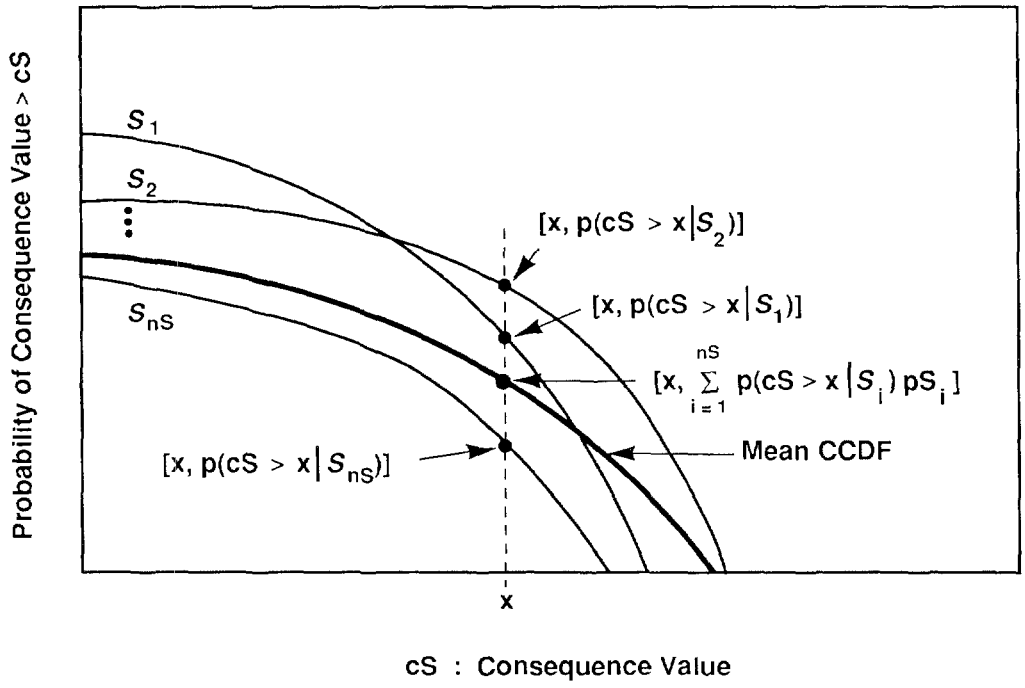

Figure 3-13. Construction of Mean CCDF from Conditional CCDFs. The expression $p(cS>x|S_i)$ is the probability of a normalized release exceeding x over 10,000 years given that scenario S_i has occurred. The ordinate displays conditional probability for the CCDFs for the individual scenarios S_i and probability for the mean CCDF. When the probabilities pS_i are small, the mean CCDF may fall far below most of the individual conditional CCDFs (Helton et al., 1991).

at the WIPP involves the characterization of the behavior of this site over a 10,000-yr period beginning at the decommissioning of the facility. Thus, the sample space would consist of all possible 10,000-yr "histories" at the WIPP for this time period. To avoid confusion with the regulatory use of the word "event," outcome or history is used for elementary event in this report. More specifically, the sample space is the set S defined by

$$S = \{x: \text{ x a single 10,000-yr history beginning at decommissioning of the WIPP}\}. \quad (3\text{-}11)$$

Each 10,000-yr history is complete in the sense that it includes a full specification, including time of occurrence, for everything of importance to performance assessment that happens in this time period. In the terminology of Cranwell et al. (1990), each history would contain a characterization for a specific sequence of "naturally occurring and/or human-induced conditions that represent realistic future states of the repository, geologic systems, and ground-water flow systems that could affect the release and transport of radionuclides from the repository to humans."

In general, the sample space will contain far too many outcomes to permit a meaningful development of probability to be based on the outcomes themselves. Crudely put, the individual outcomes are so unlikely to occur that probabilities cannot be assigned to their individual occurrences in a way that leads to a useful probabilistic structure that permits a calculation of probabilities for groups of outcomes. As a result, it is necessary to group the outcomes into sets called events, where each event is a subset of the sample space, and then to base the development of probability on these sets. An event, as used in a formal development of probability, corresponds to what is typically called a scenario in performance assessment (i.e., the S_i appearing in Equation 3-1).

An example of an event E in the probabilistic development for the WIPP would be the set of all time histories in which the first borehole to penetrate the repository occurs between 5000 and 10,000 years after decommissioning. That is,

$$E = \{x: \text{ x a 10,000-yr history at the WIPP in which the first borehole to penetrate the repository occurs between 5000 and 10,000 years after decommissioning}\}. \quad (3\text{-}12)$$

Due to the many ways in which the outcomes in a sample space might be sorted, the number of different events is infinite. In turn, each event is composed of many outcomes or, in the case of the WIPP, many 10,000-yr histories. Thus, events are "larger" than the individual outcomes contained in the sample space.

As another example, Cranwell et al. (1990) define a scenario (i.e., an event as used in the formal development of probability) to be "a set of naturally occurring and/or human-induced conditions that represent realistic future states of the repository, geologic systems, and ground-water flow systems that could affect the release and transport of radionuclides from the repository to humans." As their development shows, they include all possible ways in which this set of "conditions" could occur. Thus, they are actually using the set of all time histories in which this set of conditions occurs as their scenario. Their logic diagram for constructing scenarios (Cranwell et al., 1990, Figure 2) is equivalent to forming intersections of sets of time histories.

Probabilities are defined for events rather than for the individual outcomes in the sample space. Further, probabilities cannot be meaningfully developed for single events in isolation from other events but rather must be developed in the context of a suitable collection of events. The basic idea is to develop a logically complete representation for probability for a collection of events that is large enough to contain all events that might reasonably be of interest but, at the same time, is not so large that it contains events that result in intractable mathematical properties. As a result, the development of probability is usually restricted to a collection $\S$ of events that has the following two properties:

(1) if E is in $\S$, then E^c is in $\S$, where the superscript c is used to denote the complement of E,

and

(2) if $\{E_i\}$ is a countable collection of events from $\S$, then $\cup_i E_i$ and $\cap_i E_i$ also belong to $\S$.

A collection or set $\S$ satisfying the two preceding conditions is called a σ-algebra or a Borel algebra. The significance of such a set is that all the familiar operations with sets again lead to a set in it (i.e., it is closed with respect to set operations such as unions, intersections, and complements).

As noted earlier, an event in the probabilistic development corresponds to what is typically called a scenario in performance assessment. Thus, in the context of performance assessment, the set $\S$ would contain all allowable scenarios. However, for a given sample space S, the definition of $\S$ is not unique. This results from the fact that it is possible to develop the events in $\S$ at many different levels of detail. As described in the preceding paragraph, $\S$ is required to be a σ-algebra. The importance of this requirement with respect to performance assessment is that it results in the

complements, unions, and intersections of scenarios also being scenarios with defined probabilities.

Given that a suitably restricted set $\mathcal{S}$ is under consideration (i.e., a σ-algebra), the probabilities of the events in $\mathcal{S}$ are defined by a function p such that

(1) $p(S) = 1$,

(2) if E is in $\mathcal{S}$, then $0 \leq p(E) \leq 1$,

and

(3) if $E_1, E_2, \ldots$ is a sequence of disjoint sets (i.e., $E_i \cap E_j = \emptyset$ if $i \neq j$) from $\mathcal{S}$, then $p(\cup_i E_i) = \Sigma_i\, p(E_i)$.

All of the standard properties of probabilities can be derived from this definition.

An important point to recognize is that probabilities are not defined in isolation. Rather, there are three elements to the definition of probability: the sample space S, a collection $\mathcal{S}$ of subsets of S, and the function p defined on $\mathcal{S}$. Taken together, these quantities form a triple $(S, \mathcal{S}, p)$ called a probability space and must be present, either implicitly or explicitly, in any reasonable development of the concept of probability.

Now that the formal ideas of probability theory have been briefly introduced, the representation for risk in Equation 3-1 is revisited. As already indicated in Equation 3-11, the sample space in use when the EPA release limit for the WIPP is under consideration is the set of all possible 10,000-yr histories that begin at the decommissioning of the facility. The sets S_i appearing in Equation 3-1 are subsets of the sample space, and thus the pS_i are probabilities for sets of time histories. If an internally consistent representation for probability is to be used, the S_i must be members of a suitably defined set $\mathcal{S}$, and a probability function p must be defined on $\mathcal{S}$. Typically, the set $\mathcal{S}$ is not explicitly developed. However, if there is nothing inherently inconsistent with the probability assignments already made in Equation 3-1, it is possible to construct a set $\mathcal{S}$ and an associated probability function p such that the already assigned probabilities for the S_i remained unchanged. However, this extension is not unique unless it is made to the smallest σ-algebra that contains the already defined scenarios. Such an extension permits the assignment of probabilities to new scenarios in a manner that is consistent with the probabilities already assigned to existing scenarios.

The most important idea that the reader should take out of this section is that scenarios (i.e., the sets S_i in Equation 3-1) are sets of time histories. In particular, scenarios are arrived at by forming sets of similar time histories. There is no inherently correct grouping, and the probabilities associated with individual scenarios S_i can always be reduced by using a finer grouping. Indeed, as long as low-probability S_i are not thrown away, the use of more but lower probability S_i will improve the resolution in the estimated CCDF shown in Figure 3-1. Further, as an integrated release or some other consequence result must be calculated for each scenario S_i, the use of more S_i also results in more detailed specification of the calculations that must be performed for each scenario.

For example, a scenario S_i for the WIPP might be defined by

$$S_i = \{x: \text{ x a 10,000-yr history at the WIPP beginning at decommissioning in which a single borehole occurs}\}. \quad (3\text{-}13)$$

A more refined definition would be

$$S_{ik} = \{x: \text{ x a 10,000-yr history at the WIPP beginning at decommissioning in which a single borehole occurs between } (i\text{-}1)*10^3 \text{ and } i*10^3 \text{ yrs and no boreholes occur during any other time interval}\}. \quad (3\text{-}14)$$

Then,

$$S_{ik} \subset S_i, \; i = 1, \ldots, 10, \text{ and } S_i = \bigcup_{k=1}^{10} S_{ik}. \quad (3\text{-}15)$$

Thus, S_i and $\cup_k S_{ik}$ contain the same set of time histories. However, the individual S_{ik} contain smaller sets of time histories than does S_i. In terms of performance assessment, each S_{ik} describes a more specific set of conditions that must be modeled than does S_i. The estimated CCDF in Figure 3-1 could be constructed with either S_i or the S_{ik}, although the use of the S_{ik} would result in less aggregation error and thus provide better resolution in the resultant CCDF.

The S_i appearing in the definition of risk in Equation 3-1 should be developed to a level of resolution at which it is possible to view the analysis for each S_i as requiring a fixed, but possibly imprecisely known, vector **x** of variable values. Ultimately, this relates to how the set $\mathbb{S}$ in

the formal definition of probability will be defined. When a set S_i is appropriately defined, it should be possible to use the same model or models and the same vector of variable values to represent every occurrence (e.g., a 10,000-yr time history for WIPP) in S_i. In contrast, S_i is "too large" when this is not possible. For example, the set S_i in Equation 3-13 is probably "too large" for the assumption that a fixed time of intrusion (e.g., 5000 yr) is appropriate for all 10,000-yr histories contained in S_i, while a similar assumption about time of intrusion (e.g., $(k-1/2)*10^3$ yr) might be appropriate for S_{ik} as defined in Equation 3-14. A major challenge in structuring a performance assessment is to develop the sets S_i appearing in Equation 3-1, and hence the underlying probability space, at a suitable level of resolution.

3.2 Definition of Scenarios

As indicated in Equation 3-1, the outcome of a performance assessment for WIPP can be represented by a set of ordered triples. The first element of each triple, denoted S_i, is a set of similar occurrences or, equivalently, a scenario. As a result, an important part of the WIPP performance assessment is the development of scenarios.

The WIPP performance assessment uses a two stage procedure for scenario development. The purpose of the first stage is to develop a comprehensive set of scenarios that includes all occurrences that might reasonably take place at the WIPP. The result of this stage is a set of scenarios that summarize what might happen at the WIPP. These scenarios provide a basis for discussing the future behavior of the WIPP and a starting point for the second stage of the procedure, which is the definition of scenarios at a level of detail that is appropriate for use with the computational models employed in the WIPP performance assessment.

The first stage is directed at understanding what might happen at the WIPP and answering completeness questions. The second stage is directed at organizing the actual calculations that must be performed to obtain the consequences $\mathbf{cS}_i$ appearing in Equation 3-1, and as a result, must provide a structure that both permits the $\mathbf{cS}_i$ to be calculated at a reasonable cost and holds the amount of aggregation error that enters the analysis to a reasonable level. These two stages are now discussed in more detail.

3.2.1 DEFINITION OF SUMMARY SCENARIOS

The first stage of scenario definition for the WIPP performance assessment uses a five-step procedure proposed by Cranwell et al. (1990). The steps in

this procedure are: (1) compiling or adopting a "comprehensive" list of events[1] and processes that potentially could affect the disposal system, (2) classifying the events and processes to aid in completeness arguments, (3) screening the events and processes to identify those that can be eliminated from consideration in the performance assessment, (4) developing scenarios by combining the events and processes that remain after screening, and (5) screening scenarios to identify those that have little or no effect on the shape or location of the CCDF used for comparisons with EPA release limits.

Conceptually, the purpose of the first three steps is to develop the sample space S appearing in a formal definition of probability. As indicated in Equation 3-11, the sample space for the WIPP performance assessment is the set of all possible 10,000-yr histories beginning at decommissioning of the facility. The development of S is described in Chapter 4. For the 1991 performance assessment, this development lead to a set S in which all creditable disruptions were due to drilling intrusions.

Once the sample space S is developed, it is necessary to partition S into the subsets, or scenarios, S_i appearing in Equation 3-1. This is the fourth step in the scenario development procedure. As explained in Section 3.1.5-Probability and Risk, the S_i belong to a set $\mathcal{S}$ that, in concept, contains all scenarios for which probabilities will be defined.

The S_i are developed by decomposing S with logic diagrams of the form shown in Figure 3-14. The logic diagram shown in Figure 3-14 starts with the following three scenarios (i.e., subsets of S):

$$TS = \{x: \text{ x a 10,000-yr history in which subsidence results due to solution mining of potash}\}, \quad (3\text{-}16)$$

$$E1 = \{x: \text{ x a 10,000-yr history in which one or more boreholes pass through the repository and into a brine pocket}\}, \quad (3\text{-}17)$$

and

$$E2 = \{x: \text{ x a 10,000-yr history in which one or more boreholes pass through the repository without penetration of a brine pocket}\}. \quad (3\text{-}18)$$

---

[1] Cranwell et al. (1990) do not use the word "event" in the formal probabilistic sense used in Section 3.1.5-Probability and Risk, although their usage can be interpreted in that formal sense.

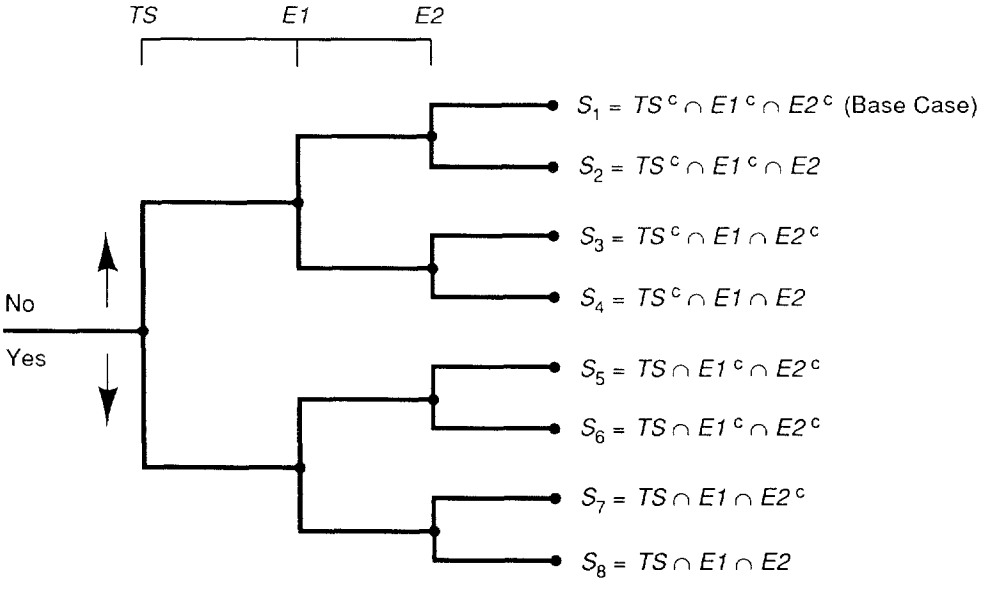

TS = {x: Subsidence Resulting From Solution Mining of Potash}

$E1$ = {x: One or More Boreholes Pass Through a Waste Panel and into a Brine Pocket}

$E2$ = {x: One or More Boreholes Pass Through a Waste Panel Without Penetration of a Brine Pocket}

Superscript c (e.g., TS^c) Denotes Set Complement

TRI-6342-576-3

Figure 3-14. Example Use of Logic Diagram to Construct Summary Scenarios.

Additional scenarios are then defined by the paths through the logic diagram shown in Figure 3-13. This results in the decomposition of S into the following eight scenarios:

$$S_1 = TS^c \cap E1^c \cap E2^c,\ S_2 = TS^c \cap E1^c \cap E2,\ S_3 = TS^c \cap E1 \cap E2^c,\ S_4 = TS^c \cap E1 \cap E2,$$

$$S_5 = TS \cap E1^c \cap E2^c,\ S_6 = TS \cap E1^c \cap E2,\ S_7 = TS \cap E1 \cap E2^c,\ S_8 = TS \cap E1 \cap E2, \qquad (3\text{-}19)$$

where the superscript c denotes the complement of a set. These eight scenarios constitute a complete decomposition of S in the sense that

$$S = \bigcup_{i=1}^{8} S_i. \qquad (3\text{-}20)$$

The development of these scenarios is discussed and more detail on their individual characteristics is given in Chapter 4 of this volume.

The last step in the development procedure is screening to remove unimportant scenarios. As discussed in Chapter 4 of this volume, screening did not remove any of the preceding eight scenarios from further consideration for the 1991 WIPP performance assessment, although the assumption is made that scenario *TS* has no impact on releases from the repository for the 1991 performance assessment. The effect of this assumption will be evaluated in the 1992 performance assessment.

3.2.2 DEFINITION OF COMPUTATIONAL SCENARIOS

Although the preceding decomposition of S is useful for discussion and the development of an understanding of what is important at the WIPP, a more detailed decomposition is needed for the actual calculations that must be performed to determine scenario consequences (i.e., the $\mathbf{cS}_i$ as shown in Equation 3-1) and to provide a basis for CCDF construction. To provide more detail for the determination of both scenario probabilities and scenario consequences, the scenarios on which the actual CCDF construction is based for the WIPP performance assessment are defined on the basis of (1) number of drilling intrusions, (2) time of the drilling intrusions, (3) whether or not a single waste panel is penetrated by two or more boreholes, of which at least one penetrates a brine pocket and at least one does not, and (4) the activity level of the waste penetrated by the boreholes. The purpose of this decomposition is to provide a systematic coverage of what might reasonably happen at the WIPP.

The preceding scenario construction procedure starts with the division of the 10,000-yr time period appearing in the EPA regulations into a sequence

$$[t_{i-1}, t_i],\ i = 1, 2, \ldots, nT, \tag{3-21}$$

of disjoint time intervals. When activity loading is not considered, these time intervals lead to scenarios of the form

$$S(\mathbf{n}) = \{x:\ x \text{ an element of } S \text{ for which exactly } n(i) \text{ intrusions occur in time interval } [t_{i-1}, t_i] \text{ for i=1, 2, ..., nT}\} \tag{3-22}$$

and

$$S^{+-}(t_{i-1},t_i) = \{x:\ x \text{ an element of } S \text{ involving two or more boreholes that penetrate the same waste panel during the time interval } [t_{i-1}, t_i], \text{ at least one of these boreholes penetrates a pressurized brine pocket and at least one does not penetrate a pressurized brine pocket}\}, \tag{3-23}$$

where

$$\mathbf{n} = [n(1), n(2), \ldots, n(nT)]. \tag{3-24}$$

When activity loading is considered, the preceding time intervals lead to scenarios of the form

$$S(\mathbf{l},\mathbf{n}) = \{x:\ x \text{ an element of } S(\mathbf{n}) \text{ for which the } j^{th} \text{ borehole encounters waste of activity level } \ell(j) \text{ for j=1, 2, ..., nBH, where nBH is the total number of boreholes associated with a time history in } S(\mathbf{n})\} \tag{3-25}$$

and

$$S^{+-}(\mathbf{l};t_{i-1},t_i) = \{x:\ x \text{ an element of } S^{+-}(t_{i-1}, t_i) \text{ for which the } j^{th} \text{ borehole encounters waste of activity level } \ell(j) \text{ for j=1, 2, ..., nBH, where nBH is the total number of boreholes associated with a time history in } S^{+-}(t_{i-1},t_i)\}, \tag{3-26}$$

where

$$\mathbf{l} = [\ell(1), \ell(2), \ldots, \ell(nBH)] \text{ and } nBH = \sum_{i=1}^{nT} n(i). \tag{3-27}$$

Further refinements on the basis of whether or not subsidence occurs and whether or not individual boreholes penetrate pressurized brine pockets are also possible. However, at present, these distinctions do not appear to be important in the determination of scenario consequences and, as a result, are not included in calculations performed for the 1991 WIPP performance assessment. In essence, the computational scenarios defined in Equation 3-21 through Equation 3-27 are defining an important sampling strategy that covers the stochastic or type A uncertainty that is characterized by the scenario probabilities pS_i appearing in Equation 3-1. Additional information on the definition of computational scenarios is given in Volume 2, Chapter 3 of this report.

3.3 Determination of Scenario Probabilities

The second element of the ordered triples shown in Equation 3-1 is the scenario probability pS_i. As with scenario definition, the probabilities pS_i have been developed at two levels of detail.

3.3.1 PROBABILITIES FOR SUMMARY SCENARIOS

The first level was for use with the summary scenarios described in Section 3.2.1-Definition of Summary Scenarios. The logic used to construct these probabilities is shown in Figures 4-10 and 4-11 in Chapter 4 of this volume. The construction shown in Figure 4-10 is based on a classical probability model in which alternative occurrences of unknown probability are assumed to have equal probability. The construction shown in Figure 4-11 is based on the use of a Poisson model. Additional discussion of these probability estimation procedures is given in Guzowski (1991). Further, Apostolakis et al. (1991) provide an extensive discussion of techniques for determining probabilities in the context of performance assessment for radioactive waste disposal.

In the WIPP performance assessment, probabilities are assigned to summary scenarios to assist in completeness arguments and to provide guidance with respect to what parts of the sample space must be considered in constructing CCDFs for comparison with the EPA release limits. The probabilities in Figure 4-11 were used to construct CCDFs for the 1990 preliminary comparison (Bertram-Howery et al., 1990). The probabilities used in the present report are now described.

3.3.2 PROBABILITIES FOR COMPUTATIONAL SCENARIOS

The second level of probability definition was for use with the computational scenarios described in Section 3.2.2-Definition of Computational Scenarios.

These are the probabilities that will actually be used in the construction of CCDFs for comparison with the EPA release limits. These probabilities are based on the assumption that the occurrence of boreholes through the repository follows a Poisson process with a rate constant λ. The probabilities $pS(\mathbf{n})$ and $pS(\mathbf{I},\mathbf{n})$ for the scenarios $S(\mathbf{n})$ and $S(\mathbf{I},\mathbf{n})$ are given by

$$pS(\mathbf{n}) = \left\{ \prod_{i=1}^{nT} \left[\frac{\lambda^{n(i)} \left(t_i - t_{i-1}\right)^{n(i)}}{n(i)!} \right] \right\} \exp\left[-\lambda \left(t_{nT} - t_0 \right) \right] \tag{3-28}$$

and

$$pS(\mathbf{I},\mathbf{n}) = \left(\prod_{j=1}^{nBH} pL_{\ell(j)} \right) pS(\mathbf{n}), \tag{3-29}$$

where $\mathbf{n}$ and $\mathbf{I}$ are defined in Equations 3-24 and 3-27, respectively, and pL_ℓ is the probability that a randomly placed borehole through a waste panel will encounter waste of activity level ℓ. The rate constant λ is a sampled variable in the 1991 WIPP performance assessment. Table 3-2 provides an example of probabilities $pS(\mathbf{n})$ calculated as shown in Equation 3-28 with $\lambda = 3.28 \times 10^{-4}\ yr^{-1}$ for the time interval from 100 to 10,000 yr, which corresponds to the maximum drilling rate suggested for use by the EPA. Because the Standard allows for 100 yr of active institutional control, λ has been set equal to zero for the time interval from 0 to 100 yr. Similar, but more involved, equations are used to obtain $pS^{+-}(t_{i-1}, t_i)$ and $pS^{+-}(\mathbf{I}; t_{i-1}, t_i)$.

The formulas for determining $pS(\mathbf{n})$, $pS(\mathbf{I},\mathbf{n})$, $pS^{+-}(t_{i-1}, t_i)$, and $pS^{+-}(\mathbf{I}; t_{i-1}, t_i)$ are derived in Volume 2, Chapter 2 of this report under the assumption that drilling intrusions follow a Poisson process (i.e., are random in time and space). The derivations are general and include both the stationary (i.e., constant λ) and nonstationary (i.e., time-dependent λ) cases.

3.4 Calculation of Scenario Consequences

The two preceding sections have discussed the development of scenarios S_i and their probabilities pS_i at two levels of detail. First, scenarios were considered at a summary level. This provides a fairly broad characterization of scenarios and their probabilities and thus provides a basis for general discussions of what might happen at the WIPP. Second, scenarios involving drilling intrusions were considered at a much finer level of detail. This additional detail facilitates the necessary calculations that must be performed to determine the scenario consequences $\mathbf{cS}_i$.

TABLE 3-2. PROBABILITIES FOR COMBINATIONS OF INTRUSIONS OVER 10,000 YRS FOR $\lambda = 0$ FROM 0 TO 100 YRS, $\lambda = 3.28 \times 10^{-4}$ YR^{-1} FROM 100 TO 10,000 YRS

The individual entries in this table correspond to computational scenarios of the form $S(\mathbf{n})$. For a specified number of intrusions, the first column indicates the time interval in which the first intrusion occurs, the second column indicates the time interval in which the second intrusion occurs, and so on, where 1 ~ [0, 2000], 2 ~ [2000, 4000], 3 ~ [4000, 6000], 4 ~ [6000, 8000], and 5 ~ [8000, 10000]; the last column lists the probability for each combination of intrusions calculated with the relationship in Eq. 3-28.

0 Intrusions
(prob = 3.888×10^{-2})
(cum prob = 3.888×10^{-2})
(comp scen = 1)

1 Intrusion
(prob = 1.263×10^{-1})
(cum prob = 1.651×10^{-1})
(comp scen = 5)

I_1	I_2	I_3	I_4	Prob
1				2.423×10^{-2}
2				2.551×10^{-2}
3				2.551×10^{-2}
4				2.551×10^{-2}
5				2.551×10^{-2}
				1.263×10^{-1}

2 Intrusions
(prob = 2.050×10^{-1})
(cum prob = 3.701×10^{-1})
(comp scen = 15)

I_1	I_2	I_3	I_4	Prob
1	1			7.551×10^{-3}
1	2			1.590×10^{-2}
1	3			1.590×10^{-2}
1	4			1.590×10^{-2}
1	5			1.590×10^{-2}
2	2			8.366×10^{-3}
2	3			1.673×10^{-2}
2	4			1.673×10^{-2}
2	5			1.673×10^{-2}
3	3			8.366×10^{-3}
3	4			1.673×10^{-2}
3	5			1.673×10^{-2}
4	4			8.366×10^{-3}
4	5			1.673×10^{-2}
5	5			8.366×10^{-3}
				2.050×10^{-1}

3 Intrusions
(prob = 2.219×10^{-1})
(cum prob = 5.920×10^{-1})
(comp scen = 35)

I_1	I_2	I_3	I_4	Prob
1	1	1		1.569×10^{-3}
1	1	2		4.953×10^{-3}
1	1	3		4.953×10^{-3}
1	1	4		4.953×10^{-3}
1	1	5		4.953×10^{-3}
1	2	2		5.214×10^{-3}
1	2	3		1.043×10^{-2}
1	2	4		1.043×10^{-2}
1	2	5		1.043×10^{-2}
1	3	3		5.214×10^{-3}
1	3	4		1.043×10^{-2}
1	3	5		1.043×10^{-2}
1	4	4		5.214×10^{-3}
1	4	5		1.043×10^{-2}
1	5	5		5.214×10^{-3}
2	2	2		1.829×10^{-3}
2	2	3		5.488×10^{-3}
2	2	4		5.488×10^{-3}
2	2	5		5.488×10^{-3}
2	3	3		5.488×10^{-3}
2	3	4		1.098×10^{-2}
2	3	5		1.098×10^{-2}
2	4	4		5.488×10^{-3}
2	4	5		1.098×10^{-2}
2	5	5		5.488×10^{-3}
3	3	3		1.829×10^{-3}
3	3	4		5.488×10^{-3}
3	3	5		5.488×10^{-3}
3	4	4		5.488×10^{-3}
3	4	5		1.098×10^{-2}
3	5	5		5.488×10^{-3}
4	4	4		1.829×10^{-3}
4	4	5		5.488×10^{-3}
4	5	5		5.488×10^{-3}
5	5	5		1.829×10^{-3}
				2.219×10^{-1}

4 Intrusions
(prob = 1.801×10^{-1})
(cum prob = 7.722×10^{-1})
(comp scen = 70)

I_1	I_2	I_3	I_4	Prob
1	1	1	1	2.444×10^{-4}
1	1	1	2	1.029×10^{-3}
.	.	.	.	.
.	.	.	.	.
.	.	.	.	.
1	2	3	4	6.841×10^{-3}
.	.	.	.	.
.	.	.	.	.
.	.	.	.	.
4	5	5	5	1.200×10^{-3}
5	5	5	5	3.000×10^{-4}
				1.801×10^{-1}

5 Intrusions
(prob = 1.170×10^{-1})
(cum prob = 8.891×10^{-1})
(comp scen = 126)

6 Intrusions
(prob = 6.331×10^{-2})
(cum prob = 9.525×10^{-1})
(comp scen = 210)

7 Intrusions
(prob = 2.937×10^{-2})
(cum prob = 9.818×10^{-1})
(comp scen = 330)

TABLE 3-2. PROBABILITIES FOR COMBINATIONS OF INTRUSIONS OVER 10,000 YRS FOR $\lambda = 0$ FROM 0 TO 100 YRS, $\lambda = 3.28 \times 10^{-4}$ YR^{-1} FROM 100 TO 10,000 YRS (concluded)

8 Intrusions (prob = 1.192×10^{-2}) (cum prob = 9.937×10^{-1}) (comp scen = 495)	11 Intrusions (prob = 4.123×10^{-4}) (cum prob = 9.999×10^{-1}) (comp scen = 1365)	14 Intrusions (prob = 6.464×10^{-6}) (cum prob =) (comp scen = 3060)
9 Intrusions (prob = 4.301×10^{-3}) (cum prob = 9.980×10^{-1}) (comp scen = 715)	12 Intrusions (prob = 1.116×10^{-4}) (cum prob =) (comp scen = 1820)	15 Intrusions (prob = 1.399×10^{-6}) (cum prob =) (comp scen = 3876)
10 Intrusions (prob = 1.397×10^{-3}) (cum prob = 9.994×10^{-1}) (comp scen = 1001)	13 Intrusions (prob = 2.787×10^{-5}) (cum prob =) (comp scen = 2380)	

An important point to bear in mind is that calculations to obtain $\mathbf{cS}_i$ are performed at the level of the individual time histories contained in the set S shown in Equation 3-11. For this reason, the computational scenarios S_i used in the construction of CCDFs should be reasonably "homogeneous"; otherwise, it is not possible to assume that a calculation performed for a specific time history in S_i is a reasonable surrogate for the calculations that might be performed for all the other time histories in S_i. However, calculations are performed at the level of individual time histories regardless of whether the previously discussed summary or computational scenarios are under consideration.

In what follows, a summary description of the models being used in the WIPP performance assessment will be given. Then, the way in which calculations are organized to provide results for comparison with the EPA release limits will be described.

3.4.1 OVERVIEW OF MODELS

The models used in the WIPP performance assessment, or any other complex analysis, actually exist at four different levels. First, there are conceptual models that characterize our perception of the site. These models provide a nonmathematical summary of our knowledge of the site and the physical processes that operate there. Development of an appropriate conceptual model, or site description as it is sometimes called, is an important part of the WIPP performance assessment. Summaries of the current conceptual model for the WIPP are given in Chapter 5 of this volume. An adequate conceptual model is essential both for the development of the sample space S appearing in Equation 3-11 and the division of the sample space into the scenarios S_i appearing in Equation 3-1.

Second, mathematical models are developed to represent the processes at the site. The conceptual models provide the context within which these mathematical models must operate and indicate the processes that they must characterize. The mathematical models are predictive in the sense that, given known properties of the system and possible perturbations to the system, they project the response of the system. The processes that are represented by these mathematical models include fluid flow, heat flow, mechanical deformation, radionuclide transport by groundwater, removal of waste by intruding boreholes, and human exposure to radionuclides released to the surface environment. Among the dependent variables predicted by these models are pressurization of the repository by gas generation, deformation of the repository due to salt creep, removal of radionuclides from the repository due to the inflow and subsequent outflow of brine, release of radionuclides to the accessible environment due to either radionuclide transport in the Culebra or cuttings removal to the surface, and human exposure to radionuclides brought to the surface. Mathematical models are often systems of ordinary or partial differential equations. However, other possibilities exist. A description of the mathematical models being used in the WIPP performance assessment is given in Volume 2, Chapters 4 through 7 of this report.

Third, numerical models are developed to approximate the mathematical models. Most mathematical models do not have closed-form solutions. Simply put, it is not possible to find simple functions that equal the solutions of the equations in the model. As a result, numerical procedures must be developed to provide approximations to the solutions of the mathematical models. In essence, these approximations provide "numerical models" that calculate results that are close to the solutions of the original mathematical models. For example, Runge-Kutta procedures are often used to solve ordinary differential equations, and finite difference and finite element methods are used to solve partial differential equations. In practice, it is unusual for

a mathematical model to have a solution that can be determined without the use of an intermediate numerical model. A brief description of the numerical models being used in the WIPP performance assessment is given in Volume 2, Chapters 4 through 7 of this report.

Fourth, computer models must be used to implement the numerical models. It is unusual for a mathematical model and its associated numerical model to be sufficiently simple to permit a "pencil-and-paper" solution. Thus, computer programs must be developed that will carry out the actual calculations. These computer models are often quite general in the sense that the user exercises a large amount of control over both the mathematical model and its numerical solution through the specific inputs supplied to the computer model. Indeed, most computer models have the capability to implement a variety of mathematical and numerical models. The computer model is where the conceptual model, mathematical model, numerical model, and analyst come together to produce predicted results.

It is the computer models that actually predict the consequences $\mathbf{cS}_i$ appearing in Equation 3-1. Further, several models are often used in a single analysis, with individual models both receiving input from a preceding model and producing output that is then used as input to another model. Figure 3-15 illustrates the sequence of linked models that was used in the 1991 WIPP performance assessment. Each of the models appearing in this figure is briefly described in Table 3-3; more information is available in Volume 2, Chapters 4 through 7 of this report and the model descriptions for the individual programs.

3.4.2 ORGANIZATION OF CALCULATIONS FOR PERFORMANCE ASSESSMENT

As shown in Table 3-2, even a fairly coarse gridding on time leads to far too many computational scenarios (e.g., $S(\mathbf{n})$ and $S(\mathbf{l},\mathbf{n})$) to perform a detailed calculation for each of them. Construction of a CCDF for comparison against the EPA release limits requires the estimation of cumulative probability through at least the 0.999 level. Thus, depending on the value for the rate constant λ in the Poisson model for drilling, this may require the inclusion of computational scenarios involving as many as 10 to 12 drilling intrusions, which results in a total of several thousand computational scenarios. Further, this number does not include the effects of different activity levels in the waste. To obtain results for such a large number of computational scenarios, it is necessary to plan and implement the overall calculations very carefully. The manner in which this can be done is not unique. The following describes the approach used in the 1991 WIPP performance assessment to calculate a CCDF for comparison with the EPA release limits.

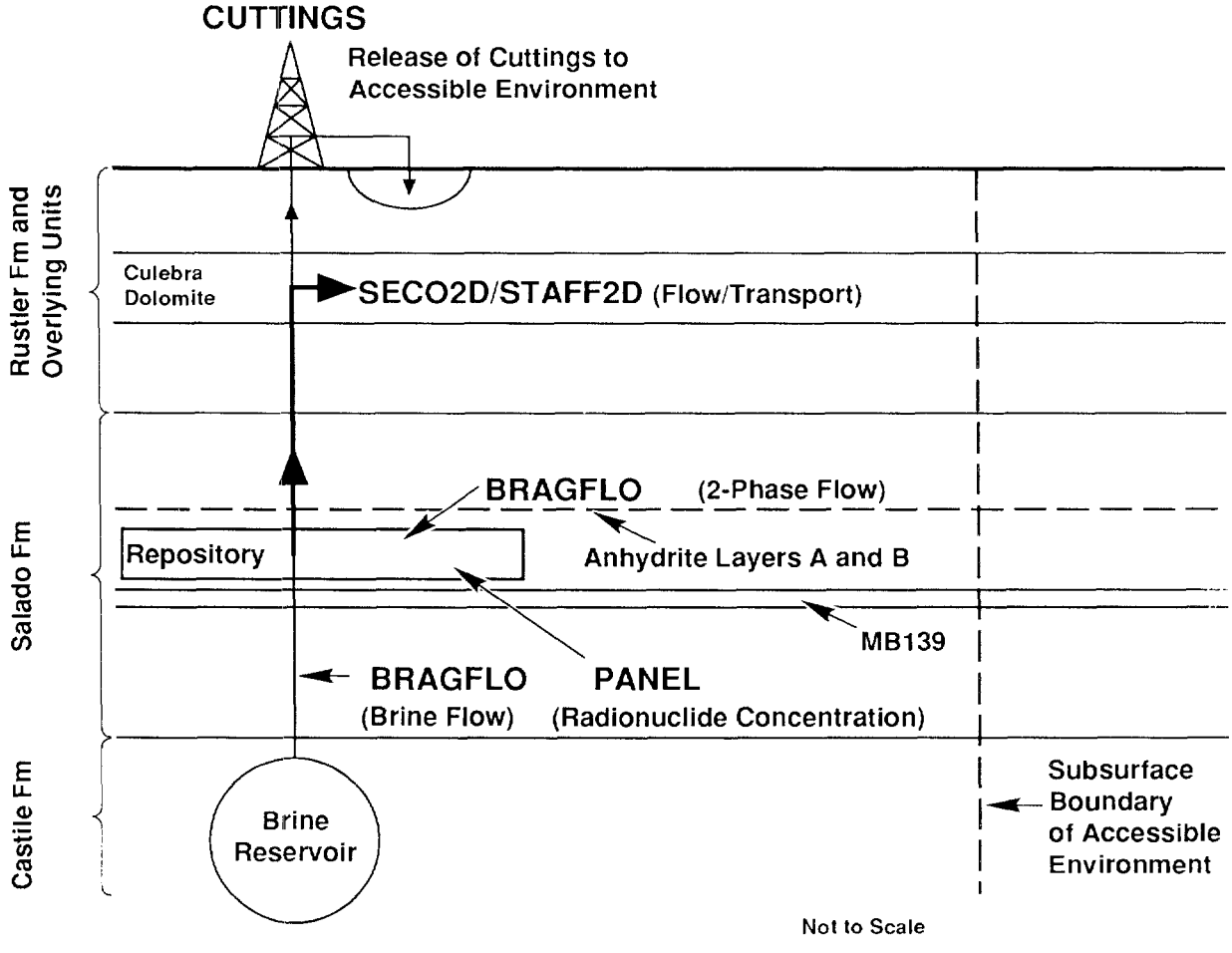

Figure 3-15. Models Used in 1991 WIPP Performance Assessment. The names for computer models (i.e., computer codes) are shown in capital letters.

TABLE 3-3. SUMMARY OF COMPUTER MODELS USED IN THE 1991 WIPP PERFORMANCE ASSESSMENT

Model	Description
CUTTINGS	Calculates the quantity of radioactive material (in curies) brought to the surface as cuttings and cavings generated by an exploratory drilling operation that penetrates a waste panel (Volume 2, Chapter 7 of this report).
BRAGFLO	Describes the multiphase flow of gas and brine through a porous, heterogenous reservoir. BRAGFLO solves simultaneously the coupled partial differential equations that describe the mass conservation of gas and brine along with appropriate constraint equations, initial conditions, and boundary conditions (Volume 2, Chapter 5 of this report).
PANEL	Calculates rate of discharge and cumulative discharge of radionuclides from a repository panel through an intrusion borehole. Discharge is a function of fluid flow rate, nuclide solubility, and remaining inventory (Volume 2, Chapter 5 of this report).
SECO2D	Calculates single-phase Darcy flow for groundwater flow problems in two dimensions. The formulation is based on a single partial differential equation for hydraulic head using fully implicit time differencing (Volume 2, Chapter 6 of this report).
STAFF2D	Simulates fluid flow and transport of radionuclides in fractured porous media. STAFF2D is a two-dimensional finite element code (Huyakorn et al., 1989; Volume 2, Chapter 6 of this report).

As indicated in Equation 3-21, the 10,000-yr time interval that must be considered for comparison with the EPA release limits can be divided into disjoint subintervals $[t_{i-1}, t_i]$, $i = 1, 2, \ldots, nT$, where nT is the number of time intervals selected for use. The following results can be calculated for each time interval:

rC_i = EPA normalized release to the surface environment for cuttings removal due to a single borehole in time interval i with the assumption that the waste is homogeneous (i.e., waste of different activity levels is not present), (3-30)

rC_{ij} = EPA normalized release to the surface environment for cuttings removal due to a single borehole in time interval i that penetrates waste of activity level j, (3-31)

$rGW1_i$ = EPA normalized release to the accessible environment for groundwater transport initiated by a single borehole in time interval i, (3-32)

and

$rGW2_i$ = EPA normalized release to the accessible environment for groundwater transport initiated by two boreholes in the same waste panel in time interval i, of which one penetrates a pressurized brine pocket and one does not (i.e., an E1E2-type scenario). (3-33)

In general, rC_i, rC_{ij}, $rGW1_i$, and $rGW2_i$ will be vectors containing a large variety of information; however, for notational simplicity, a vector representation will not be used. For the WIPP performance assessment, the cuttings release to the accessible environment (i.e., rC_i and rC_{ij}) is determined by the CUTTINGS program, and the groundwater release to the accessible environment (i.e., $rGW1_i$ and $rGW2_i$) is determined for the 1991 performance assessment through a sequence of linked calculations involving the BRAGFLO, PANEL, SECO2D, and STAFF2D programs.

The releases rC_i, rC_{ij}, $rGW1_i$ and $rGW2_i$ are used to construct the releases associated with the many individual computational scenarios that are used in the construction of a CCDF for comparison with the EPA release limits. The following assumptions are made:

(1) With the exception of E1E2-type scenarios, no synergistic effects result from multiple boreholes, and thus, the total release for a scenario involving multiple intrusions can be obtained by adding the releases associated with the individual intrusions.

(2) An E1E2-type scenario can only take place when the necessary boreholes occur within the same time interval $[t_{i-1}, t_i]$.

(3) An E1E2-type scenario involving more than two boreholes will have the same release as an E1E2-type scenario involving exactly two boreholes.

The preceding assumptions are used to construct the releases for individual computational scenarios.

The normalized releases rC_i, rC_{ij} and $rGW1_i$ can be used to construct the EPA normalized releases for the scenarios $S(\mathbf{n})$ and $S(\mathbf{l},\mathbf{n})$ defined in Equations 3-22 and 3-25, respectively. For $S(\mathbf{n})$, the normalized release to the accessible environment can be approximated by

$$cS(\mathbf{n}) = \sum_{j=1}^{nBH} (rC_{m(j)} + rGW1_{m(j)}), \tag{3-34}$$

where m(j) designates the time interval in which the j^{th} borehole occurs. The vector

$$\mathbf{m} = [m(1), m(2), \ldots, m(nBH)] \tag{3-35}$$

is uniquely determined once the vector $\mathbf{n}$ appearing in the definition of $S(\mathbf{n})$ is specified. The definition of $S(\mathbf{n})$ contains no information on the activity levels encountered by the individual boreholes, and so $cS(\mathbf{n})$ was constructed with the assumption that all waste is of the same average activity. However, the definition of $S(\mathbf{l},\mathbf{n})$ does contain information on activity levels, and the associated normalized release to the accessible environment can be approximated by

$$cS(\mathbf{l},\mathbf{n}) = \sum_{j=1}^{nBH} \left[rC_{m(j),\ell(j)} + rGW1_{m(j)} \right], \tag{3-36}$$

which does incorporate the activity levels encountered by the individual boreholes. The normalized releases for the computational scenarios $S^{+-}(t_{i-1}, t_i)$ and $S^{+-}(\mathbf{l}; t_{i-1}, t_i)$ defined in Equations 3-23 and 3-26, respectively, can be constructed in a similar manner.

Additional information on the procedures being used to construct CCDFs for the 1991 WIPP performance assessment is given in Volume 2, Chapter 3 of this report.

3.5 Uncertainty and Sensitivity Analysis

The performance of uncertainty and sensitivity analyses is an important part of the WIPP performance assessment. The need to conduct such analyses has a large effect on the overall structure of the WIPP performance assessment. In the context of this report, uncertainty analysis involves determining the uncertainty in model predictions that results from imprecisely known input variables, and sensitivity analysis involves determining the contribution of individual input variables to the uncertainty in model predictions. Specifically, uncertainty and sensitivity analyses involve the study of the effects of subjective, or type B, uncertainty. As previously discussed, the effects of stochastic, or type A, uncertainty is incorporated into the WIPP performance assessment through the scenario probabilities pS_i appearing in Equation 3-1. However, it is possible to have subjective uncertainty in quantities used in the characterization of stochastic uncertainty.

3.5.1 AVAILABLE TECHNIQUES

Review of Techniques

Four basic approaches to uncertainty and sensitivity analysis have been developed: differential analysis, Monte Carlo analysis, response surface methodology, and Fourier amplitude sensitivity test. This section provides a brief overview of these approaches and references to more detailed sources of information.

Differential analysis is based on using a Taylor series to approximate the model under consideration. Once constructed, this series is used as a surrogate for the original model in uncertainty and sensitivity studies. A differential analysis involves four steps: (1) selection of base-case values, ranges, and distributions for the input variables under consideration; (2) development of a Taylor series approximation to the original model; (3) assessment of uncertainty in model predictions through the use of variance propagation techniques with the Taylor series approximation to the model; and (4) determination of the sensitivity of model predictions to model input on the basis of fractional contributions to variance. The most demanding part of a differential analysis is often the calculation of the partial derivatives used in the Taylor series constructed in the second step. Additional sources of information on differential analysis are given in Table 3-4.

Monte Carlo analysis is based on performing multiple model evaluations with probabilistically selected model input, and then using the results of these evaluations to determine both the uncertainty in model predictions and the independent variables that give rise to this uncertainty. A Monte Carlo analysis involves five steps: (1) selection of a range and distribution for each input variable; (2) generation of a sample from the ranges and distributions assigned to the input variables; (3) evaluation of the model for each element of the sample; (4) assessment of the uncertainty in model predictions through the use of estimated means, variances, and distribution functions; and (5) determination of the sensitivity of model predictions to model input on the basis of scatterplots, regression analysis, and correlation analysis. Additional sources of information on Monte Carlo analysis are given in Table 3-4.

Response surface methodology is based on developing a response surface approximation to the model under consideration. This approximation is then used as a surrogate for the original model in subsequent uncertainty and sensitivity analyses. An analysis based on response surface methodology involves six steps: (1) selection of a range and distribution for each input variable; (2) development of an experimental design that defines the

combinations of variable values for which model evaluations will be performed; (3) evaluation of the model for each point in the experimental design; (4) construction of a response surface approximation to the original model on the basis of the model evaluations obtained in the preceding step; (5) assessment of the uncertainty in model predictions through the use of either variance propagation techniques or Monte Carlo simulation with the previously constructed response surface; and (6) determination of the sensitivity of model predictions to model input on the basis of fractional contribution to variance. Addition sources of information on response surface methodology are given in Table 3-4.

The Fourier amplitude sensitivity test (FAST) is based on performing a numerical calculation to obtain the expected value and variance of a model prediction. The basis of this calculation is a transformation that converts a multidimensional integral over all the uncertain model inputs to a one-dimensional integral. Further, a decomposition of the Fourier series representation of the model is used to obtain the fractional contribution of the individual input variables to the variance of the model prediction. An analysis based on the FAST approach involves four steps: (1) selection of a range and distribution for each input variable; (2) development of a transformation that converts the multidimensional integrals required to calculate the expected value and variance of a model prediction to one-dimensional integrals; (3) assessment of the uncertainty in model predictions by evaluation of the one-dimensional integrals constructed in the preceding step to obtain expected values and variances; and (4) determination of the sensitivity of model predictions to model inputs on the basis of fractional contributions to variance obtained from a decomposition of a Fourier series representation for the model. Additional sources of information on the FAST approach are given in Table 3-4.

Relative Merits of Individual Techniques

Differential analysis is based on developing a Taylor series approximation to the model under consideration. Ultimately, the quality of the analysis results will depend on how well this series approximates the original model. Desirable properties of differential analysis include the following: (1) the effects of small perturbations away from the base-case value about which the Taylor series was developed are revealed; (2) uncertainty and sensitivity analyses are straightforward once the Taylor series is developed; (3) specialized techniques (e.g., adjoint, Green's function, GRESS/ADGEN) exist to facilitate the calculation of derivatives; and (4) the approach has been widely studied and applied.

However, there are two important drawbacks to differential analysis that should always be considered when selecting the procedure to be used in an

TABLE 3-4. SOURCES OF ADDITIONAL INFORMATION ON UNCERTAINTY AND SENSITIVITY ANALYSIS

Topic	References
Differential Analysis	Ronen, 1988; Lewins and Becker, 1982; Frank, 1978; Dickinson and Gelinas, 1976; Tomovic and Vukobratovic, 1972; Cacuci, 1981a,b; Cacuci et al., 1980; Dougherty and Rabitz, 1979; Dougherty et al., 1979; Hwang et al., 1978; Oblow et al., 1986; Pin et al., 1986; Worley and Horwedel, 1986; Oblow, 1985
Monte Carlo Analysis	Helton et al., 1986; Helton et al., 1985; Hendry, 1984; Fedra, 1983; Gardner and O'Neill, 1983; Iman and Conover, 1982a; Iman and Conover, 1980a,b; Iman et al., 1981a; Iman et al., 1981b; Schwarz and Hoffman, 1980; Iman et al., 1978
Response Surface Methodology	Box and Draper, 1987; Kleijnen, 1987; Myers, 1971; Olivi, 1986; Morton, 1983; Mead and Pike, 1975; Kleijnen, 1974
Fourier Amplitude Sensitivity Test	Liepmann and Stephanopoulos, 1985; McRae et al., 1981; Cukier et al., 1978; Cukier et al., 1973; Schaibly and Shuler, 1973
Reviews	Helton et al., 1991; Wu et al., 1991; Zimmerman et al., 1990; Doctor, 1989; Bonano and Cranwell, 1988; NEA, 1987; Rish and Marnicio, 1988; Fischer and Ehrhardt, 1985; Iman and Helton, 1985a; Hendrickson, 1984; Rabitz et al., 1983; Cox and Baybutt, 1981; Rose and Swartzman, 1981; Tilden et al., 1981; Mazumdar et al., 1978; Mazumdar et al., 1976; Mazumdar et al., 1975
Comparative Studies	Kim et al., 1988a,b; Mishra and Parker, 1989; Doctor et al., 1988; Iman and Helton, 1988; Maerker, 1988; Seaholm et al., 1988; Sykes and Thomson, 1988; Obray et al., 1986; Downing et al., 1985; Iman and Helton, 1985b; Jacobson et al., 1985; Uliasz, 1985; Harper and Gupta, 1983; Montgomery et al., 1983; Rose, 1982; Ahmed et al., 1981; Gardner et al., 1981; Scavia et al., 1981; Cox, 1977; Burns, 1975

uncertainty/sensitivity study. First, differential analysis is inherently local. The farther a perturbation moves from the base-case value about which the Taylor series was constructed, the less reliable the analysis results become. In particular, differential analysis is a poor choice for use in estimating distribution functions and provides no information on the possible existence of thresholds or discontinuities in the relationships between independent and dependent variables. Overall, the more nonlinear the relationships between the independent and dependent variables, the more difficult it is to employ a differential analysis effectively. Second, differential analyses can be very difficult to implement and often require large amounts of human and/or computer time. This difficulty arises from the need to calculate the partial derivatives required in the Taylor series. The possible use of sophisticated techniques such as the GRESS/ADGEN procedures offers some encouragement in this area. Even so, the need to calculate the required derivatives should not be taken lightly.

Monte Carlo analysis is based on the use of a probabilistic procedure to select model input. Then, uncertainty analysis results are obtained directly from model predictions without the use of an intermediate surrogate model, and sensitivity analysis results are obtained by exploring the mapping from model input to model predictions that formed the basis for the uncertainty analysis. Desirable properties of Monte Carlo analysis include the following: (1) the full range of each input variable is sampled and subsequently used as model input; (2) uncertainty results are obtained without the use of a surrogate model; (3) extensive modifications to the original model are not necessary (such modifications are often required when adjoint or Green's function techniques are used as part of a differential analysis); (4) the full stratification over the range of each input variable facilitates the identification of nonlinearities, thresholds, and discontinuities; (5) a variety of regression-based sensitivity analysis techniques are available; and (6) the approach is conceptually simple, widely used, and easy to explain.

Two particularly appealing features of Monte Carlo analysis are the full coverage of the range of each input variable and the ease with which an analysis can be implemented. The first feature is particularly important when the input variables have large ranges and the existence of nonlinear relationships between the input and output variables is a possibility. With respect to the second feature, essentially any variable that can be supplied as an input or generated as an output can be included in a Monte Carlo analysis without any modification to the original model.

The major drawback to Monte Carlo procedures is the fact that multiple model evaluations are required. If the model is computationally expensive to evaluate or many model evaluations are required, then the cost of the

required calculations may be large. Computational cost should always be considered when selecting a technique, but it is rarely the dominant cost in performing an analysis. Special techniques such as Latin hypercube sampling and importance sampling can often be used to reduce the number of required model evaluations without compromising the overall quality of an analysis. Further, it is important to recognize that, in practice, the other analysis techniques discussed in this section can require as much computational time as Monte Carlo analysis.

Response surface methodology is based on constructing a response-surface approximation to the original model. This approximation is then used as a surrogate for the original model in subsequent uncertainty and sensitivity studies. Desirable properties of response-surface methodology include the following: (1) complete control over the structure of model input through the experimental design selected for use; (2) near optimum choice for a model whose predictions are known to be a linear or quadratic function of the input variables; and (3) uncertainty and sensitivity analyses that are inexpensive and straightforward once the necessary response surface approximation has been constructed. Further, the development of experimental designs has been widely studied, although typically for situations that are considerably less involved than those encountered in performing an uncertainty/sensitivity study for a complex model.

There are also several drawbacks to response surface methodology that should be considered when an approach to uncertainty/sensitivity analysis is being selected. These include the following: (1) difficulty in development of an appropriate experimental design because of many input variables, many output variables, unknown form for the model, or spatial/temporal variability; (2) use of few values for each input variable; (3) possible requirement of many design points; (4) difficulties in detecting thresholds, discontinuities, and nonlinearities; (5) difficulties in including correlations and restrictions between input variables; and (6) difficulty in construction of an appropriate response-surface approximation to the original model, which may require a considerable amount of statistical sophistication and/or artistry. Ultimately, the final uncertainty/ sensitivity results are no better than the response-surface approximation to the original model. Response-surface methodology will work when there are only a few (typically, less than 10) input variables, a limited number of distinct output variables (because a design that is appropriate for one output variable may not be appropriate for a different output variable), and the relationships between the input and output variables are basically linear or quadratic or involve a few cross-products. Otherwise, the structure of the input-output relationships is too complicated to be captured by a classical experimental design (or a sequence of designs if a sequential approach is being used) in an efficient manner.

The FAST approach is based on performing a numerical calculation to estimate expected value and variance. Further, sensitivity results are obtained by decomposing the variance estimate into the variances due to the individual input variables. Desirable properties of the FAST approach include the following: (1) full range of each input variable is covered; (2) estimation of expected value and variance is by a direct calculation rather than by use of a surrogate model; and (3) modifications to the original model are not required.

There are also several drawbacks to using the FAST approach. These include the following: (1) the underlying mathematics is complicated and difficult to explain; (2) the approach is not widely known or used; (3) developing the necessary space-filling curve and performing the numerical integration over this curve to obtain expected value and variance is complicated; (4) many model evaluations may be required; (5) an estimate for the cumulative distribution function of the dependent variable is not provided; and (6) it is not possible to specify correlations or other types of restrictions between variables. Fortunately, software has been developed to facilitate the implementation of an uncertainty/sensitivity study based on the FAST approach (McRae et al., 1981). As analyses are currently performed with the FAST approach, no information on discontinuities, thresholds, or nonlinearities is obtained. However, it is probably possible to investigate this type of behavior with the model evaluations that must be performed in the numerical integrations to obtain expected value and variance.

Monte Carlo as a Preferred Approach

Each approach to uncertainty and sensitivity analysis has its advantages and disadvantages, and all approaches have been successfully applied. It would be a mistake to state categorically that one approach will always be superior to the others regardless of the model under consideration. For a given analysis problem, the available approaches should be considered, and the approach that seems most appropriate for the problem should be selected. This selection should take into account the nature of the model, the type of uncertainty and sensitivity analysis results desired, the cost of modifying and/or evaluating the model, the human cost associated with mastering and implementing a technique, the time period over which an analysis must be performed, and the programmatic risk associated with unanticipated complications in the implementation of a technique.

The comments of the preceding paragraph notwithstanding, it is felt that Monte Carlo techniques provide the best overall approach for studying problems related to performance assessment for radioactive waste disposal. This statement is made for several reasons.

First, there are often large uncertainties in such problems. Due to full stratification over the range of each variable, Monte Carlo techniques are particularly appropriate for analysis problems in which large uncertainties are associated with the input variables. In particular, differential analysis and response surface methodology are likely to perform poorly when the relationships between the input and output variables are nonlinear and the input variables have large uncertainties.

Second, Monte Carlo techniques provide direct estimates for distribution functions. Neither differential analysis nor the FAST approach is intended for the estimation of distribution functions. The estimates obtained with response surface methodology are no better than the response surface approximation to the original model. It should be possible to estimate distribution functions with results generated as part of the FAST approach, but this possibility apparently has not been investigated and applied.

Third, Monte Carlo techniques do not require a large amount of sophistication that goes beyond the analysis problem of interest. In contrast, differential analysis, response surface methodology, and the FAST approach require a large amount of specialized knowledge to make them work. Developing this knowledge and making these techniques work can be very costly in terms of analyst time. Conceptually, Monte Carlo techniques are simpler and do not require modifications to the original model or additional numerical procedures. For example, both differential analysis and the FAST approach can require sophisticated numerical calculations. The application of response surface methodology can require specialized knowledge in experimental design and response surface construction. As a result, analyses based on Monte Carlo techniques are usually easier to present and explain than analyses based on the other techniques.

Fourth, Monte Carlo techniques can be used to propagate uncertainties through a sequence of separate models. Examples of this type of analysis can be found in performance assessments for radioactive waste disposal sites (Bonano et al., 1989; Cranwell et al., 1987) and probabilistic risk assessments for nuclear power plants (U.S. NRC, 1990; Helton et al., 1988; draft of NUREG/CR-4551, U.S. NRC). Due to the use of a number of independent computer programs and the necessity to handle information at model interfaces appropriately, the other methods do not seem to be applicable to this type of analysis.

Fifth, Monte Carlo techniques create a mapping from analysis input to analysis results. This mapping is rich in information because of the full stratification over the range of each input variable and the wide variety of output variables that can be generated and saved. Once produced and stored, this mapping can be explored in many ways. Differential analysis is inherently local. Response surface methodology employs a very sparse

stratification. The exact nature of the mapping produced by the FAST approach has not been investigated.

3.5.2 MONTE CARLO ANALYSIS

As previously discussed, the WIPP performance assessment uses Monte Carlo techniques to study the impact of uncertainties. A Monte Carlo analysis involves five steps. Each of these steps is now discussed in the context of the WIPP performance assessment.

Selection of Variable Ranges and Distributions

Monte Carlo analyses use a probabilistic procedure for the selection of model input. Therefore, the first step in a Monte Carlo analysis is the selection of ranges and distributions for the variables under consideration. When performed carefully, this can be the largest and most expensive part of a Monte Carlo analysis. However, the amount of effort expended here depends strongly on the purpose of the analysis.

If the analysis is primarily exploratory, then rather crude characterizations of the ranges and distributions for the input variables may be adequate. For example, physical plausibility arguments might be used to establish ranges, and uniform or loguniform distributions could be assumed within these ranges. These assumptions are often adequate to bound the ranges for output variables of interest and also to determine which input variables have the greatest influence on the output variables. The estimated range for an output variable and associated sensitivity results are primarily determined by the ranges assigned to the input variables. Thus, even for exploratory studies, care should be taken to avoid assigning unreasonably large ranges to variables. Sensitivity results are generally less dependent on the actual distributions assigned to the input variables than they are to the ranges chosen for the variables. However, distributional assumptions can have a large impact on the distributions estimated for output variables. Thus, when distributions for output variables must be estimated accurately, care must be used in developing distributions for the input variables.

Resources can often be used most effectively by performing a Monte Carlo analysis in an iterative manner. In a first iteration, rather crude range and distribution assumptions can be used to determine which input variables dominate the behavior of output variables of interest. Often, most of the variation in an output variable will be caused by a relatively small subset of the input variables. Once the most important input variables are identified, resources can be concentrated on characterizing their uncertainty. This avoids spending a large effort to characterize carefully the uncertainty in variables that have little impact on the ultimate outcome

of an analysis. This, in essence, is the approach used in the WIPP performance assessment, where an uncertainty/sensitivity study is performed each year to determine the importance of individual variables and thereby to provide guidance for future research (e.g., Helton et al., 1991).

The variables considered in Monte Carlo studies are typically input parameters to computer models. The individual variables x_j, $j = 1, \ldots, m$, can represent any parameter used in an analysis, including hydraulic conductivities, retardations, solubility limits, scenario probabilities, parameters in distributions, probabilistic cutoffs used to eliminate low probability scenarios, and parameters that characterize numerical calculations such as mesh sizes and error bounds. The defining characteristic of these variables is that the analysis requires a single value for each variable but it is uncertain as to what the value should be. Thus, the range assigned to each variable represents the set of possible values for that variable, and the corresponding distribution characterizes the likelihood that the appropriate value to use for this variable falls in various subsets of this range. As discussed in Section 3.1.3-Characterization of Uncertainty in Risk, this type of uncertainty corresponds to what is sometimes called Type B, or subjective, uncertainty.

It is very important that the range assigned to a variable be consistent with its usage in the computer program that implements the underlying model. In particular, the range assigned to a variable should be consistent with the scale on which the variable is used in the specific implementation of the model under consideration. A common mistake is to estimate a variable on a local scale and then to infer uncritically that the observed local variability is the same as the uncertainty in this variable on a much larger scale. This can lead to serious mis-estimates of the range for the "effective" variable value that is actually used in an analysis.

For example, a computer program might take a single value for the solubility limit of a radionuclide as input, with this single value being used throughout a room in a waste repository or perhaps even throughout the entire repository. Further, theoretical calculations or experimental results might be available for solubility limits under conditions that could occur in subregions of a room but which would be very unlikely to occur uniformly over the entire room. In this case, it would be a mistake to use the range of local results to characterize the range of solubility limits for a room or the repository since this range was developed for isolated sets of conditions that would not exist over large areas. The available information should be used in the construction of a range of "effective" solubility limits that is consistent with the use of this parameter in the particular analysis being performed. Similar situations can occur in the characterizations of hydraulic conductivities, retardations, and other variables where the scale

on which data are measured is very different from the scale on which estimated variables are actually used.

The preceding discussion quite naturally leads to the following question: How should the ranges and distributions for variables be determined for use in a Monte Carlo analysis? This is a reasonable question to ask, and a hard question to answer. Clearly, the answer must depend on the goals of the analysis, the time and resources available, and the type of information that exists for use in estimating ranges and distributions.

The simplest and most desirable situation would be to have a sequence

$$e_{1j}, e_{2j}, \ldots, e_{nE,j} \tag{3-37}$$

of independent, unbiased, normally and identically distributed estimates for a variable x_j exactly as it is used by a model in a particular analysis and by the computer program that implements this model. In this case, each e_{ij} is an estimate for the corresponding model input x_j, and the single best estimate for x_j is given by

$$\bar{x}_j = \sum_{i=1}^{nE} e_{ij}/nE. \tag{3-38}$$

Further, the standard deviation, or standard error as it is sometimes called when population parameters are being considered, for $\bar{x}_j$ is given by

$$SD(\bar{x}_j) = \left[\sum_{i=1}^{nE} (e_{ij} - \bar{x}_j)^2\right]^{1/2} / \sqrt{nE(nE-1)}. \tag{3-39}$$

The quantity

$$t = (\bar{x}_j - x_j)/SD(\bar{x}_j) \tag{3-40}$$

is distributed as a t-distribution with nE-1 degrees of freedom, where x_j is the appropriate but unknown variable value for use in the analysis (Iman and Conover, 1983). The preceding expression can be rearranged algebraically to obtain

$$x_j = \bar{x}_j - t\ SD(\bar{x}_j). \tag{3-41}$$

Thus, the t-distribution can be used to define a distribution for x_j. Further, a confidence interval (e.g., 95%, 99%) for x_j can also be obtained from the t-distribution and used to define the range of x_j. This is equivalent to excluding specified regions in the tails of the t-distribution when generating x_j from the expression in Equation 3-41. The justification for using the t-distribution as a probability distribution for an uncertain variable comes from applying Bayes' Theorem with a diffuse prior distribution for both the mean and standard deviation of the sampling process (Winkler, 1972).

As just illustrated, it may be possible to estimate the range and distribution for some variables with formal statistical procedures. Such procedures should always be used when data have been collected in an appropriate manner. Appropriate data collection usually requires prior knowledge of the precise variable to be estimated and use of a carefully planned experimental design. The exact statistical procedures selected for use would depend on the experimental design and the assumed relationships between the variable to be estimated and the data from the design.

Unfortunately, most parameters used in a performance assessment are not amenable to direct statistical estimation for various subsets for the following reasons: (1) The time scales over which parameters can be estimated are often much shorter than the time scales over which they will actually be used. (2) The physical scale on which parameters can be observed is often much smaller than the physical scale on which they will be used. As a result, heterogeneities in the system prevent individual observations from being used as estimates for system parameters. (3) Estimation of some parameters (e.g., distribution coefficients) requires the removal of material from the system. This removal can alter the properties of the material and thus lead to incorrect parameter estimates. (4) The exact conditions that will exist within the system (e.g., in a waste disposal room) are not known. Thus, it is not possible to design experiments to match the exact conditions for which parameter values are needed. (5) Collection of some types of data involves a degradation of the site (e.g., the drilling of boreholes). As a result, the collection of such data is necessarily limited. (6) Some data involves the occurrence of rare events (e.g., scenario probabilities). Although the geological and historical records can be searched for more information, designed experiments are not possible. (7) Some parameters are not directly measurable. For example, the time scales associated with future human activities make it impossible to design experiments to estimate parameters (e.g., drilling rates) associated with such activities.

Due to reasons of the type outlined in the preceding paragraph, ranges and distributions for most parameters used in a performance assessment cannot be obtained by formal statistical procedures. Nonetheless, there is still a

large body of relevant information that can be used in estimating ranges and distributions. Much of this information is field data collected at the site. Other sources of information include theoretical calculations, mechanistic code calculations, physical data from other sites, and knowledge of the differences between the conditions under which data were collected and the conditions under which estimated parameters are to be used.

The challenge in developing ranges and distributions for use in a Monte Carlo study is to incorporate this diverse body of information meaningfully. Indeed, the importance of such ranges and distributions is that they provide a mathematical structure that summarizes the available information in a form that can be used in further analyses. In many situations, the only practical way to develop these summary ranges and distributions is through an expert review process.

The ultimate outcome of this review process would be a distribution function F(x) of the form shown in Figure 3-16 for each independent variable of interest. For a particular variable x_j, the function F is defined such that

$$\text{prob}(x < x_j \leq x + \Delta x) = F(x + \Delta x) - F(x). \qquad (3\text{-}42)$$

That is, $F(x+\Delta x) - F(x)$ is equal to the probability that the appropriate value to use for x_j in the particular analysis under consideration falls between x and $x + \Delta x$. In most cases, the probabilities involved in this representation will be subjective in the sense that they represent a degree of belief as to where the appropriate value for x_j falls conditional on all the information available to the reviewer or reviewers. However, when formal statistical procedures can be used as is indicated in conjunction with Equation 3-41, the final result will again be a distribution of the form shown in Figure 3-16. In both cases, the data summary process will have arrived at the same place: a distribution based on available information that characterizes where the appropriate value for x_j is likely to be located.

In many situations, the most appropriate way to construct a subjective distribution of the form shown in Figure 3-16 is through the estimation of quantiles. For example, the process might start by determining minimum and maximum values for x_j, which defines the 0.00 and 1.00 quantiles. This provides estimates for the points

$$(x_{0.00}, 0.00) \text{ and } (x_{1.00}, 1.00) \qquad (3\text{-}43)$$

on the distribution function in Figure 3-16. The next point to estimate might be the median, which divides the range of x_j into two intervals of

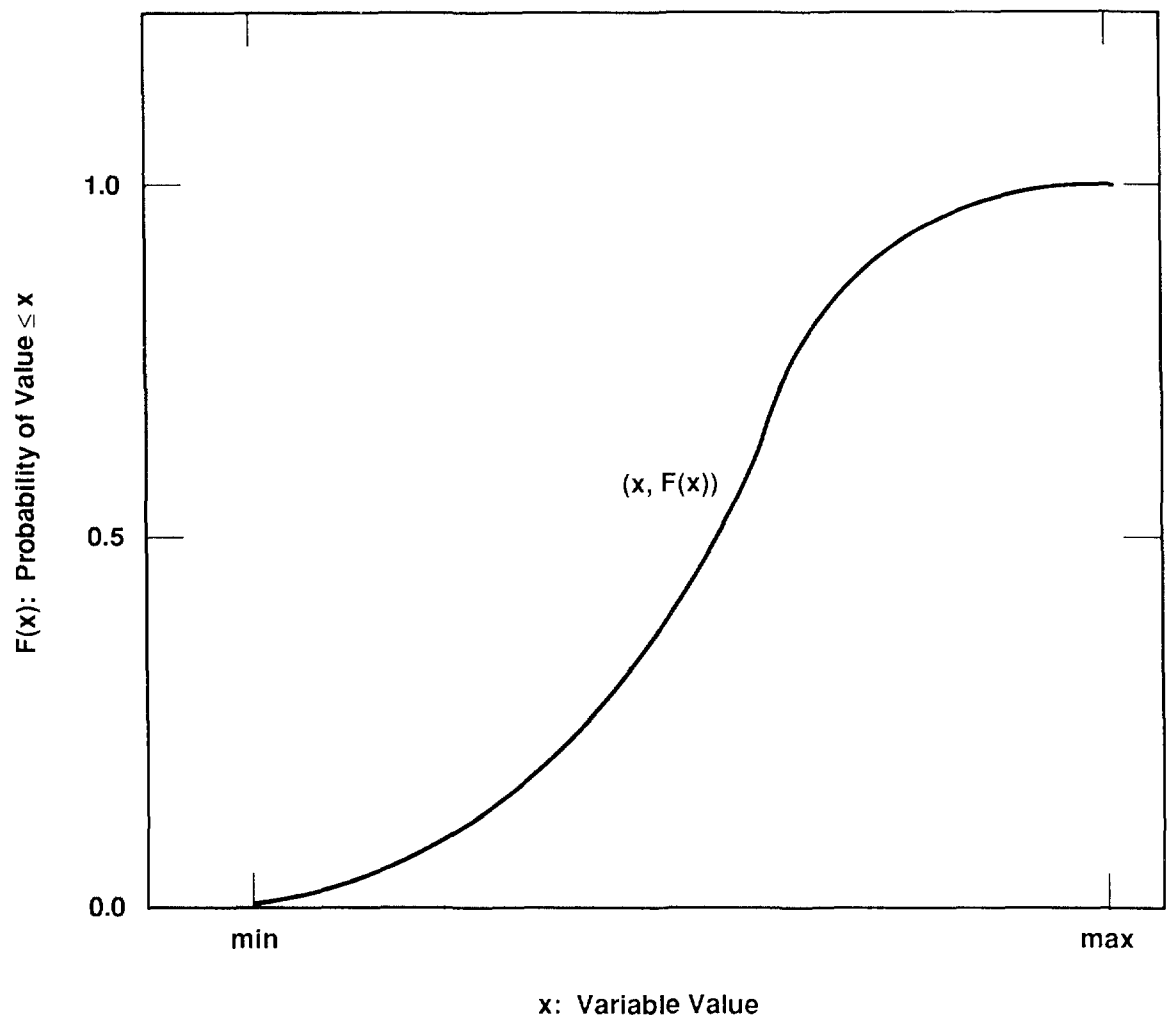

Figure 3-16. Distribution Function for an Imprecisely Known Analysis Variable. For each value x on the abscissa, the corresponding value F(x) on the ordinate is the probability that the appropriate value to use in the analysis is less than or equal to x (Helton et al., 1991).

equal probability, followed by estimates for the 0.25 and 0.75 quantiles. This produces the following additional points on the distribution function:

$$(x_{0.25}, 0.25), (x_{0.50}, 0.50), (x_{0.75}, 0.75). \quad (3\text{-}44)$$

This process would continue by estimating additional points (e.g., the 0.05, 0.10, 0.90, and 0.95 quantiles) until the shape of the distribution is reasonably characterized. The rest of the distribution could then be filled in by assuming that the distribution function is linear between the specified quantiles, which is equivalent to fitting a maximum entropy distribution (Levin and Tribus, 1978; Tierney, 1990; Cook and Unwin, 1986). Figure 3-17 illustrates what the outcome of this process might look like.

Distribution functions for imprecisely known analysis variables can also be obtained by selecting parameter values such as the mean and standard deviation for established distributions (e.g., normal, lognormal, beta). However, it is generally best to avoid this approach for several reasons.

First, there is usually no conceptual basis to pick a particular distribution. Second, it is hard to justify why a particular set of distribution parameters was selected (e.g., why a particular mean and standard deviation was selected for use with a lognormal distribution). In contrast, it is often much easier to relate the assignment of quantiles to specific information available to the reviewer. Third, most reviewers are not trained statisticians and often do not have an intuitive feeling for the relationship between the shape of a highly skewed distribution and the parameters that define it. Thus, selected parameters may not produce a distribution of the shape anticipated by the reviewer. In general, the use of formal distributions is undesirable because it puts an unnecessary transformation between the information possessed by the reviewer and the form in which this information is used in the analysis. In contrast, distributions constructed from quantiles are based on information that corresponds more closely to that available to the reviewer.

The scale of an expert review process can vary widely. At one extreme, a single individual might be involved in reviewing the available information on a particular variable and constructing the distribution shown in Figure 3-17. The actual construction of this distribution could range from being entirely subjective to using sophisticated computational procedures to relate variability in data collected at one scale to uncertainty in a parameter for use on a different scale. At the other extreme, several teams of experts could be used to estimate a distribution independently, and then the final distribution used in the analysis would be calculated by averaging the distributions obtained by the individual teams. An intermediate approach

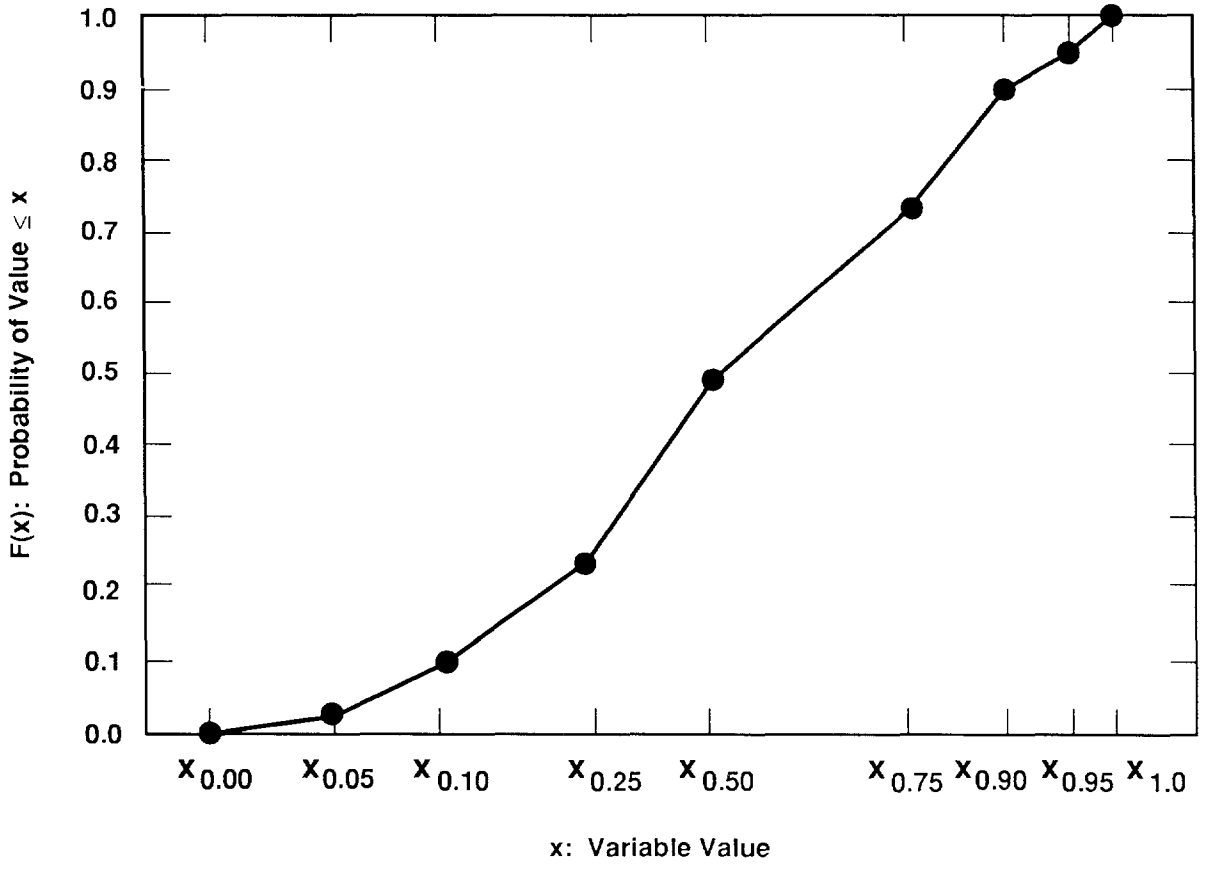

Figure 3-17. Estimated Distribution Function for an Imprecisely Known Analysis Variable. This distribution function was built up from estimates for the following quantities: 0.00, 0.05, 0.10, 0.25, 0.50, 0.75, 0.90, 0.95 and 1.00 (Helton et al., 1991).

would be to have several knowledgeable individuals independently estimate a distribution and then average these estimates. Bonano et al. (1990) provide a detailed discussion on the elicitation and use of expert judgment in performance assessment for radioactive waste disposal.

The U.S. Nuclear Regulatory Commission's reassessment of the risk from commercial nuclear power plants (NUREG-1150) provides an excellent example of the application of a formal expert review process to develop variable ranges and distributions for use in a Monte Carlo analysis (U.S. NRC, 1990). This study involves probably the most extensive use of a formal expert review process performed to date. The general approach used and the experiences gained in its implementation are summarized in several articles (Ortiz et al., 1991; Hora and Iman, 1989). Further, the actual performance of the expert review process is summarized in a sequence of technical reports (Wheeler et al., 1989; Harper et al., 1990, 1991, and other volumes in prep.). This analysis used several experts to assess independently the range and distribution for each input variable of interest; then, the distributions supplied by the individual experts were averaged, with equal weight being given to each expert. A recent study of seismic hazard curves provides an example of the use of the team approach to estimating distributions (EPRI, 1989).

A total of 45 imprecisely known variables were selected for sampling in the 1991 WIPP performance assessment. These variables are listed in Tables 6.0-1, -2, and -3 in Volume 3 of this report. Their selection was based on their perceived importance with respect to the WIPP performance assessment and was guided in part by sensitivity studies performed in conjunction with the 1990 WIPP performance assessment (Helton et al., 1991). The distributions assigned to these variables (see Tables 6.0-1, -2, and -3 in Volume 3 of this report) characterize where a fixed, but unknown, value for a variable is likely to be located. The uncertainty in most variables was characterized internally at SNL. However, a panel of experts from outside SNL was used to assess the uncertainty in solubility limits. The deliberations of this panel are described in Volume 3, Chapter 3 of this report.

Generation of Sample

The generation of a sample from the distributions developed in the first step of a Monte Carlo analysis is now discussed. For this discussion, suppose that the multidimensional variable $\mathbf{x}$ is under consideration and that the distribution function for $\mathbf{x}$ is denoted by $F(\mathbf{x})$. Many sampling procedures have been proposed for use in Monte Carlo studies to generate samples from $F(\mathbf{x})$ (McGrath et al., 1975). The following often-used techniques are

discussed below: random sampling, stratified sampling, and Latin hypercube sampling.

In random sampling, the observations

$$\mathbf{x}_i = [x_{i1}, \ldots, x_{in}], \; i = 1, \ldots, m, \tag{3-45}$$

where m is the sample size, are selected independently from the distribution defined by $F(\mathbf{x})$. In random sampling, points from different regions of the sample space of $\mathbf{x}$ occur in direct relationship to the probability of occurrence of these regions. Thus, a large sample size may be required to ensure adequate coverage of regions believed to be important but having low probabilities of occurrence.

A systematic coverage of the sample space (i.e., range) of $\mathbf{x}$ is forced in stratified sampling. Specifically, the sample space S of $\mathbf{x}$ is partitioned into nS distinct strata S_j, $j = 1, \ldots, nS$. In general each stratum has different probability p_j of occurring; that is,

$$p_j = \text{prob}(\mathbf{x} \varepsilon S_j). \tag{3-46}$$

A random sample of size m_j is then obtained from each strata S_j. That is, the points $\mathbf{x}_{jk}$, $k = 1, \ldots, m_j$, are selected at random from S_j. When all the $\mathbf{x}_{jk}$ are brought together, the result is the sequence of observations

$$\mathbf{x}_i = [x_{i1}, \ldots, x_{in}], \; i = 1, \ldots, m = \sum_{j=1}^{nS} m_j. \tag{3-47}$$

With stratified sampling, it is possible to force the selection of points from regions believed to be important even if these regions have a low probability of occurrence. This sampling technique is sometimes called importance sampling. When only one stratum is used, stratified sampling is the same as random sampling.

Stratified sampling operates to ensure the full coverage of specified regions in the sample space. This idea is carried further in Latin hypercube sampling (McKay et al., 1979) to ensure the full coverage of the range of each variable. Specifically, the range of each variable (i.e., the x_j) is divided into m intervals of equal probability and one value is selected at random from each interval. The m values thus obtained for x_1 are paired at random with the m values obtained for x_2. These m pairs are combined in a random manner with the m values of x_3 to form m triples. This process is continued until a set of m n-tuples is formed. These n-tuples are of the form

$$\mathbf{x}_i = [x_{i1}, \ldots, x_{in}], \; i = 1, \ldots, m, \tag{3-48}$$

and constitute the Latin hypercube sample. The individual x_j must be independent for the preceding construction procedure to work; a method for generating Latin hypercube and random samples from correlated variables has been developed by Iman and Conover (1982b) and will be discussed briefly.

For illustration, the results of a random sample, a stratified sample, and a Latin hypercube sample are shown in Figure 3-18. A sample of size 10 from two uniformly distributed variables is used. Ten strata are used for the stratified sample and one value is taken from each strata. The selection of strata in a stratified sample is not unique and is often made to assure that certain low probability, but high interest, subranges of the independent variables are included in an analysis.

At the end of their comparison of sampling techniques, McKay et al. (1979) conclude that Latin hypercube sampling has a number of desirable properties and recommend its consideration for use in Monte Carlo studies. These properties include (1) full stratification across the range of each variable, (2) relatively small sample sizes, (3) direct estimation of means, variances, and distribution functions, and (4) the availability of a variety of techniques for sensitivity analysis. Another desirable property of Latin hypercube sampling is that it is possible to determine the effects of different distributions for the input variables on the estimated distribution for an output variable without rerunning the model (Iman and Conover, 1980a,b). As a result of these properties, Latin hypercube sampling has become a widely used sampling technique.

Control of correlation within a sample used in a Monte Carlo analysis can be very important. If two or more variables are correlated, then it is necessary that the appropriate correlation structure be incorporated into the sample if meaningful results are to be obtained in subsequent uncertainty/sensitivity studies. On the other hand, it is equally important that variables not appear to be correlated when they are really independent.

It is often difficult to induce a desired correlation structure on a sample. Indeed, most multivariate distributions are incompatible with the majority of correlation patterns that might be proposed for them. Thus, it is fairly common to encounter analysis situations where the proposed variable distributions and the suggested correlations between the variables are inconsistent; that is, it is not possible to have both the desired variable distributions and the requested correlations between the variables.

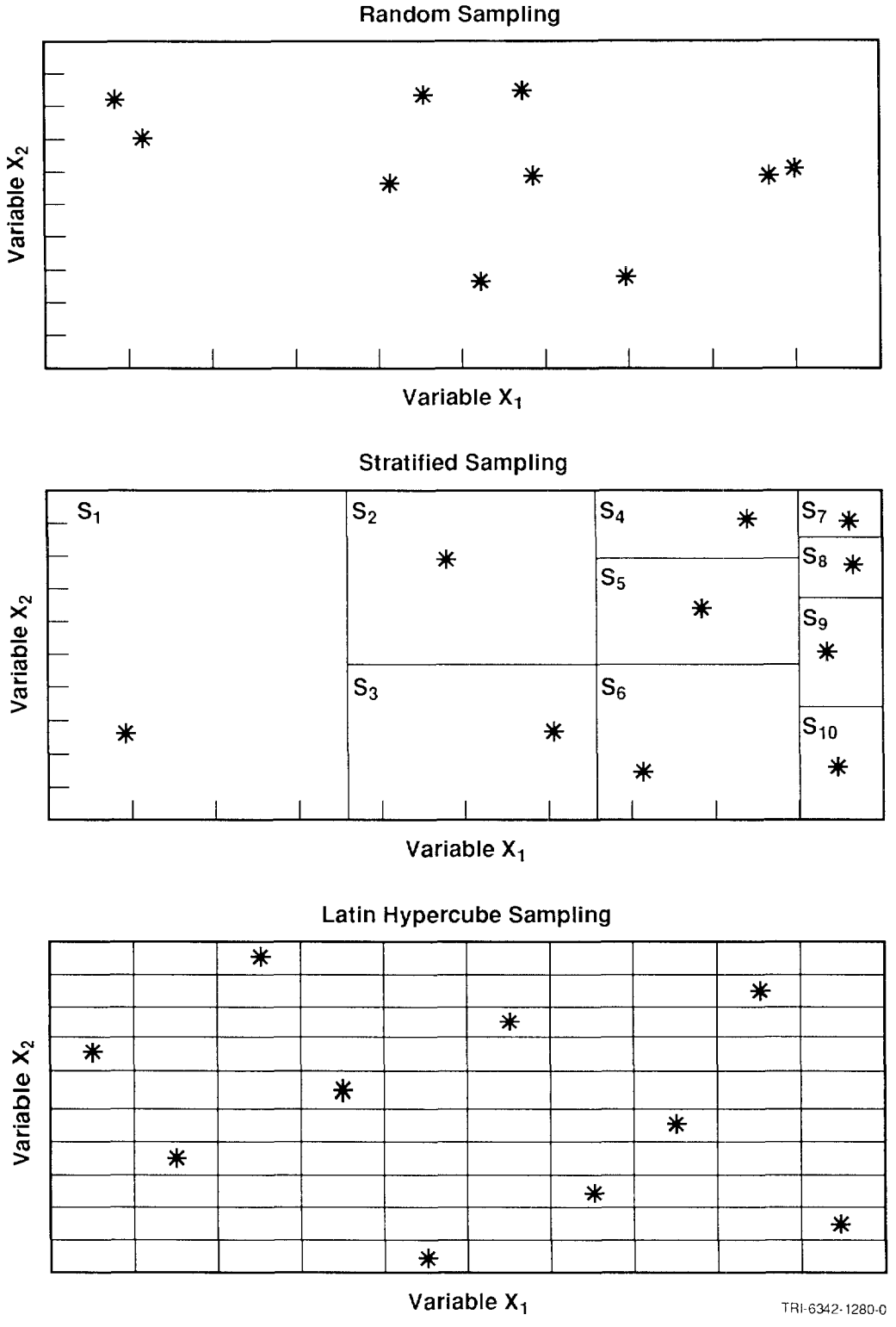

Figure 3-18. Illustration of Random Sampling, Stratified Sampling, and Latin Hypercube Sampling for a Sample of Size 10 from Two Uniformly Distributed Variables.

In response to this situation, Iman and Conover (1982b) have proposed a restricted pairing technique for controlling the correlation structure in random and Latin hypercube samples that is based on rank correlation (i.e., on rank-transformed variables) rather than sample correlation (i.e., on the original raw data). With their technique, it is possible to induce an approximation to any desired rank-correlation structure onto the sample. This technique has a number of desirable properties: (1) It is distribution free. That is, it may be used with equal facility on all types of input distribution functions. (2) It is simple. No unusual mathematical techniques are required to implement the method. (3) It can be applied to any sampling scheme for which correlated input variables can logically be considered, while preserving the intent of the sampling scheme. That is, the same numbers originally selected as input values are retained; only their pairing is affected to achieve the desired rank correlations. This means that in Latin hypercube sampling the integrity of the intervals is maintained. If some other structure is used for selection of values, that same structure is retained. (4) The marginal distributions remain intact.

For many, if not most, uncertainty/sensitivity analysis problems, rank-correlation is probably a more natural measure of congruent variable behavior than is the more traditional sample correlation. What is known in most situations is some idea of the extent to which variables tend to move up or down together; more detailed assessments of variable linkage are usually not available. It is precisely this level of knowledge that rank correlation captures.

The exact mathematical procedure used in the Iman/Conover technique to induce a desired rank-correlation structure is described in the original article (Iman and Conover, 1982b) and also in Doctor (1989). The impact of various rank-correlation assumptions is illustrated in Iman and Davenport (1982).

The WIPP performance assessment uses stratified sampling and Latin hypercube sampling. The decomposition of the sample space S shown in Equation 3-11 into scenarios S_i as indicated in Equation 3-1, and shown in more detail in Equations 3-21 through 3-27, is a form of stratified sampling. The scenario probabilities pS_i in Equation 3-1 are the strata probabilities. Thus, stratified sampling is being used to incorporate stochastic, or Type A, uncertainty into the WIPP performance assessment. Stratified sampling forces the inclusion of low probability, but possibly high consequence, scenarios.

Latin hypercube sampling is being used to incorporate subjective, or Type B uncertainty, into the WIPP performance assessment. Specifically, a Latin hypercube sample of size 60 was generated from the 45 variables in Tables 6.0-1, -2, and -3 in Volume 3 of this report. Further, the restricted

pairing technique of Iman and Conover (1982b) was used to prevent spurious correlations within the sample. The resultant sample is listed in Volume 2, Appendix A of this report.

Propagation of Sample Through Analysis

The next step is the propagation of the sample through the analysis. Conceptually, this step is quite simple. Each element of the sample is supplied to the model as input, and the corresponding model predictions are saved for use in later uncertainty and sensitivity studies. This creates a sequence of results of the form

$$y_i = f(x_{i1}, x_{i2}, \ldots, x_{in}) = f(\mathbf{x}_i), \; i = 1, 2, \ldots, m, \tag{3-49}$$

where n is the number of input (i.e., sampled) variables and m is the sample size. Typically, there are many model predictions of interest, in which case y_i would be a vector rather than a single number.

In its simplest form, this step involves little more than putting a "DO loop" around the model within which (1) each sample element is read and supplied to the model as input, (2) the model is evaluated, and (3) the results of each model evaluation are written to a file that is saved after all model evaluations have been completed. In practice, this step can be considerably more complicated than this. For example, a sampled variable may not be in exactly the form the model takes as input, or model predictions may not be in the form desired for subsequent uncertainty and sensitivity analysis. In such cases, a preprocessor and a postprocessor can be added to the loop immediately before and immediately after model evaluation to perform the necessary transformations.

A more complex situation sometimes arises when the model under consideration is actually a sequence of individual models, each of which supplies input to the next model in the sequence. When each model produces many distinct cases for analysis by the next model, it is sometimes necessary to use a clustering procedure at the interfaces to control the total number of cases that are propagated through the entire analysis. Otherwise, the number of individual cases can increase until the overall analysis becomes intractable due to computational cost. As an example, the NUREG-1150 analyses (U.S. NRC, 1990) found it necessary to group results at model interfaces to make the Monte Carlo calculations being used to propagate uncertainties practical on a computational basis (Helton et al., 1988; draft of NUREG/CR-4551, U.S. NRC).

The performance of sampling-based uncertainty/sensitivity studies is sometimes facilitated by the use of a special code package to control the

overall analysis (Campbell and Longsine, 1990; Holmes, 1987). The Compliance Assessment Methodology Controller (CAMCON) has been developed to facilitate the performance and archival storage of the many complex calculations that are required in the WIPP performance assessment (Rechard, 1989; Rechard et al., 1989). This methodology incorporates data bases, sampling procedures, model evaluations, data storage, uncertainty and sensitivity analysis procedures, and plotting capabilities into a unified structure. The structure and operation of CAMCON is illustrated in Figure 3-19.

Additional information on CAMCON and its use in the 1991 WIPP performance assessment is given in Chapter 5 of this volume.

Uncertainty Analysis

Once a sample has been generated and propagated through a model, uncertainty analysis is straightforward. If random or Latin hypercube sampling is being used, then the expected value and variance for the output variable y can be estimated by

$$E(y) \doteq \sum_{i=1}^{m} y_i/m \qquad (3\text{-}50)$$

and

$$V(y) \doteq \sum_{i=1}^{m} \left[y_i - E(y)\right]^2/(m - 1), \qquad (3\text{-}51)$$

respectively. Both estimates are unbiased for random sampling. The estimated expected value is also unbiased for Latin hypercube sampling, but the estimated variance is known to contain a bias. Empirical studies suggest that this bias is small (McKay et al., 1979; Iman and Helton, 1985a). When stratified sampling is used, the factors 1/m and 1/(m-1) in Equations 3-50 and 3-51 must be replaced by weights w_i, i = 1, ..., m, that reflect the probability and number of observations associated with each stratum.

The distributions for the output variables considered in performance assessment are often highly skewed. Due to the disproportionate impact of large but unlikely values, the estimates for the means and variances associated with such distributions tend to be unstable. Here, unstable means that there is a large amount of variation between estimates obtained from independently generated samples. Further, when skewed distributions are under consideration, means and variances give a poor characterization for distribution shape. Basically, means and variances do not contain enough information to characterize highly skewed distributions adequately.

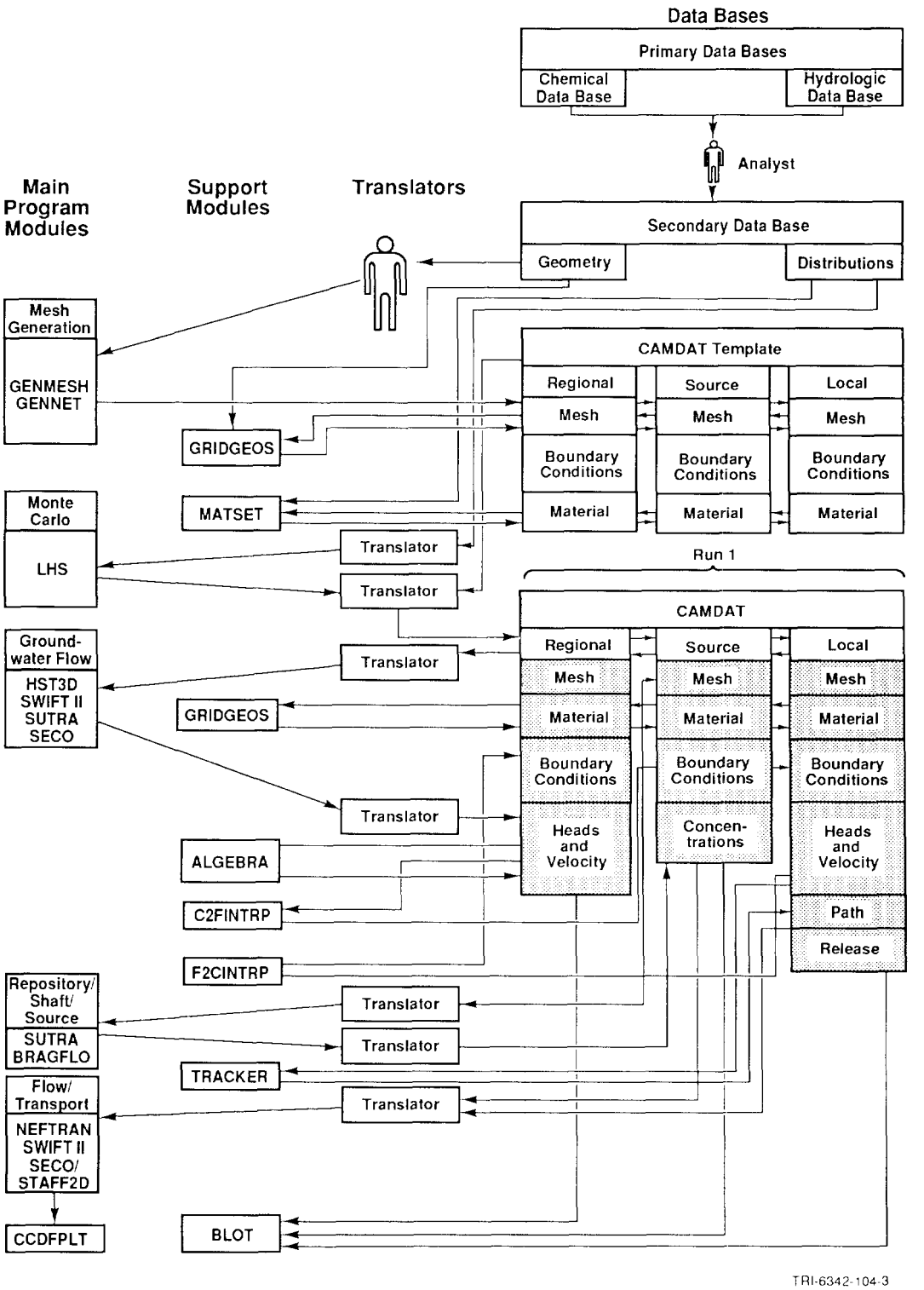

Figure 3-19. Overview of CAMCON.

An estimated distribution function gives a better characterization of the uncertainty in an output variable than a mean and a variance. The distribution function F for the output variable y appearing in Equation 3-49 can be estimated from the relationship

$$F(y) = \begin{cases} 0 & \text{if } y < y_1 \\ i/m & \text{if } y_i \le y < y_{i+1},\ i = 1, 2, \ldots, m - 1 \\ 1 & \text{if } y_n \le y, \end{cases} \qquad (3\text{-}52)$$

where it is assumed that the y_i have been ordered so that $y_i \le y_{i+1}$. This creates a plot that displays all the information contained in Equation 3-49 about the uncertainty in y. An example estimated distribution function is shown in Figure 3-20. The abscissa displays the values for the output variable, and the ordinate displays cumulative probability, which is the probability of obtaining a value equal to or less than a value on the abscissa. The step height is equal to the probability associated with the individual sample elements. If stratified sampling was being used, each observation would be assigned a weight that equalled the probability of the stratum from which it was obtained divided by the number of observations taken from that stratum.

Random sampling, stratified sampling, and Latin hypercube sampling all yield unbiased estimates for distribution functions for predicted variables. When the restricted pairing technique developed by Iman and Conover (1982b) is used to control correlations within the sample, a small bias may be introduced. However, the amount of this bias does not appear to be significant (Iman and Conover, 1982b; Iman and Helton, 1985a).

An alternate, and equivalent, way to display uncertainty is with a complementary cumulative distribution function (CCDF), which is simply 1 minus the cumulative distribution function (cdf). A common practice is to use CCDFs to display stochastic (i.e., Type A) uncertainty and cdf's to display subjective (i.e., Type B) uncertainty. CCDFs are often used to display the results of performance assessments because they answer the question "How likely is it to be this bad or worse?" Also, it is easier to read the probabilities for unlikely but high consequence events from CCDFs than from cdf's. The construction of a CCDF is described in conjunction with Figure 3-1. As discussed in Section 3.1.4-Risk and the EPA Limits, the EPA release limits can be formulated in terms of CCDFs. When both stochastic and subjective uncertainty are present in an analysis, the stochastic uncertainty can be represented with a CCDF, and the subjective uncertainty can be represented with a family or distribution of CCDFs. Examples of representations of this type are given in Figures 3-4 and 3-9.

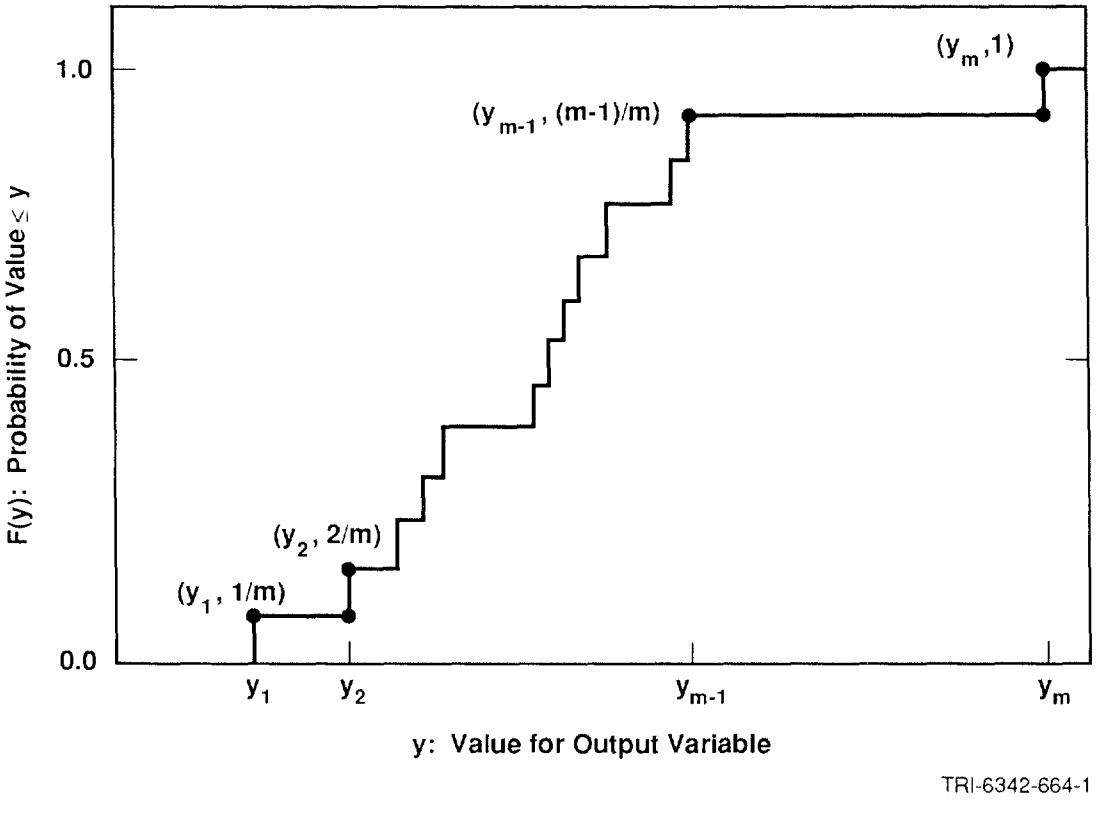

Figure 3-20. Example of an Estimated Distribution Function (Helton et al., 1991).

A cumulative distribution function readily displays the quantiles of a distribution. However, a distribution's mode (i.e., the subrange of a variable in which its probability is most concentrated) is more difficult to identify visually, although it can be done. Further, the mean is not apparent at all. Figure 3-21 shows an alternate uncertainty display that incorporates a distribution function, a density function, and a mean into a single figure (Ibrekk and Morgan, 1987). One advantage of the estimated distribution function is that it displays the results of every observation in an unaltered form. In contrast, the shape of the density function can be sensitive to the gridding selected for use unless a smoothing algorithm is used.

As illustrated in Figure 3-22, box plots (Iman and Conover, 1983) provide an alternate way to display the information in a distribution function. The endpoints of the boxes in Figure 3-22 are formed by the lower and upper quartiles of the data, that is, $x_{.25}$ and $x_{.75}$. The vertical line within the box represents the median, $x_{.50}$. The sample mean is identified by the large dot. The bar on the right of the box extends to the minimum of $x_{.75} + 1.5(x_{.75} - x_{.25})$ and the maximum observation. In a similar manner, the bar on the left of the box extends to the maximum of $x_{.25} - 1.5(x_{.75} - x_{.25})$ and the minimum observation. The observations falling outside of these bars are shown with x's. In symmetric distributions, these values would be considered as outliers. Box plots contain the same information as a distribution function, although in a somewhat reduced form. Further, their flattened shape makes it convenient to present and compare different distributions in a single figure.

Concern is often expressed with respect to the accuracy of the estimates for distribution functions obtained in Monte Carlo analyses. When random sampling is used, Kolmogorov-Smirnov bounds can be used to place confidence intervals about estimated distribution functions (Conover, 1980). Other techniques also exist for use with random sampling (Woo, 1991; Cheng and Iles, 1983). When Latin hypercube sampling is used, replicated sampling can be used to place confidence intervals about estimated distribution functions (Iman, 1982; Iman and Helton, 1991). Use of a technique called fast probability integration provides an alternative to Monte Carlo procedures for the calculation of the tails of distributions (Wu et al., 1990; Wu, 1987; Wu and Wirsching, 1987; Chen and Lind, 1983; Rackwitz and Fiessler, 1978). However, this technique does not appear to have been applied to a problem as complex as estimating the uncertainty in the results of a performance assessment.

The capability to generate means, variances, CCDFs, cdf's, and box plots has been incorporated into the CAMCON structure.

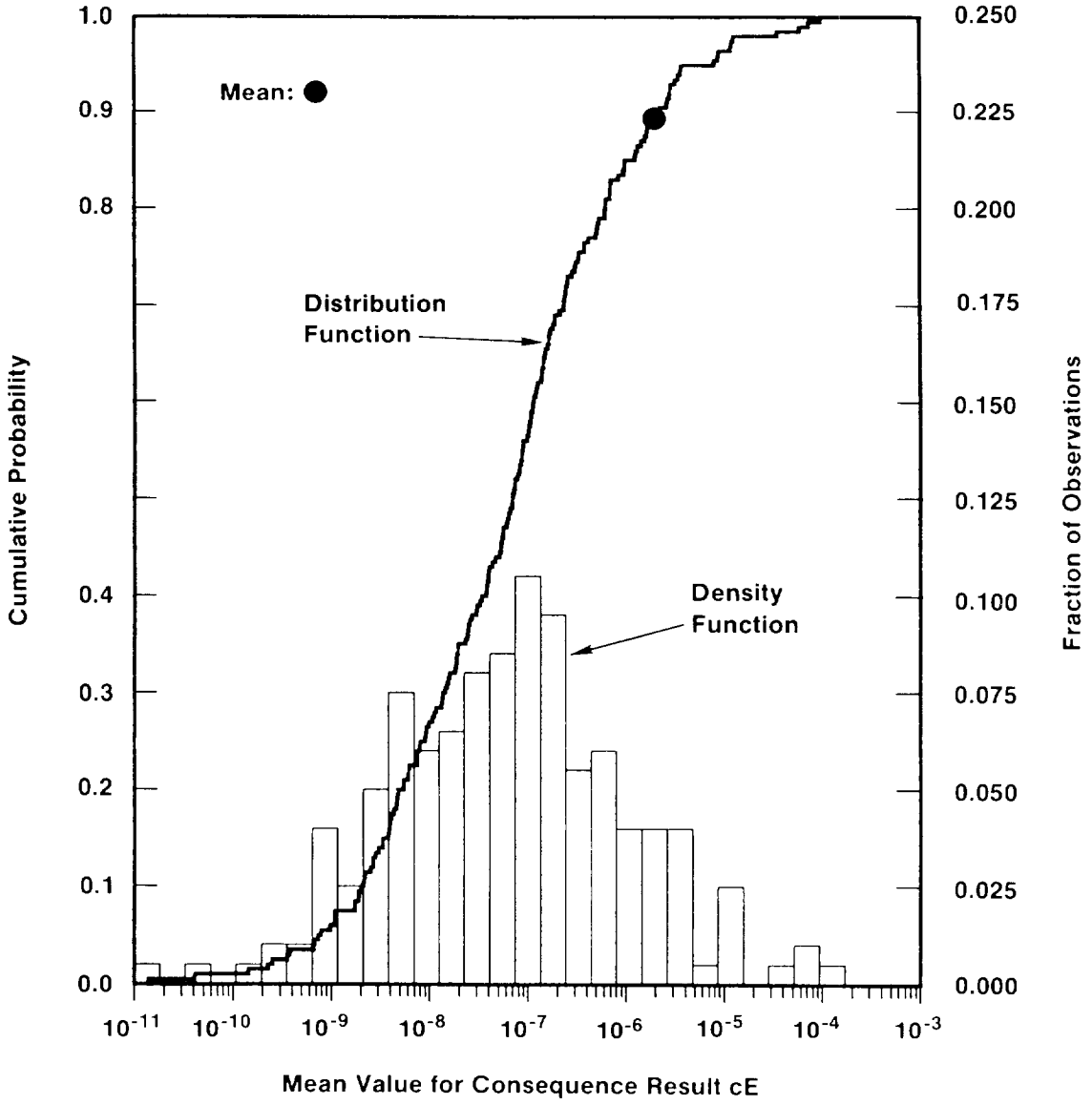

Figure 3-21. Example Uncertainty Display Including Estimated Distribution Function, Density Function, and Mean (plotted from results contained in Breeding et al., 1990).

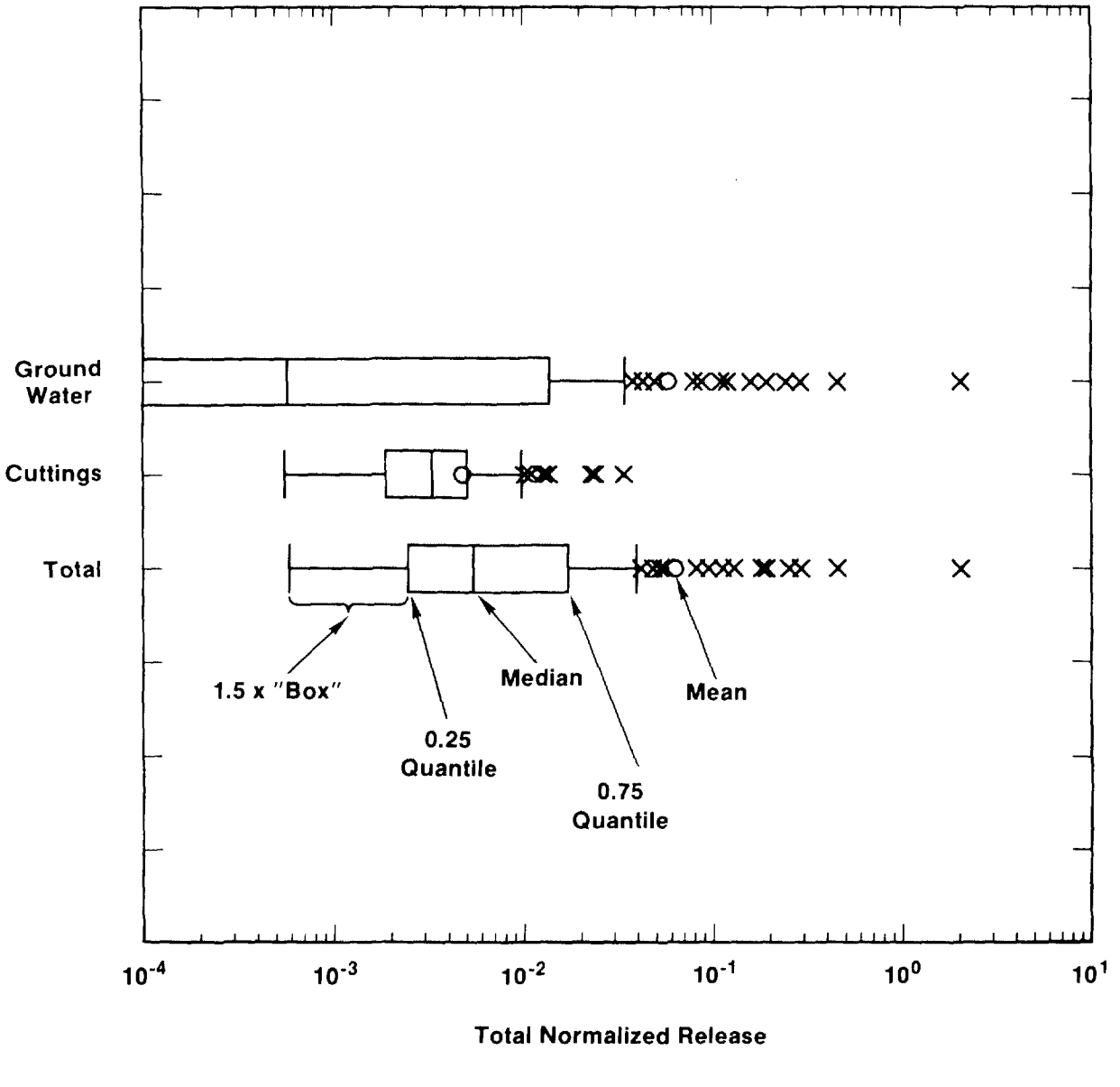

Figure 3-22. Example of Box Plots (hypothetical results).

Sensitivity Analysis

The final step in a Monte Carlo study is sensitivity analysis. The generation of scatterplots is undoubtedly the simplest sensitivity analysis technique. This approach consists of generating plots of the points (x_{ij}, y_i), $i = 1, \ldots, m$, for each input variable x_j. An example of a scatterplot showing a well-defined relationship between an input and an output variable is shown in Figure 3-23. In contrast, the individual points will be randomly spread over the plot when there is no relationship between the input and the output variable.

Sometimes scatterplots alone will completely reveal the relationships between model input and model output. This is often the case when only one or two inputs completely dominate the outcome of the analysis. Further, scatterplots often reveal nonlinear relationships, thresholds, and variable interactions that facilitate the understanding of model behavior and the planning of more sophisticated sensitivity studies. Iman and Helton (1988) provide an example where the examination of scatterplots revealed a rather complex pattern of variable interactions. The examination of scatterplots is a good starting point in any Monte Carlo sensitivity study. The examination of such plots when Latin hypercube sampling is used can be particularly revealing due to the full stratification over the range of each independent variable.

Sensitivity analyses performed as part of Monte Carlo studies are often based on regression analysis. In this approach, least squares procedures are used to construct a model of the form

$$y = b_0 + \sum_j b_j x_j \qquad (3\text{-}53)$$

from the mapping between analysis inputs and analysis results shown in Equation 3-49, where the x_j are the input variables under consideration and the b_j are coefficients that must be determined. The coefficients b_j and other aspects of the construction of the regression model shown in Equation 3-53 can be used to indicate the importance of the individual variables x_j with respect to the uncertainty in y.

The preceding regression model can be algebraically reformulated as

$$(y - \bar{y})/\hat{s} = \sum_j (b_j \hat{s}_j/\hat{s}) (x_j - \bar{x}_j)/\hat{s}_j, \qquad (3\text{-}54)$$

where

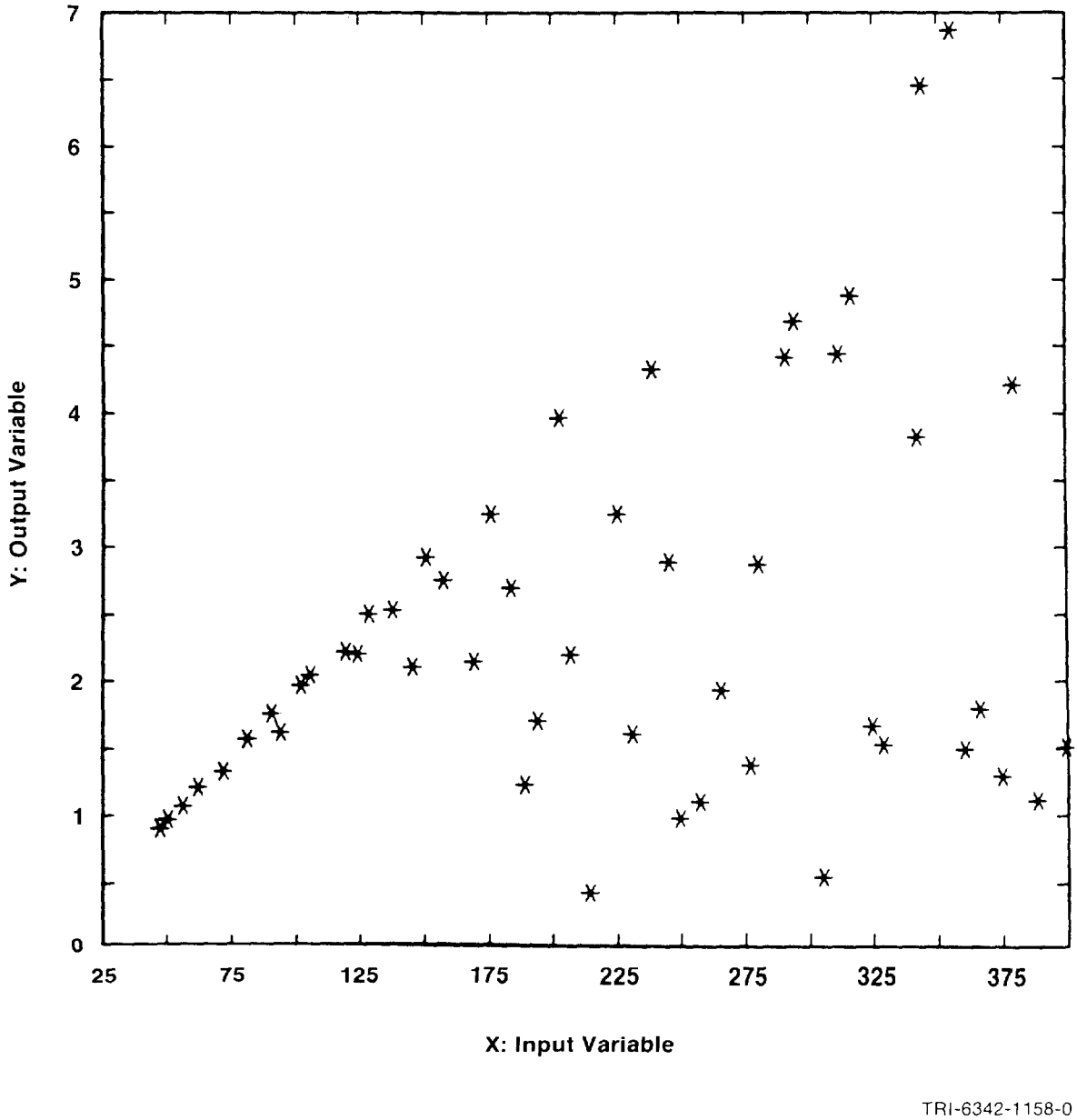

Figure 3-23. Example Scatterplot (adapted from Helton et al., 1989).

$$\bar{y} = \sum_i y_i/m, \qquad \hat{s} = \left[\sum_i (y_i - \bar{y})^2/(m - 1)\right]^{1/2},$$

$$\bar{x}_j = \sum_i x_{ij}/m, \qquad \hat{s}_j = \left[\sum_i (x_{ij} - \bar{x}_j)^2/(m - 1)\right]^{1/2}.$$

The coefficients $\hat{b}_j\hat{s}_j/\hat{s}$ appearing in Equation 3-54 are called standardized regression coefficients. When the x_j are independent, the absolute value of the standardized regression coefficients can be used to provide a measure of variable importance. Specifically, the coefficients provide a measure of importance based on the effect of moving each variable away from its expected value by a fixed fraction of its standard deviation while retaining all other variables at their expected values. Calculating standardized regression coefficients is equivalent to performing the regression analysis with the input and output variables normalized to mean zero and standard deviation one.

The following identity holds for the least square regression model shown in Equation 3-53 and plays an important role is assessing the adequacy of such models:

$$\sum_i (y_i - \bar{y})^2 = \sum_i (\hat{y}_i - \bar{y})^2 + \sum_i (y_i - \hat{y}_i)^2 , \tag{3-55}$$

where $\hat{y}_i$ denotes the estimate of y_i obtained from the regression model and $\bar{y}$ is the mean of the y_i. Since the summation $\Sigma_i (y_i - \hat{y}_i)^2$ provides a measure of variability about the regression line, the ratio

$$R^2 = \sum_i (\hat{y}_i - \bar{y}_i)^2/\sum_i (y_i - \bar{y})^2 \tag{3-56}$$

provides a measure of the extent to which the regression model can match the observed data. Specifically, when the variation about the regression line is small (i.e., when $\Sigma_i(y_i - \hat{y}_i)^2$ is small relative to $\Sigma_i(\hat{y}_i - \bar{y}_i)^2$), then the corresponding R^2 value is close to 1, which indicates that the regression model is accounting for most of the variability in the y_i. Conversely, an R^2 value close to zero indicates that the regression model is not very successful in accounting for the variability in the y_i. The designation coefficient of multiple determination is sometimes used for R^2 values.

Regression analyses often perform poorly when the relationships between the input and output variables are nonlinear. This is not surprising since

regression analysis is based on developing linear relationships between variables. The problems associated with poor linear fits to nonlinear data can often be avoided with the technique of rank regression (Iman and Conover, 1979). Rank regression is a simple concept: data are replaced with their corresponding ranks and then the usual regression procedures are performed on these ranks. Specifically, the smallest value of each variable is assigned the rank 1, the next largest value is assigned the rank 2, and so on up to the largest value, which is assigned the rank m, where m denotes the number of observations. The analysis is then performed with these ranks being used as the values for the variables in the regression model. The logarithmic and other transformations can also be used to linearize the relationships betweeen the variables in a regression analysis.

The ideas of correlation and partial correlation are useful concepts that often appear in sampling-based sensitivity studies. For a sequence of observations (x_i, y_i), $i = 1, \ldots, m$, the (sample) correlation r_{xy} between x and y is defined by

$$r_{xy} = \frac{\sum_{i=1}^{m} (x_i - \bar{x})(y_i - \bar{y})}{\left[\sum_{i=1}^{m} (x_i - \bar{x})^2\right]^{1/2} \left[\sum_{i=1}^{m} (y_i - \bar{y})^2\right]^{1/2}}, \tag{3-57}$$

where $\bar{x}$ and $\bar{y}$ are defined in conjunction with Equation 3-54. The correlation coefficient r_{xy} provides a measure of the linear relationship between x and y.

The nature of the correlation coefficient r_{xy} is most readily understood by considering the regression

$$y = b_0 + b_1 x. \tag{3-58}$$

The definition of r_{xy} in Equation 3-57 is equivalent to the definition

$$r_{xy} = \text{sign}(b_1)(R^2)^{1/2}, \tag{3-59}$$

where $\text{sign}(b_1) = 1$ if $b_1 \geq 0$, $\text{sign}(b_1) = -1$ if $b_1 < 0$, and R^2 is the coefficient of determination that results from regressing y on x (Helton et al., 1991). With respect to interpretation, the correlation coefficient r_{xy} provides a measure of the linear relationship between x and y, and the regression coefficient b_1 characterizes the effect that a unit change in x will have on y.

When more than one input variable is under consideration, partial correlation coefficients can be used to provide a measure of the linear relationships between the output variable y and the individual input variables. The partial correlation coefficient between y and an individual variable x_p is obtained from the use of a sequence of regression models. First, the following two regression models are constructed:

$$\hat{y} = b_0 + \sum_{j \neq p} b_j x_j \quad \text{and} \quad \hat{x}_p = c_0 + \sum_{j \neq p} c_j x_j. \tag{3-60}$$

Then, the results of the two preceding regressions are used to define the new variables $y - \hat{y}$ and $x_p - \hat{x}_p$. By definition, the partial correlation coefficient between y and x_p is the correlation coefficient between $y - \hat{y}$ and $x_p - \hat{x}_p$. Thus, the partial correlation coefficient provides a measure of the linear relationship between y and x_p with the linear effects of the other variables removed. The preceding provides a rather intuitive development of what a partial correlation coefficient is. A formal development of partial correlation coefficients and the relationships between partial correlation coefficients and standardized regression coefficients is provided by Iman et al. (1985).

The partial correlation coefficient provides a measure of the strength of the linear relationship between two variables after a correction has been made for the linear effects of the other variables in the analysis, and the standardized regression coefficient measures the effect on the dependent variable that results from perturbing an independent variable by a fixed fraction of its standard deviation. Thus, partial correlation coefficients and standardized regression coefficients provide related, but not identical, measures of variable importance. In particular, the partial correlation coefficient provides a measure of variable importance that tends to exclude the effects of other variables, the assumed distribution for the particular input variable under consideration, and the magnitude of the impact of an input variable on an output variable. In contrast, the value for a standardized regression coefficient is significantly influenced by both the distribution assigned to an input variable and the impact that this variable has on an output variable. However, when the input variables in an analysis are uncorrelated, an ordering of variable importance based on either the absolute value of standardized regression coefficients or the absolute value of partial correlation coefficients will yield the same ranking of variable importance, even though the standardized regression coefficients and partial correlation coefficients for individual variables may be quite different (Iman et al., 1985).

Many output variables are functions of time or location. A useful way to present sensitivity results for such variables is with plots of partial correlation coefficients or standardized regression coefficients as functions of time or location. An example of such a presentation is given in Figure 3-24. The upper set of curves in Figure 3-24 contains standardized regression coefficients (SRCs) and partial correlation coefficients (PCCs) plotted as a function of time for raw (i.e., untransformed) data. The lower set contains similar results but for analyses performed with rank-transformed data. As can be seen from the curves in Figure 3-24, the standardized regression coefficients and partial correlation coefficients display similar patterns of behavior. Further, the analysis with rank-transformed data reveals a much stronger relationship between the two variables than does the analysis with raw data.

Plots of the form shown in Figure 3-24 can be very useful in displaying the results of sensitivity studies for families of CCDFs that are used to display the uncertainty in the outcome of a performance assessment. For example, standardized regression coefficients or partial correlation coefficients can be used to determine the importance of individual input variables with respect to the exceedance probabilities for individual consequence values appearing on the abscissa in Figure 3-4. The values of these coefficients can then be plotted above the corresponding consequence values. Figure 3-25 provides an example of the results of such an analysis. As shown in this figure, variables 1, 3, and 5 are important with respect to the exceedance probabilities for smaller values of the consequence and then decrease in importance for larger consequence values. The opposite pattern of behavior is shown by variables 2 and 4.

When many input variables are involved, the direct construction of a regression model as shown in Equation 3-53 containing all input variables may not be the best approach for several reasons. First, the large number of variables makes the regression model tedious to examine and unwieldy to display. Second, it is often the case that only a relatively small number of input variables have an impact on the output variable. As a result, there is no reason to include the remaining variables in the regression model. Third, correlated variables result in unstable regression coefficients (i.e., coefficients whose values are sensitive to the specific variables included in the regression model). When this occurs, the regression coefficients in a model containing all the input variables can give a misleading representation of variable importance. Fourth, an overfitting of the data can result when variables are arbitrarily forced into the regression model. This phenomenon occurs when the regression model attempts to match the predictions associated with individual sample elements rather than match the trends shown by the sample elements collectively.

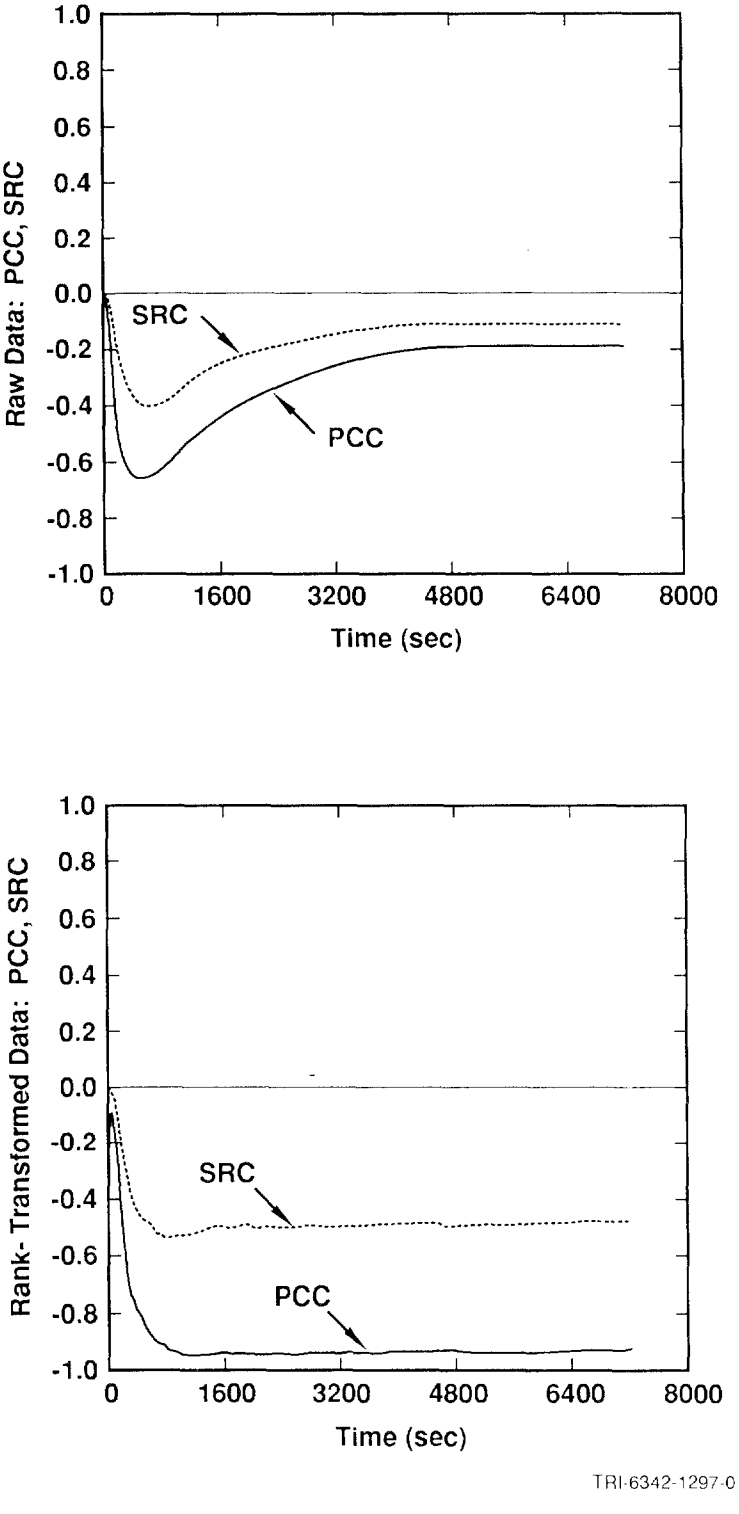

Figure 3-24. Example of Partial Correlation Coefficients (PCCs) and Standardized Regression Coefficients (SRCs) Plotted as a Function of Time for Raw and Rank-Transformed Data (adapted from Helton et al., 1989).

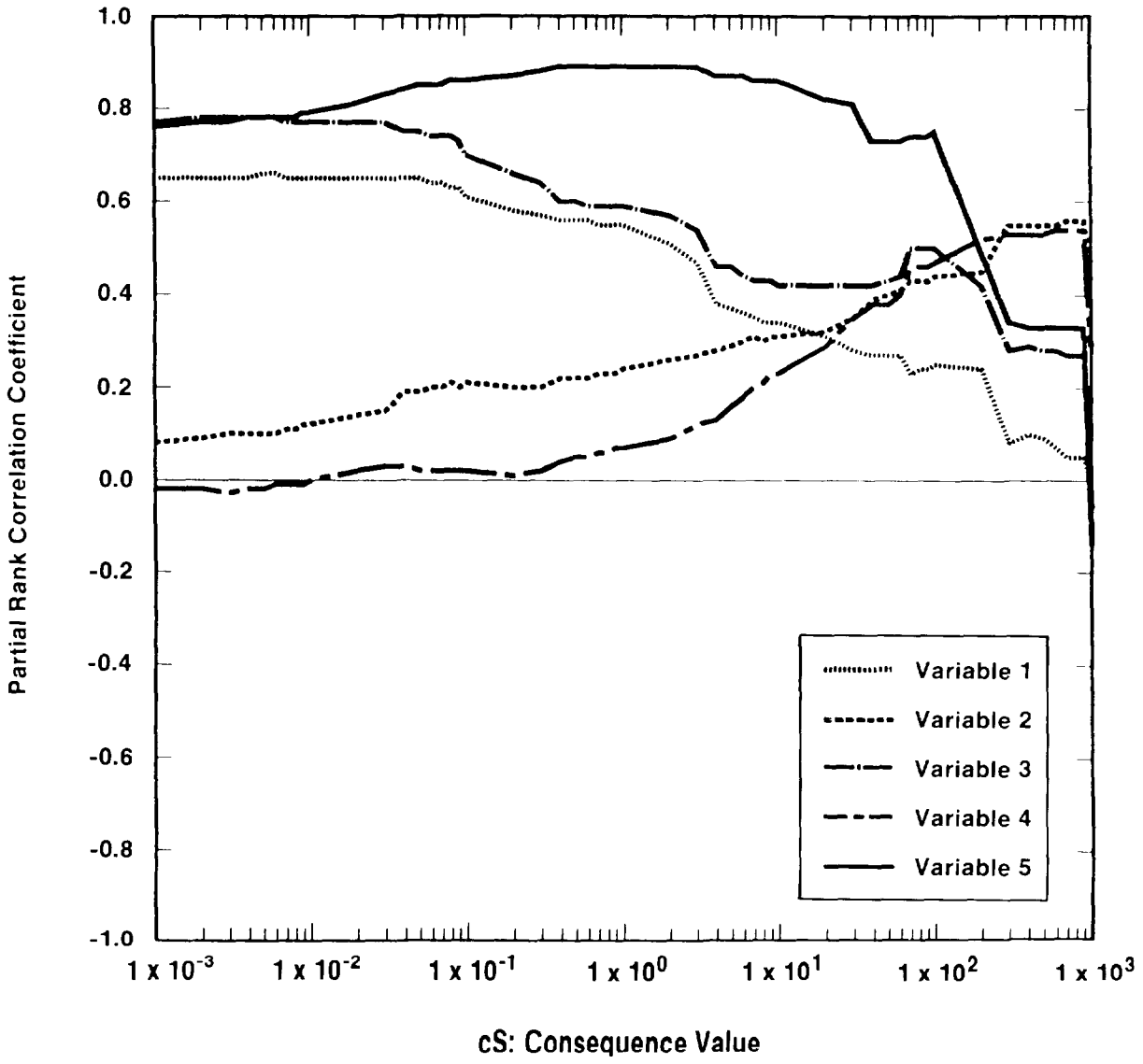

Figure 3-25. Example Sensitivity Analysis for the CCDFs in Figure 3-4 (after Breeding et al., 1990).

Stepwise regression analysis (Draper and Smith, 1981; Neter and Wasserman, 1974) provides an alternative to constructing a regression model containing all the input variables. With this approach, a sequence of regression models is constructed. The first regression model contains the single input variable that has the largest impact on the output variable. The second regression model contains the two input variables that have the largest impact on the output variable: the input variable from the first step plus whichever of the remaining variables has the largest impact on the variation not accounted for by the first variable. The third regression model contains the three input variables that have the largest impact on the output variable: the two input variables from the second step plus whichever of the remaining variables has the largest impact on the variation not accounted for by the first two variables. Additional models in the sequence are defined in the same manner until the point is reached at which further models are unable to meaningfully increase the amount of the variation in the output variable that can be accounted for. Further, at each step of the process, the possibility exists for an already selected variable to be dropped out if it no longer has a significant impact on the uncertainty in the output variable; this only occurs when correlations exist between the output variables.

Several aspects of stepwise regression analysis provide insights on the importance of the individual variables. First, the order in which the variables are selected in the stepwise procedure provides an indication of their importance, with the most important variable being selected first, the next most important variable being selected second, and so on. Second, the R^2 values (see Equation 3-69 in Helton et al., 1991) at successive steps of the analysis also provide a measure of variable importance by indicating how much of the variation in the dependent variable can be accounted for by all variables selected through each step. When the input variables are uncorrelated, the differences in the R^2 values for the regression models constructed at successive steps equal the fraction of the total variability in the output variable that can be accounted for by the individual input variables being added at each step (see Equation 3-75 in Helton et al., 1991). Third, the absolute values of the standardized regression coefficients in the individual regression models provide an indication of variable importance. Further, the sign of a standardized regression coefficient indicates whether the input and output variables tend to increase and decrease together (a positive coefficient) or tend to move in opposite directions (a negative coefficient).

A common but important situation occurs when input variables are uncorrelated. In this case, the orderings of variable importance based on order of entry into the regression model, size of the R^2 values attributable to the individual variables, the absolute values of the standardized regression coefficients, and the absolute values of the partial correlation

coefficients are the same. In situations where the input variables are believed to be uncorrelated, one of the important applications of the previously discussed restricted pairing technique of Iman and Conover (1982b) is to assure that the correlations between variables within a Latin hypercube or random sample are indeed close to zero. When variables are correlated, care must be used in the interpretation of the results of a regression analysis since the regression coefficients can change in ways that are basically unrelated to the importance of the individual variables as correlated variables are added to and deleted from the regression model.

As models involving more variables are developed in a stepwise regression analysis, the possibility exists of overfitting the data. Overfitting occurs when the regression model in essence "chases" the individual observations rather than following an overall pattern in the data. For example, it is possible to obtain a good fit on a set of points by using a polynomial of high degree. However, in doing so, it is possible to overfit the data and produce a spurious model that makes poor predictions.

To protect against overfit, the Predicted Error Sum of Squares (PRESS) criterion can be used to determine the adequacy of a regression model (Allen, 1971). For a regression model containing k variables and constructed from m observations, PRESS is computed in the following manner. For $i = 1,2,\ldots,m$, the ith observation is deleted from the original set of m observations and then a regression model containing the original k variables is constructed from the remaining m - 1 observations. With this new regression model, the value $\hat{y}_k(i)$ is estimated for the deleted observation y_i. Then, PRESS is defined from the preceding predictions and the m original observations by

$$\text{PRESS}_k = \sum_{i=1}^{m} \left[y_i - \hat{y}_k(i) \right]^2 . \qquad (3\text{-}61)$$

The regression model having the smallest PRESS value is preferred when choosing between two competing models, as this is an indication of how well the basic pattern of the data has been fit versus an overfit or an underfit.

Monte Carlo analyses generate a mapping from analysis inputs to analysis results. Once this mapping is generated and saved, it can be explored with a wide variety of techniques. This section has discussed techniques based on scatterplots, regression, correlation, partial correlation, and stepwise regression. The capability to generate sensitivity analysis results with these techniques has been incorporated into the CAMCON structure.

Acknowledgment: Substantial portions of Chapter 3 are taken from Chapters 1, 2 and 6 of the report *Sensitivity Analysis Techniques and Results for*

Performance Assessment at the Waste Isolation Pilot Plant, SAND90-7103, by J. C. Helton, J. W. Garner, R. D. McCurley, and D. K. Rudeen.

Chapter 3-Synopsis

Conceptual Model for WIPP Performance Assessment

Risk

Risk is represented by a set of ordered triples.

The first element in each triple describes things that may happen to the disposal system in the future (i.e., the scenarios).

The second element in each triple describes how likely these things are to happen (i.e., scenario probability).

The third element in each triple describes the consequences of the occurrences associated with the first element (i.e., EPA normalized releases of radionuclides to the accessible environment).

Complementary cumulative distribution functions (CCDFs) are used to display the information contained in the second and third elements of the ordered triple (scenario probability and consequence).

Uncertainty in Risk

Uncertainty in the results of the risk analysis may result from

the completeness of the occurrences considered,

the aggregation of the occurrences into scenarios for analysis,

the selection of models and imprecisely known parameters for use in the models,

stochastic variation in future occurrences.

Characterization of Uncertainty in Risk

Uncertainty resulting from imprecisely known parameter values results in a family of CCDFs. Variability in this family of CCDFs can be displayed by showing the entire family or by showing the mean and selected quantile curves.

Risk and the EPA Limits

CCDFs will be compared to the limits placed on cumulative normalized releases of radionuclides to the accessible environment by the Containment Requirements of the Standard.

Probability and Risk

The sample space for the WIPP performance assessment consists of all possible 10,000-yr histories of the WIPP following decommissioning.

The infinite number of possible 10,000-yr histories are grouped into subsets of the sample space (scenarios) for probability assignment and consequence analysis.

There is no inherently "correct" grouping of the time histories into subsets. The use of more scenarios results in finer resolution in the CCDF (more steps in a single curve) but may also result in a larger computational burden.

Definition of Scenarios

Summary Scenarios

The first stage in scenario definition for the WIPP has five steps:

- compiling or adopting a comprehensive list of events and processes that could potentially affect the disposal system during the next 10,000 years,
- classifying the events and processes,
- screening the events and processes to identify those that can be eliminated from consideration,

developing scenarios by combining the events and processes that remain after screening,

screening the scenarios to identify those that can be eliminated from consideration.

The first step corresponds to defining the sample space for the analysis. The remaining steps define the summary scenarios.

Computational Scenarios

To increase resolution in the CCDF, the summary scenarios are further decomposed into computational scenarios.

For 1991, computational scenarios are distinguished by the time and number of intrusions, whether or not a brine reservoir is encountered below the waste, and the activity level of waste intersected.

Determination of Scenario Probabilities

Probabilities for Summary Scenarios

Probabilities for summary scenarios were reported in the *1990 Preliminary Comparison*.

Probabilities for Computational Scenarios

Probabilities for the 1991 computational scenarios are based on the assumption that intrusion follows a Poisson process (i.e., boreholes are random in time and space) with a rate constant, λ, that is sampled as an uncertain parameter in the 1991 calculations.

Calculation of Scenario Consequences

Overview of Models

The models used in the WIPP performance assessment exist at four levels:

conceptual models that characterize our understanding of the system,

mathematical models that represent the processes of the conceptual model,

numerical models that provide approximations to the solutions of the selected mathematical models,

computer models that implement the numerical models.

Organization of Calculations for Performance Assessment

Calculations are organized so that results for computational scenarios can be constructed from a minimum number of calculations for each time interval.

Uncertainty and Sensitivity Analyses

Available Techniques

Available techniques for uncertainty and sensitivity analysis include differential analysis, Monte Carlo analysis, response surface methodology, and Fourier amplitude sensitivity tests.

The WIPP performance assessment uses Monte Carlo analysis techniques because

- they are appropriate for analysis problems in which large uncertainties are associated with the independent variables,
- they provide direct estimates for distribution functions,
- they do not require sophisticated techniques beyond those required for the analysis of the problem of interest,
- they can be used to propagate uncertainties through a sequence of separate models.

Monte Carlo Analysis

A Monte Carlo analysis involves five steps:

- the selection of variable ranges and distributions,
- the generation of a sample from the parameter value distributions,
- the propagation of the sample through the analysis,
- analysis of the uncertainty in results caused by variability in the sampled parameters,

sensitivity analyses to identify those parameters for which variability in the sampled value had the greatest effect on the results.

4. SCENARIOS FOR COMPLIANCE ASSESSMENT

Robert V. Guzowski[1] and Jon C. Helton[2]

[NOTE: The text of Chapter 4 is followed by a synopsis that summarizes essential information, beginning on page 4-85.]

4.1 Definition of Scenarios

4.1.1 CONCEPTUAL BASIS FOR SCENARIO DEVELOPMENT

As shown in Equation 3-1 and discussed in Chapter 3 of this volume, the results of the WIPP performance assessment can be represented by a set of ordered triples, where the first element in each triple is a set S_i of similar occurrences (i.e., a scenario), the second element is the probability pS_i for S_i, and the third element is a vector $\mathbf{cS}_i$ of consequences associated with S_i. The S_i are obtained by subdividing a set S that contains all possible occurrences during the period of regulatory concern at the WIPP. As discussed in conjunction with Equation 3-11, the set S (i.e., the sample space) consists of all possible 10,000-year time histories at the WIPP beginning at the decommissioning of the facility.

The first stage in scenario development is construction of the set S. Once S is constructed, the scenarios S_i can be obtained by subdividing S. The set S is very large; indeed, S has infinitely many elements. Thus, scenario development must proceed carefully so that excessive resources are not expended on the development and subsequent analysis of scenarios whose impact on the CCDF used for comparison with the EPA release limits can be reasonably anticipated due to low probability, low consequences, or regulatory exclusion.

The following four subsets of S (i.e., scenarios) provide a natural starting point for scenario development: S_B, called the base-case subset, which consists of all elements in S that fall within the bounds of what can be reasonably anticipated to occur at the WIPP over 10,000 years; S_M, called a minimal disruption subset, which consists of all elements in S that involve disruptions that result in no significant perturbation to the consequences associated with the corresponding element in the base-case subset S_B; S_E, a regulatory exclusion subset consisting of all elements in S that are excluded from consideration by regulatory directive (e.g., human intrusions more

---

1 Science Applications International Corporation, Albuquerque, New Mexico
2 Arizona State University, Tempe, Arizona

severe than the drilling of exploratory boreholes); and S_L, called a high consequence, low probability subset, which consists of elements of S not contained in S_B, S_M, or S_E that have the potential to result in large consequences (e.g., normalized releases to the accessible environment greater than 10) but whose collective probability is small (e.g., the probability of S_L is less than 0.0001). Everything that remains in S after the identification of S_B, S_M, S_E, and S_L now becomes a subset that can be designated S_O, where the subscript O was selected to represent the word "Other". In set notation,

$$S_O = (S_B \cup S_M \cup S_E \cup S_L)^c, \tag{4-1}$$

where the superscript c is used to designate the complement of a set. This produces a decomposition of S into five subsets.

A conceptual representation for this decomposition is shown in Figure 4-1. Due to regulatory guidance, S_E can be excluded from consideration in compliance assessment, which is equivalent to assuming that its probability pS_E is equal to zero. The actual size of S_L relative to that of S_B and S_M may be large. However, the probability of S_L is small. Thus, the possible consequences associated with S_L will not result in violation of the EPA release limits. Releases associated with S_B, and hence with S_M, are anticipated to be nonexistent or very small for the WIPP. As a result, determination of whether or not the WIPP meets the EPA release limits will depend on additional scenarios S_i, i=1, ..., nS, obtained by further refining (i.e., subdividing) the subset S_O and possibly the subset $S_B \cup S_M$. This further refinement is necessary since it is unlikely that S_O will be so homogeneous that a single normalized release will provide a suitable representation for the consequences associated with each element (i.e., time history) in S_O.

A representation of the CCDF for comparison with the EPA release limits that results from the subsets S_B, S_M, S_1, ..., S_{nS}, S_L is given in Figure 4-2. The subset S_E is not included due to its exclusion by regulatory directive. As shown in Figure 4-2, the probabilities for S_B and S_M determine the vertical drop in the CCDF above zero (with the assumption that the base-case leads to no release, which is apparently true for the WIPP (Bertram-Howery et al., 1990) but may not be true for other sites), and the right most extent of the CCDF is determined by S_L. As long as pS_L is small (e.g., less than 10^{-4}) and the releases associated with the S_i are not close to violating the EPA release limits, the actual value assigned to cS_L has no impact on whether or not the CCDF for all scenarios crosses the EPA release limits. The representation in Figure 4-2 is rather stylized. In practice, both S_B and S_L may be subdivided into additional subsets that give rise to

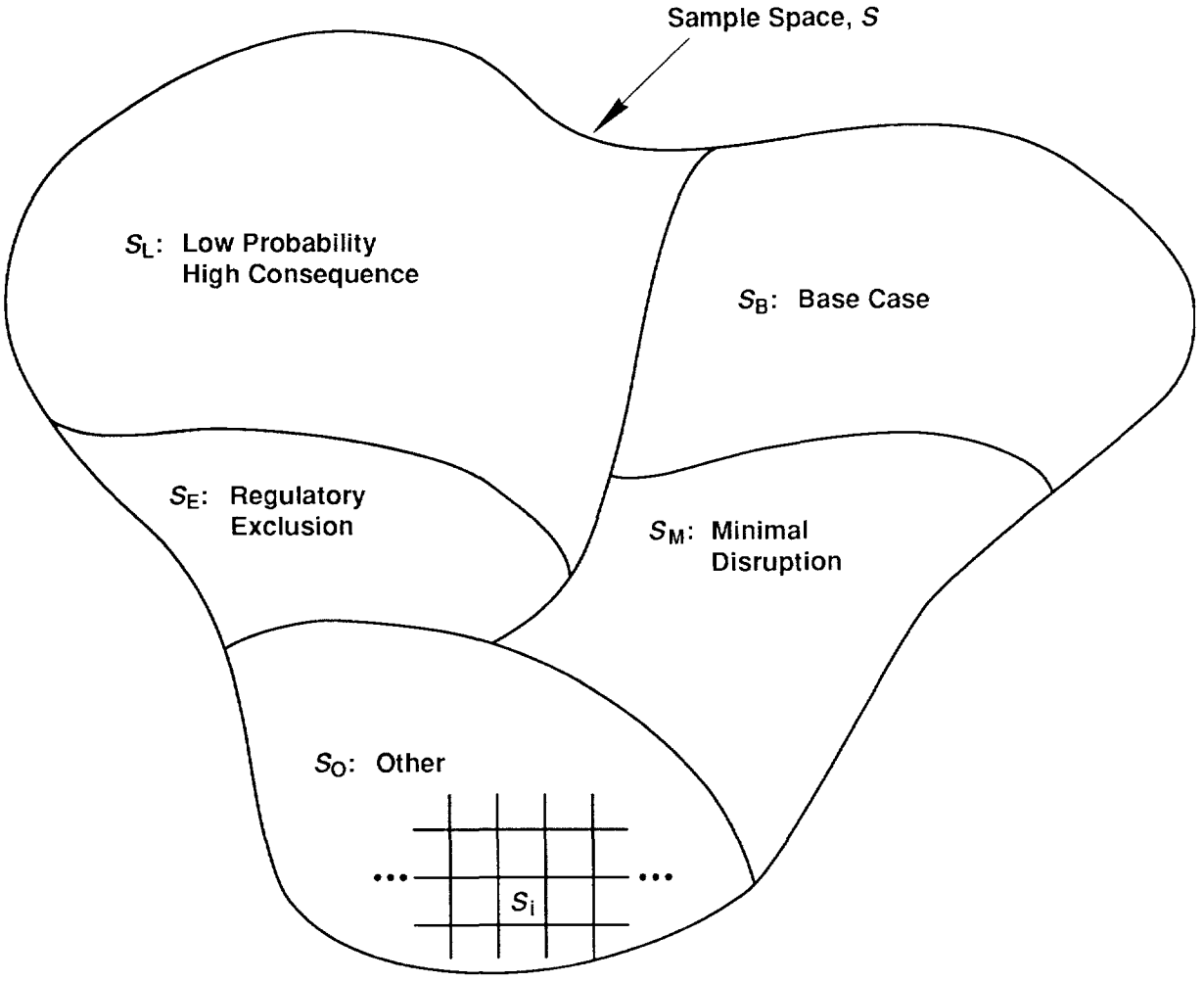

TRI-6342-1298-0

Figure 4-1. Decomposition of the Sample Space S into High-Level Subsets, where S_B Designates the Base-Case Subset, S_M Designates a Minimal Disruption Subset, S_E Designates a Regulatory Exclusion Subset, S_L Designates a Low-Probability, High-Consequence Subset, and S_O designates $(S_B \cup S_M \cup S_E \cup S_L)^c$.

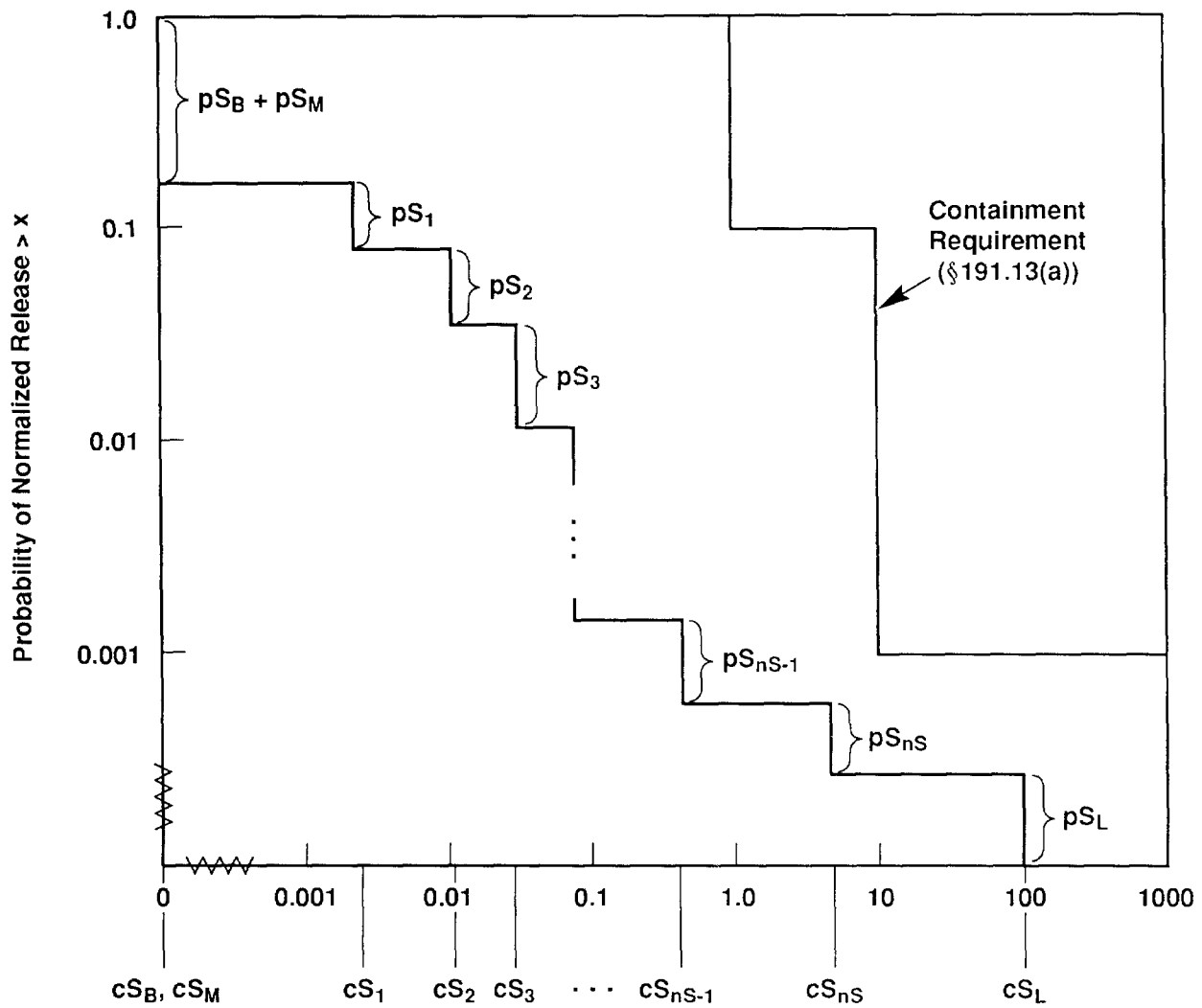

Notation: $pS_B, pS_M, pS_1, pS_2, \ldots, pS_{nS}, pS_L$ probability for corresponding scenario

$cS_B, cS_M, cS_1, cS_2, \ldots, cS_{nS}, cS_L$ consequence for corresponding scenario

$S_1, S_2, \ldots, S_{nS}$ assumed to be ordered so that $cS_1 \leq cS_2 \leq \ldots \leq cS_{nS}$

TRI-6342-1278-0

Figure 4-2. Construction of a CCDF for Comparison with the EPA Release Limits.

additional steps. Further, some of the release values for the S_i could overlap those for S_L. However, the overall pattern remains the same, with S_B and S_M determining the upper left of the CCDF, S_L determining the lower right, and the bulk of the CCDF being determined by the S_i.

Sometimes terminology is used that suggests S_M and S_L are excluded from consideration in the construction of a CCDF for comparison with the EPA release limits. Such an exclusion should not take place. The probability for S_M can be incorporated into the probability for S_B; this is usually done by simply not correcting the calculated probability of S_B for the possible occurrence of S_M. The effect of S_L is a small extension on the lower right of the CCDF. Whether or not this effect is shown on the CCDF, it was included in the construction of the CCDF through the determination that its impact was unimportant. In this regard, the EPA provides guidance that would not stand up to careful probabilistic scrutiny. They indicate that events and processes that are estimated to have less than one chance in 10,000 of occurring in 10,000 years do not have to be included in a performance assessment. By suitably defining the events and processes selected for consideration, all probabilities can be made less than the specified bound. A more reasonable specification would be on the total probability that could be ignored rather than on individual increments of probability. The intent of the WIPP performance assessment is to bound the total probability of all occurrences that are removed from detailed consideration (i.e., the probability pS_L for S_L) rather than the individual probabilities for a number of different scenarios.

Since S_B, S_M, and S_L may account for a large part of the sample space S and also have readily predicted effects on the CCDF used for comparison with the EPA release limits, an efficient strategy is to determine S_B, S_M, and S_L before the subdivision of S_O into the scenarios S_i shown in Figure 4-2 is considered. This strategy allows resolution to be built into the analysis where it is important, that is, in the construction of the S_i. In recognition of this, the WIPP performance assessment uses a two-stage approach to scenario development.

The first stage of the analysis focuses on the determination of the sample space S and the subsets S_B, S_M, S_L, and S_O. A tentative division of S_O into additional summary scenarios is also performed. This stage of the analysis uses a scenario-selection procedure suggested by Cranwell et al. (1990) that consists of the following five steps: (1) compiling or adopting a "comprehensive" list of events and processes that potentially could affect

the disposal system, (2) classifying the events and processes to aid in completeness arguments, (3) screening the events and processes to identify those that can be eliminated from consideration in the performance assessment, (4) developing scenarios by combining the events and processes that remain after screening, and (5) screening scenarios to identify those that have little or no effect on the shape or location of the mean CCDF.

The purpose of the first step is to develop the sample space S, which consists of all possible 10,000-year time histories that involve the identified events and process. The set S is infinite and, in practice, its individual elements cannot be listed. Rather, S is subdivided into the subsets S_B, S_M, S_L, and S_0. This subdivision takes place in Steps 2 and 3. The screening associated with Steps 2 and 3 also removes time histories from S that are physically unreasonable. In Step 4, a preliminary subdivision of the subset S_0 into additional summary scenarios is performed. This subdivision is accomplished through a two-part process. In the first part, subsets of S_0 (i.e., scenarios) are defined that involve specific events or processes. However, these scenarios are not mutually exclusive. In the second part, a subdivision of S_0 into mutually exclusive scenarios S_i is accomplished by forming all possible intersections of the single event/process scenarios and their complements. The fifth and final step in the process is a screening of the scenarios S_i on the basis of probability, consequence, and physical reasonableness. The purpose of this screening is to determine if some of the S_i can be removed from the analysis or assigned to S_M or S_L, with a resultant reduction in the size of S_0. Thus, this final step may involve a redefinition of S_B, S_M, S_L, and S_0.

The first stage of scenario development is described in Section 4.1.2-Definition of Summary Scenarios. If the first stage of scenario development has been performed properly, the impact of the subsets S_M and S_L on the CCDF used for comparison with the EPA release limits can be reasonably anticipated or, for S_B, determined with a small number of calculations. Compliance or noncompliance with the release limits will be determined by S_0. The summary scenarios S_i developed from S_0 in the first stage of scenario development are unlikely to be defined at a sufficiently fine level of resolution for use in the actual construction of a CCDF. Therefore, the second stage of scenario development is the division of S_0 into mutually exclusive scenarios at a sufficiently fine level of resolution for actual use in CCDF construction.

The first stage of scenario development for the 1991 WIPP performance assessment indicated that drilling intrusions are the only credible disruption associated with S_0. Therefore, the subdivision of S_0 into

mutually exclusive scenarios for CCDF construction is based on drilling intrusions. This subdivision is developed to provide good resolution at the 0.1 and 0.001 probabilities on the CCDF and is based on (1) number of drilling intrusions, (2) time of the drilling intrusions, (3) whether or not a single waste panel is penetrated by two or more boreholes, of which at least one penetrates a brine pocket and at least one does not, and (4) the activity level of the waste penetrated by the boreholes. The development of scenarios for actual use in CCDF construction is described in Section 4.1.8-Definition of Computational Scenarios.

As shown in Equation 3-1, the second element of the conceptual representation being used for the WIPP performance assessment is scenario probability pS_i. Thus, once the scenarios S_i into which S_0 is subdivided are determined, it is necessary to determine their probabilities. In addition, probabilities also must be determined for S_B and S_M. The subset S_L is constructed so that its probability is sufficiently small to have no significant impact on the CCDF used for comparison with the EPA release limits.

As with scenario development, the WIPP performance assessment uses a two-stage procedure to determine scenario probabilities. The first stage operates with the summary scenarios into which S_0 was subdivided in the first stage of scenario development. Here, the purpose is to obtain probabilities that provide guidance on what is important to performance assessment at the WIPP. For example, these probabilities provide guidance at the fifth step of scenario development (i.e., screening scenarios) as to whether or not specific scenarios S_i can be taken from S_0 and moved to S_L. The determination of probabilities in conjunction with the first stage of scenario development for the 1991 WIPP performance assessment is described in Section 4.2.1-Probabilities for Summary Scenarios.

The second stage of probability development is for the scenarios S_i actually used in CCDF construction. Thus, these probabilities are for the scenarios S_i into which S_0 is divided in the second stage of scenario development. As indicated earlier, drilling was the only disruption associated with S_0 for the 1991 WIPP performance assessment. As a result, the probabilities pS_i are derived from assumptions involving rate of drilling, area of pressurized brine under the repository, and distribution of activity levels within the waste. The values used for pS_i are described in Section 4.2.2-Probabilities for Computational Scenarios.

The determination of both scenarios and scenario probabilities is a complex process with significant uncertainties. To help assure that the WIPP

performance assessment brings a broad perspective to this task, an expert panel was formed to provide a diversity of views with respect to possible futures at the WIPP. The formation of this panel and the results obtained from its deliberations are summarized in Section 4.3-Expert Judgment on Inadvertent Human Intrusion.

4.1.2 DEFINITION OF SUMMARY SCENARIOS

A performance assessment addresses the Containment Requirements § 191.13(a) of the Standard by completing a series of analyses that predict the performance of the disposal system for 10,000 years after decommissioning and compares the performance to specific criteria within the Standard. Although the definition of performance assessment in the Standard refers only to events[3] and processes that might affect the disposal system, the occurrence of an event or process at a disposal site does not preclude the occurrence of additional events and/or processes at or near the same location. For the analyses in a performance assessment to be complete, the combinations of events and processes that define possible future states of the disposal system must be included. Combinations of events and processes are referred to as scenarios in Bertram-Howery and Hunter (1989b), Marietta et al. (1989), Cranwell et al. (1990), and Bertram-Howery et al. (1990). In the present document, these combinations are referred to as summary scenarios, including S_B and a coarse resolution of S_O into subsets of outcomes, S_i.

Appendix B of the Standard states that wherever practicable, the results of the performance assessments will be assembled into a complementary cumulative distribution function (CCDF), of which the mean CCDF (see Chapter 3 of this volume) is one possibility, in order to determine compliance. In order to construct a mean CCDF and other summary CCDFs for determining compliance with the Containment Requirements, four criteria must be met by the S_i into which S_O and possibly S_B are subdivided: (1) the set of scenarios analyzed must describe all reasonably possible future states of the disposal system, (2) the scenarios in the analyses should be mutually exclusive so that radionuclide releases and probabilities of occurrence can be conveniently associated with specific scenarios, (3) the cumulative releases of radionuclides (consequences) for each scenario must be estimated, and (4) the probability of occurrence of each scenario must be estimated. Because performance assessments are iterative analyses, the

---

[3] Event is used in the regulatory sense throughout this chapter and should not be interpreted as "event" as used in the probabilistic development of risk in Chapter 3.

results of preliminary analyses may suggest areas for additional research, which could in turn suggest new events and processes for inclusion in the performance assessment.

Identifying all possible combinations of events and processes that could affect a disposal system would result in an extremely large number of scenarios S_i, most of which would have little or no effect on the performance of the disposal system. Guidance to the Standard allows certain events and processes to be excluded from the performance-assessment analyses on the basis of low probability, which corresponds to the subset S_L. In addition, exploratory drilling for natural resources is the most severe type of human intrusion considered, so other human-intrusion modes result in possible outcomes which are contained in S_E. Each criterion is described in Appendix B of the Standard (reproduced in Appendix A of this volume).

Scenarios S_i that are within the scope of Appendix B of the Standard and meet the requirements for constructing a CCDF must be identified. Cranwell et al. (1990) developed a scenario-selection procedure that consists of five steps. These steps are (1) compiling or adopting a "comprehensive" list of events and processes that potentially could affect the disposal system, (2) classifying the events and processes to aid in completeness arguments, (3) screening the events and processes to identify those that can be eliminated from consideration in the performance assessment, (4) developing scenarios by combining the events and processes that remain after screening, and (5) screening scenarios to identify those that have little or no effect on the shape or location of the mean CCDF. This scenario-selection procedure has been adopted for the WIPP performance assessment, and a summary of its implementation follows. As discussed in Chapter 3, these scenarios are called summary scenarios, and this scenario-selection procedure is the first stage of scenario definition. The second stage is the definition of computational scenarios.

Identifying Events and Processes

Several reports have identified events and processes that could affect the integrity of generic disposal systems (e.g., Burkholder, 1980; IAEA, 1983; Andersson et al., 1989; Cranwell et al., 1990) and disposal systems at specific locations (e.g., Claiborne and Gera, 1974; Bingham and Barr, 1979). In a preliminary effort at identifying the events and processes that need to be considered for the WIPP performance assessment, Hunter (1989) developed a list of 24 events and processes primarily selected from lists published in Claiborne and Gera (1974), Bingham and Barr (1979), Arthur D. Little, Inc. (1980), and Cranwell et al. (1990). This consolidated list was found to be incomplete during preliminary scenario development (Guzowski, 1990) and from

external review of the 1990 *Preliminary Comparison with 40 CFR Part 191, Subpart B for the Waste Isolation Pilot Plant, December 1990* (Bertram-Howery et al., 1990). Several events and processes that require evaluation on a site-specific basis were not included in Hunter's (1989) list.

To address the completeness issue, the list of events and processes in Hunter (1989) was replaced, and the events and processes were rescreened. Cranwell et al. (1990) developed a scenario-selection procedure to provide specific components of performance assessments to address the Containment Requirements (§ 191.13) of the EPA Standard. For this reason, the events and processes listed in Cranwell et al. (1990) (Table 4-1) were used as a starting point in the development of disruptive scenarios for the WIPP. This list was developed by a panel of experts that met in 1976 and again in 1977 under the auspices of the U.S. Nuclear Regulatory Commission. The task of this panel was not to identify all possible events and processes that could occur in or near a waste disposal facility but to identify events and processes that could compromise the performance of an engineered disposal facility constructed in deep geologic media for nuclear waste. To address specific concerns about the WIPP, gas generation by the degradation of the waste, waste-related explosions, and nuclear criticality were added to the list produced by the panel.

The difference between an event and a process is the time interval over which a phenomenon occurs relative to the time frame of interest. Events occur over relatively short time intervals, and processes occur over much longer relative time intervals. The distinction between events and processes is not rigid. For example, in the life of a person, a volcanic eruptive cycle that lasts several years may be classified as a process, but in the 10,000 years of regulatory concern for disposal of nuclear waste, this same cycle may be considered as an event. In identifying events and processes for the WIPP performance assessment, phenomena that occur instantaneously or within a relatively short time interval are considered to be events, and phenomena that occur over a significant portion of the 10,000 years of regulatory concern are considered to be processes. The classification of a phenomenon as an event rather than as a process, or vice versa, does not affect scenario development.

Classifying Events and Processes

This step in the scenario-selection procedure is optional. The purposes for including this step in the procedure were to assist in organizing the events and processes, to assist in completeness arguments, and to provide some insights when developing conceptual models of the disposal system. Categories in the classification schemes for the generic lists mentioned in

TABLE 4-1. POTENTIALLY DISRUPTIVE EVENTS AND PROCESSES

Natural Events and Processes
Celestial Bodies
Meteorite Impact
Surficial Events and Processes
Erosion/Sedimentation
Glaciation
Pluvial Periods
Sea-Level Variations
Hurricanes
Seiches
Tsunamis
Regional Subsidence or Uplift
Mass Wasting
Flooding
Subsurface Events and Processes
Diapirism
Seismic Activity
Volcanic Activity
Magmatic Activity
Formation of Dissolution Cavities
Formation of Interconnected Fracture Systems
Faulting
Human-Induced Events and Processes
Inadvertent Intrusions
Explosions
Drilling
Mining
Injection Wells
Withdrawal Wells
Hydrologic Stresses
Irrigation
Damming of Streams and Rivers
Repository- and Waste-Induced Events and Processes
Caving and Subsidence
Shaft and Borehole Seal Degradation
Thermally Induced Stress Fracturing in Host Rock
Excavation-Induced Stress Fracturing in Host Rock
Gas Generation
Explosions
Nuclear Criticality

Source: Modified from Cranwell et al., 1990.

Step 1 are similar and can be identified as naturally occurring, human induced, and waste and repository induced. Subdivisions of the categories (Table 4-1) also may be useful.

Screening Events and Processes

Events and processes are screened using three criteria based on guidance in the Standard: probability of occurrence, physical reasonableness, and consequence. In addition, EPA's guidance concerning implementation of the Standard does not require consideration of human-intrusion events with consequences more severe than those of exploratory drilling for resources. Low probability events and processes define a set of possible outcomes that is included in S_L. Low consequence events and processes define a set of possible outcomes that is included in S_M. Modes of intrusion other than exploratory drilling define a set of possible outcomes that is included in S_E. Events and processes that are physically unreasonable may be included in S_L or removed entirely from the sample space S depending on the justification for physical unreasonableness. Probability of occurrence of an event or process must be estimated by probabilistic techniques. According to Appendix B of the Standard, events and processes that are estimated to have less than 1 chance in 10,000 of occurring in 10,000 years do not have to be included in the performance assessment. Physical reasonableness as a screening criterion is a qualitative estimate of low probability based on subjective judgment. A logical argument, possibly with supporting calculations, can be used to establish whether the occurrence of a particular event or process at a location within the time period of regulatory concern and with sufficient magnitude to affect the performance of the disposal system is physically reasonable. The third screening criterion is consequence. At this stage of the scenario-development procedure, consequence is based on whether the event or process either alone or in combination with other events or processes may affect the performance of the disposal system; many low consequence events and processes give rise to occurrences in the subset S_M. Simplified conceptual models of the disposal system and simplified mathematical models can be used to determine whether an event or process will affect the groundwater-flow system or alter possible pathways from the panels to the accessible environment.

Although quantitative screening criteria generally are preferable to qualitative criteria, the nature of the individual events and processes being screened and the availability of information and data determine how screening can proceed. On the regional scale of the northern Delaware Basin, the dynamics resulting in the low level and nonregularity of tectonic activity and other physical processes characteristic of this region are

poorly understood. Qualitative judgments of screening criteria using interpretations based on geological field relationships, natural analogs, and geographic location are required. The occurrence of human-induced events and processes is dependent on the values, needs, and technological development of future societies. While few if any of this category of events and processes can be screened out on the qualitative grounds of physical unreasonableness, qualitative judgments of the likelihood of conditions for some of these events and processes to occur or the effects of some of these occurrences on the disposal system can be made. In general, screening decisions based on qualitative judgments that are supported by strong logical arguments are as justifiable as screening decisions for certain events and processes that are based on quantitative values derived from sufficiently detailed data bases.

4.1.3 EVALUATION OF NATURAL EVENTS AND PROCESSES

This section evaluates each of the events and processes listed in Table 4-1 with regard to the screening criteria described above. Events and processes with probabilities of occurrence of 1 are part of the base-case scenario. Physically reasonable events and processes with probabilities of occurrence less than 1 and above the cutoff specified in the Standard (less than 1 chance in 10,000 of occurring in 10,000 years) are retained for scenario development. The estimation of numerical values for low-probability events and processes is difficult and often controversial, so caution should be used when screening high-consequence events and processes whose probability of occurrence is estimated to be only slightly below the regulatory cutoff. No consequence modeling was performed specifically as part of screening the events and processes. The following evaluations only consider the disposal system after it has been decommissioned.

Meteorite Impact

Meteorite impacts are a concern to nuclear-waste disposal because of the possibility that such an impact could exhume buried waste or fracture the rock overlying the waste to create pathways for groundwater to reach the waste. Several estimates have been made of the probability of an impact at a disposal site by a meteorite large enough to either exhume the waste or substantially disrupt the disposal system. Hartmann (1979) estimated the probability of a meteorite exhuming part of the waste in a repository of 10 km^2 area and a depth of 600 meters to be 6×10^{-13}/year. A Swedish study (Karnbranslesakerhet, 1978) estimated a rate of impacts large enough to create craters at least 100 meters deep to be $10^{-13}/km^2$/year. Logan and Berbano (1978) estimated the probability of direct exhumation from a depth of 800 meters for a repository of 10 km^2 to be 1×10^{-13}/year. Claiborne and Gera (1974) estimated the probability of exhumation of waste from a depth of

600 meters for a repository of 8 km^2 to be 2 x 10^{-13}/year. Cranwell et al. (1990) estimated the probability of both direct exhumation of waste from a repository of 8 km^2 at a depth of 630 meters and the fracturing of a shale aquitard at a depth of 400 meters overlying the bedded-salt unit containing the waste. The estimated probabilities are approximately 8 x 10^{-13}/year and 1 x 10^{-12}/year, respectively.

Each of these estimated probabilities is substantially below the screening limit of 1 x 10^{-8}/year (1 chance in 10,000 in 10,000 years) established in the Standard. Based on this screening criterion, meteorite impact can be eliminated from consideration in the WIPP performance assessments.

Erosion/Sedimentation

Both erosion and sedimentation as a result of wind action are ongoing processes throughout the WIPP region. Sand dunes are present at the location of the waste panels, so wind action will result in both processes occurring, although the impact on the performance of the disposal system is likely to be minimal.

No perennial drainage channels are present at the WIPP, and in addition, no intermittent channels are present at the location of the waste panels. Under current climatic conditions, erosion or deposition resulting from surficial-water movement consists of the movement of surficial sand deposits during storms. According to Bachman (1974), the presence and thickness of the Mescalero caliche, which is aerially extensive and approximately 600,000 years old, indicate that the climatic variations since that time have not resulted in significant changes in geomorphic processes.

Because no significantly high topographic features exist in the immediate vicinity of the WIPP, an influx of water-borne sediments that could cover part or all of the WIPP is not physically reasonable. Massive changes to the climatic conditions or tectonic setting within the next 10,000 years that could result in deep erosion at the WIPP are not physically reasonable. A concern about erosion is that the breaching of the Mescalero caliche, which has been interpreted by Bachman (1985) to be a barrier to infiltration of precipitation, could result in recharge elevating the water table, thereby saturating units that are currently unsaturated. According to Swift (1991a), the expected climatic conditions during the next 10,000 years are likely to be within the ranges of conditions that occurred during the past 10,000 years. The past conditions did not result in the formation of major breaches in the Mescalero caliche. Future climatic changes are not expected to cause such breaches. Wetter climatic conditions would result in an increase in the vegetative cover of the area, which could stabilize the current distribution of near-surface sedimentary deposits and protect the caliche.

Both erosion and sedimentation currently are occurring at the WIPP and are certain to occur in the future. Because of this uncertainty, these processes are part of the undisturbed conditions. Neither of these processes will occur to a degree that will affect the performance of the WIPP during the period of regulatory concern. Changes in the rates of these processes to an extent that could affect the performance of the WIPP are not physically reasonable.

Glaciation

No evidence exists to suggest that the northern part of the Delaware Basin has been covered by continental glaciers at any time since the beginning of the Paleozoic Era. During the maximum extent of continental glaciation in the Pleistocene Epoch, glaciers extended into northeastern Kansas at their closest approach to southeastern New Mexico.

According to Swift (1991a), a return to a full glacial cycle within the next 10,000 years is highly unlikely. Based on the extent of previous glaciations and the unlikely prospect that a future glaciation may occur within the period of regulatory concern, glaciation is eliminated as a process for inclusion in WIPP performance assessments based on a lack of physical reasonableness of alterations to the climatic cycle that would result in glaciers reaching or approaching the WIPP.

Pluvial Periods

The purpose of including Pluvial Periods in Table 4-1 was to assure that climatic change is considered in the screening process. Climatic change from current conditions is certain to occur for any location during the next 10,000 years, and as a result, this process has a probability of occurrence of 1.

Based on probability and physical-reasonableness arguments, climatic change is not screened out from consideration in the performance assessment. The effect of climatic change on the groundwater-flow system in the WIPP region has not been determined at this time. As a result, climatic change is retained for performance-assessment analysis.

Because climatic change has a probability of occurrence of 1, this process is considered to be part of the undisturbed performance of the diposal system and is not a separate process for inclusion in the procedure for developing disruptive scenarios.

Sea-Level Variations

Variations in sea level relative to some point on land are the result of the occurrence of other events and processes that have these changes as by-products. Examples are the rise of sea level as a result of glacial melting, which is the result of climatic change, and the uplift of continental areas by crustal rebound after the areas have been deglaciated, which is also the result of climatic change. As a result, sea-level variation is not an independent phenomenon that needs to be considered in scenario development. Another reason for excluding sea-level variation from scenario development is that the WIPP is at an elevation of approximately 3400 feet (1036 meters). No tectonic or climatic process within the next 10,000 years is likely to affect sea level to an extent that would have an effect on the performance of the WIPP.

Hurricanes

Hurricanes are storms that originate over ocean water in the tropics of the northern hemisphere (these storms are called cyclones in the southern hemisphere) and are characterized by high winds and heavy rainfall. Whereas these storms migrate to areas outside of the tropics, the distance of the WIPP from the ocean precludes hurricanes from reaching this location because they dissipate quickly over land.

Whereas hurricanes are not likely to reach the WIPP, intense storms accompanied by heavy rainfall do occur and are certain to occur in the future. These storms are short lived. The effects of these storms on the integrity of the disposal system are likely to be minor. Intense storms are common in southeastern New Mexico, and the effects of individual past storms on the geologic and hydrologic characteristics of the WIPP cannot be distinguished from the long-term geomorphic evolution of the region.

Hurricanes can be eliminated from the performance assessments because the occurrence of these events is not physically reasonable at the location of the WIPP. Intense storms are certain to occur in the future at the WIPP. As a result, intense storms are considered part of normal climate variation and are not included in the development of disruptive scenarios.

Seiches

A seiche is a "free or standing-wave oscillation of the surface of water in an enclosed or semi-enclosed basin...that is initiated chiefly by local changes in atmospheric pressure, aided by winds, tidal currents, and small earthquakes; and that continues, pendulum fashion, for a time after cessation of the originating force" (Bates and Jackson, 1980, p. 568). Seiches range

in height from several centimeters to a few meters. Whereas seiches could be of some concern to disposal facilities in certain coastal environments, the distance of the WIPP from ocean basins and other large bodies of water precludes seiches from reaching this location.

Seiches are eliminated from the WIPP performance assessments based on the lack of physical reasonableness of these phenomena at the WIPP location.

Tsunamis

A tsunami is a "gravitational sea wave produced by any large-scale, short-duration disturbance of the ocean floor, principally by a shallow submarine earthquake, but also by submarine earth movement, subsidence, or volcanic eruption" (Bates and Jackson, 1980, p. 668). Because of the elevation of the WIPP and the distance from the oceans, a wave generated by any of the mechanisms mentioned in the definition will not be of a size that could reach the WIPP.

The term tsunami perhaps can be extended to include waves produced by meteorite impacts into bodies of water. Because the WIPP is located in excess of 800 kilometers (500 miles) from the nearest large body of water (e.g., Pacific Ocean) and at an elevation of approximately 1036 meters (3400 feet), a meteorite would have to be large enough and the impact would have to be appropriately located for sufficient energy to move a large enough water volume to inundate all topographic features on the continent between the point of impact and the WIPP. Calculating the size of an appropriately large meteorite is difficult because of the dependence of the calculation on depth of water at the point of impact, water depth along the path toward the WIPP, topographic relief along the path, energy expenditure vaporizing water upon impact, and the mechanical responses of the oceanic sediments and crustal rocks to the impact. The combination of meteorite size and appropriate location makes an impact-generated tsunami reaching the WIPP a low-probability event and perhaps a physically unreasonable event. Changes in sea level caused by the melting of continental glaciers or tectonic activity during the 10,000 years of regulatory concern will not affect this screening decision.

Tsunamis of traditional origin are eliminated from the WIPP performance assessments based on the lack of physical reasonableness of events large enough to generate a wave that could reach the WIPP location. Ocean waves generated by meteorite impacts are eliminated from consideration based on the low probability of the appropriate combination of meteorite size, impact location, and adequate water depth.

Regional Subsidence or Uplift

Regional subsidence or uplift can affect groundwater-flow directions and gradients in addition to affecting erosion and deposition rates and locations. During the geologic history of the WIPP, the region has undergone several periods of regional subsidence and uplift. From early in the Paleozoic Era until approximately 100 million years ago, the stratigraphic record indicates a predominantly marine depositional environment that requires the existence of a subsiding basin in order for nearly 18,000 feet (approximately 5500 meters) of marine sediments to accumulate. The absence of units deposited from Triassic through late Tertiary time indicates either nondeposition or predominantly erosional conditions. Uplift accompanied by erosional conditions are indicated by the fact that rocks of marine origin are present at the WIPP at an elevation of greater than 3000 feet (915 meters). The absence of faults exposed at the surface in the interior of the northern Delaware Basin, which indicates a relatively intact crustal block, the relatively low rate of seismicity, which indicates an absence of or minor tectonic activity, and the wide-spread presence of the Mescalero caliche, which required relatively long-term stable conditions to form, suggest that the interior of the Delaware Basin has been and continues to be relatively stable.

The apparent long-term tectonic stability of the northern Delaware Basin suggests that neither regional subsidence nor uplift is likely to occur in the next 10,000 years on a scale that will alter the geologic or hydrologic systems and affect the performance of the disposal system. For this reason, regional subsidence and uplift do not need to be included in the WIPP performance assessments because of the lack of physical reasonableness of major changes to the tectonic regime within the time period of regulatory concern.

Mass Wasting

Mass wasting is the dislodgement and downslope movement of soil and rock under the direct application of gravitational body stresses (Bates and Jackson, 1980). This process has the potential of affecting the performance of a disposal system by damming surface drainage and impounding water. Impounded water that extends over the disposal system could affect recharge to the underlying units. An impoundment near the disposal system could affect groundwater-flow gradients, thereby altering groundwater-flow patterns.

The Pecos River, which is approximately 24 kilometers (15 miles) at closest approach to the waste panels and more than 90 meters (300 feet) lower in elevation, is the only perennial surface-water drainage feature in the WIPP

region. This river is incised, but the resulting valley is not deep enough or steep enough for mass wasting to impound water to a greater depth or aerial extent than currently results from manmade dams. No evidence indicates that past climatic conditions resulted in the existence of other perennial streams that could be dammed by mass wasting. Future climatic conditions are not likely to be substantially different from past conditions.

Because of the sparsity of perennial streams and rivers in the WIPP area and the lack of appropriate morphological features that could result in impoundments, mass wasting is not included in performance assessments for the WIPP based on a lack of physical reasonableness of such events forming large-scale impoundments.

Flooding

Flooding caused by rivers or streams overflowing their banks is a relatively short-term phenomenon. No perennial streams or standing bodies of water are present at the WIPP, and no evidence has been cited that indicates such features existed at this location during or since Pleistocene time (e.g., Powers et al., 1978a,b; Bachman, 1974, 1981, 1987). The Pecos River is approximately 24 kilometers (15 miles) from and more than 90 meters (300 feet) lower than the elevation of the land surface above the waste panels. In Nash Draw, lakes and spoil ponds associated with potash mines are located at elevations 30 meters (100 feet) or more lower than the elevation of the land surface at the location of the waste panels. No evidence has been cited in the literature to support the possibility that Nash Draw was formed by stream erosion or was at any time the location of a large body of standing water.

Because no sources of surface water exist in the WIPP region that could overflow and flood part or all of the WIPP, flooding is not included in the WIPP performance assessments because such events are not physically reasonable at this location.

Diapirism

Because of the relatively low density of salt compared to other sedimentary rocks, bedded-salt deposits at depth have a tendency to rise through and be displaced by higher density overlying rocks. This movement is facilitated by the relatively high ductility of salt when compared to other rock types. Under the appropriate conditions, bedded salt at depth will rise toward the surface and bow the overlying rocks upward, forming a salt anticline. If the overlying rocks are pierced and displaced by the upward movement of the mass of salt, the salt structure is called a salt diapir or salt dome.

The specific conditions that result in diapirism are not known, although some general conditions have been recognized. Based on evidence in German salt basins, Trusheim (1960) concluded that an overburden of 1000 meters (3300 feet) and a salt thickness of at least 300 meters (985 feet) are needed to initiate flow in salt. Similar values are used to locate areas of salt flowage in the Gulf of Mexico (Halbouty, 1979). Other factors that can affect the formation of salt domes are irregularities on the surface of the overburden, variations in the thickness of the overburden, natural variations in the density of the overburden, external stresses (tectonic stresses), depth of burial of the salt, temperature, and geologic setting (Parker and McDowell, 1951, 1955; Gussow, 1968; Trusheim, 1960).

In the northern Delaware Basin, deformation within evaporite units has been noted in disturbed zones along the margin of the Capitan Reef and at isolated locations within the interior of the basin (Borns, 1983; Borns et al., 1983). This deformation is predominantly within the anhydrite and halite of the Castile Formation with weak to nonexistent deformation in the overlying halite of the Salado Formation. Whereas the origin of this deformation is not known, Borns et al. (1983) hypothesized that the mechanism could be either gravity-driven syndepositional deformation, gravity foundering, or gravity sliding. The important thing to note about this deformation is that the thick sequence of bedded salt in the Salado Formation is not deformed. This lack of deformation indicates that the conditions required for salt diapirism to occur are absent in the northern Delaware Basin. Given the long-term stability of this part of the basin, changes in the geologic setting that could initiate diapirism are not likely to occur within the next 10,000 years.

Diapirism is excluded from the WIPP performance assessments because the development of conditions necessary to initiate diapirism are not physically reasonable within the time frame of regulatory concern.

Seismic Activity

Seismic activity refers to earth movement in response to naturally occurring or human-induced events. The most common naturally occurring event that produces earth movement on a regional scale is an earthquake. Examples of other naturally occurring sources are volcanic eruptions, landslides, and meteorite impacts. Human-induced events that can cause seismic activity on a regional scale include but are not limited to fluid extraction and injection, explosions, and rockfalls in mines.

Earthquake records for southern New Mexico date from 1923, and seismic instrumentation started in 1961 (U.S. DOE, 1980a). With the exception of three minor shocks, all shocks felt in the WIPP region prior to 1961

originated from earthquakes more than 100 miles (160 kilometers) from the WIPP and were located to the west and southwest of the WIPP (Sanford and Toppozada, 1974). Since 1961, the distribution of earthquakes remained similar to the distribution before 1961, although a cluster of earthquakes has occurred in the southeasternmost corner of New Mexico and adjacent Texas that may be the result of fluid injection for enhanced oil recovery (Shurbet, 1969). Seismic events occurring within 35 miles (56 kilometers) of the center of the WIPP were recorded in 1972, 1974, and 1978 with the maximum magnitude of 3.6 (U.S. DOE, 1980a). None of these events have been correlated with human activity.

On a seismic risk map of the United States developed for the *Uniform Building Code* (ICBO, 1979), southeastern New Mexico is located in Zone 1, which means that the region has a potential of experiencing seismic activity of Modified Mercalli intensities of V and VI. Seismic activity at these intensities can cause minor damage to some structures. Because the tectonic forces in the southwestern United States and northern Mexico that have produced and continue to produce seismic events are not likely to abruptly change and result in an aseismic region within the next 10,000 years, future regional seismic activity from naturally occurring events is certain to result in ground movement at the WIPP during the 10,000 years of regulatory concern. Ground movement at the WIPP resulting from human-induced events is likely so long as mining and the extraction of energy resources continues. Because ground movement at the WIPP from seismic activity during the next 10,000 years has a probability of occurrence of 1, seismic activity is part of the base-case scenario. No evidence has been cited in the literature of past seismic activity altering either the geologic or hydrologic systems at the WIPP. The alterations of these systems by future seismic activity is not likely to occur. Ground motion caused by seismic activity tends to rapidly dampen with increasing depth (Reiter, 1990), although the precise amount of dampening cannot be reliably predicted (Owen and Scholl, 1981). Because of the depth of the waste panels, the dampening of ground motion with depth, and the low intensity of seismic activity observed and predicted for southeastern New Mexico, future seismic activity will be of no consequence to the performance of the WIPP disposal system.

Volcanic Activity

Volcanic activity refers to magma originating in the lower crust or upper mantle that rises along fracture or fault zones through the overlying rock and is extruded onto the surface. This activity generally occurs in tectonically unstable areas such as rift zones, spreading centers and subduction zones along plate boundaries, and locations above deep-mantle thermal plumes. Volcanic activity is of interest to performance assessments because of the thermal effects of magma on groundwater flow, the possible

effects on groundwater flow of volcanic rock of low permeability in fracture or fault zones, and the possible releases of radionuclides to the accessible environment if the magma passes through a disposal facility on the way to the surface.

The Paleozoic and younger stratigraphic sequence within the Delaware Basin is devoid of volcanic rocks (Powers et al., 1978a). Within an area including eastern New Mexico, and northern, central, and western Texas, the closest Tertiary volcanic rocks with notable areal extent or tectonic significance to the WIPP are approximately 170 kilometers (105 miles) to the south in the Davis Mountains volcanic area. The closest Quaternary volcanic rocks are 250 kilometers (155 miles) to the northwest in the Sacramento Mountains. No volcanic rocks are exposed at the surface within the Delaware Basin.

Despite the lack of evidence of past volcanic activity within the Delaware Basin over a time interval of several hundred million years, Logan and Berbano (1978) estimated the probability of volcanism affecting a waste-disposal area of 10 km^2 within this basin to range from 8 x 10^{-12}/year to 8 x 10^{-11}/year. Arthur D. Little, Inc. (1980) estimated this probability to range from 1 x 10^{-10}/year to 1 x 10^{-8}/year. These ranges in probability values are at or below the cutoff probability value for eliminating events and processes from performance assessments. Because of the geologic record and the current geologic setting, a question arises as to whether these probability values are meaningful. No data exist with which to calculate probabilities. With no volcanic rocks within the Paleozoic and younger stratigraphic record, no evidence of exposed volcanic rocks within the Delaware Basin, and a tectonically stable geologic setting, the initiation of volcanic activity within the next 10,000 years is not likely to occur.

Volcanic activity is eliminated from WIPP performance assessments based on the physical unreasonableness of major changes occurring in the tectonic setting of the Delaware Basin within the time frame of regulatory concern.

Magmatic Activity

Magmatic activity as used in this report refers to molten rock (magma) that originates in the lower crust or upper mantle, migrates upward through the crust in response to buoyancy effects or stress/pressure differentials, but cools and crystallizes before reaching the surface. Existing fault or fracture zones may act as pathways for this migration. Magma that cools at considerable depth is referred to as plutonic. Because some of the igneous rocks in southeastern New Mexico and western Texas seem to have cooled relatively close to but not at the surface, all igneous rocks that have cooled before reaching the surface will be referred to as magmatic. This type of activity occurs in tectonically unstable areas. Magmatic activity is

of concern to performance assessment because of the possibility that the rising magma could reach a disposal facility, thereby disrupting the engineered barriers designed to isolate the waste, and/or the heat associated with the magma could impose significant thermal effects on groundwater flow.

According to Powers et al. (1978a), no igneous activity has occurred within 100 miles (160 kilometers) of the WIPP since mid-Tertiary time (approximately 30 million years ago). Within the northern Delaware Basin, a northeast-trending lamprophyre dike or series of en-echelon dikes has been identified in outcrop, in boreholes, and by magnetic anomaly. These various sources of information suggest that this dike or dike system is up to 20 feet (6 meters) wide and possibly extends for 80 miles (130 kilometers). Samples from one outcrop location contain vesicles, which indicate emplacement of the dike to relatively shallow depths, although no evidence of extrusion at the surface has been cited. The dike is located as close as 9 miles (14.5 kilometers) to the northwest of the WIPP (Powers et al., 1978a). Age dating of samples of the dike material have produced dates of approximately 30 million years and 35 million years.

Hunter (1989) calculated the probability of a dike of a particular length within the Delaware Basin intersecting a repository to be 2×10^{-6} during 10,000 years. This value is lower than the cutoff value of 10^{-4} in 10,000 years established in the Standard. A question arises as to the validity of one of Hunter's assumptions in making this calculation. The probability of another dike intruding into the Delaware Basin was assumed to be the period of regulatory concern (10,000 years) divided by the time interval since the last dike intruded the basin (30 million years). This assumption ignores the tectonic processes that likely contributed to the emplacement of the dike in mid-Tertiary time. Powers et al. (1978a) suggest that the coincidence of the dike's orientation with the orientation of several regional tectonic lineaments in addition to crevasses and fractures in rocks exposed near Carlsbad Caverns, which are approximately 37 miles (59 kilometers) west-southwest of the WIPP, indicates the presence of a zone of crustal weakness. Emplacement of the dike may have been along a fracture zone that formed in the early stages of mid-to-late Tertiary tectonism. Brinster (1991) suggests that uplift of the Guadalupe Mountains, which originated in late Pliocene through early Pleistocene time (Powers et al., 1978a), produced a zone of fractures in nearly the same location and of the same orientation as the dike. Groundwater flow along this fracture zone dissolved salt in the Rustler Formation. Subsidence in response to this salt dissolution produced Nash Draw. Fracturing or faulting occurred in nearly the same location in mid-Tertiary and early Pleistocene times. The fact that igneous material was emplaced along the zone of failure during mid-Tertiary time but not during early Pleistocene time suggests that a change in the geologic processes at

this location has occurred. No evidence supports the possibility of a dike being emplaced at the location of the WIPP in any time frame.

In summary, a single dike transected the northern part of the Delaware Basin during the geologic history of this basin. This event occurred approximately 30 million years ago, and a similar event has not occurred in this region since this emplacement. The occurrence of an event that results in the emplacement of another dike at or near the WIPP during the 10,000 years of regulatory concern after 30 million years of quiescence is not physically reasonable. As a result, the recurrence of the tectonic conditions that resulted in magmatic activity is eliminated from the WIPP performance assessments based on the physical unreasonableness of such changes occurring within the time frame of regulatory concern.

Formation of Dissolution Cavities

The circulation of groundwater that is undersaturated with salt can result in the dissolution of salt and the formation of a cavity. Dissolution cavities considered in a demonstration of the scenario-development procedure in Cranwell et al. (1990) were assumed to form by the dissolution of salt from a salt-bearing unit at depth, forming a cavity that resulted in the collapse of the overlying rock units into the cavity. Such debris-filled structures are called breccia pipes or breccia chimneys. In Cranwell et al. (1990), the initiation of dissolution of the salt resulted from the fracturing of an aquitard either above or below the waste panels and the flow of undersaturated groundwater through the fractures. Disruption of the unit overlying the salt has the potential of providing a pathway for groundwater to dissolve and remove the salt and eventually reach the radioactive waste, whereas disruption of the underlying unit has the potential of the waste itself being involved in the collapse into the underlying cavity where circulating groundwater could have access to disrupted waste. In addition to the formation of breccia chimneys by similar processes in the WIPP region, the possible migration of a dissolution front from Nash Draw toward the WIPP also is considered in this section.

Deep Dissolution

Hunter (1989) dismissed the formation of deep dissolution cavities using the screening criterion of low probability. Several of the assumptions used to calculate the probability cannot be justified. For this reason, an alternate approach is used to screen the formation of deep dissolution cavities. Anderson (1978, 1981, 1983) proposed that salt dissolution at depth is a major contributor to the total amount of salt removed from within the northern Delaware Basin. Davies (1983) proposed that groundwater circulating through higher-conductivity zones in the Bell Canyon Formation has resulted

in at least local areas of deep salt dissolution in the interior of the basin. Using regional well-log correlations, Borns and Shaffer (1985) concluded that the geologic features both Anderson and Davies had attributed to deep salt dissolution were more readily attributed to mass redistribution in the Castile Formation, the presence of localized depocenters in the lower Castile Formation that resulted in the deposition of thicker upper Castile and lower Salado sediments, and topographic irregularities on the top of the Bell Canyon Formation producing apparent deformational structures in the overlying units.

In the northern Delaware Basin, field work and drilling have confirmed the existence of two breccia chimneys and suggested the existence of two more. Stratigraphic relationships and active subsidence within San Simon Sink indicate that dissolution has been an ongoing process at this location (Nicholson and Clebsch, 1961; Lambert, 1983). All of the confirmed and suspected breccia chimneys and San Simon Sink are located over the Capitan Reef (Lambert, 1983). According to Snyder and Gard (1982), the origin of Hill A, which is located approximately 30 kilometers (17 miles) east-northeast of Carlsbad, is the result of dissolution of the Capitan Limestone at depth, collapse of the Salado and younger formations into the dissolution cavity, and dissolution of Salado and Rustler salts in the down-dropped blocks within the chimney, possibly by downward-moving water. The association of the other chimneys and San Simon Sink with the location of the buried Capitan Reef suggests that deep dissolution only occurs where groundwater circulates within the reef and where rocks containing evaporite minerals have collapsed into cavities within the reef.

Breccia chimneys and buried reefs have not been identified within the interior of the Delaware Basin. Based on the association of known chimneys and reefs, the deep dissolution that produces breccia chimneys is not physically reasonable at or near the WIPP.

Shallow Dissolution

Whereas deep dissolution involves processes occurring in the lower Salado and deeper formations, shallow dissolution involves processes that can affect the upper Salado and shallower formations. Shallow dissolution has the potential of occurring as a result of vertical recharge from the surface, horizontal flow along the contact zone between the Salado and Rustler Formations, and migration of the dissolution front from Nash Draw toward the WIPP. Each type of dissolution has the potential of disrupting the Rustler Formation to an extent that groundwater flow in the Rustler Formation is changed from confined to unconfined conditions. A change in groundwater-flow conditions

could have an important impact on the lengths of flow paths and the rate of groundwater flow.

In the subsurface at the WIPP, the shallowest unit that is composed of a significant soluble component is the Forty-niner Member of the Rustler Formation. With the exception of isolated sandstone lenses in the Dewey Lake Red Beds, the units overlying the Forty-niner Member are not saturated (Mercer, 1983; Brinster, 1991). The thickness of the units overlying the Rustler Formation range from approximately 80 meters (260 feet) at the western boundary of the WIPP to approximately 200 meters (650 feet) at the eastern boundary (Brinster, 1991). Tests to determine the hydrologic properties of the lower portion of the Dewey Lake Red Beds had to be stopped because of the low water content and permeability of the rocks (Beauheim, 1986, 1987a). In order for rainfall to reach the Forty-niner Member to dissolve the halite component, this water must infiltrate through the surficial wind-blown deposits and sandy Berino paleosol. Beneath the sandy material, the water must pass through the dense and generally massive, although locally fractured, Mescalero caliche. Between the caliche and the Forty-niner Member lie the sands and clays of the lower Dockum Formation and 75 to more than 150 meters (245 to 490 feet) of the Dewey Lake Red Beds. Because of the low permeability of the lower portions of the Dewey Lake Red Beds, the brine will have an extremely low flow rate, thereby blocking additional infiltrating water from reaching and dissolving the salts in the Rustler Formation. Because of the presence of both geologic and hydrologic constraints on infiltration and groundwater flow, dissolution of salt by infiltrating water at the WIPP, if this process can occur at all, will have a low consequence on the hydrologic behavior of the disposal system. Because of low consequence, this process can be eliminated from the performance assessment of the WIPP.

A layer of material is present at the contact of the Salado and Rustler Formations that has been interpreted as insoluble residue left after the dissolution of salt primarily of the Salado Formation (Robinson and Lang, 1938; Mercer and Orr, 1977; Mercer, 1983). This layer is referred to as the Salado-Rustler contact residuum. The contact residuum extends from at least the central portion of Nash Draw, across the WIPP, and into western Lea County. Based on currently available data, the thickness of the contact residuum within the WIPP ranges from 7 to 36 meters (23 to 118 feet) (Mercer, 1983; Lappin et al., 1989). Groundwater flow within the residuum is from an unidentified recharge area, north to south across the WIPP, and then to the southwest to the Pecos River (Mercer, 1983). Although the water-chemistry data compiled in Lappin et al. (1989) do not indicate a trend in increasing or decreasing total dissolved solids (TDS) or water density in the vicinity of the WIPP, Brinster (1991) states that the brine concentration generally becomes greater to the southwest and the groundwater is nearly saturated in

the portion of Nash Draw near the Pecos River. An increase in fluid density in the direction of flow indicates that dissolution of the adjacent salt is continuing, although the hydraulic properties of the residuum suggest that groundwater flow within this unit is relatively slow, and the water-chemistry data suggest little dissolution is occurring at the WIPP. Because dissolution has occurred along the Salado-Rustler contact in the past, is currently taking place to some degree, and is likely to continue into the future, this process is part of the base-case scenario. The units that overlie the contact residuum (especially the relatively brittle Mescalero caliche) in the immediate vicinity of the WIPP have not been noticeably disrupted by this dissolution process, except along the margin of Nash Draw (U.S. DOE, 1980a). In addition, the mechanically brittle anhydrite layers in the Rustler Formation tend to be unfractured. Because this long-term dissolution process seems to have had a minimal impact at the WIPP, this process is not likely to have a significant effect on the performance of the disposal system.

Nash Draw was formed by the dissolution of evaporite minerals in the Rustler and upper Salado Formations (Bachman, 1981; Lambert, 1983; Brinster, 1991). Interpretations differ as to the duration of this dissolution. Bachman (1974) estimated that Nash Draw began to form since the development of the Mescalero caliche 510,000 years ago (Bachman, 1985) and is continuing at present, although the rate of dissolution has not been a constant because of variations in the climate. With climatic conditions in southeastern New Mexico in a drying trend since the Pleistocene Epoch, the rate of dissolution has been decreasing. Brinster (1991) concluded in his synthesis of the regional geohydrology that a fracture system developed at the location of Nash Draw in association with the uplift of the Guadalupe Mountains, which is in the same time frame as the estimated age of uplift by Bachman (1974). Recharge during wetter climatic conditions and groundwater from the overlying units drained through this fracture system, dissolving the evaporite minerals and resulting in the collapse of the overlying units. Drainage of groundwater from the overlying units allowed dissolution to continue during drier climatic conditions. Once the groundwater drained from the overlying units, the dissolution process that formed Nash Draw stopped from a practical point of view. By this interpretation, the dissolution that formed Nash Draw was a relatively short-lived process that is not continuing at present. A change to a much wetter climate presumably could result in a limited resumption of dissolution, although at lower rates than during the formation of Nash Draw.

If Bachman's (1974) interpretation of the origins of Nash Draw is correct, Nash Draw is continuing to expand in width. At the closest point to the WIPP, Nash Draw is approximately 6.4 kilometers (4 miles) wide. If Nash Draw did originate 510,000 years ago and the process is continuing, the mean rate

of expansion has been 0.01 meters/year (0.4 inches/year). With symmetrical expansion from the axis of the draw, the rate of expansion toward the WIPP is half of this value, or 0.005 meters/year (0.2 inches/year). Assuming that climatic change to wetter conditions can extend this rate of expansion for the next 10,000 years, the margin of Nash Draw would be approximately 50 meters (164 feet) closer to the WIPP than the present location. With the WIPP located approximately 6.4 kilometers (4 miles) from Nash Draw, the presence of Nash Draw is unlikely to affect the performance of the disposal system. A ten-fold increase in this mean rate of expansion would result in the margin of Nash Draw being 500 meters (1640 feet) closer to the WIPP than the present location, although a climatic change of a magnitude that would produce such an increase in the rate of expansion in the relatively short time frame of 10,000 years is not physically reasonable.

If Brinster's (1991) interpretation is correct, the expansion of Nash Draw from the present location to the WIPP by dissolution is not a physically reasonable process within the time frame of regulatory concern, because the primary source of water for the dissolution of evaporites was groundwater whose source has, for practical purposes, been depleted.

Summary of Screening of Dissolution

Based on the geologic setting of confirmed and likely breccia chimneys and the lack of compelling field evidence of deep dissolution that could result in the formation of breccia chimneys at or near the WIPP, processes that could result in deep dissolution affecting the WIPP are not physically reasonable. Of the possible processes that could result in shallow dissolution, dissolution along the contact of the Salado and Rustler Formations is an ongoing process. This process is part of the undisturbed performance of the disposal system. The rate of dissolution within this zone is slow enough that no significant changes will occur to the groundwater-flow system during the time period of regulatory concern. Dissolution that could result in the margin of Nash Draw reaching the WIPP within the time frame of interest is not physically reasonable.

Formation of Interconnected Fracture Systems

Fracture systems do not spontaneously occur but instead are the product of the occurrence of events or processes. If an event or process produces fractures, the effects of these fractures on the hydrologic properties of the disposal system should be included in consequence modeling as an alteration or modification of base-case conditions. An originating event or process may be appropriate for inclusion in scenario development, whereas the inclusion of fracture systems, which are produced by events and processes, is not. No tectonic processes are occurring in the northern Delaware Basin at a rate

that would produce new fracture systems in rocks in the WIPP area within the time frame of regulatory concern.

Faulting

Faulting refers to either the creation of a new fault or renewed movement on an existing fault. The creation of a new fault is of concern to performance assessment because of the potential for the fault to pass through the disposal facility and rupture waste containers and possibly engineered barriers to groundwater flow. In addition, new faults may provide new pathways for groundwater flow or divert flow to alternate pathways. Reactivation of existing faults may modify hydraulic properties along existing pathways of groundwater flow and possibly redirect groundwater flow to alternate pathways. Modifications to existing pathways or the creation of new pathways may affect the travel time of radionuclides transported by groundwater to reach the accessible environment.

Structure-contour maps for several major units in the WIPP vicinity (Powers et al., 1978a) indicate that sedimentary units older than the Salado Formation are faulted and the Salado Formation and younger units are not. Although this change in the occurrence of faults coincides with a change in the construction of the maps from seismic-reflection data to borehole data, the quantity and spacing of the borehole data suggests that the absence of faults in the Salado and younger units is real. In addition, no tectonic fault scarps have been identified within the interior of the northern Delaware Basin. As discussed in the previous section on "Magmatic Activity," the lamprophyre dike and Nash Draw may be located along a long-lived zone of crustal weakness. The relatively undisturbed nature of the brittle rocks of the Rustler Formation indicates that this zone of weakness does not extend to the WIPP.

Movement on faults typically occurs along existing faults in tectonically active areas, and the formation of a new fault that is not subsidiary to an existing fault within such areas is a rare event (Bonilla, 1979). At the WIPP study area, faults are present in rock units older than the Salado Formation (Powers et al., 1978a). The lack of evidence for the existence of faults within the Salado Formation and younger units and the low seismic activity within the northern Delaware Basin indicate that the tectonic setting has not been suitable for faulting to occur since at least the end of Permian time 245 million years ago.

Faulting as a result of tectonic activity is excluded from the WIPP performance assessment because the establishment of tectonic conditions that would result in faulting in the vicinity of the WIPP is not physically reasonable in the time frame of regulatory concern.

4.1.4 EVALUATION OF HUMAN-INDUCED EVENTS AND PROCESSES

In addition to the three screening criteria proposed by Cranwell et al. (1990), Appendix B of the Standard limits the severity of human intrusion at the location of the waste panels that need to be included in the performance assessments. As stated in Appendix B, "...inadvertent and intermittent intrusion by exploratory drilling for resources (other than any provided by the disposal system itself) can be the most severe intrusion scenario assumed by the implementing agencies" (U.S. EPA, 1985, p. 38089). The Standard does not specifically define the term "severe" as used in Appendix B, but the preamble to the Standard does provide guidance as to the intent of the EPA. According to the preamble,

> The implementing agencies are responsible for selecting the specific information to be used in these [including the limiting assumptions regarding the frequency and severity of inadvertent human intrusion] and other aspects of performance assessments to determine compliance with 40 CFR Part 191. However, the Agency [EPA] believes it is important that the assumptions used by the implementing agencies are compatible with those used by EPA in developing this rule. Otherwise, implementation of the disposal standards may have effects quite different than those anticipated by EPA (U.S. EPA, 1985, p. 38074).

In calculating population risks as background in developing the Standard, Smith et al. (1982) considered exploratory drilling as the only realistic mode of human intrusion into the waste-storage facility. Following the example set by the EPA, exploratory drilling is the only mode of human intrusion within the boundaries of the waste panels that will be included in the performance assessments of the WIPP.

Explosions

Human-induced explosions are a concern to the WIPP performance assessment, because this type of event has the potential of breaching the engineered barriers and/or introducing disruptions to the geologic and hydrologic systems. These disruptions could alter the groundwater-flow path within the disposal system and provide shorter pathways for radionuclides to reach the accessible environment. Possible explosions associated with nuclear criticality are considered in a separate section.

Based on the current level of technology, the only type of human-induced explosion that has the potential of significantly impacting the performance of the disposal system is nuclear in origin. The deliberate use of a nuclear device to disrupt the disposal system or exhume waste would not be included in the WIPP performance assessment because Appendix B of the Standard limits

the human-intrusion events that need to be considered to those that are inadvertent.

Inadvertent explosions at the location of the waste panels also can be excluded from the WIPP performance assessments. Appendix B of the Standard limits the severity of human intrusion at the location of the repository that must be considered in performance assessments to exploratory drilling for resources. Explosions away from the location of the waste panels that potentially could result in the inadvertent disruption of the disposal system include surface or near-surface bomb detonations during war, underground testing of nuclear devices, and underground detonation of nuclear devices for peaceful purposes.

The possibility of surface or near-surface detonation of nuclear bombs during warfare requires that nations maintain nuclear arsenals into the future, a war takes place that involves nuclear weapons, and either a strategic facility worth targeting by an enemy exists in the WIPP region or the delivery system malfunctions or is damaged, causing the nontargeted area of the WIPP region to be hit. Surface nuclear detonations may affect hydrologic systems by a combination of cratering and seismic waves, whereas the effects of a near-surface detonation will primarily be the result of seismic waves. The effects of an explosion on the disposal system will be greater the closer the explosion occurs to the WIPP, but the closer an explosion occurs, the lower the probability of the occurrence because of the progressively smaller area surrounding the WIPP. Seismic effects on the source term or the disposal system are likely to be addressed within parameter uncertainty during modeling. Nuclear explosions in the WIPP region during warfare that could have significant effects on disposal-system performance are low-probability events.

The topic of future nuclear testing presumes that future societies will continue to possess nuclear devices that require testing. For this discussion, future nuclear testing is assumed to require a large area with isolation similar to the Nevada Test Site. Whereas the conditions of size and isolation are met in the northern Delaware Basin at present, future uses of this region are not known. If underground testing is conducted in the Delaware Basin, tests presumably would occur in the bedded salt of the Salado Formation because of the lack of fractures within this unit and the ability of salt to heal fractures generated during testing. The size of nuclear devices tested would have to be relatively small in order to assure that the low-permeability units that impede dissolution of the Salado Formation are not ruptured. Questions arise as to whether salt would be suitable for nuclear testing given the high potential for compromising the test site by salt dissolution, and the selection of the northern Delaware Basin instead of other areas considering the vast areas of the continental United States that

are underlain by bedded salt. The consequences of testing are likely to be limited to seismic effects on permeabilities of hydrologic units and premature rupturing of waste drums and containers. Both of these effects can be addressed with parameter uncertainties during performance modeling, although selection of the northern Delaware Basin for a future test site has a low probability, considering the numerous other locations and options for testing.

Nuclear explosions have the potential of providing a technique for fracturing oil- and natural-gas-bearing units to enhance resource recovery. Future societies may use this technique or evaluate the use of non-nuclear explosions as hydrocarbon resources become depleted. The size of explosions will be relatively small in order to maximize fracturing of the unit being exploited instead of maximizing cavity size or fracturing the surrounding rocks, which could allow the hydrocarbons to escape. In the area surrounding the WIPP, the stratigraphic units with the highest resource potential tend to be thousands of meters deeper than the waste panels. Disruptions to the WIPP disposal system and modification of the source term resulting from explosions at depth are likely to be minor to nonexistent.

Nuclear or other large-scale explosions at the location of the waste panels can be excluded from performance assessments, because these explosions would be more severe than required by the Standard for inclusion in these assessments. Accidental surface and near-surface nuclear explosions during warfare can be excluded from the assessments on the basis of low probability. Nuclear testing and/or the use of nuclear devices for enhanced resource recovery are highly speculative future human activities. The combination of the likelihood that these activities will occur in the future at a location and be of a magnitude that will affect the WIPP disposal system has a sufficiently low probability to eliminate such events from scenario development.

Drilling

Appendix B of the Standard restricts the type of drilling that needs to be included in performance assessments to exploratory drilling for resources. This restriction eliminates from consideration the higher drilling densities associated with the development of resource deposits. This appendix also discusses the frequency of exploratory drilling. In the section on Institutional Controls, the Standard states that "...the Agency [EPA] believes that passive institutional controls can never be assumed to eliminate the chance of inadvertent and intermittent human intrusion into these disposal sites" (U.S. EPA, 1985, p. 38088). This statement is interpreted here to require the probability of exploratory drilling by at least one borehole to be greater than the cutoff established in the Standard

(i.e., greater than 1 chance in 10,000 in 10,000 years). In the section of Appendix B entitled "Frequency and Severity of Inadvertent Human Intrusion into Geologic Repositories," the statement is made that "...the Agency [EPA] assumes that the likelihood of such inadvertent and intermittent drilling in 10,000 years need not be taken to be greater than 30 boreholes per square kilometer of repository area per 10,000 years for geologic repositories in proximity to sedimentary rock formations..." (U.S. EPA, 1985, p. 38089). This statement provides an upper limit on the drilling density in 10,000 years for consideration in performance assessments. The preamble to the Standard does provide an option for the use of other drilling densities by including the following statement:

> The Agency [EPA] believes that performance assessments should consider the possibilities of such intrusion, but that limits should be placed on the severity of the assumptions used to make the assessments. Appendix B to the final rule describes a set of parameters about the likelihood and consequences of inadvertent intrusion that the Agency assumed were the most pessimistic that would be reasonable in making performance assessments. The implementing agencies may adopt these assumptions or develop similar ones of their own (U.S. EPA, 1985, p. 38077).

With 30 boreholes/km^2 in 10,000 years as a "worst-case" assumption, the implication of the above statement is that the implementing agencies should strongly consider developing site-specific drilling densities. For the WIPP performance assessment, a panel of experts with a broad spectrum of backgrounds was convened to propose possible modes of inadvertent human intrusion at the WIPP during the next 10,000 years (Hora et al., 1991). Topics addressed by the panel included drilling densities and time frames of resource exploration for various possible future states of civilization. Each of the four teams within the panel estimated future drilling densities substantially lower than 30 boreholes/km^2 in 10,000 years.

Because of the wording of the Standard, exploratory drilling for resources is retained for inclusion in performance assessments. Exploratory drilling can be subdivided to identify more than one event to facilitate computer modeling and both consequence and sensitivity analyses.

Based on economic conditions and resource demands at the time of geological characterization, potash and natural gas were identified as the only two resources with economic potential at the WIPP (Powers et al., 1978b). The McNutt Potash Member of the Salado Formation, which is approximately 400 feet (120 meters) above the depth of the proposed waste panels (Nowak et al., 1990), is the only unit in the stratigraphic sequence in the northern Delaware Basin with potash in economic quantities, although economically recoverable potash is not present in this unit at all locations (Brausch et al., 1982). Keesey (1976, 1979) concluded that the Morrow

Formation at a depth in excess of 11,600 feet (3550 meters) beneath the waste panels is the only reasonable target for resource exploration for natural gas and that crude oil would not be reasonably extractable from any unit at this location. Depending on the resource needs of future societies, all exploratory drilling could be shallower than the waste panels if the target resource is potash, all exploratory drilling could be deeper than the waste panels if the target resource is natural gas, or drilling could be divided in any ratio between the two depths if both resources are targets.

Mining

During geological characterization of the WIPP location (Powers et al., 1978a,b), each of eight natural resources were evaluated for their potential occurrence in economic quantities at the WIPP. The resources investigated were caliche, gypsum, salt, uranium, sulfur, lithium, potash, and hydrocarbons. Uranium was not found to be present in even marginally economic quantities. Sulfur deposits have not been identified in the northern Delaware Basin. Lithium had been reported in marginally economic quantities in samples from a single brine reservoir, but Powers et al. (1978b) did not consider lithium as a potential resource at the WIPP because of a lack of evidence that brine of an appropriate composition and quantity exists at this location. Caliche, gypsum, and salt were not considered to be economical at the WIPP because of their widespread occurrence and the existence of more easily accessible deposits elsewhere in the region. Crude oil was not considered to be available in sufficient quantity to qualify as a potentially economically viable resource. Only natural gas and potash were concluded to be potentially exploitable resources.

Bedded-salt deposits also have the potential of being mined to form cavities for natural-gas storage. Guidance in the Standard excludes consideration of mining of storage facilities at the WIPP, because mining is a more severe disruption of the disposal system than exploratory drilling for resources. Outside the boundary of the WIPP, mining cavities for natural-gas storage can be evaluated in the same way that Powers et al. (1978b) evaluated mining salt. The existence of extensive areas underlain by bedded salt substantially reduces the likelihood of cavities being mined in the immediate vicinity of the WIPP.

Of the two potential resources at the WIPP identified in Powers et al. (1978b), potash must be recovered by mining. Langbeinite is the primary mineral mined for potash. Conventional mining currently is active in the region around the WIPP. Based on the physical properties of langbeinite, the characteristics of the ore deposits, and the limited availability of suitable water, Brausch et al. (1982) concluded that solution mining is not feasible in this area.

The Standard excludes mining of any type at the location of the waste panels from inclusion in scenarios for performance assessments. If mining beyond the boundaries of the WIPP affects the disposal system, mining needs to be included in scenario development. Brausch et al. (1982) noted that subsidence commonly occurs over potash mines in the WIPP region, although no incidence of water leaking into the mines from overlying units has been observed. Subsidence over a mine has the potential of forming a catchment basin where runoff can accumulate (Guzowski, 1990). If the underlying units are sufficiently fractured by the subsidence, accumulated water may have a pathway to recharge these underlying units. In the WIPP region, this type of recharge has the potential of affecting groundwater flow in members of the Rustler Formation at the WIPP and/or adding water to what is now the unsaturated zone.

Whether or not potash in southeastern New Mexico will continue to be mined in the long-term future is not known. The probability of future mining is assumed to be above the cutoff established in the Standard. Effects of subsidence on recharge and groundwater flow also are not known, although computer modeling by the WIPP Performance Assessment Division is in progress to estimate these effects. For preliminary scenario development, potash mining beyond the area of the waste panels is retained.

Injection Wells

Injection wells refers to the drilling of wells followed by injection of fluid. This fluid can either be water (e.g., water produced during the exploitation of resources or water injected to enhance hydrocarbon recovery) or hazardous liquids (e.g., byproducts of chemical industries). Injection wells are of interest to performance assessment because a waste-filled room or drift may be encountered during the drilling process, thereby providing a mechanism for transporting waste to the surface, an abandoned well could create a new pathway for groundwater after the well is abandoned, and the injection of a sufficient quantity of liquid may change the potentiometric field for the groundwater.

Saturated sedimentary units within a basin can be underpressured (below hydrostatic) if the basin is topographically tilted and capped by a thick sequence of low-permeability rocks (Belitz and Bredehoeft, 1988). A preliminary examination of well data for the northern Delaware Basin by Brinster (1991) found that units between the base of the Castile Formation and a depth of 1,800 meters (approximately 6,000 feet) are underpressured. Units deeper than 1,800 meters also are underpressured except where natural-gas reservoirs are present.

Whether fluid injection for any reason is a possible future event depends on the technological status and societal attitudes of future civilizations, as well as the hydrogeologic suitability of units at depth at a particular location. Although the deeper units in the basin tend to be underpressured, pressures associated with natural-gas production from deep units in the Delaware Basin tend to be greater than hydrostatic (Lambert and Mercer, 1978). Deep units beneath the WIPP have been identified as potentially containing hydrocarbon resources with natural gas possibly being present in economic quantities (Powers et al., 1978b). The presence of natural-gas reservoirs in units beneath the WIPP would limit or possibly eliminate the availability of underpressured units for injection of fluid at this location.

Unless the location of the waste panels has some uniquely favorable characteristics for injection wells that are currently not recognized, the selection of this location, which consists of an area of approximately 0.5 km^2 (0.2 mi^2), seems to be an unlikely event considering the area of the basin (33,000 km^2 (12,470 mi^2)) and the area of the region as a whole where injection wells could be located. A qualitative assessment of this location being chosen suggests that the probability is low but not positively less than the cutoff value provided in the Standard.

A borehole being drilled for an injection well could penetrate a waste-filled room or drift and possibly a brine reservoir in the Castile Formation. If the assumption is made that the geologic characteristics of the deep formations beneath the WIPP have hydrologic characteristics acceptable for injection wells, both intercepting a room or drift and/or a brine reservoir are physically reasonable. The effects of either occurrence on the performance assessment of the WIPP would be approximately the same as deep resource-exploration boreholes. For injection wells, more care might be taken in the emplacement of seals, because the use and abandonment of injection wells tend to be less routine than for oil and gas exploration boreholes.

The effects of injection wells on groundwater flow in units shallower than the Salado Formation is likely to be negligible. Units selected for injection will be thousands of feet deeper than the Rustler Formation, which is the most likely path for the groundwater transport of radionuclides to the accessible environment. The low-permeability Bell Canyon, Castile, and Salado Formations are approximately 4,000 feet (1,220 meters) thick at the WIPP (Powers et al., 1978a), and these low-permeability units will isolate the groundwater flow in the Rustler Formation from the pressure increases in the much deeper units caused by the injection of fluids.

The emplacement of injection wells cannot be immediately eliminated from consideration on the basis of probability of occurrence, although the

locations at which such wells are drilled are limited by restrictions in the Standard. Appendix B of the Standard states that the intruder's own exploration procedures will soon detect that the drilling activity is not compatible with the area. Because the candidate hydrologic units for injection are substantially deeper than the waste panels, a well being drilled for injection that penetrates a waste-filled room or drift will not be drilled for additional thousands of meters to an injectable unit if the driller soon detects the incompatibility of the area with injection.

Injection wells can be eliminated from consideration in performance assessments because of a lack of consequence. Because the units suitable for injection are separated from the waste panels and hydrologic units above the panels by the virtually impermeable evaporite sequences of the Castile and Salado Formations, the injection of fluid (e.g., brine associated with natural-gas production) at depth will have no effect on the disposal system.

Withdrawal Wells

Withdrawal wells refer to boreholes drilled and completed for the extraction of groundwater, oil, or natural gas. Wells withdrawing groundwater have the potential of altering the flow gradient in the area surrounding a well or of altering the flow on a larger scale if water is withdrawn by a field of wells. Water wells also have the potential of providing an alternate pathway for radionuclides to reach the accessible environment if the unit being pumped contains radionuclides that have escaped from the waste-filled rooms and drifts. Because the Standard restricts the severity of drilling that needs to be included in performance assessments of the WIPP to exploratory drilling for resources, oil or gas production wells, which are withdrawal wells, only need to be considered in areas outside of the repository area. Areas where oil or gas are withdrawn have the potential of surface subsidence in response to the removal of the confined fluid that supports some of the weight of the overburden.

Water Wells

Water-producing units above the Salado Formation are restricted to the Culebra Dolomite and Magenta Dolomite Members of the Rustler Formations, although the yield of the Magenta Dolomite is so low that the unit generally receives little attention (Brinster, 1991). Little is known of the specific hydrologic properties of the units deeper than the Salado Formation at the WIPP, but with the exception of possible brine reservoirs in the Castile Formation, water-producing units beneath the Salado Formation are in excess of 5,000 feet (1,500 meters) deep at this location. Because of the considerable depth to the deeper water-producing units, only the Culebra

Dolomite is regarded as a realistic candidate for water usage in this screening of events and processes.

One of the requirements for a "significant source" of groundwater as defined in the Standard is a total-dissolved-solids (TDS) content of less than 10,000 mg/ℓ, which has been used as the upper TDS limit to potable water for both people and cattle (Lappin et al., 1989). Based on the 10,000 mg/ℓ-TDS limit, no potable groundwater has been identified in the Culebra Dolomite within the land-withdrawal boundaries of the WIPP (Lappin et al., 1989). In the *Final Supplemental Environmental Impact Statement* (U.S. DOE, 1990c), no potable water was projected to occur within 5 kilometers (3.1 miles) of the waste panels. A possible exception to this TDS distribution is one of four water samples taken from well H-2 at different times. One sample had a TDS of 8,900 mg/ℓ, whereas the other three samples taken at later times ranged from 11,000 to 13,000 mg/ℓ (Lappin et al., 1989). An explanation of these changes in TDS content for the water from this well has not been verified, nor has the reason been determined for the anomalously low TDS content of the water for this particular location.

Whereas a lack of potable water within 5 kilometers of the waste panels would seem to eliminate the emplacement of water wells from scenario analyses, other considerations require that this event be retained for further evaluation. Most of the groundwater in the Culebra Dolomite is substantially more saline than seawater. At some locations (e.g., H-1, H-2, H-4, H-14, P-15), the TDS content of the water may be suitable for some types of fish or shrimp farming if the sustained yield of the Culebra Dolomite is large enough to supply such an operation. Cones of depression from pumping wells at these locations could alter the groundwater-flow pattern in the dolomite and increase the rate of groundwater flow or alter the pathway to the accessible environment.

Oil and Gas Wells

The Standard limits the severity of human intrusion at the waste panels to exploratory boreholes. Oil and gas withdrawal wells would be associated with production rather than exploration. Withdrawal wells at oil or gas fields at a distance from the waste panels need to be considered for their possible effects on the groundwater-flow system, especially those effects from subsidence that result in fracturing of shallow units and enhanced recharge.

Resource evaluation of the WIPP region was part of site characterization. Natural gas in the Morrow Formation was concluded to be the only possible hydrocarbon resource with economic potential in the area (Keesey, 1976, 1979). At the WIPP, the Morrow Formation is at a depth in excess of 13,000 feet (3,960 meters) (Powers et al., 1978a). Because of the depth and

rigidity of the possible production horizons, subsidence would not be expected to occur if gas (if present) was removed (Brausch et al., 1982).

Geothermal Wells

An assessment of the geothermal potential of the United States (Muffler, 1979) identified no potential geothermal resources in southeastern New Mexico. This conclusion was based on the lack of thermal springs and the relatively low heat flow measured in boreholes in this region.

Because favorable geothermal conditions do not exist in the northern Delaware Basin and significant changes in the geothermal regime within the time frame of regulatory concern are not physically reasonable, the drilling of geothermal wells is excluded from scenario development.

Summary of Withdrawal Wells

Poor water quality at and near the WIPP precludes the emplacement of water wells for domestic or livestock use. Depending on the tolerable water quality and sustainable water needs for fish or shrimp farming, emplacement of water wells into the Culebra Dolomite may be a realistic consideration for performance assessment because of possible alteration of the groundwater-flow field. Emplacement of water wells is retained for further evaluation and is designated Event E3.

Withdrawal of natural gas from deep reservoirs typically does not result in subsidence of the overlying units. Without subsidence, natural-gas withdrawal wells outside the boundaries of the WIPP will not affect the disposal system. This type of withdrawal well can be eliminated from consideration in the WIPP performance assessments because of low consequence. The EPA guidance for implementation of the Standard states that human intrusion at the location of the waste panels with consequences more severe than exploratory drilling for resources need not be considered. Gas-production wells at this location can be eliminated from consideration based on regulatory restriction.

Irrigation

Irrigation uses water from rivers, lakes, impoundments, and/or wells to supplement the rainfall in an area to grow crops. The amount of water needed depends on the type of crop, the amount, timing, and distribution of naturally occurring precipitation, the amount of evapotranspiration, and the type of soil or sediments being irrigated. Irrigation is of interest to performance assessment because of the possibility that the water added to the

surface will infiltrate and reach the water table, possibly affecting groundwater flow and the transport of radionuclides.

In Eddy County, irrigation of the Pecos River valley began in 1887 using water from both the river and wells (Pasztor, 1991). At present, agricultural activity in this region is restricted to areas near the Pecos and Black Rivers where water is available from either impoundments or from shallow wells in the alluvial aquifers near the rivers (Hunter, 1985).

Two major obstacles exist to the use of irrigation at the WIPP. One is the poor quality of the soil. Nearly the entire area of the WIPP is covered by stabilized sand dunes that can be as much as 100 feet (30 meters) thick (Powers et al., 1978a). Beneath these sand dunes is the Berino paleosol, which consists of up to 1.5 feet (0.4 meters) of argillaceous sand. Underlying this unit is up to 10 feet (3 meters) of the Mescalero caliche, which is a well-cemented calcareous paleosol. Any attempt at agricultural development at this location would require considerable soil modification. The other problem is the supply of water in both the quantity and quality required for crops. Water quality may be less of a concern in the future as more salt-tolerant crops are identified and developed (Gibbons, 1990), although a salt content equivalent to seawater seems to be an upper limit for most naturally occurring plants. Sources of water capable of long-term yield are few in number in the WIPP region, and the sources that do exist generally are already committed (e.g., the Pecos River) and/or are being mined and are likely to be depleted (e.g., the Capitan Limestone). Geologic units deeper than the Bell Canyon Formation are possible new sources of water for irrigation, although the several thousand foot depth to these units is considerable for irrigation wells, the amount of water available is not known, and the salinity of the water is likely to be high.

The WIPP is a relatively small area within the southeastern portion of New Mexico. By the time of the assumed loss of active institutional controls 100 years after closure of the WIPP, population pressures for more water should be intense. If technological breakthroughs have occurred and desalination is economically feasible for irrigation, vast areas of southeastern New Mexico and West Texas will be available for agricultural uses. Even with desalination, water supplies are limited in the region. The land available for irrigation is likely to outstrip the available water. As a result of limited water supplies, areas with better soils will be the primary candidates for irrigation (Swift, 1991b). Additional land at the WIPP with poor soil is unlikely to divert water from committed uses. If large-scale desalination does not develop, no uncommitted water is likely to be available to irrigate a newly available area with poor soil.

Irrigation at the WIPP is not included in the performance assessments because of the low probability of the combination of factors and necessary conditions required for this activity to be feasible.

Damming of Streams and Rivers

Damming refers to the building of a barrier across a topographically low area in order to impound water. As with mass wasting, impoundments have the potential of affecting the performance of the disposal system by altering recharge if the impoundment extends over the disposal system or by altering the groundwater gradients if the impoundment is near the disposal system.

In the WIPP area, only two topographically low features are of sufficient size to warrent consideration for damming. These features are the Pecos River and Nash Draw. During Pleistocene time, the Pecos River migrated to its present position and became incised. According to Brinster (1991), as the climate became drier and the hydraulic heads in the Capitan Reef became lower, the overall flow in the river decreased to the point where the river now has a small bed load and does little if any downward erosion. Whereas the Pecos River is incised, the depth of incision generally is not sufficient for the damming of the river to form impoundments. At a limited number of locations along the river, conditions were adequate for damming, and dams have already been constructed at these locations. The options for additional dams is severely limited. In addition, the Pecos River is approximately 24 kilometers (15 miles) from and more than 90 meters (300 feet) lower than the surface location of the waste panels. Because of the limited option of additional dams on the river and the distance of the river from the waste panels, damming of the Pecos River can be eliminated from consideration in performance assessments, because additional dams will be of no consequence to the disposal system.

Nash Draw is the most pronounced topographic feature in the vicinity of the WIPP (see Figure 7-35, U.S. DOE, 1980a). The draw is a collapse feature caused by the dissolution of underlying evaporites, and except for the southern boundary, the boundaries of the feature are relatively steep and of nearly uniform elevation. Nash Draw does not contain any perennial streams or rivers to dam. Creation of an impoundment within the draw will be considered with the possibility of water being supplied from outside of the feature. A dam across the southern end of the draw (approximately at the location of borehole WIPP-21) would have to be over 3 miles (5 kilometers) long, but such a dam would create a confined depression of approximately 40 square miles (103 square kilometers) and locally as much as 200 feet (61 meters) deep. One problem with creating this impoundment is how to confine the water. Collapse structures caused by the dissolution of evaporites beneath Nash Draw would provide pathways for water within the draw

to reach underlying fracture zones, which would act as conduits for the water to leave the draw. The rocks and sediments at the margins of the feature also could drain impounded water. To create an impoundment in Nash Draw, large-scale leakage would have to be stopped or minimized or sufficient water supplied to the impoundment to make up for the losses. Another and perhaps fatal problem to creating an impoundment in this draw is providing enough water to fill the draw and maintain the water level. Filling the draw will be ignored in this discussion. In addition to leakage, evaporation would be a major source of water loss. Pan evaporation in valleys in southeastern New Mexico is approximately 110 inches (9.2 feet, 2.8 meters) per year (Powers et al., 1978b), which for a 40-square-mile impoundment in Nash Draw would result in the loss of approximately 235,000 acre-feet of water per year to evaporation alone. Evaporation would be approximately 12 times the annual flow of the Pecos River near Malaga (based on a time-weighted average of 26 ft^3/s; Powers et al., 1978b). Based on the mean annual precipitation at Carlsbad, which is 12 inches/year (30.5 centimeters/year) (Powers et al., 1978b), the evaporated quantity of water that would have to be replaced would be approximately 11 times the annual flow volume of the Pecos River. Major aquifer depletion would occur in the region if water wells were used to maintain the water level. In the future when regional demands for water are higher than today, the possibility of piping water from the Ogallala aquifer northeast of the WIPP or a major river in another part of the country (e.g., the Mississippi River) is not realistic. Because of the limited supplies of water in southeastern New Mexico and the high demands for water that an impoundment in Nash Draw would require, damming of Nash Draw is not retained for performance assessments because this event is not physically reasonable.

The reason for eliminating damming from performance assessments depends on the location of the topographic feature being considered for damming. For the Pecos River, additional dams and impoundments will have no consequence on the disposal system. Unless a sufficiently large source of water is located to replace the water lost to leakage, evaporation, and use for human activity, the construction of a dam to form an impoundment within Nash Draw seems to have a low probability of occurring.

4.1.5 EVALUATION OF REPOSITORY- AND WASTE-INDUCED EVENTS AND PROCESSES

This category of events and processes has the potential of occurring as a result of interactions of the engineered portion of the disposal system and the surrounding rock.

Caving and Subsidence

An excavation at depth is not inherently stable because of differential stresses exerted on inhomogeneous rock surrounding the opening. The collapse of rock fragments from units above a subsurface excavation into the opening is called caving. Depending on the size and depth of the excavation, caving may result in measurable subsidence of the overlying land surface within a relatively short time interval. For excavations in salt, salt creep will be a contributing factor in the filling of the opening. Caving and subsidence have the potential of affecting groundwater-flow patterns by enhancing the vertical hydraulic conductivity between water-producing units or providing a pathway for increased recharge or discharge.

For the waste-filled rooms and drifts at the WIPP, the amount of downward movement of the overlying rock is limited by the fact that the rooms and drifts will contain waste and backfill that can be compressed to certain limits. Gas generated by corrosion of metals, bacterial action, and/or radiolysis may be of sufficient pressure to impede the downward movement of rocks into the rooms and drifts. Whereas some caving of the roof can occur into an open excavation if the opening is not specifically designed for stability, any caving that does occur will be limited by the amount of space not occupied by the waste and backfill. Salt creep without fracturing will eventually become the dominant mode of deformation in the salt surrounding the rooms and drifts as the waste and backfill exert increasing resistance to the creeping salt.

If the excavation, waste emplacement, and backfilling of the rooms and drifts occur within a relatively short time interval, caving will be minor to nonexistent. The amount of subsidence that can occur depends on the difference between the initial and compressed porosities of the various waste types and backfill, the amount of upward creep of the floor, the inward creep of the walls, the downward creep of the ceiling, and the gas pressure within the rooms and drifts.

Because of uncertainty about gas generated within the rooms and drifts, specific data do not exist with which to determine the amount of salt creep that will occur into the rooms and drifts after closure, and the amount of subsidence at the surface that will accompany this creep. Subsidence at potash mines in the northern Delaware Basin may serve as an analog for the process in the absence of pressurized gas. Mines in this region typically operate at final extraction ratios ranging from 40 to 60 percent. With 6-foot (1.8-meter) openings in production areas and no backfill, the maximum predicted subsidence at the surface is approximately 2 feet (0.7 meters) (Brausch et al., 1982). Based on data from Rechard et al. (1990a), the extraction ratio for the planned waste panels will be 0.22. This much lower

extraction ratio along with the presence of both waste and backfill within the rooms and drifts suggests that surface subsidence over the WIPP should be less, and perhaps substantially less, than the maximum predicted subsidence of 2 feet (0.7 meters) over potash mines in the area.

Predicting the specific amount of subsidence that may occur over the waste panels requires a subsidence model. Because no TRU waste-disposal facilities exist, no validated subsidence models exist for these types of facilities. An alternative approach is to adopt subsidence models developed for other types of subsurface openings, such as coal mines. The use of models for analogous openings also does not solve the problem. According to Lee and Abel (1983) with regard to subsidence over coal mines,

> The difference in rock-mass behavior caused by site conditions alone would indicate that subsidence prediction and engineering cannot be treated in purely mathematical terms. Although the NCB [British National Coal Board] has developed quantitative, practical assessments of mining effects in the United Kingdom, there is no generally applicable subsidence model for the United States, nor are there adequately tested, empirical models for any of the major U.S. coal fields... (Lee and Abel, 1983, p. 25).

In an attempt to determine rough estimates of realistic bounds on the amount of subsidence that may occur over the waste panels, some simplified calculations have been performed. As a first step, the horizontal cross-sectional area of the waste panels is converted from a rectangle to a circle to simplify the subsequent calculations. The dimensions of the waste panels are 2064 feet (629 meters) by 2545 feet (776 meters) (WEC, 1989), and a circle with an equivalent area has a radius of 1293 feet (394 meters).

The next step is to determine the area at the surface above the waste panels that will subside. Subsidence will occur over an area larger than the subsurface excavations, but at some distance laterally from the excavations, no subsidence will occur. The angle between a vertical line from the edge of the excavation to the surface and a line from the same edge of the excavation to the boundary between subsidence and nonsubsidence on the surface is called the angle of draw (α), which is also called the limit angle (Figure 4-3). A major problem is that data are insufficient in the northern Delaware Basin with which to derive or approximate a value of α for the WIPP.

Lee and Abel (1983) report that data collected by the NCB for longwall (as opposed to room and pillar) coal mines in Britain have a range of α from 25° to 35° with the range being much wider (but unspecified) when worldwide measurements are included. Although the WIPP waste panels are more analogous to room and pillar mines rather than longwall mines, no data are readily available for room and pillar mines, so the upper and lower values of the

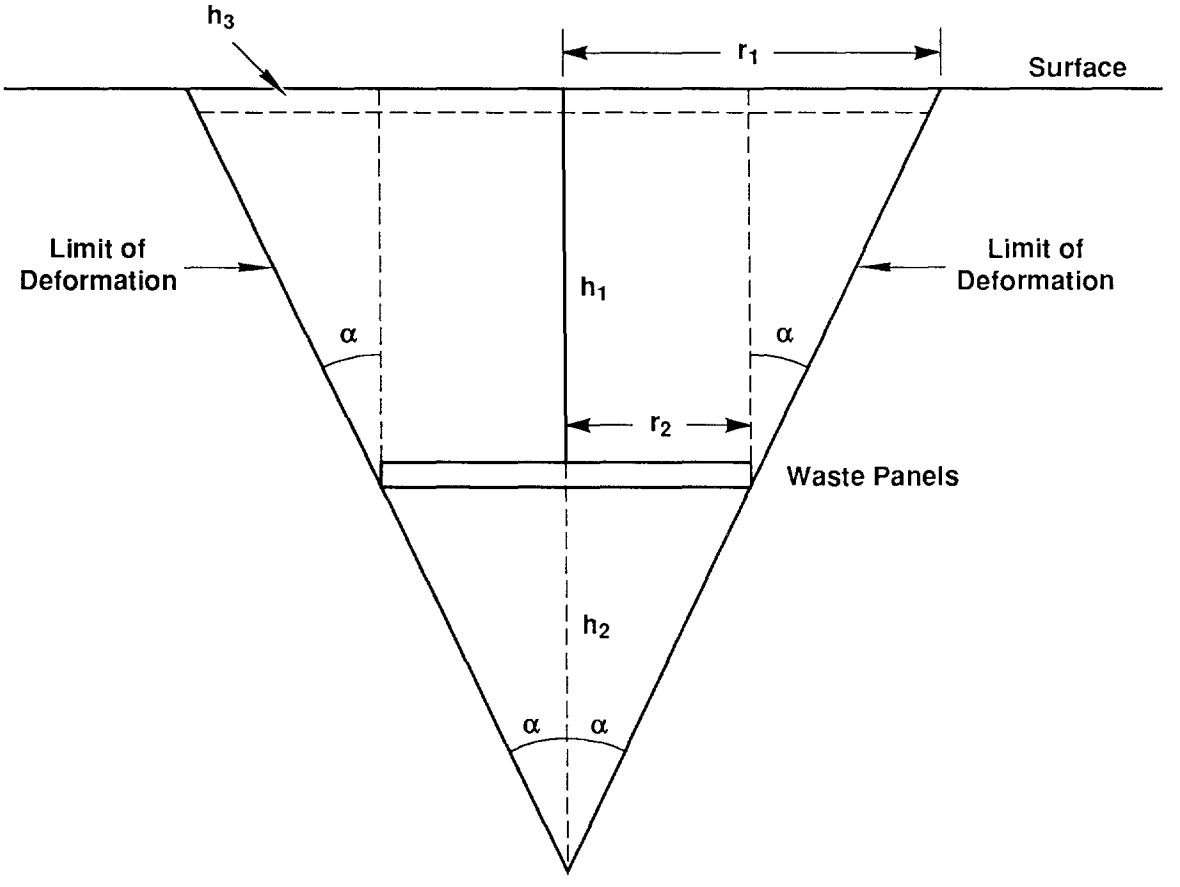

Figure 4-3. Cross-Sectional Areas of Subsidence Over Waste Panels.

range of values reported by the NCB will be used to roughly determine the area of surface subsidence.

In Figure 4-3, the radius of the subsidence area is r_1. The length of r_1 can be determined from the relationships

$$\tan \alpha = \frac{r_1}{(h_1 + h_2)} \qquad (4\text{-}2)$$

and as a result,

$$r_1 = \tan \alpha \times (h_1 + h_2) \qquad (4\text{-}3)$$

where h_1 is the depth of the waste panels beneath the surface (2150 feet) (655 meters) and h_2 is the depth from the panels to the point where the downward projection of the lateral limits of the zone of subsidence would converge at depth. Although the value of h_2 is not known directly, this distance can be calculated from the relationship

$$\tan \alpha = \frac{r_2}{h_2} \qquad (4\text{-}4)$$

which becomes

$$h_2 = \frac{r_2}{\tan \alpha} \qquad (4\text{-}5)$$

where r_2 is the radius of the circular representation of the area of the waste panels. The value of r_2 is 1293 feet (394 meters).

For a value of α equal to 25°, h_2 in Equation 4-5 equals 2774 feet (845 meters). Substituting the appropriate values into Equation 4-3,

r_1 = tan 25° x (2150 feet + 2774 feet) = 2296 feet (700 meters).

For a value of α equal to 35°, h_2 in Equation 4-5 equals 1847 feet (394 meters). Substituting the appropriate values into Equation 4-3,

r_1 = tan 35° x (2150 feet + 1847 feet) = 2799 feet (853 meters).

The next step is to determine the volume change in the waste-filled rooms and drifts that must be accommodated by subsidence. Several assumptions must be made at this point in this procedure. One assumption is that gas generated by corrosion, microbial activity, or radiolysis does not affect the compression of the waste and backfill by salt creep. Another assumption is that all of the volume change in the rooms and drifts will be expressed as

subsidence at the surface. This second assumption requires that the rock units between the waste panels and the surface have no competence. Rock units that do have competence may bend without suffering complete failure when the support of underlying units is lost, thereby causing gaps (bed separations) to form between adjacent units. The formation of these gaps distribute some of the subsidence within the subsiding volume of material rather than entirely at the surface.

Salt creep will compress the contents of the waste-filled rooms and drifts until the differential stresses have equalized. The rooms and drifts will contain a variety of waste types with the addition of backfill, which is assumed to consist of 70 percent crushed salt and 30 percent bentonite. Calculations by Butcher (1991) indicate that an average void fraction of an entire room of approximately 63 percent will be reduced to approximately 16 percent over a period of several hundred years. Rechard et al. (1990a) reported the expected volume of excavated disposal rooms and drifts at the WIPP to be 433.3 x 10^3 m^3 (1.53 x 10^7 ft^3). When the rooms and drifts are fully loaded with waste and backfill, 63 percent of the original excavated volume will remain as pore space, which will be equal to 2.72 x 10^5 m^3 (9.60 x 10^6 ft^3). Upon compaction by salt creep to a porosity of 16 percent, the rooms and drifts will contain approximately 6.93 x 10^4 m^3 (2.45 x 10^6 ft^3) of void space. The change in volume will be 2.04 x 10^5 m^3 (7.20 x 10^6 ft^3). This change in volume is assumed to be the volume of surface subsidence that will occur over the waste panels.

To accommodate the volume of subsidence, the area of subsidence is assumed to subside uniformly, thereby forming a cylinder with the amount of surface subsidence represented by the height of the cylinder. The volume of a cylinder is

$$V = \pi r^2 h_3 \qquad (4\text{-}6)$$

where h_3 is the amount of surface subsidence, and r is the r_1 in Equations 4-2 and 4-3 and Figure 4-3. From Equation 4-6,

$$h_3 = \frac{V}{\pi r^2} \; . \qquad (4\text{-}7)$$

For α equal to 25°, r_1 is equal to 2296 feet (700 meters). To accommodate a volume of subsidence V equal to 7.20 x 10^6 ft^3 (2.04 x 10^5 m^3) in Equation 4-7, h_3 equals 0.43 feet (0.13 meters). For α equal to 35°, r_1 equals 2799 feet (853 meters), and h_3 then equals 0.29 feet (0.088 meters).

Although the actual value of α for the WIPP geologic setting (including the effects of lateral salt-creep closure of the rooms and drifts), extraction

ratio, and waste and backfill conditions is not known, the above calculations indicate the approximate magnitude of subsidence that may occur over the waste panels. The next step in screening this process is to determine whether subsidence on this order of magnitude has an effect on the disposal system.

No direct information or data are available on the effects of subsidence on the overlying groundwater-flow system in the northern Delaware Basin. An alternative approach is to examine whether shallow dissolution in the WIPP has affected groundwater flow. Removal of salt by dissolution leaving the insoluble constituents reportedly is the origin for the Rustler-Salado contact residuum (Robinson and Lang, 1938; Mercer and Orr, 1977; Mercer, 1983). If the subsequent lowering of the overlying units in response to the removal of the salt has not disrupted the groundwater-flow system in these overlying units, perhaps the subsidence over the waste panels also will not affect the flow system.

Data compiled in Brinster (1991) indicate that the thickness of the contact residuum within the boundary of the WIPP ranges from 7 to 16 meters (23 to 52 feet) with a seemingly anomalous thickness in borehole H-16 of 36 meters (118 feet). A substantially thicker sequence of salt had to be removed to leave these thicknesses of insoluble residue. Based on data for nine sampled intervals of salt from borehole ERDA-9 (Powers et al., 1978b), the weighted average of the percent insoluble residue in salt is 4 percent at this location. This value was assumed to be representative of the amount of insoluble residue in salt for the Salado Formation within the boundaries of the WIPP. If a 7-meter (23-foot) thickness of insoluble residue represents 4 percent of the predissolution thickness of salt, the salt would have been 175 meters (574 feet) thick prior to dissolution. A 16-meter (52-foot) thickness of residue corresponds to 400 meters (1312 feet) of salt prior to dissolution.

The presence of the Rustler-Salado contact residuum suggests that a substantial thickness of salt has been dissolved in order to leave the thicknesses of insoluble residue that have been recorded in boreholes at the WIPP. Both the Culebra and Magenta Dolomite Members of the Rustler Formation continue to be confined water-producing units. If the units overlying the contact residuum have been lowered hundreds of meters without disrupting confined hydrologic units in the Rustler Formation, the fraction of a meter of additional lowering of units overlying the waste panels should not be expected to disrupt the confinement of the water-producing units between the waste panels and the surface.

Caving and subsidence associated with the presence of the waste panels will not be included in performance assessments of the WIPP because of the lack of consequences of these phenomena.

Shaft and Borehole Seal Degradation

The engineered facility for the WIPP includes four shafts from the surface to the level of the waste panels. At decommissioning of the facility, these shafts will be sealed in order to prevent water above the Salado Formation from reaching the waste, and to prevent water that may accumulate in the rooms and drifts from having a pathway to overlying units or to the surface. Two types of seals are planned for the shafts. One type is designed to be temporary, consisting of concrete and bentonite-based materials to prevent the downward flow of water long enough for the second type of seal to consolidate. The other type is long term and will consist of crushed salt possibly with a component of swelling clay (Nowak et al., 1990). Closure of the shafts by salt creep is expected to consolidate the seal material to a point where the hydrologic properties of the seals are approximately the same as intact salt.

Degradation of the shaft seals is of concern to performance assessments because of the possibility that the shafts could provide a pathway for groundwater flow to or from the waste-filled rooms and drifts. Because the concrete seals are designed to be temporary, their degradation is not relevant to the long-term performance of the disposal system. The lower seals are not expected to degrade, although the final properties of the seal material are not known. A degraded seal or a seal that has not fully consolidated is likely to have similar properties that can be incorporated into modeling as parameter variability. The condition of the shaft seal must be considered in every scenario analyzed in a performance assessment. For this reason, possible degradation of shaft seals is part of the base-case scenario. No mechanism for the WIPP setting has been recognized as a possible cause of massive, instantaneous failure of shaft seals.

If boreholes for resource exploration are drilled into the waste panels, these boreholes have the potential of providing pathways for groundwater flow. Whereas considerable care will be used for the proper emplacement of shaft seals at decommissioning, neither composition nor care of emplacement can be assured for borehole seals. As with shaft seals, the hydrologic properties of a degraded seal are likely to be similar to the properties of an improperly emplaced seal. The condition of the borehole seals must be considered in each scenario that contains an exploratory-drilling event. Because the properties of the seals can range from intact to totally degraded, these properties can be incorporated into the modeling of system performance as uncertainty in input variables. No mechanism for the WIPP

setting has been recognized as a possible cause of massive, instantaneous failure of borehole seals. Appendix B of the Standard provides guidance as to the "worst-case" properties of borehole seals that need to be considered in performance assessments, although alternate properties can be used.

Thermally Induced Stress Fracturing in Host Rock

If the thermal load of the radioactive waste placed in a disposal facility is sufficiently high, the potential exists for fractures to form in the host rock in response to expansion and contraction of the rock, thermal contrasts in the rock, or a large amount of thermal expansion of confined rock. These fractures could provide pathways for groundwater flow with much higher permeabilities than the intact host rock.

Because the waste destined for the WIPP will be low level, no thermal effects within the waste or on the surrounding rock are expected. Preliminary analysis (Thorne and Rudeen, 1979) assumed that drums and boxes loaded in the WIPP contain the maximum permissible plutonium content, which would result in a thermal load 25 times higher than expected for contact-handled waste (U.S. DOE, 1980a). The maximum rise in temperature at the center of the repository was calculated to be less than 2°C at 80 years after waste emplacement with the temperature quickly dropping to less than 1°C above ambient for the remainder of the analysis. Temperature increases of the magnitude determined in the analysis by Thorne and Rudeen (1979) will not result in the fracturing of the salt host rock for the WIPP.

Thermally induced fracturing of the Salado Formation can be eliminated from consideration in the WIPP performance assessments based on the physical unreasonableness of fracturing of this origin.

Excavation-Induced Stress Fracturing in Host Rock

Excavations alter the stress field in the rock surrounding the opening and provide an area into which rocks that had been under compression can expand. This expansion of the rock creates a disturbed zone of both microfractures and macrofractures within the rock that alters the mechanical and hydrologic properties around the opening. As with thermally induced fractures, excavation-induced fractures could provide pathways for groundwater flow around engineered barriers or act as sinks for the accumulation of fluids.

At the excavations for the WIPP, boreholes drilled for stratigraphic studies, experiments, and construction have encountered a zone of fractures surrounding the rooms and drifts, and the altered properties of the rock have been confirmed by geophysical surveys and gas-flow tests (Lappin et al., 1989). This zone is referred to as the disturbed-rock zone (DRZ). The DRZ

ranges from 1 to 5 feet (0.3 to 1.5 meters) in width depending on the size and age of a particular opening (Lappin et al., 1989). Drifts with relatively narrow widths do not have associated DRZs at present (U.S. DOE, 1988), although with sufficient time, a DRZ is likely to form around all of the rooms and drifts. After closure of the facility, salt creep will tend to close the DRZ once sufficient backpressure is exerted by the waste and backfill against the salt. Whether the properties of the DRZ will return to those of intact salt has not been determined.

The presence or absence of a DRZ around the waste-disposal rooms and drifts must be included in all scenarios analyzed for performance assessment. Because the DRZ is part of each scenario, this feature is part of the conceptual model for the base-case scenario.

Gas Generation

After the rooms and drifts at the WIPP are filled and sealed, various gases may be formed by the corrosion of metals in the waste and containers, microbial decomposition of organic material in the waste, reactions between the corrosion products of the metals and the microbially generated gases, and reactions between backfill constituents and gases and water (Brush and Anderson, 1988a). An additional gas-generating process is radiolysis. The generation of gas is of interest to performance assessment because sufficiently high gas pressures have the potential of re-expanding the waste-filled rooms and drifts, developing a new or maintaining an existing DRZ, and creating fractures in Marker Bed 139 and/or other marker beds along which waste could migrate (Lappin et al., 1989). Other possible effects include the limitation on the amount of brine that flows into the rooms and drifts, and the possible expulsion of degraded waste into a borehole during human intrusion.

WIPP waste is certain to contain some water as free liquid and moisture absorbed in the waste. Additional liquid water and vapor are likely to be introduced by the influx of brine from the Salado Formation. Anoxic corrosion of the waste drums and metallic waste is expected to be the dominant producer of gas, although microbial breakdown of cellulosic material and possibly plastics and other synthetic materials also is likely to occur (Lappin et al., 1989). For waste representative of the expected CH-TRU waste in rooms and drifts, radiolysis is not expected to contribute significant amounts of gas to the total amount produced (Slezak and Lappin, 1990). The amount of water available for reactions and microbial activity will have a major impact on the amounts and types of gases produced.

The generation of gases within the rooms and drifts is certain to occur. For this reason, any effects of gas generation on the disposal system must be

included in each of the scenarios analyzed in performance assessment. Because gas generation is part of each scenario, this process is an integral part of the conceptual model for the base-case scenario.

Explosions

Corrosion of metals in the waste and waste containers along with microbial breakdown of various waste constituents will produce gases that have the potential to be flammable or explosive. Explosions in the waste-filled rooms and drifts after decommissioning are of concern to performance assessments because of possible damage to engineered barriers that could generate pathways for groundwater flow.

Gases generated by corrosion and microbial activity would tend to collect in the upper portions of the rooms and drifts. To address the question of possible damage to panel seals, Slezak and Lappin (1990) assumed the "worst-case" (most potentially detonable) mixture of methane, hydrogen, and oxygen in the 1.5-foot (0.5-meter) head space of the rooms and drifts approximately five years after panel-seal emplacement. Based on several assumptions to optimize the effects of an explosion, the peak pressure pulse reaching the panel seal was calculated to be 800 psi, which would have no consequences on the performance of the panel seal. The pressure would decay to 120 psi at 0.35 seconds after impact.

Waste-induced explosions can be eliminated from consideration in the WIPP performance assessments based on the lack of consequences of such events.

Nuclear Criticality

Nuclear criticality refers to a sufficiently high concentration of radionuclides for a sustained fission reaction to occur. This type of reaction produces heat, or under a specific set of conditions, causes an explosion. Nuclear criticality is important to performance assessment because a heat source could form thermal convection cells in the groundwater, fracture brittle rocks as a result of differential thermal expansion, or possibly cause a steam explosion. A nuclear explosion would be important because such an event could result in total failure of the disposal system and directly release radionuclides to the accessible environment.

In the nuclear-waste disposal environment, the radionuclides that could result in nuclear criticality are present, although a concentration process is required to create a critical mass. The waste acceptance criteria (draft of WIPP-DOE-069-Rev. 4, as explained in Chapter 1 of this volume) for nuclear waste destined for the WIPP sets limits on the amount of fissile radionuclide content of CH- and RH-waste containers. Operations and safety criteria limit

the Pu-239 fissile gram equivalents (FGE) to less than 200 grams (0.4 pounds) in 55-gallon (0.21 m^3) drums, 100 grams (0.2 pounds) in 100-gallon (0.38 m^3) drums, 500 grams (1.1 pounds) in DOT M6 containers, and 5 grams (0.01 pounds) per ft^3 (0.028 m^3) in other waste boxes (up to a 350 gram (0.77 pounds) maximum) for CH waste. RH-waste containers are limited to no more than 600 grams (1.3 pounds) in Pu-239 FGE. Transportation standards for the waste generally are more strict in the FGE content of containers than the operations and safety criteria. The Pu-239 FGE must be less than 200 grams (0.4 pounds) for CH drums, 325 grams (0.7 pounds) for standard waste boxes, and 325 grams (0.7 pounds) for a TRUPACT-II container. RH-waste containers may be limited to less than 325 grams (0.7 pounds) per cask.

Calculations performed to support the WIPP *Final Environmental Impact Statement* (U.S. DOE, 1980a) indicated that a CH-waste drum holding 140 kilograms (308 pounds) of waste would have to contain more than 5 kilograms (11 pounds) of plutonium to potentially form a critical mass. As stated in the report, most drums will contain less than 0.01 kilograms (0.02 pounds) of plutonium, with the maximum allowed plutonium content of 0.2 kilograms (0.4 pounds) per drum. Although RH waste was not included in the calculations, the maximum allowable FGE content of RH waste per container allowed by the operations and safety criteria is far below the minimum calculated amount of plutonium required to form a critical mass under optimum dry conditions.

Because of the relatively low plutonium content of the waste containers, nuclear criticality within dry CH- and RH-waste containers has a probability of occurrence of 0. Water within the containers introduces an altered set of conditions whose effects on criticality have not been evaluated at this time. The possibility also exists that some of the plutonium will be dissolved by groundwater and transported along any of various pathways through all or part of the disposal system. Depending on the geochemical environment along any particular transport path, the plutonium could precipitate or sorb in the backfill, at certain components of the seal system, or within the Culebra Dolomite Member or other hydrologic units. The WIPP performance-assessment team has not determined at this time whether concentration of plutonium can reach critical mass at any of these locations.

For a high-yield nuclear explosion to occur within the waste containers, a critical mass of plutonium would have to undergo rapid compression to a high density (U.S. DOE, 1980a). The lack of a critical mass within the waste containers requires that the probability of a nuclear explosion occurring within the waste be assigned a value of 0, even without considering the improbability of the other required conditions. In soils, Stratton (1983) concluded that for a critical mass of plutonium to result in a high-yield explosion would require either a large amount of plutonium to be concentrated in an appropriate geometry or an unrealistically large amount of water to be

present to act as a reflectant. While not considering the WIPP disposal system directly, Stratton's analysis of the conditions required in soils for a nuclear explosion to occur indicate that explosions of this origin can be eliminated from the WIPP performance assessment on the basis of low probability.

Nuclear criticality as a possible source of heat within the disposal system is retained for additional evaluation before a screening decision is made.

4.1.6 SUMMARY OF SCREENED EVENTS AND PROCESSES

None of the natural events and processes listed in Table 4-1 is retained for scenario development (Table 4-2). Phenomena such as erosion, sedimentation, and climatic change (pluvial periods) are certain to occur during the next 10,000 years, which indicates that these phenomena are part of the conceptual model for the base-case scenario. The effects of other events (i.e., sea-level variations, hurricanes, seiches, and tsunamis) are restricted to coastal areas. Because of the geologic stability of the WIPP region, changes in the tectonic setting that would result in the occurrence or recurrence of the subsurface events and processes (except for seismic activity) are not physically reasonable in the time frame of regulatory concern. Seismic activity has the potential of affecting the source term, and these effects can be addressed in the source-term uncertainty during modeling. Regional subsidence or uplift, mass wasting, and flooding are not likely to occur to an extent that would affect the performance of the disposal system.

Of the human-induced events and processes, explosions can be eliminated from consideration because of low probability and low consequence for inadvertent explosions during warfare and nuclear testing, respectively. Irrigation and damming of valleys are not physically reasonable without major technological innovations in response to poor water quality and limited water supplies. Exploratory drilling for resources and drilling injection wells are both realistic events for the WIPP, although injection wells are expected to be of no consequence to the performance of the disposal system. Based on the geologic setting and previous resource evaluations, exploratory drilling for resources is retained for scenario development, while injection wells are excluded based on regulatory guidance and low consequence. Exploratory drilling is subdivided into two possibilities: drilling into a waste-filled room or drift and a brine reservoir in the underlying Castile Formation (Event E1), and drilling into a waste-filled room or drift but no brine reservoir (Event E2). Mining (Event TS) is limited to potash extraction by either conventional or solution methods in areas beyond the boundaries of the waste panels, and drilling of withdrawal wells (Event E3) is limited to water wells in areas where water quantity and quality will permit water use. Both

TABLE 4-2. SUMMARY OF SCREENED EVENTS AND PROCESSES

Events and Processes	RETAINED		SCREENED OUT			
	Undisturbed Conditions	For Scenario Development	Low Probability	Physically Unreasonable	Low Consequence	Regulator Requirements
Natural						
Meteorite Impact			X			
Erosion/Sedimentation	X					
Glaciation				X		
Pluvial Periods (Climate Change)	X					
Sea-Level Variations				X		
Hurricanes				X		
Seiches				X		
Tsunamis						
"Conventional"				X		
Metorite Impact			X			
Regional Subsidence or Uplift				X		
Mass Wasting				X		
Flooding				X		
Diapirism				X		
Seismic Activity	X					
Volcanic Activity				X		
Magmatic Activity				X		
Formation of Dissolution Cavities						
Deep Dissolution				X		
Shallow Dissolution						
Rustler-Salado Contact	X					
Nash Draw*			X	X		
Formation of Interconnected						
Fracture Systems				X		
Faulting				X		

*Screening criterion depends on which possible mechanisms considered for origin of Nash Draw.

TABLE 4-2. SUMMARY OF SCREENED EVENTS AND PROCESSES (continued)

Events and Processes	RETAINED		SCREENED OUT			
	Undisturbed Conditions	For Scenario Development	Low Probability	Physically Unreasonable	Low Consequence	Regulator Requirements
Human-Induced Explosions						
At Waste-Panels Location						X
Near Waste-Panels Location						
At Surface/Warfare			X			
Deep Testing			X			
Drilling (Exploratory)		X				
Mining						
At Waste-Panels Location						X
Near Waste-Panels Location		X				
Injection Wells					X	
Withdrawal Wells						
Water Wells		X				
Oil and Gas Wells						
At Waste-Panels Location						X
Near Waste-Panels Location					X	
Irrigation			X			
Damming of Streams and Rivers						
At Pecos River					X	
Near Nash Draw			X			
Repository- and Waste-Induced						
Subsidence and Caving					X	
Shaft & Borehole Seal		X				
Degradation	X					
Thermally Induced Fractures				X		

TABLE 4-2. SUMMARY OF SCREENED EVENTS AND PROCESSES (concluded)

Events and Processes	RETAINED		SCREENED OUT			
	Undisturbed Conditions	For Scenario Development	Low Probability	Physically Unreasonable	Low Consequence	Regulator Requirements
Excavation-Induced Fractures	X					
Gas Generation	X					
Explosions (Gas Ignition)					X	
Nuclear Criticality						
Critical Mass (Explosion)			X			
Sustained Reaction**						

**Retained for additional evaluation.

the mining and water wells are being evaluated for their effects on groundwater flow in the WIPP area.

In the category of waste- and repository-induced events and processes, gas generation and shaft-seal degradation are part of the conceptual model of the base-case scenario. Borehole seal degradation can be addressed through parameter uncertainty during modeling. Excavation-induced fracturing in the host rock can be handled by including the disturbed zone surrounding mined openings in the conceptual model of the base-case scenario. Caving into the rooms or drifts may occur in the short term after closure, but this process has no long-term consequences on performance because of the mechanical behavior of salt. Thermally induced fracturing of the host rock is not a physically reasonable phenomenon because of the low thermal output of WIPP waste. Subsidence caused by the mined openings and explosions caused by the ignition of gases created by waste degradation have no effect on the performance of the disposal system and can be eliminated from scenario development. Nuclear criticality requires additional evaluation before a screening decision is made.

4.1.7 DEVELOPING SUMMARY SCENARIOS

To construct a CCDF, the summary scenarios used in the performance assessment should be comprehensive and mutually exclusive subsets of the sample space S. An earlier approach to scenario development combined events and processes through the use of event trees (Bingham and Barr, 1979; Hunter, 1983; Hunter et al., 1982; Hunter et al., 1983). According to McCormick (1981), an event tree is an inductive logic method for identifying possible outcomes of a given initiating event. Once the systems that can be utilized after a failure are identified and enumerated, the failure and success states are identified through bifurcations within the tree. If partial failures are considered, a greater number of branches is needed. The result is an event tree that provides accident sequences associated with an initiating event. Analyses of this type commonly are used to assess potential accidents at nuclear power plants (e.g., U.S. NRC, 1975).

Event trees were found not to be suitable for natural systems (Burkholder, 1980). The disadvantages of using event trees to develop scenarios for natural systems are (1) the imposed temporal relationship of events and processes to one another, (2) the apparent arbitrariness of branching within the tree, (3) the inability to assure completeness of the final scenario set, and (4) the inability of the tree to handle feedback loops, whereby development along one branch may change the system to the point where the branching that resulted in that scenario will be reversed (Guzowski, 1990).

Event trees for scenario development have not been able to produce reasonable numbers of well-defined and mutually exclusive scenarios that can be analyzed probabilistically to address the current formulation of the Standard (Guzowski, 1990). An alternative approach addresses these problems through logic diagrams (Figure 4-4) (Cranwell et al., 1990). In the logic diagram, no temporal relationship between events and processes is implied by their sequence across the top of the diagram. At each junction within the diagram a yes/no decision is made as to whether the next event or process is added to the scenario. As a result, each scenario consists of a combination of occurrence and nonoccurrence of all events and processes that survive screening (Cranwell et al., 1990). To simplify scenario notation, only the events and processes that occur are used to identify the scenario. Based on the assumption that the events and processes remaining after screening define all possible futures of the disposal system that are important for a probabilistic assessment (i.e., define the sample space S), the logic diagram produces scenarios that are comprehensive, because all possible combinations of events and processes are developed; the scenarios are mutually exclusive, because each scenario is a unique set of events and processes; and feedback loops may be incorporated in models of the combinations of events and processes.

Figure 4-5 is the logic diagram for constructing all of the possible combinations of the three events (*E1*, *E2*, and *TS*) that survived the screening process for the WIPP. The base case represents the undisturbed condition, which is the expected behavior of the disposal system without disruption by human intrusion.

Screening Scenarios

The purpose of scenario screening is to identify those scenarios that will have no or a minimal impact on the shape and/or location of the mean CCDF. By inference, the criteria used to screen combinations of events and processes (scenarios) are similar to those criteria used to screen individual events and processes. These criteria are physical reasonableness of the combinations of events and processes, probability of occurrence of the scenario, and consequence.

The probability of occurrence for a scenario is determined by combining the probabilities of occurrence and nonoccurrence from the events and processes that make up the scenario. A mechanical approach to determining scenario probabilities can be implemented by assigning the probability of occurrence and nonoccurrence for each event and process to the appropriate "yes" and "no" legs at each bifurcation in the logic diagram (Figure 4-4). The probability of a scenario is the product of the probabilities along the pathway through the logic diagram that defines that scenario (see Figure 4-4

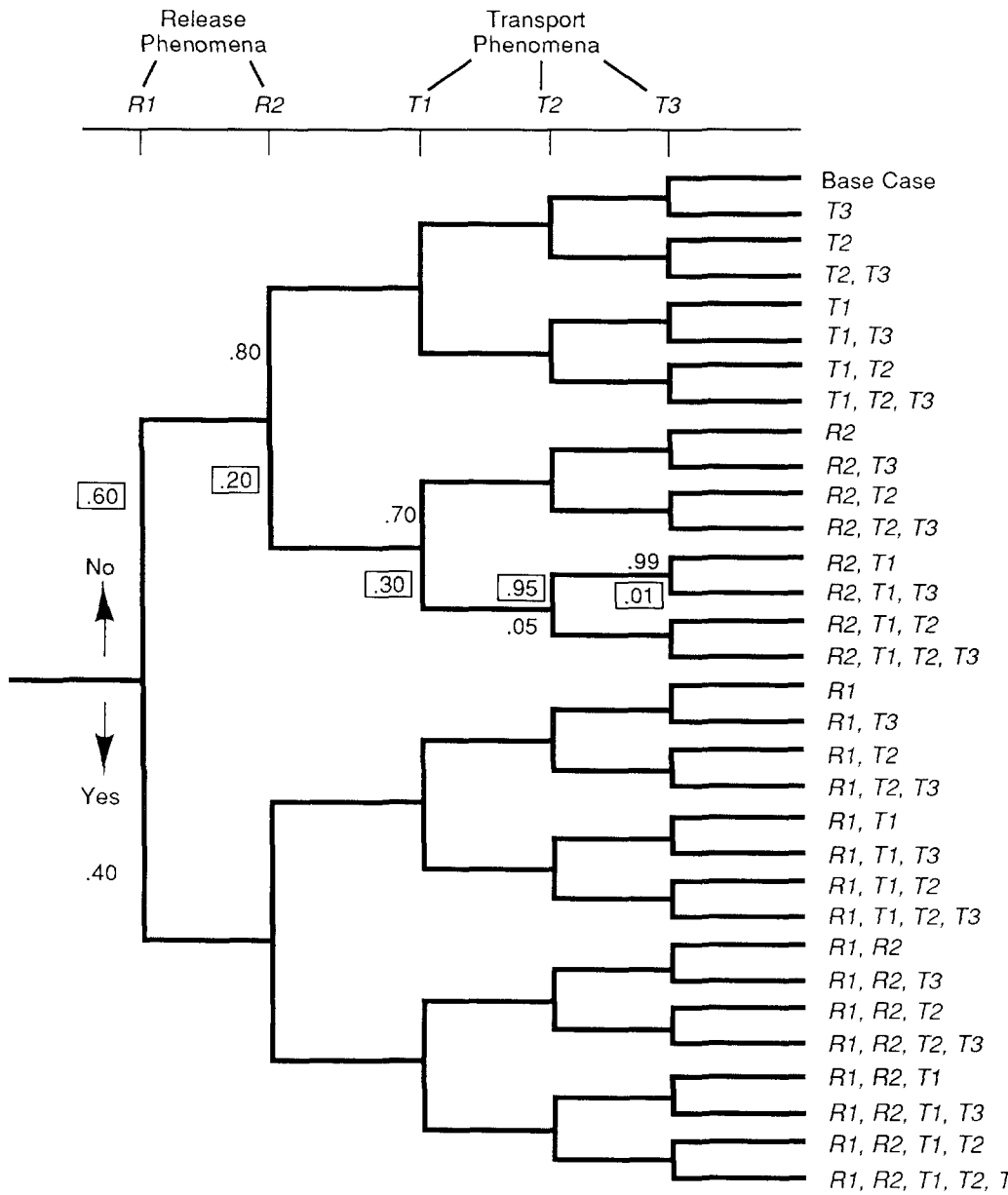

☐ Indicates Examples of Probability Values Needed to Determine Probability of Scenario *R2T1T3*
Probability of *R2T1T3* = (.60)(.20)(.30)(.95)(.01) = 3.4×10^{-4}

Notes: (1) Expressions of the form *R2, T1, T3* are an abbreviation for $R1^{c} \cap R2 \cap T1 \cap T2^{c} \cap T3$ (i.e., intersections and complements are omitted from the notation).

(2) Indicated probability calculation assumes that *R1, R2, T1, T2, T3* are independent events. That is, $p(R1 \cap R2 \cap T1 \cap T2 \cap T3) = p(R1)\,p(R2)\,p(T1)\,p(T2)\,p(T3)$.

(3) If the events *R1, R2, T1, T2, T3* are not independent, then the ordering in the tree is important because conditional probabilities must be used.

TRI-6342-222-6

Figure 4-4. **Example of a Logic Diagram with Two Events Affecting Release (R) from a Repository and Three Events Affecting Transport (T) to the Accessible Environment for the Construction of Scenarios (after Cranwell et al., 1990), Illustrating Scenario Probability Assignment.**

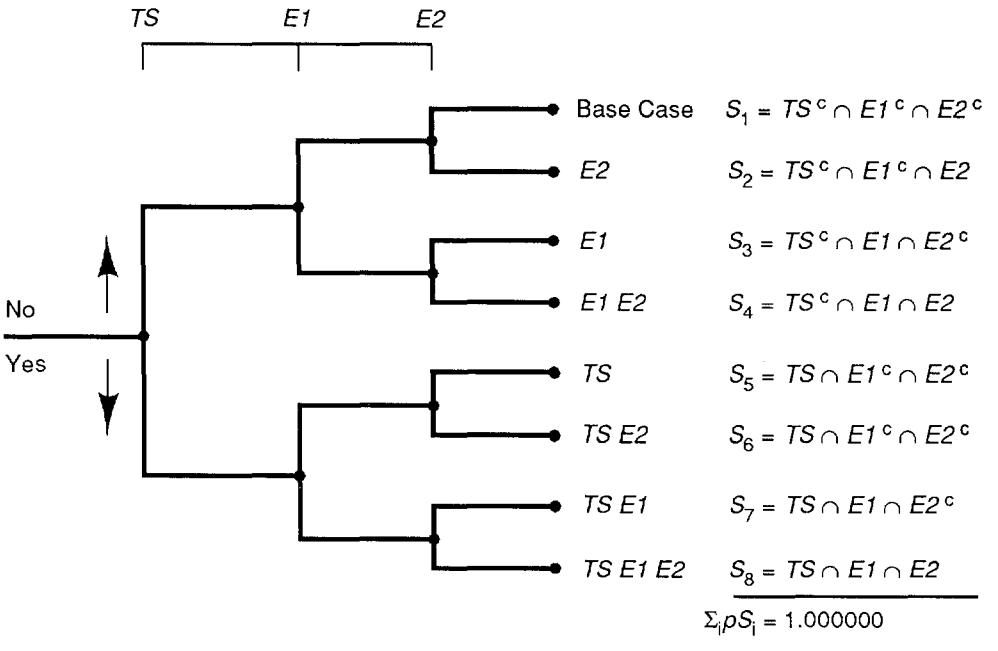

x = 10,000 yr Time History

TS = {x: Subsidence Resulting From Solution Mining of Potash}

E1 = {x: One or More Boreholes Pass Through a Waste Panel and into a Brine Pocket}

E2 = {x: One or More Boreholes Pass Through a Waste Panel Without Penetration of Brine Pocket}

Superscript c (e.g., TS^c) Denotes Set Complement

TRI-6342-578-3

Figure 4-5. Potential Scenarios for the WIPP Disposal System.

for an example). Based on the probability criterion in Appendix B of the Standard for screening out individual events and processes, scenarios with probabilities of occurrence of less than 1 chance in 10,000 in 10,000 years need not be considered in determining compliance with the Standard, and therefore, consequence calculations are not necessary.

A final screening criterion is consequence, which in this step of the procedure means integrated discharge to the accessible environment for 10,000 years. By inferring that the guidance in Appendix B of the Standard for individual events and processes also applies to scenarios, scenarios whose probability of occurrence is less than the cutoff in Appendix B can be eliminated from further consideration if their omission would not significantly change the remaining probability distribution of cumulative releases. Because the degree to which the mean CCDF will be affected by omitting such scenarios is difficult to estimate prior to constructing CCDFs, only those scenarios that have no releases should be screened out from additional consequence calculations. If significant changes are made to the data base, the conceptual models, or mathematical models of the disposal system, the latter scenarios should be rescreened.

In implementing this step of the procedure for this preliminary WIPP performance assessment, no scenarios were screened out. Because parameter values did not define the events, all combinations of events in the scenarios are physically reasonable. Because final scenario probabilities have not been estimated, no scenarios were screened out on the basis of low probability of occurrence. Final calculations of consequences have not been completed, so no scenarios were screened out on the basis of this criterion.

Descriptions of Retained Scenarios

This section describes the scenarios retained for consequence analysis.

Undisturbed Performance Summary Scenario (Base Case, S_B)

The Individual Protection Requirements of the Standard (§ 191.15) call for a reasonable expectation that the disposal system will limit annual doses to individuals for 1,000 years after disposal, assuming undisturbed performance of the disposal system. Undisturbed performance is also the base case of the scenario-development methodology (Cranwell et al., 1990; Guzowski, 1990). Although undisturbed performance is not mentioned in the Containment Requirements (§ 191.13), undisturbed performance is not precluded from the containment calculations.

As defined in the Standard (§ 191.12(p)), "'[u]ndisturbed performance' means the predicted behavior of a disposal system, including consideration of the

uncertainties in predicted behavior, if the disposal system is not disrupted by human intrusion or the occurrence of unlikely natural events." Duration of this performance is not limited by the definition. The base-case scenario describes the disposal system from the time of decommissioning and incorporates all expected changes in the system and associated uncertainties for the 10,000 years of concern for § 191.13. Expected changes are assumed to result from events and processes that are certain to occur without disrupting the disposal system. The Standard does not provide a definition of unlikely natural events to be excluded from undisturbed performance nor, by implication, likely natural events to be included. Because of the relative stability of the natural systems within the region of the WIPP disposal system, all naturally occurring events and processes that will occur are part of the base-case scenario and are nondisruptive. These conditions represent undisturbed performance (Marietta et al., 1989; Bertram-Howery et al., 1990).

Base-Case Summary Scenario

After the repository is filled with waste, the disposal rooms and drifts in the panels are backfilled and seals are emplaced in the access drifts to the panels (Figure 4-4). While excavations are open, the salt creeps inward because of the decrease in confining pressure on the salt around the rooms. The movement of floors upward and ceilings downward into rooms and drifts fractures the more brittle underlying anhydrite in MB139 and overlying anhydrite layers A and B. The anhydrite is expected to fracture directly beneath and above excavated rooms and drifts but not beneath or above the pillars because of the overburden pressure on the pillars. To control potential migration of hazardous (RCRA) wastes through MB139, seals are emplaced in MB139 directly beneath the panel seals (Stormont et al., 1987; Borns and Stormont, 1988; Nowak et al., 1990). Access drifts and the lower parts of shafts are backfilled with salt. Because of the high lithostatic pressures at the repository depth, salt creep is expected to exert sufficient pressure on the backfill to consolidate the material into low-conductivity seals with properties similar to those of the host rock. The upper parts of the shafts are also backfilled with salt, but pressure exerted by salt creep on backfill is not expected to be sufficient to cause the same degree of consolidation as is expected in lower portions of the shafts (Nowak et al., 1990).

Before the amount and direction of groundwater flow and radionuclide release from the repository can be determined, gas generation must be considered. Some waste and some waste containers will be composed of organic material. Because microbes transported into the repository with the waste are expected to be viable under sealed-repository conditions (Brush and Anderson, 1988a), organic material in the repository will biodegrade with concomitant

generation of gases. In addition, moisture in the repository, either brought in with waste or seeping in from the Salado Formation, can corrode metals in the waste and metallic waste containers themselves, with gas generated as a by-product. Radiolysis also will generate gases. The time period over which gases will be generated is uncertain. Each of these processes is dependent on the availability of water. The humidity required for microbiological activity and whether or not saturated conditions are required for corrosion and radiolysis have not been established. Moisture and microbes in waste will generate some gas prior to waste emplacement in the repository. After emplacement, the amount and rate of gas generation will depend on such factors as microbe metabolisms; relationships between gas pressure, brine inflow, room closure, and backfill and waste consolidation; and the degree to which reactions attain completion (Bertram-Howery et al., 1990).

Radionuclide migration depends on the degree of saturation within the repository. Gas pressure resulting from microbial activity and corrosion may prevent brine inflow and desaturate the nearby Salado Formation, MB139, and anhydrite layers A and B. These conditions, in addition to the consumption of water by anoxic corrosion and possibly microbial activity, also would result in a decrease in the amount of water in the waste and backfill and a lower potential for radionuclide transport.

Two pathways for groundwater flow and radionuclide transport dominate the disposal system (Figure 4-6). In the first path, brine and radionuclides enter MB139, either through fractures in salt or directly as a result of rooms and drifts intersecting the marker bed during construction or room closure. Following repository decommissioning, waste-generated gas will begin to pressurize the waste panels (Weatherby et al., 1989). Brine will drain by gravity to the lower half of the panels. Gas will saturate the DRZ above the panel and open flow paths to anhydrite layers A and B above the panel. MB139 beneath the panel will remain brine saturated, but gas will open flow paths into the MB139 beyond the panels. The more-mobile gas phase will flow outward over the less-mobile brine phase. After gas generation ceases, pressure and phase distribution will gradually equilibrate throughout the entire region. Gas will continue to expand outward, but brine flow reverses, flowing inward primarily along the lower portions of anhydrite layers A and B and MB139. Gas saturation near the waste panels will diminish. The anhydrite layers above the waste panels will be a major flow path for gas. In contrast, brine will inhibit gas inflow in the MB139 beneath the waste panels.

Because material in the upper shaft is expected to be poorly consolidated, the hydraulic pressure at the junction of the upper and lower parts of the shaft seals is assumed to approximate the pressure head of the Culebra Dolomite Member. As a result, the pressure gradient resulting from waste-

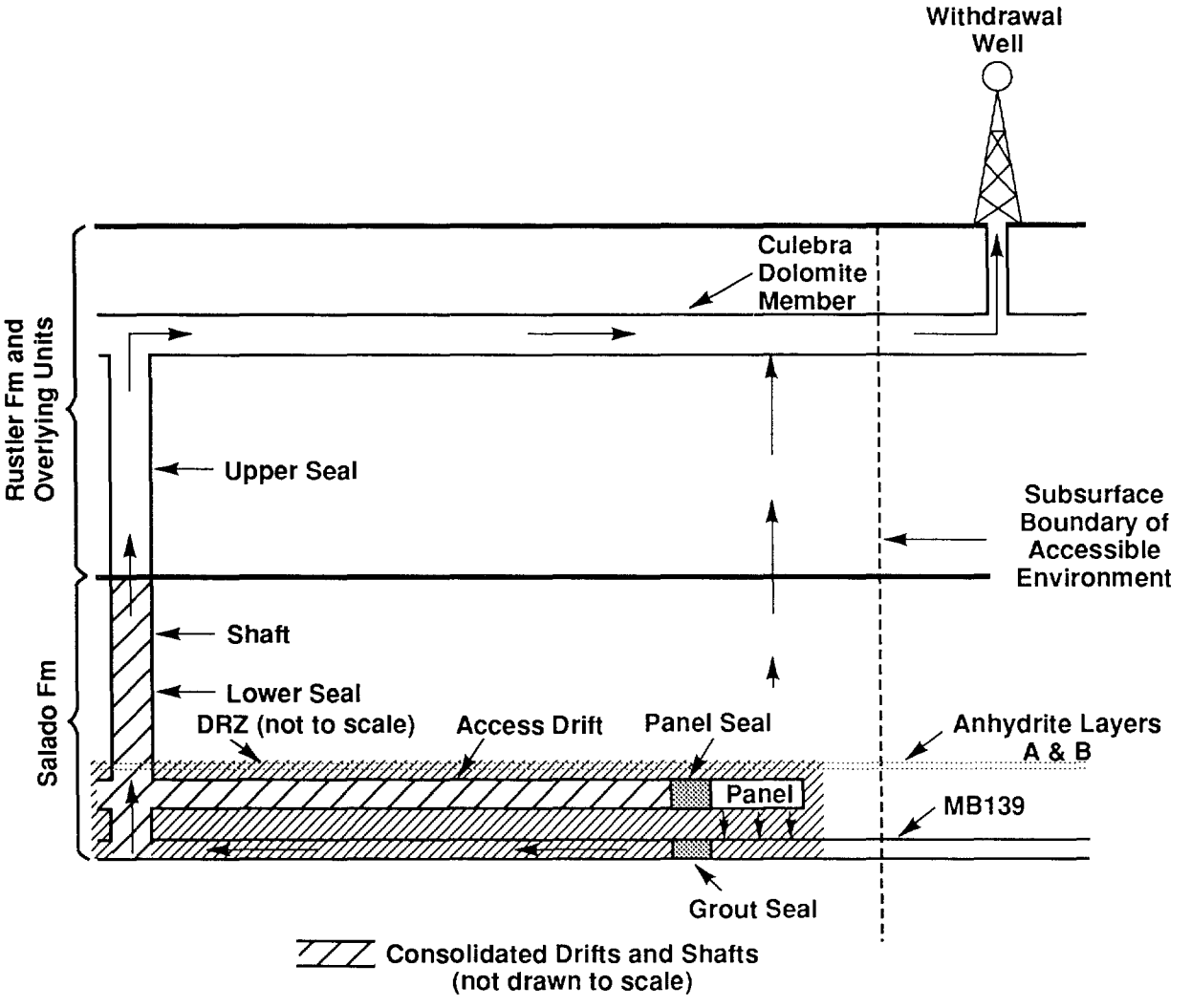

Figure 4-6. Conceptual Model Used in Simulating Undisturbed Performance.

generated gas (approximately 15 MPa+) and hydrostatic pressure at the Culebra (1 MPa) tends to force radionuclide-bearing brine from MB139 beneath the panel through the seal in the marker bed, along the fractures in MB139 to the base of the shaft. Concurrently, gas flows through the upper portion of the drifts and the anhydrite layers A and B to the shaft. Gas saturation in the shaft seals will inhibit brine migration up the shaft to the Culebra Dolomite Member. Brine and radionuclides will eventually reach the Culebra and migrate downgradient to the accessible environment.

Relative motion during salt creep and gas generation prevents MB139 from returning to its original position, and the salt-creep-induced fractures do not completely close. Flow is through MB139 instead of through the overlying access drift because of the substantially higher hydraulic conductivity in MB139. Flow in MB139 is to the north through the seal rather than to the south down the pre-excavation hydraulic gradient within MB139, because the pressure drop to the north is greater after excavation, and the flow to the south would be impeded by extremely low permeability of the intact marker bed. Therefore, the horizontal path directly through MB139 to the accessible environment is not included for this assessment, but this path is considered for other analyses (see Volume 2 of this report).

The other dominant path is assumed to be from the repository vertically through the intact Salado Formation toward the Culebra Dolomite Member (Figure 4-6) (Lappin et al., 1989). This path has the largest pressure decline over the shortest distance of any path. In addition, large potential exists for radionuclides to leave the repository along this path because of the large horizontal cross-sectional area of the waste-bearing rooms and drifts in the repository.

The methodology can determine pathways to individuals and calculate doses to humans if a release pathway is added. The pathway used in an earlier analysis (Lappin et al., 1989) is described in the next section. Because undisturbed performance releases no radionuclides in 1,000 years, these calculations are not necessary for this scenario (Marietta et al., 1989).

Release at a Livestock Pond

Livestock wells were assumed to be located downgradient from the repository for earlier analyses (Lappin et al., 1989), because these wells were believed to be the only realistic pathway for radionuclides to reach the surface under undisturbed conditions. Waste-generated gas pressurizes the waste panels, forcing radionuclide-bearing brine to seep through and around grouted seals in the marker bed and migrate through the part of MB139 that underlies drift excavations to the bottom of the sealed shafts. This material is then assumed to continue to migrate up through the lower seal system due to the

pressure gradient between the waste panels and the Culebra Dolomite Member. Material introduced into the Culebra Dolomite is entrained in the groundwater. In order to provide a route to humans, an active livestock well is assumed to penetrate the Culebra Dolomite downgradient from the sealed shafts. Radionuclides migrate through the Culebra groundwater to the livestock well where water is pumped to the surface for cattle to drink. This is the beginning of the biological pathway to humans via a beef ingestion route (Lappin et al., 1989). Other possible pathways originating from the full and later dry stock pond exist and will be considered, but for undisturbed conditions, any possibility requires a pumping well route to the surface. Because no radionuclides are released into the Culebra in 1,000 years, this route is not completed, and no need exists to consider other possible pathways for § 191.15 at this time, although this position may change when the Standard is repromulgated.

Human-Intrusion Summary Scenarios

Appendix B of the Standard (U.S. EPA, 1985) provides guidance on a number of factors concerning human intrusion. The section "Institutional Controls" in Appendix B (U.S. EPA, 1985, p. 38088) states that active controls cannot be assumed to prevent or reduce radionuclide releases for more than 100 years after disposal. Passive institutional controls can be assumed to deter systematic and persistent exploitation and to reduce the likelihood of inadvertent intrusion, but these controls cannot eliminate the chance of inadvertent intrusion. The section "Consideration of Inadvertent Human Intrusion into Geologic Repositories" in Appendix B (U.S. EPA, 1985, p. 38088) suggests that exploratory drilling for resources can be the most severe form of human intrusion considered. The section "Frequency and Severity of Inadvertent Human Intrusion into Geologic Repositories" in Appendix B (U.S. EPA, 1985, p. 38089) suggests that the likelihood and consequence of drilling should be based on site-specific factors. In keeping with the guidance, this assessment includes scenarios that contain human-intrusion events.

Intrusion Borehole into a Room or Drift (Summary Scenario *E2*)

Scenario *E2* consists of one or more boreholes that penetrate to or through a waste-filled room or drift in a panel (Figure 4-7). The borehole does not intersect pressurized brine or any other important source of water. The hole is abandoned after a plug is emplaced above the Culebra Dolomite Member. The drilling mud that remains in the borehole is assumed to degrade into sand-like material. The borehole below the plug in the Salado Formation is propped open by the sand-like material.

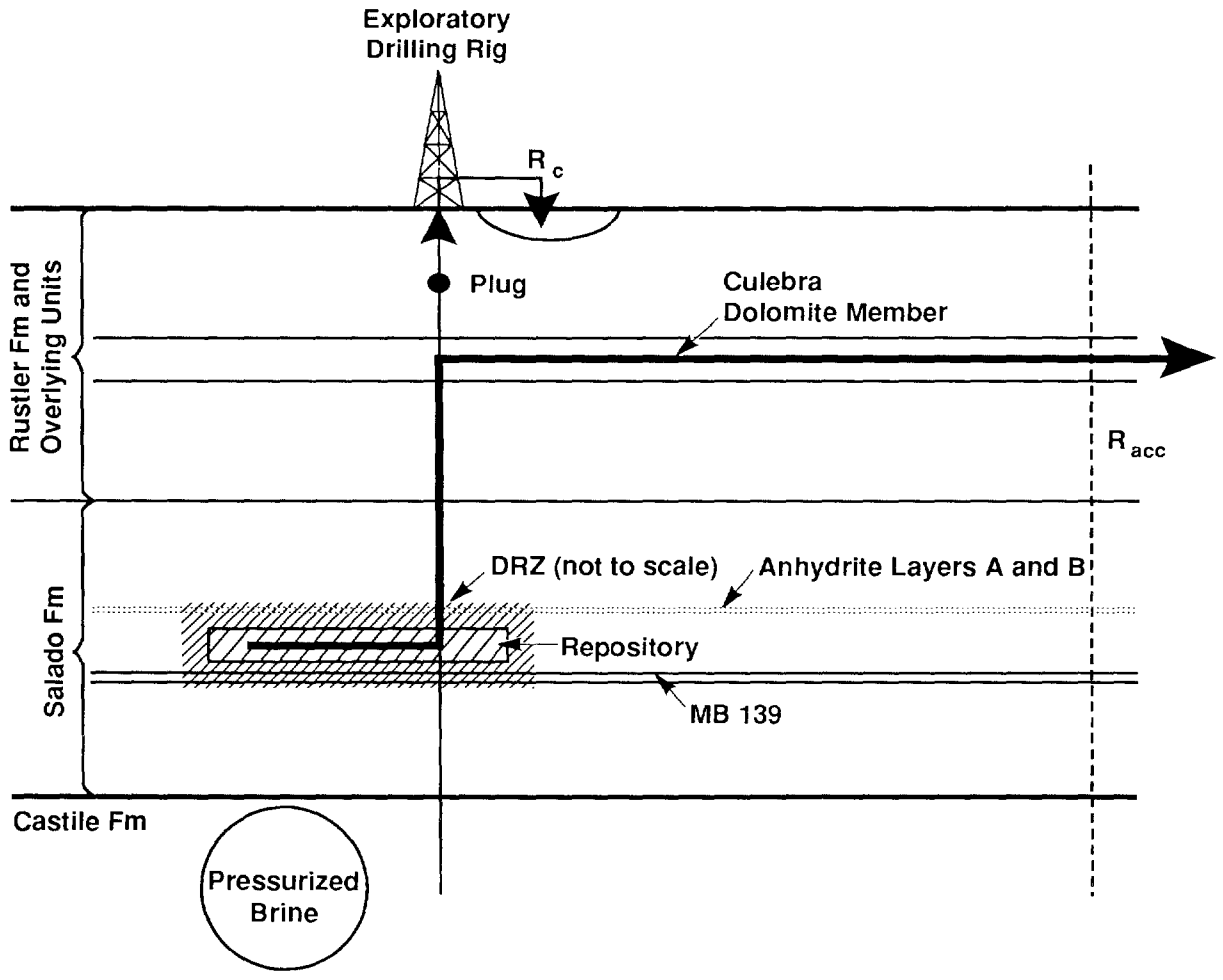

Figure 4-7. Conceptual Model for Scenario *E2*. Arrows indicate assumed direction of flow. Exploratory borehole does not penetrate pressurized brine below the repository horizon. R_C is the release of cuttings and eroded material. R_{ACC} is the release at the subsurface boundary of the accessible environment. A plug above the Culebra Dolomite Member is assumed to remain intact for 10,000 years.

After the repository is decommissioned, moisture in the waste or brine from the host rock allows microbiological activity and corrosion to occur, generating gas. Repository conditions would evolve according to the previous description of the undisturbed scenario. At the time of intrusion into a waste panel, gas could vent through the intruding borehole, thereby allowing the repository to resaturate. The rapid venting of waste-generated gas may result in spalling of waste material into the borehole and eventual removal to the surface by drilling fluid. During drilling, radionuclides are released directly to the surface as the drill penetrates a room or drift and intersects drums or boxes of waste. The waste that is ground up by the drill bit is transported to the surface by circulating drilling fluid. Additional material may be dislodged from walls of the borehole by the circulating fluid as drilling proceeds below the repository.

After drilling is completed, the hole is plugged. Because hydraulic head in the Culebra Dolomite Member is less than hydraulic head of the repository, the connection between the repository and the Culebra Dolomite provides a potential pathway for flow of water and gas from the repository to the Culebra. This process forces water and gas from the repository and nearby members (Figure 4-7) into the borehole and upward to the Culebra Dolomite Member. Brine, puddled beneath the waste in MB139, inhibits gas flow through this member towards the borehole. However, gas in the upper portion of the waste panel and overlying anhydrite layers A and B will migrate into the borehole fill, saturating the borehole. Brine flow from the lower member will be inhibited by this gas cap in the borehole. Brine flowing from the intact halite and anhydrite will eventually displace the gas. When brine saturation in the waste panel exceeds residual brine saturation (approximately 20 percent), flow through the waste will resume. When brine saturations exceed about 60 percent, significant flow into the borehole will occur. The time delay between intrusion and significant brine and radionuclide release to the Culebra Dolomite Member may be significant and will depend on a number of material property values and coupled processes discussed in Chapter 5 of this volume and Volume 2, Chapter 4 of this report. After the pressure within the repository is sufficiently reduced, brine flows in from the host rock as long as pore pressure within the host rock is greater than hydrostatic. This inflow forces brine up the borehole toward the Culebra Dolomite. The borehole plug for this scenario is located so that all flow up the borehole is diverted into the Culebra Dolomite Member. For the analysis of this scenario, it is assumed that the borehole plug does not degrade. Other analyses assumed that borehole plugs degraded in 150 years (Lappin et al., 1989; Marietta et al., 1989).

Intrusion Borehole through a Room or Drift into Pressurized Brine in the Castile Formation (Summary Scenario *E1*)

Scenario *E1* (Figure 4-8) consists of one or more boreholes that penetrate through a waste-filled room or drift and continues into or through a pressurized brine reservoir in the Castile Formation in which brine pressure is between hydrostatic and lithostatic for that depth. The borehole is plugged at a level above the Culebra Dolomite Member (Marietta et al., 1989).

A borehole that penetrates a room or a drift vents gas and intersects containers of waste as described with *E2*. This waste is incorporated into the drilling fluid and circulated directly to the mud pits at the surface. After the hole is plugged and abandoned, the brine pressure is assumed to be sufficient to drive flow up the borehole into the Culebra Dolomite Member. As in the *E2* scenario, the borehole plug is assumed to be above the Culebra Dolomite and to remain intact, diverting all flow into the Culebra. The flow rate depends on the head difference between the Culebra Dolomite and the injected brine and on the hydraulic properties of materials in the borehole. Radionuclides from the room or drift may be incorporated into the Castile brine if it circulates through the waste adjacent to the borehole. If the pressure gradient is not favorable for circulation of Castile brine through the waste, a long-term discharge of Salado brine and waste-generated gas may occur as described in *E2*. Upon reaching the Culebra Dolomite, the waste-bearing brine and gas flows down the hydraulic gradient toward the accessible environment boundary; this pressurized brine and gas injection results in temporary alterations of the flow field and chemistry in the Culebra Dolomite. Brine flow reduces the local residual pressure in the Castile Formation, thereby reducing the driving pressure of the flow. Eventually, brine stops flowing.

Intrusion Borehole through a Room or Drift into Pressurized Brine in the Castile Formation and Another Intrusion Borehole into the Same Panel (Summary Scenario *E1E2*)

Scenario *E1E2* consists of exactly two boreholes that penetrate waste-filled rooms or drifts in the same panel (Figure 4-9). One borehole also penetrates pressurized brine in the Castile Formation, whereas the other borehole does not. The borehole that penetrates the pressurized brine is plugged between the room or drift and the Culebra Dolomite Member. This plug is assumed not to degrade, forcing into the room all the brine flowing up the borehole. The other borehole is plugged above the Culebra Dolomite Member. This plug is also assumed not to degrade, forcing into the Culebra Dolomite all the brine and gas flowing up this borehole. The Castile brine is assumed to be under a greater pressure than gas or brine in rooms and drifts of the repository (Marietta et al., 1989).

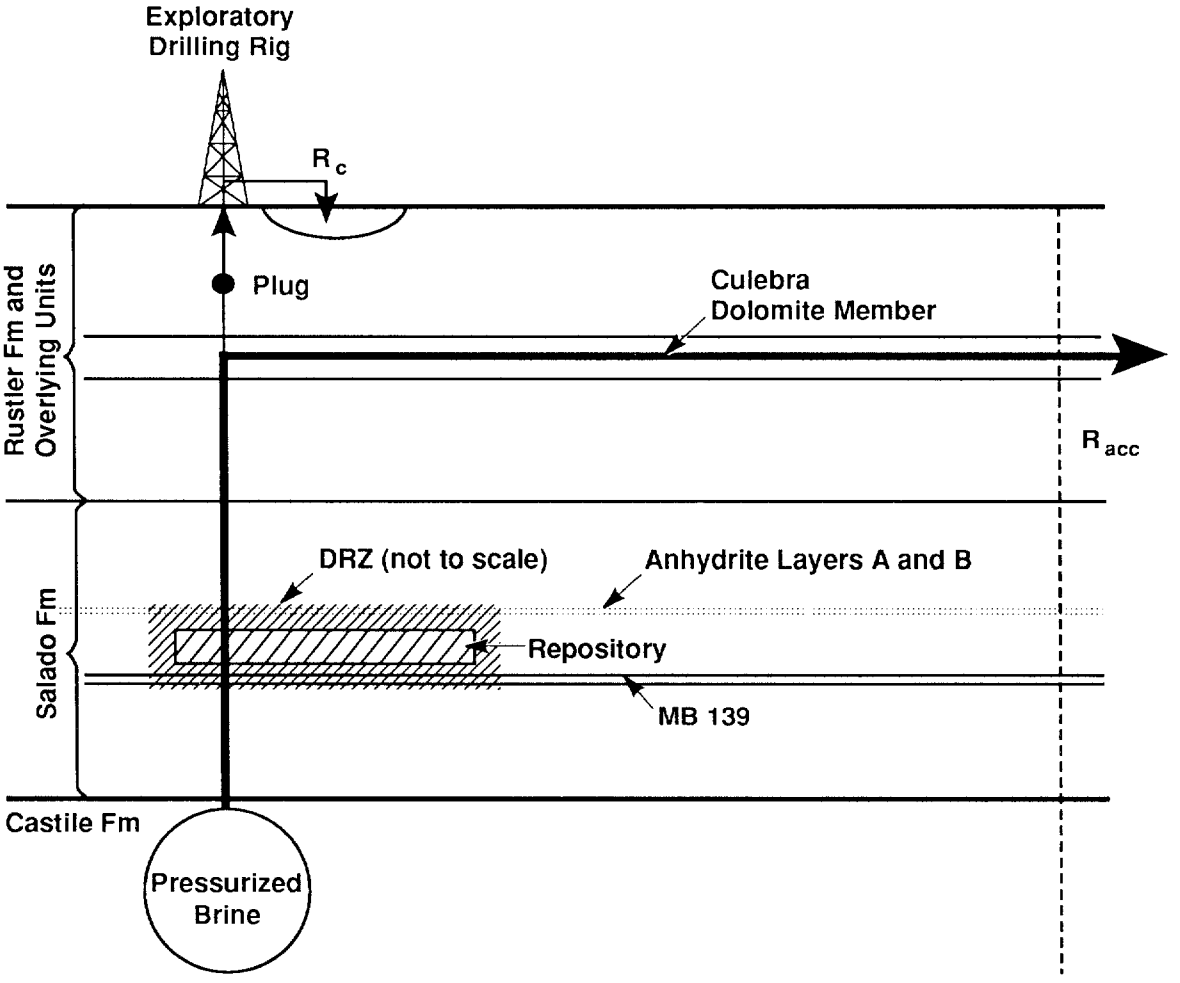

Figure 4-8. Conceptual Model for Scenario *E1*. Arrows indicate assumed direction of flow. Exploratory borehole penetrates pressurized brine below the repository horizon. R_C is the release of cuttings and eroded material. R_{acc} is the release at the subsurface boundary of the accessible environment. A plug above the Culebra Dolomite Member is assumed to remain intact for 10,000 years.

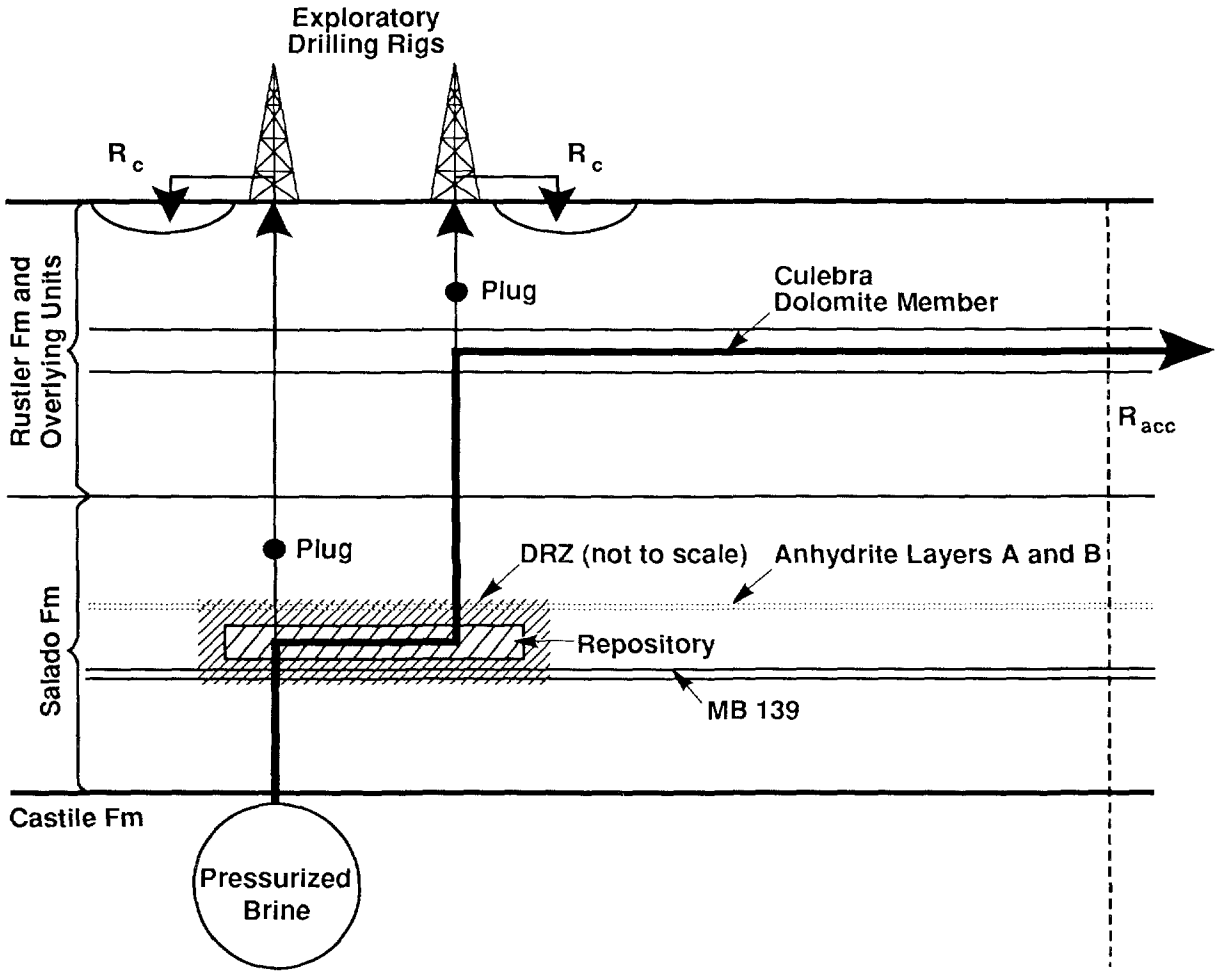

Figure 4-9. Conceptual Model for Scenario *E1E2*. Arrows indicate assumed direction of flow. One exploratory borehole penetrates pressurized brine below the repository horizon and a plug between the repository and the Culebra Dolomite Member is assumed to remain intact for 10,000 years. The second borehole does not penetrate pressurized brine below the repository, and a plug above the Culebra Dolomite Member is assumed to remain intact for 10,000 years. R_C is the release of cuttings and eroded material. R_{acc} is the release at the subsurface boundary of the accessible environment.

Radionuclides and gas are released directly to the surface during drilling of the two holes as described with *E1* and *E2*. Additional releases from this system are dependent on the sequence in which the holes are drilled. The plug in the borehole that penetrates the pressurized brine reservoir allows brine flowing up the hole to enter the repository but not leave the repository until the second hole penetrates the same panel. Once the second hole is drilled, a pathway is formed for brine and gas from the pressurized brine reservoir to flow through waste panels and nearby members to this new hole and up to the Culebra Dolomite Member. Flow in the Culebra Dolomite is downgradient (Marietta et al., 1989).

If the hole that does not penetrate pressurized brine is drilled first, gas and/or fluid pressure is relieved; this is followed by brine flow and radionuclide transport up the hole as a result of brine inflow into the panel from the host rock, possibly enhanced by creep closure of rooms and drifts. Flow is diverted into the Culebra Dolomite Member by the plug located above this unit. The subsequent drilling and plugging of the borehole that penetrates the pressurized brine reservoir results in flow through the repository and up the other borehole. After the driving pressure is depleted, Scenario *E1E2* reverts to Scenario *E2*, because the borehole that penetrates the pressurized brine no longer contributes to flow and transport (Marietta et al., 1989). Analyses of Scenario *E1E2* assume that both boreholes are drilled at or close to the same time for modeling convenience.

The sequence of drilling, time lapsed between drilling events, and distance between the two boreholes in the same panel all affect radionuclide migration. Flow through the rooms and drifts depends on the hydraulic properties of the waste backfill and seals placed in these openings and on the pressure gradient between the holes. For some configurations, flow from one hole to the other may take longer than the regulatory period or take sufficiently long to allow significant decay of radionuclides in transport. These issues are addressed in the analyses described in Chapter 6 of this volume.

4.1.8 DEFINITION OF COMPUTATIONAL SCENARIOS

A more detailed decomposition of the sample space S is desired for the actual calculations that must be performed to determine scenario consequences (i.e., $\mathbf{cS}_i$ as shown in Equation 3-1) and to provide a basis for constructing a family of CCDFs as described earlier. To provide more detail for the determination of both scenario probabilities and scenario consequences, the computational scenarios on which the actual CCDF construction is based for the WIPP performance assessment are defined on the basis of (1) number of drilling intrusions, (2) time of the drilling intrusions, (3) whether or not

a single waste panel is penetrated by two or more boreholes, of which at least one penetrates a brine pocket and at least one does not, and (4) the activity level of the waste penetrated by the boreholes. The purpose of this decomposition is to provide a systematic coverage of what might reasonably happen at the WIPP.

The procedure starts with the division of the 10,000-year time period appearing in the EPA regulations into a sequence

$$[t_{i-1}, t_i], \; i = 1, 2, \ldots, nT, \tag{4-8}$$

of disjoint time intervals. When activity loading in the waste panels is not considered, these time intervals lead to computational scenarios of the form

$$S(\mathbf{n}) = \{x: x \text{ an element of } S \text{ for which exactly } n(i) \text{ intrusions occur in the time interval } [t_{i-1}, t_i], \; i=1,2,\ldots,nT\} \tag{4-9}$$

and

$$S^{+-}(t_{i-1}, t_i) = \{x: x \text{ an element of } S \text{ involving two or more boreholes that penetrate the same waste panel during the time interval } [t_{i-1}, t_i], \text{ at least one of these boreholes penetrates a pressurized brine pocket and at least one does not penetrate a pressurized brine pocket}\}, \tag{4-10}$$

where

$$\mathbf{n} = [n(1), n(2), \ldots, n(nT)]. \tag{4-11}$$

When activity loading is considered, the preceding time intervals lead to computational scenarios of the form

$$S(\mathbf{l},\mathbf{n}) = \{x: x \text{ an element of } S(\mathbf{n}) \text{ for which the } j^{th} \text{ borehole encounters waste of activity level } \ell(j)\} \tag{4-12}$$

and

$$S^{+-}(\mathbf{l};t_{i-1}, t_i) = \{x: x \text{ an element of } S^{+-}(t_{i-1}, t_i) \text{ for which the } j^{th} \text{ borehole encounters waste of activity level } \ell(j)\}, \tag{4-13}$$

where

$$\mathbf{l} = [\ell(1), \ell(2), \ldots, \ell(nBH)] \text{ and } nBH = \sum_{i=1}^{nT} n(i). \tag{4-14}$$

Further refinements on the basis of whether or not subsidence occurs and whether or not individual boreholes penetrate pressurized brine pockets are also possible. In essence, the computational scenarios defined in Equation 4-8 through Equation 4-14 are defining an importance sampling strategy that covers the stochastic or Type A uncertainty that is characterized by the scenario probabilities pS_i appearing in Equation 3-1. Additional information on the definition of computational scenarios is given in Volume 2, Chapter 3 of this report.

4.2 Determination of Scenario Probabilities

The second element of the ordered triples shown in Equation 3-1 is the scenario probability pS_i. As with the scenarios, these probabilities have been developed at two different levels of detail. The first level is for the summary scenarios discussed in Section 4.1.2-Definition of Summary Scenarios and shown in Figure 4-5. The primary purpose of these probabilities is to provide guidance in scenario development. The development of these probabilities is described in Section 4.2.1-Probabilities for Summary Scenarios. The second level is for the computational scenarios discussed in Section 4.1.8-Definition of Computational Scenarios. These are the probabilities that will actually be used in the construction of CCDFs for comparison with the EPA release limits. These probabilities are defined in Section 4.2.2-Probabilities for Computational Scenarios.

4.2.1 PROBABILITIES FOR SUMMARY SCENARIOS

Probabilities for the summary scenarios described in Section 4.1.2-Definition of Summary Scenarios were estimated as part of a previous methodology demonstration (Marietta et al., 1989). These estimates were called weights to emphasize that they were only preliminary. Possible approaches to determining probabilities of occurrence for these scenarios were reviewed and additional probabilities were estimated by Guzowski (1991), who concluded that probability assignments for the compliance assessment should rely on expert judgment. A formal expert-judgment elicitation (e.g., Bonano et al., 1989) has begun. This elicitation focuses on identifying a set of mutually exclusive futures, modes of intrusion for each future, and frequencies of intrusion for each mode. When viewed at a high level, this process involves development of a sample space S, a collection $\S$ of subsets of S, and ultimately, a probability function defined for elements of $\S$. The status and preliminary results of effort are described in the final section of this chapter. The effects of possible markers and barriers will be considered through additional expert-judgment elicitations. Because the elicitation of expert judgments is not complete, preliminary probability estimates also must be used for this assessment.

Preliminary probability estimates for the summary scenarios are based on the current understanding of natural resources in the vicinity of the repository, projections of future drilling activity, and regulatory guidance. Two sets of probability estimates (Marietta et al., 1989; Guzowski, 1991) were compared by Bertram-Howery et al. (1990). Neither set was considered credible enough to be used as final probability estimates in the absence of formal expert-judgment elicitation (Guzowski, 1991). Both sets of preliminary probabilities, derived by using different probability techniques, were used in the 1990 preliminary assessment, and the resultant comparison of simulated performances provided a measure of the sensitivity of the modeling system to the uncertainty in scenario probability assignment. One set, obtained primarily using a classical-model approach based on the theory of indifference (Weatherford, 1982), contains estimates for event probabilities of 0.0065 for drilling into a room or drift (*E2*), 0.0033 for drilling into a room or drift and penetrating a pressurized brine occurrence (*E1*), and 0.25 for subsidence due to potash mining outside the controlled area (*TS*) (Guzowski, 1991). The scenario probabilities can be estimated from the logic diagram as before (Figure 4-10). The second set (Marietta et al., 1989) contains estimates for event probabilities of 0.17 for *E2*, 0.085 for *E1*, and 0.05 for *TS* and yields a much different set of scenario probabilities (Figure 4-11). The probability of human intrusion is 0.01 for the first set and 0.24 for the second set.

4.2.2 PROBABILITIES FOR COMPUTATIONAL SCENARIOS

Probabilities for the computational scenario refinements are now presented. These are the probabilities that will be used in the construction of CCDFs for comparison with the EPA release limits in the present report. These probabilities are based on the assumption that the occurrence of boreholes through the repository follows a Poisson process with a rate constant λ. The probabilities $pS(\mathbf{n})$ and $pS(\mathbf{l},\mathbf{n})$ for the computational scenarios $S(\mathbf{n})$ and $S(\mathbf{l},\mathbf{n})$ are given by

$$pS(\mathbf{n}) = \left\{ \prod_{i=1}^{nT} \left[\frac{\lambda^{n(i)} \left(t_i - t_{i-1} \right)^{n(i)}}{n(i)!} \right] \right\} \exp\left[-\lambda \left(t_{nT} - t_0 \right) \right] \qquad (4\text{-}15)$$

and

$$pS(\mathbf{l},\mathbf{n}) = \left(\prod_{j=1}^{nBH} pL_{\mathbf{l}(j)} \right) pS(\mathbf{n}), \qquad (4\text{-}16)$$

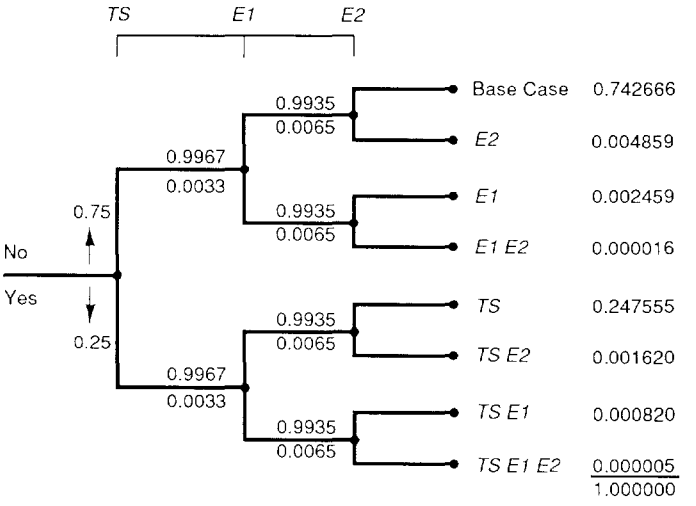

Figure 4-10. Scenario Probability Estimate Based on Guzowski (1991).

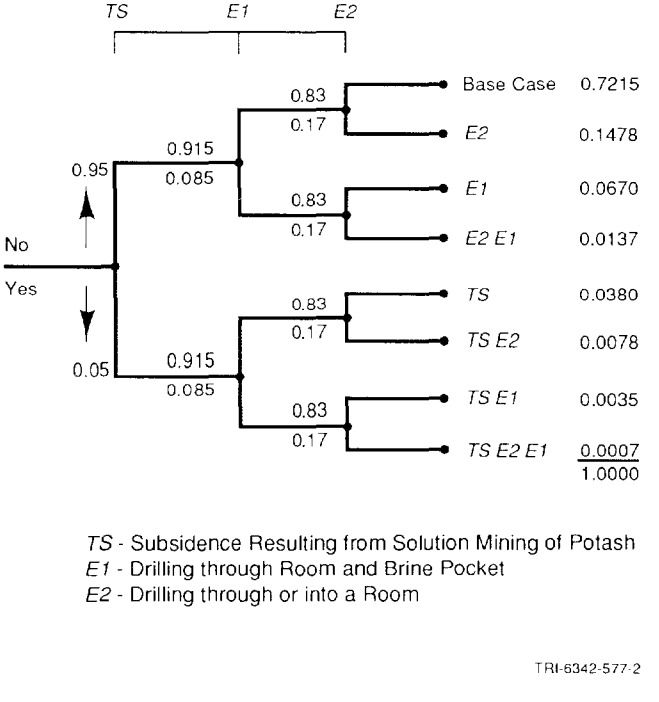

Figure 4-11. Scenario Probability Estimate Based on Marietta et al.(1989).

where $\mathbf{n}$ and $\mathbf{l}$ are defined in Equations 4-11 and 4-14, respectively, and pL_ℓ is the probability that a randomly placed borehole through a waste panel will encounter waste of activity level ℓ. The rate constant λ is a sampled variable in the 1991 WIPP performance assessment. Table 3-2 provides an example of probabilities $pS(\mathbf{n})$ calculated as shown in Equation 4-15 with $\lambda = 3.28 \times 10^{-4}\ yr^{-1}$, which corresponds to the maximum drilling rate suggested for use by the EPA. The activity level probabilities pL_ℓ used in the 1991 WIPP performance assessment are presented in Table 4.3.

The probabilities $pS^{+-}(t_{i-1},t_i)$ and $pS^{+-}(\mathbf{l};t_{i-1},t_i)$ for the computational scenarios $S^{+-}(t_{i-1},t_i)$ and $S^{+-}(\mathbf{l};t_{i-1},t_i)$ are given by

$$pS^{+-}(t_{i-1},t_i) = \sum_{\ell=1}^{nP} \{1 - \exp[-\alpha(\ell)(t_{i-1},t_i)]\}\{1 - \exp[-\beta(\ell)(t_{i-1},t_i)]\} \tag{4-17}$$

and

$$pS^{+-}(\mathbf{l};t_{i-1},t_i) = \left[\prod_{j=1}^{nBH} pL_{\ell(j)}\right] pS^{+-}(t_{i-1},t_i), \tag{4-18}$$

where

$$\alpha(\ell) = \frac{[aBP(\ell)]\lambda}{aTOT}$$

$$\beta(\ell) = \frac{[aTOT(\ell) - aBP(\ell)]\lambda}{aTOT}$$

$aBP(\ell)$ = area (m^2) of pressurized brine pocket under waste panel ℓ,

$aTOT(\ell)$ = total area (m^2) of waste panel ℓ,

$aTOT$ = total area (m^2) of waste panels,

and

nP = number of waste panels.

The probability $pS^{+-}(t_{i-1},t_i)$ can also be determined under the assumption that exactly two boreholes are involved (see Chapter 2, Volume 2 of this report).

The relations appearing in Equations 4-15 through 4-18 are derived in Volume 2, Chapter 2 of this report under the assumption that drilling intrusions follow a Poisson process (i.e., are random in time and space). The

TABLE 4-3. ACTIVITY LEVELS AND ASSOCIATED PROBABILITIES USED IN 1991 WIPP PERFORMANCE ASSESSMENT

Activity Level	Type[a]	Proba-bility[b]	Time (years) 0	1000	3000	5000	7000	9000
1	CH	0.4023	3.4833	0.2718	0.1840	0.1688	0.1575	0.1473
2	CH	0.2998	34.8326	2.7177	1.8401	1.6875	1.5748	1.4729
3	CH	0.2242	348.326	27.177	18.401	16.875	15.748	14.729
4	CH	0.0149	3483.26	271.77	184.01	168.75	157.48	147.29
5	RH	0.0588	117.6717	0.1546	0.1212	0.1139	0.1082	0.1030
Average for CH Waste:			150.7905	11.7648	7.9658	7.3053	6.8174	6.3764

[a] CH designates contact handled waste; RH designates remote handled waste

[b] Probability that a randomly placed borehole through the waste panels will intersect waste of activity level ℓ, ℓ = 1,2,3,4,5.

derivations are quite general and include both the stationary (i.e., constant λ) and nonstationary (i.e., time-dependent λ) cases.

4.3 Expert Judgment on Inadvertent Human Intrusion

Identifying the probability of future inadvertent human intrusion is at best a qualitative task. Because the Standard allows for exceptions to quantitative evaluations where qualitative judgments are the only choice and because the expertise to make the qualitative evaluations is not available within the Project, the Project has selected teams of outside experts, organized into two separate panels, to address possible modes of inadvertent intrusion and types of markers to deter intrusion. These experts evaluate the available information, reduce the problems to manageable components, and with the assistance of probability specialists, quantify their subjective conclusions to the greatest extent possible. The events and probabilities generated by these experts will be evaluated for incorporation into the performance assessment.

The activities and results of the future-intrusion panel are discussed here. The planned marker-development panel is discussed in Chapter 8 of this volume.

4.3.1 PRINCIPLES OF EXPERT-JUDGMENT ELICITATION

Expert-judgment elicitation is often used to address technical issues that cannot be practically resolved by other means (Bonano et al., 1989; Hora and Iman, 1989). Teams of experts represent the various fields that are pertinent to the issue at hand. The experts not only provide a broad perspective on the problem, but the outcome of their work can often be expressed in numerical form (events probabilities) that can be incorporated into computer models. Before beginning their task, the experts are provided with necessary background information and an explicit statement of the issue or issues to be addressed.

Training the experts to synthesize their expertise into relatively unbiased probabilities is fundamental. A common method of addressing such questions is to "decompose" each question into constituent parts that can be readily quantified. Expert interaction and the sharing of insights enhance decomposition and analysis of the questions. Individuals knowledgeable in both the topic under discussion and expert elicitation quantify the responses from each expert.

4.3.2 EXPERT SELECTION

Expert selection for the future-intrusion panel was a major activity. Sixteen experts organized into four four-member teams were selected. Their backgrounds span a variety of social and physical sciences including, for example, futures studies, demography, mining engineering, agricultural science, and resource economics. The three steps in this process were nominator identification, nominee identification, and selection of experts.

Persons with sufficient knowledge to nominate individuals to serve on the future-intrusion panel were identified. The nominators were identified through contacts with professional organizations, government organizations, and private industry. In addition, nominators were identified through literature searches in various areas such as futures research. Once the nominators were identified (71 individuals), they were formally requested to nominate candidates for the panel.

The nominators, who could also nominate themselves, submitted a total of 126 nominations. The nominees were requested to submit a description of their interests and any special qualifications relevant to this activity, along with a curriculum vitae. Letters of interest were received from 70 nominees.

The selection committee for this panel was composed of three individuals who are not members of the SNL staff. Each member of the selection committee evaluated the nominees on the following criteria: tangible evidence of

expertise; professional reputation; availability and willingness to participate; understanding of the general problem area; impartiality; lack of economic or personal stake in the potential findings; balance among team members to provide each team the needed breadth of expertise; physical proximity to other participants to facilitate interactions among team members; and balance among all participants to ensure adequate representation of various constituent groups.

4.3.3 EXPERT-JUDGMENT ELICITATION

The future-intrusion experts were asked to address issues related to societal development and human activities that could lead to inadvertent human intrusion in a time frame that extends 10,000 years after disposal. They were asked to identify reasonable, foreseeable futures for human societies, to suggest how the activities of these societies could result in intrusions into the WIPP repository, and to provide probabilities of the various futures and the degree of completeness that these foreseeable futures represent (to what extent can what could happen to society be accounted for by these foreseeable futures). For each foreseeable future, the experts were asked to identify and quantify expected modes of intrusion into the repository and to examine issues relating to persistence of information about the WIPP, the ability to detect radiological waste in the repository, and the existence of radiological waste in the repository.

The approach is a form of scenario analysis. Futures[1] can be constructed by considering alternative projections of basic trends in society. These trends may include population growth, technological development, and the use and scarcity of resources, among others. Transcending these factors are events that interrupt, modify, or reinforce the development of society. Such events include war, disease, pestilence, fortuitous discovery of new technologies, human-induced climate changes, and so forth.

Each future specifies a picture of the characteristics of society at various times. These characteristics will, in turn, provide information about those activities that are likely to take place and pose threats to the integrity of the repository. Such activities include extractive industry, particularly mining for potash or drilling for oil and gas, and drilling for water for use in agriculture, industry, or for other purposes. Other types of intrusion include various kinds of excavation or intrusive activities not currently practiced.

---

[1] The expert-elicitation scenarios are referred to here as "futures" to avoid confusion with scenarios developed for consequence analysis.

From the states of societies and their potentially intrusive activities, modes of intrusion and motivations for these intrusions can be inferred. Similarly, from futures and the resulting states of society, one can assess whether knowledge concerning underground disposal of nuclear waste would exist, whether the waste itself would continue to exist, and whether a means to detect waste before or during intrusion would exist.

Four teams of future-intrusion experts have provided written reports that discuss societal development, describe possible futures, and establish the basis for estimating the possibilities of these futures. The teams have analyzed modes of intrusion and developed probabilistic quantitative estimates of the frequencies of various intrusions. The likelihoods of various futures were also estimated by the teams with assistance from an elicitation specialist. The results of the elicitation sessions and the subsequent analysis were returned to the panelists for review and comment. A more detailed description of this process and the results can be found in Hora et al. (1991).

4.3.4 PANEL RESULTS

The material provided by the four teams falls into two categories: qualitative discussions of the future states of society and modes of intrusion found in the reports provided by each team; and a more quantitative analysis developed during the elicitation sessions. The teams were given complete freedom in addressing the issue statement, so all utilized different approaches. One important reason for convening the future-intrusion panel was to provide input to the marker-development panel regarding modes of intrusion and states of society that should be considered when examining markers to deter inadvertent human intrusion (providing design characteristics and estimating effectiveness). As such, the panelists were not limited in the issue statement to considering the mode of intrusion specified by the Standard and now being modeled—intrusion by a borehole. Thus, some modes of intrusion discussed by the teams cannot currently be modeled by computer programs.

A qualitative description of the various futures developed by the teams is presented here. The actual reports written by the four teams are reproduced as appendices in Hora et al. (1991).

Boston Team

The probability assessment developed by the Boston Team (T. Gordon, M. Baram, W. Bell, and B. Cohen) assigned probabilities to particular modes of human intrusion. They started with descriptions of possible future societies and

worked forward to develop possible modes of intrusion. This resulted in six specific modes of intrusion, four of which involve activities that directly impact the WIPP (disposal of wastes through injection wells, drilling for resources, underground storage of additional nuclear waste at the WIPP, and archaeological exploration), and two others that would have an indirect impact (the construction of dams and explosive testing in the area). Whether or not the intrusion would take place was believed to be influenced by five underlying factors (level of technology, world population, cost of materials, the persistence of knowledge concerning the WIPP, and the level of industrialization in the WIPP area). In addition, the team felt that the 10,000 year period of regulatory interest should be further divided (years 0 to 300, 300 to 3000, and 3000 to 10,000) and that factors and probabilities would be different during these intermediate periods. The Boston Team provided numerous conditional probabilities that captured all the interactions between the underlying factors and the three time periods in order to develop specific intrusion probabilities or frequencies.

Southwest Team

In contrast to the Boston Team, whose analysis was very specific and detailed, the Southwest Team (G. Benford, C. Kirkwood, H. Otway, and M. Pasqualetti) chose to focus on two broad societal factors that they felt influenced the probability of human intrusion at the WIPP, without directly linking the probability to a particular mode of intrusion. Political control, whether by the United States or by some other country, was seen as quite important, especially with regards to active control of the site and the continuation of information regarding the exact location and dangers of the WIPP. The other important underlying factor is that of the pattern of technological development (a steady increase, a steady decrease, or a seesaw between high and low levels of technology). Technological development relates to the ability to intrude upon the WIPP and to detect various warnings. While this team did not divide the 10,000 year regulatory period for the actual probability calculation, they did state that the probability of altered political control is high over the next 200 years. They also gave periods for each of the three patterns during which intrusion would be most likely (steady increase: 1000 to 2000 years; steady decrease: 100 to 500 years; and seesaw: cycles of 1000 years). This strategy resulted in a single probability of inadvertent human intrusion over the 10,000 year regulatory period. The probability is of one intrusion, for they thought that multiple intrusions were unlikely.

Several questions were handled by the team outside of the direct probability elicitation. Depending on the technological development pattern, modes of intrusion might include mole miners, nanotechnology, and deep strip mining for steady increase, or conventional drilling and excavation for steady

decline and seesaw. The question of whether the wastes would be rendered harmless was given a probability of 0.99 in the steady-increase pattern, and essentially a zero probability for the other two patterns.

Washington A Team

The Washington A Team (D. Chapman, V. Ferkiss, D. Reicher, and T. Taylor) organized their analysis by considering four alternative futures for society. The four futures are (1) continuity, where trends in population growth, technology development, and resource exploration and extraction continue along current lines; (2) radical increase, where current activities continue, but at an increased rate; (3) discontinuity, where there are shifts in political power and socioeconomic development, with a resulting loss of knowledge about the WIPP; and (4) steady-state resources, where current trends in resource extraction and consumption are reversed—recycling of resources and using renewable energy sources—so there is less need to search the earth for extractable resources. Society need not continue with one condition for the entire 10,000 years but may shift among them. Human intrusion is expected to be moderated by active controls at the WIPP (the team assumed no intrusion if there are active controls at the WIPP) and effective information regarding the location and risks of the repository. The probability of intrusion was computed separately for the two time periods of 0 to 200 years and 200 to 10,000 years and assuming that society did not shift among conditions. The first period was thought to be crucial except for the steady-state condition.

The two probabilities developed were not linked to particular modes, but the team did discuss both direct (deep tunnel that intersects the WIPP, drilling, and excavation) and indirect (dams, a water-well field, and explosions) activities that might intrude upon the repository. They also outlined which modes they thought were likely to take place with the four alternative futures: conventional drilling and excavation with the continuity future; conventional drilling and excavation, machine mining, and tunnels or pipelines with the radical-increase future; conventional drilling and excavation with the discontinuity future; and indirect means with the steady-state future.

Washington B Team

The Washington B Team (T. Glickman, N. Rosenberg, M. Singer, and M. Vinovskis) started with four specific modes of intrusion (resource exploration and extraction, development of groundwater, scientific investigation, and weather modification) that were thought to be influenced by four underlying factors in society (the overall level of wealth and technology, prudent and effective government control, climate, and resource

prices). Two significant periods of time were used in the calculations: the near future (0 to 200 years) and the far future (200 to 500 years for resource exploration and extraction, and 200 to 10,000 years for the other three modes). There were differences in the applicable underlying factors for both the modes of intrusion and the time periods, and different conditional probabilities describing the interactions between the factors. Thus, separate probabilities of intrusion were calculated for each mode and for each time period.

The findings of the future-intrusion panel were not incorporated into the 1991 calculations. Efforts are currently being made to organize the results so that they can be used in the 1992 calculations.

Chapter 4–Synopsis

Scenarios in Performance Assessment

The Containment Requirements of the Standard refer to all significant events and processes that might affect a disposal system.

For a performance assessment to be complete, combinations of events and processes (scenarios) also must be analyzed.

In order to determine compliance with the Containment Requirements,

- the set of scenarios must describe all reasonably possible, potentially disruptive future states of the disposal system,
- scenarios must be mutually exclusive,
- the consequences of each scenario must be determined,
- the probability of occurrence of each scenario must be estimated.

Certain events and processes can be excluded from performance-assessment analyses based on low probability and/or low consequence of occurrence.

Identifying Events and Processes

The WIPP performance-assessment team has adopted and modified a generic list of events and processes that could affect the performance of a waste-disposal facility.

Phenomena that occur instantaneously or within a relatively short time interval are considered events. Phenomena that occur over a significant portion of the 10,000 years of regulatory concern are considered processes.

Screening Events and Processes

Events and processes are screened based on probability of occurrence, physical reasonableness, and consequence.

Events and processes with less than one chance in 10,000 of occurring in 10,000 years do not have to be considered.

Sufficient data may not be available to calculate a probability of occurrence. A logical argument based on physical reasonableness can establish whether conditions exist or can change to a sufficient degree within the regulatory time period for a particular event or process to occur with sufficient magnitude to affect the performance of the disposal system.

Consequence is based on whether the event or process, either alone or in combination with other events or processes, may affect the performance of the disposal system.

Natural Events or Processes

None of the potentially disruptive natural events or processes considered for the WIPP were retained for scenario development of disturbed performance.

Events or processes that are part of the base-case scenario are

- erosion,
- sedimentation,
- climatic change (pluvial periods),
- seismic activity,
- shallow dissolution (Rustler-Salado contact residuum).

Events or processes that were eliminated from consideration based on low probability of occurrence are

- meteorite impact,
- tsunamis (from meteorite impacts),
- shallow dissolution (depending on theory).

Events or processes that were eliminated from consideration based on physical unreasonableness arguments are

- glaciation,
- hurricanes,
- seiches,
- tsunamis (of traditional origin),
- regional subsidence or uplift,
- mass wasting,
- flooding,
- diapirism,
- volcanic activity,
- magmatic activity,
- deep dissolution,
- shallow dissolution (depending on theory),
- faulting.

Because sea-level variation is dependent on other events or processes, it is not considered as an independent phenomenon for scenario development.

Human-Induced Events or Processes

Events or processes that were eliminated from consideration based on low probability of occurrence are

- accidental surface and near-surface nuclear explosions during warfare,
- damming of streams and rivers.

Events or processes that were eliminated from consideration based on physical unreasonableness are

- nuclear testing or enhanced oil recovery using nuclear devices,
- irrigation.

Events or processes that were eliminated from consideration based on low consequence are

- injection wells,
- drilling of deep oil or gas wells outside the WIPP boundaries.

Evaluation of deliberate, large-scale nuclear explosions at the WIPP is not required by the Standard.

Events or processes that are being evaluated for inclusion in disruptive scenarios because of their possible effects on groundwater flow are

- potash mining (outside the boundaries of the waste panels),
- drilling of water wells,
- drilling of oil or gas exploratory wells.

Exploratory drilling for resources is a realistic event for the WIPP and is retained for two possibilities of scenario development:

- drilling into a waste-filled room or drift, with a brine reservoir in the underlying Castile Formation,
- drilling into a waste-filled room or drift without breaching a brine reservoir.

Repository- and Waste-Induced Events or Processes

Events or processes that were eliminated from consideration based on physical unreasonableness are

- thermally induced stress fracturing in the host rock,
- explosions because of nuclear criticality.

Events or processes that were eliminated from consideration based on low consequence are

- caving and subsidence,
- explosions or fires within waste-filled rooms and drifts.

Events or processes that are part of the base-case scenario are

- shaft-seal degradation,
- excavation-induced stress fracturing in the host rock,
- gas generation within the repository.

A phenomenon that is being evaluated for inclusion in the development of disruptive scenarios is heat generated by nuclear criticality.

Developing Scenarios

Scenarios used in performance assessment must be comprehensive and mutually exclusive.

The WIPP performance assessment uses a logic diagram to construct scenarios. At each junction within the diagram, a yes/no decision is made as to whether the next event or process is added to the scenario. Parameter values, time of occurrence, and location of occurrence are not used to define the events and processes, and parameter uncertainty is incorporated directly into the data base. Each scenario consists of a combination of occurrence and nonoccurrence of all events and processes that survive screening.

Screening Scenarios

Scenarios are screened to identify those that have little or no effect on the mean CCDF.

Scenarios are screened on the same criteria used to screen events and processes: physical reasonableness, probability of occurrence, and consequence.

The probability of occurrence of a scenario is determined by combining the probability of occurrence and nonoccurrence of its constituent events and processes.

Descriptions

Undisturbed Performance Scenario

The undisturbed performance scenario includes all natural events and processes expected to occur at the WIPP during the next 10,000 years. It also includes undisturbed processes within the disposal system, such as gas generation within the waste panels.

The undisturbed performance scenario is used to evaluate compliance with the Individual Protection Requirements and as the base-case scenario for assessments of disturbed performance for evaluation of compliance with the Containment Requirements.

Human-Intrusion Scenarios

Three summary human-intrusion scenarios are considered:

*E*2, in which a borehole penetrates a waste panel, creating a flow path to the Culebra Dolomite,

*E*1, in which a borehole penetrates a waste panel and an underlying pressurized brine reservoir in the Castile Formation, creating a flow path to the Culebra Dolomite,

E1E2, in which two boreholes, one of each type, penetrate a single waste panel, creating a flow path for Castile brine through the waste from one hole to the other and then upward to the Culebra Dolomite.

Scenario Probability Assignments

Probabilities for the 1991 computational scenarios are based on the assumption that intrusion follows a Poisson process (i.e., boreholes are random in time and space) with a rate constant, λ, that is sampled as an uncertain parameter in the 1991 calculations.

Expert Judgment on Inadvertent Human Intrusion

The WIPP Project has selected panels of external experts to provide judgment for use in determining the probability of intrusion.

One panel has met and has addressed the possible modes of intrusion and their likelihoods.

A second panel will be convened to address types of markers that could deter intrusion, thereby lowering its probability.

Techniques of Expert-Judgment Elicitation

Judgments are elicited from experts in quantitative probabilistic forms suitable for use in performance assessments.

Expert Selection

Experts for the future-intrusion panel were selected with a three-step process:

seventy-one nominators were identified through literature searches and contacts with professional organizations, government organizations, and private industry,

one hundred and twenty six nominees were identified, of whom seventy expressed interest,

sixteen panel members were selected on the basis of expertise, professional reputation, availability and willingness to participate, understanding of the problem, impartiality, lack of an economic or personal stake in the outcome, balance of expertise, physical proximity to other panel members, and balance among various constituent groups.

Expert-Judgment Elicitation

The future-intrusion experts were asked to identify reasonable, foreseeable futures for human societies, to suggest how these futures could result in intrusions, and to provide probabilities for their futures.

Panel Results

Each of four teams on the future-intrusion panel identified possible futures and the associated probabilities of intrusion.

Findings of the panel are still being analyzed and were not incorporated into the 1991 calculations.

5. COMPLIANCE-ASSESSMENT SYSTEM

[NOTE: The text of Chapter 5 is followed by a synopsis that summarizes essential information, beginning on page 5-73.]

This chapter reviews the conceptual models used for quantitative simulations of the disposal system. A full documentation of the compliance-assessment system is beyond the scope of a single chapter, and wherever possible the reader is referred to original documents for technical details. Descriptions of specific computer programs and their applications to the WIPP performance assessment have been included in Volume 2 of this report, and are described here only briefly. Additional information about the executive controller for the computer programs within the modeling system can be found in Rechard et al. (1989). Data used in the 1991 preliminary performance assessment are available in Volume 3 of this report.

The first two major sections of this chapter describe the physical components of the disposal system and its surroundings that will provide barriers to radionuclide migration during the next 10,000 years. These barriers are of two types: natural barriers, which are features of the regional and local environment, and engineered barriers, which include designed features of the repository system, such as the panel and shaft seals. Descriptions of the physical components are followed by qualitative descriptions of the models used to simulate performance of the barrier systems.

The third section of the chapter briefly describes CAMCON, the Compliance Assessment Methodology Controller. CAMCON is the executive program which links specific numerical models into a single computational system capable of generating the Monte Carlo simulations required for probabilistic performance assessments.

5.1 The Natural Barrier System

The hydrogeologic setting of the WIPP provides excellent natural barriers to radionuclide migration. Groundwater flow, which provides the primary mechanism for radionuclide migration from the WIPP, is extremely slow in the host Salado Formation, and is slow enough in the overlying rocks to be of concern during the next 10,000 years only in the most transmissive units. If radionuclides reach the overlying units, geochemical retardation during transport may provide an additional barrier to migration.

5.1.1 REGIONAL GEOLOGY

The geology of the WIPP and the surrounding area has been summarized in Chapter 1 of this volume, and is described elsewhere in detail (e.g., Powers et al., 1978a,b; Cheeseman, 1978; Williamson, 1978; Hiss, 1975; Hills, 1984; Harms and Williamson, 1988; Ward et al., 1986; Holt and Powers, 1988; Beauheim and Holt, 1990; Brinster, 1991). The brief review presented here describes regional structural features and introduces the major stratigraphic units. Specific geologic features that affect compliance-assessment modeling are described in greater detail in subsequent sections of this chapter.

The WIPP is located in the Delaware Basin, a structural depression that formed during the Late Pennsylvanian and Permian Periods, approximately 300 to 245 million years ago (Figures 5-1, 5-2). Sedimentation within the subsiding basin resulted in the deposition of up to 4,000 m (13,000 ft) of marine strata. Organic activity at the basin margins produced massive carbonate reefs that separated deep-water facies from the shallow-water shelf sediments deposited landward.

Permian-age rocks of importance to WIPP performance-assessment modeling are those of the Guadalupian and Ochoan Series, deposited between approximately 265 and 245 million years ago (Figure 5-3). During this time subsidence in the Delaware Basin was initially rapid, resulting in deposition of deep-water shales, sandstones, and limestones of the Delaware Mountain Group. Intermittent connection with the open ocean and a decrease in clastic sediment supply, possibly in response to regional tectonic adjustments, led to the deposition of a thick evaporite sequence. Anhydrites and halites of the Castile Formation are limited to the structurally deeper portion of the basin, enclosed within the reef-facies rocks of the Capitan Limestone. Subsidence within the basin slowed in Late Permian time, and the halites of the Salado Formation, which include the host strata for the WIPP, extend outward from the basin center over the Capitan Reef and the shallow-water shelf facies. Latest Permian-age evaporites, carbonates, and clastic rocks of the Rustler Formation and the Dewey Lake Red Beds record the end of regional subsidence and include the last marine rocks deposited in southeastern New Mexico. The overlying sandstones of the Triassic-age Dockum Group reflect continental deposition and mark the onset of a period of regional tectonic stability that lasted approximately 240 million years, until late in the Tertiary Period.

Permian-age strata of the Delaware Basin now dip gently (generally less than 1°) to the east, and erosion has exposed progressively older units toward the western edge of the basin (Figures 5-1, 5-4). This tilting reflects the late Pliocene and early Pleistocene (approximately 3.5 million to 1 million years ago) uplift of the Capitan Reef to form the Guadalupe Mountains more than

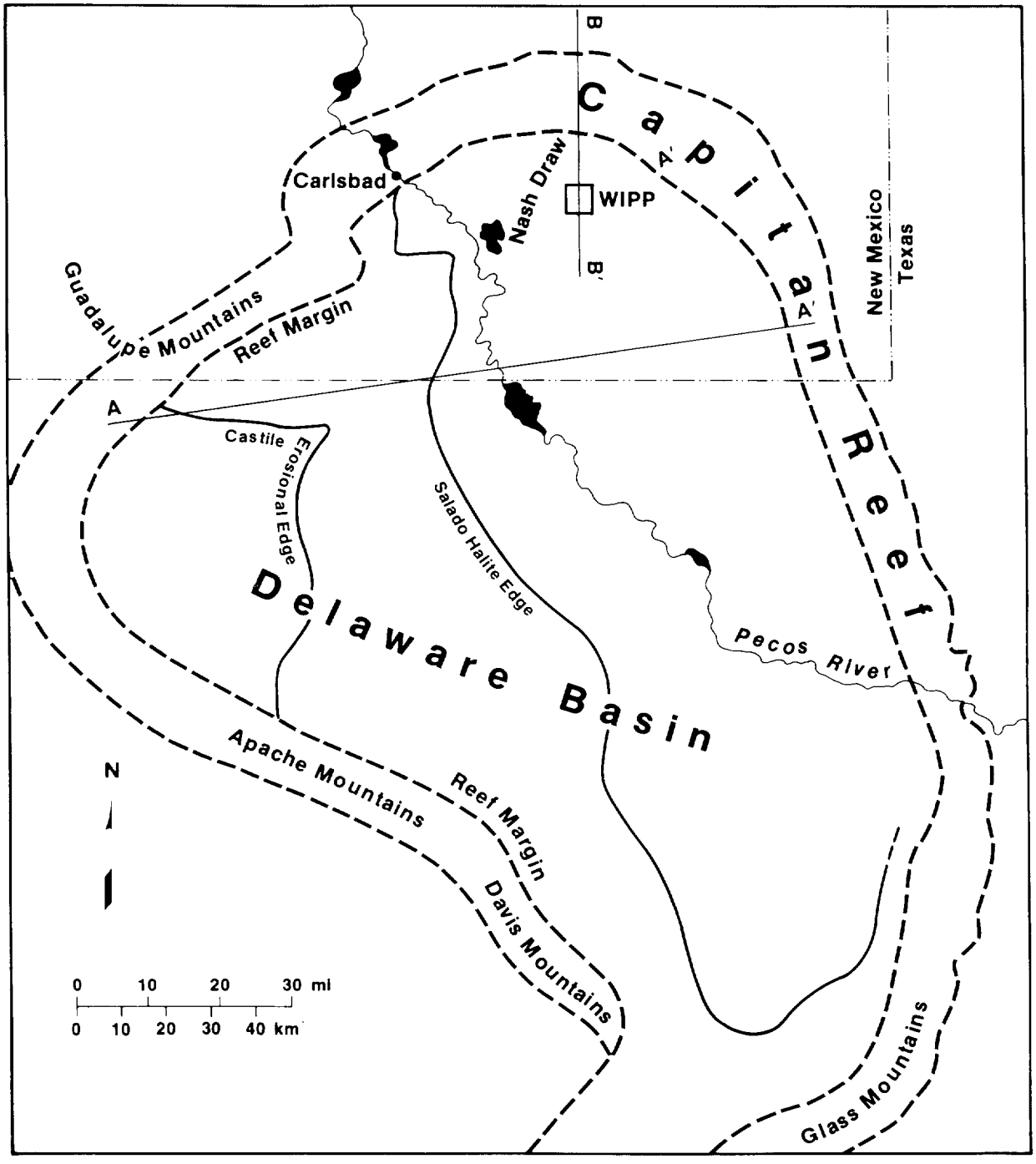

TRI-6342-237-4

Figure 5-1. Generalized Geology of the Delaware Basin, Showing the Location of the Capitan Reef and the Erosional Limits of the Basinal Formations (Lappin, 1988).

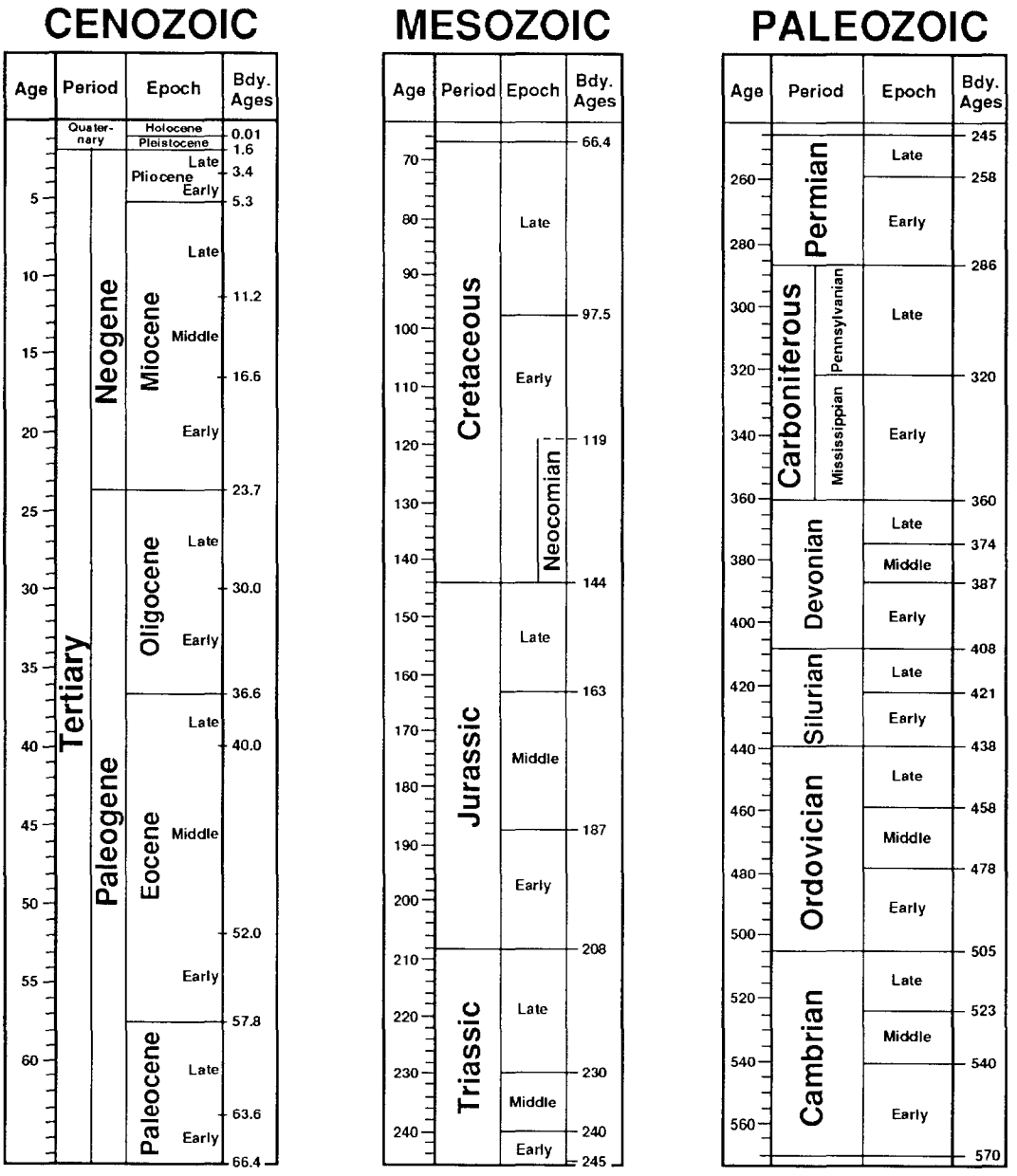

Figure 5-2. Geologic Time Scale (simplified from Geological Society of America, 1984).

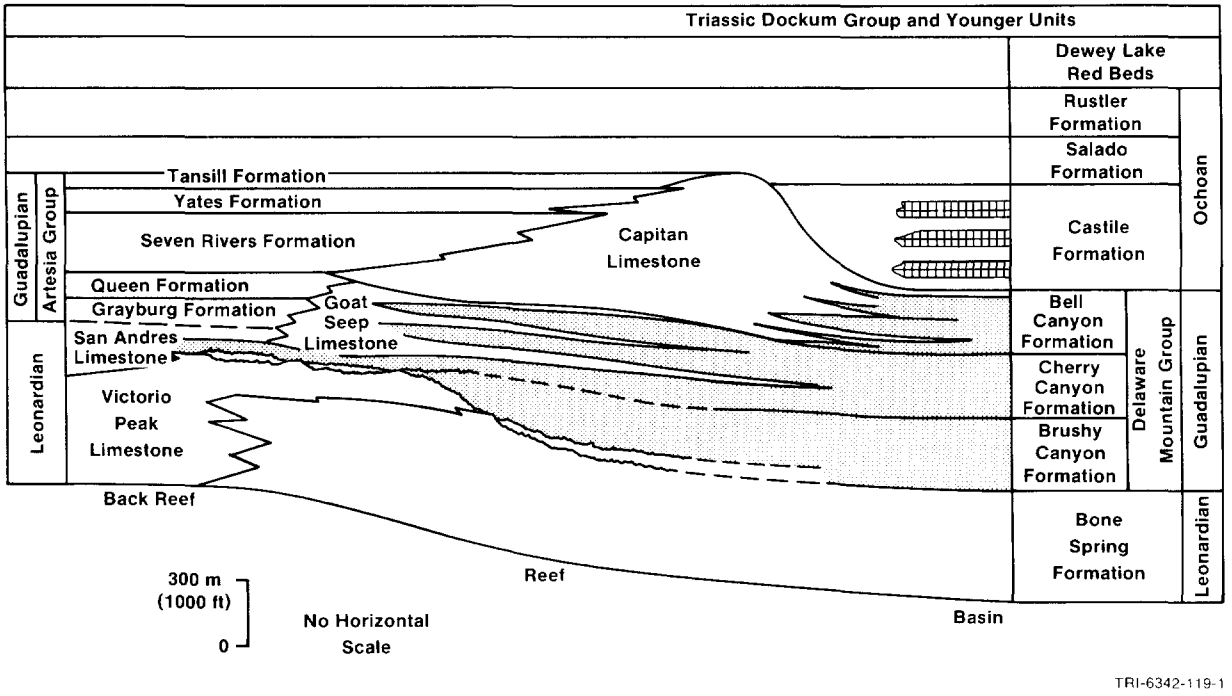

Figure 5-3. Stratigraphy of the Delaware Basin (modified from Mercer, 1983; Brinster, 1991).

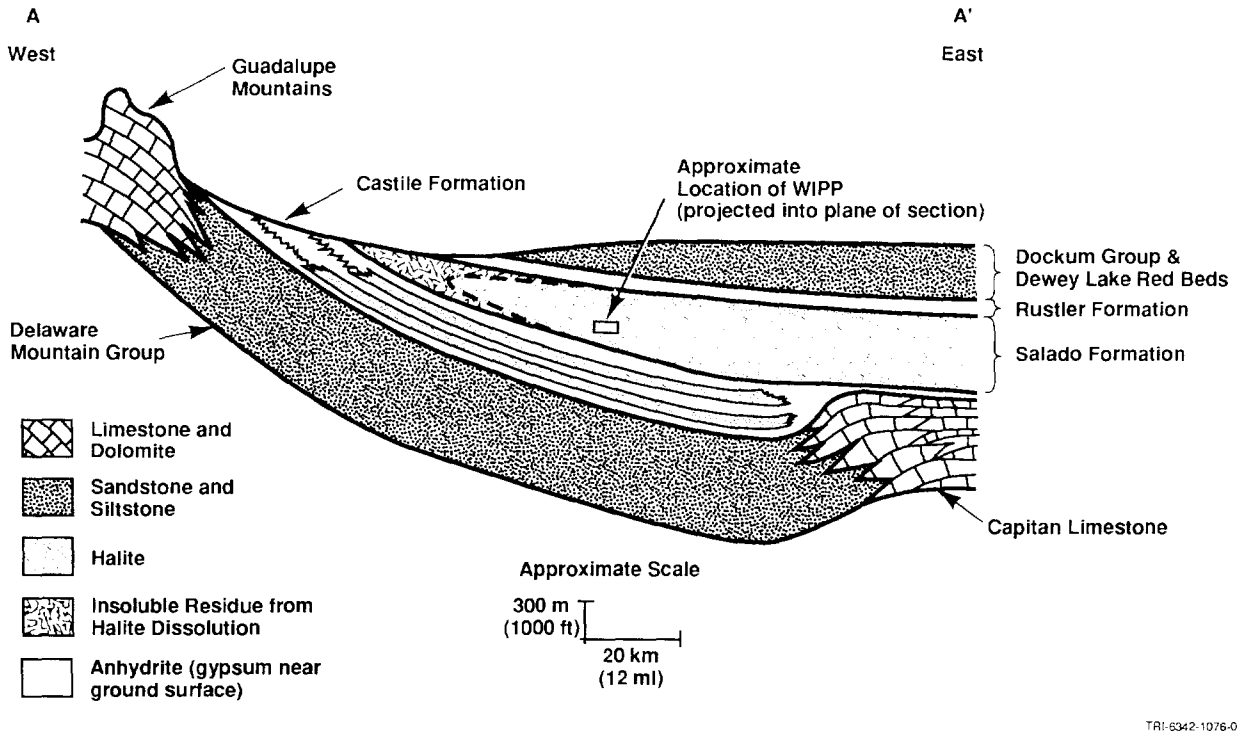

Figure 5-4. Schematic East-West Cross Section through the Northern Delaware Basin (modified from Davies, 1984). Note extreme vertical exaggeration. Approximate location of line of section shown on Figure 5-1.

60 km (37 miles) west of the WIPP (Figures 5-1, 5-4). Field evidence suggests that additional uplift may have occurred during the late Pleistocene and Holocene, and some faults of the Guadalupe Mountains may have been active within the last 1,000 years (Powers et al., 1978a,b). North and east of the WIPP the Capitan Reef has not been uplifted and remains in the subsurface (Figure 5-5).

The present landscape of the Delaware Basin has been influenced by near-surface dissolution of the evaporites (Bachman, 1984, 1987). Karst features created by dissolution include sinkholes, subsidence valleys, and breccia pipes. Most of these features formed during wetter climates of the Pleistocene, although active dissolution is still occurring wherever evaporites are exposed at the surface. Some dissolution may also be occurring at depth where circulating groundwater comes in contact with evaporites: modern subsidence in San Simon Swale east of the WIPP (Figure 1-6) may be related to localized dissolution of the Salado Formation (Anderson, 1981; Bachman, 1984; Brinster, 1991). Nash Draw, which formed during the Pleistocene by dissolution and subsidence, is the most prominent karst feature near the WIPP. As discussed again in Section 5.1.2-Stratigraphy below, evaporites in the Rustler Formation have been affected by dissolution near Nash Draw.

The largest karst feature in the Delaware Basin is the Balmorhea-Loving Trough, south of the WIPP along the axis of the basin (Figure 1-6). Dissolution of evaporites, perhaps along the course of a predecessor of the modern Pecos River, resulted in subsidence and the deposition of Cenozoic alluvium up to 300 m (984 ft) thick in southern Eddy County, and up to almost 600 m (1970 ft) thick across the state line in Texas (Bachman, 1984, 1987; Brinster, 1991).

5.1.2 STRATIGRAPHY

The stratigraphic summary presented here is based on the work of Brinster (1991) and is limited to those units that may have an important role in future performance of the disposal system. Hydrologic data about the units have been summarized by Brinster (1991), and are, in general, not repeated here. Stratigraphic relationships between the units are shown in Figure 5-3. Figure 5-6 shows the region examined in detail by Brinster (1991) and the location of wells that provide basic data.

Bell Canyon Formation

The Bell Canyon Formation consists of 210 to 260 m (690 to 850 ft) of sandstones and siltstones with minor limestones, dolomites, and conglomerates (Williamson, 1978; Mercer, 1983; Harms and Williamson, 1988). Sandstones

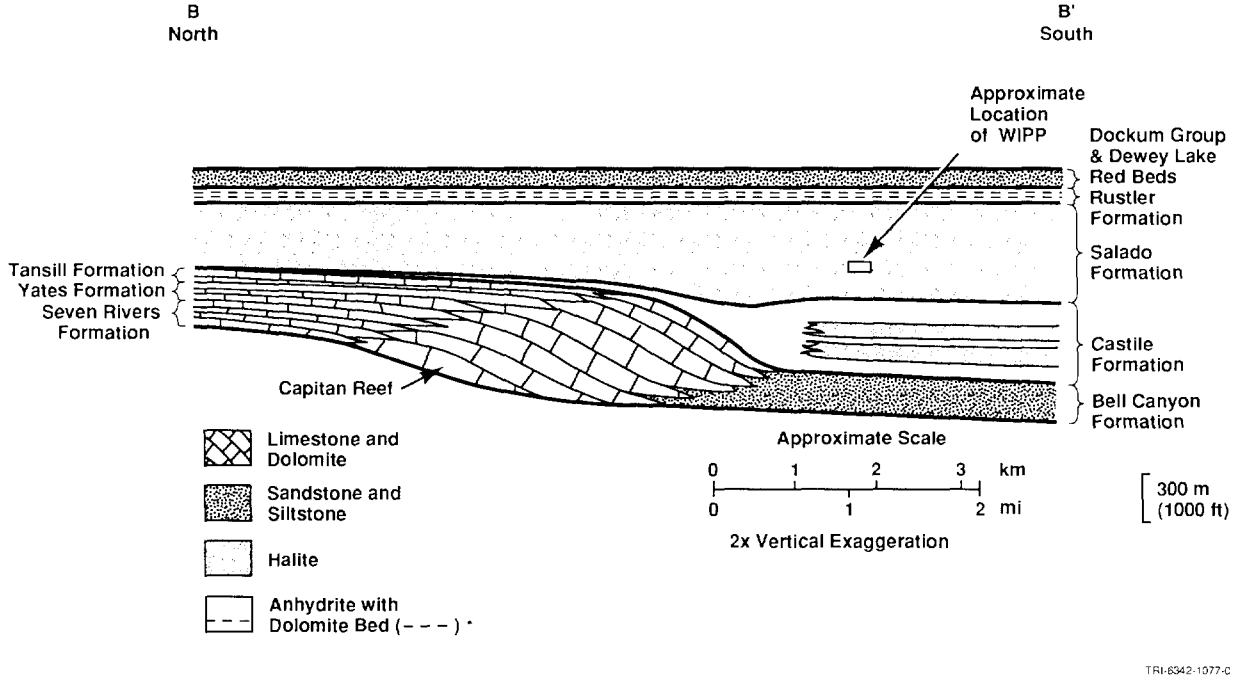

Figure 5-5. Schematic North-South Cross Section through the Northern Delaware Basin (modified from Davies, 1984). Note extreme vertical exaggeration. Approximate location of line of section shown on Figure 5-1.

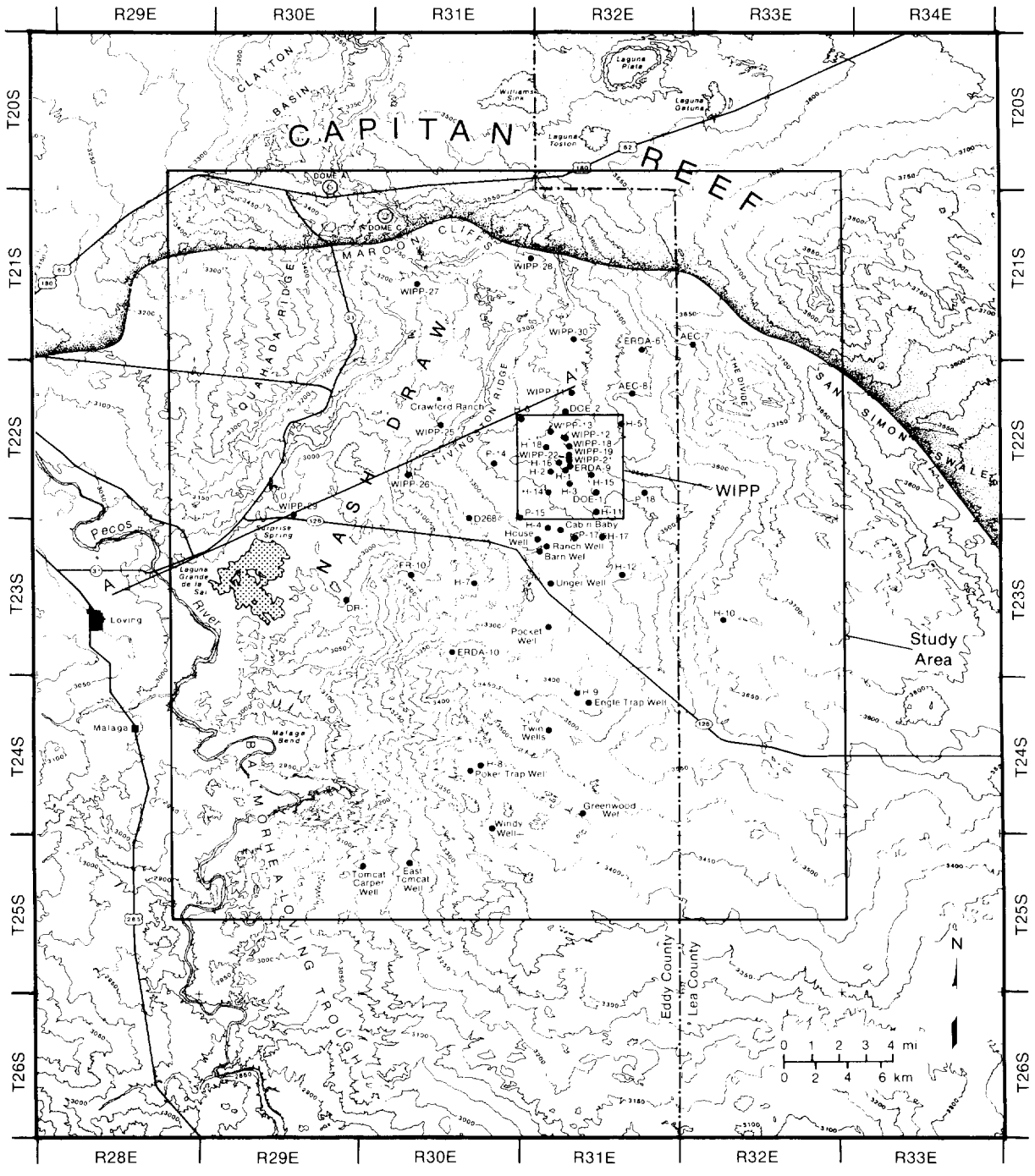

TRI-6342-612-6

Figure 5-6. Map of the WIPP Vicinity Showing the Proposed Land-Withdrawal Area, the Study Area of Brinster (1991), and the Location of Observation Wells (Haug et al., 1987; Brinster, 1991).

within the upper portion of the Bell Canyon Formation occur as long, sinuous channels separated by siltstones, reflecting their deposition by density currents that flowed into the deep basin from the Capitan Reef (Harms and Williamson, 1988). These sandstones have been targets for hydrocarbon exploration elsewhere in the Delaware Basin and are of interest for the WIPP performance assessment because they are the first units containing extensive aquifers below the evaporite sequence that hosts the repository.

Simulations of undisturbed repository performance do not include the Bell Canyon Formation because a thick sequence of evaporites with very low permeability separates the formation from the overlying units. Simulations of human intrusion scenarios do not include a borehole pathway for fluid migration between the Bell Canyon Formation (or deeper units) and the repository. Relatively little is known about the head gradient that would drive flow along this pathway, but data from five wells in the Bell Canyon Formation suggest that flow would be slight, and, in an uncased hole, downward because of brine density effects (Mercer, 1983; Beauheim, 1986; Lappin et al., 1989).

Capitan Limestone

The Capitan Limestone is not present at the WIPP but is a time-stratigraphic equivalent of the Bell Canyon and Castile Formations to the west, north, and east (Figures 5-1, 5-3). The unit is a massive limestone ranging from 76 to 230 m (250 to 750 ft) thick. Dissolution and fracturing have enhanced effective porosity, and the Capitan is a major aquifer in the region, providing the principal water supply for the city of Carlsbad. Upward flow of groundwater from the Capitan aquifer may be a factor in dissolution of overlying halite and the formation of breccia pipes. Existing breccia pipes are limited to the vicinity of the reef, as is the active subsidence in San Simon Swale (Figure 5-6) (Brinster, 1991).

Castile Formation

The Castile Formation is approximately 470 m (1540 ft) thick at the WIPP and contains anhydrites with intercalated limestones near the base and halite layers in the upper portions. Primary porosity and permeability in the Castile Formation are extremely low. However, approximately 18 wells in the region have encountered brine reservoirs in fractured anhydrite in the Castile Formation (Brinster, 1991). Hydrologic and geochemical data have been interpreted as indicating that these brine occurrences are hydraulically isolated (Lambert and Mercer, 1978; Lappin, 1988). Fluid may be derived from interstitial entrapment of connate water after deposition (Popielak et al., 1983), dehydration of the original gypsum to anhydrite (Popielak et al., 1983), or intermittent movement of meteoric waters from the Capitan aquifer

into the fractured anhydrites between 360,000 and 880,000 years ago (Lambert and Carter, 1984). Pressures within these brine reservoirs are greater than those at comparable depths in other relatively permeable units in the region and range from 7 to 17.4 MPa (Lappin et al., 1989).

Pressurized brine in the Castile Formation is of concern for performance assessment because occurrences have been found at WIPP-12 within the WIPP land-withdrawal area and at ERDA-6 and other wells in the vicinity. The WIPP-12 reservoir is at a depth of 918 m (3012 ft), about 250 m (820 ft) below the repository horizon, and is estimated to contain 2.7×10^6 m^3 (1.7×10^7 barrels) of brine at a pressure of 12.7 MPa (Lappin et al., 1989). This pressure is greater than the nominal freshwater hydrostatic pressure at that depth of 9 MPa and is slightly greater than the nominal hydrostatic pressure for a column of equivalent brine at that depth of 11.1 MPa. The brine is saturated, or nearly so, with respect to halite, and has little or no potential to dissolve the overlying salt (Lappin et al., 1989). Brine could, however, reach the repository through an intrusion borehole.

Early geophysical surveys mapped a structurally disturbed zone in the vicinity of the WIPP that may correlate with fracturing or development of secondary porosity within the Castile Formation; this zone could possibly contain pressurized brine (Borns et al., 1983). Later electromagnetic surveys indicated that the brine present at WIPP-12 could underlie part of the waste panels (Earth Technology Corporation, 1988). WIPP-12 data are therefore used to develop a conceptual model of the brine reservoir for analyzing scenarios that include the penetration of pressurized brine. The numerical model for the Castile Formation brine reservoir is described in Volume 2 of this report. Data are summarized in Volume 3 of this report.

Salado Formation

The Salado Formation is about 600 m (1970 ft) thick at the WIPP and contains bedded halite rhythmically interbedded with anhydrite, polyhalite, glauberite, and some thin mudstones (Adams, 1944; Bachman, 1981; Mercer, 1983). Unlike the underlying Castile Formation, the Salado Formation overlaps the Capitan Limestone and extends eastward beyond the reef for many kilometers into west Texas (Figure 5-3). Erosion has removed the Salado Formation from the western portion of the basin (Figure 5-1).

Where the Salado Formation is intact and unaffected by dissolution, circulation of groundwater is extremely slow because primary porosity and open fractures are lacking in the plastic salt (Mercer, 1983; Brinster, 1991). The formation is not dry, however. Interstitial brine seeps into the repository at rates up to approximately 0.01 ℓ/day/m of tunnel (Bredehoeft, 1988; Nowak et al., 1988), and the Salado is assumed to be saturated

(Brinster, 1991). Porosity is estimated to be approximately 0.001 (Mercer, 1983, 1987; Powers et al., 1978a,b; Bredehoeft, 1988). Permeability of the formation is very low but measurable, with an average value of 0.05 microdarcies (5×10^{-20} m^2) reported by Powers et al. (1978a,b) from well tests. This value corresponds approximately to a hydraulic conductivity of approximately 5×10^{-13} m/s (1×10^{-7} ft/d). In situ testing of halite in the repository indicates lower permeabilities ranging from 1 to 100 nanodarcies (10^{-22} to 10^{-20} m^2) (Stormont et al., 1987; Beauheim et al., 1990), suggesting that the higher values may reflect properties of disturbed rock (Brinster, 1991).

Rustler-Salado Contact Zone

In the vicinity of Nash Draw, the contact between the Rustler and Salado Formations is an unstructured residuum of gypsum, clay, and sandstone created by dissolution of halite. The residuum becomes thinner to the east and intertongues with clayey halite of the unnamed lower member of the Rustler Formation. Mercer (1983) concluded on the basis of brecciation at the contact that dissolution in Nash Draw occurred after deposition of the Rustler Formation. In shafts excavated at the WIPP, the residuum shows evidence of channeling and filling, fossils, and bioturbation, indicating that some dissolution occurred before Rustler deposition (Holt and Powers, 1988).

The residuum ranges in thickness in the vicinity of the WIPP from 2.4 m (7.9 ft) in P-14 east of Nash Draw to 33 m (108 ft) in WIPP-29 within Nash Draw (Mercer, 1983). Measured hydraulic conductivity values for the residuum are highest at Nash Draw (up to 10^{-6} m/s [10^{-1} ft/d]), and three to six orders of magnitude lower to the east (Brinster, 1991). Porosity estimates range from 0.15 to 0.33 (Hale and Clebsch, 1958; Robinson and Lang, 1938; Geohydrology Associates, Inc., 1979; and Mercer, 1983).

Rustler Formation

The Rustler Formation is 95 m (312 ft) thick at the WIPP (as measured in ERDA-9) and ranges in the area from a minimum of 8.5 m (28 ft) where thinned by dissolution and erosion west of the repository to a maximum of 216 m (709 ft) to the east (Brinster, 1991). Overall, the formation is composed of about 40 percent anhydrite, 30 percent halite, 20 percent siltstone and sandstone, and 10 percent anhydritic dolomite (Lambert, 1983). On the basis of outcrops in Nash Draw west of the WIPP, the formation is divided into four formally named members and a lower unnamed member (Vine, 1963). These five units (Vine, 1963; Mercer, 1983) are, in ascending order, the unnamed lower member (oldest), the Culebra Dolomite Member, the Tamarisk Member, the Magenta Dolomite Member, and the Forty-niner Member (youngest) (Figure 5-7).

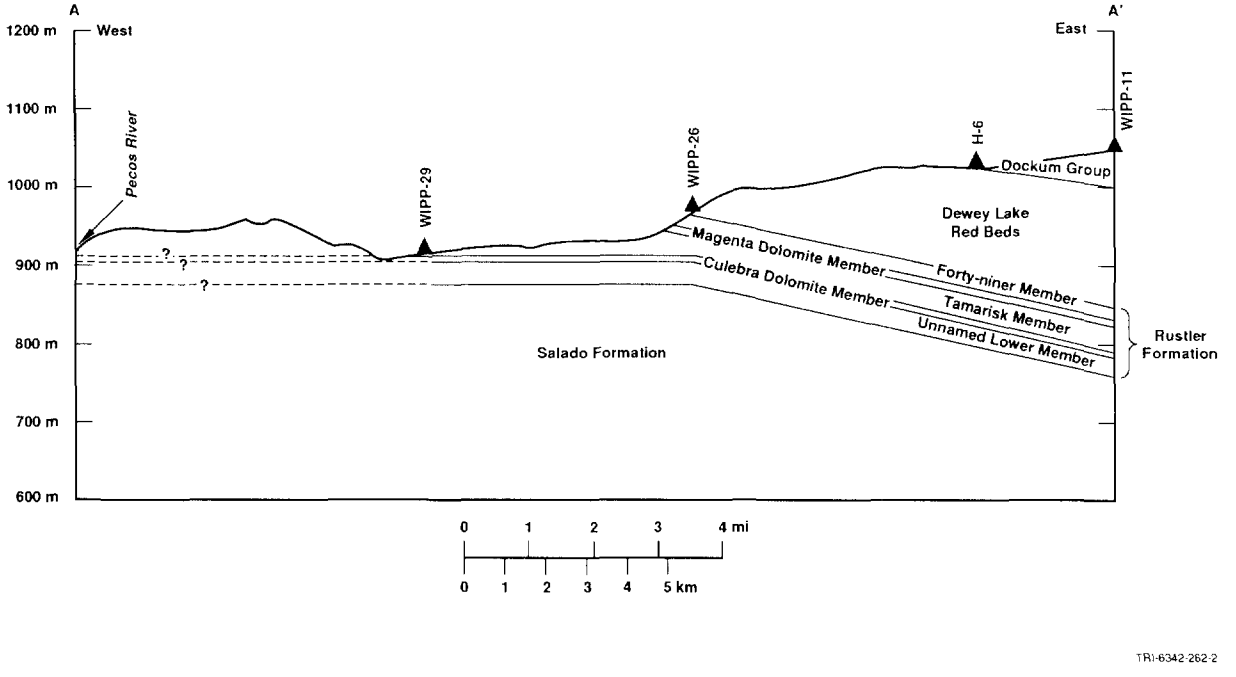

Figure 5-7. East-West Cross Section Showing Stratigraphy of the Rustler Formation and the Dewey Lake Red Beds (modified from Brinster, 1991). Note vertical exaggeration. Location of cross section is shown on Figure 5-6.

The Unnamed Lower Member

The unnamed lower member is about 36 m (118 ft) thick at the WIPP and thickens slightly to the east. The unit is composed mostly of fine-grained silty sandstones and siltstones interbedded with anhydrite (converted to gypsum at Nash Draw) west of the WIPP. Increasing amounts of halite are present to the east. Halite is present over the WIPP (Figure 5-8) but is absent north and south of the WIPP where the topographic expression of Nash Draw extends eastward. Distribution of halite within this and other members of the Rustler Formation is significant because, as is discussed in the following section, there is an apparent correlation between the absence of halite and increased transmissivity in the Culebra Dolomite Member.

The basal interval of the unnamed lower member contains siltstone and sandstone of sufficient transmissivity to allow groundwater flow. Transmissivities of 2.9×10^{-10} m^2/s (2.7×10^{-4} ft^2/d) and 2.4×10^{-10} m^2/s (2.2×10^{-4} ft^2/d) were calculated from tests at H-16 that included this interval (Beauheim, 1987a). Transmissivity in the lower portion of the unnamed member is believed to increase to the west, where dissolution in the underlying Rustler-Salado contact zone has caused fracturing of the sandstone and siltstone (Beauheim and Holt, 1990).

The remainder of the unnamed lower member contains mudstones, anhydrite, and variable amounts of halite. Hydraulic conductivity of these lithologies is extremely low: tests of mudstones and claystones in the waste-handling shaft gave hydraulic conductivity values ranging from 6×10^{-15} m/s (2×10^{-9} ft/d) to 1×10^{-13} m/s (3×10^{-8} ft/d) (Saulnier and Avis, 1988; Brinster, 1991).

Culebra Dolomite Member

The Culebra Dolomite Member of the Rustler Formation is microcrystalline dolomite or dolomitic limestone with solution cavities (Vine, 1963). In the vicinity of the WIPP, it ranges in thickness from 4 to 11.6 m (13 to 38.3 ft) and has a mean thickness of about 7 m (23 ft). Outcrops of the Culebra Dolomite occur in the southern part of Nash Draw and along the Pecos River.

The Culebra Dolomite has been identified as the most likely pathway for release of radionuclides to the accessible environment, and hydrologic research has concentrated on the unit for over a decade (Mercer and Orr, 1977; Mercer and Orr, 1979; Mercer, 1983; Mercer et al., 1987; Beauheim, 1987a,b; LaVenue et al., 1988; Davies, 1989; LaVenue et al., 1990; Cauffman et al., 1990; Brinster, 1991). Hydraulic data are available from 41 well locations in the WIPP vicinity (Cauffman et al., 1990).

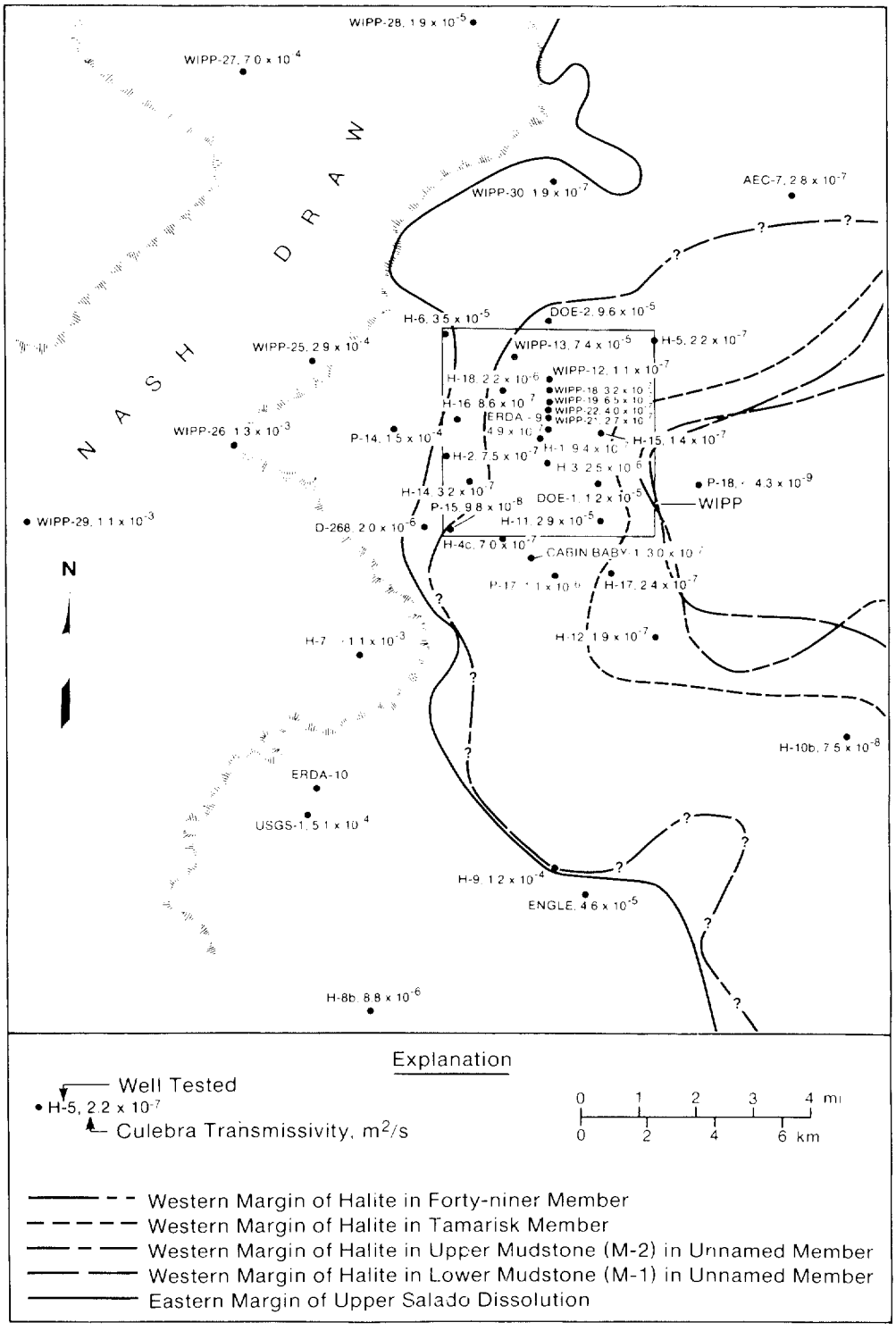

TRI-6330-94-2

Figure 5-8. Rustler Formation Halite and Culebra Dolomite Transmissivity around the WIPP (Lappin et al., 1989).

Hydraulic conductivity of the Culebra varies six orders of magnitude from east to west in the vicinity of the WIPP (Figure 5-9), ranging from 2×10^{-10} m/s (6×10^{-5} ft/d) at P-18 east of the WIPP to 1×10^{-4} m/s (6×10^{1} ft/d) at H-7 in Nash Draw (Brinster, 1991). This variation is controlled by fracturing in the Culebra caused either by subsidence associated with post-depositional dissolution of salt in the Rustler Formation (Snyder, 1985), or by stress reduction from removal of overburden (Holt and Powers, 1988), or possibly from a combination of both processes. Present distribution of halite in the Rustler Formation correlates with hydraulic conductivity in the Culebra (Figure 5-8), suggesting a causal link between the controlling processes.

Measured matrix porosities of the Culebra Dolomite range from 0.03 to 0.30 (Lappin et al., 1989; Kelley and Saulnier, 1990). Fracture porosity values have not been measured directly, but interpreted values from tracer tests at the H-3 and H-11 hydropads are 2×10^{-3} and 1×10^{-3}, respectively (Kelley and Pickens, 1986).

Tamarisk Member

The Tamarisk Member ranges in thickness from 8 to 84 m (26 to 276 ft) in southeastern New Mexico, and is about 36 m (118 ft) thick at the WIPP. The Tamarisk consists of mostly anhydrite or gypsum interbedded with thin layers of claystone and siltstone. Near Nash Draw, dissolution has removed evaporites from the Tamarisk Member, and the Magenta and Culebra Dolomites are separated only by a few meters of residue (Brinster, 1991).

Unsuccessful attempts were made in two wells, H-14 and H-16, to test a 2.4 m (7.9 ft) sequence of the Tamarisk Member that consists of claystone, mudstone, and siltstone overlain and underlain by anhydrite. Permeability was too low to measure in either well within the time allowed for testing, but Beauheim (1987a) estimated the transmissivity of the claystone sequence to be one or more orders of magnitude less than that of siltstone in the unnamed lower member, which yielded values of 2.9×10^{-10} m^2/s (2.7×10^{-4} ft^2/d) and 2.4×10^{-10} m^2/s (2.2×10^{-4} ft^2/d).

Magenta Dolomite Member

The Magenta Dolomite Member of the Rustler Formation is a fine-grained dolomite that ranges in thickness from 4 to 8 m (13 to 26 ft) and is about 6 m (19 ft) thick at the WIPP. The Magenta is saturated except near outcrops along Nash Draw, and hydraulic data are available from 14 wells. Hydraulic conductivity ranges over five orders of magnitude from 5.0×10^{-10} to 5.0×10^{-5} m/s (1×10^{-4} to 1×10^{1} ft/d).

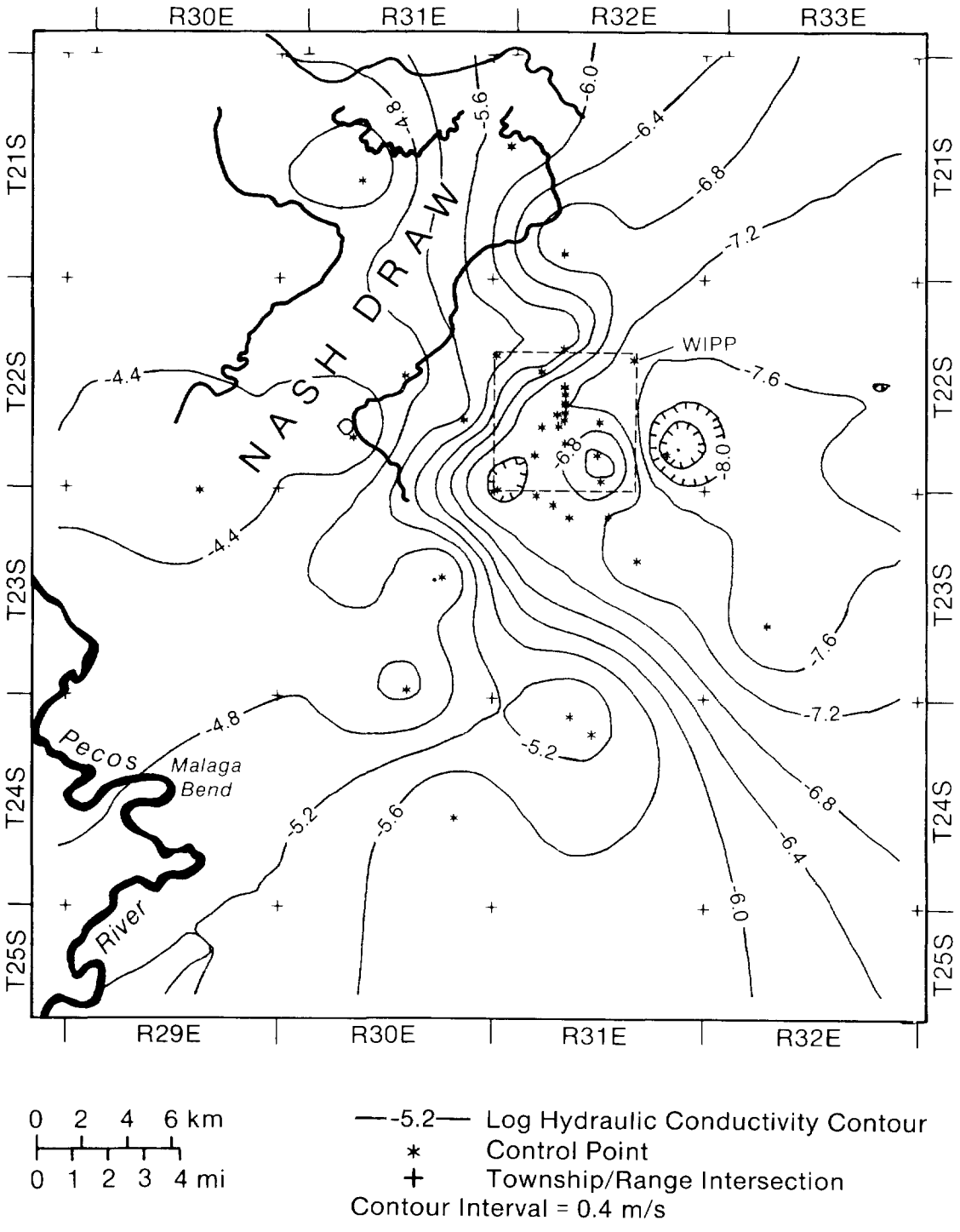

Figure 5-9. Log Hydraulic Conductivities (measured in m/s) of the Culebra Dolomite Member of the Rustler Formation (Brinster, 1991).

A contour map of log hydraulic conductivities of the Magenta Dolomite Member based on sparse data (Figure 5-10) shows a decrease in conductivity from west to east, with slight indentations of the contours north and south of the WIPP that correspond to the topographic expression of Nash Draw (Brinster, 1991). Comparison of Figures 5-9 and 5-10 show that in most locations conductivity of the Magenta is one to two orders of magnitude less than that of the Culebra.

No porosity measurements have been made on the Magenta Dolomite Member. Beauheim (1987a) assumed a representative dolomite porosity of 0.20 for interpretations of well tests.

Forty-niner Member

The uppermost member of the Rustler Formation, the Forty-niner Member, is about 20 m (66 ft) thick throughout the WIPP area and consists of low-permeability anhydrite and siltstone. Tests in H-14 and H-16 yielded hydraulic conductivities of about 5×10^{-9} m/s (1×10^{-3} ft/d) and 5×10^{-10} m/s (1×10^{-4} ft/d) respectively (Beauheim, 1987a).

Supra-Rustler Rocks

Where present, the supra-Rustler units collectively range in thickness from 4 to 536 m (13 to 1758 ft). Regionally, the supra-Rustler units thicken to the east and form a uniform wedge of overburden across the region (Brinster, 1991). Fine-grained sandstones and siltstones of the Dewey Lake Red Beds (Pierce Canyon Red Beds of Vine, 1963) conformably overlie the Rustler Formation at the WIPP and are the uppermost Permian rocks in the region. The unit is absent in Nash Draw, is as much as 60 m (196 ft) thick where present west of the WIPP, and can be over 200 m (656 ft) thick east of the WIPP (Figures 5-4, 5-7). East of the WIPP, the Dewey Lake Red Beds are unconformably overlain by Mesozoic rocks of the Triassic Dockum Group. These rocks are absent above the repository and reach a thickness of over 100 m (328 ft) in western Lea County. East of the WIPP, Triassic and, in some locations, Cretaceous rocks are unconformably overlain by the Pliocene Ogallala Formation. At the WIPP, Permian strata are overlain by discontinuous sands and gravels of the Pleistocene Gatuña Formation, the informally named Pleistocene Mescalero caliche, and Holocene soils.

Drilling in the Dewey Lake Red Beds has not identified a continuous zone of saturation. Some localized zones of relatively high permeability were identified by loss of drilling fluids at DOE-2 and H-3d (Mercer, 1983; Beauheim, 1987a). Thin and apparently discontinuous saturated sands were identified in the upper Dewey Lake Red Beds at H-1, H-2, and H-3 (Mercer and

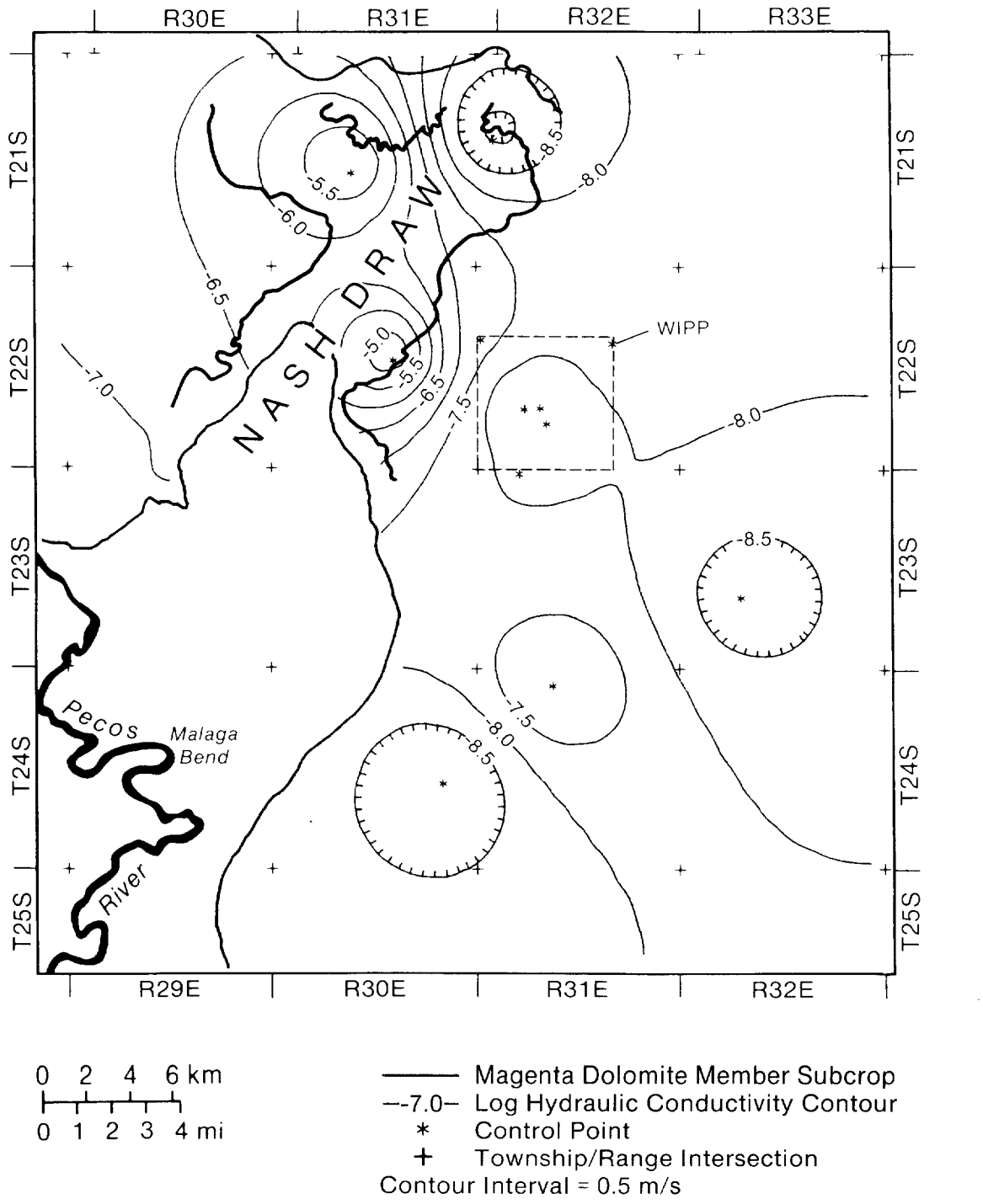

Figure 5-10. Log Hydraulic Conductivities (measured in m/s) of the Magenta Dolomite Member of the Rustler Formation (Brinster, 1991).

Orr, 1979; Mercer, 1983). Several wells operated by the J. C. Mills Ranch (James Ranch) south of the WIPP produce sufficient quantities of water from the Dewey Lake Red Beds to supply livestock (Brinster, 1991).

Hydrologic properties of supra-Rustler rocks are relatively poorly understood because of the lack of long-term hydraulic tests. Hydraulic conductivity of the Dewey Lake Red Beds, assuming saturation, is estimated to be 10^{-8} m/s (10^{-3} ft/d), corresponding to the hydraulic conductivity of fine-grained sandstone and siltstone (Mercer, 1983; Davies, 1989). Porosity is estimated to be about 0.20, which is representative of fine-grained sandstone (Brinster, 1991).

5.1.3 CLIMATE

The present climate of southeastern New Mexico is arid to semi-arid (Swift, 1991a). Annual precipitation is dominated by a late summer monsoon, when solar warming of the continent creates an atmospheric pressure gradient that draws moist air inland from the Gulf of Mexico (Cole, 1975). Winters are cool and generally dry.

Mean annual precipitation at the WIPP has been estimated to be between 28 and 34 cm/yr (10.9 and 13.5 in/yr) (Hunter, 1985). At Carlsbad, 42 km (26 mi) west of the WIPP and 100 m lower in elevation, 53-year (1931-1983) annual means for precipitation and temperature are 32 cm/yr (12.6 in/yr) and 17.1°C (63°F) (University of New Mexico, 1989). Freshwater pan evaporation in the region is estimated to be 280 cm/yr (110 in/yr) (U.S. DOE, 1980a).

Short-term climatic variability can be considerable in the region. For example, the 105-year (1878 to 1982) precipitation record from Roswell, 135 km northwest of the WIPP and 60 m higher in elevation, shows an annual mean of 27 cm/yr (10.6 in/yr) with a maximum of 84 cm/yr (32.9 in/yr) and a minimum of 11 cm/yr (4.4 in/yr) (Hunter, 1985).

5.1.4 PALEOCLIMATES AND CLIMATIC VARIABILITY

Geologic data from the American Southwest show repeated alternations of wetter and drier climates throughout the Pleistocene, which correspond to global cycles of glaciation and deglaciation (Swift, 1991a). Climates in southeastern New Mexico have been coolest and wettest during glacial maxima, when the North American ice sheet reached its southern limit roughly 1200 km (750 mi) north of the WIPP. Mean annual precipitation at these extremes was approximately twice that of the present. Mean annual temperatures may have been as much as 5°C (9°F) cooler than at present. Modeling of global circulation patterns suggests these changes resulted from the disruption and

southward displacement of the winter jet stream by the ice sheet, causing an increase in the frequency and intensity of winter storms throughout the Southwest (COHMAP members, 1988).

Data from plant and animal remains and paleo-lake levels permit quantitative reconstructions of precipitation in southeastern New Mexico during the advance and retreat of the last major ice sheet in North America. Figure 5-11 shows estimated mean annual precipitation for the WIPP for the last 30,000 years, based on an estimated present precipitation of 30 cm/yr (11.8 in/yr). The precipitation maximum coincides with the maximum advance of the ice sheet 22,000 to 18,000 years ago. Since the final retreat of the ice sheet approximately 10,000 years ago, conditions have been generally dry, with intermittent and relatively brief periods when precipitation may have approached glacial levels. Causes of these Holocene fluctuations are uncertain (Swift, 1991a).

Based on the past record, it is reasonable to assume that climate will change at the WIPP during the next 10,000 years, and the performance-assessment hydrologic model must allow for climatic variability. Presently available long-term climate models are incapable of resolution on the spatial scales required for numerical predictions of future climates at the WIPP (e.g., Hansen et al., 1988; Mitchell, 1989; Houghton et al., 1990), and simulations using these models are of limited value beyond several hundreds of years into the future. Direct modeling of climates during the next 10,000 years has not been attempted for WIPP performance assessment. Instead, performance-assessment modeling uses past climates to set limits for future variability (Swift, 1991a; Swift, October 10, 1991, memo in Volume 3, Appendix A). The extent to which unprecedented climatic changes caused by human-induced changes in the composition of the Earth's atmosphere may invalidate this assumption is uncertain. Presently available models of climatic response to an enhanced greenhouse effect (e.g., Mitchell, 1989; Houghton et al., 1990) do not predict changes of a larger magnitude than those of the Pleistocene (although predicted rates of change are far greater), suggesting the choice of a Pleistocene analog for future climatic extremes will remain appropriate. Future WIPP performance assessments will re-examine the assumption, taking into account the result of ongoing research in the fields of climate change.

Glacial periodicities have been stable for the last 800,000 years, with major peaks occurring at intervals of 19,000, 23,000, 41,000 and 100,000 years, corresponding to variations in the Earth's orbit (Milankovitch, 1941; Hays et al., 1976; Imbrie et al., 1984; Imbrie, 1985). Barring anthropogenic changes in the Earth's climate, relatively simple modeling of the nonlinear climatic response to astronomically controlled changes in the amount of solar energy reaching the Earth suggests that the next glacial maximum will occur in approximately 60,000 years (Imbrie and Imbrie, 1980). Regardless of

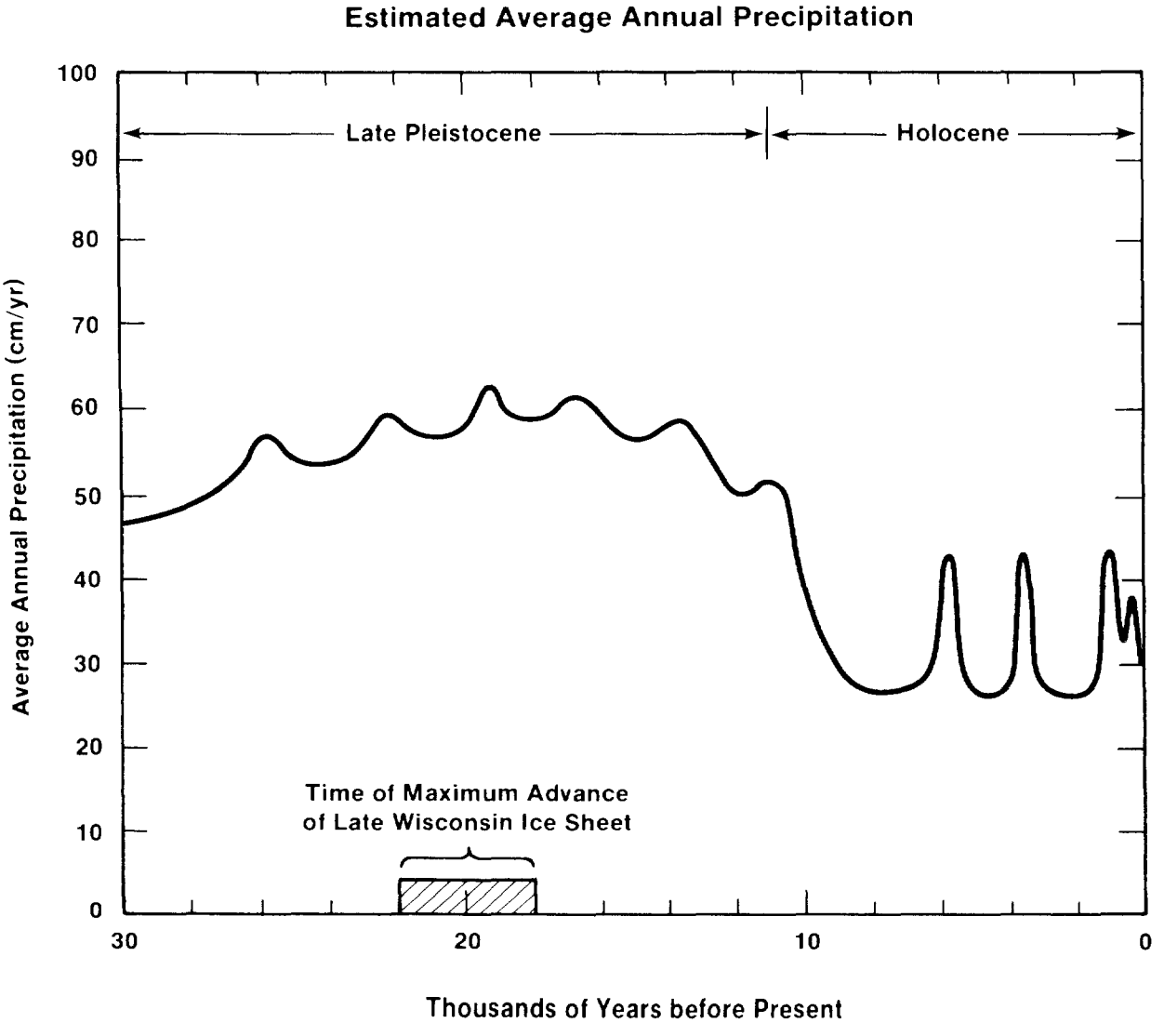

Figure 5-11. Estimated Mean Annual Precipitation at the WIPP during the Late Pleistocene and Holocene (modified from Swift, 1991a).

anthropogenic effects, short-term climatic fluctuations comparable to those of the last 10,000 years are probable during the next 10,000 years and must be included in performance-assessment modeling.

Climatic variability will be incorporated into the modeling system conceptually by varying groundwater flow into the Culebra Dolomite Member of the Rustler Formation as a scaled function of precipitation (Swift, October 10, 1991, memo in Volume 3, Appendix A). Short-term variability in precipitation is approximated with a periodic function that generates peaks of twice present precipitation every 2000 years and a future climate that is, on the average, wetter than that of the present one half of the time. Long-term, glacial increase in precipitation is approximated with a periodic function that reaches a maximum of twice present precipitation in 60,000 years. For this performance assessment, climatic variability has been included in the consequence analysis by varying boundary conditions of the Culebra groundwater-flow model as a scaled function of future precipitation. As discussed further in Section 5.1.9-Culebra Dolomite Groundwater Flow and Transport in this chapter and in Volume 2, potentiometric heads along a portion of the northern boundaries of the regional model domain were varied between present elevation and the ground surface, reaching maximum elevations at times of maximum precipitation.

5.1.5 SURFACE WATER

The Pecos River, the principal surface-water feature in southeastern New Mexico, flows southeastward in Eddy County approximately parallel to the axis of the Delaware Basin (Figure 5-1) and drains into the Rio Grande in western Texas. In the vicinity of the WIPP, the drainage system includes small ephemeral creeks and draws and has a drainage area of about 50,000 km^2 (20,000 mi^2). At its closest point the Pecos River is about 20 km (12 mi) southwest of the WIPP (Brinster, 1991).

Very little, if any, of the surface water from Nash Draw reaches the Pecos River (Robinson and Lang, 1938; Lambert, 1983). Several shallow, saline lakes in Nash Draw cover an area of about 16 km^2 (6 mi^2) southwest of the WIPP (Figure 5-6) and collect precipitation, surface drainage, and groundwater discharge from springs and seeps. The largest lake, Laguna Grande de la Sal, has existed throughout historic time. Since 1942, smaller, intermittent, saline lakes have formed in closed depressions north of Laguna Grande de la Sal as a result of effluent from potash mining and oil-well development in the area (Hunter, 1985). Effluent has also enlarged Laguna Grande de la Sal.

5.1.6 THE WATER TABLE

No detailed maps of the water table are available for the vicinity of the WIPP. Outside of the immediate vicinity of the Pecos River, where water is pumped for irrigation from an unconfined aquifer in the alluvium, near-surface rocks are either unsaturated or of low permeability and do not produce water in wells. Tests of the lower Dewey Lake Red Beds in H-14 that were intended to provide information about the location of the water table proved inconclusive because of low transmissivities (Beauheim, 1987a). Livestock wells completed south of the WIPP in the Dewey Lake Red Beds at the J. C. Mills Ranch (James Ranch) may produce from perched aquifers (Mercer, 1983; Lappin et al., 1989), or they may produce from transmissive zones in a continuously saturated zone that is elsewhere unproductive because of low transmissivities.

Regionally, water-table conditions can be inferred for the more permeable units where they are close to the surface and saturated. The Culebra Dolomite may be under water-table conditions in and near Nash Draw and near regions of Rustler Formation outcrop in Bear Grass Draw and Clayton Basin north of the WIPP (Figure 1-6). The Magenta Dolomite is unsaturated and presumably above the water table at WIPP-28 and H-7 near Nash Draw. Water-table conditions exist in the Rustler-Salado contact zone near where it discharges into the Pecos River at Malaga Bend (Brinster, 1991).

5.1.7 REGIONAL WATER BALANCE

Hunter (1985) examined the overall water budget of approximately 5180 km^2 (2000 mi^2) surrounding the WIPP. Water inflow to the area comes from precipitation, surface-water flow in the Pecos River, groundwater flow across the boundaries of the region, and water imported to the region for human use. Outflow from the water-budget model occurs as stream-water flow in the Pecos River, groundwater flow, and evapotranspiration. Volumes of water gained by precipitation and lost by evapotranspiration are more than one order of magnitude larger than volumes gained or lost by other means.

Uncertainties about precipitation, evapotranspiration, and water storage within the system limit the usefulness of estimates of groundwater recharge based on water budget analyses. Regionally, Hunter (1985) concluded that approximately 96 percent of precipitation was lost directly to evapotranspiration, without entering the surface or groundwater flow systems. Within the 1000 km^2 immediately around the WIPP, where no surface runoff occurs and all precipitation not lost to evapotranspiration must recharge groundwater, a separate analysis suggested evapotranspiration may be as high as 98 to 99.5 percent (Hunter, 1985). Direct measurements of infiltration rates are not available from the WIPP vicinity.

5.1.8 GROUNDWATER FLOW ABOVE THE SALADO FORMATION

Well tests indicate that the three most permeable units in the vicinity of the WIPP above the Salado Formation are the Culebra Dolomite and Magenta Dolomite Members of the Rustler Formation and the residuum at the Rustler-Salado contact zone. The vertical permeabilities of the strata separating these units are not known, but lithologies and the potentiometric and geochemical data summarized below suggest that for most of the region, vertical flow between the units is very slow. Although preliminary hydrologic modeling indicates that some component of vertical flow between units can be compatible with observed conditions (Haug et al., 1987; Davies, 1989), the units are assumed to be perfectly confined for the 1991 performance-assessment calculations.

Potentiometric Surfaces

Mercer (1983) and Brinster (1991) have constructed potentiometric-surface maps for the Rustler-Salado residuum, the Culebra Dolomite, and the Magenta Dolomite. Brinster's (1991) maps are reproduced here (Figures 5-12, 5-13, and 5-14). These maps show the level to which fresh water would rise in a well open to each unit. Contours are based on measured heads (water elevations in wells) that have been adjusted to freshwater-equivalent heads (the level to which fresh water would rise in the same well). Maps for the Culebra and the Magenta Dolomites are based on data from 31 and 16 wells, respectively. The map for the Rustler-Salado residuum includes data from 14 wells and water elevations in the Pecos River, reflecting an assumption that water-table conditions exist in the unit near the river.

Because the data used to construct the potentiometric maps are sparse and unevenly distributed, interpretations must be made with caution. For example, the "bullseye" patterns visible in all three maps are controlled by single data points, and would probably disappear from the maps if sufficient data were available. Contours are most reliable where data are closely spaced, particularly in the immediate vicinity of the WIPP, and are least reliable where they have been extrapolated into areas of no data, such as the southeast portion of the mapped area. With these caveats noted, however, the potentiometric maps can be useful in drawing conclusions about flow both within and between the three units.

Flow of a constant-density liquid within an isotropic medium would be perpendicular to the potentiometric contours. Near the WIPP, localized regions have been identified where variations in brine density result in non-uniform gravitational driving forces and anomalous flow directions (Davies, 1989), and the effects of anisotropy on flow patterns are not fully

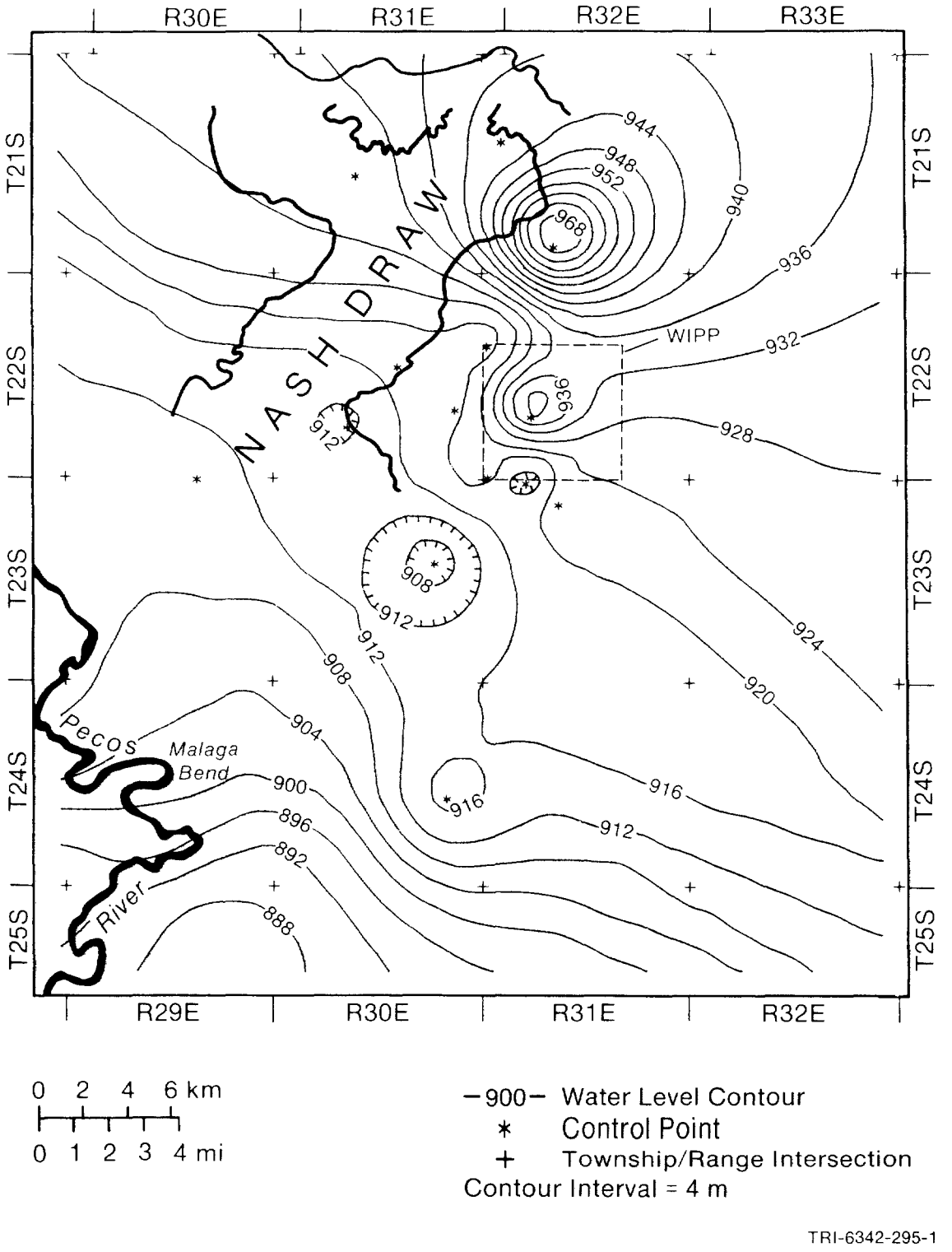

Figure 5-12. Adjusted Potentiometric Surface of the Rustler-Salado Residuum in the WIPP Vicinity (Brinster, 1991). Contours based on data from indicated wells and the elevation of the Pecos River.

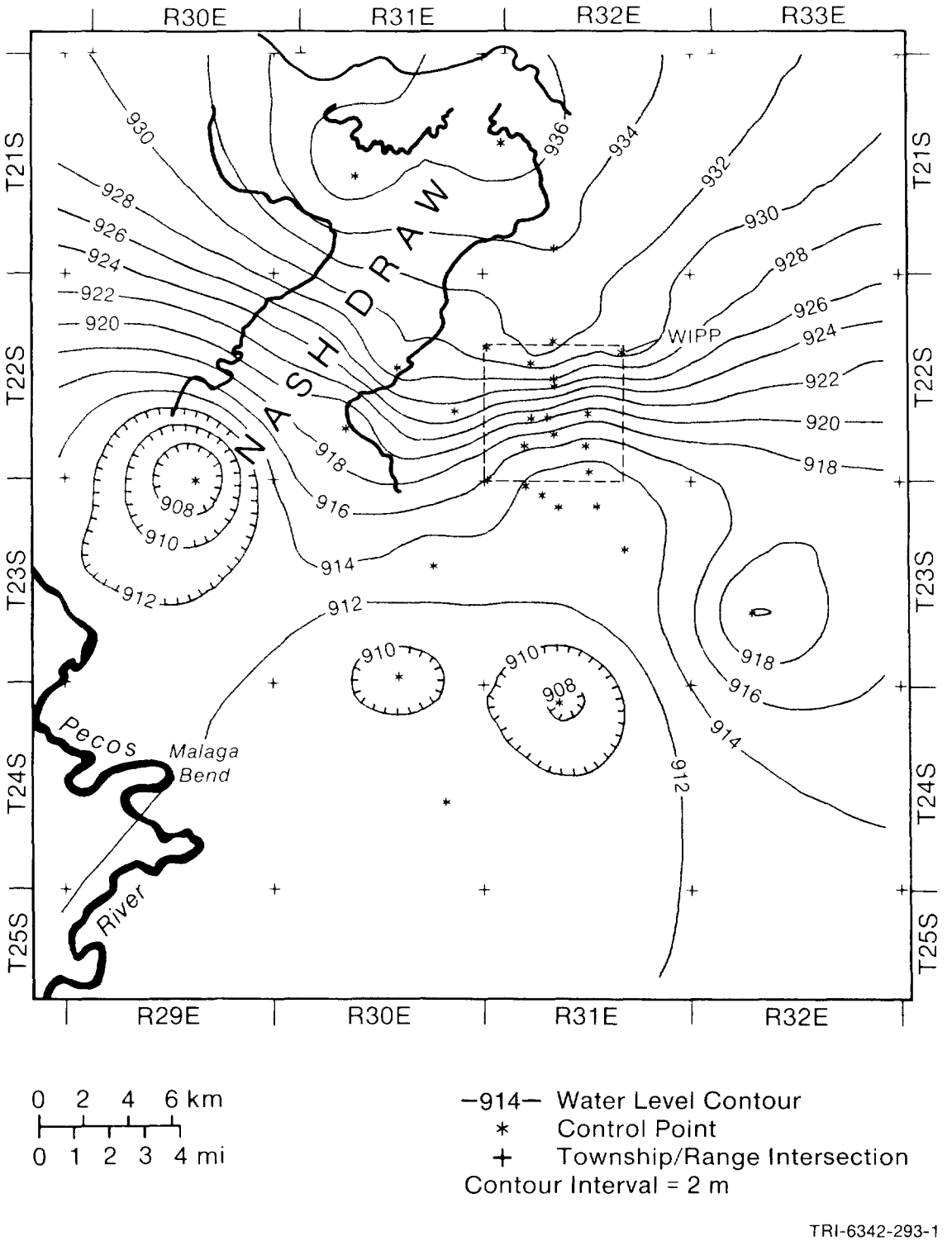

Figure 5-13. Adjusted Potentiometric Surface of the Culebra Dolomite Member of the Rustler Formation in the WIPP Vicinity (Brinster, 1991). Contours based on data from indicated wells.

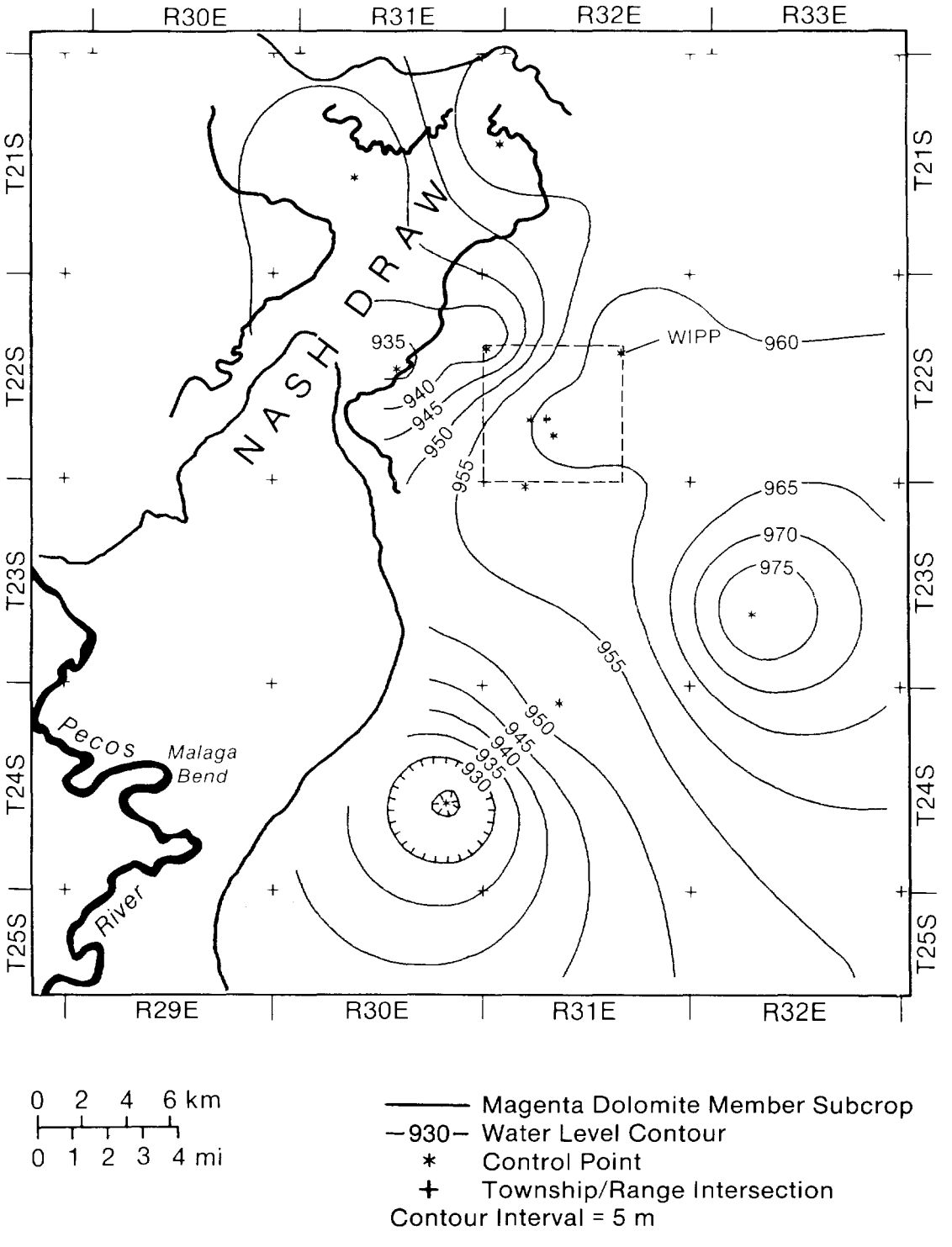

Figure 5-14. Adjusted Potentiometric Surface of the Magenta Dolomite Member of the Rustler Formation in the WIPP Vicinity (Brinster, 1991). Contours based on data from indicated wells.

understood. In general, however, flow in the Rustler-Salado residuum is from northeast to southwest. Flow in the Culebra is from north to south, and flow in the Magenta is from east to west in that portion of the map where data are sufficient to permit interpretation. Differences in flow directions may reflect long-term transient conditions (see "Recharge and Discharge" in Section 5.1.8-Confined Hydrostatigraphic Units) and indicate low permeability of the strata separating the three units: if the three functioned as a single aquifer, potentiometric maps would be similar.

Flow between units is also a function of hydraulic gradient and can be interpreted qualitatively from the potentiometric maps. Like lateral flow within units, vertical flow between units is from higher potentiometric levels to lower levels. Differences between the elevations of the potentiometric surfaces reflect low permeabilities of the intervening strata and slow rates of vertical leakage relative to rates of flow within the aquifers. Brinster (1991), Beauheim (1987a), and Holt et al. (in prep., summarized by Brinster, 1991) present analyses of vertical hydraulic gradients on a well-by-well basis. These analyses suggest that, if flow occurs, the direction of flow between the Magenta and the Culebra is downward throughout the WIPP area. Directly above the repository, flow may be upward from the Rustler-Salado residuum to the Culebra Dolomite. Elsewhere in the region, both upward and downward flow directions exist between the two units.

Groundwater Geochemistry

Major solute geochemical data are available for groundwater from the Rustler-Salado contact zone from 20 wells, from the Culebra Dolomite from 32 wells, and from the Magenta Dolomite from 12 wells (Siegel et al., 1991). Groundwater quality in all three units is poor, with total dissolved solids (TDS) exceeding 10,000 mg/ℓ (the concentration specified for regulation by the Individual Protection Requirements of the Standard) in most locations.

Waters from the Rustler-Salado residuum have the highest TDS concentrations of any groundwaters in the WIPP area. The lowest concentration reported from the unit is 70,000 mg/ℓ from H-7c southwest of the WIPP, and the highest is 410,000 mg/ℓ from H-5 at the northeast corner of the land-withdrawal area (Siegel et al., 1991).

Waters from the Magenta Dolomite are the least saline of those in the confined units. Within the land-withdrawal area, TDS concentrations range from approximately 4000 to 25,000 mg/ℓ. Higher values are reported from H-10 southeast of the WIPP, where the sample is of uncertain quality, and from WIPP 27 in Nash Draw, where groundwater chemistry has been altered by dumping of effluent from potash mines (Siegel et al., 1991).

Groundwater chemistry is variable in the Culebra Dolomite. A maximum TDS concentration of 240,000 mg/ℓ is reported from H-15 immediately east of the WIPP, and a minimum value of 2500 mg/ℓ is reported from H-8, 14 km (9 mi) southwest of the repository. Three other wells (H-7, H-9, and the Engle well), all south of the WIPP, also contain water with less than 10,000 mg/ℓ TDS. In a single test in February 1977, H-2 immediately west of the repository yielded water with a TDS concentration of 8900 mg/ℓ. Three subsequent tests over the following decade yielded TDS levels of 12,500, 13,000, and 11,000 mg/ℓ (Lappin et al., 1989).

Relative concentrations of major ions vary spatially within the Culebra Dolomite. Siegel et al. (1991) recognized four zones containing distinct hydrochemical facies (Figure 5-15) and related water chemistry to the distribution of halite in the Rustler Formation. Zone A contains a saline (about 2 to 3 molal) sodium chloride brine with a magnesium/calcium molar ratio greater than 1.2. Zone A waters occur eastward from the repository, in a region that corresponds roughly with the area of lowest transmissivity in the Culebra Dolomite. Halite is present in the unnamed lower member of the Rustler Formation throughout Zone A, and in the eastern portion of the region halite occurs in the upper members as well. Zone B is an area of dilute, calcium sulfate-rich water (ionic strength less than 0.1 molal) south of the repository. This region generally has high transmissivity in the Culebra Dolomite, and halite is absent from all members of the Rustler Formation. Zone C, extending from the repository west to Nash Draw, contains waters of variable composition with low to moderate ionic strength (0.3 to 1.6 molal), with magnesium/calcium molar ratios less than 1.2. Transmissivity is variable in this region, and halite is present in the Rustler Formation only to the east, in the unnamed lower member. Salinities are highest near the eastern edge of the zone. Zone D waters, found only in two wells in Nash Draw, are anomalously saline (3 to 6 molal) and have high potassium/sodium ratios that reflect contamination by effluent from potash mines.

Distribution of the hydrochemical facies may not be consistent with the inferred north-to-south flow of groundwater in the Culebra Dolomite. Specifically, less saline waters of Zone B are down-gradient from more saline waters in Zones A and C. Chapman (1988) suggested that direct recharge of fresh water from the surface could account for the characteristics of Zone B. As discussed in more detail below ("Recharge and Discharge" section), the inconsistency between chemical and potentiometric data could also result from a change in location and amount of recharge since the wetter climate of the last glacial maximum. Present flow in the Culebra could be transient, reflecting gradual drainage of a groundwater reservoir filled during the Pleistocene. Regional hydrochemical facies may not have equilibrated with

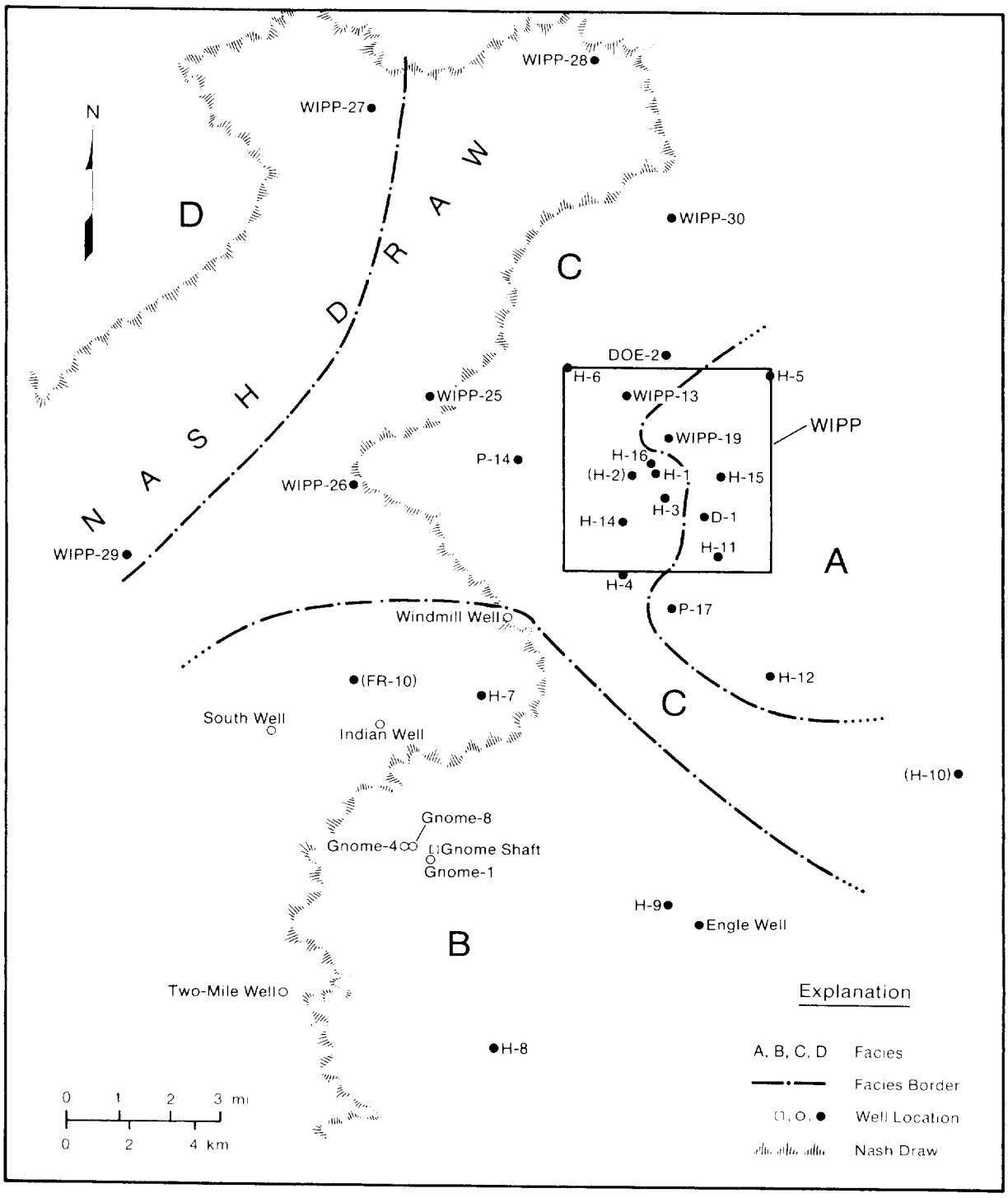

TRI-6331-78-0

Figure 5-15. Hydrochemical Facies in the Culebra Dolomite Member of the Rustler Formation (Siegel et al., 1991).

the modern flow regime and instead may reflect geographic distribution of halite during a past flow regime (Siegel and Lambert, 1991).

Recharge and Discharge

The only documented points of naturally occurring groundwater discharge in the vicinity of the WIPP are the saline lakes in Nash Draw and the Pecos River, primarily near Malaga Bend (Hunter, 1985; Brinster, 1991). Discharge into the lakes from Surprise Spring was measured at a rate of less than 0.01 m^3/s (0.35 ft^3/s) in 1942 (Hunter, 1985). Estimated total groundwater discharge into the lakes is 0.67 m^3/s (24 ft^3/s) (Hunter, 1985). Based on chemical and potentiometric data, Mercer (1983) concluded that discharge from the spring was from the Tamarisk Member of the Rustler Formation, and that the lakes were hydraulically isolated from the Culebra Dolomite and lower units. Lambert and Harvey's (1987) analysis of stable isotopes in water from Surprise Spring supports this conclusion: the isotopic compositions indicate that Surprise Spring and Laguna Grande de la Sal are not discharge points for the Culebra Dolomite.

Groundwater discharge into the Pecos River is many orders of magnitude larger than discharge into the saline lakes. Based on 1980 stream-flow gage data, Hunter (1985) estimated that groundwater discharge into the Pecos River between Avalon Dam north of Carlsbad and a point south of Malaga Bend was no more than approximately 9.2×10^{14} m^3/s (23,600 ac-ft/yr). Most of this gain in stream flow occurs near Malaga Bend and is the result of groundwater discharge from the residuum at the Rustler-Salado contact (Hale et al., 1954; Kunkler, 1980; Hunter, 1985; Brinster, 1991).

The only documented point of groundwater recharge is also near Malaga Bend, where an almost immediate water-level rise has been reported in a Rustler-Salado residuum well following a heavy rainstorm (Hale et al., 1954). This location is hydraulically down-gradient from the repository, and recharge here has little relevance to flow near the WIPP. Examination of the potentiometric-surface map for the Rustler-Salado residuum (Figure 5-12) indicates that some inflow must occur north of the WIPP, where freshwater-equivalent heads are highest. Additional inflow to the residuum may occur as leakage from overlying units, particularly where the units are close to the surface and under water-table conditions. Brinster (1991) proposed that inflow to the residuum (and other water-bearing units in the Rustler Formation) could also come from below, upward through breccia pipes from the Capitan aquifer north and east of the repository.

There is no direct evidence for the location of either recharge to or discharge from the Culebra Dolomite. The potentiometric-surface map (Figure 5-13) indicates recharge from the north and discharge to the south.

Mercer (1983) suggested that recharge from the surface probably occurred 15 to 30 km (9 to 19 mi) north of the WIPP at Clayton Basin and Bear Grass Draw, where the Rustler Formation crops out. Small amounts of inflow may also occur as leakage from overlying units throughout the region.

The potentiometric-surface map (Figure 5-13) indicates that flow in the Culebra Dolomite is toward the south. Some of this southerly flow may enter the Rustler-Salado residuum under water-table conditions near Malaga Bend and ultimately discharge into the Pecos River. Additional flow may discharge directly into the Pecos River or into alluvium in the Balmorhea-Loving Trough to the south (Figure 5-6) (Brinster, 1991).

Recharge to the Magenta Dolomite may also occur north of the WIPP in Bear Grass Draw and Clayton Basin (Mercer, 1983). The potentiometric-surface map indicates that discharge is toward the west in the vicinity of the WIPP, probably into the Tamarisk Member and the Culebra Dolomite near Nash Draw. Some discharge from the Magenta Dolomite may ultimately reach the saline lakes in Nash Draw. Additional discharge probably reaches the Pecos River at Malaga Bend or alluvium in the Balmorhea-Loving Trough (Brinster, 1991).

Isotopic data from groundwater samples suggest that groundwater travel time from the surface to the Dewey Lake Red Beds and the Rustler Formation is long and rates of flow are extremely slow. Low tritium levels in all WIPP-area samples indicate minimal contributions from the atmosphere since 1950 (Lambert and Harvey, 1987). Four modeled radiocarbon ages from Rustler Formation and Dewey Lake Red Beds groundwater are between 12,000 and 16,000 years. Observed uranium isotope activity ratios require a conservative minimum residence time in the Culebra Dolomite of several thousands of years and more probably reflect minimum ages of 10,000 to 30,000 years (Lambert and Carter, 1987). Stable-isotope data are more ambiguous: Lambert and Harvey (1987) concluded that compositions are distinct from modern surface values and that the contribution of modern recharge to the system is slight, whereas Chapman (1986, 1988) concluded that available stable-isotope data do not permit interpretations of groundwater age. Additional stable-isotope research is in progress and may resolve some uncertainty about groundwater age.

Potentiometric data from four wells support the conclusion that little infiltration from the surface reaches the water-bearing units of the Rustler Formation. Hydraulic head data are available for a claystone in the Forty-niner Member from DOE-2, H-3, H-4, H-5, and H-6. Comparison of these heads to Magenta heads in surrounding wells shows that flow between the units at all four wells may be upward (Holt et al., in prep., summarized by Brinster, 1991; Beauheim, 1987a). This observation offers no insight into the

possibility of infiltration reaching the Forty-niner Member, but it rules out the possibility of infiltration reaching the Magenta Dolomite or any deeper units at these locations.

Location and amount of groundwater recharge and discharge in the area may have been substantially different during wetter climates of the Pleistocene. Gypsiferous spring deposits on the east side of Nash Draw are of late Pleistocene age and reflect discharge from an active water table in the Rustler Formation (Bachman, 1981; 1987; Davies, 1989; Brinster, 1991). Coarse sands and gravels in the late Pleistocene Gatuña Formation indicate deposition in high-energy, through-going drainage systems unlike those presently found in the Nash Draw area (Bachman, 1987). Citing isotopic evidence for a Pleistocene age for Rustler Formation groundwater, Lambert and Carter (1987) and Lambert (1991) have speculated that during the late Pleistocene, Nash Draw may have been a principal recharge area, and flow in the vicinity of the WIPP may have been eastward. In this interpretation, there is essentially no recharge at the present, and the modern groundwater-flow fields reflect the gradual draining of the strata. Preliminary modeling of long-term transient flow in a two-dimensional, east-west cross section indicates that, although the concept remains unproven, it is not incompatible with observed hydraulic properties (Davies, 1989). As the performance-assessment groundwater-flow model (see following section) is further developed and refined, the potential significance of uncertainty in the location and amount of future recharge will be re-evaluated.

5.1.9 THE CULEBRA DOLOMITE GROUNDWATER FLOW AND TRANSPORT MODELS

Performance-assessment modeling at present simulates groundwater flow and radionuclide transport only in the Culebra Dolomite Member of the Rustler Formation, which has been identified as the most transmissive saturated unit overlying the repository. For the 1991 calculations, the unit is modeled as a perfectly confined two-dimensional aquifer. The implications of this simplifying assumption are not fully understood, and the conceptual model for groundwater flow will be re-examined in subsequent performance assessments when the computational tools for three-dimensional flow models become available.

Details of the programs used to simulate flow and transport in the Culebra Dolomite are described in Volume 2 of this report. Darcy flow is calculated for a single phase (liquid) using the SECO_2D program (Volume 2, Chapter 6 of this report). The program solves a transient equation for groundwater flow and includes capabilities for regional and local area grid solutions, generalized boundary conditions, flexible specification of initial conditions, parameterized climate variability, particle tracking, and

confined or unconfined storage coefficients. The program also has automated specification of grid spacing and times steps, options for cell-centered or node-centered grids, and efficient multigrid solvers.

Radionuclide transport is assumed to occur in a dual-porosity (fractures and matrix) medium and is calculated using the STAFF2D program (Huyakorn et al., 1989). STAFF2D is a two-dimensional finite-element program designed to simulate groundwater flow and solute transport in fractured or granular aquifers including physical and chemical retardation. The program takes into account fluid interactions between the fractures and porous matrix blocks, advective-dispersive transport in the fractures, and diffusion in the porous matrix blocks and fracture skin. The program also simulates radioactive decay during transport.

Regional and Local Model Domains for Groundwater Flow

Regional and local domains for the groundwater-flow model are shown in Figure 5-16. Flow that directly affects regulatory compliance occurs within the approximately 5-km-by-7-km local domain, which uses 125-m-by-125-m grid blocks and has relatively good control from well data. Boundary conditions for the local domain are provided by simulations within the regional domain, which uses a relatively coarser grid and has sparser well control. Initial boundary conditions for the 25-km-by-30-km regional grid are selected to be compatible with regional hydrogeologic constraints, and are adjusted during model calibration.

Uncertainty in the Transmissivity Field

Transmissivity values for the Culebra Dolomite are known from 41 well locations in the vicinity of the WIPP. These values have been used to construct and calibrate a transmissivity field that is compatible with observed head data (LaVenue et al., 1990). No calibrated field can provide a unique characterization of spatial variability in transmissivity between well locations, however, and performance-assessment calculations must take this uncertainty into account by sampling a range of transmissivity values. The 1990 calculations used a zonal approach in which the model domain was divided into coarse geographic zones, each of which was assigned a range and distribution of hydraulic conductivity values derived directly from the transmissivity values from wells. Sampling on transmissivity within the zones allowed for a probabilistic assessment of groundwater flow, but the resulting fields were not conditioned on the available head data, and transmissivity values were not correlated between zones.

In March 1991, the WIPP performance-assessment team convened a group of geostatistics consultants to advise on suitable methods for including

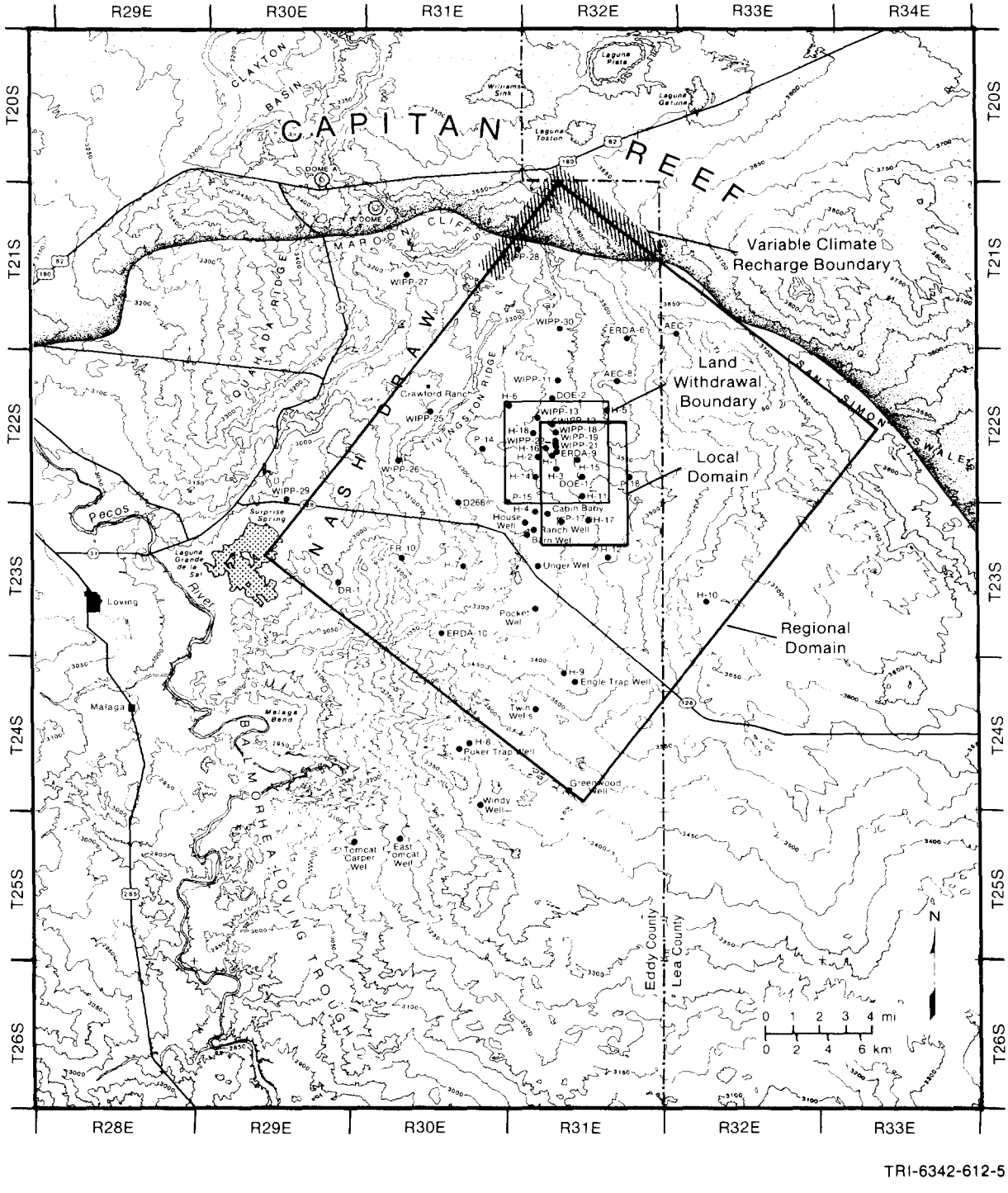

Figure 5-16. Regional and Local Domains Used for Simulations of Groundwater Flow and Transport. The regional domain is used for SECO_2D simulations of groundwater flow. The local domain is used for SECO_2D flow simulations and STAFF2D transport simulations.

uncertainty in groundwater flow and transport models. The group was requested to make suggestions that could be implemented by June 1991 to be used in the 1991 calculations. The group was also asked to suggest techniques that could be implemented in 1992 or later and to make recommendations about possible future data acquisition.

With regard to displaying the uncertainty in the transmissivity field, the consultant group proposed that a set (e.g., 100 or more) of correlated and conditioned random transmissivity fields should be generated separately, and the probabilistic sampling methodology should randomly select one of these fields for each Monte Carlo performance-assessment run. Each of these random fields should have an equal probability, or alternatively, a probability based on a "goodness-of-fit" criterion between observed and calculated heads and an assumed distribution of measurement uncertainty. For sensitivity analysis purposes, these random fields should be ordered with respect to a given criterion, such as travel time to the accessible environment.

As described in more detail in Volume 2 of this report, for the 1991 calculations 60 regional transmissivity fields have been calibrated to observed head data by adjusting boundary conditions. The multiple fields were simulated based on local estimates of transmissivity and the generalized covariance derived from them and on the pilot points used by LaVenue et al. (1990). Each simulated field was checked for consistency with pre-excavation equilibrium pressures by identifying fixed boundary pressures that minimize the squared deviation of model pressures from estimated equilibrium pressures. Boundary pressures were constrained by a prior estimate obtained through kriging the equilibrium freshwater heads. Only those fields that produced a minimum squared error of model pressures less than 2 (within the 95 percent confidence level on observed heads) were retained as plausible. These fields were assigned equal probability for Latin hypercube sampling. To facilitate sensitivity studies, the retained fields were ordered on travel time from the center of the waste panel region to the boundary of the accessible environment.

Modeling the Effects of Climatic Change

The effects of climatic change are examined in the 1991 preliminary performance assessment by varying boundary conditions for the regional model domain (see Section 5.1.4-Paleoclimates and Climatic Variability above and Swift, October 10, 1991, memo in Volume 3, Appendix A for additional information about climatic variability). As discussed further in Volume 2 of this report, groundwater flow into the model, which is assumed to be an uncertain function of mean annual precipitation, was controlled in the 1991 performance-assessment calculations by prescribing potentiometric heads along approximately 15 km of the northern boundaries of the regional model domain

(Figure 5-16). Heads within the "recharge strip" were varied between their present estimated elevations and a maximum elevation of the ground surface, using a sampled scaling factor uniformly distributed between zero and one. Maximum head values, and therefore maximum groundwater flows into the model, occurred at precipitation maximums calculated using the precipitation function described in Chapter 4 of this volume and in the October 10, 1991 memo by Swift in Volume 3, Appendix A. For those vectors with a large (close to one) scaling factor, the maximum heads were close to the ground surface. For vectors with a small (close to zero) scaling factor, the effect of climate variability was muted, and heads varied little from their present values.

This representation of variable recharge to the Culebra reflects a single, preliminary conceptual model for the effects of climatic change. Alternative conceptual models and refinement of this model will be examined in future analyses. For the 1991 preliminary comparison, variable heads were prescribed only along the northern edge of the model because, as discussed previously in "Recharge and Discharge" in Section 5.1.8-Confined Hydrostratigraphic Units in this chapter, potentiometric maps indicate north-to-south flow in the Culebra and probable recharge north of the modeled area. Maximum head elevations were limited to the ground surface because geologic evidence does not indicate the presence of widespread surface water in the region during the late Pleistocene. The sampled scaling factor reflects uncertainty in the extent to which increases in precipitation will affect heads within the model domain. As discussed in the October 10, 1991 memo by Swift in Volume 3, Appendix A, this uncertainty includes uncertainty in the location and extent of the recharge area for the Culebra, uncertainty in the relationship between precipitation and infiltration in the recharge area, and uncertainty in the flow path from the recharge area to the model domain. Future analyses will examine the sensitivity of the groundwater-flow model to uncertainty in the recharge scaling factor, to the assumptions made in determining the location and range of the prescribed head variations, and to the assumptions made in selecting the parameter values controlling the future precipitation function.

Radionuclide Transport in the Culebra Dolomite

Analysis of hydrologic tests indicates that in regions of relatively higher transmissivity, the Culebra Dolomite behaves as a dual-porosity medium, with solute transport occurring in both fractures and matrix porosity (Kelly and Pickens, 1986; Saulnier, 1987; Beauheim, 1987a,b,c, 1989). The performance-assessment model for transport uses the Darcy velocity field calculated by the local groundwater-flow model and allows for retardation during transport both by diffusion and sorption in matrix porosity and sorption by clays that line fractures.

Distribution coefficients (K_ds), defined for a given element as the amount sorbed by a gram of rock divided by the amount in a milliliter of solution, are used to calculate the partitioning of radionuclides between groundwater and rock. Distribution coefficients may be determined experimentally for individual radionuclides in specific water/rock systems (e.g., Lappin et al., 1989), but because values are strongly dependent on water chemistry and rock mineralogy and the nature of the flow system, experimental data cannot be extrapolated directly to a complex natural system. For the 1990 preliminary performance assessment, cumulative distribution functions (cdfs) for K_ds were estimated from experimental and theoretical work (Siegel, 1990). Distributions were then derived for retardation factors, which are defined as mean fluid velocity divided by mean radionuclide velocity and which take into account pore space geometry and the thickness of clay linings as well as K_d values. The derivation of retardation factors for the 1991 calculations is discussed in Volume 3 of this report.

Sensitivity analyses performed as part of the 1990 preliminary performance assessment indicated that, conditional on the models and distributions used in the 1990 calculations, variability in retardation factors was the second most important contributor (after radionuclide solubility in repository brine) to overall variability in cumulative releases through groundwater transport (Helton et al., 1991). Because the major source of uncertainty in retardation factors is in the estimation of K_ds and because directly applicable experimental data are not available, the WIPP performance-assessment team organized an expert panel to provide judgment about probability distributions for K_d values to be used in the 1991 preliminary performance assessment. Unlike other expert panels organized for WIPP performance assessment (e.g., the future intrusion panel discussed in Chapter 4 of this volume and the source term panel discussed later in this chapter), this panel consisted of SNL staff members who are currently working on retardation in the Culebra or who have done so in the past. In other regards, procedures for the presentation of the issues and the elicitation of results were as suggested by Hora and Iman (1989) and Bonano et al. (1990), as described in Chapter 4 of this volume.

The radionuclide retardation expert panel was requested to provide probability distributions for distribution (sorption) coefficients for eight elements (americium, curium, uranium, neptunium, plutonium, radium, thorium, and lead) that represent a spatial average over the total area of concern (kilometers from the repository). This was to be done for two separate cases: (1) the coefficients that result from the clay that lines the fractures in the Culebra Dolomite, and (2) the coefficients that result from the matrix pore space of the Culebra Dolomite. During the meetings, the panelists decided to further break down the problem by examining the coefficients that would result from the particular rock species and two

different transport fluids: (1) transport fluid that is predominantly relatively low-salinity Culebra brine, or (2) transport fluid that is predominantly high-salinity Salado brine. Probability distributions were thus provided for four situations for each radionuclide.

Two short meetings were held in April 1991 to discuss the physical situation and the issue statement. The period between the second and third meetings (approximately one month) was available for the panelists to examine the existing data base and discuss the results with each other. The third meeting, held at the end of May 1991, involved the expert judgment elicitation training, a discussion among the panelists as to the cases and assumptions to be used during the elicitation, and the actual elicitation sessions. The experts were elicited separately, at the request of one of the panelists. Each panelist provided distributions where they were able. Incompleteness resulted in some cases from a lack of knowledge about a particular radionuclide. Specific distributions provided by each panelist are presented in Volume 3 of this report, together with the composite distributions used in the 1991 performance-assessment calculations.

5.2 The Engineered Barrier System

The WIPP disposal system includes engineered barriers that minimize the likelihood of radionuclides migrating through the hydrogeologic setting to the accessible environment. As presently designed, the repository relies on seals in panels, drifts, and shafts to prevent migration through the excavated openings. If performance assessments indicate additional barriers are needed to reduce potential radionuclide transport up an intrusion borehole, modifications can be made to the form of the waste and backfill or to the design of the waste-disposal areas that will assure acceptable long-term performance.

5.2.1 THE SALADO FORMATION AT THE REPOSITORY HORIZON

Although the stratigraphy of the Salado Formation is consistent over much of the Delaware Basin, there are important vertical variations in lithology. Because these lithologic layers are close to horizontal at the WIPP, the repository is being excavated within a single stratigraphic horizon (rather than at a constant elevation) so that all panels within the waste-disposal area share the same local stratigraphy. As a result, the floor of the waste-disposal area will slope slightly (less than 1°) to the southeast, and there will be a difference in elevation between the highest and lowest panels of less than 10 m (33 ft).

Panels are excavated entirely within a 7.3-m (24-ft)-thick section of halite and polyhalite (Figure 5-17). Below this section and approximately 1.25 m (4 ft) below the floor of the panels lies Marker Bed 139 (MB139), which contains approximately 0.9 m (3 ft) of anhydrite with clay seams. Above the repository horizon and approximately 2.1 m (7 ft) above the roof of the panels lies anhydrite B, an approximately 6-cm (2.4-in)-thick anhydrite and clay seam. Anhydrite A, approximately 21 cm (8.3 in) of anhydrite with clay, is another 1.8 m (6 ft) above anhydrite B. A more detailed description of the stratigraphy is provided in Volume 3 of this report.

Excavation of the repository and the consequent release of lithostatic stresses has created a disturbed rock zone (DRZ) around the underground openings. The DRZ at the WIPP has been confirmed by borehole observations, geophysical surveys, and gas-flow tests, and varies in extent from 1 to 5 m (3.3 to 16.4 ft) (Stormont et al., 1987; Peterson et al., 1987; Lappin et al., 1989). Fractures and microfractures within the DRZ have increased porosity and permeability of the rock and increased brine flow from the DRZ to the excavated openings (Borns and Stormont, 1988, 1989). Fracturing has occurred in MB139 below the excavated areas and in both anhydrites A and B above the excavated area. It is not known how far fracturing in MB139 and the anhydrites A and B extends laterally from the excavations at this time, nor is the ultimate extent of the DRZ known. Most deformation related to development of the DRZ is believed to occur in the first five years after excavation (Lappin et al., 1989).

Fracturing in the DRZ, particularly in MB139 and the anhydrite layers, may provide a pathway for fluid migration out of the repository and possibly around panel and drift seals. Characterization of fracture-related permeability in these layers is essential to modeling of two-phase (gas and brine) fluid flow into and out of the repository.

5.2.2 REPOSITORY AND SEAL DESIGN

Major components of repository design that affect performance assessment are the waste itself, the underground waste-disposal area and its access drifts and shafts, and the seals that will be used to isolate the disposal area when the repository is decommissioned. The underground workings will ultimately consist of eight waste-disposal panels, access drifts and shafts, and an experimental area (Figure 5-18). Drifts in the central portion of the repository will also be used for waste disposal, providing the equivalent of an additional two panels for waste disposal. A more detailed discussion of repository design is available in Volume 3 of this report.

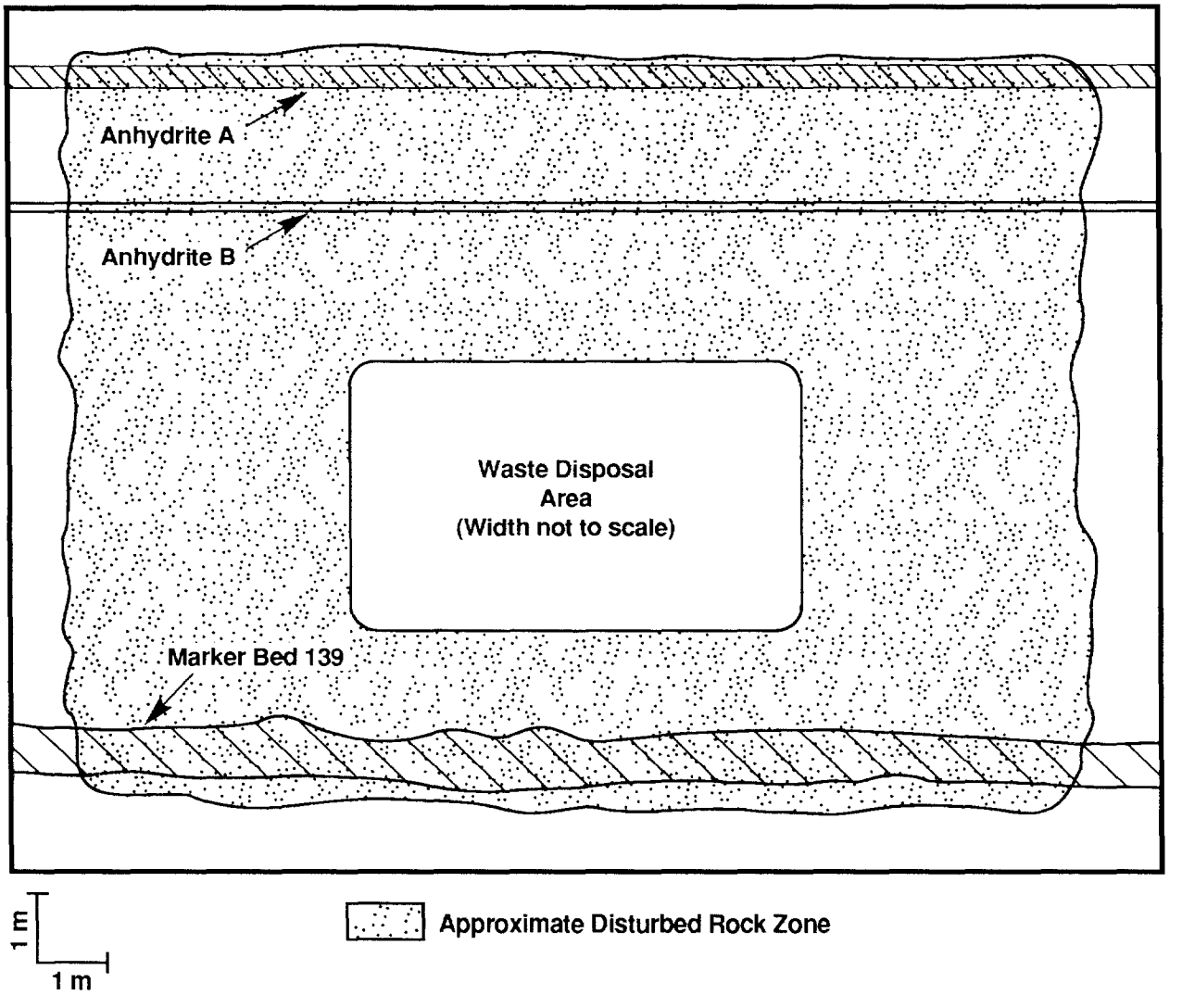

Figure 5-17. Schematic Cross Section of Salado Formation Stratigraphy at the Waste-Disposal Horizon.

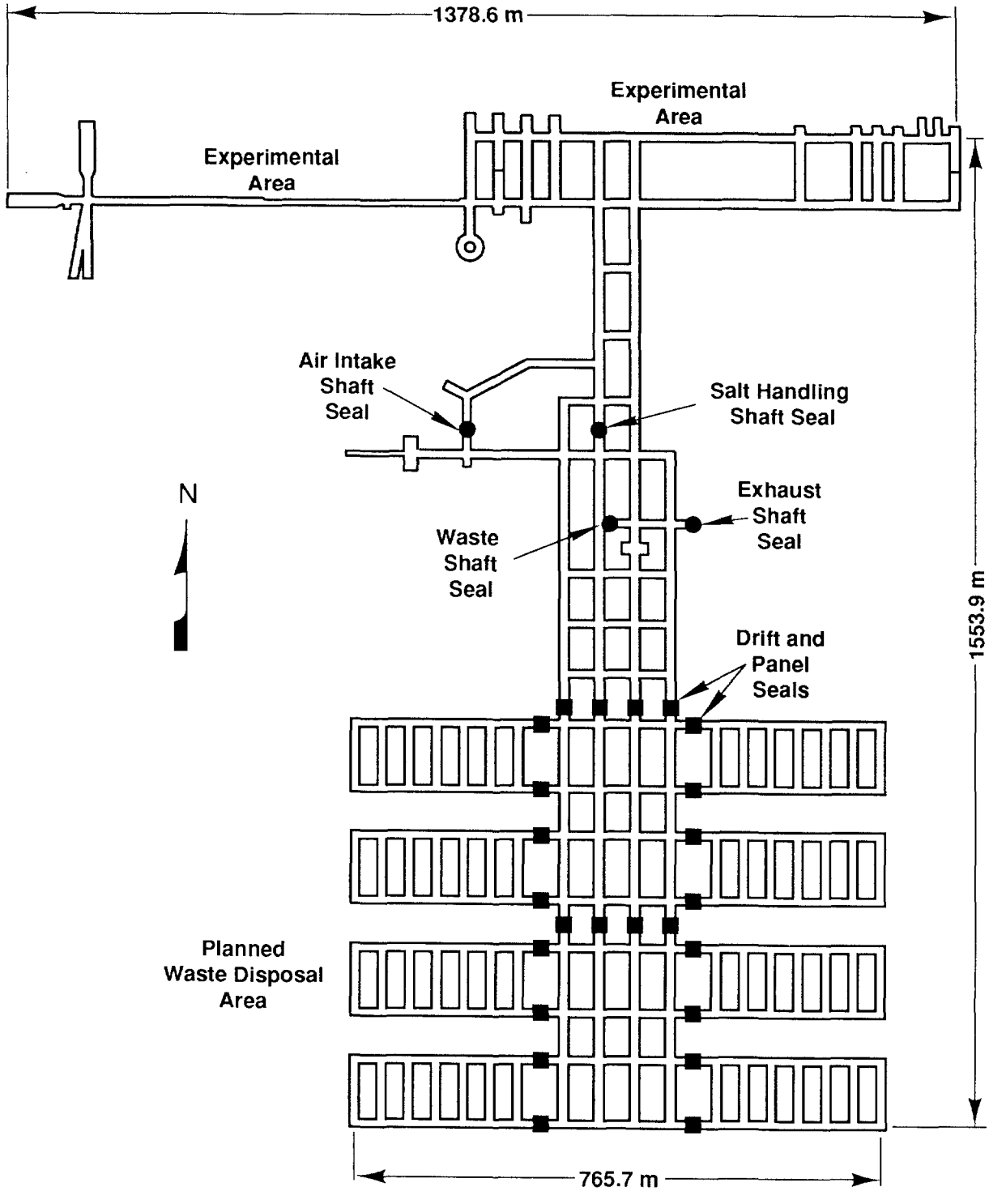

TRI-6342-229-2

Figure 5-18. Plan View of Waste-Disposal Horizon Showing Shaft, Drift, and Panel Seal Locations (after Stormont, 1988).

All underground horizontal openings are rectangular in cross section. The disposal area drifts, in the southern part of the repository, are 4.0 m (13 ft) high by 7.6 m (25 ft) wide; the disposal rooms are 4.0 m (13 ft) high, 10.1 m (33 ft) wide, and 91.4 m (300 ft) long. Pillars between rooms are 30.5 m (100 ft) wide. The eight waste-disposal panels will each have an initial volume of 46,000 m^3 (1.6 x 10^6 ft^3). The northern drift disposal area will have an initial volume of 34,000 m^3 (1.2 x 10^6 ft^3), and the southern drift disposal area will have an initial volume of 33,000 m^3 (1.2 x 10^6 ft^3) (Rechard et al., 1990a). Overall, the waste-disposal areas will have an initial volume of about 435,000 m^3 (1.5 x 10^7 ft^3).

The four access shafts are cylindrical and range in diameter from 5.8 m (19 ft) to 3.0 m (10 ft). Shafts are lined in the units above the Salado Formation to prevent groundwater inflow and provide stability; they are unlined in the salt.

Excavation of the first waste-disposal panel is complete; the remaining panels will be excavated as needed. Waste will be emplaced within the panels in drums or metal boxes, and panels will be backfilled and sealed as they are filled. Seals will be installed in panels, drifts, and the vertical shafts before the repository is decommissioned. Waste, backfill, and seals will be consolidated by creep closure after decommissioning.

Waste Characterization

The waste that will be emplaced in the WIPP must meet Waste Acceptance Certification requirements (draft of WIPP-DOE-069-Rev. 4, as explained in Chapter 1 of this volume). These requirements include that waste material containing particulates in certain size and quantity ranges will be immobilized, liquids are restricted to that remaining in well-drained containers, radionuclides in pyrophoric form are limited to less than one percent by weight of the external container, and no explosives or compressed gases are permitted. Ignitable, corrosive, and reactive wastes are not acceptable at the WIPP.

The current design of the WIPP has a total emplacement volume for CH-TRU waste of 6.2 x 10^6 ft^3 (approximately 175,000 m^3) (U.S. DOE, 1980a). The estimate of the volume of CH waste supplied by the 10 generator sites for the 1990 IDB (Integrated Data Base) was approximately 100,000 m^3 (U.S. DOE, 1990e). Current performance-assessment calculations use an initial CH-waste inventory based on the design volume for waste emplacement. To estimate the characteristics of the CH inventory for a design capacity, the 1990 IDB estimated volumes were scaled up by 64.9 percent by volume to equal the design volume. The stored waste in the 1990 IDB only represents about 34 percent of the design volume. Since 66 percent of the waste volume has not

been generated, the waste characterization must be considered an estimate with a potentially large uncertainty.

An estimation of the characterization of the CH waste for the current performance-assessment calculations was based on a scale up of weights estimated from 1987 waste characterization information (Drez, 1989). The 1987 detailed waste characterization information was used because a later update is not currently available. Based on the design capacity of the WIPP and average weights (Butcher, 1989) for the combustibles (plastics and cellulosics) and metals and glass constituents, estimates of about 13,000,000 kg of combustibles and 20,000,000 kg of metals and glass were calculated. Using the percentages of the detailed constituents in the 1987 estimated inventory and the total weight of combustibles and metals and glass for the design capacity, estimates of the total weights of the aluminum, steel, paper, cloth, wood, plastics, rubber, and other detailed constituents in CH waste for the design volume were made. The weights of metals, plastics, cellulosics, and rubbers are required for performance assessment because they may influence gas generation and potential radionuclide transport.

The weight of waste containers, drums, and boxes, and of container liners must be estimated because they also affect gas-generation potential. It was assumed in the estimation of the container weights that only 55-gallon drums and standard waste boxes will be emplaced in the WIPP. These are the only containers that can currently be transported in a TRUPACT-II (NuPac, 1989). Based on a design capacity and the assumption about the containers, it was estimated that about 532,500 drums and 33,500 standard waste boxes would be emplaced in the WIPP. The total weight of the steel in the containers is larger than the estimated total weight of metals and glass in the waste inventory.

The estimates of the total weights of the constituents in the wastes for these analyses were larger than the weights estimated for the analyses discussed in Lappin et al. (1989). This increase was primarily the result of scaling the volume of the waste to a design volume of about 175,000 m^3. Lappin et al. (1989) used a volume of 556,000 drum equivalents, which is about 115,000 m^3. The increase in the weights of the constituents also resulted from an increase in the estimates reported by Drez (1989) from an earlier inventory provided in Lappin et al. (1989).

Seals

Seals will be emplaced in the entrance to each panel, in two locations within the drifts between the panels and the vertical shafts, and in each of the four vertical shafts (Figure 5-18, 5-19) (Nowak et al., 1990). Design of these seals reflects specific functions for each type of seal. Seals in the

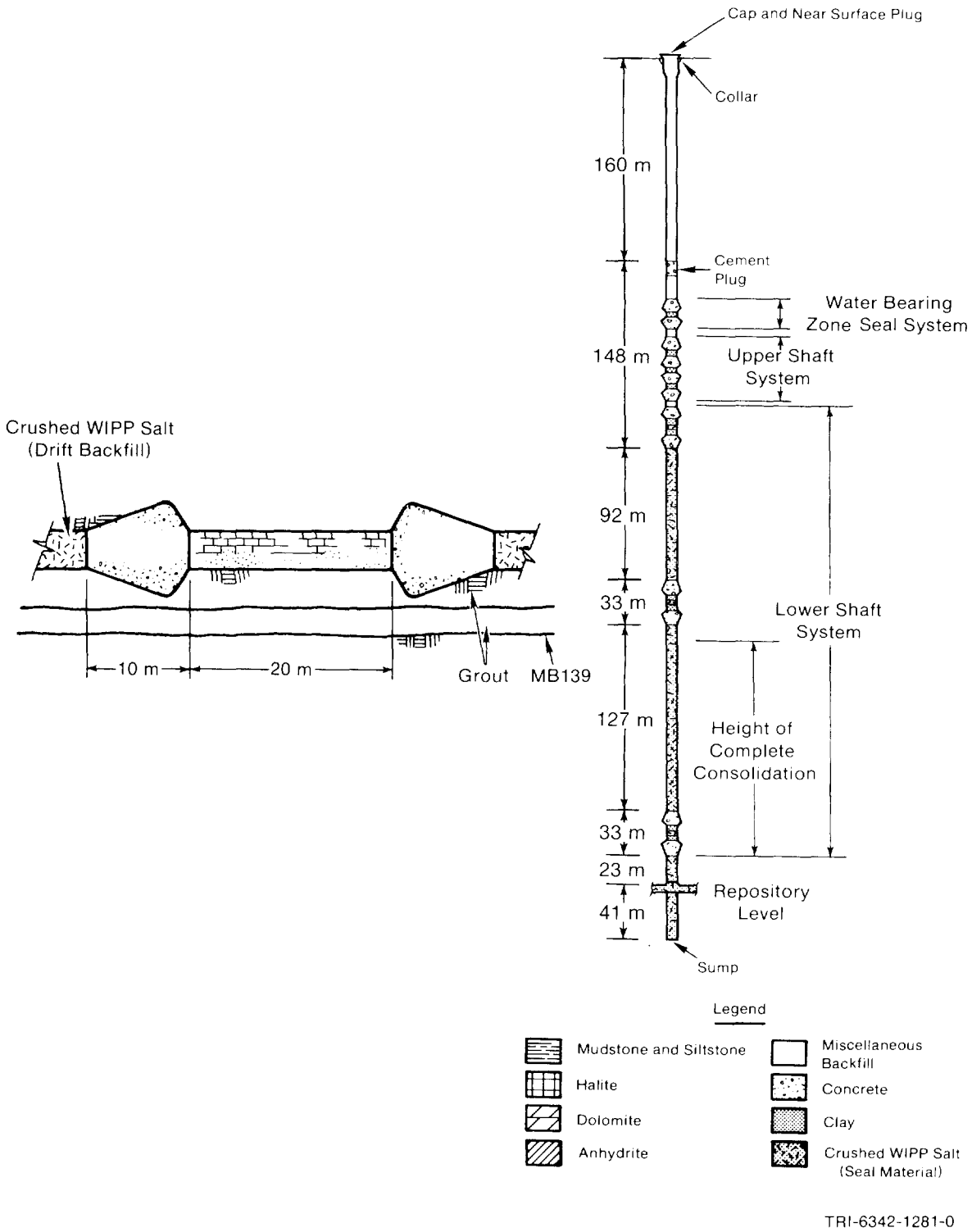

Figure 5-19. Representative Shaft and Plug Seals (after Nowak et al., 1990). Vertical distances based on stratigraphy in ERDA-9.

upper portion of the shafts must prevent groundwater flow from the water-bearing units of the Rustler Formation from reaching the lower portions of the shafts and the waste-disposal areas. Seals in the lower portion of the shafts must provide a long-term, low-permeability barrier that will prevent Salado Formation brine from migrating up the shaft. Panel seals (and drift seals) prevent long-term migration of radionuclide-contaminated brine through the drifts to the base of the shafts and must also provide safe isolation of radionuclides during the operational phase of the repository.

The primary long-term component of both lower shaft and panel seals will be crushed salt, confined between short-term rigid bulkheads that will prevent fluid flow while creep closure reconsolidates the crushed salt to properties comparable to those of the intact Salado Formation. The short-term seals will be concrete in the panels and drifts, and composite barriers of concrete, bentonite, and consolidated crushed salt in the shafts. Crushed salt in the long-term portion of the seals will be preconsolidated to approximately 80% of the density of the intact formation and will compact further to approximately 95% of initial density within 100 years, at which time permeabilities are expected to be comparable to those of the undisturbed rock (Nowak and Stormont, 1987). Panel seals will be 40 m (131 ft) long, with 20 m (66 ft) of preconsolidated crushed salt between two 10-m (33-ft) concrete barriers. Shaft seals will extend the full length of the shafts and will include composite barriers at the appropriate depths to individual lithologic units, including the Culebra Dolomite (Nowak et al., 1990). Additional information about seal design is presented in Volume 3 of this report.

Marker Bed 139 will be sealed below each panel and drift seal by grouting, either with crushed-salt-based grout, cementitious material, or bitumen. Other anhydrite layers will be sealed similarly. Salt creep is expected to close fractures in halite in the DRZ over time, and engineered seals are not planned for the DRZ outside of MB139 and other interbeds.

Backfill

Void space between waste containers and elsewhere in the underground workings will be backfilled before sealing and decommissioning (Tyler et al., 1988; Lappin et al., 1989). This backfill will reduce initial void space and permeability in the panels and will consolidate under pressure to further limit brine flow through the waste. Performance-assessment calculations to date have assumed a backfill material of pure crushed salt, which will not sorb radionuclides. Design alternatives for backfill that include bentonite as an additional barrier to retard radionuclides are under consideration (WEC, 1990; U.S. DOE, 1990d), and will be evaluated in future performance assessments.

Engineered Alternatives

The WIPP has been designed to dispose of waste in the form in which it is shipped from the generator sites. Preliminary performance-assessment calculations indicate that modifications to the waste form that limit dissolution of radionuclides in brine have the potential to improve predicted performance of the repository (Marietta et al., 1989; Bertram-Howery and Swift, 1990). Modifications to the backfill and design of the room could also reduce radionuclide releases. Modifications could also, if needed, mitigate the effects of gas generated within the repository. Present performance assessments are not complete enough to determine whether or not such modifications will be needed for regulatory compliance, but the DOE is proceeding with investigations of engineered alternatives to waste form and repository design so that alternatives will be available if needed (U.S. DOE, 1990a). The Engineered Alternatives Task Force (EATF), assembled by Westinghouse Electric Corporation, has identified 19 possible modifications to waste form, backfill, and room design that merit additional investigation (WEC, 1990; U.S. DOE, 1990d). The 1991 performance-assessment calculations do not include simulations of these alternatives. Selected alternatives will be examined in future performance-assessment calculations, however, to provide guidance to DOE on possible effectiveness of modifications.

5.2.3 THE RADIONUCLIDE INVENTORY

The radionuclide inventory for CH- and RH-TRU waste was estimated from input to the 1990 IDB (U.S. DOE, 1990e). Twelve radionuclides were identified to be in the initial CH inventory. The estimates from the 1990 IDB were based on a volume of 106,458 m^3. To estimate the curie content of the initial inventory for a design capacity, the 1990 estimated curie contents were scaled up by 64.9 percent by volume to equal the design volume. This scaling results in an initial total CH inventory of about 16,000,000 curies. Based on a design volume, the majority of the CH waste has not been generated; therefore, the radionuclide inventory is an estimate based on currently available information and has the potential for large uncertainty. The stored and newly generated RH volume in the 1990 IDB sum to a total of 5,344 m^3. The containers that will be placed in an RH canister have a different volume depending on the generator site; therefore, a canister may not contain 0.89 m^3 of RH waste. The U.S. DOE (1991c) identifies that the submittal to the 1991 IDB totals 7,622 canisters. The total volume based on the number of canisters is 6,784 m^3. The 1990 IDB indicates there may be a considerable volume of uncharacterized waste that will probably be RH. Because of the uncertainty in the RH inventory, the smaller total volume of waste and not the volume of canisters was used as a scaling factor to

estimate the RH design radionuclide inventory for these analyses. The total RH inventory was estimated to be about 1,600,000 curies. Details of the radionuclide inventory are presented in Volume 3 of this report.

Radioactive decay within the repository is simulated with a nearly complete set of decay chains, which are given in Volume 3 of this report. Decay is simulated for 20 radionuclides in the CH inventory and for an additional 3 radionuclides in the RH inventory. Only those radionuclides with short half-lives are omitted. Decay during transport, which begins when radionuclides leave the repository, is simulated using a simplified set of four decay chains that omit radionuclides with short half-lives, low toxicity, and low activity (less than 100 curies at 10,000 years). This simplification did not eliminate radionuclides that could cause significant health effects.

The only radioactive gas expected in the repository is radon-222, created from the decay of radium-226. Decay of thorium-230 will cause the amount of radium-226 to increase from about 0 to 23 curies in a panel at 10,000 years. Because radon-222, with a half-life of only 3.8 days, will exist in secular equilibrium with radium-226, its activity will be insignificant throughout the 10,000-year period. Not including releases of volatile radionuclides should not significantly affect the total radionuclide release.

5.2.4 RADIONUCLIDE SOLUBILITY AND THE SOURCE TERM FOR TRANSPORT CALCULATIONS

Previous WIPP performance assessments have calculated the source term for transport modeling using the same estimated range and distribution (loguniform from 10^{-9} to 10^{-3} M) for the solubility limit of all radionuclide species in repository brine (Lappin et al., 1989; Brush and Anderson, 1989). Sensitivity analyses performed as part of the 1990 preliminary performance assessment indicated that, conditional on the models and distributions used in the 1990 calculations, variability in the solubility limit was the most important single contributor to variability in total cumulative releases to the accessible environment resulting from groundwater transport (Helton et al., 1991). In the absence of experimental data that might better define solubility limits, a panel of experts external to the WIPP Project was convened to provide the performance-assessment team with judgment about solubility limits for specific elements under variable Eh and pH conditions.

Selection of the panel and elicitation of their judgment followed the procedure suggested by Hora and Iman (1989), described in Chapter 4 of this volume in the discussion of the future-intrusion panel. Candidates for the expert panel on source term were gathered by a two-tiered nomination process. Initial nominations were solicited from an SNL staff member and a university consultant, as well as from members of the Performance Assessment Peer Review

Panel and the National Research Council's WIPP Panel. Additional nominations were requested from all those contacted. Curriculum vitae from those who were interested in participating in such a panel and available during the entire study period were reviewed by a two-member selection committee external to SNL. Some individuals removed themselves from consideration because of prior time commitments, current contracts with SNL, a self-determined lack of expertise, or involvement in an oversight organization. Nominees were evaluated on the basis of expertise and professional reputation, and four experts were selected whose complementary areas of specialization provided the needed breadth and balance to the panel.

Rather than considering the solubility limit of the radionuclides (as was used in the 1990 calculations in lieu of concentrations), the panel was instead asked to consider explicitly the individual radionuclide concentrations that might be expected. Specifically, panel members were asked to develop probability distributions for the dissolved concentration of americium, curium, uranium, neptunium, plutonium, radium, thorium, and lead in the WIPP brines in the repository rooms and drifts (with all that implies in terms of waste and room chemistry). They were also requested to repeat the process for the concentration due to suspended materials, which was not distinguished from the dissolved fraction in the 1990 calculations.

The radionuclide source term expert panel met twice in Albuquerque during March and April 1991 and communicated with each other throughout the study period as they saw fit. The first meeting was used to acquaint the experts with the WIPP, the SNL effort in performance assessment, and the issue statement. The panelists were provided with one-half day of training in expert-judgment/probability elicitation, which is the process whereby experts are assisted in developing probability distributions by individuals experienced in decision analysis and the expert-judgment process.

The second meeting included presentations by each panelist of his or her approach in responding to the issue statement. Further discussion led to the panelists' decision to be elicited as a group in order to benefit from each panelist's particular expertise. Being elicited together required the development of a group strategy for creating the probability distributions. The panel developed a strategy based on basic solubility principles; related experimental data, where available; consideration of the impact on the concentration due to changes in environmental factors (e.g., changes in pH); and expert judgment in synthesizing the above. Individual uncertainty cannot be distinguished in a single distribution but resulted in a larger range for the composite distribution. Greater detail in the description of the panel's methodology can be found in Trauth et al. (1991). The probability distributions created by the panel are contingent upon other circumstances, such as the oxidation state of the radionuclide or the presence of other

compounds (carbonate or sulfate). Eh versus pH diagrams were provided for those radionuclides for which more than one oxidation state was thought possible. The probability distributions can be found in Trauth et al. (1991) and are reproduced in Volume 3 of this report. These distributions reflect concentrations of dissolved materials only: the panelists concluded that available data was insufficient to provide judgment about concentrations of suspended materials.

As a step in reducing the uncertainty in the estimates, the expert panel developed distributions for each specific radionuclide of interest. In addition, where the repository conditions might lead to the existence of more than one oxidation state for a radionuclide or more that one solid species containing the radionuclide (based on the presence or absence of specific complexants--carbonate and sulfate), more than one distribution was developed for a specific radionuclide. The ranges of some of the distributions developed by the panel are larger and some are smaller than the distributions used in the 1990 calculations, and the ranges reflect greater or lesser concentrations. Variations reflect differences in the chemistry of the specific radionuclide in the presence of WIPP waste and the standard A brine for the WIPP (Molecke, 1983; Lappin et al., 1989, Table 3.4).

5.2.5 PERFORMANCE-ASSESSMENT MODEL FOR THE REPOSITORY/SHAFT SYSTEM

The performance-assessment model for the repository/shaft system must simulate migration of radionuclides and hazardous materials away from the repository through all pathways. Specifically, the model simulates liquid and gas flow in the Salado Formation, particularly in the interbeds, as a function of the various processes active in the waste-disposal panels, including borehole intrusion. The model also calculates a time-dependent source term of radionuclide concentrations in repository brine for transport modeling in the Salado Formation and the overlying Culebra Dolomite.

Closure, Flow, and Room/Waste Interactions

When the repository is decommissioned, waste-disposal panels, access drifts, and the experimental area will be backfilled, and the drifts and shafts will be sealed. Free brine initially will not be present within the disposal area, and void space above the backfilled waste will be air-filled (Figure 5-20a). Brine seepage from the Salado Formation will have filled fractures in MB139 beneath the disposal area (Lappin et al., 1989; Rechard et al., 1990b).

Following decommissioning, salt creep will begin to close the repository (Figure 5-20b). In the absence of elevated gas pressures within the repository, modeling of salt creep indicates that consolidation of the waste

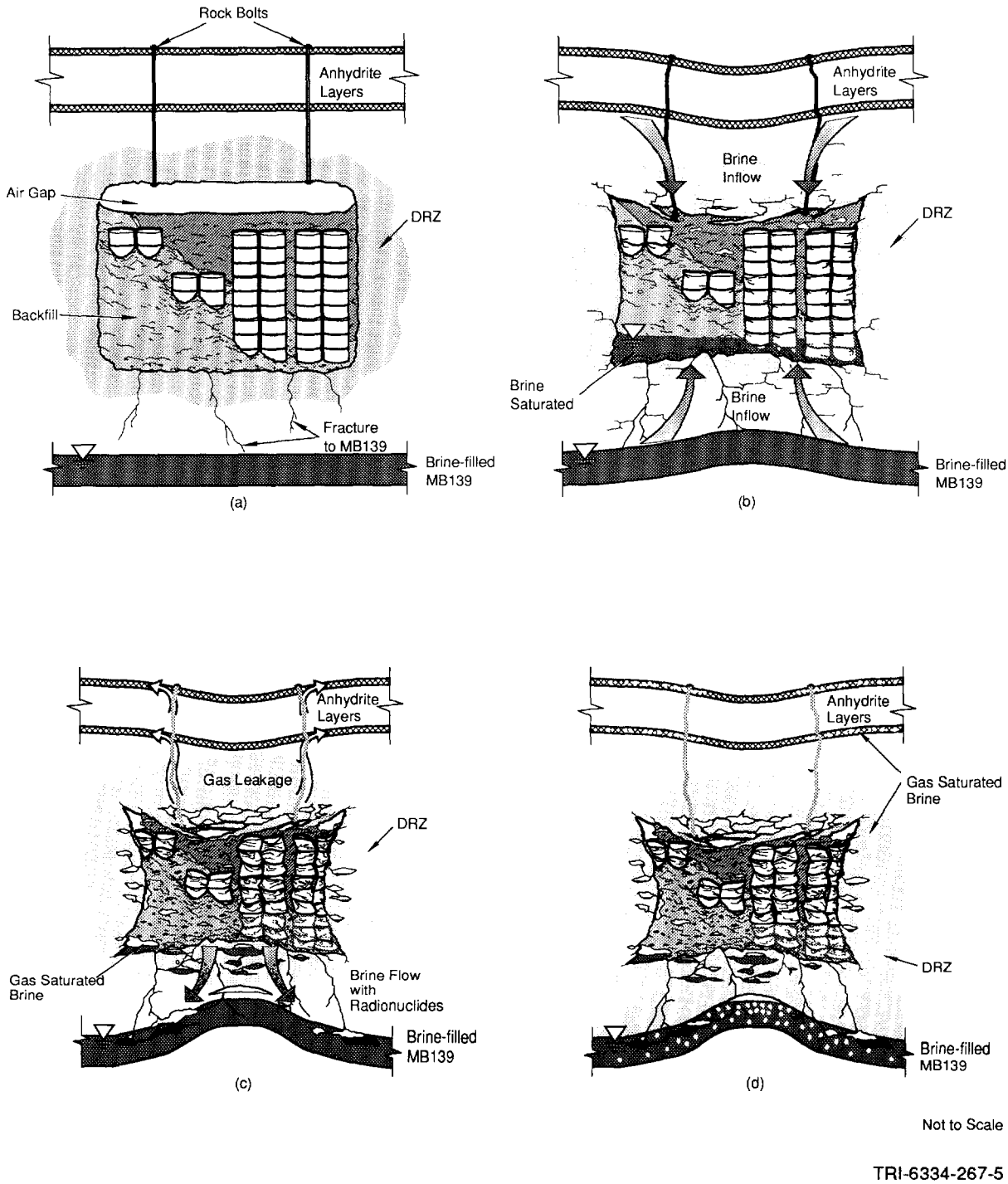

Figure 5-20. Hypothesized Episodes in Disposal Area During Undisturbed Conditions. This drawing shows (a) initial conditions after decommissioning; (b) conditions after room creep closure and brine inflow; (c) conditions after gas generation, brine outflow, and room expansion; and (d) undisturbed conditions with gas-filled room surrounded by gas-saturated brine (Rechard et al., 1990b).

in unreinforced rooms could be largely complete within 100 years (Tyler et al., 1988; Munson et al., 1989a,b). Brine will seep into the disposal area from the surrounding salt, however, and gas will be generated in the humid environment by corrosion of metals, radiolysis of brine, and microbial decomposition of organic material. Some gas will disperse into the surrounding anhydrite layers. Continued gas generation could increase pressure within the repository sufficiently to reverse brine inflow and partially or completely desaturate the waste-disposal area (Figure 5-20c). High pressure may also halt and partially reverse closure by salt creep. In the undisturbed final state, the disposal area could be incompletely consolidated and gas-filled rather than brine-filled (Figure 5-20d).

All of the major processes active in the waste-disposal area are linked, and all are rate- and time-dependent. For example, creep closure will be, in part, a function of pressure within the repository. Pressure will be in turn a function of the amount of gas generated and the volume available within the repository and the surrounding Salado Formation for gas storage. Gas-storage volume will be a function of closure rate and time, with storage volume decreasing as consolidation continues. Time and rate of gas generation, therefore, will strongly influence repository pressurization and closure. Gas-generation rates will be dependent on specific reaction rates and the availability of reactants, including water. Some water can be generated by microbial activity (Brush and Anderson, 1988b). Additional water will be provided by brine inflow, which, in the absence of a final mechanistic model, is assumed to occur according to two-phase immiscible flow through a porous medium. Other possibilities are being investigated. Whatever model is used, brine inflow will depend in large part on repository pressure, so that some gas-generation reactions could be partially self-buffering.

Responses of the disposal system to human intrusion are equally complicated. Consequences will depend on the time of intrusion, the degree to which the repository has closed, and the amount of gas generated. If intrusion occurs into a fully pressurized, dry, and partially unconsolidated waste-disposal area, venting of gas up the borehole will permit brine to resaturate available void space (Figure 5-21a,b). Following eventual deterioration of borehole plugs, brine may flow from the disposal area into the borehole, transporting radionuclides upward to the Culebra Dolomite. Upward flow from a pressurized brine pocket in the Castile Formation may contribute to flow and radionuclide transport (Figure 5-21c).

Performance assessments must model the consequences of intrusion as a function of conditions within the waste-disposal area. For example, radionuclide transport will depend, in part, on the rate of brine flow through the waste, which in turn will be a function of brine availability and waste permeability. Time- and pressure-dependent consolidation by creep

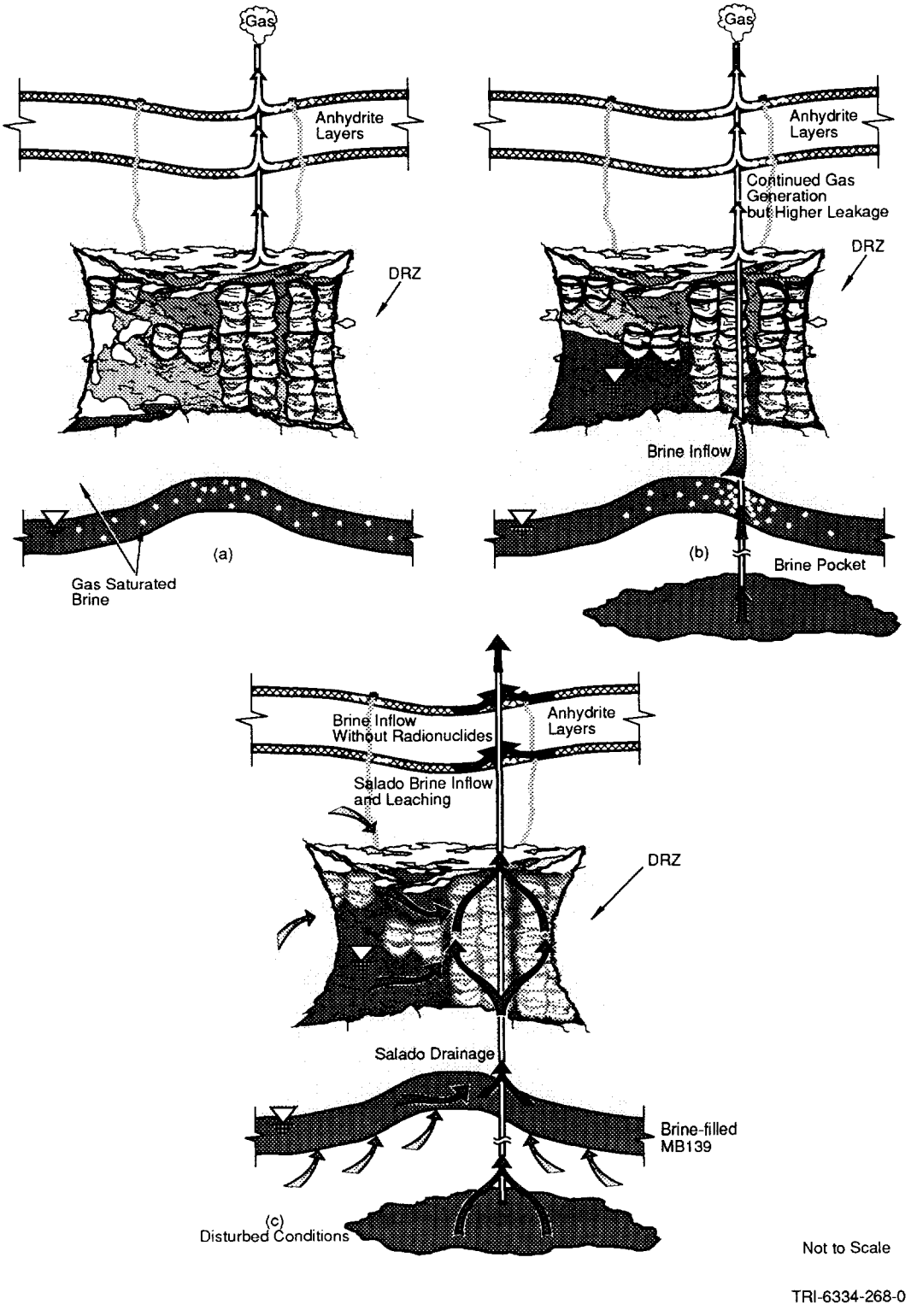

Figure 5-21. Hypothesized Episodes in Disposal Area After Human Intrusion. This drawing shows (a) initial room gas depressurization when penetrated by an exploratory borehole, (b) final gas and brine depressurization as borehole seals degrade, and (c) brine flow through the borehole to the Culebra Dolomite (Rechard et al., 1990b).

closure will be a major factor in determining waste permeability. Models and the data base needed to describe conditions within the waste-disposal area in detail are still incomplete. Present interpretations are based on simplifying assumptions that will be modified as research progresses.

Modeling of Undisturbed Performance

Modeling of the undisturbed performance of the disposal system is required to evaluate compliance with the Individual Protection Requirements of the Standard (§ 191.15) and to provide simulations of the base-case scenario for the probabilistic evaluation of compliance with the Containment Requirements of the Standard (§ 191.13). Previous estimates of undisturbed performance have indicated zero releases to the accessible environment within 10,000 years (Lappin et al., 1989; Marietta et al., 1989) (see Chapter 7 of this volume). As a result, Monte Carlo simulations of the base-case scenario are not included in the construction of the CCDFs used for preliminary comparisons with the Containment Requirements. Only those scenarios that result in releases to the accessible environment will affect the CCDF. Emphasis in modeling undisturbed performance, therefore, is on examining conservative deterministic calculations that will indicate whether or not releases could occur that would require inclusion of the base-case scenario in the Monte Carlo analysis.

Analyses of undisturbed performance reported by Lappin et al. (1989) and Marietta et al. (1989) used NEFTRAN (NEtwork Flow and TRANsport; Longsine et al., 1987), a one-dimensional flow and transport program in which the disposal system was represented by a network of discrete legs. Flow and transport was assumed to occur along MB139 to the base of the waste shaft (Figure 5-18), and then upward through the shaft seals to the Culebra Dolomite. Flow and transport was also calculated for a vertical leg through the intact Salado Formation directly to the Culebra Dolomite. The head gradient between the waste panels and the Culebra was held constant, and effects of gas generation were not considered. Neither pathway resulted in radionuclides reaching the Culebra Dolomite within 50,000 years (Marietta et al., 1989).

The 1991 preliminary assessment of undisturbed performance uses SUTRA (Saturated-Unsaturated TRAnsport; Voss, 1984) and STAFF2D (Solute Transport And Fracture Flow in 2 Dimensions; Huyakorn et al., 1989) to simulate flow and transport from the waste panels in two dimensions. Flow is assumed to occur in a single phase (brine), and gas generated within the waste panels is not included directly in the simulation. The effects of gas generation are included indirectly, however, by using elevated repository pressures calculated using the two-phase (gas and brine) flow program BOAST_II (Black

Oil Applied Simulation Tool, enhanced version; Fanchi et al., 1987). Additional details about the programs and their applications in the 1991 calculations are provided in Volume 2 of this report.

Flow and transport are simulated in two two-dimensional sections through the disposal system. One section is a horizontal plane containing the vertical projection of two waste panels onto MB139 (Figure 5-22a). This section is used to estimate lateral transport of radionuclides through the intact marker bed. The second section, a vertical profile containing a north-south drift and an access shaft, is used to estimate flow and transport along the drift and shaft pathway towards the Culebra Dolomite (Figure 5-22b). Results of these simulations are presented in detail in Volume 2 of this report and are summarized in Chapter 7 of this volume.

Modeling of Disturbed Performance

Simulations of disturbed performance use BRAGFLO (BRine And Gas FLOw; see Volume 2 of this report), a finite difference transient two-phase flow program developed for the WIPP performance assessment, to calculate brine and gas flow within a waste panel and the surrounding rock and within a borehole or boreholes connecting the panel with the Culebra Dolomite and a brine reservoir in the Castile Formation. The program PANEL (see Volume 2 of this report), also developed for the WIPP performance assessment, is used to estimate concentrations of radionuclides within repository brine and and for supplementary calculations of one-phase (brine) flow within a panel and a borehole or boreholes. Details of the programs and their application in the 1991 calculations are provided in Volume 2 of this report. Results of the simulations of disturbed performance are given in Chapter 6 of this volume.

Two-dimensional BRAGFLO simulations of two-phase (brine and gas) flow use a radially symmetric model of the disposal system with a simplified stratigraphy (Figure 5-23). Gas generation is estimated using corrosion and biodegradation reactions dependent on the availability of brine, metal, and cellulose. Gas generation ceases when reactants are consumed. Material property parameter values (e.g., porosity and absolute and relative permeability) are assigned to each of units in the simplified stratigraphy. Far-field pore pressure is held constant through time, and pressure in the repository is calculated dependent on the gas-generation rate and two-phase flow in the units shown in Figure 5-23, including the waste panel, the intact and disturbed halite and anhydrite layers, the Castile brine reservoir, the Culebra Dolomite, and the intrusion borehole.

For the 1991 preliminary comparison, uncertain parameters sampled for BRAGFLO flow simulations were porosities, permeabilities, and threshold pressures for the intrusion borehole and disturbed and undisturbed anhydrite (in anhydrite

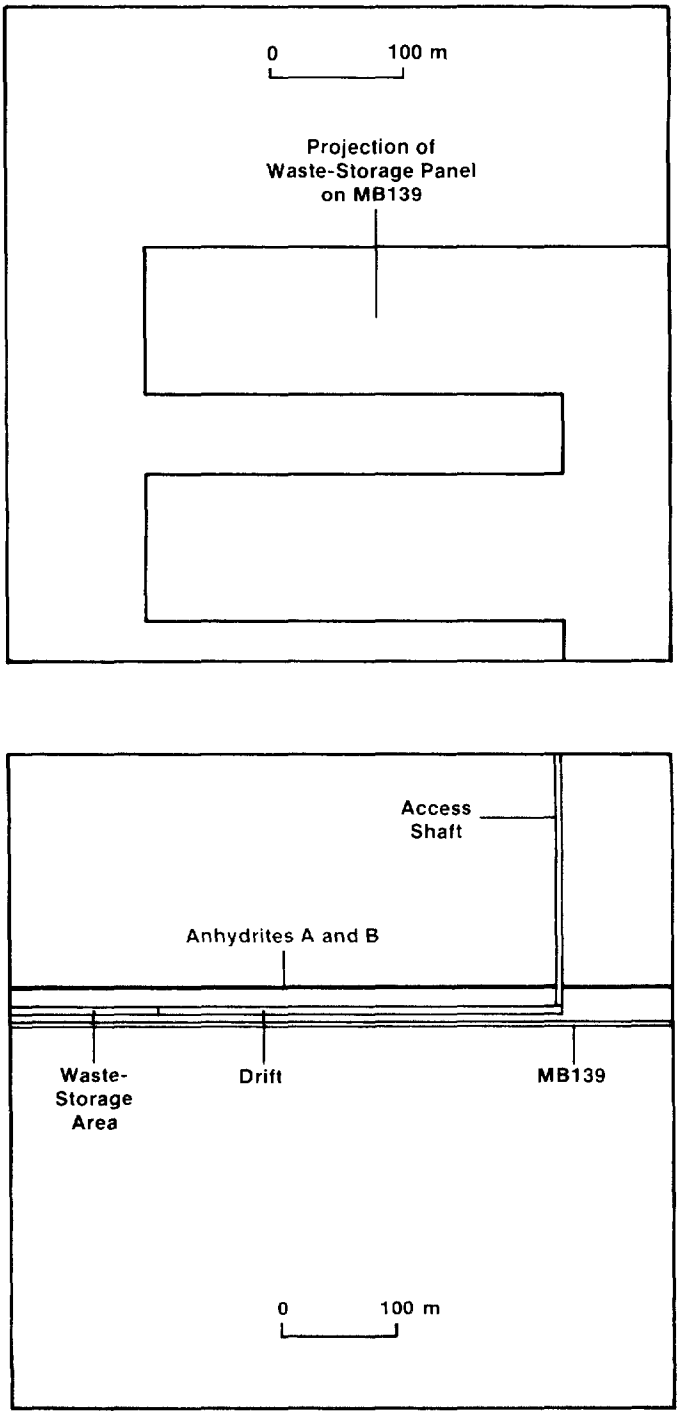

Figure 5-22. Two-Dimensional Repository Models Used for STAFF2D and SUTRA Estimations of Radionuclide Transport during Undisturbed Conditions. Figure 5-22a is a horizontal (plan) view of the projection of two waste panels onto the plane containing MB-139. Figure 5-22b is a vertical cross section containing the waste disposal area, a north-south drift, and a vertical access shaft.

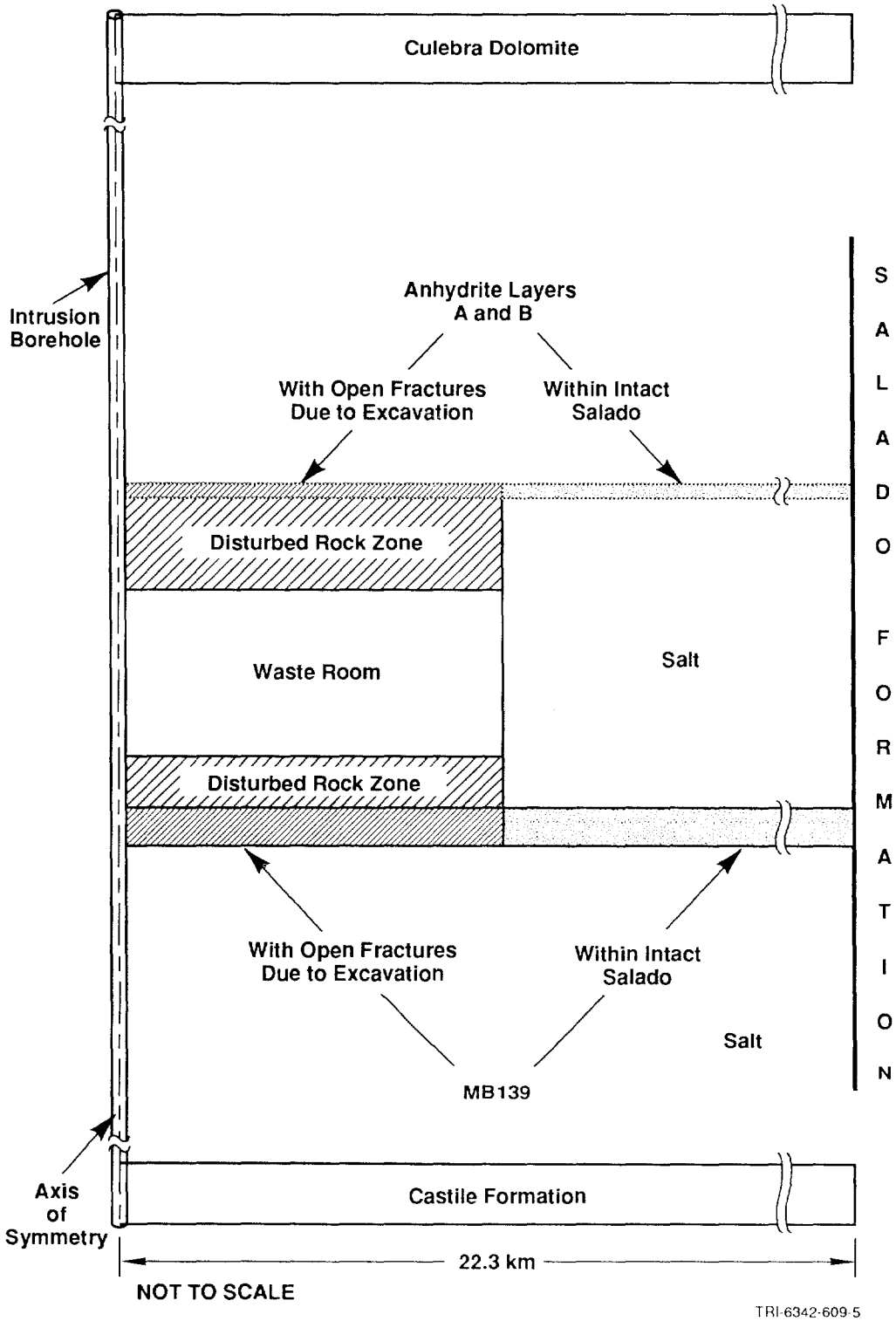

Figure 5-23. Simplified Waste-Disposal Panel Model Used in Two-Dimensional, Axially Symmetric BRAGFLO Simulations of Two-Phase (Brine and Gas) Flow (Vaughn et al., 1991).

layers A and B and in MB139), far-field pore pressure in MB139 (which was then used to fix a hydrostatic far-field pressure for all other elevations), and the initial pressure of the Castile brine reservoir. Gas-generation rates under humid and saturated conditions, the stoichiometry of the corrosion reaction, the volume fractions of the reactants (metal and cellulose), and the initial liquid saturation of the waste were also sampled. Ranges and distributions for these parameters are given in Volume 3 of this report. As described in Volume 2 of this report, reaction stoichiometry and initial volume fractions of reactants were used to derive initial room porosity and room heights.

The program PANEL estimates radionuclide concentrations in repository brine by modeling radioactive decay and dissolution within a waste panel. These calculations require an initial inventory of all radionuclides, half-lives and decay chains for all radionuclides, solubility limits for all elements, and the pore volume of the panel. The model assumes chemical equilibrium and the uniform distribution of waste within the panel. Sorption of radionuclides within the panel is not considered. For the 1991 preliminary comparison, uncertain geochemical parameters included Eh/pH conditions within the repository and solubility limits for 7 radionuclides. Ranges and distributions for these parameters are given in Volume 3 of this report.

Single-phase flow modeling using PANEL can consider four components of fluid flow separately: upward flow of brine from the Castile Formation due to the head difference between the brine reservoir and repository; brine flow from the Salado Formation into the waste panel; circulation of brine through the waste within the panel; and upward flow within the borehole from the panel to the Culebra Dolomite. Brine inflow from the Salado Formation is calculated using BRAGFLO, as described below. Required parameters for the Castile Formation include the initial pressure of the brine reservoir and the bulk storage coefficient. Other required parameters include the time of intrusion, the dimensions and locations of boreholes, and hydraulic conductivity within the waste panel and the boreholes. All flow in PANEL is assumed to occur as in a single phase (brine) and to be governed by Darcy's law. Pressure in the Culebra Dolomite is assumed to remain constant. Change in brine reservoir pressure is assumed to be proportional to the volume of fluid discharged. All components are assumed to be at steady state with respect to boundary pressures at any given time.

Modeling of Radionuclide Releases during a Borehole Intrusion

The performance-assessment model for borehole intrusion relies on a fundamental assumption that future drilling technologies will be comparable to those of the present. The reasonableness of this assumption is unknown; without it, however, estimates of the amount of waste brought to the ground surface during an intrusion would be arbitrary and purely speculative.

If a borehole intrudes the repository, waste will be brought directly to the ground surface as particulates suspended in the circulating drilling fluid. Some of this material will be cuttings, the material removed by the drill bit from a cylindrical space with a radius equal to that of the bit. An additional amount of waste will be brought to the surface as cavings, the material removed from the borehole wall. When the drill bit first penetrates the upper portion of a panel that is pressurized relative to the borehole with waste-generated gas, the escape of this gas may cause waste and backfill to spall into the borehole. As the borehole is extended below the repository, additional material will be eroded from the walls of the borehole at the repository horizon by the circulating fluid. Both cuttings and cavings will be transported to the surface in the circulated drilling fluid and released to the accessible environment in a settling pit at the surface.

The amount of waste removed as cuttings is a simple function of bit diameter. Estimating the amount of waste removed as cavings requires a more complex conceptual model, based on standard drilling technology (Figure 5-24). Drilling fluid, commonly referred to as mud, is pumped down the interior of the hollow drill pipe and out through the drill bit, where it cools the bit and removes cuttings. Fluid returns to the ground surface outside the drill pipe, in the annular space between the pipe (or collar, which is the lowest and thickest segment of pipe that supports the bit) and the borehole wall. During the return flow, fluid infiltrates into porous portions of the borehole wall and deposits a layer of muddy filter cake. In moderately porous units, filter cake typically accumulates until the unit is sealed and fluid loss is halted. Sealing of extremely porous units may require adding sealants to the drilling fluid or installing casing.

Because the drillstring (pipe, collar, and bit) rotates, fluid flow within the hole has both a rotational and axial motion (Figure 5-24). Variables controlling erosion by flowing fluid include the angular velocity of the drillstring, the fluid circulation rate, radii of the components of the drillstring, fluid viscosity, fluid density, borehole roughness, and the effective shear strength for erosion of the waste. Parameter values describing variables related to the drilling operation are determined by examining current technology. Driller's logs routinely report velocity (revolutions per minute), circulation (gallons per minute), and drillstring radii. Drilling mud exhibits non-Newtonian behavior, and viscosity must be described with two parameters. The effective shear strength for erosion of the waste will depend on several factors, including the form in which the waste is emplaced and the degree to which the waste has been consolidated by salt creep. Reference waste is a composite material, and values for the effective shear strength for erosion must be determined experimentally.

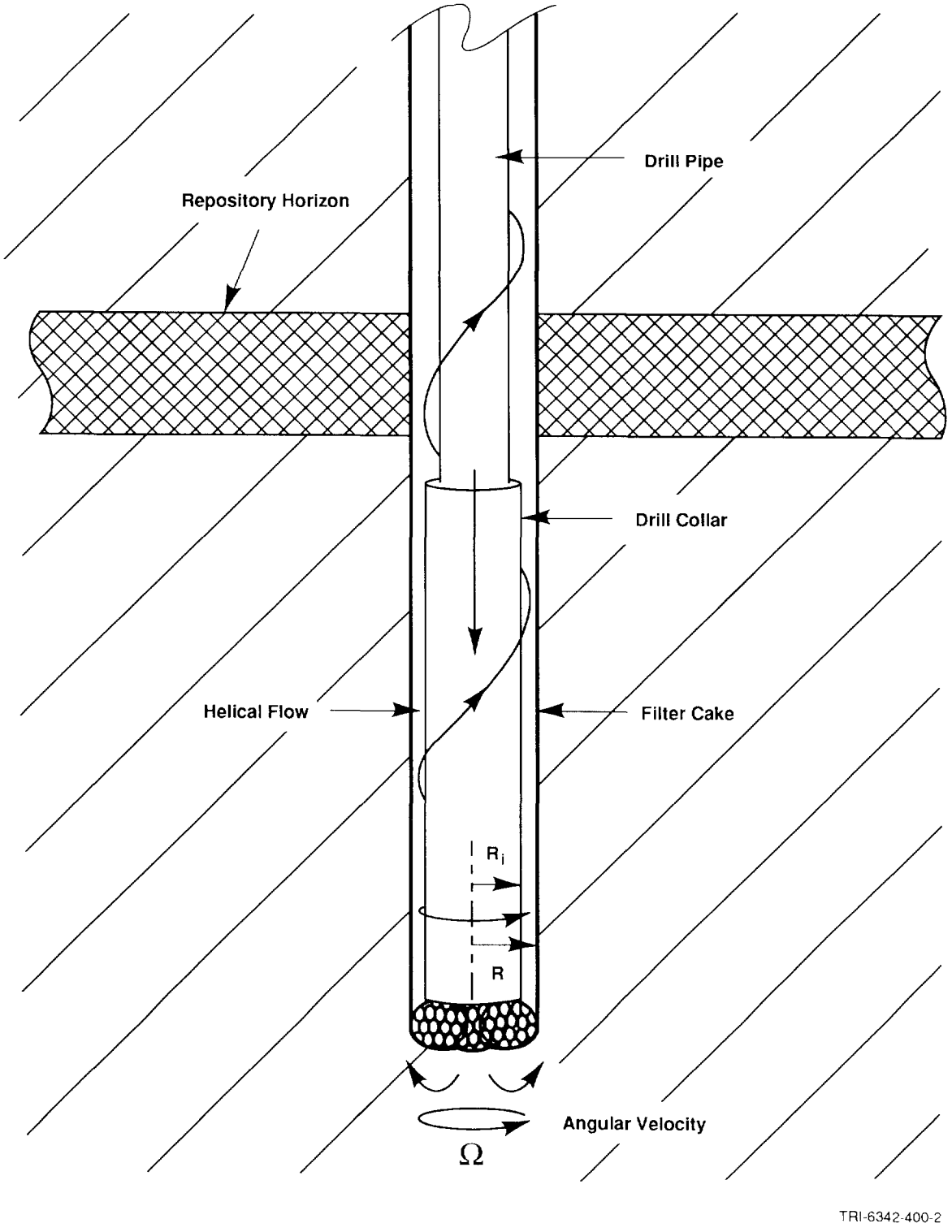

Figure 5-24. Conceptual Model of Borehole Intrusion. Not to scale (modified from Lappin et al., 1989).

As described in more detail in Volume 2 of this report, erosion of waste will occur when the fluid shear stress at the borehole wall exceeds the effective shear strength for erosion of the waste. For any given set of conditions, the fluid shear stress at the borehole wall will be a function of annular thickness: as erosion increases hole radius, shear stress will decrease (Figure 5-25a). Erosion will cease when shear stress at the borehole wall falls below a failure-shear-stress value corresponding to the effective shear strength for erosion of the waste. The total amount of waste removed, including both cuttings and eroded material, will be equal to the volume of a cylinder with a height equal to the repository thickness and a radius equal to the radius of failure by erosion (Figure 5-25b).

The program CUTTINGS (see Volume 2 of this report) is used to simulate erosion adjacent to the drill collar using fixed values for the effective shear strength for erosion for the waste corresponding to properties of as-received waste. Drill-bit radius, which in present drilling technology is primarily a function of total borehole depth, is selected by assuming that exploratory boreholes at the WIPP will be drilled for deep gas targets (see "Drilling" in Section 4.1.4-Evaluation of Human-Induced Events and Processes in Chapter 4) and then choosing the corresponding maximum bit radius at the repository depth.

Spalling of material into the borehole is not included in the analyses by CUTTINGS. This phenomenon may occur when the drill bit penetrates repository wastes pressurized by gases generated by corrosion and biodegradation. The escape of gases to the borehole causes radial effective stresses adjacent to the borehole to become tensile. The peak tensile stress is near the borehole wall, but tensile fracturing may occur away from the borehole wall, resulting in spalling of the heterogeneous composite waste and backfill material. The process of spalling is complex, involving gas flow through a moving waste matrix with changing boundaries. As a result, estimating the quantity of spalled material is not straightforward. The importance of the contribution of spalling to the total amount of cavings is still being evaluated. For the 1991 preliminary comparison, erosion by drilling fluid, rather than spalling by waste-generated gas, is assumed to be the dominant mechanism producing cavings.

5.3 CAMCON: Controller for Compliance-Assessment System

The complexity of the compliance-assessment modeling system for the WIPP requires that calculations be controlled by an executive program (Rechard, 1989; Rechard et al., 1989). CAMCON (Compliance Assessment Methodology CONtroller) controls code linkage and data flow during lengthy and iterative consequence analyses, minimizes analyst intervention during data transfer,

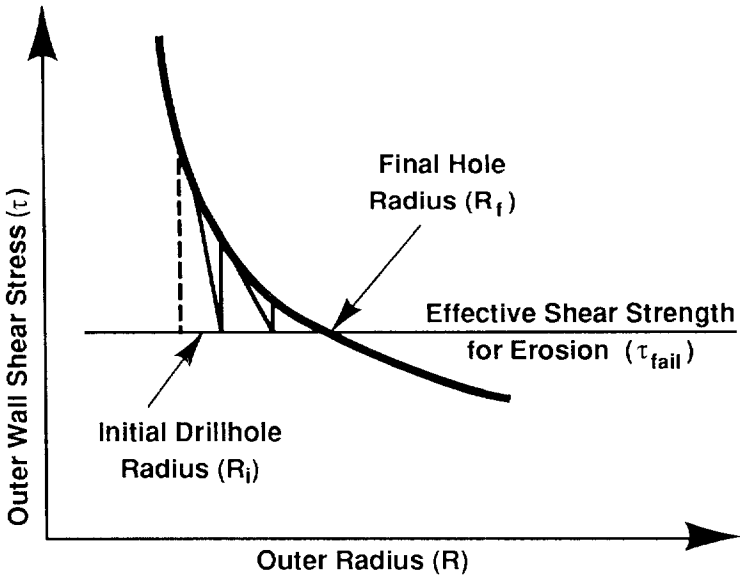

a.) Relationship Between Radius and Stress

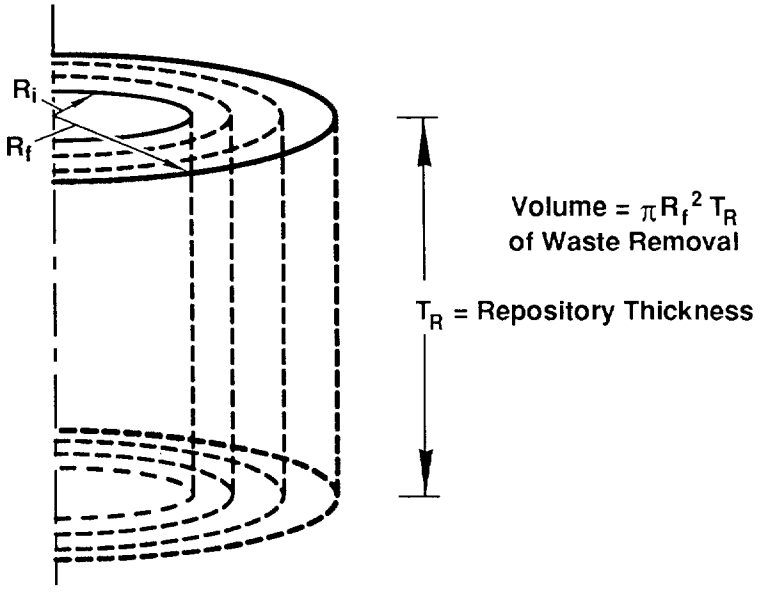

b.) Volume of Material Removed

TRI-6342-408-2

Figure 5-25. Borehole Erosion as a Function of Shear Stress.

and automatically handles quality assurance during the calculations. CAMCON currently consists of about 75 codes and FORTRAN object libraries and includes approximately 293,000 lines of FORTRAN software written specifically for the WIPP Project and another 175,000 lines of software adapted from other applications.

The controller allows easy examination of intermediate diagnostics and final results. Computer modules within the executive program can be easily replaced for model comparisons. CAMCON modularizes tasks so computer programs for a particular module are interchangeable. CAMCON is fully described in Rechard et al. (1989).

5.3.1 DATA BASES

Three data bases, primary, secondary, and computational, are included in CAMCON. The primary data base contains measured field and laboratory data gathered during the disposal-system and regional characterization. Because the analysis can be no better than these data, the data base should contain all necessary data for the compliance assessment and repository design, have as little subjective interpretation as possible, and be quality assured. Data base structure must be flexible to accommodate different organizations and unforeseen types of data. Practical experience suggests that a relational data base is best (Rautman, 1988).

The secondary data base contains interpreted data, usually interpolated onto a regular grid, and incorporates information that comprises the conceptual model of the disposal system. Levels of interpretation can vary from objective interpolation of data combined with subjective judgments to totally subjective extrapolations of data; all interpretations are well documented to ensure the secondary data is reproducible by others. Data from literature or professional judgment are used to fill knowledge gaps to complete the conceptual model. The secondary data base must be accessible to both the analyst and the executive package controlling the system.

The computational data base is CAMDAT (Compliance Assessment Methodology DATa). CAMDAT uses a neutral-file format so that a series of computer programs can be linked by a "zig-zag" connection rather than the usual serial connection. The file format chosen for CAMDAT was based on GENESIS (Taylor et al., 1987) and EXODUS and their associated data manipulation and plotting programs (Gilkey, 1986a,b, 1988; Gilkey and Flanagan, 1987). CAMDAT is fully described in Rechard et al. (1989).

5.3.2 PROGRAM LINKAGE AND MODEL APPLICATIONS

Program linkage and data flow through CAMDAT are controlled by CAMCON. Computer programs that make up the CAMCON system are major program modules, support program modules, and translators. Major program modules refer to programs that represent major tasks of the consequence modeling. Support program modules refer to programs such as interpolators that are necessary to facilitate use of major program modules. Translator program modules refer to programs that translate data either into or out of the computational data base. Figure 5-26 shows how programs within CAMCON are used to evaluate human-intrusion scenarios. Table 5-1 shows the status of the 79 composite programs now in CAMCON. Specific information on seven major CAMCON programs is provided Volume 2 of this report.

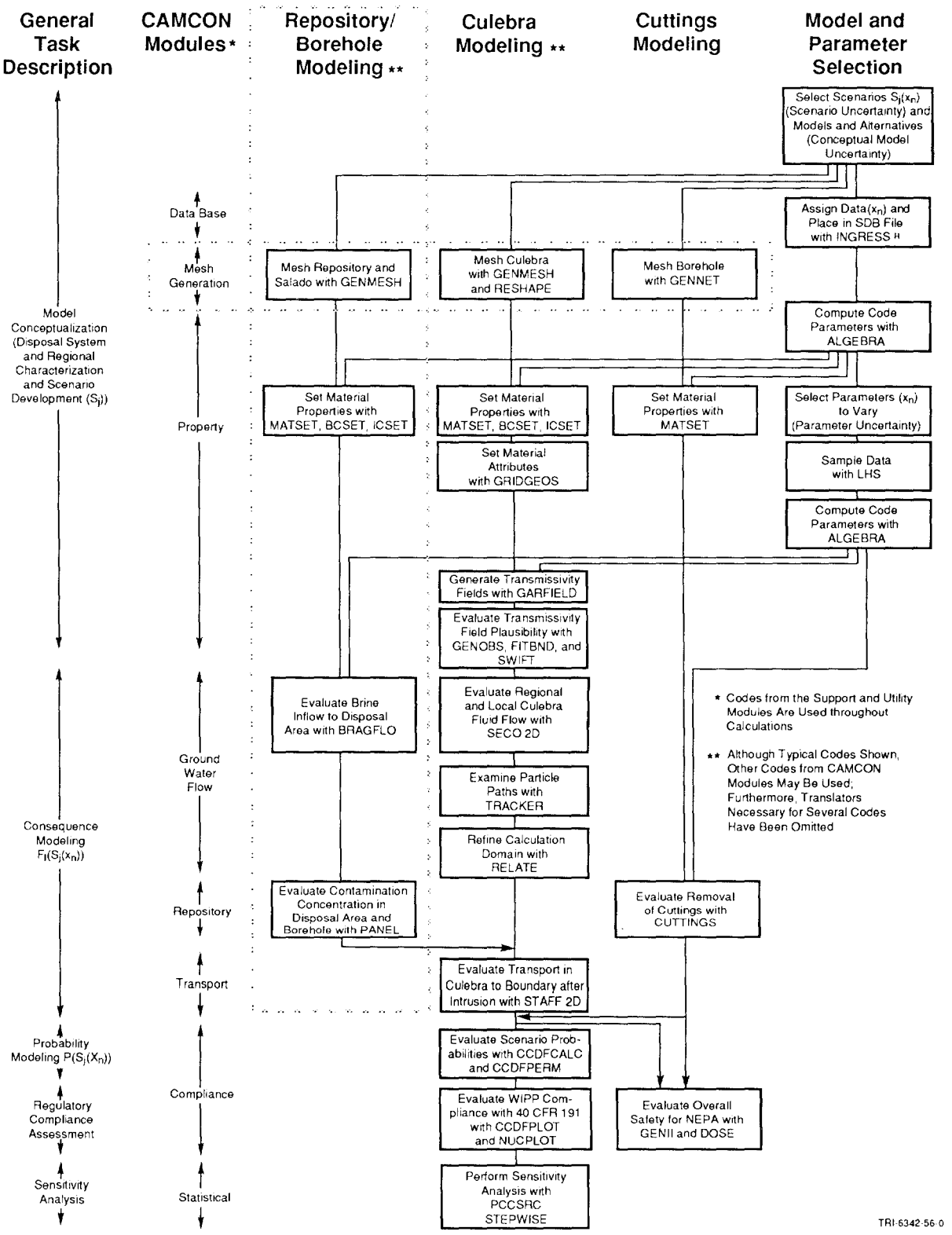

Figure 5-26. Organization of Programs in CAMCON (Rechard et al., 1989).

TABLE 5-1. SEPTEMBER 1991 STATUS OF COMPOSITE PROGRAMS IN CAMCON

Code	QA Status[1]	Work Remaining
Controller		
1. CAMCON	C	Notebook (listing); Review for Class A
Mesh Generation Module		
2. FASTQ: finite-element mesh generator	X	Add CAMDAT records
3. GENMESH: rectilinear mesh generator	A	Notebook
4. GENNET: network generator	C	Notebook; Review for Class A
5. PATEXO: PATRAN to CAMDAT transformation	X	Add CAMDAT records
Property Data Base Module		
6. GENPROP: item entry into property data base	C	Changes required by data base modification
7. INGRES™: relational data base	X	Helpfile; Notebook; Review for Class A
8. LISTSDB: data tabulation in secondary data base for reports	C	Make code more robust; SDB Reader; Update code; FLINT; Notebook
9. PLOTSDB: parameter distribution plots in secondary data base	C	SDB Reader; Document; Helpfile; FLINT; Notebook

QA Software Classifications:

1. A - Class A software has been evaluated by the Code Review Committee. The software satisfies the quality assurance requirements for traceability, retrievability, documentation, and verification. The software is available to any interested user within the WIPP Project at SNL.

   C - Class C software is a candidate for Class A, but currently satisfies only the traceability and retrievability requirements. The adequacy of documentation and verification has not been formally evaluated. An up-to-date Helpfile is maintained, a Software Abstract has been written, and internal documentation exists. However, both verification tests and external documentation are in progress. The software is available to any interested user within the WIPP Project at SNL.

   X - Class X software is currently being developed and has not been processed through any formal quality assurance procedures. The primary reason for the Class X classification is to make the existence of this software known to potential users. The software is available to any interested user within the WIPP Project at SNL.

TABLE 5-1. SEPTEMBER 1991 STATUS OF COMPOSITE PROGRAMS IN CAMCON (continued)

Code	QA Status[1]	Work Remaining
Property Module		
10. BCSET: boundary condition set up	C	Test cases; FLINT; Notebook; Review for Class A
11. FITBND: fit of pressure optimization boundary conditions	X	Helpfile; [CAMCON]; Driver
12. GARFIELD: attribute fields (e.g., transmissivity)	X	Helpfile; [CAMCON]; Driver; Test cases; FLINT; Notebook; Review for Class A
13. GENOBS: functional relationships between well heads and pressure boundary conditions	X	Helpfile; [CAMCON]; Driver
14. GRIDGEOS: interpolation from data to mesh	C	Check out kriging; Test cases; [CAMCON] FLINT; Notebook; Review for Class A
15. ICSET: initial condition set up	C	Test cases; FLINT; Notebook; Review for Class A
16. LHS: Monte Carlo sampling module	C	Test Cases; FLINT; Notebook; Review for Class A
17. PRELHS: pre-LHS translator	C	FLINT; Notebook; Review for Class A
18. POSTLHS: post-LHS translator	C	Algebraic function; FLINT; Notebook; Review for Class A
19. MATSET: material property set up	C	Test cases; FLINT; Notebook; Review for Class A
20. RELATE: interpolation from coarse to fine mesh and fine to coarse mesh (relates property and boundary conditions)	C	Document; Test cases; FLINT; Notebook; Review for Class A
21. SORTLHS: vector reordering for LHS	X	Allow user to input own order; Test cases; FLINT; Notebook; Review for Class A
Groundwater Flow Module		
22. BRAGFLO: 2-phase flow model	X	User manual

TABLE 5-1. SEPTEMBER 1991 STATUS OF COMPOSITE PROGRAMS IN CAMCON (continued)

	Code	QA Status[1]	Work Remaining
23.	PREBRAGFLO: pre-BRAGFLO translator	X	User manual
24.	POSTBRAGFLO: post-BRAGFLO translator	X	User manual
25.	BOAST_II: black oil model	X	Add semi-implicit wells; Add total velocity solution approach; Helpfile; [CAMCON]; FLINT; Test cases; Notebook; Review for Class A
26.	PREBOAST: pre-BOAST_II translator	C	(see BOAST_II, item 25)
27.	POSTBOAST: post-BOAST_II translator	C	(see BOAST_II, item 25)
28.	HST3D: hydrologic flow model	X	Add dynamic memory date and time; Add binary output
29.	PREHST: pre-HST3D translator	X	QA checkout
30.	POSTHST: post-HST3D translator	X	QA checkout
31.	SECO_2DH: 2-D hydrologic flow model, horizontal	X	Improve boundary condition capabilities; Use and Theory M; Test cases; Notebook; Review for Class A
32.	SUTRA: hydrologic flow model	C	CAMDAT source read; Test cases; Update; Helpfile; Notebook; Review for Class A
33.	PRESUTRA: pre-SUTRA translator	C	(see SUTRA, item 32)
34.	POSTSUTRA: post-SUTRA translator	C	(see SUTRA, item 32)
35.	SUTRA_GAS: SUTRA modification for fluid as gas instead of liquid	X	Helpfile; Notebook
36.	SWIFTII: hydrologic flow model	C	None at this time
37.	PRESWIFT: pre-SWIFTII translator	C	None at this time
38.	POSTSWIFT: post-SWIFTII translator	C	None at this time

TABLE 5-1. SEPTEMBER 1991 STATUS OF COMPOSITE PROGRAMS IN CAMCON (continued)

Code	QA Status[1]	Work Remaining
Repository Module		
39. CUTTINGS: evaluation of amount of material removed during drilling	C	Test cases; FLINT; Notebook; Review for Class A
40. PANEL: panel model, mixing cell for radionuclides analytic flow modeling	X	Merge versions w and w/o brine pocket models; Test cases; Document; FLINT; Notebook; Review for Class A
Containment Transport Module		
41. NEFTRAN: network transport model	C	None at this time
42. PRENEF: pre-NEFTRAN translator	C	Changes required by modifications to CAMCON
43. POSTNEF: post-NEFTRAN translator	C	None at this time
44. STAFF2D: finite-element transport model	C	Check out multi-grid solver; Define permeability and porosity attributes; Test cases; FLINT; Notebook; Review for Class A
45. PRESTAFF: pre-STAFF2D translator	C	(see STAFF2D, item 44)
46. POSTSTAFF: post-STAFF2D translator	C	(see STAFF2D, item 44)
Compliance Module		
47. CCDFCALC: CCDF calculation program	C	Test cases; Notebook; Review for Class A
48. NUCPLOT: box plot of each radionuclide contribution to CCDF	C	Make more user friendly; Test cases; Notebook; Review for Class A
49. CCDFPLOT: CCDF plotting	C	Notebook; Review for Class A
50. GENII: human dose calculations	X	Document; Helpfile; [CAMCON]; Driver
51. DOSE: dose calculations from transfer factors	X	Combine with PONDDOSE & FARMDOSE; Document; Helpfile; [CAMCON]; Driver

TABLE 5-1. SEPTEMBER 1991 STATUS OF COMPOSITE PROGRAMS IN CAMCON (continued)

	Code	QA Status[1]	Work Remaining
Support Module			
52.	ALGEBRA: CAMDAT manipulation program	C	Redo input structure; Examples; New manual; Notebook; Review for Class A
53.	BLOT: mesh and curve plotting	C	Add capability to plot geographical data; Element contours; Examples; New manual; Notebook; Review for Class A
54.	GROPE: CAMDAT file reader	C	Update helpfile; Notebook
55.	RESHAPE: redefinition of blocks (i.e., groupings of mesh elements)	C	Document; Test cases; FLINT; Notebook
56.	TRACKER: particle tracking support program	C	Add three-dimensional capability; Test cases; FLINT; Notebook; Review for Class A
57.	UNSWIFT: conversion of SWIFT input files into CAMDAT	C	Notebook
Statistical Module			
58.	PCCSRC: partial correlation coefficient statistics	C	Test cases; Notebook; Review for Class A
59.	STEPWISE: stepwise statistics	C	Document; Test cases; Notebook; Review for Class A
60.	LHS2STEP: translator from from LHS to STEPWISE or PCC/SRC	C	(see STEPWISE, item 59)
61.	CCD2STEP: translator from CCDFCALC	C	(see STEPWISE, item 59)
Utilities			
62.	CAM2TXT: binary CAMDAT to ASCII conversion	X	None at this time
63.	CHAIN: radionuclide chains	X	[CAMCON]; Notebook
64.	CHANGES: record of needed enhancements to CAMCON or codes	C	None at this time

TABLE 5-1. SEPTEMBER 1991 STATUS OF COMPOSITE PROGRAMS IN CAMCON (continued)

	Code	QA Status[1]	Work Remaining
65.	DISTRPLT: pdf's plots given parameters	X	[CAMCON]; Helpfile; Notebook
66.	FLINT: FORTRAN language analyzer	X	[CAMCON]; Helpfile
67.	HLP2ABS: conversion of helpfile to software abstract	X	Switch over from R:BASE™ to INGRES™; [CAMCON]; Helpfile
68.	LISTDCL: list of DEC command procedural files	C	None at this time
69.	LISTFOR: list of programs & sub-routines; summary of comments & active FORTRAN lines	C	None at this time
70.	NEFDIS: plot of NEFTRAN discharge history as a function of time	X	[CAMCON]
71.	SCANCAMDAT: quick summary of data in CAMDAT	X	Helpfile; Notebook
72.	TXT2CAM: ASCII to binary CAMDAT conversion	X	None at this time
Libraries			
73.	CAMCON_LIB	X	Architecture manual; Helpfile; Notebook; Review for Class A
74.	CAMSUPES	X	Add PARSE; Architecture manual; Helpfile; Notebook
75.	DVDI	X	Architecture manual; Helpfile; Notebook; Review for Class A
76.	PLOTLIB	X	Architecture manual; Helpfile; Notebook Review for Class A
77.	PLT	X	Architecture manual; Helpfile; Notebook; Review for Class A
78.	SDBREAD	X	Architecture manual; [CAMCON]; Helpfile; Notebook; Review for Class A
79.	CDBREAD	X	Under development

Chapter 5–Synopsis

The physical components of the disposal system and its surroundings provide barriers to radionuclide migration during the 10,000 years of regulatory concern.

The Natural Barrier System

Castile Formation

The Castile Formation (Late Permian), located immediately below the rock unit containing the repository, consists mostly of anhydrite and at some locations contains reservoirs of pressurized brine.

Pressurized brine in the Castile Formation could reach the repository through an intrusion borehole.

Salado Formation

The Salado Formation (Late Permian), the host rock for the repository, is about 600 m (1970 ft) thick at the WIPP and is mostly halite with some anhydrite interbeds.

Where the Salado Formation is intact and unaffected by dissolution, circulation of groundwater is extremely slow because primary porosity and open fractures are lacking.

Rustler Formation

The Rustler Formation (Late Permian), above the Salado Formation, contains five members. Two of these members, the Culebra and Magenta Dolomite Members, are considered in performance assessments because they are potential pathways for release of radionuclides to the accessible environment.

Climate

The present climate of southeastern New Mexico is arid to semi-arid. Geologic data show past alternations of wetter and drier climates that correspond to global cycles of glaciation and deglaciation.

Mean annual precipitation at the last glacial maxima was approximately twice that of the present.

Climatic variability is incorporated into the modeling system by varying boundary conditions of the two-dimensional, groundwater-flow model for the Culebra Dolomite Member of the Rustler Formation.

Surface Water

The principal surface-water feature in southeastern New Mexico is the Pecos River, which is about 20 km (12 mi) southwest of the WIPP at its closest point.

Several shallow, saline lakes in Nash Draw 8 km (5 mi) west of the WIPP collect precipitation, surface drainage, and groundwater discharge from springs and seeps.

The Water Table

Away from the immediate vicinity of the Pecos River, near-surface rocks are either unsaturated or of low permeability and do not produce water in wells.

Regionally, water-table conditions can be inferred for the more permeable units where they are close to the surface and saturated.

Regional Water Balance

Water inflow to the area comes from precipitation, surface-water flow in the Pecos River, groundwater flow across the boundaries of the region, and water imported to the region for human use.

Outflow from the water-budget model occurs as stream-water flow in the Pecos River, groundwater flow, and evapotranspiration.

Immediately around the WIPP, where no surface runoff occurs and all precipitation not lost to evapotranspiration must recharge groundwater, evapotranspiration may be as high as 98-99.5%.

Groundwater Flow above the Salado Formation

Although preliminary hydrologic modeling indicates the possibility of some vertical flow between hydrostratigraphic units, for the 1991 performance-assessment calculations units are assumed to be perfectly confined.

Potentiometric maps show differences in flow directions and indicate slow flow rates between the three major hydrostratigraphic units: they do not function as a single aquifer.

Groundwater Geochemistry

Groundwater quality of the Rustler-Salado contact residuum and the Culebra and Magenta Dolomite Members is poor, with total dissolved solids exceeding 10,000 mg/ℓ (the level set for regulation by the Individual Protection Requirements of the Standard) in most locations.

Recharge and Discharge

Potentiometric-surface mapping indicates that recharge to the Culebra Dolomite may be in an area north of the WIPP where the Rustler crops out, and through leakage from overlying units.

Discharge from the Culebra Dolomite is indicated toward the south, possibly into the Rustler-Salado contact residuum under water-table conditions near Malaga Bend and ultimately into the Pecos River. The Culebra may also discharge directly into the Pecos River or into alluvium.

Recharge to the Magenta Dolomite may also occur in an area north of the WIPP.

Discharge near the WIPP from the Magenta Dolomite is indicated toward the west, probably into the Tamarisk Member and the Culebra Dolomite near Nash Draw. Additional discharge may ultimately reach the saline lakes in Nash Draw, the Pecos River at Malaga Bend, or the alluvium in the Balmorhea-Loving Trough.

Groundwater Flow and Transport Models for the Culebra Dolomite

The Culebra Dolomite is modeled for performance assessment as a perfectly confined, two-dimensional aquifer.

Darcy flow is calculated for a single phase (liquid), and radionuclide transport is assumed to occur in a dual-porosity (fractures and matrix) medium.

The performance-assessment model allows for retardation during transport both by diffusion and sorption in matrix porosity and sorption by clays that line fractures. Retardation factors used in the 1991 preliminary comparison are based on expert judgment elicited from a panel of SNL researchers.

The Engineered Barrier System

Currently, engineered barriers in the WIPP are seals in panels, drifts, and shafts.

Other possible engineered barriers are modifications to the form of the waste and backfill or to the design of the waste-disposal areas.

The Salado Formation at the Repository Horizon

The repository has been excavated within a single stratigraphic horizon in the salt so that all panels within the waste-disposal area share the same local stratigraphy.

Excavation of the repository and the consequent release of lithostatic stresses have created a disturbed rock zone (DRZ) around the underground openings. Fracturing in the DRZ may provide a pathway for fluid migration out of the repository and possibly around panel and drift seals.

Repository and Seal Design

Waste will be emplaced within panels in drums or metal boxes, and panels will be backfilled and sealed as they are filled.

Backfill will reduce initial void space and permeability in the panels and will consolidate under pressure to further limit brine flow through the waste. Pure crushed salt, which will not sorb radionuclides, is currently assumed as backfill material.

The primary long-term component of the seals will be crushed salt, confined between short-term rigid bulkheads that will prevent fluid flow while creep closure reconsolidates the crushed salt to properties comparable to those of the intact Salado Formation.

Waste Characterization

The Waste Acceptance Certification requirements state that waste must be immobilized if it contains particulates in specified ranges. Waste must also be drained of liquids and contain no explosives or compressed gases.

Waste is characterized for the 1991 calculations by scaling 1987 data up to the design capacity of the repository. Estimates are made of the amounts of combustibles, metals, and other constituents of the waste.

The Radionuclide Inventory

Current performance-assessment calculations use an initial waste inventory that includes both CH and RH waste that currently exists or is estimated to be generated by 2013, based on 1990 data scaled up to the design volume of the repository.

The radionuclide inventory for transport calculations is a function of the initial inventory and decay within the repository before transport begins.

Radionuclide Solubility and the Source Term for Transport Calculations

Radionuclide solubility limits for the 1991 preliminary comparison are based on judgment elicited from an expert panel. Concentrations of suspended materials are not considered.

Performance-Assessment Model for the Repository/Shaft System

Liquid and gas flow in the Salado Formation is simulated as a function of the various processes active in the waste-disposal panels, including borehole intrusion.

All of the major processes active in the waste-disposal area are linked, and all are rate- and time-dependent.

Time and rate of gas generation will strongly influence repository pressurization and closure. Gas-generation rates will be dependent on specific reaction rates and the availability of reactants.

Responses of the disposal system to human intrusion will depend on the time of intrusion, the degree to which the repository has closed, and the amount of gas generated.

Modeling of Undisturbed Performance

Because estimates of undisturbed performance indicate no releases to the accessible environment, simulations of undisturbed performance are not included in the probabilistic calculations used to generate the CCDF curves.

For the 1991 preliminary comparison, the programs SUTRA and STAFF2D are used with two two-dimensional repository models (a horizontal and a vertical section through the system) to estimate radionuclide migration away from the undisturbed repository. Gas-pressurization effects are included by using elevated repository pressures calculated using the two-phase flow program BOAST_II.

Modeling of Disturbed Performance

The transient two-phase flow program BRAGFLO calculates brine and gas flow within waste panel, the surrounding rock, and an intrusion borehole. Gas-generation reactions are calculated dependent on availability of reactants (metal and cellulose) and brine saturation.

The program PANEL calculates radionuclide concentrations in repository brine as a function of solubility and decay.

Modeling of Radionuclide Releases during a Borehole Intrusion

The program CUTTINGS is used to estimate the quantity of cuttings and cavings from the drilling process released to the accessible environment in a settling pit at the surface.

CAMCON: Controller for Compliance Assessment System

The Compliance Assessment Methodology CONtroller (CAMCON) controls code linkage and data flow during lengthy and iterative consequence analyses, minimizes analyst intervention during data transfer, and automatically handles quality assurance during calculations.

6. CONTAINMENT REQUIREMENTS

[NOTE: The text of Chapter 6 is followed by a synopsis that summarizes essential information, beginning on page 6-17.]

The Containment Requirements of the Standard state that disposal systems

> shall be designed to provide a reasonable expectation, based upon performance assessments, that the cumulative releases of radionuclides to the accessible environment for 10,000 years after disposal from all significant processes and events that may affect the disposal system shall:
>
> (1) Have a likelihood of less than one chance in 10 of exceeding the quantities calculated according to Table 1 (Appendix A [of the Standard]); and
> (2) Have a likelihood of less than one chance in 1,000 of exceeding ten times the quantities calculated according to Table 1 (Appendix A [of the Standard]). (§ 191.13(a))

As indicated in Chapters 2 and 3 of this volume, compliance with the Containment Requirements will be evaluated using a family of CCDF curves that graph exceedance probability versus cumulative radionuclide releases for all significant scenarios. As discussed further in Chapters 10 and 11 of this volume, results presented here are not suitable for final compliance evaluations because portions of the modeling system and data base are incomplete, conceptual-model uncertainties are not included, final scenario probabilities remain to be determined, and the level of confidence in the results remains to be established. Uncertainty analyses required to establish the level of confidence in results will be included in future performance assessments as advances permit quantification of uncertainties in the modeling system and the data base.

Results in the form of CCDFs for the 1991 preliminary compliance assessment are presented separately for total releases (cuttings/cavings plus subsurface) to the accessible environment and for subsurface groundwater releases only. These CCDF presentations are the culmination of the application of the conceptual model for risk (performance assessment) described in Chapter 3 of this volume.

6.1 Conceptual Model for Risk

Construction of CCDFs presented in this chapter is based on the conceptual representation of performance assessment described in Chapter 3 of this volume. The outcome of the performance assessment is represented as a set of ordered triples of the form

$$R = \{(S_i, pS_i, \mathbf{cS}_i), i=1, \ldots, nS\} \quad (6\text{-}1)$$

where

S_i = a set of similar occurrences,

pS_i = probability that an occurrence in the set S_i will take place,

$\mathbf{cS}_i$ = a vector of consequences associated with S_i,

nS = number of sets selected for consideration,

and the sets S_i have no occurrences in common (i.e., the S_i are disjoint sets).

In terms of performance assessment, the S_i are scenarios, the pS_i are scenario probabilities, and the $\mathbf{cS}_i$ are vectors containing results or consequences associated with scenarios. The information contained in the pS_i and $\mathbf{cS}_i$ is summarized in the form of CCDFs as exceedance probability versus consequence curves. The construction of these curves is described in Volume 2, Chapter 3 of this report.

6.2 Scenarios Included and Probability Estimates

The representation of the performance assessment as an ordered triple involves scenario probabilities that require an underlying sample space. The introduction to Chapter 4 of this volume defined this sample space, S, as

$$S = \{x: x \text{ is a single 10,000-year history beginning at decommissioning}\}. \quad (6\text{-}2)$$

Following the screening of a comprehensive list (Table 4-1) of possible events and processes that could affect future states of the waste-barrier system, a logic diagram (Figure 4-5) was used to construct summary

scenarios, S_i, that are mutually exclusive sets of common occurrences whose union is S, i.e.,

$$S = \bigcup_{i=1}^{8} S_i \quad . \tag{6-3}$$

The base-case summary scenario, S_1, in the logic diagram is the undisturbed scenario for the Containment Requirements. Since there are no releases estimated to occur in the 10,000-year regulatory period (Volume 2, Chapter 4 of this report), S_1 is not analyzed, but it is included in CCDF construction through its estimated probability and zero consequences (Figure 4-2). In order to display the family of CCDFs such that stochastic variability and uncertainty due to imprecisely known variables are clearly separated, the summary scenarios, S_i, for human intrusion are further refined into computational scenarios denoted $S(\mathbf{n})$, $S(\mathbf{l},\mathbf{n})$, $S^{+-}(t_{i-1}, t_i)$, and $S^{+-}(\mathbf{l};t_{i-1}, t_i)$, which are disjoint sets of common occurrences defined such that it is reasonable to use the same consequences for all elements of each computational scenario and such that consequences can be estimated with reasonable computational cost.

The factors used to define $S(\mathbf{n})$, $S(\mathbf{l},\mathbf{n})$, $S^{+-}(t_{i-1}, t_i)$, and $S^{+-}(\mathbf{l};t_{i-1}, t_i)$, are: number and time of intrusions (Volume 2, Chapter 2, Tables 2-2 and 2-3), flow through a panel due to penetration of a pressurized brine reservoir in the Castile Formation (Volume 2, Chapter 2, Table 2-6), and activity level of the waste penetrated by a borehole (Volume 2, Chapter 2, Table 2-7). These factors all relate to stochastic or Type A uncertainty since they lead to values used for pS_i in constructing the CCDFs.

For the 1991 performance assessment, drilling intrusions are assumed to follow a Poisson process (i.e., intrusions occur randomly in space and time with a fixed rate constant). The rate constant is an imprecisely known variable with upper bound defined by the regulatory guidance of 30 boreholes/km^2/10,000 yr and lower bound of zero. The Poisson rate constant is assumed to be a uniformly distributed variable and is included in the set of imprecisely known variables that accounts for Type B uncertainty. Since the EPA limit requires estimation of cumulative probability through the 0.999 level, consequences of computational scenarios involving up to 10 or 12 drilling intrusions may be included in the comparison with regulatory limits. For this performance assessment, the regulatory time interval of 10,000 years is divided into five disjoint time intervals of 2,000 years each with intrusion occurring at the midpoints of these intervals (i.e., 1000, 3000, 5000, 7000, and 9000 years).

For the 1991 performance assessment, the waste panels are assumed to be underlain by one or more pressurized brine reservoirs in the Castile Formation. The possible location of these brine reservoirs is shown in Volume 3. The fraction of waste panel area underlain by brine reservoirs is included in the set of imprecisely known variables. The uncertainty in this parameter is Type B (i.e., subjective), although the parameter itself is used in the calculation of the probabilities pS_i that characterize Type A (i.e., stochastic) uncertainty.

For the 1991 performance assessment, activity loading of the waste within a panel is included. Four CH activity levels and one RH activity level are defined to represent variability in the activity level of waste penetrated by a drilling intrusion. The distribution of activity levels for existing waste to be shipped to the WIPP is contained in Volume 3 of this report. This distribution was scaled up from existing waste to the WIPP design capacity for the 1991 performance assessment. As with the rate constant λ in the model for the occurrence of drilling intrusions and the area fraction for pressurized brine, the distribution of activity loading is used in the calculation of the probabilities pS_i.

The three factors just listed (Poisson rate constant, area of brine reservoir, and variable activity loading) are used in probability models (Volume 2, Chapter 2 of this report) for estimating computational scenario probabilities, pS_i. These estimates determine the vertical step sizes of the CCDFs and therefore represent Type A or stochastic uncertainty. The probabilities used in this performance assessment are not always exact for a Poisson process because some assumptions are made to simplify the calculations. However, these assumptions are made so that probability estimates are bounding, i.e., estimates used are greater than an exact calculation (i.e., $p(\cup_i S_i) = \Sigma_i pS_i$) to simplify calculations for some S_i.

In developing the logic diagram for defining summary scenarios and setting up the design of the consequence modeling a number of additional assumptions have been made. These are summarized in Table 6-1.

Previous calculations (Marietta et al., 1989; Bertram-Howery et al., 1990) have analyzed summary scenarios, S_1, S_2, S_3, and S_4 in Figure 4-5. CCDFs were constructed as described by Cranwell et al. (1990) using fixed scenario probabilities. CCDFs presented in this report do not use the same construction technique but follow the procedure described in Volume 2, Chapter 3 of this report. Scenario probabilities are not fixed. Instead, probabilities are calculated for computational scenarios $S(\mathbf{n})$, $S(\mathbf{I},\mathbf{n})$, $S^{+-}(t_{i-1}, t_i)$, and $S^{+-}(\mathbf{I}; t_{i-1}, t_i)$ as described in Chapter 4 of this volume, using the probability models defined in Volume 2, Chapter 2 of this report.

TABLE 6-1. ASSUMPTIONS USED TO DEFINE COMPUTATIONAL SCENARIOS FOR RESULTS REPORTED IN THIS CHAPTER

1. No connections exist between panels.
2. No synergistic effects result from multiple boreholes except for $E1E2$-type computational scenarios.
3. An $E1E2$-type computational scenario only occurs when intrusions of each type happen in the same panel within the same time interval.
4. An $E1E2$-type computational scenario has the same release with more than two intrusions in one panel as with exactly two intrusions.
5. In an $E2$-type computational scenario, a plug exists directly above the Culebra Unit in the Rustler Formation that directs flow into the Culebra, and this plug is effective for 10,000 years following decommissioning.
6. In an $E1$-type computational scenario, a plug exists as in number five, and no other plug exists to retard flow from the Castile pressurized brine reservoir.
7. In an $E1E2$-type computational scenario, number five is true for one intrusion, and a similar plug exists between the repository and the Rustler Formation that directs flow through the penetrated waste panel toward the other intrusion in the same panel. Further, both intrusions are conservatively assumed to occur at the same time.
8. Computational scenarios involving subsidence events are not included in this performance assessment, which is equivalent to assuming that subsidence has no effect on the consequences calculated for the scenarios under consideration.
9. Closure of the intrusion boreholes is not included in this performance assessment.

Fundamental differences between this year's and previous years' performance assessments are the refinement of summary scenarios into computational scenarios and the use of the Poisson assumption of random intrusion in space and time for calculating scenario probabilities. The CCDF construction procedure used for this year's performance assessment results in an explicit representation for the effects of stochastic variability (Type A uncertainty).

6.3 Imprecisely Known Parameters

Forty-five imprecisely known parameters were sampled for use in consequence modeling for the Monte Carlo simulations of performance. For each of these 45 parameters, a range and distribution were assigned as discussed in Volume 3 of this report. However, Volume 3 lists approximately 300 parameters that could be used in consequence modeling. These parameters specify physical, chemical, and hydrologic properties of the rock formations (geologic barriers) and of the seals, backfill, and waste form (engineered barriers). Parameters for climate variability and future drilling intrusions are included in this list. Selection of the set of parameters to be sampled is an important decision in designing each year's preliminary compliance assessment. The present study is preliminary, so the final set of sampled parameters will probably differ from the present set. Table 6-2 lists the set of imprecisely known parameters that was sampled for the 1991

TABLE 6-2. LIST OF PARAMETERS SAMPLED FOR THE 1991 PRELIMINARY COMPARISON

Parameter Name	Volume 3 Reference
Salado Formation	
1. Far-field pore pressure	2.4.6
2. Anhydrite permeability/undisturbed	2.4.5
3. Anhydrite porosity/undisturbed	2.4.7
4. Threshold pressure/anhydrite	2.4.1
5. Halite permeability/undisturbed	2.3.5
Castile Formation	
6. Initial pressure/brine reservoir	4.3.2
7. Bulk storativity/brine reservoir	4.3.2
Rustler Formation/Culebra Dolomite Member	
8. Longitudinal dispersivity	2.6.2
9. Fracture spacing	2.6.4
10. Fracture porosity	2.6.4
11. Matrix porosity	2.6.4
12. Transmissivity conditional simulations[1]	V.2, Sec. 6.3
Partition coefficients/fracture	2.6.10
13. Am	
14. Np	
15. Pu	
16. Th	
17. U	
Partition coefficients/matrix	2.6.10
18. Am	
19. Np	
20. Pu	
21. Th	
22. U	
As-Received Waste Form	
Gas generation/corrosion	3.3.8
23. Inundated generation rate	
24. Humid generation rate[2]	
25. Stoichiometry	
Gas generation rate/biodegradation	3.3.9
26. Inundated generation rate	
27. Humid generation rate[2]	
28. Stoichiometry	

1. A sample is drawn from a uniform variate over a set of 60 fields for transmissivity, each assumed to have equal probability, and each conditioned on transmissivity measurements at well locations and pilot point values.

2. Humid generation rates are relative to inundated rates such that the upper bound for the humid rate is always the value sampled for the inundated rate for each sample element.

TABLE 6-2. LIST OF PARAMETERS SAMPLED FOR THE 1991 PRELIMINARY COMPARISON (concluded)

	Parameter Name	Volume 3 Reference
	Dissolved concentrations/solubility[3]	3.3.5
29.	Am^{3+}	
30.	Np^{4+}	
31.	Np^{5+}	
32.	Pu^{4+}	
33.	Pu^{5+}	
34.	Th^{4+}	
35.	U^{4+}	
36.	U^{5+}	
	Volume fractions of IDB categories	3.4.1
37.	Metal/glass	
38.	Combustibles	
39.	Initial waste saturation	3.4.9
40.	Eh-pH conditions	3.3.6
	Agents Acting on Disposal System	
	Human intrusion borehole	
41.	Borehole-fill permeability	4.2.1
42.	Borehole diameter	4.2.2
43.	Climate/recharge factor	4.4.3
	Probability Model for Computational Scenarios	
44.	Area fraction of pressurized brine reservoir/Castile	5.1.1
45.	Rate constant for Poisson drilling model	5.2.1

3. Each pair, (Np^{4+},Np^{5+}), (Pu^{4+},Pu^{5+}), and (U^{4+},U^{5+}), is correlated at a level of 0.99.

performance assessment. Included are the names and a reference to Volume 3 of this report for each parameter. A summary table of these parameters with a range, median, distribution, and original reference for each is given in Volume 3, Chapter 6 of this report.

Fundamental differences from last year's preliminary comparison are the addition of parameters related to two-phase flow and gas generation, parameters related to dual porosity (both chemical and physical retardation) in the Culebra, and a set of conditional simulations for transmissivity in the Culebra instead of the 1990 simple zonal approach. The 1991 calculations also include a preliminary analysis of potential effects of climatic variability on flow in the Culebra.

6.4 Sample Generation

Latin hypercube sampling is used to incorporate Type B uncertainty (i.e., uncertainty due to imprecisely known variables) into the performance assessment (Chapter 3 of this volume). Specifically, a Latin hypercube sample of size 60 was generated from the set of 45 variables listed in Table 6-2. Restricted pairing was used to prevent any spurious correlations. The resultant sample is listed in Volume 2, Appendix B of this report.

Decomposition of the sample space S into the computational scenarios described above is a form of stratified sampling (Chapter 3 of this volume), where the pS_i are the strata probabilities. This stratified sampling incorporates Type A or stochastic uncertainty into the performance assessment and forces the inclusion of low-probability, high-consequence computational scenarios (e.g., *E*1*E*2-type drilling intrusions).

6.5 Consequence Modeling

After the sample is generated, each element of the sample is propagated through the system of codes used for scenario analysis. Only human-intrusion computational scenarios are included. In the 1991 performance assessment, the major modules used to simulate flow and transport are CUTTINGS, BRAGFLO, PANEL, SECO2D, and STAFF2D. These codes are linked and the data flow controlled by the CAMCON executive package (Rechard et al., 1989). Each sample was used in the calculation of both cuttings/cavings and subsurface groundwater releases for intrusion times of 1000, 3000, 5000, 7000, and 9000 years for *E*2- and *E*1*E*2-type intrusions. Consequences, $\mathbf{cS}_i$, of *E*1-type intrusions were found to be similar to and bounded by *E*1*E*2-type intrusions, so only the latter required calculations. Therefore, 600 executions of the linked system of codes were needed to generate the required set of consequences for subsurface groundwater releases. The resulting set of consequences (cuttings/cavings plus subsurface groundwater releases) were used by the probability model, CCDFPERM, to calculate a family of CCDFs and its summary curves (median, mean, and various quantiles). The probability model calculates probabilities and consequences for computational scenarios for all combinations of the activity levels and time intervals, resulting in up to 800,000 computational scenarios included in this performance assessment.

The important assumptions for the 1991 preliminary comparison are listed in Table 6-3.

TABLE 6-3. PARTIAL LIST OF ASSUMPTIONS MADE IN CONSEQUENCE MODELING FOR RESULTS REPORTED IN THIS CHAPTER

Compliance-Assessment System Component	Assumption	Cross-Reference
REPOSITORY/SHAFT/ BOREHOLE MODELS: REPOSITORY/SHAFT DESIGN		
Panel, Drift and Lower Shaft Seals	Reconsolidate to properties close to those of intact salt	V.3,Ch.3
	No MB139 or anhydrite A and B seals	V.2,Ch.5
REPOSITORY/SHAFT/ BOREHOLE MODELS: PANEL MODEL		
Salado Formation	Homogeneous time-invariant material properties within each stratigraphic unit	V.2, Ch.5; V.3, Ch.2
	Initial brine saturation in Salado	V.2, Ch.5
Waste/Backfill	Homogeneous material properties and time-invariant porosity on a panel scale	V.2, Ch.5; V.3, Ch.3
	No sorptive retardation in backfill	V.1, Ch.5
	CH waste emplaced only in 55 gal drums and standard waste boxes	V.3, Ch.3
	IDB radionuclide inventory extrapolated to design capacity	V.1,Ch.5; V.3, Ch.3
	Volume fractions of combustibles and metals/glass extrapolated to design capacity	V.3, Ch.3
	All combustibles and 50% of rubbers biodegrade	V.3, Ch.3
	RH waste included in cuttings but not subsurface groundwater releases	V.2, Ch.2,7
	Activity loading variability included for CH waste	V.2, Ch.2
	No radionuclide transport as colloids	V.1, Ch.5; V.3, Ch.3
Panel/Waste Interactions	Panel modeled with equivalent-enclosed-volume cylindrical geometry	V.2, Ch.5

TABLE 6-3. PARTIAL LIST OF ASSUMPTIONS MADE IN CONSEQUENCE MODELING FOR RESULTS REPORTED IN THIS CHAPTER (continued)

Compliance-Assessment System Component	Assumption	Cross-Reference
	Gas generated by corrosion and biodegradation only (no radiolysis)	V.2, Ch.5 V.3, Ch.3
	Gas generation proportional to brine saturation	V.2, Ch.5
	Brine consumed during corrosion; no gas consumed within the panel	V.2, Ch.5
	Fracture flow limited to MB139/room interaction	V.3, Ch.3
	Brine and gas flow obeys generalized Darcy's Law for compressible fluids in all media	V.2, Ch.5
	No dissolved gas in brine phase	V.2, Ch.5
	Solubility limits allocated among isotopes of an element based on relative abundance	V.2, Ch.5
	Radionuclide concentrations assumed to be uniform throughout panel and in equilibrium at all times	V.2, Ch.5
Human Intrusion (see Table 6.1)	Exploratory hydrocarbon drilling only	V.1, Ch.4
	Future drilling technology comparable to present	V.1, Ch.4,5; V.3, Ch. 7
	Arbitrary plug configurations for scenarios	V.1, Ch.4
	Brine reservoirs in the Castile Fm. underlie portions of some waste panels	V.1, Ch.4; V.2, Ch.2
	Some plugs deteriorate, some remain intact from time of emplacement through remainder of 10,000 years	V.1, Ch.4; V.3, Ch.4
	Probability of intrusion follows a Poisson process (i.e., random in space and time for 9900 years)	V.1, Ch.4; V.2, Ch.2; V.3, Ch.5
	Borehole-fill properties comparable to silty sand	V.3, Ch.4
	Source for all intrusion boreholes for Culebra transport located above center of waste-disposal area	V.2, Ch.6

TABLE 6-3. PARTIAL LIST OF ASSUMPTIONS MADE IN CONSEQUENCE MODELING FOR RESULTS REPORTED IN THIS CHAPTER (continued)

Compliance-Assessment System Component	Assumption	Cross-Reference
REPOSITORY/SHAFT MODELS: REPOSITORY MODEL		
Panel and Drift Seals	Reconsolidate to properties close to those of intact salt	V.3, Ch.3
Lower Shaft Seals	Reconsolidate to properties close to those of intact salt	V.3, Ch.3
GROUNDWATER-FLOW AND TRANSPORT MODELS: GROUNDWATER-FLOW MODEL		
Regional Hydrogeology	Rock properties are time invariant	V.1, Ch.4, 5
	Future climate variability bounded by past	V.1, Ch. 5
Rustler/Dewey Lake Hydrogeology	2-D, confined,single porosity, Darcy flow model for Culebra	V.1, Ch. 5 V.2, Ch.6
	60 transmissivity fields conditioned on measured transmissivities at well locations and pilot point values represent uncertainty in field	V.2, Ch.6
	Changes in recharge restricted to northern boundary	V.1, Ch.5 V.2, Ch.6
	No flow boundary along Nash Draw, constant heads on other boundaries except for recharge strip	V.2, Ch.6
	Impact of subsidence not considered	V.2, Ch.6
	Future vertical flow through existing boreholes not considered	V.2, Ch.6
	Variable-density effects not considered	V.2, Ch.6
	Brine flow from intrusion borehole does not alter flow in Culebra	V.2, Ch.6
GROUNDWATER FLOW AND TRANSPORT MODELS: RADIONUCLIDE TRANSPORT MODEL		
Physical Retardation	Dual-porosity medium for transport	V.1, Ch.5; V.2, Ch.6

TABLE 6-3. PARTIAL LIST OF ASSUMPTIONS MADE IN CONSEQUENCE MODELING FOR RESULTS REPORTED IN THIS CHAPTER (concluded)

Compliance-Assessment System Component	Assumption	Cross-Reference
Chemical Retardation	Retardation in both clay-lined fractures and dolomite matrix	V.1, Ch.5; V.2, Ch.6
	Transport by colloids not considered	V.1, Ch.5; V.2, Ch.6
CUTTINGS/CAVINGS MODEL		
Drill Cuttings	Homogeneous waste properties	V.1, Ch.5; V.2, Ch.7
	Present-day rotary drilling methods	V.1, Ch.5; V.2, Ch.7
Erosion/Cavings	Spalling from gas-filled waste panel not considered	V.1, Ch.5; V.2, Ch.7
	Waste characterized by an effective shear strength	V.1, Ch.5; V.2, Ch.7
	Erosion occurs when drilling fluid shear stress exceeds effective shear strength	V.1, Ch.5; V.2, Ch.7

6.6 1991 Performance Assessment CCDFs

The CCDFs resulting from the 1991 analysis described above are displayed in Figures 6-1 and 6-2. Figure 6-1 is the family of CCDFs for total release (cuttings/cavings plus subsurface groundwater) to the accessible environment. Figure 6-2 is a set of summary curves (median, mean, and two quantiles) derived from this family. To illustrate the effect of cuttings and cavings, subsurface groundwater releases are displayed separately in Figures 6-3 and 6-4. Except for a few low-probability releases, cuttings and cavings dominate the CCDFs for total releases. Based on the performance-assessment data base and present understanding of the WIPP disposal system, the summary curves in Figure 6-2 are considered to be the most realistic choice for preliminary comparison with the Containment Requirements of EPA *40 CFR 191*. Additional CCDFs are presented with sensitivity analysis results and alternate displays of uncertainty analysis results in Volume 4 of this report.

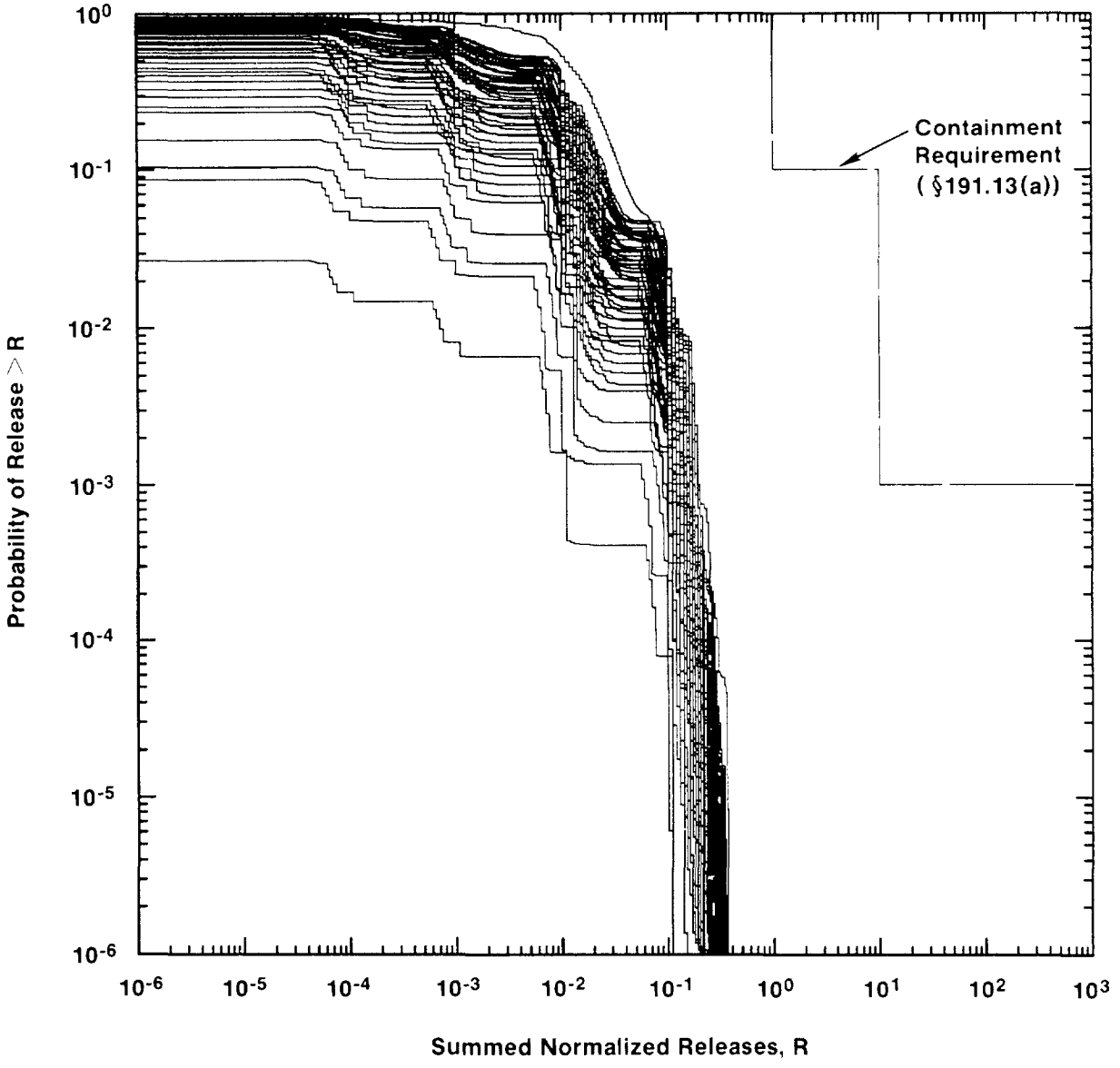

TRI-6342-1293-0

Figure 6-1. Family of CCDFs Showing Total Cumulative Normalized Releases to the Accessible Environment Resulting from Both Groundwater Transport in the Subsurface and Releases at the Surface during Drilling. CCDFs are conditional on assumed scenarios, models, and distributions for parameter values, as described in the text and in Volumes 2 and 3 of this report.

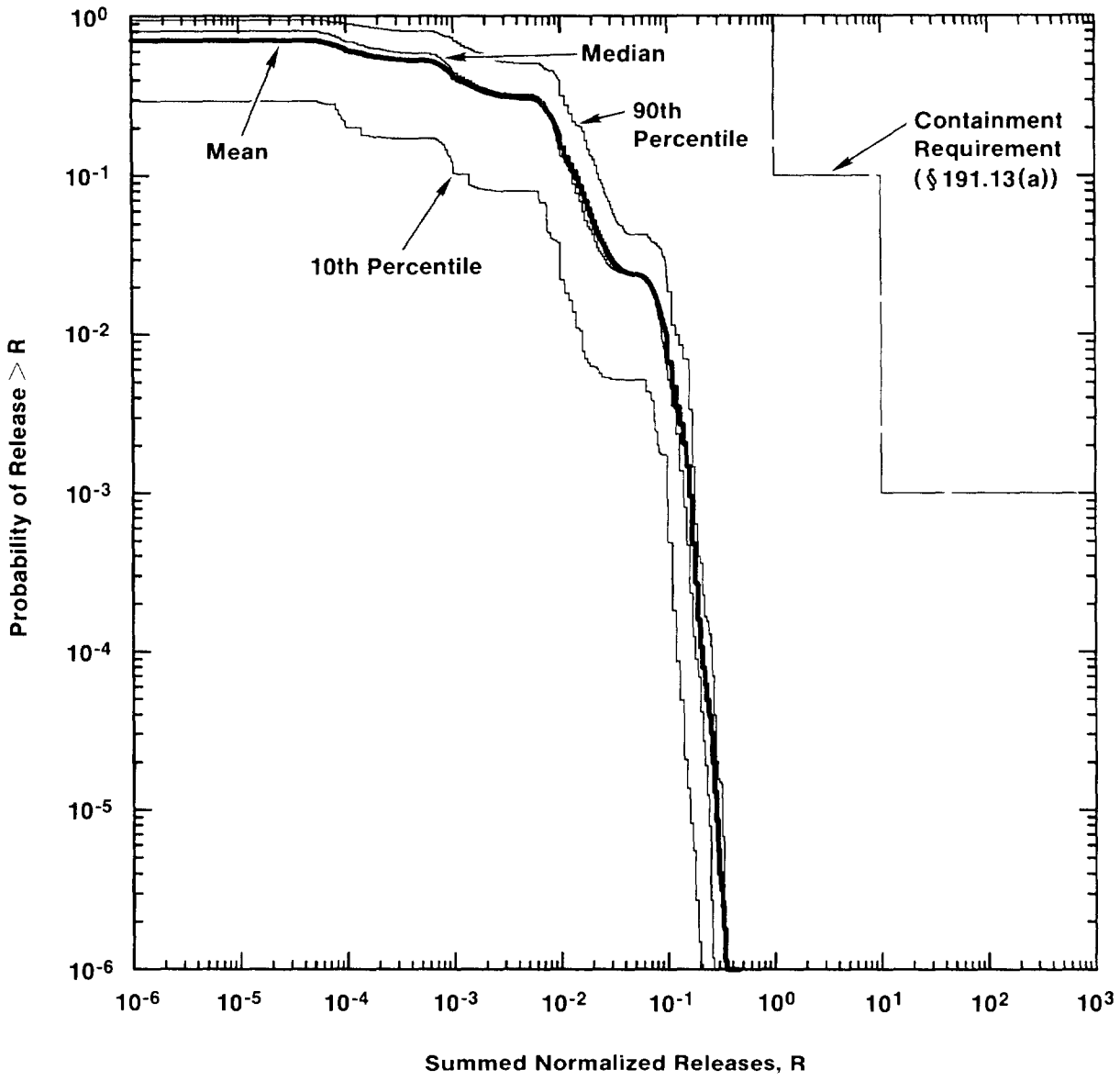

Figure 6-2. Mean, Median, 10th, and 90th Percentile CCDFs Derived from the Family of CCDFs Shown in Figure 6-1. Curves show total cumulative normalized releases to the accessible environment resulting from both groundwater transport in the subsurface and releases at the surface during drilling. CCDFs are conditional on assumed scenarios, models, and distributions for parameter values, as described in the text and in Volumes 2 and 3 of this report.

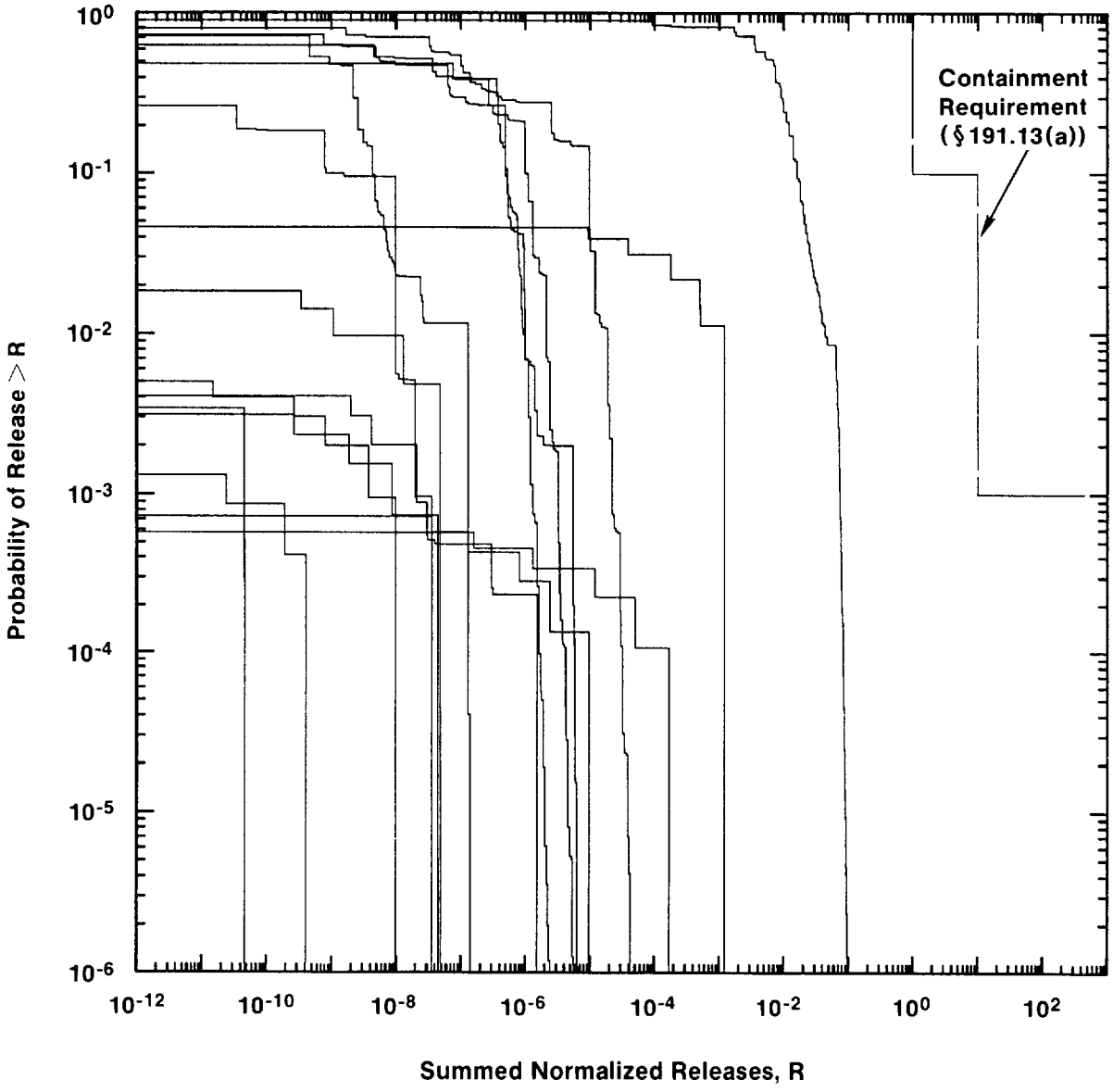

TRI-6342-1295-0

Figure 6-3. Family of CCDFs Showing Cumulative Normalized Releases to the Accessible Environment Resulting from Groundwater Transport in the Subsurface. CCDFs are conditional on assumed scenarios, models, and distributions for parameter values, as described in the text and in Volumes 2 and 3 of this report.

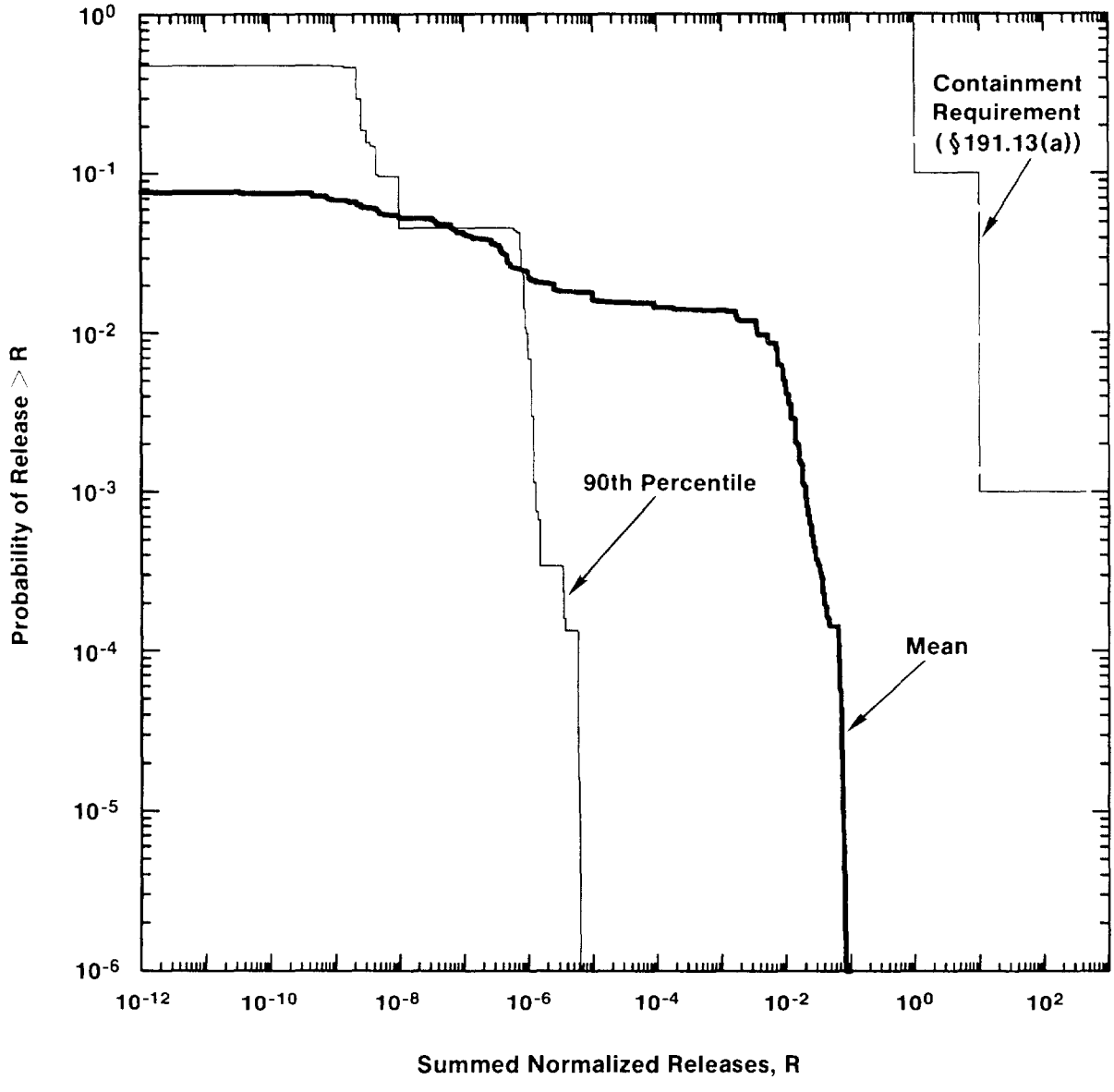

TRI-6342-1296-0

Figure 6-4. Mean and 90th Percentile CCDFs Derived from the Family of CCDFs Shown in Figure 6-3. The median and 10th percentile CCDFs are off the plot to the left. Curves show cumulative normalized releases to the accessible environment resulting from groundwater transport in the subsurface. CCDFs are conditional on assumed scenarios, models, and distributions for parameter values, as described in the text and in Volumes 2 and 3 of this report.

The main consequence modeling differences between the 1990 and 1991 preliminary comparisons are the inclusion of variable climate, dual-porosity transport, and waste-generated gas effects. The main probability modeling differences are the assumption that drilling intrusions are a Poisson process, the inclusion of uncertainty in the characterization of stochastic variability instead of using fixed probability estimates for summary scenarios, and the refinement of summary scenarios into many computational scenarios. An analysis of the effects of these changes is presented in Volume 4 of this report.

Chapter 6-Synopsis

Conceptual Model for Risk

Construction of CCDFs presented in this chapter is based on the conceptual representation of performance assessment described in Chapter 3 of this volume.

Scenarios Included and Probability Estimates

The base-case summary scenario is not analyzed for comparison with the Containment Requirements (disturbed performance) because no releases are estimated to occur in the 10,000-year regulatory period. However, the base case summary scenario is included in CCDF construction through its estimated probability and zero consequences.

Families of CCDFs are displayed so that stochastic variability and uncertainty due to imprecisely known variables are clearly separated. Portraying the summary scenarios in this manner requires further refining of the summary scenarios into computational scenarios that are separate sets of common occurrences with similar consequences for all elements of each computational scenario. In addition, separation into computational sets allows estimating consequences with reasonable computational cost.

The factors, which all relate to stochastic or Type A uncertainty, that are used to define the sets of computational scenarios are

- number and time of intrusions,
- flow through a panel due to penetration of a pressurized brine reservoir in the Castile Formation,
- activity level of the waste penetrated by a borehole.

For the 1991 performance assessment,

- drilling intrusions are assumed to occur randomly in space and time with a fixed rate constant (follow a Poisson process). For this performance assessment, the regulatory time interval of 10,000 years is divided into five time intervals of 2,000 years, with intrusion occurring at the midpoints of these intervals (at 1000, 3000, 5000, 7000, and 9000 years).

- the waste panels are assumed to be underlain by one or more pressurized brine reservoirs in the Castile Formation.

- four CH activity levels and one RH activity level are defined to represent variability in the activity level of waste penetrated by a drilling intrusion.

Fundamental differences between this year's and previous years' performance assessments are

- refinement of summary scenarios into computational scenarios,

- the use of the Poisson assumption for calculating scenario probabilities.

The CCDF construction procedure used for this year's performance assessment results in an explicit representation for the effects of stochastic variability.

Imprecisely Known Parameters

Forty-five imprecisely known parameters were sampled for use in consequence modeling for the Monte Carlo simulations of performance. For each, a range and distribution were assigned.

Fundamental differences from last year's performance assessment are the addition of

- parameters related to two-phase flow and gas generation,

- parameters related to dual porosity (both chemical and physical retardation) in the Culebra,

- a set of conditional simulations for transmissivity in the Culebra instead of the 1990 simple zonal approach,

	a preliminary analysis of potential effects of climatic variability on flow in the Culebra.
Sample Generation	Latin hypercube sampling is used to incorporate uncertainty due to imprecisely known variables, or Type B uncertainty, into the performance assessment. For the 1991 performance assessment, a Latin hypercube sample of size 60 was generated from the set of 45 variables. Decomposition into computational scenarios is a form of stratified sampling in which Type A uncertainty is incorporated into the performance assessment and forces the inclusion of low-probability, high-consequence computational scenarios.
Consequence Modeling	After the sample is generated, each element of the sample is propagated through the system of computer codes used for scenario analysis. Only computational scenarios for human intrusion are included. In the 1991 performance assessment, the major computer modules used to simulate flow and transport are CUTTINGS, BRAGFLO, SECO2D, AND STAFF2D. Each sample was used in calculating both cuttings/cavings and subsurface groundwater releases for intrusion times of 1000, 3000, 5000, 7000, and 9000 years for E1- and E2-type intrusions. Consequences of E1-type intrusion were found to be similar to and bounded by E1E2-type intrusions, so only the latter required calculations. The resulting set of consequences (cuttings/cavings plus subsurface groundwater releases) were used by the probability computer model CCDFPERM to calculate a family of CCDFs and its summary curves (median, mean, and various quantiles).
1991 Performance Assessment CCDFs	Based on the performance-assessment data base and present understanding of the WIPP disposal system, the summary curves showing total cumulative normalized releases to the accessible environment resulting from both groundwater transport in the subsurface and releases at the surface during drilling (Figure 6-2) are considered to be the most realistic choices for preliminary comparison with the Containment Requirements.

Except for a few low-probability releases, cuttings/cavings dominates the CCDFs for total releases.

The main differences in modeling consequences between the 1990 and 1991 preliminary comparisons are the inclusion of

- variable climate,
- dual-porosity transport,
- waste-generated effects.

The main differences in modeling probabilities between the 1990 and 1991 preliminary comparisons are

- the assumption that drilling intrusions are a Poisson process,
- the inclusion of uncertainty in the characterization of stochastic variability instead of using fixed probability estimates for summary scenarios,
- the refinement of summary scenarios into many computational scenarios.

7. INDIVIDUAL PROTECTION REQUIREMENTS

[*NOTE: The text of Chapter 7 is followed by a synopsis that summarizes essential information, beginning on page 7-6.*]

The Standard contains Individual Protection Requirements:

> Disposal systems for transuranic wastes shall be designed to provide a reasonable expectation that for 1000 years after disposal, undisturbed performance of the disposal system shall not cause the annual dose equivalent from the disposal system to any member of the public in the accessible environment to exceed 25 mrem to the whole body and 75 mrem to any critical organ (§ 191.15).

The Standard requires that an uncertainty analysis of undisturbed conditions be performed to assess compliance with § 191.15. In the case of the WIPP, the performance measure is dose to humans in the accessible environment. Evaluations thus far indicate that radionuclides will not migrate out of the repository/shaft system during 1000 years. Therefore, dose calculations are not expected to be a part of the WIPP assessment of compliance with *40 CFR Part 191*. However, Subpart B is in remand. The outcome of the remand could require dose calculations over longer time periods. Performance assessments will evaluate compliance with the Individual Protection Requirements of the 1985 Standard until a revised Standard is promulgated.

7.1 Previous Studies

Three previous studies reported doses to humans resulting from hypothetical releases from the WIPP for selected scenarios (U.S. DOE, 1980a; Lappin et al., 1989; Lappin et al., 1990). Although these studies employed deterministic calculations and were not concerned with assessing compliance with § 191.15, they have an important bearing on the design of probability-based dose calculations. Undisturbed performance was evaluated probabilistically by Marietta et al. (1989) in a methodology demonstration for WIPP performance assessment. Calculations for undisturbed performance of the repository were not updated in the 1990 preliminary performance assessment (Bertram-Howery et al., 1990). However, information about possible effects of gas generated within the repository was obtained from the assessment of disturbed performance.

7.1.1 EVALUATION PRIOR TO THE 1985 STANDARD (1980 FEIS)

The approach in the *WIPP Final Environmental Impact Statement* (U.S. DOE, 1980a) for analyzing the effects of radioactivity released from the WIPP was to estimate the consequence of five different hypothetical scenarios that might move radionuclides to the biosphere. The analyses of these scenarios proceeded from radionuclide movement through the geosphere to transport through the biosphere after discharge into the Pecos River at Malaga Bend, and, finally, to predicted radiation doses received by people. The human dose estimates were based on the *Report of ICRP Committee II on Permissible Dose for Internal Radiation* (ICRP, 1959), usually referred to as ICRP 2. The travel times for radionuclides arriving at Malaga Bend were on the order of a million years, but this study predates the Standard, which specifies a time scale of 1000 years for individual protection.

7.1.2 DOSE ESTIMATES (LAPPIN ET AL., 1989)

An analysis of undisturbed conditions for the WIPP was performed (Lappin et al., 1989) for two different cases in support of the WIPP supplemental environmental impact statements (SEIS) (U.S. DOE 1989b, 1990c). The exposure pathway considered was radionuclide transport through the sealed shafts and intact Salado to the Culebra Dolomite, downgradient through the Culebra to a hypothesized stockwell at the nearest location where Culebra water might be potable for cattle, and then to humans via beef ingestion. Calculations were deterministic, with one case using expected parameter values and the other case using degraded parameter values. The study indicated that, in the absence of human intrusion, there would be no releases to the Culebra in 1000 years. Therefore, no doses were calculated for undisturbed conditions.

7.1.3 1989 METHODOLOGY DEMONSTRATION

The next evaluation of undisturbed performance of the WIPP was the methodology demonstration of Marietta et al. (1989). Undisturbed performance was simulated using the base-case scenario (Guzowski, 1990). The repository was assumed to be consolidated, and all legs in the flow path were assumed to be saturated from the time of repository decommissioning. Uncertainty analysis was based on probability density functions representing realistic but preliminary estimates of minimum, maximum, and expected or median values and distributions of parameters.

In the simulations for the methodology demonstration, no releases from the repository/shaft system to the Culebra occurred during the 1000 years of regulatory concern. Because of the slow rate of radionuclide movement,

simulations were extended to 50,000 years to assess system performance. Even at this longer time interval, no significant releases to the Culebra occurred. Results were therefore presented in terms of radionuclide migration through the MB139 seal below the repository and to the base of the shaft.

The demonstration analysis for undisturbed conditions indicated no releases from the repository in either the 1000-year period for the Individual Protection Requirements (§ 191.15) or the 10,000-year period for the Containment Requirements (§ 191.13). The fact that no releases occurred indicated that no dose calculations were needed for demonstrating compliance with the Individual Protection Requirements of the 1985 Standard.

7.1.4 SENSITIVITY ANALYSES (RECHARD ET AL., 1990)

Rechard et al. (1990a) examined the relative importance of various phenomena and system components through sensitivity analyses of four different repository shaft models for undisturbed conditions. Although these simulations did not calculate EPA sums or doses to humans for either the Containment or Individual Protection Requirements, they did calculate brine flow in the lower shaft seals, which bears directly upon estimating releases to the Culebra.

The first two models considered only one-phase (brine) flow: a two-dimensional model of brine flow into MB139, and a cylindrical model of brine flow through a waste panel into a shaft. The second two models considered effects of gas flow: a two-dimensional model simulating gas flow through drifts, and a one-dimensional model of two-phase (brine and gas) flow through MB139.

The following conclusions were drawn: for brine-saturated conditions, flow from the repository occurs in all directions when expected parameter values are used, but for degraded parameter values, a primary path along MB139 exists. The two-phase calculations that assessed gas migration to the shaft indicated that brine would retard such flow unless well-fractured, high-permeability paths exist as in MB139 and anhydrite layers A and B. This work indicated that two-phase models including local stratigraphy (MB139, anhydrite layers A and B) were required for simulating undisturbed conditions.

7.1.5 DOSE ESTIMATES (LAPPIN ET AL., 1990)

The two cases reported by Lappin et al. (1989) were repeated by Lappin et al. (1990) with revised assumptions. Changes were the following: a shorter pathway from the northern equivalent panel instead of the

northeast panel was used; both hydrostatic and lithostatic driving pressures were used to bound the problem; and MB139 properties were revised to include improved understanding of the DRZ and to update seal design. Again, there were no radionuclide releases to the Culebra Dolomite in 10,000 years, and therefore, no dose calculations were performed for undisturbed conditions.

7.1.6 1990 PRELIMINARY COMPARISON

Calculations for undisturbed performance of the WIPP repository were not updated in the 1990 preliminary performance assessment (Bertram-Howery et al., 1990). However, results from preliminary simulations of two-phase (gas and brine) flow provided some data on the possible effects of gas generation within the repository during the first 1000 years after decommissioning. The analysis used two-dimensional, two-phase flow simulations with idealized room geometry and local stratigraphy to evaluate the effect of gas on repository performance. Simulations assumed panel seals that would consolidate to intact halite properties in the drift but no seal in either MB139 or the anhydrite layers A and B. The gas-generation rate was fixed at 2 moles/drum/year, the maximum rate for hydrogen generation postulated by Lappin et al. (1989). (As discussed in Volume 3 of this report, the gas-generation rate has since been revised.)

Preliminary results from the simulations suggested that in the undisturbed state, gas saturation would be high in the upper portion of the waste, MB139, and the overlying anhydrite layers. As calculated, gas migration away from a room within the excavated volume and the DRZ would occur over a length scale longer than the drift length from the northernmost panel seal to the closest shaft. In the simulations, gas saturation is near maximum at the shaft/drift interfaces, meaning that transport of dissolved radionuclides, which requires a liquid medium, would be diminished. In addition, brine content in the waste would be diminished due to the presence of gas, so less brine would be available to transport radionuclides, and very little gas or brine would move into the lower permeability, intact halite surrounding the fractured anhydrite and the DRZ.

7.2 Results of the 1991 Preliminary Comparison

All previous assessments of repository performance for undisturbed conditions have not fully addressed potential effects of waste-generated gas. Therefore, updated analyses of undisturbed conditions for Individual Protection (191.15) and Containment (191.13) Requirements were performed. As described, earlier analyses have estimated that there would be no releases to the Culebra Dolomite and, therefore, to the accessible environment 5 km downgradient (Figure 1-3) in 10,000 years. Based on these

earlier analyses, the approach adopted for the 1991 performance assessment is to perform deterministic calculations to verify that previous conclusions of no releases in 10,000 years are still valid with the 1991 modeling system including gas effects, current data, and current conceptual models. Two sets of calculations were performed and are fully described in Volume 2 of this report. These calculations have been designed to provide a conservatively large estimate of potential releases to the accessible environment. Because of the complexity of the interdependent processes being modeled, it is not possible to assert that results of these calculations bound potential releases.

First, a two-dimensional simulation to assess the migration of brine from the repository into the intact portion of MB139 was done. This calculation estimates the spatial scale that passive, neutrally bouyant particles would be transported in advecting brine as a result of maximum gas-generation rates in a waste panel. A pressure-time history was calculated for maximum corrosion and biodegradation rates with a two-phase, two-dimensional simulation using BOAST II. Brine flow, pollutant concentration, and particle transport were calculated with a one-phase, two-dimensional simulation using SUTRA with the pressure-time history from BOAST II. Assuming least-favorable bounds for important parameter values results in the 1% (of initial source) contour occurring at less than 120 m from the waste panel at 10,000 years. The accessible-environment boundary is located 5 km from the waste panels, so this pathway is not considered further.

Second, a two-dimensional vertical section simulation of the repository from waste panels to the closest shaft to assess migration of radionuclides through the DRZ, panel seals, and backfilled excavations was done. The calculation estimates the extent that radionuclides would be transported in brine flowing towards and upwards through sealed shafts as a result of the pressure gradient between the Culebra Dolomite and a waste panel that is pressurized with waste-generated gas. Again, a pressure-time history (BOAST II) resulting from maximum gas-generation rates of corrosion and biodegradation was used to calculate (STAFF2D and SUTRA) brine advection, pollutant concentration, and particle tracking (pathways and travel times). In this case, a measure of radionuclude migration at different locations should be reported. The appropriate measure for comparison to the Containment Requirements is the normalized EPA sum (EPA Sum); for the Individual Protection Requirements the measure should be peak concentration, but if there are zero releases, both measures are zero. Therefore, EPA Sums are reported 20 and 50 m up the shaft above the intersection with the repository horizon and 100 and 200 m into the intact MB139 (away from the shaft) (see Volume 2, Chapter 4 of this report). Assuming least favorable bounds for important parameter values (e.g., an inexhaustible source, no decay, no retardation, the same solubility limit for all radionuclides,

etc.) results in EPA Sums less than 10^{-2} at 20 m and less than 10^{-3} at 50 m up the shaft from the repository horizon. Therefore, there are no significant releases at the shaft/Culebra intersection at 10,000 years. The accessible-environment boundary is 5000 m downgradient in the Culebra, so this pathway results in zero releases to the accessible environment in 10,000 years. EPA Sums at 100 and 200 m into MB139 away from the shaft are less than 10^{-2} and 10^{-5}, respectively. For the Containment Requirements the undisturbed scenario is not analyzed further, and consequences (EPA Sums) of this scenario are all zero in the CCDF construction of Chapter 6 of this volume. Probability of the undisturbed scenario must still be included (Figure 3-13). For the Individual Protection Requirements, there are no releases to the accessible environment in 1000 years, so dose calculations are not required.

After performing these calculations, which are somewhat stylized, it was believed to be prudent to check diagnostic information from the Monte Carlo simulations for the Containment Requirements reported in Chapter 6 of this volume. In that set of analyses, 120 simulations of computational scenarios were run for human intrusion occurring at 1000, 3000, 5000, 7000, and 9000 years, for a total of 600 simulations. Before intrusion occurs, these calculations simulate undisturbed conditions. Simulations of the 1000-year intrusion time apply directly to the Individual Protection Requirements. The two-phase BRAGFLO calculations should be compared to the first description of calculations in the above discussion because only a waste panel and surrounding stratigraphy are modeled.

Chapter 7-Synopsis

The Standard requires that an uncertainty analysis of undisturbed conditions be performed to assess compliance with the Individual Protection Requirements. For the WIPP, the performance measure is dose to humans in the accessible environment.

Evaluations thus far indicate that radionuclides will not migrate out of the repository/shaft system during 1000 years. Therefore, dose calculations are not expected to be a part of the WIPP assessment of compliance with the Standard.

Previous Studies

Evaluation Prior to the 1985 Standard (1980 FEIS)

The Final Environmental Impact Statement (FEIS) estimated the consequence of five different hypothetical scenarios that might move radionuclides to the biosphere.

The pathway included radionuclide movement through the geosphere, transport through the biosphere after discharge into the Pecos River at Malaga Bend, and receipt of radiation doses by humans.

The travel times for radionuclides arriving at Malaga Bend were on the order of a million years.

Dose Estimates (Lappin et al., 1989)

This analysis of undisturbed conditions for the WIPP was performed in support of the supplemental environmental impact statements (SEIS).

The exposure pathway was radionuclide transport through the sealed shafts and intact Salado to the Culebra Dolomite, downgradient through the Culebra to a hypothesized stock well at the nearest location where Culebra water might be potable for cattle, and then to humans via beef ingestion.

The study indicated that, in the absence of human intrusion, no releases would occur in 1000 years.

1989 Methodology Demonstration

For this evaluation, undisturbed performance was simulated through a base-case scenario. The repository was assumed to be consolidated, and all legs in the flow path were assumed to be saturated from the time of repository decommissioning.

The simulations indicated that no releases from the repository/shaft system to the Culebra occurred during the 1000 years of regulatory concern for undisturbed performance. Even for a simulation with a longer time interval of 50,000 years, no significant releases to the Culebra occurred.

The fact that no releases occurred indicated that no dose calculations were needed for demonstrating compliance with the Individual Protection Requirements of the 1985 Standard.

Sensitivity Analysis (Rechard et al., 1990)

The relative importance of various phenomena and system components through sensitivity analyses of four different repository/shaft models for undisturbed conditions was analyzed.

Conclusions of the study were the following:

For brine-saturated conditions, flow from the repository occurs in all directions when expected parameter values are used, but for degraded parameter values, a primary path along MB139 exists.

Two-phase calculations that assessed gas migration to the shaft indicated that brine would retard such flow unless well-fractured, high-permeability paths exist as in MB139 and anhydrite layers A and B.

Two-phase models including local stratigraphy (MB139, anhydrite layers A and B) were required for simulating undisturbed conditions.

Dose Estimates (Lappin et al., 1990)

This evaluation revised the cases of Lappin et al. (1989) by using a shorter pathway within the repository, both hydrostatic and lithostatic driving pressures to bound the problem, and MB139 properties that included improved understanding of the DRZ and updated seal design.

No radionuclide releases to the Culebra Dolomite occurred in 10,000 years, and therefore, no dose calculations were performed for undisturbed conditions.

1990 Preliminary Comparison

In lieu of calculations for undisturbed performance, results from preliminary simulations of two-phase (gas and brine) flow provided some data on possible effects of gas generation within the repository during the first 1000 years after decommissioning.

Preliminary results from the simulations suggested that, in the undisturbed state,

gas saturation is near maximum at the shaft/drift interfaces, meaning that transport of dissolved radionuclides, which requires a liquid medium, would be diminished,

brine content in the waste would be diminished due to the presence of gas, so less brine would be available to transport radionuclides,

very little gas or brine would move into the lower permeability, intact halite surrounding the fractured anhydrite and the DRZ.

Results of the 1991 Preliminary Comparison

The approach adopted for the 1991 performance assessment is to perform deterministic calculations to verify that, using the 1991 modeling system, previous conclusions of no releases in 10,000 years are still valid.

First, a two-dimensional horizontal simulation to assess the migration of brine from the repository into the intact portion of MB139 was performed. The calculation estimates the spatial scale that passive, neutrally buoyant particles would be transported in advecting brine as a result of maximum gas-generation rates in a waste panel.

Second, a two-dimensional simulation of a vertical section of the repository from waste panels to the closest shaft was performed to assess migration of radionuclides through the DRZ, panel seals, and backfilled excavations. The calculation estimates the extent that radionuclides would be transported in brine flowing towards and upwards through sealed shafts as a result of the pressure gradient between the Culebra Dolomite and a waste panel that is pressurized with waste-generated gas.

Least favorable bounds for important parameter values (e.g., an inexhaustible source, no decay, no retardation, the same solubility limit for all radionuclides, etc.) are assumed.

Results of the horizontal simulation show concentrations in the intact MB139 after 10,000 years at 1% of the source 120 m from the panels. Results of the vertical simulation including the shaft show EPA normalized sums at 10,000 years of less than 10^{-2} at 20 m up the shaft and less than 10^{-3} at 50 m up the shaft. Therefore, no significant releases occur at the shaft/Culebra intersection at 10,000 years.

For the Individual Protection Requirements, no releases to the accessible environment occur in 1000 years, so dose calculations are not required.

8. ASSURANCE REQUIREMENTS PLAN

[*NOTE: The text of Chapter 8 is followed by a synopsis that summarizes essential information, beginning on page 8-10.*]

As prescribed in the Second Modification to the Consultation and Cooperation Agreement, the WIPP Project has prepared a plan for implementing the Assurance Requirements of the 1985 Standard (U.S. DOE, 1987). The plan is preliminary, because methods and technologies could evolve over the operational time period. In accordance with the Project's interpretation of the EPA's intention, the Project will select assurance measures based on the uncertainties in the final performance assessment. This chapter will be updated as the management and operating contractor, Westinghouse Electric Corporation (see Chapter 1 of this volume), updates the implementation plans. A draft of the revised *Assurance Requirements Plan* (U.S. DOE, 1987) is in review, with publication expected before year-end 1991. The current plan includes definitions and clarifications of the Standard as it applies to the WIPP, the implementation objective for each requirement, an outline of the implementation steps for each requirement, and a schedule of activities leading to final compliance. Additional information on markers as passive institutional controls comes from performance-assessment activities using expert panels. This chapter summarizes plans for implementing the Assurance Requirements.

8.1 Active Institutional Controls

Active institutional controls are expected to include evaluation of land use in the WIPP area; maintaining fences and buildings and guarding the facility during active cleanup; decontamination and decommissioning; land reclamation; and post-operational monitoring. The objectives of these activities are to provide a facility and presence at the site during active cleanup, to restore the land surface as closely to its original condition as possible to avoid future preferential selection of the area for incompatible uses, and to monitor the disposal system.

All performance-assessment calculations begin 100 years after the WIPP is decommissioned, thus assuming that active control is maintained for 100 years.

8.2 Disposal-System Monitoring

Monitoring is required until there are no significant concerns to be addressed by further monitoring. The objective of a monitoring program would be "to detect substantial and detrimental deviation from the expected performance of the disposal system" (§ 191.14(b)). Monitoring activities will be identified during the course of the performance assessment but are likely to include monitoring of hydrological, geological, geochemical, and structural performance. Numerous subsidence monuments have been installed to monitor subsidence as an indicator of unexpected changes in the disposal system.

8.3 Passive Institutional Controls

The Project will implement passive institutional controls over the entire controlled area of the WIPP. Passive institutional controls include markers warning of the presence of buried nuclear waste and identifying the boundary of the controlled area, external records about the WIPP repository, and continued federal ownership. The EPA assumes in the guidance to the Standard that passive institutional controls will reduce the possibility of inadvertent human intrusion into the repository. Compliance evaluation for the Standard must include the potential for human intrusion and the effectiveness of passive institutional controls to deter such intrusion. The remainder of this section discusses development of three types of passive institutional controls.

8.3.1 PASSIVE MARKERS

According to guidance in Appendix B of the Standard, inadvertent human intrusion can be mitigated by a number of approaches, including the use of passive controls such as markers or elements to physically deter human intrusion (and warn potential intruders that drilling, excavation, etc., should cease for safety reasons). The guidance also suggests that the effectiveness of passive institutional controls such as markers should be estimated.

In an effort to address the issue of markers for the WIPP, two expert panels have been established. Members of the first panel, whose work has already been completed, were asked to (1) identify possible future societies and how they may intrude the repository, and (2) develop probabilities of future societies and probabilities of various intrusions. The possible modes of intrusion identified by the future-intrusion experts were provided to the marker-development experts as the starting point as they (1) develop design

characteristics for "permanent" markers, and (2) judge the efficacy of the markers in deterring human intrusion.

The work of the future-intrusion panel is described in Chapter 4 of this volume, along with a discussion of the expert-judgment process. The procedure used for selection of the marker-development experts was the same as that described earlier for the future-intrusion experts. Nominations were solicited from 75 nominators, resulting in a total of 92 nominations. Letters of interest were received from 57 nominees. For the marker-development panel, 12 experts and one consultant, organized into one six-member and one seven-member team, have been selected. Their backgrounds include anthropology, archaeology, cognitive psychology, linguistics, materials science, astronomy, and architecture.

The marker-development panel met in November 1991 and will meet again in January 1992. Background information (introduction to the WIPP; performance assessment and the Standard; scenario development and modeling; the geology, hydrology, and climate of the WIPP; and a review of previous marker work) were provided to the panelists at the first meeting, and several future-intrusion experts returned to describe their efforts. These initial presentations led into a discussion of the issue statement, which delineated the specific points regarding marker development that must be addressed by the panel. Training was provided to assist the experts in the development of probability distributions describing the efficacy of markers in deterring human intrusion. In addition, the marker-development experts toured the WIPP to better understand the physical setting. The period between the two meetings will be used by the panelists to review the materials provided to them, to develop a response to the issue statement, and to prepare draft documentation describing the approach used to respond. The second meeting will involve discussion between the two teams on their respective approaches and elicitation of probability distributions. After the second meeting, the documentation will be revised based on the results of the discussions and the elicitation sessions. The probability estimates of the marker-development experts will be documented, organized, and returned to the experts for comment and review. Following concurrence by the experts, the results will be documented for performance assessment and published as a Sandia National Laboratories report (SAND report).

The marker-development experts will consider passive markers (i.e., markers that, after installation, should remain operational without further human attention) for deterring inadvertent human intrusion. These experts will be asked to define characteristics for selecting and manufacturing markers to be placed at the WIPP and to estimate the efficacy of these markers over the 10,000 years of regulatory interest. The marker characteristics should be defined so that, during the performance period, the markers and their

message(s) will have a high probability of warning potential intruders of the dangers associated with the transuranic wastes within the repository. A system of several types of markers may increase the probability that warnings about the WIPP are heeded. Judgments about the likely performance of the selected marker system will depend on the possible future states of society (incorporating judgment from the future-intrusion experts) and on the physical changes that the region surrounding the WIPP could undergo.

Determining characteristics for markers, one product of the marker-development activity, will require assessing specific marker performance for various modes of intrusion under various natural and manmade processes that may destroy or neutralize the markers. Intrusion modes identified by the future-intrusion experts will be provided to the expert panel working on characteristics for markers. The marker-development experts may, however, identify additional intrusion modes.

The marker-development panel will be asked to estimate the probabilistic performance of various types of markers. These estimates will be formally elicited.

A consultant is preparing material that describes past efforts at developing barriers to human intrusion and some considerations pertaining to such development, as a complement to the markers. An expert panel may be convened in the future to further investigate this strategy.

8.3.2 FEDERAL OWNERSHIP

In accordance with Appendix B of the Standard, the DOE or some successor agency is assumed to retain ownership and administrative control over the land. The federal agency responsible for the land will institute regulations that appropriately restrict land use and development. The Bureau of Land Management has obtained federal control of the remaining sections of former state trust lands within the boundary.

8.3.3 RECORDS

Records will be preserved of the disposal site and its contents. Though no expert-elicitation effort has yet been planned on what types of records should be preserved, the future-intrusion panel provided estimates on how effective records will be in preventing inadvertent human intrusion. Records should specify techniques for borehole plugging should exploratory drilling cause an intrusion. Such techniques could be incorporated into the legal records along with the description and location of the disposal system. The records could also contain a warning about the potential effects of drilling through the repository and into pressurized brine in the Castile Formation.

8.4 Multiple Barriers

The Standard requires that both natural and engineered barriers be used as part of the isolation system. At the WIPP, natural barriers include the favorable characteristics of the salt formation and the geohydrologic setting. Engineered barriers include backfills and seals that isolate volumes of wastes. The effectiveness of these barriers is being modeled for the performance assessment. The objective is to provide a disposal system that isolates the radioactive wastes to the levels required in the Standard. In addition, the DOE has commissioned an Engineered Alternatives Task Force to evaluate additional engineering measures for the WIPP should such measures be necessary.

8.5 Natural Resources

The Standard requires that locations containing recoverable resources not be used for repositories unless the favorable characteristics of a proposed location can be shown to compensate for the greater likelihood of being disturbed in the future. The WIPP Project met this requirement when the site was selected, and the recently published *Implementation of the Resource Disincentive in 40 CFR Part 191.14(e) at the Waste Isolation Pilot Plant* provides the supporting documentation (U.S. DOE, 1991d).

In the report, evaluation of the natural resources in the WIPP area centered on two issues. First, the denial of resources that could not be developed because such development might conflict with the long-term goal of waste isolation was considered. Second, the attractiveness to future generations of resources associated with the location was studied. Future societies might attempt to exploit natural resources near the WIPP and thereby create the potential for a release of radionuclides into the accessible environment.

These issues were evaluated in the *FEIS* (U.S. DOE, 1980a) and other reports (U.S. DOE, 1981; U.S. DOE and State of New Mexico, 1981, as modified; Brausch et al., 1982; Weart, 1983; U.S. DOE, 1990c). The *Resource Disincentive* report (U.S. DOE, 1991d) summarizes from these reports and documents the information about natural resources that the DOE used in making the decision to proceed with the WIPP Project.

In order to conduct resource analyses, the area was originally organized into four control zones (U.S. DOE, 1980a) (Figure 8-1). In 1982, the DOE released control of the outermost control zone (Vaughn, 1982). Comprehensive site characterization activities showed that the WIPP area contains potential economic quantities of both hydrocarbons and potash.

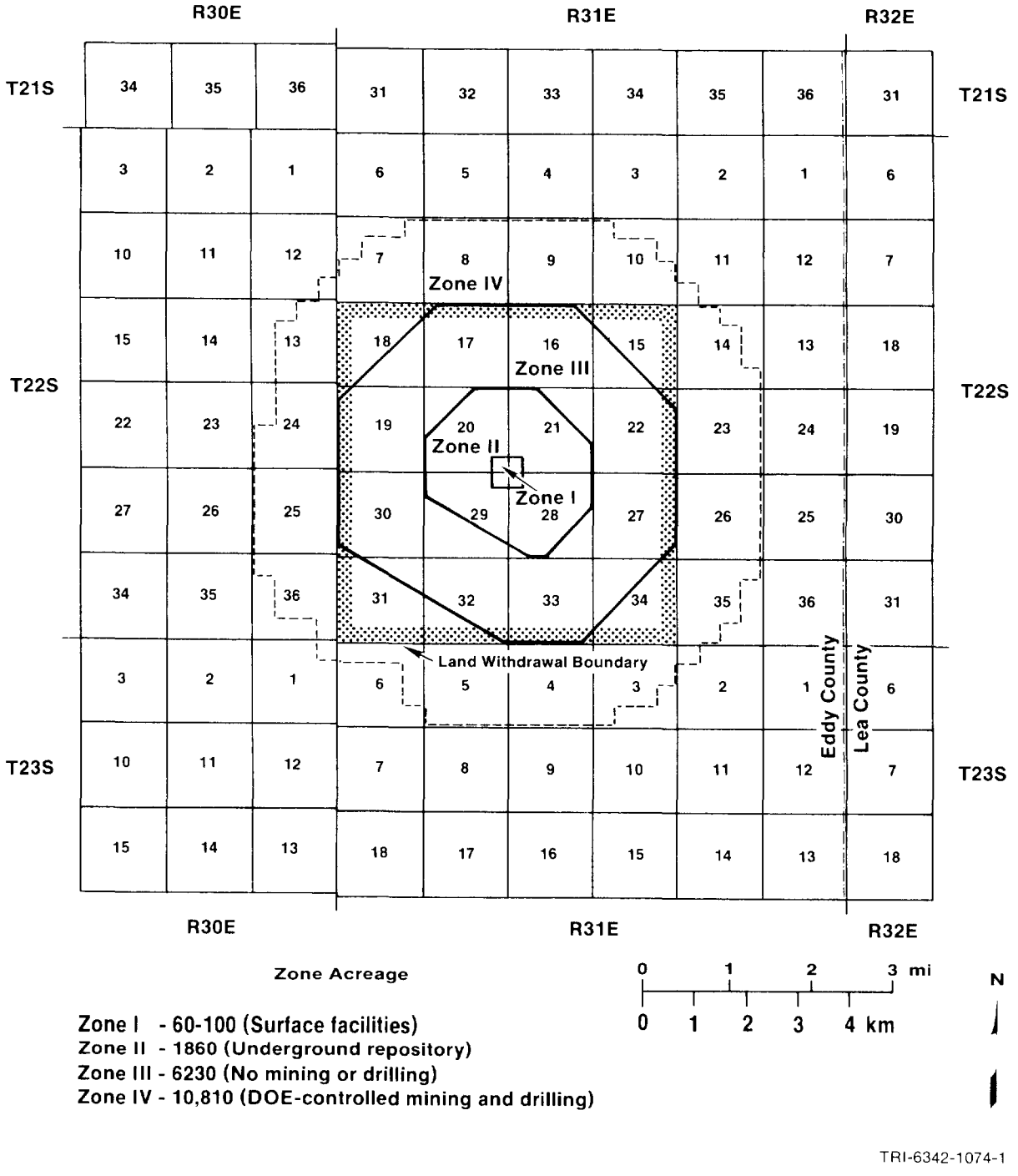

Figure 8-1. Control Zones at the WIPP (Powers et al., 1978a,b).

In order to gain control over the development of hydrocarbons at the WIPP, the DOE acquired the oil and gas leases within all the WIPP control zones. The only leases that are still intact are in Section 31 (Figure 8-1). These leases only allow resource production by entry of the proposed land withdrawal area below 6000 feet. One of these leases is currently in production. The upper 6000 feet of the leases was taken by the DOE in 1979. Current policy does not allow any further resource development inside the proposed land withdrawal boundary (U.S. DOE, 1991d). Estimates were prepared of the hydrocarbon reserves (economically producible resources) within the area (Keesey, 1976). The study was updated immediately prior to publication of the *Draft Environmental Impact Statement* (U.S. DOE, 1979), and reserve estimates were subsequently prepared (Keesey, 1979). The report on the implementation of the resource disincentive at the WIPP (U.S. DOE, 1991d) summarizes the impacts of hydrocarbon resource denial, based on information in the *FEIS* (U.S. DOE, 1980a). The projected impacts of hydrocarbon resource denial at the WIPP are shown in Table 8-1.

The principal nonhydrocarbon mineral resources that underlie the WIPP facility are caliche, gypsum, salt, lithium from brines, sylvite, and langbeinite. With the exceptions of sylvite and langbeinite (Table 8-2), however, the impact of mineral resource denial is relatively insignificant. Langbeinite, a somewhat rare mineral that contains soluble potassium used in making some fertilizers, is present in the WIPP area in limited commercial deposits. Sylvite, an additional evaporite mineral, is sometimes mixed with langbeinite to create the principal beneficial ingredient (potassium sulfate) produced from langbeinite for fertilizers. Denying langbeinite production within the WIPP boundaries would decrease the estimated 28 to 46 years of remaining mining operations in the area by only 4 years. In addition, substitutes for the potassium sulfate in langbeinite are available.

Groundwater in the WIPP area has been studied extensively, and the results have been summarized in the *FEIS* (U.S. DOE, 1980a), the *Final Safety Analysis Report* (U.S. DOE, 1990a), and in Chapters 5 and 9 of this volume. Groundwater exists both above and below the WIPP repository horizon. Below the WIPP, the groundwater in the Bell Canyon Formation is of very poor quality and is usually considered a brine. Units above the repository horizon have low groundwater yields with high concentrations of total dissolved solids (Lappin et al., 1989). Sources of drinking water for substantial populations are not impacted by the WIPP. Alternative supplies of drinking water are available from wells 30 miles north of the WIPP that are completed in the Ogallala Formation (U.S. DOE, 1990a). Groundwater near the WIPP is not vital to the preservation of unique and sensitive ecosystems. Endangered species of plants or animals are not known to inhabit the WIPP area (U.S. DOE, 1980a).

TABLE 8-1. SUMMARY OF HYDROCARBON RESOURCES AT THE WIPP

Deposit	WIPP Total*	Region	United States	World
RESOURCES				
Natural Gas (bill. ft^3)	490	25,013	855,000	N/A
Control Zones I-III	211	0.8%	0.025%	
Control Zone IV	279	1.1%	0.033%	
Distillate (mill. barrels)	5.72	293	N/A	N/A
Control Zones I-III	2.46	0.84%		
Control Zone IV	3.26	1.11%		
Crude Oil (mill. barrels)	37.5	1915	200,000	N/A
Control Zones I-III	16.12	0.84%	0.008%	
Control Zone IV	21.38	1.12%	0.0006%	
RESERVES				
Natural Gas (bill. ft^3)	44.62	3865	208,800	2,520,000
Control Zones I-III	21.05	0.54%	0.01%	0.0008%
Control Zone IV	23.57	0.61%	0.011%	0.0009%
Distillate (mill. barrels)	0.12	169.1	35,500	N/A
Control Zones I-III	0.03	0.02%	0.00008%	
Control Zone IV	0.09	0.06%	0.00024%	
Crude Oil		471.7	29,486	646,000

* Control Zones I-IV (see Figure 8-1)

Source: U.S. DOE, 1991d, based on U.S. DOE, 1980a, p. 9-19 and 9-28.

The presence of hydrocarbons, langbeinite, and other resources has been evaluated from the standpoint of resource attractiveness (U.S. DOE, 1980a; Brausch et al., 1982; U.S. DOE, 1990c). These analyses indicate that the consequence of an inadvertent intrusion into the repository in search of resources is small. The *Resource Disincentive* report (U.S. DOE, 1991d) states that the DOE believes that resource attractiveness does not appear to compromise the adequacy, safety, or reliability of the WIPP. Future studies will continue to evaluate the validity of this assumption.

TABLE 8-2. SUMMARY OF POTASH RESOURCES AT THE WIPP

Deposit	WIPP Total*	Region	United States	World
RESOURCES				
Sylvite (mill. tons ore)	133.2	4260	8550	850,000
Control Zones I-III	39.1	0.92%	0.46%	0.0046%
Control Zone IV	94.1	2.21%	1.10%	0.01%
Langbeinite (mill. tons ore)	351.0	1140	N/A	N/A
Control Zones I-III	121.9	10.7%		
Control Zone IV	229.1	20.1%		
RESERVES				
Sylvite (mill. tons K_2O)	3.66	106	206	11,206
Control Zones I-III	NIL			
Control Zone IV	3.66	3.45%	1.78%	0.33%
Langbeinite (mill. tons K_2O)	4.41	9.3	9.3	N/A
Control Zones I-III	1.21	13.0%	13.0%	
Control Zone IV	3.20	34.4%	34.4%	

* Control Zones I-IV (see Figure 8-1)

Source: U.S. DOE, 1991d, based on U.S. DOE, 1980a, p. 9-19 and 9-28.

The favorable characteristics of the WIPP location formed the basis for the DOE's decision to proceed with full construction and plans for the Test Phase. The DOE concluded that these favorable characteristics are not available at another site and that they more than compensate for the possibility that the site might be disturbed in the future (U.S. DOE, 1991d).

8.6 Waste Removal

The Standard requires that disposal systems be selected so that removal of most of the wastes is not precluded for a reasonable period of time after disposal (§ 191.14(f)). According to the preamble, "[t]he intent of this provision was not to make recovery of waste easy or cheap, but merely possible in case some future discovery or insight made it clear that the wastes needed to be relocated" (U.S. EPA, 1985, p. 38082).

A primary plan for waste removal during the operational phase of the WIPP (Subpart A of the Standard) has been prepared (U.S. DOE, 1980a). In promulgating the Standard, the EPA stated that to meet § 191.14(f) for the disposal phase (Subpart B of the Standard), it only need be technologically feasible to be able to mine the sealed repository and recover the waste, even at substantial cost and occupational risk (U.S. EPA, 1985, p. 38082). The EPA also stated that "any current concept for a mined geologic repository meets this requirement without any additional procedures or design features" (ibid.). Thus, the WIPP satisfies this requirement.

Chapter 8—Synopsis

The WIPP Project has prepared a preliminary plan for implementing the Assurance Requirements of the 1985 Standard.

Active Institutional Controls

The objectives of active institutional controls at the WIPP are to

- provide a facility and presence at the site during active cleanup,
- restore the land surface as closely to its original condition as possible to avoid future preferential selection of the area for incompatible uses,
- monitor the disposal system.

Disposal System Monitoring

The objective of a monitoring program would be to detect substantial and detrimental deviation from the expected performance of the disposal system.

Monitoring activities are likely to include monitoring of hydrological, geological, geochemical, and structural performance.

Passive Institutional Controls

The objectives of passive institutional controls at the WIPP are to deter or minimize inadvertent human intrusion into the repository, as outlined in Appendix B to the Standard.

Current plans for passive institutional controls include

- markers warning of the presence of buried nuclear waste and identifying the boundary of the controlled area,
- federal ownership,
- external records about the WIPP repository.

Passive Markers

Appendix B of the Standard assumes that

- inadvertent human intrusion into the repository can be mitigated by a number of approaches, including the use of passive controls such as markers, physical deterrents, and warnings,
- the effectiveness of passive institutional controls such as markers should be estimated.

A two-step process using expert panels addresses the issue of markers for the WIPP:

- The future-intrusion experts identified possible future societies and possible types of intrusions of the repository by those societies. The experts also developed probabilities of various intrusions based on the probability of existence of the identified societies.
- The determinations of the future-intrusion experts will be used by the marker-development experts in developing design characteristics for "permanent" markers and judging the efficacy of the markers in deterring human intrusion.

Research describing past efforts in developing barriers to human intrusion has also begun. An expert panel may be convened if this approach is deemed a necessary complement to placing markers at the WIPP.

Federal Ownership of the WIPP

In accordance with the Standard, the DOE or a successor government agency is assumed to own and control the land and institute regulations that restrict land use and development.

Records of the WIPP

Records will be preserved of the disposal site and its contents.

Records will warn about the potential effects of drilling through the repository and specify techniques for borehole plugging, should exploratory drilling cause an intrusion.

Multiple Barriers

The Standard requires that both natural and manmade barriers be used as part of the isolation system.

At the WIPP, natural barriers include

- the favorable characteristics of the salt formation,
- the features of the geohydrologic setting.

Manmade barriers include

- backfills,
- seals that isolate volumes of wastes.

The effectiveness of these barriers is being modeled for the performance assessment.

Natural Resources

The issues of denial and attractiveness of hydrocarbon and potash resources, the most significant resources in the WIPP area, have been evaluated.

Studies indicate that hydrocarbon resources represent only a small percentage of U.S. and world supplies.

Although langbeinite, a potash mineral, is relatively rare, substitutes for the soluble potassium used to make potassium sulfate for the chemical and fertilizer industries are available.

Previous analyses have indicated that the consequence of inadvertent intrusion into the repository in search of resources is small. Ongoing studies will continue to evaluate this assumption.

	The DOE has determined that the WIPP Project met the requirement that the favorable characteristics of the location outweigh the possibility of the repository being disturbed in the future.
Waste Removal	The Standard requires that it be possible to remove the waste for a reasonable period of time after disposal. The EPA has stated that current plans for mined geologic repositories meet this requirement without additional design.

9. GROUNDWATER PROTECTION REQUIREMENTS

[NOTE: The text of Chapter 9 is followed by a synopsis that summarizes essential information, beginning on page 9-5.]

The Groundwater Protection Requirements (§ 191.16) require the disposal system to provide a reasonable expectation that radionuclide concentrations in a "special source of ground water" will not exceed values specified in the regulation. This chapter shows that the requirement is not relevant to the WIPP because no groundwater near the WIPP within the maximum extent allowed by the Standard (Figure 9-1) satisfies the definition of special source of groundwater.

A special source of groundwater is defined as:

> ... those Class I groundwaters identified in accordance with the Agency's Ground-Water Protection Strategy published in August 1984 that: (1) Are within the controlled area encompassing a disposal system or are less than five kilometers beyond the controlled area; (2) are supplying drinking water for thousands of persons as of the date that the Department chooses a location within that area for detailed characterization as a potential site for a disposal system (e.g., in accordance with Section 112(b)(1)(B) of the NWPA); and (3) are irreplaceable in that no reasonable alternative source of drinking water is available to that population. (§ 191.12(o))

In accordance with the above definition, the Groundwater Protection Requirements would be relevant to the WIPP only if <u>all</u> of the criteria were met.

The following sections address these criteria.

9.1 Criteria for Special Sources of Groundwater

In its *Ground-Water Protection Strategy* (U.S. EPA, 1984), the EPA establishes groundwater protection policies for three classes of groundwater. The class definitions were developed to reflect the value of the groundwater and its vulnerability to contamination. The classes apply to groundwater having

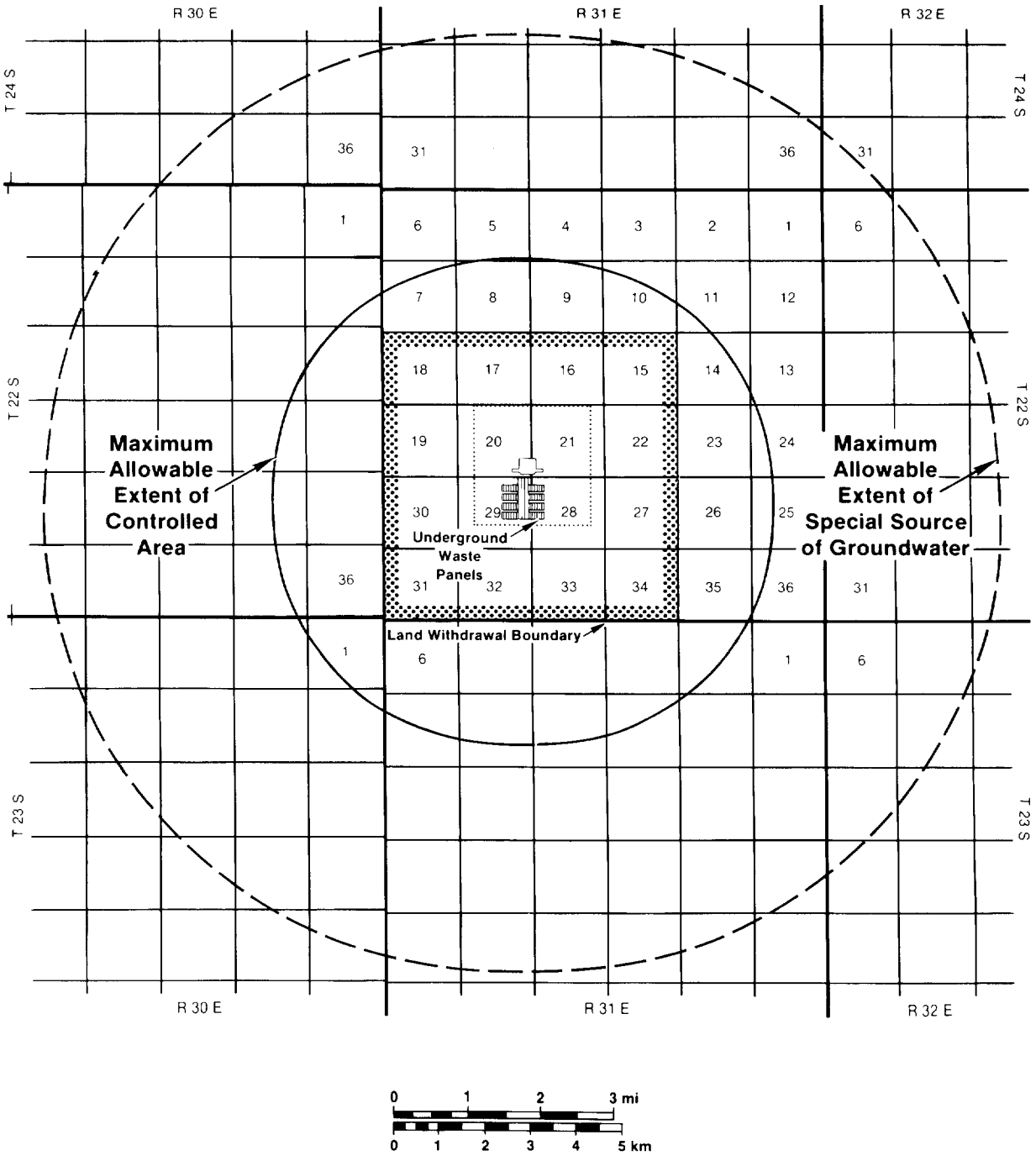

Figure 9-1. Illustration of Certain Definitions (from U.S. DOE, 1989a). The dashed line, drawn 5 km (3 mi) from the maximum allowable extent of the controlled area (§ 191.12(g)), shows the maximum area in which the occurrence of a special source of groundwater (§ 191.12(o)) is of regulatory interest.

significant water resource value. Class I groundwaters (U.S. EPA, 1984) are defined as follows:

> Certain ground-water resources are in need of special protective measures. These resources are defined to include those that are highly vulnerable to contamination because of the hydrogeological characteristics of the areas under which they occur. Examples of hydrogeological characteristics that cause groundwater to be vulnerable to contamination are high hydraulic conductivity (karst formations, sand and gravel aquifers) or recharge conditions (high water table overlain by thin and highly permeable soils). In addition, special groundwaters are characterized by one of the following two factors:
>
> (1) Irreplaceable source of drinking water. These include groundwater located in areas where there is no practical alternative source of drinking water (islands, peninsulas, isolated aquifers over bed rock) or an insufficient alternative source for a substantial population; or
>
> (2) Ecologically vital, in that the groundwater contributes to maintaining either the base flow or water level for a particularly sensitive ecological system that, if polluted, would destroy a unique habitat (e.g., those associated with wetlands that are habitats for unique species of flora and fauna or endangered species).

Based upon this EPA definition, for Class I groundwater to be present at the WIPP, the groundwater resource must be highly vulnerable to contamination because of the hydrogeological characteristics of the areas under which the resource occurs, including areas of high hydraulic conductivity or areas of groundwater recharge. Either of the following must also be true: the groundwater must be an irreplaceable source of drinking water, or the groundwater must be ecologically vital.

The hydrogeological characteristics of the WIPP have been evaluated through extensive ongoing investigations dating to 1975 (U.S. DOE, 1990f). Groundwater quality and the hydrologic conductivity of water-bearing units at the WIPP are monitored and reported annually (U.S. DOE, 1989c).

The most transmissive hydrologic unit in the WIPP area is the Culebra Dolomite Member of the Rustler Formation. Hydraulic properties of the Culebra Dolomite have been calculated from test holes in the vicinity of the WIPP. Within the approximately 10.5-km radius dictated by § 191.12(o), the Culebra has hydraulic conductivities ranging from 2×10^{-4} m/s (60 ft/d) to 2×10^{-10} m/s (6×10^{-5} ft/d) (Brinster, 1991). Horizontal groundwater flow in the Culebra is generally to the south along a decreasing gradient at a very slow rate.

Based on hydrogeological studies in the WIPP area, no geological units with high hydraulic conductivities that would require special protective measures appear to be present:

> The hydrologic system near the WIPP does not appear to be a significant groundwater recharge zone. The Culebra Dolomite is separated from overlying rocks by an anhydrite with a lower hydraulic conductivity than that of the Culebra. In wells located to the east of Livingston Ridge, the depth from the surface to the middle of the Culebra Dolomite is consistently greater than 125 m (410 ft) (Marietta et al., 1989). Available data indicate that "modern flow directions within the Rustler Formation, including the Culebra, do not reflect flow from a modern recharge area to a modern discharge area..." (Lappin et al., 1989).
>
> The WIPP area is not characterized by a high water table overlain by thin and highly permeable soils. Much of the area includes underlying beds of caliche and siltstone 10 feet or less below the ground surface that apparently prevent large volumes of water from moving downward (U.S. DOE, 1990f).

Even if groundwater that is highly vulnerable to contamination was present near the WIPP, it would not be classified as Class I because it does not meet either the second or third criterion:

> Groundwater near the WIPP is not an irreplaceable source of drinking water for a substantial population because low yields of water-bearing units and high concentrations of total dissolved solids in the groundwater severely limit its use. Uses of water from the Culebra Dolomite are restricted mostly to stock watering; none is used for domestic purposes. Total dissolved solids concentrations in Culebra groundwater in the vicinity range from 2,500 to 240,000 mg/ℓ (Lappin et al., 1989).
>
> Groundwater at the WIPP is not "ecologically vital" because it does not contribute "to maintaining base flow or water level for a particularly sensitive ecological system that, if polluted, would destroy a unique habitat..." (U.S. EPA, 1984). Endangered species of plants or animals are not known to inhabit the WIPP area (U.S. DOE, 1980a).

9.1.1 DRINKING WATER SUPPLY

Class I groundwater is not present in the vicinity of the WIPP; therefore, the Groundwater Protection Requirements are not relevant to the WIPP. If Class I groundwaters were present, however, the requirements would be relevant only if the groundwater was supplying drinking water to thousands of persons at the date DOE selected the site for development of the WIPP *and* if these groundwaters were irreplaceable.

At the time the DOE chose the WIPP location, no source of water (including Class I groundwaters) within 5 km (3 mi) beyond the maximum allowable extent of the controlled area was supplying drinking water for thousands (or even tens) of persons, a fact that remains true today. Thus, even if Class I groundwaters were present, the requirements of § 191.16 would not be relevant to the WIPP.

9.1.2 ALTERNATIVE SOURCE OF DRINKING WATER

As described above, no Class I groundwater is present in the vicinity of the WIPP. No population of thousands of people is in the vicinity of the WIPP; therefore, no alternative source of drinking water is needed.

Chapter 9–Synopsis

Groundwater Protection Requirements require the disposal system to provide a reasonable expectation that concentrations of radionuclides in a "special source of ground water" will not exceed specified values.

The Groundwater Protection Requirements would be relevant to the WIPP only if a "special source of ground water" were present at the WIPP, but none exists there.

Criteria for Special Sources of Groundwater

Presence of Class I Groundwater

For Class I groundwater to be present at the WIPP, the groundwater resource must be highly vulnerable to contamination because of the hydrogeological characteristics of the areas under which it occurs.

In addition, the groundwater must either be an irreplaceable source of drinking water, or the groundwater must be ecologically vital.

Studies indicate that such groundwater is not present in the vicinity of the WIPP.

Drinking Water Supply

At the time the DOE chose the WIPP location and at present, no source of water within 5 km (3 mi) beyond the maximum allowable extent of the controlled area was supplying drinking water for thousands (or even tens) of persons.

Alternative Source of Drinking Water

Because no Class I groundwater is present in the vicinity of the WIPP, no alternative source of drinking water is needed.

10. COMPARISON TO THE STANDARD

The preliminary performance assessment reported in this document should not be formally compared to the requirements of the Standard to determine whether the WIPP disposal system complies with Subpart B. The disposal system is not adequately characterized, and necessary models, computer programs, and data bases are incomplete. In addition, the final version of the EPA Standard has not been promulgated.

Instead, the discussion in this chapter examines the adequacy of the available information for producing a comprehensive comparison to the Containment Requirements (§ 191.13) and the Individual Protection Requirements (§ 191.15). Adequacy of repository performance will be determined primarily by qualitative judgment regarding "reasonable expectation" of meeting the requirements in § 191.13 and § 191.15. The Assurance Requirements and the Groundwater Protection Requirements are also considered here. All questions of adequacy inherently depend on the Standard. This evaluation is based on the 1985 version of the Standard.

10.1 Containment Requirements (§ 191.13)

The Containment Requirements specify probabilistically predicting cumulative releases of radionuclides to the accessible environment for 10,000 years after disposal, taking into account all significant processes and events that may affect the disposal system. Based on these and additional guidelines in the Containment Requirements, significant processes and events have been screened and combined to form the scenarios for which releases will be estimated. Judgment from an expert panel will contribute to the process of determining scenario probabilities.

Because the calculations to quantitatively assess compliance are complex, the executive computer program CAMCON is being developed to link specific numerical models into a single computational system capable of generating the Monte Carlo simulations required for probabilistic performance assessments. As Table 5-1 in Chapter 5 of this volume indicates, several of the individual computer programs required to complete CAMCON are currently under development or are incomplete.

Information continues to be added to the compliance-assessment data bases. In the absence of experimental data that might better define certain parameters, panels are being convened to provide the performance-assessment team with judgment based on the expertise of the panel members. Thus far, expert panels have provided a range of values for radionuclide solubility

and the source term for transport calculations and for distribution coefficients (K_ds) used in determining radionuclide retardation in the Culebra Dolomite Member of the Rustler Formation. Additional expert panels are planned to quantify other parameters and thus address the uncertainty in using those data sets.

The Containment Requirements state that compliance will be judged on the basis of a "reasonable expectation" of acceptable performance. Although the Standard does not define "reasonable expectation," it does indicate that compliance assessments should include both quantitative numerical simulations of disposal-system performance and qualitative expert judgment. In addition to expert evaluation of future human actions and parameter values unattainable from experimental data, expert judgment will also define the term "reasonable expectation" to guide probabilistic predictions of the WIPP's performance (Bertram-Howery and Swift, 1990).

The compliance-assessment system can be used for sensitivity and uncertainty analyses and is adequate for preliminary performance studies of the WIPP. Results of the 1991 performance-assessment calculations are in Chapter 6 of this volume.

10.2 Assurance Requirements (§ 191.14)

The Assurance Requirements were included in the Standard to provide the confidence needed for long-term compliance with the Containment Requirements. To address the provisions of the Assurance Requirements, the WIPP Project has prepared *A Plan for the Implementation of Assurance Requirements in Compliance with 40 CFR Part 191.14 at the Waste Isolation Pilot Plant*, DOE/WIPP 87-016. This plan, which was published in 1987, is currently being revised. The revised plan should be available by year-end 1991.

10.2.1 ACTIVE INSTITUTIONAL CONTROLS (§ 191.14(a))

This subsection of the Assurance Requirements specifies that active institutional controls should be maintained over disposal sites for as long as is practicable after disposal. Active institutional controls are expected to include

- evaluation of land use in the WIPP area,
- maintaining fences and buildings and guarding the facility during the operational phase,

decontamination and decommissioning,

land reclamation,

post-operational monitoring.

Many of these activities will not commence until waste disposal has been completed. All performance-assessment calculations begin 100 years after the WIPP is decommissioned. Active institutional controls are thus assumed to be maintained for 100 years, the maximum time allowed by the Standard.

10.2.2 DISPOSAL SYSTEM MONITORING (§ 191.14(b))

Monitoring the disposal system after waste disposal is expected to detect any "substantial and detrimental deviations" from expected performance if they occur. Specific monitoring activities will be identified during evaluation of the WIPP and are likely to include monitoring of hydrological, geological, geochemical, and structural performance.

Monuments have been installed to monitor subsidence as an indicator of unexpected changes in the disposal system. Additional monitoring activities will commence as the necessary types and methods of monitoring are identified.

10.2.3 PASSIVE INSTITUTIONAL CONTROLS (§ 191.14(c))

As stated in this subsection of the Assurance Requirements, the disposal site is to be designated by "the most permanent markers, records, and other passive institutional controls practicable to indicate the dangers of the wastes and their location." The EPA assumes that, for as long as passive institutional controls endure and are understood, they can be effective in deterring systematic or persistent exploitation and can reduce the likelihood of inadvertent, intermittent human intrusion. However, passive institutional controls are not expected to eliminate the possibility of inadvertent human intrusion into the repository (U.S. EPA, 1985, p. 38088). Plans for passive institutional controls include markers warning of the presence of buried nuclear waste and identifying the boundaries of the controlled area, external records about the WIPP repository, and continued federal ownership.

The marker-development panel met in November 1991 and will meet again in January 1992. The panel will define characteristics for selecting and manufacturing markers and estimate the efficacy of these markers over the 10,000-year regulatory period. The panel will also provide estimates of the probabilistic performance of various types of markers. A consultant is

preparing material that describes past efforts at developing barriers to human intrusion. An expert panel may be convened to further investigate this strategy.

Records will be preserved of the disposal site and its contents. An expert panel has not yet been planned on the types and possible content of external records that should be preserved. However, the expert panel on inadvertent human intrusion into the repository has estimated the effectiveness of records in preventing inadvertent human intrusion and suggested including specific information in external records on the potential effects of inadvertent exploratory drilling into the repository and techniques for plugging intrusion boreholes.

The Standard assumes that the DOE or some successor agency will retain ownership and administrative control over certain portions of the land around the WIPP. Withdrawal of the designated land to assure continued federal ownership has not been enacted.

10.2.4 MULTIPLE BARRIERS (§ 191.14(d))

This subsection of the Assurance Requirements specifies that different types of barriers, including engineered and natural barriers, be present in the repository to isolate the wastes from the accessible environment. At the WIPP, natural barriers include the salt formation and the geohydrologic setting. Engineered barriers include backfills and seals that isolate volumes of wastes. The effectiveness of these barriers will continue to be modeled in preliminary performance assessments until a determination is made that the barriers isolate the radioactive wastes to the levels required in the Standard.

The DOE has commissioned an Engineered Alternatives Task Force to evaluate possible additional engineering measures for the WIPP. Preliminary performance-assessment calculations indicate that modifications to the waste form that limit dissolution of radionuclides in brine have the potential to improve predicted performance of the repository (Marietta et al., 1989; Bertram-Howery and Swift, 1990). Current performance assessments are not complete enough to determine whether or not modifications will be needed for regulatory compliance. The 1991 performance-assessment calculations did not include simulations of possible alternatives. Selected alternatives will be examined in future performance-assessment calculations, however, to provide guidance to the DOE on possible effectiveness of modifications.

10.2.5 NATURAL RESOURCES (§ 191.14(e))

This subsection of the Assurance Requirements states that locations containing recoverable resources are not to be used for radioactive-waste repositories unless the favorable characteristics of a location can be shown to compensate for the greater likelihood of being disturbed in the future. The WIPP Project met this requirement when the site was selected, and the summary report *Implementation of the Resource Disincentive in 40 CFR Part 191.14(e) at the Waste Isolation Pilot Plant* (U.S. DOE, 1991d) has been published.

The report addresses the issues of denial and attractiveness of hydrocarbon and potash resources, the most significant resources in the WIPP area. Studies indicate that hydrocarbon resources near the WIPP represent only a small percentage of U.S. and world supplies. The production of the potash mineral langbeinite, the only mineral resource in significant quantities within the WIPP boundaries and a source of potassium for use in the chemical and fertilizer industries, would only be slightly impacted by removing the area from mining operations. In addition, substitutes for the potassium sulfate in langbeinite are available. The *Final Environmental Impact Statement* (U.S. DOE, 1980a) and the *Final Supplement Environmental Impact Statement* (U.S. DOE, 1990c), among other reports, have indicated that, based on available information, the consequence of an inadvertent intrusion into the repository in search of resources is small. The report on the implementation of the resource disincentive (U.S. DOE, 1991d) states that the DOE believes that resource attractiveness does not appear to compromise the adequacy, safety, or reliability of the WIPP. Future studies will continue to evaluate the validity of this assumption.

10.2.6 WASTE REMOVAL (§ 191.14(f))

This subsection of the Assurance Requirements specifies that disposal systems are to be selected so that removal of most of the wastes is not precluded for a reasonable period of time after disposal. The preamble to the Standard states that removal need not be easy or cheap, but merely possible (U.S. EPA, 1985, p. 38082). The WIPP Project has prepared a plan for waste removal during the operational phase (Subpart A of the Standard) based on the repository as designed. In addition, the EPA stated that current plans for mined geologic repositories meet this requirement without additional design (U.S. EPA, 1985, p. 38082). No further action for Subpart B of the Standard should be necessary.

10.3 Individual Protection Requirements (§ 191.15)

Repositories are expected to provide a reasonable expectation that, for 1,000 years after disposal, the undisturbed performance of the disposal system will not cause doses to any member of the public in the accessible environment to exceed certain levels. Previous and current evaluations of undisturbed performance at the WIPP have indicated no releases to the accessible environment within 10,000 years (Lappin et al., 1989; Marietta et al., 1989; Chapter 7 of this volume and Volume 2 of this report). The 1989 methodology demonstration reported that, for undisturbed performance, radionuclides did not reach the Culebra Dolomite within 50,000 years (Marietta et al., 1989). Gas generated within the waste panels was not directly included in the simulation for the 1991 preliminary performance calculations. However, the effects of gas generation were included indirectly by using elevated repository pressures calculated with a two-phase flow (gas and brine) computer program.

The compliance-assessment system for the WIPP must be used to predict releases to the accessible environment for undisturbed performance. Formal comparison to the Standard cannot be prepared until the bases of the system are judged adequate. However, analyses indicate that no releases will occur. Therefore, dose predictions are not expected to be required.

10.4 Groundwater Protection Requirements (§ 191.16)

The Groundwater Protection Requirements require the disposal system to provide a reasonable expectation that radionuclide concentrations in a "special source of ground water" will not exceed values specified in the regulation. Determining the presence of this type of groundwater relies on the definition of Class I groundwater, which is a groundwater resource that is highly vulnerable to contamination because of the hydrogeological characteristics of the areas under which the resource occurs, including areas of high hydraulic conductivity or areas of groundwater recharge. In addition, the groundwater must either be an irreplaceable source of drinking water, or the groundwater must be ecologically vital (U.S. EPA, 1984).

Studies have determined that no groundwater near the WIPP is highly vulnerable to contamination (U.S. DOE, 1989b; Lappin et al., 1989; Marietta et al., 1989; U.S. DOE, 1990f; Brinster, 1991). Groundwater flow in the Culebra Dolomite, the most transmissive hydrologic unit in the WIPP area, is generally to the south at a very slow rate, indicating that the area does not exhibit high hydraulic conductivity. Available data indicate that significant groundwater recharge does not occur near the WIPP.

Low yields from water-bearing units and high concentrations of total dissolved solids in groundwater near the WIPP severely limit groundwater use. Groundwater in the vicinity does not represent an irreplaceable source of drinking water for a substantial population. Groundwater at the WIPP does not support a particularly sensitive ecological system and, therefore, could not pollute a unique habitat.

Based on the 1985 Standard, the Groundwater Protection Requirements are not relevant to the WIPP disposal system. No further action should be necessary.

10.5 Formal Comparison to the Standard

The performance of the WIPP can be formally compared to the Standard when (U.S. DOE, 1990b)

> the complete set of significant scenarios with probabilities of occurrence has been defined,
>
> the compliance-assessment system is considered adequate, is operational, and has adequate documentation to support repetition or modification of each simulation,
>
> the data sets have undergone quality assurance, and the computational models and systems of models have been validated to the extent possible,
>
> the final analyses are complete, and a peer-review process has affirmed that the analyses are adequate.

Formal comparison to determine compliance should be based on comprehensive, practical performance assessments that incorporate all critical components and processes identified by iterative uncertainty and sensitivity analyses, results of the in situ tests, and other appropriate refinements in the system. The utility of the compliance-assessment system is conditional on how well the disposal system is understood and is reflected here for the natural barriers of the controlled area and the engineered barriers of the repository/shaft system. As test results and system refinements are incorporated into the performance assessment, their influence on the performance measures (i.e., the CCDFs and doses) will be evaluated. If successive, iterative assessments converge to a stable CCDF, the performance assessment may be considered complete.

11. STATUS

This chapter summarizes the current status of the WIPP performance assessment and indicates where work can now be identified that remains to be done before a final comparison can be made to the Standard. The summary presented here is based on the preliminary results derived from the current modeling system and may change as subsequent performance-assessment iterations shift priorities for model development and data acquisition.

11.1 Current Status of the Compliance-Assessment System

The compliance-assessment system contains models used to estimate future performance of the disposal system and the data base that supports the models. Status of models and the data base are discussed in general terms separately and then summarized in detail for each component of the modeling system.

11.1.1 COMPLIANCE-ASSESSMENT MODELS

As discussed in Chapter 3, the models used in the WIPP performance assessment exist at four distinct levels. The status of the individual models can be considered separately at each of the four levels.

At the first level, a conceptual model is used to describe the processes to be simulated for a given performance measure. This model must be based on observational information and typically involves the application of a generalized knowledge of physical processes to the available information. Thus, a conceptual model provides a simplifying framework in which information can be organized and linked to processes that can be simulated with predictive models. Only rarely is a single conceptual model uniquely compatible with the observed data, although a conceptual model is sometimes sufficiently well-established that alternatives do not need to be considered in detail. In many cases, however, alternative conceptual models may be equally appropriate given the available information. For example, the current conceptual model used in performance-assessment simulations of regional groundwater flow in the Culebra Dolomite Member of the Rustler Formation includes recharge only to the north of the repository (see Chapter 5 of this volume). This is compatible with available well data, but it is not uniquely required by the data. Alternative conceptual models for the location of recharge to the system remain to be developed and tested.

At the second level, processes defined by the conceptual models are represented by mathematical models that can be used to predict behavior of

the system through time. These mathematical models are typically systems of ordinary and partial differential equations. For example, the Darcy flow equations are used to represent the conceptual model for groundwater flow along a pressure gradient in a confined aquifer. Descriptions of the mathematical models used in the WIPP performance assessment are given in Volume 2 of this report.

At the third level, numerical models are developed that permit computational solutions that approximate the solutions of the mathematical models. In theory, this step is not always required in model development. In practice, however, it is unusual for a mathematical model based on differential equations to have a solution that can be determined without the use of an intermediate numerical model. Descriptions of the numerical solvers used in the WIPP performance assessment are given in the code manuals referenced in Volume 2 of this report.

At the fourth level, the numerical models must be translated to computer code to be implemented. A computer model could be no more than the encoding of a specific numerical model. In practice, however, computer programs typically contain options for a variety of numerical solutions for a single mathematical model and also may contain options for a variety of mathematical models corresponding to alternative conceptual models.

Ultimately, models used in the WIPP performance assessment must be verified and, to the extent possible, validated. Verification is the process by which a computer model is demonstrated to generate an acceptable numerical solution to the mathematical problem in question. For complex programs, verification is a nontrivial task and typically involves comparing benchmark test problem solutions with solutions generated by other codes and numerical models. Validation is the process by which a conceptual model and its associated mathematical model is demonstrated to provide an acceptable representation of reality. Some models can be validated experimentally. Others, however, particularly those that cover large domains with spatially varying properties and those that must simulate behavior for long time periods, are difficult to validate experimentally. In some cases, absolute validation may not be possible, and the final choice of a model will be based on subjective judgment.

11.1.2 THE COMPLIANCE-ASSESSMENT DATA BASE

The compliance-assessment data base serves two principal functions. First, it provides the essential basis for the conceptual models used to characterize the system. Conceptual models must explain the observed data. Second, the data base provides input to the computer models. Results of calculations depend directly on the data used to establish boundary

conditions and parameter values, and uncertainty in model results depends directly on uncertainty in the values selected for the input parameters. The two functions of the data base are closely linked; for example, boundary conditions for computer models may be selected based directly on observed data or on values inferred for a particular conceptual model.

The status of the data base must be evaluated with respect to both functions. Is the currently available data adequate to support the conceptual model for a particular component of the system? Is the currently available data adequate for calculations, and can it be used to characterize the uncertainty in results? For both functions, the status of the data base is evaluated relative to the needs of the performance assessment. For example, some conceptual models may be adequately supported by sparse data, whereas for other components extensive data may remain insufficient to identify the best conceptual model. For some computer model parameters, large uncertainties may have little impact on estimated performance and therefore be acceptable; for other parameters even small uncertainties may result in large uncertainties in estimated performance.

11.1.3 SUMMARY OF THE STATUS OF THE COMPLIANCE-ASSESSMENT SYSTEM

The 1991 status of individual components within the compliance-assessment system is summarized in Table 11-1. Status is evaluated with respect to 40 CFR 191, Subpart B only. Similar evaluations have not been completed for status with respect to other regulations, including 40 CFR 268 and NEPA. Status is shown for the data base for each component, as determined by researchers within the WIPP Project. Status is also indicated for the performance-assessment module that corresponds to each component and that contains the conceptual models and the computer models with their encoded and numerical models. Qualifiers used to describe the status are "preliminary," "intermediate," and "advanced." These qualifiers refer to status relative to the needs of performance assessment, which, as noted above, may not coincide with the status relative to research on the specific topic. Thus, it is possible for a simplistic model or a sparse data base to be labeled "advanced" if uncertainty about the component in question has little impact on estimated performance. Alternatively, it is possible for sophisticated models and extensive data bases to be labeled "preliminary" if uncertainty about the component remains high and has a large impact on model results.

"Preliminary," where applied to the data base, indicates that data are insufficient to distinguish conceptual models or that data are not available for some important parameters. Where applied to conceptual models, "preliminary" means that the understanding of the component is incomplete and that alternative conceptual models may remain unidentified. Where

TABLE 11-1. COMPLETENESS OF TECHNICAL BASES FOR PERFORMANCE ASSESSMENT WITH REGARD TO 40 CFR 191, SUBPART B*, CONDITIONAL ON 1991 COMPLIANCE-ASSESSMENT SYSTEM AND AS-RECEIVED WASTE

Compliance-Assessment System Component	Performance Assessment Understanding of Conceptual Model	Adequacy of Performance-Assessment Module	Adequacy of Data for Performance Assessment
REPOSITORY/SHAFT/ BOREHOLE MODELS: REPOSITORY/SHAFT DESIGN			
Repository Design			
Geometry			Intermediate
Drift Backfill			Intermediate
Performance-Assessment Module	Intermediate	Intermediate	
Panel/Drift Seals			
Concrete Seal Components			Intermediate
Grout Seal Components			Intermediate
Crushed Salt Seal Components			Intermediate
DRZ Seal Components (including fracture healing in salt)			Preliminary
Performance-Assessment Module	Intermediate	Intermediate	
Shaft Seals			
Upper Shaft Sealing System			
Concrete Seal Components			Intermediate
Grout Seal Components			Intermediate
Clay Seal Components			Intermediate
Lower Shaft Sealing System			
Concrete Seal Components			Intermediate
Clay Seal Components			Intermediate
Crushed Salt Seal Components			Intermediate
DRZ Seal Components (including fracture healing in salt)			Preliminary
Performance-Assessment Module	Intermediate	Intermediate	

* Status is evaluated with respect to 40 CFR 191, Subpart B only. Similar evaluations have not been completed for status with respect to other regulations, including 40 CFR 268 and NEPA.

TABLE 11-1. COMPLETENESS OF TECHNICAL BASES FOR PERFORMANCE ASSESSMENT WITH REGARD TO 40 CFR 191, SUBPART B, CONDITIONAL ON 1991 COMPLIANCE-ASSESSMENT SYSTEM AND AS-RECEIVED WASTE (continued)

Compliance-Assessment System Component	Performance Assessment Understanding of Conceptual Model	Adequacy of Performance-Assessment Module	Adequacy of Data for Performance Assessment
REPOSITORY/SHAFT/ BOREHOLE MODELS: PANEL MODEL			
Salado Formation			
Reference Stratigraphy			Advanced
Material Properties of Undisturbed Fm.			
Halite Absolute Permeability			Intermediate
Halite Pore Pressure			Intermediate
Anhydrite Absolute Permeability			Intermediate
Anhydrite Pore Pressure			Intermediate
Ideal Gas Solubility			Intermediate
Present Dissolved Gas Free in Fm.			Preliminary
Capillary Fingering			Preliminary
Enhanced H_2 Diffusion in Halite/Anhydrite			Preliminary
Material Properties of DRZ			
Halite Absolute Permeability			Intermediate
Halite Pore Pressure			Intermediate
Anhydrite Absolute Permeability			Preliminary
Anhydrite Pore Pressure			Preliminary
Porosity			Preliminary
Performance-Assessment Module	Intermediate	Intermediate	
Waste/Backfill			
Composite Waste/Backfill Properties			
Effective Porosity			Intermediate
Absolute Permeability			Intermediate
Initial Saturation			Intermediate
Critical Shear Strength			Preliminary
Performance-Assessment Module	Intermediate	Intermediate	
Properties of Backfill above Drums			
Effective Porosity			Intermediate
Absolute Permeability			Intermediate
Initial Saturation			Intermediate
Critical Shear Strength			Intermediate
Performance-Assessment Module	Intermediate	Intermediate	

TABLE 11-1. COMPLETENESS OF TECHNICAL BASES FOR PERFORMANCE ASSESSMENT WITH REGARD TO 40 CFR 191, SUBPART B, CONDITIONAL ON 1991 COMPLIANCE-ASSESSMENT SYSTEM AND AS-RECEIVED WASTE (continued)

Compliance-Assessment System Component	Performance Assessment Understanding of Conceptual Model	Adequacy of Performance-Assessment Module	Adequacy of Data for Performance Assessment
Inventory			
Combustibles			Intermediate
Metal/Glass			Intermediate
VOCs			Preliminary
Organics			Preliminary
Al & Fe & Heavy Metals			Preliminary
CH-Waste Inventory			Intermediate
RH-Waste Inventory			Preliminary
Performance-Assessment Module	Intermediate	Intermediate	
40 CFR 191 Source Term			
Decay			Advanced
Solubility (laboratory tests)			Preliminary
Colloid Formation/Chelation (laboratory tests)			Preliminary
Retardation in Repository			Preliminary
Performance-Assessment Module	Preliminary	Preliminary	
Panel/Waste Interactions			
Gas Generation (laboratory tests)			
Generation Processes			
Corrosion			Intermediate
Biological			Preliminary
Radiolysis			Intermediate
Gas Gettering Processes			Intermediate
Coupling of Processes to Closure/ Compaction, Brine/Gas Flow, and Gas Generation			Intermediate
Performance-Assessment Module	Intermediate	Intermediate	
Brine/Gas Flow and Transport			
Relative Permeability (to gas)			
Undisturbed Anhydrite			Preliminary
Undisturbed Halite			Preliminary
DRZ Anhydrite			Preliminary
DRZ Halite			Preliminary
Waste/Backfill			Preliminary
Capillary Pressure			
Anhydrite			Preliminary
Halite			Preliminary
Threshold Pressure for Anhydrite Fracture Opening			Preliminary

TABLE 11-1. COMPLETENESS OF TECHNICAL BASES FOR PERFORMANCE ASSESSMENT WITH REGARD TO 40 CFR 191, SUBPART B, CONDITIONAL ON 1991 COMPLIANCE-ASSESSMENT SYSTEM AND AS-RECEIVED WASTE (continued)

Compliance-Assessment System Component	Performance Assessment Understanding of Conceptual Model	Adequacy of Performance-Assessment Module	Adequacy of Data for Performance Assessment
Brine/Gas Flow and Transport (continued)			
Gas Dissolved in Brine			
Initial			Preliminary
Potential			Intermediate
Radionuclide Transport in Salado			Preliminary
Performance-Assessment Module	Preliminary	Preliminary	
Creep Closure/Expansion			
Wall Closure			Advanced
Coupling With Gas Generation and Brine/Gas Flow			Intermediate
Performance-Assessment Module	Intermediate	Intermediate	
Waste-Form and Backfill Compaction			
Waste Compaction			Intermediate
Coupling With Gas Generation and Brine/Gas Flow			Intermediate
Performance-Assessment Module	Intermediate	Intermediate	
Human Intrusion[1]			
Material Properties of Borehole			
Drilling Properties			Advanced[2]
Plug Properties			Advanced[2]
Performance-Assessment Module	Advanced	Advanced	
Castile Brine Reservoir			
Areal Extent			Intermediate
Volume of Brine			Intermediate
Pressure			Intermediate
Permeability			Intermediate
Gas			Intermediate
Performance-Assessment Module	Intermediate	Intermediate	
Intrusion Probability			Intermediate[3]
Performance-Assessment Module	Intermediate	Intermediate	

[1] Conditional on assumption of present-day drilling technology
[2] Adequacy controlled by regulation guidance
[3] Based on expert panel judgment and regulatory guidance

TABLE 11-1. COMPLETENESS OF TECHNICAL BASES FOR PERFORMANCE ASSESSMENT WITH REGARD TO 40 CFR 191, SUBPART B, CONDITIONAL ON 1991 COMPLIANCE-ASSESSMENT SYSTEM AND AS-RECEIVED WASTE (continued)

Compliance-Assessment System Component	Performance Assessment Understanding of Conceptual Model	Adequacy of Performance-Assessment Module	Adequacy of Data for Performance Assessment
GROUNDWATER FLOW AND TRANSPORT MODELS: GROUNDWATER FLOW MODEL			
Regional Hydrogeology			
3-D Regional Geology/Flow			
Understanding Present Flow			Intermediate
Predicting Future Flow			Preliminary
Climate Variability			Intermediate
Recharge Variability			
Present			Preliminary
Range in Future			Preliminary
Dissolution Processes			Intermediate
Integrate Geochemical/Isotopic Data			Intermediate
Performance-Assessment Module	Preliminary	Preliminary	
Local Hydrogeology			
2-D Groundwater (Culebra) Flow Model			
Boundary Conditions			
Present			Intermediate
Future			Intermediate
Transmissivity Distribution			
Definition of High T Zone			Intermediate
Uncertainty in T			Intermediate
Matrix/Fracture Porosity			Intermediate
Variable Brine Density Effects			
Flow Potential			Intermediate
Mixing			Preliminary
Effect of Potash Mining			Preliminary
Effect of Existing Boreholes			Preliminary
Performance-Assessment Module	Intermediate	Intermediate	
3-D Groundwater Flow Model			
Dewey Lake/Rustler Transmissivities			Preliminary
Dewey Lake/Rustler Boundary Conditions			
Vertical			Preliminary
Horizontal			Preliminary
Performance-Assessment Module	Preliminary	Preliminary	

TABLE 11-1. COMPLETENESS OF TECHNICAL BASES FOR PERFORMANCE ASSESSMENT WITH REGARD TO 40 CFR 191, SUBPART B, CONDITIONAL ON 1991 COMPLIANCE-ASSESSMENT SYSTEM AND AS-RECEIVED WASTE (concluded)

Compliance-Assessment System Component	Performance Assessment Understanding of Conceptual Model	Adequacy of Performance-Assessment Module	Adequacy of Data for Performance Assessment
GROUNDWATER FLOW AND TRANSPORT MODELS: RADIONUCLIDE TRANSPORT MODEL			
Physical Retardation			
Matrix Diffusion in Dual Porosity Transport			Intermediate
Performance-Assessment Module	Intermediate	Intermediate	
Chemical Retardation			
Radionuclide Solubility in Culebra Brine			Preliminary
Sorption by Clays			Preliminary
Performance-Assessment Module	Preliminary	Preliminary	
CUTTINGS MODELS: CUTTINGS/CAVINGS MODEL			
Drill Cuttings			
Performance-Assessment Module	Advanced[1]	Advanced[1]	
Erosion/Cavings			
Critical Shear Strength			Preliminary
Performance-Assessment Module	Preliminary	Intermediate	
Spalling			
Failure Criteria			Preliminary
Performance Assessment Module	Preliminary	Preliminary	

[1] Conditional on assumption of present-day drilling technology

applied to the performance-assessment modules, "preliminary" means work on one or more aspects of the mathematical, numerical, and computer models is either still in the planning stages or only recently initiated.

"Intermediate," where applied to the data base, means that data are sufficient for computations but that sources of uncertainty are not fully understood and uncertainty therefore has not been adequately quantified. Where applied to conceptual models, "intermediate" means that important processes are identified and understood and that significant alternative conceptual models, if any, may have been identified. Where applied to the performance-assessment modules, "intermediate" means that models are available, but that verification and validation are in the early stages and the application of the models to the WIPP performance assessment is still under development.

"Advanced," where applied to the data base, means that data for a specific component are fully adequate for performance assessments. Uncertainty is understood, quantified, and can be displayed in computational results. Where applied to conceptual models, "advanced" means that an appropriate conceptual model has been chosen and is adequately supported by the available data. Uncertainty in the conceptual model is adequately understood. Where applied to performance-assessment modules, "advanced" indicates validation and verification work is in progress and that the models are ready for use in performance assessments.

The status of the WIPP compliance-assessment system will change as the WIPP research and performance-assessment programs advance, and Table 11-1 will change accordingly in future iterations. Some changes will reflect ongoing research and the availability of new data or models. All changes will reflect performance-assessment analyses that show whether an acceptable level of information has been achieved for each component or module.

11.1.4 THE ROLE OF SENSITIVITY ANALYSES IN EVALUATING STATUS

Sensitivity analyses, as discussed in detail in Chapter 3 of this volume, provide information about the sensitivity of the modeling system to uncertainty in specific input parameters. For example, stepwise linear regression analyses can rank parameters in terms of the magnitude of the contribution to overall variability in modeled performance resulting from the variability in each parameter. These analyses are a useful tool for identifying those parameters where reductions in uncertainty (i.e., narrowing of the range of values from which the sample used in the Monte Carlo analysis is drawn) have the greatest potential to increase confidence in the estimate of disposal-system performance. Identification of sensitive parameters can help set priorities for resource allocation to allow the WIPP

Project to proceed as efficiently as possible toward a final evaluation of regulatory compliance. Sensitivity analyses performed as part of the 1990 preliminary comparison indicated that uncertainty in the values used for radionuclide solubility in the waste and retardation in the Culebra Dolomite Member dominated the variability in subsurface discharges to the accessible environment (Helton et al., 1991). As a result, expert panels were convened in 1991 to provide judgment on more suitable ranges and distributions for these parameters. Experimental programs have been accelerated for solubility and started for retardation to provide real data. However, additional research on a particular parameter will not invariably lead to a reduction in uncertainty. Reducing uncertainty in the data base is desirable, but in general the more important goal will be to determine the correct level of residual uncertainty that must be included in the analysis.

Sensitivity analyses are an important part of performance assessment, but because they are inherently conditional on the models, data distributions, and techniques used to generate them, they cannot provide insight about parameters not sampled, conceptual and computer models not used in the analysis in question, or processes that have been oversimplified during the sensitivity analyses. Qualitative judgment about the modeling system must be used in combination with sensitivity analyses to set priorities for performance-assessment data acquisition and model development.

REFERENCES

Adams, J. E. 1944. "Upper Permian Ochoa Series of Delaware Basin, West Texas and Southeastern New Mexico." *American Association of Petroleum Geologists Bulletin* **28**: 1596-1625.

Ahmed, S., D. R. Metcalf, and J. W. Pegram. 1981. "Uncertainty Propagation in Probabilistic Risk Assessment: A Comparative Study." *Nuclear Engineering and Design* **68**: 1-3.

Allen, D. M. 1971. *The Prediction Sum of Squares as a Criterion for Selecting Predictor Variables*. Report No. 23. Lexington, KY: Department of Statistics, University of Kentucky.

Anderson, R. Y. 1978. "Deep Dissolution of Salt, Northern Delaware Basin, New Mexico." Report to Sandia National Laboratories.

Anderson, R. Y. 1981. *Deep-Seated Salt Dissolution in the Delaware Basin, Texas and New Mexico*. New Mexico Geological Society Special Publication No. 10. 133-145.

Anderson, R. Y. 1983. "Evidence for Deep Dissolution in the Delaware Basin." Report prepared for the State of New Mexico Environmental Evaluation Group.

Andersson, J., T. Carlsson, T. Eng, F. Kautsky, E. Söderman, and S. Wingefors. 1989. *The Joint SKI/SKB Scenario Development Project*. TR89-35. Stockholm, Sweden: Svensk Kärnbränslehantering AB.

Apostolakis, G. 1990. "The Concept of Probability in Safety Assessments of Technological Systems." *Science* **250**: 1359-1364.

Apostolakis, G., R. Bras, L. Price, J. Valdes, K. Wahi, and E. Webb. 1991. *Techniques for Determining Probabilities of Events and Processes Affecting the Performance of Geologic Repositories*. NUREG/CR-3964. SAND86-0196/2. Washington DC: Division of High-Level Waste Management, Office of Nuclear Material Safety and Safeguards, U.S. Nuclear Regulatory Commission.

Arthur D. Little, Inc. 1980. *Technical Support of Standards for High-Level Radioactive Waste Management, Volume D, Release Mechanisms*. EPA 520/4-79-007D. Washington, DC: U.S. Environmental Protection Agency.

Ash, R. B. 1972. *Real Analysis and Probability*. New York, NY: Academic Press.

Bachman, G. O. 1974. *Geologic Processes and Cenozoic History Related to Salt Dissolution in Southeastern New Mexico*. U.S. Geological Survey Open-File Report 74-194. Denver, CO: U.S. Geological Survey.

Bachman, G. O. 1980. *Regional Geology and Cenozoic History of the Pecos Region, Southeastern New Mexico*. U.S. Geological Survey Open-File Report D-77-946. Albuquerque, NM: U.S. Geological Survey.

Bachman, G. O. 1981. *Geology of Nash Draw, Eddy County, New Mexico.* U.S. Geological Survey Open-File Report 81-31.

Bachman, G. O. 1984. *Regional Geology of Ochoan Evaporites, Northern Part of the Delaware Basin.* New Mexico Bureau of Mines and Mineral Resources Circular 184. Socorro, NM: New Mexico Bureau of Mines and Mineral Resources.

Backman, G. O. 1985. *Assessment of Near-Surface Dissolution at and near the Waste Isolation Pilot Plant (WIPP), Southeastern New Mexico.* SAND84-7178. Albuquerque, NM: Sandia National Laboratories.

Bachman, G. O. 1987. *Karst in Evaporites in Southeastern New Mexico.* SAND86-7078. Albuquerque, NM: Sandia National Laboratories.

Barnett, V. 1982. *Comparative Statistical Inference (2nd Ed.).* New York, NY: Wiley.

Bates, R. L., and J. A. Jackson, eds. 1980. *Glossary of Geology.* 2nd ed. Falls Church, VA: American Geological Institute.

Beauheim, R. L. 1986. *Hydraulic-Test Results for Well DOE-2 at the Waste Isolation Pilot Plant (WIPP) Site.* SAND86-1364. Albuquerque, NM: Sandia National Laboratories.

Beauheim, R. L. 1987a. *Interpretations of Single-Well Hydraulic Tests Conducted At and Near the Waste Isolation Pilot Plant (WIPP) Site, 1983-1987.* SAND87-0039. Albuquerque, NM: Sandia National Laboratories.

Beauheim, R. L. 1987b. *Analysis of Pumping Tests of the Culebra Dolomite Conducted at the H-3 Hydropad at the Waste Isolation Pilot Plant (WIPP) Site.* SAND86-2311. Albuquerque, NM: Sandia National Laboratories.

Beauheim, R. L. 1987c. *Interpretation of the WIPP-13 Multipad Pumping Test of the Culebra Dolomite at the Waste Isolation Pilot Plant (WIPP) Site.* SAND87-2456. Albuquerque, NM: Sandia National Laboratories.

Beauheim, R. L. 1989. *Interpretation of H-11b4 Hydraulic Tests and the H-11 Multipad Pumping Test of the Culebra Dolomite at the Waste Isolation Pilot Plant (WIPP) Site.* SAND89-0536. Albuquerque, NM: Sandia National Laboratories.

Beauheim, R. L., and R. M. Holt, 1990. "Hydrogeology of the WIPP Site," in *Geological and Hydrological Studies of Evaporites in the Northern Delaware Basin for the Waste Isolation Pilot Plant (WIPP), New Mexico. Geological Society of America 1990 Annual Meeting Field Trip #14 Guidebook. Dallas, TX: The Dallas Geological Society. 131-180.*

Beauheim, R. L., G. J. Saulnier, Jr., and J. D. Avis. 1990. Interpretation of Brine-Permeability Tests of the Salado Formation at the Waste Isolation Pilot Plant Site: First Interim Report. SAND89-0536. Albuquerque, NM: Sandia National Laboratories.

Beauheim, R. L., G. J. Saulnier, Jr., and J. D. Avis. 1991. *Interpretation of Brine-Permeability Tests of the Salado Formation at the Waste Isolation Pilot Plant Site: First Interim Report.* SAND90-0083. Albuquerque, NM: Sandia National Laboratories.

Belitz, K., and J. D. Bredehoeft. 1988. "Hydrodynamics of Denver Basin: Explanation of Subnormal Fluid Pressures." *American Association of Petroleum Geologists Bulletin* vol. 72, no. 11: 1334-1359.

Bertram-Howery, S. G., and R. L. Hunter. 1989a. *Plans for Evaluation of the Waste Isolation Pilot Plant's Compliance with EPA Standards for Radioactive Waste Management and Disposal.* SAND88-2871. Albuquerque, NM: Sandia National Laboratories.

Bertram-Howery, S. G., and R. L. Hunter, eds. 1989b. *Preliminary Plan for Disposal-System Characterization and Long-Term Performance Evaluation of the Waste Isolation Pilot Plant.* SAND89-0178. Albuquerque, NM: Sandia National Laboratories.

Bertram-Howery, S. G., and P. N. Swift. 1990. *Status Report: Potential for Long-Term Isolation by the Waste Isolation Pilot Plant Disposal System.* SAND90-0616. Albuquerque, NM: Sandia National Laboratories.

Bertram-Howery, S. G., M. G. Marietta, R. P. Rechard, P. N. Swift, D. R. Anderson, B. L. Baker, J. E. Bean, Jr., W. Beyeler, K. F. Brinster, R. V. Guzowski, J. C. Helton, R. D. McCurley, D. K. Rudeen, J. D. Schreiber, and P. Vaughn. 1990. *Preliminary Comparison with 40 CFR Part 191, Subpart B for the Waste Isolation Pilot Plant, December 1990.* SAND90-2347. Albuquerque, NM: Sandia National Laboratories.

Bingham, F. W., and G. E. Barr. 1979. *Scenarios for Long-Term Release of Radionuclides From a Nuclear-Waste Repository in the Los Medanos Region of New Mexico.* SAND78-1730. Albuquerque, NM: Sandia National Laboratories.

Bonano, E. J., and R. M. Cranwell. 1988. "Treatment of Uncertainties in the Performance Assessment of Geologic High-Level Radioactive Waste Repositories." *Mathematical Geology* 20: 543-565.

Bonano, E. J., S. C. Hora, R. L. Keeney, and D. von Winterfeldt. 1989. *The Formal Use of Expert Judgments in Performance Assessment of Radioactive Waste Repositories.* SAND89-0495C, CONF-891008-1. Albuquerque, NM: Sandia National Laboratories.

Bonano, E. J., S. C. Hora, R. L. Keeney, and D. von Winterfeldt. 1990. *Elicitation and Use of Expert Judgement in Performance Assessment for High-Level Radioactive Waste Repositories.* NUREG/CR-5411, SAND89-1821. Albuquerque, NM: Sandia National Laboratories.

Bonilla, M. G. 1979. "Historic Surface Faulting--Map Patterns, Relation to Subsurface Faulting, and Relation to Preexisting Faults" in *Proceedings of Conference VIII, Analysis of Actual Fault Zones in Bedrock, April 1-5, 1979.* U.S. Geological Survey Open-File Report 79-1239: 36-65.

Borns, D. J. 1983. *Petrographic Study of Evaporite Deformation near the Waste Isolation Pilot Plant (WIPP).* SAND83-0166. Albuquerque, NM: Sandia National Laboratories.

Borns, J. C., and S. E. Shaffer. 1985. *Regional Well-Log Correlation in the New Mexico Portion of the Delaware Basin.* SAND83-1798. Albuquerque, NM: Sandia National Laboratories.

Borns, D. J., and J. C. Stormont. 1988. *An Interim Report on Excavation Effect Studies at the Waste Isolation Pilot Plant: The Delineation of the Disturbed Rock Zone.* SAND87-1375. Albuquerque, NM: Sandia National Laboratories.

Borns, D. J., and J. C. Stormont. 1989. "The Delineation of the Disturbed Rock Zone Surrounding Excavations in Salt." *Proceedings of the Rock Mechanics Symposium at the University of West Virginia, June 19-22, 1989.* Rotterdam, Netherlands: A.A. Balkema.

Borns, D. J., L. J. Barrows, D. W. Powers, and R. P. Snyder. 1983. *Deformation of Evaporites Near the Waste Isolation Pilot Plant (WIPP) Site.* SAND82-1069. Albuquerque, NM: Sandia National Laboratories.

Box, G. E. P., and N. R. Draper. 1987. *Empirical Model-Building and Response Surfaces.* New York, NY: Wiley.

Brausch, L. M., A. K. Kuhn, and J. K. Register. 1982. *Natural Resources Study, Waste Isolation Pilot Plant (WIPP), Eddy and Lea Counties, New Mexico.* WTSD-TME-3156. Albuquerque, NM: U.S. Department of Energy.

Bredehoeft, J. D. 1988. "Will Salt Repositories Be Dry?" *EOS*, American Geophysical Union, vol. 69, no. 9.

Breeding, R. J., J. C. Helton, W. B. Murfin, and L. N. Smith. 1990. *Evaluation of Severe Accident Risks: Surry Unit 1.* NUREG/CR-4551, SAND86-1309, vol. 3, rev. 1. Albuquerque, NM: Sandia National Laboratories.

Brinster, K. F. 1991. *Preliminary Geohydrologic Conceptual Model of the Los Medaños Region near the Waste Isolation Pilot Plant for the Purpose of Performance Assessment.* SAND89-7147. Albuquerque, NM: Sandia National Laboratories.

Brush, L. H., and D. R. Anderson. 1988a. "Appendix A.1: Drum (Metal) Corrosion, Microbial Decomposition of Cellulose, Reactions Between Drum-Corrosion Products and Microbially Generated Gases, Reactions Between Possible Backfill Constituents and Gases and Water Chemical Reactions" in *System Analysis, Long-Term Radionuclide Transport, and Dose Assessments, Waste Isolation Pilot Plant (WIPP), Southeastern New Mexico, March, 1989.* Eds. A. R. Lappin, R. L. Hunter, D. P. Garber, and P. B. Davies. SAND89-0462. Albuquerque, NM: Sandia National Laboratories.

Brush, L. H., and D. R. Anderson. 1988b. "Appendix A.2: Effects of Microbial Activity on Repository Chemistry, Radionuclide Speciation, and Solubilities in WIPP Brines" in *Systems Analysis, Long-Term Radionuclide Transport, and Dose Assessments, Waste Isolation Pilot Plant (WIPP), Southeastern New Mexico; March 1989*. Eds. A. R. Lappin, R. L. Hunter, D. P. Garber, and P. B. Davies. SAND89-0462. Albuquerque, NM: Sandia National Laboratories.

Brush, L. H., and D. R. Anderson. 1989. "Appendix E: Estimates of Radionuclide Concentrations in Brines" in *Performance Assessment Methodology Demonstration: Methodology Development for Purposes of Evaluating Compliance with EPA 40 CFR Part 191, Subpart B, for the Waste Isolation Pilot Plant*. M. G. Marietta, S. G. Bertram-Howery, D. R. Anderson, K. Brinster, R. Guzowski, H. Iuzzolino, and R. P. Rechard. SAND89-2027. Albuquerque, NM: Sandia National Laboratories.

Burkholder, H. C. 1980. "Waste Isolation Performance Assessment--A Status Report" in *Scientific Basis for Nuclear Waste Management*. Volume 2. Plenum Press. 689-702.

Burns, J. R. 1975. "Error Analysis of Nonlinear Simulations: Applications to World Dynamics." *IEEE Transactions on Systems, Man, and Cybernetics* SMC-5: 331-340.

Butcher, B. M. 1989. *Waste Isolation Pilot Plant Simulated Waste Compositions and Mechanical Properties*. SAND89-0372. Albuquerque, NM: Sandia National Laboratories.

Butcher, B. M. 1990. *Preliminary Evaluation of Potential Engineered Modifications for the Waste Isolation Pilot Plant (WIPP)*. SAND89-3095. Albuquerque, NM: Sandia National Laboratories.

Butcher, B. M. 1991. *The Advantages of a Salt/Bentonite Backfill for Waste Isolation Pilot Plant Disposal Rooms*. SAND90-3074. Albuquerque, NM: Sandia National Laboratories.

Cacuci, D. G. 1981a. "Sensitivity Theory for Nonlinear Systems. I. Nonlinear Functional Analysis Approach." *Journal of Mathematical Physics* 22: 2794-2802.

Cacuci, D. G. 1981b. "Sensitivity Theory for Nonlinear Systems. II. Extensions to Additional Classes of Responses." *Journal of Mathematical Physics* 22: 2803-2812.

Cacuci, D. G., C. F. Weber, E. M. Oblow, and J. H. Marable. 1980. "Sensitivity Theory for General Systems of Nonlinear Equations." *Nuclear Science and Engineering* 75: 88-110.

Campbell, J. E., and R. M. Cranwell. 1988. "Performance Assessment of Radioactive Waste Repositories." *Science* 239: 1389-1392.

Campbell, J. E., and D. E. Longsine. 1990. "Application of Generic Risk Assessment Software to Radioactive Waste Disposal." *Reliability Engineering and System Safety* 30: 183-193.

Cauffman, T. L., A. M. LaVenue, and J. P. McCord. 1990. *Ground-Water Flow Modeling of the Culebra Dolomite: Volume II - Data Base.* SAND89-7068/2. Albuquerque, NM: Sandia National Laboratories.

Chapman, J. B. 1986. *Stable Isotopes in the Southeastern New Mexico Groundwater: Implications for Dating Recharge in the WIPP Area.* EEG-35. Santa Fe, NM: New Mexico Environmental Evaluation Group.

Chapman, J. B. 1988. *Chemical and Radiochemical Characteristics of Groundwater in the Culebra Dolomite, Southeastern New Mexico.* EEG-39. Santa Fe, NM: Environmental Evaluation Group, Environmental Improvement Division, Health and Environment Department, State of New Mexico.

Cheeseman, R. J. 1978. *Geology and Oil/Potash Resources of the Delaware Basin, Eddy and Lea Counties, New Mexico.* New Mexico Bureau of Mines and Mineral Resources Circular 159. Socorro, NM: New Mexico Bureau of Mines and Mineral Resources. 7-14.

Chen, X., and N. C. Lind. 1983. "Fast Probability Integration by Three Parameter Normal Tail Approximation." *Structural Safety* **1**: 169-176.

Cheng, R. C. H., and T. C. Iles. 1983. "Confidence Bounds for Cumulative Distribution Functions of Continuous Random Variables." *Technometrics* **25**: 77-86.

Claiborne, H. C., and F. Gera. 1974. *Potential Containment Failure Mechanisms and Their Consequences at a Radioactive Waste Repository in Bedded Salt in New Mexico.* ORNL-TM-4639. Oak Ridge, TN: Oak Ridge National Laboratory.

COHMAP (Cooperative Holocene Mapping Project) members. 1988. "Climatic Changes of the Last 18,000 years: Observations and Model Simulations." *Science* **241**: 1043-1052.

Cole, F. W. 1975. *Introduction to Meteorology Second Edition.* New York, NY: John Wiley and Sons, Inc.

Conover, W. J. 1980. *Practical Nonparametric Statistics* (2nd ed.). New York, NY: Wiley.

Cook, I., and S. D. Unwin. 1986. "Controlling Principles for Prior Probability Assignments in Nuclear Risk Assessment." *Nuclear Science and Engineering* **94**: 107-119.

Cooper, J. B., and V. M. Glanzman. 1971. "Geohydrology of Project GNOME Site, Eddy County, New Mexico" in *Hydrology of Nuclear Test Sites,* U.S. Geological Survey Professional Paper 712-A.

Cox, D. C., and P. Baybutt. 1981. "Methods for Uncertainty Analysis: A Comparative Survey." *Risk Analysis* **1**: 251-258.

Cox, N. D. 1977. "Comparison of Two Uncertainty Analysis Methods." *Nuclear Science and Engineering* **64**: 258-265.

Cranwell, R. M., J. E. Campbell, J. C. Helton, R. L. Iman, D. E. Longsine, N. R. Ortiz, G. E. Runkle, and M. J. Shortencarier. 1987. *Risk Methodology for Geologic Disposal of Radioactive Waste: Final Report*. NUREG/CR-2452, SAND81-2573. Albuquerque, NM: Sandia National Laboratories.

Cranwell, R. M., R. V. Guzowski, J. E. Campbell, and N. R. Ortiz. 1990. *Risk Methodology for Geologic Disposal of Radioactive Waste: Scenario Selection Procedure*. NUREG/CR-1667, SAND80-1429. Albuquerque, NM: Sandia National Laboratories.

Cukier, R. I., C. M. Fortuin, K. E. Shuler, A. G. Petschek, and J. H. Schiably. 1973. "Study of the Sensitivity of Coupled Reaction Systems to Uncertainties in Rate Coefficients, I. Theory." *Journal of Chemical Physics* **59**: 3873-3878.

Cukier, R. I., H. B. Levine, and K. K. Shuler. 1978. "Nonlinear Sensitivity Analysis of Multiparameter Model Systems." *Journal of Computational Physics* **26**: 1-42.

Davies, P. B. 1983. "Assessing the Potential for Deep-Seated Salt Dissolution and the Subsidence at the Waste Isolation Pilot Plant (WIPP)." Unpublished manuscript presented at the State of New Mexico Environmental Evaluation Group conference, WIPP Site Suitability for Radioactive Waste Disposal, Carlsbad, NM, May 12-13, 1983.

Davies, P. B. 1984. "Deep-Seated Dissolution and Subsidence in Bedded Salt Deposits." Ph.D. dissertation. Dept. of Applied Earth Sciences, Stanford University.

Davies, P. B. 1989. *Variable-Density Ground-Water Flow and Paleohydrology in the Region Surrounding the Waste Isolation Pilot Plant (WIPP), Southeastern New Mexico*. U.S. Geological Survey Open-File Report 88-490. Albuquerque, NM: U.S. Geological Survey.

Dickinson, R. P., and R. J. Gelinas. 1976. "Sensitivity Analysis of Ordinary Differential Equation Systems - A Direct Method." *Journal of Computational Physics* **21**: 123-143.

Doctor, P. G. 1989. "Sensitivity and Uncertainty Analyses for Performance Assessment Modeling." *Engineering Geology* **26**: 411-429.

Doctor, P. G., E. A. Jackson, and J. A. Buchanan. 1988. *A Comparison of Uncertainty Analysis Methods Using a Groundwater Flow Model*. PNL-5649. Richland, WA: Pacific Northwest Laboratory.

Dougherty, E. P., and H. Rabitz. 1979. "A Computational Algorithm for the Green's Function Method of Sensitivity Analysis in Chemical Kinetics." *International Journal of Chemical Kinetics* **11**: 1237-1248.

Dougherty, E. P., J. T. Hwang, and H. Rabitz. 1979. "Further Developments and Applications of the Green's Function Method of Sensitivity Analysis in Chemical Kinetics." *Journal of Chemical Physics* **71**: 1794-1808.

Downing, D. J., R. H. Gardner, and F. O. Hoffman. 1985. "An Examination of Response-Surface Methodologies for Uncertainty Analysis in Assessment Models." *Technometrics* **27**: 151-163.

Draper, N. R., and H. Smith. 1981. *Applied Regression Analysis, Second Edition*. New York, NY: Wiley.

Drez, P. 1989. "Preliminary Nonradionuclide Inventory of CH-TRU Waste," letter from Paul Drez, International Technology Corporation, Albuquerque, NM, to Larry Brush, Sandia National Laboratories, Albuquerque, NM.

Earth Technology Corporation. 1988. *Final Report for Time Domain Electromagnetic (TDEM) Surveys at the WIPP Site*. SAND87-7144. Albuquerque, NM: Sandia National Laboratories.

EPRI (Electric Power Research Institute). 1989. *Probabilistic Seismic Hazard Evaluations at Nuclear Plant Sites in the Central and Eastern United States: Resolution of the Charleston Earthquake Issue*. EPRI-NP-6395D. Palo Alto, CA: EPRI.

Fanchi, J. R., J. E. Kennedy, and D. L. Dauben. 1987. *BOAST II: A Three-Dimensional Three-Phase Black Oil Applied Simulation Tool*. DOE/BC-88/2/SP, DE 88001205. U.S. Department of Energy.

Fedra, K. 1983. *Environmental Modeling under Uncertainty: Monte Carlo Simulation*. RR-83-28. Laxenburg, Austria: International Institute for Applied Systems Analysis.

Feller, W. 1971. *An Introduction to Probability Theory and Its Applications, Vol. II* (2nd Ed.). New York, NY: Wiley.

Fischer, F., and J. Ehrhardt. 1985. *Uncertainty Analysis with a View Towards Applications in Accident Consequence Assessments*. KfK 3906. Karlsruhe, FRD: Kernforschungszentrum Karlsruhe.

Frank, P. M. 1978. *Introduction to System Sensitivity Theory*. New York: Academic Press.

Gardner, R. H., and R. V. O'Neill. 1983. "Parameter Uncertainty and Model Predictions: A Review of Monte Carlo Results." *Uncertainty and Forecasting of Water Quality*. Eds. M. B. Beck and G. Van Straten. New York: Springer-Verlag. 245-257.

Gardner, R. H., R. V. O'Neill, J. B. Mankin, and J. H. Carney. 1981. "A Comparison of Sensitivity Analysis and Error Analysis Based on a Stream Ecosystem Model." *Ecological Modelling* 12: 173-190.

Geohydrology Associates, Inc. 1979. *Water-Resources Study of the Carlsbad Potash Area, New Mexico*. Consultant Report for the U.S. BLM. Contract No. YA-S12-CT8-195.

Geological Society of America. 1984. *Decade of North American Geology Geologic Time Scale*. Geological Society of America Map and Chart Series MCH050.

Gibbons, A. 1990. "Growing Crops in Saltwater." *Science* **248**: 963.

Gilkey, A. P. 1986a. *SPLOT-A Distance-Versus-Variable Plot Program for the Output of a Finite Element Analysis*. SAND86-0882. Albuquerque, NM: Sandia National Laboratories.

Gilkey, A. P. 1986b. *TPLOT-A Time History or X-Y Plot Program for the Output of a Finite Element Analysis*. SAND86-0882. Albuquerque, NM: Sandia National Laboratories.

Gilkey, A. P., and D. P. Flanagan. 1987. *DETOUR-A Deformed Mesh/Contour Plot Program*. SAND86-0914. Albuquerque, NM: Sandia National Laboratories.

Gussow, W. C. 1968. "Salt Diapirism: Importance of Temperature, and Energy Source of Displacement in Diapirism and Diapirs." *American Association of Petroleum Geologists Memoir 8*, no. **8**: 16-52.

Guzowski, R. V. 1990. *Preliminary Identification of Scenarios That May Affect the Escape and Transport of Radionuclides From the Waste Isolation Pilot Plant, Southeastern New Mexico*. SAND89-7149. Albuquerque, NM: Sandia National Laboratories.

Guzowski, R. V. 1991. *Evaluation of Applicability of Probability Techniques to Determining the Probability of Occurrence of Potentially Disruptive Intrusive Events at the Waste Isolation Pilot Plant*. SAND90-7100. Albuquerque, NM: Sandia National Laboratories.

Halbouty, M. T. 1979. *Salt Domes. Gulf Region, United States & Mexico*. 2nd ed. Houston, TX: Gulf Publishing Company.

Hale, W. E., and A. Clebsch, Jr. 1958. *Preliminary Appraisal of Groundwater Conditions in Southeastern Eddy County and Southwestern Lea County, New Mexico*. U.S. Geological Survey Trace Element Memorandum Report 1045. 23.

Hale, W. E., L. S. Hughes, and E. R. Cox. 1954. *Possible Improvement of Quality of Water of the Pecos River by Diversion of Brine at Malaga Bend, Eddy County, New Mexico*. Carlsbad, NM: Pecos River Commission, New Mexico and Texas, in cooperation with USGS Water Resources Division.

Hansen, J., I. Fung, A. Lacis, D. Rind, S. Lebedeff, R. Ruedy, and G. Russell. 1988. "Global Climate Changes as Forecast by Goddard Institute for Space Studies Three-Dimensional Model." *Journal of Geophysical Research* **93**: 9341-9364.

Harms, J. C., and C. R. Williamson. 1988. "Deep-Water Density Current Deposits of Delaware Mountain Group (Permian), Delaware Basin, Texas and New Mexico." *American Association of Petroleum Geologists Bulletin* **72**: 299-317.

Harper, W. V., and S. K. Gupta. 1983. *Sensitivity/Uncertainty Analysis of a Borehole Scenario Comparing Latin Hypercube Sampling and Deterministic Sensitivity Approaches*. BMI/ONWI-516. Columbus, OH: Battelle Memorial Institute.

Harper, F. T. et al., 1990. *Evaluation of Severe Accident Risks: Quantification of Major Input Parameters; Experts' Determination of In-Vessel Issues*. NUREG/CR-4551, SAND86-1309, vol. 2, part 1, rev. 1. Albuquerque, NM: Sandia National Laboratories.

Harper, F. T. et al., 1991. *Evaluation of Severe Accident Risks: Quantification of Major Input Parameters; Experts' Determination of Containment Loads and Molten Core-Concrete Issues*. NUREG/CR-4551, SAND86-1309 vol 2, part 2, rev. 1. Albuquerque, NM: Sandia National Laboratories.

Hartmann, W. K. 1979. "Long-Term Meteorite Hazards to Buried Nuclear Waste. Report 2" in *A Summary of FY-1978 Consultant Input for Scenario Methodology Development*. Pacific Northwest Laboratories. PNL-2851: VI-1-VI-15.

Haug, A., V. A. Kelley, A. M. LaVenue, and J. F. Pickens. 1987. *Modeling of Groundwater Flow in the Culebra Dolomite at the Waste Isolation Pilot Plant (WIPP) Site: Interim Report*. SAND86-7167. Albuquerque, NM: Sandia National Laboratories.

Havens, J. S., and D. W. Wilkins. 1979. *Experimental salinity alleviation at Malaga Bend of the Pecos River, Eddy County, New Mexico*. U.S. Geological Survey Water-Resources Investigations 80-4.

Hayes, P. T. 1964. *Geology of the Guadalupe Mountains, New Mexico*. U.S. Geological Survey Professional Paper 446.

Hays, J. D., J. Imbrie, and N. J. Shackleton. 1976. "Variations in the Earth's Orbit; Pacemaker of the Ice Ages." *Science* **194**: 1121-1132.

Helton, J. C., R. L. Iman, and J. B. Brown. 1985. "Sensitivity Analysis of the Asymptotic Behavior of a Model for the Environmental Movement of Radionuclides." *Ecological Modelling* **28**: 243-278.

Helton, J. C., R. L. Iman, J. D. Johnson, and C. D. Leigh. 1986. "Uncertainty and Sensitivity Analysis of a Model for Multicomponent Aerosol Dynamics." *Nuclear Technology* **73**: 320-342.

Helton, J. C., J. M. Griesmeyer, F. E. Haskin, R. L. Iman, C. N. Amos, and W. B. Murfin. 1988. "Integration of the NUREG-1150 Analyses: Calculation of Risk and Propagation of Uncertainties." *Proceedings of the Fifteenth Water Reactor Safety Research Information Meeting:* pp. 151-176. Washington, D.C.: U.S. Nuclear Regulatory Commission.

Helton, J. C., R. L. Iman, J. D. Johnson, and C. D. Leigh. 1989. "Uncertainty and Sensitivity Analysis of a Dry Containment Test Problem for the MAEROS Aerosol Model." *Nuclear Science and Engineering* **102**: 22-42.

Helton, J. C., J. W. Garner, R. D. McCurley, and D. K. Rudeen. 1991. *Sensitivity Analysis Techniques and Results for Performance Assessment at the Waste Isolation Pilot Plant*. SAND90-7103. Albuquerque, NM: Sandia National Laboratories.

Hendrickson, R. G. 1984. *Survey of Sensitivity Analysis Methodology*. NBSIR 84-2814. Washington, D. C.: U.S. National Bureau of Standards.

Hendry, D. F. 1984. "Monte Carlo Experimentation in Econometrics," in Z. Groiliches and M. D. Intriligator (eds.), *Handbook of Econometrics, vol. II: 937-976*. New York, NY: Elsevier.

Hills, J. M. 1984. "Sedimentation, Tectonism, and Hydrocarbon Generation in the Delaware Basin, West Texas and Southeastern New Mexico." *American Association of Petroleum Geologists Bulletin* **68**: 250-267.

Hiss, W. L. 1975. "Stratigraphy and Ground-Water Hydrology of the Capitan Aquifer, Southeastern New Mexico and West Texas." Ph.D. dissertation. University of Colorado, Boulder, CO.

Holmes, R. W. 1987. "Uncertainty Analysis for the Long-Term Assessment of Uranium Mill Tailings" in *Uncertainty Analysis for Performance Assessments of Radioactive Waste Disposal Systems*, 167-190. Paris: Organization for Economic Co-Operation and Development.

Holt, R. M., and D. W. Powers. 1988. *Facies Variability and Post-Depositional Alteration Within the Rustler Formation in the Vicinity of the Waste Isolation Pilot Plant, Southeastern New Mexico*. DOE/WIPP-88-004. Carlsbad, NM: U.S. Department of Energy.

Hora, S. C., and R. L. Iman. 1989. "Expert Opinion in Risk Analysis: The NUREG-1150 Methodology." *Nuclear Science and Engineering* **102**: 323-331.

Hora, S. C., D. von Winterfeldt, and K. M. Trauth. 1991. *Expert Judgment on Inadvertent Human Intrusion into the Waste Isolation Pilot Plant*. SAND90-3063. Albuquerque, NM: Sandia National Laboratories.

Houghton, J. T., G. J. Jenkins, and J. J. Ephraums. 1990. *Climate Change: The IPCC Scientific Assessment*. Cambridge, UK: Cambridge University Press.

Hunter, R. L. 1983. *Preliminary Scenarios for the Release of Radioactive Waste From a Hypothetical Repository in Basalt of the Columbia Plateau*. NUREG/CR-3353, SAND83-1342. Albuquerque, NM: Sandia National Laboratories.

Hunter, R. L. 1985. *A Regional Water Balance for the Waste Isolation Pilot Plant (WIPP) Site and Surrounding Area*. SAND84-2233. Albuquerque, NM: Sandia National Laboratories.

Hunter, R. L. 1989. *Events and Processes for Constructing Scenarios for the Release of Transuranic Waste From the Waste Isolation Pilot Plant, Southeastern New Mexico*. SAND89-2546. Albuquerque, NM: Sandia National Laboratories.

Hunter, R. L., G. E. Barr, and F. W. Bingham. 1982. *Preliminary Scenarios for Consequence Assessments of Radioactive-Waste Repositories at the Nevada Test Site*. SAND82-0426. Albuquerque, NM: Sandia National Laboratories.

Hunter, R. L., G. E. Barr, and F. W. Bingham. 1983. *Scenarios for Consequence Assessments of Radioactive-Waste Repositories at Yucca Mountain, Nevada Test Site*. SAND82-1277. Albuquerque, NM: Sandia National Laboratories.

Hunter, R. L., R. M. Cranwell, and M. S. Y. Chu. 1986. *Assessing Compliance with the EPA High-Level Waste Standard: An Overview*. SAND86-0121, NUREG/CR-4510. Albuquerque, NM: Sandia National Laboratories.

Huyakorn, P. S., H. O. White, Jr., and S. Panday. 1989. *STAFF2D Solute Transport and Fracture Flow in Two Dimensions*. Herndon, VA: Hydrogeologic, Inc.

Hwang, J. T., E. P. Dougherty, S. Rabitz, and H. Rabitz. 1978. "The Green's Function Method of Sensitivity Analysis in Chemical Kinetics." *Journal of Chemical Physics* **69**: 5180-5191.

IAEA (International Atomic Energy Agency). 1983. *Concepts and Examples of Safety Analyses for Radioactive Waste Repositories in Continental Geological Formations*. Safety Series No. 50. Paris: International Atomic Energy Agency.

IAEA (International Atomic Energy Agency). 1989. *Evaluating the Reliability of Predictions Made Using Environmental Transfer Models*. Safety Series Report No. 100. Vienna: International Atomic Energy Agency.

Ibrekk, H., and M. G. Morgan. 1987. "Graphical Communication of Uncertain Quantities to Nontechnical People." *Risk Analysis* **7**: 519-529.

ICBO (International Conference of Building Officials). 1979. *Uniform Building Code*. Whittier, CA: International Conference of Building Officials.

ICRP (International Commission on Radiological Protection). 1959. *Report of the ICRP Committee II on Permissible Dose for Internal Radiation*. ICRP Publication 2. Pergamon Press.

Iman, R. L., 1981. "Statistical Methods for Including Uncertainty Associated with the Geologic Isolation of Radioactive Waste Which Allow For a Comparison with Licensing Criteria" in *Proceedings of the Symposium on Uncertainties Associated with the Regulation of the Geologic Disposal of High-Level Radioactive Waste, Gatlinburg, TN, March 9-13 1981*.

Iman, R. L. 1982. "Statistical Methods for Including Uncertainties Associated with Geologic Isolation of Radioactive Waste Which Allow for a Comparison with Licensing Criteria," in *Proceedings of the Symposium on Uncertainties Associated with the Regulation of the Geologic Disposal of High Level Radioactive Waste, Gatlinburg, TN March 9-13, 1981.* D. C. Hocher, ed. NUREG/CP-0022, CONF-810372: 145-157. Oak Ridge, TN: Oak Ridge National Laboratory.

Iman, R. L., and W. J. Conover. 1979. "The Use of the Rank Transform in Regression." *Technometrics* **21**: 499-509.

Iman, R. L., and W. J. Conover. 1980a. "Small Sample Sensitivity Analysis Techniques for Computer Models, with an Application to Risk Assessment." *Communications in Statistics* **A9**: 1749-1842.

Iman, R. L., and W. J. Conover. 1980b. "Rejoinder to Comments." *Communications in Statistics* **A9**: 1863-1874.

Iman, R. L., and W. J. Conover. 1982a. *Sensitivity Analysis Techniques: Self-Teaching Curriculum.* SAND81-1978, NUREG/CR-2350. Albuquerque, NM: Sandia National Laboratories.

Iman, R. L., and W. J. Conover. 1982b. "A Distribution-Free Approach to Inducing Rank Correlation Among Input Variables." *Communications in Statistics*, vol. B11, no. 3: 311-334.

Iman, R. L., and W. J. Conover. 1983. *A Modem Approach to Statistics.* New York: Wiley.

Iman, R. L., and J. M. Davenport. 1982. "Rank Correlation Plots for Use with Correlated Input Variables." *Communications in Statistics B11* **11**: 335-360.

Iman, R. L., and J. C. Helton. 1985a. *A Comparison of Uncertainty and Sensitivity Analysis Techniques for Computer Models.* NUREG/CR-3904, SAND84-1461. Albuquerque, NM: Sandia National Laboratories.

Iman, R. L. and J. C. Helton. 1985b. "Overview of Methods for Uncertainty Analysis and Sensitivity Analysis in Probabilistic Risk Assessment" in *Proceedings of the ANS/ENS International Topical Meeting on Probabilistic Safety Methods and Applications, San Francisco, CA, USA, 24 February - 1 March 1985,* vol. 1, pp. 15-1 to 15-11. La Grange Park, IL: American Nuclear Society.

Iman, R. L., and J. C. Helton. 1988. "An Investigation of Uncertainty and Sensitivity Analysis Techniques for Computer Models." *Risk Analysis* **8**: 71-90.

Iman, R. L. and J. C. Helton. 1991. "The Repeatability of Uncertainty and Sensitivity Analyses For Complex Probabilistic Risk Assessments." *Risk Analysis.* In press (December).

Iman, R. L., J. C. Helton, and J. E. Campbell. 1978. *Risk Methodology for Geologic Disposal of Radioactive Waste: Sensitivity Analysis Techniques.* NUREG/CR-0394, SAND78-0912. Albuquerque, NM: Sandia National Laboratories.

Iman, R. L., J. C. Helton, and J. E. Campbell. 1981a. "An Approach to Sensitivity Analysis of Computer Models, Part 1. Introduction, Input Variable Selection and Preliminary Variable Assessment." *Journal of Quality Technology* **13**: 174-183.

Iman, R. L., J. C. Helton, and J. E. Campbell. 1981b. "An Approach to Sensitivity Analysis of Computer Models, Part 2. Ranking of Input Variables, Response Surface Validation, Distribution Effect and Technique Synopsis." *Journal of Quality Technology* **13**: 232-240.

Iman, R. L., M. J. Shortencarier, and J. D. Johnson. 1985. *A FORTRAN 77 Program and User's Guide for the Calculation of Partial Correlation and Standardized Regression Coefficients.* NUREG/CR-4122, SAND85-0044. Albuquerque, NM: Sandia National Laboratories.

Imbrie, J. 1985. "A Theoretical Framework for the Pleistocene Ice Ages." *Journal of the Geological Society of London* **142**: 417-432.

Imbrie, J., and J. Z. Imbrie. 1980. "Modeling the Climatic Response to Orbital Variations." *Science* **207**. 943-953.

Imbrie, J., J. D. Hays, D. G. Martinson, et al. 1984. "The Orbital Theory of Pleistocene Climate: Support from a Revised Chronology of the Marine ^{18}O Record." *Milankovitch and Climate.* Eds. A. L. Berger et al. Boston, MA: D. Reidel. 269-305.

Jacobson, E. A., M. D. Freshley, and F. H. Dove. 1985. *Investigations of Sensitivity and Uncertainty in Some Hydrologic Models of Yucca Mountain and Vicinity.* SAND84-7212. Albuquerque, NM: Sandia National Laboratories.

Jones, C. L. 1978. *Test Drilling for Potash Resources: Waste Isolation Pilot Plant Site, Eddy County, New Mexico.* U.S. Geological Survey Open-File Report 78-592. Washington, DC: U.S. Geological Survey.

Kaplan, S., and B. J. Garrick. 1981. "On the Quantitative Definition of Risk." *Risk Analysis* **1**: 11-27.

Karnbranslesakerhet. 1978. *Handling of Spent Nuclear Fuel and Final Storage of Vitrified High-Level Reprocessing Waste.* Stockholm, Sweden: Karnbranslesakerhet.

Keesey, J. J. 1976. *Hydrocarbon Evaluation, Proposed Southeastern New Mexico Radioactive Storage Site, Eddy County, New Mexico.* 2 volumes. Midland, TX: Sipes, Williamson and Aycock.

Keesey, J. J. 1979. *Evaluation of Directional Drilling for Oil and Gas Reserves Underlying the WIPP Site Area, Eddy County, New Mexico.* Midland, TX: Sipes, Williamson and Associates.

Kelly, V. A., and J. F. Pickens. 1986. *Interpretation of the Convergent-Flow Tracer Tests Conducted in the Culebra Dolomite at the H-3 and H-4 Hydropads at the Waste Isolation Pilot Plant (WIPP) Site.* SAND86-7161. Albuquerque, NM: Sandia National Laboratories.

Kelly, V. A., and G. J. Saulnier, Jr. 1990. *Core Analysis From the Culebra Dolomite at the Waste Isolation Pilot Plant.* SAND90-7011. Albuquerque, NM: Sandia National Laboratories.

Kim, T. W., S. H. Chang, and B. H. Lee. 1988a. "Uncertainty and Sensitivity Analyses in Evaluating Risk of High Level Waste Repository." *Radioactive Waste Management and the Nuclear Fuel Cycle* **10**: 321-356.

Kim, T. W., S. H. Chang, and B. H. Lee. 1988b. "Comparative Study on Uncertainty and Sensitivity Analysis and Application to LOCA Model." *Reliability Engineering and System Safety* **21**: 1-26.

Kleijnen, J. P. C. 1974. *Statistical Techniques in Simulation,* Parts 1 and 2. New York, NY: Marcel Dekker.

Kleijnen, J. P. C. 1987. *Statistical Tools for Simulation Practitioners.* New York, NY: Marcel Dekker.

Kunkler, J. L. 1980. *Evaluation of the Malaga Bend Salinity Alleviation Project Eddy County, New Mexico.* U.S. Geological Survey Open-File Report 80-1111. Albuquerque, NM: U.S. Geological Survey/Water Resources Division and the Pecos River Commission.

Lambert, S. J. 1983. *Dissolution of Evaporites in and around the Delaware Basin, Southeastern New Mexico and West Texas.* SAND82-0461. Albuquerque, NM: Sandia National Laboratories.

Lambert, S. J. 1991. "Isotopic Constraints on the Rustler and Dewey Lake Groundwater Systems," Chapter 5 in *Hydrogeochemical Studies of the Rustler Formation and Related Rocks in the Waste Isolation Pilot Plant Area, Southeastern New Mexico.* M. D. Siegel, S. J. Lambert, and K. L. Robinson, eds. SAND88-0196. Albuquerque, NM: Sandia National Laboratories.

Lambert, S. J., and J. A. Carter. 1984. *Uranium-Isotope Disequilibrium in Brine Reservoirs of the Castile Fm., Northern Delaware Basin, Southeastern New Mexico, I: Principles and Methods.* SAND83-0144. Albuquerque, NM: Sandia National Laboratories.

Lambert, S. J., and J. A. Carter. 1987. *Uranium-Isotope Systematics in Groundwaters of the Rustler Formation, Northern Delaware Basin, Southeastern New Mexico.* SAND87-0388. Albuquerque, NM: Sandia National Laboratories.

Lambert, S. J., and D. M. Harvey. 1987. *Stable-Isotope Geochemistry of Groundwater in the Delaware Basin of Southeastern New Mexico.* SAND87-0138. Albuquerque, NM: Sandia National Laboratories.

Lambert, S. J., and J. W. Mercer. 1978. *Hydrologic Investigations of the Los Medaños Area, Southeastern New Mexico, 1977.* SAND77-1401. Albuquerque, NM: Sandia National Laboratories.

Lappin, A. R. 1988. *Summary of Site-Characterization Studies Conducted from 1983 through 1987 at the Waste Isolation Pilot Plant (WIPP) Site, Southeastern New Mexico.* SAND88-0157. Albuquerque, NM: Sandia National Laboratories.

Lappin, A. R., R. L. Hunter, D. P. Garber, P. B. Davies, R. L. Beauheim, D. J. Borns, L. H. Brush, B. M. Butcher, T. Cauffman, M. S. Y. Chu, L. S. Gomez, R. V. Guzowski, H. J. Iuzzolino, V. Kelley, S. J. Lambert, M. G. Marietta, J. W. Mercer, E. J. Nowak, J. Pickens, R. P. Rechard, M. Reeves, K. L. Robinson, and M. D. Siegel. 1989. *Systems Analysis, Long-Term Radionuclide Transport, and Dose Assessments, Waste Isolation Pilot Plant (WIPP), Southeastern New Mexico; March 1989.* SAND89-0462. Albuquerque, NM: Sandia National Laboratories.

Lappin, A. R., R. L. Hunter, P. B. Davies, D. J. Borns, M. Reeves, J. Pickens, and H. J. Iuzzolino. 1990. *Systems Analysis, Long-Term Radionuclide Transport, and Dose Assessments, Waste Isolation Pilot Plant (WIPP), Southeastern New Mexico; September, 1989.* SAND89-1996. Albuquerque, NM: Sandia National Laboratories.

LaVenue, A. M., A. Haug, and V. A. Kelley. 1988. *Numerical Simulation of Groundwater Flow in the Culebra Dolomite at the Waste Isolation Pilot Plant (WIPP) Site; Second Interim Report.* SAND88-7002. Albuquerque, NM: Sandia National Laboratories.

LaVenue, A. M., T. L. Cauffman, and J. F. Pickens. 1990. *Ground-Water Flow Modeling of the Culebra Dolomite: Volume 1 - Model Calibration.* SAND89-7068. Albuquerque, NM: Sandia National Laboratories.

Lee, F. T., and J. F. Abel, Jr. 1983. *Subsidence from Underground Mining: Environmental Analysis and Planning Considerations.* Circular 876. U. S. Geological Survey.

Levin, R. D., and M. Tribus, eds. 1978. *The Maximum Entropy Formalism.* Cambridge, MA: The MIT Press.

Lewins, J., and M. Becker, eds. 1982. "Sensitivity and Uncertainty Analysis of Reactor Performance Parameters." *Advances in Nuclear Science and Technology* **14**, New York, NY: Plenum Press.

Liepmann, D., and G. Stephanopoulos. 1985. "Development and Global Sensitivity Analysis of a Closed Ecosystem Model." *Ecological Modelling* **30**: 13-47.

Logan, S. E., and M. C. Berbano. 1978. *Development and Application of a Risk Assessment Method for Radioactive WAste Management, Volume II: Implementation for Terminal Storage in Reference Repository and Other Applications.* EPA 520/6-78-005. Washington, DC: U.S. Environmental Protection Agency.

Longsine, D. E., E. J. Bonano, and C. P. Harlan. 1987. *User's Manual for the NEFTRAN Computer Code*. NUREG/CR-4766, SAND86-2405. Albuquerque, NM: Sandia National Laboratories.

McCormick, N. J. 1981. *Reliability and Risk Analysis - Methods and Nuclear Power Applications*. New York: Academic Press.

McGrath, E. J., et al. 1975. *Techniques for Efficient Monte Carlo Simulation*. ORNL-RSIC-38, vols. I-III. Oak Ridge, TN: Oak Ridge National Laboratory.

McKay, M. D., W. J. Conover, and R. J. Beckman. 1979. "A Comparison of Three Methods for Selecting Values of Input Variables in the Analysis of Output From a Computer Code." *Technometrics* vol. 21, no. 2: 239-245.

McRae, G. J., J. W. Tilden, and J. H. Seinfeld. 1981. "Global Sensitivity Analysis--A Computational Implementation of the Fourier Amplitude Sensitivity Test (FAST)." *Computers and Chemical Engineering* 5: 15-25.

Marietta, M. G., S. G. Bertram-Howery, D. R. Anderson, K. Brinster, R. Guzowski, H. Iuzzolino, and R. P. Rechard. 1989. *Performance Assessment Methodology Demonstration: Methodology Development for Purposes of Evaluating Compliance with EPA 40 CFR Part 191, Subpart B, for the Waste Isolation Pilot Plant*. SAND89-2027. Albuquerque, NM: Sandia National Laboratories.

Maerker, R. E. 1988. *Comparison of Results Based on a Deterministic Versus a Statistical Sensitivity Analysis*. ORNL/TM-10773. Oak Ridge, TN: Oak Ridge National Laboratory.

Mazumdar, M., et al. 1975. *Review of the Methodology for Statistical Evaluation of Reactor Safety Analysis*. EPRI 309. Palo Alto, CA: Electric Power Research Institute.

Mazumdar, M., et al. 1976. *Methodology Development for Statistical Evaluation of Reactor Safety Analyses*. EPRI-NP-194. Palo Alto, CA: Electric Power Research Institute.

Mazumdar, M., J. A. Marshall, and S. C. Chay. 1978. "Propagation of Uncertainties in Problems of Structural Reliability." *Nuclear Engineering and Design* 50: 163-167.

Mead, R., and D. J. Pike. 1975. "A Review of Response Surface Methodology from a Biometric Viewpoint." *Biometrics* 31: 803-851.

Mercer, J. W. 1983. *Geohydrology of the Proposed Waste Isolation Pilot Plant Site, Los Medanos Area, Southeastern New Mexico*. U.S. Geological Survey, Water-Resources Investigations Report 83-4016. Albuquerque, NM: U.S. Geological Survey.

Mercer, J. W. 1987. *Compilation of Hydrologic Data from Drilling the Salado and Castile Formations Near the WIPP Site, Southeastern New Mexico*. SAND86-0954. Albuquerque, NM: Sandia National Laboratories.

Mercer, J. W., and B. R. Orr. 1977. *Review and Analysis of Hydrogeologic Conditions Near the Site of a Potential Nuclear-Waste Repository, Eddy and Lea Counties, New Mexico.* U.S. Geological Survey Open-File Report 77-123.

Mercer, J. W. and B. R. Orr. 1979. *Interim Data Report on Geohydrology of the Proposed Waste Isolation Pilot Plant, Southeast New Mexico.* U.S. Geological Survey Water Resources Investigation 79-98.

Mercer, J. W., R. L. Beauheim, R. P. Snyder, and G. M. Fairer. 1987. *Basic Data Report for Drilling and Hydrologic Testing of Drillhole DOE-2 at the Waste Isolation Pilot Plant (WIPP) Site.* SAND86-0611. Albuquerque, NM: Sandia National Laboratories.

Milankovitch, M. M. 1941. *Canon of Insolation and the Ice-age Problem.* Koniglich Serbische Akademie, Beograd. (English translation by the Israel Program for Scientific Translations; published by the U.S. Department of Commerce and the National Science Foundation, Washington, D.C.).

Mishra, S., and J. C. Parker. 1989. "Effects of Parameter Uncertainty on Predictions of Unsaturated Flow." *Journal of Hydrology* **108**: 19-33.

Mitchell, J. F. B. 1989. "The 'Greenhouse Effect' and Climate Change." *Reviews of Geophysics* **27**: 115-139.

Molecke, M. A. 1983. *A Comparison of Brines Relevant to Nuclear Waste Experimentation.* SAND83-0516. Albuquerque, NM: Sandia National Laboratories.

Montgomery, R. H., V. D. Lee, and K. H. Reckhow. 1983. "Predicting Variability in a Lake Ontario Phosphorus Model." *Journal of Great Lakes Research* **9**: 74-82.

Morton, R. H. 1983. "Response Surface Methodology." *Mathematical Scientist* **8**: 31-52.

Muffler, L. J. P., ed. 1979. *Assessment of Geothermal Resources of the United States -- 1978.* Circular 790. U.S. Geological Survey.

Munson, D. E., Fossum, A. F., and Senseny, P. E. 1989a. *Advances in Resolution of Discrepancies Between Predicted and Measured In Situ WIPP Room Closures.* SAND88-2948. Albuquerque, NM: Sandia National Laboratories.

Munson, D. E., Fossum, A. F., and Senseny, P. E. 1989b. *Approach to First Principles Model Prediction of Measured WIPP In Situ Room Closure in Salt.* SAND88-2535. Albuquerque, NM: Sandia National Laboratories.

Myers, R. H. 1971. *Response Surface Methodology.* Boston, MA: Allyn and Bacon.

Neter, J., and W. Wasserman. 1974. *Applied Linear Statistical Models.* Homewood, IL: Richard D. Irwin.

NEA (Nuclear Energy Agency). 1987. *Uncertainty Analysis for Performance Assessments of Radioactive Waste Disposal Systems*. Paris: Organization for Economic Co-Operation and Development.

Nicholson, A., Jr., and A. Clebsch, Jr. 1961. *Geology and Ground-water Conditions in Southern Lea County, New Mexico*. New Mexico Bureau of Mines and Mineral Resources Ground-Water Report No. 6. Socorro, NM: New Mexico Bureau of Mines and Mineral Resources.

Nowak, E. J., and J. C. Stormont. 1987. *Scoping Model Calculations of the Reconsolidation of Crushed Salt in WIPP Shafts*. SAND87-0879. Albuquerque, NM: Sandia National Laboratories.

Nowak, E. J., D. F. McTigue, and R. Beraun. 1988. *Brine Inflow to WIPP Disposal Rooms: Data, Modeling, and Assessment*. SAND88-0112. Albuquerque, NM: Sandia National Laboratories.

Nowak, E. J., J. R. Tillerson, and T. M. Torres. 1990. *Initial Reference Seal System Design: Waste Isolation Pilot Plan*. SAND90-0355. Albuquerque, NM: Sandia National Laboratories.

NuPac (Nuclear Packaging, Inc.). 1989. *Safety Analysis Report for the TRUPACT-II Shipping Package*. NuPac TRUPACT-II SAR Rev. 4.

Oblow, E. M. 1985. *GRESS: Gradient Enhanced Software System, Version D, User's Guide*. ORNL/TM-9658. Oak Ridge, TN: National Laboratory.

Oblow, E. M., F. G. Pin, and R. Q. Wright. 1986. "Sensitivity Analysis Using Computer Calculus: A Nuclear Waste Isolation Example." *Nuclear Science and Engineering* **94**: 46-65.

Obray, C. D, C. C. Wright, and S. J. Baldwin. 1986. "A Comparative Study of Monte-Carlo Simulation and Taylor Series Approaches to the Derivation of Uncertainty Estimates: A Case Study on Compact Heat Exchangers" in *Modelling Under Uncertainty 1986*. Eds. S. B. Jones and D. G. S. Davies. Institute of Physics Conference Series No. 80: 243-252. Bristol, England: Institute of Physics.

Olivi, L. 1986. *Response Surface Methodology Handbook for Nuclear Reactor Safety*. EUR 9600 EN. Luxembourg: Commission of the European Communities.

Ortiz, N. R., T. A. Wheeler, R. J. Breeding, S. Hora, M. A. Myer, and R. L. Keeney. 1991. "Use of Expert Judgment in NUREG-1150." *Nuclear Engineering and Design*. **126**: 313-331.

Owen, G. N., and R. E. Scholl. 1981. *Earthquake Engineering of Large Underground Structures*. FHWA/RD-80/195. Washington, D.C.: Federal Highway Administration, Department of Transportation.

Parker, T. J., and A. N. McDowell. 1951. "Scale Models as Guides to Interpretation of Salt Dome Faulting." *American Association of Petroleum Geologists Bulletin* vol. 35, no. 9: 2076-2086.

Parker, T. J., and A. N. McDowell. 1955. "Model Studies of Salt dome Tectonics." *American Association of Petroleum Geologists Bulletin* vol. 39, no. 12: 2384-2470.

Parry G. W. 1988. "On the Meaning of Probability in Probabilistic Safety Assessment." *Reliability Engineering and System Safety* **23**: 309-314.

Pasztor, S. B. 1991. "A Historical Perspective of Cultural Development in Southeastern New Mexico," Chapter IX in *Background Information Presented to the Expert Panel on Inadvertent Human Intrusion into the Waste Isolation Pilot Plant*. Eds. R. V. Guzowski and M. M. Gruebel. SAND91-0928. Albuquerque, NM: Sandia National Laboratories. In preparation.

Paté-Cornell M. E. 1986. "Probability and Uncertainty in Nuclear Safety Decisions." *Nuclear Engineering and Design* **93**: 319-327.

Pepping, R. E., M. S. Y. Chu, and M. D. Siegel. 1983. "A simplified analysis of a hypothetical repository in a basalt formation, Volume 2." *Technical Assistance for Regulatory Development: Review and Evaluation of the Draft EPA Standard 40 CFR 191 for Disposal of High-Level Waste.* NUREG/CR-3235, SAND82-1557. Albuquerque, NM: Sandia National Laboratories.

Peterson, E. W., P. L. Lagus, and K. Lie. 1987. *Fluid Flow Measurements of Test Series A and B for the Small Scale Seal Performance Tests*. SAND87-7041. Albuquerque, NM: Sandia National Laboratories.

Pin, F. G., B. A. Worley, E. M. Oblow, R. Q. Wright, and W. V. Harper. 1986. "An Automated Sensitivity Analysis Procedure for the Performance Assessment of Nuclear Waste Isolation Systems." *Nuclear and Chemical Waste Management* **6**: 255-263.

Popielak, R. S., R. L. Beauheim, S. R. Black, W. E. Coons, C. T. Ellingson, and R. L. Olson. 1983. *Brine Reservoirs in the Castile Fm., Waste Isolation Pilot Plant (WIPP) Project, Southeastern New Mexico*. TME-3153. Carlsbad, NM: U.S. Department of Energy.

Powers, D. W., S. J. Lambert, S-E Shaffer, L. R. Hill, and W. D. Weart, eds. 1978a. *Geological Characterization Report, Waste Isolation Pilot Plant (WIPP) Site, Southeastern New Mexico. Volume I*. SAND78-1596. Albuquerque, NM: Sandia National Laboratories.

Powers, D. W., S. J. Lambert, S-E Shaffer, L. R. Hill, and W. D. Weart, eds. 1978b. *Geological Characterization Report, Waste Isolation Pilot Plant (WIPP) Site, Southeastern New Mexico. Volume II*. SAND78-1596. Albuquerque, NM: Sandia National Laboratories.

Public Law 96-164. 1979. *Department of Energy National Security and Military Applications of Nuclear Energy Authorization Act of 1980.*

Public Law 100-456. 1989. *National Defense Authorization Act, Fiscal Year 1989.*

Rabitz, H., M. Kramer, and D. Dacol. 1983. "Sensitivity Analysis in Chemical Kinetics." *Annual Reviews of Physical Chemistry* **34**: 410-461.

Rackwitz, R., and B. Fiessler. 1978. "Structural Reliability Under Combined Random Load Sequences." *Journal of Computers and Structures* **9**: 489-494.

Rautman, C. 1988. *Technical Data Base Planning Strategy for the NNWSI Site & Engineering Properties Data Base.* SLTR87-5003. Albuquerque, NM: Sandia National Laboratories.

Rechard, R. P. 1989. *Review and Discussion of Code Linkage and Data Flow in Nuclear Waste Compliance Assessments.* SAND87-2833. Albuquerque, NM: Sandia National Laboratories.

Rechard, R. P., H. J. Iuzzolino, J. S. Rath, R. D. McCurley, and D. K. Rudeen. 1989. *User's Manual for CAMCON: Compliance Assessment Methodology Controller.* SAND88-1496. Albuquerque, NM: Sandia National Laboratories.

Rechard, R. P., H. J. Iuzzolino, and J. S. Sandha. 1990a. *Data Used in Preliminary Performance Assessment of the Waste Isolation Pilot Plant (1990).* SAND89-2408. Albuquerque, NM: Sandia National Laboratories.

Rechard, R. P., W. Beyeler, R. D., McCurley, D. K. Rudeen, J. E. Bean, and J. D. Schreiber. 1990b. *Parameter Sensitivity Studies of Selected Components of the WIPP Repository System.* SAND89-2030. Albuquerque, NM: Sandia National Laboratories.

Reiter, L. 1990. *Earthquake Hazard Analysis.* New York, NY: Columbia University Press.

Richey, S. F., J. G. Wells, and K. T. Stephens. 1985. *Geohydrology of the Delaware Basin and Vicinity, Texas and Mexico.* U.S. Geological Survey Water Resources Investigations Report 84-4077. Washington, DC: U.S. Geological Survey.

Rish, W. R., and R. J. Marnicio. 1988. *Review of Studies Related to Uncertainty in Risk Analysis.* ORNL/TM-10776. Oak Ridge, TN: Oak Ridge National Laboratory.

Robinson, T. W., and W. B. Lang. 1938. *Geology and Groundwater Conditions of the Pecos River Valley in the Vicinity of Laguna Grande de la Sal, New Mexico, With Special Reference to the Salt Content of the River Water.* New Mexico State Engineer 12th-13th Biennial Rpts 1934-1938. 77-100.

Ronen, Y, ed. 1988. *Uncertainty Analysis.* Boca Raton, FL: CRC Press.

Rose, K. A.. 1982. "A Simulation Comparison and Evaluation of Parameter Sensitivity Methods Applicable to Large Models" in *Analysis of Ecological Systems: State-of-the-Art in Ecological Modeling*. Eds. W. K. Lauenroth, et al. 129-140.

Rose, K. A., and G. S. Swartzman. 1981. *A Review of Parameter Sensitivity Methods Applicable to Ecosystem Models*. NUREG/CR-2016. Seattle, WA: University of Washington.

Sanford, A. R., and T. R. Toppozada. 1974. *Seismicity of Proposed Radioactive Waste Disposal Site in Southeastern New Mexico*. Circular 143. Socorro, NM: New Mexico Bureau of Mines and Mineral Resources.

Saulnier, G.J. Jr. 1987. *Analysis of Pumping Tests of the Culebra Dolomite Conducted at the H-11 Hydropad at the Waste Isolation Pilot Plant (WIPP) Site*. SAND87-7124. Albuquerque, NM: Sandia National Laboratories.

Saulnier, G. J., Jr., and J. D. Avis. 1988. Interpretation of Hydraulic Tests Conducted in the Waste-Handling Shaft at the Waste Isolation Pilot Plant (WIPP) Site. SAND87-7001. Albuquerque, NM: Sandia National Laboratories.

Scavia, D., W. F. Powers, R. P. Canale, and J. L. Moody. 1981. "Comparison of First-Order Error Analysis and Monte Carlo Simulation in Time-Dependent Lake Eutrophication Models." *Water Resources Research* **17**: 1051-1059.

Schaibly, J. H., and K. E. Shuler. 1973. "Study of the Sensitivity of Coupled Reaction Systems to Uncertainties in Rate Coefficients, II. Applications." *Journal of Chemical Physics* **59**: 3879-3888.

Schwarz, G., and F. O. Hoffman. 1980. "Imprecision of Dose Predictions for Radionuclides Released to the Environment: An Application of a Monte Carlo Simulation Technique." *Environment International* 4: 289-297.

Seaholm, S. K., E. Ackerman, and S. C. Wu. 1988. "Latin Hypercube Sampling and the Sensitivity Analysis of a Monte Carlo Epidemic Model." *International Journal of BioMedical Computing* **23**: 97-112.

Shurbet, D. H. 1969. "Increased Seismicity in Texas." *Texas Journal of Science* **21**: 37-41.

Siegel, M. D. 1990. "Appendix A, Memo 3a: Representation of Radionuclide Retardation in the Culebra Dolomite in Performance Assessment Calculations," in *Data Used in Preliminary Performance Assessment of the Waste Isolation Pilot Plant (1990)*. R. P. Rechard, H. Iuzzolino, and J. S. Sandha. SAND89-2408. Albuquerque, NM: Sandia National Laboratories.

Siegel, M. D., and S. J. Lambert. 1991. "Summary of Hydrogeochemical Constraints on Groundwater Flow and Evolution in the Rustler Formation," Chapter I in *Hydrogeochemical Studies of the Rustler Formation and Related*

Rocks in the Waste Isolation Pilot Plant Area, Southeastern New Mexico. Eds. M. D. Siegel, S. J. Lambert, and K. L. Robinson. SAND88-0196. Albuquerque, NM: Sandia National Laboratories.

Siegel, M. D., K. L. Robinson, and J. Myers. 1991. "Solute Relationships in Groundwaters from the Culebra Dolomite and Related Rocks in the Waste Isolation Pilot Plant Area, Southeastern New Mexico," Chapter 2 in *Hydrogeochemical Studies of the Rustler Formation and Related Rocks in the Waste Isolation Pilot Plant Area, Southeastern New Mexico*. SAND88-0196. Albuquerque, NM: Sandia National Laboratories.

Slezak, S., and A. Lappin. 1990. "Potential for and Possible Impacts of Generation of Flammable and/or Detonable Gas Mixtures during the WIPP Transportation, Test, and Operational Phases," memorandum to D. Mercer and C. Fredrickson (January 5). Albuquerque, NM: Sandia National Laboratories.

Smith, C. B., D. J. Egan, Jr., W. A. Williams, J. M. Grunlke, C.-Y. Hung, and B. L. Serini. 1982. *Population Risks from Disposal of High-Level Radioactive Wastes in Geologic Repositories*. EPA-520/3-80-006. Washington, D.C.: U.S. Environmental Protection Agency.

Snyder, R. P. 1985. "Dissolution of Halite and Gypsum, and Hydration of Anydrite to Gypsum, Rustler Formation, in the Vicinity of the Waste Isolation Pilot Plant, Southeastern New Mexico," Open-File Report 85-229. Denver, CO: U.S. Geological Survey.

Snyder, R. P., and L. M. Gard. 1982. *Evaluation of Breccia Pipes in Southeastern New Mexico and their Relation to the Waste Isolation Pilot Plant (WIPP) Site*. Open-File Report 82-968. Washington, D.C.: U.S. Geological Survey for the U.S. Department of Energy (Interagency Agreement E (29-2)-3627).

Stormont, J. C. 1988. *Preliminary Seal Design Evaluation for the Waste Isolation Pilot Plant*. SAND87-3083. Albuquerque, NM: Sandia National Laboratories.

Stormont, J. C., E. W. Peterson, and P. L. Lagus. 1987. *Summary of and Observations about WIPP Facility Horizon Flow Measurements through 1986*. SAND87-0176. Albuquerque, NM: Sandia National Laboratories.

Stratton, W. R. 1983. *The Myth of Nuclear Explosions at Waste Disposal Sites*. LA-9360. Los Alamos, NM: Los Alamos National Laboratory.

Sykes, J. F., and N. R. Thomson. 1988. "Parameter Identification and Uncertainty Analysis for Variably Saturated Flow." *Advances in Water Resources* 11: 185-191.

Swift, P. N. 1991a. "Long-Term Climate Variability at the Waste Isolation Pilot Plant," Chapter VII in *Background Information Presented to the Expert Panel on Inadvertent Human Intrusion into the Waste Isolation Pilot Plant*. Eds. R. V. Guzowski and M. M. Gruebel. SAND91-0928. Albuquerque, NM: Sandia National Laboratories. In preparation.

Swift, P. N. 1991b. "Agriculture and Climatic Change at the Waste Isolation Pilot Plant," Chapter VIII in *Background Information Presented to the Expert Panel on Inadvertent Human Intrusion into the Waste Isolation Pilot Plant.* Eds. R. V. Guzowski and M. M. Gruebel. SAND91-0928. Albuquerque, NM: Sandia National Laboratories. In preparation.

Taylor, L. M., D. P. Flanagan, and W. C. Mills-Curran. 1987. *The GENESIS Finite Element Mesh File Format.* SAND86-0910. Albuquerque, NM: Sandia National Laboratories.

Thorne, B. J., and D. K. Rudeen. 1979. *Regional Effects of TRU Repository Heat.* CSI-2053-05. Albuquerque, NM: Civil Systems, Inc.

Tierney, M. S. 1990. *Constructing Probability Distributions of Uncertain Variables in Models of the Performance of the Waste Isolation Pilot Plant.* SAND90-2510. Albuquerque, NM: Sandia National Laboratories.

Tilden, J. W., V. Costanza, G. J. McRae, and J. H. Seinfeld. 1981. "Sensitivity Analysis of Chemically Reacting Systems" in *Modelling of Chemical Reaction Systems.* Eds. K. H. Ebert, P. Deuflhard and W. Jaeger (eds). New York, NY: Springer-Verlag. 69-91.

Tomovic, R., and M. Vukobratovic. 1972. *General Sensitivity Theory.* New York, NY: Elsevier.

Trauth, K. M., R. P. Rechard, and S. C. Hora. 1991. "Expert Judgment as Input to Waste Isolation Pilot Plant Performance Assessment Calculations: Probability Distributions of Significant System Parameters" in *Mixed Waste: Proceedings of the First International Symposium, August 26-29, Baltimore, Maryland.* Eds. A. A. Moghissi and G. A. Benda. American Society of Mechanical Engineers, U.S. Department of Energy, U.S. Environmental Protection Agency, and the University of Maryland

Trusheim, F. 1960. "On the Mechanism of Salt Migration in Northern Germany." *American Association of Petroleum Geologists Bulletin* vol. 44, no. 9: 1519-1540.

Tyler, L. D., R. V. Matalucci, M. A. Molecke, D. E. Munson, E. J. Nowak, and J. C. Stormont. 1988. *Summary Report for the WIPP Technology Development Program for Isolation of Radioactive Waste.* SAND88-0844. Albuquerque, NM: Sandia National Laboratories.

U.S. DOE (Department of Energy). 1979. *Draft Environmental Impact Statement, Management of Commercially Generated Radioactive Waste.* DOE/EIS-0046-D. Washington, DC: U.S. Department of Energy.

U.S. DOE (Department of Energy). 1980a. *Final Environmental Impact Statement: Waste Isolation Pilot Plant.* DOE/EIS-0026. U.S. Department of Energy, October 1980.

U.S. DOE (Department of Energy). 1980b. *Subject: Radioactive Waste Management.* DOE Order 5820.2A, dated September 26, 1988.

U.S. DOE (Department of Energy). 1981. "Waste Isolation Pilot Plant (WIPP); Record of Decision." *Federal Register* **46**: 9162.

U.S. DOE (Department of Energy). 1987. *A Plan for the Implementation of Assurance Requirements in Compliance with 40 CFR Part 191.14 at the Waste Isolation Pilot Plant*. DOE/WIPP 87-016. Carlsbad, NM: U.S. Department of Energy.

U.S. DOE (Department of Energy). 1988. *Geotechnical Field Data and Analysis Report*. DOE-WIPP-87-017. Carlsbad, NM: U.S. Department of Energy.

U.S. DOE (Department of Energy). 1989a. *Waste Isolation Pilot Plant Compliance Strategy for 40 CFR Part 191*. WIPP-DOE-86-013. Carlsbad, NM: U.S. Department of Energy.

U.S. DOE (Department of Energy). 1989b. *Draft Supplement Environmental Impact Statement, Waste Isolation Pilot Plant*. DOE/EIS-0026-DS. Washington, DC: U.S. Department of Energy, Office of Enviromental Restoration and Waste Mmanagement.

U.S. DOE (Department of Energy). 1989c. *Annual Water Quality Data Report, Waste Isolation Pilot Plant*, DOE/WIPP 89-001. Carlsbad, NM: Westinghouse Electric Corporation.

U.S. DOE (Department of Energy). 1990a. *Final WIPP Safety Analysis Report, Waste Isolation Pilot Plant*. Carlsbad, NM: U.S. Department of Energy.

U.S. DOE (Department of Energy). 1990b. *WIPP Test Phase Plan: Performance Assessment*. DOE/WIPP 89-011, Rev. 0. Carlsbad, NM.

U.S. DOE (Department of Energy). 1990c. *Final Supplement Environmental Impact Statement, Waste Isolation Pilot Plant*. DOE/EIS-0026-FS. Washington, DC: U.S. Department of Energy, Office of Environmental Restoration and Waste Management.

U.S. DOE (Department of Energy). 1990d. *Recommended Initial Waste Forms for the WIPP Experimental Test Program, May 1990, Engineered Alternnatives Task Force*. DOE/WIPP 90-009. Carlsbad, NM: Westinghouse Electric Corporation.

U.S. DOE (Department of Energy). 1990e. *Integrated Data Base for 1990: Spent Fuel and Radioactive Waste Inventories, Projects and Characterizations*. DOE/RW-006, Rev. 6.

U.S. DOE (Department of Energy). 1990f. *Waste Isolation Pilot Plant No-Migration Variance Petition*. DOE/WIPP 89-003, Revision 1. Carlsbad, NM: Westinghouse Electric Corporation.

U.S. DOE (Department of Energy). 1991a. *Strategy for the Waste Isolation Pilot Plant Test Phase*. DOE/EM/48063-2. Washington, DC: Office of Waste Operations, U.S. Department of Energy.

U.S. DOE (Department of Energy). 1991b. *Waste Isolation Pilot Plant Test Phase Management Plan*. DOE/WIPP91-015. Carlsbad, NM: U.S. Department of Energy.

U.S. DOE (Department of Energy). 1991c. *Recommended Strategy for the Remote-Handled Transuranic Waste Program*. DOE/WIPP 90-058, Revision 1. Carlsbad, NM: U.S. Department of Energy.

U.S. DOE (Department of Energy). 1991d. *Implementation of the Resource Disincentive in 40 CFR Part 191.14(e) at the Waste Isolation Pilot Plant* DOE/WIPP 91-029. Carlsbad, NM: U.S. Department of Energyy.

U.S. DOE (Department of Energy) and State of New Mexico. 1981, as modified. "Agreement for Consultation and Cooperation" on WIPP by the State of New Mexico and U.S. Department of Energy, modified 11/30/84 and 8/4/87.

U.S. EPA (Environmental Protection Agency). 1984. *Ground-Water Protection Strategy*. Washington, DC: Office of Ground-Water Protection.

U.S. EPA (Environmental Protection Agency). 1985. *Environmental Standards for the Management and Disposal of Spent Nuclear Fuel, High-Level and Transuranic Radioactive Waste; Final Rule*, 40 CFR Part 191, *Federal Register* **50**: 38066-38089.

U.S. NRC (Nuclear Regulatory Commission). 1975. *Reactor Safety Study - An Assessment of Accident Risks in U.S. Commercial Nuclear Power Plants:* U.S. Nuclear Regulatory Commission Rept. WASH-1400, NUREG-75/014. Washington, DC.

U.S. NRC (Nuclear Regulatory Commission). 1990. *Severe Accident Risks: An Assessment forr Five U.S. Nuclear Power Plants*. NUREG-1150. Washington, D.C.: U.S. Nuclear Regulatory Commission.

Uliasz, M. 1985. "Comparison of the Sensitivity Analysis Methods for Meteorological Models." *Zeitschrift fuer Meteorologie* **6**: 340-348.

University of New Mexico. 1989. *New Mexico Statistical Abstract 1989*. Albuquerque, NM: Bureau of Business and Economic Research, University of New Mexico.

Vaughn, P., J. Schreiber and J. Bean. 1991. "The Modeling and Effect of Waste-Generated Gas of Probabilistic System Assessments of the Waste Isolation Pilot Plant" in *Proceedings of NEA Workshop on Gas Generation and Release from Radioactive Waste Repositories, Aix-en-Provence, France. September 23-26, 1991*. In preparation.

Vaughn, W. A. 1982. "Review of the Environmental Analysis for the Cost Reduction Proposals for the Waste Isolation Pilot Plant (WIPP) Project," letter to H. E. Roser, Assistant Secretary for Defense Programs (July 8). Washington, D.C.: Environmental Protection, U.S. Department of Energy.

Vesely, W. E. and D. M. Rasmuson. 1984. "Uncertainties in Nuclear Probabilistic Risk Analyses." *Risk Analysis* 4: 313-322.

Vine, J. D. 1963. "Surface Geology of the Nash Draw Quadrangle, Eddy County, New Mexico." *U.S. Geological Survey Bulletin* 1141-B.

Voss, C. I. 1984. *SUTRA (Saturated-Unsaturated Transport): A Finite-Element Simulation Model for Saturated-Unsaturated, Fluid-Density-Dependent Ground-Water Flow with Energy Transport or Chemically Reactive Single-Species Solute Transport*. Reston, VA. U.S. Geological Survey National Center.

Ward, R. F., C. G. St. C. Kendall, and P. M. Harris. 1986. "Upper Permian (Guadalupian) Facies and Their Association with Hydrocarbons - Permian Basin, West Texas and New Mexico." *American Association of Petroleum Geologists Bulletin* 70: 239-262.

Waste Management Technology Department. 1987. *The Scientific Program at the Waste Isolation Pilot Plant*. SAND85-1699. Albuquerque, NM: Sandia National Laboratories.

Weart, W. D. 1983. *Summary of Evaluation of the Waste Isolation Pilot Plant (WIPP) Site Suitability*. SAND83-0450. Albuquerque, NM: Sandia National Laboratories.

Weatherby, J. R., J. G. Arguello, and C. M. Stone. 1989. "The Effect of Gas Generation on Performance of CH-TRU Disposal Rooms," memorandum to B. M. Butcher (November 14). Albuquerque, NM: Sandia National Laboratories.

Weatherford, R. 1982. *Philosophical Foundations of Probability Theory*. London, UK: Routledge and Kegan Paul, Ltd.

WEC (Westinghouse Electric Corporation). 1989. *Waste Isolation Pilot Plant Underground Facility Plan*. Drawing No. 51-W-032-W, revision C, sheet 1 of 1. Carlsbad, NM: Westinghouse Waste Isolation Division.

WEC (Westinghouse Electric Corporation). 1990. *Final Program Plan for Engineered Alternatives*. April 20, 1990, Carlsbad, New Mexico.

Wheeler, T. A., S. C. Hora, W. R. Cramond, and S. D. Unwin. 1989. *Analysis of Core Damage Frequency: Expert Judgment Elicitation*. NUREG/CR-4550, SAND86-1084, vol. 2, rev. 2. Albuquerque, NM: Sandia National Laboratories.

Williamson, C. R. 1978. "Depositional Processes, Diagenesis and Reservoir Properties of Permian Deep-Sea Sandstone, Bell Canyon Formation." Ph.D. dissertation. University of Texas, Austin, TX.

Winkler, R. L. 1972. *An Introduction to Bayesian Inference and Decision*. New York: Holt, Reinhart and Winston.

Woo, G. 1991. "A Quitting Rule for Monte Carlo Simulation of Extreme Risks." *Reliability Engineering and System Safety* 31: 179-189.

Worley, B. A., and J. E. Horwedel. 1986. *A Waste Package Performance Assessment Code with Automated Sensitivity-Calculation Capability.* ORNL/TM-9976. Oak Ridge, TN: Oak Ridge National Laboratory.

Wu, Y.-T. 1987. "Demonstration of a New, Fast Probability Integration Method for Reliability Analysis." *Journal of Engineering for Industry* **109**: 24-28.

Wu, Y.-T., and P. H. Wirsching. 1987. "New Algorithm for Structural Reliability." *Journal of Engineering for Industry* **113**: 1319-1336.

Wu, Y.-T., H. R. Millwater, and T. A. Cruse. 1990. "Advanced Probabilistic Structural Method for Implicit Performance Functions." *AIAA Journal* **28**: 1663-1669.

Wu, Y. -T., A. G. Journel, L. R. Abramson, and P. K. Nair. 1991. *Uncertainty Evaluation Methods for Waste Package Performance Assessment.* NUREG/CR-5639. Washington, DC: Division of High-Level Waste Management, Office of Nuclear Material Safety and Safeguards, U.S. Nuclear Regulatory Commission.

Zimmerman, D. A., K. K. Wahi, A. L. Gutjahr, and P. A. Davis. 1990. *A Review of Techniques for Propagating Data and Parameter Uncertainties in High-Level Radioactive Waste Repository Performance Models.* NUREG/CR-5393, SAND89-1432. Albuquerque, NM: Sandia National Laboratories.

APPENDIX A:
TITLE 40, CODE OF FEDERAL REGULATIONS, SUBCHAPTER F, PART 191

APPENDIX A:
TITLE 40, CODE OF FEDERAL REGULATIONS
SUBCHAPTER F—RADIATION PROTECTION PROGRAMS

PART 191—ENVIRONMENTAL RADIATION PROTECTION STANDARDS FOR MANAGEMENT AND DISPOSAL OF SPENT NUCLEAR FUEL, HIGH-LEVEL AND TRANSURANIC RADIOACTIVE WASTES

Subpart A—Environmental Standards for Management and Storage

Authority: The Atomic Energy Act of 1954, as amended; Reorganization Plan No. 3 of 1970; and the Nuclear Waste Policy Act of 1982.

Subpart A—Environmental Standards for Management and Storage

§ 191.01 Applicability.

This Subpart applies to:

(a) Radiation doses received by members of the public as a result of the management (except for transportation) and storage of spent nuclear fuel or high-level or transuranic radioactive wastes at any facility regulated by the

Nuclear Regulatory Commission or by Agreement States, to the extent that such management and storage operations are not subject to the provisions of Part 190 of title 40; and

(b) Radiation doses received by members of the public as a result of the management and storage of spent nuclear fuel or high-level or transuranic wastes at any disposal facility that is operated by the Department of Energy and that is not regulated by the Commission or by Agreement States.

§ 191.02 Definitions.

Unless otherwise indicated in this Subpart, all terms shall have the same meaning as in Subpart A of Part 190.

(a) "Agency" means the Environmental Protection Agency.

(b) "Administrator" means the Administrator of the Environmental Protection Agency.

(c) "Commission" means the Nuclear Regulatory Commission.

(d) "Department" means the Department of Energy.

(e) "NWPA" means the Nuclear Waste Policy Act of 1982 (Pub. L. 97-425).

(f) "Agreement State" means any State with which the Commission or the Atomic Energy Commission has entered into an effective agreement under subsection 274b of the Atomic Energy Act of 1954, as amended (68 Stat. 919).

(g) "Spent nuclear fuel" means fuel that has been withdrawn from a nuclear reactor following irradiation, the constituent elements of which have not been separated by reprocessing.

(h) "High-level radioactive waste," as used in this Part, means high-level radioactive waste as defined in the Nuclear Waste Policy Act of 1982 (Pub. L. 97-425).

(i) "Transuranic radioactive waste," as used in this Part, means waste containing more than 100 nanocuries of alpha-emitting transuranic isotopes, with half-lives greater than twenty years, per gram of waste, except for: (1) High-level radioactive wastes; (2) wastes that the Department has determined, with the concurrence of the Administrator, do not need the degree of isolation required by this Part; or (3) wastes that the Commission has approved for disposal on a case-by-case basis in accordance with 10 CFR Part 61.

(j) "Radioactive waste," as used in this Part, means the high-level and transuranic radioactive waste covered by this Part.

(k) "Storage" means retention of spent nuclear fuel or radioactive wastes with the intent and capability to readily retrieve such fuel or waste for subsequent use, processing, or disposal.

(l) "Disposal" means permanent isolation of spent nuclear fuel or radioactive wastes from the accessible environment with no intent of recovery, whether or not such isolation permits the recovery of such fuel or waste. For example, disposal of waste in a mined geologic repository occurs when all of the shafts to the repository are backfilled and sealed.

(m) "Management" means any activity, operation, or process (except for transportation) conducted to prepare spent nuclear fuel or radioactive waste for storage or disposal, or the activities associated with placing such fuel or waste in a disposal system.

(n) "Site" means an area contained within the boundary of a location under the effective control of persons possessing or using spent nuclear fuel or radioactive waste that are involved in any activity, operation, or process covered by this Subpart.

(o) "General environment" means the total terrestrial, atmospheric, and aquatic environments outside sites within which any activity, operation, or process associated with the management and storage of spent nuclear fuel or radioactive waste is conducted.

(p) "Member of the public" means any individual except during the time when that individual is a worker engaged in any activity, operation, or process that is covered by the Atomic Energy Act of 1954, as amended.

(q) "Critical organ" means the most exposed human organ or tissue exclusive of the integumentary system (skin) and the cornea.

§ 191.03 Standards.

(a) Management and storage of spent nuclear fuel or high-level or transuranic radioactive wastes at all facilities regulated by the Commission or by Agreement States shall be conducted in such a manner as to provide reasonable assurance that the combined annual dose equivalent to any member of the public in the general environment resulting from: (1) Discharges of radioactive material and direct radiation from such management and storage and (2) all operations covered by Part 190; shall not exceed 25 millirems to the

whole body, 75 millirems to the thyroid, and 25 millirems to any other critical organ.

(b) Management and storage of spent nuclear fuel or high-level or transuranic radioactive wastes at all facilities for the disposal of such fuel or waste that are operated by the Department and that are not regulated by the Commission or Agreement States shall be conducted in such a manner as to provide reasonable assurance that the combined annual dose equivalent to any member of the public in the general environment resulting from discharges of radioactive material and direct radiation from such management and storage shall not exceed 25 millirems to the whole body and 75 millirems to any critical organ.

§ 191.04 Alternative standards.

(a) The Administrator may issue alternative standards from those standards established in 191.03(b) for waste management and storage activities at facilities that are not regulated by the Commission or Agreement States if, upon review of an application for such alternative standards:

(1) The Administrator determines that such alternative standards will prevent any member of the public from receiving a continuous exposure of more than 100 millirems per year dose equivalent and an infrequent exposure of more than 500 millirems dose equivalent in a year from all sources, excluding natural background and medical procedures; and

(2) The Administrator promptly makes a matter of public record the degree to which continued operation of the facility is expected to result in levels in excess of the standards specified in 191.03(b).

(b) An application for alternative standards shall be submitted as soon as possible after the Department determines that continued operation of a facility will exceed the levels specified in 191.03(b) and shall include all information necessary for the Administrator to make the determinations called for in 191.04(a).

(c) Requests for alternative standards shall be submitted to the Administrator, U.S. Environmental Protection Agency, 401 M Street, SW., Washington, DC 20460.

§ 191.05 Effective date.

The standards in this Subpart shall be effective on November 18, 1985.

Subpart B—Environmental Standards for Disposal

§ 191.11 Applicability.

(a) This Subpart applies to:

(1) Radioactive materials released into the accessible environment as a result of the disposal of spent nuclear fuel or high-level or transuranic radioactive wastes;

(2) Radiation doses received by members of the public as a result of such disposal; and

(3) Radioactive contamination of certain sources of ground water in the vicinity of disposal systems for such fuel or wastes.

(b) However, this Subpart does not apply to disposal directly into the oceans or ocean sediments. This Subpart also does not apply to wastes disposed of before the effective date of this rule.

§ 191.12 Definitions.

Unless otherwise indicated in this Subpart, all terms shall have the same meaning as in Subpart A of this Part.

(a) "Disposal system" means any combination of engineered and natural barriers that isolate spent nuclear fuel or radioactive waste after disposal.

(b) "Waste," as used in this Subpart, means any spent nuclear fuel or radioactive waste isolated in a disposal system.

(c) "Waste form" means the materials comprising the radioactive components of waste and any encapsulating or stabilizing matrix.

(d) "Barrier" means any material or structure that prevents or substantially delays movement of water or radionuclides toward the accessible environment. For example, a barrier may be a geologic structure, a canister, a waste form with physical and chemical characteristics that significantly decrease the mobility of radionuclides, or a material placed over and around waste, provided that the material or structure substantially delays movement of water or radionuclides.

(e) "Passive institutional control" means: (1) Permanent markers placed at a disposal site, (2) public records and archives, (3) government ownership and regulations regarding land or resource use, and (4) other methods of preserving knowledge about the location, design, and contents of a disposal system.

(f) "Active institutional control" means: (1) Controlling access to a disposal site by any means other than passive institutional controls; (2) performing maintenance operations or remedial actions at a site, (3) controlling or cleaning up releases from a site, or (4) monitoring parameters related to disposal system performance.

(g) "Controlled area" means: (1) A surface location, to be identified by passive institutional controls, that encompasses no more than 100 square kilometers and extends horizontally no more than five kilometers in any direction from the outer boundary of the original location of the radioactive wastes in a disposal system; and (2) the subsurface underlying such a surface location.

(h) "Ground water" means water below the land surface in a zone of saturation.

(i) "Aquifer" means an underground geological formation, group of formations, or part of a formation that is capable of yielding a significant amount of water to a well or spring.

(j) "Lithosphere" means the solid part of the Earth below the surface, including any ground water contained within it.

(k) "Accessible environment" means: (1) The atmosphere; (2) land surfaces; (3) surface waters; (4) oceans; and (5) all of the lithosphere that is beyond the controlled area.

(l) "Transmissivity" means the hydraulic conductivity integrated over the saturated thickness of an underground formation. The transmissivity of a series of formations is the sum of the individual transmissivities of each formation comprising the series.

(m) "Community water system" means a system for the provision to the public of piped water for human consumption, if such system has at least 15 service connections used by year-round residents or regularly serves at least 25 year-round residents.

(n) "Significant source of ground water," as used in this Part, means: (1) An aquifer that: (i) Is saturated with water having less than 10,000 milligrams per liter of total dissolved solids; (ii) is within 2,500 feet of the land surface; (iii) has a transmissivity greater than 200 gallons per day per foot, provided that any formation or part of a formation included within the source of ground water has a hydraulic conductivity greater than 2 gallons per day per square foot; and (iv) is capable of continuously yielding at least 10,000 gallons per day to a pumped or flowing well for a period of at least a

year; or (2) an aquifer that provides the primary source of water for a community water system as of the effective date of this Subpart.

(o) "Special source of ground water," as used in this Part, means those Class I ground waters identified in accordance with the Agency's Ground-Water Protection Strategy published in August 1984 that: (1) Are within the controlled area encompassing a disposal system or are less than five kilometers beyond the controlled area; (2) are supplying drinking water for thousands of persons as of the date that the Department chooses a location within that area for detailed characterization as a potential site for a disposal system (e.g., in accordance with Section 112(b)(1)(B) of the NWPA); and (3) are irreplaceable in that no reasonable alternative source of drinking water is available to that population.

(p) "Undisturbed performance" means the predicted behavior of a disposal system, including consideration of the uncertainties in predicted behavior, if the disposal system is not disrupted by human intrusion or the occurrence of unlikely natural events.

(q) "Performance assessment" means an analysis that: (1) Identifies the processes and events that might affect the disposal system; (2) examines the effects of these processes and events on the performance of the disposal system; and (3) estimates the cumulative releases of radionuclides, considering the associated uncertainties, caused by all significant processes and events. These estimates shall be incorporated into an overall probability distribution of cumulative release to the extent practicable.

(r) "Heavy metal" means all uranium, plutonium, or thorium placed into a nuclear reactor.

(s) "Implementing agency," as used in this Subpart, means the Commission for spent nuclear fuel or high-level or transuranic wastes to be disposed of in facilities licensed by the commission in accordance with the Energy Reorganization Act of 1974 and the Nuclear Waste Policy Act of 1982, and it means the Department for all other radioactive wastes covered by this Part.

§ 191.13 Containment requirements.

(a) Disposal systems for spent nuclear fuel or high-level or transuranic radioactive wastes shall be designed to provide a reasonable expectation, based upon performance assessments, that cumulative releases of radionuclides to the accessible environment for 10,000 years after disposal from all significant processes and events that may affect the disposal system shall:

(1) Have a likelihood of less than one chance in 10 of exceeding the quantities calculated according to Table 1 (Appendix A); and

(2) Have a likelihood of less than one chance in 1,000 of exceeding ten times the quantities calculated according to Table 1 (Appendix A).

(b) Performance assessments need not provide complete assurance that the requirements of 191.13(a) will be met. Because of the long time period involved and the nature of the events and processes of interest, there will inevitably be substantial uncertainties in projecting disposal system performance. Proof of the future performance of a disposal system is not to be had in the ordinary sense of the word in situations that deal with much shorter time frames. Instead, what is required is a reasonable expectation, on the basis of the record before the implementing agency, that compliance with 191.13(a) will be achieved.

§ 191.14 Assurance requirements.

To provide the confidence needed for long-term compliance with the requirements of 191.13, disposal of spent nuclear fuel or high-level or transuranic wastes shall be conducted in accordance with the following provisions, except that these provisions do not apply to facilities regulated by the Commission (see 10 CFR Part 60 for comparable provisions applicable to facilities regulated by the Commission):

(a) Active institutional controls over disposal sites should be maintained for as long a period of time as is practicable after disposal; however, performance assessments that assess isolation of the wastes from the accessible environment shall not consider any contributions from active institutional controls for more than 100 years after disposal.

(b) Disposal systems shall be monitored after disposal to detect substantial and detrimental deviations from expected performance. This monitoring shall be done with techniques that do not jeopardize the isolation of the wastes and shall be conducted until there are no significant concerns to be addressed by further monitoring.

(c) Disposal sites shall be designated by the most permanent markers, records, and other passive institutional controls practicable to indicate the dangers of the wastes and their location.

(d) Disposal systems shall use different types of barriers to isolate the wastes from the accessible environment. Both engineered and natural barriers shall be included.

(e) Places where there has been mining for resources, or where there is a reasonable expectation of exploration for scarce or easily accessible resources, or where there is a significant concentration of any material that is not widely available from other sources, should be avoided in selecting disposal sites. Resources to be considered shall include minerals, petroleum or natural gas, valuable geologic formations, and ground waters that are either irreplaceable because there is no reasonable alternative source of drinking water available for substantial populations or that are vital to the preservation of unique and sensitive ecosystems. Such places shall not be used for disposal of the wastes covered by this Part unless the favorable characteristics of such places compensate for their greater likelihood of being disturbed in the future.

(f) Disposal systems shall be selected so that removal of most of the wastes is not precluded for a reasonable period of time after disposal.

§ 191.15 Individual protection requirements.

Disposal systems for spent nuclear fuel or high-level or transuranic radioactive wastes shall be designed to provide a reasonable expectation that, for 1,000 years after disposal, undisturbed performance of the disposal system shall not cause the annual dose equivalent from the disposal system to any member of the public in the accessible environment to exceed 25 millirems to the whole body or 75 millirems to any critical organ. All potential pathways (associated with undisturbed performance) from the disposal system to people shall be considered, including the assumption that individuals consume 2 liters per day of drinking water from any significant source of ground water outside of the controlled area.

§ 191.16 Ground water protection requirements.

(a) Disposal systems for spent nuclear fuel or high-level or transuranic radioactive wastes shall be designed to provide a reasonable expectation that, for 1,000 years after disposal, undisturbed performance of the disposal system shall not cause the radionuclide concentrations averaged over any year in water withdrawn from any portion of a special source of ground water to exceed:

(1) 5 picocuries per liter of radium-226 and radium-228;

(2) 15 picocuries per liter of alpha-emitting radionuclides (including radium-226 and radium-228 but excluding radon); or

(3) The combined concentrations of radionuclides that emit either beta or gamma radiation that would produce an annual dose equivalent to the total body or any internal organ greater than 4 millirems per year if an individual

consumed 2 liters per day of drinking water from such a source of ground water.

(b) If any of the average annual radionuclide concentrations existing in a special source of ground water before construction of the disposal system already exceed the limits in 191.16(a), the disposal system shall be designed to provide a reasonable expectation that, for 1,000 years after disposal, undisturbed performance of the disposal system shall not increase the existing average annual radionuclide concentrations in water withdrawn from that special source of ground water by more than the limits established in 191.16(a).

§ 191.17 Alternative provisions for disposal.

The Administrator may, by rule, substitute for any of the provisions of Subpart B alternative provisions chosen after:

(a) The alternative provisions have been proposed for public comment in the Federal Register together with information describing the costs, risks, and benefits of disposal in accordance with the alternative provisions and the reasons why compliance with the existing provisions of Subpart B appears inappropriate;

(b) A public comment period of at least 90 days has been completed, during which an opportunity for public hearings in affected areas of the country has been provided; and

(c) The public comments received have been fully considered in developing the final version of such alternative provisions.

§ 191.18 Effective date.

The standards in this Subpart shall be effective on November 18, 1985.

Appendix A—Table for Subpart B

TABLE 1.—RELEASE LIMITS FOR CONTAINMENT REQUIREMENTS

(Cumulative releases to the accessible environment for 10,000 years after disposal)

Radionuclide	Release limit per 1,000 MTHM or other unit of waste (see notes) (curies)
Americium-241 or -243	100
Carbon-14	100
Cesium-135 or -137	1,000
Iodine-129	100
Neptunium-237	100
Plutonium-238, -239, -240, or -242	100
Radium-226	100
Strontium-90	1,000
Technetium-99	10,000
Thorium-230 or -232	10
Tin-126	1,000
Uranium-233, -234, -235, -236, or -238	100
Any other alpha-emitting radionuclide with a half-life greater than 20 years	100
Any other radionuclide with a half-life greater than 20 years that does not emit alpha particles	1,000

Application of Table 1

Note 1: *Units of Waste.* The Release Limits in Table 1 apply to the amount of wastes in any one of the following:

(a) An amount of spent nuclear fuel containing 1,000 metric tons of heavy metal (MTHM) exposed to a burnup between 25,000 megawatt-days per metric ton of heavy metal (MWd/MTHM) and 40,000 MWd/MTHM;

(b) The high-level radioactive wastes generated from reprocessing each 1,000 MTHM exposed to a burnup between 25,000 MWd/MTHM and 40,000 MWd/MTHM;

(c) Each 100,000,000 curies of gamma or beta-emitting radionuclides with half-lives greater than 20 years but less than 100 years (for use as discussed in Note 5 or with materials that are identified by the Commission as high-level radioactive waste in accordance with part B of the definition of high-level waste in the NWPA);

(d) Each 1,000,000 curies of other radionuclides (i.e., gamma or beta-emitters with half-lives greater than 100 years or any alpha-emitters with half-lives greater than 20 years) (for use as discussed in Note 5 or with materials that are identified by the Commission as high-level radioactive waste in accordance with part B of the definition of high-level waste in the NWPA); or

(e) An amount of transuranic (TRU) wastes containing one million curies of alpha-emitting transuranic radionuclides with half-lives greater than 20 years.

Note 2: *Release Limits for Specific Disposal Systems.* To develop Release Limits for a particular disposal system, the quantities in Table 1 shall be adjusted for the amount of waste included in the disposal system compared to the various units of waste defined in Note 1. For example:

(a) If a particular disposal system contained the high-level wastes from 50,000 MTHM, the Release Limits for that system would be the quantities in Table 1 multiplied by 50 (50,000 MTHM divided by 1,000 MTHM).

(b) If a particular disposal system contained three million curies of alpha-emitting transuranic wastes, the Release Limits for that system would be the quantities in Table 1 multiplied by three (three million curies divided by one million curies).

(c) If a particular disposal system contained both the high-level wastes from 50,000 MTHM and 5 million curies of alpha-emitting transuranic wastes, the Release Limits for that system would be the quantities in Table 1 multiplied by 55:

$$\frac{50{,}000 \text{ MTHM}}{1{,}000 \text{ MTHM}} + \frac{5{,}000{,}000 \text{ curies TRU}}{1{,}000{,}000 \text{ curies TRU}} = 55$$

Note 3: *Adjustments for Reactor Fuels with Different Burnup.* For disposal systems containing reactor fuels (or the high-level wastes from reactor fuels) exposed to an average burnup of less than 25,000 MWd/MTHM or greater than 40,000 MWd/MTHM, the units of waste defined in (a) and (b) of Note 1 shall be adjusted. The unit shall be multiplied by the ratio of 30,000 MWd/MTHM divided by the fuel's actual average burnup, except that a value of 5,000

MWd/MTHM may be used when the average fuel burnup is below 5,000 MWd/MTHM and a value of 100,000 MWd/MTHM shall be used when the average fuel burnup is above 100,000 MWd/MTHM. This adjusted unit of waste shall then be used in determining the Release Limits for the disposal system.

For example, if a particular disposal system contained only high-level wastes with an average burnup of 3,000 MWd/MTHM, the unit of waste for that disposal system would be:

$$1{,}000 \text{ MTHM} \times \frac{(30{,}000)}{(5{,}000)} = 6{,}000 \text{ MTHM}$$

If that disposal system contained the high-level wastes from 60,000 MTHM (with an average burnup of 3,000 MWd/MTHM), then the Release Limits for that system would be the quantities in Table 1 multiplied by ten:

$$\frac{60{,}000 \text{ MTHM}}{6{,}000 \text{ MTHM}} = 10$$

which is the same as:

$$\frac{60{,}000 \text{ MTHM}}{1{,}000 \text{ MTHM}} \times \frac{(5{,}000 \text{ MWd/MTHM})}{(30{,}000 \text{ MWd/MTHM})} = 10$$

Note 4: *Treatment of Fractionated High-Level Wastes.* In some cases, a high-level waste stream from reprocessing spent nuclear fuel may have been (or will be) separated into two or more high-level waste components destined for different disposal systems. In such cases, the implementing agency may allocate the Release Limit multiplier (based upon the original MTHM and the average fuel burnup of the high-level waste stream) among the various disposal systems as it chooses, provided that the total Release Limit multiplier used for that waste stream at all of its disposal systems may not exceed the Release Limit multiplier that would be used if the entire waste stream were disposed of in one disposal system.

Note 5: *Treatment of Wastes with Poorly Known Burnups or Original MTHM.* In some cases, the records associated with particular high-level waste streams may not be adequate to accurately determine the original metric tons of heavy metal in the reactor fuel that created the waste, or to determine the average burnup that the fuel was exposed to. If the uncertainties are such that the original amount of heavy metal or the average fuel burnup for particular high-level waste streams cannot be quantified, the units of waste derived from (a) and (b) of Note 1 shall no longer be used. Instead, the units of waste defined in (c) and (d) of Note 1 shall be used for such high-level waste streams. If the uncertainties in such information allow a range of values to be associated with the original amount of heavy metal or the average fuel

burnup, then the calculations described in previous Notes will be conducted using the values that result in the smallest Release Limits, except that the Release Limits need not be smaller than those that would be calculated using the units of waste defined in (c) and (d) of Note 1.

Note 6: *Uses of Release Limits to Determine Compliance with 191.13.* Once release limits for a particular disposal system have been determined in accordance with Notes 1 through 5, these release limits shall be used to determine compliance with the requirements of 191.13 as follows. In cases where a mixture of radionuclides is projected to be released to the accessible environment, the limiting values shall be determined as follows: For each radionuclide in the mixture, determine the ratio between the cumulative release quantity projected over 10,000 years and the limit for that radionuclide as determined from Table 1 and Notes 1 through 5. The sum of such ratios for all the radionuclides in the mixture may not exceed one with regard to 191.13(a)(1) and may not exceed ten with regard to 191.13(a)(2).

For example, if radionuclides A, B, and C are projected to be released in amounts Q_a, Q_b, and Q_c, and if the applicable Release Limits are RL_a, RL_b, RL_c, then the cumulative releases over 10,000 years shall be limited so that the following relationship exists:

$$\frac{Q_a}{RL_a} + \frac{Q_b}{RL_b} + \frac{Q_c}{RL_c} < 1$$

Appendix B—Guidance for Implementation of Subpart B

[Note: The supplemental information in this appendix is not an integral part of 40 CFR Part 191. Therefore, the implementing agencies are not bound to follow this guidance. However, it is included because it describes the Agency's assumptions regarding the implementation of Subpart B. This appendix will appear in the Code of Federal Regulations.]

The Agency believes that the implementing agencies must determine compliance with §§ 191.13, 191.15, and 191.16 of Subpart B by evaluating long-term predictions of disposal system performance. Determining compliance with § 191.13 will also involve predicting the likelihood of events and processes that may disturb the disposal system. In making these various predictions, it will be appropriate for the implementing agencies to make use of rather complex computational models, analytical theories, and prevalent expert judgment relevant to the numerical predictions. Substantial uncertainties are likely to be encountered in making these predictions. In fact, sole reliance on these numerical predictions to determine compliance may not be appropriate; the implementing agencies may choose to supplement such predictions with

qualitative judgments as well. Because the procedures for determining compliance with Subpart B have not been formulated and tested yet, this appendix to the rule indicates the Agency's assumptions regarding certain issues that may arise when implementing §§ 191.13, 191.15, and 191.16. Most of this guidance applies to any type of disposal system for the wastes covered by this rule. However, several sections apply only to disposal in mined geologic repositories and would be inappropriate for other types of disposal systems.

Consideration of Total Disposal System. When predicting disposal system performance, the Agency assumes that reasonable projections of the protection expected from all of the engineered and natural barriers of a disposal system will be considered. Portions of the disposal system should not be disregarded, even if projected performance is uncertain, except for portions of the system that make negligible contributions to the overall isolation provided by the disposal system.

Scope of Performance Assessments. Section 191.13 requires the implementing agencies to evaluate compliance through performance assessments as defined in § 191.12(q). The Agency assumes that such performance assessments need not consider categories of events or processes that are estimated to have less than one chance in 10,000 of occurring over 10,000 years. Furthermore, the performance assessments need not evaluate in detail the releases from all events and processes estimated to have a greater likelihood of occurrence. Some of these events and processes may be omitted from the performance assessments if there is a reasonable expectation that the remaining probability distribution of cumulative releases would not be significantly changed by such omissions.

Compliance with Section 191.13. The Agency assumes that, whenever practicable, the implementing agency will assemble all of the results of the performance assessments to determine compliance with § 191.13 into a "complementary cumulative distribution function" that indicates the probability of exceeding various levels of cumulative release. When the uncertainties in parameters are considered in a performance assessment, the effects of the uncertainties considered can be incorporated into a single such distribution function for each disposal system considered. The Agency assumes that a disposal system can be considered to be in compliance with § 191.13 if this single distribution function meets the requirements of § 191.13(a).

Compliance with Sections 191.15 and 191.16. When the uncertainties in undisturbed performance of a disposal system are considered, the implementing agencies need not require that a very large percentage of the range of estimated radiation exposures or radionuclide concentrations fall below limits established in §§ 191.15 and 191.16, respectively. The Agency assumes that

compliance can be determined based upon "best estimate" predictions (e.g., the mean or the median of the appropriate distribution, whichever is higher).

Institutional Controls. To comply with § 191.14(a), the implementing agency will assume that none of the active institutional controls prevent or reduce radionuclide releases for more than 100 years after disposal. However, the Federal Government is committed to retaining ownership of all disposal sites for spent nuclear fuel and high-level and transuranic radioactive wastes and will establish appropriate markers and records, consistent with § 191.14(c). The Agency assumes that, as long as such passive institutional controls endure and are understood, they: (1) can be effective in deterring systematic or persistent exploitation of these disposal sites; and (2) can reduce the likelihood of inadvertent, intermittent human intrusion to a degree to be determined by the implementing agency. However, the Agency believes that passive institutional controls can never be assumed to eliminate the chance of inadvertent and intermittent human intrusion into these disposal sites.

Consideration of Inadvertent Human Intrusion into Geologic Repositories. The most speculative potential disruptions of a mined geologic repository are those associated with inadvertent human intrusion. Some types of intrusion would have virtually no effect on a repository's containment of waste. On the other hand, it is possible to conceive of intrusions (involving widespread societal loss of knowledge regarding radioactive wastes) that could result in major disruptions that no reasonable repository selection or design precautions could alleviate. The Agency believes that the most productive consideration of inadvertent intrusion concerns those realistic possibilities that may be usefully mitigated by repository design, site selection, or use of passive controls (although passive institutional controls should not be assumed to completely rule out the possibility of intrusion). Therefore, inadvertent and intermittent intrusion by exploratory drilling for resources (other than any provided by the disposal system itself) can be the most severe intrusion scenario assumed by the implementing agencies. Furthermore, the implementing agencies can assume that passive institutional controls or the intruders' own exploratory procedures are adequate for the intruders to soon detect, or be warned of, the incompatibility of the area with their activities.

Frequency and Severity of Inadvertent Human Intrusion into Geologic Repositories. The implementing agencies should consider the effects of each particular disposal system's site, design, and passive institutional controls in judging the likelihood and consequences of such inadvertent exploratory drilling. However, the Agency assumes that the likelihood of such inadvertent and intermittent drilling need not be taken to be greater than 30 boreholes

per square kilometer of repository area per 10,000 years for geologic repositories in proximity to sedimentary rock formations, or more than 3 boreholes per square kilometer per 10,000 years for repositories in other geologic formations. Furthermore, the Agency assumes that the consequences of such inadvertent drilling need not be assumed to be more severe than: (1) Direct release to the land surface of all the ground water in the repository horizon that would promptly flow through the newly created borehole to the surface due to natural lithostatic pressure—or (if pumping would be required to raise water to the surface) release of 200 cubic meters of ground water pumped to the surface if that much water is readily available to be pumped; and (2) creation of ground water flow path with a permeability typical of a borehole filled by the soil or gravel that would normally settle into an open hole over time—not the permeability of a carefully sealed borehole.

APPENDIX B:
RESPONSE TO REVIEW COMMENTS

APPENDIX B: RESPONSE TO REVIEW COMMENTS

Comments in this appendix relate to SAND90-2347, *Preliminary Comparison with CFR Part 191, Subpart B for the Waste Isolation Pilot Plant, December 1990.* Responses relate to SAND91-0893, the 1991 version of SAND90-2347.

Response to Comments from New Mexico Environment Department

COMMENT 1. Page I-6, first paragraph: 2000 m equals 6560 feet.

RESPONSE: Metrication error has been corrected.

COMMENT 2. Page I-30, sixth paragraph: How important is it that the Rustler formation includes hydrostratigraphic units that provide potential pathways for radionuclide migration away from the WIPP, with so much halite of the Salado formation to cross?

RESPONSE: The Culebra Dolomite in the Rustler Formation is the primary water-producing unit between the waste panels and the surface. Although the thickness of the bedded salt between the panels and the Culebra would be expected to act as a barrier to radionuclides migrating to the Rustler, the shafts and exploratory boreholes will provide possible pathways through the salt for waste in the panels to reach the overlying units. Because of these possible pathways through the salt, possible transportation pathways within the Rustler Formation must be considered.

COMMENT 3. Page III-34: What is the meaning of CCDFs crossing the Containment Requirement?

RESPONSE: A CCDF that extends to the right of the line labeled "Containment Requirement" (see Figure 3-9 in Volume 1 of SAND91-0893) indicates that for one (or more) scenarios S_i analyzed the pair (S) ($pS_i(\mathbf{x}_k)$, cS_i ($\mathbf{x}_k$)) lies beyond the EPA limits of (0.1, 1.0) and (0.001, 10.0) for the specific sample element, $\mathbf{x}_k$.

Since the parameter values in the sample element, $\mathbf{x}_k$, are not known to be correct with certainty, the full family of CCDFs must be considered. Mean and percentile curves, e.g., median, (see Figure 3-10, Volume 1 of SAND91-0893) are suitable summary curves for comparison to the requirement.

For example, if the 90% quantile curve lies to the left of the Containment Requirement, then compliance is indicated with at least a 90% level-of-confidence conditional on the assumed conceptual and mathematical models, the assigned ranges and distributions for uncertain parameters, the scenarios, and all other assumptions used in the analyses, as discussed in Chapter 6, Volume 1 of SAND91-0893.

COMMENT 4. Page V-18, last paragraph: What method was used to convert darcies into m/s? A darcy is a unit of permeability (m^2) while m/s is a unit of conductivity.

RESPONSE: The conversion was based on Table 2.3 (Conversion Factors for Permeability and Hydraulic Conductivity Units) in *Groundwater* by R. A. Freeze and J. A. Cherry (1979).

COMMENT 5. Page V-74, second paragraph: The decay product of Radium-226 is Radon-222 (not 226) with a half-life of 3.825 days.

RESPONSE: The correction has been made.

COMMENT 6. Page VI-6, Table VI-1: Bulk Shear Stress 1 to 5 Pa?? MPa maybe.

RESPONSE: As more carefully explained in Volume 3, Section 3.4 of SAND91-0893, this effective shear stress of the waste equals the fluid stress at which sediment movement (erosion) from a bed of clay particles is general. It is smaller by several orders of magnitude from the macroscopic soil shear strength, and in the absence of real data for waste materials, is used as a conservative estimate.

COMMENT 7. Page VI-17: Abscissa should read: 10^{-15} m^2 and 10^{-13} m^2.

RESPONSE: The errors in the figure have been noted. This figure is not repeated in SAND91-0893.

COMMENT 8. Page VI-18: Time should read Time*10^3 years.

RESPONSE: The errors in the figure have been noted. This figure is not repeated in SAND91-0893.

COMMENT 9. Page VI-27: Distance should read Distance*10^3 m?

RESPONSE: The labeling errors in Figures VI-11 and VI-12 have been noted. These figures are not repeated in SAND91-0893.

Response to Comments from the Environmental Evaluation Group

COMMENT 1. Abstract (i - ii): The abstract clearly elucidates areas of uncertainty in performance assessment of the WIPP for compliance with 40 CFR Part 191, Subpart B:

a. sensitivity analysis and parameter distribution determinations;

b. construction of mean CCDF curves for scenarios included within the analysis from families of curves resulting from Latin Hypercube sampling of parameter distributions;

c. a significant increase in retardation factors due to clay-lined fractures and assumption of a dual-porosity model;

d. the effects of gas generation in the repository on brine flow and radionuclide transport and the preliminary nature of their use in performance assessment.

However, an equally important area of uncertainty not mentioned in the abstract is scenario probability assignments which have considerable influence on CCDF formulation, not only because there are significant differences in assignments between investigators, but also because they have been utilized deterministically in this PA analyses, and have significant impact on the ordinate of the CCDF curves. Also, there appears to have been a significant reduction of radionuclide release to the ground surface from human intrusion boreholes, notwithstanding scenario probability assignments, and this topic should merit attention in the abstract.

RESPONSE: These points should have been summarized in the abstract for SAND90-2347. The abstracts for the volumes of SAND91-0893 will be overviews of significant information contained in the volumes.

COMMENT 2. Page ES-3, Lines 10-13: It is stated that the "mean" CCDF's produced by this analysis are within the EPA limits. It would be equally important to note how many of the Latin Hypercube Samples (LHS) utilized in these analyses exceeded the EPA limits, and/or an exceedance frequency reported. A reported mean CCDF without a variance estimate does not convey this equally important type of information.

RESPONSE: This point was illustrated in examples of families of CCDFs in Chapter III of SAND90-2347. The subject is discussed in Volume 1, Chapter 3 of SAND91-0893 and is also illustrated in the figures in Chapter 6 of Volume 1.

COMMENT 3. Page ES-4, Lines 18-24: Whereas it is understandable that climatic change (TC) has not been incorporated into the model as part of the base case scenario at this time, the reason for exclusion of subsidence to the surface (TS) associated with potash mining is not clearly stated. Subsidence was assigned a probability of 0.05 ([Marietta et al., 1989] SAND89-2027, p. IV-46) based on the fact that it has been observed in the Delaware Basin, although it was not utilized in the methodological demonstration. It would appear that the main reason for excluding it from scenario development is that this type of event has yet to be incorporated into the modeling scheme because its effect on the Rustler Formation has not been fully conceptualized.

RESPONSE: Consequences of subsidence associated with potash mining have not been included in either the 1990 or 1991 preliminary performance assessments because, as the comment notes, "its effect on the Rustler Formation has not been fully conceptualized." Subsidence has not been excluded from scenario development, and its effects will be included in future consequence modeling.

A preliminary estimate of the effects of climatic change is included in the 1991 calculations, and will be refined and developed further in future analyses. The approach used to model the effects of subsidence may be analogous to that used in 1991 to approximate effects of climatic change.

COMMENT 4. Page I-6, Line 6: Conversion error ... about 2000 m (1,250 ft) ...

RESPONSE: Metrication error has been corrected.

COMMENT 5. Page I-38, Lines 39-40: Why was the 1987 IDB [U.S. DOE, 1987] used instead of the 1990 IDB (October 1990) [U.S. DOE, 1990a] for currently projected total radionuclide inventories by generator facility for CH and RH-TRU wastes?

RESPONSE: The CH radionuclide inventory was based on a draft of a Westinghouse report that used input to the 1987 IDB. This report had not been updated to include 1990 IDB input but was considered to be the best available CH radionuclide inventory. The RH radionuclide inventory was based on the 1990 IDB input as discussed in SAND89-2408, *Data Used in Preliminary Performance Assessment of the Waste Isolation Pilot Plant (1990)* (Rechard et al., 1990). The CH and RH radionuclide inventory in SAND89-2408, which differ somewhat from the values on Page I-38, Lines 13 to 26, were used in the analyses. The CH and RH radionuclide inventory for the 1991 analyses are based on input to the 1990 IDB.

COMMENT 6. Page II-3, Lines 22-26; Page II-11, Lines 1-4: The statement that inadvertent intrusion into the repository will lead to its detection goes beyond the guidance in the 1985 Standard and in Working Draft #3 which says "to soon detect, or be warned of, the incompatibility of the area with their activities." The thrust of their guidance seems to be that only inadvertent and intermittent intrusion need be considered, not persistent intrusion or exploitation of natural resources. Also, from a performance assessment (PA) point of view, the time interval before detection (and consequent borehole plugging) is important for some intrusion scenarios in ameliorating releases to the surface. In fact the E1 scenario depends on non-detection in the time interval it requires to reach the pressurized brine in the Castile Formation.

RESPONSE: The synopsis and text have been revised in Volume 1, Chapter 2 of SAND91-0893 to address this comment. The specific sentence in question, which was not consistent with the 1990 calculations, is not included in the 1991 report.

COMMENT 7. Page II-3, Lines 36-42; Page II-12, Lines 10-17: The statement about artificially reducing allowable releases by a factor of almost 3 suggests a misunderstanding of the EPA release limits. These rounded release limits relate to the radiological hazard of the radionuclide. Alpha-emitting transuranic elements have a higher hazard than shorter lived alpha-emitters or plutonium-241 (which is a beta emitter) and thus have a lower release limit. It is correct that some short-lived radionuclides decay to "regulated" daughter products but at a much lower curie level. For example a curie of Pu-241 will produce only 0.034 Ci of Americium-241 in its lifetime (and the maximum activity at any time would be 0.030 Ci). The inclusion of ingrowth Am-241 would increase the WIPP alpha-TRU inventory by only about 2.5%.

RESPONSE: The information in these paragraphs is no longer valid for the WIPP. Updated information is included in Volume 1, Chapter 1 of SAND91-0893.

COMMENT 8. Pages II-4 and 5, Lines 41, 45 and Lines 1-7; Page II-16, Lines 9-15: In light of the feeling that there is "reasonable confidence" that WIPP will meet the Standard, what is the purpose of this section for this report? Who is going to determine what "good isolation" means, and how will the restrictiveness of the requirements be evaluated, and by whom (EPA, DOE, ...)?

RESPONSE: This section was included to provide a complete overview of the Containment Requirements and is not intended to imply that the requirements will be modified. The EPA does not indicate who would make such determinations.

COMMENT 9. Page II-10, Lines 20-21: The statement that mining for resources need not be considered within the controlled area appears to be consistent with EPA guidance but it should be recognized that this may not be a conservative assumption for potash mining. In cases involving exploration for potash in the McNutt zone of the Salado Formation, no encounter with waste would occur and the prevention of exploitation would have to depend solely on passive institutional markers in the long term. This report references Hunter (SAND89-2546, 1989) which discusses a scenario involving solution mining of potash. This author states that Kaplan (ONWI-354, 1982) suggests that well designed markers supplemented by written records can be expected to last for 5,000 years and possibly 10,000 years. Kaplan, however, states that suitable stone markers such as exhibited by ancient monuments have survived in a variety of climates for up to 5,000 years (p. 49). In addition, the only reference to a 10,000 year marker survivability (except for the abstract) is with reference to marble and limestone markers (p. 43) which are not sufficiently durable for this period given the present levels of atmospheric pollution; and that markers constructed of modern metals such as titanium (p. 55) are not likely to survive this period of time because of recycling activities by Man. Also, this author states that about one-third to one-half of Stonehenge construction stone has been removed since it was built (p. 29). The phrase "very likely to survive 10,000 years" presented in the abstract of this report is nowhere substantiated in the report. Therefore, the exclusion of solution mining, and consequent subsidence scenario (TS) over the controlled area is seemingly not strongly supported by the Kaplan (1982) study for a 10,000 year period.

RESPONSE: The events and processes considered for scenario development have been rescreened in the 1991 report. Potash mining has been retained for further evaluation. Following the guidance in the Standard, future mining within the controlled area is excluded from consideration in performance assessment (PA) calculations. The possible effects of markers on future exploration have not been considered in the rescreening for the 1991 report. An expert panel on marker development will recommend design characteristics for "permanent" markers and judge efficacy of markers in deterring intrusion.

COMMENT 10. Page III-3, Lines 19-20; Page III-13, Lines 16-20: This statement is rather confusing because the probability of any event (for comparison with the EPA standard in this report) which constitutes part of a scenario is currently based on a binomial distribution:

$(p+q)^n$, where $q=(1-p)$, and $P(X)=(n!/X!(n-x)!)*p^X*q^{n-X}$, where $n=1$, $X=1$, and $P(X)=p$, and $q=1-p(X)$

and throughout this document, the event probabilities are held constant for PA comparisons, and both "yes" and "no" event occurrences (deterministic) are considered in the LHS sampling scheme. Hunter (SAND89-2546, 1989) describes the use of this distribution where n>1.0 for estimating the future number of borehole intrusions in the repository/rooms at WIPP over the long term. The term "probability distribution" refers to scenario LHS techniques developed for demonstration purposes, and the text should clarify that for PA in this report the term "probability" is appropriate. Furthermore, the "probability" of the probability distribution(s) utilized in this report for demonstration purposes should be documented if they are going to be used in future PA reports.

RESPONSE: The confusing text was poorly phrased and does not appear in SAND91-0893. A probability model has been developed for the 1991 performance assessment that includes stochastic variability rather than assuming fixed scenario (event) probabilities.

COMMENT 11. Page III-16, Line 16: The phrase "m input vectors," while understandable, appears awkward because "m" is undefined in the immediate vicinity of the phrase.

RESPONSE: This sentence does not appear in SAND91-0893.

COMMENT 12. Pages III-5 to III-7, Uncertainty analysis; Pages III-16 to III-37: Whereas this section is well written and understandable, there are a number of technical and philosophical concerns which create problems from both a statistical and data presentation viewpoint. Since the LHS technique permeates all aspects of uncertainty and sensitivity analysis for this PA, it is important to dwell on the advantages and disadvantages of this statistical tool because of its significant impact in the process of EPA compliance determination. As stated by Thomas (ONWI-380, 1982, p. 45): "The primary virtue of Latin Hypercube Sampling is the fact that it yields unbiased estimates of the probability density functions for computer outputs." Thomas also states that the LHS method is found to be inferior to conventional experimental designs for obtaining sensitivity coefficients for computer programs involving large numbers of equations and input parameters. The main problem with LHS utilization is in obtaining uncertainty information for individual input parameters in that it cannot control the type or extent of confounding among main effects and interactions in its operation. The problem is centered around the step-wise linear regression techniques that must be used to rank sensitivities of individual parameters which have covariances that vary with the specific magnitude of the parameters themselves. Thomas recommends an analytical approach, the adjoint method, as being superior for this purpose and it does not have the mentioned drawbacks of the LHS method in this endeavor. Although the parameter confounding issue has been mentioned in

this report to be of concern, a more extensive discussion on the justification of LHS for this purpose in comparison to other methodologies such as the adjoint should be included in the PA report.

Another concern with this section is the manner of CCDF representation. Although EPA in the remanded Standard suggests the use of the mean or median CCDF (whichever is greatest) for the undisturbed or base case scenario in PA, it does not make such a suggestion for other types. Sandia National Laboratories (SNL) has interpreted this to mean that the "mean curve" is the primary measure in PA for the WIPP for both undisturbed and human intrusion scenarios. However, such representation does not convey any further information of the CCDF distribution function which the LHS procedure generated, and it would appear that anyone attempting to make a decision on "reasonable expectation" of compliance with the Standard would require variance information on the mean. In fact the graph showing all of the CCDF's for a given LHS sampling (Figure III-6) has more information from which to make a decision on this basis than has the mean CCDF for the same sampling (Figure III-7). Criteria other than the mean CCDF such as number of LHS samples generated, the fraction of CCDF's exceeding the Standard, the CCDF's bounding the samples, and percentile CCDF's are all equally important in making such decisions. The EPA guidance on this issue was certainly not intended to restrict supplying such information, and because EPA's intent is subject to interpretation, all relevant information should be presented when possible if it may have some bearing on the decision. Ancillary information of this type becomes particularly important when the mean CCDF is very close to EPA compliance limits (such as was the case in this report), or when the Standard is exceeded.

Also, there is some question as to the use of constant scenario probabilities for comparison to the Standard at this time without addressing the issue of the possible vertical displacements of the mean CCDF's when and if probability distributions (of events) are used to generate LHS scenarios from which such a mean is estimated. Since vertical displacements of the mean CCDF's may move such curves into the non-compliance portion of the Standard, it is important that the effect(s) be documented more fully in the report. Furthermore, it is not clear from reading this section that event probability distributions will ultimately be utilized in PA, and, therefore, the relevance of some of the examples presented (see Figure III-7) to this report has not been fully established.

RESPONSE: A detailed discussion on the reasons for using LHS techniques instead of other techniques such as the adjoint method is in Volume 1, Chapter 3 of SAND91-0893.

The full range of information generated from the performance assessment will be provided in the presentation of CCDFs for preliminary and final comparisons to the Standard.

COMMENT 13. Pages III-7 to III-8, Monte Carlo Techniques; Pages III-38 to III-42: The production of the mean CCDF in Figure III-14 from the family of CCDF's in Figure III-13 is unclear with respect to the ordinate.

The procedures for developing variable distributions for use in the WIPP PA are not given adequate attention in this report. Several of the secondary references are not currently available, and the available citation (Tierney 1990, SAND90-2510), and this report do not adequately discuss:

a. sufficient criteria used for selection of a specific distribution to be used in MEF formulation (SAND90-2510) other than identification of the source;

b. number of observations (or subjective estimates) used to construct the prior distributions using MEF;

c. justification that values used for any distribution are drawn from the same population (observations), and how many (if any) of these are subjective estimates (mixed models);

d. the relationship between the number of parameter observations (if any) used in a given distribution, the uncertainty in its use for LHS, and how the MEF conservatism impacts CCDF's in the PA;

e. why some other measures such as the mean, median, or the observations themselves (assumed not to be subjective) would not be more appropriate with or without LHS application;

f. limitations outlined in SAND90-2510 pertaining to effects of spatial averaging on variances used in lumped-parameter models, and the effects of possible correlations between parameters.

Whereas it is meaningless to question whether a subjectively selected prior distribution is an unbiased estimator of the actual parameter distribution when this decision is based on personal judgement, it is important to know how it will impact on the total uncertainty of a PA run where both statistically derived prior distributions, and those based on subjective criteria are concurrently utilized for LHS. In fact the resulting LHS operation confounds these effects, and both uncertainty and (to a certain extent) sensitivity analyses are similarly affected. What proportion of subjectively derived distributions are to be admitted, before one questions whether the resulting

PA can be considered to be based primarily on quantitative observations from the site, and not on subjective (Bayesian) judgement? This question is of particular importance when "sensitive" parameters are under consideration.

The use of MEF is a well known and established Bayesian reliability analysis technique used to produce prior distributions that may be termed conservative in nature depending on their application. This is accomplished by maximizing the Shannon equation (H): ... -(p1*ln(p1) + p2*ln(p2) + ... pn*(ln(pn)), where: p1, p2, . . . pn are probabilities of observing parameter estimates: x1, x2, ... xn from given parameter functions (ki, i=1, 2, ... m, m<n) (Martz et al., 1982, p. 231). The application of Shannon's equation is well established in biostatistical analysis in the determination of species diversity on gridded areas or volumes (cells): 1, 2, ... n. A maximum diversity is obtained when: p1 = p2 = ... pn, or the measure of diversity (H) is equal to ln(n). Unfortunately, the value is affected not only by the actual diversity itself, but also by the number of categories employed (n), and users frequently employ an "evenness" or "homogeneity" Shannon index (J) which is equal to (H/ln(n)). The latter expresses the observed diversity (H) as a proportion of the maximum value obtainable (ln(n)). The theoretical maximum diversity index is obtained when the observable parameter is equally distributed in all n cells. In general a well designed experiment to measure (H) will optimize the number and size of cells required, and insure randomization of cell selection to obtain a reliable estimate of the actual value (H*); and it can be expected that as the number of randomized observations increases, that the observed value (H) will become a better estimate of the actual (H*) based on statistical sampling theory.

Although not readily apparent in the available citation (SAND90-2510), the MEF should be subject to (H) and (J) type determinations, and to the optimization techniques applied to the biostatistical example just described for comparison. Where observed values for a given parameter are representative and in good supply, it would be expected that a better representation of the actual distribution of the parameter would be obtained than when a smaller number of observations are available. The "evenness" concept would be expected to produce distributions satisfying the method of maximum entropy, however, there is no discussion in this report of the robustness of this technique with respect to prior distribution selection where the number of observables are relatively sparse. There is also some confusion when parameter distributions derived from statistical sampling theory and Bayesian MEF derived distributions involving sparse or non-existent data are given equal weighting in the LHS process. Any uncertainty and sensitivity analysis is bound to involve subjective/objective interactions that may be difficult if not impossible to identify using this mixed methodology, and will impact on decisions regarding CCDF evaluations. The references cited do not appear to address this issue.

Finally, it is not readily apparent that because MEF produced parameter distributions are conservative by design, that their application utilizing LHS for mean CCDF production are also conservative. For example, the production of large retardation factors from LHS of an MEF prior distribution factor of this parameter presented in this report would be expected to shift a given CCDF toward the compliance part of the Standard while the minimum retardation factor (1) is held constant. In fact MEF distributions which conservatively estimate upper or lower values can be shown to shift the CCDF in a non-conservative direction. It would appear that sensitive parameters that exhibit this type of behavior should be given more extensive field study based on statistical sampling theory to give possibly less conservative, but more realistic, distribution functions for use in PA. This report has not adequately justified the effects of MEF on CCDF construction.

RESPONSE: Production of a mean (or median, or p-percentile) CCDF from a family of CCDFs is discussed in some detail in the sections "Characterizing Uncertainty in Risk," pages III-23 to III-29, and "Risk and the EPA Limits," pages III-29 to III-33 in SAND90-2347.

13a. Criteria and procedures for developing probability distributions of parameters from currently available information were explained in SAND90-2510 (Tierney, 1990).

13b. The number of observations (or subjective estimates) used to construct empirical (or subjective) distributions was usually not mentioned either in SAND90-2347, or in the companion data report (Rechard et al., 1990, SAND89-2408), and is not adequately discussed in 1991. However, a thorough discussion of data is a high priority in 1992.

13c. None of the distributions in SAND89-2408 (Rechard et al., 1990) arose from mixed models; most distributions were subjective and based on range and subjective estimates of median (50th percentile).

13d. The sensitivity of CCDFs to changes in the <u>forms</u> of parameter probability distributions was not investigated in the 1990 PA exercise or in SAND91-0893.

13e. In some cases, summary measures such as mean or median would have been more appropriate choices for parameters, but distributions were nevertheless used to test for sensitivity and incorporate a (perhaps unnecessary) conservation in the analyses. See Section 1.2 in Volume 3 of SAND91-0893 for further discussion.

13f. As stated, these limitations were clearly stated in SAND90-2510 (Tierney, 1990).

Sensitivity and uncertainty analyses are "blind" to the origin of the parameter distributions that are employed in those kinds of analyses. The main question is: How sensitive are the results of, say, an uncertainty analysis to changes in the forms of the underlying parameter distributions? As stated above [13d.], no such sensitivity studies were conducted in the 1990 PA exercise.

Most comments on maximum entropy formalism (MEF) concern fine points of using MEF in Bayesian reliability analysis. The best response to these comments is the following explanation of why MEF was used in the 1990 PA exercise. The MEF was invoked in the 1990 PA exercise (Tierney, 1990, SAND90-2510) for only two reasons: 1) MEF provides an accepted technique for constructing a prior distribution when only subjective estimates of the moments (e.g., mean and variance) of the distribution are provided by experts; and 2) MEF can be used to justify connecting the points of a step-like empirical cdf (whether based on measurements or on subjective estimates of percentiles) with straight lines instead of some other curve (e.g., splines or quadratics). In actual practice, during the data gathering for the 1990 exercise, no one submitted subjective estimates of mean/variance; the MEF proved useful only in the sense of reason 2.

COMMENT 14. Page III-48, Performance Assessment Process: The reference in Table III-1 lists an improvement for 2-D radionuclide transport with a retardation submodel involving dual-porosity clay-lined fractures and other specified conditions. However, no mention is made of the C&C agreement which requires the use of a retardation factor of one (1) barring tracer experiments to make firmer estimates of this parameter. A baseline simulation where no credit is taken for retardation should be included in this report to scope out the effect of this parameter on the PA if such experiments are not forthcoming. Also, it appears that Bayesian reliability methodology has been used to make the retardation distributions which contain subjective judgement about this parameter for a specific radionuclide, and is not based purely on statistical sampling theory. How does this impact on the C & C agreement? Finally, a sensitivity analysis of retardation factors generated for use in the PA is not reported in this document.

RESPONSE: Uncertainty/sensitivity analyses of 1991 results, including parameters for chemical and physical retardation, are in Volume 4 of SAND91-0893. Construction of cdf's for these parameters is included in Volume 3. The Consultation and Cooperation (C & C) Agreement (K_d=0) is considered through a separate sensitivity analysis in Volume 4. In addition, the WIPP test plan now includes retardation experiments.

COMMENT 15. Page IV-1, Lines 4-8: Estimates of scenario probabilities for PA are to be made from expert judgement, but are the estimates to be made in a deterministic manner, or will a distribution from which to sample by LHS be constructed? It is not clear in this report whether future PA's will continue to use assigned probabilities for scenarios, or whether LHS sampling will be performed for this parameter as noted in the CCDF demonstration in Chapter 3. If the latter is the case, then a methodology for this approach should also be presented in this report including how the experts will be involved in making this determination.

RESPONSE: A summary of the results of the expert panel on inadvertent human intrusion into the WIPP is in Volume 1, Chapter 4 of SAND91-0893. The findings of this expert panel are in the recently published *Expert Judgment on Inadvertent Human Intrusion into the Waste Isolation Pilot Plant* (SAND90-3063) (Hora et al., 1991). The panel's findings were not incorporated in the 1991 calculations. In the interim, performance assessments have assumed that intrusion is a Poisson process (random in space and time) and sampled on the rate constant (see Chapter 4, Volume 1 of SAND91-0893).

COMMENT 16. Page IV-8, Lines 23-26: Comments on use of mean CCDF included in Chapter 3: it is not clear why other analysis parameters should not also be included.

RESPONSE: The full range of information generated from the performance assessments will be provided in the presentation of CCDFs for preliminary and final comparisons to the Standard.

COMMENT 17. Page IV-13, Lines 21-45; Page IV-14, Lines 1-27: The PA's in this report exclude subsidence (TS) and climatic-(base case) change as part of the scenarios; it is assumed that they will be included in future PA reports. A discussion on subsidence directly above the repository (not considered possible in this report) is criticized in Chapter 3, on the basis of secondary references used in making this determination. However, subsidence outside of the controlled area is retained for scenario development based on the possible formation of catchment basins for rainfall which could allow recharge to the unsaturated zone and the Culebra aquifer. This report as well as the cited reports (Hunter, SAND89-2546, 1989, Guzowski, SAND89-7149, 1990) do not discuss hydrological stresses to the WIPP area such as damming of streams or irrigation (Cranwell, SAND81-2573, 1987), although both reference this report. Cranwell discusses this topic in very general terms and refers to an example (p. 43) where an annual precipitation of 40 inches (compare WIPP at about 40 cm annually) is assumed. He also states that irrigation presupposes the presence of aquifers with sufficient yield to support that activity. A large mined aquifer, the Ogallala, which lies to the immediate north and east of

WIPP could be considered a prime candidate, providing future engineered recharge and expanded utilization of the Ogallala to include the WIPP area is necessary and feasible. Water could be transported from a high yield area of that aquifer. Also, local aquifers or dams along the Pecos River could be utilized pending increased moisture availability from a significant future change in precipitation (to be considered as part of the base case scenario) coupled with a concomitant favorable change in precipitation pattern. Cranwell (1987) limits his consideration of aquifers to those directly above a bedded salt repository. Since irrigation maximizes infiltration at the expense of surface runoff, it might be expected to significantly affect aquifer recharge. If the potential future hydrological stress scenarios due to irrigation activities near WIPP are to be discredited by PA in future reports, then its exclusion by screening should be justified, and not ignored as has been the case.

RESPONSE: The topics of subsidence directly above the panels and possible hydrologic stresses caused by the damming of streams and irrigation are rescreened and are discussed in more detail in Volume 1, Chapter 4 of SAND91-0893.

COMMENT 18. Page IV-15, Lines 14-17: The statement is made that a nuclear criticality scenario will be evaluated separately. A consultant to EEG in 1984 considered the possibility of a criticality incident in the Culebra. His findings indicate that under some conditions criticality was possible. The following summary is offered. . .

Criticality Considerations in the Culebra

Background

SC&A Incorporated performed Culebra criticality analyses for EEG in January 1984. These analyses considered various concentrations of fissionable material that might be in the Culebra dependent on the assumed solubilities in brine and in the distribution coefficient (Kd) value of the matrix. Also minerals in the water and brine were considered for their effect on moderating or poisoning a criticality event.

The analyses considered two geometries. One was a block of Culebra 7 m high x 5 m wide x 1 m long. The other size block was 7 m high x 0.5 m wide x 1 m long. Two plutonium solubilities were considered 0.66 mg/l and 6.6 mg/l (2.8E-6 M and 2.8E-5 M). A high and low value in adsorbed iron was also considered, since its concentration is fairly significant. A plutonium Kd value of 2,000 ml/g and a bulk rock specific gravity of 2.0 was assumed in all cases.

The results indicated that with the 5 m wide block and the high plutonium solubility the conditions could be very supercritical. For the 0.5 m wide block and high plutonium solubility the values are slightly subcritical or slightly critical. EEG concurred (in an 8/10/84 letter from Neill to W. R. Cooper) that if the plutonium solubility limit in the repository did not significantly exceed 0.66 mg/l there should not be a credible accumulation of fissile material outside of the repository that would lead to a critical configuration. Also implicit in this conclusion was that the Kd value would not significantly exceed 2,000 ml/g.

The possibility of a criticality event in the Culebra needs to be re-examined because of the possibility that both the plutonium solubility and Kd values could be greater than those used in the low fissile case.

Solubility

At present the performance assessment is assuming that solubilities could be as high as 1 E-3 M. This is 35 times the high fissile value used by SC&A. It would undoubtedly lead to k_{eff} values greater than 1.0 for all conditions evaluated. Even for 1E-4 M solubility most of the high fissile conditions would be supercritical (exception perhaps for Case C).

Kd Values

A variety of plutonium Kd values have been used. Table A-8 in Appendix A of SAND89-2408 [Rechard et al., 1990] uses 100 ml/g as the expected value for the matrix while Siegel (in a 6/12/90 memorandum that is also in Appendix A) used matrix Kd values ranging from zero (0%) to 6,000 ml/g at the 100 percentile. So, Kd values might be more or less than the 2,000 ml/g value used in the SC&A calculations.

Product of Solubility and Kd

For a given volume of aquifer the important parameter for evaluating criticality is the product of solubility and Kd since this determines the amount of plutonium in the volume with assumptions used in the SC&A calculations. A value of: KdS = 2,000 ml/g (2.8 E-5 moles/l) = 0.056 ml/g (moles/l Pu) always has a $k_{eff} > 1.0$ in a 7 m x 5 m x 1 m volume and the k_{eff} is "about 1.0" (plus or minus) in a 7 m x 0.5 m x 1.0 m volume. The 0.5 m width is probably more reasonable for a scenario where the contaminated brine is injected into the Culebra aquifer from a borehole. Therefore, criticality should be re-evaluated in the future if there is ever an indication that the KdS value exceeds about 0.05 ml/g (moles/l).

Conclusion

A 1984 analysis performed by SC&A, Inc., for EEG indicated that a criticality event in the Culebra aquifer from adsorbed plutonium following a release from the repository was not credible with the maximum values of plutonium solubility and Kd that were believed to be appropriate at the time.

Recent studies related to the Performance Assessment suggest that the solubility of plutonium in brine could be two orders of magnitude greater than that assumed in the "non-credible" determination. Also, the Kd value could be higher than the value used by SC&A, Inc.

The criticality issue needs to be thoroughly re-evaluated if Performance Assessment data indicates that the product of KdS might exceed about 0.05 ml/g (moles/l of plutonium).

RESPONSE: A performance-assessment task has been initiated to examine the potential for nuclear criticality from post-closure processes.

COMMENT 19. EEG Views on Scenarios and Assumptions Considered by Sandia [SNL] in Preliminary Performance Assessment: Analyses by Arthur D. Little (ADL), SC&A, and by EEG over the years lead to several questions about the completeness of Sandia's scenarios and the detailed assumptions used.

Parameter Uncertainty

Sandia has reached conclusions about several parameters where uncertainty exists that have had significant effects on scenarios considered, detailed assumptions made and in outcome of analyses. The parameters are discussed below.

19a. Marker Bed - 139 (MB-139) Permeability. The characteristics of MB-139 are very important in any realistic modeling of the repository room horizon. There is reason to believe that MB-139 will be the most effective conduit between waste storage rooms and: other rooms, other panels, repository shafts, and the accessible environment. ADL assumed that a disturbed area in MB-139 will extend out 50 feet horizontally from mined waste storage rooms and that this area will be in hydraulic and pressure communication with waste storage rooms. This assumption increases the sensitive area of the repository to a human intrusion drill bit by a factor of 4.4. Also, the permeability values chosen for MB-139 in both the near-field and far-field affect results in a number of undisturbed and disturbed scenarios.

EEG believes that Sandia should include a MB-139 disturbed area in the surface area available for all human intrusion scenarios unless there is field data to indicate that the disturbed area will not be in communication with waste storage rooms. Also the distance that the disturbed zone extends from waste storage rooms should be estimated from actual field data.

RESPONSE: The extent of the Disturbed Rock Zone (DRZ) in MB139 is an important factor in answering the question of whether exploratory boreholes near (0-50 m) the WIPP repository are in effective communication with the waste storage rooms through MB139. Following mining, an ellipsoidal pattern of fractures develops around the excavations. An arcuate fracture system concave toward the opening develops in the floor and roof. This DRZ varies in size and depth (1 m-5 m) (3 ft-16 ft) according to the size and age of the opening (Lappin et al., 1989). The DRZ generally extends far enough to include the MB139 directly below the repository. Currently, there is little evidence that the DRZ exists beneath unexcavated portions of the underground workings (Stormont et al. 1987).

The lack of a DRZ below unexcavated portions of the repository suggests that an intruding borehole outside the boundary of the repository would not be in effective communication for radionuclide transport in quantities important for CCDF construction with the repository wastes. This hypothesis was examined by Stormont et al. (1987) in SAND87-0176.

The principal pathway for radionuclides out of a pressurized repository is downward into MB139 and then laterally outward in MB139. If the resistance to flow of the small thickness of DRZ between MB139 and the repository is neglected, it can be assumed for computational purposes that the repository wastes lie entirely within MB139. Because excavation damage exists in MB139 only directly under the waste rooms, the permeability of MB139 beneath the rooms will be greater than MB139 regions away from the repository.

If a borehole penetrates a pressurized, brine-saturated repository panel (and in this model MB139), brine would be expected to flow into the borehole at a rate determined by the local permeability adjacent to the hole and the pressure gradient.

In the following calculations using the code SUTRA, the brine flow rates into hypothetical boreholes are calculated as a function of borehole location. Boreholes penetrating the repository and at various distances away from the repository are considered.

Spatial Grid

The analysis used the fine mesh Finite Element (FE) model used in the repository modeling of undisturbed conditions for one-phase flow and transport (Volume 2, Chapter 4 of SAND91-0893). In order to accurately model a borehole near the repository boundary, the FE mesh had to be grossly refined where simulation boreholes were to be placed. The mesh utilized symmetry and areal geometry to represent one-fourth of the WIPP repository's shadow projected onto the MB139 layer. Thus, the "footprint" of the repository on the MB139 medium was represented as material MB139DRZ, and the surrounding material was denoted as MB139FF (Far-Field). The final mesh used in the analysis consisted of 4740 elements (79 x 60 elements, and 80 x 61 nodes), shown in Figure 1. Thickness of all elements (normal to the plane) were assigned a value of 1.0 m. Simulation boreholes were then assigned to nodes located at 0.25, 0.50, 1.00, 2.00, and 1710.80 m outside the MB139DRZ, lying inside material MB139FF between the repository's footprint "toes." In addition, boreholes were modeled on the interface of MB139FF/MB139DRZ, at 0.25 m inside material MB139DRZ, and along the axis of symmetry of the FE mesh (74.00 m from the MB139FF/MB139DRZ material boundary). Simulation borehole nodes in the vicinity of interest are depicted in Figure 2.

Material Properties and Boundary Conditions

The required SUTRA flow equation properties are grain density (of solid matrix), fluid density, permeability (assumed isotropic for this calculation), bulk compressibility (of solid matrix), and fluid compressibility. Both materials' property values are listed in Table 1. Dirichlet boundary conditions (p = 11.0 MPa) for the grid were applied to the far-field boundaries. Neumann boundary conditions ($\partial p_f/\partial u = 0$; where u = outward normal direction) were applied to the one-fourth repository/MB139 symmetric boundaries, as shown in Figure 3. To simulate boreholes, a pressure of 6.5 MPa (hydrostatic) was assigned to a borehole node. The FE mesh was refined such that all elements surrounding borehole nodes were square and had a length of 0.25 m. Thus, all simulation boreholes had an effective diameter on the order of 0.25 m, as shown in Figure 4.

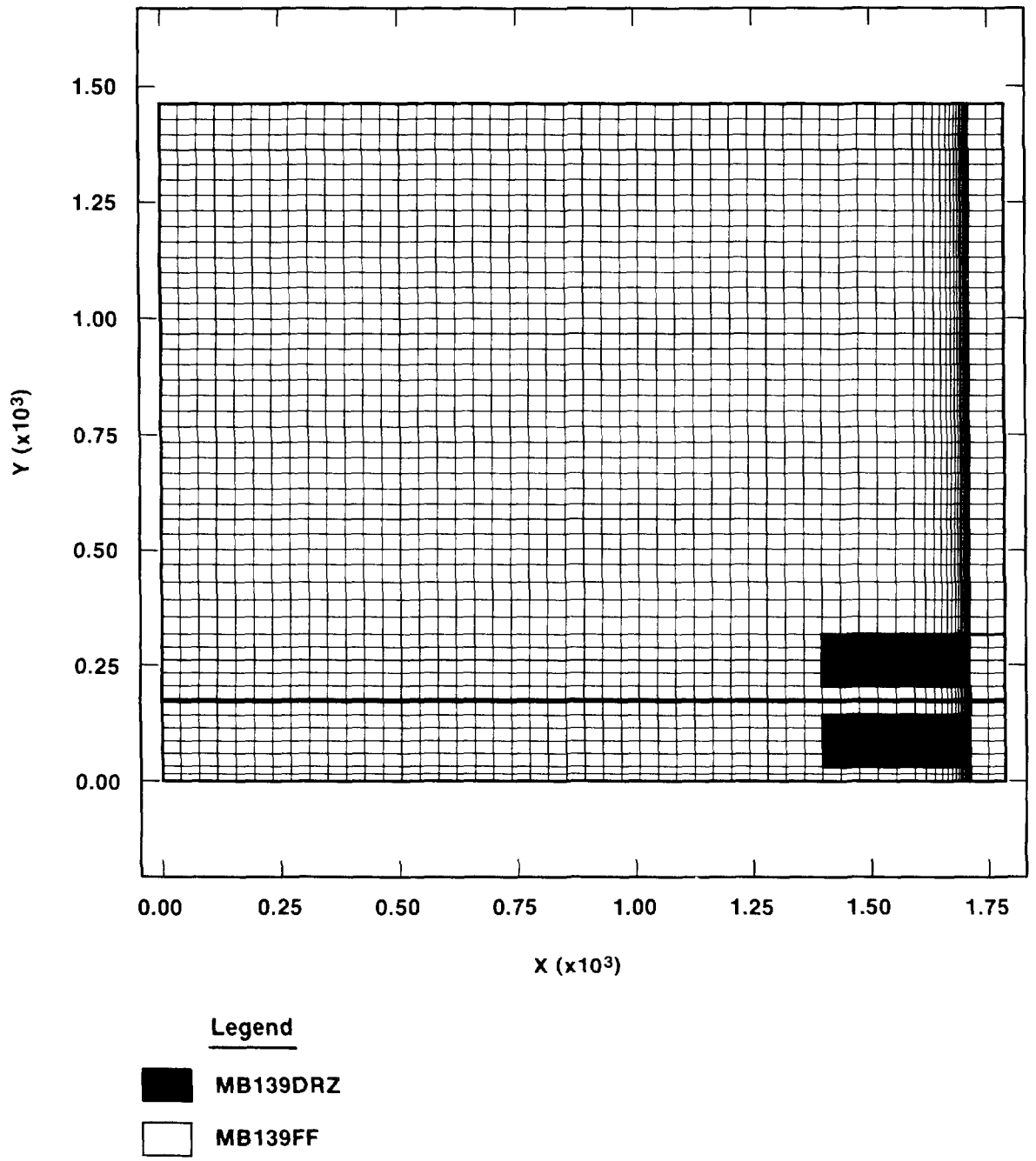

Figure 1. Final FE Mesh Used in Modeling of Undisturbed Conditions.

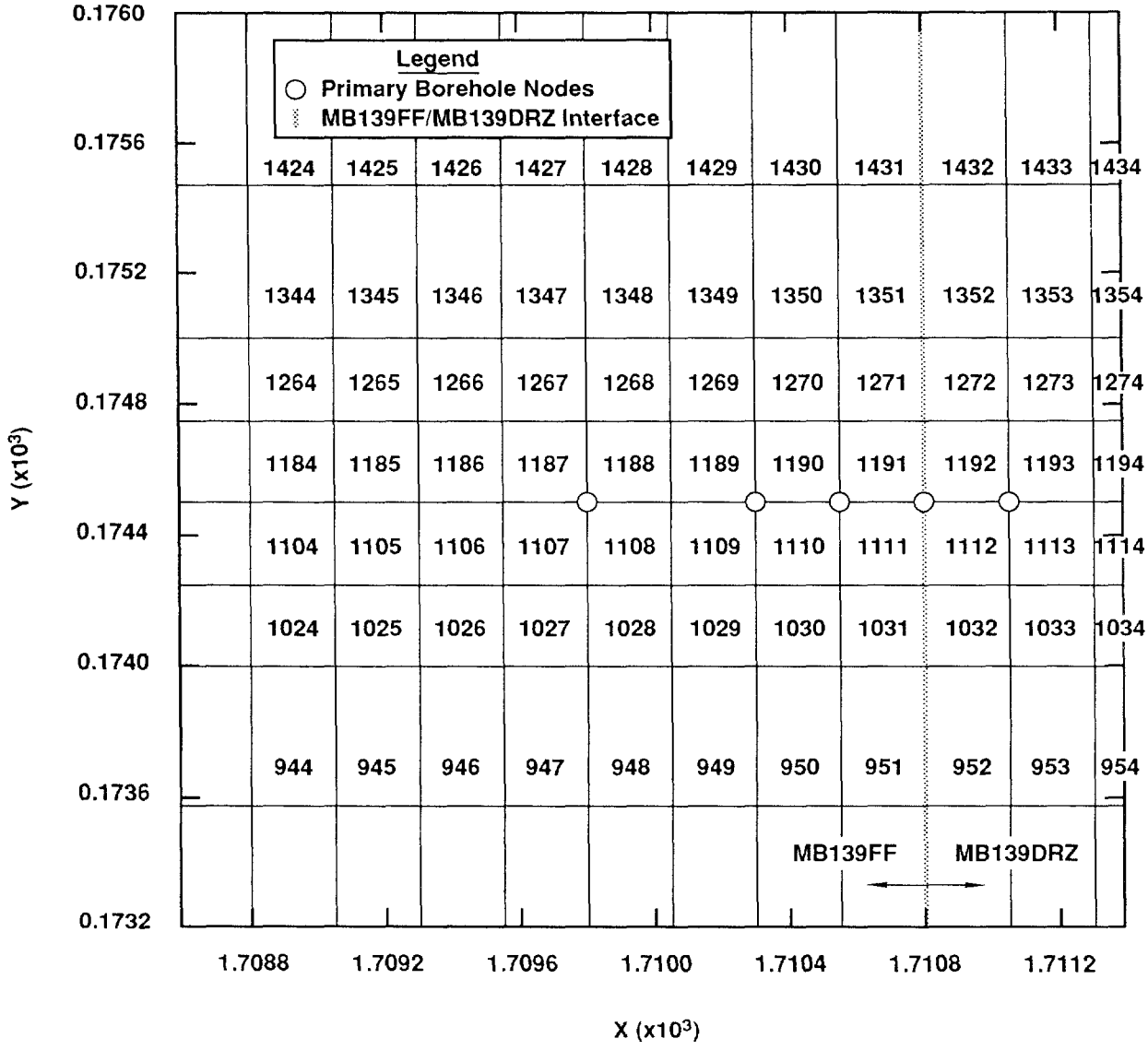

Figure 2. Simulation Borehole Nodes near the MB139FF/MB139DRZ Material Boundary.

TABLE 1. MATERIAL PROPERTIES USED FOR ONE-PHASE FLOW AND TRANSPORT CALCULATIONS

Material	Property	Value
MB139FF	Grain Density	2.963E+03 kg/m^3
	Permeability	2.870E-20 m^2
	Porosity	1.000E-02
	Bulk Compressibility	1.200E-11 Pa^{-1}
	Fluid Compressibility	2.700E-10 Pa^{-1}
	Fluid Viscosity	1.600E-03 Pa-s
MB139DRZ	Grain Density	2.963E+03 kg/m^3
	Fluid Density	1.200E+03 kg/m^3
	Permeability	1.000E-17 m^2
	Porosity	5.500E-02
	Bulk Compressibility	1.200E-11 Pa^{-1}
	Fluid Compressibility	2.700E-10 Pa^{-1}
	Fluid Viscosity	1.600E-03 Pa-s

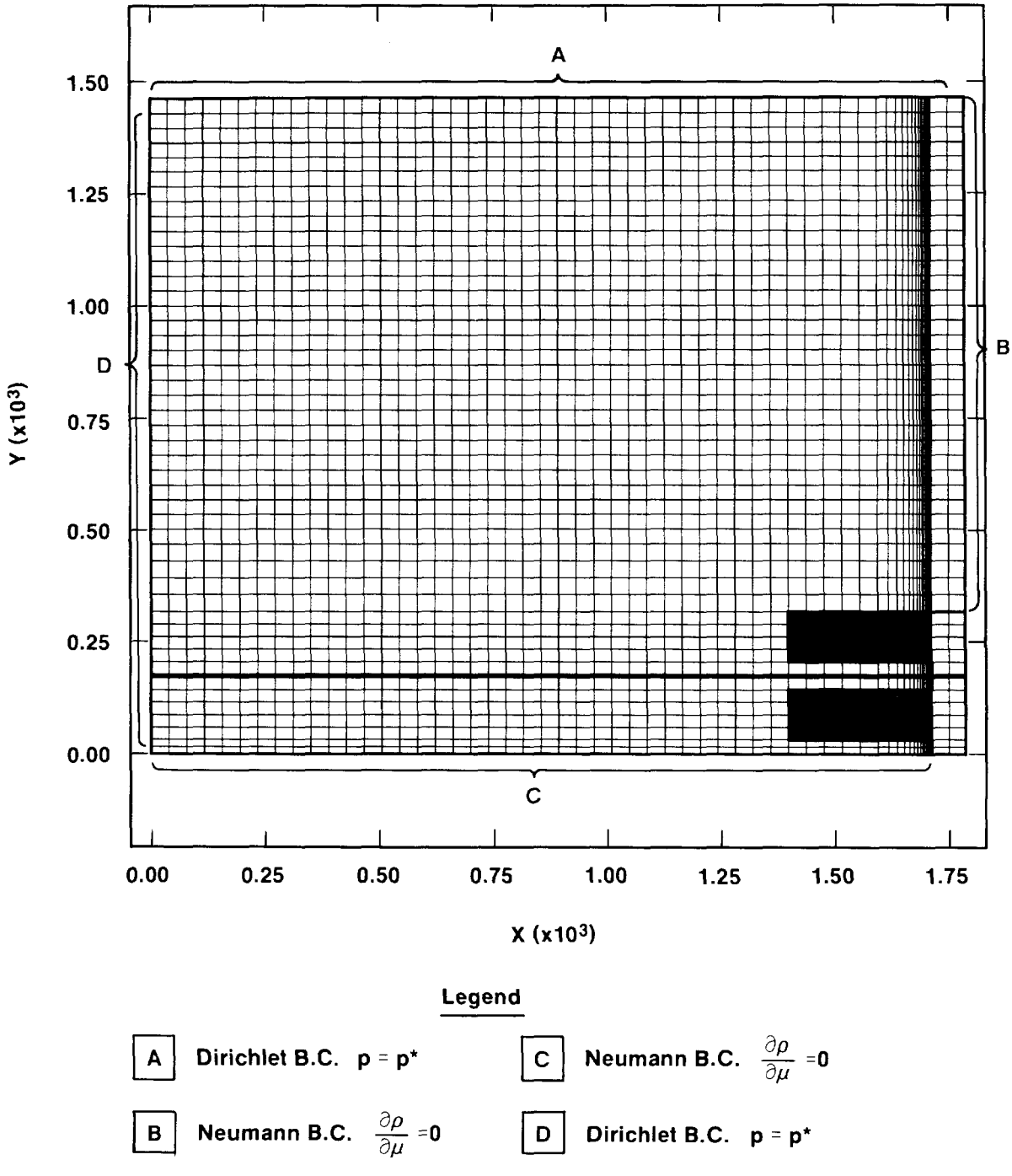

Figure 3. Application of Dirichlet and Neumann Boundary Conditions to the One-fourth Repository/MB139 Symmetric Boundaries.

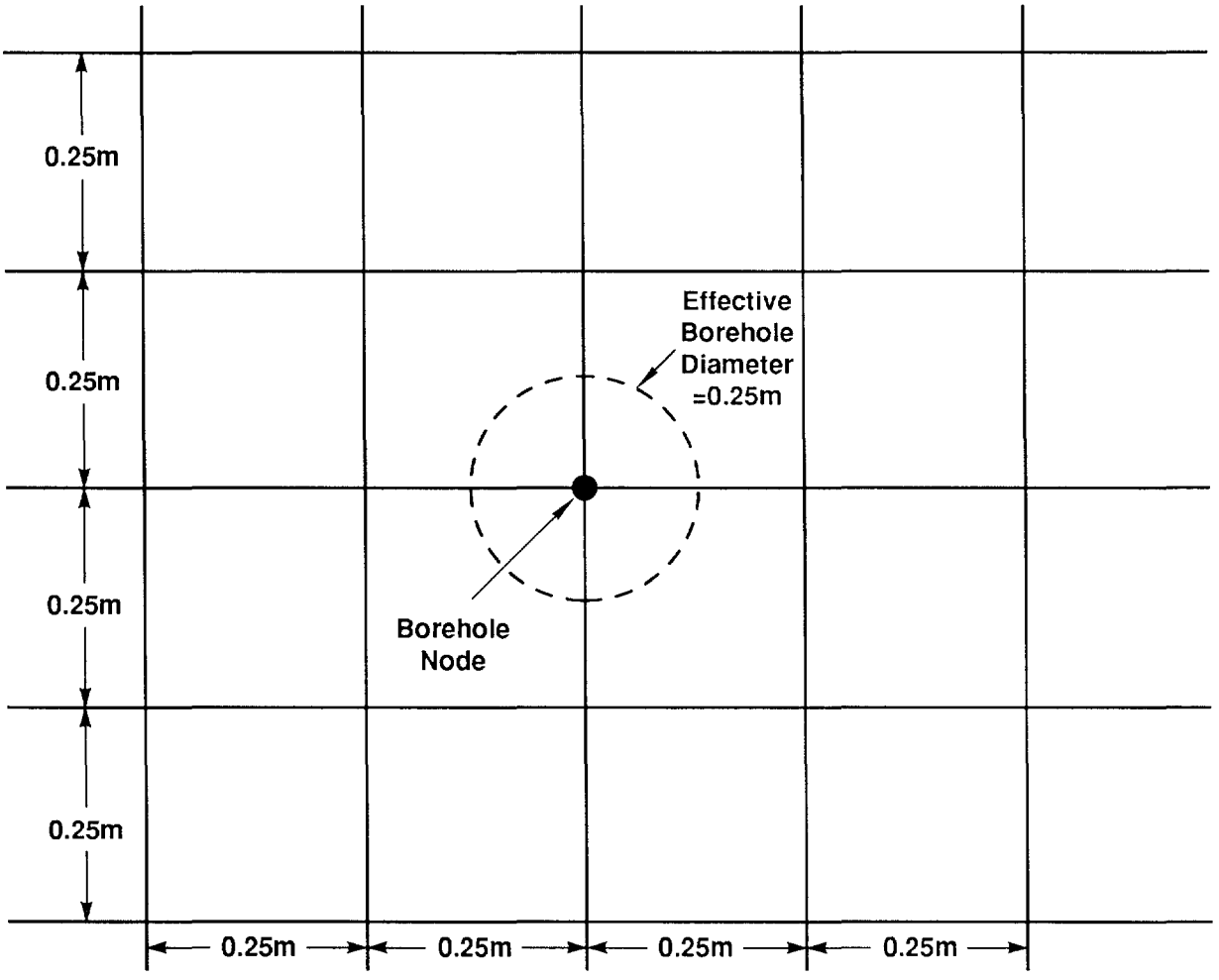

Figure 4. Effective Diameter of Simulation Boreholes.

Results and Discussion

The undisturbed calculations (Volume 2 of SAND91-0893) involving transient flow and transport into the MB139 medium used a time-varying source term, applied to interior nodes within material MB139DRZ, and was run to 10,000 years. Due to the mesh refinements in the current model, numerical stability required a very small time step. Thus to maximize computational efficiency, steady-state calculations were implemented. Instead of applying a time-varying pressure function, representing gas generation within the repository, a constant pressure of 18 MPa was used as the source term driving the fluid flow. Since transport was of no interest, the transport equations were turned off during the calculations. Therefore, seven steady-state calculations were run, a separate calculation for each borehole at a unique spatial location.

As seen in Figures 5a and 5b, the simulation borehole flow rates change dramatically as boreholes are placed outside of the "footprint" of the repository. In Figures 5a and 5b, the negative distances represent the borehole locations measured from the MB139FF/MB139DRZ interface, residing within material MB139FF. Similarly, positive distances represent the borehole locations measured from the MB139FF/MB139DRZ interface, within material MB139DRZ (i.e., the repository's "footprint"). In these figures, the flow rates represent the amount of fluid flowing into a borehole node, simulating the amount of fluid flowing up (normal to the plane of the MB139 medium) a borehole. Viewing Figure 5b, it can be seen that the simulation borehole flow rates drop approximately two and one-half orders of magnitude from inside the repository's "footprint" (MB139DRZ) to outside the "footprint" (MB139FF). Specifically, just 0.25 m inside the MB139FF/MB139DRZ interface (distance 0.25 m, node 1193), the approximated steady-state flow rate was 1.78E-07 m^3/s, and just 0.25 m outside the MB139FF/MB139DRZ interface (distance -0.25 m, node 1191), the calculated steady-state flow rate was 4.89E-10 m^3/s.

Conclusions

Based on this analysis, it seems unnecessary to enlarge the effective repository area for disturbed scenario compliance calculations to include near "hit" situations. As demonstrated by these calculations, boreholes striking outside the repository experience a significant (two orders of magnitude) decrease in volumetric flow rate.

19b. Permeability in Shaft and Borehole Seals. The appropriate value for expected and degraded permeability values in WIPP shafts and boreholes is important to the determination of whether the release to the accessible environment modeled by ADL in the undisturbed case is plausible. Also, high permeability values could influence the reasonableness and consequences of the U-Tube Scenario (Magenta - repository - Culebra) considered by SC&A.

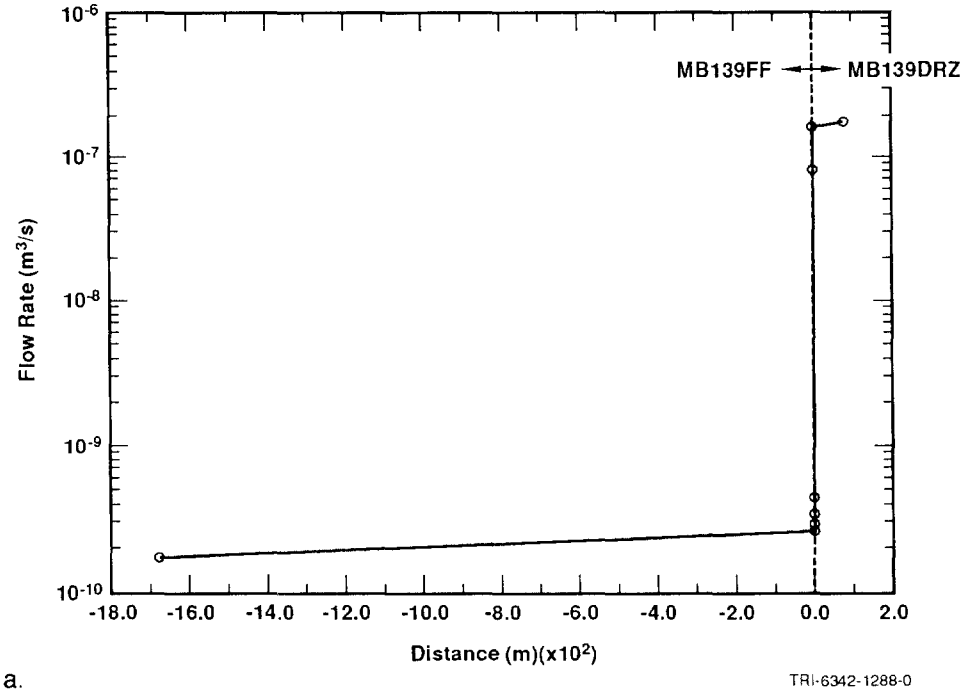

a.

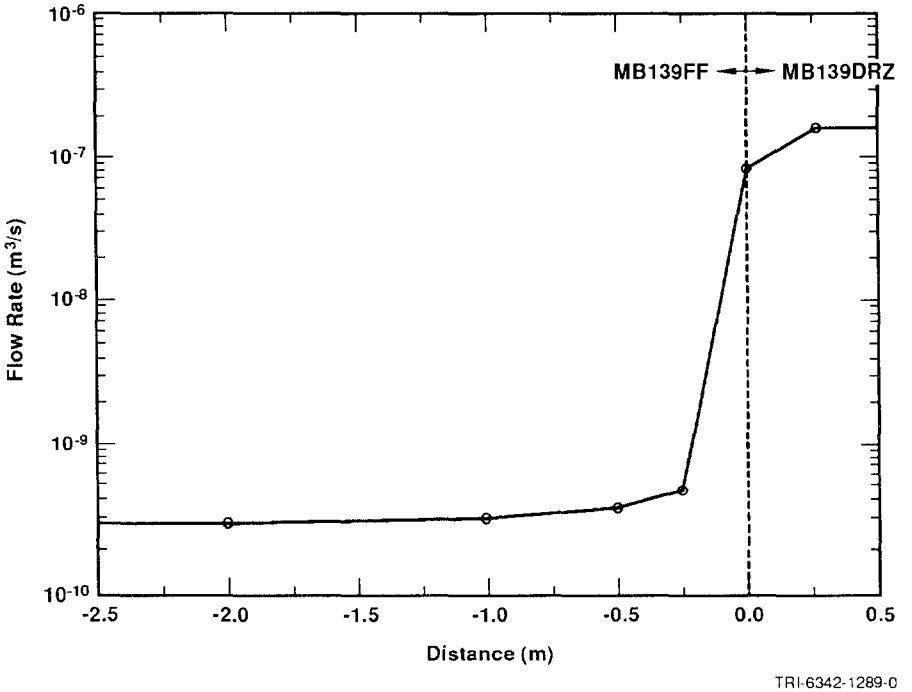

b.

Figure 5. Borehole Flow Rates versus Distance of MB139DRZ.

EEG believes that Sandia needs to justify any shaft permeability values used in any disturbed or undisturbed scenarios.

RESPONSE: The shaft backfill is an engineered barrier; consequently, the permeabilities can be specified in designs (Nowak et al., 1990). As shown in Volume 2 of SAND91-0893, the current design specifications limit the maximum allowable shaft permeability below those assumed by PA for simulating long-term performance. Justification depends on the outcome of the seal test program. Seal requirements for demonstrating compliance are discussed in Volume 4 of SAND91-0893.

19c. Climate Change. Climate change is ruled out as a variable by concluding that rainfall in a pluvial period was only double that in recent history. This estimated increase may be a reasonable conclusion from the data (EEG has not evaluated this). However, a doubling of annual precipitation is likely to lead to somewhat greater than twice the annual recharge.

A more detailed evaluation of possible recharge and Culebra transport is necessary before it can be concluded that the effects of climatic change are negligible.

RESPONSE: Climate change has not been ruled out as a variable, nor is the present understanding of the relationship between climatic change and recharge adequate to conclude that the effects of climatic change are negligible. Doubling of annual precipitation is likely to result in substantially larger increases in infiltration (see memo by Swift in Volume 3 of SAND91-0893). The 1991 groundwater-flow model does not directly link changes in infiltration to changes in model boundary flux. Instead, increased recharge was simulated by prescribing elevated heads along the northern boundary of the model domain (see Volume 1, Section 5.1.9 of SAND91-0893).

19d. Subsidence and Surface Recharge. Actions by humans have the potential to significantly increase recharge. Potash mining either within or outside the WIPP Site boundary could lead to a pathway for Culebra recharge, even without a pluvial period. Also, the present Memorandum of Understanding between the Department of Energy and the Bureau of Land Management in conjunction with the Administrative Land Withdrawal in January 1991 allows BLM to sell or give away sand, gravel, and caliche from the surface of the WIPP site (including the exclusive use area above the wastes).

These other possibilities of enhanced recharge to the Culebra need to be seriously considered in scenario assumptions.

RESPONSE: The effects of subsidence related to potash mining have been included in scenario development but are not yet sufficiently well understood to be incorporated in consequence modeling. Effects of subsidence on groundwater flow in the Culebra will be modeled in future performance assessments.

The effects of near-surface activities (e.g., removal of caliche) on flow in the Culebra have not been evaluated, but because units above the Culebra have low permeabilities at and near the WIPP, the potential for a significant change is believed to be small. The effects of vertical flux into the Culebra within the model domain, regardless of the hypothesized cause, will be evaluated in future simulations of groundwater flow.

19e. Uncertainty in Radionuclide Source Term. There is some uncertainty in the volume, number of curies, and radionuclide composition of the wastes that will eventually be brought to WIPP for disposal. All of these parameters will have some effect on the CCDF. It is realized that the WIPP Project [Site] Office is continually refining and updating data on the existing and not-yet-generated waste.

The amount of heat-source wastes (Pu-238) that will come to WIPP as well as the waste form and number of curies per container could be especially important to performance assessment calculations. About 80% of the total alpha-TRU radioactivity presently projected to be emplaced in WIPP is Pu-238 and of this total over 95% is in heat source wastes at SRS or LANL. This large amount of radioactivity greatly increases the multiplier for Table 1, thus greatly increasing the quantity of radioactivity that is allowed to reach the accessible environment.

Since Pu-238 has a half-life of only 87.7 years it figures to be of much less concern per curie during the 10,000 year evaluation period than U-233, Pu-239, Pu-240, and Am-241. Thus, the presence of heat source wastes would be expected to make compliance with 191.13 easier.

Most of the present Pu-238 wastes cannot be shipped to WIPP with the current NRC certificate of compliance for TRUPACT-II and may never be shippable without treatment. Since DOE has made no firm commitments concerning treatment of heat source wastes there is an uncertainty about whether the waste will come to WIPP at all, and (if it does come) in what form.

Sandia should perform PA calculations and plot a CCDF for two source term conditions, one with the heat source waste included and one without.

RESPONSE: Performance Assessment has considered the suggestion made by the EEG to look at inventories with and without heat-source Pu wastes. In all 1991 calculations, the WIPP is assumed to be filled to the design volume, with quantities of radionuclides scaled up from the 1990 IDB. Using a smaller inventory (without the Pu-238 in heat-source waste) would result in smaller allowable releases.

Pu-238 is not "of much less concern during the 10,000-year evaluation period than U-233, Pu-239, Pu-240, and Am-241" because Pu-238 decays to Pb-210 through the three daughter products U-234, Th-230, and Ra-226. "Thus, the presence of heat-source wastes would be expected to make compliance with 191.13 easier" only if the daughter products of Pu-238 are ignored. The Standard requires the consideration of decay products, and performance assessments therefore consider the complete design inventory.

Comment 19 (continued). Scenarios Not Considered

At the present time Sandia is not assuming that any radionuclides will be brought to the surface except in drill bit cuttings from the "effective" radius of the borehole. Furthermore, it is assumed that all wastes in drill bit cuttings contain only average concentrations of radionuclides.

Waste being brought to the surface has the potential to be a more severe test of the Standard than having the waste diverted into the Culebra Aquifer where transport to the accessible environment can be significantly delayed by ground water flow time and retardation factors. Yet at the present time Sandia has eliminated all scenarios where wastes are brought to the surface except as drill bit cuttings. The deletion of discharges to the surface is unrealistic and non-conservative.

In 1987 Sandia performed scoping and preliminary PA calculations where they considered volumes of radioactive material that might be brought to the surface from drilling into waste storage rooms in the following conditions:

(a) containing a brine slurry;
(b) in dry consolidated form;
(c) in dry nonconsolidated form.

These deterministic calculations indicated that the quantities of radioactivity brought to the surface could exceed the [EPA] standard in cases (a) and (c).

The uncertainty in waste storage room conditions reflected in Sandia's 1987 work still exists. The primary problem is that if room closure and consolidation cannot be guaranteed before brine inflow occurs and/or the 100 year control period expires then conditions (a) or (c) could be present at the time of intrusion. In 1987 the point was made that early reduction of void space alone might solve this problem. Yet, no progress has been reported in confirming this preliminary finding or in reducing void space by waste modification and/or backfill design changes.

EEG believes that Sandia must consider releases of radioactive material to the surface beyond the average radionuclide composition drill bit cuttings included in the Preliminary Comparison. Our concerns are expressed in more detail below.

Radionuclide Quantities in Drill Cuttings. The scenarios recognize there will be radioactive material brought to the surface in drilling fluid each time waste storage rooms are penetrated. This material will be both from drill bit cuttings and from "cavings" (additional material "eroded from the walls of the borehole at the repository horizon by the circulating fluid.") SAND90-2347 (pages V-83 to V-85) discusses variation in drill bit radius (is sampled probabilistically) and in shear strength of the waste which affects the amount of "cavings" (which is being studied). EEG agrees with the procedure being used to determine the final hole radius, but we point out that the bulk shear strength of the waste should also be considered for those cases where the waste is unconsolidated or in a brine slurry. The 1987 scoping studies assumed that in a dry non-consolidated room all waste in an intercepted drum would be carried to the surface and in a brine slurry room that 46 m^3 of brine would flow to the surface. These assumptions are reasonable and a good starting point for developing waste volume distributions.

The average radionuclide composition and concentration varies significantly between waste generation sites. Also, there is considerable variation between waste packages at each site. Unlike spent fuel in a high-level waste repository there is no average or typical TRU waste container. Table [2] (developed from data in DOE/RW-0006, Rev. 6, the 1990 Integrated Data Base [U.S. DOE, 1990a]) indicates the estimated averages of presently stored and newly generated wastes at the individual generating sites.

The variation at each generating site is also significant. For example, the Savannah River Site (SRS) is expected to have 5,560 drums averaging 880 Ci/m^3 (DOE/WIPP 88-005 [U.S. DOE, 1989]). Since drilling into waste is an expected event and the EPA standard requires that releases with an expected probability greater than 0.001 be considered, it is necessary that cuttings from the more concentrated packages be considered.

TABLE 2. PERCENT VOLUMES AND AVERAGE CONCENTRATIONS FROM TRU WASTES GENERATING SITES

Generator	Volume Percent	Cumulative Percent	Average Concentration (Ci/m^3)
NTS	0.6	0.6	1.17
LLNL	1.1	1.7	2.09
Mound	0.9	2.6	2.36
RFP	16.0	18.6	3.69
ANL-E	0.2	18.8	3.94
INEL	39.5	58.3	4.89
Hanford	10.3	68.6	5.28
ORNL	1.2	69.8	24.92
LANL	11.4	81.2	54.51
SRS	18.7	99.9	181.07

Ref: DOE/RW--0006, Rev. 6 [U.S. DOE, 1990a]

The effect of considering the high concentration packages in the current calculations is believed to be significant. From the CCDF plots in Figures VI-2, 3, 4 (in SAND90-2347) it appears that the quantities released during drilling are about 2 to 4 curies. This is approximately the value EEG obtained using average container concentrations and a 12 inch effective diameter borehole. However, we believe that when the SRS high-curie containers are considered there could be greater than 30 curies brought to the surface with a probability of greater than 0.001 when considering random emplacement (which may not be the actual or the most conservative mode). We recommend that this variation in radionuclide concentrations be determined as well as possible and treated probabilistically in the calculation.

RESPONSE: The analyses summarized by Lappin et al. (1989) indicated that a brine slurry would not form in a gas-free repository. The two-phase BRAGFLO calculations conducted for this report (see Volume 2 of SAND91-0893) support this conclusion: the presence of gas results in less brine in the waste. The effective shear strengths for erosion currently being used in cuttings calculations are very low, on the order of 1 Pa.

The possibility of waste removal through a borehole from a gas-pressurized and gas-saturated repository with consolidated or unconsolidated wastes is currently under study.

Comment 19 (continued). Contaminated Brine Flows to the Surface. The E1, E2, and E1E2 scenarios assume that the only material reaching the surface is from drill bit cuttings and some "cavings" from the annulus about the drill bit in the waste storage room. Brine flowing to the surface from an encounter with a pressurized Castile brine reservoir was not assumed. EEG believes that brine flows to the surface should be assumed and that the consequences could be significant for the E1E2 scenario. Our reasons follow.

Sandia and DOE have described typical drilling practices elsewhere (Appendix C of SAND89-0462 [Lappin et al., 1989] and in DOE February 7, 1990 response to EEG's comments on the Draft Supplement EIS). These responses explain how it is possible to have very little flow to the surface by closing in blow-out preventers within a few minutes, determining the pressure, and then preparing drilling mud of sufficient density to stop the flow before resuming drilling. For example, it was stated (in the 2/7/90 letter) that only 51 barrels flowed at WIPP-12 before shut in by a blow-out preventer.

The 2/7/90 DOE letter went on to say that at WIPP-12 an additional 49,224 barrels flowed during deepening, geophysical logging, and further deepening before it was finally shut in for subsequent hydrologic testing. This additional flow was described as resulting from a "conscious decision."

It appears that virtually every time a pressurized Castile brine reservoir has been encountered in the vicinity of WIPP that "conscious decisions" have been made to allow varying amounts of brine to flow at the surface. Table [3] extracted from two WIPP reports (TME-3080 and TME-3153) [U.S. DOE, 1981 and U.S. DOE, 1983] describes remedial measures taken. Although the available data are not as detailed or as quantitative as one would like, it is clear that drilling practice through 1982 included release of brine at the surface whenever pressurized Castile brine reservoirs were encountered. In the absence of any brine reservoir encountered in the Delaware Basin since 1982, where new practices might have been observed, we believe that typical commercial drilling practices should be assumed.

Brine released at the surface from the E2 scenario would be expected to increase the effective radius of the borehole and thus increase the amount of waste brought to the surface in suspension and in solution. The major effect could occur in the E1E2 scenario because brine present in the repository from the first encounter (which would be expected to be saturated in uranium, plutonium, and americium) would be discharged at the surface. The following example indicates that discharge could be significant.

There would be about 8,800 m^3 of brine in a waste panel if 20% of the original volume contained brine. If plutonium, americium, and uranium were present in the brine at 10^{-6} Molar concentration there would be about 8,000 Ci at 150

TABLE 3. CASTILE BRINE RESERVOIR INTERACTIONS IN WIPP AREA

Name of Well	Date Drilled	Initial Flow bbl/day	Remedial Action
Mascho-1	1937	8,000	No action to stop flow.
Mascho-2	1938	3,000	No action to stop flow.
Culbertson-1	1945		3,000 barrels estimated to flow to surface. No record of flow rate or duration.
Tidewater	1962	NA	12 pound per gallon drilling mud did not stop. Finally control by casing and cementing.
Shell	1964	20,000	Allowed to flow until artesian flow ceased.
Belco	1974	12,000	Brine flowed to surface for 26 hours with 14 pound per gallon drilling mud.
Gulf	1975	5,000	No records on total volume or duration of artesian flow.
ERDA-6	1975 1981-82 (testing)	660	WIPP borehole. Estimate 19,000 barrels could be produced by artesian flow.
Pogo	1979	10,000	Initial flow of 1440 bbl/day with 14.6 pound per gallon drilling mud. Stopped after 4 days with 15 pound per gallon mud.
WIPP-12	1981	12,000	WIPP borehole. Over 79,000 barrels produced. Estimate 350,000 barrels producible by artesian flow.

References

- U.S. DOE Brine Pocket Occurrences in the Castile Formation, southeastern New Mexico, TME-3080, March 1981.
- Brine Reservoirs in the Castile Formation Waste Isolation Pilot Plant (WIPP) Project Southeastern New Mexico, TME-3153, March 1983.

years after closure, 6,700 Ci at 1,500 years, and 800 Ci at 3,000 years. Permissible quantities of waste allowed in the accessible environment (assume 10 times Table 1 values) would be between about 1,700 and 5,100 Ci depending on the TRU waste equivalency definition finally used.

Although the hydraulic characteristics of many brine reservoirs are adequate to flow 8,800 m^3 at the surface (WIPP-12 would have flowed 56,000 m^3), the amount of brine flowing from a panel might be somewhat less. However, the solubility could be somewhat higher. The solubility of americium is particularly important because of its high specific activity. At 10^{-6} M americium-241 contributes about 90%, 98%, and 79% of the total activity at 150, 1500, and 3000 years. The quantities in solution are solubility limited before about 1,500 years (at 10^{-6} M) and inventory limited thereafter.

EEG believes that the Performance Assessment has to include events where contaminated brine comes to the surface. Computational details would determine whether these events should be incorporated into the E1E2 scenario or into a separate scenario.

RESPONSE: The EEG raised the question of increased quantities of waste being brought directly to the surface if flow from a penetrated brine pocket was allowed to continue unrestricted. This could happen by two mechanisms. First, some additional particulate waste could be eroded from the borehole wall. Second, waste dissolved in brine within the panel could be brought to the surface with the Castile brine. The first mechanism has been examined with calculations discussed in the next paragraph. The second mechanism, which requires an E1E2-type intrusion and flow of Castile brine through the panel, has not been modeled. It can be noted qualitatively, however, that because of the resistance provided by the relatively low-permeability waste and backfill, flow along the E1E2 pathway is less likely to result in an uncontrolled flow of brine at the surface.

The first mechanism has been examined with a CUTTINGS calculation to assess the importance on erosion of unrestricted brine flow from a Castile brine pocket in an E1 scenario. Unrestricted artesian flow from a Castile brine pocket would normally not be permitted. However, several cases of such flow have occurred in past drilling events near the WIPP site. In 1964 a well (Shell) was allowed to flow to the surface until artesian flow ceased. The initial flow rate was 20,000 bbl/day. Using this value of brine flow, borehole erosion was calculated with the CUTTINGS code assuming that the drill bit had passed the repository horizon and penetrated a Castile brine pocket. The uphole flow rate was assumed to consist of the combined drilling mud flow and brine pocket flow. The drill diameter adjacent to the repository was also assumed to be the outside drill stem diameter. All other input parameters were kept the same (see Table 4). The results indicate that for the chosen

input variables, there would be an increase in the volume of waste transported to the surface of 19.6%.

TABLE 4. INPUT AND OUTPUT VARIABLES-CUTTINGS

	With Castile Brine Flow	Without Castile Brine Flow
Drill String Angular Velocity	7.7 rad/s	7.7 rad/s
Diameter of Intrusion Drill Bit	0.4444 m	0.4444 m
Relative Roughness	0.25	0.25
Effective Shear Strength for Erosion	1 Pa	1 Pa
Fluid Density (Mud)	1200 kg/m^3	1200 kg/m^3
Viscosity	9.17×10^{-3} Pa•s	9.17×10^{-3} Pa•s
Yield Stress Point	4 Pa	4 Pa
Drill String Diameter	0.1016 m	0.1016 m
Mud and Brine Flow Rate	8.094×10^{-2} m^3/s	4.415×10^{-2} m^3/s
Final Eroded Diameter	1.0866 m	0.9935 m

Comment 19 (continued). Brine Slurry Filled Room. A brine slurry filled room could be present in scenarios that do not involve a brine reservoir. Also, because of creep closure and gas generation this brine could be under greater than hydrostatic pressure and thus have a driving force of its own (unless the gas cap was relieved by the drill bit upon initial entry to the room). The potential quantities of brine that might come to the surface would be somewhat less than with a brine reservoir (perhaps tens of cubic meters rather than hundreds or thousands of cubic meters) but the consequences could still be significant.

The brine slurry room scenario with wastes being brought to the surface in drilling fluid and/or by flow should be included unless other studies can establish that this room condition will not exist in the absence of a brine reservoir.

RESPONSE: The question of a brine-slurry-filled room was raised a number of years ago by the EEG and others. It became the impetus for extensive tests on the permeability of the Salado Formation to quantify the maximum amount of brine that could enter the repository over 10,000 years. The permeability measurements to date continue to show very low permeabilities, which prevent great quantities of brine from entering the room, which in turn precludes the possibility of forming a slurry. Furthermore, the current PA two-phase BRAGFLO code models both the gas generation and brine

movement as suggested. In the vast majority of simulations of the E2 scenario with varying permeability, there is insufficient brine entering the room to even fill the pores (and results in mostly zero releases (see Volume 2 of SAND91-0893)). Consequently, the extensive discussion refuting this hypothesized condition in Lappin et al. (1989), in the FSEIS (U.S. DOE, 1990b), and elsewhere remains valid.

Comment 19 (continued). Location and Effectiveness of Borehole Seals. The present scenarios assume that borehole plugs remain intact for the 10,000 year period and thus preclude any contaminated fluid from reaching the surface. This assumption maximizes the amount of fluid that will be injected into the Culebra aquifer but it may not maximize the amount of radionuclides that reach the accessible environment from both the Culebra and surface routes. Also, the location of the plugs is different in the E1 scenario portion of the E1E2 scenario than in the other scenarios. This change may lead to conservative (higher) release rates to the accessible environment but is not explained.

The assumed borehole permeability range of 10^{-11} to 10^{-14} m^2 is in the range that Freeze and Cherry [1979] call appropriate for silty sand. This appears to be consistent with guidance in the 4/91 Draft of 40 CFR 191.

EEG does not have a position at this time on the assumptions used about the location or the 100% effectiveness of the plugs.

RESPONSE: Because no question was asked, we can only comment on the three points raised: (1) maximizing flow to the Culebra by using 100% effective plugs above the Culebra, (2) changing locations of 100% effective plugs between E1 and E1E2 summary scenarios, and (3) selection of borehole permeability.

Concerning the first point, it is Performance Assessment's intent to be conservative in placing a 100% effective plug above the Culebra to divert the flow into the Culebra. Without the plug, contaminants could move higher in the borehole but not to the surface since the pore pressure in the Salado Formation and the Castile brine pocket are not great enough to move brine to the surface through a sand-filled borehole (see Reeves et al., 1991, SAND89-7069). Lateral transport of radionuclides in subsurface units above the Culebra (e.g., the Magenta Dolomite or the Dewey Lake Red Beds) has not been modeled but is believed to be less important than transport in the Culebra because transmissivity in these units is substantially lower.

As correctly surmised by the EEG concerning the second point, changing the locations of the 100% effective plugs between the summary scenarios does

produce higher releases by forcing 100% of any flow from the brine reservoir directly through the waste in the E1E2 summary scenario.

On the final comment, Performance Assessment concurs with the EEG that the assumed borehole permeability range of 10^{-11} to 10^{-14} m^2 is consistent with *40 CFR 191* as originally promulgated and the April 1991 draft.

COMMENT 20. Page V-2, Lines 6-42; Pages V-26, Line 26 to V-34, Line 6: The discussion of the Culebra and Magenta dolomites in the WIPP area infers that there is a source of aquifer recharge (North and East of the site) to these units. Furthermore, it is stated that the Magenta is possibly recharging the Culebra through fractures. Also, it is mentioned that the presence of a 3 meter thick caliche layer inhibits downward flow of moisture from supra-Rustler aquifer units. The recharge statements are in apparent contradiction to the discussion on the paleo-flow transient state postulated for the WIPP (summarized on p. V-53, figure V-19) which would exclude significant moisture of recent origin from entering these aquifers. The reference to a caliche moisture flow inhibitor from the surface to aquifers farther down is also perplexing. Is the Capitan Reef at the periphery of the Guadalupe Basin implicated as an ultimate source of recharge if infiltration from the surface is to be minimized? If so, how does one explain the "pleistocene" age of the water reported for the Culebra which would negate any significant modern recharge related to this discussion? Is the caliche layer compromised by sinkholes, boreholes, potash mining, or deliberate removal? The experiments and field studies (EEG is currently involved in one) to address these uncertainties should be referenced, and the state of "ignorance" on the subject should be clearly detailed in this report to accurately present the state of uncertainty in PA.

RESPONSE: Uncertainty remains high about the past and possible future changes in recharge and groundwater flow in the Culebra. The discussion of the topic in Volume 1, Chapter 5 of SAND91-0893 has been extensively rewritten. The impact of this uncertainty on the performance of the system will be evaluated in future analyses.

COMMENT 21. Pages V-2, Line 45 to V-4, Line 9; Pages V-37, Line 4 to V-51, Line 20: The section on long-term climate variability is well written and in sufficient detail in both describing paleo-climates at WIPP, and in forecasting future climates for this area. However, several important aspects are not considered which are of relevance to the WIPP area. The first aspect concerns the potential change of WIPP to a "dry-farming" region with a doubling of annual precipitation as discussed in a previous comment (p. IV-13, 14). The second aspect concerns the distribution of the precipitation throughout the year. This report indicates that the

increased moisture will occur outside of the growing season because of the southerly displacement of the jet stream during the winter. Under these conditions the doubling of annual precipitation would not produce a linear increase in soil moisture, but with reduced potential evapotranspiration rate (p.e.t.) would create significantly longer periods of water surplus in the surrounding soils and alluvium and encourage crop irrigation practices similar to those now occurring in central California. Potentially larger surface storage of moisture in surrounding dams and lakes would also encourage the latter as would potentially larger runoff from the Pecos River and its tributaries. Conversely, if the precipitation patterns were to resemble that of the midwest US, then dry farming activity would be expected to increase and to encourage irrigational supplements to overcome periods of moisture deficit currently practiced in the mid-grass region of the Great Plains. Hence PA models addressing climatic change should incorporate precipitation patterns into the analysis and model the effect on water budgets in the WIPP area. Accompanying vegetational changes through plant succession should also be modeled to determine their effect on moisture availability and their effect on WIPP integrity.

In summary, a factor of 2 increase in rainfall at the WIPP site potentially makes possible dry-farming in the area (greater than 21 inches/year precipitation is required), or increased livestock grazing. The implications of this potential effect is not discussed nor addressed in the screening of scenario possibilities at the WIPP.

RESPONSE: Doubling of precipitation may result in substantially more than doubled infiltration (see memo by Swift in Volume 3 of SAND91-0893). The performance-assessment methodology used in 1991 for simulating this increase is preliminary, and results are applicable only to the narrowly defined conceptual model for recharge at the northern edge of the model domain (see Section 5.1.9 in Volume 1, Chapter 5 of SAND91-0893). Other conceptual models for enhanced recharge will be examined in later analyses.

The WIPP performance-assessment team does not, at present, plan to model specific possible causes of increased infiltration such as changes in plant communities. Rather, the approach will be to examine the effects of varying recharge directly, with uncertainty in the recharge factor including uncertainty in the various processes that control recharge.

COMMENT 22. Page V-5, Lines 29-33; Pages V-54, Lines 35-43 to V-56, Lines 1-11: There are several areas of concern with respect to the selection of retardation factors for the Culebra dolomite: the range of values used in preparation of the CCDF (p. C-5, this document [SAND90-2347]) ranges from 1 to 16,000 (matrix), and from 1 to 50,000 (clay/fracture) for plutonium as

as provided by the "principal investigator." This presumably refers to a paper presentation by Siegel (11/19/90) in which natural uranium is the basis for a natural analog study to constrain the strength of clay/solute interactions within the Culebra Aquifer. Siegel reports retardation factors of about 1,200 for Culebra dolomite using a uniform porous-medium model, and values of about 200 for clays using the fracture flow-model. Retardation factors ranging from 200-30,000 are reported for the Palo Duro basin; however, the author states that such brines may be poor analogs for the comparatively young groundwaters of moderate salinity characteristic of the WIPP site. The latter are also under reducing conditions where uranium exists in the quadrivalent state. Siegel's paper is partly based on work by Hubbard et al. (1984) and Laul et al. (1988). Hubbard states that retardation factors greater than or equal to 40 for thorium (and indirectly for uranium) may be expected in the Palo Duro Basin based on Ra-228/Th-228 ratios observed. The uranium is again assumed to be in the quadrivalent state, and Ra-228 is considered to have a retardation factor of 1.0. Laul presents retardation factors based on U-238/Ra-226 ratios in brine ranging from about 10 to 300,000 assuming a retardation factor of 1.0 for Ra-226. Two wells, Zeeck #1 (7,140-7,172 feet deep) and J. Friemel #1 (8,168-8,204 feet deep) yielded retardation factors of about 324,000 and 132,000, respectively. Both of these wells can be considered to manifest "anoxic" or reducing environments where uranium is expected to be in the quadrivalent state. In addition, Friemel #1 yielded a retardation factor of 193,000 at another comparable depth (7,326-7,300 feet deep), again indicating a reducing environment. Laul states that wells at depths between 750 to 1,800 feet are considered to be shallow aquifers and thus may represent "oxic" or oxidizing environments. Wells ranging in depth between 750 to 2,970 feet (Zeeck #4, zone 4; Mansfield #2, Detter #2; Harman #1; and Freimel #1, zone 9) yielded retardation factor estimates between 28 to 1,897. By contrast thorium retardation factors estimated by the ratio, Ra-228/Th-228 yielded 94, 1,436, and 240 for the deep wells noted above, and a range between 70 to 870 for the shallow wells. Other wells in the study gave uranium retardation factors between 2,720 to 183,000, and thorium retardation factors between 36 to 408. The range in well depths yielding these retardation factors was between 3,100 to 7,900 feet and there was a tendency for the deepest wells to have the highest retardation factors. Furthermore, all of these wells would probably qualify as "anoxic" wells according to Laul.

It thus appears from the analysis of retardation factors based on natural-analogs U-238, Ra-226, Ra-228, and Th-228, all other conditions being met, that the Culebra at about 1,000 feet below the surface would qualify as an "oxic" aquifer and that the retardation factors estimated for these types of wells would be more applicable. The above argument suggests that a

maximum retardation factor of about 2,000 should be used for plutonium if it is a radiomimetic of uranium under these conditions, or a lower maximum retardation factor of about 1,000 should be used if it mimics thorium under oxic conditions. These estimates agree well with Siegel's and Hubbard's original estimates mentioned earlier. Thus, the maximum retardation factor of 50,000 used in PA may be high by as much as a factor of 50 for the clay/fracture environment and as much as 16 for the matrix-porosity environment. Even if the Culebra is found to be "anoxic," the retardation factor would still be under 2,000 for plutonium if it mimics thorium behavior according to these analyses. It would be desirable to take measurements of the type described for the Palo Duro Basin on the Culebra aquifer to determine the redox environment and natural-analog concentration ratios.

The use of a dual porosity model in PA involving both matrix and fracture-flow incorporating retardation factors due to both is based primarily on the work of Neretnieks and Rasmussen [1984] (Water Resources Research, V. 20, No. 12). This report is based on the flow of moisture through fissured crystalline rock which is less than exact due to insufficient knowledge of fissure orientation and frequency, intersection characteristics, and variations in these properties as stated by the authors. A discussion of application of this model to the Culebra dolomite without a comparison to crystalline rock, and adequate knowledge of fracture characteristics which might limit this application is not given enough consideration in this document. A similar criticism on the estimate of maximum retardation factors in conjunction with the clay coatings on the Culebra dolomite fractures was discussed earlier.

Overall, there remains insufficient justification for using any Kd values for the Culebra aquifer in performance assessment. EEG has urged DOE since 1979 to experimentally determine a range of Kd values for various conditions in the Culebra. Unfortunately, after all these years, there is no more experimental justification than was provided in the Geological Characterization Report in 1978 [Powers et al., 1978]. This serious deficiency in the data for performance assessment should be removed as soon as possible, either through field tests as planned in 1986 or through laboratory testing, or both. In the absence of reliable experimentally obtained results, EEG will insist on the implementation of the C & C Agreement provision of taking no credit for retardation in the performance assessment calculations.

RESPONSE: Expert judgment (whether from an individual or a panel) is always necessary to develop the probability distributions for use in the modeling systems (PA data base) from the results of experiments (sorption data base). Sandia is planning column experiments to begin preliminary

testing early in 1992. Until data required by the C & C Agreement is available, SNL will continue to include retardation in PA analyses in order to provide guidance to the data-acquisition work.

COMMENT 23. Page V-6, Lines 40-44; Pages V-59 to V-62, Lines 31-24: Exclusion of the calibrated model for the Culebra Dolomite as derived by LaVenue et al., (1990, in PA document) is of some concern, considering the amount of effort that has gone into this activity to date. The use of a "zone" approach has the advantage of using a simpler (and shorter running time) model than SWIFT II, but it appears to be uncalibrated, and it is not amenable to parameter and conceptual-model uncertainty analysis as well. In fact the use of the zone approach only for "interim" purposes should justify an analysis of how this methodology will impact on future CCDF analyses, and what one might infer from those presented in this report. It would appear that very little effort has gone into reconciling expected calibration biases of non-unique solutions on parameter and model uncertainties in PA when techniques such as "kriging" are utilized for tuning numerical models. It might be more fruitful to question either the necessity or possibility of reconciling such biases for PA over long time periods than to abandon a well documented, bench-marked and Culebra calibrated model (SWIFT II).

RESPONSE: The 1991 calculations use 60 different transmissivity fields, each calibrated to observed head data (see Sections 5.1.9 in Volume 1 and 6.3 in Volume 2 of SAND91-0893). A geostatistics expert group has been established to advise the performance-assessment team on suitable methods for including uncertainty in groundwater flow in future performance assessments (see Volume 2, Section 6.2 of SAND91-0893). Among the techniques being examined for use in future performance assessments is an extension of the pilot point approach of LaVenue et al. (1990), which will generate random fields conditioned on transmissivity data and both steady-state and transient head data, without restrictions on the variance of transmissivity and with the capability to include variable-density flow models (see Volume 2, Section 6.2 of SAND91-0893).

COMMENT 24. Page V-74, Lines 18-22: A reference is made to Radon-226 as the daughter of Ra-226 several times in this discussion. Radon-222 with a half-life of 3.8 days is the correct isotope of radon gas produced from Ra-226 (Radon-226 does not exist). Furthermore, it is stated that the activity of this radioactive gas will be insignificantly small. Because it will be in secular equilibrium with Ra-226, then the same reasoning will show that the activity of Ra-226 will be insignificantly small as well. The same logic would apply to the daughter products of Rn-222 including Pb-210. Was this the point of this discussion?

RESPONSE: The discussion of radon-222 as the only radioactive gas expected is correct in line 17. The reference to radon-226 in lines 20 and 21 were typographical errors. The point of the discussion was that the only gaseous radionuclide was radon-222, there was a very small quantity of it, and not including gaseous transport of volatile radionuclides would not significantly affect radionuclide releases.

Appendix B References

Cranwell, R. M., J. E. Campbell, J. C. Helton, R. L. Iman, D. E. Longsine, N. R. Ortiz, G. E. Runkle, and M. J. Shortencarier. 1987. *Risk Methodology for Geologic Disposal of Radioactive Waste: Final Report.* NUREG/CR-2452, SAND81-2573. Albuquerque, NM: Sandia National Laboratories.

Freeze, R. A., and J. A. Cherry. 1979. *Groundwater.* Englewood Cliffs, NJ: Prentice-Hall, Inc.

Guzowski, R. V. 1990. *Preliminary Identification of Scenarios That May Affect the Escape and Transport of Radionuclides From the Waste Isolation Pilot Plant, Southeastern New Mexico.* SAND89-7149. Albuquerque, NM: Sandia National Laboratories.

Hora, S. C., D. von Winterfeldt, and K. M. Trauth. 1991. *Expert Judgment on Inadvertent Human Intrusion into the Waste Isolation Pilot Plant.* SAND90-3063. Albuquerque, NM: SAndia National Laboratories.

Hubbard, N., D. Livingston, L. Fukui, and G. L. McVay, eds. 1984. "Composition and Stratigraphic Distribution of Materials in the Lower San Andres Salt Unit." *Materials Research Symposia Proceedings, Boston, MA, November 14, 1983.* Volume 26. New York, NY: Elsevier Science Publishing Company, Inc.

Hunter, R. L. 1989. *Events and Processes for Constructing Scenarios for the Release of Transuranic Waste From the Waste Isolation Pilot Plant, Southeastern New Mexico.* SAND89-2546. Albuquerque, NM: Sandia National Laboratories.

Kaplan, M. F. 1982. *Archeological Data as a Basis for Repository Marker Design.* ONWI-354. Washington, DC: U.S. Department of Energy.

Lappin, A. R., R. L. Hunter, D. P. Garber, P. B. Davies, R. L. Beauheim, D. J. Borns, L. H. Brush, B. M. Butcher, T. Cauffman, M. S. Y. Chu, L. S. Gomez, R. V. Guzowski, H. J. Iuzzolino, V. Kelley, S. J. Lambert, M. G. Marietta, J. W. Mercer, E. J. Nowak, J. Pickens, R. P. Rechard, M. Reeves, K. L. Robinson, and M. D. Siegel. 1989. *Systems Analysis, Long-Term Radionuclide Transport, and Dose Assessments, Waste Isolation Pilot Plant (WIPP), Southeastern New Mexico; March 1989.* SAND89-0462. Albuquerque, NM: Sandia National Laboratories.

Laul, J. C., and M. R. Smith. 1988. *Disequilibrium Study of Natural Radionuclides of Uranium and Thorium Series in Cores and Briny Groundwaters from Palo Duro Basin, Texas.* PNL/SRP-5783. Richland, WA: Pacific Northwest Laboratory.

LaVenue, A. M., T. L. Cauffman, and J. F. Pickens. 1990. *Ground-Water Flow Modeling of the Culebra Dolomite: Volume 1--Model Calibration.* SAND89-7068. Albuquerque, NM: Sandia National Laboratories.

Marietta, M. G., S. G. Bertram-Howery, D. R. Anderson, K. Brinster, G. Guzowski, H. Iuzzolino, and R. P. Rechard. 1989. *Performance Assessment*

Methodology Demonstration: Methodology Development for Purposes of Evaluating Compliance with EPA 40 CFR Part 191, Subpart B, for the Waste Isolation Pilot Plant. SAND89-2027. Albuquerque, NM: Sandia National Laboratories.

Martz, H. F., and M. C. Bryson. 1982. *Predicting Low-Probability/High-Consequence Events.* LA-UR-82-1668. Los Alamos, NM: Los Alamos National Laboratory.

Neretnieks, I., and A. Rasmussen. 1984. "An Approach to Modeling Radionuclide Migration in a Medium with Strongly Varying Velocity and Block Sizes along the Flow Path." *Water Resources Research* vol. 20, no. 12: 1823-1836.

Nowak, E. J., J. R. Tillerson, and T. M. Torres. 1990. *Initial Reference Seal System Design: Waste Isolation Pilot Plant.* SAND90-0355. Albuquerque, NM: Sandia National Laboratories.

Powers, D. W., S. J. Lambert, S-E Shaffer, L. R. Hill, and W. D. Weart, eds. 1978. *Geological Characterization Report, Waste Isolation Pilot Plant (WIPP) Site, Southeastern New Mexico.* 2 volumes. SAND78-1596. Albuquerque, NM: Sandia National Laboratories.

Rechard, R. P., H. J. Iuzzolino, and J. S. Sandha. 1990. *Data Used in Preliminary Performance Assessment of the Waste Isolation Pilot Plant (1990).* SAND89-2408. Albuquerque, NM: Sandia National Laboratories.

Reeves, M., et al. 1991. *Regional Double-Porosity Solute Transport in the Culebra Dolomite Under Brine-Reservoir-Breach Release Conditions: An Analysis of Parameter Sensitivity and Importance.* SAND89-7069. Albuquerque, NM: Sandia National Laboratories.

Stormont, J. C., E. W. Peterson, and P. L. Lagus. 1987. *Summary of and Observations about WIPP Facility Horizon Flow Measurements through 1986.* SAND87-0176. Albuquerque, NM: Sandia National Laboratories.

Thomas, R. E. 1982. *Uncertainty Analysis.* ONWI-380. Washington, DC: Office of Nuclear Waste Isolation, U.S. Department of Energy.

Tierney, M. S. 1990. *Constructing Probability Distributions of Uncertain Variables in Models of the Performance of the Waste Isolation Pilot Plant.* SAND90-2510. Albuquerque, NM: Sandia National Laboratories.

U.S. DOE (Department of Energy). 1981. *Brine Pocket Occurrences in the Castile Formation, Southeastern New Mexico.* DOE/TME-3080.

U.S. DOE (Department of Energy). 1983. *Brine Reservoirs in the Castile Forrmation, Waste Isolation Pilot Plant (WIPP) Project, Southeastern New Mexico.* DOE/TME-3153.

U.S. DOE (Department of Energy). 1987. *Integrated Data Base for 1987: Spent Fuel and Radioactive Waste Inventories, Projects and Characterizations.* DOE/RW-0006, Rev. 3.

U.S. DOE (Department of Energy). 1989. *Radionuclide Source Term for the WIPP*. DOE/WIPP-88-005. Carlsbad, NM: U.S. Department of Energy.

U.S. DOE (Department of Energy). 1990a. *Integrated Data Base for 1990: Spent Fuel and Radioactive Waste Inventories, Projects and Characterizations*. DOE/RW-0006, Rev. 6.

U.S. DOE (Department of Energy). 1990b. *Final Supplement Environmental Impact Statement, Waste Isolation Pilot Plant*. DOE/EIS-0026-FS. Washington, DC: U.S. Department of Energy, Office of Environmental Restoration and Waste Management.

WIPP PERFORMANCE ASSESSMENT BIBLIOGRAPHY

PUBLISHED

Anderson, D. R., M. G. Marietta, and S. G. Bertram-Howery. 1991. *WIPP Performance Assessment: A 1990 Snapshot of Compliance with 40 CFR 191, Subpart B*. SAND90-2338. Albuquerque, NM: Sandia National Laboratories.

Anderson, D. R., M. G. Marietta, and S. G. Bertram-Howery. 1991. "WIPP Performance Assessment: A 1990 Snapshot of Compliance with 40 CFR 191, Subpart B." *Proceedings of the Probabilistic Safety Assessment and Management (PSAM) Conference, Beverly Hills, California, February 4-7, 1991.* Amsterdam: Elsevier Science Publishers. 893-898.

Bertram-Howery, S. G., and R. L. Hunter. 1989. *Plans for Evaluation of the Waste Isolation Pilot Plant's Compliance with EPA Standards for Radioactive Waste Management and Disposal*. SAND88-2871. Albuquerque, NM: Sandia National Laboratories.

Bertram-Howery, S. G., and R. L. Hunter, eds. 1989. *Preliminary Plan for Disposal-System Characterization and Long-Term Performance Evaluation of the Waste Isolation Pilot Plant*. SAND89-0178. Albuquerque, NM: Sandia National Laboratories.

Bertram-Howery, S. G., and P. N. Swift. 1990. *Status Report: Potential for Long-Term Isolation by the Waste Isolation Pilot Plant Disposal System.* SAND90-0616. Albuquerque, NM: Sandia National Laboratories.

Bertram-Howery, S. G., and P. N. Swift. 1991. *Early-1990 Status of Performance Assessment for the Waste Isolation Pilot Plant Disposal System.* SAND90-2095. Albuquerque, NM: Sandia National Laboratories.

Bertram-Howery, S. G., and P. N. Swift. 1991. "Early-1990 Status of Performance Assessment for the Waste Isolation Pilot Plant Disposal System." *Proceedings of the Probabilistic Safety Assessment and Management (PSAM) Conference, Beverly Hills, California, February 4-7, 1991.* Amsterdam: Elsevier Science Publishers. 325-330.

Bertram-Howery, S. G., M. G. Marietta, D. R. Anderson, K. F. Brinster, L. S. Gomez, R. V. Guzowski, and R. P. Rechard. 1989. *Draft Forecast of the Final Report for the Comparison to 40 CFR Part 191, Subpart B for the Waste Isolation Pilot Plant*. SAND88-1452. Albuquerque, NM: Sandia National Laboratories.

Bertram-Howery, S. G., M. G. Marietta, R. P. Rechard, P. N. Swift, D. R. Anderson, B. L. Baker, J. E. Bean, Jr., W. Beyeler, K. F. Brinster, R. V. Guzowski, J. C. Helton, R. D. McCurley, D. K. Rudeen, J. D. Schreiber, and P. Vaughn. 1990. *Preliminary Comparison with 40 CFR Part 191, Subpart B for the Waste Isolation Pilot Plant, December 1990*. SAND90-2347. Albuquerque, NM: Sandia National Laboratories.

Brinster, K. F. 1991. *Preliminary Geohydrologic Conceptual Model of the Los Medaños Region near the Waste Isolation Pilot Plant for the Purpose of Performance Assessment.* SAND89-7147. Albuquerque, NM: Sandia National Laboratories.

Guzowski, R. V. 1990. *Preliminary Identification of Scenarios That May Affect the Escape and Transport of Radionuclides From the Waste Isolation Pilot Plant, Southeastern New Mexico.* SAND89-7149. Albuquerque, NM: Sandia National Laboratories.

Guzowski, R. V. 1991. *Evaluation of Applicability of Probability Techniques to Determining the Probability of Occurrence of Potentially Disruptive Intrusive Events at the Waste Isolation Pilot Plant.* SAND90-7100. Albuquerque, NM: Sandia National Laboratories.

Guzowski, R. V. 1991. *Preliminary Identification of Scenarios for the Waste Isolation Pilot Plant, Southeastern New Mexico.* SAND90-7090. Albuquerque, NM: Sandia National Laboratories.

Guzowski, R. V. 1991. "Preliminary Identification of Scenarios for the Waste Isolation Pilot Plant, Southeastern New Mexico." *Proceedings of the Probabilistic Safety and Management (PSAM) Conference, Beverly Hills, California, February 4-7, 1991.* Amsterdam: Elsevier Science Publishers. 337-342.

Guzowski, R. V., and M. M. Gruebel, eds. 1991. *Background Information Presented to the Expert Panel on Inadvertent Human Intrusion into the Waste Isolation Pilot Plant.* SAND91-0928. Albuquerque, NM: Sandia National Laboratories.

Helton, J. C., J. W. Garner, R. D. McCurley, and D. K. Rudeen. 1991. *Sensitivity Analysis Techniques and Results for Performance Assessment at the Waste Isolation Pilot Plant.* SAND90-7103. Albuquerque, NM: Sandia National Laboratories.

Hora, S. C., D. von Winterfeldt, and K. M. Trauth. 1991. *Expert Judgment on Inadvertent Human Intrusion into the Waste Isolation Pilot Plant.* SAND90-3063. Albuquerque, NM: Sandia National Laboratories.

Hunter, R. L. 1989. *Events and Processes for Constructing Scenarios for the Release of Transuranic Waste from the Waste Isolation Pilot Plant, Southeastern New Mexico.* SAND89-2546. Albuquerque, NM: Sandia National Laboratories.

Marietta, M. G., S. G. Bertram-Howery, D. R. Anderson, K. F. Brinster, R. V. Guzowski, H. J. Iuzzolino, and R. P. Rechard. 1989. *Performance Assessment Methodology Demonstration: Methodology Development for Evaluating Compliance with EPA 40 CFR 191, Subpart B, for the Waste Isolation Pilot Plant.* SAND89-2027. Albuquerque, NM: Sandia National Laboratories.

Marietta, M. G., S. G. Bertram-Howery, R. P. Rechard, and D. R. Anderson. 1991. "Status of WIPP Compliance with EPA 40 CFR 191, December 1990." *Proceedings of the 1991 International High-Level Radioactive Waste Management Conference - Public Safety and Technical Achievement, Las Vegas, Nevada, April 28-May 3,1991.*

Rechard, R. P. 1989. *Review and Discussion of Code Linkage and Data Flow in Nuclear Waste Compliance Assessments.* SAND87-2833. Albuquerque, NM: Sandia National Laboratories.

Rechard, R. P. 1991. *CAMCON: Computer System for Assessing Regulatory Compliance of the Waste Isolation Pilot Plant.* SAND90-2094. Albuquerque, NM: Sandia National Laboratories.

Rechard, R. P. 1991. "CAMCON: Computer System for Assessing Regulatory Compliance of the Waste Isolation Pilot Plant." *Proceedings of the Probabilistic Safety and Management (PSAM) Conference, Beverly Hills, California, February 4-7, 1991.* Amsterdam: Elsevier Science Publishers. 899-904.

Rechard, R. P. 1991. "Use of Risk to Resolve Conflicts in Assessing Hazards." *Proceedings of the First International Mixed-Waste Symposium, Baltimore, Maryland, August 26-29, 1991.*

Rechard, R. P., H. J. Iuzzolino, J. S. Rath, R. D. McCurley, and D. K. Rudeen. 1989. *User's Manual for CAMCON: Compliance Assessment Methodology Controller.* SAND88-1496. Albuquerque, NM: Sandia National Laboratories.

Rechard, R. P., H. J. Iuzzolino, and J. S. Sandha. 1990. *Data Used in Preliminary Performance Assessment of the Waste Isolation Pilot Plant (1990).* SAND89-2408. Albuquerque, NM: Sandia National Laboratories.

Rechard, R. P., W. Beyeler, R. D. McCurley, D. K. Rudeen, J. E. Bean, and J. D. Schreiber. 1990. *Parameter Sensitivity Studies of Selected Components of the Waste Isolation Pilot Plant Repository/Shaft System.* SAND89-2030. Albuquerque, NM: Sandia National Laboratories.

Rechard, R. P., P. J. Roache, R. L. Blaine, A. P. Gilkey, and D. K. Rudeen. 1991. *Quality Assurance Procedures for Computer Software Supporting Performance Assessments of the Waste Isolation Pilot Plant.* SAND90-1240. Albuquerque, NM: Sandia National Laboratories.

Roache, P. J., P. M. Knupp, S. Steinberg, and R. L. Blaine. 1990. "Experience with Benchmark Test Cases for Groundwater Flow" in *FED-Vol. 93, Benchmark Test Cases for Computational Fluid Dynamics.* Eds. I. Celik and C. J. Freitas. American Society of Mechanical Engineers.

SNL (Sandia National Laboratories) WIPP Performance Assessment Division. 1991. *Preliminary Comparison with 40 CFR Part 191, Subpart B for the Waste Isolation Pilot Plant, December 1991—Volume 1: Methodology and Results.* SAND91-0893/1. Albuquerque NM: Sandia National Laboratories.

SNL (Sandia National Laboratories) WIPP Performance Assessment Division. 1991. *Preliminary Comparison with 40 CFR Part 191, Subpart B for the Waste Isolation Pilot Plant, December 1991–Volume 2: Probability and Consequence Modeling*. SAND91-0893/2. Albuquerque, NM: Sandia National Laboratories.

SNL (Sandia National Laboratories) WIPP Performance Assessment Division. 1991. *Preliminary Comparison with 40 CFR Part 191, Subpart B for the Waste Isolation Pilot Plant, December 1991–Volume 3: Reference Data*. R. P. Rechard, A. C. Peterson, J. D. Schreiber, H. J. Iuzzolino, M. S. Tierney, and J. S. Sandha, eds. SAND91-0893/3. Albuquerque, NM: Sandia National Laboratories.

Tierney, M. S. 1990. *Constructing Probability Distributions of Uncertain Variables in the Models of the Performance of the Waste Isolation Pilot Plant*. SAND90-2510. Albuquerque, NM: Sandia National Laboratories.

Tierney, M. S. 1991. *Combining Scenarios in a Calculation of the Overall Probability Distribution of Cumulative Releases of Radioactivity from the Waste Isolation Pilot Plant, Southeastern New Mexico*. SAND90-0838. Albuquerque, NM: Sandia National Laboratories.

Trauth, K. M., S. C. Hora, and R. P. Rechard. 1991. "Expert Judgment as Input to Waste Isolation Pilot Plant Performance-Assessment Calculations, Probability Distributions of Significant System Parameters." *Proceedings of the First International Mixed-Waste Symposium, Baltimore, Maryland, August 26-29, 1991*.

IN PREPARATION

Berglund, J., and M. G. Marietta. *A Computational Model for the Direct Removal of Repository Material by Drilling*. SAND90-2977. Albuquerque, NM: Sandia National Laboratories.

Blaine, T., and D. Jackson. *Environmental Pathways Data Base for WIPP Radiological Safety Assessments*. SAND90-7101. Albuquerque, NM: Sandia National Laboratories.

Gilkey, A. *ALGEBRA User's Manual*. SAND88-1431. Albuquerque, NM: Sandia National Laboratories.

Gilkey, A. *BLOT User's Manual*. SAND88-1432. Albuquerque, NM: Sandia National Laboratories.

Marietta, M. G., D. R. Anderson, D. Scott, and P. N. Swift. *Review of Parameter Sensitivity Studies for the Waste Isolation Pilot Plant*. SAND89-2028. Albuquerque, NM: Sandia National Laboratories.

Marietta, M. G., R. P. Rechard, P. N. Swift, and others. *Preliminary Probabilistic Safety Assessment of the Waste Isolation Pilot Plant*. SAND90-2718. Albuquerque, NM: Sandia National Laboratories.

Marietta, M. G., S. G. Bertram-Howery, R. P. Rechard, and D. R. Anderson. *Status of WIPP Compliance with EPA 40 CFR 191, December 1990.* SAND90-2424. Albuquerque, NM: Sandia National Laboratories.

Rechard, R. P. *CAMCON Architectural Overview and Program Reference Manual.* SAND90-1984. Albuquerque, NM: Sandia National Laboratories.

Rechard, R. P., A. P. Gilkey, D. K. Rudeen, J. S. Rath, W. Beyeler, R. Blaine, H. J. Iuzzolino, and R. D. McCurley. *User's Reference Manual for CAMCON: Compliance Assessment Methodology Controller Version 3.0.* SAND90-1983. Albuquerque, NM: Sandia National Laboratories.

Rechard, R. P., H. J. Iuzzolino, and J. S. Sandha. *Quality Assurance Procedures for Data Supporting Performance Assessments of the Waste Isolation Pilot Plant.* SAND91-0429. Albuquerque, NM: Sandia National Laboratories.

Rechard, R. P., P. J. Roache, J. W. Berglund, D. K. Rudeen, J. E. Bean, and J. D. Schreiber. *Quality Assurance Procedures for Analyses Supporting Performance Assessments of the Waste Isolation Pilot Plant.* SAND91-0428. Albuquerque, NM: Sandia National Laboratories.

Roache, P. J., R. Blaine, and B. L. Baker. *SECO 2.1 User's Manual.* SAND90-7096. Albuquerque, NM: Sandia National Laboratories.

SNL (Sandia National Laboratories) WIPP Performance Assessment Division. *Preliminary Comparison with 40 CFR Part 191, Subpart B for the Waste Isolation Pilot Plant, December 1991—Volume 4: Uncertainty and Sensitivity Analyses.* SAND91-0893/4. Albuquerque, NM: Sandia National Laboratories.

Swift, P. N., B. L. Baker, K. F. Brinster, M. G. Marietta, and P. J. Roache. *Parameter and Boundary Conditions Sensitivity Studies Related to Climate Variability and Scenario Screening for the Waste Isolation Pilot Plant.* SAND89-2029. Albuquerque, NM: Sandia National Laboratories.

GLOSSARY

absorption - The attraction of molecules of gases or ions in solution to the surface of solids in contact with them.

accessible environment - The accessible environment means (1) the atmosphere, (2) land surfaces, (3) surface waters, (4) oceans, and (5) all of the lithosphere that is beyond the controlled area *(40 CFR 191.12[k])*.

actinide - Any element in the actinium series of elements of increasing atomic numbers beginning with actinium (89) and ending with lawrencium (103).

activation product - An isotope created from another isotope subjected to radiation.

adsorption - Adherence of gas molecules, or of ions or molecules in solution, to the surface of solids with which they are in contact.

advection - The process of transport of an aqueous property by mass motion.

algorithm - A procedure for solving a mathematical problem in a finite number of steps that frequently involves repetition of an operation.

alpha particle - A positively charged particle emitted in the radioactive decay of certain nuclides. Made up of two protons and two neutrons bound together, it is identical to the nucleus of a helium atom. It is the least penetrating of the three common types of radiation--alpha, beta, and gamma.

alternative conceptual model - Multiple working hypotheses of a system. Part of a formalized procedure of inquiry first proposed by T. C. Chamberlin in 1890. The purpose is to "divide our affection, suggest critical tests, and expose more facets of a system," thereby avoiding being too strongly swayed by one conceptual model (set of hypotheses) and unwittingly seeking only facts to support it.

anhydrite - A mineral consisting of anhydrous calcium sulfate ($CaSO_4$). It is gypsum without water, and is denser, harder, and less soluble.

anisotropic - Pertaining to any material property, such as hydraulic conductivity, that varies with direction.

anoxic - Without free oxygen.

anticline - A fold of rocks, generally concave downward (convex upward), whose core contains stratigraphically older rocks.

aperture - The open space caused by a fracture in rock.

aquifer - A body of rock that is sufficiently permeable to conduct groundwater and to yield significant quantities of groundwater to wells and springs.

aquitard - A less permeable unit in a hydrostratigraphic sequence that retards but does not prevent the flow of water to or from an adjacent aquifer.

argillaceous - Containing clay-sized particles or clay minerals.

argillic - See argillaceous.

backfill - Material filling a former excavation (e.g., salt placed around the waste containers, filling the open space in the room).

barrier - "Barrier means any material or structure that prevents or substantially delays movement of water or radionuclides toward the accessible environment. For example, a barrier may be a geologic structure, a canister, a waste form with physical and chemical characteristics that significantly decrease the mobility of radionuclides, or a material placed over and around waste, provided that the material or structure substantially delays movement of water or radionuclides." *(40 CFR 191.12[d])*

benchmark - To compare model predictions made with one applied model with those obtained with other implementations of analytic or numerical computational models. Benchmarking is a part of verification.

bentonite - A commercial term applied to expansive clay materials containing montmorillonite (smectite) as the essential mineral.

beta distribution - A useful model for random variates defined on a finite interval. The beta distribution permits representation of a wide variety of distributional shapes by selection of two shape parameters.

biodegradable - Capable of being broken down by microorganisms.

biogenic - Produced directly by the physiological activities of organisms, either plant or animal.

biosphere - The life zone of the earth, including the lower part of the atmosphere, the hydrosphere, soil, and the lithosphere to a depth of about 2 km (1 mi).

biotransformation - The changing of chemical compounds within a living system.

biotransport - Movement of radionuclides over biological pathways, such as through the food chain.

borehole - (1) A manmade hole in the wall, floor, or ceiling of a subsurface room used for verifying geology, making observations, or emplacing canisters of remote-handled transuranic (RH-TRU) waste. (2) A hole drilled from the surface for purposes of geologic or hydrologic testing, or to explore for resources; sometimes referred to as a drillhole.

breccia - A rock consisting of very angular, coarse fragments held together by a mineral cement or a fine-grained matrix (as sand or clay).

breccia pipe - A vertically cylindrical feature filled with collapse debris. It is formed when relatively fresh water from a deep aquifer moves upward dissolving more soluble rocks and causing collapse of the surrounding rock material.

brine aquifer - The Rustler-Salado residuum, a zone of residual material, left after dissolution of the original salt at the interface of the Rustler and Salado Formations, that is highly permeable and contains much brine.

brine inclusion - A small cavity in a rock mass (salt) containing brine; also, the brine included in such an opening. Some gas is often present.

brine occurrence - See brine reservoir.

brine pocket - See brine occurrence.

brine reservoir - Pressurized brine in the Castile Formation; also referred to as "brine pocket" or "brine occurrence."

calibrate - To vary parameters of an applied model within reasonable range until differences between observed data and computed values are minimized (subjective).

canister - For the WIPP, it is a container, usually cylindrical, for remotely handled waste, spent fuel, or high-level waste; affords physical containment during handling but not radiation shielding.

capacitance - In hydrology, the combined compressibility of the solid porous matrix and the fluid within the pores.

capture volume - The maximum volume of waste through which neutrally buoyant particles can pass (by means of being carried along with brine) within a given time period (usually 10,000 years).

cask - A shipping container that is radiation shielded.

cationic - Pertaining to positively charged ions.

chlorite - Any of a group of magnesium-, aluminum-, and iron-bearing hydrous silicate minerals. Their layered, sheet-like structure is similar to that of clays and micas.

clastic - Rock or sediment composed principally of broken fragments that are derived from preexisting rocks or minerals.

claystone - An indurated clay having the texture and composition of shale but lacking the fine lamination and fissility.

cokriging - Geostatistical technique for estimating two (or more) correlated variables from field measurements at different locations.

compaction - Mechanical process by which the pore space in the waste is reduced prior to waste emplacement.

complementary cumulative distribution function (CCDF) - One minus the cumulative distribution function.

compliance evaluation or assessment - The process of assessing the regulatory compliance of a mined geologic waste repository.

compressibility - A measure of the ability of a substance to be reduced in volume by application of pressure; quantitatively, the reciprocal of the bulk modulus.

computational model - The computational model is the implementation of the mathematical model. The implementation may be through analytic or numerical solution. Often the analytic solution is numerically evaluated (e.g., numerical integration or evaluation of complex functions); hence, both solution techniques are typically coded on the computer. Consequently, the computational model is often called a computer model.

computer model - The appropriately coded analytical, quasi-analytical, or numerical solution technique used to solve a mathematical model; generic, until site-specific data are used.

conceptual model - The set of hypotheses (preferably based on observed data) that postulate the description and behavior of the disposal system (e.g., structural geometry, material properties, and significant physical processes that affect behavior). For WIPP, the data pertinent for a conceptual model are stored in the secondary data base.

conductivity - A shortened form of hydraulic conductivity.

confined groundwater - Groundwater occurring in an aquifer bounded above and below by an aquitard.

confirm - To use full-scale in situ experiments to corroborate portions of parameter ranges or distributions established by laboratory or small-scale tests.

conformable - Strata or stratification characterized by an unbroken sequence in which the layers are formed one above the other by regular, uninterrupted deposition.

connectivity - The manner in which individual nodes or points connect together to form elements or legs.

consequence module - A module of the CAMCON system that assesses the consequences of radionuclides being transported from the repository.

consolidate - To cause loosely aggregated, soft, or liquid earth materials to become firm and coherent.

consolidation - Process by which backfill and waste mass loses pore space in response to the increasing weight of overlying material.

Consultation and Cooperation (C&C) Agreement - An agreement that affirms the intent of the Secretary of Energy to consult and cooperate with the State of New Mexico with respect to State public health and safety concerns. It is an appendix to a July 1981 agreement (the Stipulated Agreement) made with the State and approved by the District court when that court stayed the proceedings of a lawsuit against the DOE by the State. The C&C agreement identifies a number of "key events" and "milestones" in the construction and operation of the WIPP that must be reviewed by the State before they are started. The C&C agreement has been updated and extended as recently as March 1988.

controlled area - The controlled area means "(1) a surface location, to be identified by passive institutional controls, that encompasses no more that 100 km and extends horizontally no more than 5 km in any direction from the outer boundary of the original location of the radioactive wastes in a disposal system; and (2) the subsurface underlying such a surface location." (*40 CFR 191.12[g]*)

creep - A usually very slow deformation of solid rock resulting from constant stress; refers to the gradual flow of salt under high compressive loading.

creep closure - Closure of underground openings, especially openings in salt, by plastic flow of the surrounding rock under pressure.

criticality - The state of a mass of fissionable material when it is sustaining a chain reaction.

cumulative distribution function - The sum (or integral as appropriate) of the probability of those values of a random variable that are less than or equal to a specified value.

curie - Ci; a unit of radioactivity equal to the number of disintegrations per second of 1 pure gram of radium-226 (1 Ci = 3.7×10^{10} disintegrations per second).

cuttings - Rock chips cut by a bit in the process of drilling a borehole or well.

Darcian flow - Pertaining to a formula derived by Darcy for the flow of fluids through porous media, which states that flow is directly proportional to the hydraulic gradient, the cross-sectional area through which flow occurs, and the hydraulic conductivity.

darcy - An English standard unit of permeability, defined by a medium for which a flow of 1 cm^3/s is obtained through a section of 1 cm^2, for a fluid viscosity of 1 cP and a pressure gradient of 1 atm/cm. One darcy is equal to 9.87×10^{-13} m^2.

decommissioning - Actions taken upon abandonment of the repository to reduce potential environmental, health, and safety impacts, including repository sealing as well as activities to stabilize, reduce, or remove radioactive materials or to demolish surface structures.

decontamination - The removal of radioactive contamination from facilities, equipment, or soils by washing, heating, chemical or electrochemical treating, mechanical cleaning, or other techniques.

desaturate - To remove liquid from a material until it is no longer saturated.

deterministic - An exact mathematical relationship between the dependent and independent variables in a system.

diffusion - The transfer of mass components from a region of higher to lower concentration.

disposal - "Disposal means permanent isolation of spent nuclear fuel or radioactive waste from the accessible environment with no intent of recovery, whether or not such isolation permits the recovery of such fuel or waste. For example, disposal of waste in a mined geologic repository occurs when all of the shafts to the repository are backfilled and sealed." *(40 CFR 191.02[1])*

disposal system - Any combination of engineered and natural barriers that isolate spent nuclear fuel or radioactive waste after disposal (*40 CFR 191.12(a)*). The natural barriers extend to the accessible environment. The WIPP disposal system comprises the disposal region, shafts, and controlled area.

disturbed rock zone - That portion of the geologic barrier of which the physical or chemical properties may have changed significantly as a result of underground construction.

dolomite - A carbonate sedimentary rock consisting of more than 50% of the mineral dolomite [$CaMg(CO_3)_2$].

dose - A general term indicating the amount of energy absorbed per unit mass from incident radiation.

dose equivalent - The product of absorbed dose and modifying factors that take into account the biological effect of the absorbed dose. While dose includes only physical factors, dose equivalent includes both physical and biological factors and provides a radiation-protection scale applicable to all types of radiation. Units are rem for individual and person-rem for a population group.

dosimetry - The measurement of radiation doses.

drawdown - The lowering of water level in a well as a result of fluid withdrawal.

drift - A horizontal passageway in a mine.

dynamical - Characterized by or tending to produce continuous change or advance.

empirical - Relying explicitly upon or derived explicitly from observation or experiment.

emplacement - At WIPP, the placing of radioactive wastes within the waste rooms.

equipotential - Points with the same hydraulic head.

equivalent grams plutonium-239 - Fissionable content of radioactive waste converted to an equivalent number of grams of plutonium-239.

Eulerian - Pertaining to a mathematical representation of fluid flow in which the behavior and properties of the fluid are described at fixed points within the coordinate system.

evaporite - A sedimentary rock composed primarily of minerals produced by precipitation from a solution that has become concentrated by the evaporation of a solvent, especially salts deposited from a restricted or enclosed body of seawater or from the water of a salt lake. In addition to halite (NaCl), these salts include potassium, calcium, and magnesium chlorides and sulfates.

evapotranspiration - Loss of water from a land area through transpiration of plants and evaporation from the soil.

event - A phenomenon that occurs instantaneously or within a short time interval relative to the time frame of interest.

exploratory drilling - Drilling to an unexplored depth or in territory having unproven resources.

exponential distribution - A probability distribution whose pdf is an exponential function defined on the range of the variable in question.

facies - An areally restricted part of a rock body that differs in mineralogic composition, grain size, or fossil content from nearby beds deposited at the same time and that broadly corresponds to a certain environment or mode of deposition.

facility - The surface structures of the repository.

finding - A conclusion that is reached after an evaluation.

fission product - Any radioactive or stable nuclide resulting from fission, including both primary fission fragments and their radioactive decay products.

flowpath - The path traveled by a neutrally buoyant particle released into a groundwater-flow field.

fluvial - Of or pertaining to a river or rivers.

frequentist - One who believes that the probability of an event is the ratio of the number of times the event occurs in a series of trials of a chance experiment to the number of trials performed.

geochemistry - The study of the distribution and amounts of the chemical elements in minerals, ores, rocks, soils, water, and the atmosphere.

geohydrology - The study of the hydrologic or flow characteristics of subsurface waters.

geology - The study of the Earth, the materials of which it is made, the processes that act on these materials, the products formed, and the history of the planet and its life forms since its origin.

geomorphology - The study of the classification, description, nature, origin, and development of present landforms and their relationships to underlying structure, and of the history of geologic changes as recorded by these surface features.

geophysics - The study of the Earth by quantitative physical methods such as electric, gravity, magnetic, seismic, and thermal techniques.

geosphere - The solid portion of the Earth as compared to the atmosphere and the hydrosphere.

getter - A substance that sorbs gases.

glaciation - The formation, movement, and recession of glaciers or ice sheets. Used narrowly, the term can refer only to the growth of ice sheets.

glauberite - A brittle, light-colored, monoclinic mineral: $Na_2Ca(SO_4)_2$. It has a vitreous luster and saline taste and occurs in saline residues.

gradational - Gradual change in rock characteristics from one rock body to another.

grout - A cement slurry of high water content.

gypsum - Hydrous calcium sulfate ($CaSO_4 \cdot 2H_2O$), a mineral frequently associated with halite and anhydrite in evaporites.

halite - A dominant mineral in evaporites; salt, NaCl.

halogenated - Atoms from the halogen family of elements combined with other atoms such as carbon.

headward erosion - The lengthening and cutting upstream of a young valley or gully above the original source of its stream.

Holocene - A geologic epoch of the Quaternary Period, subsequent to the Pleistocene Epoch (about 10,000 years ago) and continuing to the present.

horizon - In geology, an interface indicative of a particular position in a stratigraphic sequence. An underground level; for instance, the waste-emplacement horizon at the WIPP is the level about 650 m (2,150 ft) deep in the Salado Formation where openings are mined for waste disposal.

host rock - The geologic medium in which radioactive waste is emplaced.

hot cell - A heavily shielded compartment in which highly radioactive material can be handled, generally by remote control.

hydraulic - Of, involving, moved, or operated by a fluid under pressure.

hydraulic conductivity - The measure of the rate of flow of water through a cross-sectional area under a unit hydraulic gradient.

hydraulic gradient - A quantity defined in the study of ground-water hydraulics that describes the rate of change of total hydraulic head per unit distance of flow in a given direction.

hydraulic head - The elevation above a datum to which water would rise at a given point in a well open to an aquifer. It is a function of the elevation of the aquifer and the fluid pressure within it.

hydrochemical - The diagnostic chemical character of ground water occurring in hydrologic systems.

hydrodynamic dispersion - The tendency of a solute to spread out from the path that it would be expected to follow according to the advective hydraulics of the solvent.

hydrogeology - The study of subsurface waters and of related geologic aspects of surface waters.

hydrologic properties - Those properties of a rock that govern the entrance of water and the capacity to hold, transmit, and deliver water, such as porosity, effective porosity, specific retention, permeability, and the directions of maximum and minimum permeabilities.

hydrology - The study of global water, its properties, circulation, and distribution.

hydropad - A complex of water wells closely spaced for testing on hydrostratigraphic units.

hydrophobic - Lacking an affinity for, repelling, or failing to adsorb or absorb water.

hydrostatic - Pressure caused by the weight of overlying fluid.

hydrostratigraphic - Pertaining to a body of rock in which lateral variations in hydraulic properties within the study area are less significant than vertical variations between it and the overlying and underlying units.

in situ - In the natural or original position; used to distinguish in-place experiments, rock properties, and so on, from those in the laboratory.

interbeds - Sedimentary beds that lie between or alternate with other beds having different characteristics.

interfinger - The disappearance of sedimentary bodies into laterally adjacent masses by splitting into many thin layers, each terminating independently.

intergranular - Between the grains or particles of a rock.

interpolators - Computer programs used to estimate an intermediate value of one (dependent) variable which is a function of a second variable.

intertonguing - The lateral intergradation of different rock types through a vertical succession of thin, interlocking or overlapping, wedge-shaped layers.

intracrystalline - Pertaining to something within a mineral crystal.

ionic strength - A measure of the average electrostatic interaction among ions in a solution; a function of both concentration and valence of the solutes.

isolation - Refers to inhibiting the transport of radioactive material so that the amounts and concentrations of this material entering the accessible environment will be kept within prescribed limits.

isopach - A line drawn on a map through points of equal thickness of a designated stratigraphic unit or group of stratigraphic units.

isotope - A species of atom characterized by the number of protons and the number of neutrons in its nucleus. In most instances, an element can exist as any of several isotopes, differing in the number of neutrons, but not the number of protons, in their nuclei. Isotopes can be either stable isotopes or radioactive isotopes (also called radioisotopes or radionuclides).

isotropic - Having the same property in all directions.

iterative - A computational procedure in which repetition of a set of operations produces results that approximate the desired result more and more closely as the number of repetitions increases.

jointing - The condition or presence of parallel fractures or partings in a rock, without displacement.

karst - A topography formed from solution of limestone, dolomite, or gypsum; characterized by sinkholes, caves, and underground drainage.

karstification - The formation of karst features by the solutional and mechanical action of water.

kriging - Geostatistical method for estimating magnitude plus uncertainty of a quantity (e.g., hydrogeological parameters), that is distributed in space and is measured in a network of points, at points other than the points of the network.

lacustrine - Pertaining to a lake or lakes.

Lagrangian - Pertaining to a mathematical representation of fluid flow in which the behavior and properties of the fluid are described for elements that move with flow.

langbeinite - A colorless to reddish mineral [$K_2Mg_2(SO_4)_3$] used as a source of potassium in fertilizers and formed as a saline residue from evaporation.

Latin hypercube sampling - A Monte Carlo sampling technique that divides the cumulative distribution function into intervals of equal probability and samples from each interval.

lenticular - Having the cross-sectional shape of a lens, esp. of a double-convex lens. The term may be applied to a body of rock or a sedimentary structure.

ligands - Ions bound to a central atom in a compound.

limey - Containing calcium carbonate ($CaCO_3$).

lithologic - The descriptive characteristics of rock composition.

lithosphere - The solid portion of the earth, including any groundwater contained within it, as opposed to the atmosphere and the hydrosphere.

lithostatic pressure - Subsurface pressure caused by the weight of overlying rock or soil; about 14.9 MPa at the WIPP repository level.

lognormal distribution - A probability distribution in which the logarithm of the variable in question follows a normal distribution.

loguniform distribution - A probability distribution in which the logarithm of the variable in question follows a uniform distribution.

low - A general geologic term for such features as a structural basin, a syncline, a saddle, or a sag.

management - "Management means any activity, operation, or process (except for transportation) conducted to prepare spent nuclear fuel or radioactive waste for storage or disposal, or the activities associated with placing such fuel or waste in a disposal system." *(40 CFR 191.02[m])*

material - Substance (e.g., rock type) with physical properties that can be expressed quantitatively.

material attribute - Material characteristic that varies at each element of a mesh of a numerical model.

material property - Characteristic of the material that remains constant throughout the mesh of a numerical model.

mathematical model - The mathematical representation of a conceptual model (e.g., as coupled algebraic, differential, or integral equations with proper

boundary conditions that approximate the physical processess in a specified domain of the conceptual model).

mean - The expectation of a random variable; i.e., the sum (or integral) of the product of the variable and the pdf over the range of the variable.

median - That value of a random variable at which its cdf takes the value 0.5; i.e., the 50th percentile point.

mesh - A subdivision of the domain of some mathematical model into cells for purposes of numerical solution.

microbiology - A branch of biology dealing especially with microscopic forms of life.

microcrystalline - Crystals too small to see with the naked eye.

microfracturing - The formation of fractures that cannot be detected with the unaided eye.

microwave - Electromagnetic radiation having wavelengths between 100 centimeters and 1 millimeter.

mode - That value of a random variable at which its pdf takes its maximum value.

modeler - One who studies a phenomenon or system by making a model of that phenomenon or system.

modular - Constructed with standardized units or dimensions for flexibility and variety in use.

module - A standardized computer program within a functional aggregation of computer programs.

molal - Concentration of a solution expressed in moles of solute per 1000 grams of solvent.

monocline - A local steepening in an otherwise uniformly gentle dip.

Monte Carlo sampling - A random sampling technique used in computer simulation to obtain approximate solutions to mathematical or physical problems.

mud - In drilling, a carefully formulated suspension, usually in water but sometimes in oil, used in drilling to lubricate and cool the drill bit, carry cuttings up from the bottom, and maintain pressure in the borehole to offset pressures of fluids in the formation.

mudstone - A blocky or massive, fine-grained sedimentary rock in which the proportion of clay and silt are approximately equal.

multipad - See hydropad.

neoprene - A synthetic rubber made by the polymerization of chloroprene.

neutron - An elementary particle that has approximately the same mass as the proton but lacks electric charge, and is a constituent of all nuclei having mass number greater than 1.

Newtonian fluid - Pertaining to a substance in which the rate of shear strain is directly proportional to the shear stress.

noncombustibles - Materials that will not burn.

normal (or Gaussian) distribution - A probability distribution in which the pdf is a symmetric, bell-shaped curve of bounded amplitude extending from minus infinity to plus infinity.

nuclide - A species of atom characterized by the construction of its nucleus.

organics - Compounds containing carbon.

ostracode - Any of various fossil and living species of marine and freshwater bivalve crustaceans, subclass Ostracoda.

overexcavation - Excavation of the disturbed rock zone prior to emplacement of a seal.

overgrowth - Secondary material deposited around a crystal grain of the same composition.

overpack (waste) - A container put around another container. In the WIPP, overpacks would be used on those damaged or otherwise non-transportable drums, boxes, and canisters that it would not be practical to decontaminate.

oxygen-18/oxygen-16 ratio - Comparison of the amount of oxygen-18 and oxygen-16 in a substance. Ratios in sea water reflect global volume of glacial ice.

oxyhydroxides - Compounds containing an oxide and a hydroxide group: e.g., goethite ($\alpha FeO \cdot OH$) and limonite ($FeO \cdot OH \cdot nH_2O$).

paleoclimate - A climate of the geologic past.

paleosol - A buried soil horizon of the geologic past.

panel - A group of several underground rooms bounded by two pillars and connected by drifts. Within the WIPP, a panel usually consists of seven rooms connected by 10-m-wide drifts at each end.

parameter - See variable.

particulate - Minute separate particles.

pascal (Pa) - Unit of pressure produced by a force of 1 newton applied over an area of 1 m^2. One pound per square inch is equal to 6.895×10^3 Pa.

passive institutional control - "Passive institutional control means (1) permanent markers placed at a disposal site, (2) public records and archives, (3) government ownership and regulations regarding land or resource use, and (4) other methods of preserving knowledge about the location, design, and contents of a disposal system." *(40 CFR 191.12[e])*

perched groundwater - Groundwater occurring in a discontinuous saturated zone and separated from an underlying body of groundwater by an unsaturated zone. Its water table is a perched water table.

performance assessment - Performance assessment is defined by Subpart B of *40 CFR 191* as "an analysis that (1) identifies the processes and events that might affect the disposal system, (2) examines the effects of these processes and events on the performance of the disposal system, and (3) estimates the cumulative releases of radionuclides, considering the associated uncertainties, caused by all significant processes and events. These estimates shall be incorporated into an overall probability distribution of cumulative release to the extent practicable." (*40 CFR 191.12(q)*)

permeability - A measurement of the ability of a rock or soil to allow fluid to pass through it.

physico-chemical - Pertaining to physical chemistry.

pillar - Rock left in place after mining to provide underground vertical support.

pintle - A cylindrical flanged device on the end of an RH-TRU waste canister used for grasping and lifting the canister.

plankton - Aquatic organisms that float passively or exhibit limited locomotor activity.

playa - An intermittently dry, vegetation-free, flat area at the lowest part of an undrained desert basin, underlain by stratified clay, silt, or sand, and commonly by soluble salts.

plutonium - A reactive metallic element, symbol Pu, atomic number 94, in the transuranium series of elements; used as a nuclear fuel, to produce radioactive nuclides for research, and as a fissile agent in nuclear weapons.

pluvial - Of a geologic episode, change, deposit, process, or feature resulting from the action or effects of rain.

polyethylene - Various partially crystalline lightweight thermo-plastics made from ethylene.

polyhalite - An evaporite mineral: $K_2MgCa_2(SO_4)_4.2H_2O$; a hard, poorly soluble mineral.

polypropylene - A plastic made from propylene.

polyvinyl - A plastic made from vinyl chloride.

porosity - The percentage of total rock volume occupied by voids.

post-depositional - Occurring after sediments have been laid down.

potash - Specifically K_2CO_3. Also loosely used for many potassium compounds, especially as used in agriculture or industry.

potential - In physics, the work required to bring a unit electrical charge, magnetic pole, or mass from an infinitely distant position to a designated point in a static electrical, magnetic, or gravitational field, respectively.

potentiometric surface - An imaginary surface representing the head of groundwater and defined by the level to which water will rise in a well.

predictive - Foretelling or predicting something; for the WIPP, predicting future states of the repository system.

probabilistic - Using or pertaining to probabilities or probability theory.

probability density function - For a continuous random variable X, the function giving the probability that X lies in the interval x to x+dx centered about a specified value x (i.e., the derivative of the cumulative distribution function).

process - A phenomenon that occurs over a significant portion of the time frame of interest.

quality assurance - All those planned and systematic actions necessary to provide adequate confidence that a structure, system, or component will perform satisfactorily in service.

rad - A basic unit of absorbed dose defined as an energy absorption of 100 erg/g by a specified material from any ionizing radiation incident upon that material.

radioactive waste - Solid, liquid, or gaseous material of negligible economic value that contains radionuclides in excess of threshold quantities.

radioactivity - The emission of energetic particles and/or radiation during radioactive decay.

radiochemistry - The chemical study of irradiated and naturally occurring radioactive materials and their behavior.

radiological - Pertaining to nuclear radiation and radioactivity.

radiolysis - The damage to a material caused by radiation.

radiometric - Pertaining to the disintegration of radioactive elements.

radionuclide - A radioactive nuclide.

radionuclide retardation - The process or processes that cause the time required for a given radionuclide to move between two locations to be greater than the ground-water travel time, because of physical and chemical interactions between the radionuclide and the geohydrologic unit through which the radionuclide travels.

recharge - The processes involved in the addition of water to the ground-water zone of saturation.

recrystallization - The formation, essentially in the solid state, of new crystalline mineral grains in a rock. The new grains are generally larger than the original grains and may have the same or a different mineralogical composition.

reentrant - A prominent, generally angular indentation in a land form.

rem - Roentgen equivalent in man - a special unit of dose equivalent which is the product of absorbed dose, a quality factor which rates the biological effectiveness of the radiation types producing the dose, and other modifying factors (usually equal to one). If the quality and modifying factors are unity, 1 rem is equal to 1 rad.

repository - The portion of the WIPP facility within the Salado Formation, including the access drifts, waste panels, and experimental areas, but excluding the shafts.

repository/shaft system - The WIPP underground workings, including the shafts, and all emplaced materials and the altered zones within the Salado Formation and overlying units resulting from construction of the underground workings.

retardation - The degree to which the rate of radionuclide migration is reduced below the velocity of fluid flow.

retardation factor - Fluid speed divided by mean speed.

retrieval - The act of intentionally removing radioactive waste before repository decommissioning from the underground location at which the waste had been previously emplaced for disposal.

risk - A representation of the potential of a system to cause harm, represented by combining the likelihood of undesirable occurrences and the negative effects associated with such occurrences. A general representation of risk is a set $R = \{(S_i, pS_i, cS_i), i = 1, \ldots, nS\}$ of ordered triples, where S_i is a set of similar occurrences, pS_i is the probability of S_i, cS_i is a vector of consequences associated with S_i, and nS is the number of sets.

room - An excavated cavity underground. Within the WIPP, a room is 10 m wide, 4 m high, and 91 m long.

saturated - All connected pores in a given volume of material contain fluid.

scenario - A combination of naturally occurring or human-induced events and processes that represents realistic future changes to the repository, geologic, and geohydrologic systems that could cause or promote the escape of radionuclides from the repository.

seal - An engineered barrier designed to isolate the waste panels or to impede groundwater flow in the shafts.

sealing - Formation of barriers within man-made penetrations (shafts, drill-holes, tunnels, drifts).

sedimentation - The action or process of forming or depositing rock particles in layers.

semilog - Graph or chart having a logarithmic scale on one axis and an arithmetic scale or uniform spacing on the other axis.

shaft - A man-made hole, either vertical or steeply inclined, that connects the surface with the underground workings of a mine.

significant source of groundwater - "Significant source of ground water means: (1) An aquifer that: (i) is saturated with water having less than 10,000 milligrams per liter of total dissolved solids; (ii) is within 2,500 feet of the land surface; (iii) has a transmissivity greater than 200 gallons per day per foot, provided, that any formation or part of a formation included within the source of ground water has a hydraulic conductivity greater than two gallons per day per square foot; and (iv) is capable of continuously yielding at least 10,000 gallons per day to a pumped or flowing well for a period of at least a year; or (2) an aquifer that provides the primary source of water for a community water system as of the effective date of this subpart." *(40 CFR 191.12[n])*

silicification - The introduction of, or replacement by, silica, generally resulting in the formation of fine-grained quartz, which may fill pores and replace existing minerals.

siliclastic - Clastic, noncarbonate rocks that contain almost exclusively quartz or other silicate minerals.

siltstone - A sedimentary rock composed of at least two-thirds silt-sized grains (1/256 to 1/16 mm); it tends to be flaggy, containing hard, durable, generally thin layers.

sinkhole - A hollow or funnel-shaped depression at the land surface generally caused by solution in a limestone region that communicates with a cavern or passage.

sludge - A muddy or slushy mass, deposit, or sediment.

smectite - A general term for clay minerals of the montmorillonite group that possess swelling properties and high cation-exchange capacities.

solubility - The equilibrium concentration of a solute when undissolved solute is in contact with the solvent.

solute - The material dissolved in a solvent.

sorb - To take up and hold by either adsorption or absorption.

source term - The kinds and amounts of radionuclides that make up the source of a potential release of radioactivity. For the performance assessment, the source term is defined as the sum of the quantities of the important radionuclides in the WIPP inventory that could be mobilized for possible transport to the accessible environment, and the rates at which these radionuclides could be mobilized.

special source of groundwater - "Special source of ground water means those Class I ground waters identified in accordance with the Agency's Ground-Water Protection Strategy published in August 1984 that: (1) are within the controlled area encompassing a disposal system or are less than five kilometers beyond the controlled area; (2) are supplying drinking water for thousands of persons as of the date that DOE chooses a location within that area for detailed characterization as a potential site for a disposal system (e.g., in accordance with Section 112(b)(1)(B) of the *NWPA* and (3) are irreplaceable in that no reasonable alternative source of drinking water is available to that population." *(40 CFR 191.12[o])*

Standard - 40 CFR Part 191, *Environmental Standards for the Management and Disposal of Spent Nuclear Fuel, High-Level and Transuranic Radioactive Wastes; Final Rule.*

stationarity - A stochastic process is said to be stationary in time (or space) if its statistical properties are invariant under arbitrary time (or space) translations.

stochastic process - Any process occurring in space and/or time whose descriptive variables are random variables; synonymous with random function, random field, or random process.

storativity - The volume of water released by an aquifer per unit surface area per unit drop in hydrologic head.

stratabound - A deposit confined to a single stratigraphic unit.

stratigraphy - The study of rock strata; concerned with the original succession and age relations of rock strata, their form, distribution, lithologic composition, fossil content, and geophysical and geochemical properties.

subjective - Proceeding from or taking place within an individual's mind (as opposed to empirical, i.e., supported by explicit records of measurements or experiments).

surfactant - A surficially active substance.

sylvite - A white or colorless mineral (KCl), the principal ore mineral of potassium compounds, that occurs in beds as a saline residue from evaporation.

syncline - A fold having stratigraphically younger rock material in its center; it is usually concave upward.

syndepositional - Forming contemporaneously with deposition.

Tamarisk Member - A sequence of anhydrite, claystone, and siltstone within the Late Permian Rustler Formation of southeastern New Mexico.

tectonic - The forces involved in, or the resulting structures and features of, movements of the Earth's crust.

thermodynamic - Pertaining to the relationship of heat to mechanical and other forms of energy.

tight - Pertaining to a rock that has all interstices filled with fine grains or with matrix material so that porosity and permeability are almost non-existent.

topography - The configuration of a land surface, including its relief and the position of its natural and man-made features.

tortuosity - A measure of the actual length of the path of flow through a porous medium.

transgressive - The spread or extension of the sea over land areas, and the consequent evidence of such an advance (such as strata deposited unconformably on older rocks).

transiency - The state or quality of being transient.

translator - A computer program that translates output from one program to input for another program. Also referred to as pre- and post-processors.

transmissivity - For a confined aquifer, the product of hydraulic conductivity and aquifer thickness.

transuranic radioactive waste (TRU waste) - Waste that, without regard to source or form, is contaminated with more than 100 nCi of alpha-emitting transuranic isotopes with half-lives greater than 20 yr, per gram of waste, except for (1) HLW; (2) wastes that the DOE has determined, with the concurrence of the EPA Administrator, do not need the degree of isolation required by *40 CFR 191*; or (3) wastes that the NRC Commission has approved for disposal on a case-by-case basis in accordance with *10 CFR 61*. Heads of DOE field organizations can determine that other alpha-contaminated wastes, peculiar to a specific site, must be managed as TRU waste.

truncated distribution - A probability distribution defined on a range of variable values that is smaller than the range normally associated with the distribution: e.g., a normal distribution defined on a finite range of variable values.

turbidity current - A density current in water, air, or other fluid, caused by different amounts of matter in suspension; specifically a bottom-flowing current laden with suspended sediment moving swiftly (under the influence of gravity) down a subaqueous slope and spreading horizontally on the floor of a body of water.

unconfined - Used to describe an aquifer that is not bounded above and below by an aquitard.

unconformably - Not conformable, i.e., a break in deposition of sedimentary material.

unconformity - A substantial break or gap in the geologic record in which a rock unit is overlain by another that is not normally next in stratigraphic succession.

unconsolidated - Material that is loosely arranged or whose particles are not cemented together.

undisturbed performance - "The predicted behavior of a disposal system, including consideration of the uncertainties in predicted behavior, if the disposal system is not disrupted by human intrusion or the occurrence of unlikely natural events." (*40 CFR 191.12(p)*)

uniform distribution - A probability distribution in which the pdf is constant over the range of variable values.

unsaturated - Refers to a rock or soil in which the pores are not completely filled with a fluid (usually water, but also other liquids and gas).

Uranium-234/Uranium-238 activity ratio - Comparison of the radioactivities of U-234 and U-238; the change in this ratio in groundwater can be related to the passage of time because U-238 decays to the more soluble Th-234, which in turn decays to U-234. As a result, the ratio of U-234 to U-238 in groundwater increases with time.

validate - To establish confidence that the model (and the associated computer program) correctly simulates the appropriate physical and chemical phenomena. Validation is accomplished through either laboratory or in situ experiments, as appropriate.

validation - The process of assuring through sufficient testing of a model using real site data that a conceptual model and the corresponding mathematical and computer models correctly simulate a physical process with sufficient accuracy.

variable - Any quantity supplied as an ingredient of a model, or a computer program that implements a model; also referred to as a parameter.

variance - The square of the standard deviation; the variance is a measure of the amount of spreading of a probability density function about its mean.

verification - The process of assuring (e.g., through tests on ideal problems) that a computer code (computational model) correctly performs the stated capabilities (such as solving the mathematical model). Given that a computer code correctly solves the mathematical model, the physical assumptions of the mathematical model must then be checked through validation.

vug - A small cavity in a rock.

water table - In saturated rock, the surface of the water that is at atmospheric pressure.

WIPP land withdrawal- Sixteen contiguous sections proposed to be withdrawn from public access to be used for the disposal of TRU waste.

NOMENCLATURE

Acronyms and Initialisms

AEC - Atomic Energy Commission

AKRIP - Computer program used for kriging

ALGEBRA - CAMDAT computer program that algebraically manipulates data and plots meshes and curves.

ASCII - American Standard Code for Information Exchange

BCSET - Computer program that sets up boundary conditions.

BLOT - A mesh-and-curve-plotting computer program.

BOAST_II - A computational computer program that simulates three-phase flow (oil, water, and gas) in a three-dimensional, porous medium.

BRAGFLO - Computer program that simulates two-phase flow (brine and gas) in a three-dimensional, porous medium.

BRWM - Board on Radioactive Waste Management of the National Research Council

CAM - Compliance Assessment Methodology

CAMCON - Compliance Assessment Methodology CONtroller; controller (driver) for compliance evaluations developed for the WIPP.

CAMDAT - Compliance Assessment Methodology DATa base; computational data base developed for the WIPP.

CAM2TXT - Computer program for binary CAMDAT to ASCII conversion.

CAS - Compliance assessment system

CCDF - See Glossary: complementary cumulative distribution function

CCDFCALC - Computer program used to calculate a CCDF

CCDFPLT - Computer program that calculates and plots the complementary cumulative distribution function.

CCD2STEP - Computer program that translates from CCDFCALC.

cdf - See Glossary: cumulative distribution function

CFR - Code of Federal Regulations

CHAIN - Computer program that generates radionuclide chains.

CHANGES - Computer program that is a record of needed enhancements to CAMCON or codes.

CH-TRU - Contact-Handled TRansUranic waste; packaged TRU waste whose external surface dose rate does not exceed 200 mrem per hour.

CUTTINGS - Computer program for evaluating the amount of material removed during drilling.

DISTRPLT - Computer program that plots a pdf's given parameters.

DOE - The U.S. Department Of Energy, established in 1978 as a successor to the Energy Research and Developmment Administration (ERDA).

DOSE - Computer program that calculates human doses from transfer factors.

DRZ - See Glossary: disturbed rock zone

DST - Drill-stem test

E1 - A scenario for the WIPP consisting of one or more boreholes that penetrate through a waste-filled room or drift and continue into or through a brine pocket in the underlying Castile Formation.

E2 - A scenario for the WIPP consisting of one or more boreholes that penetrate to or through a waste-filled room or drift in a panel but do not intersect brine or any other important source of water.

E1E2 - A scenario for the WIPP consisting of exactly two boreholes that penetrate waste-filled rooms or drifts in the same panel, with one borehole also penetrating a brine reservoir in the underlying Castile Formation.

EDTA - Ethylenediaminetetraacetic acid: an organic compound that reacts with many metallic ions to form a soluble complex.

EEG - The Environmental Evaluation Group, an agency of the State of New Mexico that reviews the safety of the WIPP.

EID - Environmental Improvement Division

EIS - Environmental impact statement

EPA - Environmental Protection Agency of the U.S. Government

ERDA - Energy Research and Development Administration

FASTQ - Computer program that generates finite element meshes.

FD - Finite difference (numerical analysis)

FE - Finite element (numerical analysis)

FEIS - Final Environmental Impact Statement

50 FR 38066 - Federal Register, Volume 50, p. 38066

FITBND - Computer program that optimizes fit-of-pressure boundary conditions.

FLINT - Computer program that is a FORTRAN language analyzer.

FORTRAN - A computer programming language; from FORmula TRANslation.

40 CFR 191 - Code of Federal Regulations, Title 40, Part 191

FRP - Fiberglass-reinforced plywood

FSAR - Final Safety Analysis Report

FSEIS - Final Supplement Environmental Impact Statement

GARFIELD - Computer program that generates attribute fields (e.g., transmissivity)

GENII - Computer program that calculates human doses.

GENMESH - Computer program that generates three-dimensional, finite difference, meshes.

GENNET - Computer program that generates networks.

GENOBS - Computer program that generates functional relationships between well heads and pressure boundary conditions.

GENPROP - Computer program for item entry into a property data base.

GRIDGEOS - Computer program that interpolates observational hydrologic or geologic data onto computational meshes.

GROPE - File reader for CAMDAT.

HEPA - High Efficiency Particulate Air (filter): usually capable of 99.97% efficiency as measured by a standard photometric test using a 0.3μm droplets (aerodynamic equivalent diameter) of DOP.

HLP2ABS - Computer program that reads a program help file and converts it into standard data base format from which the program abstract can be written.

HLW - High level waste

HST3D - Computer program that simulates three-dimensional ground-water flow systems and heat and solute transport.

ICRP - International Commission on Radiological Protection

ICSET - Computer program that sets up initial conditions.

IGIS - Interactive Graphics Information System

IMPES - Implicit pressure, explicit saturation

INGRES^{TM} - A relational data base management system used to implement the WIPP secondary property data base.

LHS - Latin hypercube sampling; computer program that selects Latin hypercube samples: A constrained Monte Carlo sampling scheme which samples n different values of a continuous random variate from n nonoverlapping intervals selected on the basis of equal probability.

LHS2STEP - Computer program that translates from LHS to STEPWISE or PCCSRC.

LISTDCL - Computer program that lists DEC command procedural files.

LISTFOR - Computer program that lists programs and subroutines and summarizes comments and active FORTRAN lines.

LISTSDB - Computer program that tabulates data in a secondary data base for reports.

MATSET - Computer program that sets material properties in CAMDAT.

MB139 - Marker Bed 139: One of 45 units within the Salado Formation composed of silica or sulfate and containing about 1 m of polyhalitic anhydrite and anhydrite. MB139 is located within the WIPP horizon.

MEF - Maximum Entropy Formalism

NAS - National Academy of Sciences

NCRP - National Council on Radiation Protection and Measurement

NEA - Nuclear Energy Agency of the Office of Economic Cooperation and Development, Paris.

NEFDIS - Computer program that plots NEFTRAN discharge history as a function of time.

NEFTRAN - Network Flow and TRANsport. Computer program that calculates flow and transport along one-dimensional legs comprising a flow network.

NRC - Nuclear Regulatory Commission

NUCPLOT - Computer program for a box plot of each radionuclide contribution to a CCDF.

NWPA - Nuclear Waste Policy Act (Public Law 97-425 & 100-203)

PA - Performance Assessment

PANEL - Computer program for a panel model that estimates radionuclide flow to the Culebra Dolomite Member through one or more boreholes.

PATEXO - Computer program that transforms PATRAN to CAMDAT.

PCCSRC - Computer program that calculates partial correlation and standardized regression coefficients.

pdf - See Glossary: probability density function.

PLOTSDB - Computer program that plots parameter distribution in a secondary data base.

POSTBOAST - Post-processor computer program (translator) for BOAST_II.

POSTBRAGFLO - Post-processor computer program (translator) for BRAGFLO.

POSTHST - Post-processor computer program (translator) for HST3D.

POSTLHS - Post-processor computer program (translator) for LHS.

POSTNEF - Post-processor computer program (translator) for POSTNEF.

POSTSTAFF - Post-processor computer program (translator) for STAFF2D.

POSTSUTRA - Post-processor computer program (translator) for SUTRA.

POSTSWIFT - Post-processor computer program (translator) for SWIFTII.

PRA - Probabilistic risk assessment

PREBOAST - Pre-processor computer program (translator) for BOAST II.

PREBRAGFLO - Pre-processor computer program (translator) for BRAGFLO.

PREHST - Pre-processor computer program (translator) for HST3D.

PRELHS - Pre-processor computer program (translator) for LHS.

PRENEF - Pre-processor computer program (translator) for NEFTRAN.

PRESTAFF - Pre-processor computer program (translator) for STAFF2D.

PRESUTRA - Pre-processor computer program (translator) for SUTRA.

PRESWIFT - Pre-processor computer program (translator) for SWIFTII.

QA - See Glossary: quality assurance

R_{acc} - Release of radioisotopes at the subsurface boundary of the accessible environment.

R_c - Release of radioisotope-bearing cuttings and eroded material to the land surface during drilling of an intrusion borehole.

RCRA - Resource, Conservation, and Recovery Act of 1976 (Public Law 94-580)

RELATE - Computer program that interpolates from coarse to fine mesh and fine to coarse mesh (relates property and boundary conditions).

RESHAPE - Computer program that redefines blocks (i.e., groupings of mesh elements).

RH-TRU - Remote-Handled TRansUranic waste: packaged TRU waste whose external surface dose rate exceeds 200 mrem per hour, but not greater than 1,000 mrem per hour.

SAR - Safety Analysis Report

SCANCAMDAT - Computer program that quickly summarizes the data in CAMDAT.

SCP - Site characterization plan

SECO_2DH - Computer program for horizontal, two-dimensional groundwater flow simulation.

SEIS - Supplement Environment Impact Statement

SNL - Sandia National Laboratories

SORTLHS - Computer program that reorders vectors for LHS (Latin hypercube sampling).

SRC - Standardized regression coefficients

STAFF2D - Computer program for a finite-element transport model.

STEPWISE - Computer program that performs stepwise regression including rank regression.

SUTRA - Finite-element simulation computer program that calculates saturated-unsaturated, fluid-density-dependent groundwater flow with energy transport or chemically reactive single-species solute transport.

SUTRAGAS - SUTRA computer program modified for fluid as a gas instead of as a liquid.

SWB - Standard waste box

SWIFTII - Sandia Waste-Isolation Flow and Transport computer program that simulates saturated flow and heat, brine, and radionuclide chain transport in porous and fractured media.

TRACKER - Computer program that tracks neutrally buoyant particles in a steady or transient flow.

TRU - TRansUranic

TS - An event considered in scenario development for the WIPP consisting of subsidence that results due to solution mining of potash.

TXT2CAM - Computer program for ASCII to binary CAMDAT conversion.

UNSWIFT - Computer translator program that converts SWIFTII input files into CAMDAT.

WAC - Waste Acceptance Criteria

WEC - Westinghouse Electric Corporation

WIPP - Waste Isolation Pilot Plant

YMP - Yucca Mountain Project

Abbreviations and Symbols

Am - americium

atm - atmosphere

Ba - barium

Ce - cerium

Cf - californium

Ci - curie

cm - centimeter

Cm - curium

Co - cobalt

Cs - cesium

Cu - copper

Eh - oxidation potential

Eu - europium

Fe - iron

ft - foot

g - gram

gal - gallon

in - inch

kg - kilogram

km - kilometer

ℓ - liter

lb - pound

m - meter

M - Molar (molarity): Concentration of a solution expressed as moles of solute per liter of solution.

mg/ℓ - milligrams per liter

mi - mile

μd - microdarcy

md - millidarcy

Mn - manganese

MPa - megapascal (10^6 Pa)

mrem - millirem (10^{-3} rem)

nCi - nanocurie

Ni - nickel

NM - New Mexico

Np - neptunium

Pa - pascal

Pb - lead

pH - the negative logarithm of the activity of hydrogen ion

Pr - praseodymium

Pu - plutonium

Ra - radium

Rn - radon

Ru - ruthenium

s - second

Sb - antimony

Si - silicon

Sm - samarium

Sr - strontium

Te - tellurium

Th - thorium

U - uranium

Y - yttrium

yr - year

§ - section of 40 CFR Part 191

Distribution

FEDERAL AGENCIES

U. S. Department of Energy (4)
Office of Environmental Restoration
and Waste Management
Attn: L. P. Duffy, EM-1
J. E. Lytle, EM-30
S. Schneider, EM-342
C. Frank, EM-50
Washington, DC 20585

U.S. Department of Energy (5)
WIPP Task Force
Attn: M. Frei, EM-34 (2)
G. H. Daly
S. Fucigna
J. Rhoderick
12800 Middlebrook Rd.
Suite 400
Germantown, MD 20874

U.S. Department of Energy (4)
Office of Environment, Safety and
Health
Attn: R. P. Berube, EH-20
C. Borgstrum, EH-25
R. Pelletier, EH-231
K. Taimi, EH-232
Washington, DC 20585

U. S. Department of Energy (4)
WIPP Project Integration Office
Attn: W. J. Arthur III
L. W. Gage
P. J. Higgins
D. A. Olona
P.O. Box 5400
Albuquerque, NM 87115-5400

U. S. Department of Energy (12)
WIPP Project Site Office (Carlsbad)
Attn: A. Hunt (4)
M. McFadden
V. Daub (4)
J. Lippis
K. Hunter
R. Becker
P.O. Box 3090
Carlsbad, NM 88221-3090

U. S. Department of Energy, (5)
Office of Civilian Radioactive Waste
Management
Attn: Deputy Director, RW-2
Associate Director, RW-10
Office of Program
Administration and
Resources Management
Associate Director, RW-20
Office of Facilities
Siting and
Development
Associate Director, RW-30
Office of Systems
Integration and
Regulations
Associate Director, RW-40
Office of External
Relations and Policy
Office of Geologic Repositories
Forrestal Building
Washington, DC 20585

U. S. Department of Energy
Attn: National Atomic Museum Library
Albuquerque Operations Office
P.O. Box 5400
Albuquerque, NM 87185

U. S. Department of Energy
Research & Waste Management Division
Attn: Director
P.O. Box E
Oak Ridge, TN 37831

U. S. Department of Energy (2)
Idaho Operations Office
Fuel Processing and Waste
Management Division
785 DOE Place
Idaho Falls, ID 83402

U.S. Department of Energy
Savannah River Operations Office
Defense Waste Processing
Facility Project Office
Attn: W. D. Pearson
P.O. Box A
Aiken, SC 29802

U.S. Department of Energy (2)
Richland Operations Office
Nuclear Fuel Cycle & Production Division
Attn: R. E. Gerton
825 Jadwin Ave.
P.O. Box 500
Richland, WA 99352

U.S. Department of Energy (3)
Nevada Operations Office
Attn: J. R. Boland
D. Livingston
P. K. Fitzsimmons
2753 S. Highland Drive
Las Vegas, NV 87183-8518

U.S. Department of Energy (2)
Technical Information Center
P.O. Box 62
Oak Ridge, TN 37831

U.S. Department of Energy (2)
Chicago Operations Office
Attn: J. C. Haugen
9800 South Cass Avenue
Argonne, IL 60439

U.S. Department of Energy
Los Alamos Area Office
528 35th Street
Los Alamos, NM 87544

U.S. Department of Energy (3)
Rocky Flats Area Office
Attn: W. C. Rask
G. Huffman
T. Lukow
P.O. Box 928
Golden, CO 80402-0928

U.S. Department of Energy
Dayton Area Office
Attn: R. Grandfield
P.O. Box 66
Miamisburg, OH 45343-0066

U.S. Department of Energy
Attn: E. Young
Room E-178
GAO/RCED/GTN
Washington, DC 20545

U.S. Bureau of Land Management
101 E. Mermod
Carlsbad, NM 88220

U.S. Bureau of Land Management
New Mexico State Office
P.O. Box 1449
Santa Fe, NM 87507

U.S. Environmental Protection Agency (2)
Office of Radiation Protection Programs (ANR-460)
Attn: Richard Guimond (2)
Washington, D.C. 20460

U.S. Nuclear Regulatory Commission
Division of Waste Management
Attn: H. Marson
Mail Stop 4-H-3
Washington, DC 20555

U.S. Nuclear Regulatory Commission (4)
Advisory Committee on Nuclear Waste
Attn: Dade Moeller
Martin J. Steindler
Paul W. Pomeroy
William J. Hinze
7920 Norfolk Avenue
Bethesda, MD 20814

Defense Nuclear Facilities Safety Board
Attn: Dermot Winters
625 Indiana Avenue NW
Suite 700
Washington, DC 20004

Nuclear Waste Technical Review Board (2)
Attn: Dr. Don A. Deere
Dr. Sidney J. S. Parry
Suite 910
1100 Wilson Blvd.
Arlington, VA 22209-2297

Katherine Yuracko
Energy and Science Division
Office of Management and Budget
725 17th Street NW
Washington, DC 20503

U.S. Geological Survey (2)
Water Resources Division
Attn: Cathy Peters
Suite 200
4501 Indian School, NE
Albuquerque, NM 87110

INSTITUTIONAL DISTRIBUTION

NEW MEXICO CONGRESSIONAL DELEGATION:

Jeff Bingaman
U.S. Senate
524 SHOB
Washington, DC 20510

Pete V. Domenici
U.S. Senate
427 SDOB
Washington, DC 20510

Bill Richardson
House of Representatives
332 CHOB
Washington, DC 20510

Steven H. Schiff
House of Representatives
1520 LHOB
Washington, DC 20510

Joe Skeen
House of Representatives
1007 LHOB
Washington, DC 20510

STATE AGENCIES

Environmental Evaluation Group (5)
Attn: Robert Neill
Suite F-2
7007 Wyoming Blvd., N.E.
Albuquerque, NM 87109

New Mexico Bureau of Mines
and Mineral Resources
Socorro, NM 87801

New Mexico Department of Energy & Minerals
Attn: Librarian
2040 S. Pacheco
Santa Fe, NM 87505

New Mexico Radioactive Task Force (2)
(Governor's WIPP Task Force)
Attn: Anita Lockwood, Chairman
Chris Wentz,
Coordinator/Policy Analyst
2040 Pacheco
Santa Fe, NM 87505

Bob Forrest
Mayor, City of Carlsbad
P.O. Box 1569
Carlsbad, NM 88221

Chuck Bernard
Executive Director
Carlsbad Department of Development
P.O. Box 1090
Carlsbad, NM 88221

Robert M. Hawk (2)
Chairman, Hazardous and Radioactive Materials Committee
Room 334
State Capitol
Sante Fe, NM 87503

New Mexico Environment Department
Secretary of the Environment
Attn: J. Espinosa (3)
P.O. Box 968
1190 St. Francis Drive
Santa Fe, NM 87503-0968

New Mexico Environment Department
Attn: Pat McCausland
WIPP Project Site Office
P.O. Box 3090
Carlsbad, NM 88221-3090

ADVISORY COMMITTEE ON NUCLEAR FACILITY SAFETY

John F. Ahearne
Executive Director, Sigma Xi
99 Alexander Drive
Research Triangle Park, NC 27709

James E. Martin
109 Observatory Road
Ann Arbor, MI 48109

Dr. Gerald Tape
Assoc. Universities
1717 Massachusetts Ave. NW
Suite 603
Washington, DC 20036

WIPP PANEL OF NATIONAL RESEARCH COUNCIL'S BOARD ON RADIOACTIVE WASTE MANAGEMENT

Charles Fairhurst, Chairman
Department of Civil and
Mineral Engineering
University of Minnesota
500 Pillsbury Dr. SE
Minneapolis, MN 55455-0220

John O. Blomeke
3833 Sandy Shore Drive
Lenoir City, TN 37771-9803

John D. Bredehoeft
Western Region Hydrologist
Water Resources Division
U.S. Geological Survey (M/S 439)
345 Middlefield Road
Menlo Park, CA 94025

Fred M. Ernsberger
1325 NW 10th Avenue
Gainsville, FL 32601

Rodney C. Ewing
Department of Geology
University of New Mexico
200 Yale, NE
Albuquerque, NM 87131

B. John Garrick
Pickard, Lowe & Garrick, Inc.
2260 University Drive
Newport Beach, CA 92660

Leonard F. Konikow
U.S. Geological Survey
431 National Center
Reston, VA 22092

Jeremiah O'Driscoll
505 Valley Hill Drive
Atlanta, GA 30350

Christopher Whipple
Clement International Corp.
160 Spear St.
Suite 1380
San Francisco, CA 94105-1535

National Research Council (3)
Board on Radioactive
Waste Management
RM HA456
Attn: Peter B. Myers, Staff
Director (2)
Dr. Geraldine J. Grube
2101 Constitution Avenue
Washington, DC 20418

PERFORMANCE ASSESSMENT PEER REVIEW PANEL

G. Ross Heath
College of Ocean and
Fishery Sciences HN-15
583 Henderson Hall
University of Washington
Seattle, WA 98195

Thomas H. Pigford
Department of Nuclear Engineering
4159 Etcheverry Hall
University of California
Berkeley, CA 94720

Thomas A. Cotton
JK Research Associates, Inc.
4429 Butterworth Place, NW
Washington, DC 20016

Robert J. Budnitz
President, Future Resources
Associates, Inc.
2000 Center Street
Suite 418
Berkeley, CA 94704

C. John Mann
Department of Geology
245 Natural History Bldg.
1301 West Green Street
University of Illinois
Urbana, IL 61801

Frank W. Schwartz
Department of Geology and Mineralogy
The Ohio State University
Scott Hall
1090 Carmack Rd.
Columbus, OH 43210

FUTURE SOCIETIES EXPERT PANEL

Theodore S. Glickman
Resources for the Future
1616 P St., NW
Washington, DC 20036

Norman Rosenberg
Resources for the Future
1616 P St., NW
Washington, DC 20036

Max Singer
The Potomac Organization, Inc.
5400 Greystone St.
Chevy Chase, MD 20815

Maris Vinovskis
Institute for Social Research
Room 4086
University of Michigan
426 Thompson St
Ann Arbor, MI 48109-1045

Gregory Benford
University of California, Irvine
Department of Physics
Irvine, CA 92717

Craig Kirkwood
College of Business Administration
Arizona State University
Tempe, AZ 85287

Harry Otway
Health, Safety, and Envir. Div.
Mail Stop K-491
Los Alamos National Laboratory
Los Alamos, NM 87545

Martin J. Pasqualetti
Department of Geography
Arizona State University
Tempe, AZ 85287-3806

Michael Baram
Bracken and Baram
33 Mount Vernon St.
Boston, MA 02108

Wendell Bell
Department of Sociology
Yale University
1965 Yale Station
New Haven, CT 06520

Bernard L. Cohen
Department of Physics
University of Pittsburgh
Pittsburgh, PA 15260

Ted Gordon
The Futures Group
80 Glastonbury Blvd.
Glastonbury, CT 06033

Duane Chapman
5025 S. Building, Room S5119
The World Bank
1818 H Street NW
Washington, DC 20433

Victor Ferkiss
23 Sage Brush Circle
Corrales, NM 87048

Dan Reicher
Senior Attorney
Natural Resources Defense Council
1350 New York Ave. NW, #300
Washington, DC 20005

Theodore Taylor
P.O. Box 39
3383 Weatherby Rd.
West Clarksville, NY 14786

MARKERS EXPERT PANEL

Dr. Dieter Ast
Department of Materials Science
Bard Hall
Cornell University
Ithaca, NY 14853-1501

Dr. Victor Baker
Department of Geosciences
Building #77, Gould-Simpson Building
University of Arizona
Tucson, AZ 85721

Mr. Michael Brill
President
BOSTI
1479 Hertel Ave.
Buffalo, NY 14216

Dr. Frank Drake
Board of Studies in Astronomy and Astrophysics
Lick Observatory
University of California, Santa Cruz
Santa Cruz, CA 95064

Dr. Ben Finney
University of Hawaii at Manoa
Department of Anthropology
Porteus Hall 346, 2424 Maile Way
Honolulu, HI 96822

Dr. David Givens
American Anthropological Association
1703 New Hampshire Ave., NW
Washington, D.C. 20009

Dr. Ward Goodenough
Department of Anthropology
University of Pennsylvania
325 University Museum
33rd and Spruce Streets
Philadelphia, PA 19104-6398

Dr. Maureen Kaplan
Eastern Research Group, Inc.
6 Whittemore Street
Arlington, MA 02174

Mr. Jon Lomberg
P.O. Box 207
Honaunau, HI 96726

Dr. Louis Narens
Department of Cognitive Sciences
School of Social Sciences
University of Califorrnia, Irvine
Irvine, CA 92717

Dr. Frederick Newmeyer
Department of Linguistics
GN-40
University of Washington
Seattle, WA 98195

Dr. Woodruff Sullivan
Department of Astonomy
FM-20
University of Washington
Seattle, WA 98195

Dr. Wendell Williams
Materials Science and Engineering
White Building
Case Western Reserve University
Cleveland, OH 44106

NATIONAL LABORATORIES

Argonne National Labs (2)
Attn: A. Smith
D. Tomasko
9700 South Cass, Bldg. 201
Argonne, IL 60439

Battelle Pacific Northwest Laboratories (3)
Attn: R. E. Westerman
S. Bates
H. C. Burkholder
Battelle Boulevard
Richland, WA 99352

Lawrence Livermore National Laboratory
Attn: G. Mackanic
P.O. Box 808, MS L-192
Livermore, CA 94550

Los Alamos National Laboratories
Attn: B. Erdal, CNC-11
P.O. Box 1663
Los Alamos, NM 87544

Los Alamos National Laboratories
Attn: A. Meijer
Mail Stop J514
Los Alamos, NM 87545

Los Alamos National Laboratories (3)
HSE-8
Attn: M. Enoris
L. Soholt
J. Wenzel
P.O. Box 1663
Los Alamos, NM 87544

Los Alamos National Laboratories (2)
HSE-7
Attn: A. Drypolcher
S. Kosciewiscz
P.O. Box 1663
Los Alamos, NM 87544

Oak Ridge National Labs
Martin Marietta Systems, Inc.
Attn: J. Setaro
P.O. Box 2008, Bldg. 3047
Oak Ridge, TN 37831-6019

Savannah River Laboratory (3)
Attn: N. Bibler
M. J. Plodinec
G. G. Wicks
Aiken, SC 29801

Savannah River Plant (2)
Attn: Richard G. Baxter
Building 704-S
K. W. Wierzbicki
Building 703-H
Aiken, SC 29808-0001

CORPORATIONS/MEMBERS OF THE PUBLIC

Benchmark Environmental Corp. (3)
Attn: John Hart
C. Frederickson
K. Lickliter
4501 Indian School Rd., NE
Suite 105
Albuquerque, NM 87110

Deuel and Associates, Inc.
Attn: R. W. Prindle
7208 Jefferson, NE
Albuquerque, NM 87109

Disposal Safety, Inc.
Attn: Benjamin Ross
Suite 314
1660 L Street NW
Washington, DC 20006

Ecodynamics Research Associates (2)
Attn: Pat Roache
Rebecca Blaine
P.O. Box 8172
Albuquerque, NM 87198

E G & G Idaho (3)
1955 Fremont Street
Attn: C. Atwood
C. Hertzler
T. I. Clements
Idaho Falls, ID 83415

Geomatrix
Attn: Kevin Coppersmith
100 Pine Street #1000
San Francisco, CA 94111

Golden Associates, Inc. (3)
Attn: Mark Cunnane
Richard Kossik
Ian Miller
4104 148th Avenue NE
Redmond, WA 98052

In-Situ, Inc. (2)
Attn: S. C. Way
C. McKee
209 Grand Avenue
Laramie, WY 82070

INTERA, Inc.
Attn: A. M. LaVenue
8100 Mountain Road NE
Suite 213
Albuquerque, NM 87110

INTERA, Inc.
Attn: J. F. Pickens
Suite #300
6850 Austin Center Blvd.
Austin, TX 78731

INTERA, Inc.
Attn: Wayne Stensrud
P.O. Box 2123
Carlsbad, NM 88221

INTERA, Inc.
Attn: William Nelson
101 Convention Center Drive
Suite 540
Las Vegas, NV 89109

IT Corporation (2)
Attn: P. Drez
J. Myers
Regional Office - Suite 700
5301 Central Avenue, NE
Albuquerque, NM 87108

IT Corporation
R. J. Eastmond
825 Jadwin Ave.
Richland, WA 99352

MACTEC (2)
Attn: J. A. Thies
D. K. Duncan
8418 Zuni Road SE
Suite 200
Albuquerque, NM 87108

Pacific Northwest Laboratory
Attn: Bill Kennedy
Battelle Blvd.
P.O. Box 999
Richland, WA 99352

RE/SPEC, Inc. (2)
Attn: W. Coons
Suite 300
4775 Indian School NE
Albuquerque, NM 87110

RE/SPEC, Inc.
Attn: J. L. Ratigan
P.O. Box 725
Rapid City, SD 57709

Reynolds Elect/Engr. Co., Inc.
Building 790, Warehouse Row
Attn: E. W. Kendall
P.O. Box 98521
Las Vegas, NV 89193-8521

Roy F. Weston, Inc.
CRWM Tech. Supp. Team
Attn: Clifford J. Noronha
955 L'Enfant Plaza, S.W.
North Building, Eighth Floor
Washington, DC 20024

Science Applications International Corporation
Attn: Howard R. Pratt,
Senior Vice President
10260 Campus Point Drive
San Diego, CA 92121

Science Applications International Corporation (2)
Attn: George Dymmel
Chris G. Pflum
101 Convention Center Dr.
Las Vegas, NV 89109

Science Applications International Corporation (2)
Attn: John Young
Dave Lester
18706 North Creek Parkway
Suite 110
Bothell, WA 98011

Southwest Research Institute
Center for Nuclear Waste Regulatory Analysis (2)
Attn: P. K. Nair
6220 Culebra Road
San Antonio, Texas 78228-0510

Systems, Science, and Software (2)
Attn: E. Peterson
P. Lagus
Box 1620
La Jolla, CA 92038

TASC
Attn: Steven G. Oston
55 Walkers Brook Drive
Reading, MA 01867

Tech. Reps., Inc. (5)
Attn: Janet Chapman
Terry Cameron
Debbie Marchand
John Stikar
Denise Bissell
5000 Marble NE
Suite 222
Albuquerque, NM 87110

Tolan, Beeson, & Associates
Attn: Terry L. Tolan
2320 W. 15th Avenue
Kennewick, WA 99337

TRW Environmental Safety Systems
(TESS)
Attn: Ivan Saks
10306 Eaton Place
Suite 300
Fairfax, VA 22030

Westinghouse Electric Corporation (4)
Attn: Library
L. Trego
C. Cox
L. Fitch
R. F. Kehrman
P.O. Box 2078
Carlsbad, NM 88221

Westinghouse Hanford Company
Attn: Don Wood
P.O. Box 1970
Richland, WA 99352

Western Water Consultants
Attn: D. Fritz
1949 Sugarland Drive #134
Sheridan, WY 82801-5720

Western Water Consultants
Attn: P. A. Rechard
P.O. Box 4128
Laramie, WY 82071

Neville Cook
Rock Mechanics Engineering
Mine Engineering Dept.
University of California
Berkeley, CA 94720

Dennis W. Powers
Star Route Box 87
Anthony, TX 79821

Shirley Thieda
P.O. Box 2109, RR1
Bernalillo, NM 87004

Jack Urich
c/o CARD
144 Harvard SE
Albuquerque, NM 87106

UNIVERSITIES

University of California
Mechanical, Aerospace, and
Nuclear Engineering Department (2)
Attn: W. Kastenberg
D. Browne
5532 Boelter Hall
Los Angeles, CA 90024

University of Hawaii at Hilo
Attn: S. Hora
Business Administration
Hilo, HI 96720-4091

University of New Mexico
Geology Department
Attn: Library
Albuquerque, NM 87131

University of New Mexico
Research Administration
Attn: H. Schreyer
102 Scholes Hall
Albuquerque, NM 87131

University of Wyoming
Department of Civil Engineering
Attn: V. R. Hasfurther
Laramie, WY 82071

University of Wyoming
Department of Geology
Attn: J. I. Drever
Laramie, WY 82071

University of Wyoming
Department of Mathematics
Attn: R. E. Ewing
Laramie, WY 82071

LIBRARIES

Thomas Brannigan Library
Attn: Don Dresp, Head Librarian
106 W. Hadley St.
Las Cruces, NM 88001

Hobbs Public Library
Attn: Marcia Lewis, Librarian
509 N. Ship Street
Hobbs, NM 88248

New Mexico State Library
Attn: Norma McCallan
325 Don Gaspar
Santa Fe, NM 87503

New Mexico Tech
Martin Speere Memorial Library
Campus Street
Socorro, NM 87810

New Mexico Junior College
Pannell Library
Attn: Ruth Hill
Lovington Highway
Hobbs, NM 88240

Carlsbad Municipal Library
WIPP Public Reading Room
Attn: Lee Hubbard, Head Librarian
101 S. Halagueno St.
Carlsbad, NM 88220

University of New Mexico
General Library
Government Publications Department
Albuquerque, NM 87131

NEA/PSAC USER'S GROUP

Timo K. Vieno
Technical Research Centre of Finland
(VTT)
Nuclear Engineering Laboratory
P.O. Box 169
SF-00181 Helsinki
FINLAND

Alexander Nies (PSAC Chairman)
Gesellschaft für Strahlen- und
Institut für Tieflagerung
Abteilung für Endlagersicherheit
Theodor-Heuss-Strasse 4
D-3300 Braunscheweig
GERMANY

Eduard Hofer
Gesellschaft für Reaktorsicherheit
(GRS) MBH
Forschungsgelände
D-8046 Garching
GERMANY

Takashi Sasahara
Environmental Assessment Laboratory
Department of Environmental Safety
Research
Nuclear Safety Research Center,
Tokai Research Establishment, JAERI
Tokai-mura, Naka-gun
Ibaraki-ken
JAPAN

Alejandro Alonso
Cátedra de Tecnología Nuclear
E.T.S. de Ingenieros Industriales
José Gutiérrez Abascal, 2
E-28006 Madrid
SPAIN

Pedro Prado
CIEMAT
Instituto de Tecnología Nuclear
Avenida Complutense, 22
E-28040 Madrid
SPAIN

Miguel Angel Cuñado
ENRESA
Emilio Vargas, 7
E-28043 Madrid
SPAIN

Francisco Javier Elorza
ENRESA
Emilio Vargas, 7
E-28043 Madrid
SPAIN

Nils A. Kjellbert
Swedish Nuclear Fuel and Waste Management Company (SKB)
Box 5864
S-102 48 Stockholm
SWEDEN

Björn Cronhjort
Swedish National Board for Spent Nuclear Fuel (SKN)
Sehlsedtsgatan 9
S-115 28 Stockholm
SWEDEN

Richard A. Klos
Paul-Scherrer Institute (PSI)
CH-5232 Villingen PSI
SWITZERLAND

NAGRA (2)
Attn: Charles McCombie
Fritz Van Dorp
Parkstrasse 23
CH-5401 Baden
SWITZERLAND

Brian G. J. Thompson
Department of the Environment
Her Majesty's Inspectorate of Pollution
Room A5.33, Romney House
43 Marsham Street
London SW1P 2PY
UNITED KINGDOM

INTERA/ECL (2)
Attn: Trevor J. Sumerling
Daniel A. Galson
Chiltern House
45 Station Road
Henley-on-Thames
Oxfordshire RG9 1AT
UNITED KINGDOM

U.S. Nuclear Regulatory Commission (2)
Attn: Richard Codell
Norm Eisenberg
Mail Stop 4-H-3
Washington, D.C. 20555

Paul W. Eslinger
Battelle Pacific Northwest Laboratories (PNL)
P.O. Box 999, MS K2-32
Richland, WA 99352

Andrea Saltelli
Commission of the European Communities
Joint Resarch Centre od Ispra
I-21020 Ispra (Varese)
ITALY

Budhi Sagar
Center for Nuclear Waste Regulatory Analysis (CNWRA)
Southwest Research Institute
P.O. Drawer 28510
6220 Culebra Road
San Antonio, TX 78284

Shaheed Hossain
Division of Nuclear Fuel Cycle and Waste Management
International Atomic Energy Agency
Wagramerstrasse 5
P.O. Box 100
A-1400 Vienna
AUSTRIA

Claudio Pescatore
Division of Radiation Protection and Waste Management
38, Boulevard Suchet
F-75016 Paris
FRANCE

FOREIGN ADDRESSES

Studiecentrum Voor Kernenergie
Centre D'Energie Nucleaire
Attn: A. Bonne
SCK/CEN
Boeretang 200
B-2400 Mol
BELGIUM

Atomic Energy of Canada, Ltd. (3)
Whiteshell Research Estab.
Attn: Michael E. Stevens
Bruce W. Goodwin
Donna Wushke
Pinewa, Manitoba
ROE 1LO
CANADA

Ghislain de Marsily
Lab. Géologie Appliqué
Tour 26, 5 étage
4 Place Jussieu
F-75252 Paris Cedex 05
FRANCE

Jean-Pierre Olivier
OECD Nuclear Energy Agency (2)
38, Boulevard Suchet
F-75016 Paris
FRANCE

D. Alexandre, Deputy Director
ANDRA
31 Rue de la Federation
75015 Paris
FRANCE

Claude Sombret
Centre D'Etudes Nucleaires
De La Vallee Rhone
CEN/VALRHO
S.D.H.A. BP 171
30205 Bagnols-Sur-Ceze
FRANCE

Bundesministerium fur Forschung und
Technologie
Postfach 200 706
5300 Bonn 2
GERMANY

Bundesanstalt fur Geowissenschaften
und Rohstoffe
Attn: Michael Langer
Postfach 510 153
3000 Hannover 51
GERMANY

Gesellschaft fur Reaktorsicherheit
(GRS) mb (2)
Attn: Bruno Baltes
Wolfgang Muller
Schwertnergasse 1
D-5000 Cologne
GERMANY

Hahn-Mietner-Institut fur
Kernforschung
Attn: Werner Lutze
Glienicker Strasse 100
100 Berlin 39
GERMANY

Institut fur Tieflagerung (2)
Attn: K. Kuhn
Theodor-Heuss-Strasse 4
D-3300 Braunschweig
GERMANY

Physikalisch-Technische Bundesanstalt
Attn: Peter Brenneke
Postfach 33 45
D-3300 Braunschweig
GERMANY

Shingo Tashiro
Japan Atomic Energy Research
Institute
Tokai-Mura, Ibaraki-Ken
319-11
JAPAN

Netherlands Energy Research
Foundation
ECN
Attn: L. H. Vons
3 Westerduinweg
P.O. Box 1
1755 ZG Petten
THE NETHERLANDS

Johan Andersson
Statens Kärnkraftinspektion
SKI
Box 27106
S-102 52 Stockholm
SWEDEN

Fred Karlsson
Svensk Karnbransleforsorjning AB
SKB
Box 5864
S-102 48 Stockholm
SWEDEN

Nationale Genossenschaft fur die
Lagerung Radioaktiver Abfalle
(NAGRA) (2)
Attn: Stratis Vomvoris
Piet Zuidema
Hardstrasse 73
CH-5430 Wettingen
SWITZERLAND

D. R. Knowles
British Nuclear Fuels, plc
Risley, Warrington, Cheshire WA3 6AS
1002607 UNITED KINGDOM

AEA Technology
Attn: J.H. Rees
D5W/29 Culham Laboratory
Abington
Oxfordshire OX14 3DB
UNITED KINGDOM

AEA Technology
Attn: W. R. Rodwell
044/A31 Winfrith Technical Centre
Dorchester
Dorset DT2 8DH
UNITED KINGDOM

AEA Technology
Attn: J. E. Tinson
B4244 Harwell Laboratory
Didcot
Oxfordshire OX11 ORA
UNITED KINGDOM

INTERNAL

1 A. Narath
20 O. E. Jones
1510 J. C. Cummings
1511 D. K. Gartling
3151 S. M. Wayland
3200 N. R. Ortiz
6000 D. L. Hartley
6233 J. C. Eichelberger
6300 T. O. Hunter
6301 E. Bonano
6310 T. E. Blejwas, Acting
6313 L. E. Shephard
6312 F. W. Bingham
6313 L. S. Costin
6315 Supervisor
6316 R. P. Sandoval
6320 R. E. Luna, Acting
6340 W. D. Weart
6340 S. Y. Pickering
6341 J. M. Covan
6341 D. P. Garber
6341 R. C. Lincoln
6341 J. Orona*
6341 Sandia WIPP Central Files (250)
6342 D. R. Anderson
6342 B. M. Butcher
6342 D. P. Gallegos
6342 L. S. Gomez
6342 M. Gruebel
6342 R. Guzowski
6342 R. D. Klett
6342 M. G. Marietta
6342 D. Morrison
6342 A. C. Peterson
6342 R. P. Rechard
6342 P. Swift
6342 M. Tierney
6342 K. M. Trauth
6342 B. L. Baker*
6342 J. Bean*
6342 J. Berglund*
6342 W. Beyeler*
6342 T. Blaine*
6342 K. Brinster*
6342 K. Byle*
6342 L. Clements*
6342 J. Garner*
6342 A. Gilkey*
6342 H. Iuzzolino*
6342 J. Logothetis*
6342 R. McCurley*
6342 J. Rath*
6342 D. Rudeen*
6342 J. Sandha*
6342 J. Schreiber*
6342 P. Vaughn*
6343 T. M. Schultheis
6344 R. L. Beauheim
6344 P. B. Davies
6344 S. J. Finley
6344 E. Gorham
6344 C. F. Novak
6344 S. W. Webb
6345 R. Beraun
6345 L. Brush
6345 A. R. Lappin
6345 M. A. Molecke
6346 D. E. Munson
6346 E. J. Nowak
6346 J. R. Tillerson
6347 A. L. Stevens
6400 D. J. McCloskey
6413 J. C. Helton
6415 R. M. Cranwell
6415 C. Leigh
6415 R. L. Iman
6622 M.S.Y. Chu
9300 J. E. Powell
9310 J. D. Plimpton
9325 J. T. McIlmoyle
9325 R. L. Rutter
9330 J. D. Kennedy
8523-2 Central Technical Files
3141 S. A. Landenberger (5)
3145 Document Processing (8) for DOE/OSTI
3151 G. C. Claycomb (3)

*6342/Geo-Centers

☆ U.S. GOVERNMENT PRINTING OFFICE: 1991—673-122/60035

SANDIA REPORT

SAND91—0893/2 • UC—721
Unlimited Release
Printed December 1991

Preliminary Comparison with 40 CFR Part 191, Subpart B for the Waste Isolation Pilot Plant, December 1991

Volume 2: Probability and Consequence Modeling

WIPP Performance Assessment Division

Prepared by
Sandia National Laboratories
Albuquerque, New Mexico 87185 and Livermore, California 94550
for the United States Department of Energy
under Contract DE-AC04-76DP00789

Issued by Sandia National Laboratories, operated for the United States Department of Energy by Sandia Corporation.

Available to DOE and DOE contractors from
Office of Scientific and Technical Information
PO Box 62
Oak Ridge, TN 37831

Prices available from (615) 576-8401, FTS 626-8401

Available to the public from
National Technical Information Service
US Department of Commerce
5285 Port Royal Rd
Springfield, VA 22161

NTIS price codes
Printed copy: A16
Microfiche copy: A01

SAND91-0893/2
Unlimited Release
Printed December 1991

Distribution
Category UC-721

PRELIMINARY COMPARISON WITH 40 CFR PART 191, SUBPART B FOR THE WASTE ISOLATION PILOT PLANT, DECEMBER 1991

VOLUME 2: PROBABILITY AND CONSEQUENCE MODELING

WIPP Performance Assessment Division
Sandia National Laboratories
Albuquerque, New Mexico 87185

ABSTRACT

This second volume documents the probability and consequence modeling done by the Performance Assessment Division of Sandia National Laboratories for the 1991 preliminary performance assessment (PA) of the Waste Isolation Pilot Plant (WIPP). The volume provides an overview of the PA calculations; discusses the mechanics of the probability modeling and construction of the complementary cumulative distribution functions (CCDFs); discusses the generic computational models and the applied (or site-specific) models used in consequence analysis and the results that these models predict for both undisturbed conditions (base case) and disturbed conditions (in which one or more hypothetical boreholes intrude the repository during the 10,000-year regulatory period); and tabulates the calculational results used to construct the CCDFs reported in Volume 1.

ACKNOWLEDGMENTS

The WIPP Performance Assessment Division is comprised of both Sandia and contractor employees working as a team to produce these annual preliminary comparisons with EPA regulations, assessments of overall long-term safety of the repository, and interim technical guidance to the program. The on-site team, affiliations, and contributions to the 1991 performance assessment are listed in alphabetical order:

Performance Assessment Division

Name	Affil.	Primary Author of Doc: Sect.	Major Code	Area of Responsibility
R. Anderson	SNL			Division Manager
B. Baker	TEC	V.2:§.6.4		SECO2D, Hydrology, Office Manager
J. Bean	UNM	V.2:§.4.2.1		BRAGFLO & BOASTII, 2-Phase Flow
J. Berglund	UNM	V.2:Ch.7 Editor V.2	CUTTINGS	Task Ldr., Undisturbed Repository, Cuttings/Cavings/ Engr. Mech.
W. Beyeler	SAI	V.2:§.5.3; 6.1;6.3	PANEL GARFIELD	Geostatistics, Analytical Models, CAMCON Systems Codes
K. Brinster	SAI			Geohydrology, Conceptual Models
R. Blaine	ECO			SECO2D & CAMCON Systems Codes
T. Blaine	EPE			Drilling Technology, Exposure Pathways Data
J. Garner	API	V.2:§.5.3	PANEL	Source Term, Sens. Anal.
A. Gilkey	UNM			CAMCON Systems Codes
L. Gomez	SNL			Task Ldr., Safety Assessments
M. Gruebel	TRI	V.1:Ch.1,2, 8,9,10		EPA Regulations
R. Guzowski	SAI	V.1:Ch.4		Geology, Scenario Construction
J. Helton	ASU	V.1:Ch.3,4 V.2:Ch.2,3	CCDFPERM	Task Ldr., Uncert./Sens. Anal., Probability Models
H. Iuzzolino	GC	Editor V.3	CCDFPERM	LHS & CAMCON System Codes
R. Klett	SNL			EPA Regulations
P. Knupp	ECO			STAFF2D & SECOTR, Comp. Fluid Dyn.
C. Leigh	SNL		GENII-S	Exposure Pathways
M. Marietta	SNL	Editor (Set)		Dep. Div. Manager, Tech. Coord.
G. de Marsily	UP	V.2:§.6.2		Task Ldr., Geostatistics
R. McCurley	UNM	V.2:§.4.2.3		SUTRA & CAMCON System Codes
A. Peterson	SNL	Editor V.3		Task Ldr., Inventory
J. Rath	UNM	V.2:§.4.2.3		SUTRA, Engr. Mech.
R. Rechard	SNL	Editor V.2 & V.3		Task Ldr., CAMCON, QA, Ref. Data, Calculations
P. Roache	ECO	V.2:§.6.4	SECO	Task Ldr., Comp. Fluid Dyn.
D. Rudeen	UNM 6.5	V.2:§.4.2.2;		STAFF2D, Transport
J. Sandha	SAI	Editor V.3		INGRES, PA Data Base
J. Schreiber	SAI	V.2:§.4.2.1; 5.2.5 Editor V.3		BRAGFLO & BOASTII, 2-Phase Flow
P. Swift	TRI	V.1:Ch.5,11		Task Ldr., Geology, Climate Var.
M. Tierney	SNL	Editor V.3		Task Ldr., CDF Constr., Probability Models
K. Trauth	SNL			Task Ldr., Expert Panels

P. Vaughn	API	V.2:§.5.1; 5.2; 5.2.5; App.A	BRAGFLO	Task Ldr., 2-Phase Flow & Waste Panel Chemistry
J. Wormeck	ECO			Comp. Fluid Dyn. & Thermodyn.

The foundation of the annual WIPP performance assessment is the underlying data set and understanding of the important processes in the engineered and natural barrier systems. The SNL Nuclear Waste Technology Department is the primary source of these data and understanding. Assistance with the waste inventory comes from WEC and its contractors. We gratefully acknowledge the support of our departmental and project colleagues. Some individuals have worked closely with the performance assessment team, and we wish to acknowledge their contributions individually:

J. Ball	ReS	Computer System Manager
H. Batchelder	WEC	CH & RH Inventories
R. Beauheim	SNL	Natural Barrier System, Hydrologic Parameters
B. Butcher	SNL	Engineered Barrier System, Unmodified Waste-Form Parameters, Disposal Room Systems Parameters
L. Brush	SNL	Engineered Barrier System, Source Term (Solubility) and Gas Generation Parameters
L. Clements	ReS	Computer System Support
T. Corbet	SNL	Natural Barrier System, Geologic & Hydrologic Parameters, Conceptual Models
P. Davies	SNL	Natural Barrier System, Hydrologic & Transport Parameters, & 2-Phase Flow Mechanistic Modeling
P. Drez	IT	CH & RH Inventories
E. Gorham	SNL	Natural Barrier System, Fluid Flow & Transport Parameters
S. Howarth	SNL	Natural Barrier System, Hydrologic Parameters
R. Kehrman	WEC	CH & RH Waste Characterization
R. Lincoln	SNL	Project Integration
F. Mendenhall	SNL	Engineered Barrier System, Unmodified Waste Form Parameters, Waste Panel Closure (Expansion)
D. Munson	SNL	Reference Stratigraphy, Constitutive Models, Physical & Mechanical Parameters
E. Nowak	SNL	Shaft/Panel Seal Design, Seal Material Properties, Reliability
J. Orona	ReS	Computer System Support
J. Tillerson	SNL	Repository Isolation Systems Parameters
S. Webb	SNL	2-Phase Flow Sensitivity Analysis & Benchmarking

API	=	Applied Physics Incorporated
ASU	=	Arizona State University
ECO	=	Ecodynamics Research Associates
EPE	=	Epoch Engineering
GC	=	Geo-Centers Incorporated
IT	=	International Technology
ReS	=	ReSpec
SAI	=	Scientific Applications International Corporation
SNL	=	Sandia National Laboratories
TEC	=	Technadyne Engineering Consultants
TRI	=	Tech Reps, Inc.
UNM	=	Univiversity of New Mexico/New Mexico Engineering Research Institute
UP	=	University of Paris
WEC	=	Westinghouse Electric Corporation

Peer Review

Internal/Sandia

T. Corbet
D. Gallegos
M. LaVenue
S. Hora

Management/Sandia

W. Weart
T. Hunter

PA Peer Review Panel

R. Heath, Chairman	University of Washington
R. Budnitz	Future Resources Associates, Inc.
T. Cotton	JK Research Associates, Inc.
J. Mann	University of Illinois
T. Pigford	University of California, Berkeley
F. Schwartz	Ohio State University

Department of Energy

R. Becker
J. Rhoderick

Expert Panels

Futures

M. Baram	Boston University
W. Bell	Yale University
G. Benford	University of California, Irvine
D. Chapman	The World Bank, Cornell University
B. Cohen	University of Pittsburgh
V. Ferkiss	Georgetown University
T. Glickman	Resources for the Future
T. Gordon	Futures Group
C. Kirkwood	Arizona State University
H. Otway	Joint Research Center (Ispra), Los Alamos National Laboratory
M. Pasqualetti	Arizona State University
D. Reicher	Natural Resources Defense Council
N. Rosenberg	Resources for the Future
M. Singer	The Potomac Organization
T. Taylor	Consultant
M. Vinovski	University of Michigan

Source Term

C. Bruton	Lawrence Livermore National Laboratory
I-Ming Chou	U.S. Geological Survey
D. Hobart	Los Alamos National Laboratory
F. Millero	University of Miami

Retardation

R. Dosch	Sandia National Laboratories
C. Novak	Sandia National Laboratories
M. Siegel	Sandia National Laboratories

Geostatistics Expert Group

G. de Marsily, Chairman	U. of Paris
R. Bras	Massachusetts Inst. of Tech.
J. Carrera	U. Politechnica de Cataluña
G. Dagan	Tel Aviv U.
A. Galli	Ecole des Mines de Paris
A. Gutjahr	New Mexico Tech.
D. McLaughlin	Massachusetts Inst. of Tech.
S. Neuman	U. of Arizona
Y. Rubin	U. of California, Berkeley

Report Preparation (TRI)

Editors:

Volume 1: M. Gruebel (text); S. Laundre-Woerner (illustrations)
Volume 2: D. Scott (text); D. Marchand (illustrations)
Volume 3: J. Chapman (text); D. Pulliam (illustrations)

D. Rivard, D. Miera, T. Allen, and the Word Processing Department
R. Rohac, R. Andree, and the Illustration and Computer Graphics Departments
S. Tullar and the Production Department

J. Stikar (compilation of PA Peer Review Panel comments)

CONTENTS

LIST OF FIGURES

LIST OF TABLES

1. INTRODUCTION—Rob P. Rechard

1.1 Role of Volume 2

The Waste Isolation Pilot Plant (WIPP) is planned as the first mined geologic repository for transuranic (TRU) wastes generated by defense programs of the United States Department of Energy (DOE). Before disposing of waste at the WIPP, the DOE must evaluate compliance with the United States Environmental Protection Agency's Standard, *Environmental Radiation Protection Standards for Management and Disposal of Spent Nuclear Fuel, High-Level and Transuranic Radioactive Wastes* (40 CFR Part 191, U. S. EPA, 1985).

This volume deals primarily with probability and consequence modeling of the WIPP disposal system for evaluating compliance with the quantitative requirements of Subpart B of the EPA Standard. Volume 1 deals primarily with scenario development and the regulations in 40 CFR Part 191 and their application to the WIPP, but also summarizes aspects of this volume. Volume 3 compiles pertinent data from disposal system characterization. Finally, uncertainty/sensitivity analysis is discussed in Volume 4.

1.2 Organization of Volume 2

This introduction to Volume 2 provides an overview of the 1991 PA calculations using the general tasks of the performance assessment methodology as a framework. It also summarizes the CAMCON (Compliance Assessment Methodology CONtroller) computer system used to perform these complex calculations.

The two chapters following the introduction discuss probability modeling and complementary cumulative distribution function (CCDF) construction for the 1991 PA:

- Chapter 2 describes the probability model for computational scenarios in the 1991 calculations.
- Chapter 3 describes the mathematical construction of the CCDF for WIPP performance assessment.

The next four chapters discuss the generic computational models and the applied (or site-specific) models used in consequence analysis and the results that these models predict:

- Chapter 4 discusses predicted undisturbed performance of the repository/shaft system (where no boreholes intrude the repository during the 10,000-year regulatory period). Because no releases beyond the repository shaft are predicted for undisturbed conditions, radionuclide release into the groundwater of the Culebra was not evaluated.
- Chapter 5 discusses disturbed performance of the repository/shaft system (in which one or more hypothetical boreholes intrude the repository during the 10,000-year regulatory period).

- Chapter 6 discusses predicted radionuclide release into the Culebra groundwater for disturbed conditions.
- Chapter 7 discusses predicted radionuclide release by transport of cuttings and eroded material to the surface during borehole intrusion.

Discussion in Chapters 4 through 7 is limited to the seven generic computational models ("codes") and the corresponding applied models used to simulate the major conceptual components of the WIPP disposal system. Details of code development and uses are not presented here; in most cases, that information is available separately in user's manuals for the various codes. Furthermore, details of CAMCON, including information about the codes that link the major models and control data flow, are also not presented here. That information is contained in the CAMCON user's manual (Rechard et al., 1989).

Finally, this volume contains two appendices:

- Appendix A discusses the theory of multiphase flow through porous media. This appendix is included in the report because two of the analysis models, BOAST II (for undisturbed conditions) and BRAGFLO (for disturbed conditions), describe simultaneous flow of brine and gas through porous media.
- Appendix B presents the input and output data for calculations reported in Volumes 1 and 2.

1.3 Background on PA Methodology

The Sandia methodology for assessing the compliance of the WIPP with the Containment Requirements, § 191.13 of 40 CFR Part 191 (U.S. EPA, 1985), hereafter referred to as performance assessment (PA), consists of six general tasks (Figure 1-1):

1. characterization of the WIPP disposal system and regional area
2. scenario development and selection of scenarios to model
3. development and execution of probability models
4. development and execution of consequence models (both generic computational and site-specific models) including uncertainty
5. regulatory compliance assessment
6. uncertainty/sensitivity analysis.

The first task is performed primarily outside the PA organization (except for estimating the radionuclide inventory), and the data are compiled in Volume 3. The other five tasks are performed inside the PA division.

For the WIPP, the PA process is conducted in annual cycles, and the 1991 PA is the second* in a series of annual "Performance Analysis and DOE Documentation" activities shown in the

* The PA process actually started in 1989, but it was primarily a demonstration with a specific example from the WIPP.

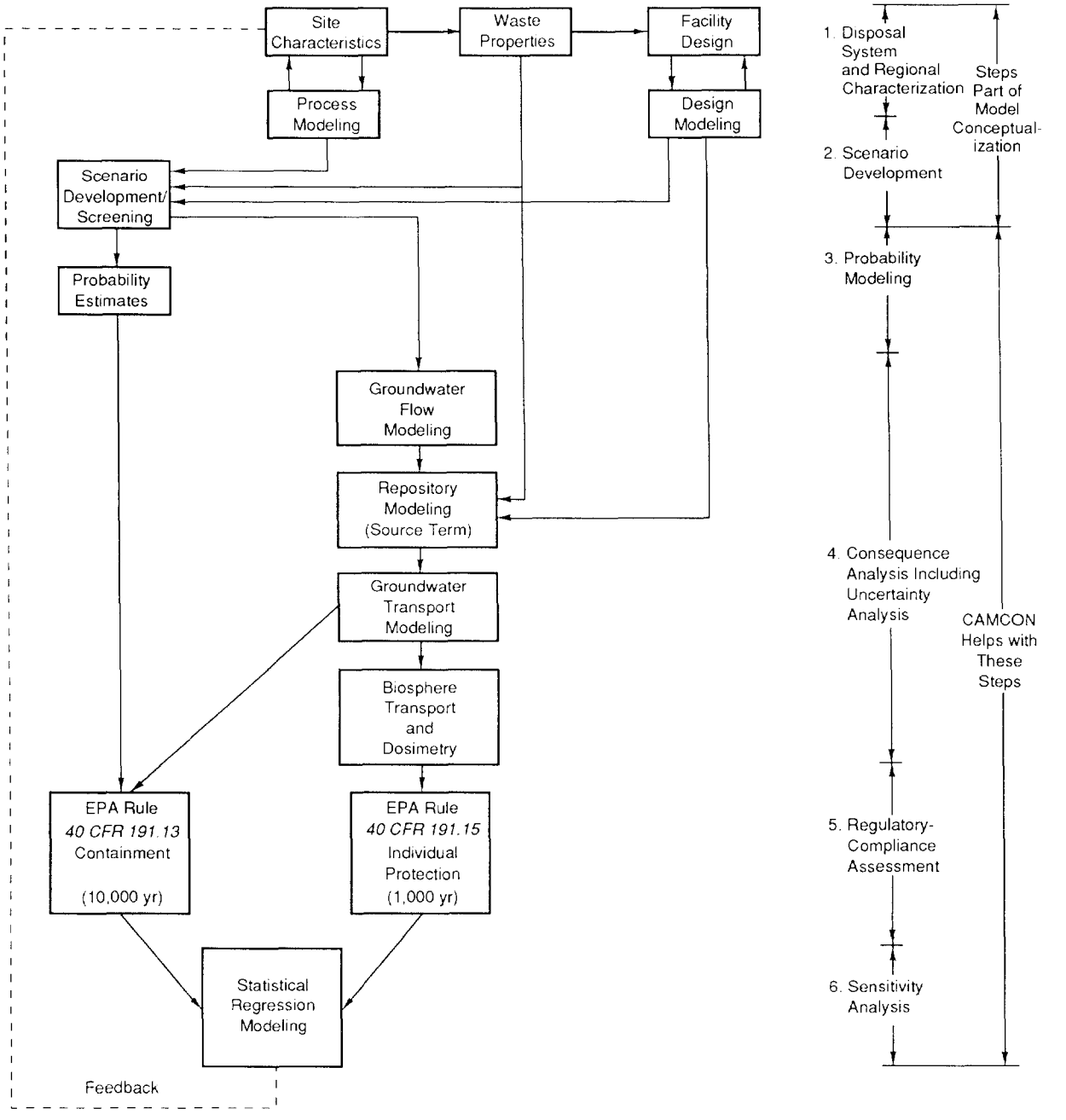

Figure 1-1. Overview of WIPP Performance Assessment Process (after Rechard, 1989, Figure 3.1)

Performance Assessment Time-Phased Activities for the Test Phase (U.S. DOE, 1991). In each cycle, data from the test program are used to update scenarios, update conceptual models (and computational models if necessary), and provide input to applied models to evaluate compliance.

The first two PA tasks listed above are referred to collectively as model conceptualization (Figure 1-1). Characterization of the disposal system and surrounding regional hydrology has been in progress since project inception in 1975 (e.g., Powers et al., 1978) and is nearing completion. Screening of events and processes that may affect performance of the system during the next 10,000 years is also nearly complete, and significant summary scenarios have been identified for consideration in consequence modeling (Guzowski, 1990; and Volume 1).

For Task 3, a probability model has been developed to evaluate probabilities of detailed computational scenarios for analysis, which are a decomposition of the summary scenarios developed above as part of Task 2. The scenarios incorporate stochastic variability (IAEA, 1989) into the performance assessment.

A major portion of the methodology consists of simulating physical processes to estimate the amount of radionuclides released to the accessible environment. This process is referred to as consequence modeling and analysis and actually is a composite function of several models (Task 4) (Figure 1-1). Construction of the modeling system begins with the development of conceptual models that identify the processes that will be simulated. These conceptual models provide a framework in which to interpret observational data and a basis for developing predictive mathematical models. In most cases, the choice of a conceptual model introduces simplifying assumptions about the real world that permit interpretation of entire components of the system using limited available data. In some cases the choice of a conceptual model may also be influenced by the availability of computational models to simulate it. For some processes, available generic computational models required adaptation. For other components of the disposal system, such as the coupled processes of gas generation, brine flow, and creep closure in the repository domain, computational models were developed specifically for the WIPP.

The complexity of the WIPP disposal system and the need to use multiple codes to describe the various components poses operational problems in performing calculations. An executive controller, CAMCON (Compliance Assessment Methodology CONtroller) (Rechard et al., 1989), links codes within the modeling system, manages data flow from one component to the next, and minimizes the opportunities for operator error.

Because of imprecisely known parameters, uncertainty is incorporated into the performance assessment through a Monte Carlo analysis (part of Task 4). As discussed in more detail in Chapter 3 of Volume 1 and compiled in Volume 3, Monte Carlo analysis consists of first identifying the important parameters to vary and assigning ranges and distributions. Second, sample elements are generated from these distributions. In the WIPP performance assessment,

Latin hypercube sampling (LHS) is used to minimize the number of sample elements needed to capture variability in the parameters adequately. And finally, each sample element is propagated through the consequence modeling system. For the 1991 calculations, 60 sample elements were drawn from the distributions assigned to 45 imprecisely known parameters. The repository performance was evaluated for each sample element (a vector of 45 parameter values).

From the consequence results using Monte Carlo analysis, the final two tasks naturally follow. In Task 5, estimated releases are combined into a complementary cumulative distribution function (CCDF) for each sample element. A CCDF (exceedance probability curve) is used for evaluating compliance with § 191.13 of 40 CFR Part 191. The CCDF from each sample element results in a distribution (family) of CCDFs. Summary statistics of the CCDFs (e.g. mean, median, and different quantiles) are also produced. The CCDFs for the WIPP are presented in Volume 1.

In Task 6, sensitivity analyses are used to analyze the results. For example, sensitivity analyses can be used to identify those parameters for which variability in the sampled value had the greatest effect on results, to provide guidance for research that may improve confidence in the estimate of performance. This sixth task is reported in Volume 4. CCDFs using several different modeling assumptions are also presented in Volume 4.

1.4 Overview of Calculations

The following discusses the calculations using the framework of the PA methodology. (Tasks 3 and 4 are particularly pertinent to Volume 2.)

1.4.1 SUMMARY SCENARIOS MODELED

Four summary scenarios from the scenario development task are examined for the 1991 PA: three disturbed (human intrusion) scenarios and the undisturbed (base case) scenario (see Chapter 4, Volume 1). (These same scenarios were examined for the 1990 PA calculations.) Disturbed performance scenarios include the possibility of human disruption of the repository by exploratory drilling or the occurrence of unlikely events. Undisturbed performance forms the base case for scenario development (Guzowski, 1990). As defined in the EPA Standard, "undisturbed performance" means "the predicted behavior of a disposal system, including consideration of the uncertainties in predicted behavior, if the disposal system is not disrupted by human intrusion or the occurrence of unlikely natural events" (U.S. EPA, 1985, § 191.12(p)).

The approach for the calculations for the human intrusion and base case scenarios differs somewhat for the WIPP disposal system. If human intrusion by drilling hypothetically occurs some time in the next 10,000 years, some releases by removal of cuttings are certain (but do not necessarily exceed EPA limits). Furthermore, the long-term consequence from disrupting the

repository must be evaluated. Consequently, a complex modeling effort is required. For undisturbed conditions, a number of deterministic calculations are performed to investigate radionuclide transport in and adjacent to the repository. It is tempting to describe the deterministic calculations as bounding since the conceptual model often appears conservative—but they are not always. For example, in one analysis the disposal region was assumed to be directly in the MB139 anhydrite layer, a potential pathway. However, the selection of conservative values for many of the parameters of these models was problematic since it was often difficult to assess their influence on such a complex system a priori. Thus, median values (not "conservative" values) were typically selected. (The Monte Carlo calculations for undisturbed conditions are described in Volume 4.) Because of the excellent isolating capabilities of the bedded salt in the Salado Formation, the undisturbed scenario has zero releases of radionuclides, and only the region directly around the repository needs to be modeled.

1.4.2 PROBABILITY MODELING AND REGULATORY COMPLIANCE EVALUATION

Following the usual sequential order of the tasks presented above, regulatory assessment (Task 5) would be discussed later. However, because probability modeling is intimately tied to regulatory evaluation, both are discussed here prior to the consequence analysis (Task 4) discussion.

Last year for the 1990 PA, probabilities for the four summary scenarios were determined from (1) professional judgment and (2) assuming a Poisson process. These probabilities were then paired with EPA-summed normalized releases, and the CCDF was constructed.

For the 1991 PA, the probabilities were also evaluated assuming drilling is a Poisson process. However, although the summary scenarios are the same as for the 1990 PA, these summary scenarios were decomposed based on (1) number of drilling intrusions (1 to 15), (2) time of intrusion (5 times—1000, 3000, 5000, 7000, and 9000 years), and (3) the activity level of the waste penetrated by the boreholes (five activity levels—four for contact-handled (CH) and one for remote-handled (RH) waste). This decomposition more fully resolves the CCDF, that is, each individual CCDF has numerous small steps rather than the four large steps (with two being identical) shown in the 1990 PA calculations (Bertram-Howery et al., 1990). The decomposition of the summary scenarios required many more simulations, as described in the following sections of this introduction.

The construction of the CCDF is possible once all the simulations are completed in each of the three modeling systems described below. The code, CCDFCALC, extracts the radionuclide concentration history and the cuttings concentration history calculated in the consequence modeling described below and evaluates cumulative releases and EPA-summed normalized releases. The

actual construction of the CCDF required a new program, CCDFPERM, in addition to CCDFCALC to decompose the summary scenarios. The Poisson probability model for evaluating decomposed scenario probabilities and the theory underlying the CCDF construction are thoroughly described in Chapters 2 and 3, respectively.

1.4.3 CONSEQUENCE MODELING OF DISTURBED CONDITIONS

The consequence modeling of disturbed conditions of the WIPP is discussed first because the modeling for undisturbed conditions is actually a simplification of this complex modeling system.

1.4.3.1 Physical Features Modeled

Of the numerous computer codes required to perform the PA, relatively few generic computational models ("codes") are necessary to simulate the major physical features of the WIPP disposal system (Figure 1-2). Five computational models are used for disturbed conditions. (Four computational models are used for undisturbed conditions, the base case summary scenario [see Section 1.4.5 of this introduction]). Except for PANEL, which implements analytic solutions to the mathematical model to model flow and radionuclide concentration in a WIPP disposal panel, the computer codes are generic and implement a variety of mathematical models using several numerical solution techniques. Hence, some codes were used to model several different physical features of the WIPP disposal system and are repeated in several places. Furthermore, the CAMCON model system was developed so that different codes could be used to model any one physical feature with relative ease; thus some WIPP disposal systems features in Figure 1-2 show more than one code being used. Specifically, three codes (BRAGFLO, STAFF2D, and SUTRA) can be used to simulate flow and transport within the repository environment. PANEL estimates radionuclide concentrations in repository brine and can analytically simulate flow near the repository. CUTTINGS estimates the amount of radioactive material brought to the surface during drilling. SECO_2DH simulates regional groundwater flow within the Culebra Dolomite Member of the Rustler Formation, and STAFF2D simulates local groundwater flow and radionuclide transport within the Culebra.

1.4.3.2 Modeling Systems

Depicting the generic computational models and the physical features they represent is fairly straightforward. However, the actual mechanics of moving through the calculations are more complicated. For modeling, the WIPP disposal system was divided into three modeling systems: repository/shaft/borehole, Culebra groundwater flow and transport, and cuttings. The seven major computational models and the systems they model are listed in Table 1-1. For disturbed conditions, all three modeling systems are used. Each of these modeling systems are analyzed in

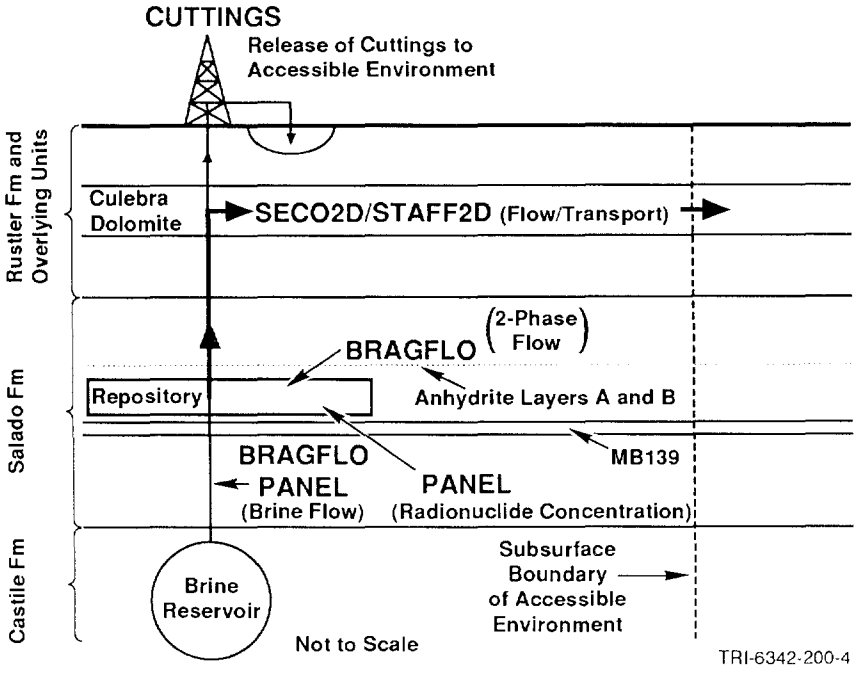

Figure 1-2. Major Computational Models and the Physical Features They Simulate in the WIPP Disposal System (Disturbed Conditions). Five generic computational models used for disturbed conditions.

Table 1-1. The Seven Major Computational Models Grouped According to the Modeling Systems Used in Modeling the WIPP Disposal System in the 1991 PA

Modeling System	Generic Computational Models ("Codes")
Repository/Shaft/Borehole	BOAST II, BRAGFLO SUTRA, STAFF2D, PANEL
Culebra Groundwater Flow and Transport	SECO_2DH, STAFF2D
Cuttings	CUTTINGS

parallel and results are combined during the regulatory compliance assessment (described in the previous section) and sensitivity analysis (described below) tasks.

The modeling systems do not correspond to the geologic and engineered barrier systems associated with physical parts of the WIPP disposal system and defined in the EPA Standard. Rather, these categories are an alternate subdivision of the WIPP disposal system done to facilitate modeling. The modeling subdivision and the identified components may change from year to year as required by the analysis whereas the physical systems described in the EPA Standard are invariant.

Twenty-nine major and support codes are used in these modeling systems (Figure 1-3). Section 1.5 provides a brief description of these codes. A more thorough discussion of the codes is provided in the CAMCON user's manual (Rechard et al., 1989).

The codes and general flow of information used in calculations of disturbed conditions has not substantially changed from the 1990 PA calculations. Specific changes for calculations of disturbed conditions are (1) the full incorporation of BOAST II and BRAGFLO, used to analyze two-phase flow, and CUTTINGS, used to analyze cuttings release, into the procedure rather than their use as subsidiary calculations as in the 1990 PA, (2) the use of the codes GARFIELD (which generates equally likely transmissivity fields), GENOBS (which generates head impulse functions at selected points along the boundary), FITBND (which determines functional relationships between well heads and pressure boundary conditions and optimizes the fit of pressure boundary conditions), and SWIFT II (which models hydrologic flow) during model conceptualization to evaluate uncertainty of the transmissivity field within the Culebra Dolomite Member of the Rustler Formation, and (3) the evaluation of scenario probabilities and the permutation of computational scenarios within CCDFPERM, which calculates decomposed scenario probabilities (Chapter 2). This last change is a result of decomposition of the summary scenarios used in the PA (mentioned earlier). Although the software tools have not substantially changed, the underlying treatment of the calculations, as represented by CCDFPERM, has changed substantially and is described in Chapters 2 and 3.

The overview of the mechanics of the 1991 PA calculations for disturbed conditions is shown in Figure 1-3. Model and parameter selection and the modeling steps in each of the modeling systems are discussed in the following sections.

1.4.3.3 Model and Parameter Selection

The calculations start with model and parameter selection. This can be a time-consuming process, but in short, the process involves evaluating data and then developing conceptual, mathematical, and computational models if necessary. It is then followed by a selection of parameters to vary (45 parameters in the 1991 PA). Following these decisions, data are entered in

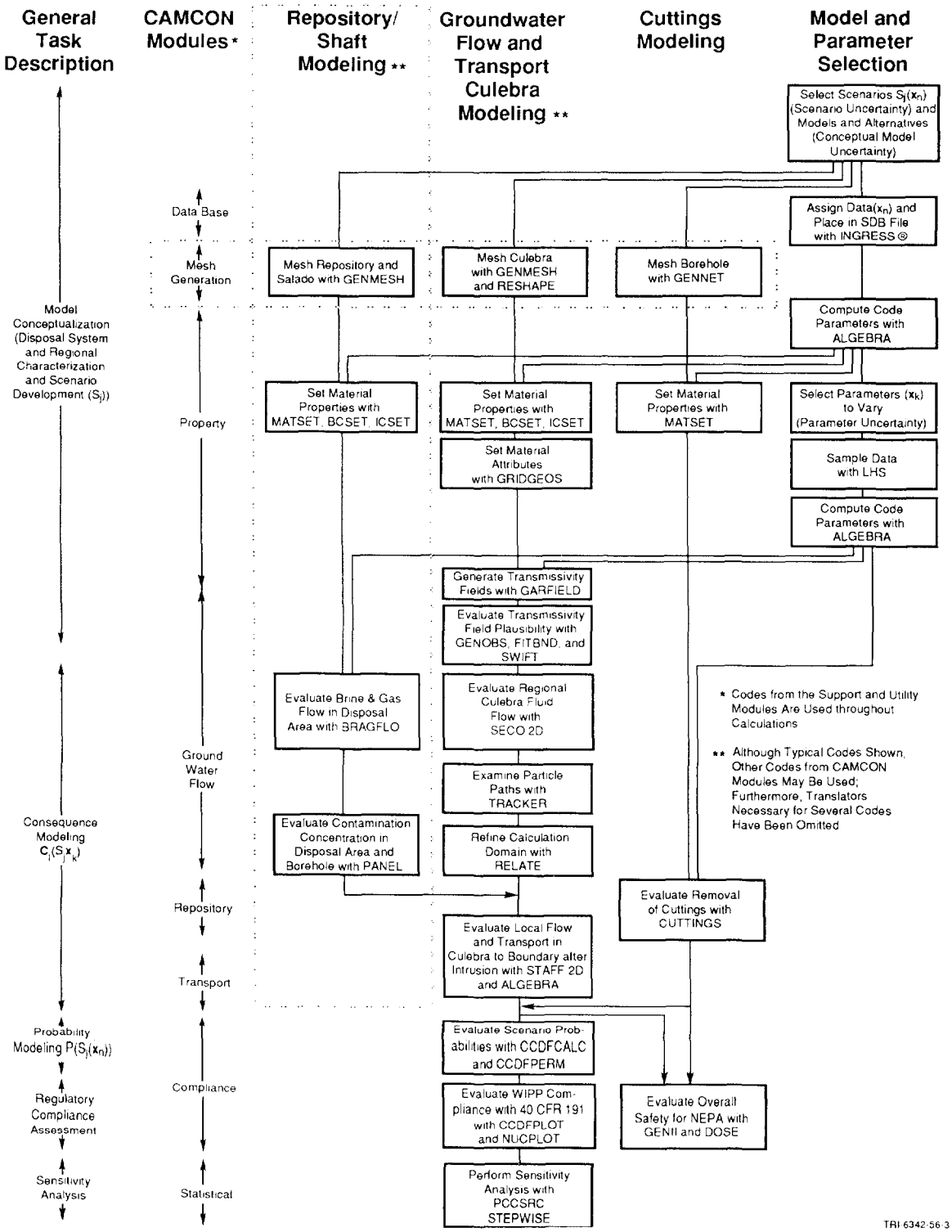

Figure 1-3. Overview of 1991 PA Calculations for Disturbed Conditions (Human Intrusion). Refer to Section 1.5 and CAMCON User's Manual (Rechard et al., 1989) for description of codes listed.

the data base and are sampled. The parameters sampled and the sampled values are presented in Tables B-1 through B-3 in Appendix B. All other data used for the 1991 PA calculations are documented in Volume 3. The fixed data are not repeated in this volume unless the data differed from what is reported in Volume 3. (Differences usually occurred only for the undisturbed calculations because they began in May 1991, prior to final decisions for some parameters.)

Once this critical step is completed, the analysts can begin the task of performing the calculations. (In this volume, the analysts have authored the parts of the calculations for which they are responsible.) As mentioned previously, the next steps are performed in parallel. In general, this consists of preparation of input with several computer codes, followed by the simulation and finally followed by examination of intermediate results and usually very little preparation for use by other codes. The intermediate results, along with the details of the applied models, are the subject of Chapters 4, 5, and 6.

1.4.3.4 Cuttings Modeling

The mechanics of modeling the initial human intrusion by drilling into the repository is fairly simple. It involves input preparation using GENMESH, the mesh generation model of CAMCON, (the mesh is a simple line representing the borehole since the analysis of cuttings is implemented with an analytic solution), extraction of pertinent data from the database using MATSET and sampled parameters from LHS using ALGEBRA. Then the CUTTINGS code is run for each sample element for each time, first assuming an intrusion into contact-handled (CH) waste and then an intrusion into remote-handled (RH) waste. (The time of intrusion was important because of radionuclide decay.) Six hundred simulations are required—two for the RH and CH wastes, five for the time intervals, and 60 for the sample elements. Once the 600* simulations are complete, the output is stored for use by CCDFCALC. The simulation release results for CH and RH waste are presented in Tables B-6 and B-7, respectively (Appendix B).

1.4.3.5 Repository/Borehole Modeling

The repository/borehole modeling system models phenomena around the repository. These phenomena include gas generation from corrosion and microbiological degradation of the waste, brine movement around the waste over time, and the possible saturation of the waste by the brine reservoir following intrusion and creep closure. The two-phase numerical code BRAGFLO and the one-phase analytic code PANEL were developed specifically to model these phenomena. (The creep closure phenomenon is not modeled in the 1991 PA calculations. Rather, constant room state corresponding to high porosity after gas generation was selected.) For most calculations

* The numerous additional simulations required for the sensitivity analysis presented in Volume 4 are not included in these or any of the following simulation counts.

reported in Chapter 5, the brine-phase flow results from the cylindrical approximation of the repository, Castile brine reservoir, and Culebra using BRAGFLO were used by PANEL to evaluate radionuclide concentrations using a equilibrium-mixing cell mathematical model. However, in one case PANEL was also used to evaluate analytically brine inflow from the Salado and brine reservoir to make comparisons with BRAGFLO.

Modeling the repository/borehole area required 600 simulations: 2x5x60; two for the E2 and E1E2 summary scenarios, five for the five time intervals selected to decompose these two scenarios, and 60 for the sample elements used to describe parameter uncertainty. (Based on one-phase and early two-phase simulations, the E1 summary scenario was assumed to be similar to the E2 summary scenario—and bounded by the E1E2 summary scenario. This assumption is more thoroughly examined in Volume 4.)

1.4.3.6 Culebra Groundwater Flow Modeling

Flow and transport are grouped into the same modeling subdivision because they model the same physical features of the same unit, the Culebra Dolomite Member at the Rustler Formation. However, the modeling and number of simulations are different and are separated in this discussion. (Transport modeling is discussed in Section 1.4.3.7 of this introduction.)

The groundwater flow component of the Culebra modeling system was quite complicated. It not only consisted of a normal data-preparation step using GENMESH to set up a planar, two-dimensional mesh at the Culebra and MATSET, BCSET, and ICSET to set fixed material properties and boundary conditions, but as indicated in Figure 1-3 it also consisted of evaluating the uncertainty of the transmissivity fields using GARFIELD, GENOBS, FITBND, and the groundwter flow code SWIFT II.

Specifically, the procedure consisted of using GARFIELD to randomly generate thousands of transmissivity fields of the Culebra, which had the general spatial variance (same variogram) as suggested by the data, after which a set of head impulse functions at selected points along the mesh boundary were generated (40 impulse functions in the 1991 PA), followed by an evaluation of the steady-state, linear response of the thousands of Culebra "systems" (including brine density variation) to these impulse functions using the hydrologic code SWIFT II. Finally, each of the generated transmissivity fields were conditioned to the steady-state equivalent head measurements at wells by using the 40 linear responses to select the optimal pressure conditions on the boundaries of the regional model using FITBND. The first 60 transmissivity fields generated by this procedure that had (1) good agreement with the head measurements and (2) agreement with known general flow directions in the area were retained. (About 1 in 5 meets these selection criteria; thus, about 12,000 simulations (60x40x5) of the steady-state Culebra system were made with SWIFT II.) Uncertainty of the transmissivity fields is the subject of the first part of Chapter 6.

Once the final 60 transmissivity fields were selected, the regional fluid flow assuming constant brine density was determined 60 times with a newly developed hydrologic code, SECO_2DH. The regional analyses included effects from varying head boundary conditions that were related to increases in precipitation. Capabilities of SECO_2DH and the results are the second topic discussed in Chapter 6.

1.4.3.7 Culebra Groundwater Transport

The second part of the Culebra modeling system is the evaluation of radionuclide transport from the intrusion borehole to the 5-km boundary of the accessible environment and through the Culebra. The code RELATE was used to evaluate fluid flow boundary conditions on a greatly decreased local mesh. STAFF2D was then used to evaluate first flow and then transport on this local two-dimensional domain. Note that no borehole model was used; rather, the radionuclide concentrations (mass flux only) from the repository/borehole modeling system were directly injected into the Culebra at a point directly above the center of the disposal area. Following the STAFF2D simulations, the support program ALGEBRA was used to evaluate radionuclide transport across the 5-km boundary of the accessible environment.

While the evaluation of local fluid flow with STAFF2D only required 60 simulations, the evaluation of transport required 600 simulations because 600 different "source terms" come from the repository/borehole modeling system. The transport conceptual model reported here and in Volume 1 is dual porosity. A fracture-porosity-only transport model is reported in Volume 4. The integrated releases from these transport simulations are reported in Tables B-4 and B-5 (Appendix B).

1.4.4 SENSITIVITY ANALYSIS

The final task, sensitivity analysis, can only start after major results have been calculated. Hence, Volume 4, where the sensitivity analysis is described, must of necessity be produced after Volumes 1, 2, and 3. It involves plotting scatter plots and developing regression models between the parameters varied (and their ranks) and various results (e.g., EPA-summed normalized releases for cumulative releases of each radionuclide from the 600 combined simulations or the 600 cuttings simulations) using the Sandia statistics codes PCCSRC (which calculates partial correlation coefficients and standardized regression coefficients) and STEPWISE (which selects the regression model using stepwise techniques). In addition, several other issues such as conceptual model uncertainty is explored in Volume 4, so the number of total simulations increases four or five times.

1.4.5 CONSEQUENCE MODELING SYSTEM FOR UNDISTURBED CONDITIONS

Preliminary results from the 1989 PA demonstration showed no releases to the accessible environment (Marietta et al., 1989) for undisturbed conditions. Consequently, simulations of undisturbed conditions were not performed in 1990; instead, the preliminary results showing no releases were summarized (Bertram-Howery et al., 1990). Simulations of undisturbed conditions were repeated in 1991 with updated data and computational models to verify these results and examine the influence of gas generation in the repository.

Prior to running the two-phase undisturbed calculations with BRAGFLO, much work was expended to gain experience in using several one-phase models (both planar and cross-sectional using STAFF2D and SUTRA) assuming a constant and varying gas drive with modifications to the porosity and permeability to examine various alternative modeling schemes. The modifications to porosity and permeability were based on preliminary calculations using BOAST II because development of BRAGFLO was not complete in May 1991, when these undisturbed calculations were being run. The alternative modeling schemes could find use in providing design criteria for panel and shaft backfill or for examining engineered modifications to the waste where detailed calculations may be necessary and approximations to the two-phase flow formulation may be desirable. The different modeling schemes are presented in Chapter 4. (The physical features modeled and the codes used are shown in Figure 1-4.) The overview of the mechanics of the 1991 PA calculations for undisturbed conditions is shown in Figure 1-5. Thirteen major codes are used in the repository/shaft modeling system.

For the undisturbed calculations incorporating two-phase flow, two cases were run using BRAGFLO. First, the 60 simulations of the cylindrical model for the E2 scenario (without a borehole) were extended to the full 10,000-year performance period. Second, a separate BRAGFLO vertical cross-section model of the repository that included the shaft was also run. This latter two-dimensional model included three-dimensional effects by gradually increasing the thickness of elements as a function of distance from the repository. (Because only fluid-flow comparisons were planned, this latter case used a new LHS sampling with only 22 sampled elements.) These undisturbed calculations with BRAGFLO are reported in Volume 4.

The conclusion has remained the same since the 1989 preliminary calculations: if no one drills into the repository during the 10,000-year performance period, there will be no radionuclide releases from WIPP to the accessible environment, and furthermore, no radionuclide movement outside the Salado Formation.

1.5 Background on the CAMCON System

As shown in Figures 1-3 and 1-5, many different types of software are necessary to investigate various events and physical processes, perform the assessment, and present the final output as a

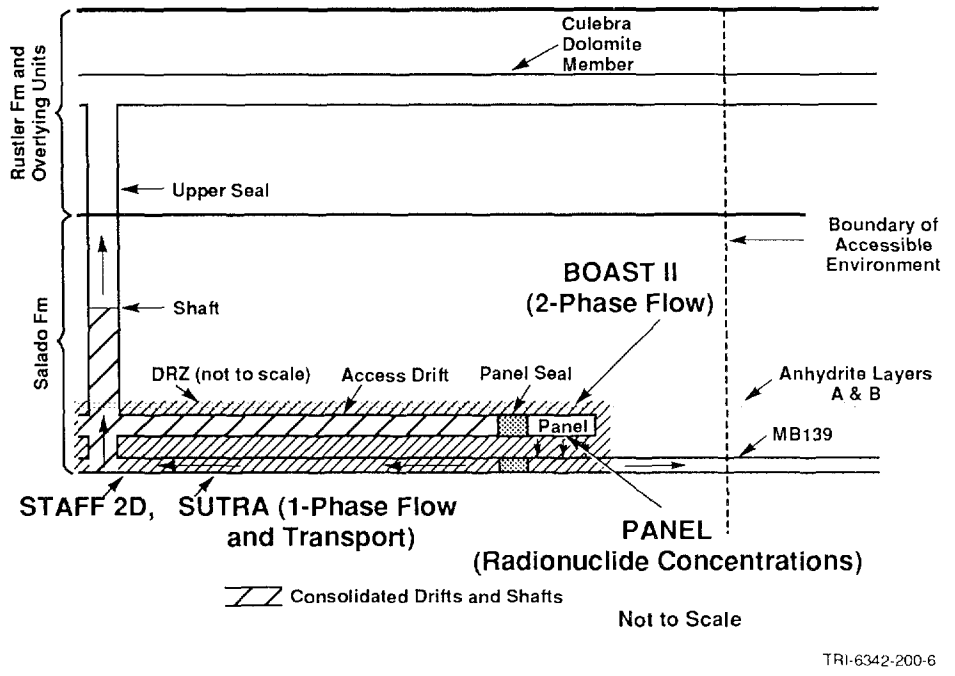

Figure 1-4. Major Computational Models and the Physical Features They Simulate in the WIPP Disposal System (Undisturbed Conditions). Four generic computational models used for undisturbed conditions.

complementary cumulative distribution function (CCDF) for comparison with the probabilistically based release limits in 40 CFR 191. While Figures 1-3 and 1-5 show the modeling mechanics of producing a CCDF, the support structure (framework) for the modeling system is CAMCON (Compliance Assessment Methodology CONtroller). CAMCON manipulates this software as an analysis system (analysis "toolbox") by assisting the flow of information between numerous codes.

1.5.1 ASSISTING THE FLOW OF INFORMATION: THE CAMCON SYSTEM

CAMCON, the analysis toolbox for running the calculations, has two important functions. First, it provides the analyst with the necessary tools and flexibility to build and execute all or portions of an assessment for the WIPP. For example, it allows an analyst to quickly identify available software and the necessary information for using individual codes, enabling the analyst to

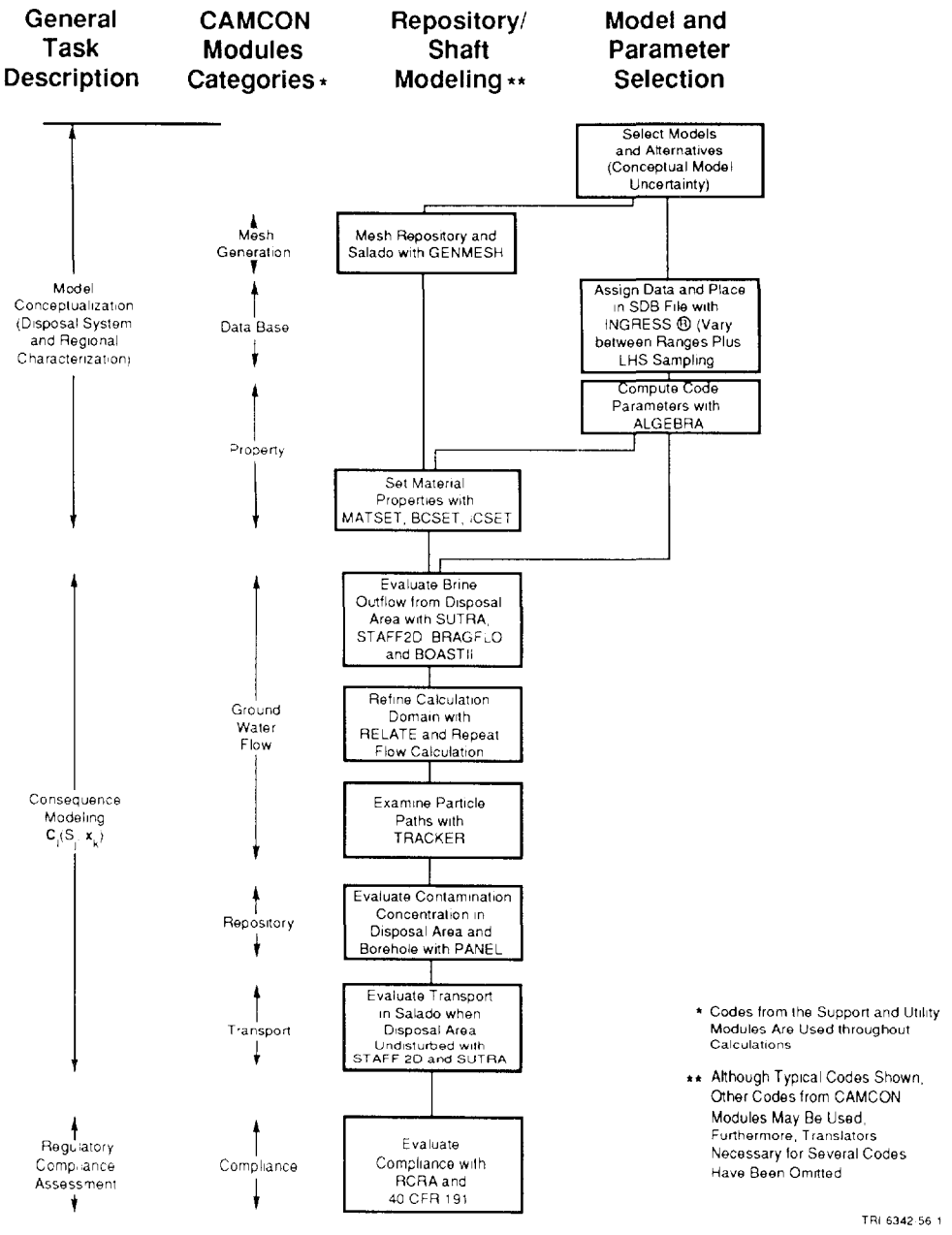

Figure 1-5. Overview of 1991 PA Calculations for Undisturbed Conditions (Base Case)

select the code(s) best suited for a particular study. Second, several of CAMCON's procedures, utility programs, and even directory structure assist in implementing software QA procedures (Rechard et al., 1989). For example, CAMCON serves as a software management system, providing (1) rudimentary configuration control, (2) FORTRAN libraries of commonly used subroutines, and (3) on-line documentation for each code, consisting of a description of the code and its capability, summary of user commands, update history, and examples.

Related to the first function, CAMCON has five main features that help the analyst perform a quality analysis: (1) the ability to read model parameters from one central data base to ensure data consistency; (2) semi-automated linkage of codes, reducing errors in keying in data, (3) a computational data base that stores all data results in one location; (4) codes to algebraically manipulate and plot any intermediate (and final) results for careful scrutiny; and (5) a procedure to help archive analysis input and output.

1.5.2 THE CAMCON SYSTEM PARTS

The primary parts of the CAMCON system consist of (Figure 1-6):

1. Code modules broken down into:
   - seven computational modules (mesh generation, property assignment and Monte Carlo sampling, etc.)
   - one support module (e.g., plotting and algebraic manipulation) (eighth module)
   - one utility module for archiving input files and results, listing programs, reporting code discrepancies, etc. (ninth module)
   - a data base module containing software for storing and/or manipulating the secondary and computational data bases
2. A computational data base, CAMDAT, and several secondary data bases
3. A collection of frequently used subroutines in FORTRAN object libraries (e.g., plot libraries)
4. A suite of procedural files (and symbols to set up the computer environment) for ready access and execution (either batch or interactively) of the computational and support modules. The VAX/VMS procedures are written in DEC (Digital Equipment Corporation) Control Language (DCL).
5. Directory structure and protocols for storing codes for rudimentary configuration control.
6. Help files for on-line documentation.

The CAMCON software (modules, procedures, help files, and libraries) is stored within its own directory on the WIPP 8810 VAX computer.

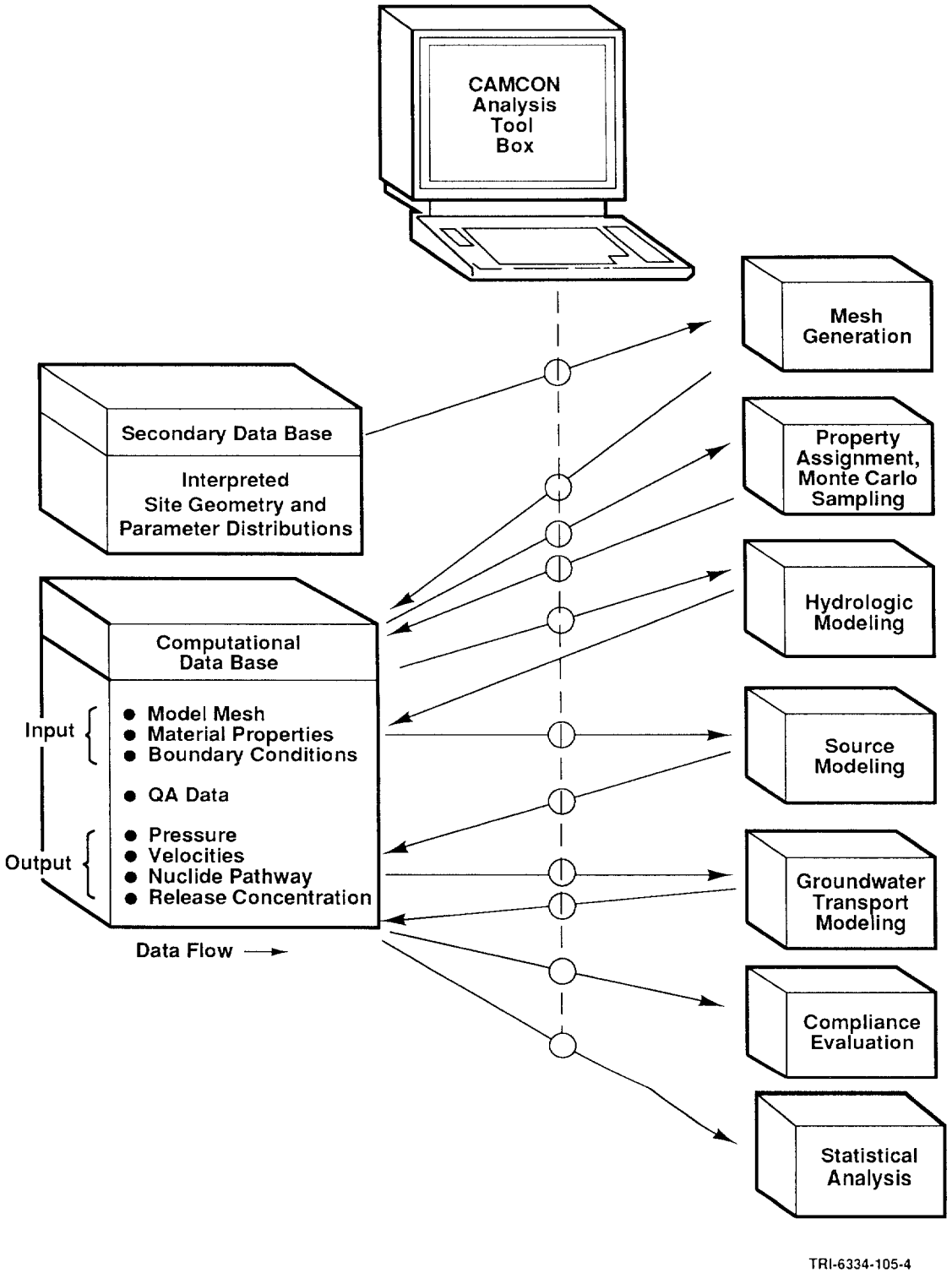

Figure 1-6. The Analysis Tool, CAMCON. CAMCON consists of (1) code modules broken down into seven computational modules, one support module (not shown), one utility module (not shown), and a data base module, a computational data base (CAMDAT), and several secondary data bases, (3) software libraries (not shown), (4) procedural files to access modules (not shown), (5) directory structures and protocols for storing codes (not shown), and (6) help files for on-line documentation (not shown).

1.5.3 CODES AVAILABLE IN THE CAMCON MODULES

The ten code modules (groupings of codes) mentioned above are the (1) mesh generation module, (2) material property module, (3) regional and local hydrologic module, (4) panel module, (5) transport module, (6) compliance calculation module, (7) statistical module, (8) support module, (9) utility module, and (10) data base module.

- The Mesh Generation Module discretizes the models needed for assessing consequences of one scenario.
- The Property (Monte Carlo sampling) Module samples distributions of geologic and hydrologic properties needed for uncertainty and sensitivity calculations.
- The Regional and Local Fluid-Flow Module establishes flow conditions within the controlled area of the repository.
- The Repository Module develops a source term for transport calculations by incorporating the complex processes in the waste container, storage room, drifts, shaft, and seals.
- The Nuclide Transport Module predicts radionuclide migration from the repository source to the accessible environment boundary for EPA standard calculations or the maximally exposed individuals for the NEPA calculations.
- The Compliance Module evaluates the cumulative distribution function (CCDF) from simulations on all scenarios to assess compliance with the EPA Standard.
- The Statistical Module evaluates parameter sensitivity through regression analysis.
- The Support Module provides data base manipulation and plotting codes to support the other modules.
- The Utility Module contains codes that assist in the operation of the CAMCON system (e.g., listing programs, etc.).
- The Property Data Base Module inputs and manipulates the data collected during disposal system characterization.

CAMCON currently consists of about 75 codes and FORTRAN object libraries, which includes those codes and libraries developed external to Sandia, those internal to Sandia but developed in other organizations, and those developed specifically for the WIPP project. The total FORTRAN lines of software written specifically for the WIPP project is about 300,000 (of which about 51% are comment lines). Imported software, much of which was modified for use in the WIPP project, totals about 175,000 (25% comments) but excludes six libraries and codes for which only executables are available. Thus, the total is about 475,000 lines of FORTRAN coding that may be selected by the analyst.

In most cases, a choice of computer codes is available within each module. For example, five codes are available in the groundwater flow module; the selection depends upon the type of problem under consideration. The codes available within each module are listed below:

Mesh Generation Module

- FASTQ: generate finite-element mesh
- GENMESH: generate rectilinear mesh
- GENNET: generate network
- PATEXO: transform PATRAN neutral file to CAMDAT data base format

Property Module

- BCSET: set up boundary condition
- FITBND: determine functional relationships between well heads and pressure boundary conditions and optimize fit of pressure boundary conditions
- GARFIELD: generate equally likely attribute fields, e.g., transmissivity
- GENOBS: generate a set of impulse functions at selected points along the boundary
- GRIDGEOS: interpolate from data to mesh
- ICSET: set up initial conditions
- LHS: sample using Latin hypercube sampling
  - PRELHS: translate from property secondary data base to LHS
  - POSTLHS: translate from LHS output to CAMDAT
- MATSET: set up material properties
- RELATE: interpolate from coarse to fine mesh and fine to coarse mesh (relates property and boundary conditions)
- SORTLHS: reorders LHS vectors

Groundwater Flow Module

- BRAGFLO: model two-phase flow
- BOAST_II: model black oil
  - PREBOAST: translate from CAMDAT to BOAST_II
  - POSTBOAST: translate from BOAST_II to CAMDAT
- HST3D: model hydrologic flow
  - PREHST: translate from CAMDAT to HST3D
  - POSTHST: translate from HST3D to CAMDAT
- SECO_2DH: model 2-D hydrologic flow using head formulation
- SUTRA: model hydrologic flow
  - PRESUTRA: translate from CAMDAT to SUTRA
  - POSTSUTRA: translate from SUTRA to CAMDAT
- SUTRA_GAS: SUTRA modified for fluid as gas instead of liquid

- SWIFT_II: model hydrologic flow
  - PRESWIFT: translate from CAMDAT to SWIFT_II
  - POSTSWIFT: translate from SWIFT_II to CAMDAT

Repository Module

- CUTTINGS: evaluate amount of material removed during drilling
- PANEL: model flow (analytically) and radionuclide concentration (mixing cell) in a WIPP disposal panel

Transport Module

- NEFTRAN: simulate transport with network model
  - PRENEF: translate from CAMDAT to NEFTRAN
  - POSTNEF: translate from NEFTRAN to CAMDAT
- STAFF2D: model transport using finite elements
  - PRESTAFF: translate from CAMDAT to STAFF2D
  - POSTSTAFF: translate from STAFF2D to CAMDAT

Compliance Module

- CCDFCALC: preprocess radionuclide time histories for CCDF
- CCDFPERM: calculate decomposed scenario probabilities
- NUCPLOT: plot box plots of each radionuclide contribution to CCDF
- CCDFPLOT: plot CCDF
- GENII: calculate human doses
- DOSE: calculate doses from transfer factors

Support Module

- ALGEBRA: manipulate data in CAMDAT
- BLOT: plot mesh and results
- GROPE: read CAMDAT file for debugging
- RESHAPE: redefine blocks (i.e., groupings of mesh elements)
- TRACKER: track a neutrally buoyant particle
- UNSWIFT: convert SWIFT_II input files into CAMDAT data base

Statistical Module

- PCCSRC: calculate partial correlation coefficients and standardized regression coefficients
- STEPWISE: select regression model using stepwise techniques

- LHS2STEP: translate from LHS output to STEPWISE or PCCSRC
- CCD2STEP: translate from CCDFCALC to STEPWISE or PCCSRC

Utility Module

- CHAIN: calculate radionuclide chains
- CHANGES: record needed enhancements to CAMCON or codes
- DISTRPLT: plots pdf's given parameters
- FLINT: analyze FORTRAN codes
- HLP2ABS: convert help file to software abstract
- LISTDCL: list DEC command procedural files
- LISTFOR: list programs; summarize comments and active FORTRAN lines
- NEFDIS: plot NEFTRAN discharge history as a function of time

Data Base Module

- GENPROP: enter item into property data base
- INGRES: store and manipulate data (commercial relational data base manager)
- LISTSDB: tabulate data in secondary data base for reports
- PLOTSDB: plot parameter distributions in property secondary data base
- CAM2TXT: convert binary CAMDAT to ASCII format file
- SCANCAMDAT: quickly summarize data in CAMDAT
- TXT2CAM: convert ASCII file to binary CAMDAT data base

2. DRILLING INTRUSION PROBABILITIES—Jon C. Helton

2.1 Introduction

The U.S. Environmental Protection Agency (EPA) has promulgated the following as a requirement for the geologic disposal of radioactive waste (U.S. EPA, 1985):

> *191.13 Containment requirements.*
> *(a) Disposal systems for spent nuclear fuel or high-level or transuranic radioactive wastes shall be designed to provide a reasonable expectation, based upon performance assessments, that the cumulative releases of radionuclides to the accessible environment for 10,000 years after disposal from all significant processes and events that may affect the disposal system shall:*
> *(1) Have a likelihood of less than one chance in 10 of exceeding the quantities calculated according to Table 1 (Appendix A); and*
> *(2) Have a likelihood of less than one chance in 1,000 of exceeding ten times the quantities calculated according to Table 1 (Appendix A).*

The term accessible environment means "(1) the atmosphere; (2) land surfaces; (3) surface waters; (4) oceans; and (5) all of the lithosphere that is beyond the controlled area" [U.S. EPA, 1985, 191.12 (k)]. Further, controlled area means "(1) a surface location, to be identified by passive institutional controls, that encompasses no more than 100 square kilometers and extends horizontally no more than 5 kilometers in any direction from the outer boundary of the original location of the radioactive wastes in a disposal system; and (2) the subsurface underlying such a surface location" [U.S. EPA, 1985, 191.12 (g)]. Table 1 (Appendix A), which is referred to in the preceding containment requirements, is reproduced here as Table 2-1.

For releases to the accessible environment that involve a mix of radionuclides, the limits in Table 2-1 are used to define normalized releases for comparison with the release limits. Specifically, the normalized release for transuranic waste is defined by

$$nR = \sum_i \left(\frac{Q_i}{L_i} \right) \left(1 \times 10^6 \text{ Ci}/C \right), \tag{2-1}$$

where

Q_i = cumulative release (Ci) of radionuclide i to the accessible environment during the 10,000-year period following closure of the repository,

L_i = the release limit (Ci) for radionuclide i given in Table 2-1,

and

C = amount of transuranic waste (Ci) emplaced in the repository.

For the 1991 WIPP performance assessment, $C = 11.87 \times 10^6$ Ci.

Table 2-1. Release Limits for the Containment Requirements
(U.S. EPA, 1985, Appendix A, Table 1)

Radionuclide	Release Limit L_i per 1,000 MTHM* or Other Unit of Waste (Curies)
Americium-231 or -243	100
Carbon 14	100
Cesium-135 or -137	1,000
Iodine-129	100
Neptunium-237	100
Plutonium-238, -239, -240, -or -242	100
Radium-226	100
Strontium-90	1,000
Technetium-99	10,000
Thorium-230, or -232	10
Tin-126	1,000
Uranium-233, -234, -235, -236, or -238	100
Any other alpha-emitting radionuclide with a half-life greater than 20 years	100
Any other radionuclide with a half-life greater than 20 years that does not emit alpha particles	1,000

* Metric tons of heavy metal exposed to a burnup between 25,000 megawatt-days per metric ton of heavy metal (MWd/MTHM) and 40,000 MWd/MTHM.

In addition, the EPA directs that the results of a performance assessment intended to show compliance with the release limits in 191.13 should be assembled into a single complementary cumulative distribution function (CCDF). Specifically, the following statement is made:

> *. . whenever practicable, the implementing agency will assemble all of the results of the performance assessments to determine compliance with [section] 191.13 into a "complementary cumulative distribution function" that indicates the probability of exceeding various levels of cumulative release. When the uncertainties in parameters are considered in a performance assessment, the effects of the uncertainties considered can be incorporated into a single such distribution function for each disposal system considered. The Agency assumes that a disposal system can be considered to be in compliance with [section] 191.13 if this single distribution function meets the requirements of [section] 191.13(a). (U.S. EPA, 1985, Appendix B, p. 38088).*

Construction of the single CCDF requires a clear conceptual representation for a performance assessment. A representation based on a set of ordered triples provides a suitable way to organize a performance assessment and leads naturally to the presentation of the outcome of a performance assessment as a CCDF (Kaplan and Garrick, 1981; Helton et al., 1991). Specifically, the outcome of a performance assessment can be represented by a set of $\mathcal{R}$ ordered triples of the form

$$\mathcal{R} = \left\{ \left(S_i, pS_i, \mathbf{cS}_i \right),\ i = 1, \ldots, nS \right\}, \tag{2-2}$$

where

S_i = a set of similar occurrences,

pS_i = probability that an occurrence in set S_i will take place,

$\mathbf{cS}_i$ = a vector of consequences associated with S_i

and

nS = number of sets selected for consideration.

In terms of performance assessment, the S_i are scenarios, the pS_i are scenario probabilities, and the $\mathbf{cS}_i$ are vectors containing results or consequences associated with scenarios.

The information contained in the pS_i and $\mathbf{cS}_i$ shown in (2-2) can be summarized in CCDFs. With the assumptions that a particular consequence result cS (e.g., normalized release to the accessible environment) is under consideration and that the values for this result have been ordered so that $cS_i \le cS_{i+1}$ for $i = 1, 2, \ldots, nE - 1$, Figure 2-1 shows the resultant CCDF. As illustrated in

Figure 2-2, the EPA containment requirement in 191.13 specifies that the CCDF for normalized release to the accessible environment should fall below a curve defined by the points (1, 0.1) and (10, 0.001). The vertical lines in Figure 2-2 have been added for visual appeal but are not really part of the CCDF. A waste disposal site can be considered to be in compliance with the EPA release limits if the CCDF for normalized release to the accessible environment falls below the bounding curve shown in Figure 2-2.

Since the representation for a performance assessment in (2-2) and the resultant CCDFs in Figures 2-1 and 2-2 involve probabilities, there must be an underlying sample space. For performance assessments conducted to provide comparisons with the EPA release limits, the sample space is the set S defined by

$$S = \{x : x \text{ a single 10,000-year time history beginning at decommissioning of the facility under consideration}\}. \tag{2-3}$$

Each 10,000-year history is complete in the sense that it provides a full specification, including time of occurrence, for everything of importance to performance assessment that happens in this time interval. The S_i appearing in (2-1) are disjoint subsets of S for which

$$S \triangleq \bigcup_{i=1}^{nS} S_i . \tag{2-4}$$

In the terminology of probability theory, the S_i are events and the pS_i are the probabilities for these events. It is the discretization of S into the sets S_i that leads to the steps in the estimated CCDFs in Figures 2-1 and 2-2. The use of more sets will reduce the step sizes but will not alter the fact that CCDFs are the basic outcome of a performance assessment (Helton et al., 1991, Chapter VI).

Important parts of any performance assessment are the discretization of S into the sets S_i, commonly referred to as scenario development (Hunter, 1989; Ross, 1989; Cranwell et al., 1990; Guzowski, 1990), and the subsequent determination of probabilities for these sets (Mann and Hunter, 1988; Hunter and Mann, 1989; Guzowski, 1991). For radioactive waste disposal in sedimentary basins, many computational scenarios (i.e., scenarios defined specifically for the construction of CCDFs) result from unintended intrusions due exploratory drilling for natural resources, particularly oil and gas. To construct CCDFs of the form shown in Figures 2-1 and 2-2, the time histories associated with these drilling intrusions must be sorted into disjoint sets such that (1) each S_i is sufficiently homogeneous that it is reasonable to use the same consequence

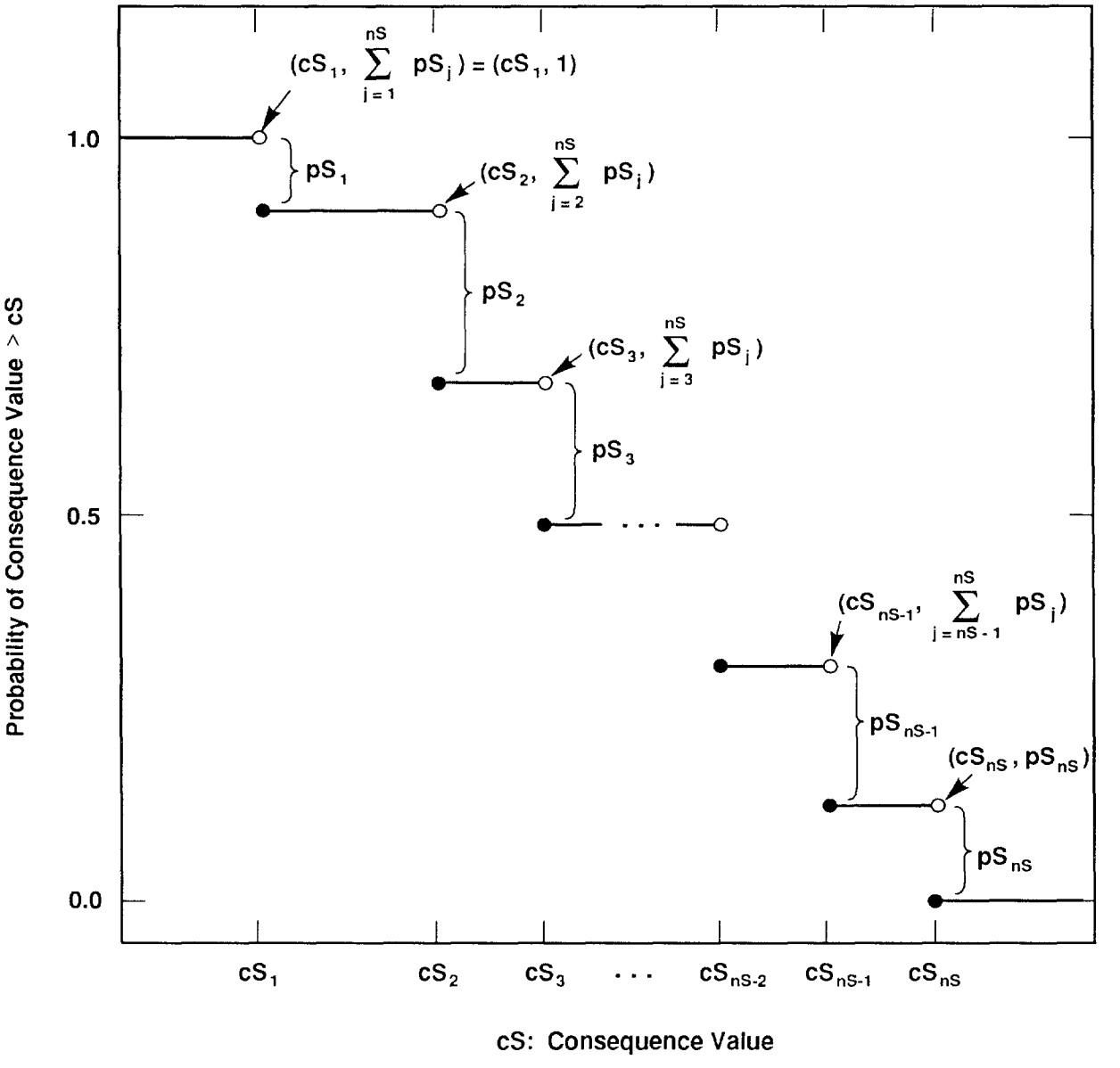

TRI-6342-730-5

Figure 2-1. Estimated Complementary Cumulative Distribution Function (CCDF) for Consequence Result cS. (Helton et al. 1991, Figure VI-1).

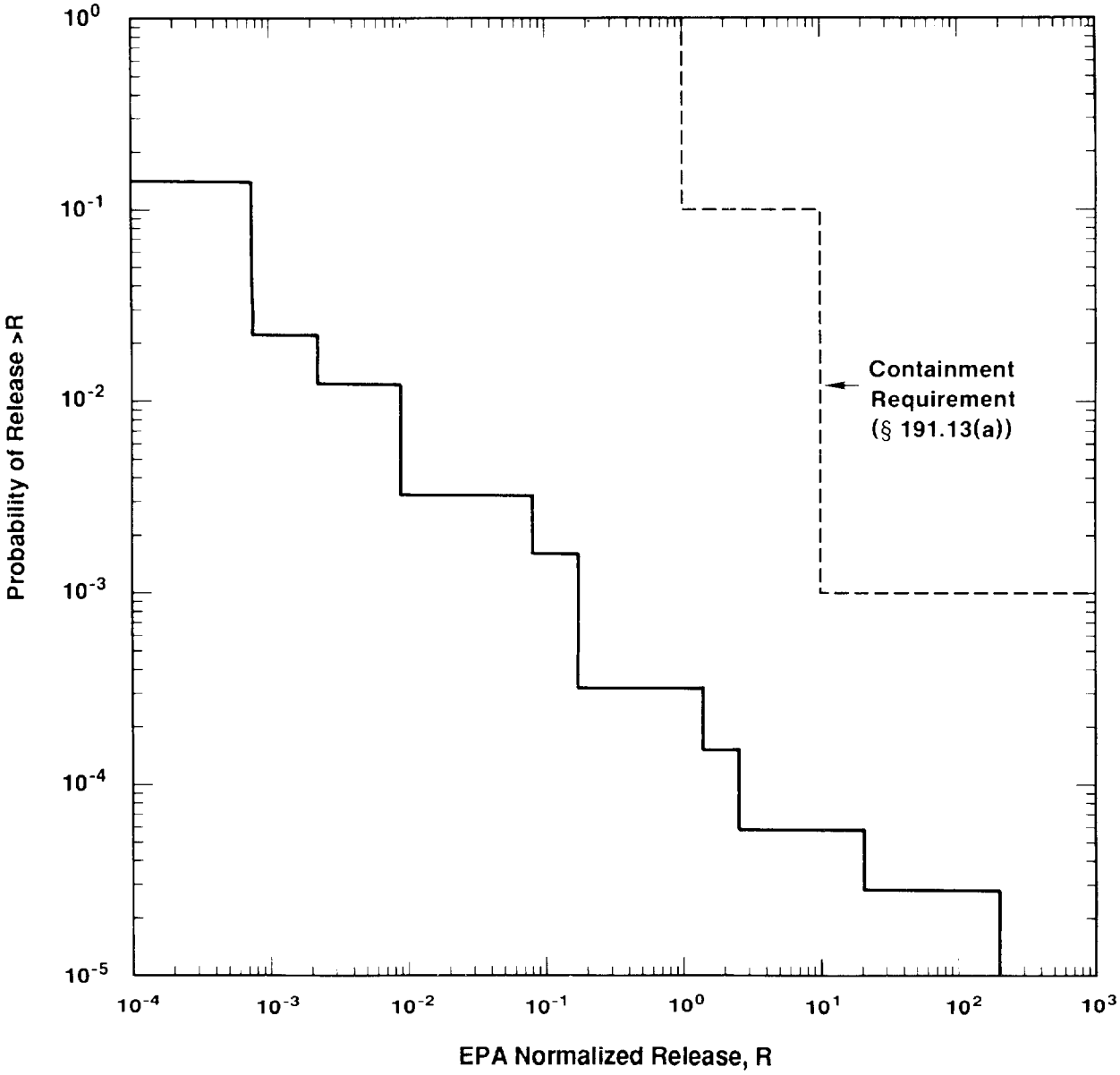

Figure 2-2. Comparison of a CCDF for Normalized Release to the Accessible Environment with the EPA Release Limits.

result $\mathbf{cS}_i$ for all elements of S_i, (2) a probability pS_i can be determined for each S_i, and (3) the computational costs for estimation of pS_i and $\mathbf{cS}_i$ are acceptable.

This chapter describes a decomposition of drilling intrusions into computational scenarios on the basis of number of intrusions and their times of occurrence and derives the necessary formulas to convert from drilling rates to scenario probabilities. For these derivations, the occurrence of individual drilling intrusions is assumed to be random in time and space, although the drilling rate is not assumed to be constant or, for that matter, even continuous through time. A following presentation will describe a computational procedure that can be used to determine CCDFs for intrusions due to drilling (Chapter 3).

2.2 Mathematical Preliminaries

The symbol $S_k(a,b)$ will be used to denote the subset of S [see (2-3)] defined by

$$S_k(a,b)=\{x:x \text{ an element of } S \text{ that involves exactly } k \text{ drilling intrusions in the time interval } [a,b]\ \}. \tag{2-5}$$

One of the objectives of this presentation is to derive a probability $p[S_k(a,b)]$ for $S_k(a,b)$. Membership in $S_k(a,b)$ only places a restriction on intrusions in the time interval $[a,b]$ and thus does not preclude intrusions in other time intervals. As a result, an additional objective will be to determine the probability $p\left[\bigcap_{i=1}^{n} S_{n(i)}(t_{i-1},t_i)\right]$ for the set $\bigcap_{i=1}^{n} S_{n(i)}(t_{i-1},t_i)$, where $t_0 < t_1 < \cdots < t_n$ and each $n(i)$, $i = 1,2,\ldots,n$, is a nonnegative integer. This corresponds to determining the probability of a computational scenario in which exactly $n(1)$ intrusions occur in time interval $[t_0,t_1]$, exactly $n(2)$ intrusions occur in time interval $[t_1,t_2]$, and so on.

The probability of having exactly one intrusion in the time interval $[u,v]$ will be approximated by a function F such that

$$p[S_1(u,v)] = F(u,v) + O\left[(v-u)^2\right], \tag{2-6}$$

where the preceding notation is a shorthand for the statement that the ratio

$$\frac{p[S_1(u,v)] - F(u,v)}{(v-u)^2} \tag{2-7}$$

is bounded as $v-u$ approaches zero. More precisely, the statement in (2-6) is satisfied on a time interval $[a,b]$ if there exists a number B and a sequence of times $a=t_0<t_1<\cdots<t_n=b$ such that, if $1\le i\le n$ and $t_{i-1}\le u<v\le b$, then

$$\left|\frac{p[S_1(u,v)]-F(u,v)}{(v-u)^2}\right|<B\,. \tag{2-8}$$

The expressions in (2-6) and (2-8) are providing a mathematical form for the statement "$F(u,v)$ is a good approximation to $p[S_1(u,v)]$ when $v-u$ is small."

The function F in (2-6) can be defined in a number of ways. The simplest definition is

$$F(u,v)=\lambda(v-u). \tag{2-9}$$

In this case, F corresponds to a Poisson process (Cox and Lewis, 1966; Haight, 1967; Cox and Isham, 1980) with a fixed rate of constant λ (i.e., a homogeneous Poisson process). A step up in complexity is

$$F(u,v)=\lambda(u)(v-u), \tag{2-10}$$

in which case F corresponds to a Poisson process with a time-dependent rate constant (i.e., a nonhomogeneous Poisson process). Results obtained in an expert review process indicate that the WIPP performance assessment may need to use time-dependent values for λ (Hora et al., 1991). Another possibility is

$$F(u,v)=f(u)[g(v)-g(u)], \tag{2-11}$$

where $g(t)$ is the probability that no intrusions will have occurred by time t and $f(t)=-1/g(t)$. As a final example, F might be defined by

$$F(u,v)=\begin{cases}p_i & \text{if } t_{i-1}<u<v=t_i\\ \lambda(v-u) & \text{otherwise,}\end{cases} \tag{2-12}$$

where $t_{i-1}<t_i$ and $0\le p_i\le 1$ for $i=1,2,\cdots$. The preceding example allows nonzero failure, or intrusion, probabilities at fixed points in time; this type of discontinuity is unlikely to arise in radioactive waste disposal problems but does help show the generality of characterizing a Poisson process with an interval function.

The following presentation will require two types of integrals involving interval functions of the type defined in (2-9) through (2-12): sum integrals and product integrals. These integrals, along with some related terminology, are now defined.

Definition 1. The statement that $\mathcal{D} = \{x_i\}_{i=0}^{m}$ is a subdivision of an interval $[a,b]$ means $a = x_0 < x_1 < \cdots < x_m = b$.

Definition 2. The statement that $\mathcal{R}$ is a refinement of a subdivision $\mathcal{D}$ of $[a,b]$ means (1) $\mathcal{R}$ is a subdivision of $[a,b]$ and (2) every point in $\mathcal{D}$ is also a point in $\mathcal{R}$.

Definition 3. The statement that the sum integral $\int_a^b F$ exists means there exists a number L such that, if $\varepsilon > 0$, then there exists a subdivision $\mathcal{D}$ of $[a,b]$ such that, if $\mathcal{R} = \{r_i\}_{i=0}^{n}$ is a refinement of $\mathcal{D}$, then $\left|L - \Sigma_{i=1}^{n} F(r_{i-1}, r_i)\right| < \varepsilon$.

Definition 4. The statement that the product integral ${}_a\prod^b(1+F)$ exists means there exists a number L such that, if $\varepsilon > 0$, then there exists a subdivision $\mathcal{D}$ of $[a,b]$ such that, if $\mathcal{R} = \{r_i\}_{i=0}^{n}$ is a refinement of $\mathcal{D}$, then $\left|L - \prod_{i=1}^{n}\left[1 + F(r_{i-1}, r_i)\right]\right| < \varepsilon$.

As indicated in the two preceding definitions, the sum and product integrals

$$\int_a^b F \text{ and } {}_a\prod^b(1+F) \tag{2-13}$$

are simply representations for limits involving

$$\sum_{i=1}^{n} F(r_{i-1}, r_i) \text{ and } \prod_{i=1}^{n}\left[1 + F(r_{i-1}, r_i)\right], \tag{2-14}$$

respectively. These definitions lead to the equalities

$$\int_a^b F = \int_a^x F + \int_x^b F \tag{2-15}$$

and

$$ {}_a\prod^b(1+F) = {}_a\prod^x(1+F)\,{}_x\prod^b(1+F) \tag{2-16} $$

for $a \le x \le b$, where

$$ \int_x^x F = 0 \text{ and } {}_x\prod^x(1+F) = 1. \tag{2-17} $$

As shown by the following two theorems, there is a reciprocal relationship between sum and product integrals.

Theorem 1 (Helton, 1973a). If F is an interval function defined on $[a,b]$ and either

(1) $\int_a^b F$ exists and $\int_a^b F^2$ exists,

or

(2) $\int_a^b F$ exists and ${}_a\prod^b(1+F)$ exists and is not zero,

or

(3) each of ${}_a\prod^b(1+F)$ and ${}_a\prod^b(1-F)$ exists and is not zero,

then $\int_x^y F$, $\int_x^y F^2$ and ${}_x\prod^y(1+F)$ exist for $a \le x \le y \le b$.

Theorem 2 (Davis and Chatfield, 1970; Helton, 1973b). If F is an interval function defined on $[a,b]$ and either $\int_a^b F$ exists or ${}_x\prod^y(1+F)$ exists for $a \le x \le y \le b$, then either of the following two statements implies the other:

(1) ${}_x\prod^y(1+F)$ and $\int_x^y F$ both exist and ${}_x\prod^y(1+F) = \exp\left(\int_x^y F\right)$ for $a \le x \le y \le b$,

and

(2) $\int_a^b F^2 = 0$.

The definition of F in (2-9) satisfies both theorems, as does the definition in (2-10) if $\lambda(u)$ is bounded and integrable on $[a,b]$. It is also possible for the definition in (2-11) to satisfy both theorems when g does not have any discontinuities. The definition in (2-12) satisfies Theorem 1 when $\sum_{i=1}^{\infty} p_i$ exists but will not satisfy Theorem 2 unless $p_i = 0$ for $i = 1,2,\cdots$. Theorem 2 is important because it presents the relationship between product integrals and exponentials of sum integrals.

In the discussions that follow, it will be assumed that F is sufficiently well-behaved for the existence of both $\int_a^b F^2$ and ${}_x\prod^y(1+F)$ for $a \le x \le y \le b$. Actually, we will be interested in the existence of ${}_x\prod^y(1-F)$, which follows from Theorem 1 if $\int_a^b F$ and ${}_x\prod^y(1+F)$ both exist, or equivalently, if $\int_a^b F$ and $\int_a^b F^2$ both exist. Further, the exponential relationship in Theorem 2 will be used to simplify relationships under the added assumption that $\int_a^b F^2 = 0$.

Although not widely used, product integrals are a very useful mathematical construction. Additional background and information can be found in several references (Masani, 1947; Helton, 1977; Dollard and Friedman, 1979; Gill and Johansen, 1990).

2.3 Computational Scenario Probabilities for Single Time Intervals

This section presents a derivation for the probability that exactly k intrusions will occur in a fixed time interval. More specifically, the purpose of this section is to determine the probability $p[S_k(a,b)]$ of $S_k(a,b)$. Notation will involve a subdivision $\{t_i\}_{i=0}^n$ of $[a,b]$. Further, limits are assumed to be of the subdivision-refinement type, although the notation does not expressly indicate this. The function F is also assumed to be sufficiently well-behaved for all indicated integrals to exist.

The probability of no intrusions in the interval $[a,b]$ is given by

$$p[S_0(a,b)] = \lim_{n\to\infty} \prod_{i=1}^{n} [1 - F(t_{i-1}, t_i)]$$

$$= {}_a\prod^b (1-F)$$

$$= \exp\left(-\int_a^b F\right) \qquad \left[\text{if } \int_a^b F^2 = 0\right]$$

$$= \exp[-\lambda(b-a)] , \qquad [\text{if } F(r,s) = \lambda(s-r)] \tag{2-18}$$

where the final expression is the usual form for a Poisson process with a fixed rate constant λ. The expressions

$$ {}_a\prod^b (1-F) \text{ and } \exp\left(-\int_a^b F\right) \tag{2-19}$$

give the probability of no intrusions under less restrictive conditions. In particular, the exponential form includes time-dependent values for λ, and the product integral form is sufficiently general to permit nonzero intrusion probabilities at fixed points in time. A discussion of similar derivations in other contexts is given in Gill and Johansen (1990), Section 4.1.

The probability of exactly one intrusion in the interval [a, b] is given by

$$p[S_1(a,b)] = \lim_{n\to\infty} \sum_{i=1}^{n} p[S_0(a,t_{i-1})]F(t_{i-1},t_i)p[S_0(t_i,b)]$$

$$= \int_a^b p[S_0(a,r)]F(r,s)\, p[S_0(s,b)]$$

$$= \int_a^b {}_a\prod^r (1-F)\, F(r,s)\, {}_s\prod^b (1-F)$$

$$= \left[\int_a^b F\right]\left[{}_a\prod^b (1-F)\right] \qquad \left[\text{if} \int_a^b F^2 = 0\right]$$

$$= \left[\int_a^b F\right]\exp\left(-\int_a^b F\right)$$

$$= [\lambda(b-a)]\exp[-\lambda(b-a)], \qquad [\text{if } F(r,s) = \lambda(s-r)] \tag{2-20}$$

where the final expression is again the usual form for a Poisson process with a fixed rate constant λ. The expressions

$$\int_a^b {}_a\prod^r (1-F)\, F(r,s)\, {}_s\prod^b (1-F) \text{ and } \left[\int_a^b F\right]\exp\left(-\int_a^b F\right) \tag{2-21}$$

give the probability of exactly one intrusion under less restrictive conditions.

The probability of exactly two intrusions in the interval $[a,b]$ is given by

$$p[S_2(a,b)] = \lim_{n\to\infty} \sum_{i=1}^{n} p[S_1(a,t_{i-1})]F(t_{i-1},t_i)p[S_0(t_i,b)]$$

$$= \int_a^b p[S_1(a,u)]F(u,v)\, p[S_0(v,b)]$$

$$= \int_a^b \left[\int_a^u {}_a\prod^{r}(1-F)F(r,s)\,{}_s\prod^{u}(1-F) \right] F(u,v)\,{}_s\prod^{b}(1-F)$$

$$= \int_a^b \left[\int_a^u F \right] \left[{}_a\prod^{u}(1-F) \right] F(u,v)\,{}_v\prod^{b}(1-F) \qquad \left[if \int_a^b F^2 = 0 \right]$$

$$= \left\{ \int_a^b \left[\int_a^u F \right] F(u,v) \right\} {}_a\prod^{b}(1-F)$$

$$= \left\{ \int_a^b \left[\int_a^u F \right] F(u,v) \right\} \exp\left(-\int_a^b F \right)$$

$$= \left[\frac{\lambda^2 (b-a)^2}{2} \right] \exp[-\lambda(b-a)], \qquad [\text{if } F(u,v) = \lambda(v-u)] \qquad (2\text{-}22)$$

where the final expression is the usual form for a Poisson process with a fixed rate constant λ. Various representations for a Poisson process under less restrictive assumptions are also given in the preceding sequence of equalities.

The preceding derivations can be continued for $k = 3,4,\cdots$. In general, the probability of exactly k intrusions, $k = 1,2,3,\cdots$, in the interval $[a,b]$ is given by

$$p[S_k(a,b)] = \lim_{n\to\infty} \sum_{i=1}^{n} p[S_{k-1}(a,t_{i-1})]F(t_{i-1},t_i)p[S_0(t_i,b)]$$

$$= \int_a^b p[S_{k-1}(a,u)]F(u,v)\, p[S_o(v,b)]$$

$$= \left[\int_a^b \left\{ \int_a^u \cdots \left[\left(\int_a^r F \right) F(r,s) \right] \cdots \right\} F(u,v) \right] \exp\left(-\int_a^b F \right) \qquad \left[if \int_a^b F^2 = 0 \right]$$

$$= \left[\frac{\lambda^k (b-a)^k}{k!} \right] \exp[-\lambda(b-a)], \qquad [\text{if } F(u,v) = \lambda(v-u)] \qquad (2\text{-}23)$$

where the preceding iterated integral involves k integrals. The final expression is the usual form for a Poisson process with a fixed rate constant λ. As before, the two preceding expressions give

representations for $p[\mathcal{S}_k(a,b)]$ with less restrictive conditions on F. For a formal development, the equalities in (2-23) could be established by mathematical induction.

2.4 Computational Scenario Probabilities for Multiple Time Intervals

This section presents a derivation for the probability of a pattern of intrusions involving multiple time intervals. Suppose $\{t_i\}_{i=0}^{n}$ is a subdivision of the time interval [a, b]. Further, for $i = 1,2,\cdots,n$, let $\mathcal{S}(t_{i-1},t_i)$ denote a subset of $\mathcal{S}$ that is defined on the basis of drilling intrusions occurring in the time interval $[t_{i-1},t_i]$. That is, the conditions that determine whether or not an element x of $\mathcal{S}$ is also an element of $\mathcal{S}(t_{i-1},t_i)$ are specified only for $[t_{i-1},t_i]$, and thus, the possible intrusions associated with x in other time intervals do not affect membership in $\mathcal{S}(t_{i-1},t_i)$.

A set of time histories satisfying the conditions imposed on $\mathcal{S}(t_{i-1},t_i)$ for all i can be obtained by forming the intersection of the sets $\mathcal{S}(t_{i-1},t_i)$. Specifically, the time histories in the set

$$\mathcal{S}(a,b) = \bigcap_{i=1}^{n} \mathcal{S}(t_{i-1},t_i) \tag{2-24}$$

satisfy the conditions imposed on each of the sets $\mathcal{S}(t_{i-1},t_i)$. The intrusion model is based on the assumption that the occurrences of boreholes are independent in time and space. Thus, the sets (i.e., events) $\mathcal{S}(t_{i-1},t_i)$ and $\mathcal{S}(t_{j-1},t_j)$ are independent for $i \neq j$. As a result, the probability of $\mathcal{S}(a,b)$ can be obtained from the relationship

$$p[\mathcal{S}(a,b)] = p\left[\bigcap_{i=1}^{n} \mathcal{S}(t_{i-1},t_i)\right] = \prod_{i=1}^{n} p\left[\mathcal{S}(t_{i-1},t_i)\right]. \tag{2-25}$$

In words, the probability of $\mathcal{S}(a,b)$ is the product of the probabilities for the sets $\mathcal{S}(t_{i-1},t_i)$.

The sets $\mathcal{S}(t_{i-1},t_i)$ are often specified by the number of drilling intrusions (i.e., boreholes) occurring within the time interval $[t_{i-1},t_i]$. As indicated in Section 2.2, $\mathcal{S}_{n(i)}(t_{i-1},t_i)$ can be used to denote the subset of $\mathcal{S}$ such that $x \in \mathcal{S}_{n(i)}(t_{i-1},t_i)$ only if x involves exactly $n(i)$ intrusions within the time interval $[t_{i-1},t_i]$. Then,

$$S(a,b) = \bigcap_{i=1}^{n} S_{n(i)}(t_{i-1}, t_i) \tag{2-26}$$

denotes the set of time histories in which exactly $n(1)$ intrusions occur in the time interval $[t_0, t_1]$, exactly $n(2)$ intrusions occur in the time interval $[t_1, t_2]$, and so on. As shown in (2-25), the probability of $S(a,b)$ is given by

$$p[S(a,b)] = \prod_{i=1}^{n} p\left[S_{n(i)}(t_{i-1}, t_i)\right]. \tag{2-27}$$

Section 2.3 provides computational formulas for the probabilities $p\left[S_{n(i)}(t_{i-1}, t_i)\right]$. These formulas in conjunction with the relationship in (2-27) provide a means to determine the probabilities of a wide variety of scenarios involving drilling intrusions.

Several examples are now presented to illustrate the use of the formula in (2-27). The first example is for a single borehole in time interval $\left[t_{j-1}, t_j\right]$ and no intrusions in all other intervals, which is equivalent to

$$n(i) = \begin{cases} 1 \text{ if } i = j \\ 0 \text{ if } i \neq j. \end{cases} \tag{2-28}$$

In this case,

$$p[S(a,b)] = \prod_{i=1}^{n} p\left[S_{n(i)}(t_{i-1}, t_i)\right] \qquad \text{[from (2-27)]}$$

$$= \left\{\prod_{i=1}^{j-1} p\left[S_0(t_{i-1}, t_i)\right]\right\}\left\{p\left[S_1(t_{j-1}, t_j)\right]\right\}\left\{\prod_{i=j+1}^{n} p\left[S_0(t_{i-1}, t_i)\right]\right\}$$

[from (2-28)]

$$= \left\{\prod_{i=1}^{j-1}\left[t_{i-1}\prod^{t_i}(1-F)\right]\right\}\left\{p\left[S_1(t_{j-1}, t_j)\right]\right\}\left\{\prod_{i=j+1}^{n}\left[t_{i-1}\prod^{t_i}(1-F)\right]\right\}$$

[from (2-18)]

$$= \left\{ {}_{a}\prod^{t_{j-1}} (1-F) \right\} \left\{ p\left[S_1\left(t_{j-1}, t_j\right) \right] \right\} \left\{ {}_{t_{i-1}}\prod^{t_i} (1-F) \right\} . \tag{2-29}$$

The value for $p\left[S_1\left(t_{j-1}, t_j\right)\right]$ is given in (2-20) and results in the equality

$$p[S(a,b)] = \left\{ {}_{a}\prod^{t_{j-1}} (1-F) \right\} \left\{ \int_{t_{j-1}}^{t} {}_{t_{j-1}}\prod^{u} (1-F) F(u,v) {}_{v}\prod^{t_j} (1-F) \right\}$$

$$\bullet \left\{ {}_{t_j}\prod^{b} (1-F) \right\}. \tag{2-30}$$

The preceding representation for $p[S(a,b)]$ was developed with no restrictions on F other than the existence of the integrals involved. Simpler representations result when additional restrictions are placed on F.

When the requirement that $\int_a^b F^2 = 0$ is added, the representation in (2-30) becomes

$$p[S(a,b)] = \left\{ \exp\left(-\int_a^{t_{j-1}} F \right) \right\} \left\{ \left[\int_{t_{j-1}}^{t_j} F \right] \exp\left(-\int_{t_{j-1}}^{t_j} F \right) \right\} \left\{ \exp\left(-\int_{t_j}^{b} F \right) \right\}$$

$$= \left[\int_{t_{j-1}}^{t_j} F \right] \exp\left(-\int_a^b F \right). \tag{2-31}$$

Further, the representation in (2-30) becomes

$$p[S(a,b)] = \left[\lambda\left(t_j - t_{j-1}\right) \right] \exp[-\lambda(b-a)] \tag{2-32}$$

when the additional requirement that $F(u,v) = \lambda(v-u)$ is added.

The intrusion pattern indicated in (2-28) is equivalent to no intrusions in the time intervals $\left[a, t_{j-1}\right]$ and $\left[t_j, b\right]$ together with exactly 1 intrusion in the time interval $\left[t_{j-1}, t_j\right]$. When this decomposition is used, the representation for $p[S(a,b)]$ is

$$p[S(a,b)] = \left\{ p\left[S_0\left(a, t_{j-1}\right) \right] \right\} \left\{ p\left[S_1\left(t_{j-1}, t_j\right) \right] \right\} \left\{ p\left[S_0\left(t_j, b\right) \right] \right\}$$

$$= \left\{ {}_a\prod^{t_j} (1-F) \right\} \left\{ p\left[S_1\left(t_{j-1}, t_j\right) \right] \right\} \left\{ {}_{t_j}\prod^{b} (1-F) \right\}, \tag{2-33}$$

[from (2-27)]

which is the same as the representation in (2-29).

The second example is for exactly k boreholes in time interval $\left[t_{j-1}, t_j\right]$ and no intrusion in all other intervals, which is equivalent to

$$n(i) = \begin{cases} k \text{ if } i = j \\ 0 \text{ if } i \neq j \end{cases}. \tag{2-34}$$

As indicated in both (2-29) and (2-33), this case leads to

$$p[S(a,b)] = \left\{ {}_a\prod^{t_{j-1}} (1-F) \right\} \left\{ p\left[S_k\left(t_{j-1}, t_j\right) \right] \right\} \left\{ {}_{t_j}\prod^{b} (1-F) \right\}. \tag{2-35}$$

The form taken by $p\left[S_k\left(t_{j-1}, t_j\right) \right]$ is shown in (2-29), which leads to

$$p[S(a,b)] = \left\{ {}_a\prod^{t_{j-1}} (1-F) \right\} \left\{ \int_{t_{j-1}}^{t_j} p\left[S_{k-1}\left(t_{j-1}, u\right) \right] F(u,v)\, p\left[S_0\left(v, t_j\right) \right] \right\} \left\{ {}_{t_j}\prod^{b} (1-F) \right\} \tag{2-36}$$

for the general case,

$$p[S(a,b)] = \left[\int_{t_{j-1}}^{t_j} \left\{ \int_{t_{j-1}}^{u} \cdots \left[\left(\int_{t_{j-1}}^{r} F \right) F(r,s) \right] \cdots \right\} F(u,v) \right] \exp\left(-\int_a^b F \right) \tag{2-37}$$

for the case $\int_a^b F^2 = 0$, and

$$p[S(a,b)] = \left[\frac{\lambda^k \left(t_j - t_{j-1}\right)^k}{k!} \right] \exp[-\lambda(b-a)] \tag{2-38}$$

for the case $F(u,v) = \lambda(v-u)$.

The third example is for exactly k boreholes in time interval $\left[t_{j-1},t_j\right]$, exactly m boreholes in time interval $\left[t_{l-1},t_l\right]$, and no intrusions in all other intervals, which is equivalent to

$$n(i)=\begin{cases}k & \text{if } i=j\\ m & \text{if } i=l\\ 0 & \text{otherwise.}\end{cases} \tag{2-39}$$

Derivations similar to those shown in (2-29) and (2-33) lead to

$$p[S(a,b)]=\left\{{}_a\prod^{t_{j-1}}(1-F)\right\}\left\{p\left[S_k\left(t_{j-1},t_j\right)\right]\right\}\left\{{}_{t_j}\prod^{t_{l-1}}(1-F)\right\}$$

$$\bullet\left\{p\left[S_m\left(t_{l-1},t_l\right)\right]\right\}\left\{{}_{t_l}\prod^{a}(1-F)\right\}, \tag{2-40}$$

with the assumption that $t_j<t_l$. The forms taken by $p\left[S_k\left(t_{j-1},t_j\right)\right]$ and $p\left[S_m\left(t_{l-1},t_l\right)\right]$ are shown in (2-29) and can be substituted into (2-40) to produce expressions corresponding to those shown in (2-36), (2-37) and (2-38). The general case and the case for $\int_a^b F^2=0$ will involve two pairs of iterated integrals. The relatively simple expression

$$p[S(a,b)]=\left[\frac{\lambda^{k+m}\left(t_j-t_{j-1}\right)^k\left(t_l-t_{l-1}\right)^m}{k!m!}\right]\exp[-\lambda(b-a)] \tag{2-41}$$

is produced for the case $F(u,v)=\lambda(v-u)$.

This section concludes by returning to the general case shown in (2-27) in which exactly $n(i)$ intrusions occur for each time interval. Equation (2-29) provides computational formulas for the probabilities $p\left[S_{n(i)}\left(t_{i-1},t_i\right)\right]$ appearing in (2-27). Thus, a general formula for $p[S(a,b)]$ could be generated by substituting the relations in (2-29) into (2-27). The resultant relationships for the general case and the case $\int_a^b F^2=0$ are notationally messy due to the many iterated integrals involved. However, the relatively compact relationship

$$p[S(a,b)]=\left\{\prod_{i=1}^{n}\left[\frac{\lambda^{n(i)}\left(t_i-t_{i-1}\right)^{n(i)}}{n(i)!}\right]\right\}\exp[-\lambda(b-a)] \tag{2-42}$$

results for the case $F(u,v) = \lambda(v-u)$.

2.5 Computational Scenario Probabilities for Pressurized Brine Pockets

Field data indicate that part of the waste panels at the WIPP may be underlain by one or more pressurized brine pockets in the Castile formation (Earth Technology Corp., 1987). The possible location of these pockets is shown in Figure 2-3. As a result, a potentially important summary scenario involves two or more boreholes through a waste panel in which at least one borehole penetrates a pressurized brine pocket and at least one borehole does not. The significance of this summary scenario results because fluid may flow up one borehole from the pressurized brine pocket, through the panel, and then out through another borehole. This was referred to as the E1E2 scenario in the 1990 WIPP performance assessment for the case involving two boreholes through a panel in which one borehole penetrates a pressurized brine pocket, one borehole does not penetrate a pressurized brine pocket, and the borehole seals fail in a pattern that induces flow through the panel as shown in Figure 2-4 (Bertram-Howery et al., 1990).

Determination of probabilities for E1E2-type computational scenarios is based on the subsets $\mathcal{BP}_k^+(l;a,b)$ and $\mathcal{BP}_k^-(l;a,b)$ of $\mathcal{S}$, where

$$\mathcal{BP}_k^+(l;a,b) = \{x : x \text{ an element of } \mathcal{S} \text{ that involves exactly } k \text{ drilling intrusions through waste panel } l \text{ in the time interval } [a,b] \text{ that penetrate a pressurized brine pocket}\} \quad (2\text{-}43)$$

and

$$\mathcal{BP}_k^-(l;a,b) = \{x : x \text{ an element of } \mathcal{S} \text{ that involves exactly } k \text{ drilling intrusions through waste panel } l \text{ in the time interval } [a,b] \text{ that do not penetrate a pressurized brine pocket}\}. \quad (2\text{-}44)$$

Computational scenarios of the E1E2-type are defined by the intersection of sets of the form shown in (2-43) and (2-44).

As shown in (2-18) and (2-23), the probabilities for $\mathcal{BP}_k^+(l;a,b)$ and $\mathcal{BP}_k^-(l;a,b)$ are given by

$$p\left[\mathcal{BP}_0^+(l;a,b)\right] = \prod_a^b \left[1 - F^+(l;u,v)\right], \quad (2\text{-}45)$$

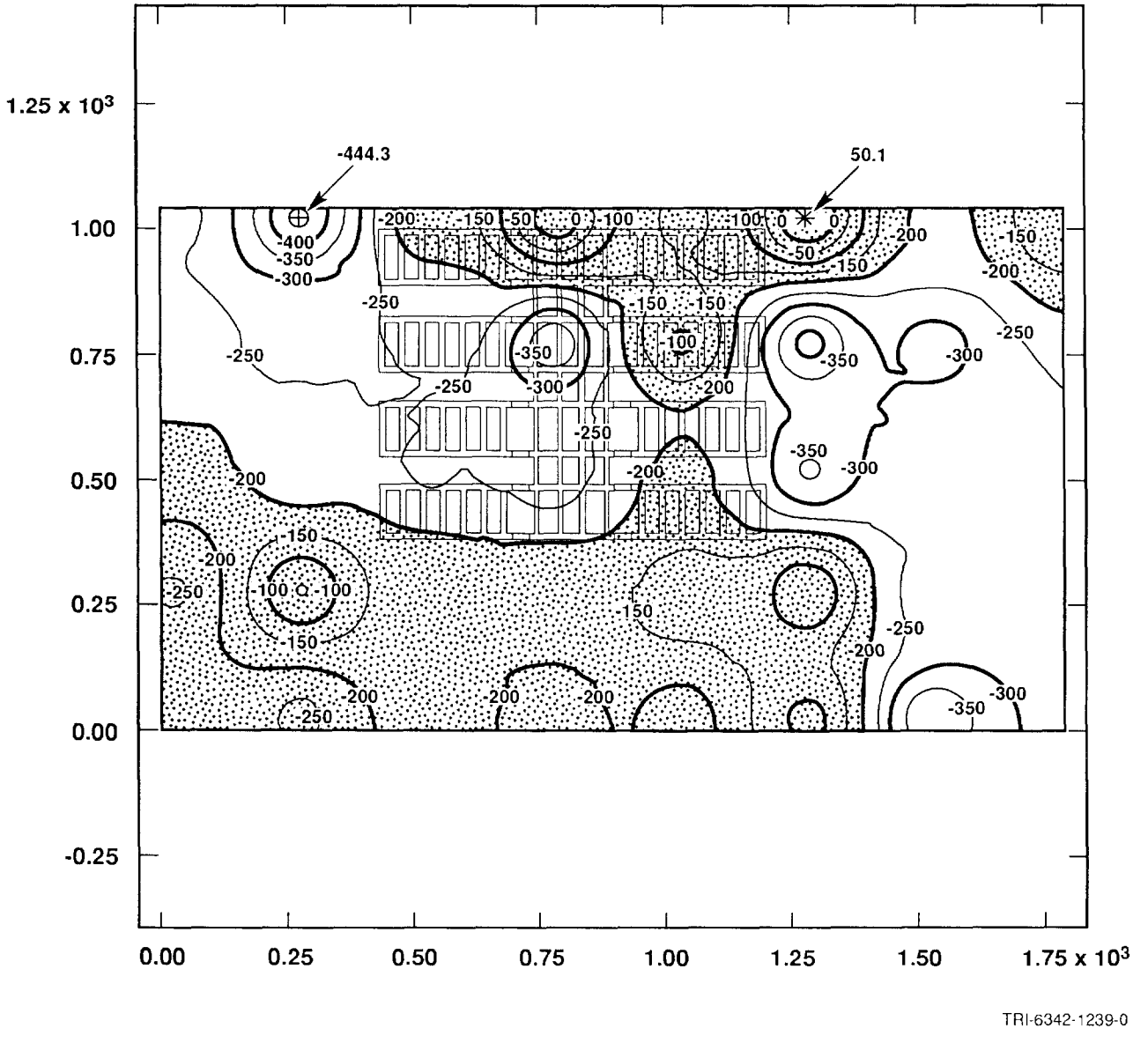

Figure 2-3. Contour Map of Elevation to First Major Conductor below WIPP Disposal Area (after Earth Technology Corp., 1987) (see Section 5.1.1 of Volume 3 of this report).

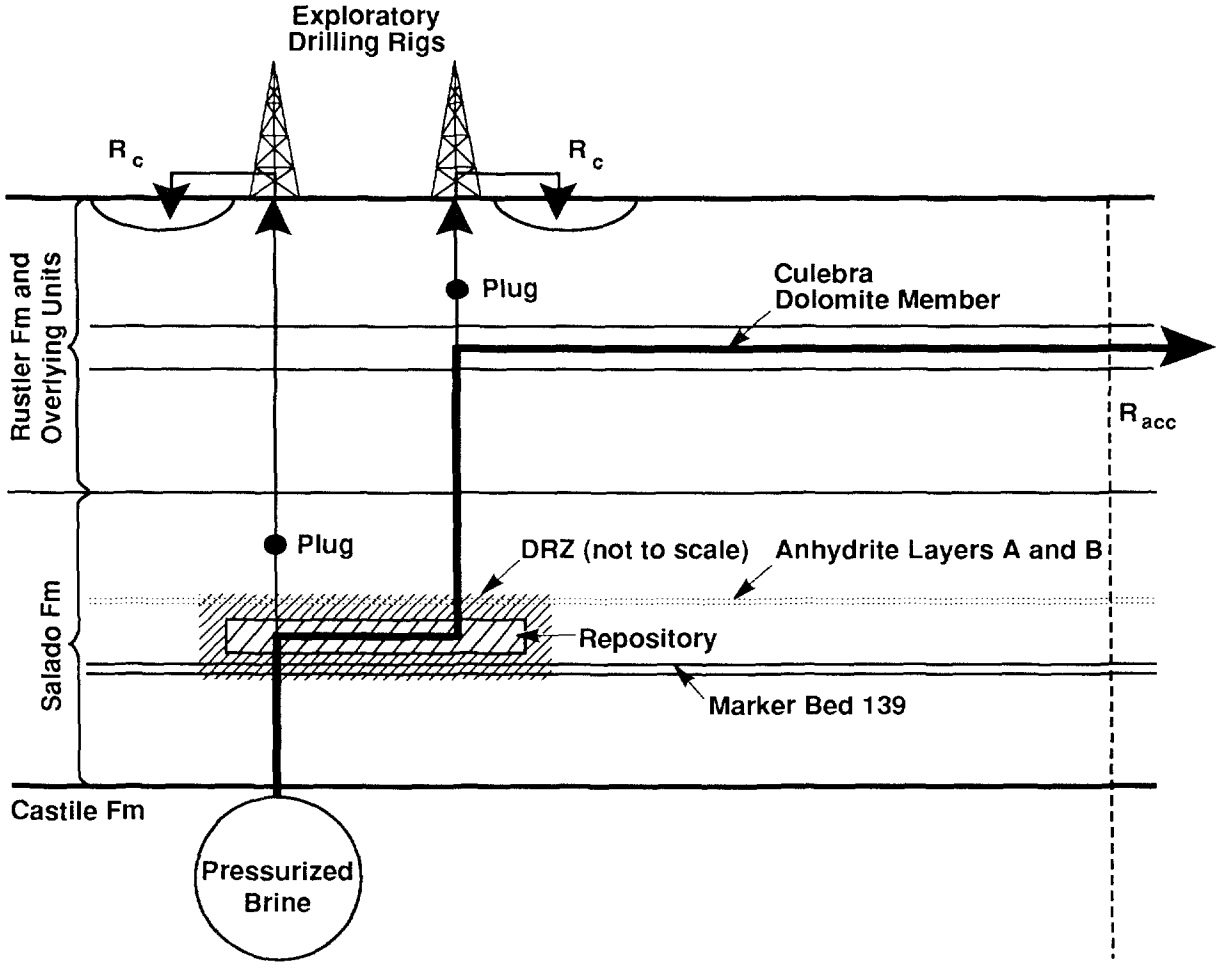

R_c = Release of Cuttings and Eroded Material

R_{acc} = Release at the Subsurface Boundary of the Accessible Environment

DRZ = Disturbed Rock Zone

TRI-6342-217-3

Figure 2-4. Conceptual Model for Scenario E1E2 (Bertram-Howery et al., 1990, Fig. IV-6). Arrows indicate direction of flow. The indicated plugs are assumed to be intact; other possible plugs are assumed to be degraded.)

$$p\left[\mathcal{BP}_k^+(l;a,b)\right] = \int_a^b p\left[\mathcal{BP}_{k-1}^+(l;a,u)\right] F^+(l;u,v)\, p\left[\mathcal{BP}_0^+(l;v,b)\right], \tag{2-46}$$

$$p\left[\mathcal{BP}_0^-(l;a,b)\right] = {}_a\prod^b \left[1 - F^-(l;u,v)\right], \tag{2-47}$$

and

$$p\left[\mathcal{BP}_k^-(l;a,b)\right] = \int_a^b p\left[\mathcal{BP}_{k-1}^-(l;a,u)\right] F^-(l;u,v)\, p\left[\mathcal{BP}_0^-(l;v,b)\right], \tag{2-48}$$

where $k = 1,2,\cdots$ in (2-46) and (2-48) and the functions $F^+(l;u,v)$ and $F^-(l;u,v)$ approximate the probability of drilling through panel l in time interval $[u,v]$ and penetrating a pressurized brine pocket $\left(F^+\right)$ and not penetrating a pressurized brine pocket $\left(F^-\right)$, respectively.

Since drilling is assumed to be random in time and space, $F^+(l;u,v)$ and $F^-(l;u,v)$ are related to the function F used in Sections 2.3 and 2.4 by

$$\begin{aligned} F^+(l;u,v) &= \left(\frac{aBP(l)}{aTOT(l)}\right)\left(\frac{aTOT(l)}{aTOT}\right)F(u,v) \\ &= \left(\frac{aBP(l)}{aTOT}\right)F(u,v) \end{aligned} \tag{2-49}$$

and

$$\begin{aligned} F^-(l;u,v) &= \left(\frac{aTOT(l) - aBP(l)}{aTOT(l)}\right)\left(\frac{aTOT(l)}{aTOT}\right)F(u,v) \\ &= \left(\frac{aTOT(l) - aBP(l)}{aTOT}\right)F(u,v), \end{aligned} \tag{2-50}$$

respectively, where

$aBP(l)$ = area (m^2) of pressurized brine pocket under waste panel l,
$aTOT(l)$ = total area (m^2) of waste panel l,

and

$aTOT$ = total area (m^2) of all waste panels.

For the special case in which $F(u,v)=\lambda(v-u)$, the functions $F^{+}(l;u,v)$ and $F^{-}(l;u,v)$ are defined by

$$F^{+}(l;u,v)=\alpha(l)(v-u) \text{ and } F^{-}(l;u,v)=\beta(l)(v-u), \tag{2-51}$$

where

$$\alpha(l)=\left(\frac{aBP(l)}{aTOT}\right)\lambda \text{ and } \beta(l)=\left(\frac{aTOT(l)-aBP(l)}{aTOT}\right)\lambda. \tag{2-52}$$

The probability of having an E1E2-type computational scenario involving waste panel l during the time interval $[a,b]$ is given by

$$p\left[\mathcal{BP}_1^{+}(l;a,b)\cap\mathcal{BP}_1^{-}(l;a,b)\right]=p\left[\mathcal{BP}_1^{+}(l;a,b)\right]p\left[\mathcal{BP}_1^{-}(l;a,b)\right], \tag{2-53}$$

where $p\left[\mathcal{BP}_1^{+}(l;a,b)\right]$ and $p\left[\mathcal{BP}_1^{-}(l;a,b)\right]$ are defined in (2-46) and (2-48). For the special case in which $F(u,v)=\lambda(v-u)$, the preceding expression becomes

$$\begin{aligned} &p\left[\mathcal{BP}_1^{+}(l;a,b)\cap\mathcal{BP}_1^{-}(l;a,b)\right] \\ &\quad=\left\{\alpha(l)(b-a)\exp[-\alpha(l)(b-a)]\right\}\left\{\beta(l)(b-a)\exp[-\beta(l)(b-a)]\right\} \\ &\quad=\alpha(l)\beta(l)(b-a)^2\exp\left\{-[\alpha(l)+\beta(l)][b-a]\right\} \\ &\quad=\left\{\frac{aBP(l)[aTOT(l)-aBP(l)]}{aTOT^2}\right\}\lambda^2(b-a)^2\exp\left\{-[aTOT(l)/aTOT]\lambda(b-a)\right\}, \end{aligned} \tag{2-54}$$

where $\alpha(l)$ and $\beta(l)$ are defined in (2-52) and the values for $p\left[\mathcal{BP}_1^{+}(l;a,b)\right]$ and $p\left[\mathcal{BP}_1^{-}(l;a,b)\right]$ follow from a derivation analogous to the one shown in (2-20).

In a similar manner the probability of having an E1E2-type computational scenario for the time interval [a, b] in which r boreholes pass through waste panel l and subsequently penetrate a pressurized brine pocket and s boreholes pass through waste panel l but do not penetrate a pressurized brine pocket is given by

$$p\left[\mathcal{BP}_r^+(l;a,b)\cap\mathcal{BP}_s^-(l;a,b)\right]=p\left[\mathcal{BP}_r^+(l;a,b)\right]\;\;p\left[\mathcal{BP}_s^-(l;a,b)\right]. \tag{2-55}$$

For the special case in which $F(u, v) = \lambda(v-u)$, the preceding expression becomes

$$\begin{aligned}
&p\left[\mathcal{BP}_r^+(l;a,b)\cap\mathcal{BP}_s^-(l;a,b)\right]\\
&\quad=\left\{\left[\alpha(l)\right]^r[b-a]^r\exp\left[\alpha(l)(b-a)\right]\right\}\left\{\left[\beta(l)\right]^s[b-a]^s\exp\left[\beta(l)(b-a)\right]\right\}\\
&\quad=\left\{\left[aBP(l)\right]^r\left[aTOT(l)-aBP(l)\right]^s/aTOT^{r+s}\right\}\lambda^{r+s}(b-a)^{r+s}\\
&\qquad\bullet\exp\left\{\left[aTOT(l)/aTOT\right]\lambda(b-a)\right\},
\end{aligned} \tag{2-56}$$

which reduces to the expression in (2-54) when $r = s = 1$.

Rather than basing the probability of an E1E2-type computational scenario for waste panel l on the sets $\mathcal{BP}_1^+(l;a,b)$ and $\mathcal{BP}_1^-(l;a,b)$, a more conservative (i.e., larger) probability can be obtained by using the sets

$$\mathcal{BP}^+(l;a,b)=\{x:x \text{ an element of } \mathcal{S} \text{ that involves one or more drilling intrusions through waste panel } l \text{ in the time interval } [a,b] \text{ that penetrate a pressurized brine pocket}\} \tag{2-57}$$

and

$$\mathcal{BP}^-(l;a,b)=\{x:x \text{ an element of } \mathcal{S} \text{ that involves one or more drilling intrusions through waste panel } l \text{ in the time interval } [a,b] \text{ that do not penetrate a pressurized brine pocket}\}. \tag{2-58}$$

In this case, the probability for an E1E2-type computational scenario is given by

$$\begin{aligned}
&p\left[\mathcal{BP}^+(l;a,b)\cap\mathcal{BP}^-(l;a,b)\right]=p\left[\mathcal{BP}^+(l;a,b)\right]\;\;p\left[\mathcal{BP}^-(l;a,b)\right]\\
&\quad=\left\{1-\prod_a^b\left[1-F^+(l;u,v)\right]\right\}\left\{1-\prod_a^b\left[1-F^-(l;u,v)\right]\right\},
\end{aligned} \tag{2-59}$$

where the second equality follows from (2-18). For the special case in which $F(u,v) = \lambda(v-u)$, the preceding expression becomes

$$p\left[\mathcal{BP}^{+}(l;a,b) \bigcap \mathcal{BP}^{-}(l;a,b)\right] = \left\{1-\exp\left[-\alpha(l)(b-a)\right]\right\}\left\{1-\exp\left[-\beta(l)(b-a)\right]\right\}, \tag{2-60}$$

where $\alpha(l)$ and $\beta(l)$ are defined in (2-52).

Thus far, this section has dealt with E1E2-type computational scenarios that involve a single waste panel. A complete performance assessment requires consideration of all waste panels. This leads to computational scenarios defined by sets of the form

$$\mathcal{BP}_{11}^{+-}(a,b) = \{x : x \text{ an element of } S \text{ in which at least one waste panel is penetrated by exactly two boreholes during the time interval } [a,b], \text{ of which one penetrates a pressurized brine pocket and one does not}\}.$$

$$= \bigcup_{l=1}^{nP} \left\{\mathcal{BP}_1^{+}(l;a,b) \bigcap \mathcal{BP}_1^{-}(l;a,b)\right\}, \tag{2-61}$$

where nP is the number of waste panels in the repository. The probability of $\mathcal{BP}_{11}^{+-}(a,b)$ is then given by

$$p\left[\mathcal{BP}_{11}^{+-}(a,b)\right] = p\left[\bigcup_{l=1}^{nP} \left\{\mathcal{BP}_1^{+}(l;a,b) \bigcap \mathcal{BP}_1^{-}(l;a,b)\right\}\right]$$

$$\stackrel{\bullet}{=} \sum_{l=1}^{nP} p\left[\left\{\mathcal{BP}_1^{+}(l;a,b) \bigcap \mathcal{BP}_1^{-}(l;a,b)\right\}\right]$$

$$= \sum_{l=1}^{nP} p\left[\mathcal{BP}_1^{+}(l;a,b)\right] p\left[\mathcal{BP}_1^{-}(l;a,b)\right]. \tag{2-62}$$

As indicated in (2-54), the preceding relation becomes

$$p\left[\mathcal{BP}_{11}^{+-}(a,b)\right] \stackrel{\bullet}{=} \sum_{l=1}^{nP} \left[\alpha(l)\beta(l)(b-a)^2 \exp\left\{-\left[\alpha(l)+\beta(l)\right][b-a]\right\}\right] \tag{2-63}$$

when $F(u,v)=\lambda(v-u)$, where $\alpha(l)$ and $\beta(l)$ are defined in (2-52).

As shown in conjunction with (2-60), it is also possible to determine a more conservative probability for E1E2-type computational scenarios by considering one or more boreholes rather than the single boreholes associated with the sets $\mathcal{BP}_1^+(l;a,b)$ and $\mathcal{BP}_1^-(l;a,b)$. This leads to computational scenarios defined by sets of the form

$\mathcal{BP}^{+-}(a,b)=\{x: x$ an element of $\mathcal{S}$ in which at least one waste panel is penetrated by two or more boreholes during the time interval $[a,b]$, of which at least one penetrates a pressurized brine pocket and at least one does not$\}$

$$= \bigcup_{l=1}^{nP} \left\{ \mathcal{BP}^+(l;a,b) \bigcap \mathcal{BP}^-(l;a,b) \right\}. \tag{2-64}$$

As shown in (2-62), the probability of $\mathcal{BP}^{+-}(a,b)$ can be approximated by

$$p\left[\mathcal{BP}^{+-}(a,b)\right] \doteq \sum_{l=1}^{nP} p\left[\mathcal{BP}^+(l;a,b)\right] p\left[\mathcal{BP}^-(l;a,b)\right]. \tag{2-65}$$

Further, when the condition that $F(u,v)=\lambda(v-u)$ is added, it follows from (2-60) that

$$p\left[\mathcal{BP}^{+-}(a,b)\right] \doteq \sum_{l=1}^{nP} \left\{1-\exp[-\alpha(l)(b-a)]\right\}\left\{1-\exp[-\beta(l)(b-a)]\right\}, \tag{2-66}$$

where $\alpha(l)$ and $\beta(l)$ are defined in (2-52).

The approximations appearing in (2-62), (2-63), (2-65) and (2-66) result from use of the identity

$$p\left(\bigcup_{i=1}^{N} S_i\right) = \sum_{i=1}^{N} p(S_i) - \sum_{i_1<i_2} p\left(S_{i_1} \bigcap S_{i_2}\right) + \cdots + (-1)^{n+1} \sum_{i_1<i_2<\cdots<i_n} p\left(S_{i_1} \bigcap S_{i_2} \bigcap \cdots \bigcap S_{i_n}\right)$$

$$+ \cdots + (-1)^{N+1} p\left(S_1 \bigcap S_2 \bigcap \cdots \bigcap S_N\right), \tag{2-67}$$

which leads to the inequality

$$p\left(\bigcup_{i=1}^{N} S_i\right) \le \sum_{i=1}^{N} p(S_i). \tag{2-68}$$

Thus, the relations in (2-62), (2-63), (2-65) and (2-66) actually provide bounds on the probabilities involved. Strict equalities could be derived. However, as indicated by (2-67), the resultant relationships would be very cumbersome.

As indicated in (2-52), $\alpha(l)$ and $\beta(l)$ depend on the ratios

$$aBP(l)/aTOT \text{ and } \left[aTOT(l) - aBP(l)\right]/aTOT. \tag{2-69}$$

Thus, as shown in (2-63) and (2-66) for $F(u,v) = \lambda(v-u)$, $p\left[\mathcal{BP}_{11}^{+-}(a,b)\right]$ and $p\left[\mathcal{BP}^{+-}(a,b)\right]$ also depend on these ratios. When only an estimate for

$$aBP = \sum_{l=1}^{nP} aBP(l) \tag{2-70}$$

is available, where aBP is the total brine pocket area under the waste panels, $aBP(l)$ can be estimated by

$$aBP(l) = aBP/nP, \tag{2-71}$$

which leads to

$$\alpha(l) = \left(\frac{aBP}{nP\ aTOT}\right)\lambda \text{ and } \beta(l) = \left(\frac{aTOT(l) - aBP/nP}{aTOT}\right)\lambda. \tag{2-72}$$

The preceding values for $\alpha(l)$ and $\beta(l)$ can be used in conjunction with (2-63) and (2-66) to estimate the probabilities for $\mathcal{BP}_{11}^{+-}(a,b)$ and $\mathcal{BP}^{+-}(a,b)$, which correspond to E1E2-type computational scenarios involving exactly one intrusion of each type and one or more intrusions of each type, respectively.

2.6 Example Results

The 1990 WIPP performance assessment (Bertram-Howery et al., 1990) used a value of

$$\lambda = 3.28 \times 10^{-4}\ \mathrm{yr}^{-1} \tag{2-73}$$

for drilling intrusions, which was derived from an assumption of 30 boreholes per square kilometer per 10,000-years (U.S. EPA, 1985) and an excavated disposal area of 1.09 x 10^5 m^2 (Volume 3 of this report). For illustration, Table 2-2 shows the probability of various computational scenarios involving drilling during different 2,000-year time intervals over a 10,000-year time period.

For a specified number of intrusions, the first column in Table 2-2 indicates the time interval in which the first intrusion takes place, the second column indicates the time interval in which the second intrusion takes place, and so on. The last column lists the probability for each combination of intrusions. For example, the row

I_1	I_2	I_3	I_4	Prob
⋮	⋮	⋮	⋮	⋮
1	3	4		1.062×10^{-2}
⋮	⋮	⋮	⋮	⋮

under 3 Intrusions indicates that the first, second and third intrusions occur during the time intervals [0, 2000], [4000, 6000] and [6000, 8000], respectively, and that the probability of this pattern of intrusions (i.e., scenario) is 1.062×10^{-2}. When expressed with previously used notation, this row indicates that

$$p\Big[S_1(0,2000) \bigcap S_0(2000,4000) \bigcap S_1(4000,6000) \bigcap S_1(6000,8000) \bigcap S_0(8000,10000)\Big] = 1.062 \times 10^{-2}. \tag{2-74}$$

The probabilities appearing in Table 2-2 were calculated with the relationship shown in (2-42).

For each specified number of intrusions, say k, in Table 2-2, the resultant number of cases, or scenarios, is the total number of combinations of the 2,000-year intervals taken k at a time with repetition. In general, the number of combinations of n elements taken k at a time with repetition is given by (Gellert et al., 1977, p. 578)

$$^{n}C_{k} = \binom{n+k-1}{k}. \tag{2-75}$$

For Table 2-2, $n = 5$ and $k = 1, 2, ..., 15$.

The EPA standard allows a 100-year period of administrative control to be assumed after the decommissioning of a waste disposal facility in which no disruptions due to human intrusion can

occur. Table 2-3 shows the result of recalculating the scenario probabilities in Table 2-2 with an assumed 100-year period of administration control (i.e., no drilling intrusions can occur in the first 100-years after decommissioning, which is equivalent to assuming that $\lambda = 0$ in the time interval [0, 100]). As comparison of Tables 2-2 and 2-3 shows, the assumption of a 100-year period of administrative control has little effect on scenario probabilities defined by a Poisson process over a 10,000-year period.

Probabilities for E1E2-type computational scenarios are shown in Table 2-4. The probabilities in this table are actually approximations due to the use of the relations in (2-62), (2-65) and (2-66). Exact results can be obtained but the formulas are very involved. The values used for $aBP(\ell)$, $aTOT(\ell)$ and $aTOT$ in the generation of Table 2-4 are shown in Table 2-5. For comparison, Table 2-6 shows the probabilities that result when an initial 100-year period of administrative control is assumed. As previously seen in Tables 2-2 and 2-3, the exclusion of drilling for a 100-year period does not have a large impact when a 10,000-year period is under consideration.

Probabilities for various types of drilling scenarios are shown in Tables 2-2, 2-3, 2-4 and 2-6. Another factor that can enter into computational scenario definition is the distribution of activity levels (i.e., Ci/m^2) within the waste emplaced in the repository. A projected distribution for the activity levels in waste that will be shipped to the WIPP is shown in Table 2-7. Chapter 3 of this volume discusses how activity loading can be incorporated into both the definition and probability of individual computational scenarios and the CCDF that can be determined for comparison with the EPA release limits.

Table 2-2. Probabilities for Computational Scenarios Involving Multiple Intrusions over 10,000-years for $\lambda = 3.28 \times 10^{-4} yr^{-1}$ and 2,000-Year Time Intervals. For a specified number of intrusions, the first column indicates the time interval in which the first intrusion occurs, the second column indicates the time interval in which the second intrusion occurs, and so on, where 1 ~ [0,2000], 2 ~ [2000,4000], 3 ~ [4000,6000], 4 ~ [6000,8000] and 5 ~ [8000,10000]; the last column lists the probability for each pattern of intrusions calculated with the relationship in (2-42).

0 Intrusions
(prob = 3.763E-02)
(cum prob = 3.763E-02)
(comb of intrusions = 1)

1 Intrusion
(prob = 1.234E-01)
(cum prob = 1.610E-01)
(comb of intrusions = 5)

I_1	I_2	I_3	I_4	Prob
1				2.468E-02
2				2.468E-02
3				2.468E-02
4				2.468E-02
5				2.468E-02
				1.234E-01

2 Intrusions
(prob = 2.024E-01)
(cum prob = 3.635E-01)
(comb of intrusions = 15)

I_1	I_2	I_3	I_4	Prob
1	1			8.096E-03
1	2			1.619E-02
1	3			1.619E-02
1	4			1.619E-02
1	5			1.619E-02
2	2			8.096E-03
2	3			1.619E-02
2	4			1.619E-02
2	5			1.619E-02
3	3			8.096E-03
3	4			1.619E-02
3	5			1.619E-02
4	4			8.096E-03
4	5			1.619E-02
5	5			8.096E-03
				2.024E-01

3 Intrusions
(prob = 2.213E-01)
(cum prob = 5.848E-01)
(comb of intrusions = 35)

I_1	I_2	I_3	I_4	Prob
1	1	1		1.770E-03
1	1	2		5.311E-03
1	1	3		5.311E-03
1	1	4		5.311E-03
1	1	5		5.311E-03
1	2	2		5.311E-03
1	2	3		1.062E-02
1	2	4		1.062E-02
1	2	5		1.062E-02
1	3	3		5.311E-03
1	3	4		1.062E-02
1	3	5		1.062E-02
1	4	4		5.311E-03
1	4	5		1.062E-02
1	5	5		5.311E-03
2	2	2		1.770E-03
2	2	3		5.311E-03
2	2	4		5.311E-03
2	2	5		5.311E-03
2	3	3		5.311E-03
2	3	4		1.062E-02
2	3	5		1.062E-02
2	4	4		5.311E-03
2	4	5		1.062E-02
2	5	5		5.311E-03
3	3	3		1.770E-03
3	3	4		5.311E-03
3	3	5		5.311E-03
3	4	4		5.311E-03
3	4	5		1.062E-02
3	5	5		5.311E-03
4	4	4		1.770E-03
4	4	5		5.311E-03
4	5	5		5.311E-03
5	5	5		1.770E-03
				2.213E-01

4 Intrusions
(prob = 1.815E-01)
(cum prob = 7.662E-01)
(comb of intrusions = 70)

I_1	I_2	I_3	I_4	Prob
1	1	1	1	2.903E-04
1	1	1	2	1.161E-03
.	.	.	.	.
.	.	.	.	.
.	.	.	.	.
1	2	3	4	6.968E-03
.	.	.	.	.
.	.	.	.	.
.	.	.	.	.
4	5	5	5	1.161E-03
5	5	5	5	2.903E-04
				1.815E-01

5 Intrusions
(prob = 1.190E-01)
(cum prob = 8.853E-01)
(comb of intrusions = 126)

6 Intrusions
(prob = 6.508E-02)
(cum prob = 9.503E-01)
(comb of intrusions = 210)

7 Intrusions
(prob = 3.049E-02)
(cum prob = 9.808E-01)
(comb of intrusions = 330)

Table 2-2. Probabilities for Computational Scenarios Involving Multiple Intrusions over 10,000-years for $\lambda = 3.28 \times 10^{-4} yr^{-1}$ and 2,000-Year Time Intervals. (Concluded)

8 Intrusions (prob = 1.250E-02) (cum prob = 9.933E-01) (comb of intrusions = 495)	11 Intrusions (prob = 4.456E-04) (cum prob = 9.998E-01) (comb of intrusions =1365)	14 Intrusions (prob = 7.200E-06) (cum prob = 1.000E+00) (comb of intrusions =3060)
9 Intrusions (prob = 4.556E-03) (cum prob = 9.979E-01) (comb of intrusions = 715)	12 Intrusions (prob = 1.218E-04) (cum prob = 1.000E+00) (comb of intrusions =1820)	15 Intrusions (prob = 1.574E-06) (cum prob = 1.000E+00) (comb of intrusions =3876)
10 Intrusions (prob = 1.494E-03) (cum prob = 9.994E-01) (comb of intrusions =1001)	13 Intrusions (prob = 3.073E-05) (cum prob = 1.000E+00) (comb of intrusions =2380)	

Table 2-3. Probabilities for Computational Scenarios Involving Multiple Intrusions over 10,000-years for $\lambda = 3.28 \times 10^{-4} yr^{-1}$, a 100-year Period Of Administrative Control During Which No Drilling Intrusions Can Occur, and 2,000-Year Time Intervals. For a specified number of intrusions, the first column indicates the time interval in which the first intrusion occurs, the second column indicates the time interval in which the second intrusion occurs, and so on, where 1 ~ [0,2000], 2 ~ [2000,4000], 3 ~ [4000,6000], 4 ~ [6000,8000] and 5 ~ [8000,10000]; the last column lists the probability for each pattern of intrusions calculated with the relationship in (2-42).

0 Intrusions
(prob = 3.888E-02)
(cum prob = 3.888E-02)
(comb of intrusions = 1)

1 Intrusion
(prob = 1.263E-01)
(cum prob = 1.651E-01)
(comb of intrusions = 5)

I_1	I_2	I_3	I_4	Prob
1				2.423E-02
2				2.551E-02
3				2.551E-02
4				2.551E-02
5				2.551E-02
				1.263E-01

2 Intrusions
(prob = 2.050E-01)
(cum prob = 3.701E-01)
(comb of intrusions = 15)

I_1	I_2	I_3	I_4	Prob
1	1			7.551E-03
1	2			1.590E-02
1	3			1.590E-02
1	4			1.590E-02
1	5			1.590E-02
2	2			8.366E-03
2	3			1.673E-02
2	4			1.673E-02
2	5			1.673E-02
3	3			8.366E-03
3	4			1.673E-02
3	5			1.673E-02
4	4			8.366E-03
4	5			1.673E-02
5	5			8.366E-03
				2.050E-01

3 Intrusions
(prob = 2.219E-01)
(cum prob = 5.920E-01)
(comb of intrusions = 35)

I_1	I_2	I_3	I_4	Prob
1	1	1		1.569E-03
1	1	2		4.953E-03
1	1	3		4.953E-03
1	1	4		4.953E-03
1	1	5		4.953E-03
1	2	2		5.214E-03
1	2	3		1.043E-02
1	2	4		1.043E-02
1	2	5		1.043E-02
1	3	3		5.214E-03
1	3	4		1.043E-02
1	3	5		1.043E-02
1	4	4		5.214E-03
1	4	5		1.043E-02
1	5	5		5.214E-03
2	2	2		1.829E-03
2	2	3		5.488E-03
2	2	4		5.488E-03
2	2	5		5.488E-03
2	3	3		5.488E-03
2	3	4		1.098E-02
2	3	5		1.098E-02
2	4	4		5.488E-03
2	4	5		1.098E-02
2	5	5		5.488E-03
3	3	3		1.829E-03
3	3	4		5.488E-03
3	3	5		5.488E-03
3	4	4		5.488E-03
3	4	5		1.098E-02
3	5	5		5.488E-03
4	4	4		1.829E-03
4	4	5		5.488E-03
4	5	5		5.488E-03
5	5	5		1.829E-03
				2.219E-01

4 Intrusions
(prob = 1.801E-01)
(cum prob = 7.722E-01)
(comb of intrusions = 70)

I_1	I_2	I_3	I_4	Prob
1	1	1	1	2.444E-04
1	1	1	2	1.029E-03
.	.	.	.	.
.	.	.	.	.
.	.	.	.	.
1	2	3	4	6.841E-03
.	.	.	.	.
.	.	.	.	.
.	.	.	.	.
4	5	5	5	1.200E-03
5	5	5	5	3.000E-04
				1.801E-01

5 Intrusions
(prob = 1.170E-01)
(cum prob = 8.891E-01)
(comb of intrusions = 126)

6 Intrusions
(prob = 6.331E-02)
(cum prob = 9.525E-01)
(comb of intrusions = 210)

7 Intrusions
(prob = 2.937E-02)
(cum prob = 9.818E-01)
(comb of intrusions = 330)

Table 2-3. Probabilities for Computational Scenarios Involving Multiple Intrusions over 10,000-years for $\lambda = 3.28 \times 10^{-4} yr^{-1}$, a 100-year Period Of Administrative Control During Which No Drilling Intrusions Can Occur, and 2,000-Year Time Intervals. (Concluded)

8 Intrusions (prob = 1.192E-02) (cum prob = 9.937E-01) (comb of intrusions = 495)	11 Intrusions (prob = 4.123E-04) (cum prob = 9.999E-01) (comb of intrusions =1365)	14 Intrusions (prob = 6.464E-06) (cum prob = 1.000E+00) (comb of intrusions =3060)
9 Intrusions (prob = 4.301E-03) (cum prob = 9.980E-01) (comb of intrusions = 715)	12 Intrusions (prob = 1.116E-04) (cum prob = 1.000E+00) (comb of intrusions =1820)	15 Intrusions (prob = 1.399E-06) (cum prob = 1.000E+00) (comb of intrusions =3876)
10 Intrusions (prob = 1.397E-03) (cum prob = 9.994E-01) (comb of intrusions =1001)	13 Intrusions (prob = 2.787E-05) (cum prob = 1.000E+00) (comb of intrusions =2380)	

Table 2-4. Probabilities for E1E2-Type Computational Scenarios (i.e., boreholes through a single panel in which at least one borehole penetrates a pressurized brine pocket and at least one borehole does not penetrate a pressurized brine pocket) over 10,000-years for $\lambda = 3.28 \times 10^{-4} yr^{-1}$ and 2,000-Year Time Intervals.

Time Intervals	2 Boreholes[a] (Eqs 2-63, 2-52)	≥2 Boreholes[b] (Eqs 2-66, 2-52)	2 Boreholes[c] (Eqs 2-63, 2-72)	≥ 2 Boreholes[d] (Eqs.2-66, 2-72)
[0, 2000]	0.005635	0.005825	0.009964	0.010304
[2000, 4000]	0.005635	0.005825	0.009964	0.010304
[4000, 6000]	0.005635	0.005825	0.009964	0.010304
[6000, 8000]	0.005635	0.005825	0.009964	0.010304
[8000, 10000]	0.005635	0.005825	0.009964	0.010304

a. At least one waste panel penetrated by exactly two boreholes during the indicated time interval, of which one penetrates a pressurized brine pocket and one does not. Calculation uses approximation in (2-63) with $\alpha(l)$ and $\beta(l)$ defined in (2-52). Values for aBP(l), aTOT(l) and aTOT consistent with Figure 2-3.

b. At least one waste panel penetrated by two or more boreholes during the indicated time interval, of which at least one penetrates a pressurized brine pocket and at least one does not. Calculation uses approximation in (2-66) with $\alpha(l)$ and $\beta(l)$ defined in (2-52). Values for aBP(l), aTOT(l) and aTOT consistent with Figure 2-3.

c. Same as a. but $\alpha(l)$ and $\beta(l)$ defined in (2-72) and aBP(l), aTOT(l) and aTOT defined to be consistent with Figure 2-3.

d. Same as b. but $\alpha(l)$ and $\beta(l)$ defined in (2-71) and aBP(l), aTOT(l) and aTOT defined to be consistent with Figure 2-3.

Table 2-5. Parameter Values Used in Example Calculation of Probabilities for E1E2-type Computational Scenarios (Source: Table 5.1-1 of Vol. III of this report with depth to pressurized brine assumed to be less than 1250 m).

	$aTOT(l)^a$	$aBP(l)^b$	$aBP(l) / aTOT(l)$
Panel 1	11,530	11,530	1.0000
Panel 2	11,530	8,249	0.7154
Panel 3	11,530	3,548	0.3077
Panel 4	11,530	8,869	0.7692
Panel 5	11,530	4,833	0.4192
Panel 6	11,530	0	0.0000
Panel 7	11,530	0	0.0000
Panel 8	11,530	7,432	0.6446
Southern Panel	8,413	3,786	0.4500
Northern Panel	8,701	1,044	0.1200

Additional Values:

$$aTOT = \sum_{l=1}^{10} aTOT(l) = 109,354$$

$$aBP = \sum_{l=1}^{10} aBP(l) = 49,291$$

$$aBP \,/\, aTOT = 0.45075$$

[a] $aTOT(l)$ = area (m^2) of waste panel l

[b] $aBP(l)$ = area (m^2) of pressurized brine under waste panel l

Table 2-6. Probabilities for E1E2-Type Computational Scenarios (i.e., boreholes through a single panel in which at least one borehole penetrates a pressurized brine pocket and at least one borehole does not penetrate a pressurized brine pocket) over 10,000-years for $\lambda = 3.28 \times 10^{-4} yr^{-1}$, a 100-year Period of Administrative Control During Which No Drilling Intrusions Can Occur, and 2,000-Year Time Intervals.

Time Intervals	2 Boreholes[a] (Eqs 2-63, 2-52)	≥2 Boreholes[b] (Eqs 2-66, 2-52)	2 Boreholes[c] (Eqs 2-63, 2-72)	≥ 2 Boreholes[d] (Eqs 2-66, 2-72)
[0, 2000]	0.005102	0.005266	0.009022	0.009315
[2000, 4000]	0.005635	0.005825	0.009964	0.010304
[4000, 6000]	0.005635	0.005825	0.009964	0.010304
[6000, 8000]	0.005635	0.005825	0.009964	0.010304
[8000, 10000]	0.005635	0.005825	0.009964	0.010304

a. At least one waste panel penetrated by exactly two boreholes during the indicated time interval, of which one penetrates a pressurized brine pocket and one does not. Calculation uses approximation in (2-63) with $\alpha(l)$ and $\beta(l)$ defined in (2-52). Values for aBP(l), aTOT(l) and aTOT consistent with Figure 2-3.

b. At least one waste panel penetrated by two or more boreholes during the indicated time interval, of which at least one penetrates a pressurized brine pocket and at least one does not. Calculation uses approximation in (2-66) with $\alpha(l)$ and $\beta(l)$ defined in (2-52). Values for aBP(l), aTOT(l) and aTOT consistent with Figure 2-3.

c. Same as a. but $\alpha(l)$ and $\beta(l)$ defined in (2-72) and aBP(l), aTOT(l) and aTOT defined to be consistent with Figure 2-3.

d. Same as b. but $\alpha(l)$ and $\beta(l)$ defined in (2-71) and aBP(l), aTOT(l) and aTOT defined to be consistent with Figure 2-3.

Table 2-7. Projected Activity Levels (Ci/m^2) in Waste That is Currently Stored and May be Shipped to the WIPP (based on Table 3.4-11 in Volume 3 of this report).

Activity Level	Type[a]	Probability[b]	Time (years) 0	1000	3000	5000	7000	9000
1	CH	0.4023	3.4833	0.2718	0.1840	0.1688	0.1575	0.1473
2	CH	0.2998	34.8326	2.7177	1.8401	1.6875	1.5748	1.4729
3	CH	0.2242	348.326	27.177	18.401	16.875	15.748	14.729
4	CH	0.0149	3483.26	271.77	184.01	168.75	157.48	147.29
5	RH	0.0588	117.6717	0.1546	0.1212	0.1139	0.1082	0.1030
Average for CH Waste:			150.7905	11.7648	7.9658	7.3053	6.8174	6.3764

[a] CH designates contact handled waste; RH designates remote handled waste

[b] Probability that a randomly placed borehole through the waste panels will intersect waste of activity level (l), $l = 1,2,3,4,5$.

3. CONSTRUCTION OF COMPLEMENTARY CUMULATIVE DISTRIBUTION FUNCTIONS—Jon C. Helton

3.1 Introduction

Sandia National Laboratories is conducting an ongoing performance assessment for the Waste Isolation Pilot Plant (WIPP) in southeastern New Mexico (Bertram-Howery and Hunter, 1989; Lappin et al., 1989). At present, a performance assessment is performed each year to summarize what is known about the WIPP and to provide guidance for future work (Marietta et al., 1989; Bertram-Howery et al., 1990). It is anticipated that these iterative performance assessments will continue until the WIPP is either licensed for the disposal of transuranic wastes or found to be unsuitable for such disposal.

The result of greatest interest obtained in these performance assessments is a complementary cumulative distribution function (CCDF) that is used for comparison with the U. S. Environmental Protection Agency (EPA) release limits for radioactive waste disposal (U.S. EPA, 1985). As discussed in the preceding chapter (Chapter 2 of this volume), the EPA standard requires that the normalized releases to the accessible environment be expressed as a single CCDF and that this CCDF fall under certain specified bounds. At present, drilling intrusions are believed to be the most severe potential disruptions that need be considered at the WIPP (Guzowski, 1990 and 1991). Thus, the construction of this CCDF for the WIPP is based on summary scenarios that result from drilling intrusions.

This presentation will describe how a CCDF can be constructed for comparison against the EPA release limits when the disruptions to the waste disposal site under consideration result from drilling intrusions. For the results presented here, the drilling intrusions are assumed to follow a Poisson process (i.e., occur randomly in time and space) (Cox and Lewis, 1966; Haight, 1967; Cox and Isham, 1980) with a fixed rate constant. However, the described approach would work with any probability model for drilling intrusions.

With regard to the risk representation

$$\mathcal{R} = \{(\mathcal{S}_i, pS_i, \mathbf{cS}_i), i = 1, \ldots, nS\} \tag{3-1}$$

described in the preceding chapter and elsewhere (Kaplan and Garrick, 1981; Helton et al., 1991), $\mathcal{S}_i$ is a set of similar time histories defined on the basis of drilling intrusions, pS_i is the probability for $\mathcal{S}_i$, and $\mathbf{cS}_i$ contains the EPA normalized release for $\mathcal{S}_i$. The $\mathcal{S}_i$ appearing in (3-1) are obtained by discretizing a suitable sample space. For comparisons with the EPA release limits, this sample space is

$S = \{x: x$ a single 10,000-year time history beginning at decommissioning of the facility under consideration$\}$. (3-2)

In what follows, an approach will be described for defining the S_i, assigning probabilities pS_i and consequences $\mathbf{cS}_i$ to these S_i, and then constructing the resultant CCDF.

3.2 Construction of a CCDF

The following factors will be used to define the computational scenarios S_i appearing in (3-1): number and time of the intrusions (see Tables 2-2 and 2-3), flow through a panel due to penetration of a pressurized brine pocket in the Castile formation (see Tables 2-4 and 2-6), and activity level of the waste penetrated by a borehole (see Table 2-7). The preceding factors all relate to stochastic or type A uncertainty (Kaplan and Garrick, 1981; Helton et al., 1991; International Atomic Energy Agency, 1989) since they lead to values for the probabilities appearing in (3-1) and ultimately to a CCDF. Scenarios defined at this level of detail are referred to as computational scenarios in the WIPP performance assessment due to their role in defining the actual calculations that must be performed in the construction of a CCDF for comparison with the EPA release limits.

As shown in Tables 2-2 and 2-3 of this volume, even a fairly coarse gridding on time leads to far too many computational scenarios to perform a detailed calculation for each of them. Construction of a CCDF for comparison against the EPA release limits requires the estimation of cumulative probability through the 0.999 level. Thus, depending on the value for the rate constant λ in the Poisson model for drilling, this may require the inclusion of computational scenarios involving as many as 10 to 12 drilling intrusions, which results in a total of several thousand computational scenarios. Further, this number does not include the effects of different activity levels in the waste. To obtain results for such a large number of computational scenarios, it is necessary to plan and implement the overall calculations very carefully. The manner in which this can be done is not unique. In the following, one computational procedure for calculating a CCDF for comparison with the EPA release limits is described.

The 10,000-year time interval that must be considered for comparison with the EPA release limits can be divided into disjoint subintervals

$$[t_{i-1}, t_i], \quad i = 1, 2, \ldots, nT, \tag{3-3}$$

where nT is the number of time intervals selected for use. The following results can be calculated for each time interval (e.g., with the assumption the intrusion takes place at the middle of the time interval):

rC_i = EPA normalized release to the surface environment for cuttings removal due to a single borehole in time interval i with the assumption that the waste is homogeneous (i.e., waste of different activity levels is not present), (3-4)

rC_{ij} = EPA normalized release to the surface environment for cuttings removal due to a single borehole in time interval i that penetrates waste of activity level j, (3-5)

$rGW1_i$ = EPA normalized release to the surface environment for groundwater transport initiated by a single borehole in time interval i, (3-6)

and

$rGW2_i$ = EPA normalized release to the surface environment for groundwater transport initiated by two boreholes in the same waste panel in time interval i, of which one penetrates a pressurized brine pocket and one does not [i.e., an E1E2-type summary scenario (Bertram-Howery et al., 1990)]. (3-7)

In general, rC_i, rC_{ij}, $rGW1_i$ and $rGW2_i$ will be vectors containing a large variety of information; however, for notational simplicity, a vector representation will not be used.

For the WIPP performance assessment, the cuttings release to the accessible environment (i.e., rC_i and rC_{ij}) is determined by the CUTTINGS (Rechard et al., 1989) program, and the groundwater release to the accessible environment (i.e., $rGW1_i$ and $rGW2_i$) is determined through a sequence of linked calculations involving the SECO_2DH (draft of SAND90-7096, Roache et al., in preparation; also see Chapter 6 of this volume), BRAGFLO (Chapter 5 of this volume), PANEL (Rechard et al., 1989) and STAFF2D (Huyakorn et al., 1989) programs. The overall operation of these programs is controlled by a driver called CAMCON (Rechard et al., 1989). Additional information on the actual calculations that must be performed to obtain rC_i, rC_{ij}, $rGW1_i$ and $rGW2_i$ is available elsewhere (Chapters 5 through 7 of this volume).

The releases rC_i, rC_{ij}, $rGW1_i$ and $rGW2_i$ can be used to construct the releases associated with the many individual scenarios that must be used in the construction of a CCDF for comparison with the EPA release limits. The following assumptions are made:

1. With the exception of E1E2-type computational scenarios, no synergistic effects result from multiple boreholes, and thus, the total release for a scenario involving multiple intrusions can be obtained by adding the releases associated with the individual intrusions.

2. An E1E2-type computational scenario can only take place when the necessary boreholes occur within the same time interval $[t_{i-1}, t_i]$.

3. An E1E2-type computational scenario involving more than two boreholes will have the same release as an E1E2-type computational scenario involving exactly two boreholes.

The preceding assumptions can now be used systematically to construct the releases for individual computational scenarios.

Computational scenarios that involve *nBH* intrusions, but not an E1E2-type intrusion, are considered first. For a time history involving exactly *nBH* intrusions over 10,000 yrs, let

$$\mathbf{l} = [l(1), l(2), \ldots, l(nBH)] \tag{3-8}$$

$$\mathbf{m} = [m(1), m(2), \ldots, m(nBH)] \tag{3-9}$$

and

$$\mathbf{n} = [n(1), n(2), \ldots, n(nT)] \tag{3-10}$$

represent vectors such that $l(j)$ designates the activity level penetrated by the j^{th} borehole, $m(j)$ designates the time interval in which the j^{th} borehole occurs, and $n(i)$ equals the number of intrusions that occur in the i^{th} time interval. Each element $l(j)$ of $\mathbf{l}$ will take on an integer value between 1 and nL, where nL is the number of activity levels into which the waste has been classified, and each element $m(j)$ of $\mathbf{m}$ will take on an integer value between 1 and nT, where nT is the number of time intervals in use. Similarly, each element $n(i)$ of $\mathbf{n}$ will take on an integer value between 0 and nBH. The elements of $\mathbf{m}$ satisfy the ordering $m(j) \le m(j+1)$, and the elements of $\mathbf{n}$ satisfy the equality $\Sigma_i n(i) = nBH$. Further, a reciprocal relationship exists between $\mathbf{m}$ and $\mathbf{n}$ in the sense that, if either is known, then the other can be determined.

The vectors $\mathbf{l}$, $\mathbf{m}$ and $\mathbf{n}$ can be used to define computational scenarios in a manner that will lead naturally to the calculation of their probabilities and consequences. Specifically, let

$$\mathcal{S}(\mathbf{n}) = \{x: x \text{ an element of } \mathcal{S} \text{ for which exactly } n(i) \text{ intrusions occur in time interval } [t_{i-1}, t_i] \text{ for } i = 1,2,\ldots,nT\} \quad (3\text{-}11)$$

and

$$\mathcal{S}(\mathbf{l},\mathbf{n}) = \{x: x \text{ an element of } \mathcal{S} \text{ for which the } j^{th} \text{ borehole encounters waste of activity } l(j) \text{ and exactly } n(i) \text{ intrusions occur in time interval } [t_{i-1}, t_i] \text{ for } i = 1,2,\ldots,nT\}. \quad (3\text{-}12)$$

The computational scenarios $\mathcal{S}(\mathbf{n})$ and $\mathcal{S}(\mathbf{l},\mathbf{n})$ are related by

$$\mathcal{S}(\mathbf{n}) = \bigcup_{\mathbf{l}} \mathcal{S}(\mathbf{l},\mathbf{n}), \quad (3\text{-}13)$$

where, for a fixed value of $\mathbf{n}$, the union is taken over all possible values for $\mathbf{l}$ (i.e., over all possible combinations of activity loading that the boreholes specified by $\mathbf{n}$ might encounter).

It follows from Eq. (2-42) that the probability $pS(\mathbf{n})$ for $\mathcal{S}(\mathbf{n})$ is given by

$$pS(\mathbf{n}) = \left\{ \prod_{i=1}^{nT} \left[\frac{\lambda^{n(i)} (t_i - t_{i-1})^{n(i)}}{n(i)!} \right] \right\} \exp\left[-\lambda (t_{nT} - t_0) \right] \quad (3\text{-}14)$$

when drilling follows a Poisson process with a rate constant λ. Further, the probability $pS(\mathbf{l},\mathbf{n})$ for $\mathcal{S}(\mathbf{l},\mathbf{n})$ is given by

$$pS(\mathbf{l},\mathbf{n}) = \left(\prod_{j=1}^{nBH} pL_{l(j)} \right) pS(\mathbf{n}), \quad (3\text{-}15)$$

where $pS(\mathbf{n})$ is defined in (3-14) and $pL_{l(j)}$ is the probability that a randomly placed borehole in the repository will encounter waste of activity level $l(j)$.

The normalized releases rC_i, rC_{ij} and $rGW1_i$ can be used to construct the EPA normalized releases for computational scenarios $\mathcal{S}(\mathbf{n})$ and $\mathcal{S}(\mathbf{l},\mathbf{n})$. For $\mathcal{S}(\mathbf{n})$, the normalized release to the accessible environment can be approximated by

$$cS(\mathbf{n}) = \sum_{j=1}^{nBH} \left(rC_{m(j)} + rGW1_{m(j)} \right), \tag{3-16}$$

where $\mathbf{m}$ is the vector defined in (3-9). As indicated earlier, $\mathbf{m}$ is uniquely determined once $\mathbf{n}$ is specified. The computational scenario $S(\mathbf{n})$ contains no information on the activity levels encountered by the individual boreholes, and so $cS(\mathbf{n})$ was constructed with the assumption that all waste is of the same average activity. However, $S(\mathbf{l},\mathbf{n})$ does contain information on activity levels, and the associated normalized release to the accessible environment can be approximated by

$$cS(\mathbf{l},\mathbf{n}) = \sum_{j=1}^{nBH} \left(rC_{m(j),l(j)} + rGW1_{m(j)} \right), \tag{3-17}$$

which does incorporate the activity levels encountered by the individual boreholes.

Computational scenarios of the E1E2-type are now considered. This is a relatively unlikely type of computational scenario (see Tables 2-4 and 2-6) but has the potential to cause large releases due to flow between two boreholes within a single panel. Specifically, E1E2-type computational scenarios are defined by

$$S^{+-}(t_{k-1},t_k) = \{x : x \text{ an element of } S \text{ involving two or more boreholes that penetrate the same waste panel during the time interval } [t_{k-1},t_k], \text{ at least one of these boreholes penetrates a pressurized brine pocket and at least one does not penetrate a pressurized brine pocket}\}. \tag{3-18}$$

Further, the computational scenario $S^{+-}(t_{k-1},t_k)$ can be subdivided on the basis of the activity levels encountered by the boreholes, which produces computational scenarios of the form

$$S^{+-}(\mathbf{l};t_{k-1},t_k) = \{x : x \text{ an element of } S^{+-}(t_{k-1},t_k), \text{ for which the } jth \text{ borehole encounters waste of activity level } l(j)\}. \tag{3-19}$$

It follows from Eqs. (2-63) and (2-66) that the probability for $S^{+-}(t_{k-1},t_k)$ can be approximated by

$$pS^{+-}(t_{k-1},t_k) \triangleq \sum_{l=1}^{nP}\left[\alpha(l)\beta(l)(t_k - t_{k-1})^2\right]\exp\left\{-[\alpha(l)+\beta(l)][t_k - t_{k-1}]\right\} \tag{3-20}$$

or

$$pS^{+-}(t_{k-1},t_k) \triangleq \sum_{l=1}^{nP}\left\{1-\exp\left[-\alpha(l)(t_k - t_{k-1})\right]\right\}\left\{1-\exp\left[-\beta(l)(t_{k-1},t_k)\right]\right\}, \tag{3-21}$$

where

$\alpha(l)$ = $[aBP(l)]\lambda / aTOT$,

$\beta(l)$ = $[aTOT(l) - aBP(l)]\lambda / aTOT$,

$aBP(l)$ = area (m^2) of pressurized brine pocket under waste panel l,

$aTOT(l)$ = total area (m^2) of waste panel l,

$aTOT$ = total area (m^2) of waste panels,

nP = number of waste panels,

and drilling is assumed to follow a Poisson process with a rate constant λ. The expression for $pS^{+-}(t_{k-1},t_k)$ in (3-21) was derived for two or more drilling intrusions and thus provides a somewhat larger value for $pS^{+-}(t_{k-1},t_k)$ than the expression in (3-20), which was derived for exactly two intrusions. However, as illustrated in Tables 2-4 and 2-6, there is not a large difference in the values for $pS^{+-}(t_{k-1},t_k)$ obtained for these two expressions. If desired, an exact probability can be obtained with the relationship in Eq. (2-67) in Chapter 2 of this volume. Further,

$$pS^{+-}(\mathrm{I};t_{k-1},t_k) = \left(\prod_{j=1}^{nB} pL_{l(j)}\right) pS^{+-}(t_{k-1},t_k). \tag{3-22}$$

Before continuing, it is pointed out that the expression in (3-21) is actually greater than $pS^{+-}(t_{k-1},t_k)$ (see Eqs. (2-67) and (2-68)) and also incorporates the probability for the occurrence of an E1E2-type computational scenario in two different waste panels during the time interval $[t_{k-1},t_k]$.

The normalized release to the accessible environment for $S^{+-}(t_{k-1},t_k)$ can be approximated by

$$cS^{+-}(t_{k-1},t_k) = 2\ rC_k + rGW2_k, \tag{3-23}$$

where it is assumed that all waste is of the same average activity for cuttings removal. Similarly, the normalized release $cS^{+-}(\mathbf{l};t_{k-1},t_k)$ for $S^{+-}(\mathbf{l};t_{k-1},t_k)$ can be approximated by

$$cS^{+-}(\mathbf{l};t_{k-1},t_k) = \sum_{j=1}^{2} rC_{k,l(j)} + rGW2_k, \tag{3-24}$$

which incorporates the activity level of the waste. The approximations for $cS^{+-}(t_{k-1},t_k)$ and $cS^{+-}(\mathbf{l};t_{k-1},t_k)$ in (3-23) and (3-24) are based on exactly two intrusions in the time interval $[t_{k-1},t_k]$. More complicated expressions could be developed to define releases for multiple E1E2-type intrusions. However, due to the low probability of such patterns of intrusion (e.g., compare the probabilities for 2 and ≥2 boreholes in Tables 2-4 and 2-6), the use of such expressions would have little impact on the CCDFs used for comparison with the EPA release limits.

The results contained in this section can be used in conjunction with the risk representation in (3-1) to calculate CCDFs for comparison with the EPA release limits. The choices for S_i, pS_i and $\mathbf{cS}_i$ with and without the consideration of activity level for cuttings removal are summarized in Table 3-1.

Table 3-1. Calculation of a CCDF for Comparison with the EPA Release Limits with and without the Effects of Activity Loading

	S_i	pS_i	$\mathbf{cS}_i$
Without Activity Loading	$S(\mathbf{n})$, $S^{+-}(t_{k-1},t_k)$ (Eqs. 3-11, 3-18)	$pS(\mathbf{n})$, $pS^{+-}(t_{k-1},t_k)$ (Eqs. 3-14, 3-20, 3-21)	$cS(\mathbf{n})$, $cS^{+-}(t_{k-1},t_k)$ (Eqs. 3-16, 3-23)
With Activity Loading	$S(\mathbf{l},\mathbf{n})$, $S^{+-}(\mathbf{l};t_{k-1},t_k)$ (Eqs. 3-12, 3-19)	$pS(\mathbf{l},\mathbf{n})$, $pS^{+-}(\mathbf{l};t_{k-1},t_k)$ (Eqs. 3-15, 3-22)	$cS(\mathbf{l},\mathbf{n})$, $cS^{+-}(\mathbf{l};t_{k-1},t_k)$ (Eqs. 3-17, 3-24)

Example CCDFs calculated with the techniques discussed in this section are given in Section 3.4. However, there is a numerical problem that must be addressed first. The computational scenarios $\mathcal{S}(\mathbf{l},\mathbf{n})$ are based on taking all possible combinations of activity levels that might be encountered by the boreholes associated with $\mathcal{S}(\mathbf{n})$. As the number of boreholes increases, the number of activity level combinations increases rapidly and becomes too large to permit a systematic consideration of every possible combination. A numerical procedure for determining the distribution of cuttings releases that results from the consideration of activity loading is presented in Section 3.3. This procedure is then used in the generation of the CCDFs presented in Section 3.4.

3.3 Computation of Activity Loading Effects

The computational scenario $\mathcal{S}(\mathbf{n})$ defined in (3-11) involves nBH drilling intrusions (i.e., $\Sigma_i n(i) = nBH$) and nT time intervals; in addition, the computational scenario $\mathcal{S}(\mathbf{l},\mathbf{n})$ defined in (3-12) involves nL levels for activity loading. This results in

$$\binom{nT+nBH-1}{nBH} \text{ and } nL^{nBH}\binom{nT+nBH-1}{nBH} \tag{3-25}$$

possible values for $\mathcal{S}(\mathbf{n})$ and $\mathcal{S}(\mathbf{l},\mathbf{n})$, respectively [Eq. (2-75)]. As illustrated in Table 3-2, the number of possible computational scenarios increases rapidly with increases in nBH.

Construction of the CCDF for comparison with the EPA release limits may require the consideration of as many as 10 to 12 drilling intrusions when the suggested default drilling rate of 30 boreholes/km^2/10,000 yrs is used (Tables 2-2 and 2-3). As examination of Table 3-2 shows, use of the computational scenarios $\mathcal{S}(\mathbf{n})$ and their associated consequences in the construction of a CCDF should be possible. However, a systematic incorporation of each computational scenario $\mathcal{S}(\mathbf{l},\mathbf{n})$ into a CCDF is likely to require an unreasonable amount of computation. This is especially true when sampling-based uncertainty/sensitivity studies are used to investigate the possible variation in the CCDF used for comparison with the EPA release limits (Helton et al., 1991, Chapter VI).

Table 3-2. Number of Possible Computational Scenarios for Varying Numbers of Intrusions (nBH), Time Intervals (nT) and Levels for Activity Loading (nL)

nBH	$nT = 3$, $nL = 3$		$nT = 5$, $nL = 5$		$nT = 10$, $nL = 5$	
	$\mathcal{S}(\mathbf{n})$	$\mathcal{S}(\mathbf{l},\mathbf{n})$	$\mathcal{S}(\mathbf{n})$	$\mathcal{S}(\mathbf{l},\mathbf{n})$	$\mathcal{S}(\mathbf{n})$	$\mathcal{S}(\mathbf{l},\mathbf{n})$
0	1	1	1	1	1	1
1	3	9	5	25	10	50
2	6	54	15	375	55	1375
3	10	270	35	4375	220	27500
4	15	1215	70	43750	715	446875
5	21	5103	126	393750	2002	6.26×10^{6}
6	28	20412	210	3.28×10^{6}	5005	7.82×10^{7}
7	36	78732	330	2.58×10^{7}	11440	8.94×10^{8}
8	45	295245	495	1.93×10^{8}	24310	9.50×10^{9}
9	55	1.08×10^{6}	715	1.40×10^{9}	48620	9.50×10^{10}
10	66	3.90×10^{6}	1001	9.78×10^{9}	92378	9.02×10^{11}
11	78	1.38×10^{7}	1365	6.67×10^{10}	167960	8.20×10^{12}
12	91	4.84×10^{7}	1820	4.44×10^{11}	293930	7.18×10^{13}
13	105	1.67×10^{8}	2380	2.91×10^{12}	497420	6.07×10^{14}
14	120	5.74×10^{8}	3060	1.87×10^{13}	817190	4.99×10^{15}
15	136	1.95×10^{9}	3876	1.18×10^{14}	1307504	3.99×10^{16}

Computational costs associated with the construction of a CCDF involving the computational scenarios $\mathcal{S}(\mathbf{l},\mathbf{n})$ can be controlled by considering all computational scenarios for relatively small values of nBH and then switching to a Monte Carlo procedure for larger values of nBH. Further, storage requirements can be significantly reduced by sorting the individual consequence results into groups based on size and accumulating the associated probability as the calculation progresses. In essence, this constructs the desired CCDF as the calculation progresses and removes the need to save results for the large number of individual computational scenarios until the end of the calculation. These ideas are now elaborated on.

First, a "binning" system must be established to accumulate the probabilities for the individual computational scenarios as the calculation progresses. To this end, the range of possible

consequence results (i.e., normalized releases to the accessible environment) is partitioned by a sequence of values of the form

$$cS_0 < cS_1 < \cdots < cS_{m-1} < cS_m, \tag{3-26}$$

where cS_0 is less than or equal to the smallest anticipated consequence value and cS_m is greater than or equal to the largest anticipated consequence value. The increments

$$\Delta(cS_i) = cS_i - cS_{i-1} \tag{3-27}$$

will determine the horizontal step sizes in the final CCDF. After each consequence value cS in the integrated calculation has been determined, the integer i such that

$$cS_{i-1} < cS \le cS_i \tag{3-28}$$

is determined and the probability for the associated computational scenario is accumulated in a variable pS_i. At the end of the calculation, the pS_i will determine the vertical step sizes in the final CCDF.

Second, a systematic coverage of the computational scenarios $\mathcal{S}(\mathbf{l},\mathbf{n})$ is performed for small values of nBH (e.g., ≤5). For each of these computational scenarios, $cS(\mathbf{l},\mathbf{n})$ will be calculated, an integer i will be determined such that

$$cS_{i-1} < cS(\mathbf{l},\mathbf{n}) \le cS_i, \tag{3-29}$$

and $pS(\mathbf{l},\mathbf{n})$ will be accumulated in pS_i. Since there are relatively few of them, the scenarios $\mathcal{S}^{+-}(\mathbf{l};t_{k-1},t_k)$ can be handled similarly at this point.

Third, a Monte Carlo procedure can be used to incorporate computational scenarios for larger values of nBH (e.g., >5). For a fixed nBH and each associated computational scenario $\mathcal{S}(\mathbf{n})$, a distribution must be estimated for the releases $cS(\mathbf{l},\mathbf{n})$ defined in (3-17). The variable in this estimation is the vector $\mathbf{l}$, which characterizes the activity levels encountered by the individual boreholes. Each element $l(j)$ of $\mathbf{l}$ is an integer-valued variable defined by the discrete distribution

$$(1,pL_1),(2,pL_2),\ldots,(nL,pL_{nL}). \tag{3-30}$$

Specifically, $l(j) = l$ occurs with probability pL_l and indicates that the j^{th} borehole encountered waste of activity level l. Since drilling is assumed to be random in time and space, the individual elements of $\mathbf{l}$ have the same distribution but are independent of each other. Random or Latin hypercube sampling (McKay et al., 1979) in conjunction with the distribution indicated in (3-8) can be used to generate a sample

$$\mathbf{l}_s = [l_s(1), l_s(2), \ldots, l_s(nBH)], \quad s = 1,2,\ldots,nR, \tag{3-31}$$

from the set of all possible values for $\mathbf{l}$, where nBH is the total number of boreholes associated with $\mathcal{S}(\mathbf{n})$ and nR is the sample size. The following assignments are made for each sample element $\mathbf{l}_s$:

$$pS_s = \frac{p\mathcal{S}(\mathbf{n})}{nR} \text{ and } cS_s = cS(\mathbf{l}_s, \mathbf{n}). \tag{3-32}$$

For each sample element $\mathbf{l}_s$, the integer i such that

$$cS_{i-1} < cS_s \leq cS_i \tag{3-33}$$

is determined and pS_s is accumulated in pS_i. The preceding procedure must be repeated for all nBH selected for consideration and all $\mathcal{S}(\mathbf{n})$ associated with each nBH. The number of $\mathcal{S}(\mathbf{n})$ associated with various values of nBH is shown in Table 3-2.

Fourth, once the calculations are completed for all nBH, the probabilities pS_i and the associated consequence values cS_i can be used to construct the desired CCDF. Specifically, this CCDF is given by the function

$F(x)$ = probability that cS exceeds a specific consequence value x

$$= \sum_{j=i}^{m} pS_j, \tag{3-34}$$

where i is the smallest integer such that $cS_i > x$.

An observation on computational logistics with respect to the sampling procedure in the third step is now made. The most computationally efficient approach would be to generate the sample shown in (3-31) for a large value of nBH (e.g., nBH = 15) and then use this sample for all values of nBH and associated computational scenarios in the analysis. For any specific value of nBH, only the first nBH values in each vector would be used. The advantage of this approach is that the

generation of only one sample is required. Another approach would be to generate a new sample for each computational scenario, which has the advantages that (1) the systematic biases that might result from the repeated use of the same sample would not be present and (2) a fuller coverage of the possible combinations of activity loadings would be obtained. However, as shown in Table 3-2, many thousands of samples would be required for large values of nBH. For example, 1001 samples would be required to provide a different sample for each $\mathcal{S}(\mathbf{n})$ when $nT = 5$ and $nBH = 10$. An intermediate approach would be to generate a new sample for each value of nBH and then to use this sample for all computational scenarios $\mathcal{S}(\mathbf{n})$ associated with nBH. Examples of CCDFs constructed with the techniques described in this section are given in Section 3.4.

3.4 Examples of CCDF Construction

As indicated in (3-1), the outcome of a performance assessment for the WIPP can be represented by a set $\mathcal{R}$ of ordered triples. In practice, many imprecisely known variables are required in the determination of $\mathcal{R}$. When these variables are included, the representation for $\mathcal{R}$ becomes

$$\mathcal{R}(\mathbf{x}) = \left\{\left[\mathcal{S}_i(\mathbf{x}), pS_i(\mathbf{x}), \mathbf{cS}_i(\mathbf{x})\right], \quad i = 1, \cdots, nS(\mathbf{x})\right\} \tag{3-35}$$

where the vector $\mathbf{x}$ denotes these imprecisely known variables. The 1991 WIPP performance assessment considered the 45 imprecisely known variables listed in Tables 6.01-1, 6.0-2 and 6.0-3 of Volume 3 of this report. The impact of these variables on $\mathcal{R}$ was assessed by generating a Latin hypercube sample (McKay et al., 1979) of size 60 from these variables and then evaluating $\mathcal{R}$ for each sample element $\mathbf{x}_j$. This produced the sequence of sets

$$\mathcal{R}(\mathbf{x}_j) = \left\{\left[\mathcal{S}_i(\mathbf{x}_j), pS_i(\mathbf{x}_j), \mathbf{cS}_i(\mathbf{x}_j)\right], \quad i = 1, \cdots, nS(\mathbf{x}_j)\right\} \tag{3-36}$$

for $j = 1, \cdots, 60$.

One or more CCDFs can be constructed for each set $\mathcal{R}(\mathbf{x}_j)$. In particular, Figure 3-1 shows the distribution of CCDFs for releases to the accessible environment due to groundwater transport, and Figure 3-2 shows the distribution of CCDFs for releases to the accessible environment due to cuttings removal. Further, Figure 3-3 shows the distribution of CCDFs for total release to the accessible environment (i.e., groundwater transport and cuttings removal combined). Each set $\mathcal{R}(\mathbf{x}_j)$ shown in (3-36) leads to a single CCDF in Figures 3-1, 3-2 and 3-3, although Figure 3-1

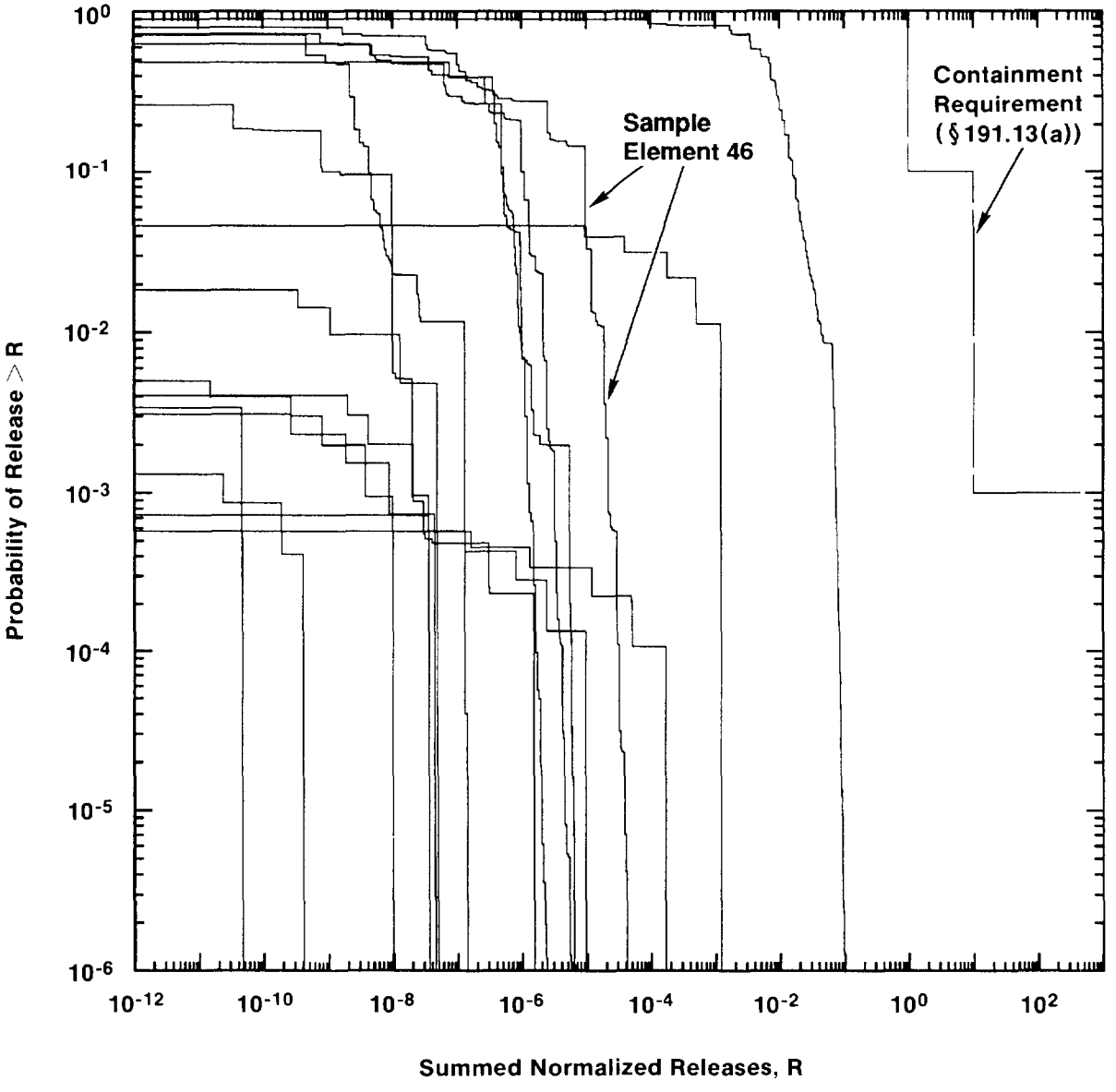

TRI-6342-1295-1

Figure 3-1. Distribution of CCDFs For Normalized Releases to the Accessible Environment Due to Groundwater Transport with a Dual Porosity Model for the Culebra Formation. Each CCDF shown in this figure results from one of the sets $\mathcal{R}(\mathbf{x}_j)$ shown in (3-36).

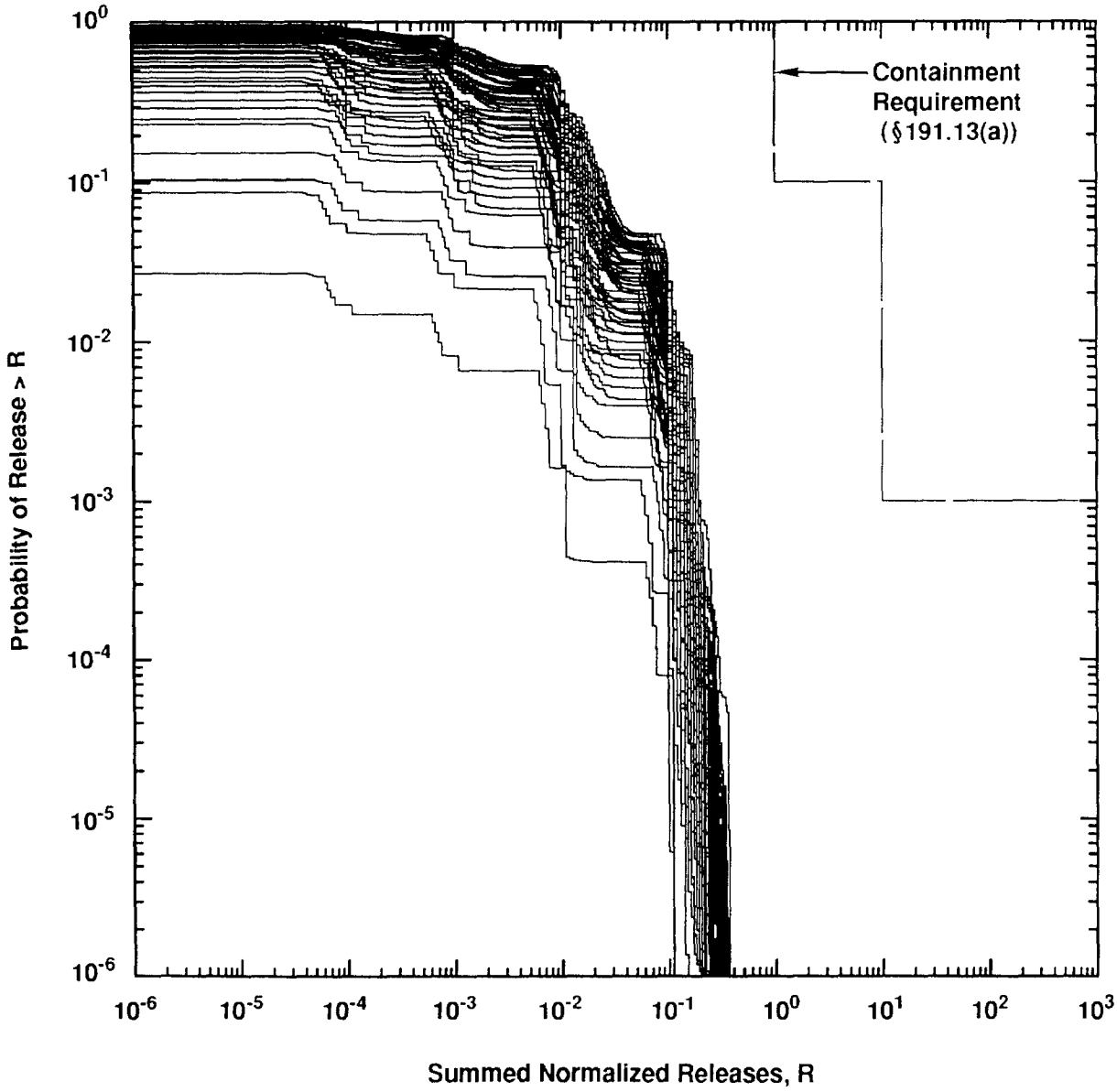

TRI-6342-1383-0

Figure 3-2. Distribution of CCDFs For Normalized Releases to the Accessible Environment Due to Cuttings Removal. Each CCDF shown in this figure results from one of the sets $\mathcal{R}(\mathbf{x}_j)$ shown in (3-36).

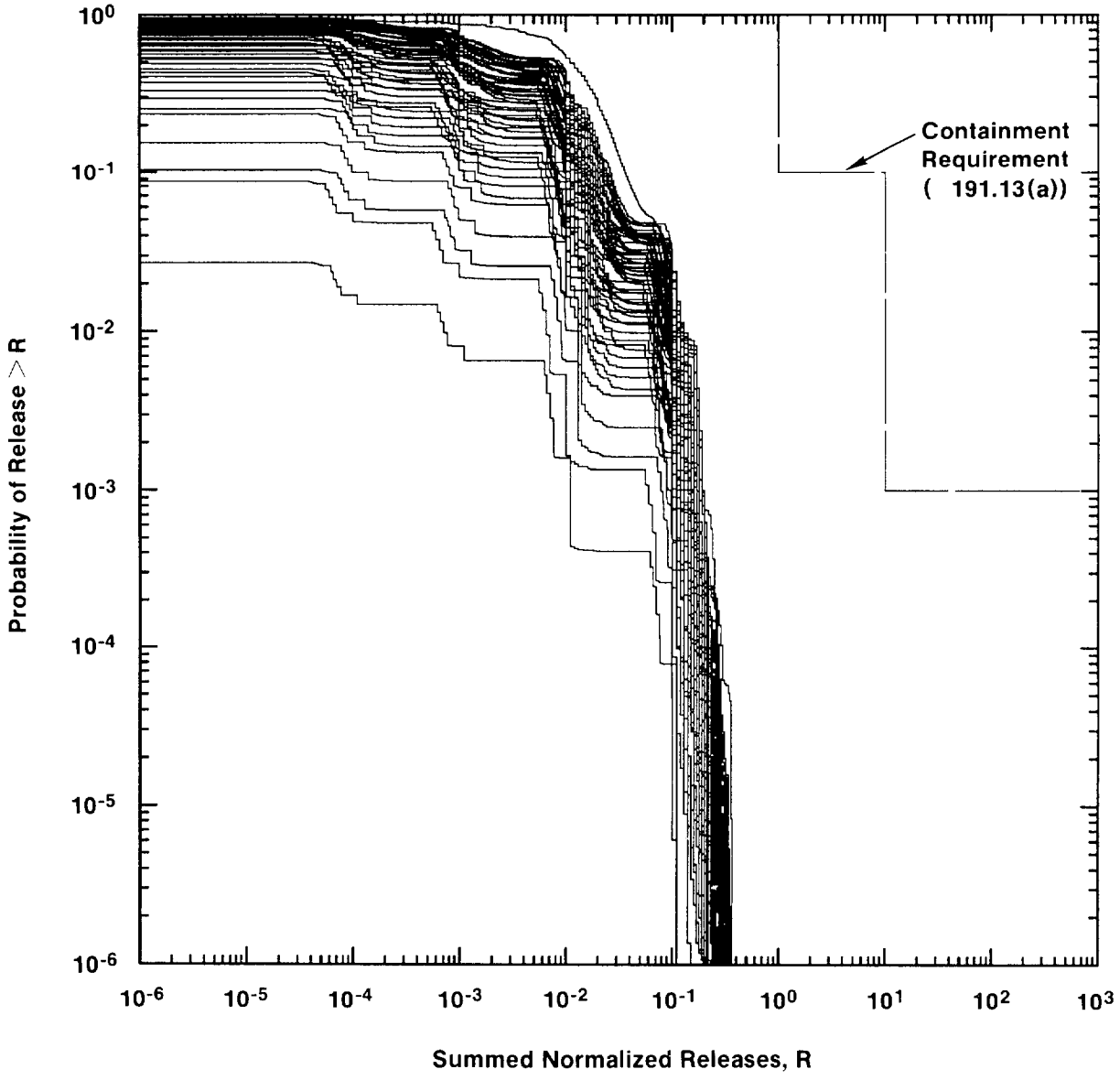

TRI-6342-1293-0

Figure 3-3. Distribution of CCDFs For Normalized Releases to the Accessible Environment Due to Both Cuttings Removal and Groundwater Transport with a Dual Porosity Model for the Culebra. Each CCDF shown in this figure results from one of the sets $\mathcal{R}(\mathbf{x}_j)$ shown in (3-36).

contains less than 60 CCDFs because some sample elements result in no groundwater releases to the accessible environment.

This section will use results associated with one of the sample elements on which Figures 3-1, 3-2 and 3-3 are based to illustrate CCDF construction. In particular, results associated with sample element $j = 46$ will be used. The variable values associated with sample element 46 are listed in Appendix B of this volume. For perspective, the CCDF for groundwater releases associated with this sample element is identified in Figure 3-1; further, sample element 46 results in one of the higher-probability CCDFs in Figure 3-2 for cuttings releases and also in Figure 3-3 for the total release due to both groundwater transport and cuttings removal.

As discussed in Section 3.2, the cuttings releases rC_i and rC_{ij} indicated in (3-4) and (3-5) and the groundwater releases $rGW1_i$ and $rGW2_i$ indicated in (3-6) and (3-7) are used to construct CCDFs for comparison with the EPA release limits. The values that resulted for these variables for sample element 46 are listed in Table 3-3.

The computational scenarios $\mathcal{S}(\mathbf{n})$ and $\mathcal{S}^{+-}(t_{k-1},t_k)$ are defined in (3-11) and (3-18), respectively. Further, probabilities for these scenarios are defined in (3-14) and (3-21), respectively, and the associated releases to the accessible environment under the assumption that all waste is of the same average activity level are defined in (3-16) and (3-23), respectively. The ratio of brine pocket area to total repository area (i.e., $aBP/aTOT$, where aBP is the area (m^2) of pressurized brine under the panels and $aTOT$ (m^2) is the total area of the panels) was a sampled variable in the 1991 WIPP performance assessment. As examination of the terms $\alpha(l)$ and $\beta(l)$ appearing in the approximations for $pS^{+-}(t_{k-1},t_k)$ in (3-20) and (3-21) shows, calculation of $pS^{+-}(t_{k-1},t_k)$ requires the ratio of brine pocket area under waste panel l to total area under waste panel l (i.e., $aBP(l)/aTOT(l)$). As only the ratio $aBP/aTOT$ is known for each sample element, the approximations

$$aBP(l)/aTOT(l) = aBP/aTOT \text{ and } aTOT(l) = aTOT/nP \tag{3-37}$$

are used in the determination of $\alpha(l)$ and $\beta(l)$, where $nP = 10$ is the number of waste panels. With the preceding approximations,

$$\alpha(l) = \lambda(aBP/aTOT)/nP,\ \beta(l) = \lambda(1 - aBP/aTOT)/nP, \tag{3-38}$$

and the representations for $pS^{+-}(t_{k-1},t_k)$ in (3-20) and (3-21) become

$$pS^{+-}(t_{k-1},t_k) \overset{\bullet}{=} \left[\left(\frac{aBP}{aTOT}\right)\left(1-\frac{aBP}{aTOT}\right)(t_k-t_{k-1})^2\lambda^2 \Big/ nP\right]\exp\left[-\lambda(t_k-t_{k-1})/nP\right] \quad (3\text{-}39)$$

and

$$pS^{+-}(t_{k-1},t_k) \overset{\bullet}{=} nP\left\{1-\exp\left[-\lambda\frac{aBP}{aTOT}(t_k-t_{k-1})\Big/nP\right]\right\}$$

$$\bullet\left\{1-\exp\left[-\lambda\left(1-\frac{aBP}{aTOT}\right)(t_k-t_{k-1})\Big/nP\right]\right\}, \quad (3\text{-}40)$$

respectively. It is the form of (3-21) given in (3-40) that was actually used in the construction of CCDFs in the 1991 WIPP performance assessment.

The results of the indicated probability and release calculations are illustrated in Table 3-4 for sample element 46. Examples of the computational scenarios $\mathcal{S}(\mathbf{n})$ appear in the first column of Table 3-4 as $\mathcal{S}(0,0,0,0,0), \mathcal{S}(1,0,0,0,0), \cdots, \mathcal{S}(1,0,0,0,15)$. As a reminder, five time intervals are being used, and so the vector $\mathbf{n}$ has five elements (i.e., $\mathbf{n} = (0,0,0,0,0),(1,0,0,0,0),\cdots,(0,0,0,0,15)$ in Table 3-4). The scenarios $\mathcal{S}^{+-}(t_{k-1},t_k)$ appear as the last five entries in the first column (i.e., $\mathcal{S}^{+-}(0,2000),\cdots,\mathcal{S}^{+-}(8000,10000)$). The remaining columns present the probabilities and normalized releases for the individual scenarios. Probabilities are presented with and without a 100 year period of administrative control in which drilling intrusions cannot take place. As comparison of the two probability columns shows, assumption of a 100 year period of administrative control has little effect on the scenario probabilities.

The computational scenarios $\mathcal{S}(\mathbf{I},\mathbf{n})$ and $\mathcal{S}^{+-}(\mathbf{I};t_{k-1},t_k)$ incorporating activity loading effects for the cuttings releases are defined in (3-12) and (3-19), respectively. Further, probabilities for these scenarios are defined in (3-15) and (3-22), respectively, and the associated releases to the accessible environment are defined in (3-17) and (3-24), respectively. The results of the indicated probability and release calculations are illustrated for $\mathcal{S}(\mathbf{I},\mathbf{n})$ in Table 3-5 for sample element 46. The calculations for $\mathcal{S}^{+-}(\mathbf{I};t_{k-1},t_k)$ are similar and are not shown.

The CCDFs appearing in the 1991 WIPP performance assessment are constructed from computational scenarios with probabilities and normalized releases of the form shown in Tables 3-4 and 3-5. When only groundwater releases are under consideration, it is possible to systematically incorporate all the computational scenarios indicated in Table 3-4 into a CCDF.

Table 3-3. Normalized Radionuclide Releases Used to Illustrate Scenario Construction Procedures. The releases presented in this table were calculated for sample element 46 in the 1991 WIPP performance assessment (see Appendix B, Vol. 2).

Time[a]	$rGW1_i$[b]	$rGW2_i$[c]	rC_i[d]	rC_{i1}[e]	rC_{i2}[e]	rC_{i3}[e]	rC_{i4}[e]	rC_{i5}[e]
1	9.92E-06	1.48E-05	7.39E-03	1.71E-04	1.71E-03	1.71E-02	1.71E-01	6.96E-03
2	2.51E-06	5.08E-06	5.01E-03	1.16E-04	1.16E-03	1.16E-02	1.16E-01	4.72E-03
3	3.61E-07	1.34E-06	4.60E-03	1.06E-04	1.06E-03	1.06E-02	1.06E-01	4.33E-03
4	7.72E-08	3.16E-07	4.29E-03	9.92E-05	9.92E-04	9.92E-03	9.92E-02	4.04E-03
5	0.00E+00	5.08E-08	4.02E-03	9.28E-05	9.28E-04	9.28E-03	9.28E-02	3.78E-03

a Time at which intrusion occurs, where 1~1000 yr, 2~3000 yr, 3~5000 yr, 4~7000 yr, 5~9000 yr.

b EPA normalized release (dimensionless) to the accessible environment for groundwater transport (with a dual porosity model in the Culebra Formation) initiated by a single borehole in time interval i.

c EPA normalized release (dimensionless) to the accessible environment for groundwater transport (with a dual porosity model in the Culebra Formation) initiated by two boreholes in the same waste panel in time interval i, of which one penetrates a pressurized brine pocket and one does not (i.e., an E1E2-type scenario).

d EPA normalized release (dimensionless) to the surface environment for cuttings removal due to a single borehole in time interval i with the assumption that the waste is homogeneous (i.e., waste of different activity levels is not present). Calculation of the rC_i used the average activity level shown in Table 2-7.

e EPA normalized release (dimensionless) to the surface environment for cuttings removal due to a single borehole in time interval i that penetrates waste of activity level j. Calculation of the rC_{ij} used the activity levels corresponding to j=1,2,3,4,5 shown in Table 2-7.

Table 3-4. Probabilities and Normalized Releases for Computational Scenarios Used to Illustrate Scenario Construction Procedures without the Inclusion of Activity Loading Effects on the Cuttings Releases. The probabilities presented in this table were calculated for sample element 46 in the 1991 WIPP performance assessment (see Appendix B, Vol. 2), which resulted in the rate constant in the Poisson model for drilling (i.e., λ) equaling 8.4424E-05 yr^{-1} and the area ratio for the pressurized brine pocket (i.e., aBP/aTOT) equaling 0.44981; the normalized releases were constructed from the values shown for $rGW1_i$, $rGW2_i$, and rC_i in Table 3-3.

a Computational Scenario	b Probability w/o Control	c Probability w Control	d Cuttings Release	e Groundwater Release	f Total Release
$\mathcal{S}(0,0,0,0,0)$	0.429886	0.433530	0.000E+00	0.000E+00	0.000E+00
$\mathcal{S}(1,0,0,0,0)$	0.072585	0.069540	6.961E-03	9.922E-06	6.971E-03
$\mathcal{S}(0,1,0,0,0)$	0.072585	0.073200	4.716E-03	2.507E-06	4.719E-03
$\mathcal{S}(0,0,1,0,0)$	0.072585	0.073200	4.329E-03	3.610E-07	4.329E-03
$\mathcal{S}(0,0,0,1,0)$	0.072585	0.073200	4.042E-03	7.724E-08	4.042E-03
$\mathcal{S}(0,0,0,0,1)$	0.072585	0.073200	3.784E-03	0.000E+00	3.784E-03
$\mathcal{S}(2,0,0,0,0)$	0.006128	0.005577	1.392E-02	1.984E-05	1.394E-02
$\mathcal{S}(1,1,0,0,0)$	0.012256	0.011742	1.168E-02	1.243E-05	1.169E-02
$\mathcal{S}(1,0,1,0,0)$	0.012256	0.011742	1.129E-02	1.028E-05	1.130E-02
$\mathcal{S}(1,0,0,1,0)$	0.012256	0.011742	1.100E-02	1.000E-05	1.101E-02
$\mathcal{S}(1,0,0,0,1)$	0.012256	0.011742	1.074E-02	9.922E-06	1.075E-02
$\mathcal{S}(0,2,0,0,0)$	0.006128	0.006180	9.433E-03	5.013E-06	9.438E-03
$\mathcal{S}((0,1,1,0,0)$	0.012256	0.012360	9.045E-03	2.868E-06	9.048E-03
$\mathcal{S}(0,1,0,1,0)$	0.012256	0.012360	8.759E-03	2.584E-06	8.761E-03
$\mathcal{S}(0,1,0,0,1)$	0.012256	0.012360	8.500E-03	2.507E-06	8.503E-03
$\mathcal{S}(0,0,2,0,0)$	0.006128	0.006180	8.657E-03	7.220E-07	8.658E-03
$\mathcal{S}(0,0,1,1,0)$	0.012256	0.012360	8.371E-03	4.382E-07	8.371E-03
$\mathcal{S}(0,0,1,0,1)$	0.012256	0.012360	8.112E-03	3.610E-07	8.113E-03
$\mathcal{S}(0,0,0,2,0)$	0.006128	0.006180	8.085E-03	1.545E-07	8.085E-03
$\mathcal{S}(0,0,0,1,1)$	0.012256	0.012360	7.826E-03	7.724E-08	7.826E-03
$\mathcal{S}(0,0,0,0,2)$	0.006128	0.006180	7.568E-03	0.000E+00	7.568E-03
$\mathcal{S}(3,0,0,0,0)$	0.000345	0.000298	2.088E-02	2.977E-05	2.091E-02
$\mathcal{S}(2,1,0,0,0)$	0.001035	0.000942	1.864E-02	2.235E-05	1.866E-02
$\mathcal{S}(2,0,1,0,0)$	0.001035	0.000942	1.825E-02	2.021E-05	1.827E-02
$\mathcal{S}(2,0,0,1,0)$	0.001035	0.000942	1.796E-02	1.992E-05	1.798E-02
$\mathcal{S}(2,0,0,0,1)$	0.001035	0.000942	1.771E-02	1.984E-05	1.773E-02
$\mathcal{S}(1,2,0,0,0)$	0.001035	0.000991	1.639E-02	1.494E-05	1.641E-02
$\mathcal{S}(1,1,1,0,0)$	0.002069	0.001983	1.601E-02	1.279E-05	1.602E-02
$\mathcal{S}(1,1,0,1,0)$	0.002069	0.001983	1.572E-02	1.251E-05	1.573E-02

Table 3-4 (Continued).

a Computational Scenario	b Probability w/o Control	c Probability w Control	d Cuttings Release	e Groundwater Release	f Total Release
$\mathcal{S}(1,1,0,0,1)$	0.002069	0.001983	1.546E-02	1.243E-05	1.547E-02
$\mathcal{S}(1,0,2,0,0)$	0.001035	0.000991	1.562E-02	1.064E-05	1.563E-02
$\mathcal{S}(1,0,1,1,0)$	0.002069	0.001983	1.533E-02	1.036E-05	1.534E-02
$\mathcal{S}(1,0,1,0,1)$	0.002069	0.001983	1.507E-02	1.028E-05	1.508E-02
$\mathcal{S}(1,0,0,2,0)$	0.001035	0.000991	1.505E-02	1.008E-05	1.506E-02
$\mathcal{S}(1,0,0,1,1)$	0.002069	0.001983	1.479E-02	1.000E-05	1.480E-02
$\mathcal{S}(1,0,0,0,2)$	0.001035	0.000991	1.453E-02	9.922E-06	1.454E-02
$\mathcal{S}(0,3,0,0,0)$	0.000345	0.000348	1.415E-02	7.520E-06	1.416E-02
$\mathcal{S}(0,2,1,0,0)$	0.001035	0.001043	1.376E-02	5.374E-06	1.377E-02
$\mathcal{S}(0,2,0,1,0)$	0.001035	0.001043	1.347E-02	5.091E-06	1.348E-02
$\mathcal{S}(0,2,0,0,1)$	0.001035	0.001043	1.322E-02	5.013E-06	1.322E-02
$\mathcal{S}(0,1,2,0,0)$	0.001035	0.001043	1.337E-02	3.229E-06	1.338E-02
$\mathcal{S}(0,1,1,1,0)$	0.002069	0.002087	1.309E-02	2.945E-06	1.309E-02
$\mathcal{S}(0,1,1,0,1)$	0.002069	0.002087	1.283E-02	2.868E-06	1.283E-02
$\mathcal{S}(0,1,0,2,0)$	0.001035	0.001043	1.280E-02	2.661E-06	1.280E-02
$\mathcal{S}(0,1,0,1,1)$	0.002069	0.002087	1.254E-02	2.584E-06	1.255E-02
$\mathcal{S}(0,1,0,0,2)$	0.001035	0.001043	1.228E-02	2.507E-06	1.229E-02
$\mathcal{S}(0,0,3,0,0)$	0.000345	0.000348	1.299E-02	1.083E-06	1.299E-02
$\mathcal{S}(0,0,2,1,0)$	0.001035	0.001043	1.270E-02	7.992E-07	1.270E-02
$\mathcal{S}(0,0,2,0,1)$	0.001035	0.001043	1.244E-02	7.220E-07	1.244E-02
$\mathcal{S}(0,0,1,2,0)$	0.001035	0.001043	1.241E-02	5.155E-07	1.241E-02
$\mathcal{S}(0,0,1,1,1)$	0.002069	0.002087	1.215E-02	4.382E-07	1.216E-02
$\mathcal{S}(0,0,1,0,2)$	0.001035	0.001043	1.190E-02	3.610E-07	1.190E-02
$\mathcal{S}(0,0,0,3,0)$	0.000345	0.000348	1.213E-02	2.317E-07	1.213E-02
$\mathcal{S}(0,0,0,2,1)$	0.001035	0.001043	1.187E-02	1.545E-07	1.187E-02
$\mathcal{S}(0,0,0,1,2)$	0.001035	0.001043	1.161E-02	7.724E-08	1.161E-02
$\mathcal{S}(0,0,0,0,3)$	0.000345	0.000348	1.135E-02	0.000E+00	1.135E-02
$\mathcal{S}(4,0,0,0,0)$	0.000015	0.000012	2.784E-02	3.969E-05	2.788E-02
$\mathcal{S}(3,1,0,0,0)$	0.000058	0.000050	2.560E-02	3.227E-05	2.563E-02
.					
.					
.					
$\mathcal{S}(1,1,1,1,0)$	0.000349	0.000335	2.005E-02	1.287E-05	2.006E-02
.					
.					
.					
$\mathcal{S}(0,0,0,0,4)$	0.000015	0.000015	1.514E-02	0.000E+00	1.514E-02
.					
.					
.					
$\mathcal{S}(0,0,0,0,15)$	8.497E-25	8.569E-25	5.676E-02	0.000E+00	5.676E-02

Table 3-4 (Concluded).

Computational Scenario [a]	Probability w/o Control [b]	Probability w Control [c]	Cuttings Release [d]	Groundwater Release [e]	Total Release [f]
$\mathcal{S}^{+-}(0, 2000)$	0.000700	0.000632	1.392E-02	1.480E-05	1.394E-02
$\mathcal{S}^{+-}(2000, 4000)$	0.000700	0.000700	9.433E-03	5.082E-06	9.438E-03
$\mathcal{S}^{+-}(4000, 6000)$	0.000700	0.000700	8.657E-03	1.342E-06	8.659E-03
$\mathcal{S}^{+-}(6000, 8000)$	0.000700	0.000700	8.085E-03	3.162E-07	8.085E-03
$\mathcal{S}^{+-}(8000,10000)$	0.000700	0.000700	7.568E-03	5.080E-08	7.568E-03

a $\mathcal{S}(\mathbf{n})$ and $\mathcal{S}^{+-}(t_{k-1},t_k)$ are defined in (3-11) and (3-18), respectively.

b Probabilities for $\mathcal{S}(\mathbf{n})$ (defined in 3-14)) and $\mathcal{S}^{+-}(t_{k-1},t_k)$ (defined in (3-21) and (3-40)), without a 100 yr period of administrative control in which drilling intrusions cannot take place.

c Same as b but with a 100 yr period of administrative control in which drilling intrusions cannot take place.

d Cuttings releases for $\mathcal{S}(\mathbf{n})$ and $\mathcal{S}^{+-}(t_{k-1},t_k)$ are defined in (3-16) and (3-23), respectively, with the groundwater component of the release set to zero.

e Groundwater releases for $\mathcal{S}(\mathbf{n})$ and $\mathcal{S}^{+-}(t_{k-1},t_k)$ are defined in (3-16) and (3-23), respectively, with the cuttings component of the release set to zero.

f Total releases for $\mathcal{S}(\mathbf{n})$ and $\mathcal{S}^{+-}(t_{k-1},t_k)$ are defined in (3-16) and (3-23), respectively.

Table 3-5. Probabilities and Normalized Releases for Computational Scenarios Used to Illustrate Scenario Construction Procedures with the Inclusion of Activity Loading Effects on the Cuttings Releases. The probabilities presented in this table were calculated for observation number 46 in the 1991 WIPP performance assessment (see Appendix B, Vol. 2), which resulted in the rate constant in the Poisson model for drilling (i.e., λ) equaling 8.4424E-05 yr^{-1}, and the activity loading distribution given in Table 2-7; the normalized releases were constructed from the values shown for $rGW1_i$ and rC_{ij} in Table 3-3.

a	b	c	d	e	f
Computational Scenario	Probability w/o Control	Probability w Control	Cuttings Release	Groundwater Release	Total Release
$\mathcal{S}$(0,0,0,0,0)	0.429886	0.433530	0.000E+00	0.000E+00	0.000E+00
$\mathcal{S}$(I;1,0,0,0,0)					
I=(1)	0.029201	0.027976	1.708E-04	9.922E-06	1.807E-04
I=(2)	0.021761	0.020848	1.708E-03	9.922E-06	1.718E-03
I=(3)	0.016274	0.015591	1.708E-02	9.922E-06	1.709E-02
I=(4)	0.001082	0.001036	1.708E-01	9.922E-06	1.708E-01
I=(5)	0.004268	0.004089	9.712E-05	9.922E-06	1.070E-04
	---	---			
	0.072585	0.069540			
$\mathcal{S}$(I;0,1,0,0,0)					
I=(1)	0.029201	0.029449	1.157E-04	2.507E-06	1.182E-04
I=(2)	0.021761	0.021945	1.157E-03	2.507E-06	1.160E-03
I=(3)	0.016274	0.016412	1.157E-02	2.507E-06	1.157E-02
I=(4)	0.001082	0.001091	1.157E-01	2.507E-06	1.157E-01
I=(5)	0.004268	0.004304	7.615E-05	2.507E-06	7.865E-05
	---	---			
	0.072585	0.073200			
$\mathcal{S}$(I;0,0,1,0,0)					
.					
.					
.					
$\mathcal{S}$(I;0,0,0,1,0)					
.					
.					
.					
$\mathcal{S}$(I;0,0,0,0,1)					
.					
.					
.					
$\mathcal{S}$(I;2,0,0,0,0)					
I=(1,1)	0.000992	0.000903	3.416E-04	1.984E-05	3.615E-04
I=(1,2)	0.000739	0.000673	1.879E-03	1.984E-05	1.899E-03
I=(1,3)	0.000553	0.000503	1.725E-02	1.984E-05	1.727E-02
I=(1,4)	0.000037	0.000033	1.710E-01	1.984E-05	1.710E-01
I=(1,5)	0.000145	0.000132	2.679E-04	1.984E-05	2.878E-04
I=(2,1)	0.000739	0.000673	1.879E-03	1.984E-05	1.899E-03
I=(2,2)	0.000551	0.000501	3.416E-03	1.984E-05	3.436E-03

Table 3-5 (Continued)

a Computational Scenario	b Probability w/o Control	c Probability w Control	d Cuttings Release	e Groundwater Release	f Total Release
.					
.					
.					
I=(5,5)	0.000021	0.000019	1.942E-04	1.984E-05	2.141E-04
	---	---			
	0.006128	0.005577			
$\mathcal{S}$(I;1,1,0,0,0)					
I=(1,1)	0.001984	0.001900	2.865E-04	1.243E-05	2.989E-04
I=(1,2)	0.001478	0.001416	1.328E-03	1.243E-05	1.340E-03
I=(1,3)	0.001105	0.001059	1.174E-02	1.243E-05	1.175E-02
I=(1,4)	0.000073	0.000070	1.159E-01	1.243E-05	1.159E-01
I=(1,5)	0.000290	0.000278	2.470E-04	1.243E-05	2.594E-04
I=(2,1)	0.001478	0.001416	1.824E-03	1.243E-05	1.836E-03
I=(2,2)	0.001102	0.001055	2.865E-03	1.243E-05	2.878E-03
.					
.					
.					
I=(5,5)	0.000042	0.000041	1.733E-04	1.243E-05	1.857E-04
	---	---			
	0.012256	0.011742			
$\mathcal{S}$(I;1,0,1,0,0)					
.					
.					
.					
$\mathcal{S}$(I;0,0,0,0,2)					
.					
.					
.					
$\mathcal{S}$(I;3,0,0,0,0)					
I=(1,1,1)	0.000022	0.000019	5.124E-04	2.977E-05	5.422E-04
I=(1,1,2)	0.000017	0.000014	2.050E-03	2.977E-05	2.079E-03
I=(1,1,3)	0.000013	0.000011	1.742E-02	2.977E-05	1.745E-02
.					
.					
.					
I=(2,3,5)	0.000001	0.000001	1.889E-02	2.977E-05	1.892E-02
.					
.					
.					
I=(5,5,5)	0.000000	0.000000	2.914E-04	2.977E-05	3.211E-04
	---	---			
	0.000345	0.000298			
$\mathcal{S}$(I;2,1,0,0,0)					
.					
.					
.					
$\mathcal{S}$(I;0,0,0,0,3)					

Table 3-5 (Concluded)

a Computational Scenario	b Probability w/o Control	c Probability w Control	d Cuttings Release	e Groundwater Release	f Total Release
.					
.					
.					
$S(\mathbf{I};4,0,0,0,0)$					
.					
.					
.					

a $S(\mathbf{I},\mathbf{n})$ is defined in (3-12).

b Probability for $S(\mathbf{I},\mathbf{n})$ as defined in (3-15) without a 100 yr period of administrative control in which drilling intrusions cannot take place.

c Same as b but with a 100 yr period of administrative control in which drilling intrusions cannot take place.

d Cuttings release for $S(\mathbf{I},\mathbf{n})$ from (3-17) with the groundwater component of the release set to zero.

e Groundwater release for $S(\mathbf{I},\mathbf{n})$ from (3-17) with the cuttings component of the release set to zero.

f Total release for $S(\mathbf{I},\mathbf{n})$ from (3-17).

The result of this calculation is shown in Figure 3-4. Specifically, the CCDF labeled "Groundwater" in Figure 3-4 was constructed from the probabilities and releases in the columns "Probability w Control" and "Groundwater Release" in Table 3-4. This is also the CCDF identified in Figure 3-1 as resulting from sample element 46. Similarly, when activity loading effects on the cuttings releases are not considered (i.e., all waste is assumed to be of the same average activity level), it is possible to systematically incorporate all the computational scenarios indicated in Table 3-4 into a CCDF for cuttings release and also into a CCDF for total release (i.e., cuttings release and groundwater release combined). The CCDF labeled "Cuttings without Activity Loading" in Figure 3-4 was constructed from the probabilities and releases in the columns "Probability w Control" and "Cuttings Release" in Table 3-4. Due to the small releases for groundwater transport, the CCDF constructed with the releases in the column "Total Release" is identical in appearance to the "Cuttings without Activity Loading" CCDF in Figure 3-4.

When activity loading effects for the cuttings releases are considered, it is necessary to use results of the form shown in Table 3-5. Due to the large number of computational scenarios that result from the many possible combinations of cuttings releases, it is not possible to systematically cover all scenarios of the form listed in Table 3-5. Rather, as described in Section 3.3, these computational scenarios are covered systematically up to a certain number of intrusions and then a switch is made to a Monte Carlo procedure. For the 1991 WIPP performance assessment, computational scenarios of the form shown in Table 3-5 were systematically covered up to $nB = 4$ boreholes; then, a switch was made to a Monte Carlo procedure that used a Latin hypercube sample of size $nR = 100$ for each computational scenario involving more than $nB = 4$ boreholes. The results of this calculation for cuttings release is shown in Figure 3-4. Specifically, the CCDF labeled "Cuttings with Activity Loading" in Figure 3-4 was constructed from the probabilities and releases in the columns "Probability w Control" and "Cuttings Release" in Table 3-5. This is also the CCDF for sample element 46 in Figure 3-2, although its exact identification is difficult due to the large number of closely placed CCDFs in this figure.

Activity loading effects can also be incorporated into the CCDF for total release. This involves use of the results in the column "Total Release" in Table 3-5 together with similar results for computational scenarios of the form $\mathcal{S}^{+-}(\mathbf{I}; t_{k-1}, t_k)$. Due to the small groundwater releases associated with sample element 46, this results in a CCDF for total release that is identical in appearance to the CCDF labeled "Cuttings with Activity Loading" in Figure 3-4. The CCDF that results from this construction procedure for sample 46 also appears in Figure 3-3, but is difficult to identify.

The CCDFs appearing in Figures 3-1 through 3-4 were constructed with the program CCDFPERM, which is part of the CAMCON system. Probabilities and normalized releases for computational scenarios are determined by CCDFPERM with the procedures illustrated in this section. To reduce storage requirements, CCDFPERM uses a binning algorithm of the type indicated in conjunction with (3-28) to accumulate the probabilities associated with individual computational scenarios. For the 1991 WIPP performance assessment, the binning algorithm used 100 increments per order of magnitude on the release axis. To reduce unnecessary calculations, CCDFPERM provides a mechanism to stop the CCDF construction procedure. Specifically, CCDFPERM determines the smallest integer n such that the probability of having exactly n boreholes over 10,000 years is less than B, where B is a user-specified quantity. Then, CCDFPERM only uses computational scenarios that involve less than or equal to n boreholes. For the 1991 WIPP performance assessment, B was specified to be 1×10^{-6}, which resulted in the omitted scenario probability being far below the 0.001 point used in defining the EPA release limits. Since the λ in the Poisson model was a sampled variable in the 1991 WIPP performance

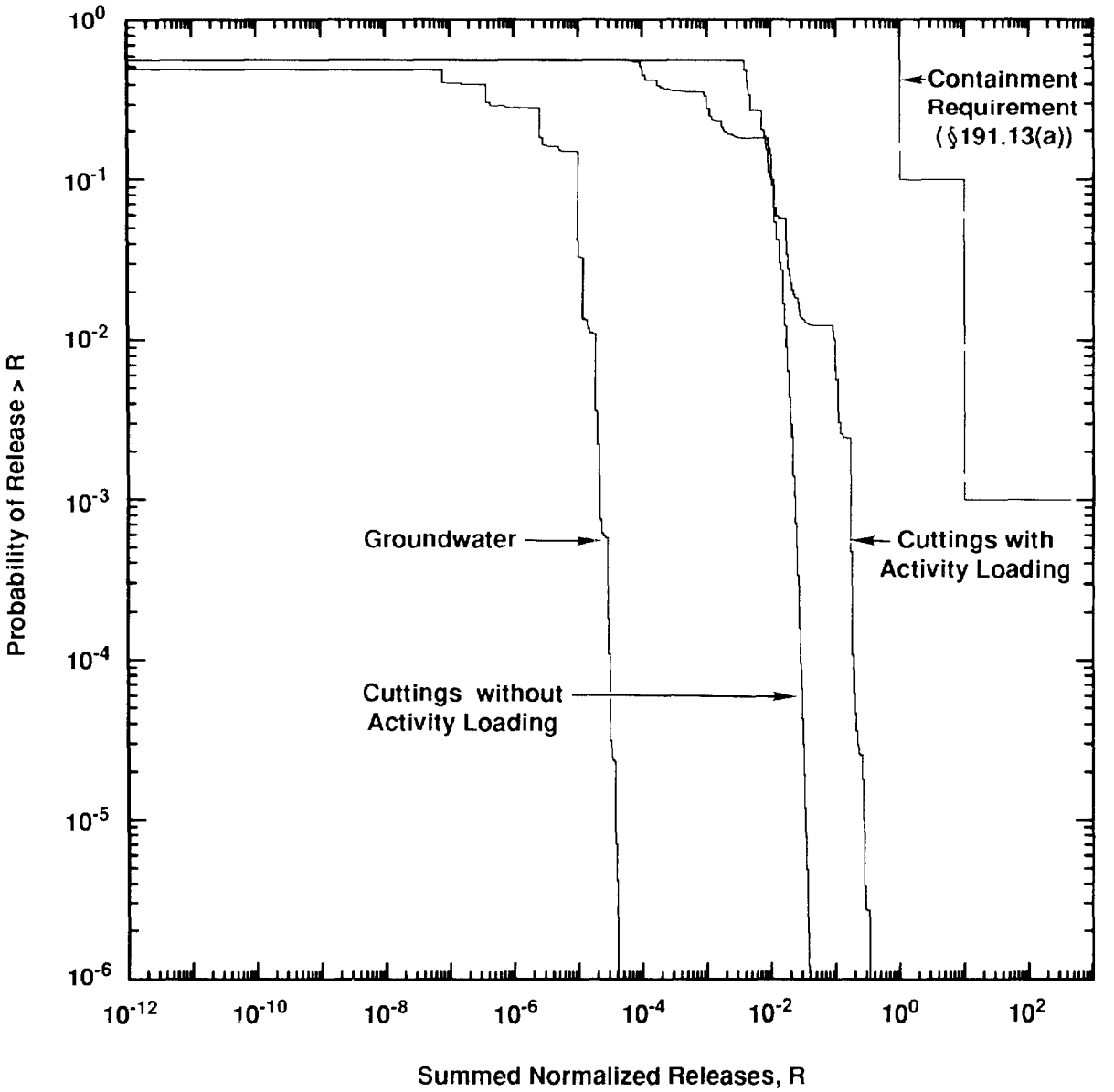

TRI-6342-1382-0

Figure 3-4. Estimated CCDFs for Sample Element 46.

assessment, the maximum number of boreholes used in CCDF construction varied from sample element to sample element.

There is actually some overlap (i.e., intersection) between the computational scenarios $S(\mathbf{n})$ and $S^{+-}(t_{k-1},t_k)$. That is, no correction has been made for the fact that some time histories in computational scenarios of the form $S(\mathbf{n})$ also belong to computational scenarios of the form $S^{+-}(t_{k-1},t_k)$. Further, as indicated in conjunction with (2-68), probabilities for the $S^{+-}(t_{k-1},t_k)$ are approximated with conservative relationships that actually bound the probabilities. As the probabilities for the scenarios $S(\mathbf{n})$ sum to 1, the total estimated probabilities for the computational scenarios $S(\mathbf{n})$ and $S^{+-}(t_{k-1},t_k)$ will be somewhat greater than 1. For example, the total probability for the computational scenarios indicated in Table 3-4 is 1.003432 when 100 years of administrative control is assumed. If desired, the probabilities for the individual computational scenarios could be defined with greater resolution, but the resultant relationship would be very complicated (e.g., see (2-67)). At present, the added complexity that these refined probabilities would require is not justified. Specifically, they would produce few visually identifiable shifts in the CCDFs shown in Figures 3-1 through 3-4, and the effects that they did produce would tend to shift the CCDFs downward. However, as a low-level correction, CCDFPERM does normalize the probabilities for computational scenarios involving two or more boreholes so that total computational scenario probability sums to 1.

The probability normalization performed by CCDFPERM is based on the ratio

$$R = \frac{\sum_{k=1}^{nT} pS^{+-}(t_{k-1},t_k)}{\sum_{\mathbf{n}\in\mathcal{A}} pS(\mathbf{n})}, \tag{3-41}$$

where $\mathbf{n}\in\mathcal{A}$ only if $\mathbf{n}$ has an element greater than or equal to 2 (i.e., if $S(\mathbf{n})$ designates a set of time histories in which two or more drilling intrusions can occur in the same time interval). Thus, R is the ratio between the estimated probability for all E1E2-type computational scenarios and the probability for all computational scenarios $S(\mathbf{n})$ that could contain an E1E2-type intrusion.

Once R is determined, CCDFPERM systematically goes through all computational scenarios $S(\mathbf{l},\mathbf{n})$ selected for consideration. For each $S(\mathbf{l},\mathbf{n})$, the probability $pS(\mathbf{l},\mathbf{n})$ and release $cS(\mathbf{l},\mathbf{n})$ are determined as shown in (3-15) and (3-17), respectively. If $\mathbf{n}\notin\mathcal{A}$, no modification to $pS(\mathbf{l},\mathbf{n})$ is made. If $\mathbf{n}\in\mathcal{A}$, then the probability $pS(\mathbf{l},\mathbf{n})$ is redefined to be (1-R) $pS(\mathbf{l},\mathbf{n})$. Further, $S^{+-}(\mathbf{l},\mathbf{n})$ is assigned the probability

$$pS^{+-}(\mathbf{l},\mathbf{n}) = R\, pS(\mathbf{l},\mathbf{n}), \tag{3-42}$$

where $pS(\mathbf{l},\mathbf{n})$ is the initial probability for $S(\mathbf{l},\mathbf{n})$ defined in (3-15) and

$$S^{+-}(\mathbf{l},\mathbf{n}) = \{x: x \text{ an element of } S(\mathbf{l},\mathbf{n}) \text{ in which at least one waste panel is penetrated by two or more boreholes during a time interval } [t_{i-1},t_i], \text{ of which at least one penetrates a pressurized brine pocket and at least one does not}\}. \tag{3-43}$$

The set $S^{+-}(\mathbf{l},\mathbf{n})$ is assigned the normalized release $S^{+-}(\mathbf{l};t_{k-1},t_k)$ in (3-24), where k is the smallest integer such that $S^{+-}(\mathbf{l},\mathbf{n}) \subset S^{+-}(\mathbf{l};t_{k-1},t_k)$. As $pS(\mathbf{l},\mathbf{n})$, $cS(\mathbf{l},\mathbf{n})$, $pS^{+-}(\mathbf{l},\mathbf{n})$ and $cS^{+-}(\mathbf{l},\mathbf{n})$ are determined, the probabilities $pS(\mathbf{l},\mathbf{n})$ and $pS^{+-}(\mathbf{l},\mathbf{n})$ are accumulated within the binning algorithm used in CCDFPERM.

The outcome of the preceding normalization procedure is that (1) probabilities for computational scenarios $S(\mathbf{l},\mathbf{n})$ that do not contain time histories also contained in a set $S^{+-}(\mathbf{l};t_{k-1},t_k)$ are unchanged, (2) probabilities for computational scenarios $S(\mathbf{l},\mathbf{n})$ that do contain time histories also contained in a set $S^{+-}(\mathbf{l};t_{k-1},t_k)$ are scaled down by a factor of $1-R$, (3) total probability for the computational scenarios $S^{+-}(\mathbf{l};t_{k-1},t_k)$ is unchanged, and (4) total probability for all computational scenarios sums to 1. Other normalizations are also possible. For example, a normalization could be used that also produces a downward scaling in the probabilities for $S^{+-}(\mathbf{l};t_{k-1},t_k)$, which are known to be overestimates. However, no "reasonable" normalization would have had a significant impact on the CCDFs produced for the 1991 WIPP performance assessment.

4. UNDISTURBED PERFORMANCE OF REPOSITORY/SHAFT

4.1 Conceptual Model

The overall hypothesized sequence of events in the disposal area for undisturbed conditions is summarized in the scenario discussion in Chapter 4 of Volume 1 and is repeated in more detail in Chapter 5 of Volume 1. The reader is encouraged to refer to the figures and the discussion in Volume 1 when reading about the models discussed in the remainder of Volume 2.

Generally, the repository/shaft system models for the undisturbed case consist of at most six components (or features): (1) a room or disposal region, (2) a panel and drift seal, (3) drift backfill, (4) shaft backfill and seal, (5) Salado Formation salt, and (6) anhydrite interbeds (MB139 and layers a and b, which are combined). These features comprise both the natural and engineered barriers to migration from waste panels during undisturbed conditions.

Groundwater flow and radionuclide migration are driven by gas generation in the waste disposal panels. Creep closure of the repository can also affect brine flow; however, the dynamics of this effect are not currently modeled. Two pathways for groundwater flow and radionuclide transport will likely dominate the disposal system (Figure 4-6 in Volume 1). In both, radionuclides enter MB139, either through fractures in salt or directly as a result of rooms and drifts intersecting the marker bed during construction or room closure. The head gradient tends to force radionuclide-bearing brine into MB139 beneath the panel, along the fractures in MB139 to the base of the shaft. Radionuclides may then move up the shaft to the Culebra dolomite member, and downgradient in the Culebra to the accessible environment. The second conceivable pathway is along MB139 to the subsurface extension of the accessible environment (5 km boundary) from the waste-disposal area (Figure 4-6 in Volume 1).

For the undisturbed scenario type, four primary generic computational models were used to assess the response of the repository/shaft system to this base case: BOAST II, a three-dimensional, multiphase code for isothermal Darcy flow; PANEL, an analytical model that estimates the discharge of radionuclides from a repository panel breached by a borehole; SUTRA, a two-dimensional, saturated or unsaturated, coupled flow and transport code; and STAFF2D, a two-dimensional, single-phase, flow or transport code.

The simulations described examine the importance of the principal migration pathways for radionuclides to reach the accessible environment during the undisturbed scenario. The hypothesized migration paths assume that under undisturbed conditions brine with dissolved radionuclides is expelled from the storage rooms by gas generated from anoxic corrosion of the containers and microbiological degradation of the waste. Because the computer codes SUTRA and STAFF2D model single-phase-flow instead of two-phase flow, liquid (brine) replaces gas in these simulations and the pores of the waste are assumed to be completely filled with liquid. An effect

of substituting a liquid source for the gas drive is that the liquid tends to leave the storage area in all directions, while gas-driven brine would be expected to leave the repository mainly through the floor (because the waste-generated gas rises to the top of the waste panels). To account for the presence of undissolved gas in an approximate sense using the single-phase codes SUTRA and STAFF2D, the material properties (permeability and porosity) can be modified to reflect the changes that occur as the result of varying gas saturation. These changes, in terms of brine (or gas) saturation, relative permeability, and porosity can be determined from a separate calculation with the two-phase code BOAST II, which does account for both gas generation and combined brine and gas flow.

SUTRA, STAFF2D, and PANEL were used to evaluate the flow of brine and the transport of dissolved radionuclides from the repository in the undisturbed case. Vertical cross-sections through the repository, anhydrite layers a and b, MB139, the drift, and the shaft were modeled to determine the path and extent of transport from the repository. Calculations assuming single-phase flow with and without properties modified by the effects of gas were performed.

Recognizing that radionuclide migration from the repository is three dimensional, additional calculations were performed with SUTRA modeling a horizontal plane through the repository. MB139 has been hypothesized to be the principal brine pathway out of the repository. In these calculations it was assumed that the entire waste repository was located within MB139. This conservative assumption eliminated any resistance to flow afforded by the DRZ between the repository and MB139, maximizing the advective flow in MB139.

STAFF2D and PANEL were the two codes used to quantify the transport of radionuclides up the shaft and away from the repository within MB139. Using these codes it was determined that the quantity of radionuclides passing a point 20 m up the shaft from the repository horizon and through a boundary 100 m away from the repository within MB139 were several orders of magnitude less than the EPA normalized limit of one. The SUTRA code was used primarily to verify the extent of transport calculated by STAFF2D and to assess the importance of transient gas pressures. SUTRA was also used to investigate some of the three-dimensional aspects of flow away from the repository. The BOAST II code was used to calculate the transient pressure from waste-generated gas and to provide relative permeabilities and porosities for use in the single-phase codes SUTRA and STAFF2D.

Subpart B of 40 CFR Part 191 (The Standard) limits the probabilities of cumulative releases of radionuclides to the accessible environment for 10,000 years and limits the dose to individuals for 1000 years after disposal (Volume 1, Chapter 1). Bounding calculations that show that no releases reach the accessible environment can be used to satisfy the requirement of the Standard for undisturbed conditions. It is not always intuitively obvious, however, that the selection of

extreme values for input parameters for computation have the effect of providing an upper bound on radionuclide transport.

In the following calculations for undisturbed performance, many of the assumptions were indeed conservative, tending to maximize transport away from the waste panel. However, this was not wholly true for all parameters; often average or median properties were used. Therefore, it cannot be claimed that these calculations are truly bounding. Indeed, it may not be possible to prove that any fixed set of assumed input parameters will produce a bounding result.

These calculations had several objectives:

- To determine the path and extent of migration of radionuclides from the waste panels, and to quantify the magnitude of radionuclide transport up the shaft.
- To evaluate (in an approximate sense) the effect of waste-generated undissolved gas on migration of radionuclides for undisturbed conditions.
- To assess the importance of three-dimensional effects on radionuclide migration in MB139.
- To cross-verify the results from the two single-phase codes SUTRA and STAFF2D.

4.2 Consequence Models

4.2.1 BOAST II AXISYMMETRIC APPROXIMATION OF TWO-PHASE FLOW—James E. Bean and James D. Schreiber

4.2.1.1 Model Overview

For undisturbed conditions, the generation of gas by corrosion and microbial degradation of waste is the principal driving force that moves brine and dissolved radionuclides out of the repository. The presence of an undissolved gas phase also affects the brine saturation and other material properties governing flow in and around the repository.

To account for these effects, the three-phase code BOAST II was used to calculate the pressure history, brine saturations and relative permeabilities within and adjacent to the repository waste panel. These parameters could then be used to modify material parameters (e.g., porosity and permeability) and calculate brine flow using the single-phase codes SUTRA and STAFF2D.

Since BOAST II was originally written as a petroleum reservoir model, the three phases normally considered are gas, oil, and water. In using BOAST II to simulate flow of brine and gas in and adjacent to the repository, only two of the three phases in the model are used. What is referred to as "oil" in BOAST II is given properties of brine. "Gas" is given properties of hydrogen gas. "Water" is not used. "Oil," rather than "water," is used to simulate brine simply as a matter of convenience. As long as the correct properties are used, the same results will be obtained regardless of which phase is used to simulate brine.

The following description of BOAST II hinges largely on a conceptualization of multiphase flow through porous media described in detail in Appendix A. The reader is encouraged to refer to Appendix A for a broader view of the underlying assumptions.

4.2.1.2 Model Description

Nomenclature

Symbols may appear with subscripts g (gas), o (oil), or w (water) substituted for phase subscript symbol p.

B_p = Formation volume factor for phase p [m^3 @ reservoir conditions/m^3 @ reference conditions]
CG_p = Collections of terms for phase p, defined by equations (4-15), (4-16), and 4-17 [s^{-1}]
c_p = Compressibility of phase p [Pa^{-1}]
c_r = Compressibility of rock [Pa^{-1}]
c_t = Total compressibility [Pa^{-1}]
g = Gravitational acceleration [m/s^2]
K = Absolute permeability [m^2]
k_{rp} = Relative permeability of phase p [dimensionless]
p_p = Pressure of phase p [Pa]
q_p = Well injection rate for phase p [m^3/s]
R_{sp} = Solubility of gas in phase p [m^3 gas/m^3 phase p]
S_p = Saturation of phase p [m^3 phase p/m^3 void]
v_p = Darcy velocity (or flux) of phase p [m^3 phase p/(s•m^2 cross-section flow area)]
λ_p = Mobility of phase p [$(Pa•s)^{-1}$]
μ_p = Viscosity of phase p [Pa•s]
ρ_p = Density of phase p [kg/m^3]
ϕ = Porosity [m^3 void/m^3 rock]
∇ = Gradient operator [m^{-1}]
$\nabla \bullet$ = Divergence operator [m^{-1}]

Description

BOAST II (Black Oil Applied Simulation Tool, enhanced version) is a petroleum reservoir model that simulates isothermal Darcy flow in three dimensions. BOAST II assumes that reservoir fluids can be described by three fluid phases, two that are immiscible fluids and a third that is conceptually a gas soluble in each of the other two. Each phase has a constant composition with physical properties that depend only on pressure. All three phases, as well as the porous medium, are assumed to be compressible. A complete description of BOAST II and its capabilities

is found in Fanchi et al. (1987). The model description that follows is based closely on the presentation in Fanchi et al. (1982).

BOAST II uses a finite-difference, implicit-pressure, explicit-saturation (IMPES) numerical technique to solve the three differential mass balance equations that describe the simultaneous flow of the three phases. In the IMPES procedure, the mass balance for gas is recast in terms of fluid pressures, and the equations for the other two phases are written in terms of the saturations of each phase. This procedure simplifies the solution, but the explicit solution of the pressure equation results in certain limitations. For example, neither the pressure or the saturations can change rapidly (as in "coning" situations where liquid flow converges rapidly toward a well) because the IMPES solution technique then requires an impracticably small time step. This problem will also occur if the capillary pressure is not constant. The system of algebraic equations resulting from discretizing the differential equations can be solved using either direct or iterative techniques. Boundary conditions other than no-flow conditions must be specified by wells. Well models in BOAST II allow rate or pressure constraints on well performance to be specified so that gas generation and brine sinks can be simulated in a variety of realistic ways. Time steps are adjusted automatically to ensure accurate solutions. Permeabilities can be varied in each of the three orthogonal directions, and porosities can vary from cell to cell.

BOAST II solves the flow equations for three fluid phases in three dimensions in a porous medium. In the discussion that follows, the three fluid phases are referred to as oil, water, and gas, in keeping with the original development of BOAST II as an oil reservoir simulator (Fanchi et al., 1982). The flow, or mass conservation, equations for each phase, in their simplest form, are:

$$-\nabla \bullet \frac{\vec{v}_o}{B_o} - \frac{q_o}{\rho_{osc}} = \frac{\partial}{\partial t}\left(\phi S_o / B_o\right) , \tag{4-1}$$

$$-\nabla \bullet \frac{\vec{v}_w}{B_w} - \frac{q_w}{\rho_{wsc}} = \frac{\partial}{\partial t}\left(\phi S_w / B_w\right) , \tag{4-2}$$

and

$$-\nabla \bullet \left(\frac{\vec{v}_g}{B_g} + \frac{R_{so}}{B_o}\vec{v}_o + \frac{R_{sw}}{B_w}\vec{v}_w \right) - \frac{q_g}{\rho_{gsc}} = \frac{\partial}{\partial t}\left[\phi \left(\frac{S_g}{B_g} + \frac{R_{so}\, S_o}{B_o} + \frac{R_{sw}\, S_w}{B_w} \right) \right] . \tag{4-3}$$

where the symbol $\nabla \bullet \vec{v}_p$ is shorthand for the divergence of the velocity of phase p:

$$\nabla \bullet \vec{v}_p = \frac{\partial}{\partial x} v_{xp} + \frac{\partial}{\partial y} v_{yp} + \frac{\partial}{\partial z} v_{zp} . \tag{4-4}$$

The parameters B_o, B_w, and B_g are formation volume factors in units of volume at reservoir conditions/volume at reference or standard conditions. (The subscript *sc* refers to standard conditions.) R_{so} and R_{sw} are solubilities of gas in oil and water, respectively.

The phase densities are related to formation volume factors and gas solubilities by

$$\rho_o = \frac{1}{B_o}\left[\rho_{osc} + R_{so}\rho_{gsc}\right], \tag{4-5}$$

$$\rho_w = \frac{1}{B_w}\left[\rho_{wsc} + R_{sw}\rho_{gsc}\right], \tag{4-6}$$

and

$$\rho_g = \frac{\rho_{gsc}}{B_g}. \tag{4-7}$$

The velocities $\vec{v}_p$ are assumed to be Darcy velocities and their x-components are

$$v_{xp} = -K_x\lambda_p\frac{\partial}{\partial x}\left[p_p - \rho_p gz\right]. \tag{4-8}$$

Similar expressions can be written for the y and z components. This equation is generally valid for incompressible fluids (oil and water). It is also valid for compressible fluids (gas), as long as the flow is irrotational and the fluid density is a function of pressure only (Bear, 1972), which is true for the simulations done using BOAST II.

The phase mobility λ_p is defined as the ratio of the relative permeability to flow of the phase divided by its viscosity; thus,

$$\lambda_p = k_{rp}/\mu_p. \tag{4-9}$$

The presence of oil, water, and gas phase pressures in (4-8) complicates the problem. For many situations, the difference between phase pressures is much smaller than the individual phase potentials and can be either ignored or treated less rigorously mathematically. The handling of the phase pressures and potentials in the flow equations can be simplified by using the capillary pressure concept. BOAST II defines the difference in phase pressures as

$$p_{cow} = p_o - p_w \tag{4-10}$$

and

$$p_{cgo} = p_g - p_o \,. \tag{4-11}$$

The differences p_{cow} and p_{cgo} are the capillary pressures of oil-to-water and gas-to-oil phases, respectively. Experimentally p_{cow} and p_{cgo} have been observed to be principally functions of water and gas saturations, respectively.

Combining (4-1) through (4-3) with (4-8), (4-9), (4-10), and (4-11) and rearranging yields

Oil

$$\nabla \bullet \left[\vec{K} \bullet \left(\frac{\lambda_o}{B_o} \right) \nabla p_o \right] + CG_o - \frac{q_o}{\rho_{osc}} = \frac{\partial}{\partial t} \left(\phi \frac{S_o}{B_o} \right) \tag{4-12}$$

Water

$$\nabla \bullet \left[\vec{K} \bullet \left(\frac{\lambda_w}{B_w} \right) \nabla p_o \right] + CG_w - \frac{q_w}{\rho_{wsc}} = \frac{\partial}{\partial t} \left(\phi \frac{S_w}{B_w} \right) \tag{4-13}$$

and Gas

$$\nabla \bullet \left[\vec{K} \bullet \left(\frac{\lambda_g}{B_g} + \frac{R_{so}\lambda_o}{B_o} + \frac{R_{sw}\lambda_w}{B_w} \right) \nabla p_o \right] + CG_g - \frac{q_g}{\rho_{gsw}}$$

$$= \frac{\partial}{\partial t} \left[\phi \left(\frac{S_g}{B_g} + \frac{R_{so}S_o}{B_o} + \frac{R_{sw}S_w}{B_w} \right) \right] \tag{4-14}$$

The notation $\vec{K}$ signifies that permeability is a second-order tensor. The common assumption is made that the coordinate axes of the reference system are aligned along the principal axes of $\vec{K}$. The gravity and capillary contributions to the phase pressures have been collected in the terms CG_o, CG_w, and CG_g:

$$CG_o = -\nabla \bullet \left[\vec{K} \bullet \left(\frac{\lambda_o}{B_o} \right) \nabla (\rho_o g z) \right] \tag{4-15}$$

$$CG_w = -\nabla \bullet \left[\vec{K} \bullet \left(\frac{\lambda_w}{B_w} \right) \nabla (\rho_w g z + p_{cow}) \right] \tag{4-16}$$

and

$$CG_g = \nabla \bullet \left\{ \vec{K} \bullet \left(\frac{\lambda_g}{B_g} \nabla \left(p_{cgo} - \rho_g g z \right) - \frac{R_{so} \lambda_o}{B_o} \nabla (\rho_o g z) - \frac{R_{sw} \lambda_w}{B_w} \nabla \left(p_{cow} + \rho_w g z \right) \right) \right\} \tag{4-17}$$

Essentially BOAST II's task is to solve (4-12) through (4-14) and (4-18) (discussed below) for the four unknowns p_o, S_o, S_w, and S_g. All other physical properties in the equations are known, in principle, as functions of the four unknowns, or from field and laboratory data.

The procedure BOAST II uses to solve the flow equations requires combining (4-12) through (4-14) with the equality

$$S_o + S_w + S_g = 1 \tag{4-18}$$

such that only one equation for the unknown pressure p_o remains:

$$\left(B_o - R_{so} B_g \right) \left[\nabla \bullet \left(\vec{K} \bullet \frac{\lambda_o}{B_o} \nabla p_o \right) + CG_o - \frac{q_o}{\rho_{osc}} \right]$$

$$+ \left(B_w - R_{sw} B_g \right) \left[\nabla \bullet \left(\vec{K} \bullet \frac{\lambda_w}{B_w} \nabla p_o \right) + CG_w - \frac{q_w}{\rho_{wsc}} \right]$$

$$+ B_g \left\{ \nabla \bullet \left[\vec{K} \bullet \left(\frac{\lambda_g}{B_g} + \frac{R_{so} \lambda_o}{B_o} + \frac{R_{sw} \lambda_w}{B_w} \right) \nabla p_o \right] + CG_g - \frac{q_g}{\rho_{gsc}} \right\} = \frac{\phi c_t \partial p_o}{\partial t} \tag{4-19}$$

The equation in (4-19) is called the pressure equation because no explicit time derivatives of saturations are present. BOAST II solves the three-dimensional, three-phase flow equations by first numerically solving the pressure equation for p_o, then using the results in (4-20), (4-21), and (4-18) to find the phase saturations.

Oil

$$\frac{\partial}{\partial t}\left(\phi\frac{S_o}{B_o}\right)=\nabla\bullet\left(\vec{\vec{K}}\bullet\frac{\lambda_o}{B_o}\nabla p_o\right)+CG_o-\frac{q_o}{\rho_{osc}} \tag{4-20}$$

Water

$$\frac{\partial}{\partial t}\left(\phi\frac{S_w}{B_w}\right)=\nabla\bullet\left(\vec{\vec{K}}\bullet\frac{\lambda_w}{B_w}\nabla p_o\right)+CG_w-\frac{q_w}{\rho_{wsc}} \tag{4-21}$$

The oil, water, gas, rock, and total compressibilities are identified as

$$c_o=-\frac{1}{B_o}\frac{\partial B_o}{\partial p_o}+\frac{B_g}{B_o}\frac{\partial R_{so}}{\partial p_o}\ , \tag{4-22}$$

$$c_w=-\frac{1}{B_w}\frac{\partial B_w}{\partial p_o}+\frac{B_g}{B_w}\frac{\partial R_{sw}}{\partial p_o}\ , \tag{4-23}$$

$$c_g=-\frac{1}{B_g}\frac{\partial B_g}{\partial p_o}\ , \tag{4-24}$$

$$c_r=\frac{1}{\phi}\frac{\partial\phi}{\partial p_o}\ , \tag{4-25}$$

and

$$c_t=c_r+c_oS_o+c_wS_w+c_gS_g \tag{4-26}$$

respectively.

Code Modifications for CAMCON Version

A number of improvements have been incorporated into the version used in CAMCON.

- BOAST II has been tied into CAMCON via the preprocessor, PREBOAST, and the postprocessor, POSTBOAST.
- Darcy velocities of each phase in each direction can be calculated and included in the output along with time-dependent phase pressures and saturations.
- Interpolation between values of physical properties in lookup tables has been improved for greater speed.
- Rock compressibility calculations have been modified from the original version. Non-zero capillary pressures can now be used although the IMPES formulation may require the capillary pressure to be constant to maintain reasonable time steps.

- An algebraic multigrid (AMG) solver (Ruge and Stuben, 1987) has been added; it is much faster and requires far less memory than the direct solver and is more accurate and robust than the other iterative solvers in BOAST II. The multigrid solution is checked by following it with at least one iteration of a point-successive overrelaxation solver. The advantage of AMG over simple iterative or even direct methods commonly used in groundwater flow and transport programs is more pronounced with finer meshes.

4.2.1.3 Spatial Grid

Although BOAST II has three-dimensional capabilities, the complexity of the WIPP repository or even of a waste panel precludes using BOAST II in three dimensions. Consequently, the geometry used in the two-phase model for undisturbed performance represents a cylindrical, equivalent panel surrounded by the Salado Formation with anhydrite layers above and below (Figure 4-1). The region modeled extends upward to the Culebra, downward to the Castile Formation, and outward approximately 21 kilometers. The Castile and Culebra were included because they represent the major sources and sinks for brine flow to and from the repository. The far-field boundary is intended to be far enough away to justify the use of a no-flow boundary without the boundary affecting the behavior of the repository. Anhydrite layers a and b immediately above the repository have been consolidated into a single layer with a thickness equal to the combined thicknesses of a and b and located at the elevation of layer b. The panel thickness was chosen to be 2 m. The floor area of the cylindrical panel is the same as the enclosed area of an actual equivalent panel, including the area occupied by pillars. To account for the inclusion of the pillars, the porosity of the panel is adjusted (decreased) from the original waste porosity. The initial brine saturation is also adjusted for the presence of pillars fully saturated with brine. The disturbed rock zone (DRZ) extends vertically upward through the anhydrite layer and downward through MB139. Beyond the outer radius of the panel, both the anhydrite layers and the Salado are intact.

4.2.1.4 Material Properties, Boundary Conditions, and Initial Conditions

The generation of hydrogen as a result of corrosion and microbial action was simulated by means of gas injection wells in the repository grid blocks. Gas generation resulting from anoxic corrosion was assumed to occur for the first 450 years at a fixed rate of 2 moles per equivalent drum per year (Brush and Lappin, 1990), with the repository capacity being 556,000 equivalent drums. During the first 600 years, microbial action was assumed to generate gas at a fixed rate of 1 mole per equivalent drum per year (Brush and Lappin, 1990). Thus, the total gas generation rate from 0 to 450 years was 3 moles per drum per year, and from 450 to 600 years, the rate was 1 mole per drum per year. All corrodible metal was assumed to be reacted in 450 years, so corrosion

ceased then. Biodegradable material in the waste was completely consumed in 600 years, so gas generation by microbial processes ended then. The injection rates actually used in the model were on the basis of a unit volume of repository, or panel, grid block: 2.5×10^{-9} m^3 H_2/ ($s \cdot m^3$ panel) for years 0 to 450, 8.3×10^{-10} m^3 H_2/ ($s \cdot m^3$ panel) for years 450 to 600, and 0 m^3 H_2/ ($s \cdot m^3$ panel) for years 600 to 10,000. The gas generation rates used for anoxic corrosion and biodegradation were based on values available at the time the calculations were performed and do not necessarily correspond to values given in Volume 3 of this report. Currently, anoxic corrosion at 2 moles per drum equivalent corresponds to twice the maximum rate for humid conditions and a biodegradation rate of 1 mole per drum equivalent corresponds to the maximum rate for humid conditions (see Brush, July 8, 1991, memo, Volume 3).

For initial conditions, the brine saturation in the waste was assumed to be 13%; when averaged in with the pillars in the enclosed panel, which were assumed to be fully saturated with brine, the panel average saturation was 19.2% (80.8% gas saturation). The value chosen for initial brine saturation (13%) was selected from literature values reported for analogous materials. The uncertainty in this value was addressed in the calculations for Disturbed Conditions by varying it from zero to the residual saturation of the waste, 27.6%, but for the Undisturbed Conditions, the fixed value of 13% was used. In all other regions, an initial brine saturation of 100% was used.

The initial pressure in the equivalent panel was 0.1 MPa (1 atm). Initial far-field pressures were not known with any certainty, so a value midway between hydrostatic (~7 MPa at the repository elevation) and lithostatic pressure (~15 MPa at the elevation of the repository) was chosen, 11 MPa. An average gradient midway between hydrostatic and lithostatic was used to vary the far-field pressure with depth. No-flow boundary conditions were used on all six sides of the region modeled.

Because of the Implicit Pressure-Explicit Saturation formulation used in BOAST II, stability requirements initially resulted in time steps that were too small for 10,000-year simulations. To overcome this limitation, the capillary pressure, which is a nonlinear function of saturation, was assumed to be constant and equal to the threshold displacement pressure. The threshold displacement pressure is the pressure that is just large enough for gas to enter and move through a fully brine-saturated porous medium and displace some brine from it. This assumption allows simulations to proceed at a reasonable time step size. A fully implicit code, such as BRAGFLO (see Chapter 5), is less sensitive to the nonlinearities of the capillary pressure function; however, this code was not ready for use when these calculations were done, and was used only for the calculations for disturbed conditions with borehole intrusion.

4.2.1.5 Results and Discussion

Figure 4-2 illustrates the pressure in the repository as a function of time. As a result of gas generation, the pressure increases from 0.1 MPa initially to approximately 15.5 MPa after about 500 years. The pressure at that time exceeds lithostatic (~15 MPa). The effect of internal pressure near lithostatic would cause an actual waste panel to inflate slightly, forcing salt to creep outward to relieve the rising pressure in the repository. BOAST II ignores these creep effects.

Figures 4-3 and 4-4 provide vertical slices through the grid near the repository panel boundary of the brine relative permeability and the brine saturation. It can be seen in Figure 4-4 that gas has moved up into the DRZ and anhydrite layers within the first 1000 years (31.5×10^9 s). At 1000 years and later, the brine saturation was greater than residual saturation (0.276). Because the initial brine saturation in the waste was below residual saturation, there had to be a period of time during the first 1000 years in which brine flowed into the waste, some of it draining from the DRZ and some flowing in from the anhydrite layers and MB 139. This brought the brine saturation in the waste above residual saturation, thus allowing brine to brine flow. After 1000 years, the relative permeability to brine flow in the waste decreases continuously to 10,000 years, which indicates that brine saturation is decreasing. Therefore, brine is flowing out of the waste, transporting radionuclides away from the repository.

To determine the amount of radionuclides that leave the repository, a transport model such as SUTRA or STAFF2D, rather than just a flow model such as BOAST II, was needed. However, since SUTRA and STAFF2D are single-phase models, it was necessary to modify the material properties to simulate the effect of gas generation on brine flow. The relative permeability results from these BOAST II calculations, as shown in Figure 4-3, were used to modify the waste, DRZ, and anhydrite permeabilities used by STAFF2D and SUTRA in order to model the effects of gas on radionuclide transport. These calculations are discussed in Sections 4.2.2 and 4.2.3.

4.2.2 STAFF2D VERTICAL CROSS SECTION SIMULATIONS—David K. Rudeen

4.2.2.1 Model Overview

Gas generation within the repository is expected to be the primary driving force causing radionuclides to be driven out of the waste repository into the adjacent halite and anhydrite layers. To determine the primary pathways and estimate the magnitude of the release, finite-element flow and transport calculations were performed in a vertical cross section that passed through the repository, drift, shaft, and surrounding geology. The intent of these calculations is *not* to predict the actual behavior of the repository, but to show with conservative calculations that release to the accessible environment will not exceed current EPA standards. Models and most parameters were chosen to maximize release yet still be within expected ranges.

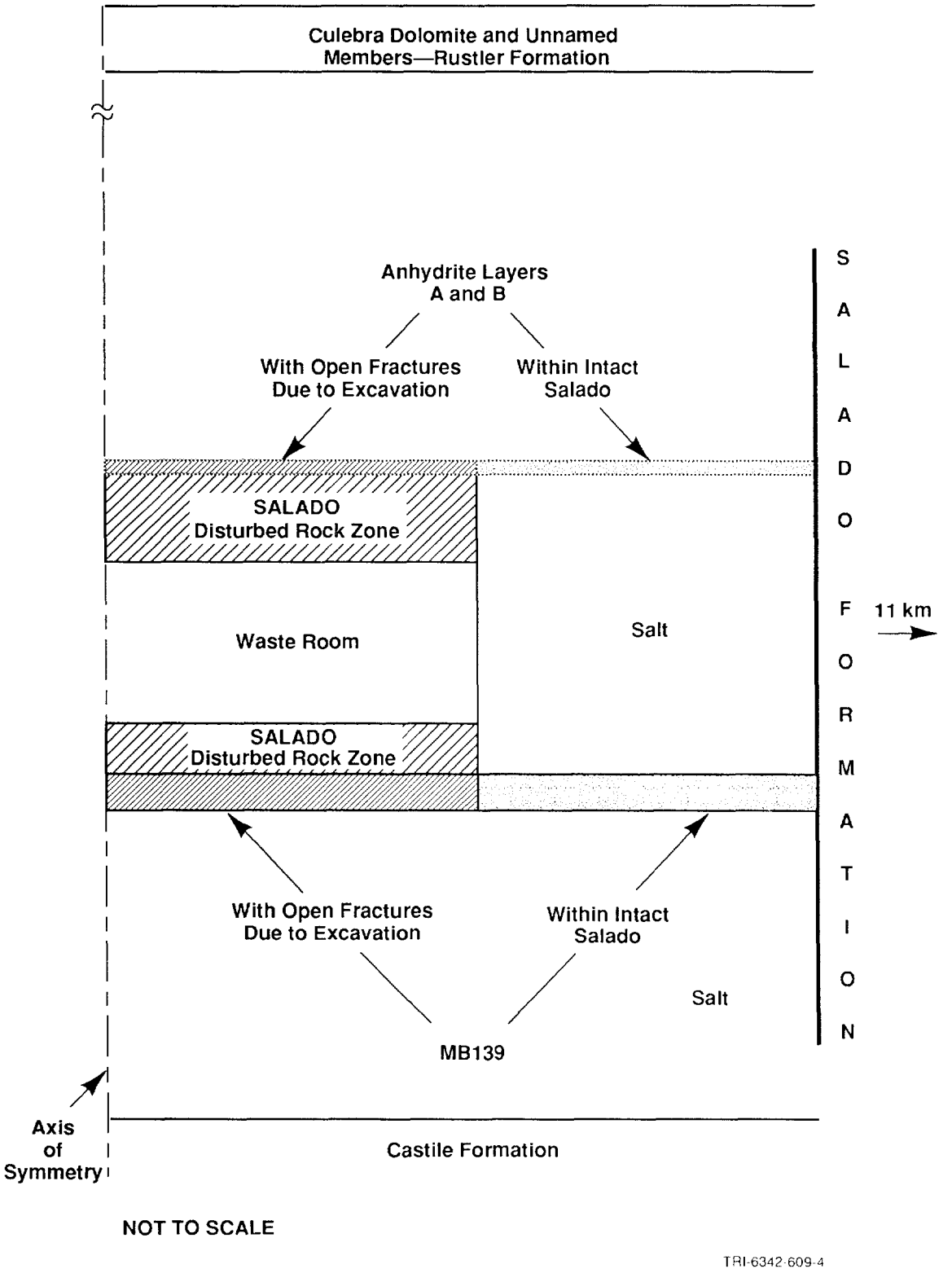

Figure 4-1. BOAST II Geologic/Waste Panel.

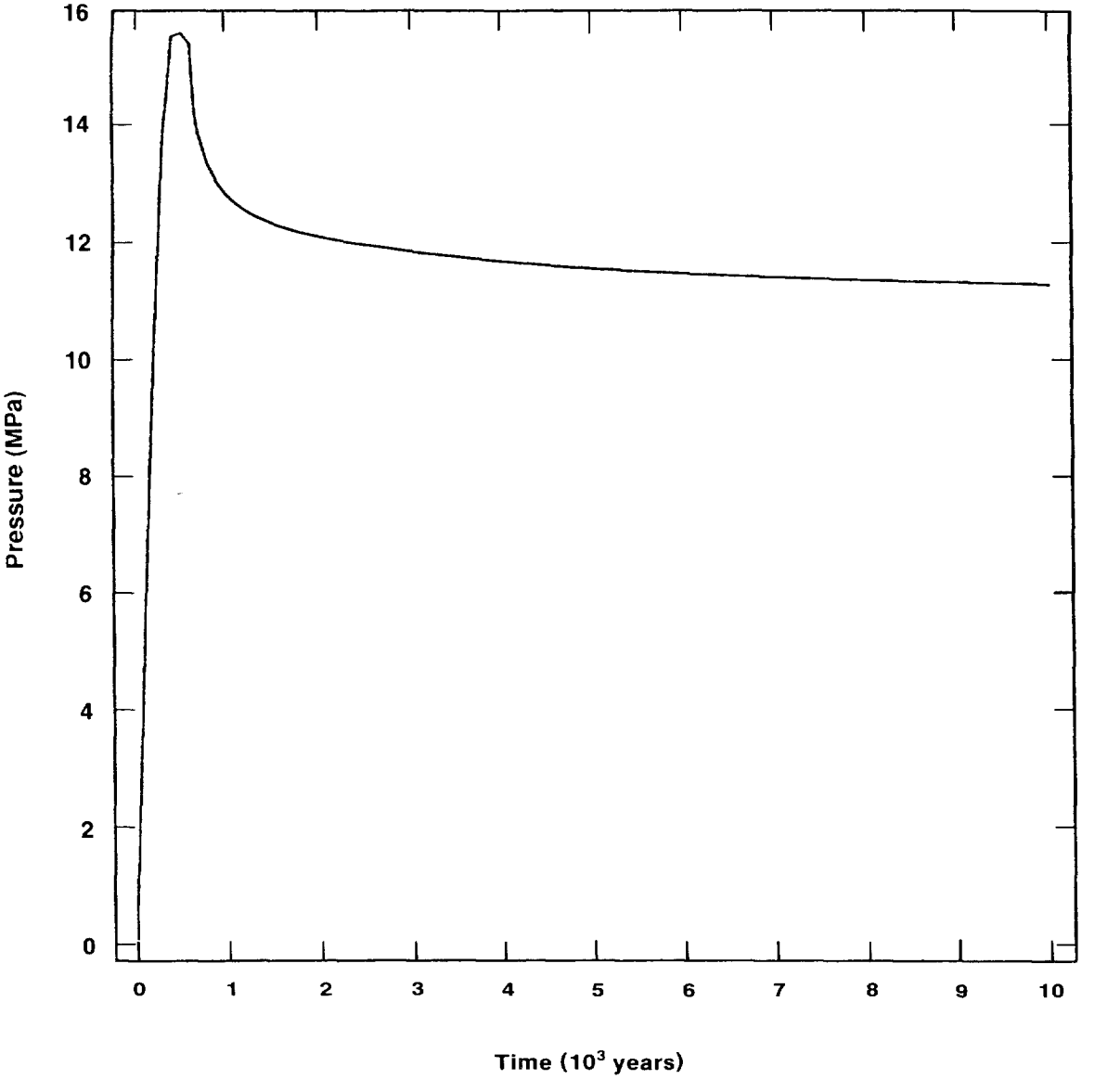

Figure 4-2. Equivalent Panel Pressure as a Function of Time

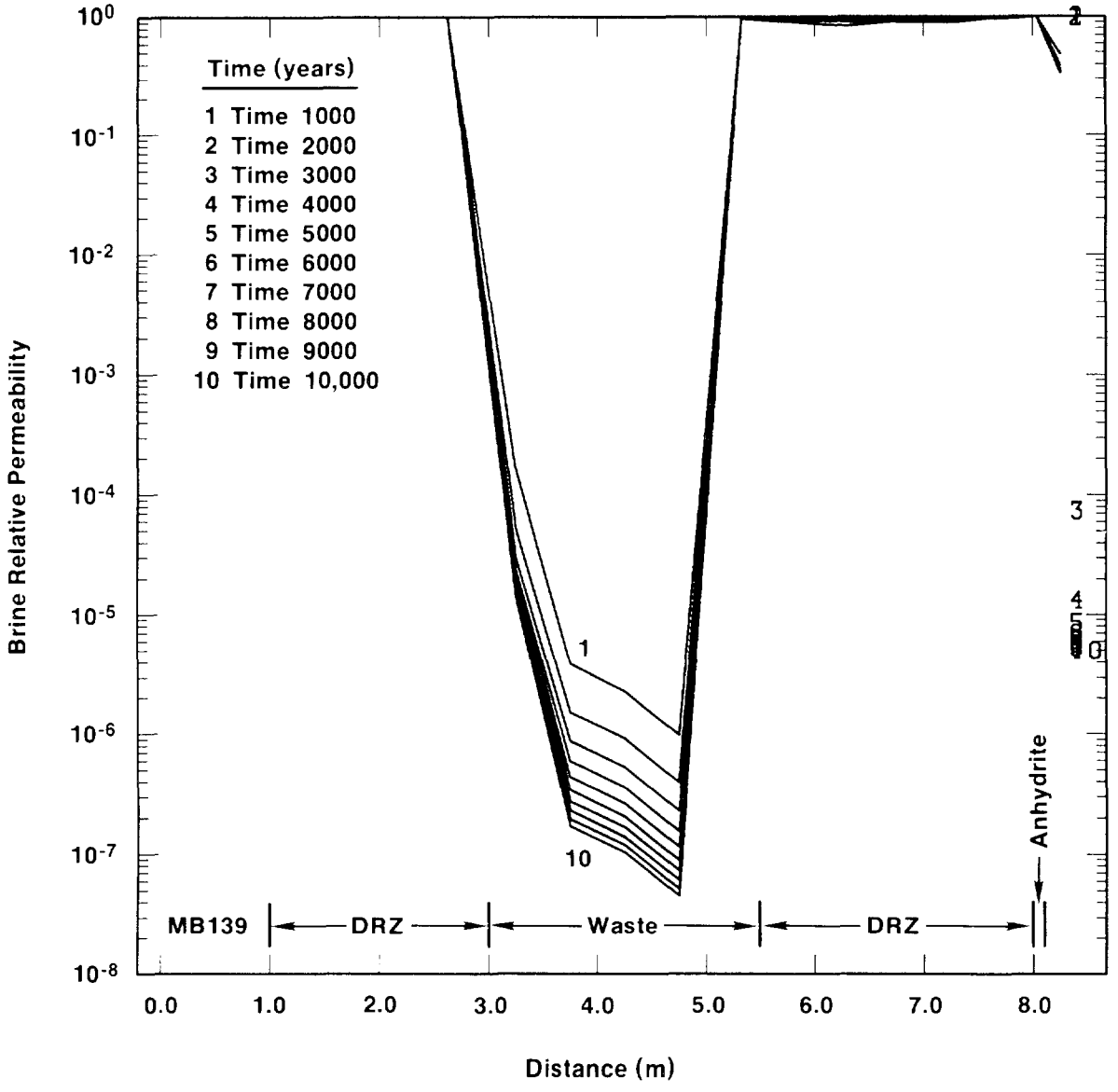

TRI-6342-1303-0

Figure 4-3. Brine Relative Permeability Profile From Bottom of MB139 to Top of Anhydrite

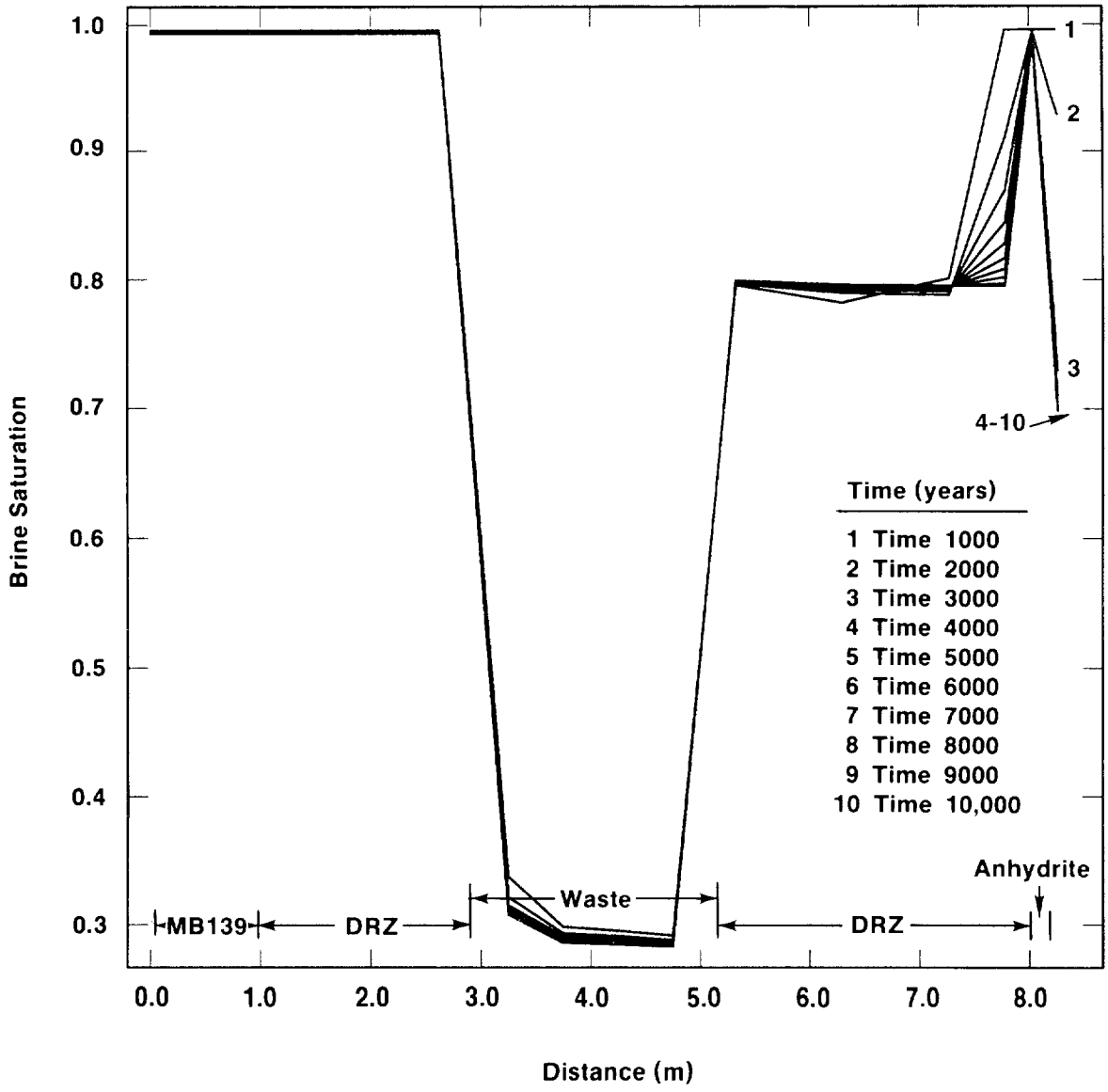

Figure 4-4. Brine Saturation Vertical Profile from Bottom of MB139 to Top of Anhydrite

The simulations in the model described here are designed to study the effect of the repressurization of the repository as the result of gas generation. The hypothesized episodes described in Section 4.1 assume that under undisturbed conditions, the repository remains in a gas-filled state after brine is expelled. Brine is expelled from the repository by the gas, which is generated from anoxic corrosion of the containers and microbiological degradation of the waste. The generation of gas causes a decrease in the brine volume in the pores. There is less brine available for transport and it is more disconnected; therefore the effective porosity, effective permeability, and effective diffusion are reduced. Because STAFF2D models saturated groundwater flow instead of gas, liquid (brine) replaces the gas in these simulations, and the repository is assumed to be completely saturated. Pressurized pore liquid becomes the force driving brine out of the repository. The brine generation is not realistic but an artifact of the pressure boundary condition applied to the nodes in the interior of the repository. An influx of brine is required to maintain the pressure above ambient. The effect of substituting a brine source for the gas drive is that brine leaves the storage area in all directions; gas-driven brine would be expected to leave primarily through the floor (because gas rises to the top of the repository) and then circle outward and up within the DRZ and host rock. The effect of gas generation on effective properties will be examined in later sections of this report (see Section 4.2.3 and Pseudo-Unsaturated Flow discussion in Section 4.2.2.6).

These calculations are an extension of those reported in the parameter sensitivity studies of Rechard et al. (1990b). In the current calculations, (1) the undisturbed MB139 is included beyond the repository, (2) the anhydrite layers above the repository are also included, (3) the drift seals have been removed, (4) the entire repository is modeled rather than only one room, (5) material properties have been updated to the current best estimates (Volume 3), particularly the effective diffusion coefficient, which includes tortuosity. STAFF2D requires the input of an effective diffusion coefficient ($D^o\tau$) where D^o (length^2/time) is the free water diffusion coefficient and τ (length/length) is the tortuosity. Including tortuosity has the effect of dropping the effective diffusion by about one order of magnitude. This results in less radionuclide diffusion into the surrounding host rock making more radionuclides available for advective transport along (or "within") MB139. Solute diffusing into the surrounding rock does not diffuse back because, with the constant pressure and concentration source, there is no solute pulse propagating away from the repository. Diffusion is constantly away from the repository, which is another conservative aspect of the model.

Analysis was performed primarily with two computer codes: STAFF2D and PANEL. The STAFF2D finite-element code calculated the steady-state flow and transient transport of a passive solute from the waste repository assuming a constant panel pressure. The choice of a constant

pressure tends to maximize flow away from the repository over 10,000 years.* Calculations with STAFF2D used either median properties or effective properties adjusted to account for desaturation. The source concentration of the passive solute was 1 kg/m^3. Simple scaling was then be used to estimate field concentrations for radionuclides with specific source concentration determined by their solubility limits. Steady-state flow was driven by a constant pressure of 17 MPa within the repository. The value chosen was the peak pressure seen from preliminary two-phase calculations similar to Section 4.2.1.5 that had been completed at the time this analysis was initiated. The PANEL code was used to calculate the quantity of radionuclides dissolved in the brine passing through the repository. The PANEL results, which take into account repository and radionuclide properties, were assumed to be source values that were scaled by the STAFF2D normalized concentrations to obtain conservative estimates of concentrations for specific radionuclides.

4.2.2.2 Model Description

STAFF2D (Solute Transport and Fracture Flow in 2 Dimensions) is a two-dimensional, finite-element code designed to simulate groundwater flow and solute transport in fractured or porous aquifers (Huyakorn et al., 1991). The original version was developed through a joint effort by HydroGeoLogic, Inc., and the International Ground Water Modeling Center of the Holcomb Research Institute. Improved versions of the code have since been commercially available through HydroGeoLogic, the latest being Version 3.2. CAMCON originally adapted Version 2.0 of the code and has since included upgrades from Version 3.2. Additional changes to the code have been made to accommodate CAMCON input/output requirements and tailor code inputs to the WIPP database (Rechard et al., 1989). The model description that follows is based closely on the presentation in Huyakorn et al. (1991).

Governing Physical Equations

Fluid Flow. The model description for fluid flow that follows is based closely on the presentation in Huyakorn et al. (1991). The governing equation for fluid flow in STAFF2D is

$$\frac{\partial}{\partial x_i}\left(T_{ij}\frac{\partial h}{\partial x_j}\right) = S\frac{\partial h}{\partial t} - \Lambda - q, \; i = 1,2 \tag{4-27}$$

where,

* Steady-state calculations neglect the effects of flow transients. To address this, transient STAFF2D flow and transport calculations using a constant repository pressure were performed after the bulk of this report went to press and consequently could not be reported here in detail. Briefly, the transient integrated flow and transport results were within 10% of the results determined using a steady flow assumption. The reader is also directed to the SUTRA calculations of Section 4.3.3.2, where fully transient calculations were performed.

h = hydraulic head (length)

T_{ij} = transmissivity tensor (length^2/time)

S = storage coefficient (dimensionless)

Λ = volumetric rate of fluid transfer per unit area from porous matrix blocks to the fracture when using dual-porosity flow (length^3/(time•length^2))

q = volumetric rate of fluid flow per unit area for sources or sinks (length^3/(time•length^2))

In accordance with standard definitions for transmissivity and storage coefficient, T_{ij} and S can be expressed as

$$T_{ij} = \phi_f H K_{ij} \tag{4-28}$$

and

$$S = \phi_f H S_s \text{ for confined aquifers} \tag{4-29}$$

where,

H = formation thickness (length)

K_{ij} = hydraulic conductivity tensor (length/time)

ϕ_f = porosity (fracture or secondary porosity for dual porosity) (dimensionless)

S_s = specific storage coefficient (1/length).

The term Λ represents the interaction between the porous rock matrix and fractures and is analogous to the Γ_ℓ in the transport equation. For the flow calculated here, Λ is assumed to be zero. The fluid exchange between the matrix and fractures in the Culebra dolomite is assumed to negligible. The q term is also zero. The fluid injected into the Culebra at the intrusion borehole that carries dissolved nuclides is assumed to have negligible effect on the existing flow field.

Transport. STAFF2D can perform both fluid flow and transport problems. The governing equations for transport in STAFF2D are

$$\frac{\partial}{\partial x_i}\left(D_{ij}\frac{\partial c_\ell}{\partial x_j}\right) - V_i\frac{\partial c_\ell}{\partial x_i} = \phi R_\ell \frac{\partial c_\ell}{\partial t} + \phi R_\ell \lambda_\ell c_\ell - \sum_{m=1}^{M} \xi_{\ell m}\phi R_m \lambda_m c_m - q\left(c_\ell^* - c_\ell\right) - \Gamma_\ell$$

$$\ell = 1, 2, \ldots, M \text{ species}, \tag{4-30}$$

where,

c_ℓ = concentration (mass/volume) of species ℓ,

D_{ij} = hydrodynamic dispersion tensor (length^2/time),

V_i = Darcy velocity (length/time) of the flow field,

ϕ = porosity (dimensionless),

λ_ℓ = first order decay constant (time^{-1}) of species ℓ,

R_ℓ = retardation coefficient (dimensionless) of species ℓ,

$\xi_{\ell m}$ = fraction of parent species m (dimensionless) that transforms into daughter species ℓ,

q = rate of fluid injection per unit volume of formation (time^{-1}),

c_ℓ^* = concentration of species ℓ in the injected fluid, and

Γ_ℓ = rate of material transfer of component ℓ from the rock matrix to the fracture (mass/(volume•time)) (see dual-porosity model, Section 6.5)

In the transport mode, the Darcy velocity is considered as input to the code and is obtained from STAFF2D or other flow codes. The dispersion tensor is defined as (Scheidegger, 1960),

$$D_{11} = \frac{\alpha_L V_1^2 + \alpha_T V_2^2}{|V|} + \phi D_1^*$$

$$D_{12} = (\alpha_L - \alpha_T)\frac{V_1 V_2}{|V|}$$

$$D_{22} = \frac{\alpha_L V_2^2 + \alpha_T V_1^2}{|V|} + \phi D_2^* \qquad (4\text{-}31)$$

where α_L and α_T are the longitudinal and transverse dispersivities, and D_1^* and D_2^* are the effective coefficients of molecular diffusion.

The decay constant is

$$\lambda = \frac{\ln(2)}{T_{1/2}} \qquad (4\text{-}32)$$

where $T_{1/2}$ is the half-life of species ℓ.

Retardation is given by

$$R_\ell = 1 + \frac{\rho_s(1-\phi)}{\phi} K_{d,\ell} \qquad (4\text{-}33)$$

where $K_{d,\ell}$ is the distribution coefficient, and ρ_s is the solid density.

In (4-30), Γ_ℓ represents a source term modeling the matrix-fracture interaction when using the dual-porosity model. The undisturbed calculations did not use the dual porosity capability, so $\Gamma_\ell = 0$. Also, for a passive solute with an infinite half-life and no retardation, $\lambda_\ell = 0$ and $R_\ell = 1.0$.

The finite-element approximation technique applied to the convective-dispersive equation is an upstream-weighted residual technique (Huyakorn and Pinder, 1983) designed to overcome oscillations of the numerical solutions when the convective terms are dominant.

Physical Assumptions and Limitations

Assumptions are as follows:

- The code is limited to two dimensions.
- Transport is governed by Fick's Law.
- The dispersivity is assumed to correspond to an isotropic porous medium so that only two constants, the longitudinal and transverse dispersivity, are important.
- Adsorption and decay of radionuclides obey a linear equilibrium isotherm.
- Solute concentration effects on fluid density are ignored.

CAMCON Enhancement: Spatially Varying Material Properties

The HydroGeoLogic version of STAFF2D is limited to having distinct material regions over which physical properties do not vary. In the transport case, these include porosity and tortuosity. In addition, the free-water molecular diffusion parameter is independent of species in Version 3.2. The CAMCON data base contains spatially varying data for tortuosity and porosity and species-dependent molecular diffusion parameters. The CAMCON version of STAFF2D was modified to permit input and use of these data.

Benchmark Tests

Several benchmark calculations have been performed to compare STAFF2D with analytical solutions. Generally, good agreement with the analytic solutions is claimed. Unfortunately, for the case of multiple species transport, analytic solutions are confined to one-dimensional model problems. The following list of documented benchmark problems is discussed in Huyakorn et al. (1991):

- longitudinal transport in fractures and transverse matrix diffusion
- longitudinal transport in fractures and spherical matrix diffusion
- one-dimensional transport of a three-member radioactive decay chain
- radial transport in fractures and transverse matrix diffusion
- two-well transport in a porous medium system

4.2.2.3 Summary of Results

A brief summary of results and conclusion is presented here. Details of the calculations including spatial and temporal grids, material properties, and boundary conditions follow. Results from STAFF2D indicate that the primary migration pathway is from the repository down into

MB139, and within MB139 to the shaft. Solute is transported up the shaft at concentrations much less than 1% of the source. The effect of desaturation via effective properties on flow and transport was minimal. An estimate of the normalized EPA sum of radionuclides passing a point 20 m up the shaft was several orders of magnitude less than the normalized EPA limit of 1, during the 10,000-year regulatory period. A similar result was obtained for radionuclides moving in MB139 away from the repository and shaft.

Flow rates up the shaft are less than 0.03 m^3 /yr with no shaft seal system, and concentrations in the shaft are much less than 1% of the source. A six order-of-magnitude decrease in shaft permeability, from 10^{-12} m^2 (permeability of sand) to 10^{-18} m^2 (permeability of initially placed salt), drops the flux up the shaft by only a factor of three. The shaft seals were not included in the original model, again to maximize flow up the shaft. Varying the shaft permeability in a parameter study showed that the properties of an engineered shaft seal would have to approach the properties of the intact Salado before it would have an effect on the undisturbed performance.

4.2.2.4 Spatial and Temporal Grids

Two grids were initially used for these simulations. A very large, coarse grid was used for a regional simulation to establish boundary conditions on a much smaller, finely zoned local simulation. Comparisons of both pressure and concentration contours from both calculations show that the extra step was not necessary. The large regional grid adequately resolved the flow and transport within MB139 and up the shaft. Therefore, all remaining results are for the large, coarse grid.

The region covered by the grid extended from 1,000 m below the MB139 to the top of the Culebra dolomite and for 1,000 m downgradient from the shaft to 1,500 m up gradient from the repository (Figure 4-5). Details of the grid are shown in Figure 4-6 at the shaft/drift intersection. The MB139 and anhydrite layers were modeled using one element through the thickness. Two and three elements were used through the thickness of the Salado DRZ below and above the repository respectively. Three zones were used through the thickness of the repository. One element was used through the thickness of the shaft. Along the drift, the zones increased in length from 5 to about 40 m; in the repository they were approximately 30 m long. Zones expanded in all directions away from the repository/shaft system. The zoning resulted in some rather large aspect ratios (e.g., greater than 30). However, they did not cause numerical problems for flow, as evidenced by a comparison with the fine-zoned mesh discussed above.

The two-dimensional calculations are for a 1-meter-thick cross section through the center of the repository, drift, and shaft. The code calculates specific flux ($m^3/(s \cdot m^2)$) or Darcy velocity (m/s) per unit thickness. The reported fluxes are scaled to the actual shaft dimension by assuming

a 25-m^2 shaft cross-sectional area. The assumption is conservative in that the repository, drift, and shaft are assumed to be infinite in the direction orthogonal to the plane of the calculation.

4.2.2.5 Material Properties, Boundary Conditions, and Initial Conditions

Material properties used in the simulations are given in Volume 3 of this report. The entire shaft has been modeled with upper shaft properties (no lower shaft seal system) to maximize flow up the shaft. The shaft permeability was varied between 10^{-12} and 10^{-18} m^2 in a parameter study to obtain a possible bound on properties of the engineered barrier-shaft seal system. The region below the repository is assumed to be entirely Salado. The Castile formation has been excluded. The effect is assumed to be minimal.

Boundary conditions are shown schematically in Figure 4-7. It has been hypothesized that the initial fluid pore pressure at the repository is between Salado brine hydrostatic (7.0 MPa) and lithostatic (14.9 MPa); a value of 11 MPa has been selected. Generating the quasi-hydrostatic conditions using a fluid density of 1200 kg/m^3 and a pressure of 11 MPa at the repository horizon results in a hydrostatic pressure of about 6 MPa at the Culebra dolomite. The other choices required either an artificially high fluid density to get realistic fluid pressure at the Culebra or result in boundary-condition-induced vertical flow. To enhance the flow up the shaft, a no-flow boundary was used along the top of the Culebra, except at the shaft, which had a 2.8 MPa pressure corresponding to the actual hydrostatic pressure due to a column of brine extending to the ground surface. Flow is induced by an 17-MPa pressure boundary condition in the waste part of the repository. For the STAFF2D simulations, these pressure, boundary, and initial conditions were converted to hydraulic head. A steady-state governing equation was used. The solute source in the repository was modeled with a constant normalized concentration boundary condition of 1.0 kg/m^3.

4.2.2.6 Results and Discussion

The results are summarized in Figure 4-8 as pressure and total hydraulic head contours and in Figure 4-9 as normalized solute contours at 10,000 years. The pressure and head contours show the gradients away from the repository, between the repository and the shaft, and up the shaft. Compared to other regions near the repository in the computational plane, there is very little gradient between the base of the shaft and the Culebra and therefore very little flow. The solute contours show that vertical transport into surrounding host rock adjacent to the waste panel is small compared to transport along MB139 (note the magnified vertical scale in Figure 4-9). The primary migration pathway is from the repository to MB139, and within MB139 to the shaft. Concentrations in the shaft are less than 1% of the source. Solute under the influence of increased

pressure primarily moves into the disturbed region (Salado and MB139) below the repository and drift.

The fluid flux up the shaft is about 0.026 m^3/yr. For U234 with a current median solubility limit of $1.0x10^{-4}$ molar, this corresponds to $4.68x10^{-6}$ kg/yr or $4.68x10^{-2}$ kg/10,000 yr. For PU239 with a current median solubility of $6x10^{-10}$ molar, it corresponds to $2.86x10^{-5}$ kg/10,000 yr. U234 and Pu239 are the primary radionuclides contributing to the normalized EPA sum.

The permeability and porosity values of the shaft (10^{-12} m^2 and 0.10, respectively) are for unconsolidated salt. To estimate the properties of an engineered shaft seal system that would be effective in reducing transport up the shaft, a series of simulations was performed with varying shaft permeabilities. Two and four order-of-magnitude decreases in permeability (10^{-14} m^2 and 10^{-16} m^2) resulted in essentially no change in the flow up the shaft. A permeability of 10^{-18} m^2 resulted in a factor-of-three decrease in flow. This implies for undisturbed conditions an engineered shaft seal has little effect unless the permeability approaches that of the intact Salado.

In conclusion, for fully saturated conditions, no significant quantity of radionuclides move up a shaft, even when it is filled with a material with a permeability of 10^{-12} m^2. The permeability of the shaft backfill must be within a few (2 to 3) orders of magnitude of the surrounding host rock to reduce this already insignificant migration even further. These results are consistent with results reported earlier by Rechard et al., 1990.

Release Estimates

Nuclide release up the shaft was estimated conservatively by combining the normalized concentration from STAFF2D with actual source concentration for radionuclides as calculated using the PANEL code (Section 5.3). PANEL uses the repository inventory, radionuclide properties, repository properties and intrusion borehole flow history to calculate radionuclide mass flux up an intrusion borehole. For this problem the steady-state flow up the shaft of 0.026 m^3/yr as calculated in the undisturbed simulations discussed above was used as an intrusion borehole flow history. The flow rate was calculated from the Darcy velocity times the shaft cross-sectional area. Transport up the shaft as calculated by PANEL assumes that the shaft intersects a waste panel. The effect is that there is no time delay or diffusion due to travel down the MB139 from the repository to the shaft and consequently no concentration gradient; what comes out of the repository goes directly up the shaft. The resulting radionuclide discharge is very conservative. PANEL-calculated discharges up a shaft are much larger than they would be up a shaft 366 m away. Releases calculated by PANEL were then scaled by the normalized concentrations at locations of interest up the shaft as calculated in the STAFF2D undisturbed simulations to account for the transport and time delay due to transport down the MB139.

Three PANEL calculations were run using two sets of radionuclide solubilities (median and maximum, see Volume 3) and two values of repository pore water volume (1 m^3 and 4000 m^3). The pore water volume of 4000 m^3 corresponds to an inundated waste panel and was used in the December 1990 PA. The value of 1 m^3 was used to generate concentration of the radionuclides near their solubility limits. It provides a bound to release but not a least upper bound or a maximum. PANEL mixes the in-flowing fluid with the fluid in the repository and then releases it with dissolved radionuclides. Larger volumes of pore water result in lower release concentrations.

The normalized EPA sum (Section 2.1) for the three calculations are shown in Table 4-1 for the release as calculated by PANEL (column 4). These releases are then reduced to account for the actual 366 m separation of the repository and shaft by combining the PANEL and STAFF2D results. For Case 1 (column 4), 99% of the EPA sum comes from the activity of AM241, which is released from the repository in the first 200 yr. AM241 can be excluded from the EPA sum since the average travel time down the MB139 is over 10,000 years and the half-life of AM241 is 432 years. This results in the values shown in column 5. There are similar results for Case 2 where AM241 contributes 70% of the EPA sum. The values shown in columns 6 and 7 have been scaled by the normalized concentrations 366 m from the repository and 20 and 50 m up the shaft (above the repository horizon)—0.001 and 0.0001, respectively.

Other factors that would significantly reduce radionuclide release up the shaft would be retardation, reduced solubilities, larger pore water volume, travel time delays for all radionuclides, and time varying concentrations. For the analysis presented the concentration scale factors are constant at their value at 10,000 yr. They are actually much smaller early in time when releases from PANEL are large.

Another pathway for release from the undisturbed scenario is within MB139 directly to the accessible environment. Darcy velocities 100 m from the far side of the repository (away from the shaft) are 0.03 times the velocities in the shaft; however the flux area is significantly larger—on the order of 3600 m^2 assuming discharge at 100 m from all four sides of the repository. Normalized concentrations are $5x10^{-5}$ 100 m from the repository within MB139. The associated EPA sum would be $2.2x10^{-4}$ ($5x10^{-5}$*0.03*3600/25) times the release calculated by PANEL or one-fifth as large as the release 20 m up the shaft, column 8. Concentrations drop off considerably with distance away from the repository. At 200 m the scale factor is $8.4x10^{-7}$ or 250 times smaller than at 100 m, column 9. In summary, the results in Table 4-1 show that normalized EPA sums for release up the shaft and out the MB139 when conservatively estimated by PANEL and appropriately scaled to account for diffusion and travel time down the MB139 are several orders of magnitude below the EPA limit.

Verification

The STAFF2D calculations were verified by performing the same simulations with the SUTRA code and comparing results. The CAMCON system made this process quite simple as only the CAMDAT data base had to be modified to include a few properties required by SUTRA. Figure 4-10 shows a comparison of the 1% contour for both the SUTRA and STAFF2D simulations at 10,000 years. The comparison shows SUTRA transporting solute slightly farther from the repository due to the subtle modeling differences and/or different numerics. The main difference between the two models is that the porosity fields are slightly different. STAFF2D uses element-centered porosity as it is stored in the CAMDAT Data Base. SUTRA interpolates the porosities to the nodes resulting in average porosities at material boundaries.

Table 4-1. Normalized EPA Sums for Release up the Shaft in the Undisturbed Scenario From All Waste Panels

			EPA SUM					
Case	Solu-	Pore - Water		No	shaft		MB139	
	bility	Vol.	PANEL	AM241	20m	50m	100m	200m
(1)	(2)	(3)	(4)	(5)	(6)	(7)	(8)	(9)
1	max.	1	1407	4.6	4.6×10^{-3}	4.6×10^{-4}	1.0×10^{-3}	4.0×10^{-6}
2	max.	4000	6.25	1.8	1.8×10^{-3}	1.8×10^{-4}	3.9×10^{-4}	1.6×10^{-6}
3	median	4000	0.11	0.11	1.1×10^{-4}	1.1×10^{-5}	2.4×10^{-5}	9.6×10^{-8}

Notes on columns 4 through 9:

(4) PANEL results including AM241 for shaft intersecting repository.
(5) Same as (4) but without AM241 in EPA sum.
(6) (5) scaled by relative concentration 20 m up shaft from STAFF2D.
(7) (5) scaled by relative concentration 50 m up shaft from STAFF2D.
(8) (5) scaled by relative concentration 100 m from repository within MB 139.
(9) (5) scaled by relative concentration 200 m from repository within MB 139.

Nuclides used in EPA sum: AM241, NP237, PB210, PU238, PU239, PU240, PU242, RA226, RA228, TH229, TH230, TH232, U233, U234, U236, U238.

Pseudo-Unsaturated Flow

In the previous calculations, STAFF2D was run assuming that the permeability and porosity were unaffected by the presence of waste-generated gas. The effect of gas was included only in so far as it provided a pressure of 17 MPa to nodes within the repository. In the following calculations with STAFF2D, gas generation effects on effective properties were included in a second STAFF2D simulation by modifying the properties of the waste, Salado DRZ, and MB139DRZ based on results of two-phase flow simulations performed with BOAST II (Section 4.2.1). Gas-generation effects are accounted for by effective properties that arise due to desaturation of the pores and by a constant 17 MPa repository source pressure. Note that saturation refers to the ratio of volume of brine to volume of pores. Saturation of 1 is fully brine saturated; a value of 0 implies the pores are void (empty). Effective porosity and effective diffusion were calculated based on brine saturation in the pores. Effective permeability was calculated using relative permeability, which is a function of brine saturation in the pores. Profiles of relative permeability on a vertical slice through the repository were shown in Figure 4-3. The waste material was broken into three layers. Permeability in the three layers was decreased by seven, six, and five orders of magnitude from top to bottom based on relative permeability. This reflects the higher gas saturations (lower brine saturation) near the ceiling. To maximize desaturation effects, permeabilities in the Salado-DRZ and MB139-DRZ were decreased by a factor of 10. Porosity in the waste, Salado DRZ and MB139DRZ were decreased by a factor of three based on the saturation profiles shown in Figure 4-4. Effective diffusion, which is a strong function of fluid saturation, was decreased by a factor of 100. Dispersivity coefficients were unchanged since saturation effects on dispersion are accounted for via the flow velocity.

The results, summarized as a concentration contour of 1% of the source value, are compared to the original saturated flow simulations in Figure 4-11. The effective property changes due to gas generation and desaturation as modeled here had little effect on solute transport; a little more solute is transported downward and a little less solute is transported laterally along MB139. The results above the repository appear to be noisy. Very little change in results will occur until effective waste and DRZ properties approach those of the intact Salado properties. This conclusion is consistent with effects of shaft seal properties on flow up the shaft. The solute transport is advection- and dispersion- (fluid velocity) dominated. The velocities are a function of hydraulic conductivity and head gradient. One would expect the fluid velocity and transport to decrease with decreased hydraulic conductivity; however, head gradients increased resulting in velocities similar to the those using unmodified properties. Gas generation in the *undisturbed* repository is *not* expected to cause releases to the accessible environment or beyond the 5-km boundary in excess of the EPA limit. In fact, the releases calculated here are several orders of magnitude lower than the limit only a few hundred meters away from the repository. Gas generation effects on radionuclide

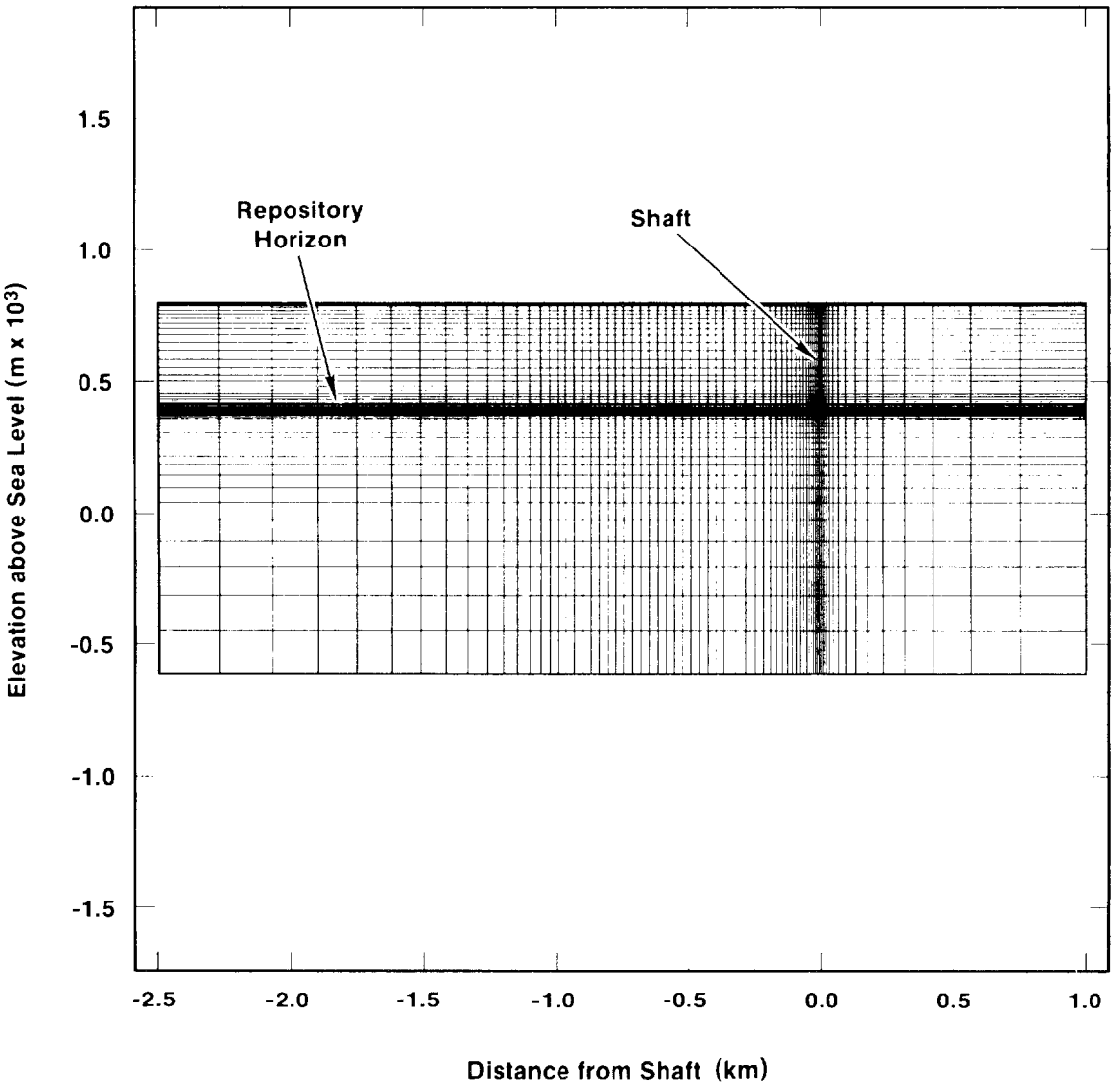

Figure 4-5. Spatial Grid for Undisturbed Simulation with Saturated Flow

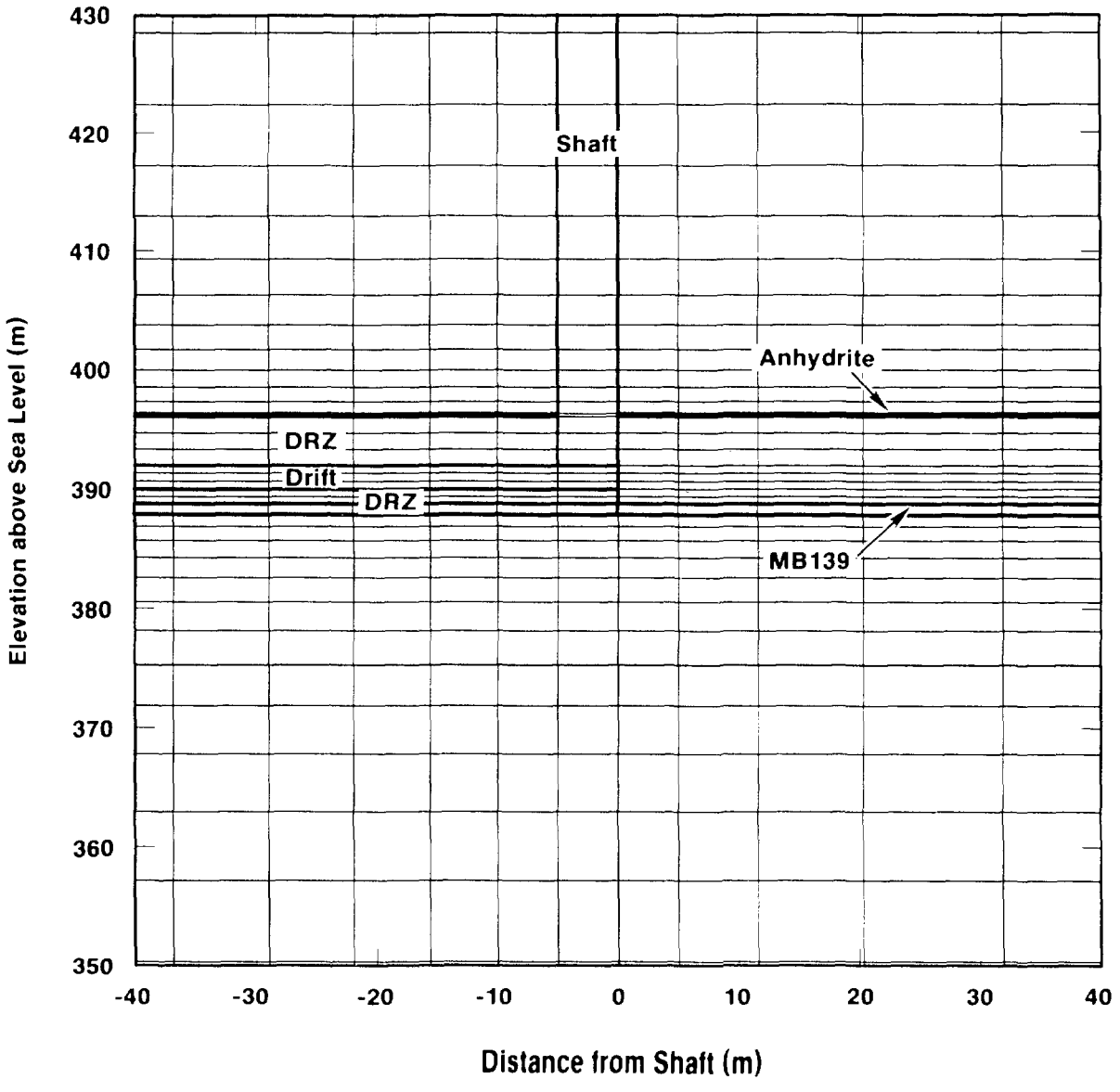

TRI-6342-1306-0

Figure 4-6. Spatial Grid Details Near Shaft/Drift Intersection

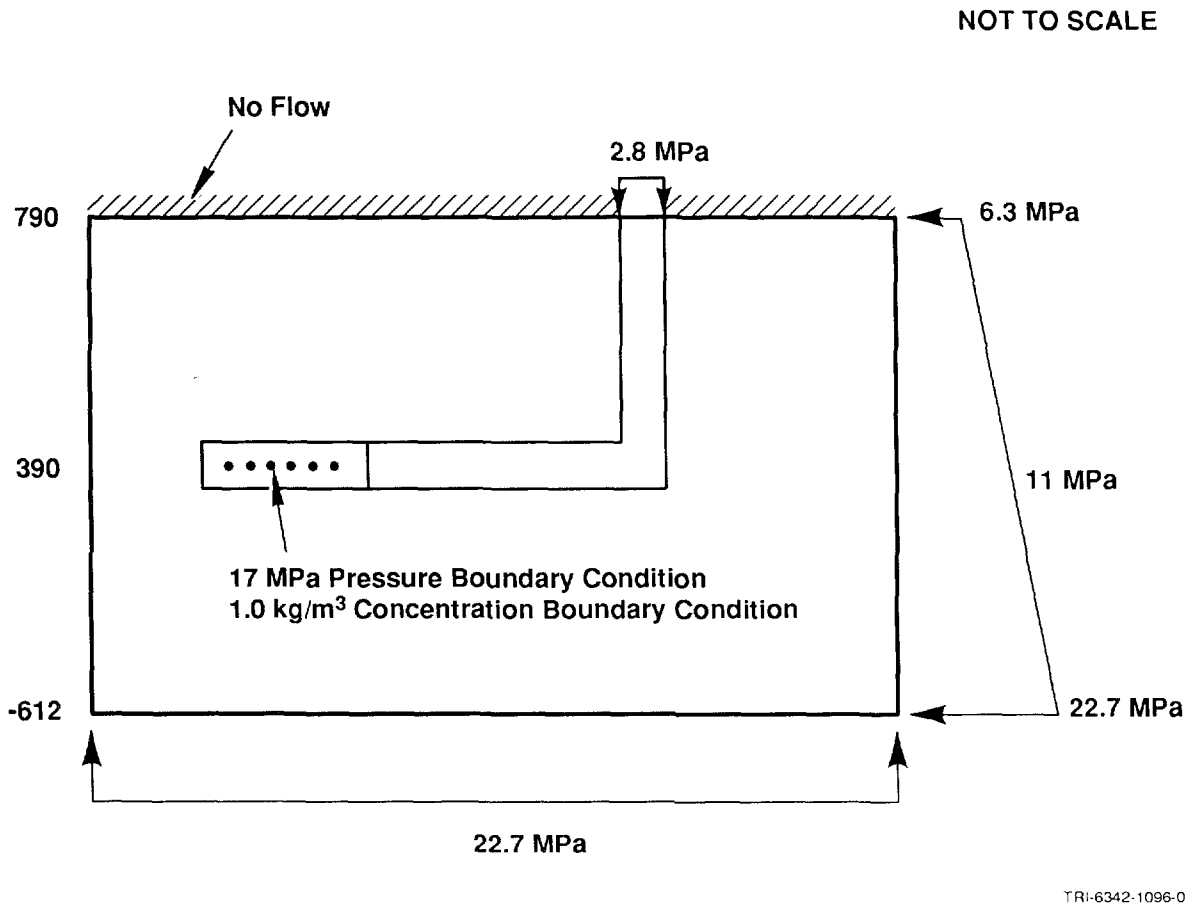

Figure 4-7. Boundary Conditions for Undisturbed Repository Performance

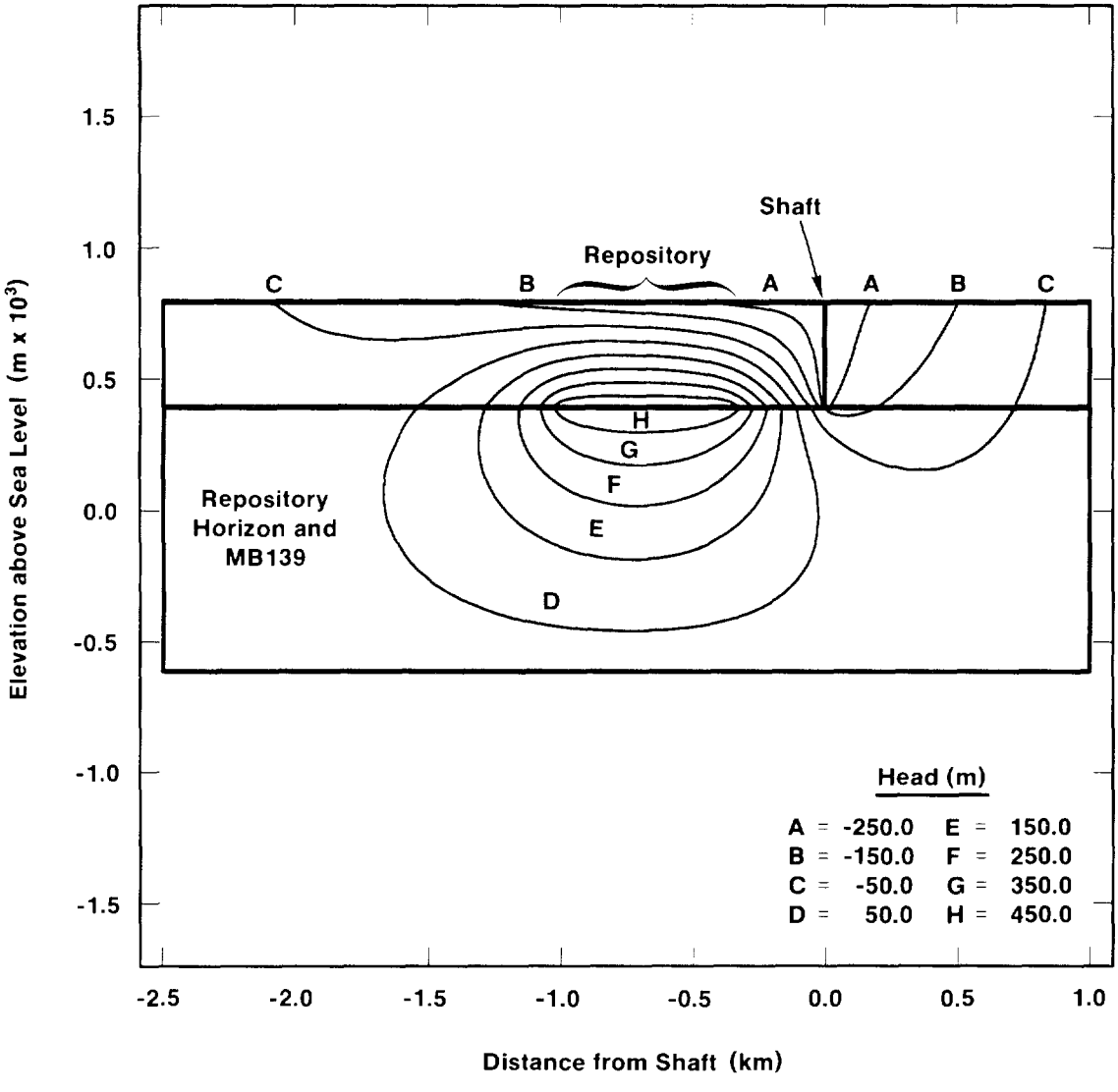

Figure 4-8a. Hydraulic Head Contours for Undisturbed Simulation with Steady-State Saturated Flow

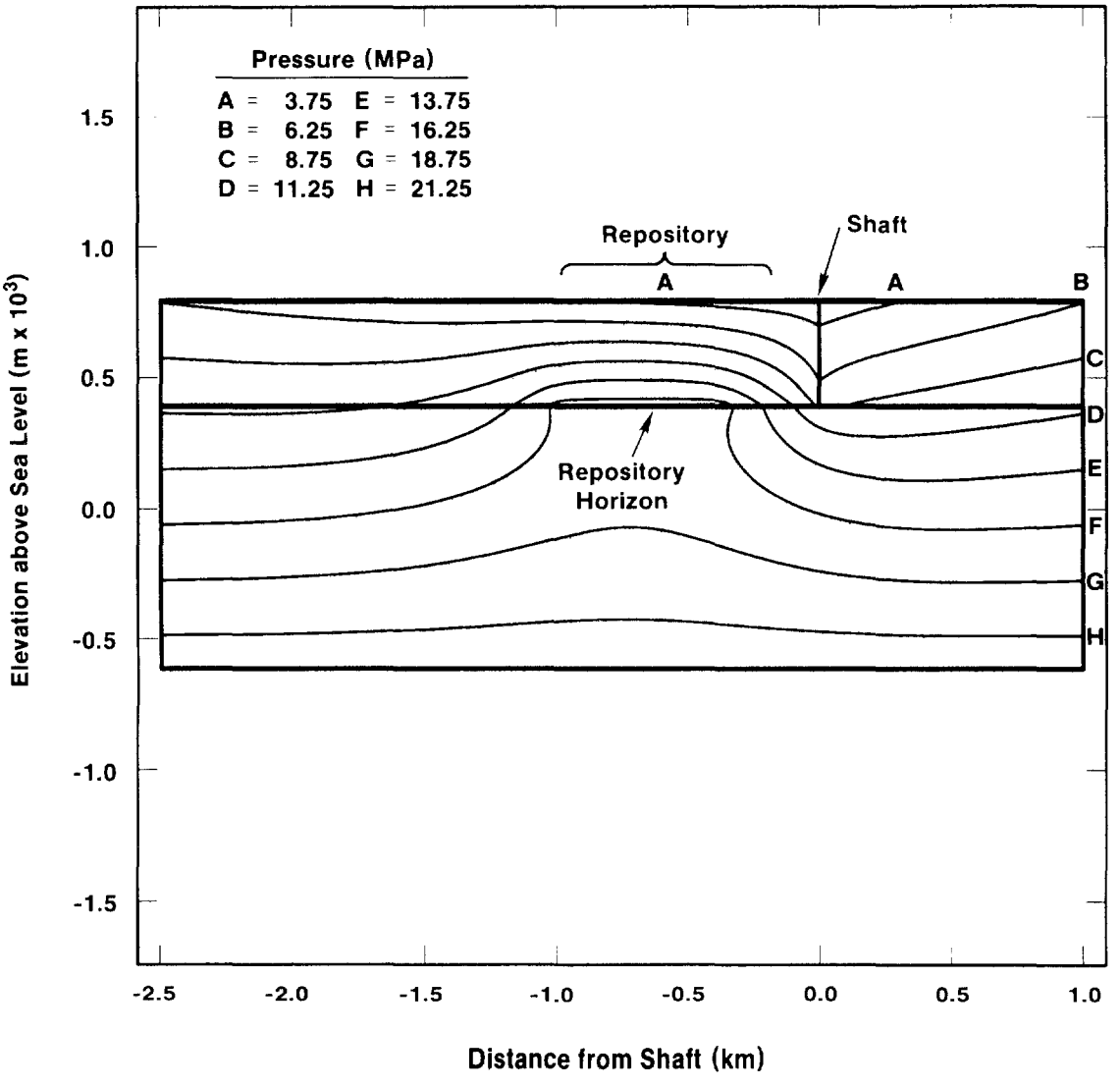

Figure 4-8b. Pressure Contours for Steady-State Saturated Flow for Undisturbed Repository Performance

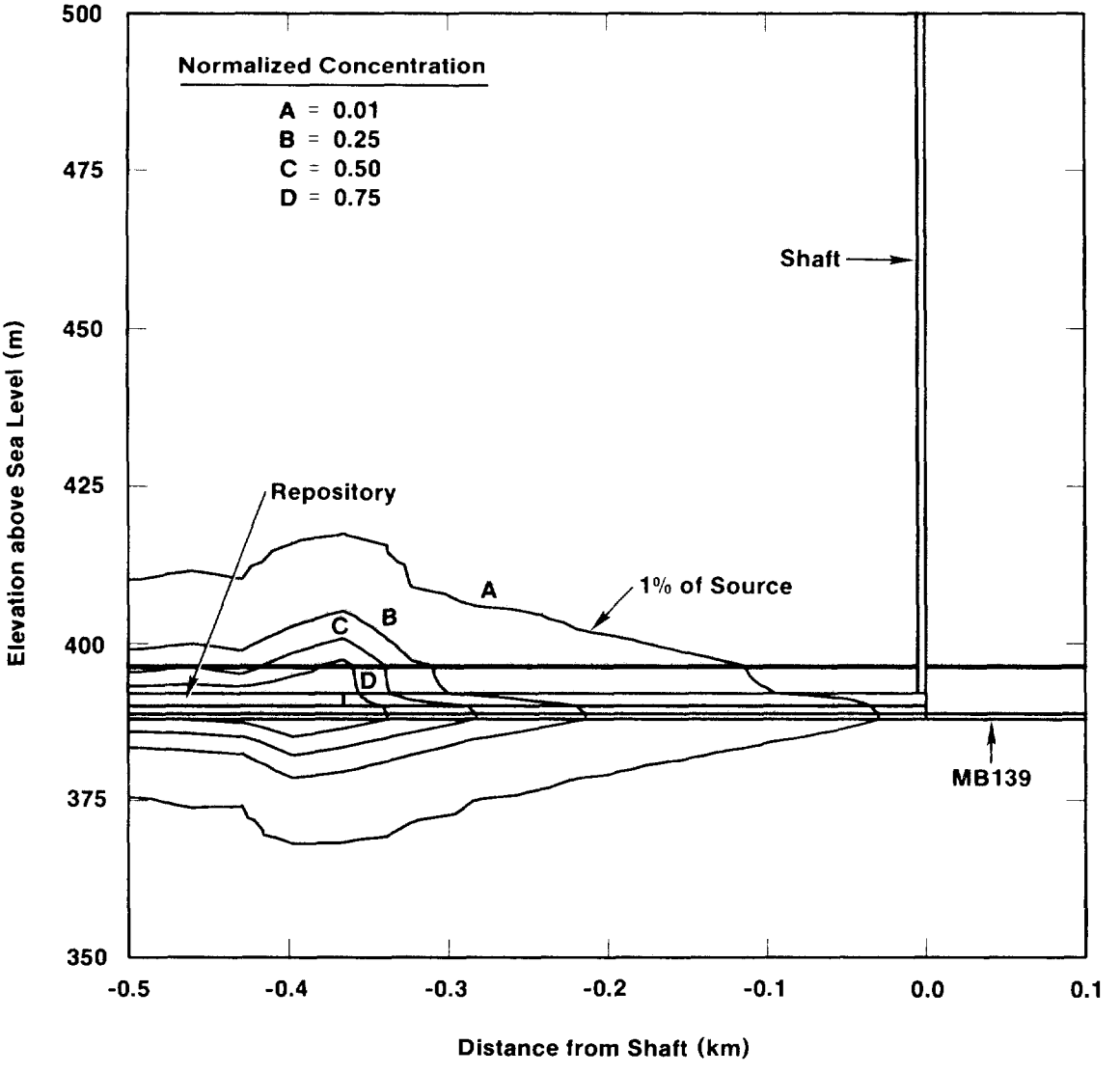

Figure 4-9. Normalized Solute Concentration Contours at 10,000 Years

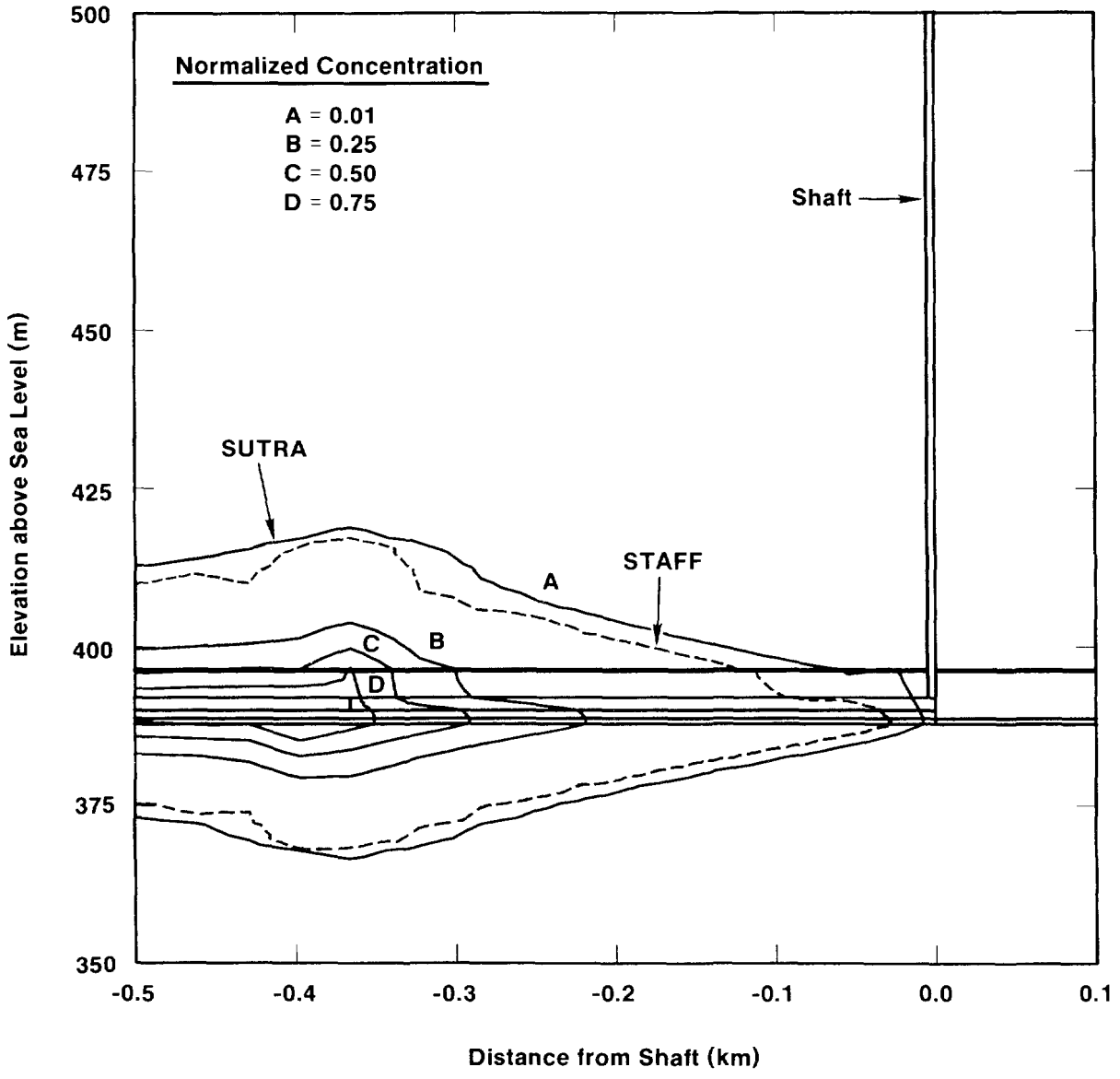

Figure 4-10. Solute Concentration Contours at 10,000 Years for SUTRA Undisturbed Simulation and Comparison with STAFF

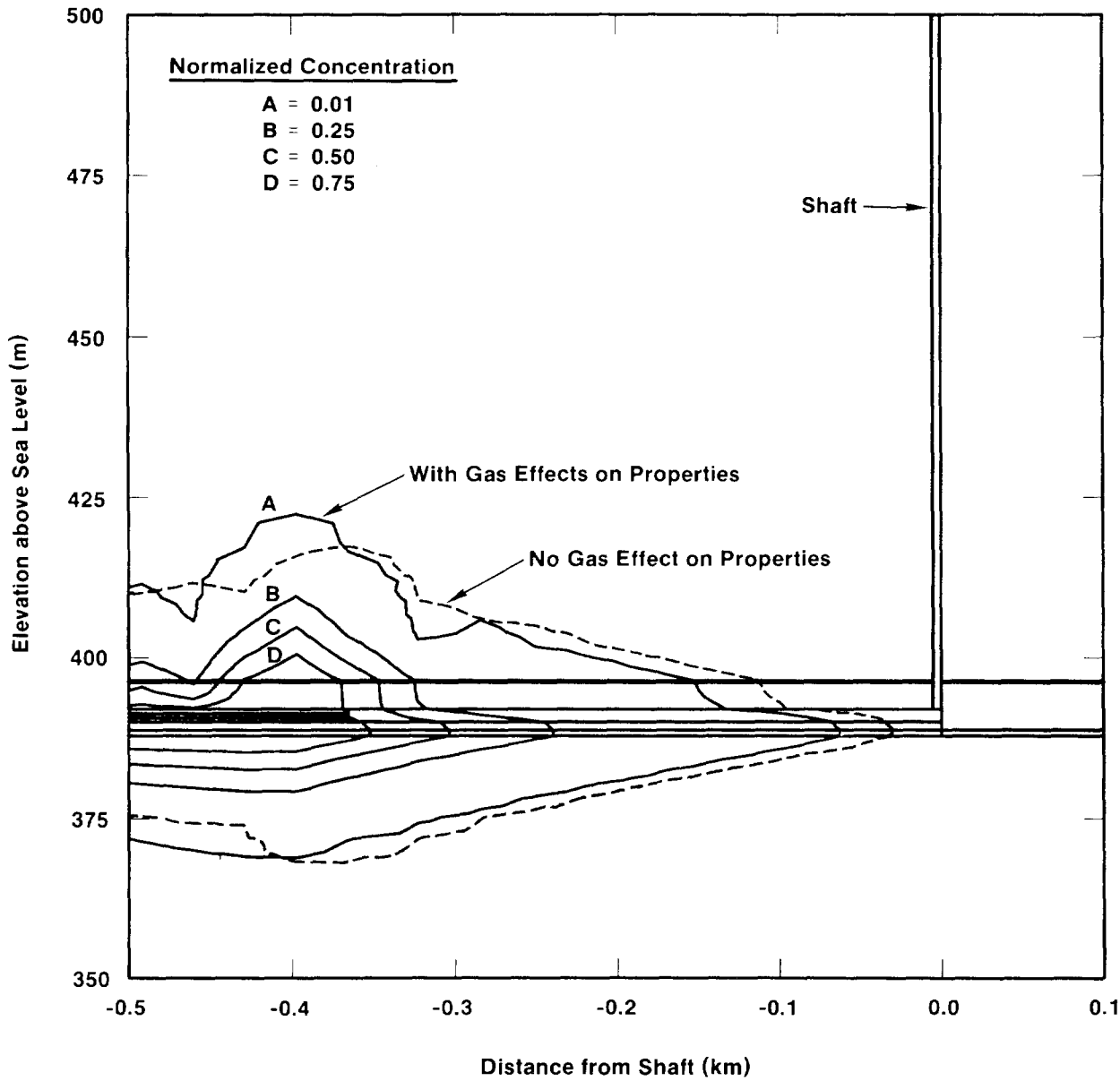

Figure 4-11. Solute Concentration Contours with Properties Modified Based on Two-Phase Simulation with BOAST (at 10,000 Years)

transport (due to property changes) are confined to a region between the repository and access shafts. The results presented here for time-constant "effective" properties are preliminary, for demonstration purposes only. They are the initial effort in an ongoing investigation into possible methods of calculating transport in the presence of two-phase flow. Other areas include fully coupling transport into a two-phase flow code (such as BRAGFLO), uncoupling two-phase flow and transport, or coupling the two-phase flow to a single-phase transport code and using time-dependent transport properties that are derived from the two-phase flow field.

4.2.3 SUTRA SIMULATIONS—Jonathan S. Rath and Ron D. McCurley

In addition to the STAFF2D calculations, the SUTRA code was also used in a vertical cross-section through the repository to verify further the results of STAFF2D (see the steady-state verification discussion in Section 4.2.2.6) and to study in greater detail the effects of transient gas pressures and time-varying material properties as generated by BOAST II. The SUTRA calculations for the vertical cross-section (Section 4.2.3.2), as opposed to STAFF2D, were run in a fully transient mode utilizing the time-varying gas pressure and material permeabilities. Additional calculations were carried out with SUTRA modeling a horizontal plane through the repository (Section 4.2.3.3). The purpose of these calculations was to investigate some of the three-dimensional aspects of flow out of the waste repository.

4.2.3.1 Model Description

The model description that follows is based closely on the presentation in Voss (1984). SUTRA (Saturated-Unsaturated TRAnsport) (Voss, 1984) evaluates density-dependent, saturated or unsaturated groundwater flow in rigid, porous media with either (1) transport of a single-species solute subject to non-linear equilibrium adsorption and zero- and first-order production or decay or (2) transport of thermal energy in the groundwater and solid matrix of an aquifer. SUTRA employs a two-dimensional hybrid finite-element and integrated finite-difference method to approximate the governing equations. The primary results are fluid pressures, velocities, and either solute mass fractions or temperatures as they vary with time. SUTRA solves partial differential equations for coupled flow and transport using backwards finite differencing time discretization for time derivatives appearing in the conservation equations. Groundwater flow is simulated through the numerical solution of a fluid mass balance. Similarly, transport of either solute mass or energy is solved numerically by satisfying a solute mass or energy balance equation. SUTRA's finite element approximation equations are derived by using the Galerkin-type method of weighted residuals. Isoparametric, bilinear, 4-node quadrilateral elements are used exclusively by SUTRA.

In addition, SUTRA allows (1) steady or transient flow, (2) radial or Cartesian coordinate systems, (3) areal (in plane) or cross-sectional solution domains, (4) equilibrium non-linear

adsorption, (5) zero and first-order production or decay for a single species, (6) saturated or unsaturated flow, (7) material-dependent storativity and grain density, (8) time-dependent boundary conditions and/or sources and sinks, and (9) time-dependent material properties. Items 7, 8, and 9 are enhancements developed for the CAMCON version.

Groundwater Flow Equation

The governing partial differential equation describing conservation of fluid mass in an unsaturated porous medium is given by (Voss, 1984),

$$\left\{S_l \rho_f G + \left(\varepsilon \rho_f\right)\frac{\partial S_l}{\partial p}\right\}\frac{\partial p}{\partial t} + \left\{\left(\varepsilon S_l\right)\frac{\partial \rho_f}{\partial \hat{C}}\right\}\frac{\partial \hat{C}}{\partial t} = \nabla \bullet \left\{\left[\frac{\underline{\underline{k}} k_{rl} \rho_f}{\mu_l}\right] \bullet \left[\nabla p - \rho_f \underline{g}\right]\right\} + Q_l \qquad (4\text{-}34)$$

where,

S_l = ratio of fluid saturation to total void volume (dimensionless),

ρ_f = fluid density (M/L^3),

G = specific storativity (t^2/M),

ε = porosity (dimensionless),

p = pore pressure ($M/(Lt^2)$),

t = time (t),

$\hat{C}$ = solute mass fraction (M/M),

$\underline{\underline{k}}$ = permeability tensor (L^2),

k_r = relative permeability (dimensionless),

μ_l = fluid kinematic viscosity (ML/t),

∇p = pressure gradient ($M/(L^2t^2)$),

$\underline{g}$ = gravitational acceleration vector (L/t^2), and

Q_l = fluid mass source or sink (including pure fluid plus solute mass dissolved in fluid) ($M/(L^3t)$.

k_{rl} = relative permeability (dimensionless)

Relative permeability, k_{rl}, expresses what fraction of the total permeability remains when the void space is partially fluid-filled. Thus, for a saturated fluid, $S_l = 1$, and $k_{rl} = 1$. If the fluid density is not allowed to vary as a function of solute mass fraction ($\partial \rho_f / \partial \hat{C} = 0$), the second term of (4-34) drops out. Thus, the resulting fluid mass balance equation is no longer coupled to solute transport.

Solute Transport Equation

SUTRA allows a single solute species to be transported conservatively, or the single solute species may be subjected to equilibrium sorption (through linear, Freundlich, or Langmuir

isotherms). Single species solute may also be produced or decay through first- or zero-order reaction processes. SUTRA's solute transport simulation allows for a single species mass stored in fluid solution as solute and species mass stored as adsorbate on the surfaces of solid matrix grains. Solute concentration, $\hat{C}$, and adsorbate concentration, C_s, are related through equilibrium adsorption isotherms. Assuming that species mass stored as adsorbate on the surfaces of solid matrix grains does not occur, $C_s = 0$ (i.e., no adsorbate mass transfer occurs, and thus solute is transported conservatively). The governing partial differential equation describing conservation of solute mass fraction in a saturated, $S_l = 1$, porous medium is given by Voss (1984),

$$\varepsilon\rho_f \frac{\partial \hat{C}}{\partial t} = \nabla \bullet \left\{ \left[\varepsilon\rho_f \left(D_p \underline{\underline{I}} + \underline{\underline{D}} \right) \right] \bullet \nabla \hat{C} \right\} - \varepsilon\rho_f \underline{v} \bullet \nabla \hat{C} + Q_l \left(C^* - \hat{C} \right) \tag{4-35}$$

where,

D_p = molecular diffusion coefficient in porous media (L^2/t),

$\underline{\underline{I}}$ = identity tensor (dimensionless),

$\underline{\underline{D}}$ = dispersion tensor (L^2/t)

$\nabla \hat{C}$ = gradient of solute mass fraction (L^{-1}),

$\underline{v}$ = interstitial velocity vector (L/t), and

C^* = solute mass fraction of fluid mass source (M/M).

The term involving the interstitial fluid velocity vector, $\underline{v}$, of (4-35) represents the average advection into or out of the local volume. For saturated flow, $S_l = k_{rl} = 1$, this velocity term is calculated in SUTRA from a generalized form of Darcy's law as,

$$\underline{v} = -\left[\frac{\underline{\underline{k}}}{\varepsilon\mu_l} \right] \bullet \left(\nabla p - \rho_f \underline{g} \right) \tag{4-36}$$

SUTRA employs an algorithm for determination of fluid velocities that alleviates typical spurious numerical errors common with standard finite element methods for systems with variable fluid density. Such errors are a result of fundamental numerical inconsistencies in spatial and temporal approximations for the pressure gradient, ∇p, and the density-gravity term, $\rho_f \underline{g}$, of (4-36), which are used in computing the velocity field (Voss, 1984). Consistent evaluation of the velocity is also necessary for the assembly of the dispersion tensor, $\underline{\underline{D}}$. SUTRA's method of velocity calculation applies a consistent spatial and temporal discretization to the term $(\nabla p - \rho_f \underline{g})$. Thus, SUTRA produces consistently evaluated velocities and allows stable and accurate transport modeling.

The term involving molecular diffusivity of the solute, D_p, and the dispersion tensor, $\underline{\underline{D}}$, of (4-35) represents the contribution of solute diffusion and dispersivity to the temporal solute mass

gradient. The diffusion contribution is based on a true physical process frequently neglected at the field scale. The dispersion term approximates the irregularity of the velocity field and the flow field's mixing, which are not accounted for by average solute advection. Subsequent mixing is due to the presence of non-uniform, convective velocities in three dimensions about the average interstitial velocity, $\underline{v}$, and is conceptualized in two dimensions as a diffusion-like process with anisotropic dispersivities.

For a system with isotropic permeabilities, SUTRA's dispersion tensor, $\underline{\underline{D}}$, components can be written in matrix form as,

$$[D] = \begin{bmatrix} D_{LL} & D_{TL} \\ D_{LT} & D_{TT} \end{bmatrix}, \tag{4-37}$$

where the tensor components are symmetric, defined as,

$$D_{LL} = \frac{1}{v^2}\left(\alpha_L v_L^2 + \alpha_T v_T^2\right),$$

$$D_{TT} = \frac{1}{v^2}\left(\alpha_T v_L^2 + \alpha_L v_T^2\right), \text{ and}$$

$$D_{TL} = D_{LT} = \frac{1}{v^2}\left(\alpha_L v_L v_T - \alpha_T v_L v_T\right),$$

where

α_L = longitudinal dispersivity of solid matrix (L),

α_T = transverse dispersivity of solid matrix (L), and

v = magnitude of the velocity vector, $\|\underline{v}\|$.

When such an isotropic media model is applied to a particular field situation where aquifer inhomogeneities are much smaller than the field transport scale, dispersivities α_L and α_T may be considered to be fundamental transport properties of a system in the same sense that permeability is a fundamental property of flow through porous media (Voss, 1984).

For an anisotropic permeability field, SUTRA uses an ad-hoc model of flow-direction-dependent longitudinal dispersion. SUTRA's anisotropic-media dispersion algorithm splits longitudinal dispersivity into two principal space directions aligned with the principal directions of permeability. Since anisotropic permeability's transverse dispersivity is typically only a fraction of the longitudinal dispersivity, the transverse dispersivity is ignored. Dropping the transverse dispersivity term can also be justified by the limitations of mesh refinement for accurate simulation of low transverse dispersion. Thus, the effect of any direction-dependence of tranverse dispersivity would be obscured by the numerical discretization errors in a typical mesh. SUTRA's value of longitudinal dispersivity as dependent on the flow direction for an anisotropic permeability media is given as

$$\alpha_L = \frac{\alpha_{L\min}\alpha_{L\max}}{\alpha_{L\min}(\cos\theta_{kv})^2 + \alpha_{L\max}(\sin\theta_{kv})^2}, \quad (4\text{-}38)$$

where

$\alpha_{L\min}$ = longitudinal dispersivity in the minimum permeability direction (L),

$\alpha_{L\max}$ = longitudinal dispersivity in the maximum permeability direction (L), and

θ_{kv} = angle from maximum permeability direction to the local flow direction ($\underline{v}/\|\underline{v}\|$).

4.2.3.2 Vertical Cross Section Simulations

Model Overview

Introduction. The following describes SUTRA calculations using vertical cross-sectional geometry to examine the phenomenology of solute transport in and near the repository. This phenomenology includes transport due to advection and dispersion related to the movement of fluid (brine) through the repository and surrounding rock matrix, and to molecular diffusion.

The SUTRA simulations described in this section differ from the STAFF2D calculations (described in Section 4.2.2) in the following ways: (1) The SUTRA calculations solved for transient flow and transient transport simultaneously; STAFF2D used a two-step process—steady-state flow followed by transient transport. (2) SUTRA used smaller time steps (100 years). (3) The modeled pressure in the waste (due to gas-generation) is time-dependent in SUTRA calculations, (4) In one SUTRA calculation, the permeabilities in several materials are allowed to vary with time. Otherwise, mesh geometry, material properties, and boundary and initial conditions are the same as those of the STAFF2D calculations.

The results of the SUTRA calculations confirm and augment the findings of other studies of transport in the undisturbed scenario. One significant and unique result of this study shows qualitatively different and quantitatively less transport than STAFF2D, due to time-varying permeabilities (from gas invasion into porous spaces generated by waste decomposition, etc.) and due to time-varying gas pressure.

Summary of Results. The results from SUTRA are consistent with those generated by STAFF2D (Sections 4.2.2.3 and 4.2.2.6). Again, as with STAFF2D, the primary migration pathway is down into MB139 and laterally within MB139 towards the shaft. When SUTRA used the transient gas pressures generated by BOAST II and no gas modified material properties, the 1% source concentration contour at 10,000 years did not extend as far down MB139 as the STAFF2D 1% source concentration contour run steady state with a constant, higher repository driving pressure (17 MPa). When SUTRA and STAFF2D were both run with steady-state pressures (Section 4.2.2.6), the 1% SUTRA contours preceded the STAFF2D contour. It should be noted

that the normalized concentrations calculated in STAFF2D (given as a percent of the initial concentration) are equivalent to normalized mass fractions (given as a percent of the initial mass fraction) as calculated by SUTRA. When the repository and surrounding geologic permeabilities are modified as a function of time as the result of gas generation, the SUTRA generated concentration contours show further retardation; the 1% source concentration contour in this case is approximately 50 m farther from the shaft than for the unmodified material case. Transport along MB139 without the effects of a shaft present reveals that the 1% source concentration contour extends out from the repository by approximately 120 m (see in-plane SUTRA calculation, Section 4.2.3.3).

Geometry, Spatial Grid, and Temporal Grid

For undisturbed conditions, SUTRA was exercised with a constant source term of solute mass fractions, no adsorption, and no decay. The modeled geologic matrix defined a slice perpendicular to the plane (referred to, hereafter, as the out-of-plane geometry) of and through the axis of the repository. This vertical slice included, in addition to the waste, the drift and the lower shaft, the surrounding intact host rock, the nearby disturbed rock zones, an anhydrite layer (combining layers a and b), and MB139. Disturbed rock zone regions (in the Salado) and disturbed regions in the anhydrite and MB139 layers underlying and overlying the repository are distinct materials with distinct flow properties.

The physical domain included the geological strata below the waste up to the top of the Culebra dolomite member. To simplify modeling the geometry of the geology, no account was taken for bending or changing thickness of layers. The thickness of the consolidated waste was assumed to be 2.0 meters in the vertical direction. Adjustments were required to preserve the elevation (or depth) of the repository (the original thickness is 4.0 meters). The layer thickness of the disturbed rock zone in the Salado above the repository was increased by 2.0 meters to preserve elevations of other layers. The far-field boundaries and computational mesh was the same as those used for the STAFF2D calculations (Section 4.2.2).

Two computational domains, a coarse and a fine grid, were created. The coarse grid was intended to establish and examine transient flow and concentration fields over a large domain. Due to constraints such as the large extent of the modeled domain and relative thicknesses of modeled geologic layers, there was a large variation of element size and aspect ratio (refer to Figures 4-12, and 4-13.). A finely meshed grid was created to examine flow and transport more accurately and to study the effect of mesh geometry (e.g., element aspect ratios) on transport. The results from the coarse grid were used to establish boundary conditions for a fine grid. These analyses involved several individual SUTRA calculations utilizing several pre-and post-processors. The entire series of calculations may be summarized in the following sequence (refer to Figure 1-4 in Chapter 1:

1. A coarse mesh with boundary conditions and material properties was developed using CAMCON tools GENMESH, MATSET, BCSET, and ICSET. The size of the computational domain was chosen to be the same as that used in the STAFF2D calculations (see Section 4.2.2.4).

2. Transient flow transport calculations using the computational domain developed in Step 1 were used to investigate transport phenomena and sensitivity to variations of time-step and diffusivity. (The term diffusivity used here and by SUTRA is the product of the pure fluid molecular diffusivity and the tortuosity of the porous media [sometimes referred to as the coefficient of molecular diffusion].) These transient calculations used no-flow ($\partial Q/\partial n = 0$, $\partial \hat{C}/\partial n = 0$, where n = outward or normal direction) far-field boundary conditions. Results from BOAST II (Section 4.2.1) for gas-generated time-dependent pore pressures were used as internal boundary conditions inside the waste. The rationale for the particular gas-generation rate used to determine BOAST II results used here is discussed in Section 4.2.1.5. In some cases time-dependent effective permeabilities and porosities were implemented. Care was taken to use time steps sufficiently small to reflect adequately the time-dependent functionality of results from BOAST II. The time step used in most of the calculations done here was 100 years. A smaller time step of 10 years was used only to study the effect of smaller time steps on the transport results.

3. Finally ALGEBRA, BLOT, and TRACKER were used to display results.

Material Properties, Boundary and Initial Conditions

As noted above, in some calculations the effective permeabilities of selected materials were allowed to vary with time. The time variation was determined by relative brine permeabilities predicted by BOAST II due to gas-generation in the waste. Plots of results predicted by BOAST II showing changes in relative brine permeability as a function of time for different regions in and near the repository are shown in Figures 4-14a, b, c, d. These time-dependent relative permeabilities were used to modify geologic permeabilities in SUTRA in order to make them time-dependent. The expression used to do this was $k(t) = k_0 k_r(t)$, where $k(t)$ is the derived time-dependent permeability, k_0 is the permeability and $k_r(t)$ is the time-dependent relative permeability from BOAST II. In all calculations SUTRA was used in the fully saturated mode (S_l = 1). The time variation in permeabilities was introduced to account for some of the effects of gas generation in the waste and two-phase flow in the surrounding geology.

A plot showing changes in drift permeability, due to time-dependent consolidation, is also included as Figure 4-14e. This figure is taken from Rechard et al. (1990b). The waste material

was subdivided into lower and upper regions in the model using time-varying permeabilities (see Figure 4-15). This was both reasonable and desirable because results from BOAST II showed significantly different permeability variations in the two regions. The upper region had dramatic decreases (many orders of magnitude) in brine permeability due to gas saturation; the lower region (the bottom row of elements) showed only small changes (less than an order of magnitude). Refer to Figures 4-14a and 14b.

The material and fluid properties used in these calculations were identical to those listed in the data report (Volume 3), with the exception of those shown in Tables 4-2 and 4-3. Included in these tables are material properties of the lower shaft that are to be determined by engineering design (Table 4-2). Also, as already indicated, the diffusivity used is a representative value of inventory radionuclides (Table 4-3).

Table 4-2. SUTRA Material Properties that Differ from those Found in Volume 3

	Property Value			
Zone	Dns Grain (kg/m^3)	Perm x (m^2)	Perm y (m^2)	Porosity (dimensionless)
Anhydrite (DRZ)	___	___	___	0.1
Anhydrite (FF)	___	$1.00x10^{-19}$	$1.00x10^{-19}$	___
Culebra	___	___	___	$1.50x10^{-3}$
Drift	$2.19x10^{3}$	___	___	___
MB139 (DRZ)	___	___	___	___
MB139 (FF)	___	$1.00x10^{-19}$	$1.00x10^{-19}$	___
Salado (DRZ)	___	___	___	___
Salado (FF)	___	$3.50x10^{-21}$	$3.50x10^{-21}$	___
Shaft	___	$1.00x10^{-12}$*	$1.00x10^{-12}$*	$1.00x10^{-1}$*
Waste	$2.70x10^{3}$	___	___	___

* Undetermined engineered value.

Table 4-3. SUTRA Brine Properties that Differ from those Found in Volume 3

Brine Property	Value
Compressibility (Pa^{-1})	2.70×10^{-10}
Density (kg/m^3)	1.20×10^{3}
Viscosity (Pa•sec)	1.60×10^{-3}
Diffusivity (m^2/sec)	1.40×10^{-11}*

* Generic radionuclide.

The initial flow field for the coarse-zoned transport calculations was established in the following way. The pore pressure at the repository elevation was assigned a value of 11.0 MPa. This value represents a median value between hydrostatic pore pressure at that depth (7.0 MPa) and lithostatic pressure (15.0 MPa). The pressure in the repository itself is initially 0.1 MPa (atmospheric). The pore pressures at other elevations in the grid are determined by using a brine density of 1200 kg/m^3, gravitational acceleration of 9.8 m/s^2 and the relation

$$p(z) = p|_{z=391m} + \rho g(z - 391\,\mathrm{m}) \tag{4-39}$$

where z is the elevation of a node in the grid, g is the gravitational constant, ρ is the brine density and p is pore pressure (see Figure 4-16). (The repository is located at an elevation of 391 m above sea level.)

Far-field boundary conditions are no-flow ($\partial Q/\partial n = 0$), except at the top boundary of the shaft where the pressure is brine hydrostatic (due to a column of brine up to the surface). The boundary pressures inside the repository were determined by BOAST II calculations and were applied uniformly to all internal nodes of the waste in these calculations. Nodes on the edges of the waste are excluded because this would introduce artificially large flow velocities in the elements in surrounding regions having these nodes as corners. Gas-generation predictions from BOAST II show pressures building quite rapidly initially (a peak pressure of about 15.5 MPa is attained by 500 years) and then decaying gradually to ambient pressure (11 MPa) in 10,000 years (see Section 4.2.1 and Figure 4-2). Pressure contours at 600 years are shown in Figure 4-17.

A constant solute source term of 2.0×10^{-7} kg solute/kg solution (mass fraction) was input at those nodes in the waste where a gas pressure boundary has been applied. The value, 2.0×10^{-7} comes from using an arbitrary source of atomic weight 240 (specifically Pu-240). The solubility

limit for $^{240}Pu^{+4}$ is about 10^{-6} molar. A simple calculation gives the value of 2×10^{-7} for mass fractions.

Results and Discussion

Figures 4-18 and 4-19 show the combined effects of advection, dispersion, and diffusion on mass fraction (the ratio of solute mass to total fluid mass) contours at 10,000 years for calculations with both time-dependent pressure and time-dependent properties and with time-dependent gas-generated pressures only (no time-dependent properties), respectively. (To obtain concentrations as used in STAFF2D, mass-fraction must be multiplied by fluid density.) In Figures 4-18 through 4-23 the scale on the *Y* axis has been magnified by four to show the contours more clearly. Results show that (1) contours of 1% of original waste concentrations do not intersect the shaft at 10,000 years, and (2) when changes in brine permeability due to gas generation are taken into account, that transport of the solute is reduced relative to calculations with constant (in time) brine permeability.

Interestingly, if one examines mass fraction contours where permeability in the anhydrite above the repository has changed due to gas invading the pore spaces, a notable effect can be seen. Transport along the anhydrite layers above the repository is enhanced for the case of no-gas-modified properties (Figure 4-19). This enhancement disappears when gas-modified properties are introduced (Figure 4-18).

Calculations using diffusivities of zero, 1.4×10^{-11}, and 1.4×10^{-9}, and with advection essentially turned off (by eliminating head gradients in the near field of the waste) were done to study both the effect of changing the value of diffusivity on solute transport and the relative effect of diffusion compared to advection (advection includes dispersion). The middle value (of diffusivity) was chosen as representative of a generic radionuclide (Rechard et al., 1990a). The upper value was chosen merely to show clearly the effect of increasing the diffusivity.

Plots (Figures 4-20 and 4-21) of mass fraction contours at 1000 years show a dramatic spreading of plume widths using diffusivity of 1.4×10^{-9} rather than 1.4×10^{-11}. No other effects are evident. Comparisons of Figures 4-20 and 4-22 (diffusivity=0.0 in Figure 4-22) indicate that the value of 1.4×10^{-11} used for diffusivity gave a negligible diffusion effect (note negligible differences in mass-fraction contours).

It is unclear how important diffusion is in specific local regions. The value of diffusivity used in SUTRA is a global value and does not attempt to reflect local geologic differences due to variations of tortuosity. Along the marker bed, diffusion may be relatively more significant with respect to vertical movement of particles, especially for larger values of diffusivity (refer to the statements above regarding plume width).

Comparisons of transport results in SUTRA calculations using the in-plane (of the repository) geometry (see discussion of calculations in Section 4.2.3.3) and the out-of-plane (vertical cross-section) geometry used in these calculations, show that both configurations predict similar transport away from the repository, but that the in-plane geometry predicts somewhat different transport plume dimensions. The in-plane geometry models predict more uniform movement in all in-plane directions away from the repository. The out-of-plane calculations described here and calculations done using STAFF2D all show eccentricities in the direction of the shaft. However, the in-plane geometry does not include simulation of the shaft. To see the effect of the presence of the shaft in the out-of-plane geometry, a calculation was done with the shaft absent (Figure 4-23). This calculation shows that without the shaft, the vertical model produced transport results comparable to the in-plane results (see Section 4.2.3.3). A closer examination of contour plots of mass-fractions indicates that the (small) differences may be due, in part, to the relatively large dimensions of elements along the direction parallel to the repository. Because of the limitations of computational resources and the increase of computational time with grid size, large aspect ratios in a large number of mesh elements are unavoidable.

Effects due to reduction of time step in coarse mesh were studied. A limited study of time step change show a small effect on the spread of the concentration plume (of particulates). Smaller time steps result in slight (less than 1%) magnification of plume intensity (i.e., the contours spread further from the source with 10 year time steps as compared to 100 year time steps). In all calculations a constant time step was used.

4.2.3.3 In-Plane Calculations

Model Overview

Introduction. Calculations with SUTRA (vertical cross section) and STAFF2D (Sections 4.2.3.2 and 4.2.2.3) showed that the principal pathway for radionuclides driven out of the waste panels by waste-generated gas was downward from a waste panel, into MB139 and then laterally through MB139. These results are based on a vertical two-dimensional model of an essentially three-dimensional phenomenon. Of course, once brine from the repository reaches MB139 the flow spreads in all directions in the plane defined by the thin (approximately 1.0 m thick) MB139.

To assess transport in this horizontal plane the SUTRA code was used to model several waste panels assuming that its entire contents were located in MB139. This assumption essentially neglects any flow resistance afforded by the DRZ in the small thickness of halite between the repository and MB139. SUTRA was run with the transient gas pressure history generated within the repository by the BOAST II code. See Section 4.2.1.5 and Figure 4-2. No gas-modified material properties were used and the shaft was not included. These calculations provide an estimate of the spatial extent of transport in the MB139 medium and can be compared to results

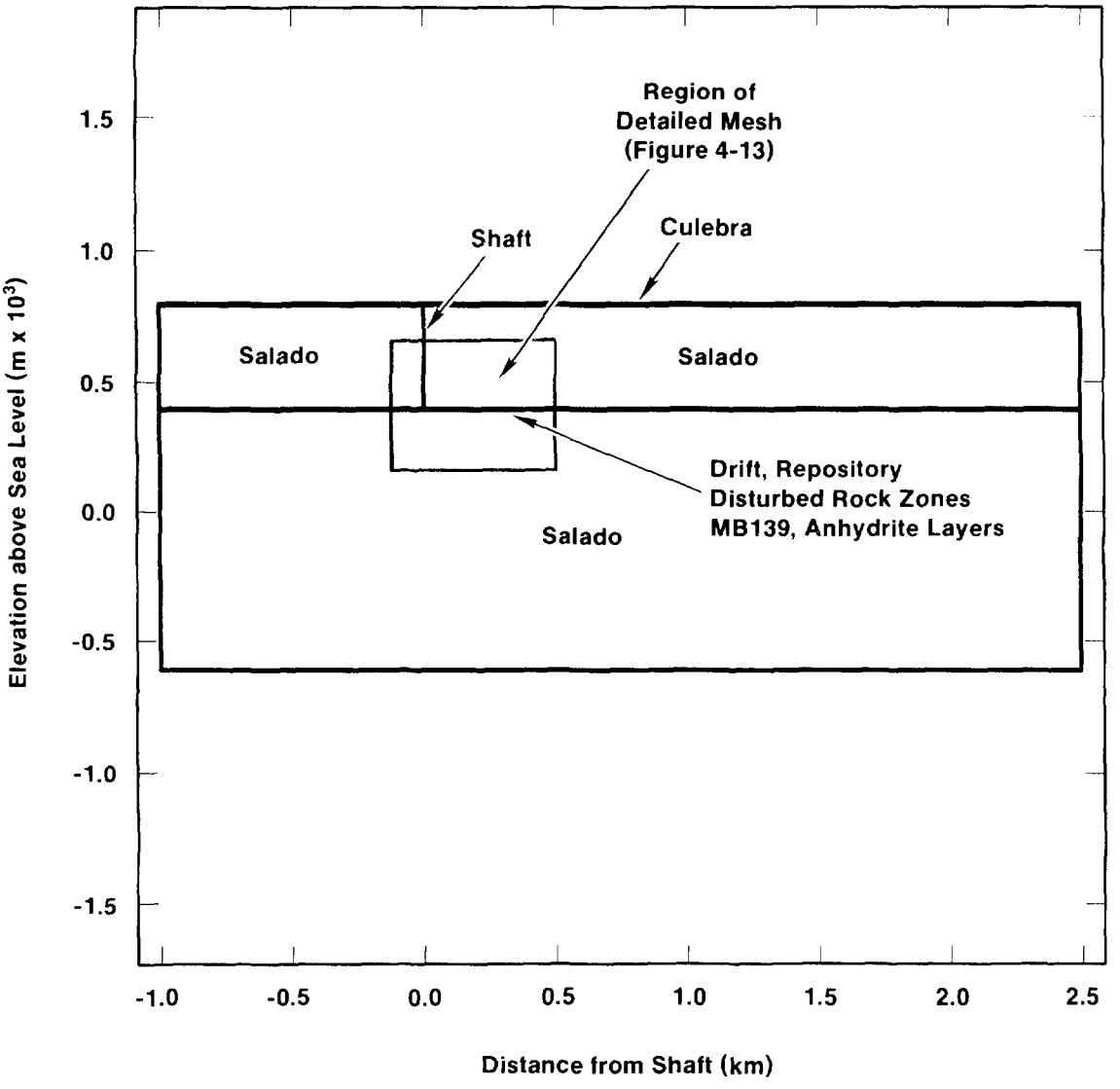

TRI-6342-1312-0

Figure 4-12. Large-Scale View of Coarse Mesh for SUTRA Boundary Conditions

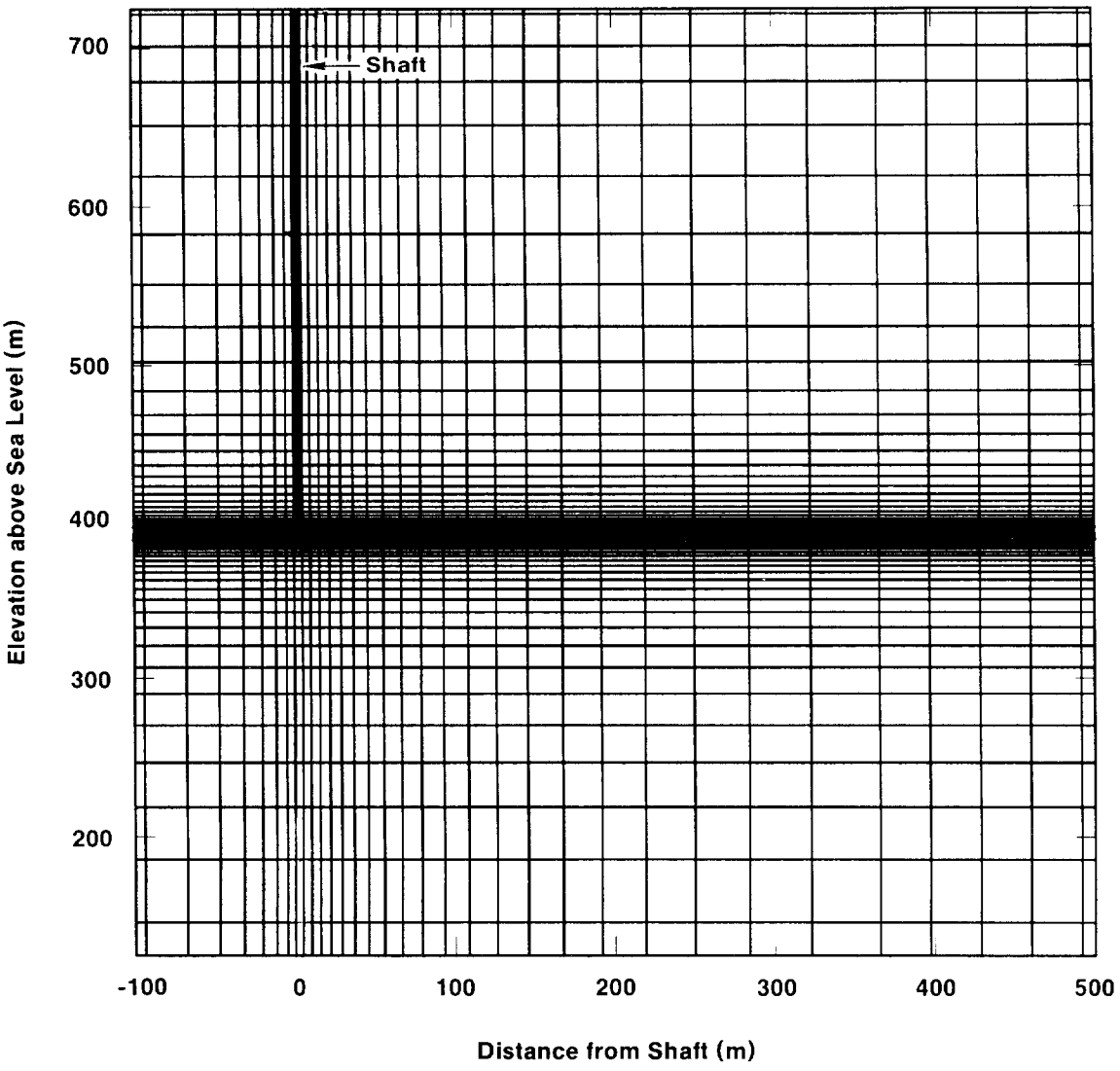

TRI-6342-1313-0

Figure 4-13. Detailed View of Coarse Mesh for SUTRA Boundary Conditions

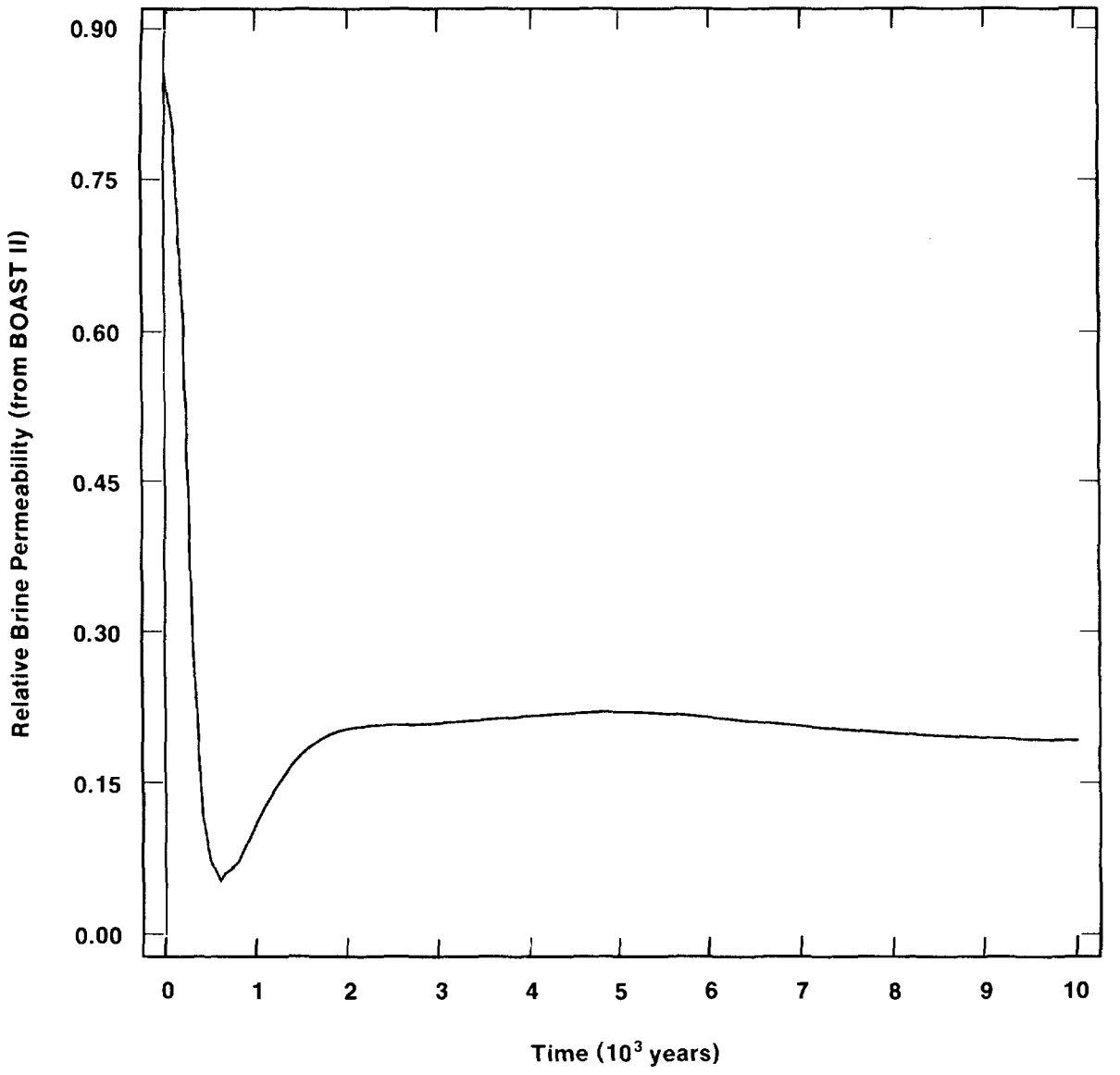

Figure 4-14a. Relative Permeability in Lower Region of Waste Due to Gas Generation

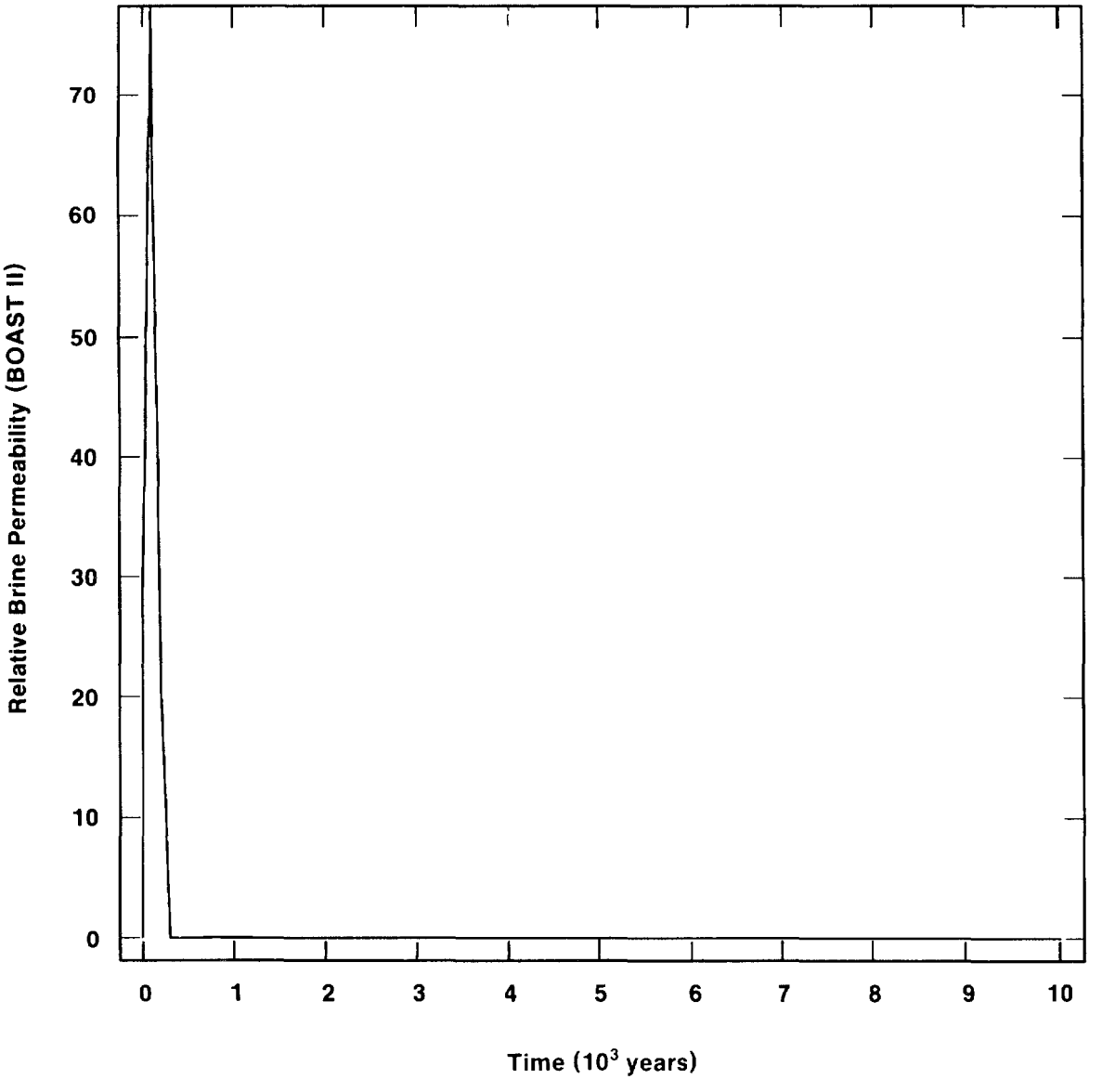

Figure 4-14b. Relative Permeability in Upper Region of Waste Due to Gas Generation

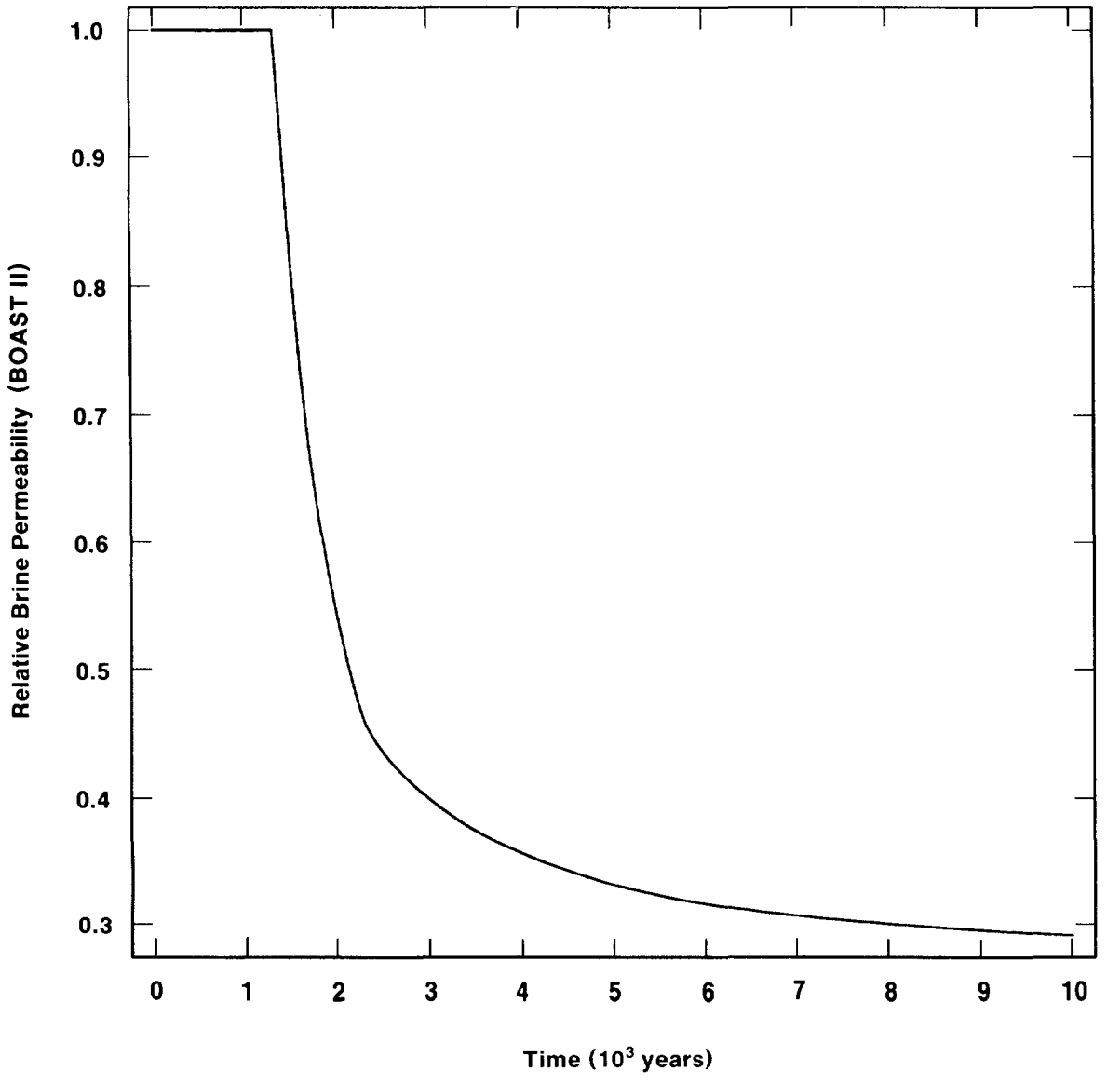

Figure 4-14c. Relative Permeability in Anhydrite

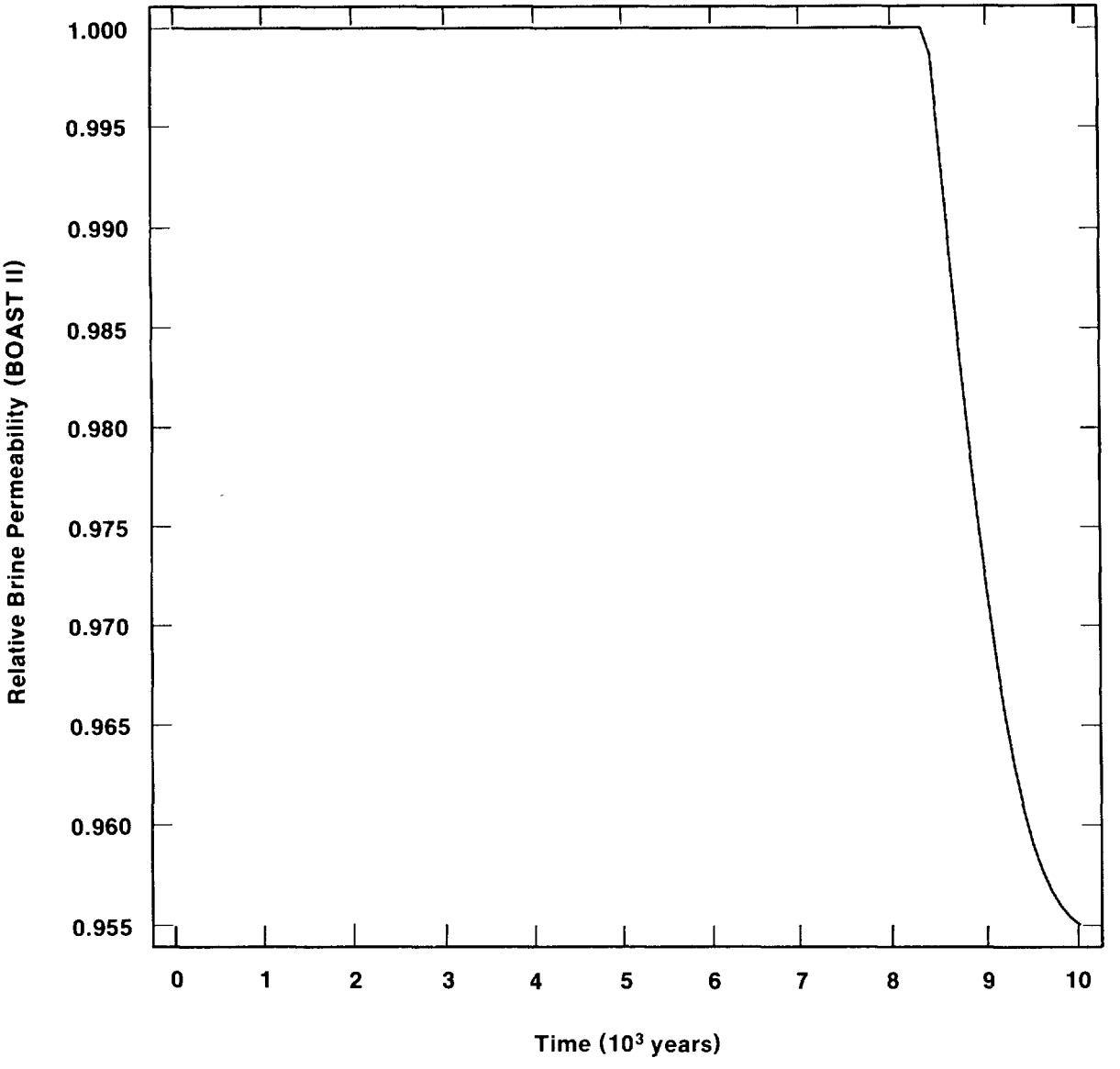

Figure 4-14d. Relative Permeability in Upper Salado DRZ (Above Repository)

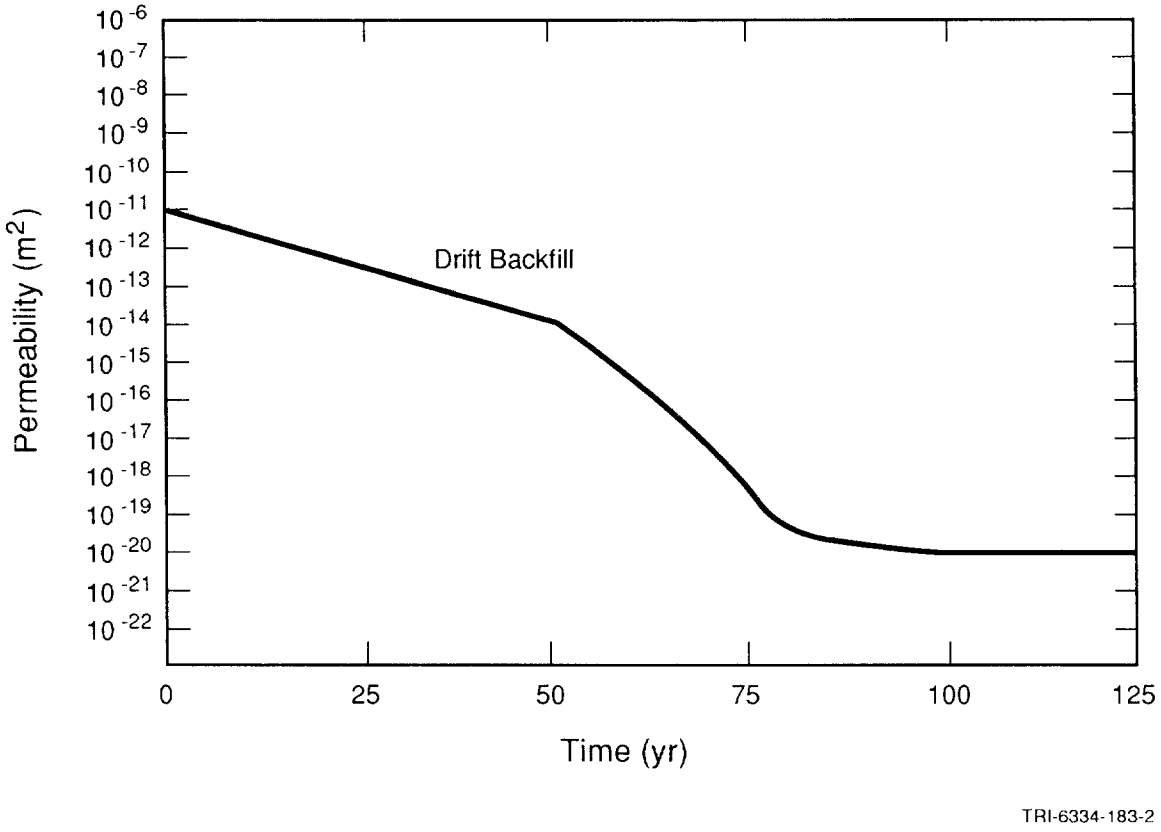

Figure 4-14e. Time Variation of Drift Permeability Due to Consolidation of Drift (from Rechard et al., 1990b, p. 74))

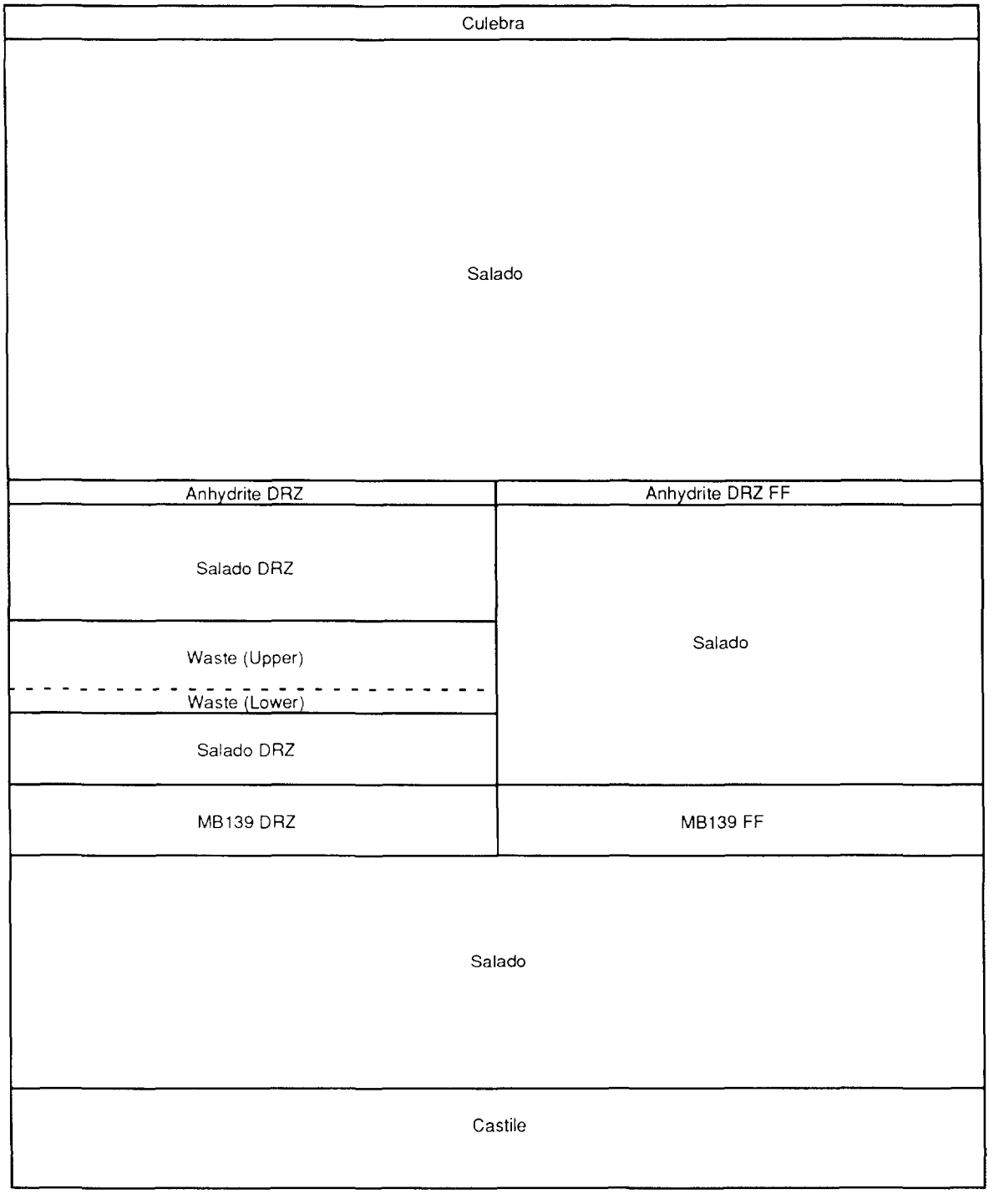

TRI-6342-1376-0

Figure 4-15. BOAST Regions

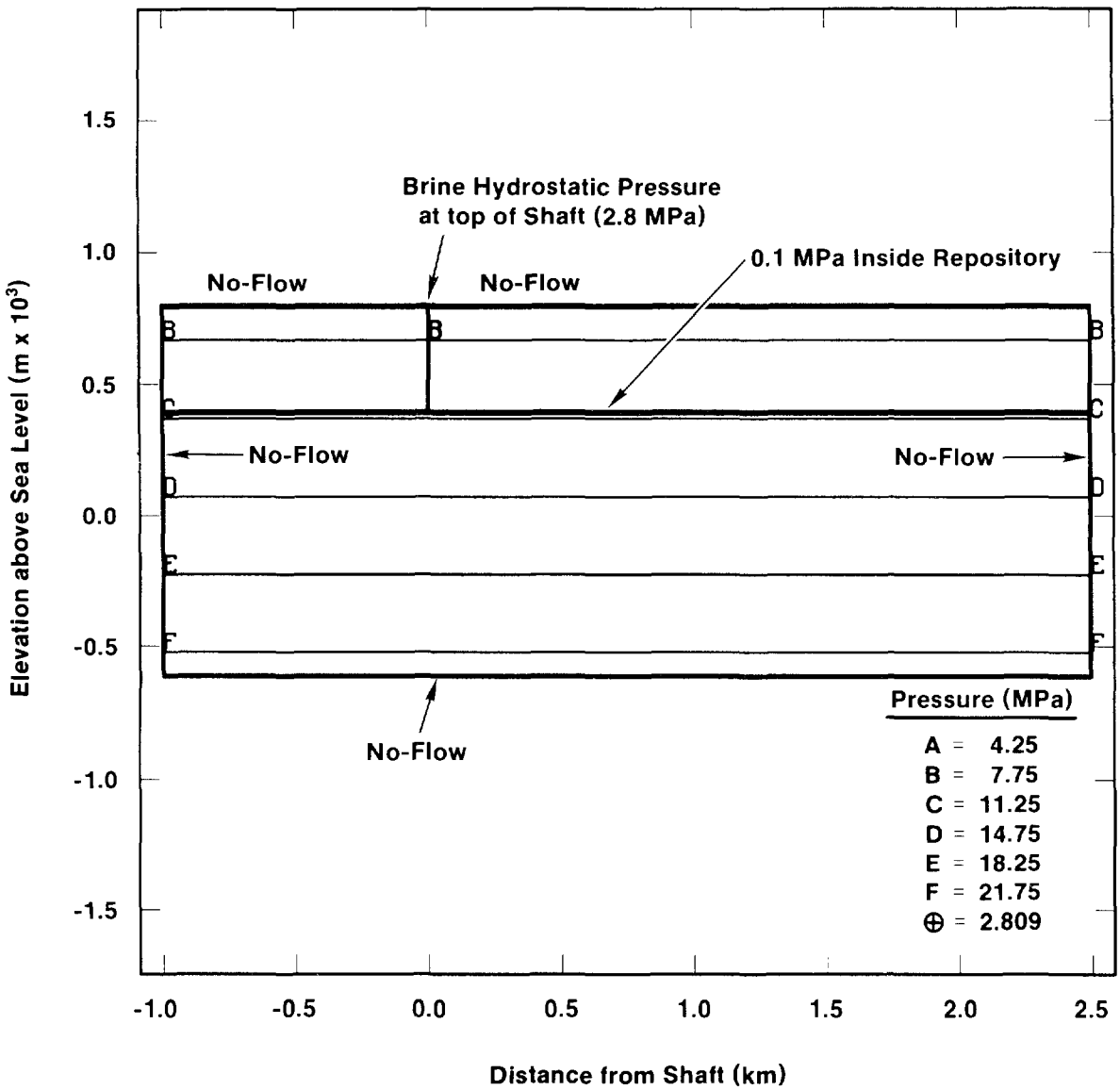

TRI-6342-1319-0

Figure 4-16. Initial Pressure Conditions

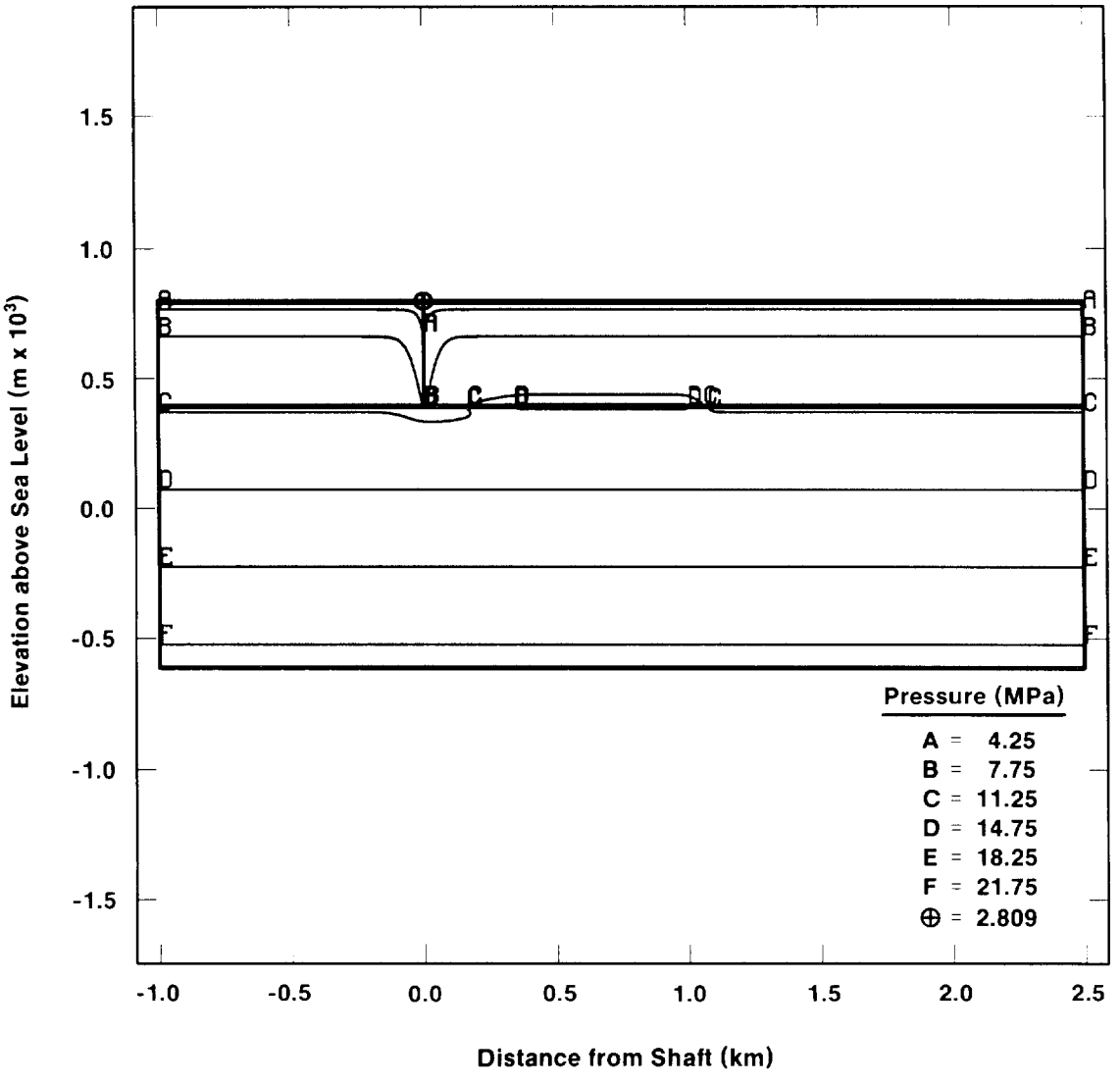

Figure 4-17. Pressures at 600 Years

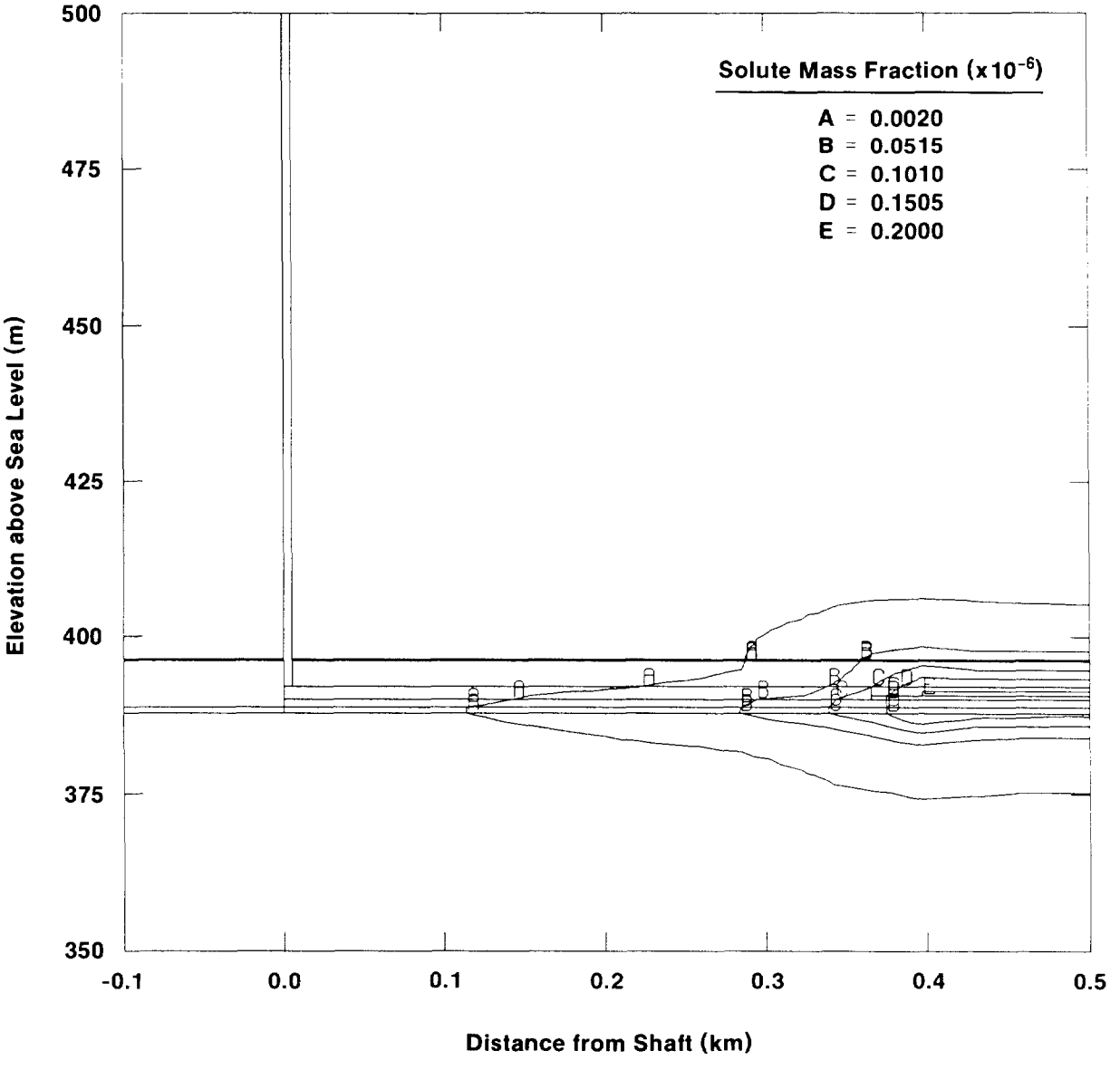

TRI-6342-1322-0

Figure 4-18. Mass Fraction Contours for Undisturbed Vertical Cross Section, Time-Dependent Gas Pressures and Permeabilities (from BOAST II), Step=100 Years, Diffusivity=1.4e-11, Total Time=10,000 years

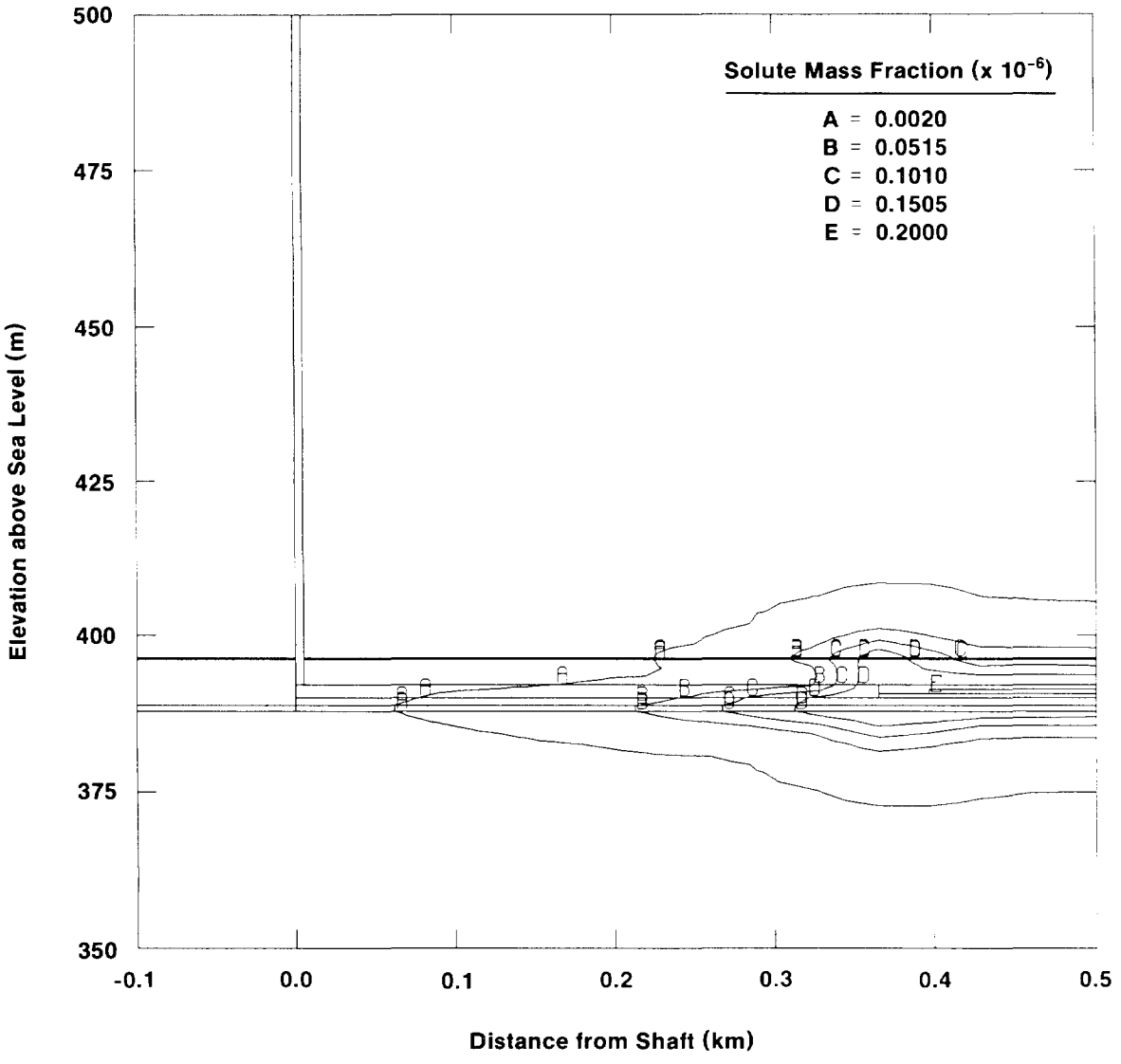

Figure 4-19. Mass Fraction Contours for Undisturbed Vertical Cross Section, Time-Dependent Gas Pressure Only (BOAST II), Time Step=100 Years, Diffusivity = 1.4e-11, Total Time=10,000 years

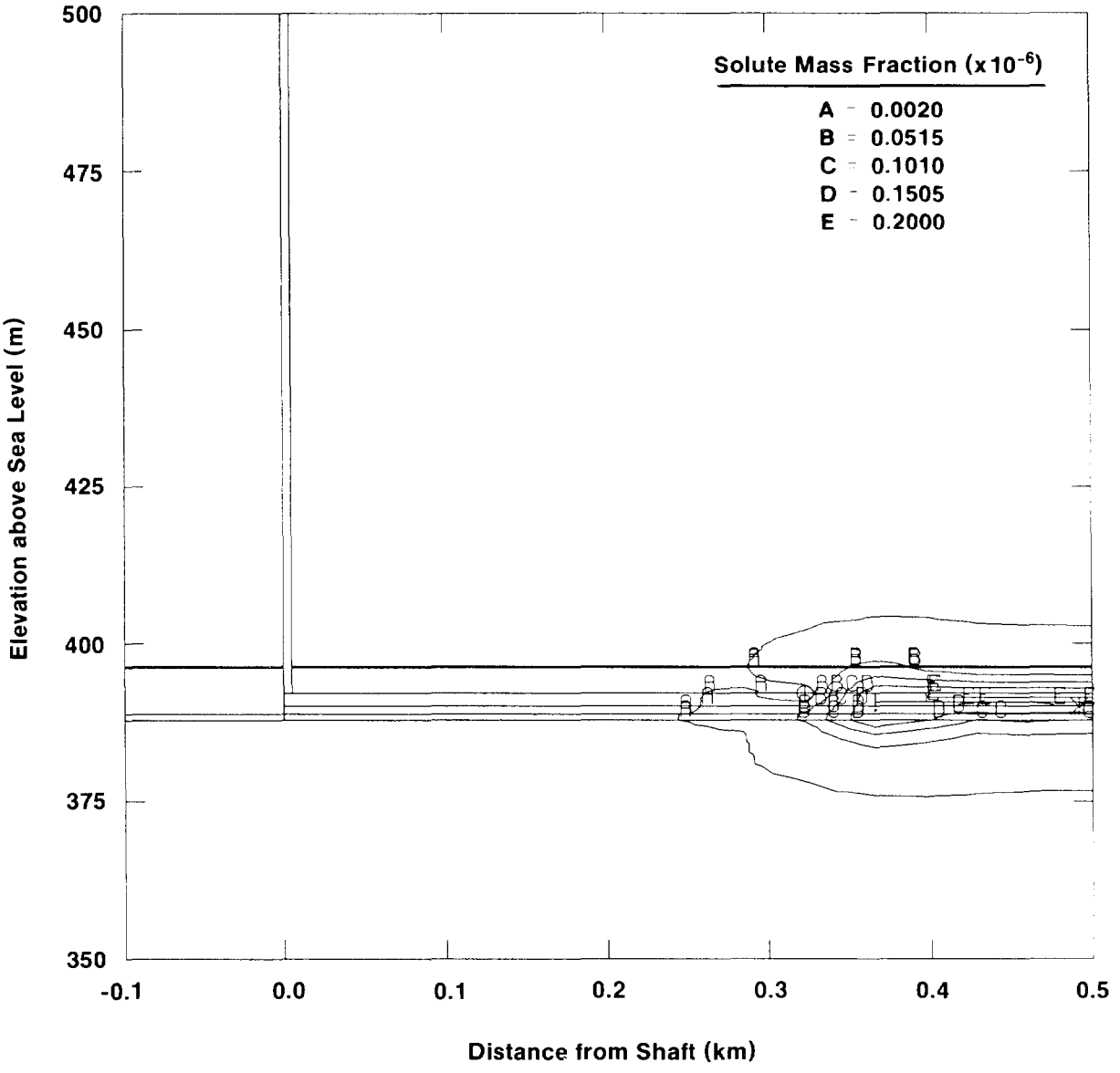

Figure 4-20. Mass Fraction Contours for Undisturbed Vertical Cross Section, Time-Dependent Gas Pressure Only (BOAST II), Diffusivity=1.4e-11, Total Time=1000 years

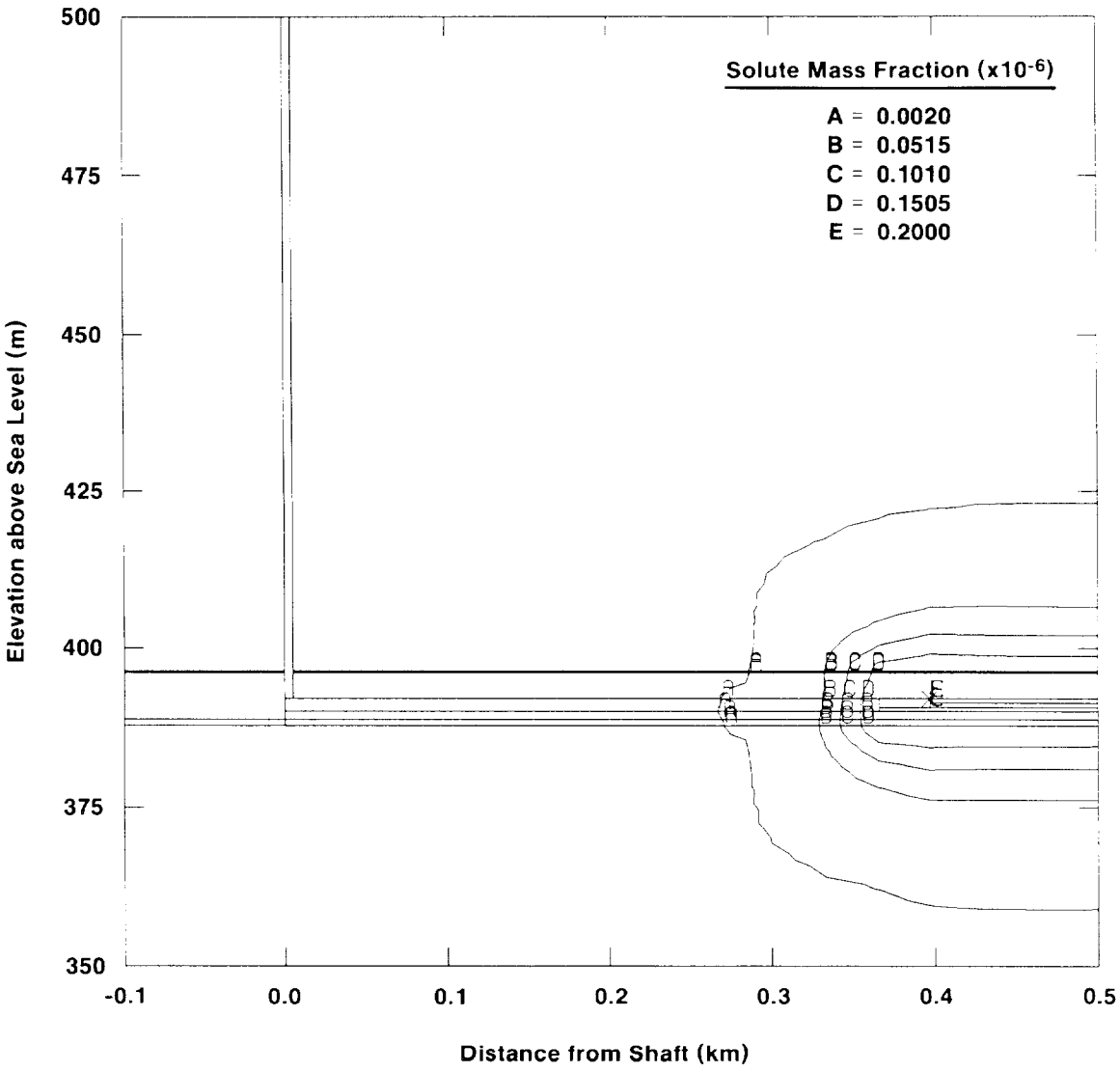

Figure 4-21. Mass Fraction Contours for Undisturbed Vertical Cross Section, Time-Dependent Gas Pressure Only (BOAST II), Diffusivity=1.4e-9, Total Time=1000 years

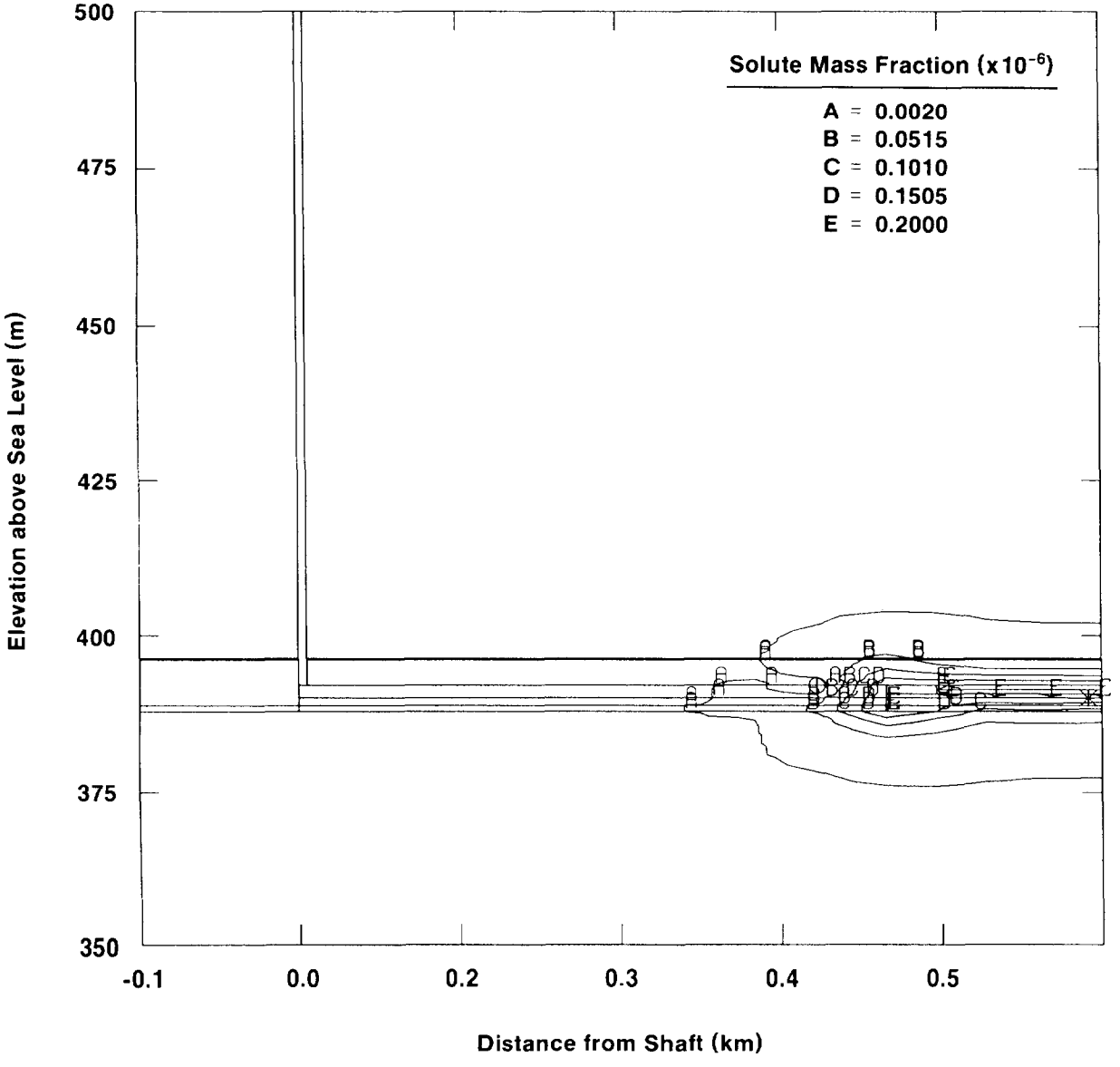

Figure 4-22. Mass Fraction Contours for Undisturbed Vertical Cross Section, Time-Dependent Gas Pressure Only (BOAST II), No Diffusion, Total Time=1000 years

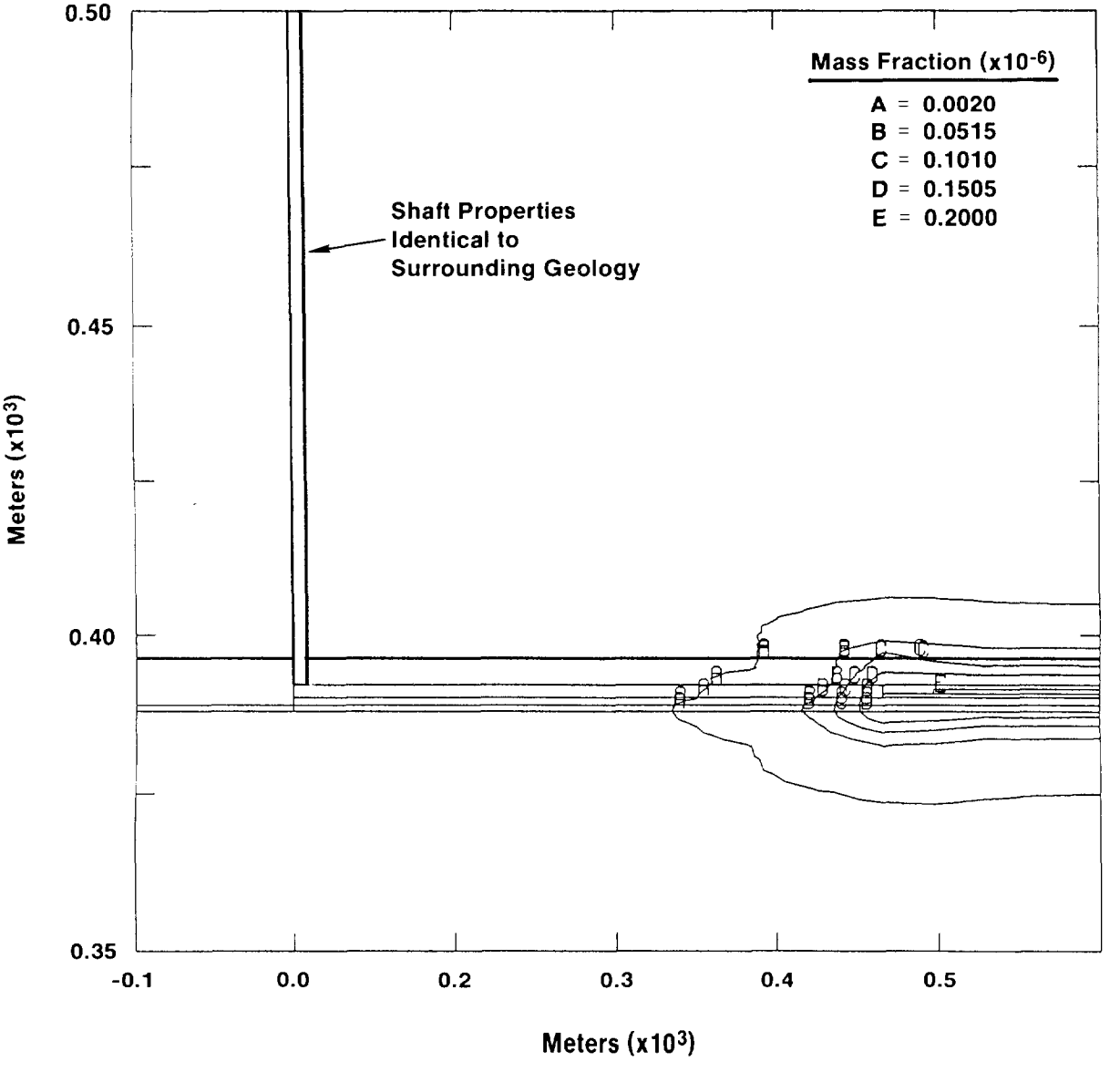

TRI-6342-1327-0

Figure 4-23. Mass Fraction Contours for Undisturbed Vertical Cross Section, Time-Dependent Gas Pressure Only (BOAST II), No Shaft, Total Time 10,000 Years

obtained from calculations performed in a vertical cross section (Section 4.2.3.2). Since the calculations have been performed utilizing single-phase groundwater flow theory, no adsorbate mass transfer, and since the panels are assumed to lie within MB139, the following results represent a conservative estimate of transport phenomena away from the panels in the MB139 medium. References to variables and equations used in SUTRA correspond to definitions provided in Section 4.2.3.1.

Summary of Results. Contours of solute concentrations were plotted at different times and at the end of the 10,000 year regulatory period. At 10,000 years the 1% source-concentration contour extended 75 to 110 m from the repository boundary. These results are consistent with the SUTRA results obtained in a vertical cross-section (approximately 120 m, Section 4.2.3.2) and tend to confirm the validity of the two-dimensional methods used.

Spatial and Temporal Grids

SUTRA was used to investigate transport phenomena as if the WIPP repository fed directly into the fractured anhydrite of MB139. This assumption eliminates the resistance to brine flow that exists in the DRZ just below the repository and maximizes the flow in MB139. Using symmetry and areal geometry (in plane), only one-fourth of the waste panel's shadow projected onto the MB139 layer needs to be modeled. To simulate accurately the gas-generation effects, a pressure history (obtained from BOAST II; see Figure 4-2) was applied to interior repository nodes that lie in the disturbed zone. All calculations were run to 10,000 years. The effect of the shaft is not included.

Simulations using SUTRA were performed assuming single-phase, saturated flow ($S_l = 1$), no adsorbate mass production (i.e., $C_s = 0$), single-species solute without decay, and no density change with concentration. Since density was not allowed to vary as a function of concentration change, ($\partial \rho_f / \partial \hat{C} = 0$), SUTRA's coupling process between flow and transport was eliminated. This is a valid assumption since the initial mass fraction is quite small compared to the initial brine solution density. The assumption that adsorption does not occur is conservative. The model used SUTRA's time-dependent boundary-condition capability to handle the transient pressure condition from BOAST II calculated due to gas generation (Figure 4-2).

Two different spatial and temporal grids were used to model the repository/MB139 medium. A coarse finite-element (FE) mesh used 2,160 elements (45 x 48 elements and 46 x 49 nodes) with a maximum element length (E_l) of 78.50 m (Figure 4-24). The fine FE mesh of 2,116 elements (46 x 46 elements and 47 x 47 nodes) modeled a smaller domain within the coarse mesh. With a maximum element length of 39.25 m, the exterior boundaries of the fine mesh are also shown in Figure 4-24. The coarse mesh calculation was run to provide boundary conditions for the fine mesh calculations. The first temporal grid used 100 100-year time steps. The second temporal

grid used 200 50-year time steps. The coarse spatial mesh was initially constructed to maintain a mesh Peclet number (Pe_m) less than 10 (the mesh Peclet number estimates the ratio of advection to transport, and can be approximated as $Pe_m=MAX(E_l)/\alpha_L$). The fine mesh was used to study the sensitivity of the model to smaller mesh Peclet numbers. The first temporal scale of 100-year time steps was chosen to handle accurately the pressure history simulating gas generation. Although SUTRA uses an implicit time integration scheme (backwards time-differencing method), a finer temporal scale of 50-year time steps was applied to both coarse and fine spatial grids. The smaller time-step runs were used to investigate sensitivity of time-step size when using time-dependent boundary conditions. The SUTRA codes states that spatial stability is usually guaranteed when $Pe_m \leq 4$. Since the E_ℓ of the fine mesh was 39.25 m and the longitudinal dispersivity of both MB139 materials modeled was 15.00 m, the resulting $Pe_m \approx 2.619$.

Material Properties, Boundary Conditions, and Initial Conditions

Excavation damage and creep damage is expected to modify the properties of MB139 directly under the repository (Lappin et al., 1989). Consequently, two material regions were modeled with both the fine and coarse FE grids: MB139FF and MB139DRZ. (The suffix FF represents "Far Field"; DRZ denotes "Disturbed Rock Zone.") The required SUTRA flow properties are (1) grain density (of solid matrix), (2) fluid density, (3) permeability (assumed isotropic for this calculation), (4) bulk compressibility (of solid matrix), and (5) fluid compressibility. The required SUTRA transport properties are (1) dispersivity, (2) diffusion, (3) fluid density, and (4) fluid viscosity. The material property values of both MB139FF and MB139DRZ are for the most part given in Volume 3 of this report. Certain parameters differed, however, from those found in Volume 3 of this report. For MB139FF a permeability of $1.0\text{x}10^{-19}$ m^2 was used (as opposed to the report value of $2.87\text{x}10^{-20}$ m^2) and for MB139DRZ a porosity of 0.06 was used as opposed to a value of 0.055 reported in Volume 3 of this report. The SUTRA input variable for solid (bulk) compressibility, corresponding to the MB139 bulk compressibility was calculated as the inverse of the solid mechanics bulk modulus (K_{bulk}). Therefore the bulk compressibility equals $3(1-2\nu)/E$, where ν and E are Poisson's ratio and Young's modulus, respectively. It is assumed that the anhydrite material and MB139 material have equivalent bulk compressibilities. Both ν and E values are referenced from Table A-8 of Rechard et al. (1990a). The MB139 fluid's molecular diffusion, density, compressibility, and viscosity were assumed equivalent to Salado brine properties found in Table A-9 of Rechard et al. (1990b).

The SUTRA code uses a coefficient of apparent molecular diffusivity of solute in solution in a porous medium, including tortuosity effects (D_p, Section 4.2.3.1), for the diffusion term of the transport partial differential equation (PDE). Thus, for diffusive/dispersion-dominated transport, solute concentration is highly sensitive to the input diffusion and dispersivity values. The

apparent molecular diffusivity term used in SUTRA calculations was computed as the product of the free-water molecular diffusion in a pure fluid, D^*, and tortuosity, τ (1.000×10^{-10} m^2/s and 0.140, respectively).

Dirichlet boundary conditions (of p=11.00 MPa and $\hat{C}$ = 0.000 kg/kg) for the coarse grid were applied to the far-field boundaries. The far-field pressure of 11.00 MPa was taken as the median value of brine pressure at the repository level found in Rechard et al. (1990b). Neumann boundary conditions ($\partial p/\partial u = 0$ and $\partial \hat{C}/\partial u = 0$, where u = outward normal direction) were applied to the one-fourth repository/MB139 symmetric boundaries as shown in Figure 4-25. In addition, time-dependent pressure conditions were applied at interior nodes of the MB139DRZ to simulate gas generation effects. The time-dependent conditions (a pressure history function) from BOAST II (see Figure 4-2) were applied exclusively to interior nodes of the MB139DRZ because SUTRA computes an associated fluid-flux term at each pressure boundary condition node. According to Voss (1984), SUTRA computes specified pressures at nodes through cellwise addition of fluid flux, Q_{bc}^i (where i denotes a node number) [L^3/t], as

$$Q_{bc}^i = v\left(p_{bc} - p^i\right) \tag{4-40}$$

where v is the conductance [$L^4 t/M$], p^i is the specified pressure node [M/Lt^2], and p_{bc} is the specified pressure value [M/Lt^2].

SUTRA defines a "cell" as a node centered among four separate quadrants of four neighboring elements. Thus for a cell in which a large number is assigned to v, the flux term Q_{bc}^i dominates the fluid mass balance equation. This results in $p^i \cong p_{bc}$ and achieves the specified pressure at the node representing cell i. It is because of this "cellwise" fluid-flux terminology involving fluid sources and flows across boundaries that the time-dependent pressures were applied only to the interior nodes of material MB139DRZ. Thus, applying a pressure condition on the material boundary of MB139FF/MB139DRZ would invoke unrealistic fluid-flux terms. Figures 4-26a and 4-26b display the MB139DRZ material and the interior nodes at which the BOAST II pressure function was applied for both spatial grids. In conjunction with the pressure function, a constant concentration (SUTRA's concentration is actually a mass fraction: mass solute per mass total solution) of 2.000×10^{-7} kg/kg was also set at the interior MB139DRZ nodes. This value of concentration is about the maximum solubility limit of brine solution transporting radionuclide $^{240}Pu^{+4}$.

At first, the fine FE mesh calculations used two sets of time-dependent conditions, transient boundary conditions and a transient source function (pressure history and constant concentration applied on the MB139DRZ interior nodes). To remain consistent with the coarse FE mesh

calculations, the fine grid's boundary pressures and concentrations were interpolated at each time step from the coarse mesh solution. (Note that the fine mesh is nested completely within the coarse mesh as shown in Figure 4-24). However, the interpolated fine mesh boundary values at each time step were found to be identical to the coarse mesh constant boundary values. Thus, the same constant coarse mesh boundary conditions were applied to the fine mesh boundaries and the coarse grid calculations were, in fact, not necessary.

Initial conditions of the two primary variables (pressure and concentration) for both the coarse and fine grids were p = 11.00 MPa and $\hat{C}$ = 0.000 kg/kg, applied at the nodes of the MB139FF material and at nodes of the MB139FF/MB139DRZ boundary.

Results and Discussion

Because the interior nodes of MB139DRZ are initially at a lower pressure than the nodes of MB139FF (MB139DRZ at atmospheric pressure and MB139FF at a far-field pore pressure of p=11.00 MPa), the SUTRA solution resulted in flow into the MB139DRZ material until the gas generation source function (pressure history) reached 11.00 MPa. After that time, the MB139DRZ pressure exceeded the MB139FF far-field pore pressure, and flow was driven outward from the MB139DRZ material.

Viewing the concentration contour plots, it can be seen that both grid size and time-step size have a noticeable effect on transport. Studying the coarse mesh analyses, it was found that decreasing the time-step size from 100 to 50 years had no affect on the transport distance of the 1% source concentration contour line (2.0×10^{-9} kg/kg) after 10,000 years (Figures 4-27a and 4-27b). In contrast, the fine mesh SUTRA calculations were more sensitive to smaller size time steps. The fine mesh analyses resulted in a greater transport distance of the 1% source-concentration line for 50-year time steps than for 100-year time steps. Yet, decreasing the time-step size even further (10-year time steps) showed no difference from using the 50-year time steps. The effects of concentration transport due to decreased time-step size on the fine mesh after 1,000 years are shown in Figures 4-28a, 28b, and 28c. Comparing the coarse and fine mesh calculations for 50-year time steps, it can be seen in Figures 4-27b and 4-29 that the fine mesh shows the 1% source-concentration contour line traveling much further and around both "fingers" of the one-fourth repository's shadow in the MB139 layer. Since the fine mesh SUTRA calculations revealed that decreasing the time step to 10 years had no effect compared to the calculations using 50-year time steps, it follows that 50-year time steps are adequate for temporal discretization. This SUTRA transport calculation (fine mesh and 50-year time steps) predicts that after 10,000 years the 1% source-concentration contour line (2.000×10^{-9} kg/kg) has traveled approximately 75 m from the MB139DRZ-MB139FF material intersection (Figure 4-29).

To verify that this model is not diffusion/dispersion dominant, additional calculations setting the velocity field equal to zero would be necessary. If the velocity contribution of the transport PDE were omitted from equation (4-35), the resultant PDE becomes more parabolic,

$$\varepsilon\rho_f \frac{\partial \hat{C}}{\partial t} = \nabla \bullet \left\{ \left[\varepsilon\rho_f \left(D_p \underline{\underline{I}} + \underline{\underline{D}} \right) \right] \bullet \nabla \hat{C} \right\} \tag{4-41}$$

where,

ε = porosity (dimensionless),

ρ_f = fluid density (M/L^3),

∇ = del operator,

$\bullet$ = dot product,

D_p = diffusion coefficient (L^2/t),

$\underline{\underline{I}}$ = identity tensor (dimensionless),

$\underline{\underline{D}}$ = dispersivity tensor (L^2/t), and

$\nabla \hat{C}$ = concentration gradient (L^{-1}).

Equation (4-41) reveals that if the dispersivity tensor, $\underline{\underline{D}}$, components were small (functions of the velocity components), the transport PDE would be diffusion, D_p, dominated. A brief study was made to investigate the influence of diffusion on contaminated groundwater transport. Rather than use a zero-velocity field ($\underline{v}$=0) to study the uncoupled effects of diffusion, a calculation was performed using an order-of-magnitude increase in the apparent molecular diffusion coefficient, D_p (1.400×10^{-10} m^2/s), with the fine FE mesh and a temporal grid of 100-year time steps. As seen in Figure 4-30a, the resulting calculation's increased diffusion in the transport is noticeable when compared to the fine mesh calculation with the original diffusion coefficient(1.4×10^{-11} m^2/s of Figure 4-30b (especially between the "fingers" where the 1% source-concentration contour line has traveled farther). However, the increased diffusion does not dominate the solution (concentration-contour lines), and since Pe_m = 2.619, the model is not completely diffusion-dominated and advection should not be ignored.

An additional calculation was performed to study the effect of placing source concentration nodes on the boundary of the MB139FF and MB139DRZ materials. This slight modification to the boundary conditions retained the flow equation's time-varying Dirichlet conditions applied to the interior MB139DRZ nodes, while extending the transport equation's constant Dirichlet conditions to all interior MB139DRZ nodes and MB139DRZ/MB139FF boundary nodes. Previous calculations assumed that the source terms for transport were applied only to the interior MB139DRZ nodes. Thus employing the fine mesh, a temporal discretization of 50-year time steps, identical initial conditions, and these slightly modified boundary conditions, the calculation was run to 10,000 years. As displayed in Figure 4-31, the 1% source concentration contour line

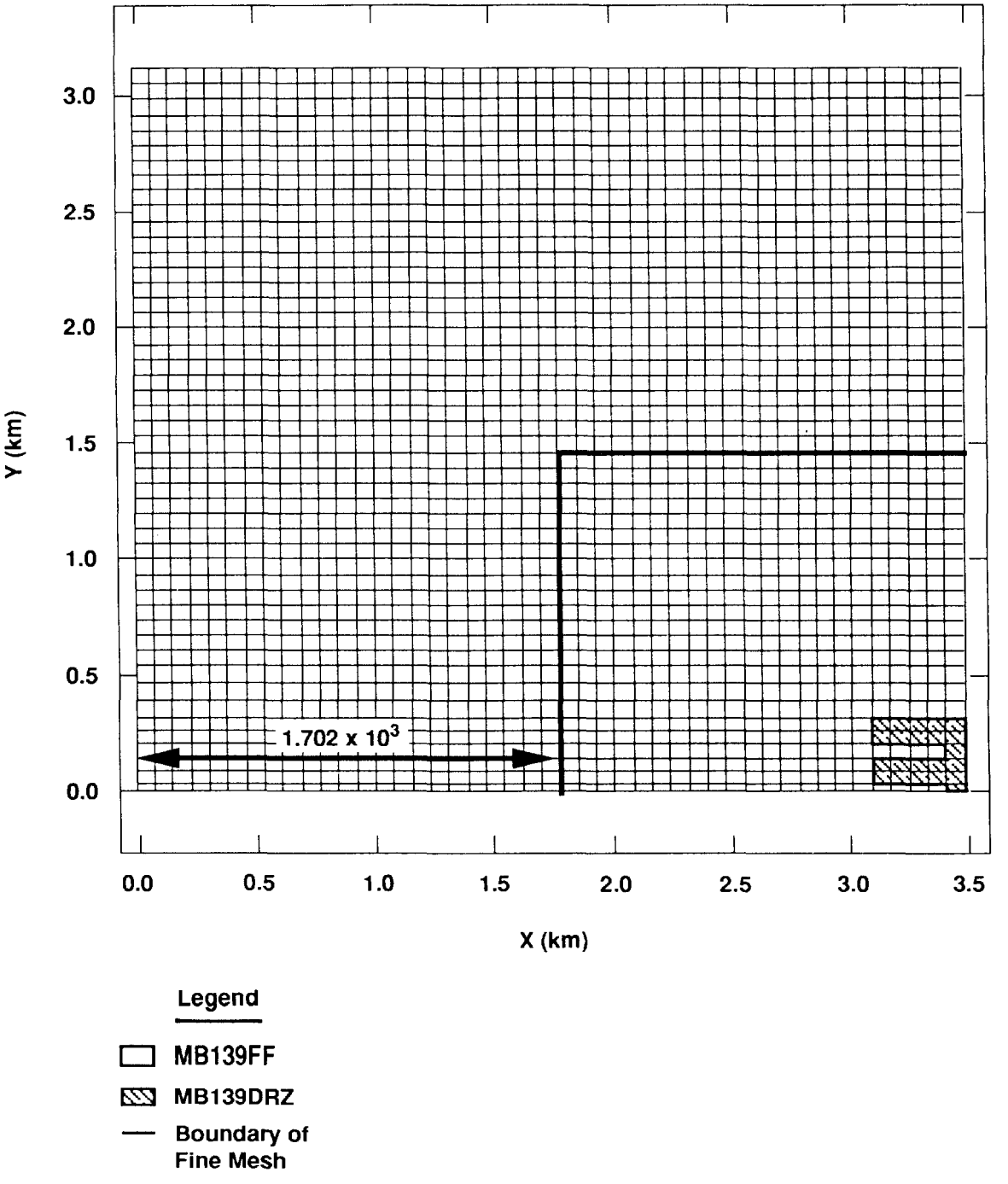

TRI-6342-1386-0

Figure 4-24. Coarse FE Mesh for In-Plane Calculations

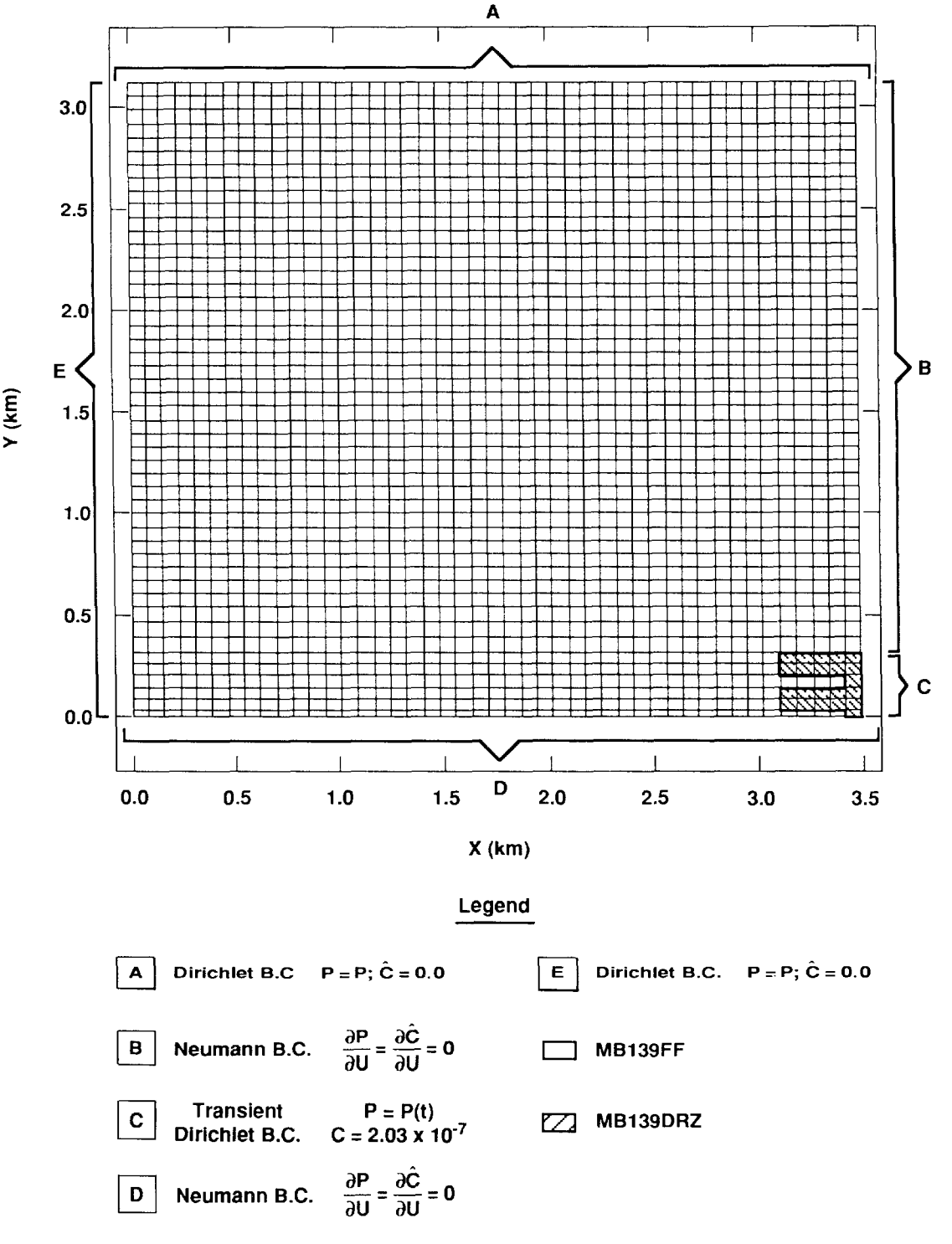

Figure 4-25. Boundary Conditions for In-Plane Calculations

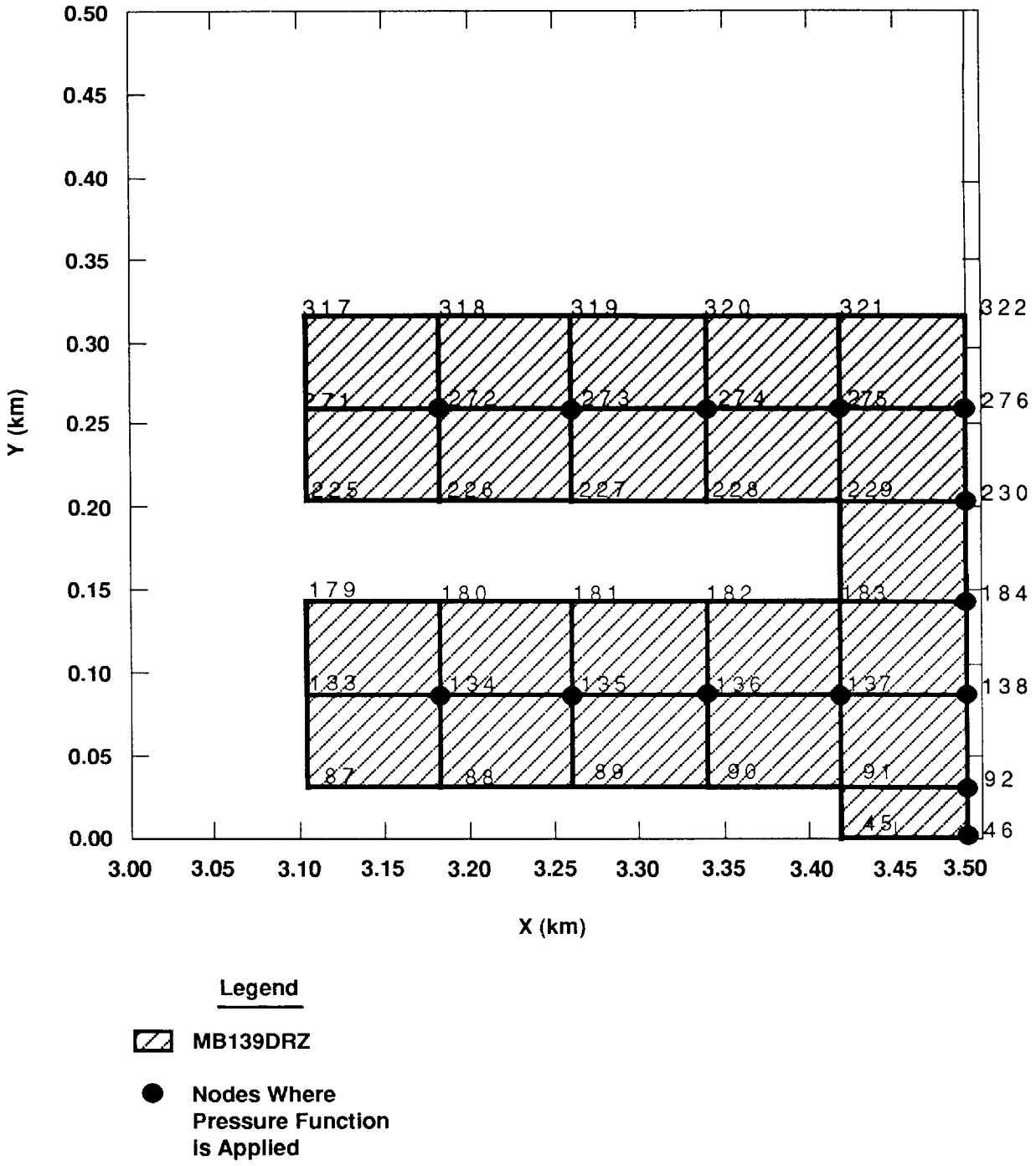

TRI-6342-1384-0

Figure 4-26a. Location of Nodes of Coarse FE Mesh for Applied Pressure Function

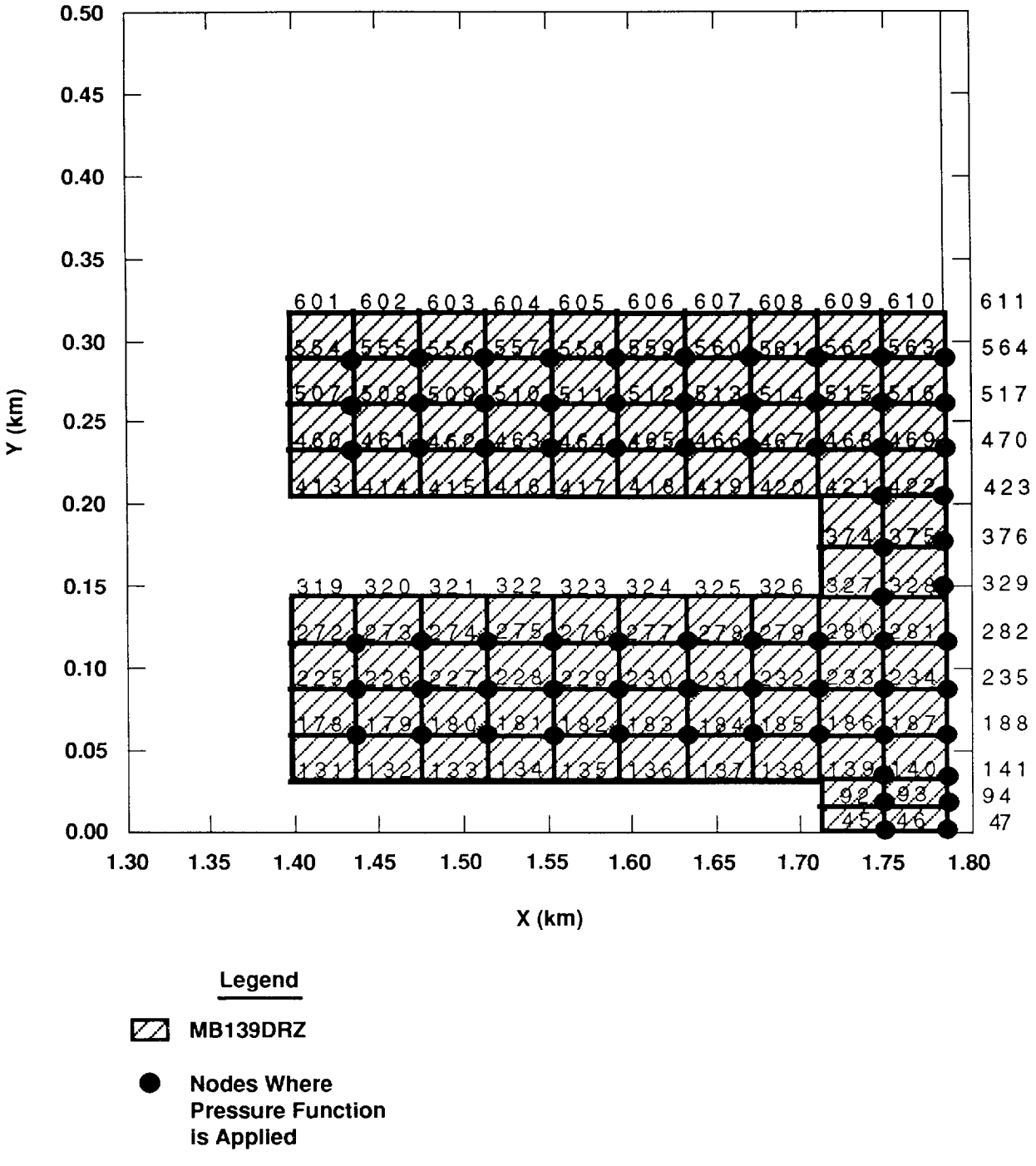

TRI-6342-1385

Figure 4-26b. Location of Nodes of Fine FE Mesh for Applied Pressure Function

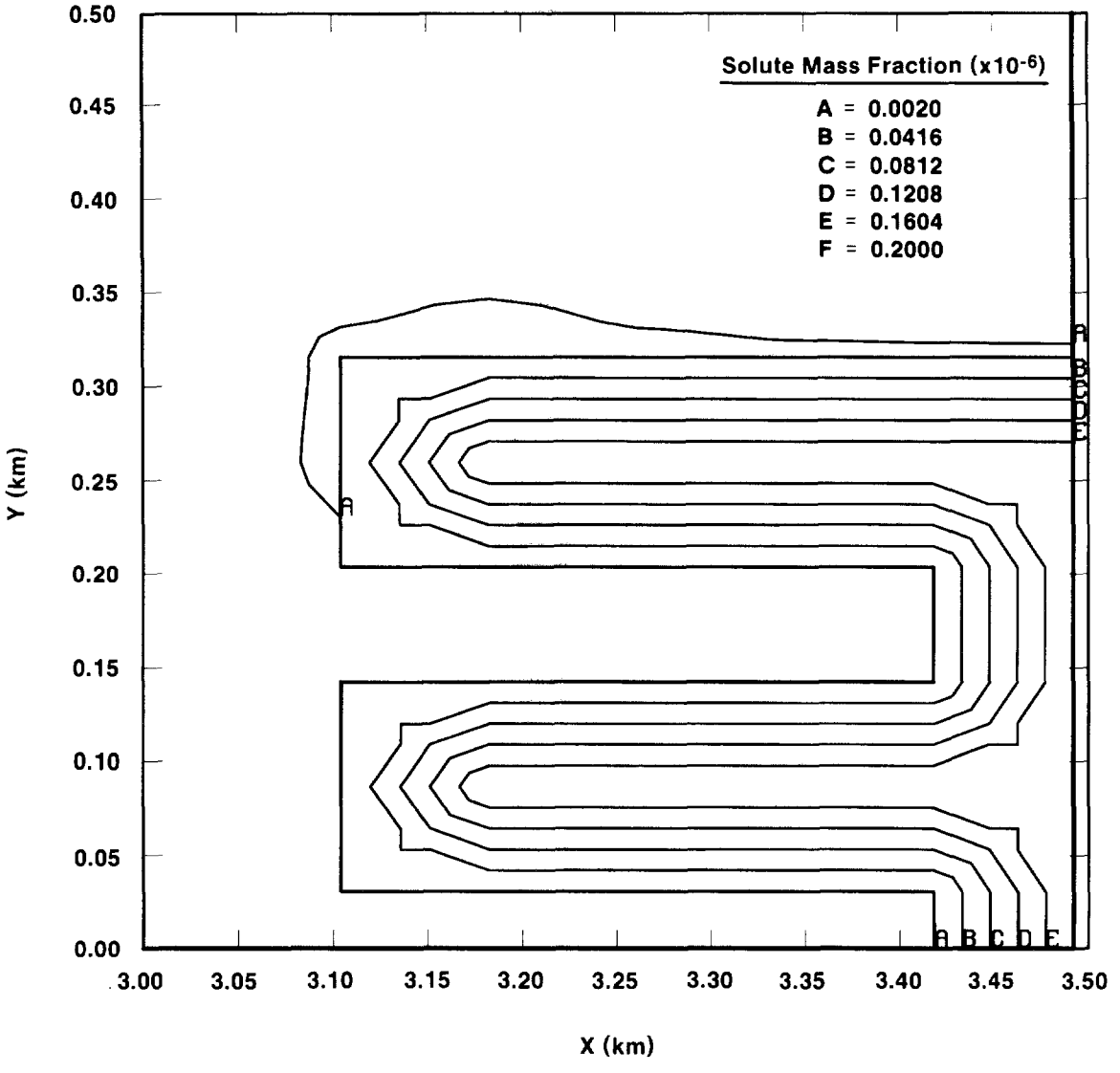

TRI-6342-1332-0

Figure 4-27a. Solute Concentration Contours at 10,000 Years (Coarse Mesh, Δt = 100 Years)

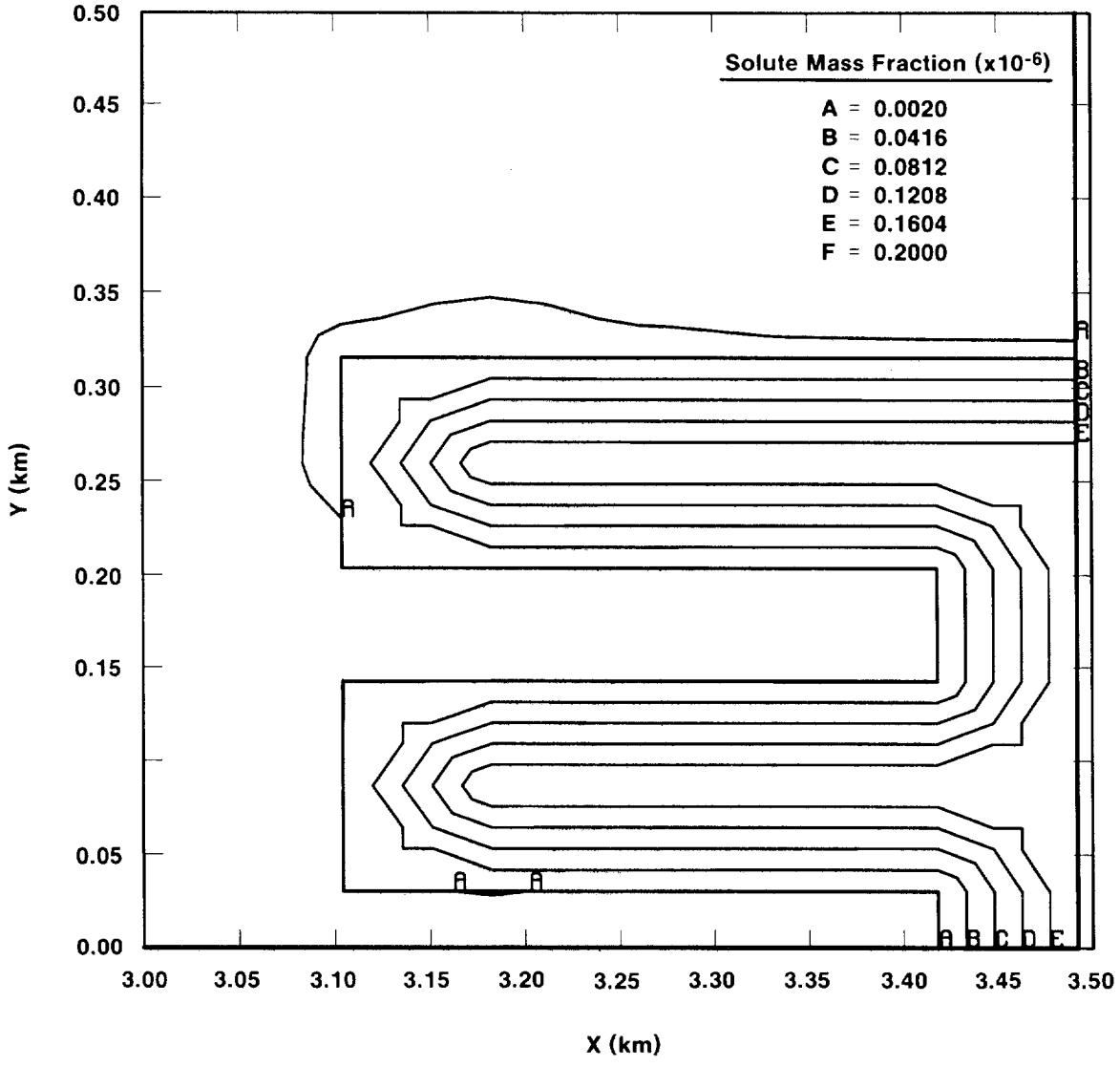

TRI-6342-1333-0

Figure 4-27b. Solute Concentration Contours at 10,000 Years (Coarse Mesh, Δt = 50 Years)

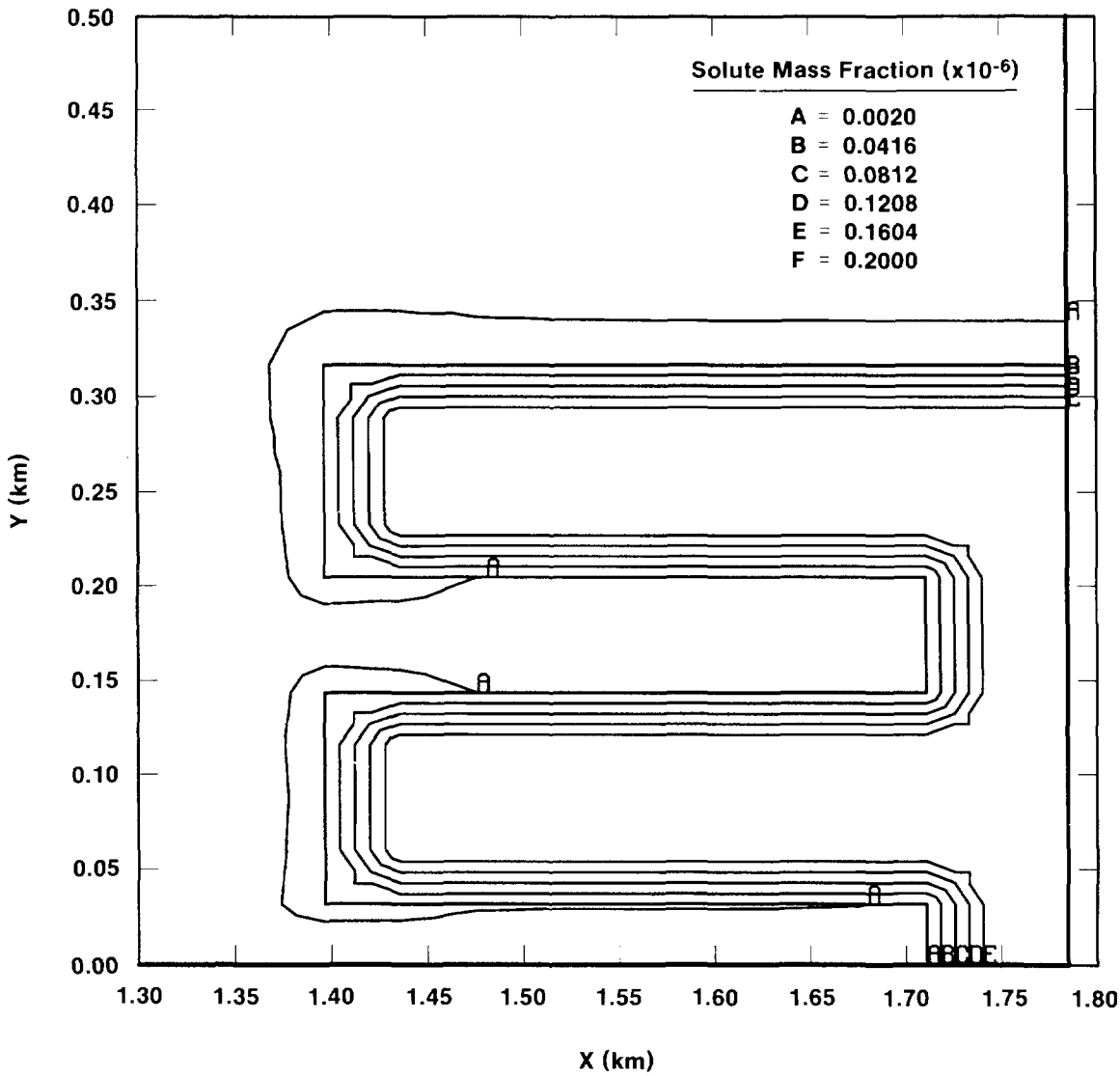

Figure 4-28a. Solute Concentration Contours at 1000 Years (Fine Mesh, Δt = 100 Years)

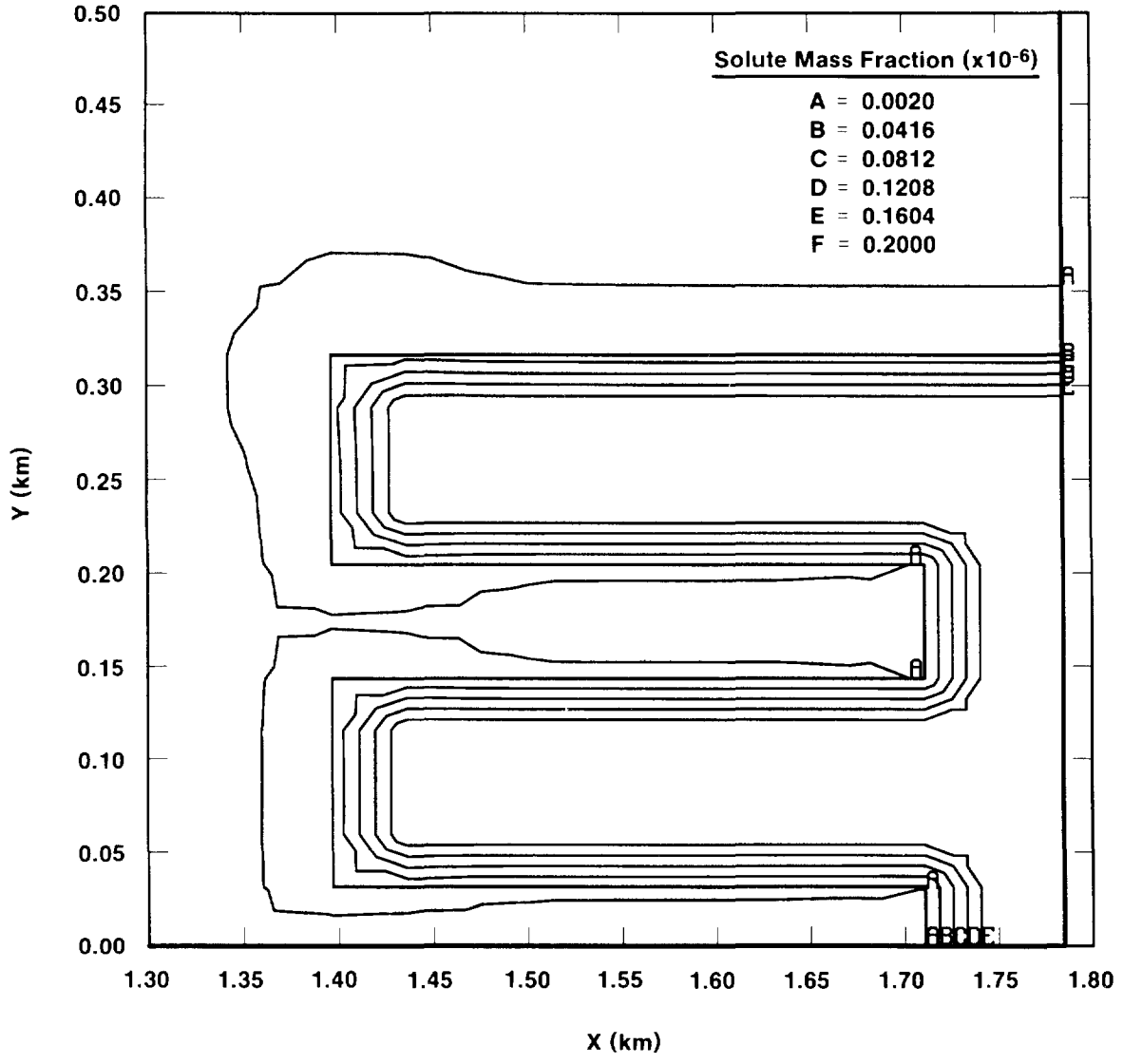

Figure 4-28b. Solute Concentration Contours at 1000 Years (Fine Mesh, Δt = 50 Years)

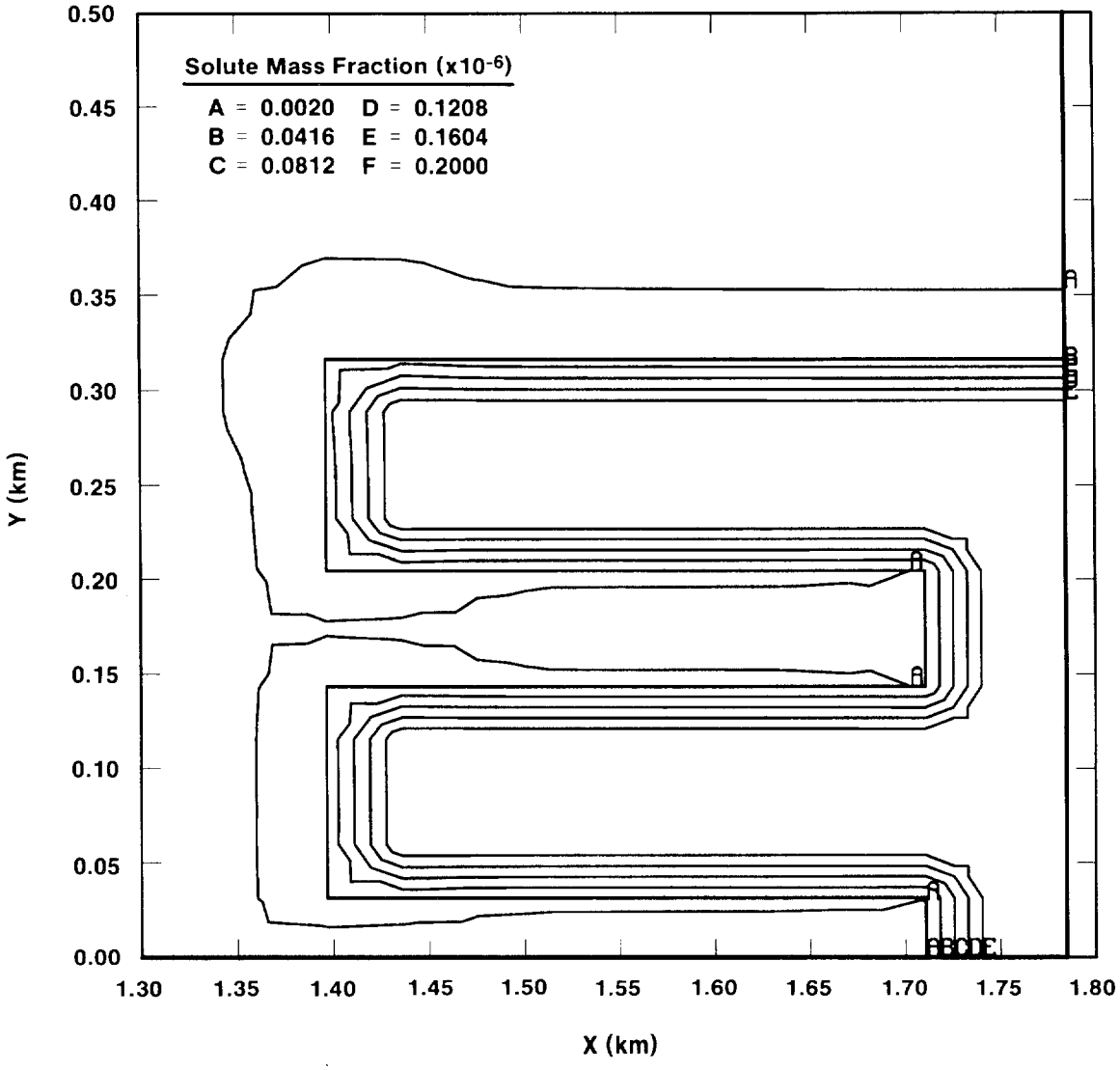

Figure 4-28c. Solute Concentration Contours at 1000 Years (Fine Mesh, Δt = 10 Years)

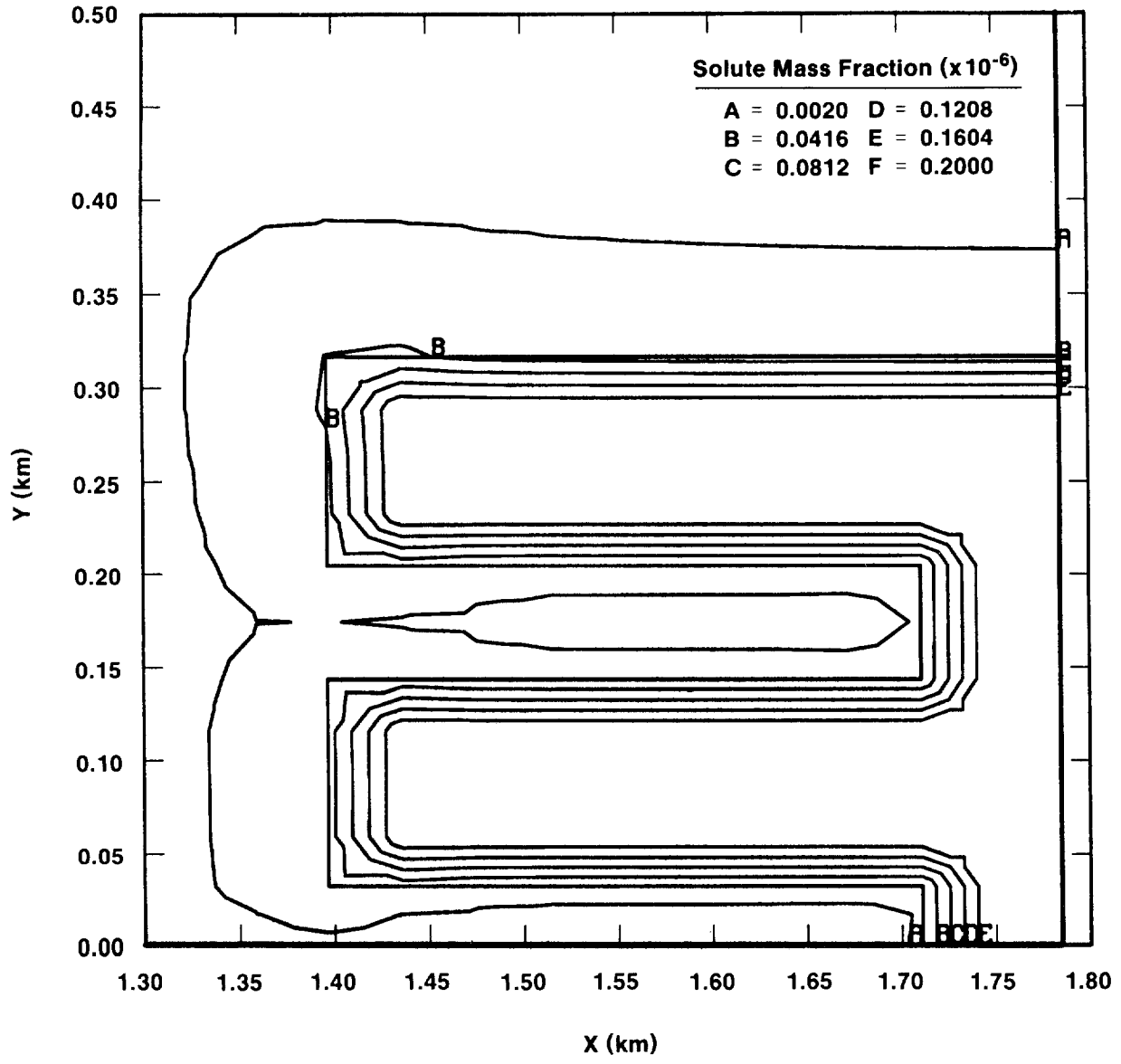

TRI-6342-1337-0

Figure 4-29. Solute Concentration Contours at 10,000 Years (Fine Mesh, Δt = 50 Years)

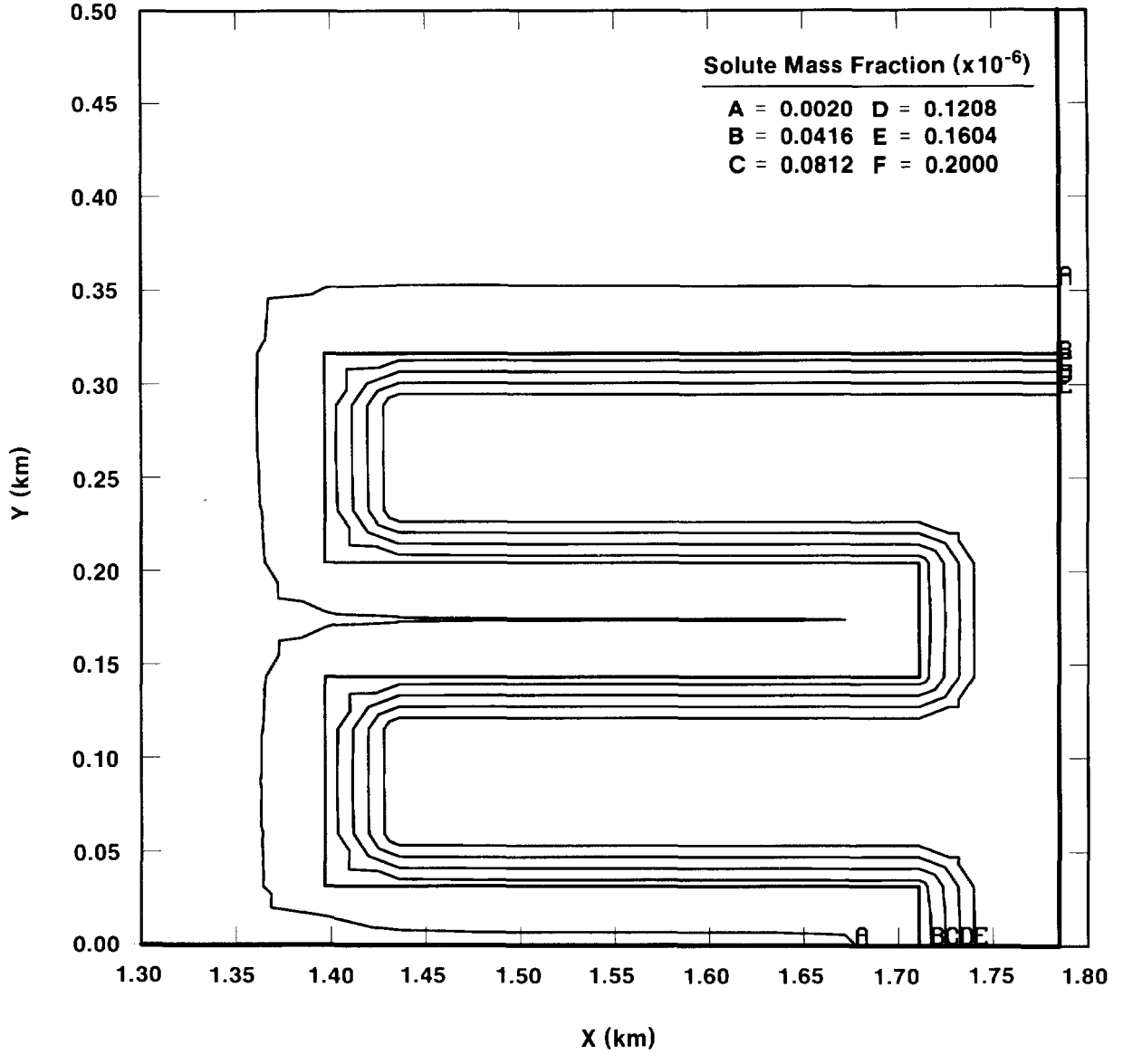

Figure 4-30a. Solute Concentration Contours at 10,000 Years With Increased Diffusion Coefficient (Fine Mesh, Δt = 100 Years)

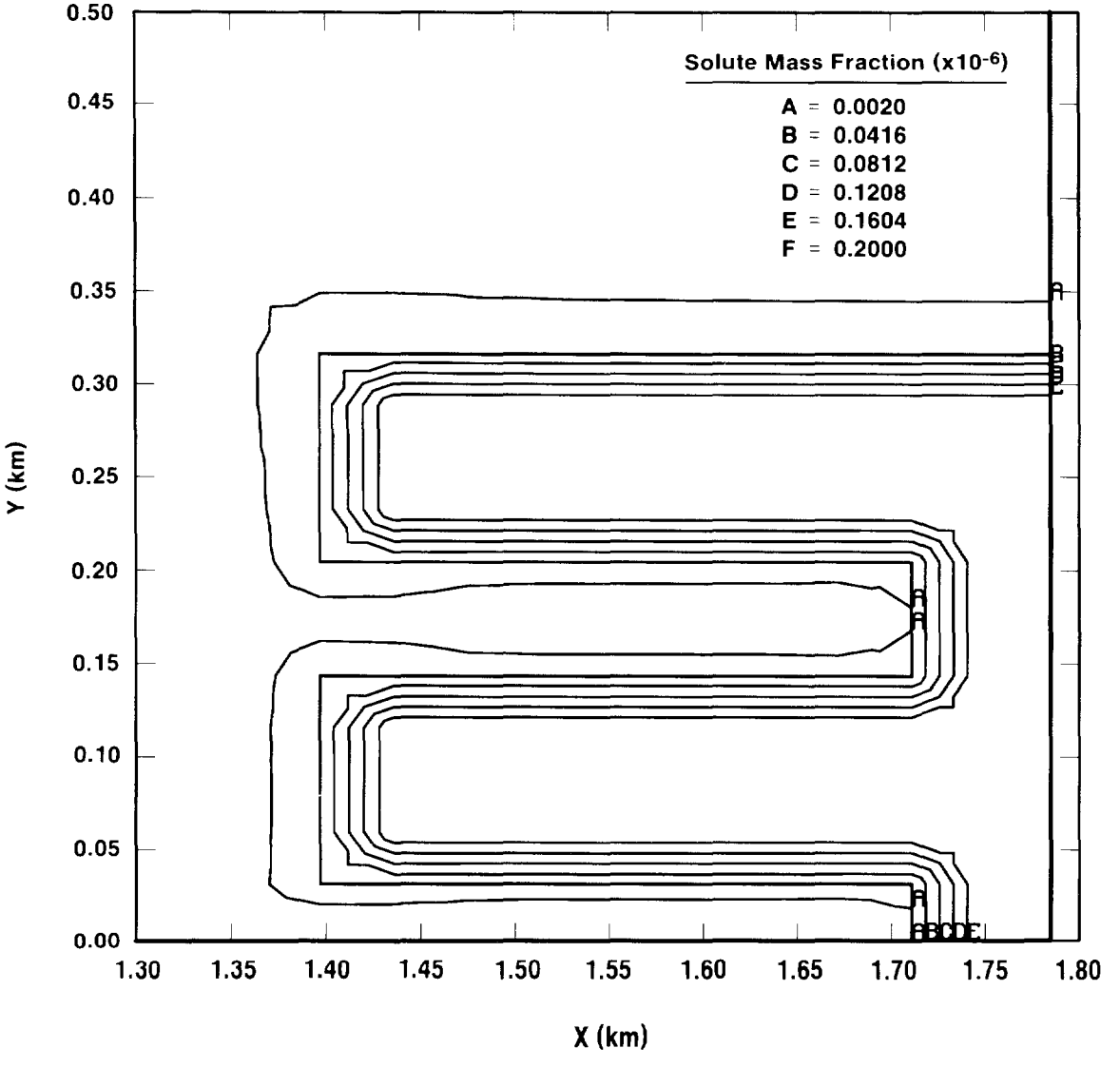

TRI-6342-1339-0

Figure 4-30b. Solute Concentration Contours at 10,000 Years With Original Diffusion Coefficient (Fine Mesh, Δt = 100 Years)

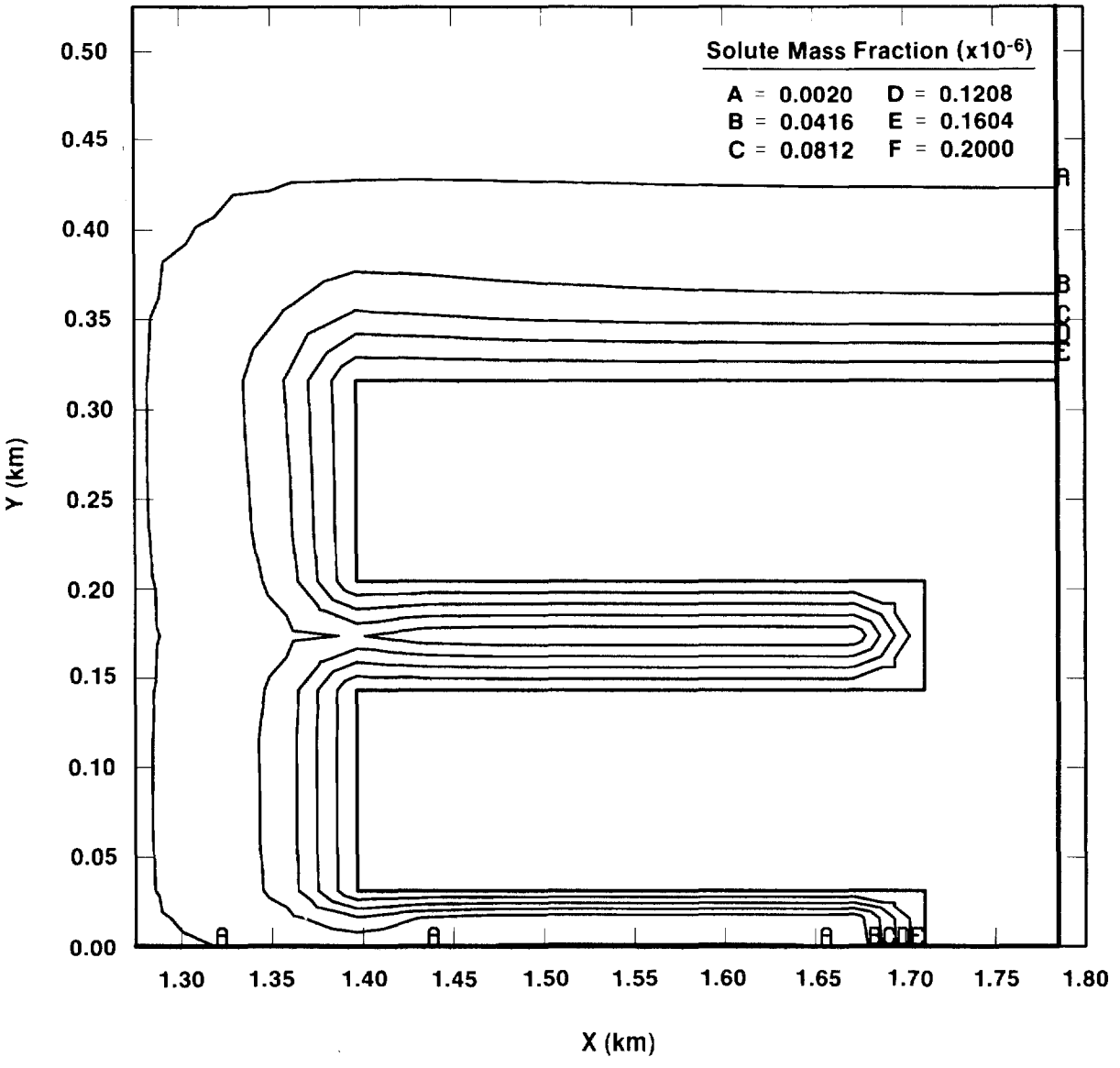

Figure 4-31. Solute Concentration Contours at 10,000 Years With Modified Concentration Source Placement (Fine Mesh, Δt = 50 Years)

has traveled 110 m into the MB139FF material, whereas previous calculations indicated a distance of 75 m (Figure 4-29). In addition, the concentration contours of Figure 4-31 depict no internal concentration gradients within the MB139DRZ material. This calculation is more conservative and provides an upper bound for transport phenomena in the MB139FF medium for this set of calculations.

4.3 Summary of Results for Undisturbed Performance of the Repository/Shaft

The calculations performed to assess the undisturbed performance of the Repository/Shaft System had four objectives

- To determine the path and extent of migration of radionuclides from the waste panel, and to quantify the magnitude of radionuclide transport up the shaft.
- To evaluate (in an approximate sense) the effect of waste-generated, undissolved gas on migration of radionuclides for undisturbed conditions.
- To assess the importance of three-dimensional effects on radionuclide migration in MB139.
- To cross-verify the results from the two single-phase codes SUTRA and STAFF2D.

To address these objectives, the four codes BOAST II, STAFF2D, SUTRA and PANEL were used in one or more configurations with varying material properties and operational assumptions. In utilizing these codes an attempt was made to use conservative assumptions that tend to maximize migration of dissolved radionuclides away from the waste panels. However, this was not done for all parameters where often average or median values were used. Thus the results from the calculations cannot be claimed to be a worst-case or a bounding result. In fact, it may not be possible to prove that any set of assumed input parameters will produce a bounding result. The results from the calculations are summarized below.

1. In determining the pathway and extent of movement of radionuclides from the repository an effort was made to use assumptions that were believed to be conservative and that would tend to maximize the extent of migration. Using STAFF2D as the principal computational tool and aided with results from BOAST II and PANEL, it was determined that the primary pathway of dissolved radionuclides out of the repository, as the result of pressurized gas generated by the corrosion and biodegradation of the waste, is downward through the small thickness of fractured Salado halite below the repository into MB139. The greater permeability of MB139 compared to the surrounding Salado channels the movement of dissolved radionuclides along the MB139 primarily toward the shaft. Movement of radionuclides along MB139 in the direction away from the shaft is slower than toward the shaft by approximately a factor of 2. Radionuclide concentrations

decrease steadily toward the shaft and also after the primary flow path turns upward into the shaft. The quantity of radionuclides passing a level of 20 m up the shaft from the repository in 10,000 years was calculated and shown to be several orders of magnitude less than the EPA limit of 1 for releases to the accessible environment at five kilometers from the waste emplacement panels. Similar results were shown for radionuclide migration away from the repository and shaft in MB139 at distances of 100 m from the repository.

Decreases in shaft permeabilities of 2 and 4 orders of magnitude (10^{-12} m^2 to 10^{-14} m^2 and 10^{-12} m^2 to 10^{-16} m^2) resulted in essentially no change in flow up the shaft. This implies that for undisturbed conditions the presence of an engineered shaft seal has little effect in restricting flow up the shaft unless the permeability of the seal approaches that of the intact surrounding Salado.

2. As configured in the undisturbed calculations, both SUTRA and STAFF2D considered only a single phase (brine) in assessing flow in and around the repository. The two-phase BOAST II code was used in the undisturbed calculations to provide input source pressures for the SUTRA calculations, and gas-modified material properties for both SUTRA and STAFF2D. The use of gas-modified material properties in SUTRA and STAFF2D allowed these single-phase codes to account for (in an approximate sense) the presence of undissolved gas in the waste and surrounding geology. Calculations with gas-modified material properties in SUTRA and STAFF2D revealed that the presence of undissolved gas has little effect on solute transport compared to the unmodified (fully saturated) case. The principal effect of the presence of gas is to delay the transport of dissolved radionuclides along the primary pathway to the shaft (MB139).

3. The majority of calculations for the undisturbed case were performed using a two-dimensional vertical cross-section through the repository, drift, and shaft. This two-dimensional representation neglects potential three-dimensional effects that may be important. In an effort to investigate this, two-dimensional SUTRA calculations were performed using a computational grid based on a horizontal plane through the repository and surrounding geology. Moreover, an additional conservative assumption was made that divided the permeabilities in the computational plane into two regions—one that corresponds to the excavation-disturbed MB139 and the other to the undisturbed MB139. These assumptions had the effect of placing the contents of the waste repository within MB139, the primary transport medium. In this configuration, the magnitude of the radial solute transport away from the repository (in MB139) was found to be entirely consistent with SUTRA vertical cross-section calculations, which were run with the same source pressure and where the shaft was assumed to be absent. These results suggest that the

two-dimensional vertical cross-section calculations with SUTRA and STAFF2D performed to ascertain the pathway and spatial extent of migration of solute are valid.

4. The calculations performed for a vertical cross-section through the waste panel, drift, and shaft were accomplished with the two codes, SUTRA and STAFF2D. These codes, based on the same governing equations, nevertheless use different centering schemes for some element variables such as porosity. A comparison of results from the two codes, modeling the same problem, reveal similar results based on solute-concentration contours. The SUTRA solution is somewhat more numerically dispersive than the STAFF2D solutions. In spite of these slight differences, for the calculations performed, the two codes tend to cross-verify one another.

5. DISTURBED CONDITIONS OF REPOSITORY/SHAFT

In addition to the undisturbed performance, the Standard (40 CFR 191, Subpart B) requires a study of combinations of hypothetical events and processes (scenarios) in which a waste repository is intruded by humans (see Chapter 4 of Volume 1). In these scenarios, the primary component of the geologic barrier (the Salado Formation) has been breached leaving only the waste form, possibly intervening panel and borehole seals, and the Culebra Dolomite as barriers. Thus, characterizing the behavior of the disposal system is much more important under these conditions than for the undisturbed scenario and requires the use of several additional simulation models (e.g., CUTTINGS, SECO_2DH, GENOBS, BRAGFLO and others) (see Figure 1-3 in Chapter 1).

5.1 Conceptual Model—Palmer Vaughn

In Sections 5.1 and 5.2 the term "flow" is used repeatedly. Unless otherwise stated, "flow" is meant to represent the cumulative volume of contaminated brine that has flowed up the intrusion borehole in 10,000 years and enters the Culebra. The term "flow rate" is the rate of this flow.

Currently, two summary scenarios are directly used in performance-assessment analysis during disturbed conditions: (1) one or more intrusion boreholes terminating in a disposal panel (E2) and (2) one intrusion borehole terminating in a disposal panel followed by a second borehole penetrating the same panel and terminating in a lower Castile brine pocket (E1E2). The computational scenarios used in modeling consequences of these summary scenarios are further distinguished by the number of intrusions and the time of intrusion. Consequences of the E1 summary scenario, in which an intrusion borehole intersects both a disposal panel and a lower Castile brine pocket, are not calculated for the 1991 analysis and are assumed to be the same as E2 consequences (see Section 5.1.2). The E1, E2, and E1E2 summary scenarios are defined in detail in Chapter 4, Volume 1 of the report.

The E2 summary scenario consists of one or more boreholes that penetrate a waste-filled room or drift in a panel. Shortly after completion, plugs are placed to isolate any aquifers (i.e., above and below the Culebra) and the well is abandoned and packed with concrete. The concrete remaining in the borehole degrades with time into a sand-like material. The borehole below the Culebra creeps partially closed due to movement of halite in the surrounding Salado. All plugs except the one above the Culebra degrade thus forcing any flow out through the Culebra. This maximizes the possible release through the Culebra. During multiple E2 well intrusions no interaction between wells occurs (Volume 1, Chapter 5).

The E1E2 summary scenario consists of one or more boreholes that penetrate a waste-filled room or drift in a panel and another borehole that penetrates a panel and a pressurized brine pocket in the Castile formation. The boreholes are abandoned, plugged, and creep partially closed as in the E2 summary scenario. The plugs also degrade as before except that a plug located between the

panel and Culebra in all but one of the wells that terminate in the panel remains intact. This forces all brine leaving the pressurized brine pocket through the waste panel before it flows out a well connected to the Culebra (Volume 1, Chapter 5).

When an intrusion of a waste panel first occurs, the room quickly depressurizes (the entire panel does not) and gas escapes through the borehole. As suggested in Appendix B of the Standard, the intruders "soon" (interpreted as less than one month) detect that the area is incompatible with their intended use and they seal and abandon the well. The room repressurizes either from continued gas generation or from a redistribution of pressure and saturation from the surrounding formation. Over time (less than 75 years) the borehole degrades and partially creeps closed. The net effect is a permeable and porous borehole that provides communication between the repository and the Culebra formation. After this period of degradation, the remaining gas moves out of the panel and brine will flow toward the panel and well bore. During the E2 scenario the primary path of this brine in-flow is along MB139 from the far field and up through the DRZ into the panel near the panel/Salado boundary. During an E1E2 scenario the primary source of brine in-flow is from the Castile brine pocket, although some Salado brine flows along MB139 toward the panel. Little brine flows into the panel from the intact Salado during the E2 or E1E2 scenarios because of its low permeability. Brine flowing through the upper anhydrite layers takes longer to reach the panel because the gas drive during room pressurization forces brine out the anhydrite farther than it is forced out MB139 and gravity drainage tends to saturate the lower MB139 to a greater extent than the upper anhydrite. Once brine saturations in the room exceed residual, interconnected brine pathways are formed in the void space and brine eventually reaches the well. Brine may then be forced out the well, up toward the Culebra against hydrostatic pressures in the well. Exactly how far up the well or how much brine reaches the Culebra during the regulatory 10,000 years depends, in part, upon how much gas flow can dissipate room pressure.

5.1.1 APPROXIMATION TO E1E2 SUMMARY SCENARIO

The E1E2 summary scenario is modeled by BRAGFLO (see Section 5.2) as an E1 scenario with the important conservative assumption that all of the Castile brine mixes with all of the waste. This conservative approximation is a necessary result of the limitations in modeling the waste panel in two dimensions as a cylinder with an axis of symmetry coincident with the intrusion well (Section 5.2.3). While a second borehole in the E1E2 summary scenario could be modeled in three-dimensional Cartesian or radial geometry, there is no convenient way of locating a second well in the two-dimensional radial representation while accurately describing well interactions and individual well flow. The assumption of total mixing of Castile brine with the waste overestimates the contamination of the brine compared to a true two-well E1E2 scenario

since the flow paths between two separated wells located anywhere in the panel results in less than 100% of the waste volume being in contact with brine.

The cumulative "flow" of brine in a true two-well E1E2 summary scenario also cannot exceed this conservative single-well approximation. In a true E1E2 summary scenario, the two intrusion wells are spatially separated. The flow path in this case is longer and is through the less permeable waste material (compared to the borehole) than in the single well E1 approximation to the E1E2 scenario. This lengthens the time required for brine to reach the Culebra through the borehole and increases pressure drop requirements to maintain flow up the borehole in the true E1E2 compared to the conservative E1E2 approximation. The existence of a second borehole in the true E1E2 scenario also increases the total void space available for brine. More time is required to saturate the panel with brine. Except for occasional gas pockets, the panel must be brine saturated before brine can flow up the borehole that connects the panel to the Culebra. Therefore, in a true E1E2 summary scenario, less brine reaches the Culebra after 10,000 years than would for the conservative E1 scenario approximation of an E1E2 scenario.

5.1.2 APPROXIMATION TO E1 SUMMARY SCENARIO

The consequences of E1 summary scenarios have been assumed to fall in the same consequence "bin" as those of the E2 summary scenarios. Results from the two-phase flow calculations using BRAGFLO indicate that for many scenario vectors the "flow" resulting from the E2 summary scenario bounds that from the E1 scenarios. The "flow" associated with the E1 summary scenarios is obtained from the E1E2 BRAGFLO simulation results assuming that the Castile brine does not mix with the waste after the waste panel becomes saturated with brine. In Figure 5-1 the "flow" from the E1 scenario vectors is compared to the "flow" from the E2 scenario vectors for each of the five intrusion times (1000, 3000, 5000, 7000, 9000 years). Points above the indicated 45 degree line correspond to E2 scenario "flows" in excess of E1 scenario flows. The cases where the "flows" from the E1 scenario exceed those from the E2 scenario either occur at low or zero E2 "flow" or are close to each other (near the 45 degree line).

In Figure 5-1 a clustering of data points according to intrusion time is also observed. For instance, the large releases tend to be dominated by the 1000-year intrusion scenarios followed by 3000-, 5000- and 7000-year intrusions. All 9000-year intrusion vectors produce no release. In addition, the relative degree to which the E2 "flows" exceed the E1 "flows" for the high E2 "flow" vectors is qualitatively preserved among the various intrusion times. This suggests some scaling or correlation factor may exist to relate "flow" at one intrusion time to "flow" at another intrusion time.

In the case assuming single-phase flow of brine and a fully brine-saturated panel, the "flows" from E2 summary scenarios bound those from the E1 summary scenarios if Castile brine bypasses

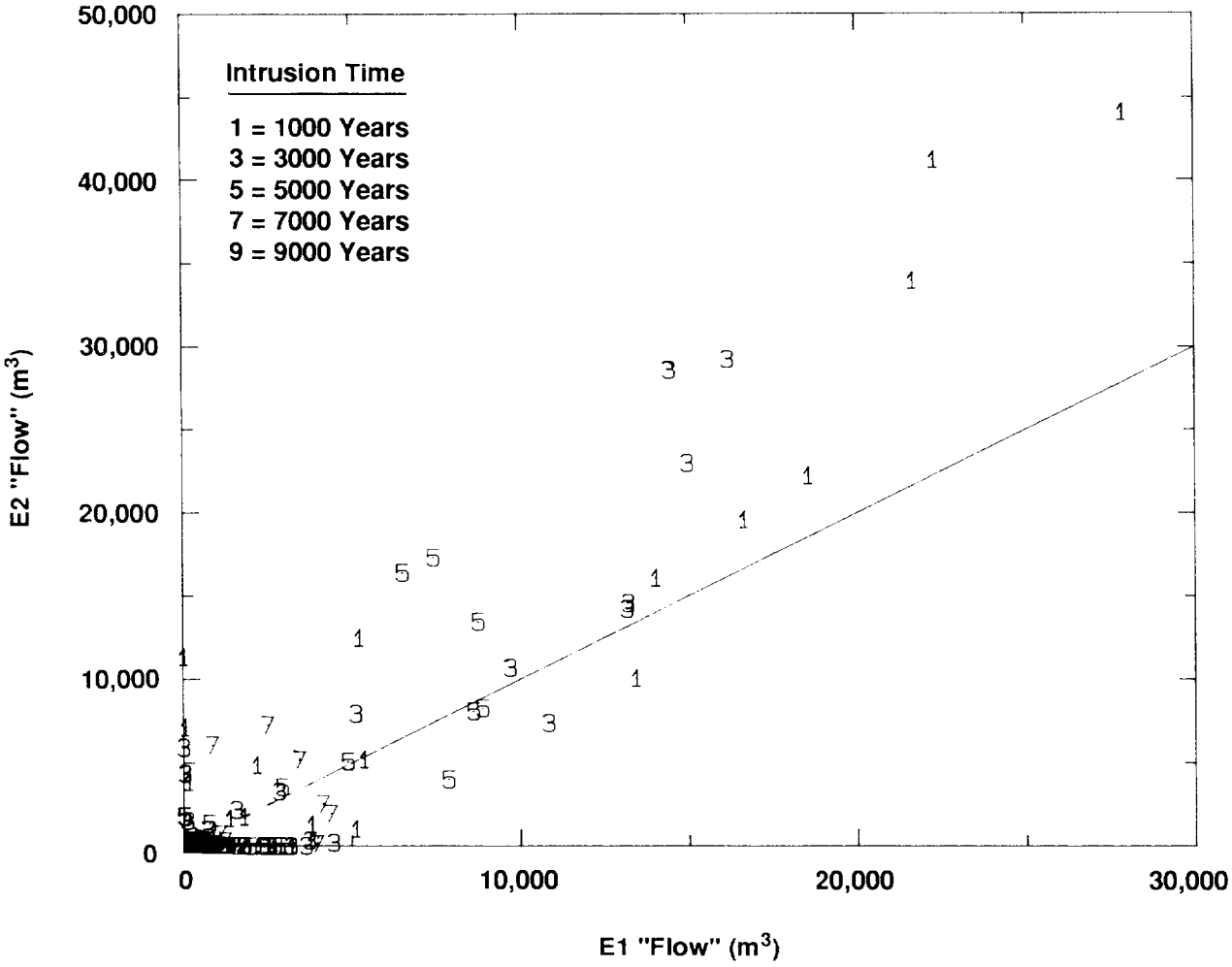

"Flow" = Volume of contaminated brine entering Culebra and accumulated over 10,000 years

TRI-6342-1356-0

Figure 5-1. Comparisons of E1 Flows with E2 Flows Assuming Two-Phase Flow at 1000-, 3000-, 5000-, 7000-, and 9000-Year Intrusion Times

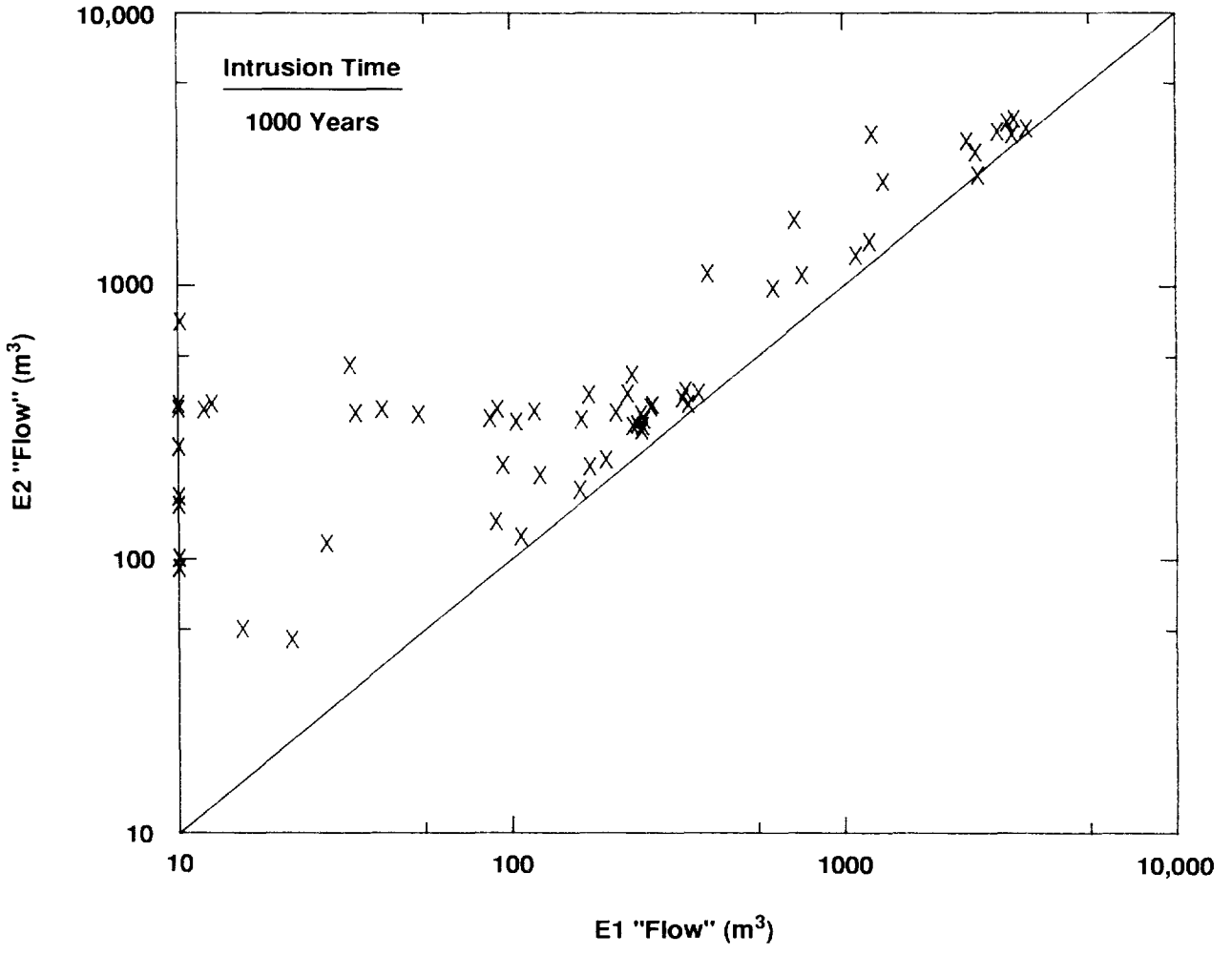

Figure 5-2. Comparisons of E1 and E2 Flows (Full Brine Saturation and No Castile Brine Mixing Assumed) at 1000-Year Intrusion Time

the contaminated waste in the panel. Figure 5-2 compares the "flow," resulting from E1 summary scenarios with that resulting from E2 summary scenarios. The "flows" are accumulated over 10,000 years for a well intrusion at 1000 years. On the figure the E2 "flows" are plotted on the vertical axis against the E1 "flows" on the horizontal axis; logarithmic scales are used for both axes. All data pairs fall above the indicated 45 degree-sloped line, indicating that the E2 "flows" bound the E1 "flows" under the conditions and assumptions used. These results are obtained from the analytic model, PANEL, a single-phase flow model (Section 5.3) in which it is assumed that the waste panel is fully saturated with brine and that a negligible amount of Castile brine mixes with waste panel brine.

When two-phase flow is considered, E2 scenarios do not necessarily bound E1 scenarios, particularly at lower levels of "flow." When considering two-phase flow, brine does not flow up the intrusion shaft from the panel to the Culebra until the portion of the panel surrounding the shaft becomes highly saturated with brine. Those E2 scenario vectors that result in no "flow" are vectors in which the panel is not brine filled in 10,000 years. When the panel is connected to a pressured brine pocket by an intrusion well, less time is required to fill the panel with brine and flow toward the Culebra may begin earlier.

At the higher release levels, the E2 "flows" bound the E1 "flows." This primarily reflects the higher brine pocket pressure retarding the flow of brine into the waste panel from the far field along the anhydrite layers. Once the intrusion occurs, the Culebra, panel, and Castile become connected. When the gas is displaced from the panel and the panel is brine-filled a nearly linear pressure gradient will be established between Culebra pressure and brine pocket pressure. This can result in the establishment of a higher panel pressure in the E1 summary scenarios compared to the panel pressure established in the E2 summary scenarios. The higher panel pressures reduce the pressure gradient between the panel and far field, and consequently less Salado brine flows into the panel from the far field along the anhydrite layers. For the high "flow" vectors compared to the low "flow" vectors, the panel becomes brine saturated earlier and the Culebra to Castile pressure gradient is established and remains for a longer period of time.

In summary, E2 "flows" bound E1 "flows" for large release vectors because the established panel pressure retards or reverses Salado brine in-flow toward the panel. E1 "flows" bound E2 "flows" for small release vectors because the flow of Castile brine decreases the time required to fill the panel with brine so that brine may begin to flow toward the Culebra.

5.2 Two-Phase Flow: BRAGFLO—Palmer Vaughn

5.2.1 MODEL OVERVIEW

BRAGFLO is used to evaluate the effect of gas on the flow of brine through the repository and up an intrusion borehole. (BRAGFLO is based on conceptualizations of porous media and multiphase flow presented in Appendix A.) The presence of gas and its rate of production may be extremely important in evaluating the flow characteristics of the repository. With respect to contaminants transported primarily in the brine phase (radionuclides and dissolved chemicals) gas may have negative and positive impacts. A potential negative impact is the increased brine phase mobility because of increased dissolved gas, possibly causing lower brine viscosity and higher relative permeability. Gas may additionally increase the driving force for moving brine away from the repository and may increase permeability through fracture development. Positive impacts associated with gas include the partial occupation of pore space by gas and the associated reduction in brine relative permeability and its mobility. Gas pressurization may drive brine from the room along the anhydrite layers to the far field creating unsaturated conditions around the waste. In addition, if the mechanism for gas generation consumes brine, then brine saturation may be reduced well below residual levels in the waste resulting in immobile brine at the time of intrusion.

In addition to quantifying the brine and gas flow fields in and around the repository for consequence analysis calculations, BRAGFLO is used to evaluate the effect of gas generation on the flow of brine. The comparisons are made to evaluate our hypothesis that the assumptions of no gas generation and predominantly single-phase brine flow is conservative with respect to predicting brine flow through the repository and borehole.

5.2.2 MODEL DESCRIPTION

5.2.2.1 Nomenclature

The following nomenclature is used throughout the model description of the two-phase flow model BRAGFLO:

English

$C_{M\ell}$	mass fraction of component M dissolved or miscible in phase ℓ
D	depth in reservoir measured from surface [L], [m]
g	gravitational acceleration constant [$L\,t^{-2}$], [m s^{-2}]

G	vector obtained in evaluating the finite differences analogs of the conservation equations at each grid block location [$ML^{-3}t^{-1}$], [kg m^{-3} s^{-1}]
H	length in the direction normal to the flow phase [L], [m]
J	shorthand notation for the Jacobian Matrix
k	absolute permeability of the reservoir [L^2], [m^2]
k_x	absolute permeability in the x direction [L^2], [m^2]
k_y	absolute permeability in the y direction [L^2], [m^2]
$k_{r\ell}$	relative permeability to phase ℓ [dimensionless]
P_C	capillary pressure [$ML^{-1}t^{-2}$], [Pa]
P_ℓ	pressure of phase ℓ [$ML^{-1}t^{-2}$], [Pa]
P_ℓ^*	potential of phase ℓ defined as $P_\ell - \rho_\ell\ g\ D$ [$ML^{-1}t^{-2}$], [Pa]
q_ℓ	mass rate of well injection (or production, if negative) per unit volume of reservoir [$ML^{-3}\ t^{-1}$], [kg m^{-3} s^{-1}]
$q_{r\ell}$	mass rate of products produced (or reactant consumed, if negative) per unit volume of reservoir due to chemical reaction [$ML^{-3}\ t^{-1}$], [kg m^{-3} s^{-1}]
q_v	volumetric flow rate of water per unit cross sectional area normal to the flow direction [$L^3\ L^{-2}\ t^{-1}$]
S_ℓ	saturation of phase ℓ [dimensionless]
$T_{\ell x}$	shorthand for the group $\rho_\ell\ k_x\ k_{r\ell}\ /\ u_\ell$ for phase ℓ
$T_{\ell y}$	shorthand for the group, $\rho_\ell\ k_y\ k_{re}\ /\ u_\ell$ for phase ℓ
x,y	spatial dimensions (x-horizontal, y-vertical)

Greek

α	geometric factor (in three dimensions, α = 1; in two dimensions, α = length; in one dimension, α = area
∇	gradient, shorthand for vector $\partial / \partial x$, $\partial / \partial y$ in two dimensions
$\nabla \bullet$	divergence, shorthand for $\partial / \partial x + \partial / \partial y$ in two dimensions
Δt	time step [t], [s]
Δz_m^k	maximum change in dependent variable values during time step, k (see equation (5-9))

Δz^*		the change in dependent variable values during a time step such that the new estimate for time step size remains the same as the current time step size (see equation (5-9))
$\bar{\delta}^k$		solution vector of dependent variable changes for time step k
ϕ		reservoir porosity [dimensionless]
ρ_ℓ		density of phase ℓ [$M^1\ L^{-3}$], [kg^1 m^{-3}]
u_ℓ		viscosity of phase ℓ [$ML^{-1}\ t^{-1}$], [cp]

Subscripts

B	brine component
b	brine phase
G	gas component
g	gas phase
N	nonwetting component
n	nonwetting phase
W	wetting component
w	wetting phase

5.2.2.2 Background

BRAGFLO is a computational model that describes the multiphase flow of gas and brine through a porous, heterogeneous reservoir. BRAGFLO was developed in-house for the Sandia National Laboratories WIPP Performance Assessment (PA) Division and is used by PA to simulate two-phase flow in and around the WIPP repository waste rooms. The roots of the BRAGFLO formulation are in TSRS, a multiphase compositional thermal reservoir simulator used to model the in-situ processing of tar sand (Vaughn, 1986). TSRS was developed for the DOE through an agreement with Western Research Institute, Laramie, WY. The version of BRAGFLO currently used by PA represents a significant improvement beyond its predecessor. A technical user's manual for BRAGFLO is being prepared and should become available in the latter part of 1992.

BRAGFLO is a necessary tool for PA primarily because no other public domain model was available for simulating the convergent flow of brine and gas to an intrusion well in a heterogeneous reservoir under conditions of gas generation and brine consumption. Repeated attempts using BOAST II during disturbed conditions resulted in excessively small time steps and unstable oscillations in saturations. The causes of these problems are characteristic of the IMPES

(implicit-pressure, explicit-saturation) solution technique, which BOAST II uses. BRAGFLO, because of its fully implicit numerical formulation, does not suffer from the stability and time-step restrictions that hamper BOAST II.

BRAGFLO was developed as a research tool capable of expanding and evolving to accommodate our changing conceptual models. Its highly structured architecture facilitates making future enhancements. The description that follows is a summary of the version of BRAGFLO used for this year's calculation, BRAGFLO 1.0; additional enhancements to the model are anticipated. Because the theory of BRAGFLO has not been previously documented, the summary for BRAGFLO is more extensive than the summaries presented in this volume on the other WIPP PA consequence analysis models.

5.2.2.3 Benchmark Results

Prior to its use in PA calculations, BRAGFLO was put through a series of benchmark tests. This verification process consisted of running three multiphase reservoir codes (BRAGFLO, BOAST II, and TOUGH) and comparing the results. The results of four one-dimensional, radial benchmarks (with/without dissolved gas and with/without gas generation) showed excellent agreement between the three codes, supporting our confidence in using BRAGFLO. For example, in Figures 5-3 and 5-4 the results of repository pressure and brine saturation are compared among BRAGFLO, BOAST, and TOUGH for the one-dimensional, constant gas generation benchmark. In this problem the repository is initially fully gas saturated and gas is generated at a rate of 2×10^{-7} kg/s/m^3. No well intrusion occurs and the simulation continues for 700 years. Pressure in the repository rises due to gas generation from the initial pressure of 0.1 MPa to 13 MPa at 700 years. The gas saturation (initially 100%) in the room falls to 15% in the first 100 years as brine flows into the repository from the Salado, after which increased pressure in the repository reverses the direction of brine flow. Gas saturation increases for the remainder of the simulation.

The results of a more realistic two-dimensional simulation with an intrusion well and the inclusion of the repository stratification and material zoning also showed excellent agreement between BOAST II and BRAGFLO up until the time of intrusion. (BOAST was unable to proceed beyond intrusion.) In the two-dimensional benchmark the repository is bounded top and bottom by a disturbed rock zone, anhydrite layers, and Salado and is surrounded by Salado in the horizontal direction. Gas is generated at two rates to simulate differing corrosion and biodegradation reaction rates: 1.7×10^{-10} kg/s/m^3 for 525 years followed by 5.7×10^{-11} kg/s/m^3 for 185 years. The repository panel volume is 5.6×10^4 m^3. The panel is initially 80% gas saturated with a porosity of 8.4%. In Figure 5-5 the repository pressures predicted by BRAGFLO are compared to those of BOAST for the first 1200 years (the time of well intrusion). The high pressures predicted by both models are primarily a result of the gas generation rates and the low repository porosity used. The

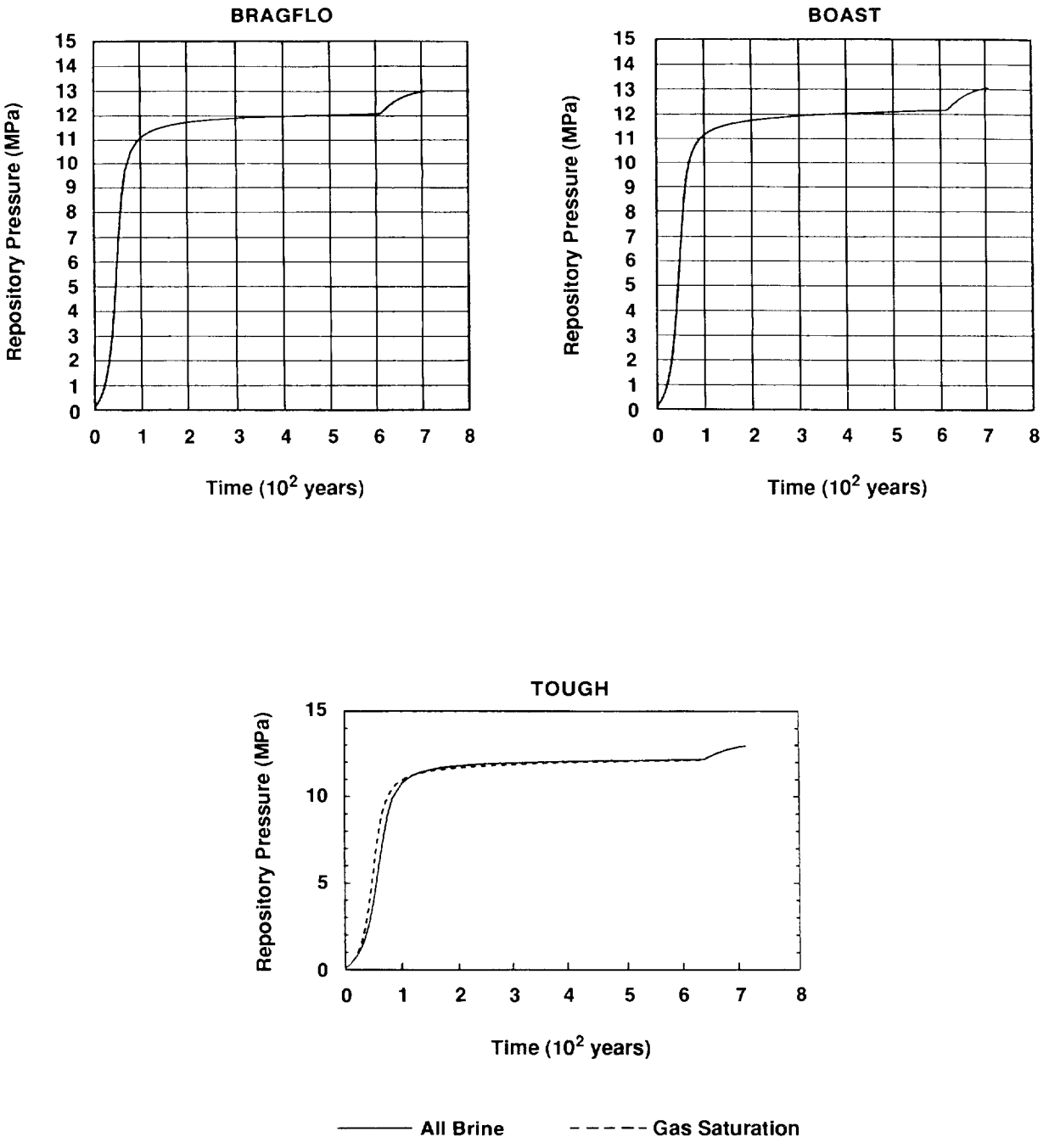

Figure 5-3. Repository Pressure Comparisons for Benchmark 2

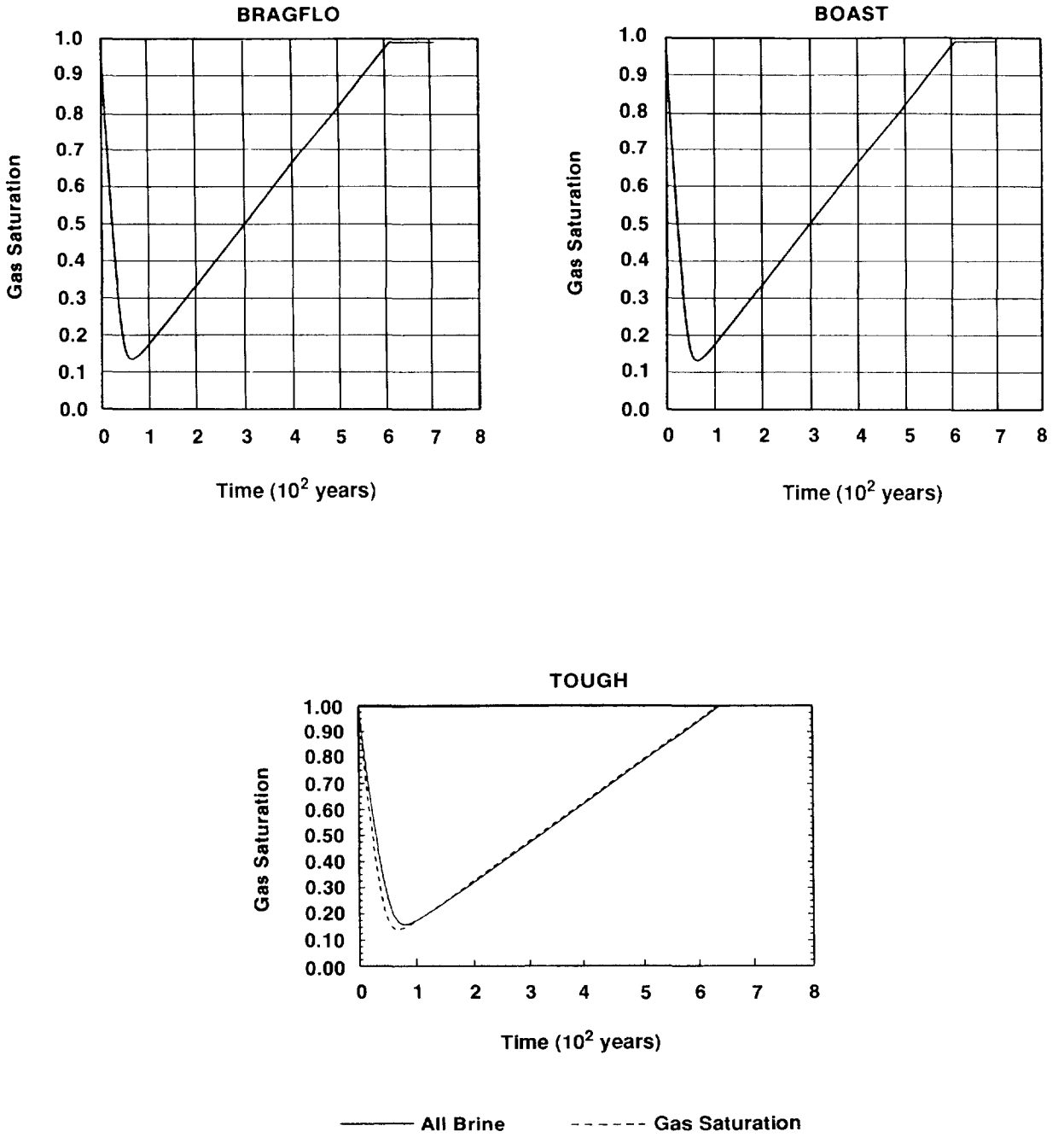

Figure 5-4. Repository Gas Saturation Comparisons for Benchmark 2

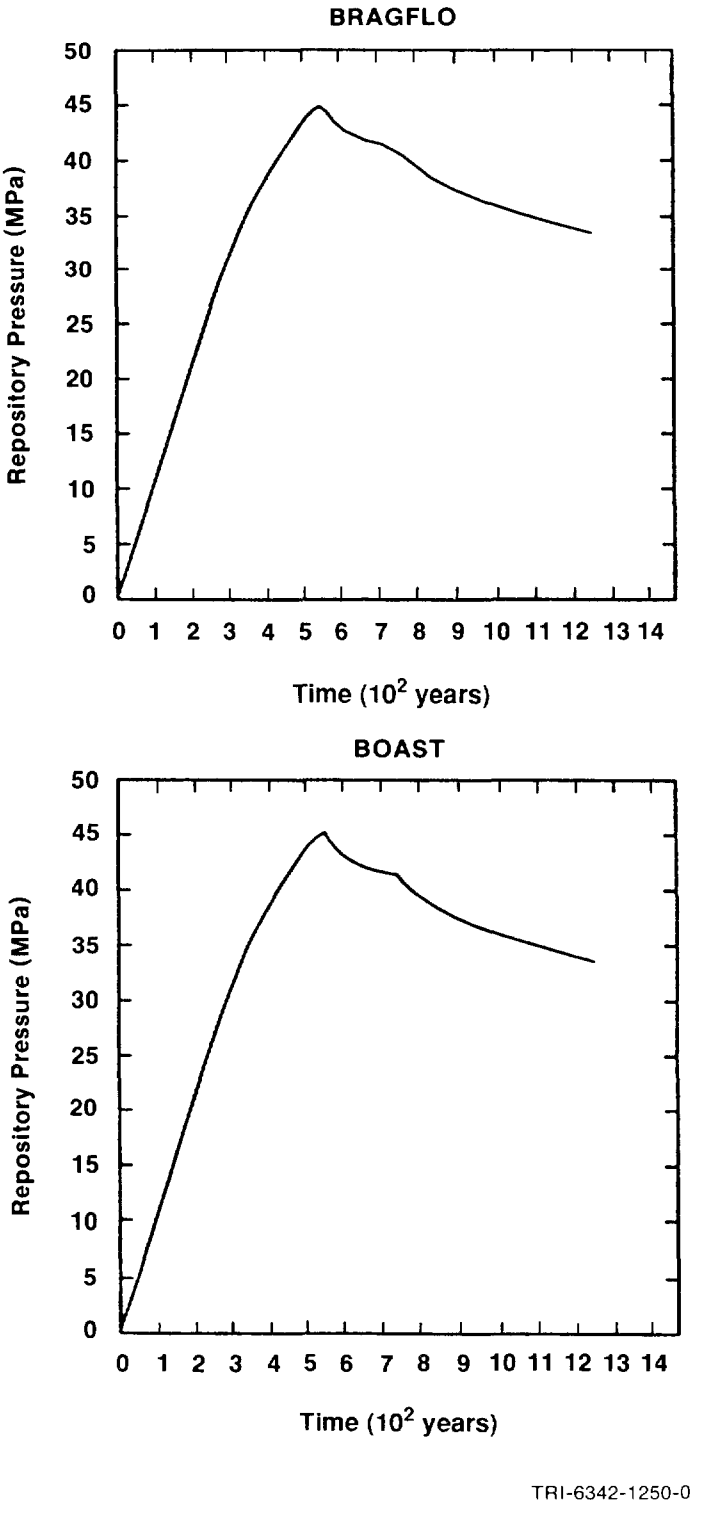

Figure 5-5. Repository Pressure Comparisons for Two-Dimensional Benchmark

comparisons of other resulting parameters such as saturations similarly showed excellent agreement. Results from TOUGH on this two-dimensional benchmark are unavailable at this time.

5.2.2.4 Fundamental Equations

BRAGFLO solves simultaneously the partial differential equations (PDEs) that describe the mass conservation of each mobile component (gas and brine) along with appropriate constraint equations, initial conditions, and boundary conditions. The fundamental equations can be found in Peaceman (1977) and Crichlow (1977). A total of five independent equations (two component mass conservation PDEs and three constraints) can be written to define the two-phase flow phenomena:

Gas Component Conservation:

$$\nabla \bullet \left[\frac{\alpha \rho_n K k_{rn}}{\mu_n} \left(\nabla P_n - \rho_n g \nabla D \right) + \frac{\alpha C_{Nw} \rho_w K k_{rw}}{\mu_w} \left(\nabla P_w - \rho_w g \nabla D \right) \right] + \alpha q_n + \alpha q_{rn}$$

$$= \alpha \frac{\partial \left(\phi \rho_n S_n + \phi C_{Nw} \rho_w S_w \right)}{\partial t} \tag{5-1}$$

Brine Component Conservation:

$$\nabla \bullet \left[\frac{\alpha C_{Ww} \rho_w K k_{rw}}{\mu_w} \left(\nabla P_w - \rho_w g \nabla D \right) \right] + \alpha q_w + \alpha q_{rw} = \alpha \frac{\partial \left(\phi C_{Ww} \rho_w S_w \right)}{\partial t} \tag{5-2}$$

Saturation Constraint:

$$S_n + S_w = 1 \tag{5-3}$$

Mass Fraction Constraint:

$$C_{Nw} + C_{Ww} = 1.0 \tag{5-4}$$

Capillary Pressure Constraint:

$$P_n - P_w = P_c \tag{5-5}$$

In the above equations uppercase subscripts refer to components while lowercase subscripts refer to phases. The subscript n or N refers to the nonwetting phase or component (assumed to be gas), while the subscript w or W refers to the wetting phase or component (assumed to be brine). In the case of the mass fraction terms (C_{Nw}, C_{Ww}), the first subscript refers to the component while the second refers to phase. In other words, C_{Nw} is the mass fraction of the nonwetting component (gas) in the wetting phase (brine), and C_{Ww} is the mass fraction of the wetting component (brine) in the wetting phase (brine). The term α in (5-1) and (5-2) is a geometric factor that generalizes the equations regardless of spatial dimension. In two dimensions, α is the "thickness" in the direction perpendicular to flow. The rest of the nomenclature is defined in Section 5.2.2.1.

In casting the PDEs in this form, a number of assumptions have been made. For instance, the conservation equations are balances on components and not phases. Because of the possibility of transfer of components between phases, it would not be appropriate to conserve the mass of each phase. Instead, the total mass of each component must be conserved. Equations (5-1) and (5-2) describe the simplest two-component, two-phase compositional mode. We have assumed that gas may exist in the gas phase as well as in the brine phase (as dissolved gas). We have further assumed that brine only exists in the brine phase (zero vapor pressure) so that $C_{Nn} = 1$ and $C_{Wn} = 0$. The amount of gas which is dissolved in the brine is described by a gas solubility parameter which may vary with pressure. The gas solubility parameter is defined as the ratio of the volume of dissolved gas (measured at standard conditions) to a unit volume of brine and can be related to C_{Gb}, the mass fraction of gas dissolved in brine. Imbedded in the PDEs is the assumption that Darcy's law, which linearly relates flow rate and pressure drop, remains valid.

The equation in (5-1) states that the net change in gas flow rate into and out of a control volume in pure or dissolved form, plus any gas added to or taken out of the control volume due to well or chemical reaction, equals the rate of gas accumulation in the control volume. The equation in (5-2) states the same for the brine component except there is no gas phase contribution to brine flow. The equation in (5-3) states that the volumes of the two mobile phases must occupy all of the void space. The equation in (5-4) states that the oil phase consists of brine and dissolved gas. Finally, (5-5) defines the concept of capillary pressure.

Because the amount of dissolved gas can be expressed as a function of pressure and the capillary pressure can be expressed as a function of saturation, the six unknowns can be reduced to four (brine and gas pressure and brine and gas saturations); two of these unknowns can be aligned with two PDEs and the other two found by application of the constraints expressed in (5-3) and (5-5). Other combinations of alignment may be more efficient. In the current version of BRAGFLO, (5-1) is aligned with gas saturation while (5-2) is aligned with brine pressure. We

have found no difference when (5-1) and (5-2) are aligned with gas pressure and brine saturation respectively during test cases.

In two dimensions (5-1) and (5-2) become respectively:

$$\frac{\partial}{\partial x}\left(HT_{gx}\frac{\partial P_g^*}{\partial x}\right)+\frac{\partial}{\partial y}\left(HT_{gy}\frac{\partial P_g^*}{\partial y}\right)+\frac{\partial}{\partial x}\left(HT_{bx}C_{Gb}\frac{\partial P_b^*}{\partial x}\right)+\frac{\partial}{\partial y}\left(HT_{by}C_{Gb}\frac{\partial P_b^*}{\partial y}\right)+Hq_g+Hq_{rg}$$

$$=H\frac{\partial}{\partial x}\left(\phi\rho_g S_g+\phi\rho_b S_b C_{Gb}\right) \tag{5-6}$$

and

$$\frac{\partial}{\partial x}\left(HT_{bx}C_{Bb}\frac{\partial P_b^*}{\partial x}\right)+\frac{\partial}{\partial y}\left(HT_{by}C_{Bb}\frac{\partial P_b^*}{\partial y}\right)+Hq_b+Hq_{rb}=H\frac{\partial}{\partial t}\left(\phi\rho_b S_b C_{Bb}\right). \tag{5-7}$$

In (5-6) and (5-7) the n, N, w and W subscripts have been replaced with g, G (gas) and b, B (brine) respectively. In addition, H (thickness in meters) has replaced α, T is shorthand for the group $\rho K k_r/\mu$ and P^* is $P-\rho gD$. In writing (5-6) and (5-7) we distinguish anisotropic permeability by expressing it in terms of k_x and k_y, which are contained in the groupings for T_x and T_y.

The equations in (5-6), (5-7), (5-3), (5-4), and (5-5), along with appropriate boundary and initial conditions and material physical property relationships, form the basis of the model's fundamental equations. All of the physical properties may be functions of any of the dependent variables (saturations and pressures) or independent variables (spatial position and time).

5.2.2.5 Wells

In reservoir models, wells are used to inject or withdraw fluids at specific locations in the reservoir. In BRAGFLO wells may be accommodated by using simple well models or by directly including well geometry and properties into the numerical mesh. In addition to describing the human intrusion borehole, wells can be used to approximate the gas generation process in the waste during corrosion and biodegradation and to modify the boundary condition from no-flow to fixed pressure or non-zero flow.

The well models treat a well as a point source or sink. Because of the finite size of the grids making up the numerical mesh of the reservoir, a true point source or sink can only be approximated. A true point source has infinite flow rate per unit volume of reservoir at the well and zero elsewhere (Peaceman, 1977). Instead, for finite-sized grids, the well is assumed to be

located in the center of a grid block of volume V_B. The mass flow rate per unit volume of reservoir into the grid block then is the well flow rate divided by the block volume. Outside the block the well does not directly contribute to flow rate. Wells are described according to type (injection or production) and operation (pressure or rate controlled). Injection wells may be of either operation while production wells are always pressure controlled. Injection wells only inject, and production wells only produce. If a production well is specified, but the well pressure exceeds reservoir pressure, fluid will not be drawn into the reservoir from the well; flow will be zero. If a well is to function as both an injector or producer, two wells are specified at the same location. This may be desirable when specifying a pressure along a boundary. Flow may then occur in either direction dependent on the direction of the pressure gradient.

In BRAGFLO wells may be accommodated by using simple well models or by directly including the well geometry and properties into the numerical mesh. The well model approach is more computationally efficient; however, the parameters that describe the flow properties of the well are unknown in advance. These parameters are typically determined from historical production or reservoir pressure and flow data. Because collection of such data at the WIPP is not feasible, current calculations do not use the well models to simulate the human intrusion boreholes. Instead the borehole dimensions, permeability, and porosity are directly incorporated into the numerical grid.

The well model, however, is used in certain areas along the far-field boundary where a constant pressure condition rather than a no-flow condition is desirable. Such an area is in the Culebra zone. The no-flow boundary condition is valid only to the extent its location is far enough removed such that events in the repository do not produce responses at the boundary over the simulated time frame. This may be questionable in the Culebra zone for some of the vectors associated with human intrusion scenarios. The relatively high permeability in the borehole and throughout the Culebra may cause pressure and saturation to fluctuate at the Culebra's far-field boundary. By specifying both an injection well and a production well characterized by a large injectivity and productivity index, constant pressure and saturation can be maintained at the Culebra boundary. This allows for the possibility of flow across the Culebra far-field boundary, thus avoiding unrealistic pressure buildup in the Culebra.

While wells can also be used to approximate gas generation in the waste, more sophisticated descriptions of the gas-generating reactions and their dependence on brine saturation have been included in BRAGFLO. Inclusion of separate corrosion and biodegradation reaction descriptions allow sensitivities associated with inventory variability and brine saturation variability to be evaluated. These sensitivities cannot be evaluated directly using a well model representation for reaction sources.

5.2.2.6 Numerical Solution Techniques

The numerical techniques in BRAGFLO are based on a fully implicit finite difference representation of the nonlinear conservation equations. In implicit methods the dependent variable at a particular location is evaluated as a function of the current values of its neighbors and the current value of any coefficients. In explicit methods current values of the dependent variables are evaluated as a function of previously determined (or past-dated) values of dependent variables and coefficients. Implicit methods are inherently more numerically stable compared to their explicit or hybrid (IMPES) counterparts (Fanchi et al., 1982; Carnahan et al., 1969; and Smith, 1965). The penalty for this increased stability is the increased computational effort associated with the simultaneous solution of the resulting finite difference analogs of the conservation equations at each grid block center.

In BRAGFLO the Newton-Raphson (Hildebrand, 1974; Carnahan et al., 1969; and Peaceman, 1977) iteration technique is used to generate solutions to the nonlinear partial differential equations. In the Newton-Raphson method a sequence of dependent variable values are produced which come increasingly close to the solution of the nonlinear analogs. The Newton-Raphson technique is chosen because of its quadratic convergence behavior (provided a good initial guess is available), its robustness (Carnahan, 1969; and Hildebrand, 1974), and its proven track record in solving multi-phase flow problems arising in petroleum reservoir modeling (Peaceman, 1977; Rubin, Vinsom, 1980; Coats, 1980; Crookston, Culham, Chen, 1979; Vaughn, 1986; and Price and Coats, 1974).

Five steps comprise our implementation of the Newton-Raphson solution method. The first is the linearization of the finite difference analogs of the conservation equations by truncation of a Taylor series expansion around the solution at each grid block center.

The second step is forming the recurrence formulas which relate values at successive intra-time step iteration levels. In matrix notation the recurrence equations become

$$J\left(\overline{Z}^{k}\right)\overline{\delta}^{k} = -G\left(\overline{Z}^{k}\right) \tag{5-8}$$

where k is the iteration level, $\overline{\delta}^{k}$ is the solution vector of corrections to the dependent variables $\overline{Z}$, $G\left(\overline{Z}^{k}\right)$ is a vector of the finite difference analogs evaluated at each grid block position, and $J\left(\overline{Z}^{k}\right)$ is the Jacobian matrix (Smith, 1965; and Hildebrand, 1974). The Jacobian matrix consists of the values of the partial derivative of finite difference analogs with respect to each dependent variable evaluated at each grid block center. In our implementation, the recurrence formula relates the changes in dependent variable values at successive iterations rather than the values themselves. This simplifies the computational process somewhat. The solutions to this system of equations

are then the changes in (or updated corrections to) the dependent variable values from the values converged to in the previous time step.

The third step is the evaluation of the elements in the Jacobian matrix. If the nonlinear analog functions are known analytically, then in principle analytical forms of their partial derivatives with respect to the dependent variables may be obtained. If the functions are not analytic or are complicated through coefficients which depend nonlinearly on the dependent variables, it becomes more practical or necessary to evaluate the Jacobian elements numerically. We choose the numerical approach in BRAGFLO for the reasons above as well as the increased flexibility which results from the ability to replace or modify property (coefficient) functionalities without requiring re-derivation of the analytical partial derivatives. The numerical evaluation of the Jacobian elements does not significantly affect the convergence characteristics provided the change in dependent variables for calculating the derivatives numerically is small enough that it captures the true nature of the slope at the point required. The change should not be so small; however, that machine precision errors dominate. We have found that changes on the order of 0.1 to 0.01 percent of the dependent variable values are satisfactory.

The fourth step is the solution of the system of equations resulting from the recurrence equations in step 2. The finite difference analog functions which appear in the recurrence equations and are used in forming the Jacobian relate the value of a dependent variable (or its change), a grid block (i, j) to values of the dependent variable evaluated at the four closest grid blocks: $(i-1, j)$, $(i+1, j)$, $(i, j-1)$, and $(i, j+1)$. This may be represented by a 5-point stencil (Figure 5-6) (Smith, 1965). The structure of the Jacobian made from the 5-point stencil is sparse (contains many 0 elements), consisting of five diagonal bands with a minimum bandwidth that may be calculated from grid block dimensions (Price and Coats, 1974; and Smith, 1965). The solution techniques available in BRAGFLO take advantage of the sparseness. For large problems this becomes a necessity from both storage and computational considerations.

Four solution options are available in BRAGFLO for solving the matrix equations. Two techniques are iterative solvers (Smith, 1965), PSOR (Point Successive Over Relaxation) and a Multi-Grid Algorithm. The third and fourth options are direct solvers using a banded LU decomposition (Conte and de Boor, 1972) and an LU decomposition routine from LINPACK (Dongarra et al., 1979). The Multi-Grid solver has the potential for being the most efficient technique for meshes in excess of 16 by 16 blocks while the LU solver is less efficient for large systems. Unfortunately for the current WIPP application, modeling matrix conditioning numbers (an indication of the determinant of the Jacobian matrix) are such that both iterative solvers suffer from extremely slow convergence to a solution. These conditioning numbers are calculated during

the LINPACK implementation of the LU decomposition method. This results in the LU solver being the most efficient and robust solver of the three options for this particular application.

In general the Jacobian matrix must be evaluated and solved for each intra-time step iteration. Fortunately, experience has shown for this particular application that the Jacobian can be evaluated only once at the start of each time step and left unchanged throughout the time step without significant impact on convergence or on the results. This results in a great computational savings since only one matrix evaluation and decomposition is required for each time step. All other intra-time step iterations only require the right-hand side of the matrix equation (5-8) to be updated and a back substitution to obtain the iterate solution vector, $\overline{\delta}^k$.

The fifth step in Newton-Raphson procedure is to update the dependent variables and check for convergence. The updating is done as $\overline{Z}^{k+1} = \overline{Z}^k + \overline{\delta}^k$, where k is the iteration level. Convergence is assumed when the right-hand side function vector of (5-8) is within a small tolerance of zero and all the δ^k's are within a specified tolerance of zero.

There are a few caveats associated with the application of Newton-Raphson technique to the multiphase flow of brine and gas at the WIPP. One is that the if the time step is too large an overshoot of gas saturation ($S_g > 1$) or an undershoot ($S_g < 0$) can occur during the iterations. It is not appropriate to accept these values even if they occur when convergence is satisfied. Internal checks in BRAGFLO flag these situations and cause the time step calculations to be repeated at a reduced time step. The selection of time step is another important issue.

Secondly, during the simulation when saturation and/or pressure are changing rapidly smaller time steps are required than when variables change slowly. In BRAGFLO the time step is updated continuously and is proportional to the change in dependent variables by

$$\Delta t^{k+1} = \Delta t^k \left[\frac{2\Delta z^*}{\Delta z^* + \Delta z_m^k} \right] \tag{5-9}$$

In (5-9), Δz^* is input and is the change in dependent variable (pressure and saturation) such that $\Delta t^{k+1} = \Delta t^k$. Δz_m^k is the maximum change in a dependent variable across all grid blocks defined as $z^{k+1} - z^k$. The time step is further restricted such that $\Delta t_{\min} < \Delta t^k < \Delta t_{\max}$ and $\Delta t^{k+1} / \Delta t^k < \Delta t_r$. $\Delta t_{\min}$, $\Delta t_{\max}$ and Δt_r are all user specified. The time step calculated above is reduced if required so that the resulting elapsed simulation time is coincident with the times required for specifying a change in well data, material property data, or for printing output.

A third issue concerns the spatial location where the various coefficients in the finite difference analogs of the conservation equations, (5-6) and (5-7), are evaluated. These coefficients involve the

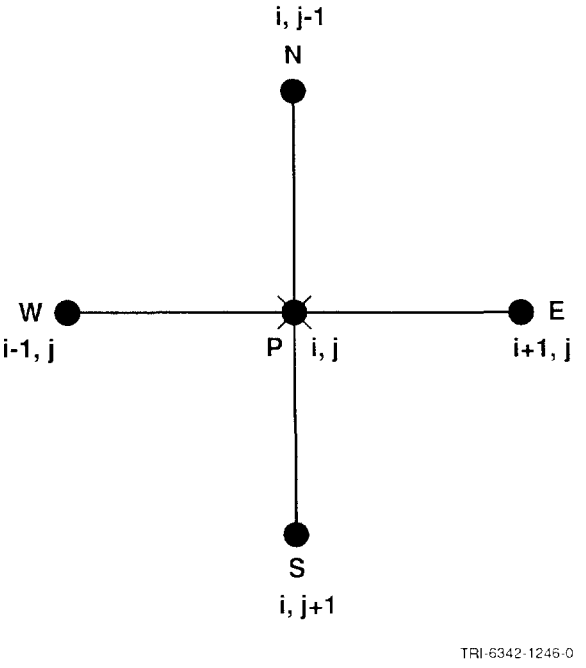

Figure 5-6. Five-Point Finite Difference Stencil.

grouping of parameters, $(\rho_b k_\ell C_{Bb}/\mu_b)\bullet(k_{rb})$ in the brine phase and $(\rho_g k_\ell C_{Gb}/\mu_b)\bullet(k_{rg})$ in the gas phase in the direction ℓ. The discretization of (5-6) and (5-7) about a grid block center located at i, j as used in BRAGFLO necessitates the evaluation of these coefficients at the interfaces between i, j and its four neighboring grid block centers (i.e., at $(i+1, j)$, $(i-1, j)$, $(i, j+1)$, and $(i, j-1)$). This raises the following question: How should the values of the coefficients evaluated at adjacent grid block centers be correctly averaged to obtain the interface value?

Mass balances about the interface between two grid blocks indicate that a harmonic average of its coefficients evaluated at adjacent grid block centers conserves mass, (Fanchi et al., 1982; Peaceman, 1977). Furthermore, experience (Crichlow, 1977; Rubin and Vinsome, 1980; Peaceman, 1977; Crookston et al., 1979; Coats, 1980) has shown that use of a relative permeability in the block that has the larger phase potential of the two neighboring blocks yields more reliable results. This is called "upstream weighting" in the reservoir modeling literature. The formulation in BRAGFLO combines the upstream weighted relative permeability with the harmonic average of remaining grouping of parameters in the coefficients to yield interface coefficient values.

Upstream weighting of relative permeability produces more realistic results compared to complete harmonic averaging. This can be best understood by considering the flow of a phase

between two adjacent grid blocks for the case when the grid block having the lower potential also has none of the flowing phase present (i.e., relative permeability = 0). In this case, using a straight harmonic average would never allow any of the phase to flow into the lower potential block. In other words, assuming only potential flow, once a phase saturation in part of the reservoir is reduced to below its residual saturation it will remain below residual saturation regardless of the potential gradient. Upstream weighting eliminates this unrealistic behavior. Upstream weighting also produces more stable results allowing larger time steps to be taken. Unfortunately, upstream weighting also tends to increase numerical dispersion producing a smoothing of sharp fronts (in saturation and pressure fields) particularly around interfaces between differing materials. The shape and magnitude of the fronts may become distorted (broadened); however, the area under (or spatial integral of) the saturation or pressure distribution is conserved.

5.2.3 SPATIAL AND TEMPORAL GRIDS—James D. Schreiber

The geometry used in the two-phase disturbed conditions modeling is similar to that used in the undisturbed calculations. It represents an axisymmetric approximation to an equivalent panel. Cylindrical geometry was necessary for two reasons. First, the actual geometry of the WIPP repository is too complex for PA modeling; a mesh having all the detail of the repository, or even of a single panel, would be prohibitively large and would require more computation time than is available for a single year's PA calculation. Second, BRAGFLO is currently a two-dimensional model; cylindrical geometry allows the most important aspects of flow over a large areal extent to be simulated in only two dimensions. Specifically, the convergence of flow radially toward a point sink can be modeled more accurately in cylindrical geometry than in rectangular geometry. This is important because on a large scale the flow is radial toward the intrusion borehole, which is located along the axis of symmetry. Even within a panel, because of the relatively high permeability of the waste, flow will be essentially radial, though constrained by the pillars to be more rectilinear. For flow into a panel from the far field, the most important features of a panel are its perimeter, both the length and the distance of the perimeter from the center where an intrusion well is assumed located, and the enclosed volume. How these parameters are averaged into a cylinder is somewhat arbitrary, and compromises are necessary.

In modeling a panel for PA purposes, the panel is treated as a cylinder having the same enclosed floor area as an actual panel, including the area occupied by the pillars. This results in a cylinder having a radius of 96.78 m. To account for the inclusion of the pillars, which have a very low porosity, the porosity of the panel is adjusted from the final porosity of the waste alone. The initial brine saturation is also adjusted for the presence of pillars that are fully saturated with brine. These calculations are discussed in Section 3.4.8 of Volume 3.

The region modeled includes the cylindrical equivalent panel and the surrounding Salado formation with anhydrite layers above and below (see Figure 4-1). The borehole is coincident with the axis of symmetry. The region extends upward to the top of the Culebra, downward to the bottom of the Castile brine reservoir, and outward approximately 22.3 km. By including the Castile and Culebra, the major sources and sinks for brine flow to and from the repository are represented in a single model. The far-field boundary is intended to be far enough away to justify the use of a no-flow boundary, which is required in BRAGFLO, without the boundary affecting the behavior of the repository. While a further removed boundary might be desirable for greater accuracy with this model, the formations being modeled actually extend only about 10 km north of the repository (see Figure 1.5-2, Volume 3). Anhydrite layers a and b immediately above the repository have been consolidated into a single layer with a thickness equal to the combined thicknesses of a and b and located at the elevation of layer b, the one closer to the repository. The panel thickness was varied, depending on the final porosity of the waste, which in turn depends on the composition of the waste and the total gas generation potential. The procedure for calculating the panel height and porosity, and the assumptions used, are described in Section 3.4.8 of Volume 3. The DRZ extends vertically upward through the anhydrite layer and downward through MB139. Beyond the outer radius of the panel, both the anhydrite layers and the Salado are intact. The center of the intrusion borehole is located at the axis of symmetry.

5.2.4 MATERIAL PROPERTIES AND BOUNDARY AND INITIAL CONDITIONS

Specification of boundary and initial conditions are required to complete the formulation. Upon examination of equations (5-6) and (5-7) it is evident that they are second-order with respect to gas pressure (P_g) and brine pressure (P_b). Thus two boundary conditions are required for each phase pressure in each dimension (two on P_g and P_b in x and two on P_g and P_b in y). BRAGFLO handles boundary conditions in a way that typifies reservoir models; that is the reservoir of interest is enclosed by a boundary across which there is no flow in the direction normal to it. Mathematically these types of conditions are Neumann boundary conditions in which the normal derivative of pressure to the boundary is zero. In BRAGFLO this is accomplished by assigning a zero value to the normal transmissibilities along each of the boundaries for both the gas and brine phase.

Through the use of wells, BRAGFLO has the capability to override the no-flow conditions. By locating pressure-constrained or flow-constrained fictitious wells along the boundaries, fixed pressures along the boundary or non-zero flow into or out of the reservoir across the boundary can be approximated.

The calculations of this report are based on the assumption of no-flow boundaries with the exception of a constant pressure condition located at the far field in the Culebra. The no-flow conditions occur on two types of boundary lines: (1) along the far-field boundary and above and below the repository and (2) along a vertical line of symmetry that passes through the center of a panel (the smallest unit of the repository that is assumed to be hydrologically isolated). For application to WIPP, an implicit assumption is that the boundaries of the no-flow type are located far enough away from the repository that they have a negligible influence on the flow behavior in and around the repository over the 10,000-year time span. A constant-pressure well is located at the far-field Culebra boundary because the Culebra zone is the most permeable material in our reservoir model. The constant pressure well allows for the possibility of flow across the boundary in the event that the flow fields affect the pressures and saturation near this boundary.

A number of variables and properties must be specified at time t=0. These initial conditions consist of: (1) the two dependent variables aligned with (5-6) and (5-7) (S_g and P_b), (2) the reservoir properties of porosity and the directional permeabilities, and (3) the concentrations of metal and cellulose. These variables must be specified throughout the simulation volume and along the boundaries. All other material (fluid and reservoir properties) must also be specified; however, properties such as relative permeabilities, capillary pressures, densities, viscosities, dissolved gas, etc., are functions of the previously specified dependent variables and are calculated in BRAGFLO. (Details on material, fluid, and reservoir properties used in BRAGFLO calculations are provided in Volume 3 of this report.)

5.2.5 RESULTS AND DISCUSSION—Palmer Vaughn and James D. Schreiber

5.2.5.1 Overall Results

PA calculations using BRAGFLO have been completed for the 1991 "snap-shot." The results from the 600 two-phase-flow simulations quantify the flow fields in and around the repository over 10,000 years for all the vectors comprising the E2 and E1E2 summary scenarios. A vector is a set of model input parameter values obtained from one particular sampling of parameter value probability distributions. The flow fields from the E1 scenarios are inferred from the E1E2 results as justified earlier, in Section 5.1.2. In addition to the 600 simulations used in the consequence analysis, an additional 120 simulations were completed for comparing the effects of gas generation with no gas generation.

A detailed analysis of all the BRAGFLO results is an ambitious task and is not available at this time. Such an analysis is focused on analyzing the output of all 600 simulations with respect to pressures, saturations, gas generation, iron concentrations, and cellulosic concentrations in order

that phenomenological differences resulting from the wide disparity in parameter values associated with each vector may be evaluated.

A number of general conclusions that have important impact and implications on the final CCDFs can be made at this time. The discussion of results in this section is focused on the intermediate flow-field results from BRAGFLO and not on final CCDFs. A discussion of the final CCDFs and the effect of gas on radionuclide release is summarized in Chapter 6, Volume 1 of this report. Unless otherwise defined, the term "flow" in this section is used to represent the cumulative amount of contaminated brine (in m^3) that flows up an intrusion well and enters the Culebra over the 10,000 years following emplacement.

The first conclusion is that for each vector of the E2 and E1E2 scenarios the "flow" decreases for later-occurring intrusions. In Figures 5-7 and 5-8 the "flows" are plotted for each vector at the selected intrusion times of 1000, 3000, 5000, 7000, and 9000 years after the repository is sealed. Figure 5-7 corresponds to the E2 scenario while Figure 5-8 corresponds to the E1E2 summary scenario. In all cases the flow not only decreases with increasing intrusion time but it decreases at an increasing rate as the time of intrusion increases.

This is an important conclusion. The trend in "flow" versus intrusion time had been observed in the case of single-phase, fully brine-saturated flow, but was unverified, until now, for the case of simultaneous flow of brine and gas with gas generation. This suggests that the release of brine from early intrusion times may bound that of latter times. As long as CCDFs based on early time release comply with the regulation there may be no need to consider late intrusion time scenarios. This conclusion does not apply when considering Resource Conservation and Recovery Act (RCRA) compliance and may not hold for other conceptual models or other combinations of parameters.

A second conclusion is that the "flows" from the E1E2 summary scenario exceed the "flows" from the E2 scenarios in all vectors for each intrusion time investigated. Figures 5-7 and 5-8 described earlier support this conclusion. The larger E1E2 "flows" compared to E2 are dominated by the flow of Castile brine rather than the flow of Salado brine. The flow of Castile brine into the waste panel and up the intrusion borehole is larger than that from the Salado for a number of reasons. First, the borehole connecting the Castile brine pocket to the waste panel is much more permeable (4 to 6 orders of magnitude in m^2 units) than are the anhydrite layers (the primary flow paths for Salado brine to reach the panel). Second, the Castile rock compressibility, which is calculated from the bulk storage coefficient, is larger than that of the anhydrite. The larger rock compressibility results in a smaller pressure decline per unit volume of brine removal from the brine pocket than that which occurs in the anhydrite. Thus the potential difference (the potential for flow) between the brine pocket and the waste panel does not decline as rapidly as that difference between the anhydrite and the panel. Third, the brine volume available in the anhydrite is small

compared to that of the brine pocket and the brine which flows out of the anhydrite is replaced slowly by the surrounding Salado due to low Salado permeability. Finally, good connectivity between the panel and the brine pocket and the high brine pocket pressure generally causes the panel to pressurize more rapidly and to a higher level in the E1E2 compared to the E2, thus reducing further the component of flow from the far field along the anhydrite in the E1E2 compared to the E2. However, this is more than offset by the large contribution to borehole flow from the brine pocket.

A third conclusion is that gas generation produces lower "flow" than in the absence of gas generation for all of the vectors in the E2 and E1E2 1000-year intrusion time summary scenarios. Comparisons for the E1 scenario are believed to result in the same conclusion. In Figures 5-9 and 5-10, the flows from the 120 input vectors are compared to the flow from the same input vectors with zero gas generation rates. The zero reaction rates are the only differences between the two input vector sets. Figure 5-9 corresponds to the E2 scenario class, while Figure 5-10 corresponds to the E1E2 scenario class. The intrusion time is 1000 years (the intrusion time which produces the highest releases). The "flows" from the gas generation simulation are lower and the amount or percentage of reduction in "flow" differs from vector to vector.

The effect of gas generation on "flow" is more pronounced in the E2 scenarios than in the E1E2 with respect to the percent reduction in "flow" because of the smaller "flows" associated with the E2 cases. The amount of the reductions are, however, consistently larger for the E1E2 scenarios. An analysis of the results presented in Figures 5-9 and 5-10 indicate that for the E2 scenario the average "flow" of the 60 vectors is reduced from $9.0 \times 10^3 m^3$ to $4.0 \times 10^3 m^3$, a reduction of $5.0 \times 10^3 m^3$ or 55% when gas generation occurs. The number of E2 vectors resulting in zero "flow" increases from 0 to 22 when gas is considered. The average "flow" of the 60 E1E2 vectors is reduced from 8.2×10^4 to 7.0×10^4, a reduction of 1.2×10^4 or 15%. The large flow rates of Castile brine into the panel compared to the flow rates of brine from Salado into the panel once the repository and brine pocket is breached is partially responsible for the lower percentage reduction in flow observed in the E1E2 scenario compared to E2. The large flow from the brine pocket occurs in spite of rising gas pressure in the waste panel because at the 1000 year time of intrusion the pressure in the panel is still significantly lower than that of the brine pocket and the connection between the brine pocket and panel is quite permeable.

The percent reduction in "flow" is expected to be larger in E1E2 scenarios at later intrusion times provided gas generation still occurs for at least two reasons. First, the higher pressures from continued gas generation at the latter intrusion times will slow the flow of Castile brine. Second, the longer reaction times before intrusion result in increased brine consumption and gas generation. The larger presence of gas in the panel at the time of intrusion results in lower brine

mobilities so not only must a larger amount of gas be displaced from the panel before brine flows up the intrusion well but it is displaced at a slower rate.

Conclusion 4 is that the "flows" produced during E2 summary scenarios do not bound the flows produced during the E1 summary scenario in some vectors. For reasons discussed earlier in Section 4.2.3, the E2 "flows" exceed those from E1 at the higher E2 "flow" vectors except for many of the vectors that produced little or no E2 flow. In those vectors where E1 "flow" exceeds E2 flow, the "flows" are close in magnitude to each other. In generating the final CCDFs, the releases from E1 are approximated by those from the E2 scenario. This is justified since the E2 releases either bound those of E1 or the magnitudes of the E1 releases are sufficiently close to those of E2 that they fall in the same discretized release "bins" used in calculating the CCDFs.

Conclusion 5 is that the "flow" produced during E1 summary scenarios at early intrusion times does not bound that which is produced at later intrusion times for some vectors. This is different behavior than is seen for flows produced from E2 and E1E2 summary scenarios. In Figure 5-11 "flow" produced during E1 summary scenarios is presented for each vector at the five intrusion times (1000, 3000, 5000, 7000, and 9000 years). At the higher "flow" magnitudes (in excess of 5000 m^3) the early intrusion "flows" exceed the "flows" at later intrusion times for all vectors. At low "flow" magnitudes (less than 5000 m^3) the early intrusion "flows" do not necessarily exceed the "flows" at later intrusion times when comparing "flows" resulting from the 1000-, 3000-, and 5000-year intrusion times (vector 18 and 38 for example). Because the releases for these particular vectors are low this behavior does not appreciably affect the CCDFs. The causes of these trends at low "flow" magnitude are being investigated and while interesting from a phenomenological or mechanistic point of view, they are not at this time believed to be important with respect to compliance assessment.

Preliminary examination of some of the details in pressure, saturation, and reaction rate profiles from vector 58 (a vector where "flow," although small, is greater for the 3000-, 5000-, and 7000-year intrusion time than for the 1000-year intrusion time) suggest that the increase in E1 "flow" at later intrusion times may be a result of increased gas generation. In this vector a large gas pocket forms in the panel shortly after flow from the panel through the intrusion well begins. The gas pocket is located in the upper part of the panel some 20 to 50 m from the well, isolating a portion of the panel from the brine. The gas pocket continues to expand throughout the 10,000 years and drives brine predominantly toward the well but also out along the MB 139 as well. During the 1000-year intrusion time scenario this gas pocket does not form and the subsequent "gas drive" does not occur. The additional contribution to "flow" from the gas drive is believed to result in some of the later intrusion times having larger releases. Gas pockets typically do not persist throughout the 10,000 years. They tend to dissipate shortly after intrusion. Exactly how they form and under what conditions they form is being investigated.

5.2.5.2 Results for a Typical Vector

A "typical" vector is analyzed to illustrate the significant features and behavior of two-phase flow under disturbed conditions when an intrusion borehole opens at 1000 years. Vector 18 was chosen as typical in that brine releases were very low, but nonzero, in the E2 scenario (the majority of the 60 vectors showed zero release) when gas generation was included. Without gas generation, the release was higher by a factor of about 6, well within the range of differences seen among the 60 E2 scenario vectors. In the E1E2 scenario, the release for vector 18 was near the mean for the 60 vectors when gas generation was modeled. With no gas generation, the release was just slightly higher, as was generally the case.

The behavior seen in vector 18 appears typical, particularly the pressure history in the waste, which, in the case of gas generation, shows a rapid buildup followed by an even more rapid pressure release when the intrusion borehole opens at 1000 years. The pressure builds up again, rapidly in the E1E2 scenario, and very slowly in the E2 scenario. Without gas generation, the pressure in the waste simply rises monotonically approximately to hydrostatic pressure at the time of borehole opening, then the pressure levels off and remains nearly constant for the remainder of the 10,000-year period.

Comparison of E2 With E1E2, With Gas Generation

During the first 1000 years, the behavior of the two scenarios is identical, since the Castile brine reservoir is modeled as being completely isolated from the Salado by an impermeable layer of Castile anhydrite. Pressure in the waste rises rapidly to 9.2 MPa primarily as a result of gas generation. Small amounts of brine also flow in from the anhydrite layer above the repository and from MB139, which tends to equalize the pressure in the waste with the pressure in the far field, which is at 12.8 MPa. In this vector, gas generation by anoxic corrosion occurs rapidly compared to other vectors; approximately 55% of the corrodible metal in the waste is consumed by 1000 years. The biodegradation rate is slower, but the amount of biodegradable material is one of the lowest among the 60 vectors, and it is fully consumed in about 350 years.

The intrusion borehole opens at 1000 years, resulting in rapid depressurization in both scenarios. In the E1E2 scenario, the pressure (Figure 5-12) bottoms out at 2.5 MPa 280 years later. (It should be noted that in the WIPP repository and the surrounding geologic media, "rapid" changes occur over centuries, not days, weeks, or a few years.) During this period, a gas column (i.e., a gas-filled degraded borehole plug) connects the waste panel with the Culebra. Since the pressure in the Culebra remains fairly constant at about 1.05 MPa, the pressure in the waste could continue to drop to this level. Countering the drop in pressure is continued gas generation by anoxic corrosion, which finally consumes all corrodible metal by 1630 years. At the same time,

brine flow from the Castile is rapidly filling the panel. By 1540 years, the waste panel is connected to the Culebra by a column of brine, and the pressure in the waste rises above hydrostatic. Because the pressure in the Castile (11.57 MPa) is above hydrostatic, a gradient higher than hydrostatic is maintained in the borehole, resulting in the pressure being higher than hydrostatic in the waste. The panel pressure peaks at 7.9 MPa immediately after connection is made with the Culebra, and drops very slowly over the rest of the 10,000-year period to 7.7 MPa. Hydrostatic pressure at the repository level, with the Culebra pressure fixed at 1.053 MPa and brine density of 1230 kg/m^3, is 6.04 MPa. The pressure in the waste is actually slightly greater than even the gradient from the Castile would impose. This is probably caused by brine flow from the far field, which will tend to elevate the pressure closer to the far field pressure of 12.8 MPa, as long as there is some resistance to flow up the borehole. The pressure in the waste drops slowly over time because the Castile brine reservoir pressure is slowly decreasing as brine is withdrawn. Because of the high storage capacity of the brine reservoir, the pressure there drops only from 11.57 MPa initially to 11.51 MPa after 10,000 years. During the 8500 years that brine flows upward from the waste panel, about 31,500 m^3 of brine is released (Figure 5-13).

In the E2 scenario, the pressure in the panel (Figure 5-14) continues to decrease long after the borehole opens. Gas continues to be generated by anoxic corrosion until all corrodible metal is reacted after 4100 years, but the production rate is low because the brine saturation is low owing to the slow recharge from the far field and consumption of brine by the corrosion reaction. The borehole is filled with gas and offers little resistance to gas flow, so as gas is generated, it simply flows up to the Culebra, where the relatively high permeability results in nearly constant pressures of 1.05 MPa. Thus, waste pressure bottoms out at 1.09 MPa after 5400 years. Brine is flowing in from MB139 and from the anhydrite layer during this time, and once corrosion ceases, the panel slowly fills up. After 7700 years, the panel is finally filled and a brine column fills the borehole to the Culebra after 7700 years, at which time the pressure in the waste climbs to just above hydrostatic. It continues to rise very slowly for the remainder of the 10,000 years, presumably as a result of inflow from the far field and some resistance to flow in the borehole. Until the panel and borehole are filled with brine, there is actually a downward flow of brine from the borehole into the panel (see Figure 5-15). This brine is seeping into the borehole from the Salado along the 400 m of Salado between the repository and the Culebra. Once the panel is filled, at 7700 years, the direction of brine flow in the borehole reverses, and 1300 m^3 of brine flows from the panel over the next 2300 years.

There are clearly some major differences in behavior between the E2 and the E1E2 scenarios, owing to the high pressure in the Castile brine reservoir. Without that large source of brine, releases from the waste panel are delayed 6700 years, and the rate of release is far lower. Over the

10,000-year regulatory period, the amount of brine released in the E2 scenario is only 1300 m^3, compared with 31,500 m^3 when a pressurized brine reservoir is intercepted.

Comparison of E1E2, With Gas Generation, With E1E2, Without Gas Generation

Without gas generation, the pressure in the waste rises slowly at first (Figure 5-16), the only mechanism for increasing pressure being inflow of brine from MB139 and the anhydrite layer. Only when the panel is nearly full of brine does the pressure rise rapidly. This occurs just prior to the borehole opening. When the borehole does open at 1000 years, the pressure in the panel has not yet reached hydrostatic. Brine then drains into the panel by way of the borehole from the Salado DRZ, the anhydrite layer and the lower Salado above the repository, and pressure in the neighborhood of hydrostatic is achieved. Only a small amount of the gas that was present initially flows into the borehole (less than 0.2 m^3 at reference conditions); the rest has been compressed to less than residual saturation and remains trapped in the waste. The borehole then fills with brine up to the Culebra. The pressure holds nearly constant for the remainder of the 10,000 years, as was the case with gas generation, except that the pressure is very slightly lower without gas generation than with gas generation. The greatest effect of gas generation is on the brine flow out of the waste (Figure 5-17). Although the time when the brine first flows out is about the same in both cases, the flow rate is higher (4.32 m^3/yr at 10,000 years, vs. 4.08 m^3/yr) and the total flow out over the 10,000 years is greater when no gas is generated. Cumulative releases of brine are 31,500 m^3 with gas generation and 37,300 m^3 without. The process of filling the panel, driving out enough gas for brine to make the connection to the Culebra, and starting flow out of the panel seems to take nearly as long whether or not gas is generated.

There are several reasons for the higher releases when no gas is generated. With gas generation, the panel initially fills with gas over the first 1000 years; and at the same time, brine is consumed by anoxic corrosion, further reducing the brine content of the panel. Gas production via corrosion consumes about 2660 m^3 of brine. The rapid pressure buildup with gas generation restricts the flow of brine from the anhydrite layer and MB139 during the first 1000 years preventing another 150 m^3 of brine from coming in through MB139, compared with when gas is generated. (Flow through the anhydrite layer is largely unaffected during this time period.) Without gas generation, essentially all the gas that is present is compressed down to residual saturation or less before the borehole opens. Thus, there is no resistance to brine flow imposed by the presence of gas. With gas generation, there is gas present in some part of the panel at saturations greater than residual for the full 10,000 years. This restricts flow from the far field and flow through the panel from the Castile, even after the panel is sufficiently filled with brine that it flows upward to the Culebra, which is delayed 540 years while the panel fills. The result is

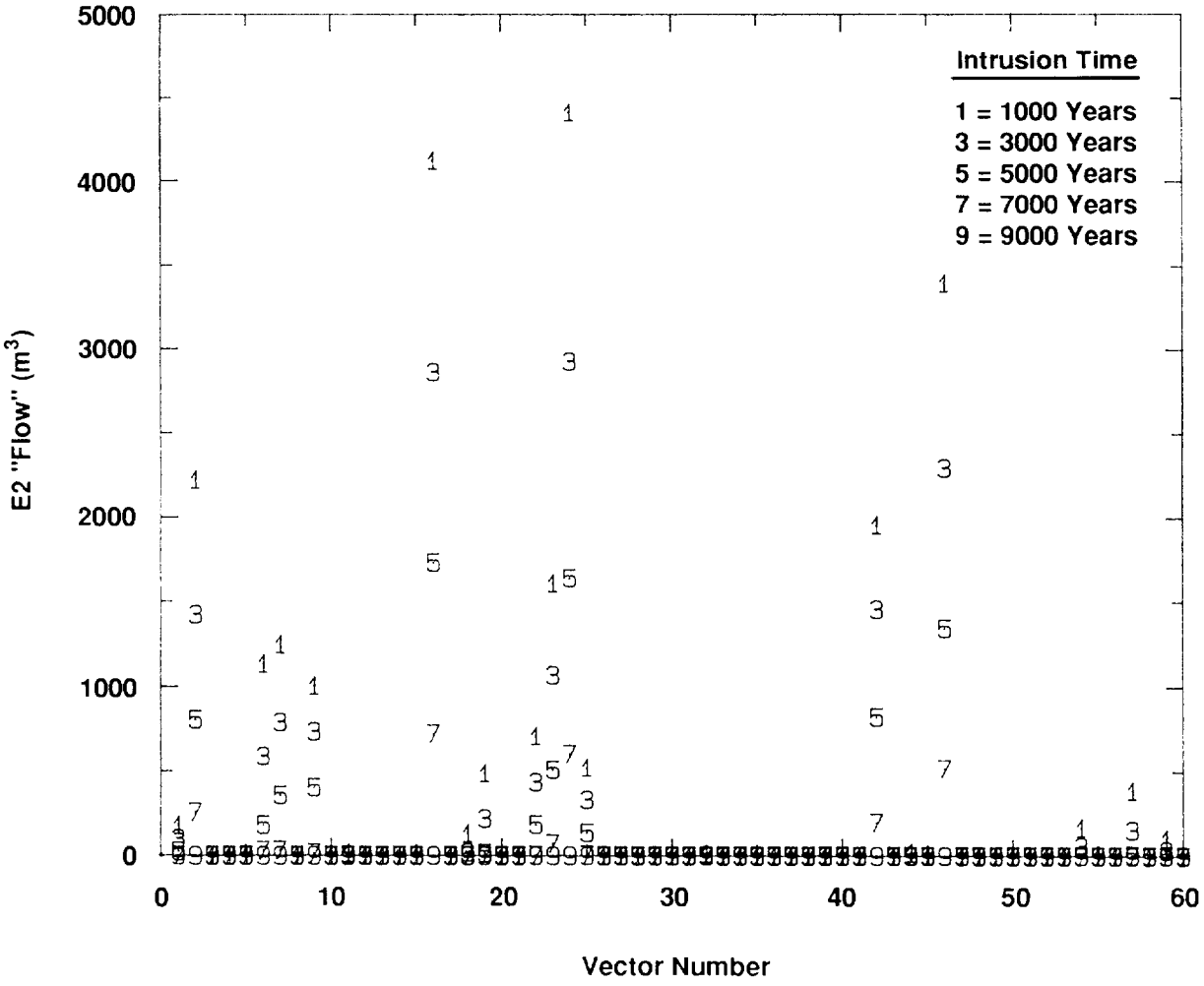

"Flow" = Volume of contaminated brine entering
Culebra and accumulated over 10,000 years

TRI-6342-1397-0

Figure 5-7. Borehole "Flow" From BRAGFLO During E2 Summary Scenarios

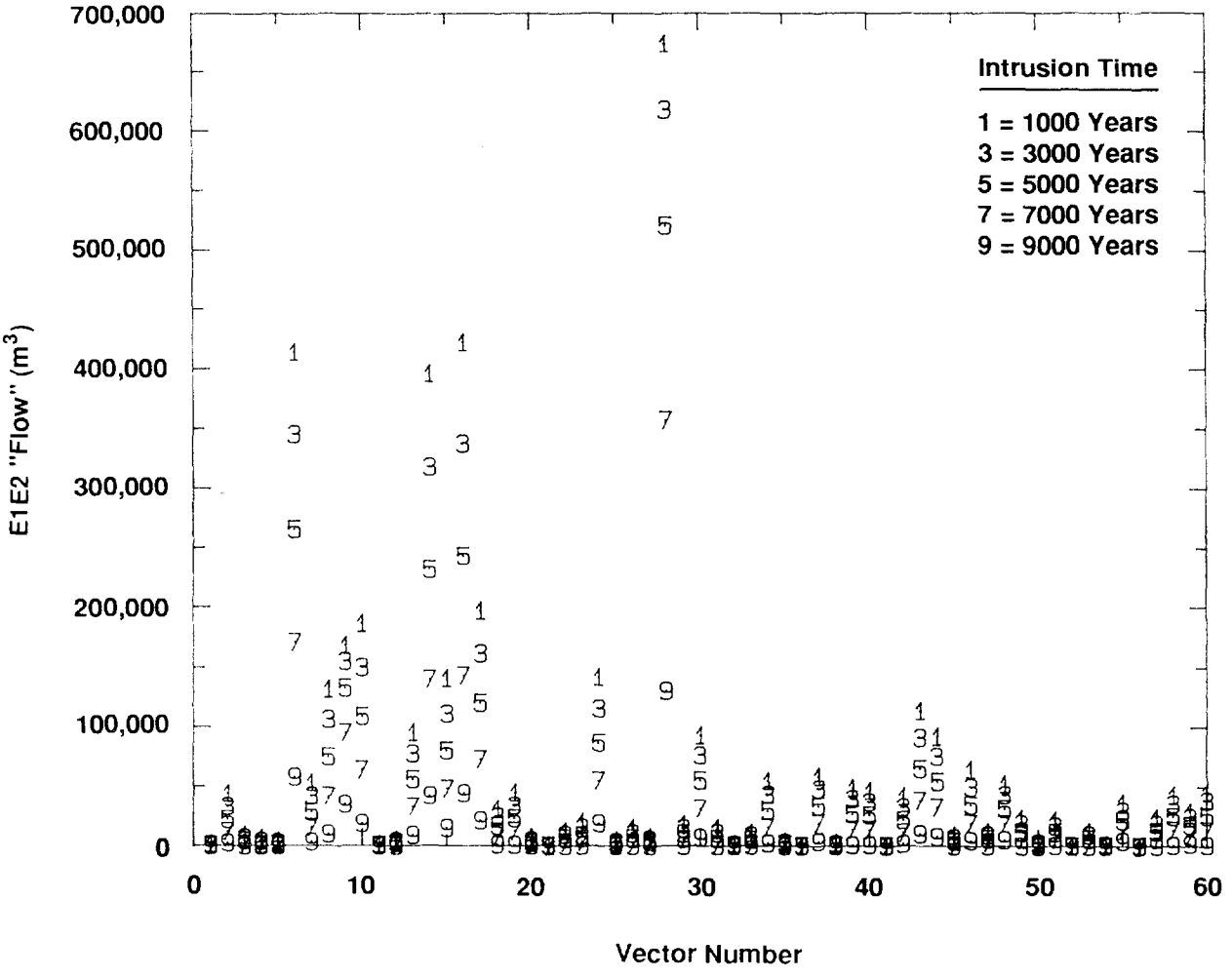

Figure 5-8. Borehole "Flow" From BRAGFLO During E1E2 Summary Scenarios

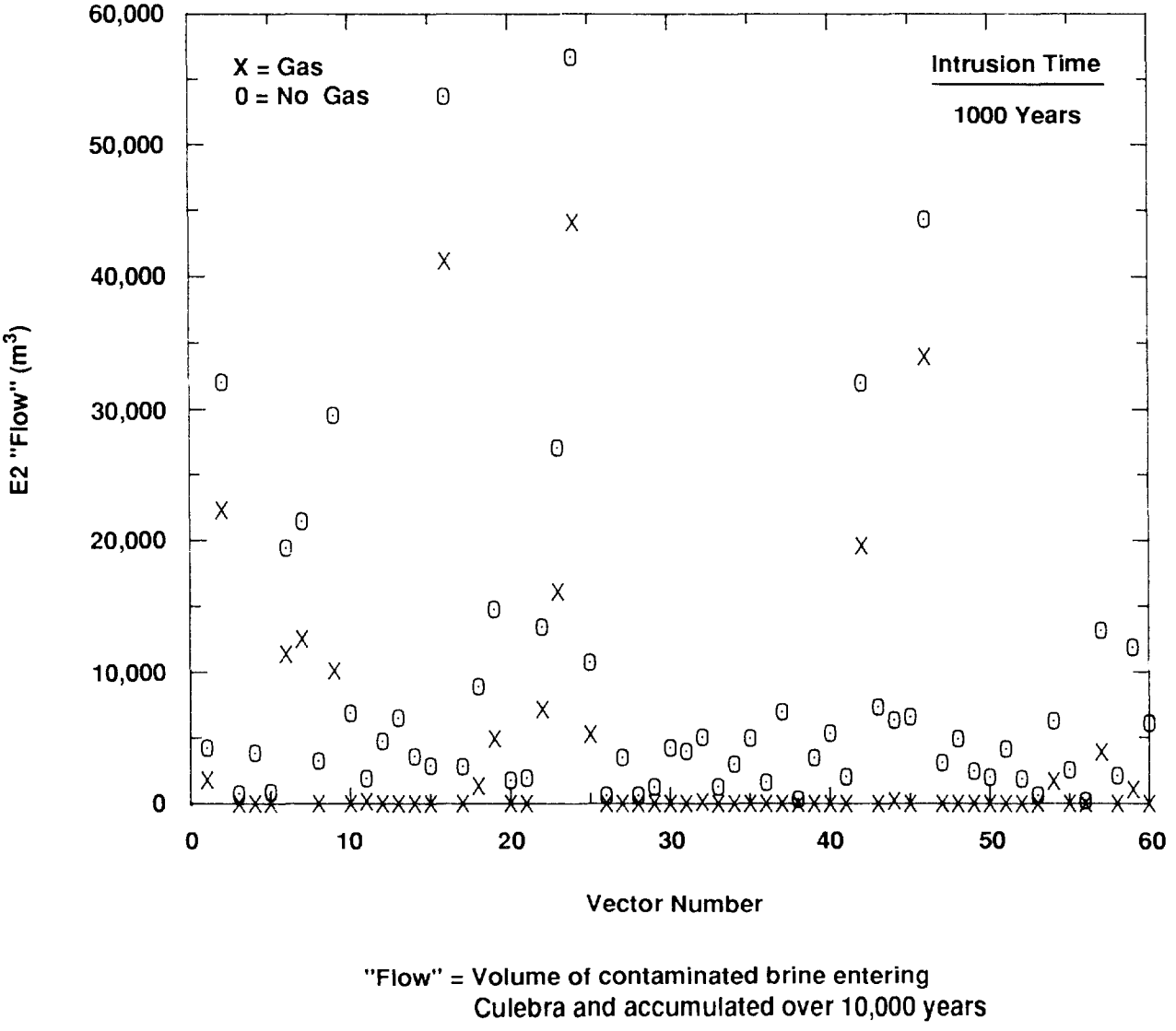

Figure 5-9. Borehole "Flow" Results From BRAGFLO: Effect of Gas Generation In E2 1000-Year Intrusion Summary Scenario

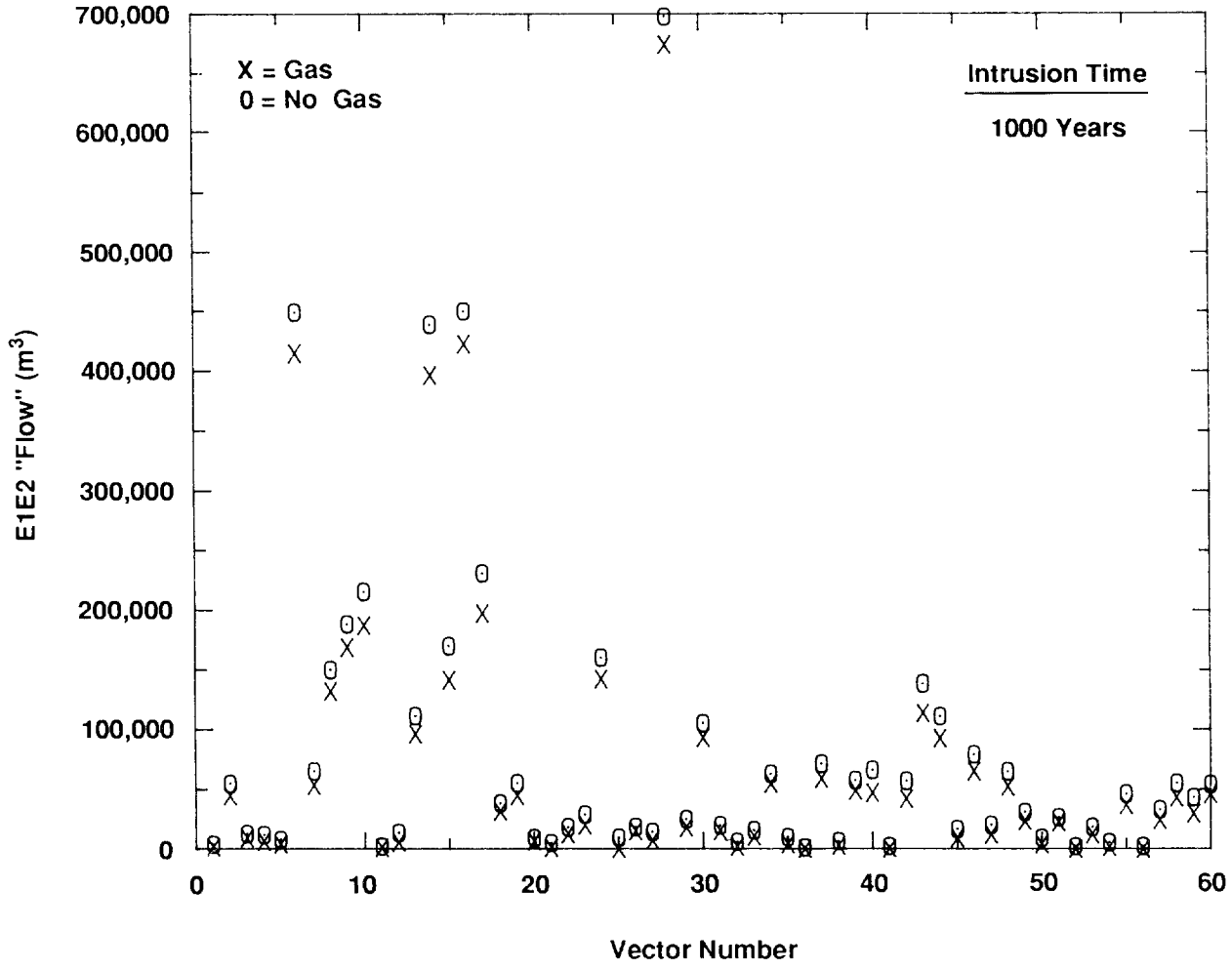

"Flow" = Volume of contaminated brine entering Culebra and accumulated over 10,000 years

TRI-6342-1359-0

Figure 5-10. Borehole "Flow" Results From BRAGFLO: Effect of Gas Generation In E1E2 1000-Year Intrusion Summary Scenario

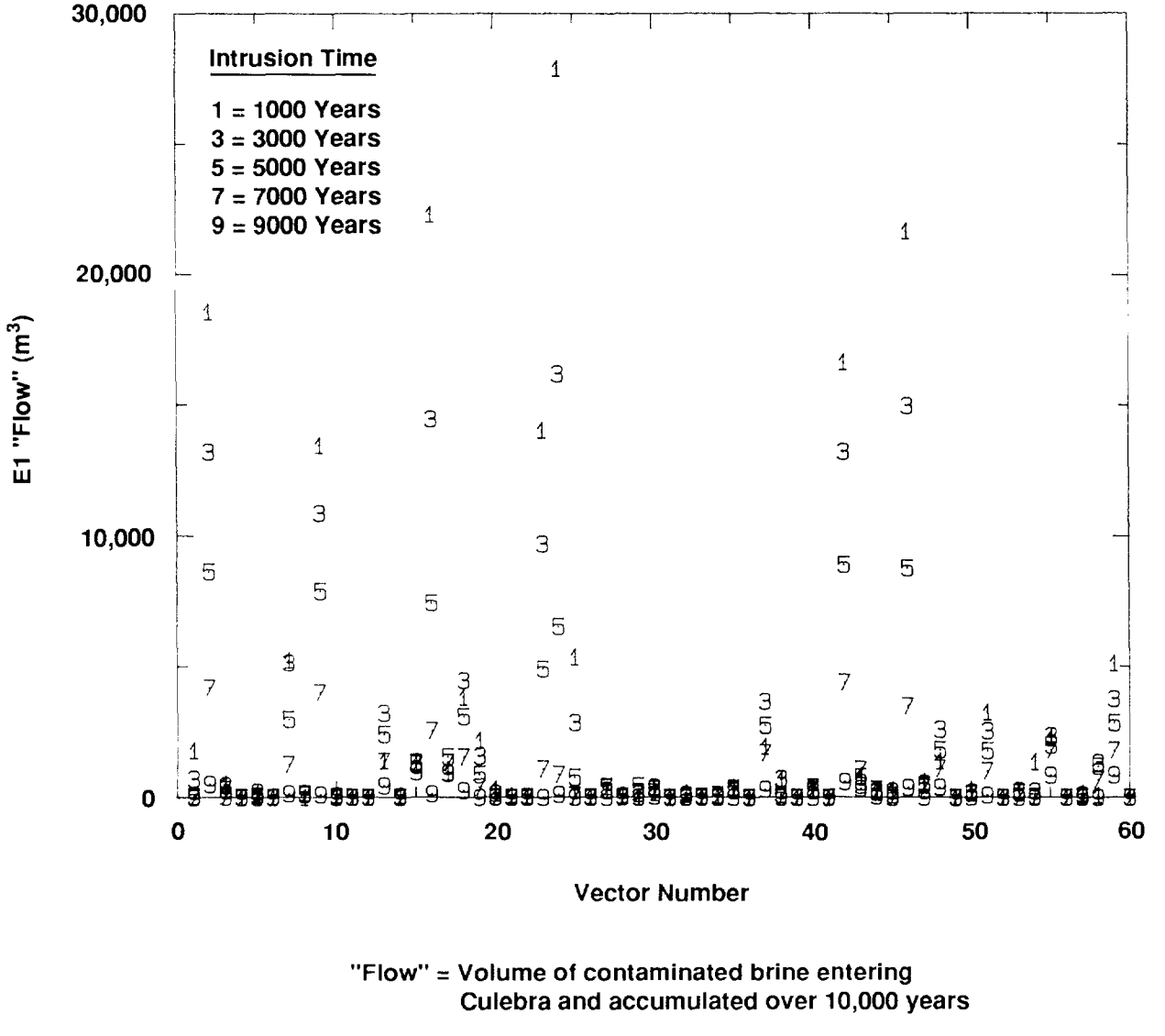

Figure 5-11. Borehole "Flow" Results From BRAGFLO During E1 Summary Scenarios

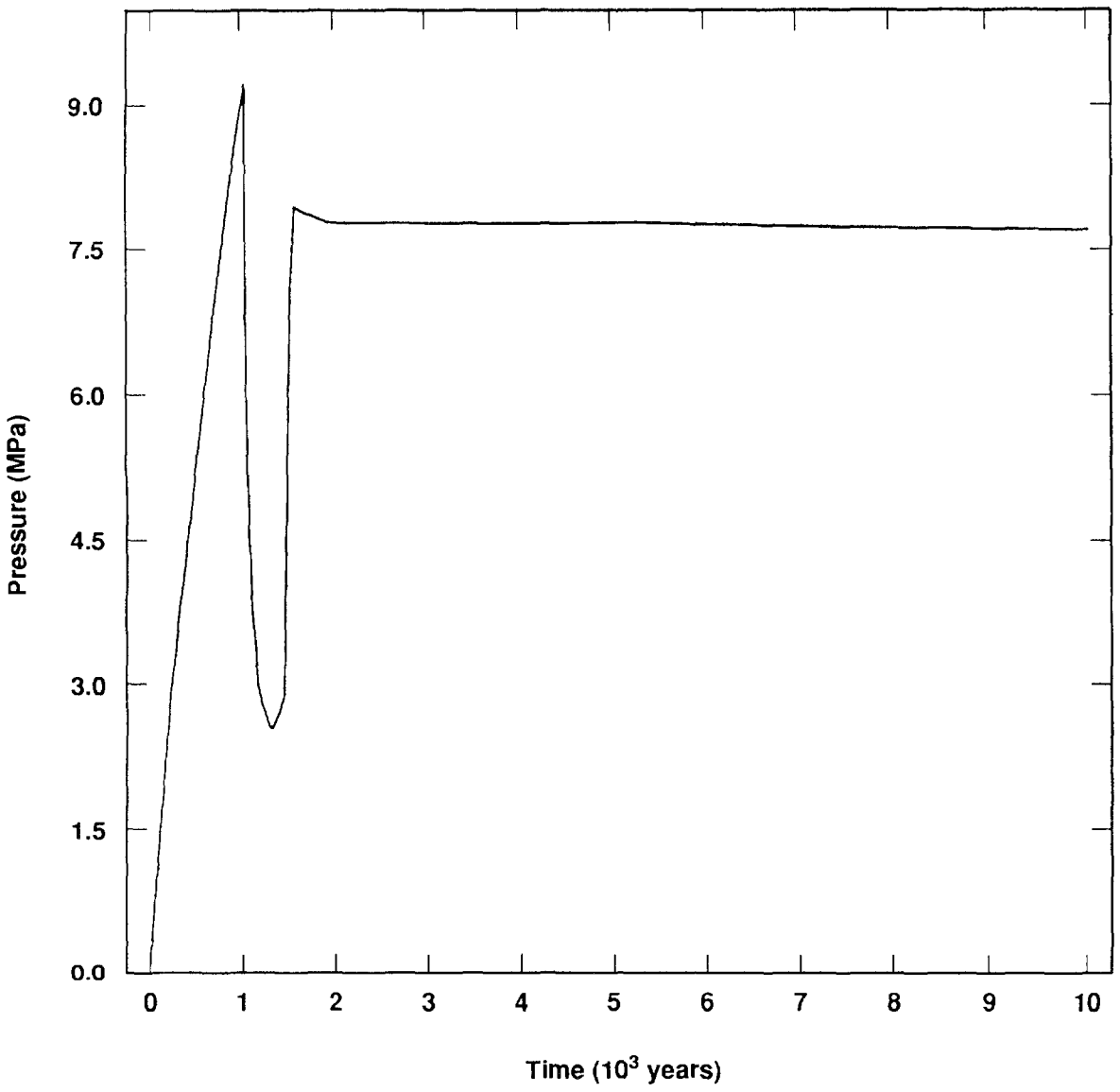

Figure 5-12. Pressure in Waste (E1E2 Scenario, With Gas Generation)

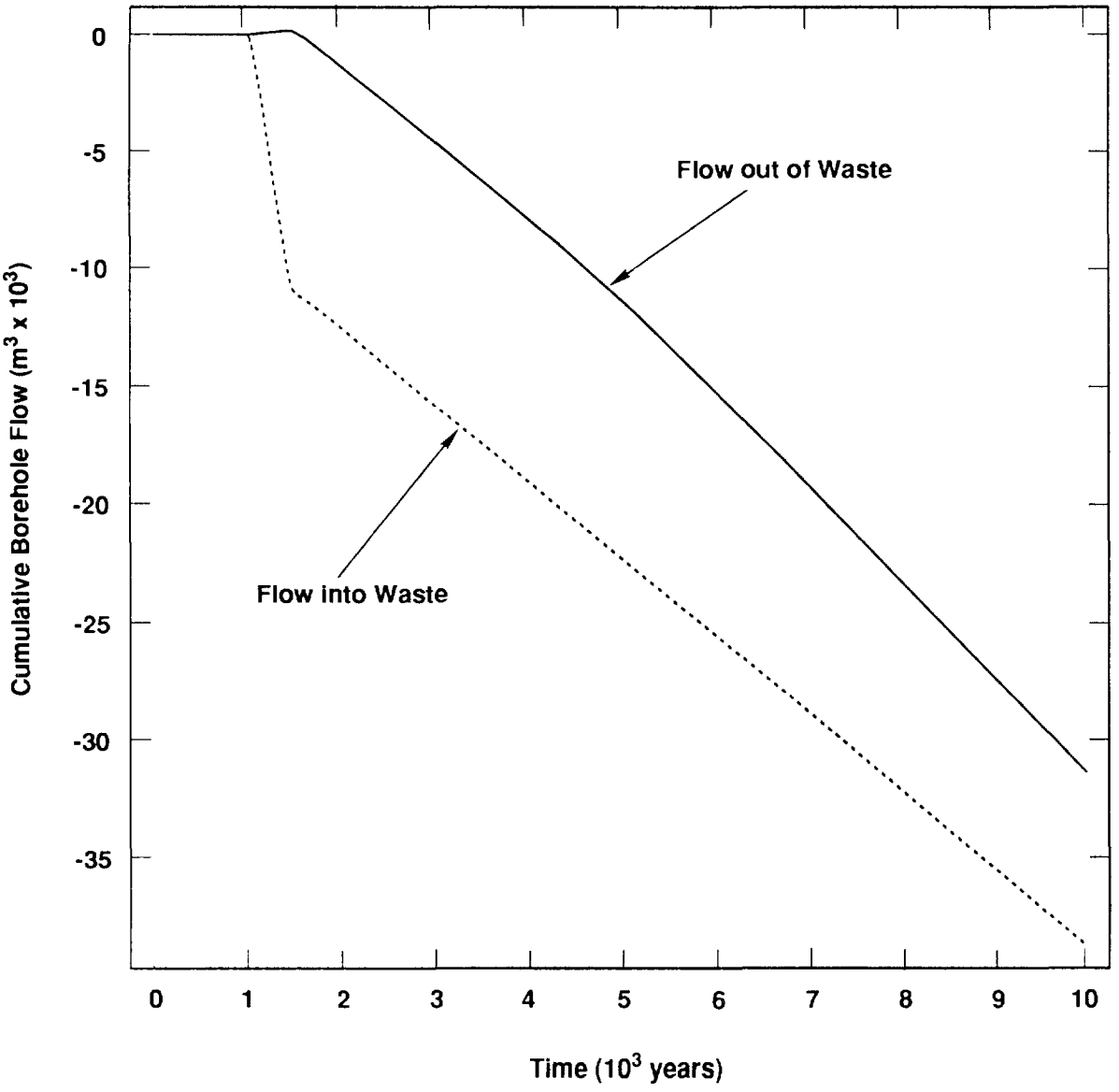

Figure 5-13. Cumulative Borehole Flows Into and Out of Waste (E1E2 Scenario, With Gas Generation)

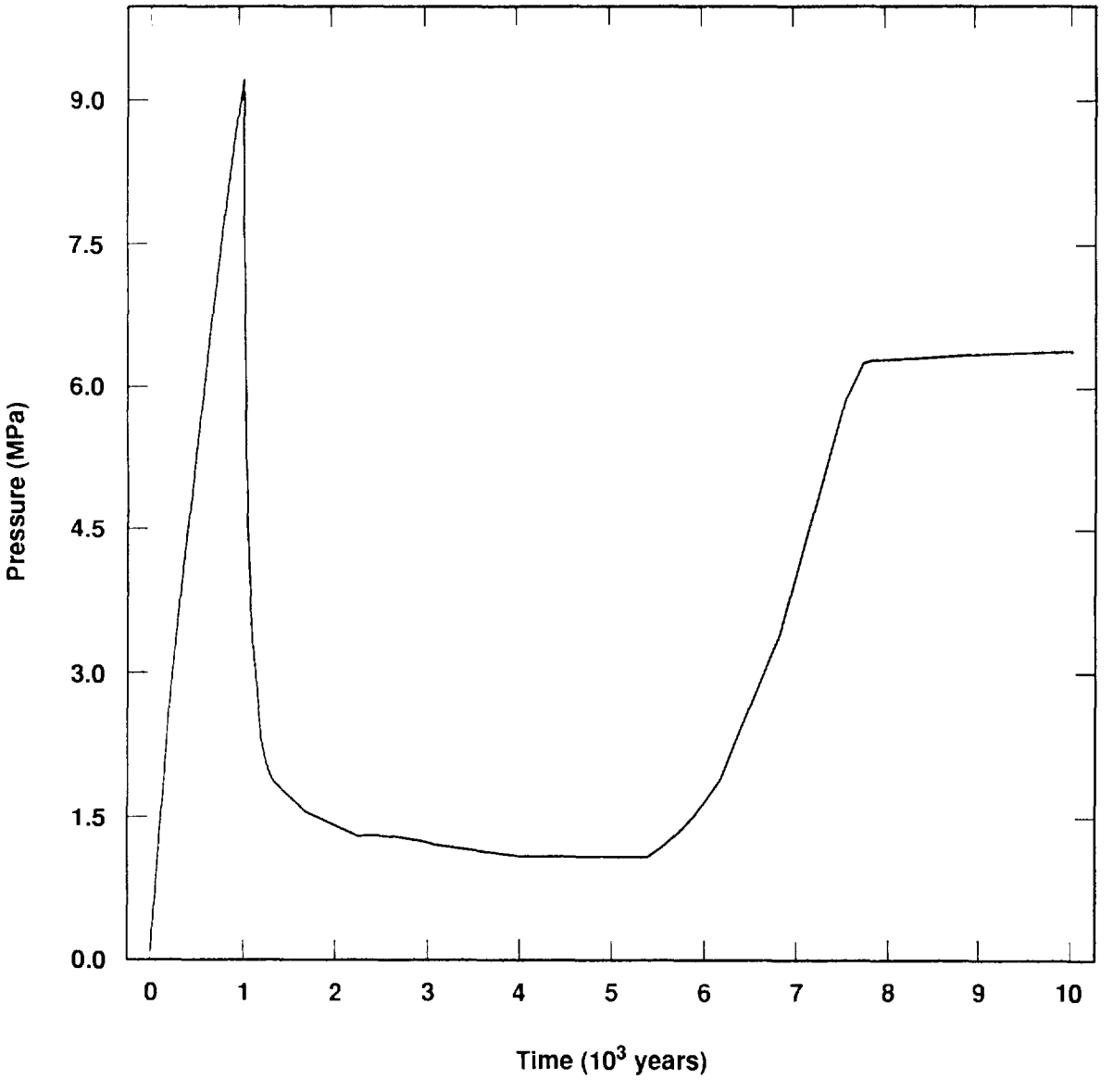

Figure 5-14. Pressure in Waste (E2 Scenario, With Gas Generation)

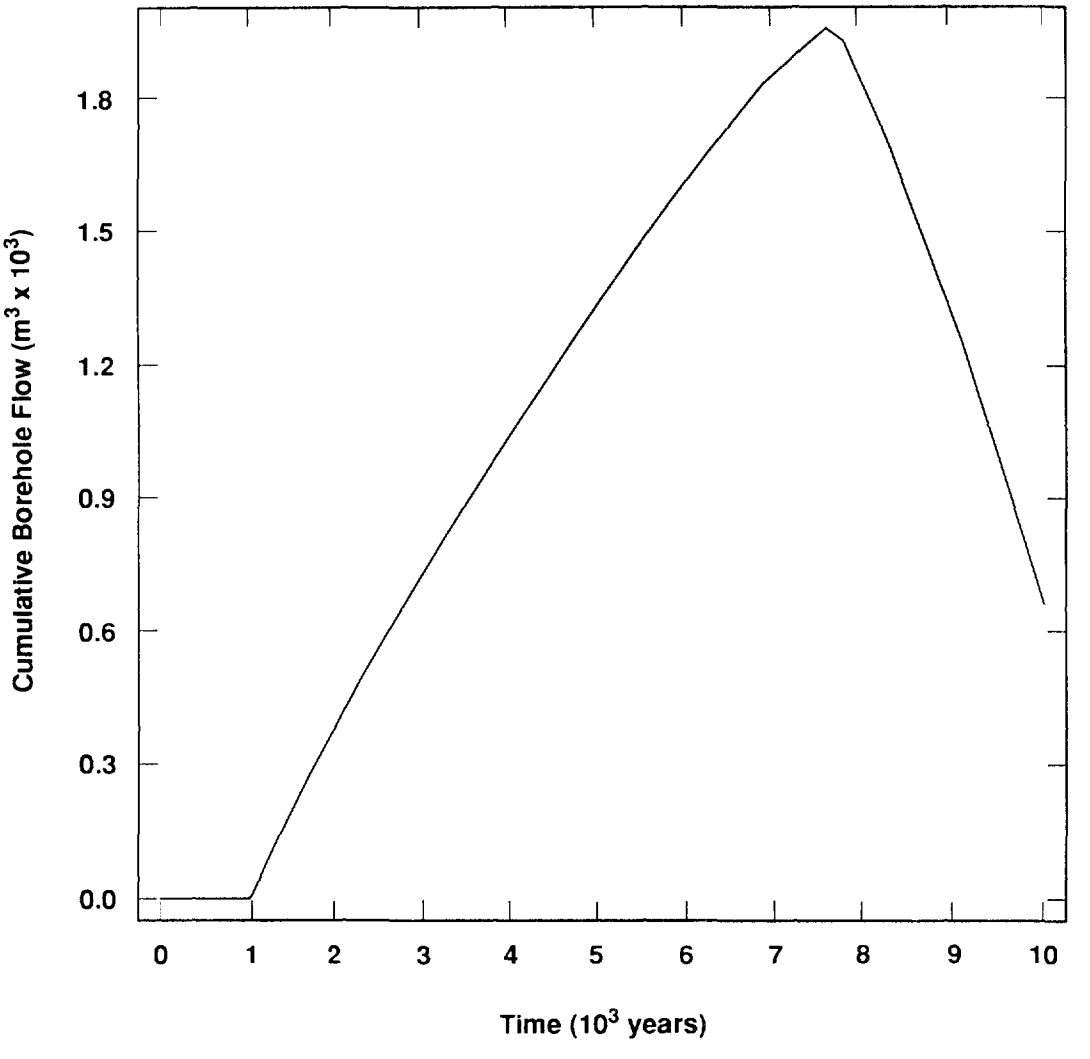

TRI-6342-1351-0

Figure 5-15. Cumulative Borehole Flow Out of Waste (E2 Scenario, With Gas Generation)

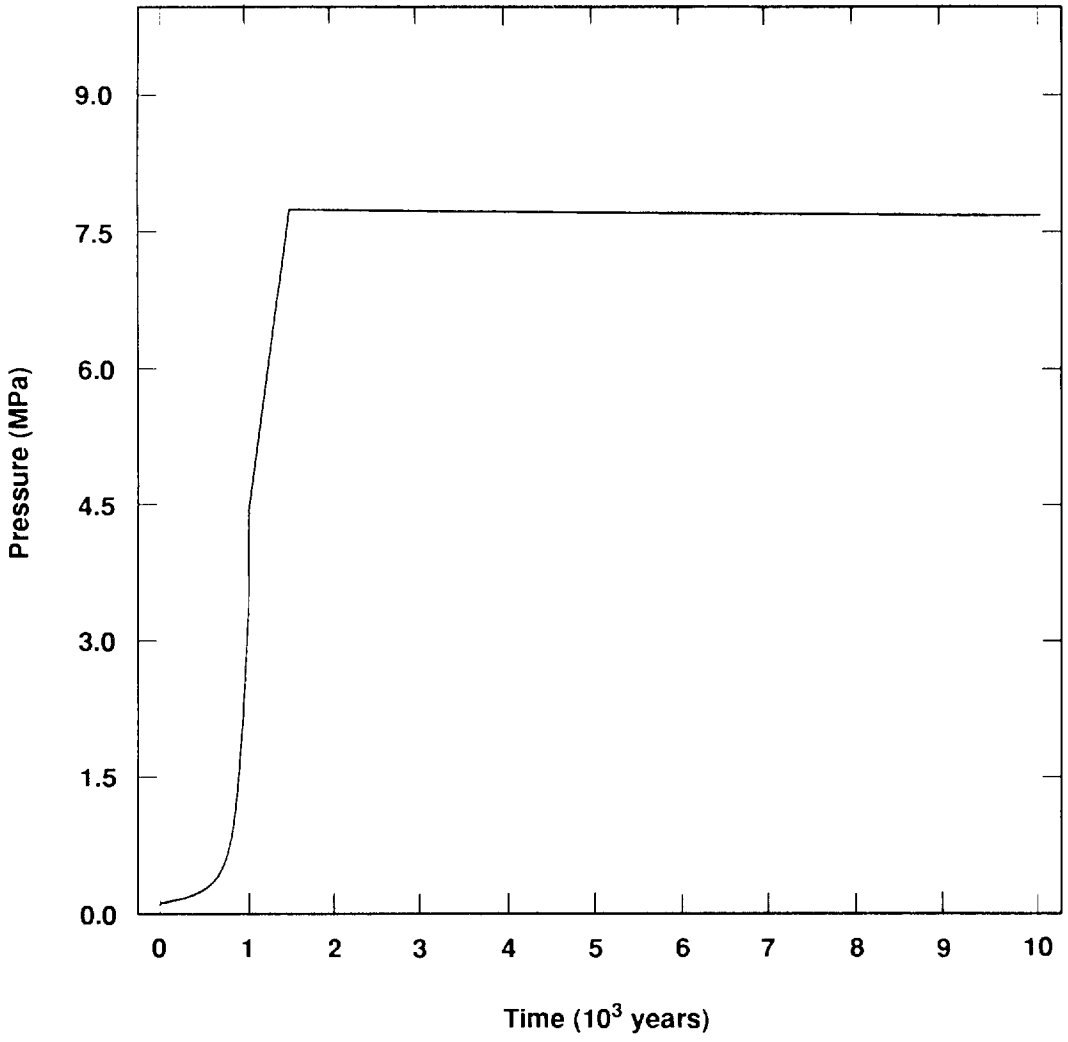

Figure 5-16. Pressure In Waste (E1E2 Scenario, Without Gas Generation)

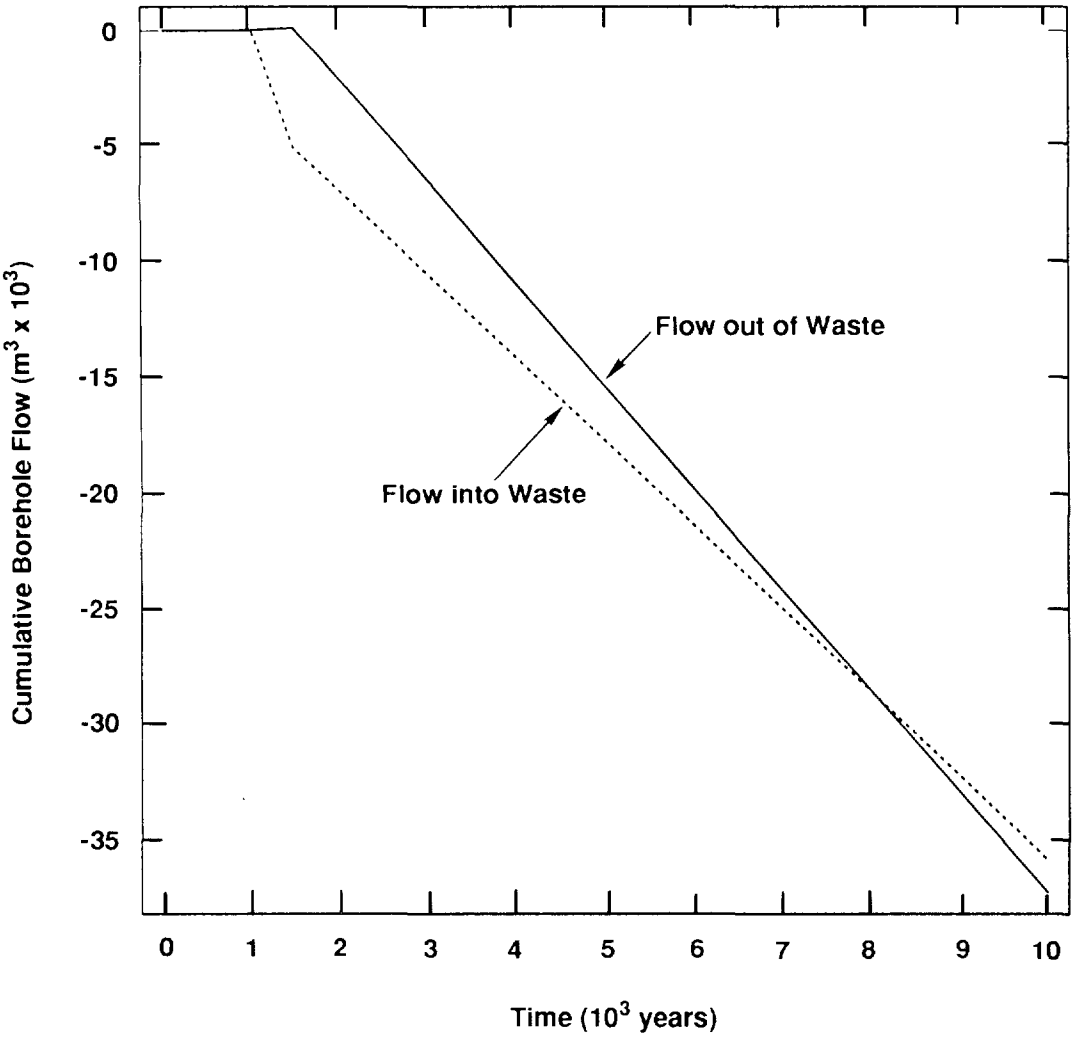

TRI-6342-1353-0

Figure 5-17. Cumulative Borehole Flows Into and Out of Waste (E1E2 Scenario, Without Gas Generation)

slightly higher pressure in the panel. At the same time, the gas bubble driven up into the Culebra is restricting flow there, resulting in higher pressures in the Culebra at the top of the borehole. The pressure there is high enough that the pressure drop from the panel to the Culebra is lower than when no gas is generated, which also reduces the flow rate of brine from the panel.

Comparison of E2, With Gas Generation, With E2, Without Gas Generation

As with the E1E2 scenario, the E2 scenario shows no pressure spike when no gas is generated (Figure 5-18). The pressure in the panel reaches hydrostatic in about 1850 years. When the borehole opens at 1000 years, the pressure is still below hydrostatic, and brine drains down from above to fill and pressurize the panel. The source of this brine is the Salado DRZ, the overlying anhydrite layer, and the lower Salado Formation above the repository. Flow upward to the Culebra (Figure 5-19) begins after 1760 years. The effect of gas generation is clear in this case: With gas generation, the time lag between borehole intrusion and brine flow out of the panel is 6730 years; without gas generation, the time lag is only 760 years. This shorter lag time results in far greater releases of brine: 8430 m^3 vs. 1300 m^3 with gas generation. When no gas has been generated, only residual saturation remains a short time after the borehole opens, so gas imposes no resistance to flow of brine through the waste from the anhydrite layer or MB139, as it does when gas is generated. Thus, the flow rate out of the panel is higher even after 10,000 years when no gas is generated: 0.92 m^3/yr vs. 0.68 m^3/yr with gas.

5.3 Repository Discharge (PANEL)—Walt Beyeler and James W. Garner

Boreholes penetrating a waste panel and possibly a Castile brine pocket can initiate the flow of brine and dissolved radionuclides between the repository and the Culebra Dolomite. Based on coupled models of fluid flow and the geochemical processes occurring within the repository, the discharge rate can be calculated with the code PANEL.

This model estimates rates of discharge of radionuclides and brine to the Culebra resulting from interconnection by one or more boreholes of the Culebra, repository, and possibly a Castile brine pocket underlying the repository. Radionuclide discharge depends on flow through the waste. Flow rates may be calculated internally in PANEL, or may be specified from a separate model (e.g., BRAGFLO). The 1991 calculations of the consequence analysis for disturbed conditions used flow rates calculated by BRAGFLO and not those of PANEL. Only the waste mobilization and transport model of PANEL is used.

Figure 5-20 is a schematic diagram of the Castile, repository panels, and Culebra following penetration.

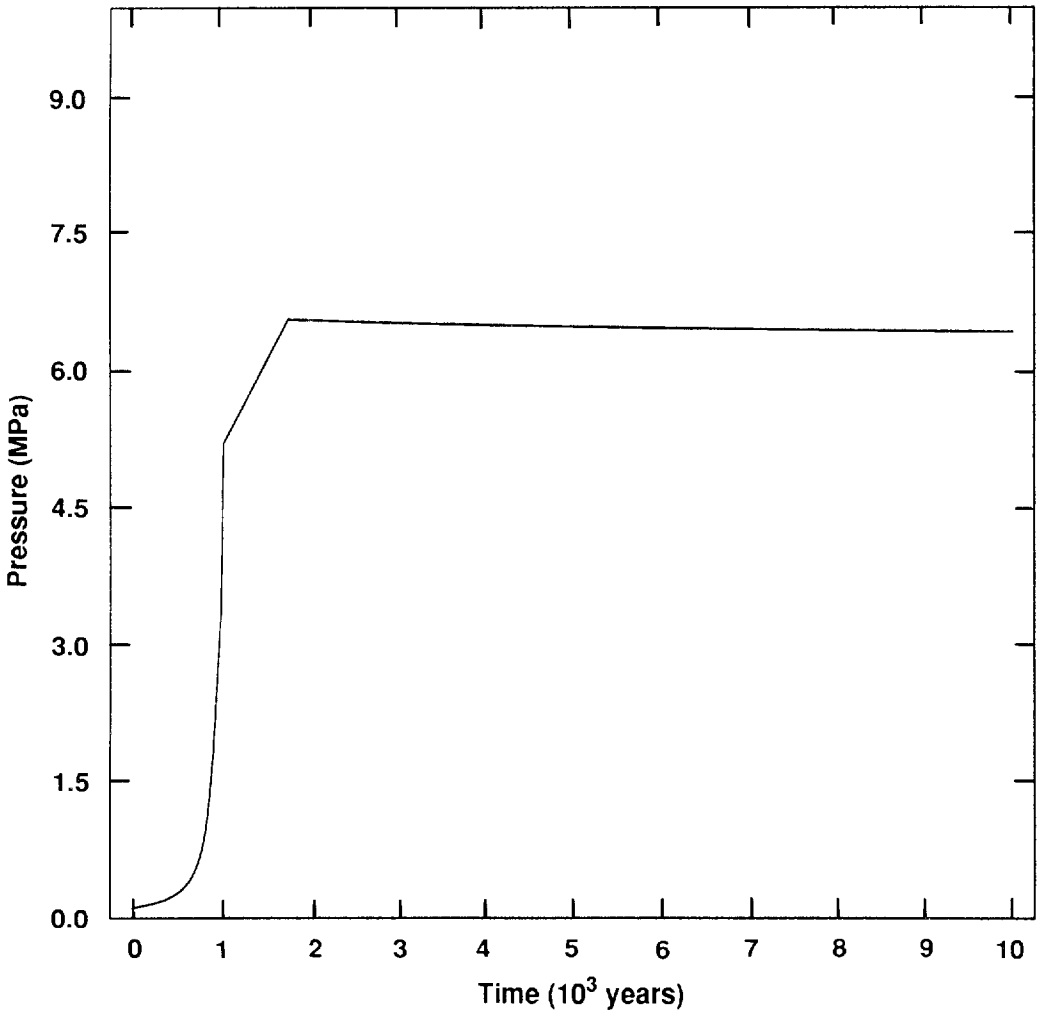

TRI-6342-1354-0

Figure 5-18. Pressure in Waste (E2 Scenario, Without Gas Generation)

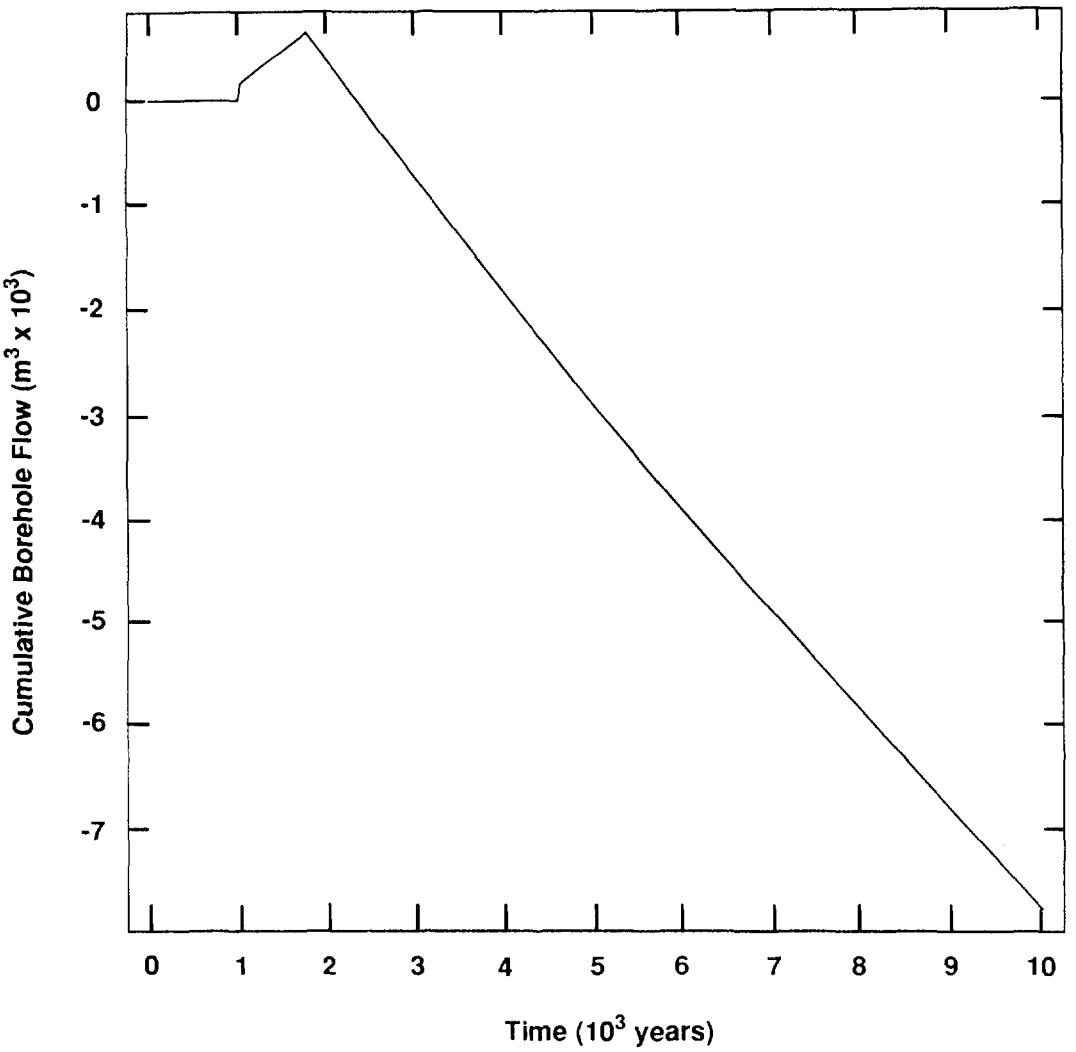

Figure 5-19. Cumulative Borehole Flow Out of Waste (E2 Scenario, Without Gas Generation)

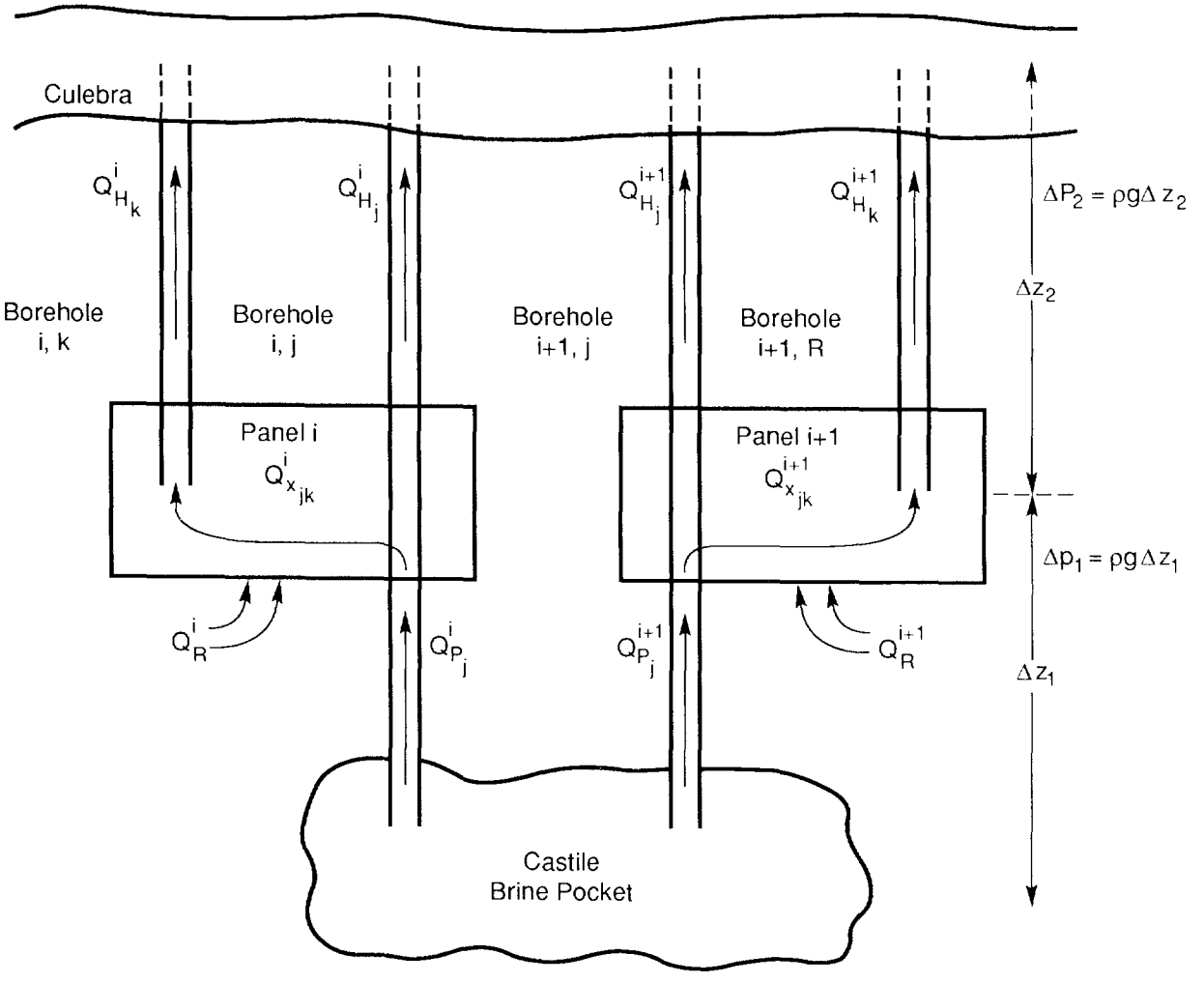

TRI-6342-840-0

Figure 5-20. Borehole Penetration of Repository Panels and Brine Pockets

Chemical/physical processes governing radionuclide flux are:

a. Dissolution of solid waste in the repository,

b. Radioactive decay, and

c. Advection of dissolved radionuclides from the repository to the Culebra.

Processes considered in the internal flow model are:

a. Upward flow through each borehole (Q_p^i $[L^3T^{-1}]$) from the Castile reservoir due to the difference between the reservoir pressure and the pressure in the panel at the borehole location;

b. Flow into each repository panel from the Salado (Q_R^i $[L^3T^{-1}]$);

c. Flow between boreholes k and j within a panel ($Q_{X_{kj}}^i$ $[L^3T^{-1}]$),

d. Upward flow through each borehole from the repository to the Culebra ($Q_{H_j}^i$ $[L^3T^{-1}]$).

The following describes the mathematical models used to represent the above process.

5.3.1 FLUID FLOW MODEL

5.3.1.1 Assumptions

While the fluid-flow model of PANEL was not used during the consequence analysis calculations, it was used for preliminary screening and comparison calculations. For this reason a discussion of PANEL's fluid-flow model follows.

All flow is assumed to occur as a single fluid phase. Possibly relevant processes which are neglected in this simplified approach include gas generation within the waste, exsolution of gases from Castile brine, and precipitation in the wellbore resulting from chemical or thermal disequilibrium between Castile brine and borehole fluid. All components of the flow system which are explicitly included in the model (see below) are assumed to be governed by Darcy's law. Hydrologic properties of each component are therefore completely characterized by hydraulic conductivity, specific storativity, and component geometry.

Volume 3 discusses ranges of values of these properties for the Castile, borehole fill, waste, and Culebra.

Using these properties, an analysis of the hydrologic response of these components following interconnection by a borehole of the Castile, repository, and Culebra suggests the following (Rechard et al., 1990b):

a. During discharge, pressure in the Culebra is not significantly elevated above its initial value;

b. Time constants for internal pressure transients in the Castile (both large and small fracture sets), borehole, and waste range from less than a year to tens of years;

c. The discharge time of the Castile reservoir ranges from thousands to hundreds of thousands of years.

On this basis, the following assumptions about the Castile, boreholes, waste, and Culebra have been made in the fluid flow model:

a. The Culebra acts as a fixed pressure discharge for all boreholes.

b. The transient behavior of the system over the period of interest is governed by the depletion of the brine reservoir, rather than by internal pressure transients within any component. Accordingly, all components are assumed to be at steady state with respect to boundary pressures at any given time.

c. The evolution of boundary pressures is controlled by depletion of the brine reservoir. Pressure change is assumed to be a linear function of the change in reservoir brine volume (e.g., due to linear elastic expansion of reservoir fluid and anhydrite):

$$\Delta V_p = S_b \Delta P_p \tag{5-10}$$

In terms of parameters of the Darcy flow model, the storativity of all components other than the brine reservoir is assumed to be zero. The conductivities of the brine reservoir and Culebra are assumed to be infinite.

Brine inflow rates from the Salado are assumed to be described by a differential equation which is linear in boundary pressure (such as the Darcian flow equation). In addition, pressure gradients within the panel due to flow from the Salado are assumed to be small, so that the pressure at the waste/Salado interface is effectively equal to an equivalent panel pressure P_{0_i}. Salado brine inflow for an arbitrary pressure history in the panel can be estimated by convolution.

5.3.1.2 Mathematical Formulation

Volume balance expressions are written for each borehole at the point of penetration of the waste panel (Figure 5-21) as follows:

$$Q^i_{H_j} = Q^i_{R_j} + Q^i_{X_j} + Q^i_{P_j} \tag{5-11}$$

where Q^i_R is that portion of Q^i_R discharged through the control volume.

Darcy's law allows all flow components at each junction to be expressed in terms of the discharge (Culebra) pressure (p_D), pressure in the panel at each wellbore (P^i_j), the pressure in the panel at other wellbores (P^i_k) and the instantaneous pressure in the brine reservoir (P_p):

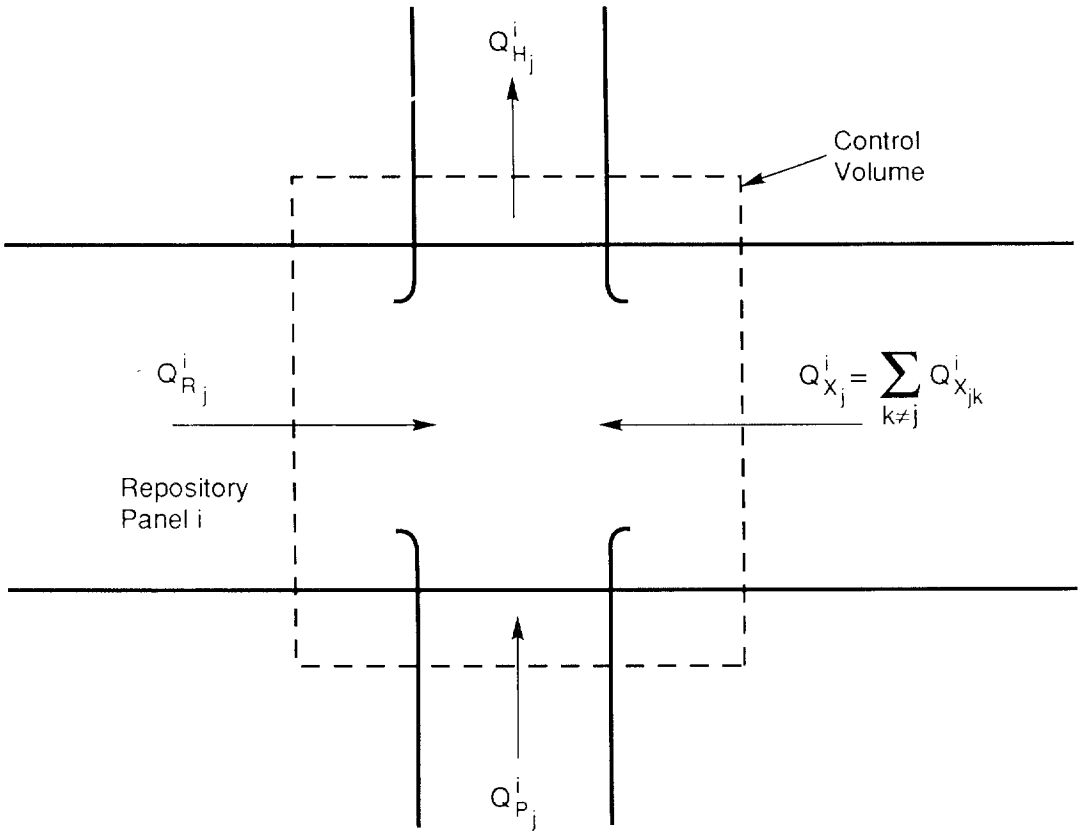

Figure 5-21. Waste Panel Penetration

$$Q_{H_j}^i = \zeta_{\omega_j}^i \left(P_j^i - P_D - \Delta P_2 \right) \tag{5-12}$$

$$Q_{R_j}^i = \zeta_{W_j}^i \left(P_0^i - P_j^i \right) \tag{5-13}$$

$$Q_{X_j}^i = \sum_{k \neq j} Q_{X_{kj}}^i = \sum_{k \neq j} \zeta_{X_{jk}}^i \left(P_k^i - P_j^i \right) \tag{5-14}$$

$$Q_{P_j}^i = \zeta_{L_j}^i \left(P_p - P_j^i - \Delta P_1 \right) \tag{5-15}$$

The connection terms $\zeta \bullet$ are the effective hydraulic conductances (in units of $m^3/s/Pa$) of the pathways associated with each flow component. $\zeta_{U_j}^i$ and $\zeta_{L_j}^i$ are the conductances of the upper and lower portions of wellbore is as follows:

$$\zeta_{U_j}^i = \frac{KA_j^i}{\Delta Z_2 \rho g} \tag{5-16}$$

$$\zeta_{L_j}^i = \frac{KA_j^i}{\Delta Z_1 \rho g} \tag{5-17}$$

where,

- K = hydraulic conductivity of the borehole fills,
- A = borehole cross-sectional area,
- ΔZ_1 = lengths of the lower segment of the borehole,
- ΔZ_2 = lengths of the upper segment of the borehole,
- ρ = fluid density, and
- g = gravitational acceleration.

The effects of alteration of borehole hydraulic properties through plug degradation and closure may be included by varying the product KA for each borehole with time.

Q_R^i is allocated among wellbores in panel i based on the wellbore radius (via the wellbore/waste conductance term $\zeta_{W_j}^i$) and the pressure at the wellbore (via the far-field waste pressure p_0). Accordingly, the individual discharges $Q_{R_j}^i$ must collectively satisfy

$$Q_R^i = \sum_j Q_{R_j}^i \tag{5-18a}$$

The instantaneous inflow rate to the panel, Q_R^i, is given by the pressure history in panel i and the unit pressure response function h(t):

$$Q_R^i = \left(P_I - P_0^i\right) * h \tag{5-18b}$$

where P_I is the equilibrium (far field) pressure at the repository elevation.

The wellbore/waste conductance is estimated as the steady-state conductance between the wellbore radius $r_{W_j}^i$ and a radius r_∞ equal to one-half the width of a panel excavation:

$$\zeta_{W_j}^i = \frac{2\pi K_R b}{\ln\left(\frac{r_\infty}{r_{W_j}^i}\right)\rho g} \tag{5-19}$$

where K_R is the hydraulic conductivity of the waste, and b is the panel height.

ζ is the conductance between boreholes within the same waste panel, and is given by:

$$\left(\zeta_{X_{jk}}^i\right)^{-1} = \left(\zeta_{W_j}^i\right)^{-1} + \left(\zeta_{W_k}^i\right)^{-1} + \left(\zeta_{R_{jk}}^i\right)^{-1} \tag{5-20}$$

where $\zeta_{R_{jk}}^i$ is that portion of the inter-borehole conductance due to borehole separation, i.e., the conductance of the paths between the far fields of each borehole (Figure 5-22).

Substituting for flow terms in (5-11) gives:

$$\zeta_{U_j}^i\left(P_j^i - P_D - \Delta P_2\right) = \zeta_{W_j}^i\left(P_0^i - P_j^i\right) + \sum_{k \neq j} \zeta_{X_{jk}}^i\left(P_k^i - P_j^i\right)$$

$$+\zeta_{L_j}^i\left(P_p - P_j^i - \Delta P_1\right) \tag{5-21}$$

The linear relationship between Castile brine reservoir pressure decline and total reservoir discharge volume can be written:

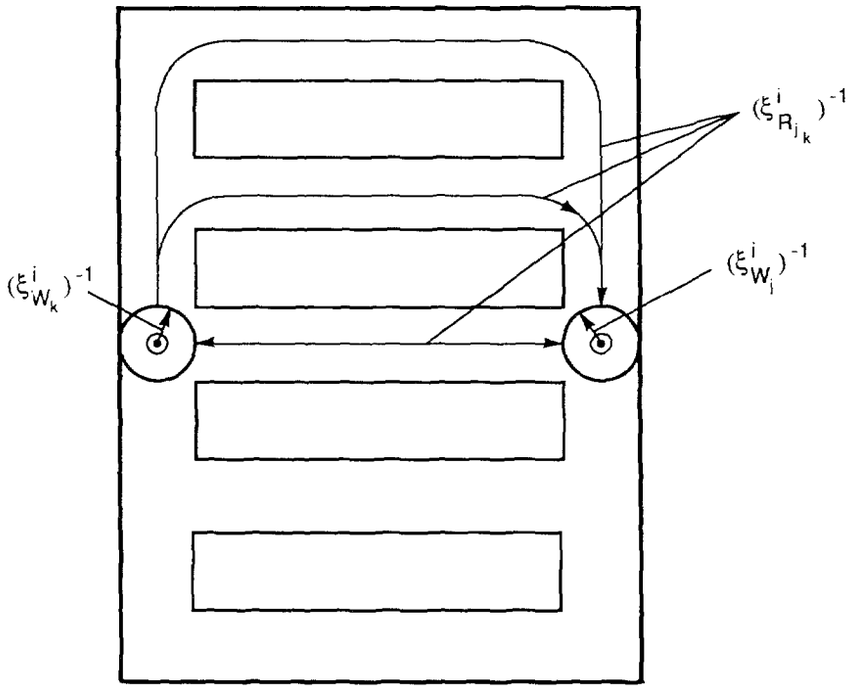

Figure 5-22. Conductance Between Boreholes Within the Same Waste Panel

$$P_p(t_2) = P_p(t_1) - \frac{1}{S_b}\int_{t_1}^{t_2} \sum_i \sum_j Q_{p_j}^i \, dt \tag{5-22}$$

Because of the possibility of time-varying borehole properties (see above), coefficients of (5-21) are not constant. The system is therefore solved numerically using a semi-implicit expression for $Q_{p_j}^i$ in (5-22) to approximate P_p:

$$P_p(t_2) = P_p(t_1) - \frac{t_2 - t_1}{S_b} \sum_i \sum_j Q_{p_j}^i \tag{5-23}$$

$$\overline{Q}_{P_j}^i = \overline{\zeta}_{L_j}^i \left\{ \frac{1}{2}\left[P_p(t_1) + P_p(t_2)\right] - \frac{1}{2}\left[P_j^i(t_1) + P_j^i(t_2)\right] - \Delta P_1 \right\} \tag{5-24}$$

where $\overline{\zeta}_{L_j}^i$ is an effective conductance for the lower portion of the borehole over the interval $(t_1 \rightarrow t_2)$, estimated from the harmonic mean of the end point values:

$$\overline{\zeta}_{L_j}^i = \frac{\zeta_{L_j}^i(t_1) * \zeta_{L_j}^i(t_2)}{\frac{1}{2}\left[\zeta_{L_j}^i(t_1) + \zeta_{L_j}^i(t_2)\right]} \tag{5-25}$$

Substituting (5-24) into (5-23) and defining

$$\overline{W}_L(x) = \frac{\Delta t}{2S_b} \sum_{\ell} \sum_m \overline{\zeta}_{L\ell m} \cdot x \tag{5-26a}$$

$$\Delta t = t_2 - t_1 \tag{5-26b}$$

yields

$$P_p(t_2) = \frac{1}{1 + \overline{W}_l(1)} \left\{ \left[1 - \overline{W}_L(1)\right] P_p(t_1) + \overline{W}_L\left[P_{\ell m}(t_1)\right] + \overline{W}_L\left[P_{\ell m}(t_2)\right] + 2\Delta P_1 \overline{W}_L(1) \right\} \tag{5-27}$$

Collecting junction pressure terms p_j^i in (5-21) gives:

$$\left(\zeta^i_{U_j}+\zeta^i_{W_j}+\sum_{k\neq j}\zeta^i_{X_{kj}}+\zeta^i_{L_j}\right)P^i_j-\sum_{k\neq j}\zeta^i_{X_{kj}}P^i_k-\zeta^i_{L_j}P_p$$

$$=\zeta^i_{U_j}\left(P_D+\Delta P_2\right)+\zeta^i_{W_j}P^i_0-\zeta^i_{L_j}\Delta P_1 \tag{5-28}$$

Substituting for P_p in (5-28) and collecting pressure terms at time t_2 on the left hand side yields:

$$\left(\zeta^i_{U_j}+\zeta^i_{W_j}+\sum_{k\neq j}\zeta^i_{X_{kj}}+\zeta^i_{L_j}\right)P^i_j(t_2)-\frac{\zeta^i_{L_j}}{1+\overline{W}_L(1)}\overline{W}_L\left[P_m(t_2)\right]$$

$$-\sum_{k\neq j}\zeta^i_{X_{kj}}P^i_k(t_2)$$

$$=\zeta^i_{U_j}\left(P_D+\Delta P_2\right)+\zeta^i_{W_j}P^i_0-\zeta^i_{L_j}\Delta P_1$$

$$+\frac{\zeta^i_{L_j}}{1+\overline{W}_L(1)}\left\{P_p(t_1)\left[1-\overline{W}_L(1)\right]+\overline{W}_L\left[P_m(t_1)\right]+2\Delta P_1\overline{W}_L(1)\right\} \tag{5-29a}$$

Substituting for $Q^i_{R_j}$ from (5-13) into (5-18),

$$\sum_j\zeta^i_{W_j}\left(P^i_0-P^i_j\right)=Q^i_R=\left(P_I-P^i_0\right)*h \tag{5-29b}$$

Convolution in (5-29b) is approximated from tabulated values of $h(t)$ and accumulated values of P^i_0, expanded around $P^i_0(t)$:

$$\left(P_I-P^i_0\right)*h=Q^i_0+\alpha^i\left[P_I-P^i_0(t)\right] \tag{5-30}$$

giving

$$\sum_j\zeta^i_{W_j}\left(P^i_0-P^i_j\right)=Q^i_0+\alpha^i\left[P_I-P^i_0\right] \tag{5-31}$$

or

$$\sum_j \zeta^i_{W_j}\left(P^i_0 - P^i_j\right) + \alpha^i P^i_0 = Q^i_0 + \alpha P_I \tag{5-32}$$

Equations (5-29a) and (5-29b) can then be solved for the pressures at each junction in each panel P^i_j and for the equivalent far-field pressure in each panel P^i_0.

In practice, the waste conductance terms $\zeta^i_{X_{jk}}$, $\zeta^i_{W_j}$ are usually much larger than the borehole conductance terms. Small inaccuracies in calculated junction pressures can produce large mass balance errors within the waste panel. To overcome this problem, flow rates in each borehole are first calculated assuming infinite waste conductivity (pressure equilibrium in the waste). These flow rates are then used with the waste conductivity and borehole locations to calculate an upper bound on pressure variation induced at each borehole as a result of resistance to flow through the waste. If this variation is within some specified tolerance, the infinite-conductivity approximation is retained. If not, the full system, including waste permeability [i.e., equation (5-29)], is solved.

5.3.1.3 Required Parameters

The following parameters are required by the model:

a. Culebra discharge pressure;
b. Length, area, location, fill hydraulic conductivity, and time of construction for each borehole;
c. Waste hydraulic conductivity;
d. Rate of brine inflow from the Salado as a function of time for some fixed pressure change at the waste/Salado boundary;
e. Castile reservoir initial pressure and bulk storage coefficient (change in volume per unit change in pressure).

In addition, the product of the hydraulic conductivity and area of the borehole may be made to vary in an arbitrary way with time, in order to represent (e.g.) the effects of plug degradation and closure.

5.3.2 WASTE MOBILIZATION AND TRANSPORT MODEL

Assumptions. The following are the waste mobilization and transport assumptions:

a. Concentrations of all species are assumed to be uniform throughout the waste panel.
b. Concentrations of all species are assumed to be in equilibrium at any time.

c. Solubility limits for a given element are allocated among its isotopes on the basis of relative abundance.

5.3.2.1 Mathematical Formulation

Radionuclide concentration and discharge are calculated at discrete time steps as follows:

a. The total volume of fluid entering the panel over the interval displaces an identical volume of fluid with the appropriate concentrations of all isotopes. This volume is limited to no more than 10% of the pore volume of a panel by selection of the time step.

b. Concentrations within the panel are updated by:

   1. Mixing the remaining panel pore fluid with the introduced fluid volume;

   2. Updating the existing inventory of all species from radioactive decay during the interval; the amount of each radionuclide at time $T + \Delta T$ is $A_I(T + \Delta T)$ with decay constant λ_I is defined as $A_I(T + \Delta T) = A_I(T)\ell^{\lambda_I \Delta T}$ + Parental, Grandparental and Great-Grandparental contributions as defined by Bateman Equations (see discussion in CUTTINGS, Chapter 7).

   3. Calculating the new equilibrium concentrations of all species with respect to dissolution. The amount in solution for each element is the solubility limit (molar) * 1,000 liters/m^3 * volume of panel (m^3). If this amount is more than the amount of the element in the panel, the amount in solution is the entire amount of the element.

   The concentration of each radionuclide is the mass of its corresponding element in solution times the moles of this radionuclide in the panel/the total moles for its corresponding element in the panel. Since this is a mixing-cell model, there are no local variations.

5.3.2.2 Parameters

The following are the waste mobilization and transport required parameters:

a. Initial inventory of all isotopes in each panel;

b. Half-lives and daughters for each isotope;

c. Solubility limits for each element;

d. Pore volume of each panel;

e. Rate of fluid flow through the waste (derived from the fluid model discussed above or specified from results of another model, e.g. BRAGFLO).

5.3.3 FLUID-FLOW/WASTE MODEL COUPLING

Two components of the flow system may potentially mobilize waste; flow from the Salado to a borehole, and flow from one borehole to another. The sum of these components at any time provides an estimate of the rate of flow through the waste. In the event of a single intrusion, only

provides an estimate of the rate of flow through the waste. In the event of a single intrusion, only flow from the Salado is assumed to pass through the waste. In the E1E2 scenario, flow from the Castile is also assumed to pass through the waste. Integration of fluid flow rate through the waste over some time interval provides an estimate of the volume of contaminated fluid (with concentrations calculated as described under waste mobilization) discharged to the Culebra through the intrusion boreholes. Final flow rates and concentrations discharged to the Culebra from a given borehole are estimated from the mixing of fluid entering the borehole from the waste with fluid flowing through the borehole from the Castile. This procedure ignores any decay or sorption in transport through the upper half of the borehole. Short travel times and expected borehole fill material suggest that the effect of these would be negligible.

5.3.4 RESULTS

The total flow input to PANEL from the BRAGFLO (Section 5.2.5.1) calculations varied from 0 m^3 to 44,000 m^3 for intrusions that did not intersect a brine pocket and from 0 m^3 to 675,000 m^3 for intrusions that intersected a brine pocket. These flows, coupled with solubilities that varied over many orders of magnitude produced releases of the various radionuclides from PANEL that varied from zero to the inventory of one panel. These releases were then used as input to the program STAFF2D. The EPA normalized releases from PANEL are shown in Figures 5-23 and 5-24. A comparison of Figure 5-23 with 5-7 (the "flows" from BRAGFLO) reveals that large flows are a necessary condition for large releases, but not a sufficient condition (compare vectors 16 and 24). Also, comparing E2 releases and E1E2 releases for vectors 15 and 16 indicates that vector 16 has large releases for both E2 and E1E2, but vector 15 has a near zero release for E2 and a maximum release for E1E2.

PANEL can also be run in a mode that does not require fluid flows produced by BRAGFLO. In this mode, it calculates internally the flows through the waste. The runs made in this mode were used as a diagnostic tool for BRAGFLO. This type of calculation was not used in any of the results reported.

5.4 Summary of Results for Disturbed Performance of the Repository/Shaft

The calculations performed to assess the disturbed performance of the Repository/Shaft System had two primary objectives:

- To determine the path and extent of flow of contaminated brine and to determine migration and transport of radionuclides from the waste panel up an intrusion borehole.
- To evaluate the effect of waste-generated gas on the flow of contaminated brine and on the migration of radionuclides.

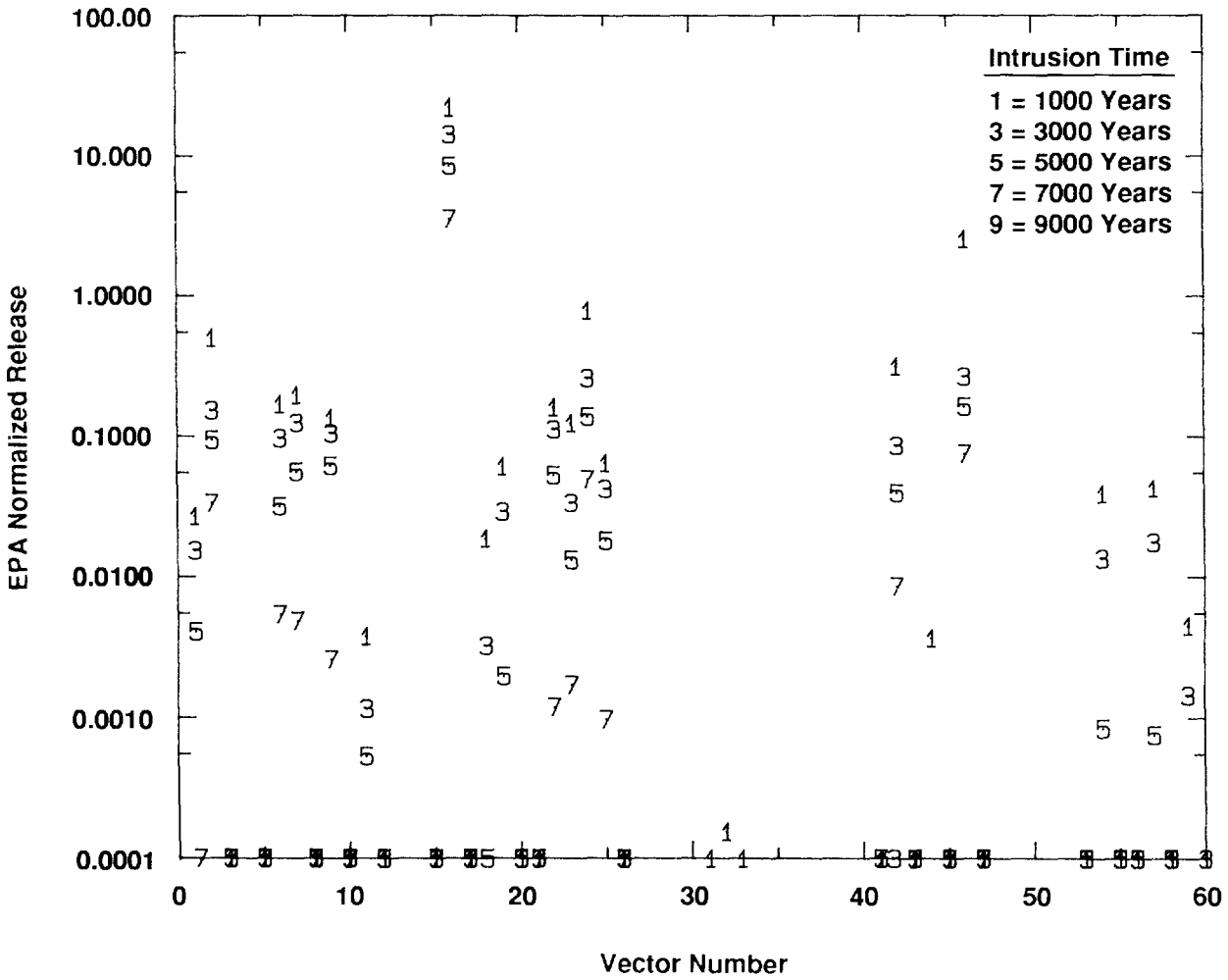

Figure 5-23. E2 Releases from PANEL at Various Times of Intrusion

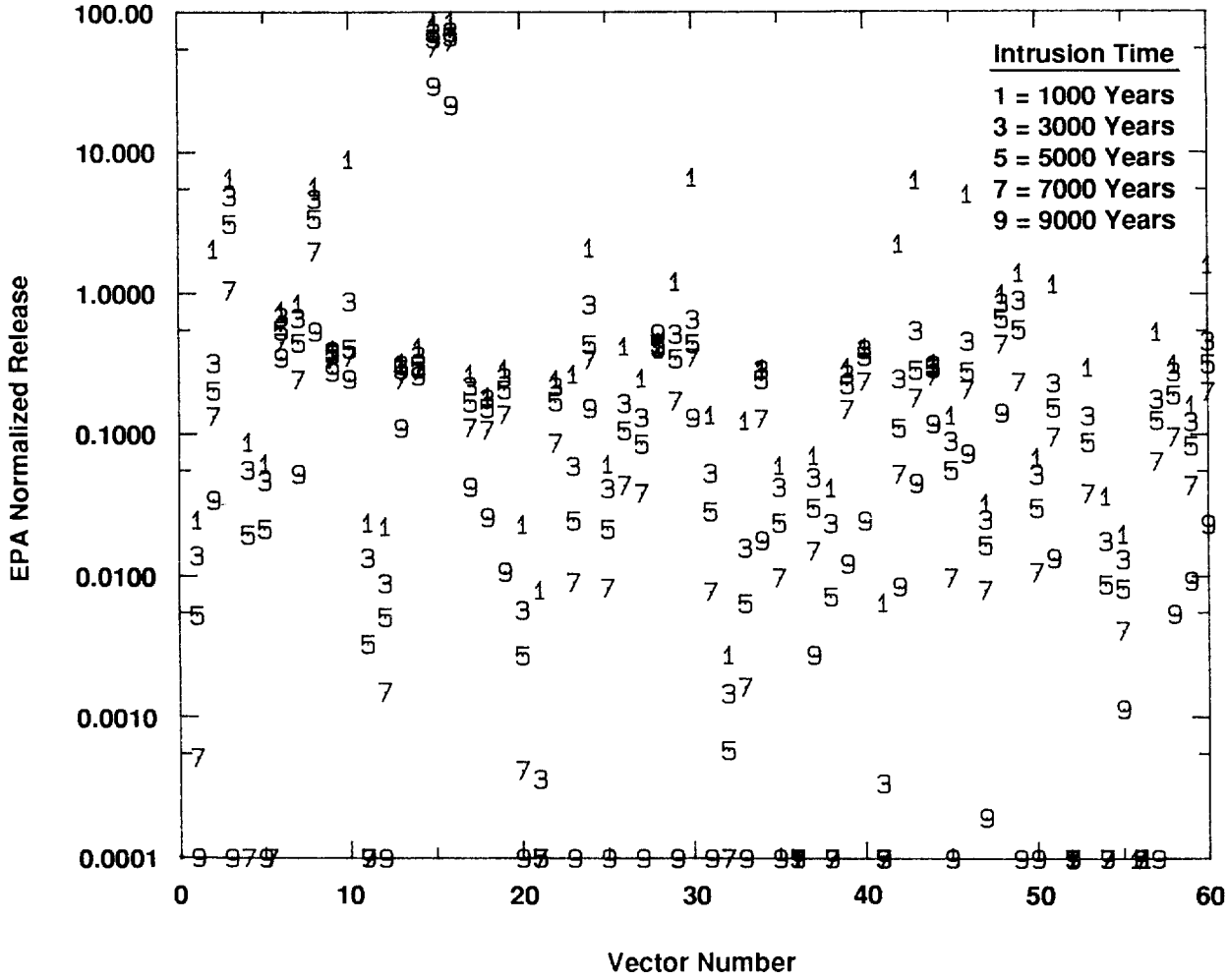

Figure 5-24. E2 Releases from PANEL at Various Times of Intrusion

To address these objectives, two computer codes (BRAGFLO and PANEL) were used with varying material, reservoir, and waste properties. A Latin hypercube sampling procedure was used for selection of the parameter values from parameter probability distributions documented in Volume 3 of this report. The sampling procedure resulted in 60 vectors (differing sets of sampled input parameter values) for each of two summary scenarios E2 and E1E2. The E2 summary scenario is single intrusion of the waste panel, the E1E2 summary scenario is a multiple intrusion of the repository with one well terminating in the waste panel and a second well passing through the panel and terminating in a pressurized brine pocket. The consequences of a third scenario summary the E1 (in which a single borehole penetrates the waste and a brine pocket) was assumed identical to the E2 summary scenario. All three summary scenarios were further sub-divided according to the time of intrusion (1000, 3000, 4000, 7000, and 9000 years). A total of 600 BRAGFLO and PANEL simulations were performed for assessing the disturbed performance of the repository 300 E2 and 300 E1E2 simulation sets.

In PA the calculations, BRAGFLO was used to quantify the two-phase flow fields in and around the repository. PANEL was used for calculating the radionuclide concentration and discharge of radionuclide from the waste through the intrusion borehole. The time-dependent flow fields, phase saturations, and waste porosity from BRAGFLO served as input to PANEL. The well bore flow rates and radionuclide concentrations in the brine resulting from BRAGFLO and PANEL are source terms for models such as SECO2D and STAFF2D (Chapter 6), which quantify the flow fields and radionuclide transport in the Culebra dolomite member of the Rustler formation, considered to be the most likely subsurface pathway to the accessible environment during human intrusion.

Results for a typical vector were described to illustrate the significant features and behavior of two-phase flow under disturbed conditions when an intrusion borehole opens at 1000 years. The E2 and E1E2 scenarios, with gas generation occurring, were compared. Then the effects of gas generation were examined by comparing the results of each scenario with and without gas being generated.

The following general conclusions are based on analysis of the BRAGFLO and PANEL intermediate results. (The term "flow" is defined as the accumulated volume of contaminated brine which enters the Culebra from an intrusion borehole during a 10,000-year interval following panel sealing.)

- "Flow" and radionuclide release decreased for later- occurring intrusions.
- "Flow" and radionuclide release was larger during E1E2 summary scenarios than during E2 summary scenarios.

- Waste generated gas reduced "flow" and radionuclide release during the 1000-year intrusion E2 and E1E2 summary scenarios for the range in waste properties and gas generation rates sampled.
- The "flows" produced during E2 summary scenarios were of similar magnitude to those of E1 summary scenarios but did not necessarily bound the E1 produced "flows" for all vectors.
- Large "flow" was a necessary but not a sufficient condition for producing a large radionuclide release from the waste panel.

6. DISTURBED GROUNDWATER FLOW AND TRANSPORT

6.1 Conceptual Model—Walt Beyeler

The Culebra Dolomite member of the Rustler Formation is considered to be the most likely subsurface pathway for radionuclide transport to the accessible environment in the event of human intrusion into the repository (Volume 1 of this report). Because of its perceived importance to site performance, conceptual and numerical models of the Culebra continue to receive much attention. The conceptual model of the Culebra Dolomite underlying the current performance assessment calculations describes the hydrologic state and behavior of the Culebra Dolomite within the model domain shown on Figure 6-1. The conceptual model consists of the following assumptions:

- **Single-porosity Darcian flow.** Results of hydrologic tests on wells completed in the Culebra are consistent with the response of a heterogeneous medium obeying Darcy's law. Results of some well tests indicate double-porosity response during the early part of the tests (see, for example, Beauheim, 1987). This is interpreted to be caused by disequilibrium between pressure in coextensive fracture and matrix porosity sets. Because the time of pressure equilibration between the porosity sets is much smaller than the time scale of processes considered in the human-intrusion scenario, the Culebra Dolomite is modeled as a heterogeneous single-porosity medium for the purpose of fluid flow calculations. (Dual porosity effects on transport are considered, however).

- **Two-dimensional flow.** Most hydrologic test wells in the Culebra Dolomite are completed across the entire vertical extent of the Culebra. Parameters derived from tests on these wells are therefore composite or average values over the vertical extent of the member. Although flow is known to be localized to particular elevations within the Culebra at several wells (Mercer and Orr, 1979), there is insufficient information to characterize vertical variability of hydrologic properties within the Culebra Dolomite. A vertically integrated two-dimensional model has therefore been adopted.

- **No flow through upper and lower boundaries.** Potentiometric differences between the Culebra and other members of the Rustler suggest that vertical flow between the members is extremely slow over the WIPP and in much of the surrounding study area. The present conceptual model includes impermeable upper and lower boundaries on the Culebra.

- **Parallel-to-axis-flow along the axis of Nash Draw.** Nash Draw is believed to be a major sub-surface drain for the Rustler in the vicinity of the WIPP (Davies, 1989;

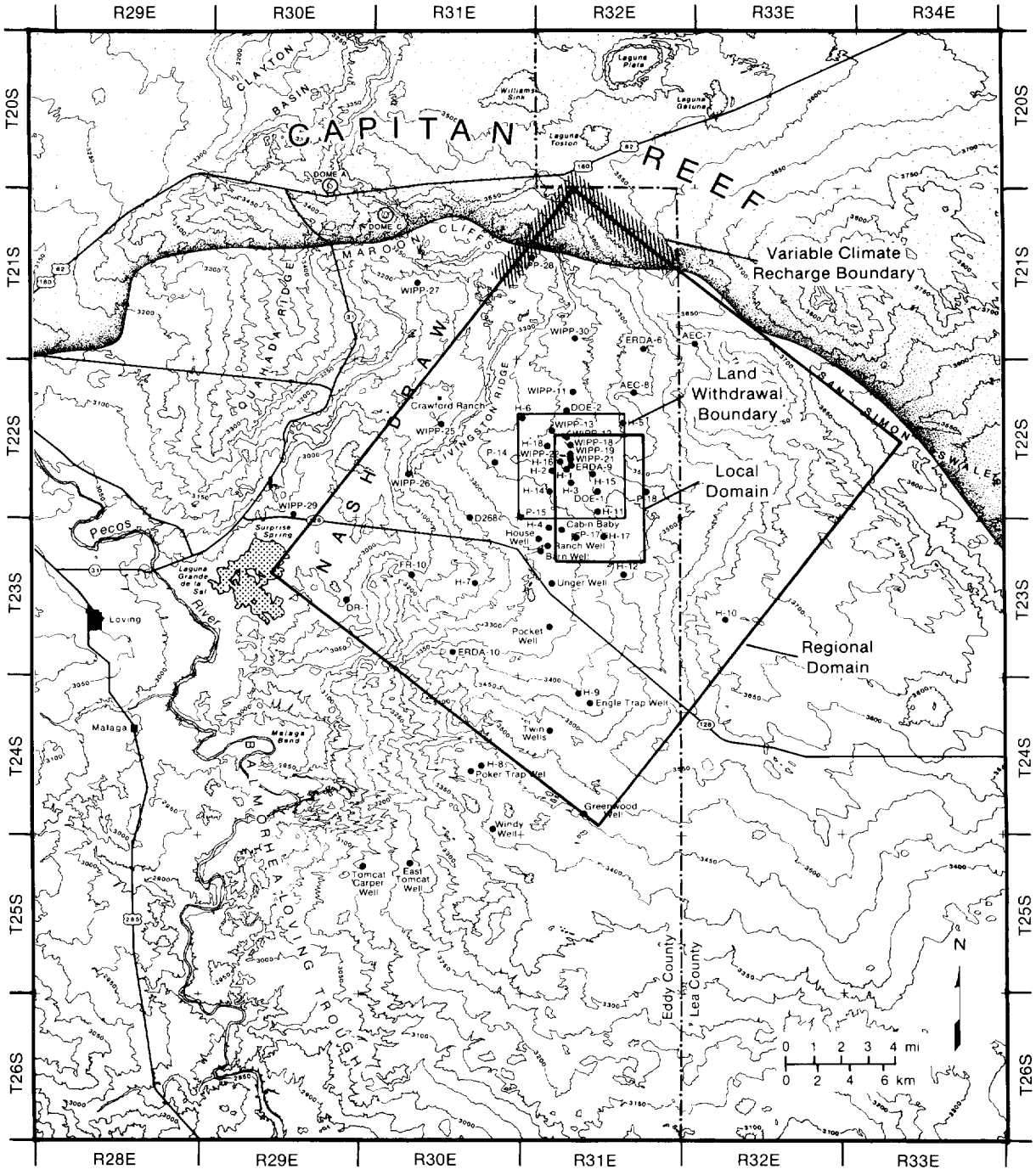

TRI-6342-612-5

Figure 6-1. Model Domain of the Culebra Dolomite Member

Brinster, 1991). Flow in the Rustler would therefore follow the axis of Nash Draw; the axis of the draw is treated as a streamline (no-flow) boundary.

- **Pressure equilibrium and flow prior to WIPP construction.** Time constants of pressure changes due to compression of the fluid and matrix are small compared to time constants of fluid density change, transmissivity evolution, or other transient processes affecting pressure. For any subdomain of the Culebra, and in the absence of fluid sources or sinks within the subdomain, the Culebra pressure is assumed to be currently in equilibrium with pressures around the boundary of the subdomain.

- **Future flow-field transients induced by external changes.** The future state of the Culebra flow field is assumed to differ from the present state through regional climate change. Climate change is assumed to affect recharge and discharge rates external to the model domain, and therefore to influence flow within the model domain through a change in boundary pressures.

- **Transport decoupled from flow.** In the human intrusion scenario, one or more boreholes create a long-term connection between the repository and the Culebra. Hydrologic properties of the borehole fill limit potential fluid discharge to the Culebra to approximately 80 m^3/yr. This rate of fluid injection is assumed to have no impact on the prevailing Culebra flow field (Reeves et al., 1991). In addition, fluid injected from the repository is assumed to have negligible effect on the Culebra fluid density. Estimation of the Culebra flow field, and estimation of radionuclide transport through this flow field resulting from intrusion, are therefore considered as separate problems.

- **Dual-porosity transport.** Matrix and fracture porosities that are coextensive and communicating can result in local disequilibrium in radionuclide concentrations between the fracture and matrix. The time constant associated with this disequilibrium is determined by the rate of exchange of radionuclides between the two porosity sets, and the radionuclide storage capacity of the fracture and matrix. Because this equilibration time may be significant in comparison to the time scale of source-term concentration change, a dual-porosity transport model has been adopted.

- **Linear equilibrium sorption of radionuclides.** In addition to hydrodynamic processes, radionuclide concentrations in Culebra groundwater are assumed to be affected by geochemical interactions with the host rock. Reversible sorption is assumed to be the only

mechanism of interaction of the radionuclides with the Culebra Dolomite. Sorption is further assumed to follow a linear Freundlich isotherm, with different coefficients describing sorption on the Culebra matrix and on clays in Culebra fractures.

Several assumptions made in the present conceptual model are tentative and may be revised after evaluation of more comprehensive models of the regional flow system. Specific areas being investigated by Sandia's Fluid Flow and Transport research group include:

- The extent to which leakage between the Culebra and adjacent units can be neglected. While this assumption may be acceptable in many areas, it is not universally valid. For example, extensive dissolution of Rustler halite and anhydrite in lower Nash Draw has resulted in the Rustler becoming highly fractured, forming a single unconfined aquifer. A more accurate description of vertical flow may be made on the basis of existing data, regional fluid balance requirements, and geologic considerations.
- Geochemical interaction of radionuclides with the Culebra may not be adequately described by a linear sorption model A more detailed representation of the specific interactions between radionuclides, pore fluid, and matrix may be required to predict potential migration rates.

6.1.1 PARAMETERS OF THE CULEBRA MODEL

The Darcian flow model requires values for transmissivity, storage coefficient, fluid density, and initial pressure defined throughout the model domain, in addition to boundary conditions and internal fluid sources and sinks. The dual-porosity transport model requires a fluid seepage velocity field (derived from the Darcian flow model), fracture and matrix porosities, effective matrix diffusivity, fracture dispersivity and diffusivity, and isotope-specific geochemical parameters (retardation factors in both porosity sets) defined over the model domain, as well as specification of internal sources. Parameter values used in the performance assessment are discussed in Volume 3.

6.1.2 MODEL IMPLEMENTATION

Separability of the flow and transport problems allows the release associated with intrusion to be estimated as follows:

- estimation of the prevailing Culebra flow field
- estimation of integrated release due to radionuclide sources introduced into the Culebra flow field.

Because of the complexity of the spatial distribution of transmissivity, and the resulting spatial variability of the flow field, numerical approximations are used to simulate flow and transport processes. Uncertainty in release due to uncertainty in model parameters is addressed by

creating equally likely realizations of the set of parameters controlling transport. Most parameters are assumed to have a single value over the entire model domain for each realization. Because of the large variability of transmissivity, the dependence of transmissivity on location, and the large number of estimates of transmissivity over the site, spatial variability of transmissivity is explicitly included in the model. Realizations of transmissivity are required to honor the point estimates at well locations as well as indirect constraints imposed by the Culebra head distribution, as described below.

6.2 Generation of Transmissivity Fields by Geostatistics—Walt Beyeler

Previous WIPP Performance Assessments used a simple zonal approach for including uncertainty in the transmissivity (T) field within the Culebra Dolomite Member of the Rustler Formation. The zonal method divides the regional and local computational domains into geographic regions; 8, 13, and 15 regions have been used for different analyses reported in Marietta et al. (1989) and Bertram-Howery et al. (1990). In each region, a distribution was constructed using transmissivity measurements from available wells. This empirical distribution was sampled and one constant value used for the transmissivity in each zone. Each zone was sampled independently, so a single simulation used 8 (or 13 or 15) transmissivity values to represent the regional T field. Some simulations used distributions constructed from pilot point values (LaVenue et al., 1990) at locations assigned during calibration in addition to actual measurements at well locations.

This approach can be improved in two ways:

- The reason for varying transmissivity over geographic zones is to include spatial variability in the T field. Correlations exist in the T field over distances greater than five kilometers; however, assuming that the 8 (or 13 or 15) zones are independent during sampling is only a first approximation. Spatial dependence should be included over the whole model domain.
- The T fields generated by the simple zonal approach directly used transmissivity measurements whereas other information was included indirectly through pilot point values. Many other data are available, and it would be better to incorporate these data directly, e.g. hydraulic head measurements and geologic information.

Several methods have been proposed in the scientific literature to resolve these two issues. Most suggestions have relied on geostatistical techniques combined with inverse methods (de Marsily, 1986; Yeh, 1986). To obtain fast guidance on development of a package for WIPP PA to use in the final compliance assessment, a Geostatistics eXpert Group (GXG) was convened. The GXG was asked to provide advice given the modeling work completed, calibrated transmissivity

field, data collected, and the above two objectives listed for improvement of the earlier zonal approach. The group's recommendations were organized into three categories:

- Proposing methods for generating conditional random fields to be used in the present assessment.
- Proposing methods for including conceptual model uncertainty.
- Proposing methods for including geological information.

These recommendations are summarized in the following discussion.

6.2.1 GENERATION OF CONDITIONAL RANDOM FIELDS

Transmissivities display a variability in space that can be characterized using measured data, e.g. pump tests, by geostatistical analyses. This spatial variability was found to be stationary in the mean (LaVenue et al., 1990), but intrinsic in the second moment (IRF = 0) with a linear variogram without nugget effect (i.e., locally described by a constant with random perturbations that increase in variance with distance. Several techniques are available to generate random fields having this spatial structure: turning bands, inversion of the full covariance matrix, and spectral methods. Many such realizations could be generated and each realization could be used as one input for a system simulation. Each realization would then have the correct spatial structure of the true field, and would satisfy the first objective above.

However, these realizations would not be fully coherent with the actual measurements, and would overestimate the uncertainty in the T field. Making realizations of random fields coherent with measured information is called conditioning, which was the major focus of the GXG. For WIPP PA, conditioning can be performed on at least four types of information:

- Measured T values at the wells.
- Measured or estimated head values at the wells in pre-excavation steady-state conditions.
- Measured head values during various transient hydraulic tests (e.g., long-term pump tests, shaft excavation).
- Indirect geologic data that can be correlated with transmissivity (such as overburden thickness, or presence of evaporites in the Culebra or Rustler).

Conditioning on the measured T values is one available technique (Delhomme, 1979). A second technique, conditioning on steady-state and transient head data is discussed below. Conditioning on geologic information will be discussed later.

Six methods of conditioning on head data were discussed by the GXG. These methods range from the simple to the complex. Each method has potential advantages and disadvantages. The GXG will compare these methods on the WIPP data base, and make a recommendation for the final compliance assessment. Given the time constraints for the present PA, only the first method could be implemented. A brief description of the six methods follows.

1. The first method considered by the GXG was used in the 1991 Preliminary Comparison reported in Volume 1 of this document set. Random fields conditioned on T measurements at well locations and on values assigned during manual calibration were assigned to pilot point locations where no measurements were available (LaVenue et al., 1990). Forty-one measured-T and 41 pilot-point values are available. The pilot point values were assigned to insure coherence of the calibrated T field with the measured head data (both steady-state and transient conditions) so conditioning on head data is indirectly included.

   This approach still needs to be validated on the transient data. An advantage of this method is that it does not require any assumption on the acceptable range of variability of T ($\mathrm{Var}(T)$). Many methods require that the $\mathrm{Var}(\ln T) > 1$, and in the Culebra the $\mathrm{Var}(\ln T)$ is about 3.5. This first method also allows using a variable-density fluid-flow model which may be important in the Culebra (Davies, 1989). Other methods are linear, but can only accommodate constant-density fluid-flow models. A second advantage is computational efficiency because the Cholesky decomposition only needs to be performed once regardless of the number of simulations.

2. The second method considered by the GXG was to apply method one only on measured T values. Conditioning on head values (steady-state and transient) would be accomplished simply by screening out T fields not satisfying an assigned acceptance criterion on observed head. Upon testing, the rejection rate proved to be high, so this method was not pursued further.

3. The third method considered by the GXG was to use an available code, INVS (Bras and Kitanidis, 1991; Kitanidis and Vomvoris, 1983; Hoeksema and Kitanidis, 1984, 1985 a and b), that conditions on both measured T values and also steady-state head values, with or without using pilot point values. However, this method is restricted to $\mathrm{Var}(\ln T) < 1$ because of linearization of the flow equations (only constant-density fluid flow). The present code assumes full stationarity of $\ln T$ with an exponential covariance function, and automatically fits the corresponding covariance of the head and cross-covariance functions. The relationship between these covariances is derived analytically assuming that average flow direction and gradient are constant. Uniform rectilinear grids with less than about 10^3 blocks are also required. After automatic fitting of the covariances, an optimal T field can be estimated by co-kriging, and conditional simulations can be generated.

   A similar method relying on spectral techniques (Gutjahr, 1989) is also part of the ongoing comparison exercise between methods 1 and 3.

4. The fourth method considered by the GXG is an extension of the pilot point approach used for the calibration of the Culebra T field. This method should generate random fields conditioned on T measurements, steady-state, and transient head data without restriction on $\mathrm{Var}(\ln T)$ and with variable-density fluid-flow models. This method, if successful, will be used for the 1992 PA.

   First, random T fields conditioned only on the measured T values are generated. These fields are further conditioned on the head data by calibrating them with the pilot point approach both on steady-state and transient data. To generate a large number of calibrated random fields, the procedure will be automated. Order of pilot point selection and the uniqueness of the resulting T field are issues to be examined during operational tests and sensitivity analyses.

5. The fifth method considered by the GXG was a semi-analytical approach (Rubin and Dagan, 1987a and b, 1988; Rubin, 1990; Rubin 1991, in press). This method is similar to method 3, but uses semi-analytical expressions. It will be added to the comparison exercise with methods 1, 3, and 4.

6. The sixth method considered by the GXG is complex relying on a maximum likelihood approach (Carrera and Neuman, 1986 a,b, and c). This method conditions on both steady-state and transient head data, assumes linearity iteratively (in the vicinity of the optimal solution), and constant-density fluid-flow. It may also be added to the comparison exercise.

The comparison exercise will expose potential discrepancies among these six methods. Depending upon the resolution of these discrepancies, the GXG will recommend a method(s) for use in the final PA.

6.2.2 INCLUDING GEOLOGICAL INFORMATION

Geological information should be included in the estimation of the T field because of

- An apparent non-stationarity of the T field; an increasing trend from east to west exists in the data.
- An observed difference between kriged T field and the conditionally simulated fields above.
- A large amount of available geologic information that has not been directly used in either the calibration or the conditional simulations.

The GXG discussed two proposals. First, relevant geologic information such as thickness of the overburden, total estimated thickness of evaporites in the Rustler, slope or curvature of Culebra, density of lineaments, chemical data, etc. should be tested by co-kriging with transmissivity. If a candidate geologic data set(s) is found to improve the T estimation, it can be

retained, and a new T estimation procedure developed. Second, after a new co-kriging procedure using geologic data sets is developed, co-kriged estimates should be compared with measured values at well locations to look for any systematic bias. If a bias is found, the quality of those measurements would be questioned. This would allow well measurements which have been questioned (e.g., well P-18) to be evaluated objectively.

6.2.3 INCLUDING CONCEPTUAL MODEL UNCERTAINTY

After considering the detailed problem of residual uncertainty in the *T* field of the Culebra, the GXG discussed the general problem of how to include conceptual model uncertainty in WIPP PA. The approach discussed was the same as used in previous analyses (Marietta et al, 1989; Bertram-Howery et al., 1990). For each conceptual model, the underlying parameter uncertainty is characterized, and different sets of CCDFs are produced as described in Volume 1, Chapter III. These sets of CCDFs are compared with respect to potential impact on a compliance decision that would be based on a mean CCDF constructed from one or more of these conceptual model sets of CCDFs with an assigned weighting. If a conceptual model produces a set of CCDFs that would have negligible impact on the eventual compliance decision, it can be discarded. The goal is then to identify possible alternative conceptual models that are qualitatively different, and can be calibrated on the available data.

Preliminary approaches for identifying such alternative conceptual models were discussed:

- A fractal model of the Culebra transmissivity was proposed (Grindrod and Capon, 1991). Using a fractal approach allows an extension of the spatial variability in the transmissivity fields to scales less than the measured scale. In this way the effect of possible smaller scale features than have been observed can be evaluated.
- Basin-scale hydrologic modeling over past geologic time scales could evaluate the steady-state assumption of the present PA modeling. Sensitivity studies with such a model would assess different conceptual models for both recharge/infiltration and geologic framework of the Culebra, other Rustler units, and overlying formations.
- A lithofacies modeling approach was proposed (Ravennes et al., 1991). Instead of describing spatial variability by just parameter variability, lithofacies models represent geometric descriptions of geologic strata by sequential stratigraphy in a stochastic framework. These models can be conditioned by geologic information.
- Upscaling block properties and modifying the governing equations appropriately is an approach that was also proposed.

These proposed methods will be assessed by the GXG after the results of the variability studies in the Culebra are available.

6.3 Selection of Transmissivity Fields—Walt Beyeler

At least three types of information are available for estimating values of Culebra transmissivity (T): slug tests, drill stem tests, and short-term pumping tests are interpreted to give estimates of T in the neighborhood of the tested well; long-term pumping tests with pressure observations made at several wells can yield a T value integrated over a large region surrounding the pumped well; and the distribution of pressures over the aquifer is related to the distribution of transmissivities by the flow equation.

The estimation procedure used in the present PA is intended to identify transmissivity fields which are consistent with both point observations of T and the equilibrium pressure distribution. An approach being developed for the 1992 PA (method 4, described above) will allow transmissivities to be constrained by both short- and long-term transient pressure data, in addition to the transmissivity observations and equilibrium pressures used in the present method. As an interim means of incorporating information about transmissivity from long-term transient observations, pilot points derived during calibration of the Culebra flow model (LaVenue et al., 1990) were introduced as additional observations of T.

The present method consists of four steps: generation of candidate transmissivities constrained by point data; determination of the sensitivity of pressure at all observation wells to changes in boundary pressure; assembly of an optimal boundary pressure function which minimizes the deviation of model pressures from estimated equilibrium pressures; and evaluation of acceptability of the resulting model. Detailed information on these four steps follows.

The CAMCON program GARFIELD (draft of SAND90-1983, Rechard et al., in preparation) was used to simulate transmissivity fields over the discretized model domain. GARFIELD uses a set of point observations, and a generalized covariance describing the spatial variability of the observations, to simulate any number of alternative fields conditioned by the point observations. The point observations of transmissivity, and the associated generalized covariance function, were identical to those used in the final calibrated flow model of LaVenue et al. (1990). Conditioning on both measured and pilot point values was done by a Cholesky decomposition of the full covariance matrix of the kriging estimation error. An IRF = 0 random function was considered with the linear variogram determined by LaVenue et al. (1990). Point simulations on a 32 x 25 km^2 grid (52 by 44 elements) were produced. The resulting realizations honor the point estimates of transmissivity (within bounds established by the variance of the point estimate), and the spatial variability of transmissivity reflected in the generalized covariance.

Since this conditioning on head measurements is only indirect, a systematic measurement of the coherence of the calculated heads with the measured heads was performed, but given the time constraint, only steady-state heads could be considered. Uncertainty in the value of the prescribed heads on the boundary was also taken into account. These prescribed heads on the boundary are

estimated by kriging the local head measurements at well locations. Therefore, they are given a variance of their estimation error. Programs GENOBS and SWIFT were then used to calculate sensitivity of steady-state model pressure with respect to pressure changes on segments of the model boundary. In order to reduce the number of independent pressures, the pressure distribution along a boundary segment was assumed to be piecewise linear.

Program FITBND then used the above sensitivity coefficients to derive fixed-pressure boundary conditions which optimized model agreement with estimates of pre-construction Culebra pressure at the 36 control points used in the LaVenue et al. (1990) study. The resulting pressure fields are optimal in the sense of minimizing the following objective function:

$$X^2 = \frac{1}{N_{obs} + N_{bound}} \left\{ \sum_{i=1}^{N_{obs}} \left(\frac{P_{obs} - P_{\mathrm{mod}}}{\sigma_{obs}} \right)^2 + \sum_{i=1}^{N_{bound}} \left(\frac{P_{bound} - P_{\mathrm{mod}}}{\sigma_{bound}} \right)^2 \right\} \qquad (6\text{-}1)$$

where N is the number of elements of a particular type, P is pressure, σ is the estimated standard deviation of the error of the observation, *obs* denotes an observation well location, *bound* denotes a model boundary element, and *mod* denotes a model-calculated pressure.

To decide on the acceptability of a conditionally simulated field, the boundary conditions of the calculated head fields were first optimized within their uncertainty range. Then, two acceptance criteria were used:

- The average standard deviation of the model error over all wells where steady-state head data are available should not exceed $\sqrt{2} \bullet s$ where s is the standard deviation of the measured head error.
- The corresponding flow field should be globally coherent with known flow in the area including general direction, recharge and discharge zones

6.3.1 RATIONALE FOR FIRST CRITERION

The value of model error (X^2) at the minimum was used as an indication of the plausibility of the underlying T field. X^2 is the average normalized squared deviation of the model pressure from the observed pressure or prior estimate of boundary pressure. If the variance of the observation and boundary errors have been correctly estimated, and the observation errors are normally distributed, the expected value of X^2 for the correct model would be 1. If the observation error distribution is less compact than the normal distribution, X^2 for the correct model would be larger than 1. To allow for this possibility, a threshold value of 2 was selected for X^2 (as discussed below, the particular threshold value selected has little effect on release). If the model error for a given transmissivity field was greater than this threshold, the transmissivity was considered irreconcilable

with pre-construction equilibrium pressures. Transmissivity fields (along with optimal boundary conditions) which produce an error less than the threshold were considered to be plausible. All plausible transmissivity fields were considered to be equally likely.

6.3.2 RATIONALE FOR SECOND CRITERION

Because pressure data near the model boundaries are sparse, the optimizing procedure has considerable latitude in assigning some boundary values. In a few cases, the location of minimum pressure in otherwise plausible fields was believed to be unrealistically located along the southeastern boundary. For this reason, a further screening of flow fields satisfying the maximum error criterion was made on the subjective basis of requiring discharge to occur along the southwestern boundary.

6.3.3 TRAVEL TIMES FOR RETAINED FIELDS

The procedure described above was applied to produce 60 plausible transmissivity fields and associated equilibrium boundary pressures. About 350 simulations conditioned on point transmissivities were generated. The first criterion selected 88 acceptable T fields. The second criterion, although subjective, reduced that number to 76.

The resulting flow fields control advection of radionuclides released into the Culebra Dolomite from an intrusion borehole. For this reason, the travel time of a neutrally buoyant particle from the hypothesized location of an intrusion borehole to the accessible environment boundary is an appropriate index of the influence of the flow field on discharge. The first 60 of the 76 T fields were retained and then ordered by travel time to the accessible environment. This travel time was calculated for each plausible flow field using the program TRACKER. Figure 6-2 is a cumulative distribution of travel times of the 60 flow fields. Figure 6-3 shows a scatter plot of model error X^2 versus travel time. There is no apparent relationship between the model error and travel time, so that the distribution of travel times is independent of the threshold model error used to define plausible flow fields. Figure 6-4 (part a through part o) shows the transmissivity distribution in each of the retained fields.

Flow fields were selected for the 1991 PA calculations using a single uniformly distributed random variable as an index of the flow field to be used in conjunction with all other parameters defining a sample vector. Travel time from the center of the waste panel region was used to impose a natural ordering on the flow fields to facilitate future sensitivity analyses (for example, the tenth smallest value of the sampled index was associated with the flow field having the tenth smallest travel time). Because the flow fields are considered to be equally likely, the rank of the sampled index value was used an an index of the flow field. The particular shape and range of the distribution is therefore irrelevant.

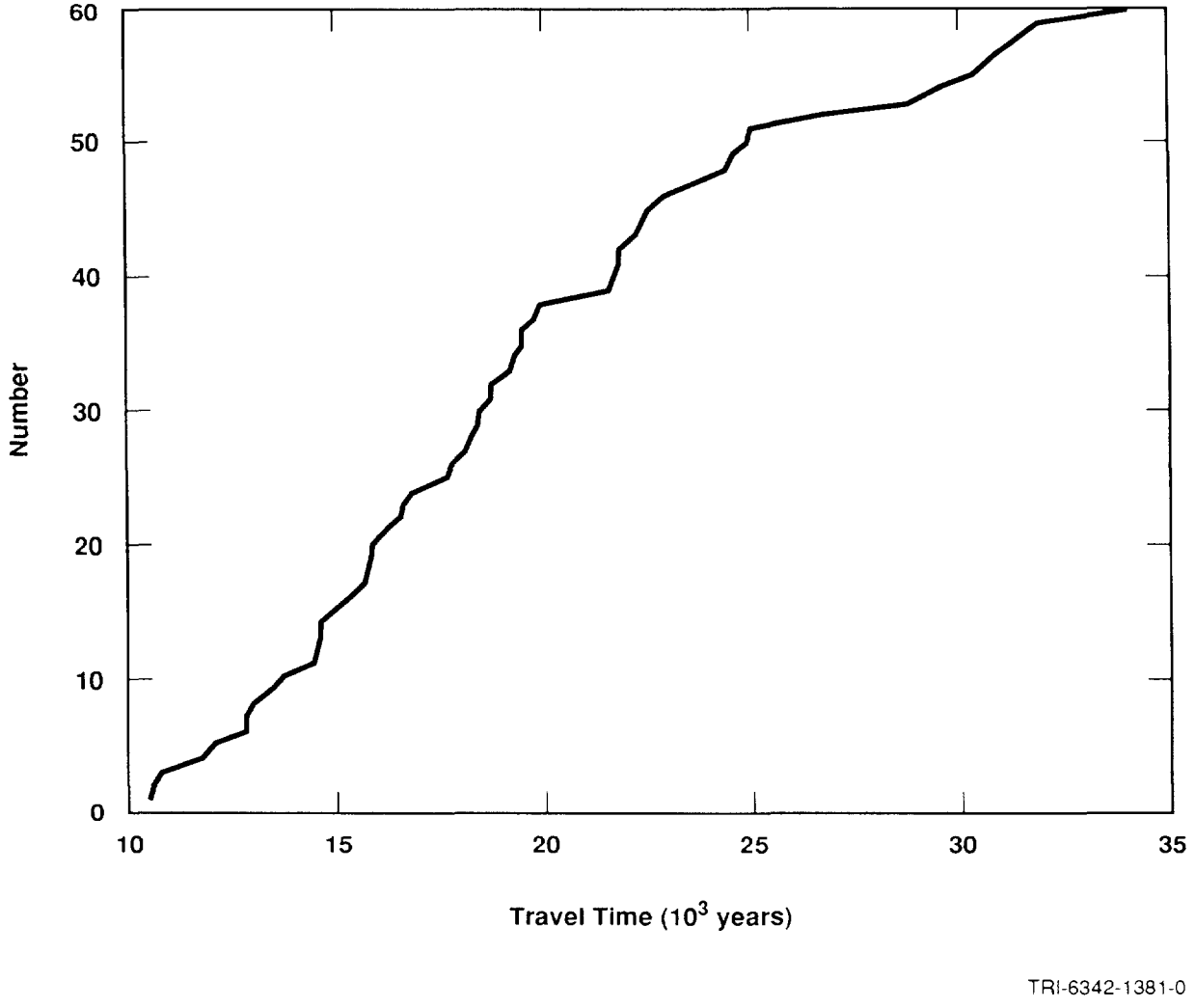

Figure 6-2. Cumulative Distribution of Travel Times of the 60 Flow Fields

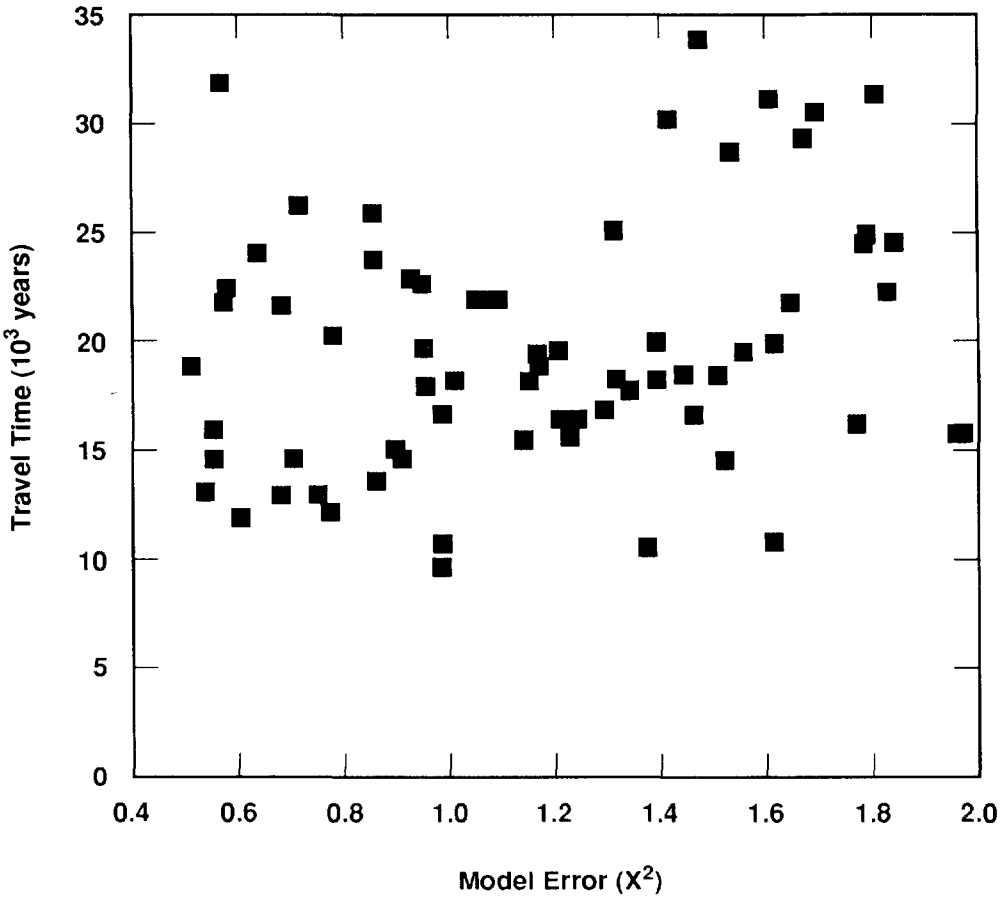

Figure 6-3. Scatter Plot of Model Error X^2 versus Travel Time

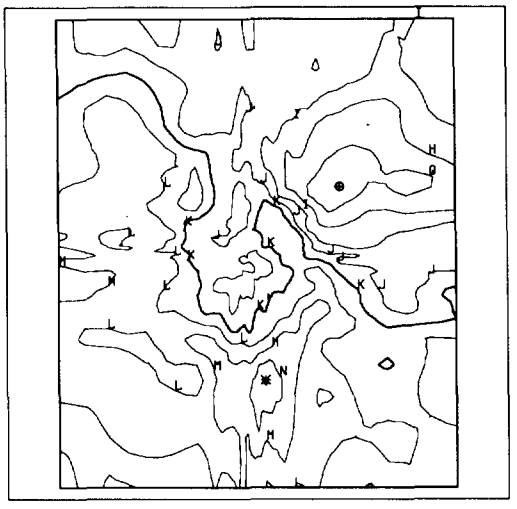

Field 1
⊕ = -9.781
★ = -0.875

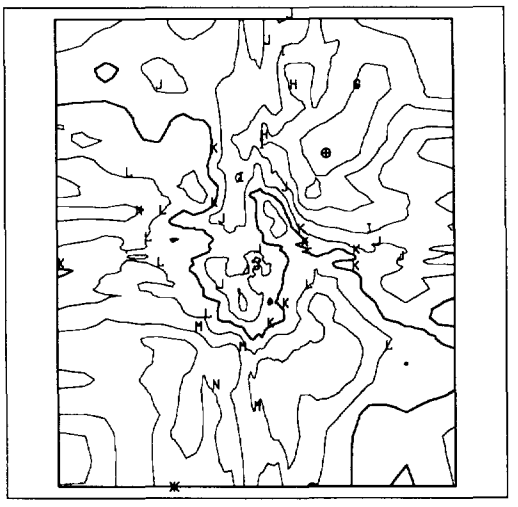

Field 2
⊕ = -9.627
★ = -1.231

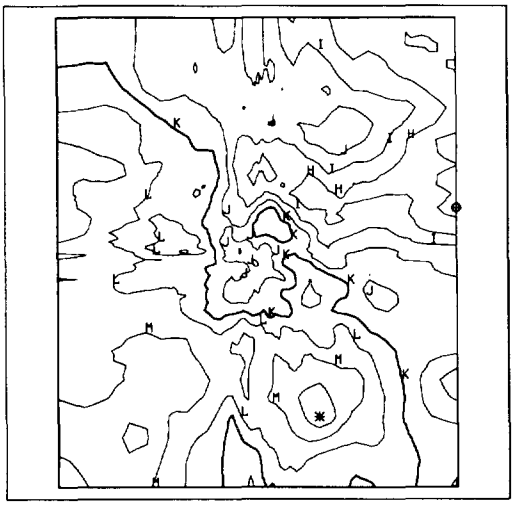

Field 3
⊕ = -9.502
★ = -1.141

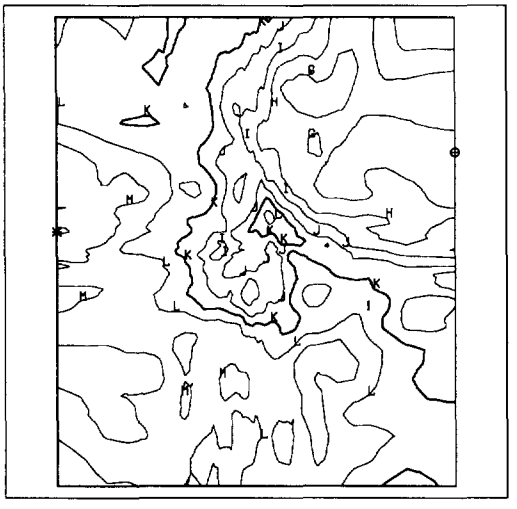

Field 4
⊕ = -9.972
★ = -1.860

Legend

LOGT (log_{10} m^2/s)

A = -15.00	D = -12.00	G = -9.00	J = -6.00
B = -14.00	E = -11.00	H = -8.00	●●●
C = -13.00	F = -10.00	I = -7.00	Q = 1.00

TRI-6342-1367-0

Figure 6-4a. Transmissivity Field Distribution (Fields 1-4)

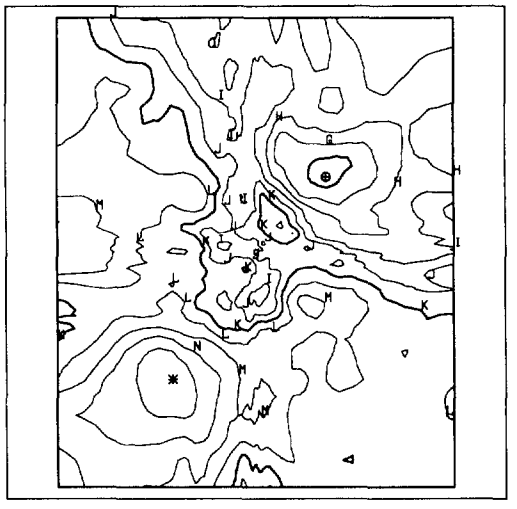

Field 5
⊕ = -10.74
★ = -0.16

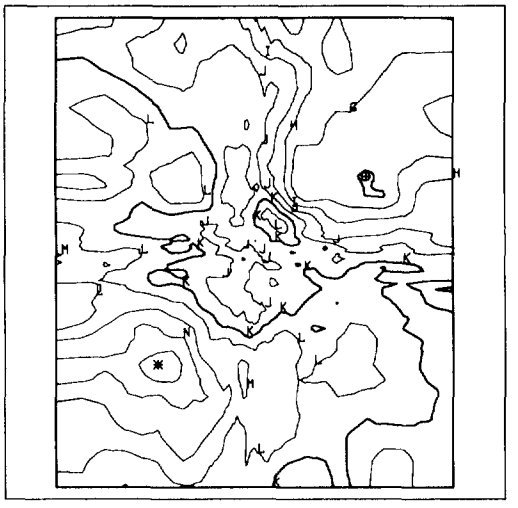

Field 6
⊕ = -10.22
★ = -0.24

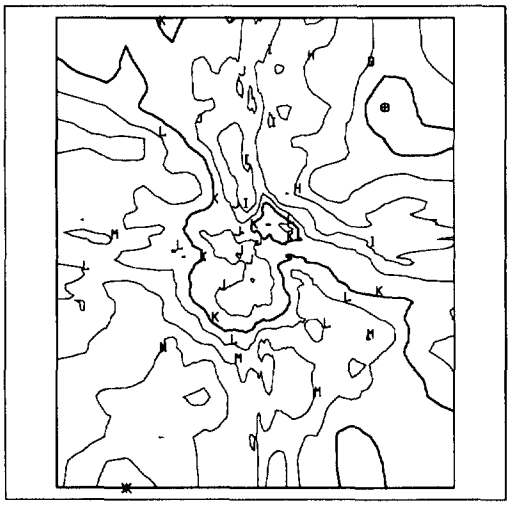

Field 7
⊕ = -10.78
★ = -0.23

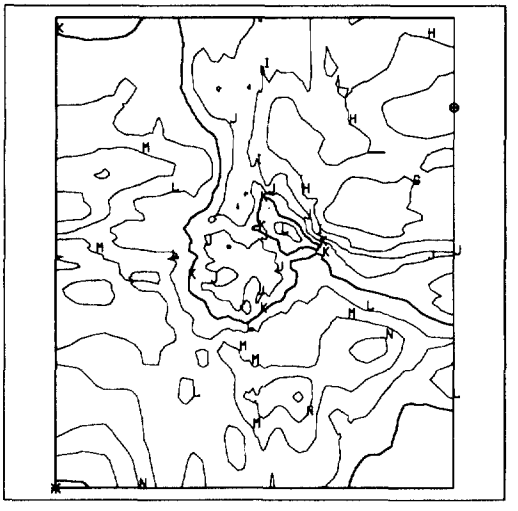

Field 8
⊕ = -10.01
★ = 0.28

Legend

LOGT (log_{10} m^2/s)

A = -15.00	D = -12.00	G = -9.00	J = -6.00
B = -14.00	E = -11.00	H = -8.00	●●●
C = -13.00	F = -10.00	I = -7.00	Q = 1.00

TRI-6342-1368-0

Figure 6-4b. Transmissivity Field Distribution (Fields 5-8)

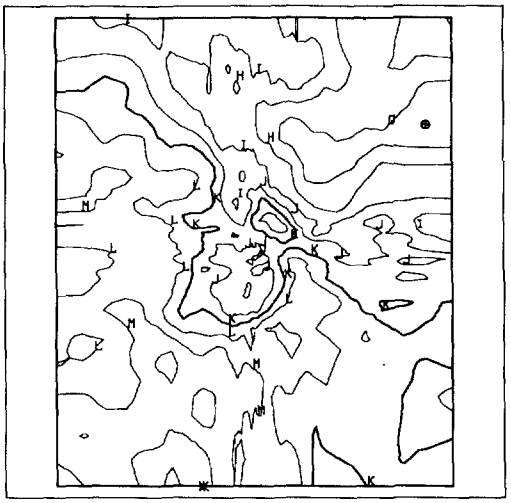

Field 9
⊕ = -9.722
★ = -1.186

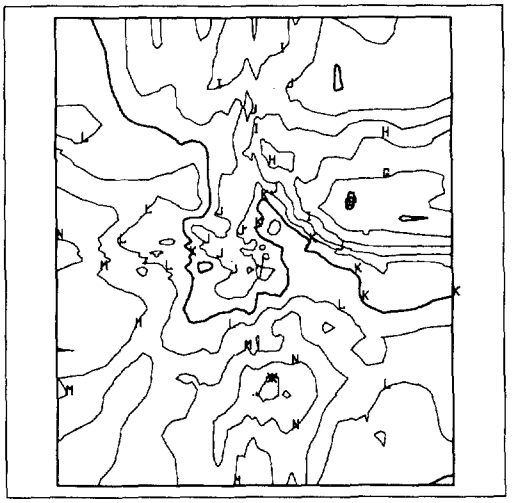

Field 10
⊕ = -10.13
★ = -0.72

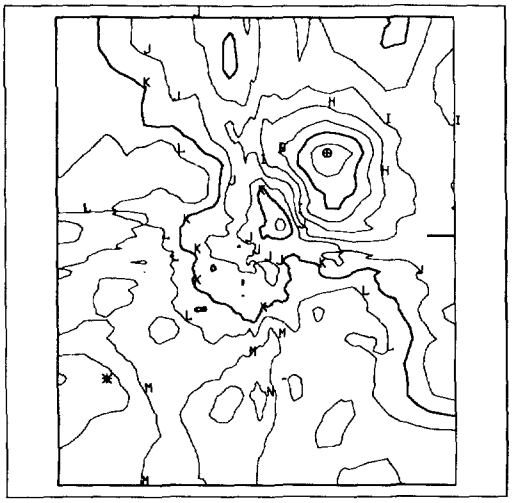

Field 11
⊕ = -11.72
★ = -1.57

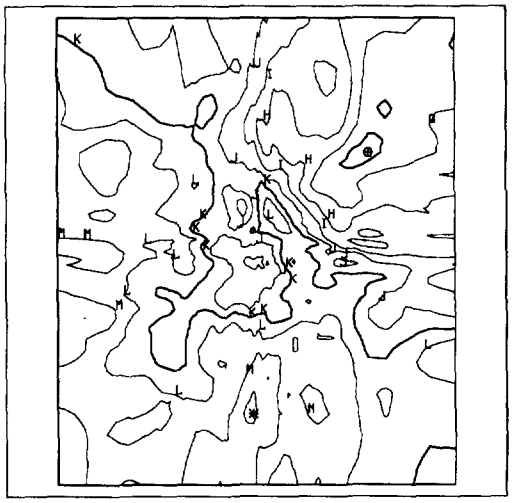

Field 12
⊕ = -10.39
★ = -1.61

Legend

LOGT ($\log_{10}$ m^2/s)

A = -15.00	D = -12.00	G = -9.00	J = -6.00
B = -14.00	E = -11.00	H = -8.00	⋮
C = -13.00	F = -10.00	I = -7.00	Q = 1.00

TRI-6342-1369-0

Figure 6-4c. Transmissivity Field Distribution (Fields 9-12)

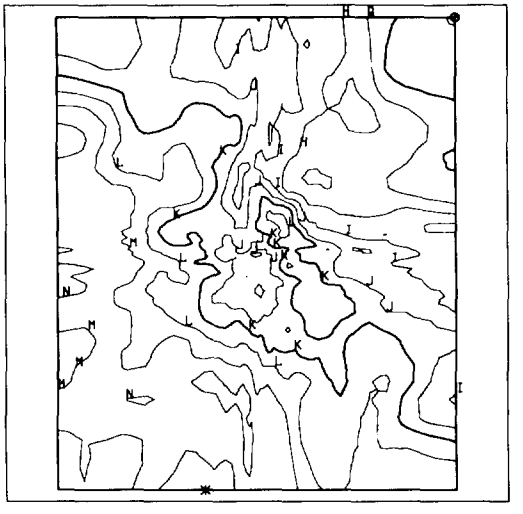

Field 13
⊕ = -11.13
★ = -1.21

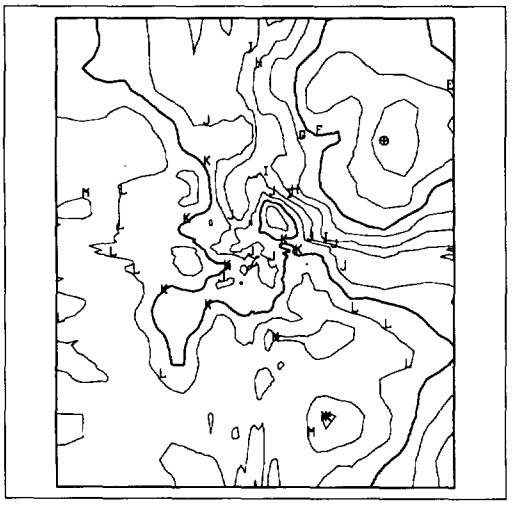

Field 14
⊕ = -12.57
★ = -1.79

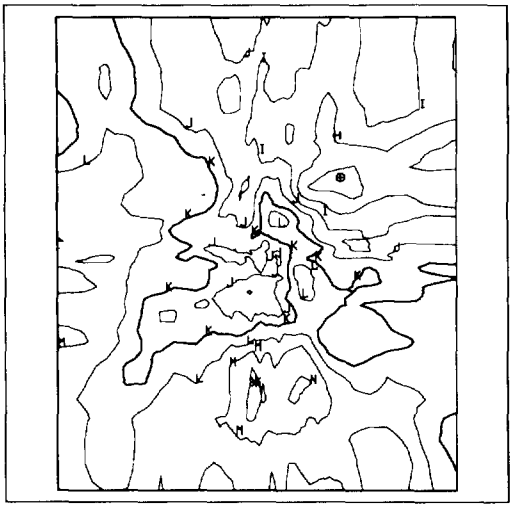

Field 15
⊕ = -9.351
★ = -1.664

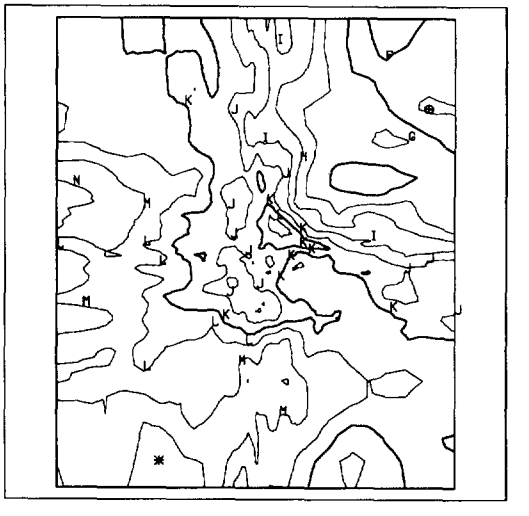

Field 16
⊕ = -11.15
★ = -1.10

Legend

LOGT ($\log_{10}$ m^2/s)

A = -15.00	D = -12.00	G = -9.00	J = -6.00
B = -14.00	E = -11.00	H = -8.00	⋮
C = -13.00	F = -10.00	I = -7.00	Q = 1.00

TRI-6342-1370-0

Figure 6-4d. Transmissivity Field Distribution (Fields 13-16)

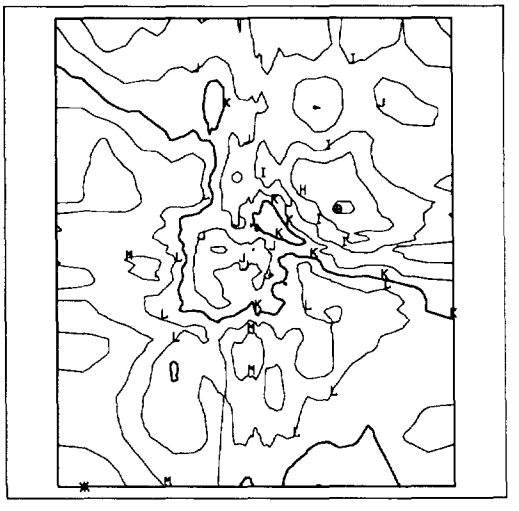

Field 17
⊕ = -9.306
★ = -1.206

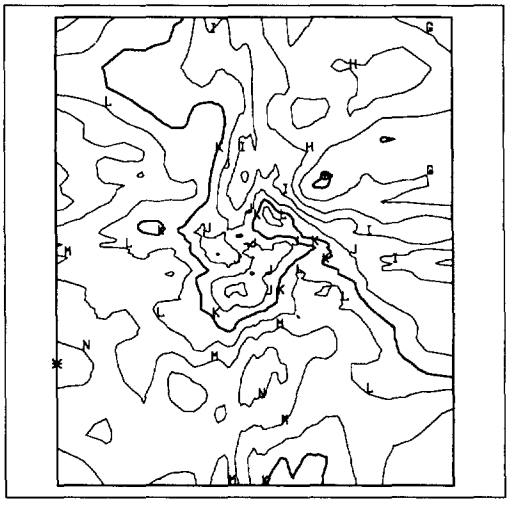

Field 18
⊕ = -10.16
★ = -1.41

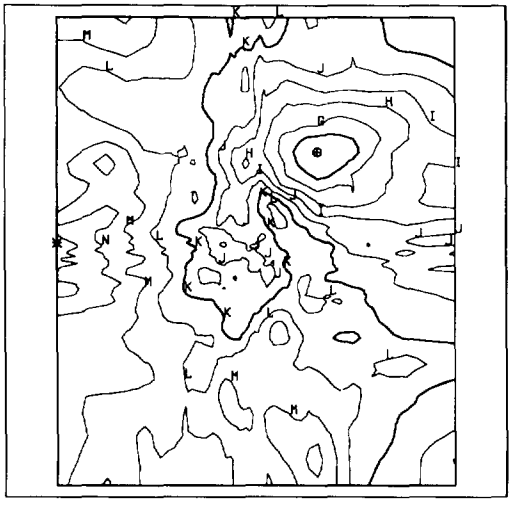

Field 19
⊕ = -10.99
★ = -0.43

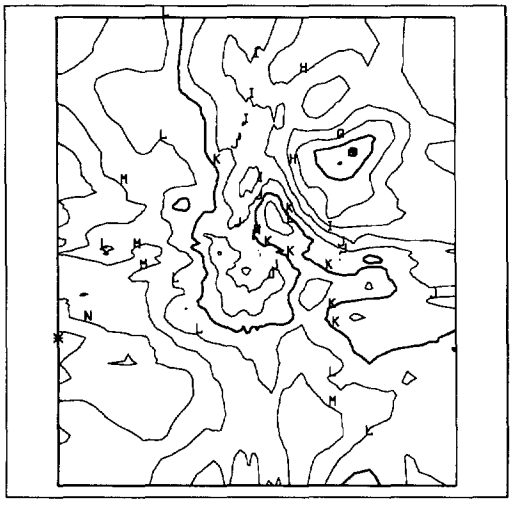

Field 20
⊕ = -11.15
★ = -0.46

Legend

LOGT ($\log_{10}$ m^2/s)

A = -15.00	D = -12.00	G = -9.00	J = -6.00
B = -14.00	E = -11.00	H = -8.00	⋮
C = -13.00	F = -10.00	I = -7.00	Q = 1.00

TRI-6342-1371-0

Figure 6-4e. Transmissivity Field Distribution (Fields 17-20)

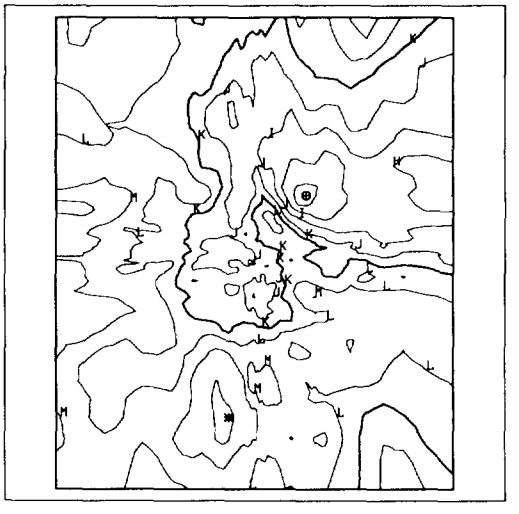

Field 21
⊕ = -9.431
★ = -1.579

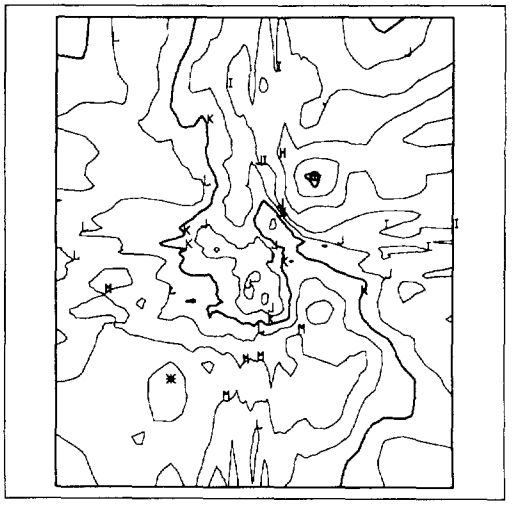

Field 22
⊕ = -10.17
★ = -1.36

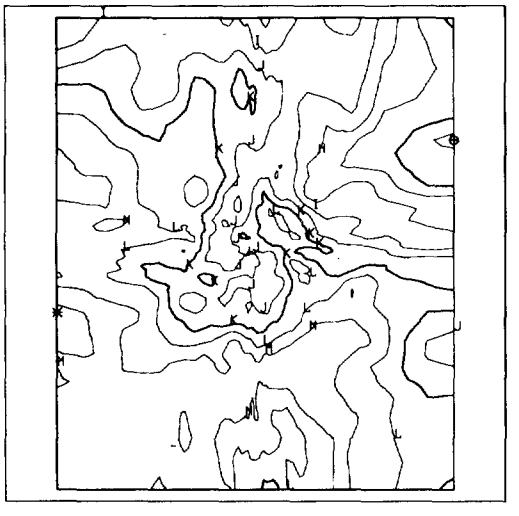

Field 23
⊕ = -11.41
★ = -1.71

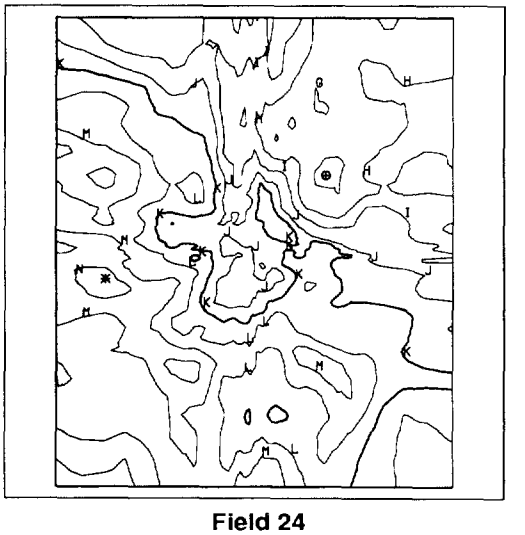

Field 24
⊕ = -9.337
★ = -1.438

Legend

LOGT (log_{10} m^2/s)

A = -15.00	**D = -12.00**	**G = -9.00**	**J = -6.00**
B = -14.00	**E = -11.00**	**H = -8.00**	**⋮**
C = -13.00	**F = -10.00**	**I = -7.00**	**Q = 1.00**

TRI-6342-1372-0

Figure 6-4f. Transmissivity Field Distribution (Fields 21-24)

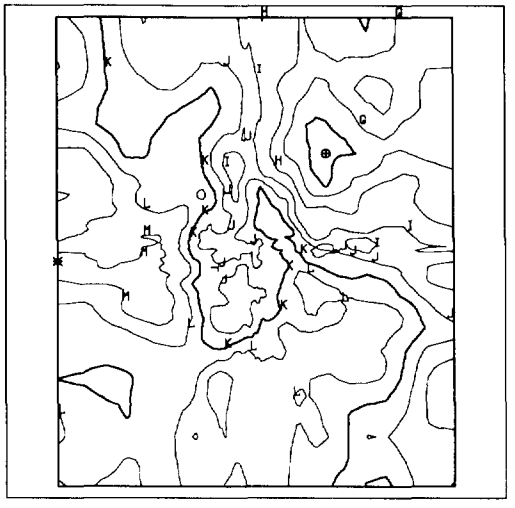

Field 25
⊕ = -10.48
★ = -1.93

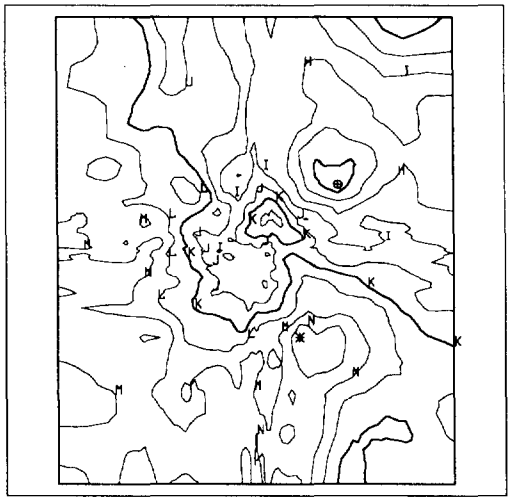

Field 26
⊕ = -10.62
★ = -1.10

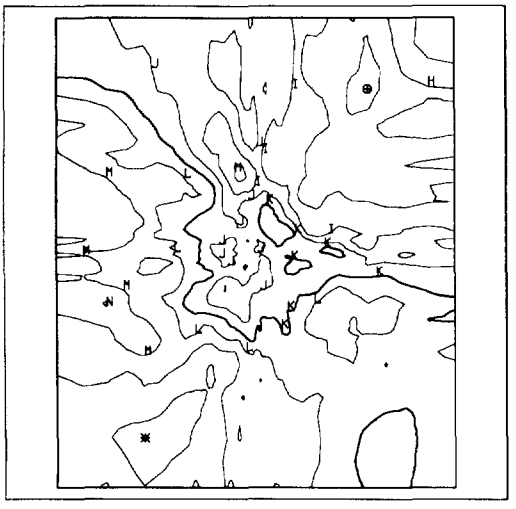

Field 27
⊕ = -9.388
★ = -1.168

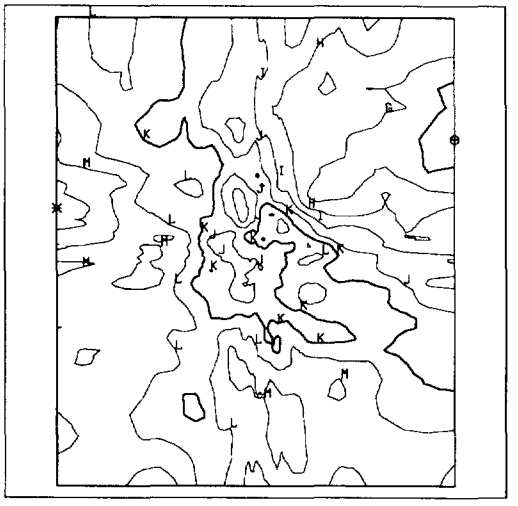

Field 28
⊕ = -11.03
★ = -1.19

Legend

LOGT (log_{10} m^2/s)

A = -15.00	**D = -12.00**	**G = -9.00**	**J = -6.00**
B = -14.00	**E = -11.00**	**H = -8.00**	⋮
C = -13.00	**F = -10.00**	**I = -7.00**	**Q = 1.00**

TRI-6342-1373-0

Figure 6-4g. Transmissivity Field Distribution (Fields 25-28)

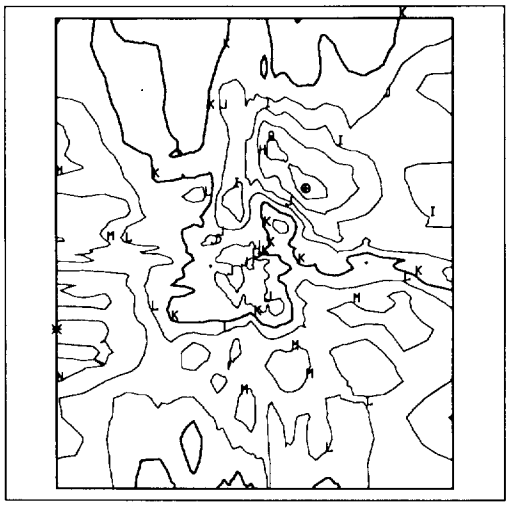

Field 29
⊕ = -9.654
★ = -1.620

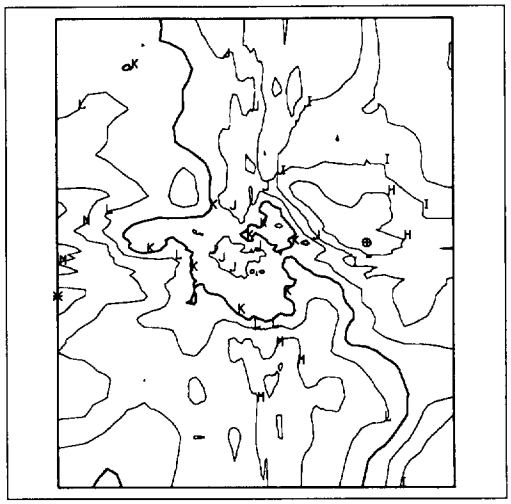

Field 30
⊕ = -8.811
★ = -1.466

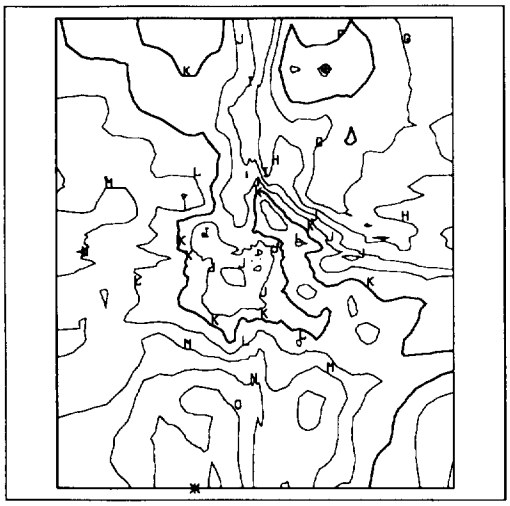

Field 31
⊕ = -11.19
★ = -0.06

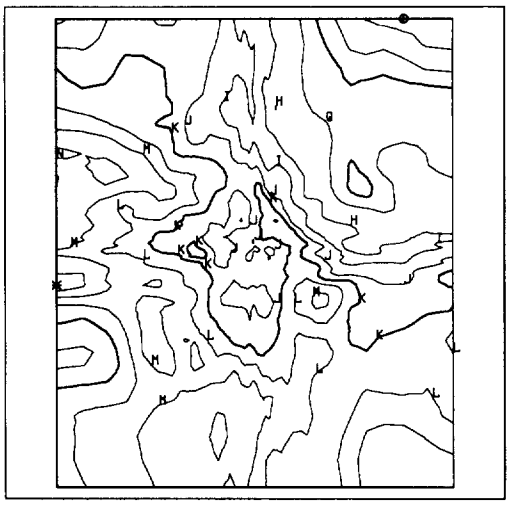

Field 32
⊕ = -12.42
★ = -1.53

Legend

LOGT ($\log_{10}$ m^2/s)

A = -15.00	D = -12.00	G = -9.00	J = -6.00
B = -14.00	E = -11.00	H = -8.00	⋮
C = -13.00	F = -10.00	I = -7.00	Q = 1.00

TRI-6342-1374-0

Figure 6-4h. Transmissivity Field Distribution (Fields 29-32)

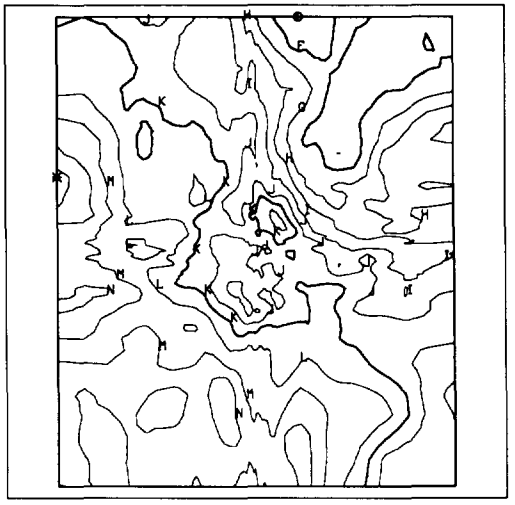

Field 33
⊕ = -11.03
★ = -0.52

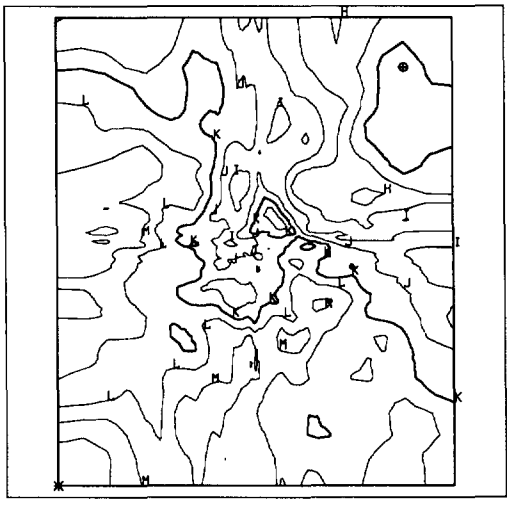

Field 34
⊕ = -10.67
★ = -1.27

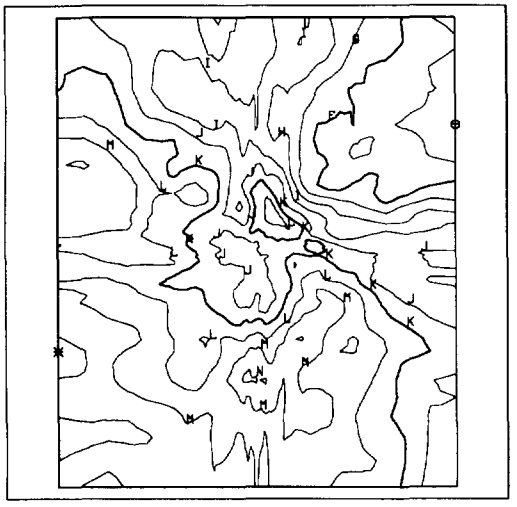

Field 35
⊕ = -11.46
★ = -1.56

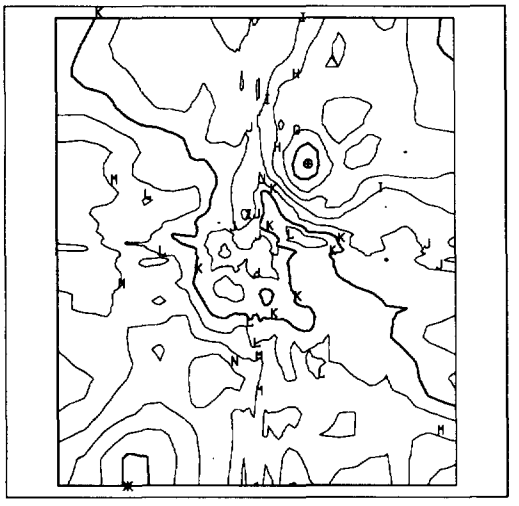

Field 36
⊕ = -10.71
★ = 0.25

Legend

LOGT (log_{10} m^2/s)

A = -15.00	D = -12.00	G = -9.00	J = -6.00
B = -14.00	E = -11.00	H = -8.00	⋮
C = -13.00	F = -10.00	I = -7.00	Q = 1.00

TRI-6342-1375-0

Figure 6-4i. Transmissivity Field Distribution (Fields 33-36)

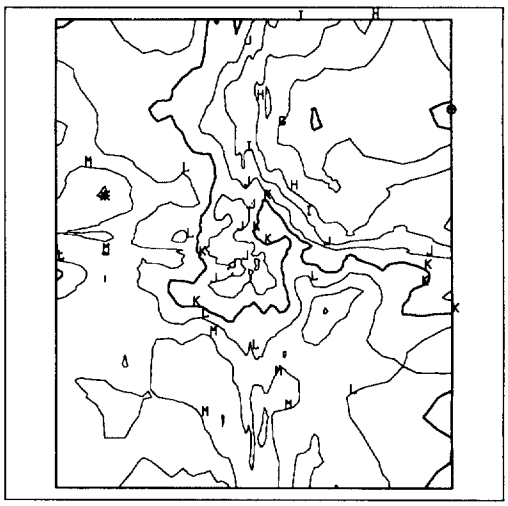

Field 37
⊕ = -10.33
★ = -1.88

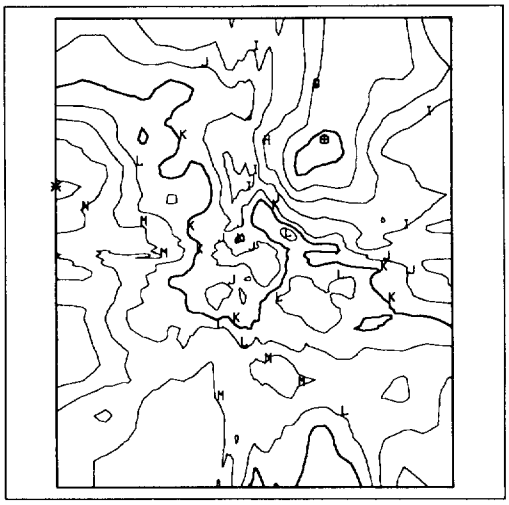

Field 38
⊕ = -10.41
★ = -0.48

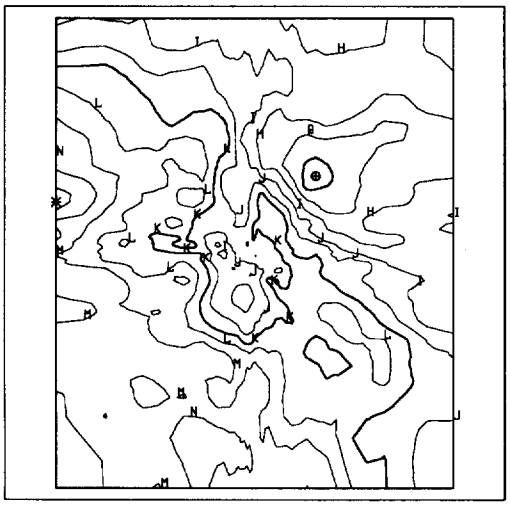

Field 39
⊕ = -10.49
★ = -0.58

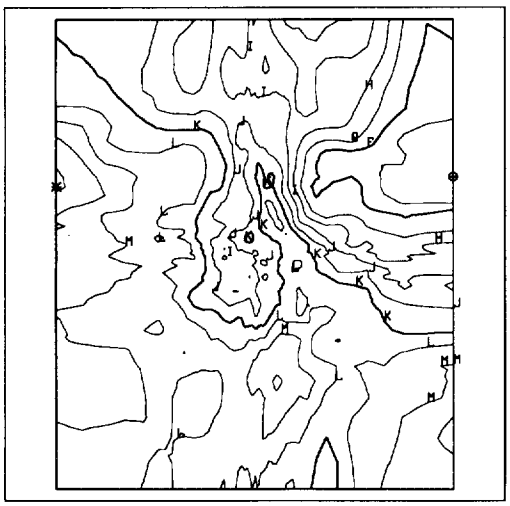

Field 40
⊕ = -11.69
★ = -0.79

Legend

LOGT ($\log_{10}$ m^2/s)

A = -15.00	**D = -12.00**	**G = -9.00**	**J = -6.00**
B = -14.00	**E = -11.00**	**H = -8.00**	**⋮**
C = -13.00	**F = -10.00**	**I = -7.00**	**Q = 1.00**

TRI-6342-1376-0

Figure 6-4j. Transmissivity Field Distribution (Fields 37-40)

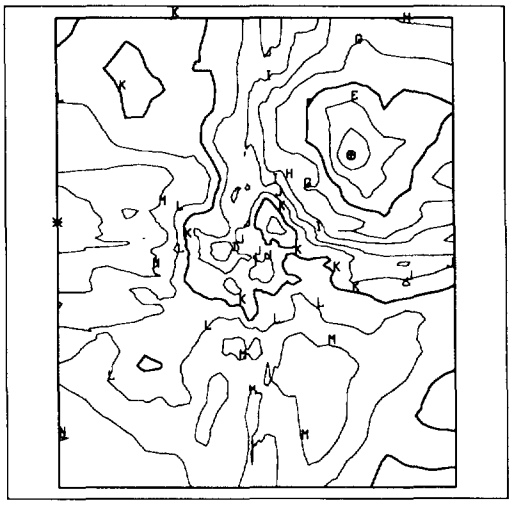

Field 41
⊕ = -13.08
★ = -0.94

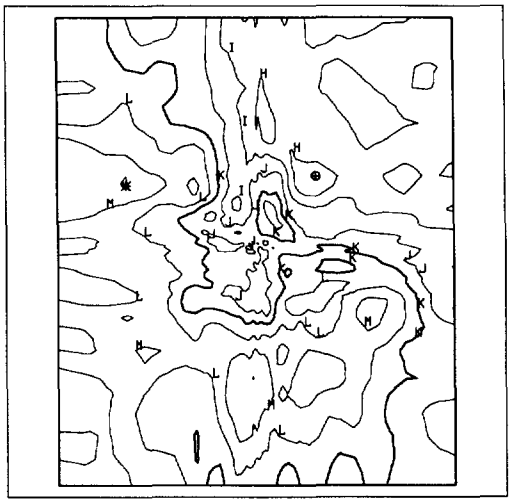

Field 42
⊕ = -8.797
★ = -1.963

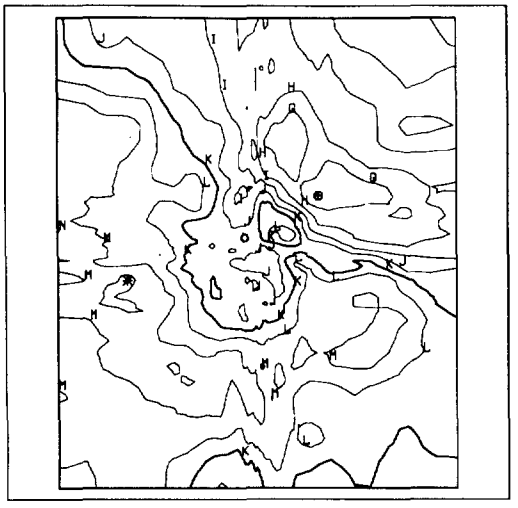

Field 43
⊕ = -10.04
★ = -1.80

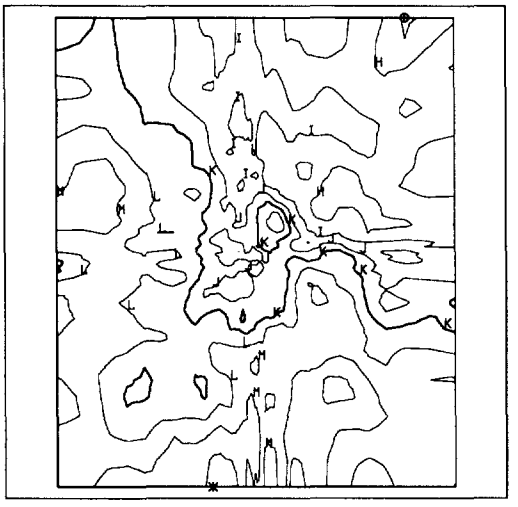

Field 44
⊕ = -9.172
★ = -1.630

Legend

LOGT ($\log_{10}$ m^2/s)

A = -15.00	**D = -12.00**	**G = -9.00**	**J = -6.00**
B = -14.00	**E = -11.00**	**H = -8.00**	**⋮**
C = -13.00	**F = -10.00**	**I = -7.00**	**Q = 1.00**

TRI-6342-1377-0

Figure 6-4k. Transmissivity Field Distribution (Fields 41-44)

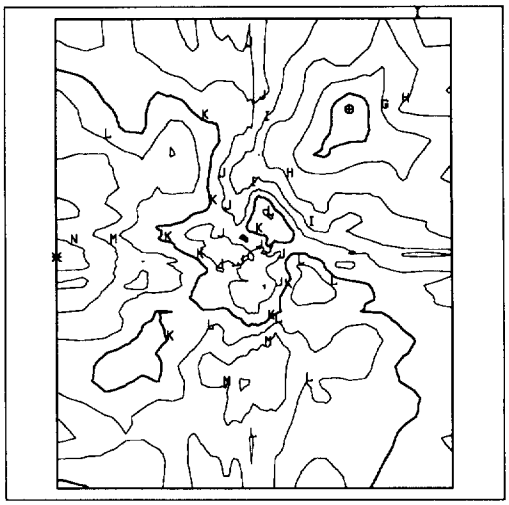

Field 45
⊕ = -10.68
★ = -1.46

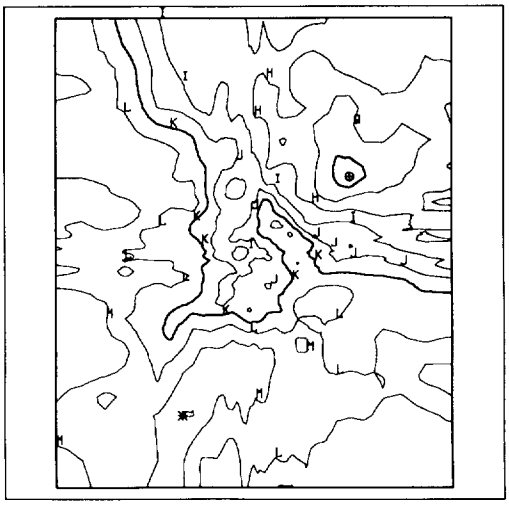

Field 46
⊕ = -10.62
★ = -1.96

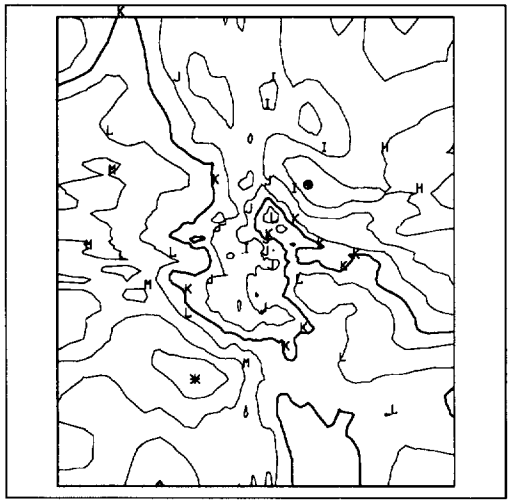

Field 47
⊕ = -9.118
★ = -1.194

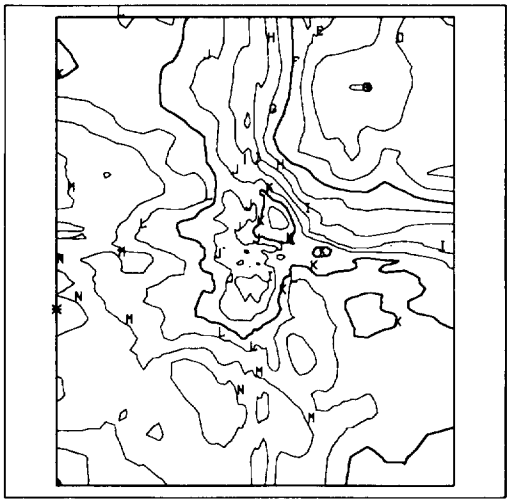

Field 48
⊕ = -13.06
★ = -1.13

Legend

LOGT (log_{10} m^2/s)

A = -15.00	**D = -12.00**	**G = -9.00**	**J = -6.00**
B = -14.00	**E = -11.00**	**H = -8.00**	⋮
C = -13.00	**F = -10.00**	**I = -7.00**	**Q = 1.00**

TRI-6342-1378-0

Figure 6-4l. Transmissivity Field Distribution (Fields 45-48)

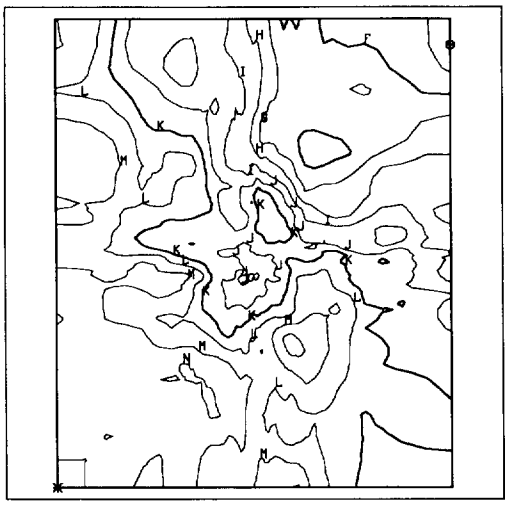

Field 49
⊕ = -11.45
★ = -1.24

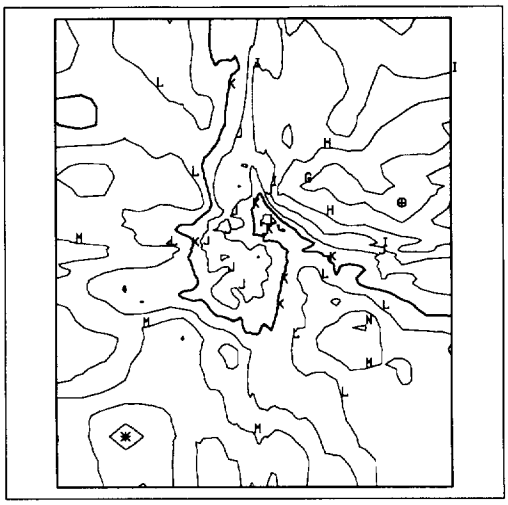

Field 50
⊕ = -9.929
★ = -0.655

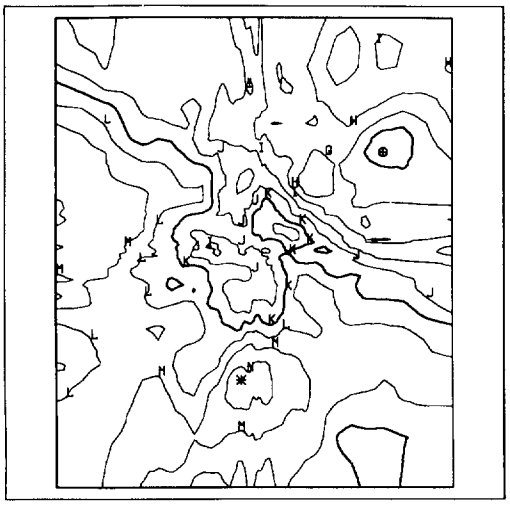

Field 51
⊕ = -10.80
★ = -1.22

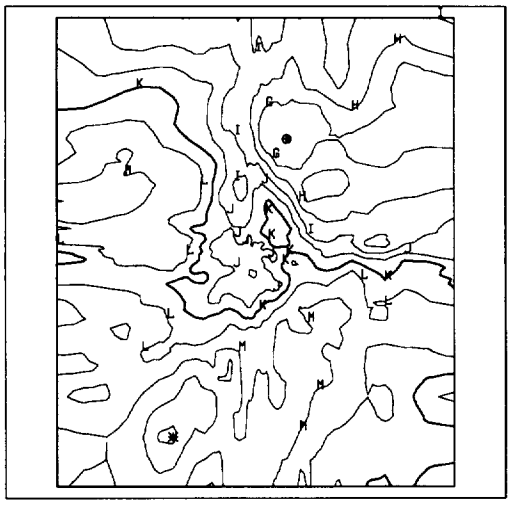

Field 52
⊕ = -10.02
★ = -0.72

Legend

LOGT ($\log_{10}$ m^2/s)

A = -15.00	D = -12.00	G = -9.00	J = -6.00
B = -14.00	E = -11.00	H = -8.00	⋮
C = -13.00	F = -10.00	I = -7.00	Q = 1.00

TRI-6342-1379-0

Figure 6-4m. Transmissivity Field Distribution (Fields 49-52)

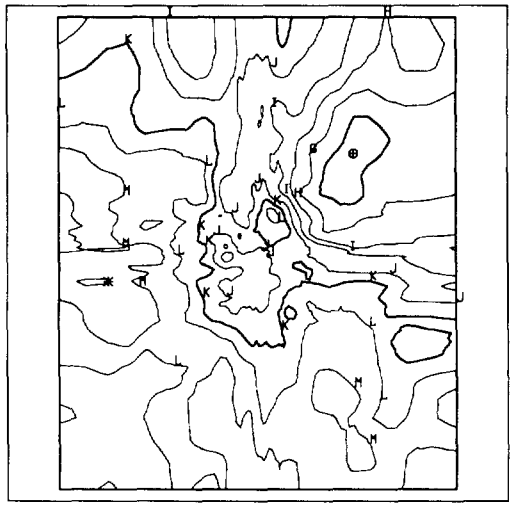

Field 53
⊕ = -10.66
★ = -1.88

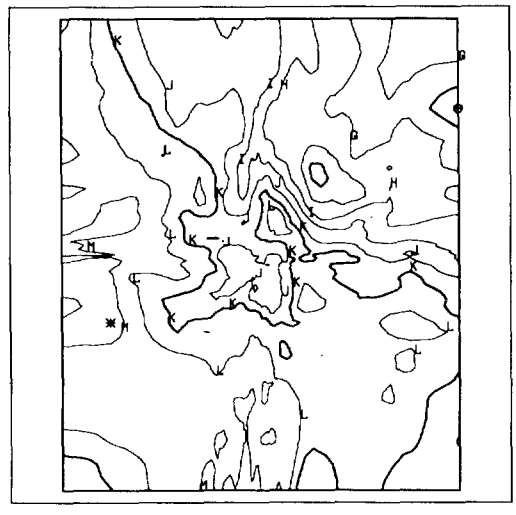

Field 54
⊕ = -10.78
★ = -2.33

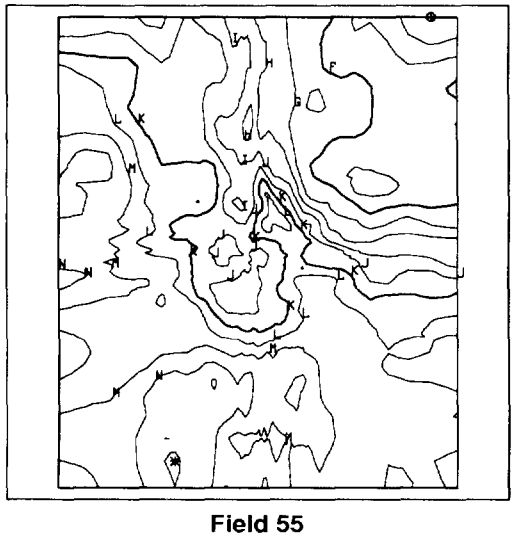

Field 55
⊕ = -12.67
★ = -0.81

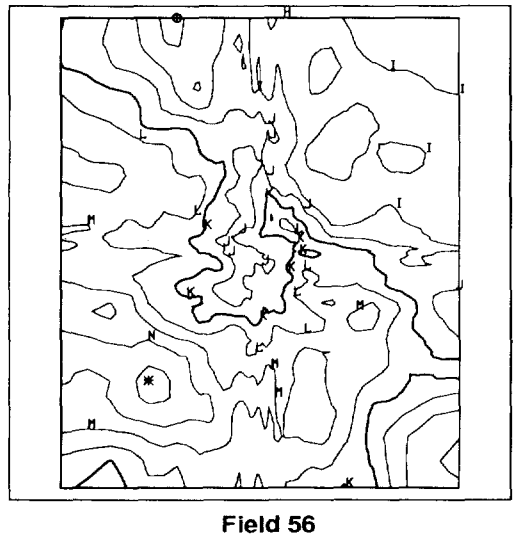

Field 56
⊕ = -8.359
★ = -0.562

Legend

LOGT ($\log_{10}$ m^2/s)

A = -15.00	D = -12.00	G = -9.00	J = -6.00
B = -14.00	E = -11.00	H = -8.00	⋮
C = -13.00	F = -10.00	I = -7.00	Q = 1.00

TRI-6342-1380-0

Figure 6-4n. Transmissivity Field Distribution (Fields 53-56)

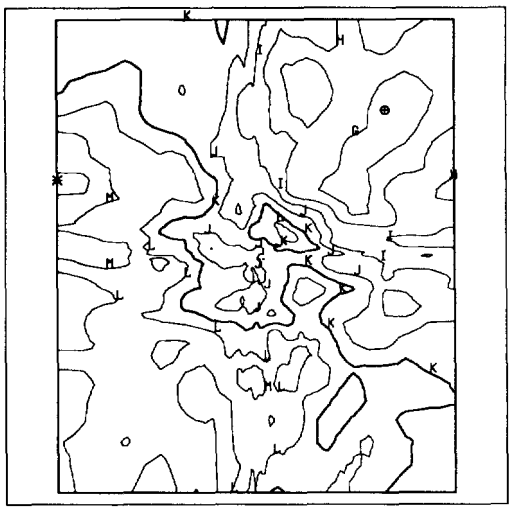

Field 57
⊕ = -9.951
★ = -1.383

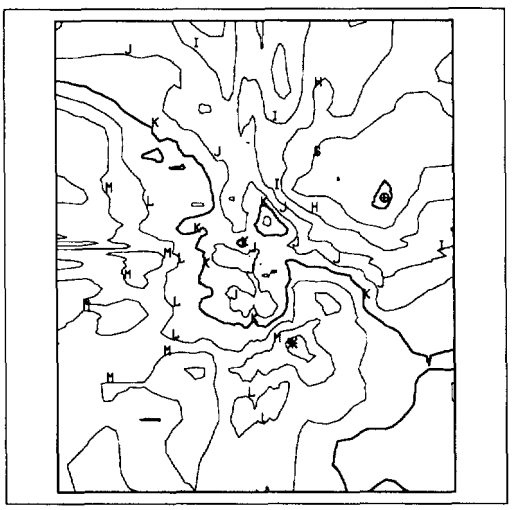

Field 58
⊕ = -10.36
★ = -1.30

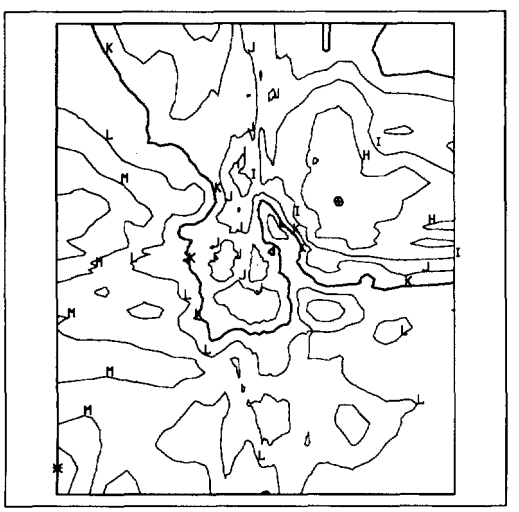

Field 59
⊕ = -8.787
★ = -1.298

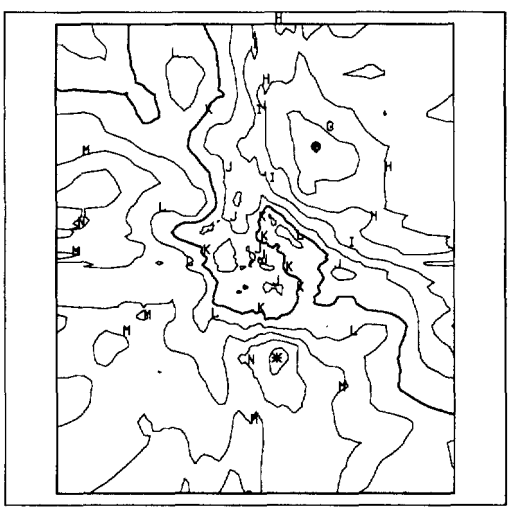

Field 60
⊕ = -10.09
★ = -0.47

Legend

LOGT ($\log_{10}$ m^2/s)

A = -15.00	**D = -12.00**	**G = -9.00**	**J = -6.00**
B = -14.00	**E = -11.00**	**H = -8.00**	**⋮**
C = -13.00	**F = -10.00**	**I = -7.00**	**Q = 1.00**

TRI-6342-1381-0

Figure 6-4o. Transmissivity Field Distribution (Fields 57-60)

6.4 Fluid Flow Modeling with SECO2D—Bruce L. Baker and Patrick J. Roache

The SECO_2DH code was used to model the effect of climate on groundwater flow in the Culebra Dolomite Member. Capabilities of SECO_2DH are fully documented in the SECO 2.1 User's Manual (draft of SAND90-7096, Roache et al., in preparation). A brief overview the SECO_2DH code is first described and then the specific options utilized to model the Culebra aquifer are detailed.

6.4.1 MODEL DESCRIPTION

SECO_2DH, a single-phase, two-dimensional flow code, was developed specifically for the WIPP project. For the 1991 PA calculations, SECO_2DH was used to estimate the regional steady-state flow fields for present and climatically perturbed boundaries.

6.4.1.1 Governing Equation

The partial differential equation solved for potentiometric head, h, is the following:

$$S_s \frac{\partial h}{\partial t} = \nabla \bullet (K \nabla h) - W \tag{6-2}$$

where K is the (tensor) hydraulic conductivity, S_s is the specific storage of the porous material, t is time, and W is a volumetric flux (out of the porous material) percent volume representing wells. The principal axes of K must be aligned along the coordinate directions x and y. S_s, K, and W may be functions of (x, y, t).

6.4.1.2 Discretization and Solvers

The above equation (or the steady-state version with $\partial h/\partial t = 0$) is discretized using standard second-order differences in space and first-order backward (fully implicit) differences in time (McDonald and Harbaugh, 1988; Roache, 1976). The fully implicit time differencing produces unconditional stability for this linear equation but requires solution of an elliptic (Helmholtz) equation at each time step. In MODFLOW and other common groundwater hydrology codes, this linear, elliptic equation is solved by either the 2-line successive over-relaxation (SOR) iterative method or by a direct solver. The direct solver is not considered to be practical for realistic grids (sufficiently fine resolution), being excessively sensitive to computer round-off error (especially on VAX class computers) and very slow. In SECO_2DH, the solver options are point SOR, (single)

line SOR (e.g., see Roache, 1976), and the semi-coarsening multigrid solver MGSS2, which was developed at Ecodynamics (Schaffer, 1991).

The semi-coarsening multigrid solver (MGSS2) is the default option. For very coarse resolution (e.g., a 6x6 grid that might be used for development of code enhancements), the point SOR solver is fastest. However, MGSS2 results in significantly increased efficiency for problems with fine resolution and strongly varying conductance (due to either hydraulic conductivity variations or highly stretched grids). Further, the MGSS2 solver does not require that the user estimate an optimum relaxation factor, as SOR solvers do.

6.4.1.3 Block-Centered Discretization

SECO_2DH has been written with an option flag called MAC to select either the most common block-centered discretization (MAC=1), with the cell edge coincident with the aquifer edge, or node-centered discretization (MAC=0), with the cell center (or node) on the aquifer edge. Unless required by a specific study, the default cell configuration is MAC=1. This configuration clearly more accurately locates the aquifer edge for both Dirichlet (fixed head) and Neumann (fixed gradient) boundary conditions. For QA purposes, MAC=0 is unsupported in SECO_2DH.

6.4.1.4 Problem Decoupling

To make the problem definition convenient and to facilitate the running of grid convergence tests and local-area simulations within the larger regional-area simulation, the problem definition is decoupled from the computational grid. The aquifer properties are defined on a discrete data base that can be independent of the computational grids. A sequence of grid solutions does not require the user to define aquifer properties point by point in each computational grid; likewise, the regional computational grid is decoupled from the local computational grid, both in space and time. A number of parameters, including the boundaries of the computational regions, the spatial increments (cell sizes), the simulation times, and the time steps, are all decoupled in both space and time. The only requirement is that the local grid problem domain of definition must lie within the regional grid problem domain of definition. Likewise, definition of boundary conditions (types and values) and wells (locations and pumping schedules) are decoupled from the computational grid and are defined in the continuum.

6.4.1.5 Initial Conditions

Initial conditions on hydraulic head may be specified by one of three methods: (1) by using the values set in the aquifer-defining grid; (2) by specifying other values by way of linear variations in

the x and y directions (the initial condition subroutine, SET IC, may be readily modified for other distributions); or (3) by solving the steady-state problem with the specified boundary conditions and all wells turned off.

6.4.1.6 Boundary Conditions

Unlike most groundwater hydrology codes, SECO_2DH allows a fairly general specification of boundary conditions. The SECO_2DH boundary conditions can be of the following types: Dirichlet (specified head), non-homogeneous Neumann (specified, possibly non-zero gradient), or Robin (mixed) conditions. A further option is an adaptive boundary condition, which sets specified flux at inflow boundaries and specified head at outflow boundaries. These types of boundaries may be set independently along each of the four rectangular boundaries of the grid or along an arbitrary number of user-specified sections on each boundary. (Following the basic philosophy of the SECO codes, the specification of these boundary sections is done in the continuum rather than being tied into the discretization.) In particular, sections of specified-gradient boundaries can be used to simulate recharge boundaries; these values can be modified by climatic variation.

Constant-head regions may also be set on interior regions, as can time-independent wells and lake/river levels, which differ from simple constant-head regions in that they affect the cell block heads via a riverbed conductance term. The specification of these interior boundaries is not automated at present: the user must specify each interior boundary on a cell-by-cell basis in the aquifer-defining grid, as is the case with other aquifer properties. However, once established, these values can be used without further user specification in any regional or local grid. In this sense, the interior boundaries are still defined independently of the discretization of the computational grids.

6.4.1.7 Additional Capabilities

Although the SECO codes solve the same equation for hydraulic head as the United States Geological Survey (USGS) code MODFLOW (McDonald and Harbaugh, 1988), the SECO codes have the following additional capabilities:

- Regional and local grid solutions
- General boundary conditions
- Interactive problem definition and output
- Options for initial condition specification
- Options for either cell-centered or node-centered grids

- Automated specification of grid spacing, including uniform spacing or power-law stretching for increased resolution near physical features
- Automated specification of time steps, including uniform spacing or power-law stretching for increased time resolution near events
- Parameterized climatic variations
- Particle-tracking capability

The regional and local grid capabilities include the following:

- Independent specification of aquifer properties in an aquifer-defining grid (independent of the computational grids)
- User-friendly specification of regional and local grid translation and rotation without the need for redefining aquifer properties
- A single specification of well properties and locations applicable to both the regional and local grids
- Independent specification of time stepping
- Time events such as well schedules, climatic variability, and time-dependent boundaries are defined independent of the modeled time.
- Automated, conservative interpolation of time-dependent or steady boundary conditions from the regional grid solution to the local grid boundaries
- Automated particle tracking from the local into the regional grid with the entire particle history expressed conveniently in the regional grid

Particle tracking is accomplished by the SECO Tracker codes (which are separate from the SECO_2DH flow codes) for the local and regional grid flow solutions with either time-dependent or steady-state solutions. For time-dependent solutions, the particle-tracking time intervals are equal to the flow-solution time intervals as output to a file. There is no requirement for separate time intervals because the nature of Darcy flow assures that the characteristic time for the particle motion will always be significantly less than the characteristic time for the flow solution. For steady-state flows, the particle-tracking time intervals are defined separately.

The particle-tracking algorithm is based on a linear interpolation of the Darcy velocities in space (consistent with the second-order spatial accuracy of the flow solution) and an adaptive fifth-order (Runge-Kutta-Fehlberg) integration in time. Note that the tracker integrator is a much higher order in time than the flow solution. This is not inconsistent or unbalanced because the flow solution involves an Eulerian description, whereas the particle solution is inherently Lagrangian. For example, even a steady-state flow solution with zero time truncation error and a velocity field linearly varying in space produces a particle path that involves exponential time functions, which justifies the higher order accuracy in time.

Three options govern the code performance if the tracked particle exits the computational grid within the simulation time: the code can simply stop computing as soon as the particle exits; it can continue the calculation over the entire tracking time step by extrapolation of the velocity field; or the code can repeat the previous step with a new time step adjusted so as to approximately place the particle at the grid boundary. Provision is made should the particle exit the grid within the first time step.

The particle history (position vs. time) is written to a file. The output file from the local grid particle tracker may be read by the regional grid tracker to set the initial position of the particle in the regional grid. In this option, the entire history in the local grid coordinates is read and translated to the regional grid coordinates, and the tracking is continued. The output file from the regional grid tracker then contains the entire particle history (local and regional grid) expressed in the regional grid coordinates.

The accuracy of the flow codes in SECO_2DH and the particle tracking codes SECO_TRACKER have been verified on model problems. The flow codes experimentally exhibit the expected $O(\Delta x^2, \Delta t)$ accuracy, and the particle tracking codes exhibit the expected $O(\Delta x^2, \Delta t^5)$ accuracy. See the internal code documentation or Roache et al. (1990).

6.4.2 OPTIONS USED FOR 1991 CALCULATIONS

The specific options utilized in the current calculations are mentioned here. Semi-coarsening multigrid solvers are used to increase solution efficiency. A point SOR solver is then used to check the convergence of the finite difference formulation of the fluid flow. Independent regional and local grid definition and orientation keep boundary effects from unduly influencing the fluid flow field input to the STAFF2D transport equations. Initial conditions on hydraulic head are set by solving the steady-state problem with the specified boundary conditions and all wells turned off. The user-modifiable nature of SECO_2DH is utilized to include a customized climatic variation for boundary recharge. The boundary conditions used include fixed head, fixed flux, and time-varying head. The SECO_2DH particle tracking capability is utilized to estimate path lines and fluid travel times for diagnostic analysis.

6.4.2.1 Spatial Grid

Regional gridding for SECO_2DH used for 1991 calculations is the same as used for the transmissivity sampling and is shown in Figure 6-5. The regional domain is shown in Figure 6-1. As this figure shows, the regional domain of the previous year's calculations has been shortened from 40 to 30 kilometers in length. Greater accuracy in modeling of the transmissivity

fields results because of the lack of control well data in this southern 10 km portion. The resulting 25 km by 30 km grid is still of sufficient size to keep effects of the regional boundary from adversely influencing the solution of the local domain simulation. The region retains its orientation along the natural boundary of Nash Draw but now has a power-law-stretched rectangular gridding. Initial testing has shown difficulties in utilizing the finite difference results of a SECO2 local fluid flow solution to solve the finite element transport equations of STAFF2D. For consistency, the local fluid flow and mass transport are both solved using STAFF2D using the regional SECO2D solutions as input boundary conditions. Saline concentration density and mass transport features are being added to SECO2D to solve these difficulties for next year's calculations.

6.4.2.2 Changing Climate Models

The climate model was planned to utilize the user-modifiable climate factor routines to input a modified sinusoidal variability of flux, including an LHS-sampled, uniformly distributed factor. This climatic variability was entered as a boundary recharge along 15 kilometers of the north and west regional boundaries. Difficulties arose from trying to apply a single average flux value along the entire recharge boundary. The variability of sampled transmissivities changed this property by six orders of magnitude along this boundary, requiring a similar range of head values. This required us to look at other ways to incorporate climatic change in the model. For preliminary analysis a steady-state simulation with heads along the same recharge boundary set to the land surface elevation was used to represent the effects on climatic change.

6.4.2.3 Climate Factors and Climatic Variability Calculations

For the 1991 preliminary comparison, climate variability was modeled by varying head along the recharge boundary. The amplitude of the climate function was bounded between present values and the land surface elevation, multiplied by a uniformly sampled value, ClimtIdx, ranging from zero to one. The user-modifiable climate function routine was utilized to model an equation with three peaks in ten thousand years (see Volume 3). This does not match the data base definition of five peaks in ten thousand years because it was written before the data base was defined. However, the integrated effect will be the same and the historical data show three minor climate peaks in the last ten thousand years. This model with its peaks occurring at exactly four thousand year intervals is not intended to predict the exact climatic change but only to model its effect.

6.4.2.4 Material Properties, Boundary Conditions, and Initial Conditions

The western regional boundary that corresponds to the center of Nash Draw is modeled as a no-flow symmetry boundary, except for the small portion (7.3 km) of the northern end that takes climatic boundary recharge. The head boundaries of the north, south, and east sides are fixed as part of the transmissivity sampling process. Each sample has a set of fixed head boundaries associated with it as part of the constraints on the transmissivity field. Initial conditions for interior head values are taken from a preliminary steady-state solution step computed by SECO_2DH.

6.4.3 RESULTS AND DISCUSSION

The sampled transmissivities resulted in a greater spatial variation of aquifer properties than were present in previous calculations. The variability in flow fields, travel times, and path lines were more realistic than the 1990 zoned calculations. There were no unphysical or unrealistic flow problems revealed by solving for these synthetically generated fields. The effect of the climatic variability calculations were shown to be less than 5000 years reduction in travel times, averaging about 3000 years. Characteristics of all modeled flows are illustrated by displaying results of the vector containing the largest sampled climate factor. Since this is an LHS uniformly sampled variable, the effect is to randomly select a synthetic transmissivity field.

The results of these calculations are shown in Figures 6-6 through 6-11:

- Figure 6-6 shows the 10,000-year history of the climate function, sampled at 1000-year time steps.
- The head contours in Figure 6-7 describe all time steps with a climate head boundary factor (HEAD_VAR) of 1. (See Figure 6-6 for the plot of HEAD_VAR.)
- Figure 6-8 shows the resulting flux vector representation of the velocity flow field. Small values of flux are thresholded to blanks. This illustrates the channelized nature of the flow in response to the transmissivity field which is described in Figure 6-9.
- Figure 6-10 has the elevated heads at the northwest corner set to the land surface elevation times ClimtIdx (=.985), which is the LHS sampled climate factor. These elevated heads are applied at 2000, 6000, and 10,000 years.
- The resulting increased flux is shown in Figure 6-11. Note the no-flow symmetry boundary on the west face representing the center of Nash Draw. The highly channelized flow was present in single or multiple flow paths for all the characterized fields.

This model of climatic variability will be refined for next year's calculations.

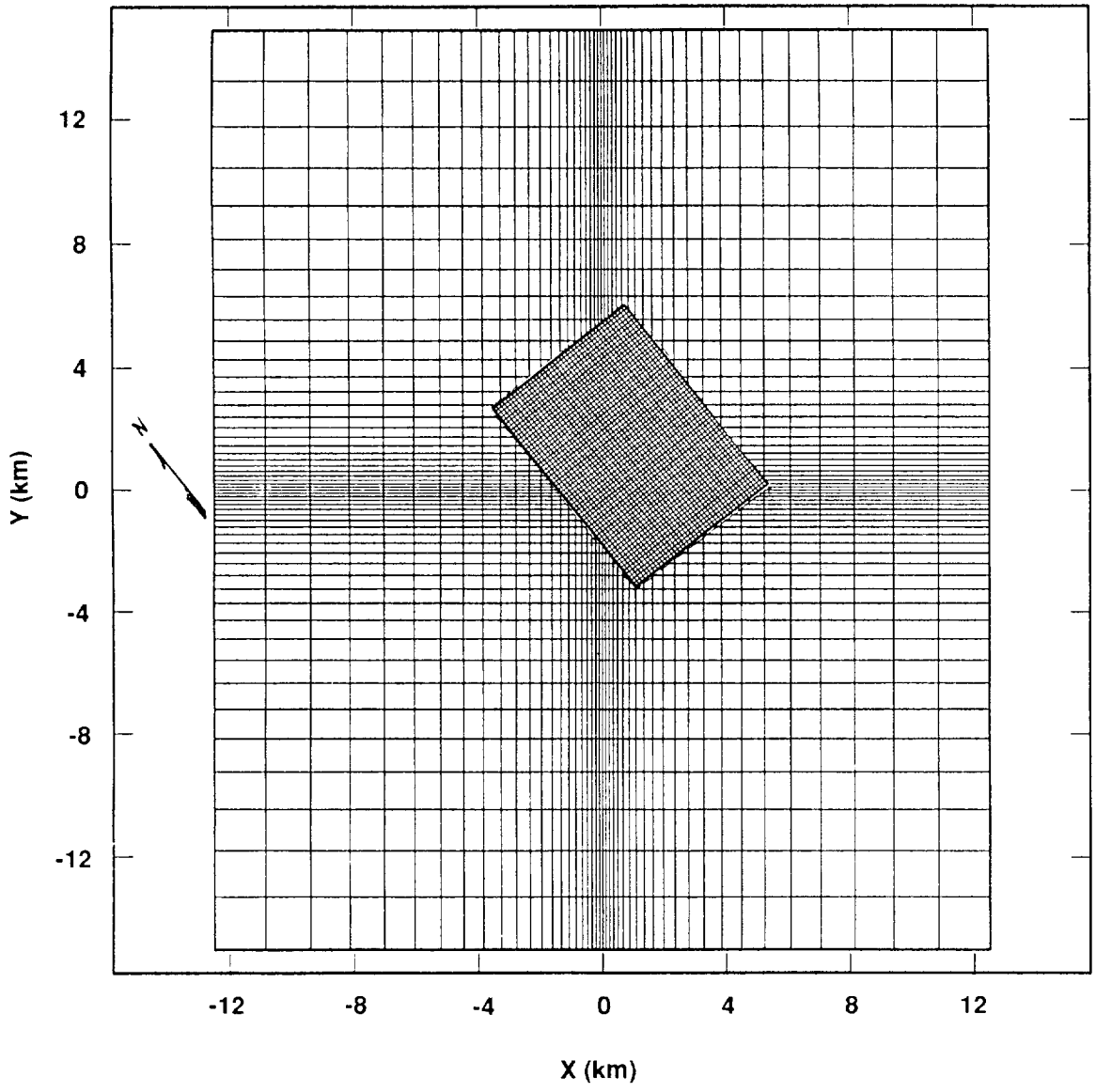

TRI-6342-1360-0

Figure 6-5. Regional and Local Grids Used for Disturbed Fluid Flow and Transport Calculations

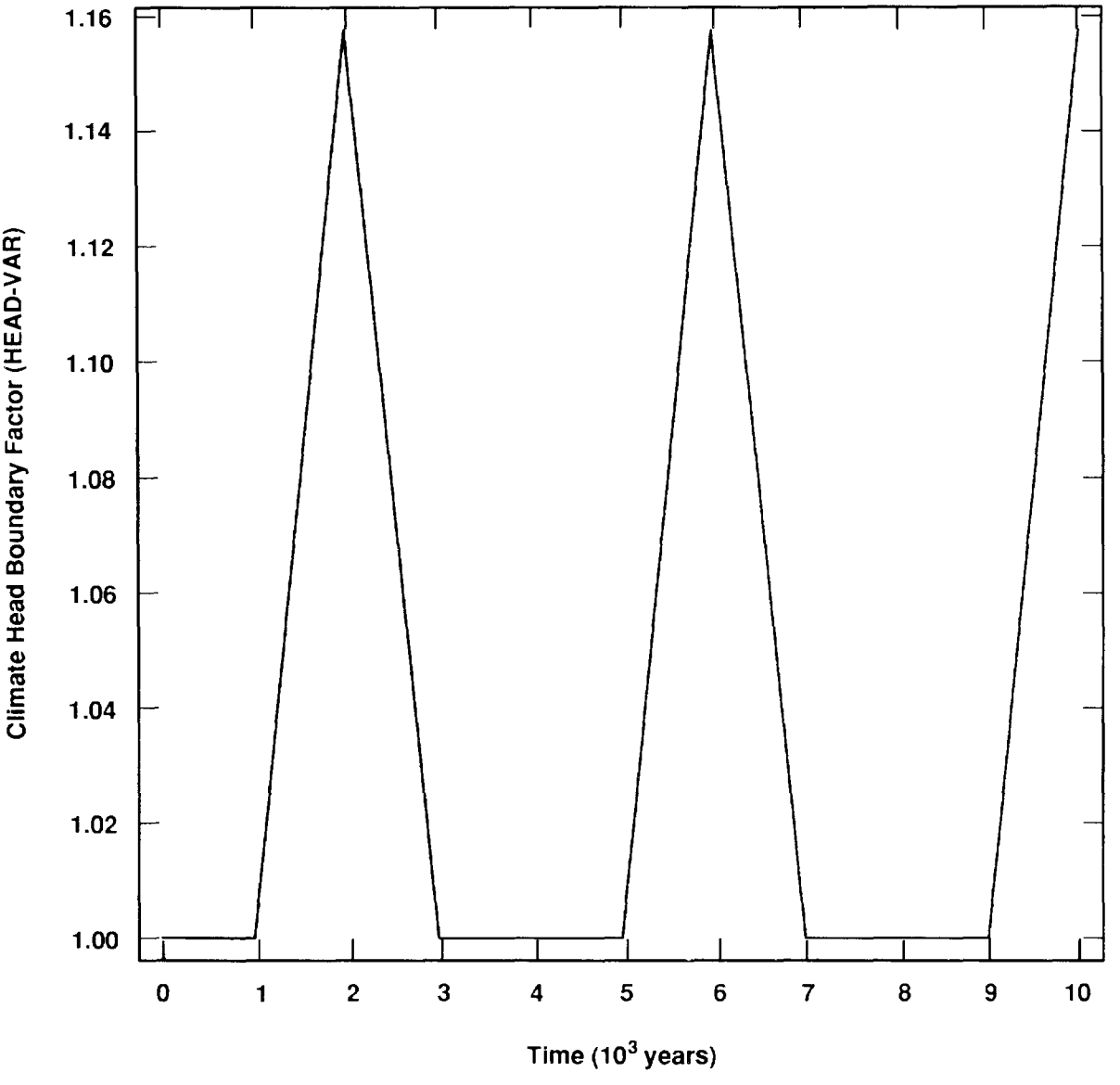

Figure 6-6. 10,000-Year History of Climate Function, Sampled at 1000-Year Time Steps

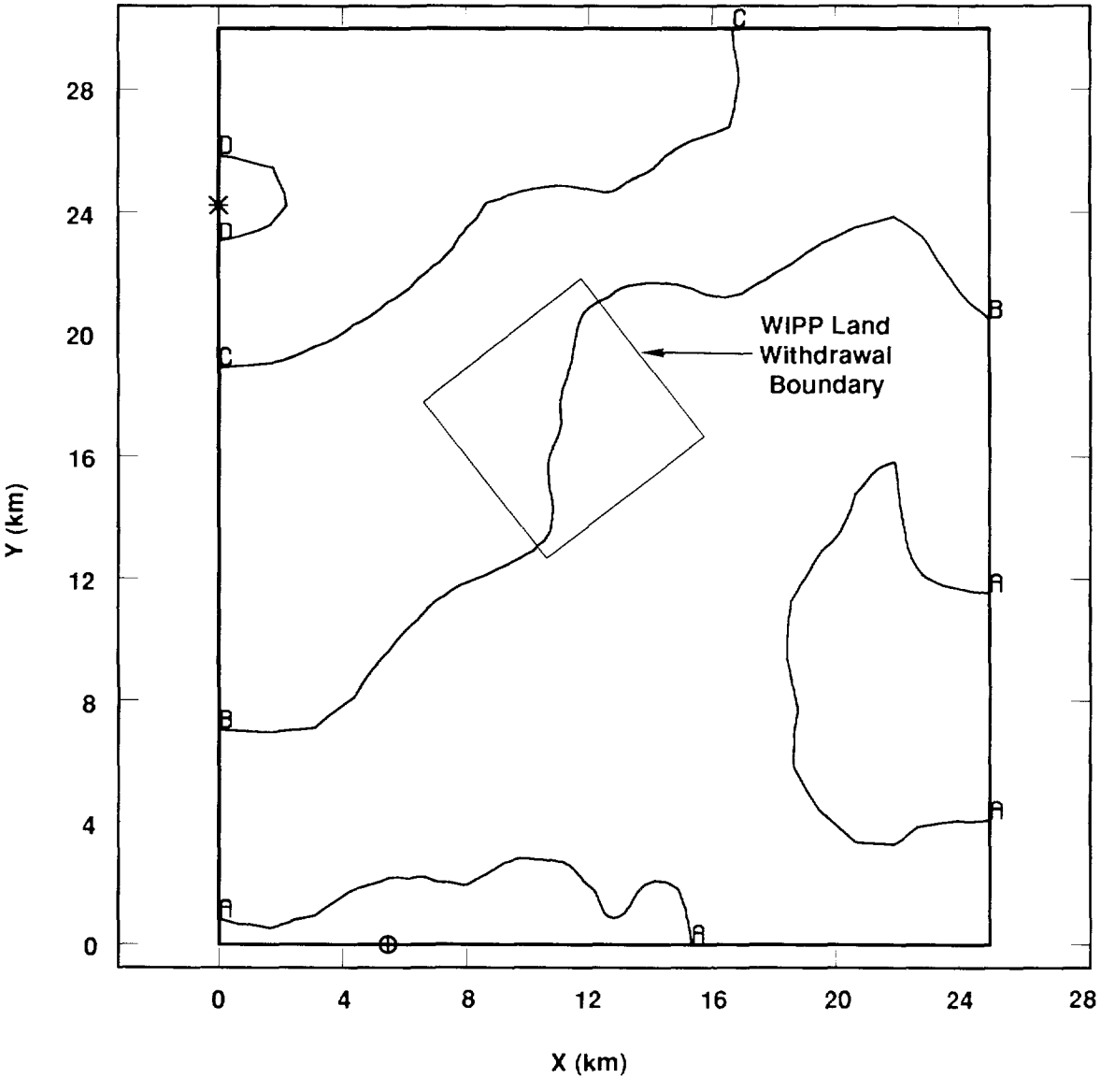

HEADEL (m x 10^{3})

A = 0.91	G = 0.97	M = 1.03
B = 0.92	H = 0.98	N = 1.04
C = 0.93	I = 0.99	0 = 1.05
D = 0.94	J = 1.00	P = 1.06
E = 0.95	K = 1.01	Q = 1.07
F = 0.96	L = 1.02	⊕ = 906.7
		★ = 942.2

TRI-6342-1362-0

Figure 6-7. Head Contours at 1000 Years, Climate Minimum

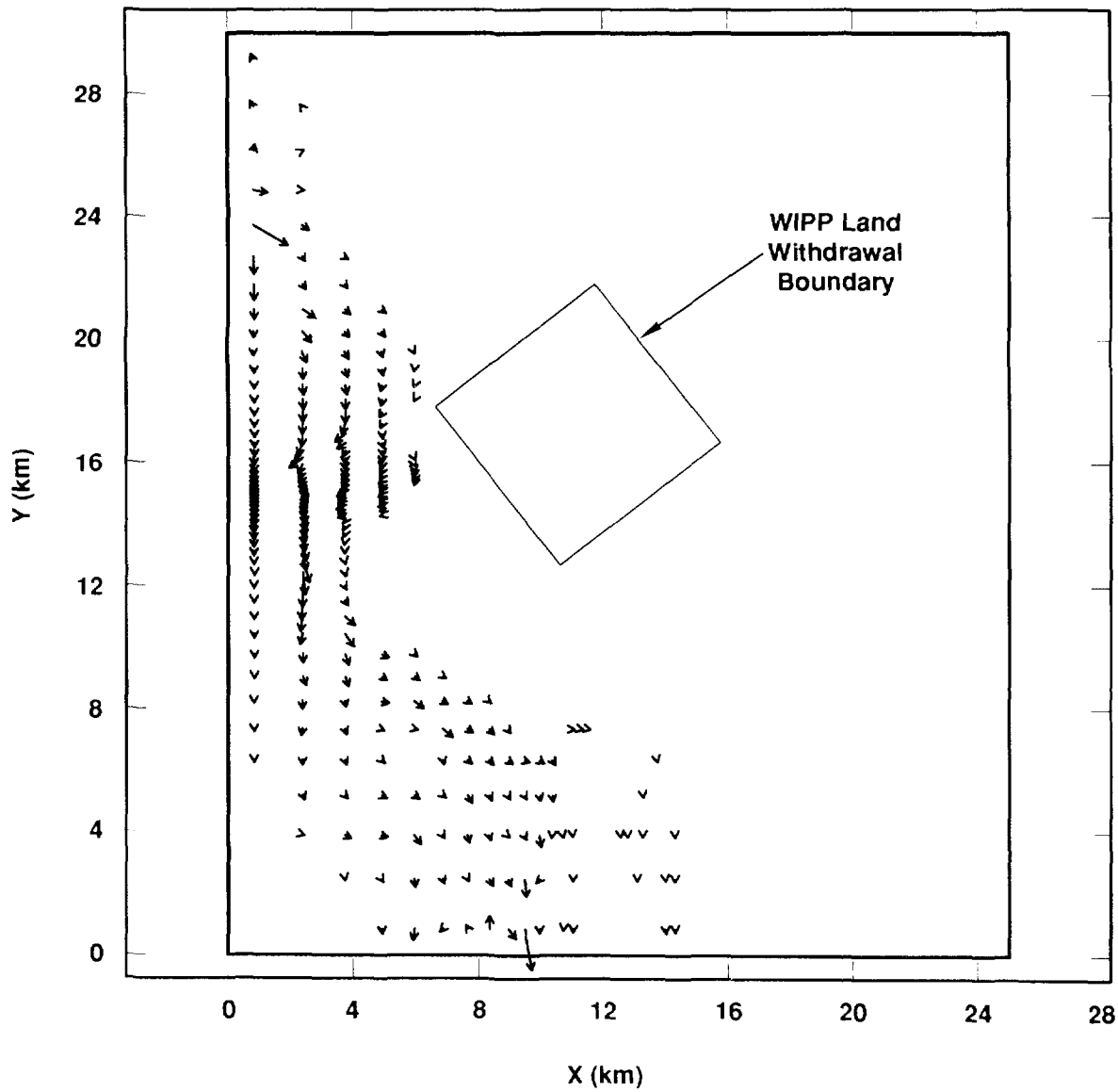

TRI-6342-1363-0

Figure 6-8. Flux Vector Representation of the Velocity Flow Field at 1000 Years, Climate Minimum

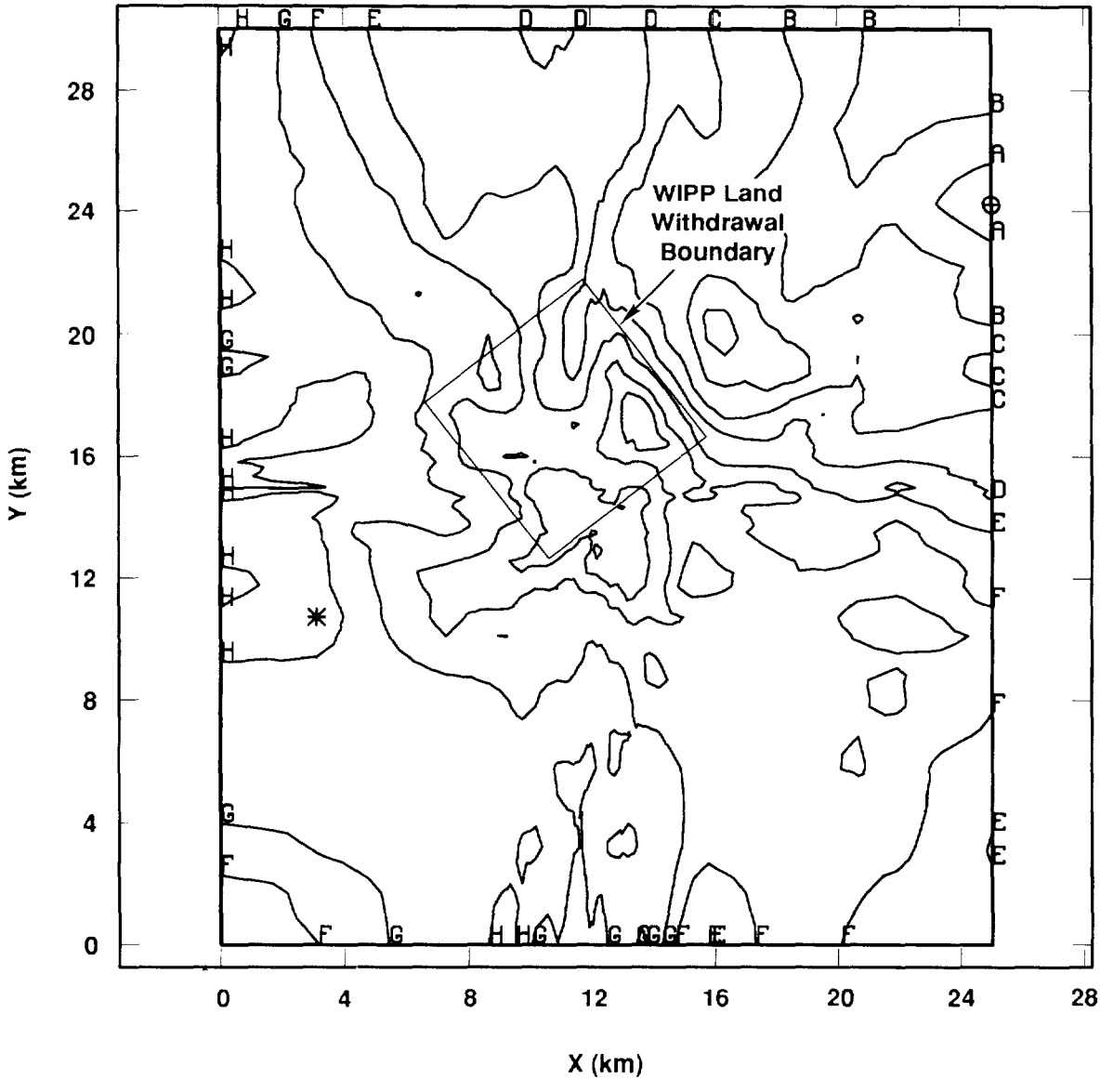

LOGT (log_{10} m^2/s)

A = -10.00 E = -6.00
B = -9.00 F = -5.00
C = -8.00 ⊕ = -10.75
D = -7.00 ★ = -2.33

TRI-6342-1364-0

Figure 6-9. Log_{10} of Transmissivity Field for Vector 54

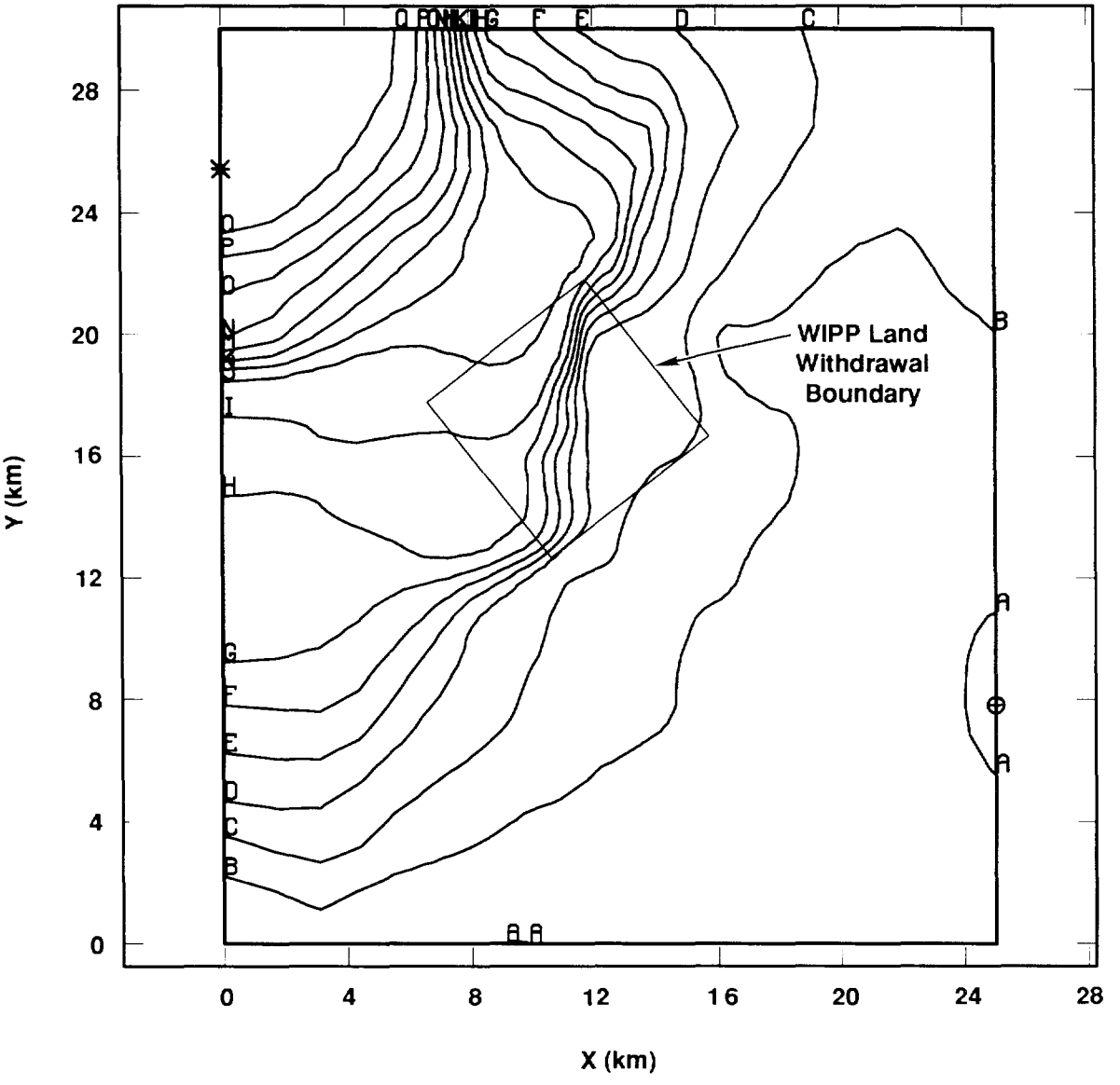

HEADEL (m x 10^3)

A = 0.910	H = 0.980	O = 1.05
B = 0.920	I = 0.990	P = 1.06
C = 0.930	J = 1.00	Q = 1.07
D = 0.940	K = 1.01	⊕ = 0.909
E = 0.950	L = 1.02	* = 1.084
F = 0.960	M = 1.03	
G = 0.970	N = 1.04	

TRI-6342-1365-0

Figure 6-10. Elevated Heads at the Northwest Corner Set to the Land Surface Elevation at 10,000 Years, Climate Maximum

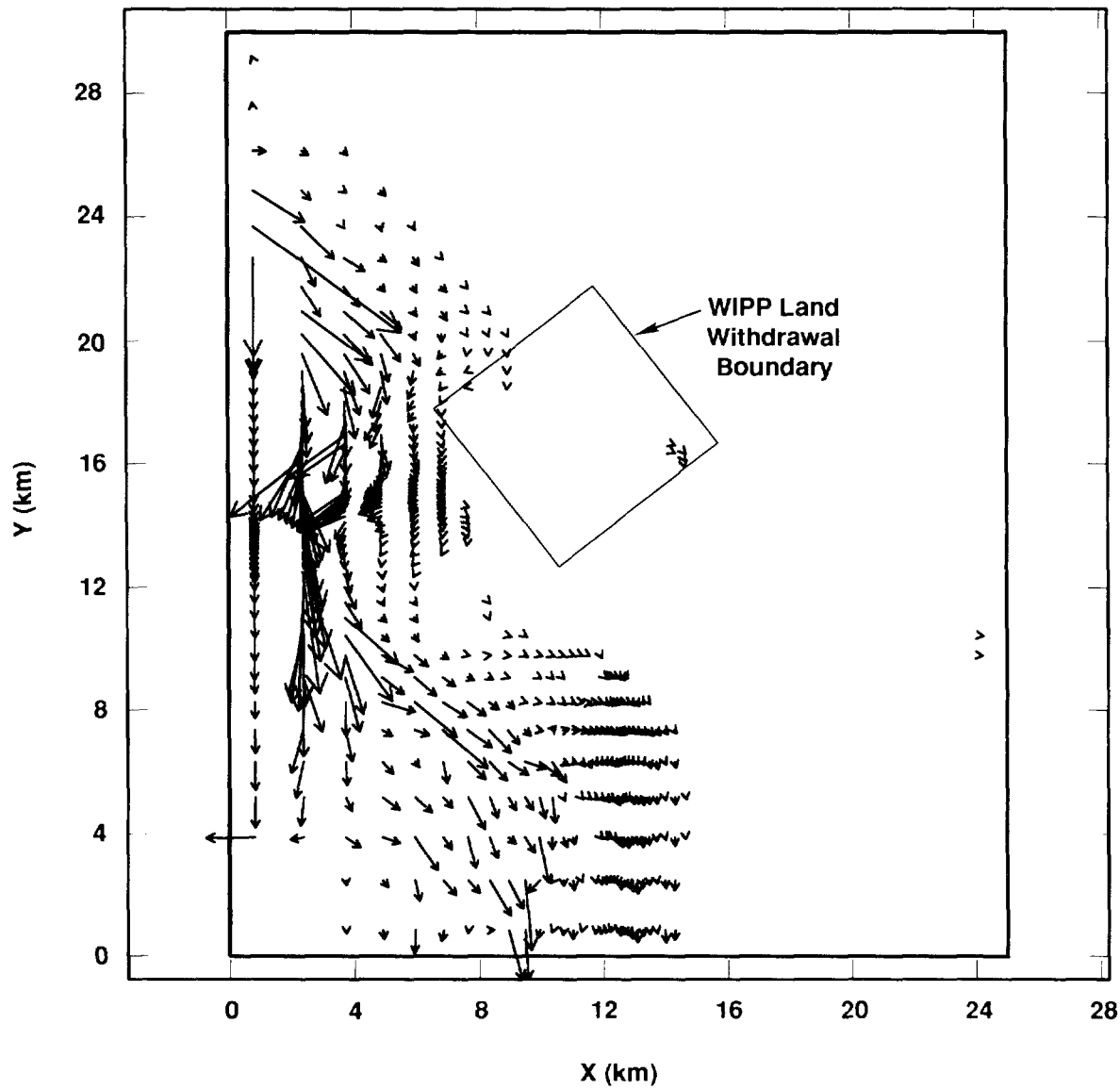

Figure 6-11. Resulting Increased Flux, Climate Maximum

6.5 Transport Modeling (STAFF2D)—David K. Rudeen

6.5.1 Local Flow Modeling With STAFF2D

The local flow fields calculations were generated with the STAFF2D finite element program. STAFF2D calculates either Darcy flow or radionuclide transport in two-dimensions. The flow and transport could be uncoupled because the rate of fluid injection into the Culebra from an intrusion borehole was assumed to have no impact on the prevailing flow-field and the injected nuclide concentration was assumed to be so small as to have no effect on Culebra fluid density. The local flow simulations were each run in two steps. The first step was a steady state calculation of initial conditions for a second transient calculation. The resulting transient flow fields were used for transport discussed below.

6.5.1.1 Fluid Flow Model Description

The model description that follows is based closely on the presentation in Huyakorn et al. (1991). The governing equation for fluid flow in STAFF2D is

$$\frac{\partial}{\partial x_i}\left(T_{ij}\frac{\partial h}{\partial x_j}\right) = S\frac{\partial h}{\partial t} - \Lambda - q,\ i = 1,2 \tag{6-3}$$

where,

h = hydraulic head (length)

T_{ij} = transmissivity tensor (length^2/time)

S = storage coefficient (dimensionless)

Λ = volumetric rate of fluid transfer per unit area from porous matrix blocks to the fracture when using dual-porosity flow (length^3/(time•length^2))

q = volumetric rate of fluid flow per unit area for sources or sinks (length^3/(time•length^2))

In accordance with standard definitions for transmissivity and storage coefficient, T_{ij} and S can be expressed as

$$T_{ij} = \phi_f H K_{ij} \tag{6-4}$$

and

$$S = \phi_f H S_s \text{ for confined aquifers} \tag{6-5}$$

where,

H = formation thickness (length)

K_{ij} = hydraulic conductivity tensor (length/time)

ϕ_f = porosity (fracture or secondary porosity for dual porosity) (dimensionless)

S_s = specific storage coefficient (1/length).

The term Λ represents the interaction between the porous rock matrix and fractures and is analogous to the Γ_ℓ in the transport equation. For the flow calculated here, Λ is assumed to be zero. The fluid exchange between the matrix and fractures in the Culebra dolomite is assumed to negligible. The q term is also zero. The fluid injected into the Culebra at the intrusion borehole that carries dissolved nuclides is assumed to have negligible effect on the existing flow field.

6.5.1.2 Space and Time Discretization

The spatial grid used for the fluid flow modeling in the Culebra was a subregion of the regional flow field (Section 6.4). The extent of the local grid region was chosen to minimize the size of the simulation and still cover the expected transport region to a boundary 5 km south of the center of the repository. TRACKER flow paths for a neutrally buoyant particle released at the intrusion borehole for all regional flow fields were examined to determine the extent of the east and west particle path positions. All zones in the grid were 125 m square. The region covered extended form 1500 m east to 3750 m west of the borehole and 1750 m north to 5375 m south. The grid and its relation to the regional and local flow fields is shown in Figure 6-5. UTM coordinates for the grid origin (south west corner) are 612094 m east and 3576025 m north. Equal times of 1000 years to the maximum time of 10,000 yr were used in all transient simulations.

6.5.1.3 Boundary and Initial Conditions

The zones (elements) in the local grid did not coincided with the zones in the regional grid so interpolation of the heads on to the boundaries of the grid was required. The head boundary conditions for the steady state calculation of initial conditions were interpolated from time zero SECO_2DH regional calculations using the RELATE computer program. The resulting steady-state hydraulic heads were used as initial conditions for the second step, which was a transient flow calculation with time dependent boundary heads interpolated from subsequent SECO_2DH time step results.

6.5.1.4 Results and Discussion

The resulting flow fields were used for radionuclide transport as discussed below. Figure 6-12 shows the spatial range of particle paths for a neutrally buoyant particle released at time 0 at the intrusion borehole. The 5 chosen paths are representative of the spread in the 60 sampled flow

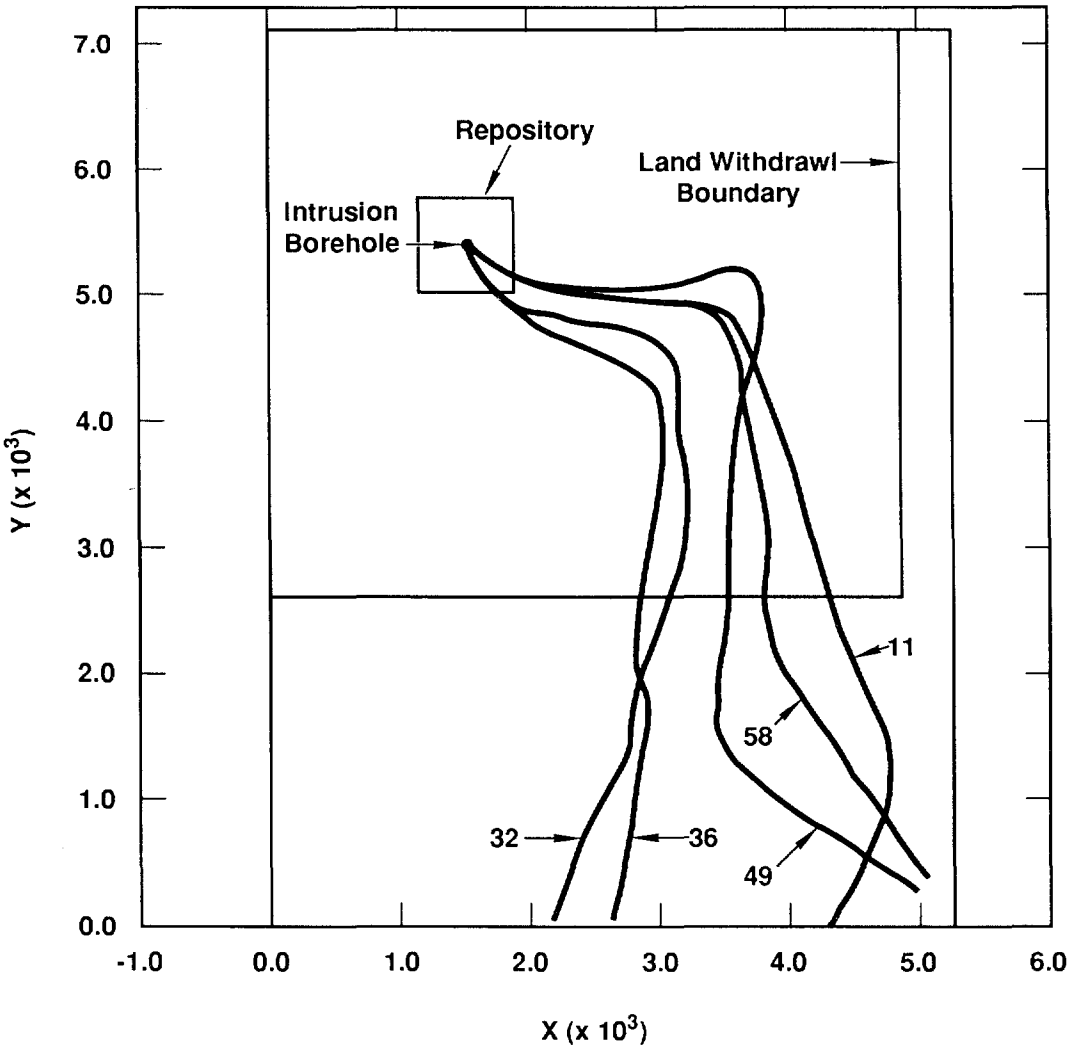

Figure 6-12. Representative Particle Paths for Local Fluid Flow Calculations

fields. Travel time variations were discussed in the section on transmissivity field generation (Section 6.3.3).

6.5.2 LOCAL TRANSPORT MODELING WITH STAFF2D

The local transport modeling was performed with the STAFF2D finite element program. STAFF2D calculates either Darcy fluid flow or radionuclide transport. The flow fields used in the transport calculations were also calculated with STAFF2D as discussed above. Transport was calculated using the dual-porosity conceptual model. The flow and transport are assumed to take place in the fractures with a solute exchange between the fractures and matrix controlled by a one-dimensional diffusion equation. Single porosity fracture transport was calculated using a fracture field derived from the specific discharge by scaling by fracture porosity. Dual porosity transport used the fracture flow field but included diffusion into the matrix. Transport was also calculated using single-porosity fracture transport with no diffusion into the matrix.

6.5.2.1 Transport Model Description

STAFF2D (Solute Transport and Fracture Flow in 2 Dimensions) is a two-dimensional, finite-element code designed to simulate groundwater flow and solute transport in fractured or granular aquifers (Huyakorn et al., 1991). The original version was developed through a joint effort by HydroGeoLogic, Inc., and the International Ground Water Modeling Center of the Holcomb Research Institute. Improved versions of the code have since been commercially available through HydroGeoLogic, the latest being Version 3.2. CAMCON originally adapted Version 2.0 of the code and has since included upgrades from Version 3.2. Additional changes to the code have been made to accommodate CAMCON input/output requirements and tailor code inputs to the WIPP database (Rechard et al., 1989). The model description that follows is based closely on the presentation in Huyakorn et al. (1991).

6.5.2.2 Governing Physical Equations

STAFF2D can perform both fluid flow and transport problems. The governing equations for transport in STAFF2D are

$$\frac{\partial}{\partial x_i}\left(D_{ij}\frac{\partial c_\ell}{\partial x_j}\right) - V_i\frac{\partial c_\ell}{\partial x_i} = \phi R_\ell\frac{\partial c_\ell}{\partial t} + \phi R_\ell\lambda_\ell c_\ell - \sum_{m=1}^{M}\xi_{\ell m}\phi R_m\lambda_m c_m - q\left(c_\ell^* - c_\ell\right) - \Gamma_\ell$$

$$\ell = 1, 2, \ldots, M \quad \textit{species} \tag{6-6}$$

where,

c_ℓ = concentration (mass/volume) of species ℓ,

D_{ij} = hydrodynamic dispersion tensor (length^2/time),

V_i = Darcy velocity (length/time) of the flow field,

ϕ = porosity (dimensionless),

λ_ℓ = first order decay constant (time^{-1}) of species ℓ,

R_ℓ = retardation coefficient (dimensionless) of species ℓ,

$\xi_{\ell m}$ = fraction of parent species m (dimensionless) that transforms into daughter species ℓ,

q = rate of fluid injection per unit volume of formation (length^3/(time•length^3)),

c_ℓ^* = concentration of species ℓ in the injected fluid, and

Γ_ℓ = rate of material transfer of component ℓ from the rock matrix to the fracture (see dual porosity model below).

In the transport mode, the Darcy velocity is considered as input to the code and is obtained from STAFF2D or other flow codes. The dispersion tensor is defined as (Scheideger, 1960),

$$D_{11} = \frac{\alpha_L V_1^2 + \alpha_T V_2^2}{|V|} + \phi D_1^*, \text{ [length}^2\text{/time]}$$

$$D_{12} = (\alpha_L - \alpha_T)\frac{V_1 V_2}{|V|}, \text{ [length}^2\text{/time]}$$

$$D_{22} = \frac{\alpha_L V_2^2 + \alpha_T V_1^2}{|V|} + \phi D_2^*, \text{ [length}^2\text{/time]} \qquad (6\text{-}7)$$

where α_L and α_T [length] are the longitudinal and transverse dispersivities, and D_1^* and D_2^* [length^2/time] are the effective coefficients of molecular diffusion, including tortuosity effects ($D_\ell^o \bullet \tau$) where D_ℓ^o is the free water molecular diffusion of species ℓ and τ [dimensionless] is the tortuosity.

The decay constant is

$$\lambda = \frac{\ln(2)}{T_{1/2}}, \text{ [time}^{-1}\text{]} \qquad (6\text{-}8)$$

where $T_{1/2}$ is the half-life of species ℓ.

Retardation is given by

$$R_\ell = 1 + \frac{\rho_s(1-\phi)}{\phi} K_{d,\ell}, \text{ [dimensionless]} \tag{6-9}$$

where K_d is the distribution coefficient, and ρ_s is the solid density.

In (6-6), Γ represents a source term modeling the matrix-fracture interaction. The dual porosity model involves the solution of both the two-dimensional, advective-dispersion equation for transport in the fracture (6-6) and a one-dimensional diffusion equation derived by assuming Fick's Law for solute exchange between the fracture and the matrix,

$$\frac{\partial}{\partial \chi'}\left(D' \frac{\partial c'_\ell}{\partial \chi'} \right) = \phi' R'_\ell \frac{\partial c'_\ell}{\partial t} + \phi' R'_\ell \lambda_\ell c'_\ell - \sum_{m=1}^{M} \xi_{lm} \phi' R'_m \lambda_m c'_m \tag{6-10}$$

where the prime indicates matrix properties and with the boundary condition requirement that the concentrations match at the interface. Refinements are made depending on the assumed geometry. For slab geometry:

$$\Gamma_\ell = \frac{2}{-b} D' \frac{\partial C'_\ell}{\partial \chi'}\bigg|_{\chi'=\alpha} \tag{6-11}$$

where,

b = fracture aperture (length)

α = fracture matrix interface.

The initial and boundary conditions for (6-10) are given by

$$C'_\ell(\chi', t=0) = C'^{o}_\ell \tag{6-12}$$

$$D' \frac{\partial C'}{\partial \chi}(0, y) = 0 \tag{6-13}$$

$$C'_\ell(b', t) = C_\ell - \zeta D' \frac{\partial C'}{\partial \chi'} \tag{6-14}$$

where ζ is a parameter characterizing the resistance of a thin skin adjacent to the fracture surface. The parameter is defined as $\zeta = b_s / D_s$, where b_s (length) and D_s (length^2/time) are the skin thickness and the effective skin diffusion coefficient, respectively.

The purpose of the dual-porosity term is to simulate solute storage within the matrix through diffusion processes. If the concentration in the fractures decreases with time, solute is returned to the fractures through diffusion out of the matrix. Note that there is no transport through the matrix; there is only an exchange between the fracture and matrix at discrete points. Details are given in Huyakorn et al. (1991, 1983a, and 1983b).

6.5.2.3 Physical Assumptions and Limitations

Assumptions are as follows:

- The code is limited to two dimensions.
- Transport is governed by Fick's Law.
- The dispersivity is assumed to correspond to an isotropic porous medium so that it can be represented by two constants in the principal direction of flow.
- In the fracture-flow-only model, the fractures are modeled as an equivalent porous medium.
- In the dual-porosity model, there is no flow or transport through the matrix, only an exchange between the matrix and fracture.
- Adsorption and decay of radionuclides obey a linear equilibrium isotherm.
- Solute concentration effects on fluid density are ignored.
- There is local chemical equilibrium between the liquid and the solid.

CAMCON Enhancement: Spatially Varying Material Properties. The HydroGeoLogic version of STAFF2D is limited to having distinct material regions over which physical properties do not vary. In the transport case, these include porosity and tortuosity. In addition, the free-water molecular diffusion parameter is independent of species in Version 3.2. The CAMCON database contains spatially varying data for tortuosity and porosity and species-dependent molecular diffusion parameters. The CAMCON version of STAFF2D was modified to permit input of these data.

6.5.2.4 Numerical Approach

As used in CAMCON, the fractured porous medium is represented by a "double-continuum" idealization, with a two-dimensional continuum representing the domain of fractures and a one-dimensional continuum representing the porous matrix (Figure 6-13). Transport is thus described by equations (6-6) and (6-10). These equations are solved using a finite-element technique, combining upstream weighting for the fracture domain and a Galerkin approximation for the porous medium. At each time level, tri-diagonal sets of algebraic equations for the matrix blocks are generated and solved using the standard Thomas algorithm to obtain the relation between the solute mass flux from the matrix and the nodal concentrations in the fractures. These flux terms

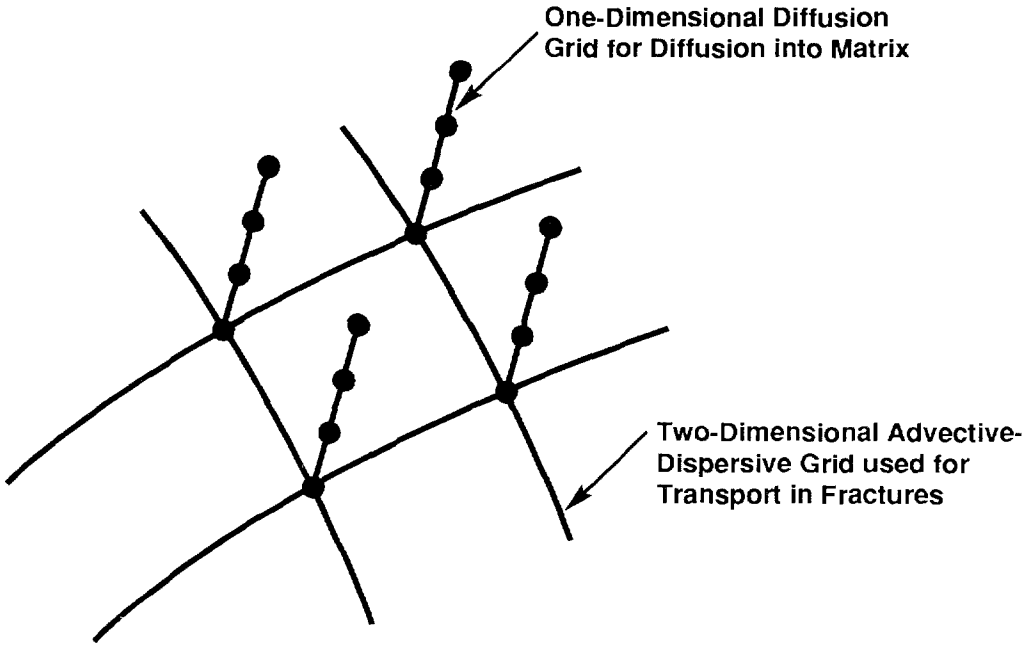

Note: No Transport Through Matrix

TRI-6342-1375-0

Figure 6-13. Schematic of Dual Porosity Double Continuum Idealization Used in STAFF2D

are treated implicitly when the equations for the two-dimensional fracture domain are generated and solved. The nodal concentrations in the matrix blocks can then be updated by performing the back-substitution step of the Thomas algorithm. The finite-element approximation technique applied to the convective-dispersive equation is an upstream-weighted residual technique (Huyakorn and Pinder, 1983) designed to overcome oscillations of the numerical solutions when the convective terms are dominant.

6.5.2.5 Benchmark Tests

Several benchmark calculations have been performed to compare STAFF2D with analytical solutions. Generally, good agreement with the analytic solutions is claimed. For the case of multiple decaying and interacting species transport, analytic solutions are currently confined to one-dimensional model problems. The following list of documented benchmark problems is discussed in Huyakorn et al. (1991):

- Longitudinal transport in fractures and transverse matrix diffusion
- Longitudinal transport in fractures and spherical matrix diffusion
- One-dimensional transport of a three-member radioactive decay chain
- Radial transport in fractures and transverse matrix diffusion
- Two-well transport in a porous medium system

6.5.2.6 Space and Time Discretization

The spatial grid used for the transport modeling in the Culebra was identical to the local flow field discussed above and is shown overlayed on the regional grid in Figure 6-5.

A time step of 1000 years was used in all simulations. The simulations were run from the time of intrusion (1000, 3000, 5000, 7000, 9000 yr) to 10,000 yr.

6.5.2.7 Boundary Conditions

The four boundaries surrounding the grid permitted flow. The discharge was determined by the velocities at the boundary. Flow out of the grid results in loss of fluid and solute. Flow into the grid had a solute concentration of zero.

A single intrusion borehole was modeled as a time dependent flux boundary (or source term) at a single node at the center of the repository with UTM coordinates of 613594 m east and 3581400 m north. The flux boundary requires the input of both the fluid flux rate and the solute flux rate. The STAFF code integrates the flux rates to obtain a total mass injected over the time step and determines an average rate to preserve total mass. The fluid flux into the Culebra from the borehole was assumed to have negligible effect on the Culebra flow field and was therefore set to 0. Solute mass flux history was supplied by the PANEL calculations. The simulations therefore

modeled the direct dumping of nuclides into Culebra flow. Transport effects between the repository and the Culebra has been ignored.

6.5.2.8 Material Properties

Up to three sets of properties are required for STAFF2D simulations of transport depending on wether the single or dual porosity conceptual models are used. For the the single porosity simulations only the fracture properties and solute (nuclide) properties are used. For the dual porosity simulations fracture, matrix and nuclide properties are required. Property values can found in Vol III. Fracture transport properties include porosity*, tortuosity, longitudinal dispersivity*, transverse dispersivity, retardations*, and effective diffusion coefficient. Matrix properties include porosity*, tortuosity, retardations*, fracture spacing*, and skin resistance effective diffusion coefficients. (Starred properties were sampled.) Nuclide properties include half life, specific activity, and chain description.

6.5.2.9 Nuclide Chains

A total of seven species broken down into 4 chains were transported. The chains are as follows:

- PU240
- AM241 -> NP237 -> U233
- U234 -> TH230
- PU239

6.5.2.10 Results

The primary results from the transport simulations is the integrated discharge across boundaries 3 and 5 km south of the repository. The 3 km boundary is actually located at the southern land withdrawal boundary. Each species flux is calculated from the y-component (south) of Darcy velocity, zone flux area (DX * thickness) and the species concentrations. The mass flux rate for each of the species is converted to activity rates across each boundary and stored for subsequent use in generating the CCDF curves. Results are tabulated for all scenarios and all vectors in Appendix B.

A typical solute plume is shown in Figure 6-14 at times of 2000 and 10,000 years. The results are for vector 9 (dual-porosity scenario E1E2 with an intrusion time of 1000 years). The effects of artificial numerical dispersion can be seen at the northeast and southwest corners of the repository. The oscillations are minimal and decrease with time. The results are typical of numerical algorithms that generate numerical oscillation transverse to the primary flow. The oscillations can be reduced by using more upwinding but only at the expense of increased dispersion throughout the entire problem. The current solution error is assumed to be more

localized near the source where concentration gradients are largest. This particular vector had the largest normalized EPA release (0.065) to the accessible environment, which was calculated as discharge across the 5-km boundary south of the repository. Normalized EPA release varied from 0 to 0.065. For the E1E2 dual-porosity scenario with a time of intrusion of 1000 years, only 10 vectors had EPA normalized releases greater than 10^{-7}. For the E2 scenario there were only five. The number of vectors with releases greater than 10^{-7} decreased with later times of intrusion. Fracture-only-transport releases were generally 150 times larger.

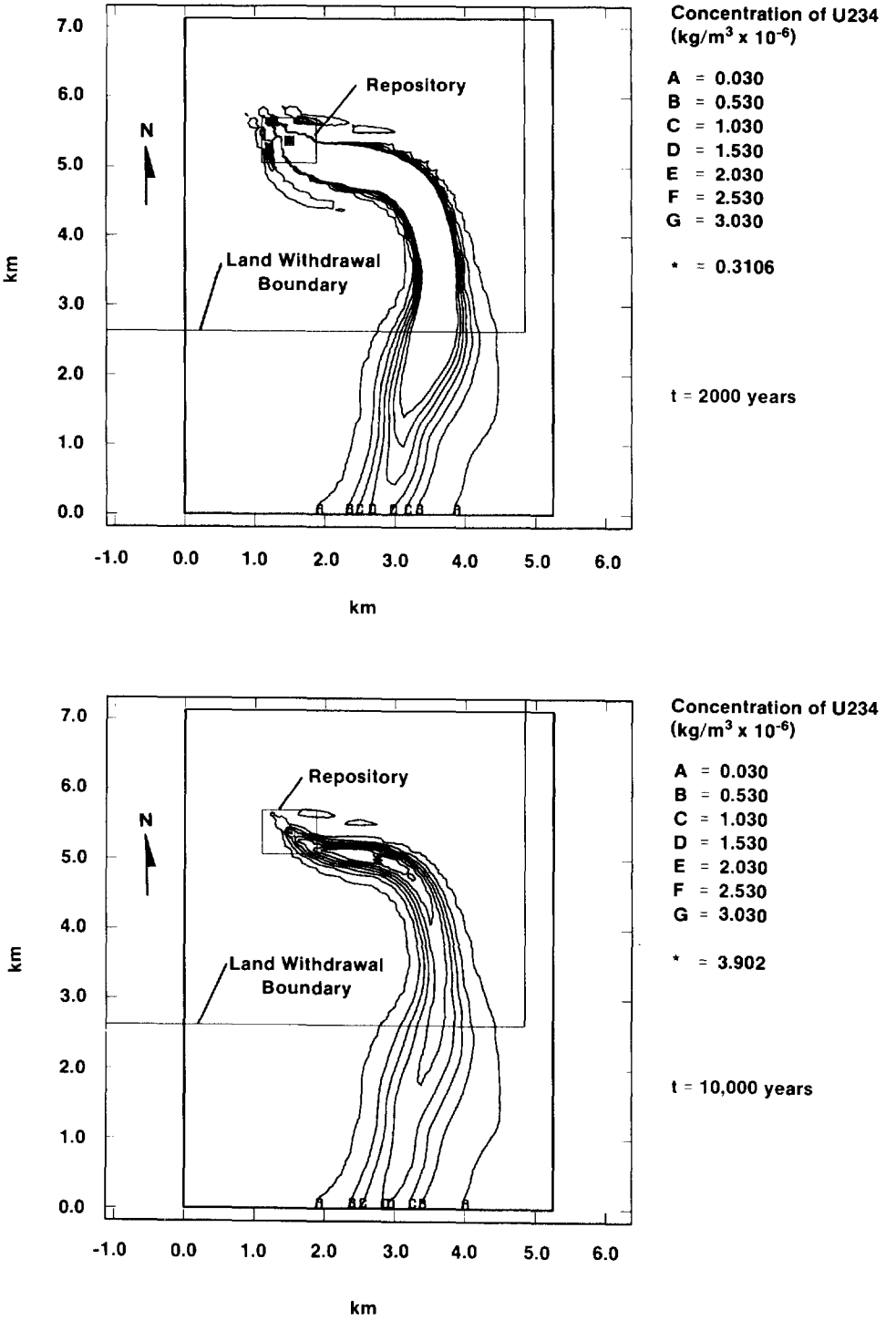

Figure 6-14. Sample Concentration Contours for Culebra Transport (Vector 9, E1E2, Dual Porosity, t_{int} = 1000 years)

7. CUTTINGS REMOVAL DURING DISTURBANCES—Jerry W. Berglund

One of the more important considerations in assessing the long term behavior of the WIPP repository involves the transport of radionuclides from the WIPP repository as the result of penetrating a panel by an exploratory borehole. If a borehole intrudes the repository, waste will be brought directly to the surface as particulates suspended in the circulating drilling fluid. This section addresses the assumptions, theory, and computational procedures governing direct waste removal due to drilling and summarizes some of the results obtained for the 1991 comparison to 40 CFR 191.

7.1 General Considerations

In the human intrusion type scenario, a hydrocarbon exploration well is drilled through a WIPP repository panel and into the underlying pressurized brine Castile formation. If rotary drilling is assumed, a volume of repository wastes is removed from the breached panel and is transported to the surface as cuttings and cavings suspended in the drilling fluid. The minimum volume of repository material removed is equal to the cross-sectional area of the drill bit multiplied by the repository thickness (cuttings). This minimum volume must be increased by material eroded from the borehole wall (cavings) by the scouring action of the swirling drilling fluid. Both cuttings and cavings will be released to the accessible environment in a settling pit at the surface.

In traditional rotary drilling, a cutting bit attached to a series of hollow drill collars and pipes is rotated at a fixed angular velocity and is directed to cut downward through the underlying strata. To remove the drill cuttings a fluid is pumped down the drill pipe through and around the drill bit and up to the surface within the annulus formed by the drill pipe and the borehole wall (Figure 7-1). In addition to the removal of cuttings, the drilling fluid (mud) serves to cool and clean the bit, reduce drilling friction, maintain borehole stability, prevent the inflow of unwanted fluids from permeable formations, and form a thin, low permeability filter cake on penetrated formations.

The volume of repository wastes removed by the cutting action of the bit is simple to calculate and is equal to the cross-sectional area of the drill bit multiplied by the thickness of the compacted repository panel. Calculating the volume of eroded waste, however, requires a more complex model. In the oil and gas drilling industry, it has been suggested (Broc, 1982) that drill hole wall erosion may be influenced by a number of factors:

- the shear stresses of the drilling fluid against the hole wall during circulation
- suction effect during pipe movement
- eccentricity of pipe with respect to the hole
- impact of the solid particles in the mud on the walls
- physical and chemical interaction between the mud and the exposed formation

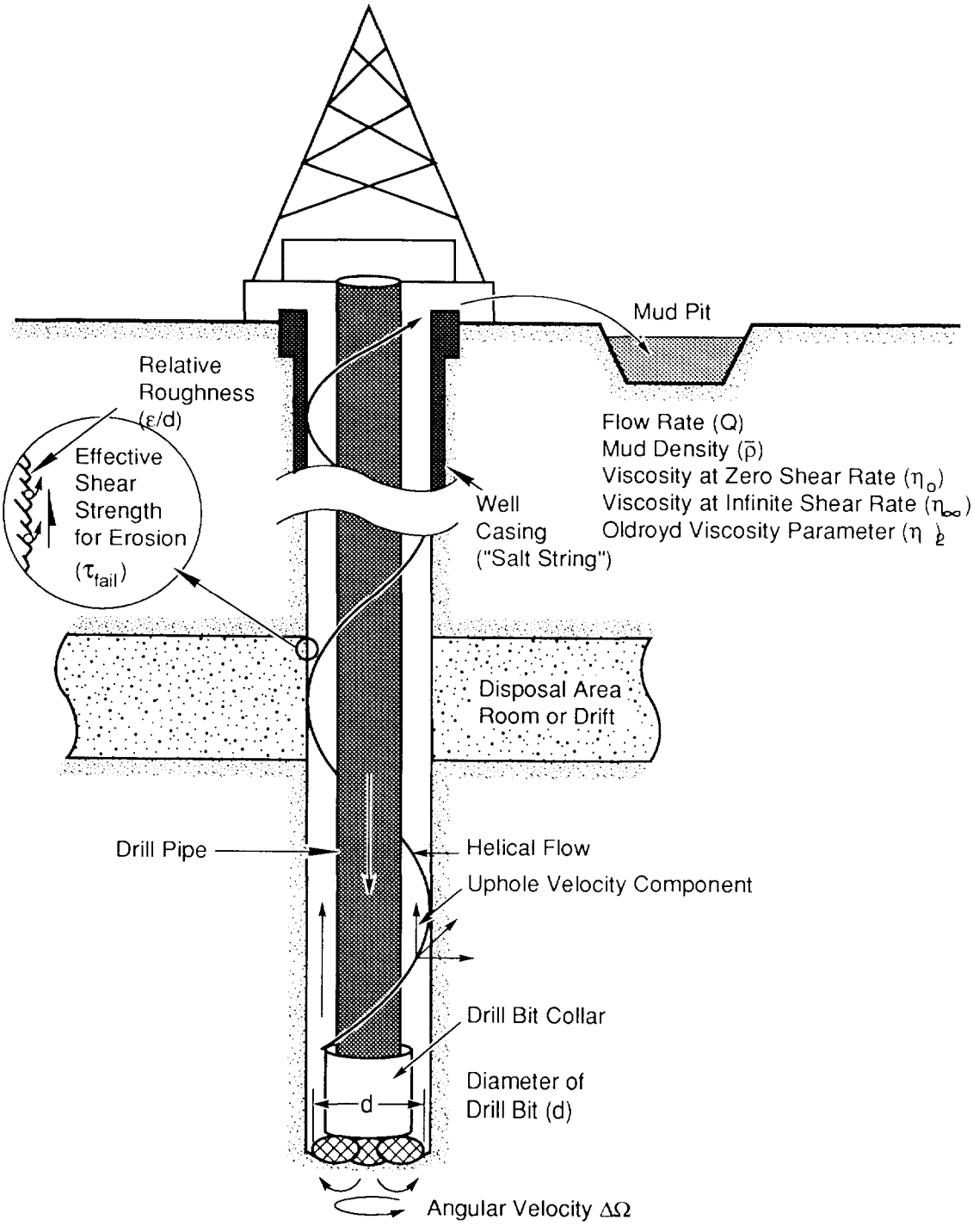

Figure 7-1. Rotary Drilling

- time of contact between the mud and the formation.

A number of investigators maintain that the flow pattern has a major effect on the stability of the walls. Walker and Holman (1971) defined an index of erosion that is a function of the shear stress acting on the walls and the type of flow opposite the drill collars. They postulated that erosion occurs primarily opposite the drill collars where the mud flow rates are greatest and is considerably more prevalent when the flow is turbulent rather than laminar. Darley (1969), in a number of laboratory experiments also showed that for aqueous drill fluids, erosion was sensitive to flow rates. For certain types of shales Darley showed that the material in the exposed borehole wall can undergo a swelling due to the decrease in the lateral effective stress and by undergoing surface hydration and osmotic action. In such cases the circulation of clear liquids caused severe erosion of the walls. Erosion was much less when colloidal suspensions were circulated partly because the formation of a filter cake inhibited the formation of a soft swollen zone. Brittle shales also exhibited a weakening when penetrated by a drill hole due in part to the infiltration of drilling fluid into old fracture or cleavage planes.

The mechanical and chemical properties of the compacted wastes in a WIPP panel sometime in the distant future will undoubtedly be quite different than any material encountered in today's oil and gas drilling industry. However, the behaviors that influence erosion are likely to be similar.

Although there are a number of factors that may influence borehole erosion, industry opinion appears to single out the effects of fluid shear stress acting on the borehole wall and the character of the fluid flow regime (laminar or turbulent). To consider these effects it is necessary to know the threshold fluid shear stress acting on the borehole wall that will initiate erosion. This "effective" borehole shear strength for erosion must be determined by experiment and may be different for laminar and turbulent flow. In the following analysis it is assumed that borehole erosion is caused primarily by the magnitude of the fluid shear stress acting on the borehole wall. Caving or spalling effects that may be caused by an encounter with gas-pressurized wastes are ignored. These effects will be addressed in a later study.

7.2 Analysis

In the annulus formed by the collars or drill pipe and the borehole wall, the flow of the drilling fluid has both a vertical and rotational component. Within this helical flow pattern shear stresses are generated by the relative motion of adjacent fluid regions and also by the motion of the fluid directly adjacent to the borehole wall and the borehole wall itself. In this analysis it is assumed that if the shear stress at the wall exceeds the effective shear strength for erosion of the wall material (filter cake or compacted repository wastes) erosion of the wall material will occur, increasing the diameter of the bored hole. The eroded material will be passed to the surface in the flowing drilling fluid.

Flow in the annulus between the drill pipe and borehole wall is usually laminar (Darley and Gray, 1988). Adjacent to the collar, however, the flow may be either laminar or turbulent as a consequence of the larger collar diameter and resulting higher mud velocities (Pace, 1990). For laminar flow, the analysis lends itself to classical solution methods. Turbulent flow requires a more approximate approach where the flow is assumed to be axial with no rotational component. Finally, the amount of radioactive material that is extracted from the repository depends on the extent of radioactive decay. A discussion on these three topics follows.

7.2.1 LAMINAR FLOW

Below Reynolds numbers of about 2100 for newtonian fluids and 2400 for some non-newtonian fluids (Walker, 1976), experiments have shown that the flow of a fluid in a circular pipe or annulus is well behaved and can be described using a well defined relationship between the velocity field and the fluid shear stress. This type of flow is called laminar.

Some of the early work on laminar, helical flow of a non-newtonian fluid in an annulus was performed by Coleman and Noll (1959) and Fredrickson (1960). The laminar helical flow solution procedure outlined below is, for the most part, an adaptation of methods described in a paper by Savins and Wallick (1966).

One of the principal difficulties in solving for the shear stresses within a helically flowing drilling fluid is the shear rate dependence of the fluid viscosity. This non-newtonian fluid behavior necessitates choosing a functional form for the variation of viscosity with shear rate for the fluid. There are several functional forms for the viscosity of drilling fluids that can be assumed. For example, in the oil and gas industry, the Bingham and power law models are often used to approximate the shear rate dependence of the fluid viscosity. A less common function is a form chosen by Oldroyd (1958) and used in the analyses by Savins and Wallick (1966). Oldroyd assumed that the viscosity varies according to the functional relation.

$$\eta = \eta_o \left[\frac{1 + \sigma_2 \Gamma^2}{1 + \sigma_1 \Gamma^2} \right] \tag{7-1}$$

where σ_1 and σ_2 are constants, η_o is the limiting viscosity at zero rate of shear, η_∞—defined as $\eta_o(\sigma_2/\sigma_1)$—is the limiting viscosity at infinite rate of shear, and Γ is the shear rate.

Viscous shear stress is described by

$$\tau = \eta \Gamma . \tag{7-2}$$

The above expression, developed using the Oldroyd viscosity equation (7-1), can be illustrated graphically as shown in Figure 7-2 This is a rate softening (pseudoplastic) model that has an initial slope of η_o and a limiting slope of η_∞ for large shear rates.

The Oldroyd model cannot account for drilling fluids that exhibit a yield stress. However, above a shear rate of zero, parameters can be chosen so that the model approximates the pseudoplastic rate response of many drilling fluids (see Figure 7-2).

Savins and Wallick (1966), expanding on the work of Coleman and Noll (1959) and Fredrickson (1960), showed that the solution for laminar helical flow of a non-newtonian fluid in an annulus could be written in terms of three nonlinear integral equations

$$F_1 = \int_{\alpha}^{1} \left(\frac{\rho^2 - \lambda^2}{\rho} \right) \frac{d\rho}{\eta} = 0$$

$$F_2 = C \int_{\alpha}^{1} \frac{d\rho}{\rho^3 \eta} - \Delta\Omega = 0$$

$$F_3 = \frac{4Q}{\pi R^3} + 4\left(\frac{RJ}{2}\right) \int_{\alpha}^{1} \left(\frac{\alpha^2 - \rho^2}{\eta} \right) \left(\frac{\rho^2 - \lambda^2}{\rho} \right) d\rho = 0 \qquad (7\text{-}3)$$

where α is the ratio of the collar radius over the cutting radius (R_i/R) (Figure 7-3), $\Delta\Omega$ is the drill string angular velocity, Q is the drilling fluid flow rate, r is the radial coordinate, and ρ is the non-dimensional radial coordinate representing the ratio r/R. The unknown parameters λ^2, $RJ/2$, and C are related to the fluid shear stresses through the relations

$$\tau_{r\theta} = \frac{C}{\rho^2}$$

$$\tau_{rz} = \frac{RJ}{2} \left(\frac{\rho^2 - \lambda^2}{\rho} \right)$$

$$\tau^2 = \tau_{r\theta}^2 + \tau_{rz}^2 \qquad (7\text{-}4)$$

where r, θ, and z represent radial, tangential, and vertical coordinates associated with the cylindrical geometry (Figure 7-3).

The three nonlinear integral equations represented by (7-3) in general must be solved numerically. By expanding each of the integral equations into a Taylor series and retaining only the linear terms, a recursive solution procedure can be used (Newton-Raphson) to find the solution for the unknowns $\delta\lambda^2$, $\delta(RJ/2)$, and δC. The three linear equations are

$$\frac{\partial F_1}{\partial \lambda^2} \delta\lambda^2 + \frac{\partial F_1}{\partial C} \delta C + \frac{\partial F_1}{\partial \left(\frac{RJ}{2}\right)} \delta\left(\frac{RJ}{2}\right) = -F_1$$

$$\frac{\partial F_2}{\partial \lambda^2} \delta\lambda^2 + \frac{\partial F_2}{\partial C} \delta C + \frac{\partial F_2}{\partial \left(\frac{RJ}{2}\right)} \delta\left(\frac{RJ}{2}\right) = -F_2$$

$$\frac{\partial F_3}{\partial \lambda^2}\delta\lambda^2 + \frac{\partial F_3}{\partial C}\delta C + \frac{\partial F_3}{\partial\left(\frac{RJ}{2}\right)}\delta\left(\frac{RJ}{2}\right) = -F_3 \tag{7-5}$$

The solution procedure consists of assuming initial values for λ^2, $RJ/2$, and C and solving the three linear equations in (7-5) for the corrections $\delta\lambda^2$, $\delta(RJ/2)$, and δC. The unknowns λ^2, $RJ/2$, and C are then replaced by $\lambda^2+\delta\lambda^2$, $(RJ/2)+\delta(RJ/2)$, and $C+\delta C$. This recursive solution procedure is repeated until $|\delta\lambda^2|$, $|\delta(RJ/2)|$, and $|\delta C|$ are all less than some specified limit. The coefficients of the unknowns $\delta\lambda^2$, $\delta(RJ/2)$, and δC in (7-5) are determined by differentiating the equations in (7-3):

$$\frac{\partial F_1}{\partial \lambda^2} = -\int_\alpha^1 \frac{1}{\eta\rho}\left[1+\frac{\left(\rho^2-\lambda^2\right)}{\eta}\frac{\partial\eta}{\partial\lambda^2}\right]d\rho$$

$$\frac{\partial F_1}{\partial C} = -\int_\alpha^1 \frac{1}{\eta\rho}\frac{\left(\rho^2-\lambda^2\right)}{\eta}\frac{\partial\eta}{\partial C}d\rho$$

$$\frac{\partial F_1}{\partial\left(\frac{RJ}{2}\right)} = -\int_\alpha^1 \frac{1}{\eta\rho}\frac{\left(\rho^2-\lambda^2\right)}{\eta}\frac{\partial\eta}{\partial\left(\frac{RJ}{2}\right)}d\rho$$

$$\frac{\partial F_2}{\partial \lambda^2} = -C\int_\alpha^1 \frac{1}{\eta^2\rho^3}\frac{\partial\eta}{\partial\lambda^2}d\rho$$

$$\frac{\partial F_2}{\partial C} = \int_\alpha^1 \frac{1}{\eta\rho^3}\left[1-\frac{C}{\eta}\frac{\partial\eta}{\partial C}\right]d\rho$$

$$\frac{\partial F_2}{\partial\left(\frac{RJ}{2}\right)} = -C\int_\alpha^1 \frac{1}{\eta^2\rho^3}\frac{\partial\eta}{\partial\left(\frac{RJ}{2}\right)}d\rho$$

$$\frac{\partial F_3}{\partial \lambda^2} = -4\left(\frac{RJ}{2}\right)\int_\alpha^1 \frac{\alpha^2-\rho^2}{\eta\rho}\left[1+\frac{\left(\rho^2-\lambda^2\right)}{\eta}\frac{\partial\eta}{\partial\lambda^2}\right]d\rho$$

$$\frac{\partial F_3}{\partial C} = -4\left(\frac{RJ}{2}\right)\int_\alpha^1 \frac{\left(\alpha^2-\rho^2\right)}{\eta\rho}\frac{\left(\rho^2-\lambda^2\right)}{\eta}\frac{\partial\eta}{\partial C}d\rho$$

$$\frac{\partial F_3}{\partial\left(\frac{RJ}{2}\right)} = 4\int_\alpha^1 \frac{\left(\alpha^2-\rho^2\right)}{\eta\rho}\left(\rho^2-\lambda^2\right)d\rho - 4\left(\frac{RJ}{2}\right)\int_\alpha^1 \frac{\left(\alpha^2-\rho^2\right)}{\eta\rho}\frac{\left(\rho^2-\lambda^2\right)}{\eta}\frac{\partial\eta}{\partial\left(\frac{RJ}{2}\right)}d\rho \tag{7-6}$$

The viscosity is related to the the shear rate function $Y(\Gamma)$ by the equation

$$\eta^2 Y = 2\left[\left(\frac{RJ}{2}\right)^2\left(\frac{\rho^2-\lambda^2}{\rho}\right)^2 + \frac{C^2}{\rho^4}\right] \tag{7-7}$$

where $Y = 2\Gamma^2$. (7-8)

For the Oldroyd viscosity function (7-1) the unknown derivatives of the viscosity in (7-6) can be determined by using the chain rule of differentiation and (7-7):

$$\frac{\partial\eta}{\partial\lambda^2} = \frac{\partial(\eta^2 Y)}{\partial\lambda^2}\frac{\partial\eta}{\partial(\eta^2 Y)} = -4\left(\frac{RJ}{2}\right)^2\left(\frac{\rho^2-\lambda^2}{\rho^2}\right)\frac{\partial\eta}{\partial(\eta^2 Y)}$$

$$\frac{\partial\eta}{\partial C} = \frac{\partial(\eta^2 Y)}{\partial C}\frac{\partial\eta}{\partial(\eta^2 Y)} = \frac{4C}{\rho^4}\frac{\partial\eta}{\partial(\eta^2 Y)}$$

$$\frac{\partial\eta}{\partial\left(\frac{RJ}{2}\right)} = \frac{\partial(\eta^2 Y)}{\partial\left(\frac{RJ}{2}\right)}\frac{\partial\eta}{\partial(\eta^2 Y)} = 4\left(\frac{RJ}{2}\right)\left(\frac{\rho^2-\lambda^2}{\rho}\right)^2\frac{\partial\eta}{\partial(\eta^2 Y)} \tag{7-9}$$

The derivative $\partial\eta/\partial(\eta^2 Y)$ can be determined by combining (7-1) and (7-8) and differentiating to obtain

$$\frac{\partial\eta}{\partial(\eta^2 Y)} = \frac{\left(\frac{\sigma_2}{2}\eta_o - \frac{\sigma_1}{2}\eta\right)^2}{\left(\frac{\sigma_2}{2}\eta_o - \frac{\sigma_1}{2}\eta\right)\left[\eta^2 + 2(\eta-\eta_o)\eta\right] + (\eta-\eta_o)\eta^2\frac{\sigma_1}{2}} \tag{7-10}$$

Based upon the preceding equations, a Fortran computer code was written to perform the necessary computations for a solution to the problem of laminar helical flow in an annulus.

For the specific case of borehole erosion, once a solution to the three integral equations in (7-3) is found, the shear stress in the fluid at the wall can be calculated by setting $\rho = 1$ in the equations in (7-4). By changing the outer radius of the hole, the fluid shear stress can be forced to equal the repository effective shear strength for erosion. The required outer hole radius is determined by iteration as shown in Figure 7-4. The derivatives required for the iteration $(d\tau/dR)$ are found numerically.

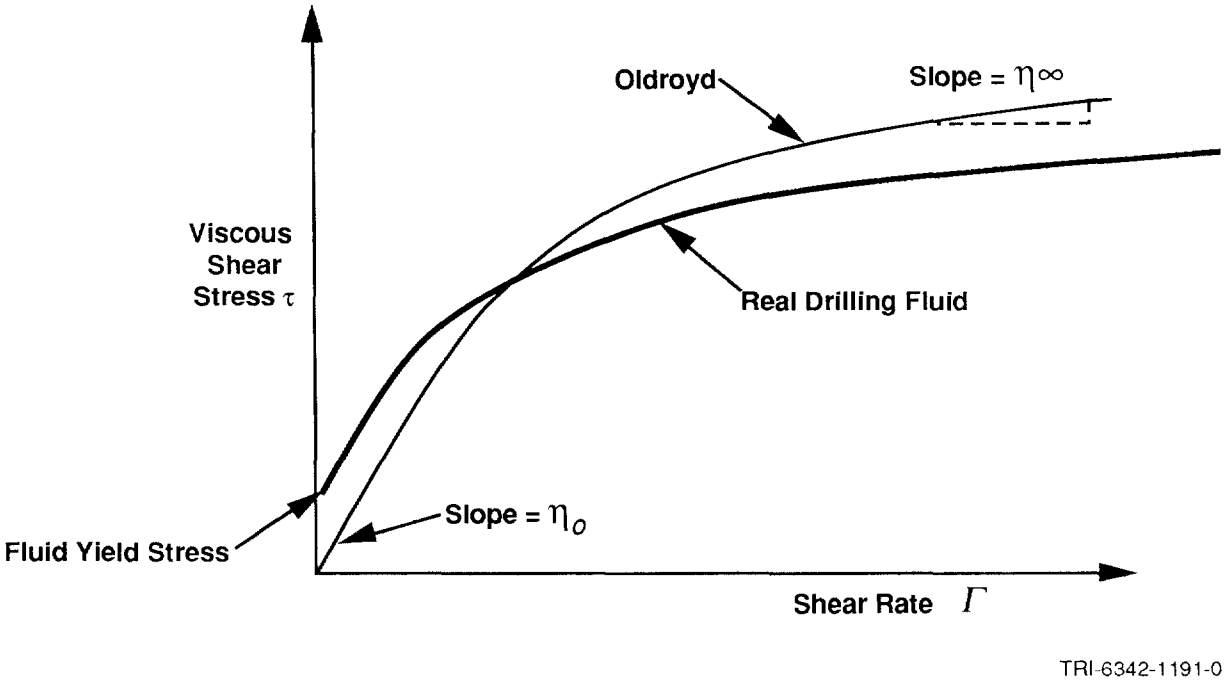

Figure 7-2. Viscous Shear Stress for Oldroyd and Real Drilling Fluid

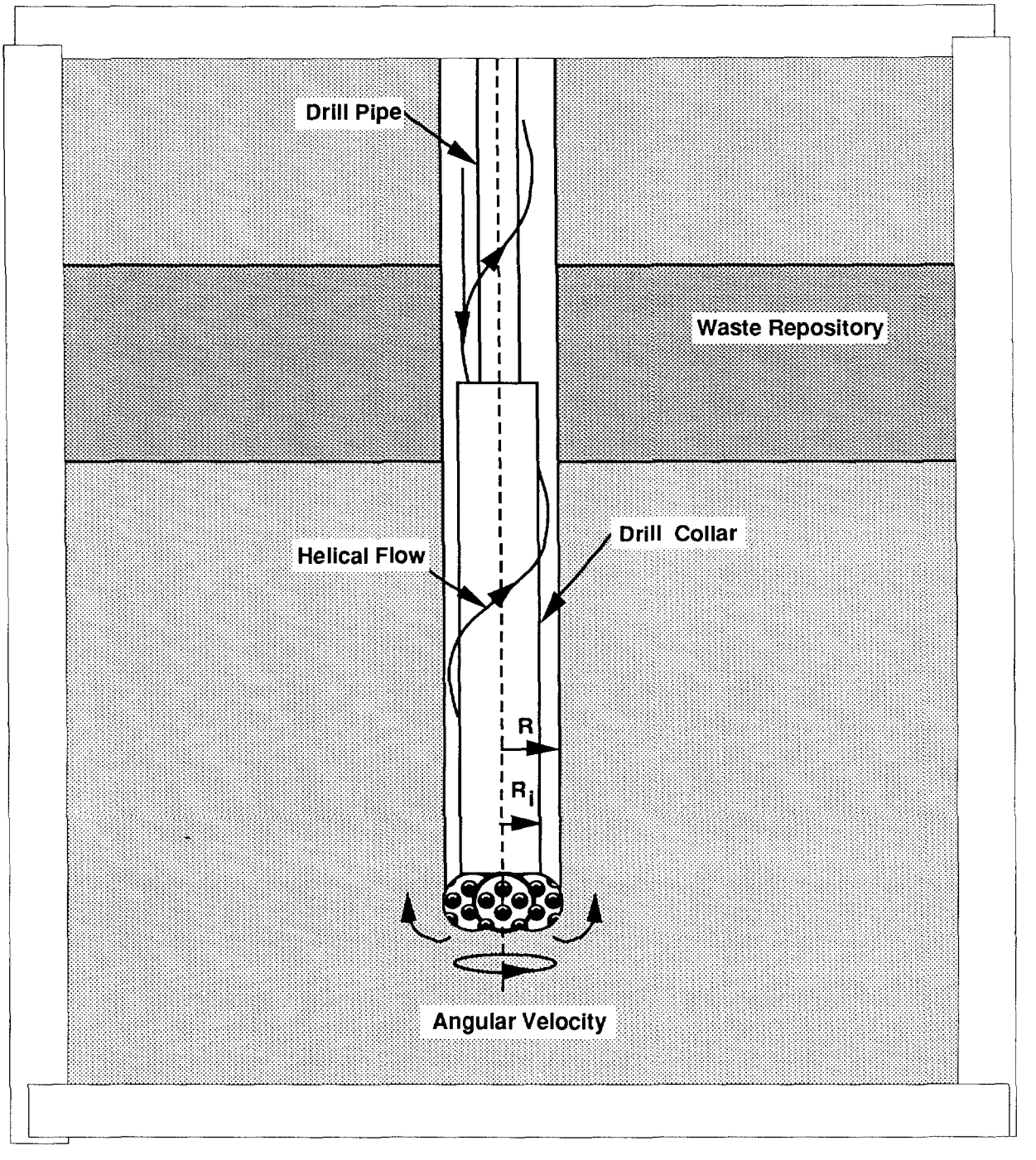

TRI-6342-1190-0

Figure 7-3. Detail of Rotary Drill String Adjacent to Drill Bit

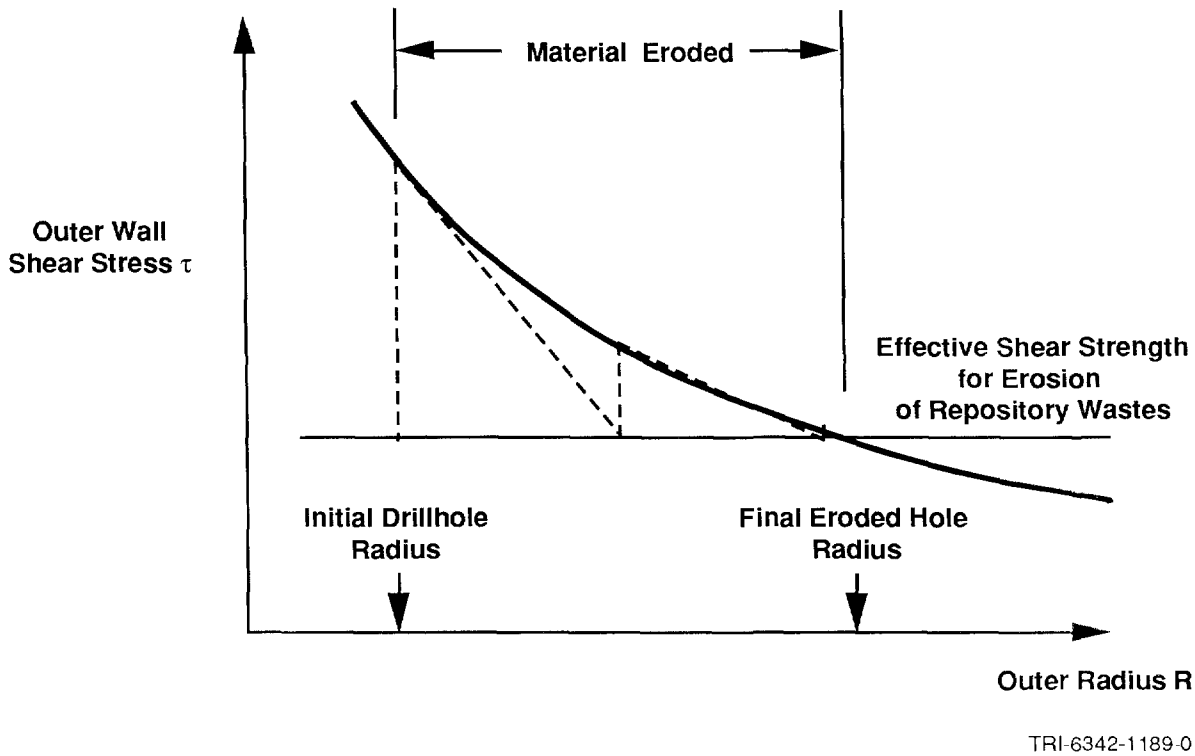

Figure 7-4. Iteration Procedure for Finding the Final Hole Radius

7.2.2 TURBULENT FLOW

For fluids with Reynolds numbers greater than about 2100, flow in a circular pipe or annulus starts to become more or less random in character, which makes orderly mathematical analysis of the flow difficult if not impossible. With increasing Reynolds numbers this random behavior increases until at a Reynolds number of about 3000 the flow becomes fully turbulent. In fully turbulent flow, momentum effects dominate and the fluid viscosity is no longer important in characterizing pressure losses.

The Reynolds number is defined as

$$R_e = \frac{\overline{\rho}\overline{V}D_e}{\overline{\eta}} \tag{7-11}$$

where D_e is the equivalent hydraulic diameter, $\overline{\rho}$ is the drill fluid density, $\overline{V}$ is the average fluid velocity, and $\overline{\eta}$ is the average fluid viscosity.

For newtonian fluids the value to use for the viscosity is clear since the viscosity is constant for all rates of shear. Non-newtonian fluids, which exhibit a changing viscosity with shear rate, present a special problem in calculating R_e.

For fluids that exhibit a limiting viscosity at high rates of shear (such as the Bingham model and in our case the Oldroyd model) it has been suggested (Broc, 1982) that the limiting viscosity ($\overline{\eta} = \eta_\infty$) be used in calculating the Reynolds number.

The Reynolds number for an Oldroyd fluid in an annulus can then be written as (Broc, 1982)

$$R_e = \frac{0.8165D\overline{V}\overline{\rho}}{\overline{\eta}} \tag{7-12}$$

where the hydraulic diameter is expressed as $D = 2(R - R_i)$ (see Figure 7-3).

The most important influence viscosity has on the calculation of pressure losses in fully turbulent flow of non-newtonian fluids appears to be in the calculation of the Reynolds number. A far more important parameter is the surface roughness past which the fluid must flow. The Reynolds number, however, does have a role in determining the onset of turbulence. For newtonian fluids this number is about 2100. For non-newtonian, rate thinning fluids the critical value of R_e tends to be greater than 2100 but less than 2400 (Walker, 1976). For our purposes a value of 2100 will be used to represent R_{e_c} (critical Reynolds number) for the Oldroyd fluid model. Since turbulent flow is more effective in generating fluid shear stresses at the borehole wall, this assumption is conservative.

There is a transition region beyond R_{e_c} before the development of fully turbulent flow. In this regime the flow has the character of both laminar and turbulent flow. However, since pressure

losses increase rapidly in turbulent flow and affect borehole shear stresses more severely it will be assumed that beyond R_{ec} the flow is fully turbulent.

To characterize the turbulent flow regime, the great bulk of analysis has concentrated on empirical procedures.

For axial flow in an annulus, the pressure loss under turbulent conditions can be written as (Whittaker, 1985)

$$\Delta P = \frac{2fL\bar{\rho}\bar{V}^2}{D} \tag{7-13}$$

where f is the Fanning friction factor and L is the borehole length.

If the shear stress due to the flowing fluid is uniformly distributed on the inner and outer surfaces of the annulus, it can be easily shown using equation (7-13) that the shear stress acting on the borehole wall is related to the average velocity through the relation

$$\tau = \frac{f\bar{\rho}\bar{V}^2}{2} \tag{7-14}$$

The Fanning friction factor is empirically related to the Reynolds number and relative roughness for pipe flow by the equation (Whittaker, 1985)

$$\frac{1}{\sqrt{f}} = -4\log_{10}\left[\frac{\varepsilon}{3.72D} + \frac{1.255}{R_e\sqrt{f}}\right] \tag{7-15}$$

where ε/D is the relative roughness. For pipes, D in this equation represents the inside diameter and ε is the absolute roughness or the average depth of pipe wall irregularities. In the absence of a similar equation for flow in an annulus, it will be assumed that this equation also applies here, where D is the hydraulic diameter as defined earlier and ε is the absolute roughness of the waste-borehole interface.

Based upon a calculated Reynolds number, a Fanning friction factor can be determined by numerically solving (7-15). The value of the shear stress acting on the borehole wall can then be determined from (7-14). Using an iterative procedure similar to that for the laminar flow problem (Figure 7-4), the fluid shear stress can be forced to equal the repository effective shear strength for erosion to obtain the final eroded borehole radius.

7.2.3 RADIOACTIVE DECAY

The quantity of radioactive material deposited in the settling pit as the result of drilling must be modified by the growth and decay of component radionuclides in the cuttings and cavings at the time of intrusion. The Bateman equations (Wehr et al., 1984) are used to calculate this decay.

For example, consider a chain of five radionuclides A, B, C, D, and E directly brought to the surface as the result of drilling. If N_a , N_b , N_c , N_d , and N_e represent the number of atoms of each of the radionuclides, then the differential equations that govern the decay and growth are (Wehr et al., 1984)

$$\frac{dN_a}{dt} = -\lambda_a N_a \qquad \frac{dN_b}{dt} = \lambda_a N_a - \lambda_b N_b$$

$$\frac{dN_c}{dt} = \lambda_b N_b - \lambda_c N_c \qquad \frac{dN_d}{dt} = \lambda_c N_c - \lambda_d N_d$$

$$\frac{dN_e}{dt} = \lambda_d N_d - \lambda_e N_e \tag{7-16}$$

If the initial number of atoms of radionuclide A is N_{a0} , the initial number of daughter atoms are N_{b0} , N_{c0} , N_{d0} , and N_{e0}, and the disintegration constants are λ_a, λ_b, λ_c, λ_d, and λ_e, then the half-lives of the radionuclides are related to the disintegration constants through the relation half-life = $\ln 2/\lambda$. Solving the differential equations in (7-16) sequentially yields.

$$N_a = N_{a0} \exp(-\lambda_a t)$$

$$N_b = \frac{\lambda_a N_{a0}}{\lambda_b - \lambda_a}\exp(-\lambda_a t) + C_1 \exp(-\lambda_b t)$$

$$N_c = \frac{\lambda_b \lambda_a N_{a0}}{\lambda_b - \lambda_a}\frac{\exp(-\lambda_a t)}{\lambda_c - \lambda_a} + C_1 \frac{\lambda_b}{\lambda_c - \lambda_b}\exp(-\lambda_b t) + C_2 \exp(-\lambda_c t)$$

$$N_d = \frac{\lambda_c \lambda_b \lambda_a N_{a0}}{(\lambda_b - \lambda_a)(\lambda_c - \lambda_a)}\frac{\exp(-\lambda_a t)}{(\lambda_d - \lambda_a)} + C_1 \frac{\lambda_c \lambda_b}{(\lambda_c - \lambda_b)}\frac{\exp(-\lambda_b t)}{(\lambda_d - \lambda_b)} + C_2 \frac{\lambda_c}{(\lambda_d - \lambda_c)}\exp(-\lambda_c t)$$

$$+C_3 \exp(-\lambda_d t)$$

and

$$N_e = \frac{\lambda_d \lambda_c \lambda_b \lambda_a N_{a0}}{(\lambda_b - \lambda_a)(\lambda_c - \lambda_a)}\frac{\exp(-\lambda_a t)}{(\lambda_d - \lambda_a)(\lambda_e - \lambda_a)} + C_1 \frac{\lambda_d \lambda_c \lambda_b}{(\lambda_c - \lambda_b)}\frac{\exp(-\lambda_b t)}{(\lambda_d - \lambda_b)(\lambda_e - \lambda_b)}$$

$$+C_2 \frac{\lambda_d \lambda_c \exp(-\lambda_c t)}{(\lambda_d - \lambda_c)(\lambda_e - \lambda_c)} + C_3 \frac{\lambda_d}{(\lambda_e - \lambda_d)}\exp(-\lambda_d t) + C_4 \exp(-\lambda_e t) \tag{7-17}$$

The constants of integration are

$$C_1 = -\frac{\lambda_a N_{a0}}{\lambda_b - \lambda_a} + N_{b0}$$

$$C_2 = -\frac{\lambda_b \lambda_a N_{a0}}{(\lambda_b - \lambda_a)(\lambda_c - \lambda_a)} - C_1 \frac{\lambda_b}{\lambda_c - \lambda_b} + N_{c0}$$

$$C_3 = -\frac{\lambda_c \lambda_b \lambda_a N_{a0}}{(\lambda_b - \lambda_a)(\lambda_c - \lambda_a)(\lambda_d - \lambda_a)} - C_1 \frac{\lambda_c \lambda_b}{(\lambda_c - \lambda_b)(\lambda_d - \lambda_b)} - C_2 \frac{\lambda_c}{(\lambda_d - \lambda_c)} + N_{d0}$$

$$C_4 = -\frac{\lambda_d \lambda_c \lambda_b \lambda_a N_{a0}}{(\lambda_b - \lambda_a)(\lambda_c - \lambda_a)(\lambda_d - \lambda_a)(\lambda_e - \lambda_a)} - C_1 \frac{\lambda_d \lambda_c \lambda_b}{(\lambda_c - \lambda_b)(\lambda_d - \lambda_b)(\lambda_e - \lambda_b)}$$

$$-C_2 \frac{\lambda_d \lambda_c}{(\lambda_d - \lambda_c)(\lambda_e - \lambda_c)} - C_3 \frac{\lambda_d}{(\lambda_e - \lambda_d)} + N_{e0} \qquad (7\text{-}18)$$

Since the above equations are based upon the number of atoms of each radionuclide, initial quantities in terms of activities would have to be changed to use these equations. The relative number of radionuclide atoms of each constituent can be obtained from the activities by multiplying each daughter activity by the ratio of daughter half-life to the half-life of the oldest parent. After the above equations are solved in terms of the relative number of atoms, the activities can be retrieved by inverting the above procedure, i.e., by multiplying the relative number of atoms by the ratio of the half-life of the oldest parent to the half-life of the daughter product.

7.3 Code Description

The CUTTINGS code, developed specifically for the WIPP, calculates the quantity of radioactive material (in curies) brought to the surface as cuttings generated by an exploratory drilling operation that penetrates the repository during the human intrusion type scenario. The code determines the amount of cuttings removed by drilling and mud erosion, and accounts for radioactive decay that has occurred up to the intrusion time.

It is assumed that the drilling operation uses techniques similar to the rotary drilling methods in use today and that the waste can be characterized as having an effective shear strength for erosion. When the effective shear strength for erosion of the compacted waste is exceeded by the drilling fluid shear stress acting on the borehole wall, it is assumed that erosion of the wall (waste) occurs and continues until a state of equilibrium exists between the effective shear strength for erosion and the applied fluid shear stress. Primary erosion occurs adjacent to the largest diameter of the drill string, namely the drill collar, which is assumed to be aligned concentrically with the hole. It is also assumed that erosion occurs during drilling operations when the drill bit lies on the

hole bottom and drilling mud is flowing up the annulus. Drilling time is not a variable in the analysis. It is assumed that if conditions are conducive to causing erosion, sufficient time is available to complete the erosion process.

The total volume of material removed by drilling is the sum of the eroded material and the material directly cut by the drill bit. Multiple borehole intrusions are permissible. The code is based on an exact analytical solution for laminar helical flow of a non-newtonian fluid in an annulus and on empirical equations for turbulent flow. Input for the code includes rotational speed of the drill string; drilling mud flow rate; cutting bit diameter; shear rate dependent viscosity parameters for the drilling mud; borehole roughness; compacted repository thickness and porosity; effective failure shear strength of the compacted repository material, radionuclide inventory, and the number of intrusions. If the Reynolds number is greater than 2100, the calculation is based on turbulent, axial, annular flow. If the Reynolds number is less than 2100, the calculation assumes that the flow is laminar and is governed by equations for the helical flow of a non-newtonian fluid. An Oldroyd type fluid is assumed.

The volume of material removed as the result of each intrusion is used with the intrusion times and the repository radionuclide inventory to calculate the total amount (in curies) of decayed radionuclides brought to the surface. The radioactive decay process is solved using the Bateman equations.

7.4 Drilling Parameters

The direct removal of wastes to the accessible environment is based on the assumption that rotary drilling will be used. The parameters associated with drilling are dependent upon the well type, predicted depth, and materials through which the drill will penetrate.

The ranges and distributions for the input variables used in generating the CCDF were chosen from data gathered from a number of sources:

- For drilling operations through salt in the Delaware basin (WIPP site), the drilling mud most likely to be used is a brine (Pace, 1990), with the density cut somewhat with an emulsified oil. The density and viscosity related variables were chosen for the calculations based on the assumption of the use of such a brine-based drilling mud.
- For drilling through salt, the drilling speeds can vary from 40 to 220 rpm (Austin, 1983; Pace, 1990), with the most probable speed about 70 rpm (Pace, 1990).
- Mud flow rates are usually selected to be from 30 to 50 gallons/minute per inch of drill diameter (Austin, 1983) and usually result in flow velocities in the annulus between the drill collars and the hole wall at or near the critical flow state (laminar-turbulent transition) (Pace, 1990).

- The drill diameter is related to the total planned depth of the hole to be drilled. For gas wells in the 4000- to 10000-foot range, it is likely that the drill used that passes through the repository would have a diameter of 10.5 to 17.5 inches. The collar diameter is assumed to be 2 inches less than the drill diameter.
- The amount of material eroded from the borehole wall is dependent upon the magnitude of the fluid-generated shear stress acting on the wall and the effective shear strength for erosion of the repository material. In the absence of experimental data, the effective shear strength for erosion of the repository material is assumed to be similar to that of a montmorillonite clay, with an effective shear strength for erosion of 1 Pa (Sargunam et al., 1973).
- For turbulent flow, the shear stress acting on the borehole wall at the repository is dependent upon the absolute surface roughness. The value chosen for the calculations exceeds that of very rough concrete or riveted steel piping (Streeter, 1958).
- For most input parameters the median values were chosen. However, to maximize cuttings removal, a lower bound for the effective shear strength for erosion was chosen. The drill bit diameter was sampled over its range. The specific input values chosen for the cuttings calculations appear in Volume 3.

7.5 Results and Discussion

Except for the five different times of intrusion and the sampling of the drill bit diameter, the input data used in the CUTTINGS code to characterize the drilling mud, drill string, and waste properties was fixed for all cases (see Volume 3). As an example of the type of results obtained from the 600 CUTTINGS calculations required to calculate a CCDF, one specific calculation set for the five intrusion times is shown in Tables 7-1 and 7-2 for a drill bit diameter of 0.4445 m (17.5 inches). The calculations indicated that borehole erosion increased the diameter of the borehole from an initial value of 0.4445 m to a final diameter of 0.994 m. During the erosion process the flow between the drill collar and borehole wall remained turbulent. The initial value of the Reynolds number was 7165, which decreased to 4319 when erosion ceased. Radionuclide release to the surface (in curies) from contact-handled (CH) and remote-handled (RH) waste for the five intrusion times are shown in Tables 7-1 and 7-2, respectively. The releases are ordered according to magnitude at the 1000-year intrusion.

Table 7-1. Radionuclide Release (CI) From Contact-Handled (CH) Waste Based on Eroded Volume and Intrusion Time

	1000 yrs	3000 yrs	5000 yrs	1000 yrs	9000 yrs
PU239	0.5817×10^{1}	0.5492×10^{1}	0.5184×10^{1}	0.4894×10^{1}	0.4620×10^{1}
AM241	0.2571×10^{1}	0.1040×10^{0}	0.4209×10^{-2}	0.1703×10^{-3}	0.6888×10^{-3}
PU240	0.6818×10^{0}	0.5515×10^{0}	0.4461×10^{0}	0.3608×10^{0}	0.2919×10^{0}
PU238	0.2433×10^{-1}	0.3344×10^{-8}	0.4596×10^{-15}	0.6317×10^{-22}	0.8682×10^{-29}
U234	0.2348×10^{-1}	0.2336×10^{-1}	0.2323×10^{-1}	0.2310×10^{-1}	0.2297×10^{-1}
NP237	0.2070×10^{-2}	0.2567×10^{-2}	0.2585×10^{-2}	0.2584×10^{-2}	0.2583×10^{-2}
U233	0.7375×10^{-3}	0.7523×10^{-3}	0.7682×10^{-3}	0.7840×10^{-3}	0.7997×10^{-3}
TH230	0.1842×10^{-3}	0.5989×10^{-3}	0.1004×10^{-2}	0.1399×10^{-2}	0.1785×10^{-2}
TH229	0.6628×10^{-4}	0.1831×10^{-3}	0.2824×10^{-3}	0.3674×10^{-3}	0.4405×10^{-3}
RA226	0.3141×10^{-4}	0.2577×10^{-3}	0.5900×10^{-3}	0.9612×10^{-3}	0.1343×10^{-2}
PB210	0.2934×10^{-4}	0.2530×10^{-3}	0.5842×10^{-3}	0.9551×10^{-3}	0.1337×10^{-2}
U236	0.2129×10^{-4}	0.5766×10^{-4}	0.8707×10^{-4}	0.1109×10^{-3}	0.1301×10^{-3}
PU242	0.1528×10^{-4}	0.1523×10^{-4}	0.1517×10^{-4}	0.1512×10^{-4}	0.1506×10^{-4}
U235	0.6824×10^{-5}	0.1796×10^{-4}	0.2847×10^{-4}	0.3839×10^{-4}	0.4776×10^{-4}
CM248	0.1014×10^{-5}	0.1010×10^{-5}	0.1006×10^{-5}	0.1002×10^{-5}	0.9974×10^{-6}
U238	0.2373×10^{-11}	0.7106×10^{-11}	0.1182×10^{-10}	0.1652×10^{-10}	0.2120×10^{-10}
TH232	0.5344×10^{-12}	0.4493×10^{-11}	0.1168×10^{-10}	0.2149×10^{-10}	0.3341×10^{-10}
CM244	0.3002×10^{-17}	0.0000	0.0000	0.0000	0.0000
PU241	0.4060×10^{-19}	0.0000	0.0000	0.0000	0.0000
CF252	0.0000	0.0000	0.0000	0.0000	0.0000

Table 7-2. Radionuclide Release (Ci) From Remote-Handled (RH) Waste Based on Eroded Volume and Intrusion Time

	1000 yrs	3000 yrs	5000 yrs	1000 yrs	9000 yrs
PU239	0.7065×10^{-1}	0.6669×10^{-1}	0.6296×10^{-1}	0.5943×10^{-1}	0.5611×10^{-1}
AM241	0.2145×10^{-1}	0.8678×10^{-3}	0.3511×10^{-4}	0.1420×10^{-5}	0.5746×10^{-7}
PU240	0.1547×10^{-1}	0.1251×10^{-1}	0.1012×10^{-1}	0.8189×10^{-2}	0.6624×10^{-2}
U233	0.1111×10^{-1}	0.1101×10^{-1}	0.1092×10^{-1}	0.1082×10^{-1}	0.1073×10^{-1}
TH229	0.1003×10^{-2}	0.2734×10^{-2}	0.4150×10^{-2}	0.5306×10^{-2}	0.6247×10^{-2}
NP237	0.8828×10^{-4}	0.9237×10^{-4}	0.9248×10^{-4}	0.9243×10^{-4}	0.9237×10^{-4}
PU238	0.2730×10^{-4}	0.3753×10^{-11}	0.5158×10^{-18}	0.7089×10^{-25}	0.9743×10^{-32}
U234	0.2635×10^{-4}	0.2622×10^{-4}	0.2607×10^{-4}	0.2592×10^{-4}	0.2577×10^{-4}
U238	0.4824×10^{-5}	0.4824×10^{-5}	0.4824×10^{-5}	0.4824×10^{-5}	0.4824×10^{-5}
U235	0.8403×10^{-6}	0.9756×10^{-6}	0.1103×10^{-5}	0.1224×10^{-5}	0.1337×10^{-5}
U236	0.4826×10^{-6}	0.1308×10^{-5}	0.1975×10^{-5}	0.2515×10^{-5}	0.2952×10^{-5}
PU242	0.2251×10^{-6}	0.2243×10^{-6}	0.2235×10^{-6}	0.2226×10^{-6}	0.2218×10^{-6}
TH230	0.2067×10^{-6}	0.6721×10^{-6}	0.1127×10^{-5}	0.1570×10^{-5}	0.2003×10^{-5}
CM248	0.5384×10^{-7}	0.5362×10^{-7}	0.5340×10^{-7}	0.5319×10^{-7}	0.5297×10^{-7}
RA226	0.3525×10^{-7}	0.2892×10^{-6}	0.6621×10^{-6}	0.1079×10^{-5}	0.1507×10^{-5}
PB210	0.3293×10^{-7}	0.2839×10^{-6}	0.6556×10^{-6}	0.1072×10^{-5}	0.1501×10^{-5}
CS137	0.3348×10^{-8}	0.2858×10^{-28}	0.0000	0.0000	0.0000
SR90	0.1327×10^{-8}	0.2803×10^{-29}	0.0000	0.0000	0.0000
TH232	0.1210×10^{-13}	0.1019×10^{-12}	0.2650×10^{-12}	0.4875×10^{-12}	0.7580×10^{-12}
CM244	0.6113×10^{-17}	0.0000	0.0000	0.0000	0.0000
PU241	0.9313×10^{-21}	0.0000	0.0000	0.0000	0.0000
PM147	0.0000	0.0000	0.0000	0.0000	0.0000
CF252	0.0000	0.0000	0.0000	0.0000	0.0000

REFERENCES

Austin, E. H. 1983. *Drilling Engineering Handbook.* Boston: International Human Resources Development Corporation.

Bear, J. 1972. Dynamics of Fluids in Porous Media. Elsevier, New York.

Beauheim, Richard L. 1987. *Interpretations of Single-Well Hydraulic Tests Conducted At and Near The Waste Isolation Pilot Plant (WIPP) Site, 1983-1987.* SAND87-0039. Albuquerque, NM: Sandia National Laboratories.

Bertram-Howery, S. G., and R. L. Hunter, eds. 1989. *Preliminary Plan for Disposal-System Characterization and Long-Term Performance Evaluation of the Waste Isolation Pilot Plant.* SAND89-0178. Albuquerque, NM: Sandia Naitonal Laboratories.

Bertram-Howery, S. G., M. G. Marietta, R. P. Rechard, P. N. Swift, D. R. Anderson, B. L. Baker, J. E. Bean, Jr., W. Beyeler, K. F. Brinster, R. V. Guzowski, J. C. Helton, R. D. McCurley, D. K. Rudeen, J. D. Schreiber, and P. Vaughn. 1990. *Preliminary Comparison with 40 CFR Part 191, Subpart B for the Waste Isolation Pilot Plant, December 1990.* SAND90-2347. Albuquerque, NM: Sandia National Laboratories.

Bras, R. L., and P. K. Kitanidis. 1991. *User's Manual for the INVS Computer Code.* SAND number not available. Albuquerque, NM: Sandia National Laboratories.

Brinster, Kenneth F. 1991. *Preliminary Geohydrologic Conceptual Model of the Los Medanos Region Near the Waste Isolation Pilot Plant for the Purpose of Performance Assessment.* SAND89-7147. Albuquerque, NM: Sandia National Laboratories.

Broc, R., ed. 1982. *Drilling Mud and Cement Slurry Rheology Manual.* Houston, Texas: Gulf Publishing Company.

Brush, L. H., and A. L. Lappin. 1990. *Appendix A, Memo 4: Additional Estimates of Gas Production Rates and Radionuclide Solubilities for Use in Models of WIPP Disposal Rooms* in Data Used in Preliminary Performance Assessment of the Waste Isolation Pilot Plant (1990). R. P. Rechard, H. Iuzzolino, and J. S. Sandha. SAND89-2408. Albuquerque, NM: Sandia National Laboratories.

Carnahan, B., H. A. Luther, J. O. Wilkes. 1969. "Applied Numerical Methods." John Wiley & Sons, Inc. New York, 1969.

Carrera, J., and S. P. Neuman. 1986a. "Estimation of Aquifer Parameters Under Transient and Steady State Conditions: 1. Maximum Likelihood Method Incorporating Prior Information." *Water Resources Research 22*: 199-210.

Carrera, J., and S. P. Neuman. 1986b. "Estimation of Aquifer Parameters Under Transient and Steady State Conditions: 2. Uniqueness, Stability, and Solution Algorithms." *Water Resources Research 22*: 211-227.

Carrera, J., and S. P. Neuman. 1986c. "Estimation of Aquifer Parameters Under Transient and Steady State Conditions: 3. Application to Synthetic and Field Data." *Water Resources Research 22*: 228-242.

Coats, K. H. 1980. "In-Situ Combustion Model." *Soc. Pet. Eng. J.* (Dec. 1980) 533-554.

Coleman, B. D., and W. Noll. 1959. "Helical Flow of General Fluids." *Journal of Applied Physics* vol. 30, no. 10: 1508.

Conte, S. D., and C. de Boor. 1972. *Elementary Numerical Analysis and Algorithm Approach.* McGraw Hill Book Company, New York, 1972.

Cox, D. R., and P. A. W. Lewis. 1966. *The Statistical Analysis of Series of Events.* London: Chapman and Hall.

Cox, D. R., and V. Isham. 1980. *Point Processes.* London: Chapman and Hall.

Cranwell, R. M., R. V. Guzowski, J. E. Campbell, and N. R. Ortiz. 1990. *Risk Methodology for Geologic Disposal of Radioactive Waste: Scenario Selection Procedure.* SAND80-1429, NUREG/CR-1667. Albuquerque, NM: Sandia National Laboratories.

Crichlow, H. B. 1977. *Modern Reservoir Engineering–A Simulation Approach.* Englewood Cliffs, NJ: Prentice Hall.

Crookston, H. B., W. E. Culham, and W. H. Chen. 1979. "Numerical Simulation Model for Thermal Recovery Processes". *Soc. Pet. Eng. J.* (Feb 1979) 37-58.

Darley, H. C. H. 1969. *"A Laboratory Investigation of Borehole Stability."* Journal of Petroleum Technology. Trans. AIME. Vol. 246 (July): 883-892.

Darley, H. C. H., and G. R. Gray. 1988. *Composition and Properties of Drilling and Completion Fluids.* Houston, TX: Gulf Publishing Company. 243.

Davies, Peter B. 1989. *Variable-Density Ground-Water Flow and Paleohydrology in the Waste Isolation Pilot Plant (WIPP) Region, Southeastern New Mexico.* U.S. Geological Survey Open-File Report 88-490. Albuquerque, NM: U.S. Geological Survey.

Davis, W. P., and J. A. Chatfield. 1970. "Concerning Product Integrals and Exponentials." *Proceeding of the American Mathematical Society 25*: 743-747.

Delhomme, J. P.. 1979. "Spatial Variability and Uncertainty in Groundwater Flow Parameters: a Geostatistical Approach." *Water Resources Research,* Vol. 15, No. 2: 269-289.

de Marsily, G. 1986. *Quantitative Hydrogeology.* Orlando, FL: Academic Press, Inc.

Dollard, J. D., and C. N. Friedman. 1979. *Product Integration with Applications to Differential Equations* (with an appendix by P. R. Masani). Reading, MA: Addison-Wesley.

Dongarra, J. J., J. R. Bonch, C. B. Moler, G. W. Stewart. 1979. *LINPACK User's Guide.* Philadelphia, PA. SIAM.

Earth Technology Corp. 1987. *Final Report for Time Domain Electromagnetic (TDEM) Survey of the WIPP.* SAND87-7144. Albuquerque, NM: Sandia National Laboratories.

Fanchi, J. R., K. J. Harpole, and S. W. Bujnowski. 1982. *BOAST III: A Three-Dimensional Three-Phase Black Well Applied Simulation Tool.* DOE/BC-10033-3. U.S. Department of Energy.

Fanchi, J. R., J. E. Kennedy, and D. L. Dauben. 1987. *BOAST II: A Three-Dimensional Three-Phase Black Oil Applied Simulation Tool.* DOE/BC-88/2/SP, DE 88001205. U.S. Department of Energy.

Fredrickson, A. G. 1960. "Helical Flow of an Annular Mass of Visco-Elastic Fluid." *Chemical Engineering Science 11*: 252-259.

Gellert, W., H. Guestner, M. Hellwich, and H. Kaestner, eds. 1977. *The VNR Concise Encyclopedia of Mathematics*. 1st American ed. New York: Van Nostrand Reinhold.

Gill, R. D., and S. Johansen. 1990. "A Survey of Product-Integration with a View Toward Application in Survival Analysis." *The Annals of Statistics 18*: 1501-1555.

Grindrod, P., and Capon, P. 1991. *Flow Through Fractured Rock: What Does the WIPP Site Culebra Data Reveal*. Draft report, version 2. NSARP 55(91)R9(IMI898-26). United Kingdom: INTERA SCIENCES.

Gutjahr, A. L. 1989. *Fast Fourier Transforms for Random Field Generation*. Socorro, NM: New Mexico Tech. Report. 106.

Guzowski, R. V. 1990. *Preliminary Identification of Scenarios that May Affect the Escape and Transport of Radionuclides from the Waste Isolation Pilot Plant, Southeastern New Mexico*. SAND89-7149. Albuquerque, NM: Sandia National Laboratories.

Guzowski, R. V. 1991. *Evaluation of Applicability of Probability Techniques to Determining the Probability of Occurrence of Potentially Disruptive Intrusive Events at the Waste Isolation Pilot Plant*. SAND90-7100. Albuquerque, NM: Sandia National Laboratories. In preparation.

Haight, F. A. 1967. *Handbook of the Poisson Distribution*. New York: Wiley.

Helton, J. C. 1973a. "Existence of Sum and Product Integrals." *Transactions of the American Mathematical Society 182*: 165-174.

Helton, J. C. 1973b. "Some Interdependencies of Sum and Product Integrals." *Proceedings of the American Mathematical Society 37*: 201-206.

Helton, J. C. 1977. "Existence of Integrals and the Solution of Integral Equations." *Transactions of the American Mathematical Society 229*: 307-327.

Helton, J. C., J. W. Garner, R. D. McCurley, and D. K. Rudeen. 1991. *Sensitivity Analysis Techniques and Results for Performance Assessment at the Waste Isolation Pilot Plant*. SAND90-7103. Albuquerque, NM: Sandia National Laboratories.

Hildebrand , F. B. 1974 *Introduction to Numerical Analysis*. McGraw-Hill, Inc. 1974.

Hoeksema, R. J., and P. K. Kitanidis. 1984. "An Application of the Geostatistical Approach to the Inverse Problem in Two-Dimensional Groundwater Modeling." *Water Resources Research 20*: 1003-1020.

Hoeksema, R. J., and P. K. Kitanidis. 1985a. "Analysis of the Spatial Structure of Properties of Selected Aquifers." *Water Resources Research 21*: 563-572.

Hoeksema, R. J., and P. K. Kitanidis. 1985b. "Comparison of Gaussian Conditional Mean and Kriging Estimation in the Geostatistical Solution of the Inverse Problem." *Water Resources Research 21*: 825-836.

Hora, S. C., D. von Winterfeldt, and K. Trauth. 1991. *Expert Judgment on Inadvertent Human Intrusion into the Waste Isolation Pilot Plant*. SAND90-3063. Albuquerque, NM: Sandia National Laboratories.

Hunter, R. L. 1989. *Events and Processes for Constructing Scenarios for the Release of Transuranic Waste from the Waste Isolation Pilot Plant, Southeastern New Mexico*. SAND89-2546. Albuquerque, NM: Sandia National Laboratories.

Hunter, R. L., and C. J. Mann, eds. 1989. *Techniques for Determining Probabilities of Events and Processes Affecting the Performance of Geologic Repositories: Literature Review*. Vol. 1. SAND86-0196, NUREG/CR-3964. Albuquerque, NM: Sandia National Laboratories.

Huyakorn, P. S., and G. F. Pinder. 1983. *Computational Methods in Subsurface Flow*. New York: Academic Press.

Huyakorn, P. S., B. H. Lester, and J. W. Mercer. 1983a. "An Efficient Finite Element Technique for Modeling Transport in Fractured Porous Media, 1, Single Species Transport." *Water Resources Research vol. 19, no. 3*: 841-854.

Huyakorn, P. S., B. H. Lester, and J. W. Mercer. 1983b. "An Efficient Finite Element Technique for Modeling Transport in Fractured Porous Media, 2, Nuclide Decay Chain Transport." *Water Resources Research vol. 19, no. 5*: 1286-1296.

Huyakorn, P. S., H. O. White, Jr., and S. Panday. 1989. *STAFF2D Solute Transport and Fracture Flow in Two Dimensions*. Herndon, VA: HydroGeologic, Inc.

Huyakorn, P. S., H. O. White, Jr., and S. Panday. 1991. *STAFF2D. Solute Transport and Fracture Flow in 2-Dimensions*. Herndon, VA: HydroGeoLogic, Inc.

IAEA (International Atomic Energy Agency). 1989. *Evaluating the Reliability of Predictions Made Using Environmental Transfer Models*. Vienna, Austria: Safety Series Report No. 100.

Kaplan, S., and B. J. Garrick. 1981. "On the Quantitative Definition of Risk." *Risk Analysis 1*: 11-27.

Kitanidis, P. K. and E. G. Vomvoris. 1983. "A Geostatistical Approach to the Inverse Problem in Groundwater Modeling (Steady State) and One-Dimensional Simulations." *Water Resources Research 19*: 677-690.

Lappin, A. R., R. L. Hunter, D. P. Garber, P. B. Davies, R. L. Beauheim, D. J. Borns, L. H. Brush, B. M. Butcher, T. Cauffman, M. S. Y. Chu, L. S. Gomez, R. V. Guzowski, H. J. Iuzzolino, V. Kelley, S. J. Lambert, M. G. Marietta, J. W. Mercer, E. J. Nowak, J. Pickens, R. P. Rechard, M. Reeves, K. L. Robinson, and M. D. Siegel. 1989. *Systems Analysis, Long-Term Radionuclide Transport, and Dose Assessments, Waste Isolation Pilot Plant (WIPP), Southeastern New Mexico; March 1989*. SAND89-0462. Albuquerque, NM: Sandia National Laboratories.

LaVenue, A. M., T. L. Cauffman, and J. F. Pickens. 1990. *Ground-Water Flow Modeling of the Culebra Dolomite - Volume I: Model Calibration*. SAND89-7068/1. Albuquerque, NM: Sandia National Laboratories.

McDonald, M. G., and A. W. Harbaugh. 1988. *A Modular Three-Dimensional Finite-Difference Ground-Water Flow Model*. Techniques of Water-Resources Investigations of the United States Geological Survey, Book 6, Modeling Techniques. Washington, D.C.: Scientific Software Group.

McKay, M. D., W. J. Conover, and R. J. Beckman. 1979. "A Comparison of Three Methods for Selecting Values of Input Variables in the Analysis of Output from a Computer Code." *Technometrics 21*: 239-245.

Mann, C. J., and R. L. Hunter. 1988. "Probabilities of Geologic Events and Processes in Natural Hazards." *Zeitschrift fuer Geomorphologie N.F. 67*: 39-52.

Marietta, M. G., S. G. Bertram-Howery, D. R. Anderson, K. Brinster, R. Guzowski, H. Iuzzolino, and R. P. Rechard. 1989. *Performance Assessment Methodology Demonstration: Methodology Development for Purposes of Evaluating Compliance with EPA 40 CFR Part 191, Subpart B, for the Waste Isolation Pilot Plant.* SAND89-2027. Albuquerque, NM: Sandia National Laboratories.

Masani, P. R. 1947. "Multiplicative Riemann Integration in Normed Rings." *Transactions of the American Mathematical Society 16*: 147-192.

Mercer, J. W. and B. R. Orr. 1979. *Interim Data Report on the Geohydrology of the Proposed Waste Isolation Pilot Plant Site Southeast New Mexico.* U.S. Geological Survey Water Resources Investigation, 79-98. Albuquerque, NM: U.S. Geological Survey.

Oldroyd, J. G. 1958. *Proceedings of the Royal Society* (London) A245: 278.

Pace, R. O. 1990. Manager, Technology Exchange Technical Services, Baroid Drilling Fluids, Inc., 3000 N. Sam Houston Pkwy. E , Houston, Texas. (Expert Opinion), Letter of 18 September 1990.

Peaceman, D. W. 1977. *Fundamentals of Numerical Reservoir Simulation: Developments in Petroleum Science, 6, Elsevier Scientific Publishing Company.* New York, 1977.

Powers, D. W., S. J. Lambert, S. E. Shaffer, L. R. Hill, and W. D. Weart, eds. 1978. *Geological Characterization Report, Waste Isolation Pilot Plant (WIPP) Site, Southeastern New Mexico.* SAND78-1596, Volume 1 and 2. Albuquerque, NM: Sandia National Laboratories.

Price, H. S., and K. H. Coats. 1974. "Direct Methods in Reservoir Simulation". *Soc. Pet. Eng. J.* (June 1974) 195-308.

Ravenne, C., A. Galli, H. Beucher, R. Eschard, D. Guerillot, and Heresim Group. 1991. *Outcrop Studies and Geostatistical Modelling of a Middle Jurassic Brent Analogue.* Paper distributed at the meeting of the WIPP performance-assessment geostatistics consultant group, April 22-23, 1991, Albuquerque, New Mexico.

Rechard, R. P., H. J. Iuzzolino, J. S. Rath, R. D. McCurley, and D. K. Rudeen. 1989. *User's Manual for CAMCON: Compliance Assessment Methodology Controller.* SAND88-1496. Albuquerque, NM: Sandia National Laboratories.

Rechard, R. P., H. J. Iuzzolino, and J. S. Sandha. 1990a. *Data Used in Preliminary Performance Assessment of the Waste Isolation Pilot Plant (1990).* SAND89-2408. Albuquerque, NM: Sandia National Laboratories.

Rechard, R. P., W. Beyeler, R. D., McCurley, D. K. Rudeen, J. E. Bean, and J. D. Schreiber. 1990b. *Parameter Sensitivity Studies of Selected Components of the WIPP Repository System.* SAND89-2030. Albuquerque, NM: Sandia National Laboratories.

Rechard, R. P., P. J. Roache, R. L. Blaine, A. P. Gilkey, and D. K. Rudeen. 1991. *Quality Assurance Procedures for Computer Software Supporting Performance Assessments of the Waste Isolation Pilot Plant.* SAND90-1240. Albuquerque, NM: Sandia National Laboratories.

Reeves, M., G. A. Freeze, V. A. Kelley, J. F. Pickens, and D. T. Upton. 1991. *Regional Double-Porosity Solute Transport in the Culebra Dolomite Under Brine-Rerservoir-Breach Release Conditions: An Analysis of Parameter Sensitivity and Importance.* SAND89-7069. Albuquerque, NM: Sandia National Laboratories.

Roache, P. J. 1976. *Computational Fluid Dynamics.* Rev. ed. Albuquerque, NM: Hermosa Publishers.

Roache, P. J., P. M. Knupp, S. Steinberg, and R. L. Blaine. 1990. *Experience with Benchmark Test Cases for Groundwater Flow in ASME FED. Benchmark Test Cases for Computational Fluid Dynamics.* Eds. I. Celik and C. J. Freitas. Vol. 93, no. H00598, (June): 49-56.

Ross, B. 1989. "Scenarios for Repository Safety Analysis." *Engineering Geology 26*: 285-299.

Rubin, B., and P. K. W. Vinsome. 1980. "The Simulation of the In Situ Combustion Process in One Dimension Using a Highly Implicit Finite-Difference Scheme". *J. Col. Pet. Tech* (Oct/Dec. 1980) 68-76.

Rubin, Y. 1990. "Stochastic Modeling of Macrodispersion in Heterogeneous Porous Media." *Water Resources Research 26*: 133-141.

Rubin, Y. 1991. "Prediction of Tracer Plume Migration in Disordered Porous Media by the Method of Conditional Probabilities." *Water Resources Research.* In press.

Rubin, Y., and G. Dagan. 1987a. "Stochastic Identification of Transmissivity and Effective Recharge in Steady Groundwater Flow: 1. Theory." *Water Resources Research 23*: 1185-1192.

Rubin, Y., and G. Dagan. 1987b. "Stochastic Identification of Transmissivity and Effective Recharge in Steady Groundwater Flow: 2. Case Study." *Water Resources Research 23*: 1193-1200.

Rubin, Y., and G. Dagan. 1988. "Stochastic Analysis of Boundary Effects on Head Spatial Variability in Heterogeneous Aquifers: 1. Constant Head Boundary." *Water Resources Research 24*: 1689-1697.

Ruge, J. W., and K. Stuben. 1987. *Algebraic Multigrid* in Multigrid Methods. Ed. S. McCormick. Philadelphia: SIAM.

Sargunam, A., P. Riley, K. Arulanandan, and R. B. Krone. 1973. "Physico-Chemical Factors in Erosion of Cohesive Soils." *Proceedings of the American Society of Civil Engineers, Journal of the Hydraulics Division vol. 99, no. HY3 99,* (March): 555-558.

Savins, J. G. and G. C. Wallick. 1966. "Viscosity Profiles, Discharge Rates, Pressures, and Torques for a Rheologically Complex Fluid in Helical Flow." *A.I.Ch.E. Journal vol. 12,* no. 2.

Schaffer, S. 1991. *An Efficient 'Black Box' Semi-coarsening Multigrid Algorithm for Two and Three Dimensional Symmetric Elliptic PDE's with Highly Varying Coefficients.* Proceedings of the Fifth Copper Mountain Conference on Multigrid Methods, March 31-April 5, 1991. Also, submitted to SIAM Journal of Numerical Analysis.

Scheideger, A. E. 1960. *The Physics of Flow Through Porous Media.* Toronto, Canada: University of Toronto Press.

Smith, G. D. 1965. *Numerical Solution of Partial Differential Equations.* Oxford University Press, New York, 1965.

Streeter, V. L. 1958. *Fluid Mechanics.* New York: McGraw-Hill.

U.S. EPA (Environmental Protection Agency). 1985. *Environmental Standards for the Management and Disposal of Spent Nuclear Fuel, High-Level and Transuranic Radioactive Waste*; Final Rule, 40 CFR Part 191, Federal Register 50: 38066-38089.

U.S. DOE (Department of Energy). 1991. *Strategy for the Waste Isolation Pilot Plant Test Phase*. Department of Energy Office of Waste Operations, DOE/EM/48063-2.

Vaughn, P. 1986. *A Numerical Model for Thermal Recovery Processes in Tar Sand: Description and Application*. April 1986, DOE Report #DOE/FE/60177-2219.

Voss, C. I. 1984. *SUTRA (Saturated-Unstaturated TRAnsport): A Finite-Element Simulation Model for Saturated-Unsaturated, Fluid-Density-Dependent Ground-Water Flow with Energy Transport or Chemically Reactive Single-Species Solute Transport*. Reston, VA: U.S. Geological Survey National Center.

Walker, R. E. 1976. "Hydraulic Limits Are Set by Flow Restrictions." *Oil and Gas Journal*. (October 4): 86-90.

Walker, R. E. and W. E. Holman. 1971. "Computer Program Predicting Drilling-Fluid Performance." Oil and Gas Journal (March 29): 80-90.

Wehr, R. M., J. A. Richards, Jr., and T. W. Adair III. 1984. *Physics of the Atom*. Reading, Massachusetts: Addison-Wesley.

Whittaker, A., ed. 1985. *Theory and Application of Drilling Fluid Hydraulics*. Boston: International Human Resources Development Corporation.

Yeh, W. W-G. 1986. "Review of Parameter Identification Procedures in Groundwater Hydrology: The Inverse Problem." *Water Resources Research* February 1986, Vol. 22, No. 2., 95-108

A. MULTIPHASE FLOW THROUGH POROUS MEDIA—Palmer Vaughn

Consequence modeling of WIPP for compliance assessment under both undisturbed and disturbed conditions involves quantification of the flow fields in and around the repository. Many of the models used by performance assessment (PA) rely on simulating the nature of the flow fields and are based on mathematical formulations that describe flow through porous media. Two models, BOAST (for undisturbed conditions) and BRAGFLO (for undisturbed and disturbed conditions) describe the simultaneous flow of brine and gas through porous media. Table A-1 provides list of terms commonly used when discussing multiphase flow through porous media. These PA models are based on the following general conceptualization of porous media flow.

A description of multi-phase porous media flow is necessary to understand the assumptions involved in modeling multi-phase flow through porous media. Details of equations of motion for multi-phase flow describing assumptions, derivations, and implementation are wide-spread throughout the petroleum and hydrology literature (Bear et al., 1968; Bear, 1975; Bear, 1979; Dake, 1978; Crichlow, 1977; Collins, 1961; Aziz, Settari, 1979; Peaceman, 1977; Crookston, Culhan, and Chen, 1979; Coats, 1980; Vaughn, 1986; Rubin, Vinsome, 1980; Scheidegger, 1960). The interested reader is referred to this literature for this background information. The nomenclature, assumptions, and conceptualization used here are typical with those found in much of the multiphase reservoir modeling literature referenced above.

BRAGFLO and BOAST are based on a description of porous media presented by Bear (1975) and Bear, Zaslavsky, and Irmay (1968). Bear (1975) points out that "no precise definition of porous media exists; however, the following characteristics, even though they are subjective, convey something about the nature of porous media:"

1. A portion of the space is occupied by heterogeneous or multiphase matter, with at least one of the phases being fluid.
2. The space within the porous media domain that is not part of the solid matrix is referred to as void space or pore space. The openings comprising the void space are relatively narrow. Some of the pores comprising the void space are interconnected (effective pore space) while unconnected pores are considered part of the solid matrix.
3. The solid phase is distributed throughout the porous media and solid must be present inside each representative elementary volume.
4. The specific surface (surface area of the pores per unit bulk volume) is relatively high.
5. "Any two points within the effective pore space may be connected by a curve that lies completely within it."

6. With respect to fluid flow, the porous media restricts the transport of the fluid to well defined channels and the velocity of a fluid particle at a point in the void space is parallel to the walls.

The term "distributed" in characteristic 3 above is somewhat general. PA adopts the Bear and Bachmat (1966 and 1967) visualization that "the void space of a porous media is composed of a spatial network of interconnected random passages of varying length, cross-section, orientation, and functions" (Bear, 1975, p. 93). Flow in the void space is laminar and each channel defines a stream tube in which the pattern of streamlines is fixed although the direction of flow along them may be reversed. The junctions where channels intersect occupy negligible pore space volume.

The fluids (either individually or combined) all occupy the pore space and are viscous and Newtonian and may be compressible. The active forces on the fluids are those due to pressure, gravity, capillarity, and shear resulting from the fluid's velocity. The fluid loses energy only during passage through the narrow channels and not through a junction. The network of channels connected to each other by junctions produces average gradients of pressure, density, and viscosity in any elementary volume that includes a sufficiently large number of channels and junctions. These average gradients are practically independent of the geometric shape of a single channel within the elementary volume (Bear 1975, p. 93).

BRAGFLO and BOAST simulate the flow of brine and gas through porous media. Two types of multi-phase flow are possible, miscible and immiscible. The PA conceptual models consider immiscible displacement only. In this case both fluids flow simultaneously through the porous network. The gas and brine phases are separated by an interface whose curvature and surface tension give rise to a capillary pressure difference across the interface (Brook, Corey, 1964; Corey, 1986; Peaceman, 1977; Dake, 1978; Crichlow, 1977; Collins, 1961). The interface is assumed to be abrupt and any transitions from one phase to another occur over a distance of negligible length compared to the channel diameter (Bear, 1975).

When brine and gas occupy void space, the concept of saturation is introduced. Saturation is defined as the volume fraction of void space occupied by a particular fluid. Interfacial tension exists where the two immiscible fluids contact each other. The shape of the resulting meniscus defines the wettability of the system (Brook, Corey, 1964; Bear, 1975). For example, the convex side of the meniscus faces toward the wetting phase while the concave side faces toward the non-wetting phase. The wetting phase for all the strata surrounding the WIPP is assumed to be brine. Interfacial tension and wettability may depend on the direction the interface is moving. This phenomenon is called hysteresis. Hysteresis is a secondary effect and is not currently modeled (Brook, Corey, 1964).

Three saturation regions are differentiated in the two-phase (brine and gas) system. Assuming a brine-wet reservoir, at low brine saturations water forms in isolated rings or exists as a thin film

of molecular thickness. As brine saturation increases, a condition is reached where the brine forms a continuous phase that is capable of transmitting pressure. Above this critical saturation or "irreducible saturation," brine flow is possible. Potential flow of brine below the irreducible brine saturation will not occur. At high brine saturation brine isolates the gas and the gas no longer forms a continuous phase. This occurs at the irreducible gas saturation.

In formulating the equations of motion for the simultaneous flow of two immiscible fluids through porous media, it is assumed that "each fluid establishes its own tortuous path, forming very stable channels, and that a unique set of channels corresponds to each degree of saturation" (Bear, 1975). Bear's continuum approach is used when two immiscible fluids simultaneously flow through porous media. Under these conditions "each of the fluids is regarded as a continuum completely filling the flow domain (at a fluid content that is a function of space coordinates and of time). The various continua occupy the entire flow domain simultaneously" (Bear, 1975 p. 457). The equations of motion for multi-phase flow used here are based on heuristic extensions of Darcy's law (Hubbert, 1956; Bear, 1975; Bear, 1979; Dake, 1978; Crichlow, 1977; Collins, 1961; Dullien, 1979; Hiatt, 1968); deMarsily, 1986; DeWest, 1965; Aziz, Settari, 1979).

The following is a statement of Darcy's law in differential form:

$$q_v = -\frac{k}{\mu}\left[\nabla P - \rho g\right] \tag{A-1}$$

where q_v is the volumetric flow rate per unit cross sectional area, k is the absolute or intrinsic permeability of the porous media, μ is the fluid viscosity, ρ is the fluid density, g is the gravitational constant, and P is the fluid pressure.

Darcy's original observations were made on the one-dimensional vertical flow of water through a fully saturated porous media (Hubbert, 1956). Darcy postulated the law, which states that the flow of water under these conditions is proportional to the change in potential. Many generalizations of Darcy's law can be found in the literature (Bear, 1975; Bear, 1979; Bear, 1968; Bear, 1966; Bear, 1967; Dake, 1978; Crichlow, 1977; Collins, 1961; Dullien, 1979; Hiatt, 1968; deMarsily, 1986; DeWest, 1965; Aziz, Settari, 1979). These generalizations extend Darcy's observation to other fluids, to the simultaneous flow of immiscible fluids, to multiple dimensions, and to compressible fluids. These generalizations are used in obtaining the equations of motion governing the two-phase flow assumed here and are discussed below.

The first extension is a generalization from an isotropic to an anisotropic medium. This extension is developed heuristically as well as theoretically in Bear (1975). Implicit in this generalization is the extension to two and three dimensions.

The second extension is that of accounting for fluid compressibility effects. Hubbert (1940) shows that extensions of Darcy's law to compressible fluids such as gas are valid provided the density of the fluid is only a function of pressure and the flow is irrotational "Darcy's law in its differential form is the same for a gas as for a liquid, provided that the flow behavior of a gas in small pore spaces, other than expansion, is similar to that of a liquid" (Hubbert, 1956). The two flows (of liquid and gas) for a given potential are not similar. Klinkenberg (1941) has shown that in general the permeability to gas (k_g) based on the assumed validity of Darcy's law for gases is not the same as the permeability to liquid (k_L) and is a function of pressure. This is a result of boundary slip associated with gas and the lower frictional resistances to flow of gas compared to a liquid of the same viscosity and velocity. However, at pressures in excess of 30 atm, k_g and k_L differ by only 1%. This Klinkenberg effect is assumed to be negligible in the WIPP environment and the equations of motion that are developed in Sections 4.2.1.2 and 5.2.2 are assumed to hold for compressible gas as well as the slightly compressible brine.

The third extension of Darcy's law accounts for the presence and flow of multiple immiscible phases. Once steady-state flow is achieved, Darcy's law may be extended to describe the separate flow of each phase (Bear, 1975). This extension introduces the concept of effective permeabilities, relative permeabilities, and capillary pressure.

For each phase, the absolute permeability of (A-1) is replaced by the effective phase permeability and the pressure of (A-1) is replaced by the phase pressure. These effective permeabilities are empirically determined by pressure drop and flow measurements. Numerous experiments verify the validity of this extension and suggest that the effective permeability depends on characteristics of the rock, the wettability characteristics, surface tension, the shape of the interface separating the phases, and on phase saturation. The effective permeabilities do not appear to depend on fluid viscosity or their specific discharges (Bear, 1975; Scheideggar, 1960). Instead of using effective permeabilities it is more convenient to refer to relative permeabilities, which are defined for each phase as the ratio of the effective phase permeability to the absolute or intrinsic permeability of the medium (measured when the medium is saturated with a single fluid).

As stated above, the relative permeabilities are empirical fits of pressure drop and flow data to extensions of Darcy's law. Measurements taken at different degrees of saturation result in differing relative permeabilities. The dependence on saturation results in the sum of the effective permeabilities being less than the absolute permeability at all values of saturation as long as more than one phase is present (Bear, 1975; Dake, 1978; Corey, 1986; Scheideggar, 1960). The typical dependence of relative permeability on saturation is shown in Figure A-1. For each phase its relative permeability increases with that phase's saturation. Below each phase's residual or irreducible saturation (S_{wo} for wetting and S_{nwo} for non-wetting) the relative permeability is zero,

indicating flows due to potential gradients in that phase will not occur. The effective permeability and its saturation dependence is an empirical way of accounting for the interference that one fluid makes on the other as they simultaneously flow through the porous media. Some researchers suggest that there may be a transfer of viscous forces across this interface and that a finite velocity exist at the interface (Russell and Charles, 1959; Yuster, 1953). This would result in effective permeabilities being dependent on the difference in the viscosities or viscosity ratio of the phases. Rose (1960) shows theoretically that this effect is secondary and most experimental data fail to substantiate this dependence (Bear, 1975 p. 462). Therefore the relative permeabilities used here are assumed independent of the viscosity ratio of the brine and gas phases. The relative permeabilities are assumed to depend on saturation according to relationships presented by Brooks and Corey (1964). Volume 3 of this report presents the Brooks and Corey parameters that define the relative permeabilities assumed for WIPP Brine and Gas.

Table A-1. Definitions for Terms Used to Describe Flow Through Porous Media.

permeability	Defined by Darcy's law as a conductivity of 1.0 darcy ($9.87 \times 10^{-13} m^2$) if a pressure difference of 1 atm produces a flow rate of 1 cm^3/sec of a fluid with 1 cp viscosity through a cube having sides 1 cm in length (Dullen, 1979). It is determined under single phase saturated flow conditions and is independent of the fluid used. Also the absolute permeability or specific permeability of porous media. [L^2], [m^2]
effective permeability	Defined for each phase and determined experimentally and defined by extensions of Darcy's law to immiscible multiple phase flow. It is dependent on both fluid and rock properties as well as fluid saturation. Assumed to vary with saturation according to Brooks and Corey relationship Brook and Corey (1964). [L^2], [m^2]
relative permeability	Defined for each phase as the ratio of effective permeability of a phase to the absolute permeability of the rock. [dimensionless]
saturation	Defined for each phase as the ratio of the volume of a phase to the pore volume. The volume of a fluid in a reservoir is then the product of that fluid's saturation, rock porosity, and reservoir volume. [dimensionless]
porosity	Volume fraction of the reservoir that is void (non-rock). The quantity 1.0-porosity is the reservoir's rock volume. [dimensionless]
Irreducible Saturation	Also the residual saturation and is defined for each phase as the saturation corresponding to the formation of a continuous flow path of that phase. Below irreducible saturation that phase will not flow under a potential gradient. [dimensionless]

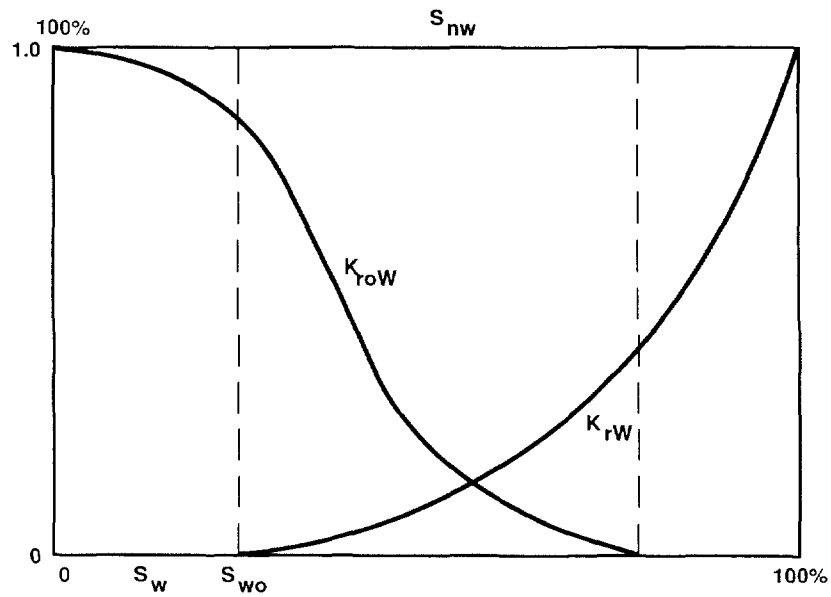

Figure A-1. Typical Relative Permeability Dependence on Saturation

References

Aziz, K., and A. Settari. 1979. *Petroleum Reservoir Simulation.* Applied Science, London.

Bear, J. 1975. *Dynamics of Fluids in Porous Media.* Elsevier Publishing Company, 1975, NY.

Bear, J. 1979. *Hydraulics of Groundwater.* McGraw-Hill, Inc., 1979, NY.

Bear, J., and Y. Bachmat. 1966. *Hydrodynamic Dispersion in Non-uniform Flow Through Porous Media, Taking into Account Density and Viscosity Differences (in Hebrew with English Summary),* Hydraulic Lab., Technion, Haifa, Israel, IASH, P.N. 4/66, 1966.

Bear, J., and Y. Bachmat. 1967. "A Generalized Theory on Hydrodynamic Dispersion in Porous Media," *I.A.S.H. Symp. Artificial Recharge and Management of Aquifers,* Haifa, Israel, IASH, P.N. 72, 7-16 (1967).

Bear, J., D. Zaslowsky, and S. Irmay. 1968. *Physical Principles of Water Percolation and Seepage,* UNESCO, Paris, 1968.

Brook, R. H., and A. T. Corey. 1964. *Hydraulic Properties of Porous Media.* Civil Engineering Department, Colorado State University, Fort Collins. Hydrology Paper No. 3.

Coats, K. H. 1980. "In-Situ Combustion Model." *Soc. Pet. Eng. J.,* Dec. 1980, 533-554.

Collins, R. E. 1961. *Flow of Fluids Through Porous Materials.* Reinhold Publishing Corporation, NY.

Corey, A. T. 1986. *Mechanics of Immiscible Fluids in Porous Media.* Water Resources Publication, Littleton, CO.

Crichlow, H. B. 1977. *Modern Reservoir Engineering - A Simulation Approach.* Prentice - Hall, Inc. 1977 Englewood Cliffs, NJ.

Crookston, H. B., W. E. Culham, and W. H. Chen. 1979. "Numerical Simulation Model for Thermal Recovery Processes." *Soc. Pet. Eng. J.,* Feb, 1979, 37-58.

Dake, L. P. 1978. *Fundamentals of Reservoir Engineering.* Elsevier Scientific Publishing Co., 1978, NY.

deMarsily, G. 1986. *Quantitative Hydrogeology.* Academic Press, Inc., Orlando, Florida, 440 pp.

DeWest, R. J. M. 1965. *Geohydrology.* John Wiley and Sons, New York, NY, 366 pp.

Dullien, F. A. L. 1979. *Porous Media Fluid Transport and Pore Structure.* Academic Press, 1979, NY.

Hiatt, W. N. 1968. *Mathematical Basis of Two-Phase, Incompressible, Vertical Flow Through Porous Media and Its Implications in the Study of Gravity-Drainage-Type Petroleum Reservoirs.*

Hubbert, M. K. 1956. "The Theory of Ground Water Motion." *J. Geol.* 48: 785-944 (1940).

Hubbert, M. K. 1956. "Darcy Law and the Field Equations of the Flow of Underground Fluids." *Trans. Amer. Inst. Min. Metal. Eng.* 207: 222-239 (1956).

Klinkenberg, L. J. 1941. "The Permeability of Porous Media to Liquids and Gases." *Amer. Petrol. Inst. Drilling Prod. Pract.* 200-213 (1941).

Peaceman, D. W. 1977. *Fundamentals of Numerical Reservoir Simulation.* Elsevier Scientific Publishing Company, New York.

Rose, W. 1953. "Fluid Flow in Petroleum Reservoirs III. Effect of Fluid-Fluid Interfacial Boundary Condition," *Ill. Geol. Survey Circ.* 291 (1960).

Rubin, B., and P. K. W. Vinsome. 1980. "The Simulation of the In-Situ Combustion Process in One Dimension Using a Highly Implicit Finite Difference Scheme." *J. Col. Pet. Tech.* (Oct/Dec 1980), 68-76.

Russell, T. W. F. and E. Charles. 1959. "Effect of the Less Viscous Liquid in the Laminar Flow of Two Immiscible Liquids." *Canad. J. Chem. Eng.* 37: 18-24 (1959).

Scheideggar, A. E. 1960. *The Physics of Flow Through Porous Media,* 2nd ed. University of Toronto Press, Toronto, 1960.

Vaughn, P. 1986. *A Numerical Model for Thermal Recovery Processes in Tar Sand: Description and Application.* April 1986, DOE Report #DOE/FE/60177-2219.

Yuster, S. T. 1953 "Theoretical Considerations of Multiphase Flow in Idealized Capillary Systems," *Proc. 3rd World Petrol., The Hague* 2: 437-445 (1953).

B. LHS SAMPLES AND CALCULATED NORMALIZED RELEASES

This appendix contains the 60 sample elements for each of the 45 parameters varied and sampled by LHS and summaries of radionuclide release to the 5-km, accessible environment boundary south of the WIPP for the E1 and E1E2 scenarios with intrusions at 1000, 3000, 5000, 7000, and 9000 yr. The simulations are run assuming a dual porosity model for transport in the Culebra Dolomite Member of the Rustler Formation.

This appendix also contains the summaries of release to the accessible environment from initially drilling into the repository and bringing up cuttings from one average activity of CH waste and one average activity of RH waste. (The CH waste activity is subsequently multiplied by a factor to account for the four CH activity levels. This modified activity along with the probability of actually hitting these various CH activity levels are used when constructing the CCDF.

Cuttings were calculated for the five different intrusion times but there is no difference between the E1, E2 or E1E2 scenarios. The different scenarios are accounted for by the CCDFPERM program. The output tables were created by the CCDFCALC computer code after reading the output databases created by STAFF2D and CUTTINGS and are the input to the CCDFPERM program which calculates the final CCDF.

Table B-1 lists the 45 parameters sampled and the distribution type used.

Table B-1. Numerical ID and Distributions of 45 Sampled Parameters in December 1991 WIPP PA Calculations

Parameter	Range		Distribution Type
Unmodified Waste Form			
1. Initial waste saturation	0	2.76×10^{-1}	Uniform
Gas Generation			
Corrosion			
2. Stoichiometry	0	1	Uniform
3. Relative humid rate	0	5×10^{-1}	Cumulative
4. Inundated rate, mol/m^2/s*	0	1.2×10^{-8}	Cumulative
Microbiological			
5. Relative humid rate	0	2×10^{-1}	Uniform
6. Inundated rate, mol/m^2/s**	0	1.6×10^{-8}	Cumulative
9. Stoichiometry	0	1.67	Uniform
Volume Fractions of IDB Categories			
7. Metal/Glass	2.76×10^{-1}	4.76×10^{-1}	Normal
8. Combustibles	2.84×10^{-1}	4.84×10^{-1}	Normal

* mole/m^2 surface area steel/s

** mole/kg cellulosics/s

Table B-1. Numerical ID and Distributions of 45 Sampled Parameters in December 1991 WIPP PA Calculations (Continued)

Parameter	Range		Distribution Type
18. Relative areas in Eh-pH Space (index)	0	1.0	Uniform
Dissolved Concentrations (Solubility)*			
19. Am3+, Molar	$5x10^{-14}$	1.4	Cumulative
20. Np4+, Molar	$3x10^{-16}$	$2x10^{-5}$	Cumulative
21. Np5+, Molar	$3x10^{-11}$	$1.2x10^{-2}$	Cumulative
22. Pu4+, Molar	2.0×10^{-16}	4×10^{-6}	Cumulative
23. Pu5+, Molar	$2.5x10^{-17}$	$5.5x10^{-4}$	Cumulative
24. Th4+, Molar	$5.5x10^{-16}$	$2.2x10^{-6}$	Cumulative
25. U4+, Molar	$1x10^{-15}$	$5x10^{-2}$	Cumulative
26. U6+, Molar	$1x10^{-7}$	1	Cumulative
Halite within Salado Formation			
10. Permeability (k), m^2	8.6×10^{-22}	5.4×10^{-20}	Data
Anhydrite Layers within Salado Formation			
11. Pore pressure (p), Pa	9.3×10^{6}	1.39×10^{7}	Data
12. Undisturbed, Permeability (k), m^{2**}	6.8×10^{-20}	9.5×10^{-19}	Data
13. Undisturbed Porosity (ϕ)	1×10^{-3}	3×10^{-2}	Cumulative
45. Threshold displacement index (p_t)	0	1	Normal
Castile Formation Brine Reservoir			
14. Initial pressure (p), Pa	1.1×10^{7}	2.1×10^{7}	Cumulative
15. Storativity, bulk (S_b), m^3	2×10^{-2}	2	Lognormal
16. Permeability (k), m^2	1×10^{-14}	1×10^{-11}	Lognormal
17. Diameter, m	2.67×10^{-1}	4.44×10^{-1}	Uniform
Culebra Dolomite Member			
27. Transmissivity field	0	60	Uniform
28. Climate index	0	1.0	Uniform
29. Dispersivity, longitudinal (α_L), m	5×10^{1}	3×10^{2}	Cumulative
30. Fracture porosity (ϕ_f)	1×10^{-4}	1×10^{-2}	Lognormal
Fracture Partition Coefficients, m^3/kg			
31. Americium	0.0	1×10^{3}	Cumulative

* For the following elements – Np, Pu, and Th – only one species was used in each sample. The species were rank correlated at r = 0.99.

** Permeability of the halite and anhydrite were rank correlated with an r = 0.80.

Table B-1. Numerical ID and Distributions of 45 Sampled Parameters in December 1991 WIPP PA Calculations (Concluded)

Parameter	Range		Distribution Type
32. Neptunium	0.0	1×10^{3}	Cumulative
33. Plutonium	0.0	1×10^{3}	Cumulative
34. Thorium	0.0	1×10^{1}	Cumulative
35. Uranium	0.0	1	Cumulative
36. Fracture spacing (2B), m	6×10^{-2}	8	Cumulative
37. Matrix porosity (ϕ_m)	9.6×10^{-2}	2.08×10^{-1}	Spatial
Matrix Partition Coefficients (m^3/kg)			
40. Am	0.0	1×10^{2}	Cumulative
41. Np	0.0	1×10^{2}	Cumulative
42. Pu	0.0	1×10^{2}	Cumulative
43. Th	0.0	1	Cumulative
44. U	0.0	1	Cumulative
Probability Model for Scenarios			
38. Rate constant in Poisson drilling model, $\Lambda(t)$, s-1	0 <	1.04×10^{-11}	Uniform
39. Area of pressurized brine reservoir	2.5×10^{-1}	5.52×10^{-1}	Cumulative

Table B-2 lists the Latin Hypercube sampled (LHS) values for each of the 45 parameters.

Table B-2. Sixty Values Sampled By LHS For 45 Parameters which Were Varied in December 1991 WIPP PA Calculations

Material Parameter RUN NO.	WastRef Brine Sat X(1)	WastRef CorRatFr X(2)	WastRef G RatCor H X(3)	WastRef GRatCorI X(4)	WastRef GRatMicH X(5)	WastRef GRatMicI X(6)
1	0.854	0.315	3.454E-02	6.775E-09	0.122	4.706E-09
2	0.810	0.459	0.436	7.461E-09	0.165	9.441E-10
3	0.611	0.850	0.372	1.128E-10	0.152	2.845E-09
4	0.139	0.254	0.194	4.313E-09	7.819E-02	3.106E-09
5	0.123	0.383	0.359	8.924E-09	0.198	1.265E-08
6	0.945	0.942	8.686E-02	2.106E-09	0.116	3.953E-10
7	0.725	0.653	5.686E-02	9.723E-09	0.138	1.608E-09
8	0.151	0.402	6.637E-02	1.164E-08	0.118	1.147E-09
9	0.469	0.818	7.563E-02	3.244E-09	0.146	1.392E-08
10	0.109	0.536	4.467E-02	1.073E-08	0.168	2.787E-10
11	0.236	0.361	1.606E-02	5.732E-09	8.184E-02	1.166E-08
12	4.723E-02	0.614	9.739E-02	7.308E-10	0.104	1.355E-08
13	0.738	0.478	2.705E-03	1.286E-08	6.507E-02	2.939E-09
14	0.259	0.892	1.952E-02	7.067E-09	8.896E-02	1.091E-08
15	0.923	4.737E-02	9.478E-02	6.221E-10	3.021E-02	1.019E-08

Table B-2. Sixty Values Samples By LHS For 45 Parameters Which Were Varied In December 1991 WIPP PA Calculations (Continued)

Material Parameter RUN NO.	WastRef Brine Sat X(1)	WastRef CorRatFr X(2)	WastRef GRadCorH X(3)	WastRef GRatCorI X(4)	WastRef GRatMicH X(5)	WastRef GRatMicI X(6)
16	0.288	0.212	0.327	1.172E-08	5.353E-02	2.291E-09
17	0.532	0.233	0.475	2.921E-09	4.978E-02	8.301E-10
18	0.331	0.671	8.471E-02	1.264E-08	0.173	5.550E-09
19	0.390	5.652E-02	0.464	9.104E-09	6.868E-02	1.206E-08
20	0.229	0.190	0.495	6.679E-09	1.346E-02	3.723E-09
21	0.960	0.447	0.413	4.429E-09	0.177	1.736E-09
22	0.355	0.523	0.157	7.330E-09	7.233E-02	2.464E-09
23	8.905E-02	0.152	0.232	3.525E-09	5.874E-02	5.234E-09
24	0.537	0.574	0.421	1.194E-08	0.162	2.172E-09
25	0.650	0.905	0.300	1.084E-08	3.453E-02	9.966E-10
26	0.847	1.134E-02	9.080E-03	1.140E-08	9.785E-02	6.680E-09
27	1.635E-02	0.563	8.296E-02	1.600E-09	0.189	3.508E-09
28	0.446	0.732	6.049E-02	9.515E-09	4.091E-03	1.586E-08
29	0.278	0.285	0.271	3.914E-09	5.248E-02	2.067E-09
30	0.817	0.789	0.325	4.136E-09	7.454E-02	2.424E-09
31	0.967	0.685	9.240E-02	1.232E-08	0.148	1.474E-08
32	0.404	0.427	5.519E-03	8.680E-09	9.438E-02	2.646E-09
33	0.787	0.986	0.192	2.488E-09	4.027E-02	1.367E-09
34	5.649E-02	0.933	0.142	5.351E-09	3.841E-02	5.767E-09
35	2.096E-02	0.328	3.873E-02	1.140E-09	2.195E-02	5.228E-10
36	0.773	8.698E-02	6.932E-02	9.337E-09	0.100	6.373E-10
37	0.760	0.170	0.385	6.332E-09	0.193	1.515E-08
38	0.496	0.588	2.427E-02	7.912E-09	9.186E-02	1.554E-10
39	0.454	0.500	0.398	4.872E-09	1.698E-02	6.403E-09
40	0.341	0.134	0.114	2.099E-09	0.142	1.184E-09
41	0.554	0.781	0.249	8.331E-09	6.304E-02	1.435E-09
42	0.697	0.649	1.021E-02	1.834E-09	2.670E-02	1.430E-08
43	0.372	0.125	7.764E-02	5.941E-09	0.130	1.599E-09
44	0.575	0.766	0.127	3.583E-09	0.185	1.906E-09
45	0.679	0.342	0.108	5.081E-09	2.491E-02	1.313E-08
46	0.883	0.383	4.118E-02	2.651E-09	0.110	7.384E-10
47	0.642	0.868	2.058E-02	1.438E-09	0.156	2.737E-09
48	0.707	0.742	0.288	7.857E-09	7.898E-03	1.076E-08
49	0.624	0.486	2.742E-02	5.668E-09	0.195	9.775E-09
50	0.432	0.862	7.281E-02	9.637E-10	0.173	8.372E-09
51	0.906	0.983	0.450	8.089E-09	0.111	7.530E-09
52	0.209	0.816	0.353	1.112E-08	1.258E-02	1.254E-08
53	0.182	0.627	0.217	1.237E-08	0.128	4.370E-09
54	0.190	0.961	4.961E-02	6.227E-09	0.159	7.458E-09
55	0.890	0.104	3.077E-02	2.446E-10	4.374E-02	9.474E-09
56	0.989	0.271	0.274	1.036E-08	8.555E-02	8.150E-09
57	7.286E-02	0.243	0.172	1.020E-08	0.136	8.908E-09
58	0.507	0.701	5.553E-02	9.999E-09	3.208E-03	1.051E-10
59	0.303	3.048E-02	5.130E-02	3.006E-09	0.124	1.937E-09
60	0.586	7.983E-02	0.242	4.754E-09	0.182	3.053E-09

Table B-2. Sixty Values Sampled By LHS For 45 Parameters which Were Varied in December 1991 WIPP PA Calculations (Continued)

RUN NO.	Wast Ref VolMetal X(7)	Wast Ref Vol Wood X(8)	Wast Ref SH2Mic X(9)	Salado Prm_X_U X(10)	MB139 Pressure X(11)	MB139 Prm_X_U X(12)
1	0.358	0.316	0.595	1.027E-19	1.473E+07	1.077E-18
2	0.350	0.301	1.48	3.989E-20	1.267E+07	1.530E-18
3	0.385	0.284	1.11	2.341E-21	8.502E+06	5.455E-20
4	0.334	0.339	1.17	5.593E-21	1.280E+07	1.309E-19
5	0.385	0.376	0.200	3.348E-22	1.277E+07	3.839E-20
6	0.412	0.396	0.785	1.207E-19	8.415E+06	8.435E-19
7	0.339	0.401	0.773	2.347E-20	1.208E+07	1.035E-18
8	0.380	0.340	0.888	1.544E-21	1.308E+07	6.800E-20
9	0.321	0.351	0.856	6.585E-21	1.425E+07	1.170E-18
10	0.345	0.358	0.335	5.878E-21	1.280E+07	6.800E-20
11	0.314	0.388	0.927	1.115E-19	9.027E+06	1.257E-18
12	0.371	0.374	1.47	7.331E-21	1.262E+07	7.853E-20
13	0.361	0.370	1.03	5.402E-21	1.280E+07	6.800E-20
14	0.318	0.395	1.66	1.337E-21	1.396E+07	7.291E-20
15	0.336	0.382	1.33	6.438E-21	9.176E+06	7.900E-20
16	0.352	0.413	7.328E-02	7.433E-20	1.280E+07	1.319E-18
17	0.432	0.378	1.58	1.120E-21	1.445E+07	2.595E-20
18	0.368	0.305	0.331	5.046E-21	1.280E+07	4.760E-19
19	0.392	0.384	0.650	1.416E-20	1.235E+07	6.631E-19
20	0.344	0.404	0.464	5.972E-21	8.738E+06	8.099E-20
21	0.399	0.409	1.23	1.429E-21	1.264E+07	7.665E-20
22	0.404	0.329	0.153	3.508E-20	1.406E+07	1.395E-18
23	0.326	0.414	1.00	5.577E-20	1.417E+07	7.307E-20
24	0.382	0.434	1.50	1.334E-19	1.280E+07	1.659E-18
25	0.424	0.446	1.27	9.770E-20	1.272E+07	1.798E-18
26	0.398	0.360	0.479	7.504E-22	8.542E+06	6.949E-20
27	0.427	0.409	0.817	3.469E-21	1.154E+07	8.143E-20
28	0.378	0.439	1.07	6.086E-22	8.816E+06	4.557E-20
29	0.293	0.387	1.13	4.162E-22	1.186E+07	7.475E-20
30	0.330	0.424	3.803E-02	2.715E-21	1.286E+07	6.800E-20
31	0.390	0.353	1.21	8.079E-21	1.082E+07	8.161E-20
32	0.395	0.399	0.299	1.571E-20	1.012E+07	7.446E-19
33	0.369	0.365	0.133	4.489E-22	1.358E+07	6.623E-20
34	0.365	0.379	2.110E-02	8.179E-21	9.254E+06	7.930E-20
35	0.356	0.334	0.432	4.234E-21	1.336E+07	7.568E-20
36	0.413	0.453	1.28	3.414E-21	1.428E+07	7.031E-20
37	0.388	0.322	0.956	6.083E-21	1.280E+07	7.837E-20
38	0.440	0.406	1.35	7.230E-22	8.220E+06	3.247E-20
39	0.476	0.350	0.383	7.050E-21	9.657E+06	1.946E-19
40	0.423	0.362	1.63	4.941E-21	1.274E+07	7.742E-20
41	0.283	0.443	1.60	4.762E-20	9.389E+06	2.843E-19
42	0.465	0.356	1.43	2.632E-20	1.457E+07	8.934E-19
43	0.365	0.455	0.726	5.509E-21	1.388E+07	5.972E-20
44	0.379	0.428	9.182E-02	5.749E-21	1.269E+07	6.800E-20
45	0.363	0.422	1.15	6.070E-21	1.467E+07	8.059E-20
46	0.407	0.369	0.516	8.084E-20	1.297E+07	1.574E-18
47	0.298	0.346	1.37	1.881E-21	1.257E+07	6.800E-20
48	0.453	0.371	0.614	3.919E-21	1.280E+07	3.026E-20
49	0.374	0.466	0.671	1.258E-21	1.326E+07	6.834E-20
50	0.402	0.484	0.407	9.420E-22	1.280E+07	8.007E-20
51	0.347	0.384	0.572	1.702E-21	1.442E+07	6.800E-20
52	0.393	0.416	0.705	7.265E-21	1.280E+07	5.837E-19
53	0.442	0.398	1.42	2.025E-22	1.376E+07	1.397E-20
54	0.417	0.392	0.995	6.918E-20	1.259E+07	6.800E-20
55	0.373	0.430	0.269	1.929E-21	1.098E+07	6.800E-20

Table B-2. Sixty Values Samples By LHS For 45 Parameters Which Were Varied In December 1991 WIPP PA Calculations (Continued)

RUN NO.	Wast Ref VolMetal X(7)	Wast Ref Vol Wood X(8)	Wast Ref SH2Mil X(9)	Salado Prm_X_U X(10)	MB139 Pressure X(11)	MB139 Prm_X_U X(12)
56	0.341	0.345	0.538	5.744E-22	8.910E+06	1.867E-20
57	0.420	0.366	1.55	4.587E-20	1.029E+07	7.999E-20
58	0.354	0.331	0.891	8.206E-22	1.318E+07	6.800E-20
59	0.407	0.391	0.171	7.766E-21	1.280E+07	4.111E-19
60	0.311	0.419	0.225	5.680E-21	1.348E+07	7.135E-20

RUN NO.	MB139 Pore_U X(13)	Castile_R Pressure X(14)	Castile_R StorBulk X(15)	Borehole Prm_X X(16)	Borehole DiamMod X(17)	Wast Ref RelAEhpH X(18)
1	2.337E-02	1.232E+07	0.118	2.050E-14	0.410	0.276
2	2.329E-02	1.202E+07	0.156	1.047E-12	0.294	0.160
3	2.840E-02	1.426E+07	1.08	1.019E-13	0.377	0.841
4	2.413E-02	1.940E+07	0.465	3.905E-14	0.424	0.666
5	6.626E-03	1.174E+07	5.452E-02	2.271E-13	0.273	0.977
6	3.835E-03	1.486E+07	0.212	4.515E-12	0.361	0.588
7	1.423E-02	1.408E+07	0.143	6.181E-13	0.339	0.389
8	4.976E-03	1.890E+07	0.808	7.856E-13	0.329	0.473
9	2.194E-02	1.147E+07	8.365E-02	1.000E-11	0.333	0.576
10	2.797E-02	1.544E+07	0.191	2.681E-12	0.277	0.870
11	2.062E-03	1.172E+07	0.566	4.298E-14	0.345	0.715
12	1.298E-02	1.654E+07	9.906E-02	1.116E-13	0.307	0.209
13	1.080E-02	1.242E+07	0.138	1.200E-12	0.420	0.381
14	1.831E-02	1.575E+07	0.373	2.276E-12	0.422	0.623
15	7.069E-03	1.503E+07	0.269	1.578E-12	0.328	0.903
16	9.040E-03	1.321E+07	0.541	3.537E-12	0.434	0.789
17	8.390E-03	1.607E+07	0.113	1.462E-12	0.387	0.820
18	1.706E-02	1.157E+07	0.655	5.053E-13	0.405	0.945
19	1.487E-02	1.548E+07	0.411	2.393E-13	0.442	0.284
20	6.341E-03	1.117E+07	0.501	2.491E-13	0.318	9.611E-02
21	2.927E-02	1.271E+07	0.157	4.819E-14	0.390	2.648E-02
22	4.805E-03	1.833E+07	9.589E-02	1.309E-13	0.286	0.329
23	1.893E-02	1.222E+07	0.177	3.888E-13	0.311	0.998
24	8.745E-03	1.362E+07	3.996E-02	1.714E-12	0.427	0.695
25	1.142E-02	1.167E+07	1.81	1.462E-13	0.283	0.648
26	2.559E-02	1.243E+07	0.174	2.628E-13	0.349	0.429
27	5.575E-03	1.154E+07	0.257	2.004E-13	0.398	0.510
28	8.070E-03	1.993E+07	0.122	5.495E-12	0.363	0.526
29	1.360E-02	1.124E+07	0.126	5.953E-13	0.337	0.342
30	2.517E-02	1.762E+07	0.228	4.873E-13	0.380	0.739
31	1.423E-03	1.790E+07	0.295	1.366E-13	0.311	0.403
32	9.893E-03	1.191E+07	3.792E-02	7.621E-14	0.365	0.923
33	7.770E-03	1.851E+07	9.060E-02	7.112E-14	0.369	0.866
34	2.105E-02	1.811E+07	0.326	4.470E-13	0.299	5.813E-02
35	1.131E-03	1.129E+07	0.284	1.162E-13	0.439	0.230
36	1.941E-02	1.141E+07	0.637	2.267E-14	0.270	0.893
37	2.930E-03	1.258E+07	0.370	8.042E-13	0.375	4.848E-02
38	2.650E-02	1.188E+07	0.224	9.055E-14	0.391	0.246
39	1.631E-02	2.033E+07	6.140E-02	1.806E-13	0.415	0.759
40	2.335E-03	1.911E+07	0.134	3.546E-13	0.326	0.810
41	9.117E-03	1.266E+07	2.229E-02	3.225E-14	0.352	0.546
42	1.266E-02	1.227E+07	1.40	9.110E-13	0.305	0.683

Table B-2. Sixty Values Sampled By LHS For 45 Parameters Which Were Varied In December 1991 WIPP PA Calculations (Continued)

RUN NO.	MB139 Pore_U X(13)	Castile_R Pressure X(14)	Castile_R StorBulk X(15)	Borehole Prm_X X(16)	Borehole DiamMod X(17)	Wast Ref RelAEhpH X(18)
43	2.551E-03	1.463E+07	0.973	9.961E-13	0.372	0.134
44	4.061E-03	1.685E+07	0.197	5.514E-13	0.384	0.185
45	1.038E-02	1.686E+07	6.910E-02	1.622E-13	0.268	7.773E-02
46	3.131E-03	1.261E+07	4.850E-02	6.654E-13	0.431	0.610
47	5.274E-03	1.216E+07	7.638E-02	2.959E-13	0.355	0.307
48	2.973E-02	1.122E+07	7.937E-02	2.038E-12	0.320	0.365
49	1.539E-02	2.046E+07	0.315	9.869E-14	0.396	0.255
50	4.433E-03	1.249E+07	0.761	1.770E-13	0.288	0.726
51	5.830E-03	1.101E+07	0.411	4.306E-13	0.417	0.438
52	6.889E-03	1.721E+07	0.105	1.088E-14	0.401	0.780
53	3.539E-03	1.136E+07	6.601E-02	2.975E-13	0.407	0.178
54	2.214E-02	1.185E+07	0.206	6.375E-14	0.315	0.127
55	2.691E-02	1.109E+07	0.169	7.211E-13	0.436	0.461
56	1.662E-03	1.208E+07	0.343	5.933E-14	0.291	0.960
57	1.752E-02	1.338E+07	0.255	3.631E-13	0.342	0.559
58	7.443E-03	1.972E+07	0.438	3.211E-13	0.300	1.443E-02
59	9.428E-03	1.205E+07	2.587E-02	1.289E-12	0.281	0.108
60	2.006E-02	2.088E+07	0.245	2.084E-13	0.356	0.489

RUN NO.	Am^{+3} Solm X(19)	Np^{+4} Sol M X(20)	Np^{+5} Sol M X(21)	Pu^{+4} Sol M X(22)	Pu^{+5} Sol M X(23)	Th^{+4} Sol M X(24)
1	1.080E-10	1.850E-09	1.680E-07	1.909E-09	8.394E-10	9.272E-11
2	0.203	2.844E-09	2.737E-07	4.096E-12	2.675E-13	8.644E-09
3	6.019E-07	3.912E-11	1.812E-08	3.772E-07	5.302E-05	1.736E-06
4	5.557E-04	2.247E-07	3.421E-06	1.518E-12	1.207E-13	6.645E-11
5	3.634E-10	3.763E-09	3.346E-07	1.071E-08	1.656E-08	7.327E-09
6	9.860E-10	5.273E-07	9.456E-06	4.490E-08	1.361E-07	5.318E-09
7	5.988E-11	3.122E-07	5.483E-06	1.185E-06	1.819E-04	1.681E-11
8	2.781E-10	2.321E-09	2.480E-07	3.083E-06	4.131E-04	4.808E-13
9	1.671E-11	5.633E-09	5.552E-07	4.300E-08	1.491E-07	2.787E-13
10	8.132E-07	1.117E-06	4.670E-04	1.524E-08	4.692E-08	2.532E-11
11	2.993E-11	1.024E-05	5.006E-03	1.176E-07	9.552E-06	9.457E-08
12	9.701E-07	1.441E-05	8.102E-03	3.231E-08	1.084E-07	8.285E-16
13	2.183E-10	1.151E-11	3.920E-09	3.652E-10	3.954E-10	4.555E-09
14	8.734E-10	4.735E-11	2.490E-08	2.283E-10	1.333E-10	7.170E-11
15	4.189E-07	2.963E-11	1.570E-08	3.920E-06	5.035E-04	4.317E-11
16	3.680E-07	5.202E-06	3.436E-03	3.186E-07	3.679E-05	6.307E-09
17	3.626E-12	1.274E-06	6.182E-04	1.686E-08	6.375E-08	2.722E-09
18	7.520E-10	1.384E-05	8.770E-03	1.239E-11	3.273E-11	6.262E-07
19	1.798E-10	3.306E-06	2.750E-03	1.449E-10	2.012E-10	3.824E-13
20	3.046E-04	1.716E-07	2.557E-06	8.286E-08	3.996E-06	9.174E-10
21	8.743E-11	7.438E-08	1.383E-06	5.463E-10	5.535E-10	5.955E-11
22	7.906E-10	1.626E-09	1.827E-07	4.900E-08	1.664E-07	2.065E-06
23	1.956E-07	3.346E-08	7.398E-07	1.628E-15	1.981E-16	2.966E-15
24	4.831E-08	3.268E-16	4.467E-11	2.953E-08	8.233E-08	1.470E-07
25	3.420E-11	2.614E-10	4.306E-08	2.426E-12	1.677E-13	8.038E-11
26	0.264	5.686E-07	8.172E-06	7.384E-16	7.319E-17	1.183E-07
27	6.281E-04	1.146E-07	2.131E-06	4.139E-10	4.138E-10	1.345E-06
28	1.896E-10	5.198E-07	8.881E-06	1.036E-13	1.769E-14	3.244E-07
29	9.571E-07	5.595E-09	5.869E-07	1.747E-06	2.312E-04	8.050E-13
30	1.09	4.793E-07	8.085E-06	3.012E-10	3.010E-10	5.456E-08

Table B-2. Sixty Values Samples By LHS For 45 Parameters Which Were Varied In December 1991 WIPP PA Calculations (Continued)

RUN NO.	Am^{+3} SolM X(19)	Np^{+4} Sol M X(20)	Np^{+5} Sol M X(21)	Pu^{+4} Sol M X(22)	Pu^{+5} Sol M X(23)	Th^{+4} Sol M X(24)
31	1.174E-03	3.317E-07	6.160E-06	3.382E-07	4.807E-05	1.400E-15
32	1.811E-05	4.613E-09	4.694E-07	2.079E-08	6.791E-08	3.560E-15
33	8.906E-04	4.398E-09	4.301E-07	4.995E-12	3.209E-13	5.334E-15
34	4.235E-11	1.209E-15	1.473E-10	4.091E-16	5.546E-17	3.534E-11
35	9.258E-10	1.835E-11	7.314E-09	7.517E-09	3.293E-08	3.322E-09
36	7.585E-11	1.508E-07	3.933E-06	4.428E-10	4.665E-10	9.268E-13
37	1.517E-10	2.665E-09	3.169E-07	9.479E-13	4.702E-14	4.353E-15
38	7.496E-07	1.881E-06	1.083E-03	5.445E-08	1.890E-07	9.794E-14
39	4.825E-10	5.145E-09	5.039E-07	5.188E-10	5.098E-10	5.993E-13
40	5.348E-10	1.723E-06	9.840E-04	8.352E-16	1.028E-16	1.782E-07
41	9.668E-04	5.750E-11	2.749E-08	2.695E-12	1.861E-13	7.915E-09
42	1.25	2.348E-15	2.503E-10	5.757E-10	5.648E-10	6.032E-09
43	0.729	2.517E-07	4.545E-06	3.763E-12	2.398E-13	4.818E-10
44	4.592E-10	4.237E-07	7.075E-06	1.277E-15	1.722E-16	2.925E-11
45	3.467E-04	1.931E-05	1.113E-02	1.895E-10	1.724E-10	9.875E-07
46	0.645	6.832E-07	1.195E-04	9.900E-11	8.268E-11	1.599E-13
47	1.384E-11	1.394E-06	7.828E-04	3.232E-10	3.259E-10	6.413E-08
48	6.415E-10	1.538E-06	8.646E-04	9.944E-07	6.953E-05	3.658E-09
49	5.225E-07	9.042E-07	1.942E-04	2.764E-06	3.780E-04	1.073E-08
50	1.268E-10	4.502E-11	2.249E-08	2.637E-08	9.569E-08	4.453E-12
51	1.105E-06	1.030E-06	3.380E-04	2.551E-10	2.792E-10	1.213E-11
52	6.115E-10	3.229E-09	3.990E-07	2.451E-07	2.753E-05	1.594E-07
53	1.160E-06	5.299E-12	2.819E-09	1.850E-07	2.362E-05	4.930E-11
54	1.332E-03	3.842E-07	6.378E-06	3.963E-08	1.299E-07	1.994E-07
55	1.494E-10	2.916E-15	2.994E-10	7.244E-11	5.394E-11	9.515E-11
56	1.168E-07	2.439E-11	1.034E-08	1.827E-15	2.238E-16	8.833E-09
57	6.740E-07	1.756E-15	1.884E-10	5.735E-12	3.906E-13	7.314E-13
58	3.571E-10	7.851E-10	8.756E-08	5.673E-08	1.806E-07	7.562E-11
59	7.249E-10	8.958E-10	1.155E-07	1.599E-07	1.526E-05	9.512E-09
60	3.166E-07	9.088E-16	1.095E-10	2.707E-07	3.460E-05	1.940E-09

RUN NO.	U^{+4} SolM X(25)	U^{+6} SolM X(26)	Culebra FieldIdx X(27)	Culebra ClimtIdx X(28)	Culebra Disp_Ing X(29)	Culebra FPore X(30)
1	5.674E-03	3.843E-02	0.612	4.754E-02	59.3	3.373E-04
2	1.097E-02	6.729E-02	0.842	0.153	72.2	6.051E-03
3	9.926E-07	2.984E-05	0.506	0.846	165.	7.606E-04
4	6.936E-04	6.966E-03	0.597	0.464	282.	2.647E-03
5	8.458E-05	1.690E-03	0.701	0.470	206.	1.304E-03
6	2.561E-03	2.338E-02	0.896	0.222	77.8	1.554E-03
7	4.323E-09	5.469E-07	3.516E-03	0.969	272.	4.447E-03
8	4.543E-03	4.310E-02	0.243	3.045E-02	208.	1.676E-04
9	4.988E-02	0.914	4.062E-02	0.833	61.4	1.048E-03
10	1.221E-02	8.384E-02	0.285	0.125	131.	3.211E-04
11	3.876E-02	0.790	0.820	0.813	238.	1.487E-03
12	6.470E-07	2.179E-05	0.216	5.657E-02	52.8	7.358E-03
13	2.796E-04	3.463E-03	0.186	0.381	50.0	5.535E-04
14	6.245E-04	6.241E-03	0.973	0.789	241.	1.208E-03
15	2.420E-02	0.361	0.344	0.605	232.	4.104E-04
16	8.701E-07	1.851E-05	0.562	0.204	82.8	1.343E-03
17	8.932E-09	9.753E-07	0.173	0.728	118.	9.504E-04
18	1.215E-09	2.477E-07	0.687	0.587	74.5	1.760E-03

Table B-2. Sixty Values Sampled By LHS For 45 Parameters which Were Varied in December 1991 WIPP PA Calculations (Continued)

RUN NO.	U^{+4} SolM X(25)	U^{+6} SolM X(26)	Culebra Field Idx X(27)	Culebra ClimtIdx X(28)	Culebra Disp_lng X(29)	Culebra FPore X(30)
19	1.425E-02	0.173	0.964	0.940	89.4	1.868E-03
20	2.912E-07	8.830E-06	0.374	0.660	54.7	2.624E-04
21	4.443E-05	9.478E-04	0.464	0.716	159.	9.785E-04
22	8.125E-03	5.940E-02	0.311	0.536	213.	1.000E-02
23	4.534E-07	1.426E-05	0.815	0.739	153.	3.304E-03
24	3.771E-07	1.278E-05	0.399	0.233	276.	1.041E-03
25	3.158E-05	5.836E-04	0.662	0.417	90.1	5.374E-04
26	8.859E-05	1.820E-03	0.490	0.755	188.	7.807E-04
27	9.102E-04	9.377E-03	0.223	0.438	81.4	1.057E-04
28	1.477E-03	1.812E-02	8.122E-02	0.674	63.5	2.506E-03
29	4.153E-04	5.334E-03	0.914	0.626	126.	4.657E-04
30	5.708E-05	1.120E-03	2.404E-02	0.334	86.4	1.099E-03
31	6.229E-09	6.672E-07	0.351	0.502	184.	6.819E-04
32	7.956E-09	8.273E-07	0.778	0.868	220.	4.368E-04
33	1.298E-07	6.962E-06	0.628	0.523	57.3	4.906E-04
34	4.829E-05	9.888E-04	0.861	0.485	292.	2.950E-04
35	7.281E-05	1.466E-03	0.166	0.366	265.	2.212E-03
36	7.892E-04	8.364E-03	0.413	0.896	84.6	8.208E-04
37	4.445E-06	1.240E-04	0.325	0.297	97.3	6.090E-04
38	9.433E-04	9.696E-03	9.229E-02	9.709E-03	258.	4.138E-03
39	3.127E-02	0.402	0.281	0.768	113.	2.490E-04
40	7.894E-05	1.529E-03	0.647	0.695	75.4	3.947E-04
41	7.015E-04	7.338E-03	0.528	0.389	61.9	8.872E-04
42	7.791E-07	2.551E-05	0.785	0.327	95.0	2.086E-03
43	2.738E-05	4.406E-04	0.436	0.416	67.9	6.894E-04
44	8.777E-04	8.649E-03	0.872	0.191	99.3	2.870E-03
45	2.079E-05	4.199E-04	0.149	0.146	296.	2.151E-04
46	1.333E-02	9.681E-02	0.728	0.932	167.	8.718E-04
47	3.163E-09	2.668E-07	0.767	0.306	138.	1.604E-04
48	3.208E-04	4.162E-03	0.984	7.205E-02	198.	6.467E-04
49	9.799E-05	1.958E-03	0.945	0.559	68.9	7.244E-04
50	3.567E-04	4.030E-03	0.549	0.167	87.1	1.968E-03
51	3.656E-02	0.600	0.127	0.912	248.	5.944E-04
52	6.680E-05	1.319E-03	0.431	0.106	70.4	1.647E-03
53	4.857E-04	4.822E-03	0.919	0.647	141.	3.767E-03
54	1.385E-04	2.415E-03	0.104	0.985	92.0	1.458E-03
55	1.176E-07	1.638E-06	0.261	9.896E-02	178.	2.335E-03
56	8.334E-03	7.984E-02	0.469	0.278	105.	3.189E-03
57	5.626E-04	6.579E-03	6.127E-02	0.264	79.2	3.790E-04
58	3.794E-05	7.308E-04	0.742	0.959	66.3	1.234E-03
59	1.077E-05	2.459E-04	0.583	0.854	56.2	1.807E-03
60	1.715E-04	2.653E-03	0.675	0.578	93.7	1.138E-03

RUN NO.	Culebra FKd_Am_C X(31)	Culebra FKd_Np_C X(32)	Culebra FKd_Pu_C X(33)	Culebra FKd_Th_C X(34)	Culebra FKd_U_C X(35)	Culebra FrctrSp X(36)
1	39.8	419.	494.	6.560E-02	5.791E-04	7.31
2	247.	690.	690.	2.64	0.992	0.329
3	77.9	9.821E-03	180.	1.240E-02	3.464E-03	0.546
4	1.28	202.	1.97	7.925E-04	1.156E-02	7.12
5	1.141E-02	5.075E-03	728.	0.893	3.841E-03	1.40
6	577.	1.365E-02	69.0	1.704E-02	9.744E-03	5.59
7	647.	201.	825.	1.52	7.360E-03	0.298
8	1.10	991.	0.178	4.030E-02	6.461E-03	0.273

Table B-2. Sixty Values Samples By LHS For 45 Parameters Which Were Varied In December 1991 WIPP PA Calculations (Continued)

RUN NO.	Culebra FKd_Am_C X(31)	Culebra FKd_Np_C X(32)	Culebra FKd_Pu_C X(33)	Culebra FKd_Th_C X(34)	Culebra FKd_U_C X(35)	Culebra FrctrSp X(36)
9	2.49	7.655E-04	541.	4.526E-02	1.095E-02	4.56
10	733.	333.	145.	7.714E-02	1.183E-02	0.356
11	1.06	27.4	910.	8.19	0.392	0.776
12	412.	2.326E-03	306.	3.005E-02	1.300E-02	0.192
13	525.	1.676E-03	4.27	2.122E-02	4.144E-03	0.283
14	7.79	595.	565.	8.80	1.487E-02	3.75
15	477.	6.809E-03	394.	5.028E-02	9.550E-03	0.165
16	0.482	286.	5.18	2.501E-02	0.885	0.115
17	2.06	129.	351.	3.26	0.573	4.86
18	824.	8.876E-02	576.	0.217	9.142E-04	0.248
19	561.	343.	1.43	9.376E-02	2.982E-03	0.215
20	697.	643.	230.	4.925E-02	5.271E-03	6.80
21	0.836	5.578E-03	2.94	2.18	8.966E-03	0.201
22	0.878	558.	1.20	0.426	6.140E-03	0.238
23	1.43	134.	0.480	0.837	2.968E-04	5.37
24	379.	90.0	812.	2.723E-02	1.405E-03	0.393
25	0.626	1.637E-03	0.591	6.779E-02	0.133	6.25
26	193.	4.429E-03	0.370	0.151	0.801	6.18
27	0.295	0.263	7.37	4.03	5.564E-03	8.236E-02
28	2.24	833.	319.	1.623E-02	1.159E-03	0.352
29	346.	64.4	459.	9.065E-02	2.117E-03	2.95
30	16.5	8.359E-03	161.	9.02	1.035E-02	7.82
31	0.424	8.528E-04	3.600E-03	6.79	2.373E-03	4.10
32	856.	507.	262.	8.353E-02	0.643	0.287
33	0.967	625.	943.	9.904E-02	0.307	8.809E-02
34	302.	2.558E-03	890.	3.856E-02	6.744E-03	0.375
35	772.	1.584E-04	7.73	0.956	1.277E-02	3.20
36	5.33	395.	776.	9.255E-03	1.349E-02	0.138
37	121.	733.	974.	6.023E-02	1.426E-02	2.53
38	1.53	1.311E-02	852.	0.530	1.985E-04	1.97
39	6.53	7.243E-03	99.3	0.729	0.204	2.25
40	990.	4.154E-03	431.	0.332	7.072E-04	0.336
41	1.25	1.096E-02	1.79	0.273	5.420E-03	0.141
42	9.23	7.525E-03	657.	0.377	4.273E-03	0.121
43	0.181	1.468E-02	966.	0.520	5.984E-03	5.92
44	507.	3.378E-03	0.733	4.61	7.163E-03	6.751E-02
45	617.	0.923	203.	5.644E-02	8.681E-03	0.254
46	1.39	937.	499.	7.216E-02	1.644E-03	6.62
47	3.02	792.	2.644E-02	5.968E-02	1.055E-02	1.84
48	3.89	0.445	374.	5.80	1.963E-03	1.09
49	715.	6.182E-03	618.	8.906E-02	0.448	4.22
50	924.	860.	4.605E-02	7.509E-02	4.654E-03	7.68
51	956.	0.781	2.55	0.781	2.606E-03	0.103
52	888.	496.	743.	5.77	5.088E-02	1.50
53	218.	1.019E-02	5.78	5.650E-03	0.694	5.10
54	3.36	900.	11.5	3.466E-02	8.154E-03	2.76
55	3.76	736.	2.38	0.637	1.232E-02	0.155
56	332.	451.	632.	8.234E-02	7.691E-03	0.378
57	807.	883.	3.29	9.49	1.406E-02	0.311
58	152.	264.	72.6	7.29	3.160E-03	0.227
59	173.	1.171E-02	9.15	3.82	4.964E-03	3.61
60	436.	0.514	35.8	0.655	1.736E-03	0.176

Table B-2. Sixty Values Samples By LHS For 45 Parameters Which Were Varied In December 1991 WIPP PA Calculations (Continued)

RUN NO.	Culebra Porosity X(37)	Culebra Kd_Am_C X(38)	Culebra Kd_Np_C X(39)	Culebra Kd_Pu_C X(40)	Culebra Kd_Th_C X(41)	Culebra Kd_U_C X(42)
1	0.133	3.609E-02	3.549E-02	0.116	6.603E-02	3.237E-02
2	0.185	0.333	91.2	0.938	7.053E-03	6.583E-04
3	9.854E-02	8.183E-02	4.062E-03	40.0	1.304E-03	6.137E-04
4	0.207	0.998	4.849E-04	92.7	8.686E-03	0.194
5	0.178	0.169	0.121	7.642E-03	8.653E-03	9.397E-04
6	0.163	0.136	9.27	0.694	0.438	2.061E-04
7	0.121	1.356E-02	5.16	2.551E-02	5.029E-03	1.087E-02
8	0.115	0.150	87.3	32.1	0.863	5.635E-04
9	0.122	0.130	5.562E-02	0.381	5.662E-03	1.233E-04
10	0.120	0.347	5.154E-05	4.398E-04	4.605E-03	9.050E-02
11	0.118	53.7	4.957E-02	47.3	1.333E-02	0.462
12	0.138	57.2	1.798E-04	6.307E-02	0.594	0.261
13	0.172	26.7	1.92	0.133	5.899E-03	6.630E-02
14	0.163	9.28	7.942E-04	4.185E-02	0.580	9.994E-02
15	0.127	3.01	5.651E-04	1.633E-03	2.108E-02	3.970E-02
16	0.147	2.285E-02	6.25	7.772E-02	9.823E-03	0.868
17	0.203	77.1	1.082E-03	1.887E-02	0.668	2.298E-04
18	0.179	87.3	1.476E-03	0.186	2.294E-02	1.460E-03
19	9.539E-02	4.874E-02	1.312E-03	3.274E-03	8.440E-02	5.483E-05
20	0.154	39.7	1.195E-03	8.434E-02	6.482E-03	1.077E-03
21	0.101	0.892	69.4	5.077E-03	0.803	0.672
22	0.121	4.91	2.688E-04	0.488	4.851E-03	4.451E-02
23	0.140	2.802E-02	51.1	0.210	7.909E-03	8.371E-04
24	0.106	0.182	1.426E-04	8.96	4.954E-02	9.392E-02
25	0.180	0.105	1.085E-04	0.456	6.317E-02	2.458E-02
26	8.716E-02	0.200	0.107	1.418E-02	4.187E-02	1.278E-03
27	0.138	6.201E-02	3.811E-04	4.911E-02	0.706	4.344E-04
28	0.139	0.142	8.994E-02	61.5	9.644E-03	2.714E-03
29	0.175	9.405E-02	0.184	0.963	3.327E-03	7.931E-02
30	7.623E-02	0.159	7.131E-04	70.4	5.371E-02	5.547E-02
31	0.179	8.15	6.753E-02	0.332	4.306E-03	0.171
32	0.131	6.41	1.410E-02	82.2	0.981	2.157E-05
33	0.120	5.884E-02	0.136	0.531	7.392E-02	0.704
34	0.164	0.393	20.1	6.405E-03	3.292E-02	0.125
35	0.158	9.895E-02	0.195	0.269	0.181	3.412E-02
36	0.123	12.4	1.115E-03	79.1	1.484E-03	5.997E-02
37	0.116	6.892E-02	2.141E-04	16.4	7.680E-02	1.560E-02
38	0.199	0.148	2.704E-02	0.630	3.740E-02	8.225E-04
39	0.211	0.752	28.6	0.767	2.164E-03	4.912E-02
40	0.111	7.509E-02	11.3	0.797	9.168E-03	0.963
41	0.120	0.115	7.210E-02	7.407E-02	9.183E-02	1.056E-03
42	0.126	0.129	3.80	9.461E-02	8.103E-03	4.007E-04
43	0.130	72.3	59.2	0.217	2.844E-03	3.562E-04
44	0.121	0.300	6.381E-04	46.6	7.663E-05	1.614E-04
45	0.166	8.802E-02	0.102	0.166	6.933E-03	4.879E-04
46	0.145	6.56	6.736E-04	1.181E-03	1.844E-03	7.486E-02
47	0.143	0.536	8.125E-02	0.846	4.462E-04	1.173E-03
48	0.119	0.247	9.876E-04	2.15	9.892E-02	0.183
49	0.222	3.250E-03	4.349E-04	0.301	6.014E-03	1.340E-03
50	0.119	0.645	0.709	8.558E-03	0.284	0.163
51	0.204	1.59	8.578E-02	54.6	0.276	0.135
52	0.124	30.7	7.87	2.796E-03	2.634E-03	2.579E-04
53	0.100	0.122	4.651E-02	0.239	3.503E-03	8.507E-02
54	0.178	0.191	0.147	4.400E-03	0.157	0.111
55	0.179	0.271	8.473E-04	3.573E-02	3.700E-03	0.152
56	0.214	3.176E-02	3.086E-04	9.532E-03	0.922	2.324E-02
57	0.179	4.474E-02	2.752E-02	26.0	8.412E-04	7.041E-02

Table B-2. Sixty Values Samples By LHS For 45 Parameters Which Were Varied In December 1991 WIPP PA Calculations (Continued)

RUN NO.	Culebra Porosity X(37)	Culebra Kd_Am_C X(38)	Culebra Kd_Np_C X(39)	Culebra Kd_Pu_C X(40)	Culebra Kd_Th_C X(41)	Culebra Kd_U_C X(42)
58	0.122	9.340E-02	4.317E-06	5.528E-02	7.517E-03	7.079E-04
59	0.180	0.113	1.355E-03	99.9	0.350	0.474
60	0.179	97.2	0.172	0.651	0.471	8.230E-03

RUN NO.	Global Lambda X(43)	Castile_R AreaFrc X(44)	MB139 ThrsPIdx X(45)
1	9.787E-12	0.443	0.215
2	8.358E-12	0.489	0.286
3	6.893E-12	0.416	0.517
4	4.289E-12	0.354	0.747
5	5.988E-12	0.407	0.709
6	5.181E-12	0.257	0.898
7	5.544E-12	0.362	0.163
8	2.465E-12	0.348	0.111
9	9.137E-12	0.368	0.823
10	1.795E-12	0.462	0.611
11	8.574E-13	0.418	0.374
12	9.401E-12	0.361	0.236
13	9.402E-13	0.342	0.589
14	7.739E-12	0.352	0.594
15	6.288E-12	0.483	0.434
16	7.511E-12	0.439	0.813
17	1.287E-12	0.345	0.258
18	2.946E-12	0.429	0.190
19	1.659E-12	0.372	0.488
20	2.857E-12	0.432	0.783
21	5.290E-12	0.470	0.961
22	8.232E-12	0.306	0.642
23	4.004E-12	0.382	0.580
24	7.884E-12	0.423	0.385
25	6.472E-12	0.456	0.308
26	7.221E-12	0.340	0.331
27	7.001E-12	0.336	0.405
28	8.930E-12	0.491	0.506
29	5.471E-12	0.318	8.115E-02
30	1.118E-12	0.385	0.477
31	7.402E-12	0.366	0.525
32	1.017E-11	0.425	0.688
33	3.789E-12	0.410	0.527
34	1.917E-12	0.325	0.418
35	8.128E-12	0.514	0.632
36	4.408E-12	0.392	0.650
37	5.373E-13	0.377	0.537
38	1.481E-12	0.412	0.761
39	3.220E-12	0.464	-1.192E-07
40	9.590E-12	0.331	0.566
41	3.511E-13	0.402	0.297
42	8.838E-14	0.445	0.561
43	1.030E-11	0.358	0.358
44	5.872E-12	0.476	0.271
45	3.828E-12	0.420	0.616
46	2.675E-12	0.450	0.549
47	2.141E-12	0.453	0.703
48	9.991E-12	0.458	0.439

Table B-2. Sixty Values Samples By LHS For 45 Parameters Which Were Varied In December 1991 WIPP PA Calculations (Concluded)

RUN NO.	Global Lambda X(43)	Castile_R Area Frc X(44)	MB139 ThrsPIdx X(45)
49	3.318E-12	0.386	0.413
50	3.483E-12	0.468	0.396
51	4.560E-12	0.333	0.449
52	4.821E-12	0.324	0.728
53	2.393E-12	0.394	0.499
54	8.728E-12	0.435	0.354
55	8.595E-12	0.311	0.339
56	6.666E-12	0.397	0.465
57	6.100E-12	0.374	0.877
58	9.295E-12	0.399	0.678
59	2.908E-13	0.390	0.464
60	4.940E-12	0.441	0.659

Table B-3 lists the ranks of samples.

Table B-3. Ranks of Sixty Values Sampled

Material Parameter RUN NO.	WastRef Brine Sat X(1)	WastRef CorRatFr X(2)	WastRef GRatCorH X(3)	WastRef GRatCorI X(4)	WastRef GRatMicH X(5)	WastRef G Rat Mic I X(6)	Wast Ref VolMetal X(7)	Wast Ref VolWood X(8)
1	52.	19.	11.	33.	37.	34.	21.	4.
2	49.	28.	56.	36.	50.	9.	17.	2.
3	37.	51.	51.	1.	46.	27.	36.	1.
4	9.	16.	38.	21.	24.	30.	10.	9.
5	8.	23.	50.	42.	60.	53.	35.	26.
6	57.	57.	27.	11.	35.	4.	48.	37.
7	44.	40.	18.	46.	42.	16.	12.	40.
8	10.	25.	20.	54.	36.	11.	33.	10.
9	29.	50.	23.	16.	44.	56.	7.	14.
10	7.	33.	14.	50.	51.	3.	15.	17.
11	15.	22.	5.	28.	25.	50.	5.	33.
12	3.	37.	30.	4.	32.	55.	28.	25.
13	45.	29.	1.	60.	20.	28.	22.	23.
14	16.	54.	6.	34.	27.	49.	6.	36.
15	56.	3.	29.	3.	10.	47.	11.	29.
16	18.	13.	48.	55.	17.	22.	18.	45.
17	32.	14.	59.	14.	15.	8.	55.	27.
18	20.	41.	26.	59.	52.	36.	26.	3.
19	24.	4.	58.	43.	21.	51.	39.	30.
20	14.	12.	60.	32.	5.	32.	14.	41.
21	58.	27.	54.	22.	54.	17.	43.	44.
22	22.	32.	35.	35.	22.	24.	45.	6.
23	6.	10.	40.	17.	18.	35.	8.	46.
24	33.	35.	55.	56.	49.	21.	34.	53.
25	40.	55.	46.	51.	11.	10.	53.	56.
26	51.	1.	3.	53.	30.	39.	42.	18.
27	1.	34.	25.	8.	57.	31.	54.	43.
28	27.	44.	19.	45.	2.	60.	31.	54.
29	17.	18.	43.	19.	16.	20.	2.	32.
30	50.	48.	47.	20.	23.	23.	9.	50.
31	59.	42.	28.	57.	45.	58.	38.	15.
32	25.	26.	2.	41.	29.	25.	41.	39.

Table B-3. Ranks of Sixty Values Sampled (Continued)

Material Parameter RUN NO.	WastRef Brine Sat X(1)	WastRef CorRatFr X(2)	WastRef GRatCorH X(3)	WastRef GRatCorI X(4)	WastRef GRatMicH X(5)	WastRef GRatMicI X(6)	Wast Ref VolMetal X(7)	Wast Ref VolWood X(8)
33	48.	60.	37.	12.	13.	13.	27.	20.
34	4.	56.	34.	26.	12.	37.	25.	28.
35	2.	20.	12.	6.	7.	5.	20.	8.
36	47.	6.	21.	44.	31.	6.	49.	57.
37	46.	11.	52.	31.	58.	59.	37.	5.
38	30.	36.	8.	38.	28.	2.	56.	42.
39	28.	31.	53.	24.	6.	38.	60.	13.
40	21.	9.	32.	10.	43.	12.	52.	19.
41	34.	47.	42.	40.	19.	14.	1.	55.
42	42.	39.	4.	9.	9.	57.	59.	16.
43	23.	8.	24.	29.	40.	15.	24.	58.
44	35.	46.	33.	18.	56.	18.	32.	51.
45	41.	21.	31.	25.	8.	54.	23.	49.
46	53.	24.	13.	13.	33.	7.	46.	22.
47	39.	53.	7.	7.	47.	26.	3.	12.
48	43.	45.	45.	37.	3.	48.	58.	24.
49	38.	30.	9.	27.	59.	46.	30.	59.
50	26.	52.	22.	5.	53.	43.	44.	60.
51	55.	59.	57.	39.	34.	41.	16.	31.
52	13.	49.	49.	52.	4.	52.	40.	47.
53	11.	38.	39.	58.	39.	33.	57.	38.
54	12.	58.	15.	30.	48.	40.	50.	35.
55	54.	7.	10.	2.	14.	45.	29.	52.
56	60.	17.	44.	49.	26.	42.	13.	11.
57	5.	15.	36.	48.	41.	44.	51.	21.
58	31.	43.	17.	47.	1.	1.	19.	7.
59	19.	2.	16.	15.	38.	19.	47.	34.
60	36.	5.	41.	23.	55.	29.	4.	48.

RUN NO.	Wast Ref SH2Mil X(9)	Salado Prm_X_U X(10)	MB139 Pressure X(11)	MB139 Prm_X_U X(12)	MB139 Pore_U X(13)	Castile_R Pressure X(14)	Castile_R StorBulk X(15)	Borehole Prm_X X(16)
1	22.	57.	60.	52.	51.	24.	18.	2.
2	54.	49.	25.	57.	50.	18.	24.	48.
3	40.	19.	3.	8.	58.	36.	58.	14.
4	43.	29.	36.	41.	52.	55.	49.	5.
5	8.	2.	29.	6.	19.	14.	6.	25.
6	29.	59.	2.	49.	10.	38.	32.	58.
7	28.	46.	19.	51.	37.	35.	23.	41.
8	32.	15.	43.	16.	14.	53.	56.	44.
9	31.	37.	54.	53.	48.	9.	12.	60.
10	13.	32.	36.	16.	57.	40.	29.	56.
11	34.	58.	8.	54.	4.	13.	52.	6.
12	53.	40.	23.	32.	35.	44.	15.	15.
13	38.	27.	36.	16.	32.	25.	22.	49.
14	60.	13.	51.	25.	43.	42.	45.	55.
15	48.	36.	9.	33.	21.	39.	38.	52.
16	3.	54.	36.	55.	27.	32.	51.	57.
17	57.	11.	57.	3.	25.	43.	17.	51.
18	12.	26.	36.	45.	41.	11.	54.	38.
19	24.	44.	20.	47.	38.	41.	47.	26.
20	17.	33.	5.	38.	18.	3.	50.	27.
21	45.	14.	24.	29.	59.	31.	25.	7.
22	6.	48.	52.	56.	13.	51.	14.	17.

Table B-3. Ranks of Sixty Values Sampled (Continued)

RUN NO.	Wast Ref SH2Mil X(9)	Salado Prm_X_U X(10)	MB139 Pressure X(11)	MB139 Prm_X_U X(12)	MB139 Pore_U X(13)	Castile_R Pressure X(14)	Castile_R StorBulk X(15)	Borehole Prm_X X(16)
23	37.	52.	53.	26.	44.	22.	28.	34.
24	55.	60.	36.	59.	26.	34.	4.	53.
25	46.	56.	27.	60.	33.	12.	60.	19.
26	18.	8.	4.	22.	54.	26.	27.	28.
27	30.	22.	17.	39.	16.	10.	37.	23.
28	39.	6.	6.	7.	24.	57.	19.	59.
29	41.	3.	18.	27.	36.	5.	20.	40.
30	2.	20.	41.	16.	53.	48.	34.	37.
31	44.	42.	15.	40.	2.	49.	40.	18.
32	11.	45.	13.	48.	30.	17.	3.	11.
33	5.	4.	48.	10.	23.	52.	13.	10.
34	1.	43.	10.	34.	47.	50.	42.	36.
35	16.	24.	46.	28.	1.	6.	39.	16.
36	47.	21.	55.	23.	45.	8.	53.	3.
37	35.	35.	36.	31.	7.	28.	44.	45.
38	49.	7.	1.	5.	55.	16.	33.	12.
39	14.	38.	12.	42.	40.	58.	7.	22.
40	59.	25.	28.	30.	5.	54.	21.	32.
41	58.	51.	11.	43.	28.	30.	1.	4.
42	52.	47.	58.	50.	34.	23.	59.	46.
43	27.	28.	50.	9.	6.	37.	57.	47.
44	4.	31.	26.	16.	11.	45.	30.	39.
45	42.	34.	59.	37.	31.	46.	9.	20.
46	19.	55.	42.	58.	8.	29.	5.	42.
47	50.	17.	21.	16.	15.	21.	10.	29.
48	23.	23.	36.	4.	60.	4.	11.	54.
49	25.	12.	45.	21.	39.	59.	41.	13.
50	15.	10.	36.	36.	12.	27.	55.	21.
51	21.	16.	56.	16.	17.	1.	46.	35.
52	26.	39.	30.	46.	20.	47.	16.	1.
53	51.	1.	49.	1.	9.	7.	8.	30.
54	36.	53.	22.	16.	49.	15.	31.	9.
55	10.	18.	16.	16.	56.	2.	26.	43.
56	20.	5.	7.	2.	3.	20.	43.	8.
57	56.	50.	14.	35.	42.	33.	36.	33.
58	33.	9.	44.	16.	22.	56.	48.	31.
59	7.	41.	36.	44.	29.	19.	2.	50.
60	9.	30.	47.	24.	46.	60.	35.	24.

RUN NO.	Borehole DiamMod X(17)	Wast Ref RelAEhpH X(18)	Am^{+3} Sol M X(19)	Np^{+4} Sol M X(20)	Np^{+5} Sol M X(21)	Pu^{+4} Sol M X(22)	Pu^{+5} Sol M X(23)	Th^{+4} Sol M X(24)
1	49.	17.	10.	20.	19.	31.	31.	29.
2	10.	10.	55.	23.	22.	13.	13.	43.
3	38.	51.	38.	12.	12.	54.	54.	59.
4	54.	40.	49.	36.	35.	9.	9.	25.
5	3.	59.	19.	25.	24.	33.	32.	41.
6	32.	36.	30.	44.	45.	42.	41.	38.
7	25.	24.	7.	38.	38.	56.	56.	18.
8	22.	29.	17.	21.	21.	59.	59.	11.
9	23.	35.	3.	30.	29.	41.	42.	9.
10	4.	53.	41.	49.	49.	34.	34.	19.
11	27.	43.	4.	57.	57.	47.	47.	49.
12	14.	13.	43.	59.	58.	39.	39.	1.

Table B-3. Ranks of Sixty Values Sampled (Continued)

RUN NO.	Borehole DiamMod X(17)	Wast Ref RelAEhpH X(18)	Amt^{+3} Sol M X(19)	Np^{+4} Sol M X(20)	Np^{+5} Sol M X(21)	Pu^{+4} Sol M X(22)	Pu^{+5} Sol M X(23)	Th^{+4} Sol M X(24)
13	52.	23.	16.	8.	8.	25.	25.	37.
14	53.	38.	28.	14.	14.	21.	19.	26.
15	21.	55.	36.	11.	11.	60.	60.	22.
16	57.	48.	35.	56.	56.	52.	52.	40.
17	41.	50.	1.	50.	50.	35.	35.	34.
18	47.	57.	26.	58.	59.	16.	16.	56.
19	60.	18.	14.	55.	55.	19.	21.	10.
20	18.	6.	47.	35.	34.	46.	46.	32.
21	42.	2.	9.	32.	32.	29.	29.	24.
22	7.	20.	27.	19.	20.	43.	43.	60.
23	16.	60.	33.	31.	31.	5.	5.	3.
24	55.	42.	31.	1.	1.	38.	37.	51.
25	6.	39.	5.	16.	16.	10.	10.	28.
26	28.	26.	56.	45.	43.	2.	2.	50.
27	45.	31.	50.	33.	33.	26.	26.	58.
28	33.	32.	15.	43.	44.	7.	7.	55.
29	24.	21.	42.	29.	30.	57.	57.	14.
30	39.	45.	59.	42.	42.	23.	23.	47.
31	15.	25.	53.	39.	39.	53.	53.	2.
32	34.	56.	46.	27.	27.	36.	36.	4.
33	35.	52.	51.	26.	26.	14.	14.	6.
34	11.	4.	6.	3.	3.	1.	1.	21.
35	59.	14.	29.	9.	9.	32.	33.	35.
36	2.	54.	8.	34.	36.	27.	27.	15.
37	37.	3.	13.	22.	23.	8.	8.	5.
38	43.	15.	40.	54.	54.	44.	45.	7.
39	50.	46.	21.	28.	28.	28.	28.	12.
40	20.	49.	22.	53.	53.	3.	3.	53.
41	29.	33.	52.	15.	15.	11.	11.	42.
42	13.	41.	60.	5.	5.	30.	30.	39.
43	36.	9.	58.	37.	37.	12.	12.	31.
44	40.	12.	20.	41.	41.	4.	4.	20.
45	1.	5.	48.	60.	60.	20.	20.	57.
46	56.	37.	57.	46.	46.	18.	18.	8.
47	30.	19.	2.	51.	51.	24.	24.	48.
48	19.	22.	24.	52.	52.	55.	55.	36.
49	44.	16.	37.	47.	47.	58.	58.	46.
50	8.	44.	11.	13.	13.	37.	38.	16.
51	51.	27.	44.	48.	48.	22.	22.	17.
52	46.	47.	23.	24.	25.	50.	50.	52.
53	48.	11.	45.	7.	7.	49.	49.	23.
54	17.	8.	54.	40.	40.	40.	40.	54.
55	58.	28.	12.	6.	6.	17.	17.	30.
56	9.	58.	32.	10.	10.	6.	6.	44.
57	26.	34.	39.	4.	4.	15.	15.	13.
58	12.	1.	18.	17.	17.	45.	44.	27.
59	5.	7.	25.	18.	18.	48.	48.	45.
60	31.	30.	34.	2.	2.	51.	51.	33.

Table B-3. Ranks of Sixty Values Sampled (Continued)

RUN NO.	U^{+4} Sol M X(25)	U^{+6} Sol M X(26)	Culebra Field Idx X(27)	Culebra Climt Idx X(28)	Culebra Disp_lng X(29)	Culebra FPore X(30)	Culebra FKd_Am_C X(31)	Culebra FKd_Np_C X(32)
1	49.	48.	37.	3.	6.	9.	29.	43.
2	52.	51.	51.	10.	14.	58.	36.	51.
3	15.	15.	31.	51.	40.	24.	30.	18.
4	40.	40.	36.	28.	58.	51.	13.	37.
5	28.	28.	43.	29.	46.	37.	1.	11.
6	47.	47.	54.	14.	17.	41.	47.	23.
7	3.	3.	1.	59.	56.	57.	49.	36.
8	48.	49.	15.	2.	47.	3.	11.	60.
9	60.	60.	3.	50.	7.	32.	19.	2.
10	53.	53.	18.	8.	35.	8.	52.	40.
11	59.	59.	50.	49.	51.	40.	10.	31.
12	12.	13.	13.	4.	2.	59.	41.	6.
13	33.	33.	12.	23.	1.	17.	45.	5.
14	39.	38.	59.	48.	52.	35.	26.	48.
15	56.	56.	21.	37.	50.	12.	43.	14.
16	14.	12.	34.	13.	20.	38.	5.	39.
17	6.	6.	11.	44.	33.	29.	17.	34.
18	1.	1.	42.	36.	15.	43.	55.	25.
19	55.	55.	58.	57.	24.	45.	46.	41.
20	9.	9.	23.	40.	3.	6.	50.	50.
21	22.	22.	28.	43.	39.	30.	7.	12.
22	50.	50.	19.	33.	48.	60.	8.	47.
23	11.	11.	49.	45.	38.	54.	15.	35.
24	10.	10.	24.	15.	57.	31.	40.	33.
25	20.	20.	40.	26.	25.	16.	6.	4.
26	29.	29.	30.	46.	44.	25.	34.	10.
27	44.	44.	14.	27.	19.	1.	3.	26.
28	46.	46.	5.	41.	9.	50.	18.	55.
29	36.	37.	55.	38.	34.	14.	39.	32.
30	24.	24.	2.	21.	22.	33.	28.	17.
31	4.	4.	22.	31.	43.	21.	4.	3.
32	5.	5.	47.	53.	49.	13.	56.	46.
33	8.	8.	38.	32.	5.	15.	9.	49.
34	23.	23.	52.	30.	59.	7.	37.	7.
35	26.	26.	10.	22.	55.	48.	53.	1.
36	42.	42.	25.	54.	21.	26.	24.	42.
37	16.	16.	20.	18.	29.	19.	31.	52.
38	45.	45.	6.	1.	54.	56.	16.	22.
39	57.	57.	17.	47.	32.	5.	25.	15.
40	27.	27.	39.	42.	16.	11.	60.	9.
41	41.	41.	32.	24.	8.	28.	12.	20.
42	13.	14.	48.	20.	28.	47.	27.	16.
43	19.	19.	27.	25.	11.	22.	2.	24.
44	43.	43.	53.	12.	30.	52.	44.	8.
45	18.	18.	9.	9.	60.	4.	48.	30.
46	54.	54.	44.	56.	41.	27.	14.	59.
47	2.	2.	46.	19.	36.	2.	20.	54.
48	34.	35.	60.	5.	45.	20.	23.	27.
49	30.	30.	57.	34.	12.	23.	51.	13.
50	35.	34.	33.	11.	23.	46.	58.	56.
51	58.	58.	8.	55.	53.	18.	59.	29.
52	25.	25.	26.	7.	13.	42.	57.	45.
53	37.	36.	56.	39.	37.	55.	35.	19.
54	31.	31.	7.	60.	26.	39.	21.	58.
55	7.	7.	16.	6.	42.	49.	22.	53.
56	51.	52.	29.	17.	31.	53.	38.	44.

Table B-3. Ranks of Sixty Values Sampled (Continued)

RUN NO.	U^{+4} Sol M X(25)	U^{+6} Sol M X(26)	Culebra Field Idx X(27)	Culebra Climt Idx X(28)	Culebra Disp_lng X(29)	Culebra FPore X(30)	Culebra FKd_Am_C X(31)	Culebra FKd_Np_C X(32)
57	38.	39.	4.	16.	18.	10.	54.	57.
58	21.	21.	45.	58.	10.	36.	32.	38.
59	17.	17.	35.	52.	4.	44.	33.	21.
60	32.	32.	41.	35.	27.	34.	42.	28.

RANKS OF LATIN HYPERCUBE SAMPLE INPUT VECTORS

RUN NO.	Culebra FKd_Pu_C X(33)	Culebra FKd_Th_C X(34)	Culebra FKd_U_C X(35)	Culebra FrctrSp X(36)	Culebra Porosity X(37)	Culebra Kd_Am_C X(38)	Culebra Kd_Np_C X(39)	Culebra Kd_Pu_C X(40)
1	41.	20.	3.	58.	28.	6.	29.	24.
2	49.	48.	60.	24.	53.	36.	60.	44.
3	30.	4.	16.	31.	4.	13.	25.	51.
4	12.	1.	40.	57.	57.	43.	11.	59.
5	50.	44.	17.	34.	45.	29.	40.	9.
6	25.	6.	36.	51.	39.	24.	52.	40.
7	54.	46.	30.	22.	18.	2.	49.	14.
8	4.	13.	27.	19.	9.	27.	59.	50.
9	43.	14.	39.	47.	20.	23.	32.	34.
10	28.	24.	41.	27.	15.	37.	2.	1.
11	57.	57.	53.	32.	11.	55.	31.	53.
12	34.	10.	44.	12.	29.	56.	5.	19.
13	17.	7.	18.	20.	42.	52.	47.	25.
14	44.	58.	48.	44.	38.	50.	16.	16.
15	38.	16.	35.	10.	25.	45.	12.	3.
16	18.	8.	59.	5.	35.	3.	50.	21.
17	36.	49.	55.	48.	55.	58.	19.	13.
18	45.	32.	5.	17.	48.	59.	24.	27.
19	10.	29.	14.	14.	3.	8.	22.	5.
20	32.	15.	22.	56.	36.	54.	21.	22.
21	15.	47.	34.	13.	6.	42.	58.	7.
22	9.	36.	26.	16.	17.	46.	7.	36.
23	6.	43.	2.	50.	32.	4.	56.	28.
24	53.	9.	7.	30.	7.	30.	4.	47.
25	7.	21.	50.	54.	52.	18.	3.	35.
26	5.	31.	58.	53.	2.	32.	39.	12.
27	20.	51.	24.	2.	30.	10.	9.	17.
28	35.	5.	6.	26.	31.	25.	37.	55.
29	40.	28.	11.	41.	43.	16.	44.	45.
30	29.	59.	37.	60.	1.	28.	15.	56.
31	1.	55.	12.	45.	48.	49.	33.	33.
32	33.	26.	56.	21.	27.	47.	26.	58.
33	58.	30.	52.	3.	14.	9.	41.	37.
34	56.	12.	28.	28.	40.	38.	54.	8.
35	21.	45.	43.	42.	37.	17.	45.	31.
36	52.	3.	45.	7.	22.	51.	20.	57.
37	60.	19.	47.	39.	10.	11.	6.	48.
38	55.	38.	1.	37.	54.	26.	27.	38.
39	27.	41.	51.	38.	58.	41.	55.	41.
40	39.	34.	4.	25.	8.	12.	53.	42.
41	11.	33.	23.	8.	16.	20.	34.	20.
42	48.	35.	19.	6.	24.	22.	48.	23.
43	59.	37.	25.	52.	26.	57.	57.	29.
44	8.	52.	29.	1.	19.	35.	13.	52.
45	31.	17.	33.	18.	41.	14.	38.	26.
46	42.	22.	8.	55.	34.	48.	14.	2.

Table B-3. Ranks of Sixty Values Sampled (Continued)

RUN NO.	Culebra FKd_Pu_C X(33)	Culebra FKd_Th_C X(34)	Culebra FKd_U_C X(35)	Culebra FrctrSp X(36)	Culebra Porosity X(37)	Culebra Kd_Am_C X(38)	Culebra Kd_Np_C X(39)	Culebra Kd_Pu_C X(40)
47	2.	18.	38.	36.	33.	39.	35.	43.
48	37.	54.	10.	33.	12.	33.	18.	46.
49	46.	27.	54.	46.	60.	1.	10.	32.
50	3.	23.	20.	59.	13.	40.	46.	10.
51	14.	42.	13.	4.	56.	44.	36.	54.
52	51.	53.	49.	35.	23.	53.	51.	4.
53	19.	2.	57.	49.	5.	21.	30.	30.
54	23.	11.	32.	40.	44.	31.	42.	6.
55	13.	39.	42.	9.	46.	34.	17.	15.
56	47.	25.	31.	29.	59.	5.	8.	11.
57	16.	60.	46.	23.	49.	7.	28.	49.
58	26.	56.	15.	15.	21.	15.	1.	18.
59	22.	50.	21.	43.	51.	19.	23.	60.
60	24.	40.	9.	11.	50.	60.	43.	39.

RUN NO.	Culebra Kd_Th_C X(41)	Culebra Kd_U_C X(42)	Global Lambda X(43)	Castile_R AreaFrc X(44)	MB139 ThrsPIdx X(45)
1	40.	31.	57.	46.	6.
2	22.	14.	49.	58.	10.
3	4.	13.	40.	36.	32.
4	27.	53.	25.	15.	53.
5	26.	18.	35.	33.	51.
6	51.	5.	30.	1.	59.
7	16.	27.	33.	18.	4.
8	58.	12.	15.	13.	3.
9	17.	3.	53.	20.	57.
10	14.	43.	11.	52.	42.
11	31.	55.	5.	37.	17.
12	54.	54.	55.	17.	7.
13	18.	38.	6.	11.	40.
14	53.	45.	45.	14.	41.
15	32.	33.	37.	57.	23.
16	30.	59.	44.	44.	56.
17	55.	6.	8.	12.	8.
18	33.	24.	18.	41.	5.
19	43.	2.	10.	21.	29.
20	20.	20.	17.	42.	55.
21	57.	57.	31.	55.	60.
22	15.	34.	48.	2.	45.
23	24.	17.	24.	24.	39.
24	37.	44.	46.	39.	18.
25	39.	30.	38.	50.	12.
26	36.	22.	42.	10.	13.
27	56.	10.	41.	9.	20.
28	29.	25.	52.	59.	31.
29	10.	41.	32.	4.	2.
30	38.	36.	7.	25.	28.
31	13.	51.	43.	19.	33.
32	60.	1.	59.	40.	49.
33	41.	58.	22.	34.	34.
34	34.	47.	12.	6.	22.
35	47.	32.	47.	60.	44.
36	5.	37.	26.	28.	46.

Table B-3. Ranks of Sixty Values Sampled (Concluded)

RUN NO.	Culebra Kd_Th_C X(41)	Culebra Kd_U_C X(42)	Global Lambda X(43)	Castile_R Area Frc X(44)	MB139 ThrsPIdx X(45)
37	42.	28.	4.	23.	35.
38	35.	16.	9.	35.	54.
39	7.	35.	19.	53.	1.
40	28.	60.	56.	7.	38.
41	44.	19.	3.	32.	11.
42	25.	9.	1.	47.	37.
43	9.	8.	60.	16.	16.
44	1.	4.	34.	56.	9.
45	21.	11.	23.	38.	43.
46	6.	40.	16.	48.	36.
47	2.	21.	13.	49.	50.
48	45.	52.	58.	51.	24.
49	19.	23.	20.	26.	21.
50	49.	50.	21.	54.	19.
51	48.	48.	27.	8.	25.
52	8.	7.	28.	5.	52.
53	11.	42.	14.	29.	30.
54	46.	46.	51.	43.	15.
55	12.	49.	50.	3.	14.
56	59.	29.	39.	30.	27.
57	3.	39.	36.	22.	58.
58	23.	15.	54.	31.	48.
59	50.	56.	2.	27.	26.

Table B-4 lists the total and percentage release for the 3 radionuclides contributing the most for each vector showing integrated discharge to the accessible environment for the E2 scenario assuming the dual porosity conceptual model for contaminant transport in the Culebra Dolomite Member. Values are normalized by the EPA factor for each radionuclide. Vectors are ordered from most to least release. Vectors which have no release are omitted.

Table B-4. Vectors with Integrated Discharge through the Culebra Dolomite Member to the Accessible Environment for E2 Scenario and Assuming a Dual Porosity Conceptual Model.

Comp. Scen ID	Vector	Total Integrated Discharge	Top 3 Radionuclides Contribution to Integrated Discharge								
(Time of Intrusion, 1000 years)											
00	9	7.4111E-03	U234	7.0062E-03	95%	U233	3.6317E-04	5%	TH230	4.1754E-0	51%
	46	9.9224E-06	TH230	9.9224E-06	100%	NP237	1.5441E-29	0%			
	23	1.0705E-06	U234	9.4263E-07	88%	U233	1.1494E-07	11%	TH230	1.2899E-0	81%
	6	4.8043E-07	U234	3.8823E-07	81%	U233	9.2155E-08	19%	TH230	4.6176E-1	10%
	25	3.8288E-07	NP237	3.8286E-07	100%	U233	2.3849E-11	0%			
	19	1.0095E-08	U234	9.7562E-09	97%	U233	3.3807E-10	3%	TH230	1.2177E-1	20%
	32	2.2144E-09	U234	2.1328E-09	96%	U233	8.1490E-11	4%	TH230	7.6370E-1	40%
	59	2.1210E-14	NP237	2.1210E-14	100%	U233	3.2312E-19	0%			
	44	2.6502E-17	U234	2.5213E-17	95%	U233	8.7023E-19	3%	TH230	4.1842E-1	92%
	42	9.1316E-22	U234	8.7683E-22	96%	U233	3.0992E-23	3%	TH230	5.3350E-2	41%
	7	1.7848E-24	TH230	1.7848E-24	100%	U233	8.1346E-30	0%			
(Time of Intrusion, 3000 years)											
01	9	3.5231E-03	U234	3.3285E-03	94%	U233	1.7981E-04	5%	TH230	1.4770E-0	50%
	46	2.5066E-06	TH230	2.5066E-06	100%	NP237	1.7962E-29	0%			
	23	2.7330E-07	U234	2.4171E-07	88%	U233	2.8615E-08	10%	TH230	2.9758E-0	91%
	25	1.0827E-07	NP237	1.0827E-07	100%	U233	4.6077E-12	0%			
	6	6.3414E-08	U234	5.0573E-08	80%	U233	1.2837E-08	20%	TH230	4.7593E-1	20%
	19	8.0444E-10	U234	7.7627E-10	96%	U233	2.8085E-11	3%	TH230	8.1208E-1	40%
	32	4.6991E-10	U234	4.5277E-10	96%	U233	1.7118E-11	4%	TH230	.6213E-1	40%
	59	5.4216E-15	NP237	5.4215E-15	100%	U233	7.4345E-20	0%			
	42	1.5283E-22	U234	1.4662E-22	96%	U233	5.3403E-24	3%	TH230	8.7202E-2	51%
	7	2.5804E-25	TH230	2.5804E-25	100%	U233	8.4656E-31	0%			
(Time of Intrusion, 5000 years)											
02	9	1.7559E-03	U234	1.6583E-03	94%	U233	9.2364E-05	5%	TH230	5.2346E-06	0%
	46	3.6100E-07	TH230	3.6100E-07	100%	NP2371	.2852E-29	0%			
	23	3.7514E-08	U234	3.3300E-08	89%	U2333.	9436E-09	11%	TH230	2.6985E-10	1%
	25	3.3973E-08	NP237	3.3972E-08	100%	U2331.	0815E-12	0%			
	6	4.9214E-09	U234	3.8830E-09	79%	U2331.	0382E-09	21%	TH230	2.4932E-13	0%
	19	3.5557E-11	U234	3.4292E-11	96%	U2331.	2618E-12	4%	TH230	3.5873E-15	0%
	59	3.3202E-16	NP237	3.3201E-16	100%	U2334	.5529E-21	0%			
	42	2.3845E-24	U234	2.2851E-24	96%	U2338	.7434E-26	4%	TH230	1.2055E-26	1%
	7	3.0110E-26	TH230	3.0110E-26	100%						
(Time of Intrusion, 7000 years)											
03	9	9.1063E-05	U234	8.6037E-05	94%	U233	4.7559E-06	5%	TH230	2.7082E-07	0%
	46	7.7239E-08	TH230	7.7239E-08	100%	NP23	74.2876E-30	0%			
	23	4.6506E-09	U234	4.1516E-09	89%	U233	4.6541E-10	10%	TH230	3.3642E-11	1%
	25	1.7391E-09	NP237	1.7391E-09	100%	U233	5.5235E-14	0%			
	6	7.6023E-10	U234	6.0262E-10	79%	U233	1.5757E-10	21%	TH230	3.7913E-14	0%
	42	2.4243E-25	U234	2.3209E-25	96%	U233	9.1288E-27	4%	TH230	1.2172E-27	1%
	7	2.0199E-27	TH230	2.0199E-27	100%						
(Time of Intrusion, 9000 years)											
04	No Release										

Table B-5 lists the total and percentage release for the 3 radionuclides contributing the most for each vector showing integrated discharge to the accessible environment for the E1E2 scenario assuming the dual porosity conceptual model for contaminant transport in the Culebra Dolomite Member. Values are normalized by the EPA factor for each radionuclide. Vectors are ordered from most to least release. Vectors which have no release are omitted.

Table B-5. Vectors with Integrated Discharge through the Culebra Dolomite Member to the Accessible Environment for E1E2 Scenario and Assuming a Dual Porosity Conceptual Model. (Time of Intrusion, 1000 yr)

Comp. Scen ID	Vector	Total Integrated Discharge	Top 3 Radionuclides Contribution to Integrated Discharge								
			(Time of Intrusion, 1000 years)								
05	9	6.5082E-02	U234	6.1583E-02	95%	U233	2.7365E-03	4%	TH230	7.6209E-04	1%
	43	1.2666E-03	U234	1.1239E-03	89%	U233	9.9814E-05	8%	TH230	4.2823E-05	3%
	30	1.7067E-04	NP237	1.7065E-04	100%	U233	2.1216E-08	0%			
	46	1.4798E-05	TH230	1.4798E-05	100%	NP23	71.5120E-29	0%			
	17	9.6709E-06	U234	8.6384E-06	89%	U233	1.0299E-06	11%	TH230	2.5980E-09	0%
	6	5.4014E-06	U234	4.4395E-06	82%	U233	9.6131E-07	18%	TH230	6.2036E-10	0%
	23	1.6703E-06	U234	1.4698E-06	88%	U233	1.7879E-07	11%	TH230	2.1675E-08	1%
	19	1.5696E-06	U234	1.5197E-06	97%	U233	4.9715E-08	3%	TH230	2.2826E-10	0%
	25	3.5095E-07	NP237	3.5093E-07	100%	U233	2.1724E-11	0%			
	32	1.3396E-07	U234	1.2926E-07	96%	U233	4.6924E-09	4%	TH230	6.3923E-12	0%
	26	4.9229E-08	U234	4.5890E-08	93%	U233	3.0312E-09	6%	TH230	3.0864E-10	1%
	20	4.5796E-08	U234	4.0527E-08	88%	U233	3.9738E-09	9%	TH230	1.2953E-09	3%
	49	3.6983E-08	NP237	3.6838E-08	100%	U233	1.1942E-10	0%	U234	2.3882E-11	0%
	39	1.0609E-08	TH230	1.0609E-08	100%						
	47	4.1081E-10	TH230	4.1081E-10	100%	U233	4.9310E-18	0%	U234	1.1139E-18	0%
	44	4.7679E-11	U234	4.5269E-11	95%	U233	1.3956E-12	3%	TH230	1.0151E-12	2%
	59	6.6671E-12	NP237	6.6669E-12	100%	U233	1.6261E-16	0%			
	3	2.1841E-13	U234	1.3545E-13	62%	TH230	5.1161E-14	23%	U233	3.1807E-14	15%
	12	1.4713E-13	NP237	1.4713E-13	100%	U233	7.5906E-19	0%			
	53	6.6924E-14	TH230	6.6924E-14	100%						
	15	5.2519E-14	NP237	5.2514E-14	100%	U233	5.2241E-18	0%	PU239	1.8186E-29	0%
	45	2.0295E-14	U234	1.9207E-14	95%	U233	9.0038E-16	4%	TH230	1.8702E-16	1%
	58	1.1489E-14	U234	1.0746E-14	94%	U233	6.2401E-16	5%	TH230	1.1905E-16	1%
	29	8.6867E-17	TH230	8.6867E-17	100%						
	5	4.2155E-17	U233	2.8583E-17	68%	U234	1.3338E-17	32%	TH230	2.3335E-19	1%
	38	2.5094E-18	U233	1.8804E-18	75%	U234	6.2730E-19	25%	TH230	1.7421E-21	0%
	4	7.9147E-19	TH230	7.9147E-19	100%	NP237	9.5638E-31	0%			
	27	3.6659E-19	U234	2.5720E-19	70%	NP237	9.6979E-20	26%	U233	1.2401E-20	3%
	42	1.4259E-20	U234	1.3698E-20	96%	U233	4.7139E-22	3%	TH230	9.0300E-23	1%
	8	2.1725E-22	U234	2.0266E-22	93%	U233	1.4567E-23	7%	TH230	1.6082E-26	0%
	7	3.2895E-23	TH230	3.2895E-23	100%	U233	1.6574E-28	0%	U234	1.6483E-29	0%
	31	2.4636E-23	TH230	2.4636E-23	100%						
	48	1.3068E-23	NP237	1.3067E-23	100%	U233	6.2704E-28	0%			
	28	5.4726E-26	U233	3.8690E-26	71%	U234	1.4905E-26	27%	TH230	1.1309E-27	2%
	50	1.5237E-26	PU239	1.5147E-26	99%	PU240	8.9241E-29	1%			
	37	4.6066E-30	U234	4.6066E-30	100%						

Table B-5. (Continued)

Comp. Scen ID	Vector	Total Integrated Discharge	Top 3 Radionuclides Contribution to Integrated Discharge								
			(Time of Intrusion, 3000 years)								
06	9	2.6392E-02	U234	2.4918E-02	94%	U233	1.2978E-03	5%	TH230	1.7603E-04	1%
	43	5.1662E-04	U234	4.5947E-04	89%	U233	4.4436E-05	9%	TH230	1.2714E-05	2%
	30	5.1104E-05	NP237	5.1099E-05	100%	U233	5.1087E-09	0%			
	46	5.0816E-06	TH230	5.0816E-06	100%	NP237	2.3186E-29	0%			
	17	2.4671E-06	U234	2.1575E-06	87%	U233	3.0909E-07	13%	TH230	5.2258E-10	0%
	6	9.7589E-07	U234	7.7604E-07	80%	U233	1.9976E-07	20%	TH230	8.1581E-11	0%
	23	6.2387E-07	U234	5.5077E-07	88%	U233	6.5860E-08	11%	TH230	7.2476E-09	1%
	19	3.0330E-07	U234	2.9333E-07	97%	U233	9.9359E-09	3%	TH230	3.9213E-11	0%
	25	1.3413E-07	NP237	1.3413E-07	100%	U233	6.7511E-12	0%			
	32	2.4762E-08	U234	2.3841E-08	96%	U233	9.2059E-10	4%	TH230	8.5369E-13	0%
	49	2.1552E-08	NP237	2.1472E-08	100%	U233	6.6478E-11	0%	U234	1.3549E-11	0%
	26	1.3023E-08	U234	1.2163E-08	93%	U233	7.8152E-10	6%	TH230	7.8647E-11	1%
	20	8.7469E-09	U234	7.7873E-09	89%	U233	7.5096E-10	9%	TH230	2.0867E-10	2%
	39	3.8495E-09	TH230	3.8495E-09	100%						
	47	1.9020E-10	TH230	1.9020E-10	100%	U233	1.6989E-18	0%	U234	3.9167E-19	0%
	44	3.9860E-12	U234	3.7902E-12	95%	U233	1.2082E-13	3%	TH230	7.4998E-14	2%
	59	2.5793E-12	NP237	2.5793E-12	100%	U233	5.2276E-17	0%			
	3	6.6863E-14	U234	3.9930E-14	60%	TH230	1.6579E-14	25%	U233	1.0354E-14	15%
	53	1.5144E-14	TH230	1.5144E-14	100%						
	12	9.2273E-15	NP237	9.2273E-15	100%	U233	4.5082E-20	0%			
	58	2.3430E-15	U234	2.1859E-15	93%	U233	1.3523E-16	6%	TH230	2.1813E-17	1%
	45	2.0100E-15	U234	1.8998E-15	95%	U233	9.2425E-17	5%	TH230	1.7740E-17	1%
	15	7.2103E-16	NP237	7.2097E-16	100%	U233	6.1399E-20	0%	PU239	1.7431E-29	0%
	29	2.1674E-17	TH230	2.1674E-17	100%						
	5	4.7979E-18	U233	3.4424E-18	72%	U234	1.3376E-18	28%	TH230	1.7910E-20	0%
	27	1.0718E-19	U234	7.5530E-20	70%	NP237	2.7985E-20	26%	U233	3.6592E-21	3%
	38	9.2118E-20	U233	7.1491E-20	78%	U234	2.0578E-20	22%	TH230	4.9476E-23	0%
	4	7.0047E-20	TH230	7.0047E-20	100%	NP237	4.7296E-31	0%			
	42	6.8662E-22	U234	6.5899E-22	96%	U233	2.3691E-23	3%	TH230	3.9367E-24	1%
	8	1.0383E-23	U234	9.6239E-24	93%	U233	7.5799E-25	7%	TH230	6.3983E-28	0%
	7	5.5810E-24	TH230	5.5809E-24	100%	U233	2.7528E-29	0%	PU239	1.7850E-29	0%
	31	3.1870E-24	TH230	3.1870E-24	100%						
	48	1.2971E-24	NP237	1.2970E-24	100%	U233	5.0439E-29	0%			
	28	2.9754E-27	U233	2.2082E-27	74%	U234	7.4297E-28	25%	TH230	2.4159E-29	1%
	50	1.4106E-27	PU239	1.4106E-27	100%						
	14	3.7900E-32	NP237	3.7900E-32	100%						

Table B-5. (Continued)

Comp. Scen ID	Vector	Total Integrated Discharge	Top 3 Radionuclides Contribution to Integrated Discharge (Time of Intrusion, 5000 years)								
07	9	3.6213E-02	U234	3.4237E-02	95%	U233	1.7311E-03	5%	TH230	2.4524E-04	1%
	43	1.8519E-04	U234	1.6547E-04	89%	U233	1.5778E-05	9%	TH230	3.9396E-06	2%
	30	1.2139E-05	NP237	1.2138E-05	100%	U233	1.0635E-09	0%			
	46	1.3415E-06	TH230	1.3415E-06	100%	NP237	2.2848E-29	0%			
	17	8.1064E-07	U234	7.0772E-07	87%	U233	1.0275E-07	13%	TH230	1.6014E-10	0%
	6	7.6053E-07	U234	6.1091E-07	80%	U233	1.4956E-07	20%	TH230	6.2342E-11	0%
	23	7.2613E-08	U234	6.4280E-08	89%	U233	7.8127E-09	11%	TH230	5.2095E-10	1%
	25	3.8589E-08	NP237	3.8587E-08	100%	U233	1.2360E-12	0%			
	19	3.0801E-08	U234	2.9760E-08	97%	U233	1.0364E-09	3%	TH230	3.6252E-12	0%
	32	7.4968E-09	U234	7.2230E-09	96%	U233	2.7353E-10	4%	TH230	2.5864E-13	0%
	49	4.2624E-09	NP237	4.2523E-09	100%	U233	8.7013E-12	0%	U234	1.4183E-12	0%
	20	1.9746E-09	U234	1.7719E-09	90%	U233	1.6741E-10	8%	TH230	3.5369E-11	2%
	26	1.1727E-09	U234	1.0977E-09	94%	U233	6.9746E-11	6%	TH230	5.2587E-12	0%
	39	8.2784E-10	TH230	8.2784E-10	100%						
	47	2.4072E-11	TH230	2.4072E-11	100%	U233	1.5621E-19	0%	U234	2.6333E-20	0%
	59	8.4104E-13	NP237	8.4103E-13	100%	U233	1.5783E-17	0%			
	44	4.6382E-13	U234	4.4103E-13	95%	U233	1.4391E-14	3%	TH230	8.3947E-15	2%
	3	5.9903E-15	U234	3.2579E-15	54%	TH230	1.7440E-15	29%	U233	9.8838E-16	16%
	53	1.1622E-15	TH230	1.1622E-15	100%						
	12	1.9101E-16	NP237	1.9101E-16	100%	U233	8.5407E-22	0%			
	58	1.8512E-16	U234	1.7228E-16	93%	U233	1.1252E-17	6%	TH230	1.5877E-18	1%
	45	1.0401E-16	U234	9.7996E-17	94%	U233	5.2142E-18	5%	TH230	8.0178E-19	1%
	15	9.3804E-17	NP237	9.3796E-17	100%	U233	7.7804E-21	0%	PU239	1.1183E-29	0%
	5	2.2931E-18	U233	1.6703E-18	73%	U234	6.1464E-19	27%	TH230	8.1531E-21	0%
	29	1.5233E-18	TH230	1.5233E-18	100%						
	4	9.9425E-21	TH230	9.9425E-21	100%	NP237	1.0015E-31	0%			
	27	3.7151E-21	U234	2.5701E-21	69%	NP237	1.0187E-21	27%	U233	1.2617E-22	3%
	38	2.2066E-21	U233	1.7398E-21	79%	U234	4.6573E-22	21%	TH230	1.0354E-24	0%
	42	7.4086E-23	U234	7.1043E-23	96%	U233	2.6250E-24	4%	TH230	4.1849E-25	1%
	7	1.0809E-24	TH230	1.0809E-24	100%	PU239	1.6208E-29	0%	U233	7.3469E-30	0%
	8	3.9691E-25	U234	3.6534E-25	92%	U233	3.1568E-26	8%			
	31	1.6184E-25	TH230	1.6184E-25	100%						
	48	1.3572E-25	NP237	1.3572E-25	100%	U233	3.5373E-30	0%			
	28	2.8333E-27	U233	2.1761E-27	77%	U234	6.3627E-28	22%	TH230	2.0733E-29	1%
	50	2.4960E-29	PU239	2.4960E-29	100%						

Table B-5. (Continued)

Comp. Scen ID	Vector	Total Integrated Discharge	Top 3 Radionuclides Contribution to Integrated Discharge								
			(Time of Intrusion, 7000 years)								
08	9	6.5008E-03	U234	6.1261E-03	94%	U233	3.5508E-04	5%	TH230	1.9603E-05	0%
	43	3.9312E-05	U234	3.5309E-05	90%	U233	3.5109E-06	9%	TH230	4.9273E-07	1%
	30	1.3132E-06	NP237	1.3131E-06	100%	U233	8.1087E-11	0%			
	46	3.1618E-07	TH230	3.1618E-07	100%	NP237	1.4399E-29	0%			
	17	1.3816E-07	U234	1.1817E-07	86%	U233	1.9966E-08	14%	TH230	1.9207E-11	0%
	6	6.0202E-08	U234	4.7013E-08	78%	U233	1.3186E-08	22%	TH230	2.9586E-12	0%
	23	2.5024E-08	U234	2.2265E-08	89%	U233	2.5786E-09	10%	TH230	1.8042E-10	1%
	25	1.4402E-08	NP237	1.4401E-08	100%	U233	4.5752E-13	0%			
	19	3.9838E-09	U234	3.8442E-09	96%	U233	1.3919E-10	3%	TH230	4.0215E-13	0%
	49	2.0283E-09	NP237	2.0234E-09	100%	U233	4.1459E-12	0%	U234	7.1708E-13	0%
	26	3.4243E-10	U234	3.2110E-10	94%	U233	1.9792E-11	6%	TH230	1.5382E-12	0%
	39	2.7854E-10	TH230	2.7854E-10	100%						
	20	2.7115E-10	U234	2.4478E-10	90%	U233	2.1486E-11	8%	TH230	4.8862E-12	2%
	47	9.8228E-12	TH230	9.8228E-12	100%	U233	4.8780E-20	0%	U234	9.4011E-21	0%
	59	1.5256E-13	NP237	1.5255E-13	100%	U233	2.0920E-18	0%			
	44	1.0365E-14	U234	9.8679E-15	95%	U233	3.3335E-16	3%	TH230	1.6389E-16	2%
	3	1.9539E-15	U234	9.7441E-16	50%	TH230	6.5519E-16	34%	U233	3.2431E-16	17%
	53	2.2807E-16	TH230	2.2807E-16	100%						
	58	3.7253E-17	U234	3.4576E-17	93%	U233	2.3892E-18	6%	TH230	2.8786E-19	1%
	45	7.2069E-18	U234	6.7808E-18	94%	U233	3.7069E-19	5%	TH230	5.5477E-20	1%
	15	5.3191E-18	NP237	5.3187E-18	100%	U233	3.6843E-22	0%			
	12	3.7488E-18	NP237	3.7488E-18	100%	U233	1.6490E-23	0%			
	29	4.0059E-19	TH230	4.0059E-19	100%						
	27	9.8198E-22	U234	6.8113E-22	69%	NP237	2.6707E-22	27%	U233	3.3734E-23	3%
	5	2.4982E-22	U233	1.8242E-22	73%	U234	6.6519E-23	27%	TH230	8.8236E-25	0%
	42	2.3004E-24	U234	2.2035E-24	96%	U233	8.5296E-26	4%	TH230	1.1625E-26	1%
	7	1.4039E-25	TH230	1.4038E-25	100%	PU239	8.8810E-30	0%			
	31	1.6678E-26	TH230	1.6678E-26	100%						
	48	4.6182E-27	NP237	4.6182E-27	100%						
	8	4.0428E-27	U234	3.6903E-27	91%	U233	3.5247E-28	9%			
	28	7.6283E-29	U233	6.0913E-29	80%	U234	1.5370E-29	20%			
	10	1.3532E-29	NP237	1.3532E-29	100%						
	14	1.9103E-31	NP237	1.9103E-31	100%						

Table B-5. (Concluded)

Comp. Scen ID	Vector	Total Integrated Discharge	Top 3 Radionuclides Contribution to Integrated Discharge								
			(Time of Intrusion, 9000 years)								
09	9	9.3121E-03	U234	8.7988E-03	94%	U233	4.8564E-04	5%	TH230	2.7696E-05	0%
	43	9.4847E-06	U234	8.5607E-06	90%	U233	8.0461E-07	8%	TH230	1.1932E-07	1%
	30	1.6783E-07	NP237	1.6782E-07	100%	U233	1.0297E-11	0%			
	46	5.0795E-08	TH230	5.0795E-08	100%	NP237	3.3970E-30	0%			
	6	4.3087E-08	U234	3.4178E-08	79%	U233	8.9065E-09	21%	TH230	2.1503E-12	0%
	17	3.6881E-08	U234	3.1801E-08	86%	U233	5.0747E-09	14%	TH230	5.1686E-12	0%
	19	1.9423E-10	U234	1.8731E-10	96%	U233	6.8974E-12	4%	TH230	1.9595E-14	0%
	39	1.5154E-11	TH230	1.5154E-11	100%						
	47	2.3617E-13	TH230	2.3617E-13	100%	U233	9.4620E-22	0%	U234	2.1175E-22	0%
	59	3.6621E-14	NP237	3.6621E-14	100%	U233	5.0218E-19	0%			
	44	8.3026E-16	U234	7.8985E-16	95%	U233	2.7302E-17	3%	TH230	1.3108E-17	2%
	58	1.9070E-18	U234	1.7663E-18	93%	U233	1.2592E-19	7%	TH230	1.4705E-20	1%
	15	9.8113E-19	NP237	9.8106E-19	100%	U233	6.7959E-23	0%			
	42	2.1272E-25	U234	2.0359E-25	96%	U233	8.0601E-27	4%	TH230	1.0677E-27	1%
	7	2.1828E-26	TH230	2.1824E-26	100%	PU239	3.3538E-30	0%			
	48	3.0377E-28	NP237	3.0377E-28	100%						
	28	7.9241E-29	U233	6.4883E-29	82%	U234	1.4229E-29	18%	NP237	1.2864E-31	0%
	8	4.5490E-29	U234	4.1792E-29	92%	U233	3.6982E-30	8%			
	10	7.6689E-30	NP237	7.6689E-30	100%						

CCDFCALC C-4.06VV (09/23/91) 10/07/91 14:09:58

Table B-6 lists total EPP summed normalized release and the percentages contribution for the 3 radionuclides contributing the most release for each vector when drilling into a CH waste drum with an average activity level. Vectors are ordered from most to least release. All vectors have some release when intruding into the repository from drilling.

Table B-6. Integrated Discharge to the Accessible Environment by Bringing Average CH-Activity Cuttings to the Surface when Initially Drilling through the Repository.

Comp. Scen ID	Vector	Total Integrated Discharge	Top 3 Radionuclides Contribution to Integrated Discharge (Time of Intrusion, 1000 years)								
00	19	7.6179E-03	PU239	4.8576E-03	64%	AM241	2.1471E-03	28%	PU240	5.6927E-04	7%
	35	7.5567E-03	PU239	4.8185E-03	64%	AM241	2.1299E-03	28%	PU240	5.6470E-04	7%
	55	7.4956E-03	PU239	4.7796E-03	64%	AM241	2.1127E-03	28%	PU240	5.6013E-04	7%
	16	7.4550E-03	PU239	4.7537E-03	64%	AM241	2.1012E-03	28%	PU240	5.5710E-04	7%
	46	7.3941E-03	PU239	4.7149E-03	64%	AM241	2.0841E-03	28%	PU240	5.5255E-04	7%
	24	7.3132E-03	PU239	4.6633E-03	64%	AM241	2.0612E-03	28%	PU240	5.4650E-04	7%
	4	7.2527E-03	PU239	4.6247E-03	64%	AM241	2.0442E-03	28%	PU240	5.4198E-04	7%
	14	7.2124E-03	PU239	4.5990E-03	64%	AM241	2.0328E-03	28%	PU240	5.3897E-04	7%
	13	7.1722E-03	PU239	4.5734E-03	64%	AM241	2.0215E-03	28%	PU240	5.3596E-04	7%
	51	7.1120E-03	PU239	4.5350E-03	64%	AM241	2.0045E-03	28%	PU240	5.3147E-04	7%
	39	7.0719E-03	PU239	4.5094E-03	64%	AM241	1.9932E-03	28%	PU240	5.2847E-04	7%
	1	6.9720E-03	PU239	4.4457E-03	64%	AM241	1.9651E-03	28%	PU240	5.2101E-04	7%
	53	6.9123E-03	PU239	4.4076E-03	64%	AM241	1.9482E-03	28%	PU240	5.1654E-04	7%
	18	6.8725E-03	PU239	4.3823E-03	64%	AM241	1.9370E-03	28%	PU240	5.1357E-04	7%
	52	6.7932E-03	PU239	4.3317E-03	64%	AM241	1.9147E-03	28%	PU240	5.0764E-04	7%
	27	6.7338E-03	PU239	4.2939E-03	64%	AM241	1.8980E-03	28%	PU240	5.0321E-04	7%
	49	6.6944E-03	PU239	4.2687E-03	64%	AM241	1.8868E-03	28%	PU240	5.0026E-04	7%
	38	6.5959E-03	PU239	4.2059E-03	64%	AM241	1.8591E-03	28%	PU240	4.9290E-04	7%
	21	6.5763E-03	PU239	4.1934E-03	64%	AM241	1.8535E-03	28%	PU240	4.9143E-04	7%
	17	6.5174E-03	PU239	4.1559E-03	64%	AM241	1.8370E-03	28%	PU240	4.8704E-04	7%
	44	6.4587E-03	PU239	4.1184E-03	64%	AM241	1.8204E-03	28%	PU240	4.8265E-04	7%
	30	6.3807E-03	PU239	4.0687E-03	64%	AM241	1.7984E-03	28%	PU240	4.7682E-04	7%
	3	6.3223E-03	PU239	4.0314E-03	64%	AM241	1.7820E-03	28%	PU240	4.7246E-04	7%
	37	6.2835E-03	PU239	4.0067E-03	64%	AM241	1.7710E-03	28%	PU240	4.6955E-04	7%
	43	6.2253E-03	PU239	3.9696E-03	64%	AM241	1.7546E-03	28%	PU240	4.6521E-04	7%
	33	6.1673E-03	PU239	3.9326E-03	64%	AM241	1.7383E-03	28%	PU240	4.6087E-04	7%
	32	6.0902E-03	PU239	3.8834E-03	64%	AM241	1.7165E-03	28%	PU240	4.5511E-04	7%
	28	6.0517E-03	PU239	3.8589E-03	64%	AM241	1.7057E-03	28%	PU240	4.5223E-04	7%
	6	6.0132E-03	PU239	3.8344E-03	64%	AM241	1.6949E-03	28%	PU240	4.4936E-04	7%
	60	5.9175E-03	PU239	3.7733E-03	64%	AM241	1.6679E-03	28%	PU240	4.4220E-04	7%
	47	5.8984E-03	PU239	3.7611E-03	64%	AM241	1.6625E-03	28%	PU240	4.4077E-04	7%
	41	5.8411E-03	PU239	3.7246E-03	64%	AM241	1.6463E-03	28%	PU240	4.3650E-04	7%
	26	5.7840E-03	PU239	3.6882E-03	64%	AM241	1.6302E-03	28%	PU240	4.3223E-04	7%
	11	5.7081E-03	PU239	3.6398E-03	64%	AM241	1.6088E-03	28%	PU240	4.2655E-04	7%
	57	5.6513E-03	PU239	3.6036E-03	64%	AM241	1.5928E-03	28%	PU240	4.2231E-04	7%
	7	5.5946E-03	PU239	3.5674E-03	64%	AM241	1.5769E-03	28%	PU240	4.1808E-04	7%
	29	5.5569E-03	PU239	3.5434E-03	64%	AM241	1.5662E-03	28%	PU240	4.1526E-04	7%
	9	5.4817E-03	PU239	3.4954E-03	64%	AM241	1.5450E-03	28%	PU240	4.0964E-04	7%
	8	5.4068E-03	PU239	3.4476E-03	64%	AM241	1.5239E-03	28%	PU240	4.0404E-04	7%
	15	5.3881E-03	PU239	3.4357E-03	64%	AM241	1.5186E-03	28%	PU240	4.0264E-04	7%
	40	5.3507E-03	PU239	3.4119E-03	64%	AM241	1.5081E-03	28%	PU240	3.9985E-04	7%
	48	5.2390E-03	PU239	3.3406E-03	64%	AM241	1.4766E-03	28%	PU240	3.9150E-04	7%
	20	5.2019E-03	PU239	3.3170E-03	64%	AM241	1.4662E-03	28%	PU240	3.8873E-04	7%
	54	5.1463E-03	PU239	3.2815E-03	64%	AM241	1.4505E-03	28%	PU240	3.8457E-04	7%
	31	5.0724E-03	PU239	3.2344E-03	64%	AM241	1.4297E-03	28%	PU240	3.7905E-04	7%
	23	5.0724E-03	PU239	3.2344E-03	64%	AM241	1.4297E-03	28%	PU240	3.7905E-04	7%
	12	4.9988E-03	PU239	3.1875E-03	64%	AM241	1.4089E-03	28%	PU240	3.7355E-04	7%
	42	4.9621E-03	PU239	3.1641E-03	64%	AM241	1.3986E-03	28%	PU240	3.7081E-04	7%
	58	4.8705E-03	PU239	3.1057E-03	64%	AM241	1.3728E-03	28%	PU240	3.6396E-04	7%
	34	4.8522E-03	PU239	3.0940E-03	64%	AM241	1.3676E-03	28%	PU240	3.6260E-04	7%
	2	4.7611E-03	PU239	3.0359E-03	64%	AM241	1.3419E-03	28%	PU240	3.5579E-04	7%
	56	4.7066E-03	PU239	3.0012E-03	64%	AM241	1.3266E-03	28%	PU240	3.5172E-04	7%

Table B-6. (Continued)

Comp. Scen ID	Vector	Total Integrated Discharge	Top 3 Radionuclides Contribution to Integrated Discharge								
			(Time of Intrusion, 1000 years)								
	50	4.6523E-03	PU239	2.9665E-03	64%	AM241	1.3113E-03	28%	PU240	3.4766E-04	7%
	22	4.6161E-03	PU239	2.9435E-03	64%	AM241	1.3011E-03	28%	PU240	3.4496E-04	7%
	25	4.5620E-03	PU239	2.9090E-03	64%	AM241	1.2858E-03	28%	PU240	3.4091E-04	7%
	59	4.5260E-03	PU239	2.8860E-03	64%	AM241	1.2757E-03	28%	PU240	3.3822E-04	7%
	10	4.4542E-03	PU239	2.8402E-03	64%	AM241	1.2554E-03	28%	PU240	3.3285E-04	7%
	5	4.3826E-03	PU239	2.7946E-03	64%	AM241	1.2352E-03	28%	PU240	3.2750E-04	7%
	36	4.3290E-03	PU239	2.7604E-03	64%	AM241	1.2201E-03	28%	PU240	3.2350E-04	7%
	45	4.2934E-03	PU239	2.7377E-03	64%	AM241	1.2101E-03	28%	PU240	3.2084E-04	7%

Comp. Scen ID	Vector	Total Integrated Discharge	Top 3 Radionuclides Contribution to Integrated Discharge								
			(Time of Intrusion, 3000 years)								
01	19	5.1607E-03	PU239	4.5856E-03	89%	PU240	4.6049E-04	9%	AM241	8.6864E-05	2%
	35	5.1193E-03	PU239	4.5488E-03	89%	PU240	4.5679E-04	9%	AM241	8.6166E-05	2%
	55	5.0779E-03	PU239	4.5120E-03	89%	PU240	4.5310E-04	9%	AM241	8.5470E-05	2%
	16	5.0504E-03	PU239	4.4876E-03	89%	PU240	4.5064E-04	9%	AM241	8.5006E-05	2%
	46	5.0091E-03	PU239	4.4509E-03	89%	PU240	4.4696E-04	9%	AM241	8.4313E-05	2%
	24	4.9543E-03	PU239	4.4022E-03	89%	PU240	4.4207E-04	9%	AM241	8.3390E-05	2%
	4	4.9133E-03	PU239	4.3658E-03	89%	PU240	4.3841E-04	9%	AM241	8.2700E-05	2%
	14	4.8860E-03	PU239	4.3416E-03	89%	PU240	4.3598E-04	9%	AM241	8.2241E-05	2%
	13	4.8588E-03	PU239	4.3173E-03	89%	PU240	4.3355E-04	9%	AM241	8.1782E-05	2%
	51	4.8180E-03	PU239	4.2811E-03	89%	PU240	4.2991E-04	9%	AM241	8.1096E-05	2%
	39	4.7909E-03	PU239	4.2570E-03	89%	PU240	4.2749E-04	9%	AM241	8.0639E-05	2%
	1	4.7232E-03	PU239	4.1969E-03	89%	PU240	4.2145E-04	9%	AM241	7.9500E-05	2%
	53	4.6827E-03	PU239	4.1609E-03	89%	PU240	4.1784E-04	9%	AM241	7.8818E-05	2%
	18	4.6558E-03	PU239	4.1370E-03	89%	PU240	4.1543E-04	9%	AM241	7.8365E-05	2%
	52	4.6020E-03	PU239	4.0892E-03	89%	PU240	4.1064E-04	9%	AM241	7.7461E-05	2%
	27	4.5618E-03	PU239	4.0535E-03	89%	PU240	4.0705E-04	9%	AM241	7.6784E-05	2%
	49	4.5351E-03	PU239	4.0297E-03	89%	PU240	4.0466E-04	9%	AM241	7.6334E-05	2%
	38	4.4684E-03	PU239	3.9705E-03	89%	PU240	3.9871E-04	9%	AM241	7.5211E-05	2%
	21	4.4551E-03	PU239	3.9586E-03	89%	PU240	3.9753E-04	9%	AM241	7.4987E-05	2%
	17	4.4152E-03	PU239	3.9232E-03	89%	PU240	3.9397E-04	9%	AM241	7.4316E-05	2%
	44	4.3755E-03	PU239	3.8879E-03	89%	PU240	3.9042E-04	9%	AM241	7.3647E-05	2%
	30	4.3226E-03	PU239	3.8409E-03	89%	PU240	3.8570E-04	9%	AM241	7.2757E-05	2%
	3	4.2831E-03	PU239	3.8058E-03	89%	PU240	3.8217E-04	9%	AM241	7.2091E-05	2%
	37	4.2567E-03	PU239	3.7824E-03	89%	PU240	3.7983E-04	9%	AM241	7.1648E-05	2%
	43	4.2173E-03	PU239	3.7474E-03	89%	PU240	3.7631E-04	9%	AM241	7.0985E-05	2%
	33	4.1780E-03	PU239	3.7124E-03	89%	PU240	3.7280E-04	9%	AM241	7.0324E-05	2%
	32	4.1258E-03	PU239	3.6660E-03	89%	PU240	3.6814E-04	9%	AM241	6.9444E-05	2%
	28	4.0997E-03	PU239	3.6428E-03	89%	PU240	3.6581E-04	9%	AM241	6.9005E-05	2%
	6	4.0737E-03	PU239	3.6197E-03	89%	PU240	3.6349E-04	9%	AM241	6.8567E-05	2%
	60	4.0088E-03	PU239	3.5621E-03	89%	PU240	3.5770E-04	9%	AM241	6.7475E-05	2%
	47	3.9958E-03	PU239	3.5506E-03	89%	PU240	3.5655E-04	9%	AM241	6.7257E-05	2%
	41	3.9571E-03	PU239	3.5161E-03	89%	PU240	3.5309E-04	9%	AM241	6.6604E-05	2%
	26	3.9184E-03	PU239	3.4817E-03	89%	PU240	3.4963E-04	9%	AM241	6.5953E-05	2%
	11	3.8669E-03	PU239	3.4360E-03	89%	PU240	3.4504E-04	9%	AM241	6.5087E-05	2%
	57	3.8285E-03	PU239	3.4018E-03	89%	PU240	3.4161E-04	9%	AM241	6.4440E-05	2%
	7	3.7901E-03	PU239	3.3677E-03	89%	PU240	3.3819E-04	9%	AM241	6.3794E-05	2%
	29	3.7645E-03	PU239	3.3450E-03	89%	PU240	3.3591E-04	9%	AM241	6.3364E-05	2%
	9	3.7136E-03	PU239	3.2998E-03	89%	PU240	3.3136E-04	9%	AM241	6.2506E-05	2%
	8	3.6628E-03	PU239	3.2546E-03	89%	PU240	3.2683E-04	9%	AM241	6.1652E-05	2%
	15	3.6501E-03	PU239	3.2434E-03	89%	PU240	3.2570E-04	9%	AM241	6.1438E-05	2%
	40	3.6248E-03	PU239	3.2209E-03	89%	PU240	3.2344E-04	9%	AM241	6.1012E-05	2%
	48	3.5491E-03	PU239	3.1536E-03	89%	PU240	3.1669E-04	9%	AM241	5.9738E-05	2%
	20	3.5240E-03	PU239	3.1313E-03	89%	PU240	3.1444E-04	9%	AM241	5.9315E-05	2%
	54	3.4864E-03	PU239	3.0979E-03	89%	PU240	3.1108E-04	9%	AM241	5.8682E-05	2%
	31	3.4363E-03	PU239	3.0534E-03	89%	PU240	3.0662E-04	9%	AM241	5.7839E-05	2%
	23	3.4363E-03	PU239	3.0534E-03	89%	PU240	3.0662E-04	9%	AM241	5.7839E-05	2%

Table B-6. (Continued)

Comp. Scen ID	Vector	Total Integrated Discharge	Top 3 Radionuclides Contribution to Integrated Discharge								
			(Time of Intrusion, 3000 years)								
	12	3.3864E-03	PU239	3.0091E-03	89%	PU240	3.0217E-04	9%	AM241	5.6999E-05	2%
	42	3.3615E-03	PU239	2.9869E-03	89%	PU240	2.9995E-04	9%	AM241	5.6581E-05	2%
	58	3.2995E-03	PU239	2.9318E-03	89%	PU240	2.9441E-04	9%	AM241	5.5537E-05	2%
	34	3.2871E-03	PU239	2.9208E-03	89%	PU240	2.9331E-04	9%	AM241	5.5328E-05	2%
	2	3.2254E-03	PU239	2.8660E-03	89%	PU240	2.8780E-04	9%	AM241	5.4290E-05	2%
	56	3.1885E-03	PU239	2.8332E-03	89%	PU240	2.8451E-04	9%	AM241	5.3668E-05	2%
	50	3.1517E-03	PU239	2.8005E-03	89%	PU240	2.8122E-04	9%	AM241	5.3049E-05	2%
	22	3.1272E-03	PU239	2.7787E-03	89%	PU240	2.7904E-04	9%	AM241	5.2636E-05	2%
	25	3.0905E-03	PU239	2.7461E-03	89%	PU240	2.7577E-04	9%	AM241	5.2019E-05	2%
	59	3.0661E-03	PU239	2.7245E-03	89%	PU240	2.7359E-04	9%	AM241	5.1609E-05	2%
	10	3.0175E-03	PU239	2.6812E-03	89%	PU240	2.6925E-04	9%	AM241	5.0789E-05	2%
	5	2.9690E-03	PU239	2.6381E-03	89%	PU240	2.6492E-04	9%	AM241	4.9973E-05	2%
	36	2.9327E-03	PU239	2.6059E-03	89%	PU240	2.6168E-04	9%	AM241	4.9363E-05	2%
	45	2.9086E-03	PU239	2.5844E-03	89%	PU240	2.5953E-04	9%	AM241	4.8956E-05	2%

Comp. Scen ID	Vector	Total Integrated Discharge	Top 3 Radionuclides Contribution to Integrated Discharge								
			(Time of Intrusion, 5000 years)								
02	19	4.7364E-03	PU239	4.3289E-03	91%	PU240	3.7249E-04	8%	U234	1.9395E-05	0%
	35	4.6984E-03	PU239	4.2942E-03	91%	PU240	3.6950E-04	8%	U234	1.9239E-05	0%
	55	4.6604E-03	PU239	4.2595E-03	91%	PU240	3.6651E-04	8%	U234	1.9084E-05	0%
	16	4.6351E-03	PU239	4.2364E-03	91%	PU240	3.6453E-04	8%	U234	1.8980E-05	0%
	46	4.5973E-03	PU239	4.2018E-03	91%	PU240	3.6155E-04	8%	U234	1.8825E-05	0%
	24	4.5470E-03	PU239	4.1558E-03	91%	PU240	3.5759E-04	8%	U234	1.8619E-05	0%
	4	4.5093E-03	PU239	4.1214E-03	91%	PU240	3.5464E-04	8%	U234	1.8465E-05	0%
	14	4.4843E-03	PU239	4.0985E-03	91%	PU240	3.5267E-04	8%	U234	1.8363E-05	0%
	13	4.4593E-03	PU239	4.0757E-03	91%	PU240	3.5070E-04	8%	U234	1.8260E-05	0%
	51	4.4219E-03	PU239	4.0415E-03	91%	PU240	3.4776E-04	8%	U234	1.8107E-05	0%
	39	4.3970E-03	PU239	4.0187E-03	91%	PU240	3.4580E-04	8%	U234	1.8005E-05	0%
	1	4.3349E-03	PU239	3.9619E-03	91%	PU240	3.4091E-04	8%	U234	1.7751E-05	0%
	53	4.2977E-03	PU239	3.9280E-03	91%	PU240	3.3799E-04	8%	U234	1.7598E-05	0%
	18	4.2730E-03	PU239	3.9054E-03	91%	PU240	3.3605E-04	8%	U234	1.7497E-05	0%
	52	4.2237E-03	PU239	3.8603E-03	91%	PU240	3.3217E-04	8%	U234	1.7295E-05	0%
	27	4.1868E-03	PU239	3.8266E-03	91%	PU240	3.2927E-04	8%	U234	1.7144E-05	0%
	49	4.1622E-03	PU239	3.8041E-03	91%	PU240	3.2734E-04	8%	U234	1.7044E-05	0%
	38	4.1010E-03	PU239	3.7482E-03	91%	PU240	3.2252E-04	8%	U234	1.6793E-05	0%
	21	4.0888E-03	PU239	3.7370E-03	91%	PU240	3.2156E-04	8%	U234	1.6743E-05	0%
	17	4.0522E-03	PU239	3.7036E-03	91%	PU240	3.1868E-04	8%	U234	1.6593E-05	0%
	44	4.0157E-03	PU239	3.6703E-03	91%	PU240	3.1581E-04	8%	U234	1.6444E-05	0%
	30	3.9672E-03	PU239	3.6259E-03	91%	PU240	3.1200E-04	8%	U234	1.6245E-05	0%
	3	3.9309E-03	PU239	3.5927E-03	91%	PU240	3.0914E-04	8%	U234	1.6096E-05	0%
	37	3.9067E-03	PU239	3.5706E-03	91%	PU240	3.0724E-04	8%	U234	1.5997E-05	0%
	43	3.8706E-03	PU239	3.5376E-03	91%	PU240	3.0440E-04	8%	U234	1.5849E-05	0%
	33	3.8345E-03	PU239	3.5046E-03	91%	PU240	3.0156E-04	8%	U234	1.5702E-05	0%
	32	3.7865E-03	PU239	3.4608E-03	91%	PU240	2.9779E-04	8%	U234	1.5505E-05	0%
	28	3.7626E-03	PU239	3.4389E-03	91%	PU240	2.9591E-04	8%	U234	1.5407E-05	0%
	6	3.7387E-03	PU239	3.4171E-03	91%	PU240	2.9403E-04	8%	U234	1.5310E-05	0%
	60	3.6792E-03	PU239	3.3627E-03	91%	PU240	2.8935E-04	8%	U234	1.5066E-05	0%
	47	3.6673E-03	PU239	3.3518E-03	91%	PU240	2.8841E-04	8%	U234	1.5017E-05	0%
	41	3.6317E-03	PU239	3.3193E-03	91%	PU240	2.8561E-04	8%	U234	1.4871E-05	0%
	26	3.5962E-03	PU239	3.2868E-03	91%	PU240	2.8282E-04	8%	U234	1.4726E-05	0%
	11	3.5490E-03	PU239	3.2437E-03	91%	PU240	2.7911E-04	8%	U234	1.4533E-05	0%
	57	3.5137E-03	PU239	3.2114E-03	91%	PU240	2.7633E-04	8%	U234	1.4388E-05	0%
	7	3.4785E-03	PU239	3.1792E-03	91%	PU240	2.7356E-04	8%	U234	1.4244E-05	0%
	29	3.4550E-03	PU239	3.1578E-03	91%	PU240	2.7172E-04	8%	U234	1.4148E-05	0%
	9	3.4083E-03	PU239	3.1151E-03	91%	PU240	2.6804E-04	8%	U234	1.3956E-05	0%
	8	3.3617E-03	PU239	3.0725E-03	91%	PU240	2.6438E-04	8%	U234	1.3765E-05	0%
	15	3.3500E-03	PU239	3.0618E-03	91%	PU240	2.6346E-04	8%	U234	1.3718E-05	0%
	40	3.3268E-03	PU239	3.0406E-03	91%	PU240	2.6163E-04	8%	U234	1.3623E-05	0%
	48	3.2573E-03	PU239	2.9771E-03	91%	PU240	2.5617E-04	8%	U234	1.3338E-05	0%
	20	3.2343E-03	PU239	2.9560E-03	91%	PU240	2.5436E-04	8%	U234	1.3244E-05	0%

Table B-6. (Continued)

Comp. Scen ID	Vector	Total Integrated Discharge	Top 3 Radionuclides Contribution to Integrated Discharge								
			(Time of Intrusion, 5000 years)								
	54	3.1997E-03	PU239	2.9244E-03	91%	PU240	2.5164E-04	8%	U234	1.3102E-05	0%
	31	3.1538E-03	PU239	2.8825E-03	91%	PU240	2.4803E-04	8%	U234	1.2914E-05	0%
	23	3.1538E-03	PU239	2.8825E-03	91%	PU240	2.4803E-04	8%	U234	1.2914E-05	0%
	12	3.1080E-03	PU239	2.8406E-03	91%	PU240	2.4443E-04	8%	U234	1.2727E-05	0%
	42	3.0852E-03	PU239	2.8197E-03	91%	PU240	2.4263E-04	8%	U234	1.2633E-05	0%
	58	3.0282E-03	PU239	2.7677E-03	91%	PU240	2.3815E-04	8%	U234	1.2400E-05	0%
	34	3.0169E-03	PU239	2.7573E-03	91%	PU240	2.3726E-04	8%	U234	1.2354E-05	0%
	2	2.9602E-03	PU239	2.7056E-03	91%	PU240	2.3281E-04	8%	U234	1.2122E-05	0%
	56	2.9263E-03	PU239	2.6746E-03	91%	PU240	2.3014E-04	8%	U234	1.1983E-05	0%
	50	2.8926E-03	PU239	2.6437E-03	91%	PU240	2.2748E-04	8%	U234	1.1845E-05	0%
	22	2.8701E-03	PU239	2.6232E-03	91%	PU240	2.2572E-04	8%	U234	1.1753E-05	0%
	25	2.8364E-03	PU239	2.5924E-03	91%	PU240	2.2307E-04	8%	U234	1.1615E-05	0%
	59	2.8140E-03	PU239	2.5719E-03	91%	PU240	2.2131E-04	8%	U234	1.1523E-05	0%
	10	2.7694E-03	PU239	2.5311E-03	91%	PU240	2.1780E-04	8%	U234	1.1340E-05	0%
	5	2.7249E-03	PU239	2.4904E-03	91%	PU240	2.1430E-04	8%	U234	1.1158E-05	0%
	36	2.6916E-03	PU239	2.4600E-03	91%	PU240	2.1168E-04	8%	U234	1.1022E-05	0%
	45	2.6694E-03	PU239	2.4398E-03	91%	PU240	2.0994E-04	8%	U234	1.0931E-05	0%

Comp. Scen ID	Vector	Total Integrated Discharge	Top 3 Radionuclides Contribution to Integrated Discharge								
			(Time of Intrusion, 7000 years)								
03	19	4.4232E-03	PU239	4.0866E-03	92%	PU240	3.0131E-04	7%	U234	1.9285E-05	0%
	35	4.3876E-03	PU239	4.0538E-03	92%	PU240	2.9889E-04	7%	U234	1.9130E-05	0%
	55	4.3522E-03	PU239	4.0210E-03	92%	PU240	2.9648E-04	7%	U234	1.8976E-05	0%
	16	4.3286E-03	PU239	3.9992E-03	92%	PU240	2.9487E-04	7%	U234	1.8873E-05	0%
	46	4.2933E-03	PU239	3.9666E-03	92%	PU240	2.9246E-04	7%	U234	1.8719E-05	0%
	24	4.2463E-03	PU239	3.9232E-03	92%	PU240	2.8926E-04	7%	U234	1.8514E-05	0%
	4	4.2111E-03	PU239	3.8907E-03	92%	PU240	2.8687E-04	7%	U234	1.8361E-05	0%
	14	4.1877E-03	PU239	3.8691E-03	92%	PU240	2.8527E-04	7%	U234	1.8259E-05	0%
	13	4.1644E-03	PU239	3.8475E-03	92%	PU240	2.8368E-04	7%	U234	1.8157E-05	0%
	51	4.1294E-03	PU239	3.8152E-03	92%	PU240	2.8130E-04	7%	U234	1.8004E-05	0%
	39	4.1062E-03	PU239	3.7937E-03	92%	PU240	2.7972E-04	7%	U234	1.7903E-05	0%
	1	4.0482E-03	PU239	3.7401E-03	92%	PU240	2.7577E-04	7%	U234	1.7650E-05	0%
	53	4.0135E-03	PU239	3.7081E-03	92%	PU240	2.7340E-04	7%	U234	1.7499E-05	0%
	18	3.9904E-03	PU239	3.6868E-03	92%	PU240	2.7183E-04	7%	U234	1.7398E-05	0%
	52	3.9443E-03	PU239	3.6442E-03	92%	PU240	2.6869E-04	7%	U234	1.7197E-05	0%
	27	3.9099E-03	PU239	3.6124E-03	92%	PU240	2.6635E-04	7%	U234	1.7047E-05	0%
	49	3.8870E-03	PU239	3.5912E-03	92%	PU240	2.6478E-04	7%	U234	1.6947E-05	0%
	38	3.8298E-03	PU239	3.5384E-03	92%	PU240	2.6089E-04	7%	U234	1.6698E-05	0%
	21	3.8184E-03	PU239	3.5278E-03	92%	PU240	2.6011E-04	7%	U234	1.6648E-05	0%
	17	3.7842E-03	PU239	3.4963E-03	92%	PU240	2.5779E-04	7%	U234	1.6499E-05	0%
	44	3.7501E-03	PU239	3.4648E-03	92%	PU240	2.5546E-04	7%	U234	1.6351E-05	0%
	30	3.7048E-03	PU239	3.4229E-03	92%	PU240	2.5238E-04	7%	U234	1.6153E-05	0%
	3	3.6709E-03	PU239	3.3916E-03	92%	PU240	2.5007E-04	7%	U234	1.6005E-05	0%
	37	3.6484E-03	PU239	3.3708E-03	92%	PU240	2.4853E-04	7%	U234	1.5907E-05	0%
	43	3.6146E-03	PU239	3.3396E-03	92%	PU240	2.4623E-04	7%	U234	1.5760E-05	0%
	33	3.5809E-03	PU239	3.3084E-03	92%	PU240	2.4394E-04	7%	U234	1.5613E-05	0%
	32	3.5361E-03	PU239	3.2671E-03	92%	PU240	2.4089E-04	7%	U234	1.5418E-05	0%
	28	3.5138E-03	PU239	3.2464E-03	92%	PU240	2.3936E-04	7%	U234	1.5320E-05	0%
	6	3.4915E-03	PU239	3.2258E-03	92%	PU240	2.3784E-04	7%	U234	1.5223E-05	0%
	60	3.4359E-03	PU239	3.1744E-03	92%	PU240	2.3406E-04	7%	U234	1.4980E-05	0%
	47	3.4248E-03	PU239	3.1642E-03	92%	PU240	2.3330E-04	7%	U234	1.4932E-05	0%
	41	3.3915E-03	PU239	3.1335E-03	92%	PU240	2.3104E-04	7%	U234	1.4787E-05	0%
	26	3.3584E-03	PU239	3.1028E-03	92%	PU240	2.2878E-04	7%	U234	1.4643E-05	0%
	11	3.3143E-03	PU239	3.0621E-03	92%	PU240	2.2577E-04	7%	U234	1.4450E-05	0%
	57	3.2813E-03	PU239	3.0316E-03	92%	PU240	2.2353E-04	7%	U234	1.4307E-05	0%
	7	3.2484E-03	PU239	3.0012E-03	92%	PU240	2.2129E-04	7%	U234	1.4163E-05	0%
	29	3.2265E-03	PU239	2.9810E-03	92%	PU240	2.1980E-04	7%	U234	1.4068E-05	0%
	9	3.1829E-03	PU239	2.9407E-03	92%	PU240	2.1682E-04	7%	U234	1.3877E-05	0%
	8	3.1393E-03	PU239	2.9005E-03	92%	PU240	2.1386E-04	7%	U234	1.3688E-05	0%
	15	3.1285E-03	PU239	2.8904E-03	92%	PU240	2.1312E-04	7%	U234	1.3640E-05	0%

Table B-6. (Continued)

Comp. Scen ID	Vector	Total Integrated Discharge	Top 3 Radionuclides Contribution to Integrated Discharge							
			(Time of Intrusion, 7000 years)							
	40	3.1068E-03	PU239	2.8704E-03	92%	PU240	2.1164E-04	7%	U234	1.3546E-05	0%
	48	3.0419E-03	PU239	2.8105E-03	92%	PU240	2.0722E-04	7%	U234	1.3263E-05	0%
	20	3.0204E-03	PU239	2.7905E-03	92%	PU240	2.0575E-04	7%	U234	1.3169E-05	0%
	54	2.9881E-03	PU239	2.7607E-03	92%	PU240	2.0355E-04	7%	U234	1.3028E-05	0%
	31	2.9452E-03	PU239	2.7211E-03	92%	PU240	2.0063E-04	7%	U234	1.2841E-05	0%
	23	2.9452E-03	PU239	2.7211E-03	92%	PU240	2.0063E-04	7%	U234	1.2841E-05	0%
	12	2.9024E-03	PU239	2.6816E-03	92%	PU240	1.9772E-04	7%	U234	1.2655E-05	0%
	42	2.8811E-03	PU239	2.6619E-03	92%	PU240	1.9627E-04	7%	U234	1.2562E-05	0%
	58	2.8280E-03	PU239	2.6128E-03	92%	PU240	1.9264E-04	7%	U234	1.2330E-05	0%
	34	2.8174E-03	PU239	2.6030E-03	92%	PU240	1.9192E-04	7%	U234	1.2284E-05	0%
	2	2.7645E-03	PU239	2.5541E-03	92%	PU240	1.8832E-04	7%	U234	1.2053E-05	0%
	56	2.7328E-03	PU239	2.5249E-03	92%	PU240	1.8616E-04	7%	U234	1.1915E-05	0%
	50	2.7013E-03	PU239	2.4957E-03	92%	PU240	1.8401E-04	7%	U234	1.1778E-05	0%
	22	2.6803E-03	PU239	2.4763E-03	92%	PU240	1.8258E-04	7%	U234	1.1686E-05	0%
	25	2.6488E-03	PU239	2.4473E-03	92%	PU240	1.8044E-04	7%	U234	1.1549E-05	0%
	59	2.6279E-03	PU239	2.4280E-03	92%	PU240	1.7902E-04	7%	U234	1.1458E-05	0%
	10	2.5862E-03	PU239	2.3894E-03	92%	PU240	1.7618E-04	7%	U234	1.1276E-05	0%
	5	2.5447E-03	PU239	2.3510E-03	92%	PU240	1.7335E-04	7%	U234	1.1095E-05	0%
	36	2.5136E-03	PU239	2.3223E-03	92%	PU240	1.7123E-04	7%	U234	1.0959E-05	0%
	45	2.4929E-03	PU239	2.3032E-03	92%	PU240	1.6982E-04	7%	U234	1.0869E-05	0%

Table B-6. (Concluded)

Comp. Scen ID	Vector	Total Integrated Discharge	Top 3 Radionuclides Contribution to Integrated Discharge (Time of Intrusion, 9000 years)								
04	19	4.1403E-03	PU239	3.8579E-03	93%	PU240	2.4373E-04	6%	U234	1.9176E-05	0%
	35	4.1070E-03	PU239	3.8269E-03	93%	PU240	2.4178E-04	6%	U234	1.9022E-05	0%
	55	4.0738E-03	PU239	3.7959E-03	93%	PU240	2.3982E-04	6%	U234	1.8868E-05	0%
	16	4.0517E-03	PU239	3.7753E-03	93%	PU240	2.3852E-04	6%	U234	1.8766E-05	0%
	46	4.0186E-03	PU239	3.7445E-03	93%	PU240	2.3657E-04	6%	U234	1.8613E-05	0%
	24	3.9747E-03	PU239	3.7036E-03	93%	PU240	2.3399E-04	6%	U234	1.8409E-05	0%
	4	3.9418E-03	PU239	3.6729E-03	93%	PU240	2.3205E-04	6%	U234	1.8257E-05	0%
	14	3.9199E-03	PU239	3.6525E-03	93%	PU240	2.3076E-04	6%	U234	1.8155E-05	0%
	13	3.8980E-03	PU239	3.6321E-03	93%	PU240	2.2947E-04	6%	U234	1.8054E-05	0%
	51	3.8653E-03	PU239	3.6017E-03	93%	PU240	2.2755E-04	6%	U234	1.7903E-05	0%
	39	3.8435E-03	PU239	3.5814E-03	93%	PU240	2.2627E-04	6%	U234	1.7802E-05	0%
	1	3.7892E-03	PU239	3.5308E-03	93%	PU240	2.2307E-04	6%	U234	1.7550E-05	0%
	53	3.7568E-03	PU239	3.5005E-03	93%	PU240	2.2116E-04	6%	U234	1.7400E-05	0%
	18	3.7352E-03	PU239	3.4804E-03	93%	PU240	2.1989E-04	6%	U234	1.7300E-05	0%
	52	3.6920E-03	PU239	3.4402E-03	93%	PU240	2.1735E-04	6%	U234	1.7100E-05	0%
	27	3.6598E-03	PU239	3.4102E-03	93%	PU240	2.1545E-04	6%	U234	1.6951E-05	0%
	49	3.6383E-03	PU239	3.3902E-03	93%	PU240	2.1419E-04	6%	U234	1.6851E-05	0%
	38	3.5848E-03	PU239	3.3403E-03	93%	PU240	2.1104E-04	6%	U234	1.6604E-05	0%
	21	3.5742E-03	PU239	3.3304E-03	93%	PU240	2.1041E-04	6%	U234	1.6554E-05	0%
	17	3.5422E-03	PU239	3.3006E-03	93%	PU240	2.0853E-04	6%	U234	1.6406E-05	0%
	44	3.5103E-03	PU239	3.2708E-03	93%	PU240	2.0665E-04	6%	U234	1.6258E-05	0%
	30	3.4679E-03	PU239	3.2313E-03	93%	PU240	2.0415E-04	6%	U234	1.6062E-05	0%
	3	3.4361E-03	PU239	3.2017E-03	93%	PU240	2.0228E-04	6%	U234	1.5915E-05	0%
	37	3.4150E-03	PU239	3.1821E-03	93%	PU240	2.0104E-04	6%	U234	1.5817E-05	0%
	43	3.3834E-03	PU239	3.1526E-03	93%	PU240	1.9918E-04	6%	U234	1.5671E-05	0%
	33	3.3519E-03	PU239	3.1232E-03	93%	PU240	1.9732E-04	6%	U234	1.5525E-05	0%
	32	3.3100E-03	PU239	3.0842E-03	93%	PU240	1.9485E-04	6%	U234	1.5330E-05	0%
	28	3.2890E-03	PU239	3.0647E-03	93%	PU240	1.9362E-04	6%	U234	1.5234E-05	0%
	6	3.2682E-03	PU239	3.0452E-03	93%	PU240	1.9239E-04	6%	U234	1.5137E-05	0%
	60	3.2161E-03	PU239	2.9967E-03	93%	PU240	1.8933E-04	6%	U234	1.4896E-05	0%
	47	3.2057E-03	PU239	2.9870E-03	93%	PU240	1.8872E-04	6%	U234	1.4848E-05	0%
	41	3.1746E-03	PU239	2.9581E-03	93%	PU240	1.8689E-04	6%	U234	1.4704E-05	0%
	26	3.1436E-03	PU239	2.9291E-03	93%	PU240	1.8506E-04	6%	U234	1.4560E-05	0%
	11	3.1023E-03	PU239	2.8907E-03	93%	PU240	1.8263E-04	6%	U234	1.4369E-05	0%
	57	3.0714E-03	PU239	2.8619E-03	93%	PU240	1.8081E-04	6%	U234	1.4226E-05	0%
	7	3.0406E-03	PU239	2.8332E-03	93%	PU240	1.7900E-04	6%	U234	1.4083E-05	0%
	29	3.0202E-03	PU239	2.8141E-03	93%	PU240	1.7779E-04	6%	U234	1.3988E-05	0%
	9	2.9793E-03	PU239	2.7761E-03	93%	PU240	1.7539E-04	6%	U234	1.3799E-05	0%
	8	2.9385E-03	PU239	2.7381E-03	93%	PU240	1.7299E-04	6%	U234	1.3610E-05	0%
	15	2.9284E-03	PU239	2.7286E-03	93%	PU240	1.7239E-04	6%	U234	1.3563E-05	0%
	40	2.9081E-03	PU239	2.7097E-03	93%	PU240	1.7120E-04	6%	U234	1.3469E-05	0%
	48	2.8473E-03	PU239	2.6531E-03	93%	PU240	1.6762E-04	6%	U234	1.3188E-05	0%
	20	2.8272E-03	PU239	2.6343E-03	93%	PU240	1.6643E-04	6%	U234	1.3094E-05	0%
	54	2.7970E-03	PU239	2.6062E-03	93%	PU240	1.6466E-04	6%	U234	1.2955E-05	0%
	31	2.7568E-03	PU239	2.5688E-03	93%	PU240	1.6229E-04	6%	U234	1.2769E-05	0%
	23	2.7568E-03	PU239	2.5688E-03	93%	PU240	1.6229E-04	6%	U234	1.2769E-05	0%
	12	2.7168E-03	PU239	2.5315E-03	93%	PU240	1.5994E-04	6%	U234	1.2583E-05	0%
	42	2.6968E-03	PU239	2.5129E-03	93%	PU240	1.5876E-04	6%	U234	1.2491E-05	0%
	58	2.6471E-03	PU239	2.4665E-03	93%	PU240	1.5583E-04	6%	U234	1.2260E-05	0%
	34	2.6371E-03	PU239	2.4573E-03	93%	PU240	1.5525E-04	6%	U234	1.2214E-05	0%
	2	2.5876E-03	PU239	2.4111E-03	93%	PU240	1.5233E-04	6%	U234	1.1985E-05	0%
	56	2.5580E-03	PU239	2.3835E-03	93%	PU240	1.5059E-04	6%	U234	1.1848E-05	0%
	50	2.5285E-03	PU239	2.3560E-03	93%	PU240	1.4885E-04	6%	U234	1.1711E-05	0%
	22	2.5088E-03	PU239	2.3377E-03	93%	PU240	1.4769E-04	6%	U234	1.1620E-05	0%
	25	2.4794E-03	PU239	2.3103E-03	93%	PU240	1.4596E-04	6%	U234	1.1484E-05	0%
	59	2.4598E-03	PU239	2.2921E-03	93%	PU240	1.4481E-04	6%	U234	1.1393E-05	0%
	10	2.4208E-03	PU239	2.2557E-03	93%	PU240	1.4251E-04	6%	U234	1.1212E-05	0%
	5	2.3819E-03	PU239	2.2194E-03	93%	PU240	1.4022E-04	6%	U234	1.1032E-05	0%
	36	2.3528E-03	PU239	2.1923E-03	93%	PU240	1.3851E-04	6%	U234	1.0897E-05	0%
	45	2.3334E-03	PU239	2.1743E-03	93%	PU240	1.3737E-04	6%	U234	1.0808E-05	0%

Table B-7 lists total EPA summed normalized release and the percentage contribution for the top 3 radionuclides for each vector when drilling into an RH waste cask with an average activity level. Vectors are ordered from most to least release. All vectors have some small release when intruding into the repository from drilling.

Table B-7. Integrated Discharge to the Accessible Environment by Bringing Average RH-Activity Cuttings to the Surface when Initially Drilling through the Repository.

Comp. Scen ID	Vector	Total Integrated Discharge	Top 3 Radionuclides Contribution to Integrated Discharge (Time of Intrusion, 1000 years)								
00	19	1.0006E-04	PU239	5.8991E-05	59%	AM241	1.7911E-05	18%	PU240	1.2919E-05	13%
	35	9.9256E-05	PU239	5.8517E-05	59%	AM241	1.7767E-05	18%	PU240	1.2815E-05	13%
	55	9.8453E-05	PU239	5.8044E-05	59%	AM241	1.7624E-05	18%	PU240	1.2711E-05	13%
	16	9.7919E-05	PU239	5.7730E-05	59%	AM241	1.7528E-05	18%	PU240	1.2642E-05	13%
	46	9.7120E-05	PU239	5.7259E-05	59%	AM241	1.7385E-05	18%	PU240	1.2539E-05	13%
	24	9.6057E-05	PU239	5.6632E-05	59%	AM241	1.7195E-05	18%	PU240	1.2402E-05	13%
	4	9.5262E-05	PU239	5.6163E-05	59%	AM241	1.7053E-05	18%	PU240	1.2299E-05	13%
	14	9.4733E-05	PU239	5.5851E-05	59%	AM241	1.6958E-05	18%	PU240	1.2231E-05	13%
	13	9.4205E-05	PU239	5.5540E-05	59%	AM241	1.6863E-05	18%	PU240	1.2163E-05	13%
	51	9.3414E-05	PU239	5.5074E-05	59%	AM241	1.6722E-05	18%	PU240	1.2061E-05	13%
	39	9.2888E-05	PU239	5.4764E-05	59%	AM241	1.6628E-05	18%	PU240	1.1993E-05	13%
	1	9.1576E-05	PU239	5.3990E-05	59%	AM241	1.6393E-05	18%	PU240	1.1823E-05	13%
	53	9.0791E-05	PU239	5.3527E-05	59%	AM241	1.6252E-05	18%	PU240	1.1722E-05	13%
	18	9.0269E-05	PU239	5.3219E-05	59%	AM241	1.6159E-05	18%	PU240	1.1655E-05	13%
	52	8.9227E-05	PU239	5.2605E-05	59%	AM241	1.5972E-05	18%	PU240	1.1520E-05	13%
	27	8.8448E-05	PU239	5.2146E-05	59%	AM241	1.5833E-05	18%	PU240	1.1419E-05	13%
	49	8.7929E-05	PU239	5.1840E-05	59%	AM241	1.5740E-05	18%	PU240	1.1352E-05	13%
	38	8.6636E-05	PU239	5.1078E-05	59%	AM241	1.5508E-05	18%	PU240	1.1185E-05	13%
	21	8.6378E-05	PU239	5.0925E-05	59%	AM241	1.5462E-05	18%	PU240	1.1152E-05	13%
	17	8.5605E-05	PU239	5.0470E-05	59%	AM241	1.5324E-05	18%	PU240	1.1052E-05	13%
	44	8.4834E-05	PU239	5.0015E-05	59%	AM241	1.5186E-05	18%	PU240	1.0953E-05	13%
	30	8.3809E-05	PU239	4.9411E-05	59%	AM241	1.5002E-05	18%	PU240	1.0820E-05	13%
	3	8.3042E-05	PU239	4.8959E-05	59%	AM241	1.4865E-05	18%	PU240	1.0721E-05	13%
	37	8.2532E-05	PU239	4.8658E-05	59%	AM241	1.4774E-05	18%	PU240	1.0656E-05	13%
	43	8.1768E-05	PU239	4.8208E-05	59%	AM241	1.4637E-05	18%	PU240	1.0557E-05	13%
	33	8.1006E-05	PU239	4.7758E-05	59%	AM241	1.4501E-05	18%	PU240	1.0459E-05	13%
	32	7.9993E-05	PU239	4.7161E-05	59%	AM241	1.4319E-05	18%	PU240	1.0328E-05	13%
	28	7.9488E-05	PU239	4.6863E-05	59%	AM241	1.4229E-05	18%	PU240	1.0263E-05	13%
	6	7.8983E-05	PU239	4.6565E-05	59%	AM241	1.4138E-05	18%	PU240	1.0197E-05	13%
	60	7.7725E-05	PU239	4.5824E-05	59%	AM241	1.3913E-05	18%	PU240	1.0035E-05	13%
	47	7.7474E-05	PU239	4.5676E-05	59%	AM241	1.3868E-05	18%	PU240	1.0003E-05	13%
	41	7.6722E-05	PU239	4.5232E-05	59%	AM241	1.3734E-05	18%	PU240	9.9054E-06	13%
	26	7.5972E-05	PU239	4.4790E-05	59%	AM241	1.3599E-05	18%	PU240	9.8086E-06	13%
	11	7.4974E-05	PU239	4.4202E-05	59%	AM241	1.3421E-05	18%	PU240	9.6798E-06	13%
	57	7.4229E-05	PU239	4.3762E-05	59%	AM241	1.3287E-05	18%	PU240	9.5835E-06	13%
	7	7.3484E-05	PU239	4.3324E-05	59%	AM241	1.3154E-05	18%	PU240	9.4874E-06	13%
	29	7.2989E-05	PU239	4.3032E-05	59%	AM241	1.3066E-05	18%	PU240	9.4235E-06	13%
	9	7.2001E-05	PU239	4.2449E-05	59%	AM241	1.2889E-05	18%	PU240	9.2960E-06	13%
	8	7.1017E-05	PU239	4.1869E-05	59%	AM241	1.2712E-05	18%	PU240	9.1689E-06	13%
	15	7.0771E-05	PU239	4.1724E-05	59%	AM241	1.2668E-05	18%	PU240	9.1371E-06	13%
	40	7.0280E-05	PU239	4.1435E-05	59%	AM241	1.2581E-05	18%	PU240	9.0738E-06	13%
	48	6.8813E-05	PU239	4.0570E-05	59%	AM241	1.2318E-05	18%	PU240	8.8843E-06	13%
	20	6.8325E-05	PU239	4.0282E-05	59%	AM241	1.2231E-05	18%	PU240	8.8214E-06	13%
	54	6.7596E-05	PU239	3.9852E-05	59%	AM241	1.2100E-05	18%	PU240	8.7272E-06	13%
	31	6.6625E-05	PU239	3.9280E-05	59%	AM241	1.1926E-05	18%	PU240	8.6019E-06	13%
	23	6.6625E-05	PU239	3.9280E-05	59%	AM241	1.1926E-05	18%	PU240	8.6019E-06	13%
	12	6.5658E-05	PU239	3.8710E-05	59%	AM241	1.1753E-05	18%	PU240	8.4770E-06	13%
	42	6.5176E-05	PU239	3.8425E-05	59%	AM241	1.1667E-05	18%	PU240	8.4147E-06	13%
	58	6.3973E-05	PU239	3.7716E-05	59%	AM241	1.1452E-05	18%	PU240	8.2594E-06	13%
	34	6.3733E-05	PU239	3.7575E-05	59%	AM241	1.1409E-05	18%	PU240	8.2285E-06	13%
	2	6.2536E-05	PU239	3.6869E-05	59%	AM241	1.1194E-05	18%	PU240	8.0740E-06	13%
	56	6.1821E-05	PU239	3.6447E-05	59%	AM241	1.1066E-05	18%	PU240	7.9816E-06	13%
	50	6.1107E-05	PU239	3.6026E-05	59%	AM241	1.0939E-05	18%	PU240	7.8894E-06	13%
	22	6.0632E-05	PU239	3.5746E-05	59%	AM241	1.0853E-05	18%	PU240	7.8281E-06	13%

Table B-7. (Continued)

Comp. Scen ID	Vector	Total Integrated Discharge	Top 3 Radionuclides Contribution to Integrated Discharge								
			(Time of Intrusion, 1000 years)								
00	25	5.9921E-05	PU239	3.5327E-05	59%	AM241	1.0726E-05	18%	PU240	7.7363E-06	13%
	59	5.9448E-05	PU239	3.5048E-05	59%	AM241	1.0642E-05	18%	PU240	7.6752E-06	13%
	10	5.8505E-05	PU239	3.4492E-05	59%	AM241	1.0473E-05	18%	PU240	7.5534E-06	13%
	5	5.7564E-05	PU239	3.3938E-05	59%	AM241	1.0304E-05	18%	PU240	7.4320E-06	13%
	36	5.6861E-05	PU239	3.3523E-05	59%	AM241	1.0178E-05	18%	PU240	7.3412E-06	13%
	45	5.6393E-05	PU239	3.3247E-05	59%	AM241	1.0095E-05	18%	PU240	7.2808E-06	13%

Table B-7. (Continued)

Comp. Scen ID	Vector	Total Integrated Discharge	Top 3 Radionuclides Contribution to Integrated Discharge (Time of Intrusion, 3000 years)								
01	19	7.8452E-05	PU239	5.5689E-05	71%	PU240	1.0450E-05	13%	U233	9.1950E-06	12%
	35	7.7822E-05	PU239	5.5242E-05	71%	PU240	1.0366E-05	13%	U233	9.1211E-06	12%
	55	7.7193E-05	PU239	5.4795E-05	71%	PU240	1.0282E-05	13%	U233	9.0474E-06	12%
	16	7.6774E-05	PU239	5.4498E-05	71%	PU240	1.0226E-05	13%	U233	8.9983E-06	12%
	46	7.6148E-05	PU239	5.4053E-05	71%	PU240	1.0143E-05	13%	U233	8.9249E-06	12%
	24	7.5314E-05	PU239	5.3462E-05	71%	PU240	1.0032E-05	13%	U233	8.8272E-06	12%
	4	7.4691E-05	PU239	5.3019E-05	71%	PU240	9.9489E-06	13%	U233	8.7541E-06	12%
	14	7.4276E-05	PU239	5.2725E-05	71%	PU240	9.8937E-06	13%	U233	8.7055E-06	12%
	13	7.3862E-05	PU239	5.2431E-05	71%	PU240	9.8385E-06	13%	U233	8.6570E-06	12%
	51	7.3242E-05	PU239	5.1991E-05	71%	PU240	9.7559E-06	13%	U233	8.5843E-06	12%
	39	7.2830E-05	PU239	5.1698E-05	71%	PU240	9.7009E-06	13%	U233	8.5360E-06	12%
	1	7.1801E-05	PU239	5.0968E-05	71%	PU240	9.5639E-06	13%	U233	8.4154E-06	12%
	53	7.1186E-05	PU239	5.0531E-05	71%	PU240	9.4820E-06	13%	U233	8.3433E-06	12%
	18	7.0776E-05	PU239	5.0240E-05	71%	PU240	9.4274E-06	13%	U233	8.2953E-06	12%
	52	6.9959E-05	PU239	4.9660E-05	71%	PU240	9.3186E-06	13%	U233	8.1995E-06	12%
	27	6.9348E-05	PU239	4.9227E-05	71%	PU240	9.2372E-06	13%	U233	8.1279E-06	12%
	49	6.8941E-05	PU239	4.8938E-05	71%	PU240	9.1830E-06	13%	U233	8.0803E-06	12%
	38	6.7928E-05	PU239	4.8218E-05	71%	PU240	9.0480E-06	13%	U233	7.9614E-06	12%
	21	6.7725E-05	PU239	4.8075E-05	71%	PU240	9.0211E-06	13%	U233	7.9377E-06	12%
	17	6.7119E-05	PU239	4.7645E-05	71%	PU240	8.9404E-06	13%	U233	7.8667E-06	12%
	44	6.6515E-05	PU239	4.7215E-05	71%	PU240	8.8598E-06	13%	U233	7.7959E-06	12%
	30	6.5711E-05	PU239	4.6645E-05	71%	PU240	8.7528E-06	13%	U233	7.7016E-06	12%
	3	6.5110E-05	PU239	4.6218E-05	71%	PU240	8.6727E-06	13%	U233	7.6312E-06	12%
	37	6.4710E-05	PU239	4.5934E-05	71%	PU240	8.6194E-06	13%	U233	7.5843E-06	12%
	43	6.4111E-05	PU239	4.5509E-05	71%	PU240	8.5396E-06	13%	U233	7.5141E-06	12%
	33	6.3514E-05	PU239	4.5085E-05	71%	PU240	8.4600E-06	13%	U233	7.4441E-06	12%
	32	6.2719E-05	PU239	4.4521E-05	71%	PU240	8.3542E-06	13%	U233	7.3510E-06	12%
	28	6.2323E-05	PU239	4.4240E-05	71%	PU240	8.3014E-06	13%	U233	7.3045E-06	12%
	6	6.1927E-05	PU239	4.3959E-05	71%	PU240	8.2487E-06	13%	U233	7.2581E-06	12%
	60	6.0941E-05	PU239	4.3259E-05	71%	PU240	8.1173E-06	13%	U233	7.1425E-06	12%
	47	6.0744E-05	PU239	4.3119E-05	71%	PU240	8.0911E-06	13%	U233	7.1194E-06	12%
	41	6.0154E-05	PU239	4.2700E-05	71%	PU240	8.0126E-06	13%	U233	7.0504E-06	12%
	26	5.9566E-05	PU239	4.2283E-05	71%	PU240	7.9342E-06	13%	U233	6.9814E-06	12%
	11	5.8784E-05	PU239	4.1728E-05	71%	PU240	7.8301E-06	13%	U233	6.8898E-06	12%
	57	5.8199E-05	PU239	4.1313E-05	71%	PU240	7.7522E-06	13%	U233	6.8212E-06	12%
	7	5.7616E-05	PU239	4.0899E-05	71%	PU240	7.6745E-06	13%	U233	6.7528E-06	12%
	29	5.7228E-05	PU239	4.0623E-05	71%	PU240	7.6228E-06	13%	U233	6.7073E-06	12%
	9	5.6453E-05	PU239	4.0073E-05	71%	PU240	7.5196E-06	13%	U233	6.6166E-06	12%
	8	5.5681E-05	PU239	3.9525E-05	71%	PU240	7.4168E-06	13%	U233	6.5261E-06	12%
	15	5.5489E-05	PU239	3.9388E-05	71%	PU240	7.3911E-06	13%	U233	6.5035E-06	12%
	40	5.5104E-05	PU239	3.9115E-05	71%	PU240	7.3399E-06	13%	U233	6.4584E-06	12%
	48	5.3953E-05	PU239	3.8299E-05	71%	PU240	7.1866E-06	13%	U233	6.3236E-06	12%
	20	5.3571E-05	PU239	3.8027E-05	71%	PU240	7.1357E-06	13%	U233	6.2788E-06	12%
	54	5.2999E-05	PU239	3.7621E-05	71%	PU240	7.0595E-06	13%	U233	6.2117E-06	12%
	31	5.2238E-05	PU239	3.7081E-05	71%	PU240	6.9581E-06	13%	U233	6.1225E-06	12%
	23	5.2238E-05	PU239	3.7081E-05	71%	PU240	6.9581E-06	13%	U233	6.1225E-06	12%
	12	5.1480E-05	PU239	3.6543E-05	71%	PU240	6.8571E-06	13%	U233	6.0336E-06	12%
	42	5.1101E-05	PU239	3.6274E-05	71%	PU240	6.8067E-06	13%	U233	5.9893E-06	12%
	58	5.0158E-05	PU239	3.5605E-05	71%	PU240	6.6811E-06	13%	U233	5.8788E-06	12%
	34	4.9970E-05	PU239	3.5471E-05	71%	PU240	6.6561E-06	13%	U233	5.8567E-06	12%
	2	4.9032E-05	PU239	3.4805E-05	71%	PU240	6.5311E-06	13%	U233	5.7468E-06	12%
	56	4.8471E-05	PU239	3.4407E-05	71%	PU240	6.4564E-06	13%	U233	5.6810E-06	12%
	50	4.7911E-05	PU239	3.4010E-05	71%	PU240	6.3818E-06	13%	U233	5.6154E-06	12%
	22	4.7539E-05	PU239	3.3745E-05	71%	PU240	6.3322E-06	13%	U233	5.5718E-06	12%
	25	4.6982E-05	PU239	3.3350E-05	71%	PU240	6.2580E-06	13%	U233	5.5064E-06	12%
	59	4.6611E-05	PU239	3.3087E-05	71%	PU240	6.2086E-06	13%	U233	5.4630E-06	12%
	10	4.5871E-05	PU239	3.2561E-05	71%	PU240	6.1100E-06	13%	U233	5.3763E-06	12%
	5	4.5134E-05	PU239	3.2038E-05	71%	PU240	6.0118E-06	13%	U233	5.2899E-06	12%
	36	4.4582E-05	PU239	3.1647E-05	71%	PU240	5.9384E-06	13%	U233	5.2252E-06	12%
	45	4.4215E-05	PU239	3.1386E-05	71%	PU240	5.8895E-06	13%	U233	5.1822E-06	12%

Table B-7. (Continued)

Comp. Scen ID	Vector	Total Integrated Discharge	Top 3 Radionuclides Contribution to Integrated Discharge (Time of Intrusion, 5000 years)								
02	19	7.3751E-05	PU239	5.2572E-05	71%	U233	9.1156E-06	12%	PU240	8.4530E-06	11%
	35	7.3158E-05	PU239	5.2149E-05	71%	U233	9.0423E-06	12%	PU240	8.3851E-06	11%
	55	7.2567E-05	PU239	5.1728E-05	71%	U233	8.9692E-06	12%	PU240	8.3173E-06	11%
	16	7.2173E-05	PU239	5.1447E-05	71%	U233	8.9206E-06	12%	PU240	8.2722E-06	11%
	46	7.1584E-05	PU239	5.1028E-05	71%	U233	8.8478E-06	12%	PU240	8.2047E-06	11%
	24	7.0801E-05	PU239	5.0469E-05	71%	U233	8.7510E-06	12%	PU240	8.1149E-06	11%
	4	7.0215E-05	PU239	5.0051E-05	71%	U233	8.6785E-06	12%	PU240	8.0478E-06	11%
	14	6.9825E-05	PU239	4.9773E-05	71%	U233	8.6303E-06	12%	PU240	8.0031E-06	11%
	13	6.9436E-05	PU239	4.9496E-05	71%	U233	8.5822E-06	12%	PU240	7.9584E-06	11%
	51	6.8853E-05	PU239	4.9080E-05	71%	U233	8.5102E-06	12%	PU240	7.8916E-06	11%
	39	6.8465E-05	PU239	4.8804E-05	71%	U233	8.4622E-06	12%	PU240	7.8472E-06	11%
	1	6.7498E-05	PU239	4.8115E-05	71%	U233	8.3427E-06	12%	PU240	7.7363E-06	11%
	53	6.6919E-05	PU239	4.7702E-05	71%	U233	8.2712E-06	12%	PU240	7.6700E-06	11%
	18	6.6535E-05	PU239	4.7428E-05	71%	U233	8.2237E-06	12%	PU240	7.6259E-06	11%
	52	6.5767E-05	PU239	4.6880E-05	71%	U233	8.1287E-06	12%	PU240	7.5379E-06	11%
	27	6.5192E-05	PU239	4.6471E-05	71%	U233	8.0577E-06	12%	PU240	7.4721E-06	11%
	49	6.4810E-05	PU239	4.6198E-05	71%	U233	8.0105E-06	12%	PU240	7.4282E-06	11%
	38	6.3857E-05	PU239	4.5519E-05	71%	U233	7.8927E-06	12%	PU240	7.3190E-06	11%
	21	6.3667E-05	PU239	4.5384E-05	71%	U233	7.8692E-06	12%	PU240	7.2972E-06	11%
	17	6.3097E-05	PU239	4.4978E-05	71%	U233	7.7988E-06	12%	PU240	7.2319E-06	11%
	44	6.2529E-05	PU239	4.4572E-05	71%	U233	7.7285E-06	12%	PU240	7.1668E-06	11%
	30	6.1773E-05	PU239	4.4034E-05	71%	U233	7.6351E-06	12%	PU240	7.0802E-06	11%
	3	6.1208E-05	PU239	4.3631E-05	71%	U233	7.5653E-06	12%	PU240	7.0154E-06	11%
	37	6.0832E-05	PU239	4.3363E-05	71%	U233	7.5188E-06	12%	PU240	6.9723E-06	11%
	43	6.0269E-05	PU239	4.2961E-05	71%	U233	7.4492E-06	12%	PU240	6.9078E-06	11%
	33	5.9707E-05	PU239	4.2561E-05	71%	U233	7.3798E-06	12%	PU240	6.8434E-06	11%
	32	5.8960E-05	PU239	4.2029E-05	71%	U233	7.2875E-06	12%	PU240	6.7578E-06	11%
	28	5.8588E-05	PU239	4.1763E-05	71%	U233	7.2414E-06	12%	PU240	6.7151E-06	11%
	6	5.8216E-05	PU239	4.1498E-05	71%	U233	7.1955E-06	12%	PU240	6.6725E-06	11%
	60	5.7288E-05	PU239	4.0837E-05	71%	U233	7.0808E-06	12%	PU240	6.5662E-06	11%
	47	5.7103E-05	PU239	4.0705E-05	71%	U233	7.0580E-06	12%	PU240	6.5450E-06	11%
	41	5.6549E-05	PU239	4.0310E-05	71%	U233	6.9895E-06	12%	PU240	6.4815E-06	11%
	26	5.5996E-05	PU239	3.9916E-05	71%	U233	6.9211E-06	12%	PU240	6.4181E-06	11%
	11	5.5261E-05	PU239	3.9392E-05	71%	U233	6.8303E-06	12%	PU240	6.3338E-06	11%
	57	5.4711E-05	PU239	3.9000E-05	71%	U233	6.7623E-06	12%	PU240	6.2708E-06	11%
	7	5.4163E-05	PU239	3.8609E-05	71%	U233	6.6945E-06	12%	PU240	6.2079E-06	11%
	29	5.3798E-05	PU239	3.8349E-05	71%	U233	6.6494E-06	12%	PU240	6.1661E-06	11%
	9	5.3070E-05	PU239	3.7830E-05	71%	U233	6.5594E-06	12%	PU240	6.0827E-06	11%
	8	5.2344E-05	PU239	3.7313E-05	71%	U233	6.4697E-06	12%	PU240	5.9995E-06	11%
	15	5.2163E-05	PU239	3.7184E-05	71%	U233	6.4474E-06	12%	PU240	5.9787E-06	11%
	40	5.1802E-05	PU239	3.6926E-05	71%	U233	6.4026E-06	12%	PU240	5.9373E-06	11%
	48	5.0720E-05	PU239	3.6155E-05	71%	U233	6.2690E-06	12%	PU240	5.8133E-06	11%
	20	5.0361E-05	PU239	3.5899E-05	71%	U233	6.2245E-06	12%	PU240	5.7721E-06	11%
	54	4.9823E-05	PU239	3.5515E-05	71%	U233	6.1581E-06	12%	PU240	5.7105E-06	11%
	31	4.9107E-05	PU239	3.5005E-05	71%	U233	6.0697E-06	12%	PU240	5.6285E-06	11%
	23	4.9107E-05	PU239	3.5005E-05	71%	U233	6.0697E-06	12%	PU240	5.6285E-06	11%
	12	4.8394E-05	PU239	3.4497E-05	71%	U233	5.9815E-06	12%	PU240	5.5468E-06	11%
	42	4.8039E-05	PU239	3.4244E-05	71%	U233	5.9376E-06	12%	PU240	5.5060E-06	11%
	58	4.7152E-05	PU239	3.3612E-05	71%	U233	5.8280E-06	12%	PU240	5.4044E-06	11%
	34	4.6976E-05	PU239	3.3486E-05	71%	U233	5.8062E-06	12%	PU240	5.3842E-06	11%
	2	4.6094E-05	PU239	3.2857E-05	71%	U233	5.6972E-06	12%	PU240	5.2831E-06	11%
	56	4.5566E-05	PU239	3.2481E-05	71%	U233	5.6320E-06	12%	PU240	5.2226E-06	11%
	50	4.5040E-05	PU239	3.2106E-05	71%	U233	5.5669E-06	12%	PU240	5.1623E-06	11%
	22	4.4690E-05	PU239	3.1856E-05	71%	U233	5.5237E-06	12%	PU240	5.1222E-06	11%
	25	4.4166E-05	PU239	3.1483E-05	71%	U233	5.4589E-06	12%	PU240	5.0621E-06	11%
	59	4.3817E-05	PU239	3.1234E-05	71%	U233	5.4158E-06	12%	PU240	5.0222E-06	11%
	10	4.3122E-05	PU239	3.0739E-05	71%	U233	5.3299E-06	12%	PU240	4.9425E-06	11%
	5	4.2429E-05	PU239	3.0245E-05	71%	U233	5.2442E-06	12%	PU240	4.8630E-06	11%
	36	4.1910E-05	PU239	2.9875E-05	71%	U233	5.1801E-06	12%	PU240	4.8036E-06	11%
	45	4.1566E-05	PU239	2.9629E-05	71%	U233	5.1375E-06	12%	PU240	4.7641E-06	11%

Table B-7. (Continued)

Comp. Scen ID	Vector	Total Integrated Discharge	Top 3 Radionuclides Contribution to Integrated Discharge								
			(Time of Intrusion, 7000 years)								
03	19	7.0056E-05	PU239	4.9629E-05	71%	U233	9.0369E-06	13%	PU240	6.8377E-06	10%
	35	6.9493E-05	PU239	4.9230E-05	71%	U233	8.9642E-06	13%	PU240	6.7828E-06	10%
	55	6.8931E-05	PU239	4.8832E-05	71%	U233	8.8918E-06	13%	PU240	6.7279E-06	10%
	16	6.8557E-05	PU239	4.8567E-05	71%	U233	8.8436E-06	13%	PU240	6.6915E-06	10%
	46	6.7998E-05	PU239	4.8171E-05	71%	U233	8.7714E-06	13%	PU240	6.6369E-06	10%
	24	6.7254E-05	PU239	4.7644E-05	71%	U233	8.6754E-06	13%	PU240	6.5642E-06	10%
	4	6.6697E-05	PU239	4.7250E-05	71%	U233	8.6036E-06	13%	PU240	6.5099E-06	10%
	14	6.6327E-05	PU239	4.6987E-05	71%	U233	8.5558E-06	13%	PU240	6.4737E-06	10%
	13	6.5957E-05	PU239	4.6725E-05	71%	U233	8.5081E-06	13%	PU240	6.4377E-06	10%
	51	6.5403E-05	PU239	4.6333E-05	71%	U233	8.4367E-06	13%	PU240	6.3836E-06	10%
	39	6.5035E-05	PU239	4.6072E-05	71%	U233	8.3892E-06	13%	PU240	6.3477E-06	10%
	1	6.4116E-05	PU239	4.5421E-05	71%	U233	8.2707E-06	13%	PU240	6.2580E-06	10%
	53	6.3567E-05	PU239	4.5032E-05	71%	U233	8.1998E-06	13%	PU240	6.2044E-06	10%
	18	6.3201E-05	PU239	4.4773E-05	71%	U233	8.1526E-06	13%	PU240	6.1687E-06	10%
	52	6.2472E-05	PU239	4.4256E-05	71%	U233	8.0585E-06	13%	PU240	6.0975E-06	10%
	27	6.1926E-05	PU239	4.3870E-05	71%	U233	7.9881E-06	13%	PU240	6.0442E-06	10%
	49	6.1563E-05	PU239	4.3612E-05	71%	U233	7.9413E-06	13%	PU240	6.0088E-06	10%
	38	6.0657E-05	PU239	4.2971E-05	71%	U233	7.8245E-06	13%	PU240	5.9204E-06	10%
	21	6.0477E-05	PU239	4.2843E-05	71%	U233	7.8012E-06	13%	PU240	5.9028E-06	10%
	17	5.9936E-05	PU239	4.2460E-05	71%	U233	7.7314E-06	13%	PU240	5.8500E-06	10%
	44	5.9396E-05	PU239	4.2077E-05	71%	U233	7.6618E-06	13%	PU240	5.7973E-06	10%
	30	5.8678E-05	PU239	4.1569E-05	71%	U233	7.5692E-06	13%	PU240	5.7272E-06	10%
	3	5.8141E-05	PU239	4.1188E-05	71%	U233	7.5000E-06	13%	PU240	5.6748E-06	10%
	37	5.7784E-05	PU239	4.0935E-05	71%	U233	7.4539E-06	13%	PU240	5.6400E-06	10%
	43	5.7249E-05	PU239	4.0557E-05	71%	U233	7.3849E-06	13%	PU240	5.5878E-06	10%
	33	5.6716E-05	PU239	4.0179E-05	71%	U233	7.3161E-06	13%	PU240	5.5357E-06	10%
	32	5.6006E-05	PU239	3.9676E-05	71%	U233	7.2246E-06	13%	PU240	5.4664E-06	10%
	28	5.5652E-05	PU239	3.9425E-05	71%	U233	7.1789E-06	13%	PU240	5.4319E-06	10%
	6	5.5299E-05	PU239	3.9175E-05	71%	U233	7.1333E-06	13%	PU240	5.3974E-06	10%
	60	5.4418E-05	PU239	3.8551E-05	71%	U233	7.0197E-06	13%	PU240	5.3114E-06	10%
	47	5.4242E-05	PU239	3.8427E-05	71%	U233	6.9970E-06	13%	PU240	5.2943E-06	10%
	41	5.3716E-05	PU239	3.8054E-05	71%	U233	6.9291E-06	13%	PU240	5.2429E-06	10%
	26	5.3191E-05	PU239	3.7682E-05	71%	U233	6.8614E-06	13%	PU240	5.1916E-06	10%
	11	5.2493E-05	PU239	3.7187E-05	71%	U233	6.7713E-06	13%	PU240	5.1235E-06	10%
	57	5.1970E-05	PU239	3.6817E-05	71%	U233	6.7039E-06	13%	PU240	5.0725E-06	10%
	7	5.1449E-05	PU239	3.6448E-05	71%	U233	6.6367E-06	13%	PU240	5.0217E-06	10%
	29	5.1103E-05	PU239	3.6202E-05	71%	U233	6.5920E-06	13%	PU240	4.9878E-06	10%
	9	5.0411E-05	PU239	3.5712E-05	71%	U233	6.5028E-06	13%	PU240	4.9203E-06	10%
	8	4.9722E-05	PU239	3.5224E-05	71%	U233	6.4139E-06	13%	PU240	4.8530E-06	10%
	15	4.9550E-05	PU239	3.5102E-05	71%	U233	6.3917E-06	13%	PU240	4.8363E-06	10%
	40	4.9206E-05	PU239	3.4859E-05	71%	U233	6.3474E-06	13%	PU240	4.8027E-06	10%
	48	4.8179E-05	PU239	3.4131E-05	71%	U233	6.2148E-06	13%	PU240	4.7024E-06	10%
	20	4.7837E-05	PU239	3.3889E-05	71%	U233	6.1708E-06	13%	PU240	4.6691E-06	10%
	54	4.7326E-05	PU239	3.3527E-05	71%	U233	6.1049E-06	13%	PU240	4.6192E-06	10%
	31	4.6647E-05	PU239	3.3046E-05	71%	U233	6.0172E-06	13%	PU240	4.5529E-06	10%
	23	4.6647E-05	PU239	3.3046E-05	71%	U233	6.0172E-06	13%	PU240	4.5529E-06	10%
	12	4.5970E-05	PU239	3.2566E-05	71%	U233	5.9299E-06	13%	PU240	4.4868E-06	10%
	42	4.5632E-05	PU239	3.2327E-05	71%	U233	5.8863E-06	13%	PU240	4.4539E-06	10%
	58	4.4790E-05	PU239	3.1730E-05	71%	U233	5.7777E-06	13%	PU240	4.3717E-06	10%
	34	4.4622E-05	PU239	3.1611E-05	71%	U233	5.7560E-06	13%	PU240	4.3553E-06	10%
	2	4.3784E-05	PU239	3.1018E-05	71%	U233	5.6480E-06	13%	PU240	4.2735E-06	10%
	56	4.3283E-05	PU239	3.0663E-05	71%	U233	5.5833E-06	13%	PU240	4.2246E-06	10%
	50	4.2783E-05	PU239	3.0309E-05	71%	U233	5.5189E-06	13%	PU240	4.1758E-06	10%
	22	4.2451E-05	PU239	3.0073E-05	71%	U233	5.4760E-06	13%	PU240	4.1434E-06	10%
	25	4.1953E-05	PU239	2.9720E-05	71%	U233	5.4118E-06	13%	PU240	4.0948E-06	10%
	59	4.1622E-05	PU239	2.9486E-05	71%	U233	5.3690E-06	13%	PU240	4.0625E-06	10%
	10	4.0961E-05	PU239	2.9018E-05	71%	U233	5.2838E-06	13%	PU240	3.9980E-06	10%
	5	4.0303E-05	PU239	2.8551E-05	71%	U233	5.1989E-06	13%	PU240	3.9337E-06	10%
	36	3.9811E-05	PU239	2.8203E-05	71%	U233	5.1354E-06	13%	PU240	3.8857E-06	10%
	45	3.9483E-05	PU239	2.7971E-05	71%	U233	5.0931E-06	13%	PU240	3.8537E-06	10%

Table B-7. (Concluded)

Comp. Scen ID	Vector	Total Integrated Discharge	Top 3 Radionuclides Contribution to Integrated Discharge (Time of Intrusion, 9000 years)								
04	19	6.6682E-05	PU239	4.6851E-05	70%	U233	8.9588E-06	13%	PU240	5.5311E-06	8%
	35	6.6146E-05	PU239	4.6474E-05	70%	U233	8.8868E-06	13%	PU240	5.4866E-06	8%
	55	6.5611E-05	PU239	4.6099E-05	70%	U233	8.8150E-06	13%	PU240	5.4423E-06	8%
	16	6.5256E-05	PU239	4.5849E-05	70%	U233	8.7672E-06	13%	PU240	5.4128E-06	8%
	46	6.4723E-05	PU239	4.5475E-05	70%	U233	8.6957E-06	13%	PU240	5.3686E-06	8%
	24	6.4015E-05	PU239	4.4977E-05	70%	U233	8.6005E-06	13%	PU240	5.3099E-06	8%
	4	6.3485E-05	PU239	4.4605E-05	70%	U233	8.5293E-06	13%	PU240	5.2659E-06	8%
	14	6.3132E-05	PU239	4.4357E-05	70%	U233	8.4820E-06	13%	PU240	5.2367E-06	8%
	13	6.2780E-05	PU239	4.4110E-05	70%	U233	8.4347E-06	13%	PU240	5.2075E-06	8%
	51	6.2253E-05	PU239	4.3739E-05	70%	U233	8.3639E-06	13%	PU240	5.1638E-06	8%
	39	6.1903E-05	PU239	4.3493E-05	70%	U233	8.3168E-06	13%	PU240	5.1347E-06	8%
	1	6.1028E-05	PU239	4.2879E-05	70%	U233	8.1993E-06	13%	PU240	5.0621E-06	8%
	53	6.0505E-05	PU239	4.2511E-05	70%	U233	8.1290E-06	13%	PU240	5.0188E-06	8%
	18	6.0157E-05	PU239	4.2267E-05	70%	U233	8.0823E-06	13%	PU240	4.9899E-06	8%
	52	5.9463E-05	PU239	4.1779E-05	70%	U233	7.9890E-06	13%	PU240	4.9323E-06	8%
	27	5.8944E-05	PU239	4.1414E-05	70%	U233	7.9192E-06	13%	PU240	4.8892E-06	8%
	49	5.8598E-05	PU239	4.1171E-05	70%	U233	7.8727E-06	13%	PU240	4.8605E-06	8%
	38	5.7736E-05	PU239	4.0566E-05	70%	U233	7.7570E-06	13%	PU240	4.7891E-06	8%
	21	5.7564E-05	PU239	4.0445E-05	70%	U233	7.7339E-06	13%	PU240	4.7748E-06	8%
	17	5.7049E-05	PU239	4.0083E-05	70%	U233	7.6647E-06	13%	PU240	4.7321E-06	8%
	44	5.6535E-05	PU239	3.9722E-05	70%	U233	7.5957E-06	13%	PU240	4.6895E-06	8%
	30	5.5852E-05	PU239	3.9242E-05	70%	U233	7.5039E-06	13%	PU240	4.6328E-06	8%
	3	5.5341E-05	PU239	3.8883E-05	70%	U233	7.4352E-06	13%	PU240	4.5904E-06	8%
	37	5.5001E-05	PU239	3.8644E-05	70%	U233	7.3895E-06	13%	PU240	4.5622E-06	8%
	43	5.4492E-05	PU239	3.8286E-05	70%	U233	7.3211E-06	13%	PU240	4.5200E-06	8%
	33	5.3984E-05	PU239	3.7929E-05	70%	U233	7.2529E-06	13%	PU240	4.4779E-06	8%
	32	5.3309E-05	PU239	3.7455E-05	70%	U233	7.1622E-06	13%	PU240	4.4218E-06	8%
	28	5.2972E-05	PU239	3.7218E-05	70%	U233	7.1169E-06	13%	PU240	4.3939E-06	8%
	6	5.2636E-05	PU239	3.6982E-05	70%	U233	7.0717E-06	13%	PU240	4.3660E-06	8%
	60	5.1797E-05	PU239	3.6393E-05	70%	U233	6.9591E-06	13%	PU240	4.2965E-06	8%
	47	5.1630E-05	PU239	3.6275E-05	70%	U233	6.9366E-06	13%	PU240	4.2826E-06	8%
	41	5.1129E-05	PU239	3.5923E-05	70%	U233	6.8693E-06	13%	PU240	4.2410E-06	8%
	26	5.0629E-05	PU239	3.5572E-05	70%	U233	6.8021E-06	13%	PU240	4.1996E-06	8%
	11	4.9965E-05	PU239	3.5105E-05	70%	U233	6.7128E-06	13%	PU240	4.1444E-06	8%
	57	4.9467E-05	PU239	3.4756E-05	70%	U233	6.6461E-06	13%	PU240	4.1032E-06	8%
	7	4.8972E-05	PU239	3.4408E-05	70%	U233	6.5794E-06	13%	PU240	4.0621E-06	8%
	29	4.8642E-05	PU239	3.4176E-05	70%	U233	6.5351E-06	13%	PU240	4.0347E-06	8%
	9	4.7983E-05	PU239	3.3713E-05	70%	U233	6.4467E-06	13%	PU240	3.9801E-06	8%
	8	4.7327E-05	PU239	3.3252E-05	70%	U233	6.3585E-06	13%	PU240	3.9257E-06	8%
	15	4.7163E-05	PU239	3.3137E-05	70%	U233	6.3365E-06	13%	PU240	3.9121E-06	8%
	40	4.6836E-05	PU239	3.2907E-05	70%	U233	6.2926E-06	13%	PU240	3.8850E-06	8%
	48	4.5858E-05	PU239	3.2220E-05	70%	U233	6.1612E-06	13%	PU240	3.8038E-06	8%
	20	4.5534E-05	PU239	3.1992E-05	70%	U233	6.1175E-06	13%	PU240	3.7769E-06	8%
	54	4.5047E-05	PU239	3.1650E-05	70%	U233	6.0522E-06	13%	PU240	3.7365E-06	8%
	31	4.4400E-05	PU239	3.1196E-05	70%	U233	5.9653E-06	13%	PU240	3.6829E-06	8%
	23	4.4400E-05	PU239	3.1196E-05	70%	U233	5.9653E-06	13%	PU240	3.6829E-06	8%
	12	4.3756E-05	PU239	3.0743E-05	70%	U233	5.8787E-06	13%	PU240	3.6294E-06	8%
	42	4.3434E-05	PU239	3.0517E-05	70%	U233	5.8355E-06	13%	PU240	3.6028E-06	8%
	58	4.2633E-05	PU239	2.9954E-05	70%	U233	5.7278E-06	13%	PU240	3.5363E-06	8%
	34	4.2473E-05	PU239	2.9842E-05	70%	U233	5.7063E-06	13%	PU240	3.5230E-06	8%
	2	4.1676E-05	PU239	2.9281E-05	70%	U233	5.5992E-06	13%	PU240	3.4569E-06	8%
	56	4.1199E-05	PU239	2.8946E-05	70%	U233	5.5351E-06	13%	PU240	3.4173E-06	8%
	50	4.0723E-05	PU239	2.8612E-05	70%	U233	5.4712E-06	13%	PU240	3.3779E-06	8%
	22	4.0406E-05	PU239	2.8390E-05	70%	U233	5.4287E-06	13%	PU240	3.3516E-06	8%
	25	3.9933E-05	PU239	2.8057E-05	70%	U233	5.3650E-06	13%	PU240	3.3123E-06	8%
	59	3.9618E-05	PU239	2.7835E-05	70%	U233	5.3227E-06	13%	PU240	3.2862E-06	8%
	10	3.8989E-05	PU239	2.7394E-05	70%	U233	5.2382E-06	13%	PU240	3.2340E-06	8%
	5	3.8362E-05	PU239	2.6953E-05	70%	U233	5.1540E-06	13%	PU240	3.1820E-06	8%
	36	3.7893E-05	PU239	2.6624E-05	70%	U233	5.0910E-06	13%	PU240	3.1432E-06	8%
	45	3.7582E-05	PU239	2.6405E-05	70%	U233	5.0492E-06	13%	PU240	3.1173E-06	8%

Distribution

FEDERAL AGENCIES

U. S. Department of Energy (4)
Office of Environmental Restoration
and Waste Management
Attn: L. P. Duffy, EM-1
J. E. Lytle, EM-30
S. Schneider, EM-342
C. Frank, EM-50
Washington, DC 20585

U.S. Department of Energy (5)
WIPP Task Force
Attn: M. Frei, EM-34 (2)
G. H. Daly
S. Fucigna
J. Rhoderick
12800 Middlebrook Rd.
Suite 400
Germantown, MD 20874

U.S. Department of Energy (4)
Office of Environment, Safety and
Health
Attn: R. P. Berube, EH-20
C. Borgstrum, EH-25
R. Pelletier, EH-231
K. Taimi, EH-232
Washington, DC 20585

U. S. Department of Energy (4)
WIPP Project Integration Office
Attn: W. J. Arthur III
L. W. Gage
P. J. Higgins
D. A. Olona
P.O. Box 5400
Albuquerque, NM 87115-5400

U. S. Department of Energy (12)
WIPP Project Site Office (Carlsbad)
Attn: A. Hunt (4)
M. McFadden
V. Daub (4)
J. Lippis
K. Hunter
R. Becker
P.O. Box 3090
Carlsbad, NM 88221-3090

U. S. Department of Energy, (5)
Office of Civilian Radioactive Waste
Management
Attn: Deputy Director, RW-2
Associate Director, RW-10
Office of Program
Administration and
Resources Management
Associate Director, RW-20
Office of Facilities
Siting and
Development
Associate Director, RW-30
Office of Systems
Integration and
Regulations
Associate Director, RW-40
Office of External
Relations and Policy
Office of Geologic Repositories
Forrestal Building
Washington, DC 20585

U. S. Department of Energy
Attn: National Atomic Museum Library
Albuquerque Operations Office
P.O. Box 5400
Albuquerque, NM 87185

U. S. Department of Energy
Research & Waste Management Division
Attn: Director
P.O. Box E
Oak Ridge, TN 37831

U. S. Department of Energy (2)
Idaho Operations Office
Fuel Processing and Waste
Management Division
785 DOE Place
Idaho Falls, ID 83402

U.S. Department of Energy
Savannah River Operations Office
Defense Waste Processing
Facility Project Office
Attn: W. D. Pearson
P.O. Box A
Aiken, SC 29802

U.S. Department of Energy (2)
Richland Operations Office
Nuclear Fuel Cycle & Production
Division
Attn: R. E. Gerton
825 Jadwin Ave.
P.O. Box 500
Richland, WA 99352

U.S. Department of Energy (3)
Nevada Operations Office
Attn: J. R. Boland
D. Livingston
P. K. Fitzsimmons
2753 S. Highland Drive
Las Vegas, NV 87183-8518

U.S. Department of Energy (2)
Technical Information Center
P.O. Box 62
Oak Ridge, TN 37831

U.S. Department of Energy (2)
Chicago Operations Office
Attn: J. C. Haugen
9800 South Cass Avenue
Argonne, IL 60439

U.S. Department of Energy
Los Alamos Area Office
528 35th Street
Los Alamos, NM 87544

U.S. Department of Energy (3)
Rocky Flats Area Office
Attn: W. C. Rask
G. Huffman
T. Lukow
P.O. Box 928
Golden, CO 80402-0928

U.S. Department of Energy
Dayton Area Office
Attn: R. Grandfield
P.O. Box 66
Miamisburg, OH 45343-0066

U.S. Department of Energy
Attn: E. Young
Room E-178
GAO/RCED/GTN
Washington, DC 20545

U.S. Bureau of Land Management
101 E. Mermod
Carlsbad, NM 88220

U.S. Bureau of Land Management
New Mexico State Office
P.O. Box 1449
Santa Fe, NM 87507

U.S. Environmental Protection
Agency (2)
Office of Radiation Protection Programs
(ANR-460)
Attn: Richard Guimond (2)
Washington, D.C. 20460

U.S. Nuclear Regulatory Commission
Division of Waste Management
Attn: H. Marson
Mail Stop 4-H-3
Washington, DC 20555

U.S. Nuclear Regulatory Commission (4)
Advisory Committee on Nuclear Waste
Attn: Dade Moeller
Martin J. Steindler
Paul W. Pomeroy
William J. Hinze
7920 Norfolk Avenue
Bethesda, MD 20814

Defense Nuclear Facilities Safety Board
Attn: Dermot Winters
625 Indiana Avenue NW
Suite 700
Washington, DC 20004

Nuclear Waste Technical Review Board (2)
Attn: Dr. Don A. Deere
Dr. Sidney J. S. Parry
Suite 910
1100 Wilson Blvd.
Arlington, VA 22209-2297

Katherine Yuracko
Energy and Science Division
Office of Management and Budget
725 17th Street NW
Washington, DC 20503

U.S. Geological Survey (2)
Water Resources Division
Attn: Cathy Peters
Suite 200
4501 Indian School, NE
Albuquerque, NM 87110

INSTITUTIONAL DISTRIBUTION

NEW MEXICO CONGRESSIONAL DELEGATION:

Jeff Bingaman
U.S. Senate
524 SHOB
Washington, DC 20510

Pete V. Domenici
U.S. Senate
427 SDOB
Washington, DC 20510

Bill Richardson
House of Representatives
332 CHOB
Washington, DC 20510

Steven H. Schiff
House of Representatives
1520 LHOB
Washington, DC 20510

Joe Skeen
House of Representatives
1007 LHOB
Washington, DC 20510

STATE AGENCIES

Environmental Evaluation Group (5)
Attn: Robert Neill
Suite F-2
7007 Wyoming Blvd., N.E.
Albuquerque, NM 87109

New Mexico Bureau of Mines
and Mineral Resources
Socorro, NM 87801

New Mexico Department of Energy & Minerals
Attn: Librarian
2040 S. Pacheco
Santa Fe, NM 87505

New Mexico Radioactive Task Force (2)
(Governor's WIPP Task Force)
Attn: Anita Lockwood, Chairman
Chris Wentz, Coordinator/Policy Analyst
2040 Pacheco
Santa Fe, NM 87505

Bob Forrest
Mayor, City of Carlsbad
P.O. Box 1569
Carlsbad, NM 88221

Chuck Bernard
Executive Director
Carlsbad Department of Development
P.O. Box 1090
Carlsbad, NM 88221

Robert M. Hawk (2)
Chairman, Hazardous and Radioactive Materials Committee
Room 334
State Capitol
Sante Fe, NM 87503

New Mexico Environment Department
Secretary of the Environment
Attn: J. Espinosa (3)
P.O. Box 968
1190 St. Francis Drive
Santa Fe, NM 87503-0968

New Mexico Environment Department
Attn: Pat McCausland
WIPP Project Site Office
P.O. Box 3090
Carlsbad, NM 88221-3090

ADVISORY COMMITTEE ON NUCLEAR FACILITY SAFETY

John F. Ahearne
Executive Director, Sigma Xi
99 Alexander Drive
Research Triangle Park, NC 27709

James E. Martin
109 Observatory Road
Ann Arbor, MI 48109

Dr. Gerald Tape
Assoc. Universities
1717 Massachusetts Ave. NW
Suite 603
Washington, DC 20036

WIPP PANEL OF NATIONAL RESEARCH COUNCIL'S BOARD ON RADIOACTIVE WASTE MANAGEMENT

Charles Fairhurst, Chairman
Department of Civil and
Mineral Engineering
University of Minnesota
500 Pillsbury Dr. SE
Minneapolis, MN 55455-0220

John O. Blomeke
3833 Sandy Shore Drive
Lenoir City, TN 37771-9803

John D. Bredehoeft
Western Region Hydrologist
Water Resources Division
U.S. Geological Survey (M/S 439)
345 Middlefield Road
Menlo Park, CA 94025

Fred M. Ernsberger
1325 NW 10th Avenue
Gainsville, FL 32601

Rodney C. Ewing
Department of Geology
University of New Mexico
200 Yale, NE
Albuquerque, NM 87131

B. John Garrick
Pickard, Lowe & Garrick, Inc.
2260 University Drive
Newport Beach, CA 92660

Leonard F. Konikow
U.S. Geological Survey
431 National Center
Reston, VA 22092

Jeremiah O'Driscoll
505 Valley Hill Drive
Atlanta, GA 30350

Christopher Whipple
Clement International Corp.
160 Spear St.
Suite 1380
San Francisco, CA 94105-1535

National Research Council (3)
Board on Radioactive
Waste Management
RM HA456
Attn: Peter B. Myers, Staff Director (2)
Dr. Geraldine J. Grube
2101 Constitution Avenue
Washington, DC 20418

PERFORMANCE ASSESSMENT PEER REVIEW PANEL

G. Ross Heath
College of Ocean and
Fishery Sciences HN-15
583 Henderson Hall
University of Washington
Seattle, WA 98195

Thomas H. Pigford
Department of Nuclear Engineering
4159 Etcheverry Hall
University of California
Berkeley, CA 94720

Thomas A. Cotton
JK Research Associates, Inc.
4429 Butterworth Place, NW
Washington, DC 20016

Robert J. Budnitz
President, Future Resources
Associates, Inc.
2000 Center Street
Suite 418
Berkeley, CA 94704

C. John Mann
Department of Geology
245 Natural History Bldg.
1301 West Green Street
University of Illinois
Urbana, IL 61801

Frank W. Schwartz
Department of Geology and Mineralogy
The Ohio State University
Scott Hall
1090 Carmack Rd.
Columbus, OH 43210

FUTURE SOCIETIES EXPERT PANEL

Theodore S. Glickman
Resources for the Future
1616 P St., NW
Washington, DC 20036

Norman Rosenberg
Resources for the Future
1616 P St., NW
Washington, DC 20036

Max Singer
The Potomac Organization, Inc.
5400 Greystone St.
Chevy Chase, MD 20815

Maris Vinovskis
Institute for Social Research
Room 4086
University of Michigan
426 Thompson St
Ann Arbor, MI 48109-1045

Gregory Benford
University of California, Irvine
Department of Physics
Irvine, CA 92717

Craig Kirkwood
College of Business Administration
Arizona State University
Tempe, AZ 85287

Harry Otway
Health, Safety, and Envir. Div.
Mail Stop K-491
Los Alamos National Laboratory
Los Alamos, NM 87545

Martin J. Pasqualetti
Department of Geography
Arizona State University
Tempe, AZ 85287-3806

Michael Baram
Bracken and Baram
33 Mount Vernon St.
Boston, MA 02108

Wendell Bell
Department of Sociology
Yale University
1965 Yale Station
New Haven, CT 06520

Bernard L. Cohen
Department of Physics
University of Pittsburgh
Pittsburgh, PA 15260

Ted Gordon
The Futures Group
80 Glastonbury Blvd.
Glastonbury, CT 06033

Duane Chapman
5025 S. Building, Room S5119
The World Bank
1818 H Street NW
Washington, DC 20433

Victor Ferkiss
23 Sage Brush Circle
Corrales, NM 87048

Dan Reicher
Senior Attorney
Natural Resources Defense Council
1350 New York Ave. NW, #300
Washington, DC 20005

Theodore Taylor
P.O. Box 39
3383 Weatherby Rd.
West Clarksville, NY 14786

MARKERS EXPERT PANEL

Dr. Dieter Ast
Department of Materials Science
Bard Hall
Cornell University
Ithaca, NY 14853-1501

Dr. Victor Baker
Department of Geosciences
Building #77, Gould-Simpson Building
University of Arizona
Tucson, AZ 85721

Mr. Michael Brill
President
BOSTI
1479 Hertel Ave.
Buffalo, NY 14216

Dr. Frank Drake
Board of Studies in Astronomy and
Astrophysics
Lick Observatory
University of California, Santa Cruz
Santa Cruz, CA 95064

Dr. Ben Finney
University of Hawaii at Manoa
Department of Anthropology
Porteus Hall 346, 2424 Maile Way
Honolulu, HI 96822

Dr. David Givens
American Anthropological Association
1703 New Hampshire Ave., NW
Washington, D.C. 20009

Dr. Ward Goodenough
Department of Anthropology
University of Pennsylvania
325 University Museum
33rd and Spruce Streets
Philadelphia, PA 19104-6398

Dr. Maureen Kaplan
Eastern Research Group, Inc.
6 Whittemore Street
Arlington, MA 02174

Mr. Jon Lomberg
P.O. Box 207
Honaunau, HI 96726

Dr. Louis Narens
Department of Cognitive Sciences
School of Social Sciences
University of Califorrnia, Irvine
Irvine, CA 92717

Dr. Frederick Newmeyer
Department of Linguistics
GN-40
University of Washington
Seattle, WA 98195

Dr. Woodruff Sullivan
Department of Astonomy
FM-20
University of Washington
Seattle, WA 98195

Dr. Wendell Williams
Materials Science and Engineering
White Building
Case Western Reserve University
Cleveland, OH 44106

NATIONAL LABORATORIES

Argonne National Labs (2)
Attn: A. Smith
D. Tomasko
9700 South Cass, Bldg. 201
Argonne, IL 60439

Battelle Pacific Northwest Laboratories (3)
Attn: R. E. Westerman
S. Bates
H. C. Burkholder
Battelle Boulevard
Richland, WA 99352

Lawrence Livermore National Laboratory
Attn: G. Mackanic
P.O. Box 808, MS L-192
Livermore, CA 94550

Los Alamos National Laboratories
Attn: B. Erdal, CNC-11
P.O. Box 1663
Los Alamos, NM 87544

Los Alamos National Laboratories
Attn: A. Meijer
Mail Stop J514
Los Alamos, NM 87545

Los Alamos National Laboratories (3)
HSE-8
Attn: M. Enoris
L. Soholt
J. Wenzel
P.O. Box 1663
Los Alamos, NM 87544

Los Alamos National Laboratories (2)
HSE-7
Attn: A. Drypolcher
S. Kosciewiscz
P.O. Box 1663
Los Alamos, NM 87544

Oak Ridge National Labs
Martin Marietta Systems, Inc.
Attn: J. Setaro
P.O. Box 2008, Bldg. 3047
Oak Ridge, TN 37831-6019

Savannah River Laboratory (3)
Attn: N. Bibler
M. J. Plodinec
G. G. Wicks
Aiken, SC 29801

Savannah River Plant (2)
Attn: Richard G. Baxter
Building 704-S
K. W. Wierzbicki
Building 703-H
Aiken, SC 29808-0001

CORPORATIONS/MEMBERS OF THE PUBLIC

Benchmark Environmental Corp. (3)
Attn: John Hart
C. Frederickson
K. Lickliter
4501 Indian School Rd., NE
Suite 105
Albuquerque, NM 87110

Deuel and Associates, Inc.
Attn: R. W. Prindle
7208 Jefferson, NE
Albuquerque, NM 87109

Disposal Safety, Inc.
Attn: Benjamin Ross
Suite 314
1660 L Street NW
Washington, DC 20006

Ecodynamics Research Associates (2)
Attn: Pat Roache
Rebecca Blaine
P.O. Box 8172
Albuquerque, NM 87198

E G & G Idaho (3)
1955 Fremont Street
Attn: C. Atwood
C. Hertzler
T. I. Clements
Idaho Falls, ID 83415

Geomatrix
Attn: Kevin Coppersmith
100 Pine Street #1000
San Francisco, CA 94111

Golden Associates, Inc. (3)
Attn: Mark Cunnane
Richard Kossik
Ian Miller
4104 148th Avenue NE
Redmond, WA 98052

In-Situ, Inc. (2)
Attn: S. C. Way
C. McKee
209 Grand Avenue
Laramie, WY 82070

INTERA, Inc.
Attn: A. M. LaVenue
8100 Mountain Road NE
Suite 213
Albuquerque, NM 87110

INTERA, Inc.
Attn: J. F. Pickens
Suite #300
6850 Austin Center Blvd.
Austin, TX 78731

INTERA, Inc.
Attn: Wayne Stensrud
P.O. Box 2123
Carlsbad, NM 88221

INTERA, Inc.
Attn: William Nelson
101 Convention Center Drive
Suite 540
Las Vegas, NV 89109

IT Corporation (2)
Attn: P. Drez
J. Myers
Regional Office - Suite 700
5301 Central Avenue, NE
Albuquerque, NM 87108

IT Corporation
R. J. Eastmond
825 Jadwin Ave.
Richland, WA 99352

MACTEC (2)
Attn: J. A. Thies
D. K. Duncan
8418 Zuni Road SE
Suite 200
Albuquerque, NM 87108

Pacific Northwest Laboratory
Attn: Bill Kennedy
Battelle Blvd.
P.O. Box 999
Richland, WA 99352

RE/SPEC, Inc. (2)
Attn: W. Coons
Suite 300
4775 Indian School NE
Albuquerque, NM 87110

RE/SPEC, Inc.
Attn: J. L. Ratigan
P.O. Box 725
Rapid City, SD 57709

Reynolds Elect/Engr. Co., Inc.
Building 790, Warehouse Row
Attn: E. W. Kendall
P.O. Box 98521
Las Vegas, NV 89193-8521

Roy F. Weston, Inc.
CRWM Tech. Supp. Team
Attn: Clifford J. Noronha
955 L'Enfant Plaza, S.W.
North Building, Eighth Floor
Washington, DC 20024

Science Applications International Corporation
Attn: Howard R. Pratt,
Senior Vice President
10260 Campus Point Drive
San Diego, CA 92121

Science Applications International Corporation (2)
Attn: George Dymmel
Chris G. Pflum
101 Convention Center Dr.
Las Vegas, NV 89109

Science Applications International Corporation (2)
Attn: John Young
Dave Lester
18706 North Creek Parkway
Suite 110
Bothell, WA 98011

Southwest Research Institute
Center for Nuclear Waste Regulatory Analysis (2)
Attn: P. K. Nair
6220 Culebra Road
San Antonio, Texas 78228-0510

Systems, Science, and Software (2)
Attn: E. Peterson
P. Lagus
Box 1620
La Jolla, CA 92038

TASC
Attn: Steven G. Oston
55 Walkers Brook Drive
Reading, MA 01867

Tech. Reps., Inc. (5)
Attn: Janet Chapman
Terry Cameron
Debbie Marchand
John Stikar
Denise Bissell
5000 Marble NE
Suite 222
Albuquerque, NM 87110

Tolan, Beeson, & Associates
Attn: Terry L. Tolan
2320 W. 15th Avenue
Kennewick, WA 99337

TRW Environmental Safety Systems (TESS)
Attn: Ivan Saks
10306 Eaton Place
Suite 300
Fairfax, VA 22030

Westinghouse Electric Corporation (4)
Attn: Library
L. Trego
C. Cox
L. Fitch
R. F. Kehrman
P.O. Box 2078
Carlsbad, NM 88221

Westinghouse Hanford Company
Attn: Don Wood
P.O. Box 1970
Richland, WA 99352

Western Water Consultants
Attn: D. Fritz
1949 Sugarland Drive #134
Sheridan, WY 82801-5720

Western Water Consultants
Attn: P. A. Rechard
P.O. Box 4128
Laramie, WY 82071

Neville Cook
Rock Mechanics Engineering
Mine Engineering Dept.
University of California
Berkeley, CA 94720

Dennis W. Powers
Star Route Box 87
Anthony, TX 79821

Shirley Thieda
P.O. Box 2109, RR1
Bernalillo, NM 87004

Jack Urich
c/o CARD
144 Harvard SE
Albuquerque, NM 87106

UNIVERSITIES

University of California
Mechanical, Aerospace, and
Nuclear Engineering Department (2)
Attn: W. Kastenberg
D. Browne
5532 Boelter Hall
Los Angeles, CA 90024

University of Hawaii at Hilo
Attn: S. Hora
Business Administration
Hilo, HI 96720-4091

University of New Mexico
Geology Department
Attn: Library
Albuquerque, NM 87131

University of New Mexico
Research Administration
Attn: H. Schreyer
102 Scholes Hall
Albuquerque, NM 87131

University of Wyoming
Department of Civil Engineering
Attn: V. R. Hasfurther
Laramie, WY 82071

University of Wyoming
Department of Geology
Attn: J. I. Drever
Laramie, WY 82071

University of Wyoming
Department of Mathematics
Attn: R. E. Ewing
Laramie, WY 82071

LIBRARIES

Thomas Brannigan Library
Attn: Don Dresp, Head Librarian
106 W. Hadley St.
Las Cruces, NM 88001

Hobbs Public Library
Attn: Marcia Lewis, Librarian
509 N. Ship Street
Hobbs, NM 88248

New Mexico State Library
Attn: Norma McCallan
325 Don Gaspar
Santa Fe, NM 87503

New Mexico Tech
Martin Speere Memorial Library
Campus Street
Socorro, NM 87810

New Mexico Junior College
Pannell Library
Attn: Ruth Hill
Lovington Highway
Hobbs, NM 88240

Carlsbad Municipal Library
WIPP Public Reading Room
Attn: Lee Hubbard, Head Librarian
101 S. Halagueno St.
Carlsbad, NM 88220

University of New Mexico
General Library
Government Publications Department
Albuquerque, NM 87131

NEA/PSAC USER'S GROUP

Timo K. Vieno
Technical Research Centre of Finland (VTT)
Nuclear Engineering Laboratory
P.O. Box 169
SF-00181 Helsinki
FINLAND

Alexander Nies (PSAC Chairman)
Gesellschaft für Strahlen- und
Institut für Tieflagerung
Abteilung für Endlagersicherheit
Theodor-Heuss-Strasse 4
D-3300 Braunscheweig
GERMANY

Eduard Hofer
Gesellschaft für Reaktorsicherheit (GRS)
MBH
Forschungsgelände
D-8046 Garching
GERMANY

Takashi Sasahara
Environmental Assessment Laboratory
Department of Environmental Safety Research
Nuclear Safety Research Center,
Tokai Research Establishment, JAERI
Tokai-mura, Naka-gun
Ibaraki-ken
JAPAN

Alejandro Alonso
Cátedra de Tecnología Nuclear
E.T.S. de Ingenieros Industriales
José Gutiérrez Abascal, 2
E-28006 Madrid
SPAIN

Pedro Prado
CIEMAT
Instituto de Tecnología Nuclear
Avenida Complutense, 22
E-28040 Madrid
SPAIN

Miguel Angel Cuñado
ENRESA
Emilio Vargas, 7
E-28043 Madrid
SPAIN

Francisco Javier Elorza
ENRESA
Emilio Vargas, 7
E-28043 Madrid
SPAIN

Nils A. Kjellbert
Swedish Nuclear Fuel and Waste Management Company (SKB)
Box 5864
S-102 48 Stockholm
SWEDEN

Björn Cronhjort
Swedish National Board for Spent Nuclear Fuel (SKN)
Sehlsedtsgatan 9
S-115 28 Stockholm
SWEDEN

Richard A. Klos
Paul-Scherrer Institute (PSI)
CH-5232 Villingen PSI
SWITZERLAND

NAGRA (2)
Attn: Charles McCombie
Fritz Van Dorp
Parkstrasse 23
CH-5401 Baden
SWITZERLAND

Brian G. J. Thompson
Department of the Environment
Her Majesty's Inspectorate of Pollution
Room A5.33, Romney House
43 Marsham Street
London SW1P 2PY
UNITED KINGDOM

INTERA/ECL (2)
Attn: Trevor J. Sumerling
Daniel A. Galson
Chiltern House
45 Station Road
Henley-on-Thames
Oxfordshire RG9 1AT
UNITED KINGDOM

U.S. Nuclear Regulatory Commission (2)
Attn: Richard Codell
Norm Eisenberg
Mail Stop 4-H-3
Washington, D.C. 20555

Paul W. Eslinger
Battelle Pacific Northwest Laboratories (PNL)
P.O. Box 999, MS K2-32
Richland, WA 99352

Andrea Saltelli
Commission of the European Communities
Joint Resarch Centre od Ispra
I-21020 Ispra (Varese)
ITALY

Budhi Sagar
Center for Nuclear Waste Regulatory Analysis (CNWRA)
Southwest Research Institute
P.O. Drawer 28510
6220 Culebra Road
San Antonio, TX 78284

Shaheed Hossain
Division of Nuclear Fuel Cycle and Waste Management
International Atomic Energy Agency
Wagramerstrasse 5
P.O. Box 100
A-1400 Vienna
AUSTRIA

Claudio Pescatore
Division of Radiation Protection and Waste Management
38, Boulevard Suchet
F-75016 Paris
FRANCE

FOREIGN ADDRESSES

Studiecentrum Voor Kernenergie
Centre D'Energie Nucleaire
Attn: A. Bonne
SCK/CEN
Boeretang 200
B-2400 Mol
BELGIUM

Atomic Energy of Canada, Ltd. (3)
Whiteshell Research Estab.
Attn: Michael E. Stevens
Bruce W. Goodwin
Donna Wushke
Pinewa, Manitoba
ROE 1L0
CANADA

Ghislain de Marsily
Lab. Géologie Appliqué
Tour 26, 5 étage
4 Place Jussieu
F-75252 Paris Cedex 05
FRANCE

Jean-Pierre Olivier
OECD Nuclear Energy Agency (2)
38, Boulevard Suchet
F-75016 Paris
FRANCE

D. Alexandre, Deputy Director
ANDRA
31 Rue de la Federation
75015 Paris
FRANCE

Claude Sombret
Centre D'Etudes Nucleaires
De La Vallee Rhone
CEN/VALRHO
S.D.H.A. BP 171
30205 Bagnols-Sur-Ceze
FRANCE

Bundesministerium fur Forschung und Technologie
Postfach 200 706
5300 Bonn 2
GERMANY

Bundesanstalt fur Geowissenschaften und Rohstoffe
Attn: Michael Langer
Postfach 510 153
3000 Hannover 51
GERMANY

Gesellschaft fur Reaktorsicherheit (GRS) mb (2)
Attn: Bruno Baltes
Wolfgang Muller
Schwertnergasse 1
D-5000 Cologne
GERMANY

Hahn-Mietner-Institut fur Kernforschung
Attn: Werner Lutze
Glienicker Strasse 100
100 Berlin 39
GERMANY

Institut fur Tieflagerung (2)
Attn: K. Kuhn
Theodor-Heuss-Strasse 4
D-3300 Braunschweig
GERMANY

Physikalisch-Technische Bundesanstalt
Attn: Peter Brenneke
Postfach 33 45
D-3300 Braunschweig
GERMANY

Shingo Tashiro
Japan Atomic Energy Research Institute
Tokai-Mura, Ibaraki-Ken
319-11
JAPAN

Netherlands Energy Research Foundation
ECN
Attn: L. H. Vons
3 Westerduinweg
P.O. Box 1
1755 ZG Petten
THE NETHERLANDS

Johan Andersson
Statens Kärnkraftinspektion
SKI
Box 27106
S-102 52 Stockholm
SWEDEN

Fred Karlsson
Svensk Karnbransleforsorjning AB
SKB
Box 5864
S-102 48 Stockholm
SWEDEN

Nationale Genossenschaft fur die Lagerung
Radioaktiver Abfalle (NAGRA) (2)
Attn: Stratis Vomvoris
Piet Zuidema
Hardstrasse 73
CH-5430 Wettingen
SWITZERLAND

D. R. Knowles
British Nuclear Fuels, plc
Risley, Warrington, Cheshire WA3 6AS
1002607 UNITED KINGDOM

AEA Technology
Attn: J.H. Rees
D5W/29 Culham Laboratory
Abington
Oxfordshire OX14 3DB
UNITED KINGDOM

AEA Technology
Attn: W. R. Rodwell
O44/A31 Winfrith Technical Centre
Dorchester
Dorset DT2 8DH
UNITED KINGDOM

AEA Technology
Attn: J. E. Tinson
B4244 Harwell Laboratory
Didcot
Oxfordshire OX11 ORA
UNITED KINGDOM

INTERNAL

1	A. Narath
20	O. E. Jones
1510	J. C. Cummings
1511	D. K. Gartling
3151	S. M. Wayland
3200	N. R. Ortiz
6000	D. L. Hartley
6233	J. C. Eichelberger
6300	T. O. Hunter
6301	E. Bonano
6310	T. E. Blejwas, Acting
6313	L. E. Shephard
6312	F. W. Bingham
6313	L. S. Costin
6315	Supervisor
6316	R. P. Sandoval
6320	R. E. Luna, Acting
6340	W. D. Weart
6340	S. Y. Pickering
6341	J. M. Covan
6341	D. P. Garber
6341	R. C. Lincoln
6341	J. Orona*
6341	Sandia WIPP Central Files (250)
6342	D. R. Anderson
6342	B. M. Butcher
6342	D. P. Gallegos
6342	L. S. Gomez
6342	M. Gruebel
6342	R. Guzowski
6342	R. D. Klett
6342	M. G. Marietta
6342	D. Morrison
6342	A. C. Peterson
6342	R. P. Rechard
6342	P. Swift
6342	M. Tierney
6342	K. M. Trauth
6342	B. L. Baker*
6342	J. Bean*
6342	J. Berglund*
6342	W. Beyeler*
6342	T. Blaine*
6342	K. Brinster*
6342	K. Byle*
6342	L. Clements*
6342	J. Garner*
6342	A. Gilkey*
6342	H. Iuzzolino*
6342	J. Logothetis*
6342	R. McCurley*
6342	J. Rath*
6342	D. Rudeen*
6342	J. Sandha*
6342	J. Schreiber*
6342	P. Vaughn*
6343	T. M. Schultheis
6344	R. L. Beauheim
6344	P. B. Davies
6344	S. J. Finley
6344	E. Gorham
6344	C. F. Novak
6344	S. W. Webb
6345	R. Beraun
6345	L. Brush
6345	A. R. Lappin
6345	M. A. Molecke
6346	D. E. Munson
6346	E. J. Nowak
6346	J. R. Tillerson
6347	A. L. Stevens
6400	D. J. McCloskey
6413	J. C. Helton
6415	R. M. Cranwell
6415	C. Leigh
6415	R. L. Iman
6622	M.S.Y. Chu
9300	J. E. Powell
9310	J. D. Plimpton
9325	J. T. McIlmoyle
9325	R. L. Rutter
9330	J. D. Kennedy
8523-2	Central Technical Files
3141	S. A. Landenberger (5)
3145	Document Processing (8) for DOE/OSTI
3151	G. C. Claycomb (3)

*6342/Geo-Centers

☆ U.S. GOVERNMENT PRINTING OFFICE: 1991—673-122/60036

SANDIA REPORT

SAND91-0893/3 • UC-721
Unlimited Release
Printed December 1991

Preliminary Comparison with 40 CFR Part 191, Subpart B for the Waste Isolation Pilot Plant, December 1991

Volume 3: Reference Data

WIPP Performance Assessment Division

Prepared by
Sandia National Laboratories
Albuquerque, New Mexico 87185 and Livermore, California 94550
for the United States Department of Energy
under Contract DE-AC04-76DP00789

Issued by Sandia National Laboratories, operated for the United States Department of Energy by Sandia Corporation.

Available to DOE and DOE contractors from
Office of Scientific and Technical Information
PO Box 62
Oak Ridge, TN 37831

Prices available from (615) 576-8401, FTS 626-8401

Available to the public from
National Technical Information Service
US Department of Commerce
5285 Port Royal Rd
Springfield, VA 22161

NTIS price codes
Printed copy: A99
Microfiche copy: A01

SAND91-0893/3
Unlimited Release
Printed December 1991

Distribution
Category UC-721

PRELIMINARY COMPARISON WITH 40 CFR PART 191, SUBPART B FOR THE WASTE ISOLATION PILOT PLANT, DECEMBER 1991

VOLUME 3: REFERENCE DATA

WIPP Performance Assessment Division
Editors: Rob P. Rechard, Andrew C. Peterson, James D. Schreiber,[1]
Harold J. Iuzzolino[2], Martin S. Tierney, Jim S. Sandha[1]
Sandia National Laboratories
Albuquerque, New Mexico 87185

ABSTRACT

This volume documents the data available as of August 1991, which were used by the Performance Assessment Division of Sandia National Laboratories in its 1991 preliminary performance assessment of the Waste Isolation Pilot Plant (WIPP). Ranges and distributions for about 300 modeling parameters, several of which are spatially varying parameters with between 15 and 80 point values, and about 500 well locations and corresponding stratigraphic elevations are presented in both tables and graphics for the geologic and engineered barriers, global materials (e.g., fluid properties), and agents that act upon the WIPP disposal system such as climate variability and human-intrusion boreholes. Sources for the data and a brief discussion of each parameter are also provided.

[1] Science Applications International, Albuquerque, NM 87106
[2] Geo-Centers, Inc., Albuquerque, NM 87106

ACKNOWLEDGMENTS

The WIPP Performance Assessment Division is comprised of both Sandia and contractor employees working as a team to produce these annual preliminary comparisons with EPA regulations, assessments of overall long-term safety of the repository, and interim technical guidance to the program. The on-site team, affiliations, and contributions to the 1991 performance assessment are listed in alphabetical order:

Performance Assessment Division

Name	Affil.	Primary Author of Doc: Sect.	Major Code	Area of Responsibility
R. Anderson	SNL			Division Manager
B. Baker	TEC	V.2:§6.4		SEC02D, Hydrology, Office Manager
J. Bean	UNM	V.2:§4.2.1		BRAGFLO & BOASTII, 2-Phase Flow
J. Berglund	UNM	V.2:Ch.7 Editor V.2	CUTTINGS	Task Ldr., Undisturbed Repository, Cuttings/Cavings/ Engr. Mech.
W. Beyeler	SAI	V.2:§5.3; 6.1;6.3	PANEL GARFIELD	Geostatistics, Analytical Models, CAMCON Systems Codes
K. Brinster	SAI			Geohydrology, Conceptual Models
R. Blaine	ECO			SEC02D & CAMCON Systems Codes
T. Blaine	EPE			Drilling Technology, Exposure Pathways Data
J. Garner	API	V.2:§5.3	PANEL	Source Term, Sens. Anal.
A. Gilkey	UNM			CAMCON Systems Codes
L. Gomez	SNL			Task Ldr., Safety Assessments
M. Gruebel	TRI	V.1:Ch.1,2, 8,9,10		EPA Regulations
R. Guzowski	SAI	V.1:Ch.4		Geology, Scenario Construction
J. Helton	ASU	V.1:Ch.3,4 V.2:Ch.2,3	CCDFPERM	Task Ldr., Uncert./Sens. Anal., Probability Models
H. Iuzzolino	GC	Editor V.3	CCDFPERM	LHS & CAMCON System Codes
R. Klett	SNL			EPA Regulations
P. Knupp	ECO			STAFF2D & SECOTR, Comp. Fluid Dyn.
C. Leigh	SNL		GENII-S	Exposure Pathways
M. Marietta	SNL	Editor (Set)		Dep. Div. Manager, Tech. Coord.
G. de Marsily	UP	V.2:§6.2		Task Ldr., Geostatistics
R. McCurley	UNM	V.2:§4.2.3		SUTRA & CAMCON System Codes
A. Peterson	SNL	Editor V.3		Task Ldr., Inventory
J. Rath	UNM	V.2:§4.2.3		SUTRA, Engr. Mech.
R. Rechard	SNL	Editor V.2 & V.3		Task Ldr., CAMCON, QA, Ref. Data
P. Roache	ECO	V.2:§6.4	SECO	Task Ldr., Comp. Fluid Dyn.
D. Rudeen	UNM	V.2:§4.2.2; 6.5		STAFF2D, Transport
J. Sandha	SAI	Editor V.3		INGRES, PA Data Base
J. Schreiber	SAI	V.2:§4.2.1; 5.2.5 Editor V.3		BRAGFLO & BOASTII, 2-Phase Flow
P. Swift	TRI	V.1:Ch.5,11		Task Ldr., Geology, Climate Var.

M. Tierney	SNL	Editor V.3			Task Ldr., CDF Constr., Probability Models
K. Trauth	SNL				Task Ldr., Expert Panels
P. Vaughn	API	V.2:§5.1; 5.2;5.2.5; App.A		BRAGFLO	Task Ldr., 2-Phase Flow & Waste Panel Chemistry
J. Wormeck	ECO				Comp. Fluid Dyn. & Thermodyn.

The foundation of the annual WIPP performance assessment is the underlying data set and understanding of the important processes in the engineered and natural barrier systems. The SNL Nuclear Waste Technology Department is the primary source of these data and understanding. Assistance with the waste inventory comes from WEC and its contractors. We gratefully acknowledge the support of our departmental and project colleagues. Some individuals have worked closely with the performance assessment team, and we wish to acknowledge their contributions individually:

J. Ball	ReS	Computer System Manager
H. Batchelder	WEC	CH & RH Inventories
R. Beauheim	SNL	Natural Barrier System, Hydrologic Parameters
B. Butcher	SNL	Engineered Barrier System, Unmodified Waste-Form Parameters, Disposal Room Systems Parameters
L. Brush	SNL	Engineered Barrier System, Source Term (Solubility) and Gas Generation Parameters
L. Clements	ReS	Computer System Support
T. Corbet	SNL	Natural Barrier System, Geologic & Hydrologic Parameters, Conceptual Models
P. Davies	SNL	Natural Barrier System, Hydrologic & Transport Parameters, & 2-Phase Flow Mechanistic Modeling
P. Drez	IT	CH & RH Inventories
E. Gorham	SNL	Natural Barrier System, Fluid Flow & Transport Parameters
S. Howarth	SNL	Natural Barrier System, Hydrologic Parameters
R. Kehrman	WEC	CH & RH Waste Characterization
R. Lincoln	SNL	Project Integration
F. Mendenhall	SNL	Engineered Barrier System, Unmodified Waste Form Parameters, Waste Panel Closure (Expansion)
D. Munson	SNL	Reference Stratigraphy, Constitutive Models, Physical & Mechanical Parameters
E. Nowak	SNL	Shaft/Panel Seal Design, Seal Material Properties, Reliability
J. Orona	ReS	Computer System Support
J. Tillerson	SNL	Repository Isolation Systems Parameters
S. Webb	SNL	2-Phase Flow Sensitivity Analysis & Benchmarking

API = Applied Physics Incorporated
ASU = Arizona State University
ECO = Ecodynamics Research Associates
EPE = Epoch Engineering
GC = Geo-Centers Incorporated
IT = International Technology
ReS = ReSpec
SAI = Scientific Applications International Corporation
SNL = Sandia National Laboratories
TEC = Technadyne Engineering Consultants
TRI = Tech Reps, Inc.
UNM = Univ. of New Mexico/New Mexico Engineering Research Institute
UP = University of Paris
WEC = Westinghouse Electric Corporation

Peer Review

Internal/Sandia

T. Corbet
D. Gallegos
M. LaVenue
S. Hora

Management/Sandia

W. Weart
T. Hunter

PA Peer Review Panel

R. Heath, Chairman	University of Washington
R. Budnitz	Future Resources Associates, Inc.
T. Cotton	JK Research Associates, Inc.
J. Mann	University of Illinois
T. Pigford	University of California, Berkeley
F. Schwartz	Ohio State University

Department of Energy

R. Becker
J. Rhoderick

Expert Panels

Futures

M. Baram	Boston University
W. Bell	Yale University
G. Benford	University of California, Irvine
D. Chapman	The World Bank, Cornell University
B. Cohen	University of Pittsburgh
V. Ferkiss	Georgetown University
T. Glickman	Resources for the Future
T. Gordon	Futures Group
C. Kirkwood	Arizona State University
H. Otway	Joint Research Center (Ispra), Los Alamos National Laboratory
M. Pasqualetti	Arizona State University
D. Reicher	Natural Resources Defense Council
N. Rosenberg	Resources for the Future
M. Singer	The Potomac Organization
T. Taylor	Consultant
M. Vinovski	University of Michigan

Source Term

C. Bruton	Lawrence Livermore National Laboratory
I-Ming Chou	U.S. Geological Survey
D. Hobart	Los Alamos National Laboratory
F. Millero	University of Miami

Retardation

R. Dosch	Sandia National Laboratories
C. Novak	Sandia National Laboratories
M. Siegel	Sandia National Laboratories

Geostatistics Expert Group

G. de Marsily, Chairman	U. of Paris
R. Bras	Massachusetts Inst. of Tech.
J. Carrera	U. Politechnica de Cataluña
G. Dagan	Tel Aviv U.
A. Galli	Ecole des Mines de Paris
A. Gutjahr	New Mexico Tech.
D. McLaughlin	Massachusetts Inst. of Tech.
S. Neuman	U. of Arizona
Y. Rubin	U. of California, Berkeley

Report Preparation (TRI)

Editors:

Volume 1: M. Gruebel (text); S. Laundre-Woerner (illustrations)
Volume 2: D. Scott (text); D. Marchand (illustrations)
Volume 3: J. Chapman (text); D. Pulliam (illustrations)

D. Rivard, D. Miera, T. Allen, and the Word Processing Department
R. Rohac, R. Andree, and the Illustration and Computer Graphics Departments
S. Tullar and the Production Department

J. Stikar (compilation of PA Peer Review Panel comments)

PREFACE

This volume documents the data and other pertinent information used by the Performance Assessment (PA) Division of Sandia National Laboratories in its 1991 preliminary comparison of the Waste Isolation Pilot Plant (WIPP) with the Environmental Protection Agency's (EPA's) *Environmental Standards for the Management and Disposal of Spent Nuclear Fuel, High-Level, and Transuranic Radioactive Wastes (40 CFR 191).*

Besides the DOE project office in Carlsbad, New Mexico, which oversees the project, the WIPP currently has two major participants: Sandia National Laboratories in Albuquerque, New Mexico, which functions as scientific investigator; and Westinghouse Electric Company, which is responsible for the management of WIPP operations. The specific tasks of Sandia are (1) characterizing the disposal system and surrounding region and responding to specific concerns of the State of New Mexico, (2) assessing the performance of the WIPP (i.e., assessing regulatory compliance with *40 CFR 191*, except the Assurance Requirements), (3) performing analytic, laboratory, field experiments, and applied research to nuclear waste disposal in salt, relevant to support tasks 1 and 2 (disposal system characterization and performance assessment), and (4) providing ad hoc scientific and engineering support (e.g., supporting environmental assessments such as Resource, Conservation, and Reentry Act (1976) and the National Environmental Policy Act (1969). This volume helps fulfill the performance assessment task.

For the performance assessment, the PA Division at Sandia maintains a data base, the secondary data base, which contains interpreted data from many primary sources. The data are used to form a conceptual model of the WIPP disposal system. The secondary data base provides a set of parameter values (median, range, and distribution type where appropriate) and the source of these values. As better information becomes available, the parameter values reported herein will be updated. Thus, this volume is only a snapshot of the data in the secondary data base compiled as of August 1991. At a minimum, updated data reports will be issued annually as a separate volume of the *Preliminary Comparison with 40 CFR Part 191, Subpart B for the Waste Isolation Pilot Plant.* A previous data report was published in December 1990 (Rechard et al., 1990a).

The 1991 comparison and background information on the comparison are reported in Volumes 1, 2, and 4 of this report:

SNL (Sandia National Laboratories) WIPP Performance Assessment Division. 1991. *Preliminary Comparison with 40 CFR Part 191, Subpart B for the Waste Isolation Pilot Plant, December 1991—Volume 1: Methodology and Results.* SAND91-0893/1. Albuquerque, NM: Sandia National Laboratories.

SNL (Sandia National Laboratories) WIPP Performance Assessment Division. 1991. *Preliminary Comparison with 40 CFR Part 191, Subpart B for the Waste Isolation Pilot Plant, December 1991—Volume 2: Probability and Consequence Modeling.* SAND91-0893/2. Albuquerque, NM: Sandia National Laboratories.

SNL (Sandia National Laboratories) WIPP Performance Assessment Division. 1991. *Preliminary Comparison with 40 CFR Part 191, Subpart B for the Waste Isolation Pilot Plant, December 1991—Volume 4: Sensitivity Analyses.* SAND91-0893/4. Albuquerque, NM: Sandia National Laboratories. (In preparation)

Other compilations of data used by the WIPP Project are reported in:

Bayley, S. G., M. D. Siegel, M. Moore, and S. Faith. 1990. *Sandia Sorption Data Management System Version 2 (SSDMSII).* SAND89-0371. Albuquerque, NM: Sandia National Laboratories.

Krieg, R. D. 1984. *Reference Stratigraphy and Rock Properties for the Waste Isolation Pilot Plant (WIPP) Project.* SAND83-1908. Albuquerque, NM: Sandia National Laboratories.

Munson, D. E., J. R. Ball, and R. L. Jones. 1990a. "Data Quality Assurance Controls through the WIPP In Situ Data Acquisition, Analysis, and Management System" in *Proceedings of the International High-Level Radioactive Waste Management Conference, Las Vegas, NV, April 8-12.* Sponsored by American Nuclear Society and ASCE, New York, p. 1337-1350.

Providing the data as ranges and distributions to the PA Division is a major task. Although the PA Division is responsible for comparing the WIPP with *40 CFR 191, Subpart B*, the majority of data used for these comparisons is supplied by experimenters and analysts characterizing the disposal system and surrounding regional geology as noted in the acknowledgments.

In addition to individual contributors who established current data (and are listed in Appendix A of this volume), earlier contributors are also acknowledged. Much of the data provided prior to 1991 is summarized in *Systems Analysis Long-Term Radionuclide Transport, and Dose Assessments, Waste Isolation Pilot Plant (WIPP), Southeastern New Mexico; March 1989*, edited by Lappin et al. (1989). Because of this report's wide circulation, we found it convenient to refer to this report as a data source, although in many cases it only summarizes others' work. Its selection as a source is not meant to diminish the contributions of the original authors. However, Lappin et al. (1989) is the first report in which ranges were assigned for many parameters, so it does provide a primary reference for these ranges. Furthermore, some of the data has not yet been published and thus Lappin et al. (1989) may be the only source until the reports are complete.

We appreciate the time and suggestions supplied by the final peer reviewers: T. F. Corbet (6344) and A. M. LaVenue (INTERA, Inc.). Furthermore, K. Byle's and J. C. Logothetis' (New Mexico Engineering Research Institute) efforts in producing the tables and distribution figures, respectively, from the PA secondary data base for this report are greatly appreciated. In addition, the editorial help on the text and over 140 illustrations provided respectively by J. Chapman and D. Pulliam of Tech Reps, Inc., Albuquerque, New Mexico, greatly improved the report.

CONTENTS

FIGURES

TABLES

1. INTRODUCTION

1.1 Purpose and Organization of Report

The purpose of this volume is to present data and information compiled and available in August 1991 for use by the Performance Assessment (PA) Division of Sandia National Laboratories in its 1991 evaluation of the long-term performance ("performance assessment") of the Waste Isolation Pilot Plant (WIPP). The data are critical for generating a well-founded and defensible analysis. In this volume, performance assessment refers to the prediction of all long-term performance. For example, the data compiled can be used to compare WIPP performance with the requirements of the Environmental Protection Agency's (EPA's) *Environmental Standards for the Management and Disposal of Spent Nuclear Fuel, High-Level, and Transuranic Radioactive Wastes (40 CFR 191)*, with long-term safety goals for individual exposure (doses) which may be necessary for environmental impact statements (National Environmental Policy Act [NEPA, 1969]), and with hazardous waste regulations (Resource, Conservation, Recovery Act of 1976 [RCRA, 1976]).

About 300 distinct parameters are listed in this report for use in the consequence and probability models used in simulations of the WIPP. Most of these parameters specify the physical, chemical, or hydrologic properties of the rock formations (geologic barriers) in which the WIPP is placed; a substantial number of the parameters specify physical, chemical, or hydrologic properties of the seals, backfill, and waste form (engineered barriers); and some pertain to future climatic variability or future episodes of exploratory drilling at the WIPP. Dimensions of selected engineered features of the WIPP underground facility are also listed, although these dimensions are not counted as part of the 300 parameters.

The EPA Standard, *40 CFR 191*, explicitly acknowledges the uncertainties associated with scientific predictions, especially when predictions cover thousands of years, and mandates that this uncertainty be reported when making comparisons with *40 CFR 191*. One of several sources of uncertainty in scientific predictions is uncertainty in the data; consequently, this report not only tabulates median values and sources for these values but also lists estimates of the range and distribution (uncertainty) of the parameters. A brief discussion accompanies each parameter description.

The organization of this volume is as follows:

- The remainder of Chapter 1 presents conventions used in the data tables, and background information on the selection of distributions, performance assessments, and the WIPP. Chapter 1 is arranged so that information specific to the data is presented first, followed by more general information (e.g., background on the WIPP)

- Chapter 2 provides consequence-model parameters for geologic barriers

- Chapter 3 provides consequence-model parameters for the engineered barriers
- Chapter 4 provides consequence-model parameters for global materials such as fluid properties (e.g., Salado Formation brine compressibility) and properties of agents that act upon the WIPP disposal system such as climate variability and human-intrusion boreholes
- Chapter 5 provides probability model parameters for scenario-probability estimation
- Chapter 6 lists the specific parameters that were varied for the December 1991 preliminary comparison of the WIPP with *40 CFR 191*
- Appendices A and B provide endorsements of the data currently in use and tabulated data from numerous wells near the disposal system
- Following the cited references is a table of conversion factors between SI and common English units; a glossary of terms; and a list of variables, acronyms, and initialisms.

1.2 Conventions

Chapters 2 through 5 provide the data that make up the 1991 conceptual model of the WIPP. The tables in these chapters list modeling parameters by their median (x_{50}), range (a,b), units, distribution type, and data source. Plots of both probability and cumulative distribution functions (pdfs and cdfs) of these parameters depict the mean ($\bar{x}$) and median (x_{50}). These terms are defined below.

1.2.1 Median

The median (x_{50}), a measure of the central tendency of the distribution, represents the value in the cumulative distribution function (cdf) of the parameter that occupies the position at which 50% of the data lie above and below it (i.e., 0.5 quantile).

1.2.2 Mean

The mean ($\bar{x}$), another measure of the central tendency of the distribution, is the expected value (E) (first moment about the origin) of the x-variable with respect to a continuous or discrete probability distribution function (pdf).

$$\bar{x} = \int_{-\infty}^{\infty} f(x)dx \sim \sum_{\text{all } x} x_i f(x)_i = E(x) \qquad (1.2\text{-}1)$$

Because the mean is strongly influenced by the tails of the distribution, it is not tabulated; however, it is shown on plots of cdfs.

The sample mean, also denoted by $\bar{x}$, is the arithmetic average of sample data pertaining to a modeling parameter.

1.2.3 Range

The range of a distribution, (a,b), is the pair of numbers in which a and b are respectively the minimum and the maximum values that are taken by the random variable x.

Continuous Distribution

For PA work, continuous distributions with range $(-\infty,+\infty)$(e.g., the normal distribution) are truncated at the 0.01 and 0.99 quantiles.

Constructed Distribution (Empirical)

Empirical distributions, cdfs and pdfs, are constructed from sets of measurements of a variable. Empirical cdfs are represented by histograms, which are piecewise constant functions based on the empirical percentiles derived from a set of measurements; an empirical cdf constructed in this way is an unbiased estimator of the unknown cdf associated with the variable (Blom, 1989, p. 216). The PA Division may modify empirical distributions in one or more of the four ways described below.

(1) Since the range of measurements in a data set may not reflect the true range of the random variable underlying the measurements, the PA Division may estimate the range by $\bar{x}$ + 2.33s, where $\bar{x}$ is the *sample* mean and s is the *sample* standard deviation. (The lower limit of this estimate is not allowed to be less than zero for an intrinsically positive variable: both the upper and lower limit are not allowed to exceed physical limits.) This estimate of range is justified by the fact that the indicated end-points are estimates of the 0.01 and 0.99 quantiles if the variable is normally distributed. If the variable is not normally distributed, the quantiles will differ in inessential ways (Table 1.2-1). For any distribution with finite mean and variance, Chebyshev's inequality states that the probability that the random variable x lies outside the interval $(\bar{x} - hs, \bar{x} + hs)$, h > 0, is a quantity less than $1/h^2$ (Blom, 1989, p. 121); i.e.,

$$P(|x - \bar{x}| \geq hs) \leq \frac{1}{h^2} \qquad (1.2\text{-}2)$$

If the pdf of the unknown distribution is known to be unimodal and symmetric about the mean value, then the right-hand side of Eq. 1.2-2 can be replaced with $4/(9h^2)$ (Gauss' inequality); i.e.,

$$P(|x - \bar{x}| \geq hs) \leq \frac{4}{9h^2} \qquad (1.2\text{-}3)$$

(2) If only two data points are available, the PA Division may estimate the range by $(\bar{x} \pm \sqrt{3}s)$ (see uniform distribution, Table 1.2-2).

Table 1.2-1. Probability of Parameters Lying within Range Defined by $\bar{x} \pm hs$ (after Harr, 1987, Table 1.8.2)

h	Chebyshev's Inequality	Gauss' Inequality	Exponential pdf	Normal pdf	Uniform pdf
1	0	0.56	0.86	0.68	0.58
2	0.75	0.89	0.95	0.96	1.00
2.33	0.82	0.92	0.964	0.9901	1.00
3	0.89	0.95	0.982	0.9973	1.00
4	0.94	0.97	0.993	0.99993	1.00

(3) Empirical cdfs for intrinsically continuous variables are always converted to piecewise linear cdfs by joining the empirical percentile points (including extrapolated end points) with straight lines in linear space (Tierney, 1990a, p. II-5). (Cumulative distribution functions in log space will be piecewise exponential.)

Constructed Distribution (Subjective)

Subjective distributions are histograms constructed from subjective estimates of range (the 0 and 1.0 quartiles) and at least one interior quartile (usually the 0.5 quartile) provided by experts in the subject matter of the variable of concern. The subjective cdf of an intrinsically continuous variable is always converted to a piecewise linear cdf by joining the subjective quartile points with straight lines in linear space (not log space). (Cumulative distribution functions in log space will be piecewise exponential.)

Variance and Coefficient of Variation

The variance, s^2, a measure of the width of a distribution, is the expected value of the square of the difference of the variable and its mean value (i.e., the second moment about the mean):

$$s^2 = \int_{-\infty}^{\infty} (x - \bar{x})^2 f(x)dx, \text{ or } s^2 = \sum_i (x_i - \bar{x})^2 f(x_i) \qquad (1.2\text{-}4)$$

The standard deviation, s, is the positive square root of the variance. The coefficient of variation, $s/\bar{x}$, is the ratio of the standard deviation to the mean value. The sample variance of a set of measurements of the x-variable, say x_1, x_2, x_3, ..., x_n, is the sum

$$\frac{1}{(N-1)} \sum_{n=1}^{N} (x_n - [\text{sample mean}])^2$$

The sample variance is an unbiased estimator of the variance (Blom, 1989, p. 197).

Table 1.2-2 Description of Several Probability Distributions

Probability Density Function f(x)	Cumulative Distribution Function F(x)	Expected Value μ	Variance σ^2
1. Beta $\frac{1}{B(\alpha,\lambda)} \frac{(x-a)^{\alpha-1} (b-x)^{\lambda-1}}{(b-a)^{\alpha+\lambda-2}}$ $a < x < b,\ \alpha > 0,\ \lambda > 0$ where $B(\alpha,\lambda) = \frac{\Gamma(\alpha)\,\Gamma(\lambda)}{\Gamma(\alpha+\lambda)}$ and $\Gamma(\gamma) = \int_0^\infty x^{\gamma-1} e^{-x} dx$ $= \frac{\alpha!\ \lambda!}{(\alpha+\lambda-1)!}$ if α and λ are integers	$\int_a^x f(\chi)\, d\chi$	$a = \frac{\alpha}{\alpha+\lambda}$	$\frac{(b-a)^2\,\alpha\lambda}{(\alpha+\lambda)^2(\alpha+\lambda+1)}$
2. Gamma $\frac{\lambda^\alpha x^{\alpha-1} e^{-\lambda x}}{\Gamma(\alpha)}$	$\int_0^x f(\chi) d\chi$	$\frac{\alpha}{\lambda}$	$\frac{\alpha}{\lambda^2}$
3. Exponential $\lambda e^{-\lambda x}$ $x \geq 0$	$1-e^{-\lambda x}$	$\frac{1}{\lambda}$	$\frac{1}{\lambda^2}$

Table 1.2-2 Description of Several Probability Distributions (Continued)

Probability Density Function f(x)	Cumulative Distribution Function F(x)	Expected Value μ	Variance σ^2
4. Normal $N(\mu, \sigma^2)$			
$\frac{1}{\sigma\sqrt{2\pi}} \exp\left[-\frac{(x-\mu)^2}{2\sigma^2}\right]$	$\int_{-\infty}^{x} f(\chi)d\chi$	μ	σ^2
$-\infty \le x \le \infty$			
but for WIPP PA			
$a \le x \le b$ where $P(x>a) = 0.99$ and $P(x>b) = 0.01$		$\mu = \frac{a+b}{2}$	$\left(\frac{b-a}{4.66}\right)^2$
5. Lognormal		$\exp\left[\mu(y) + \frac{\sigma^2(y)}{2}\right]$	
$\frac{1}{\sigma x\sqrt{2\pi}} \exp\left[-\frac{1}{2\sigma^2}(\ln x-\mu)^2\right]$	$\int_{o}^{x} f(\chi)d\chi$	Median $= e^{\mu(y)}$	$e^{2\mu(y)+\sigma^2(y)}\left(e^{\sigma^2(y)} - 1\right)$
$x \ge 0$			
$x = e^{y}$ where $y = N(\mu, \sigma^2)$			
but for WIPP PA			
$P(y>a) = 0.99$ and			
$P(y>b) = 0.01$		$\mu(y) = \frac{a+b}{2}$	$\sigma^2(y) = \left(\frac{b-a}{4.66}\right)^2$

Table 1.2-2 Description of Several Probability Distributions (Concluded)

	Probability Density Function f(x)	Cumulative Distribution Function F(x)	Expected Value μ	Variance σ^2
6.	Uniform		$\frac{a+b}{2} = \mu$	$\frac{(b-a)^2}{12}$
	$\frac{1}{b-a}$ $a \le x \le b$	$\frac{x-a}{b-a}$	$a = \mu - \sqrt{3\sigma}$	
			$b = \mu + \sqrt{3\sigma}$	
7.	Loguniform			
	$\frac{1}{x(\ln b - \ln a)}$	$\frac{\ln x - \ln a}{\ln b - \ln a}$	$\frac{b-a}{\ln b - \ln a}$	$(b-a)\left[\frac{(\ln b - \ln a)(b+a) - 2(b-a)}{2(\ln b - \ln a)^2}\right]$
	$a < x < b$		Median $= \sqrt{ab}$	
8.	Binomial (discrete)			
	$\frac{n!}{x!(n-x)!} \rho^x \left(1-\rho\right)^{n-x}$	$\sum_{\chi=0}^{x} f(\chi)$	np	np(1-p)
	$x = 0,1,2,\ldots,N;$			
9.	Poisson (discrete)			
	$\frac{u^x e^{-\mu}}{x!}$ $x = 0,1,2,\ldots,n$	$\sum_{\chi=0}^{x} f(\chi)$	μ	μ

1.2.4 Units

The units indicate how the parameter is expressed quantitatively. Only SI units are used in the tables and the PA secondary data base (except for radionuclide inventory activity, which is expressed in curies since EPA release limits for *40 CFR 191* are expressed in curies). However equivalent values in English units are given in the text. In addition, conversion factors for SI and English units are listed at the end of the report.

1.2.5 Distribution Type

The distribution types listed in the tables are grouped into four major categories (Table 1.2-2):

1. Continuous pdf: beta, normal, lognormal, uniform, or loguniform (Figure 1.2-1a)

2. Discrete pdf: Poisson (Figure 1.2-1b)

3. Constructed distributions: a piecewise linear cdf designated as "cumulative" (subjective); a piecewise uniform pdf designated as "data" or a piecewise uniform cdf designated as "delta" (Figure 1.2-1b)

4. Miscellaneous categories (null distributions): constant, spatial, and table.

The figures in the text emphasize the cdf of the distribution--the form of the distribution from which samples are taken; however, the pdf of the distribution is also shown.

Continuous Probability Density Functions

Five continuous pdfs are described below:

Beta. Beta designates the beta pdf, which is a versatile density function specified by two parameters (α, λ) that can assume numerous shapes in a specified range (a,b) (Harr, 1987, p. 79; Johnson and Kotz, 1970b, p. 37; Miller and Freund, 1977, p. 119).

Normal. Normal designates the normal pdf, a good approximation of many physical parameters. Most arguments for the use of the normal distribution are based on the central limit theorem (Miller and Freund, 1977, p. 104; Johnson and Kotz, 1970a, p. 40). The distribution is truncated at the 0.01 and 0.99 quantiles (i.e., the probability that the parameter will be smaller or larger is 1%), which corresponds to $\bar{x} \pm 2.33s$.

Lognormal. Lognormal designates a lognormal pdf, a distribution of a variable whose logarithm follows a normal distribution. The distribution is truncated at the 0.01 and 0.99 quantiles.

Uniform. Uniform designates a pdf that is constant in the interval (a,b) and zero outside of that interval.

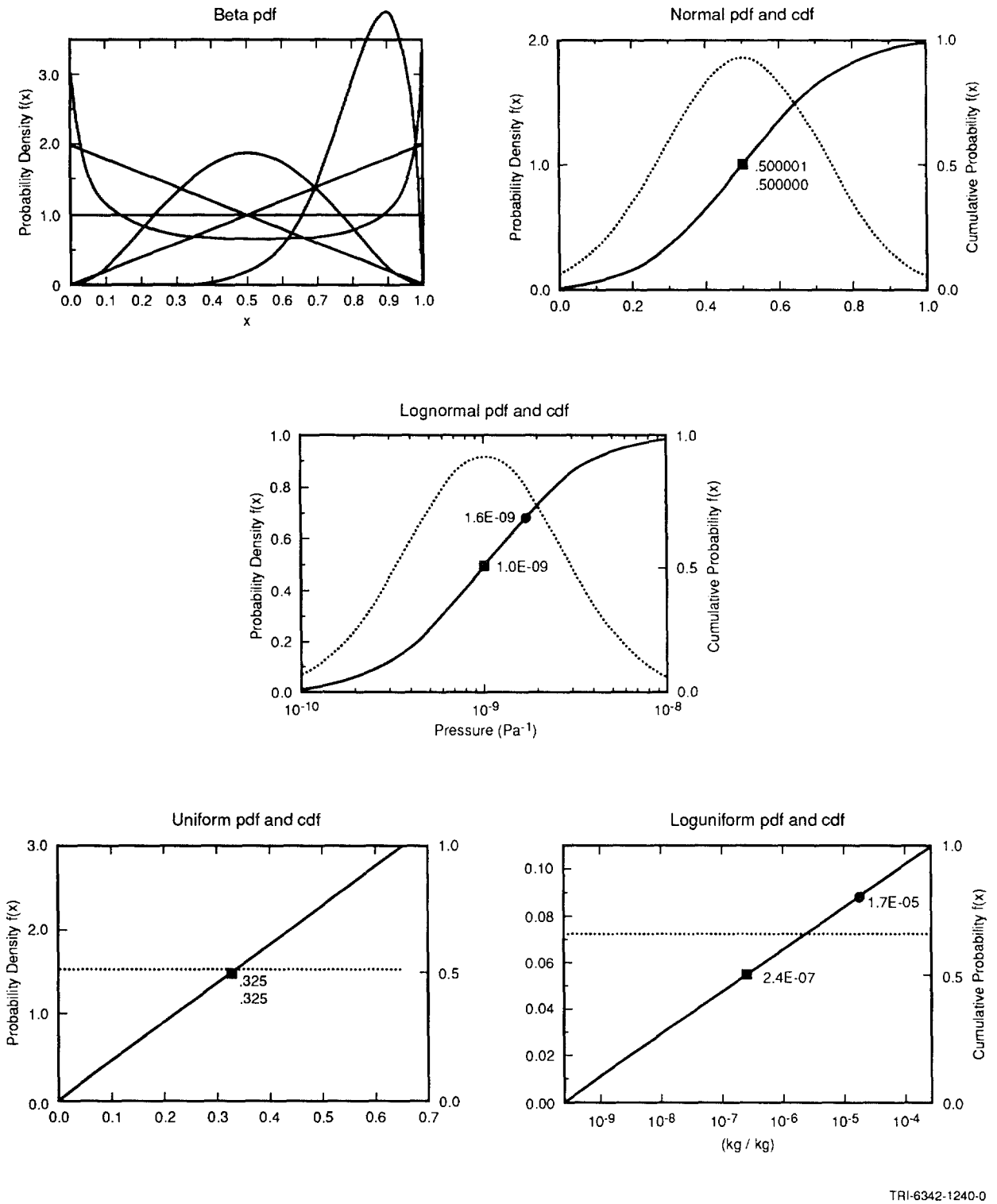

(a) Continuous Distribution Plots

Figure 1.2-1. Examples of Distribution Plots

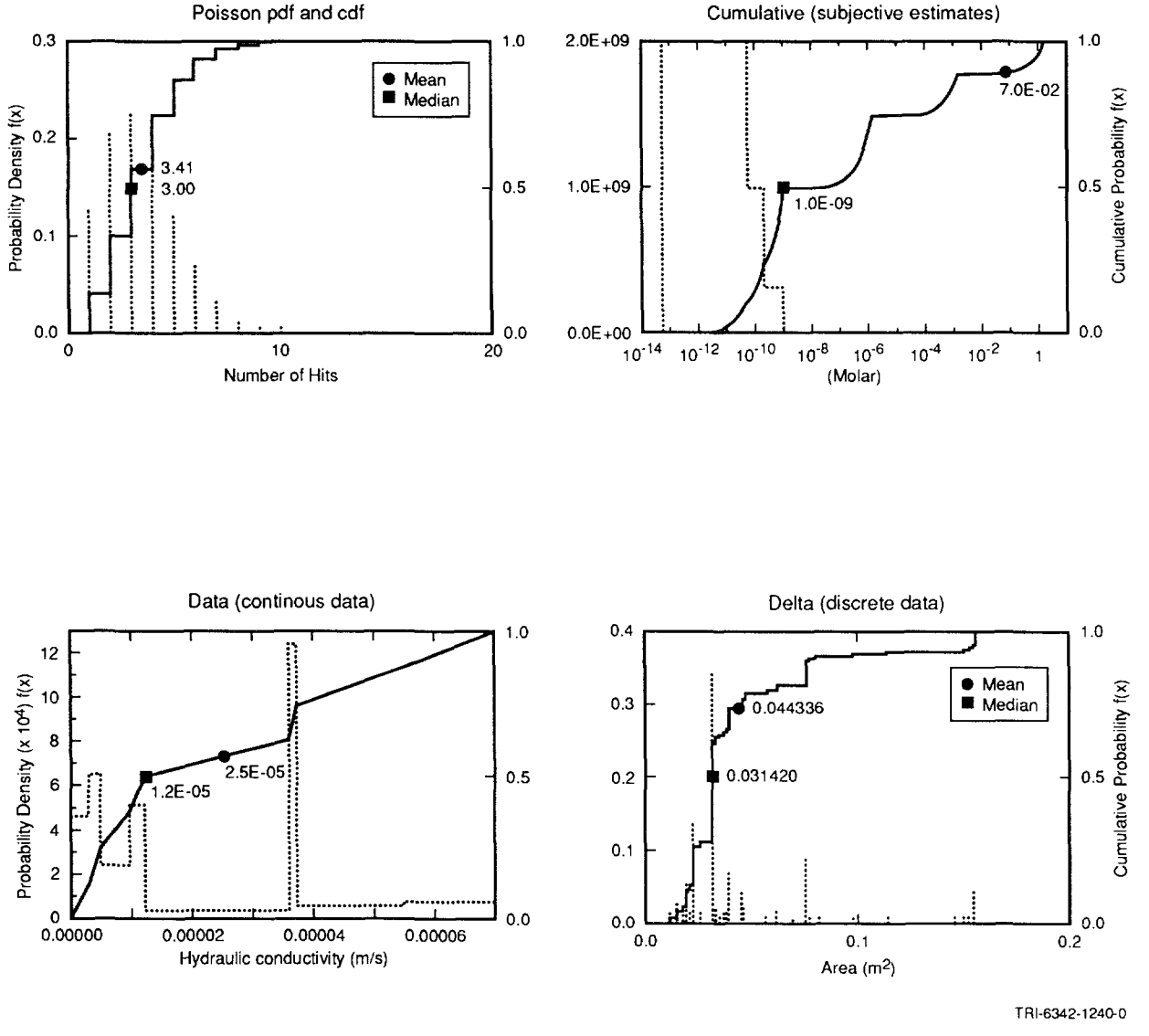

(b) Discrete and Constructed Distribution Plots

Figure 1.2-1. Examples of Distribution Plots (Concluded)

Loguniform. Loguniform designates a loguniform pdf, a distribution of a variable whose logarithm follows a uniform distribution.

Discrete Probability Density Function

One discrete probability density function, the Poisson, was used.

Poisson. Poisson designates a discrete Poisson pdf. The Poisson pdf is often used to model processes taking place over continuous intervals of time such as the arrival of telephone calls at a switch station (queuing problem) or the number of imperfections continuously produced in a bolt of cloth. The Poisson pdf is used in the probability model for human intrusion by exploratory drilling.

Constructed Distributions

The cumulative, data, and delta distributions are described below:

Cumulative. The cumulative distribution type refers to the piecewise linear cdf constructed by linearly connecting subjective point estimates of the distribution percentiles supplied by experts (Tierney, 1990a, Section 3.1). Distributions are stored in the secondary data base as a cdf when the distribution is subjectively estimated from sparse or no data. Plots of the subjectively estimated distributions show a corresponding piecewise uniform pdf, but the pdf is not used for calculations.

Data. The data distribution type indicates an empirical distribution (i.e., measured data points are stored in the data base and used to form the distribution). The pdf is piecewise uniform; the cdf, which is constructed from this data for purposes of Monte Carlo sampling, is piecewise linear (see Cumulative). However, the name indicates that the distribution is based on empirical information rather than subjective estimates.

Delta. The delta distribution type refers to a pdf where parameters must be assigned discrete values (i.e., the pdf is a series of dirac delta functions ($\Sigma\ \delta(x_i-x)$); the cdf is a series of step functions). As an example, in the 1990 preliminary comparison (Bertram-Howery et al., 1990) the drill-bit diameters used for the human-intrusion borehole were not assumed to vary continuously between the minimum and maximum drill bit sizes, but were fixed at diameters of bits that are actually available.

Miscellaneous Categories

The constant, spatial, and table distributions are described below:

Constant. When a distribution type is listed as constant, a distribution has not been assigned and a constant value is used in all PA calculations.

Spatial. The spatial category of data indicates that the parameter varies spatially. This spatial variation is shown on an accompanying figure. The median value recorded is a typical value for simulations that use the parameter as a lumped parameter in a model; however, the value varies depending upon the scale of the model. The range of a spatially varying parameter is also scale dependent.

Table. The table category of data indicates that the parameter varies with another property and the result is a tabulated value. For example, relative permeability varies with saturation; its distribution type is listed as table (also, the median value is not meaningful and is therefore omitted in the table).

Note on Correlations. Most of the uncertain variables studied during the 1991 PA calculations were assumed to be independent random variables, although it was known some were interdependent, i.e., correlated in some way. Correlations of the model variables may arise from the fact that there are natural correlations between the local quantities used to determine the form of the model variable (e.g., local porosity could be strongly correlated with local permeability); or correlations of model variables may be implicit in the form of the mathematical model in which they are used.

1.2.6 Sources

The source indicates the document in which the parameter value is cited. Several sources are cited when one source cannot supply all the data or information (e.g., median, range, distribution type, or explanatory information).

1.2.7 Note on Unnecessary Conservatism of Material-Property Parameters

The following arguments attempt to show why some of the current assignments of probability distributions to material-property parameters of WIPP performance models are unnecessarily conservative, given the present level of detail and spatial resolution of the models. Current methods of assigning uncertainty to some of the material-property parameters (e.g., including small-scale spatial variability as a source of uncertainty) may distort results of sensitivity analyses performed to identify those important model variables that are material-property parameters and result in unnecessary expense, but will probably not affect validity of results of the uncertainty analyses that are used to make preliminary comparisons with EPA standards.

WIPP performance models described in Volume 2 of this report are based on the numerical solution of one or more of three types of equations:

(a) Partial differential equations - which are reduced to a set of algebraic equations or ordinary differential equations in order to effect a solution by finite-difference or finite-element methods. Examples: the equations of groundwater and brine flow, solute transport, gas flow, and salt creep.

(b) Ordinary differential equations - which may be the result of a reduction of a partial differential equation or may directly model the dynamics of a lumped-parameter system, e.g., punctured brine reservoirs, leaching and decay of radioactive waste stored in a panel.

(c) Algebraic equations of the form

$$F(x_1, x_2, x_3, ..., x_n; y) = 0$$

which may arise indirectly from equilibrium solutions of ordinary differential equations (i.e., solutions for time $\rightarrow \infty$) or may directly express a model of some physical relationship between WIPP performance-model variables (x_1, x_2, x_3, ..., x_n) and y.

In addition to dependent variables and independent variables of position and time, certain constants, or free parameters, will appear in each of the three types of equations. In most cases, these free parameters are intended to represent physical and chemical properties of real materials of the WIPP system: e.g., the hydraulic conductivity, porosity, and specific storage in models of fluid flow in the Salado Fm.; the fracture spacing, dispersivity, diffusivity, and chemical distribution coefficients in models of solute transport in the Culebra Fm.; the porosity, permeability and solubility of waste forms emplaced in a typical WIPP panel. This kind of free parameter will be called a material-property parameter in the remainder of this note.

Many of the material-property parameters of WIPP performance models were included in the set of uncertain variables that was sampled in a recent study of variable sensitivity of performance models (Helton et al., 1991) and in a recent preliminary assessment of WIPP system performance (Rechard et al., 1990a). (Note: In these two reports, all uncertain model parameters were usually called "variables" or "independent variables.") In these studies, uncertainty associated with a sampled variable was quantified by assigning an empirical or subjective probability distribution to the values taken on by that variable within a predetermined range of values. Current procedures for the assignment of probability distributions are described in Section 3.1 of Tierney (1990a); these procedures include construction of empirical cumulative distribution functions (cdfs) from data sets or, if there is little or no data, construction of cdfs from subjective quantiles obtained by elicitation of expert opinion. Tierney (1990a; Chapter III) also briefly noted the problems involved in scaling uncertainty from measured data to model parameters and he suggested some rules for estimating the mean and variance of a material-property parameter using the sample mean and variance of a set of measurements of the material property.

The distribution of a material-property parameter needs to reflect spatial variability of the material property and also the scale of the model. The zones or cells of numerical models (finite-element, finite-difference, or lumped-parameter models) must be few in number in order to minimize computational time and expense; in a typical problem involving geologic media, these cells will have dimensions of tens of meters or more and volumes of thousands

of cubic meters. Material-property parameters must therefore represent the effects of a physical or chemical property of matter in these relatively large, arbitrarily defined volumes of space. It follows that material-property parameters are model dependent and usually not observable quantities, i.e., quantities that can be measured in the field or in the laboratory. On the other hand, with few exceptions (e.g., formation transmissivity measured by pumping tests) most physical and chemical properties of geologic or anthropogenic materials are actually measured on spatial scales typical of the laboratory or an exploratory borehole, a matter of at most a few tens of centimeters. In addition, natural materials and many man-made materials (e.g., defense waste) tend to be inhomogeneous on spatial scales characteristic of model cell sizes; accordingly, a set of measurements of a material property taken randomly from large volumes of real material may show wide variability. The question is: How to assign values to material-property parameters in a way that correctly reflects both cell size and the small-scale variability that may appear in measurements of the corresponding material property?

To begin to answer this question, assume that the material property can be represented as a scalar field in space, say $\phi(\mathbf{x})$, where $\mathbf{x} = (x,y,z)$ denotes position in space. (The assumptions of a scalar quantity in three dimensions are for the sake of simplicity of argument and involve no loss of generality; the property could be a vector or tensor.) It is argued in some modern textbooks that the material-property parameter, say Φ, to be used in type (a) equations (above) should be taken as a spatial average of ϕ over the cell or zone; for instance, in a cell or zone of volume V,

$$\Phi(V) = \frac{1}{V} \int_V \phi\ (\mathbf{x})\ d\mathbf{x} \qquad (1.2\text{-}5)$$

where dx is the volume element dxdydz. (Again, no loss of generality is involved; a line or surface average could replace the volume average.) The arguments for this choice of material-property parameter are highly technical and limitations of time and space preclude their inclusion in this note; however, see the discussion in de Marsily (1986, Chapter 3 and Section 4.4).

To account for spatial variability of $\phi(\mathbf{x})$, it can be assumed that ϕ is a *stationary, random scalar field* within a cell volume V, with realizations $\phi(\mathbf{x},\mu)$ and the following statistical properties:

$$\text{Expectation of } \phi(\mathbf{x},\mu) = E[\phi(\mathbf{x})] = \bar{\phi}, \text{ a constant,} \qquad (1.2\text{-}6)$$

and

$$\begin{aligned}\text{Covariance of } \phi(\mathbf{x},\mu) &= E\{[\phi(\mathbf{x}) - \bar{\phi}][\phi(\mathbf{y}) - \bar{\phi}]\} \\ &= \sigma^2 \rho(|\mathbf{x} - \mathbf{y}|),\end{aligned} \qquad (1.2\text{-}7)$$

where σ^2 is a constant (called the variance of ϕ), and $\rho(\bullet)$ is a function of $r = |x - y|$ with the properties

$$\begin{aligned} &\rho(r) \geq 0 \text{ for } r \in (0,\infty), \\ &\rho(r) \to 1 \text{ as } r \to 0 \\ &\rho(r) \to 0 \text{ as } r \to \infty. \end{aligned} \tag{1.2-8}$$

The function $\rho(\bullet)$ is called the autocorrelation function (Yaglom, 1962); it is a measure of the statistical dependence of the values of ϕ measured at two different points x and y. The assumptions of constant mean value $\bar{\phi}$ and variance σ^2 can be slightly weakened by allowing these quantities to depend on the coordinates of the center of the volume V; i.e., $\bar{\phi}$ and σ^2 may vary from cell to cell.

Treating $\phi(x)$ as a stationary random field with statistical properties 1.2-6 through 1.2-8 allows estimates of the mean value and variance of the volume average of ϕ, $\Phi(V)$, to be made. It is shown in many textbooks (see for instance Yaglom, 1962, pgs. 23-24) that

$$\text{Expectation of } \Phi(V) = E[\Phi(V)] = \bar{\phi}, \tag{1.2-9}$$

and

$$\text{Variance of } \Phi(V) = \frac{\sigma^2}{V^2} \int_V \int_V \rho(|x - y|)\, dx\, dy. \tag{1.2-10}$$

If $\bar{\phi}$, σ^2 and $\rho(r)$ were known, the problem would be essentially solved in that the distribution of the material-property parameter, $\Phi(V)$, could be approximated by a normal distribution with mean and variance given respectively by Eqs. 1.2-9 and 1.2-10. In general, $\bar{\phi}$, σ^2 and the function $\rho(r)$ must be estimated using sets of measurements of the material property ϕ, say $(\phi_1, \phi_2, \ldots, \phi_N)$. The estimators of $\bar{\phi}$ and σ^2 are the usual unbiased estimators of mean and variance (see Tierney, 1990a, pp. II-4,5) and, given a sufficiently large set of spatially coordinated measurements of ϕ, approximations to the autocorrelation function could be constructed and used in the numerical evaluation of the volume integrals in Eq. 1.2-10. This ideal solution to the problem cannot be implemented, however, since there are few measurements of the material properties appearing in WIPP performance models (and most are not spatially indexed; measured transmissivity, grain density, porosity, and tortuosity of the Culebra Formation are exceptions). Thus, one must try to use available measurements and insight to infer the statistical properties, given by Eqs. 1.2-9 and 1.2-10, of material-property parameters $\Phi(V)$. The following observations may be useful in inferring statistical properties of material-property parameters.

(1) The variance of a material-property parameter is less than or equal to the apparent variance of the material property. Note that because of the properties of $\rho(r)$ (Eq. 1.2-8), the integrand in the double volume integral of Eq. 1.2-10 is always less than one so that

$$\text{Variance of } \Phi(V) \leq \sigma^2.$$

In particular, if we take the special form of autocorrelation function ("cookie cutter"),

$$\rho(|\mathbf{x} - \mathbf{y}|) = 1 \text{ if } |\mathbf{x} - \mathbf{y}| \leq a,$$
$$= 0 \text{ otherwise,} \qquad (1.2\text{-}11)$$

then

$$\text{Variance of } \Phi(V) \approx \frac{v}{V} \sigma^2 \qquad (1.2\text{-}12)$$

where $v = \frac{4\pi}{3} a^3$ can be called the *volume of correlation.* Equation 1.2-12 suggests that if the volume of correlation is <<V, then the distribution of $\Phi(V)$ is peaked about the mean value of the material property, $\bar{\phi}$. If the coefficient of variation of the material property, $\sigma/\bar{\phi}$, is not large (say, of the order of one), the distribution of $\Phi(V)$ is more sharply peaked about the mean value, $\bar{\phi}$, than is the distribution of the material property, $\phi(\mathbf{x})$. If this tendency is strong enough, then $\Phi(V)$ can simply be assigned the mean value,

$$\Phi(V) \approx \bar{\phi}$$

This is what is usually done in studies with numerical models that are not probabilistic; that is, not directed explicitly towards sensitivity and uncertainty analyses.

(2) If, as suggested above, $\Phi(V) \approx \bar{\phi}$, then one must consider the uncertainty inherent in estimating the mean value $\bar{\phi}$ that arises from (a) a limited number of measurements of the material property, and (b) relationships between $\bar{\phi}$ and other uncertain problem parameters. Uncertainty of type (a) can be handled by fitting available data to a "t-distribution" (Blom, 1989) which, in a Bayesian approach, gives the distribution of the true mean of the material property about the sample mean of measurements. However, this was not done in assigning ranges to parameters and thus introduces conservatism. Uncertainty of type (b) is model dependent and must be handled on a case-by-case basis.

The standard techniques of statistical estimation cannot be directly applied when the distribution of the material property, $\phi(\mathbf{x})$, must be gained by subjective means, i.e., the elicitation of expert judgment. In such cases, the PA Division must make the unnecessarily conservative assumption that the distribution of the material property, $\phi(\mathbf{x})$, is also the distribution of the material-property parameter, $\Phi(V)$.

1.3 Background on Selecting Parameter Distribution

1.3.1 Requests for Data from Sandia Investigators and Analysts

When evaluating long-term performance, the PA Division follows a fairly well-defined procedure for acquiring and controlling the data used in consequence and probability models. A data base, called the secondary data base, contains the interpreted data and in essence embodies the conceptual model(s) of the disposal system. The data provided in this report are from the secondary data base as of July 1991 and are used in the 1991 preliminary performance assessment of the WIPP (Volume 1 of this report).

The major sources of the data are the task leaders and investigators at Sandia and from Westinghouse.

Identify Necessary Data

Each year, the PA Division identifies data that are necessary to perform the calculations for the preliminary performance assessment. Members of the PA Division informally compile data from published reports, personal communications with investigators, and other sources.

Request Median Value and Distribution

The PA Division then requests that the investigators provide a median value and distribution for each parameter in a large subset of the parameters. Some model parameters are specific to the PA calculations and so individuals in the PA Division are considered the experts for these parameters (e.g., probability model parameters).

Initially, the investigator is responsible for providing the median value and distribution for all parameters. As this procedure for acquiring data is repeated, a few parameters are evaluated through formal elicitation.

Update Secondary Data Base

The PA Division enters the endorsed or elicited data into the secondary data base. The PA Division then selects a subset of the data to sample, keeping all other values constant at the median or mean value, unless specifically noted.

Perform Consequence Simulations and Sensitivity Analyses

The PA Division runs consequence simulations and sensitivity analyses with the selected subsets of data from the updated secondary data base. The sensitivity analysis may evaluate either or both the sensitivity and the importance of a parameter in determining variation of the result (i.e., CCDF). During this time, the PA Division prepares a report that lists the data in the secondary data base at the time of these calculations (i.e., this data report).

Determine Whether Parameter Is Important in Analysis

By means of the sensitivity analyses, the PA Division can determine whether the parameter is significant in the calculations. If the parameter does not appear to be significant in the sensitivity analyses, and the review process of the Data Report does not question the parameter value, then the parameter is flagged as not likely to change or be sampled.

1.3.2 Construction of Distributions

The steps below describe the procedure developed by the PA Division to construct probability distributions (cdfs or pdfs) for the uncertain independent variables in consequence and probability models (Figure 1.3-1) (modified from Tierney, 1990a).

Step 1

Determine whether site-specific data for the variable in question exists, i.e., find a set of site-specific sample values of the variable. Data are usually either documented in a formal report or are described in an internal memorandum (see Appendix A). If data sets exist, go to Step 3; if no data sets are found, go to Step 2.

Step 2

Request that the investigator supply a specific shape (e.g., normal, lognormal) and associated numerical parameters for the distribution of the variable. If the investigator assigns a specific shape and numerical parameters, go to Step 5; if the investigator cannot assign a specific shape and appropriate parameters, go to Step 4. In responding to this request, the investigator may use his or her knowledge of global data to form an answer.

Step 3

Determine the size of the combined data sets. If the number of values in the combined data set is >3, use the combined data to evaluate the data range as $\bar{x} \pm 2.33s$ and construct a piecewise-linear cumulative distribution function or, alternatively, a discrete cumulative distribution function, and then go to Step 5. If the number of variables in the combined data set is ≤ 3, evaluate the data range as $\bar{x} \pm \sqrt{3}s$ and go to Step 4.

Step 4

Request that the investigator provide subjective estimates of (a) the range of the variable (i.e., the minimum and maximum values taken by the variable with at least 99% confidence and preferably 100% confidence) and (b) if possible, one of the following (in decreasing order of preference): (1) percentile points for the distribution of the variable (e.g., the 25th, 50th [median], and 75th percentiles), (2) the mean value and standard deviation of the distribution, or (3) the mean value. Again, in responding to this request, the investigator may use his or her knowledge of global data to form an answer. Then, using the maximum entropy formalism (MEF), construct one of the following distributions depending upon the kind of subjective estimate that has been provided (Tierney, 1990a; Harr, 1987):

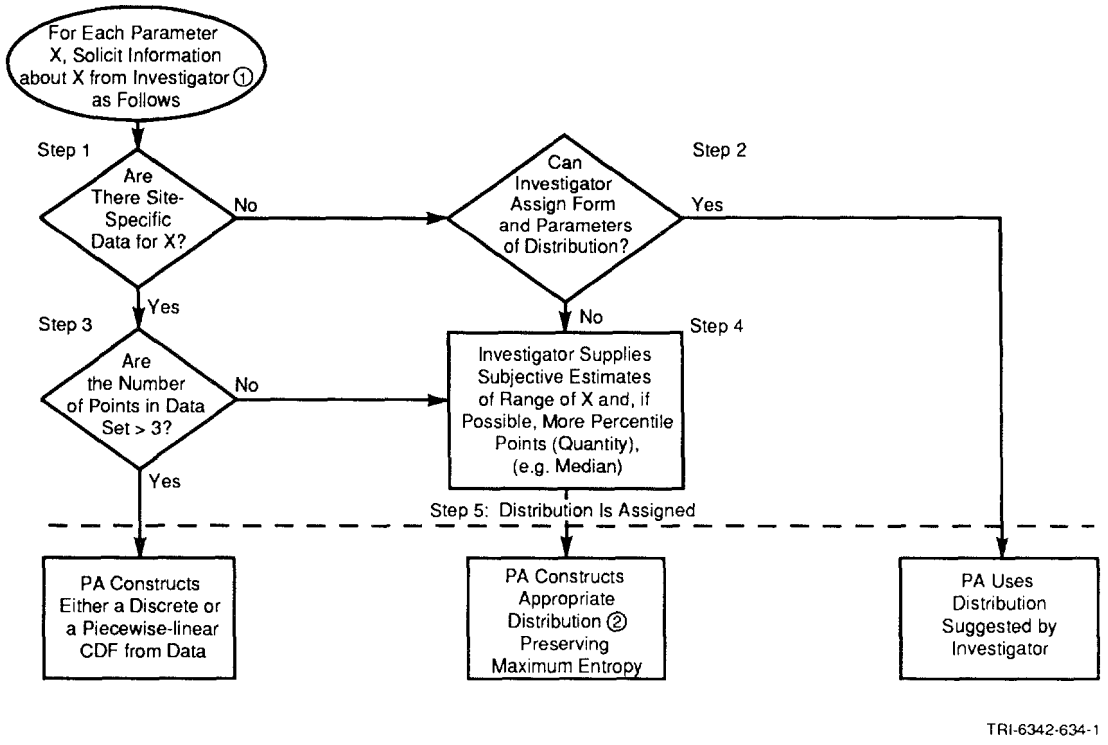

Figure 1.3-1. Five-Step Procedure Used to Construct Cumulative Distribution Functions (cdf) for the 1991 Performance Simulations. Investigator refers to expert in subject matter; MEF refers to maximum entropy formalism (after Tierney, 1990a).

- Uniform pdf over the range of the variable
- Piecewise-linear cdf based on the subjective percentiles
- Exponential pdf (truncated) based on the subjective range and mean value
- Normal pdf based on subjective mean value and standard deviation
- Beta pdf based on the subjective range, mean value, and standard deviation. (The beta distribution is not a maximum-entropy distribution under these constraints.)

Then go to Step 5.

Step 5

End of procedure; distribution is assigned. Computational restrictions may require later modification to some distributions and are discussed with each parameter.

1.3.3 Selection of Parameters for Sampling

For the 1991 preliminary performance assessment of the WIPP, the 45 parameters that were selected for variation (sampling) together with a brief description of why they were selected are discussed in Chapter 6. Other studies on subsystems of the WIPP disposal system (e.g., sensitivity of the repository to gas generation) may use different subsets of the approximately 300 parameters for which distributions are reported herein.

1.3.4 Elicitation of Distributions from Experts

This section discusses formal elicitation of probability distributions for model parameters that are uncertain and are considered significant in the performance assessment (e.g., estimate of radionuclide concentration in the disposal region [Trauth et al., 1991]). Formal elicitation is also being used in the performance assessment of the WIPP to hypothesize about possible futures of society and the effects of appropriate markers to warn future societies about the WIPP; these elicitation efforts are discussed elsewhere (Hora et al., 1991).

In all aspects of data gathering, professional judgment (i.e., opinion) must bridge the gaps in knowledge that invariably exist in scientific explanations. For example, the selection of methods to collect data (characterizing a site), interpretation of data, development of conceptual models, and selection of model parameters all require professional judgment by the investigator. This volume summarizes these judgments.

When data are lacking, either because of the complexity of processes or the time and resources it would take to collect data or when data have a major impact on the performance assessment, a formal elicitation of expert judgment is pursued. The procedure has the following advantages. First, formal elicitation offers a structured procedure for gathering opinions. Second, it encourages diversity in opinions and thus guards against understating the uncertainty. Finally, it promotes clear and thorough documentation of how the results were achieved (Hora and Iman, 1989).

The judgments that result from formal elicitation are a snapshot of the current state of knowledge. As new observations are made, the state of knowledge is refined. Even though the compilation of information through formal elicitation is often enlightening and helps to prevent bias, it does not create information. An important aspect of the elicitation, which occurs either during or following the procedure, is to examine how new data collected may improve understanding.

A successful formal elicitation of expert opinion includes the following five components (Hora and Iman, 1989):

Selection of Issue and Issue Statement

The first component of the formal elicitation process is a clear statement of the issue that cannot be practically resolved by other means. For example, the issue may not be resolved

For example, the issue may not be resolved either because of time (the judgment may be a temporary solution until laboratory or field data become available) or because the complexity of the issue prevents a resolution regardless of the resources applied.

Selection of Experts

The second component is the selection of experts with the recognized training and experience to address the issue. The experts should be free from motivational biases and represent a diversity of opinions. (Experts in a subject who may be motivationally biased can give testimony to the selected expert(s) as part of the training described below.) For controversial issues, the selection may require that an external committee select individuals from a list of nominees provided by diverse groups such as universities, the government, consulting firms, and intervenor groups.

Once selected, the experts may be asked to respond to a single question individually, respond to similar questions as a group, or become part of a team of experts who are expected to fully analyze a complex problem. The strategy selected is based on the importance of the issue and the time and resources available.

Elicitation Sessions

The third component consists of the elicitation sessions. Elicitation training includes informing the experts about the methods that will be used to process and propagate their subjective beliefs, introducing the assessment tools and practicing with these tools, providing calibration training using almanac questions, and introducing the psychological aspects of probability elicitation.

At the session (or a subsequent session), the issues are presented to the analysts. Included in each presentation is a proposed decomposition of the problem. Problem decomposition improves the quality of assessments by structuring the analysis so that the expert is required to make a series of simpler assessments rather than one complex assessment. Decomposition also provides a form of self-documentation since the expert's thought process is made explicit. The elicitation sessions are led by a normative analyst (i.e., an expert trained in decision analysis). The session may include a substantive analyst, who is an expert in the subject matter under discussion.

Recomposition and Aggregation

The fourth component is the recomposition of an expert's opinions and the aggregation of the diverse opinions from several experts. The tools employed in recomposing the assessments vary from issue to issue. In most issues, however, three levels of action are required. The first level is the modification of the assessed values to obtain cumulative distribution functions for any continuous quantities. The second level of action is the recomposition of

each expert's individual assessments to obtain a recomposed distribution for the specific issue in question. The final level is the aggregation of the experts' judgments to obtain the aggregated distribution.

Documentation

The final component is documentation of the elicitation process. Documentation usually includes a record of problem decomposition, the diversity of opinion, and the recomposition and aggregation performed.

1.4 Performance-Assessment Methodology

The Containment Requirements of the Standard state that:

> Disposal systems for spent nuclear fuel or high-level or transuranic radioactive wastes shall be designed to provide a reasonable expectation, based upon performance assessments, that the cumulative releases of radionuclides to the accessible environment for 10,000 years after disposal from all significant processes and events that may affect the disposal system shall:
>
> (1) Have a likelihood of less than one chance in 10 of exceeding the quantities calculated according to Table 1 (Appendix A); and
>
> (2) Have a likelihood of less than one chance in 1,000 of exceeding ten times the quantities calculated according to Table 1 (Appendix A). (§ 191.13(a))

As defined by the Standard, the term accessible environment means "(1) the atmosphere; (2) land surfaces; (3) surface waters; (4) oceans; and (5) all of the lithosphere that is beyond the controlled area" (191.12(k)). Controlled area is defined to be "(1) a surface location, to be identified by passive institutional controls, that encompasses no more than 100 square kilometers and extends horizontally no more than 5 kilometers in any direction from the outer boundary of the original location of the radioactive wastes in a disposal system; and (2) the subsurface underlying such a surface location" (191.12(g)). Table 1 of Appendix A of the Standard, which is referred to in the preceding Containment Requirements, is reproduced here as Table 1.4-1. The complete text of the Standard is reproduced as Appendix A of Volume 1 of this report.

For releases to the accessible environment that involve a mix of radionuclides, the limits in Table 1.4-1 are used to define normalized releases for comparison with the release limits. Specifically, the normalized release for transuranic waste is defined by

$$R = \sum_{i=1}^{nR} \left[\frac{Q_i}{L_i}\right] \cdot (1 \times 10^6 \text{ Ci/C}) \qquad (1.4\text{-}1)$$

where

Table 1.4-1. Release Limits for Containment Requirements (40 CFR 191, Appendix A, Table 1)

	Release limits (L_i) per 1000 MTHM* or Other Unit of Waste (Ci)
Americium (Am) -241 or -243	100
Carbon (C) -14	100
Cesium (Cs) -135 or -137	1000
Iodine (I) -129	100
Neptunium (Np) -237	100
Plutonium (Pu) -238, -239, -240, or -242	100
Radium (Ra) -226	100
Strontium (Sr) -90	1000
Technetium (Tc) -99	10000
Thorium (Th) -230 or -232	10
Tin (Sn) -126	1000
Uranium (U) -233, -234, -235, -236, or -238	100
Any other α-emitting radionuclide with $t_{1/2}$ > 20 yr	100
Any other non α-emitting radionuclide with $t_{1/2}$ > 20 yr	1000

* Metric tons of heavy metal exposed to a burnup between 25,000 megawatt-days per metric ton of heavy metal (MWd/MTHM) and 40,000 MWd/MTHM.

nR = number of radionuclides included in the analysis,
C = amount of TRU waste with half-lives greater than 20 years (1 x 10^6 Ci/C is the reciprocal of the waste unit factor f_w used in Chapter 3) (Ci) emplaced in the repository,
Q_i = cumulative release (Ci) of radionuclide i to the accessible environment during the 10,000-yr period following closure of the repository,

and

L_i = the release limit (Ci) for radionuclide i given in Table 1.4-1.

In addition, the EPA suggests that the results of a performance assessment intended to show compliance with the release limits in § 191.13 can be assembled into a single complementary cumulative distribution function (CCDF). Specifically, the nonbinding guidance contained in Appendix B of the Standard indicates that

> ... whenever practicable, the implementing agency will assemble all of the results of the performance assessments to determine compliance with § 191.13 into a "complementary cumulative distribution function" that indicates the probability of exceeding various levels of cumulative release. When the uncertainties in parameters are considered in a performance assessment, the effects of the

uncertainties considered can be incorporated into a single such distribution function for each disposal system considered. The Agency assumes that a disposal system can be considered to be in compliance with § 191.13 if this single distribution function meets the requirements of § 191.13(a). (U.S. EPA, 1985, p. 38088).

1.4.1 Conceptual Model for WIPP Performance Assessment

Construction of a CCDF for comparison to the Standard requires a clear conceptual representation for a performance assessment. A representation based on a set of ordered triples provides a suitable way to organize a performance assessment and leads naturally to the presentation of the outcome of a performance assessment as a CCDF (Kaplan and Garrick, 1981; Helton et al., 1991; Volume 1, Chapter 3). Specifically, the outcome of a performance assessment can be represented by a set R of ordered triples of the form

$$R = \{(S_i, pS_i, \mathbf{cS}_i), i = 1, ..., nS\}, \quad (1.4\text{-}2)$$

where

S_i = a set of similar occurrences,
pS_i = probability that an occurrence in set S_i will take place,
$\mathbf{cS}_i$ = a vector of consequences associated with S_i,

and

nS = number of sets selected for consideration.

In terms of performance assessment, the S_i are scenarios, the pS_i are scenario probabilities, and the $\mathbf{cS}_i$ are vectors containing results or consequences associated with scenarios.

The information contained in the pS_i and $\mathbf{cS}_i$ shown in Eq. 1.4-2 can be summarized in CCDFs. With the assumptions that a particular consequence result **cS** (e.g., normalized release to the accessible environment) is under consideration and that the values for this result have been ordered so that $\mathbf{cS}_i$ is less than or equal to $\mathbf{cS}_{i+1}$ for i = 1,2,...,nS-1, the resultant CCDF is shown in Figure 1.4-1. As illustrated in Figure 1.4-2, the EPA containment requirement in 191.13 specifies that the CCDF for normalized release to the accessible environment should fall below a CCDF defined by the points (1, 0.1) and (10, 0.001). The vertical lines in Figure 1.4-2 have been added for visual appeal but are not really part of the CCDF. A waste disposal site can be considered to be in compliance with the EPA release limits if the CCDF for normalized release to the accessible environment falls below the bounding curve shown in Figure 1.4-2.

Since the representation for a performance assessment in Eq. 1.4-2 and the resultant CCDFs in Figures 1.4-1 and 1.4-2 involve probabilities, there must be an underlying sample space. For performance assessments conducted to provide comparisons with the EPA release limits, the sample space is the set $\mathcal{S}$ defined by

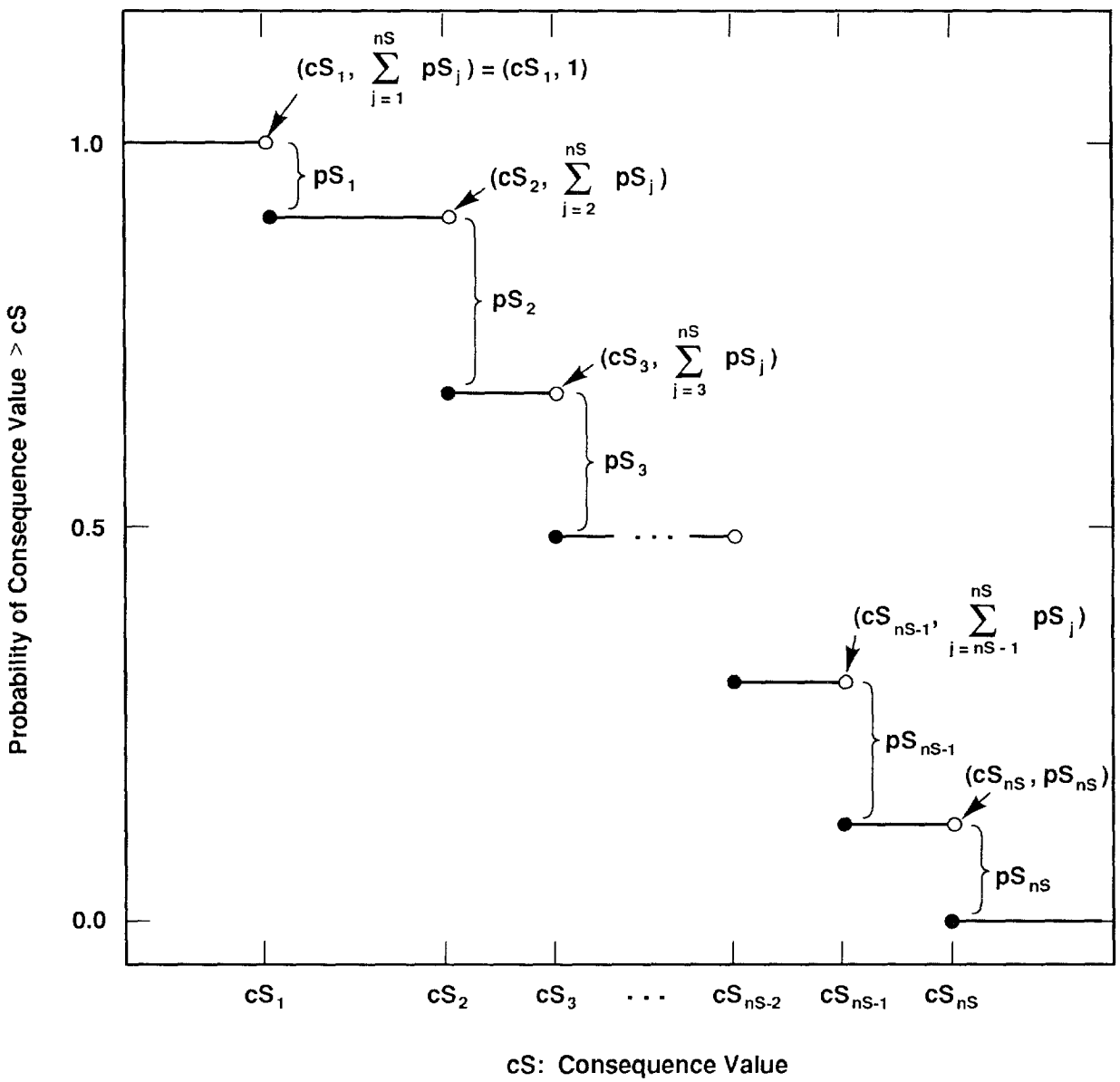

TRI-6342-730-5

Figure 1.4-1. Estimated Complementary Cumulative Distribution Function (CCDF) for Consequence Result **cS**. (Helton et al., 1991, Figure VI-1).

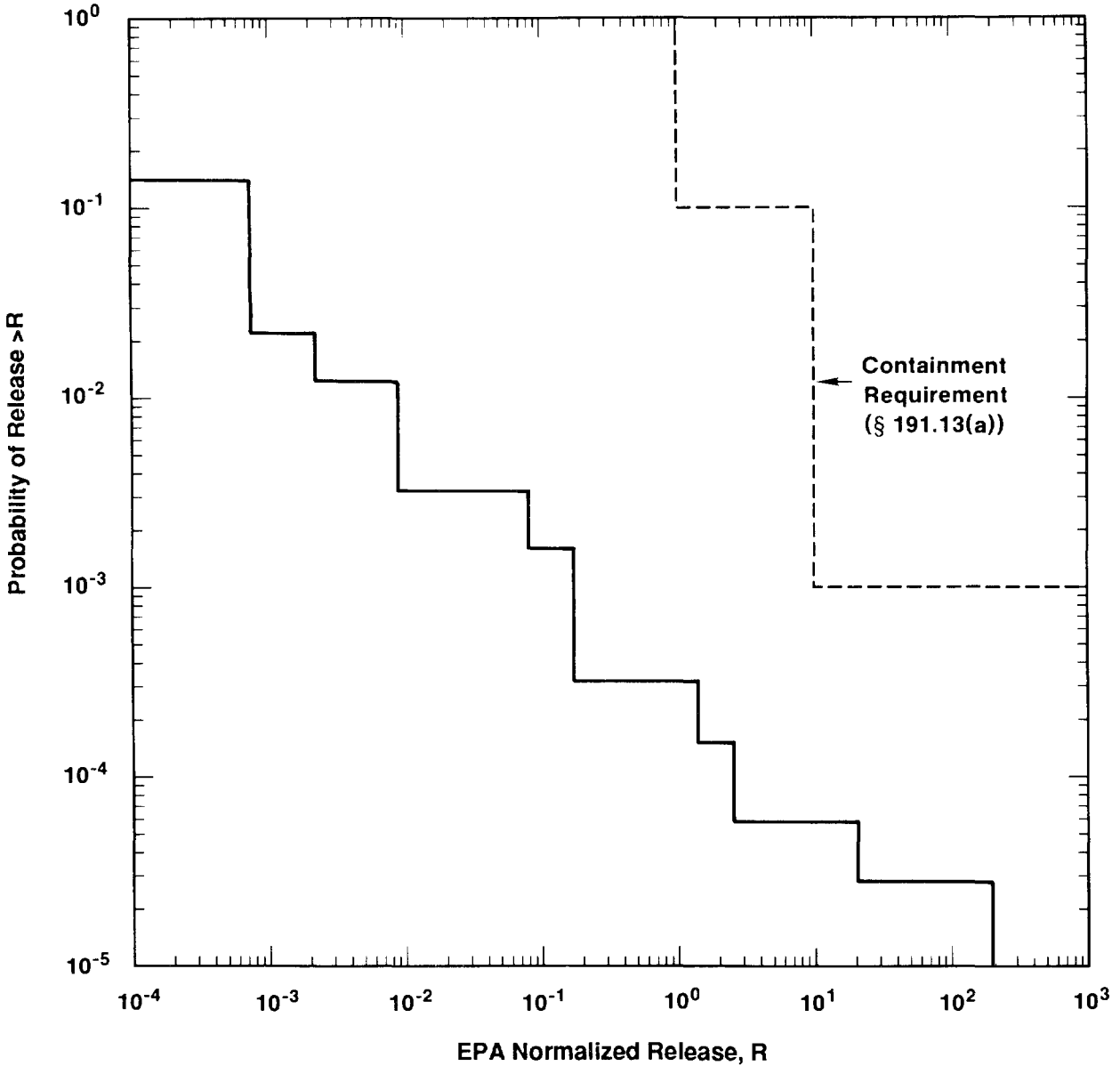

Figure 1.4-2. Comparison of a CCDF for Normalized Release to the Accessible Environment with the EPA Release Limits.

$$\mathcal{S} = \{x : x \text{ a single 10,000-yr time history beginning at decommissioning of the facility under consideration}\}. \quad (1.4\text{-}3)$$

Each 10,000-yr history is complete in the sense that it provides a full specification, including time of occurrence, for everything of importance to performance assessment that happens in this time interval. The S_i appearing in Eq. 1.4-2 are disjoint subsets of $\mathcal{S}$ for which

$$\mathcal{S} = \bigcup_{i=1}^{nS} S_i. \quad (1.4\text{-}4)$$

In the terminology of probability theory, the S_i are events and the pS_i are the probabilities for these events. It is the discretization of into the sets S_i that leads to the steps in the estimated CCDFs in Figures 1.4-1 and 1.4-2. The use of more sets will reduce the step sizes but will not alter the fact that CCDFs are the basic outcome of a performance assessment (Helton et al., 1991, Chapter VI).

Important parts of any performance assessment are the discretization of S into the sets S_i, commonly referred to as scenario development (Hunter, 1989; Ross, 1989; Cranwell et al., 1990; Guzowski, 1990), and the subsequent determination of probabilities for these sets (Mann and Hunter, 1988; Hunter and Mann, 1989; Guzowski, 1991). For radioactive waste disposal in sedimentary basins, many S_i result from unintended intrusions due to exploratory drilling for natural resources, particularly oil and gas. To construct CCDFs of the form shown in Figures 1.4-1 and 1.4-2, the time histories associated with these drilling intrusions must be sorted into disjoint sets such that (1) each S_i is sufficiently homogeneous that it is reasonable to use the same consequence result $\mathbf{cS}_i$ for all elements of S_i, (2) a probability can be determined for each S_i, and (3) estimation of pS_i and $\mathbf{cS}_i$ is computationally feasible.

Chapter 2, Volume 2 of this report describes a decomposition of drilling intrusions into computational scenarios on the basis of number of intrusions and their times of occurrence, and derives the necessary formulas to convert from drilling rates to scenario probabilities. Chapter 3, Volume 2 describes a computational procedure that can be used to determine CCDFs for intrusions due to drilling.

1.4.2 Uncertainty in Risk

A number of factors affect uncertainty in risk results, including completeness, aggregation, model selection, imprecisely known variables, and stochastic variation. The risk representation in Eq. 1.4-2 provides a convenient structure in which to discuss these uncertainties.

Completeness refers to the extent that a performance assessment includes all possible occurrences for the system under consideration. In terms of the risk representation in Eq. 1.4-2, completeness deals with whether or not all possible occurrences are included in the union of the sets S_i (i.e., in $U_i S_i$). Aggregation refers to the division of the possible occurrences into the sets S_i, and thus relates to the logic used in the construction of the sets S_i. Resolution is lost if the S_i are defined too coarsely (e.g., nS is too small) or in some other

inappropriate manner. Model selection refers to the actual choice of the models for use in a risk assessment. Appropriate model choice is sometimes unclear and can affect both pS_i and $\mathbf{cS}_i$. Similarly, once the models for use have been selected, imprecisely known variables required by these models can affect both pS_i and $\mathbf{cS}_i$. Due to the complex nature of risk assessment, model selection and imprecisely known variables can also affect the definition of the S_i. Stochastic variation is represented by the probabilities pS_i, which are functions of the many factors that affect the occurrence of the individual sets S_i. The CCDFs in Figures 1.4-1 and 1.4-2 display the effects of stochastic uncertainty. Even if the probabilities for the individual S_i were known with complete certainty, the ultimate result of a risk assessment would still be CCDFs of the form shown in Figures 1.4-1 and 1.4-2.

The calculation of risk is driven by the determination of the sets S_i. Once these sets are determined, their probabilities of pS_i and associated consequences $\mathbf{cS}_i$ must be determined. In practice, development of the S_i is a complex and iterative process that must take into account the procedures required to determine the probabilities pS_i and the consequences $\mathbf{cS}_i$. Typically, the overall process is organized so that pS_i and $\mathbf{cS}_i$ will be calculated by various models whose exact configuration will depend on the individual S_i. These models will also require a number of imprecisely known variables. It is also possible that imprecisely known variables could affect the definition of the S_i.

These imprecisely known variables can be represented by a vector

$$\mathbf{x} = [x_1, x_2, \ldots, x_{nV}], \tag{1.4-5}$$

where each x_j is an imprecisely known input required in the analysis and nV is the total number of such inputs. In concept, the individual x_j could be almost anything, including vectors or functions required by an analysis. However, an overall analysis, including uncertainty and sensitivity studies, is more likely to be successful if the risk representation in Eq. 1.4-2 has been developed so that each x_j is a real-valued quantity for which the overall analysis requires a single value, but it is not known with preciseness what this value should be. With the preceding ideas in mind, the representation for risk in Eq. 1.4-2 can be restated as a function of $\mathbf{x}$:

$$R(\mathbf{x}) = \{(S_i(\mathbf{x}), pS_i(\mathbf{x}), \mathbf{cS}_i(\mathbf{x})), \quad i=1, \ldots, nS(\mathbf{x})\} \tag{1.4-6}$$

As $\mathbf{x}$ changes, so will $R(\mathbf{x})$ and all summary measures that can be derived from $R(\mathbf{x})$. Thus, rather than a single CCDF for each consequence value contained in $\mathbf{cS}$, a distribution of CCDFs results from the possible values that $\mathbf{x}$ can take on.

The individual variables x_j in $\mathbf{x}$ can relate to different types of uncertainty. Individual variables might relate to completeness uncertainty (e.g., the value for a cutoff used to drop low-probability occurrences from the analysis), aggregation uncertainty (e.g., a bound on the

value for nS), model uncertainty (e.g., a 0-1 variable that indicates which of two alternative models should be used), stochastic uncertainty (e.g., a variable that helps define the probabilities for the individual S_i), or variable uncertainty (e.g., a solubility limit or a retardation for a specific element). Variable uncertainty may include uncertainty resulting from the incompleteness of data and measurement uncertainty resulting from systematic or random errors that may occur in the data. Measurement uncertainty has, in general, received little attention in this report because, as discussed in the following section, values for most variable parameters used in the performance assessment are assessed subjectively, not empirically. Even for those parameters for which values are derived empirically, the conservative use of total variability rather than variability about the mean discussed in Section 1.2 limits the potential to expand parameter uncertainty.

1.4.3 Characterization of Uncertainty in Risk

If the inputs to a performance assessment as represented by the vector **x** in Eq. 1.4-5 are uncertain, then so are the results of the assessment. Characterization of the uncertainty in the results of a performance assessment requires characterization of the uncertainty in **x**. Once the uncertainty in **x** has been characterized, then Monte Carlo techniques can be used to characterize the uncertainty in the risk results.

The outcome of characterizing the uncertainty in **x** is a sequence of probability distributions

$$D_1, D_2, \ldots, D_{nV}, \tag{1.4-7}$$

where D_j is the distribution developed for the variable x_j, $_j$=1, 2, ..., nV, contained in **x**. (Elsewhere in this volume these distributions are indicated by $F(x_j)$.) The definition of these distributions may also be accompanied by the specification of correlations and various restrictions that further define the possible relations among the x_j. These distributions and other restrictions probabilistically characterize where the appropriate input to use in the performance assessment might fall given that the analysis is structured so that only one value can be used for each variable under consideration. In most cases, each D_j will be a subjective distribution that is developed from available information through a suitable review process and serves to assemble information from many sources into a form appropriate for use in an integrated analysis. However, it is possible that the D_j may be obtained by classical statistical techniques for some variables. Details related to the probability distributions D_j used by WIPP PA are provided in the previous section.

Once the distributions in Eq. 1.4-7 have been developed, Monte Carlo techniques can be used to determine the uncertainty in $R(\mathbf{x})$ from the uncertainty in **x**. First, a sample

$$\mathbf{x}_k = [x_{k1}, x_{k2}, \ldots, x_{k,nV}], \; k=1, \ldots, nK \tag{1.4-8}$$

is generated according to the specified distributions and restrictions, where nK is the size of the sample. The performance assessment is then performed for each sample element $\mathbf{x}_k$, which yields a sequence of risk results of the form

$$R(\mathbf{x}_k) = \{(S_i(\mathbf{x}_k), pS_i(\mathbf{x}_k), \mathbf{cS}_i(\mathbf{x}_k)), i=1, ..., nS(\mathbf{x}_k)\} \quad (1.4\text{-}9)$$

for k=1, ..., nK. Each set $R(\mathbf{x}_k)$ is the result of one complete performance assessment performed with a set of inputs (i.e., $\mathbf{x}_k$) that the review process producing the distributions in Eq. 1.4-7 concluded was possible. Further, associated with each risk result $R(\mathbf{x}_k)$ in Eq. 1.4-9 is a probability or weight* that can be used in making probabilistic statements about the distribution of $R(\mathbf{x})$.

In most performance assessments, CCDFs are the results of greatest interest. For a particular consequence result, a CCDF will be produced for each set $R(\mathbf{x}_k)$ of results shown in Eq. 1.4-9. This yields a distribution of CCDFs of the form shown in Figure 1.4-3.

Although Figure 1.4-3 provides a complete summary of the distribution of CCDFs obtained for a particular consequence result by propagating the sample shown in Eq. 1.4-8 through a performance assessment, the figure is hard to read. A less crowded summary can be obtained by plotting the mean value and selected percentile values for each consequence value on the abscissa. For example, the mean plus the 5th, 50th (i.e., median) and 95th percentile values might be used. The mean and percentile values can be obtained from the exceedance probabilities associated with the individual consequence values and the weights or "probabilities" associated with the individual sample elements. If the mean and percentile values associated with individual consequence values are connected, a summary plot of the form shown in Figure 1.4-4 is obtained.

A point of possible confusion involving the risk representation in Eq. 1.4-2 is the distinction between the uncertainty that gives rise to a single CCDF and the uncertainty that gives rise to a distribution of CCDFs. A single CCDF arises from the fact that a number of different occurrences have a real possibility of taking place. This type of uncertainty is referred to as stochastic variation in this report. A distribution of CCDFs arises from the fact that fixed, but unknown, quantities are needed in the estimation of a CCDF. The development of distributions that characterize what the values for these fixed quantities might be leads to a distribution of CCDFs. In essence, a performance assessment can be viewed as a very complex function that estimates a CCDF. Since there is uncertainty in the values of some of the independent variables operated on by this function, there will also be uncertainty in the dependent variable produced by this function, where this dependent variable is a CCDF.

Both Kaplan and Garrick (1981) and a recent report by the International Atomic Energy Agency (IAEA, 1989) distinguish between these two types of uncertainty. Specifically, Kaplan and Garrick distinguish between probabilities derived from frequencies and probabilities that

---

* In random or Latin hypercube sampling, this weight is the reciprocal of the sample size (i.e, 1/nK) and can be used in estimating means, cumulative distribution functions, and other statistical properties. This weight is often referred to as the probability for each observation (i.e., each sample element x_k). However, this is not technically correct. If continuous distributions are involved, the actual probability of each observation is zero.

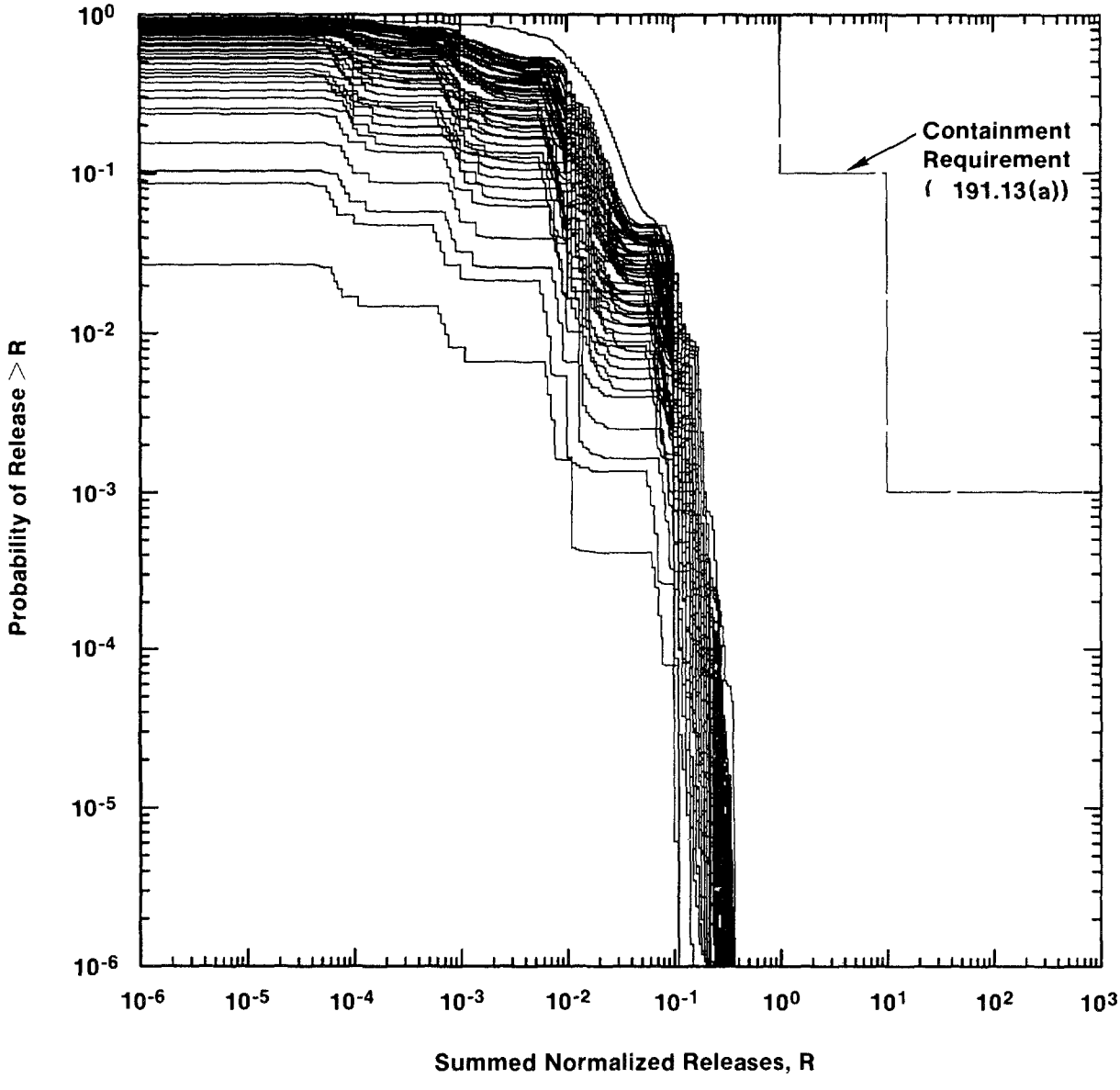

Figure 1.4-3. Example of CCDF Distribution Produced for Results Shown in Eq. 1.4-9.

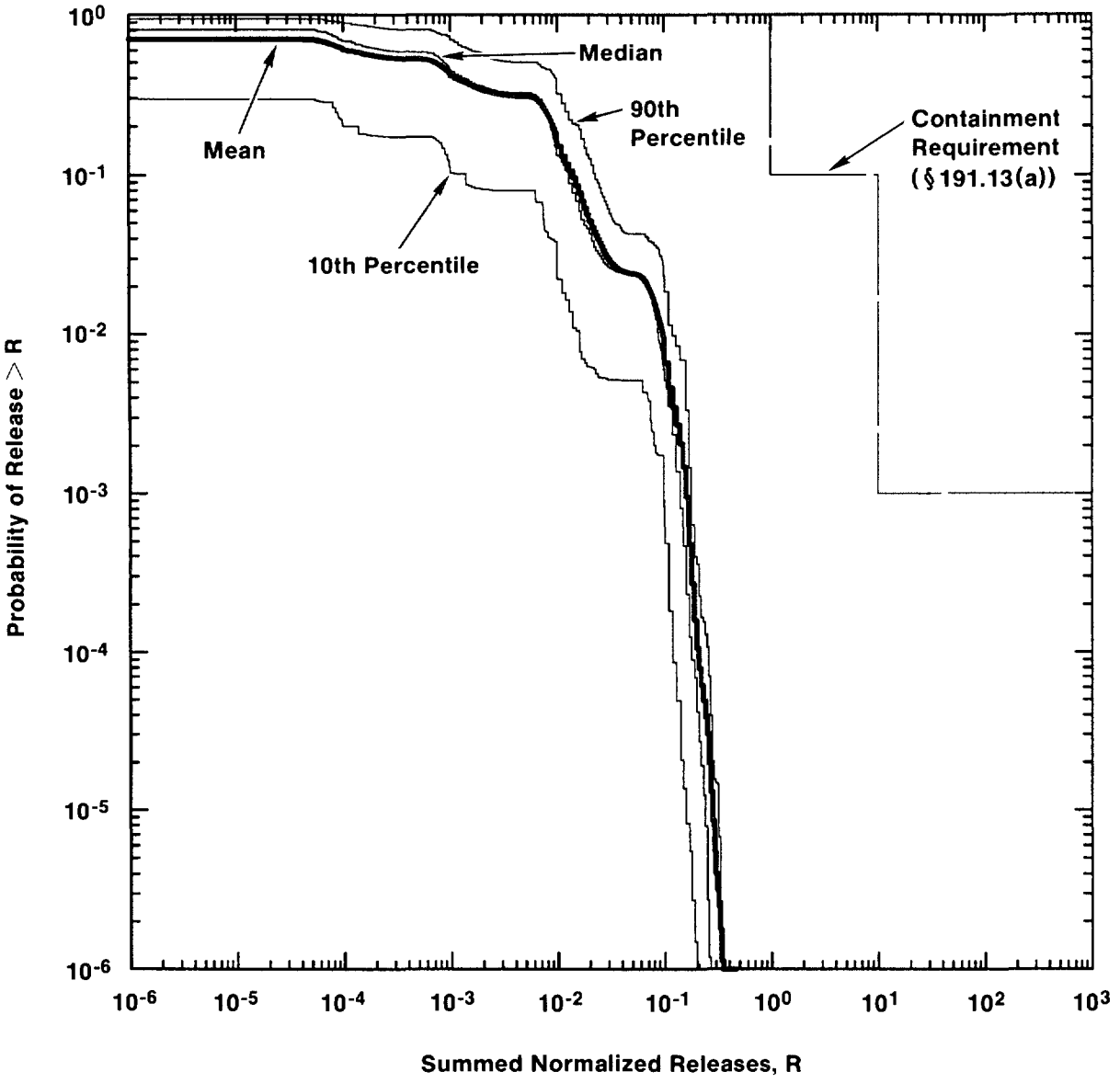

Figure 1.4-4. CCDF Summary Plot.

characterize degrees of belief. Probabilities derived from frequencies correspond to the probabilities pS_i in Eq. 1.4-2 while probabilities that characterize degrees of belief (i.e., subjective probabilities) correspond to the distributions indicated in Eq. 1.4-7. The IAEA report distinguished between what it calls Type A uncertainty and Type B uncertainty. The IAEA report defines Type A uncertainty to be stochastic variation; as such, this uncertainty corresponds to the frequency-based probability of Kaplan and Garrick and the pS_i of Eq. 1.4-7. Type B uncertainty is defined to be uncertainty that is due to lack of knowledge about fixed quantities; thus, this uncertainty corresponds to the subjective probability of Kaplan and Garrick and the distributions indicated in Eq. 1.4-7. This distinction has also been made by other authors including Vesely and Rasmuson (1984), Paté-Cornell (1986), and Parry (1988).

1.4.4 Calculation of Scenario Consequences

The $\mathbf{cS}_i$ in Eq. 1.4-2 are estimated for each sample element $\mathbf{x}_k$ using computer codes that comprise the consequence model. This model is deterministic and predicts an EPA normalized release to the accessible environment for each scenario S_i. The consequence model is actually composed of many individual models C_ℓ, ℓ = 1, ..., nM. The collective operation of these models can be represented by the relationship

$$\mathbf{cS}_i = C_{nM}\{...;C_2[\mathbf{x}_k;C_1(\mathbf{x}_k, S_i)]\} \qquad (1.4\text{-}10)$$

where

C_ℓ = consequence model ℓ,

$C_\ell(\mathbf{x}_k,S_i)$ = vector containing consequence results predicted by model ℓ for sample element $\mathbf{x}_k$ and scenario S_i,

and

nM = number of consequence models.

As indicated in the preceding relationship, the individual models predict results that depend on the $\mathbf{x}_k$ and S_i and also generate input to the next model in the computational sequence.

The consequence models C_ℓ are separate computational models (usually computer models) that are selected from several categories that represent physical processes and phenomena such as groundwater flow, dissolution of radionuclides in repository brine, and groundwater transport. As part of the 1991 WIPP performance assessment system, about 75 FORTRAN codes are grouped into 10 model categories, which are called modules. CAMCON is the software package designed and used by the PA Division to assemble the computational models from the various modules into the structure indicated in Eq. 1.4-10 (Rechard, 1989; Rechard et al., 1989). Chapter 4 (Volume 2) describes the C_ℓ and their application to undisturbed conditions. Chapters 5, 6, and 7 (Volume 2) describe the application of the C_ℓ to disturbed conditions for the S_i defined in Chapter 2 (Volume 2).

1.4.5 Uncertainty and Sensitivity Analyses

In the context of this report, uncertainty analysis involves determining the uncertainty in model predictions that results from imprecisely known input variables, and sensitivity analysis involves determining the contribution of individual input variables to the uncertainty in model predictions. Specifically, uncertainty and sensitivity analyses involve the study of the effects of subjective, or type B, uncertainty. As previously discussed, the effects of stochastic, or type A, uncertainty is incorporated into the WIPP performance assessment through the scenario probabilities pS_i appearing in Eq. 1.4-2. Sensitivity and uncertainty analyses for the results from the 1991 preliminary performance assessment are reported in Volume 4.

1.5 Background on WIPP

1.5.1 Purpose

The DOE was authorized by Congress in 1979 to build the WIPP as a research and development facility to demonstrate the safe management, storage, and eventual disposal of transuranic (TRU) waste generated by DOE defense programs (WIPP Act, 1979). Only after demonstrating compliance with *40 CFR 191* and other laws and regulations (e.g., RCRA [1976] and NEPA [1969]) will the DOE permanently dispose of TRU waste at the WIPP repository.

1.5.2 Location

The WIPP is located within a large sedimentary basin, the Delaware Basin, in southeastern New Mexico, an area of low population density approximately 38 km (24 mi) east of Carlsbad (Figure 1.5-1). Topographically, the WIPP is between the high plains of West Texas and the Guadalupe and Sacramento Mountains of southeastern New Mexico.

Four prominent surface features are found in the area--Los Medanos ("The Dunes"), Nash Draw, Laguna Grande de la Sal, and the Pecos River. Los Medanos is a region of gently rolling hills that slopes upward to the northeast from the eastern boundary of Nash Draw to a low ridge called "The Divide." The WIPP is in Los Medanos. Nash Draw, 8 km (5 mi) west of the WIPP, is a broad shallow topographic depression with no external surface drainage. Laguna Grande de la Sal, about 9.5 km (6 mi) west-southwest of the WIPP, is a large playa about 3.2 km (2 mi) wide and 4.8 km (3 mi) long formed by coalesced collapse sinks that were created by dissolution of evaporate deposits. The Pecos River, the principal surface-water feature in southeastern New Mexico, flows southeastward, draining into the Rio Grande in western Texas.

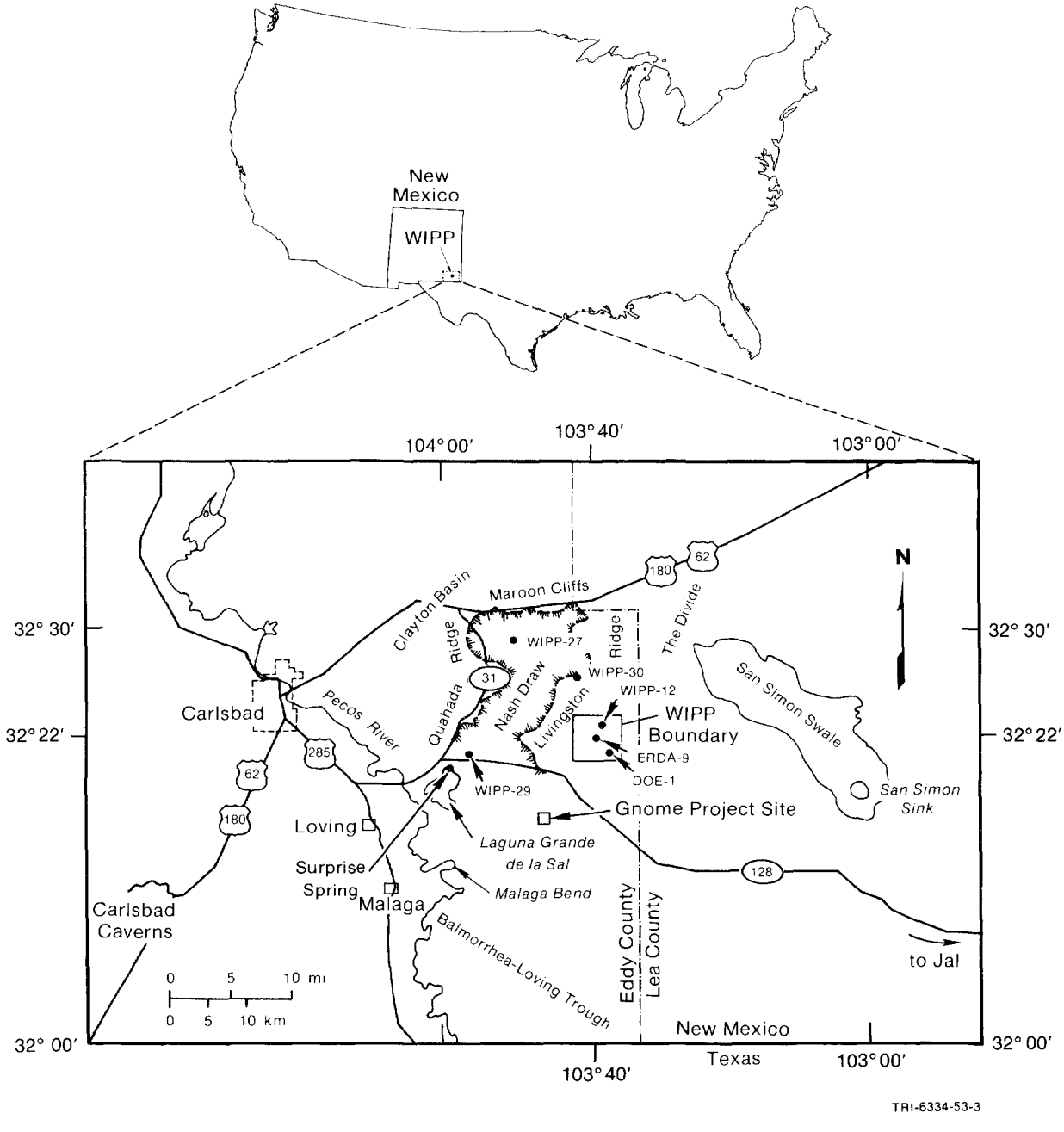

Figure 1.5-1. WIPP Location in Southeastern New Mexico (after Rechard, 1989, Figure 1.2).

1.5.3 Geologic History of the Delaware Basin

The Delaware Basin, an elongated, geologically confined depression, extends from just north of Carlsbad, New Mexico, into Texas west of Fort Stockton (Figure 1.5-2). The basin covers 33,000 km^2 (12,750 mi^2) and is filled with sedimentary rocks to depths as great as 7,300 m (24,000 ft) (Hills, 1984). Geologic history of the Delaware Basin began about 450 to 500 million years ago when a broad, low depression formed during the Ordovician Period as transgressing seas deposited clastic and carbonate sediments (Powers et al., 1978; Cheeseman, 1978; Williamson, 1978; Hiss, 1975; Hills, 1984; Harms and Williamson, 1988; Ward et al., 1986). After a long period of accumulation and subsidence, the depression separated into the Delaware and Midland Basins when the area now called the Central Basin Platform uplifted during the Pennsylvanian Period, about 300 million years ago.

During the Early and Middle Permian Period, the Delaware Basin subsided rapidly, resulting in a sequence of clastic rocks rimmed by reef limestone. The thickest of the reef deposits, the Capitan Limestone, is buried north and east of the WIPP but is exposed at the surface in the Guadalupe Mountains to the west (Figure 1.5-2). Evaporite deposits (marine bedded salts) of the Castile Formation and the Salado Formation, which hosts the WIPP, filled the basin during the late Permian Period and extended over the reef margins. Evaporites, carbonates, and clastic rocks of the Rustler Formation and the Dewey Lake Red Beds were deposited above the Salado Formation before the end of the Permian Period.

1.5.4 Repository

The repository is located in the Delaware Basin because the 600-m (2,000-ft)-thick Salado Formation of marine bedded salts (Late Permian Period) eventually encapsulates the nuclear waste through salt creep. The bedded salts, consisting of thick halite and interbeds of minerals such as clay and anhydrites, do not contain flowing water.

The repository level is located within these bedded salts 655 m (2,150 ft) below the surface and 384 m (1,260 ft) above sea level. The WIPP repository is composed of a single underground disposal level connected to the surface by four shafts (Figure 1.5-3). The repository level consists of an experimental area at the north end and a disposal area at the south end.

1.5.5 WIPP Waste Disposal System

The WIPP relies on three approaches to contain waste: geologic barriers, engineered barriers, and institutional controls. The third approach, institutional controls, consists of many parts, e.g., the legal ownership and regulations of the land and resources by the U.S. Government, the fencing and signs around the property, permanent markers, public records and archives, and other methods of preserving knowledge about the disposal system.

The WIPP disposal system, as defined by *40 CFR 191*, includes the geologic and engineered barriers. The physical features of the repository (e.g., stratigraphy, design of repository, waste form) are components of these barriers.

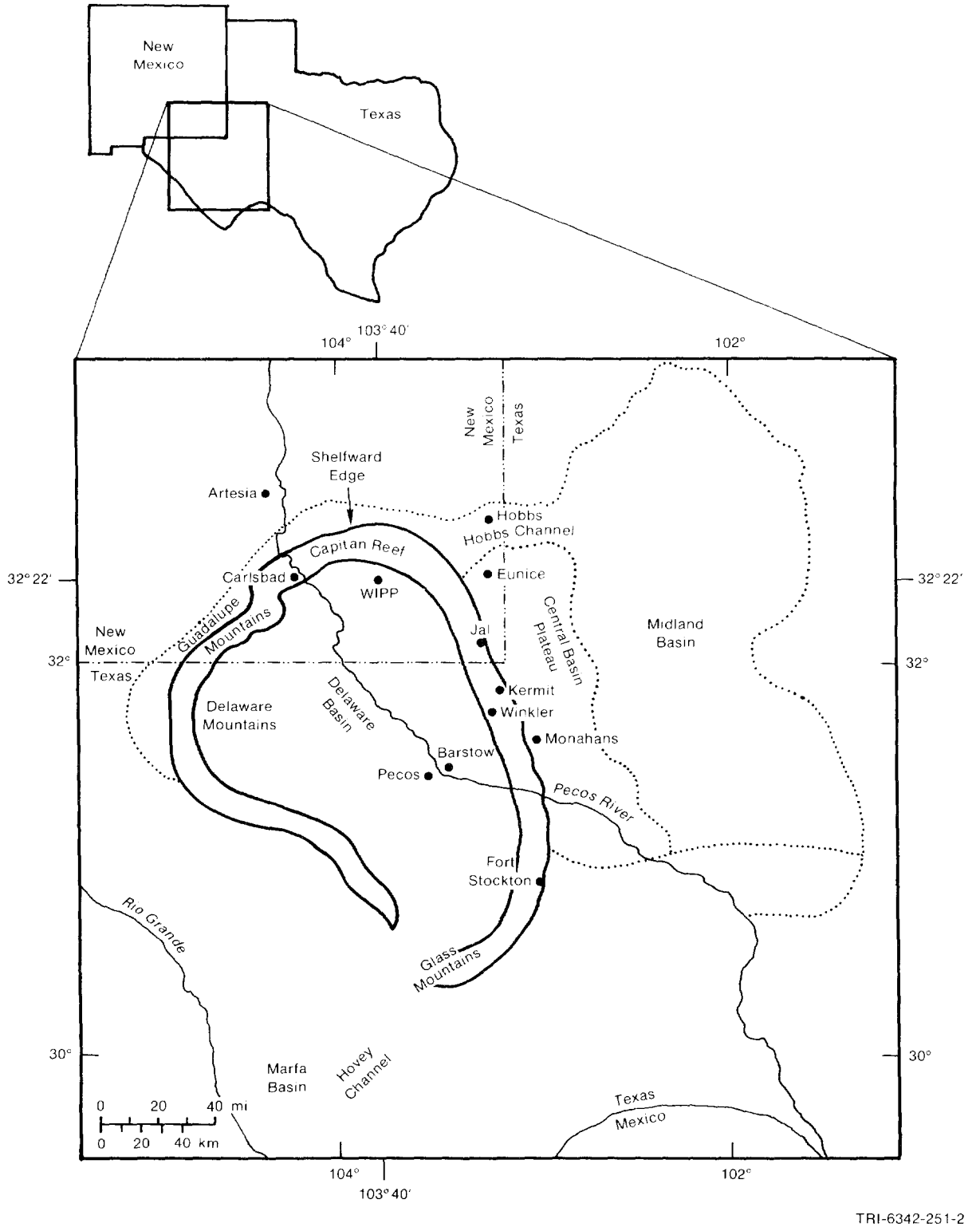

Figure 1.5-2. Location of the WIPP in the Delaware Basin (modified from Richey et al., 1985 and Lappin, 1988, Figure 1.4).

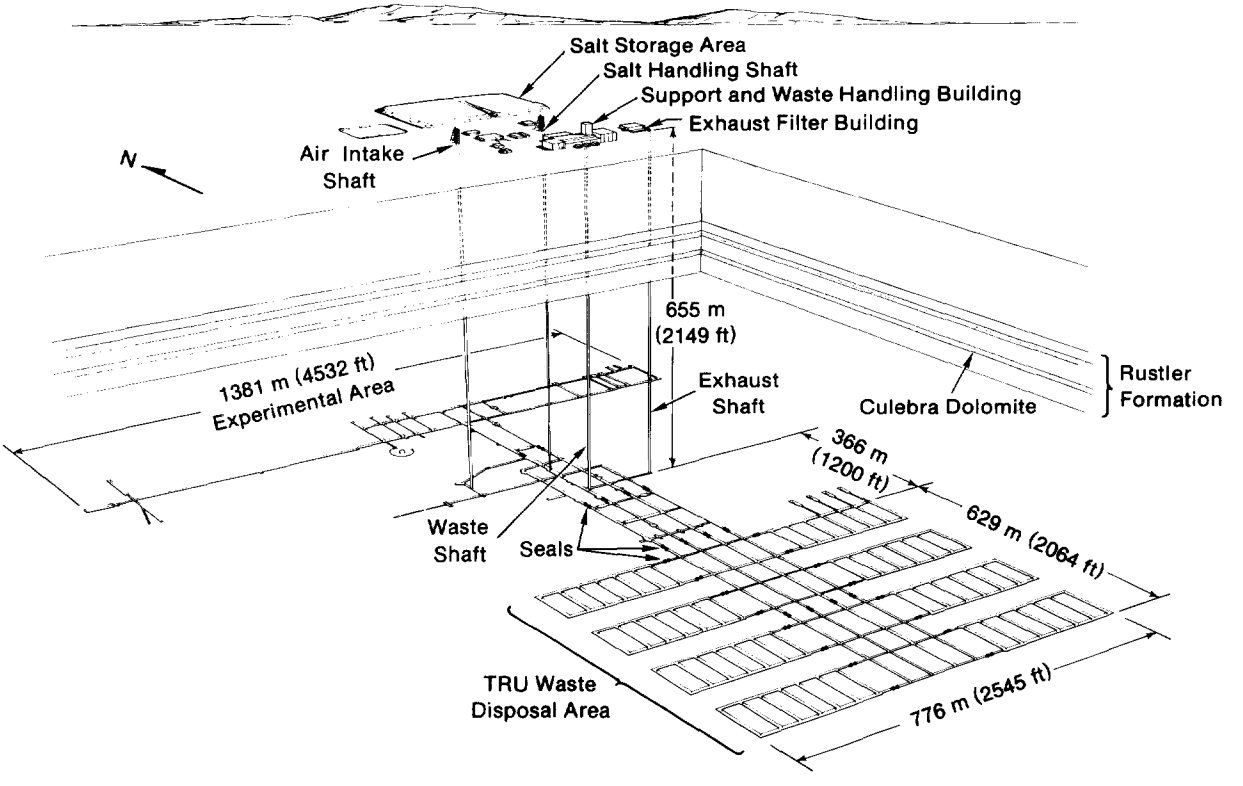

Figure 1.5-3. WIPP Repository, Showing Surface Facilities, Proposed TRU Disposal Areas, and Experimental Areas (after Nowak et al., 1990, Figure 2).

The geologic barriers are limited to the lithosphere up to the surface and no more than 5 km (3 mi) from the outer boundary of the WIPP waste-emplacement panels (Figure 1.5-4). The boundary of this maximum-allowable geologic subsystem is greater than the currently proposed boundary of the WIPP land withdrawal. The extent of the WIPP controlled area will be defined during performance assessment but will not be less than the area withdrawn, which will be under U.S. DOE administrative control (Bertram-Howery and Hunter, 1989).

Data for components of the geologic and engineered barriers are the subject of this volume. No data on institutional controls are contained in this volume.

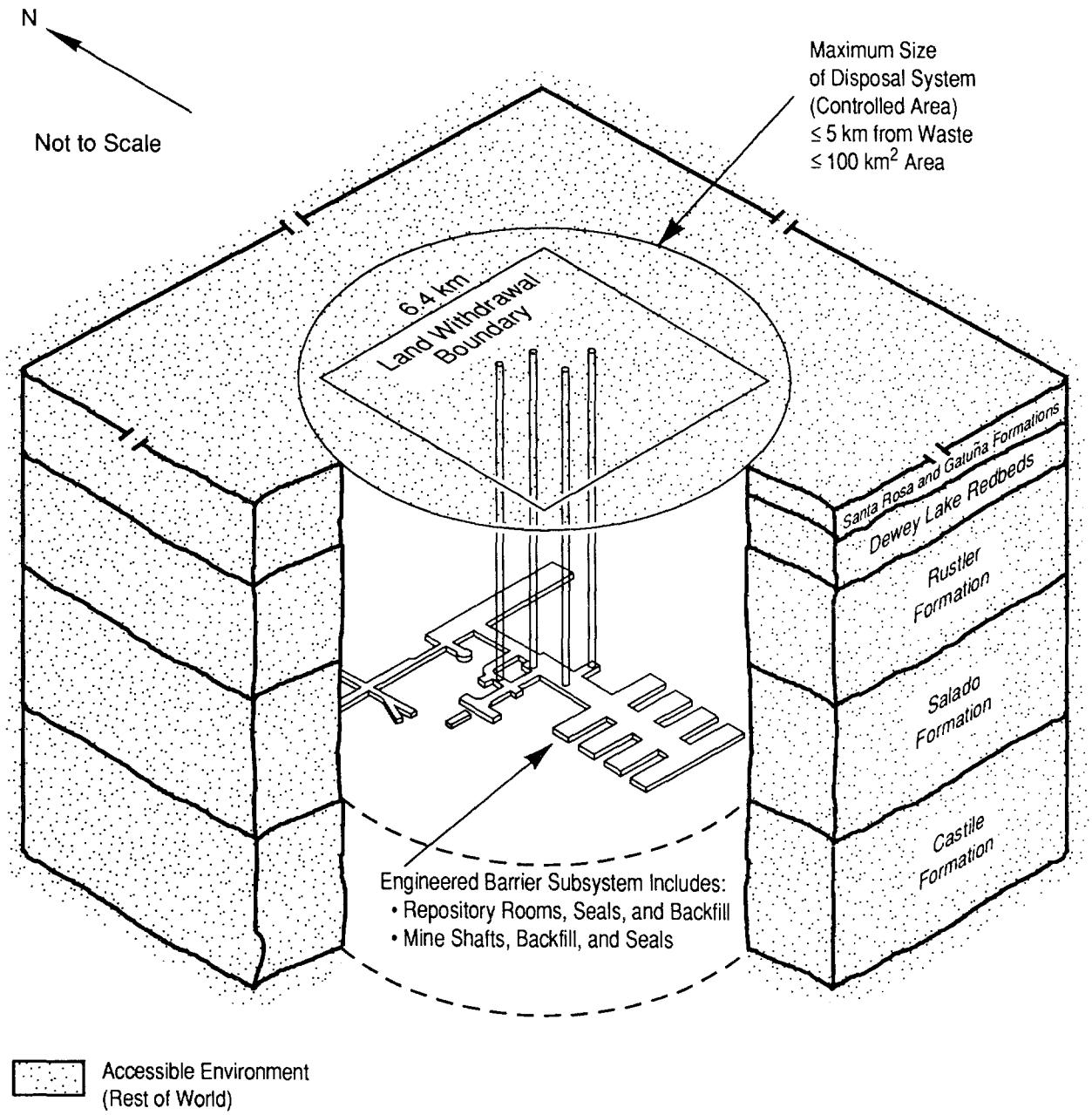

Figure 1.5-4 Geologic and Engineered Barriers of the WIPP Disposal System.

2. GEOLOGIC BARRIERS

The geologic barriers consist of the physical features of the repository, such as stratigraphy and geologic components.

2.1 Areal Extent of Geologic Barriers

Figure 2.1-1 shows the maximum areal extent of the geologic barriers. Figure 2.1-2 shows the UTM coordinates of the modeling domains. The UTM coordinates for the northeast and southeast corners of the land-withdrawal boundary were derived from values reported in Gonzales (1989). Because the township ranges shift at the land-withdrawal border, the UTM coordinates for the northwest and southwest corners were derived from information on the wells nearest the corners (i.e., Well H-6A for the northwest corner and Well D-15 for the southwest corner).

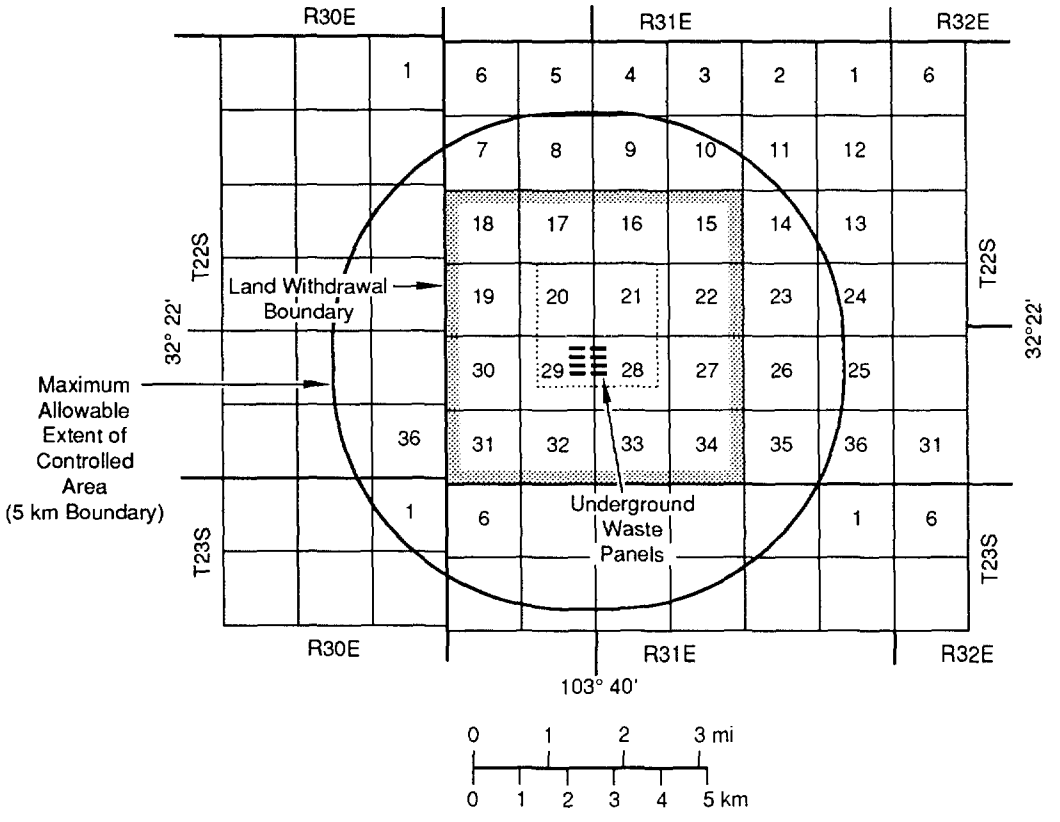

Figure 2.1-1. Position of the WIPP Waste Panels Relative to Land Withdrawal Boundary (16 Contiguous Sections), 5-km Boundary (40 CFR 191.12y), and Surveyed Section Lines (after U.S. DOE, 1989a, Figure 2.2).

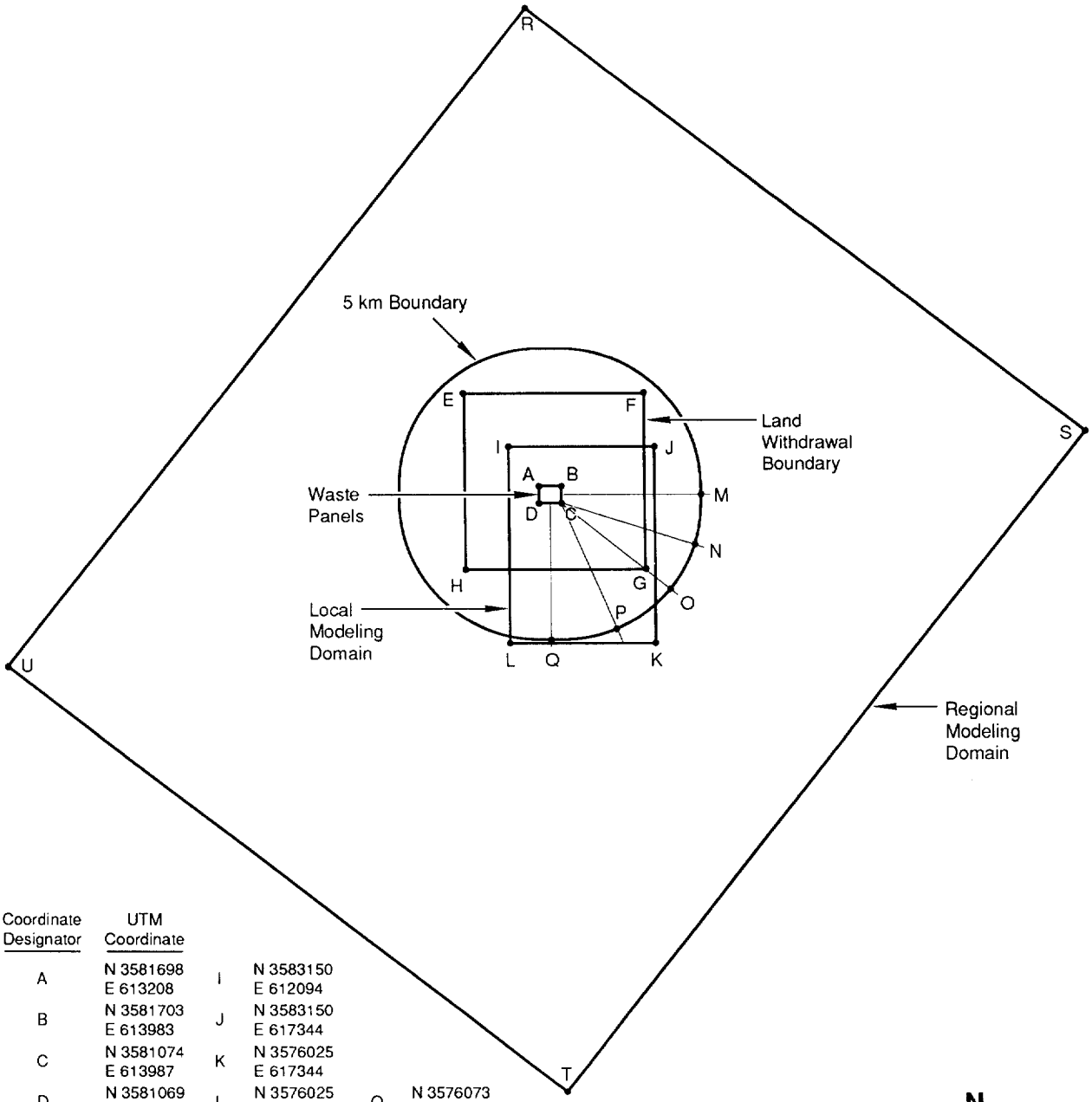

Coordinate Designator	UTM Coordinate				
A	N 3581698 E 613208	I	N 3583150 E 612094		
B	N 3581703 E 613983	J	N 3583150 E 617344		
C	N 3581074 E 613987	K	N 3576025 E 617344		
D	N 3581069 E 613212	L	N 3576025 E 612094	Q	N 3576073 E 613631
E	N 3585057 E 610496	M	N 3581420 E 618984	R	N 3598943 E 612819
F	N 3585109 E 616941	N	N 3579579 E 618791	S	N 3583551 E 632519
G	N 3578681 E 617015	O	N 3577945 E 617856	T	N 3559911 E 614049
H	N 3578612 E 610566	P	N 3576436 E 615991	U	N 3575303 E 594349

TRI-6342-1406-0

Figure 2.1-2. UTM Coordinates of the Modeling Domains.

Figure 2.1-3 shows the topography, the locations of wells used for defining the general stratigraphy, and the modeling domains near the WIPP typically plotted in the report. The well locations by universal transverse mercator (UTM), state plan coordinates, and survey sections are provided in Table B.1 (Appendix B). The elevations of the stratigraphic layers in each of the wells are tabulated in Table B.2 (Appendix B).

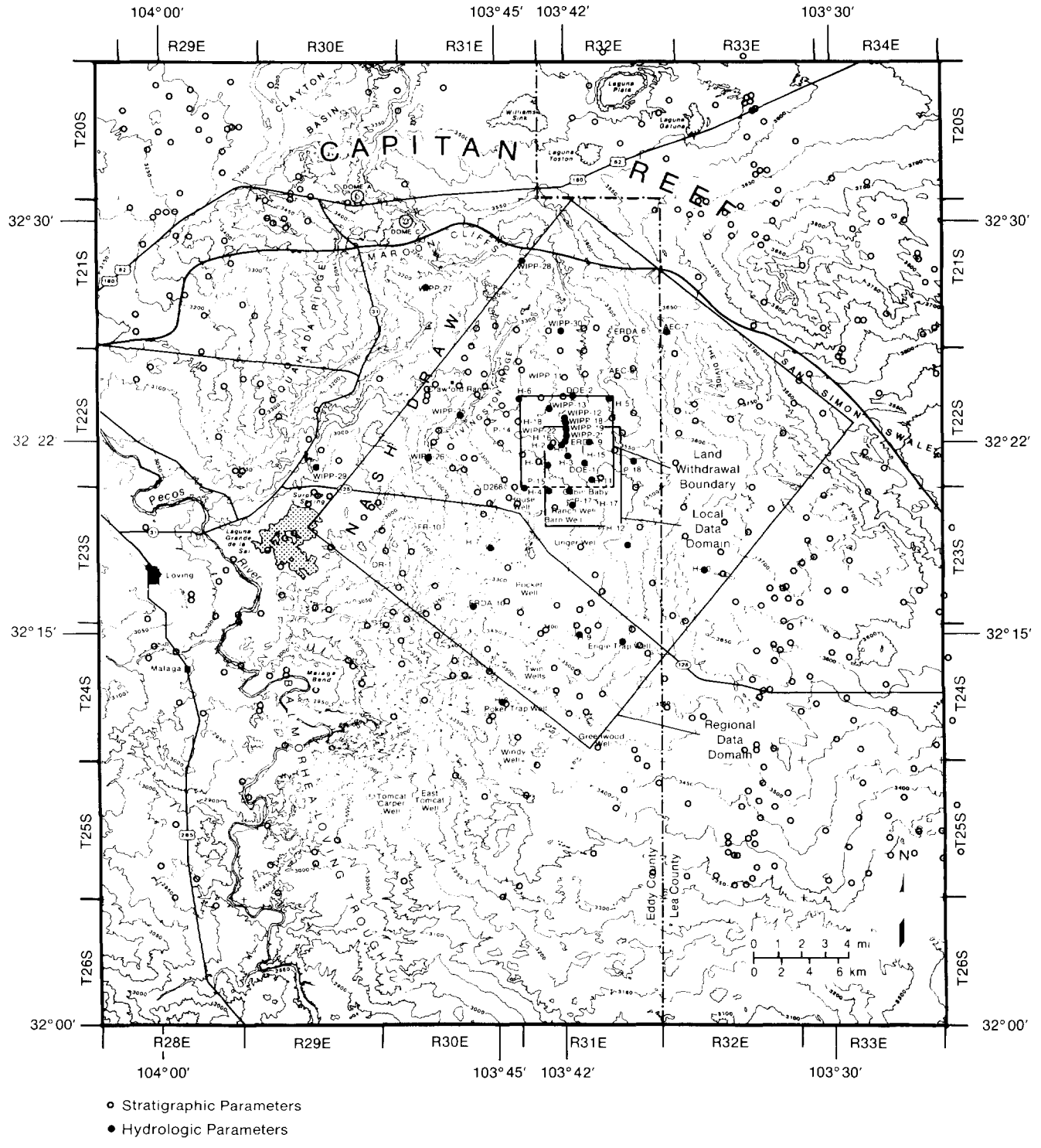

○ Stratigraphic Parameters
● Hydrologic Parameters

TRI-6342-612-1

Figure 2.1-3. Locations of Wells for Defining General Stratigraphy and Regional and Local Data Domains Typically Plotted in Report.

2.2 Stratigraphy at the WIPP

The level of the WIPP repository is located within bedded salts 655 m (2,150 ft) below the surface and 384 m (1,260 ft) above sea level (Figures 2.2-1 and 2.2.2). The bedded salts consist of thick halite and interbeds of minerals such as clay and anhydrites of the late Permian period (Ochoan series) (approximately 255 million yr old)* (Figure 2.2-3). An interbed that forms a potential transport pathway, Marker Bed 139 (MB139), located about 1 m (3 ft) below the repository interval (Figure 2.2-3), is about 1 m (3 ft) thick, and is one of about 45 siliceous or sulfatic units within the Salado Formation consisting of polyhalitic anhydrite (Figure 2.2-4) (Lappin, 1988; Tyler et al., 1988). Figure 2.2-5 shows the lithostatic and hydrostatic pressure with depth.

Parameter:	**Anhydrite III elevation @ ERDA-9**
Median:	105
Range:	70
	140
Units:	m
Distribution:	Uniform
Source(s):	See text.

Parameter:	**Bell Canyon elevation @ ERDA-9**
Median:	-200
Range:	-170
	-230
Units:	m
Distribution:	Uniform
Source(s):	See text.

For most strata above the repository, the elevations (though varying) are well known because of numerous wells; however, the elevations of the Anhydrite III in the Castile Formation and the Bell Canyon directly below the repository can only be inferred from a geologic cross section (Figure 2.2-1). The geologic structure is uncomplicated, thus the uncertainty is likely small on the regional geologic scale. Yet the information is important to evaluating the potential and the corresponding size of any brine reservoirs under the repository. Hence, uncertainty bounds have been placed on these two elevations inferred from the geologic cross section. For the 1991 PA calculations, a uniform distributon with a mean of the elevation of the strata was inferred from using WIPP-12, and Cabin Baby-1, ERDA-10, or DOE-1 for the Anhydrite III strata and DOE, and Cabin Baby-1 or ERDA-10 for the Bell Canyon. The endpoints were estimated at $\overline{x} \pm \sqrt{3}s$.

* This age reflects the revised 1983 geologic timetable (Palmer, 1983).

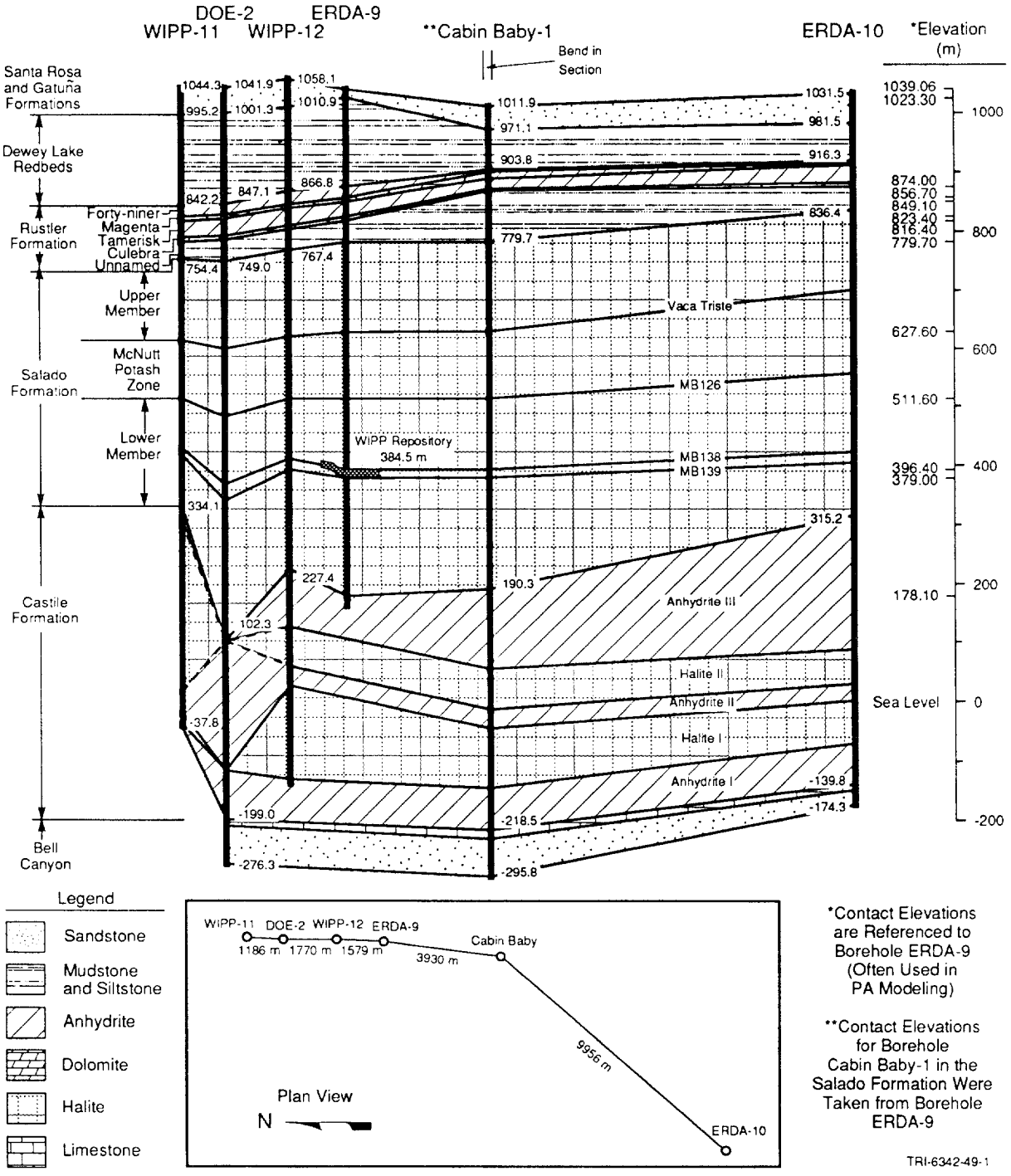

Figure 2.2-1. Level of WIPP Repository, Located in the Salado Formation. The Salado Formation is composed of thick halite with thin interbeds of clay and anhydrite deposited as marine evaporites about 255 million years ago (Permian period) (after Lappin, 1988, Figure 3.1).

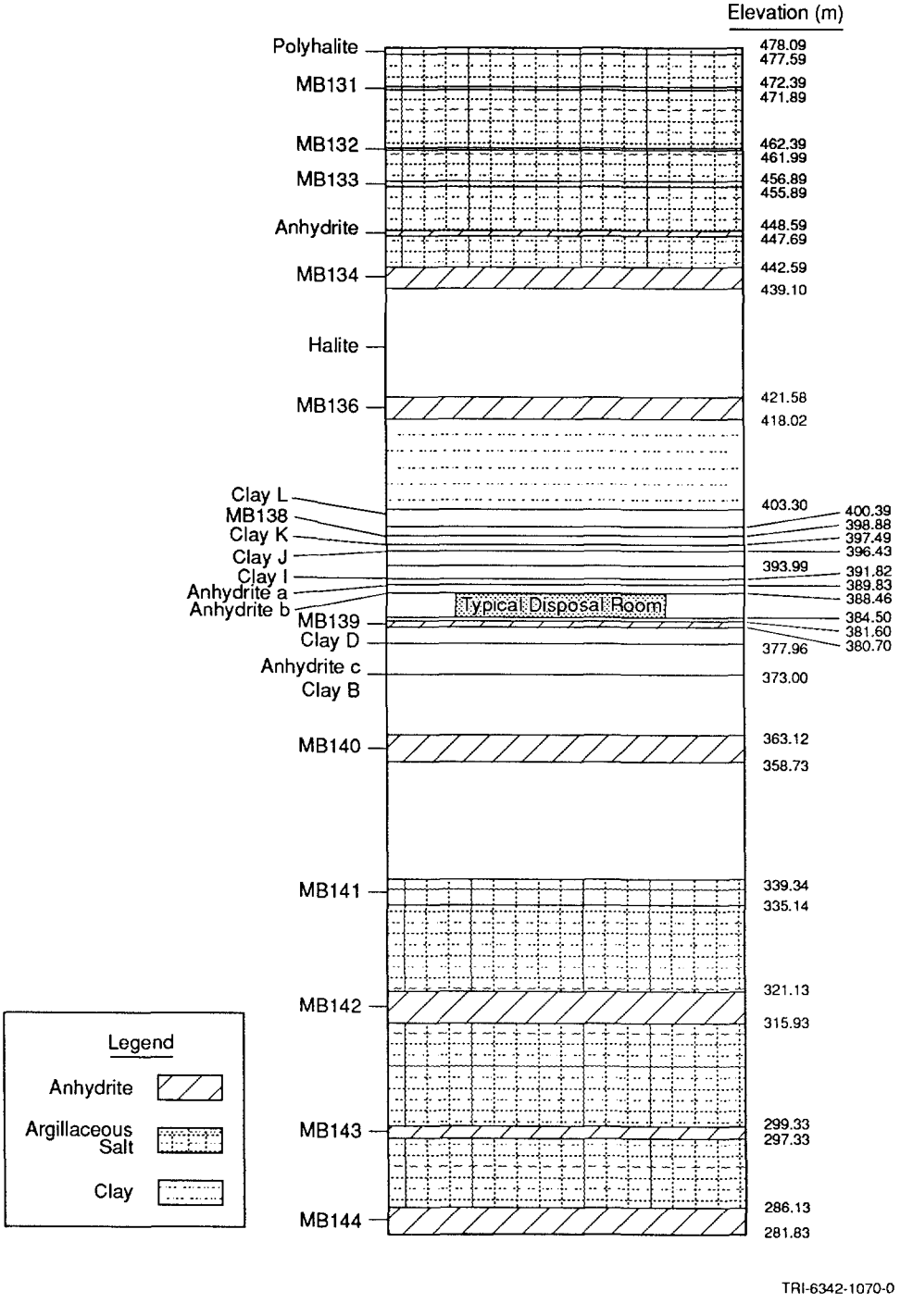

Figure 2.2-2. Reference Local Stratigraphy near Repository (after Munson et al., 1989, Figure 3-3).

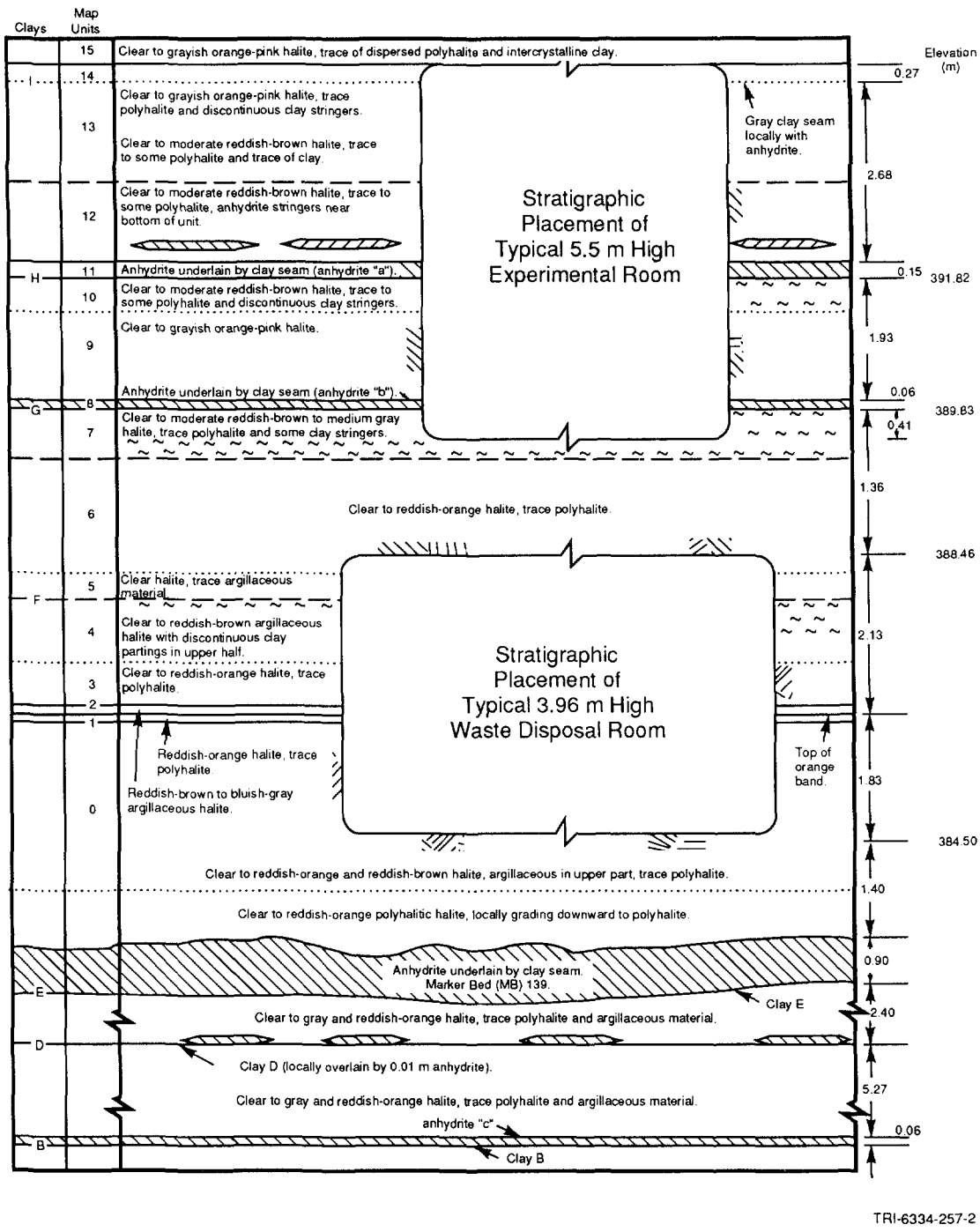

Figure 2.2-3. Stratigraphy at the Repository Horizon (after Bechtel, 1986, Figures 6-2, 6-3 and Lappin et al., 1989, Figure 4-12). Units in the disposal area dip slightly to the south, but disposal excavations are always centered about the orange marked band (reddish-orange halite).

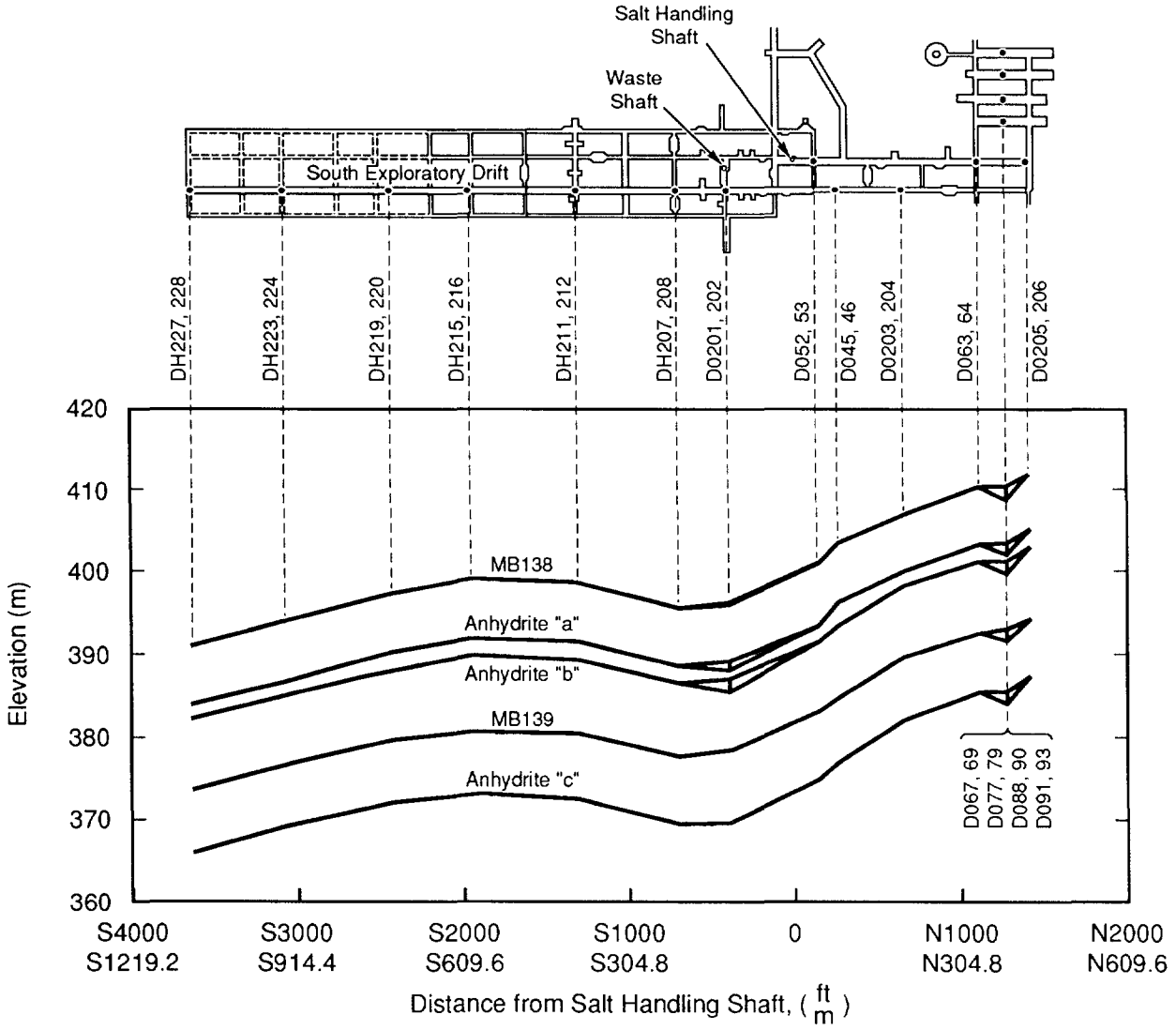

Figure 2.2-4. Marker Bed 139, One of Many Anhydrite Interbeds near the WIPP Repository Horizon (after Krieg, 1984, Figure 2).

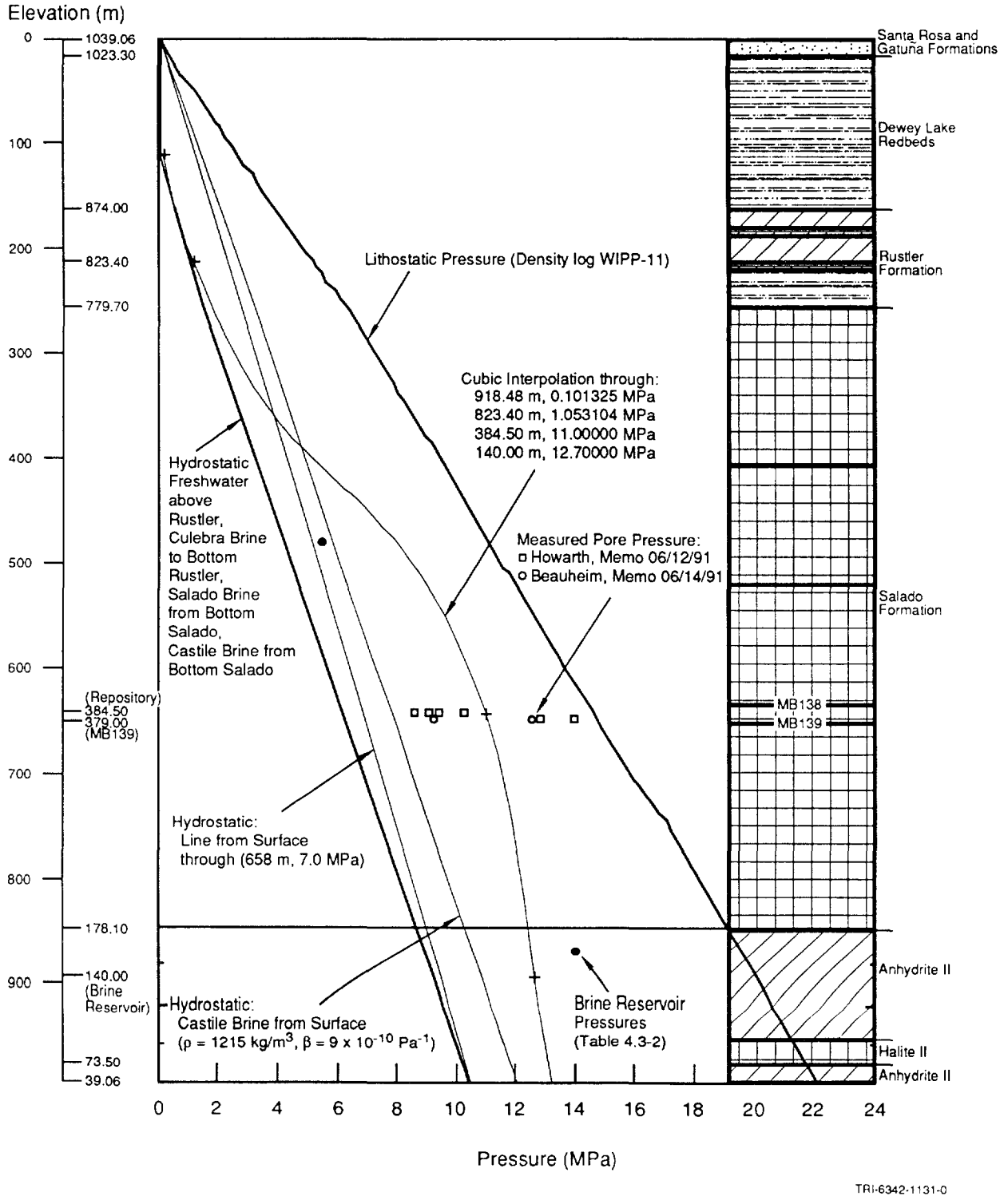

Figure 2.2-5. Lithostatic and Hydrostatic Pressure with Depth.

2.3 Hydrologic Parameters for Halite and Polyhalite within Salado Formation

The WIPP repository is located in the Salado Formation. The Salado Formation is composed of thick halite with thin interbeds of clay and anhydrite deposited as marine evaporites about 255 million years ago (Permian period). The parameters for the Salado Formation near the repository are given in Table 2.3-1.

Table 2.3-1. Parameter Values for Halite and Polyhalite within Salado Formation Near Repository

Parameter	Median	Range		Units	Distribution Type	Source
Capillary pressure (p_c) and relative permeability (k_{rw})						
Threshold displacement pressure (p_t)	2.3×10^7	2.3×10^5	2.3×10^9	Pa	Lognormal	Davies, June 2, 1991, Memo (see Appendix A); Brooks and Corey, 1964
Residual Saturations						
Wetting phase ($S_{\ell r}$)	2×10^{-1}	1×10^{-1}	4×10^{-1}	none	Cumulative	Davies and LaVenue, 1990b
Gas phase (S_{gr})	2×10^{-1}	1×10^{-1}	4×10^{-1}	none	Cumulative	Davies and LaVenue, 1990b
Brooks-Corey Exponent (η)	7×10^{-1}	3.5×10^{-1}	1.4	none	Cumulative	Davies and LaVenue, 1990b
Density						
Grain (ρ_g) Halite	2.163×10^3			kg/m^3	Constant	Carmichael, 1984, Table 2; Krieg, 1984, p. 14; Clark, 1966, p. 44
Grain (ρ_g) Polyhalite	2.78×10^3			kg/m^3	Constant	Shakoor and Hume, 1981 (p. 103-203)
Bulk (ρ_{bulk})	2.14×10^3			kg/m^3	Constant	Holcomb and Shields, 1987, p.17
Average (ρ_{ave})	2.3×10^3			kg/m^3	Constant	Krieg, 1984, Table 4
Dispersivity						
Longitudinal (α_L)	1.5×10^1	1	4×10^1	m	Cumulative	Pickens and Grisak, 1981; Lappin et al., 1989, Table D-2
Transverse (α_T)	1.5	1×10^{-1}	4	m	Cumulative	Pickens and Grisak, 1981; Freeze and Cherry, 1979, Figure 9.6
Partition Coefficient						
All species	0			m^3/kg	Constant	Lappin et al., 1989, p. D-17
Permeability (k)						
Undisturbed	5.7×10^{-21}	8.6×10^{-22}	5.4×10^{-20}	m^2	Data	Beauheim, June 14, 1991, Memo (see Appendix A)
Disturbed	1×10^{-19}	1×10^{-20}	1×10^{-18}	m^2	Lognormal	Beauheim, 1990
Pore pressure (p)	1.28×10^7	9.3×10^6	1.39×10^7	Pa	Data	Beauheim, June 14, 1991, Memo (see Appendix A); Howarth, June 12, 1991, Memo (see Appendix A)
Porosity (ϕ)						
Undisturbed	1×10^{-2}	1×10^{-3}	3×10^{-2}	none	Cumulative	Skokan et al.,1988; Powers et al.,1978; Black et al., 1983
Disturbed	6×10^{-2}			none	Constant	See text.
Specific storage	9.5×10^{-8}	2.8×10^{-8}	1.4×10^{-6}	m^{-1}	Cumulative	Beauheim, June 14, 1991, Memo (Appendix A)
Tortuosity	1.4×10^{-1}	1×10^{-2}	6.67×10^{-1}	none	Cumulative	See Culebra, text; Freeze and Cherry, 1979, p. 104

2.3.1 Capillary Pressure and Relative Permeability

Threshold Displacement Pressure, p_t

Parameter:	**Threshold displacement pressure (p_t)**
Median:	2.3×10^7
Range:	2.3×10^5
	2.3×10^9
Units:	Pa
Distribution:	Lognormal
Source(s):	Davies, P. B. 1991. *Evaluation of the Role of Threshold Pressure in Controlling Flow of Waste-Generated Gas into Bedded Salt at the Waste Isolation Pilot Plant.* SAND90-3246. Albuquerque, NM: Sandia National Laboratories.
	Davies, P. B. 1991. "Uncertainty Estimates for Threshold Pressure for 1991 Performance Assessment Calculations Involving Waste-Generated Gas." Internal memo to D. R. Anderson (6342), June 2, 1991. Albuquerque, NM: Sandia National Laboratories. (In Appendix A of this volume)

Discussion:

Threshold pressure plays an important role in controlling which Salado lithologies are accessible to gas and at what pressure gas will flow. The Salado Formation's thick halite beds with anhydrite and clay interbeds are similar in many respects to the consolidated lithologies presented in Figure 2.3-1. Similarities in pore structure exist between halite, anhydrite, and low-permeability carbonates; low-permeability sandstones and crystalline cements; and clay interbeds and shales. Given the general similarities, a best-fit power curve through the combined data set for consolidated lithologies was judged to provide the best available correlation for estimates of threshold pressure for the Salado Formation (Figure 2.3-1). Threshold pressure is also a key parameter in the Brooks and Corey (1964) model used to characterize the 2-phase properties of analogue materials for preliminary gas calculations (Davies and LaVenue, 1990). Because threshold pressure is strongly related to intrinsic permeability, an empirical estimate is used as follows:

$$p_t \text{ (MPa)} = 5.6 \times 10^{-7} [k \text{ (m}^2\text{)}]^{-0.346}$$

p_t is commonly referred to as the threshold displacement pressure. Hence, the capillary pressure can be evaluated given p_t, λ, $s_{\ell r}$, and s_{gr}. Some investigators define threshold pressure as the capillary pressure associated with first penetration of a nonwetting phase into the largest pores near the surface of the medium, which means that threshold pressure is equal to the capillary pressure at a water saturation of 1.0 (Davies, 1991, p. 9). Others define threshold pressure as the capillary pressure associated with the incipient development of a

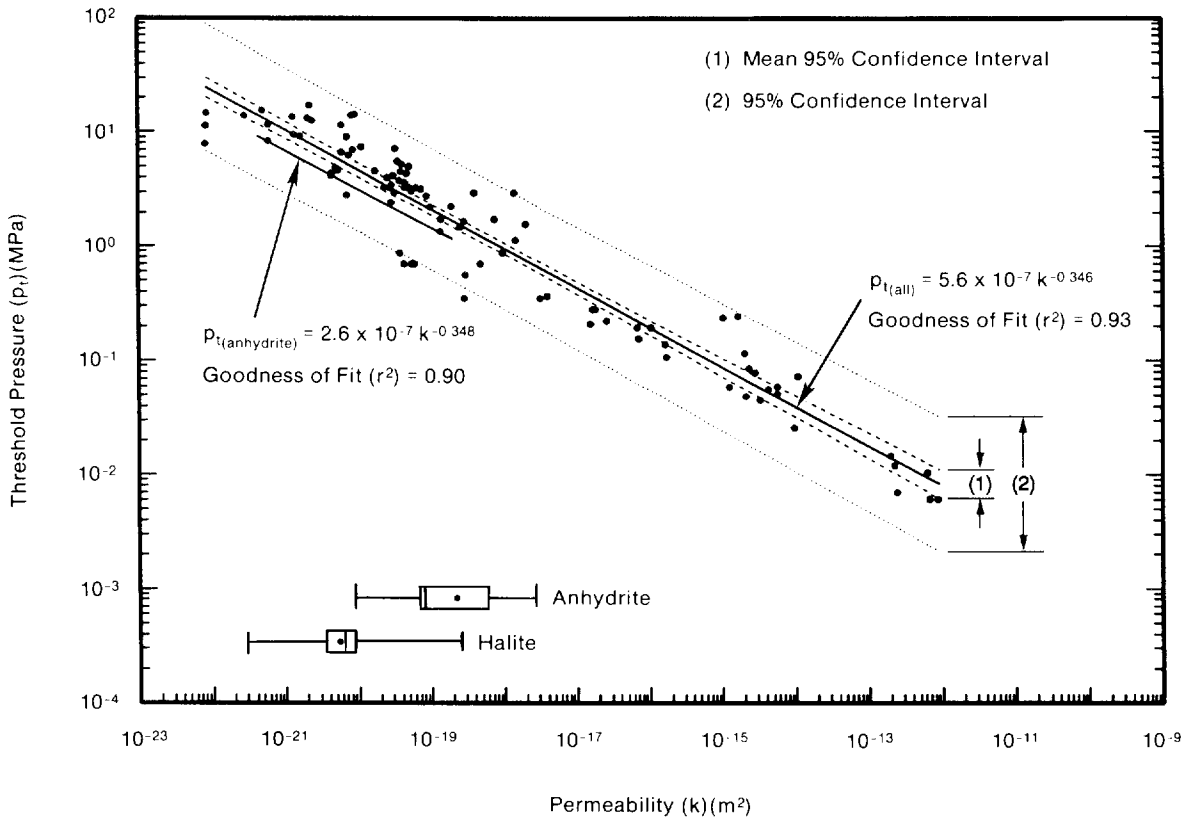

TRI-6344-730-1

Figure 2.3-1. Correlation of Threshold Pressure with Permeability for a Composite of Data from All Consolidated Rock Lithologies. Data from Ibrahim et al., 1970; Rose and Bruce, 1949; Thomas et al., 1968; and Wyllie and Rose, 1950. (after Davies, 1991, Figures 5 and 8)

continuum of the nonwetting phase through a pore network, providing gas pathways not only through relatively large pores, but also through necks between pores. This latter definition means that threshold pressure is equal to the capillary pressure at a saturation equal to the residual gas saturation (dashed lines in Figure 2.3-2).

Because flow of waste-generated gas outward from the WIPP repository will require that outward flowing gas penetrate and establish a gas-filled network of flow paths in the surrounding bedded salt, the latter definition has been adopted here.

Capillary Pressure and Relative Permeability

Figure 2.3-2a shows the values estimated for relative permeability for Salado salt. Figure 2.3-2b shows the estimated capillary pressure curve for Salado salt. Figure 2.3-3 is an example of variation in relative permeability and capillary pressure when Brooks and Corey parameters are varied.

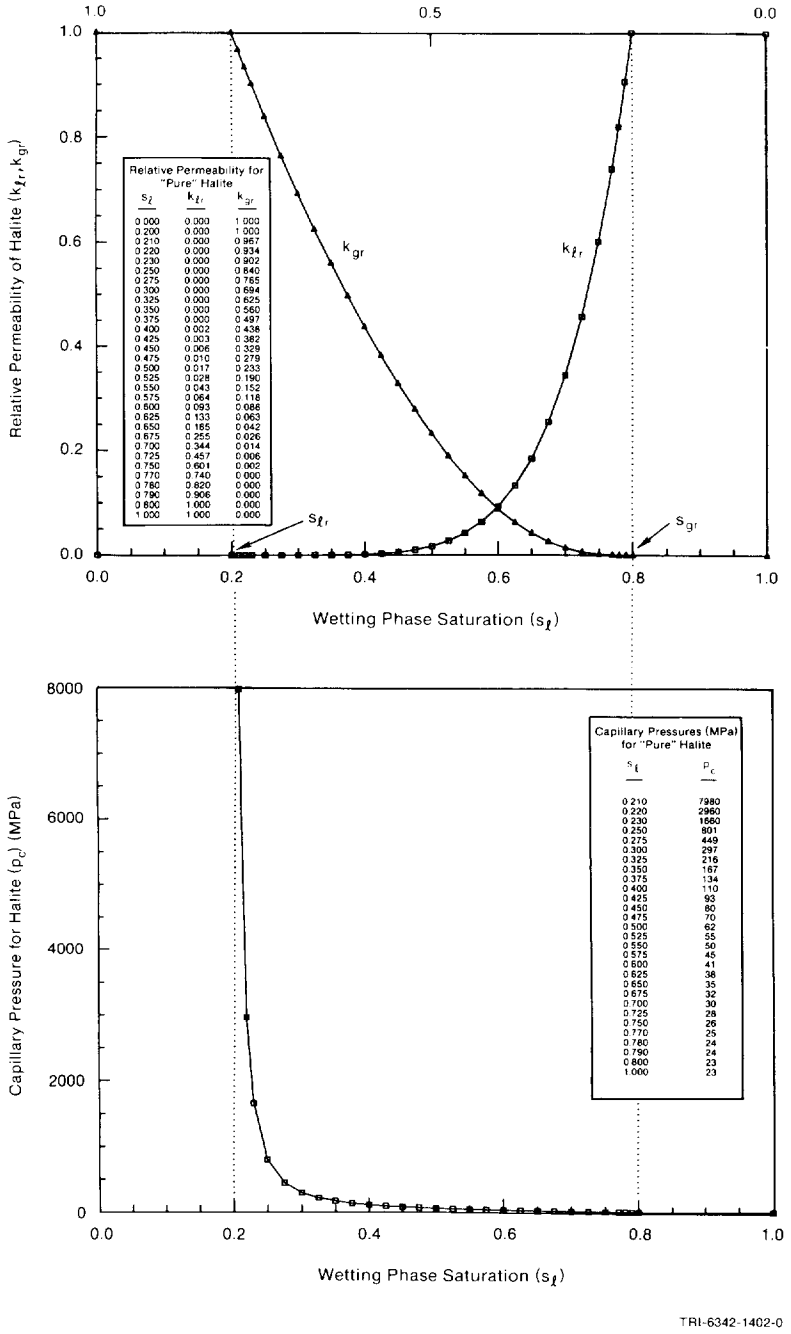

Figure 2.3-2. Estimated Capillary Pressure and Relative Permeability Curves.

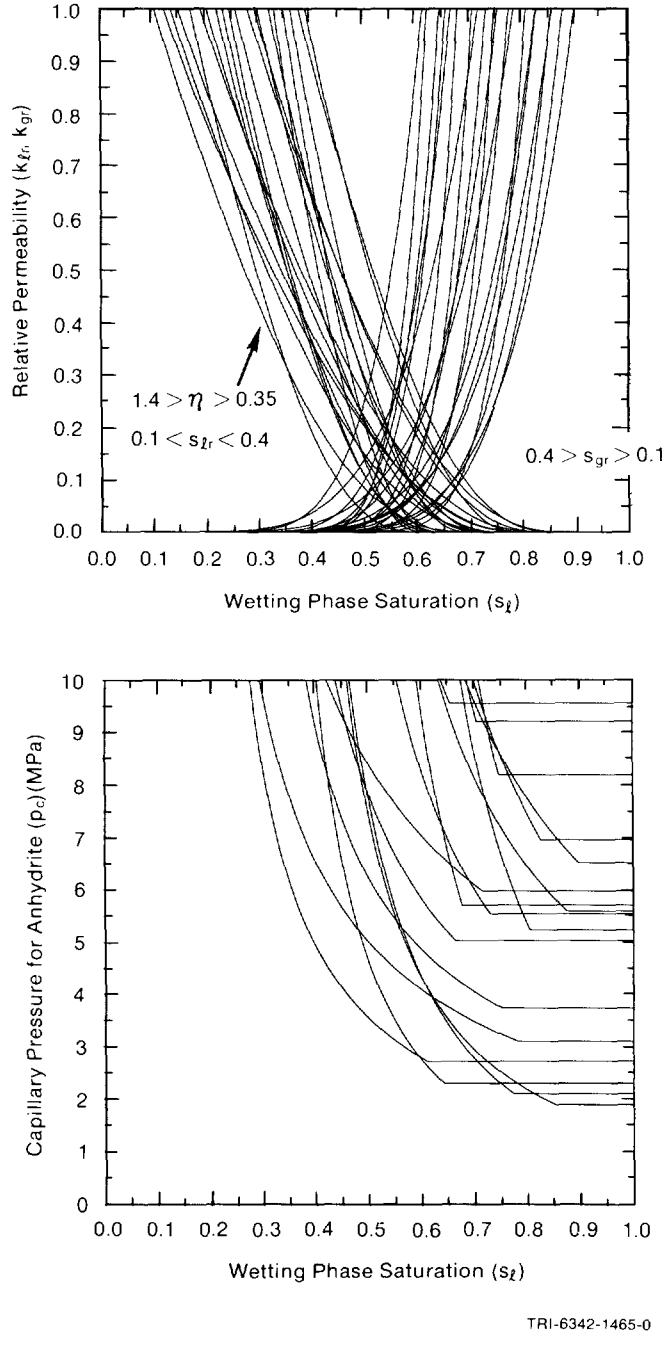

Figure 2.3-3. Example of Variation in Relative Permeability and Capillary Pressure When Brooks and Corey Parameters are Varied.

Residual Saturations

Parameter:	**Residual wetting phase (liquid) saturation ($S_{\ell r}$)**
Median:	2×10^{-1}
Range:	1×10^{-1}
	4×10^{-1}
Units:	Dimensionless
Distribution:	Cumulative
Source(s):	Davies, P. B. and A. M. LaVenue. 1990b. "Additional Data for Characterizing 2-Phase Flow Behavior in Waste-Generated Gas Simulations and Pilot Point Information for Final Culebra 2-D Model." Memo 11 in Appendix A of Rechard et al. 1990. *Data Used in Preliminary Performance Assessment of the Waste Isolation Pilot Plant.* SAND89-2408. Albuquerque, NM: Sandia National Laboratories.

Parameter:	**Residual gas saturation (S_{gr})**
Median:	2×10^{-1}
Range:	1×10^{-1}
	4×10^{-1}
Units:	Dimensionless
Distribution:	Cumulative
Source(s):	Davies, P. B. and A. M. LaVenue. 1990b. "Additional Data for Characterizing 2-Phase Flow Behavior in Waste-Generated Gas Simulations and Pilot Point Information for Final Culebra 2-D Model." Memo 11 in Appendix A of Rechard et al. 1990. *Data Used in Preliminary Performance Assessment of the Waste Isolation Pilot Plant.* SAND89-2408. Albuquerque, NM: Sandia National Laboratories.

Brooks and Corey Exponent

Parameter:	**Brooks and Corey exponent (η)**
Median:	7×10^{-1}
Range:	3.5×10^{-1}
	1.4
Units:	Dimensionless
Distribution:	Cumulative
Source(s):	Davies, P. B. and A. M. LaVenue. 1990b. "Additional Data for Characterizing 2-Phase Flow Behavior in Waste-Generated Gas Simulations and Pilot Point Information for Final Culebra 2-D Model." Memo 11 in Appendix A of Rechard et al. 1990. *Data Used in Preliminary Performance Assessment of the Waste Isolation Pilot Plant.* SAND89-2408. Albuquerque, NM: Sandia National Laboratories.

Discussion:

Capillary pressures and relative permeabilities for the Salado halite, the anhydrite layers, and waste have not been measured. As presented and discussed in Davies (1991), natural analogs were used to provide capillary pressure and relative permeability curves for these lithologies as follows:

Brooks and Corey defined s_e as

$$s_e = \frac{s_\ell - s_{\ell r}}{1 - s_{\ell r}} \qquad (2.3\text{-}1)$$

where s_ℓ is the wetting phase saturation (brine) and $s_{\ell r}$ is the residual wetting phase saturation, below which the wetting phase no longer forms a continuous network through the pore network and therefore does not flow, regardless of the pressure gradient. This has been modified to account for residual (or critical) gas saturation, s_{gr}:

$$s_e = \frac{s_\ell - s_{\ell r}}{1 - s_{gr} - s_{\ell r}} \qquad (2.3\text{-}2)$$

Brooks and Corey observed that the effective saturation of a porous material, s_e, can be related to the capillary pressure, p_c, by

$$s_e = \left(\frac{p_t}{p_c}\right)^\lambda \quad \text{or} \quad p_c = \frac{p_t}{s_e^{1/\lambda}} \qquad (2.3\text{-}3)$$

where

λ and p_t = characteristic constants of the material.

p_c = $p_g - p_\ell$

p_g = pressure of the gas

p_ℓ = pressure of the wetting phase

In addition, after obtaining the effective saturation from Eq. 2.3-1 the relative permeability of the wetting phase ($k_{r\ell}$) is obtained from

$$k_{r\ell} = s_e^{\frac{2 + 3\lambda}{\lambda}} \qquad (2.3\text{-}4)$$

For the gas phase, the relative permeability (k_{rg}) is

$$k_{rg} = \left(1 - s_e\right)^2 \left[1 - s_e^{\frac{2 + \lambda}{\lambda}}\right] \qquad (2.3\text{-}5)$$

Although none of the four parameters that are used in Eqs. 2.3-2, 2.3-3, 2.3-4 and 2.3-5 has been measured for either the Salado halite, anhdyrites, or waste room, they were estimated from values that were obtained from the natural analogs (Davies, 1991; Davies and LaVenue, 1990b). The natural analogs consist of alternate materials that possess some of the same characteristics (i.e., permeability and porosity) as the anhydrite, halite, and waste room. The natural analogs applicable to the very low permeability of the halite and anhydrite were sands that were investigated during the Multiwell Tight Gas Sands Project (Ward and Morrow, 1985). The permeability for these sands typically ranges from 1 x 10^{-16} to 1 x 10^{-19} m^2 (1 x 10^{-1} to 1 x 10^{-4} mD). Although these permeabilities are higher than those of the anhdyrites and halites, no other material was found with a lower permeability for which capillary pressure and relative permeability curves had been measured. The following values have been selected for Salado halite: $\lambda = 0.7$, $s_{\ell r} = 0.2$, $s_{gr} = 0.2$. The values selected for the anhydrites and waste room are discussed in later sections.

The resulting curves for capillary pressure and relative permeability were shown in Figure 2.3-2.

The uncertainty surrounding these parameters is unknown. An initial range was selected for the purpose of being able to run sensitivity parameter studies. The ranges shown for the parameters are arbitrary, corresponding to a simple doubling and halving of the median values. The range of curves produced by sampling 20 times from the assigned distribution using LHS (Volume 2) is shown in Figure 2.3-3.

2.3.2 Density

Grain Density of Halite in Salado Formation

Parameter:	**Density, grain (ρ_g)**
Median:	2.163×10^3
Range:	None
Units:	kg/m^3
Distribution:	Constant
Source(s):	Carmichael, R. S., ed. 1984. *CRC Handbook of Physical Properties of Rocks*, Vol III. Boca Raton, FL: CRC Press, Inc. (Table 2) Krieg, R. D. 1984. *Reference Stratigraphy and Rock Properties for the Waste Isolation Pilot Plant (WIPP) Project.* SAND83-1908. Albuquerque, NM: Sandia National Laboratories. (p. 14) Clark, S. P. 1966. *Handbook of Physical Constants.* New York, NY: The Geological Society of America, Inc. (p. 44)

Discussion:

The published grain density of halite (NaCl) is 2,163 kg/m^3 (135 lb/ft^3) (Carmichael, 1984, Table 2; Krieg, 1984, p. 14; Clark, 1966, p. 44).

Grain Density of Polyhalite in Salado Formation

Parameter:	**Density, grain (ρ_g)**
Median:	2.78×10^3
Range:	None
Units:	kg/m^3
Distribution:	Constant
Source(s):	Shakoor, A. and H. R. Hume. 1981. "Chapter 3: Mechanical Properties," in *Physical Properties Data for Rock Salt*. NBS Monograph 167. Washington, DC: National Bureau of Standards. (p. 103-203)

Discussion:

The published grain density of polyhalite is 2,780 kg/m^3 (173.6 lb/ft^3) (Shakoor and Hume, 1981).

Bulk Density of Halite in Salado (Halite)

Parameter:	**Density, bulk** (ρ_{bulk})
Median:	2.14×10^3
Range:	None
Units:	kg/m^3
Distribution:	Constant
Source(s):	Holcomb, D. J. and M. Shields. 1987. *Hydrostatic Creep Consolidation of Crushed Salt with Added Water.* SAND87-1990. Albuquerque, NM: Sandia National Laboratories. (p. 17)

Discussion:

The PA Division uses a bulk density of halite near the repository of 2,140 kg/m^3 (133.6 lb/ft^3) as reported by Holcomb and Shields (1987, p. 17). This value corresponds to a porosity of 0.01 ($\phi = 1 - (\rho_b/\rho_g)$).

Average Density near Repository

Parameter:	**Density, average (ρ_{ave})**
Median:	2.3×10^3
Range:	None
Units:	kg/m^3
Distribution:	Constant
Source(s):	Krieg, R. D. 1984. *Reference Stratigraphy and Rock Properties for the Waste Isolation Pilot Plant (WIPP) Project.* SAND83-1908. Albuquerque, NM: Sandia National Laboratories. (Table 4)

Discussion:

The average density of the Salado Formation in a 107.06-m (351.25-ft) interval straddling the repository is 2,300 kg/m^3 (143.6 lb/ft^3). The interval includes anhydrite marker beds 134, 136, and 138 (above the repository) and anhydrite marker beds 139, 140, and polyhalite marker bed 141 (below the repository) (see Figure 2.2-4). (Marker beds 135 and 137 are very thin and not found in every borehole; therefore these marker beds are not included.) The sum of the thicknesses of all layers of halite and argillaceous halite is 90.92 m (298.29 ft). Assuming that 83.5% of this thickness is pure halite (89.12 m [292.39 ft]) with a grain density of 2,163 kg/m^3 (135 lb/ft^3) (see Table 2.4-1) and that the remaining thickness (17.94 m [58.86 ft]) (16.5% of total thickness) is anhydrite with a density of 2,963 kg/m^3 (185 lb/ft^3) (see Table 2.4-1) yields a weighted average density of 2,300 kg/m^3 (144 lb/ft^3) (Krieg, 1984, p. 14).

2.3.3 Dispersivity

Parameter:	**Dispersivity, longitudinal (α_L)**
Median:	1.5×10^1
Range:	1
	4×10^1
Units:	m
Distribution:	Cumulative
Source(s):	Pickens, J. F., and G. E. Grisak. 1981. Modeling of Scale-Dependent Dispersion in Hydrogeologic Systems. *Water Resources Research*, vol. 17, no. 6, pp. 1701-11.
	Lappin, A. R., R. L. Hunter, D. P. Garber, and P. B. Davies, eds. 1989. *Systems Analysis Long-Term Radionuclide Transport, and Dose Assessments, Waste Isolation Pilot Plant (WIPP), Southeastern New Mexico; March 1989*. SAND 89-0462. Albuquerque, NM: Sandia National Laboratories. (Table D-2)

Parameter:	**Dispersivity, transverse (α_T)**
Median:	1.5
Range:	1×10^{-1}
	4
Units:	m
Distribution:	Cumulative
Source(s):	Pickens, J. F., and G. E. Grisak. 1981. Modeling of Scale-Dependent Dispersion in Hydrogeologic Systems. *Water Resources Research*, vol. 17, no. 6, pp. 1701-11.
	Freeze, R. A. and J. C. Cherry. 1979. *Groundwater*. Englewood Cliffs, NJ: Prentice-Hall, Inc.

Discussion:

No solute transport tests have been run in the Salado Formation, and no relevant solute transport data exist for very low permeability media from which to estimate dispersivity (α). However, current models show limited fluid movement away from the disposal area (Rechard et al., 1989); hence, the rule of thumb applied in standard porous media (Pickens and Grisak, 1981) is assumed to apply, that is, the longitudinal dispersivity $\alpha_L \simeq 0.1 d_s$ where d_s is the distance traveled by the solute. For typical distances traveled, α_L is between 1 and 40 m (3 and 130 ft). The distribution for α_L is shown in Figure 2.3-4.

Transverse dispersivity (α_T) is usually linearly related to α_L. The ratio of α_L to α_T typically varies between 5 and 20 (see, for example, Bear and Verruijt, 1987; Freeze and Cherry, 1979, Figure 9.6; Dullien, Figure 7.13). However, at very low velocities the ratio can approach 1, while in some strata the ratio has been reported to approach 100 (de Marsily, 1986). Transverse dispersivity was assumed to be ten times smaller than α_L ($\alpha_T \sim 0.1\alpha_L$) for PA transport calculations. The current range for sensitivity studies is 1 to 25 (Figure 2.3-5).

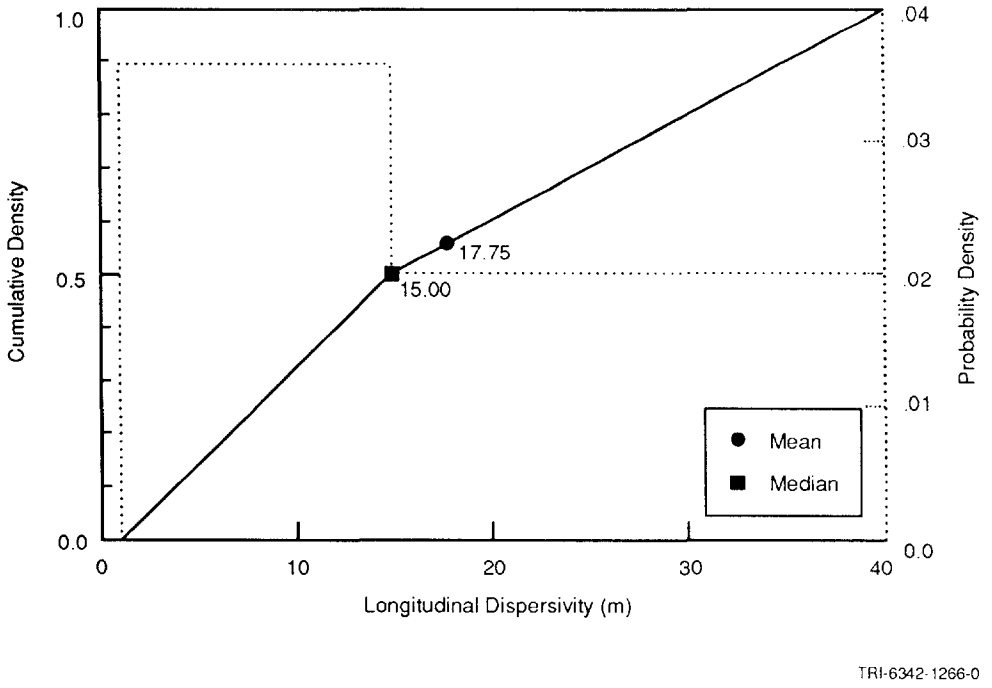

Figure 2.3-4. Estimated Distribution (pdf and cdf) for Longitudinal Dispersivity in Halite, Salado Formation.

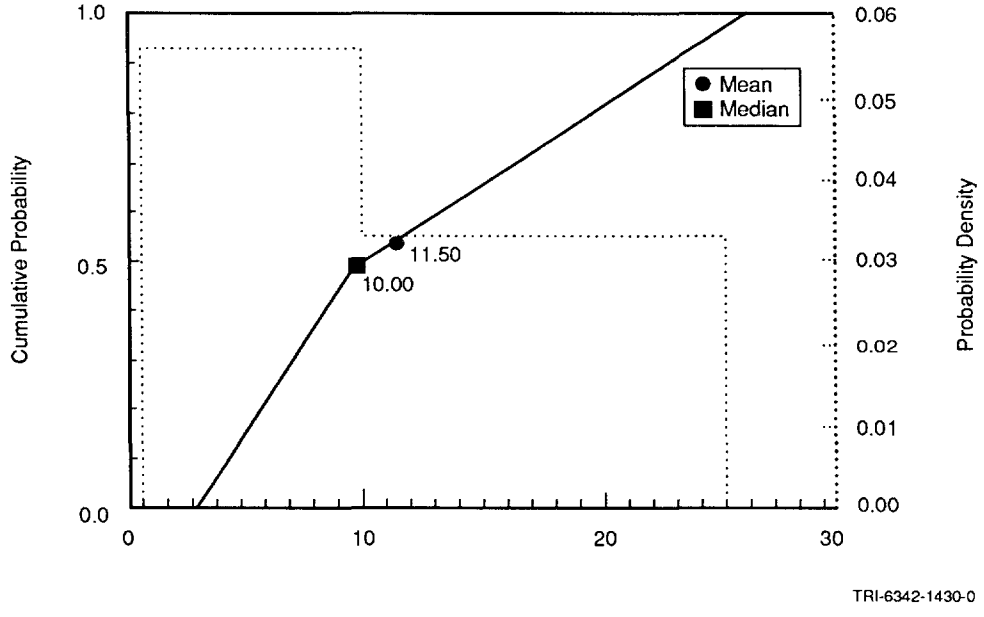

Figure 2.3-5. Estimated Distribution (pdf and cdf) for Transverse Dispersivity in Halite, Salado Formation.

2.3.4 Partition Coefficients and Retardation

Parameter:	**Partition coefficient for halite and polyhalite**
Median:	0
Range:	None
Units:	m^3/kg
Distribution:	Constant
Source(s):	Lappin, A. R., R. L. Hunter, D. P. Garber, and P. B. Davies, eds. 1989. *Systems Analysis Long-Term Radionuclide Transport, and Dose Assessments, Waste Isolation Pilot Plant (WIPP), Southeastern New Mexico; March 1989.* SAND89-0462. Albuquerque, NM: Sandia National Laboratories. (p. D-17)

Discussion:

The halite and polyhalite in the Salado Formation are assumed to not adsorb any contaminants; only clay layers in the Salado Formation are assumed to have this capability (see Sections 2.4.4 and 3.2.4).

2.3.5 Permeability

Undisturbed Permeability

Parameter:	**Permeability, undisturbed** (k)
Median:	5.7×10^{-21}
Range:	8.6×10^{-22}
	5.4×10^{-20}
Units:	m^2
Distribution:	Data
Source(s):	Beauheim, R. 1991. "Review of Salado Parameter Values To Be Used in 1991 Performance Assessment Calculations," Internal memo to Rob Rechard (6342), June 14, 1991. Albuquerque, NM: Sandia National Laboratories. (In Appendix A of this volume)

Figure 2.3-6 shows the values for permeability assuming no correlation with distance from excavation. Figure 2.3-7 shows a non-linear fit of halite permeability with distance from the excavation.

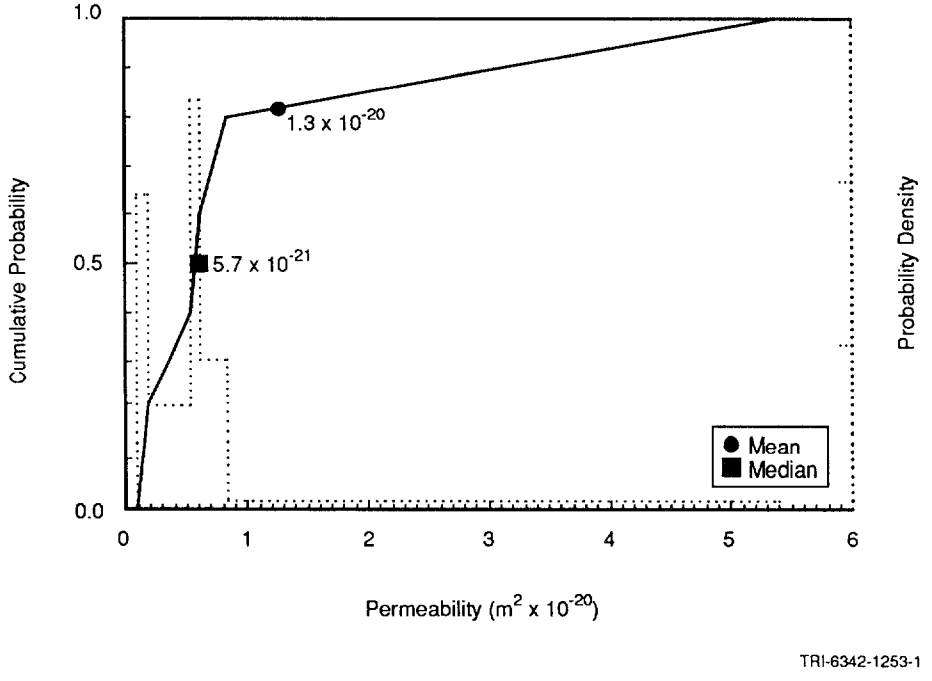

Figure 2.3-6. Estimated Distribution (pdf and cdf) for Salado Undisturbed Permeability.

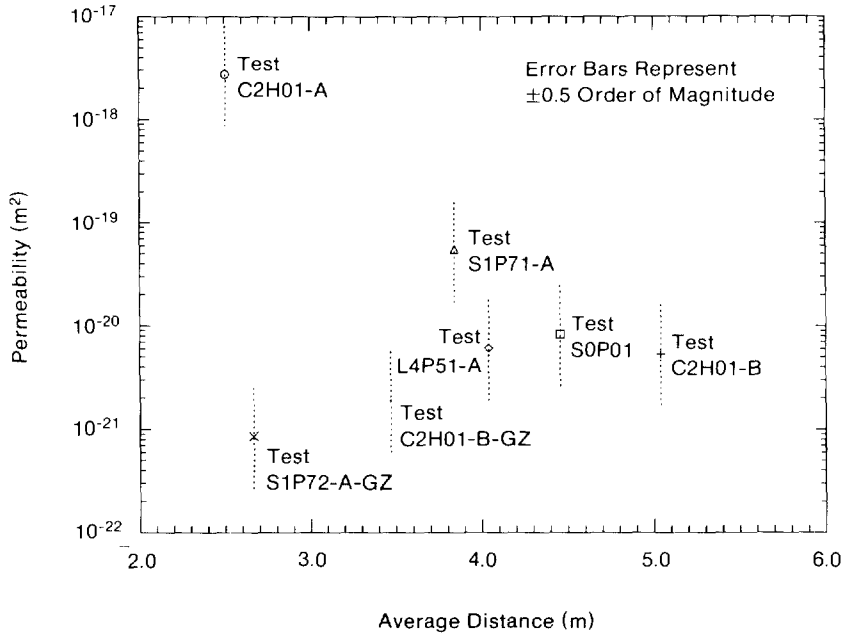

Figure 2.3-7. Logarithm of Halite Permeability Fitted to Distance from the Excavation.

Discussion:

Three experimental programs (Room Q, Small-Scale Brine Inflow, and Permeability Tests, described in the draft of the "Sandia National Laboratories Waste Isolation Pilot Plant Program Plan for Fiscal Year 1992") are evaluating permeability (and storativity and pore pressure) in the halite and anhydrite layers of the Salado Formation. In both 1990 and 1991 PA calculations (Rechard et al., 1990a, p II-13), we used values from the Permeability Test program (Beauheim et al., 1990; Beauheim, June 14, 1991, Memo [Appendix A]) until the Fluid Flow and Transport Division standardizes the interpretation of permeability tests.

Interestingly, over the past several years, the distribution of permeability in the halite has remained generally similar to a lognormal distribution with a range between 10^{-23} and 10^{-18} and a median of 3×10^{-21} m^2 (e.g., McTigue, 1988 in Lappin et al., 1989, p. A-97).

A fit of Beauheim's data to distance from excavation (Figure 2.3-6) shows that the $\log_{10}$ of the asymptotic value of undisturbed halite permeability is -20.83 ± 1.64. The probable error in this estimate can be construed as a one-sigma confidence limit on the asymptotic value.

Rank Correlation Between Halite and Anhydrite Permeability in Salado Formation. Available data are recorded in Table 2.3-2 (from Gorham, July 2, 1991, Memo, and Beauheim, June 14, 1991, Memo [Appendix A]):

Table 2.3-2. Data for Calculating a Rank Correlation between Halite and Anhydrite Permeability In Salado Formation.

Test[a]	Interval[a] (m)	Lithology[a]	Permeability (m^2)[b] Halite	Permeability (m^2)[b] Anhydrite
C2H01-A	2.09 - 2.92	halite	2.7×10^{-18}	
C2H01-A-GZ	0.50 - 1.64	halite		
C2H01-B	4.50 - 5.58	halite	5.3×10^{-21}	
C2H01-B-GZ	2.92 - 4.02	halite	1.9×10^{-21}	
C2H01-C	6.80 - 7.76	MB139		9.5×10^{-19}
C2H02	9.47 - 10.86	MB139		7.8×10^{-20}
L4P51-A	3.33 - 4.75	halite	6.1×10^{-21}	
L4P51-A-GZ	1.50 - 2.36	MB139		
S0P01	3.74 - 5.17	halite	8.3×10^{-21}	
S0P01-GZ	1.80 - 2.76	MB139		$<5.7 \times 10^{-18}$
S1P71-A	3.12 - 4.56	halite	5.4×10^{-20}	
S1P71-A-GZ	1.40 - 2.25	MB139		
S1P71-B	9.48 - 9.80	Anhydrite "c"		
S1P72	4.40 - 6.00	MB139		6.8×10^{-20}
S1P72-GZ	2.15 - 3.18	halite	8.6×10^{-22}	
SCP01	10.50 - 14.78	MB139		
L4P51-B	9.62 - 9.72	Anhydrite "c"		6.8×10^{-20}
S1P73-B	10.86 - 11.03	MB138		

[a] Gorham, July 2, 1991, Memo, Appendix A
[b] Beauheim June 14, 1991, Memo, Appendix A

Note that there are only *two* (halite, anhydrite) pairs of measurements from comparable intervals:

halite, 2.7×10^{-18} m^2 (2.09-2.92 m) + anhydrite, $<5.7 \times 10^{-18}$ m^2 (1.80-2.76 m)

and

halite, 5.3×10^{-21} m^2 (4.50-5.58 m) + anhydrite, 6.8×10^{-20} m^2 (4.40-6.00 m)

To compute a rank correlation with these data, we first make the following table (Table 2.3-3):

Table 2.3-3. Ranks Halite and Anhydrite Data

	(Halite)		Anhydrite	
i	x_i	$R(x_i)$	y_i	$R(y_i)$
1	2.7×10^{-18}	2	5.7×10^{-18}	2
2	5.3×10^{-21}	1	6.8×10^{-20}	1

where

$R(x_i)$ is the rank of x_i in the data set $x_1, x_2, ..., x_n$, and

$R(y_i)$ is the rank of y_i in the data set $y_1, y_2, ..., y_n$.

Conover (1980, p. 252, Eq. 6) suggests using the following formula for computing rank correlation (r_{rank}) when there are many "ties" in the paired data:

$$r_{rank} = \frac{\sum_{i=1}^{n} R(x_i)\, R(y_i) - n\left(\frac{n+1}{2}\right)^2}{\left[\sum_{i=1}^{n} R(x_i)^2 - n\left(\frac{n+1}{2}\right)^2\right]^{1/2} \cdot \left[\sum_{i=1}^{n} R(y_i)^2 - n\left(\frac{n+1}{2}\right)^2\right]^{1/2}}$$

Using the data for $R(x_i)$, $R(y_i)$ given in the table above, it can be seen that $r_{rank}=1$. (This result is expected since limited data are all tied.)

The most important information from the above result is that the correlation coefficient is positive. The actual value is most likely less than one. For current PA calculations, the rank correlation coefficient is assumed to be 0.80 (Figure 2.3-6). This value is high enough to greatly limit the probability that the anhydrite will have a lower permeability than the halite and thereby change the current conceptual model of brine flow within the Salado Formation.

Disturbed Permeability

Parameter:	**Permeability, disturbed** (k)
Median:	1×10^{-19}
Range:	1×10^{-20}
	1×10^{-18}
Units:	m^2
Distribution:	Lognormal
Source(s):	Beauheim, R. L. 1990. "Review of Parameter Values to be Used in Performance Assessment," Memo 3c in Appendix A of Rechard et al. 1990. *Data Used in Preliminary Performance Assessment of the Waste Isolation Pilot Plant (1990).* SAND89-2408. Albuquerque, NM: Sandia National Laboratories.

Discussion:

The disturbed permeability and porosity of the Salado Formation and interbeds vary from the intact properties to large, open fractures. These two disturbed properties also change as the stress field around the excavations change with time. Furthermore, the halite will likely heal to intact conditions over time (Lappin et al., 1989, p. 4-45; Sutherland and Cave, 1978). Often the PA Division does not model the disturbed zone when it is conservative to do so; however, when necessary the following values are typically used.

The disturbed permeability after consolidation and healing is assumed to vary between 1×10^{-20} m^2 (1×10^{-5} mD) (permeability at 0.95 of intact density [see Figure 3.2-3]) and the highest value measured. Beauheim et al. (1990, Table 7-1) reports one measurement from the disturbed rock zone in the Salado Formation of about 1×10^{-18} m^2 (1×10^{-3} mD). The median value was set about one and one-half orders of magnitude higher than the corresponding median value for the intact Salado Formation.

Figure 2.3-8 shows the estimated distribution for the disturbed permeability of the Salado.

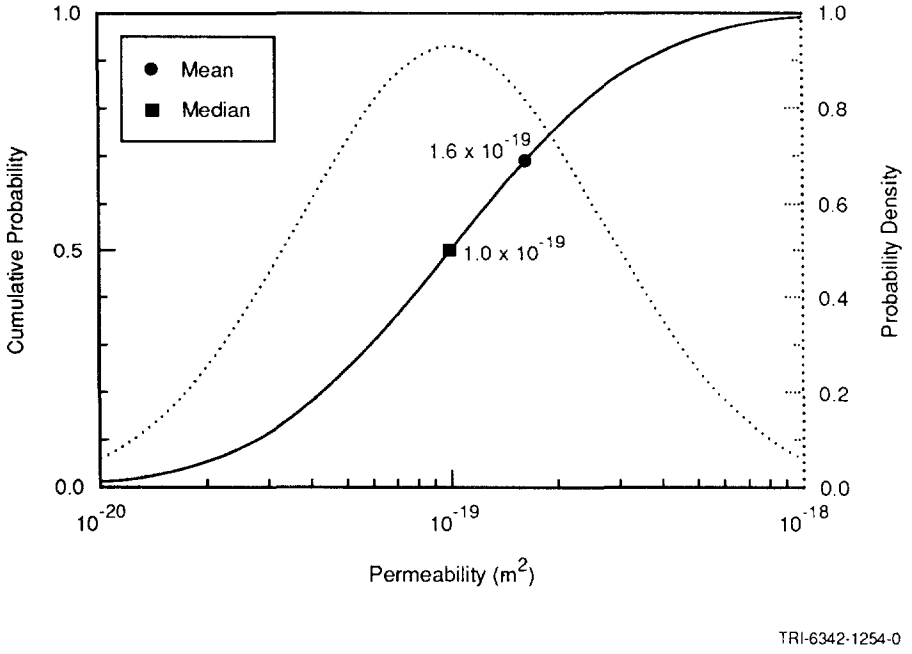

Figure 2.3-8. Estimated Distribution (pdf and cdf) for Disturbed Permeability in Halite, Salado Formation.

2.3.6 Pore Pressure at Repository Level in Halite

Parameter:	**Pore pressure** (p)
Median:	1.28×10^7
Range:	9.3×10^6
	1.39×10^7
Units:	Pa
Distribution:	Data
Source(s):	Beauheim, R. L. 1991. "Review of Salado Parameter Values to be Used in 1991 Performance Assessment Calculations," Internal memo to Rob Rechard (6342), June 14, 1991. Albuquerque, NM: Sandia National Laboratories. (In Appendix A of this volume)
	Howarth, S. 1991. "Pore Pressure Distributions for 1991 Performance Assessment Calculations," Internal memo to Elaine Gorham (6344), June 12, 1991. Albuquerque, NM: Sandia National Laboratories. (In Appendix A of this volume).

Figure 2.3-9 shows the estimated distribution for brine pore pressure in halite. Figure 2.3-10 shows two non-linear fits of brine pore pressure to distance from the excavation.

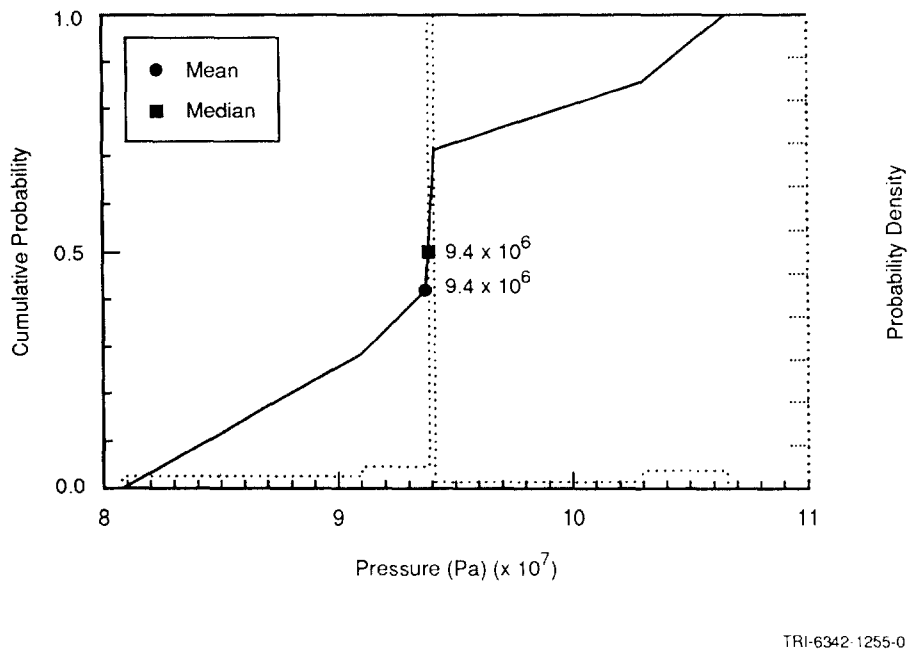

Figure 2.3-9. Estimated Distribution (pdf and cdf) for Brine Pore Pressure at Repository Level in Halite, Salado Formation.

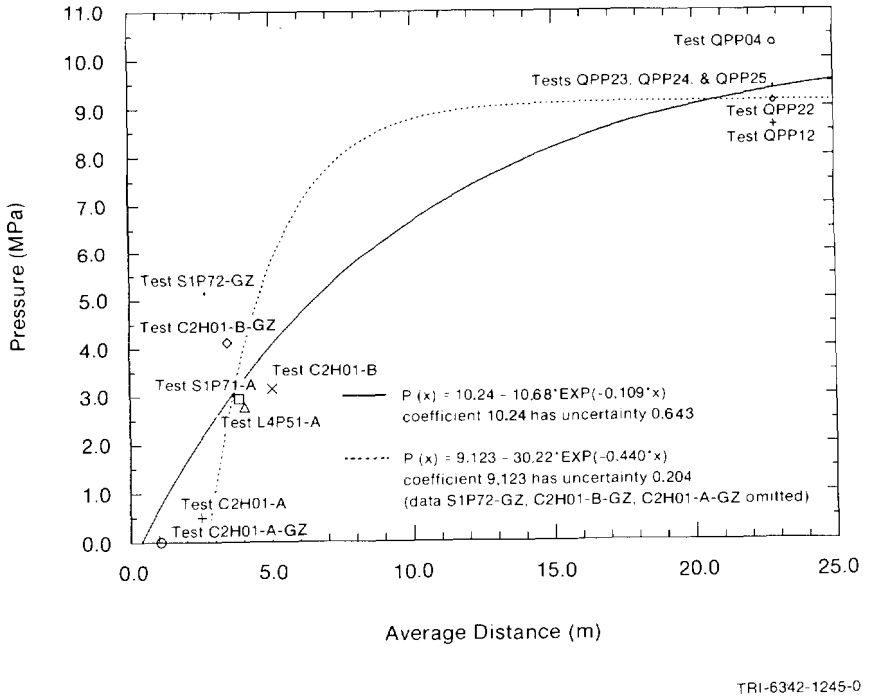

Figure 2.3-10. Non-Linear Fit of Halite Pore Pressure to Distance from Excavation.

Discussion:

In 1991, seven pore pressure measurements from borehole tests taken prior to excavation and located 22.9 m (75 ft) from any existing excavation were available from Room Q (Howarth, June 12, 1991, Memo [Appendix A]). (Beauheim [June 14, 1991, Memo, Appendix A] suggested that none of his pore pressure measurements in the halite be considered to represent far-field conditions.) One Room Q measurement (1 MPa) clearly showed the effects of depressurization. Although all remaining Room Q values are at or above hydrostatic pressure (~6 MPa [$z \bullet \rho_{brine} \bullet g$ $\rho_{Culebra}$] pore pressures, assuming 1 MPa at the Culebra), they are distinctly lower than measurements taken at the same time in the anhydrite layer, suggesting some depressurization. Consequently, the 1991 PA calculations use the pore pressure measured in the anhydrite where data suggest less depressurization.

Non-linear fits of pore pressure to distance (Figure 2.3-10) show that the asymptotic value of pore pressure is about 10 MPa with a probable error of about 0.6 MPa. The probable error can be construed as a one-sigma confidence limit.

2.3.7 Porosity

Undisturbed Porosity

Parameter:	**Porosity, undisturbed (ϕ)**
Median:	1×10^{-2}
Range:	1×10^{-3}
	3×10^{-2}
Units:	Dimensionless
Distribution:	Cumulative
Source(s):	Skokan, C., J. Starrett, and H. T. Andersen. 1988. *Final Report: Feasibility Study of Seismic Tomography to Monitor Underground Pillar Integrity at the WIPP Site.* SAND88-7096. Albuquerque, NM: Sandia National Laboratories.
	Powers, D. W., S. J. Lambert, S. E. Shaffer, L. R. Hill, and W. D. Weart, ed. 1978. *Geological Characterization Report, Waste Isolation Pilot Plant (WIPP) Site, Southeastern New Mexico.* SAND78-1596, vol. 1 and 2. Albuquerque, NM: Sandia National Laboratories.
	Black, S. R., R. S. Newton, and D. K. Shukla, eds. 1983. "Brine Content of the Facility Interval Strata" in *Results of the Site Validation Experiments,* Vol. II, Supporting Document 10. Waste Isolation Pilot Plant, U.S. Department of Energy.

Discussion:

The median porosity is assumed to be 0.01 based on electromagnetic and DC resistivity measurements (Skokan et al., 1989). This median value is identical to that calculated from a grain density of 2,163 kg/m^3 (135 lb/ft^3) for halite (see Table 2.7-1) and a bulk density of 2,140 kg/m^3 (133.6 lb/ft^3) ($\rho_b = (1-\phi)\rho_g$) (see Table 2.2-1). Although not varied in current PA calculations, the low of 0.001 is based on drying experiments (Powers et al., 1978), while the high of 0.03 is based on the low end of the DC resistivity measurements (Skokan et al., 1988).

Figure 2.3-11 shows the estimated distribution for the undisturbed porosity.

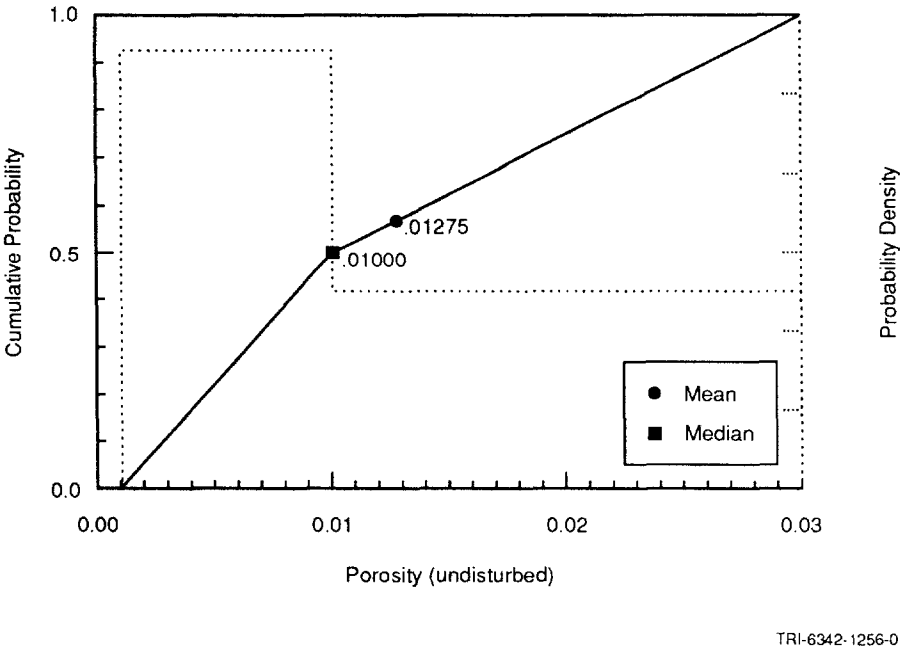

Figure 2.3-11. Estimated Distribution (pdf and cdf) for Undisturbed Porosity in Halite, Salado Formation.

Disturbed Porosity

Parameter:	**Porosity, disturbed (ϕ)**
Median:	6×10^{-2}
Range:	None
Units:	Dimensionless
Distribution:	Constant
Source(s):	See text below.

Discussion:

The disturbed porosity of 0.06 (after consolidation and healing [Lappin et al., 1989, p. 4-45; Sutherland and Cave, 1978]) is calculated assuming that the final density is 0.95 of the intact density ($0.95\rho_b = (1-\phi)\rho_g$) (refer to Figure 3.2-3).

2.3.8 Specific Storage

Parameter:	**Specific storage**
Median:	9.5×10^{-8}
Range:	2.8×10^{-8}
	1.4×10^{-6}
Units:	m^{-1}
Distribution:	Cumulative
Source(s):	Beauheim, R. 1991. "Review of Salado Parameter Values To Be Used in 1991 Performance Assessment Calculations," Internal memo to Rob Rechard (6342), June 14, 1991. Albuquerque, NM: Sandia National Laboratories. (In Appendix A of this volume).

Figure 2.3-12 shows the estimated distribution for specific storage.

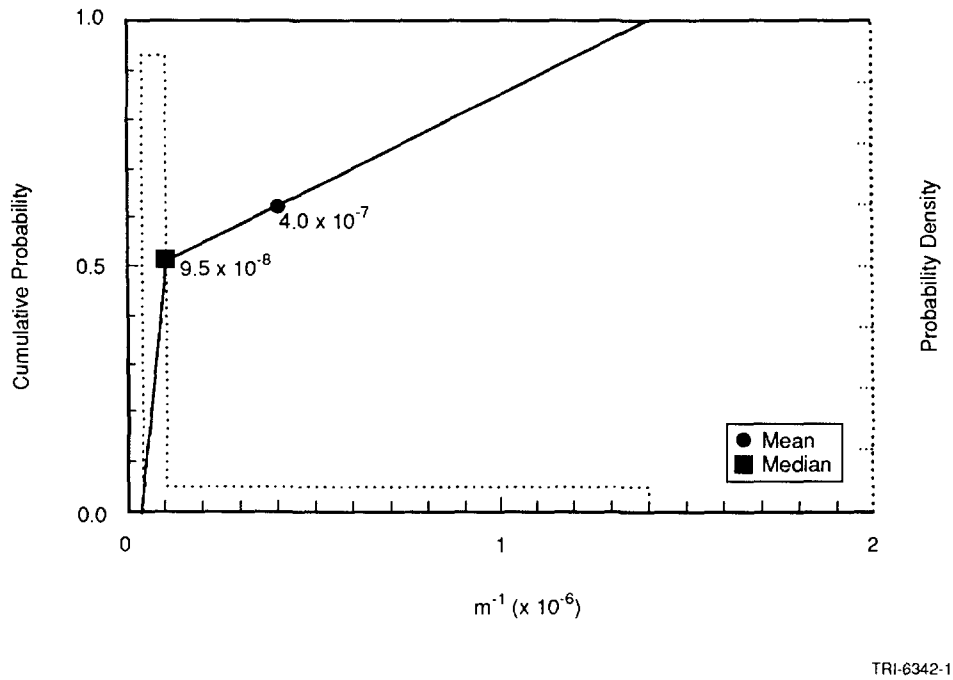

Figure 2.3-12. Estimated Distribution (pdf and cdf) for Specific Storage of Halite, Salado Formation.

The median and range on specific storage are based on laboratory measurements of rock and fluid properties (ϕ, ρ_f, β_f reported herein) and the theoretical definition of specific storage, which is the current procedure for interpreting permeability tests (Beauheim et al., 1991, p. 38).

Beauheim has combined constant-pressure flow tests with pulse tests. This combination allows him to identify the particular values of specific storage that best fit our data. As yet, however, he does not have many of these combined interpretations. Significantly, all of our preliminary values fall within the range established from laboratory experiments, though at the high end. Next year, Beauheim may be able to refine the range somewhat. For the 1991 PA calculations, we used the high end of the laboratory range.

The PA modeling codes all use a slightly different definition of specific storage. To clarify these differences, a detailed discussion of the specific storage term follows.

Derivation of Specific Storage Including Effects of Fluid, Matrix, and Solid Compressibility. Biot (1941) presented a theory for the combined effects of matrix deformation and fluid movement in a porous medium. Rice and Cleary (1976) reformulated Biot's equations in terms of physically identifiable parameters. In this section, we use the notation of Rice and Cleary to derive a general expression for specific storage allowing for fluid, matrix, and solid compressibilities. Direct notation is used with a single underline to identify vectors and double underline to identify 2nd order tensors. Assuming isotropic, linear elastic behavior, Biot's equations for strain, $\underline{\underline{E}}$, written in terms of total stress, $\underline{\underline{\sigma}}$ and fluid pressure p were given in Rice and Cleary as

$$2G\underline{\underline{E}} = \underline{\underline{\sigma}} + P\underline{\underline{I}} - \frac{\nu}{1+\upsilon}\,(\mathrm{tr}\,(\underline{\underline{\sigma}}) + 3p)\,\underline{\underline{I}} - \frac{2G}{3K_s}\,p\underline{\underline{I}} \qquad (2.3\text{-}6)$$

where

- G = drained shear modulus of elasticity
- ν = drained Poisson's ratio
- K_s = bulk modulus of elasticity of solid particles
- $\underline{\underline{I}}$ = identity tensor with components δij
  where $\delta ij = 1$ if $i = j$
  $= 0$ if $i \neq j$
- tr( ) = trace operator such that $\mathrm{tr}\,(\underline{\underline{\sigma}}) = \sigma_{11} + \sigma_{22} + \sigma_{33}$

Equation (2.3-6) can be rewritten using the drained bulk modulus of elasticity, K, for the porous matrix as

$$2G\underline{\underline{E}} = \underline{\underline{\sigma}} - \frac{1}{3}\left(1 - \frac{2G}{3K}\right)\mathrm{tr}\left(\underline{\underline{\sigma}}\right)\underline{\underline{I}} + \frac{2G}{3}\left(\frac{1}{K} - \frac{1}{K_s}\right)p\underline{\underline{I}} \qquad (2.3\text{-}7)$$

This expression can be further simplified by defining the "effective stress" tensor $\bar{\underline{\underline{\sigma}}}$

$$2G\underline{\underline{E}} = \bar{\underline{\underline{\sigma}}} - \frac{1}{3}\left(1 - \frac{2G}{3K}\right)\mathrm{tr}\left(\bar{\underline{\underline{\sigma}}}\right)\underline{\underline{I}} \qquad (2.3\text{-}8)$$

where

$$\bar{\underline{\underline{\sigma}}} = \underline{\underline{\sigma}} + \alpha \, p\underline{\underline{I}} \qquad (2.3\text{-}9)$$

$$\alpha = 1 - K/K_s \qquad (2.3\text{-}10)$$

This illustrates the fact that the deformation of the porous material is governed by the "effective stresses." It should be noted that $\underline{\underline{\sigma}}$ and p are increments of stress and fluid pressure from an unstressed state and it has also been assumed in Eqs. 2.3-7 and 2.3-8 that fluid pressure affects only the normal strain components and not the shear strain components.

Introducing the porosity, ϕ of a porous material where

ϕ = volume of voids in a unit volume of porous material

Rice and Cleary give an expression for porosity change in terms of total stress and fluid pressure

$$\phi - \phi_o = \frac{1}{3}\left(\frac{1}{K} - \frac{1}{K_s}\right)\left[\mathrm{tr}\,(\underline{\underline{\sigma}}) + 3p\right] - \frac{\phi_o}{K_s}\,p \qquad (2.3\text{-}11)$$

where, in this work, it is assumed that the compressibility of the solids making up the matrix can be described by a single bulk elastic modulus K_s. Biot however did not make this assumption. ϕ_o is the porosity in the unstressed state.

The mass of fluid, m_f, in a unit volume of the porous medium is given by

$$m_f = \rho_f \, \phi \qquad (2.3\text{-}12)$$

where

ρ_f = mass density of the fluid.

The continuity equation for fluid mass balance can be expressed by

$$\nabla \cdot \left(\rho_f \, \underline{q}\right) + \frac{\partial m_f}{\partial t} = 0 \qquad (2.3\text{-}13)$$

where

$\underline{q}$ = specific discharge

t = time

$\nabla\bullet$ = divergence operator

The specific discharge $\underline{q}$ is defined in terms of the average velocity of the fluid

$$\underline{q} = \phi \, \underline{v}_f \tag{2.3-14}$$

Darcy's law may be stated as follows

$$\underline{v}_f - \underline{v}_s = - \frac{\underline{\underline{K}}}{\phi \mu_f} \cdot \left(\nabla p + \rho_f g \, \nabla z \right) \tag{2.3-15}$$

where

$\underline{v}_s$ = the average solid phase velocity
$\underline{\underline{K}}$ = permeability tensor
∇ = gradient operator
g = gravitation constant
z = elevation

The specific discharge *relative* to the deforming solid is given by

$$\underline{q}_r = \underline{q} - \phi \, \underline{v}_s$$
$$\underline{q}_r = -\frac{\underline{\underline{K}}}{\mu_f} \cdot (\nabla p + \rho g \nabla z) \tag{2.3-16}$$

Specific storage is defined as the volume of fluid released from storage in a unit volume due to expansion of the fluid and compression of the porous matrix due to a decrease in hydraulic head.

In a non-deforming porous medium $\underline{V}_s = 0$ and $\underline{q}_r = \underline{q}$. This assumption is made in all PA code, however the effects of matrix compressibility are accounted for in the definition of specific storage. This assumption greatly simplifies the problem. Thus with $\underline{V}_s \approx \underline{0}$ the continuity equation becomes

$$- \nabla \cdot \left[\frac{\rho_f \underline{\underline{K}}}{\mu_f} (\nabla p + pg \, \nabla z) \right] + \frac{\partial m_f}{\partial t} = 0 \tag{2.3-17}$$

Since $m_f = \rho_f \phi$, we may express the second term in 2.3-17

$$\frac{\partial m_f}{\partial t} = \rho_f \frac{\partial \phi}{\partial t} + \phi_o \frac{\partial \rho_f}{\partial t} \tag{2.3-18}$$

Introducing the fluid bulk modulus K_f which is the inverse of fluid compressibility β_f where

$$K_f = \rho_f \frac{\partial P}{\partial \rho_f} = \frac{1}{\beta} \qquad (2.3\text{-}19)$$

$$\frac{\partial \rho_f}{\partial t} = \frac{\partial \rho_f}{\partial p} \frac{\partial p}{\partial t} = \frac{\rho_f}{K_f} \frac{\partial p}{\partial t}$$

$$\text{or } \frac{\partial m_f}{\partial t} = \rho_f \frac{\partial \phi}{\partial t} + \rho_f \frac{\phi_o}{K_f} \frac{\partial p}{\partial t} \qquad (2.3\text{-}20)$$

From Eq. 2.3-11 get an expression for $\partial\phi/\partial t$ such that

$$\frac{\partial m_f}{\partial t} = \rho_f \left[\frac{1}{3} \left(\frac{1}{K} - \frac{1}{K_s} \right) \left[tr \left(\frac{\partial \underline{\underline{\sigma}}}{\partial t} \right) + 3 \frac{\partial p}{\partial t} \right] - \frac{\phi_o}{K_s} \frac{\partial p}{\partial t} + \frac{\phi}{K_f} \frac{\partial p}{\partial t} \right] \qquad (2.3\text{-}21)$$

From this expression, it can be concluded that in general fluid mass changes are influenced by the stress changes as well as the fluid pressure changes.

If only vertical deformation is allowed, ($E_{11} = E_{22} = 0$), along with constant vertical total stress, $\sigma_{33} = 0$ with $\sigma_{11} = \sigma_{22}$, using Eq. 2.3-7, it is possible to derive an expression relating the horizontal σ_{11} (or σ_{22}) components of total stress with the fluid pressure. This relationship is given by

$$\sigma_{11} = \sigma_{22} = \frac{-2G \left(\frac{1}{K} - \frac{1}{Ks} \right)}{1 + (4G/3K)}$$

Also we may now compute $tr \left(\frac{\partial \underline{\underline{\sigma}}}{\partial t} \right)$

$$tr \left(\frac{\partial \underline{\underline{\sigma}}}{\partial t} \right) = 2 \frac{\partial \sigma_{11}}{\partial t} = \frac{-4G \left(\frac{1}{K} - \frac{1}{K_s} \right)}{1 + (4G/3K)} \frac{\partial p}{\partial t}$$

Substitution of this result into Eq. 2.3-21 gives

$$\frac{\partial m_f}{\partial t} = \rho_f \left[\left(\frac{1}{K} - \frac{1}{K_s} \right) \left(1 - \frac{4G}{3} \left(\frac{1 - \left(K / K_s \right)}{K + (4G/3K)} \right) + \phi \left(\frac{1}{K_f} - \frac{1}{K_s} \right) \right] \frac{\partial p}{\partial t} \qquad (2.3\text{-}22)$$

or

$$\frac{\partial m_f}{\partial t} = \rho_f c \frac{\partial p}{\partial t}$$

where c is the capacitance (specific pressure storativity).

Under the conditions specified above, the specific storage (S_s) is defined as

$$\frac{\partial m_f}{\partial t} = \rho_f S_s \frac{\partial h}{\partial t} \qquad (2.3\text{-}23)$$

where

h = hydraulic head.

Our result is written in terms of fluid pressure, p, instead of hydraulic head; however, the two are related by

$$\frac{\partial h}{\partial t} = \frac{1}{\rho_f g} \frac{\partial p}{\partial t}$$

$$\frac{\partial m_f}{\partial t} = \frac{1}{g} S_s \frac{\partial p}{\partial t} \text{ and } S_s = \rho_f g c$$

$$\therefore S_s = \rho_f g \left[\left(\frac{1}{K} - \frac{1}{K_s} \right) \left(\frac{1 - \frac{4G}{3}(1-K/Ks)}{K + (4G/3)} \right) + \phi \left(\frac{1}{K_f} - \frac{1}{K_s} \right) \right] \qquad (2.3\text{-}24)$$

This is the equation for specific storage including the effects of pore fluid compressibility ($1/K_f$), matrix compressibility ($1/K$), and solid compressibility ($1/K_s$).

Typically, $K_s >> K$ and $K_s >> K_f$ and Eq. 2.3-24 may be simplified to

$$S_s = \rho_f g \left(\frac{1}{K + (4G/3)} + \frac{\phi}{K_f} \right) \qquad (2.3\text{-}25)$$

The term $\frac{1}{K + (4G/3)}$ is the inverse of the drained constrained modulus of elasticity porous media and is often denoted by β_s, the vertical compressibility. Letting $1/K_f = \beta_f$ gives the familiar result for specific storage.

$$S_s = \rho_f g (\beta_s + \phi \beta_f).$$

Some confusion may result because groundwater models often employ different definitions for the matrix compressibility β_s. For example SUTRA (Voss, 1984) defines β_s

$$\beta_s = \frac{1}{1 - \phi} \frac{\partial \phi}{\partial p}$$

but defines capacitance (specific pressure storativity) as

$$c = (1 - \phi)\beta_s + \phi\beta_f$$

thus

$$c = \frac{\partial \phi}{\partial p} + \phi\beta$$

STAFF 2D (Huyakorn et al., 1989) and HST3D (Kipp, 1987) defines β_s as

$$\beta_s = \frac{\partial \phi}{\partial p}$$

while BOAST II (Fanchi et al., 1987) and BRAGFLO (Volume 2 of this report) use

$$\beta_s = \frac{1}{\phi} \frac{\partial \phi}{\partial p}$$

It is important to recognize that each code uses a different definition of matrix compressibility and all ignore solid compressibility. Beauheim et al. (1991) note that the assumption that $K_s >> K$ may not be valid for halite (due to low porosity and compressibility).

2.3.9 Tortuosity

Parameter:	**Tortuosity** (τ)
Median:	1.4×10^{-1}
Range:	1×10^{-2}
	6.67×10^{-1}
Units:	Dimensionless
Distribution:	Cumulative
Source(s):	See text (Culebra, Section 2.6.7)
	Freeze, R. A. and J. C. Cherry. 1979. *Groundwater.* Englewood Cliffs, NJ: Prentice-Hall, Inc.

Discussion:

No direct measurements of tortuosity are available in the anhydrite (or halite) layers of the Salado Formation. The range reported is the maximum typical theoretical value of 0.667 for uniform-sized grains at low Peclet numbers (N_p) (Dullien, 1979, Figure 7.12) down to 0.01 observed in laboratory experiments of nonadsorbing solutes in porous materials (Freeze and Cherry, 1979, p. 104). The PA Division selected a median value equal to that of the Culebra Dolomite Member. This parameter primarily influences diffusion-dominated transport, a condition occurring only when the repository is undisturbed. The influence of the tortuosity on results was explored in a few 1991 PA calculations of the undisturbed summary scenario class (Volume 2 of this report).

2.4 Hydrologic Parameters for Anhydrite Layers within Salado Formation

Table 2.4-1 provides the parameter values for anhydrite layers near the repository within the Salado Formation. Marker Bed 139 (MB139), a potential transport pathway, is an interbed located about 1 m (3.3 ft) below the repository interval and thus is an anhydrite layer of particular interest. Figure 2.4-1 shows a cross section of MB139.

Table 2.4-1. Hydrologic Parameter Values for Anhydrite Layers within Salado Formation

Parameter	Median	Range		Units	Distribution Type	Source
Capillary pressure (p_c) and relative permeability (k_{rw})						
Threshold displacement pressure (p_t)	3×10^5	3×10^3	3×10^7	Pa	Lognormal	Davies, 1991; Davies, June 2, 1991, Memo (see Appendix A)
Residual Saturations						
Wetting phase ($S_{\ell r}$)	2×10^{-1}	1×10^{-1}	4×10^{-1}	none	Cumulative	Davies and LaVenue, 1990b
Gas phase (S_{gr})	2×10^{-1}	1×10^{-1}	4×10^{-1}	none	Cumulative	Davies and LaVenue, 1990b
Brooks-Corey Exponent (η)	7×10^{-1}	3.5×10^{-1}	1.4	none	Cumulative	Davies and LaVenue, 1990b
Density, grain (ρ_g)	2.963×10^3			kg/m^3	Constant	See text (anhydrite).
Dispersivity						
Longitudinal (αL)	1.5×10^1	1	4×10^1	m	Cumulative	Pickens and Grisak, 1981; Lappin et al., 1989, Table D-2
Transverse (α_T)	1.5	1×10^{-1}	4	m	Cumulative	Pickens and Grisak, 1981
Partition coefficient						
Am	2.5×10^{-2}			m3/kg	Constant	Lappin et al., 1989, Table D-4
Np	1×10^{-3}			m3/kg	Constant	Lappin et al., 1989, Table D-4
Pb	1×10^{-3}			m3/kg	Constant	Lappin et al., 1989, Table D-4
Pu	1×10^{-1}			m3/kg	Constant	Lappin et al., 1989, Table D-4
Ra	1×10^{-3}			m3/kg	Constant	Lappin et al., 1989, Table D-4
Th	1×10^{-1}			m3/kg	Constant	Lappin et al., 1989, Table D-4
U	1×10^{-3}			m3/kg	Constant	Lappin et al., 1989, Table D-4
Permeability (k)						
Undisturbed	7.8×10^{-20}	6.8×10^{-20}	9.5×10^{-19}	m^2	Cumulative	Beauheim, June 14, 1991, Memo (see Appendix A)
Disturbed	1×10^{-17}	1×10^{-19}	1×10^{-13}	m^2	Cumulative	Beauheim, 1990
Pore pressure	1.28×10^7	9.3×10^6	1.39×10^7	Pa	Data	Beauheim, June 14, 1991, Memo; Howarth, June 12, 1991, Memo (see Appendix A)
Porosity (ϕ)						
Undisturbed	1×10^{-2}	1×10^{-3}	3×10^{-2}	none	Cumulative	See text.
Disturbed	5.5×10^{-2}	1×10^{-2}	1×10^{-1}	none	Normal	See text.
Specific storage	1.4×10^{-7}	9.7×10^{-8}	1×10^{-6}	m^{-1}	Cumulative	Beauheim, June 14, 1991, Memo (see Appendix A)
Thickness (Δz)	9×10^{-1}	4×10^{-1}	1.25	m	Cumulative	Borns, 1985, Figure 3; WEC, 1989b; Krieg, 1984, Table I
Tortuosity	1.4×10^{-1}	1×10^{-2}	6.67×10^{-1}	none	Cumulative	See text (Culebra); Freeze and Cherry, 1979, p. 104

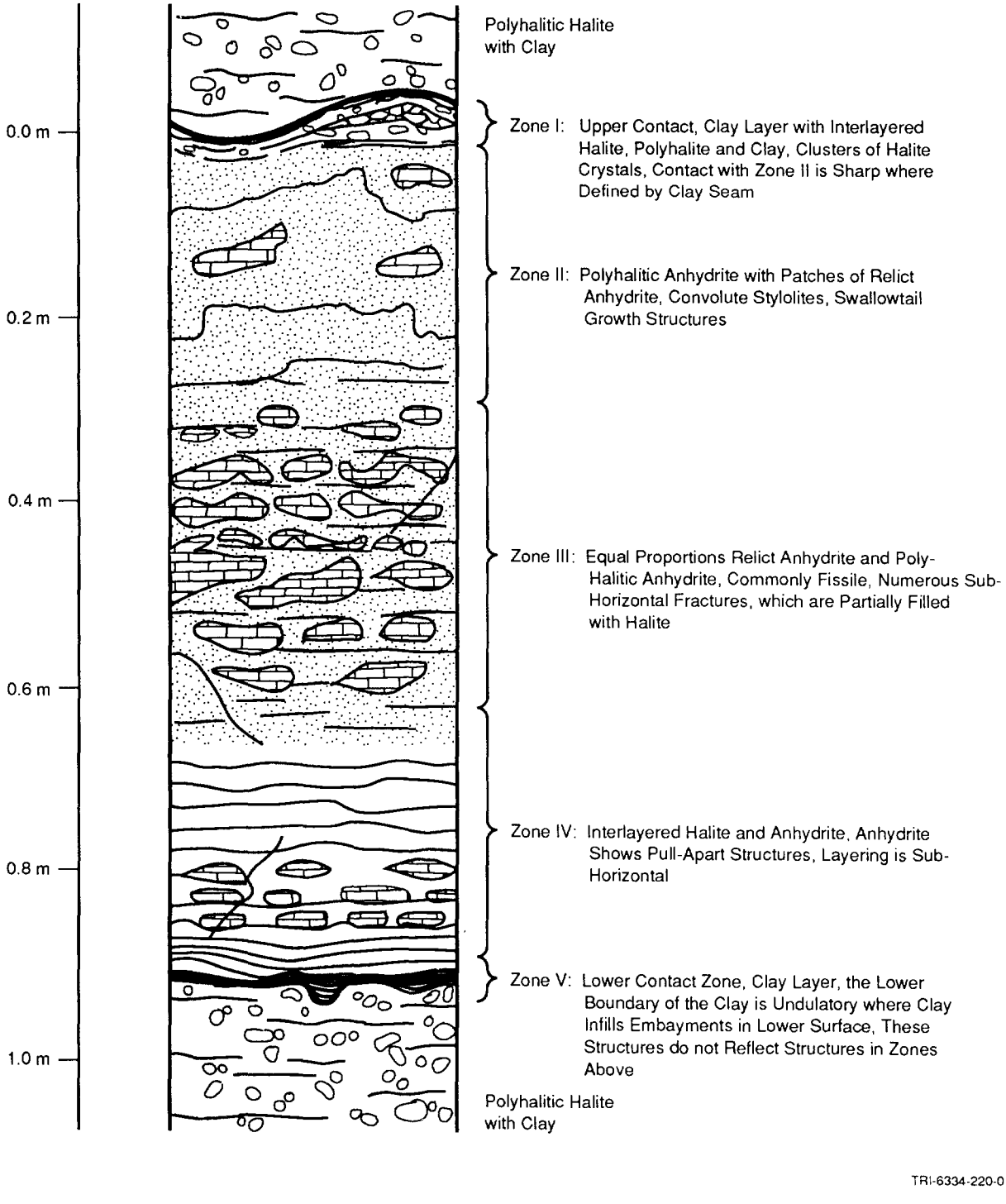

Figure 2.4-1. Generalized Cross Section of Marker Bed 139. The figure shows the internal variability of the unit and the character of both the upper and lower contacts (after Borns, 1985). The thickness varies spatially between 0.4 and 1.25 m with a reference thickness of 0.99 (WEC, 1989b; Krieg, 1984, Table I).

2.4.1 Capillary Pressure and Relative Permeability

Threshold Displacement Pressure, p_t

Parameter:	**Threshold displacement pressure (p_t)**
Median:	3×10^5
Range:	3×10^3
	3×10^7
Units:	Pa
Distribution:	Lognormal
Source(s):	Davies, P. B. 1991. *Evaluation of the Role of Threshold Pressure in Controlling Flow of Waste-Generated Gas into Bedded Salt at the Waste Isolation Pilot Plant.* SAND90-3246. Albuquerque, NM: Sandia National Laboratories.
	Davies, P. B. 1991. "Uncertainty Estimates for Threshold Pressure for 1991 Performance Assessment Calculations Involving Waste-Generated Gas." Internal memo to D. R. Anderson (6342), June 2, 1991. Albuquerque, NM: Sandia National Laboratories. (In Appendix A of this volume)

Residual Saturations

Parameter:	**Residual wetting phase (liquid) saturation ($S_{\ell r}$)**
Median:	2×10^{-1}
Range:	1×10^{-1}
	4×10^{-1}
Units:	Dimensionless
Distribution:	Cumulative
Source(s):	Davies, P. B. and A. M. LaVenue. 1990b. "Additional Data for Characterizing 2-Phase Flow Behavior in Waste-Generated Gas Simulations and Pilot Point Information for Final Culebra 2-D Model." Memo 11 in Appendix A of Rechard et al. 1990. *Data Used in Preliminary Performance Assessment of the Waste Isolation Pilot Plant.* SAND89-2408. Albuquerque, NM: Sandia National Laboratories.

Parameter:	**Residual gas saturation (S_{gr})**
Median:	2×10^{-1}
Range:	1×10^{-1}
	4×10^{-1}
Units:	Dimensionless
Distribution:	Cumulative
Source(s):	Davies, P. B. and A. M. LaVenue. 1990b. "Additional Data for Characterizing 2-Phase Flow Behavior in Waste-Generated Gas Simulations and Pilot Point Information for Final Culebra 2-D Model." Memo 11 in Appendix A of Rechard et al. 1990. *Data Used in Preliminary Performance Assessment of the Waste Isolation Pilot Plant.* SAND89-2408. Albuquerque, NM: Sandia National Laboratories.

Brooks and Corey Exponent

Parameter:	**Brooks and Corey exponent (η)**
Median:	7×10^{-1}
Range:	3.5×10^{-1}
	1.4
Units:	Dimensionless
Distribution:	Cumulative
Source(s):	Davies, P. B. and A. M. LaVenue. 1990b. "Additional Data for Characterizing 2-Phase Flow Behavior in Waste-Generated Gas Simulations and Pilot Point Information for Final Culebra 2-D Model." Memo 11 in Appendix A of Rechard et al. 1990. *Data Used in Preliminary Performance Assessment of the Waste Isolation Pilot Plant.* SAND89-2408. Albuquerque, NM: Sandia National Laboratories.

Capillary Pressure and Relative Permeability

Figure 2.4-2a shows the estimated relative permeability for anhydrite layers. Figure 2.4-2b shows the estimated capillary pressure for anhydrite layers. Figure 2.4-3 is an example of variation of relative permeability and capillary pressure when Brooks and Corey parameters are varied.

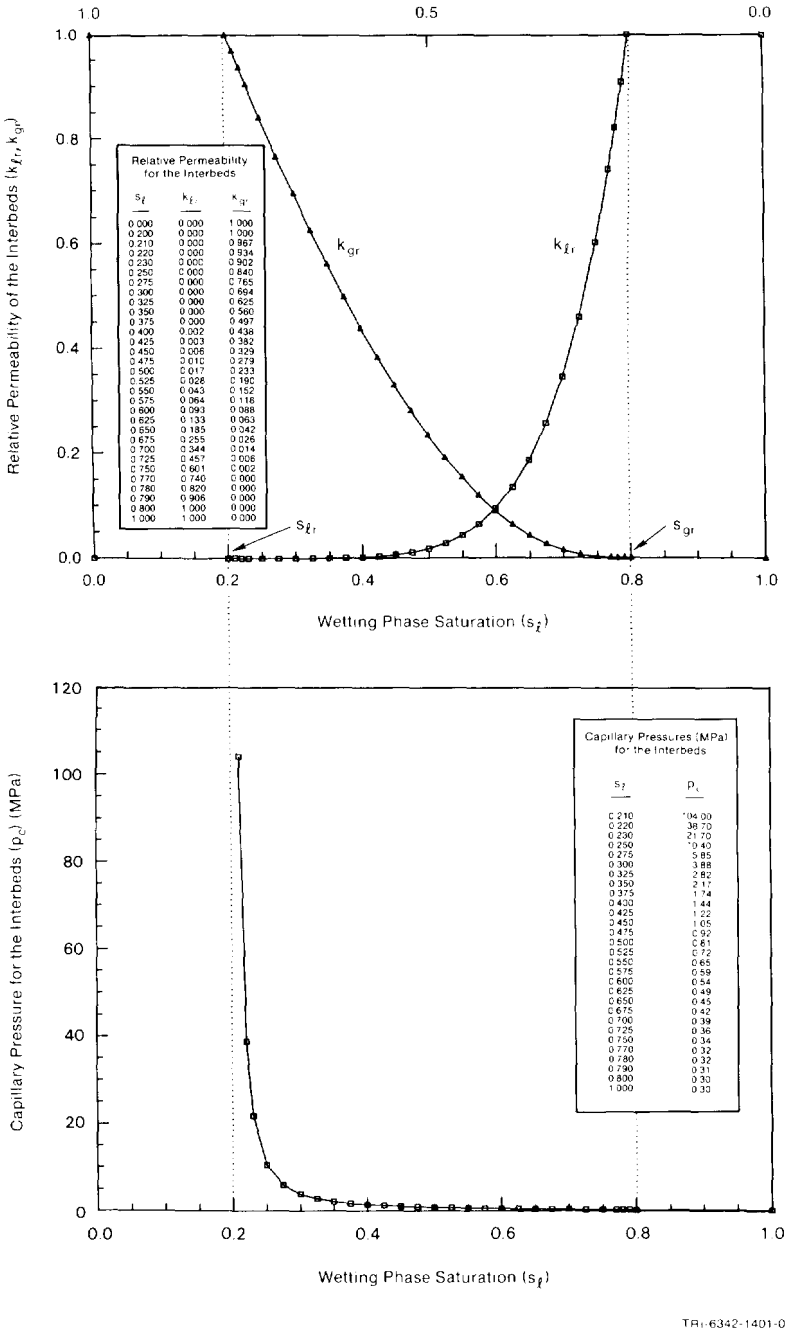

Figure 2.4-2. Estimated Capillary Pressure and Relative Permeability Curves for Anhydrite Layers.

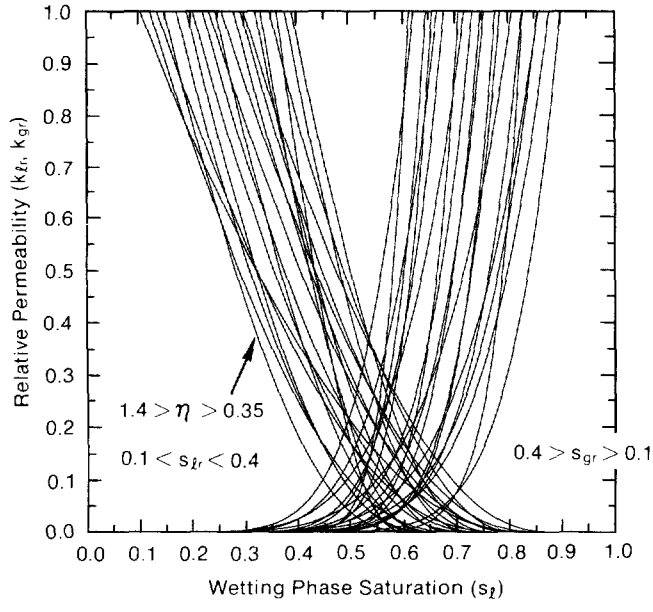

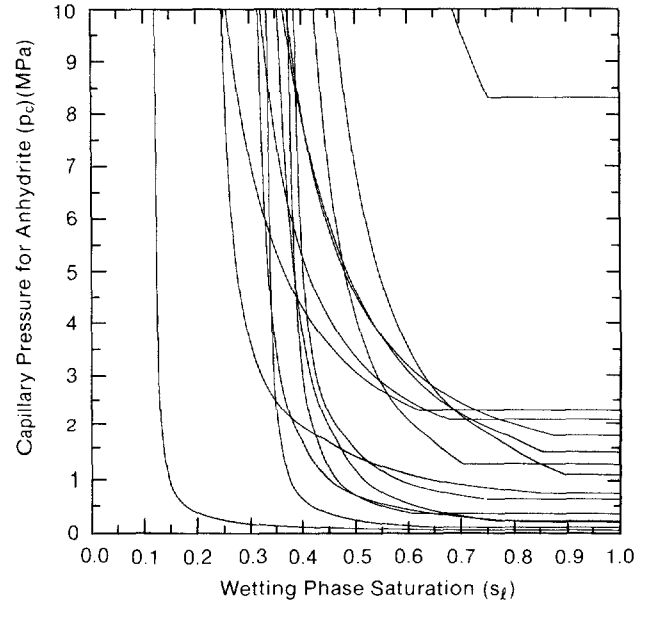

TRI-6342-1466-0

Figure 2.4-3. Example of Variation of Relative Permeability and Capillary Pressure for Anhydrite Layers in Salado Formation When Brooks and Corey Parameters Are Varied.

Discussion:

The correlations for these values were developed as discussed in the section, "Hydrologic Parameters for Halite and Polyhalite within the Salado Formation." Preliminary parameter values selected for MB139 and other anhydrite beds are the same as for Salado halite, except for a lower threshold displacement pressure (p_t), and were taken from experimental data measured for the tight gas sands (Davies and LaVenue, 1990; Ward and Morrow, 1985).

An initial range was selected for the purpose of being able to run sensitivity parameter studies. The ranges shown for the parameters are quite arbitrary, corresponding to a simple doubling and halving of the median values as discussed in Section 2.3.1, "Hydrologic Parameters for Halite in the Salado Formation." The relative permeability curves are identical to those of halite. Only the capillary curves differ because of the different range assumed for the threshold displacement pressure (Figure 2.4-3).

2.4.2 Anhydrite Density

Parameter:	**Density, grain (ρ_g)**
Median:	2.963×10^3
Range:	None
Units:	kg/m^3
Distribution:	Constant
Source(s):	Clark, S. P. 1966. *Handbook of Physical Constants.* New York, NY: The Geological Society of America, Inc. (p. 46) Krieg, R. D. 1987. *Reference Stratigraphy and Rock Properties for the Waste Isolation Pilot Plant (WIPP) Project.* SAND83-1908. Albuquerque, NM: Sandia National Laboratories. (p. 14)

Discussion:

The published grain density of anhydrite ($CaSO_4$) is 2,963 kg/m^3 (185 lb/ft^3) (Clark, 1966, p.46; Krieg, 1987, p. 14).

2.4.3 Dispersivity

Parameter:	**Dispersivity, longitudinal (α_L)**
Median:	1.5×10^1
Range:	1
	4×10^1
Units:	m
Distribution:	Cumulative
Source(s):	Pickens, J. F., and G. E. Grisak. 1981. Modeling of Scale-Dependent Dispersion in Hydrogeologic Systems. *Water Resources Research*, vol. 17, no. 6, pp. 1701-11.
	Lappin, A. R., R. L. Hunter, D. P. Garber, and P. B. Davies, eds. 1989. *Systems Analysis Long-Term Radionuclide Transport, and Dose Assessments, Waste Isolation Pilot Plant (WIPP), Southeastern New Mexico; March 1989*. SAND 89-0462. Albuquerque, NM: Sandia National Laboratories. (Table D-2)

Parameter:	**Dispersivity, transverse (α_T)**
Median:	1.5
Range:	1×10^{-1}
	4
Units:	m
Distribution:	Cumulative
Source(s):	Pickens, J. F., and G. E. Grisak. 1981. Modeling of Scale-Dependent Dispersion in Hydrogeologic Systems. *Water Resources Research*, vol. 17, no. 6, pp. 1701-11.

Discussion:

The dispersivity values are discussed in Section 2.3.3.

2.4.4 Partition Coefficients and Retardations

Table 2.4-2 provides the partition coefficients for anhydrite layers.

Table 2.4-2. Partition Coefficients for Anhydrite Layers (after Lappin et al., 1989, Table D-4)

Radionuclide	Partition coefficient* (m^3/kg)
Am	2.5×10^{-2}
Np	1×10^{-3}
Pb	1×10^{-3}
Pu	1×10^{-1}
Ra	1×10^{-3}
Th	1×10^{-1}
U	1×10^{-3}

* Assumed constant

Discussion:

The sorption of trace radionuclides onto salt-like minerals such as anhydrite is poorly understood; thus, current PA calculations assume partition coefficients of zero (the lower limit). However, because sensitivity studies require ranges of values, the upper limit was arbitrarily chosen to keep the calculated retardation below 10. The rough estimates on median values are those reported by Lappin et al. (1989). Generally, the reported experimental K_d data was reduced by several orders of magnitude as explained below.

Americium. K_d values for americium are decreased by factors of 3 to 1000 from values in Paine (1977), Dosch (1979), and Tien et al. (1983), because of the potential effects of organic complexation. (As a conservative measure, the likely degradation of the organic compounds was neglected.) For example, Swanson (1986) found that moderate concentrations (4×10^{-6} to 10^{-4} M) of EDTA significantly decreased americium sorption onto kaolinite and montmorillonite. The magnitude of this effect was a function of the pH and concentration of EDTA, calcium, magnesium, and iron in solution.

Uranium and Neptunium. In general, low K_ds for uranium and thorium have been measured in waters relevant to the WIPP repository. The K_d of uranium depends strongly on the pH, concentration of competing ions, and the extent of complexation by carbonate and organic ligands (Lappin et al., 1989). A low value (K_d = 1) has been assumed to account for these effects. Theoretical calculations (Leckie, 1989) and arguments based on similarities in speciation, ionic radii, and valence (Chapman and Smellie, 1986) suggest that the behavior of neptunium will be similar to that of uranium.

Plutonium. K_d values for plutonium are decreased by two to three orders of magnitude from the values in Paine (1977), Dosch (1979), and Tien et al. (1983), because of the potential effect of carbonate complexation.

Thorium. There are very few data for thorium under conditions relevant to the WIPP. Thorium K_d values were estimated from data for plutonium, a reasonable homolog element (Krauskopf, 1986). Data describing sorption of thorium onto kaolinite (Riese, 1982) suggest that high concentrations of calcium and magnesium will prevent significant amounts of sorption onto clays in the repository. Stability constants for organo-thorium complexes suggest that organic complexation could be important in the repository and may inhibit sorption (Langmuir and Herman, 1980).

Radium and Lead. There are very few sorption data for radium and lead under conditions relevant to the WIPP. K_d values were estimated by assuming homologous radium-palladium behavior (cf. Tien et al., 1983). Data from Riese (1982) suggest that radium will sorb onto clays but that high concentrations of calcium and magnesium will inhibit sorption. Langmuir and Riese (1985) presented theoretical and empirical arguments that suggest that radium will be coprecipitated in calcite, gypsum, and anhydrite in solutions close to saturation with respect to these minerals.

Retardation. See Section 2.6.10 for the discussion of retardation.

2.4.5 Permeability

Undisturbed Permeability

Parameter:	**Permeability, undisturbed** (k)
Median:	7.8×10^{-20}
Range:	6.8×10^{-20}
	9.5×10^{-19}
Units:	m^2
Distribution:	Data
Source(s):	Beauheim, R. 1991. "Review of Salado Parameter Values To Be Used in 1991 Performance Assessment Calculations," Internal memo to Rob Rechard (6342), June 14, 1991. Albuquerque, NM: Sandia National Laboratories. (In Appendix A of this volume)

Discussion:

The distribution of anhydrite permeability in the far field is based on five measurements from the Permeability Testing Program (Beauheim, June 14, 1991, Memo [Appendix A]). In the past, the general consensus for the permeability of anhydrite layers in general, and MB139 in particular, has been a median value of 1×10^{-19} (Rechard et al., 1990, p. II-16). The current data show an insignificant but somewhat smaller median value of 7.8×10^{-20}.

Figure 2.4-4 shows the distribution for undisturbed permeability in the anhydrite assuming no correlation with distance from excavation. However, a non-linear fit of permeability to distance shows an asymtoptic value near 8×10^{-20} m^2 (Figure 2.4-5). More specifically, the asymptotic value of $\log_{10}$ of anhydrite permeability is about -19, with a probable error of ± 0.6. The probable error can be interpreted as a one-sigma confidence interval.

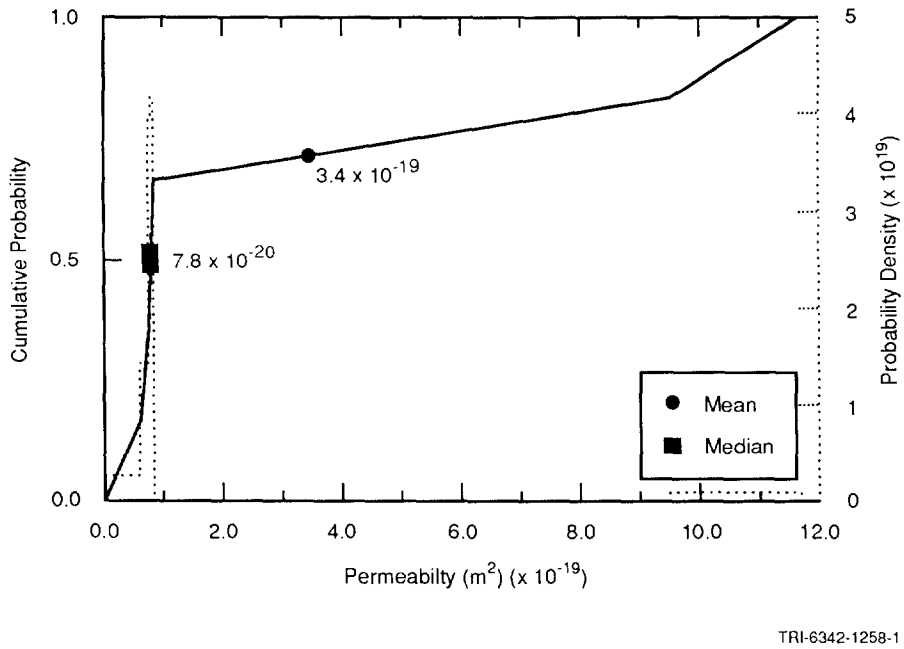

Figure 2.4-4. Estimated Distribution (pdf and cdf) for Undisturbed Permeability, Anhydrite Layers in Salado Formation.

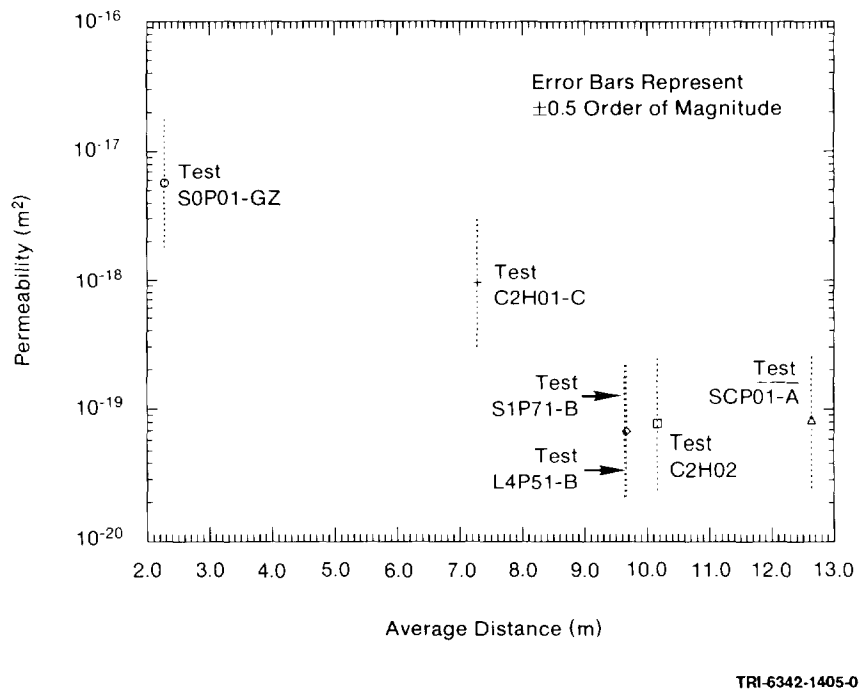

Figure 2.4-5. Non-Linear Fit of Anhydrite Permeability to Distance from Excavation.

Disturbed Permeability

Parameter:	**Permeability, disturbed** (k)
Median:	1×10^{-17}
Range:	1×10^{-19}
	1×10^{-13}
Units:	m^2
Distribution:	Cumulative
Source(s):	Beauheim, R. L. 1990. "Review of Parameter Values to be Used in Performance Assessment," Memo 3c in Appendix A of Rechard et al. 1990. *Data Used in Preliminary Performance Assessment of the Waste Isolation Pilot Plant (1990).* SAND89-2408. Albuquerque, NM: Sandia National Laboratories.

Discussion:

Following the logic described for permeability for the Salado halite, the disturbed permeability is assumed to vary between the median intact value and the highest measured value; the median value is set about two orders of magnitude below the undisturbed median value. The highest permeability measured to date in MB139 is 3.2×10^{-13} m^2 (3.2×10^2 mD) (from draft report by M. E. Crawley, "Hydraulic Testing of Marker Bed 139 at the Waste Isolation Pilot Plant, Southeastern New Mexico," Westinghouse Electric Co., Carlsbad, NM), but was rounded down to 1×10^{-13} m^2 (1×10^2 mD), the value used for unmodified TRU waste.

Figure 2.4-6 shows the estimated distribution for disturbed permeability for the anhydrite layers.

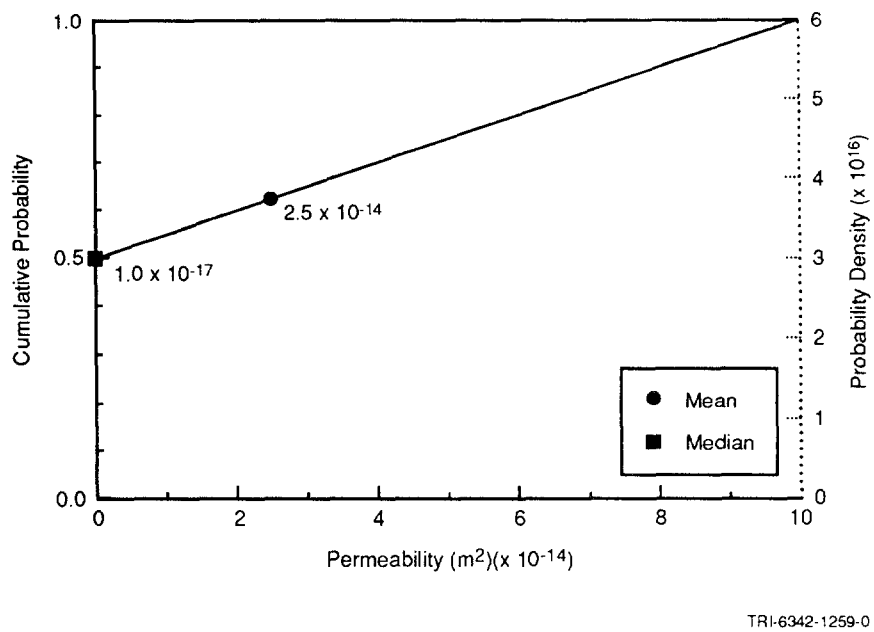

Figure 2.4-6. Estimated Distribution (pdf and cdf) for Disturbed Permeability, Anhydrite Layers in Salado Formation.

2.4.6 Pore Pressure at Repository Level in Anhydrite

Parameter:	**Pore pressure at repository level** (p)
Median:	1.28×10^7
Range:	9.3×10^6
	1.39×10^7
Units:	Pa
Distribution:	Data
Source(s):	Beauheim, R. L. 1991. "Review of Parameter Values to be Used in 1991 Performance Assessment." Internal memo to R. Rechard, June 14, 1991. Albuquerque, NM: Sandia National Laboratories. (In Appendix A of this volume)
	Howarth, S. 1991. "Pore Pressure Distributions for 1991 Performance Assessment Calculations," Internal memo to Elaine Gorham (6344), June 12, 1991. Albuquerque, NM: Sandia National Laboratories. (In Appendix A of this volume).

Figure 2.4-7 shows the distribution for brine pore pressure. Figure 2.4-8 shows the variation of pore pressure with distance from the excavation.

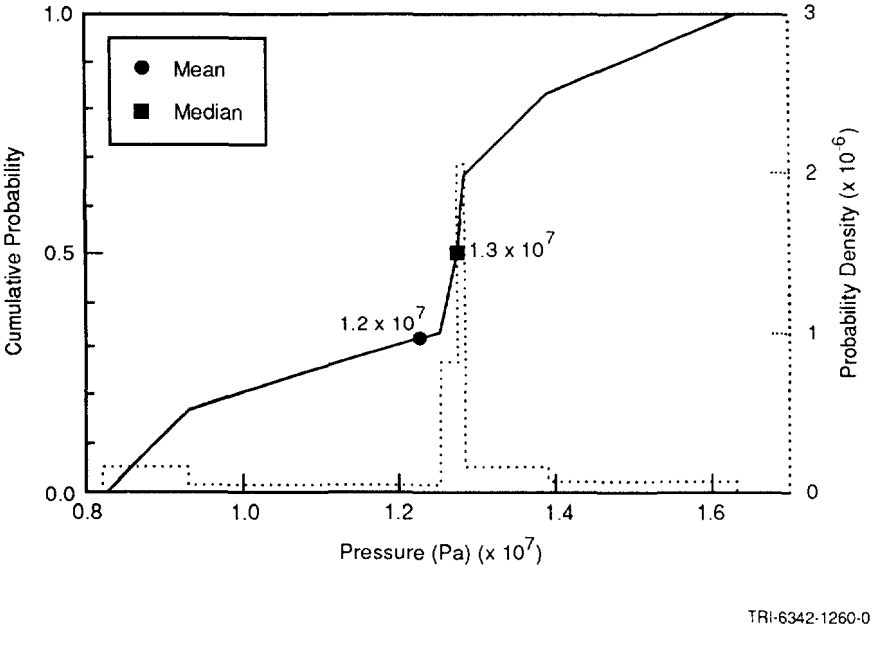

Figure 2.4-7. Estimated Distribution (pdf and cdf) for Brine Pore Pressure in Anhydrite MB139 at Repository Level.

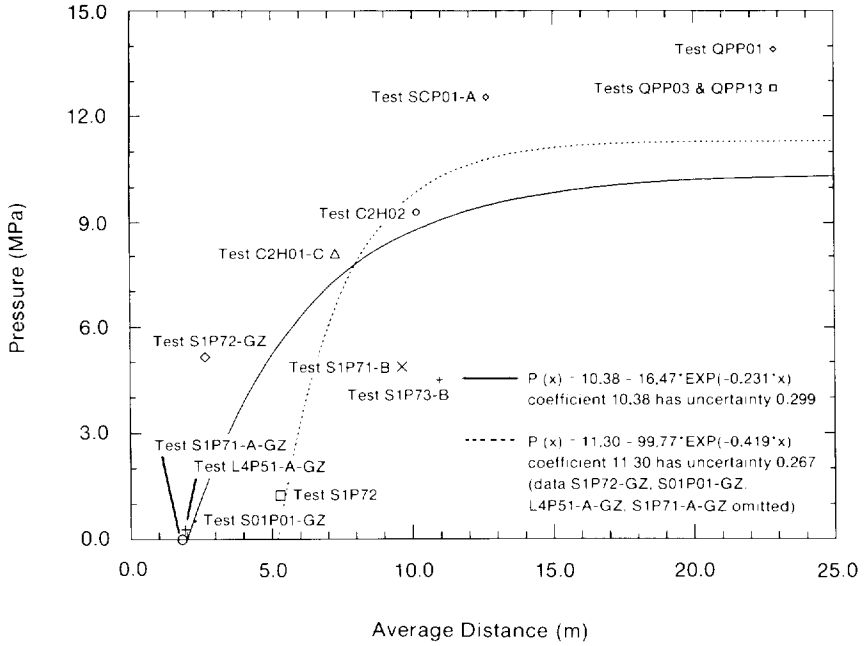

Figure 2.4-8. Non-Linear Fits of Pore Pressure in Anhydrite to Distance from Excavation. (Data from Beauheim, June 14, 1991, Memo and Howarth, June 12, 1991, Memo [Appendix A]).

Discussion:

For the 1991 PA calculations, the pore pressure measurements of investigator Beauheim (June 14, 1991, Memo [Appendix A]) and Howarth (June 12, 1991, Memo [Appendix A]) were combined to form a data distribution with a median of 12.8 MPa (128 atm) and a data range of 9.3 and 13.9 MPa (93 and 139 atm). (The sample range was 8.21 to 15 MPa [Figure 2.4-7].)

In comparison, for the 1990 PA calculations, two pore pressure measurements were reported for Anhydrite MB139: 9.3 MPa (93 atm) (Beauheim et al., 1990) and 12.6 MPa (126 atm). Assuming a uniform distribution, the mean and median were 11.0 MPa, and the range was $\bar{x} + \sqrt{3}s$ or 7 MPa (70 atm) and 15 MPa (150 atm) (Figure 2.4-6). The maximum corresponded to lithostatic pressure based on hydraulic fracturing experiments (Wawersik and Stone, 1985) and density log for WIPP-11 (Figure 2.2-5). The minimum of 7.0 MPa was the average of a pure water hydrostatic of 6.4 MPa and a Salado brine hydrostatic of 7.9 (Figure 2.2-5) or equivalently, the hydrostatic pressure of a column of fluid that linearly varied between pure water at the surface and Salado brine at 655 m (2,142 ft).

The non-linear fits of pore pressure (in anhydrite) to distance (Figure 2.4-8) indicate an asymptotic value of about 10 MPa with probable error of the order of 0.3 MPa. The probable error can be construed as a one-sigma confidence level.

2.4.7 Porosity

Undisturbed Porosity

Parameter:	**Porosity, undisturbed (ϕ)**
Median:	1×10^{-2}
Range:	1×10^{-3}
	3×10^{-2}
Units:	Dimensionless
Distribution:	Cumulative
Source(s):	See text.

Discussion:

PA calculations have assumed an undisturbed porosity similar to the undisturbed porosity of the Salado Formation as a whole.

Figure 2.4-9 shows the estimated distribution for undisturbed porosity for the anhydrite layers.

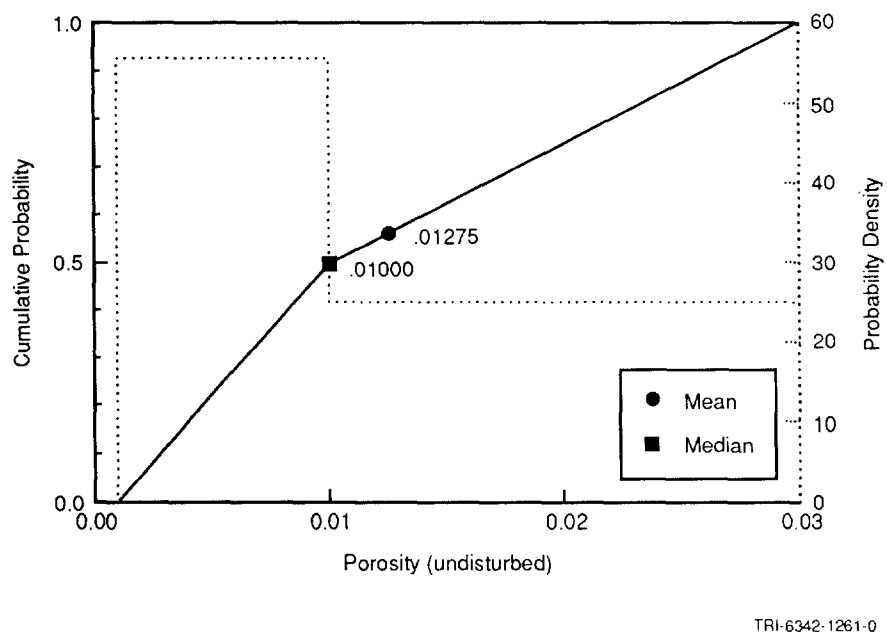

Figure 2.4-9. Estimated Distribution (pdf and cdf) for Undisturbed Porosity for Anhydrite Layers in Salado Formation.

Disturbed Porosity

Parameter:	**Porosity, disturbed (ϕ)**
Median:	5.5×10^{-2}
Range:	1×10^{-2}
	1×10^{-1}
Units:	Dimensionless
Distribution:	Normal
Source(s):	See text.

Discussion:

The lower range for disturbed porosity of the anhydrite layers after reconsolidation was set at 0.1. This value is an order of magnitude increase above the undisturbed porosity lower range and equal to the undisturbed median value. The reason for the increase is that the fractures that form within the brittle anhydrite beds during excavations will not heal completely. Shear displacement will likely cause abutment of asperities in the fractures which, in turn, will prop them open (Lappin et al., 1989, p. 4-62). The upper value of the range was set an order of magnitude above the lower value. Finally, the porosity was assumed to be normally distributed as in many materials (Harr, 1987, Table 1.8.1).

Figure 2.4-10 shows the distribution for the disturbed porosity for the anhydrite layers.

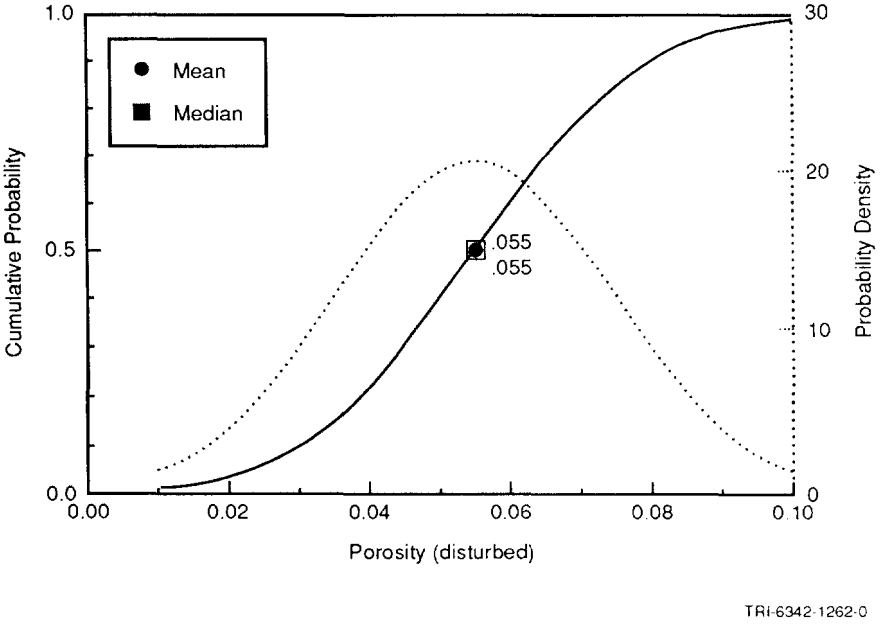

Figure 2.4-10. Estimated Distribution (pdf and cdf) for Disturbed Porosity for Anhydrite Layers in Salado Formation.

2.4.8 Specific Storage

Parameter:	**Specific storage**
Median:	1.4×10^{-7}
Range:	9.7×10^{-8}
	1×10^{-6}
Units:	m^{-1}
Distribution:	Cumulative
Source(s):	Beauheim, R. 1991. "Review of Salado Parameter Values To Be Used in 1991 Performance Assessment Calculations," Internal memo to Rob Rechard (6342), June 14, 1991. Albuquerque, NM: Sandia National Laboratories. (In Appendix A of this volume).

Figure 2.4-11 shows the estimated distribution for specific storage.

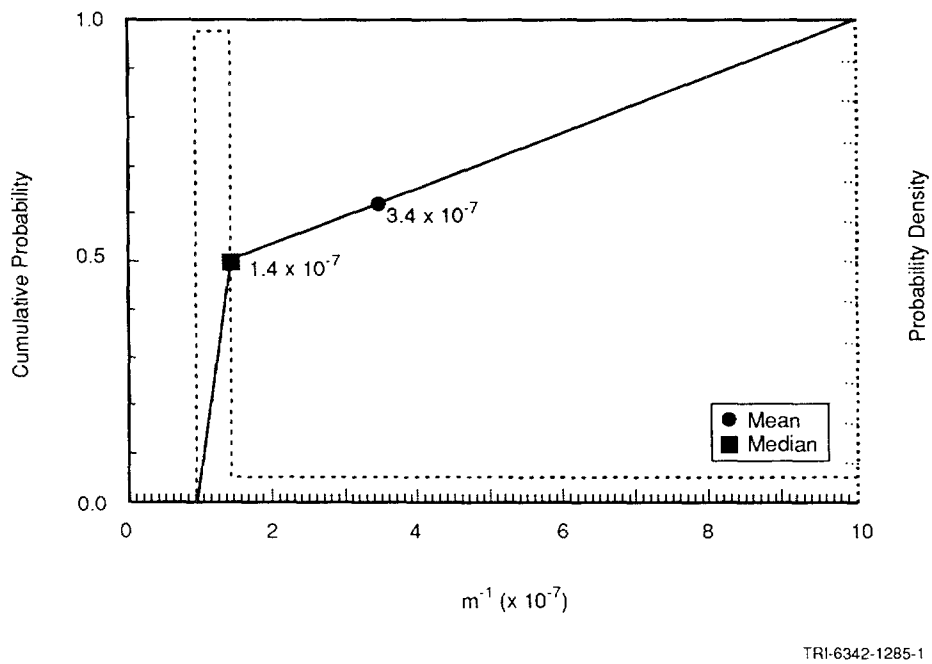

Figure 2.4-11. Estimated Distribution (pdf and cdf) for Anhydrite Specific Storage.

Discussion:

See Section 2.3.8 for complete discussion of specific storage.

2.4.9 Thickness of MB139 Interbed

Parameter:	**MB139 thickness** (Δz)
Median:	9×10^{-1}
Range:	4×10^{-1}
	1.25
Units:	m
Distribution:	Cumulative
Source(s):	Borns, D. J. 1985. *Marker Bed 139: A Study of Drillcore From a Systematic Array.* SAND85-0023. Albuquerque, NM: Sandia National Laboratories. (Figure 3)
	WEC (Westinghouse Electric Corporation). 1989b. *Geotechnical Field Data and Analysis Report, July 1987 through June 1988*, vols. 1 and 2. DOE/WIPP-89-009. Prepared for U.S. Department of Energy. Carlsbad, NM: Westinghouse Electric Corporation.
	Krieg, R. D. 1984. *Reference Stratigraphy and Rock Properties for the Waste Isolation Pilot Plant (WIPP) Project.* SAND83-1908. Albuquerque, NM: Sandia National Laboratories.

Discussion:

The thickness for MB139 in the generalized stratigraphy of the site is about 0.9 m (3 ft) (WEC, 1989b) and is used as the median value. Because the upper contact is irregular and undulates (caused from reworking of the interbed prior to further halite deposition), the thickness varies between 0.40 and 1.25 m (1.3 and 4.1 ft) (Borns, 1985, Figure 3; Krieg, 1984, Table I). Figure 2.4-12 shows the distribution for the thickness of the anhydrite layers in the Salado.

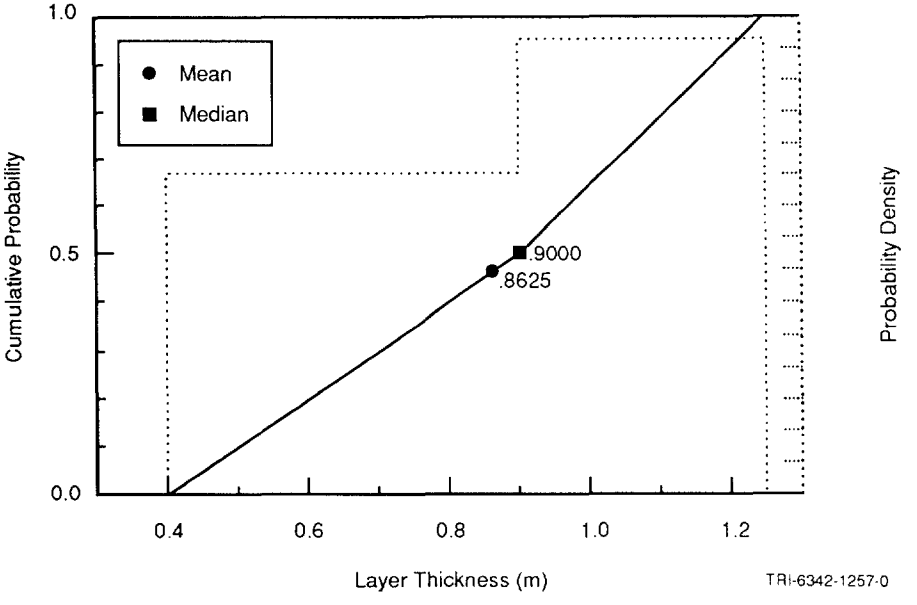

Figure 2.4-12. Estimated Distribution (pdf and cdf) for Thickness of Interbed.

2.4.10 Tortuosity

Parameter:	**Tortuosity** (τ)
Median:	1.4×10^{-1}
Range:	1×10^{-2}
	6.67×10^{-1}
Units:	Dimensionless
Distribution:	Cumulative
Source(s):	See text (Culebra, Section 2.6.7)
	Freeze, R. A. and J. C. Cherry. 1979. *Groundwater*. Englewood Cliffs, NJ: Prentice-Hall, Inc.

Discussion:

No direct measurements of tortuosity are available in the anhydrite (or halite) layers of the Salado Formation. The range reported is the maximum typical theoretical value of 0.667 for uniform-sized grains at low Peclet numbers (N_p) (Dullien, 1979, Figure 7.12) down to 0.01 observed in laboratory experiments of nonadsorbing solutes in porous materials (Freeze and Cherry, 1979, p. 104). The PA Division selected a median value equal to that of the Culebra Dolomite Member. This parameter primarily influences diffusion-dominated transport, a condition occurring only when the repository is undisturbed. The influence of the tortuosity on results was explored in a few 1991 PA calculations of the undisturbed summary scenario class (Volume 2 of this report).

2.5 Mechanical Parameters for Materials in Salado Formation

2.5.1 Halite and Argillaceous Halite

Elastic Constants

Salt Creep Constitutive Model Constants

Polyhalite Elastic Constants

Anhydrite Elastic Constants

2.6 Parameters for Culebra Dolomite Member of Rustler Formation

The Culebra Dolomite Member of the Rustler Formation is a finely crystalline, locally argillaceous (containing clay) and arenaceous (containing sand), vuggy dolomite ranging in thickness near the WIPP from about 7 m (23 ft) (at DOE-1 and other locations) to 14 m (46 ft) (at H-7). Figure 2.6-1 shows a detailed lithology of the Rustler Formation. Figure 2.6-2 is a cross-section across the WIPP disposal system. The Culebra Dolomite is generally considered to provide the most important potential groundwater-transport pathway for radionuclides that may be released to the accessible environment provided human intrusion occurs. Accordingly, the WIPP Project has devoted much attention to understanding the hydrogeology and hydraulic properties of the Culebra. Figure 2.6-3 shows the locations of wells used to define the hydrologic parameters for the Culebra Dolomite. Detailed hydrogeologic information is available in reports by Brinster (1991) and Holt and Powers (1988). The Culebra Dolomite has been tested at 41 locations in the vicinity of the WIPP. Results of these tests and interpretations have been reported by Beauheim (1987a,b,c; 1989), Saulnier (1987), and Avis and Saulnier (1990).

One early observation (Mercer and Orr, 1979) was that the transmissivity of the Culebra Dolomite varies by six orders of magnitude in the vicinity of the WIPP. This variation in transmissivity appears to be the result of differing degrees of fracturing within the Culebra Dolomite. The cause of the fracturing, however, is unresolved. Culebra transmissivities of about 1×10^{-6} m^2/s (0.93 ft^2/d) or greater appear to be related to fracturing. Where the transmissivity of the Culebra Dolomite is less than 1×10^{-6} m^2/s (0.93 ft^2/d), few or no open fractures have been observed in core, and the Culebra's hydraulic behavior during pumping or slug tests is that of a single-porosity medium. Where transmissivities are between 1×10^{-6} m^2/s (0.93 ft^2/d) and at least 1×10^{-4} m^2/s (93 ft^2/d), open fractures are observed in core, and the hydraulic behavior of the Culebra Dolomite during pumping tests is that of a dual-porosity medium (Beauheim, 1987a, b, c; Saulnier, 1987).

Parameter values for the Culebra Dolomite Member are given in Table 2.6-1.

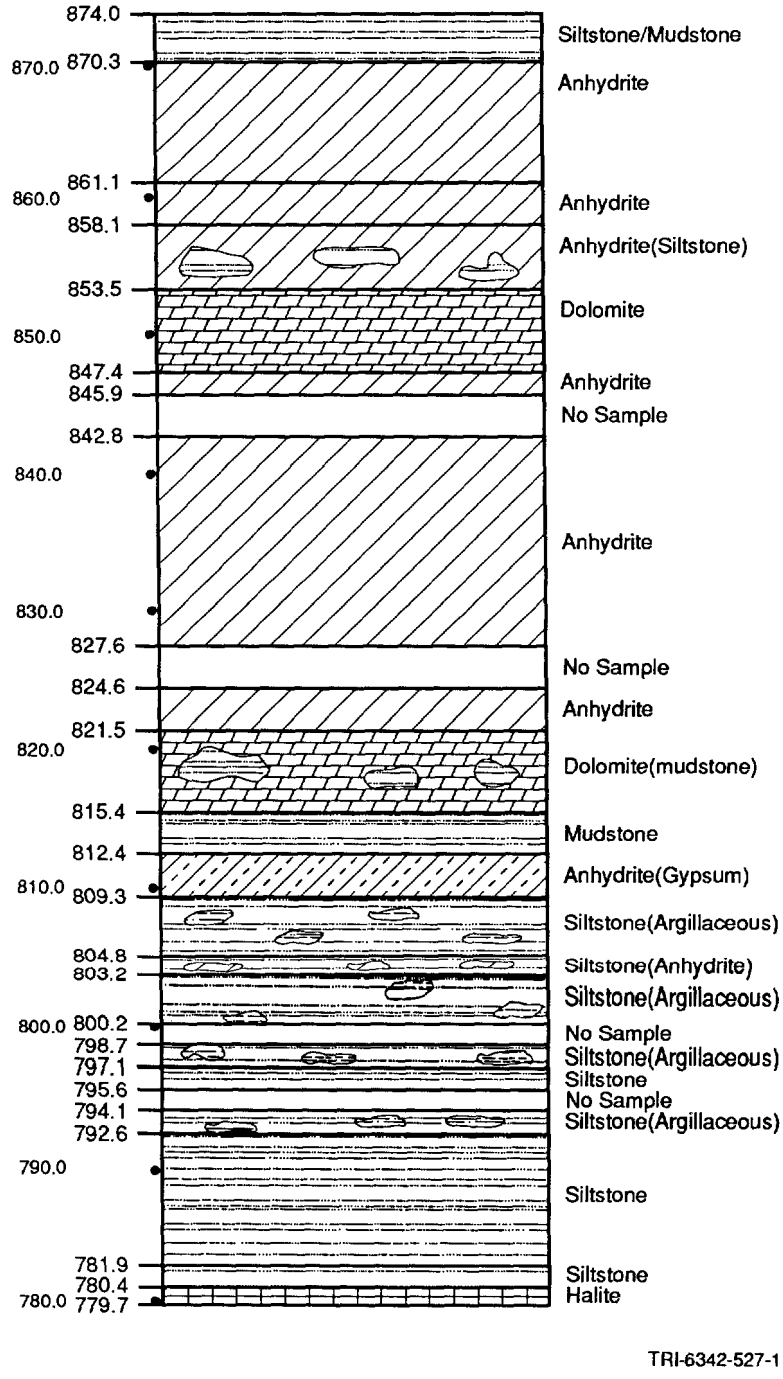

Figure 2.6-1. Detailed Lithology of Rustler Formation at ERDA-9 (after SNL and USGS, 1982b).

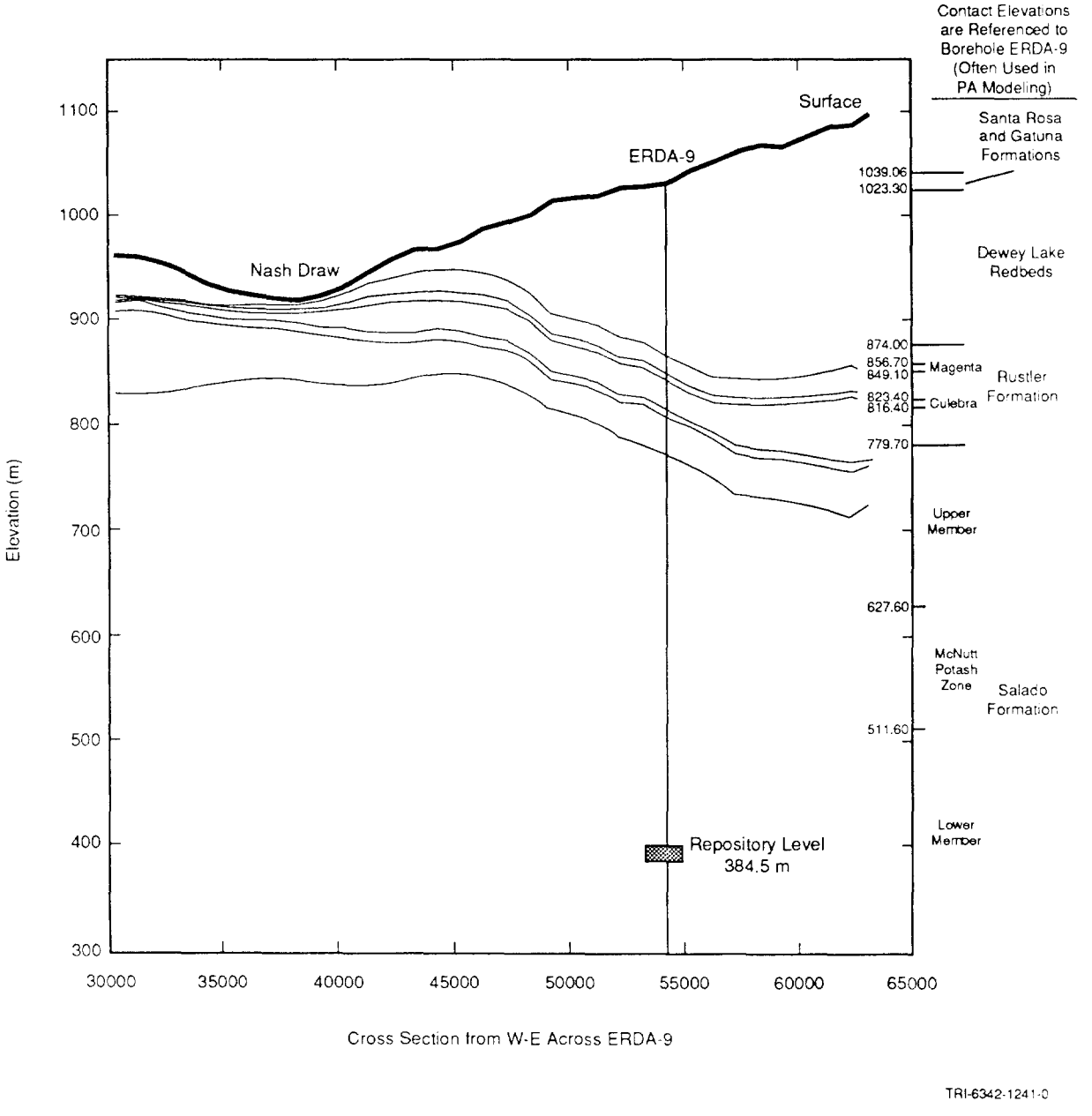

Figure 2.6-2. Interpolated Geologic West-East Cross Section across the WIPP Disposal System (after Mercer, 1983; Davies, 1989, Figure 53).

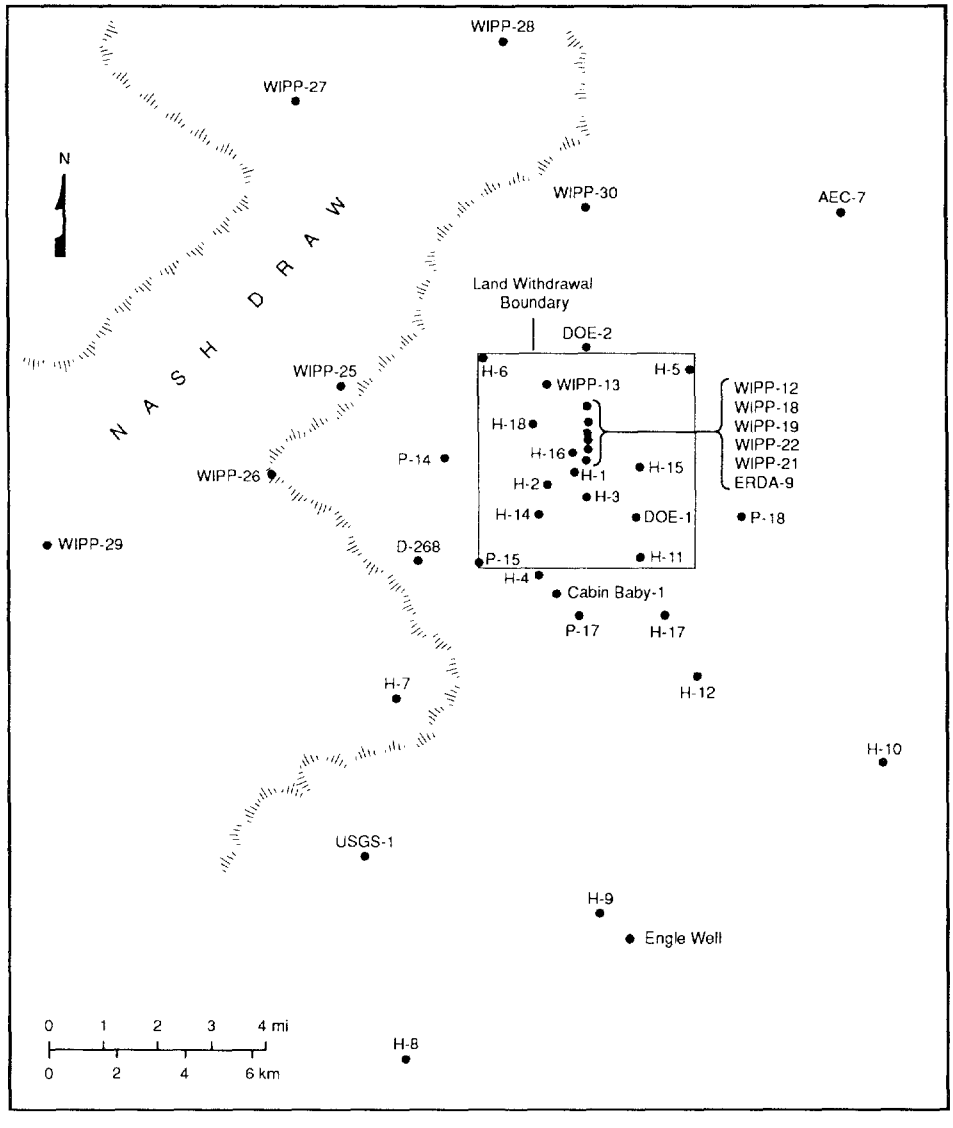

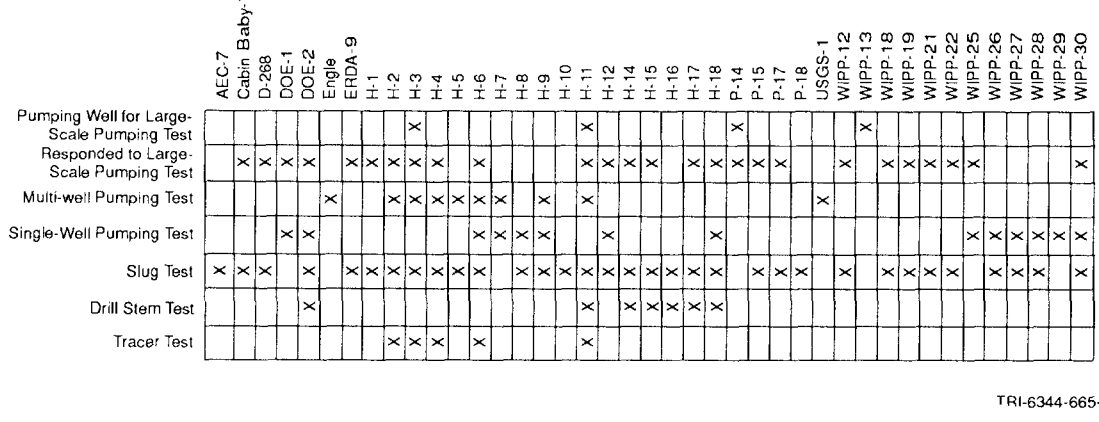

TRI-6344-665-2

Figure 2.6-3. Location of Wells Used to Define Hydrologic Parameters for Culebra Dolomite.

Table 2.6-1. Parameter Values for Culebra Dolomite Member of Rustler Formation

Parameter	Median	Range		Units	Distribution Type	Source
Density						
Dolomite, grain (ρ_g)	2.82×10^3	2.78×10^3	2.86×10^3	kg/m^3	Normal	Kelley and Saulnier, 1990, Tables 4.1, 4.2, 4.3
Clay, bulk (ρ_b)	2.5×10^3			kg/m^3	Constant	Siegel, 1990
Dispersivity,						
longitudinal (α_L)	1×10^2	5×10^1	3×10^2	m	Cumulative	Lappin et al.,1989, Table E-6
transverse (α_T)	1×10^1	5	3×10^1	m	Cumulative	Lappin et al., 1989, Table E-6
Fracture spacing (2B)	4×10^{-1}	6×10^{-2}	8	m	Cumulative	Beauheim et al., June 10, 1991, Memo (see Appendix A)
Clay filling fraction (b_c/b)	0.5	0.1	0.9	none	Normal	Siegel, 1990
Heads	9.32×10^2	9×10^2	9.4×10^2	m	Spatial	See text.
Hydraulic Conductivity						
Avg. pathway - 5 k	1.4574×10^{-6}	1.77×10^{-7}	1.2×10^{-5}	m/s	Lognormal	
Partition Coefficients						
Matrix						
Am	1.86×10^{-1}	0.0	1×10^2	m^3/kg	Cumulative	See text.
Cm	1.86×10^{-1}	0.0	1×10^2	m^3/kg	Cumulative	See text.
Np	4.8×10^{-2}	0.0	1×10^2	m^3/kg	Cumulative	See text.
Pb	1×10^{-2}	0.0	1×10^1	m^3/kg	Cumulative	See text.
Pu	2.61×10^{-1}	0.0	1×10^2	m^3/kg	Cumulative	See text.
Ra	1×10^{-2}	0.0	1×10^1	m^3/kg	Cumulative	See text.
Th	1×10^{-2}	0.0	1	m^3/kg	Cumulative	See text.
U	2.58×10^{-2}	0.0	1	m^3/kg	Cumulative	See text.
Fracture						
Am	9.26×10^1	0.0	1×10^3	m^3/kg	Cumulative	See text.
Cm	9.26×10^1	0.0	1×10^3	m^3/kg	Cumulative	See text.
Np	1	0.0	1×10^3	m^3/kg	Cumulative	See text.
Pb	1×10^{-1}	0.0	1×10^2	m^3/kg	Cumulative	See text.
Pu	2.02×10^2	0.0	1×10^3	m^3/kg	Cumulative	See text.
Ra	3.41×10^{-2}	0.0	1×10^2	m^3/kg	Cumulative	See text.
Th	1×10^{-1}	0.0	1×10^1	m^3/kg	Cumulative	See text.
U	7.5×10^{-3}	0.0	1	m^3/kg	Cumulative	See text.
Porosity						
Fracture (ϕ_f)	1×10^{-3}	1×10^{-4}	1×10^{-2}	none	Lognormal	Lappin et al.,1989, Table 1-2, Table E-6
Matrix (ϕ_m)	1.39×10^{-1}	9.6×10^{-2}	2.08×10^{-1}	none	Data	Kelley and Saulnier, 1990, Table 4.4
Storage coefficient (S)	2×10^{-5}	5×10^{-6}	5×10^{-4}	none	Cumulative	LaVenue et al.,1990, p. 2-18; Haug et al.,1987
Thickness (Δz)	7.7	5.5	1.13×10^1	m	Spatial	LaVenue et al.,1988, Table B-1
Tortuosity (τ)						
Dolomite	1.2×10^{-1}	3×10^{-2}	3.3×10^{-1}	none	Data	Kelley and Saulnier, 1990, Table 4.6; Lappin et al.,1989, Table E-9
Clay	1.2×10^{-2}	3×10^{-3}	3.3×10^{-2}	none	Cumulative	Kelley and Saulnier, 1990, Table 4.6; Lappin et al., 1989, Table E-9
Transmissivity	-4.9	-3.5	-8.9	log (m^2/s)	Spatial	See text.

2.6.1 Density

Parameter:	**Density, grain (ρ_g): Dolomite**
Median:	2.82×10^3
Range:	2.78×10^3
	2.86×10^3
Units:	kg/m^3
Distribution:	Normal
Source(s):	Kelley, V. A., and G. J. Saulnier, Jr. 1990. *Core Analysis for Selected Samples from the Culebra Dolomite at the Waste Isolation Pilot Plant Site.* SAND90-7011. Albuquerque, NM: Sandia National Laboratories. (Tables 4.1, 4.2, and 4.3)

Parameter:	**Density, bulk (ρ_b): Clay**
Median:	2.5×10^3
Range:	None
Units:	kg/m^3
Distribution:	Constant
Source(s):	Siegel, M. D. 1990. "Representation of Radionuclide Retardation in the Culebra Dolomite in Performance Assessment Calculations," Memo 3a in Appendix A of Rechard et al. 1990. *Data Used in Preliminary Performance Assessment of the Waste Isolation Pilot Plant (1990).* SAND89-2408. Albuquerque, NM: Sandia National Laboratories.

Discussion:

The grain density (ρ_g) of the Culebra Dolomite Member was evaluated for 73 core samples from 20 boreholes. For the 20 boreholes, the average and median are 2,815 kg/m^3 (175.7 lb/ft^3) with a range between 2,792 and 2,835 kg/m^3 (174.3 and 177.0 lb/ft^3). The 73 values varied between 2,780 and 2,840 kg/m^3 (173.5 and 177.3 lb/ft^3) with an average of 2,810 kg/m^3 (173.4 lb/ft^3) and a median of 2,830 kg/m^3 (176.7 lb/ft^3) (Kelley and Saulnier, 1990, Tables 4.1, 4.2, and 4.3).

The bulk density (ρ_b) of the minerals (gypsum and corrensite) lining the fractures of the Culebra Dolomite is 2500 kg/m^3 (156 lb/ft^3) (Siegel, 1990).

Figure 2.6-4 shows the spatial variation of density in Culebra based on averages from 20 boreholes.

Table 2.6-2 provides the average grain density of intact dolomite at 20 wells in the Culebra Dolomite Member.

Table 2.6-2. Average Grain Density of Intact Dolomite at 20 Wells in Culebra Member (Kelly and Saulnier, 1990, Tables 4.1 and 4.3)

Well ID	Average Grain Density* (kg/m^3)
H3B3	2.728×10^3
H2B	2.7925×10^3
H10B	2.7933×10^3
H11	2.795×10^3
WIPP30	2.8067×10^3
H2A	2.81×10^3
WIPP12	2.81×10^3
H2B1	2.8125×10^3
H3B2	2.815×10^3
H5B	2.815×10^3
WIPP26	2.8167×10^3
AEC8	2.8233×10^3
H7B2	2.83×10^3
H7C	2.83×10^3
WIPP28	2.83×10^3
H11B3	2.835×10^3
WIPP13	2.835×10^3
H6B	2.8375×10^3
H7B1	2.84×10^3
H4B	2.845×10^3

*Average of measurements from indicated well

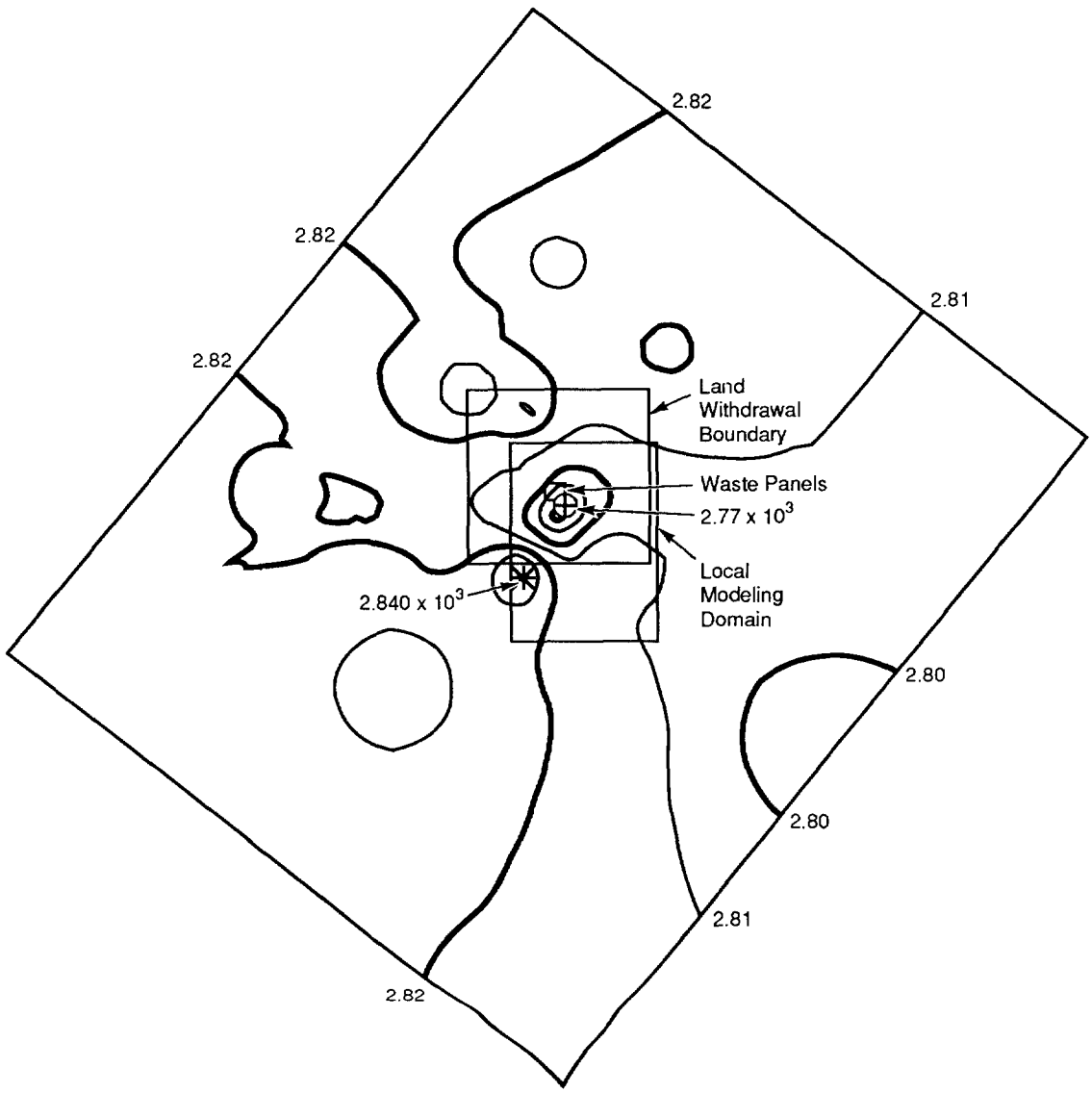

Figure 2.6-4. Spatial Variation of Grain Density in Culebra Based on Averages from 20 Boreholes.

2.6.2 Dispersivity

Parameter:	**Dispersivity, longitudinal (α_L)**
Median:	1×10^2
Range:	5×10^1
	3×10^2
Units:	m
Distribution:	Cumulative
Source(s):	Lappin, A. R., R. L. Hunter, D. P. Garber, and P. B. Davies, eds. 1989. *Systems Analysis Long-Term Radionuclide Transport, and Dose Assessments, Waste Isolation Pilot Plant (WIPP), Southeastern New Mexico; March 1989.* SAND89-0462. Albuquerque, NM: Sandia National Laboratories. (Table E-6)

Parameter:	**Dispersivity, transverse (α_T)**
Median:	1×10^1
Range:	5
	3×10^1
Units:	m
Distribution:	Cumulative
Source(s):	Lappin, A. R., R. L. Hunter, D. P. Garber, and P. B. Davies, eds. 1989. *Systems Analysis Long-Term Radionuclide Transport, and Dose Assessments, Waste Isolation Pilot Plant (WIPP), Southeastern New Mexico; March 1989.* SAND89-0462. Albuquerque, NM: Sandia National Laboratories. (Table E-6)

Discussion:

For moderate travel distances (on the order of kilometers), longitudinal dispersivity (α_L) roughly varies between 0.01 and 0.1 of the mean travel distance of the solute (Lallemand-Barres and Peaudecerf, 1978; Pickens and Grisak, 1981). As first adopted by Lappin et al. (1989), the PA Division has assumed α_L can vary between 50 and 300 m (164 and 984 ft) with a median value of 100 m (328 ft). The distribution for α_L is shown in Figure 2.6-5.

Transverse dispersivity (α_T) is usually linearly related to α_L. The ratio of α_L to α_T typically varies between 5 and 20 (see, for example, Bear and Verruijt, 1987; Freeze and Cherry, 1979, Figure 9.6; Dullien, Figure 7.13). However, at very low velocities the ratio can approach 1, while in some strata the ratio has been reported to approach 100 (de Marsily, 1986). Transverse dispersivity was assumed to be ten times smaller than α_L ($\alpha_T \sim 0.1\alpha_L$) for PA transport calculations. The current range for sensitivity studies is 1 to 25 (Figure 2.6-6).

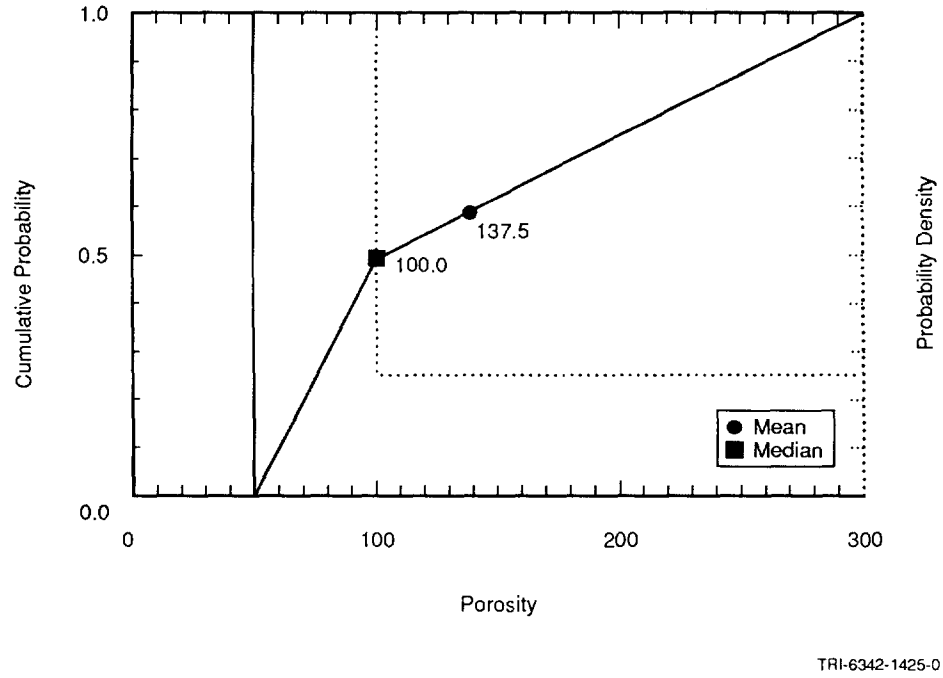

Figure 2.6-5. Estimated Distribution (pdf and cdf) for Longitudinal Dispersivity, Culebra Dolomite Member.

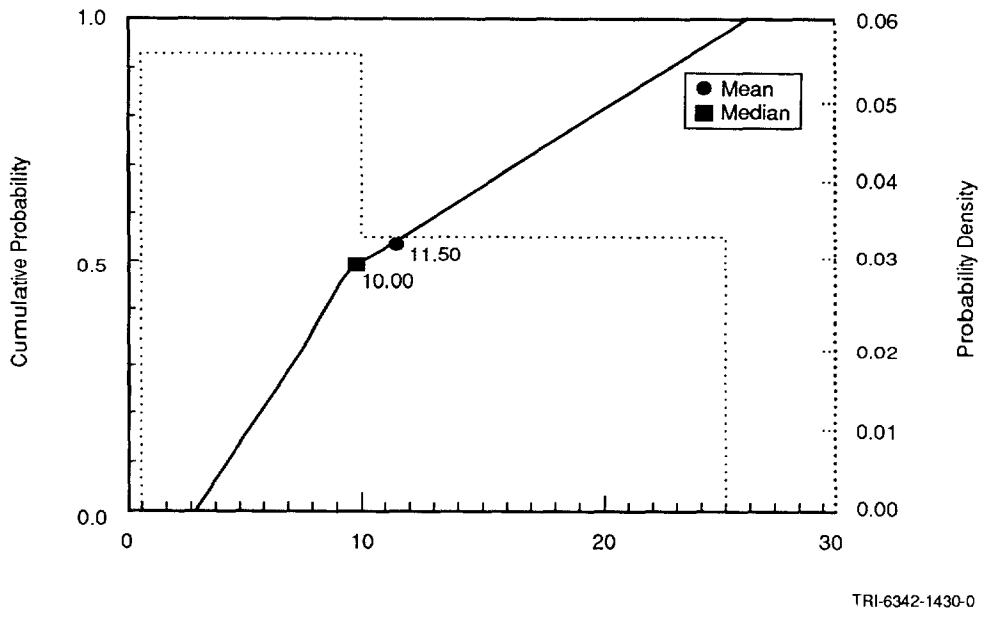

Figure 2.6-6. Estimated Distribution (pdf and cdf) for Transverse Dispersivity, Culebra Dolomite Member.

2.6.3 Fraction of Clay Filling in Fractures

Parameter:	**Clay filling fraction** (b_c/b)
Median:	0.5
Range:	0.1
	0.9
Units:	Dimensionless
Distribution:	Normal
Source(s):	Siegel, M. D. 1990. "Representation of Radionuclide Retardation in the Culebra Dolomite in Performance Assessment Calculations," Memo 3a in Appendix A of Rechard et al. 1990. *Data Used in Preliminary Performance Assessment of the Waste Isolation Pilot Plant (1990).* SAND89-2408. Albuquerque, NM: Sandia National Laboratories.

Discussion:

Within fractures of the Culebra Dolomite Member, gypsum and corrensite (alternating layers of chlorite and smectite) are observed. To evaluate the retardation of radionuclides within the fractures (caused by interaction with this material lining the fractures), the fraction of lining material (b_c/b) is needed, where b_c is the total thickness of clays and b is fracture aperture. At present, data are not available to estimate the true range or distribution of b_c/b in the Culebra. Siegel (1990) recommended a normal distribution with a maximum of 0.9 and a minimum of 0.1. Current PA calculations used a median of 0.5 to estimate the fracture retardation.

Figure 2.6-7 shows the estimated distribution for the fraction of clay filling.

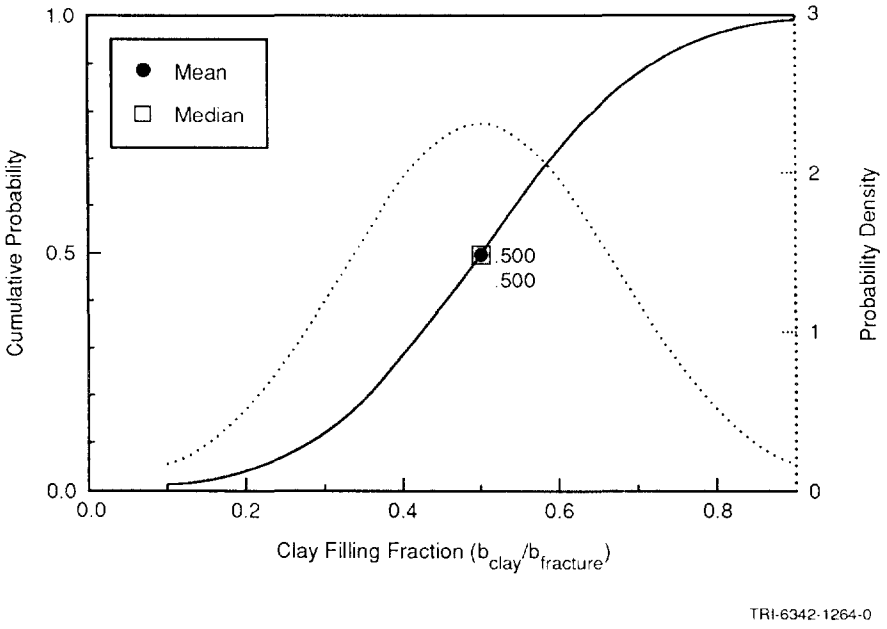

Figure 2.6-7. Estimated Distribution (pdf and cdf) for Clay Filling Fraction, Culebra Dolomite Member.

2.6.4 Porosity

Fracture Porosity

Parameter:	**Fracture porosity (ϕ_f)**
Median:	1×10^{-3}
Range:	1×10^{-4}
	1×10^{-2}
Units:	Dimensionless
Distribution:	Lognormal
Source(s):	Lappin, A. R., R. L. Hunter, D. P. Garber, and P. B. Davies, eds. 1989. *Systems Analysis Long-Term Radionuclide Transport, and Dose Assessments, Waste Isolation Pilot Plant (WIPP), Southeastern New Mexico; March 1989.* SAND89-0462. Albuquerque, NM: Sandia National Laboratories. (Table 1-2; Table E-6)

Discussion:

The fracture porosities interpreted from the tracer tests at the H-3 and H-11 hydropads are 2×10^{-3} (Kelley and Pickens, 1986) and 1×10^{-3}, respectively.

Both H-3 and H-11 lie near the expected transport pathway. The average value rounded to one significant figure was selected as the median and used for PA calculations. Similar to Lappin et al. (1989), the PA Division set the minimum and maximum one order of magnitude to either side of this median.

Figure 2.6-8 shows the estimated distribution for the fracture porosity.

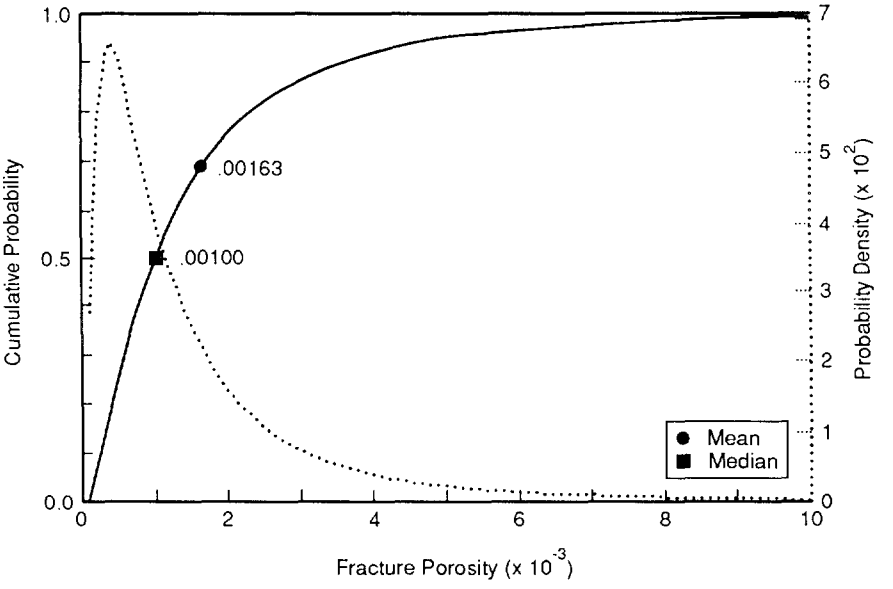

Figure 2.6-8. Estimated Distribution (pdf and cdf) for Fracture Porosity, Culebra Dolomite Member.

Matrix Porosity

Parameter:	**Matrix porosity (ϕ_m)**
Median:	1.39×10^{-1}
Range:	9.6×10^{-2}
	2.08×10^{-1}
Units:	Dimensionless
Distribution:	Data
Source(s):	Kelley, V. A., and G. J. Saulnier, Jr. 1990. *Core Analysis for Selected Samples from the Culebra Dolomite at the Waste Isolation Pilot Plant Site.* SAND90-7011. Albuquerque, NM: Sandia National Laboratories. (Table 4.4)
	Lappin, A. R., R. L. Hunter, D. P. Garber, and P. B. Davies, eds. 1989. *Systems Analysis Long-Term Radionuclide Transport, and Dose Assessments, Waste Isolation Pilot Plant (WIPP), Southeastern New Mexico; March 1989.* SAND89-0462. Albuquerque, NM: Sandia National Laboratories. (Table E-8)

Discussion:

Matrix porosity has been evaluated by the Boyles' law technique using helium or air on 79 samples taken from the *intact* portion of core from 20 borehole or hydropad locations near the WIPP and also by water-resaturation for 30 of the samples. The agreement between the two techniques was excellent with an r^2 of 0.99 (Kelley and Saulnier, 1990, p. 4-7). From the Boyles' law technique, an average porosity for the 20 wells of 0.139 was obtained, with a range of 0.096 to 0.208 (Kelley and Saulnier, 1990, Table 4.4). (Lappin et al., [1989, Table E-8] report an average of 0.153 with a range of 0.028 and 0.303 assuming each of the 79 measurements is independent.) For many of the wells, a large amount of core was lost in highly porous (vuggy) and/or fractured portions of the Culebra Dolomite Member. Thus only intact matrix porosity, the porosity not contributing to fluid flow in dual porosity computational models (e.g., STAFF2D or SWIFT [Rechard et al., 1989]) is reported here.

Table 2.6-3 provides a summary of porosity measurements of intact Culebra Dolomite at selected wells. Figure 2.6-9 shows the assumed density function for porosity of the Culebra Dolomite member. Figure 2.6-10 shows the spatial variation of the intact matrix porosity.

Table 2.6-3. Average of Porosity Measurements of Intact Culebra Dolomite at Selected Wells (after Kelley and Saulnier, 1990, Table 4.4)

Well ID	Median (m)	Low Range (m)	High Range (m)
AEC8	0.10333	0.05195	0.15471
H10B	0.0955	0.04228	0.14872
H11B	0.1618	0.00506	0.31854
H2A	0.1235	0.10512	0.14188
H2B	0.129	0.07576	0.18224
H2B1	0.1205	0.04391	0.19709
H3B2	0.178	0.15351	0.20249
H3B3	0.20775	0.14575	0.26975
H4B	0.2525	0.1435	0.3615
H5B	0.1784	0.04839	0.30841
H6B	0.11033	0.09884	0.12182
H7B1	0.2025	0.0733	0.3317
H7B2	0.1385	0.08829	0.18871
H7C	0.14433	0.1016	0.18706
WIPP12	0.1074	0.00213	0.21267
WIPP13	0.1796	0.03141	0.32779
WIPP25	0.115	0.115	0.115
WIPP26	0.12225	0.10606	0.13844
WIPP28	0.1616	0.10451	0.21869
WIPP30	0.16517	0.07372	0.25662

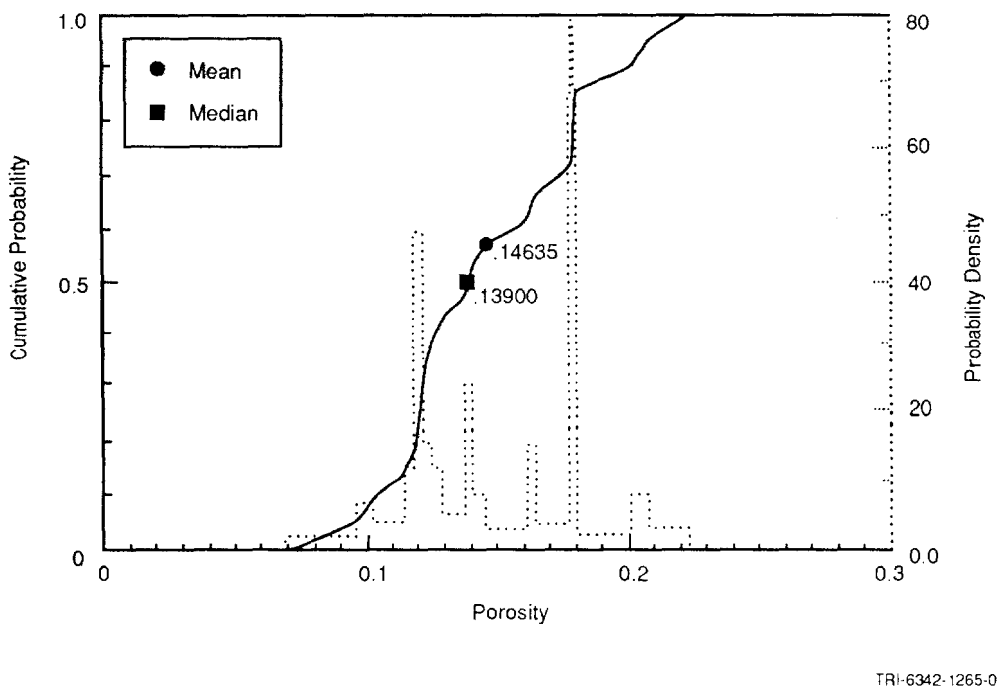

Figure 2.6-9. Assumed Distribution (pdf and cdf) for Intact Matrix Porosity of Culebra Dolomite Member Assuming No Spatial Correlation.

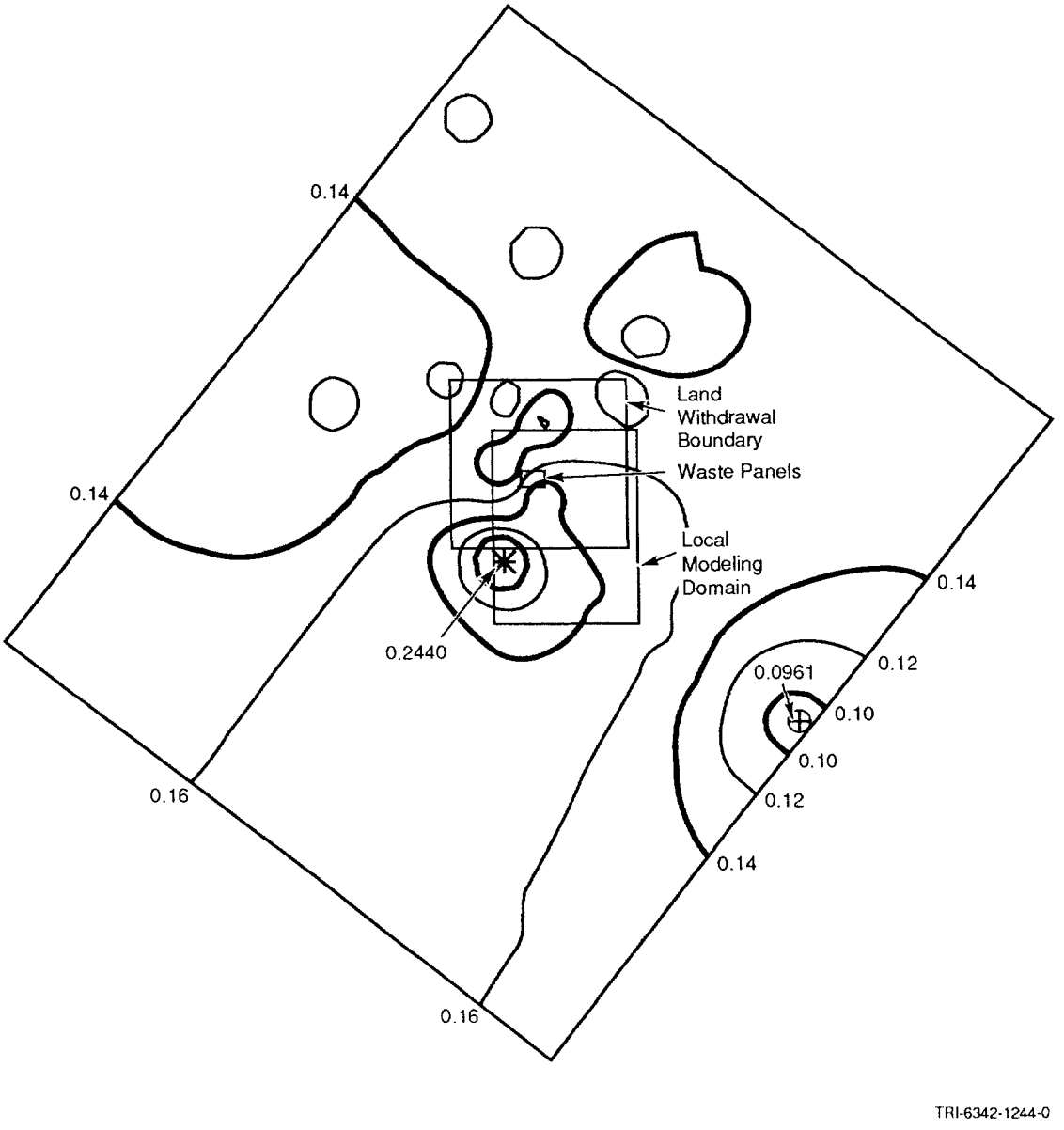

Figure 2.6-10. Variation of Intact Matrix Porosity of Culebra Dolomite Member as Estimated by 10 Nearest Neighbors Using Inverse-Distance-Squared Weighting.

Fracture Spacing

Parameter:	**Fracture spacing** (2B)
Median:	4×10^{-1}
Range:	6×10^{-2}
	8
Units:	m
Distribution:	Cumulative
Source(s):	Beauheim, R. L., T. F. Corbet, P. B. Davies, and J. F. Pickens. 1991. "Recommendations for the 1991 Performance Assessment Calculations on Parameter Uncertainty and Model Implementation for Culebra Transport Under Undisturbed and Brine-Reservoir-Breach Conditions." Internal memo to D. R. Anderson, June 10, 1991. Albuquerque, NM: Sandia National Laboratories. (In Appendix A of this volume).

Figure 2.6-11 shows the estimated distribution for fracture spacing.

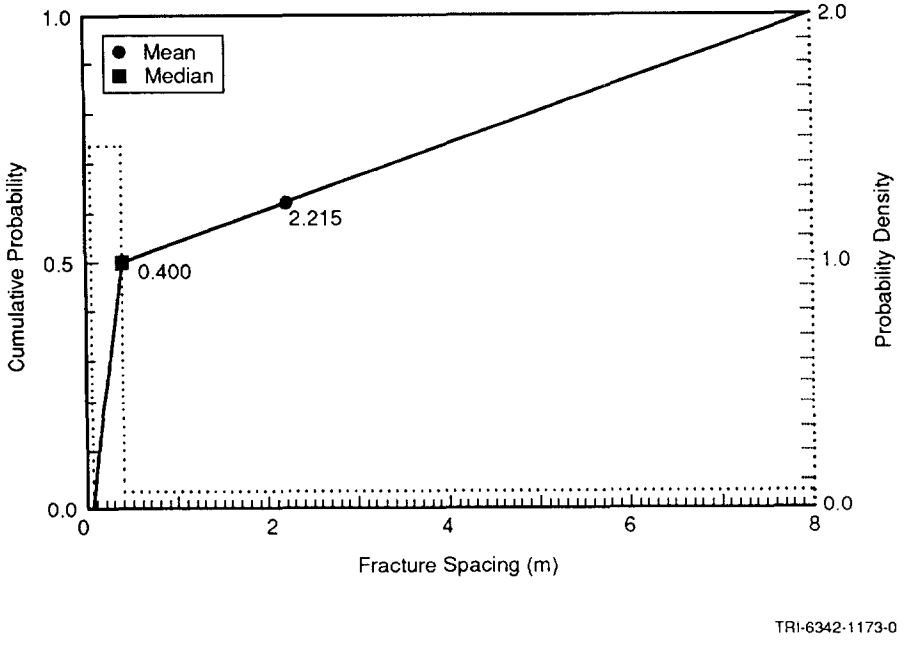

Figure 2.6-11. Estimated Distribution (pdf and cdf) for Culebra Fracture Spacing.

Discussion:

Both horizontal and vertical fracture sets have been observed in core samples, shaft excavations, and outcrops. A fracture spacing varying between 0.23 and 1.2 m (0.75 and 3.9 ft) has been interpreted for two travel paths at the H-3 borehole (Kelley and Pickens, 1986). Preliminary evaluation of the breakthrough curves for the H-6 borehole tracer test suggests a fracture spacing between 0.056 and 0.44 m (0.18 and 1.44 ft), and the H-11 borehole tracer test suggests a fracture spacing between 0.11 and 0.32 m (0.36 and 1.05 ft) (Beauheim et al., June 10, 1991 Memo [Appendix A]). From these data, Beauheim et al. (June 10, 1991, Memo [Appendix A]) suggested a minimum of 0.06 m (0.2 ft) and a maximum equivalent to the assumed uniform thickness of the Culebra (8 m [26.2 ft]). Finally, the average fracture spacing at the three wells (H-3, H-6, and H-11) is 0.4 m (1.3 ft).

2.6.5 Storage Coefficient

Parameter:	**Storage coefficient** (S)
Median:	2×10^{-5}
Range:	5×10^{-6}
	5×10^{-4}
Units:	Dimensionless
Distribution:	Cumulative
Source(s):	LaVenue, A. M., T. L. Cauffman, and J. F. Pickens. 1990. *Groundwater Flow Modeling of the Culebra Dolomite, Volume I: Model Calibration.* SAND89-7068/1. Albuquerque, NM: Sandia National Laboratories. (p. 2-18)
	Haug, A., V. A. Kelley, A. M. LaVenue, and J. F. Pickens. 1987. *Modeling of Groundwater Flow in the Culebra Dolomite at the Waste Isolation Pilot Plant (WIPP) Site: Interim Report.* Contractor Report SAND86-7167. Albuquerque, NM: Sandia National Laboratories.

Discussion:

Model studies of the Culebra (LaVenue et al., 1990, 1988; Haug et al., 1987) have used a storage coefficient (S) of 2×10^{-5}. The storage coefficient near the WIPP ranges over two orders of magnitude (5×10^{-6} to 5×10^{-4}) and is the basis for the range in Table 2.6-1. However, based on sparse well test data from 13 wells, the storage coefficient can range over four orders of magnitude (1×10^{-6} to 1×10^{-2}) in the Culebra (LaVenue et al., 1990, p. 2-18). Table 2.6-4 provides the storage coefficients at wells within the Culebra Dolomite Member. Figure 2.6-12 gives the estimated distribution for the storage coefficient. Figure 2.6-13 shows the spatial variation of the storage coefficient.

Table 2.6-4. Storage Coefficients at Wells within Culebra Dolomite Member (Cauffman et al., 1990, Table D.1)

Well ID	Storage Coefficients
H2	1.28×10^{-5}
H4	4.62×10^{-6}
H5	2.79×10^{-5}
H6	2.35×10^{-4}
H9	3.82×10^{-4}
H11	1.58×10^{-4}
H16	1×10^{-5}
P14	2×10^{-5}
USGS1	2×10^{-5}
WIPP25	1×10^{-2}
WIPP26	4.8×10^{-3}
WIPP27	1×10^{-6}
WIPP28	5×10^{-2}

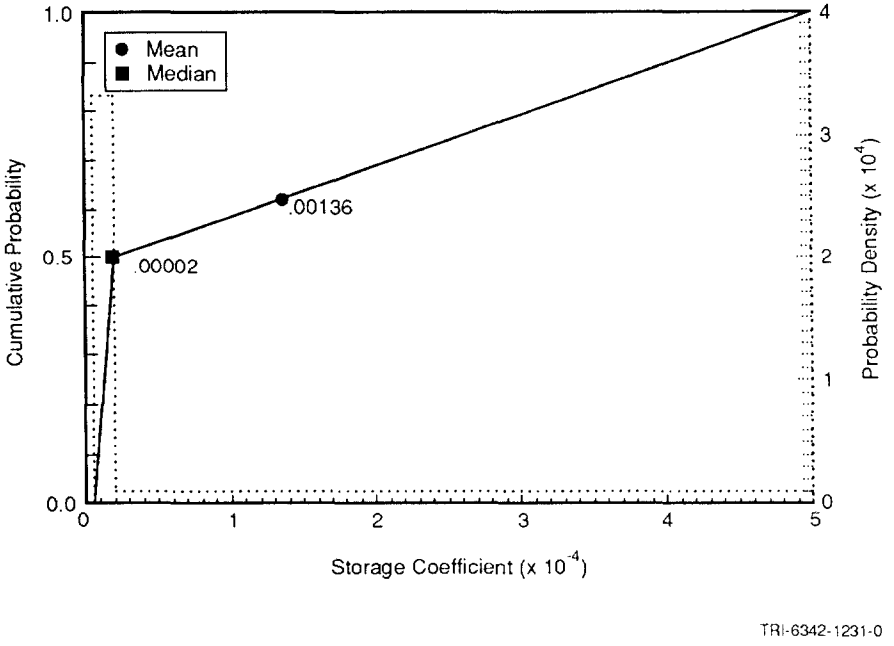

Figure 2.6-12. Estimated Distribution (pdf and cdf) for Storage Coefficient.

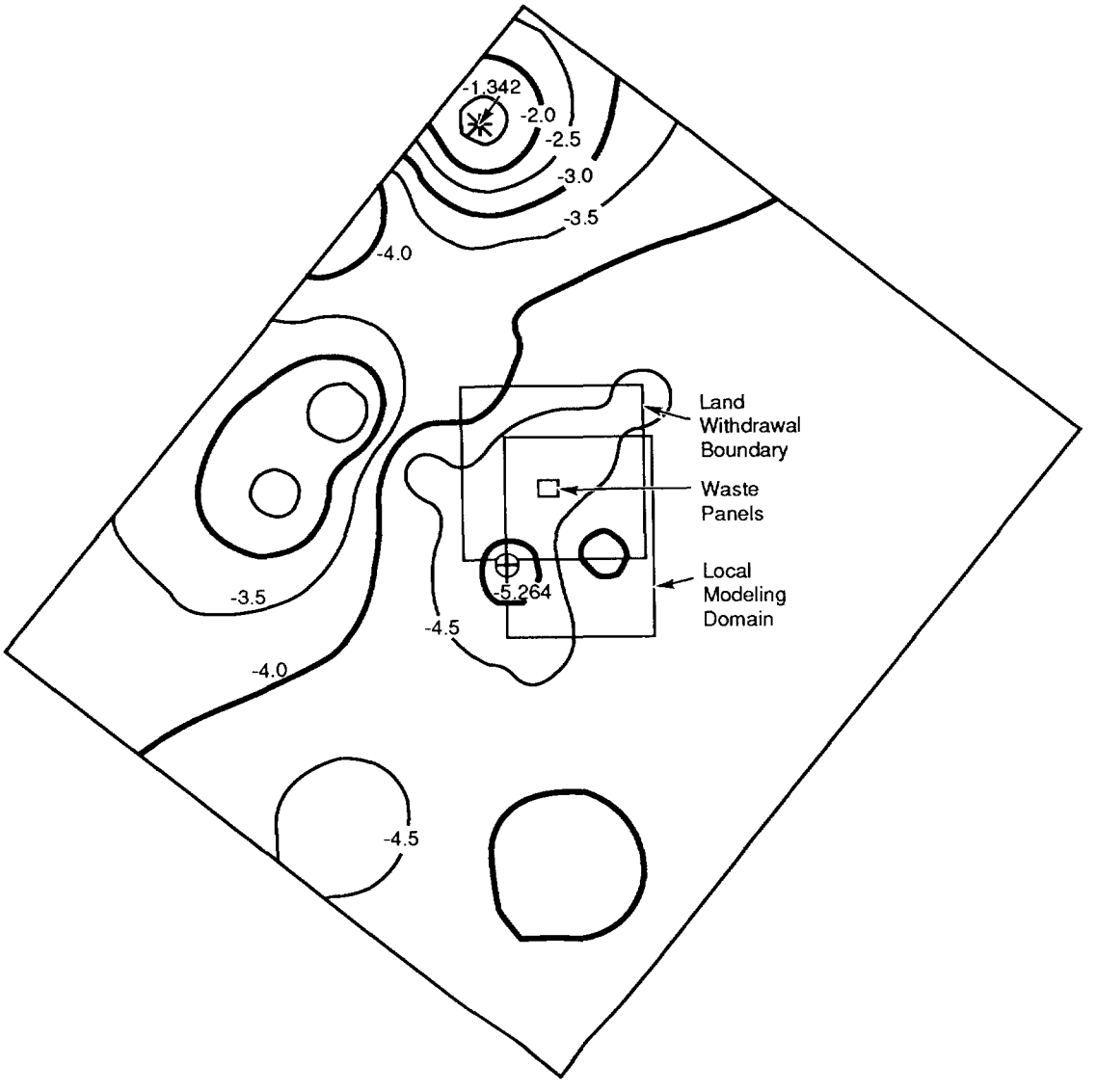

Figure 2.6-13. Spatial Variation of Logarithm of Storage Coefficients within Culebra.

2.6.6 Thickness

Parameter:	**Thickness** (Δz)
Median:	7.7
Range:	5.5
	11.3
Units:	m
Distribution:	Spatial
Source(s):	LaVenue, A. M., A. Haug, and V. A. Kelley. 1988. *Numerical Simulation of Ground-Water Flow in the Culebra Dolomite at the Waste Isolation Pilot Plant (WIPP) Site: Second Interim Report.* SAND88-7002. Albuquerque, NM: Sandia National Laboratories. (Table B-1)

Discussion:

The Culebra thickness reported in Table 2.6-1 is the constant thickness used in modeling studies reported by LaVenue et al. (1988, 1990) and used in PA calculations. Figure 2.6-14 shows the spatial variation of thickness (Δz) in the Culebra Dolomite Member estimated by kriging followed by two passes of a moving average of 15 nearest neighbors with a center weight of zero on a 500-m (1,635-ft) grid.

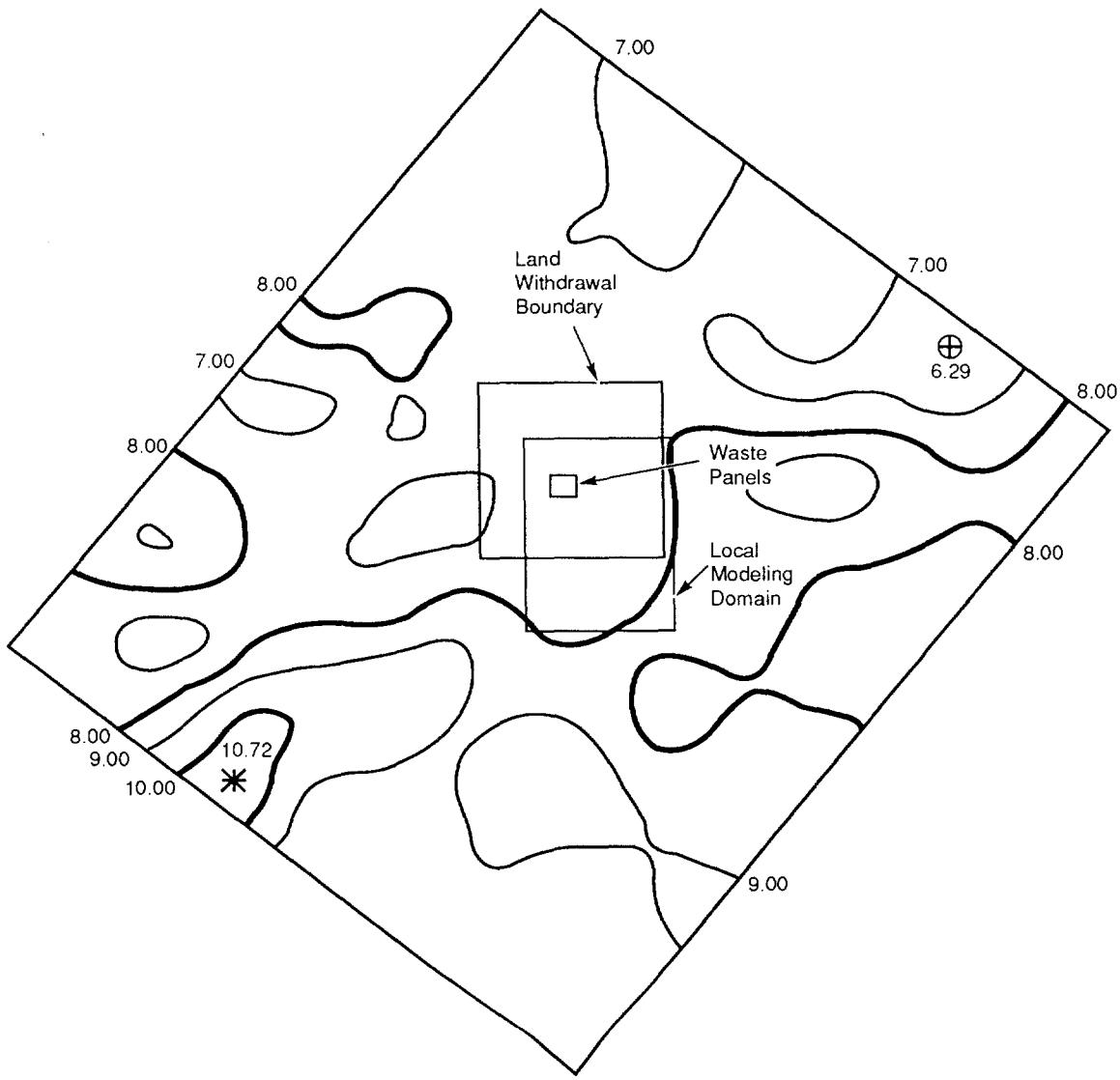

Figure 2.6-14. Variation of Culebra Member Thickness in Regional Modeling Domain. Estimate used kriging followed by two passes of a moving average of 15 nearest neighbors with a center weight of zero on a 500-m grid.

2.6.7 Tortuosity

Parameter:	**Matrix tortuosity (τ), Dolomite**
Median:	1.2×10^{-1}
Range:	3×10^{-2}
	3.3×10^{-1}
Units:	Dimensionless
Distribution:	Data
Source(s):	Kelley, V. A., and G. J. Saulnier, Jr. 1990. *Core Analysis for Selected Samples from the Culebra Dolomite at the Waste Isolation Pilot Plant Site.* SAND90-7011. Albuquerque, NM: Sandia National Laboratories. (Table 4.6)
	Lappin, A. R., R. L. Hunter, D. P. Garber, and P. B. Davies, eds. 1989. *Systems Analysis Long-Term Radionuclide Transport, and Dose Assessments, Waste Isolation Pilot Plant (WIPP), Southeastern New Mexico; March 1989.* SAND89-0462 Albuquerque, NM: Sandia National Laboratories. (Table E-9)

Parameter:	**Tortuosity in clay lining (τ_{clay})**
Median:	1.2×10^{-2}
Range:	3×10^{-3}
	3.3×10^{-2}
Units:	Dimensionless
Distribution:	Cumulative
Source(s):	See text.

Figure 2.6-15 shows the measured distribution for Culebra Dolomite Member tortuosity. Figures 2.6-16 gives the variation of matrix tortuosity measured from intact core samples of the Culebra Dolomite Member.

Discussion:

Intact Matrix Tortuosity. Intact matrix tortuosity is used to evaluate the effective molecular diffusion coefficient (D_m) from the coefficient of molecular diffusion ($D^{\square}$) in the pure saturating fluid ($D_m = \tau D^{\square}$), where τ equals $(\ell/\ell_{path})^2$, ℓ is the linear length, and ℓ_{path} is the length of the [tortuous] path that a fluid particle would take (Bear, 1972, p. 111).

Intact matrix tortuosity for the Culebra Dolomite Member was calculated from 15 core samples from 15 borehole locations using the helium porosity (ϕ_m) and a formation factor (R_ℓ/R_m) determined from electrical-resistivity measurements as follows: $\tau_m^2 = [(1/\phi_m)(R_\ell/R_m)]$, where R_m is the intact porous media saturated with a fluid of resistivity, R_ℓ. (For the Culebra core samples, a 100-g NaCl solution was used with an ambient pressure of 1.4 MPa.) Kelley and Saulnier (1990) state that "... the formation factor (R_ℓ/R_m)

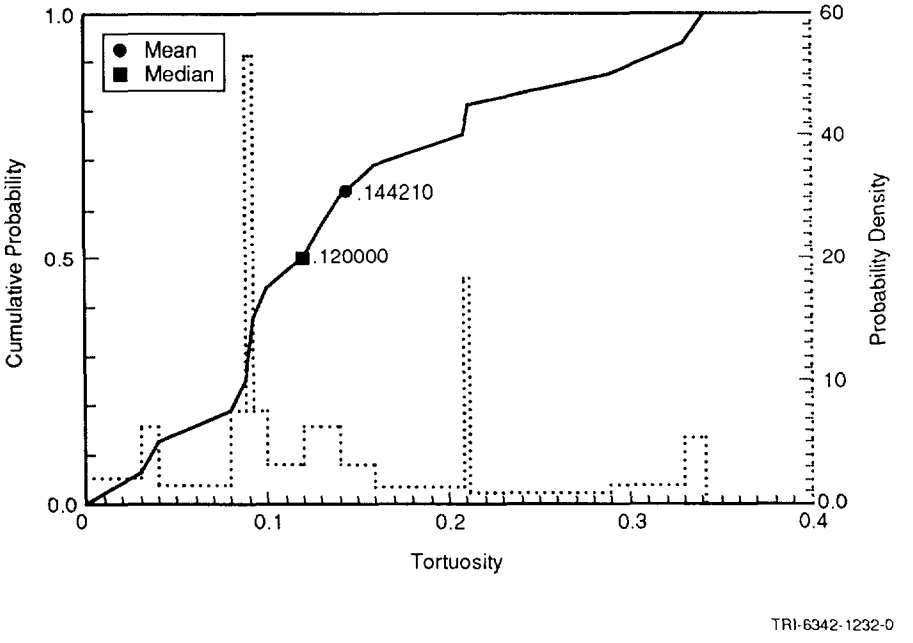

Figure 2.6-15. Measured Distribution (pdf and cdf) for Tortuosity of Culebra Matrix.

determined from electrical-resistivity measurements is usually smaller than that determined by diffusion studies." The values range from 0.03 to 0.33 with a median of 0.12 and an average of 0.14 (Kelley and Saulnier, 1990, Table 4.6; Lappin et al., 1989, Table E-9) (Figure 2.6-9). The spatial variation of tortuosity is shown in Figure 2.6-16. Within the local transport modeling domain, the tortuosity is near the median, 0.12.

Matrix Skin Resistance and Clay Tortuosity. In the dual porosity mathematical model implemented by STAFF2D (Rechard et al., 1989), the boundary condition for the matrix at the fracture matrix interface (Figure 2.6-17) is given by

$$C_i'(B,T) = C_i - \zeta D_n^* \frac{\partial C'}{\partial x}$$

where

C_i', C_i = concentrations of the ith nuclide in the matrix and fracture, respectively
$2B$ = the fracture spacing
D_n^* = diffusion coefficient in matrix
ζ = a parameter characterizing the resistance of a thin skin (e.g., clay lining adjacent to the fracture).

ζ is defined by

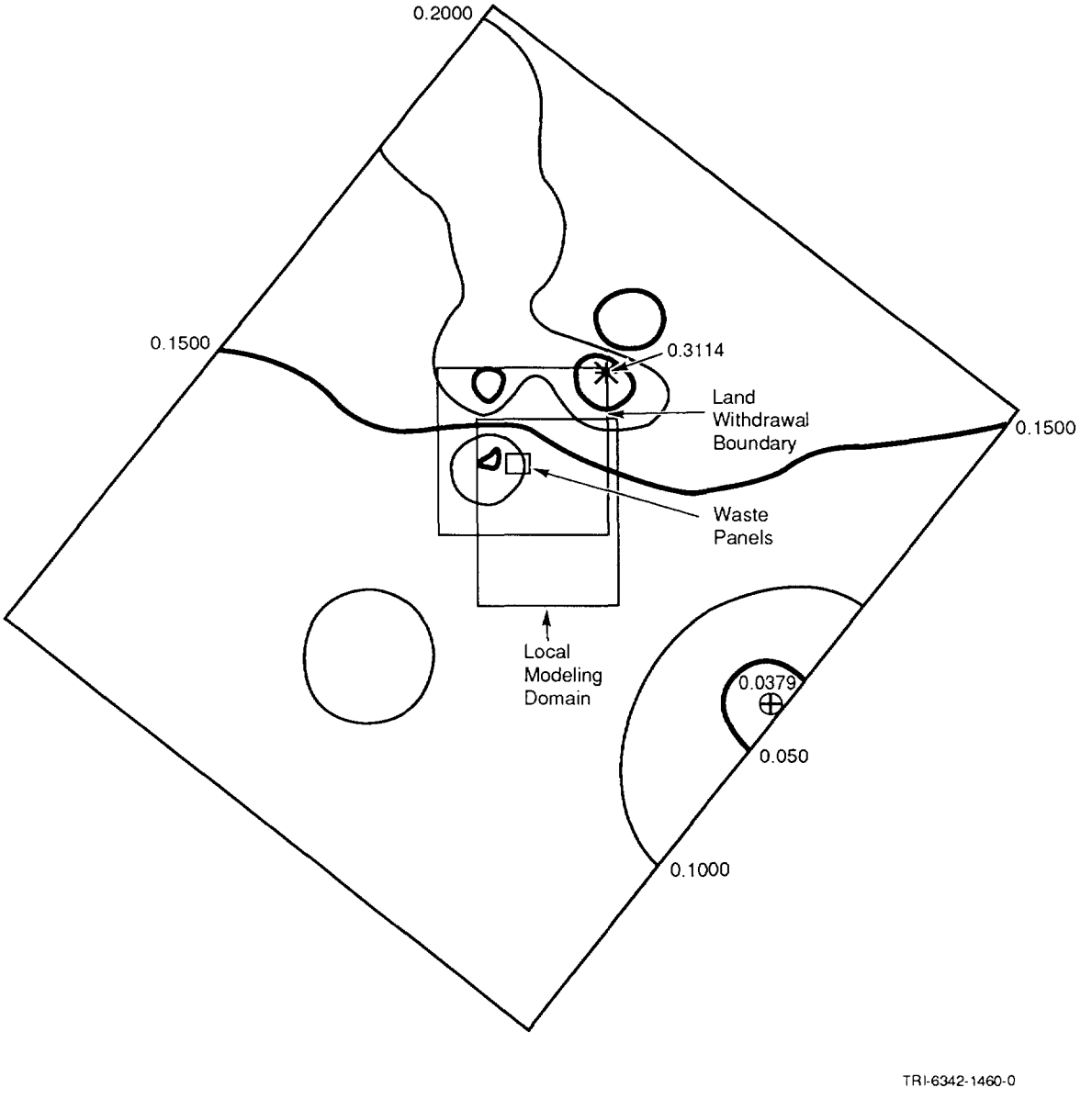

Figure 2.6-16. Variation of Matrix Tortuosity Measured from Intact Core Samples of Culebra Dolomite Member by 10 Nearest Neighbors Using Inverse-Distance-Squared Weighting.

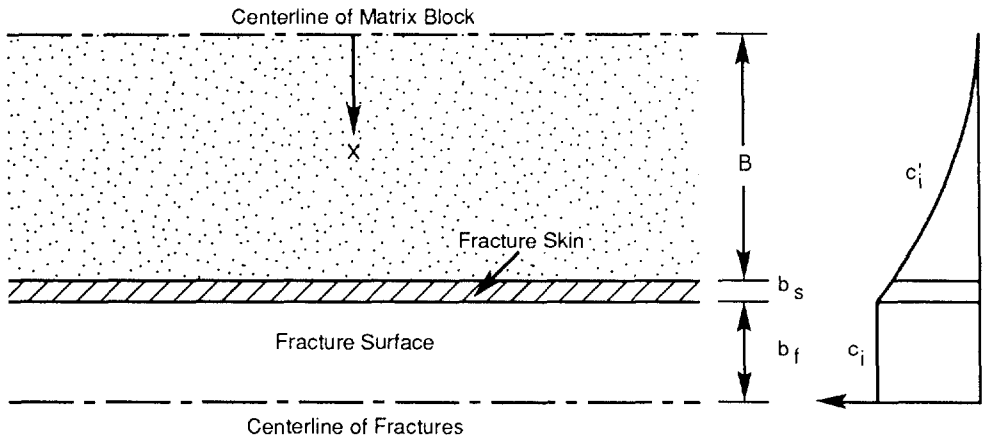

Figure 2.6-17. Boundary Condition for the Matrix at the Fracture Matrix Interface.

$$\zeta = \frac{b_s}{D_s}$$

where

b_s = the skin thickness
D_s = skin diffusion coefficient

For the current PA calculations, the following estimate of the skin resistance is used because of the clay lining in the fractures:

$$\zeta = \frac{f\phi_f(B + b_f)}{\tau_{clay} D^{\alpha}}$$

where

f = clay lining, fracture aperature ratio (b_s/b_f)
ϕ_f = fracture or secondary porosity ($b_f/[B + b_f]$) ~ b_f/B, $B >> b_f$

and as defined above, the diffusion coefficient D_s is skin (e.g., clay),

$$D_s = \tau_{clay} D^{¤}$$

where

τ_{clay} = tortuosity of clay lining
$D^{¤}$ = full molecular diffusion coefficient in the pure saturating fluid.

For 1991 PA calculations, the clay tortuosity is assumed to be one order of magnitude smaller than the Culebra Dolomite Member matrix tortuosity consistent with the generally observed apparent diffusion coefficients in clayey materials (i.e., 0.012). This conservative assumption reduces the amount of contaminants moving through the clay lining and ultimately being absorbed onto the matrix. Furthermore, only the median value of the molecular diffusion coefficient for the actinides was used (Section 3.3.6), rather than a value for each separate contaminant.

2.6.8 Freshwater Heads at Wells

Table 2.6-5 provides the freshwater head measurements in the Culebra Dolomite Member.

Table 2.6-5. Summary of Selected Steady-State Freshwater Head Measurements in Culebra Dolomite Member (after Cauffman et al., 1990, Table 6.2)

Well ID	Median (m)	Low Range (m)	High Range (m)
AEC7	9.3200×10^2	9.3014×10^2	9.3386×10^2
CABIN1	9.1120×10^2	9.0980×10^2	9.1260×10^2
D268	9.1520×10^2	9.1462×10^2	9.1578×10^2
DOE1	9.1390×10^2	9.0831×10^2	9.1949×10^2
DOE2	9.3530×10^2	9.3181×10^2	9.3880×10^2
H1	9.2330×10^2	9.1860×10^2	9.2796×10^2
H10B	9.2140×10^2	9.1627×10^2	9.2653×10^2
H11B1	9.1280×10^2	9.1000×10^2	9.1560×10^2
H12	9.1360×10^2	9.1080×10^2	9.1640×10^2
H14	9.1550×10^2	9.1457×10^2	9.1643×10^2
H15	9.1560×10^2	9.1234×10^2	9.1886×10^2
H17	9.1100×10^2	9.0890×10^2	9.1310×10^2
H18	9.3190×10^2	9.2887×10^2	9.3493×10^2
H2C	9.2400×10^2	9.2167×10^2	9.2633×10^2
H3B1	9.1710×10^2	9.1267×10^2	9.2153×10^2
H4B	9.1280×10^2	9.1140×10^2	9.1420×10^2
H5B	9.3400×10^2	9.3074×10^2	9.3726×10^2
H6B	9.3260×10^2	9.3027×10^2	9.3493×10^2
H7B1	9.1270×10^2	9.1200×10^2	9.1340×10^2
H8B	9.1240×10^2	9.1147×10^2	9.1333×10^2
H9B	9.0820×10^2	9.0680×10^2	9.0960×10^2
P14	9.2690×10^2	9.2480×10^2	9.2900×10^2
P15	9.1680×10^2	9.1494×10^2	9.1866×10^2
P17	9.1160×10^2	9.0997×10^2	9.1323×10^2
USGS1	9.0980×10^2	9.0922×10^2	9.1038×10^2
USGS4	9.0970×10^2	9.0947×10^2	9.0993×10^2
USGS8	9.1110×10^2	9.1087×10^2	9.1133×10^2
WIPP12	9.3310×10^2	9.3147×10^2	9.3473×10^2
WIPP13	9.3400×10^2	9.3120×10^2	9.3680×10^2
WIPP18	9.3000×10^2	9.2720×10^2	9.3280×10^2
WIPP25	9.2870×10^2	9.2637×10^2	9.3103×10^2
WIPP26	9.1940×10^2	9.1882×10^2	9.1998×10^2
WIPP27	9.3810×10^2	9.3647×10^2	9.3973×10^2
WIPP28	9.3700×10^2	9.3467×10^2	9.3933×10^2
WIPP29	9.0540×10^2	9.0482×10^2	9.0598×10^2
WIPP30	9.3510×10^2	9.3254×10^2	9.3766×10^2

2.6.9 Transmissivities for Wells

Table 2.6-6 provides the logarithms of selected transmissivity measurements in the Culebra Dolomite Member (Cauffman et al., 1990, Table C.1). Table 2.6-7 provides the logarithms of the calibrating points.

Table 2.6-6. Logarithms of Selected Transmissivity Measurements in Culebra Dolomite Member (after Cauffman et al., 1990, Table C.1)

Well ID	Median	Low Range	High Range
AEC7	-6.5535	-7.7185	-5.3885
CABIN1	-6.5213	-7.6863	-5.3563
D268	-5.6897	-6.8547	-4.5247
DOE1	-4.4271	-5.0096	-3.8466
DOE2	-4.0191	-4.6016	-3.4366
ENGLE	-4.3350	-4.9175	-3.7525
ERDA9	-6.2964	-7.4614	-5.1314
H1	-6.0290	-7.1940	-4.8640
H10B	-7.1234	-8.2884	-5.9584
H11B1	-4.5057	-5.0882	-3.9232
H12	-6.7132	-7.8782	-5.5482
H14	-6.4842	-7.6492	-5.3192
H15	-6.3804	-7.5454	-5.2154
H16	-6.1149	-7.2799	-4.9499
H17	-6.6361	-7.8011	-5.4471
H18	-5.7775	-6.3600	-5.1950
H2B1	-6.2005	-6.7830	-5.6180
H3	-5.6089	-6.1914	-5.0264
H4B	-5.9960	-6.5785	-5.4135
H5B	-7.0115	-7.5940	-6.4290
H6B	-4.4500	-5.0325	-3.8675
H7B1	-2.8125	-3.3950	-2.2300
H8B	-5.0547	-5.6372	-4.4722
H9B	-3.9019	-4.4844	-3.3194
USGS1	-3.2584	-3.8409	-2.6759
WIPP12	-6.9685	-8.1355	-5.8035
WIPP13	-4.1296	-5.2946	-2.9646
WIPP18	-6.4913	-7.6563	-5.3263
WIPP19	-6.1903	-7.3553	-5.0253
WIPP21	-6.5705	-7.7355	-5.4055
WIPP22	-6.4003	-7.5653	-5.2353
WIPP25	-3.5412	-4.1237	-2.9587
WIPP26	-2.9136	-3.4961	-2.3311

Table 2.6-6. Logarithms of Selected Transmissivity Measurements in Culebra Dolomite Member (after Cauffman et al., 1990, Table C.1) (Concluded)

Well ID	Median	Low Range	High Range
WIPP27	-3.3692	-3.9517	-2.7867
WIPP28	-4.6839	-5.2664	-4.1014
WIPP29	-2.9685	-3.5510	-2.3860
WIPP30	-6.6023	-7.7673	-5.4373
P14	-3.5571	-4.5124	-2.6018
P15	-7.0354	-8.2004	-5.8704
P17	-5.9685	-7.1335	-4.8035
P18	-1.0123×10^{1}	-1.1288×10^{1}	-8.9584

Table 2.6-7. Logarithms of Transmissivity of Calibrating Points (Pilot Points) for Culebra Dolomite Member (after Davies and LaVenue, 1990)

Well ID	Median	Low Range	High Range
PP1	-2.0700	-4.4233	2.833×10^{-1}
PP2	-2.2500	-4.5334	3.340×10^{-2}
PP3	-2.3200	-4.6267	-1.330×10^{-2}
PP4	-3.6200	-5.3442	-1.8958
PP5	-3.5800	-5.2576	-1.9024
PP6	-6.0200	-7.7675	-4.2725
PP7	-6.4200	-8.0044	-4.5656
PP8	-3.4100	-4.8779	-1.9421
PP9	-2.7100	-3.8913	-1.5217
PP11	-7.7200	-9.1413	-6.2987
PP12	-8.0800	-9.0353	-7.1247
PP13	-5.6400	-6.5953	-4.6847
PP14	-8.3400	-9.7846	-6.8954
PP15	-6.4900	-7.7482	-5.2318
PP16	-5.1300	-6.5280	-3.7320
PP17	-6.6000	-8.1378	-5.0622
PP18	-2.6300	-4.5173	-7.427×10^{-1}
PP19	-2.8600	-4.7939	-9.261×10^{-1}
PP20a	-2.9400	-4.8972	-9.828×10^{-1}
PP21a	-3.0000	-4.8407	-1.1593
PP23	-3.8500	-5.1548	-2.5452
PP24	-3.5000	-4.2689	-2.7311
PP25	-6.0000	-7.0718	-4.9282
PP26	-5.5000	-6.3388	-4.6612
PP27	-4.2500	-5.3684	-3.1316
PP28	-3.5000	-4.7582	-2.2418
PP29	-3.2500	-4.3451	-2.1549
PP30	-6.1600	-7.3250	-4.9950
PP31	-5.8700	-7.0350	-4.7050
PP32	-5.0000	-5.7223	-4.2777
PP34	-3.5900	-4.5453	-2.6347
PP35	-2.6700	-3.6253	-1.7147
PP36	-5.1700	-6.0787	-4.2613
PP37	-4.3100	-6.0342	-2.5858
PP38	-3.9000	-5.3446	-2.4554
PP39	-3.9000	-5.3446	-2.4554
PP40	-5.9300	-6.8853	-4.9747
PP41	-4.0000	-4.9553	-3.0447
PP42	-3.5000	-4.5951	-2.4049
PP43	-5.0000	-5.9553	-4.0447
PP44	-5.0000	-5.9553	-4.0447

2.6.10 Partition Coefficients and Retardations

A partitioning or distribution coefficient (K_d), which describes the intensity of sorption, is used to calculate the partitioning of species such as radionuclides between the groundwater and rock and, thereby, calculate the sorption capacity or retardation (R). A K_d value cannot be extrapolated with confidence to physiochemical conditions that differ from those under which the experimental data were obtained.

The recommended K_d cumulative distributions reported in Tables 2.6-8 and 2.6-9 are considered to be realistic in light of available data, but require a number of subjective assumptions that ongoing experiments may invalidate. The distributions were derived from an internal expert-judgment process regarding radionuclide retardation in the Culebra, which convened in April and May, 1991. The three Sandia experts involved were Robert G. Dosch (6212), Craig F. Novak (6344), and Malcolm D. Siegel (6315). The three experts participated in individual elicitation sessions for the purpose of developing probability distributions for the distribution coefficients for americium, curium, lead, neptunium, plutonium, radium, thorium, and uranium, for two sets of conditions. The first is the nature of the transport fluid: essentially Culebra or Salado brine. The second is whether the retardation takes place in the dolomite matrix or in the clay lining the fractures.

The K_d cumulative distributions that resulted from this panel are provided in Tables 2.6-8 and 2.6-9. The distributions are derived from a combination of values from two of the participants; a decision was made to not use Siegel's values in the 1991 PA calculations, as explained in the discussion that follows the tables. The rationales behind Dosch' and Novak's values are briefly described below; a more thorough description of Novak's values is provided in Appendix A of this report (Novak, September 4, 1991, Memo).

Dosch reviewed data from several experiments on distribution coefficients for various actinides in a variety of mediums. His own work (Lynch and Dosch, 1980) was included in his data set. He believed that even though some experiments were conducted using mediums different from the Culebra matrix and the Culebra clay, most of the data could not be discounted (personal communication from S. Hora, September 1991 regarding expert panel elicitation on May 1991). His justification for this was that experimental data directly applicable to the issue at hand was so scarce that no relevant data should be disregarded. In general, Dosch remarked that most of the experimental data deserved equal weight in any judgments about the behavior of actinides in the Culebra matrix and clay. Dosch declined to give any probability distributions for thorium and lead because he did not believe himself qualified to make enlightened assessments for those elements (personal communication from S. Hora, September 1991, regarding expert panel elicitation on May 1991).

Novak examined available research that detailed the experimental measurement of K_ds using substrates and water compositions pertinent to transport in the WIPP system (Novak, 1991). He showed that (1) data are not available for all elements of interest, (2) almost no data exist for clay substrates in the Culebra, and (3) existing data may not be applicable to current human-intrusion scenarios. In this study (Novak, 1991), Novak also questioned the use of the K_d model for estimating radionuclide retardation in the Culebra. Despite the limitations in existing data, Novak attempted to provide K_d values for use in the 1991 PA calculations.

Novak believes that the water composition called "Culebra H_2O" is the most representative among available data for Case One, which assumed that water reaching the Culebra would not change the composition of Culebra water significantly, except for the presence of radionuclides. Brine A best represented Case Two, which assumed that water reaching the Culebra would not be diluted and a concentrated brine contaminated with radionuclides would flow through the Culebra. Within each case, K_d estimates were needed for radionuclide sorption on the matrix (i.e., the dolomitic Culebra substrates), and in the fractures (i.e., on clay materials lining fractures). Each type of water was used for both matrix and fractures. Thus, for Case One, data from "Culebra H_2O" studies were used to estimate K_d values where actual data were not available. Similarly, Brine A data were used to estimate K_ds for Case Two.

Novak offered K_ds of 0 m^3/kg for all cdfs because he thought it possible that any of the elements could be transported with the fluid velocity. Upper bounds represent Novak's opinions on maximum values for K_ds observable under human-intrusion scenarios (Novak, September 4, 1991, Memo [see Appendix A]). Novak chose different sets of fractiles for different radionuclides. These represent his best estimates resulting from his studies of existing data and literature.

Novak further states that values obtained through the expert elicitation process are subjective estimates only because of large uncertainties in water composition, mixing within the Culebra, and the questionable utility of the K_d model. Finally, Novak argues that these cdfs for K_ds do not substitute for actual data, and believes that additional study is needed to quantify the potential for radionuclide retardation in the Culebra (Novak, September 4, 1991, Memo [Appendix A]).

Table 2.6-8. Cumulative Density Function for Partition Coefficients for Culebra Dolomite Member within Matrix Dominated by Culebra Brine (average of Dosch and Novak estimates)

Element	Median	Range		Partition Coefficient	Probability	Units	Source
Am	1.86×10^{-1}	0.0	1×10^{2}	0.0	0.0	m^3/kg	See text.
				1×10^{-2}	0.0139		
				9×10^{-2}	0.236		
				1×10^{-1}	0.271		
				1.5×10^{-1}	0.437		
				2×10^{-1}	0.525		
				4×10^{-1}	0.627		
				1	0.71		
				1×10^{1}	0.829		
				1×10^{2}	1		
Cm	1.86×10^{-1}	0.0	1×10^{2}	0.0	0.0	m^3/kg	See text.
				1×10^{-2}	0.0139		
				9×10^{-2}	0.236		
				1×10^{-1}	0.271		
				1.5×10^{-1}	0.437		
				2×10^{-1}	0.525		
				4×10^{-1}	0.627		
				1	0.71		
				1×10^{1}	0.829		
				1×10^{2}	1		
Np	4.8×10^{-2}	0.0	1×10^{2}	0.0	0.0	m^3/kg	See text.
				2.5×10^{-4}	0.1		
				7.5×10^{-4}	0.25		
				1.5×10^{-3}	0.4		
				1×10^{-2}	0.409		
				1×10^{-1}	0.625		
				2×10^{-1}	0.75		
				1×10^{1}	0.875		
				1×10^{2}	1		
Pb	1×10^{-2}	0.0	1×10^{1}	0.0	0.0	m^3/kg	See text.
				1×10^{-3}	0.25		
				1×10^{-2}	0.5		
				1×10^{-1}	0.75		
				1	0.99		
				1×10^{1}	1		
Pu	2.61×10^{-1}	0.0	1×10^{2}	0.0	0.0	m^3/kg	See text.
				1×10^{-4}	0.001		
				5×10^{-3}	0.112		
				1×10^{-2}	0.18		
				8×10^{-2}	0.347		
				1×10^{-1}	0.386		
				3×10^{-1}	0.528		
				1	0.75		
				1×10^{2}	1		

Table 2.6-8. Cumulative Density Function for Partition Coefficients for Culebra Dolomite Member within Matrix Dominated by Culebra Brine (average of Dosch and Novak estimates) (Concluded)

Element	Median	Range		Partition Coefficient	Probability	Units	Source
Ra	1×10^{-2}	0.0	1×10^{1}	0.0	0.0	m^3/kg	See text.
				1×10^{-3}	0.25		
				1×10^{-2}	0.5		
				2×10^{-2}	0.639		
				1×10^{-1}	0.85		
				1	0.972		
				1×10^{1}	1		
Th	1×10^{-2}	0.0	1	0.0	0.0	m^3/kg	See text.
				5×10^{-3}	0.25		
				1×10^{-2}	0.5		
				1×10^{-1}	0.75		
				1	1		
U	2.58×10^{-2}	0.0	1	0.0	0.0	m^3/kg	See text.
				2.5×10^{-4}	0.101		
				7.5×10^{-4}	0.252		
				1.5×10^{-3}	0.404		
				5×10^{-2}	0.574		
				1×10^{-1}	0.75		
				2×10^{-1}	0.875		
				1	1		

Table 2.6-9. Cumulative Density Function for Partition Coefficients for Culebra Dolomite Member within Fracture Dominated by Culebra Brine (average of Dosch and Novak estimates)

Element	Median	Range		Partition Coefficient	Probability	Units	Source
Am	9.26×10^{1}	0.0	1×10^{3}	0.0	0.0	m^3/kg	See text.
				9×10^{-1}	0.125		
				1	0.146		
				1.5	0.250		
				4	0.376		
				1×10^{1}	0.454		
				1×10^{3}	1		
Cm	9.26×10^{1}	0.0	1×10^{3}	0.0	0.0	m^3/kg	See text.
				9×10^{-1}	0.125		
				1	0.146		
				1.5	0.250		
				4	0.376		
				1×10^{1}	0.454		
				1×10^{3}	1		
Np	1	0.0	1×10^{3}	0.0	0.0	m^3/kg	See text.
				2.5×10^{-3}	0.1		
				7.5×10^{-3}	0.25		
				1.5×10^{-2}	0.4		
				1	0.5		
				1×10^{3}	1		
Pb	1×10^{-1}	0.0	1×10^{2}	0.0	0.0	m^3/kg	See text.
				1×10^{-2}	0.25		
				1×10^{-1}	0.5		
				1	0.75		
				1×10^{1}	0.99		
				1×10^{2}	1		
Pu	2.02×10^{2}	0.0	1×10^{3}	0.0	0.0	m^3/kg	See text.
				5×10^{-2}	0.05		
				8×10^{-1}	0.125		
				1	0.136		
				3	0.251		
				1×10^{1}	0.379		
				1×10^{3}	1		
Ra	3.41×10^{-2}	0.0	1×10^{2}	0.0	0.0	m^3/kg	See text.
				1×10^{-2}	0.225		
				5×10^{-2}	0.680		
				1×10^{-1}	0.75		
				1	0.875		
				1×10^{1}	0.995		
				1×10^{2}	1		

Table 2.6-9. Cumulative Density Function for Partition Coefficients for Culebra Dolomite Member within Fracture Dominated by Culebra Brine (average of Dosch and Novak estimates) (Concluded)

Element	Median	Range		Partition Coefficient	Probability	Units	Source
Th	1×10^{-1}	0.0	1×10^{1}	0.0	0.0	m^3/kg	See text.
				5×10^{-2}	0.25		
				1×10^{-1}	0.5		
				1	0.75		
				1×10^{1}	1		
U	7.5×10^{-3}	0.0	1	0.0	0.0	m^3/kg	See text.
				2.5×10^{-3}	0.2		
				7.5×10^{-3}	0.5		
				1.5×10^{-2}	0.8		
				1	1		

Discussion (Siegel, 1991):

The estimates provided by Siegel are similar to those he provided for the 1990 PA calculations and are shown in Tables 2.6-10 and 2.6-11. The decision to not incorporate these numbers into the 1991 panel's distributions was based on discussions with Steve Hora (University of Hawaii at Hilo) who conducted Siegel's elicitation session and who has worked extensively in the area of expert-judgment elicitation (e.g., U.S. NRC, 1990). The decision to not combine Siegel's values with the other two participants' responses was based on Siegel's values being fundamentally different from those provided by the other experts.

For example, two of the experts, Dosch and Novak, provided points on probability distributions that reflected their best judgments about the possible levels of retardation. Siegel chose, instead, to provide upper bounds on the fractiles of a probability distribution. Thus, the information obtained from Siegel is inherently different than the information obtained from the other two experts. The strategy that Siegel employed was to examine experimental evidence, determine a range of values for a specific quantile such as the median of the uncertainty distribution, and select the most conservative value from this range. Because experimental evidence is meager, Siegel did not believe that a sufficient scientific basis was available to justify forming a complete uncertainty distribution. He thus chose to bound the distribution.

Because the responses are fundamentally different, any attempt to aggregate Siegel's responses with the other participants would have led to an end product with no interpretable meaning. For this reason, Siegel's responses were not combined with those of the other experts and are not used in the 1991 performance assessment. The assessments provided by Siegel, however, are similar to those provided in 1990, which were used in the 1990 performance assessment.

Table 2.6-10. Cumulative Density Function for Partition Coefficients for Culebra Dolomite Member within Matrix Dominated by Culebra Brine (estimated by Siegel, 1991, 1990)

Element	Median		Range	Partition Coefficient[a] 1991	(1990)	Probability	Units	Source[b]
Am	1.2×10^{-1}	0.0	3.8×10^{-1}	0.0		0.0	m^3/kg	Anderson et al., 1991;
				1×10^{-1}		0.25		Siegel, 1990; Lappin
				1.2×10^{-1}	(1.1×10^{-1})	0.50		et al., 1989, Table
				2×10^{-1}		0.75		3-14, E-10, E-11, E-12
				3.80×10^{-1}		1.0		
Cm	8×10^{-1}	0.0	1.6	0.0			m^3/kg	Anderson et al., 1991;
				4×10^{-1}	(1×10^{-1})	0.25		Siegel, 1990; Lappin
				8×10^{-1}	ng	0.50		et al., 1989, Table
				1.2	(2×10^{-1})	0.75		3-14, E-10, E-11, E-12
				1.6	(1.2×10^{1})	1.0		
Np	6×10^{-4}	0.0	7.4×10^{-3}	0.0			m^3/kg	Anderson et al., 1991;
				3×10^{-4}	(5×10^{-5})	0.25		Siegel, 1990; Lappin
				6×10^{-4}	(1×10^{-4})	0.50		et al., 1989, Table
				1.5×10^{-3}	ng	0.75		3-14, E-10, E-11, E-12
				7.4×10^{-3}	(1×10^{-2})	1.0		
Pu = Th	8×10^{-2}	0.0	1	0.0			m^3/kg	Anderson et al., 1991;
				2.5×10^{-2}		0.25		Siegel, 1990; Lappin
				8×10^{-2}		0.50		et al., 1989, Table
				2×10^{1}	(1×10^{-1})	0.75		3-14, E-10, E-11, E-12
				1	(1.05)	1.0		
Ra = Pb	5×10^{-4}	0.0	1×10^{-3}	0.0			m^3/kg	Siegel, July 14, 1989 and
				2.5×10^{-4}	ng	0.25		June 25, 1991, Memos
				5×10^{-4}	(6×10^{-4})	0.50		(see Appendix A);
				7.5×10^{-4}	(1×10^{-3})	0.75		Siegel, 1990; Lappin
				1×10^{-3}	(7.5×10^{-3})	1.0		et al., 1989, Table 3-15
U	6×10^{-4}	0.0	7.4×10^{-3}	0.0			m^3/kg	Anderson et al., 1991;
				3×10^{-4}	ng	0.25		Siegel, 1990; Lappin
				6×10^{-4}		0.5		et al., 1989, Table
				1.5×10^{-3}	(1×10^{-3})	0.75		3-14, E-10, E-11, E-12
				7.4×10^{-3}	(7.5×10^{-3})	1.0		

[a] The parenthesis indicates the 1990 value; a blank indicates no change; and "ng" indicates that a value was not given in 1990.

[b] Anderson et al., 1991 is the source for the 1991 data; Siegel, 1990 and Lappin et al., 1989, are sources for the 1990 data.

Table 2.6-11. Cumulative Density Function for Partition Coefficients for Culebra Dolomite Member within Fracture Dominated by Culebra Brine (estimated by Siegel, 1991, 1990)

Element	Median	Range		Partition Coefficient[a] 1991	(1990)	Probability	Units	Source[b]
Am	2.3	0.0	4.1	0.0			m^3/kg	Anderson et al., 1991;
				5×10^{-1}	(2×10^{-1})	0.25		Siegel, 1990; Lappin
				2.3	(3×10^{-1})	0.5		et al., 1989, Table
				3	(5×10^{-1})	0.75		3-14, E-10, E-11, E-12
				4.1		1.0		
Cm	2.7	0.0	1.6×10^2	0.0			m^3/kg	Anderson et al., 1991;
				1.35	(2×10^{-1})	0.25		Siegel, 1990; Lappin
				2.7	(5×10^{-1})	0.5		et al., 1989, Table
				1.9×10^1	(2.7)	0.75		3-14, E-10, E-11, E-12
				1.6×10^2		1.0		
Np	5×10^{-2}	0.0	1.25	0.0			m^3/kg	Anderson et al., 1991;
				2×10^{-2}	(1×10^{-3})	0.25		Siegel, 1990; Lappin
				5×10^{-2}	(1×10^{-2})	0.5		et al., 1989, Table
				6.5×10^{-1}	(2×10^{-2})	0.75		3-14, E-10, E-11, E-12
				1.25	(5×10^{-2})	1.0		
Pu=Th	3×10^{-1}	0.0	4×10^1	0.0			m^3/kg	Anderson et al., 1991;
				1.5×10^{-1}	(1×10^{-1})	0.25		Siegel, 1990; Lappin
				3×10^{-1}		0.5		et al., 1989, Table
				2.3		0.75		3-14, E-10, E-11, E-12
				4×10^1		1 x 10		
Ra=Pb	5×10^{-2}	0.0	1×10^{-1}	0.0			m^3/kg	Seigel, July 14, 1989,
				2.5×10^{-2}	(1×10^{-3})	0.25		and June 25, 1991,
				5×10^{-2}	(1×10^{-2})	0.50		Memos (see Appendix
				7.5×10^{-2}	(2×10^{-2})	0.75		A); Siegel, 1990; Lappin
				1×10^{-1}	(5×10^{-2})	1.0		et al., 1989, Table 3-15
U	5×10^{-2}	0.0	1.25	0.0			m^3/kg	Anderson et al., 1991;
				2×10^{-2}	(1×10^{-3})	0.25		Siegel, 1990; Lappin
				5×10^{-2}	(1×10^{-2})	0.5		et al., 1989, Table
				6.5×10^{-1}	(2×10^{-2})	0.75		3-14, E-10, E-11, E-12
				1.25	(5×10^{-2})	1.0		

[a] The parenthesis indicates the 1990 value; a blank indicates no change; and "ng" indicates that a value was not given in 1990.

[b] Anderson et al., 1991 is the source for the 1991 data; Siegel, 1990 and Lappin et al., 1989, are sources for the 1990 data.

General Rationale for Values Recommended by Siegel (1990)

The general rationale for selecting the K_d value in each percentile of the cdf follows (Tables 2.6-10 and 2.6-11). Separate K_d distributions are given for the dolomite matrix and the clays lining the fractures in the Culebra Dolomite Member. In general, the recommended K_d values were reduced by several orders of magnitude from experimental K_d data. Many of the K_ds reported for the actinides are in the range of 10,000 to 100,000 mL/g (Lappin et al., 1989, Table 3-14). The following summarizes the discussion presented in Lappin et al. (1989).

The uncertainties in the composition of water in the Culebra Dolomite that will be produced by mixing fluids from the repository and aquifer require that large ranges of pH, Eh, organic content, and carbonate content of the groundwaters be considered in choosing K_d values. These possible variations in solution chemistry could result in order-of-magnitude changes of the K_ds from the values obtained in the experimental studies. The K_d values chosen for each element are explained further below.

Culebra brine is assumed to dominate the groundwater chemistry. The Culebra brine is represented by the average composition of a brine sample from well H-2b and H-2c.

Plutonium, Americium, and Curium. K_d values for plutonium are decreased from the values in Paine (1977), Dosch (1979), and Tien et al. (1983), because of the potential effect of carbonate complexation and competition for sorption sites by competing cations. K_d values for americium are decreased from cited values because of the potential effects of organic complexation and competition. K_d values for curium were decreased from the values listed in Tien et al. (1983) based on the assumption of behavior similar to americium and europium.

Uranium and Neptunium. In general, low K_ds for uranium and thorium have been measured in waters relevant to the WIPP repository. Low values (K_d = 1 or 10) have been assumed here to account for the possible effects of complexation and competition.

Thorium. There are very few data for thorium under conditions relevant to the WIPP. Thorium K_d values were estimated from data for plutonium, a reasonable homolog element for thorium (Krauskopf, 1986).

Radium and Lead. Siegel assumed that sorption of lead and radium will be controlled by the amount of clay in the matrix (1%) and fracture-filling clay (100%). (Note the fractures are assumed to be 50% filled by clays in the calculation of the retardation factor.) The matrix K_ds are obtained from the clay K_ds by multiplying by a utilization factor of 0.01 as discussed in Lappin et al. (1989). The maximum values are based on Tien et al. (1983) as cited in Lappin et al., (1989, Table 3-15).

Available data suggest that radium will sorb onto clays that are similar to those identified within the matrix and lining fractures in the Culebra Dolomite. The same data indicate that the degree of sorption is dependent upon the solution composition. Based on this information, values of 100 and 5 ml/g were chosen to represent the sorption of radium and lead onto clays in the Culebra. These K_d values correspond to sorption in dilute to moderately saline Culebra groundwaters (Case 1) and solutions with high contents of salt and organic ligands (Case 2), respectively. Retardation factors for the bulk matrix were calculated using the K_d values and a utilization factor of 0.01 to account for the occurrence of the clay as a trace constituent in the dolomite matrix.

General Rationale for Constructing Cumulative Distributions

The general rationale for selecting the K_d value in each percentile of the cumulative distribution follows (Tables 2.6-9 and 2.6-10).

Dolomite Matrix. A description of distributions for dolomite matrix is given below.

100th percentile: The highest K_d value for each radionuclide for the Culebra brine was used for the 100th percentile. If data for this brine were not available, the highest minimum value of the ranges from experiments carried out in WIPP Solutions A, B, and C (see Table 3-16 in Lappin et al., 1989) was used. The use of the minimum values introduces a degree of conservatism in the distributions. Data from experiments that include organic ligands were not considered.

75th percentile: The K_d values for the 75th percentile represent a compromise between the empirical data that show that sorption will occur under WIPP-specific conditions and theoretical calculations that suggest that many factors can decrease the extent of sorption significantly under other conditions that are possible in the Culebra. The values are identical to those used in Case I of Lappin et al. (1989, Table E-10).

50th percentile: The lowest reported K_d value for Culebra brine was used for the 50th percentile. If no data for Culebra brine were available, the lowest of the values reported for organic-free WIPP Solutions A, B, and C was used.

25th percentile: The 25th percentile represents conditions under which the solution chemistry is dominated by the influx of inorganic salts from the Salado and Castile Formations and includes the additional effects of organic ligands. The K_d values are identical to those of Case IIB of Lappin et al. (1989, Table E-10).

0th percentile: The use of a K_d value of zero increases the conservatism of the distribution because there is evidence some sorption will occur (Lappin et al., 1989, Table 3-14).

Clay in Fractures. A description of distributions for clay in fractures is given below. For the 1990 calculations, the fracture K_d values used were 3 orders of magnitude lower than the estimates provided.

75th and 50th percentiles: The values in Table E-11 in Lappin et al. (1989) and the lowest value for Culebra brine were compared; the larger of the two values was used for the 75th percentile. The smaller value was used for the 50th percentile. If no data for Culebra brine were available, the lowest value reported for WIPP Solutions A, B, and C (organic-free) was compared to the value in Table E-11, and the smaller value was used for the 50th percentile.

25th percentile: The 25th percentile represents conditions under which the solution chemistry is dominated by the influx of inorganic salts from the Salado and Castile Formations and includes the additional effects of organic ligands. The K_d values are identical to those of Case IIB of Lappin et al. (1989, Table E-11).

0th percentile: The use of a K_d value of zero increases the conservatism of the distribution because there is evidence some sorption will occur (Lappin et al., 1989, Table 3-14).

Retardation

For codes requiring retardation, the retardation for the matrix was calculated using the standard expression for retardation in a porous matrix (Freeze and Cherry, 1979, p. 404):

$$R_m = 1 + \rho_b K_d / \phi_m \qquad (2.6\text{-}1)$$

The retardation factor for the fractures was calculated from (Neretnieks and Rasmusson, 1984):

$$R_f = 1 + \rho_b K_d b_c / b \qquad (2.6\text{-}2)$$

where

- b_c = thickness of the minerals (e.g., clay) lining both sides of the fracture ($b_c/b = 0.5$, Table 2.6-1)
- b = fracture aperature
- K_d = partition coefficient (Tables 2.6-8 and 2.6-9)
- ϕ_m = matrix porosity (Table 2.6-1)
- ρ_b = bulk density of material (Table 2.6-1) = $(1 - \phi)\rho_g$

3. ENGINEERED BARRIERS AND SOURCE TERM

The engineered barriers consist of the repository design, waste form, seals, and backfill. Also discussed in this chapter are characteristics of the waste such as inventory of radionuclides and hazardous chemicals, solubility, and gas production potential.

3.1 Dimensions of Underground Facility

The WIPP repository is composed of a single 15-ha (38-acre) underground disposal level constructed in one stratigraphic interval, which dips slightly to the south. The repository level consists of an experimental region at the north end, the operations region in the center for waste-handling and repository equipment maintenance, and a disposal region at the south end. Figures 3.1-1 and 3.1-2 show the excavated and enclosed areas in the WIPP repository, and the planned dimensions of the WIPP disposal region and access drifts. The UTM coordinates shown in Figure 3.1-2 are derived from the state plane coordinates reported in Gonzales, 1989. To maintain consistency with coordinate values reported elsewhere in this volume, the UTM coordinates were computed by the Technology Application Center, University of New Mexico, Albuquerque, New Mexico 87106. Table 3.1-1 provides a summary of the excavated and enclosed areas and initial volumes of excavated regions (not considering disturbed rock zone [DRZ] or closure). At present, only the first panel has been excavated.

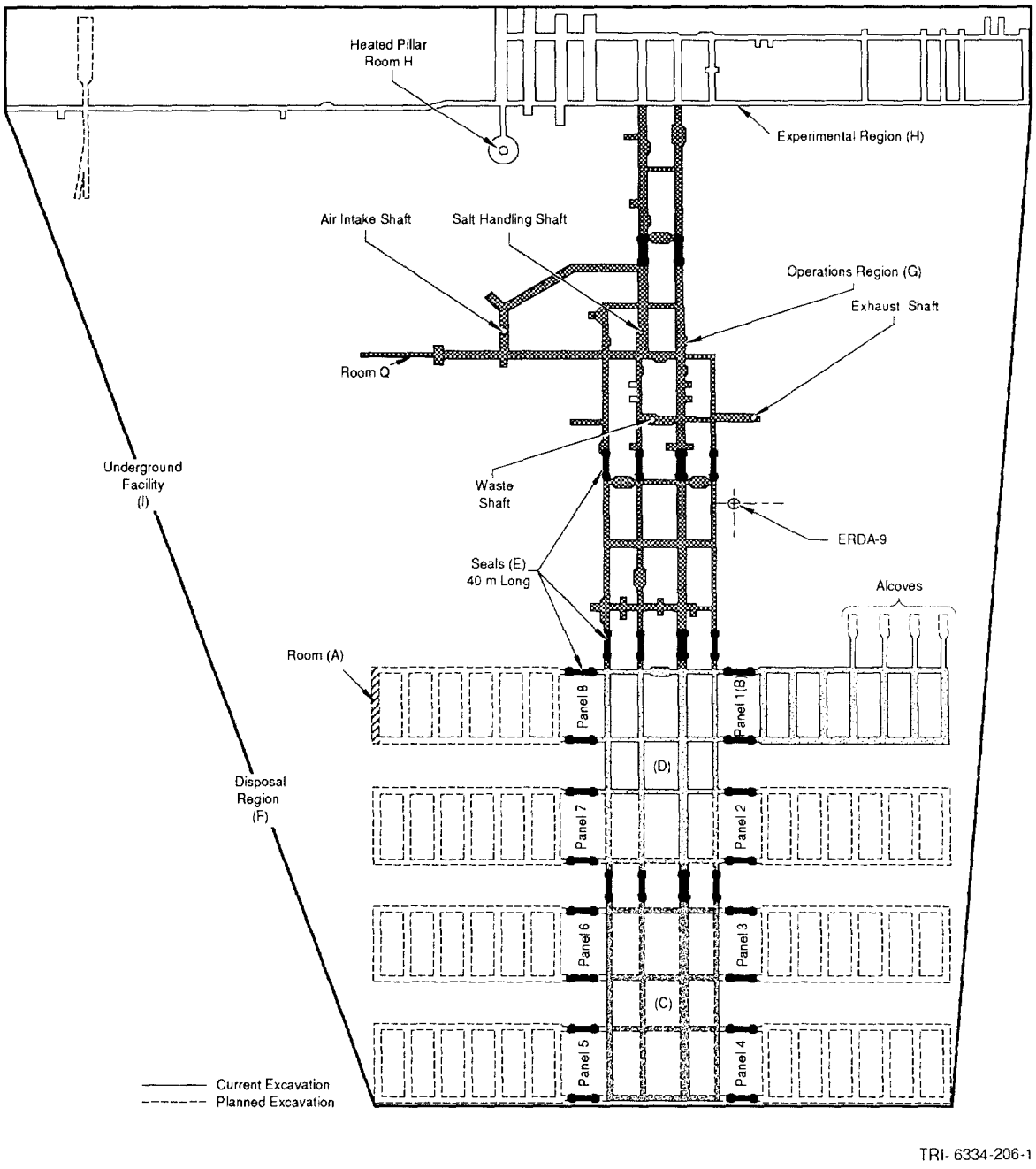

Figure 3.1-1. Excavated and Enclosed Areas in the WIPP Repository.

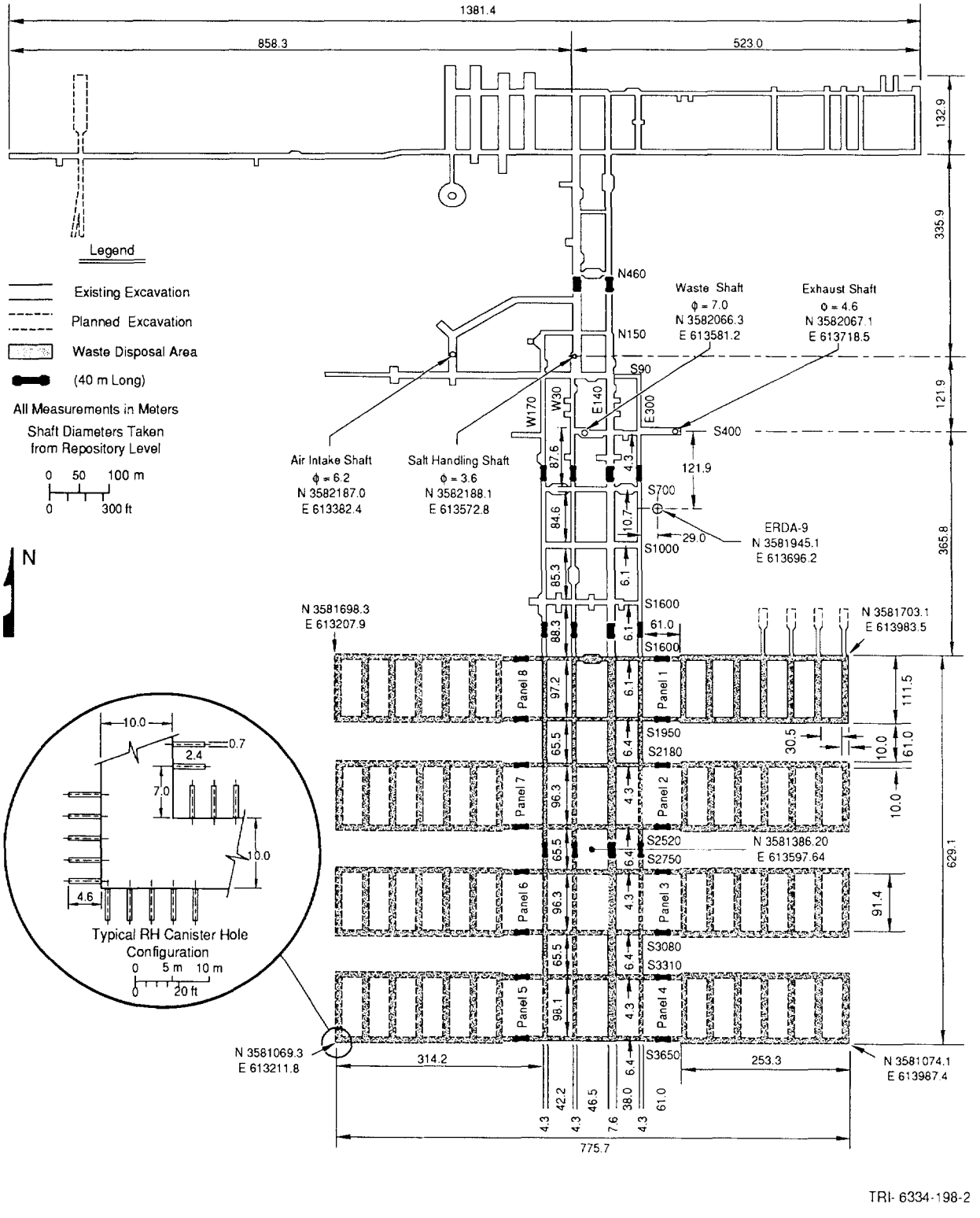

TRI-6334-198-2

Figure 3.1-2. Planned Dimensions of WIPP Disposal Region and Access Drifts. (Dimensions originally specified in units of feet.) (after Bechtel, 1986)

Table 3.1-1. Summary of Excavated and Enclosed Areas and Initial Volumes of Excavated Regions within the WIPP Repository, Not Considering the DRZ or Closure (Rechard et al., 1990b, Table A-12)

Region*	Areas		Volume	
	Excavated (10^3 m^2)	Enclosed (10^3 m^2)	Excavated (10^3 m^3)	Enclosed (10^3 m^3)
Room (A)	0.9197	0.9197	3.644	3.644
One panel excluding seals (B)	11.64	29.42	46.10	116.59
Southern equivalent panel excluding seals (C)	8.820	49.46	32.26	180.90
Northern equivalent panel excluding seals (D)	9.564	53.68	34.98	196.34
Panel seals (20) (E)	4.133		15.119	
Total disposal region (F)	111.52	506.8	436.0	2008.0
Operations region (G)	21.84	283.6	78.07	1037.2
Four shafts (only) to base of Rustler Fm.	0.08691	0.08691	34.76	34.76
Experimental region (H)	21.61	298.1	71.90	1090
Total facility (I)	152.83	1748	583.4	6926

*Regions shown in Figure 3.1-1; detailed dimensions shown in Figure 3.1-2.

3.1.1 Disposal Region

All of the underground openings are rectangular in cross section. The disposal area drifts are generally 3.96 m (13 ft) high by 4.3 m (14 ft) wide; the disposal rooms are 4 m (13 ft) high, 10 m (33 ft) wide, and 91.4 m (300 ft) long. The width of the pillars between rooms is 30.5 m (100 ft). The total excavated volume in the disposal region is 4.334×10^5 m^3 (1.53×10^7 ft^3). The reported design disposal volume is 1.756×10^5 m^3 (6.2×10^6 ft^3) or about 36% of the excavated volume (Bechtel, 1986). The disposal volume, however, for waste changes depending on the type of containers, waste form, and volume of panel seals. Hence, the design volume is discussed in the description of the containers (Section 3.1.5).

3.1.2 Experimental Region

The experimental region (Figure 3.1-2) is located in the northern portion of the underground facility and consists of over ten rooms, which are used for in situ testing of salt creep and brine inflow (Matalucci, 1987, pp. 3,15). The sizes of the rooms vary, depending on the experiment. The excavated area of the experimental region is about 21.61 x 10^3 m^2 (23.2 x 10^4 ft^2), and its volume is about 71.90 x 10^3 m^3 (25.3 x 10^5 ft^3) (Table 3.1-1).

3.1.3 Operations Region

The operations region (Figure 3.1-2) consists of the access drifts located in the center of the underground facility. The drifts are used for transport of equipment and personnel to the experimental area and disposal region. All four shafts are connected to the operations region. The excavated area of the operations region is 21.84 x 10^3 m^2 (23.4 x 10^4 ft^2), and its volume is 78.07 x 10^3 m^3 (27.6 x 10^5 ft^3) (Table 3.1-1).

3.1.4 Shafts

The four shafts connecting the underground facility to the surface are (1) the Air Intake Shaft, 6.2 m (20 ft) in diameter; (2) the Exhaust Shaft, 4.6 m (15 ft) in diameter, (3) the Salt Handling (C&SH) Shaft, 3.6 m (12 ft) in diameter, and (4) the Waste Shaft, 7 m (23 ft) in diameter (Figure 3.1-2).

During operations, the Salt-Handling Shaft will transport personnel, equipment, and salt. The Waste Shaft will transport the waste, and the Air Intake and Exhaust Shafts will provide air flow. The Air Intake Shaft will also serve as a backup for transporting personnel and equipment.

At present, the shaft functions are the same as those described above, except that the Waste Shaft is not currently used to transport waste. It serves as a backup for transport of personnel and materials.

The Air Intake Shaft, the most recently constructed shaft (1988), provides fresh air to the underground. It also serves as a backup for transporting personnel and materials. In addition, in situ testing is being performed to investigate the disturbed rock zone (DRZ) surrounding the shaft and hydrologic properties of the Rustler Formation (Nowak et al., 1990).

The Exhaust Shaft, drilled in 1983-84, serves as the primary air exhaust for the underground facility (Bechtel, 1985).

The Salt-Handling Shaft (formerly called the Construction and Salt-Handling [C&SH] Shaft and the Exploratory Shaft [Bechtel, 1985]) was drilled in 1981. It was used during construction of the WIPP repository to remove salt and serve as the primary transport for personnel and equipment. The Salt-Handling Shaft continues to serve as the primary transport for personnel and equipment and as a secondary air supply to the underground facility.

The Waste Shaft (initially called the Ventilation Shaft) is designed to move radioactive waste between the surface waste-handling facilities and the underground facility. The Ventilation Shaft was enlarged from 2 m (6 ft) diameter to 6 m (20 ft) diameter in 1983-84, when it was renamed the Waste Shaft (Bechtel, 1985). Until waste transport begins, the Waste Shaft serves as a secondary means to transport personnel, materials, large, equipment, and diesel fuel. The Waste Shaft can continue to serve as backup for transporting personnel and materials whenever waste is not being transported.

All four shafts will be backfilled upon decommissioning of the WIPP (Nowak et al., 1990).

3.1.5 Waste Containers

Contact-handled (CH) transuranic (TRU) waste to be shipped to the WIPP is currently stored in 55-gal. drums, metal boxes, and fiberglass-reinforced plywood (FRP) boxes of various sizes (Table 3.1-2). The WIPP *Waste Acceptance Criteria* (see Section 3.4, Table 3.4-2) requires a metal overpack for all combustible boxes as a fire prevention measure, so FRP boxes and any other non-metal boxes will be overpacked and subsequently handled and disposed of in these overpacks. Furthermore, TRUPACT II, the transportation container for trucking TRU waste to the WIPP has space only for 7-pack drums and SWBs; hence, large boxes will have to be repacked unless a new transportation container is built in later years. CH-TRU waste in drums will be stacked three high in the waste-storage rooms.

The reference canister for the remotely handled (RH) TRU waste is a 0.65-m (26-in.) O.D. (outside diameter) right-circular cylinder made of 1/4-in. carbon steel plate. Caps are welded at both ends. The canister is 3 m (10 ft) in length, including the handling pintle. Inside, the waste occupies about 0.89 m^3 (30 ft^3) (U.S. DOE, 1990d).

Table 3.1-2. CH-TRU Waste Containers (U.S. DOE, 1990a, Dwg 165-F-001-W)

Container Description	Approximate Dimensions (h x w x l) m	Volume		
		Internal m^3	External m^3	Packing m^3
Approved for transportation:				
DOT 17C (metal) 55-gal steel drums	0.9 x 0.1 dia.	0.208	0.21	
7-Pack of 55-gal steel drums		1.451	1.47	2.2
Standard waste box (Dwg 165-F-001-W)	0.94 x 1.8 x 1.3	1.90	1.95	2.34
Other storage containers:				
Steel box	1.2 x 1.2 x 1.2		2.3	
Steel box	2.0 x 1.7 x 2.8		9.5	
Steel box (FRP box overpacked)	1.4 x 1.4 x 2.2		4.1	
Plywood Box	1.2 x 1.2 x 1.7		3.17	

3.1.6 Waste Placement and Backfill in Rooms

Figure 3.1-3 shows the ideal packing configuration of drums in the rooms and drifts. At the waste storage room, the waste packages (7-packs) will be removed from the transporter and stacked 3 high and 6 wide across the room. In the ideal packing configuration, a total of 6,804 drums (972 7-pack units) can be placed in one room. A 0.711-m air gap exists above the drums; also a thin plastic pallet is set between layers. For the 1991 calculations, the plastic sheet was assumed to be 0.30-m thick, consistent with the Bechtel initial reference design report (1986). Recently developed final plans (U.S. DOE, 1990d) for the plastic sheet call for 0.004-m-thick plastic on the top and bottom; hence, slightly more salt backfill will be used.

The standard waste box stacking (SWB) configuration depends upon the box size (Figure 3.1-4). Seven-packs and SWBs may be intermixed, as practical. To reach the original design capacity of 175,600 m^3 (6.2 x 10^6 ft^3), the SWBs were also assumed to be stacked three high. However, current plans call for stacking the SWBs only two high, which substantially reduces the disposal capacity of the WIPP.

The current placement technique for RH TRU waste in the WIPP is to emplace one canister horizontally every 2.4 m (8 ft) into the drift and room walls. Based on this technique, the capacity in each panel for RH-TRU canisters along drifts and rooms 10-m wide is 874 canisters or about 6,000 m^3. The intended capacity for RH-TRU waste is 7,080 m^3 (250,000 ft^3); hence, additional methods will be explored. Current PA calculations assume a capacity of 7,080 m^3.

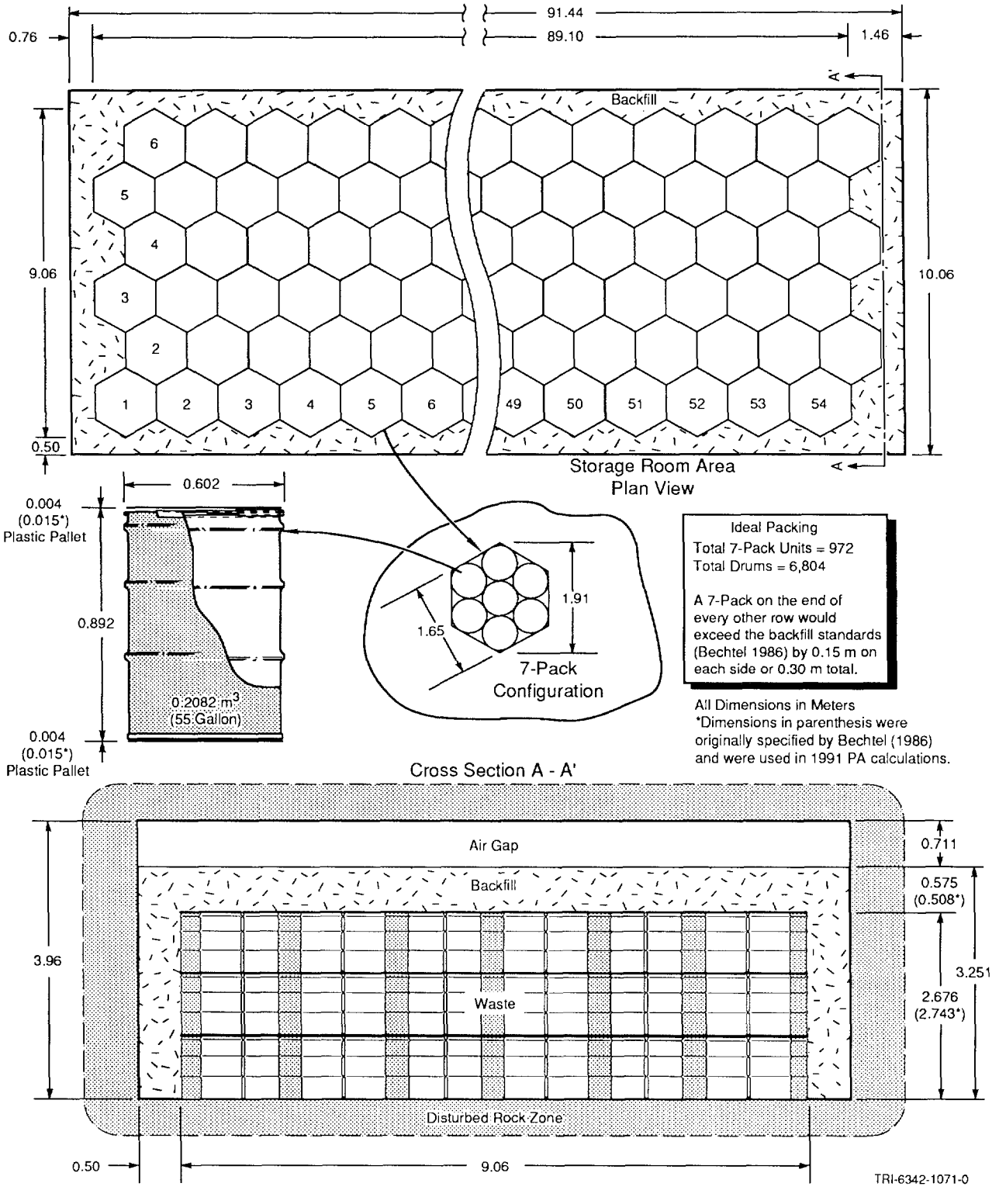

Figure 3.1-3. Ideal Packing of Drums in Rooms and 10-m-wide Drifts.

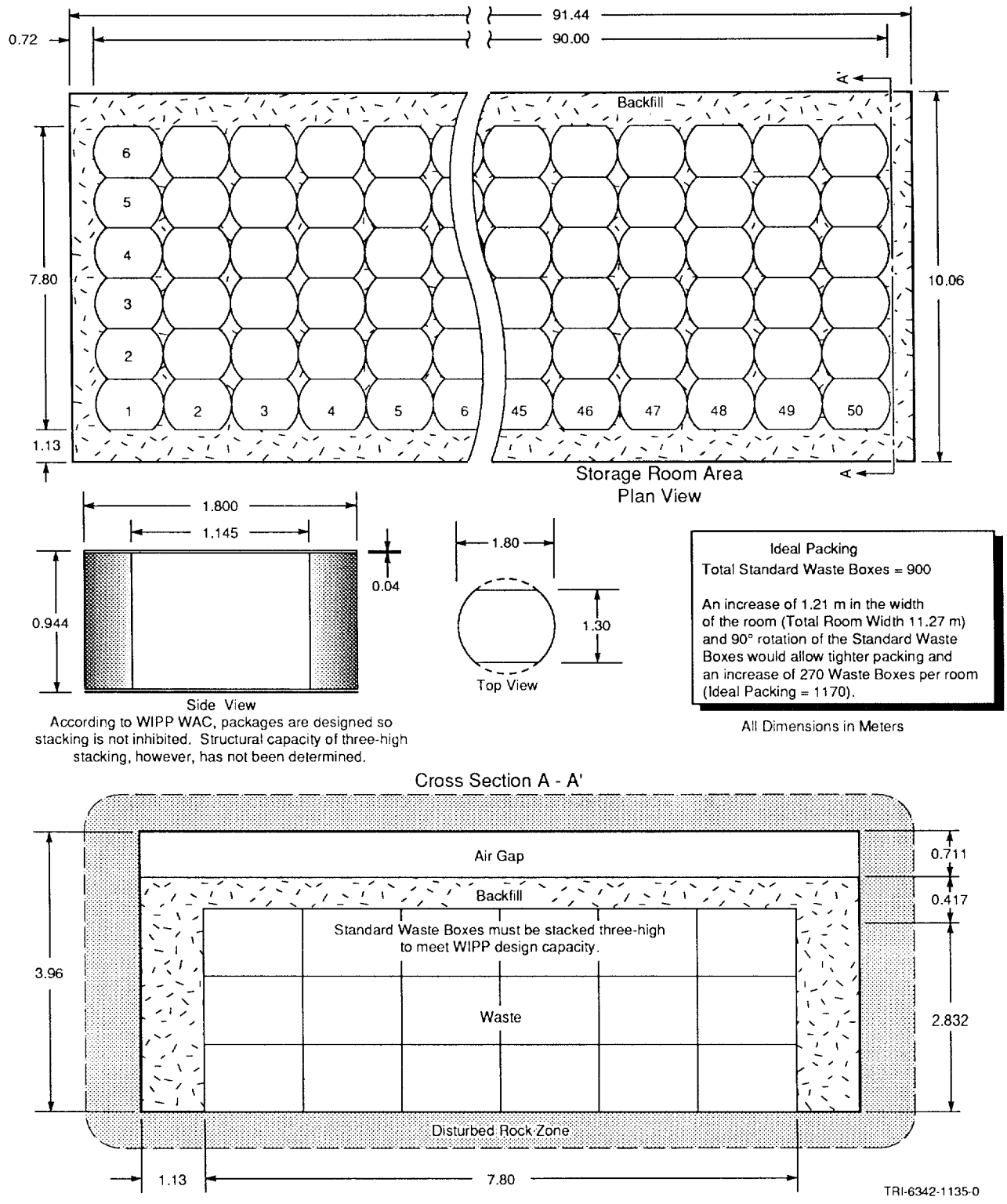

Figure 3.1-4. Ideal Packing of Standard Waste Boxes in Rooms and Drifts.

3.2 Parameters for Backfill Outside Disposal Region

This section presents parameters (such as permeability and porosity) for backfill placed in the shafts and access drifts when WIPP is decommissioned (Table 3.2-1).

Table 3.2-1. Parameter Values for Backfill Outside Disposal Region

Parameter	Median	Range		Units	Distribution Type	Source
Preconsolidated Salt (Lower shaft, drifts, panels)						
Density (ρ)						
Initial	1.71×10^3 ($0.8\rho_{Salado}$)			kg/m^3	Constant	Nowak et al., 1990, Figure 11
Final	2.03×10^3 ($0.95\rho_{Salado}$)			kg/m^3	Constant	Sjaardema and Krieg, 1987; Arguello, 1988
Height (Lower shaft)	2×10^2	1×10^2	3×10^2	m	Uniform	Nowak et al., 1990, p. 14.
Permeability (k)						
Initial	1×10^{-14}			m^2	Constant	Holcomb and Shields, 1987, Figure 4
Final	1×10^{-20}	3.3×10^{-21}	3.3×10^{-20}	m^2	Lognormal	Holcomb and Shields, 1987 Figure 4; Nowak et al., 1990, Figure 11, p. 14.
Salt Backfill in Drifts						
Density (ρ)						
Initial	1.28×10^3 ($0.6\rho_{Salado}$)			kg/m^3	Constant	Nowak et al., 1990, Figure 11
Final	2.03×10^3 ($0.95\rho_{Salado}$)			kg/m^3	Constant	Sjaardema and Krieg, 1987; Arguello, 1988
Permeability (k)						
Initial	1×10^{-11}			m^2	Constant	Holcomb and Shields, 1987, Figure 4
Final	1×10^{-20}	3.3×10^{-21}	3.3×10^{-20}	m^2	Lognormal	Holcomb and Shields, 1987, Figure 4; Nowak et al., 1990, Figure 11, p. 14.
Partition Coefficients for Salt Backfill						
Am	1×10^{-4}			m^3/kg	Constant	Lappin et al., 1989, Table D-5 ($K_{dclay}/1000$)
Np	1×10^{-5}			m^3/kg	Constant	Lappin et al., 1989, Table D-5 ($K_{dclay}/1000$)
Pb	1×10^{-6}			m^3/kg	Constant	Lappin et al., 1989, Table D-5 ($K_{dclay}/1000$)
Pu	1×10^{-4}			m^3/kg	Constant	Lappin et al., 1989, Table D-5 ($K_{dclay}/1000$)
Ra	1×10^{-6}			m^3/kg	Constant	Lappin et al., 1989, Table D-5 ($K_{dclay}/1000$)
Th	1×10^{-4}			m^3/kg	Constant	Lappin et al., 1989, Table D-5 ($K_{dclay}/1000$)
U	1×10^{-6}			m^3/kg	Constant	Lappin et al., 1989, Table D-5 ($K_{dclay}/1000$)
Concrete and Bentonite						
Permeability (k)						
Concrete	2.7×10^{-19}			m^2	Constant	Nowak et al., 1990, Figure 11, p. 13
Bentonite	1.4×10^{-19}			m^2	Constant	Nowak et al., 1990, Figure 11, p. 13

3.2.1 Description of the Reference Design for Backfill

The purpose of the reference backfill design, which Sandia has developed for backfilling the WIPP repository, is to provide a common basis for calculations performed in modeling tasks such as performance assessment and sensitivity analysis (Nowak et al., 1990; Nowak and Tyler, 1989). The reference design is a starting point for developing experiments and analysis from which a detailed design will evolve.

General Backfill Strategy

In general, the entire underground facility and shafts will be backfilled. As part of the reference design, portions of the backfill emplaced at several locations within the shafts and various drifts, which are specially prepared (i.e., preconsolidated salt with concrete plugs), are often termed "seals." However, the purpose of these prepared portions is not to act as the sole seal for the shaft or drift (in general, all the backfill fulfills this function), but instead to protect sections of the backfill from fluids (gases or liquids). Inhibiting fluids hastens backfill consolidation and thus greatly increases the probability that the salt backfill will rapidly (< 200 yr) assume properties similar to the surrounding host rock. Consequently, the term seal is misleading; however, since it has been used throughout the WIPP Project, it is also used here.

The strategy for backfilling specially prepared portions of the drift and shaft combines short- and long-term seal components; preconsolidated crushed salt is the principal long-term component in the Salado Formation salt. Clay -- a swelling clay material shown to be stable and to have low permeability to brines -- is the principal long-term component in the Rustler Formation. Concrete is the principal short-term component in both locations.

The combination of short- and long-term seals (backfill) is used so that short-term seals provide the initial sealing functions necessary until the long-term seal components become adequately reconsolidated (Nowak et al., 1990). Preconsolidated crushed-salt and clay components are expected to become fully functional for sealing within 100 yr after emplacement (Nowak and Stormont, 1987; Arguello, 1988). Then the long-term seals take over all sealing functions.

Short-term seal components consist of concretes developed specifically for the WIPP. The concrete components provide flow resistance to control the effects of possible gas generation in the waste disposal area and limit water inflow from above to protect the crushed salt from saturation with brine; they also provide physical containment for the swelling clay and consolidating crushed-salt materials (Nowak et al., 1990).

The long-term seals in the Salado consist of preconsolidated WIPP crushed salt in the shafts, drifts, and panel entries. The emplaced crushed-salt material is intended to have an initial density equal to 80% of the density of the intact WIPP host rock salt (80% relative density) (Nowak et al., 1990). Within 100 yr of emplacement, the preconsolidated salt backfill will be fully consolidated by creep closure of the host-rock salt to a state of low permeability, approximately 1×10^{-20} m^2 (Nowak and Stormont, 1987; Arguello, 1988; Lappin et al., 1989). This permeability value is in the expected permeability range for the host-rock salt (1×10^{-21} to 1×10^{-20}) (Nowak et al., 1988; Lappin et al., 1989). There is very little compositional difference between the reconsolidated WIPP crushed-salt material and the surrounding host rock from which it was mined. The crushed-salt seals, therefore, are expected to be mechanically and chemically stable in the WIPP environment (Nowak et al., 1990).

Seal Locations

In the reference design, multicomponent seals between 30 and 40 m (100 and 130 ft) long will be located in each of the four shafts, the entrances to the waste disposal panels, and selected access drifts (Nowak et al., 1990). (See Figures 3.1-1 and 3.1-2 for seal locations.) Seals near the Rustler Formation (upper shaft and water-bearing zone seals) serve to limit brine flow from water-bearing zones down into the crushed-salt backfill. Seals in the drifts serve to reduce fluid flow (gas and brine) from the repository area and thus limit the creation of a preferred pathway for contaminant migration. The drift entries to each filled disposal panel will be sealed during operations. The disturbed rock zone (DRZ), which occurs in the host-rock salt at the excavated openings, is expected to heal by creep closure (Nowak et al., 1990). The extent of a DRZ in the drift entries may be reduced by the use of concrete liners during operations. If necessary, however, the conceptual design for sealing the DRZ (both in drifts and shafts) and anhydrite interbeds (e.g., MB139 directly underneath the disposal area) envisions a salt-based grout (Nowak and Tyler, 1989) using grouting techniques that are currently under development (Figure 3.2-3). When all disposal panels are filled, the drift entries to the entire disposal area will be sealed. The shafts will be backfilled upon decommissioning of the WIPP (Figures 3.2-1 and 3.2-2) (Nowak et al., 1990).

Backfill in Upper Shaft, Water-Bearing Zone, and Dewey Lake Red Beds

According to current calculations, movement of radionuclides does not reach the upper shaft in 10,000 yr. Therefore, the actual properties of the backfill in the upper shaft and above have not been used in the 1991 PA calculations and properties are not given. Instead the initial placement properties of the lower shaft have been used.

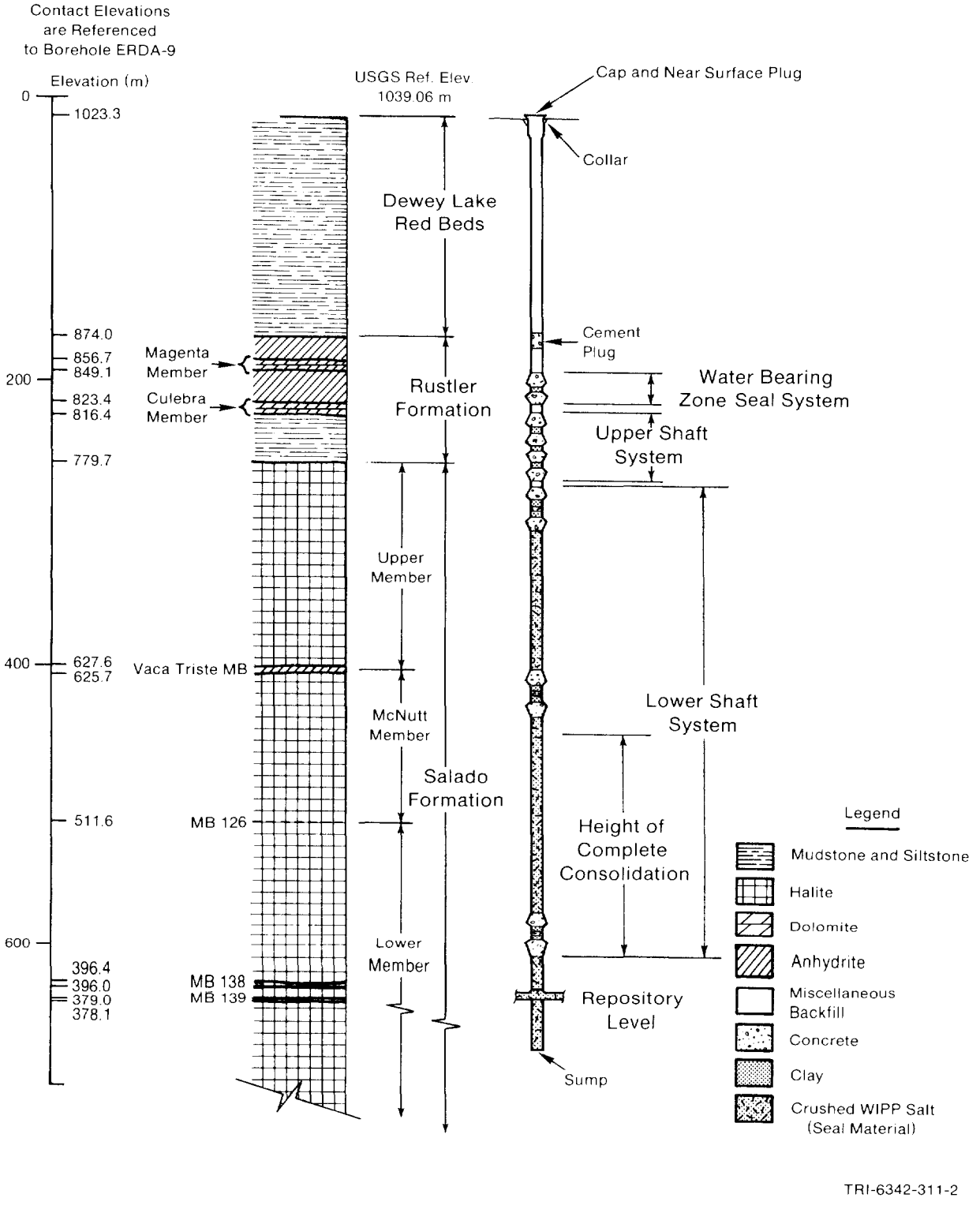

Figure 3.2-1. Diagram of Typical Backfilled Access Shaft (after Nowak et al., 1990).

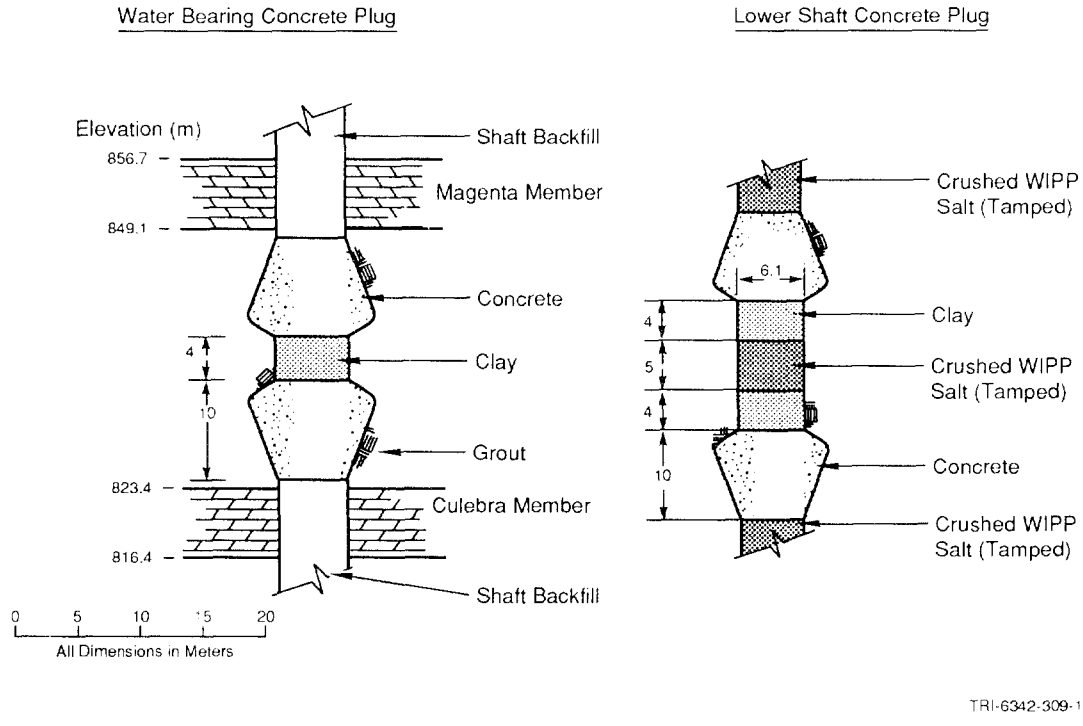

Figure 3.2-2. Diagram of Typical Concrete Plugs in Backfilled Shafts. The drawing shows concrete plugs between water-bearing units (e.g., Culebra Dolomite) (left) and for the Lower Shaft Backfill (e.g., at Vaca Triste) for Waste Shaft (right) (after Nowak et al., 1990).

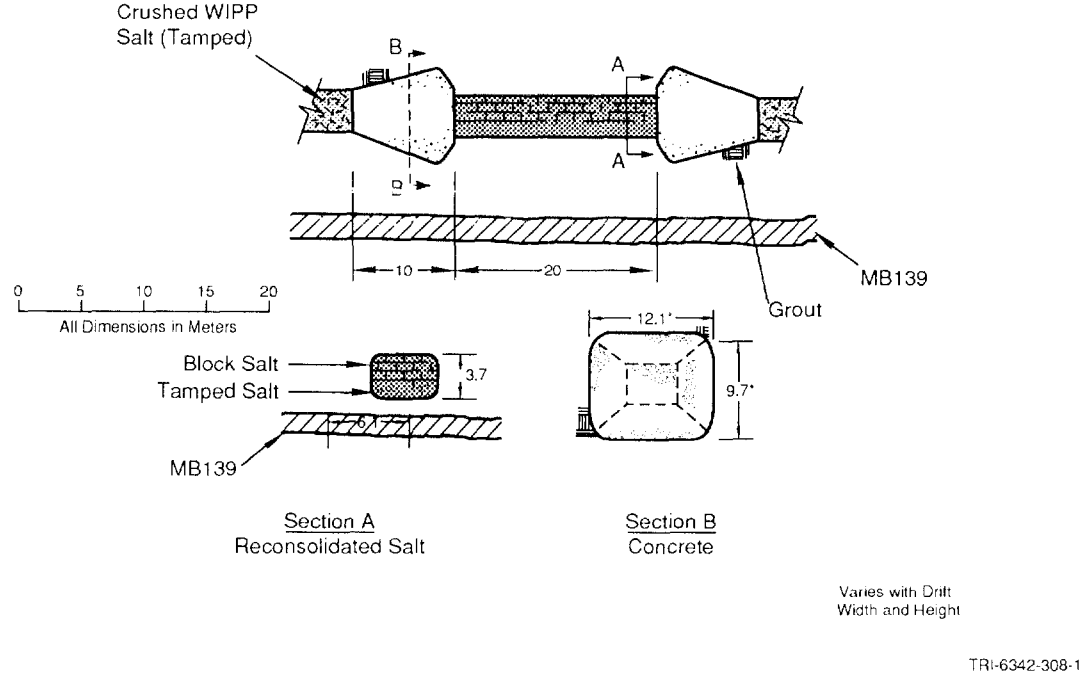

Figure 3.2-3. Diagram of Typical Concrete and Preconsolidated Salt Backfill for Drifts and Panels (after Nowak et al., 1990).

3.2.2 Preconsolidated Salt Backfill in Lower Shaft, Drifts, and Panels

The reference seal uses preconsolidated (tamped) crushed WIPP salt as the primary long-term seal material. For redundancy, concrete plugs and clay (Figure 3.2-2) are emplaced at three locations in the shaft: (1) near the bottom of the shaft, (3) at an intermediate position in the shaft just below the Vaca Triste Marker Bed, and (3) near the top of the Salado Formation.

The emplaced WIPP crushed salt is intended to have an initial density equal to 80% of the density of the intact WIPP host rock salt (80% relative density). Salt with 80% relative density will be created either by pouring and tamping crushed salt or by laying preconsolidated salt blocks. Creep closure of the lower part of the shaft will continue to consolidate this crushed salt.

Density for Preconsolidated Backfill ("Seals")

Parameter:	**Density, initial (ρ)**
Median:	1.71×10^3 ($0.8\rho_{Salado}$)
Range:	None
Units:	kg/m^3
Distribution:	Constant
Source(s):	Nowak, E. J., J. R. Tillerson, and T. M. Torres. 1990. *Initial Reference Seal System Design: Waste Isolation Pilot Plant.* SAND90-0355. Albuquerque, NM: Sandia National Laboratories. (Figure 11)

Parameter:	**Density, final (ρ)**
Median:	2.03×10^3 ($0.95\rho_{Salado}$)
Range:	None
Units:	kg/m^3
Distribution:	Constant
Source(s):	Sjaardema, G. D. and R. D. Krieg. 1987. *A Constitutive Model for the Consolidation of WIPP Crushed Salt and Its Use in Analysis of Backfilled Shaft and Drift Configurations.* SAND87-1977. Albuquerque, NM: Sandia National Laboratories. Arguello, J. G. 1988. *WIPP Panel Entryway Seal - Numerical Simulation of Seal Composite Interaction for Preliminary Seal Design Evaluation.* SAND87-2804. Albuquerque, NM: Sandia National Laboratories.

Discussion:

The initial placement density for the crushed-salt backfill is specified in the reference design as 0.8 of the intact Salado density ($0.8\rho_{Salado}$) (Nowak et al., 1990). A higher initial compaction than in the drift and panel backfill is specified to ensure faster consolidation. The estimated final density of 0.95 of the intact Salado density ($0.95\rho_{Salado}$) comes from salt creep modeling (Sjaardema and Krieg, 1987; Arguello, 1988). The initial and final porosity can be calculated directly from the densities. Assuming that the intact Salado density is 2.14×10^3 kg/m^3 with a porosity of 0.01 (see Table 2.3-1), the resulting initial and final porosities are 0.21 and 0.069, respectively.

Height of Complete Consolidation in Lower Shaft

Parameter:	**Height of complete consolidation in lower shaft**
Median:	2×10^2
Range:	1×10^2
	3×10^2
Units:	m
Distribution:	Uniform
Source(s):	Nowak, E. J., J. R. Tillerson, and T. M. Torres. 1990. *Initial Reference Seal System Design: Waste Isolation Pilot Plant.* SAND90-0355. Albuquerque, NM: Sandia National Laboratories. (p. 14)

Discussion:

The estimated range for the height of the final column of consolidated salt with 1×10^{-20} m^2 permeability is between 100 and 300 m, with an expected height of 200 m in each shaft (Nowak and Stormont, 1987; Lappin et al., 1989, p. 4-57). Figure 3.2-4 gives the distribution for height.

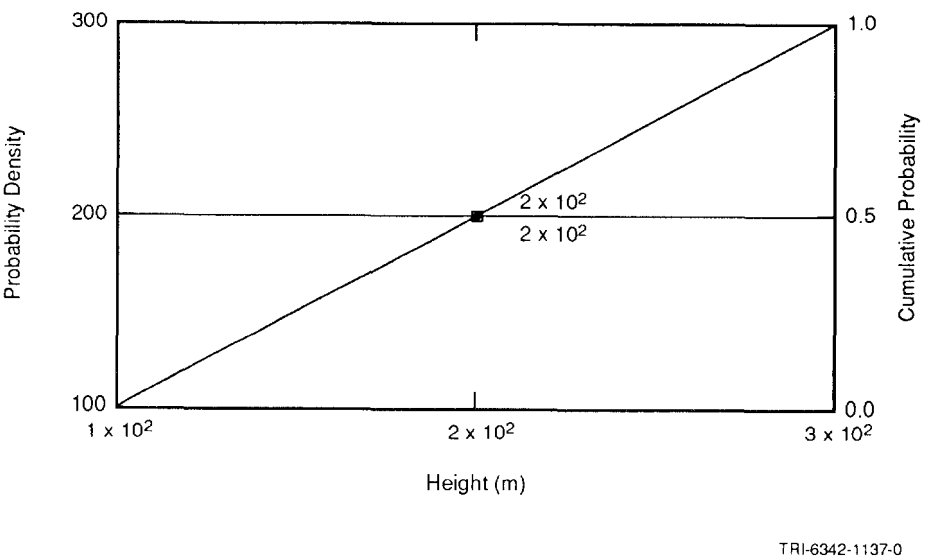

Figure 3.2-4. Estimated Distribution (pdf and cdf) for Height of Complete Consolidation in Lower Shaft.

Permeability for Preconsolidated Backfill ("Seals")

The initial and final permeability, porosity, and density of the salt component in the shaft, drift, and panel seals are as follows:

Parameter:	**Permeability, initial** (k)
Median:	1×10^{-14}
Range:	None
Units:	m^2
Distribution:	Constant
Source(s):	Holcomb, D. J. and M. Shields. 1987. *Hydrostatic Creep Consolidation of Crushed Salt with Added Water.* SAND87-1990. Albuquerque, NM: Sandia National Laboratories. (Figure 4)

Parameter:	**Permeability, final** (k)
Median:	1×10^{-20}
Range:	3.3×10^{-21}
	3.3×10^{-20}
Units:	m^2
Distribution:	Lognormal
Source(s):	Holcomb, D. J. and M. Shields. 1987. *Hydrostatic Creep Consolidation of Crushed Salt with Added Water.* SAND87-1990. Albuquerque, NM: Sandia National Laboratories. (Figure 4) Nowak, E. J., J. R. Tillerson, and T. M. Torres. 1990. *Initial Reference Seal System Design: Waste Isolation Pilot Plant.* SAND90-0355. Albuquerque, NM: Sandia National Laboratories. (Figure 11, p. 14)

Discussion:

Knowing the initial and final salt density, the final permeability was estimated from laboratory experiments (Holcomb and Shields, 1987, Figure 4) (Figure 3.2-5). The resulting initial and final permeabilities were 1×10^{-14} and 1×10^{-20} m^2. Nowak et al. (1990, p. 14) places a range of 3×10^{-21} to 3×10^{-20} m^2 on the final permeability. The lower limit is equivalent to that found by extrapolating the data in Figure 3.2-5 to a relative density of 0.95. Figure 3.2-6 illustrates the assumed time-dependent permeability relationship of the preconsolidated and normal backfill.

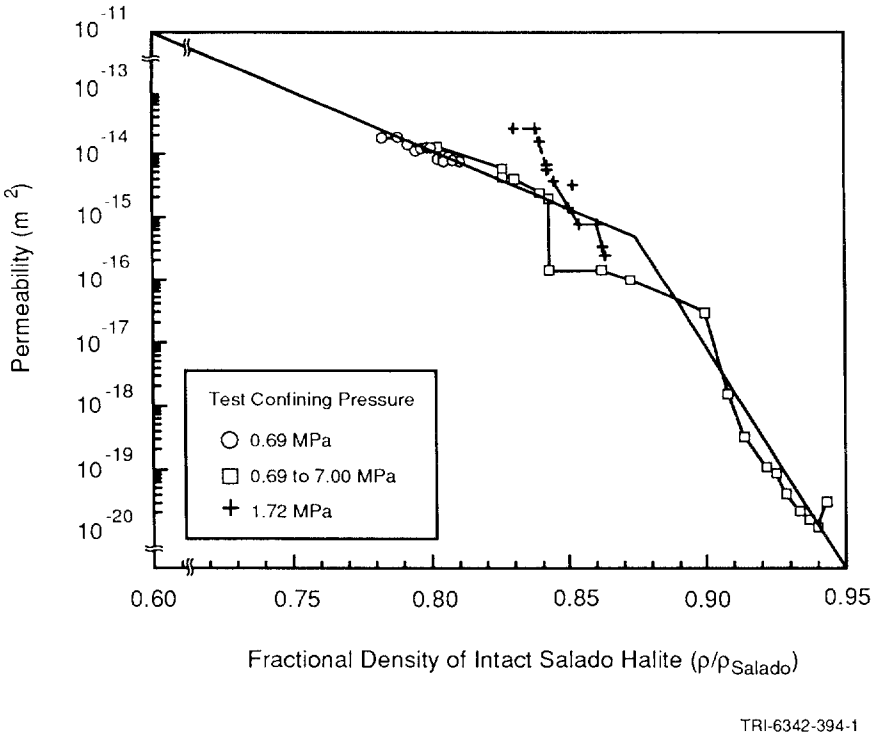

Figure 3.2-5. Permeability as a Function of Relative Halite Density (after Holcomb and Shields, 1987, Figure 4).

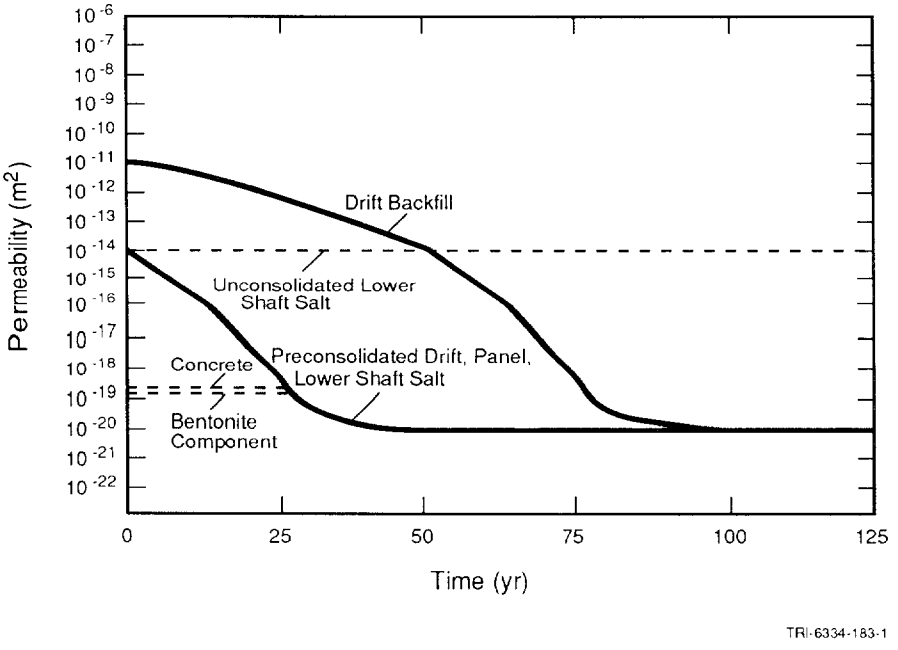

Figure 3.2-6. Time Variation of Permeability Decrease from Consolidation for Disposal Area, Drift, and Seal. Dashed line indicates seal permeability including the concrete/bentonite component (after Rechard et al., 1990b, Figure 3-30).

3.2.3 Salt Backfill in Drifts

Density for Backfill

Parameter:	**Density, initial (ρ)**
Median:	1.28×10^3 ($0.6\rho_{Salado}$)
Range:	None
Units:	kg/m^3
Distribution:	Constant
Source(s):	Nowak, E. J., J. R. Tillerson, and T. M. Torres. 1990. *Initial Reference Seal System Design: Waste Isolation Pilot Plant.* SAND90-0355. Albuquerque, NM: Sandia National Laboratories. (Figure 11)

Parameter:	**Density, final (ρ)**
Median:	2.03×10^3 ($0.95\rho_{Salado}$)
Range:	None
Units:	kg/m^3
Distribution:	Constant
Source(s):	Sjaardema, G. D. and R. D. Krieg. 1987. *A Constitutive Model for the Consolidation of WIPP Crushed Salt and Its Use in Analysis of Backfilled Shaft and Drift Configurations.* SAND87-1977. Albuquerque, NM: Sandia National Laboratories. Arguello, J.G. 1988. *WIPP Panel Entryway Seal - Numerical Simulation of Seal Composite Interaction for Preliminary Seal Design Evaluation.* SAND87-2804. Albuquerque, NM: Sandia National Laboratories.

Discussion:

The initial placement density for the crushed salt backfill is specified in the reference design as 0.6 of the intact Salado density ($0.6\rho_{Salado}$) (Nowak et al., 1990). The estimated final density of 0.95 of the intact Salado density ($0.95\rho_{Salado}$) comes from modeling (Sjaardema and Krieg, 1987; Arguello, 1988). The initial and final porosity can be calculated directly from the densities, assuming that the intact Salado density of 2.14×10^3 kg/m^3 with a porosity of 0.01 (see Table 2.3-1). The resulting initial and final porosities are 0.38 and 0.069, respectively.

Permeability

Parameter:	**Permeability, initial** (k)
Median:	1×10^{-11}
Range:	None
Units:	m^2
Distribution:	Constant
Source(s):	Holcomb, D. J. and M. Shields. 1987. *Hydrostatic Creep Consolidation of Crushed Salt with Added Water.* SAND87-1990. Albuquerque, NM: Sandia National Laboratories. (Figure 4)

Parameter:	**Permeability, final** (k)
Median:	1×10^{-20}
Range:	3.3×10^{-21} 3.3×10^{-20}
Units:	m^2
Distribution:	Lognormal
Source(s):	Holcomb, D. J. and M. Shields. 1987. *Hydrostatic Creep Consolidation of Crushed Salt with Added Water.* SAND87-1990. Albuquerque, NM: Sandia National Laboratories. (Figure 4) Nowak, E. J., J. R. Tillerson, and T. M. Torres. 1990. *Initial Reference Seal System Design: Waste Isolation Pilot Plant.* SAND90-0355. Albuquerque, NM: Sandia National Laboratories. (Figure 11, p. 14)

Discussion:

Knowing the initial and final salt density, the final permeability was estimated from laboratory experiments (Holcomb and Shields, 1987, Figure 4) (Figure 3.2-5); the initial permeability was found by extrapolating this data to the initial placement density of $0.6\rho_{Salado}$. The resulting initial and final permeabilities were 1×10^{-11} and 1×10^{-20} m^2. Nowak et al. (1990, p. 14) places a range of 3×10^{-21} to 3×10^{-20} m^2 on the final permeability. The lower limit can be found by extrapolating to a density of $0.95\rho_{Salado}$.

Figure 3.2-6 shows the assumed time variation of the decrease in permeability as the result of consolidation used in many current PA calculations. A linear permeability decrease over 50 yr was assumed until the drift backfill reached a density (and permeability) equal to the initial preconsolidated ("seal") permeability (1×10^{-14} m^2). Afterwards, the backfill permeability was assumed to decrease similar to the "seals."

3.2.4 Partition Coefficients for Salt Backfill

Table 3.2-2 provides the partition coefficients for salt backfill.

Table 3.2-2. Partition Coefficients for Salt Backfill Containing Trace (0.1%) Amounts of Clay (after Lappin et al., 1989, Table D-5)

Radionuclide	Partition Coefficient* (m^3/kg)
Am	1×10^{-4}
Np	1×10^{-5}
Pb	1×10^{-6}
Pu	1×10^{-4}
Ra	1×10^{-6}
Th	1×10^{-4}
U	1×10^{-6}

* Assumed constant

Discussion:

As mentioned for halite, none of the radionuclides is assumed to sorb onto halite ($K_d = 0$), but the crushed salt from the excavation will have small amounts of clay, which does sorb radionuclides. For those studies exploring the influence of retardation near the repository, partition coefficients similar to those for anhydrite (Section 2.4) are used, with the following exceptions: (1) americium and neptunium had larger values by a factor of 10 and (2) the values for anhydrite with clay were reduced by 1000 to account for only 0.1% clay volume in the backfill.

As a conservative assumption, the 1991 PA calculations do not consider adsorption of radionuclides in the salt backfill (similar to halite and anhydrite interbeds, Section 2.4).

3.2.5 Concrete and Bentonite

Parameter:	**Concrete permeability** (k)
Median:	2.7×10^{-19}
Range:	None
Units:	m^2
Distribution:	Constant
Source(s):	Nowak, E. J., J. R. Tillerson, and T. M. Torres. 1990. *Initial Reference Seal System Design: Waste Isolation Pilot Plant.* SAND90-0355. Albuquerque, NM: Sandia National Laboratories. (Figure 11, p. 13)

Parameter:	**Bentonite permeability** (k)
Median:	1.4×10^{-19}
Range:	None
Units:	m^2
Distribution:	Constant
Source(s):	Nowak, E. J., J. R. Tillerson, and T. M. Torres. 1990. *Initial Reference Seal System Design: Waste Isolation Pilot Plant.* SAND90-0355. Albuquerque, NM: Sandia National Laboratories. (Figure 11, p. 13)

Discussion:

Nowak et al. (1990, Figure 11) has specified maximum permissible permeabilities (as well as strength and expansion characteristics) for the concrete and bentonite (saturated in brine) components of the seals. The maximum permeabilities are 2.7×10^{-19} and 1.4×10^{-19} m^2 for the concrete and bentonite, respectively. Because all PA calculations have considered only the long-term salt components in the lower and upper shaft system and not examined the water-bearing zone shaft seal, these values have not been used to date.

3.3 Parameters for Contaminants Independent of Waste Form

The TRU waste for which the WIPP is designed is defense-program waste that has been generated at ten facilities since 1970. The waste consists of laboratory and production trash such as glassware, metal pipes, solvents, disposable laboratory clothing, cleaning rags, and solidified sludges. Current plans specify that most of the TRU waste generated since 1970 will be placed in the WIPP repository, with the remainder to be disposed of at other DOE facilities.

The ten defense facilities ("generators") that eventually will ship TRU waste to the WIPP are (1) Argonne National Laboratory-East (ANL-E), Illinois; (2) Hanford Reservation (HANF), Washington; (3) Idaho National Engineering Laboratory (INEL), Idaho; (4) Los Alamos National Laboratory (LANL), New Mexico; (5) Lawrence Livermore National Laboratory (LLNL), California; (6) Mound Laboratory, Ohio; (7) Nevada Test Site (NTS), Nevada; (8) Oak Ridge National Laboratory (ORNL), Tennessee; (9) Rocky Flats Plant (RFP), Colorado; and (10) Savannah River Site (SRS), South Carolina (U.S. DOE, 1990c).

The trash is contaminated by alpha-emitting transuranic elements, defined as having atomic numbers greater than uranium-92, half-lives greater than 20 yr, and curie contents greater than 100 nCi/g. Other contaminants include uranium and several radionuclides with half-lives less than 20 yr. Approximately 60% of the waste may be co-contaminated with waste considered hazardous under the RCRA, e.g., lead (WEC, 1989a).

Radioactive waste that emits alpha radiation, although dangerous if inhaled or ingested, is not hazardous externally. Most of the waste, therefore, can be contact handled (CH) because the external dose rate (5.6×10^{-7} Sv/s [200 mrem/h] or less) permits people to handle properly sealed drums and boxes without any special shielding.

A small portion of the TRU waste must be transported and handled in shielded casks (remotely handled [RH]), i.e., the surface dose rate exceeds 5.6×10^{-7} Sv/s (200 mrem/h). The surface dose rate of RH-TRU canisters cannot exceed 2.8×10^{-3} Sv/s (1000 rem/h); however, no more than 5% of the canisters can exceed 2.8×10^{-4} Sv/s (100 rem/h) (U.S. DOE, 1990d). The total curie content is being determined but the volume must be less than 250,000 m^3 and the curie content must be less than 5.1×10^6 Ci (1.89×10^{17} Bq) according to the agreement between DOE and the State of New Mexico (U.S. DOE/NM, 1984).

Subpart B of the Standard sets release limits in curies for isotopes of americium, carbon, cesium, iodine, neptunium, plutonium, radium, strontium, technetium, thorium, tin, and uranium, as well as for certain other radionuclides (Section 3.3.4 of this volume). Although the initial WIPP inventory contains little or none of some of the listed nuclides, they may be produced as a result of radioactive decay and must be accounted for in the compliance evaluation; moreover, any radionuclides not listed in Subpart B must be accounted for if those radionuclides would contribute to doses used in NEPA calculations (e.g., Pb-210).

Figure 3.3-1 shows the total activity for all stored, projected, and scaled CH waste. Figure 3.3-2 gives the same information for RH waste. Table 3.3-1 provides the parameters for TRU radionuclides. Table 3.3-2 provides the parameter values for TRU waste.

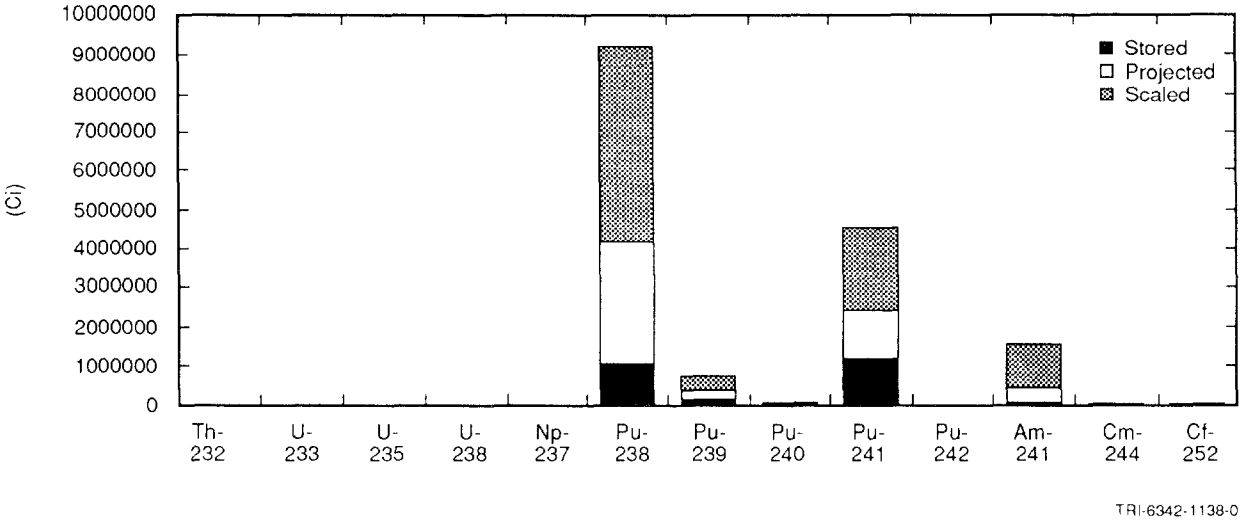

Figure 3.3-1. Total Activity for Stored, Projected, and Scaled CH Waste Activities.

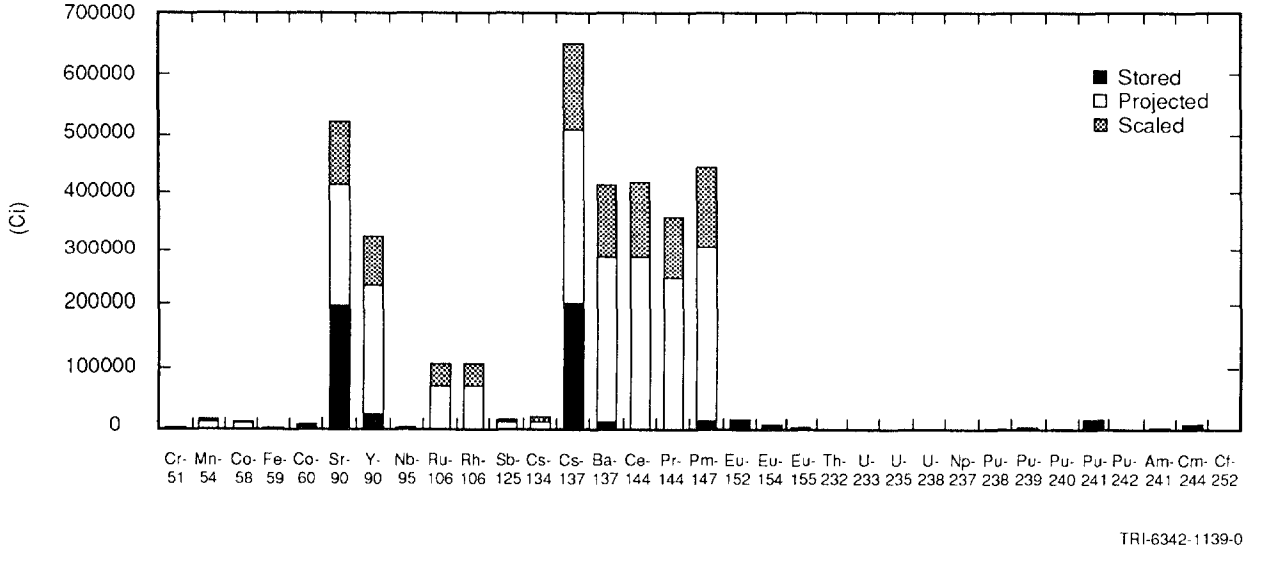

Figure 3.3-2. Total Activity for Stored, Projected, and Scaled RH Waste Activities.

Table 3.3-1. Inventory and Parameter Values for TRU Radioisotopes

Parameter	Median	Units	Source
Ac225			
Half-life	8.640×10^{5}	s	ICRP, Pub 38, 1983
Ac227			
Half-life	6.871×10^{8}	s	ICRP, Pub 38, 1983
Ac228			
Half-life	2.207×10^{4}	s	ICRP, Pub 38, 1983
Am241			
Activity conversion	3.43×10^{3}	Ci/kg	1.1281×10^{16}/(half-life(s)xAt.Wt.)
Half-life	1.364×10^{10}	s	ICRP, Pub 38, 1983
Inventory, Anticipated (1990)			
CH	6.65×10^{6}	Ci	See text.
RH	1.29×10^{3}	Ci	IDB, 1990; Peterson, 1990
Inventory, Design (1990)			
CH	1.65×10^{6}	Ci	See text.
RH	1.46×10^{3}	Ci	IDB, 1990; Peterson, 1990
Am243			
Half-life	5.822×10^{11}	s	ICRP, Pub 38, 1983
At217			
Half-life	3.230×10^{-2}	s	ICRP, Pub 38, 1983
Bi210			
Half-life	4.330×10^{5}	s	ICRP, Pub 38, 1983
Bi211			
Half-life	1.284×10^{2}	s	ICRP, Pub 38, 1983
Bi212			
Half-life	3.633×10^{3}	s	ICRP, Pub 38, 1983
Bi213			
Half-life	2.739×10^{3}	s	ICRP, Pub 38, 1983
Bi214			
Half-life	1.194×10^{3}	s	ICRP, Pub 38, 1983

Table 3.3-1. Inventory and Parameter Values for TRU Radioisotopes (Continued)

Parameter	Median	Units	Source
Cf252			
Activity conversion	5.38×10^{5}	Ci/kg	1.1281×10^{16}/(half-life(s)xAt.Wt.)
Half-life	8.325×10^{7}	s	ICRP, Pub 38, 1983
Inventory, Anticipated (1990)			
CH	1.27×10^{4}	Ci	See text.
RH	2.39×10^{3}	Ci	IDB, 1990; Peterson, 1990
Inventory, Design (1990)			
CH	1.84×10^{4}	Ci	See text.
RH	1.25×10^{2}	Ci	IDB, 1990; Peterson, 1990
Cm244			
Activity conversion	8.09×10^{4}	Ci/kg	1.1281×10^{16}/(half-life(s)xAt.Wt.)
Half-life	5.715×10^{8}	s	ICRP, Pub 38, 1983
Inventory, Anticipated (1990)			
CH	1.23×10^{4}	Ci	See text.
RH	8.75×10^{3}	Ci	IDB, 1990; Peterson, 1990
Inventory, Design (1990)			
CH	1.78×10^{4}	Ci	See text.
RH	4.63×10^{3}	Ci	IDB, 1990; Peterson, 1990
Cs137			
Activity conversion	8.70×10^{4}	Ci/kg	1.1281×10^{16}/(half-life(s)xAt.Wt.)
Half-life	9.467×10^{8}	s	ICRP, Pub 38, 1983
Inventory, Anticipated (1990)			
RH	3.33×10^{5}	Ci	IDB, 1990; Peterson, 1990
Inventory, Design (1990)			
RH	6.54×10^{5}	Ci	IDB, 1990; Peterson, 1990
Fr221			
Half-life	2.880×10^{2}	s	ICRP, Pub 38, 1983

Table 3.3-1. Inventory and Parameter Values for TRU Radioisotopes (Continued)

Parameter	Median	Units	Source
Np237			
Activity conversion	7.05×10^{-1}	Ci/kg	1.1281×10^{16}/(half-life(s)xAt.Wt.)
Half-life	6.753×10^{13}	s	ICRP, Pub 38, 1983
Inventory, Anticipated (1990)			
CH	1.47	Ci	See text.
RH	8.87×10^{-1}	Ci	IDB, 1990; Peterson, 1990
Inventory, Design (1990)			
CH	2.14	Ci	See text.
RH	1.29	Ci	IDB, 1990; Peterson, 1990
Np239			
Half-life	2.035×10^{5}	s	ICRP, Pub 38, 1983
Pa231			
Half-life	1.034×10^{12}	s	ICRP, Pub 38, 1983
Pa233			
Half-life	2.333×10^{6}	s	ICRP, Pub 38, 1983
Pb209			
Half-life	1.171×10^{4}	s	ICRP, Pub 38, 1983
Pb210			
Activity conversion	7.63×10^{4}	Ci/kg	1.1281×10^{16}/(half-life(s)xAt.Wt.)
Half-life	7.037×10^{8}	s	ICRP, Pub 38, 1983
Pb211			
Half-life	2.166×10^{3}	s	ICRP, Pub 38, 1983
Pb212			
Half-life	3.830×10^{4}	s	ICRP, Pub 38, 1983
Pb214			
Half-life	1.608×10^{3}	s	ICRP, Pub 38, 1983
Pm147			
Activity conversion	9.27×10^{5}	Ci/kg	1.1281×10^{16}/(half-life(s)xAt.Wt.)
Half-life	8.279×10^{7}	s	ICRP, Pub 38, 1983
Inventory, Anticipated (1990)			
RH	3.15×10^{5}	Ci	IDB, 1990; Peterson, 1990

Table 3.3-1. Inventory and Parameter Values for TRU Radioisotopes (Continued)

Parameter	Median	Units	Source
Inventory, Design (1990)			
RH	4.49×10^{5}	Ci	IDB, 1990; Peterson, 1990
Po210			
Half-life	1.196×10^{7}	s	ICRP, Pub 38, 1983
Po212			
Half-life	3.050×10^{-7}	s	ICRP, Pub 38, 1983
Po213			
Half-life	4.200×10^{-6}	s	ICRP, Pub 38, 1983
Po214			
Half-life	1.643×10^{-4}	s	ICRP, Pub 38, 1983
Po215			
Half-life	1.780×10^{-3}	s	ICRP, Pub 38, 1983
Po216			
Half-life	1.500×10^{-1}	s	ICRP, Pub 38, 1983
Po218			
Half-life	1.830×10^{2}	s	ICRP, Pub 38, 1983
Pu238			
Activity conversion	1.71×10^{4}	Ci/kg	1.1281×10^{16}/(half-life(s)xAt.Wt.)
Half-life	2.769×10^{9}	s	ICRP, Pub 38, 1983
Inventory, Anticipated (1990)			
CH	4.26×10^{6}	Ci	See text.
RH	5.14×10^{2}	Ci	IDB, 1990; Peterson, 1990
Inventory, Design (1990)			
CH	9.26×10^{6}	Ci	See text.
RH	1.33×10^{3}	Ci	IDB, 1990; Peterson, 1990
Pu239			
Activity conversion	6.22×10^{1}	Ci/kg	1.1281×10^{16}/(half-life(s)xAt.Wt.)
Half-life	7.594×10^{11}	s	ICRP, Pub 38, 1983

Table 3.3-1. Inventory and Parameter Values for TRU Radioisotopes (Continued)

Parameter	Median	Units	Source
Inventory, Anticipated (1990)			
CH	4.37×10^{5}	Ci	See text.
RH	1.45×10^{3}	Ci	IDB, 1990; Peterson, 1990
Inventory, Design (1990)			
CH	8.45×10^{5}	Ci	See text.
RH	1.31×10^{3}	Ci	IDB, 1990; Peterson, 1990
Pu240			
Activity conversion	2.28×10^{2}	Ci/kg	1.1281×10^{16}(half-life(s)xAt.Wt.)
Half-life	2.063×10^{11}	s	ICRP, Pub 38, 1983
Inventory, Anticipated (1990)			
CH	5.91×10^{4}	Ci	See text.
RH	2.89×10^{2}	Ci	IDB, 1990; Peterson, 1990
Inventory, Design (1990)			
CH	1.07×10^{5}	Ci	See text.
RH	2.98×10^{2}	Ci	IDB, 1990; Peterson, 1990
Pu241			
Activity conversion	1.03×10^{5}	Ci/kg	1.1281×10^{16}/half-life(s)xAt.Wt.)
Half-life	4.544×10^{8}	s	ICRP, Pub 38, 1983
Inventory, Anticipated (1990)			
CH	2.54×10^{6}	Ci	See text.
RH	1.32×10^{4}	Ci	IDB, 1990; Peterson, 1990
Inventory, Design (1990)			
CH	4.60×10^{6}	Ci	See text.
RH	1.35×10^{4}	Ci	IDB, 1990; Peterson, 1990
Pu242			
Activity conversion	3.93	Ci/kg	1.1281×10^{16}/(half-life(s)xAt.Wt.)
Half-life	1.187×10^{13}	s	ICRP, Pub 38, 1983
Inventory, Anticipated (1990)			
CH	1.84	Ci	See text.
RH	3.31×10^{-3}	Ci	IDB, 1990; Peterson, 1990
Inventory, Design (1990)			
CH	2.16	Ci	See text.
RH	4.07×10^{-3}	Ci	IDB, 1990; Peterson, 1990

Table 3.3-1. Inventory and Parameter Values for TRU Radioisotopes (Continued)

Parameter	Median	Units	Source
Ra223			
Half-life	9.879×10^{5}	s	ICRP, Pub 38, 1983
Ra224			
Half-life	3.162×10^{5}	s	ICRP, Pub 38, 1983
Ra225			
Half-life	1.279×10^{6}	s	ICRP, Pub 38, 1983
Ra226			
Activity conversion	9.89×10^{2}	Ci/kg	1.1281×10^{16}/(half-life(s)xAt.Wt.)
Half-life	5.049×10^{10}	s	ICRP, Pub 38, 1983
Ra228			
Half-life	1.815×10^{8}	s	ICRP, Pub 38, 1983
Rn219			
Half-life	3.960	s	ICRP, Pub 38, 1983
Rn220			
Half-life	5.560×10^{1}	s	ICRP, Pub 38, 1983
Rn222			
Half-life	3.304×10^{5}	s	ICRP, Pub 38, 1983
Sr90			
Activity conversion	1.36×10^{5}	Ci/kg	1.1281×10^{16}/(half-life(s)xAt.Wt.)
Half-life	9.189×10^{8}	s	ICRP, Pub 38, 1983
Inventory, Anticipated (1990)			
RH	2.80×10^{5}	Ci	IDB, 1990; Peterson, 1990
Inventory, Design (1990)			
RH	5.21×10^{5}	Ci	IDB, 1990; Peterson, 1990
Th227			
Half-life	1.617×10^{6}	s	ICRP, Pub 38, 1983
Th228			
Half-life	6.037×10^{7}	s	ICRP, Pub 38, 1983

Table 3.3-1. Inventory and Parameter Values for TRU Radioisotopes (Continued)

Parameter	Median	Units	Source
Th229			
Activity conversion	2.13×10^{2}	Ci/kg	1.1281×10^{16}/(half-life(s)xAt.Wt.)
Half-life	2.316×10^{11}	s	ICRP, Pub 38, 1983
Th230			
Activity conversion	2.02×10^{1}	Ci/kg	1.1281×10^{16}/(half-life(s)xAt.Wt.)
Half-life	2.430×10^{12}	s	ICRP, Pub 38, 1983
Th231			
Half-life	9.187×10^{4}	s	ICRP, Pub 38, 1983
Th232			
Activity conversion	1.10×10^{-4}	Ci/kg	1.1281×10^{16}/(half-life(s)xAt.Wt.)
Half-life	4.434×10^{17}	s	ICRP, Pub 38, 1983
Inventory, Anticipated (1990)			
CH	0.0	Ci	See text.
RH	0.0	Ci	IDB, 1990; Peterson, 1990
Inventory, Design (1990)			
CH	0.0	Ci	See text.
RH	0.0	Ci	IDB, 1990; Peterson, 1990
Th234			
Half-life	2.082×10^{6}	s	ICRP, Pub 38, 1983
Tl207			
Half-life	2.862×10^{2}	s	ICRP, Pub 38, 1983
U233			
Activity conversion	9.68	Ci/kg	1.1281×10^{16}/(half-life(s)xAt.Wt.)
Half-life	5.002×10^{12}	s	ICRP, Pub 38, 1983
Inventory, Anticipated (1990)			
CH	7.18×10^{1}	Ci	See text.
RH	2.86×10^{1}	Ci	IDB, 1990; Peterson, 1990
Inventory, Design (1990)			
CH	1.04×10^{2}	Ci	See text.
RH	2.02×10^{2}	Ci	IDB, 1990; Peterson, 1990
U234			
Activity conversion	6.25	Ci/kg	1.1281×10^{16}/(half-life(s)xAt.Wt.)
Half-life	7.716×10^{12}	s	ICRP, Pub 38, 1983

Table 3.3-1. Inventory and Parameter Values for TRU Radioisotopes (Concluded)

Parameter	Median	Units	Source
U235			
Activity conversion	2.16×10^{-3}	Ci/kg	1.1281×10^{16}/(half-life(s)xAt.Wt.)
Half-life	2.221×10^{16}	s	ICRP, Pub 38, 1983
Inventory, Anticipated (1990)			
CH	5.54×10^{-2}	Ci	See text.
RH	1.23×10^{-2}	Ci	IDB, 1990; Peterson, 1990
Inventory, Design (1990)			
CH	1.43×10^{-1}	Ci	See text.
RH	1.39×10^{-2}	Ci	IDB, 1990; Peterson, 1990
U236			
Half-life	7.389×10^{14}	s	ICRP, Pub 38, 1983
U238			
Activity conversion	3.36×10^{-4}	Ci/kg	1.1281×10^{16}/(half-life(s)xAt.Wt.)
Half-life	1.410×10^{17}	s	ICRP, Pub 38, 1983
Inventory, Anticipated (1990)			
CH	0.0	Ci	See text.
RH	7.83×10^{-2}	Ci	IDB, 1990; Peterson, 1990
Inventory, Design (1990)			
CH	0.0	Ci	See text.
RH	8.71×10^{-2}	Ci	IDB, 1990; Peterson, 1990

Table 3.3-2. Parameter Values for TRU Waste Radioelements

Parameter	Median	Range		Units	Distribution Type	Source
Gas generation						
Corrosion						
Inundated rate	6.3×10^{-9}	0	1.3×10^{-8}	mol/m^2/s*	Cumulative	Brush, July 8, 1991, Memo (Appendix A)
Relative humid rate	1×10^{-1}	0	5×10^{-1}	none	Cumulative	Brush, July 8, 1991, Memo (Appendix A)
Microbiological						
Inundated rate	3.2×10^{-9}	0	1.6×10^{-8}	mol/kg/s**	Cumulative	Brush, July 8, 1991, Memo (Appendix A)
Relative humid rate	1×10^{-1}	0	2×10^{-1}	none	Uniform	Brush, July 8, 1991, Memo (Appendix A)
Radiolysis	1×10^{-4}	1×10^{-7}	1×10^{-1}	mol/drum/yr	Constant	Brush, July 8, 1991, Memo (Appendix A)
Gas generation stoichiometry factor						
Corrosion	5×10^{-1}	0	1	none	Uniform	Brush and Anderson in Lappin et al., 1989, p. A-6
Microbiological	8.35×10^{-1}	0	1.67	none	Uniform	Brush and Anderson in Lappin et al., 1989, p. A-10
Am						
Diffusion coefficient***	1.76×10^{-10}	5.3×10^{-11}	3×10^{-10}	m^2/s	Uniform	Lappin et al.,1989, Table E-7
Am^{3+}						
Solubility	1×10^{-9}	5×10^{-14}	1.4	Molar	Cumulative	Trauth et al., 1991
Cm						
Diffusion coefficient	1.76×10^{-10}	5.3×10^{-11}	3×10^{-10}	m^2/s	Uniform	Lappin et al.,1989, Table E-7
Cm^{3+}						
Solubility	1×10^{-9}	5×10^{-14}	1.4	Molar	Cumulative	Trauth et al., 1991
Np						
Diffusion coefficient	1.76×10^{-10}	5.2×10^{-11}	3×10^{-10}	m^2/s	Uniform	Lappin et al.,1989, Table E-7
Np^{4+}						
Solubility	6×10^{-9}	3×10^{-16}	2×10^{-5}	Molar	Cumulative	Trauth et al., 1991
Np^{5+}						
Solubility	6×10^{-7}	3×10^{-11}	1.2×10^{-2}	Molar	Cumulative	Trauth et al., 1991
Pb						
Diffusion coefficient	4×10^{-10}	2×10^{-10}	8×10^{-10}	m^2/s	Cumulative	Lappin et al.,1989, Table E-7

* mole/m^2 surface area steel/s
** mole/kg cellulosics/s
*** Free liquid diffusion coefficient of the indicated species

Table 3.3-2. Parameter Values for TRU Waste Radioelements (Concluded)

Parameter	Median	Range		Units	Distribution Type	Source
Pb^{2+}						
Solubility						
Absence of CO^3	1.64	$1x10^{-2}$	$1x10^{1}$	Molar	Cumulative	Trauth et al., 1991
Presence of CO^3	$8x10^{-3}$	$1x10^{-9}$	$8x10^{-2}$	Molar	Cumulative	Trauth et al., 1991
Pu						
Diffusion coefficient	$1.74x10^{-10}$	$4.8x10^{-11}$	$3x10^{-10}$	m^2/s	Uniform	Lappin et al.,1989, Table E-7
Pu^{4+}						
Solubility	$6x10^{-10}$	$2.0x10^{-16}$	$4x10^{-6}$	molar	Cumulative	Trauth et al., 1991
Pu^{5+}						
Solubility	$6x10^{-10}$	$2.5x10^{-17}$	$5.5x10^{-4}$	Molar	Cumulative	Trauth et al., 1991
Ra						
Diffusion coefficient	$3.75x10^{-10}$	$1.88x10^{-10}$	$7.5x10^{-10}$	m^2/s	Cumulative	Lappin et al.,1989, Table E-7
Ra^{2+}						
Solubility						
Absence of CO^3 and SO^4	$1.1x10^{1}$	2	$1.8x10^{1}$	Molar	Cumulative	Trauth et al., 1991
Presence of CO^3	$1.6x10^{-6}$	$1.6x10^{-9}$	1	Molar	Cumulative	Trauth et al., 1991
Presence of SO^4	$1x10^{-8}$	$1x10^{-11}$	$1x10^{-6}$	Molar	Cumulative	Trauth et al., 1991
Th						
Diffusion coefficient	$1x10^{-10}$	$5x10^{-11}$	$1.5x10^{-10}$	m^2/s	Uniform	Lappin et al.,1989, Table E-7
Th^{4+}						
Solubility	$1x10^{-10}$	$5.5x10^{-16}$	$2.2x10^{-6}$	Molar	Cumulative	Trauth et al., 1991
U						
Diffusion coefficient	$2.7x10^{-10}$	$1.1x10^{-10}$	$4.3x10^{-10}$	m^2/s	Uniform	Lappin et al.,1989, Table E-7
U^{4+}						
Solubility	$1x10^{-4}$	$1x10^{-15}$	$5x10^{-2}$	Molar	Cumulative	Trauth et al., 1991
U^{6+}						
Solubility	$2x10^{-3}$	$1x10^{-7}$	1	Molar	Cumulative	Trauth et al., 1991

3.3.1 Inventory of Radionuclides in Contact-Handled Waste

The inventory (curie content) of radionuclides in the contact-handled (CH) waste was estimated from input submitted to the 1990 Integrated Date Base (IDB) (IDB, 1990). The information submitted to the IDB is separated into retrievably stored and newly generated (future generation), referred to herein as projected inventory. The anticipated total volume (stored plus projected) of CH waste submitted to the 1990 IDB was 1.06 x 10^5 m^3 (3.76 x 10^6 ft^3), which is less than the current design volume for the WIPP of about 1.8 x 10^5 m^3 (6.2 x 10^6 ft^3). To estimate the total curie content in the WIPP, if it contained a design volume of CH waste, the future-generated radionuclide inventories of the five largest future generators listed in the 1990 IDB were volume scaled to reach a design volume of waste. (Details of this volume scaling are discussed in Section 3.4.) This inventory per generator site is only a projected estimate and should not be considered a statement of what they will generate.

The weight fractions reported in the 1990 IDB were used to calculate the major radionuclides of the mixes reported. The IDB did not report the inventory of each radionuclide. Rather the inventory of each radionuclide at each site was based on the mix of waste streams reported. The Hanford submittal to the 1990 IDB indicated that the activity of some of the CH waste was currently unknown. Rather than underestimate the potential inventory, the Hanford input to the 1987 IDB was used. These inventories have not been independently checked and should be considered preliminary estimates.

The estimate of the radionuclide inventory for the retrievably stored waste at the 10 generator/storage sites is listed in Table 3.3-3. The estimated total curie content of the retrievably stored waste was 2.6 x 10^6 Ci (9.7 x 10^{16} Bq). The projected radionuclide inventory is also listed in Table 3.3-4. The estimated total curie content of the projected waste is 5.4 x 10^6 Ci (1.99 x 10^{17} Bq).

The estimated inventory of radionuclides, based on volume scaling, that could be emplaced in the WIPP if the total design volume were used is shown in Table 3.3-5; the total is about 1.65 x 10^7 Ci (6.1 x 10^{17} Bq). This inventory is different from that reported in Lappin et al. (1989, 1990). The input for this estimate was based on input to the 1990 IDB, whereas the earlier estimate was based on input to the 1987 IDB. Note that the estimate for Hanford was based on the 1987 input since the 1990 IDB input indicated that the total was unknown.

The estimated radionuclide inventory of CH waste by site and isotope is illustrated in Figure 3.3-3.

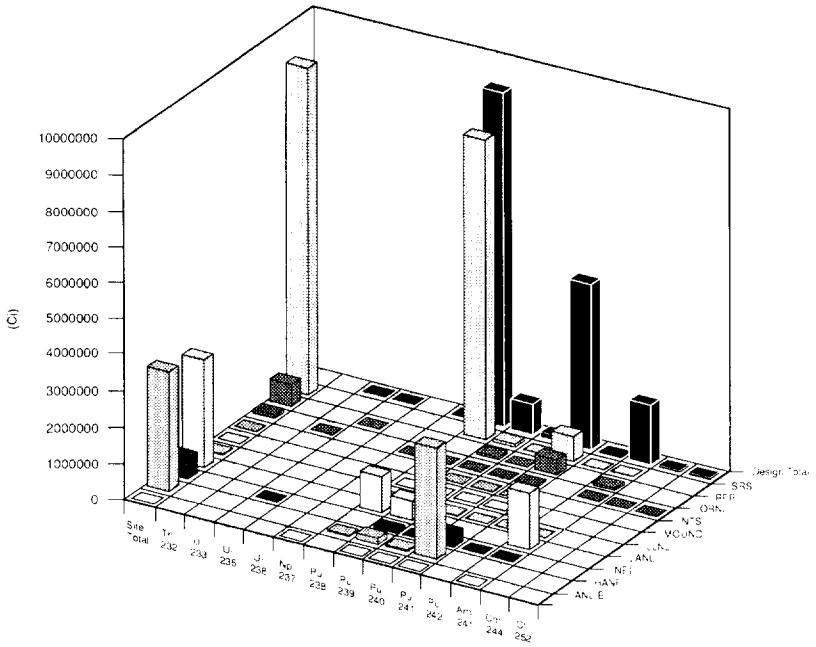

(a)

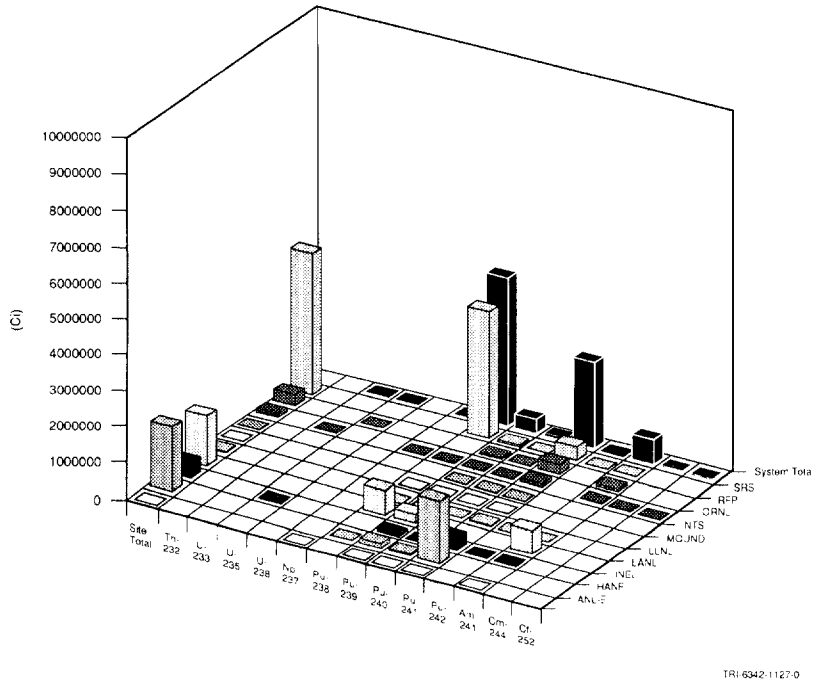

(b)

Figure 3.3-3. Estimate of Radionuclide Inventory of CH Waste by Site and Isotope for (a) Design Total, (b) Anticipated System Total, (c) Projected Total, and (d) Stored Total.

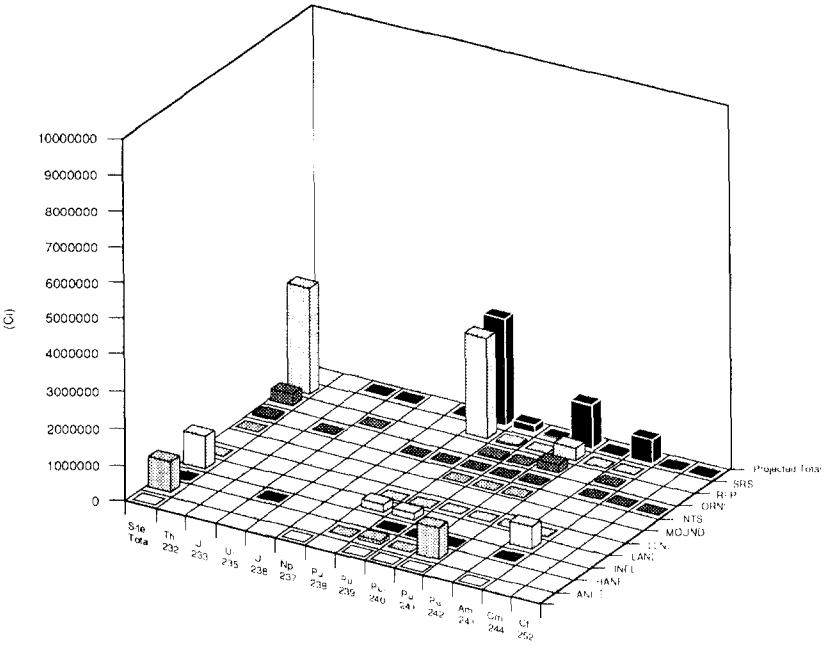

(c)

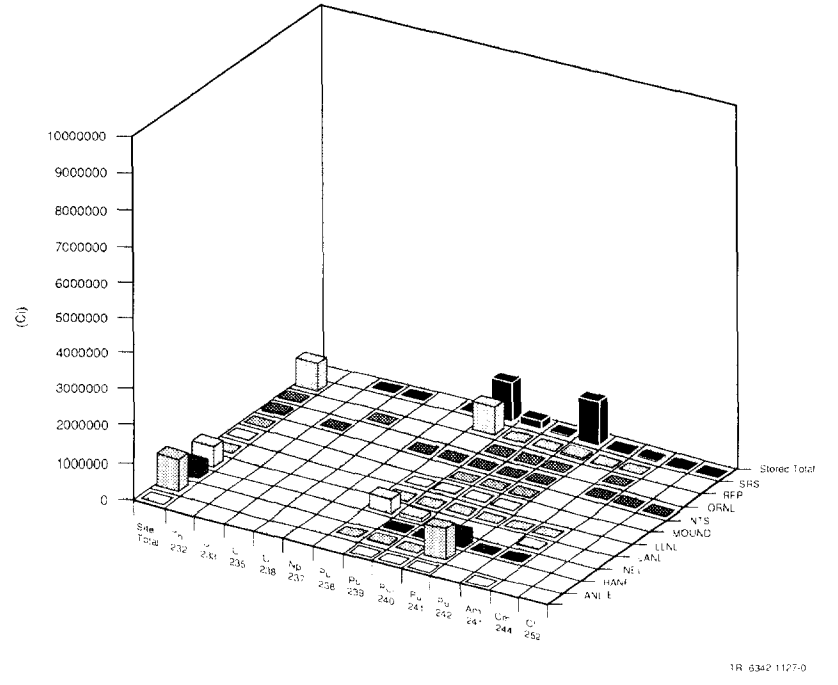

(d)

Figure 3.3-3. Estimate of Radionuclide Inventory of CH Waste by Site and Isotope for (a) Design Total, (b) Anticipated System Total, (c) Projected Total, and (d) Stored Total. (Concluded)

Table 3.3-3. Retrievably Stored[a] Design Radionuclide Inventory by Waste Generator for Contact-Handled Waste

Radionuclide	Half-Life (s)	ANL-E (Ci)	HANF[b] (Ci)	INEL (Ci)	LANL (Ci)	LLNL (Ci)	MOUND (Ci)	NTS (Ci)	ORNL (Ci)	RFP (Ci)	SRS (Ci)	Stored Total (Ci)
Th-232	4.4337×10^{17}	--	--	--	--	--	--	--	--	--	--	0.0
U-233	5.0018×10^{12}	--	--	--	--	--	--	--	4.0×10^{1}	--	--	4.0×10^{1}
U-235	2.221×10^{16}	--	--	--	--	--	--	--	--	4.69×10^{-4}	--	4.69×10^{-4}
U-238	1.41×10^{17}	--	--	--	--	--	--	--	--	--	--	0.0
Np-237	6.753×10^{13}	--	--	--	--	--	--	--	8.0×10^{-1}	--	--	8.0×10^{-1}
Pu-238	2.7688×10^{9}	--	3.819×10^{3}	--	3.558×10^{5}	9.377×10^{1}	2.312×10^{3}	--	6.86×10^{3}	--	7.460×10^{5}	1.115×10^{6}
Pu-239	7.5492×10^{11}	1.0	4.242×10^{4}	5.012×10^{4}	7.886×10^{4}	1.673×10^{3}	1.79	6.586×10^{1}	6.23×10^{2}	2.045×10^{3}	3.677×10^{3}	1.795×10^{5}
Pu-240	2.0629×10^{11}	4.3×10^{-1}	1.511×10^{4}	1.146×10^{4}	--	5.431×10^{2}	1.15	1.517×10^{1}	3.062×10^{2}	4.686×10^{2}	1.015×10^{3}	2.892×10^{4}
Pu-241	4.5422×10^{8}	1.922×10^{1}	7.687×10^{5}	3.571×10^{5}	--	1.308×10^{4}	1.04	6.31×10^{2}	3.405×10^{4}	1.119×10^{4}	5.283×10^{4}	1.238×10^{6}
Pu-242	1.1875×10^{13}		--	1.02	--	4.3×10^{-1}	--	--	--	--	1.7×10^{-1}	1.62
Am-241	1.3639×10^{10}	6.4×10^{-1}	--	2.722×10^{3}	4.022×10^{4}	1.371×10^{3}	--	--	5.045×10^{2}	2.113×10^{3}	5.687×10^{2}	4.75×10^{4}
Cm-244	5.715×10^{8}	--	--	--	--	--	--	--	6.796×10^{3}	--	--	6.796×10^{3}
Cf-252	8.3247×10^{7}	--	--	--	--	--	--	--	7.055×10^{3}	--	--	7.055×10^{3}
TOTALS		2.129×10^{1}	8.301×10^{5}	4.214×10^{5}	4.749×10^{5}	1.676×10^{4}	2.316×10^{3}	7.12×10^{2}	5.624×10^{4}	1.581×10^{4}	8.041×10^{5}	2.622×10^{6}

[a] Stored as of December 31, 1989 such that containers can be retrieved and shipped to the WIPP.

[b] Based on 1987 input since 1990 total was unknown.

Table 3.3-4. Projected[a] Radionuclide Inventory by Waste Generator for Contact-Handled Waste (Curies)

Radionuclide	ANL-E	HANF[b,c]	INEL[c]	LANL[c]	LLNL	MOUND	NTS	ORNL	RFP[c]	SRS[c]	Projected Total	(Projected + Stored) System Total 1990	(Projected + Stored) System Total 1987
Th-232	--	--	--	--	--	--	--	--	--	--	--	0.0	$2.74x10^{-1}$
U-233	--	--	--	--	--	--	--	$3.185x10^{1}$	--	--	$3.185x10^{1}$	$7.185x10^{1}$	$7.7x10^{3}$
U-235	--	--	$4.8x10^{-2}$	--	--	--	--	--	$6.924x10^{-3}$	--	$5.492x10^{-2}$	$5.539x10^{-2}$	$3.73x10^{-1}$
U-238	--	--	--	--	--	--	--	--	--	--	0.0	0.0	1.49
Np-237	$2.0x10^{-2}$	--	--	--	--	--	--	$6.5x10^{-1}$	--	--	$6.7x10^{-1}$	1.47	8.01
Pu-238	--	$4.362x10^{3}$	--	$2.231x10^{5}$	9.15	--	--	$5.529x10^{3}$	--	$2.913x10^{6}$	$3.146x10^{6}$	$4.261x10^{6}$	$3.91x10^{6}$
Pu-239	$3.212x10^{1}$	$4.742x10^{4}$	$4.415x10^{2}$	$1.554x10^{5}$	$1.876x10^{2}$	--	--	$5.053x10^{2}$	$3.016x10^{4}$	$2.288x10^{4}$	$2.571x10^{5}$	$4.366x10^{5}$	$4.24x10^{5}$
Pu-240	$1.148x10^{1}$	$1.689x10^{4}$	$1.824x10^{2}$	--	$4.574x10^{1}$	--	--	$2.468x10^{2}$	$6.912x10^{3}$	$5.897x10^{3}$	$3.02x10^{4}$	$5.912x10^{4}$	$1 x 10^{5}$
Pu-241	$6.255x10^{2}$	$8.593x10^{5}$	$6.409x10^{2}$	--	$1.302x10^{3}$	--	--	$2.744x10^{4}$	$1.65x10^{5}$	$2.509x10^{5}$	$1.306x10^{6}$	$2.54x10^{6}$	$4.1 x 10^{6}$
Pu-242	--	--	--	--	$5.0x10^{2}$	--	--	--	--	$1.7x10^{-1}$	$2.2x10^{-1}$	1.84	$1.83x10^{1}$
Am-241	$2.085x10^{1}$	--	$1.211x10^{2}$	$5.815x10^{5}$	$2.534x10^{1}$	--	--	$4.066x10^{2}$	$3.118x10^{4}$	$3.76x10^{3}$	$6.17x10^{5}$	$6.645x10^{5}$	$6.34x10^{5}$
Cm-244	--	--	--	--	--	--	--	$5.477x10^{3}$	--	--	$5.477x10^{3}$	$1.227x10^{4}$	$1.27x10^{4}$
Cf-252	--	--	--	--	--	--	--	$5.685x10^{3}$	--	--	$5.685x10^{3}$	$1.274x10^{4}$	$2.02x10^{3}$
Projected Totals	$6.9x10^{2}$	$9.28x10^{5}$	$1.386x10^{3}$	$9.6x10^{5}$	$1.57x10^{3}$	0.0	0.0	$4.532x10^{4}$	$2.333x10^{5}$	$3.196x10^{6}$	$5.367x10^{6}$	$7.99 x 10^{6}$	$9.19 x 10^{6}$
Percent of Design Total	0.0	5.63	0.01	5.82	0.01	0.0	0.0	0.27	1.41	19.38	32.54		
System Total		$1.401x10^{3}$	$3.233x10^{6}$	$4.25x10^{5}$	$2.961x10^{6}$	$1.99x10^{4}$	$7.12x10^{2}$	$2.139x10^{-3}$	$1.469x10^{5}$	$6.2x10^{5}$	$9.082x10^{6}$		

[a] Generated between 1990 and 2013

b Based on 1987 input since 1990 total was unknown.

[c] One of five DOE defense facilities, which produce the largest volume of waste and are used to scale the inventory.

Table 3.3-5. Design Radionuclide Inventory by Waste Generator for Contact-Handled Waste (Curies)

Radionuclide	ANL-E	HANF	INEL	LANL	LLNL	MOUND	NTS	ORNL	RFP	SRS	PA Calculations Design 1990	Waste Unit Factor
Th-232	--	--	--	--	--	--	--	--	--	--	0.0	0.0
U-233	--	--	--	--	--	--	--	1.037×10^{2}	--	--	1.037×1^{2}	--
U-235	--	--	1.243×10^{-1}	--	--	--	--	--	1.84×10^{-2}	--	1.427×10^{-1}	--
U-238	--	--	--	--	--	--	--	--	--	--	0.0	--
Np-237	4.0×10^{-2}	--	--	--	--	--	--	2.1	--	--	2.14	2.14
Pu-238	--	1.512×10^{4}	--	9.336×10^{5}	1.121×10^{2}	2.312×10^{3}	--	1.792×10^{4}	--	8.29×10^{6}	9.259×10^{6}	9.259×10^{6}
Pu-239	6.524×10^{1}	1.652×10^{5}	5.126×10^{4}	4.813×10^{5}	2.048×10^{3}	1.79	2.003×10^{2}	1.634×10^{3}	8.016×10^{4}	6.293×10^{4}	8.448×10^{5}	8.448×10^{5}
Pu-240	2.339×10^{1}	5.885×10^{4}	1.193×10^{4}	--	6.346×10^{2}	1.15	4.551×10^{1}	7.998×10^{2}	1.837×10^{4}	1.629×10^{4}	1.069×10^{5}	1.069×10^{5}
Pu-241	1.27×10^{3}	2.994×10^{6}	3.588×10^{5}	--	1.568×10^{4}	1.04	1.893×10^{3}	8.893×10^{4}	4.386×10^{5}	7.026×10^{5}	4.602×10^{6}	--
Pu-242	--	--	1.02	--	5.3×10^{-1}	--	--	--	--	6.103×10^{-1}	2.16	2.16
Am-241	4.234×10^{1}	--	3.036×10^{3}	1.546×10^{6}	1.422×10^{3}	--	--	1.318×10^{3}	8.285×10^{4}	1.031×10^{4}	1.645×10^{6}	1.645×10^{6}
Cm-244	--	--	--	--	--	--	--	1.775×10^{4}	--	--	1.775×10^{4}	1.775×10^{4}
Cf-252	--	--	--	--	--	--	--	1.843×10^{4}	--	--	1.843×10^{4}	--
TOTALS	1.401×10^{3}	3.233×10^{6}	4.25×10^{5}	2.961×10^{6}	1.99×10^{4}	2.316×10^{3}	2.139×10^{3}	1.469×10^{5}	6.2×10^{5}	9.082×10^{6}	1.649×10^{7}	1.187×10^{7}

3.3.2 Inventory of Remotely Handled Waste

The inventory of TRU waste that must be transported and handled in shielded casks because of dose rates at the surface above 200 mrem/hr (remotely handled [RH]) was estimated from the input submitted to the 1990 IDB (IDB, 1990). Estimates were made using a similar method to that used for the CH waste (discussed in Section 3.3.1).* Some differences between the methods for estimating CH and RH were in the estimation of the activity for RH waste reported as mixed fission products and the "unknown" distribution from Hanford. For the mixed fission products, a mixture of 10-yr-old fission products was assumed as the source term. For the Hanford "unknown," a slurry mixture from the Hanford high level waste tanks provided the isotopic distribution; it was estimated that a 2.15 x 10^{-6} C/(kg•s) canister will contain about 450 Ci of gamma emitters. For other mixtures reported in the 1990 IDB, the weight fractions reported were used to calculate the major radionuclides. A volume scaling method similar to that used for CH waste was used to increase the volume from about 5,300 m^3 (estimated from the 1990 IDB) to the maximum volume of 7,079 m^3.

The estimates of the radionuclide inventory for stored waste at the five generator sites are tabulated in Table 3.3-6. The estimated inventory of the stored RH waste was about 5.3 x 10^5 Ci (2.0 x 10^{16} Bq). The projected generated inventory is listed in Table 3.3-7 and the design radionuclide inventory is listed in Table 3.3-8. The estimated total curies content of the projected RH waste was 2.1 x 10^6 Ci (7.0 x 10^{16} Bq).

To estimate the inventory for the maximum volume of RH waste, the projected volumes at each site were volume scaled to provide the additional volume. The projected radionuclide inventory was also volume scaled to estimate the total inventory. The total additional scaled inventory was about 9.4 x 10^5 Ci (3.5 x 10^{17} Bq). Not including the radionuclides with short half-lives, the estimated inventory was 1.6 x 10^6 Ci (3.6 x 10^{16} Bq). By agreement with the State of New Mexico, the DOE will not emplace more than 5.2 x 10^6 Ci (1.9 x 10^{17} Bq) (U.S. DOE and NM, 1989). The current estimate was less than the allowed curie content.

Figure 3.3-4 provides a summary of the estimated activity of the stored, projected, and design radionuclide inventory. These are estimates for PA analyses and should not be considered as a statement of what each site will generate.

For the 1991 PA calculations, the RH-TRU waste was included in the cuttings releases. The RH-TRU waste has not been included in the long-term performance assessment inventory for most previous calculations (Marietta et al., 1989; Lappin et al., 1989; U.S. DOE, 1990b), because RH-TRU waste constituted less than 2% of the activity. Furthermore, as discussed in Section 3.5, the current procedure for emplacing RH waste in the pillar walls will minimize the interaction of the RH waste canisters and the CH waste rooms. Also a large amount of the activity in RH waste is from radionuclides with relatively short half-lives, which have a small consequence over the long term.

---

* An alternate method would be to scale the radionuclides so that the activity limit agreed upon by the State of New Mexico and the DOE--5.2 x 10^6 Ci--would be emplaced instead of the agreed upon volume limit.

Table 3.3-6. Retrievably Stored* Design Radionuclide Inventory by Waste Generator for Remotely Handled Waste

Radionuclide	Half-Life (s)	ANL-E (Ci)	HANF (Ci)	INEL (Ci)	LANL (Ci)	ORNL (Ci)	Stored Total (Ci)
Cr-51	2.3936×10^{6}	--	--	--	--	--	0.0
Mn-54	2.7×10^{7}	--	--	1.703×10^{2}	--	--	1.703×10^{2}
Co-58	6.1171×10^{6}	--	--	5.288×10^{1}	--	--	5.288×10^{1}
Fe-59	3.8473×10^{6}	--	--	--	--	--	0.0
Co-60	1.6634×10^{8}	--	1.667×10^{3}	--	--	4.794×10^{3}	6.461×10^{3}
Sr-90	9.1894×10^{8}	3.582×10^{1}	2.466×10^{4}	--	5.408×10^{2}	1.728×10^{5}	1.98×10^{5}
Y-90	2.304×10^{5}	3.582×10^{1}	2.466×10^{4}	--	5.408×10^{2}	--	2.523×10^{4}
Nb-95	3.037×10^{6}	--	--	8.963×10^{-1}	--	--	8.963×10^{-1}
Ru-106	3.1812×10^{7}	--	1.468	--	--	--	1.468
Rh-106	2.99×10^{1}	--	1.468	--	--	--	1.468
Sb-125	8.7413×10^{7}	--	--	--	--	--	0.0
Cs-134	6.507×10^{7}	--	--	--	--	--	0.0
Cs-137	9.4671×10^{8}	2.687×10^{1}	1.851×10^{4}	2.996×10^{3}	4.056×10^{2}	1.825×10^{5}	2.044×10^{5}
Ba-137m	1.5312×10^{2}	2.388×10^{1}	1.645×10^{4}	--	3.605×10^{2}	--	1.683×10^{4}
Ce-144	2.4564×10^{7}	--	1.468×10^{2}	1.603×10^{3}	--	--	1.75×10^{3}
Pr-144	1.0368×10^{3}	--	1.468×10^{2}	--	--	--	1.468×10^{2}
Pm-147	8.2786×10^{7}	2.687×10^{1}	1.868×10^{4}	--	4.056×10^{2}	--	1.911×10^{4}
Eu-152	4.2065×10^{8}	--	--	--	--	2.397×10^{4}	2.397×10^{4}
Eu-154	2.777×10^{8}	--	--	--	--	1.438×10^{4}	1.438×10^{4}
Eu-155	1.5652×10^{8}	--	--	--	--	--	0.0
Th-232	4.4337×10^{17}	--	--	--	--	--	--
U-233	5.0018×10^{12}	--	--	--	--	1.918×10^{2}	1.918×10^{2}
U-235	2.221×10^{16}	7.351×10^{-5}	5.429×10^{-3}	1.769×10^{-3}	2.916×10^{-3}	--	1.019×10^{-2}
U-238	1.41×10^{17}	--	6.145×10^{-2}	2.386×10^{-4}	2.723×10^{-4}	--	6.196×10^{-2}
Np-237	6.7532×10^{13}	--	--	--	--	--	0.0
Pu-238	2.7688×10^{9}	--	5.066×10^{2}	--	2.334	8.137×10^{2}	1.323×10^{3}
Pu-239	7.5942×10^{11}	1.508	4.801×10^{2}	4.306×10^{1}	2.57×10^{1}	2.876×10^{2}	8.38×10^{2}
Pu-240	2.0629×10^{11}	2.356×10^{-1}	2.589×10^{2}	1.667	8.608	--	2.694×10^{2}
Pu-241	4.5442×10^{8}	--	1.21×10^{4}	--	3.611×10^{2}	--	1.246×10^{4}
Pu-242	1.1875×10^{13}	--	--	--	1.609×10^{-3}	--	1.609×10^{-3}
Am-241	1.3639×10^{10}	--	--	--	--	--	0.0
Cm-244	5.7515×10^{8}	--	--	--	--	3.452×10^{3}	3.452×10^{3}
Cf-252	8.3247×10^{7}	--	--	--	--	--	0.0
TOTALS		1.51×10^{2}	1.183×10^{5}	4.868×10^{3}	2.651×10^{3}	4.032×10^{5}	5.291×10^{5}

* Stored as of December 31, 1989; these estimates were based on 1990 IDB input and were made by H. Batchelder (Westinghouse, WIPP) and transmitted by personal communication.

Table 3.3-7. Projected* Radionuclide Inventory by Waste Generator for Remotely Handled Waste (Curies)

Radiounculide	ANL-E	HANF	INEL	LANL	ORNL	Projected Total	(Stored + Projected) Anticipated System Total
Cr-51	--	--	$1.976x10^{2}$	--	--	$1.976x10^{2}$	$1.976x10^{2}$
Mn-54	--	--	$1.196x10^{4}$	--	--	$1.196x10^{4}$	$1.213x10^{-4}$
Co-58	--	--	$7.707x10^{3}$	--	--	$7.707x10^{3}$	$7.759x10^{3}$
Fe-59	--	--	$1.976x10^{2}$	--	--	$1.976x10^{2}$	$1.976x10^{2}$
Co-60	--	$1.889x10^{2}$	$1.559x10^{3}$	--	--	$1.748x10^{3}$	$8.209x10^{3}$
Sr-90	$4.403x10^{2}$	$2.067x10^{5}$	$1.558x10^{4}$	$5.519x10^{1}$	$2.088x10^{1}$	$2.228x10^{5}$	$4.209x10^{5}$
Y-90	$4.403x10^{2}$	$2.067x10^{5}$	--	$5.519x10^{1}$	--	$2.072x10^{5}$	$2.325x10^{5}$
Nb-95	--	$1.629x10^{3}$	--	--	--	$1.629x10^{3}$	$1.63x10^{3}$
Ru-106	--	$7.573x10^{4}$	--	--	--	$7.573x10^{4}$	$7.573x10^{4}$
Rh-106	--	$7.573x10^{4}$	--	--	--	$7.573x10^{4}$	$7.573x10^{4}$
Sb-125	--	$1.369x10^{4}$	--	--	--	$1.369x10^{4}$	$1.369x10^{4}$
Cs-134	--	$8.91x10^{3}$	$7.68x10^{3}$	--	--	$1.659x10^{4}$	$1.659x10^{4}$
Cs-137	$3.302x10^{2}$	$2.939x10^{5}$	$1.548x10^{4}$	$4.139x10^{1}$	$1.623x10^{2}$	$3.099x10^{5}$	$5.144x10^{5}$
Ba-137m	$2.935x10^{2}$	$2.779x10^{5}$	--	$3.679x10^{1}$	--	$2.782x10^{5}$	$2.95x10^{5}$
Ce-144	--	$2.53x10^{5}$	$3.825x10^{4}$	--	--	$2.913x10^{5}$	$2.93x10^{5}$
Pr-144	--	$2.53x10^{5}$	--	--	--	$2.53x10^{5}$	$2.531x10^{5}$
Pm-147	$3.302x10^{2}$	$2.957x10^{5}$	--	$4.139x10^{1}$	--	$2.961x10^{5}$	$3.152x10^{5}$
Eu-152	--	$1.149x10^{1}$	--	--	--	$1.149x10^{1}$	$2.398x10^{4}$
Eu-154	--	$1.607x10^{3}$	--	--	--	$1.607x10^{3}$	$1.599x10^{4}$
Eu-155	--	$2.939x10^{3}$	--	--	--	$2.939x10^{3}$	$2.939x10^{3}$
Th-232	--	--	--	--	--	--	--
U-233	--	--	--	--	6.696	6.696	$1.985x10^{2}$
U-235	$9.036x10^{-4}$	$8.782x10^{-4}$	--	$2.663x10^{-4}$	$5.079x10^{-4}$	$2.556x10^{-3}$	$1.276x10^{-2}$
U-238	--	$1.627x10^{-2}$	--	$2.486x10^{-5}$	$1.035x10^{-3}$	$1.733x10^{-2}$	$7.929x10^{-2}$
Np-237	--	$6.986x10^{-1}$	--	--	$1.881x10^{-1}$	$8.867x10^{-1}$	$8.867x10^{-1}$
Pu-238	--	5.275	--	$7.105x10^{-2}$	$3.305x10^{-2}$	5.379	$1.328x10^{3}$
Pu-239	$1.853x10^{1}$	$5.898x10^{1}$	$1.975x10^{2}$	$7.826x10^{-1}$	$5.14x10^{1}$	$3.272x10^{2}$	$1.165x10^{3}$
Pu-240	2.896	$1.6x10^{1}$	--	$2.001x10^{-1}$	$4.496x10^{-1}$	$1.955x10^{1}$	$2.89x10^{2}$
Pu-241	--	$7.075x10^{2}$	--	$1.099x10^{1}$	$1.053x10^{-2}$	$7.185x10^{2}$	$1.318x10^{4}$
Pu-242	--	$1.648x10^{-3}$	--	$4.899x10^{-5}$	--	$1.697x10^{-3}$	$3.306x10^{-3}$
Am-241	--	$9.409x10^{2}$	--	--	$6.481x10^{1}$	$1.006x10^{3}$	$1.006x10^{3}$
Cm-244	--	2.209	--	--	$8.073x10^{2}$	$8.095x10^{2}$	$4.262x10^{3}$
Cf-252	--	--	--	--	$8.629x10^{1}$	$8.629x10^{1}$	$8.629x10^{1}$
TOTALS	$1.856x10^{3}$	$1.969x10^{6}$	$9.88x10^{4}$	$2.42x10^{2}$	$1.20x10^{3}$	$2.071x10^{6}$	$2.6x10^{6}$

* Generated between 1990 and 2013; these estimates were based on 1990 IDB input and were made by H. Batchelder (Westinghouse, WIPP) and transmitted by personal communication.

Table 3.3-8. Design Radionuclide Inventory by Waste Generator for Remotely Handled Waste (Curies)

Radionuclide	ANL-E	HANF	INEL	LANL	ORNL	PA Calculations Design 1990	Waste Unit Factor
Cr-51	--	--	2.869×10^{2}	--	--	--	
Mn-54	--	--	1.753×10^{4}	--	--	--	
Co-58	--	--	1.124×10^{4}	--	--	--	
Fe-59	--	--	2.869×10^{2}	--	--	--	
Co-60	--	1.941×10^{3}	2.263×10^{3}	--	4.794×10^{3}	--	
Sr-90	6.747×10^{2}	3.247×10^{5}	2.262×10^{4}	6.213×10^{2}	1.728×10^{5}	5.214×10^{5}	
Y-90	6.747×10^{2}	3.247×10^{5}	--	6.213×10^{2}	--	--	
Nb-95	--	2.364×10^{3}	8.963×10^{-1}	--	--	--	
Ru-106	--	1.099×10^{5}	--	--	--	--	
Rh-106	--	1.099×10^{5}	--	--	--	--	
Sb-125	--	1.987×10^{4}	--	--	--	--	
Cs-134	--	1.293×10^{4}	1.115×10^{4}	--	--	--	
Cs-137	5.06×10^{2}	4.451×10^{5}	2.547×10^{4}	4.66×10^{2}	1.827×10^{5}	6.543×10^{5}	
Ba-137m	4.498×10^{2}	4.199×10^{5}	--	4.142×10^{2}	--	--	
Ce-144	--	3.673×10^{5}	5.713×10^{4}	--	--	--	
Pr-144	--	3.673×10^{5}	--	--	--	--	
Pm-147	5.06×10^{2}	4.479×10^{5}	--	4.66×10^{2}	--	4.489×10^{5}	
Eu-152	--	1.668×10^{1}	--	--	2.397×10^{4}	--	
Eu-154	--	2.333×10^{3}	--	--	1.438×10^{4}	--	
Eu-155	--	4.266×10^{3}	--	--	--	--	
Th-232	--	--	--	--	--	--	
U-233	--	--	--	--	2.015×10^{2}	2.015×10^{2}	
U-235	1.385×10^{-3}	6.704×10^{-3}	1.769×10^{-3}	3.298×10^{-3}	7.372×10^{-4}	1.389×10^{-2}	
U-238	--	8.507×10^{-2}	2.386×10^{-4}	3.086×10^{-4}	1.502×10^{-3}	8.712×10^{-2}	
Np-237	--	1.014	--	--	2.73×10^{-1}	1.287	1.287
Pu-238	--	5.143×10^{2}	--	2.438	8.137×10^{2}	1.33×10^{3}	1.33×10^{3}
Pu-239	2.84×10^{1}	5.657×10^{2}	3.298×10^{2}	2.684×10^{1}	3.622×10^{2}	1.313×10^{3}	1.313×10^{3}
Pu-240	4.438	2.821×10^{2}	1.667	8.9	6.525×10^{-1}	2.978×10^{2}	2.978×10^{2}
Pu-241	--	1.313×10^{4}	--	3.771×10^{2}	1.101×10^{-1}	1.350×10^{4}	
Pu-242	--	2.392×10^{-3}	--	1.68×10^{-3}	--	4.072×10^{-3}	4.072×10^{-3}
Am-241	--	1.366×10^{3}	--	--	9.406×10^{1}	1.46×10^{3}	1.46×10^{3}
Cm-244	--	3.206	--	--	4.624×10^{3}	4.627×10^{3}	
Cf-252	--	--	--	--	1.252×10^{2}	1.252×10^{2}	
TOTALS	2.844×10^{3}	2.976×10^{6}	1.483×10^{5}	3.004×10^{3}	4.049×10^{5}	1.697×10^{6}	4.410×10^{3}

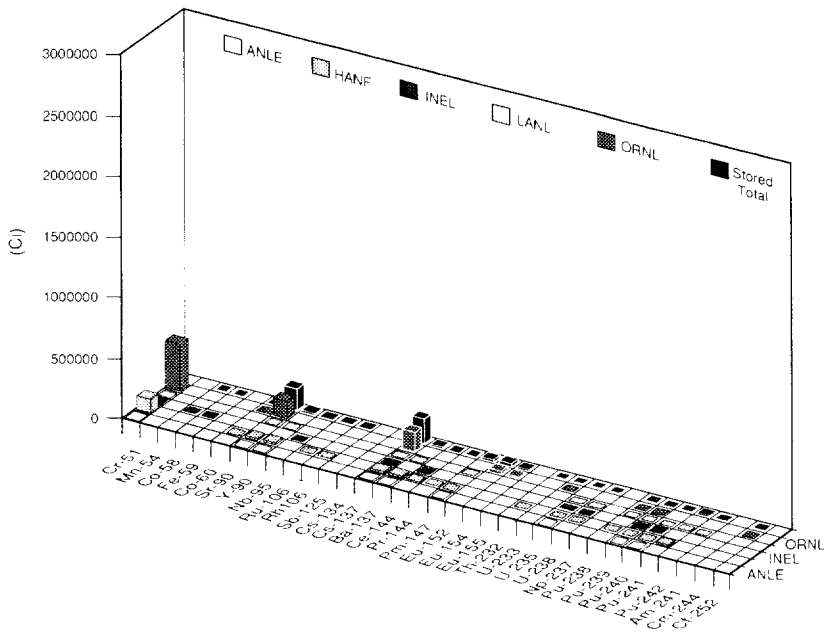

(a)

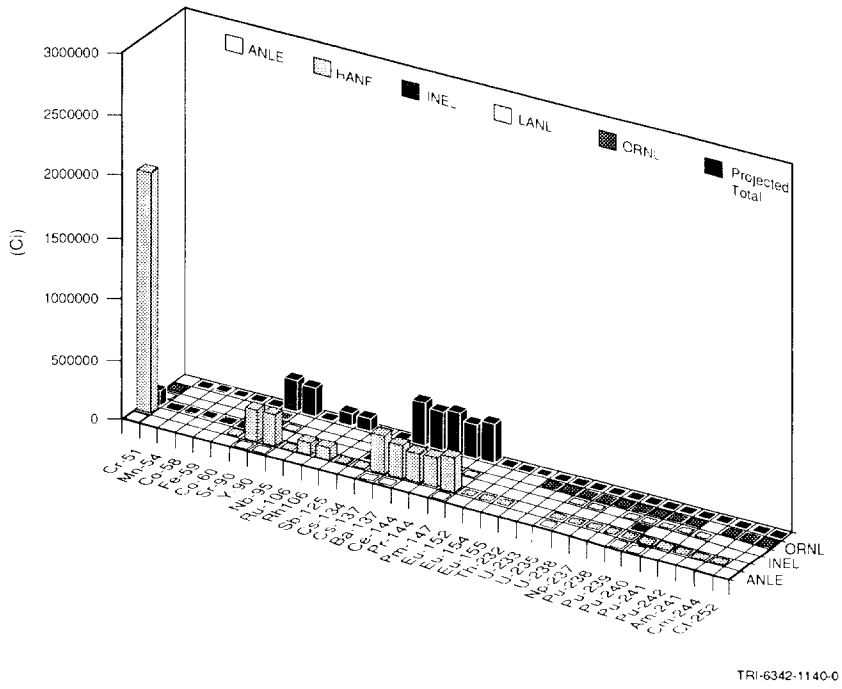

(b)

Figure 3.3-4. Activity of (a) Stored, (b) Projected, (c) Anticipated Actual System Total, and (d) Design Radionuclide Inventory of RH Waste.

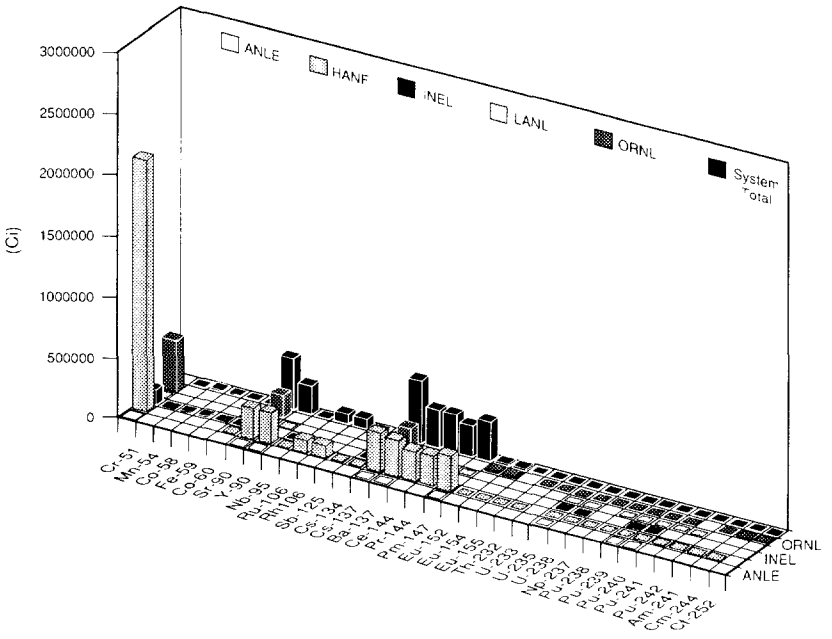

(c)

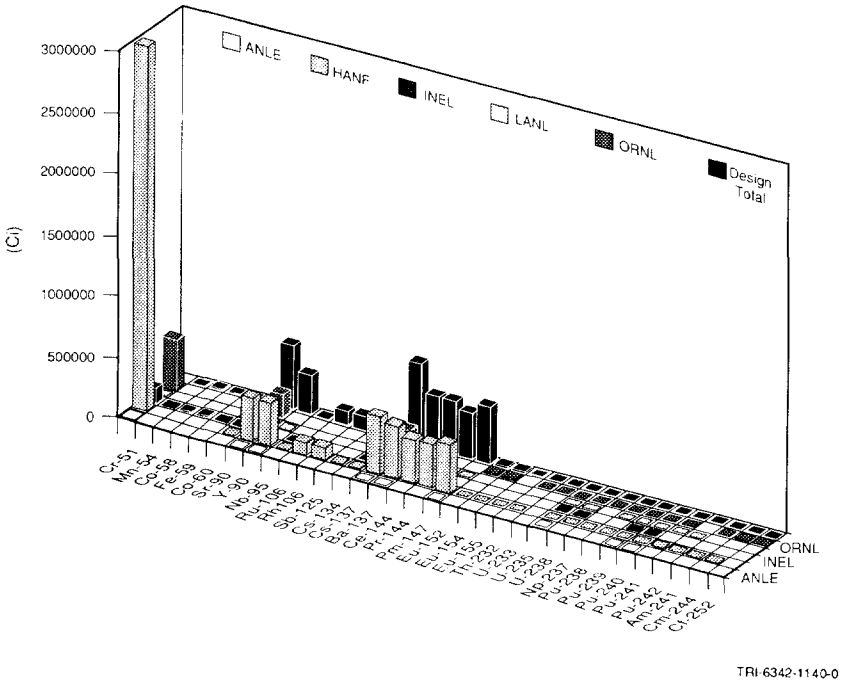

(d)

Figure 3.3-4. Activity of (a) Stored, (b) Projected, (c) Anticipated Actual System Total, and (d) Design Radionuclide Inventory of RH Waste (Concluded).

3.3.3 Radionuclide Chains and Half-Lives

The decay chains for the initial radionuclides in the CH and RH inventory are shown in Figures 3.3-5 and 3.3-6, respectively. The half-lives for each radionuclide as listed in the literature by ICRP Publication 38 (ICRP, Pub 38, 1983) and the mass of the initial inventory are also on Figure 3.3-5. For reference, the half-lives of the radionuclides in the initial WIPP inventory and decay products are tabulated in Table 3.3-9.

Many of the daughter radionuclides have extremely short half-lives, low activities, and make a small contribution to the curie inventory. Shortened chains are used when modeling as follows.

Radionuclides for Cuttings and Repository Modeling

From the 70 radionuclides shown in Figure 3.3-5, 23 are considered major contributors to the inventory and are used in calculating the radionuclide releases from drilling into the repository and bringing cuttings to the surface and when calculating concentrations within the repository prior to transport to the Culebra. In general, most radionuclides of plutonium, thorium, americium, curium, neptunium, californium, radon, and uranium are considered.

The RH inventory decay chains include the chains in the CH inventory shown in Figure 3.3-5 plus the three chains shown in Figure 3.3-6. The radionuclides in the RH cuttings releases included cesium-137, promethium-147, and strontium-90 in addition to all of the radionuclides in the CH releases.

Radionuclides for Transport Modeling

Seven radionuclides are considered in PA transport calculations for CH waste and are highlighted on Figure 3.3-5.

Figure 3.3-7 shows the change with time in radionuclide activity in one panel normalized to the EPA release limits for 11 of the 23 radionuclides not included in the transport calculations. The curies of each radionuclide may be calculated by multiplying the normalized activity by the EPA release limit and the total curies in the initial inventory (11.87×10^6 Ci). Figure 3.3-7 indicates that the total activity at 10,000 yr in a panel for all radionuclides omitted, except for radium-226, is less than 1% of the EPA limit. The normalized activity including radium-226 is less than 2% of the EPA limit.

Five additional radionuclides were not included. Californium-252, curium-244, and plutonium-241 were not included for transport because of their small initial quantities and relatively short half-lives, all less than 20 yr. Curium-248, a daughter of californium-252, was not included because of the small quantity and low radiological toxicity. Plutonium-244 was not included because of its small quantity also.

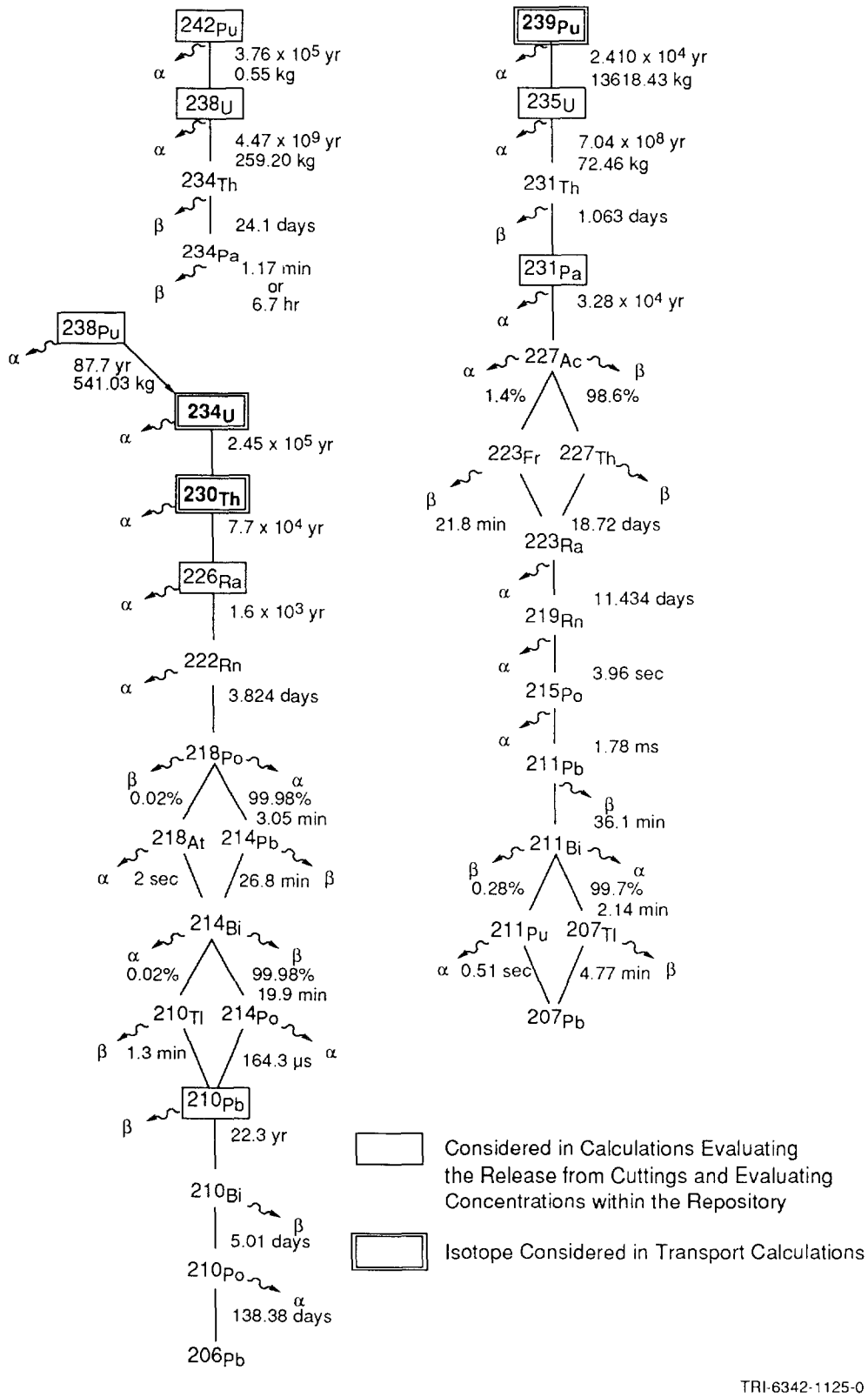

Figure 3.3-5. Decay of CH Radionuclide Chain in TRU-Contaminated Waste.

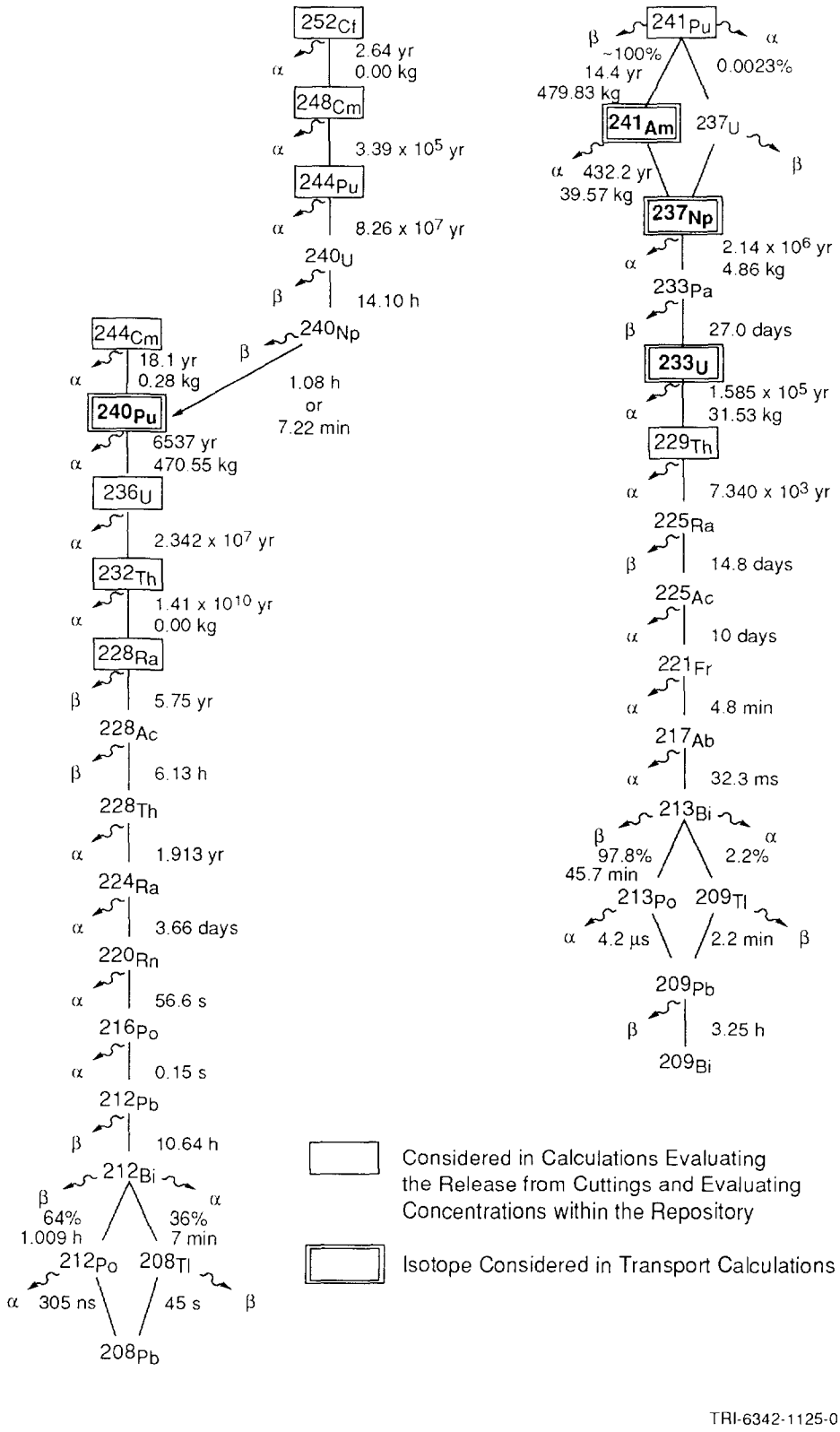

Figure 3.3-5. Decay of CH Radionuclide Chain in TRU-Contaminated Waste (Concluded).

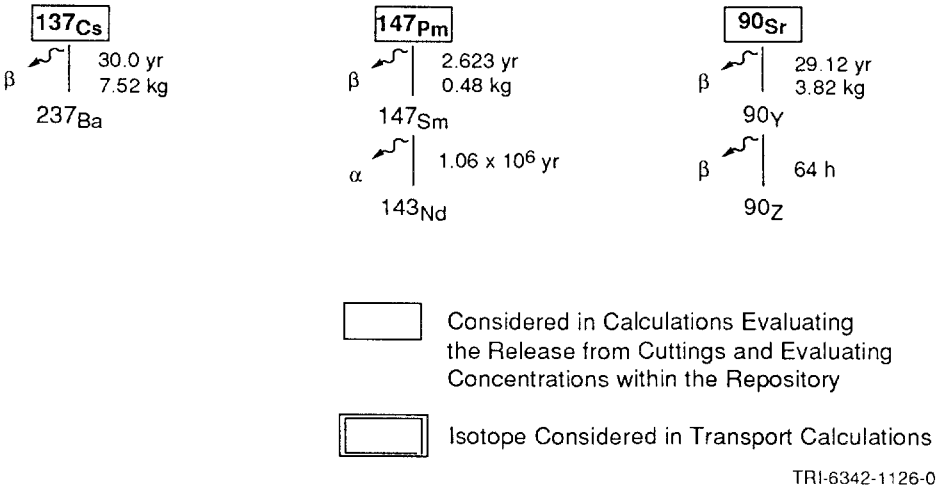

Figure 3.3-6. Decay of RH Radionuclide Chain in TRU-Contaminated Waste.

Table 3.3-9. Half-Lives of Isotopes Disposed or Created in WIPP (ICRP, 1983)

Radioisotope		Half-life ($t_{1/2}$) (s)	Reported
Actinium	^{228}Ac	2.207×10^{4}	6.13 h
	^{227}Ac	6.871×10^{8}	2.177×10^{1} yr
	^{225}Ac	8.64×10^{5}	10 day
Americium	^{243}Am	5.822×10^{11}	7.38×10^{3} yr
	^{241}Am	**1.364×10^{10}**	4.322×10^{2} yr
Antimony	^{125}Sb	8.741×10^{7}	2.77 yr
Astatine	^{217}At	3.23×10^{-2}	3.23×10^{-2} s
Barium	^{137m}Ba	1.531×10^{2}	2.552 min
Bismuth	^{214}Bi	1.194×10^{3}	19.9 min
	^{213}Bi	2.739×10^{3}	45.65 min
	^{212}Bi	3.633×10^{3}	60.55 min
	^{211}Bi	1.284×10^{2}	2.14 min
	^{210}Bi	4.33×10^{5}	5.012 day
Californium	**^{252}Cf**	**8.325×10^{7}**	2.638 yr
Cerium	^{144}Ce	2.456×10^{7}	284.3 day
Cesium	**^{137}Cs**	**9.467×10^{8}**	30.0 yr
	^{134}Cs	6.507×10^{7}	2.062 yr
Chromium	^{51}Cr	2.394×10^{6}	27.7 day
Cobalt	^{60}Co	1.663×10^{8}	5.221 yr
	^{58}Co	6.117×10^{6}	70.8 day
Curium	^{248}Cm	1.070×10^{13}	3.39×10^{5} yr
	^{244}Cm	**5.715×10^{8}**	18.11 yr
Europium	^{155}Eu	1.565×10^{8}	4.96 yr
	^{154}Eu	2.777×10^{8}	8.80 yr
	^{152}Eu	4.207×10^{8}	13.53 yr
Francium	^{221}Fr	2.88×10^{2}	4.8 min
Iron	^{59}Fe	3.847×10^{6}	44.53 day
Lead	^{214}Pb	1.608×10^{3}	26.8 min
	^{212}Pb	3.83×10^{4}	10.64 h
	^{211}Pb	2.166×10^{3}	3.61 min
	^{210}Pb	7.037×10^{8}	22.3 yr
	^{209}Pb	1.171×10^{4}	3.253 h
Manganese	^{54}Mn	2.7×10^{7}	312.5 day
Neptunium	^{239}Np	2.035×10^{5}	2.355 day
	^{237}Np	**6.753×10^{13}**	2.14×10^{6} yr
Niobium	^{95}Nb	3.037×10^{6}	35.15 day
Plutonium	^{244}Pu	2.607×10^{15}	8.76×10^{7} yr
	^{242}Pu	**1.187×10^{13}**	3.763×10^{5} yr
	^{241}Pu	**4.544×10^{8}**	14.4 yr
	^{240}Pu	**2.063×10^{11}**	6.537×10^{3} yr
	^{239}Pu	**7.594×10^{11}**	2.407×10^{4} yr
	^{238}Pu	**2.769×10^{9}**	87.74 yr
Polonium	^{218}Po	1.83×10^{2}	3.05 min
	^{216}Po	1.5×10^{-1}	1.5×10^{-1} s
	^{215}Po	1.78×10^{-3}	1.78×10^{-3} s
	^{214}Po	1.643×10^{-4}	1.643×10^{-4} s
	^{213}Po	4.2×10^{-6}	4.2×10^{-6} s
	^{212}Po	3.05×10^{-7}	3.05×10^{-7} s
	^{210}Po	1.196×10^{7}	138.4 day
Praseodymium	^{144}Pr	1.037×10^{3}	17.28 min
Promethium	**^{147}Pm**	**8.279×10^{7}**	2.623 yr

* Bolding indicates isotopes assumed in inital inventory for PA calculations

Table 3.3-9. Half-Lives of Isotopes Disposed or Created in WIPP (ICRP, 1983) (Concluded)

Radioisotope		Half-life ($t_{1/2}$) (s)	Half-life ($t_{1/2}$) Reported
Protactinium	^{233}Pa	2.333×10^{6}	27 day
	^{231}Pa	1.034×10^{12}	3.276×10^{4} yr
Radium	^{228}Ra	1.815×10^{8}	5.75 yr
	^{226}Ra	5.049×10^{10}	1.6×10^{3} yr
	^{225}Ra	1.279×10^{6}	14.8 day
	^{224}Ra	3.162×10^{5}	3.66 day
	^{223}Ra	9.879×10^{5}	11.43 day
Radon	^{222}Rn	3.304×10^{5}	3.824 day
	^{220}Rn	5.56×10^{1}	5.56×10^{1} s
	^{219}Rn	3.96	3.96 s
Rhodium	^{106}Rh	2.99×10^{1}	2.99×10^{1} s
Ruthenium	^{106}Ru	3.181×10^{7}	3.682×10^{2} day
Strontium	**^{90}Sr***	**9.189×10^{8}**	29.12 yr
Thallium	^{207}Tl	2.862×10^{2}	4.77 min
Thorium	^{234}Th	2.082×10^{6}	24.1 day
	^{232}Th	**4.434×10^{17}**	1.405×10^{10} yr
	^{231}Th	9.187×10^{4}	25.52 h
	^{230}Th	2.43×10^{12}	7.7×10^{4} yr
	^{229}Th	2.316×10^{11}	7.34×10^{3} yr
	^{228}Th	6.037×10^{7}	1.913 yr
	^{227}Th	1.617×10^{6}	18.72 day
Uranium	^{240}U	5.076×10^{4}	1.41×10^{1} hr
	^{238}U	**1.41×10^{17}**	4.468×10^{9} yr
	^{236}U	7.389×10^{14}	2.342×10^{7} yr
	^{235}U	**2.221×10^{16}**	7.038×10^{8} yr
	^{234}U	7.716×10^{12}	2.445×10^{5} yr
	^{233}U	**5.002×10^{12}**	1.585×10^{5} yr
Yttrium	^{90}Y	2.304×10^{5}	64.0 h

* Bolding indicates isotopes assumed in inital inventory for PA calculations

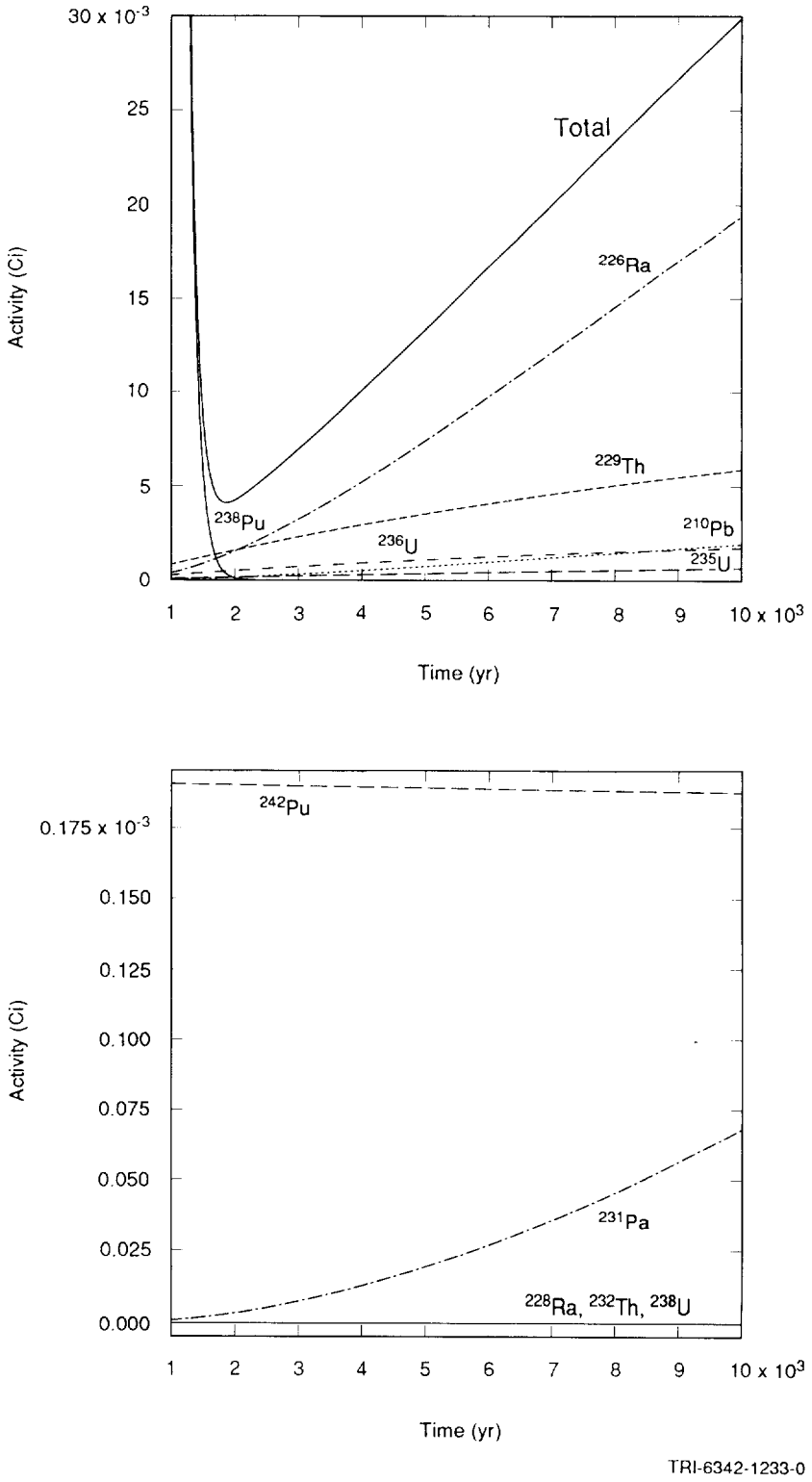

Figure 3.3-7. Radionuclides in One Panel Normalized by EPA Release Limits, Which Were Eliminated from Transport Calculations.

3.3.4 40 CFR 191 Release Limits and Waste Unit Factor

40 CFR 191 Release Limits

The release limits (L_i) for evaluating compliance with *40 CFR 191 § 13* are provided in Table 3.3-10.

Table 3.3-10. Cumulative Release Limits (L_i) to the Accessible Environment 10,000 Yr after Disposal for Evaluating Compliance with Containment Requirements (40 CFR 191, Appendix B, Table 1)

Radionuclide	Release limit (L_i) per 1 x 10^6 Ci α-emitting TRU nuclide with $t_{1/2}$ > 20 yr* (Ci)	1991 PA Release Limits $f_m L_i$ (Ci)
Americium (Am) -241 or -243	100	1187
Carbon (C) -14	100	1187
Cesium (Cs) -135 or -137	1000	11870
Iodine (I) -129	100	1187
Neptunium (Np) -237	100	1187
Plutonium (Pu) -238, -239, -240, or -242	100	1187
Radium (Ra) -226	100	1187
Strontium (Sr) -90	1000	11870
Technetium (Tc) -99	10000	118700
Thorium (Th) -230 or -232	10	118.7
Tin (Sn) -126	1000	11870
Uranium (U) -233, -234, -235, -236, or -238	100	1187
Any other α-emitting radionuclide with $t_{1/2}$ > 20 yr	100	1187
Any other non α-emitting radionuclide with $t_{1/2}$ > 20 yr	1000	11870

* Other units of waste described in 40 CFR 191, Appendix A

Waste Unit Factor

The waste unit factor (f_w) is the inventory in curies of transuranic (TRU) α-emitting radionuclides in the waste with half-lives greater than 20 yr divided by 10^6 Ci, where TRU is defined as radionuclides with atomic weights *greater* than uranium (92). Consequently, as currently defined in *40 CFR 191*, all TRU radioactivity in the waste cannot be included when calculating the waste unit factor. For the WIPP, 1.187 x 10^7 Ci of the radioactivity design total of 1.814 x 10^7 Ci comes from TRU α-emitting radionuclides with half-lives greater than 20 yr (see Tables 3.3-5 and 3.3-8).* Regardless of the waste unit, the WIPP has assumed that all nuclides listed in Tables 3.3-5 and 3.3-8 are regulated and must be included in the release calculations. Therefore, the release limits (L_i) used by the WIPP are reduced somewhat (i.e., more restrictive).

EPA Sums for Each nS Scenario Set

See discussion in Chapter 1, Section 1.4.1.

* For the remanded regulation, the following change has been suggested: Include all radionuclides in the inventory but use the activity (curie content) of the first daughter with a half-life greater than 20 yr for radionuclides with half-lives of less than 20 yr.

3.3.5 Solubility

The solubility of specific radionuclides was estimated by a panel of experts (outside Sandia) in the fields of actinide and brine chemistry (Trauth et al., 1991). Supporting calculations with EQ3/6 were performed using a standard brine that simulates the brine in the Salado Formation as the solvent (Lappin et al., 1989, Table 3-4). These efforts resulted in the estimation of the oxidation state(s) in which the radionuclides would exist in the environment of the WIPP disposal area, and corresponding solid species that would exist with that particular oxidation state.

Figure 3.3-8 depicts the estimated distributions of solubility for americium, curium, lead, neptunium, plutonium, radium, thorium, and uranium.

The points on the probability distributions that were elicited during the expert panel session are found in Figure 3.3-8 and Table 3.3-11.

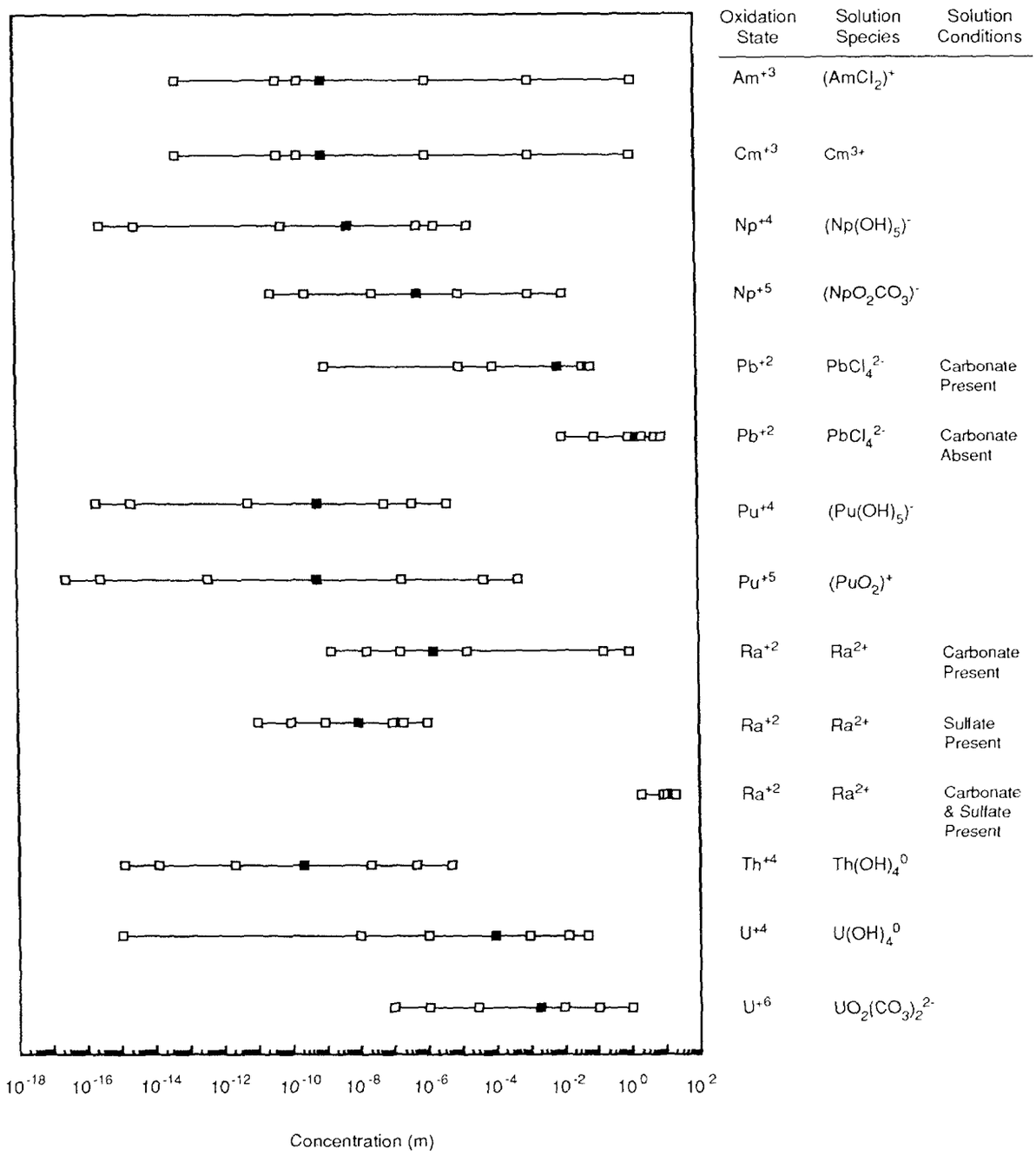

The blocks represent, from left to right, the 0.00, 0.10, 0.25, 0.50, 0.75, 0.90 and 1.00 fractiles

TRI-6342-1410-0

Figure 3.3-8. Subjective Distribution (cdf) of Solubility for Americium, Curium, Lead, Neptunium, Plutonium, Radium, Thorium, and Uranium (after Trauth et al., 1991).

Table 3.3-11. Estimated Solubilities of Radionuclides (from Trauth et al., 1991, Table 1)

Element	Solution Species	Solid Species Maximum and Minimum	Condition	Cumulative Probabilities of Concentrations (M) 0.0	0.10	0.25	0.50	0.75	0.90	1.00
Am^{3+}	$(AmCl_2)^+$	$Am(OH)_3$ $AmOHCO_3$		5.0×10^{-14}	5.0×10^{-11}	2.0×10^{-10}	1.0×10^{-9}	1.2×10^{-6}	1.4×10^{-3}	1.4
Cm^{3+}	Cm^{III}	$Cm(OH)_3$ CmO_2		5.0×10^{-14}	5.0×10^{-11}	2.0×10^{-10}	1.0×10^{-9}	1.2×10^{-6}	1.4×10^{-3}	1.4
Np^{5+}	$(NpO_2CO_3)^-$	$NpO_2(OH)$ (amorphous) $NaNpO_2CO_3 \cdot 3.5H_2O$		3.0×10^{-11}	3.0×10^{-10}	3.0×10^{-8}	6.0×10^{-7}	1.0×10^{-5}	1.2×10^{-3}	1.2×10^{-2}
Np^{6+}	$(Np(OH)_5)^-$	$Np(OH)_4$ NpO_2		3.0×10^{-16}	3.0×10^{-15}	6.0×10^{-11}	6.0×10^{-9}	6.0×10^{-7}	2.0×10^{-6}	2.0×10^{-5}
Pb^{2+}	$PbCl_4^{2-}$	$PbCO_3$	Carbonate Present	1.0×10^{-9}	1.0×10^{-5}	1.0×10^{-4}	8.0×10^{-3}	4.4×10^{-2}	6.2×10^{-2}	8.0×10^{-2}
		$PbCl_2$	Carbonate Absent	0.01	0.10	1.0	1.64	2.5	6.0	10.0
Pu^{4+}	$(Pu(OH)_5)^-$	$Pu(OH)_4$ PuO_2		2.0×10^{-16}	2.0×10^{-15}	6.0×10^{-12}	6.0×10^{-10}	6.0×10^{-8}	4.0×10^{-7}	4.0×10^{-6}
Pu^{5+}	$(PuO_2)^+$	$Pu(OH)_4$ PuO_2		2.5×10^{-17}	2.5×10^{-16}	4.0×10^{-13}	6.0×10^{-10}	2.0×10^{-7}	5.5×10^{-5}	5.5×10^{-4}
Ra^{2+}	Ra^{2+}	$RaSO_4$ and $(Ra/Ca)SO_4$	Sulfate Present	1.0×10^{-11}	1.0×10^{-10}	1.0×10^{-9}	1.0×10^{-8}	1.0×10^{-7}	2.0×10^{-7}	1.0×10^{-6}
		$RaCO_3$ and $(Ra/Ca)CO_3$	Carbonate Present	1.6×10^{-9}	1.6×10^{-8}	1.6×10^{-7}	1.6×10^{-6}	1.6×10^{-5}	1.6×10^{-1}	1.0
		$RaCl_2 \cdot 2H_2O$	Carbonate and Sulfate Absent	2.0	4.0	8.6	11.0	14.5	17.2	18.0
Th^{4+}	$Th(OH)_4^0$	$Th(OH)_4$ ThO_2		5.5×10^{-16}	5.5×10^{-15}	1.0×10^{-12}	1.0×10^{-10}	1.0×10^{-8}	2.2×10^{-7}	2.2×10^{-6}
U^{4+}	$U(OH)_4^0$	UO_2 (amorphous) U_3O_8		1.0×10^{-15}	1.0×10^{-8}	1.0×10^{-6}	4.0×10^{-3}	1.0×10^{-3}	1.4×10^{-2}	5.0×10^{-2}
U^{6+}	$UO_2(CO_3)_2^{2-}$	$UO_3 \cdot 2H_2O$ UO_2		1.0×10^{-7}	1.0×10^{-6}	3.0×10^{-5}	2.0×10^{-3}	1.0×10^{-2}	0.1	1.0

General Rationale for Constructing Cumulative Distributions

The assessment of each distribution began by establishing the upper and lower solubility regimes. The first regime was based on the solid species with the highest solubility, and thus, the highest concentration of the actinide, and the second regime was based on the solid species with the lowest solubility, and thus, the lowest concentration. The regime depends upon the chemical properties within the repository, which are uncertain. The conditions considered included the pH and ionic strength of the brine, and the presence of carbonate and sulfate. The factor(s) controlling each regime differed for each actinide.

Each of these probability distributions represents the uncertainty in estimating a fixed, but unknown, quantity. In this case, the quantity is the concentration of a particular radionuclide given a particular condition. Thus, uncertainty cannot be assigned to the concentration for a particular fractile. The uncertainty inherent in these distributions includes that due to uncertainty in the pH of the solvent in contact with the waste. When the impact of variation in pH was included, the ranges of the distributions increased. Likewise, the distributions encompass the differences of opinion of the experts. These differences also resulted in larger ranges for the distributions. Because the distributions were developed by the panel as a whole, the uncertainty in the judgments of the individual panel members cannot be quantified.

10th, 90th and 0th, 100th Percentiles. Typically, the calculated value of each actinide for each regime was used to establish a fractile, often either the 0.10 or 0.90 fractile, of the distribution. The absolute lower, or upper, end point of the distribution was obtained by considering the sensitivity of solubility to the underlying brine chemistry. For example, the calculated lower solubility limit for Am^{3+} (solid species $AmOHCO_3$) was 5×10^{-11} M. The absolute lower limit of the distribution was judged to be 5×10^{-14} M. This judgment was obtained through consideration and discussion of the sensitivity of solubility to pH. In a similar manner, the upper 0.90 fractile was set equal to the calculated solubility with the solid speciation $Am(OH)_3$. The calculated value was 1.4×10^{-3} M. The absolute upper limit was judged to be 1.4 M.

25th and 75th Percentiles. The interior fractiles (0.25 and 0.75) were obtained after the 0.10 and 0.90 fractiles and the endpoints were established and based on speciation. In some cases, one speciation was thought to be more likely, resulting in a skewed distribution. In other cases, both speciations were thought to be likely, or to perhaps coexist, so that the assessed distribution was more symmetric and either bimodal or flat.

50th Percentile. Where possible, concentration data from a well (J-13) at the Nevada Yucca Mountain site, with a correction made for the ionic strength difference between the J-13 water and the WIPP A brine (Lappin et al., 1989, Table 3-4), was used as the 0.50 fractile.

Radium and Lead

The assessments for radium and lead require special comment because they are the only ones based on the presence or absence of specific compounds—carbonateand sulfate. For radium, the solubility is controlled by the solid species $RaSO_4$ and $(Ra/Ca)SO_4$ if sulfate is present. In the absence of sulfate, but in the presence of carbonate, $RaCO_3$ and $(Ra/Ca)CO_3$ control the solubility. If neither sulfate nor carbonate is present, then $RaCl_2$ $2H_2O$ will be the solid species. In the case of lead, the solid speciation depends upon the presence of carbonate but not sulfate. If carbonate is present, the solid speciation is $PbCO_3$, otherwise, $PbCl_2$.

Colloids

The expert panel had considerable difficulty dealing with colloids because of a lack of experimental data and physical principles governing their formation. There was some diversity of opinion about the significance of colloids. One expert placed an upper limit on the concentration of colloids of 10% of the concentration due to solubility. Another expert suggested that for some actinides, such as plutonium, the concentration due to colloidal formation may be greater than that due to solubility. Another suggestion was that the activity coefficients embody some colloid formation and thus the assessed distributions reflect the presence of both dissolved and suspended materials. The panel did not believe they could make judgments about suspended solids concentrations at the present time. They plan to include recommendations for future experiments related specifically to colloids in a final panel report.

Correlations

Correlations between the concentrations assigned to the radionuclides were discussed briefly by the panel. The consensus was that correlations do exist, possibly between Am^{3+} and Cm^{3+}, and between Np^{4+} and Pu^{4+}. The panel will address this issue in their final panel report.

3.3.6 Eh - pH Conditions

Parameter:	**Relative areas of radionuclide oxidation state**
Median:	0.5
Range:	0
	1.0
Units:	Dimensionless (A_i/A_{total})
Distribution:	Uniform
Source(s):	See text.

Discussion:

From estimates of constituents in the waste, inventory estimates of radionuclide concentration in brine as a function of Eh and pH are theoretically possible. However, the work remains to be done. Currently, radionuclide solubility estimates include variations in pH when assigning the 0th and 100th percentiles (Section 3.3.5, Solubility). For Eh, the oxidizing or reducing potential of the solution is sampled from a uniform distribution with ranges dependent on the stability of water. For 1991 PA calculations, an index variable between 0 and 1 was used to select the relative areas of the estimated regimes of stability for the various oxidation states of neptunium (Np), plutonium (Pu), and uranium (U) (Figure 3.3-9).

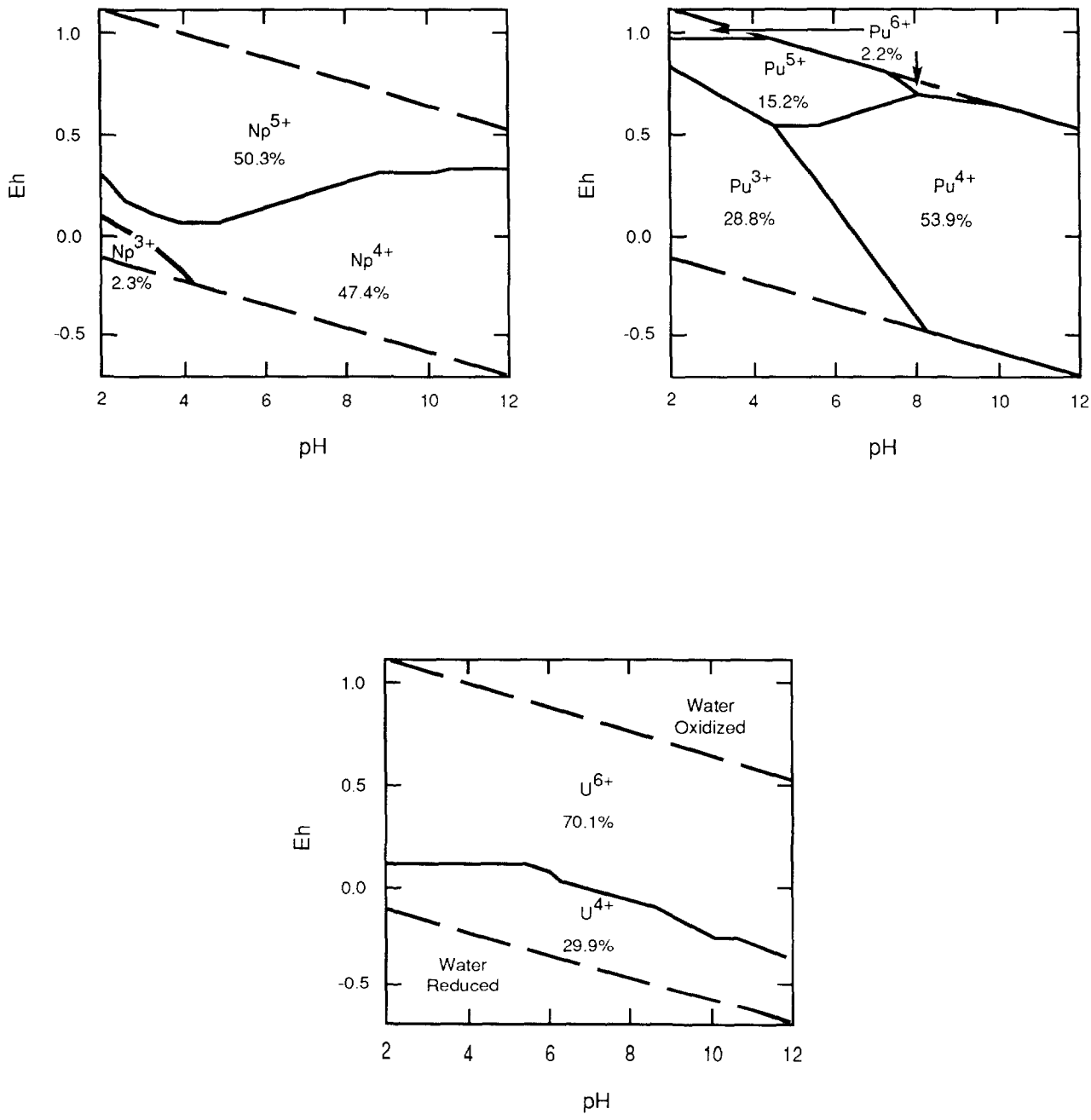

Figure 3.3-9. Estimated Regimes of Stability in the Eh-pH Space for Neptunium, Plutonium, and Uranium and Percentage of Area of Stable Water.

3.3.7 Molecular Diffusion Coefficient*

Table 3.3-12 provides estimated values of the free liquid diffusion coefficient of important actinides. Figure 3.3-10 provides the uniform distribution assumed for the average actinide.

Table 3.3-12. Estimated Molecular Diffusion Coefficient for Radionuclide Transport in Culebra Dolomite (after Lappin et al., 1989, Table E-7).

Parameter	Median	Range		Units	Distribution Type
Actinide, average	2.4×10^{-10}	4.8×10^{-11}	4.3×10^{-10}	m^2/s	Uniform
Am	1.765×10^{-10}	5.3×10^{-11}	3×10^{-10}	m^2/s	Uniform
Cm	1.765×10^{-10}	5.3×10^{-11}	3×10^{-10}	m^2/s	Uniform
Np	1.76×10^{-10}	5.2×10^{-11}	3×10^{-10}	m^2/s	Uniform
Pb	4×10^{-10}	2×10^{-10}	8×10^{-10}	m^2/s	Cumulative
Pu	1.74×10^{-10}	4.8×10^{-11}	3×10^{-10}	m^2/s	Uniform
Ra	3.75×10^{-10}	1.875×10^{-10}	7.5×10^{-10}	m^2/s	Cumulative
Th	1×10^{-10}	5×10^{-11}	1.5×10^{-10}	m^2/s	Uniform
U	2.7×10^{-10}	1.1×10^{-10}	4.3×10^{-10}	m^2/s	Uniform

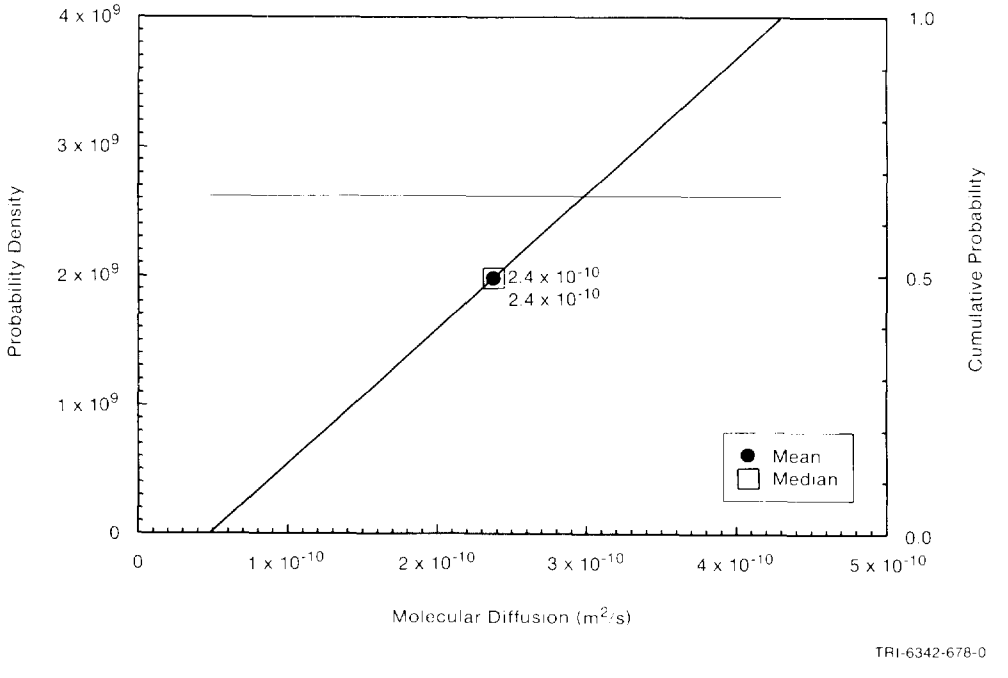

Figure 3.3-10. Uniform Distribution (pdf and cdf) for Molecular Diffusion Coefficient, D^{α}.

* This section provides data for free-liquid diffusion coefficients; the diffusion coefficient for an actual porous media is the free-liquid coefficient times the tortuosity factor for that media.

Discussion:

Table 3.3-12 provides values of the molecular diffusion estimated both from the Nernst equation at infinite dilution (upper range) (Brush, 1988; Li and Gregory, 1974) and data obtained in experiments (lower range). For cases with both experimental and Nernst equation estimates, the molecular diffusion was assumed to be uniformly distributed between the two values.

Because the experimental values were obtained from apparent diffusion coefficients in granitic ground waters and sodium bentonite, they required assumptions about retardation factors for the radionuclides, porosity, and tortuosity (Torstenfelt et al., 1982; Lappin et al., 1989, Table E-7). Therefore, considerable but unquantifiable uncertainty is associated with all the values of the actinide diffusion coefficients reported in the literature. Furthermore, there are few data to guide predictions of radionuclide diffusion coefficients in the concentrated brines. Consequently, extrapolation of the measured diffusion coefficients to the range of conditions assumed for the Salado and Culebra Dolomite brines introduces more uncertainty.

Some data suggest that diffusion coefficients for divalent cations (alkaline earth chlorides, transitions metal chlorides) decrease by a factor of 2 with increasing ionic strength over the range 0 to 6 M (Miller, 1982). This factor of 2 was used to establish ranges for Ra and Pb, for which only a single value (the upper range) is available from the Nernst expression (Li and Gregory, 1974). Specifically, the median value selected is smaller than the Nernst equation value by a factor of 2 to include some salinity effects. The lower range is smaller than the median by a factor of 2 to account for greater salinity and miscellaneous uncertainties.

Although molecular diffusion varies with each species and the concentration of ions (e.g., Na^+ from brackish water), some of the computational models used by the PA Division require a single value. For these cases, molecular diffusion is assumed to be uniformly distributed (Figure 3.3-11) with a range chosen to encompass the extremes for the actinide radionuclides, 4.8×10^{-11} to 4.3×10^{-10} m^2/s (4.5×10^{-5} to 4.0×10^{-4} ft^2/d) with a mean of 2.4×10^{-10} m^2/s (2.2×10^{-4} ft^2/d).

3.3.8 Gas Production from Corrosion

Parameter:	**Gas production rates, corrosion, inundated rate**
Median:	6.3×10^{-9}
Range:	0
	1.3×10^{-8}
Units:	mol H_2/(m^2 surface area steel • s)
Distribution:	Cumulative
Source(s):	Brush, L. H. 1991. "Current Estimates of Gas Production Rates, Gas Production Potentials, and Expected Chemical Conditions Relevant to Radionuclide Chemistry for the Long-Term WIPP Performance Assessment," Internal memo to D.R. Anderson (6342), July 8, 1991. Albuquerque, NM: Sandia National Laboratories. (Memo 3 in Appendix A of this volume)

Parameter:	**Gas production rates, corrosion, relative humid rate**
Median:	1×10^{-1}
Range:	0
	5×10^{-1}
Units:	Dimensionless
Distribution:	Cumulative
Source(s):	Brush, L. H. 1991. "Current Estimates of Gas Production Rates, Gas Production Potentials, and Expected Chemical Conditions Relevant to Radionuclide Chemistry for the Long-Term WIPP Performance Assessment," Internal memo to D.R. Anderson (6342), July 8, 1991. Albuquerque, NM: Sandia National Laboratories. (Memo 3 in Appendix A of this volume)

Parameter:	**Anoxic iron corrosion stoichiometry**
Median:	0.5
Range:	0
	1
Units:	None (mol fraction)
Distribution:	Uniform
Source(s):	Brush, L. H. and D. R. Anderson. 1989. In Lappin et al., 1989. *Systems Analysis Long-Term Radionuclide Transport and Dose Assessments, Waste Isolation Pilot Plant (WIPP), Southeastern New Mexico; March 1989.* SAND89-0462. Albuquerque, NM: Sandia National Laboratories.

Figures 3.3-11, 3.3-12, and 3.3-13 provide the assumed distributions for gas production rates from corrosion under inundated conditions; gas production rates from corrosion under humid conditions; and anoxic iron corrosion stoichiometry, respectively. These distributions were constructed using information from Brush (July 8, 1991, Memo, Appendix A).

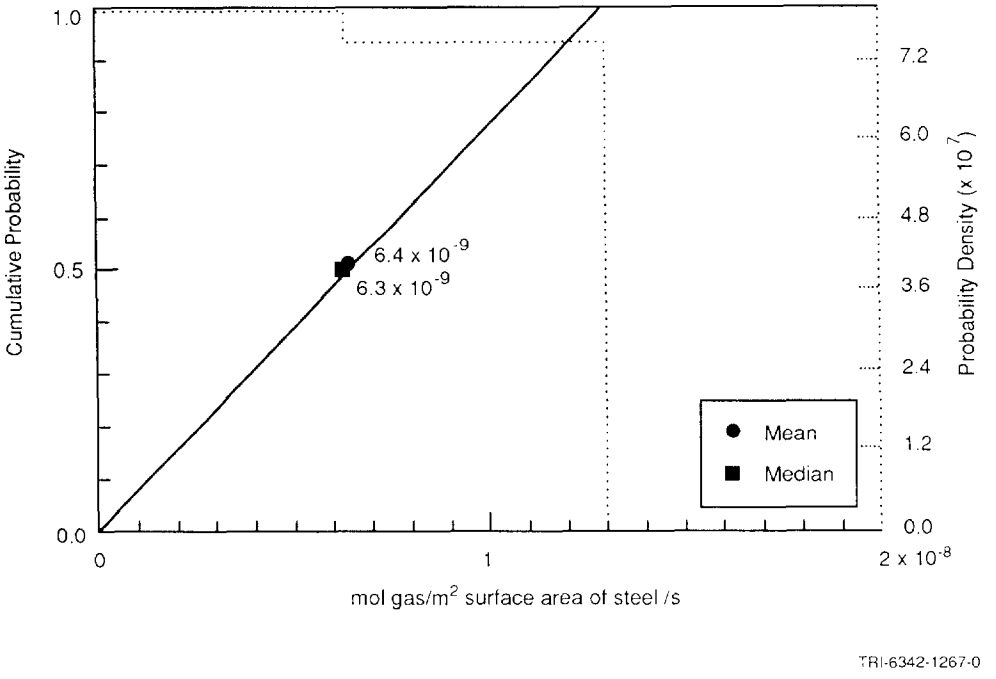

Figure 3.3-11. Assumed Distribution (pdf and cdf) for Gas Production Rates from Corrosion under Inundated Conditions.

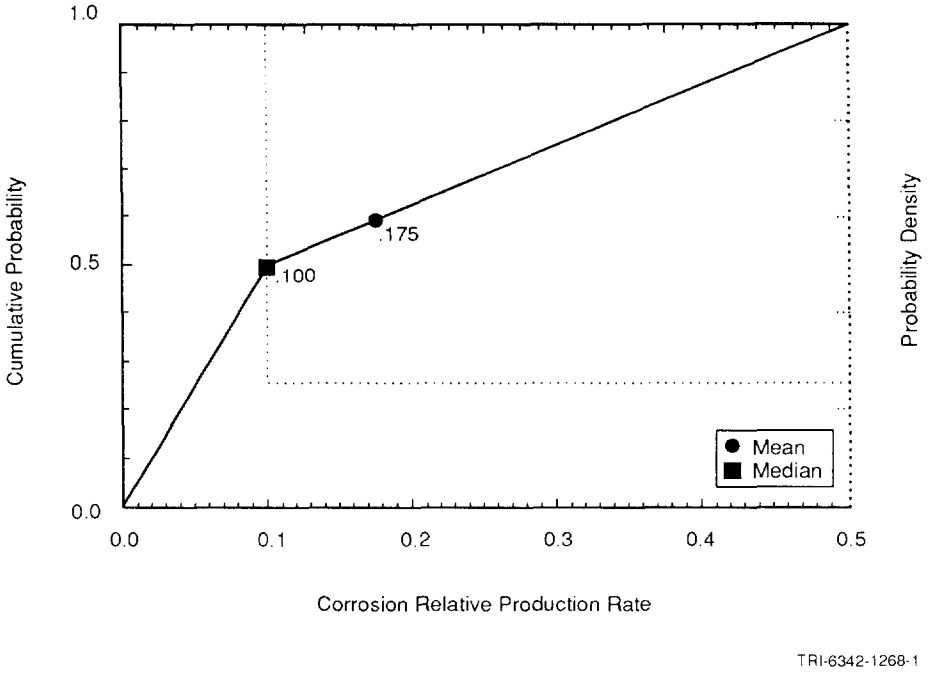

Figure 3.3-12. Assumed Distribution (pdf and cdf) for Relative Gas Production Rates from Corrosion under Humid Conditions.

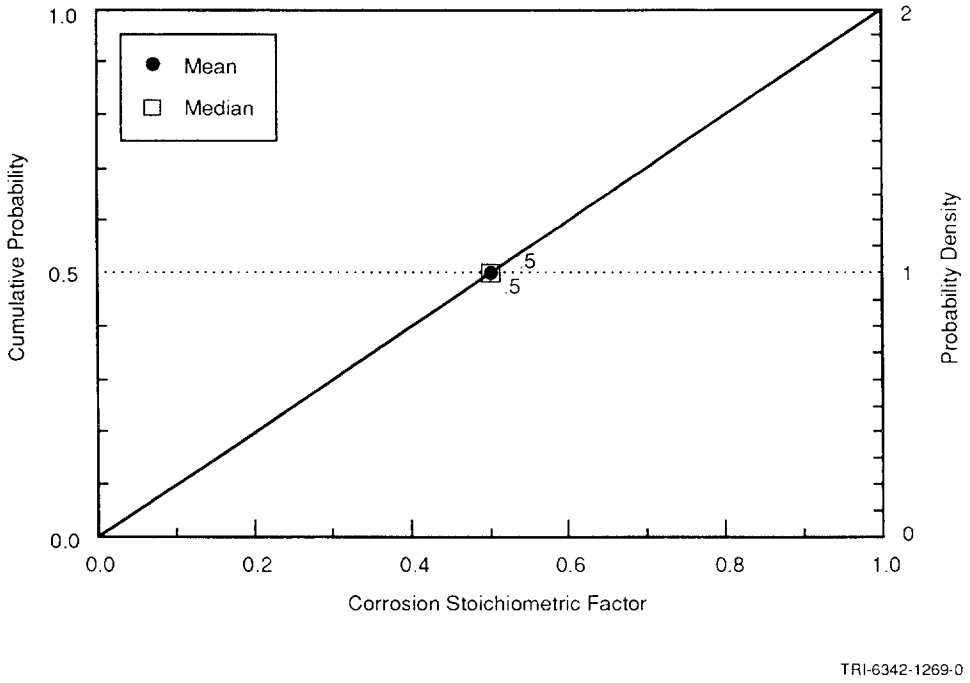

Figure 3.3-13. Assumed Distribution (pdf and cdf) for Anoxic Iron Corrosion Stoichiometric Factor, x.

Discussion:

After waste is emplaced in the WIPP repository, some gas is expected to be generated from three types of chemical reactions: (1) anoxic corrosion, (2) biodegradation, and (3) radiolysis. In theory, the rates are dependent upon several factors, such as the chemical makeup of the waste (both organic and inorganic), the types of bacteria present, interactions among the products of the reactions, characteristics of WIPP brine, pH, and Eh. Experimental data describing these dependencies are incomplete at this time. However, some rough estimates of the range of gas generation rate values under possible WIPP environmental conditions have been made using available data.

Brush (July 8, 1991, Memo [Appendix A]) estimates gas production from corrosion for inundated and humid conditions. The estimates for inundated conditions are based on 3- and 6-month experiments by R. E. Westerman of Pacific Northwest Laboratory (PNL) on ASTM A 366 and ASTM A 570 steels by WIPP Brine A when N_2 is present at low pressures (~ 0.105 MPa [150 psig]) (Brush, July 8, 1991, Memo [Appendix A]) (Figure 3.3-14). The following are estimated gas production and corrosion rates for inundated conditions: minimum, 0 mol H_2/m^2 steel/yr (0 mol H_2/drum/yr); best estimate, 0.2 mol H_2/m^2 steel/yr (1 mol/drum/yr); and maximum, 0.4 mol H_2/m^2 steel/yr (2 mol/drum/yr) with N_2 at 0.698 MPa (1000 psig) (Brush, July 8, 1991, Memo [Appendix A]).

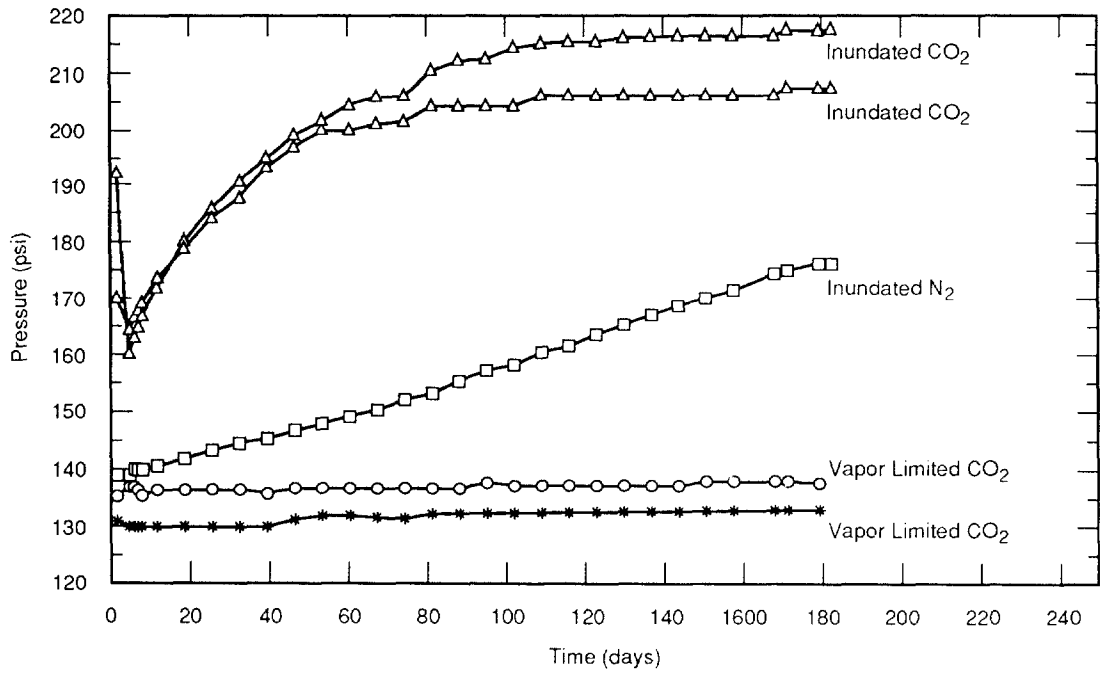

Figure 3.3-14. Pressure-Time Plots for 6-Month Anoxic Corrosion Experiments Under Brine-Inundated and Vapor-Limited ("Humid") Conditions (Davies et al., 1991).

Westerman also performed 3- and 6-month low-pressure humid experiments with either CO_2 or N_2 atmospheres (Brush, July 8, 1991, Memo [Appendix A]). No H_2 production was observed except for very limited quantities from corrosion of the bottom 10% of the specimens splashed with brine during pretest preparation of the containers. Westerman is currently quantifying H_2 production from anoxic corrosion of steels in contact with noninundated backfill materials; results are expected in late 1991. Until these results are available, the estimated rates for humid conditions are as follows: minimum, 0 mol H_2/m^2 steel/yr (0 mol H_2/drum/yr); best estimate, 0.02 mol H_2/m^2 steel/yr (0.1 mol H_2/drum/yr); and maximum, 0.2 mol H_2/m^2 steel/yr (1 mol H_2/drum/yr) with N_2 at 0.698 MPa (1000 psig) (Brush, July 8, 1991, Memo [Appendix A]). When expressed in terms of relative rates, the values are 0 to 0.5 with a median of 0.1.

Previous Simulations. Previous simulations used ficticious wells in the waste as a way to introduce reaction-generated gas. The various gas generation rates were assumed to be constant for a specified length of time after which the "wells" were turned off. However, the corrosion and biodegradation rates are dependent on brine saturation (distinguishing brine-inundated conditions from humid conditions). While it is not known if the biodegradation reactions will consume or produce water, it is believed that water will be consumed during corrosion and radiolysis.

Current Procedure. To handle the rate of reactant consumption (brine, steel, and cellulosics) and product generation (gas) in a more realistic fashion, chemical reactions, reaction mechanisms, kinetics, and stoichiometry are used in PA calculations (i.e., BRAGFLO) and replace the use of wells.

Anoxic Corrosion Stoichiometry. Brush and Anderson (Lappin et al., 1989, p. A-6) describe four possible anoxic corrosion reactions likely to occur when waste drums are exposed to WIPP brines:

$$Fe + 2H_2O = Fe(OH)_2 + H_2 \qquad (3.3\text{-}1)$$

$$3Fe + 4H_2O = Fe_3O_4 + 4H_2 \qquad (3.3\text{-}2)$$

$$Fe + H_2O = FeO + H_2 \qquad (3.3\text{-}3)$$

$$(x + y)Fe + (2(x + y) + z)H_2O + yNacl = xFe(OH)2.yFeOCl.zH_2O + yNa^+ + yOH^- + (x + 3y)H_2 \qquad (3.3\text{-}4)$$

Brush and Anderson believed that FeO would not be stable under low-temperature conditions, so reaction 3.3-3 was discounted. Sufficient data are not available to characterize reaction 3.3-4, so it, too, is ignored in current PA calculations.

The average stoichiometry of reactions 3.3-1 and 3.3-2 is

$$Fe + ((4+2x)/3)H_2O = ((4-x)/3)H_2 + (3x)Fe(OH)_2 + ((1-x)/3)Fe_3O_4 \qquad (3.3\text{-}5)$$

where x mole fraction of iron is consumed by reaction 3.3-1. The PA calculations sample the parameter x from a uniform distribution between 0 and 1.

Reaction Rate Constant. The reaction rate for corrosion under inundated conditions is sampled from the distribution shown in Figure 3.3-11, ranging from 0 to 0.4 mol H_2/m^2 steel/yr = 1.268 x 10^{-8} mol H_2/m^2 steel/s. The rate under humid conditions is sampled as a fraction of the inundated rate, the fraction ranging from 0 to 1, with the distribution shown in Figure 3.3-12. This forces the humid rate always to be less than the inundated rate as observed in preliminary tests (Figure 3.3-14).

For use in BRAGFLO, the corrosion rate (mol H_2/m^2) for both humid and inundated conditions is converted to units of mol Fe/m^3 panel/s by the following formula:

$$\text{ñ}_{CI} = (\text{ñ}'_{CI})(A_d)(n_d)/x_{CH2}/V_{pf} \qquad (3.3\text{-}6)$$

$$\text{ñ}_{CH} = (\text{ñ}'_{CH})(A_d)(n_d)/x_{CH2}/V_{pf} \qquad (3.3\text{-}7)$$

where

ñ_{CH}, ñ_{CI} = humid and inundated corrosion reaction rate, respectively (mol Fe/m^3 panel/s)

$\text{ñ}'_{CH}$, $\text{ñ}'_{CI}$ = humid and inundated corrosion reaction rate, respectively (mol H_2/m^2 steel/s)

A_d = surface area of steel in an equivalent drum, including both the drum and its contents (Brush, July 8, 1991, Memo [Appendix A, p. A-25]) (6 m^2 steel/drum; 4.5 m^2 for drum surfaces alone)

n_d = number of equivalent drums per panel (6,804 drum/panel, Section 3.1.6)

x_{CH2} = stoichiometric coefficient in reaction 3.3-5
= (4-x)/3, where x is a sampled parameter (mol H_2/mol Fe)

V_{pf} = final enclosed volume of a panel (m^3 panel)
= $(V_{pI})(\Delta z_f/\Delta z_i)$

V_{pi} = initial enclosed volume of a panel (Table 3.1-1)
= (116.39 x 10^3 m^3 panel)

Δz_i = initial height of a panel (3.9624 m, Section 3.1.6)

Δz_f = final height of a gas-tight panel after the full potential of gas has been generated (see discussion under Waste Porosity Calculation, Section 3.4.8) (m)

Implicit in the use of average stoichiometry from Eq. 3.3-5 to determine a reaction rate is the assumption that each of the reactions (comprising the average) react at the same rate.

Model Usage. Collection of data describing the kinetic rate expressions for corrosion in the WIPP environment is continuing at this time. The available data suggest that as long as inundated conditions (liquid phase brine in contact with metal) exist, corrosion proceeds at a constant rate (e.g., in N_2 atmosphere and, at least early in the corrosion process, in a CO_2 atmosphere) (Figure 3.3-14). This suggests zero-order kinetics with respect to steel (independent of the steel concentration in the waste). Future data may suggest that the reaction rate may be a function of surface area, film resistance, gas pressure or gas composition. For the 1991 PA calculations, we assume that the rate of corrosion is independent of the parameters mentioned above as well as the concentration of steel in the waste.

Data also suggest that corrosion under humid conditions (no liquid phase brine in contact with metal) may proceed at a slower rate than that under inundated conditions. The humid rate could be dependent on the moisture content in the vapor which contacts the metal; however, in absence of data to support this, we assume that as long as brine is present the humid corrosion rate is independent of humidity. We further assume that any water consumed during corrosion under humid conditions is replenished from the brine pool as long as liquid phase brine is present.

Throughout the course of a calculation, BRAGFLO determines and uses an effective corrosion rate. Both the inundated and humid rate contribute to the effective rate. BRAGFLO calculates the effective corrosion rate from a weighted average of the inundated and humid rates. This weighting is assumed to be dependent on the portion of steel which is in contact with liquid and gas phases. BRAGFLO and numerical models in general are characterized by finite sized homogenous volumes of uniform properties called grid blocks. A typical grid block in the waste can be divided to include 4 material types: brine, gas, steel, and other (rock, backfill, other waste components, etc.) Since each block is assumed homogenous, the steel will be in contact with the brine, gas, steel, and "other." The portion of steel in contact with brine in a given grid block is assumed propotional to the volume fraction of brine in the block and similarly for the portions of steel in contact with gas, steel, and "other." These volume fractions are determined from porosity and saturation; brine volume fraction = $\phi\ s_\ell$, gas volume fraction = $\phi\ s_g$, and "other" (including steel) volume fraction = $1 - \phi$, where ϕ is the porosity (volume fraction of grid block that is void space), s_ℓ is the brine saturation (volume fraction of void space occupied by brine, and s_g is the gas saturation. The portion of steel in contact with brine is assumed to react at the inundated rate while the portion of steel in contact with gas reacts at the humid rate as long as there is some liquid phase brine present to be in equilibrium with the brine in the gas phase.

The portion of steel which is in contact with "other" does not corrode at all. The effective corrosion rate under these assumptions becomes

$$r_{Ce} = r_{CI}\ \phi\ s_\ell + r_{CH}\ \phi\ s_g + 0\ (1 - \phi) \qquad (3.3\text{-}8)$$

where

$\dot{n}_{Ce}$ = effective corrosion rate (moles of steel consumed/reservoir volume/second)

$\dot{n}_{CI}$ = inundated corrosion rate (mol/(m^3•s))

$\dot{n}_{CH}$ = humid corrosion rate (mol/(m^3•s))

Other expressions for obtaining an effective corrosion rate can be envisioned. For example, if the materials in a grid block are not uniformly distributed, all of the steel could always be in contact with either the brine phase or only the gas phase. In addition, moisture in the gas phase could condense on the metal. Nevertheless, Eq. 3.3-8 is used in BRAGFLO for the 1991 PA calculation to determine corrosion rate because (1) it is most consistent with the homogenous assumption, (2) no data are currently available to support any other relationship, and (3) it lies between the bounds set by fully inundated and humid conditions. It should be kept in mind that any uncertainty in the value of the effective rate calulated from Eq. 3.3-8 is captured by the large range of inundated and humid rate values sampled on during the calculations. It should further be pointed out that Eq. 3.3-8 implies that the corrosion rate will vary with time and position in the waste since porosity and saturation vary temporally and spatially. This is a departure from last year when corrosion rates were asumed to be constant in time and space.

The kinetic expression for inundated corrosion assuming zero-order kinetics with aspect to steel concentration in the waste is

$$k_{CI} = -\frac{\partial C_{Fe}}{\partial t} = \dot{n}_{CI} = -\dot{n}_{Fe} \qquad (3.3\text{-}9)$$

where

k_{CI} = rate constant for corrosion under inundated conditions (mole Fe/(m^3 panel•s))

$-\dot{n}_{Fe}$ = rate of steel consumption (mole Fe/(m^3 panel•s))

C_{Fe} = steel concentration (mole Fe/(m^3 panel)

A similar expression results for humid corrosion kinetics. A characteristic of zero-order kinetics is that the rate constant has the same units as the reaction rate (r_{CI}).

From Eqs. 3.3-8 and 3.3-9, the amount of iron per unit volume of panel consumed by corrosion is given by

$$(C_{Fe}^{k+1} - C_{Fe}^{k}) = (k_{CI}\ \phi\ s_{\ell} + k_{CH}\ \phi\ s_{g})\ \Delta t \qquad (3.3\text{-}10)$$

where

Δt = the time step size (s)
k = the time step level

The amount of gas produced and brine consumed by corrosion over a specified time step depends on the rate constant and stoichiometry of reaction. Assuming the stoichiometry of Eq. 3.3-5 remains valid for both humid and inundated conditions and the effective corrosion reaction rate is determined as in Eq. 3.3-8, the rate of gas production and water consumption are calculated from Eqs. 3.3-11 and 3.3-12, respectively.

$$q_{CH_2} = (k_{CI}\ \phi\ s_{\ell} + k_{CH}\ \phi\ s_{g})\ (x_{CH_2})(M_{H_2}) \qquad (3.3\text{-}11)$$

$$q_{CH_2O} = (k_{CI}\ \phi\ s_{\ell} + k_{CH}\ \phi\ s_{g})\ (x_{CH_2O})(M_{H_2O}) \qquad (3.3\text{-}12)$$

where

q_{CH_2} = rate of H_2 produced from corrosion per unit volume of panel (kg/m³s)

q_{CH_2O} = rate of H_2O consumed by corrosion per unit volume of panel (kg/m³s)

x_{CH_2} = corrosion stoichiometry for H_2 = (4 - x)/3 (see Eq. 3.3-5)

x_{CH_2O} = corrosion stoichiometry for H_2O = -(4 + 2x)3 (see Eq. (3.3-5)

M_{H_2} = molecular weight for H_2(kg/gmol)

M_{H_2O} = molecular weight for H_2O (kg/gmol)

Since we are concerned with brine removal rather than water, we convert the water consumption rate of Eq. 3.3-12 to that of brine using Eq. 3.3-13.

$$q_{cb} = (q_{CH_2O})/(1.0 - w_s) \qquad (3.3\text{-}13)$$

where

q_b = rate of brine consumption (kg brine/(m³ panel • s)

w_s = weight fraction of NaCl in brine (kg NaCl/kg brine) assumed to be 25%

We do not adjust the salinity of the brine nor do we deposit salt in the pore space as water is consumed. The corrosion reaction rates, the concentration of steel, and the rates of production and consumption of the various species are computed in BRAGFLO as outlined above.

3.3.9 Gas Production from Microbiological Degradation

Parameter:	**Gas production rates, microbiologial, inundated rate**
Median:	3.2×10^{-9}
Range:	0
	1.6×10^{-8}
Units:	mol gas/kg cellulosics/s
Distribution:	Cumulative
Source(s):	Brush, L. H. 1991. "Current Estimates of Gas Production Rates, Gas Production Potentials, and Expected Chemical Conditions Relevant to Radionuclide Chemistry for the Long-Term WIPP Performance Assessment," Internal memo to D.R. Anderson (6342), July 8, 1991. Albuquerque, NM: Sandia National Laboratories. (In Appendix A of this volume)

Parameter:	**Gas production rates, microbiologial, relative humid rate**
Median:	1×10^{-1}
Range:	0
	2×10^{-1}
Units:	Dimensionless
Distribution:	Cumulative
Source(s):	Brush, L. H. 1991. "Current Estimates of Gas Production Rates, Gas Production Potentials, and Expected Chemical Conditions Relevant to Radionuclide Chemistry for the Long-Term WIPP Performance Assessment," Internal memo to D.R. Anderson (6342), July 8, 1991. Albuquerque, NM: Sandia National Laboratories. (In Appendix A of this volume)

Parameter:	**Gas generation, stoichiometry factor**
Median:	8.35×10^{-1}
Range:	0
	1.67
Units:	Dimensionless
Distribution:	Uniform
Source(s):	Brush, L. H. and D. R. Anderson. 1989. In Lappin et al., 1989. *Systems Analysis Long-Term Radionuclide Transport and Dose Assessments, Waste Isolation Pilot Plant (WIPP), Southeastern New Mexico; March 1989.* SAND89-0462. Albuquerque, NM: Sandia National Laboratories.

Figures 3.3-15 and 3.3-16 provide distributions for gas production rates from microbiological degradation under inundated and humid conditions, respectively.

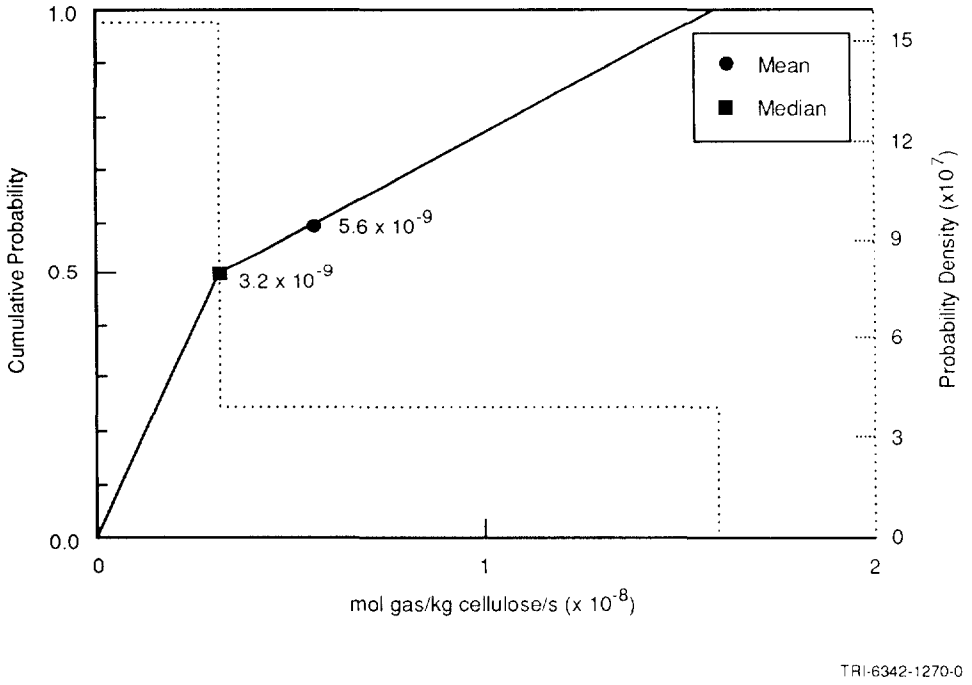

Figure 3.3-15. Estimated Distribution (pdf and cdf) for Gas Production Rates from Microbiological Degradation under Inundated Conditions.

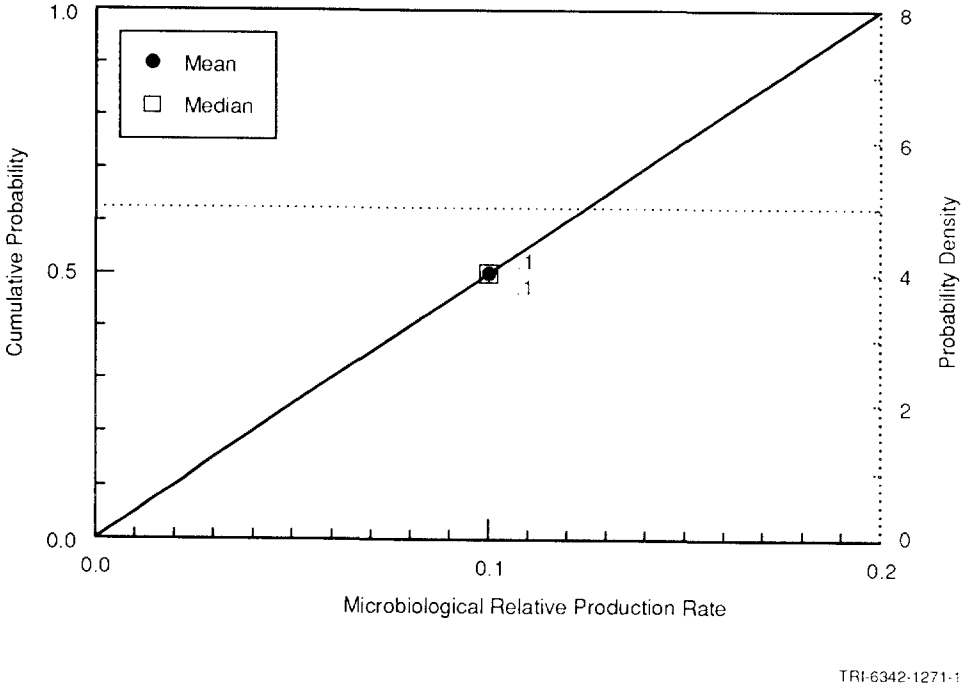

Figure 3.3-16. Estimated Distribution (pdf and cdf) for Relative Gas Production Rates from Microbiological Degradation under Humid Conditions.

Discussion:

Brush (July 8, 1991, Memo [Appendix A]) estimates activity from microbiological degradation based on a recent study at Stanford University and studies carried out during the 1970s (Barnhart et al., 1980; Caldwell, 1981; Caldwell et al., 1988; Molecke, 1979; Sandia National Laboratories, 1979). A test plan for laboratory experiments (Brush, 1990) and in-situ gas production experiments using real waste at the WIPP (Lappin et al., 1989) describe experiments currently underway. Although the Stanford tests seemed to suggest that microbial gas production may be significant under overtest conditions but not under realistic conditions, results from the earlier tests implied significant microbial gas production under both realistic and overtest conditions. However, until the Stanford tests are corroborated, the best estimate for microbial gas production has remained the same as first proposed by Brush and Anderson (in Lappin et al., 1989; Brush, 1990), 0.1 mole of various gases per kg cellulosics per year (1 mol gas/(drum•yr)). However, new minimum and maximum rates for inundated conditions are 0 and 0.5 mol/(kg•yr) (5 mol per drum per year), respectively.

For humid conditions, new minimum and best estimates for microbial gas production rates are 0 and 0.01 mol/(kg cellulosics•yr) (0.1 mol/(drum•yr)). The maximum estimate under humid conditions remains unchanged from the value estimated by Brush and Lappin (1990), 0.1 mol/(kg•yr) (1 mol/(drum•yr)). Expressed in terms of relative rates, the values are 0 to 0.2 with a median of 0.1.

Microbiologic Degradation Stoichiometry. The stoichiometry of the net biodegradation reaction is uncertain. About 20 reactions have been postulated and others may be possible, according to Brush and Anderson (Lappin et al., 1989, p. A-10). The reactions depend on such factors as what electron donors are available, the solubility of CO_2, interaction with products of corrosion, pH, and Eh. It is not known at this time what effect biodegradation has on water (brine) inventory, so it is assumed to have no net effect, neither consuming water nor producing it. Some of the postulated reactions produce gas; others consume it. At present, we know that some gas (CO_2 and some H_2, H_2S, and CH_4) may be produced and that cellulose (CH_2O) will be consumed. Using the stoichiometry recommended in Lappin et al. (1989, Supplement to Appendix A.1, p. A-30) that yields the maximum gas generation per unit of cellulose (5/3 mol gas/mol CH_2O), the biodegradation reaction may be written

$$CH_2O + \text{unknowns} + \text{microbes} = 5/3 \text{ gas} + \text{unknowns} \qquad (3.3\text{-}14)$$

However, in view of the wide variety of reactions that may occur, together with our current lack of knowledge as to precisely which reactions do occur, it is prudent to sample on the stoichiometric coefficient for gas in reaction 3.3-14. If the assumption is also made that any CO_2 that is produced will dissolve in the WIPP brine, then of the reactions presented in Lappin et al., (1989) only one reaction will consume gas, that one being

$$CH_2O + O_2 = H^+ + HCO^{3-} \qquad (3.3\text{-}15)$$

This reaction requires oxygen, which will be present initially in air and will be produced by radiolysis. Neither source of oxygen is sufficient to oxidize all of the cellulose in the inventory, and oxic corrosion will compete strongly for this oxygen, so this reaction is expected to be of minor importance. None of the other reactions consumes gas, whereas most produce gas, with the net gas production ranging from 0 to 5/3 mol gas/mol CH_2O. Therefore, the stoichiometric coefficient is sampled from a uniform distribution ranging from 0 to 5/3.

Model Usage. As with corrosion, the rate of gas generation from the biodegradation of cellulosics differs depending on whether inundated or humid conditions exist in the repository. In BRAGFLO an effective rate of biodegradation is calculated, as described in the previous corrosion rate discussion, from a weighted average of the inundated and humid rates.

There are insufficient data available at this time to quantify any biodegradation kinetics other than zero-order kinetics with respect to the concentration of cellulosic in the waste panel (rate is independent of the concentration of cellulosics). One might expect the reaction rate to depend in some way on the concentration of the reactants (organisms and cellulose) and perhaps on the concentration or partial pressure of the products as well as the gas composition, all of which vary with time. However, until such data become available, we use the zero-order assumption.

The kinetic expression for inundated biodegradation assuming zero-order kinetics with respect to the concentration of cellulosics in the waste panel is

$$k_{BI} = -\frac{\partial C_c}{\partial t} = \dot{n}_{BI} = -\dot{n}_c \qquad (3.3\text{-}16)$$

where

k_{BI} = rate constant for biodegradation under inundated conditions [mol/(m³•s)]

$-\dot{n}_c$ = consumption rate of cellulosics [mol/(m³•s)]

$\dot{n}_{BI}$ = Reaction rate for biodegradation under inundated conditions [mol/(m³•s)]

C_c = Concentration of cellulosics (mol/m³ of panel)

A similar expression results for the humid biodegradation kinetics.

The amount of cellulosics consumed and the rate of gas production follow from a development similar to that outlined in the corrosion section, Eqs. 3.3-17 and 3.3-18, respectively.

$$(C_c^{k+1} - C_c^k) = (k_{BI}\ \phi\ s_\ell + k_{BH}\ \phi\ s_g)\Delta t \qquad (3\text{-}3.17)$$

$$q_{BH_2} = (k_{BI}\ \phi\ s_\ell + k_{BH}\ \phi\ s_g)\ (s_{BH_2})(M_{wc}) \qquad (3\text{-}3.18)$$

where

q_{BH_2} = rate of H_2 produced from biodegradation per unit volume [kg/(m³•s)]

s_{BH_2} = biodegradation stoichiometry for H_2 (moles H_2 produced/moles cellulosics consumed)

(See Section 3.3.8 for definitions of remaining variables.)

Because some potential biodegradation reactions consume water while others produce water and in absence of any experimental data, we currently assume that biodegradation does not impact brine inventory. The reaction rates, cellulosics concentration, and the rates of production and consumption of the various species are calculated in BRAGFLO as described above.

3.3.10 Radiolysis

Parameter:	**Radiolysis of brine**
Median:	1×10^{-4}
Range:	1×10^{-7}
	1×10^{-1}
Units:	mol/drum/yr
Distribution:	Constant
Source(s):	Brush, L. H. 1991. "Current Estimates of Gas Production Rates, Gas Production Potentials, and Expected Chemical Conditions Relevant to Radionuclide Chemistry for the Long-Term WIPP Performance Assessment," Internal memo to D.R. Anderson (6342), July 8, 1991. Albuquerque, NM: Sandia National Laboratories. (In Appendix A of this volume)

Early indications from experimental data that are currently being collected show that the rate of gas production from radiolysis is very small compared to that from corrosion and biodegradation. A current study is investigating gas production at low pressures by alpha radiolysis of WIPP Brine A as a function of dissolved plutonium concentration (Brush, July 8, 1991, Memo [Appendix A]). Small linear pressure increases from the solution with the highest dissolved plutonium concentration, 1×10^{-4} M, have been observed but there are not enough data to convert these rates to moles of gas per drum per year. Pressure increases were not observed with lower dissolved plutonium concentrations (1×10^{-6} and 1×10^{-8} M). Two-month runs with a dissolved plutonium concentration of 1×10^{-4} M in other WIPP brines are planned.

Until results are available from longer term studies, the radiolytic gas production rates are the same as those proposed by Brush and Lappin (1990): minimum, 1×10^{-7} mole/gases/drum/yr; best estimate, 1×10^{-4} mol/drum/yr, and maximum of 1×10^{-1} mol/drum/yr.

The PA calculations do not separately break out the radiolysis reaction, but will include its contribution to gas generation in the biodegradation reaction. Furthermore, we neglect the consumption of brine by radiolysis.

3.4 Parameters for Unmodified Waste Form Including Containers

As of 1990, the currently stored CH-TRU waste that will be disposed of in the WIPP, if authorized, is estimated to be about 60,000 m^3 (2.1 x 10^6 ft^3), which is about 34% of the design storage volume of 170,000 m^3 (6.2 x 10^6 ft^3). The stored waste consists of about 110,000 0.21-m^3 (55-gal) drums, 5,000 1.8-m^3 (64 ft^3) Standard Waste Boxes (SWBs), and 7,000 3.2-m^3 (113-ft^3) miscellaneous containers, mostly steel and fiberglass reinforced wood boxes. Drums and SWBs are the only containers that can currently be transported in a TRUPACT-II. If the waste in boxes other than SWBs were repackaged into SWBs, it was estimated that 533,000 0.21-m^3 (55-gal) drums and 33,500 1.8-m^3 (64-ft^3) SWBs could be emplaced in the WIPP repository containing 170,000 m^3 (6.2 x 10^6 ft^3) of waste, the design volume for CH-TRU waste.

The volume of RH-TRU waste is limited by the agreement between DOE and the State of New Mexico to 7,079 m^3 (0.25 x 10^6 ft^3) (U.S. DOE and NM, 1984). RH waste will likely be placed in 0.89-m^3 (31.4-ft^3) canisters in the walls of the rooms and access drifts. (Placement of canisters is discussed in Section 3.1.6.)

The parameter values for unmodified waste that is expected to be shipped (i.e., to meet the current waste acceptance criteria discussed below) are provided in Table 3.4-1. The basis for these values is provided in the tables included in this section (see Tables 3.4-3 through 3.4-14). However, the significant figures for masses that are reported in these tables should not be interpreted as known accuracy. (Indeed, the majority of waste to be emplaced in the WIPP has not been generated; hence, the amounts are uncertain.) The significant figures in the tables for masses are presented as a means to trace the work until a report detailing the assumptions and calculations pertaining to these amounts has been prepared. On the other hand, the significant figures on design volumes are important since the limits on volumes agreed upon by the DOE and the State of New Mexico (U.S. DOE and NM, 1984) were in English units and are an exact conversion.

All CH- and RH-TRU waste must meet the WIPP *Waste Acceptance Criteria* (WEC, 1989). This criteria includes requirements for the waste form. For example, the waste material shall (1) include only residual liquids in well-drained containers and limit this waste to less than 1% (volume), (2) not permit explosives or compressed gases, and (3) limit radionuclides in pyrophoric form to less than 1% by weight in each waste package. There also are limitations on the curie content in a drum, SWB, and canister based on transportation considerations (Table 3.4-2). These criteria were summarized from a draft of the *TRU Waste Acceptance Criteria for the Waste Isolation Pilot Plant*, Revision 4, WIPP-DOE-069.

Table 3.4-1. Parameter Values for Unmodified TRU Waste Categories, Containers, and Salt Backfill

Parameter	Median	Range		Units	Distribution Type	Source
CH Waste						
Molecular weight						
Cellulose	0.030			kg/mol	Constant	CH_2; Weast and Astle, 1981
Iron	0.05585			kg/mol	Constant	Fe; Weast and Astle, 1981
Density, grain (ρ_g)						
Metal/glass	3.44×10^3			kg/m^3	Constant	Butcher, 1990, Table 2
Combustibles	1.31×10^3			kg/m^3	Constant	Butcher, 1990, Table 2
Sludge	2.15×10^3			kg/m^3	Constant	Butcher, 1990, Table 2
Salt backfill	2.14×10^3			kg/m^3	Constant	See Table 2.3-1
Steel, cold-drawn	7.83×10^3			kg/m^3	Constant	Perry et al., 1969, Table 3-137
Air @ 300.15K, 1 atm	1.177			kg/m^3	Constant	Vennard and Street, 1975, p. 709
Volumes of IDB Categories						
Metal/glass fraction	3.76×10^{-1}	2.76×10^{-1}	4.76×10^{-1}	none	Normal	See Table 3.4-10
Combustibles fraction	3.84×10^{-1}	2.84×10^{-1}	4.84×10^{-1}	none	Normal	See Table 3.4-10
Salt backfill	1.712×10^5			m^3	Constant	See Figure 3.1-3
Air @ 300.15K, 1 atm	8.908×10^4			m^3	Constant	See Figure 3.1-3
Average per Drum						
Metal/glass	6.44×10^1	3.05×10^1	9.83×10^1	kg/drum	Normal	Butcher, 1989, Table 7
Combustibles	4.00×10^1	1.73×10^1	6.26×10^1	kg/drum	Normal	Butcher, 1989, Table 6
Sludge	2.25×10^2			kg/drum	Constant	See Table 3.4-10
Mass of IDB Categories						
Metal/glass	1.984×10^7					See Tables 3.4-10 and 3.4-12
Combustibles	1.348×10^7					See Tables 3.4-10 and 3.4-12
Mass of Steel Containers in IDB Categories						
Metal/glass	1.076×10^7			kg	Constant	See Table 3.4-10
Combustibles	1.178×10^7			kg	Constant	See Table 3.4-10
Sludge	3.598×10^6			kg	Constant	See Table 3.4-10
Mass of Steel Containers and Liners in IDB Categories						
Metal/glass	4.458×10^6			kg	Constant	See Table 3.4-10
Combustibles	1.214×10^7			kg	Constant	See Table 3.4-10
Sludge	1.329×10^7			kg	Constant	See Table 3.4-10
Mass of Contents						
Iron, steel, paint cans, shipping cans	1.431×10^7			kg	Constant	See Table 3.4-12
Steel in containers	2.613×10^7			kg	Constant	See Table 3.4-10
Cellulosics, + 50% gloves, Hypalon, Neoprene, rubber	7.475×10^6			kg	Constant	See Table 3.4-12
Capillary pressure (p_c) and relative permeability ($k_{\ell r}$)						
Threshold displacement pressure (p_t)	2.02×10^3	2.02×10^1	2.02×10^5	Pa	Lognormal	Davies, 1991; Davies, June 2, 1991, Memo (see Appendix A)
Residual Saturations						
Wetting phase ($S_{\ell r}$)	2.76×10^{-1}	1.38	5.52×10^{-1}	none	Cumulative	Brooks and Corey, 1964
Gas phase (S_{gr})	7×10^{-2}	3.5×10^{-2}	1.4×10^{-1}	none	Cumulative	Brooks and Corey, 1964
Brooks-Corey Exponent (η)	2.89	1.44	5.78	none	Cumulative	Brooks and Corey, 1964

Table 3.4-1. Parameter Values for Unmodified TRU Waste Categories, Containers, and Salt Backfill (Concluded)

Parameter	Median	Range		Units	Distribution Type	Source
Drilling Erosion Parameters						
Absolute roughness (ε)	2.5×10^{-2}	1×10^{-2}	4×10^{-2}	m	Uniform	Streeter and Wylie, 1975, Figure 5.32.
Shear strength (τ_{fail})	1	1×10^{-1}	1×10^{1}	Pa	Cumulative	Sargunam et al., 1973; Henderson, 1966
Partition Coefficient for clays in salt backfill						
Am	1×10^{-4}			m^3/kg	Constant	Lappin et al., 1989, Table D-5 ($K_{dclay}/1000$)
Np	1×10^{-5}			m^3/kg	Constant	Lappin et al., 1989, Table D-5 ($K_{dclay}/1000$)
Pb	1×10^{-6}			m^3/kg	Constant	Lappin et al., 1989, Table D-5 ($K_{dclay}/1000$)
Pu	1×10^{-4}			m^3/kg	Constant	Lappin et al., 1989, Table D-5 ($K_{dclay}/1000$)
Ra	1×10^{-6}			m^3/kg	Constant	Lappin et al., 1989, Table D-5 ($K_{dclay}/1000$)
Th	1×10^{-4}			m^3/kg	Constant	Lappin et al., 1989, Table D-5 ($K_{dclay}/1000$)
U	1×10^{-6}			m^3/kg	Constant	Lappin et al., 1989, Table D-5 ($K_{dclay}/1000$)
Permeability (k)						
Average	1×10^{-13}			m^2	Constant	Lappin et al., 1989, Table 4-6
Combustibles	1.7×10^{-14}	2×10^{-15}	2×10^{-13}	m^2	Cumulative	Butcher et al., 1991
Metals/glass	5×10^{-13}	4×10^{-14}	1.2×10^{-12}	m^2	Cumulative	Butcher et al., 1991
Sludge	1.2×10^{-16}	1.1×10^{-17}	1.7×10^{-16}	m^2	Cumulative	Butcher et al., 1991
Porosity (ϕ)						
Average	1.9×10^{-1}			none	Constant	See text; Butcher, 1990; Lappin et al., 1989, Table 4-6
Combustibles	1.4×10^{-2}	8.7×10^{-2}	1.8×10^{-1}	none	Data	Butcher et al., 1991
Metals/glass	4×10^{-1}	3.3×10^{-1}	4.4×10^{-1}	none	Data	Butcher et al., 1991
Sludge	1.1×10^{-1}	1×10^{-2}	2.2×10^{-1}	none	Data	Butcher et al., 1991
Saturation, initial ($S_{\ell i}$)	1.38×10^{-1}	0	2.76×10^{-1}		Uniform	See text.

Table 3.4-2. Summary of Waste Acceptance Criteria and Requirements Applicable to Performance Assessment

Description	Waste Type	WAC Criterion or Requirement
Particulates	CH	Immobilize if greater than 1% by weight below 10 microns
	RH	Immobilize if greater than 15% by weight below 200 microns
Liquids	CH & RH	Liquids that result from liquid residues remaining in well-drained containers; condensation moisture; and liquid separation from sludges or resin settling shall be less than 1% by volume of the waste container
Pyrophoric Materials	CH	Radionuclides in pyrophoric form are limited to less than 1% by weight in each waste package. No non-radionuclide pyrophorics permitted.
	RH	
Explosives and compressed gas	CH & RH	No explosives or compressed gases are permitted.
Specific Activity	CH	The specific activity shall be greater than 100 nCi/g TRU radionuclides, excluding the weight of added shielding, rigid liners, and waste containers.
	RH	The specific activity shall be greater than 100 nCi/g TRU radionuclides, excluding the weight of external shielding, rigid liners, and the waste containers. The container average maximum activity concentration shall not exceed 23 curies/liter.
Nuclear Criticality* (Pu-239 FGE)**	CH	The fissile or fissionable radionuclide content shall be less than 200 FGE for a 55-gallon drum. The fissile or fissionable radionuclide content shall be less than 325 FGE for a SWB. The fissile or fissionable radionuclide content shall be less than 325 FGE for a TRUPACT-II
	RH	The fissile or fissionable radionuclide content shall be less than 325 FGE.
Pu-239 Activity*	CH & RH	Waste packages shall not exceed 1000 Ci to Pu-239 equivalent activity.

* Transportation requirement
** Fissile gram equivalent of Pu-239

3.4.1 Composition of CH-TRU Contaminated Trash (Non-Radionuclide/ Non-RCRA Inventory)

TRU waste destined for the WIPP is generated or currently stored by ten DOE nuclear weapon facilities. Although we know that this TRU waste consists in general of laboratory and production line trash, such as glassware, metal pipes, solvents, disposal laboratory clothing, cleaning rags, and solidified sludges, the precise composition of the trash (e.g., percentages by weight and volume) is not well defined. Estimates of metals/glass combustible and sludge reported here were made based on information on volumes submitted annually to the IDB by the generator sites and therefore are from the same source as the radionuclide inventory. (A potential source in the future is the data collected specifically for the PA Division from the generators.)

Volumes of Various Categories of CH-TRU Contaminated Trash

Parameter:	**Volume fraction, combustibles**
Median:	3.84
Range:	2.84
	4.84
Units:	Dimensionless
Distribution:	Normal
Source(s):	See text and Table 3.4-10.

Parameter:	**Volume fraction, metals/glass**
Median:	3.76
Range:	2.76
	4.76
Units:	Dimensionless
Distribution:	Normal
Source(s):	See text and Table 3.4-10.

Parameter:	**Volume, backfill**
Median:	1.712×10^5
Range:	None
Units:	m^3
Distribution:	Constant
Source(s):	See Figure 3.1-3 and text.

Parameter:	**Air @ 300.15 K, 1 atm**
Median:	8.908×10^4
Range:	None
Units:	m^3
Distribution:	Constant
Source(s):	See Figure 3.1-3 and text.

Figure 3.4-1 indicates CH waste volumes by site and status.

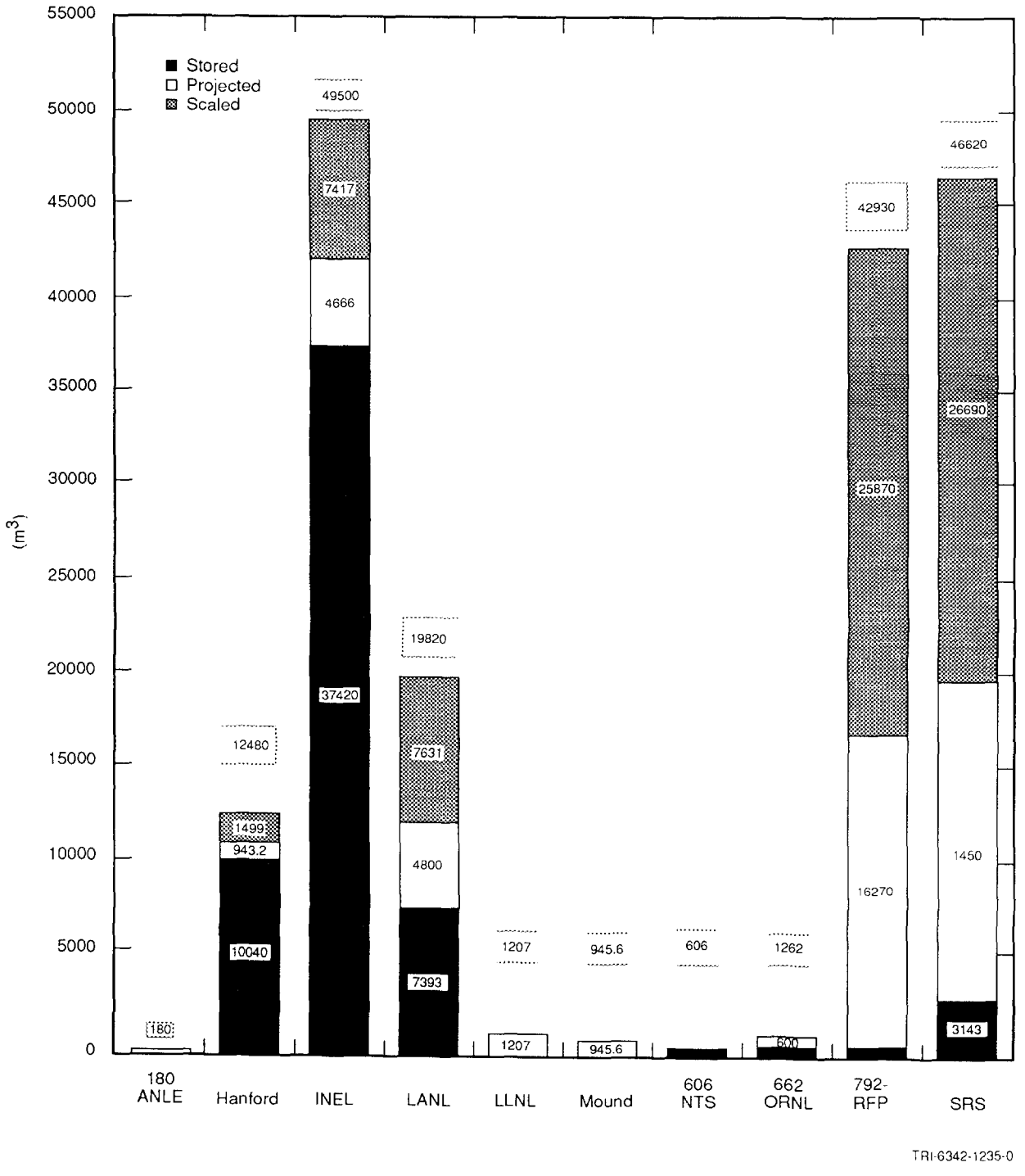

Figure 3.4-1. Estimates of CH Waste Volumes by Site and Status

Discussion:

Estimates of the masses and volumes of the constituents of TRU waste that affect gas generation, transport, and room properties are required for performance assessment. Since the majority of the waste to be emplaced in the WIPP has not been generated, the waste characterization is an estimate with a potentially large uncertainty. The estimated waste characterization is used as a base for analyses that include the uncertainty in waste characterization. The following discussion presents the method that was used to estimate the characterization of the waste. The intent was to use available information and to use a reasonable method to scale it up to a design volume, which was used in performance assessment. This method resulted in estimates of volumes and masses of waste by generator site; however, these results should not necessarily be considered as indicative of the actual masses and volumes that the sites will generate.

The total anticipated volume (stored waste and projected annual volumes) of the TRU waste calculated from information reported in the yearly IDB has been decreasing over the last four years (Table 3.4-3 and Figure 3.4-2). The most significant change from 1987 to 1990 is the percentage of concreted or cemented sludge; the estimated volume decrease was about 30%. Furthermore, the information contained in the 1990 IDB indicates that generators anticipate there will be less volume of absorbed sludges and more volume of concreted and cemented sludges in the projected waste than is contained in the stored waste.

The 1990 IDB was used as the basis for the estimate of the total volume of CH-TRU waste for the 1991 PA calculations. Table 3.4-4 lists the stored and projected (generated in the future) waste volume by generator site listed in the 1990 IDB. The IDB uses the terms "stored" and "newly generated" waste. In the discussion that follows, the term "projected" is used in place of "newly generated."

For performance assessment calculations, we assume that a design volume of 175,564 m^3 (6.2 x 10^6 ft^3) will be emplaced in the WIPP. The following discussion presents the method that was used to estimate the volumes of the waste types if the current design volume of waste was emplaced. To estimate the volume of waste by generator site to fill the WIPP, it was assumed that the five largest generators* of projected waste would provide the additional volume. The percentage of the total projected waste for each site was calculated and, based on this percentage, volumes for the five sites were calculated to provide an additional 69,105 m^3 (2.4 x 10^6 ft^3). The scaled volume for the five sites is shown in Table 3.4-4.

Details of the volumes and physical composition of CH waste as calculated from the information from the 1990 IDB (Tables 3.5, 3.7, and 3.10) are listed in Table 3.4-5.

* These five DOE defense facilities for 1990 are Hanford Reservation (HANF), Washington; Idaho National Engineering Laboratory (INEL), Idaho; Los Alamos National Laboratory (LANL), New Mexico; Rocky Flats Plant (RFP), Colorado; and Savannah River Site (SRS), South Carolina. In 1991, INEL was reclassified as a storage site rather than a generator site because a project that would generate waste was indefinitely delayed/cancelled.

For performance assessment calculations, room properties are required. To estimate the volume fraction of the sludges, combustibles, and metals and glass in CH waste, it was assumed the volume of the sludges included the absorbed liquid and sludges, concreted or cemented sludges, and dirt, gravel and asphalt categories of Table 3.4-5. The volume of filter, filter media, and "other" categories of Table 3.4-5 were distributed into the volume of sludges, combustibles, and metals and glass based on the relative volume of the initial amounts of each of these categories. Estimates for the volume fraction of stored; projected; projected plus scaled; and stored, projected, and scaled are tabulated in Table 3.4-6. The $\pm 10\%$ ranges on the volume fractions for the various categories in Table 3.4-6 were based on the historical change observed in the categories over the past 4 yr (Table 3.4-3; Figure 3.4-2).

Table 3.4-3. Estimated Composition by Volume of CH-TRU Contaminated Trash from 1987 to 1990.

	Combustibles (%)	Metal and Glass (%)	Absorbed Liquid and Sludge (%)	Concrete/ Cemented Sludge (%)	Dirt/ Gravel/ Asphalt (%)	Filters/ Filter Media (%)	Other (%)	Total Volume* (m^3)
1987	38.87	31.53	8.99	7.37	1.33	5.81	6.11	158,526
1988	39.84	34.18	7.28	8.00	2.44	4.53	3.73	136,402
1989	32.01	36.41	6.09	16.41	1.31	3.00	4.78	120,243
1990	34.24	34.31	6.28	14.43	1.30	3.67	5.77	106,459

* Design volume is 175,564 m^3.

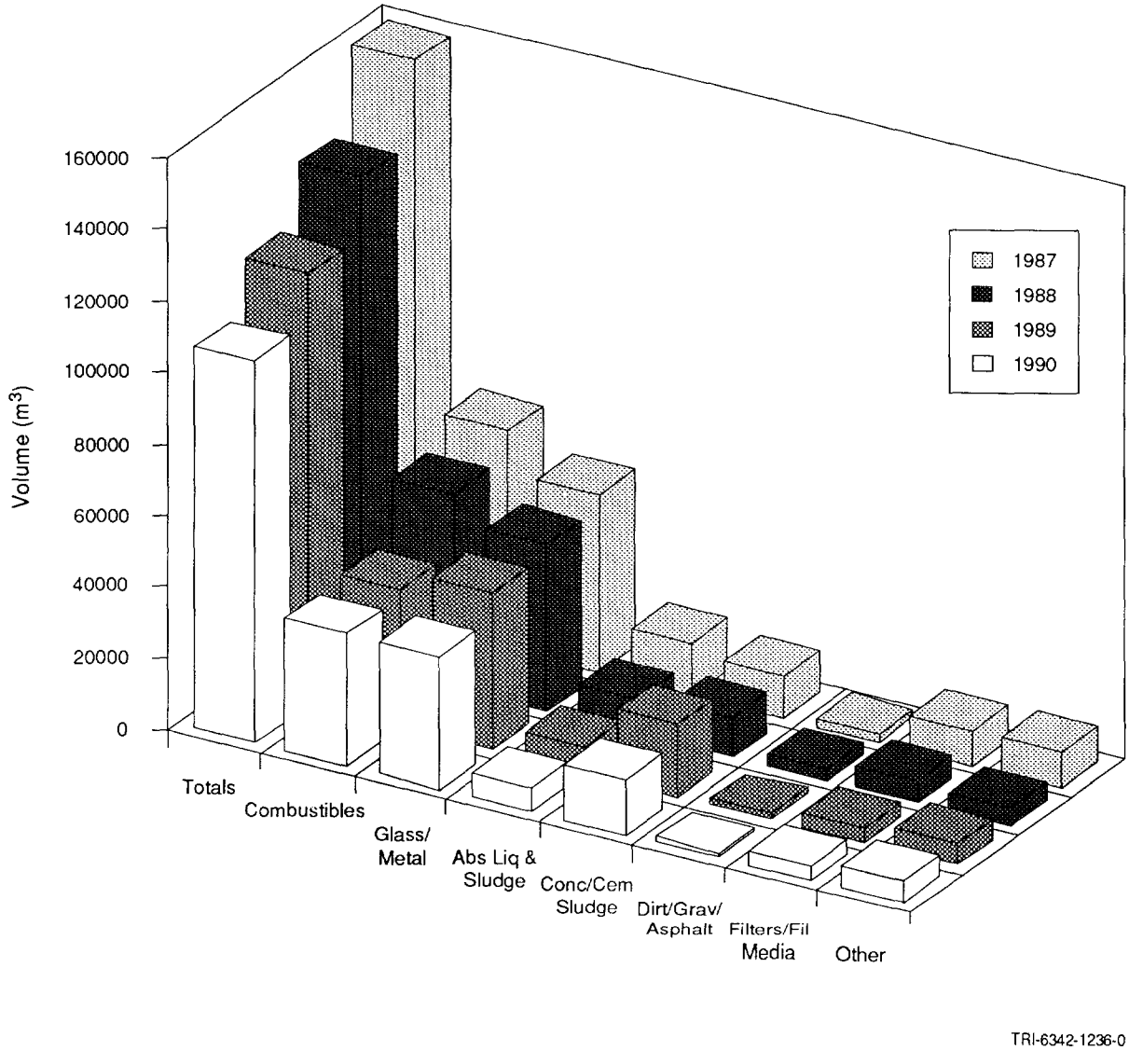

Figure 3.4-2. Changes in Volume Estimates of CH-TRU Contaminated Trash Between 1987 and 1990.

Table 3.4-4. Estimate of a Design Volume for CH-TRU Waste

Site	Stored Volume (1990 IDB) (m^3)	Projected Volume (1990 IDB) (m^3)	Total Volume (1990 IDB) (m^3)	Scaled Volume* (m^3)	Estimated Design Volume (m^3)
ANL-E	--	180	180	--	180
HANF	10,041	943	10,984	1,499	12,484
INEL	37,420	4,666	42,086	7,417	49,503
LANL	7,393	4,800	12,193	7,631	19,824
LLNL	--	1,207	1,207	--	1,207
MOUND	--	945	945	--	945
NTS	606	--	606	--	606
ORNL	662	600	1,262	--	1,262
RFP	792	16,272	17,064	25,869	42,933
SRP	3,143	16,788	19,931	26,689	46,620
Total	60,057	46,402	106,459	69,105	175,564

* Assuming that HANF, INEL, LANL, RFP, and SRP provide the difference between the current total inventory and the design volume. The difference between the total volume of 106,458 m^3 in the 1990 IDB and the design volume of 175,564 m^3 (6.2×10^6 ft^3) was ratioed between the five sites based on their estimated annual generation rates. These five sites provide 94% of the estimated total annual volume of 1,993.4 m^3 per year.

Table 3.4-5. Estimated Composition of CH-TRU Contaminated Trash in 1990 by Generator (IDB, 1990, Tables 3.5, 3.7, 3.10)

Category	ANL-E	HANF	INEL	LANL	LLNL	NTS	MOUND	ORNL	RFP	SRS	Percent	Total (m^3)	Percent of Total
STORED													
Absorbed Liquid and Sludge	--	0.0	4490.4	1626.5	--	0.0	--	0.0	122.8	0.0	10.39	--	--
Combustibles	--	4317.6	9355.0	961.1	--	312.2	--	390.3	287.5	2200.1	29.68	--	--
Concreted or Cemented Sludge	--	602.5	4864.6	2217.9	--	6.1	--	0.0	5.5	0.0	12.82	--	--
Dirt, Gravel, or Asphalt	--	301.2	0.0	0.0	--	0.0	--	6.6	5.5	0.0	0.52	--	--
Filters or Filter Media	--	0.0	1871.0	369.7	--	0.0	--	33.1	327.1	0.0	4.33	--	--
Glass/Metal/Similar Noncombustibles	--	4819.7	13097.0	2217.9	--	288.0	--	231.6	43.6	942.9	36.03	--	--
Other	--	0.0	3742.0	0.0	--	0.0	--	0.0	0.0	0.0	6.23	--	--
TOTAL	--	10041.0	37420.0	7393.1	--	606.3	--	661.6	792.0	3143.0	--	--	--
Percent of Total	--	9.43	35.15	6.94	--	0.57	--	0.62	0.74	2.95	--	--	--
PROJECTED													
Absorbed Liquid and Sludge	64.8	0.0	0.0	48.0	0.0	--	0.0	0.0	0.0	335.8	0.97	6688.2[a]	6.28[a]
Combustibles	57.6	377.3	2020.2	1944.0	881.3	--	9.5	72.0	2522.2	10744.3	40.15	36452.2	34.24
Concreted or Cemented Sludge	0.0	132.0	737.2	864.0	12.1	--	9.5	0.0	5906.7	0.0	16.51	15358.1	14.43
Dirt, Gravel, or Asphalt	0.0	113.2	0.0	0.0	0.0	--	841.6	6.0	113.9	0.0	2.32	1388.1	1.30
Filters or Filter Media	0.0	94.3	23.3	120.0	84.5	--	0.0	30.0	113.9	839.4	2.81	3906.3	3.67
Glass/Metal/Similar Noncombustibles	57.6	226.4	681.2	1824.0	181.1	--	85.1	492.0	6720.3	4616.7	32.08	36525.0	34.31
Other	0.0	0.0	1203.7	0.0	48.3	--	0.0	0.0	895.0	251.8	5.17	6140.8	5.77
TOTAL	180.0	943.2	4665.6	4800.0	1207.2	--	945.6	600.0	16272.0	16788.0		106458.6	100.00
Percent of Total	0.17	0.89	4.38	4.51	1.13	--	0.89	0.56	15.28	15.77		100.00	
PROJECTED PLUS SCALED													
Absorbed Liquid and Sludge	64.8	0.0	0.0	124.3	0.0	0.0	0.0	0.0	0.0	869.5	0.92	7298.3[b]	4.16[b]
Combustibles	57.6	977.1	5231.9	5034.5	881.3	0.0	9.5	72.0	6531.8	27825.3	40.36	64444.8	36.71
Concreted or Cemented Sludge	0.0	342.0	1909.1	2237.6	12.1	0.0	9.5	0.0	15297.1	0.0	17.15	27503.8	15.67
Dirt, Gravel, or Asphalt	0.0	293.1	0.0	0.0	0.0	0.0	841.6	6.0	295.0	0.0	1.24	1749.1	1.00
Filters or Filter Media	0.0	244.3	60.4	310.8	84.5	0.0	0.0	30.0	295.0	2173.9	2.77	5799.6	3.30
Glass/Metal/Similar Noncombustibles	57.6	586.2	1764.1	4723.7	181.1	0.0	85.1	492.0	17404.1	11956.2	32.25	58890.8	33.54
Other	0.0	0.0	3117.4	0.0	48.3	0.0	0.0	0.0	2317.7	652.2	5.31	9877.5	5.63
TOTAL	180.0	2442.7	12082.8	12430.9	1207.2	0.0	945.6	600.0	42140.7	43477.1	--	175564.0	100.00
Percent of Total	0.1	1.39	6.88	7.08	0.69	0.0	0.54	0.34	24.00	24.76	--	100.00	--

[a] Stored plus projected

[b] Stored, plus projected, plus scaled

Table 3.4-6. Calculation of Constituent Volume Distribution in CH Waste*

Category	Initial	Distributed Amount of Filter and Filter Media	Total
Stored			
Sludge**	0.2373	0.0280	0.265
Combustible	0.2968	0.0350	0.332
Glass/Metal	0.3603	0.0425	0.403
Total	0.8944	--	1.000
Projected			
Sludge**	0.1980	0.0171	0.215
Combustible	0.4015	0.0348	0.436
Glass/Metal	0.3208	0.0278	0.349
Total	0.9203	--	1.000
Stored plus Projected			
Sludge**	0.2201	0.0229	0.243
Combustible	0.3424	0.0357	0.378
Glass/Metal	0.3431	0.0358	0.379
Total	0.9056	--	1.000
Stored, Projected, plus Scaled			
Sludge**	0.2083	0.0204	0.229
Combustible	0.3671	0.0360	0.403
Glass/Metal	0.3354	0.0328	0.368
Total	0.9108	--	1.000

* The values for the initial volume percents were obtained from Table 3.4-5.
** Total of absorbed liquid and sludge, concreted and cemented sludge, and dirt, gravel, or asphalt.

Masses of Various Categories of CH-TRU Contaminated Trash

Figure 3.4-3 shows the breakdown of CH waste mass by status, IDB waste categories, and gas-producing components.

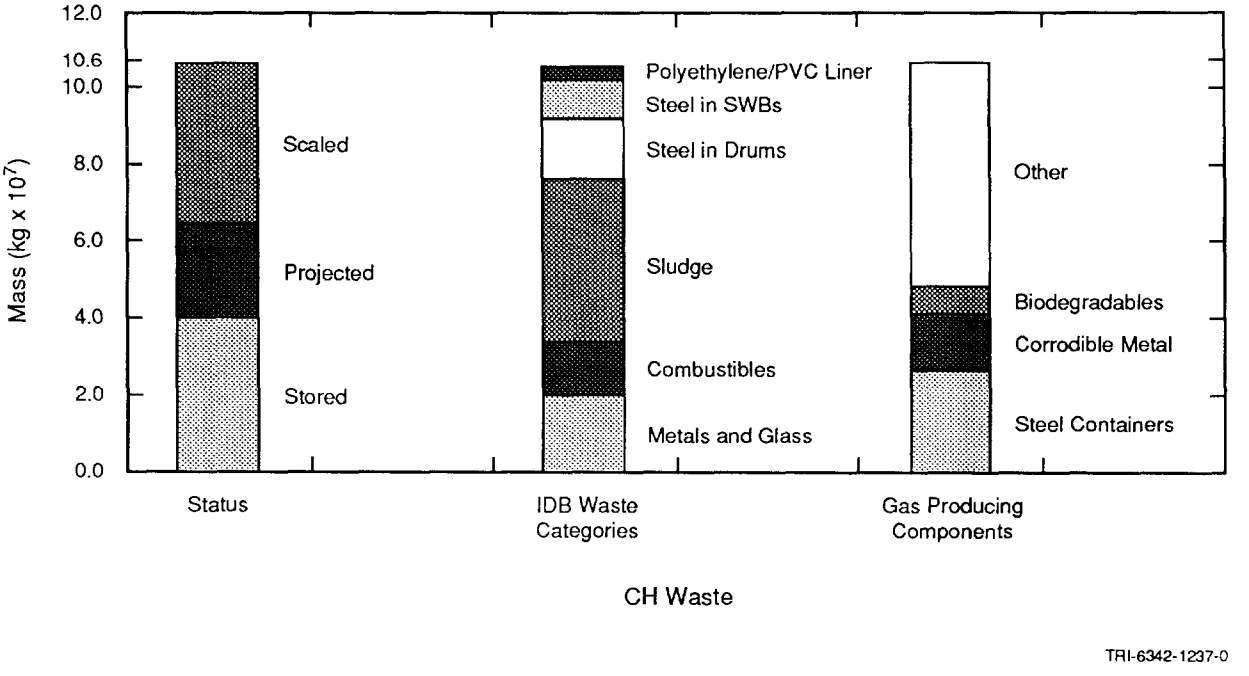

Figure 3.4-3. Breakdown of CH Waste Masses by Status, IDB Waste Categories, and Gas-Producing Components.

Discussion:

The PA calculations require an estimate of the mass of the major constituents of CH-TRU waste that affect gas generation. Because the PA analyses are based on a design volume, the mass of the waste constituents for a design volume were estimated. The generator sites provided estimates of the number, total volume, and mass of stored and projected waste to the 1990 IDB. Based on the number of containers, the masses of container steel, PVC liners, polyethylene liners, fiberglass reinforced wood, and plywood were estimated. Drez (May 9, 1989, Letter [Appendix A]) provided masses for these components.

Since detailed information was not available, it was assumed that each drum had one 4-kg polyvinyl chloride liner bag and each standard waste box (SWB) had one high-density 6.8-kg polyethylene liner. Masses for the larger boxes and bins were estimated by volume scaling to the mass of a 1.2 x 1.2 x 2.1 m (4 x 4 x 7 ft) box, which was obtained from Drez (May 9, 1989, Letter [Appendix A]). The empty mass of a drum was estimated to be 29.5 kg (65 lbm); a SWB, 310.7 kg (685 lbm). Table 3.4-7 summarizes the estimated masses.

Since currently only drums and SWBs can be transported in a TRUPACT II, excluding test bins, an estimate was made of the number of SWBs that would be required if the bins and boxes were repackaged in SWBs. The details of the masses and volumes of the waste in boxes and bins other than SWBs are summarized in Table 3.4-8. A total of 12,152 SWBs would be required to repackage the waste in the bins and boxes. Because of the mass of the SWBs, this repackaging would significantly increase the amount of steel emplaced in the WIPP. The calculations for repackaging in SWBs show (1) number of SWBs (1.9 m^3 volume), 12,150; (2) mass of SWB steel, 3.776 Gg (8.3 x 10^6 lbm); (3) mass of SWB PVC, 0.0486 Gg (1.1 x 10^5 lbm); (4) mass of waste, 5.591 Gg (1.2 x 10^7 lbm); and (5) total repackaged mass of about 9.0 Gg (2.0 x 10^7 lbm).

To obtain an estimate of the number of drums and SWBs that could be emplaced in the WIPP, the number of drums and SWBs at each generator site listed in Table 3.4-4 for stored and projected waste was calculated. Since the estimated volume for each generator from the number of containers was not consistent with the volume in Table 3.4-4, the number of containers for both stored and projected waste was adjusted to the volume of Table 3.4-4. To calculate this adjustment, the ratio of the volume of waste in each type of container in Table 3.4-7 was calculated and the number of containers increased or decreased to make the total volume consistent with the values in Table 3.4-4. The results of this estimate are summarized in Table. 3.4-9. Based on these assumptions, and assuming that the waste that cannot be currently transported is repackaged into SWBs, the inventory would contain 532,600 drums and 33,540 SWBs.

Estimates of the mass fractions were made based on the volume fractions tabulated in Table 3.4-6. Since the information that was available was the total mass of the waste and the volume fraction of sludge, combustibles, and glass/metals, other information was required to make estimates of the mass fraction. For these estimates, it was assumed that the combustible and metal and glass components had the average density listed in Butcher, 1989. An average mass of 40 kg (88.2 lbm) per drum for the combustibles and 64.5 kg (142.2 lbm) per drum for metals and glass was assumed. The mass of combustibles and metals/glass was estimated by calculating the number of drums in each category and multiplying by the average mass. The difference between the total mass of 30.18 Gg (6.6×10^7 lbm) of stored waste from Table 3.4-7 and the mass of the combustibles, metals/glass, polyethylene/PVC liners, and container steel was assumed to be the mass of the sludge, which resulted in the average mass of a sludge drum being 282.8 kg (623.6 lbm). A similar estimate was made for projected waste. The total mass of projected waste was estimated to be 17.48 Gg (3.9×10^7 lbm) as shown in Table 3.4-7. The estimated average mass of a drum of sludge of projected waste was 190.7 kg (420.5 lbm).

For the mass fraction for the design volume estimate, the mass of the sludge was estimated from the average masses of stored and projected waste. The volume of stored sludge and of projected and scaled sludge was estimated. Based on these volumes and the average masses, an average mass of 225 kg (496.1 lbm) per drum was calculated. The mass of sludge was estimated by calculating the number of drums of sludge and multiplying by the average mass. The same average mass of combustibles and metals/glass was assumed for the design volume as for the stored and projected volumes.

The calculated mass fractions for stored waste, projected waste, combined stored and projected waste, and combined stored, projected, and scaled waste are shown in Table 3.4-10. These results indicate the range of mass fractions that could be emplaced in the WIPP. As expected, the mass fraction for sludge is considerably less for projected waste than for stored waste. Note that the mass fraction for combined stored and projected waste has a somewhat higher mass fraction for sludge than was used in Lappin et al., 1989. As indicated in Table 3.4-6, the volume fraction of sludges has increased somewhat from 1987, on which earlier estimates were made, to 1990.

Table 3.4-7. Estimated Inventory of Containers in 1990

Description	Volume (m^3)	Number	Total Mass (Gg)	Total Volume (m^3)	Mass Steel (kg)	Mass PVC (kg)	Mass Polyethelene (kg)	Mass Fiberglass Reinforced Wood (kg)	Mass Plywood (kg)
Stored CH Inventory									
Drums	0.208	110120	25.060	23125	3.249	0.7488	--	--	--
SWBs	1.9	5327	5.198	10121	1.655	--	0.0213	--	--
Boxes	3.17	5925	6.819	18782	0.360	0.0296	--	1.3759	0.2899
Bins	3.4	415	0.421	1411	0.097	0.0022	--	--	--
Boxes	3.8	672	0.600	2554	0.175	0.0040	--	--	--
Boxes	3.9	35	0.036	137	0.009	0.0002	--	--	--
Boxes	5.9	23	0.047	136	0.009	0.0002	--	--	--
Boxes	6.35	11	0.025	70	0.005	0.0001	--	--	--
TOTALS			38.206	56335	5.559	0.7852	0.0213	1.3759	0.2899
Estimated mass of stored waste (Gg) 30.18									
Projected CH Inventory									
Drums	0.208	155420	18.882	32638	4.585	--	1.057	--	--
SWBs	1.9	6105	6.166	11600	1.897	0.2442	--	--	--
TOTALS			25.046	44238	6.489	0.2442	1.057	--	--
Estimated mass of projected waste (Gg) 17.48									

TOTALS	
Total Mass (Gg)	63.252
Total Volume (m^3)	0.101
Total Mass Steel (Gg)	12.04
Total Mass PVC (Gg)	0.810
Total Mass Polyethylene (Gg)	1.078
Total Mass Fiberglass Reinforced Wood (Gg)	1.376
Total Mass Plywood (Gg)	0.29
Estimated Total Mass of Waste (Gg)	47.658
Total Drums	265,540
Total SWBs	11,432
Total Bins & Boxes	7,081

Table 3.4-8. Summary of Bins and Boxes

Description	Volume (m^3)	Number	Total Mass (Gg)	Container Volume (m^3)	Mass Steel (Gg)	Mass PVC (Gg)	Mass Fiberglass Reinforced Wood (Gg)	Mass Plywood (Gg)
Boxes	3.17	5925	6.8193	18782.2	3.60	0.0296	1.3759	0.2899
Bins (1)	3.4	415	0.4210	1411.0	0.96	0.0022	--	--
Boxes (2)	3.8	672	0.6000	2553.6	1.75	0.0040	--	--
Boxes (3)	3.9	35	0.0362	136.5	0.09	0.0002	--	--
Boxes (4)	5.9	23	0.0468	135.7	0.09	0.0002	--	--
Boxes (5)	6.35	11	0.0254	69.9	0.05	0.0001	--	--
TOTALS			7.9487	23088.9	6.55	0.0364	1.3759	0.2899

Estimated metal box masses:
(1) 233.5 kg
(2) 261 kg
(3) 268 kg
(4) 405 kg
(5) 436 kg

Calculations for repackaging in SWBs:

Number of SWBs (1.9 m^3 vol)	0.012
Mass of SWB steel (Gg)	3.776
Mass of SWB PVC (Gg)	0.049
Mass of waste (Gg)	5.591
Total repackaged mass (Gg)	9.379

Table 3.4-9. Estimate of the Number of Drums and SWBs in a Design Volume

Category	Volume	Total	Adjusted Total
Stored Drums	23113	110064	121113
Stored SWBs	10121	5327	6007
Adjustment to stored* Drums	2320	11049	--
Adjustment to stored* SWBs	1425	750	--
Projected Drums	32717	155795	161294
Projected SWBs	12132	6385	6595
Adjustment to Projected* Drums	1155	5499	--
Adjustment to Projected* SWBs	399	210	--
Scaled Drums	52534	250164	250164
Scaled SWBs	16566	8719	8719
Repackaged SWBs**	23089	12152	12152
Total Drums	532571		
Total SWBs	33543		

* Adjusted to make total volume equal volume in Table 3.4-3.
** Assumed volume in Bins and Boxes were repackaged into SWBs.

Table 3.4-10. Estimated Composition of CH-TRU Contaminated Trash Including Containers in 1990

	Mass (Gg)	Volume (m^3)	Volume Fraction	Steel Containers (Gg)	SWB Steel (Gg)	Poly/ PVC (Gg)	Total Mass (Gg)	Mass Fraction
Stored Inventory								
Sludge[a]	20.106	14,928.9	0.265	2.300	--	0.217	22.623	0.570
Metals and Glass[b]	5.745	18,703.4	0.332	2.881	--	0.272	8.898	0.224
Combustibles[c]	4.324	22,703.2	0.403	3.498	--	0.330	8.152	0.205
Steel Containers	8.679							
Polyethylene/PVC liner	0.819							
Total	39.673	56,335.4		8.679	--	0.819	39.673	
Projected								
Sludge	8.618	9,511.1	0.215	1.394	--	0.227	10.239	0.409
Metals and Glass[b]	5.924	19,287.6	0.436	2.826	--	0.461	9.211	0.368
Combustibles[c]	2.941	15,439.0	0.349	2.262	--	0.369	5.572	0.223
Steel Containers	6.482							
Polyethylene/PVC liner	1.057							
Total	25.022	44,237.7		6.482	--	1.057	25.022	
Stored and Projected								
Sludge	28.717	24,444.1	0.243	3.684	--	0.462	32.863	0.508
Metals and Glass[b]	11.679	38,024.2	0.378	5.731	--	0.718	18.128	0.280
Combustibles[c]	7.262	38,124.8	0.379	5.746	--	0.720	13.728	0.212
Steel Containers	15.161							
Polyethylene/PVC liner	1.900							
Total	64.719	100,593.1		15.161	--	1.900	64.719	
Stored, Projected, and Scaled								
Sludge[d]	43.076	40,204.2	0.229	3.598	--	0.860	47.534	0.447
Metals and Glass[b]	19.844	64,607.6	0.368	5.782	4.974	1.382	31.982	0.301
Combustibles[c]	13.477	70,752.3	0.403	6.331	5.447	1.513	26.769	0.252
Steel in drums	15.711							
Steel in SWBs	10.422							
Polyethylene/ PVC liner	3.755							
Total	106.285	175,564.0		15.711	10.422	3.755	106.285	

a The mass of sludge is the difference between a total estimated mass of 30.18 Gg for the total waste package and the mass of the combustibles and metals and glass.

b The mass of metals and glass is based on an average mass of 64.5 kg per drum (Butcher, 1989).

c The mass of combustibles is based on an average mass of 40 kg per drum (Butcher, 1989).

d The mass of sludge is based on the ratio of the 14,929 m^3 of stored waste with an average mass of 282.8 kg per drum and the 25,275 m^3 of projected and scaled waste with an average mass of 190.7 kg per drum. This ratio results in an average mass of 225 kg per drum for sludge.

Estimated Curie Content of Drums and Standard Waste Boxes

Submittals from the generator sites to the 1990 IDB included estimates of the number of stored and projected waste containers in a range of total initial plutonium curie content. The current analyses were based on the design volume of waste emplaced in the WIPP. To estimate the number of drums and SWBs in the four ranges of total plutonium curie content used in the analyses, the estimates from the ranges from the generators were combined and estimates were made for total quantity of drums and SWBs for a design volume based on the quantities from Table 3.4-9. The estimated number of drums and SWBs for the stored, projected, and scaled inventory are shown in Figure 3.4-4 and listed in Table 3.4-11. Since it was assumed for the current analyses that the waste in bins and boxes would be repackaged, an estimate for the repackaged boxes was also made. The current analyses further combined the number of drums and boxes in the range of curie content. It was assumed for the removal of cuttings during drilling for human intrusion that the surface area encountered by the drill for a SWB was about 8.2 times the surface area of a drum. Therefore, the curies removed by drilling into a SWB would be about 8.2 times less than for a drum in the same range. To combine them into an equivalent number of drums, the total number of SWBs was increased by a factor of 8.22 and the curie range was decreased by a factor of ten. This results in no contribution of SWBs in the range above 100 curies and the total SWBs in the 0-to-1 and 1-to-10 range being combined in the 0-to-1 curie category for the combined drums and SWBs shown in Table 3.4-11.

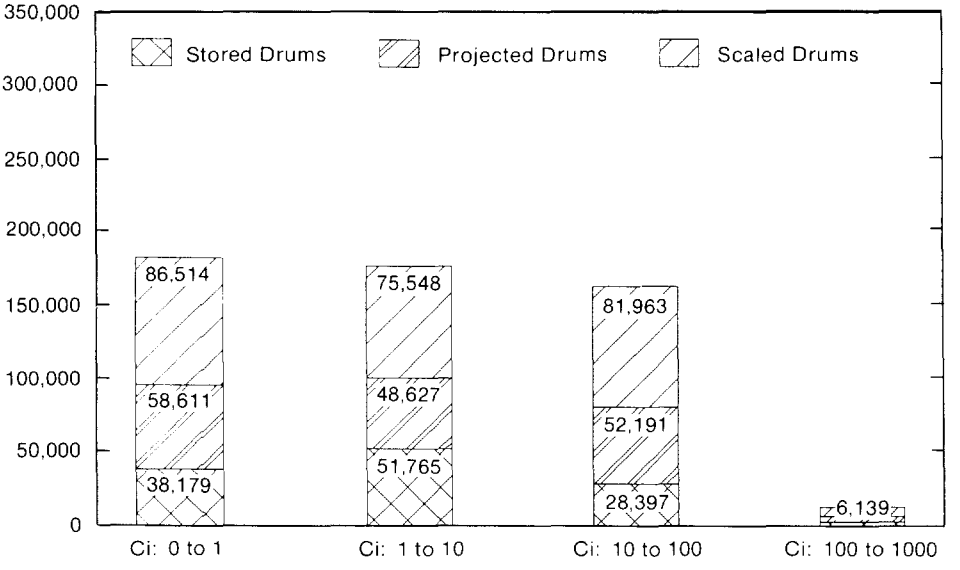

(a) Drums

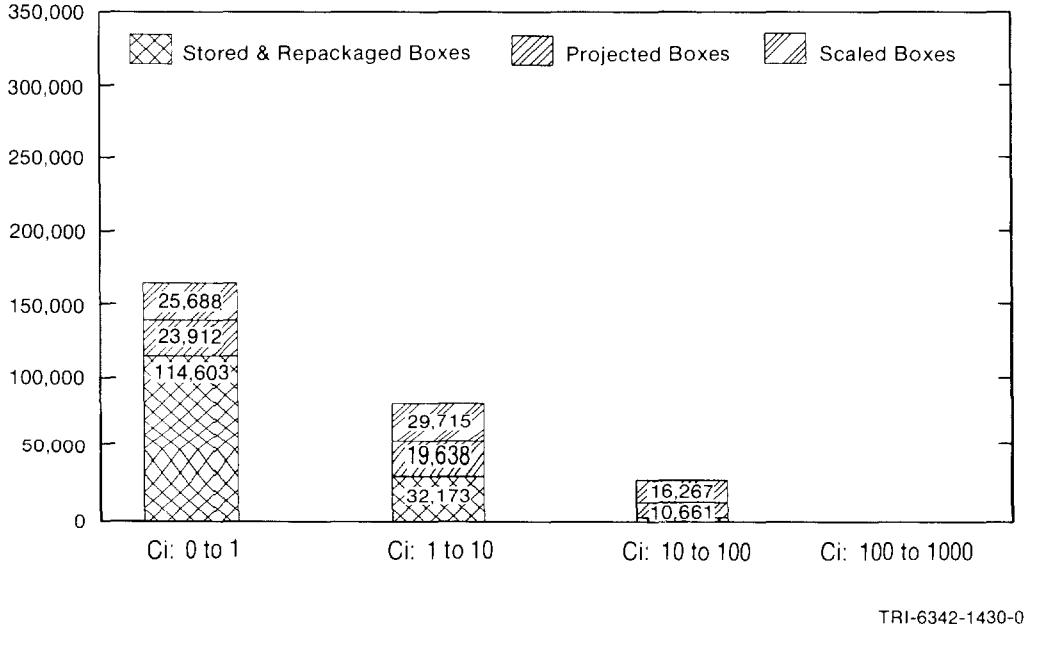

(b) SWBs

Figure 3.4-4. Estimated Number of Drums and SWBs for Stored, Projected, and Scaled Inventory in Each Activity Range.

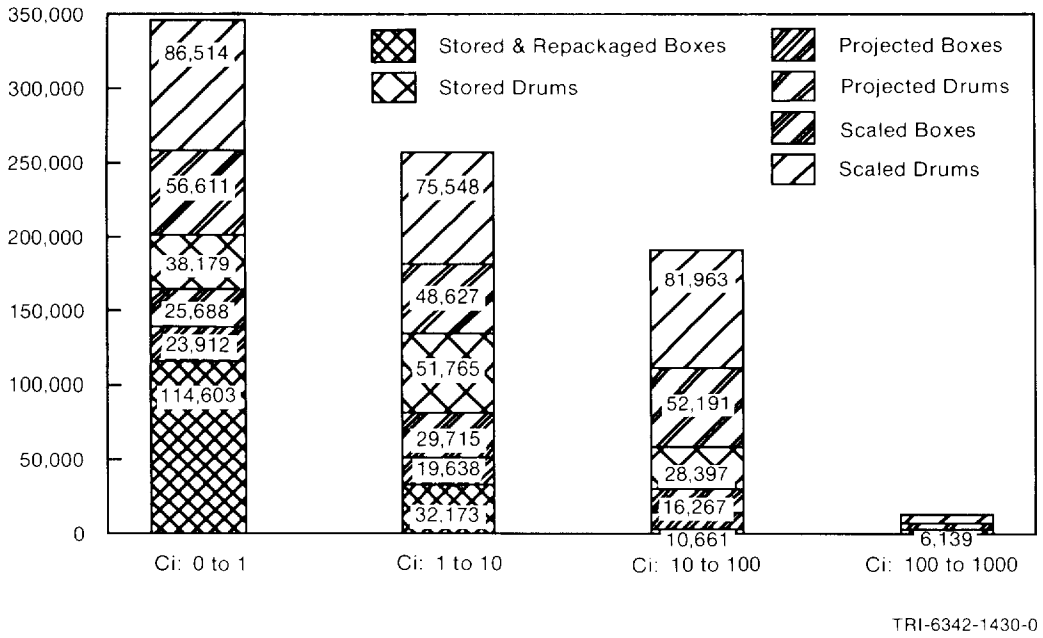

(c) Total, Drums and Boxes

Figure 3.4-4. Estimated Number of Drums and SWBs for Stored, Projected, and Scaled Inventory in Each Activity Range (Concluded).

Table 3.4-11. Estimate of Curie Content of Drums and Standard Waste Boxes in a Design Volume

	0 to 1 (Ci)	1 to 10 (Ci)	10 to 100 (Ci)	100 to 1000 (Ci)	Total (Ci)
Stored Drums					
Totals	38179	51765	28397	2772	121113
Percent	31.5	42.7	23.4	2.3	
Projected Drums					
Totals	56611	48627	52191	3865	161294
Percent	35.1	30.1	32.4	2.4	
Scaled Drums					
Totals	86514	75548	81963	6139	250164
Percent	34.6	30.2	32.8	2.5	
Total Drums					
Totals	181304	175940	162551	12776	532571
Percent	34.0	33.0	30.5	2.4	
Stored Boxes					
Totals	4070	1222	596	189	6077
Percent	67.0	20.1	9.8	3.1	
Projected Boxes					
Totals	1234	1675	2389	1297	6595
Percent	18.7	25.4	36.2	19.7	
Scaled Boxes					
Totals	775	2350	3615	1979	8719
Percent	8.9	27.0	41.5	22.7	
Repackaged (Stored) Boxes					
Totals	1608	7042	3318	184	12152
Percent	13.2	57.9	27.3	1.5	
Total Boxes					
Totals	7687	12289	9918	3649	33543
Percent	22.9	36.6	29.6	10.9	
Combination of Drums and Boxes (Equivalent Drums)					
Totals	345507	257466	192546	12776	808294
Percent	42.7	31.9	23.8	1.6	

Gas Generation Potential

Without a detailed knowledge of the mechanisms by which gas may be produced, the gas generation potentials can only be calculated based on the amount of waste received at the WIPP. Based on information in 1988 (IDB, 1988; Lappin et al., 1989, p. A-119), Sandia estimated a gas generation potential from corrosion of about 900 mole/drum equivalent and from microbial degradation of about 600 mole/drum equivalent. Because estimates of the volume of CH waste are decreasing, but the volume of RH waste is increasing, these values have changed.

An estimate of the amounts of waste that contribute to gas generation are required for PA calculations. The masses of the constituents in combustible and metals/glass were estimated in Drez (May 9, 1989, Letter [Appendix A]). The results of these estimates are shown in column 2 of Table 3.4-12. The total volume for the current PA analysis is based on the design volume of 175,564 m^3 (6.2 x 10^6 ft^3). The total volume on which the estimates in Drez (May 9, 1989, Letter [Appendix A]) were made was 95,111 m^3 (3.4 x 10^6 ft^3). Volume scaling the masses from 95,111 m^3 (3.4 x 10^6 ft^3) to a design volume of 175,564 m^3 (6.2 x 10^6 ft^3), a factor of 1.846, results in the masses listed in column 4 of Table 3.4-12. Butcher (1989) reported estimates of the percentage of various components of combustible and metals/glass. Based on these percentages and volume scaling the masses to a design volume results in the masses listed in column 6.

Another method for estimating the masses is to base the total mass of the combustibles and metals and glass on the mass estimated in Table 3.4-10 for the stored, projected, and scaled estimates. Scaling the masses of the combustibles in column 1 by the ratio of the total combustible mass of 8.593 Gg (1.9 x 10^7 lbm) to 13.467 Gg (3.0 x 10^7 lbm) from Table 3.4-10, a factor of 1.567, the estimated masses shown in columns 7 and 8 were calculated. A similar scaling was calculated for the metals and glass based on the total mass of metals and glass in Table 3.4-10 and are also tabulated in columns 7 and 8. The significant figures in Table 3.4-12 should not be interpreted as an indication of the accuracy of the estimates. These are estimates with a potentially large uncertainty and were made as a base for uncertainty analyses. The significant figures were included only for consistency with Table 3.4-10. The results listed in column 8 of Table 3.4-12 were used as the estimates of these constituents in the PA calculations because they are the same as were used in the estimates of the mass fractions for a design volume in Table 3.4-10. Figure 3.4-3 displays the breakdown of the CH waste mass including the gas-producing components. Not all of the components listed in Table 3.4-12 were included as gas-producing components. The components for microbial activity included the total cellulosics mass and one-half of the mass of surgeon's gloves, Hypalon, Neoprene, and other undefined rubber. The components for corrosion included iron, paint cans, steel, and shipping cans.

Table 3.4-12. Estimates of Masses for a CH Design Volume[a]

	Source 1[b] (kg)	Source 1 (%)	Design (kg)	Source 2[c] (%)	Source 2 (kg)	Source 2[d] (kg)	Design[d] (kg)
COMBUSTIBLES							
Cellulosics							
Paper/Kimwipes	3,890,000	45.27	7,223,730	24.0	3,829,619	3,234,390	6,100,964
Cloth	226,000	2.63	419,682	4.0	638,270	539,065	354,452
Other paper	51	0.00	95	--	--	--	80
Lumber (untreated)	73,100	0.85	135,747	--	--	--	114,648
Lumber (treated)	36,700	0.43	68,152	--	--	--	57,559
Plywood	98,400	1.15	182,729	--	--	--	154,328
Other wood (rulers)	--	0.00	0	--	--	--	0
Other wood (all types)	23,700	0.28	44,011	--	--	--	37,170
Other cellulose (phenolic binder)	1,720	0.02	3194	--	--	--	2,698
Cellulosics subtotal	4,349,671	50.62	8,077,339	28.0	4,467,888	3,773,456	6,821,898
Plastics				38.0	6,063,563	5,121,118	
Polyethylene	1,540,000	17.92	2,859,780	--	--	--	2,415,291
PVC	1,040,000	12.10	1,931,280	--	--	--	1,631,106
Surgeon's gloves (latex)	582,000	6.77	1,080,774	15.0	2,393,512	2,021,494	912,792
Leaded rubber gloves	596,000	6.94	1,106,772	2.0	319,135	269,533	934,749
(Lead-Hypalon-Neoprene)	--	0.00	0	--	--	--	0
Hypalon	114,000	1.33	211,698	--	--	--	178,794
Neoprene	129,000	1.50	239,553	--	--	--	202,320
Viton	133	0.00	247	--	--	--	209
Teflon	41,000	0.48	76,137	--	--	--	64,303
Plexiglass	18,900	0.22	35,097	--	--	--	29,642
Styrofoam	330	0.00	613	--	--	--	518
Plastic prefilters	33,600	0.39	62,395	--	--	--	52,697
Polystyrene	2,560	0.03	4,754	--	--	--	4,015
Conwed pads	2,030	0.02	3,770	--	--	--	3,184
Other plastics	75,500	0.88	140,204	--	--	--	118,412
Other rubber (kalrez)	--	0.00	0	--	--	--	0
Other rubber undefined	7,530	0.09	13,983	--	--	--	11,810
Plastics subtotal	4,182,583	48.68	7,767,057	55.0	8,776,209	7,412,145	6,559,842

[a] The estimated mass of the INEL and LANL containers (3.590 Gg) was subtracted from the 9.170 Gg of metal (Drez, May 9, 1989, Letter [Appendix A]) to obtain the estimated steel mass of 5.580 Gg.

The volume of the inventory for the estimates from Drez (1989) was based on 283,298 drums, 0.21 m^3, 5,541 4x4x7 boxes, 3.17 m^3, and 9,502 SWBs 1.9 m^3. Using this estimate results in the volume as 95,111 m^3. The ratio between the estimated volume and the design volume is 1.846.

[b] Drez. P. 1989. "Preliminary Nonradionuclide Inventory of CH-TRU waste," letter to L. Brush, May 9, 1989 (Appendix A).

[c] Butcher, B. 1989. Waste Isolation Pilot Plant Simulated Waste Compositions and Mechanical Properties. SAND89-0372. Albuquerque, NM: Sandia National Laboratories.

[d] For these estimates, the percentages were assumed to be correct and the total mass was based on combustibles having an average mass of 40 kg per drum for a total mass of 13.477 Gg; the metals and glass having an average mass of 64.5 kg per drum for a total mass of 19.844 Gg.

Table 3.4-12. Estimates of Masses for a CH Design Volume (Concluded)[a]

	Source 1[b] (kg)	Source 1 (%)	Design (kg)	Source 2[c] (%)	Source 2 (kg)	Source 2[d] (kg)	Design[d] (kg)
Other							
Blacktop	18,800	0.22	34,912	--	--	--	29,485
Other	41,700	0.49	77,437	17.0	2,712,647	2,291,027	65,401
Other subtotal	60,500	0.70	112,349	17.0	2,712,647	--	94,886
Total Combustible	8,592,754		15,956,744	--	15,956,744	13,476,627	13,476,627
METALS							
Aluminum	666,000	5.44	1,229,436	14.0	3,164,476	2,778,125	1,079,334
Beryllium	8,640	0.07	15,949	--	--	--	14,002
Cadmium	5	0.00	9	--	--	--	8
Chromium	5	0.00	9	--	--	--	8
Copper	300,000	2.45	553,800	11.0	2,486,374	2,182,812	486,187
Iron	2,620,000	21.40	4,836,520	--	--	--	4,246,029
Lead		0.00	0	7.0	1,582,238	1,389,062	0
Metallic	513,000	4.19	946,998	--	--	--	831,379
Glass (including glass mass)	1,120,000	9.15	2,067,520	--	--	--	1,815,096
Glove (including glove mass)	596,000	4.87	1,100,216	--	--	--	965,891
Lithium	1,030	0.01	1,901	--	--	--	1,669
Mercury	120	0.00	222	--	--	--	194
Paint cans	547,000	4.47	1,009,762	--	--	--	886,480
Platinum	1,500	0.01	2,769	--	--	--	2,431
Selenium	5	0.00	9	--	--	--	8
Silver	5	0.00	9	--	--	--	8
Steel	5,580,000	45.57	10,300,680	64.0	14,466,174	12,699,999	9,043,070
Shipping cans	217	0.00	401	--	--	--	352
Tantalum	125,000	0.02	230,750	4.0	904,136	793,750	202,578
Tungsten	20,000	0.16	36,920	--	--	--	32,412
Other	146,000	1.19	269,516	--	--	--	236,611
Total Metals	12,244,527	--	22,603,397	--	22,603,397	19,843,748	19,843,748

[a] The estimated mass of the INEL and LANL containers (3.590 Gg) was subtracted from the 9.170 Gg of metal (Drez, May 9, 1989, Letter [Appendix A]) to obtain the estimated steel mass of 5.580 Gg.

The volume of the inventory for the estimates from Drez (1989) was based on 283,298 drums, 0.21 m^3, 5,541 4x4x7 boxes, 3.17 m^3, and 9,502 SWBs 1.9 m^3. Using this estimate results in the volume as 95,111 m^3. The ratio between the estimated volume and the design volume is 1.846.

[b] Drez. P. 1989. "Preliminary Nonradionuclide Inventory of CH-TRU waste," letter to L. Brush, May 9, 1989 (Appendix A).

[c] Butcher, B. 1989. Waste Isolation Pilot Plant Simulated Waste Compositions and Mechanical Properties. SAND89-0372. Albuquerque, NM: Sandia National Laboratories.

[d] For these estimates, the percentages were assumed to be correct and the total mass was based on combustibles having an average mass of 40 kg per drum for a total mass of 13.477 Gg; the metals and glass having an average mass of 64.5 kg per drum for a total mass of 19.844 Gg.

Comparison with Other Estimates

The estimates that were made and discussed for the combustibles and the metals and glass for Table 3.4-10 used the average mass from Butcher (1989) for these components. The total volume for the stored and projected waste in Table 3.4-10 was 100,593 m^3 (3.6 x 10^6 ft^3). The estimates from Drez (May 9, 1989, Letter [Appendix A]) were based on a total waste volume of 95,111 m^3 (3.4 x 10^6 ft^3). A comparison of the results of the two estimates indicates some consistency. The total mass of combustibles was 8.59 Gg (1.9 x 10^7 lbm) in Drez (May 9, 1989, Letter [Appendix A]) and the estimates in Table 3.4-10 were about 7.30 Gg (1.6 x 10^7 lbm). The mass of the metals and glass in Table 3.4-10 is about 11.60 Gg (2.6 x 10^7 lbm). The estimate in Drez (1989) was a total mass of 15.80 Gg (3.5 x 10^7 lbm). This estimate included the mass of the containers for the INEL and LANL. If the estimated mass of the INEL and LANL containers in Table 3.4-7 (3.59 Gg [7.9 x 10^6 lbm] is subtracted from the total in Drez (1989), the estimated mass of the glass and metal waste is 12.21 Gg (2.7 x 10^7 lbm).

3.4.2 Composition of RH-TRU Contaminated Trash (Non-Radionuclide/ Non-RCRA Inventory)

Volumes of Various Categories of RH-TRU Contaminated Waste

Estimates of the weights and volumes of RH-TRU constituents that affect gas generation, transport, and room properties are required for performance assessment. However, the weight of RH inventory was not included in the current analyses. The total RH inventory has changed considerably in the last several years. The following discussion presents a method that was used to estimate the characterization of the RH inventory. The method resulted in estimates of the volume and weights of waste by generator site; however, these results should not be interpreted as indicative of the weights and volumes that a specific site may generate.

From the information in the IDBs, an estimate of the total volume and the percentage of selected constituent forms may be identified. Table 3.4-13 summarizes the information for the last four years and shows that the estimated total volume increase from 2,500 m^3 (8.83 x 10^4 ft^3) in 1988 to about 5,300 m^3 (1.87 x 10^5 ft^3) in 1990 (Figure 3.4-5). The reasons for the large increase are discussed in the 1990 IDB.

For the current PA calculations, it was assumed that the maximum allowed RH volume of 7,079 m^3 (0.25 x 10^6 ft^3) will be emplaced in the WIPP. The following discussion presents the method that was used to estimate the total volumes of the waste constituents if the maximum volume of RH waste was emplaced. Input to the 1990 IDB was used as the basis for these estimates. The IDB presents estimates of the stored volume and projected (newly generated) volume for each generator site. The stored and projected volumes for the five sites that have or will generate RH waste are tabulated in Table 3.4-14. To estimate the additional volume required to reach the maximum volume, it was assumed that the generators of projected waste would provide the additional volume. The percentage of projected waste for each site was calculated and, based on this percentage, volumes for the five sites were calculated to provide an additional 1,735 m^3 (6.13 x 10^4 ft^3). The scaled volumes for the five sites are shown in Table 3.4-14.

The stored and newly generated (projected) RH volume in the 1990 IDB sum to about 5,300 m^3 (8.83 x 10^4 ft^3). The containers that will be placed in an RH canister have a different volume depending on the generator site. Therefore, a canister may not contain 0.89 m^3 (31.4 ft^3) of RH waste. U.S. DOE (1991) indicates that the submittals to the 1990 IDB total 7,622 canisters. The total volume based on this number of canisters is 6,784 m^3 (2.4 x 10^5 ft^3). U.S. DOE (1991) also discusses the number of uncertainties in the projection of the RH inventory and acknowledges that the details of the RH-TRU waste canister design should be revisited for re-evaluation. Because of the uncertainty in the RH inventory and the discussion in U.S. DOE (1991) on canister design, the smaller total stored plus projected volume of waste —not the volume of the canisters —was used as a scaling factor to estimate the RH radionuclide inventory for an RH design volume.

Table 3.4-13. Estimated Composition by Volume of RH-TRU Contaminated Trash from 1987 to 1990

	Combustibles (%)	Metal and Glass (%)	Absorbed Liquid and Sludge (%)	Concrete/ Cemented Sludge (%)	Dirt/ Gravel/ Asphalt (%)	Filters/ Filter Media (%)	Other (%)	Total Volume* (m^3)
1987	45.10	19.00	30.60	2.2	0.0	0.7	2.3	2690
1988	41.20	21.80	33.00	0.0	0.0	1.4	2.5	2500
1989	41.40	17.40	33.60	0.0	0.0	7.6	0.0	2812
1990	10.50	66.50	15.70	0.1	0.0	7.1	0.3	5344

* Design volume is 7,079 m^3.

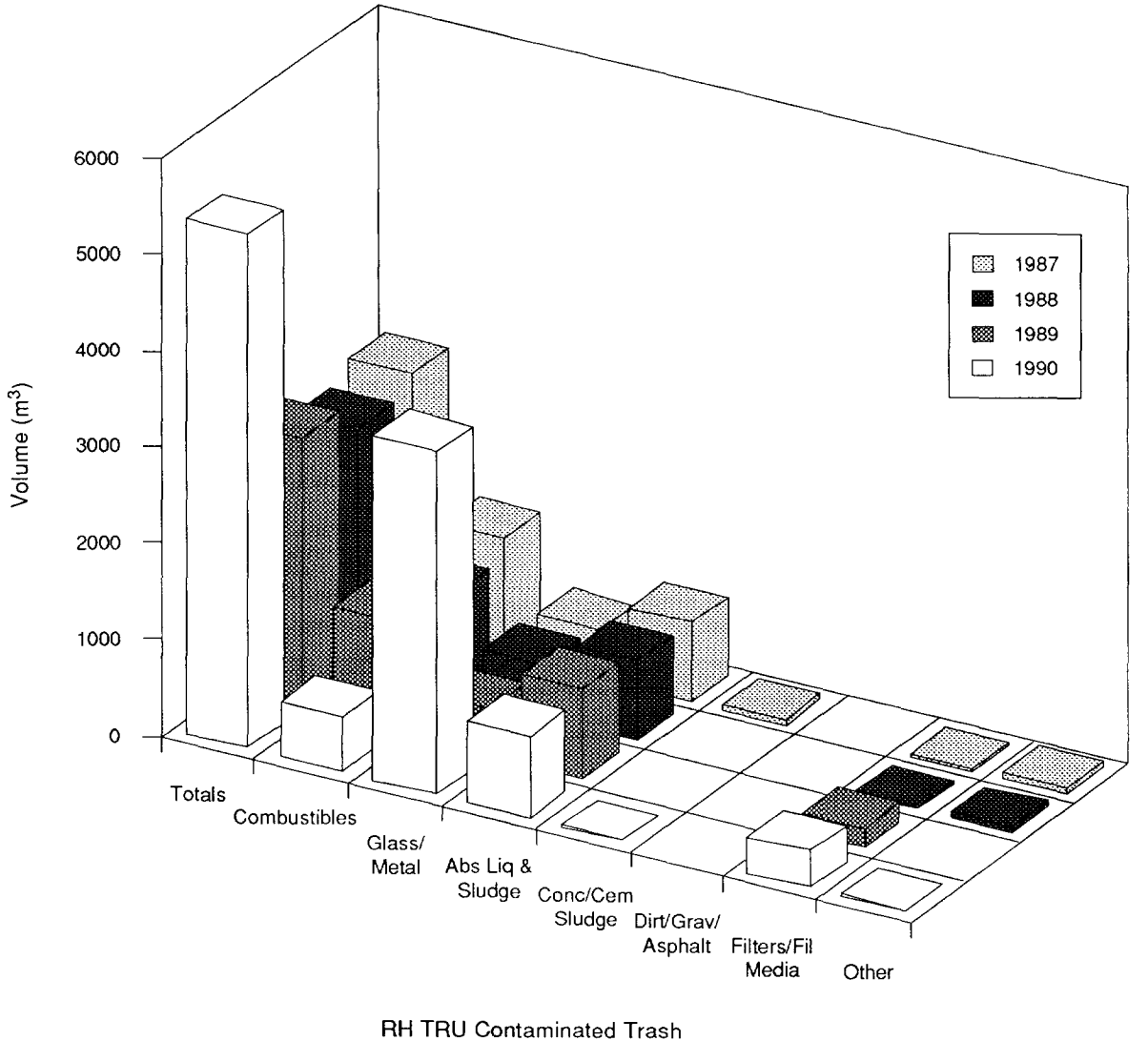

Figure 3.4-5. Changes in RH Waste Volume Estimates Between 1987 and 1990.

Table 3.4-14. Estimate of a Design Volume for RH-TRU Waste

Site	Stored Volume (1990 IDB) (m^3)	Projected Volume (1990 IDB) (m^3)	Total Volume (1990 IDB) (m^3)	Scaled Volume* (m^3)	Estimated Design Volume (m^3)
ANL-E	--	81.6	81.6	36.8	118.4
HANF	137	3535.2	3672.2	1,596.0	5,268.2
INEL	29.5	76.8	106.3	34.7	141.0
LANL	28.4	4.8	33.2	2.2	35.4
ORNL	1307	144.0	1,451.0	65.0	1,516.0
Total	1,501.9	3,842.4	5,344.3	1,734.7	7,079

* Assuming that ANL, HANF, INEL, LANL, and ORNL provide the difference between the current total inventory and the design volume. The difference between the total volume of 5,344 m^3 in the 1990 IDB and the design volume of 7,079 m^3 (0.25×10^6 ft^3) was ratioed between the five sites based on their estimated annual generation rates.

3.4.3 Inventory of Organic RCRA Contaminants

Hazardous materials are not regulated under *40 CFR 191*, but are regulated separately by the EPA and New Mexico. Some trace organic chemicals could affect the ability of radionuclides to migrate out of the repository, at least initially, until microbial activity destroyed them.

A major RCRA constituent of CH-TRU waste is lead that is present as incidental shielding, glovebox parts, and linings of gloves and aprons (U.S. DOE, 1990d). Trace quantities of mercury, barium, chromium, and nickel have also been reported in some sludges (U.S. DOE, 1990d).

Two RH-TRU waste forms contain hazardous chemical constituents. A solid waste containing mixtures of combustibles and noncombustibles was removed from a hot cell facility at Oak Ridge National Laboratory. This waste will not contain free liquids or particulates. In addition, fuel sludges and process sludges will be solidified. This waste will be a solid monolith (U.S. DOE, 1990d). Quantities of the above-mentioned RCRA constituents are being compiled for calculations necessary for the No-Migration Variance Petition but are not available at this time.

3.4.4 Capillary Pressure and Relative Permeability

Threshold Displacement Pressure, p_t

Parameter:	**Threshold displacement pressure (p_t)**
Median:	2.02×10^3
Range:	2.02×10^2
	2.02×10^5
Units:	Pa
Distribution:	Lognormal
Source(s):	Davies, P. B. 1991. *Evaluation of the Role of Threshold Pressure in Controlling Flow of Waste-Generated Gas into Bedded Salt at the Waste Isolation Pilot Plant.* SAND90-3246. Albuquerque, NM: Sandia National Laboratories.
	Davies, P. B. 1991. "Uncertainty Estimates for Threshold Pressure for 1991 Performance Assessment Calculations Involving Waste-Generated Gas." Internal memo to D. R. Anderson (6342), June 2, 1991. Albuquerque, NM: Sandia National Laboratories. (In Appendix A of this volume)

Residual Saturations

Parameter:	**Residual wetting phase (liquid) saturation ($S_{\ell r}$)**
Median:	2.76×10^{-1}
Range:	5.52×10^{-1}
	1.38
Units:	Dimensionless
Distribution:	Cumulative
Source(s):	Brooks, R. H. and A. T. Corey. 1964. "Hydraulic Properties of Porous Media," Hydrology Papers, No. 3. Fort Collins, CO: Colorado State University
	Davies, P. B. and A. M. LaVenue. 1990b. "Additional Data for Characterizing 2-Phase Flow Behavior in Waste-Generated Gas Simulations and Pilot Point Information for Final Culebra 2-D Model," Memo 11 in Appendix A of Rechard et al., 1990. *Data Used in Preliminary Performance Assessment of the Waste Isolation Pilot Plant.* SAND89-2408. Albuquerque, NM: Sandia National Laboratories

Parameter:	**Residual gas saturation (S_{gr})**
Median:	7×10^{-2}
Range:	3.5×10^{-2}
	1.4×10^{-1}
Units:	Dimensionless
Distribution:	Cumulative
Source(s):	Brooks, R. H. and A. T. Corey. 1964. "Hydraulic Properties of Porous Media," Hydrology Papers, No. 3. Fort Collins, CO: Colorado State University
	Davies, P. B. and A. M. LaVenue. 1990b. "Additional Data for Characterizing 2-Phase Flow Behavior in Waste-Generated Gas Simulations and Pilot Point Information for Final Culebra 2-D Model," Memo 11 in Appendix A of Rechard et al., 1990. *Data Used in Preliminary Performance Assessment of the Waste Isolation Pilot Plant.* SAND89-2408. Albuquerque, NM: Sandia National Laboratories.

Brooks and Corey Exponent

Parameter:	**Brooks and Corey exponent (η)**
Median:	2.89
Range:	1.44
	5.78
Units:	Dimensionless
Distribution:	Cumulative
Source(s):	Based on information in Brooks, R. H. and A. T. Corey. 1964. "Hydraulic Properties of Porous Media," Hydrology Papers, No. 3. Fort Collins, CO: Colorado State University.

Capillary Pressure and Relative Permeability

Figures 3.4-6a and 3.4-6b show the assumed values for capillary pressure and relative permeability, respectively. Figure 3.4-7 is an example of the variation in relative permeability and capillary pressure when Brooks and Corey parameters are varied.

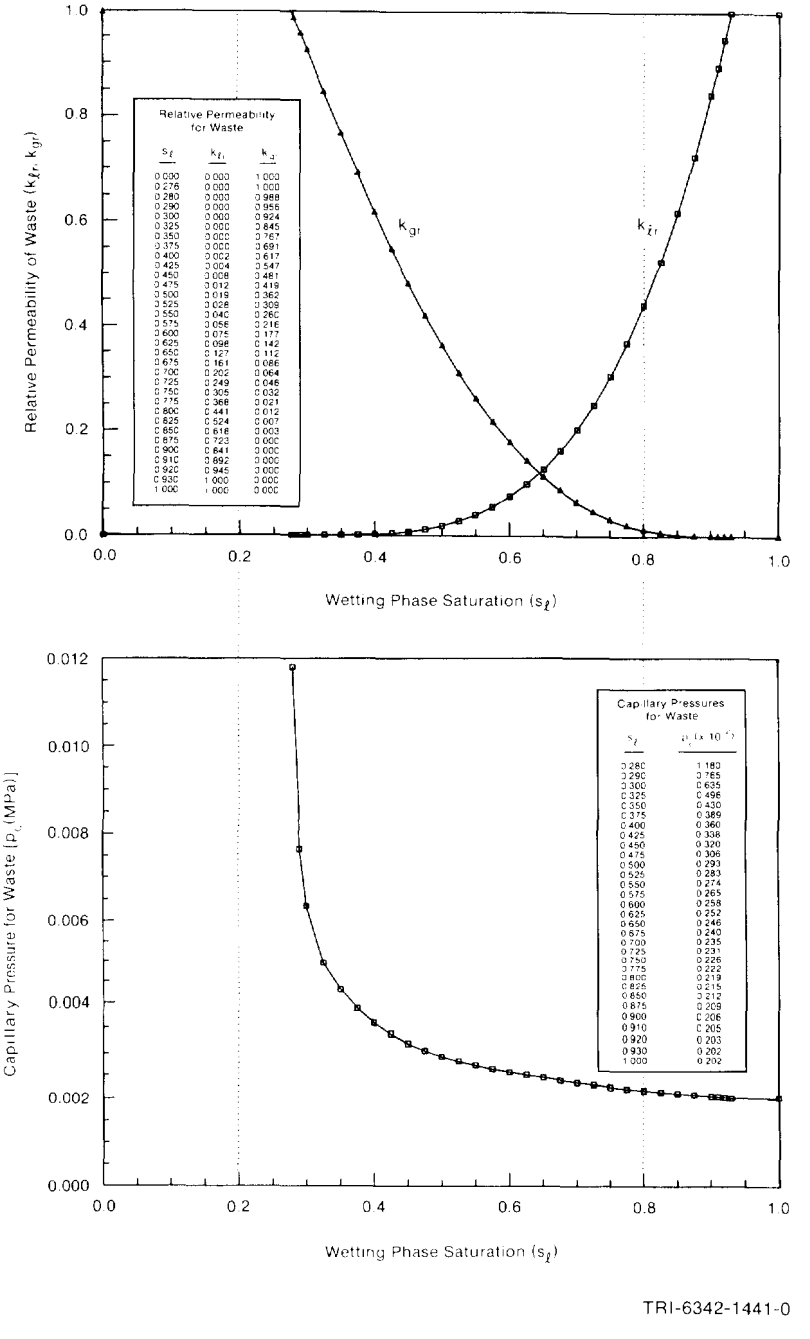

Figure 3.4-6. Estimated Capillary Pressure and Relative Permeability for Unmodified Waste.

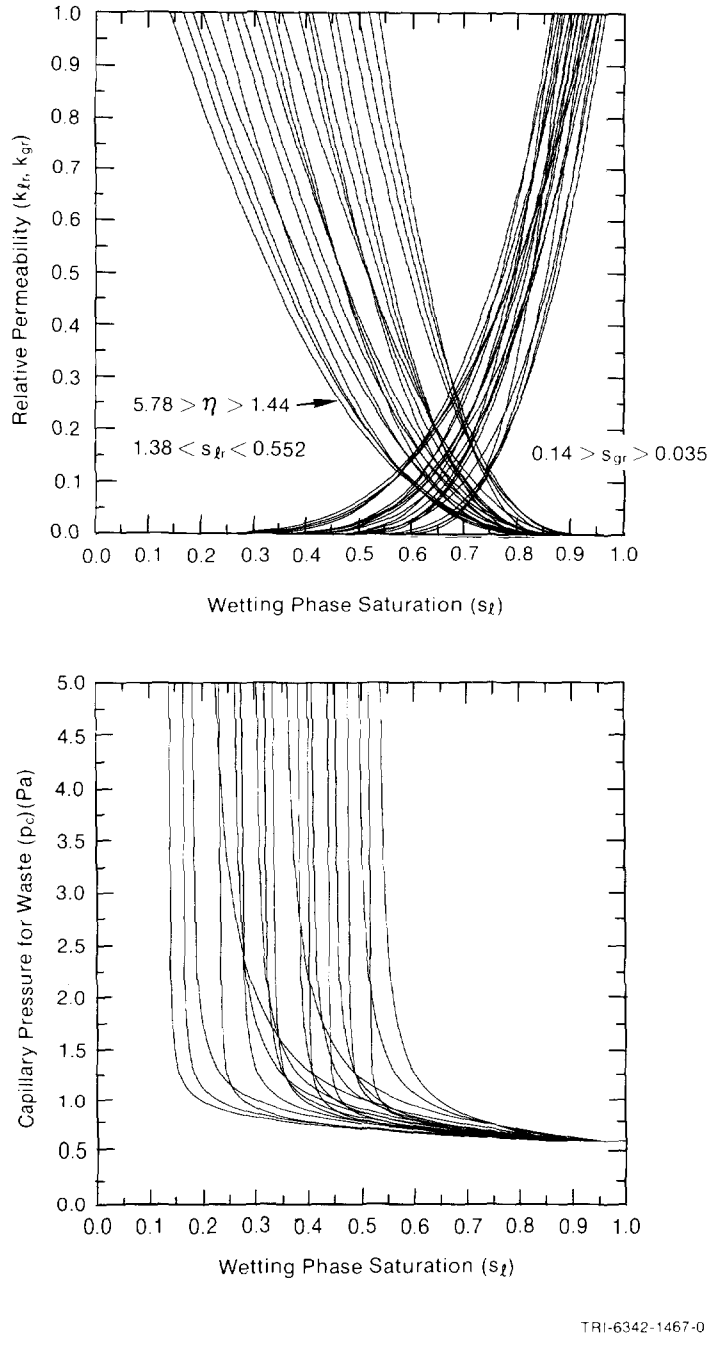

Figure 3.4-7. Example of Variation in Relative Permeability and Capillary Pressure for Unmodified Waste When Brooks and Corey Parameters Are Varied.

Discussion:

The correlations for these values were developed as discussed in the Chapter 2 section, "Hydrologic Parameters for Halite and Polyhalite within the Salado Formation." Preliminary parameter values were obtained from Brooks and Corey (1964). Their experimental data for a "poorly sorted, fragmented mixture of granulated clay, fragmented sandstone, and volcanic sand" were used as the natural analog.

An initial range was selected for the purpose of being able to run sensitivity parameter studies. The ranges shown for the parameters are quite arbitrary, corresponding to a simple doubling and halving of the median values.

Because the threshold displacement pressure (p_t) is so small, current PA calculations set the value to zero (only in the waste). This allows pressure to equilibrate faster within the waste by permitting the easy movement of phases throughout the waste and thereby reducing the computational burden of codes modeling the two-phase phenomenon.

3.4.5 Drilling Erosion Parameters

Two waste-dependent parameters influencing the amount of material that erodes from the borehole wall during drilling are shear stress generated by the drilling fluid (mud) and waste shear strength.

Absolute Roughness

Parameter:	**Absolute roughness of waste (ε)**
Median:	2.5×10^{-2}
Range:	1×10^{-2}
	4×10^{-2}
Units:	m
Distribution:	Uniform
Source(s):	Streeter, V. L., and E. B. Wylie. 1975. *Fluid Mechanics*. Sixth Edition. New York, NY: McGraw-Hill Book Co. (Figure 5.32)

Discussion:

For turbulent flow, the shear stress of the drilling fluid (mud) acting on the borehole wall is dependent upon the relative surface roughness (ε/d) at the repository level, where ε is the absolute roughness or the average depth of well irregularities, and for flow within an annulus d is the hydraulic diameter. The variable, d, is defined as the difference in borehole diameter and collar diameter. As erosion increases the borehole diameter, the relative roughness decreases if ε is fixed. The current value chosen for PA calculations exceeds that of riveted steel piping, one of the roughest pipes for which data is frequently given (Moody diagram) (Streeter and Wylie, 1975, Figure 5.32).

Figure 3.4-8 provides the distribution for waste absolute roughness.

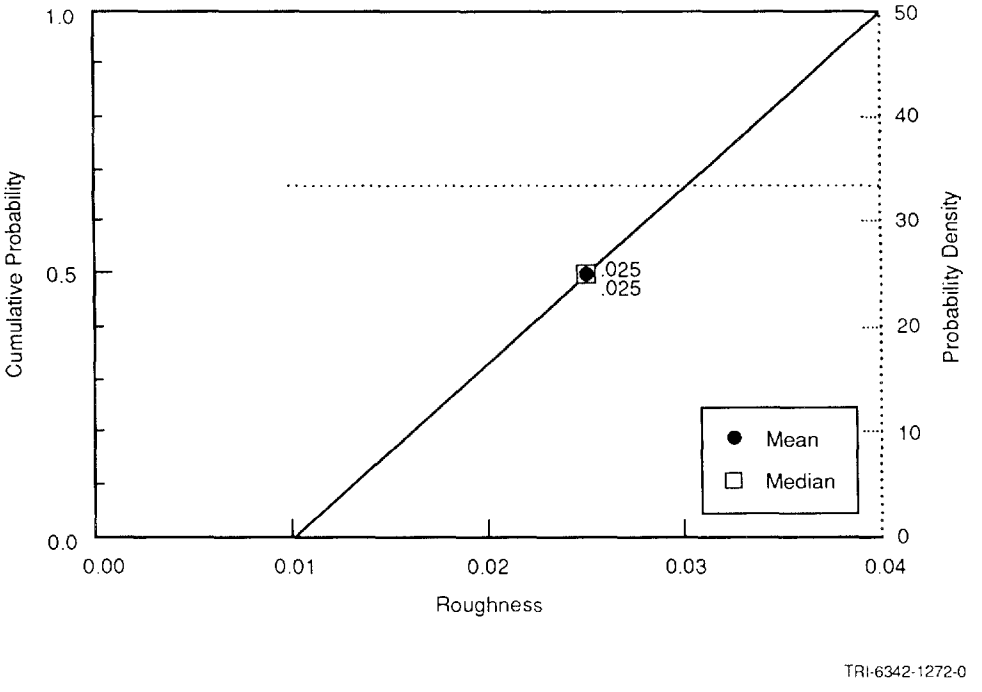

Figure 3.4-8. Estimated Distribution (pdf and cdf) for Waste Absolute Roughness.

Effective Shear Strength for Erosion

Parameter:	**Effective shear strength for erosion (τ_{fail})**
Median:	1
Range:	1×10^{-1}
	1×10^{1}
Units:	Pa
Distribution:	Cumulative
Source(s):	Sargunam, A., P. Riley, K. Arulanadum, and R. B. Krone. 1973. "Physico-Chemical Factors in Erosion of Cohesive Soils." *Journal of the Hydraulics Division, American Society of Civil Engineers* 99: 555-558.
	Henderson, F. M. 1966. *Open Channel Flow.* New York: Macmillan Publishing Co. (Figure 10-5)

Discussion:

The effective shear strength for erosion (allowable tractive force) equals the threshold* value of fluid shear stress required to sustain general erosion at the borehole wall. Parthenaides and Paaswell (1970), in discussing investigations on the erosion of seabed sediments and in channels, has noted that this effective soil shear strength is not related to the soil shear strength as normally determined from conventional soil tests. The effective shear strength for erosion is smaller by several orders of magnitude than the macroscopic soil shear strength.

Following the experimental work of Sargunam et al. (1973) on erosion of cohesive soils (see Figure 4.2-6 in Chapter 4), the PA Division assumed an effective shear strength for erosion (τ_{fail}) for the unmodified waste of 1 Pa (1.45×10^{-4} psi), a value at the low end of the range for loose (uncompacted) montmorillonite clay. The erodible shear strength of a noncohesive, fine sand (diameter near 2.5×10^{-4}) is also about 1 Pa (1.45×10^{-4} psi) (Henderson, 1966, Figure 10-5). Because the erodibility of the material at any given velocity is highly dependent on the effective diameter of the material—and for cohesive materials, its degree of compaction and plasticity index (Henderson, 1966)—the upper limit can be quite large (greater than 100 Pa). However, PA calculations assume only an order-of-magnitude range since values much greater than 10 Pa preclude erosion.

* The threshold of sediment movement (erosion) cannot be defined with absolute precision, because as the fluid shear stress gradually increases (due to velocity increase) there is no precise point at which sediment movement suddenly becomes general. Rather, at first only a few grains are dislodged every few seconds, then grain movement becomes more frequent until it affects the entire bed.

3.4.6 Partition Coefficients for Clays in Salt Backfill

Table 3.4-15 provides assumed partition coefficients for salt backfill.

Table 3.4-15. Partition Coefficients for Salt Backfill Containing Trace (0.1%) Amounts of Clay (after Lappin et al., 1989, Table D-5)

Radionuclide	Partition Coefficient* (m^3/kg)
Am	1×10^{-4}
Np	1×10^{-5}
Pb	1×10^{-6}
Pu	1×10^{-4}
Ra	1×10^{-6}
Th	1×10^{-4}
U	1×10^{-6}

* Assumed constant

Discussion:

See discussion in Section 3.2.4.

3.4.7 Permeability

Parameter:	**Permeability (k), combustibles**
Median:	1.7×10^{-14}
Range:	2×10^{-15}
	2×10^{-13}
Units:	m^2
Distribution:	Cumulative
Source(s):	Butcher, B. M., T. W. Thompson, R. G. Van Buskirk, and N. C. Patti. 1991. *Mechanical Compaction of WIPP Simulated Waste.* SAND90-1206. Albuquerque, NM: Sandia National Laboratories.

Parameter:	**Permeability (k), metals/glass**
Median:	5×10^{-13}
Range:	4×10^{-14}
	1.2×10^{-12}
Units:	m^2
Distribution:	Cumulative
Source(s):	Butcher, B. M., T. W. Thompson, R. G. Van Buskirk, and N. C. Patti. 1991. *Mechanical Compaction of WIPP Simulated Waste.* SAND90-1206. Albuquerque, NM: Sandia National Laboratories.

Parameter:	**Permeability (k), sludge**
Median:	1.2×10^{-16}
Range:	1.1×10^{-17}
	1.7×10^{-16}
Units:	m^2
Distribution:	Cumulative
Source(s):	Butcher, B. M., T. W. Thompson, R. G. Van Buskirk, and N. C. Patti. 1991. *Mechanical Compaction of WIPP Simulated Waste.* SAND90-1206. Albuquerque, NM: Sandia National Laboratories.

Discussion:

The permeability for the combustibles was estimated from a few tests on simulated waste (Butcher, 1990). After crushing a mixture of 60% by weight of pine cubes and 40% of rags for 30 days at 14 MPa, the permeability started at 2 x 10^{-13} m^2 (200 mD) and dropped to 2 x 10^{-15} m^2 (2 mD), which defined the maximum range for combustibles. (A similar test had a steady permeability of 1.3 x 10^{-14} m^2 (13 mD); two tests on a mixture of 40% plastic bottles, 40% PVC parts, and 20% gloves had permeabilities of 0 and 2.5 x 10^{-4} m^2 [0 and 25 mD].) The median permeability of 1.7 x 10^{-14} m^2 (17 mD) for combustible waste was estimated from the average of two tests on a simulated waste mixture consisting of 45% of the above plastics and 37% of the above wood mixture plus 9% 1-inch metal parts and 9% dry Portland cement.

The maximum and median values for permeability of the metals and glass component of the waste were estimated using 50% 1-inch metal parts and 50% magnetite that were crushed for one day. The latter material represented the corroded metal. One test had an initial permeability of 5.0 x 10^{-13} m^2 (500 mD) (used as the median value), but dropped to 4 x 10^{-15} m^2 (4 mD) (used as the minimum value). (A second test had a steady permeability of 1.1 x 10^{-14} m^2 [11 mD].) The maximum permeability is the value estimated for uncorroded metal waste in Lappin et al. (1989, p 4-56).

Mean Permeability of Drum. For computational ease, the PA Division assumed that the permeabilities of each component were uniformly distributed from the minimum to the maximum values given above in evaluating the permeability of an average drum. Consequently, the distribution of local permeability (i.e., the effective permeability of a collapsed drum) was the weighted sum of uniform distributions, the weights being percent by volume of each component.

Assuming that the volume fractions of the components are 40% combustibles, 40% metals/glass, and 20% sludge (values reported in Table 3.4-1 rounded to one significant digit), it is easily calculated that the expected permeability on the scale of a drum (0.27 m^3 or 9.5 ft^3) is

$$E(k) = \mu_{perm} = \int k f(\eta) d\eta = 1.7 \times 10^{-13}\ m^2 \qquad (3.4\text{-}1)$$

and the coefficient of variation $[V(k)]^{1/2}/E(k)$ is

$$([V(k)]^{1/2}/E(k)^2 = (\sigma/\mu_{perm})$$

$$= (\int m^2 f(\eta) d\eta)^{1/2}/\mu_{perm} = E(k - \mu)^2]^{1/2}/\mu_{perm} = 1.22 \qquad (3.4\text{-}2)$$

where

E(k) = expectation of k
V(k) = variance of k

The foregoing estimates establish the statistical properties of the permeability of a *single*, typical collapsed waste drum. These properties are next used to estimate the distribution of the material-property parameter: effective hydraulic conductivity of an entire, collapsed WIPP room. To estimate distribution of effective hydraulic conductivity of a room, we must make further assumptions about the way waste drums are sorted and placed into particular rooms: in the absence of any firm plans for sorting waste drums, we are forced to assume that any waste drum is equally likely to be placed in any of the (approximately) 120 rooms. Hence, there is no spatial correlation between two adjacent drums in the same room, and the "cookie cutter" autocorrelation function (see Chapter 1) is applicable with a correlation volume, a^3, of the order of the volume of a collapsed waste drum.

Model of WIPP Room. The collapsed WIPP room is modeled as a rectangular parallelopiped composed of many, small rectangular parallelopipeds (the collapsed drums) (Figure 3.4-9).

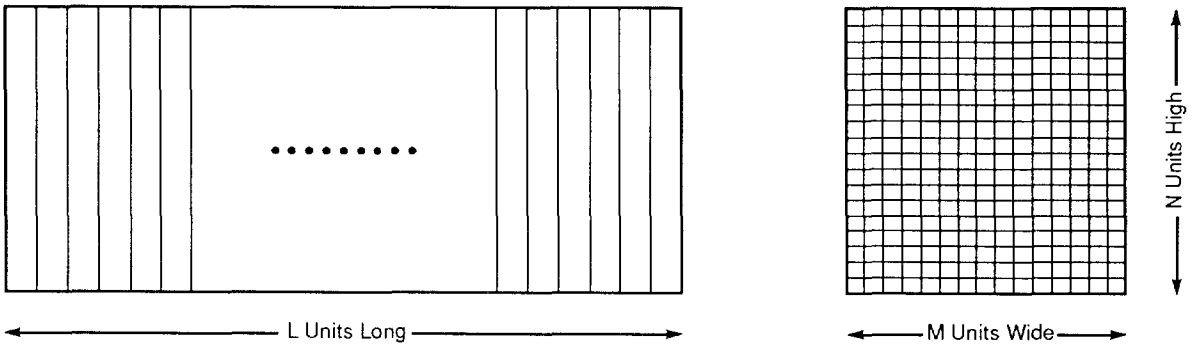

Figure 3.4-9. Model of Collapsed WIPP Room

The collapsed drums will be called "units." In Figure 3.4-8 above, LMN = 6804, or

L = number of replications of the unit down length of a room (~162, Figure 3.1-3)
M = number of replications of the unit across a room (~14, Figure 3.1-3)
N = number of replications of the unit veritically (3, Figure 3.1-3).

With each unit is associated a local porosity

$\phi_{\ell mn}$ - local porosity (assumed isotropic)

and a local hydraulic conductivity

$k_{\ell mn}$ - local hydraulic conductivity (assumed isotropic)

As previously stated, it is assumed that $\phi_{\ell mn}$ and $k_{\ell mn}$ are independent, identically distributed random variables; i.e., the $\phi_{\ell mn}$ have a density function f(c) and the $k_{\ell mn}$ have density function g(k).

Effective Permeability. The first problem is to find the distribution of k_{eff}, where

$$J = k_{eff} \frac{\Delta h}{x},$$

Δh being the applied pressure-head difference across the room in the x-direction. Now, from Freeze & Cherry (1979, p. 34, Eq. 2.32), the effective permeability, k_ℓ, of the ℓ^{th} slab follows (flow parallel to layering):

$$k_\ell = \frac{1}{MN} \sum_{m=1}^{M} \sum_{n=1}^{N} k_{\ell mn} \qquad (3.4\text{-}3)$$

Thus, viewing the slabs $\ell = 1,2,...L$ as layers and the flow being perpendicular to these layers, we have from Freeze & Cherry (1979, p. 34, Eq. 2.31)

$$k_{eff} = \frac{1}{\frac{1}{L} \sum_{\ell=1}^{L} \frac{1}{k_\ell}} \qquad (3.4\text{-}4)$$

Now if $E[k_{\ell mn}] = \mu$ and Var $[k_{\ell mn}] = \sigma^2$ (i.e., it is assumed that the $k_{\ell mn}$ are independent, identically distributed [iid] random variables with mean μ and variance σ^2), and if MN >> 1, then by the Central Limit Theorem (Ross, 1985, p. 70), the random variable K_ℓ is approximately normally distributed, i.e.,

$$Pr(k_\ell \leq x) \rightarrow \Phi\left(\frac{\sqrt{MN}\,(x-\mu)}{\sigma}\right) \text{ as } MN \rightarrow \infty$$

where

$$\Phi(y) = \frac{1}{\sqrt{2\pi}} \int_{-\infty}^{y} e^{-x^2/2} dx \text{ (the standard normal distribution)}$$

In other words, k_ℓ is approximately normally distributed with mean μ and variance $\sigma_k^2 = \sigma^2/MN$.

Gauss' approximation formulae (Blom, 1989, p. 125) are next used to estimate the mean and variance of the distribution of k_{eff}, given that the mean and variance of the k_ℓ are respectively μ and σ^2/MN. Using these formulae and Eq. 3.4-4 gives, for the mean value,

$$E\left[k_{eff}\right] \sim \frac{1}{\frac{1}{L} \sum_{\ell=1}^{L} \frac{1}{\mu}} = \mu \qquad (3.4\text{-}5)$$

and for the variance,

$$\mathrm{Var}\left[k_{eff}\right] \sim \sum_{\ell=1}^{L} \mathrm{Var}[k_\ell] \cdot \left[\left(\frac{\delta k_{eff}}{\delta k_\ell}\right)_{k_\ell=\mu}\right]^2 = \sum_{\ell=1}^{L} \frac{\sigma^2}{MN} \cdot \frac{1}{L^2} = \frac{\sigma^2}{MNL} \qquad (3.4\text{-}6)$$

Magnitudes of these quantities can be estimated using the preliminary permeability estimates (Eqs. 3.4-1 and 3.4-2),

$$\mu_{perm} = 1.7 \times 10^{-13}\ m^2\ (1.25 \times 10^{-6}\ m/s)$$

$$\sigma_{perm} = 2.07 \times 10^{-13}\ m^2\ (1.52 \times 10^{-6}\ m/s),$$

and taking L = 162, M = 14, and N=3. The results are

$$E[k_{eff}] \sim \mu = 1.7 \times 10^{-13}\ m^2\ (1.25 \times 10^{-6}\ m/s)$$

and coefficient of variation of

$$\frac{E(k_{eff})}{V(k_{eff})} \sim [(MNL)^{-1/2}] \cdot (\sigma/\mu) = 1.48 \times 10^{-2}.$$

The small coefficient of variation suggests that the distribution of k_{eff} is highly concentrated about the mean value, μ. The mean varies only slightly with the permeability estimate in Lappin et al., 1989. To be consistent with this and other previous work, the PA Division used a value of $1 \times 10^{-13}\ m^2$ (100 mD).

Because the coefficient of variation is so small, the PA Division did not sample on waste permeability nor adjust its value according to the waste composition as was done for porosity. The waste permeability was so high that a large decrease (~4 orders of magnitude) would be required to have a noticeable effect on results (Rechard et al., 1989, Figure 4-2), too large a decrease to be obtained from the currently assumed variation in waste composition. (The variance of the volume fraction of waste components adds directly [not reduced by the Central Limit Theorem] to the waste unit variance.)

3.4.8 Porosity

Parameter:	**Porosity (ϕ), combustibles**
Median:	0.014
Range:	0.087
	0.18
Units:	Dimensionless
Distribution:	Data
Source(s):	Butcher, B. M., T. W. Thompson, R. G. Van Buskirk, and N. C. Patti. 1991. *Mechanical Compaction of WIPP Simulated Waste.* SAND90-1206. Albuquerque, NM: Sandia National Laboratories.

Parameter:	**Porosity (ϕ), metals/glass**
Median:	0.40
Range:	0.33
	0.44
Units:	Dimensionless
Distribution:	Data
Source(s):	Butcher, B. M., T. W. Thompson, R. G. Van Buskirk, and N. C. Patti. 1991. *Mechanical Compaction of WIPP Simulated Waste.* SAND90-1206. Albuquerque, NM: Sandia National Laboratories.

Parameter:	**Porosity (ϕ), sludge**
Median:	0.11
Range:	0.01
	0.22
Units:	Dimensionless
Distribution:	Data
Source(s):	Butcher, B. M., T. W. Thompson, R. G. Van Buskirk, and N. C. Patti. 1991. *Mechanical Compaction of WIPP Simulated Waste.* SAND90-1206. Albuquerque, NM: Sandia National Laboratories.

Discussion:

The objective of the procedure described here for calculating panel porosity is to enable Performance Assessment to determine initial and final porosities of the panel in a manner that is consistent with the estimated actual inventory of the repository and with the need to vary the composition of the waste in PA calculations. First, the initial porosity will be calculated based on the design capacity of the repository and the design waste inventory estimates discussed in Section 3.4.1. Then the final porosity of a perfectly sealed panel (no gas escapes) will be determined. Finally, the procedure will be extended to variable waste compositions.

Initial Porosity. The waste inventory is broken down into three IDB categories: metals and glass, combustibles, and sludge. In Section 3.4.1, a volume fraction of each of these categories, $f_m = 0.368$, $f_c = 0.403$, and $f_s = 0.229$, respectively, was estimated from which the volume of each category is calculated:

$$V_m = f_m V_w = 64{,}610 \text{ m}^3$$
$$V_c = f_c V_w = 70{,}750 \text{ m}^3$$
$$V_s = f_s V_w = 40{,}200 \text{ m}^3$$

where $V_w = 175{,}600$ m^3 (6.2×10^6 ft^3), the design capacity of the repository.

The mass of each category is then computed assuming a fixed average mass of waste category in each drum and the known volume of a drum, $V_d = 0.21$ m^3. The average mass of each category per drum (not including the containers), as used in Table 3.4-9, is:

$$M_{dm} = 64.5 \text{ kg/drum}$$
$$M_{dc} = 40.0 \text{ kg/drum}$$
$$M_{ds} = 225. \text{ kg/drum}$$

A fixed average mass of container is also assumed to be portioned to each category, the values obtained from Table 3.4-9 being:

$$M_{cm} = 12.40 \text{ Gg}$$
$$M_{cc} = 13.29 \text{ Gg}$$
$$M_{cs} = 4.458 \text{ Gg}$$

The total mass of each category, including containers, in the full repository is then:

$$M_m = M_{dm} V_m / V_d + M_{cm} = 31.98 \text{ Gg}$$
$$M_c = M_{dc} V_c / V_d + M_{cc} = 26.77 \text{ Gg}$$
$$M_s = M_{ds} V_s / V_d + M_{cs} = 47.53 \text{ Gg}$$

The total mass of waste, including containers, is the sum of the masses of these three categories:

$$M_w = M_m + M_c + M_s = 106.3 \text{ Gg}$$

These figures can all be found in Table 3.4-9 (under the heading "Stored, Projected, and Scaled") and in Table 3.4-1, which summarizes the data.

In addition to the waste, the repository will also contain salt backfill and an air gap between the top of the backfill and the ceiling of the repository. The masses of backfill and the initial air gap are:

$$M_b = \rho_{bb} V_b = 219.2 \text{ Gg}$$
$$M_a = \rho_a V_a = 0.1051 \text{ Gg}$$

where ρ_{bb} and ρ_a are, respectively, the bulk density of backfill and the density of air (ideal gas with molecular weight 0.02897 kg/mol at atmospheric pressure [101.3 kPa] and 300.15 K):

$$\rho_{bb} = 1280 \text{ kg/m}^3$$
$$\rho_a = 1.18 \text{ kg/m}^3$$

and the volume of salt backfill and air gap initially present when the repository is filled are (see Section 3.1.6):

$$V_b = 171{,}200 \text{ m}^3$$

$$V_a = 89{,}080 \text{ m}^3$$

The total mass of waste, backfill, and air gap initially present in the repository is:

$$M_t = M_w + M_b + M_a = 325.6 \text{ Gg}$$

The bulk density of each category (including containers) and of the waste are:

$$\rho_{bm} = M_m/V_m = 495 \text{ kg/m}^3$$
$$\rho_{bc} = M_c/V_c = 378 \text{ kg/m}^3$$
$$\rho_{bs} = M_s/V_s = 1182 \text{ kg/m}^3$$
$$\rho_{bw} = V_w = 605 \text{ kg/m}^3$$

The initial porosity of each category (including containers) and of the backfill are calculated from the above bulk densities and assumed values for the solid (grain) densities of each category (Butcher et al., 1991):

ρ_m = 3440 kg/m^3
ρ_c = 1310 kg/m^3
ρ_s = 2150 kg/m^3
ρ_b = 2140 kg/m^3

The solid densities of the three waste categories presumably include containers; this enables calculation of porosities in which a bulk density (including containers) is divided by a solid density (also including containers). The solid density of salt includes a 1% irreducible porosity that remains in compacted halite. To be fully consistent, the true grain density, 2,160 kg/m^3, should be used. This minor inconsistency will be corrected in the 1992 PA calculations. The porosities are then

$\phi_m = 1 - \rho_{bm}/\rho_m = 0.856$
$\phi_c = 1 - \rho_{bc}/\rho_c = 0.711$
$\phi_s = 1 - \rho_{bs}/\rho_s = 0.450$
$\phi_b = 1 - \rho_{bb}/\rho_b = 0.402$

Now the initial pore volumes of each category can be determined:

$V_{pm} = \phi_m V_m = 55{,}310$ m^3
$V_{pc} = \phi_c V_c = 50{,}320$ m^3
$V_{ps} = \phi_s V_s = 18{,}100$ m^3
$V_{pb} = \phi_b V_b = 68{,}820$ m^3
$V_{pa} = V_a = 89{,}080$ m^3

Summing, the net waste pore volume (including containers) is

$V_{pw} = V_{pm} + V_{pc} + V_{ps} = 123{,}700$ m^3

and the pore volume of the entire repository is initially

$V_{pt} = V_{pw} + V_{pb} + V_{pa} = 281{,}600$ m^3

The initial porosity of the repository for the design inventory is then

$\phi_t = V_{pt}/V_t = 0.646$

where V_t is the initial excavated volume of the repository, excluding seals (Table 3.1-1)

$V_t = 436{,}000$ m^3.

A number also of interest, though not needed for PA calculations, is the porosity of the waste alone, including containers, but excluding backfill and air gap:

$\phi_w = V_{pw}/V_w = 0.705$

Table 3.4-16 summarizes the calculation of initial porosity of the repository.

Table 3.4-16. Summary of Initial Porosity Calculations

	Waste Volume Fraction	Initial Volume (m^3)	Initial Mass (kg)	Bulk Density (kg/m^3)	Solid Density (kg/m^3)	Initial Porosity --	Pore Volume (m^3)	Solids Volume (m^3)
Metal + Glass	0.368	64,608	31,981,774	495	3,440	0.856	55,311	9,297
Combustibles	0.403	70,752	26,769,084	378	1,310	0.711	50,318	20,434
Sludge	0.229	40,204	47,533,716	1,182	2,150	0.450	18,095	22,109
Waste subtotal	1.000	175,564	106,284,574	605	2,050	0.705	123,724	51,840
Backfill		171,241	219,188,480	1,280	2,140	0.402	68,816	102,425
Air Gap		89,081	105,116	1	--	1.000	89,081	--
Total		436,023	325,578,170	747	2,109	0.646	281,621	154,265

Note: Figures for waste categories and subtotal include containers.

Final Porosity. The final porosity is calculated by assuming that no gas leaks from the repository and that the final gas pressure is equal to lithostatic pressure, 14.9 MPa. It is also assumed that the volume of solids in the repository is conserved. Knowing the corrodible metal content of the waste and the amount of biodegradables enables the total gas potential to be calculated. Adjusting for lithostatic pressure, this final potential gas volume, together with the air initially present (both in the air gap and in the initial pore spaces), constitutes the final pore volume of the repository.

The initial solids volume is the difference between the bulk volume and the pore volume of each category:

$$V_{sm} = V_m - V_{pm} = 9{,}297 \text{ m}^3$$

$$V_{sc} = V_c - V_{pc} = 20{,}430 \text{ m}^3$$

$$V_{ss} = V_s - V_{ps} = 22{,}110 \text{ m}^3$$

The initial solids volume in the waste is:

$$V_{sw} = V_w - V_{pw} = 51{,}840 \text{ m}^3$$

and the initial backfill solids volume is:

$$V_{sb} = V_b - V_{pb} = 102{,}400 \text{ m}^3$$

The total solids volume is the sum of waste solids volume and backfill solids volume:

$$V_{st} = V_{sw} + V_{sb} = 154{,}300 \text{ m}^3$$

Additional assumptions concerning the composition of the waste are needed. In the metals and glass category, only a portion of the total mass is corrodible and thus capable of producing gas. Of the metals listed in Table 3.4-11 (Design column), the following are considered corrodible: Iron, paint cans, steel, and shipping cans. The total mass of these materials in the Design inventory is

$$M_{Few} = 14.31 \text{ Gg}$$

and for gas potential calculations, the materials are assumed to be pure iron (Fe). The waste containers contain an even greater amount of corrodible metal. From Table 3.4-8, the container steel in the repository Design volume is

$$M_{Fec} = 26.13 \text{ Gg}$$

This mass is also assumed to be pure iron for gas potential purposes. The total iron in the repository is

$$M_{Fet} = M_{Few} + M_{Fec} = 40.44 \text{ Gg}$$

In the Combustibles category, only a portion is believed to be biodegradable. This portion includes all cellulosics and 50% of certain rubbers, including surgeon's gloves (latex), hypalon, neoprene, and other rubber undefined. The total mass of biodegradables in the Design inventory, from Table 3.4-11, is

$$M_{Bio} = 7.475 \text{ Gg}$$

Details of the gas potential from iron corrosion are discussed in Section 3.3.8. It is assumed that corrosion and biodegradation reactions produce hydrogen gas. The median stoichiometric coefficient for hydrogen using the average corrosion reaction, Eq. 3.3-4, is

$$s_{Fe} = 7/6 = 1.167 \text{ mol H2/mol Fe}$$

and the molecular weight of iron is

$$M_{Fe} = 0.055\,85 \text{ kg/mol Fe}$$

Then the gas potential from corrosion is

$$M_{H_2Fe} = M_{Fet} s_{Fe} / M_{Fe} = 844.8 \text{ Mmol } H_2$$

Details of the gas potential from biodegradation are discussed in Section 3.3.9. The median stoichiometric coefficient for hydrogen using the average biodegradation reaction, Eq. 3.3-6, is

$$s_{Bio} = 0.835 \text{ mol } H_2/\text{mol cellulose is}$$

and the molecular weight of cellulose is

$$M_{cell} = 0.030 \text{ kg/mol cellulose}$$

Then the gas potential from corrosion is

$$m_{H_2 Bio} = M_{Bio} s_{Bio} / M_{cell} = 208 \text{ Mmol } H_2$$

The total gas potential using the design inventory and median reaction parameters is

$$m_{H_2 t} = m_{H_2 Fe} + m_{H_2 Bio} = 1.053 \text{ Gmol } H_2$$

Using a molar volume for H_2 of 1.822 x 10^{-4} m^3/mol H_2 (see Section 4.1.4), the volume of this hydrogen at 14.9 MPa and 300.15 K is

$$V_{H_2} = 191{,}800 \text{ m}^3$$

In addition, the air initially present in the repository both in the air gap and in pore space is compressed from initial pressure, p_i, of 101.325 kPa to final lithostatic pressure, p_f, of 14.9 MPa, resulting in a volume (assuming ideal gas behavior) of

$$V_{af} = V_{pt} p_i / p_f = 1{,}915 \text{ m}^3$$

The total gas volume in the final repository at 14.9 MPa is

$$V_g = V_{H_2} + V_{af} = 193{,}700 \text{ m}^3$$

Then the final porosity of a gas-tight repository containing the full amount of gas that is potentially producible is

$$\phi_f = V_g/(V_g + V_{st}) = 0.557$$

Final Porosity for Variable Waste Composition. The porosity of a room or panel will vary with time as salt creep compresses the pore spaces while gas generation creates a time-dependent resistance to creep closure. These phenomena cannot yet be simulated accurately within the PA calculations, so some simplifying assumptions must be made. The first is that the porosity will not change over time, but instead will immediately attain the final porosity.

Second, it is assumed that the final porosity is the porosity of a gas-tight, perfectly sealed repository. Although this second assumption appears somewhat arbitrary, since almost any porosity between a sealed-room porosity and a completely open porosity (i.e., all gas escapes and causes no additional resistance to creep closure beyond what the solids impose) might be justified, preliminary calculations indicated that, barring any pressure release resulting from intrusions, the pressure in the repository generally reaches a value close to lithostatic, quite rapidly, and stays there for the duration of the 10,000-yr period. Furthermore, the permeabilities of the likeliest gas flow paths (the anhydrite layers and Marker Bed 139) are so low that little gas will escape over the 10,000 yr. Therefore, the repository will generally behave more like a gas-tight enclosure than like a very leaky one, so assuming it is gas-tight is reasonable.

Because the composition of the waste that will ultimately fill the repository is not known with complete certainty, it is varied in the 1991 PA calculations. Variations in the composition of the waste result in different final porosities, because the gas potential changes, depending on how much corrodible metal and biodegradable material is present. In addition to the volume fractions of metals and glass and of combustibles, two other parameters that effect the final porosity are also varied in the PA calculation: the stoichiometric coefficients x_{Fe} and x_{Bio}.

The procedure described above is used to calculate the final porosity. Three additional assumptions are required. First, the mass of containers is assumed to remain fixed; in particular, the mass of iron in the containers, M_{cm}, is assumed constant. Second, the mass fraction of metals and glass that is corrodible metal is assumed to be constant. This fraction is

$$f_{mc} = M_{Few}/(M_m - M_{cm}) = 14.31 \text{ Gg}/19.84 \text{ Gg} = 0.721$$

Third, the mass fraction of combustibles that is biodegradable is assumed to be constant. This fraction is

$$f_{cb} = M_{Bio}/(M_c - M_{cc}) = 7.475 \text{ Gg}/13.48 \text{ Gg} = 0.555$$

Then the total iron content in the repository is

$$M_{Fet} = f_{mc}M_{dm}V_m/V_d + M_{Fec}$$

and the total biodegradable mass is

$$M_{Bio} = f_{cb}M_{dc}V_c/V_d + M_{Bioc}$$

where M_{Bioc}, the mass of biodegradable container material, is currently zero. The rest of the porosity calculation is the same as described above (except that the stoichiometric coefficients vary).

Brine saturation will also affect the final porosity. This effect has not been taken into account in these calculations because the brine saturation varies greatly during the 10,000 yr, and a consistent and accurate way to incorporate this effect has not been developed.

Final room or panel height is calculated from the initial and final porosity. It is assumed that creep closure occurs only in the vertical direction, not horizontally. While not correct, this assumption has little effect on the results, except to make calculation of the final panel height much easier, since the floor area does not change.

Assuming solids volume is conserved during closure,

$$(1 - \phi_i)Ah_i = (1 - \phi_f)Ah_f$$

where A is the floor area, h_i is the initial panel height, and h_f is the final panel height. The final panel height is then

$$h_f = h_i(1 - \phi_i)/(1 - \phi_f)$$

Panel Averaging. Some PA calculations, done on a panel scale, require that certain properties be averaged over the entire panel. This is particularly true for the two-phase flow calculations, which, because of time and size constraints, must be done using two-dimensional cylindrical geometry. This necessitates using properties for a full panel that combine properties of the waste and backfill with those of the intact salt pillars that separate rooms in a panel. Properties used in the models are generally area-weighted averages of the waste properties and the pillar properties. (A notable exception is permeability; waste permeability is used as the average permeability of a panel.)

The average porosity of a panel is calculated from

$$\phi_{pav} = \frac{\phi_f A_{panx} + \phi_p A_{pil}}{A_{panx} + A_{pil}}$$

where A_{panx} is the excavated floor area of a panel (11,640 m^2, from Table 3.1-1), ϕ_p is the constant median porosity of an undisturbed halite pillar (0.01, from Table 2.3-1), and A_{pil} is the area of the pillars in a panel,

$$A_{pil} = A_{pann} - A_{panx} = 17{,}780 \text{ m}^2$$

where A_{pann} is the enclosed area of a panel (29,420 m^2, from Table 3.1-1). Note that the height of the panel does not enter into the equation. This is true because of the assumption the salt creep occurs only vertically.

The average initial brine saturation of a panel is calculated from S_{bw}, the initial brine saturation of the waste (a varied parameter), and the fixed brine saturation of undisturbed halite, S_{bpil} (1.0, i.e., fully saturated):

$$S_{bpav} = (S_{bw}\phi_f A_{panx} + S_{bpil}\phi_p A_{pil})/(\phi_f A_{panx} + \phi_p A_{pil})$$

Minimum Porosity. The minimum porosity is the porosity of the waste that is reached within about 200 yr without gas generation and sometime later (perhaps after 10,000 yr) with gas generation.

Similar to the calculations presented for permeability, the porosity of the overall waste was estimated by combining, by volume, the estimated individual porosities (on the scale of a drum) of combustibles (plastic, gloves, pine wood, and rags), metal/glass (including corroded and uncorroded steel), and sludges (liquid waste mixed with cement). Estimates for the individual components from estimates of the density at 15 MPa (148 atm) are shown above (Butcher et al., 1991).

Performance Assessment assumed that the porosities of each component were uniformly distributed between the minimum and maximum values given above. Consequently the distribution of local porosity (i.e., the porosity of a collapsed drum) was the weighted sum of uniform distributions.

The resulting mean porosity depends on the final volume fraction of the individual components, which varies in the current PA calculations. For example, we may assume that the initial volume fractions are 40% combustibles, 40% metals/glass, and 20% sludge.

Using the ranges of component porosity (Table 3.4-9), the pdf for porosity of a collapsed drum becomes

$$p(\phi)d\phi = f_c \frac{d\phi}{0.093} + f_m \frac{d\phi}{0.11} + f_s \frac{d\phi}{0.21}$$

where

f_c, f_m, f_s = volume fractions of combustibles, metals/glass, and sludges, respectively

Holding these fractions fixed, the expected value of porosity of a collapsed drum, μ_e, can be calculated:

$$\mu_e = \frac{f_c}{0.093} \int_{0.087}^{0.18} \phi d\phi + \frac{f_m}{0.11} \int_{0.33}^{0.44} \phi d\phi + \frac{f_s}{0.21} \int_{0.01}^{0.22} \phi d\phi \qquad (3.4\text{-}7)$$

$$= 0.134\, f_c + 0.385\, f_m + 0.115\, f_s$$

If the waste-component volume fractions are those given in Table 3.4-1, then

$$\mu_e = 0.134\ (.40) + 0.385(.40) + 0.115\ (.20) = 0.23$$

The variance of the porosity of a collapsed drum, σ_e^2, can also be calculated:

$$\sigma_e^2 = \frac{f_c}{0.093}\int_{0.087}^{0.18}\phi^2 d\phi + \frac{f_m}{0.11}\int_{0.33}^{0.44}\phi^2 d\phi + \frac{f_s}{0.21}\int_{0.01}^{0.22}\phi^2 d\phi - \mu_e^2$$

$$= 1.85 \times 10^{-2} f_c + 1.49 \times 10^{-1} f_m + 1.69 \times 10^{-2} f_s - \mu_e^2 \qquad (3.4\text{-}8)$$

If the waste-component volume fractions are those given in Table 3.4-1, $\sigma_e = 0.13$ and the coefficient of variation is 0.56.

Effective Minimum Porosity. The effective porosity of the collapsed WIPP room is given by (see Section 3.4.6, Permeability)

$$\phi_{eff} = \frac{1}{MN}\sum_{m=1}^{M}\sum_{n=1}^{N}\phi_{\ell mn} \qquad (3.4\text{-}9)$$

where

M = number of replications of units (waste drums) across a room (~14)
N = number of replications of units vertically (3)

Thus, if $E[\phi_{\ell mn}] = \mu_e$ and Var $[\phi_{\ell mn}] = \sigma_e^2$, the Central Limit Theorem (Ross, 1985, p. 70) guarantees that

$$P_r\left\{\phi_{eff} \le x\right\} \to \Phi\left[\frac{\sqrt{MN}\left(x - \mu_e\right)}{\sigma_e}\right] \text{ as } MN \to \infty$$

In other words, ϕ_{eff} is approximately normally distributed with mean μ_e and variance = σ_e^2/MN.

The coefficient of variation of the effective porosity is therefore

$$(MN)^{-1/2}\sigma_e/\mu_e \qquad (3.4\text{-}10)$$

where μ_e and σ_e are given respectively by Eqs. 3.4-7 and 3.4-8. Numerical exploration of Eq. 3.4-10 with M=14 and N=3, using several possible values of f_c and f_m will show that the coefficient of variation of the effective porosity is small enough (less than 10%) to justify not sampling on it. Instead, in the 1991 preliminary comparison, the PA Division sampled on the waste component volume fractions, f_c, f_m, and f_s.

Figure 3.4-10 shows predicted consolidation curves for specific waste types.

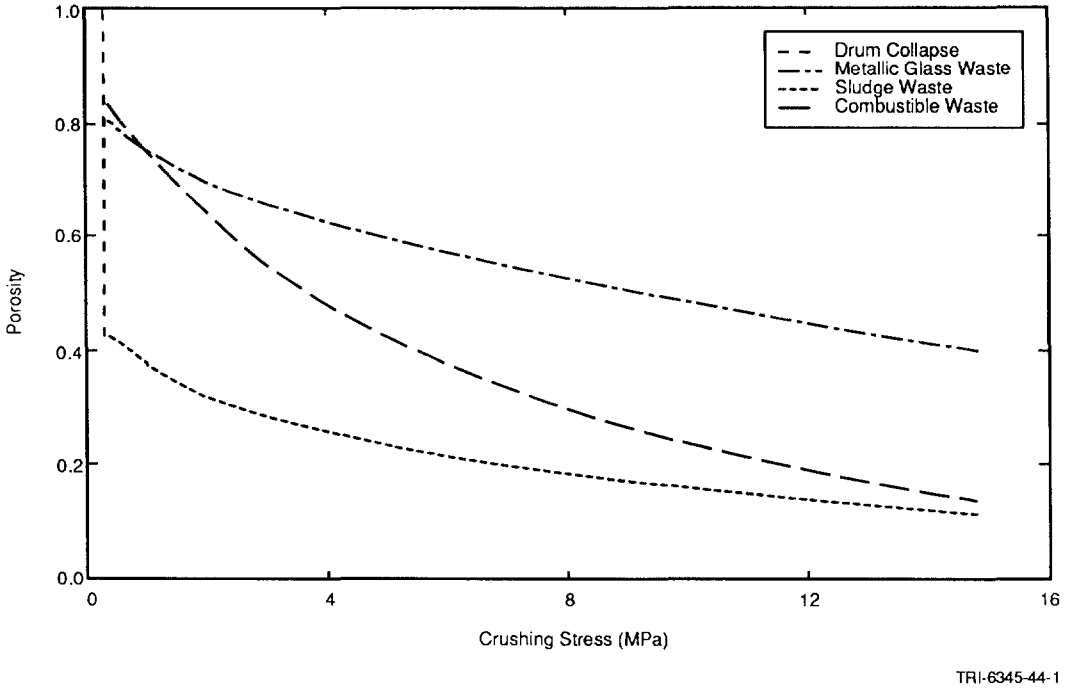

Figure 3.4-10. Predicted Consolidation Curves for Specific Waste Types, including Combustibles, Metals/Glass, and Sludge Wastes (after Butcher et al., 1991, Figure 4-1).

3.4.9 Saturation

Parameter:	**Saturation, initial ($s_{\ell i}$)**
Median:	1.38×10^{-1}
Range:	0
	2.76×10^{-1}
Units:	Dimensionless
Distribution:	Uniform
Source(s):	See text.

Discussion:

The initial fluid saturation ($s_{\ell i}$) of the waste (trash, containers, and backfill) could conceivably vary from 0 up to the residual saturation ($s_{r\ell}$) assumed for the waste provided no fluid is purposefully added. Although these endpoints are probably less likely than some intermediate point, the PA Division did not attempt to more preceisely define this distribution and thus used a uniform distribution.

3.5 Parameters for Salt-Packed Waste Form

Preliminary calculations suggest compliance with *40 CFR 191, Subpart B* can be achieved for the repository as currently designed (Volume 1 of this report; Bertram-Howery et al., 1990; Bertram-Howery and Swift, 1990). However, potential modifications to the present design of the repository and waste are being explored. In last year's PA calculations, waste modification was simulated using modified values for waste permeability, porosity, and shear strength (Table 3.5-1). These values correspond to hypothetical properties of combustible and metallic waste that has been shredded, mixed with crushed salt to reduce void space, and repackaged in new containers. All other parameters for the modified waste remained identical to those of the unmodified waste (Table 3.4-1).

Table 3.5-1. Parameter Values for Salt-Packed Waste

Parameter	Median	Range	Units	Distribution Type	Source
Drilling Erosion Parameter					
Shear strength (τ_{fail})	5		Pa	Constant	Sargunam et al., 1973
Permeability(k)	2.4×10^{-17}		m^2	Constant	See text
Porosity (ϕ)	8.5×10^{-2}		none	Constant	See text; Butcher, 1990a

3.5.1 Drilling Erosion Parameter

Effective Shear Strength for Erosion

Parameter:	**Effective shear strength for erosion (τ_{fail})**
Median:	5
Range:	None
Units:	Pa
Distribution:	Constant
Source(s):	Sargunam, A., P. Riley, K. Arulanadum, and R. B. Krone. 1973. "Physico-Chemical Factors in Erosion of Cohesive Soils." *Journal of the Hydraulics Division, American Society of Civil Engineers* 99: 555-558.

Discussion:

The PA Division assumed a shear strength for erosion (τ_{fail}) for the modified waste of 5 Pa (49 atm), a value at the upper end of the range for montmorillonite clay (Sargunam et al., 1973).

(See also Section 3.4.5.)

3.5.2 Permeability and Porosity

Permeability

Parameter:	**Permeability** (k)
Median:	2.4×10^{-17}
Range:	None
Units:	m^2
Distribution:	Constant
Source(s):	See text.

Porosity

Parameter:	**Porosity** (ϕ)
Median:	8.5×10^{-2}
Range:	None
Units:	Dimensionless
Distribution:	Constant
Source(s):	See text.
	Butcher, B. M., T. W. Thompson, R. G. Van Buskirk, and N. C. Patti. 1991. *Mechanical Compaction of WIPP Simulated Waste.* SAND90-1206. Albuquerque, NM: Sandia National Laboratories. In preparation.

Discussion:

Effective permeability and porosity of a collapsed WIPP room filled with modified waste were calculated in a manner similar to the calculations for unmodified waste (Section 3.4.6, Permeability; Section 3.4.7, Porosity); i.e., the Central Limit Theorem (Ross, 1985, p. 70) was used to show that the distributions of effective permeability and porosity are highly concentrated about the mean values of permeability and porosity that apply to a waste unit (collapsed waste drum). Hypothetical distributions of permeability and porosity for a modified waste unit are tabulated in Table 3.5-2.

Table 3.5-2. Estimated Permeability and Porosity Distributions

Permeability	Porosity	Probability
10^{-16}	0.12	1.0
10^{-19}	0.08	0.5
10^{-21}	0.06	0.0

Using information in Table 3.5-2, it is easily verified that expected permeability (μ_{perm}) and porosity (μ_{por}) on the scale of a drum (0.27 m^3 or 9.4 ft^3) are

$$\mu_{perm} = 2.4 \times 10^{-17}\ m^2 \qquad (3.5\text{-}1)$$

$$\mu_{por} = 0.085 \qquad (3.5\text{-}2)$$

and the coefficients of variation (σ/μ) are approximately 0.20.

The effective porosity of a collapsed WIPP room filled with modified waste is therefore (Section 3.4.7) approximately normally distributed with mean $\mu_{por} = 0.085$ and coefficient of variation $\sim 0.20(MN)^{-1/2} = 2.7 \times 10^{-2}$; the effective permeability is also approximately normally distributed (Section 3.4.6) with mean $\mu_{perm} = 2.4 \times 10^{-17}\ m^2$ and coefficient of variation $\sim 0.20(LMN)^{-1/2} = 2.2 \times 10^{-3}$.

Because the coefficients of variation are so small, the PA Division did not sample on either effective waste permeability or porosity.

3.5.3 Solubility

Discussion:

The solubility and leachability of the radionuclides will likely change, because the repository conditions (e.g., pH, Eh) will change. However, quantifying this change is difficult and has not yet been attempted for the PA calculations. Consequently, as with the unmodified, reference waste, the overall solubility ranges are the same as the extreme local scale (subregions within the drum) solubility; the leach rate from the contaminated material is assumed infinite.

4. PARAMETERS OF GLOBAL MATERIALS AND AGENTS ACTING ON DISPOSAL SYSTEM

This chapter contains parameters for fluid properties, climate variability, and intrusion characteristics.

4.1 Fluid Properties

The fluid parameters tabulated in Table 4.1-1 include Salado and Culebra brine, drilling mud, and hydrogen gas.

Table 4.1-1. Fluid Properties

Parameter	Median	Range		Units	Distribution Type	Source
Brine, Salado (T = 27°C [300.15 K], p = 1 atm [0.101325 MPa])						
Compressibility	2.5×10^{-10}	2.4×10^{-10}	2.6×10^{-10}	Pa^{-1}	Normal	McTigue et al., March 14, 1991, Memo (see Appendix A).
Density (ρ_f)	1.23×10^{3}	1.207×10^{3}	1.253×10^{3}	kg/m^3	Normal	McTigue et al., March 14, 1991, Memo (see Appendix A).
Viscosity (μ)	1.8×10^{-3}			Pa•s	Constant	Kaufman, 1960, p. 622
Brine, Culebra (T = 27°C [300.15 K], p = 1 atm [0.101325 MPa])						
Density (ρf)	1.09×10^{3}	9.99×10^{2}	1.154×10^{3}	kg/m^3	Spatial	Cauffman et al., 1990, Table E.1
Viscosity (μ)	1×10^{-3}			Pa•s	Constant	Haug et al.,1987, p.3-20
Brine, Castile (T = 27°C [300.15 K], p = 1 atm [0.101325 MPa])						
Compressibility	9×10^{-10}			Pa^{-1}	Constant	Popielak et al., 1983, p. H-32
Density	1.215×10^{3}			kg/m^3	Constant	Popielak et al., 1983, Table C-2
Hydrogen (T = 27°C [300.15 K])						
Density	1.1037×10^{1}	8.1803×10^{-2}	1.4442×10^{1}	kg/m^3	Table	See text (Density and Formation Volume Factor)
Viscosity (μ)	9.2×10^{-6}	8.92×10^{-6}	9.33×10^{-6}	Pa•s	Table	Vargaftik, 1975, p. 39.
Solubility in brine (χ)	3.84×10^{-4}	6.412×10^{-6}	4.901×10^{-4}	none	Table	See text (Hydrogen Solubility). Cygan, 1991.
Drilling Mud Properties (T = 22°C [295.15 K], p = 1 atm [0.101325 MPa])						
Density (ρ_f)	1.211×10^{3}	1.139×10^{3}	1.378×10^{3}	kg/m^3	Cumulative	Pace, 1990
Viscosity	9.17×10^{-3}	5×10^{-3}	3×10^{-2}	Pa•s	Cumulative	Pace, 1990
Yield stress	4	2.4	1.92×10^{1}	Pa	Cumulative	Fredrickson, 1960, p.252; Savins et al., 1966; Pace, 1990

4.1.1 Salado Brine

Salado Brine Compressibility

Parameter:	**Compressibility** @ 27°C (300.15 K)
Median:	2.5×10^{-10}
Range:	2.4×10^{-10}
	2.6×10^{-10}
Units:	Pa^{-1}
Distribution:	Normal
Source(s):	McTigue, D. F., S. J. Finley, J. H. Gieske, and K. L. Robinson. "Compressibility Measurements on WIPP Brines." Internal memorandum to Distribution, March 14, 1991. Albuquerque, NM: Sandia National Laboratories. (In Appendix A of this volume)

Discussion:

McTigue et al. (March 14, 1991, Memo [Appendix A]) measured the compressibility of Salado Formation brines over a temperature range of 20 to 40°C. They found that brine compressibility exhibits no significant dependence on temperature over this range. The compressibilities of six Salado brines ranged from 2.40×10^{-10} Pa^{-1} to 2.54×10^{-10} Pa^{-1}, with the error in each measurement estimated at 0.6%. They found a strong correlation with brine density, in that compressibility decreased with increasing density. The following linear relationship correlates well for the data for Salado brines over the small range of densities tested.

$$\beta_f = 7.662 \times 10^{-10} - 4.217 \times 10^{-13} \rho_f \qquad (4.1\text{-}1)$$

where

β_f = the compressibility (Pa^{-1}) (defined as $\frac{1}{\rho}\frac{\partial \rho_f}{\partial p}$

ρ_f = the brine density (kg/m^3).

The correlation coefficient is $r^2 = 0.91$. McTigue et al. also developed a quadratic relationship that gives β_f for densities that include pure water and lower-concentration NaCl brines as well as Salado brines:

$$\beta_f = 4.492 \times 10^{-10} - 1.138 \times 10^{-12}(\rho_f - 1000) + 1.155 \times 10^{-15}(\rho_f - 1000)^2 \qquad (4.1\text{-}2)$$

For a Salado brine density of 1230 kg/m^3 (see Salado Brine Density discussion), both Eqs. 4.1-1 and 4.1-2 give a compressibility of 2.5×10^{-10} Pa^{-1}.

Salado Brine Formation Volume Factor

The formation volume factor is the ratio of the volume at reservoir conditions to the volume at reference conditions (300.15 K [27°C], 0.101325 MPa [1 atm]). Equivalently, it is the ratio of density at reference conditions to the density at reservoir conditions. Assuming the temperature and brine compressibility do not vary, the pressure dependence of Salado brine can be obtained from the definition of compressibility:

$$\beta_f = \frac{1}{\rho_f} \frac{\partial \rho_f}{\partial p} \qquad (4.1\text{-}3)$$

Integrating

$$\int \frac{d\rho_f}{\rho_f} = \int \beta_f dp$$

gives the brine density, ρ_f, as a function of pressure, p:

$$\rho_f = \rho^o e^{\beta_f (p - p^o)} \qquad (4.1\text{-}4)$$

where

- ρ^o = brine density at reference condition (1,230 kg/m^3) (see Salado Brine Density discussion)
- p^o = reference pressure (0.101325 MPa)
- β_f = compressibility of Salado brine (2.5 x 10^{-10} Pa^{-1}) (see Salado Brine Compressibility discussion)

From the definition of formation volume factor, B_b,

$$B_b = \frac{\rho^o}{\rho_f} = e^{-\beta_f (p - p^o)}$$

Figure 4.1-1 shows the variation of Salado brine density and formation volume factor with pressure.

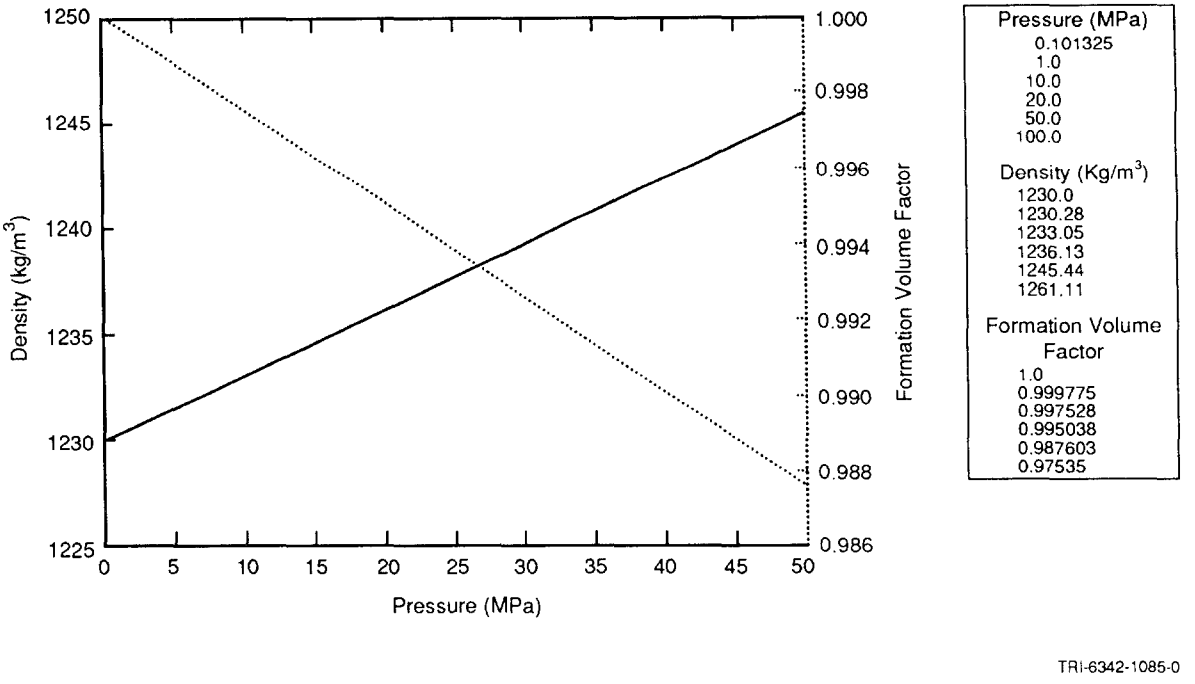

Figure 4.1-1. Variation of Salado Brine Density and Formation Volume Factor with Pressure.

Salado Brine Density

Parameter:	**Density** (ρ_f) @ 0.101325 MPa, 300.15 K
Median:	1.230 x 10^3
Range:	1.207 x 10^3
	1.253 x 10^3
Units:	kg/m^3
Distribution:	Normal
Source(s):	McTigue, D. F., S. J. Finley, J. H. Gieske, and K. L. Robinson. "Compressibility Measurements on WIPP Brines." Internal memorandum to Distribution, March 14, 1991. Albuquerque, NM: Sandia National Laboratories. (In Appendix A of this volume)

Discussion:

The density of brine in the Salado Formation at the repository level was reported by McTigue et al. (March 14, 1991, Memo [Appendix A]). They measured the density of six samples at 22°C and 1 atm pressure, with values ranging from 1,224 to 1,249 kg/m^3. To determine the precision of the density measurement of each individual sample, they repeated the measurement on one sample 14 times; for that sample, the average brine density was 1,249 kg/m^3 with a standard deviation of 2.6 kg/m^3 and a 95% confidence interval on the mean of 1,247 to 1,251 kg/m^3, based on Student's t distribution. The average density for the six samples was 1,232 kg/m^3 at 22°C with an overall range of 1,208 to 1,255 kg/m^3 (s = 10.1 kg/m^3). These values were corrected to the temperature of the Salado Formation at the repository level, assumed to be a uniform and constant 27°C. McTigue et al. developed the following expression to correct the densities measured at 22°C:

$$\frac{\rho_f}{\rho_{fo}} = 1 + a_1(T - 22) + a_2(T - 22)^2 + a_3(T - 22)^3 \qquad (4.1\text{-}5)$$

where

ρ_{fo} = density at 22°C
T = temperature of interest (°C)
a_1, a_2, a_3 = coefficients (a_1 = -4.4294 x 10^{-4}, a_2 = -6.3703 x 10^{-7}, and a_3 = -1.3148 x 10^{-9}.

This expression is based on pure saturated NaCl solutions, rather than on WIPP brines; however, McTigue et al. believe the behavior of the brines will not differ significantly from pure NaCl brines. With this correction, the density of Salado brine at 27°C and 1 atm pressure is 1,230 kg/m^3 with an overall range of 1,207 to 1,253 kg/m^3 (s = 10.0 kg/m^3).

Factors Affecting Brine Density

Empirical correlations developed for petroleum reservoir brines give the dependence of brine density on salinity, gas content, temperature, and pressure (Numbere et al., 1977; Hewlett Packard, 1984). The correlation of Numbere et al. is valid over the range of conditions (temperature, pressure, and salinity) encountered in the Salado Formation, but does not agree with the measured values discussed above. At 27°C, 1 atm, and 26.5 wt% NaCl, the Numbere correlation gives a density of 1,197 kg/m^3, compared with the measured value (corrected to 27°C) of 1,230 kg/m^3.

Because the composition of Salado brines varies considerably (Krumhansl et al., 1991), simple correlations for the dependence of density on salinity (such as the Numbere and HP correlations) do not offer more accuracy or reliability than assuming that the composition does not vary from that of McTigue et al.'s samples.

The effect of dissolved gas on the density of Salado brine cannot be predicted at present. The HP correlations presumably are for natural gas, rather than H_2, N_2, and CO_2, which are relevant to the WIPP. Water (not brine) density is calculated using correlations for either gas-free or gas-saturated water. This density is then corrected for salinity. The effect of salinity on the degree of gas saturation is ignored, yet, as Cygan (1991) shows, the solute composition and concentration both have major effects on the amount of gas that dissolves in the brine, which in turn should affect the density of the brine.

The Salado Formation is assumed to have a constant and uniform temperature of 27°C, so the temperature dependence of brine density is not considered.

The effect of pressure on brine density is discussed under Salado Brine Compressibility.

Salado Brine Viscosity

Parameter:	**Viscosity (μ) @ 300 K**
Median:	1.8×10^{-3}
Range:	None
Units:	Pa•s
Distribution:	Constant
Source(s):	Kaufman, D. W. ed. 1960. *Sodium Chloride, the Production and Properties of Salt and Brine*, Monograph No. 145. Washington, DC: American Chemical Society. (p. 622)

Discussion:

Literature values for brines extrapolating to density of 1,230 kg/m^3 and a temperature of 300 K yields a viscosity of 1.8×10^{-3} Pa•s (3.76×10^{-3} lbf•ft/s) (Kauffman, 1960, p. 622).

4.1.2 Culebra Brine

Culebra Brine Density

Parameter:	**Density** (ρ_f) @ 0.101325 MPa, 300.15 K
Median:	1.09×10^3
Range:	9.99×10^2
	1.154×10^3
Units:	kg/m^3
Distribution:	Spatial
Source(s):	Cauffman, T. L., A. M. LaVenue, and J. P. McCord. 1990. *Ground-Water Flow Modeling of the Culebra Dolomite: Volume II - Data Base.* SAND89-7068/2. Albuquerque, NM: Sandia National Laboratories. (Table E.1)

Table 4.1-2 provides the brine densities at wells within the Culebra Dolomite Member. Figure 4.1-2 shows the spatial variation of brine densities.

Table 4.1-2. Average Brine Density at Wells within Culebra Dolomite Member (after Cauffman et al., 1990, Table E.1)

Well ID	Fluid Density* (kg/m^3)
DOE1	1.088×10^3
DOE2	1.041×10^3
ENGLE	1.001×10^3
H1	1.022×10^3
H2	1.006×10^3
H3	1.035×10^3
H4	1.014×10^3
H5	1.102×10^3
H6	1.038×10^3
H7B	0.999×10^3
H8B	1×10^3
H9B	1×10^3
H10B	1.047×10^3
H11	1.078×10^3
H12	1.095×10^3
H14	1.01×10^3
H15	1.154×10^3
H17	1.1×10^3
H18	1.017×10^3
P14	1.018×10^3
P15	1.015×10^3
P17	1.061×10^3
USGS1	1×10^3
USGS4	1×10^3
USGS8	1×10^3
WIPP13	1.046×10^3
WIPP19	1.059×10^3
WIPP25	1.009×10^3
WIPP26	1.009×10^3
WIPP28	1.032×10^3
WIPP30	1.018×10^3

* Average of measurements from indicated well

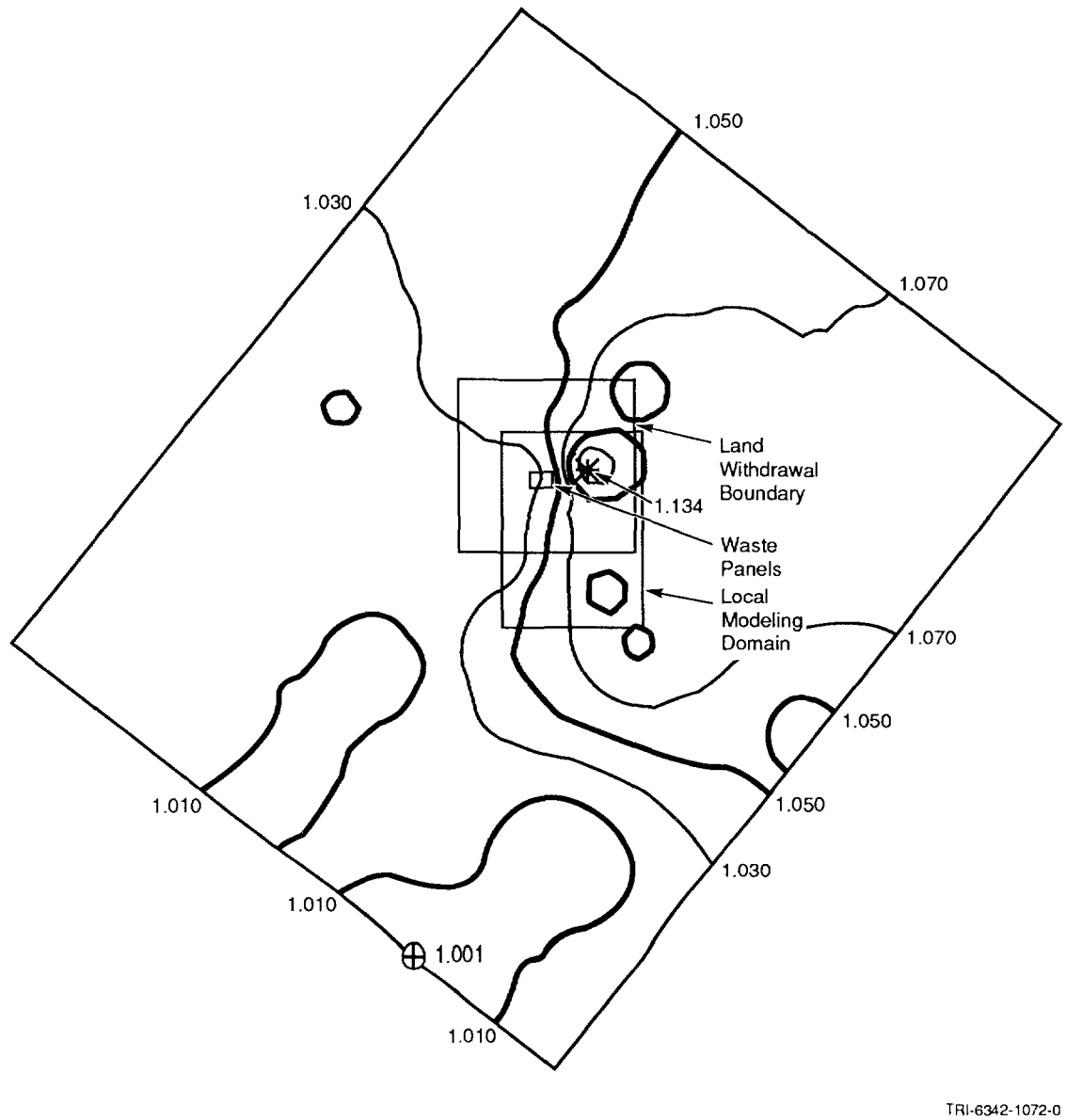

Figure 4.1-2. Variation of Brine Density within Culebra Member Estimated by 10 Nearest Neighbors Using Inverse-Distance-Squared Weighting.

Culebra Brine Viscosity

Parameter:	**Viscosity (μ)**
Median:	1×10^{-3}
Range:	None
Units:	Pa•s
Distribution:	Constant
Source(s):	Haug, A., V. A. Kelley, A. M. LaVenue, and J. F. Pickens. 1987. *Modeling of Groundwater Flow in the Culebra Dolomite at the Waste Isolation Pilot Plant (WIPP) Site: Interim Report.* Contractor Report SAND86-7167. Albuquerque, NM: Sandia National Laboratories. (p. 3-20)

Discussion:

Similar to other modeling studies of the Culebra Dolomite (LaVenue et al., 1990, 1988; Haug et al., 1987), PA calculations assume that the Culebra Brine viscosity is identical to pure water, 1.0×10^{-3} Pa•s (2.089×10^{-3} lbf•ft/s).

4.1.3 Castile Brine

Castile Brine Compressibility

Parameter:	**Compressibility (β_f)**
Median:	9×10^{-10}
Range:	None
Units:	Pa^{-1}
Distribution:	Constant
Source(s):	Popielak, R. S., R. L. Beauheim, S. R. Black, W. E. Coons, C. T. Ellingson, and R. L. Olsen. 1983. *Brine Reservoirs in the Castile Formation, Southeastern New Mexico, Waste Isolation Pilot Plant (WIPP) Project.* TME-3153. Carlsbad, NM: U.S. Department of Energy.

Discussion:

Popielak et al. (1983) estimated the compressibility,

$$\beta_f = \frac{1}{\rho_f} \frac{\partial \rho_f}{\partial p}$$

of Castile Formation brine to be 9×10^{-10} Pa^{-1} (6×10^{-6} psi^{-1}) for brine from well WIPP-12. Only a single value is reported with no estimate of its precision. Some indication of accuracy is obtained by comparing the value with the compressibility value cited for the nearby well ERDA-6: 3×10^{-10} Pa^{-1} (2×10^{-6} psi^{-1}) (Popielak et al., 1983). (Note, however, that Popielak et al. concluded that there was no hydraulic connection between the Castile brine reservoir encountered by WIPP-12 and ERDA-6.)

Castile Brine Formation Volume Factor

Following the discussion and assumptions under Salado Brine Formation Volume Factor, the formation volume factor, B_b, for Castile brine is given by

$$B_b = e^{-\beta_f(p - p^o)}$$

where

β_f = compressibility (9×10^{-10} Pa^{-1}) See discussion under Castile Brine Compressibility.
p = pressure (Pa)
p^o = reference pressure (0.101325 MPa)

Figure 4.1-3 shows the variation of Castile brine density and formation volume factor with pressure.

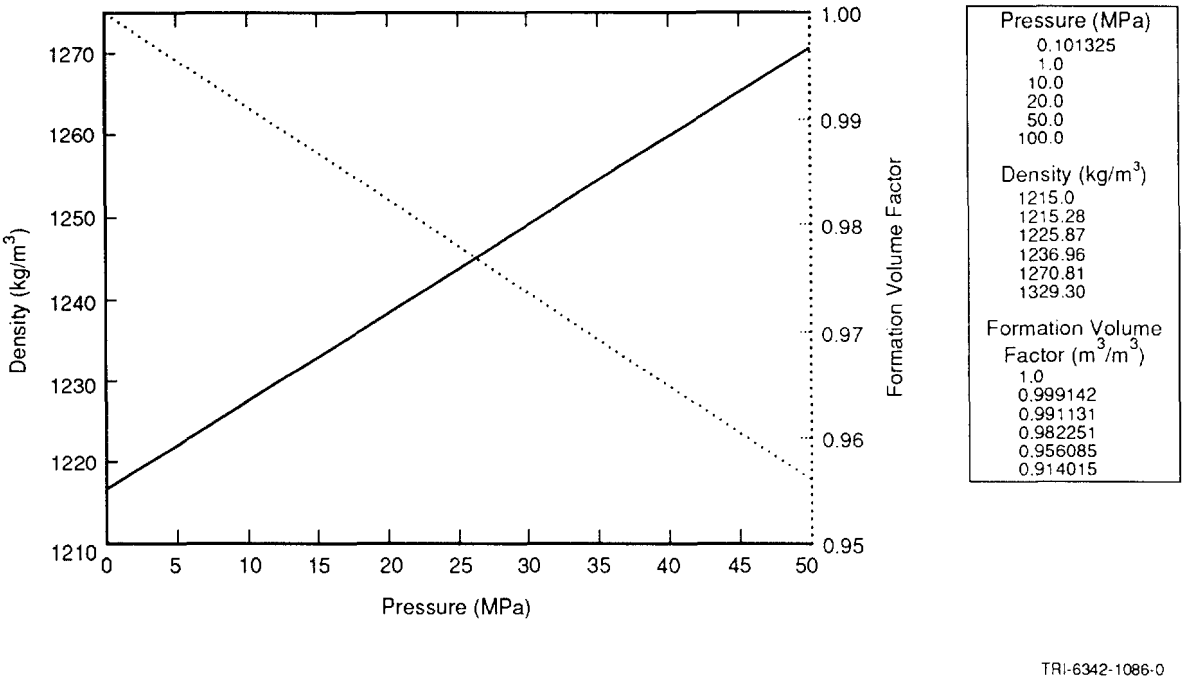

Figure 4.1-3. Variation of Castile Brine Density and Formation Volume Factor with Pressure.

Castile Brine Density

Parameter:	**Density (ρ_f) @ 0.101325 MPa, 300.15 K**
Median:	1.215×10^3
Range:	1.209×10^3
	1.221×10^3
Units:	kg/m^3
Distribution:	Constant
Source(s):	Popielak, R. S., R. L. Beauheim, S. R. Black, W. E. Coons, C. T. Ellingson, and R. L. Olsen. 1983. *Brine Reservoirs in the Castile Formation, Southeastern New Mexico, Waste Isolation Pilot Plant (WIPP) Project.* TME-3153. Carlsbad, NM: U.S. Department of Energy.

Discussion:

Popielak et al. (1983) measured the density of 59 flow samples of Castile Formation brine from well WIPP-12. The density at atmospheric pressure ranged from 1,210 to 1,220 kg/m^3. At an average temperature of 26.7°C, the average density was 1,215 kg/m^3 with a standard deviation of 2.4 kg/m^3 and a 95% confidence interval, based on Student's t distribution, of 1,214 to 1,216 kg/m^3. Using the expression discussed under Salado Brine Density, the average density corrected to 27°C is 1,215 kg/m^3 at 1 atm (0.101325 MPa) pressure. The WIPP-12 brine reservoir is the closest to the disposal region and is assumed representative of Castile brines in any reservoir under the WIPP. Other Castile brine reservoirs have minor differences, e.g., ERDA-6 brine has an average density of 1,216 kg/m^3 at 26.7°C and 1 atm pressure (Popielak et al., 1983).

4.1.4 Hydrogen Gas

Hydrogen Density and Formation Volume Factor

Parameter:	**Density**
Median:	11.037 @ 15 MPa
Range:	0.081803 @ 0.101325 MPa
	14.442 @ 20 MPa
Units:	kg/m^3
Distribution:	Table
Source(s):	See text.

Figure 4.1-4 shows the variation with pressure of density (ρ_f) and the formation volume factor for hydrogen gas (B_g). The formation volume factor, B_g, is the ratio of specific volume of a gas at reservoir conditions to specific volume of the gas at reference or standard conditions (ρ/ρ_f).

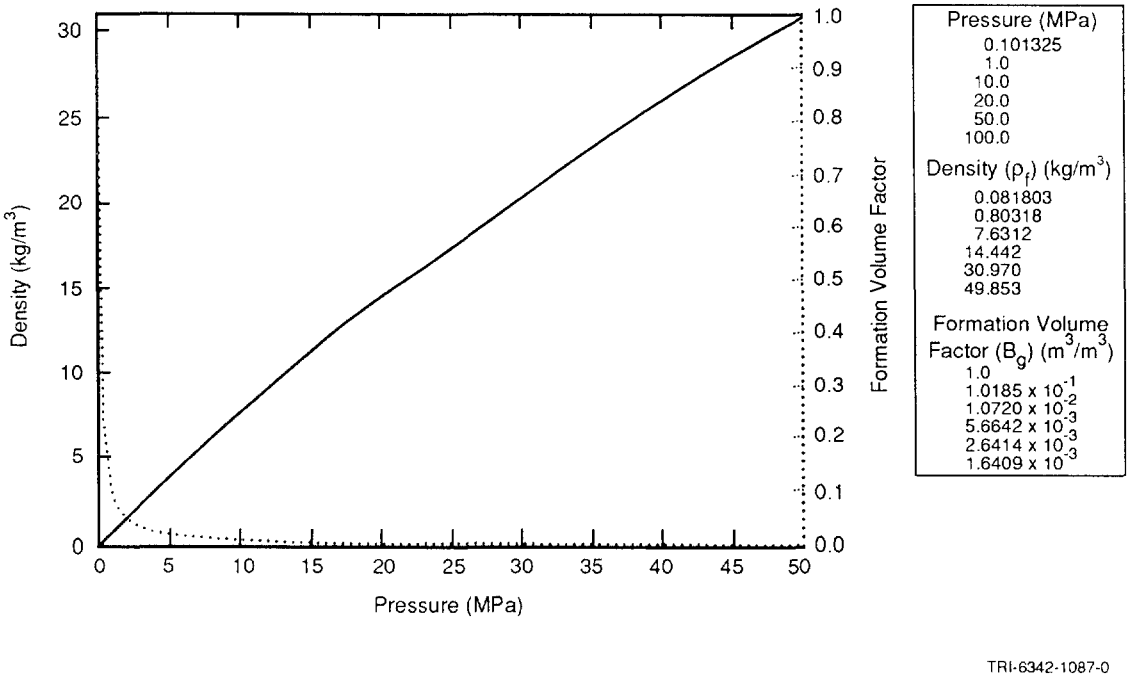

Figure 4.1-4. Formation Volume Factor for Hydrogen Gas.

Discussion:

The formation volume factor is the ratio of the volume at reservoir conditions to the volume at reference conditions (300.15 K [27°C], 0.101325 MPa [1 atm]). The molar volume of hydrogen gas is computed using the Redlich-Kwong-Soave equation of state (Walas, 1985):

$$Z = \frac{p\upsilon}{R^*T} = \frac{\upsilon}{\upsilon - b_R} - \frac{a_R \alpha_R}{R^*T(\upsilon + b_R)} \qquad (4.1\text{-}6)$$

where

a_R = $0.42747\ R^* T_{cr}^2 / p_{cr}$ ($cm^6 \cdot bar/mol^2$)

b_R = $0.08664\ R^* T_{cr} / p_{cr}$ (cm^3/mol)

p = pressure (bar)

R^* = universal gas constant = 83.1441 ($cm^3 \cdot bar/mol \cdot K$)

T = temperature (K)

υ = molar volume (cm^3/mol)

p_{cr} = critical pressure (bar)

T_{cr} = critical temperature (K)

α_R = $[1 + (0.48508 + 1.55171\ \omega_R - 0.1561\ \omega_R)(1 - T_r^{0.5} 1)]^2$ (dimensionless)

ω_R = acentric factor (dimensionless)

T_r = reduced temperature = T/T_{cr} (dimensionless)

Z = compressibility factor (dimensionless)

for hydrogen:

$$T_{cr} = \frac{43.6}{1 + \frac{21.8}{TM}} \quad (K)$$

$$Pcr = \frac{20.47}{1 + \frac{44.2}{TM}} \quad (bar)$$

M = molecular weight = 2.01594 g/mol

α_R = $1.202 \exp(-0.30288\ T_r)$

ω_R = 0.0

Note that temperature-dependent effective critical properties are used for hydrogen (Prausnitz, 1969). Hydrogen also requires a special expression for (α_R) (Graboski and Daubert, 1979), and an acentric factor (ω_R) of zero (Knapp et al., 1982).

Equation 4.1-6 is solved numerically for molar volume, v, at the reference condition and at reservoir conditions to provide the values used to calculate the formation volume factor (Figure 4.1-1). At the reference conditions (300.15 K, 0.101325 MPa), the density (ρ_{H_2}) of H_2 gas is 0.081803 kg/m^3 and the molar volume (v) is 0.024644 m^3/mol.

Alternative Gas Equation of State

At pressures near lithostatic, the gas in the repository deviates significantly from the behavior described by the ideal gas law, p V = n R T. The behavior is described accurately by several real gas equations. A simple yet moderately accurate gas law was developed by Iuzzolino (1983):

$$p = \frac{n\,R\,T}{V}\,\frac{(V + b_I V_{cr})}{(V - b_I V_{cr})} - a_i p_c\,(V_{cr}/V)^2 \qquad (4.1\text{-}7)$$

where

- p = pressure (Pa)
- n = number of moles
- R^* = gas constant = 8.31441 Pa•m^3/mol-K
- V = volume (m^3)
- T = temperature (K)
- T_c = critical temperature (K) for the gas
- p_c = critical pressure (Pa) for the gas
- V_{cr} = n R T_{cr}/p_{cr}
- a_I and b_I = constants.

The constants a and b are obtained from a least-squared-error fit to standard gas compressibility curves. The results from the original curve fit (1981) were a_I = 0.4184 and b_I = 0.078104. A recent fit (1990) using more accurate compressibility data gives a_I = 0.4377 and b_I = 0.08186. The fit is good to within about 5% at temperatures above 1.3 T_{cr} and pressures up to 40 p_{cr}. Near the critical point the errors are about 25%. Since repository gases are at temperatures above 0°C (273 K), they will be significantly above 1.3 T_{cr}, and the fit should be good to within about 5%.

The gas equation fits compressibility data with about half the mean-squared error of the standard Redlich-Kwong-Soave equation of state (EOS) (discussed earlier). The error of this gas equation is larger than that of the Redlich-Kwong-Soave EOS near the critical point and smaller at higher temperatures.

Derivation of the Gas Equation. Iuzzolino's gas equation is derived from a real-gas modification of the canonical partition function for a gas. The partition function Z for an ideal gas is

$$Z = \frac{1}{N!}\left[\left(\frac{2\,\pi\,m_A k^* T}{h^{*2}}\right)^{3/2} V\right]^N \qquad (4.1\text{-}8)$$

where

N = number of molecules
m_A = atomic mass (kg)
k^* = Boltzmann's constant
h^* = Planck's constant.

The ideal gas equation is derived using the thermodynamic relation

$$p = k^* T \frac{\delta \ln Z}{\delta V} \qquad (4.1\text{-}9)$$

applying this relation to the partition function gives p = N k* T / V. Since N k* = n R, the usual form p V = n R T is obtained.

Iuzzolino uses two modifications to the partition function. The volume term is multiplied by $(1 - b_I V_{cr}/V)^2$ to provide a quadratic (soft-molecule) correction for the volume taken up by the molecules. The parameter b_I is proportional to the volume of the gas at the critical point and is an excluded-volume correction. Earlier work using a two-constant quadratic correction of the form $1 - b_I V_{cr}/V + c (V_{cr}/V)^2$ indicated that a factor of the form $(1 - b_I V_{cr}/V)^2$ gave the better fit.

A second correction is applied to take into account attractive forces between molecules: the volume term is multiplied by exp $(a_I p_{cr} V_{cr}^2/Nk^*T V)$. The form of this correction is the best result of several arbitrary trials. The real-gas partition function is

$$Z = \frac{1}{N!}\left[\left(\frac{2 \pi m_A k^* T}{(h^*)^2}\right)^{3/2} V(1 - b_I V_{cr}/V)^2 \, e^{(a_I P_{cr} V_{cr}^2/N k^* T V)}\right]^N \qquad (4.1\text{-}10)$$

Gas Mixtures. To preserve the form of the gas equation for a mixture of gases, the critical pressure of the mixture should be

$$p_{cr} = \sum_i n_i \, p_{cr_i}$$

where

p_{cr_i} = the critical pressure of the i-th gas

n_i = the number of moles of the i-th gas.

The summation runs over each gas in the mixture.

To preserve the concept that V_{cr} is proportional to an excluded volume, for a mixture

$$V_{cr} = \sum_{I} \frac{n_i R T_{cr_i}}{p_{cr_i}} \qquad (4.1\text{-}11)$$

where

T_{cr_i} = the critical temperature of the i-th gas.

Then

$$\frac{n R T_{cr}}{p_{cr}} = \sum_{i} \frac{n_i R T_{cr_i}}{p_{cr_i}} \qquad (4.1\text{-}12)$$

implies that

$$\frac{T_{cr}}{p_{cr}} = \sum_{i} n_i \left(\frac{T_{cr_i}}{p_{cr_i}} \right) \qquad (4.1\text{-}13)$$

so that, for the mixture,

$$T_{cr} = p_{cr} \sum_{i} n_i \left(\frac{T_{cr_i}}{p_{cr_i}} \right) \qquad (4.1\text{-}14)$$

Quantum Effects. Several gases deviate significantly from the real gas compressibility curves, most notably very light gases and highly polar gases. For H_2 and He, the deviation is primarily a result of quantum effects. For NH_3 the deviation is caused by hydrogen bonding. In both cases the fit to the real gas equation can be improved by using values of p_{cr} and T_{cr} that are not the actual critical constants. For H_2, a good fit results using T_{cr} = 50 K and p_{cr} = 2.35 X 10^6 Pa.

Viscosity

Parameter:	**Viscosity (μ) @ 300.15 K**
Median:	9.20×10^{-6} @ 15 MPa
Range:	8.92×10^{-6} @ 0.101325 MPa
	9.33×10^{-6} @ 20 MPa
Units:	Pa•s
Distribution:	Table
Source(s):	Vargaftik, N. B. 1975. *Tables on the Thermophysical Properties of Liquids and Gases in Normal and Dissociated States.* New York: John Wiley & Sons, Inc.

Discussion:

Vargaftik (1975) tabulates numerous measurements of hydrogen viscosity covering a wide range of temperatures and pressures. At pressures of 0.100 MPa (1 bar) to 0.101325 MPa (1 atm), eight independent measurements are reported at 293 to 293.15 K (20°C), with values ranging from 8.73×10^{-6} to 8.86×10^{-6} Pa•s. Hydrogen viscosity increases with temperature; two values reported at 300 K are 8.89×10^{-6} and 8.91×10^{-6} Pa•s. Vargaftik (1975, p. 39) presents two tables with hydrogen viscosity ranging from -200°C to 1000°C and 0.1 MPa to 50 MPa. (The table value of viscosity at 20°C and 0.1 MPa is 8.80×10^{-6} Pa•s.) Linear interpolation within these tables between 0 and 100°C provides sufficiently precise viscosity values at the temperatures of interest; at 20°C, the viscosity is 8.79×10^{-6} Pa•s, which is in the middle of the range of measured values cited above. At 300 K, the temperature of the repository, the viscosity at 0.1 MPa is 8.92×10^{-6} Pa•s. Quadratic interpolation based on table values at pressures of 0.1, 10, and 20 MPa (interpolated linearly to 300.15 K) results in the following expression giving H_2 viscosity at 300.15 K (27°C, 80.6°F) as a function of pressure:

$$\mu = 8.920074 \times 10^{-6} + 1.020892 \times 10^{-8}\ p + 5.273692 \times 10^{-10}\ p^2 \qquad (4.1\text{-}15)$$

where

μ = viscosity (Pa•s)
p = pressure (MPa)

Figure 4.1-5 shows the variation of hydrogen viscosity with pressure.

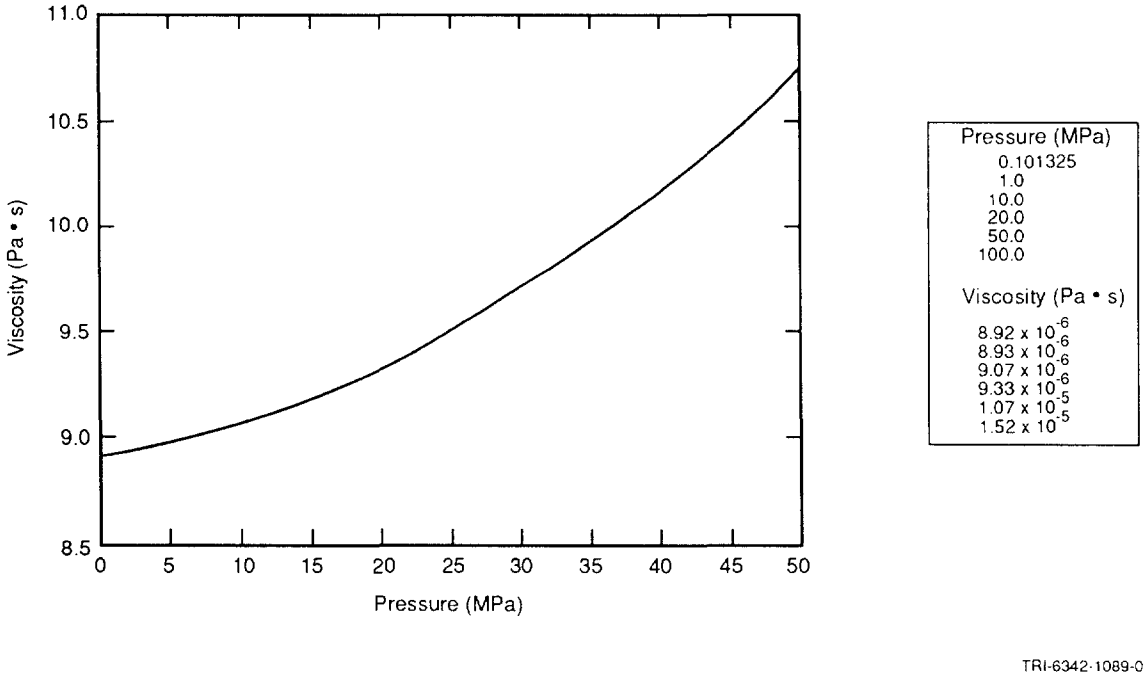

Figure 4.1-5. Variation of Hydrogen Viscosity with Pressure.

Hydrogen Solubility

Parameter:	**H_2 Solubility in brine**
Median:	3.84×10^{-4}
Range:	6.412×10^{-6}
	4.901×10^{-4}
Units:	Dimensionless
Distribution:	Table
Source(s):	Cygan, R. T. 1991. *The Solubility of Gases in NaCl Brine and a Critical Evaluation of Available Data.* SAND90-2848. Albuquerque, NM: Sandia National Laboratories.

Discussion:

Cygan (1991) estimated the solubility of H_2 in NaCl solutions at elevated pressure and developed the following correlation relating H_2 mole fraction in solution, χ_{H_2}, to pressure, p, in MPa:

$$\ln\chi_{H_2} = a_0 + a_1 \ln p \qquad (4.1\text{-}16)$$

where

a_0 = -8.8980 (pure water); -10.0789 (5 N NaCl brine at 298.15 K)
a_1 = 0.9538 (pure water); 0.8205 (5 N NaCl brine at 298.15 K)

Cygan emphasizes that this correlation is only an "educated estimate," but probably we are justified in applying it to Salado brine at 300.15 K.

Some multiphase flow models, e.g., BOAST and BRAGFLO (Rechard et al., 1989), require gas solubility expressed in terms of gas volume at reference conditions per unit volume of solution (brine), also at reference conditions. This "gas/brine ratio," $r_{g/\ell}$, is calculated from

$$r_{g/\ell} = \chi_{H_2} \frac{V^\circ_{H_2}}{V^\circ_b} \qquad (4.1\text{-}17)$$

where

V°_b = volume of a mole of brine at reference conditions ($\overline{M}/\rho^\circ$)

$V^\circ_{H_2}$ = volume of a mole of H_2 gas at reference conditions, 300.15 K and 0.101325 MPa

ρ° = density of Salado brine (1230 kg/m^3)

$\overline{M}$ = molar average molecular weight of brine.

For NaCl brine, $\overline{M}$ is calculated as follows:

$$\overline{M} = \chi_{NaCl} M_{NaCl} + \chi_{H_2O} M_{H_2O} = \chi_{NaCl}(M_{NaCl} - M_{H_2O}) + M_{H_2O} \quad (4.1\text{-}18)$$

where

χ = mole fraction of NaCl and H_2O
$\chi_{H_2O} = 1 - \chi_{NaCl}$

Molecular weights are M_{NaCl} = 58.44 g/mol and M_{H_2O} = 18.015 g/mol.

$$\chi_{NaCl} = \frac{\omega}{\omega + 1} \quad (4.1\text{-}19)$$

where

ω = molar ratio of NaCl to H_2O ($M_{H_2O}N/C_w$)
N = molarity of the solution (5 mol NaCl/ℓ)
C_w = total water concentration in the solution.

C_w is obtained by quadratic interpolation from tabulated data relating C_w to molarity for NaCl solutions (Weast and Astle, 1981, p. D-232). For N equals 5 mol NaCl/ℓ, C_w equals 893.53 g H_2O/ℓ brine, which in turn gives ω = 0.10081 mol NaCl/mol H_2O; χ_{NaCl} = 0.09158 mol NaCl/mol brine; $\overline{M}$ = 21.718 g/mol brine molecular weight; and $V_b^\circ = \overline{M}/\rho^\circ$ = 1.7657 x 10^{-5} m^3/mol. The molar volume of H_2 at reference conditions (see discussion under Hydrogen Density) is $V_{H_2}^\circ$ = 0.0246347 m^3/mol. Applying Eqs. 4.1-18 and 4.1-19 for 5N NaCl brine results in the following values for gas/brine ratio, $r_{g/\ell}$, at 300.15 K (Figure 4.1-6).

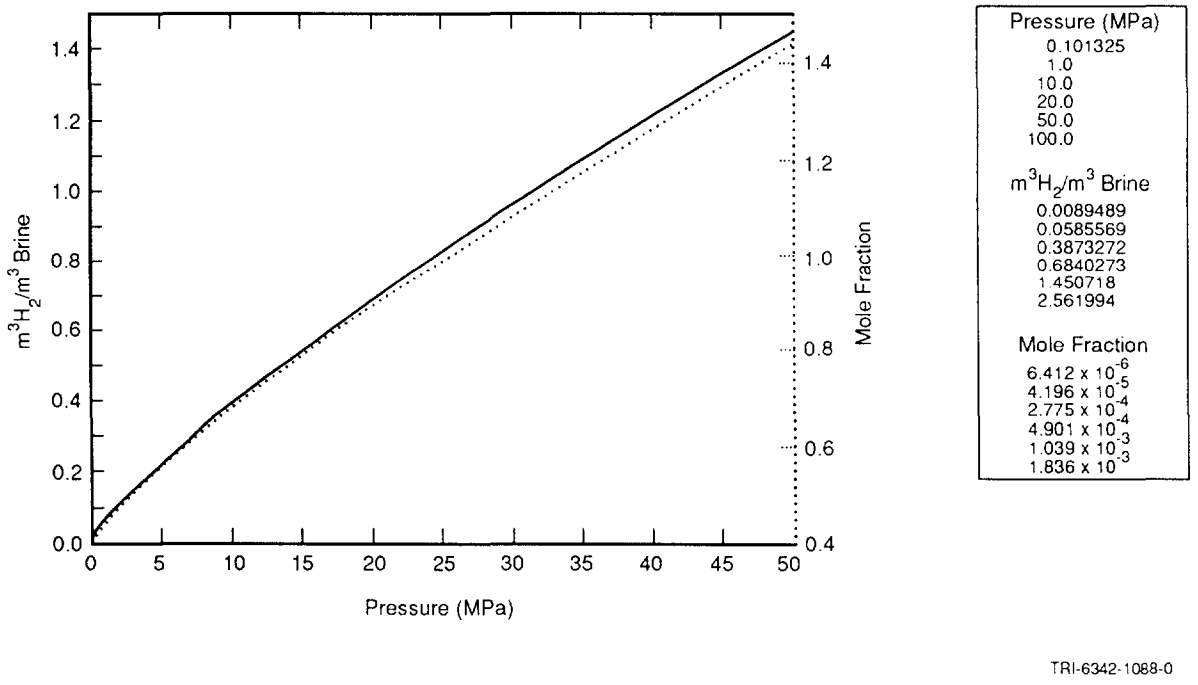

TRI-6342-1088-0

Figure 4.1-6. Variation of Hydrogen Solubility with Pressure.

4.1.5 Drilling Mud Properties

In assessing the long-term performance of the WIPP containment system, we must predict the transport of radionuclides to the accessible environment during and after a drilling procedure in which a company drills an exploratory drillhole through the underground disposal region in search of resources *(40 CFR 191, Appendix B)*. Given two assumptions -- (1) the resource is either gas or oil and (2) standard rotary drilling equipment in use today will be used in the future -- an important consideration in determining the consequence of the drilling is an estimation of the amount of material brought to the surface during the drilling procedure. The parameters for drilling mud density, viscosity, and yield point are shown below. A discussion of these parameters follows.

Density

Parameter:	**Density, mud** (ρ_f) @ 225.15 K, p = 0.101325 MPa
Median:	1.2×10^3
Range:	1.14×10^3
	1.38×10^3
Units:	kg/m^3
Distribution:	Cumulative
Source(s):	Pace, R. O. 1990. "Letter 1b: Changes to bar graphs," in Rechard et al. 1990. *Data Used in Preliminary Performance Assessment of the Waste Isolation Pilot Plant (1990)*. SAND89-2408. Albuquerque, NM: Sandia National Laboratories.

Viscosity

Parameter:	**Viscosity** (μ) @ 225.15 K, p = 0.101325 MPa
Median:	9.17×10^{-3}
Range:	5×10^{-3}
	3×10^{-2}
Units:	Pa•s
Distribution:	Cumulative
Source(s):	Pace, R. O. 1990. "Letter 1b: Changes to bar graphs," in Rechard et al. 1990. *Data Used in Preliminary Performance Assessment of the Waste Isolation Pilot Plant (1990)*. SAND89-2408. Albuquerque, NM: Sandia National Laboratories.

Yield Stress Point

Parameter:	**Yield stress point**
Median:	4
Range:	2.4
	1.92×10^1
Units:	Pa
Distribution:	Cumulative
Source(s):	Pace, R. O. 1990. "Letter 1b: Changes to bar graphs," in Rechard et al. 1990. *Data Used in Preliminary Performance Assessment of the Waste Isolation Pilot Plant (1990)*. SAND89-2408. Albuquerque, NM: Sandia National Laboratories.

Discussion:

Standard Rotary Drilling. In standard rotary drilling, a cutting bit is attached to a series of hollow drill pipe and then rotated and directed downward to cut through underlying strata. To remove the cuttings, a fluid ("mud") is pumped down the hollow drill pipe, through the bit, and up the annulus formed by the drill pipe and borehole wall. In addition to removing the cuttings, the mud cools and cleans the bit, reduces drilling friction, and helps to support the borehole. The mud also forms a thin, low-permeability filter cake on the borehole walls, thus preventing inflow of unwanted fluids from permeable formations.

Although the amount of waste removed by direct cutting is simple to calculate, calculating the amount of waste eroded from the borehole wall is more difficult. A number of factors may influence borehole erosion (e.g., eccentricity of pipe and hole, impact of solid particles in mud on the walls, physical and chemical interaction between mud and walls, and time of contact between the mud and walls [Broc, 1982]); however, industry opinion singles out fluid shear stress as the most important factor (Walker and Holman, 1971; Darley, 1969).

Three drilling mud properties (density, viscosity, and yield stress) are necessary to evaluate the fluid shear stress, which in turn is one of several parameters used to evaluate the amount of material eroded from the borehole wall by scouring from the swirling drilling fluid (e.g., CUTTINGS [Rechard et al., 1989]). (Section 4.3, Intrusion Borehole Characteristics; Chapter 3, Engineered Barriers; and Chapter 6, Probability Models, present other parameters for this anthropogenic event.)

Flow Regime. The flow regime within the annulus (laminar or turbulent) is governed by the Reynolds number, N_R. The Reynolds number is dependent upon the properties of the drilling mud (density, viscosity, and velocity) and the size of the annulus. The Reynolds number is defined as

$$N_R = \frac{\bar{\rho}\ \bar{V} d_e}{\bar{\mu}} \qquad (4.1\text{-}20)$$

where

d_e = length dimension = equivalent diameter for annulus = d_{hole}-d_{collar}

$\bar{\rho}$ = average fluid density

$\bar{V}$ = average fluid velocity

$\bar{\mu}$ = average fluid viscosity (for non-newtonian fluids, the average viscosity will depend upon the viscosity model used)

The ultimate diameter of the hole, d_{hole}, is the quantity to be evaluated, and is determined through an iterative process. The velocity is estimated from the drilling pump rates provided in Section 4.3. The fluid density and viscosity (and yield stress for non-newtonian fluids) are discussed below.

Density. The current drilling procedure for an exploratory oil or gas well in the Delaware Basin (see Figure 1.6-2) involves using a drilling fluid, which is usually a saturated brine. The brine density is maintained during the transport of cuttings by adding an emulsified oil (Pace, 1990). Consequently, the fluid density is near 1,200 kg/m^3 (75 lb/ft^3 or 10 lb/gal) with a narrow range between 1,138 and 1,377 kg/m^3 (9.5 and 11.5 lb/gal) (Figure 4.1-7).

When drilling for oil or gas, particularly in the area around the WIPP, there is the possibility of encountering a blowout. The drilling companies can respond in a relatively short time. If the drill hole intercepts a brine reservoir with sufficient pressure to cause copious amounts of brine flow to the surface, the company will add weight (usually barite) to the drilling fluid to stop the flow from the reservoir. The mud density could increase to as much as 1900 kg/m^3 (16 lb/gal). This density increase would occur long after the drill passed through the repository area, the time of greatest erosion.

Shear Stress. For both laminar and turbulent flow, the shear stress can be expressed as (Vennard and Street, 1975, p. 381):

$$\tau = \frac{f\rho V^2}{2} \qquad (4.1\text{-}21)$$

The fanning friction factor, f, is discussed below for turbulent and laminar shear stress.

Turbulent Shear Stress. In turbulent flow (Reynolds number $N_{R>} N_{R_{crit}}$ where $N_{R_{crit}}$ varies between 2,100 for newtonian fluids and 2,400 for some non-newtonian fluids [Vennard and Street, 1975, p. 384; Walker, 1976, p. 89]) the fanning friction factor is dependent on both N_R, and surface roughness (e.g., Moody diagram [Vennard and Street, 1975, Figure 9.5; Streeter and Wylie, 1975, Figure 5.32]), with N_R having a minor influence. Consequently, the shear stress is dependent primarily upon absolute surface roughness, ε, and kinetic energy ($\rho V^2/2$). An empirical expression for f is (Colebrook, 1938):

$$\frac{1}{\sqrt{f}} = -4 \log \left[\frac{\varepsilon/d}{3.72} + \frac{1.255}{N_R\sqrt{f}} \right] \qquad (4.1\text{-}22)$$

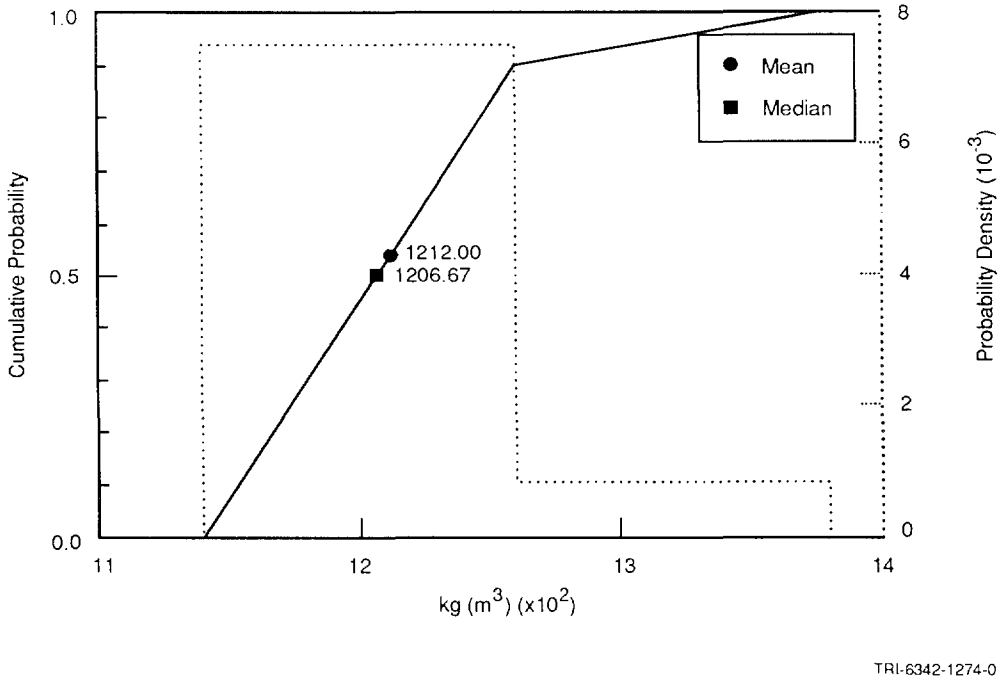

Figure 4.1-7. Distribution of Drilling Mud (Saturated Brine) Density.

where

ε = absolute roughness of material

d = hydraulic diameter = difference between borehole diameter and collar diameter

The assumed absolute roughness of waste (ε) is tabulated in the description of the waste in Chapter 3, Engineered Barriers.

Laminar Shear Stress. For laminar flow, the fanning friction factor, f, is a function of only N_R. The shear stress in laminar flow (Reynolds number N_R < 2,100 [Vennard and Street, 1975, p. 384]) depends solely on the fluid viscosity and strain rate (velocity gradient); however, for a non-newtonian fluid such as drilling mud, the viscosity varies with strain rate (Figure 4.1-8). Several functional forms are used to model this variation (Ideal Bingham Plastic, Power Law, and Oldroyd Model). The PA Division currently uses the Oldroyd model.

Ideal Bingham Plastic -- A linear (Ideal Bingham Plastic) model approximates the actual yield stress (τ_o) (Figure 4.1-8) at high strain rate

$$\tau = \tau'_o + \mu_\ell \Gamma \qquad (4.1\text{-}23)$$

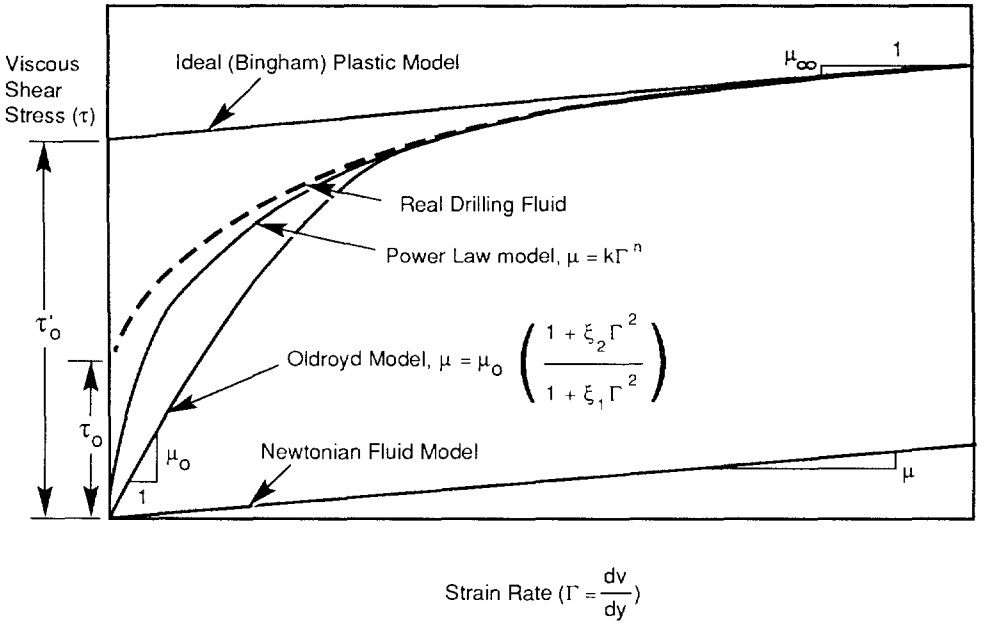

Figure 4.1-8. Various Models for Modeling Drilling Fluid Shear Stress.

where

μ_ℓ = linear viscosity (= "average" viscosity for evaluating N_R)
τ'_o = yield point (shear stress at zero strain rate)
Γ = strain rate

Oldroyd Model -- Oldroyd's (1958) shear softening model of the viscosity can also approximate the drilling fluid behavior away from the yield stress (τ_o) by the appropriate choice of parameters:

$$\tau = \mu_0 \left[\frac{1 + \zeta_2 \Gamma^2}{1 + \zeta_1 \Gamma^2} \right] \Gamma \qquad (4.1\text{-}24)$$

where

μ_∞ = $\mu_o(\zeta_2/\zeta_1)$ = limiting viscosity at infinite strain rate = μ_ℓ (= "average" viscosity for evaluating N_R)
Γ = strain rate
ζ_1, ζ_2 = Oldroyd model parameters
μ_0 = limiting viscosity at zero rate of strain

Note that for the PA calculations, ζ_1 was assumed equal to 2 ζ_2, based on viscosity measurements for an oil-based, 1.7-kg/m^3 (14-lb/gal) mud (Darley and Gray, 1988, Table 5-2). The assumption can be somewhat arbitrary since the behavior at high strain rate (away from the yield point) is of primary interest.

Using the above assumption, the parameter ζ_2 was estimated by equating the linear ideal plastic model, Eq. 4.1-23 with the Oldroyd model, Eq. 4.1-24, at a high strain rate. After simple algebraic manipulation

$$\zeta_2 = (\mu_\infty \Gamma_m - \tau_o')/2\Gamma_m^2 \tau_o' \qquad (4.1\text{-}25)$$

The high strain rate selected for the match point (Γ_m) was 1020 s^{-1}.

Linear Viscosity. For a saturated brine with the density maintained by emulsified oil and modeled as an ideal Bingham plastic, Pace (1990) estimates that μ_ℓ varies between 0.005 and 0.030 Pa•s (0.003 and 0.020 lbf•s/ft^2) with a median of 0.009 Pa•s (0.006 lbf•s/ft^2). Figure 4.1-9 shows the estimated pdf and cdf for drilling mud viscosity.

Yield Stress. For a saturated brine with the density maintained by emulsified oil and modeled as an ideal Bingham plastic, Pace (1990) estimates the yield point (τ_o') varies between 2.4 and 19 Pa (5 and 42 lb/100 ft^2) with a median of 4 Pa (9.2 lb/100 ft^2) (Figure 4.1-10).

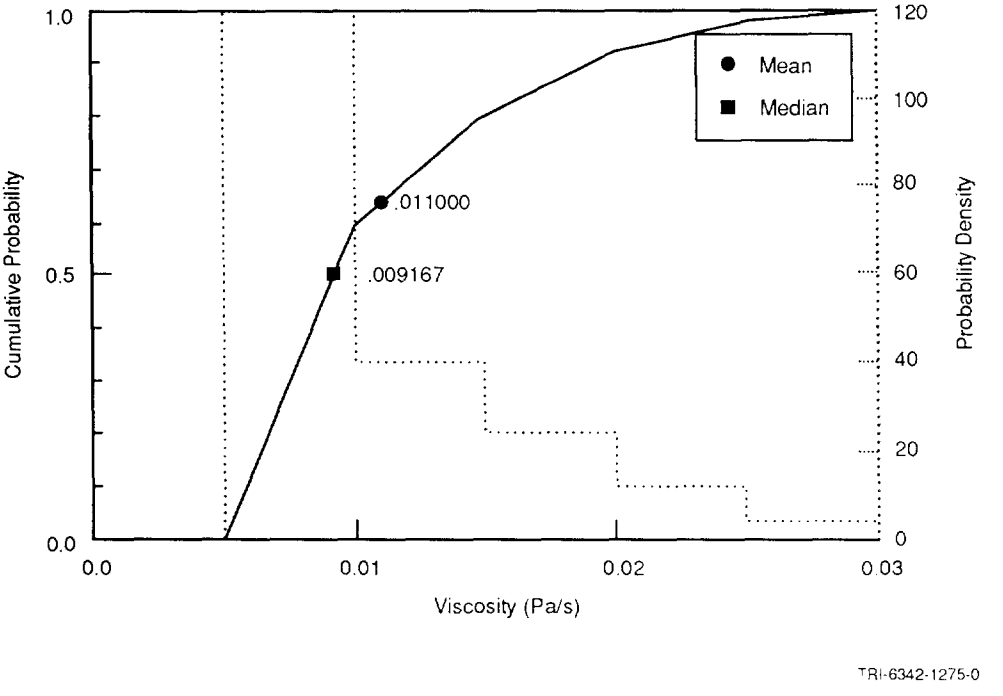

Figure 4.1-9. Estimated Distribution (pdf and cdf) for Drilling Mud Viscosity.

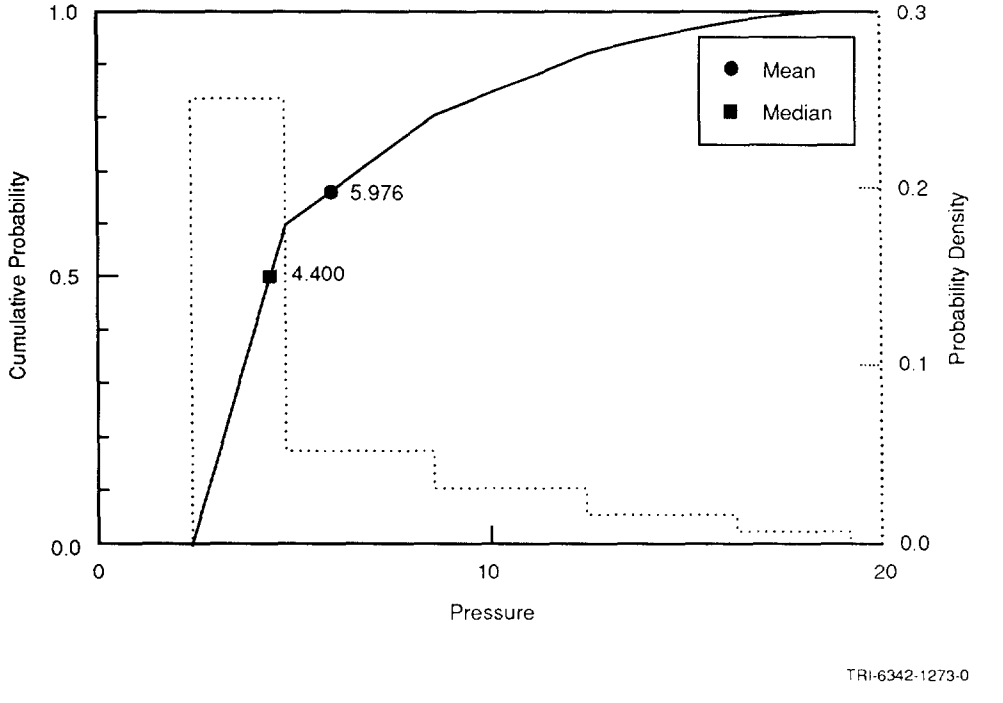

Figure 4.1-10. Estimated Distribution (pdf and cdf) for Drilling Mud Yield Stress (Ideal Plastic).

4.2 Human-Intrusion Borehole

Table 4.2-1. Characteristics of Human-Intrusion Borehole

Parameter	Median	Range		Units	Distribution Type	Source
Borehole Fill Properties						
Creep (r_o-r/r_o)		2×10^{-2}	8×10^{-1}	none	Table	Sjaardema and Krieg, 1987, Figure 4.6
Density, average (ρ_{ave})	2.3×10^{3}			kg/m^3	Constant	See text (Salado).
Density, bulk (ρ_{bulk})	2.14×10^{3}			kg/m^3	Constant	See text (Salado).
Permeability, final (k)	3.16×10^{-12}	1×10^{-14}	1×10^{-11}	m^2	Lognormal	Freeze and Cherry, Table 2.2 (silty sand)
Initial						
Plug in Castile Fm.	10^{-15}			m^2	Constant	Lappin et al., 1989, Table C-1
Plugs in Salado Fm.	10^{-18}			m^2	Constant	Lappin et al., 1989, Table C-1
Porosity (ϕ)	3.75×10^{-1}	2.5×10^{-1}	5×10^{-1}	none	Normal	Freeze and Cherry, Table 2.4 (sand)
Drilling Characteristics						
Drill bit diameter (d)						
Intrusion	3.55×10^{-1}	2.67×10^{-1}	4.44×10^{-1}	m	Uniform	See text.
Historical	2×10^{-1}	1.21×10^{-1}	4.45×10^{-1}	m	Delta	Brinster, 1990c
Drill string angular velocity ($\dot{\theta}$)	7.7	4.2	2.3×10^{1}	rad/s	Cumulative	Pace, 1990; Austin, 1983
Drilling mud flowrate (Q_f)	9.935×10^{-2}	7.45×10^{-2}	1.24×10^{-1}	$m^3/(s \cdot m)$	Uniform	Pace, 1990; Austin, 1983

4.2.1 Borehole Fill Properties

Creep

Parameter:	**Creep**
Median:	None
Range:	2×10^{-2}
	8×10^{-1}
Units:	Dimensionless
Distribution:	Table
Source(s):	Sjaardema, G. D. and R. D. Krieg. 1987. *A Constitutive Model for the Consolidation of WIPP Crushed Salt and Its Use in Analysis of Backfilled Shaft and Drift Configurations.* SAND87-1977. Albuquerque, NM: Sandia National Laboratories. (Figure 4.6)

Storage Density near Repository

Parameter:	**Density, average (ρ_{ave})**
Median:	2.3×10^3
Range:	None
Units:	kg/m^3
Distribution:	Constant
Source(s):	Krieg, R. D. 1984. *Reference Stratigraphy and Rock Properties for the Waste Isolation Pilot Plant (WIPP) Project.* SAND83-1908. Albuquerque, NM: Sandia National Laboratories. (Table 4)

Bulk Density of Halite in Salado

Parameter:	**Density, bulk (ρ_{bulk})**
Median:	2.14×10^3
Range:	None
Units:	kg/m^3
Distribution:	Constant
Source(s):	Holcomb, D. J. and M. Shields. 1987. *Hydrostatic Creep Consolidation of Crushed Salt with Added Water.* SAND87-1990. Albuquerque, NM: Sandia National Laboratories. (p. 17)

Final Permeability

Parameter:	**Permeability, final** (k)
Median:	3.16×10^{-12}
Range:	1×10^{-14}
	1×10^{-11}
Units:	m^2
Distribution:	Lognormal
Source(s):	Freeze, R. A. and J. C. Cherry. 1979. *Groundwater*. Englewood Cliffs, NJ: Prentice-Hall, Inc. (Table 2.4, silty sand)

Porosity

Parameter:	**Porosity** (ϕ)
Median:	3.75×10^{-1}
Range:	2.5×10^{-1}
	5×10^{-1}
Units:	Dimensionless
Distribution:	Normal
Source(s):	Freeze, R. A. and J. C. Cherry. 1979. *Groundwater*. Englewood Cliffs, NJ: Prentice-Hall, Inc. (Table 2.4, sand)

Discussion:

Because of the speculative nature of inadvertent human intrusion, PA calculations depend on the guidance provided by regulations on factors such as length, severity, and resulting conditions after intrusion. The EPA Standard, *40 CFR 191*, in Appendix B states

> "...the implementing agency can assume that passive institutional controls or the intruders' own exploratory procedures are adequate for the intruders to soon detect, or be warned of, the incompatibility of the area with their activities ... Furthermore, the Agency assumes that the consequences of such inadvertent drilling need not be assumed to be more severe than: ... (2) creation of a ground water flow path with a permeability typical of a borehole filled by the soil or gravel that would normally settle into an open hole over time--not the permeability of a carefully sealed borehole."

Thus while intruders "soon detect" the repository, the guidance in Appendix B suggests that the implementing agency should not take credit for any special precautions that the drilling company might pursue as the result of detection that could alter long-term borehole behavior.

Initial Conditions after Abandonment. Some PA calculations require that initial conditions be established for the time period immediately after intrusion; no regulatory guidance has been provided for these conditions. In defining initial conditions in the borehole, the PA calculations assume that future societies establish government regulations on drilling similar to those in effect today to protect natural resources. Thus, for any borehole through the repository and hypothetical brine reservoir, drillers would be required to place casing and several cement and sand plugs as follows:

Casing. The normal procedure for drilling an oil and gas well is to drill the hole to the base of the Rustler Formation (the top of salt) and set casing, called a salt string. The State Engineer Office dictates the use of this casing because the WIPP is located in a closed ground-water basin, and all hydrocarbon wells are required to protect the aquifers in the basin (e.g., Culebra Dolomite). After the hole has been drilled and the casing placed in the hole, the casing is cemented from bottom to top with an API Class C grout (intended for use in oil and gas wells from surface to a depth of 2,400 m [8,000 ft] and having a sulfate resistance).

Plug Locations. The Energy, Minerals, and Natural Resources Department, Oil Conservation Division (OCD) controls plugging when abandoning a borehole in the Delaware Basin in and around the WIPP. Exact specifications are negotiated between the drilling company and the OCD. The OCD then inspects for compliance. Because the WIPP repository is located in the potash enclave, recommended plugging procedures protect the potash horizon from foreign

fluids. Prior to 1988, specifications likely included sealing off any encountered brine reservoir in the Castile Formation with cement grout and capping the seal with a 60-m (200-ft) cement-grout plug. About 15 m (50 ft) of sand was usually emplaced above grout plugs. Weighted drilling fluid above the sand was usually emplaced to ~60 m (~200 ft) below the potash horizon, where another plug extended through the potash horizon. A second sand cap was emplaced, followed by weighted drilling mud to within ~60 m (~200 ft) of the top of the Salado Formation salt, where another plug of cement grout was emplaced, followed by sand and weighted mud. When the base of the casing was reached, the specifications either required grouting or filling with weighted mud to the surface, where a cap and abandonment marker were often placed (Lappin et al, 1989, Appendix C).

In April 1988, the OCD amended order R-111 and specified that the plug be a "solid cement plug through the salt section" (Salado Formation); the amendment was in response to conflicts between the potash and oil/gas industries (OCD, 1988, p. 10). The 1991 PA calculations assumed these latter plugging conditions.

Initial Plug Permeability. The initial plug permeabilities depend strongly on the host rock in which the plug is emplaced (e.g., clean vs. chemically altered steel casing or ahydrite vs. halite). Because most experimental studies of plug-borehole interactions extend for only hundreds of days or less, data are limited (Christensen and Petersen, 1981; Buck, 1985; Bush and Piele, 1986; Scheetz et al., 1986). Any PA calculations starting from initial conditions assume permeabilities of 10^{-15} m^2 (1 mD) for plugs in the Castile Formation and 10^{-18} m^2 (10^{-3} mD) in the Salado and Rustler Formations (Lappin et al., 1989, Table C-1).

Borehole Permeability and Porosity. Of primary concern to the PA calculations is the borehole permeability over most of the 10,000 yr. Three components of these calculations are (1) the length of time that the plug and casing remain intact, (2) the change in permeability of the deteriorating plugs with time, and (3) the ultimate deformation of the borehole.

Plug Life. Cementing companies suggest that the cement plugs should last for at least 100 yr, as would casing. PA calculations assume a life of 75 yr followed by 75 yr of degredation (Figure 4.2-2).

Degraded Plugs and Borehole Debris Permeability. PA calculations assume that the degrading concrete plugs and other debris initially present in the hole would have a permeability (Figure 4.2-3) and porosity (Figure 4.2-4) of silty sand (Freeze and Cherry, 1979), but with a bulk and average density equal to that of the Salado Formation (Table 4.2-1). The permeability and porosity were assumed to vary lognormally and normally, respectively, between the typical range for silty sand, typical of distributions of the parameters in the literature (Harr, 1987, Table 1.8.1).

Note that any drilling mud initially in the borehole or brine that drains into the borehole would have to be able to migrate through the degrading plugs before the borehole could be a viable conduit. In other words, if the fluid is trapped, the borehole is not a conduit.

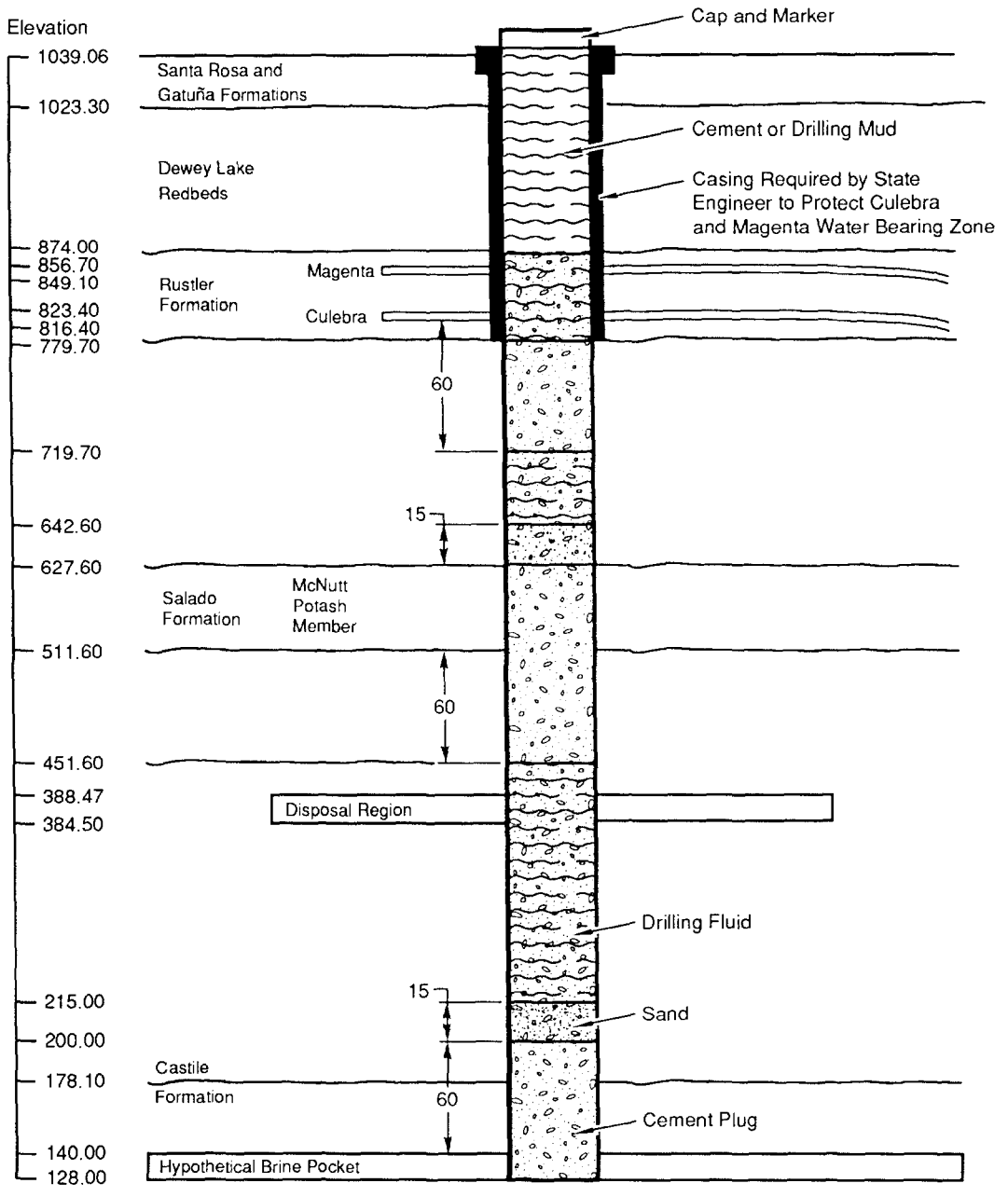

Contact Elevations (in Meters) are Taken from Borehole ERDA - 9, Typically Used in Modeling

Not to Scale

TRI-6330-69-1

Figure 4.2-1. Required Casing and Plugs. New Mexico State Engineer requires casing through Rustler Fm. when drilling exploratory boreholes; New Mexico Energy, Mineral, and Natural Resources Department currently requires solid cement plugs in Salado Fm. to protect potash horizon when abandoning a borehole.

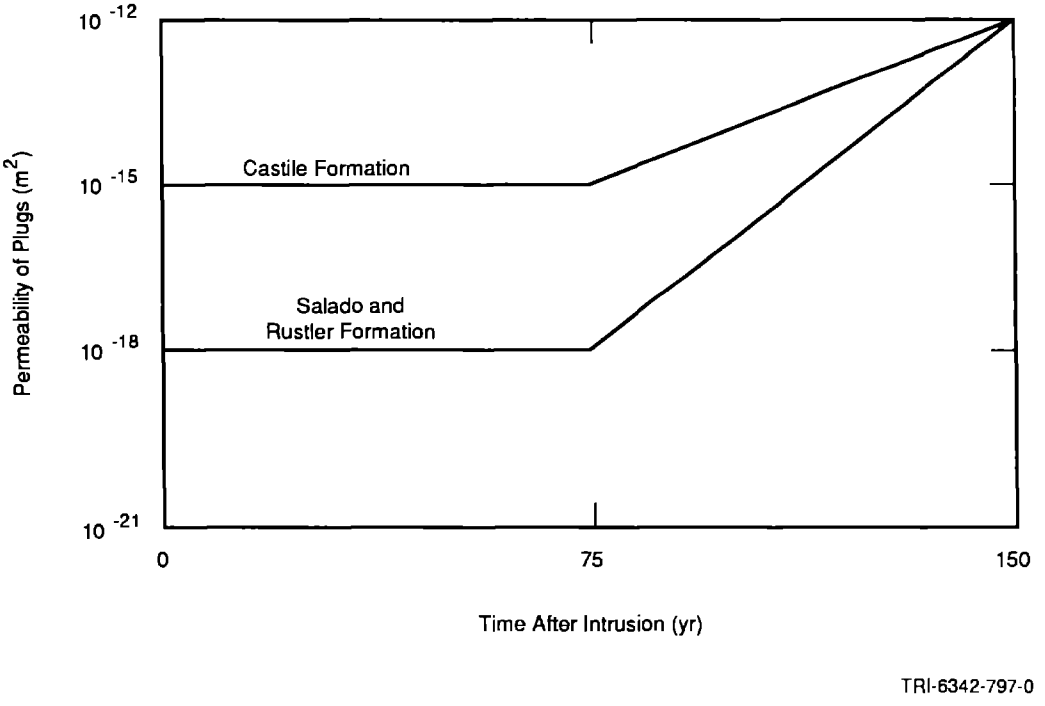

Figure 4.2-2. Increased Permeability of Cement Grout Plugs in Intrusion Borehole with Time because of Degradation.

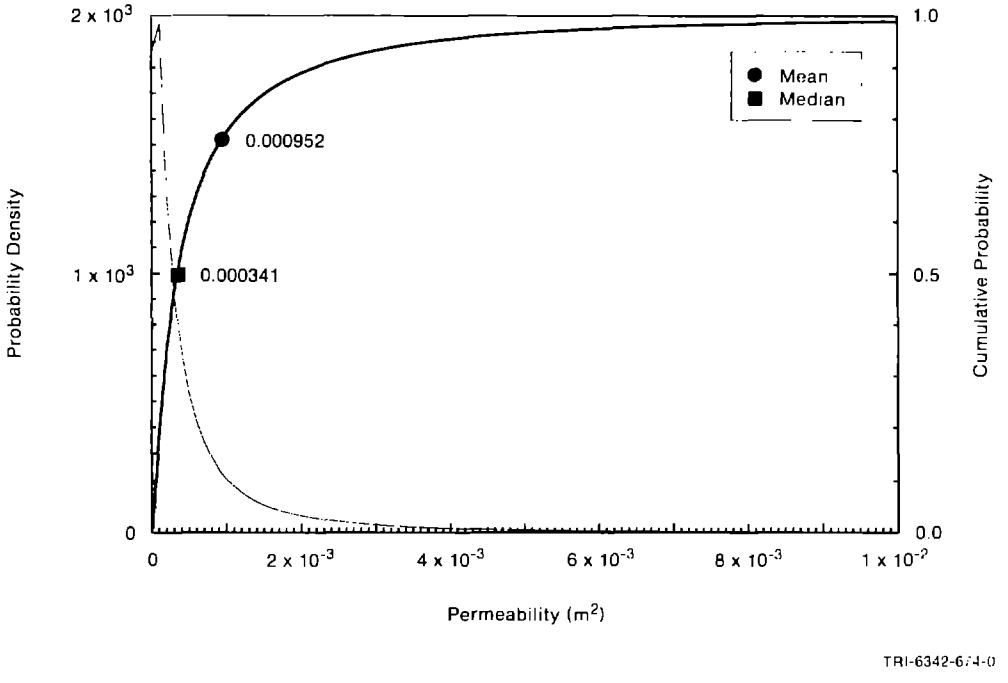

Figure 4.2-3. Lognormal Distribution (pdf and cdf) for Borehole Permeability after Degradation but before Creep Deformation.

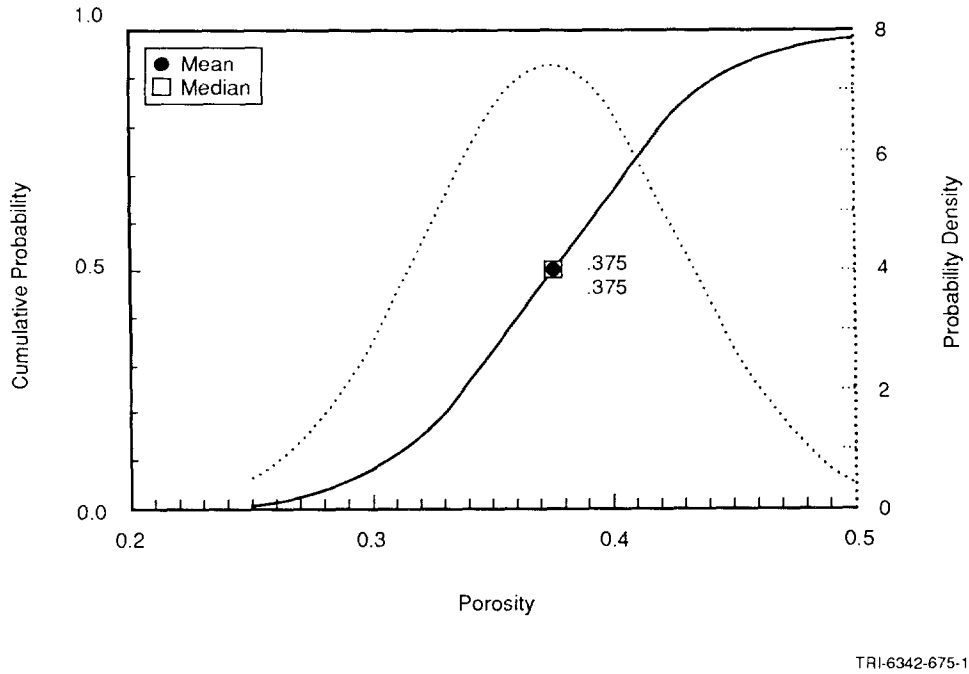

Figure 4.2-4. Normal Distribution (pdf and cdf) for Borehole Porosity after Degradation but before Creep Deformation.

Borehole Deformation. Because of the change in borehole abandonment procedures, the 1991 PA calculations did not assume any borehole deformation. This assumption contributed to a more conservative calculation.

With the previous order, salt "would normally settle into an open hole" and naturally seal the hole shut in the uncemented section of the borehole. Thus, with time, the borehole would attain very low permeabilities similar to the host salt. However, if the amended orders are followed and the borehole is filled, the use of a solid cement plug through the Salado Formation greatly decreases the likelihood that the borehole will be permanently sealed by salt creep over the long term (>100 yr).

The numerically predicted creep closure used in the 1990 PA calculations is shown in Figure 4.2-5 (Sjaardema and Krieg, 1987, Figure 4.6). Although a homogenous transient creep model may not completely predict borehole closure -- because local variations such as anhydrite layers and clay lenses play an important role in the ultimate deformation -- the homogenous model of creep will err on the conservative side, predicting much slower creep closure than actually occurs (Munson et al., 1988; 1989; 1990c). On the other hand, Figure 4.2-5 assumes no fluid is in the hole. The presence of hydrostatic pressure will greatly decrease the closure rate.

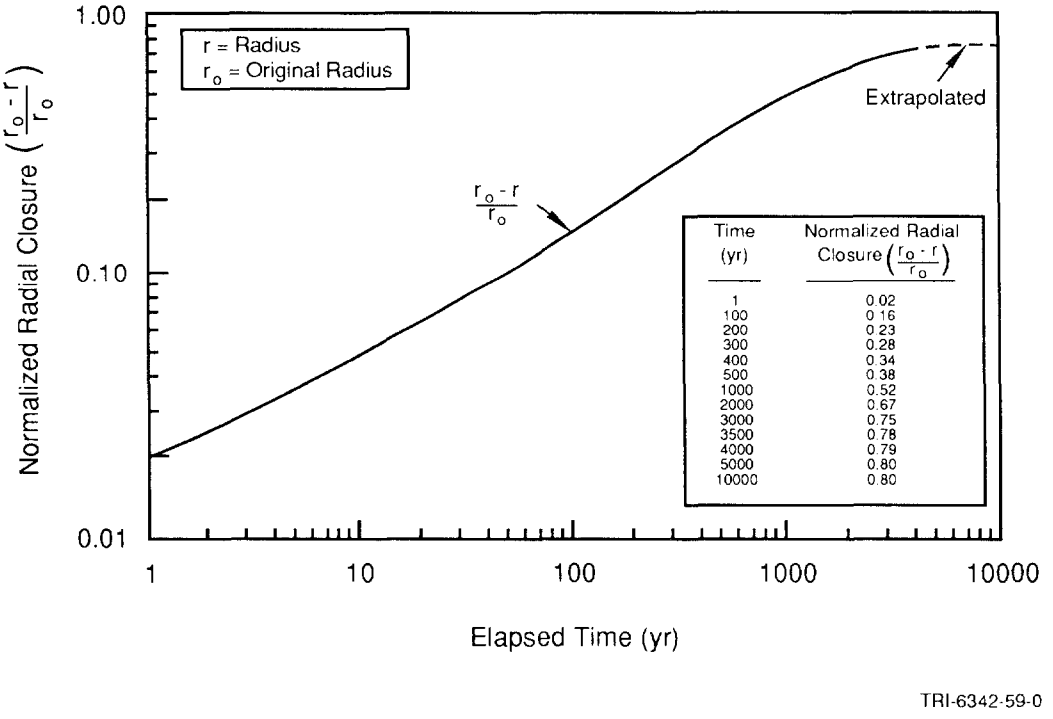

Figure 4.2-5. Normalized Closure for Shaft (Sjaardema and Krieg, 1987, Figure 4.6).

4.2.2 Drilling Characteristics

Diameter of Intrusion Drill Bit (Deep Hydrocarbon Target)

Parameter:	**Intrusion drill bit diameter** (d)
Median:	3.55×10^{-1}
Range:	2.67×10^{-1}
	4.44×10^{-1}
Units:	m
Distribution:	Uniform
Source(s):	See text.

Historical Drill Bit Diameter

Parameter:	**Historical drill bit diameters** (d)
Median:	2×10^{-1}
Range:	1.21×10^{-1}
	4.45×10^{-1}
Units:	m
Distribution:	Delta
Source(s):	Brinster, K. 1990c. "Well data from electric logs," Memo 10 in Appendix A of Rechard et al. 1990. *Data Used in Preliminary Performance Assessment of the Waste Isolation Pilot Plant (1990).* SAND89-2408. Albuquerque, NM: Sandia National Laboratories.

Figure 4.2-6 shows the uniform distribution for the diameter of the intrusion drill bit.

Figure 4.2-7 shows the distribution of drill bits used in the past.

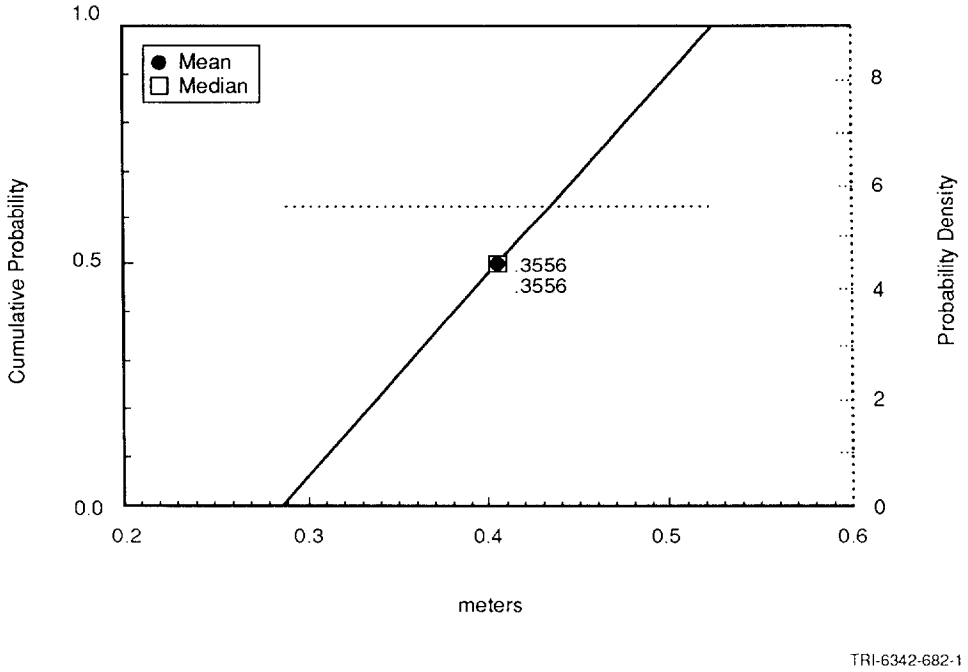

Figure 4.2-6. Estimated Probability of Drilling an Intrusion Borehole with a Specific Diameter.

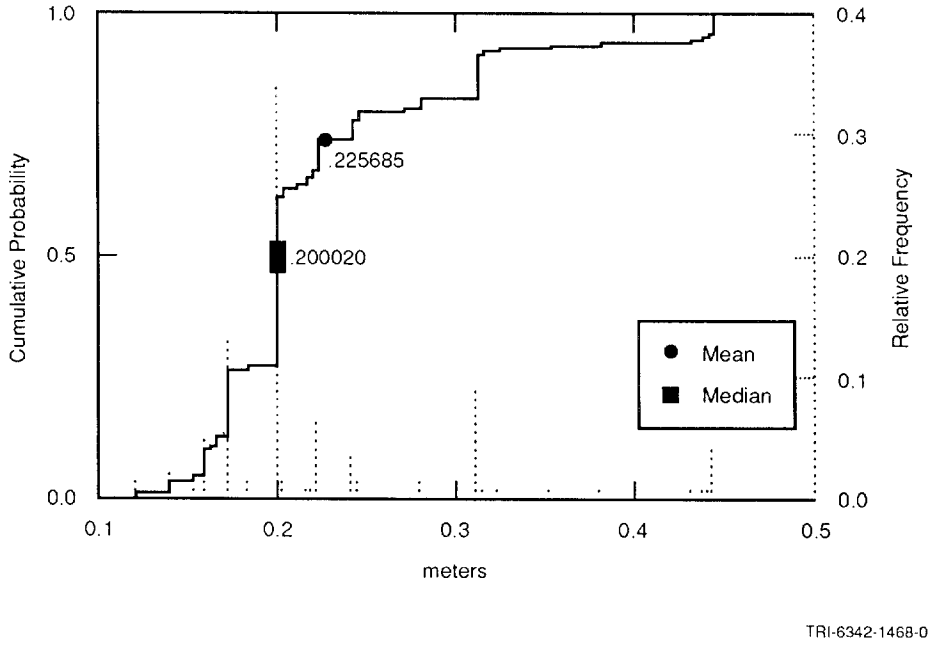

Figure 4.2-7. Distribution of Historical Drill Bit Diameter.

Discussion:

The guidance for the EPA Standard, *40 CFR 191*, (Appendix B) states that the EPA

> "...believes that the most productive consideration of inadvertent intrusion concerns those realistic possibilities that may be usefully mitigated by repository design, site selection, or use of passive controls (although passive institutional controls should not be assumed to completely rule out the possibility of intrusion). Therefore, inadvertent and intermittent intrusion by exploratory drilling for resources (other than any provided by the disposal system itself) can be the most severe intrusion scenario assumed..."

The future histories (scenarios) that must be considered are not necessarily exhaustive, but rather those that if examined might differentiate between repository sites or perhaps identify ways to improve repository design.

Consequently, the PA Division of the WIPP assumes that current standard drilling procedures for gas and oil exploration will continue into the future, and that future drillers will observe regulations similar to those currently imposed by federal and state agencies to protect resources.

Drilling for oil and gas has two main objectives: to drill the hole to the production zone as quickly and economically as safely possible, and to install casing from the reservoir to the surface for well production. The procedures used to accomplish these objectives are fairly well standardized in the drilling industry.

Currently when a company drills an exploratory oil or gas well, the operation uses a standard rotary drill rig with a mud circulation system. The differences between drilling for oil and gas depend on the depth of the well, which controls the size of casing used. Figures 4.2-6 and 4.2-7 show the distribution used in the past in the Delaware Basin for oil and gas exploration. The data are reported as a discrete distribution because bit diameters cannot vary continuously between 0.1206 m and 0.4445 m diameter (4-3/4 in. and 17-1/2 in.), but must be the diameter of a bit that was actually used (Brinster, 1990c). The median bit diameter is 0.2000 m (7-7/8 in. diameter) (Figures 4.2-6 and 4.2-7).

Currently, the normal depth for an oil well in the Delaware Basin near the WIPP site ranges from 1,200 to 1,800 m (4,000 to 6,000 ft), but gas-well depths usually exceed 3,000 m (10,000 ft). Consequently, oil wells normally have a standard 0.413-m (16 1/4-in.) drilled hole to the top of salt to accommodate 0.340-m (13 3/8-in.) steel casing, and gas wells normally have a standard 0.4445-m (17 1/2-in.) drilled hole to accommodate 0.356-m (14-in.) casing. After casing is set with grout, the company drills either a standard 0.311-m (12 1/4-in.) hole, if the target is oil, or a 0.356-m (14-in.) hole, if the target is gas (Table 4.2-2). Rather than sample from the historical diameters for evaluating the borehole as was done in the 1990 PA calculations, the 1991 PA calculations sample from a perturbation about the currently used diameter for deep gas wells (i.e., 0.356 m $\pm$ 0.0889 [14 in. $\pm$ 3.5]). This practice ensures that fairly large borehole diameters are used and thus is more conservative than the 1990 calculations.

From the bit diameter, the drilled diameter through the waste is predicted based on strength properties of the waste (e.g., shear strength) and angular velocity of the drillstring, viscosity of the drilling fluid, fluid density, and annular uphole fluid velocity (Rechard et al., 1989) (Figure 4.2-8). Shear strength and surface roughness of the waste also influence the drilled area and are discussed with waste properties.

Table 4.2-2. Specifications for Gas and Oil Exploratory Boreholes

Parameter	Value	Units
Drilled diameter		
In Rustler Formation (oil well)	0.413	m
(gas well)	0.444	m
In Salado and Castile Formations, (oil well)	0.311	m
(gas well)	0.356	m

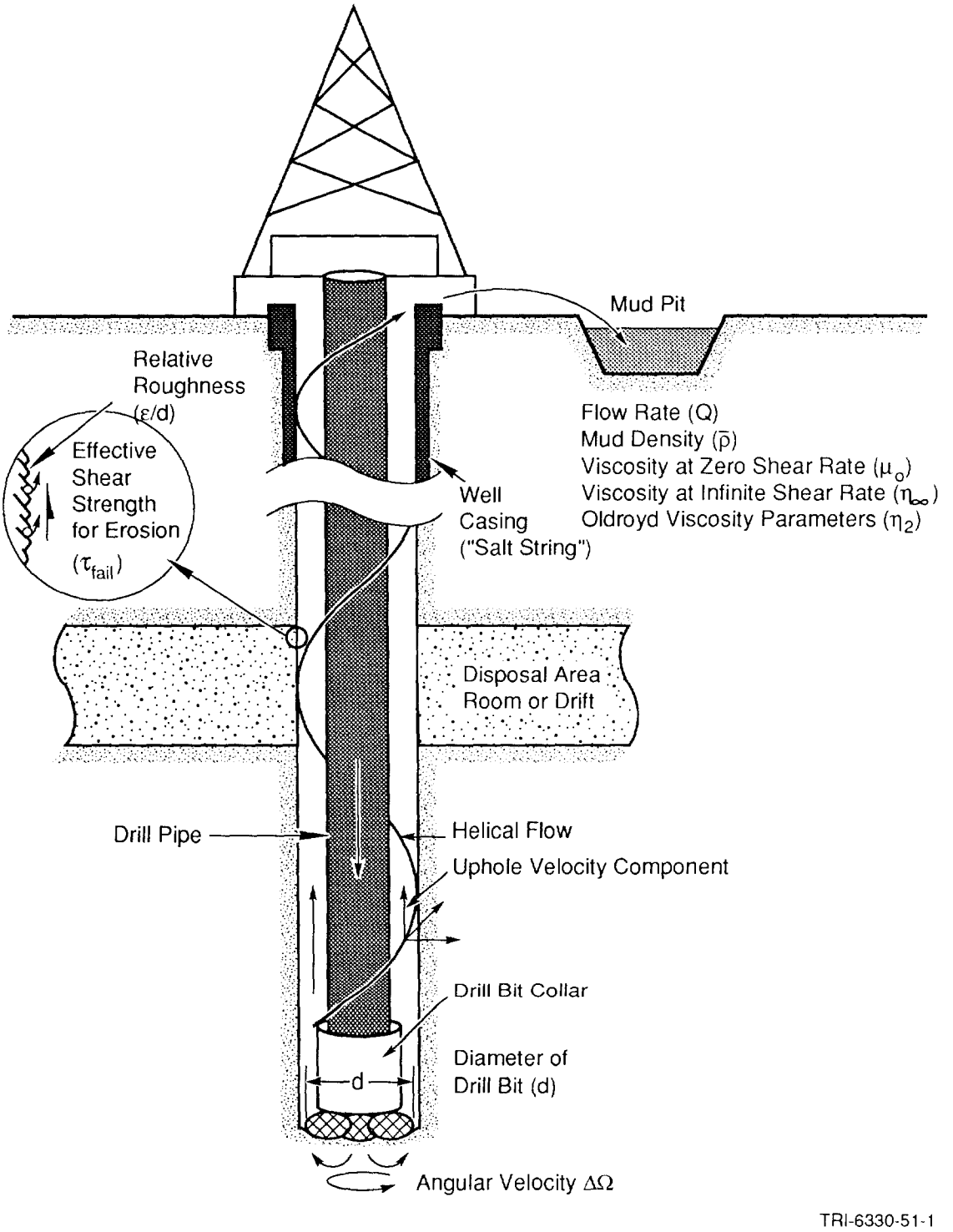

Figure 4.2-8. Definition of Parameters Describing Human Intrusion by Drilling.

Drill String Angular Velocity

Parameter:	**Drill string angular velocity ($\dot{\theta}$)**
Median:	7.7
Range:	4.2
	2.3×10^1
Units:	rad/s
Distribution:	Cumulative
Source(s):	Pace, R. O. 1990. Manager, Technology Exchange Technical Services, Baroid Drillng Fluids, Inc., 3000 N. Sam Houston Pkwy. E., Houston, TX. (Expert Opinion). Letter of 18 September 1990. Letter 1b in Appendix A of Rechard et al. 1990. *Data Used in Preliminary Performance Assessment of the Waste Isolation Pilot Plant (1990)*. SAND89-2408. Albuquerque, NM: Sandia National Laboratories.
	Austin, E. H. 1983. *Drilling Engineering Handbook*. Boston, MA: International Human Resources Development Corporation.

Figure 4.2-9 shows the distribution of the drill string angular velocity.

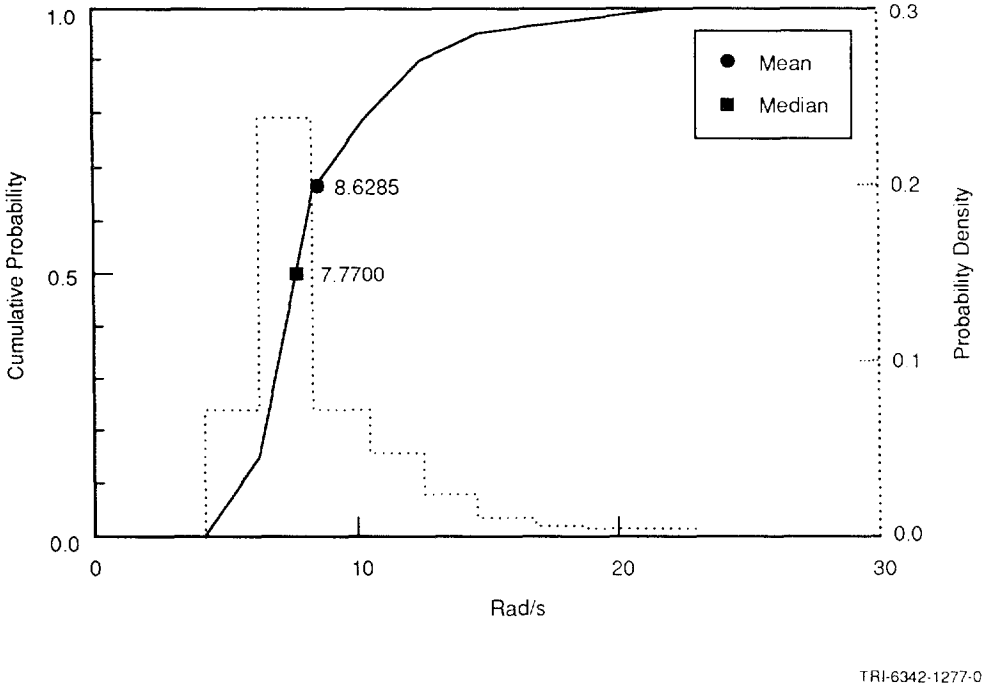

Figure 4.2-9. Distribution (pdf and cdf) of Drill String Angular Velocity.

Discussion:

For drilling through salt, the drill string angular velocity ($\dot{\theta}$) can vary between 4.18 and 23 rad/s (40 and 220 rpm) (Austin, 1983, Figure 4.5), with a median speed of about 7.75 rad/s (75 rpm) (Pace, 1990).

Mud Flowrate

Parameter:	**Drilling mud flowrate (Q_f)**
Median:	9.925×10^{-2}
Range:	7.45×10^{-2}
	1.24×10^{-1}
Units:	$m^3/(s \cdot m)$
Distribution:	Uniform
Source(s):	Austin, E. H. 1983. *Drilling Engineering Handbook.* Boston, MA: International Human Resources Development Corporation.

Discussion:

Flowrates of the drilling fluid usually vary between 7.45×10^{-2} and 1.24×10^{-1} $m^3/(s \cdot m)$ of drill diameter (30 and 50 gal/min/in.) (Austin, 1983, Table 1.15). PA calculations assumed that the annulus between the drill collar and borehole was initially about 2.5 cm (1 in.). Thus, for the minimum and maximum diameters typically used in the drilling near the WIPP, the uphole velocity varies between 0.99 and 1.73 m/s (3.2 and 5.7 ft/s).

4.3 Parameters for Castile Formation Brine Reservoir

Pressurized brine in the northern Delaware Basin has been encountered in fractured anhydrites of the Castile Formation in boreholes both north and northeast of the WIPP over the past 50 yr. In addition, Castile brines were encountered southwest of the WIPP at the Belco Well, about 6.5 km (4 mi) from the center of the WIPP. During WIPP site characterization, Castile Formation brine reservoirs were encountered in the WIPP-12 borehole, about 1.6 km (1 mi) north of the center of the WIPP, and the ERDA-6 borehole, about 8 km (5 mi) northeast of the center of the WIPP (Figure 4.3-1).

Also, a geophysical study that correlated with the known occurrence of brine at WIPP-12 indicated the presence of brine fluid within the Castile Formation under the WIPP (Earth Technology Corp., 1988). Based on borehole experience and the geophysical study, the PA calculations assume that a brine reservoir exists underneath at least a portion of the disposal region. The assumed presence of a Castile brine reservoir beneath the repository is of concern only in the event of human intrusion. (The area and thus the probability of hitting a brine reservoir and the disposal area are discussed in Chapter 5.)

Table 4.3-1 provides the parameter values for the Castile Formation Brine Reservoir.

Table 4.3-1. Parameter Values for Castile Formation Brine Reservoir

Parameter	Median	Range		Units	Distribution Type	Source
Elevation, top	1.4×10^{2}	-2.00×10^{2}	1.78×10^{2}	m	Cumulative	See text.
Density, grain (ρ_g)	2.963×10^{3}			kg/m^3	Constant	See anhydrite, Section 24.
Analytic Model						
Pressure, initial (p_i)	1.26×10^{7}	1.1×10^{7}	2.1×10^{7}	Pa	Cumulative	$\rho_f g \Delta z$, $\rho_b g \Delta z$; Lappin et al.,1989, Table 3-19; Popielak et al.,1983, p. H-52
Storativity, bulk $\hat{S}_b$	2×10^{-1}	2×10^{-2}	2×10^{1}	m^3/Pa	Loguniform	See text.
Numerical Model						
Permeability						
Intact matrix	1×10^{-19}	1×10^{-20}	1×10^{-18}	m^2	Cumulative	See Table 2.4-1.
Fractured matrix	1×10^{-13}	1×10^{-16}	1×10^{-10}	m^2	Cumulative	Freeze and Cherry, 1979; Reeves et al., 1991.
Porosity	5×10^{-3}	1×10^{-3}	1×10^{-2}	none	Cumulative	Reeves et al., 1991.
Radius, equivalent	2.32×10^{2}	3×10^{1}	8.6×10^{3}	m	Cumulative	Reeves et al., 1991.
Thickness	1.2×10^{1}	7	6.1×10^{1}	m	Constant	Reeves et al., 1991.

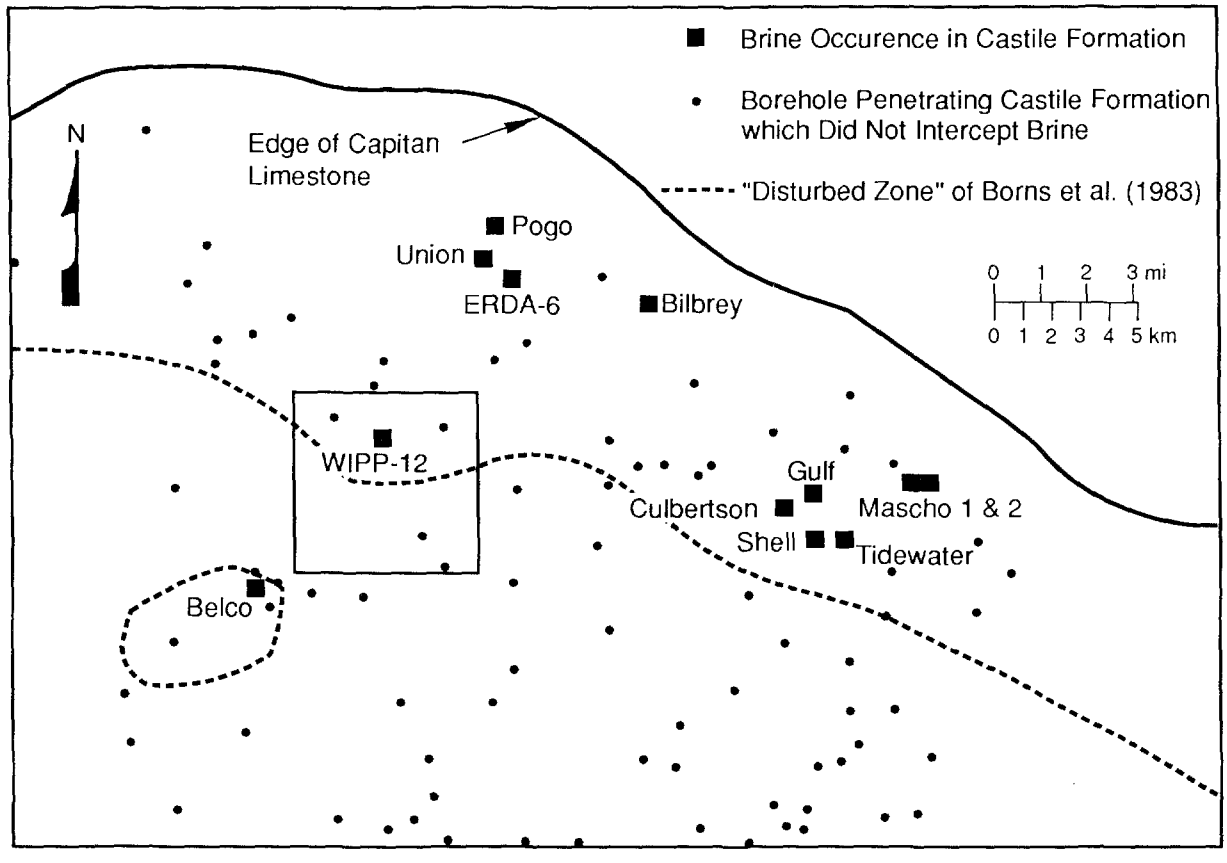

Figure 4.3-1. Deep Boreholes that Encountered Brine Reservoirs within the Castile Formation, Northern Delaware Basin (Lappin et al., 1989, Figure 3-26).

4.3.1 Analytic Brine Reservoir Model

Elevation of Top

Parameter:	**Elevation of top**
Median:	1.4×10^2
Range:	-2.0×10^2
	1.78×10^2
Units:	m
Distribution:	Cumulative
Source(s):	See Figure 2.2-1.
	Lappin, A. R., R. L. Hunter, D. P. Garber, and P. B. Davies, eds. 1989. *Systems Analysis Long-Term Radionuclide Transport, and Dose Assessments, Waste Isolation Pilot Plant (WIPP), Southeastern New Mexico: March 1989.* SAND89-0462. Albuquerque, NM: Sandia National Laboratories. (Table 3-19)

Discussion:

As discussed in Section 5.1.1, the elevation of the brine reservoir is directly tied to the areal extent. The elevation of the brine reservoir potentially varies between -200 and 178 m (-656 and 584 ft), the estimated bottom and measured top elevation, respectively, of the Castile Formation in ERDA-9. The elevation of the top of the WIPP-12 brine reservoir (140 m [457.8 ft]) was chosen as the median. For 1991 PA calculations, the hypothetical brine reservoir elevation was fixed at the median, while the areal extent was allowed to vary, independently.

Figure 4.3-2 shows the estimated distribution for elevation.

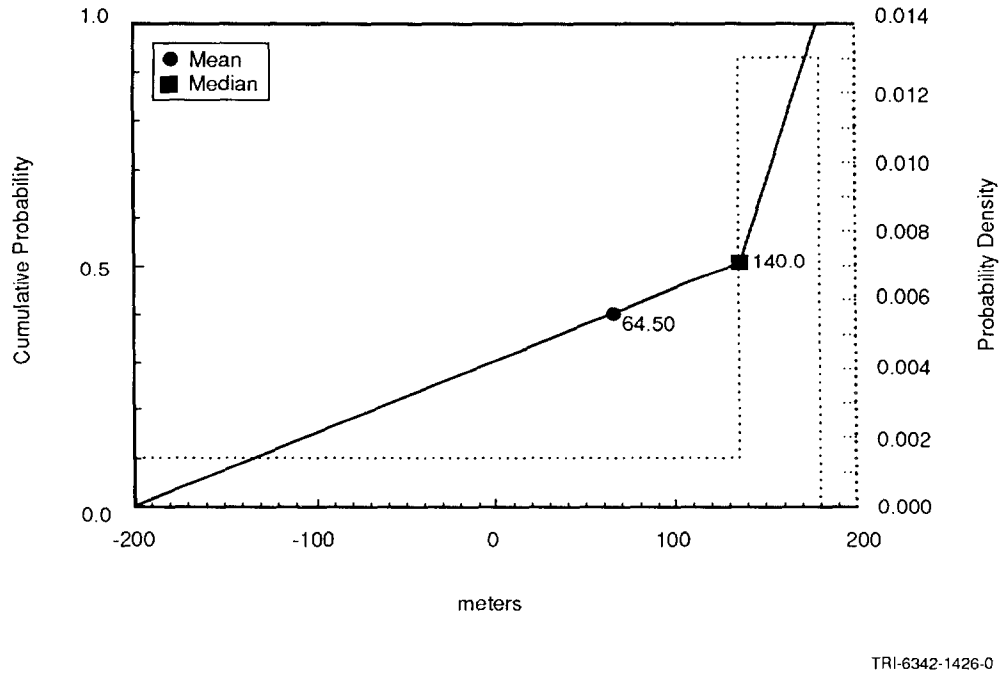

Figure 4.3-2. Estimated Distribution (pdf and cdf) for Elevation of Castile Formation Brine Reservoir.

Brine Pressure

Parameter:	**Pressure, initial** (p_i)
Median:	1.26×10^7
Range:	1.1×10^7
	2.1×10^7
Units:	Pa
Distribution:	Cumulative
Source(s):	Popielak, R. S., R. L. Beauheim, S. R. Black, W. E. Coons, C. T. Ellingson, and R. L. Olsen. 1983. *Brine Reservoirs in the Castile Fm., Waste Isolation Pilot Plant (WIPP) Project, Southeastern New Mexico.* TME-3153. Carlsbad, NM: U.S. Department of Energy.
	Lappin, A. R., R. L. Hunter, D. P. Garber, and P. B. Davies, eds. 1989. *Systems Analysis Long-Term Radionuclide Transport, and Dose Assessments, Waste Isolation Pilot Plant (WIPP), Southeastern New Mexico; March 1989.* SAND89-0462. Albuquerque, NM: Sandia National Laboratories. (Table 3-19)

Figure 4.3-3 shows the estimated distribution for initial brine reservoir pressure.

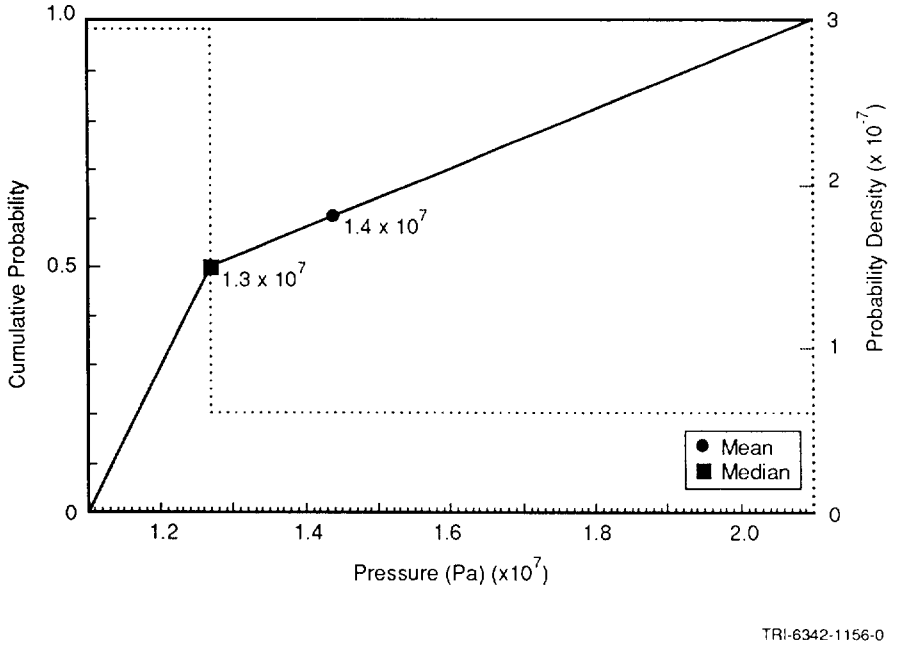

Figure 4.3-3. Estimated Distribution (pdf and cdf) for Castile Brine Reservoir Initial Pressure.

Discussion:

Median. The measured initial pressure of 12.6 MPa (125 atm) for WIPP-12 (Popielak, 1983, p. H-52) was used as the median brine reservoir initial pressure.

Range. Lappin et al. (Table 3-19, 1989, derived from Popielak et al., 1983, Table H.1) estimated the initial brine reservoir pressure from several wellhead measurements at WIPP-12 and other boreholes that encountered pressurized Castile brine. The range was between 7.0 and 17.4 MPa (69 and 172 atm). Because the range of pressures includes measurements in wells completed at various elevations, a correction for differences in elevation is required.

The origin of Castile brine reservoirs is not conclusively known. Present interpretations are that their origin is either local, by limited movement of intergranular brines from adjacent Castile halites, or regional, by the previous existence of a lateral hydraulic connection of the Castile Formation with the Capitan reef (Lappin et al., 1989). However, the initial pressure observations at other wells are only directly pertinent if (1) the reservoir fluids are from the same source (past interconnection of reservoir fluid) or (2) they had a common genesis (e.g., brine trapped along bedding planes in areas of high permeability).

For the first case (interconnection), an elevation correction assuming a hydrostatic variation with depth is most appropriate. For the second case (common genesis), an elevation correction assuming a lithostatic variation depth is most appropriate. The range using both types of elevation corrections is 10.7 to 16.8 MPa (106 to 166 atm) (Table 4.3-2). A brine density of 1,215 kg/m^3 (75.85 lb/ft^3) (Section 4.1) was assumed for the first case; an average formation density of 2,400 kg/m^3 (149.8 lb/ft^3) was assumed for the second case. Elevations (except WIPP-12 and ERDA-6) were estimated from the well location and a topographic map of the area (USGS 15 min quads, Carlsbad, NM, 1971, Nash Draw, NM, 1965).

This calculated range is similar to the maximum and minimum possible range of 11 and 21 MPa assuming hydrostatic and lithostatic pressures at the elevation of the WIPP-12 brine reservoir (140 m [457.8 ft]) (see Figure 2.2-3) and consequently this latter range was used in the PA calculations.

Table 4.3-2. Estimated Initial Pressures of Brine Reservoirs Encountered in the Region around the WIPP Corrected to the Depth at the WIPP-12 Brine Reservoir (after Popielak et al., 1983)

Well Name	Pressure with Hydrostatic Correction (MPa)	Pressure with Lithostatic Correction (MPa)	Reported Pressure at Observation (MPa)	Elevation of Observation (m)	Depth to Observation (m)	Surface Elevation* (m)
WIPP-12	12.7	12.7	12.7	140	918	1058
ERDA-6	15.5	16.8	14.1	253	826	1079
Belco	14.5	14.6	14.3	152	854	1006
Gulf	12.1	10.7	13.6	16	1097	1113
Pogo	>16.6	>15.8	>17.4	69	1013	1082
Tidewater	>14.0	>12.2	>16.0	-24	1137	1113
Union	>11.2	>12.2	>10.1	226	856	1082
H&W Danford 1	11.5	15.8	7.0	512	588	1100(?)
**Bilbrey	12.1	13.8	11.2	209	942	1151
**Culbreston	11.8	10.9	12.8	57	1071	1128
**Mascho 1	11.6	10.8	12.4	69	1013	1082
**Mascho 2	11.3	10.6	12.0	77	1005	1082
**Shell	11.8	10.4	13.4	9	1119	1128

* Elevation from well location and USGS 15 min quad topographic map, Carlsbad, NM, 1971, Nash

** According to Popielak et al. (1983, Table H.1), these wells should not be used to estimate static pressure.

Bulk Storativity

Parameter:	**Bulk storativity (S_b)**
Median:	2×10^{-1}
Range:	2×10^{-2}
	2
Units:	m^3/Pa
Distribution:	Lognormal
Source(s):	See text.
	Popielak, R. S., R. L. Beauheim, S. R. Black, W. E. Coons, C. T. Ellingson, and R. L. Olsen. 1983. *Brine Reservoirs in the Castile Formation, Southeastern New Mexico, Waste Isolation Pilot Plant (WIPP) Project.* TME-3153. Carlsbad, NM: U.S. Department of Energy.

Figure 4.3-4 shows the estimated distribution for bulk storativity.

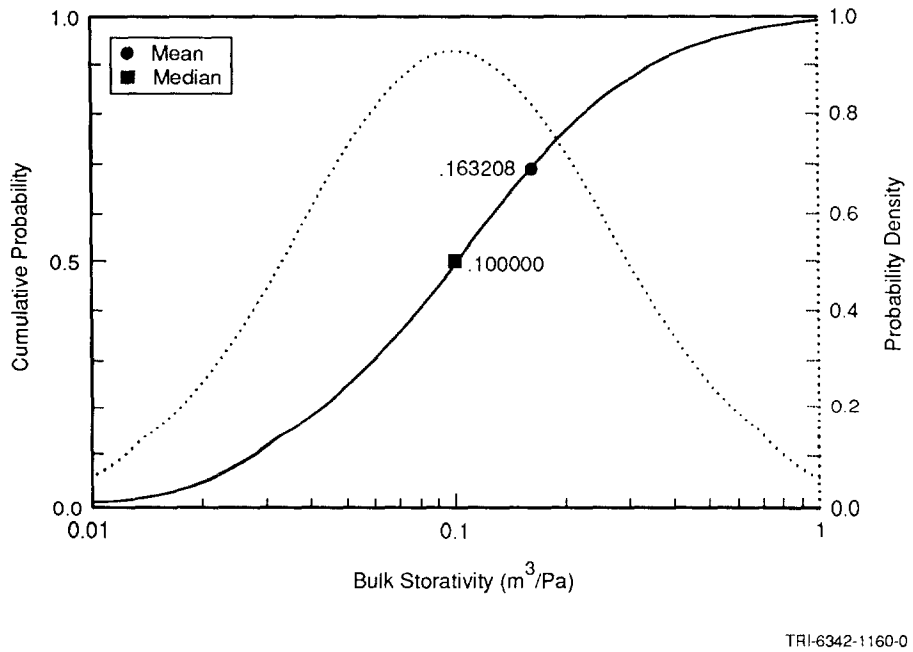

Figure 4.3-4. Estimated Distribution (pdf and cdf) for Bulk Storativity of Castile Brine Reservoir.

Discussion:

Bulk storativity (S_b) as defined herein is the total volume of fluid discharged from the reservoir per unit decrease in reservoir pressure ($\Delta V/\Delta p$). The bulk storativity can be estimated from wellhead measurements (long-term change in pressure and total discharge volume), or from the compressibility of the reservoir matrix and fluid and the total volume and porosity of the reservoir.

The pressure recovery of the WIPP-12 reservoir is characteristic of a dual-porosity medium. An initial rapid response is attributed to a highly permeable fracture set, while a more gradual component of recovery is due to repressurization of the higher permeability fracture set by intersecting lower permeability fractures. Because the human-intrusion scenarios contemplate that the Castile will be connected to the Culebra over the long term (compared to the duration of well tests), estimates of bulk storativity from long-term pressure changes are more appropriate than those made using short-term pressure changes, which may represent only the storativity of the highest permeability fractures. Estimates of bulk storativity using wellhead measurements range from 5 x 10^{-4} m^3/Pa (from ERDA-6 testing through October, 1982) to 2 x 10^{-1} m^3/Pa (from estimated total discharge volume, maximum estimated formation pressure, and apparent long-term recovery pressure at WIPP-12). Because WIPP-12 is closer to the waste disposal areathan ERDA-6, the latter number is considered more appropriate for a sub-repository reservoir.

Reservoir compressibility ($\beta_{s/\phi}$) and total volume (V_{tot}) may also be used to estimate bulk storativity:

$$S_b = \frac{\Delta V}{\Delta p} = V_{tot} \frac{1}{V_{tot}} \frac{\Delta V}{\Delta p} = V_{tot} \frac{1}{K} = V_{tot} \beta_s \qquad (4.3\text{-}1)$$

The area of the anticline associated with the WIPP-12 reservoir is approximately 1.7 x 10^6 m^2 (Popielak et. al., 1982 p. H-53). Popielak depicts brine occurrence in the lower 40% of the 100-m thickness of Anhydrite III-IV at WIPP-12 (Popielak et al., 1983, Figure G-2), giving a rough estimate of the reservoir total volume of 6.5 x 10^7 m^3. (Note that other published estimates of reservoir volume [e.g., Lappin et al., 1989, p. E-32] were made from wellhead measurements assuming some value of compressibility. These volume estimates will therefore not lead to independent estimates of S_b). Estimates of the bulk modulus $K_{bulk} = E/3(1-2\nu)$ (where E is Young's modulus and ν is Poisson's ratio) of Anhydrite III at WIPP-12 were used by Popielak et al. (1983, p. G-34) to derive a range of β_s from 3 x 10^{-11} Pa^{-1} to 1.4 x 10^{-10} Pa^{-1}. The resulting range in bulk storativity from Eq. 4.3-1 is 2 x 10^{-3} to 9 x 10^{-3} m^3/Pa. The reason this range does not include the wellhead estimate from WIPP-12 may be due to errors in the estimate of bulk volume or compressibility. For example, the apparent β_s may be larger than estimated here because of fractures in the anhydrite or trapped gas in the reservoir. However, at present there is no reason to suppose that bulk storativity is substantially higher than estimated from WIPP-12 wellhead measurements.

Based on the above considerations, the bulk storativity is assumed to lie between 2 x 10^{-2} and 2 x 10 m^3/Pa. The likelihood of the actual value falling in a given interval is described by a loguniform distribution between these limits. The median of this distribution is 0.2 m^3/Pa.

The high effective transmissivity of the Castile brine reservoir inferred from flow tests at the WIPP-12 borehole (Lappin et al., 1989; Popielak et al., 1983) implies that, in the event of its connection to the Culebra Dolomite through a sand-filled borehole, fluid flow rates from the brine reservoir will be controlled by the conductivity of the borehole fill and the area of the borehole (Rechard et al., 1990b, Figure 4-14; Reeves et al., 1991); pressure gradients within the brine reservoir will be small compared to gradients along the intrusion borehole. Observed correlation between brine occurrence and anticlines in the Castile (Lappin, 1988), and the larger differences in pressure among brine reservoirs at various locations, imply that Castile brine reservoirs have finite extent and are effectively isolated from one another over the long term. These observations suggest that in the context of discharge through an intrusion borehole(s) during the regulatory lifetime of the repository, Castile brine reservoirs would behave as finite reservoirs with effectively infinite conductivity. The reservoir state at any time could therefore be characterized by a single pressure.

Assuming constant compressibility of the brine reservoir components (fluid, matrix, and gas), the pressure in the brine reservoir will vary linearly with the volume of brine removed as follows: $dp/dV = 1/S_b$ where dp is the change in brine reservoir pressure, dV is the change in brine volume in the brine reservoir, and S_b is the bulk storage coefficient for the whole brine reservoir.

Therefore, the essential characteristics of the brine reservoir are contained in two parameters (Figure 4.3-5): the initial pressure of the brine reservoir, p_i, and bulk storativity, S_b.

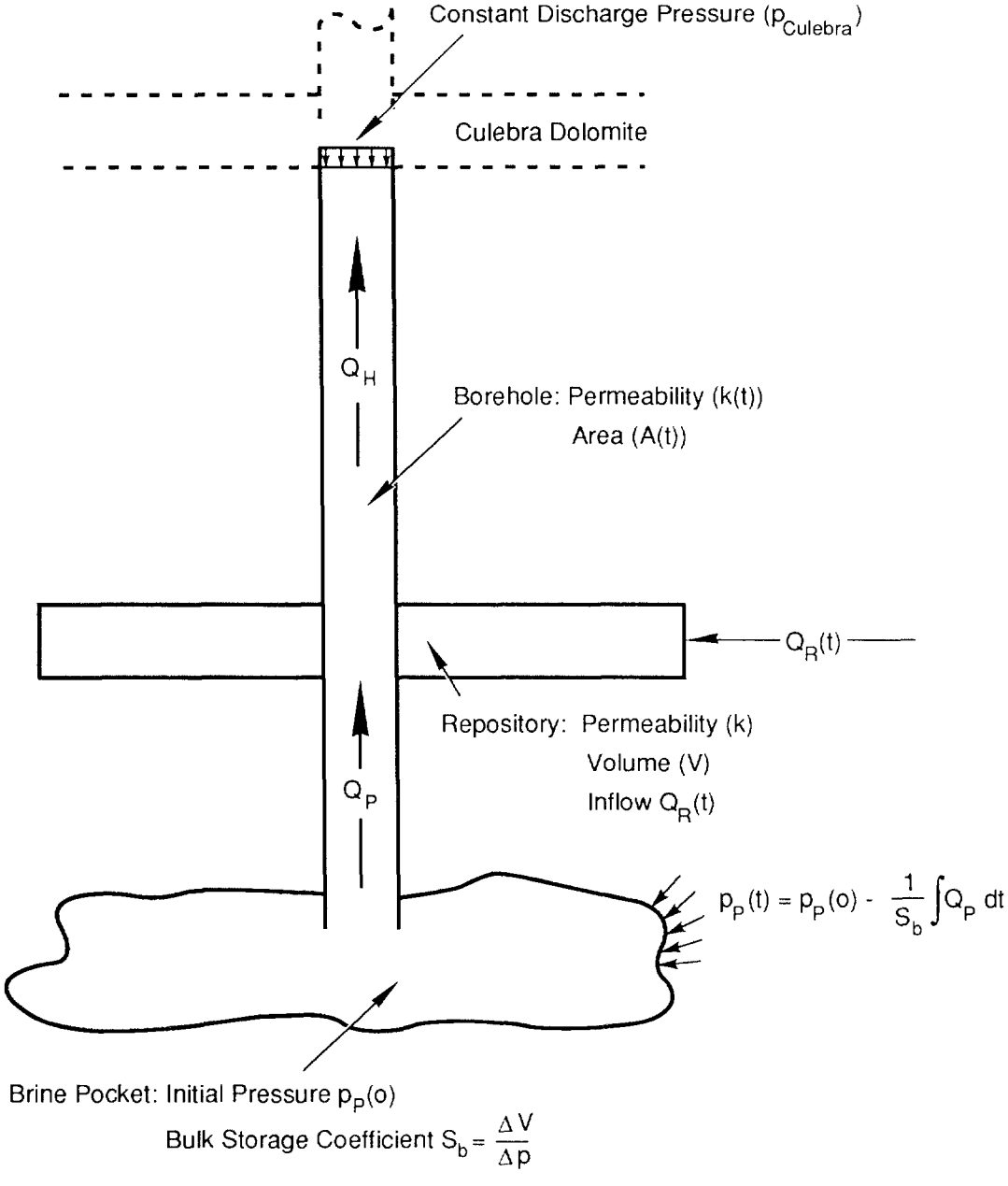

Figure 4.3-5. Conceptual Model of Castile Brine Reservoir, Repository, and Borehole Requires a Specified Initial Brine Reservoir Pressure and a Bulk Storage Coefficient (Change in Discharge Volume with Change in Brine Reservoir Pressure).

4.3.2 Numerical Brine Reservoir Model

Permeability, Intact Matrix

Parameter:	**Permeability, intact matrix**
Median:	1×10^{-19}
Range:	1×10^{-20}
	1×10^{-18}
Units:	m^2
Distribution:	Cumulative
Source(s):	See Table 2.4-1.

Permeability, Fractured Matrix

Parameter:	**Permeability, fractured matrix**
Median:	1×10^{-13}
Range:	1×10^{-16}
	1×10^{-10}
Units:	m^2
Distribution:	Cumulative
Source(s):	Freeze, R. A. and J. C. Cherry. 1979. *Groundwater.* Englewood Cliffs, NJ: Prentice-Hall, Inc. (Table 2.6)
	Reeves, M., G. Freeze, V. Kelley, J. Pickens, D. Upton, and P. Davies. 1991. *Regional Double-Porosity Solute Transport in the Culebra Dolomite under Brine-Reservoir-Breach Release Conditions: An Analysis of Parameter Sensitivity and Importance.* SAND89-7069. Albuquerque, NM: Sandia National Laboratories. (Table 2.1)

Discussion:

The mesh for the numerical model used two layers for the Castile Formation (see Figure 4.3-6). The upper layer and the lower layer beyond a radius of 2,320 m (7,586 ft) were intact Castile anhydrite matrix. The lower layer out to a radius of 2,320 m (7,586 ft) was the fractured brine reservoir. The permeability used for the reservoir was 1×10^{11} m^2. Test simulations using the median permeability of intact anhydrite, 1×10^{-19} m^2, and pressures in the brine reservoir within the range of sampled values (11 MPa to 21 MPa), showed that those pressures decayed relatively quickly by flow through the intact matrix (upper layer) and into the Salado Formation. It was apparent that, when using the reported median permeability of Castile anhydrite and assuming Darcy flow everywhere, one cannot maintain a pressurized brine reservoir in the Castile for more than a few hundred years. In order to

simulate a pressurized brine reservoir, it was necessary to isolate it completely from the Salado and from the far field by assigning a permeability of zero to the intact Castile matrix (upper Castile mesh layer and far field lower layer). When isolated in this manner, the numerical model of the Castile brine reservoir can simulate the behavior observed during well tests done by Popielak et al. (1983) with the properties described in this section and in Sections 4.3 and 4.3.2.

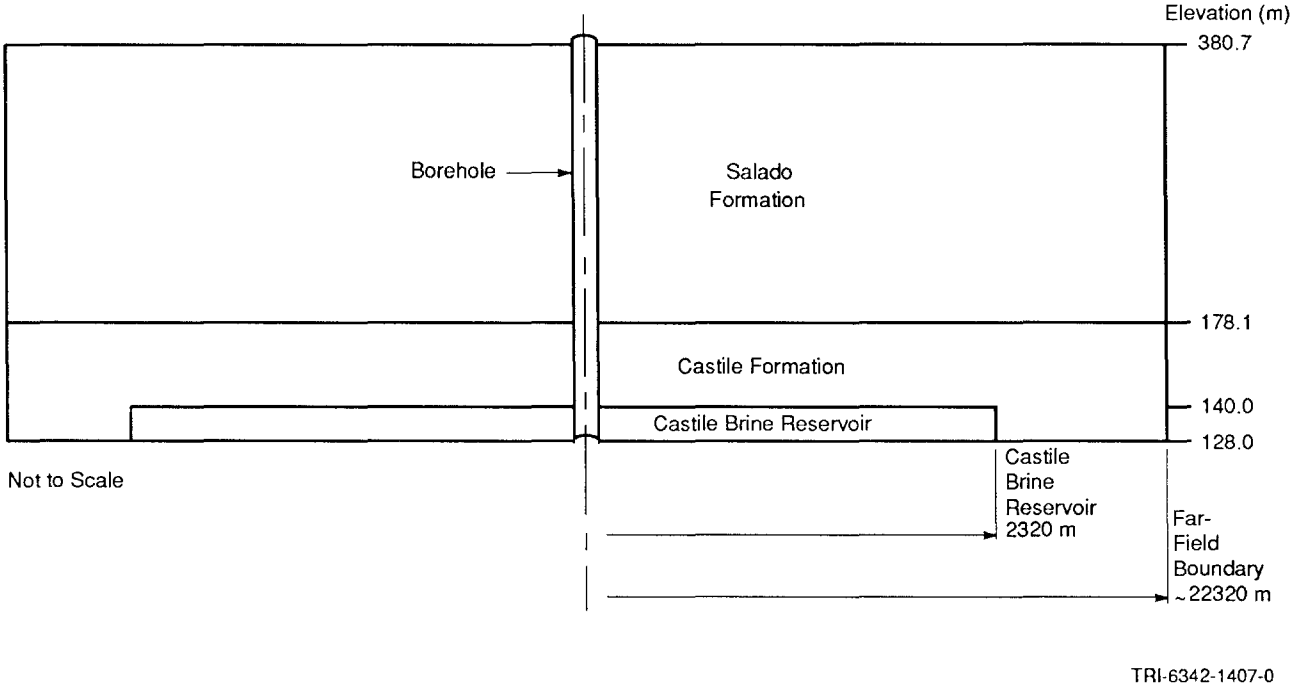

Figure 4.3-6. Numerical Model of Castile Brine Reservoir.

Porosity

Parameter:	**Porosity**
Median:	0.005
Range:	0.001
	0.01
Units:	Dimensionless
Distribution:	Cumulative
Source(s):	Reeves, M., G. Freeze, V. Kelly, J. Pickens, D. Upton, and P. Davies. 1991. *Regional Double-Porosity Solute Transport in the Culebra Dolomite under Brine-Reservoir-Breach Release Conditions: An Analysis of Parameter Sensitivity and Importance.* SAND89-7069. Albuquerque, NM: Sandia National Laboratories. (Table 2.1)

Discussion:

Bulk storativity was varied in the 1991 PA calculations. However, calculations done using the two-dimensional, two-phase porous flow model, BRAGFLO, require compressibilities of brine and rock, rather than bulk storativity to determine the storage capacity of a porous medium. A porosity, ϕ, of 0.005 was used for both the brine reservoir and the Castile Formation, and the brine compressibility, S_b, was 2.5 x 10^{-10} Pa^{-1} (Salado brine was used in the model, since brine density has to be constant in BRAGFLO; see Section 4.1.1). Brine reservoir matrix compressibility, β_s, was obtained from sampled values of bulk storativity, S_b, using the formula

$$\phi = S_b/V - \phi\beta$$

where V is the volume of the reservoir, $\pi r^2 L$. Dimensions of the reservoir (radius, r, and the thickness, L) are discussed below. The compressibility discussed here is defined by

$$\beta_s = \frac{1}{1-\phi}\frac{d\phi}{dp}$$

whereas BRAGFLO requires a compressibility, β_s', defined as

$$\beta_s' = \frac{1}{\phi}\frac{d(\phi)}{dp}$$

so one more step is needed to obtain β_s':

$$\beta_s' = \beta_s(1-\phi)/\phi$$

For the brine reservoir, the bulk storativity ranged from 0.02 to 2.0, resulting in matrix compressibility, β_s', ranging from 2.2×10^{-8} to 1.8×10^{-6} Pa^{-1}.

The value used in the two-phase flow model for the intact Castile matrix compressibility was 1.99×10^{-7} Pa^{-1}, although the zero permeability meant that this parameter was effectively unused.

Values of other material properties for the Castile Formation and the brine reservoir are discussed elsewhere in Sections 4.3 and 2.4 (Hydrologic Parameters for Anhydrite Layers within Salado Formation). Parameters used in the two-phase flow model for the intact Castile matrix include: residual brine saturation of 0.2; residual gas saturation of 0.2; Brooks-Corey relative permeability correlation exponent of 0.7; and threshold capillary pressure of 1.869 MPa. Because the permeability of the intact matrix was set to zero, none of these parameters has any effect; however, if nonzero permeabilities were used, these are the values that would be used. For the fractured brine reservoir, the following were used: residual brine and gas saturations of 0.2; Brooks-Corey exponent of 0.7; and a threshold capillary pressure of zero. Zero capillary pressure in the brine reservoir proved to be necessary for numerical stability; nonzero values caused excessively long run times, but otherwise had little effect on the results.

Radius and Thickness

Parameter:	**Radius**
Median:	2320
Range:	30
	8600
Units:	m
Distribution:	Cumulative
Source(s):	Reeves, M., G. Freeze, V. Kelly, J. Pickens, D. Upton, and P. Davies. 1991. *Regional Double-Porosity Solute Transport in the Culebra Dolomite under Brine-Reservoir-Breach Release Conditions: An Analysis of Parameter Sensitivity and Importance.* SAND89-7069. Albuquerque, NM: Sandia National Laboratories. (Table 2.1)

Parameter:	**Thickness**
Median:	12.0
Range:	7.0
	61
Units:	m
Distribution:	Constant
Source(s):	Reeves, M., G. Freeze, V. Kelly, J. Pickens, D. Upton, and P. Davies. 1991. *Regional Double-Porosity Solute Transport in the Culebra Dolomite under Brine-Reservoir-Breach Release Conditions: An Analysis of Parameter Sensitivity and Importance.* SAND89-7069. Albuquerque, NM: Sandia National Laboratories. (Table 2.1) Popielak, R. S., R. L. Beauheim, S. R. Black, W. E. Coons, C. T. Ellingson, and R. L. Olsen. 1983. *Brine Reservoirs in the Castile Formation, Southeastern New Mexico, Waste Isolation Pilot Plant (WIPP) Project.* TME-3153. Carlsbad, NM: U.S. Department of Energy. (p. H-55)

Discussion:

The size of the brine reservoir was based on several factors, including the bulk storativity (which was varied in the 1991 PA calculations), earlier estimates of the extent of the reservoir (specifically, the radius of the "outer ring" of the brine reservoir, as determined in Reeves et al. [1989]), and the size of grid blocks in the mesh. The dimensions finally used were arrived at iteratively and somewhat arbitrarily as the conceptual model and the mesh were developed and as the original data of Popielak et al. (1983) were reexamined. After establishing the grid and selecting a radius for the reservoir, the value for the thickness of the reservoir was chosen in order to accommodate the sampled range of storativities. A value of 12 m (39 ft) was selected as appropriate for use in the numerical

storativities. A value of 12 m (39 ft) was selected as appropriate for use in the numerical model for the Castile brine reservoir. As a comparison, Popielak et al. (1983) originally assumed a thickness of 61 m (199 ft), which coincided with the thickness tested during their drill stem tests, whereas Reeves et al. estimated an effective thickness of 7 to 24 m (23 to 78 ft) in their analysis of the data for Popielak et al., (1983).

4.4 Climate Variability and Culebra Member Recharge

Climate variability is a continuous process (agent) acting on and thus affecting the state of the disposal system. The primary concerns are precipitation variation and, ultimately, recharge to strata above the Salado Formation, specifically, to the Culebra Dolomite Member. The parameters for climate variability and Culebra Member recharge are shown in Table 4.4-1.

Table 4.4-1. Climate Variability and Culebra Member Recharge

Parameter	Median	Range		Units	Distribution Type	Source
Annual precipitation ($\bar{r}_p$)	3.436×10^{-1}	3.09×10^{-2}	6.563×10^{-1}	m	Normal	Hunter, 1985
Precipitation variation						
Amplitude factor (A_m)	2			none	Constant	Swift, October 10, 1991, Memo (see Appendix A).
Short-term fluctuation (Φ)	2×10^{-10}			Hz	Constant	Swift, October 10, 1991, Memo (see Appendix A).
Glacial fluctuation (Θ)	1.7×10^{-12}			Hz	Constant	Swift, October 10, 1991, Memo (see Appendix A).
Recharge amplitude factor (A_m)	8×10^{-2}	0	1.6×10^{-1}	none	Uniform	See text.

Precipitation variability is modeled as a simple combination of sine and cosine functions representing high-frequency precipitation fluctuations and low-frequency glacial (e.g., Pleistocene) fluctuations. The function is not a prediction of future precipitation but rather is a simple way to explore the influence of precipitation variation:

$$\frac{\bar{r}_f}{\bar{r}_p} = \left[\left(\frac{3A_m + 1}{4}\right) - \left(\frac{A_m - 1}{2}\right)\left(\cos\Theta t + \frac{1}{2}\cos\Phi t - \sin\frac{\Phi}{2}t\right)\right] \qquad (4.4\text{-}1)$$

4.4.1 Annual Precipitation

Parameter:	**Mean annual precipitation**
Mean median:	3.436×10^{-1}
Range:	3.09×10^{-2}
	6.563×10^{-1}
Units:	m
Distribution:	Normal
Source(s):	Hunter, R. L. 1985. *A Regional Water Balance for the Waste Isolation Pilot Plant (WIPP) Site and Surrounding Area.* SAND84-2233. Albuquerque, NM: Sandia National Laboratories. (Table 2)

Figure 4.4-1 shows the distribution for mean annual precipitation at the WIPP station. Figure 4.4-2 shows the contours for the mean annual precipitation near the WIPP.

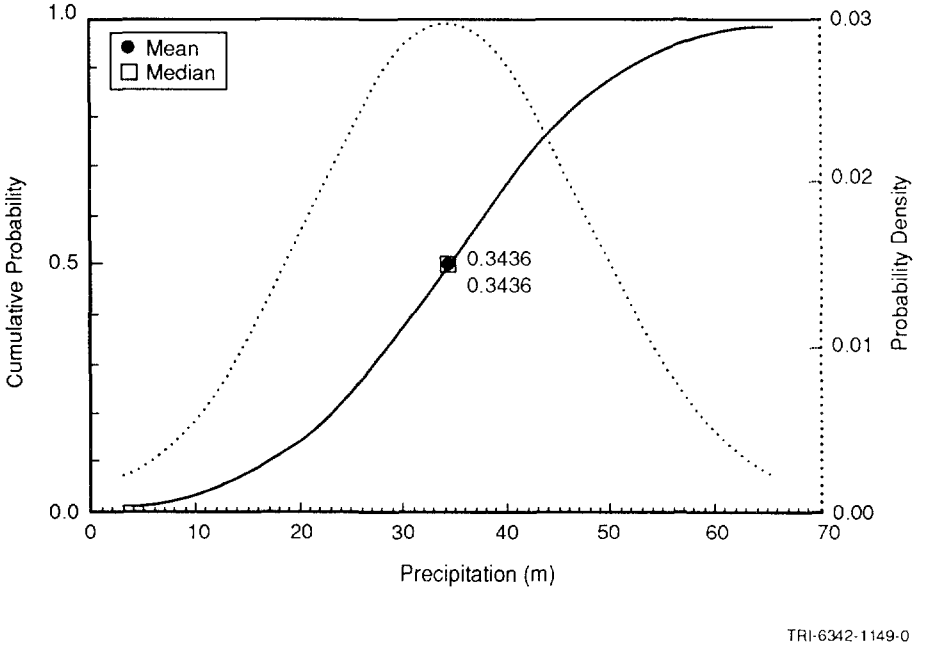

Figure 4.4-1. Normal Distribution (pdf and cdf) for Mean Annual Precipitation.

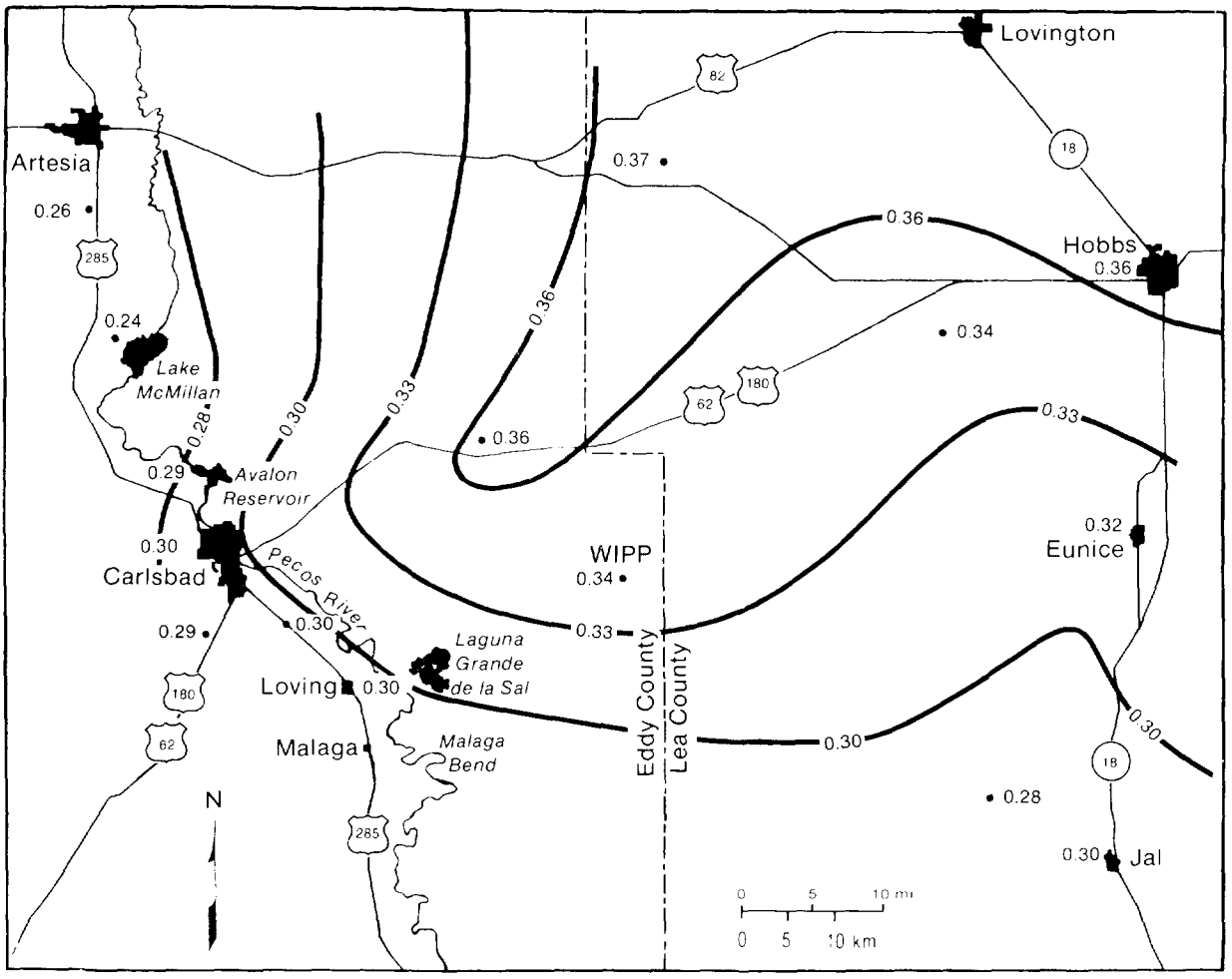

• Mean Precipitation in Meters

TRI-6342-123-1

Figure 4.4-2. Contours of Normal (Mean Annual between 1940 and 1970) Precipitation near the WIPP (after Hunter, 1985, Figure 3).

Discussion:

Southeastern New Mexico is an arid-to-semiarid fringe of the Chihuahuan Desert that receives about 0.30 m (12 in.) of annual precipitation. Three complete years of record (1977 through 1979) collected at a station located at the WIPP for the Environmental Impact Statement show that the average annual precipitation is 0.3436 m (13.53 in.), with a range of 0.0309 and 0.6563 m (1.22 and 25.84 in.), assuming a normal distribution (Figure 4.4-1) (EIS, 1980).* In general, most of the precipitation falls in the summer between May and September (Hunter, 1985, Table 2). The range of the mean from stations close to the WIPP varies between 0.28 and 0.38 m (11 and 15 in.) (Figure 4.4-2).

Precipitation at weather stations near the WIPP varies greatly from year to year. For example, Roswell's record low annual precipitation since 1878 is about 0.11 m (4.4 in.); the record annual high is about 0.84 m (33 in.) (Hunter, 1985, Figure 2). Consequently, an average precipitation for the WIPP based on three complete years of record is only a rough estimate of the long-term mean. However, this estimate is adequate for typical PA calculations.

Precipitation in the vicinity of the WIPP for years 1977 and 1979 was near normal, and 1978 was very wet. (The National Weather Service defines "normal precipitation" as the mean value for the past 30 yr, updated every 10 yr.) Hunter calculated an adjusted mean precipitation of 0.2771 m (10.91 in.) (20% difference) for the WIPP based on the mean departure during the years 1977 through 1979 of precipitation measurements from seven nearby stations (Hunter, 1985, p. 12).

---

* The WIPP began collecting precipitation data on a regular basis in 1986. This additional data will be reported in future volumes.

4.4.2 Precipitation Variation

The basic premise for assessing climatic change at the WIPP is the assumption that, because of the long-term stability of glacial cycles, future climates will remain within the range defined by the Pleistocene and Holocene. Data from deep-sea sediments indicate that fluctuations in global climate corresponding to glaciation and deglaciation of the northern hemisphere have been regular in both frequency and amplitude for at least 780,000 yr. Published results of global-warming models do not predict climatic changes of greater magnitude than those of the Pleistocene (Bertram-Howery et al., 1990).

Amplitude Factor

Parameter:	**Amplitude factor (A_m)**
Median:	2
Range:	None
Units:	Dimensionless
Distribution:	Constant
Source(s):	Swift, P. 1991. "Climate Recharge Variability Parameters for the 1991 WIPP PA Calculations, Internal memo to distribution, October 10, 1991. Albuquerque, NM: Sandia National Laboratories. (In Appendix A of this volume)

Discussion:

Field data from the American Southwest and global-climate models indicate that the wettest conditions in the past at the WIPP occurred when the North American ice sheet reached its southern limit (roughly 1,200 km [746 mi] north of the WIPP during the last glacial maximum 18,000 to 22,000 yr before present), which moved the jet stream much further south than now. The average precipitation in the Southwest increased to about twice its present value. Wet periods have occurred since the retreat of the ice sheet, but none has exceeded glacial limits.

Although the amplitude of the glacial precipitation is relatively well constrained by data (Bertram-Howery et al., 1990, p. V-37; Swift, October 10, 1991, Memo, [Appendix A]), amplitudes of the Holocene peaks are less easily determined. However, data indicate that none of the Holocene precipitation peaks exceeded glacial levels. Continuous climatic data from ice cores in Antarctica and Greenland suggest that at these locations temperature fluctuated significantly during glacial maximums (e.g., Jouzel et al., 1987). These fluctuations may reflect global climatic changes, and in the absence of high-resolution data from the American Southwest for precipitation fluctuations during glacial maximums, we have assumed that peaks comparable to those of the Holocene could have been superimposed on the glacial maximum. Therefore, there may have been relatively brief (i.e., on the order of hundreds to perhaps thousands of years) periods during the glacial maximum when precipitation at the WIPP may have averaged three times present levels.

Model of Precipitation Variation. Paleoclimatic data permit reconstruction of a precipitation curve for the WIPP for the last 30,000 yr (Figure 4.4-3). This curve shows two basic styles of climatic fluctuation: relatively low-frequency increases in precipitation that coincide with the maximum extent of the North American ice sheet; and higher-frequency precipitation increases of uncertain causes that have occurred several times in the last 10,000 yr since the retreat of the ice sheet. Variability has also occurred in the seasonality and intensity of precipitation. Most of the late Pleistocene moisture fell as winter rain. Most of the Holocene moisture falls during during a summer monsoon, in local and often intense thunderstorms.

The curve shown in Figure 4.4-3 cannot be extrapolated into the future with any confidence. The curve can be used, however, in combination with the general understanding of glacial periodicity (see Bertram-Howery et al., 1990), to make a reasonable approximation of likely future variability. The proposed function does not in any sense predict precipitation at a future time. Rather, it is a function to approximate the variability in precipitation that may occur.

Specifically, the currently proposed precipitation function is as follows:

$$\frac{\bar{r}_f}{\bar{r}_p} = \left[\left(\frac{3A_m + 1}{4}\right) - \left(\frac{A_m - 1}{2}\right)\left(\cos\Theta t + \frac{1}{2}\cos\Phi t - \sin\frac{\Phi}{2}t\right)\right] \qquad (4.4\text{-}1)$$

where

r_f = future mean annual precipitation
r_p = present mean annual precipitation
A_m = amplitude scaling factor (i.e., past precipitation maximum was A_m times the present)
Θ = frequency parameter for Holocene-type climatic fluctuations (Hz)
Φ = frequency parameter for Pleistocene glaciations (Hz)
t = time (s)

The preferred values for Θ and Φ have been chosen from examination of the past precipitation curve (Figure 4.4-3) and the glacial record. If $\Phi = 2 \times 10^{-10}$ Hz, wet maximums will occur every 2,000 yr, approximately with the same frequency shown on Figure 4.4-3. Note that we are presently near a dry minimum, and the last wet maximum occurred roughly 1000 yr ago. If $\Theta = 1.7 \times 10^{-12}$ Hz, the next full glacial maximum will occur in 60,000 yr, approximately the time predicted by simple models of the astronomical control of glacial periodicity (e.g., Imbrie and Imbrie, 1980). Figure 4.4-4 shows a plot of the climate function for these values.

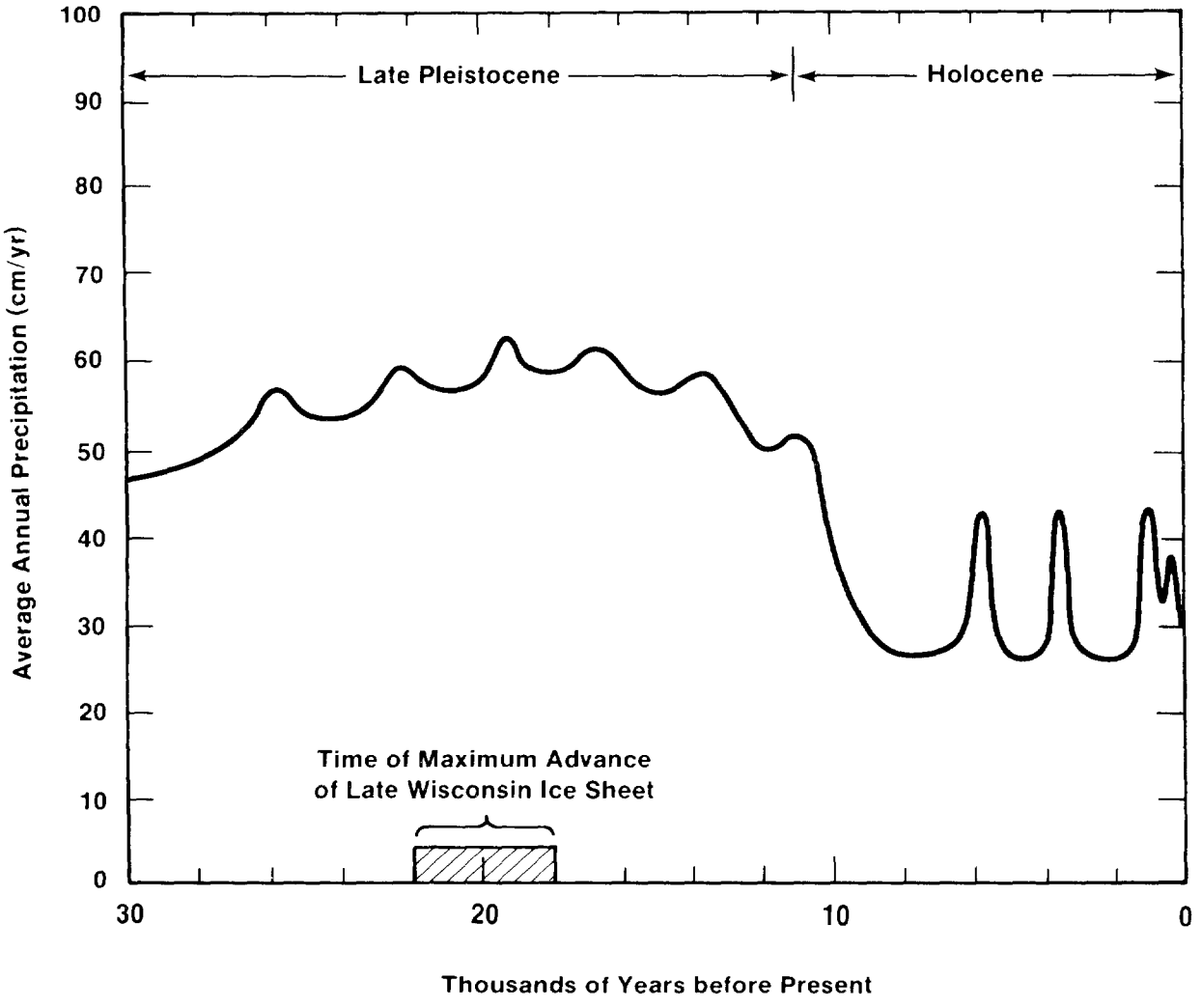

Figure 4.4-3. Estimated Mean Annual Precipitation at the WIPP during the Late Pleistocene and Holocene (after Bertram-Howery et al., 1990, Figure V-18).

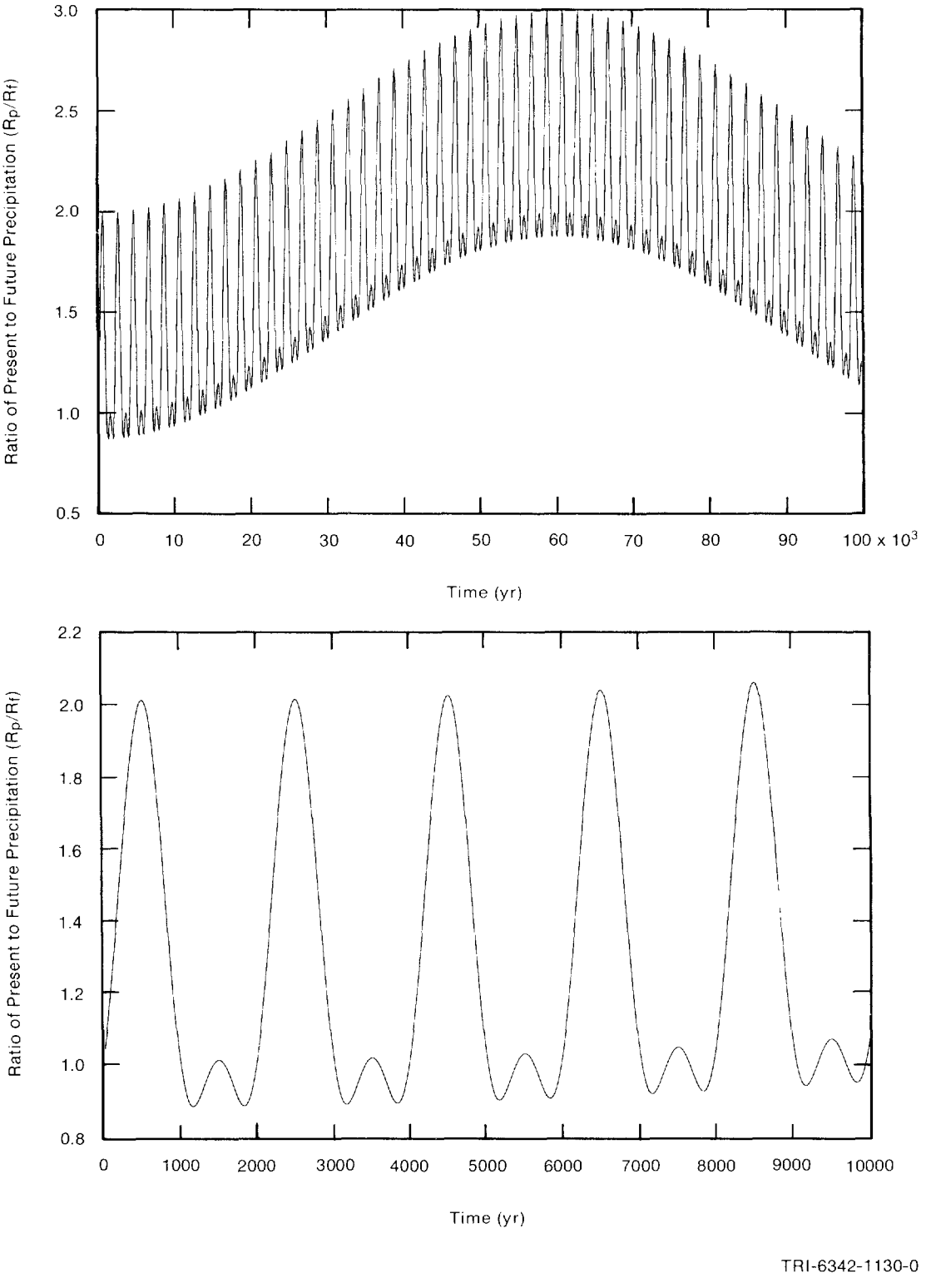

Figure 4.4-4. Precipitation Fluctuations Assumed at the WIPP for Next 10,000 Yr.

Short-Term Fluctuation

Parameter:	**Short-term precipitation fluctuation frequency (Φ)**
Median:	2×10^{-10}
Range:	None
Units:	Hz
Distribution:	Constant
Source(s):	Swift, P. 1991. "Climate and Recharge Variability Parameters for the 1991 WIPP PA Calculations," Internal memo to distribution, October 10, 1991. Albuquerque, NM: Sandia National Laboratories. (In Appendix A of this volume)

Discussion:

The approximate frequency of wet maximum is every 2,000 yr, or a value of Φ of about 0.2 nHz ($2\pi/(1000 \text{ yr} \bullet 3.155 \bullet 10^7 \text{ s/yr})$. Note that we are presently near a dry minimum; the last wet maximum occurred roughly 1,000 yr ago.

Holocene climates have been predominantly dry, with wet peaks much briefer than dry minimums (Figure 4.4-3). The Φ terms in the model equation (4.4-1) give an oscillation in which the future climate is wetter than the present one-half of the time. This value appears to be somewhat greater than the actual ratio, and, assuming that wet conditions are more likely to result in releases from the WIPP, these terms provide a conservative approximation of Holocene variability. The functions and values used give an "average" precipitation roughly 1.3 times present precipitation, with peaks of just over 2 times present precipitation.

Glacial Fluctuation

Parameter:	**Glacial fluctuation (Θ)**
Median:	1.7×10^{-12}
Range:	None
Units:	Hz
Distribution:	Constant
Source(s):	Swift, P. 1991. "Climate and Recharge Variability Parameters for the 1991 WIPP PA Calculations," Internal memo to distribution, October 10, 1991. Albuquerque, NM: Sandia National Laboratories. (In Appendix A of this volume)

Discussion:

The approximate time predicted by simple models assuming astronomical control of glacial periodicity suggest the next glacial maximum may occur in about 60,000 yr or a value of Θ of about 1.7 pHz (π/60,000 yr) (Imbrie and Imbrie, 1980). A value of Θ of 10 pHz (π/10,000 yr) gives a wet maximum in 10,000 yr, and results in extreme precipitation values 3 times those of the present. This is not a realistic value for Θ -- ice sheets grow relatively slowly, and it would be difficult to achieve full continential glaciation within 10,000 yr.

4.4.3 Boundary Recharge Variation

Parameter:	**Recharge amplitude factor (A_m)**
Median:	0.08
Range:	0
	0.16
Units:	Dimensionless
Distribution:	Uniform
Source(s):	See text.

Figure 4.4-5 shows the distribution for the recharge amplitude factor.

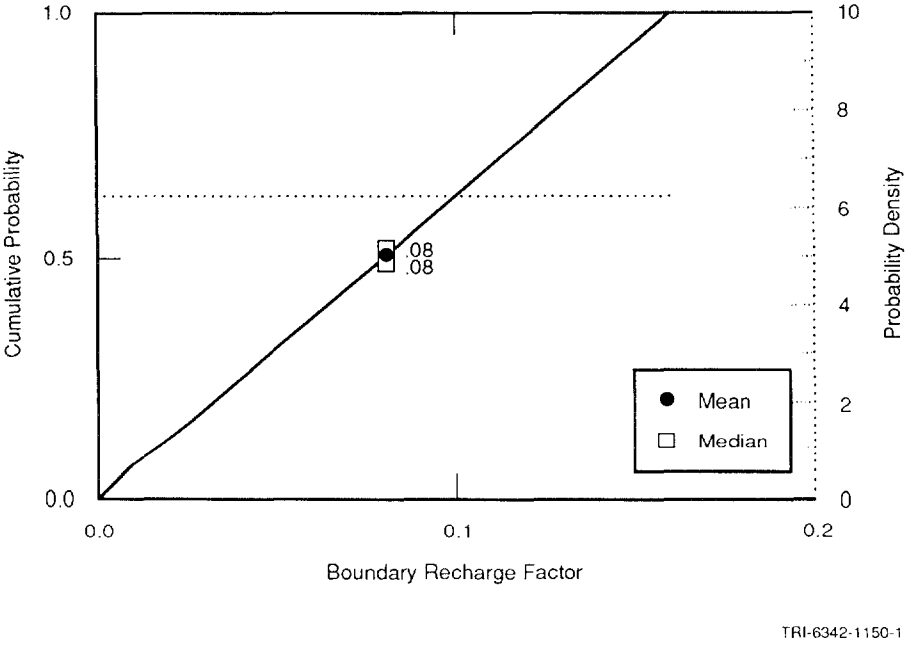

Figure 4.4-5. Uniform Distribution (pdf and cdf) for Recharge Boundary Amplitude Factor for Culebra Dolomite Member.

Discussion:

At present, the location and areal extent of the surface recharge area for the Culebra and the present amount of infiltration are not known. Hydraulic head and isotopic data indicate that very little, if any, moisture reaches the Culebra directly from the ground surface above the WIPP (Lambert and Harvey, 1987; Lambert and Carter, 1987; Lappin et al., 1989; Beauheim, 1987c). Researchers believe that regional recharge occurs several tens of kilometers to the north of the WIPP, where the Culebra is near the ground surface (Mercer, 1983; Brinster, 1991). Whether water from this hypothesized recharge area could reach the current model domain area is not known (Swift, October 10, 1991, Memo [Appendix A]).

Available literature on the relationship between precipitation and recharge is limited to examinations of recharge to a water table by direct infiltration. There is no particular reason to assume a 1-to-1 correlation between increases in precipitation and increases in model recharge. Environmental tracer research (e.g., Allison, 1988) suggests that long-term increases in precipitation in deserts may result in significantly larger increases in infiltration, particularly if the increases in precipitation coincide with lower temperatures and decreased evapotranspiration. As an extreme example, Stone (1984) estimated a 28-fold increase in infiltration for one location at the Salt Lake coal field in western New Mexico during the late Pleistocene wet maximum. Bredenkamp (1988a,b) compared head-levels in wells and sinkholes with short-term (decade-scale) precipitation fluctuations in the Transvaal, and suggested that for any specific system there may be a minimum precipitation level below which recharge does not occur. Above this uncertain level, recharge to the water table may be a linear function of precipitation.

Both the range and the distribution for the recharge factor are preliminary and should be adjusted as new data or interpretations warrant.

Recharge Model. Because of the unknown factors regarding recharge, a very simple model of recharge to the Culebra is used. The model consists of evaluating the head by scaling the relative change in precipitation with a recharge factor. The head is then applied at the hypothesized recharge area.

The current model is

$$\frac{h_f}{h_p} = \frac{3A_m + 1}{4} - \frac{A_m - 1}{2}\left(\cos \Theta t + \frac{1}{2}\cos \Phi t - \sin \frac{1}{2}\Phi t\right) \qquad (4.4\text{-}2)$$

Recharge Amplitude Factor. The recharge amplitude factor represents uncertainty in numerous parameters, including (a) the location and extent of the surface recharge area, (b) groundwater flow between the surface recharge area and the boundary of the model domain, and (c) the relationship between precipitation and infiltration in the surface recharge area, which in turn is dependent on factors such as vegetation, temperature, local topography, and soil characteristics.

To cover variability in model recharge, the PA Division incorporates recharge uncertainty in the 1991 calculations by sampling a uniformly distributed amplitude parameter (A_m) over a range that permits the range to vary from present hydraulic heads to heads equal to the land surface. Justification for the range is as follows:

Lower bound, r = 1. This value corresponds to present hydraulic head conditions. Circumstances can be imagined in which increases in precipitation result in a decrease in infiltration (e.g., development of plant cover on previously barren land, or changes in topography resulting in runoff from a previously closed drainage), but none appears likely for the WIPP area. It is more likely that an increase in the cool-season component of precipitation will result in higher infiltration.

Upper bound, r = 0.16. This value sets hydraulic heads equal to the land surface. This value is consistent with fossil evidence that springs existed in the region near the northwest corner of the regional grid (Bachman, 1981; Brinster, 1991, p. IV-7).

5. PARAMETERS FOR SCENARIO PROBABILITY MODELS

This chapter presents data used in those probability models that estimate elementary probabilities of events and processes that appear in future WIPP histories, specifically, those histories in which the WIPP is penetrated by exploratory boreholes. Elementary probabilities furnished by these models are used to calculate probabilities $P(S_j)$ of computational scenarios S_j. The mathematical approach to scenario-based performance assessment is discussed in Volume 1, Chapter 3, and Volume 2, Chapters 2 and 3, of this report; Tierney (1991); Helton et al. (1991); and Section 1.4 of this volume.

Because innumerable scenarios exist, an infinite number of groupings of scenarios exist. As in 1990, the analyzed scenarios for 1991 were grouped into four summary scenarios (see Volume 1): one base-case scenario (without human intrusion) and three human-intrusion scenarios (i.e., E1, E2, and E1E2). To more carefully explore the cause and effect relationship from hypothetical events and processes (as opposed to those that will occur but for which we do not know the precise parameter values), the three human-intrusion summary scenarios have been further refined (discretized) into computational scenarios. While this partitioning of summary scenario space is new and, consequently, the details of the probability model, are dramatically different in 1991, the parameters ($\mathbf{x}$) of the probability model $P(S_j(\mathbf{x}))$ are the same as in 1990 and the same Poisson probability model was used to evaluate the time and number of potential intrusions. The parameters are discussed in the following sections.

5.1 Area of Brine Reservoirs

5.1.1 Area of Castile Brine Reservoir below WIPP Disposal Area

Parameter:	**Areal extent of brine reservoir**
Median:	0.40
Range:	0.25
	0.552
Units:	Dimensionless (%)
Distribution:	Cumulative
Source(s):	See text.

Figure 5.1-1 shows the distribution of the areal extent.

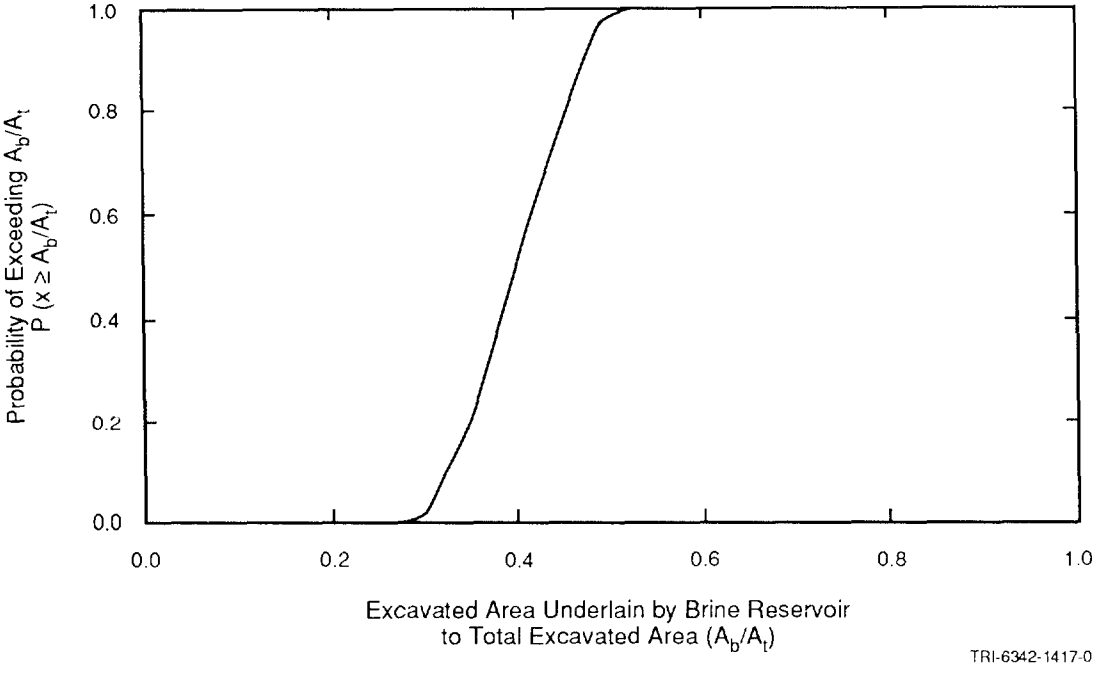

Figure 5.1-1. Distribution of Fraction of WIPP Disposal Area Overlapped by Brine Reservoir. Simulated construction uses inclusive definition of brine reservoir and block model (see text).

Discussion:

A geophysical survey, using transient electromagnetic methods, was made in 1987 to determine the presence or absence of brines within the Castile Formation under the WIPP disposal area (Earth Technology Corp., 1988). Briefly, the electromagnetic method associates high electric conductivity with fluid. (The stated precision was to within ±75 m.) The entire Bell Canyon Formation directly beneath the Castile Formation is a good conductor. However, in several places underneath the WIPP disposal area, the elevation to the first major conducting media detected lay above the top of the Bell Canyon Formation (~-200 ± 30 m [-654 ± 100 ft] in the ERDA-9 well) but below the bottom of the Salado Formation (178 m [582 ft] in ERDA-9) (see Figure 2.2-1 and Section 2.2).

The probability of hitting a brine reservoir can be evaluated for the waste disposal area as a whole or for subunits such as the panels. The current human-intrusion probability model (Volume 2, Chapters 1 and 2) uses the former data (the probability of hitting a brine reservoir over the entire waste panel) and assumes that this same probability applies to each panel. However, an examination of this assumption required the probability for each panel as well (Volume 2, Chapters 1 and 2). The following discussion emphasizes the probability over the entire disposal area, but provides data on a per panel basis as well.

Two methods were considered for determining the area of the brine reservoir. The first involved using the interpolated conductor elevations and the Anhydrite III of the Castile Formation and the Bell Canyon Formation elevations without considering uncertainty in the data. Although not used, it is discussed first because of its simplicity. The second method considers uncertainty in the data through geostatistics.

Area Estimate Assuming No Uncertainty in Data. Contours of the depth or elevation to the first major conductor are plotted in Figures 5.1-2 and 5.1-3. The data in Figure 5.1-2 was the interpretation originally reported (Earth Technology Corporation, 1988). However, Figure 5.1-3 is an equally valid interpretation of the data; it is somewhat more conservative and was computer generated from the same data.

Minimum Area (Anhydrite III Level). The brine reservoirs are usually found in fracture zones of anticlimal structures in the uppermost anhydrite layer in the Castile (Lappin, 1988) (e.g., Anhydrite III as in WIPP-12 or when Anhydrite III is absent such as Anhydrite II in ERDA-6).

In ERDA-9, the elevation to the bottom of Anhydrite III in the Castile Formation is estimated at 105 m (250 ft). Consequently, there is a possibity that no brine is present beneath the disposal area (Figure 5.1-1).

Maximum Area (Bell Canyon Level). Pressurized brine reservoirs cannot be entirely discounted until the Bell Canyon Formation is reached at about -200 m (-660 ft) (Figure 2.2-1), implying that conductors higher than about -200 m (-660 ft) could indicate brine within the Castile Formation. PA calculations use the -200 m (-660 ft) contour for defining the maximum area of any brine reservoirs under the WIPP disposal area (Figure 5.1-2), resulting in a maximum area at 45% (Table 5.1-1).

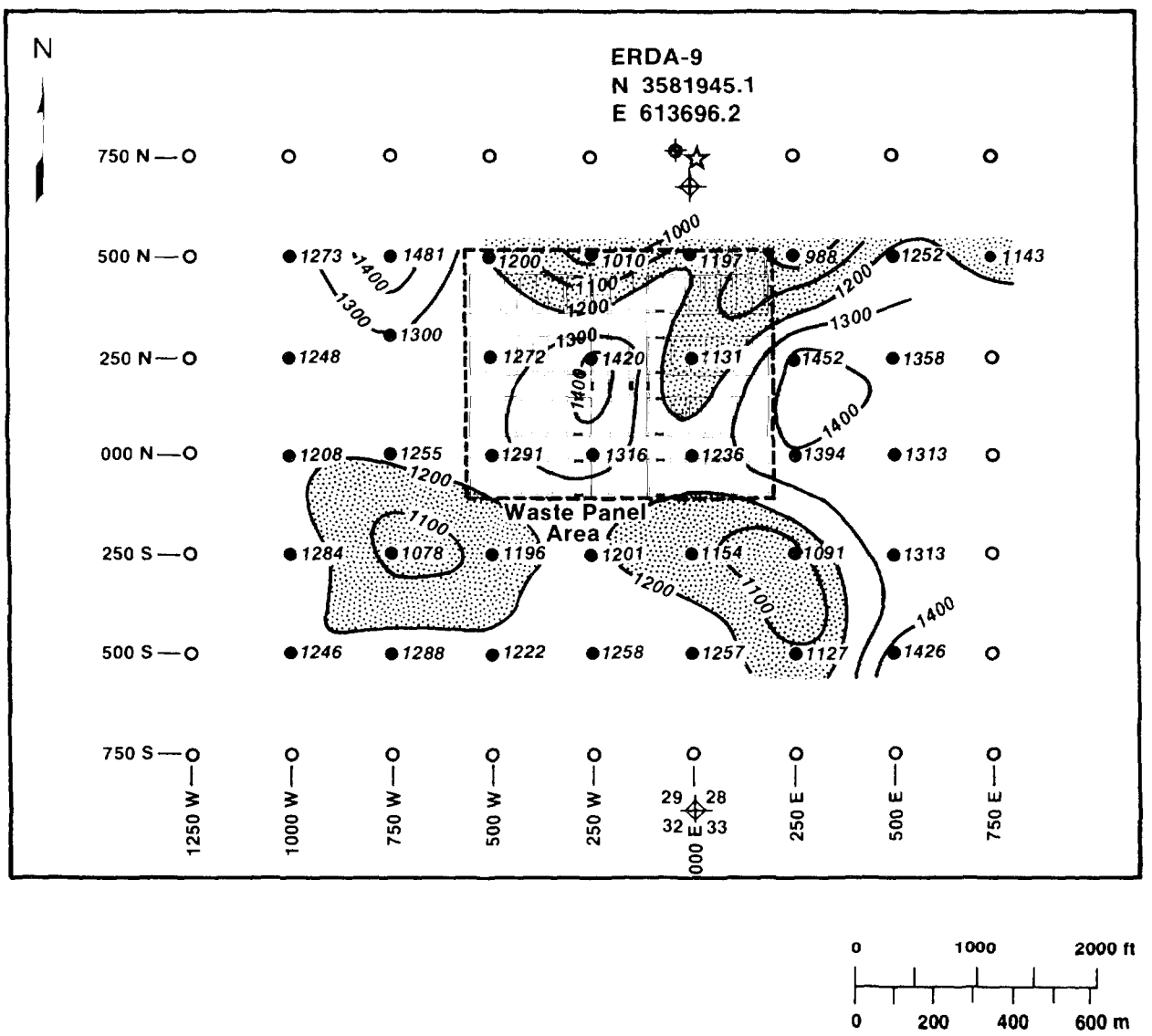

TRI-6342-256-2

Figure 5.1-2. Frequently Reported Contour Map of Depth of First Major Conductor below WIPP Disposal Area. (Map drawn by hand.) (after Earth Technology Corp., 1988).

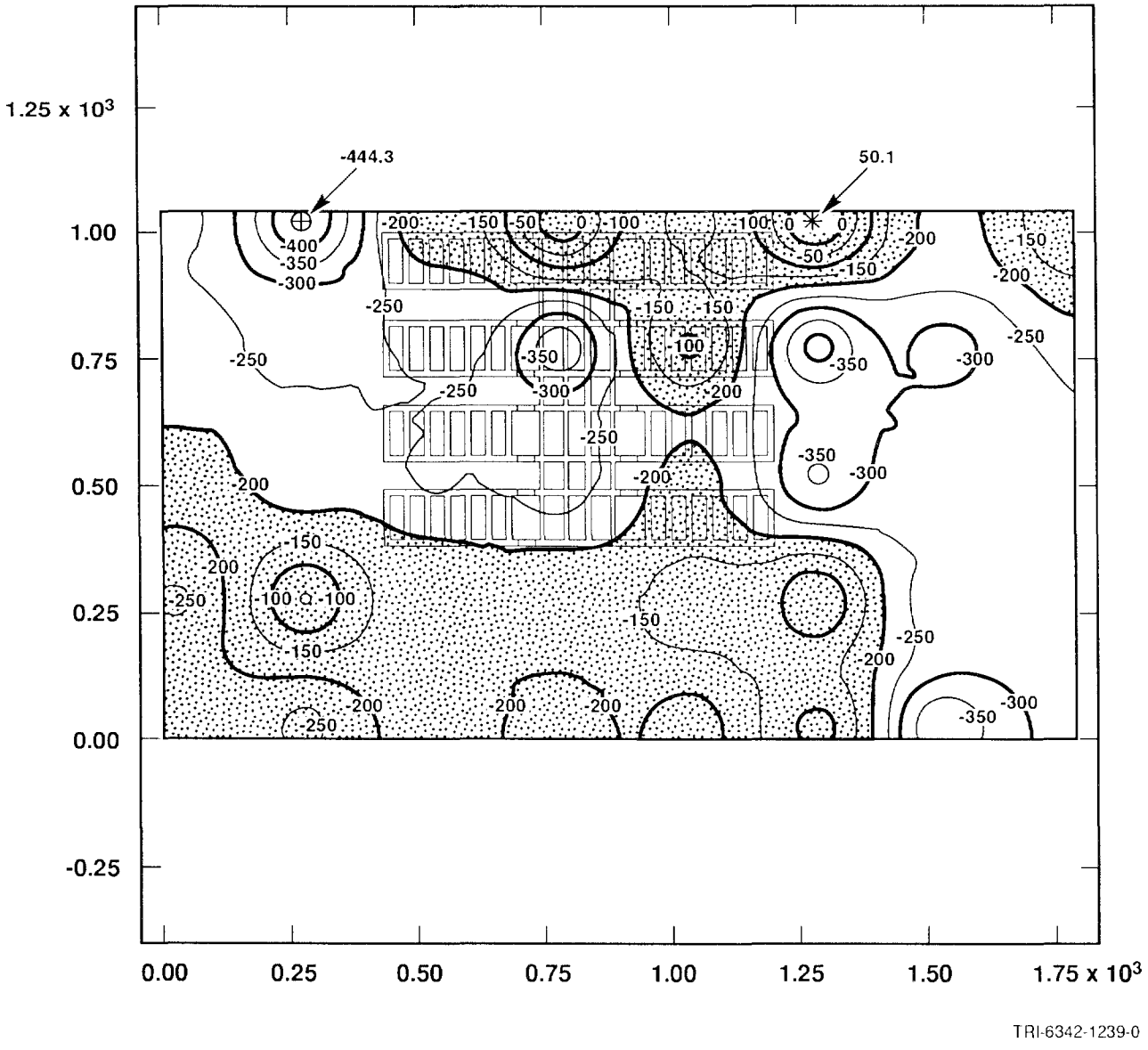

Figure 5.1-3. Conservative Contour Map of Elevation of First Major Conductor below WIPP Disposal Area.

Table 5.1-1. Cumulative Percentages of the Disposal Region Underlain by a Brine Reservoir, Assuming Various Maximum Depths

	Cumulative Percent (%) at Indicated Maximum Depths										Area
Depth (m)	0	-50	-100	-150	-180	-200	-250	-300	-350	-400	(m^2)
Panel 1			5.37	61.95	97.80	100.00	100.00	100.00	100.00	100.00	11,530.0
Panel 2			4.00	44.57	69.33	73.08	87.47	100.00	100.00	100.00	11,530.0
Panel 3						18.23	85.73	100.00	100.00	100.00	11,530.0
Panel 4					35.85	75.57	96.17	100.00	100.00	100.00	11,530.0
Panel 5						19.76	94.80	100.00	100.00	100.00	11,530.0
Panel 6							26.57	100.00	100.00	100.00	11,530.0
Panel 7							67.45	100.00	100.00	100.00	11,530.0
Panel 8			0.79	9.01	34.64	52.86	100.00	100.00	100.00	100.00	11,530.0
Southern						3.24	45.01	100.00	100.00	100.00	8,413.0
Northern	3.97	12.49	21.67	27.49	34.86	45.29	54.79	69.25	94.52	100.00	8,701.0
Cumulative Percent	0.316	0.994	2.796	14.367	27.828	39.648	77.219	97.553	99.564	100.000	
Cumulative Area (m^2)	345.3	1,086.8	3,057.6	15,711.1	30,431.4	43,357.1	84,442.3	106,678.2	108,877.4	109,354.0	

Combined Distribution. Without knowing the likelihood that either endpoint is more valid, a discrete distribution with points at 0 and 45% of equal probability is suggested.

Area Estimate Incorporating Uncertainty in the Data. Described above is a method of estimating the fractional area of the waste-panel region underlain by a Castile brine reservoir using contours of the conductor elevation. This method assumes that elevation contours drawn from the observed data correctly represent the variation of conductor depth between observation locations. The following discussion describes an alternative method that does not rely on reported depth contours, and the resulting area fraction distribution.

Conductor elevation measurements are available at 36 points (Figure 5.1-3). These data were used to estimate conductor elevation at all points within the waste panel region. Any estimate of the conductor depth at an unmeasured location had an uncertainty associated with it. The objective of this procedure is to incorporate relevant uncertainties in the estimate of area fraction.

Spatial Variability and Interpolation. Uncertainty in interpolated elevations is a consequence of spatial variability of the observed data. Quantifying spatial variability helps in estimating the error of an interpolated value. If two observations are made close together, it is reasonable to expect that similar values will be obtained (autocorrelation function, Chapter 1). As the distance between observations increases, the similarity of observed values decreases. This behavior of spatially varying fields is often represented as a variogram (Figure 5.1-4). The variogram shows the average squared difference in observed values between observations separated by a given distance vs. the distance between observations. For a given separation distance h, the average is taken over all pairs of observations that are separated by distance h.

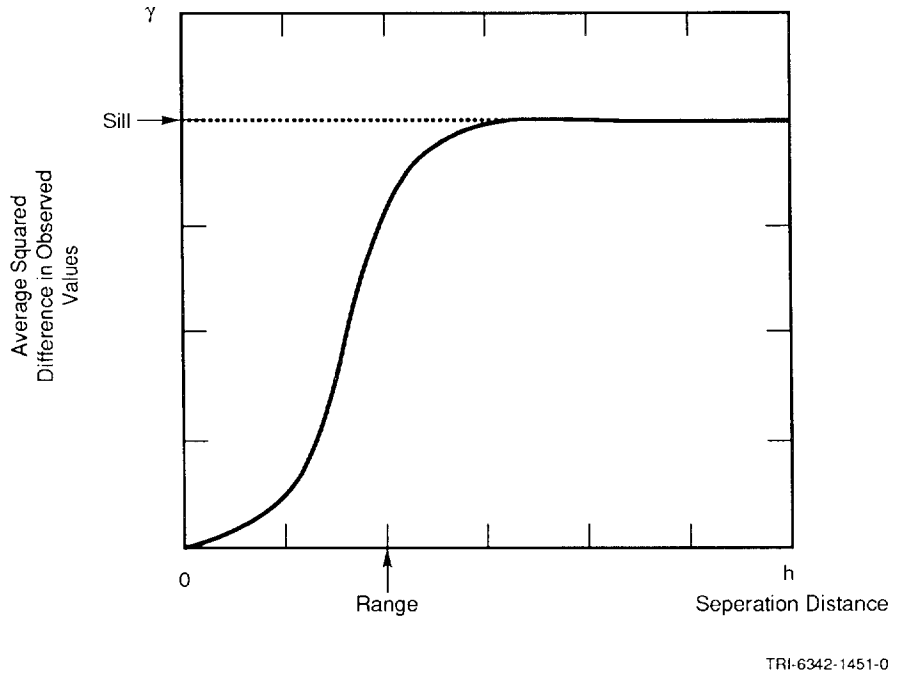

Figure 5.1-4. Example Variogram Illustrating Typical Behavior of γ with h.

The variogram in Figure 5.1.4 is a generic example illustrating two common features seen in real data. Close to the origin (i.e., small separation distances), values are similar, so that the average squared difference is small. As the distance between observations increases, observed values tend to become uncorrelated, resulting in an increase in average squared difference in observed values. The distance at which observations tend to become uncorrelated is referred to as the range of the variogram. As separation distance increases beyond the range, the average squared difference tends to a limiting value, called the sill.

Not all fields exhibit clearly defined range and sill. Systematic trends in the data, for example, can produce variograms that continually increase with separation distance. In addition, the spatial variability of the data may be different along different directions, so that a variogram constructed from separations along one direction may be different from a variogram constructed along another direction.

Information contained in the variogram is useful in interpolating from observed values for two reasons:

(1) The range of the variogram identifies the maximum distance over which observations tend to be correlated. This information is important for selecting the data points near the interpolation location having values that may be related to the actual value at the interpolation location.

(2) The average squared difference between data values, along with the distances between the interpolation location and the locations of the selected observations, may be used to estimate the potential variability of the real value from the interpolated value.

Analysis of TDEM Data. Figure 5.1-2 shows conductor elevations interpreted from the TDEM survey at 36 locations near and within the waste panel region. Figure 5.1-5 shows a cumulative distribution of observed elevations, along with the average elevation and sample standard deviation. Scatter plots of conductor elevation vs. X (E-W) location and Y (N-S) location are shown in Figure 5.1-6. There is no suggestion of a significant simple trend in elevation along either direction.

A variogram of elevations was constructed in the E-W, N-S, NE-SW, and NW-SE directions. The regular arrangement of observation points facilitates this calculation: the variogram value for a separation of 250 m in the E-W direction, for example, is simply the average of the squared difference of elevation values at points adjacent to each other in the E-W direction. Similar averages can be made for multiples of the observation grid spacing (250 m) in the E-W and N-S directions. Points in the NE-SW and NW-SE directions area separated by multiples of ~353 m. In calculating the elevation variogram, the observation at (750W, 290N) was assumed to have been made at (750W, 250N). This displacement has no important effect on the resulting variogram.

Figure 5.1-7 shows the variogram of the elevation data along the directions mentioned. The separation distances considered were 250 m and 500 m in the E-W and N-S directions, and 353 m in the diagonal directions. Larger separations have too few pairs to provide a reliable estimate of mean squared difference. The horizontal line, which shows the average squared difference over all pairs of points regardless of separation, is an estimate of the variogram sill.

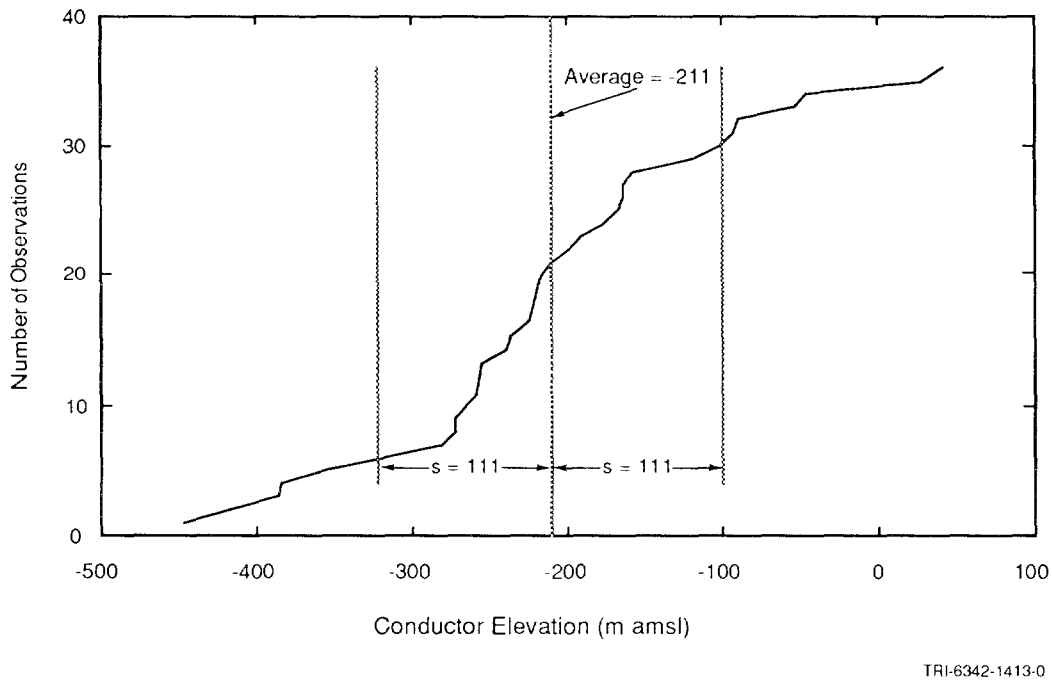

Figure 5.1-5. Population Distribution and Statistics for Conductor Elevations.

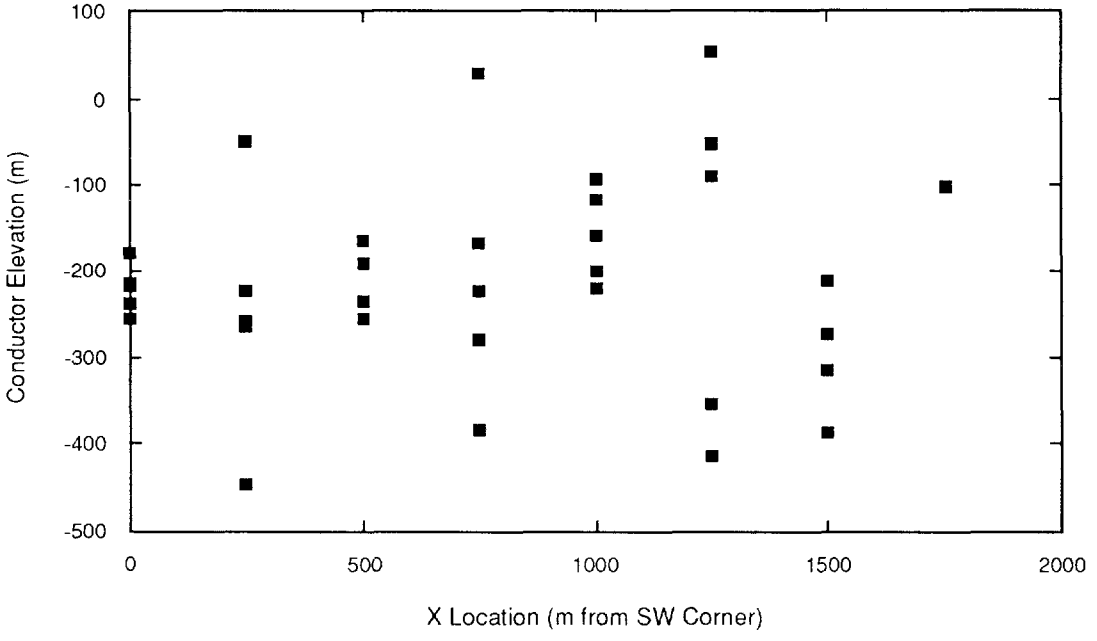

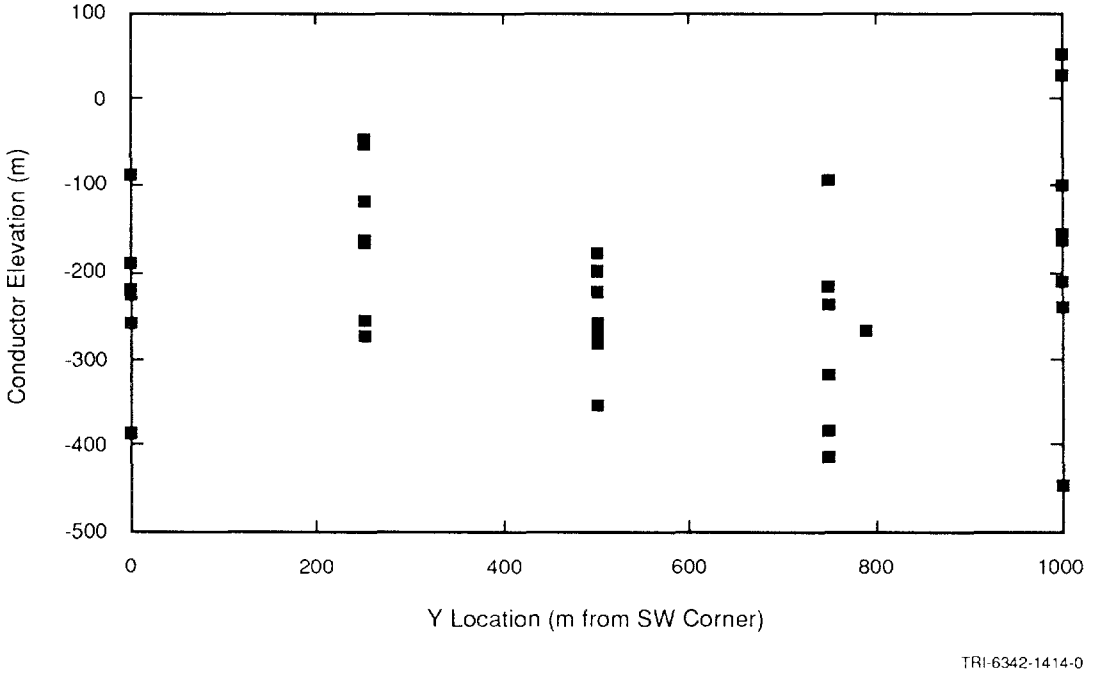

Figure 5.1-6. Scatter Plots of Conductor Elevation vs. X and Y Location.

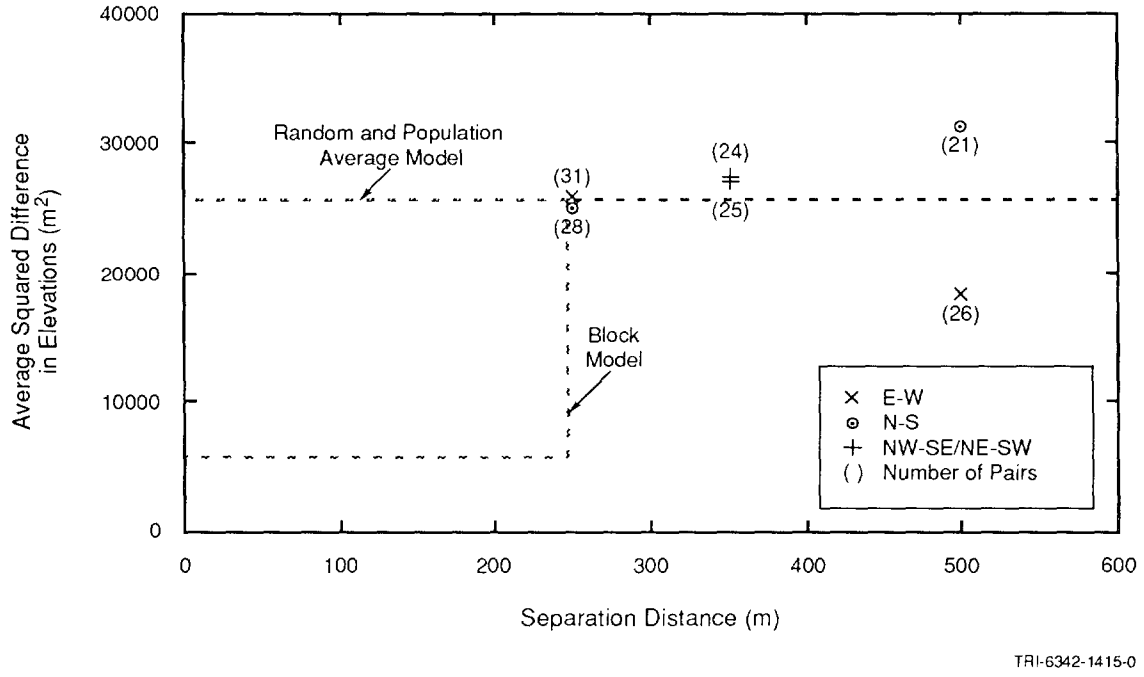

Figure 5.1-7. Empirical Variogram of Conductor Elevations.

The striking feature of the variogram is the lack of evidence for a range of correlation of observations. The average squared difference for adjacent measurements and the expected squared difference for randomly selected measurements (i.e., the sill) are indistinguishable. In other words, there is no evidence for spatial correlation of elevation over distances as small as 250 m. (In a separate analysis, the program AKRIP was used to estimate a generalized covariance for the elevation data. The identified model contained only a "nugget" term, i.e., the generalized covariance was not found to depend on separation distance.)

Estimation of Conductor Elevation. The variogram suggests that, in attempting to estimate conductor elevation at non-measured locations, observations made 250 m from the interpolation location contain no more information about the real value at the interpolation location than more distant observations. For all points within the waste panel region, at least one observation less than 250 m away will be available. The variogram analysis does not indicate whether observations less than 250 m distant can be expected to provide information about elevation at the interpolation point. In particular, the assumption of linear variation of elevation between data points made in constructing contours of conductor elevation has no support (i.e., Figures 5.1-2 and 5.1-3).

Two bounding alternatives, corresponding to different assumptions about the behavior of the variogram between 0 and 250 m have been considered (see Figure 5.1-7):

(1) "Random elevation" assumption: Conductor elevation correlation length is very small <<250 m. The variogram is equal to the sill value between 0 and 250 m.

(2) "Block elevation" assumption: The observation grid spacing is just outside the actual correlation length. Below 250 m, observations become highly correlated, with an expected squared difference equal to twice the measurement error variance ("cookie cutter" autocorrelation).

These assumptions lead to two different methods of estimating conductor elevation. Both assumptions have been carried through in estimating brine reservoir area fraction.

In the random elevation assumption, nearby data points contribute no special information about the real value at the interpolation point in virtue of their proximity. The best estimate for elevation at any point is simply the average elevation over all observations. The variance of the error of this estimate is the population variance.

In the block elevation assumption, elevation is highly correlated over distances smaller than the measurement interval. The estimate of elevation at an interpolation point is simply the observed value at the nearest observation point. The variance of the error of this estimate is the variance of the error of the observation (75 m^2).

If the interpolated value is thought of as a weighted linear combination of observed values (as in inverse distance interpolation or in kriging), the random and block assumptions lead to the extremes of uniform weighting of all observations and exclusive weighting of the nearest observation.

Estimation of Area Fraction. The area fraction is defined as the area of the waste panel excavation overlying a brine reservoir divided by the total excavation area. A point is considered to overlie a brine reservoir if there is an electrically conductive zone in a hydrologically conductive layer of the Castile Formation. Although Castile brine reservoirs encountered during drilling appear to be always associated with the uppermost Castile anhydrite (Anhydrite III at the WIPP site), there is the possibility that brine reservoirs may occur in lower Castile Anhydrites. For the purpose of estimating area fraction using the existing data, two formulations are possible:

(1) A point overlies a brine reservoir if the sub-Salado conductor elevation is greater than the elevation of the base of Anhydrite III, or
(2) A point overlies a brine reservoir if the sub-Salado conductor elevation is greater than the elevation of the base of the Castile.

For any point in the waste panel region, none of the elevations used to identify a brine reservoir by either formulation are known with certainty. In addition, there is uncertainty in which of the above formulations is appropriate. The area fraction estimate should incorporate these uncertainties.

Description of Method. Uncertainties associated with estimation of the area fraction were addressed through Monte Carlo simulations as follows:

- 200 samples from two uncorrelated uniformly distributed random variables were taken as possible values for the base elevations of the Castile and Anhydrite III. These distributions ranged from -230 m to -170 m for the base of the Castile, and from 70 m to 140 m for the base of Anhydrite III. The estimates of base elevation were uniformly distributed over the given range and were not correlated. The base elevation for the Castile and for Anhydrite III were assumed to be constant over the waste panel area.

- Along with these elevations, one of the two formulations for identifying a brine reservoir were selected at random.

- For each set of sampled base elevations and brine reservoir definition, 2000 realizations of conductor elevation were created on a uniform mesh. The relative area overlying the brine reservoir was then calculated using the sampled realizations and the selected definition of a brine reservoir.

- The relative number of simulations having a given area fraction was then used to construct an area fraction distribution. The derived area fraction distribution reflects uncertainty in conductor elevation, lithology, and the existence of brine reservoirs in lower Castile anhydrites.

The above process was applied twice, using the "random" and "block" assumptions for spatial correlation of conductor elevation in the generation of conductor realizations. In either case, conductor elevations at each mesh cell were assumed to be normally distributed around the estimated value.

Maximum Area (Bell Canyon Level). Based on the geostatistical analysis and data uncertainty described above, the use of the more conservative block model, and the assumption that a brine reservoir cannot be discounted until the Bell Canyon is reached, there is a chance that the brine reservoir has an area between 25 and 55% of the excavated area with a median of 40%. This contrasts with the best estimate of 45% from the contour method. The distribution is bell-shaped (Figure 5.1-1).

Minimum Area (Anhydrite III Level). Based on the geostatistical analysis and data uncertainty described above, the probability of the brine reservoir residing in the uppermost anhydrite layer is very small.

50% Combination. Figure 5.1.8 shows the derived cumulative distribution of area fraction using both the "random" and "block" assumptions and assuming that 50% of the time Anhydrite III is the maximum depth and 50% of the time the Bell Canyon is the maximum depth. Both distributions show a distinct bi-modality assuming very small values of area fraction correspond to the requirement that the brine reservoir be in Anhydrite III, while larger area fractions correspond to the requirement that the brine reservoir must be in the Castile Formation. The relative weighting of the two formulations for the brine reservoir controls the elevation of the plateau in the cumulative distribution, and is clearly more important than the model of spatial variability of conductor elevation (random or block).

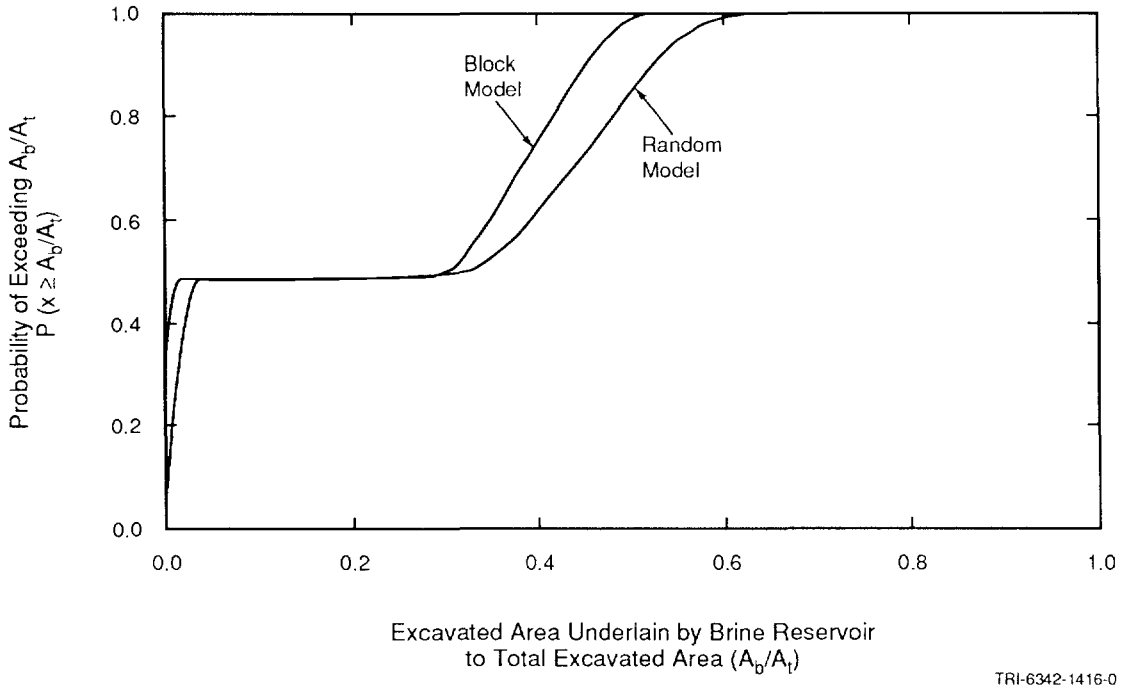

Figure 5.1-8. Cumulative Distribution of Area Fraction using the "Random" and "Block" Assumptions.

In the 1991 PA calculations, we used the maximum area distribution of 25 to 55% because the results are more conservative. We could not readily establish the likelihood that the elevation of Anhydrite III in the Castile Formation could be used as a cutoff for indicating whether a brine reservoir existed under the disposal area without further examination of the occurrence of brine reservoirs in the region.

Lack of Spatial Correlation of Conductor Elevations. The variogram analysis suggests that conductor elevations are not correlated over a distance of 250 m. Aside from ramifications for interpolation, this result appears to place limits on the areal extent of brine reservoirs beneath WIPP. This conclusion is not entirely justified. Figure 5.1-9 shows a hypothetical arrangement of measurement points, and an underlying structure dominated by narrow features at an angle to the measurement array. Although the features are continuous over the region, observations of particular features are randomly distributed through the measurement array. In order for the underlying correlation structure of the oblong features to be revealed in this hypothetical case, the measurement array must be able to resolve the minimum characteristic dimension of the features. Note that it may still be possible for the original sampling to provide a good estimate of the relative area of each feature type.

Although the above illustration is hypothetical, geologic considerations argue that brine reservoir location may be controlled by fracturing along Castile anticlines. In this situation, it is not unreasonable to expect brine reservoirs to be defined by long, narrow fracture zones along the anticline axis. Lack of correlation at a scale of 250 m would then place an upper limit on the minimum dimension of these fracture zones, but would not constraint maximum area extent.

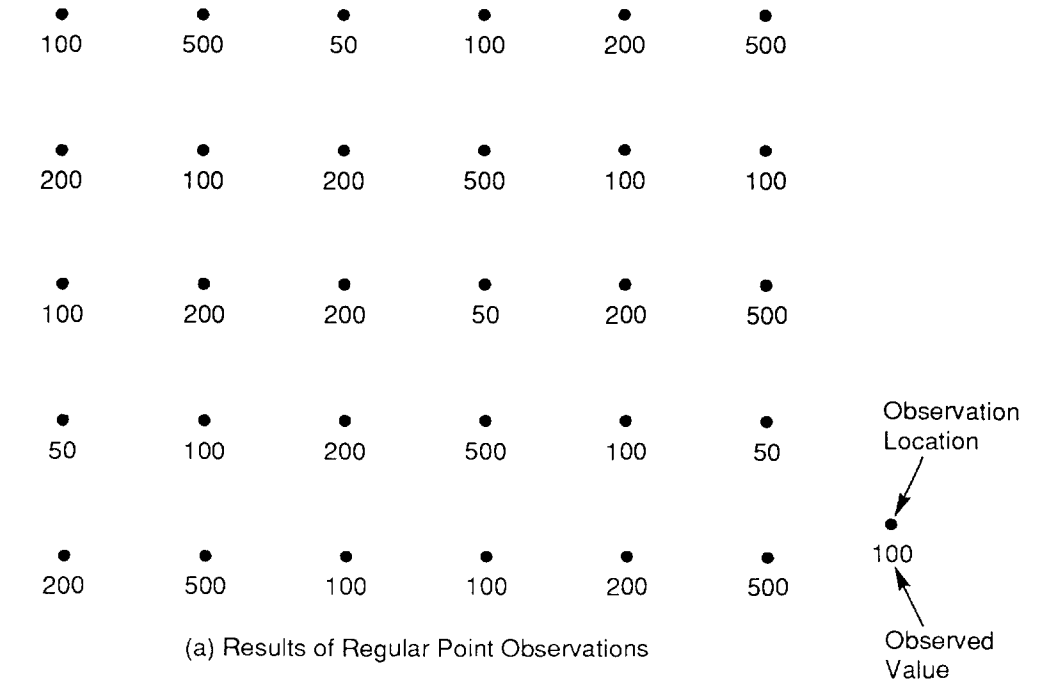

(a) Results of Regular Point Observations

(b) Underlying Structure

TRI-6342-1419-0

Figure 5.1-9. Illustration of Hypothetical Variability of Regular Sampling of Extensive Narrow Features.

5.1.2 Location of Intrusion

In 1991, the location of the borehole was fixed at the center of the disposal region (see Figure 3.1-2) to reduce the computational burden in the transport calculations until the influence of the variable transmissivity fields on fluid flow could be determined. (The most conservative position was not known a priori.) Next year's PA calculations will either use a variable position of the borehole or select a conservative location.

5.2 Human-Intrusion Probability (Drilling) Models

5.2.1 Drilling Rate Function

Parameter:	**Drilling rate function** $\Lambda(t)$
Median:	5.2×10^{-12}
Range:	$0 <$ 1.04×10^{-11}
Units:	s^{-1}
Distribution:	Uniform
Source(s):	Tierney, M. S. 1991. *Combining Scenarios in a Calculation of the Overall Probability Distribution of Cumulative Releases of Radioactivity from the Waste Isolation Pilot Plant, Southeastern New Mexico.* SAND90-0838. Albuquerque, NM: Sandia National Laboratories. (Appendix C)

Figure 5.2-1 shows the distribution for the constant failure rate function for exploratory drilling.

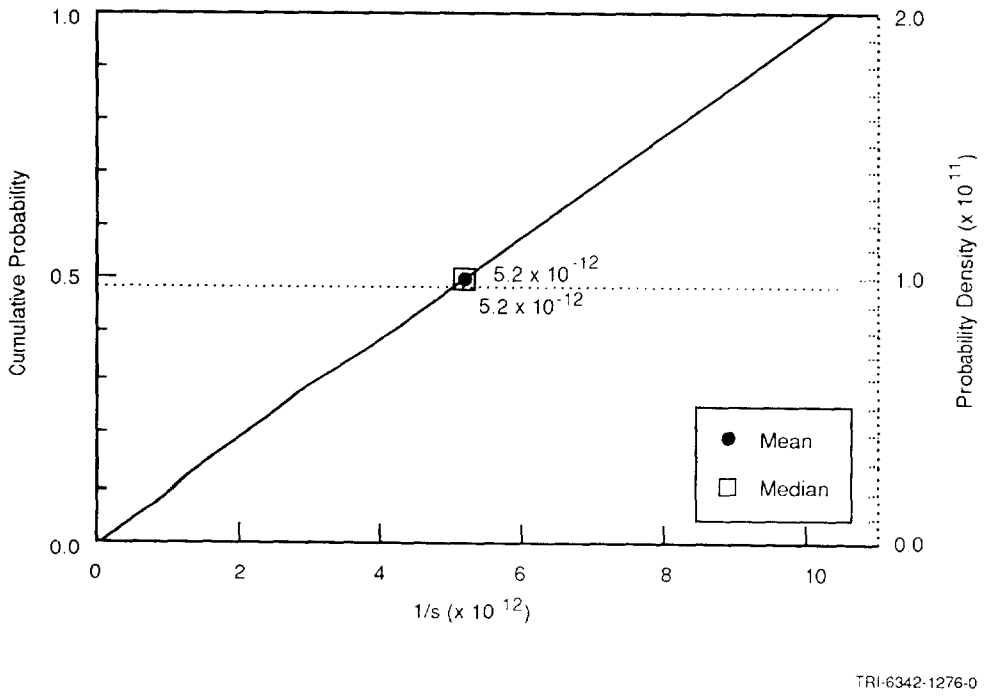

Figure 5.2-1. Estimated Distribution (pdf and cdf) of Constant Failure Rate.

Discussion:

The model for determining the probabilities of human intrusions (drilling) is based upon a general failure rate function ($\Lambda(t)$):

$$\Lambda(t) = \begin{cases} 0, & 0 < t < t_0 \\ -d/dt\ \ell n[1-F(t)], & t_0 < t \end{cases} \qquad (5.2\text{-}1)$$

where

t = time elapsed since disposal system placed in operation
t_0 = time when active government control ceases (100 yr [40 CFR 191])
$F(t)$ = cumulative distribution for first time of disturbing event.

40 CFR 191, Appendix B, places an upper bound on $\Lambda(t)$:

> ... the Agency assumes that the likelihood of such inadvertent and intermittent drilling need not be taken to be greater than 30 boreholes per square kilometer per 10,000 years for geologic repositories in proximity to sedimentary rock formations...

or

$$\lambda = \frac{30 \text{ boreholes}}{10^6 m^2\ 10^4 yr} \cdot \text{area of excavated disposal region} \qquad (5.2\text{-}2)$$

Hence for the WIPP, $\lambda = 3.28 \times 10^{-4}$ yr^{-1} assuming an excavated disposal region of about 1.09×10^5 m^2 (1.1×10^6 ft^2). The mean time of the first intrusion is $1/\lambda$ or about 3,000 yr. The number of intrusions is sampled from an associated Poisson distribution.

Similarly, *40 CFR 191*, Appendix B, places a lower bound on $\Lambda(t)$:

> ... passive institutional controls should not be assumed to completely rule out the possibility of intrusion ...

The actual variation of the drilling (failure) rate function with time is unknown but can be conservatively approximated by a piecewise linear function (Tierney, 1991, Appendix C) (Curve A, Figure 5.2-2). Currently, PA calculations assume $\Lambda(t)$ is a constant ($\Lambda(t) = \lambda$) for each simulation and uniformly distributed between certain maximum and minimum values.* The failure rate, $\Lambda(t)$, is used in estimating, for example, probabilities for multiple intrusions or evaluating the time of the first intrusion.

---

* Though conservative, the constant failure rate is unrealistic because the effects of markers (required by 40 CFR 191 to warn of the presence of the repository) are ignored.

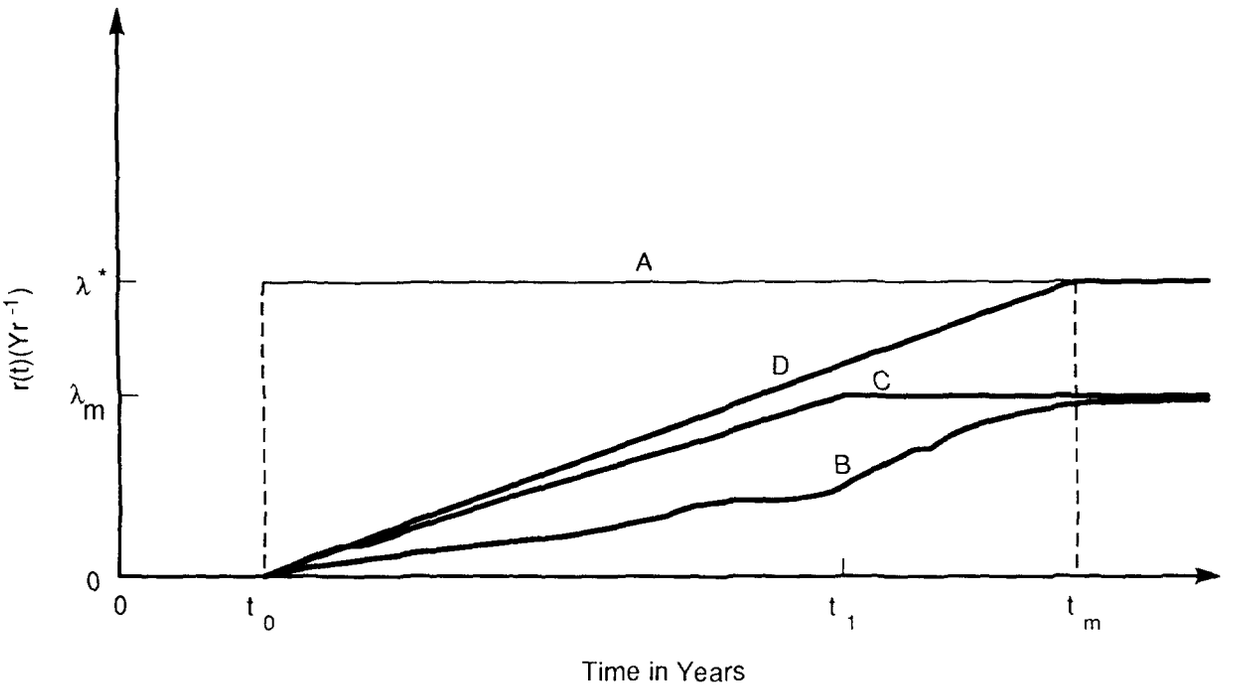

Figure 5.2-2. Alternative Forms of a Failure Rate for Exploratory Drilling (after Tierney, 1991, Appendix C).

Assuming that the times of attempted drilling are independent of each other and that the failure rate $\Lambda(t)$ is a constant λ, the probability that drilling will occur exactly n times in the time interval t is given by the Poisson distribution (Ross, 1985, Chapter 7):

$$P\{N=n\} = \frac{(\lambda t)^n}{n!} \exp(-\lambda t), \quad n=0,1,2,\ldots \qquad (5.2\text{-}3)$$

where

t = time
$1/\lambda + t_0$ = average time one must wait until first drilling occurs
N = number of intrusions (a random variable).

Because the PA Division grouped the occurrence of human intrusion into separate scenarios, PA calculations used the conditional probability. The conditional probability that drilling will occur more than once ($N > 0$) is

$$P\{N=n \mid N>0\} = P\{N=n\}/P\{N>0\} \qquad (5.2\text{-}4)$$

where

$$P\{N>0\} = 1 - P\{N=0\} = 1 - \exp(-\lambda t)$$

Hence,

$$P\{N=n \mid N>0\} = \left(\frac{(\lambda t)^n}{n!} \exp(-\lambda t)\right)/[1-\exp(-\lambda t)] \qquad (5.2\text{-}5)$$

The discrete probability of intrusion, $P\{N=n \mid N>0\}$, is given in Table 5.2-1 and Figure 5.2-2 for between 1 and 13 intrusions for $\Lambda(t) - \lambda_{max} = 3.28 \times 10^{-4}$ yr^{-1}.

Table 5.2-1. Probability of Multiple Hits into Disposal Region of Repository

Median	Range		Value	Probability	Units	Source
3	1	13	1	1.2810×10^{-1}	none	Tierney, 1991, Appendix C
			2	2.1020×10^{-1}		
			3	2.2990×10^{-1}		
			4	1.8860×10^{-1}		
			5	1.2380×10^{-1}		
			6	6.77×10^{-2}		
			7	3.17×10^{-2}		
			8	1.30×10^{-2}		
			9	4.70×10^{-3}		
			10	1.60×10^{-3}		
			11	5.00×10^{-4}		
			12	1.00×10^{-4}		
			13	1.00×10^{-4}		

5.2.2 Time of First Intrusion for Scenarios

Parameter:	**Time of first intrusion**
Median:	7×10^{10}
Range:	3.156×10^{9}
	3.156×10^{11}
Units:	s
Distribution:	Exponential
Source(s):	Tierney, M. S. 1991. *Combining Scenarios in a Calculation of the Overall Probability Distribution of Cumulative Releases of Radioactivity from the Waste Isolation Pilot Plant, Southeastern New Mexico.* SAND90-0838. Albuquerque, NM: Sandia National Laboratories. (Appendix C)

Figure 5.2-3 shows the distribution for time of intrusion.

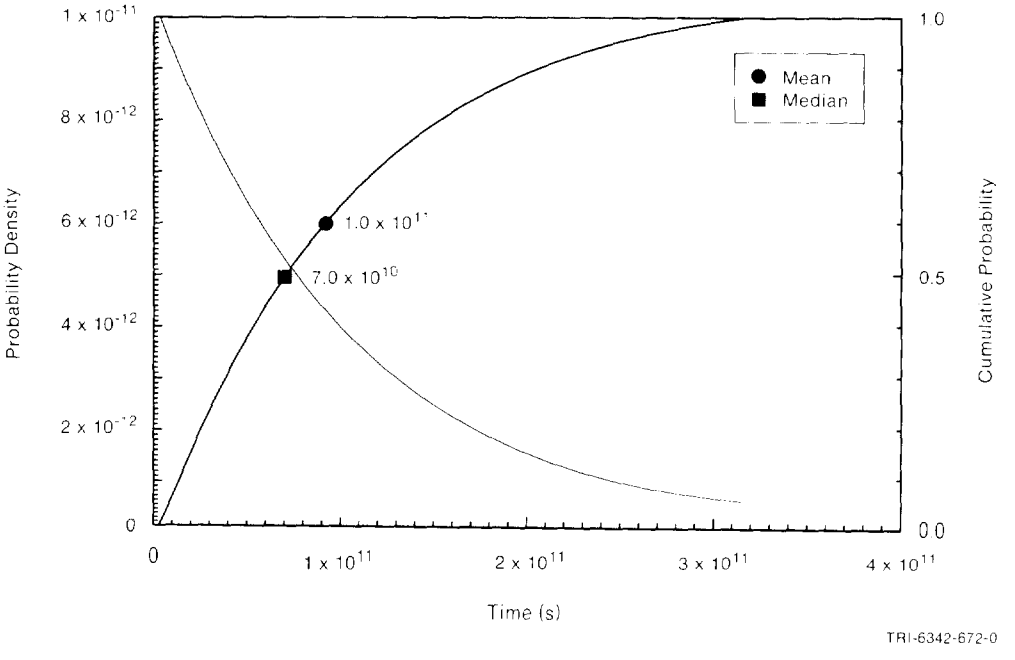

Figure 5.2-3. Estimated Distribution (pdf and cdf) for Time of Intrusion for E1, E2, and E1E2 Scenarios.

Discussion:

The time of first intrusion is evaluated from failure rate function $\Lambda(t)$ (Eq. 5.2-1). Integrating Eq. 5.2-1 to evaluate F(t) yields

$$F(t) = 1 - \exp\left[-\int_{t_o}^{t} \Lambda(\tau)\, d\tau\right] \qquad (5.2\text{-}6)$$

Since PA calculations assume $\Lambda(t)$ is a constant (λ) for each simulation, F(t) is a cumulative exponential distribution

$$F(t) = \begin{cases} 0 \\ 1 - \exp(-\lambda t), \end{cases} \quad \begin{array}{l} \text{if } 0 < t < t_0 \\ \text{if } t \geq t_0 \end{array} \qquad (5.2\text{-}7)$$

$$= \Pr\{\text{time of hit} < t\}$$

where

$1/\lambda + t_0$ = the average time one must wait either until the first drilling occurs that intersects the disposal region or between intrusions.

Thus, for a Poisson process, the waiting time between successive intrusions has an exponential distribution.

Because the PA Division grouped the occurrence of human intrusion into separate scenarios, PA calculations used the conditional probability. The conditional probability on the time when drilling will occur given that drilling occurs at least once before $t > t_1$, where t_1 is the regulatory period of 10,000 yr is (Miller and Freund, 1977, p. 34)

$$P\{\text{time of hit} < t \mid \text{time of hit} < t_1\}$$
$$= P\{\text{time of hit} < t\}/P\{\text{time of hit} < t_1\} \qquad (5.2\text{-}8)$$

where

$P\{\text{time of hit}$ $1 - \exp[-\lambda(t_1 - t_0)]$

Hence,

$$P\{\text{time of hit} < t \mid \text{time of hit} < t_1\}$$
$$= \{1 - \exp[-\lambda(t - t_0)]\}/\{1 - \exp[-\lambda(t_1 - t_0)]\} \qquad (5.2\text{-}9)$$

5.2.3 Times of Multiple Intrusions

Parameter:	**Time of intrusion**
Median:	1.5936×10^{11}
Range:	3.156×10^{9}
	3.156×10^{11}
Units:	s
Distribution:	Uniform
Source(s):	Tierney, M. S. 1991. *Combining Scenarios in a Calculation of the Overall Probability Distribution of Cumulative Releases of Radioactivity from the Waste Isolation Pilot Plant, Southeastern New Mexico.* SAND90-0838. Albuquerque, NM: Sandia National Laboratories. (Appendix C)

Figure 5.2-4 shows the distribution for time of intrusion used in 1990.

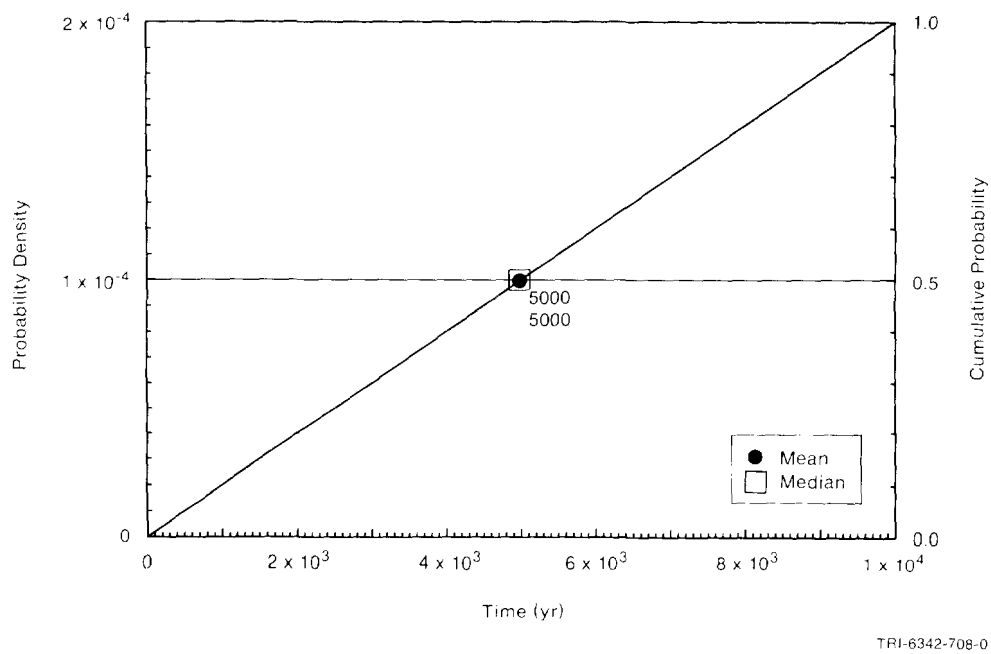

Figure 5.2-4. Estimated Distribution (pdf and cdf) for Time of Intrusion for Multiple Hits Used in 1990.

Discussion:

In 1990, the times of the N intrusions were evaluated from a uniform distribution between 100 and 10,000 yr* (Figure 5.2-4). The N random samples from the uniform distribution were then ordered from the smallest to the largest. Identical times for intrusions were permitted. Because the waiting times between successive intrusions have exponential distributions for a Poisson process, the mean time of intrusion (or mean time between intrusions) was $1/\lambda + t_0$ or about 3,000 yr.

In 1991, the time of intrusion is used to define computational scenarios. To simplify the discretization, the time of intrusion was divided into five equal intervals of 2,000 yr and the intrusion or multiple intrusions in each interval set at the midpoint (e.g., 1,000 yr).

---

* For compliance calculations, 100 yr is the time period after which active government control of the WIPP must be assumed to stop (40 CFR 191); 10,000 yr is the end of the regulatory period.

6. SUMMARY OF PARAMETERS SAMPLED IN 1991

Tables 6.0-1, 6.0-2, and 6.0-3 summarize the parameters that were sampled for the 1991 PA calculations for the geologic barriers, engineered barriers, and agents acting on the disposal system and probability models for scenarios, respectively. Figure 6.0-1 shows the rank correlation for halite and anhydrite permeability (Table 6.0-1).

Table 6.0-1. Distributions of Sample Parameters in December 1991 WIPP Performance Assessment for Geologic Barriers

Parameter	Median	Range		Units	Distribution Type	Source
Halite within Salado Formation						
Permeability (k)	5.7×10^{-21}	8.6×10^{-22}	5.4×10^{-20}	m^2	Data	Beauheim, June 14, 1991, Memo (see Appendix A)
Pore pressure (p)	1.28×10^{7}	9.3×10^{6}	1.39×10^{7}	Pa	Data	See anhydrite.
Anhydrite Layers within Salado Formation						
Pore pressure (p)	1.28×10^{7}	9.3×10^{6}	1.39×10^{7}	Pa	Data	Beauheim, June 14, 1991, Memo; Howarth, June 12, 1991, Memo (see Appendix A)
*Permeability (k)						
Undisturbed	7.8×10^{-20}	6.8×10^{-20}	9.5×10^{-19}	m^2	Data	Beauheim, June 14, 1991, Memo (see Appendix A)
Porosity (ϕ)						
Undisturbed	1×10^{-2}	1×10^{-3}	3×10^{-2}	none	Cumulative	See text.
Threshold displacement pressure (p_t)	3×10^{5}	3×10^{3}	3×10^{7}	Pa	Lognormal	Davies, 1991; Davies, June 2, 1991, Memo (see Appendix A)
Castile Formation Brine Reservoir						
Initial pressure (p)	1.26×10^{7}	1.1×10^{7}	2.1×10^{7}	Pa	Cumulative	Popielak et al., 1983, p. H-52; Lappin et al., 1989, Table 3-19
Storativity, bulk (S_b)	2×10^{-1}	2×10^{-2}	2	m^3	Lognormal	See text.
Culebra Dolomite Member						
Dispersivity, longitudinal (α_L)	1×10^{2}	5×10^{1}	3×10^{2}	m	Cumulative	Lappin et al., 1990, Table E-6
Fracture spacing (2B)	4×10^{-1}	6×10^{-2}	8	m	Cumulative	Beauheim et al., June 10, 1991, Memo (see Appendix A)
Porosity						
Fracture (ϕ_f)	1×10^{-3}	1×10^{-4}	1×10^{-2}	none	Lognormal	Lappin et al., 1989, Table 1-2, Table E-6
Matrix (ϕ_m)	1.39×10^{-1}	9.6×10^{-2}	2.08×10^{-1}	none	Spatial	Kelley and Saulnier, 1990, Table 4.4; Lappin et al., 1989 Table E-8

* Permeability of the halite and anhydrite were rank correlated with an r = 0.80 (Figure 6.0-1).

Table 6.0-1. Distributions of Sample Parameters in December 1991 WIPP Performance Assessment for Geologic Barriers (Continued)

Parameter	Median	Range		Units	Distribution Type	Source
Partition Coefficients						
Fracture						
Am	9.26×10^{1}	0.0	1×10^{3}	m^3/kg	Cumulative	See text.
Np	1	0.0	1×10^{3}	m^3/kg	Cumulative	See text.
Pu	2.02×10^{2}	0.0	1×10^{3}	m^3/kg	Cumulative	See text.
Th	1×10^{-1}	0.0	1×10^{1}	m^3/kg	Cumulative	See text.
U	7.5×10^{-3}	0.0	1	m^3/kg	Cumulative	See text.
Matrix						
Am	1.86×10^{-1}	0.0	1×10^{2}	m^3/kg	Cumulative	See text.
Np	4.8×10^{-2}	0.0	1×10^{2}	m^3/kg	Cumulative	See text.
Pu	2.61×10^{-1}	0.0	1×10^{2}	m^3/kg	Cumulative	See text.
Th	1×10^{-2}	0.0	1	m^3/kg	Cumulative	See text.
U	2.58×10^{-2}	0.0	1	m^3/kg	Cumulative	See text.
Transmissivity field	3.5×10^{1}	0	60	none	Uniform	See text.

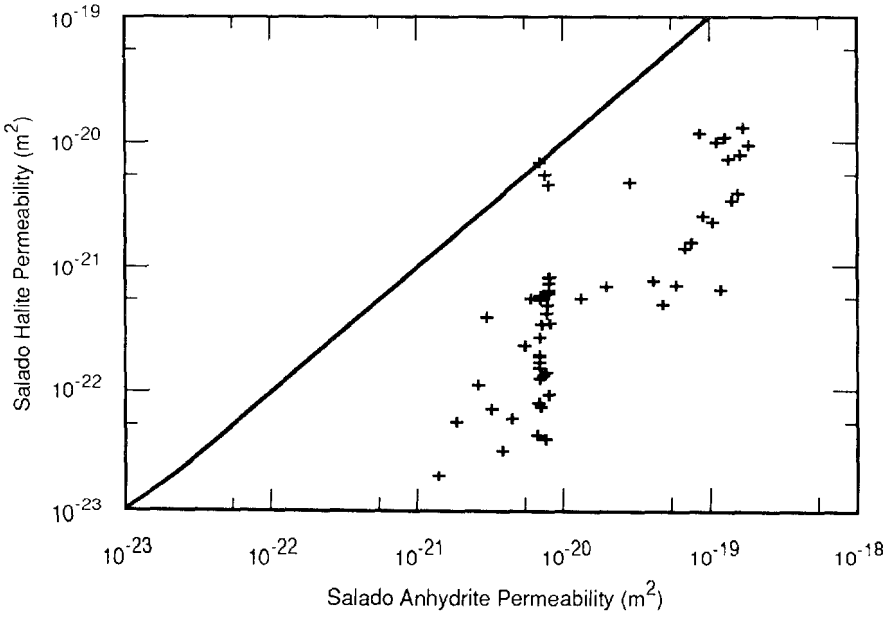

Figure 6.0-1. General Relationship Maintained between Halite and Anhydrite Permeabilities of Salado Formation Using a Rank Correlation Coefficient (r) of 0.80.

Table 6.0-2. Distributions of Sample Parameters in December 1991 WIPP Performance Assessment for Engineered Barriers

Parameter	Median		Range	Units	Distribution Type	Source
Unmodified Waste Form						
Gas Generation						
Corrosion						
Inundated rate	6.3×10^{-9}	0	1.3×10^{-8}	$mol/m^2/s$*	Cumulative	Brush, July 8, 1991, Memo (see Appendix A)
Relative humid rate	1×10^{-1}	0	5×10^{-1}	none	Cumulative	Brush, July 8, 1991, Memo (see Appendix A)
Stoichiometry	5×10^{-1}	0	1	none	Uniform	Brush and Anderson in Lappin et al., 1989, p. A-6
Microbiological						
Inundated rate	3.2×10^{-9}	0	1.6×10^{-8}	mol/kg/s**	Cumulative	Brush, July 8, 1991, Memo (see Appendix A)
Relative humid rate	1×10^{-1}	0	2×10^{-1}	none	Uniform	Brush, July 8, 1991, Memo (see Appendix A)
Stoichiometry	8.35×10^{-1}	0	1.67	none	Uniform	Brush and Anderson in Lappin et al., 1989, p. A-10.
Dissolved Concentrations (Solubility)***						
Am^{3+}	$1x10^{-9}$	$5x10^{-14}$	1.4	Molar	Cumulative	Trauth et al., 1991
Np^{4+}	$6x10^{-9}$	$3x10^{-16}$	$2x10^{-5}$	Molar	Cumulative	Trauth et al., 1991
Np^{5+}	$6x10^{-7}$	$3x10^{-11}$	$1.2x10^{-2}$	Molar	Cumulative	Trauth et al., 1991
Pu^{4+}	6×10^{-10}	2.0×10^{-16}	4×10^{-6}	Molar	Cumulative	Trauth et al., 1991
Pu^{5+}	$6x10^{-10}$	$2.5x10^{-17}$	$5.5x10^{-4}$	Molar	Cumulative	Trauth et al., 1991
Th^{4+}	$1x10^{-10}$	$5.5x10^{-16}$	$2.2x10^{-6}$	Molar	Cumulative	Trauth et al., 1991
U^{4+}	$1x10^{-4}$	$1x10^{-15}$	$5x10^{-2}$	Molar	Cumulative	Trauth et al., 1991
U^{6+}	$2x10^{-3}$	$1x10^{-7}$	1	Molar	Cumulative	Trauth et al., 1991
Volume Fractions of IDB Categories						
Metal/Glass	3.76×10^{-1}	2.76×10^{-1}	4.76×10^{-1}	none	Normal	See text, Table 3.4-9
Combustibles	3.84×10^{-1}	2.84×10^{-1}	4.84×10^{-1}	none	Normal	See text, Table 3.4-9
Initial waste saturation	1.38×10^{-1}	0	2.76×10^{-1}		Uniform	See text.
Eh-pH Conditions	0.5	0	1.0	none	Uniform	See text.

* $mole/m^2$ surface area steel/s

** mole/kg cellulosics/s

*** For the following elements —Np, Pu, and Th —only one species was used in each sample. The species were rank correlated at r = 0.99.

Table 6.0-3. Distributions of Sample Parameters in December 1991 WIPP Performance Assessment for Agents Acting on Disposal System and Probability Models for Scenarios

Parameter	Median	Range		Units	Distribution Type	Source
Agents Acting on Disposal System						
Intrusion Borehole Flow Parameters						
Diameter	3.55×10^{-1}	2.67×10^{-1}	4.44×10^{-1}	m	Uniform	See text.
Permeability (k)	3.16×10^{-12}	1×10^{-14}	1×10^{-11}	m^2	Lognormal	Freeze and Cherry, Table 2.2 (clean sand)
Climate parameter						
Recharge amplitude factor	8×10^{-2}	0	1.6×10^{-1}	none	Uniform	See text.
Probability Model for Scenarios						
Area of pressurized brine reservoir	4.0×10^{-1}	2.5×10^{-1}	5.52×10^{-1}	none	Cumulative	See text.
Rate constant in Poisson drilling model, $\Lambda(t)$	5.2×10^{-12}	0 <	1.04×10^{-11}	s^{-1}	Uniform	40 CFR 191.

Selection Procedure for Parameters Sampled in 1991

A parameter was chosen for sampling in the 1991 PA calculations if it fulfilled one of two criteria: (1) the parameter proved to be sensitive in the 1990 sensitivity analyses (Helton et al., 1991); or (2) the parameter was an imprecisely known quantity in a consequence model first formally used in the present (1991) series of calculations. Examples of parameters that fulfilled Criterion 1 are Culebra partition coefficients and dissolved concentrations (solubilities including Eh-pH conditions). Examples of parameters that fulfilled Criterion 2 are the parameters of dual-porosity transport in the Culebra (dispersivity, fracture spacing, matrix and fracture porosities); material properties of the anhydrite layers within the Salado Formation (pore pressure, permeability, porosity); gas generation rates in unmodified waste forms; volume fractions of unmodified waste forms; and constants in probability model for human intrusion scenarios (area of pressurized brine reservoir, rate constant in Poisson model of exploratory drilling). Some imprecisely known parameters must be sampled in any PA exercise that uses the results of certain models; examples of this kind of parameter are the transmissivity field, intrusion-borehole flow parameters (permeability, porosity), and the recharge factor for climatic change (Swift, October 10, 1991, Memo [Appendix A]).

Consequence Models for WIPP Disposal System (42 + 3 Variables)

Geologic Barriers (22 Variables)

Halite within Salado Formation Near Repository (1 variable)
- **Permeability** (1)
- Sampled in 1990 But Omitted in 1991
  - *Compressibility* — not very important in 1990

Anhydrite Layers within Salado Formation (4 variables)
- **Brine Pressure at Repository Level** (1)
- **Permeability, Intact** (1)
- **Porosity, Intact** (1)
- **Threshold pressure** (1)

Castile Formation Brine Reservoir (2 variables)
- **Bulk Storativity (S_b)** (1)
- **Initial Pressure** (1)

Culebra Dolomite Member (13 variables)
- **Dispersivity** (1)
- **Matrix Porosity** (1)
- **Fracture Porosity** (1) (no quantitative correlation with T)
- **Fracture Spacing** (1) (no quantitative correlation with T)
- **Retardation, Matrix and Fracture** (10=5x2)
- **Transmissivity Field** (1) (0 - 60, uniform distribution)
- Sampled in 1990 But Omitted in 1991
  - *Tortuosity* — not much spatial change in transport model domain

Engineered Barriers (15 + 3 Variables)

Unmodified Waste Form
- **Gas Generation Rates for Corrosion and Degradation in Humid and Saturated Conditions** (4)
- **Corrosion stoichiometry** (1)
- **Microbial stoichiometry** (1)
- **Dissolved Concentrations (Solubility)** (5 + 3) — 3 correlated at r = 0.99 for modeling convenience
- **Volumes of Metal and Combustibles** (2)
- **Initial Waste Saturation** (1)
- **Eh-pH Conditions** (1)
- Sampled in 1990 But Omitted in 1991
  - *Molecular Diffusion* -- Species dependent in 1991

Agents Acting on Disposal System (3 Variables)

- **Recharge** (1) (includes leakage from subsidence)
- **Intrusion Borehole Permeability and Drill Bit Diameter** (2) (based on deep gas reservoir target in 1991)

Probability Model for Scenarios (2 Variables)

Area of Pressurized Brine Reservoir (1)
Rate Constant in Poisson Drilling Model (1)
Sampled in 1990 but Omitted in 1991
Number of Hits -- Defining variable for computational scenario
Room Number -- Area of brine reservoir determines probability of hitting brine reservoir in 1991; location for transport is fixed at the center of the Disposal Region
Time of Intrusion -- Defining variable for computational scenario

REFERENCES

Allison, G. B. 1988. "A Review of Some of the Physical, Chemical, and Isotopic Techniques Available for Estimating Groundwater Recharge," in I. Simmers (ed.), *Estimation of Natural Groundwater Recharge.* NATO ASI series, series C, vol. 222. Dordrecht, Holland: D. Reidel. pp. 49-72.

Anderson, D. R., M. G. Marietta, and M. S. Tierney. 1990. "Request for Assistance in Assigning Probability Distribution to the Parameters Being Used for the Preliminary Performance Assessment of the WIPP relating to EPA 40 CFR 191," Memo 2 in Appendix A of Rechard et al. 1990. *Data Used in Preliminary Performance Assessment of the Waste Isolation Pilot Plant (1990).* SAND89-2408. Albuquerque, NM: Sandia National Laboratories.

Anderson, D. R., K. M. Trauth, and S. C. Hora. 1991. "The Use of Expert Elicitation to Quantify Uncertainty in Incomplete Sorption Data Bases for Waste Isolation Pilot Plant Performance Assessment." SAND91-7099C. Presented at the *Organization for Economic Cooperation and Development, Nuclear Energy Agency Sorption Workshop '91, Interlaken, Switzerland, October 16, 1991.*

Arguello, J. G. 1988. *WIPP Panel Entryway Seal-Numerical Simulation of Seal Composite Interaction for Preliminary Seal Design Evaluation.* SAND87-2804. Albuquerque, NM: Sandia National Laboratories.

Austin, E. H. 1983. *Drilling Engineering Handbook.* Boston, MA: International Human Resources Development Corporation.

Avis, J. D., and G. J. Saulnier, Jr. 1990. *Analysis of the Fluid-Pressure Responses of the Rustler Formation at H-16 to the Construction of the Air-Intake Shaft at the Waste Isolation Pilot Plant (WIPP) Site.* SAND89-7067. Albuquerque, NM: Sandia National Laboratories.

Bachman, G. O. 1981. *Geology of Nash Draw, Eddy County, New Mexico.* U.S. Geological Survey Open-File Report 81-31. Albuquerque, NM: U. S. Geological Survey.

Barnhart, B. J., E. W. Campbell, E. Martinez, D. E. Caldwell, and R. Hallett. 1980. *Potential Microbial Impact on Transuranic Wastes Under Conditions Expected in the Waste Isolation Pilot Plant (WIPP), Annual Report, October 1, 1978-September 30, 1979.* LA-8297-PR. Los Alamos, NM: Los Alamos National Laboratories.

Bayley, S. G., M. D. Siegel, M. Moore, and S. Faith. 1990. *Sandia Sorption Data Management System Version 2 (SSDMS11).* SAND89-0371. Albuquerque, NM: Sandia National Laboratories.

Bear, J. 1972. *Dynamics of Fluids in Porous Media.* New York: American Elsevier Publishing Company, Inc.

Bear, J., and A. Verruijt. 1987. *Modeling Groundwater Flow and Pollution.* Boston, MA: D. Reidel Publishing Company, p. 126.

Beauheim, R. L. 1987a. *Analysis of Pumping Tests of the Culebra Dolomite Conducted at the H-3 Hydropad at the Waste Isolation Pilot Plant (WIPP) Site.* SAND86-2311. Albuquerque, NM: Sandia National Laboratories.

Beauheim, R. L. 1987b. *Interpretation of the WIPP-13 Multipad Pumping Test of the Culebra Dolomite at the Waste Isolation Pilot Plant (WIPP) Site.* SAND87-2456. Albuquerque, NM: Sandia National Laboratories.

Beauheim, R. L. 1987c. *Interpretations of Single-Well Hydraulic Tests Conducted at and Near the Waste Isolation Pilot Plant (WIPP) Site, 1983-1987.* SAND87-0039. Albuquerque, NM: Sandia National Laboratories.

Beauheim, R. L. 1989. *Interpretation of H-11b4 Hydraulic Tests and the H-11 Multipad Pumping Test of the Culebra Dolomite at the Waste Isolation Pilot Plant (WIPP) Site.* SAND89-0536. Albuquerque, NM: Sandia National Laboratories.

Beauheim, R. L. 1990. "Review of Parameter Values to be Used in Performance Assessment," Memo 3c in Appendix A of Rechard et al. 1990. *Data Used in Preliminary Performance Assessment of the Waste Isolation Pilot Plant (1990).* SAND89-2408. Albuquerque, NM: Sandia National Laboratories.

Beauheim, R. L., G. J. Saulnier, and J. D. Avis. 1990. *Interpretation of Brine-Permeability Tests of the Salado Formation at the Waste Isolation Pilot Plant Site: First Interim Report.* SAND90-0083. Albuquerque, NM: Sandia National Laboratories.

Beauheim, R. L., G. J. Saulnier, and J. D. Avis. 1991. *Interpretation of Brine-Permeability Tests of the Salado Formation at the Waste Isolation Pilot Plant: First Interim Report.* SAND90-0083. Albuquerque, NM: Sandia National Laboratories.

Bechtel, Inc. 1985. *Quarterly Geotechnical Field Data Report, December 1985.* WIPP-DOE-211. Prepared for the U.S. Department of Energy. San Francisco, CA: Bechtel National, Inc.

Bechtel, Inc. 1986. *WIPP Design Validation Final Report.* DOE/WIPP-86-010. Prepared for U.S. Department of Energy. San Francisco, CA: Bechtel National, Inc.

Bertram-Howery, S. G., M. G. Marietta, D. R. Anderson, K. F. Brinster, L. S. Gomez, R. V. Guzowski, and R. P. Rechard. 1988. *Draft Forecast of the Final Report for the Comparison to 40 CFR Part 191, Subpart B for the Waste Isolation Pilot Plant.* SAND88-1452. Albuquerque, NM: Sandia National Laboratories.

Bertram-Howery, S. G., M. G. Marietta, R. P. Rechard, P. N. Swift, D. R. Anderson, B. Baker, J. Bean, W. Beyeler, K. F. Brinster, R. V. Guzowski, J. Helton, R. D. McCurley, D. K. Rudeen, J. Scheiber, and P. Vaughn. 1990. *Preliminary Comparison with 40 CFR Part 191, Subpart B for the Waste Isolation Pilot Plant, December 1990.* SAND90-2347. Albuquerque, NM: Sandia National Laboratories.

Bertram-Howery, S. G., and R. L. Hunter. 1989. *Preliminary Plan for Disposal-System Characterization and Long-Term Performance Evaluation of the Waste Isolation Pilot Plant.* SAND89-0178. Albuquerque, NM: Sandia National Laboratories.

Bertram-Howery, S. G., and P. Swift. 1990. *Status Report: Potential for Long-Term Isolation by the Waste Isolation Pilot Plant Disposal System, 1990.* SAND90-0616. Albuquerque, NM: Sandia National Laboratories.

Biot, M. A. 1991. "General Theory of Three-Dimensional Consolidation." *Journal of Applied Physics* vol. 12, February 1941, pp. 155-164.

Black, S. R., R. S. Newton, and D. K. Shukla, eds. 1983. "Brine Content of the Facility Interval Strata" in *Results of the Site Validation Experiments*, Vol. II, Supporting Document 10. Carlsbad, NM: U.S. Department of Energy.

Blom, G. 1989. *Probability and Statistics: Theory and Applications*. New York: Springer-Verlag.

Borns, D. J. 1985. *Marker Bed 139: A Study of Drillcore From a Systematic Array*. SAND85-0023. Albuquerque, NM: Sandia National Laboratories.

Bredenkamp, D. B. 1988a. "Quantitative Estimation of Ground-Water Recharge in Dolomite," in I. Simmers (ed.), *Estimation of Natural Groundwater Recharge*. NATO ASI series, series C, Vol. 222. Dordrecht, Holland: D. Reidel. pp. 449-460.

Bredenkamp, D. B. 1988b. "Quantitative Estimation of Ground-Water Recharge in the Pretoria-Rietondale Area," in I. Simmers (ed.), *Estimation of Natural Groundwater Recharge*. NATO ASI series, series C, vol. 222. Dordrecht, Holland: D. Reidel. pp. 461-476.

Brinster, K. F. 1990a. "Transmissivity Zones in Culebra Dolomite Member of Rustler Formation," Memo 8 in Appendix A of Rechard et al. 1990. *Data Used in Preliminary Performance Assessment of the Waste Isolation Pilot Plant (1990)*. SAND90-2408. Albuquerque, NM: Sandia National Laboratories.

Brinster, K. F. 1990b. "Transmissivities and Pilot Points for the Culebra Dolomite Member," Memo 9 in Appendix A of Rechard et al. 1990. *Data Used in Preliminary Performance Assessment of the Waste Isolation Pilot Plant (1990)*. SAND90-2408. Albuquerque, NM: Sandia National Laboratories.

Brinster, K. F. 1990c. "Well Data from Electric Logs," Memo 10 in Appendix A of Rechard et al. 1990. *Data Used in Preliminary Performance Assessment of the Waste Isolation Pilot Plant (1990)*. SAND89-2408. Albuquerque, NM: Sandia National Laboratories.

Brinster, K. F. 1991. *Preliminary Geohydrologic Conceptual Model of the Los Medaños Region Near the Waste Isolation Pilot Plant for the Purpose of Performance Assessment*. SAND89-7147. Albuquerque, NM: Sandia National Laboratories.

Broc, R., ed. 1982. *Drilling Mud and Cement Slurry Rheology Manual*. Houston, TX: Gulf Publishing Company.

Brooks, R. H., and A. T. Corey. 1964. "Hydraulic Properties of Porous Media," Hydrology Papers, No. 3. Fort Collins, CO: Colorado State University.

Brush, L. H. 1988. *Feasibility of Disposal of High-Level Radioactive Wastes into the Seabed: Review of Laboratory Investigations of Radionuclide Migration Through Deep-Sea Sediments*. SAND87-2438. Albuquerque, NM: Sandia National Laboratories.

Brush, L. H. 1990. *Test Plan for Laboratory and Modeling Studies of Repository and Radionuclide Chemistry for the Waste Isolation Pilot Plant*. SAND90-0266. Albuquerque, NM: Sandia National Laboratories.

Brush, L. H., and D. R. Anderson. 1989. "Appendix E: Estimates of Radionuclide Concentrations in Brines" in Marietta et al. 1989. *Performance Assessment Methodology Demonstration: Methodology Development for Purposes of Evaluating Compliance with EPA 40 CFR Part 191, Subpart B. for the Waste Isolation Pilot Plant*. SAND89-2027. Albuquerque, NM: Sandia National Laboratories.

Brush, L. H., and A. R. Lappin. 1990. "Additional Estimates of Gas Production Rates and Radionuclide Solubility for Use in Models of WIPP Disposal Rooms," Memo 4 in Appendix A of Rechard et al. 1990. *Data Used in Preliminary Performance Assessment of the Waste Isolation Pilot Plant (1990).* SAND89-2408. Albuquerque, NM: Sandia National Laboratories.

Buck, A. D. 1985. *Development of a Sanded Nonsalt Expansive Grout for Repository Sealing Application.* Miscellaneous Paper SL-85-6. Vicksburg, MS: Department of the Army, Waterways Experimental Station.

Buddenberg, J. W., and C. R. Wilke. 1949. *Ind. Eng. Chem.* 41: 1345-1347.

Bush, D. D., and S. Piele. 1986. *A Full Scale Borehole Sealing Test in Salt Under Simulated Downhole Conditions: Volume 1.* BMI/ONWI-573(2). Columbus, OH: Office of Nuclear Waste Isolation, Battelle Memorial Institute.

Butcher, B. M. 1989. *Waste Isolation Pilot Plant Simulated Waste Compositions and Mechanical Properties.* SAND89-0372. Albuquerque, NM: Sandia National Laboratories.

Butcher, B. M. 1990. "Disposal Room Porosity and Permeability Values for Disposal Room Performance Assessment," Memo 5 in Appendix A of Rechard et al. 1990. *Data Used in Preliminary Performance Assessment of the Waste Isolation Pilot Plant (1990).* SAND89-2408. Albuquerque, NM: Sandia National Laboratories.

Butcher, B. M., T. W. Thompson, R. G. VanBuskirk, and N. C. Patti. 1991. *Mechanical Compaction of WIPP Simulated Waste.* SAND90-1206. Albuquerque, NM: Sandia National Laboratories.

Caldwell, D. E. 1981. *Microbial Biogeochemistry of Organic Matrix Transuranic Waste.* Unpublished Report submitted to M. A. Molecke, June 17, 1981. Albuquerque, NM: University of New Mexico.

Caldwell, D. E., R. C. Hallett, M. A. Molecke, E. Martinez, and B. J. Barnhart. 1988. *Rates of Co2 Production from the Microbial Degradation of Transuranic Wastes under Simulated Geologic Isolation Conditions.* SAND87-7170. Albuquerque, NM: Sandia National Laboratories.

Carmichael, R. S., ed. 1984. *CRC Handbook of Physical Properties of Rocks,* Vol. III. Boca Raton, FL: CRC Press, Inc.

Cauffman, T. L., A. M. LaVenue, and J. P. McCord. 1990. *Ground-Water Flow Modeling of the Culebra Dolomite: Volume II Data Base.* SAND89-7068/2. Albuquerque, NM: Sandia National Laboratories.

Chapman, N. A., and J. A. T. Smellie. 1986. "Natural Analogues to the Conditions around a Final Repository for High-Level Radioactive Waste." *Chemical Geology* vol. 55, no. 3/4.

Cheeseman, R. J. 1978. *Geology and Oil/Potash Resources of the Delaware Basin, Eddy and Lea Counties, New Mexico.* New Mexico Bureau of Mines and Mineral Resources Circular 159. Socorro, NM: New Mexico Bureau of Mines and Mineral Resources. 7-14.

Christensen, C. L., and W. W. Petersen. 1981. *The Bell Canyon Test Summary Report.* SAND80-1375. Albuquerque, NM: Sandia National Laboratories.

Clark, S. P. 1966. *Handbook of Physical Constants.* New York: The Geological Society of America, Inc.

Colebrook, C. F. 1938. "Turbulent Flow in Pipes, with Particular Reference to the Transition Region Between the Smooth and Rough Pipe Laws," *J. Inst. Civ. Eng. Long.* **11**: 133-156.

Conover, W. J. 1980. *Practical Nonparametric Statistics.* 2nd ed. New York: John Wiley and Sons.

Cranwell, R. M., and J. C. Helton. 1981. "Uncertainty Analysis for Geologic Disposal of Radioactive Waste," in D. C. Kocher, ed., *Proceedings of the Symposium on Uncertainties Associated with the Regulation of the Geologic Disposal of High-Level Radioactive Waste, Gatlinburg, TN, March 9-13, 1981.*

Cranwell, R. M., R. V. Guzowski, J. E. Campbell, and N. R. Ortiz. 1990. *Risk Methodology for Geologic Disposal of Radioactive Waste: Scenario Selection Procedure.* SAND80-1429, NUREG/CR-1667. Albuquerque, NM: Sandia National Laboratories.

Cygan, R. T. 1991. *The Solubility of Gases in NaCl Brine and a Critical Evaluation of Available Data.* SAND90-2848. Albuquerque, NM: Sandia National Laboratories.

Darley, H. C. H. 1969. "A Laboratory Investigation of Borehole Stability." *Journal of Petroleum Technology*, July, 883-392.

Darley, H. C. H., and G. R. Gray. 1988. *Composition and Properties of Drilling and Completion Fluids.* Houston, TX: Gulf Publishing Company.

Davies, P. B. 1989. *Variable-Density Ground-water Flow and Palehydrology in the Waste Isolation Pilot Plant (WIPP) Region, Southeastern New Mexico.* Open File Report 88-490. Albuquerque, NM: U.S. Geological Survey, Dept. of the Interior.

Davies, P. B. 1991. *Evaluation of the Role of Threshold Pressure in Controlling Flow of Waste-Generated Gas into Bedded Salt at the Waste Isolation Pilot Plant.* SAND90-3246. Albuquerque, NM: Sandia National Laboratories.

Davies, P. B., and A. M. LaVenue. 1990a. "Comments on Model Implementation and Data for Use in August Performance Assessment Calculations," Memo 3b in Appendix A of Rechard et al. 1990. *Data Used in Preliminary Performance Assessment of the Waste Isolation Pilot Plant (1990).* SAND89-2408. Albuquerque, NM: Sandia National Laboratories.

Davies, P. B., and A. M. LaVenue. 1990b. "Additional Data for Characterizing 2-Phase Flow Behavior in Waste-Generated Gas Simulations and Pilot Point Information for Final Culebra 2-D Model," Memo 11 in Appendix A of Rechard et al. 1990. *Data Used in Preliminary Performance Assessment of the Waste Isolation Pilot Plant.* SAND89-2408. Albuquerque, NM: Sandia National Laboratories.

Davies, P. B., L. H. Brush, and F. T. Mendenhall. 1991. "Assessing the Impact of Waste-Generated Gas from the Degradation of Transuranic Waste at the Waste Isolation Pilot Plant (WIPP): An Overview of Strongly Coupled Chemical, Hydrologic, and Structural Processes." *Proceedings of NEA Workshop on Gas Generation and Release from Radioactive Waste Repositories, Aix-en-Provence, France, September 23, 1991.* Organisation for Economic Co-operation and Development (OECD).

Dosch, R. G. 1979. "Radionuclide Migration Studies Associated with the WIPP Site in Southern New Mexico" in G. J. McCarthy, ed., *Scientific Basis for Nuclear Waste Management.* New York: Plenum Publishing Company 1: 395-398.

Dullien, F. A. L. 1979. *Porous Media Fluid Transport and Pore Structure.* New York: Academic Press.

Earth Technology Corporation. 1988. *Final Report for Time Domain Electromagnetic (TDEM) Surveys at the WIPP Site.* SAND87-7144. Albuquerque, NM: Sandia National Laboratories.

Fanchi, J. R., J. E. Kennedy, and D. L. Dauben. 1987. *BOASTII: A Three-Dimensional Three-Phase Black Oil Applied Simulation Tool.* DOE/BC-88/2/SP. U.S. Department of Energy.

Frederickson, A. G. 1960. "Helical Flow of an Annular Mass of Visco-Elastic Fluid." *Chemical Engineering Science* vol. II: 252-259.

Freeze, R. A. and J. C. Cherry. 1979. *Groundwater.* Englewood Cliffs, NJ: Prentice-Hall, Inc.

Gorham, E. 1990. "Data for Use in August Performance Assessment Calculations," Memo 3 in Appendix A of Rechard et al. 1990. *Data Used in Preliminary Performance Assessment of the Waste Isolation Pilot Plant (1990).* SAND89-2408. Albuquerque, NM: Sandia National Laboratories.

Gonzales, M. M. 1989. *Compilation and Comparison of Test - Hole Location Surveys in the Vicinity of the Waste Isolation Pilot Plant Site.* SAND88-1065. Albuquerque, NM: Sandia National Laboratories.

Graboski, M. S., and T. E. Daubert. 1979. "A Modified Soave Equation of State for Phase Equilibrium Calculations. 3. Systems Containing Hydrogen," in *Ind. Eng. Chem. Process Des. Dev.* vol. 18, no. 2: 300-306.

Guzowski, R. V. 1990. *Preliminary Identification of Scenarios that May Affect the Release and Transport of Radionuclides from the Waste Isolation Pilot Plant, Southeastern New Mexico.* SAND89-7149. Albuquerque, NM: Sandia National Laboratories.

Guzowski, R. V. 1991. *Applicability of Probability Techniques to Determining the Probability of Occurrence of Potentially Disruptive Intrusive Events at the Waste Isolation Pilot Plant.* SAND90-7100. Albuquerque, NM: Sandia National Laboratories.

Harms, J. C., and C. R. Williamson. 1988. "Deep-water Density Current Deposits of Delaware Mountain Group (Permian), Delaware Basin, Texas and New Mexico." *American Association of Petroleum Geologists Bulletin* vol. 72, no. 3: 299-317.

Harr, M. E. 1987. *Reliability Based Design in Civil Engineering.* New York: McGraw Hill Book Co.

Haug, A., V. A. Kelley, A. M. LaVenue, and J. F. Pickens. 1987. *Modeling of Groundwater Flow in the Culebra Dolomite at the Waste Isolation Pilot Plant (WIPP) Site: Interim Report.* Contractor Report SAND86-7167. Albuquerque, NM: Sandia National Laboratories.

Helton, J. C., J. M. Griesmeyer, F. E. Haskin, R. L. Iman, C. N. Amos, and W. B. Murfin. 1988. "Integration of the NUREG-1150 Analyses: Calculation of Risk and Propagation of Uncertainties." *Proceedings of the Fifteenth Water Reactor Safety Research Information Meeting, Washington, D.C.* U.S. Nuclear Regulatory Commission. 151-176.

Helton. J. C., J. W. Garner, R. D. McCurley, and D. K. Rudeen. 1991. *Sensitivity Analysis Techniques and Results for Performance Assessment at the Waste Isolation Pilot Plant.* Contractor Report SAND90-7103. Albuquerque, NM: Sandia National Laboratories.

Henderson, F. M. 1966. *Open Channel Flow.* New York: Macmillan Publishing Co.

Hills, J. M. 1984. "Sedimentation, Tectonism, and Hydrocarbon Generation in Delaware Basin, West Texas and Southeastern New Mexico." *American Association of Petroleum Geologist Bulletin* **68**: 250-267.

Hiss, W. L. 1975. *Stratigraphy and Ground-Water Hydrology of the Capitan Aquifer, Southeastern New Mexico and West Texas.* Ph.D. Dissertation. Hydrology Dept, University of Colorado, Boulder.

Holcomb, D. J., and M. Shields. 1987. *Hydrostatic Creep Consolidation of Crushed Salt with Added Water.* SAND87-1990. Albuquerque, NM: Sandia National Laboratories.

Holt, R. M., and D. W. Powers. 1988. *Facies Variability and Post-Depositional Alteration Within the Rustler Formation in the Vicinity of the Waste Isolation Pilot Plant, Southeastern New Mexico.* DOE-WIPP 88-004. Carlsbad, NM: U.S. Department of Energy.

Holt, R. M., and D. W. Powers. 1990. *Geologic Mapping of the Air Intake Shaft at the Waste Isolation Pilot Plant.* DOE-WIPP 90-051. Carlsbad, NM: U.S. Department of Energy.

Hora, S. C., and R. L. Iman. 1989. "Expert Opinion in Risk Analysis: The NUREG-1150 Methodology." *Nuclear Science and Engineering* **102**: 323-331.

Hora, S. C., D. von Winterfeldt, and K. M. Trauth. 1991. *Expert Judgment on Inadvertent Human Intrusion into the Waste Isolation Pilot Plant.* SAND90-3063. Albuquerque, NM: Sandia National Laboratories.

HP (Hewlett-Packard). 1984. *Petroleum Fluids PAC for HP-41C.* Corvallis, OR: Hewlett-Packard.

HSWA. 1984. *Hazardous and Solid Waste Amendments of 1984.* Pub. L. No. 98-616.

Hunter, R. L. 1985. *A Regional Water Balance for the Waste Isolation Pilot Plant (WIPP) Site and Surrounding Area.* SAND84-2233. Albuquerque, NM: Sandia National Laboratories.

Hunter, R. L. 1989. *Events and Processes for Constructing Scenarios for the Release of Transuranic Waste from the Waste Isolation Pilot Plant, Southeastern New Mexico.* SAND89-2546. Albuquerque, NM: Sandia National Laboratories.

Hunter, R. L., and C. J. Mann, eds. 1989. *Techniques for Determining Probabilities of Events and Processes Affecting the Performance of Geologic Repositories: Literature Review.* Vol. 1. SAND86-0196, NUREG/CR-3964. Albuquerque, NM: Sandia National Laboratories.

Huyakorn, P. S., H. O. White, Jr., and S. Panday. 1989. STAFF2D. Herndon, VA: Hydrogeologic, Inc.

IAEA (International Atomic Energy Agency). 1989. *Evaluating the Reliability of Predictions Made Using Environmental Transfer Models.* Safety Series Report No. 100. Vienna: International Atomic Energy Agency.

Ibrahim, M. A., M. R. Tek, and D. L. Katz. 1970. *Threshold Pressure in Gas Storage.* Arlington, VA: American Gas Association, Inc.

ICRP, Pub 38. 1983. Radionuclide Transformations Energy and Intensity of Emissions, ICRP Publication 38, *Annals of the International Commission on Radiological Protection (ICRP),* Vols. 11-13.

IDB (Integrated Data Base). 1987. *1987 Integrated Data Base: Spent Fuel and Radioactive Waste Inventories, Projection and Characteristics, DOE/RW-0006 Revision 3.* Oak Ridge, TN: Oak Ridge National Laboratory for U.S. Department of Energy.

IDB (Integrated Data Base). 1988. *1988 Integrated Data Base: Spent Fuel and Radioactive Waste Inventories, Projection and Characteristics, DOE/RW-0006 Revision 4.* Oak Ridge, TN: Oak Ridge National Laboratory for U.S. Department of Energy.

IDB (Integrated Data Base). 1990. *1990 Integrated Data Base: Spent Fuel and Radioactive Waste Inventories, Projection and Characteristics. DOE/RW-0006 Revision 6.* Oak Ridge, TN: Oak Ridge National Laboratory for U.S. Department of Energy.

Iman, R. L., and W. J. Conover. 1980. "Small Sample Sensitivity Analysis Techniques for Computer Models, with and Application to Risk Assessment." *Communications in Statistics A9:* 1749-1842. Rejoinder to comments, pp. 1863-74.

Iman, R. L., and J. C. Helton. 1985. *A Comparison of Uncertainty and Sensitivity Analysis Techniques for Computer Models.* SAND84-1461, NUREG/CR-3904. Albuquerque, NM: Sandia National Laboratories.

Imbrie, J., and J. Z. Imbrie. 1980. "Modeling the Climatic Response to Orbital Variations," *Science* **207**: 943-953.

Iuzzolino, H. J. 1983. *Equation of State Development from Shock Tube Calculations.* AFWL TR 82-57. Kirtland AFB, NM: Air Force Weapons Laboratory.

Johnson, N. L., and S. Kotz, 1970a. *Continuous Univariate Distributions-1.* New York: John Wiley & Sons.

Johnson, N. L., and S. Kotz, 1970b. *Continuous Univariate Distributions-2.* New York: John Wiley & Sons.

Jouzel, J., C. Lorius, J. R. Petit, C. Genton, N. I. Barkow, V. M. Kotlyakov, and V. M. Petrov. 1987. "Vostok Ice Core; A Continuous Isotope Temperature Record Over the Last Climatic Cycle (160,000 Years)." *Nature* **329**: 403-408.

Kaplan, S., and B. J. Garrick. 1981. "On the Quantitative Definition of Risk," *Risk Analysis* **1**: 11-27.

Kaufman, D. W., ed. 1960. *Sodium Chloride, the Production and Properties of Salt and Brine*, Monograph No. 145. Washington, DC: American Chemical Society.

Kelley, V. A., and J. F. Pickens. 1986. *Interpretation of the Convergent-Flow Tracer Tests Conducted in the Culebra Dolomite at the H-3 and H-4 Hydropads at the Waste Isolation Pilot Plant (WIPP) Site*. SAND86-7161. Albuquerque, NM: Sandia National Laboratories.

Kelley, V. A., and G. J. Saulnier, Jr. 1990. *Core Analysis for Selected Samples from the Culebra Dolomite at the Waste Isolation Pilot Plant Site*. SAND90-7011. Albuquerque, NM: Sandia National Laboratories.

Kipp, K. L. 1987. *HST3D: A Computer Code for Simulation of Heat and Solute Transport in Three-Dimensional Groundwater Flow Systems*. WRIR 86-4095. Denver, CO: U.S. Geological Survey.

Knapp, H., R. Doring, L. Oellrich, U. Plocker, and J. M. Prausnitz. 1982. "Vapor-Liquid Equilibria for Mixtures of Low Boiling Substances" in *Chemistry Data Series*, Vol. 6. DECHEMA

Krauskopf, K. B. 1986. "Thorium and Rare-Earth Metals as Analogs for Actinide Elements" in *Chemical Geology* **55**: 323-336.

Krieg, R. D. 1984. *Reference Stratigraphy and Rock Properties for the Waste Isolation Pilot Plant (WIPP) Project*. SAND83-1908. Albuquerque, NM: Sandia National Laboratories.

Krumhansl, J. L., K. M. Kimball, and C. L. Stein. 1991. *Intergranular Fluid Compositions from the Waste Isolation Pilot Plant (WIPP), Southeastern New Mexico*. SAND90-0584. Albuquerque, NM: Sandia National Laboratories.

Lallemand-Barres, J. and P. Peaudecerf. 1978. Recherche des Relations Entre les Valeurs Mesurèesde la Dispersivitè Macroscropique d'un Milieu Aquifère, Ses Autres Charactèristiques et ales Conditions de Mesure. Eude Bibliograaphique. *Rech. Bull. Bur. Geol. Min.* Sèr. 2, Sec. III, 4-1978. 277-284.

Lambert, S. J., and J. A. Carter. 1987. *Uranium-Isotope Systematics in Groundwaters of the Rustler Formation, Northern Delaware Basin, Southeastern New Mexico*. SAND87-0388. Albuquerque, NM: Sandia National Laboratories.

Lambert, S. J., and D. M. Harvey. 1987. *Stable-Isotope Geochemistry of Groundwater in the Delaware Basin of Southeastern New Mexico*. SAND87-0138. Albuquerque, NM: Sandia National Laboratories.

Langmuir, D., and J. S. Herman. 1980. "The Mobility of Thorium in Natural Waters at Low Temperatures." *Geochimica et Cosmochimica Acta* **44**: 1753-1766.

Langmuir, D., and A. C. Riese. 1985. "The Thermodynamic Properties of Radium." *Geochimica et Cosmochimica Acta* **49**: 1593-1601.

Lappin, A. R. 1988. *Summary of Site Characterization Studies Conducted from 1983 through 1987 at Waste Isolation Pilot Plant (WIPP) Site, Southeastern New Mexico*. SAND88-0157. Albuquerque, NM: Sandia National Laboratories.

Lappin, A. R., R. L. Hunter, D. P. Garber, and P. B. Davies, eds. 1989. *Systems Analysis Long-Term Radionuclide Transport, and Dose Assessments, Waste Isolation Pilot Plant (WIPP), Southeastern New Mexico; March 1989.* SAND89-0462. Albuquerque, NM: Sandia National Laboratories.

LaVenue, A. M., A. Haug, and V. A. Kelley. 1988. *Numerical Simulation of Ground-Water Flow in the Culebra Dolomite at the Waste Isolation Pilot Plant (WIPP) Site: Second Interim Report.* SAND88-7002. Albuquerque, NM: Sandia National Laboratories.

LaVenue, A. M., T. L. Cauffman, and J. F. Pickens. 1990. *Ground-Water Flow Modeling of the Culebra Dolomite. Volume I: Model Calibration.* SAND89-7068. Albuquerque, NM: Sandia National Laboratories.

Leckie, J. O. 1989. "Simulations of Distribution Coefficients Using Surface Complexation Models," Appendix C in M.D. Siegel, ed., *Progress in Development of a Methodology for Geochemical Sensitivity Analysis for Performance Assessment: Volume 2. Speciation, Sorption, and Transport in Fractured Media*, Letter Report to the U.S. Nuclear Regulatory Commission.

Li, Y., and S. Gregory. 1974. "Diffusion of Ions in Seawater and in Deep-Sea Sediments," *Geochimica et Cosmochimica Acta.* **38**: 703-714.

Lynch, A. W., and R. G. Dosch. 1980. *Sorption Coefficients for Radionuclides on Samples from the Water-Bearing Magenta and Culebra Members of the Rustler Formation.* SAND80-1064. Albuquerque, NM: Sandia National Laboratories.

McKay, M. D., W. J. Conover, and R. J. Beckman. 1979. "A Comparison of Three Methods for Selecting Values of Input Variables in the Analysis of OUtput from a Computer Code" in *Techometrics*, vol. 21, no. 2.

Mann, C. J., and R. L. Hunter. 1988. "Probabilities of Geologic Events and Processes in Natural Hazards." *Zeitschrift fuer Geomorphologie* N.F. **67**: 39-52.

Marietta, M. G., S. G. Bertram-Howery, D. R. Anderson, K. F. Brinster, R. V. Guzowski, H. J. Iuzzolino, and R. P. Rechard. 1989. *Performance Assessment Methodology Demonstration: Methodology Development for Purposes of Evaluating Compliance with EPA 40 CFR 191, Subpart B, for the WIPP.* SAND89-2027. Albuquerque, NM: Sandia National Laboratories.

Marsily, G. de. 1986. *Quantitative Hydrogeology: Groundwater Hydrology for Engineers.* Orlando, FL: Academic Press, Inc.

Matalucci, R. V. 1987. *In Situ Testing at the Waste Isolation Pilot Plant.* SAND87-2382. Albuquerque, NM: Sandia National Laboratories.

Mercer, J. W. 1983. *Geohydrology of the Proposed Waste Isolation Pilot Plant Site, Los Medaños Area, Southeastern New Mexico.* U.S. Geological Survey Water Resources Investigation 83-4016.

Mercer, J. W., and B. R. Orr. 1979. *Interim Data Report on the Geohydrology of the Proposed Waste Isolation Pilot Plant Site, Southeastern New Mexico.* USGS Water-Resources Investigations 79-98. Albuquerque, NM: U.S. Geological Survey.

Mercer, J. W., R. L. Beauheim, R. P. Snyder, and G. M. Fairer. 1987. *Basic Data Report for Drilling and Hydrologic Testing of Drillhole DOE-2 at the Waste Isolation Pilot Plant (WIPP) Site.* SAND86-0611. Albuquerque, NM: Sandia National Laboratories.

Miller, D. G. 1982. *Estimation of Tracer Diffusion Coefficients of Ions in Aqueous Solution.* UCRL-53319. Livermore, CA: Lawrence Livermore National Laboratory.

Miller, I., and J. E. Freund. 1977. *Probabilities and Statistics for Engineers.* 2nd ed. Englewood Cliffs, NJ: Prentice-Hall.

Molecke, M. A. 1979. *Gas Generation from Transuranic Waste Degradation: Data Summary and Interpretation.* SAND79-1245. Albuquerque, NM: Sandia National Laboratories.

Munson, D. E., A. F. Fossum, and P. E. Senseny. 1989. *Advances in Resolution of Discrepancies between Predicted and Measured In Situ Room Closures.* SAND88-2948. Albuquerque, NM: Sandia National Laboratories.

Munson, D. E., J. R. Ball, and R. L. Jones. 1990a. "Data Quality Assurance Controls through the WIPP In Situ Data Acquisition, Analysis and Management System" in *Proceedings of the International High-Level Radioactive Waste Management Conference, Las Vegas, NV, April 8-12.* Sponsored by American Nuclear Society and ASCE, New York, pp. 1337-1350.

Munson, D. E., R. V. Matalucci, J. R. Ball, and R. L. Jones. 1990b. *WIDSAAM: The WIPP In Situ Data Acquisition, Analysis, and Management System.* SAND87-2258. Albuquerque, NM: Sandia National Laboratories.

Munson, D. E., K. L. DeVries, and G. D. Gallahan. 1990c. "Comparison of Calculations and In Situ Results for a Large, Heated Test Room at the Waste Isolation Pilot Plant (WIPP)." *Proceedings of 31th U.S. Symposium on Rock Mechanics, Golden, CO, June 18-20.*

NEPA. 1969. National Environmental Policy Act of 1969. Pub. L. No. 91-190, 83 Stat. 852.

Neretnieks, I., and A. Rasmussen. 1984 "An Approach to Modeling Radionuclide Migration in a Medium with Strongly Varying Velocity and Block Sizes along the Flow Path," *Water Resources Research* vol. 20, no. 12: 1823-1836.

Novak, C. F. 1991. *An Evaluation of Radionuclide Batch Sorption Data on Culebra Dolomite for Aqueous Compositions Relevant to the Human Intrusion Scenario for the Waste Isolation Pilot Plant (WIPP).* SAND91-1299. Albuquerque, NM: Sandia National Laboratories.

Nowak, E. J., and J. C. Stormont. 1987. *Scoping Model Calculations of the Reconsolidation of Crushed Salt in WIPP Shafts.* SAND87-0879. Albuquerque, NM: Sandia National Laboratories.

Nowak, E. J., and L. D. Tyler. 1989. "The Waste Isolation Pilot Plant (WIPP) Seal System Performance Program," *Proceedings of the Joint NEA/CEC Repositories, Braunschweig, FRG, May 22-25, 1989.*

Nowak, E. J., D. F. McTigue, and R. Beraun. 1988. *Brine Inflow to WIPP Disposal Rooms: Data, Modeling and Assessment.* SAND88-0112. Albuquerque, NM: Sandia National Laboratories.

Nowak, E. J., J. R. Tillerson, and T. M. Torres. 1990. *Initial Reference Seal System Design: Waste Isolation Pilot Plant (WIPP).* SAND90-0355. Albuquerque, NM: Sandia National Laboratories.

Numbere, D., W. E. Grigham, and M. B. Standing. 1977. *Correlations for Physical Properties of Petroleum Reservoir Brines.* Palo Alto, CA: Petroleum Research Institute, Stanford University.

OCD. 1988. *State of New Mexico, Energy, Minerals, and Natural Resources Department, Oil Conservation Commission of Oil Conservation Division,* Order No. R-111-P, April 21, 1988.

Oldroyd, J. G. 1958. *Proceedings of the Royal Society (London)* **A245**: 278.

Pace, R. O. 1990. Manager, Technology Exchange Technical Services, Baroid Drilling Fluids, Inc., 3000 N. Sam Houston Pkwy. E., Houston, Texas. (Expert Opinion). Letter 1b in Appendix A of Rechard et al. 1990. *Data Used in Preliminary Performance Assessment of the Waste Isolation Pilot Plant (1990).* SAND89-2408. Albuquerque, NM: Sandia National Laboratories.

Paine, R. T. 1977. *Chemistry Related to the WIPP Site, Draft Final Report*, Sandia Contract GTK/07-1488. Albuquerque, NM: Chemistry Department, University of New Mexico.

Palmer, A. R. 1983. *The Decade of North American Geology, 1983 Geologic Time Scale.* Geological Society of North America.

Parry, G. W. 1988. "On the Meaning of Probability in Probabilistic Safety Assessment." *Reliability Engineering and System Safety* **23**: 309-314.

Parthenaides, E., and R. E. Paaswell. 1970. "Erodibility of Channels with Cohesive Boundary," *Proceedings of the American Society of Civil Engineers, Journal of the Hydraulics Division,* **99**: 555-558.

Paté-Cornell, M. E. 1986. "Probability and Uncertainty in Nuclear Safety Decisions." *Nuclear Engineering and Design* **93**: 319-327.

Perry, R. H., C. H. Chilton, and S. D. Kirkpatrick. 1969. *Chemical Engineer's Handbook.* New York: McGraw-Hill Book Company.

Peterson, A. C. 1990. "Preliminary Contact Handled (CH) and Remote Handled (RH) Radionuclide Inventories," Memo 7 in Appendix A of Rechard et al. 1990. *Data Used in Preliminary Performance Assessment of the Waste Isolation Plant (1990).* SAND89-2408. Albuquerque, NM: Sandia National Laboratories.

Pickens, J. F., and G. E. Grisak. 1981. "Modeling of Scale-Dependent Dispersion in Hydrolgeologic Systems." *Water Resources Research* vol. 17, no. 6: 1701-11.

Popielak, R. S., R. L. Beauheim, S. R. Black, W. E. Coons, C. T. Ellingson, and R. L. Olsen. 1983. *Brine Reservoirs in the Castile Formation, Southeastern New Mexico, Waste Isolation Pilot Plant (WIPP) Project.* TME-3153. Carlsbad, NM: U.S. Department of Energy.

Powers, D. W., S. J. Lambert, S. E. Shaffer, L. R. Hill, and W. D. Weart, ed. 1978. *Geological Characterization Report, Waste Isolation Pilot Plant (WIPP) Site, Southeastern New Mexico.* SAND78-1596, vols. 1 and 2. Albuquerque, NM: Sandia National Laboratories.

Prausnitz, J. M. 1969. *Molecular Thermodynamics of Fluid-Phase Equilibria.* Englewood Cliffs, NJ: Prentice-Hall, Inc.

Public Law 96-164. 1979. *Department of Energy National Security and Military Applications of Nuclear Energy Authorization Act of 1980.*

RCRA. 1976. *Resource, Conservation, and Recovery Act of 1976.* Pub. L. No. 94-580, 90 Stat. 2795.

Rechard, R. P. 1989. *Review and Discussion of Code Linkage and Data Flow in Nuclear Waste Compliance Assessments.* SAND87-2833. Albuquerque, NM: Sandia National Laboratories.

Rechard, R. P., H. J. Iuzzolino, J. S. Rath, R. D. McCurley, and D. K. Rudeen. 1989. *User's Manual for CAMCON: Compliance Assessment Methodology Controller.* SAND88-1496. Albuquerque, NM: Sandia National Laboratories.

Rechard, R. P., H. J. Iuzzolino, and J. Sandha. 1990a. *Data Used in Preliminary Performance Assessment at the Waste Isolation Pilot Plant (1990).* SAND89-2408. Albuquerque, NM: Sandia National Laboratories.

Rechard, R. P., W. Beyeler, R. D. McCurley, D. K. Rudeen, J. E. Bean, and J. D. Schreiber. 1990b. *Parameter Sensitivity Studies of Selected Components of the Waste Isolation Pilot Plant Repository/Shaft System.* SAND89-2030. Albuquerque, NM: Sandia National Laboratories.

Reeves, M., G. Freeze, V. Kelly, J. Pickens, D. Upton, and P. Davies. 1991. *Regional Double-Porosity Solute Transport in the Culebra Dolomite under Brine-Reservoir-Breach Release Conditions: An Analysis of Parameter Sensitivity and Importance.* SAND89-7069. Albuquerque, NM: Sandia National Laboratories.

Rice, J. R., and M. P. Cleary. "Stress Diffusion Solutions for Fluid-Saturated Elastic Porous Media with Compressible Constituents." *Review of Geophysics and Space Physics* vol. 14, no. 2 (May 1976): 227-241.

Richey, S. F., J. G. Wells, K. T. Stephens. 1985. *Geohydrology of the Delaware Basin and Vicinity, Texas and New Mexico.* U.S. Geological Survey Water Resources Investigations Report 84-4077. Washington, DC: U.S. Geological Survey.

Riese, A. C. 1982. "Adsorption of Radium and Thorium onto Quartz and Kaolinite: A Comparison of Solution/Surface Equilibria Models," Ph.D. Thesis. Colorado School of Mines, Golden, CO.

Rose, W., and W. A. Bruce. 1949. "Evaluation of Capillary Character in Petroleum Reservoir Rock." *Transactions of the American Institute of Mining and Metallurgical Engineers* **186:** 127-142.

Ross, S. M. 1985. *Introduction to Probability Models.* 3rd ed. New York: Academic Press, Inc.

Ross, B. 1989. "Scenarios for Repository Safety Analysis." *Engineering Geology* **26:** 285-299.

Sargunam, A., P. Riley, K. Arulanadum, and R. B. Krone. 1973. "Physico-Chemical Factors in Erosion of Cohesive Soils." *Journal of the Hydraulics Division, American Society of Civil Engineers* 99: 555-558.

Saulnier, G. J., Jr. 1987. *Analysis of Pumping Tests of the Culebra Dolomite Conducted at the H-11 Hydropad at the Waste Isolation Pilot Plant (WIPP) Site.* SAND87-7124. Albuquerque, NM: Sandia National Laboratories.

Savins, J. G., and G. C. Wallick. 1966. "Viscosity Profiles, Discharge Rates, Pressures, and Torques for a Rheologically Complex Fluid in Helical Flow." *A.I.Ch.E. Journal* vol. 12, no. 2 (March 1966).

Scheetz, B. E., P. H. Licastro, and D. M. Roy. 1986. *A Full Scale Borehole Sealing Test in Anhydrite Under Simulated Downhole Conditions*, vols. 1 and 2. BMI/ONWI-573(2). Columbus, OH: Office of Nuclear Waste Isolation, Battelle Memorial Institute.

Shakoor, A., and H. R. Hume. 1981. *Physical Properties Data for Rock Salt: Chapter 3, Mechanical Properties, NBS Monograph 167.* Washington, DC: National Bureau of Standards: 103-203.

Siegel, M. D. 1990. "Representation of Radionuclide Retardation in the Culebra Dolomite in Performance Assessment Calculations," Memo 3a in Appendix A of Rechard et al. 1990. *Data Used in Preliminary Performance Assessment of the Waste Isolation Pilot Plant (1990).* SAND89-2408. Albuquerque, NM: Sandia National Laboratories.

Sjaardema, G. D., and R. D. Krieg. 1987. *A Constitutive Model for the Consolidation of WIPP Crushed Salt and Its Use in Analysis of Backfilled Shaft and Drift Configurations.* SAND87-1977. Albuquerque, NM: Sandia National Laboratories.

Skokan, C., J. Starrett, and H. T. Andersen. 1988. *Final Report: Feasibility Study of Seismic Tomography to Monitor Underground Pillar Integrity at the WIPP Site.* SAND88-7096. Albuquerque, NM: Sandia National Laboratories.

SNL (Sandia National Laboratories). 1979. *Summary of Research and Development Activities in Support of Waste Acceptance Criteria for the WIPP.* SAND79-1305. Albuquerque, NM: Sandia National Laboratories.

SNL (Sandia National Laboratories) and U.S. Geological Survey. 1982a. *Basic Data Report for Drillhole WIPP 11 (Waste Isolation Pilot Plant - WIPP).* SAND79-0272. Albuquerque, NM: Sandia National Laboratories.

SNL (Sandia National Laboratories) and U.S. Geological Survey. 1982b. *Basic Data Report for Drillhole ERDA 9 (Waste Isolation Pilot Plant - WIPP).* SAND79-0270. Albuquerque, NM: Sandia National Laboratories.

SNL (Sandia National Laboratories) and D'Appolonia Consulting Engineers. 1983. *Basic Data Report for Drillhole WIPP 12 (Waste Isolation Pilot Plant - WIPP).* SAND82-2336. Albuquerque, NM: Sandia National Laboratories.

Stone, W. J. 1984. *Recharge in the Salt Lake Coal Field Based on Chloride in the Unsaturated Zone.* Open File Report 214. Socorro, NM: New Mexico Bureau of Mines and Mineral Resources.

Streeter, V. L., and E. B. Wylie. 1975. *Fluid Mechanics.* 6th ed. New York: McGraw-Hill Book Co.

Sutherland, H. J., and S. Cave. 1978. *Gas Permeability of SENM Rock Salt.* SAND78-2287. Albuquerque, NM: Sandia National Laboratories.

Swanson, J. L., 1986. *Organic Complexant-Enhanced Mobility of Toxic Elements in Low-Level Wastes: Final Report.* NUREG/CR-4660, PNL-4965-10. Richland, WA: Pacific Northwest Laboratory.

Thomas, L. K., D. L. Katz, and M. R. Tek. 1968. "Threshold Pressure Phenomena in Porous Media." *Society of Petroleum Engineers Journal* vol. 8, no. 2: 174-184.

Tien, P. L., F. B. Nimick, A. B. Muller, P. A. Davis, R. V. Guzowski, L. E. Duda, and R. L. Hunter. 1983. *Repository Site Data and Information in Bedded Salt: Palo Duro Basin, Texas.* SAND82-2223, NUREG/CR-3129. Albuquerque, NM: Sandia National Laboratories.

Tierney, M. S. 1990a. *Constructing Probability Distributions of Uncertain Variables in the Models of the Performance of the Waste Isolation Pilot Plant (WIPP).* SAND90-2510. Albuquerque, NM: Sandia National Laboratories.

Tierney, M. S. 1990b. "Values of Room Porosity and Hydraulic Conductivity," Memo 6 in Appendix A of Rechard et al. 1990. *Data Used in Preliminary Performance Assessment of the Waste Isolation Pilot Plant (1990).* SAND89-2408. Albuquerque, NM: Sandia National Laboratories.

Tierney, M. S. 1991. *Combining Scenarios in a Calculation of the Overall Probability Distribution of Cumulative Releases of Radioactivity from the Waste Isolation Pilot Plant, Southeastern New Mexico.* SAND90-0838. Albuquerque, NM: Sandia National Laboratories.

Tomovic, R. 1963. *Sensitivity Analysis of Dynamic Systems.* New York: McGraw Hill.

Torstenfelt, B., H. Kipatsi, K. Anderson, B. Allard, and U. Olofsson. 1982. "Transport of Actinides Through a Bentonite Backfill" in W. Lutze, ed., *Scientific Basis for Radioactive Waste Management V.* New York: Elsevier Science Publishing Co.

Trauth, K. M., S. C. Hora, and R. P. Rechard. 1991. "Expert Judgment as Input to Waste Isolation Pilot Plant Performance-Assessment Calculations: Probability Distributions of Significant System Parameters" in *Proceedings of the First International Mixed Waste Symposium, Baltimore, MD, August 26-29, 1991.*

Tyler, L. D., R. V. Matalucci, M. A. Molecke, D. E. Munson, E. J. Nowak, and J. C. Stormont. 1988. *Summary Report for the WIPP Technology Development Program for Isolation of Radioactive Waste.* SAND88-0844. Albuquerque, NM: Sandia National Laboratories.

U.S. DOE (Department of Energy). 1982a. *Basic Data Report for Borehole DOE-1, Waste Isolation Pilot Plant (WIPP) Project, Southeastern New Mexico.* TME 3159. Albuquerque, NM: Sandia National Laboratories.

U.S. DOE (Department of Energy). 1982b. *Basic Data Report for Borehole WIPP-12 Deepening, Waste Isolation Pilot Plant (WIPP) Project, Southeastern, New Mexico.* TME 3148. Albuquerque, NM: Sandia National Laboratories.

U.S. DOE (Department of Energy). 1983a. Drawing number 35-R-004-01D Rev. A. San Francisco, CA: Bechtel National, Inc.

U.S. DOE (Department of Energy). 1983b. Drawing number 31-R-013-01D Rev. A. San Francisco, CA: Bechtel National, Inc.

U.S. DOE (Department of Energy). 1987a. *Radioactive Source Term for Use at the Waste Isolation Pilot Plant.* DOE/WIPP88-005. In preparation.

U.S. DOE (Department of Energy). 1987b. Drawing number 33-R-012-34A Rev. 5. San Francisco, CA: Bechtel National, Inc.

U.S. DOE (Department of Energy). 1989a. *Waste Isolation Pilot Plant Compliance Strategy for 40 CFR Part 191.* WIPP-DOE-86-013. Carlsbad, NM: U.S. Department of Energy.

U.S. DOE (Department of Energy). 1989b. *Addendum to No-Migration Variance Petition for WIPP.* DOE/WIPP 89-003. Carlsbad, NM: U.S. Department of Energy.

U.S. DOE (Department of Energy). 1990a. *WIPP Test Phase Plan: Performance Assessment.* DOE/WIPP 89-011, Rev. O. Carlsbad, NM: U.S. Department of Energy.

U.S. DOE (Department of Energy). 1990b. *Final Supplemental Environmental Impact Statement, Waste Isolation Pilot Plant.* DOE/EIS-0026-FS. Washington, DC: U.S. Department of Energy, Office of Environmental Restoration and Waste Management.

U.S. DOE (Department of Energy). 1990c. *Geologic Mapping of the Air Intake Shaft at the Waste Isolation Pilot Plant.* DOE-WIPP-90-051. Albuquerque, NM: IT Corporation.

U.S. DOE (Department of Energy). 1990d. *Final WIPP Safety Analysis Report, Waste Isolation Pilot Plant.* Carlsbad, NM: U.S. Department of Energy.

U.S. DOE (Department of Energy). 1991. *Recommended Strategy for the Remote-Handled Transuranic Waste Program.* DOE/WIPP 90-058, Revision 1. Carlsbad, NM: Waste Isolation Pilot Plant.

U.S. DOE (Department of Energy) and State of New Mexico. 1984. U.S. Department of Energy and State of New Mexico, 1981, First Modification to the July 1, 1981 "Agreement for Consultation and Cooperation" on WIPP by the State of New Mexico and U.S. Department of Energy, November 30, 1984.

U.S. NRC (Nuclear Regulatory Commission). 1990. *Severe Accident Risks: An Assessment of Five U.S. Nuclear Power Plants.* Summary Report of NUREG 1150. Washington, D.C.: U.S. Nuclear Regulatory Commission.

Vargaftik, N. B. 1975. *Tables on the Thermophysical Properties of Liquids and Gases in Normal and Dissociated States.* New York: John Wiley & Sons, Inc.

Vennard, J. K., and R. L. Street. 1975. *Elementary Fluid Mechanics*, 5th ed. New York: John Wiley & Sons.

Vesely, W. E., and D. M. Rasmuson. 1984. "Uncertainties in Nuclear Probabilistic Risk Analyses." *Risk Analysis* **4**: 313-322.

Voss, C. I. 1984. *SUTRA (Saturated-Unsaturated TRAnsport): A Finite-Element Simulation Model for Saturated-Unsaturated Fluid Density Dependent Groundwater Flow and Energy Transport or Chemically Reactive Single Species Solute Transport.* Reston, VA: U.S. Geological Survey National Center.

Walas, S. M. 1985. *Phase Equilibrium in Chemical Engineering.* Boston, MA: Butterworth Publishers. 52-54.

Walker, R. E., and W. E. Holman. 1971. "Computer Program Predicting Drilling-Fluid Performance." *Oil and Gas Journal* (March 29, 1971): 80-90.

Ward, J. S., and N. R. Morrow. 1985. "Capillary Pressures and Gas Permeabilities of Low-Permeability Sandstone." SPE/DOE 13882. Paper presented at the *SPE/DOE 1985 Low Permeability Gas Reservoirs, Denver, CO, May 19-22, 1985.*

Ward, R. G., C. G. St. C. Kendall, and P. M. Harris. 1986. "Upper Permian (Guadalupian) Facies and Their Association with Hydrocarbons - Permian Basin, West Texas and New Mexico." *American Association of Petroleum Geologists Bulletin* **70**: 239-262.

Wawersik, W. R., and C. M. Stone. 1985. *Application of Hydraulic Fracturing to Determine Virgin In Situ Stress Around Waste Isolation Pilot Plant--In Situ Measurements.* SAND85-1776. Albuquerque, NM: Sandia National Laboratories.

Weast, R. C., and M. J. Astle, eds. 1981. *Handbook of Chemistry and Physics.* 62nd ed. Cleveland, OH: CRC Press.

WEC (Westinghouse Electric Corporation). 1985a. *TRU Waste Acceptance Criteria for the Waste Isolation Pilot Plant,* Revision 2. WIPP-DOE-069-Rev. 2. Carlsbad, NM: Westinghouse Electric Corporation.

WEC (Westinghouse Electric Corporation). 1989. *TRU Waste Acceptance Criteria for the Waste Isolation Pilot Plant,* Revision 3. WIPP-DOE-069-Rev. 2. Prepared for U.S. Department of Energy. Carlsbad, NM: Westinghouse Electric Corporation.

WEC (Westinghouse Electric Corporation). 1990. *Waste Isolation Pilot Plant No-Migration Variance Petition.* DOE/WIPP 89-003. Prepared for U.S. Department of Energy. Carlsbad, NM: Westinghouse Electric Corporation.

Williamson, C. R. 1978. *Depositional Processes, Diagenesis and Reservoir Properties of Permian Deep-Sea Sandstone, Bell Canyon Formation,* Ph.D. Dissertation. University of Texas, Austin, TX.

WIPP Act. 1980. *Department of Energy National Security and Military Applications of Nuclear Energy Authorization Act of 1980, Title II - General Provisions: Waste Isolation Pilot Plant, Delaware Basin, NM.* Pub. L. No. 96-164, 93 Stat. 1259. (Clarify 79 or 80).

Wyllie, M. R. J., and W. D. Rose. 1950. "Some Theoretical Considerations Related to the Quantitative Evaluation of the Physical Characteristics of Reservoir Rock from Electric Log Data." *Transactions of the American Institute of Mining and Metallurgical Engineers* **189:** 105-118.

Yaglom, A. M. 1962. *An Introduction to the Theory of Stationary Random Functions.* Englewood Cliffs, NJ: Prentice-Hall, Inc.

40 CFR 191. Environmental Radiation Protection Standards for Management and Disposal of Spent Nuclear Fuel, High-Level, and Transuranic Radioactive Wastes. U.S. Environmental Protection Agency (EPA), Title 40 Code of Federal Regulations Part 191 (*40 CFR 191*).

APPENDIX A:
MEMORANDA REGARDING REFERENCE DATA

Referenced Memoranda

Related Memoranda

APPENDIX A:
MEMORANDA REGARDING REFERENCE DATA

Referenced Memoranda

The memoranda referenced are as follows:

Beauheim et al., June 10, 1991

Date: 6/10/91
To: D. R. Anderson (6342)
From: R. L. Beauheim (6344), T. F. Corbet (6344), P. B. Davies (6344), J. F. Pickens (INTERA)
Subject: Recommendations for the 1991 Performance Assessment Calculations on Parameter Uncertainty and Model Implementation for Culebra Transport Under Undisturbed and Brine-Reservoir-Breach Conditions

Beauheim, June 14, 1991

Date: 6/14/91
To: Rob Rechard (6342)
From: Rick Beauheim (6344)
Subject: Review of Salado Parameter Values to be Used in 1991 Performance Assessment Calculations

Brush, July 8, 1991

Date: 7/8/91
To: D. R. Anderson (6342)
From: L. H. Brush (6345)
Subject: Current Estimates of Gas Production Rates, Gas Production Potentials, and Expected Chemical Conditions Relevant to Radionuclide Chemistry for the Long-Term WIPP Performance Assessment

Davies, June 2, 1991

Date: 6/2/91
To: D. R. Anderson (6342)
From: P. B. Davies (6344)
Subject: Uncertainty Estimates for Threshold Pressure for 1991 Performance Assessment Calculations Involving Waste-Generated Gas

Drez, May 9, 1989

Date: 5/9/89
To: L. Brush (6334)
From: Paul Drez (International Technology Corporation)
Subject: Preliminary Nonradionuclide Inventory of CH-TRU Waste

Finley and McTigue, June 17, 1991

Date: 6/17/91
To: Elaine Gorham, 6344
From: S. J. Finley, 6344, and
D. F. McTigue, 1511
Subject: Parameter Estimates from the Small-Scale Brine Inflow Experiments

Howarth, June 12, 1991

Date: 6/12/91
To: Elaine Gorham (6344)
From: Susan Howarth (6344)
Subject: Pore Pressure Distributions for 1991 Performance Assessment Calculations

Howarth, June 13, 1991

Date: 6/13/91
To: Elaine Gorham (6344)
From: Susan Howarth (6344)
Subject: Permeability Distributions for 1991 Performance Assessment Calculations

McTigue et al., March 14, 1991

Date: 3/14/91
To: Distribution
From: D. F. McTigue, 1511; S. J. Finley, 6344, J. H. Gieske, 7552; K. L. Robinson, 6345
Subject: Compressibility Measurements on WIPP Brines

Novak, September 4, 1991

Date: 9/4/91
To: K. M. Trauth, 6342
From: Craig F. Novak, 6344
Subject: Rationale for K_d Values Provided During Elicitation of the Retardation Expert Panel, May 1991

Swift, October 10, 1991

Date: 10/10/91
To: R. P. Rechard
From: Peter Swift, 6342/Tech Reps
Subject: Climate and recharge variability parameters for the 1991 WIPP PA calculations

Related Memoranda

Gorham, July 2, 1991

Date: 7/2/91
To: Rob Rechard (6342)
From: Elaine Gorham (6344)
Subject: Aggregated Frequency Distributions for Permeability, Pore Pressure and Diffusivity in the Salado Formation

Anderson, October 25, 1991

Date: 10/25/91
To: File
From: D. R. (Rip) Anderson (6342)
Subject: Modifications to Reference Data for 1991 Performance Assessment

Mendenhall and Butcher, June 1, 1991

Date: 6/1/91
To: R. P. Rechard (6342)
From: F. T. Mendenhall (6345) and B. M. Butcher
Subject: Disposal room porosity and permeability values for use in the 1991 room performance assessment calculations

Siegel, July 14, 1989

Date: 7/14/89
To: P. Davies (6331) and A. R. Lappin (6331)
From: M. D. Siegel
Subject: Supplementary Information Concerning Radionuclide Retardation

Siegel, June 25, 1991

Date: 6/25/91
To: K. Trauth (6342)
From: M. D. Siegel
Subject: K_d Values for Ra and Pb

Beauheim et al., June 10, 1991

Date: 6/10/91
To: D. R. Anderson (6342)
From: R. L. Beauheim (6344), T. F. Corbet (6344), P. B. Davies (6344), J. F. Pickens (INTERA)
Subject: Recommendations for the 1991 Performance Assessment Calculations on Parameter Uncertainty and Model Implementation for Culebra Transport Under Undisturbed and Brine-Reservoir-Breach Conditions

Sandia National Laboratories

Albuquerque, New Mexico 87185

Date: June 10,1991

To: D.R. Anderson (6342)

From: R.L. Beauheim (6344)
T.F. Corbet (6344)
P.B. Davies (6344)
J. F. Pickens (INTERA)

Subject: Recommendations for the 1991 Performance Assessment Calculations on Parameter Uncertainty and Model Implementation for Culebra Transport Under Undisturbed and Brine-Reservoir-Breach Conditions

This memo provides input for modeling radionuclide transport for the 1991 Performance Assessment calculations. Recommendations are divided into two segments, one on double porosity-transport parameters and one on model implementation for brine-reservoir-breach scenarios.

Double-Porosity Transport

Several of the parameters used for double-porosity transport calculations are specific to a given transport code. We recommend that at some time, the code being used for performance assessment calculations be analyzed and benchmarked with the double-porosity transport code used to interpret tracer tests (SWIFT II, Reeves et al., 1986). Also, we note that the effect of many of the double-porosity parameters can be concisely characterized using dimensionless parameter groups (Reeves et al., 1991). We recommend that in future years, consideration be given to parameter sampling structured around dimensionless groups. This may save significant computational effort and eliminate inconsistencies associated with sampling correlated parameters.

The following comments on transport parameters follow the format in the data document for the 1990 PA calculations (Rechard et al., 1990).

Bulk Density

The values reported from laboratory analyses of Culebra core in Kelley and Saulnier, 1990 and in Lappin et al., 1989 are grain densities, not bulk densities. Correct range in text and table to 2.76×10^3 to 2.86×10^3 kg/m^3. Also correct arithmetic mean to

2.82×10^3 kg/m^3 and median to 2.83×10^3 kg/m^3. Change table source reference to Kelley and Saulnier, 1990, Tables 4.1, 4.2 and 4.3.

Dispersivity

No new information.

Fracture Spacing

The most recent results of tracer test interpretations for the H-3, H-6, and H-11 hydropads to obtain best-fit double-porosity parameters (fracture spacing and fracture porosity) are summarized in Table 1 (Cauffman, et al., in prep.). It is our opinion that there are too few data to construct a meaningful distribution for fracture spacing. Therefore, we recommend that the low end of the range be represented by the smallest fracture spacing interpreted from field experiments (0.06 meters) and be assigned to the 5th percentile. For the median value, we recommend the use of the average value from the limited number of available tests, 0.4 meters. For the upper end of the range, we recommend the continued use of the total Culebra thickness, 8 meters, and that this value be assigned to the 95th percentile.

Fracture Porosity

Fracture porosity is derived from the same analysis of tracer tests that produces fracture spacing (Table 1). Therefore, it is our opinion that there are too few data to construct a meaningful distribution for fracture porosity. Therefore, we recommend that the average value, 0.001, be used for the median of the distribution. Given the absence of additional data, the range should continue to be taken as one order of magnitude above and below this average value.

Matrix Porosity

The most comprehensive and up to date information on Culebra matrix porosity is Kelley and Saulnier, 1990. Table 2 is a list of porosity measurements on 79 core samples from 15 locations. The mean value is 0.15 and the median value is 0.14. The range is from 0.03 to 0.30. Note error in value reported in Table II-6 of SAND89-2408 where median value is reported as 15.2. This should be 0.152.

Storage Coefficient

No change from previous year. Correct reference in last sentence to LaVenue et al.,

1990, Table 2.5.

Thickness

Note error in Table II-6, where Culebra thickness is reported as 77 meters.

Tortuosity

The most comprehensive and up to date information on Culebra tortuosity is Kelley and Saulnier, 1990. Table 3 is a list of tortuosity measurement on 15 core samples from 11 locations. The mean value is 0.14 and the median value is 0.12. The range is from 0.03 to 0.3. Note that tortuosity is strongly related to fracture spacing. Dimensional analysis of Reeves et al. (1991) shows that the half-fracture spacing squared interpreted from a tracer test is inversely proportional to the assumed tortuosity. Therefore, we recommend that these parameters not be sampled independently.

Modeling of Brine-Reservoir Breach Scenarios

We have reviewed the draft text on proposed brine reservoir modeling and have the following comments:

The discussion of the justification for the simplified representation of brine-reservoir response to a borehole should cite the analysis of Reeves et al. (1991) that develops and tests the technical basis for this assumption. Also the limitations of the simplified approach should be stated. For example, while this approach is valid for time scales of less than 10,000 years, for longer time periods, there is increased sensitivity to intact Castile properties (transmissivity and storage).

The rationale for estimating a range of initial pressures is unnecessarily complex and may not be defensible. As an alternative approach, we suggest the following. The data show that pressures in the brine pockets are all greater than or equal to hydrostatic. No upper limit is indicated by the data, however lithostatic pressure is a defensible limit. Therefore, we suggest using the range from hydrostatic to lithostatic, calculated for the depth of the brine pocket at WIPP 12. This range is approximately 11 to 22 MPa (which compares with 10.4 to >16.6 MPa for the original approach).

One general comment is that for technical accuracy, this discussion should cite original sources rather that second or third generation material.

cc: W.D. Weart (6340)
M.G. Marietta (6342)
R.P. Rechard (6342)
E.D. Gorham (6344)

Path	Interpreted Parameters (1)		Assumed Parameters (2)		
	Fracture Porosity	Fracture Spacing	Matrix Porosity	Tortuosity	Dispersivity
H-3 Test					
H-3b1 to H-3b3	1.2E-3	1.2 m	0.20	0.15	1.5 m
H-3b2 to H-3b3	1.2E-3	0.23 m	0.20	0.15	1.5 m
H-6 Test #1					
H-6b to H-6c	1.5E-3	0.41 m	0.16	0.15	1.5 m
H-6a to H-6c	1.5E-3	0.056 m	0.16	0.15	1.5 m
H-6 Test #2					
H-6b to H-6c	1.5E-3	0.44 m	0.16	0.15	1.5 m
H-11 Test					
H-11b3 to H-11b1	5.0E-4	0.32 m	0.16	0.11	1.5 m
H-11b2 to H-11b1	5.0E-4	0.11 m	0.16	0.11	1.5 m
H-11b4 to H-11b1	5.0E-4	0.28 m	0.16	0.11	1.5 m

Footnotes: (1) Parameters derived from interpretations that assume that variations in Culebra hydrologic response during tracer tests are due to a heterogeneous distribution of isotropic transmissivities (Cauffman, et al., in prep.).

(2) Matrix porosity and tortuosity values are devrived from core tests at each specific hydropad. Dispersivity is assumed to be approximately 5 percent of a typical transport path length.

Table 1. Summary of best-fit double-porosity model-input parameters from Cauffman et al. (in prep).

Borehole Number	Sample Number	Porosity
H-2a	H-2a-1	0.116
	H-2a-2	0.131 *
H-2b	1-1	0.141
	2-1/3-1	0.154 **
	1-2	0.118
	2-2/3-2	0.103 **
H-2b1	H2b1-1	0.082
	H2b1-1F	0.105
	H2b1-2	0.142 *
	H2b1-3	0.153
H-3b2	1-3	0.188
	1-4	0.168
H-3b3	2-3/3-3	0.180 **
	2-4/3-4V	0.202 **
	1-6/3-6V	0.244
	2-5/3-5	0.205 **
H-4b	1-9	0.297
	2-6/3-6V	0.208 **
H-5b	H-5b-1a	0.128 *
	H-5b-1b	0.155
	H-5b-2	0.228
	H-5b-2F	0.248
	H-5b-3	0.133
H-6b	2-7	0.108
	2-8	0.116
	1-7	0.107
	1-8/3-8V	0.255
H-7b1	H-7b1-1	0.177
	H-7b1-1F	0.149
	H-7b1-2a	0.206 *
	H-7b1-2b	0.278

Table 2. Porosity measured on 79 Culebra core samples representing 15 locations (Saulnier and Kelley, 1990, Table 4.4).

Borehole Number	Sample Number	Porosity
H-7b2	H-7b2-1	0.159 *
	H-7b2-2	0.118
H-7c	H-7c-1a	0.130 *
	H-7c-1b	0.165
	H-7c-1f	0.138
H-10b	H-10b-1	0.089 *
	H-10b-2	0.115
	H-10b-2f	0.066
	H-1-b-3	0.112
H-11	H-11-1	0.155
	H-11-2	0.105 *
	H-11-2f	0.104
	H-11b3-1	0.303
	H-11b3-1f	0.223
	H-11b3-2	0.099
	H-11b3-2f	0.123
	H-11b3-3	0.130
	H-11b3-4	0.152 *
	H-11b3-4f	0.224
WIPP-12	W-12-1a	0.028
	W-12-1b	0.114 *
	W-12-2	0.126 *
	W-12-2f	0.135
	W-12-3	0.134
WIPP-13	W-13-1	0.143
	W-13-2	0.219
	W-13-2f	0.260
	W-13-3a	0.179 *
	W-13-3b	0.097

Table 2 (continued). Porosity measured on 79 Culebra core samples representing 15 locations (Saulnier and Kelley, 1990, Table 4.4).

Borehole Number	Sample Number	Porosity
WIPP-25	W-25-1	0.115
WIPP-26	W-26-1	0.124
	W-26-1F	0.112
	W-26-2	0.126
	W-26-3	0.127 *
WIPP-28	W-28-1a	0.142
	W-28-1b	0.130 *
	W-28-2	0.187
	W-28-3	0.170
	W-28-3F	0.179
WIPP-30	W-30-1	0.128
	W-30-2	0.150
	W-30-3a	0.176
	W-30-3b	0.149 *
	W-30-3F	0.149
	W-30-4	0.239 *
AEC-8	AEC-8-1	0.079
	AEC-8-1F	0.122
	AEC-8-2	0.109

Number of samples = 79
Average porosity = 0.153
Standard deviation = 0.053
Range = 0.028 - 0.303

* Represents an average value from porosity determinations from Terra Tek Laboratories and K & A Laboratories.

** Represents an average of porosity values determined using sample bulk volume estimated from pressured sample dimensions and from fluid displacement.

Table 2 (continued). Porosity measured on 79 Culebra core samples representing 15 locations (Saulnier and Kelley, 1990, Table 4.4).

Sample Number	Helium Porosity	Formation Factor	Tortuosity *
AEC-8-1F	0.122	90.09	0.091
H-2b1-1F	0.105	326.77	0.029
H-5b-2F	0.248	12.2	0.331
H-7b1-1F	0.149	73.49	0.091
H-7C-1F	0.138	79.61	0.091
H-10b-2F	0.066	406.78	0.037
H-11-2F	0.104	94.82	0.101
H-11b3-1F	0.223	36.35	0.123
H-11b3-2F	0.123	101.93	0.080
H-11b3-4F	0.224	32.74	0.136
W-12-2F	0.135	47.3	0.157
W-13-2F	0.26	13.26	0.290
W-26-1F	0.112	68.77	0.130
W-28-3F	0.179	26.3	0.212
W-30-3F	0.149	31.49	0.213

* Tortuosity calculated from Equation (9) using formation factor determined from electrical-resistivity measurements.

Table 3. Tortuosity estimated from values of formation factor and porosity for 15 Culebra core samples representing 11 locations (Saulnier and Kelley, 1990, Table 4.6).

REFERENCES

Cauffman, T.L., V.A. Kelley, J.F. Pickens, and D.T. Upton. (in preparation). *Integration of Interpretation Results of Tracers Tests Performed in the Culebra Dolomite at the Waste Isolation Pilot Plant Site.* SAND91-7076. Albuquerque, New Mexico: Sandia National Laboratories.

Kelley, V.A., and G.J. Saulnier. 1990. *Core Analysis for Selected Samples from the Culebra Dolomite at the Waste Isolation Pilot Plant Site.* SAND90-7011. Albuquerque, New Mexico: Sandia National Laboratories.

Lappin, A.R., R.L. Hunter, D.P. Garber, and P.B. Davies (editors). 1989. *Systems Analysis, Long-Term Radionuclide Transport, and Dose Assessments, Waste Isolation Pilot Plant (WIPP), Southeastern New Mexico; March, 1989.* SAND89-0462. Albuquerque, New Mexico: Sandia National Laboratories.

Rechard, R.P., H. Iuzzolino, and J.S. Sandha. 1990. *Data Used in Preliminary Performance Assessment of the Waste Isolation Pilot Plant (1990).* SAND89-2408. Albuquerque, New Mexico: Sandia National Laboratories.

Reeves, M., D.S. Ward, N.D. Johns, and R.M. Cranwell. 1986. *Theory and Implementation for SWIFT II, the Sandia Waste-Isolation Flow and Transport Model, Release 4.84.* NUREG/CR-3328 and SAND83-1159. Albuquerque, New Mexico: Sandia National Laboratories.

Reeves M., G.A. Freeze, V.A. Kelley, J.F. Pickens, D.T. Upton, and P.B. Davies. 1991. *Regional Double-Porosity Solute Transport in the Culebra Dolomite Under brine-Reservoir-Breach Release Conditions: An Analysis of Parameter Sensitivity and Importance.* SAND89-7069. Albuquerque, New Mexico: Sandia National Laboratories.

Beauheim, June 14, 1991

Date: 6/14/91
To: Rob Rechard (6342)
From: Rick Beauheim (6344)
Subject: Review of Salado Parameter Values to be Used in 1991 Performance Assessment Calculations

Sandia National Laboratories

Albuquerque, New Mexico 87185

Date: June 14, 1991

To: Rob Rechard, 6342

From: Rick Beauheim, 6344

Subject: Review of Salado Parameter Values to be Used in 1991 Performance Assessment Calculations

From the Salado permeability testing program, we produce three types of data used in PA calculations: permeabilities, pore pressures, and specific storage/compressibility values. Presented below are the latest data in each of these three categories. At this time, I do not have a good feel for how to assign probabilities across the uncertainty ranges. I generally feel that the middle or base-case values are more probable than the extremes, particularly in the case of pore pressure.

Permeability

Permeability data can be divided on the basis of rock type (halite vs. anhydrite) and on the basis of whether they represent conditions in the far field or in the DRZ. All permeabilities presented below are considered to have an uncertainty of ± one-half order of magnitude.

Halite Data:

Test	Permeability (m^2)	Uncertainty Range (m^2)	Comments	Reference
C2H01-A	2.7E-18	8.6E-19 to 8.6E-18	DRZ	SAND90-0083
C2H01-B	5.3E-21	1.7E-21 to 1.7E-20	far field?	SAND90-0083
C2H01-B-GZ	1.9E-21	6.0E-22 to 6.0E-21	far field?	SAND90-0083
L4P51-A	6.1E-21	1.9E-21 to 1.9E-20	far field?	SAND90-0083
S0P01	8.3E-21	2.6E-21 to 2.6E-20	far field?	SAND90-0083
S1P71-A	5.4E-20	1.7E-20 to 1.7E-19	far field?	SAND90-0083
S1P72-A-GZ	8.6E-22	2.7E-22 to 2.7E-21	far field?	preliminary

Anhydrite Data:

Test	Permeability (m^2)	Uncertainty Range (m^2)	Comments	Reference
C2H01-C	9.5E-19	3.0E-19 to 3.0E-18	far field?	SAND90-0083
C2H02	7.8E-20	2.5E-20 to 2.5E-19	far field	SAND90-0083
S0P01-GZ	<5.7E-18	<1.8E-18 to <1.8E-17	DRZ	SAND90-0083
SCP01-A	8.2E-20	2.6E-20 to 2.6E-19	far field	preliminary
L4P51-B	6.8E-20	2.2E-20 to 2.2E-19	far field	preliminary
S1P71-B	6.8E-20	2.2E-20 to 2.2E-19	far field	preliminary

Pore Pressure

To date, most of our pore-pressure data appear to reflect some degree of depressurization around the repository. Only two tests provided estimates of pore pressure that I think might be representative of far-field conditions. Both of these tests were of Marker Bed 139. From C2H02, we estimated a pressure of 9.3 MPa (SAND90-0083), and from SCP01-A we estimated a pressure of 12.55 MPa (preliminary). Our estimated uncertainty is $\pm$ 0.5 MPa.

Specific Storage/Compressibility

For our test interpretations, we typically input a value of specific storage based on laboratory measurements of rock properties. We use the range of laboratory measurements to define a range of uncertainty in specific storage, and this uncertainty is one of the factors leading to our uncertainty in permeability. When we have performed only pressure-pulse tests, we have no way of telling where within the expected range for specific storage a particular test actually falls. For those tests, we simply use our base-case values of specific storage. More recently, we have been combining constant-pressure flow tests with the pulse tests. This combination allows us to identify the particular values of specific storage that best fit our data. We do not as yet have many of these combined interpretations, however, and those that we do have are still preliminary. Significantly, all of our preliminary values fall within the range established from laboratory measurements. For this year's PA calculations, therefore, I think you are safe using the laboratory range. Next year we may be able to refine the range somewhat.

For halite, we use a specific storage range from 2.8E-8 to 1.4E-6 m^{-1}, with a base-case value of 9.5E-8 m^{-1}. For anhydrite, we use a specific storage range from 9.7E-8 to 1.0E-6 m^{-1}, with a base-case value of 1.4E-7 m^{-1}.

To get from specific storage to compressibility, you can rearrange the following equation:

$$S_s = \rho_f g(\alpha + \phi\beta)$$

where: ρ_f = fluid density
g = acceleration of gravity
α = formation compressibility
ϕ = formation porosity
β = fluid compressibility

To define our ranges for specific storage, we used the following ranges of parameter values:

ρ_f: 1200 to 1250 kg/m^3, base-case value of 1220 kg/m^3
ϕ: 0.001 to 0.03, base-case value of 0.01
β: 2.9E-10 to 3.3E-10 Pa^{-1}, base-case value of 3.1E-10 Pa^{-1}

You can use these values to get to a range for formation compressibility. The reason I can't just give you the range is that we use a more complicated expression for specific storage than the one I presented above. I expect,

however, that your model does use the expression presented above, and therefore you need to go through this calculation exercise to get at the right values for your model. All of this specific-storage information can be referenced to SAND90-0083.

I hope you find this information useful. Please contact me if you have any questions.

cc: W.D. Weart, 6340
E.D. Gorham, 6344
S.M. Howarth, 6344
S.J. Finley, 6344
D.R. Anderson, 6342

Brush, July 8, 1991

Date: 7/8/91
To: D. R. Anderson (6342)
From: L. H. Brush (6345)
Subject: Current Estimates of Gas Production Rates, Gas Production Potentials, and Expected Chemical Conditions Relevant to Radionuclide Chemistry for the Long-Term WIPP Performance Assessment

Sandia National Laboratories

Albuquerque, New Mexico 87185

date July 8, 1991

to D. R. Anderson, 6342

L. H. Brush

from L. H. Brush, 6345

subject Current Estimates of Gas Production Rates, Gas Production Potentials, and Expected Chemical Conditions Relevant to Radionuclide Chemistry for the Long-Term WIPP Performance Assessment

This memorandum justifies the estimates of gas production rates, gas production potentials, and expected chemical conditions relevant to radionuclide chemistry in WIPP disposal rooms for design-basis transuranic (TRU) waste provided to R. P. Rechard last month (Table 1). Many of these estimates are new; some are based on recently obtained data from laboratory studies of anoxic corrosion.

I will provide similar estimates for the Engineered Alternatives Task Force's (in prep.) Alternatives 2 and 6 by August 1, 1991.

ANOXIC CORROSION

R. E. Westerman (1990, 1991a) of Pacific Northwest Laboratory (PNL) has observed significant H_2 production from anoxic corrosion of two heats each of ASTM A 366 and ASTM A 570 steels by WIPP Brine A under inundated conditions when N_2 is present at low pressures (about 150 psig) in the headspace above the brine. The low-C, cold-rolled steel alloy ASTM A 366 simulates the drums to be emplaced in the repository; the medium-C, hot-rolled steel alloy ASTM A 570 simulates the boxes. The H_2 production rate was essentially constant during 3- and 6-month experiments; the average value for all four heats obtained from the 6-month experiments is 0.21 moles per m^2 of steel per year. Based on my estimate of 6 m^2 of steels per equivalent drum of waste, which includes steels used to fabricate waste containers (drums and boxes) and steels contained in the waste, this is equivalent to 1.26 mole of H_2 per drum per year. Westerman also reported an average corrosion rate of 1.72 μm of steel per year for the 6-month runs. The H_2 production rates of 0.2 moles per m^2 per year or 1 mole per drum per year and the corrosion rate of 2 μm per year are my best estimates for inundated conditions, rounded to one significant figure (Table 1).

Strictly speaking, the H_2 production rates and the corrosion rate are not equivalent. Although he obtained both rates from each

experiment, Westerman used independent techniques to obtain them (pressure measurements and posttest analysis of the headspace gases for the H_2 production rate and gravimetric, or weight-loss, analysis for the corrosion rate). These techniques agreed well, but not exactly, when applied to the 6-month experiments, but not as well for the 3-month experiments. (The best estimates described above are from the 6-month runs.) The discrepancies between these techniques probably result from uncertainties as to the identity and composition of the corrosion product or products formed during these experiments. (Characterization of the corrosion product is necessary to write the chemical reactions used to convert corrosion rates to H_2 production rates.) We are still attempting to characterize the corrosion product from these runs.

Although the H_2 production rate has been constant for 6 months when N_2 is present at low-pressures, the results of high-pressure experiments at PNL imply that the build-up of H_2 pressure would eventually reduce this rate significantly (Westerman, 1991b). After 6 months, the corrosion rate of two heats of ASTM A 366 steel under inundated conditions with H_2 at a pressure of 1,000 psig was 0.356 μm per year, 21.8% of the rate of 1.63 μm per year observed for the same two heats of ASTM A 366 steel under low-pressure, inundated conditions with N_2. Multiplying 1.72 μm per year, the average rate for all four heats, by 0.218 gives 0.375 μm per year, my estimate of the average corrosion rate for all four heats of steel at 1,000 psig H_2. However, at an N_2 pressure of 1,000 psig the corrosion rate of two heats of ASTM A 366 steel was 2.96 μm per year, 81.6% higher than the low-pressure, inundated rate of 1.63 μm per year observed for the same two heats of ASTM A 366 steel. The product of 1.72 μm per year and 1.82 is 3.13 μm per year, my estimated average corrosion rate for all four heats of steel at 1,000 psig N_2. Westerman did not report H_2 production rates for the high-pressure experiments. Furthermore, we have still not identified the corrosion product or products yet. However, the corrosion product appears to be the same phase that formed in the 6-month, low pressure experiments. It is thus possible to estimate an H_2 production rate by multiplying the 6-month, low-pressure rates of 0.21 moles per m^2 or 1.26 moles per drum of waste by 0.218 (1,000 psig H_2) and 1.82 (1,000 psig N_2) to obtain 0.046 moles per m^2 per year or 0.275 moles per drum per year (1,000 psig H_2) and 0.38 moles per m^2 per year or 2.29 moles per drum per year (1,000 psig N_2). At present, we do not have corrosion rates for any pressures other than 150 and 1,000 psig. Westerman will, however, report 12-month data for 500 psig H_2 and 1,000 psig H_2 in November or December 1991. The adjusted, measured corrosion rate of 3 μm per year and the estimated H_2 production rate of 0.4 mole per m^2 per year or 2 moles per drum per year with N_2 at 1,000 psig are my maximum estimates for inundated conditions, rounded to one significant figure (Table 1).

Under low-pressure, inundated conditions with CO_2, H_2 production occurred for about 3 months, then virtually stopped after 3 or 4 months due to formation of a passivating layer of $FeCO_3$, or siderite

(Westerman, 1991a). This suggests that, if microbially produced CO_2 were present, passivation of steel surfaces by $FeCO_3$ could stop H_2 production before the generation of significant quantities of this gas. However, we do not know the partial pressure of CO_2 required to form $FeCO_3$. Furthermore, crushing of drums and boxes during room closure could disrupt the layer of $FeCO_3$ and lead to some additional H_2 production. Nevertheless, the passivation observed after 3 or 4 months is the basis for my minimum estimates of 0 moles of H_2 per m^2 per year or 0 moles of H_2 per drum per year and 0 μm of steel per year for inundated conditions (Table 1).

Because we have still not identified the corrosion product or products, we cannot calculate the number moles of H_2O consumed per mole of Fe consumed or the number moles of H_2O consumed per mole of H_2 produced from anoxic corrosion of steels. However, the corrosion reaction that produces $Fe(OH)_2$ (amakinite) a possible corrosion product identified by Brush and Anderson (1988) and Brush (1990), would consume 2 moles of H_2O per mole of Fe consumed, or consume 2 moles of H_2O per mole of H_2 produced. The corrosion reaction that produces Fe_3O_4 (magnetite), another possible corrosion product, would consume 1.33 mole of H_2O per mole of Fe consumed, or consume 1 mole of H_2O per mole of H_2 produced. These values are probably typical of other corrosion reactions.

In 3- and 6-month, low-pressure, humid experiments with either CO_2 or N_2, Westerman (1990, 1991a) observed no H_2 production except for very limited quantities from corrosion of the bottom 10% of the specimens splashed with brine during pretest preparation of the containers. These results and modeling studies conducted by Davies (personal communication) suggested to me that anoxic corrosion could be self-limiting; small quantities of brine in the repository could produce H_2, increase the pressure, prevent additional brine inflow or even cause brine outflow, and thus prevent additional H_2 production. However, the thin film of brine introduced by capillary rise or condensation followed by dissolution of salts from the backfill, or H_2O absorbed by crushed salt or bentonite in the backfill, which will be in contact with drums and boxes, could cause additional anoxic corrosion of steels and H_2 production after brine is driven away from corroding steels.

Westerman (1991c) has just started a study to quantify H_2 production from anoxic corrosion of steels in contact with noninundated backfill materials and will report preliminary results by the end of September 1991. Until then, I propose the following arbitrarily estimated rates for humid conditions: minimum estimates of 0 moles of H_2 per m^2 of steel per year or 0 moles per drum of waste per year and 0 μm of steel per year; best estimates of 0.02 moles of H_2 per m^2 per year or 0.1 moles of H_2 per drum per year and 0.2 μm per year; and maximum estimates of 0.2 moles of H_2 per m_2 per year or 1 moles of H_2 per drum per year and 2 μm per year (Table 1).

Finally, I propose that the estimated gas production potential from

anoxic corrosion remain at 900 moles per drum of waste. This value, estimated by Brush and Anderson (1989), Lappin et al. (1989), and Brush (1990), is 60% of the total gas production potential.

MICROBIAL ACTIVITY

D. Grbic-Galic and her colleagues at Stanford University observed significant microbial gas production by halophilic microorganisms in brine collected from G Seep in the WIPP underground workings with glucose, a relatively biodegradable substrate, but did not report significant gas production with cellulose, a much less biodegradable substrate. Furthermore, brine from G Seep inhibited significant gas production by nonhalophilic microorganisms, although a few experiments did show some evidence for possible microbial activity. These results seem to suggest that microbial gas production may be significant under overtest conditions (relatively biodegradable substrates, amendment of brine with nutrients, etc.), but not under realistic conditions. However, I believe that, for the reasons described below, the results obtained by Grbic-Galic and her colleagues do not rule out significant microbial gas production.

First, N. Black of Stanford University, R. H. Vreeland of West Chester University, and I compared the recent study at Stanford University and studies carried out during the 1970s (Barnhart et al., 1980; Caldwell, 1981; Caldwell et al., 1988; Molecke, 1979; Sandia National Laboratories, 1979). We concluded, as others have before us (Molecke, 1979; Brush and Anderson, 1989; Lappin et al., 1989), that the earlier results implied significant microbial gas production under both realistic and overtest conditions.

Second, Vreeland observed significant degradation of filter paper by his enrichments of halophilic and halotolerant microorganisms from the salt lakes in Nash Draw. Although he could not quantify gas production rates from these experiments, the results suggest that microorganisms could consume paper under realistic conditions in WIPP disposal rooms. Paper constitutes 70% of the 10 kg of cellulosics per equivalent drum of contact handled TRU waste to be emplaced in the repository (Brush, 1990).

Third, Black, Vreeland, and I reviewed the methods used in the earlier and recent studies in detail. We concluded that the study at Stanford University was not sensitive enough to detect gas production rates equivalent to a few tenths of a mole of gas per drum of waste per year. Davies (1990) has demonstrated that gas production rates greater than about 0.1 mole per equivalent drum of waste per year are significant from the standpoint of the long-term performance of the repository.

Because the results obtained at Stanford University do not rule out significant microbial gas production under realistic conditions, I

propose using the same best estimate for the microbial gas production rate under inundated conditions proposed by Brush and Anderson (1989), Lappin et al. (1989), and Brush (1990), 1 mole of various gases per drum per year. However, I propose new minimum and maximum rates for inundated conditions, 0 and 5 moles per drum per year, respectively. The minimum estimate is analogous to the minimum estimate for anoxic corrosion under inundated conditions. The maximum estimate is Molecke's (1979) maximum estimate for microbial activity under inundated conditions. I also propose new minimum and best estimates for microbial gas production rates under humid conditions, 0 and 0.1 moles per drum per year. These estimates, both arbitrary, are analogous to the arbitrary minimum and best estimates for anoxic corrosion under humid conditions. The maximum estimate for microbial activity under humid conditions remains unchanged from the value estimated by Brush and Lappin (1990), 1 mole per drum per year (Table 1).

To convert these estimates of microbial gas production rates to units of moles per kg of cellulosics per year, I divided each rate by 10 kg of cellulosics per drum, the estimate used by Brush (1990), to obtain the estimates given in Table 1. Strictly speaking, this is inconsistent with the fact that the rate of 1 mole per drum per year is based on experiments carried out with simulated waste that included materials other than cellulosics (Molecke, 1979). It is also inconsistent with the assumption of Molecke (1979), Brush and Anderson (1979), and Lappin et al. (1989) that microorganisms will degrade 100% of the cellulosics, 50% of the Hypalon, and 50% of the Neoprene in the waste. However, about 90% of the microbial gas production potential (below) and hence 90% of the microbial gas production rate estimated by Brush and Anderson (1989) and Lappin et al. (1989) would result from biodegradation of cellulosics and only 5% each from Hypalon and Neoprene. Furthermore, Francis will use cellulosics as the sole substrate in his study of microbial gas production, at least initially. Finally, it will be much easier to use rates normalized only to the mass of cellulosics present than rates normalized to cellulosics, Hypalon, and Neoprene in performance-assessment calculations.

I also propose that the estimated gas production potential from microbial activity stay at 600 moles per drum of waste, the value estimated by Brush and Anderson (1989), Lappin et al. (1989), and Brush (1990). This is 40% of the total gas production potential.

RADIOLYSIS

D. T. Reed of Argonne National Laboratory is carrying out a low-pressure study of gas production by α radiolysis of Brine A as a function of dissolved Pu concentration. He has observed small, linear pressure increases from the solution with the highest dissolved Pu concentration, $1 \cdot 10^{-4}$ M, but does not have enough data to convert these rates to moles of gas per drum of waste per year yet. As

expected, he has not observed pressure increases yet from the solutions with lower dissolved Pu concentrations, $1 \cdot 10^{-6}$ and $1 \cdot 10^{-8}$ M. After completion of these 3-month experiments, Reed will carry out 2-month runs with a dissolved Pu concentration of $1 \cdot 10^{-4}$ M in other WIPP brines to determine the effect of compositional variations on the radiolytic gas production rate.

As soon as he obtains longer-term data from Brine A with a dissolved Pu concentration of $1 \cdot 10^{-4}$ M, data with lower dissolved Pu concentrations in Brine A, and results from other WIPP brines with a dissolved Pu concentration of $1 \cdot 10^{-4}$ M, Reed will calculate experimentally based radiolytic gas-production rates for the radionuclide concentrations estimated by the Radionuclide Source Term Expert Panel. In addition to rates in units of moles of gas per drum of waste per year, he will provide rates in moles per cubic meter of brine for various concentrations. Until then, I propose using the radiolytic gas production rates proposed by Brush and Lappin (1990), who estimated a minimum rate of $1 \cdot 10^{-7}$ mole of various gases per drum of waste per year, a best rate of $1 \cdot 10^{-4}$ mole per drum per year, and a maximum rate of $1 \cdot 10^{-1}$ mole per drum per year (Table 1).

EXPECTED CHEMICAL CONDITIONS RELEVANT TO RADIONUCLIDE CHEMISTRY

Development of the source term for radionuclide-transport calculations will require: (1) estimates of the quantity of each nonradioactive constituent of design-basis TRU waste to be emplaced in the repository; (2) predictions of the microenvironments (Eh, pH, and the concentrations of organic and inorganic ligands) for each nonradioactive waste constituent; (3) quantification of the chemical behavior of the important radionuclides in the waste for each of these microenvironments; (4) construction of a frequency distribution of radionuclide concentrations based on the relative quantity of each nonradioactive waste constituent and the concentration associated with that constituent.

Currently, inventories of radioactive and nonradioactive waste constituents and estimates of radionuclide concentrations in brines as a function of Eh and pH are available. However, the high priority placed on the gas issue in laboratory studies of repository chemistry has precluded efforts to predict microenvironment for waste constituents. Therefore, I propose that oxidizing, acidic conditions, oxidizing, basic conditions, reducing, acidic conditions, and reducing, basic conditions be considered equally probable for interpreting Eh-pH-dependent estimates of radionuclide concentrations in WIPP brines.

REFERENCES

Barnhart, B. J., E. W. Campbell, E. Martinez, D. E. Caldwell, and R. Hallett (1980). **Potential Microbial Impact on Transuranic Wastes Under Conditions Expected in the Waste Isolation Pilot Plant (WIPP), Annual Report, October 1, 1978-September 30, 1979.** LA-8297-PR, Los Alamos Scientific Laboratory, Los Alamos, NM.

Brush, L. H. (1990). **Test Plan for Laboratory and Modeling Studies of Repository and Radionuclide Chemistry for the Waste Isolation Pilot Plant**, SAND90-0266, Sandia National Laboratories, Albuquerque, NM.

Brush, L. H., and D. R. Anderson (1989). Estimates of Gas Production Rates, Potentials, and Periods, and Dissolved Radionuclide Concentrations for the WIPP Supplemental Environmental Impact Statement, unpublished memorandum to B. M. Butcher, February 14, 1989. Sandia National Laboratories, Albuquerque, NM.

Brush, L. H., and A. R. Lappin (1990). Additional Estimates of Gas Production Rates and Radionuclide Solubilities for Use in Models of WIPP Disposal Rooms, unpublished memorandum to D. R. Anderson, August 1, 1990. Sandia National Laboratories, Albuquerque, NM.

Caldwell, D. E. (1981). Microbial Biogeochemistry of Organic Matrix Transuranic Waste, unpublished report submitted to M. A. Molecke, June 17, 1981, University of New Mexico, Albuquerque, NM.

Caldwell, D. E., R. C. Hallett, M. A. Molecke, E. Martinez, and B. J. Barnhart (1988). **Rates of CO_2 Production From the Microbial Degradation of Transuranic Wastes under Simulated Geologic Isolation Conditions**. SAND87-7170, Sandia National Laboratories, Albuquerque, NM.

Davies, P. B. (1990). Results from Recent Variable-Rate Gas Simulations that Examine the Impact of Vapor-Limited ("Humid") Gas-Generation Rates, unpublished memorandum to L. H. Brush and A. R. Lappin, December 6, 1990. Sandia National Laboratories, Albuquerque, NM.

Engineered Alternatives Task Force (in prep.). **Evaluation of the Effectiveness and Feasibility of the Waste Isolation Pilot Plant Engineered Alternatives: Final Report of the Engineered Alternatives Task Force, Vol. I and II**, DOE/WIPP 91-007, Rev. 2, US Department of Energy Waste Isolation Pilot Plant, Carlsbad, NM.

Lappin, A. R., R. L. Hunter, D. P. Garber, and P. B. Davies, Eds. (1989). **Systems Analysis, Long-Term Radionuclide Transport, and Dose Assessments, Waste Isolation Pilot Plant (WIPP), Southeastern New Mexico; March, 1989**. SAND89-0462, Sandia National Laboratories, Albuquerque, NM.

Molecke, M. A. (1979). **Gas Generation from Transuranic Waste Degradation: Data Summary and Interpretation**. SAND79-1245, Sandia National Laboratories, Albuquerque, NM.

Sandia National Laboratories (1979). **Summary of Research and Development Activities in Support of Waste Acceptance Criteria for the WIPP**. SAND79-1305, Sandia National Laboratories, Albuquerque, NM.

Westerman, R. E. (1990). Corrosion of Low-Carbon Steel in Simulated Waste Isolation Pilot Plant (WIPP) Environments, Quarterly Progress Report for the Period July 1 - September 30, 1990, unpublished report submitted to L. H. Brush, September 28, 1990. Pacific Northwest Laboratory, Richland, WA.

Westerman, R. E. (1991a). Corrosion of Low-Carbon Steel in Simulated Waste Isolation Pilot Plant (WIPP) Environments, Progress Report for the Period October 1, 1990 to March 31, 1991, unpublished report submitted to L. H. Brush, March 29, 1991. Pacific Northwest Laboratory, Richland, WA.

Westerman, R. E. (1991b). April 1991 Monthly Report, Corrosion of Low-Carbon Steel in Simulated WIPP Environments, unpublished report submitted to L. H. Brush, April 26, 1991. Pacific Northwest Laboratory, Richland, WA.

Westerman, R. E. (1991c). May 1991 Monthly Report, Corrosion of Low-Carbon Steel in Simulated WIPP Environments, unpublished report submitted to L. H. Brush, May 28, 1991. Pacific Northwest Laboratory, Richland, WA.

TABLE 1. CURRENT ESTIMATES OF GAS PRODUCTION RATES

Process	Gas Production Rate (various units)		
	Minimum	Best	Maximum
Anoxic corrosion, inundated:[1]			
moles/m^2 · year	0	0.2	0.4
moles/drum · year	0	1	2
μm/year	0	2	3
Anoxic corrosion, humid:[1]			
moles/m^2 · year	0	0.02	0.2
moles/drum · year	0	0.1	1
μm/year	0	0.2	2
Microbial activity, inundated:			
moles/drum · year	0	1	5
moles/kg cellulosics · year	0	0.1	0.5
Microbial activity, humid:			
moles/drum · year	0	0.1	1
moles/kg cellulosics · year	0	0.01	0.1
Radiolysis of brine:			
moles/drum · year	0.0000001	0.0001	0.1

1. See text for estimates of H_2O consumption by anoxic corrosion of steels.

Distribution:

V. Daub, DOE/WPO
J. Carr, DOE/WPO
D. Blackstone, DOE/WPO
W. D. Arnold, Oak Ridge National Laboratory
J. N. Butler, Harvard University
G. R. Choppin, Florida State University
A. J. Francis, Brookhaven National Laboratory
J. B. Gillow, Brookhaven National Laboratory
J. K. Lanyi, University of California at Irvine
R. E. Meyer, Oak Ridge National Laboratory
H. Nitsche, Lawrence Livermore National Laboratory
D. T. Reed, Argonne National Laboratory
R. H. Vreeland, West Chester University
R. E. Westerman, Pacific Northwest Laboratory
6340 W. D. Weart
6341 R. C. Lincoln
6341 SWCF (6): XXXRC, XXXRC/AC, XXXRC/MA, XXXRC/R, XXXRNC, XXXRNC/SOL
6342 Staff
6343 T. M. Schultheis
6344 E. D. Gorham
6344 P. B. Davies
6345 B. M. Butcher
6345 Staff
6346 J. R. Tillerson

Davies, June 2, 1991

Date: 6/2/91
To: D. R. Anderson (6342)
From: P. B. Davies (6344)
Subject: Uncertainty Estimates for Threshold Pressure for 1991 Performance Assessment Calculations Involving Waste-Generated Gas

Sandia National Laboratories

Albuquerque, New Mexico 87185

Date: June 6, 1991

To: D.R. Anderson (6342)

P.B. Davies

From: P.B. Davies (6344)

Subject: Uncertainty Estimates for Threshold Pressure for 1991 Performance Assessment Calculations Involving Waste-Generated Gas

This memorandum contains the recommended uncertainty distribution for the threshold pressure for 1991 performance assessment calculations involving waste-generated gas. Threshold pressure may play an important role in controlling which Salado lithologies are accessible as gas migration flow paths and at what gas pressures gas flow will be initiated. Threshold pressure is also a key parameter in the Brooks and Corey (1964) model used to characterize the 2-phase properties of analogue materials for preliminary gas calculations (Davies and LaVenue, 1990). Threshold pressure is strongly related to intrinsic permeability and, therefore, these parameters should not be sampled independently. The recommended approach for 1991 calculations is as follows. First sample for the intrinsic permeability for a given unit (either interbed or halite), then use the following the empirical correlation for threshold pressure from Davies (1991) to compute a median value for threshold pressure:

$$P_t\ [\text{MPa}] = 5.6 \times 10^{-7} \left(k\ [\text{m}^2] \right)^{-0.346}$$

As noted in Davies (1991), threshold pressure estimates based on this empirical correlation have uncertainty associated with the correlation itself and with factors external to the correlation. One uncertainty in the correlation is the error associated with estimating the true mean value of the threshold pressure for a given intrinsic permeability. Because of the relatively strong correlation (goodness-of-fit, R^2, is equal to 0.93), the estimation error is fairly small. A second uncertainty in the correlation is prediction error due to random variations in threshold pressure in any given rock type and to measurement error in the original data. Because measurement error in the original data was not quantified, these two sources of uncertainty cannot be evaluated independently. The interval between the bounds of this prediction error is approximately three times the estimated mean threshold pressure. One source of uncertainty that is external to the correlation is the uncertainty associated with measurements of intrinsic permeability in various lithologies of the Salado Formation. Presumably, this uncertainty will be accounted for in performance assessment calculations by sampling on permeability. Another very important source of uncertainty is the fact that while the data for the correlation span a wide range of consolidated rock types (shale, anhydrite, carbonate, and sandstone), the data do not include any actual measurements from the Salado Formation at the WIPP repository nor do the data include any actual measurements on halite.

Clearly the total uncertainty in the estimates described in the previous paragraph is quite large. Given the present lack of any WIPP-specific data, it is not possible to rigorously quantify this uncertainty. Therefore,

it is recommended that a relatively simple representation of uncertainty should be used for purposes of the 1991 performance assessment calculations. For these calculations, it is recommended that a log normal distribution be assumed, with plus/minus one order of magnitude for one standard deviation and plus/minus two orders of magnitude for two standard deviations (Figure 1). This large uncertainty should produce a wide range of hydrologic responses to waste-generated gas, which is appropriate given the present lack of WIPP-specific data.

REFERENCES

Brooks, R.H., and A.T. Corey. 1964. Hydraulic Properties of Porous Media. Colorado State University, Hydrology Paper No. 3.

Davies, P.B. 1991. Evaluation of the Role of Threshold Pressure in Controlling Flow of Waste-Generated Gas into the Bedded Salt at the Waste Isolation Pilot Plant. SAND90-3246. Albuquerque, New Mexico: Sandia National Laboratories.

Davies, P.B. and LaVenue, A.M. 1990. "Additional Data for Characterizing 2-Phase Flow Behavior in Waste-Generated Gas Simulations and Pilot Point Information for Final Culebra 2-D Model (SAND89-7068/1)." memorandum to R.P. Rechard (11-19-91). Albuquerque, New Mexico: Sandia National Laboratories.

cc: W.D. Weart (6340)
M.G. Marietta (6342)
R.P. Rechard (6342)
P. Vaughn (Applied Physics Inc.)
E.D. Gorham (6344)
S.M. Howarth (6344)
S.W. Webb (6344)

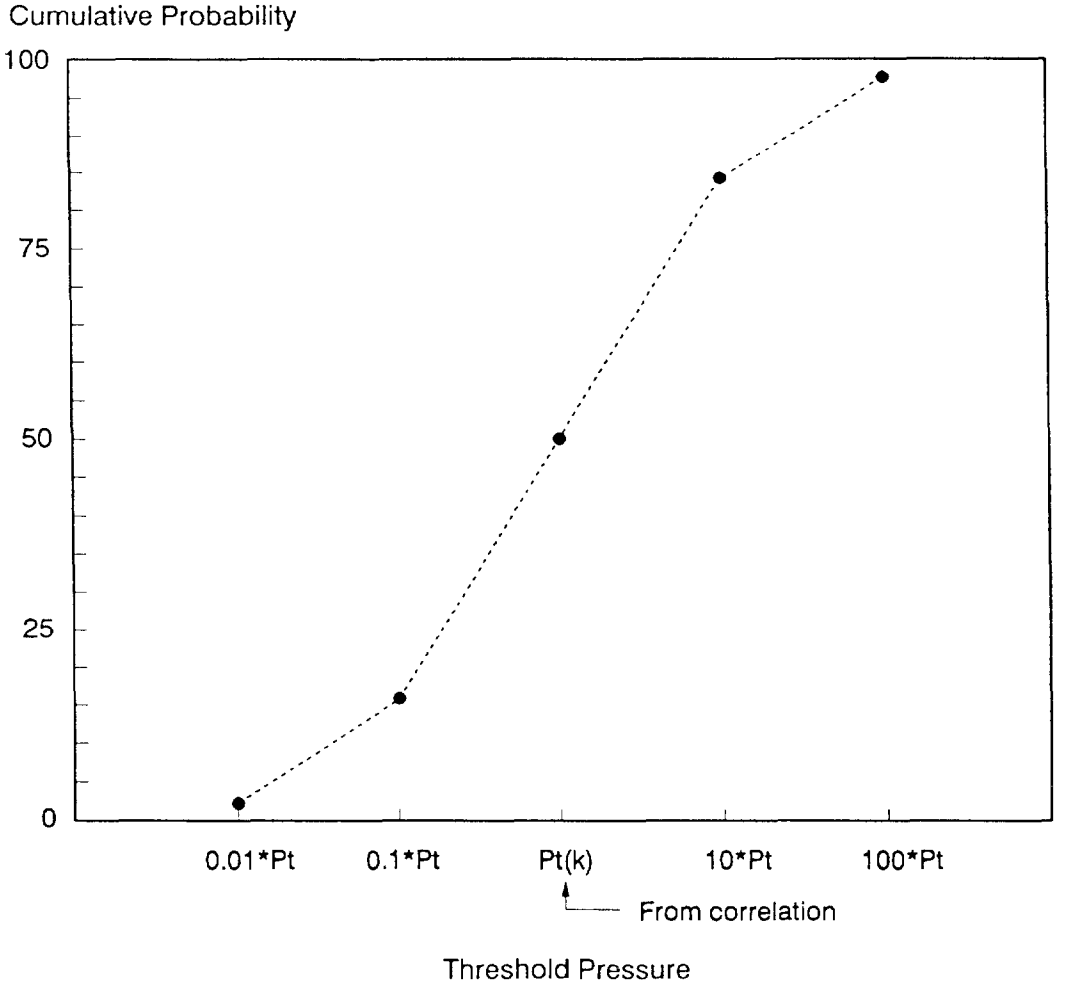

Figure 1. Uncertainty distribution for threshold pressure.

Drez, May 9, 1989

Date: 5/9/89
To: L. Brush (6334)
From: Paul Drez (International Technology Corporation)
Subject: Preliminary Nonradionuclide Inventory of CH-TRU Waste
(Note: Following the letter are Tables 3.5, 3.6, and 3.9, which were taken from the draft report, "Preliminary Nonradionuclide Inventory for CH-TRU Waste," by P. E. Drez and P. James-Lipponer, International Technology Corporation, Albuquerque, NM, May, 1989.)

INTERNATIONAL TECHNOLOGY CORPORATION

May 9, 1989

Project No. 301192.88.01

Dr. L. Brush
Sandia National Laboratories
Division 6334
P. O. Box 5800
Albuquerque, NM 87185

Preliminary Nonradionuclide Inventory of CH-TRU Waste

Dear Dr. Brush:

Attached is a preliminary report on the status of the Nonradionuclide Inventory Database and detailed tabulations of waste materials as requested in the last amendment to the IT Sandia Support contract. I am sorry for the slight delay in completing the report, but the CH-TRU generator/storage sites were late in their responses and the process of tabulating the appropriate data proved to be a difficult task. Part of the difficulty has to do with the slight variations in the way the sites report data.

Listed below is the information contained in this package:

- Report entitled: "Preliminary Nonradionuclide Inventory for CH-TRU Waste." The report includes a description of how the data was collected from the CH-TRU waste generator/storage sites, a description of the database used to compile the data, and examples of how the calculations were made including any limitations (Item 7 in Statement of Work).

- Table 3-5 in the report summarizes the total quantity of combustible materials in the waste, including cellulosics, plastics and other combustibles (Item 3 in Statement of Work).

  Although only total cellulosics were requested, data on plastics and other combustibles were also tabulated, anticipating their eventual need to support the Performance Assessment program.

- Table 3-5 in the report estimates the quantity of various types of cellulosic materials in the total cellulosic inventory (Item 4 in Statement of Work).

  A breakdown of the various types of plastic and rubber materials has also been provided in Table 3-5. Caution is advised in the interpretation of the plastics in the tables, since two sites choose to report the weight of plastic bagging and rigid liners as part of the waste totals.

- Table 3-6 in the report estimates the total quantity of metals in the CH-TRU waste and also provides a breakdown of the various types of metals in the waste (Item 5 in Statement of Work).

  Caution is advised in the interpretation of this table, since two sites choose to report the amount of metal in the waste packaging as part of the waste contents in this table. I have no way of separating out the weight of the waste cannister from the database at this time.

  In an attempt to provide a complete inventory (including waste packaging), Table 3-8 provides a preliminary estimate of the amount of plastic and other internal packaging in addition to an estimate of the metal included in the waste. Variations in the method of packaging from site to site have been accounted for in the tabulation of the data.

- Table 3-7 in the report estimates the total quantity of nitrates and total inorganic carbon (TIC) in the waste (Items 2 and 6 in Statement of Work). Graphite or charcoal is not considered part of this summary, only inorganic carbonate.

- Table 4-2 in the report lists quantitative information on selected chelating agents that occur in the waste. All chelating agents requested in your statement of work (Item 1) have been included plus any additional chelating agents that have been reported by the sites.

- Printouts for each generator/storage site that represent complete data dumps of the Nonradionuclide Inventory Database (Item 7 of Statement of Work).

- Floppy disks containing all the dBASE files for the database. An explanation of the files is provided in Appendix 2.0 of the report (Item 7 of Statement of Work).

I am very pleased to transmit this preliminary report on the Nonradionuclide Inventory Database to you. This database is important step towards an understanding of the composition and quantities of CH-TRU waste to be emplaced in WIPP. This is a "living" database that should be updated periodically as more precise information is provided by the CH-TRU waste generator/storage sites.

Do not hesitate to contact me at 262-8800 if you need any clarification of the data contained in this packet of information. Pamela James (262-8800) can provide any information about the structure and output of the database.

Sincerely,

Paul E. Drez

Paul E. Drez
Senior Technical Associate

Enclosures

cc: M. Devarakonda, IT-Albuquerque (report only)
P. James, IT-Albuquerque (report only)
J. Myers, IT-Albuquerque (report only)

Do not hesitate to contact me at 262-8800 if you need any clarification of the data contained in this packet of information. Pamela James (262-8800) can provide any information about the structure and output of the database.

Sincerely,

Paul E. Drez

Paul E. Drez
Senior Technical Associate

Enclosures

cc: M. Devarakonda, IT-Albuquerque (report only)
P. James, IT-Albuquerque (report only)
J. Myers, IT-Albuquerque (report only)

Table 3-5. Total Quantity of CH-TRU Combustible Waste to be Shipped to WIPP

Waste Material	Weight (Kilograms)
COMBUSTIBLES	
-Cellulosics	
-Paper/Kimwipes	3,890,000*
-Cloth	226,000
-Other Paper	51
-Lumber (untreated)	73,100
-Lumber (treated)	36,700
-Plywood	98,400
-Other Wood (rulers)	<1
-Other Wood (all types)	23,700
-Other Cellulose (with phenolic binder)	1,720
-Cellulosics Subtotal	4,350,000

* All numbers, including totals, rounded off to a maximum of three significant number.

Table 3-5. Total Quantity of CH-TRU Combustible Waste to be Shipped to WIPP (Continued)

Waste Material	Weight (Kilograms)
COMBUSTIBLES	
-Plastics	
-Polyethylene	1,540,000*
-Polyvinyl Chloride	1,040,000
-Surgeon's Gloves (latex)	582,000
-Leaded Rubber Gloves (Lead-Hypalon-Neoprene)	596,000
-Hypalon	114,000
-Neoprene	129,000
-Viton	133
-Teflon	41,000
-Plexiglas (including Lucite)	18,900
-Styrofoam	330
-Plastic Prefilters (polypropylene?)	33,600
-Polystyrene	2,560
-Conwed Pads (plastic fibers)	2,030
-Other Plastic	75,500
-Other Rubber (Kalrez)	<1
-Other Rubber (undefined)	7,530
-Plastics Subtotal	4,180,000

* All numbers, including totals, rounded off to a maximum of three significant number.

Table 3-5. Total Quantity of CH-TRU Combustible Waste to be Shipped to WIPP (Continued)

Waste Material	Weight (Kilograms)
COMBUSTIBLES	
-Other	
-Blacktop	18,800*
-Other	41,700
-Other Subtotal	60,500
-Cellulosics Subtotal	4,350,000
-Plastics Subtotal	4,180,000
-Other Subtotal	60,500
COMBUSTIBLES TOTAL IN CH-TRU WASTE	8,590,000

* All numbers, including totals, rounded off to a maximum of three significant number.

Table 3-6. Total Quantity of CH-TRU Metal Waste to be Shipped To WIPP

Waste Material	Weight (Kilograms)
Metals	
-Aluminum	666,000*
-Beryllium	8,640
-Cadmium	5
-Chromium	5
-Copper	300,000
-Iron	2,620,000
-Lead	
- Metallic	513,000
- Glass (includes weight of glass)	1,120,000#
- Gloves (includes weight of gloves)	596,000#
-Lithium (batteries)	1,030
-Mercury	120
-Paint Cans	547,000
-Platinum	1,500
-Selenium	5
-Silver	5

* All numbers, including totals, rounded off to a maximum of three significant number.

The reported weights for lead include the weight of the matrix, therefore, the values are conservative (too high).

Table 3-6. Total Quantity of CH-TRU Metal Waste to be Shipped To WIPP (Continued)

Waste Material	Weight (Kilograms)
Metals	
-Steel (including stainless, crushed drums inner drums, carbon steel, etc.)	9,170,000*#
-Shipping Cans	217
-Tantalum	125,000
-Tungsten	20,000
-Other	146,000
Total Metals	15,800,000

* All numbers, including totals, rounded off to a maximum of three significant number.

The weight of steel quoted in the table includes the weight of the waste containers (drums and boxes) for INEL and LANL.

Table 3-9. Average Weights Used for Calculation of Container and Packaging Materials

Type of Packaging Material	Weight (Kilograms)
Drums -	
Weight of 17C drum	29.5*
Weight of 90-mil high-density polyethylene liner	6.8
Weight of Polyvinyl Chloride drum liner bag	0.7
Weight of Polyethylene drum liner bag	0.7
Weight of Fiberboard liner for 55 gallon drum	2.0
4x4x7 Boxes -	
Weight of 4x4x7 metal box	217.7
Weight of Plywood liner for 4x4x7 metal box	175.5
Weight of PVC liner bag for 4x4x7 box	5.0
Weight of fiberboard liner for 4x4x7 box	11.8
Weight of wooden 4x4x7 box	208.7
Weight of fiberglass reinforced wooden box	322.0
Standard Waste Boxes -	
Weight of Standard Waste Box	310.7#
Weight of PVC liner bag	4.0

* All weights are based on containers and packaging materials used at the Rocky Flats Plant, except for the weight of the Standard Waste Box.

Trupact-II Safety Analysis Report, Appendix 1.3.4, Revision 0, 1989.

Finley and McTigue, June 17, 1991

Date: 6/17/91
To: Elaine Gorham, 6344
From: S. J. Finley, 6344, and D. F. McTigue, 1511
Subject: Parameter Estimates from the Small-Scale Brine Inflow Experiments

Sandia National Laboratories

Albuquerque, New Mexico 87185

date: June 17, 1991

to: Elaine Gorham, 6344

from: S. J. Finley, 6344 and D. F. McTigue, 1511

subject: Parameter Estimates from The Small-Scale Brine Inflow Experiments

Data from the small-scale brine inflow experiments has been analyzed using the one-dimensional, radial, Darcy flow model. Brine inflow data from 10 boreholes in halite and 3 boreholes testing Marker Bed 139 has been used to estimate permeability and hydraulic diffusivity. The diffusivity is determined from the time scale of the decay of the flux (inflow rate/unit area), and the product of the pore pressure and permeability is determined from the magnitude of the flux.

All of the results of the two parameter fit to the flux data are given in Table 1. Permeability values reported are estimated by assuming a uniform pore pressure of 10 MPa, 5 MPa, and 1 Mpa. (Susan Howarth and Rick Beauheim have both made measurements of pore pressure in the WIPP underground and should be consulted about the pore pressure assumptions.) Uncertainty in all parameter estimates is reported as plus or minus one standard deviation. This uncertainty is a measure of how good the fit is assuming a random error of the order of the expected measurement error is included in the data set. Any uncertainty in the model itself or the pore pressure assumed are not included in the uncertainty measure reported.

All of the boreholes included in this set of experiments are drilled from an underground excavation. Boreholes vary from 3 m to 6 m in length. For all halite tests, brine inflow was averaged over the entire length of the borehole. For the boreholes testing Marker Bed 139, the brine inflow was averaged over the thickness of Marker Bed 139 (3-feet).

Attachment

Copy to:
W. D. Weart, 6340
D. R. Anderson, 6342
R. P. Rechard, 6342
R. L. Beauheim, 6344
S. M. Howarth, 6344

Table 1: Parameter Estimates from Borehole Experiments

Borehole #	Rock Type	Permeability @Po = 10 MPa (m^2)	Permeability @Po = 5 MPa (m^2)	Permeability @Po = 1 MPa (m^2)	Diffusivity (m^2/sec)
DBT10	Halite	2.9E-22±.18E-22	5.8E-22±.36E-22	2.9E-21±.18E-21	4.7E-11 ±.78E-11
DBT11	Halite	1.1E-21±.09E-21	2.3E-21±.18E-21	1.1E-20±.09E-20	3.5E-9 ±.63E-9
DBT12	Halite	6.4E-22±.72E-22	1.3E-21±.14E-21	6.4E-21±.72E-21	1.0E-8 ±.65E-8
DBT13	Halite	1.7E-22±.26E-22	3.4E-22±.52E-22	1.7E-21± .26E-21	5.9E-11 ± 2.3E-11
DBT14A	Halite	7.8E-22±2.4E-22	1.6E-21±.48E-21	7.8E-21±2.4E-21	2.8E-8 ±4.6E-8*
DBT14B	Halite	2.2E-20±.28E-21	4.5E-21±.56E-21	2.2E-21±.28E-21	4.3E-8 ±3.3E-8
DBT15A	Halite	3.2E-22±.55E-22	6.4E-22±1.1E-22	3.2E-21±.55E-21	1.8E-10 ±.86E-10
DBT15B	Halite	1.8E-22±.59E-22	3.6E-22±1.1E-22	1.8E-21±.59E-21	1.3E-10 ±1.2E-10
L4B01	Halite	.67E-22±.43E-22	1.3E-22±.86E-22	.67E-21±.43E-21	5.8E-11 ±9.1E-11*
DBT31A	Halite	9.0E-22±2.4E-22	1.8E-21±.48E-21	9.0E-21±2.4E-21	1.27E-10±1.22E-11
QPB01 *1	Anhydrite	4.8E-21±.3E-21	9.6E-21±.06E-21	4.8E-20±.3E-20	1.1E-8 ±.34E-8
QPB02 *1	Anhydrite	8.2E-20±.03E-20	1.6E-19±.006E-19	8.2E-19±.03E-19	1.2E-9 ±.014E-9
QPB03 *1	Anhydrite	4.8E-21±1.5E-21	9.6E-21±3E-21	4.8E-20±1.5E-20	6.4E-7 ±18.8E-7*

* The lower limit of these uncertainty bounds should be assumed to be zero.

*1 For all of these borehole tests, the length of the productive unit was assumed to be equal to the average thickness of Marker Bed 139 (3-feet).

Howarth, June 12, 1991

Date: 6/12/91
To: Elaine Gorham (6344)
From: Susan Howarth (6344)
Subject: Pore Pressure Distributions for 1991 Performance Assessment Calculations

Sandia National Laboratories

Albuquerque, New Mexico 87185

DATE: June 12, 1991

TO: Elaine Gorham, 6344

FROM: Susan Howarth, 6344

SUBJECT: Pore Pressure Distributions for 1991 Performance Assessment Calculations

Attached are the Relative Frequency and Cumulative Frequency distributions for pore pressure as determined from the pre-excavation borehole tests at Room Q. There are three sets of graphs: 1) all data, 2) halite only tests, and 3) anhydrite only tests. On each frequency distribution graph, the vertical bars are centered above a pore pressure value which represents the midpoint of the pressure range. For example, the bar above the 9.5 value represents the data in the 9.0 to 9.9 range.

In determining pore pressure from a shut in (pressure build up) pressure test, pressure is extrapolated to the pore pressure using the Horner method. For each Room Q borehole, a range of pore pressure values is given: the low number is the highest pre-excavation pressure recorded for the test zone and the high number is the Horner extrapolated value. All data within the range is weighed equally. A list of the boreholes and pressure ranges is found below in Table 1.

During the pre-excavation time period, each Room Q borehole test region was located 75 feet from an existing excavation. Because these pressure tests are located farther from an excavation than any similar tests, they are thought to be most representative of far-field conditions. However, these data should be combined with data from the Small-Scale Brine Inflow Program and the Permeability Testing Program for use in Performance Assessment calculations.

TABLE 1.
Room Q Pre-excavation Pore Pressure Ranges

Borehole	Pore Pressure (MPa)
QPP01	9.3-13.9
QPP02	1.1-1.1
QPP03	11.5-12.8
QPP04	7.0-10.3
QPP05	Indeterminate
QPP11	Indeterminate
QPP12	5.8-8.6
QPP13	10.5-12.8
QPP14	Indeterminate
QPP15	Indeterminate
QPP21	Indeterminate
QPP22	8.5-9.1
QPP23	7.1-9.4
QPP24	8.7-9.4
QPP25	7.2-9.4

Copy to:

W. D. Weart, 6340 (w/o attachments)
D. R. Anderson, 6342
R. P. Rechard, 6342
R. L. Beauheim, 6344
S. J. Finley, 6344

ROOM Q

PORE PRESSURE (ALL DATA)

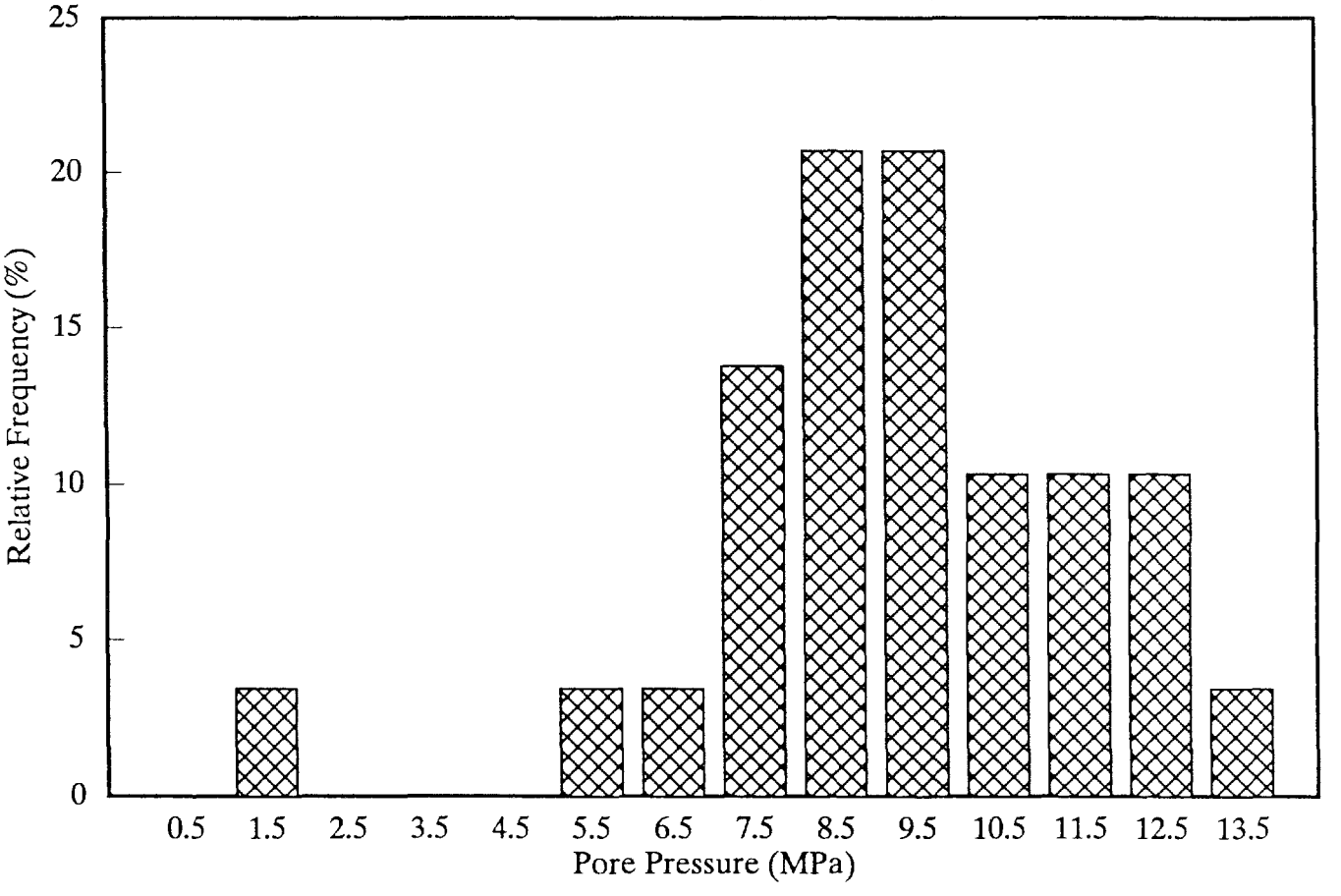

ROOM Q

PORE PRESSURE (ALL DATA)

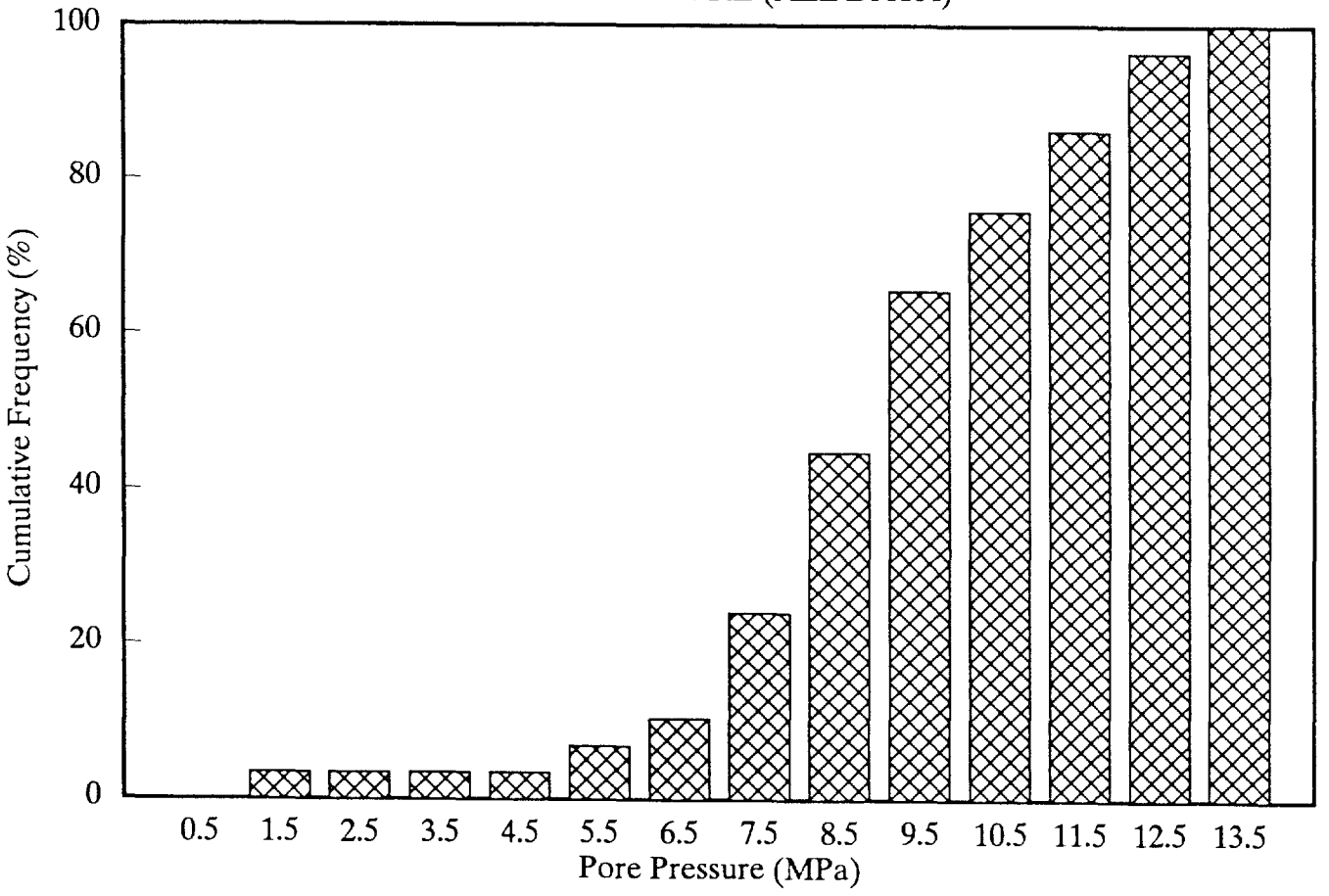

ROOM Q

PORE PRESSURE (HALITE)

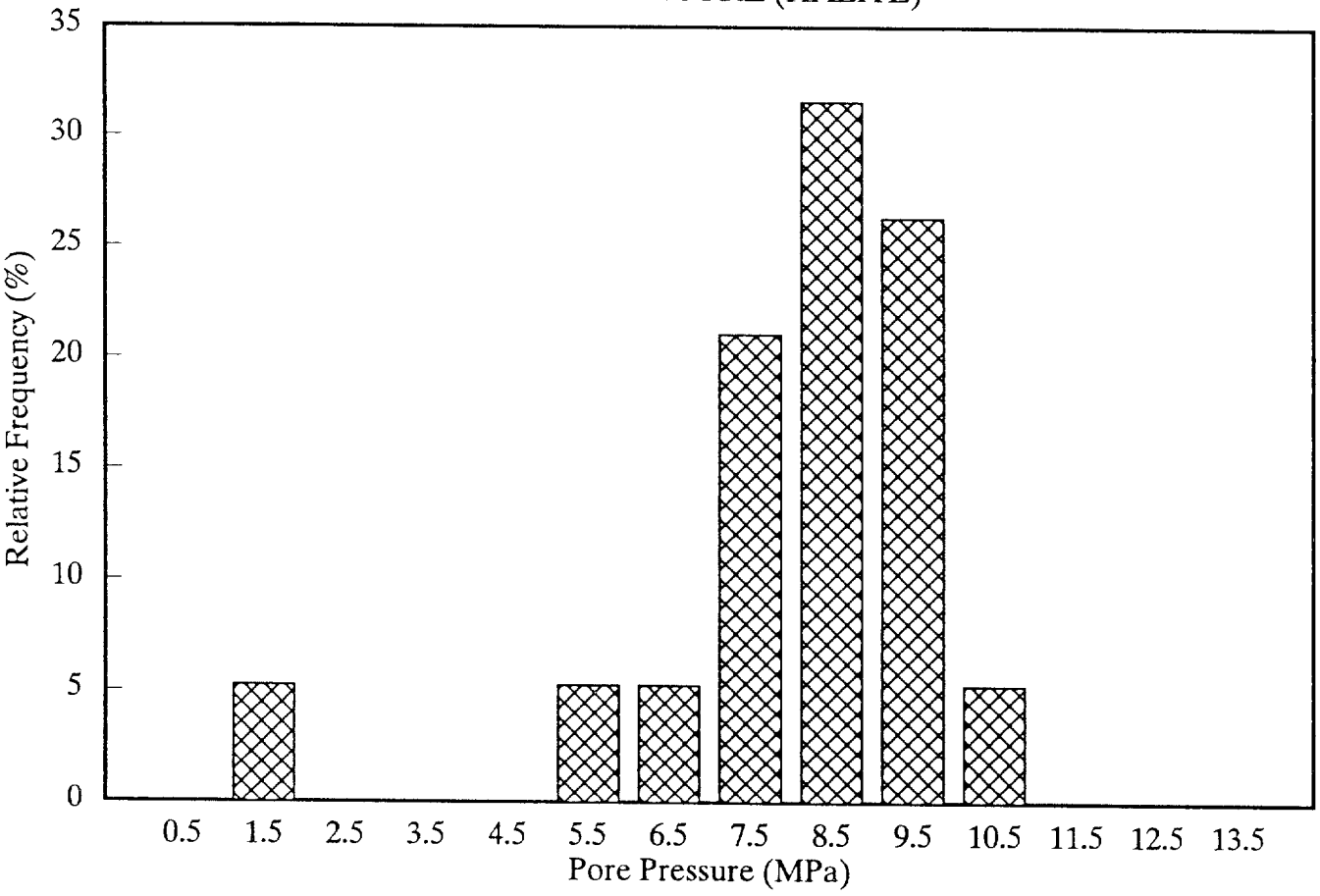

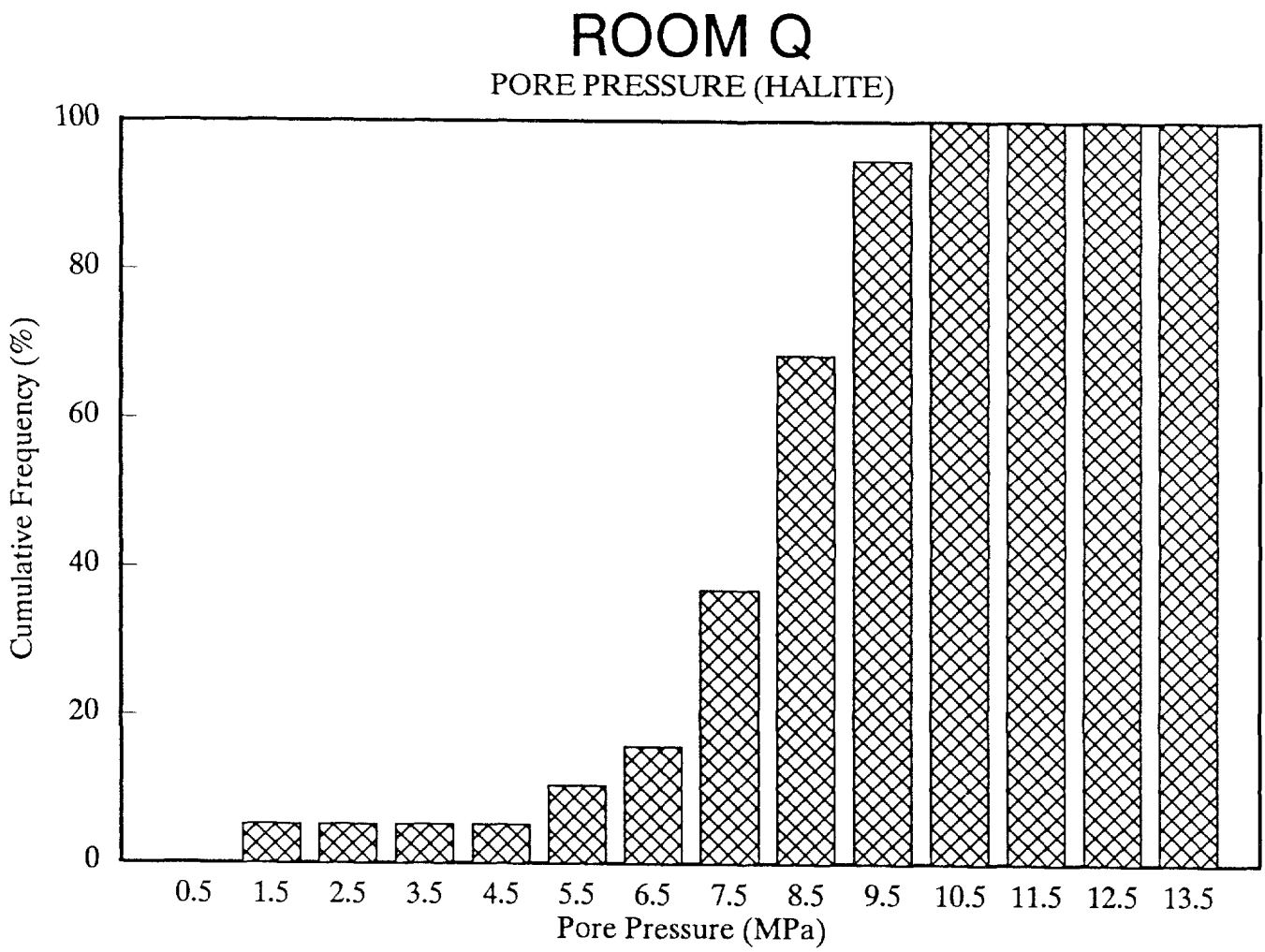
ROOM Q
PORE PRESSURE (HALITE)
Cumulative Frequency (%)
100
80
60
40
20
0
0.5
1.5
2.5
3.5
4.5
5.5
6.5
7.5
8.5
9.5
10.5
11.5
12.5
13.5
Pore Pressure (MPa)

ROOM Q

PORE PRESSURE (ANHYDRITE)

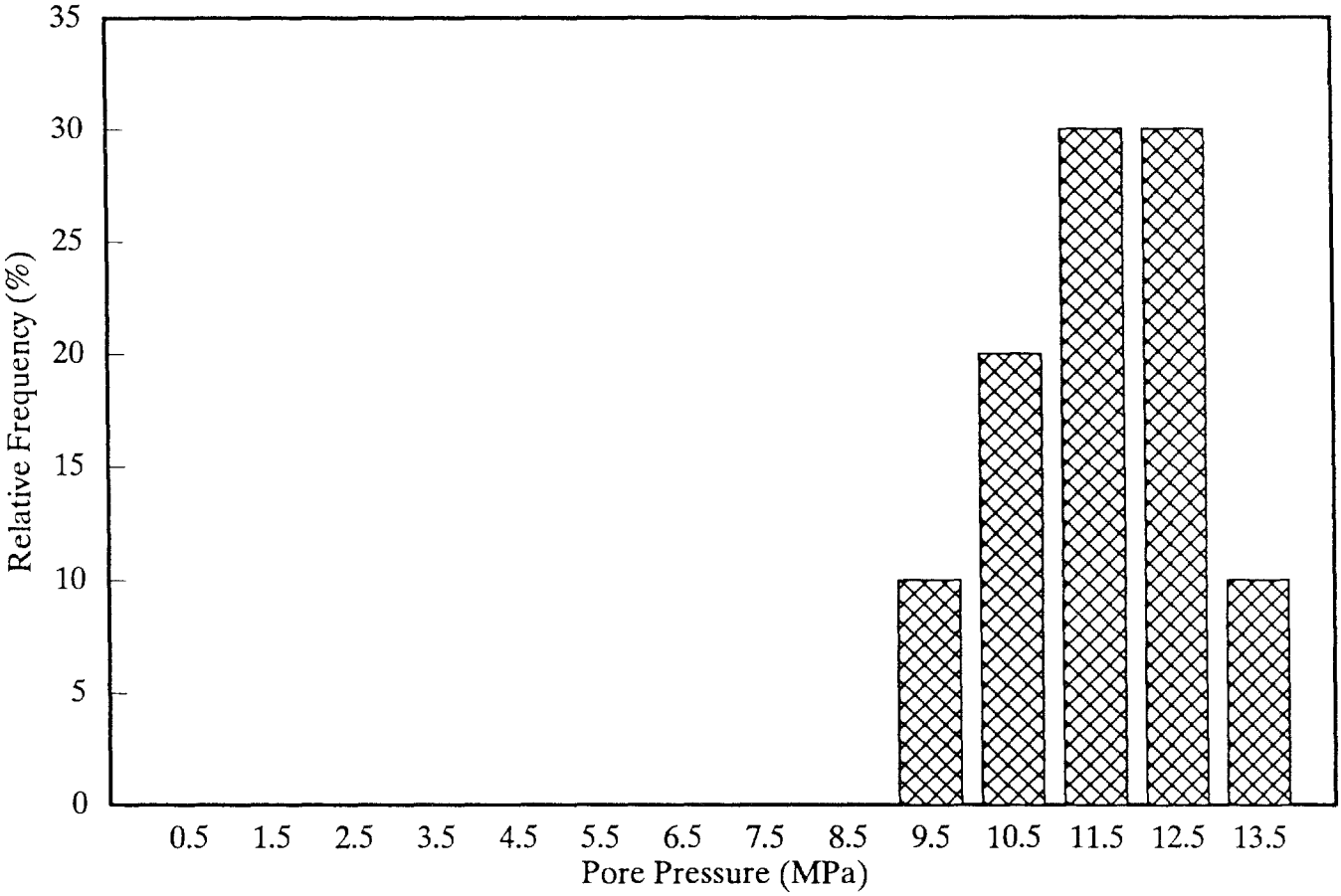

ROOM Q

PORE PRESSURE (ANHYDRITE)

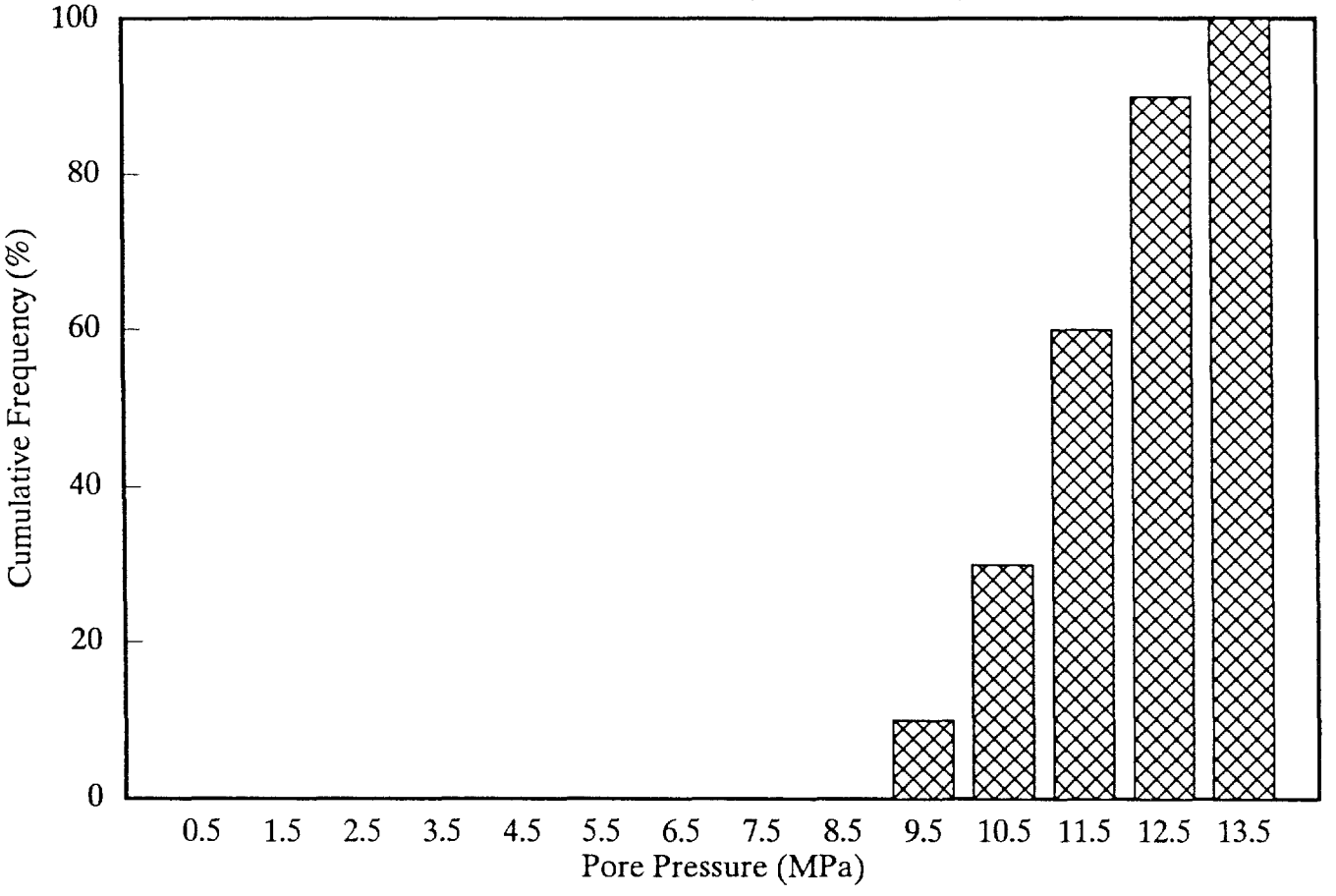

Howarth, June 13, 1991

Date: 6/13/91
To: Elaine Gorham (6344)
From: Susan Howarth (6344)
Subject: Permeability Distributions for 1991 Performance Assessment Calculations

Sandia National Laboratories

Albuquerque, New Mexico 87185

DATE: June 13, 1991

TO: Elaine Gorham, 6344

FROM: Susan Howarth, 6344

SUBJECT: Permeability Distributions for 1991 Performance Assessment Calculations

Attached are the Relative Frequency and Cumulative Frequency distributions for permeability as determined from the pre-excavation borehole tests at Room Q. There are three sets of graphs: 1) all tests, 2) halite only tests, and 3) anhydrite only tests. On each frequency distribution graph, the vertical bars are centered above a number which represents data within that order of magnitude. For example, the bar above the -23 value represents permeabilities within the LOG($1*10^{-23}$) to LOG($9.9*10^{-23}$) m^2 range.

Permeabilities were calculated using a 1-D radial Darcy-flow model with the following assumptions: 1) no damage zone, 2) constant capacitance (stiff-matrix), and 3) test zone fluid compressibility equals brine compressibility. Permeabilities calculated using these assumptions for the Room Q pre-excavation borehole tests are found in Table 1.

Division 6344 is in the process of standardizing permeability test interpretation. The current Standard Model has two important assumptions that differ from those used in the permeabilities shown in Table 1 which could significantly change the inferred permeabilities. The Standard Model assumes that the material is poroelastic (not stiff-matrix) and uses measured values for test zone fluid compressibility (not brine compressibility). Re-analysis of the Room Q pre-excavation data using the current Standard Model is not complete but it is expected that permeability values may increase by 1 to 2 orders of magnitude when re-analyzed.

In order to account for this expected[1] change, uncertainty tails were added to the Table 1 permeability values in the following manner. Because using the measured test zone fluid compressibility instead of the brine compressibility will result in larger (1 to 2 orders of magnitude) permeabilities, a 2 order of magnitude increase uncertainty tail was added. Then, because using a stiff-matrix results in a higher permeability (by 0.5 to 1 orders of magnitude) than would be calculated using the poroelastic model a 1 order of magnitude decrease uncertainty tail was added. For example, for the QPP01 data, Table 1 lists the permeability as $1.5*10^{-21}$ m^2. When uncertainty tails are added, the QPP01 permeability range becomes $1.5*10^{-22}$ to $1.5*10^{-19}$ m^2.

Confidence intervals were subsequently assigned to the permeabilities for each borehole. A 10% confidence was assigned to lowest permeability order of magnitude, 20% was assigned to the next larger order of magnitude, 50% to the next higher order of magnitude and 20% was assigned to the highest order of magnitude. Again using QPP01 as an example, a 10% confidence was assigned to permeabilities in the 1 to $9.9*10^{-22}$ m^2 range, 20% was assigned to permeabilities in the 1 to $9.9*10^{-21}$ m^2 range, 50% was assigned to permeabilities in the 1 to $9.9*10^{-20}$ m^2 range, and 20% was assigned to permeabilities in the 1 to $9.9*10^{-19}$ m^2 range.

[1] R. L. Beauheim, Personal Communication, June 12, 1991.

Frequency distributions were calculated by assigning points equal to the confidence percentage for each permeability range for each borehole test. The points assigned to each range were then summed.

During the pre-excavation time period, each Room Q borehole test region was located 75 feet from an existing excavation. Because these pressure tests are located farther from an excavation than any similar tests, they are thought to be most representative of far-field conditions. However, these data should be combined with data from the Small-Scale Brine Inflow Program and the Permeability Testing Program for use in Performance Assessment calculations.

TABLE 1.
Room Q Pre-excavation Permeability

Borehole	Permeability (m^2)
QPP01	$1.5*10^{-21}$
QPP02	TLTM
QPP03	$2.4*10^{-22}$
QPP04	$5.0*10^{-23}$
QPP05	TLTM
QPP11	TLTM
QPP12	$2.0*10^{-23}$
QPP13	$3.0*10^{-22}$
QPP14	TLTM
QPP15	TLTM
QPP21	TLTM
QPP22	$1.0*10^{-22}$
QPP23	$1.0*10^{-21}$
QPP24	$1.0*10^{-21}$
QPP25	$1.0*10^{-22}$

Copy to:

W. D. Weart, 6340 (w/o attachments)
D. R. Anderson, 6342
R. P. Rechard, 6342
R. L. Beauheim, 6344
S. J. Finley, 6344

ROOM Q

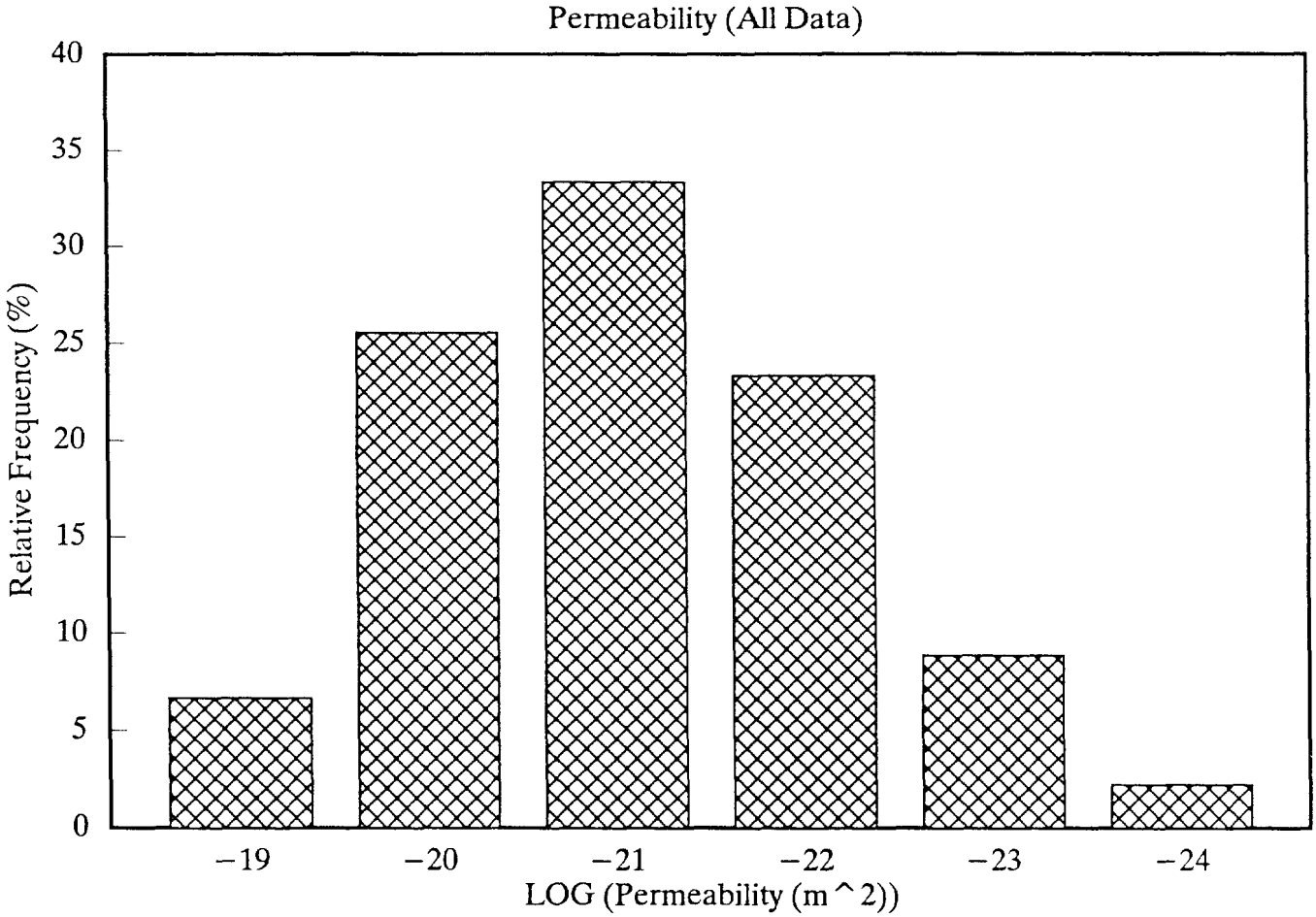
Permeability (All Data)
Relative Frequency (%)
40
35
30
25
20
15
10
5
0
−19
−20
−21
−22
−23
−24
LOG (Permeability (m ^ 2))

ROOM Q

Permeability (All Data)

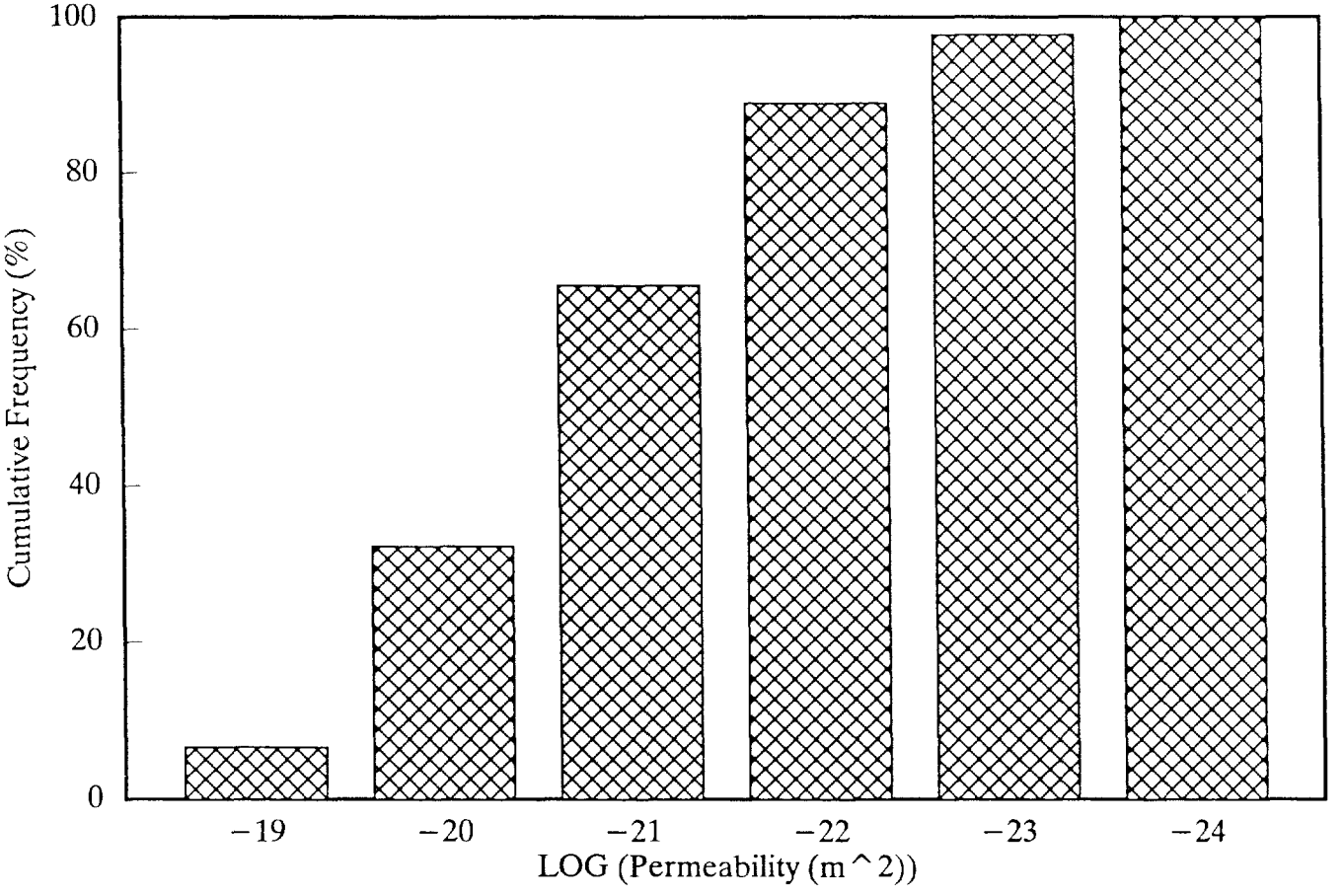

ROOM Q

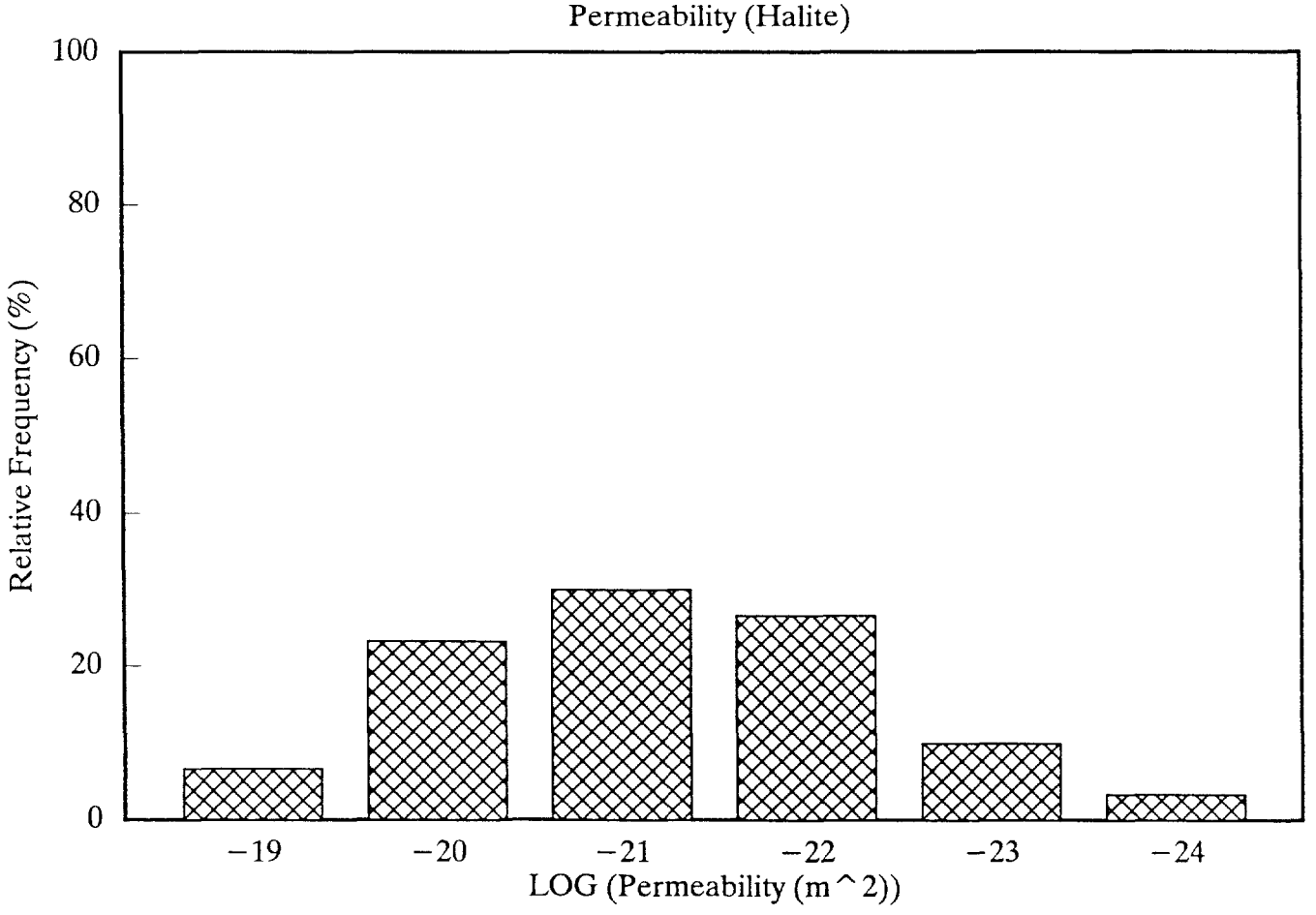
Permeability (Halite)
100
80
60
40
20
0
Relative Frequency (%)
−19
−20
−21
−22
−23
−24
LOG (Permeability (m ^ 2))

ROOM Q

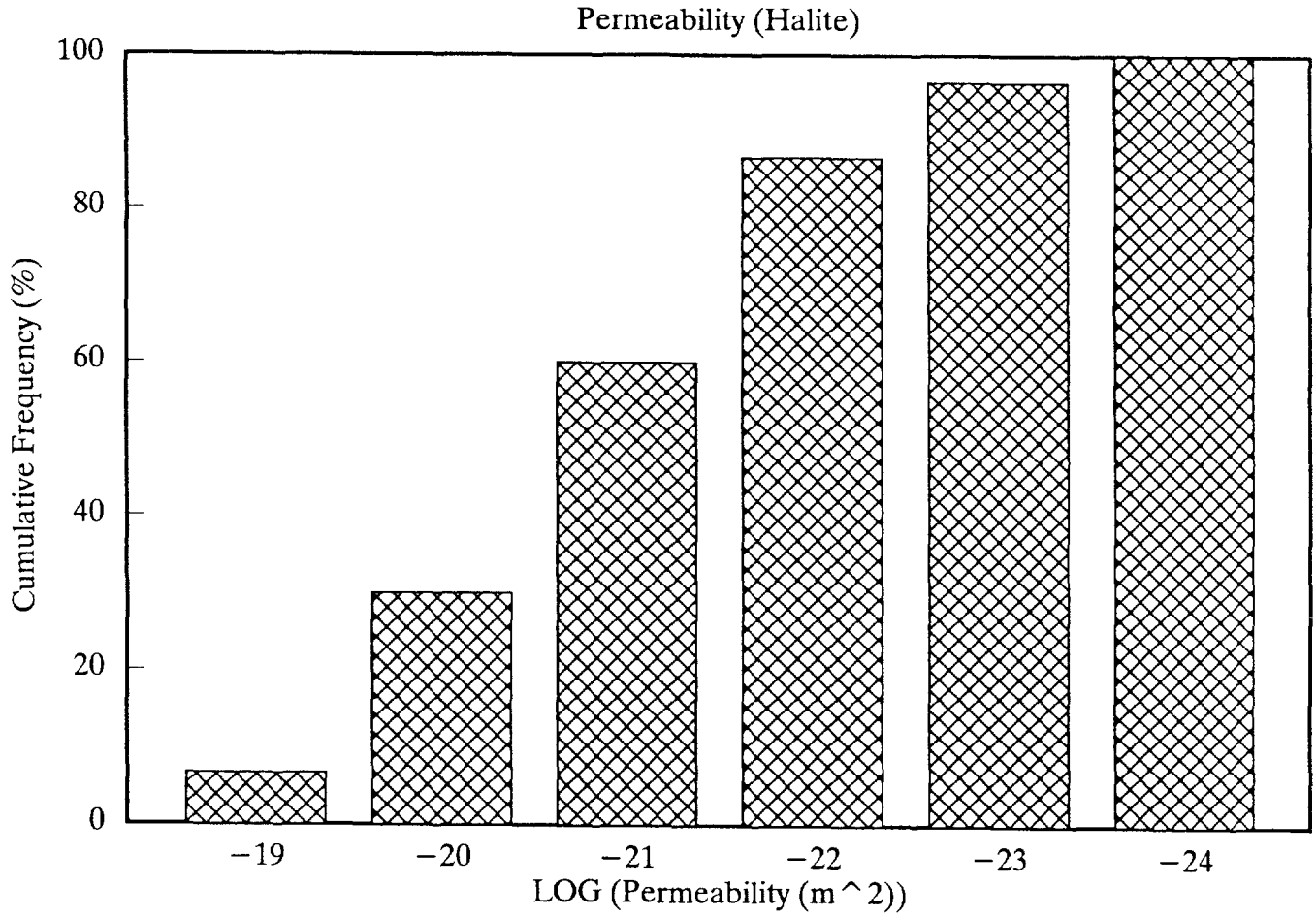
Permeability (Halite)
100
80
60
40
20
0
Cumulative Frequency (%)
−19
−20
−21
−22
−23
−24
LOG (Permeability (m ^ 2))

ROOM Q

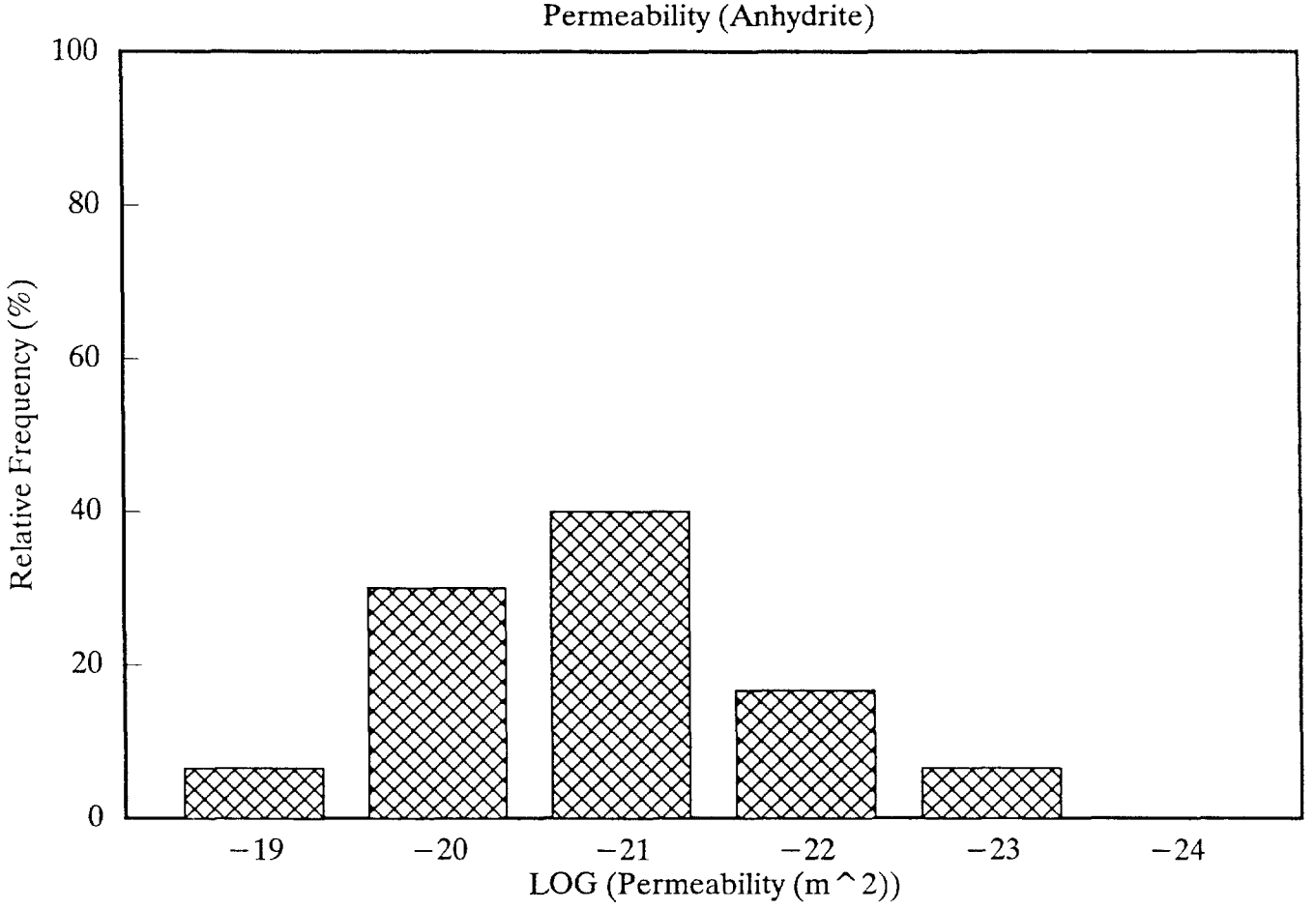
Permeability (Anhydrite)
100
80
60
40
20
0
Relative Frequency (%)
−19
−20
−21
−22
−23
−24
LOG (Permeability (m ^ 2))

ROOM Q

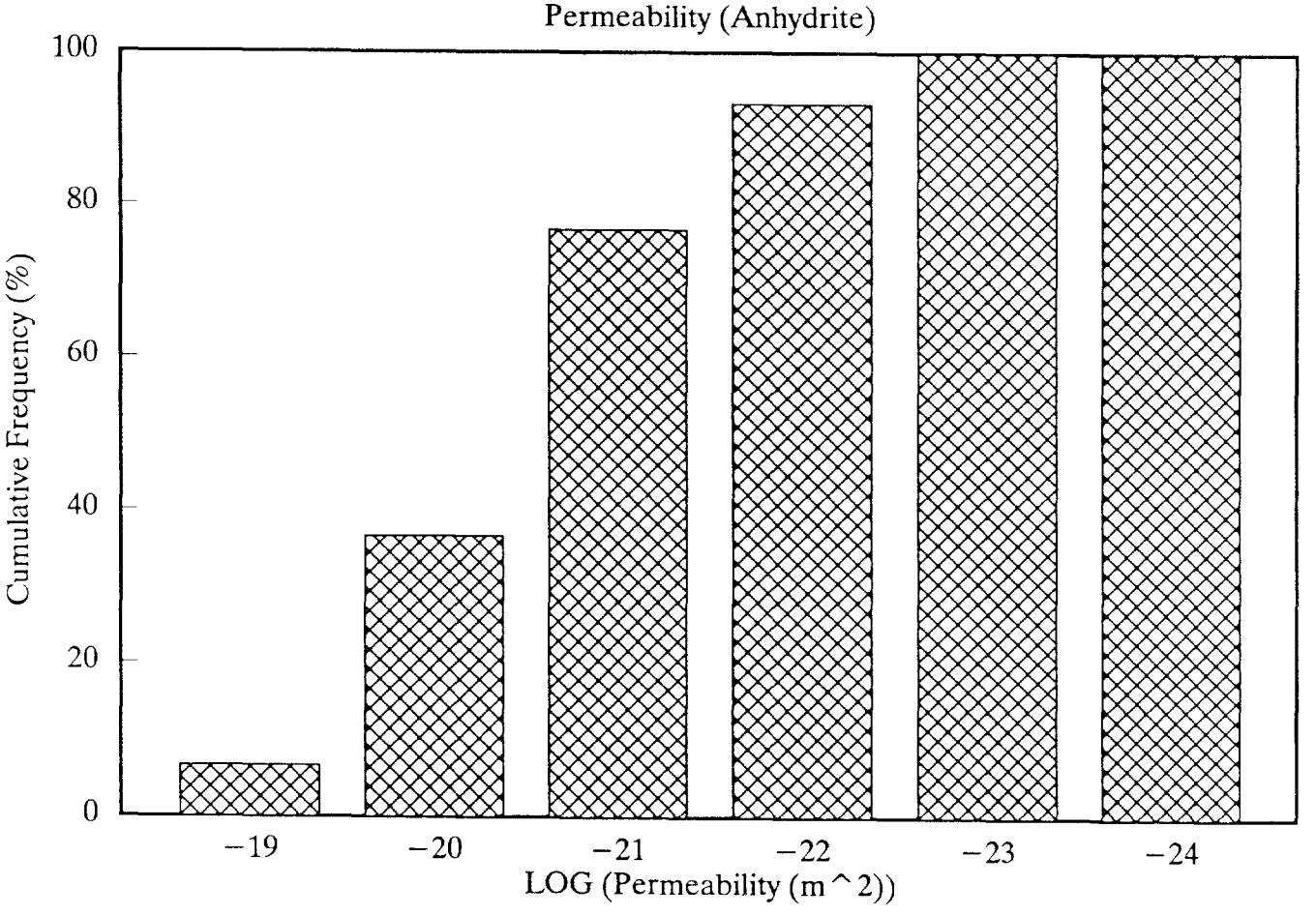
Permeability (Anhydrite)
100
80
60
40
20
0
Cumulative Frequency (%)
−19
−20
−21
−22
−23
−24
LOG (Permeability (m^2))

McTigue et al., March 14, 1991

Date: 3/14/91
To: Distribution
From: D. F. McTigue, 1511; S. J. Finley, 6344, J. H. Gieske, 7552; K. L. Robinson, 6345
Subject: Compressibility Measurements on WIPP Brines

Sandia National Laboratories
Albuquerque, New Mexico 87185

date: March 14, 1991

to: Distribution

D.F. McTigue J.F. Finley J.H. Gieske Karen Robinson

from: D. F. McTigue, 1511; S. J. Finley, 6344; J. H. Gieske, 7552; K. L. Robinson, 6345

subject: Compressibility Measurements on WIPP Brines

Preview Summary

The compressibility of WIPP brines has been measured using an acoustic method. For six samples collected from Room D and the Room Q access drift, measured compressibilities fall in the range $(2.40\text{–}2.54)\times10^{-10}$ Pa^{-1} at temperatures from 20 to 40 °C. The measurement error is estimated to be less than 1%.

Introduction

Most models for transient flow in porous media take into account the compressibility of the pore fluid. Compressibility allows for "storage" of fluid mass, *i.e.*, changes of fluid mass per unit volume of the medium in response to changes of fluid pressure. In a saturated medium in which the porous skeleton and the solid pore walls can be approximated as rigid, fluid compressibility is the only source of storage (or "capacitance"). In a deformable medium, there are contributions to the storage from compression of the fluid, compression of the pores, and compression of the solid comprising the pore walls. Virtually every model currently used to represent brine flow in WIPP salt requires a numerical value for the brine compressibility. To our knowledge, no direct compressibility measurements have been made previously on WIPP brines.

The purpose of this memo is to report recent measurements of the compressibility of Salado Formation brines collected from the WIPP underground. The method used exploits the simple relationship between compressibility and the sound speed in a liquid, and thus allows the use of highly developed ultrasonics technology. The direct measurement of compressibility in a static test, although very simple conceptually, is relatively difficult in practice. The compressibility of brine is of the order of 10^{-10} Pa^{-1}, indicating that one would need to resolve a volume change of the order of one part in 10^4 in order to obtain a compressibility measurement through an applied pressure change of 1 MPa (10 bars).

Definitions

As noted above, models for flow in porous media often take into account compressibilities of the fluid, the solid mineral constituent, and the porous skeleton. Thus, we adopt a subscript f here to emphasize that the present considerations address only the fluid phase.

The coefficient of compressibility, β_f, is defined by:

$$\beta_f = \frac{1}{\rho_f}\frac{\partial \rho_f}{\partial p} \quad , \tag{1}$$

where ρ_f is density and p is pressure. The compressibility is also simply the inverse of the bulk modulus, K_f:

$$\beta_f = \frac{1}{K_f} \quad . \tag{2}$$

The longitudinal wave speed, v_L, in an elastic body is given by

$$v_L = \sqrt{\frac{1}{\rho}\left(K + \frac{4}{3}G\right)} \quad , \tag{3}$$

where K and G are the bulk and shear moduli, respectively. In a fluid, in which $G = 0$, and we identify $K \equiv K_f$ and $\rho \equiv \rho_f$, (3) can be reduced and rearranged to give

$$K_f = \rho_f v_L^2 \quad . \tag{4}$$

Thus, the bulk modulus of a fluid is determined by measurements of its density and longitudinal wave speed.

Sample Selection

Six samples of Salado brine collected at the WIPP site were used for these measurements. The samples were selected from the brine sample inventory for the small-scale brine-inflow experiments. During the course of these experiments, brine flowing into boreholes in the underground is periodically pumped out of the boreholes, weighed, and saved in plastic sample bottles. The sample bottles are currently stored in metal cabinets in a building on the surface at the WIPP site.

The six samples used are listed in Table 1. After pumping, all brine samples are labeled with the borehole number and the date the sample was pumped out of the borehole. For example, the brine sample designated DBT31 12-7-88 was pumped out of borehole DBT31 on December 7, 1988. All of the DBT boreholes are vertical boreholes collared in the floor of Room D, which is situated in the northeastern corner of the WIPP underground experimental area. All of the QPB boreholes are vertical boreholes collared in the floor of the Q access drift, halfway between Room Q and the Air Intake Shaft. Brine samples 3 and 4 in Table 1, labeled QPB05A and QPB05C, respectively, were pumped from the same borehole on December 10, 1990. The letter designators A and C indicate that multiple sample bottles were filled when borehole QPB05 was pumped.

The particular samples chosen were from the subset of samples that are greater than 100 milliliters in volume, as this was assumed to be the minimum volume required for the sound speed measurements. Within this subset of larger-volume samples, those selected are believed to be representative of the Salado brine collected. Three of the samples are from Room D. These boreholes are collecting brine from the waste facility horizon, which includes Map Unit 6 and extends down through the top of Map Unit 0. The boreholes in Room D were drilled in the fall of 1987, and the brine collecting in those boreholes has been pumped out periodically since the drilling date. The Room D brine samples selected were considered to be representative of the time interval over which the brine has been collected. The other three samples are from the Q access drift, where the boreholes have been collecting brine from the lower section of Map Unit 0 and Marker Bed 139. These boreholes were drilled in the spring of 1989. All of the Q access drift samples were collected in December, 1990.

Density Measurements

The procedure used to measure the density of the brine samples is a standard laboratory procedure for measuring the density of liquids. An empty 50 ml beaker and watch glass were weighed and then filled with an aliquot of brine from the sample bottle. The aliquot was either 10 or 5 ml in volume, and was extracted from the sample bottle with a class A volumetric pipet. The beaker and watch glass with the brine sample were weighed again, and the weight of the empty beaker and watch glass was subtracted to obtain a weight for the brine itself. The weight of the brine was divided by the aliquot volume to obtain a density in grams per milliliter. These measured densities were converted to units of kg/m^3 and are listed in Table 1.

The ambient temperature of the laboratory where all density measurements were made was 22 °C. The temperature of the air in the boreholes in Room D fluctuates between 28 °C and 32 °C. Temperatures have not been measured in the QPB boreholes, but are assumed to be in the same range as in the Room D boreholes.

In order to determine the standard deviation associated with any one density measurement, the above-mentioned procedure was repeated 14 times on sample 1 (DBT31 12-7-88). The average brine density calculated was 1.249 g/ml, with a standard deviation of 0.0026 g/ml. The 95% confidence interval based on the Student's t distribution is 1.247 g/ml to 1.251 g/ml.

Table 1. Measured density; 22 °C.

Sample No.	Sample Loc. & Date	Density (kg/m^3)
1	DBT31 12-7-88	1.249×10^3
2	QPB02A 12-7-90	1.225×10^3
3	QPB05A 12-7-90	1.229×10^3
4	QPB05C 12-10-90	1.226×10^3
5	DBT32 1-18-90	1.240×10^3
6	DBT11 10-7-87	1.224×10^3

Sound Speed Measurements

The sound speed measurements reported here were obtained by the "pulse-echo-delay" method. An acoustic reflector in the shape of a "stair step" is placed in a vessel containing the brine sample (Figure 1). An acoustic transducer is positioned an arbitrary distance away from the step. The transducer is pulsed with a given waveform, and the reflections from the first and second step surfaces are recorded. The difference in travel time for the acoustic pulse can be determined very accurately from a digitized waveform of the two pulse echoes. The wave speed is related to the height of the step, L, and the time delay between echoes, T, by

$$v_L = \frac{2L}{T}. \tag{5}$$

The measurements reported here were made with a Lucite reflector with step height $L = 0.955$ cm. A 25 MHz transducer 0.635 cm in diameter was used, and the data were recorded with a LeCroy TR8828B 200 MHz transient recorder. The acoustic pulse was measured to have a frequency of 16 MHz. The pulse-echo time delay procedure was carried out on a 386 PC using a QuickBasic program. Temperatures were varied by placing the vessel in a heated water bath, and the temperature at the time of the subsequent test was recorded with a mercury thermometer with 0.1 °C graduations.

Temperature Corrections for Density

The fluid densities, ρ_f, used to compute the bulk moduli reported here are based on temperature corrections applied to a reference state.

For the pure water, densities are tabulated at discrete temperatures in [1, Table F-10]. In the temperature range from 15 to 45 °C, these data are very well represented by a four-term Taylor series expansion about a reference temperature of 30 °C:

$$\rho_f = \rho_{f0}[1 + d_1(\theta - 30) + d_2(\theta - 30)^2 + d_3(\theta - 30)^3], \tag{6}$$

where $\rho_{f0} = 0.99567$ is the density at the reference temperature of 30 °C, θ is the temperature of interest, and the coefficients take the values $d_1 = -3.0332 \times 10^{-4}$, $d_2 = -4.3866 \times 10^{-6}$, and $d_3 = 2.6828 \times 10^{-8}$. The fit was performed with the parameter-estimation code ESTIM [2]. The densities used to compute the compressibilities of distilled water shown in Table 4 were calculated from equation (6) using these parameters.

For the brines, it was assumed that each sample was saturated with respect to its dissolved species at the 22 °C laboratory temperature at which the initial density determinations were done. The thermal expansion of NaCl brines was discussed in a recent memo [3]. Based on data reported by Kaufmann [4, Table 46, p. 612], it is estimated that a saturated NaCl brine at 22 °C contains about 26.5 weight % salt. Extrapolation of the coefficients reported in [3], which were determined for brines at lower concentrations, yields the following expression for the density of brine saturated with respect to NaCl at 22 °C:

$$\frac{\rho_f}{\rho_{f0}} = 1 + d_1(\theta - 22) + d_2(\theta - 22)^2 + d_3(\theta - 22)^3, \tag{7}$$

where ρ_{f0} is the density at the reference temperature of 22 °C, and the coefficients take the values $d_1 = -4.4294 \times 10^{-4}$, $d_2 = -6.3703 \times 10^{-7}$, and $d_3 = -1.3148 \times 10^{-9}$. This expression was used to correct the reference densities measured at 22 °C (Table 1) for calculations of the compressibility at different temperatures (Tables 2, 3, 5, 6). We emphasize that the thermal expansion correction for brine is based on pure NaCl solutions rather than on WIPP brines. However, the behavior of WIPP brines is not expected to differ significantly. In any case, the density corrections are at most less than 1%.

Results

Results of the bulk modulus and compressibility determinations are shown in Tables 2–6. Tables 2 and 3 show data for all six brine samples at 20 °C and 25 °C, respectively. Table 4 shows results for distilled water at temperatures from 20 to 40 °C. The data from Table 4 are plotted as a function of temperature in Figure 2 along with reference compressibility data from the *CRC Handbook* [1, Table F-15] for comparison. The data from both the present study and the *CRC Handbook* appear to define a trend of decreasing compressibility with increasing temperature. Both data sets exhibit roughly the same degree of scatter about the general trend, suggesting that the data from the present study are of an accuracy comparable to that of the reference data. Quantitative error estimates for this study are discussed in the following section.

Tables 5 and 6 show results for two brines at temperatures from 20 to 40 °C. The brines show no significant variation in compressibility over this temperature range. This is

in contrast to pure water (Table 4; Figure 2), which shows a distinct decrease in β_f with increasing θ. Thus, the presence of a high concentration of dissolved salt serves to moderate the temperature sensitivity of the compressibility.

Figure 4 shows all compressibility measurements made on WIPP brines, regardless of temperature, plotted against density (Tables 2, 3, 5, 6). There is a strong correlation, indicating decreasing compressibility with increasing density. A linear regression on the data shown in Figure 4 yields

$$\beta_f = 7.662 \times 10^{-10} - 4.217 \times 10^{-13} \rho_f, \tag{8}$$

with a correlation coefficient of $r^2 = 0.91$. (Here, β_f has dimension Pa^{-1} and ρ_f dimension $\mathrm{kg/m^3}$.) This may provide a reasonable estimate for β_f for WIPP brines based solely on a density determination.

Table 2. Acoustic velocity; 20 °C.

Sample No.	Velocity, v_L m/s, $\times 10^{-3}$	Density, ρ_f $\mathrm{kg/m^3}$, $\times 10^{-3}$	Bulk Modulus, K_f Pa, $\times 10^{-9}$	Compressibility, β_f $\mathrm{Pa^{-1}}$, $\times 10^{10}$
1	1.825	1.250	4.163	2.402
2	1.803	1.226	3.984	2.510
3	1.806	1.230	4.013	2.492
4	1.805	1.227	3.998	2.501
5	1.811	1.241	4.071	2.456
6	1.808	1.225	4.003	2.498

Table 3. Acoustic velocity; 25 °C.

Sample No.	Velocity, v_L m/s, $\times 10^{-3}$	Density, ρ_f kg/m^3, $\times 10^{-3}$	Bulk Modulus, K_f Pa, $\times 10^{-9}$	Compressibility, β_f Pa^{-1}, $\times 10^{10}$
1	1.828	1.247	4.166	2.400
2	1.807	1.223	3.993	2.504
3	1.818	1.227	4.056	2.466
4	1.814	1.224	4.027	2.483
5	1.813	1.238	4.070	2.457
6	1.811	1.224	4.009	2.494
pure water	1.493	0.997	2.223	4.498

Table 4. Acoustic velocity; distilled water.

Temperature °C	Velocity, v_L m/s, $\times 10^{-3}$	Density, ρ_f kg/m^3, $\times 10^{-3}$	Bulk Modulus, K_f Pa, $\times 10^{-9}$	Compressibility, β_f Pa^{-1}, $\times 10^{10}$
19.9	1.478	0.9983	2.181	4.586
21.0	1.483	0.9980	2.195	4.556
24.8	1.493	0.9971	2.223	4.499
30.7	1.494	0.9955	2.222	4.501
40.0	1.516	0.9922	2.280	4.385

Table 5. Acoustic velocity; sample #1, DBT31.

Temperature °C	Velocity, v_L m/s, $\times 10^{-3}$	Density, ρ_f kg/m^3, $\times 10^{-3}$	Bulk Modulus, K_f Pa, $\times 10^{-9}$	Compressibility, β_f Pa^{-1}, $\times 10^{10}$
20.0	1.825	1.250	4.163	2.402
24.9	1.828	1.247	4.167	2.400
29.7	1.827	1.245	4.156	2.406
35.1	1.830	1.242	4.159	2.404
39.6	1.820	1.239	4.104	2.437

Table 6. Acoustic velocity; sample #2, QPB02A.

Temperature °C	Velocity, v_L m/s, $\times 10^{-3}$	Density, ρ_f kg/m^3, $\times 10^{-3}$	Bulk Modulus, K_f Pa, $\times 10^{-9}$	Compressibility, β_f Pa^{-1}, $\times 10^{10}$
20.0	1.803	1.226	3.985	2.509
25.5	1.807	1.224	3.997	2.502
29.6	1.808	1.222	3.994	2.503
35.0	1.797	1.219	3.936	2.540
37.6	1.798	1.217	3.934	2.542

Propagation of Error

Estimates of the error in the compressibilities reported here were made in the following manner. The error estimate, $\lambda(x)$, for the measurement of each quantity x is given in Table 7.

In terms of measured quantities, the sound speed is given by equation (5). The error estimate for the sound speed, $\lambda(v_L)$, is then given by [5]:

$$\lambda^2(v_L) = \left(\frac{\partial v_L}{\partial L}\right)^2 \lambda^2(L) + \left(\frac{\partial v_L}{\partial T}\right)^2 \lambda^2(T), \tag{9}$$

or,

$$\lambda^2(v_L) = v_L^2 \left[\frac{\lambda^2(L)}{L^2} + \frac{\lambda^2(T)}{T^2}\right]. \tag{10}$$

For typical values of the measured quantities and the error estimates given in Table 7, equation (10) gives an estimated error for the reported wave speeds of about ±5 m/s (Table 8).

Table 7. Error estimates for measurements.

		$\lambda(x)$	
Quantity (x)	Symbol	Error Est. (As Reported)	Error Est. (SI Units)
Fluid density	ρ_f	±0.003 g/ml	±3.0 kg/m^3
Step Height	L	±0.001"	$\pm 2.5 \times 10^{-5}$ m
Time Delay	T	±0.01 μs	$\pm 1.0 \times 10^{-8}$ s
Temperature	θ	±0.1 °C	±0.1 K

In a similar fashion, the error estimates for the bulk modulus and compressibility can be shown to be:

$$\frac{\lambda^2(K_f)}{K_f^2} = \frac{\lambda^2(\beta_f)}{\beta_f^2} = \frac{\lambda^2(\rho_f)}{\rho_f^2} + \frac{4\lambda^2(L)}{L^2} + \frac{4\lambda^2(T)}{T^2}. \tag{11}$$

Evaluation of (11) using typical values of the measured quantities and the error estimates from Table 7 yields an error of about 0.6% for the bulk modulus and compressibility, or about ±0.025 GPa and $\pm 1.5 \times 10^{-12}$ Pa^{-1}, respectively (Table 8).

Table 8. Error estimates for calculated quantities.

Quantity (x)	Symbol	Error Est. $\lambda(x)$
Sound Speed	v_L	± 5.0 m/s
Bulk Modulus	K_f	$\pm 2.5 \times 10^7$ Pa
Compressibility	β_f	$\pm 1.5 \times 10^{-12}$ Pa^{-1}

Consistency with Independent Data

In addition to the test against tabulated properties for pure water discussed above, a check for consistency of the present measurements with independent values from the literature can be made for brines. The data presented here indicate a strong correlation of compressibility with fluid density (Figure 4). In fact, compressibility is reduced by nearly 50% by the addition of salt up to full saturation. The *CRC Handbook* [1, Table F-15] reports reference compressibilities for pure water, and Kaufmann [4, Table 40, p. 609] reports compressibilities determined acoustically for NaCl brines of varying concentrations. These data are shown in Figure 5 along with the present results for measurements at 25 °C, plotted against density. The conversion of weight-percent NaCl to density applied to the Kaufmann data was obtained from Kaufmann [4 Table 44, p. 611]. All the available data fall on a very smooth trend; a second-order polynomial fits this trend very well:

$$\beta_f = 4.492 \times 10^{-10} - 1.138 \times 10^{-12}(\rho_f - 1000.) + 1.155 \times 10^{-15}(\rho_f - 1000.)^2, \quad (12)$$

where ρ_f is in units of kg/m^3, and β_f is in units of Pa^{-1}.

Summary

The principal results outlined in this memo are:

- The compressibilities of six Salado brines from Room D and the Room Q access drift fall in the range $(2.40\text{–}2.54)\times 10^{-10}$ Pa^{-1}.
- The measurements were carried out over a temperature range of 20 to 40 °C; brine compressibility exhibits no significant dependence on temperature over this range.
- Compressibility exhibits a strong correlation with brine density, with β_f decreasing with increasing ρ_f; a linear relationship (eq. 8) correlates the data for WIPP brines well over the small range of densities tested.

- The results from this study are consistent with published results for NaCl brines at lower concentration; a smooth trend of decreasing β_f with increasing density (concentration) encompasses pure water, published data for lower-concentration NaCl brines, and the WIPP brines considered here (Figure 5). A quadratic relationship (eq. 12) describes this trend very well.

- The acoustic method was validated by measurements made on distilled water. Results compare very well with reference data.

- Error in the compressibility measurements is estimated to be approximately 0.6%.

Note that a number of previous calculations of flow in WIPP salt [*e.g.*, 6–8] used values for brine compressibility of 5.0×10^{-10} Pa^{-1} (bulk modulus 2.0×10^{9} Pa). This high value for β_f (low K_f) was based on an estimate for pure water (one-place accuracy for K_f). The results shown here indicate that the presence of a high concentration of salt reduces the compressibility by nearly a factor of two.

References

1. Weast, R. C., ed., *CRC Handbook of Chemistry and Physics*, CRC Press, Boca Raton, 1985.

2. Hills, R. G., ESTIM: A parameter estimation computer program, **SAND87–7063**, *Sandia National Laboratories Technical Report*, August 1987.

3. McTigue, D. F., "Thermal expansion coefficient for brine," memo to Distribution, January 22, 1991.

4. Kaufmann, D. W., Physical properties of sodium chloride in crystal, liquid, gas, and aqueous solution states, in *Sodium Chloride: The Production and Properties of Salt and Brine*, D. W. Kaufmann, ed., American Chemical Society, Washington, D. C. 587–626, 1960.

5. Shoemaker, D. F., Garland, C. W., and Steinfeld, J. I., "Propagation of errors," *Experiments in Physical Chemistry*, McGraw-Hill, New York, 1974, 51–55.

6. Nowak, E. J., and McTigue, D. F., "Interim results of brine transport studies in the Waste Isolation Pilot Plant (WIPP), *Sandia National Laboratories Technical Report*, **SAND87–0880**, May 1987.

7. McTigue, D. F., and Nowak, E. J., "Brine transport in the bedded salt of the Waste Isolation Pilot Plant (WIPP): Field Measurements and a Darcy Flow Model," *Scientific Basis for Nuclear Waste Management XI*, M. J. Apted and R. E. Westerman, eds., Materials Research Society, Pittsburgh, 209–218, 1987.

8. Nowak, E. J., McTigue, D. F., and Beraun, R., "Brine inflow to WIPP disposal rooms: data, modeling, and assessment," *Sandia National Laboratories Technical Report*, **SAND88–0112**, September 1988.

DFM:1511:dfm

Key Words: **radioactive waste, Waste Isolation Pilot Plant (WIPP), material properties, brine, compressibility**

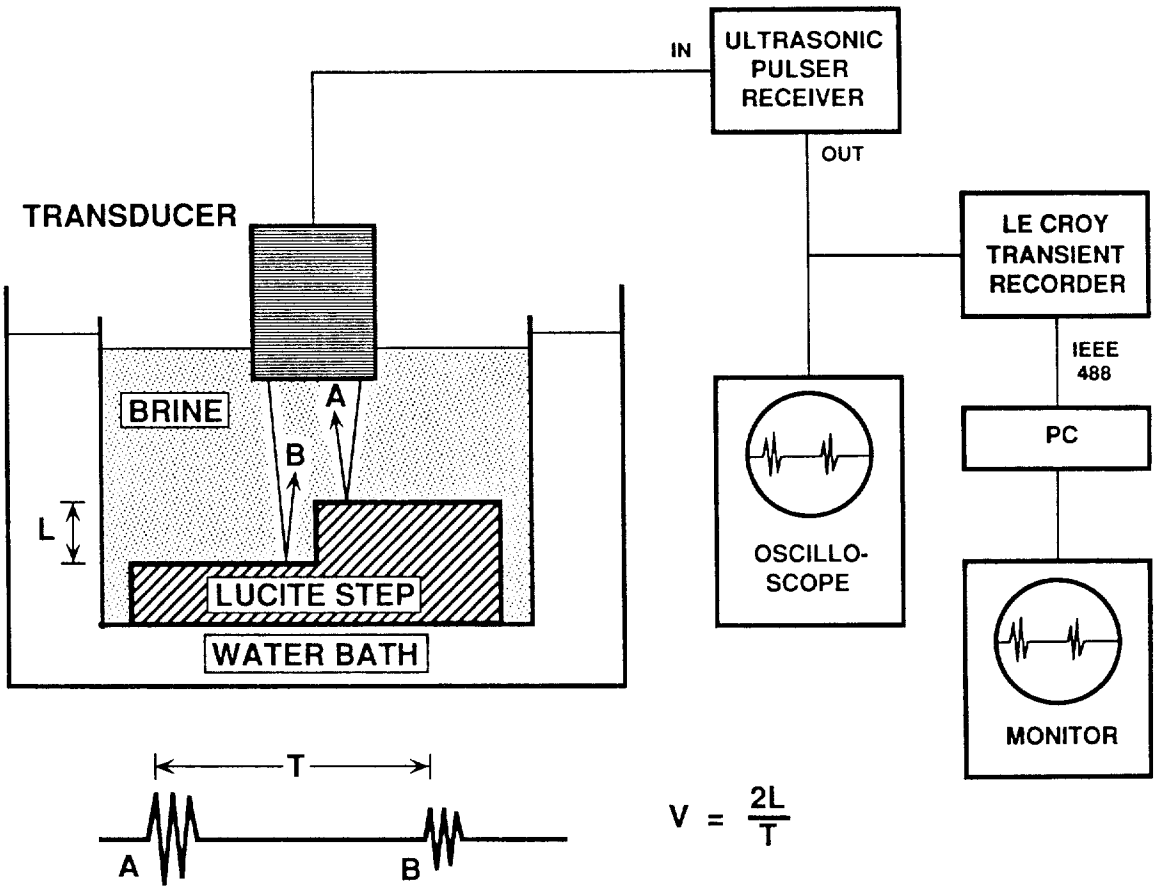

Figure 1. Schematic of the pulse-echo delay time technique for measuring acoustic velocity in a liquid.

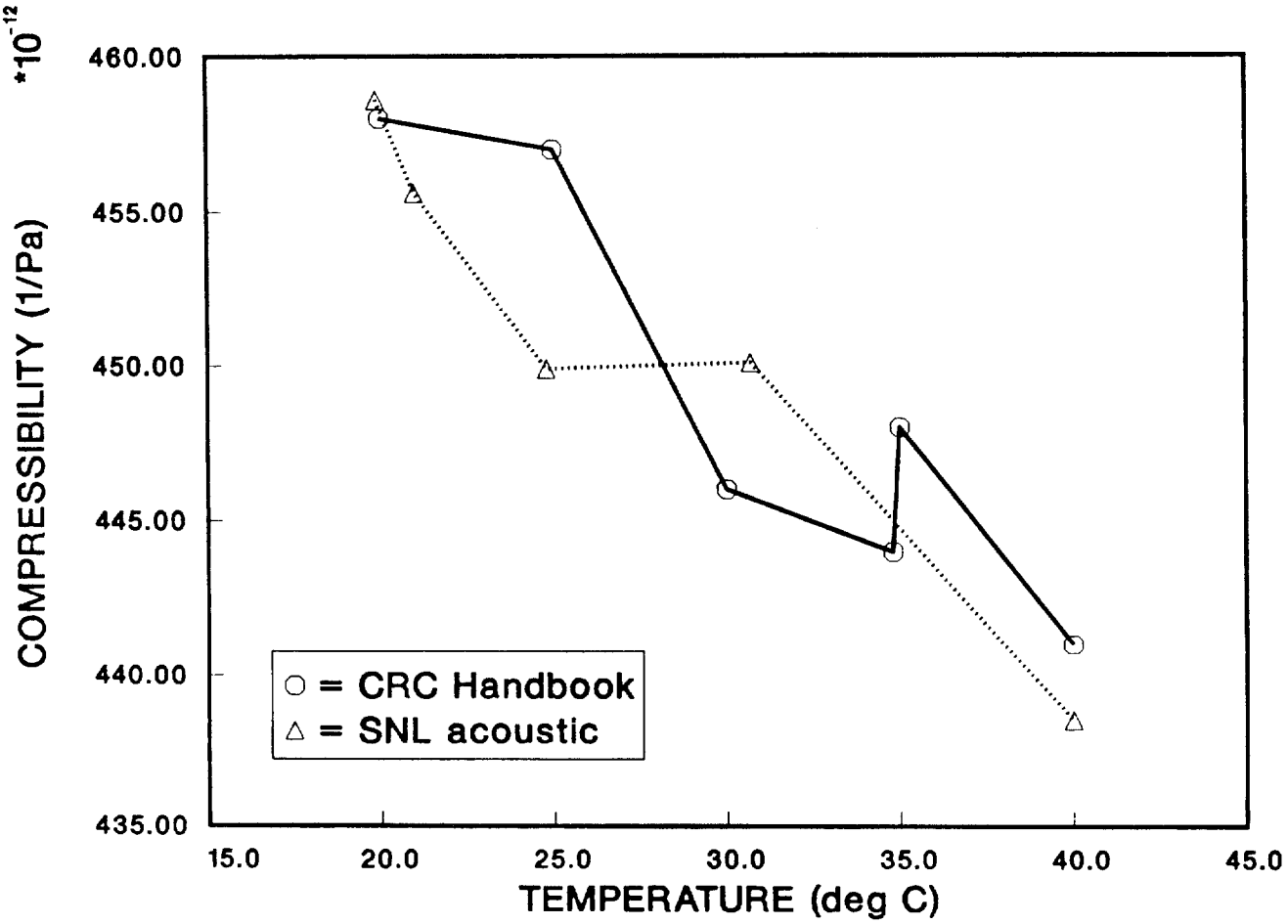

Figure 2. Comparison of compressibilities determined in this study with tabulated values [1] for distilled water.

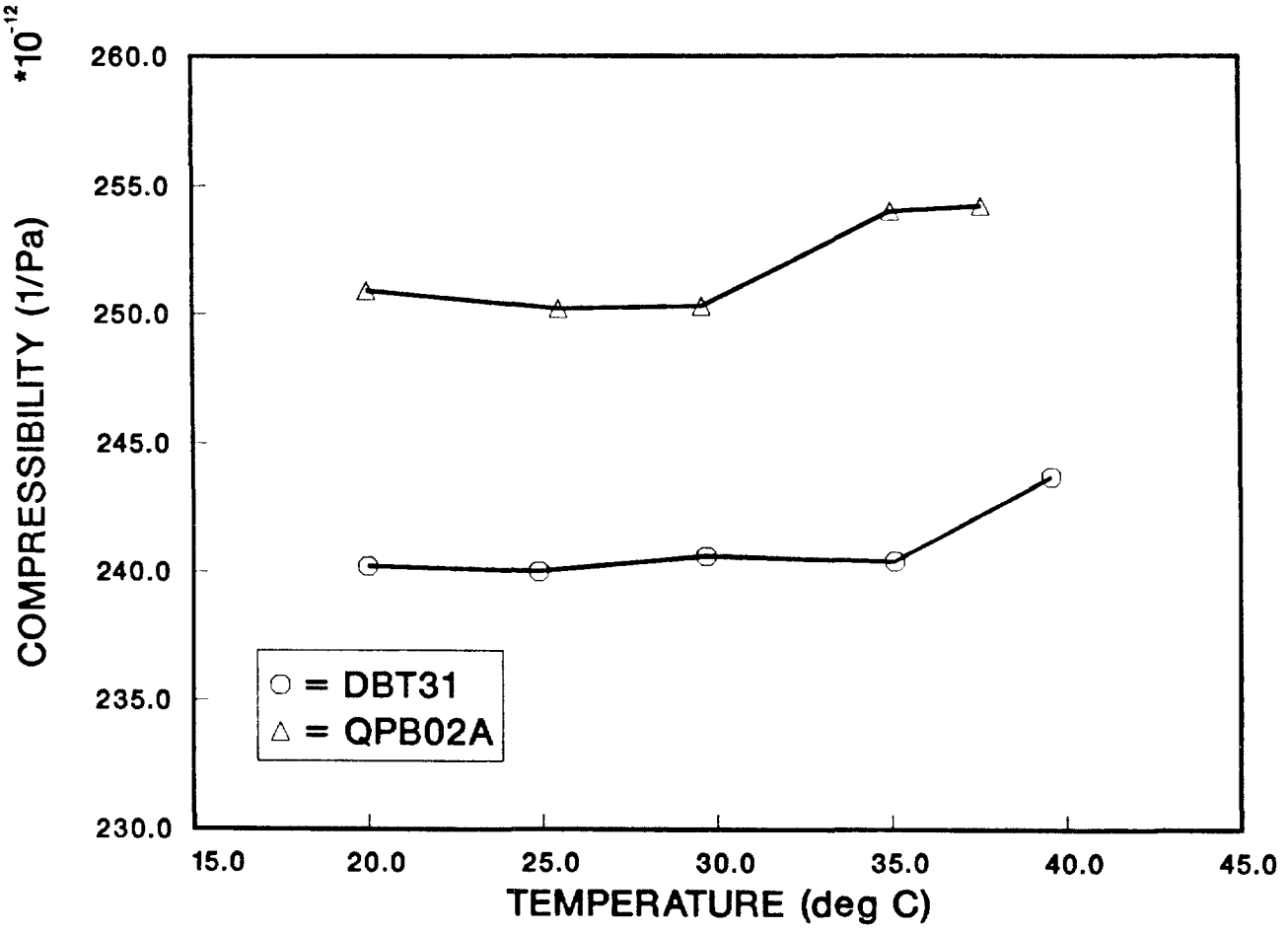

Figure 3. Compressibility of WIPP brines plotted against temperature.

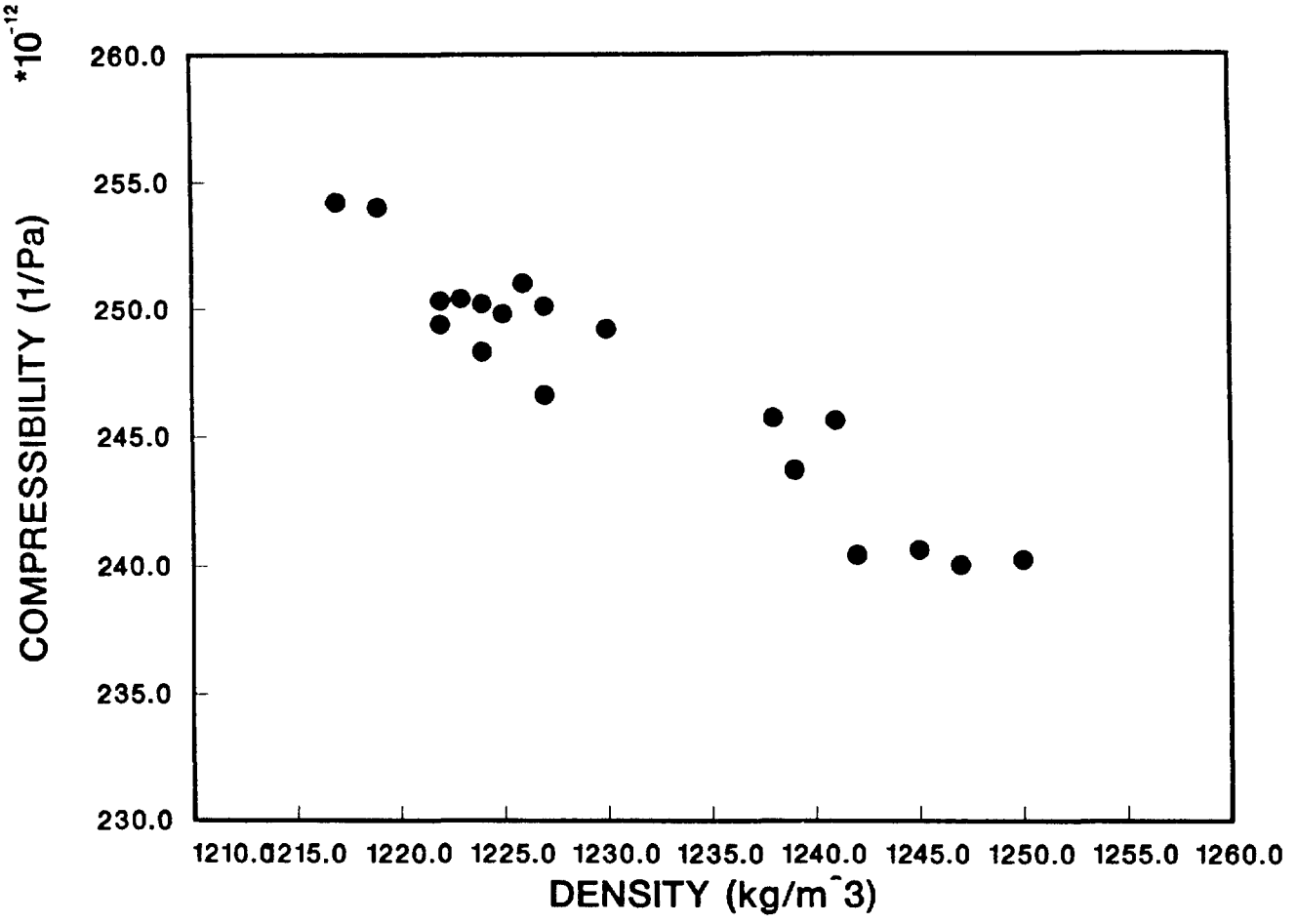

Figure 4. Compressibilities of WIPP brines plotted against fluid density.

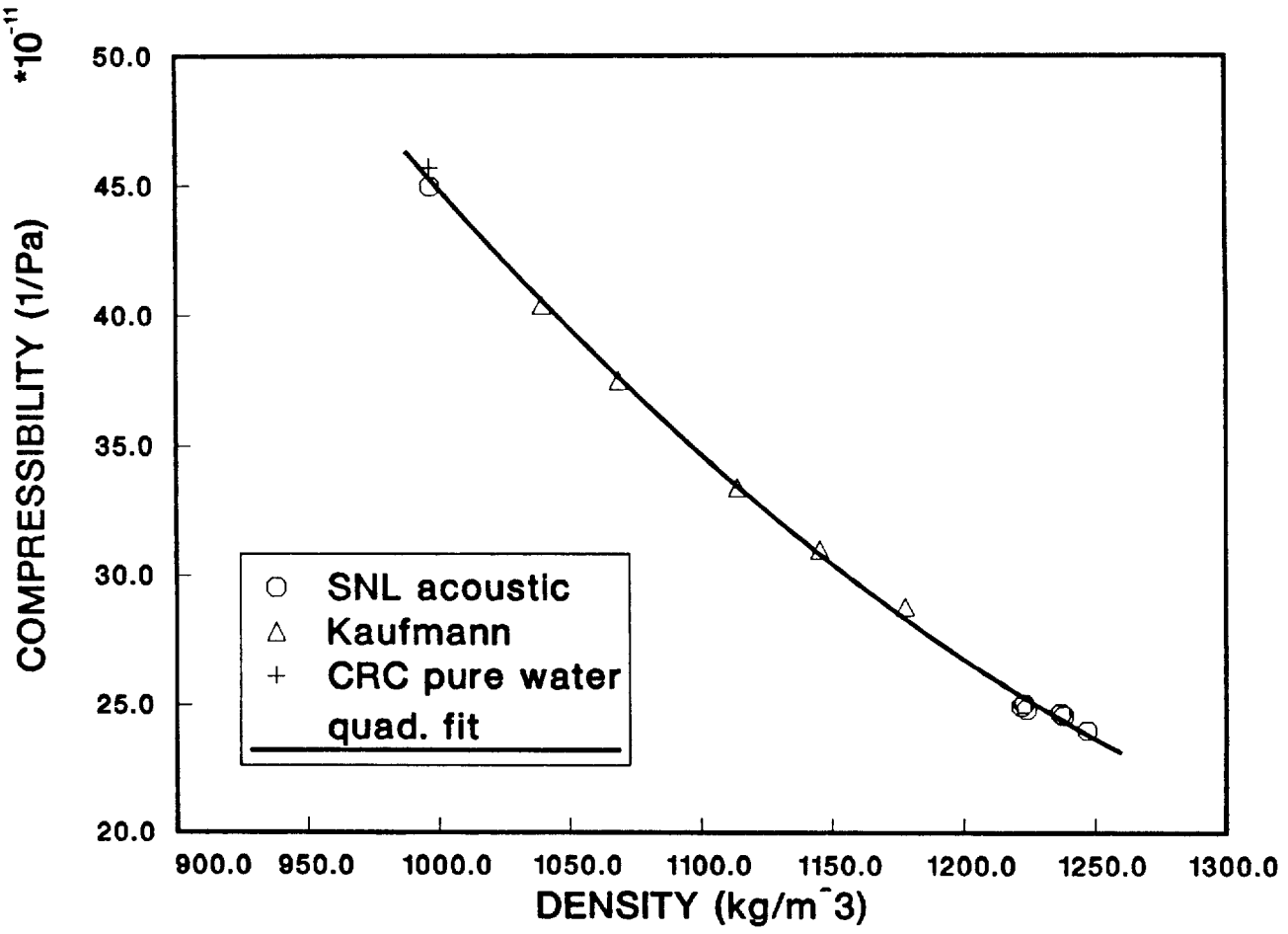

Figure 5. Compressibilities of WIPP brines and pure water determined in this study and literature values [1, 4] at 25 °C, plotted against density. Solid line shows a quadratic fit (eq. 12) to the 13 points shown. WIPP brine compressibilities appear to be on a consistent trend with the literature values.

Copy to:
1510 J. C. Cummings
1511 D. K. Gartling
1511 D. F. McTigue (day file)
1512 A. C. Ratzel
1513 Acting Supervisor
1514 H. S. Morgan
1514 J. G. Arguello, Jr.
1514 C. M. Stone
1514 J. R. Weatherby
1540 J. R. Asay
1550 C. W. Peterson, Jr.
6232 W. R. Wawersik
6257 J. L. Todd, Jr.
6340 W. D. Weart
6340 A. R. Lappin
6340 S. Y. Pickering
6341 R. C. Lincoln
6341 R. D. Klett
6342 D. R. Anderson
6342 R. P. Rechard
6344 E. D. Gorham
6344 R. L. Beauheim
6344 P. B. Davies
6344 S. J. Finley
6344 S. Howarth
6344 S. W. Webb
6345 B. M. Butcher
6345 F. T. Mendenhall
6345 K. L. Robinson
6346 J. R. Tillerson
6346 E. J. Nowak
6346 J. C. Stormont
7551 B. D. Hansche
7552 W. W. Shurtleff
7552 J. H. Gieske

Novak, September 4, 1991

Date: 9/4/91
To: K. M. Trauth, 6342
From: Craig F. Novak, 6344
Subject: Rationale for K_d Values Provided During Elicitation of the Retardation Expert Panel, May 1991
(Note: Includes addendum with correction for typographical error in Table 2.)

Sandia National Laboratories

Albuquerque, New Mexico 87185

date: 4 September 1991

to: K.M. Trauth, 6342

from: Craig F. Novak, 6344

subject: Rationale for K_d Values Provided During Elicitation of the Retardation Expert Panel, May 1991

In May 1991, I was asked to participate on a panel for estimating values of radionuclide retardation in the Culebra Dolomite Member of the Rustler Formation. Estimates were to be made using the K_d model for retardation, and according to an "expert judgement" methodology (Tierney, 1991). This memorandum summarizes my preparation for this task, and the thought processes used in responding to this request. The cumulative probability functions (CDFs) for K_d values resulting from this elicitation are given in Tables 1 and 2.

I performed a detailed examination of available research reports describing experimental measurement of K_d's using substrates and water compositions pertinent to transport in the WIPP system. This study is documented in Novak (1991). Novak showed that data are not available for all elements of interest, almost no data exist for clay substrates in the Culebra, and existing data may not be applicable to current human intrusion scenarios. Novak (1991) also questions the utility of the K_d model for estimating retardation in the Culebra. Despite these limitations, I endeavored to provide K_d values for use in the 1991 performance assessment calculations.

Estimates of K_d's were requested for two scenarios differing only in water composition. Within each scenario, K_d estimates were needed for radionuclide sorption on the matrix (i.e. dolomitic Culebra substrates) and in the fractures (i.e. on clay materials lining fractures). Scenario One assumed that water reaching the Culebra would not change the composition of Culebra water significantly, except for the presence of radionuclides. Scenario Two assumed that water reaching the Culebra would not be diluted, and thus a concentrated brine contaminated with radionuclides would flow

through the Culebra. These scenarios were chosen as bounding cases for hydrologic and chemical behavior in the Culebra under breach scenarios. Scenarios One and Two reflect the uncertainty involved with mixing in the Culebra and the observation that measured K_d values depend on water composition.

The eight elements for which K_d estimates were requested were plutonium (Pu), americium (Am), curium (Cm), uranium (U), neptunium (Np), thorium (Th), radium (Ra), and lead (Pb). I chose to group Am with Cm, U with Np, and Ra with Pb, and to provide a single CDF for each group. This choice was made because of the limited amount of data and because of analogies between the chemical behavior of the grouped elements (Lappin et al., 1989).

Among the existing data, I feel that the water composition called "Culebra H2O" is the most representative for Scenario One, while Brine A is the most representative for Scenario Two. Thus, for Scenario One, data in "Culebra H2O" were used to estimate K_d values where the data were available. Similarly for Scenario Two and data in Brine A. In the absence of these data, values were provided based on subjective "expert judgement" and interpretation of other data. The same CDFs were given for both scenarios for Th, and for Ra and Pb, because of the lack of data.

The lower bounds for K_d's in all CDFs are 0 ml/g because it is possible that any of the elements could be transported with the fluid velocity. The upper bounds in Tables 1 and 2 represent my opinions on the maximum values for K_d's that could be observed for these elements under the human intrusion scenarios. K_d values for cumulative probabilities of 0.25, 0.5, etc., represent best estimates resulting from my assimilation of data and literature on this topic.

There is a paucity of data for sorption of radionuclides on clays for solutions with water compositions pertinent to WIPP breach scenarios. However, clays are known to have large adsorption capacities, and therefore should exhibit high K_d values for radionuclides. For these reasons, CDFs for the fractures were estimated to be a factor of ten larger than for the matrix.

The values provided through the elicitation process are subjective estimates only. The human intrusion scenarios contain large uncertainties with respect to water compositions and mixing in the Culebra. Few experimental measurements of K_d's have been performed. In addition, the K_d model may have limited applicability to the WIPP Culebra system. These factors could render the CDFs given for K_d's inadequate to represent the actual values for K_d's that would occur under human intrusion scenarios.

The CDFs for K_d's are not a substitute for actual data, and should not be interpreted as such. Additional study is needed to quantify the potential for radionuclide retardation in the Culebra Dolomite Member of the Rustler Formation.

References

Lappin, A.R., and R.L. Hunter, eds. 1989. *Systems Analysis, Long-Term Radionuclide Transport, and Dose Assessments, Waste Isolation Pilot Plant (WIPP), Southeastern New Mexico; March 1989.* SAND89-0462. Albuquerque, New Mexico: Sandia National Laboratories.

Novak, C.F. 1991. *An Evaluation of Radionuclide Batch Sorption Data on Culebra Dolomite for Aqueous Compositions Relevant to the Human Intrusion Scenario for the Waste Isolation Pilot Plant (WIPP).* SAND91-1299. Albuquerque, New Mexico: Sandia National Laboratories.

Tierney, M.S. 1991. *Issue Statement for Elicitation of Expert Judgement Concerning Magnitudes of Culebra Distribution Coefficients for Use in the 1991 WIPP Performance Assessment.* 8 May 1991. Albuquerque, New Mexico: Sandia National Laboratories.

CFN:6344

Distribution:

6340 W.D. Weart
6342 D.R. Anderson
6344 E.D. Gorham
6344 C.F. Novak
DOE/WPO B. Becker

Table 1. Estimates of Matrix K_d Values from Expert Elicitation

Cumulative Probability	Scenario One, Pu Matrix K_d, ml/g	Scenario Two, Pu Matrix K_d, ml/g
0	0	0
0.1	5	0.55
0.25	80	10
0.5	300	50
0.75	1000	150
1	100000	100000

Cumulative Probability	Scenario One, Am and Cm Matrix K_d, ml/g	Scenario Two, Am and Cm Matrix K_d, ml/g
0	0	0
0.25	90	10
0.5	150	40
0.75	400	100
0.9	1000	
0.99		1000
1	100000	100000

Cumulative Probability	Scenario One, U and Np Matrix K_d, ml/g	Scenario Two, U and Np Matrix K_d, ml/g
0	0	0
0.2	0.25	1
0.5	0.75	3.3
0.8	1.5	8
1	100	100

Cumulative Probability	Scenarios One and Two, Th Matrix K_d, ml/g
0	0
0.25	5
0.5	10
0.75	100
1	1000

Cumulative Probability	Scenarios One and Two, Ra and Pb Matrix K_d, ml/g
0	0
0.25	1
0.5	10
0.75	100
0.99	1000
1	10000

Table 2. Estimates of Fracture K_d Values from Expert Elicitation

Cumulative Probability	Scenario One, Pu Fracture K_d, ml/g	Scenario Two, Pu Fracture K_d, ml/g
0	0	0
0.1	50	5.5
0.25	800	100
0.5	3000	500
0.75	10000	1500
1	1000000	1000000

Cumulative Probability	Scenario One, Am and Cm Fracture K_d, ml/g	Scenario Two, Am and Cm Fracture K_d, ml/g
0	0	0
0.25	900	100
0.5	1500	400
0.75	4000	1000
0.9	10000	
0.99		10000
1	1000000	1000000

Cumulative Probability	Scenario One, U and Np Fracture K_d, ml/g	Scenario Two, U and Np Fracture K_d, ml/g
0	0	0
0.2	2.5	10
0.5	7.5	33
0.8	15	80
1	1000	1000

Cumulative Probability	Scenarios One and Two, Th Fracture K_d, ml/g
0	0
0.25	50
0.5	100
0.75	1000
1	10000

Cumulative Probability	Scenarios One and Two, Ra and Pb Fracture K_d, ml/g
0	0
0.25	1
0.5	10
0.75	100
0.99	1000
1	10000

Sandia National Laboratories

Albuquerque, New Mexico 87185

date: 9 September 1991

to: K.M. Trauth, 6342

from: Craig F. Novak, 6344

subject: Typographical Error in Memo of 4 September 1991

My memorandum of 4 September contained a typographical error in Table 2, the fracture Kd values for Ra and Pb for Scenarios One and Two. As the test states, the fracture Kd's were estimated to be a factor of ten larger than the matrix Kd's. Thus, the Ra and Pb section of Table 2 should read

Cumulative Probability	Scenarios One and Two, Ra and Pb Fracture K_d, ml/g
0	0
0.25	10
0.5	100
0.75	1000
0.99	10000
1	100000

CFN:6344

Distribution:

6340 W.D. Weart
6342 D.R. Anderson
6344 E.D. Gorham
6344 C.F. Novak
DOE/WPO B. Becker

Swift, October 10, 1991

Date: 10/10/91
To: R. P. Rechard
From: Peter Swift, 6342/Tech Reps
Subject: Climate and recharge variability parameters for the 1991 WIPP PA calculations

TECH REPS, INC.
5000 Marble Avenue NE
Albuquerque, New Mexico 87110
505 266 5678
fax 505 260 1163

October 10, 1991

to: R. P. Rechard
Sandia National Laboratories Division 6342

from: P. N. Swift
6342/Tech Reps

subject: Climate and recharge variability parameters for the 1991 WIPP PA calculations

Summary of Recommendations for the 1991 PA Calculations

The uncertain input parameter of interest here is recharge to the regional domain of the Culebra Dolomite groundwater-flow model.

I recommend separating recharge into two component functions: variability in mean annual precipitation and variability in the amount of precipitation that reaches our Culebra model domain as recharge. For the 1991 *Preliminary Comparison*, I recommend sampling on the recharge parameter only, and using a fixed function for climatic variability. Specific functions are as follows.

Recommended function for future mean annual precipitation (P_f) as a function of time (t, measured in units of 10^4 years):

$$P_f(\text{cm/yr}) = 52.5 - 15(\cos\beta t - \sin 0.5\alpha t + 0.5\cos\alpha t)] ,$$

with $\alpha = 20\pi$, $\beta = \pi/6$.

Recommended function for future model recharge (R_f) as a function of nominal present model recharge (R_p), assuming that model recharge can be expressed as boundary flux into the regional model domain:

$$R_f = R_p \times [1 + (2r - 1)(\frac{P_f - 30}{30})] ,$$

if $P_f \geq P_p$, or

$R_f = R_p$ if $P_f < P_p$;

with P_f calculated according to the previous equation, in cm/yr, and r sampled on a uniform distribution from 1 to 10.

Introduction

Ideally, it could be possible to describe variability in recharge within a single conceptual model for flow in the Culebra using a single parameter—future recharge as a function of present recharge. I recommend, however, separating recharge into two component functions: variability in mean annual precipitation and variability in the amount of precipitation that reaches our Culebra model domain as recharge. This distinction allows examining model sensitivity to climatic change independently of the uncertainty in the physical recharge process. The distinction is meaningful because we can assess climatic variability relatively confidently, whereas uncertainty about the recharge process is high. Sampling on separate parameters will permit us to perform sensitivity analyses (to be reported by Swift et al. [in prep.], separately from the 1991 ***Preliminary Comparison***) on both climate variability and the assumed recharge function.

This memo defines climate and recharge functions and the associated parameters to be sampled. The memo does not address conceptual model uncertainty about the location or amount of present recharge to the model domain, or about the location of future recharge. These model uncertainties will be addressed in 1992 or later, as results become available from the geostatistics project addressing uncertainty in the Culebra flow model. The assumption is made here that future model recharge will be expressed as a function of nominal present flux into a calibrated steady-state flow model.

For the 1991 PA calculations, there appears to be little need to sample on a distribution of climate parameter values. As explained below, we can select "best estimate" values for climate variability for the full-system simulations, and wait for the separate sensitivity analysis report to examine the impact of the assumptions. This does not mean that the 1991 calculations will not include climate variability. Climate variability will be incorporated, and the results will reflect the knowledge that some future climates will be wetter than that of the present. The function and values I am recommending will give us an "average" future precipitation roughly 1.3 times present, with peaks of just over 2 times present.

I do recommend sampling on the recharge function parameter. As defined here, this parameter is a simple multiplier that is applied to the nominal increase in precipitation, yielding the change in model recharge. The multiplier represents uncertainty in numerous parameters, including (i) the location and extent of the surface recharge area, (ii) groundwater flow between the surface recharge area and the boundary of the model domain, and (iii) the relationship between precipitation and infiltration in the surface recharge area, which in turn is dependent on factors such as vegetation, temperature, local topography, and soil characteristics. There is no particular reason to assume a 1-to-1 correlation between increases in precipitation and increases in model recharge, and limited evidence for water-table conditions in semi-arid climates suggests that increases in precipitation may result in substantially larger increases in infiltration. I recommend that we incorporate recharge uncertainty in the 1991 calculations by sampling a uniformly distributed recharge parameter (defined below) over a range that permits the relationship between mean annual precipitation and model recharge to vary between 1-to-1 and 10-to-1. This

would mean that with precipitation at a maximum of 2x present, model recharge could range from 2x to 20x present. Both the range and the distribution are preliminary, and should be adjusted as new data or interpretations warrant.

Description of Climate Variability

The basic premise for assessing climatic change at the WIPP is the assumption that, because of the long-term stability of glacial cycles, future climates will remain within the range defined by Pleistocene variation. Present understanding does not suggest that short-term (century-scale) anthropogenic changes in the Earth's greenhouse effect will invalidate this premise: published results of global-warming models do not predict climatic changes of greater magnitude than those of the Pleistocene (Swift, in prep.; Bertram-Howery et al., 1990).

Paleoclimatic data permit reconstruction of a precipitation curve for the WIPP for the last 30,000 years (Figure 1). This curve shows two basic styles of climatic fluctuation: relatively low-frequency increases in precipitation that coincide with the maximum extent of the North American ice sheet; and higher-frequency precipitation increases of uncertain causes that have occurred both during the glacial maximum and in the 10,000 years since the retreat of the ice sheet. Variability has also occurred in the seasonality and intensity of precipitation. Most of the late Pleistocene moisture fell as winter rain. Most of the Holocene precipitation falls during during a summer monsoon, in local and often intense thunderstorms. This variability probably has affected recharge: no WIPP-specific data are available, but, in general, higher temperatures increase evapotranspiration and decrease infiltration. The resulting variability in recharge is included in the recharge function described below, however, and I have made no effort to distinguish between winter and summer precipitation in the climate function.

The amplitude of the low-frequency glacial precipitation peak is relatively well-constrained by data from multiple sources. Amplitudes of the higher-frequency are less easily determined, but data indicate that none of the Holocene precipitation peaks exceeded average glacial levels. I recommend that we assume that high-frequency peaks with amplitudes comparable to those of the Holocene could have been superimposed on the glacial maximum. Therefore, there may have been relatively brief (i.e., on the order of hundreds to perhaps thousands of years) periods during the glacial maximum when precipitation at the WIPP may have averaged three times present levels.

The curve shown in Figure 1 cannot be extrapolated into the future with any confidence. The curve can be used, however, in combination with the general understanding of glacial periodicity (see Swift, in prep.) to make a reasonable approximation of likely future variability. The function I propose is not in any sense a predictive function for future precipitation. Rather, it is an admittedly simplistic function that can be readily adjusted to approximate the variability that may occur.

Specifically, my proposed precipitation function is as follows:

$$P_f = P_p \times \left[\left(\frac{3A + 1}{4}\right) - \left(\frac{A - 1}{2}\right)\left(\cos\beta t - \sin\frac{\alpha}{2}t + \frac{1}{2}\cos\alpha t\right)\right] ,$$

where

P_f = future mean annual precipitation
P_p = present mean annual precipitation
A = amplitude scaling factor (i.e., past precipitation maximum was A times the present)
α = frequency parameter for Holocene-type climatic fluctuations
β = frequency parameter for Pleistocene glaciations
t = time (after present, in 10^4 years).

The equation can be simplified considerably by using available data. The three-year precipitation record from the site is too brief to be useful for determining a long-term mean, but examination of regional data suggests an approximate value of 30 cm/yr (estimated from data presented by Hunter, 1985). Past precipitation maximums were approximately twice present (Swift, in prep.), and the amplitude scaling factor, A, can therefore be set at 2. The equation then becomes:

$$P_f(\text{cm/yr}) = 52.5 - 15(\cos\beta t - \sin 0.5\alpha + 0.5\cos\alpha t)].$$

My preferred values for α and β have been chosen from examination of the past precipitation curve (Figure 1) and the glacial record. If $\alpha = 20\pi$, wet maximums will occur every 2000 years, approximately with the same frequency shown on Figure 1. Note that we are presently near a dry minimum, and the last wet maximum occurred roughly 1000 years ago. If $\beta = \pi/6$, the next full glacial maximum will occur in 60,000 years, approximately the time predicted by simple models of the astronomical control of glacial periodicity (e.g., Imbrie and Imbrie, 1980). Figure 2 shows a plot of the climate function for these values.

Figure 3 shows how varying β can affect the curve. Choosing $\beta = \pi$ gives a wet maximum in 10,000 years, and results in extreme precipitation values 3 times those of the present. This is not a realistic value for β—ice sheets grow relatively slowly, and it would be difficult to achieve full continental glaciation within 10,000 years. I do not recommend sampling on variations in β for the 1991 calculations, but I do plan to consider the case in the separate sensitivity analyses.

Figure 4 shows the effect of varying α, in this case to yield wet peaks every 4000 years. Changes in α vary the frequency of the shorter-term fluctuations, but they do not change the ratio between wet and dry climates, and the average precipitation over 10,000 years remains the same.

Examination of Figure 1 shows that Holocene climates have been predominantly dry, with wet peaks much briefer than dry minimums. The α terms in the above equation give an oscillation in which the future climate is wetter than the present one-half of the time. I believe this value to be somewhat greater than the actual ratio, and, assuming that wet conditions are more

likely to result in releases from the WIPP, these terms provide a conservative approximation of Holocene variability. Furthermore, the choice of a single amplitude scaling factor for both Holocene and glacial peaks results in α peaks that are probably higher than all Holocene peaks and certainly higher than most.

Minor fluctuations during the dry minimums shown in Figures 2 through 4 are an artifact of the three-term function, and are not intended to represent any particular climatic variability. The minimum values of the "overshoots" do, however, correspond reasonably well to the minimum values shown in Figure 1 for the middle Holocene. Paleoclimatic data indicate that minimum Holocene precipitation may have been approximately 90% of present values (Swift, in prep.).

Glacial cycles have not been symmetric. Precipitation increases during glacial advances have been gradual, whereas decreases at the end of glaciation have been abrupt, giving a sawtooth characteristic to the curve. The assumption of a cosine function for glacial cycles may therefore not be conservative for WIPP performance assessment: precipitation during glacial advances may be underestimated. The significance of this possible underestimation will be examined in the separate sensitivity analyses by using larger β values, and accelerating the next glacial peak (Swift et al., in prep.).

Description of Recharge Variability

We know little about recharge to the Culebra. Hydraulic head and isotopic data (e.g., Holt et al., in prep.; Lambert and Harvey, 1987; Lambert and Carter, 1987, Lappin et al., 1989) indicate that very little if any moisture reaches the Culebra directly from the ground surface within the model domain. Regionally, it is believed that recharge occurs several tens of kilometers to the north, where the Culebra is near the ground surface (Mercer, 1983; Brinster, 1991). It is unknown if water from this recharge area presently reaches the model domain. Nominal recharge to the two-dimensional Culebra model has, in the past, been a prescribed boundary condition estimated from head and density data from WIPP-area wells (LaVenue et al., 1990).

Available literature on the relationship between precipitation and recharge is limited to examinations of recharge to a water table by direct infiltration. Environmental tracer research (e.g., Allison, 1988) suggests that long-term increases in precipitation in deserts may result in significantly larger increases in infiltration, particularly if the increases in precipitation coincide with lower temperatures and decreased evapotranspiration. As an extreme example, Stone (1984) estimated a 28-fold increase in infiltration for one location at the Salt Lake coal field in western New Mexico during the late Pleistocene wet maximum. Bredenkamp (1988a,b) compared head levels in wells and and sinkholes with short-term (decade-scale) precipitation fluctuations in the Transvaal, and suggested that for any specific system there may be a minimum precipitation level below which recharge does not occur. Above this uncertain level recharge to the water table may be a linear function of precipitation.

Data of this sort could perhaps be applied quantitatively to the WIPP if we (i) knew the location and extent of the surface recharge area for the Culebra, (ii) knew how much, if any, infiltration occurs there at present, and (iii) could include the recharge area in the model domain. We do not know the first two, and it is not feasible to attempt the third. Even if we could map the recharge area, uncertainty would remain about the extent of the larger area in which significant inflow to the Culebra occurs as leakage from overlying units. Even if we could quantify recharge from the surface and inflow from overlying units, extending the model domain to include the necessary area does not appear realistic.

Therefore, I recommend assigning a wide range to model recharge. The specific function I suggest is:

$$R_f = R_p \times \left[1 + \left(\frac{Ar - 1}{A - 1}\right)\left(\frac{P_f - P_p}{P_p}\right)\right] ,$$

if $P_f \geq P_p$, or

$R_f = R_p$ if $P_f < P_p$;

with terms defined to be:

R_f = future nominal flux into the modeled Culebra
R_p = present nominal flux into the modeled Culebra
r = recharge scaling parameter
P_f = future mean annual precipitation, as calculated from the above climate variability equation
P_p = present mean annual precipitation
A = precipitation amplitude scaling factor as in the climate variability function above (i.e., past precipitation maximum was A times the present).

Using values of 2 for A and 30 cm/yr for P_p, the recharge function simplifies to:

$$R_f = R_p \times \left[1 + (2r - 1)\left(\frac{P_f - 30}{30}\right)\right] ,$$

if $P_f \geq P_p$, or

$R_f = R_p$ if $P_f < P_p$.

This function applies the recharge scaling factor only to that portion of future precipitation that represents an increase over present precipitation. Thus, to achieve a 10-fold increase in recharge from a doubling of precipitation (i.e., $A = 2$, $P_f = 2P_p$), it would be necessary to use an r value of 5. Regardless of the selected r value, if precipitation remains constant, recharge also remains constant. The function does not allow for a time lag between changes in precipitation and model recharge. This is unrealistic, but of little consequence unless the lag is long relative to

the 10,000-year period of interest, in which case the assumption of instantaneous model recharge response is conservative.

The decision to hold recharge at the present level when calculated precipitation falls below present avoids "negative" recharge for large values of r. Flux across the model domain boundary may in fact have been less in the past, during times when precipitation was slightly less than present, but variation was probably slight, and it is unrealistic to assume that the same function applies for lower levels of precipitation.

I recommend sampling a uniform distribution of r values from 1 to 10 to cover variability in model recharge. Justification for the range and distribution are as follows:

Lower bound, r = 1. This value yields a 1-to-1 correspondence between precipitation and model recharge, which I believe to be a conservatively high lower bound. A less than 1-to-1 correspondence (r values less than 1) could occur if the transmissivity field between the surface recharge area and the model domain is such that precipitation fluctuations reach the model domain with strongly muted amplitudes. An improved understanding of regional hydrology may indicate that it is appropriate to include these lower values in future calculations. Circumstances can also be imagined in which increases in precipitation result in a decrease in infiltration (e.g., development of plant cover on previously barren land, or changes in topography resulting in runoff from a previously closed drainage), but none appear plausible for the WIPP area. It is more likely that an increase in the cool-season component of precipitation will result in higher infiltration and r values greater than 1.

Upper bound, r = 10. This value yields a 20-fold increase in model recharge with a doubling of mean annual precipitation and a shift from a monsoonal climate to a climate dominated by winter storms. This value is arbitrary, but is generally representative of the infiltration data reported by Stone (1984). It is less than his maximum value recorded at a single point, reflecting my belief that it is improbable that local-scale variability in infiltration will have a significant effect on confined groundwater flow tens of kilometers down-gradient. It is greater than the mean value for his study area of a 12.5-fold increase in infiltration during the late Pleistocene. My decision to use surface infiltration for an upper bound is based on the observation that the area of surface recharge is apparently relatively small compared to the area in which the Culebra is confined, and there is no reason to assume a preferential flow path from the recharge area to the model domain.

Distribution. I suggest a uniform distribution in the absence of data indicating otherwise. Choosing any distribution other than uniform would imply a greater understanding of the recharge process than we presently have.

Both the range and distribution of the recharge parameter are preliminary, and may be adjusted for future calculations if new data or interpretations warrant.

References Cited

Allen, B. D. 1991. "Effect of Climatic Change on Estancia Valley, New Mexico: Sedimentation and Landscape Evolution in a Closed-Drainage Basin," in B. Julian and J. Zidek, eds., *Field Guide to Geologic Excursions in New Mexico and Adjacent Areas of Texas and Colorado*. New Mexico Bureau of Mines and Mineral Resources Bulletin 137. Socorro, New Mexico. pp. 166-171.

Allison, G. B. 1988. "A Review of Some of the Physical, Chemical, and Isotopic Techniques Available for Estimating Groundwater Recharge," in I. Simmers (ed.), *Estimation of Natural Groundwater Recharge*. NATO ASI series, series C, vol. 222. Dordrecht, Holland: D. Reidel. pp. 49-72.

Bertram-Howery, S. G., M. G. Marietta, R. P. Rechard, P. N. Swift, D. R. Anderson, B. L. Baker, J. E. Bean, Jr., W. Beyeler, K. Brinster, R. V. Guzowski, J. C. Helton, R. D. McCurley, D. K. Rudeen, J. D. Schreiber, and P. Vaughn. 1990. *Preliminary Comparison with 40 CFR Part 191, Subpart B for the Waste Isolation Pilot Plant, December 1990*. SAND90-2347. Albuquerque, NM: Sandia National Laboratories.

Bredenkamp, D. B. 1988a. "Quantitative Estimation of Ground-Water Recharge in Dolomite," in I. Simmers (ed.), *Estimation of Natural Groundwater Recharge*. NATO ASI series, series C, vol. 222. Dordrecht, Holland: D. Reidel. pp. 449-460.

Bredenkamp, D. B. 1988b. "Quantitative Estimation of Ground-Water Recharge in the Pretoria-Rietondale Area," in I. Simmers (ed.), *Estimation of Natural Groundwater Recharge*. NATO ASI series, series C, vol. 222. Dordrecht, Holland: D. Reidel. pp. 461-476.

Brinster, K. F. 1991. *Preliminary Geohydrologic Conceptual Model of the Los Medaños Region Near the Waste Isolation Pilot Plant for the Purpose of Performance Assessment*. SAND89-7147. Albuquerque, NM: Sandia National Laboratories.

Holt, R. M., D. W. Powers, R. L. Beauheim, and M. E. Crawley. in prep. *Conceptual Hydrogeologic Model of the Rustler Formation in the Vicinity of the Waste Isolation Pilot Plant Site, Southeastern New Mexico*. SAND89-0862. Albuquerque, NM: Sandia National Laboratories.

Hunter, R. L. 1985. *A Regional Water Balance for the Waste Isolation Pilot Plant (WIPP) Site and Surrounding Area*. SAND84-2233. Albuquerque, NM: Sandia National Laboratories.

Imbrie, J., and J. Z. Imbrie. 1980. "Modeling the Climatic Response to Orbital Variations." *Science* 207: 943-953.

Lambert, S. J., and J. A. Carter. 1987. *Uranium-Isotope Systematics in Groundwaters of the Rustler Formation, Northern Delaware Basin, Southeastern New Mexico. I: Principles and Methods*. SAND87-0388. Albuquerque, NM: Sandia National Laboratories.

Lambert, S. J., and D. M. Harvey. 1987. *Stable-Isotope Geochemistry of Groundwaters in the Delaware Basin of Southeastern New Mexico.* SAND87-0138. Albuquerque, NM: Sandia National Laboratories.

Lappin, A. R., R. L. Hunter, D. P. Garber and P. B. Davies, eds. 1989. *Systems Analysis, Long-Term Radionuclide Transport, and Dose Assessments, Waste Isolation Pilot Plant (WIPP), Southeastern New Mexico; March 1989.* SAND89-0462. Albuquerque, NM: Sandia National Laboratories.

LaVenue, A. M., T. L. Cauffman, and J. F. Pickens. 1990. *Ground-Water Flow Modeling of the Culebra Dolomite. Volume I: Model Calibration.* SAND89-7068. Albuquerque, NM: Sandia National Laboratories.

Mercer, J. W. 1983. *Geohydrology of the Proposed Waste Isolation Pilot Plant Site, Los Medaños Area, Southeastern New Mexico.* Albuquerque, NM: United States Geological Survey Water Resources Investigation 83-4016.

Phillips, F. M., A. R. Campbell, C. Kruger, P. S. Johnson, R. Roberts, and E. Keyes. in prep. *A Reconstruction of the Response to Climate Change of the Water Balance in Western United States Lake Basins.* New Mexico Water Resources Research Institute Report. Socorro, New Mexico.

Pierce, H. G. 1987. "The Gastropods, with Notes on Other Invertebrates," in E. Johnson (ed.) *Lubbock Lake: Late Quaternary Studies on the Southern High Plains.* College Station, TX: Texas A&M University Press. pp. 41-48.

Swift, P. N. in prep. *Long-Term Climate Variability at the Waste Isolation Pilot Plant.* SAND91-7055J. Albuquerque, NM: Sandia National Laboratories.

Swift, P. N., B. L. Baker, K. F. Brinster, M. G. Marietta, and P. J. Roache. in prep. *Parameter and Boundary Conditions Sensitivity Studies Related to Climate Variability and Scenario Screening for the Waste Isolation Pilot Plant.* SAND89-2029. Albuquerque, NM: Sandia National Laboratories.

Stone, W. J. 1984. *Recharge in the Salt Lake Coal Field Based on Chloride in the Unsaturated Zone.* Open File Report 214. Socorro, NM: New Mexico Bureau of Mines and Mineral Resources.

Van Devender, T. R., R. S. Thompson, and J. L. Betancourt. 1987. "Vegetation History of the Deserts of Southwestern North America; the Nature and Timing of the Late Wisconsin–Holocene Transition," in W. F. Ruddiman and H. E. Wright, Jr. (eds.), *North America and Adjacent Oceans During the Last Deglaciation.* The Geology of North America Volume K-3. Boulder, CO: Geological Society of America. pp. 323-352.

Waters, M. R. 1988. "Late Quaternary Lacustrine History and Paleoclimatic Significance of Pluvial Lake Cochise, Southeastern Arizona," *Quaternary Research* 32: 1-11.

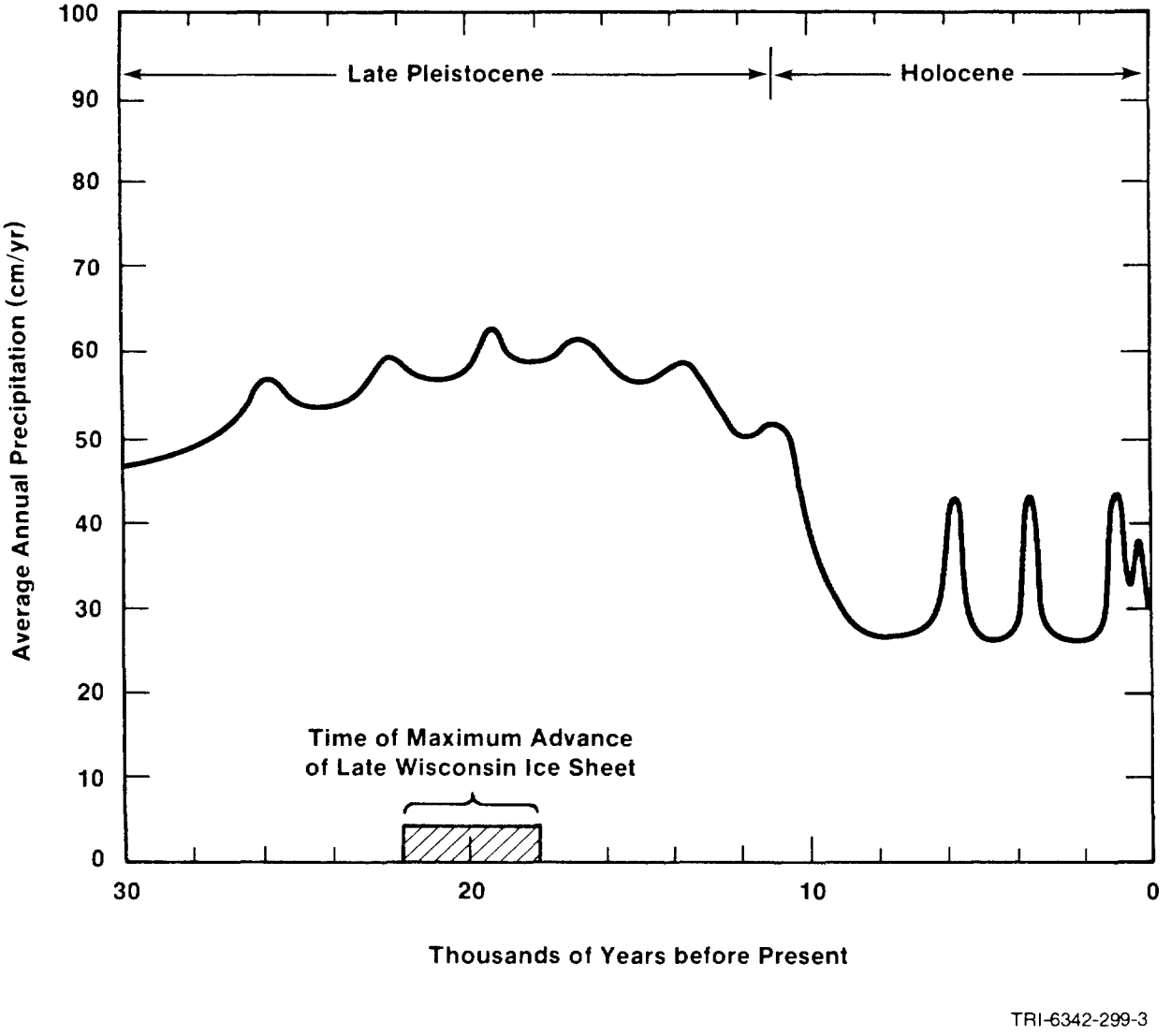

Figure 1. Estimated mean annual precipitation at the WIPP during the late Pleistocene and Holocene (Swift, in prep.). Data from Van Devender et al. (1987), Pierce (1987), Waters (1989), Phillips et al. (in prep.), Allen (1991), and other sources cited by Swift (in prep.).

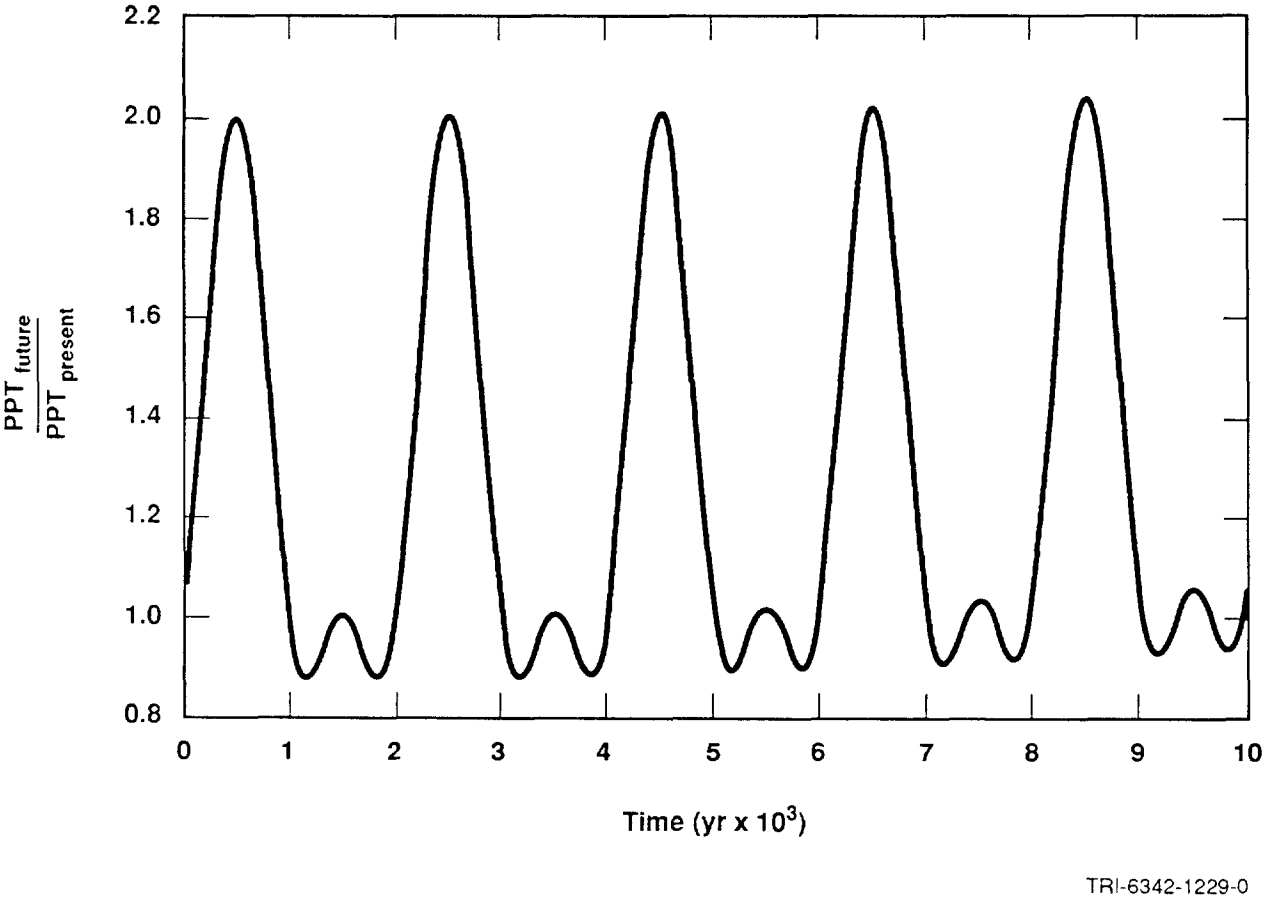

Figure 2. Ratio between future and present mean annual precipitation at the WIPP, calculated using the climate function suggested in the text and the suggested constants that yield a full glacial maximum in 60,000 years and interglacial peaks every 2000 years.

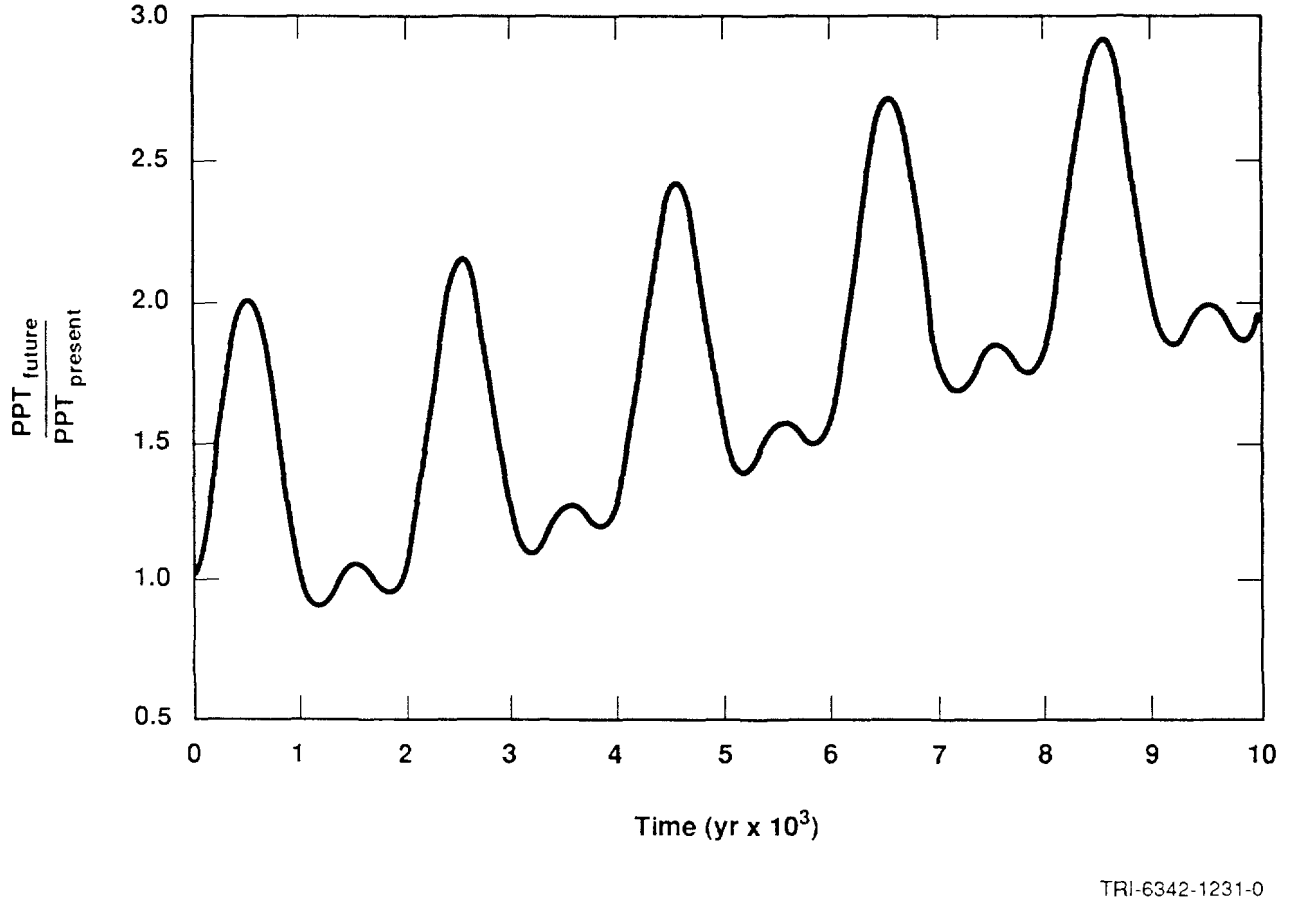

Figure 3. Ratio between future and present mean annual precipitation at the WIPP, calculated using the climate function suggested in the text and constants that yield a full glacial maximum in 10,000 years and interglacial peaks every 2000 years.

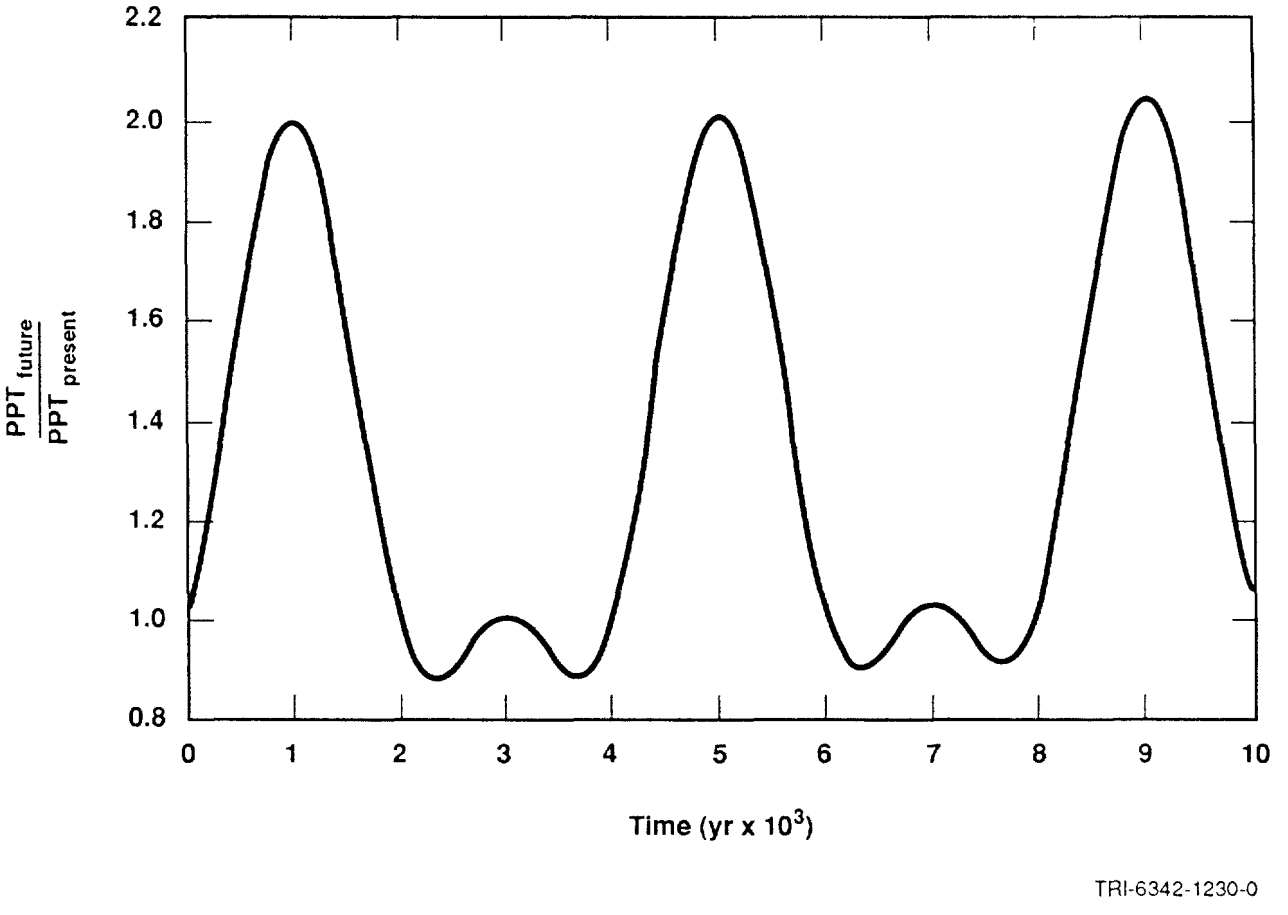

Figure 4. Ratio between future and present mean annual precipitation at the WIPP, calculated using the climate function suggested in the text and constants that yield a full glacial maximum in 60,000 years and interglacial peaks every 4000 years.

Gorham, July 2, 1991

Date: 7/2/91
To: Rob Rechard (6342)
From: Elaine Gorham (6344)
Subject: Aggregated Frequency Distributions for Permeability, Pore Pressure and Diffusivity in the Salado Formation

Sandia National Laboratories

Albuquerque, New Mexico 87185

date: July 2, 1991

to: Rob Rechard, 6342

Elaine Gorham

from: Elaine Gorham, 6344

subject: Aggregated Frequency Distributions for Permeability, Pore Pressure and Diffusivity in the Salado Formation

Attached are the frequency distributions we recommend that you use in the December 91 calculations for values of the brine permeability, pore pressure and specific storage for the Salado formation. Separate frequency distributions have been derived for halite and anhydrite layers. As we have discussed in previous meetings, the data base cannot currently support a model that clearly differentiates a disturbed rock zone from the far field. Therefore we have included data that we believe may be representative of a DRZ in formulating our property distributions for the far field.

Data and suggested frequency distributions from various experiments supported by 6344 that have been included in formulation of the recommended distributions have been transmitted to you in the following memos:

1. "Pore Pressure Distributions for 1991 Performance Assessment Calculations", S. Howarth to E. Gorham, June 12, 1991.

2. "Permeability Distributions for 1991 Performance Assessment Calculations", S. Howarth to E. Gorham, June 13, 1991.

3. "Review of Salado Parameter Values to be Used in 1991 Performance Assessment Calculations", R. Beauheim to R. Rechard, June 14, 1991.

4. "Parameter Estimates from the Small Scale Brine Inflow Experiments", S. Finley and D. McTigue, June 17, 1991.

This memo combines the information in the memos listed above in a consistent manner with the attached table of pore pressure information from the Permeability Testing Program to produce aggregated distributions for the relevant parameters. I will provide you with a publishable description of the aggregation process by your August deadline.

Permeability values inferred from the Permeability Testing Program and from the Room Q tests depend upon the assumed specific storage. At this time we have not succeeded in quantifying the correlation between these two parameters and

therefore recommend that you sample from the permeability and specific storage distributions independently.

The formation compressibility α can be obtained from the values of specific storage using the formula:

$$\alpha = S_S/\rho/g - \phi\beta,$$

where g is the gravitational acceleration, ρ the fluid density, ϕ the formation porosity and β the fluid compressibility. I recommend using average values recommended by Beauheim in Reference 3 above for the parameters in this conversion formula, since I have included considerable parameter uncertainty in the frequency distribution for the specific storage. Thus, I recommend using the expression

$$\alpha = S_S * 8.5\text{x}10^{-5}/\text{Pa} - 3.1\text{x}10^{-12}/\text{Pa}$$

to obtain formation compressibility from specific storage. Further, for values of specific storage smaller than $3.6\text{x}10^{-8}$, α may become negative. I recommend allowing it to become negative for values of specific storage larger then $3.4\text{x}10^{-8}$ at which value the total compressibility will equal the lowest recommended value of fluid compressibility ($2.9\text{x}10^{-10}$/Pa). For values of specific storage less than $3.4\text{x}10^{-8}$, which comprise less than five percent of the frequency distributions, I recommend using a formation compressibility of zero and a value of fluid compressibility of $2.9\text{x}10^{-10}$/Pa.

If you have any questions please contact me.

Copies:

1511 D. McTigue
6340 W. D. Weart
6342 D. R. Anderson
6344 R. Beauheim
6344 S. Finley
6344 S. Howarth

AGGREGATED FREQUENCY DISTRIBUTIONS FOR PERMEABILITY IN THE SALADO FORMATION:

-LOG(Permeability(m^2))	HALITE Cumulative Frequency	ANHYDRITE Cumulative Frequency
16.50		0.0
17.00	0.0	0.018481
17.50	0.018481	0.036963
18.00	0.036963	0.073959
18.50	0.065434	0.126273
19.00	0.093906	0.247036
19.50	0.154012	0.476356
20.00	0.269430	0.636369
20.50	0.416616	0.819516
21.00	0.645037	0.922176
21.50	0.826056	0.948816
22.00	0.939442	0.975456
22.50	0.964834	0.987111
23.00	0.985230	0.998766
23.50	0.991890	0.998766
24.00	0.998550	0.998766

AGGREGATED FREQUENCY DISTRIBUTIONS FOR FORMATION PRESSURE IN THE SALADO FORMATION:

Pressure (MPa)	HALITE Cumulative Frequency	ANHYDRITE Cumulative Frequency
0.0	0.000	0.0
1.0	.1250	0.15
2.0	.1500	0.20
3.0	.2750	0.20
4.0	.3375	0.20
5.0	.4625	0.30
6.0	.5500	0.35
7.0	.5750	0.35
8.0	.6800	0.35
9.0	.8400	0.40
10.0	.9750	0.50
11.0	1.000	0.60
12.0	1.000	0.75
13.0	1.000	0.95
14.0	1.000	1.00

AGGREGATED FREQUENCY DISTRIBUTIONS FOR SPECIFIC STORAGE IN THE SALADO FORMATION:

-LOG(Specific Storage(/m))	HALITE Cumulative Frequency	ANHYDRITE Cumulative Frequency
0.0		
2.3	0.050	0.027
2.4	0.053	0.042
2.9	0.070	0.11
3.0	0.075	0.12
3.1	0.084	0.15
3.3	0.10	0.20
4.0	0.17	0.21
4.4	0.24	0.25
4.5	0.26	0.26
4.7	0.28	0.27
4.8	0.29	0.28
5.1	0.33	0.30
5.2	0.34	0.31
5.4	0.36	0.34
5.8	0.40	0.40
5.9	0.40	0.41
5.9	0.41	0.41
6.0	0.44	0.41
6.4	0.54	0.53
6.8	0.66	0.67
7.0	0.70	0.92
7.1	0.77	0.93
7.5	0.98	0.95
7.7	0.99	0.96
8.0	0.99	0.97
8.5	1.0	1.0

FORMATION PORE PRESSURES FROM PERMEABILITY TESTING PROGRAM

TEST	INTERVAL (m)	PRESSURE (MPa)	LITHOLOGY
C2H01-A	2.09-2.92	0.50	halite
C2H01-A-GZ	0.50-1.64	0.00	halite
C2H01-B	4.50-5.58	3.15	halite
C2H01-B-GZ	2.92-4.02	4.12	halite
C2H01-C	6.80-7.76	8.05	MB139
C2H02	9.47-10.86	9.30	MB139
L4P51-A	3.33-4.75	2.75	halite
L4P51-A-GZ	1.50-2.36	0.28	MB139
S0P01	3.74-5.17	4.45	halite
S0P01-GZ	1.80-2.76	0.52	MB139
S1P71-A	3.12-4.56	2.95	halite
S1P71-A-GZ	1.40-2.25	0.00	MB139
S1P71-B	9.48-9.80	4.88	anhydrite "c"
S1P72	4.40-6.00	1.24	MB139
S1P72-GZ	2.15-3.18	5.15	halite
SCP01	10.50-14.78	12.55	MB139
L4P51-B	9.62-9.72	5.10	anhydrite "c"
S1P73-B	10.86-11.03	4.50	MB138

Anderson, October 25, 1991

Date: 10/25/91
To: File
From: D. R. (Rip) Anderson (6342)
Subject: Modifications to Reference Data for 1991 Performance Assessment

Sandia National Laboratories

Albuquerque, New Mexico 87185

date: 25-OCT-91

to: File

D. R. Anderson

from: D. R. (Rip) Anderson, 6342

subject: Modifications to Reference Data for 1991 Performance Assessment

Memoranda regarding reference data were provided to performance assessment from principal investigators for use in the 1991 preliminary comparison. Data were requested early in the performance assessment year (March) because consequence modeling depends on early definition of conceptual models, division of summary scenarios into computational scenarios, and robustness of different flow and transport codes. Once the conceptual and computational model(s) and the ranges and distributions of imprecisely known input parameters are defined, the annual performance assessment calculations can be designed and tested.

Concerns related to calculational design include distinguishing conceptual models so CCDF comparisons, ceteris paribus, can be made; ability to perform the calculations (i.e., acknowledging code limitations); and the need to design consequence modeling so sensitivity analysis results are interpretable. Consideration of these concerns sometimes requires modification of data ranges and distributions. For example, comparison of two different conceptual models is best performed by comparing summary CCDFs derived from two independent analyses using the same sample. Therefore, submitted data may be divided between two different conceptual models, e.g., dual- and single-porosity (fracture) transport in the Culebra.

The flow and transport codes have fundamental limitations in their ability to compute realistic results over wide parameter ranges especially when there are orders of magnitude variations in material properties between adjacent zones. Data must be made available in a timely way so that codes can be tested before Monte Carlo simulations have to start. Because last-minute adjustments cannot always be made, new data or new interpretations of old data that are delivered late may not be included until the next year's calculations.

For interim performance assessments like the 1991 preliminary comparison, sensitivity analyses must be as realistic and interpretable as possible because the comparison forms the basis for providing guidance to DOE on the experimental program. The performance assessment calculations must be designed so that different

conceptual models and different sources of uncertainty (e.g., stochastic vs. subjective, various imprecisely known parameters, etc.) can be clearly distinguished. Most important, data must be consistent with model scales, e.g., measurements may be on a m^3 scale, but the model needs information on a computational cell volume of 10^3 m^3. Therefore, realistic distribution functions on the right model scales are required for providing meaningful sensitivity results on which to base our guidance to DOE. Too much or too little emphasis on distribution tails (e.g., arbitrarily wide ranges on uncertainty) can skew results. In such cases for a parameter or submodel, more than one distribution can be tested and results compared and documented in the sensitivity analysis report. The CCDFs reported in the preliminary comparison, however, must rely on realistic conceptual models and parameter CDFs.

The following discussion lists changes in parameter distributions from recommendations in submitted memoranda for the 1991 Preliminary Comparison.

1. **Pore Pressure Distribution** (ref. E. Gorham to R. Rechard, Memo, July 2, 1991)

The distribution as provided in Gorham, Memo, June 2, 1991, includes data taken from Salado halite and anhydrite. The 10 measurements included in the data and described in Howarth, Memo, June 12, 1991, are from 7 experiments in halite and three in anhydrite. For each experiment, two pressure values are reported: (1) a "shut-in" value obtained during a pressure build-up test and (2) a Horner extrapolation of this value. The Horner extrapolation provides an estimate of a steady-state pore pressure by extrapolation to infinite time.

For the 1991 PA calculations, we are using only the Horner extrapolated pressure values for the anhydrite material (reported in Howarth, Memo, June 12, 1991) and the two anhydrite values (recommended in Beauheim, Memo, June 14, 1991) for our "far-field" pore pressure distribution at the MB139 elevation. Because doing so results in using only five experimental data, the distribution is constructed using the PA standard procedure for sparse data. This procedure involves determining the mean of the data and then extending the range to $\pm 2.33\sigma$ about the mean. Since the maximum pressure of the resulting range exceeds lithostatic pressure, we limit the maximum to lithostatic. The following supports the changes made to the pore pressure distributions of Gorham, Memo, July 2, 1991.

Reason 1: One difficulty with the Gorham distribution is that both the shut-in and Horner values of each test were weighted equally and used in the construction of the distribution. This "doubling up" of data is not consistent with PA's understanding of capturing data uncertainty with probability distributions. PA methodology requires that the data points to be used in the construction of the parameter cdfs be from independent experiments.

Reason 2: The model requires steady-state or long time estimates of pore pressure that exist in the host rock prior to excavation. The early time data or shut-in values obtained during the experiments are not consistent with the model's application and should be excluded from the distribution. The transient nature of pressure response to the excavation is calculated by the model.

Reason 3: The pressure the model expects is one which is representative of the pressure at repository elevation at a horizontal distance far removed from the repository. Far removed as defined in the model is a location where neither pressure nor saturation is affected by changes occurring in the repository. The key words are "far removed." During the course of the calculations, the model BRAGFLO determines the changing pressure and saturation profiles as a function of time and position. Results from BRAGFLO indicate that a depressurized zone surrounding the waste is created at early times. This depressurized zone is created in response to the low pressure initially in the excavation. This zone is not to be confused with the DRZ (disturbed rock zone) which, if it exists, is due to mechanical stress in the surrounding rock. The size of this depressurized zone varies with time and material properties, but it can extend tens of meters into the Salado. For example, in vector 6 of this year's input, sampling the simulated pressure field 25 m from the repository into the Salado at a time 8 yr after the excavation results in a value of 5.5 MPa, while the far-field pressure remains at 8.5 MPa. Using the value of 5.5 MPa as representative of the "far-field" value, in this case, would underestimate the potential for brine inflow into the panel from the "far field" and would be 35% low. The distance from the repository where the experiments were conducted is 23 m.

Reason 4: The data are not consistent with the models' intended use. The model uses this pressure as the initial pressure at a particular elevation in the reservoir. The key word is "initial." As mentioned above, BRAGFLO calculates the magnitude and extent of the depressurized zone as a function of time. The initial time is assumed to be the time of excavation so that there is no depressurization due to the presence of the excavation. The data, of course, are taken some time after excavation.

Reason 5: The data are not consistent with our (PA) current conceptual model assumption that the Salado and other materials are homogeneous and consist of a network of interconnected pore space. Many of the data fall below their hydrostatic pressure values at the location of measurement. Assume for the moment that the low pressures (as low as 1.1 MPa) that were measured were not influenced by the presence of the excavation and that no leakage through the equipment or unseen fractures occurred. This suggests an alternative conceptual model for the Salado: one in which isolated pockets are separated by impermeable material or by material of nonconnected porosity. While our numerical models can handle this type of conceptual model, (1) some mechanism should be postulated for the formation of low-pressure

pockets in the deformable halite, (2) additional data probably should be collected to support this alternate conceptual model, and (3) these pockets should be quantified with respect to properties as well as location and spatial extent. As discussed above, when alternative conceptual models are well supported in the documented technical basis, the PA approach for including conceptual model uncertainty is to perform independent Monte Carlo simulations, compare CCDFs, ceteris paribus, then make a judgment on whether more than one conceptual model needs to be included in later CCDF construction.

2. Permeability

Two distributions are provided: one for the halite, which has a range of 1.0E-24 to 1.0E-17 and one for the anhydrite, which has a range of 1.0E-24 to 3.2E-17. For this year's calculations, PA will use instead a range of 2.0E-22 to 1.4E-19 for intact halite and 8.5E-21 to 1.8E-18 for intact anhydrite. The PA ranges are based on the data of Beauheim, Memo, June 14, 1991. In determining the PA distributions, the two values (one for each material) that are believed to be in the DRZ, are excluded. The support of PA distributions are $\pm 2.33\sigma$ about the mean of the remaining data. The following arguments support the position for not using the distributions of Gorham, July 2, 1991.

Reason 1: The support of the permeability distributions reported in Gorham, Memo, July 2, 1991, are artificially broad for reasons outlined in Howarth, Memo, June 13, 1991. In essence, the data of Howarth, June 13, 1991, were calculated using properties of a "test zone fluid" and not brine. In addition, the values are based on the assumption of a rigid matrix as opposed to the "poroelastic" assumption currently used in the standard model for determining permeability from test data by Division 6344. Both of these factors can significantly affect the calculated permeabilities and at the very least raise questions as to their appropriateness for PA calculations. In Howarth, June 13, 1991, it is estimated that the assumptions used in determining these permeabilities may be in error by 1/2 to 2 orders of magnitude.

Reason 2: The distributions as provided are not consistent with the current conceptual model. Conceptually, the anhydrite layers are thought to be the major flow paths between the "far-field" and the repository while the halite is believed to be the more impermeable material. Sampling on Gorham, July 2, 1991 distributions resulted in the halite being more permeable than the anhydrite in nearly 25% of the vectors. Again, if different conceptual models are postulated, independent and internally consistent analyses should be performed by PA and appropriate uncertainty included later. PA can do this if the more permeable halite and tighter anhydrite is a viable alternative conceptual model.

Reason 3: While the existence of a DRZ is apparently the subject of some debate, there is still some evidence that may support the existence of a DRZ. PA models are capable of differentiating a DRZ

from intact material. Beauheim, Memo, June 14, 1991 clearly states that the high permeability measurements for halite and anhydrite are representative of a DRZ. The existence or not of the DRZ could also be analyzed as conceptual model uncertainty. PA believes that this approach is preferred over identifying near-excavation permeability measurements with estimates of far-field permeabilities.

3. Specific Storage

Specific storage of the halite and anhydrite is not sampled during this year's PA calculations. The value of specific storage selected for the calculations is the upper end of the range in specific storage values suggested in Beauheim, Memo, June 14, 1991, for the halite and anhydrite materials. The upper end value of the Gorham, July 2, 1991 range was not selected because the formation compressibility used by PA models and calculated from the specific storage would become negative for some combinations of porosity and fluid compressibility. A negative formation compressibility is contrary to our conceptual model of the matrix response to pore pressure changes in the halite and anhydrite. Current PA understanding is that matrix porosity increases with increasing pore pressure. Negative rock compressibility reverses this behavior.

Mendenhall and Butcher, June 1, 1991

Date: 6/1/91
To: R. P. Rechard (6342)
From: F. T. Mendenhall (6345) and B. M. Butcher
Subject: Disposal room porosity and permeability values for use in the 1991 room performance assessment calculations

date: June 1, 1991

to: R.P. Rechard

F. T. Mendenhall B. M. Butcher

from: F.T. Mendenhall, 6345 and B.M. Butcher

subject: Disposal room porosity and permeability values for use in the 1991 room performance assessment calculations

The following information has been prepared as input for material property value distribution for the 1991 performance assessment. The approach used for determining the properties for this years calculation differs significantly from last years information because of the of gas in both the disposal room model and the use of two phase fluid flow in modeling the room in the performance assessment calculations. **All values in this memorandum refer to the values for a single disposal room.**

In the case where it is assumed no gas is generated (total gas potential of less than 1.4×10^6 moles is assumed to be the same as no gas generation), the recommended distributions of permeability and porosity are the same as recommended last year.[1] For the cases where the expected gas generated is more than 1.4×10^6 moles, the recommended porosity (50% probability) can be defined from:

(Eq 1)

$$\phi_{(Prob=50\%)} = \frac{1}{1 + \frac{P \cdot V_s}{N_{Total} \cdot R \cdot T}}$$

Where

ϕ=*porosity*
P=14.8×10^6 *Pa* — lithostatic
V_s=1330 M^3
R=8.23 $\frac{M^3\text{-}Pa}{g\text{-}mole\text{-}K}$
T=300*K*
N_{Total}=*Total Moles Gas*

N_{Total} is the total potential number of moles of gas contained in a disposal room. This is determined by the amount and type of waste in a room as sampled in your performance assessment model. Note that the porosity is a long term equilibrium value based on the ideal gas law and assumes that the final pressure in a room will be the lithostatic pressure of the overburden. The ideal gas law is expected to be accurate at lithostatic pressure (14.8 MPa). If your

code allows a significant amount of gas to leak out of the disposal room, we recommend that you compute the amount of moles of gas in the room at a point in time three times after all gas generation has stopped, e.g. if the total gas generation stops at 700 years, determine the number of moles in the room at 2100 years and used that value, N_{3*tend}, instead of the total potential amount of gas in the room. This should allow some influence of gas migration and leakage to be accounted for in your simulations. Again if N_{Total} or if N_{3*tend} are less than $1.4x10^6$ moles the porosity and permeability ranges revert to those given last year.

Having defined the porosity for the 50% probability level, the 10% probability level remains at 0.15 as it was last year. The lowest the porosity ever expected would be the porosity of the host halite. We see no reason to change the median value of 0.01 or range of the porosity,(.001 - .03), of the host halite from those defined last year in Table II-2 of the Data Used in Preliminary Performance Assessment of the Waste Isolation Pilot Plant (1990), SAND89-2408 by Rob P. Rechard, et.al..

Porosity at the 90% probability level would be the value determined in Equation 1 by exchanging N_{Total} with $2xN_{Total}$ (or $2xN_{3*tend}$ if that was the value used). The value of twice the base line value was selected because for corrosion the most aggressive reaction in the list of potential reactions in the DSEIS report will generate two moles of hydrogen for each mole of iron and iron corrosion has the maximum gas production potential in the waste inventory.

The large range on gas generation potentials and, hence, the porosity is expected to narrow as better information regarding gas generation becomes available from laboratory and bin scale tests.

Similarly, the permeability recommendations remain unchanged from last year in the case where no gas generation, (less than $1.4x10^6$ moles of gas), is expected. Also, as you are sampling on phi if the average room porosity is less than 0.15 , then again you should use the permeability values as determined last year.

However, when significant gas occurs and in the sampling process the room porosity exceed 0.15, the recommended permeability should be determined by averaging the expected components of materials in the room. Since the composite flow is likely to be dominated by the flow of the most permeable member, a harmonic averaging process seems most appropriate. For example, let K_b, K_c, K_m, and K_s represent the permeabilities of the backfill, combustible waste, metallic waste, and sludges respectively. Furthermore, define the following values of R as

$$V_b K_b = R1$$
$$V_c K_c = R2$$
$$V_m K_m = R3$$
$$V_s K_s = R4$$

with V_b, V_c, V_m, and V_s representing the per cent volume of the backfill, combustible waste, metallic waste, and sludges respectively. Then the expected room average permeability would be defined as

$$R_{ave} = \frac{1}{\frac{1}{R1} + \frac{1}{R2} + \frac{1}{R3} + \frac{1}{R4}}$$

$$K_{ave} = \frac{R_{ave}}{Total\ Initial\ Volume}$$

The values of the individual components of permeability should be determined from the average room porosity in the following fashion.

$$K_i = (K_0) \sqrt[3]{\frac{\phi}{\phi_0}}\ Meters^2$$

Where the values of K_0 and phi_0 are given in Table 1 for the various room components. Also note, that as you are sampling on room porosity, phi, you will automatically be sampling on the room permeability.

Component	K_0 m^2	ϕ_0
Backfill	10^{-21}	0.05
Combustibles	1.7×10^{-14}	0.136
Metallic	5×10^{-13}	0.4
Sludges	1.2×10^{-16}	.113

Table 1

Caveat

This averaging scheme for the permeability is based on the assumption of a significant amount of metallic waste, nominally 30-40%, uniformly distributed throughout the disposal room. That being the case we would expect the permeability of the metallic waste to dominate the flow though the room. If these conditions are not true, that is if the metallic waste is less than 10% of room volume or if the waste is localized in one section of the room, the average technique suggested here is not appropriate and another scheme will have to be developed.

1.B.M. Butcher and A.R. Lappin, July 24, 1990, "Disposal room porosity and permeability values for disposal room performance assessment," Memorandum of Record to M.G. Marietta.

Siegel, July 14, 1989

Date: 7/14/89
To: P. Davies (6331) and A. R. Lappin (6331)
From: M. D. Siegel
Subject: Supplementary Information Concerning Radionuclide Retardation

Date: July 14, 1989

To: P. Davies, 6331
A. R. Lappin, 6331

From: M. D. Siegel

Subject: Supplementary Information Concerning Radionuclide Retardation

The purpose of this memo is to provide supplementary information supporting the choice of distribution coefficients (K_d's) for lead and diffusion coefficients for actinides for transport calculations in the FSEIS.

DISTRIBUTION COEFFICIENTS FOR LEAD

A preliminary literature review in support of the Draft Supplemental Environmental Impact Statement (DSEIS) failed to locate lead sorption data for conditions relevant to the WIPP site. The distribution coefficients (K_d's) for lead used in the transport calculations described in Lappin et al (1989) were based on the assumption that the chemical behavior of lead was similar to that of radium. Available data suggest that radium will sorb onto clays which are similar to those identified within the matrix and lining fractures in the Culebra Dolomite. The same data indicate that the degree of sorption is dependent upon the solution composition. For example, high concentrations of competing cations such as calcium will inhibit the uptake of radium onto model clays such as kaolinite.

Based on the above information, values of 100, 10 and 5 ml/gm were chosen to represent the sorption of radium and lead onto clays in the Culebra. These K_d values correspond to sorption in dilute to moderately saline Culebra groundwaters (Case I), more saline groundwaters (Case IIA) and solutions with high contents of salts and organic ligands (Cases IIB, IIC, IID) respectively. Retardation factors for the bulk matrix were calculated using the above K_d values and a utilization factor of 0.01 to account for the occurrence of the clay as a trace constituent in the dolomite matrix.

Recently, a more extensive literature review has revealed studies of lead sorption that provide some support for the above K_d values. Hem (1976) developed an ion exchange model for the uptake of lead by a simple aluminosilicate (halloysite) in river and lake waters. The model has been partially validated by comparison to experimental data in dilute (ionic strength < 0.02 M) solutions. The model predicts that in systems of moderate concentrations of the substrate (cation exchange capacity = 10^{-3} to 10^{-5} equivalents/liter solution), 60 -100% of aqueous lead will be removed from solution by ion exchange at pH 7. At pH 9, 80% of the aqueous lead will be removed when the CEC is 10^{-3} equivalents/liter but that at low concentrations of the substrate (CEC = 10^{-5} equivalents/liter) little lead is adsorbed.

Hem's model cannot be used to quantitatively assess the effect of changes in solution composition upon the K_d. The model predicts that in systems with appreciable sodium and/or chloride concentrations (> 0.1 M), very little lead adsorbs and the K_d would be close to zero. However, the model only considers sorption of Pb^{+2} and does not include the $PbCO_3$ complex which may be adsorbed much more strongly. (Bilinsky and Stumm, 1973). In addition, it is important to note that the predictions about lead sorption at the higher ionic strengths are made for conditions that fall outside the ranges of experimental conditions used to formulate the ion exchange model. In other words, they were in no way validated against experimental data. It is also important to note that even at low ionic strengths, under conditions wherein Pb-Na exchange was predicted to dominate the lead uptake, the ion exchange model underpredicted the extent of sorption by factors of 30 to 200%.

A number of other studies indicate that lead is strongly sorbed by simple oxides such as amorphous iron oxyhydroxide ($am\text{-}Fe(OH)_3$), goethite, alumina ($\gamma\text{-}Al_2O_3$) and silica ($\alpha\text{-}SiO_2$) (Davis and Leckie, 1978; Leckie et al., 1980; Hayes and Leckie; 1986). Hayes and Leckie (1986) formulated a surface complexation model (SCM) to describe the sorption of lead by goethite. The model was validated over a wide range of ionic strengths (0.01 to

1.0 M $NaNO_3$) and lead concentrations (2 to 30 mM). The experimental data show that lead is quantitatively removed from solution by sorption onto goethite in the pH range 6 - 7. These data cannot be applied directly to the WIPP, however, because no data were obtained at pH greater that 7.0, or in the presence of chloride or carbonate.

The data of Hayes and Leckie (1986) show that the extent of lead sorption is not affected appreciably by changes in ionic strength over the range 0.01 to 1.0 M $NaNO_3$. The authors show that this type of behavior is consistent with the formation of an inner sphere surface complex by lead during sorption. This kind of complex does not compete with the outer sphere complexes formed by sodium. The surface complexation model of Hayes and Leckie probably more accurately predicts lead sorption at the WIPP than does the ion exchange model of Hem (1976). This is because the former was formulated from data taken over a wider range of solution conditions. In fact, the model of Hayes and Leckie suggests that the uptake of lead by surface hydrolysis sites is not adequately represented by an ion exchange model because the two "exchanging" cations (Pb-Na) do not occupy or compete for the same type of sorption site.

If the properties of the surface hydrolysis sites on goethite are similar to those of clays, then the sorption of lead onto goethite provides a useful analog for sorption onto clays. If we assume that the Culebra has a grain density of 2.5 gm/cc, a porosity of 10%, and a clay content of 1% by weight, then a K_d of 100 ml/gm for pure clay (DSEIS Case I) corresponds to sorption of 75% of available lead onto the bulk matrix.[1] This

---

1. The relationship between K_d and percent adsorbed is:

% adsorbed = 100% x $K_d/(Y+K_d)$

(Footnote continues on next page)

may be a reasonable estimate for lead sorption in the Culebra groundwaters in Hydrochemical Facies Zones B and C (Siegel et al., 1989). The data presented above suggest that the extent of lead sorption will be lower in saline waters in the presence of complexing ligands. For such waters (Case II), the K_d's of 5 to 10 ml/gm for pure clay (corresponding to 13% to 23 % sorption onto the bulk matrix) may be reasonable, however this estimate is highly uncertain.

The above discussion demonstrates the large uncertainties associated with the choice of any single K_d value to represent sorption of lead at the WIPP. The data do not suggest that the K_d will be zero in the Culebra. There is theoretical and experimental evidence to suggest that some sorption of lead will occur in dilute, near-neutral groundwaters and that less lead will be sorbed in saline, organic-rich waters. However, the available data should not be considered adequate to predict the K_d values for use in the final performance assessment.

(Footnote continued from previous page)

where Y = solution to substrate ratio of the system in ml/gm.

Y = 33 ml/gm for batch experiments of Hayes and Leckie (1986).

For a porous matrix:

$$Y = \frac{\phi}{(1-\phi)\rho_s \psi}$$

Y = 0.17 ml/gm clay for Culebra assuming matrix porosity (ϕ) of 10%, density (ρ_s) of 2.5 gm/cc, and 1% by weight clay in the bulk matrix (ψ) is accessible to the ground water.

Siegel, June 25, 1991

Date: 6/25/91
To: K. Trauth (6342)
From: M. D. Siegel
Subject: K_d Values for Ra and Pb

Date: June 25, 1991

To: K. Trauth, 6342

From: M. D. Siegel, 6315

Subject: K_d values for Ra and Pb

Suggested Distribution for Case II (Saline Waters)

Percentile	K_d for Ra and Pb (matrix)	K_d for Ra and Pb (fracture)
100	0.3	30
75	0.23	23
50	0.15	15
25	0.07	7
0	0	0

Justification for Chosen Values:

I have assumed that Pb and Ra sorption will be controlled by the amount of clay in the matrix (1%) and fracture-filling clay (100%) (note the fractures are assumed to be 50% filled by clays in the calculation of the retardation factor.). The matrix K_d's are obtained from the clay K_d's by multiplying by a utilization factor of 0.01 as discussed in SAND89-0462. I suggested using the same values for Ra and Pb based a suggestions of Tien et al (1983) as discussed in that report. The maximum values are based on Tien et al (1983) as cited in Table 3-15 of SAND89-0462. Radium sorption has been studied by Riese (1983) and indicated that sorption will be very low in saline waters. (see SAND89-0462 for discussion and references). Attached is a memo that I wrote for P. Davies for the FSEIS discussing sorption data for lead. (I can provide the cited references if you need them.) The memo indicates that although one can wave one's arms and talk about chemical behaviour in general terms, attempts to provide meaningful probability distributions for K_d's of lead and radium are hampered by the paucity of experimental data in relevant chemical systems.

cc. (w/o encl.)

6315 F. B. Nimick
6344 E. D. Gorham

APPENDIX B:
WELL LOCATION DATA
AND
ELEVATIONS OF STRATIGRAPHIC LAYERS NEAR WIPP

Table B.1. Location of Wells used by WIPP (Universal Transverse Mercator [UTM], State Plan Coordinates [stpln], and Survey Sections [township, range and section])

	Well ID	x-UTM	y-UTM	x-STPLN	y-STPLN	Township	Range	Section	Source
2	AEC7	621117	3589387	691810	523142	21	32	31	Mercer, 1983, Table 1
3	AEC8	617522	3586435	679945	513555	22	31	11	Mercer, 1983, Table 1
4	B25	611695	3580609	660759	494504	22	31	20	Mercer, 1983, Table 1
5	CABIN1	613191	3578049	665559	486111	23	31	5	Gonzales, 1989, Tables 3-6 and 3-7
6	DH207	613634	3581973	667074	498589	0	0	0	Krieg, 1984, Table I
7	DH211	613637	3581784	667082	497966	0	0	0	Krieg, 1984, Table I
8	DH215	613634	3581588	667072	497326	0	0	0	Krieg, 1984, Table I
9	DH219	613636	3581448	667081	496864	0	0	0	Krieg, 1984, Table I
10	DH223	613634	3581247	667073	496207	0	0	0	Krieg, 1984, Table I
11	DH227	613632	3581071	667066	495630	0	0	0	Krieg, 1984, Table I
12	DH77	613476	3582573	666554	500556	0	0	0	Krieg, 1984, Table I
13	DO201	613581	3582062	666900	498880	0	0	0	Krieg, 1984, Table I
14	DO203	613630	3582376	667059	499910	0	0	0	Krieg, 1984, Table I
15	DO205	613587	3582616	667066	500696	0	0	0	Krieg, 1984, Table I
16	DO45	613632	3582263	667066	499540	0	0	0	Krieg, 1984, Table I
17	DO52	613586	3582231	666915	499432	0	0	0	Krieg, 1984, Table I
18	DO56	613587	3582375	666919	499907	0	0	0	Krieg, 1984, Table I
19	DO63	613587	3582524	666919	500396	0	0	0	Krieg, 1984, Table I
20	DO67	613516	3582572	666687	500551	0	0	0	Krieg, 1984, Table I
21	DO88	613435	3582572	666421	500551	0	0	0	Krieg, 1984, Table I
22	DO91	613395	3582575	666288	500561	0	0	0	Krieg, 1984, Table I
23	DOE1	615203	3580333	672206	493563	22	31	28	Gonzales, 1989, Tables 3-6 and 3-7
24	DOE2	613683	3585294	667317	509876	22	31	8	Gonzales, 1989, Tables 3-6 and 3-7
25	ENGLE	614953	3567454	671122	451297	24	31	4	Gonzales, 1989, Tables 3-6 and 3-7
26	ERDA10	606684	3570523	644057	461534	23	30	34	Mercer, 1983, Table 1
27	ERDA6	618226	3589011	682292	521975	21	31	35	Mercer, 1983, Table 1
28	ERDA9	613697	3581958	667297	498929	22	31	20	Mercer, 1983, Table 1
29	FFG_002	627231	3608400	712258	585415	20	33	3	Richey, 1989, Table 2
30	FFG_004	622022	3605526	695095	576082	20	33	7	Richey, 1989, Table 2
31	FFG_005	627356	3605486	712599	575853	20	33	10	Richey, 1989, Table 2
32	FFG_006	627658	3605587	713589	576183	20	33	11	Richey, 1989, Table 2
33	FFG_007	627758	3604682	713919	573213	20	33	14	Richey, 1989, Table 2
34	FFG_009	627959	3604782	714579	573543	20	33	14	Richey, 1989, Table 2
35	FFG_011	627658	3605184	713589	574863	20	33	14	Richey, 1989, Table 2
36	FFG_012	627255	3605184	712269	574863	20	33	15	Richey, 1989, Table 2
37	FFG_013	625249	3605163	705684	574827	20	33	16	Richey, 1989, Table 2
38	FFG_014	621225	3604704	692478	573420	20	33	18	Richey, 1989, Table 2
39	FFG_016	627303	3602758	712361	566901	20	33	22	Richey, 1989, Table 2

Table B.1. Location of Wells used by WIPP (Universal Transverse Mercator [UTM], State Plan Coordinates [stpln], and Survey Sections [township, range and section])

	Well ID	x-UTM	y-UTM	x-STPLN	y-STPLN	Township	Range	Section	Source
1	FFG_017	628494	3603697	716300	569948	20	33	23	Richey, 1989, Table 2
2	FFG_018	630636	3602305	723296	565346	20	33	24	Richey, 1989, Table 2
3	FFG_019	627720	3600778	713695	560402	20	33	26	Richey, 1989, Table 2
4	FFG_020	621672	3601468	693880	562799	20	33	30	Richey, 1989, Table 2
5	FFG_023	633058	3599616	731178	556481	20	33	33	Richey, 1989, Table 2
6	FFG_024	635469	3599257	739089	555233	20	33	34	Richey, 1989, Table 2
7	FFG_025	628538	3600381	716379	559068	20	33	35	Richey, 1989, Table 2
8	FFG_026	628122	3600375	715015	559082	20	33	35	Richey, 1989, Table 2
9	FFG_027	627820	3600074	714025	558092	20	33	35	Richey, 1989, Table 2
10	FFG_039	616468	3606754	676902	580244	20	32	10	Richey, 1989, Table 2
11	FFG_040	620041	3603892	688561	570786	20	32	13	Richey, 1989, Table 2
12	FFG_041	616805	3604246	677942	572014	20	32	15	Richey, 1989, Table 2
13	FFG_042	615263	3604535	672914	572994	20	32	16	Richey, 1989, Table 2
14	FFG_043	614824	3602618	671406	566704	20	32	21	Richey, 1989, Table 2
15	FFG_044	618435	3602658	683256	566770	20	32	23	Richey, 1989, Table 2
16	FFG_105	609126	3590258	652461	526265	21	30	25	Richey, 1989, Table 2
17	FFG_106	607630	3591218	647587	529450	21	30	26	Richey, 1989, Table 2
18	FFG_107	607832	3590109	648217	525810	21	30	26	Richey, 1989, Table 2
19	FFG_108	610586	3589854	657254	524908	21	31	31	Richey, 1989, Table 2
20	FFG_109	612822	3589796	664589	524686	21	31	32	Richey, 1989, Table 2
21	FFG_110	613636	3588341	667229	519875	21	31	32	Richey, 1989, Table 2
22	FFG_111	616209	3589857	675705	524786	21	31	34	Richey, 1989, Table 2
23	FFG_112	615312	3588335	672729	519825	21	31	34	Richey, 1989, Table 2
24	FFG_113	615319	3589869	672784	524858	21	31	34	Richey, 1989, Table 2
25	FFG_114	609458	3586996	653485	515558	22	30	1	Richey, 1989, Table 2
26	FFG_115	608243	3586900	649498	515244	22	30	2	Richey, 1989, Table 2
27	FFG_116	606902	3588008	645132	519179	22	30	3	Richey, 1989, Table 2
28	FFG_117	607132	3587086	645854	515889	22	30	3	Richey, 1989, Table 2
29	FFG_119	604055	3585149	635724	509600	22	30	9	Richey, 1989, Table 2
30	FFG_120	604750	3586261	638038	513251	22	30	9	Richey, 1989, Table 2
31	FFG_121	604134	3585930	636016	512165	22	30	9	Richey, 1989, Table 2
32	FFG_122	604165	3585505	636083	510770	22	30	9	Richey, 1989, Table 2
33	FFG_123	606439	3586110	643580	512686	22	30	10	Richey, 1989, Table 2
34	FFG_124	608252	3586096	649528	512608	22	30	11	Richey, 1989, Table 2
35	FFG_125	607631	3585457	647458	510544	22	30	11	Richey, 1989, Table 2
36	FFG_126	609341	3584606	653068	507720	22	30	13	Richey, 1989, Table 2
37	FFG_127	608226	3583523	649376	504163	22	30	14	Richey, 1989, Table 2
38	FFG_128	605614	3581894	640772	498885	22	30	21	Richey, 1989, Table 2

Table B.1. Location of Wells used by WIPP (Universal Transverse Mercator [UTM], State Plan Coordinates [stpln], and Survey Sections [township, range and section])

	Well ID	x-UTM	y-UTM	x-STPLN	y-STPLN	Township	Range	Section	Source
1	FFG_129	604814	3583050	638181	502679	22	30	21	Richey, 1989, Table 2
2	FFG_130	604412	3582244	636828	500068	22	30	21	Richey, 1989, Table 2
3	FFG_132	606479	3581068	643582	496139	22	30	27	Richey, 1989, Table 2
4	FFG_133	606462	3580266	643522	493544	22	30	27	Richey, 1989, Table 2
5	FFG_134	605663	3580407	640899	494006	22	30	27	Richey, 1989, Table 2
6	FFG_135	607211	3580978	645983	495845	22	30	27	Richey, 1989, Table 2
7	FFG_136	609279	3579410	652734	490667	22	30	36	Richey, 1989, Table 2
8	FFG_137	609955	3578869	654952	488858	22	30	36	Richey, 1989, Table 2
9	FFG_138	610827	3587071	657978	515773	22	31	6	Richey, 1989, Table 2
10	FFG_139	610665	3587722	657478	517912	22	31	6	Richey, 1989, Table 2
11	FFG_140	613648	3585123	667200	509316	22	31	8	Richey, 1989, Table 2
12	FFG_141	612120	3585114	662187	509317	22	31	8	Richey, 1989, Table 2
13	FFG_142	615288	3586667	672617	514350	22	31	9	Richey, 1989, Table 2
14	FFG_143	616006	3579286	674808	490129	22	31	34	Richey, 1989, Table 2
15	FFG_144	599879	3577828	621856	485641	23	29	1	Richey, 1989, Table 2
16	FFG_145	599320	3577132	620020	483389	23	29	1	Richey, 1989, Table 2
17	FFG_146	600363	3578186	623476	486818	23	29	1	Richey, 1989, Table 2
18	FFG_147	595499	3578188	607513	486922	23	29	4	Richey, 1989, Table 2
19	FFG_148	600569	3576193	624120	480278	23	29	12	Richey, 1989, Table 2
20	FFG_149	600707	3574718	624539	475434	23	29	13	Richey, 1989, Table 2
21	FFG_155	596597	3570664	610951	462232	23	29	27	Richey, 1989, Table 2
22	FFG_156	595692	3570883	607981	462952	23	29	28	Richey, 1989, Table 2
23	FFG_157	599212	3569453	619500	458190	23	29	35	Richey, 1989, Table 2
24	FFG_158	600510	3569436	623761	458104	23	29	36	Richey, 1989, Table 2
25	FFG_159	609539	3578101	653588	486370	23	30	1	Richey, 1989, Table 2
26	FFG_160	610084	3577670	655343	484923	23	30	1	Richey, 1989, Table 2
27	FFG_161	607676	3577068	647439	483015	23	30	2	Richey, 1989, Table 2
28	FFG_162	607342	3578605	646376	488059	23	30	2	Richey, 1989, Table 2
29	FFG_163	608127	3577850	648955	485549	23	30	2	Richey, 1989, Table 2
30	FFG_164	602541	3574598	630556	475010	23	30	17	Richey, 1989, Table 2
31	FFG_165	601827	3573070	628182	469995	23	30	19	Richey, 1989, Table 2
32	FFG_166	609182	3573205	652317	470305	23	30	24	Richey, 1989, Table 2
33	FFG_167	609012	3570846	651726	462566	23	30	26	Richey, 1989, Table 2
34	FFG_168	604202	3570581	635911	461795	23	30	28	Richey, 1989, Table 2
35	FFG_169	604034	3572065	635389	466662	23	30	29	Richey, 1989, Table 2
36	FFG_170	601537	3572060	627194	466716	23	30	30	Richey, 1989, Table 2
37	FFG_171	601959	3569718	628551	458995	23	30	31	Richey, 1989, Table 2
38	FFG_172	603366	3570098	633169	460209	23	30	32	Richey, 1989, Table 2

Table B.1. Location of Wells used by WIPP (Universal Transverse Mercator [UTM], State Plan Coordinates [stpln], and Survey Sections [township, range and section])

	Well ID	x-UTM	y-UTM	x-STPLN	y-STPLN	Township	Range	Section	Source
1	FFG_173	609960	3569937	654805	459582	23	30	36	Richey, 1989, Table 2
2	FFG_177	591351	3563822	593606	439877	24	29	19	Richey, 1989, Table 2
3	FFG_179	593084	3561340	599224	431698	24	29	29	Richey, 1989, Table 2
4	FFG_180	607488	3567427	646628	451374	24	30	2	Richey, 1989, Table 2
5	FFG_181	604028	3568585	635304	455245	24	30	5	Richey, 1989, Table 2
6	FFG_182	601542	3568281	627146	454314	24	30	6	Richey, 1989, Table 2
7	FFG_183	605177	3566738	639041	449147	24	30	9	Richey, 1989, Table 2
8	FFG_184	607564	3565857	646845	446225	24	30	11	Richey, 1989, Table 2
9	FFG_185	605866	3565683	641274	445686	24	30	15	Richey, 1989, Table 2
10	FFG_186	605016	3565698	638484	445736	24	30	16	Richey, 1989, Table 2
11	FFG_188	602948	3564040	631660	440361	24	30	20	Richey, 1989, Table 2
12	FFG_189	608405	3563679	649573	439043	24	30	23	Richey, 1989, Table 2
13	FFG_190	607685	3562746	647176	436015	24	30	23	Richey, 1989, Table 2
14	FFG_191	609337	3561151	652564	430748	24	30	25	Richey, 1989, Table 2
15	FFG_192	607401	3562442	646246	435019	24	30	27	Richey, 1989, Table 2
16	FFG_194	617718	3568422	680232	454446	24	31	2	Richey, 1989, Table 2
17	FFG_195	616941	3567615	677649	451793	24	31	3	Richey, 1989, Table 2
18	FFG_196	615316	3568812	672350	455759	24	31	4	Richey, 1989, Table 2
19	FFG_197	614612	3568483	670036	454709	24	31	4	Richey, 1989, Table 2
20	FFG_198	613807	3568888	667396	456038	24	31	5	Richey, 1989, Table 2
21	FFG_199	611628	3568640	660244	455257	24	31	6	Richey, 1989, Table 2
22	FFG_200	611273	3568414	659080	454549	24	31	6	Richey, 1989, Table 2
23	FFG_201	612154	3565951	661905	446431	24	31	7	Richey, 1989, Table 2
24	FFG_202	618692	3566653	683393	448607	24	31	11	Richey, 1989, Table 2
25	FFG_203	618143	3567223	681591	450478	24	31	11	Richey, 1989, Table 2
26	FFG_204	619790	3564834	686932	442604	24	31	13	Richey, 1989, Table 2
27	FFG_205	613734	3565566	667090	445140	24	31	17	Richey, 1989, Table 2
28	FFG_206	612171	3564340	661929	441145	24	31	18	Richey, 1989, Table 2
29	FFG_207	613776	3563957	667198	439860	24	31	20	Richey, 1989, Table 2
30	FFG_208	612992	3562725	664590	435847	24	31	20	Richey, 1989, Table 2
31	FFG_209	615380	3563980	672461	439901	24	31	21	Richey, 1989, Table 2
32	FFG_210	614199	3562745	668548	435879	24	31	21	Richey, 1989, Table 2
33	FFG_212	619811	3562825	686967	436012	24	31	24	Richey, 1989, Table 2
34	FFG_213	614915	3560252	670865	427664	24	31	33	Richey, 1989, Table 2
35	FFG_214	617438	3559994	679114	426785	24	31	35	Richey, 1989, Table 2
36	FFG_215	610576	3559150	656597	424152	25	30	1	Richey, 1989, Table 2
37	FFG_216	604853	3558664	637816	422688	25	30	4	Richey, 1989, Table 2
38	FFG_217	617694	3559360	679954	424705	25	31	2	Richey, 1989, Table 2

Table B.1. Location of Wells used by WIPP (Universal Transverse Mercator [UTM], State Plan Coordinates [stpln], and Survey Sections [township, range and section])

	Well ID	x-UTM	y-UTM	x-STPLN	y-STPLN	Township	Range	Section	Source
1	FFG_218	618235	3558795	681730	422820	25	31	2	Richey, 1989, Table 2
2	FFG_219	616649	3557179	676493	417552	25	31	10	Richey, 1989, Table 2
3	FFG_220	619057	3557584	684393	418848	25	31	12	Richey, 1989, Table 2
4	FFG_221	616028	3555913	674422	413427	25	31	15	Richey, 1989, Table 2
5	FFG_222	614248	3552703	668515	402929	25	31	28	Richey, 1989, Table 2
6	FFG_224	629257	3598870	718704	554099	21	32	1	Richey, 1989, Table 2
7	FFG_225	629076	3597979	718112	551174	21	32	1	Richey, 1989, Table 2
8	FFG_226	628708	3596750	716853	547172	21	32	1	Richey, 1989, Table 2
9	FFG_228	626669	3597926	710210	551066	21	32	2	Richey, 1989, Table 2
10	FFG_229	625894	3596724	707620	547120	21	32	3	Richey, 1989, Table 2
11	FFG_230	625486	3597502	706279	549709	21	32	3	Richey, 1989, Table 2
12	FFG_231	624249	3598303	702273	552336	21	32	4	Richey, 1989, Table 2
13	FFG_232	623880	3597479	701011	549665	21	32	4	Richey, 1989, Table 2
14	FFG_233	623730	3598370	700570	552588	21	32	4	Richey, 1989, Table 2
15	FFG_234	622268	3597867	695720	550968	21	32	5	Richey, 1989, Table 2
16	FFG_235	623075	3597479	698371	549665	21	32	5	Richey, 1989, Table 2
17	FFG_236	620626	3597834	690380	550899	21	32	6	Richey, 1989, Table 2
18	FFG_237	624279	3595893	702319	544429	21	32	9	Richey, 1989, Table 2
19	FFG_238	625894	3595919	707620	544480	21	32	10	Richey, 1989, Table 2
20	FFG_239	627919	3595147	714233	541912	21	32	11	Richey, 1989, Table 2
21	FFG_240	627501	3595945	712893	544532	21	32	11	Richey, 1989, Table 2
22	FFG_241	628322	3595549	715553	543232	21	32	12	Richey, 1989, Table 2
23	FFG_242	623510	3593053	699730	535143	21	32	21	Richey, 1989, Table 2
24	FFG_243	627958	3591122	714296	528704	21	32	26	Richey, 1989, Table 2
25	FFG_244	627169	3589486	711671	523370	21	32	35	Richey, 1989, Table 2
26	FFG_245	634293	3596014	735183	544627	21	33	9	Richey, 1989, Table 2
27	FFG_246	636300	3596435	741767	545977	21	33	11	Richey, 1989, Table 2
28	FFG_247	638785	3593673	749855	536845	21	33	13	Richey, 1989, Table 2
29	FFG_248	638754	3594075	749755	538165	21	33	13	Richey, 1989, Table 2
30	FFG_249	635538	3594033	739201	538094	21	33	15	Richey, 1989, Table 2
31	FFG_250	630707	3593573	723350	536681	21	33	18	Richey, 1989, Table 2
32	FFG_251	639185	3592056	751137	531538	21	33	24	Richey, 1989, Table 2
33	FFG_252	631978	3589148	727420	522161	21	33	32	Richey, 1989, Table 2
34	FFG_253	634373	3589591	735313	523550	21	33	33	Richey, 1989, Table 2
35	FFG_254	634776	3589591	736633	523550	21	33	34	Richey, 1989, Table 2
36	FFG_255	636385	3590012	741913	524900	21	33	35	Richey, 1989, Table 2
37	FFG_264	624541	3575777	702753	478415	23	32	9	Richey, 1989, Table 2
38	FFG_265	626158	3575003	708059	475842	23	32	15	Richey, 1989, Table 2

Table B.1. Location of Wells used by WIPP (Universal Transverse Mercator [UTM], State Plan Coordinates [stpln], and Survey Sections [township, range and section])

	Well ID	x-UTM	y-UTM	x-STPLN	y-STPLN	Township	Range	Section	Source
1	FFG_266	629827	3572644	720033	468035	23	32	24	Richey, 1989, Table 2
2	FFG_267	632644	3570662	729244	461468	23	33	32	Richey, 1989, Table 2
3	FFG_268	636682	3569503	742460	457597	23	33	35	Richey, 1989, Table 2
4	FFG_272	621266	3580141	692103	492804	22	32	31	Richey, 1989, Table 2
5	FFG_273	621714	3576972	693509	482402	23	32	7	Richey, 1989, Table 2
6	FFG_274	627262	3583857	711844	504897	22	32	14	Richey, 1989, Table 2
7	FFG_275	626055	3584259	707884	506217	22	32	15	Richey, 1989, Table 2
8	FFG_276	622836	3584196	697320	506076	22	32	17	Richey, 1989, Table 2
9	FFG_277	621627	3583775	693354	504725	22	32	18	Richey, 1989, Table 2
10	FFG_278	621646	3582157	693382	499416	22	32	19	Richey, 1989, Table 2
11	FFG_279	622836	3582989	697320	502116	22	32	20	Richey, 1989, Table 2
12	FFG_280	625245	3583022	705224	502190	22	32	22	Richey, 1989, Table 2
13	FFG_281	628878	3581872	717114	498350	22	32	25	Richey, 1989, Table 2
14	FFG_283	638822	3588438	749880	519668	22	33	1	Richey, 1989, Table 2
15	FFG_284	633260	3587655	731596	517227	22	33	4	Richey, 1989, Table 2
16	FFG_285	632916	3587152	730466	515577	22	33	5	Richey, 1989, Table 2
17	FFG_286	630045	3585511	721010	510259	22	33	7	Richey, 1989, Table 2
18	FFG_287	630815	3585934	723537	511615	22	33	7	Richey, 1989, Table 2
19	FFG_288	633218	3586749	731456	514257	22	33	9	Richey, 1989, Table 2
20	FFG_289	635668	3584383	739429	506427	22	33	15	Richey, 1989, Table 2
21	FFG_290	631649	3583118	726240	502376	22	33	20	Richey, 1989, Table 2
22	FFG_291	631716	3579091	726360	489157	22	33	32	Richey, 1989, Table 2
23	FFG_292	634513	3580338	735574	493186	22	33	33	Richey, 1989, Table 2
24	FFG_293	635741	3579152	739570	489260	22	33	34	Richey, 1989, Table 2
25	FFG_313	621557	3587797	693224	517925	22	32	6	Richey, 1989, Table 2
26	FFG_314	629670	3583902	719747	504978	22	32	13	Richey, 1989, Table 2
27	FFG_315	626522	3578214	709318	486382	23	32	3	Richey, 1989, Table 2
28	FFG_316	627739	3576635	713279	481164	23	32	11	Richey, 1989, Table 2
29	FFG_317	621734	3574920	693542	475670	23	32	18	Richey, 1989, Table 2
30	FFG_318	622977	3572533	697554	467800	23	32	20	Richey, 1989, Table 2
31	FFG_319	624161	3573735	701471	471749	23	32	21	Richey, 1989, Table 2
32	FFG_320	629107	3572102	717668	466290	23	32	25	Richey, 1989, Table 2
33	FFG_321	628524	3571093	715723	462981	23	32	25	Richey, 1989, Table 2
34	FFG_322	628222	3570892	714733	462321	23	32	26	Richey, 1989, Table 2
35	FFG_323	627420	3570965	712100	462590	23	32	26	Richey, 1989, Table 2
36	FFG_324	624184	3572130	701514	466480	23	32	28	Richey, 1989, Table 2
37	FFG_325	620546	3569268	689509	457154	23	32	31	Richey, 1989, Table 2
38	FFG_326	625008	3570140	704185	459917	23	32	33	Richey, 1989, Table 2

Table B.1. Location of Wells used by WIPP (Universal Transverse Mercator [UTM], State Plan Coordinates [stpln], and Survey Sections [township, range and section])

	Well ID	x-UTM	y-UTM	x-STPLN	y-STPLN	Township	Range	Section	Source
1	FFG_327	626737	3569761	709825	458640	23	32	34	Richey, 1989, Table 2
2	FFG_328	627719	3570289	713083	460341	23	32	35	Richey, 1989, Table 2
3	FFG_329	628625	3570188	716053	460011	23	32	36	Richey, 1989, Table 2
4	FFG_330	629464	3569834	718778	458813	23	32	36	Richey, 1989, Table 2
5	FFG_331	634557	3577522	735655	483942	23	33	4	Richey, 1989, Table 2
6	FFG_332	631443	3577384	725434	483557	23	33	6	Richey, 1989, Table 2
7	FFG_333	630183	3575856	721264	478574	23	33	7	Richey, 1989, Table 2
8	FFG_334	631791	3574262	726509	473313	23	33	17	Richey, 1989, Table 2
9	FFG_335	630204	3574250	721301	473303	23	33	18	Richey, 1989, Table 2
10	FFG_336	630611	3573046	722603	469355	23	33	19	Richey, 1989, Table 2
11	FFG_337	633022	3572674	730519	468066	23	33	20	Richey, 1989, Table 2
12	FFG_338	631435	3570650	725277	461460	23	33	31	Richey, 1989, Table 2
13	FFG_339	637863	3570326	746370	460265	23	33	35	Richey, 1989, Table 2
14	FFG_340	639497	3569942	751700	458973	23	33	36	Richey, 1989, Table 2
15	FFG_361	591407	3608036	594694	584951	20	29	1	Richey, 1989, Table 2
16	FFG_362	588581	3607624	585423	583663	20	29	3	Richey, 1989, Table 2
17	FFG_363	586158	3608022	577470	585038	20	29	4	Richey, 1989, Table 2
18	FFG_364	583878	3605062	569923	575355	20	29	7	Richey, 1989, Table 2
19	FFG_366	588498	3606300	585115	579318	20	29	10	Richey, 1989, Table 2
20	FFG_367	589516	3605699	588421	577345	20	29	11	Richey, 1989, Table 2
21	FFG_370	591027	3604798	593382	574358	20	29	13	Richey, 1989, Table 2
22	FFG_371	591334	3604826	594392	574416	20	29	13	Richey, 1989, Table 2
23	FFG_372	589730	3604102	589095	572070	20	29	14	Richey, 1989, Table 2
24	FFG_373	586192	3604773	577514	574376	20	29	16	Richey, 1989, Table 2
25	FFG_374	585392	3603561	574858	570394	20	29	17	Richey, 1989, Table 2
26	FFG_376	590555	3601690	591768	564155	20	29	25	Richey, 1989, Table 2
27	FFG_381	599172	3599246	619978	555961	20	29	36	Richey, 1989, Table 2
28	FFG_383	601077	3606916	626395	581073	20	30	1	Richey, 1989, Table 2
29	FFG_384	594213	3607648	603902	583643	20	30	5	Richey, 1989, Table 2
30	FFG_385	597883	3602444	615814	566466	20	30	22	Richey, 1989, Table 2
31	FFG_387	595912	3600331	609313	559598	20	30	28	Richey, 1989, Table 2
32	FFG_388	595864	3601219	609189	562513	20	30	28	Richey, 1989, Table 2
33	FFG_389	593453	3599602	601245	557239	20	30	31	Richey, 1989, Table 2
34	FFG_390	595208	3600029	607003	558608	20	30	32	Richey, 1989, Table 2
35	FFG_391	595208	3599627	607003	557288	20	30	32	Richey, 1989, Table 2
36	FFG_392	596612	3599732	611609	557599	20	30	33	Richey, 1989, Table 2
37	FFG_393	606297	3606985	643526	581199	20	31	4	Richey, 1989, Table 2
38	FFG_394	603077	3606946	632959	581140	20	31	6	Richey, 1989, Table 2

Table B.1. Location of Wells used by WIPP (Universal Transverse Mercator [UTM], State Plan Coordinates [stpln], and Survey Sections [township, range and section])

	Well ID	x-UTM	y-UTM	x-STPLN	y-STPLN	Township	Range	Section	Source
1	FFG_395	603098	3605631	632997	576823	20	31	7	Richey, 1989, Table 2
2	FFG_396	603243	3600398	633370	559652	20	31	30	Richey, 1989, Table 2
3	FFG_398	588017	3597286	583323	549759	21	28	2	Richey, 1989, Table 2
4	FFG_399	587111	3597387	580353	550089	21	28	3	Richey, 1989, Table 2
5	FFG_402	590847	3595289	592582	543138	21	28	12	Richey, 1989, Table 2
6	FFG_403	586424	3593240	578030	536512	21	28	15	Richey, 1989, Table 2
7	FFG_404	583988	3592021	570006	532548	21	28	20	Richey, 1989, Table 2
8	FFG_407	583988	3590814	570006	528588	21	28	29	Richey, 1989, Table 2
9	FFG_408	582473	3590320	565002	526999	21	28	30	Richey, 1989, Table 2
10	FFG_411	584828	3588367	572695	520558	21	28	33	Richey, 1989, Table 2
11	FFG_413	588470	3589234	584681	523337	21	28	35	Richey, 1989, Table 2
12	FFG_418	596362	3598010	610756	551972	21	29	3	Richey, 1989, Table 2
13	FFG_419	594776	3597648	605505	550814	21	29	4	Richey, 1989, Table 2
14	FFG_420	594662	3598348	605178	553113	21	29	4	Richey, 1989, Table 2
15	FFG_421	593556	3598412	601548	553321	21	29	5	Richey, 1989, Table 2
16	FFG_422	593958	3598000	602868	551971	21	29	5	Richey, 1989, Table 2
17	FFG_426	592398	3591591	597601	530971	21	29	19	Richey, 1989, Table 2
18	FFG_432	607401	3588903	646769	521852	21	30	35	Richey, 1989, Table 2
19	FFG_433	588569	3588121	584969	519682	22	28	2	Richey, 1989, Table 2
20	FFG_438	618629	3586910	683580	515081	22	31	1	Richey, 1989, Table 2
21	FFG_445	590526	3580760	591228	495462	22	28	25	Richey, 1989, Table 2
22	FFG_453	618415	3578487	682715	487442	23	31	2	Richey, 1989, Table 2
23	FFG_455	618558	3575680	683119	478229	23	31	11	Richey, 1989, Table 2
24	FFG_456	617677	3574462	680195	474264	23	31	14	Richey, 1989, Table 2
25	FFG_457	614456	3574425	669624	474210	23	31	16	Richey, 1989, Table 2
26	FFG_458	615274	3572430	672278	467629	23	31	21	Richey, 1989, Table 2
27	FFG_459	619295	3571652	685468	465012	23	31	25	Richey, 1989, Table 2
28	FFG_462	615699	3571221	673637	463662	23	31	27	Richey, 1989, Table 2
29	FFG_463	612475	3570378	663055	460962	23	31	32	Richey, 1989, Table 2
30	FFG_464	614894	3570416	670997	461022	23	31	33	Richey, 1989, Table 2
31	FFG_465	614090	3569999	668355	459685	23	31	33	Richey, 1989, Table 2
32	FFG_474	628677	3568183	716158	453428	24	32	1	Richey, 1989, Table 2
33	FFG_475	628244	3568580	714774	454733	24	32	2	Richey, 1989, Table 2
34	FFG_476	621409	3568885	692341	455866	24	32	6	Richey, 1989, Table 2
35	FFG_477	626275	3566554	708244	448117	24	32	10	Richey, 1989, Table 2
36	FFG_478	627890	3566569	713543	448132	24	32	11	Richey, 1989, Table 2
37	FFG_479	627468	3566954	712193	449429	24	32	11	Richey, 1989, Table 2
38	FFG_480	628677	3566976	716158	449468	24	32	12	Richey, 1989, Table 2

Table B.1. Location of Wells used by WIPP (Universal Transverse Mercator [UTM], State Plan Coordinates [stpln], and Survey Sections [township, range and section])

	Well ID	x-UTM	y-UTM	x-STPLN	y-STPLN	Township	Range	Section	Source
1	FFG_481	629921	3564597	720180	441628	24	32	13	Richey, 1989, Table 2
2	FFG_482	627482	3565749	712204	445477	24	32	14	Richey, 1989, Table 2
3	FFG_483	625893	3564517	706958	441463	24	32	15	Richey, 1989, Table 2
4	FFG_484	626601	3563741	709281	438885	24	32	22	Richey, 1989, Table 2
5	FFG_485	626323	3563337	708336	437561	24	32	22	Richey, 1989, Table 2
6	FFG_486	627104	3563741	710931	438885	24	32	23	Richey, 1989, Table 2
7	FFG_487	627003	3563842	710601	439215	24	32	23	Richey, 1989, Table 2
8	FFG_488	628618	3564276	715902	440608	24	32	24	Richey, 1989, Table 2
9	FFG_489	629141	3562161	717583	433668	24	32	25	Richey, 1989, Table 2
10	FFG_490	622290	3562046	695099	433421	24	32	29	Richey, 1989, Table 2
11	FFG_491	621485	3562046	692459	433421	24	32	30	Richey, 1989, Table 2
12	FFG_492	625107	3559688	704284	425618	24	32	33	Richey, 1989, Table 2
13	FFG_493	625912	3560090	706924	426938	24	32	34	Richey, 1989, Table 2
14	FFG_494	625912	3559688	706924	425618	24	32	34	Richey, 1989, Table 2
15	FFG_495	627126	3559716	710904	425675	24	32	35	Richey, 1989, Table 2
16	FFG_496	639095	3568735	750380	455013	24	33	1	Richey, 1989, Table 2
17	FFG_497	631494	3566228	725373	446949	24	33	7	Richey, 1989, Table 2
18	FFG_498	631883	3567428	726679	450888	24	33	8	Richey, 1989, Table 2
19	FFG_499	639536	3565513	751762	444438	24	33	13	Richey, 1989, Table 2
20	FFG_500	632702	3565844	729335	445656	24	33	17	Richey, 1989, Table 2
21	FFG_501	632345	3563004	728097	436369	24	33	20	Richey, 1989, Table 2
22	FFG_502	635140	3563849	737302	439075	24	33	22	Richey, 1989, Table 2
23	FFG_503	635586	3561835	738701	432466	24	33	27	Richey, 1989, Table 2
24	FFG_504	632771	3561413	729465	431115	24	33	29	Richey, 1989, Table 2
25	FFG_505	630239	3562683	721189	435349	24	33	30	Richey, 1989, Table 2
26	FFG_506	631576	3560189	725511	427131	24	33	31	Richey, 1989, Table 2
27	FFG_507	639607	3561088	751898	429920	24	33	36	Richey, 1989, Table 2
28	FFG_548	601155	3608819	626682	587316	19	30	36	Richey, 1989, Table 2
29	FFG_552	596378	3554488	609903	409146	25	29	15	Richey, 1989, Table 2
30	FFG_562	614317	3546624	668609	382978	26	31	9	Richey, 1989, Table 2
31	FFG_563	618774	3547092	683237	384417	26	31	11	Richey, 1989, Table 2
32	FFG_568	619132	3541724	684313	366799	26	31	25	Richey, 1989, Table 2
33	FFG_569	619132	3542127	684313	368119	26	31	25	Richey, 1989, Table 2
34	FFG_584	606879	3557091	644432	417458	25	30	10	Richey, 1989, Table 2
35	FFG_585	609769	3557118	653916	417516	25	30	12	Richey, 1989, Table 2
36	FFG_600	608992	3550622	651237	396198	25	30	35	Richey, 1989, Table 2
37	FFG_601	607790	3549783	647256	393477	25	30	35	Richey, 1989, Table 2
38	FFG_602	618235	3558795	681730	422820	25	31	2	Richey, 1989, Table 2

Table B.1. Location of Wells used by WIPP (Universal Transverse Mercator [UTM], State Plan Coordinates [stpln], and Survey Sections [township, range and section])

	Well ID	x-UTM	y-UTM	x-STPLN	y-STPLN	Township	Range	Section	Source
1	FFG_606	618324	3551156	681858	397752	25	31	35	Richey, 1989, Table 2
2	FFG_618	599392	3546376	619633	382460	26	29	11	Richey, 1989, Table 2
3	FFG_638	607809	3548155	647284	388134	26	30	2	Richey, 1989, Table 2
4	FFG_639	606187	3548136	641961	388102	26	30	3	Richey, 1989, Table 2
5	FFG_640	604548	3549331	636618	392062	26	30	4	Richey, 1989, Table 2
6	FFG_643	610657	3546572	656602	382873	26	30	12	Richey, 1989, Table 2
7	FFG_644	605816	3544896	640681	377470	26	30	16	Richey, 1989, Table 2
8	FFG_648	609863	3544129	653961	374890	26	30	24	Richey, 1989, Table 2
9	FFG_685	592502	3586828	597845	515341	22	29	6	Richey, 1989, Table 2
10	FFG_689	626339	3558413	708291	421399	25	32	3	Richey, 1989, Table 2
11	FFG_690	625251	3556776	704687	416062	25	32	9	Richey, 1989, Table 2
12	FFG_691	626238	3557256	707961	417604	25	32	10	Richey, 1989, Table 2
13	FFG_692	627982	3556520	713651	415154	25	32	11	Richey, 1989, Table 2
14	FFG_693	627068	3555594	710652	412151	25	32	14	Richey, 1989, Table 2
15	FFG_694	625965	3554867	706999	409798	25	32	15	Richey, 1989, Table 2
16	FFG_695	625955	3556071	706997	413752	25	32	15	Richey, 1989, Table 2
17	FFG_696	625955	3556134	706997	413957	25	32	15	Richey, 1989, Table 2
18	FFG_697	624748	3555669	703037	412432	25	32	16	Richey, 1989, Table 2
19	FFG_698	620989	3555992	690703	413589	25	32	18	Richey, 1989, Table 2
20	FFG_699	623679	3553534	699465	405455	25	32	20	Richey, 1989, Table 2
21	FFG_700	623679	3553131	699465	404135	25	32	20	Richey, 1989, Table 2
22	FFG_701	625090	3553358	704095	404846	25	32	21	Richey, 1989, Table 2
23	FFG_702	625492	3553761	705415	406166	25	32	22	Richey, 1989, Table 2
24	FFG_703	628006	3554508	713698	408555	25	32	23	Richey, 1989, Table 2
25	FFG_704	625492	3552956	705415	403526	25	32	27	Richey, 1989, Table 2
26	FFG_705	624099	3552123	700810	400825	25	32	28	Richey, 1989, Table 2
27	FFG_706	624300	3552123	701470	400825	25	32	28	Richey, 1989, Table 2
28	FFG_707	623679	3552427	699465	401825	25	32	29	Richey, 1989, Table 2
29	FFG_708	623679	3552930	699465	403475	25	32	29	Richey, 1989, Table 2
30	FFG_709	620746	3550770	689804	396452	25	32	31	Richey, 1989, Table 2
31	FFG_710	622771	3550799	696450	396515	25	32	32	Richey, 1989, Table 2
32	FFG_711	624012	3550012	700490	393900	25	32	33	Richey, 1989, Table 2
33	FFG_712	625263	3550440	704596	395271	25	32	33	Richey, 1989, Table 2
34	FFG_713	624830	3550038	703176	393951	25	32	33	Richey, 1989, Table 2
35	FFG_714	625626	3551242	705819	397905	25	32	34	Richey, 1989, Table 2
36	FFG_715	626840	3551268	709807	397957	25	32	34	Richey, 1989, Table 2
37	FFG_716	638420	3559464	747968	424622	25	33	1	Richey, 1989, Table 2
38	FFG_717	633193	3559403	730818	424522	25	33	5	Richey, 1989, Table 2

Table B.1. Location of Wells used by WIPP (Universal Transverse Mercator [UTM], State Plan Coordinates [stpln], and Survey Sections [township, range and section])

	Well ID	x-UTM	y-UTM	x-STPLN	y-STPLN	Township	Range	Section	Source
1	FFG_718	633234	3556994	730887	416614	25	33	8	Richey, 1989, Table 2
2	FFG_719	636829	3557836	742712	419312	25	33	11	Richey, 1989, Table 2
3	FFG_720	639698	3555152	752066	410438	25	33	13	Richey, 1989, Table 2
4	FFG_721	636045	3555837	740111	412751	25	33	15	Richey, 1989, Table 2
5	FFG_723	630458	3553740	721708	406002	25	33	19	Richey, 1989, Table 2
6	FFG_724	632860	3554578	729624	408686	25	33	20	Richey, 1989, Table 2
7	FFG_725	634859	3554589	736187	408691	25	33	21	Richey, 1989, Table 2
8	FFG_726	636908	3553407	742876	404776	25	33	23	Richey, 1989, Table 2
9	FFG_727	638515	3553426	748148	404806	25	33	24	Richey, 1989, Table 2
10	FFG_728	639741	3551836	752140	399555	25	33	25	Richey, 1989, Table 2
11	FFG_729	636519	3551797	741568	399493	25	33	27	Richey, 1989, Table 2
12	FFG_730	634908	3551777	736280	399460	25	33	28	Richey, 1989, Table 2
13	FFG_731	634882	3552983	736227	403421	25	33	28	Richey, 1989, Table 2
14	FFG_732	632068	3552542	726993	402039	25	33	29	Richey, 1989, Table 2
15	FFG_733	630508	3550122	721809	394129	25	33	31	Richey, 1989, Table 2
16	FFG_734	633325	3550558	731054	395493	25	33	32	Richey, 1989, Table 2
17	FFG_735	638531	3551412	748168	398200	25	33	36	Richey, 1989, Table 2
18	H1	613420	3581687	666391	498039	22	31	29	Mercer, 1983, Table 1
19	H10A	622949	3572457	697463	467561	23	32	20	Gonzales, 1989, Tables 3-6 and 3-7
20	H10B	622975	3572473	697549	467613	23	32	20	Gonzales, 1989, Tables 3-6 and 3-7
21	H10C	622976	3572449	697552	467525	23	32	20	Mercer, 1983, Table 1
22	H11B1	615346	3579130	672647	489617	22	31	33	Gonzales, 1989, Tables 3-6 and 3-7
23	H11B2	615348	3579107	672653	489542	22	31	33	Gonzales, 1989, Tables 3-6 and 3-7
24	H11B3	615367	3579127	672716	489608	22	31	33	Gonzales, 1989, Tables 3-6 and 3-7
25	H11B4	615301	3579131	672501	489620	22	31	33	Gonzales, 1989, Tables 3-6 and 3-7
26	H12	617023	3575452	678079	477535	23	31	15	Gonzales, 1989, Tables 3-6 and 3-7
27	H14	612341	3580354	662815	493697	22	31	29	Gonzales, 1989, Tables 3-6 and 3-7
28	H15	615315	3581859	672606	498572	22	31	28	Gonzales, 1989, Tables 3-6 and 3-7
29	H16	613369	3582212	666231	499726	22	31	20	Gonzales, 1989, Tables 3-6 and 3-7
30	H17	615718	3577513	673837	484304	23	31	3	Gonzales, 1989, Tables 3-6 and 3-7
31	H18	612264	3583166	662621	502926	22	31	20	Gonzales, 1989, Tables 3-6 and 3-7
32	H2A	612663	3581641	663897	497912	22	31	29	Gonzales, 1989, Tables 3-6 and 3-7
33	H2B1	612651	3581651	663860	497943	22	31	29	Gonzales, 1989, Tables 3-6 and 3-7
34	H2B2	612661	3581649	663890	497938	22	31	29	Gonzales, 1989, Tables 3-6 and 3-7
35	H2C	612663	3581662	663904	497992	22	31	29	Mercer, 1983, Table 1
36	H3	613735	3580895	667389	495440	22	31	29	Mercer, 1983, Table 1
37	H3B1	613729	3580895	667377	497440	22	31	29	Gonzales, 1989, Tables 3-6 and 3-7
38	H3B2	613701	3580906	667283	495476	22	31	29	Gonzales, 1989, Tables 3-6 and 3-7

Table B.1. Location of Wells used by WIPP (Universal Transverse Mercator [UTM], State Plan Coordinates [stpln], and Survey Sections [township, range and section])

	Well ID	x-UTM	y-UTM	x-STPLN	y-STPLN	Township	Range	Section	Source
1	H3B3	613705	3580876	667298	495376	22	31	29	Gonzales, 1989, Tables 3-6 and 3-7
2	H3D	613721	3580890	667350	495421	22	31	29	Gonzales, 1989, Tables 3-6 and 3-7
3	H4A	612407	3578469	662993	486962	23	31	5	Gonzales, 1989, Tables 3-6 and 3-7
4	H4B	612380	3578483	662906	487554	23	31	5	Gonzales, 1989, Tables 3-6 and 3-7
5	H4C	612404	3578497	662988	487603	23	31	5	Mercer, 1983, Table 1
6	H5A	616888	3584776	677828	508111	22	31	15	Gonzales, 1989, Tables 3-6 and 3-7
7	H5B	616872	3584801	677777	508194	22	31	15	Gonzales, 1989, Tables 3-6 and 3-7
8	H5C	616900	3584802	677873	508198	22	31	15	Mercer, 1983, Table 1
9	H6A	610580	3584982	657132	508881	22	31	18	Gonzales, 1989, Tables 3-6 and 3-7
10	H6B	610594	3585008	657180	508969	22	31	18	Gonzales, 1989, Tables 3-6 and 3-7
11	H6C	610609	3585027	657231	509066	22	31	18	Mercer, 1983, Table 1
12	H7A	608102	3574670	648790	475132	23	30	14	Gonzales, 1989, Tables 3-6 and 3-7
13	H7B1	608124	3574648	648862	475061	23	30	14	Gonzales, 1989, Tables 3-6 and 3-7
14	H7B2	608111	3574612	648837	474965	23	30	14	Gonzales, 1989, Tables 3-6 and 3-7
15	H7C	608086	3574632	648751	475020	23	30	14	Mercer, 1983, Table 1
16	H8A	608658	3563566	650392	438678	24	30	23	Gonzales, 1989, Tables 3-6 and 3-7
17	H8B	608683	3563556	650473	438646	24	30	23	Gonzales, 1989, Tables 3-6 and 3-7
18	H8C	608656	3563541	650397	438590	24	30	23	Mercer, 1983, Table 1
19	H9A	613958	3568260	667879	453977	24	31	4	Gonzales, 1989, Tables 3-6 and 3-7
20	H9B	613989	3568261	667979	453978	24	31	4	Gonzales, 1989, Tables 3-6 and 3-7
21	H9C	613965	3568233	667914	453889	24	31	4	Mercer, 1983, Table 1
22	MB139_1	613585	3582210	666913	499365	0	0	0	Krieg, 1984, Table I
23	MB139_2	613633	3582061	667069	498876	0	0	0	Krieg, 1984, Table I
24	MB139_3	613635	3582155	667076	499185	0	0	0	Krieg, 1984, Table I
25	MB139_4	613582	3582156	666902	499187	0	0	0	Krieg, 1984, Table I
26	P1	612339	3580339	662807	493649	22	31	29	Mercer, 1983, Table 1
27	P10	617074	3581193	678380	496355	22	31	26	Mercer, 1983, Table 1
28	P11	617016	3583462	678222	503799	22	31	23	Mercer, 1983, Table 1
29	P12	610454	3583452	656688	503899	22	30	24	Mercer, 1983, Table 1
30	P13	610539	3585079	657003	509237	22	31	18	Mercer, 1983, Table 1
31	P14	609083	3581974	652158	499079	22	30	24	Mercer, 1983, Table 1
32	P15	610624	3578793	657148	488609	22	31	31	Mercer, 1983, Table 1
33	P16	612704	3577312	663938	483715	23	31	5	Mercer, 1983, Table 1
34	P17	613929	3577459	667959	484166	23	31	4	Mercer, 1983, Table 1
35	P18	618367	3580352	682589	493561	22	31	26	Mercer, 1983, Table 1
36	P19	617687	3582410	680392	500348	22	31	23	Mercer, 1983, Table 1
37	P2	615315	3581850	672609	498541	22	31	28	Mercer, 1983, Table 1
38	P20	618541	3583770	683226	504775	22	31	14	Mercer, 1983, Table 1

Table B.1. Location of Wells used by WIPP (Universal Transverse Mercator [UTM], State Plan Coordinates [stpln], and Survey Sections [township, range and section])

	Well ID	x-UTM	y-UTM	x-STPLN	y-STPLN	Township	Range	Section	Source
1	P21	616901	3584847	677877	508345	22	31	15	Mercer, 1983, Table 1
2	P3	612799	3581888	664349	498733	22	31	20	Mercer, 1983, Table 1
3	P4	614936	3580324	671330	493533	22	31	28	Mercer, 1983, Table 1
4	P5	613686	3583535	667292	504105	22	31	17	Mercer, 1983, Table 1
5	P6	610591	3581133	657104	496288	22	31	30	Mercer, 1983, Table 1
6	P7	612305	3578476	662663	487535	23	31	5	Mercer, 1983, Table 1
7	P8	613827	3578467	667656	487472	23	31	4	Mercer, 1983, Table 1
8	P9	615365	3579125	672704	489600	22	31	33	Mercer, 1983, Table 1
9	SaltShft	613587	3582186	666919	499286	0	0	0	Krieg, 1984, Table I
10	USGS1	606462	3569459	643297	458066	23	30	34	Gonzales, 1989, Tables 3-6 and 3-7
11	USGS4	605841	3569887	641277	459483	23	30	34	Gonzales, 1989, Tables 3-6 and 3-7
12	USGS8	605879	3569888	641402	459483	23	30	34	Gonzales, 1989, Tables 3-6 and 3-7
13	WIPP11	613819	3586474	667796	513749	22	31	9	Mercer, 1983, Table 1
14	WIPP12	613709	3583524	667368	504067	22	31	17	Mercer, 1983, Table 1
15	WIPP13	612652	3584241	663901	506454	22	31	17	Mercer, 1983, Table 1
16	WIPP15	590057	3574585	589590	475231	23	35	18	Mercer, 1983, Table 1
17	WIPP16	602380	3597026	630458	548607	21	30	5	Mercer, 1983, Table 1
18	WIPP18	613731	3583179	667441	502935	22	31	20	Mercer, 1983, Table 1
19	WIPP19	613747	3582787	667461	501649	22	31	20	Mercer, 1983, Table 1
20	WIPP21	613747	3582349	667462	500213	22	31	20	Mercer, 1983, Table 1
21	WIPP22	613747	3582652	667462	501206	22	31	20	Mercer, 1983, Table 1
22	WIPP25	606391	3584037	643354	505885	22	30	15	Mercer, 1983, Table 1
23	WIPP26	604006	3581161	635496	496516	22	30	29	Mercer, 1983, Table 1
24	WIPP27	604425	3593073	637102	535603	21	30	21	Mercer, 1983, Table 1
25	WIPP28	611265	3594687	659578	540736	21	31	18	Mercer, 1983, Table 1
26	WIPP29	596981	3578700	612380	488570	22	29	34	Mercer, 1983, Table 1
27	WIPP30	613718	3589700	667532	524335	21	31	33	Mercer, 1983, Table 1
28	WIPP32	595909	3579081	608858	489850	22	29	33	Mercer, 1983, Table 1
29	WIPP33	609629	3584019	653981	505789	22	30	13	Mercer, 1983, Table 1
30	WIPP34	614333	3585141	669449	509375	22	31	9	Mercer, 1983, Table 1
31	WastShft	613595	3582061	666944	498876	0	0	0	Krieg, 1984, Table I

Table B.2. Elevations of Stratigraphic Layers Near WIPP

	Layer	Well ID	Elevation	Source
2	Anhydrt1	DOE2	-199.00	Mercer et al., 1987, Table 3-2
3	Anhydrt1	DOE2	-119.10	Mercer et al., 1987, Table 3-2
4	Anhydrt1	REF	-199.00	Rechard et al.,1991, Figure 2.2-1
5	Anhydrt1	REF	-119.10	Rechard et al.,1991, Figure 2.2-1
6	Anhydrt1	WIPP11	-43.90	SNL and USGS, 1982a, Table 2
7	Anhydrt1	WIPP11	-37.80	SNL and USGS, 1982a, Table 2
8	Anhydrt1	WIPP12	-139.00	SNL and D'Appolonia Consulting, 1983, Table 2
9	Anhydrt1	WIPP12	-131.10	SNL and D'Appolonia Consulting, 1983, Table 2
10	Anhydrt2	DOE1	-71.60	U.S. DOE, Sep 1982, Table 2
11	Anhydrt2	DOE1	-38.60	U.S. DOE, Sep 1982, Table 2
12	Anhydrt2	DOE2	-116.40	Mercer et al., 1987, Table 3-2
13	Anhydrt2	REF	-116.40	Rechard et al.,1991, Figure 2.2-1
14	Anhydrt2	WIPP11	-22.20	SNL and USGS, 1982a, Table 2
15	Anhydrt2	WIPP11	14.40	SNL and USGS, 1982a, Table 2
16	Anhydrt2	WIPP12	24.50	SNL and D'Appolonia Consulting, 1983, Table 2
17	Anhydrt2	WIPP12	57.80	SNL and D'Appolonia Consulting, 1983, Table 2
18	Anhydrt3	DOE1	30.00	U.S. DOE, Sep 1982, Table 2
19	Anhydrt3	DOE1	163.60	U.S. DOE, Sep 1982, Table 2
20	Anhydrt3	DOE2	102.30	Mercer et al., 1987, Table 3-2
21	Anhydrt3	ERDA9	162.00	SNL and USGS, 1982b, Table 2
22	Anhydrt3	ERDA9	178.10	SNL and USGS, 1982b, Table 2
23	Anhydrt3	REF	162.00	Rechard et al.,1991, Figure 2.2-1
24	Anhydrt3	REF	178.10	Rechard et al.,1991, Figure 2.2-1
25	Anhydrt3	WIPP11	309.40	SNL and USGS, 1982a, Table 2
26	Anhydrt3	WIPP11	334.10	SNL and USGS, 1982a, Table 2
27	Anhydrt3	WIPP12	127.30	SNL and D'Appolonia Consulting, 1983, Table 2
28	Anhydrt3	WIPP12	227.40	SNL and D'Appolonia Consulting, 1983, Table 2
29	Anhydrta	AirShft	386.41	Holt and Powers, 1990, Figure 22
30	Anhydrta	AirShft	386.70	Holt and Powers, 1990, Figure 22
31	Anhydrta	DH207	386.86	Krieg, 1984, Table I
32	Anhydrta	DH207	388.78	Krieg, 1984, Table I
33	Anhydrta	DH211	389.81	Krieg, 1984, Table I
34	Anhydrta	DH211	391.67	Krieg, 1984, Table I
35	Anhydrta	DH215	390.11	Krieg, 1984, Table I
36	Anhydrta	DH215	391.97	Krieg, 1984, Table I
37	Anhydrta	DH219	390.39	Krieg, 1984, Table I
38	Anhydrta	DH219	390.57	Krieg, 1984, Table I
39	Anhydrta	DH223	386.88	Krieg, 1984, Table I
40	Anhydrta	DH223	387.18	Krieg, 1984, Table I
41	Anhydrta	DH227	384.02	Krieg, 1984, Table I
42	Anhydrta	DH227	384.26	Krieg, 1984, Table I
43	Anhydrta	DH77	402.79	Krieg, 1984, Table I
44	Anhydrta	DH77	402.88	Krieg, 1984, Table I
45	Anhydrta	DO201	389.23	Krieg, 1984, Table I
46	Anhydrta	DO201	389.44	Krieg, 1984, Table I
47	Anhydrta	DO203	400.02	Krieg, 1984, Table I
48	Anhydrta	DO203	400.26	Krieg, 1984, Table I
49	Anhydrta	DO205	405.17	Krieg, 1984, Table I
50	Anhydrta	DO205	405.38	Krieg, 1984, Table I
51	Anhydrta	DO45	396.69	Krieg, 1984, Table I
52	Anhydrta	DO45	396.87	Krieg, 1984, Table I
53	Anhydrta	DO52	393.92	Krieg, 1984, Table I
54	Anhydrta	DO52	394.07	Krieg, 1984, Table I
55	Anhydrta	DO56	399.74	Krieg, 1984, Table I
56	Anhydrta	DO56	399.92	Krieg, 1984, Table I
57	Anhydrta	DO63	403.61	Krieg, 1984, Table I
58	Anhydrta	DO63	403.98	Krieg, 1984, Table I
59	Anhydrta	DO67	403.58	Krieg, 1984, Table I
60	Anhydrta	DO67	403.85	Krieg, 1984, Table I
61	Anhydrta	DO88	402.36	Krieg, 1984, Table I
62	Anhydrta	DO88	402.51	Krieg, 1984, Table I
63	Anhydrta	DO91	402.07	Krieg, 1984, Table I
64	Anhydrta	DO91	402.28	Krieg, 1984, Table I
65	Anhydrta	ExhtShft	389.78	Bechtel, Inc., 1986, Appendix F
66	Anhydrta	ExhtShft	390.03	Bechtel, Inc., 1986, Appendix F
67	Anhydrta	MB139_2	388.84	Krieg, 1984, Table I
68	Anhydrta	MB139_2	389.05	Krieg, 1984, Table I
69	Anhydrta	SaltShft	392.51	Bechtel, Inc., 1986, Appendix D
70	Anhydrta	SaltShft	392.74	Bechtel, Inc., 1986, Appendix D
71	Anhydrta	SaltShft	392.53	Krieg, 1984, Table I
72	Anhydrta	SaltShft	392.76	Krieg, 1984, Table I
73	Anhydrta	WastShft	388.76	Bechtel, Inc., 1986, Appendix E
74	Anhydrta	WastShft	388.97	Bechtel, Inc., 1986, Appendix E
75	Anhydrta	WastShft	389.01	Krieg, 1984, Table I
76	Anhydrta	WastShft	389.25	Krieg, 1984, Table I
77	Anhydrtb	DH207	386.65	Krieg, 1984, Table I

Table B.2. Elevations of Stratigraphic Layers Near WIPP (Continued)

	Layer	Well ID	Elevation	Source
2	Anhydrtb	DH207	386.70	Krieg, 1984, Table I
3	Anhydrtb	DH211	389.63	Krieg, 1984, Table I
4	Anhydrtb	DH211	389.66	Krieg, 1984, Table I
5	Anhydrtb	DH215	389.96	Krieg, 1984, Table I
6	Anhydrtb	DH215	390.02	Krieg, 1984, Table I
7	Anhydrtb	DH219	388.41	Krieg, 1984, Table I
8	Anhydrtb	DH219	388.42	Krieg, 1984, Table I
9	Anhydrtb	DH223	385.05	Krieg, 1984, Table I
10	Anhydrtb	DH223	385.05	Krieg, 1984, Table I
11	Anhydrtb	DH227	382.25	Krieg, 1984, Table I
12	Anhydrtb	DH227	382.25	Krieg, 1984, Table I
13	Anhydrtb	DH77	400.75	Krieg, 1984, Table I
14	Anhydrtb	DH77	400.83	Krieg, 1984, Table I
15	Anhydrtb	DO201	387.07	Krieg, 1984, Table I
16	Anhydrtb	DO201	387.13	Krieg, 1984, Table I
17	Anhydrtb	DO203	398.13	Krieg, 1984, Table I
18	Anhydrtb	DO203	398.19	Krieg, 1984, Table I
19	Anhydrtb	DO205	403.13	Krieg, 1984, Table I
20	Anhydrtb	DO205	403.19	Krieg, 1984, Table I
21	Anhydrtb	DO45	393.92	Krieg, 1984, Table I
22	Anhydrtb	DO45	393.95	Krieg, 1984, Table I
23	Anhydrtb	DO52	391.88	Krieg, 1984, Table I
24	Anhydrtb	DO52	391.94	Krieg, 1984, Table I
25	Anhydrtb	DO56	397.64	Krieg, 1984, Table I
26	Anhydrtb	DO56	397.70	Krieg, 1984, Table I
27	Anhydrtb	DO63	401.45	Krieg, 1984, Table I
28	Anhydrtb	DO63	401.51	Krieg, 1984, Table I
29	Anhydrtb	DO67	401.45	Krieg, 1984, Table I
30	Anhydrtb	DO67	401.53	Krieg, 1984, Table I
31	Anhydrtb	DO88	400.23	Krieg, 1984, Table I
32	Anhydrtb	DO88	400.30	Krieg, 1984, Table I
33	Anhydrtb	DO91	399.91	Krieg, 1984, Table I
34	Anhydrtb	DO91	399.96	Krieg, 1984, Table I
35	Anhydrtb	ExhtShft	387.66	Bechtel, Inc., 1986, Appendix F
36	Anhydrtb	ExhtShft	387.75	Bechtel, Inc., 1986, Appendix F
37	Anhydrtb	MB139_2	386.58	Krieg, 1984, Table I
38	Anhydrtb	MB139_2	386.61	Krieg, 1984, Table I
39	Anhydrtb	SaltShft	390.58	Bechtel, Inc., 1986, Appendix D
40	Anhydrtb	SaltShft	390.66	Bechtel, Inc., 1986, Appendix D
41	Anhydrtb	SaltShft	390.37	Krieg, 1984, Table I
42	Anhydrtb	SaltShft	390.45	Krieg, 1984, Table I
43	Anhydrtb	WastShft	386.57	Bechtel, Inc., 1986, Appendix E
44	Anhydrtb	WastShft	386.70	Bechtel, Inc., 1986, Appendix E
45	Anhydrtb	WastShft	386.91	Krieg, 1984, Table I
46	Anhydrtb	WastShft	386.97	Krieg, 1984, Table I
47	Anhydrtc	DH207	369.49	Krieg, 1984, Table I
48	Anhydrtc	DH207	369.55	Krieg, 1984, Table I
49	Anhydrtc	DH211	372.71	Krieg, 1984, Table I
50	Anhydrtc	DH211	372.80	Krieg, 1984, Table I
51	Anhydrtc	DH215	373.14	Krieg, 1984, Table I
52	Anhydrtc	DH215	373.20	Krieg, 1984, Table I
53	Anhydrtc	DH219	372.13	Krieg, 1984, Table I
54	Anhydrtc	DH219	372.19	Krieg, 1984, Table I
55	Anhydrtc	DH223	369.08	Krieg, 1984, Table I
56	Anhydrtc	DH223	369.17	Krieg, 1984, Table I
57	Anhydrtc	DH227	366.16	Krieg, 1984, Table I
58	Anhydrtc	DH227	366.22	Krieg, 1984, Table I
59	Anhydrtc	DH77	384.75	Krieg, 1984, Table I
60	Anhydrtc	DH77	384.81	Krieg, 1984, Table I
61	Anhydrtc	DO201	369.91	Krieg, 1984, Table I
62	Anhydrtc	DO201	370.03	Krieg, 1984, Table I
63	Anhydrtc	DO203	381.95	Krieg, 1984, Table I
64	Anhydrtc	DO203	382.01	Krieg, 1984, Table I
65	Anhydrtc	DO205	387.37	Krieg, 1984, Table I
66	Anhydrtc	DO205	387.43	Krieg, 1984, Table I
67	Anhydrtc	DO45	377.22	Krieg, 1984, Table I
68	Anhydrtc	DO45	377.28	Krieg, 1984, Table I
69	Anhydrtc	DO52	375.18	Krieg, 1984, Table I
70	Anhydrtc	DO52	375.24	Krieg, 1984, Table I
71	Anhydrtc	DO56	381.00	Krieg, 1984, Table I
72	Anhydrtc	DO56	381.09	Krieg, 1984, Table I
73	Anhydrtc	DO63	385.66	Krieg, 1984, Table I
74	Anhydrtc	DO63	385.84	Krieg, 1984, Table I
75	Anhydrtc	DO67	385.54	Krieg, 1984, Table I
76	Anhydrtc	DO67	385.63	Krieg, 1984, Table I
77	Anhydrtc	DO88	384.01	Krieg, 1984, Table I

Table B.2. Elevations of Stratigraphic Layers Near WIPP (Continued)

	Layer	Well ID	Elevation	Source
1	Anhydrtc	DO88	384.06	Krieg, 1984, Table I
2	Anhydrtc	DO91	384.03	Krieg, 1984, Table I
3	Anhydrtc	DO91	384.12	Krieg, 1984, Table I
4	Anhydrtc	SaltShft	373.09	Krieg, 1984, Table I
5	Anhydrtc	SaltShft	373.20	Krieg, 1984, Table I
6	B_CANyon	DOE2	-276.30	Mercer et al., 1987, Table 3-2
7	B_CANyon	DOE2	-199.00	Mercer et al., 1987, Table 3-2
8	B_CANyon	REF	-276.30	Rechard et al.,1991, Figure 2.2-1
9	B_CANyon	REF	-199.00	Rechard et al.,1991, Figure 2.2-1
10	Culebra	AEC7	848.50	Mercer, 1983, Table 1
11	Culebra	AEC8	822.70	Mercer, 1983, Table 1
12	Culebra	AirShft	824.48	Holt and Powers, 1990, Figure 22
13	Culebra	B25	824.50	Mercer, 1983, Table 1
14	Culebra	DOE1	806.10	U.S. DOE, Sep 1982, Table 2
15	Culebra	DOE2	790.80	Mercer et al., 1987, Table 3-2
16	Culebra	ERDA10	882.40	Mercer, 1983, Table 1
17	Culebra	ERDA6	862.60	Mercer, 1983, Table 1
18	Culebra	ERDA9	827.50	Mercer, 1983, Table 1
19	Culebra	ERDA9	823.40	SNL and USGS, 1982b, Table 2
20	Culebra	ExhtShft	821.57	Bechtel, Inc., 1986, Appendix F
21	Culebra	FFG_002	624.80	Richey, 1989, Table 2, p.21
22	Culebra	FFG_004	666.60	Richey, 1989, Table 2, p.21
23	Culebra	FFG_005	628.50	Richey, 1989, Table 2, p.21
24	Culebra	FFG_006	616.60	Richey, 1989, Table 2, p.21
25	Culebra	FFG_007	602.00	Richey, 1989, Table 2, p.21
26	Culebra	FFG_009	604.10	Richey, 1989, Table 2, p.21
27	Culebra	FFG_011	609.90	Richey, 1989, Table 2, p.21
28	Culebra	FFG_012	613.90	Richey, 1989, Table 2, p.21
29	Culebra	FFG_013	646.20	Richey, 1989, Table 2, p.21
30	Culebra	FFG_014	667.80	Richey, 1989, Table 2, p.21
31	Culebra	FFG_016	587.90	Richey, 1989, Table 2, p.21
32	Culebra	FFG_017	594.90	Richey, 1989, Table 2, p.22
33	Culebra	FFG_018	598.60	Richey, 1989, Table 2, p.22
34	Culebra	FFG_019	588.60	Richey, 1989, Table 2, p.22
35	Culebra	FFG_020	662.00	Richey, 1989, Table 2, p.22
36	Culebra	FFG_023	596.20	Richey, 1989, Table 2, p.22
37	Culebra	FFG_024	579.10	Richey, 1989, Table 2, p.22
38	Culebra	FFG_025	598.50	Richey, 1989, Table 2, p.22
39	Culebra	FFG_026	592.50	Richey, 1989, Table 2, p.22
40	Culebra	FFG_027	585.50	Richey, 1989, Table 2, p.22
41	Culebra	FFG_028	578.60	Richey, 1989, Table 2, p.22
42	Culebra	FFG_029	563.50	Richey, 1989, Table 2, p.22
43	Culebra	FFG_030	563.00	Richey, 1989, Table 2, p.22
44	Culebra	FFG_031	554.40	Richey, 1989, Table 2, p.22
45	Culebra	FFG_032	549.40	Richey, 1989, Table 2, p.22
46	Culebra	FFG_033	549.20	Richey, 1989, Table 2, p.22
47	Culebra	FFG_034	548.60	Richey, 1989, Table 2, p.23
48	Culebra	FFG_035	533.90	Richey, 1989, Table 2, p.23
49	Culebra	FFG_036	541.40	Richey, 1989, Table 2, p.23
50	Culebra	FFG_037	534.00	Richey, 1989, Table 2, p.23
51	Culebra	FFG_038	523.60	Richey, 1989, Table 2, p.23
52	Culebra	FFG_039	731.90	Richey, 1989, Table 2, p.23
53	Culebra	FFG_040	655.40	Richey, 1989, Table 2, p.23
54	Culebra	FFG_041	733.70	Richey, 1989, Table 2, p.23
55	Culebra	FFG_042	740.60	Richey, 1989, Table 2, p.23
56	Culebra	FFG_043	735.70	Richey, 1989, Table 2, p.23
57	Culebra	FFG_044	689.10	Richey, 1989, Table 2, p.23
58	Culebra	FFG_047	561.10	Richey, 1989, Table 2, p.23
59	Culebra	FFG_048	580.30	Richey, 1989, Table 2, p.23
60	Culebra	FFG_049	567.50	Richey, 1989, Table 2, p.23
61	Culebra	FFG_050	582.50	Richey, 1989, Table 2, p.24
62	Culebra	FFG_051	573.90	Richey, 1989, Table 2, p.24
63	Culebra	FFG_052	595.20	Richey, 1989, Table 2, p.24
64	Culebra	FFG_053	563.00	Richey, 1989, Table 2, p.24
65	Culebra	FFG_054	562.70	Richey, 1989, Table 2, p.24
66	Culebra	FFG_055	565.70	Richey, 1989, Table 2, p.24
67	Culebra	FFG_056	564.50	Richey, 1989, Table 2, p.24
68	Culebra	FFG_057	564.80	Richey, 1989, Table 2, p.24
69	Culebra	FFG_058	569.30	Richey, 1989, Table 2, p.24
70	Culebra	FFG_059	569.70	Richey, 1989, Table 2, p.24
71	Culebra	FFG_060	569.30	Richey, 1989, Table 2, p.24
72	Culebra	FFG_061	570.60	Richey, 1989, Table 2, p.24
73	Culebra	FFG_062	513.90	Richey, 1989, Table 2, p.24
74	Culebra	FFG_063	470.70	Richey, 1989, Table 2, p.24
75	Culebra	FFG_064	497.50	Richey, 1989, Table 2, p.24
76	Culebra	FFG_065	471.80	Richey, 1989, Table 2, p.24

Table B.2. Elevations of Stratigraphic Layers Near WIPP (Continued)

	Layer	Well ID	Elevation	Source
1	Culebra	FFG_066	434.30	Richey, 1989, Table 2, p.24
2	Culebra	FFG_067	470.00	Richey, 1989, Table 2, p.25
3	Culebra	FFG_068	430.10	Richey, 1989, Table 2, p.25
4	Culebra	FFG_069	447.50	Richey, 1989, Table 2, p.25
5	Culebra	FFG_070	484.60	Richey, 1989, Table 2, p.25
6	Culebra	FFG_071	755.00	Richey, 1989, Table 2, p.25
7	Culebra	FFG_072	681.20	Richey, 1989, Table 2, p.25
8	Culebra	FFG_073	659.30	Richey, 1989, Table 2, p.25
9	Culebra	FFG_074	666.40	Richey, 1989, Table 2, p.25
10	Culebra	FFG_075	717.90	Richey, 1989, Table 2, p.25
11	Culebra	FFG_076	777.60	Richey, 1989, Table 2, p.25
12	Culebra	FFG_078	814.70	Richey, 1989, Table 2, p.25
13	Culebra	FFG_079	787.00	Richey, 1989, Table 2, p.25
14	Culebra	FFG_080	765.60	Richey, 1989, Table 2, p.25
15	Culebra	FFG_081	683.10	Richey, 1989, Table 2, p.26
16	Culebra	FFG_082	711.10	Richey, 1989, Table 2, p.26
17	Culebra	FFG_083	638.10	Richey, 1989, Table 2, p.26
18	Culebra	FFG_084	661.40	Richey, 1989, Table 2, p.26
19	Culebra	FFG_085	655.40	Richey, 1989, Table 2, p.26
20	Culebra	FFG_086	665.00	Richey, 1989, Table 2, p.26
21	Culebra	FFG_087	636.70	Richey, 1989, Table 2, p.26
22	Culebra	FFG_088	626.10	Richey, 1989, Table 2, p.26
23	Culebra	FFG_089	613.90	Richey, 1989, Table 2, p.26
24	Culebra	FFG_091	652.30	Richey, 1989, Table 2, p.26
25	Culebra	FFG_092	670.90	Richey, 1989, Table 2, p.26
26	Culebra	FFG_093	673.60	Richey, 1989, Table 2, p.26
27	Culebra	FFG_094	674.20	Richey, 1989, Table 2, p.26
28	Culebra	FFG_095	651.60	Richey, 1989, Table 2, p.26
29	Culebra	FFG_096	635.50	Richey, 1989, Table 2, p.26
30	Culebra	FFG_097	614.80	Richey, 1989, Table 2, p.27
31	Culebra	FFG_098	587.90	Richey, 1989, Table 2, p.27
32	Culebra	FFG_099	582.50	Richey, 1989, Table 2, p.27
33	Culebra	FFG_100	564.80	Richey, 1989, Table 2, p.27
34	Culebra	FFG_101	533.70	Richey, 1989, Table 2, p.27
35	Culebra	FFG_102	549.00	Richey, 1989, Table 2, p.27
36	Culebra	FFG_103	609.30	Richey, 1989, Table 2, p.27
37	Culebra	FFG_104	508.10	Richey, 1989, Table 2, p.27
38	Culebra	FFG_105	867.50	Richey, 1989, Table 2, p.27
39	Culebra	FFG_106	902.60	Richey, 1989, Table 2, p.27
40	Culebra	FFG_107	887.90	Richey, 1989, Table 2, p.27
41	Culebra	FFG_108	878.70	Richey, 1989, Table 2, p.27
42	Culebra	FFG_109	862.30	Richey, 1989, Table 2, p.27
43	Culebra	FFG_110	832.10	Richey, 1989, Table 2, p.27
44	Culebra	FFG_111	836.60	Richey, 1989, Table 2, p.27
45	Culebra	FFG_112	824.50	Richey, 1989, Table 2, p.28
46	Culebra	FFG_113	838.50	Richey, 1989, Table 2, p.28
47	Culebra	FFG_114	870.50	Richey, 1989, Table 2, p.28
48	Culebra	FFG_115	857.40	Richey, 1989, Table 2, p.28
49	Culebra	FFG_116	871.40	Richey, 1989, Table 2, p.28
50	Culebra	FFG_117	868.70	Richey, 1989, Table 2, p.28
51	Culebra	FFG_119	870.90	Richey, 1989, Table 2, p.28
52	Culebra	FFG_120	874.20	Richey, 1989, Table 2, p.28
53	Culebra	FFG_121	882.40	Richey, 1989, Table 2, p.28
54	Culebra	FFG_122	876.30	Richey, 1989, Table 2, p.28
55	Culebra	FFG_123	867.10	Richey, 1989, Table 2, p.28
56	Culebra	FFG_124	837.90	Richey, 1989, Table 2, p.28
57	Culebra	FFG_125	851.20	Richey, 1989, Table 2, p.28
58	Culebra	FFG_126	852.70	Richey, 1989, Table 2, p.28
59	Culebra	FFG_127	860.70	Richey, 1989, Table 2, p.28
60	Culebra	FFG_128	887.00	Richey, 1989, Table 2, p.28
61	Culebra	FFG_129	858.30	Richey, 1989, Table 2, p.28
62	Culebra	FFG_130	897.60	Richey, 1989, Table 2, p.28
63	Culebra	FFG_132	898.60	Richey, 1989, Table 2, p.29
64	Culebra	FFG_133	901.60	Richey, 1989, Table 2, p.29
65	Culebra	FFG_134	904.40	Richey, 1989, Table 2, p.29
66	Culebra	FFG_135	880.90	Richey, 1989, Table 2, p.29
67	Culebra	FFG_136	882.50	Richey, 1989, Table 2, p.29
68	Culebra	FFG_137	892.80	Richey, 1989, Table 2, p.29
69	Culebra	FFG_138	844.10	Richey, 1989, Table 2, p.29
70	Culebra	FFG_139	855.60	Richey, 1989, Table 2, p.29
71	Culebra	FFG_140	792.70	Richey, 1989, Table 2, p.29
72	Culebra	FFG_141	820.10	Richey, 1989, Table 2, p.29
73	Culebra	FFG_142	795.90	Richey, 1989, Table 2, p.29
74	Culebra	FFG_143	804.00	Richey, 1989, Table 2, p.29
75	Culebra	FFG_144	894.30	Richey, 1989, Table 2, p.29
76	Culebra	FFG_145	893.10	Richey, 1989, Table 2, p.29

Table B.2. Elevations of Stratigraphic Layers Near WIPP (Continued)

	Layer	Well ID	Elevation	Source
1	Culebra	FFG_146	906.80	Richey, 1989, Table 2, p.29
2	Culebra	FFG_147	882.70	Richey, 1989, Table 2, p.29
3	Culebra	FFG_148	900.10	Richey, 1989, Table 2, p.29
4	Culebra	FFG_149	910.70	Richey, 1989, Table 2, p.30
5	Culebra	FFG_155	901.30	Richey, 1989, Table 2, p.30
6	Culebra	FFG_156	906.50	Richey, 1989, Table 2, p.30
7	Culebra	FFG_157	904.10	Richey, 1989, Table 2, p.30
8	Culebra	FFG_158	928.10	Richey, 1989, Table 2, p.30
9	Culebra	FFG_159	898.60	Richey, 1989, Table 2, p.30
10	Culebra	FFG_160	895.20	Richey, 1989, Table 2, p.30
11	Culebra	FFG_161	901.00	Richey, 1989, Table 2, p.30
12	Culebra	FFG_162	891.90	Richey, 1989, Table 2, p.30
13	Culebra	FFG_163	897.40	Richey, 1989, Table 2, p.30
14	Culebra	FFG_164	937.60	Richey, 1989, Table 2, p.30
15	Culebra	FFG_165	912.80	Richey, 1989, Table 2, p.30
16	Culebra	FFG_166	900.00	Richey, 1989, Table 2, p.31
17	Culebra	FFG_167	887.00	Richey, 1989, Table 2, p.31
18	Culebra	FFG_168	906.50	Richey, 1989, Table 2, p.31
19	Culebra	FFG_169	919.20	Richey, 1989, Table 2, p.31
20	Culebra	FFG_170	903.70	Richey, 1989, Table 2, p.31
21	Culebra	FFG_171	922.10	Richey, 1989, Table 2, p.31
22	Culebra	FFG_172	915.30	Richey, 1989, Table 2, p.31
23	Culebra	FFG_173	876.90	Richey, 1989, Table 2, p.31
24	Culebra	FFG_177	889.10	Richey, 1989, Table 2, p.31
25	Culebra	FFG_178	718.10	Richey, 1989, Table 2, p.31
26	Culebra	FFG_179	886.60	Richey, 1989, Table 2, p.31
27	Culebra	FFG_180	883.00	Richey, 1989, Table 2, p.31
28	Culebra	FFG_181	930.50	Richey, 1989, Table 2, p.32
29	Culebra	FFG_182	812.60	Richey, 1989, Table 2, p.32
30	Culebra	FFG_183	904.40	Richey, 1989, Table 2, p.32
31	Culebra	FFG_184	891.20	Richey, 1989, Table 2, p.32
32	Culebra	FFG_185	899.50	Richey, 1989, Table 2, p.32
33	Culebra	FFG_186	827.90	Richey, 1989, Table 2, p.32
34	Culebra	FFG_188	845.80	Richey, 1989, Table 2, p.32
35	Culebra	FFG_189	867.80	Richey, 1989, Table 2, p.32
36	Culebra	FFG_190	843.60	Richey, 1989, Table 2, p.32
37	Culebra	FFG_191	845.50	Richey, 1989, Table 2, p.32
38	Culebra	FFG_192	774.50	Richey, 1989, Table 2, p.32
39	Culebra	FFG_194	788.50	Richey, 1989, Table 2, p.33
40	Culebra	FFG_195	803.50	Richey, 1989, Table 2, p.33
41	Culebra	FFG_196	837.00	Richey, 1989, Table 2, p.33
42	Culebra	FFG_197	841.00	Richey, 1989, Table 2, p.33
43	Culebra	FFG_198	840.90	Richey, 1989, Table 2, p.33
44	Culebra	FFG_199	827.00	Richey, 1989, Table 2, p.33
45	Culebra	FFG_200	838.20	Richey, 1989, Table 2, p.33
46	Culebra	FFG_201	838.20	Richey, 1989, Table 2, p.33
47	Culebra	FFG_202	773.80	Richey, 1989, Table 2, p.33
48	Culebra	FFG_203	776.00	Richey, 1989, Table 2, p.33
49	Culebra	FFG_204	813.50	Richey, 1989, Table 2, p.33
50	Culebra	FFG_205	825.10	Richey, 1989, Table 2, p.33
51	Culebra	FFG_206	837.00	Richey, 1989, Table 2, p.33
52	Culebra	FFG_207	833.60	Richey, 1989, Table 2, p.33
53	Culebra	FFG_208	843.10	Richey, 1989, Table 2, p.34
54	Culebra	FFG_209	838.20	Richey, 1989, Table 2, p.34
55	Culebra	FFG_210	827.50	Richey, 1989, Table 2, p.34
56	Culebra	FFG_212	817.50	Richey, 1989, Table 2, p.34
57	Culebra	FFG_213	837.90	Richey, 1989, Table 2, p.34
58	Culebra	FFG_214	818.40	Richey, 1989, Table 2, p.34
59	Culebra	FFG_215	793.10	Richey, 1989, Table 2, p.34
60	Culebra	FFG_216	688.80	Richey, 1989, Table 2, p.34
61	Culebra	FFG_217	814.80	Richey, 1989, Table 2, p.34
62	Culebra	FFG_218	803.50	Richey, 1989, Table 2, p.34
63	Culebra	FFG_219	848.80	Richey, 1989, Table 2, p.34
64	Culebra	FFG_220	798.60	Richey, 1989, Table 2, p.34
65	Culebra	FFG_221	756.50	Richey, 1989, Table 2, p.34
66	Culebra	FFG_222	713.30	Richey, 1989, Table 2, p.34
67	Culebra	FFG_224	597.80	Richey, 1989, Table 2, p.35
68	Culebra	FFG_225	603.50	Richey, 1989, Table 2, p.35
69	Culebra	FFG_226	601.80	Richey, 1989, Table 2, p.35
70	Culebra	FFG_228	588.30	Richey, 1989, Table 2, p.35
71	Culebra	FFG_229	614.70	Richey, 1989, Table 2, p.35
72	Culebra	FFG_230	601.10	Richey, 1989, Table 2, p.35
73	Culebra	FFG_231	619.90	Richey, 1989, Table 2, p.35
74	Culebra	FFG_232	631.50	Richey, 1989, Table 2, p.35
75	Culebra	FFG_233	624.00	Richey, 1989, Table 2, p.35
76	Culebra	FFG_234	660.20	Richey, 1989, Table 2, p.35

Table B.2. Elevations of Stratigraphic Layers Near WIPP (Continued)

	Layer	Well ID	Elevation	Source
1	Culebra	FFG_235	635.50	Richey, 1989, Table 2, p.35
2	Culebra	FFG_236	682.70	Richey, 1989, Table 2, p.35
3	Culebra	FFG_237	646.20	Richey, 1989, Table 2, p.35
4	Culebra	FFG_238	628.50	Richey, 1989, Table 2, p.36
5	Culebra	FFG_239	620.50	Richey, 1989, Table 2, p.36
6	Culebra	FFG_240	609.90	Richey, 1989, Table 2, p.36
7	Culebra	FFG_241	605.10	Richey, 1989, Table 2, p.36
8	Culebra	FFG_242	732.20	Richey, 1989, Table 2, p.36
9	Culebra	FFG_243	668.40	Richey, 1989, Table 2, p.36
10	Culebra	FFG_244	721.30	Richey, 1989, Table 2, p.36
11	Culebra	FFG_245	510.80	Richey, 1989, Table 2, p.36
12	Culebra	FFG_246	516.00	Richey, 1989, Table 2, p.36
13	Culebra	FFG_247	501.30	Richey, 1989, Table 2, p.36
14	Culebra	FFG_248	506.60	Richey, 1989, Table 2, p.36
15	Culebra	FFG_249	505.30	Richey, 1989, Table 2, p.36
16	Culebra	FFG_250	587.50	Richey, 1989, Table 2, p.36
17	Culebra	FFG_251	477.30	Richey, 1989, Table 2, p.36
18	Culebra	FFG_252	619.60	Richey, 1989, Table 2, p.36
19	Culebra	FFG_253	566.70	Richey, 1989, Table 2, p.36
20	Culebra	FFG_254	562.00	Richey, 1989, Table 2, p.36
21	Culebra	FFG_255	514.50	Richey, 1989, Table 2, p.37
22	Culebra	FFG_256	477.90	Richey, 1989, Table 2, p.37
23	Culebra	FFG_257	523.30	Richey, 1989, Table 2, p.37
24	Culebra	FFG_258	546.20	Richey, 1989, Table 2, p.37
25	Culebra	FFG_259	503.20	Richey, 1989, Table 2, p.37
26	Culebra	FFG_260	556.30	Richey, 1989, Table 2, p.37
27	Culebra	FFG_261	542.20	Richey, 1989, Table 2, p.37
28	Culebra	FFG_262	485.60	Richey, 1989, Table 2, p.37
29	Culebra	FFG_263	456.50	Richey, 1989, Table 2, p.37
30	Culebra	FFG_264	703.80	Richey, 1989, Table 2, p.37
31	Culebra	FFG_265	686.10	Richey, 1989, Table 2, p.37
32	Culebra	FFG_266	665.40	Richey, 1989, Table 2, p.37
33	Culebra	FFG_267	641.30	Richey, 1989, Table 2, p.37
34	Culebra	FFG_268	613.60	Richey, 1989, Table 2, p.37
35	Culebra	FFG_269	627.70	Richey, 1989, Table 2, p.38
36	Culebra	FFG_270	730.30	Richey, 1989, Table 2, p.38
37	Culebra	FFG_271	773.90	Richey, 1989, Table 2, p.38
38	Culebra	FFG_272	751.80	Richey, 1989, Table 2, p.38
39	Culebra	FFG_273	753.20	Richey, 1989, Table 2, p.38
40	Culebra	FFG_274	793.10	Richey, 1989, Table 2, p.38
41	Culebra	FFG_275	800.70	Richey, 1989, Table 2, p.38
42	Culebra	FFG_276	802.80	Richey, 1989, Table 2, p.38
43	Culebra	FFG_277	795.50	Richey, 1989, Table 2, p.38
44	Culebra	FFG_278	776.60	Richey, 1989, Table 2, p.38
45	Culebra	FFG_279	776.90	Richey, 1989, Table 2, p.38
46	Culebra	FFG_280	788.80	Richey, 1989, Table 2, p.38
47	Culebra	FFG_281	762.60	Richey, 1989, Table 2, p.38
48	Culebra	FFG_283	496.20	Richey, 1989, Table 2, p.39
49	Culebra	FFG_284	648.00	Richey, 1989, Table 2, p.39
50	Culebra	FFG_285	669.60	Richey, 1989, Table 2, p.39
51	Culebra	FFG_286	773.80	Richey, 1989, Table 2, p.39
52	Culebra	FFG_287	738.20	Richey, 1989, Table 2, p.39
53	Culebra	FFG_288	668.70	Richey, 1989, Table 2, p.39
54	Culebra	FFG_289	680.60	Richey, 1989, Table 2, p.39
55	Culebra	FFG_290	770.90	Richey, 1989, Table 2, p.39
56	Culebra	FFG_291	668.70	Richey, 1989, Table 2, p.39
57	Culebra	FFG_292	724.80	Richey, 1989, Table 2, p.39
58	Culebra	FFG_293	718.10	Richey, 1989, Table 2, p.39
59	Culebra	FFG_294	504.50	Richey, 1989, Table 2, p.39
60	Culebra	FFG_295	489.50	Richey, 1989, Table 2, p.39
61	Culebra	FFG_297	469.10	Richey, 1989, Table 2, p.39
62	Culebra	FFG_298	528.10	Richey, 1989, Table 2, p.40
63	Culebra	FFG_299	497.80	Richey, 1989, Table 2, p.40
64	Culebra	FFG_300	480.60	Richey, 1989, Table 2, p.40
65	Culebra	FFG_301	435.90	Richey, 1989, Table 2, p.40
66	Culebra	FFG_302	443.50	Richey, 1989, Table 2, p.40
67	Culebra	FFG_303	449.00	Richey, 1989, Table 2, p.40
68	Culebra	FFG_304	445.90	Richey, 1989, Table 2, p.40
69	Culebra	FFG_305	443.20	Richey, 1989, Table 2, p.40
70	Culebra	FFG_306	413.00	Richey, 1989, Table 2, p.40
71	Culebra	FFG_307	432.20	Richey, 1989, Table 2, p.40
72	Culebra	FFG_308	376.10	Richey, 1989, Table 2, p.40
73	Culebra	FFG_309	434.60	Richey, 1989, Table 2, p.40
74	Culebra	FFG_310	475.20	Richey, 1989, Table 2, p.40
75	Culebra	FFG_311	428.60	Richey, 1989, Table 2, p.40
76	Culebra	FFG_312	429.80	Richey, 1989, Table 2, p.40

Table B.2. Elevations of Stratigraphic Layers Near WIPP (Continued)

	Layer	Well ID	Elevation	Source
1	Culebra	FFG_313	870.30	Richey, 1989, Table 2, p.41
2	Culebra	FFG_314	788.90	Richey, 1989, Table 2, p.41
3	Culebra	FFG_315	701.50	Richey, 1989, Table 2, p.41
4	Culebra	FFG_316	678.40	Richey, 1989, Table 2, p.41
5	Culebra	FFG_317	732.40	Richey, 1989, Table 2, p.41
6	Culebra	FFG_318	710.20	Richey, 1989, Table 2, p.41
7	Culebra	FFG_319	704.60	Richey, 1989, Table 2, p.41
8	Culebra	FFG_320	669.40	Richey, 1989, Table 2, p.41
9	Culebra	FFG_321	668.40	Richey, 1989, Table 2, p.41
10	Culebra	FFG_322	669.80	Richey, 1989, Table 2, p.41
11	Culebra	FFG_323	675.20	Richey, 1989, Table 2, p.41
12	Culebra	FFG_324	699.50	Richey, 1989, Table 2, p.41
13	Culebra	FFG_325	762.30	Richey, 1989, Table 2, p.41
14	Culebra	FFG_326	706.50	Richey, 1989, Table 2, p.41
15	Culebra	FFG_327	689.80	Richey, 1989, Table 2, p.42
16	Culebra	FFG_328	673.80	Richey, 1989, Table 2, p.42
17	Culebra	FFG_329	669.00	Richey, 1989, Table 2, p.42
18	Culebra	FFG_330	669.50	Richey, 1989, Table 2, p.42
19	Culebra	FFG_331	652.90	Richey, 1989, Table 2, p.42
20	Culebra	FFG_332	639.50	Richey, 1989, Table 2, p.42
21	Culebra	FFG_333	650.60	Richey, 1989, Table 2, p.42
22	Culebra	FFG_334	644.90	Richey, 1989, Table 2, p.42
23	Culebra	FFG_335	663.30	Richey, 1989, Table 2, p.42
24	Culebra	FFG_336	658.10	Richey, 1989, Table 2, p.42
25	Culebra	FFG_337	641.90	Richey, 1989, Table 2, p.42
26	Culebra	FFG_338	646.90	Richey, 1989, Table 2, p.42
27	Culebra	FFG_339	611.70	Richey, 1989, Table 2, p.42
28	Culebra	FFG_340	617.80	Richey, 1989, Table 2, p.42
29	Culebra	FFG_342	682.70	Richey, 1989, Table 2, p.43
30	Culebra	FFG_344	659.10	Richey, 1989, Table 2, p.43
31	Culebra	FFG_345	678.60	Richey, 1989, Table 2, p.43
32	Culebra	FFG_347	699.50	Richey, 1989, Table 2, p.43
33	Culebra	FFG_348	738.50	Richey, 1989, Table 2, p.43
34	Culebra	FFG_349	714.50	Richey, 1989, Table 2, p.43
35	Culebra	FFG_350	745.20	Richey, 1989, Table 2, p.43
36	Culebra	FFG_351	629.40	Richey, 1989, Table 2, p.43
37	Culebra	FFG_352	629.40	Richey, 1989, Table 2, p.43
38	Culebra	FFG_353	651.10	Richey, 1989, Table 2, p.43
39	Culebra	FFG_354	762.00	Richey, 1989, Table 2, p.43
40	Culebra	FFG_361	955.20	Richey, 1989, Table 2, p.44
41	Culebra	FFG_362	919.30	Richey, 1989, Table 2, p.44
42	Culebra	FFG_363	947.00	Richey, 1989, Table 2, p.44
43	Culebra	FFG_364	918.30	Richey, 1989, Table 2, p.44
44	Culebra	FFG_366	911.60	Richey, 1989, Table 2, p.44
45	Culebra	FFG_367	931.70	Richey, 1989, Table 2, p.44
46	Culebra	FFG_370	968.70	Richey, 1989, Table 2, p.44
47	Culebra	FFG_371	965.70	Richey, 1989, Table 2, p.44
48	Culebra	FFG_372	949.10	Richey, 1989, Table 2, p.45
49	Culebra	FFG_373	909.00	Richey, 1989, Table 2, p.45
50	Culebra	FFG_374	908.30	Richey, 1989, Table 2, p.45
51	Culebra	FFG_376	947.60	Richey, 1989, Table 2, p.45
52	Culebra	FFG_381	914.70	Richey, 1989, Table 2, p.45
53	Culebra	FFG_383	908.30	Richey, 1989, Table 2, p.45
54	Culebra	FFG_384	921.10	Richey, 1989, Table 2, p.45
55	Culebra	FFG_385	915.90	Richey, 1989, Table 2, p.45
56	Culebra	FFG_387	911.10	Richey, 1989, Table 2, p.45
57	Culebra	FFG_388	900.70	Richey, 1989, Table 2, p.46
58	Culebra	FFG_389	924.80	Richey, 1989, Table 2, p.46
59	Culebra	FFG_390	919.60	Richey, 1989, Table 2, p.46
60	Culebra	FFG_391	919.20	Richey, 1989, Table 2, p.46
61	Culebra	FFG_392	910.50	Richey, 1989, Table 2, p.46
62	Culebra	FFG_393	785.60	Richey, 1989, Table 2, p.46
63	Culebra	FFG_394	882.40	Richey, 1989, Table 2, p.46
64	Culebra	FFG_395	874.50	Richey, 1989, Table 2, p.46
65	Culebra	FFG_396	853.80	Richey, 1989, Table 2, p.46
66	Culebra	FFG_398	771.70	Richey, 1989, Table 2, p.46
67	Culebra	FFG_399	785.20	Richey, 1989, Table 2, p.46
68	Culebra	FFG_401	839.70	Richey, 1989, Table 2, p.46
69	Culebra	FFG_402	947.10	Richey, 1989, Table 2, p.46
70	Culebra	FFG_403	914.60	Richey, 1989, Table 2, p.47
71	Culebra	FFG_404	873.30	Richey, 1989, Table 2, p.47
72	Culebra	FFG_407	908.00	Richey, 1989, Table 2, p.47
73	Culebra	FFG_408	907.10	Richey, 1989, Table 2, p.47
74	Culebra	FFG_409	943.10	Richey, 1989, Table 2, p.47
75	Culebra	FFG_411	887.30	Richey, 1989, Table 2, p.47
76	Culebra	FFG_413	915.10	Richey, 1989, Table 2, p.47

Table B.2. Elevations of Stratigraphic Layers Near WIPP (Continued)

	Layer	Well ID	Elevation	Source
1	Culebra	FFG_418	930.30	Richey, 1989, Table 2, p.48
2	Culebra	FFG_419	942.80	Richey, 1989, Table 2, p.48
3	Culebra	FFG_420	936.90	Richey, 1989, Table 2, p.48
4	Culebra	FFG_421	923.30	Richey, 1989, Table 2, p.48
5	Culebra	FFG_422	923.20	Richey, 1989, Table 2, p.48
6	Culebra	FFG_426	926.90	Richey, 1989, Table 2, p.48
7	Culebra	FFG_432	884.50	Richey, 1989, Table 2, p.48
8	Culebra	FFG_433	897.60	Richey, 1989, Table 2, p.48
9	Culebra	FFG_438	835.60	Richey, 1989, Table 2, p.49
10	Culebra	FFG_445	920.20	Richey, 1989, Table 2, p.49
11	Culebra	FFG_453	782.30	Richey, 1989, Table 2, p.50
12	Culebra	FFG_455	770.20	Richey, 1989, Table 2, p.50
13	Culebra	FFG_456	776.60	Richey, 1989, Table 2, p.50
14	Culebra	FFG_457	831.20	Richey, 1989, Table 2, p.50
15	Culebra	FFG_458	833.30	Richey, 1989, Table 2, p.50
16	Culebra	FFG_459	761.40	Richey, 1989, Table 2, p.50
17	Culebra	FFG_462	828.60	Richey, 1989, Table 2, p.50
18	Culebra	FFG_463	854.40	Richey, 1989, Table 2, p.51
19	Culebra	FFG_464	843.40	Richey, 1989, Table 2, p.51
20	Culebra	FFG_465	844.90	Richey, 1989, Table 2, p.51
21	Culebra	FFG_467	430.90	Richey, 1989, Table 2, p.51
22	Culebra	FFG_468	377.70	Richey, 1989, Table 2, p.51
23	Culebra	FFG_470	408.10	Richey, 1989, Table 2, p.51
24	Culebra	FFG_471	426.10	Richey, 1989, Table 2, p.51
25	Culebra	FFG_472	501.70	Richey, 1989, Table 2, p.51
26	Culebra	FFG_473	390.40	Richey, 1989, Table 2, p.51
27	Culebra	FFG_474	677.50	Richey, 1989, Table 2, p.51
28	Culebra	FFG_475	686.30	Richey, 1989, Table 2, p.51
29	Culebra	FFG_476	760.20	Richey, 1989, Table 2, p.51
30	Culebra	FFG_477	726.70	Richey, 1989, Table 2, p.51
31	Culebra	FFG_478	702.60	Richey, 1989, Table 2, p.52
32	Culebra	FFG_479	706.80	Richey, 1989, Table 2, p.52
33	Culebra	FFG_480	688.00	Richey, 1989, Table 2, p.52
34	Culebra	FFG_481	681.60	Richey, 1989, Table 2, p.52
35	Culebra	FFG_482	711.70	Richey, 1989, Table 2, p.52
36	Culebra	FFG_483	741.20	Richey, 1989, Table 2, p.52
37	Culebra	FFG_484	725.90	Richey, 1989, Table 2, p.52
38	Culebra	FFG_485	730.30	Richey, 1989, Table 2, p.52
39	Culebra	FFG_486	716.00	Richey, 1989, Table 2, p.52
40	Culebra	FFG_487	715.40	Richey, 1989, Table 2, p.52
41	Culebra	FFG_488	698.30	Richey, 1989, Table 2, p.52
42	Culebra	FFG_489	717.30	Richey, 1989, Table 2, p.52
43	Culebra	FFG_490	806.80	Richey, 1989, Table 2, p.52
44	Culebra	FFG_491	799.80	Richey, 1989, Table 2, p.52
45	Culebra	FFG_492	765.60	Richey, 1989, Table 2, p.52
46	Culebra	FFG_493	752.40	Richey, 1989, Table 2, p.53
47	Culebra	FFG_494	754.00	Richey, 1989, Table 2, p.53
48	Culebra	FFG_495	749.80	Richey, 1989, Table 2, p.53
49	Culebra	FFG_496	616.00	Richey, 1989, Table 2, p.53
50	Culebra	FFG_497	649.90	Richey, 1989, Table 2, p.53
51	Culebra	FFG_498	645.60	Richey, 1989, Table 2, p.53
52	Culebra	FFG_499	612.40	Richey, 1989, Table 2, p.53
53	Culebra	FFG_500	643.40	Richey, 1989, Table 2, p.53
54	Culebra	FFG_501	673.00	Richey, 1989, Table 2, p.53
55	Culebra	FFG_502	638.20	Richey, 1989, Table 2, p.53
56	Culebra	FFG_503	624.00	Richey, 1989, Table 2, p.53
57	Culebra	FFG_504	674.30	Richey, 1989, Table 2, p.53
58	Culebra	FFG_505	702.30	Richey, 1989, Table 2, p.53
59	Culebra	FFG_506	700.10	Richey, 1989, Table 2, p.53
60	Culebra	FFG_507	607.00	Richey, 1989, Table 2, p.53
61	Culebra	FFG_508	688.90	Richey, 1989, Table 2, p.53
62	Culebra	FFG_509	668.10	Richey, 1989, Table 2, p.54
63	Culebra	FFG_510	670.10	Richey, 1989, Table 2, p.54
64	Culebra	FFG_511	629.10	Richey, 1989, Table 2, p.54
65	Culebra	FFG_512	643.70	Richey, 1989, Table 2, p.54
66	Culebra	FFG_513	667.00	Richey, 1989, Table 2, p.54
67	Culebra	FFG_514	645.90	Richey, 1989, Table 2, p.54
68	Culebra	FFG_515	617.20	Richey, 1989, Table 2, p.54
69	Culebra	FFG_516	612.60	Richey, 1989, Table 2, p.54
70	Culebra	FFG_517	755.30	Richey, 1989, Table 2, p.54
71	Culebra	FFG_518	742.20	Richey, 1989, Table 2, p.54
72	Culebra	FFG_519	704.10	Richey, 1989, Table 2, p.54
73	Culebra	FFG_520	590.90	Richey, 1989, Table 2, p.54
74	Culebra	FFG_521	633.10	Richey, 1989, Table 2, p.54
75	Culebra	FFG_522	434.20	Richey, 1989, Table 2, p.54
76	Culebra	FFG_523	449.30	Richey, 1989, Table 2, p.54

Table B.2. Elevations of Stratigraphic Layers Near WIPP (Continued)

	Layer	Well ID	Elevation	Source
1	Culebra	FFG_524	616.00	Richey, 1989, Table 2, p.55
2	Culebra	FFG_525	443.90	Richey, 1989, Table 2, p.55
3	Culebra	FFG_526	950.70	Richey, 1989, Table 2, p.55
4	Culebra	FFG_527	894.20	Richey, 1989, Table 2, p.55
5	Culebra	FFG_528	896.10	Richey, 1989, Table 2, p.55
6	Culebra	FFG_530	965.90	Richey, 1989, Table 2, p.55
7	Culebra	FFG_531	894.90	Richey, 1989, Table 2, p.55
8	Culebra	FFG_532	879.70	Richey, 1989, Table 2, p.55
9	Culebra	FFG_534	892.80	Richey, 1989, Table 2, p.55
10	Culebra	FFG_535	882.10	Richey, 1989, Table 2, p.55
11	Culebra	FFG_536	892.50	Richey, 1989, Table 2, p.55
12	Culebra	FFG_537	879.90	Richey, 1989, Table 2, p.55
13	Culebra	FFG_543	932.20	Richey, 1989, Table 2, p.56
14	Culebra	FFG_548	883.30	Richey, 1989, Table 2, p.56
15	Culebra	FFG_552	732.70	Richey, 1989, Table 2, p.56
16	Culebra	FFG_562	621.80	Richey, 1989, Table 2, p.57
17	Culebra	FFG_563	537.40	Richey, 1989, Table 2, p.57
18	Culebra	FFG_568	631.90	Richey, 1989, Table 2, p.57
19	Culebra	FFG_569	632.80	Richey, 1989, Table 2, p.57
20	Culebra	FFG_584	742.70	Richey, 1989, Table 2, p.58
21	Culebra	FFG_585	686.70	Richey, 1989, Table 2, p.58
22	Culebra	FFG_600	700.10	Richey, 1989, Table 2, p.58
23	Culebra	FFG_601	580.00	Richey, 1989, Table 2, p.58
24	Culebra	FFG_602	803.50	Richey, 1989, Table 2, p.58
25	Culebra	FFG_606	673.70	Richey, 1989, Table 2, p.58
26	Culebra	FFG_607	681.30	Richey, 1989, Table 2, p.59
27	Culebra	FFG_608	663.20	Richey, 1989, Table 2, p.59
28	Culebra	FFG_609	656.50	Richey, 1989, Table 2, p.59
29	Culebra	FFG_610	649.20	Richey, 1989, Table 2, p.59
30	Culebra	FFG_611	644.00	Richey, 1989, Table 2, p.59
31	Culebra	FFG_612	679.10	Richey, 1989, Table 2, p.59
32	Culebra	FFG_613	677.90	Richey, 1989, Table 2, p.59
33	Culebra	FFG_618	686.70	Richey, 1989, Table 2, p.59
34	Culebra	FFG_638	536.80	Richey, 1989, Table 2, p.60
35	Culebra	FFG_639	508.10	Richey, 1989, Table 2, p.60
36	Culebra	FFG_640	597.80	Richey, 1989, Table 2, p.60
37	Culebra	FFG_643	642.30	Richey, 1989, Table 2, p.60
38	Culebra	FFG_644	677.20	Richey, 1989, Table 2, p.60
39	Culebra	FFG_648	513.30	Richey, 1989, Table 2, p.60
40	Culebra	FFG_652	822.90	Richey, 1989, Table 2, p.60
41	Culebra	FFG_653	822.70	Richey, 1989, Table 2, p.61
42	Culebra	FFG_654	845.80	Richey, 1989, Table 2, p.61
43	Culebra	FFG_655	847.30	Richey, 1989, Table 2, p.61
44	Culebra	FFG_656	845.20	Richey, 1989, Table 2, p.61
45	Culebra	FFG_657	862.90	Richey, 1989, Table 2, p.61
46	Culebra	FFG_658	849.40	Richey, 1989, Table 2, p.61
47	Culebra	FFG_659	856.80	Richey, 1989, Table 2, p.61
48	Culebra	FFG_660	873.40	Richey, 1989, Table 2, p.61
49	Culebra	FFG_662	843.40	Richey, 1989, Table 2, p.61
50	Culebra	FFG_664	836.40	Richey, 1989, Table 2, p.61
51	Culebra	FFG_666	890.00	Richey, 1989, Table 2, p.62
52	Culebra	FFG_667	875.70	Richey, 1989, Table 2, p.62
53	Culebra	FFG_668	926.10	Richey, 1989, Table 2, p.62
54	Culebra	FFG_669	912.90	Richey, 1989, Table 2, p.62
55	Culebra	FFG_670	897.30	Richey, 1989, Table 2, p.62
56	Culebra	FFG_671	900.00	Richey, 1989, Table 2, p.62
57	Culebra	FFG_672	897.10	Richey, 1989, Table 2, p.62
58	Culebra	FFG_673	894.20	Richey, 1989, Table 2, p.62
59	Culebra	FFG_674	893.40	Richey, 1989, Table 2, p.62
60	Culebra	FFG_675	851.50	Richey, 1989, Table 2, p.62
61	Culebra	FFG_676	862.30	Richey, 1989, Table 2, p.62
62	Culebra	FFG_677	889.70	Richey, 1989, Table 2, p.62
63	Culebra	FFG_679	891.20	Richey, 1989, Table 2, p.62
64	Culebra	FFG_685	918.10	Richey, 1989, Table 2, p.63
65	Culebra	FFG_689	764.50	Richey, 1989, Table 2, p.63
66	Culebra	FFG_690	768.70	Richey, 1989, Table 2, p.63
67	Culebra	FFG_691	760.80	Richey, 1989, Table 2, p.63
68	Culebra	FFG_692	749.90	Richey, 1989, Table 2, p.63
69	Culebra	FFG_693	760.40	Richey, 1989, Table 2, p.63
70	Culebra	FFG_694	750.40	Richey, 1989, Table 2, p.63
71	Culebra	FFG_695	756.50	Richey, 1989, Table 2, p.63
72	Culebra	FFG_696	758.30	Richey, 1989, Table 2, p.63
73	Culebra	FFG_697	760.20	Richey, 1989, Table 2, p.64
74	Culebra	FFG_698	802.00	Richey, 1989, Table 2, p.64
75	Culebra	FFG_699	755.60	Richey, 1989, Table 2, p.64
76	Culebra	FFG_700	749.30	Richey, 1989, Table 2, p.64

Table B.2. Elevations of Stratigraphic Layers Near WIPP (Continued)

	Layer	Well ID	Elevation	Source
1	Culebra	FFG_701	749.60	Richey, 1989, Table 2, p.64
2	Culebra	FFG_702	755.60	Richey, 1989, Table 2, p.64
3	Culebra	FFG_703	761.70	Richey, 1989, Table 2, p.64
4	Culebra	FFG_704	745.60	Richey, 1989, Table 2, p.64
5	Culebra	FFG_705	679.70	Richey, 1989, Table 2, p.64
6	Culebra	FFG_706	702.30	Richey, 1989, Table 2, p.64
7	Culebra	FFG_707	686.80	Richey, 1989, Table 2, p.64
8	Culebra	FFG_708	736.70	Richey, 1989, Table 2, p.64
9	Culebra	FFG_709	632.80	Richey, 1989, Table 2, p.64
10	Culebra	FFG_710	631.60	Richey, 1989, Table 2, p.64
11	Culebra	FFG_711	634.60	Richey, 1989, Table 2, p.65
12	Culebra	FFG_712	678.30	Richey, 1989, Table 2, p.65
13	Culebra	FFG_713	620.70	Richey, 1989, Table 2, p.65
14	Culebra	FFG_714	731.50	Richey, 1989, Table 2, p.65
15	Culebra	FFG_715	741.80	Richey, 1989, Table 2, p.65
16	Culebra	FFG_716	604.90	Richey, 1989, Table 2, p.65
17	Culebra	FFG_717	672.20	Richey, 1989, Table 2, p.65
18	Culebra	FFG_718	664.70	Richey, 1989, Table 2, p.65
19	Culebra	FFG_719	626.00	Richey, 1989, Table 2, p.65
20	Culebra	FFG_720	625.80	Richey, 1989, Table 2, p.65
21	Culebra	FFG_721	646.20	Richey, 1989, Table 2, p.65
22	Culebra	FFG_723	762.80	Richey, 1989, Table 2, p.65
23	Culebra	FFG_724	686.50	Richey, 1989, Table 2, p.65
24	Culebra	FFG_725	652.90	Richey, 1989, Table 2, p.65
25	Culebra	FFG_726	648.60	Richey, 1989, Table 2, p.65
26	Culebra	FFG_727	639.20	Richey, 1989, Table 2, p.66
27	Culebra	FFG_728	646.70	Richey, 1989, Table 2, p.66
28	Culebra	FFG_729	648.90	Richey, 1989, Table 2, p.66
29	Culebra	FFG_730	673.60	Richey, 1989, Table 2, p.66
30	Culebra	FFG_731	670.40	Richey, 1989, Table 2, p.66
31	Culebra	FFG_732	686.40	Richey, 1989, Table 2, p.66
32	Culebra	FFG_733	749.80	Richey, 1989, Table 2, p.66
33	Culebra	FFG_734	707.40	Richey, 1989, Table 2, p.66
34	Culebra	FFG_735	638.90	Richey, 1989, Table 2, p.66
35	Culebra	FFG_736	676.40	Richey, 1989, Table 2, p.66
36	Culebra	FFG_737	620.30	Richey, 1989, Table 2, p.66
37	Culebra	FFG_738	662.00	Richey, 1989, Table 2, p.66
38	Culebra	FFG_739	694.80	Richey, 1989, Table 2, p.66
39	Culebra	FFG_740	662.60	Richey, 1989, Table 2, p.66
40	Culebra	FFG_741	658.70	Richey, 1989, Table 2, p.66
41	Culebra	FFG_742	700.70	Richey, 1989, Table 2, p.67
42	Culebra	FFG_743	686.10	Richey, 1989, Table 2, p.67
43	Culebra	FFG_744	677.20	Richey, 1989, Table 2, p.67
44	Culebra	FFG_745	657.70	Richey, 1989, Table 2, p.67
45	Culebra	FFG_746	645.50	Richey, 1989, Table 2, p.67
46	Culebra	H1	829.70	Mercer, 1983, Table 1
47	Culebra	H10C	709.30	Mercer, 1983, Table 1
48	Culebra	H2C	839.70	Mercer, 1983, Table 1
49	Culebra	H3	828.50	Mercer, 1983, Table 1
50	Culebra	H4C	866.80	Mercer, 1983, Table 1
51	Culebra	H5C	794.90	Mercer, 1983, Table 1
52	Culebra	H6C	836.40	Mercer, 1983, Table 1
53	Culebra	H7C	891.90	Mercer, 1983, Table 1
54	Culebra	H8C	867.20	Mercer, 1983, Table 1
55	Culebra	H9C	840.90	Mercer, 1983, Table 1
56	Culebra	P1	855.60	Mercer, 1983, Table 1
57	Culebra	P10	785.70	Mercer, 1983, Table 1
58	Culebra	P11	790.00	Mercer, 1983, Table 1
59	Culebra	P12	835.50	Mercer, 1983, Table 1
60	Culebra	P13	835.50	Mercer, 1983, Table 1
61	Culebra	P14	849.40	Mercer, 1983, Table 1
62	Culebra	P15	883.00	Mercer, 1983, Table 1
63	Culebra	P16	858.90	Mercer, 1983, Table 1
64	Culebra	P17	846.70	Mercer, 1983, Table 1
65	Culebra	P18	782.70	Mercer, 1983, Table 1
66	Culebra	P19	785.80	Mercer, 1983, Table 1
67	Culebra	P2	799.20	Mercer, 1983, Table 1
68	Culebra	P20	792.50	Mercer, 1983, Table 1
69	Culebra	P21	795.50	Mercer, 1983, Table 1
70	Culebra	P3	835.40	Mercer, 1983, Table 1
71	Culebra	P4	813.50	Mercer, 1983, Table 1
72	Culebra	P5	812.90	Mercer, 1983, Table 1
73	Culebra	P6	858.60	Mercer, 1983, Table 1
74	Culebra	P7	864.40	Mercer, 1983, Table 1
75	Culebra	P8	846.10	Mercer, 1983, Table 1
76	Culebra	P9	816.30	Mercer, 1983, Table 1

Table B.2. Elevations of Stratigraphic Layers Near WIPP (Continued)

	Layer	Well ID	Elevation	Source
1	Culebra	REF	823.40	Rechard et al.,1991, Figure 2.2-1
2	Culebra	SaltShft	822.81	Bechtel, Inc., 1986, Appendix D
3	Culebra	WIPP11	786.90	Mercer, 1983, Table 1
4	Culebra	WIPP11	787.00	SNL and USGS, 1982a, Table 2
5	Culebra	WIPP12	811.30	SNL and D'Appolonia Consulting, 1983, Table 2
6	Culebra	WIPP12	811.40	Mercer, 1983, Table 1
7	Culebra	WIPP13	824.10	Mercer, 1983, Table 1
8	Culebra	WIPP16	679.70	Mercer, 1983, Table 1
9	Culebra	WIPP18	813.80	Mercer, 1983, Table 1
10	Culebra	WIPP19	816.00	Mercer, 1983, Table 1
11	Culebra	WIPP21	819.30	Mercer, 1983, Table 1
12	Culebra	WIPP22	818.00	Mercer, 1983, Table 1
13	Culebra	WIPP25	843.10	Mercer, 1983, Table 1
14	Culebra	WIPP26	904.00	Mercer, 1983, Table 1
15	Culebra	WIPP27	879.30	Mercer, 1983, Table 1
16	Culebra	WIPP28	892.20	Mercer, 1983, Table 1
17	Culebra	WIPP29	903.70	Mercer, 1983, Table 1
18	Culebra	WIPP30	852.60	Mercer, 1983, Table 1
19	Culebra	WIPP32	902.80	Mercer, 1983, Table 1
20	Culebra	WIPP33	845.30	Mercer, 1983, Table 1
21	Culebra	WIPP34	792.20	Mercer, 1983, Table 1
22	Culebra	WastShft	823.64	Bechtel, Inc., 1986, Appendix E
23	DeweyLk	AirShft	1022.02	Holt and Powers, 1990, Figure 22
24	DeweyLk	DOE1	1018.10	U.S. DOE, Sep 1982, Table 2
25	DeweyLk	DOE2	1001.30	Mercer et al., 1987, Table 3-2
26	DeweyLk	ERDA9	1023.30	SNL and USGS, 1982b, Table 2
27	DeweyLk	ExhtShft	1022.73	Bechtel, Inc., 1986, Appendix F
28	DeweyLk	REF	1023.30	Rechard et al.,1991, Figure 2.2-1
29	DeweyLk	SaltShft	1025.35	Bechtel, Inc., 1986, Appendix D
30	DeweyLk	WIPP11	995.20	SNL and USGS, 1982a, Table 2
31	DeweyLk	WIPP12	1010.90	SNL and D'Appolonia Consulting, 1983, Table 2
32	DeweyLk	WastShft	1009.97	Bechtel, Inc., 1986, Appendix E
33	Halite1	DOE1	-170.40	U.S. DOE, Sep 1982, Table 2
34	Halite1	DOE1	-71.60	U.S. DOE, Sep 1982, Table 2
35	Halite1	DOE2	-119.10	Mercer et al., 1987, Table 3-2
36	Halite1	DOE2	-116.40	Mercer et al., 1987, Table 3-2
37	Halite1	REF	-119.10	Rechard et al.,1991, Figure 2.2-1
38	Halite1	REF	-116.40	Rechard et al.,1991, Figure 2.2-1
39	Halite1	WIPP11	-37.80	SNL and USGS, 1982a, Table 2
40	Halite1	WIPP11	-22.20	SNL and USGS, 1982a, Table 2
41	Halite1	WIPP12	-131.10	SNL and D'Appolonia Consulting, 1983, Table 2
42	Halite1	WIPP12	24.50	SNL and D'Appolonia Consulting, 1983, Table 2
43	Halite2	DOE1	-38.60	U.S. DOE, Sep 1982, Table 2
44	Halite2	DOE1	30.00	U.S. DOE, Sep 1982, Table 2
45	Halite2	WIPP11	14.40	SNL and USGS, 1982a, Table 2
46	Halite2	WIPP11	309.40	SNL and USGS, 1982a, Table 2
47	Halite2	WIPP12	57.80	SNL and D'Appolonia Consulting, 1983, Table 2
48	Halite2	WIPP12	127.30	SNL and D'Appolonia Consulting, 1983, Table 2
49	L_Member	DOE1	163.60	U.S. DOE, Sep 1982, Table 2
50	L_Member	DOE2	102.30	Mercer et al., 1987, Table 3-2
51	L_Member	ERDA9	178.10	SNL and USGS, 1982b, Table 2
52	L_Member	REF	178.10	Rechard et al.,1991, Figure 2.2-1
53	L_Member	WIPP11	334.10	SNL and USGS, 1982a, Table 2
54	L_Member	WIPP12	227.40	SNL and D'Appolonia Consulting, 1983, Table 2
55	M49er	AEC7	911.90	Mercer, 1983, Table 1
56	M49er	AEC8	875.40	Mercer, 1983, Table 1
57	M49er	AirShft	877.42	Holt and Powers, 1990, Figure 22
58	M49er	B25	876.60	Mercer, 1983, Table 1
59	M49er	DOE1	855.20	U.S. DOE, Sep 1982, Table 2
60	M49er	DOE2	847.10	Mercer et al., 1987, Table 3-2
61	M49er	ERDA6	915.60	Mercer, 1983, Table 1
62	M49er	ERDA9	878.10	Mercer, 1983, Table 1
63	M49er	ERDA9	874.00	SNL and USGS, 1982b, Table 2
64	M49er	ExhtShft	872.52	Bechtel, Inc., 1986, Appendix F
65	M49er	FFG_002	686.10	Richey, 1989, Table 2, p.21
66	M49er	FFG_004	739.10	Richey, 1989, Table 2, p.21
67	M49er	FFG_005	693.80	Richey, 1989, Table 2, p.21
68	M49er	FFG_006	688.90	Richey, 1989, Table 2, p.21
69	M49er	FFG_007	678.20	Richey, 1989, Table 2, p.21
70	M49er	FFG_009	678.10	Richey, 1989, Table 2, p.21
71	M49er	FFG_011	684.60	Richey, 1989, Table 2, p.21
72	M49er	FFG_012	687.00	Richey, 1989, Table 2, p.21
73	M49er	FFG_013	696.80	Richey, 1989, Table 2, p.21
74	M49er	FFG_014	741.90	Richey, 1989, Table 2, p.21
75	M49er	FFG_016	666.90	Richey, 1989, Table 2, p.21
76	M49er	FFG_017	669.60	Richey, 1989, Table 2, p.22

Table B.2. Elevations of Stratigraphic Layers Near WIPP (Continued)

	Layer	Well ID	Elevation	Source
1	M49er	FFG_018	672.40	Richey, 1989, Table 2, p.22
2	M49er	FFG_019	666.30	Richey, 1989, Table 2, p.22
3	M49er	FFG_020	740.70	Richey, 1989, Table 2, p.22
4	M49er	FFG_023	678.50	Richey, 1989, Table 2, p.22
5	M49er	FFG_024	662.00	Richey, 1989, Table 2, p.22
6	M49er	FFG_025	674.10	Richey, 1989, Table 2, p.22
7	M49er	FFG_026	670.80	Richey, 1989, Table 2, p.22
8	M49er	FFG_027	664.20	Richey, 1989, Table 2, p.22
9	M49er	FFG_028	629.80	Richey, 1989, Table 2, p.22
10	M49er	FFG_029	616.00	Richey, 1989, Table 2, p.22
11	M49er	FFG_030	616.60	Richey, 1989, Table 2, p.22
12	M49er	FFG_031	609.60	Richey, 1989, Table 2, p.22
13	M49er	FFG_032	611.90	Richey, 1989, Table 2, p.22
14	M49er	FFG_033	607.20	Richey, 1989, Table 2, p.22
15	M49er	FFG_034	601.30	Richey, 1989, Table 2, p.23
16	M49er	FFG_035	590.30	Richey, 1989, Table 2, p.23
17	M49er	FFG_036	602.60	Richey, 1989, Table 2, p.23
18	M49er	FFG_037	592.90	Richey, 1989, Table 2, p.23
19	M49er	FFG_038	579.40	Richey, 1989, Table 2, p.23
20	M49er	FFG_039	798.60	Richey, 1989, Table 2, p.23
21	M49er	FFG_040	740.70	Richey, 1989, Table 2, p.23
22	M49er	FFG_041	801.00	Richey, 1989, Table 2, p.23
23	M49er	FFG_042	805.50	Richey, 1989, Table 2, p.23
24	M49er	FFG_043	810.00	Richey, 1989, Table 2, p.23
25	M49er	FFG_044	762.30	Richey, 1989, Table 2, p.23
26	M49er	FFG_047	633.40	Richey, 1989, Table 2, p.23
27	M49er	FFG_048	653.20	Richey, 1989, Table 2, p.23
28	M49er	FFG_049	641.90	Richey, 1989, Table 2, p.23
29	M49er	FFG_050	648.00	Richey, 1989, Table 2, p.24
30	M49er	FFG_051	648.90	Richey, 1989, Table 2, p.24
31	M49er	FFG_052	651.60	Richey, 1989, Table 2, p.24
32	M49er	FFG_053	642.80	Richey, 1989, Table 2, p.24
33	M49er	FFG_054	641.90	Richey, 1989, Table 2, p.24
34	M49er	FFG_055	641.60	Richey, 1989, Table 2, p.24
35	M49er	FFG_056	644.30	Richey, 1989, Table 2, p.24
36	M49er	FFG_057	645.60	Richey, 1989, Table 2, p.24
37	M49er	FFG_058	641.00	Richey, 1989, Table 2, p.24
38	M49er	FFG_059	643.40	Richey, 1989, Table 2, p.24
39	M49er	FFG_060	645.50	Richey, 1989, Table 2, p.24
40	M49er	FFG_061	645.90	Richey, 1989, Table 2, p.24
41	M49er	FFG_062	574.30	Richey, 1989, Table 2, p.24
42	M49er	FFG_063	534.70	Richey, 1989, Table 2, p.24
43	M49er	FFG_064	559.70	Richey, 1989, Table 2, p.24
44	M49er	FFG_065	542.90	Richey, 1989, Table 2, p.24
45	M49er	FFG_066	496.80	Richey, 1989, Table 2, p.24
46	M49er	FFG_067	537.10	Richey, 1989, Table 2, p.25
47	M49er	FFG_068	496.50	Richey, 1989, Table 2, p.25
48	M49er	FFG_069	524.30	Richey, 1989, Table 2, p.25
49	M49er	FFG_070	553.80	Richey, 1989, Table 2, p.25
50	M49er	FFG_071	811.10	Richey, 1989, Table 2, p.25
51	M49er	FFG_072	739.70	Richey, 1989, Table 2, p.25
52	M49er	FFG_073	717.80	Richey, 1989, Table 2, p.25
53	M49er	FFG_074	723.70	Richey, 1989, Table 2, p.25
54	M49er	FFG_075	773.30	Richey, 1989, Table 2, p.25
55	M49er	FFG_076	836.40	Richey, 1989, Table 2, p.25
56	M49er	FFG_078	874.40	Richey, 1989, Table 2, p.25
57	M49er	FFG_079	848.00	Richey, 1989, Table 2, p.25
58	M49er	FFG_080	827.50	Richey, 1989, Table 2, p.25
59	M49er	FFG_081	746.80	Richey, 1989, Table 2, p.26
60	M49er	FFG_082	779.10	Richey, 1989, Table 2, p.26
61	M49er	FFG_083	693.00	Richey, 1989, Table 2, p.26
62	M49er	FFG_084	721.10	Richey, 1989, Table 2, p.26
63	M49er	FFG_085	714.20	Richey, 1989, Table 2, p.26
64	M49er	FFG_086	722.60	Richey, 1989, Table 2, p.26
65	M49er	FFG_087	698.00	Richey, 1989, Table 2, p.26
66	M49er	FFG_088	694.40	Richey, 1989, Table 2, p.26
67	M49er	FFG_089	675.80	Richey, 1989, Table 2, p.26
68	M49er	FFG_091	720.00	Richey, 1989, Table 2, p.26
69	M49er	FFG_092	734.90	Richey, 1989, Table 2, p.26
70	M49er	FFG_093	737.30	Richey, 1989, Table 2, p.26
71	M49er	FFG_094	740.60	Richey, 1989, Table 2, p.26
72	M49er	FFG_095	706.50	Richey, 1989, Table 2, p.26
73	M49er	FFG_096	689.50	Richey, 1989, Table 2, p.26
74	M49er	FFG_097	671.20	Richey, 1989, Table 2, p.27
75	M49er	FFG_098	645.50	Richey, 1989, Table 2, p.27
76	M49er	FFG_099	641.60	Richey, 1989, Table 2, p.27

Table B.2. Elevations of Stratigraphic Layers Near WIPP (Continued)

	Layer	Well ID	Elevation	Source
1	M49er	FFG_100	624.90	Richey, 1989, Table 2, p.27
2	M49er	FFG_101	593.10	Richey, 1989, Table 2, p.27
3	M49er	FFG_102	613.90	Richey, 1989, Table 2, p.27
4	M49er	FFG_103	674.60	Richey, 1989, Table 2, p.27
5	M49er	FFG_104	572.50	Richey, 1989, Table 2, p.27
6	M49er	FFG_105	926.90	Richey, 1989, Table 2, p.27
7	M49er	FFG_106	954.70	Richey, 1989, Table 2, p.27
8	M49er	FFG_107	945.20	Richey, 1989, Table 2, p.27
9	M49er	FFG_108	933.60	Richey, 1989, Table 2, p.27
10	M49er	FFG_109	917.20	Richey, 1989, Table 2, p.27
11	M49er	FFG_110	887.00	Richey, 1989, Table 2, p.27
12	M49er	FFG_111	896.70	Richey, 1989, Table 2, p.27
13	M49er	FFG_112	879.30	Richey, 1989, Table 2, p.28
14	M49er	FFG_113	893.40	Richey, 1989, Table 2, p.28
15	M49er	FFG_114	924.20	Richey, 1989, Table 2, p.28
16	M49er	FFG_115	913.80	Richey, 1989, Table 2, p.28
17	M49er	FFG_116	929.30	Richey, 1989, Table 2, p.28
18	M49er	FFG_117	935.70	Richey, 1989, Table 2, p.28
19	M49er	FFG_120	944.30	Richey, 1989, Table 2, p.28
20	M49er	FFG_121	946.40	Richey, 1989, Table 2, p.28
21	M49er	FFG_122	944.90	Richey, 1989, Table 2, p.28
22	M49er	FFG_123	928.10	Richey, 1989, Table 2, p.28
23	M49er	FFG_124	900.40	Richey, 1989, Table 2, p.28
24	M49er	FFG_125	912.20	Richey, 1989, Table 2, p.28
25	M49er	FFG_126	904.50	Richey, 1989, Table 2, p.28
26	M49er	FFG_127	909.50	Richey, 1989, Table 2, p.28
27	M49er	FFG_128	948.00	Richey, 1989, Table 2, p.28
28	M49er	FFG_129	923.80	Richey, 1989, Table 2, p.28
29	M49er	FFG_130	954.00	Richey, 1989, Table 2, p.28
30	M49er	FFG_132	956.50	Richey, 1989, Table 2, p.29
31	M49er	FFG_133	959.50	Richey, 1989, Table 2, p.29
32	M49er	FFG_134	963.80	Richey, 1989, Table 2, p.29
33	M49er	FFG_135	937.30	Richey, 1989, Table 2, p.29
34	M49er	FFG_136	934.30	Richey, 1989, Table 2, p.29
35	M49er	FFG_137	946.80	Richey, 1989, Table 2, p.29
36	M49er	FFG_138	897.40	Richey, 1989, Table 2, p.29
37	M49er	FFG_139	907.70	Richey, 1989, Table 2, p.29
38	M49er	FFG_140	849.10	Richey, 1989, Table 2, p.29
39	M49er	FFG_141	873.10	Richey, 1989, Table 2, p.29
40	M49er	FFG_142	849.30	Richey, 1989, Table 2, p.29
41	M49er	FFG_143	855.80	Richey, 1989, Table 2, p.29
42	M49er	FFG_159	956.20	Richey, 1989, Table 2, p.30
43	M49er	FFG_160	950.10	Richey, 1989, Table 2, p.30
44	M49er	FFG_161	957.40	Richey, 1989, Table 2, p.30
45	M49er	FFG_162	955.90	Richey, 1989, Table 2, p.30
46	M49er	FFG_163	955.30	Richey, 1989, Table 2, p.30
47	M49er	FFG_166	954.30	Richey, 1989, Table 2, p.31
48	M49er	FFG_167	936.70	Richey, 1989, Table 2, p.31
49	M49er	FFG_168	967.50	Richey, 1989, Table 2, p.31
50	M49er	FFG_169	980.20	Richey, 1989, Table 2, p.31
51	M49er	FFG_170	933.60	Richey, 1989, Table 2, p.31
52	M49er	FFG_173	934.80	Richey, 1989, Table 2, p.31
53	M49er	FFG_180	943.90	Richey, 1989, Table 2, p.31
54	M49er	FFG_182	856.50	Richey, 1989, Table 2, p.32
55	M49er	FFG_189	922.70	Richey, 1989, Table 2, p.32
56	M49er	FFG_190	901.60	Richey, 1989, Table 2, p.32
57	M49er	FFG_191	901.30	Richey, 1989, Table 2, p.32
58	M49er	FFG_192	834.50	Richey, 1989, Table 2, p.32
59	M49er	FFG_194	839.70	Richey, 1989, Table 2, p.33
60	M49er	FFG_195	855.30	Richey, 1989, Table 2, p.33
61	M49er	FFG_196	897.60	Richey, 1989, Table 2, p.33
62	M49er	FFG_197	899.50	Richey, 1989, Table 2, p.33
63	M49er	FFG_198	898.20	Richey, 1989, Table 2, p.33
64	M49er	FFG_199	888.80	Richey, 1989, Table 2, p.33
65	M49er	FFG_200	902.50	Richey, 1989, Table 2, p.33
66	M49er	FFG_201	894.60	Richey, 1989, Table 2, p.33
67	M49er	FFG_202	834.20	Richey, 1989, Table 2, p.33
68	M49er	FFG_203	841.30	Richey, 1989, Table 2, p.33
69	M49er	FFG_204	864.80	Richey, 1989, Table 2, p.33
70	M49er	FFG_205	880.60	Richey, 1989, Table 2, p.33
71	M49er	FFG_206	895.80	Richey, 1989, Table 2, p.33
72	M49er	FFG_207	892.20	Richey, 1989, Table 2, p.33
73	M49er	FFG_208	902.80	Richey, 1989, Table 2, p.34
74	M49er	FFG_210	885.80	Richey, 1989, Table 2, p.34
75	M49er	FFG_212	870.50	Richey, 1989, Table 2, p.34
76	M49er	FFG_213	903.50	Richey, 1989, Table 2, p.34

Table B.2. Elevations of Stratigraphic Layers Near WIPP (Continued)

	Layer	Well ID	Elevation	Source		Layer	Well ID	Elevation	Source
1	M49er	FFG_214	877.80	Richey, 1989, Table 2, p.34	39	M49er	FFG_254	651.00	Richey, 1989, Table 2, p.36
2	M49er	FFG_215	852.50	Richey, 1989, Table 2, p.34	40	M49er	FFG_255	609.90	Richey, 1989, Table 2, p.37
3	M49er	FFG_216	737.00	Richey, 1989, Table 2, p.34	41	M49er	FFG_256	557.80	Richey, 1989, Table 2, p.37
4	M49er	FFG_217	873.60	Richey, 1989, Table 2, p.34	42	M49er	FFG_257	600.40	Richey, 1989, Table 2, p.37
5	M49er	FFG_218	863.50	Richey, 1989, Table 2, p.34	43	M49er	FFG_258	615.00	Richey, 1989, Table 2, p.37
6	M49er	FFG_219	910.40	Richey, 1989, Table 2, p.34	44	M49er	FFG_259	584.90	Richey, 1989, Table 2, p.37
7	M49er	FFG_220	859.90	Richey, 1989, Table 2, p.34	45	M49er	FFG_260	621.80	Richey, 1989, Table 2, p.37
8	M49er	FFG_221	814.40	Richey, 1989, Table 2, p.34	46	M49er	FFG_261	610.20	Richey, 1989, Table 2, p.37
9	M49er	FFG_222	770.60	Richey, 1989, Table 2, p.34	47	M49er	FFG_263	553.40	Richey, 1989, Table 2, p.37
10	M49er	FFG_224	677.00	Richey, 1989, Table 2, p.35	48	M49er	FFG_264	777.60	Richey, 1989, Table 2, p.37
11	M49er	FFG_225	683.70	Richey, 1989, Table 2, p.35	49	M49er	FFG_265	775.40	Richey, 1989, Table 2, p.37
12	M49er	FFG_226	683.20	Richey, 1989, Table 2, p.35	50	M49er	FFG_266	758.90	Richey, 1989, Table 2, p.37
13	M49er	FFG_228	673.70	Richey, 1989, Table 2, p.35	51	M49er	FFG_267	736.40	Richey, 1989, Table 2, p.37
14	M49er	FFG_229	701.60	Richey, 1989, Table 2, p.35	52	M49er	FFG_268	716.00	Richey, 1989, Table 2, p.37
15	M49er	FFG_230	688.60	Richey, 1989, Table 2, p.35	53	M49er	FFG_269	729.20	Richey, 1989, Table 2, p.38
16	M49er	FFG_231	704.00	Richey, 1989, Table 2, p.35	54	M49er	FFG_270	791.80	Richey, 1989, Table 2, p.38
17	M49er	FFG_232	717.80	Richey, 1989, Table 2, p.35	55	M49er	FFG_271	833.90	Richey, 1989, Table 2, p.38
18	M49er	FFG_233	709.30	Richey, 1989, Table 2, p.35	56	M49er	FFG_272	846.60	Richey, 1989, Table 2, p.38
19	M49er	FFG_234	745.80	Richey, 1989, Table 2, p.35	57	M49er	FFG_273	816.90	Richey, 1989, Table 2, p.38
20	M49er	FFG_235	722.40	Richey, 1989, Table 2, p.35	58	M49er	FFG_274	851.00	Richey, 1989, Table 2, p.38
21	M49er	FFG_236	768.40	Richey, 1989, Table 2, p.35	59	M49er	FFG_275	858.60	Richey, 1989, Table 2, p.38
22	M49er	FFG_237	735.30	Richey, 1989, Table 2, p.35	60	M49er	FFG_276	861.60	Richey, 1989, Table 2, p.38
23	M49er	FFG_238	716.60	Richey, 1989, Table 2, p.36	61	M49er	FFG_277	853.50	Richey, 1989, Table 2, p.38
24	M49er	FFG_239	703.10	Richey, 1989, Table 2, p.36	62	M49er	FFG_278	868.40	Richey, 1989, Table 2, p.38
25	M49er	FFG_240	695.20	Richey, 1989, Table 2, p.36	63	M49er	FFG_279	860.10	Richey, 1989, Table 2, p.38
26	M49er	FFG_241	688.90	Richey, 1989, Table 2, p.36	64	M49er	FFG_280	858.60	Richey, 1989, Table 2, p.38
27	M49er	FFG_242	799.80	Richey, 1989, Table 2, p.36	65	M49er	FFG_281	835.80	Richey, 1989, Table 2, p.38
28	M49er	FFG_243	763.80	Richey, 1989, Table 2, p.36	66	M49er	FFG_283	584.60	Richey, 1989, Table 2, p.39
29	M49er	FFG_244	798.40	Richey, 1989, Table 2, p.36	67	M49er	FFG_284	730.30	Richey, 1989, Table 2, p.39
30	M49er	FFG_245	597.10	Richey, 1989, Table 2, p.36	68	M49er	FFG_285	760.20	Richey, 1989, Table 2, p.39
31	M49er	FFG_246	601.70	Richey, 1989, Table 2, p.36	69	M49er	FFG_286	837.50	Richey, 1989, Table 2, p.39
32	M49er	FFG_247	589.10	Richey, 1989, Table 2, p.36	70	M49er	FFG_287	812.00	Richey, 1989, Table 2, p.39
33	M49er	FFG_248	594.70	Richey, 1989, Table 2, p.36	71	M49er	FFG_288	765.70	Richey, 1989, Table 2, p.39
34	M49er	FFG_249	593.70	Richey, 1989, Table 2, p.36	72	M49er	FFG_289	736.30	Richey, 1989, Table 2, p.39
35	M49er	FFG_250	674.10	Richey, 1989, Table 2, p.36	73	M49er	FFG_290	825.70	Richey, 1989, Table 2, p.39
36	M49er	FFG_251	568.70	Richey, 1989, Table 2, p.36	74	M49er	FFG_291	766.20	Richey, 1989, Table 2, p.39
37	M49er	FFG_252	708.60	Richey, 1989, Table 2, p.36	75	M49er	FFG_292	774.20	Richey, 1989, Table 2, p.39
38	M49er	FFG_253	660.50	Richey, 1989, Table 2, p.36	76	M49er	FFG_293	766.00	Richey, 1989, Table 2, p.39

Table B.2. Elevations of Stratigraphic Layers Near WIPP (Continued)

	Layer	Well ID	Elevation	Source
1	M49er	FFG_294	595.30	Richey, 1989, Table 2, p.39
2	M49er	FFG_295	582.80	Richey, 1989, Table 2, p.39
3	M49er	FFG_297	567.50	Richey, 1989, Table 2, p.39
4	M49er	FFG_298	569.20	Richey, 1989, Table 2, p.40
5	M49er	FFG_299	594.40	Richey, 1989, Table 2, p.40
6	M49er	FFG_300	543.70	Richey, 1989, Table 2, p.40
7	M49er	FFG_301	514.80	Richey, 1989, Table 2, p.40
8	M49er	FFG_302	542.50	Richey, 1989, Table 2, p.40
9	M49er	FFG_303	535.90	Richey, 1989, Table 2, p.40
10	M49er	FFG_304	540.40	Richey, 1989, Table 2, p.40
11	M49er	FFG_305	534.60	Richey, 1989, Table 2, p.40
12	M49er	FFG_306	492.20	Richey, 1989, Table 2, p.40
13	M49er	FFG_307	517.90	Richey, 1989, Table 2, p.40
14	M49er	FFG_308	491.30	Richey, 1989, Table 2, p.40
15	M49er	FFG_309	535.20	Richey, 1989, Table 2, p.40
16	M49er	FFG_310	564.20	Richey, 1989, Table 2, p.40
17	M49er	FFG_311	498.70	Richey, 1989, Table 2, p.40
18	M49er	FFG_312	537.40	Richey, 1989, Table 2, p.40
19	M49er	FFG_313	934.30	Richey, 1989, Table 2, p.41
20	M49er	FFG_314	862.30	Richey, 1989, Table 2, p.41
21	M49er	FFG_315	782.90	Richey, 1989, Table 2, p.41
22	M49er	FFG_316	771.40	Richey, 1989, Table 2, p.41
23	M49er	FFG_317	792.20	Richey, 1989, Table 2, p.41
24	M49er	FFG_318	758.00	Richey, 1989, Table 2, p.41
25	M49er	FFG_319	769.30	Richey, 1989, Table 2, p.41
26	M49er	FFG_320	762.30	Richey, 1989, Table 2, p.41
27	M49er	FFG_321	760.50	Richey, 1989, Table 2, p.41
28	M49er	FFG_322	755.10	Richey, 1989, Table 2, p.41
29	M49er	FFG_323	751.10	Richey, 1989, Table 2, p.41
30	M49er	FFG_324	761.70	Richey, 1989, Table 2, p.41
31	M49er	FFG_325	819.60	Richey, 1989, Table 2, p.41
32	M49er	FFG_326	754.40	Richey, 1989, Table 2, p.41
33	M49er	FFG_327	748.30	Richey, 1989, Table 2, p.42
34	M49er	FFG_328	757.00	Richey, 1989, Table 2, p.42
35	M49er	FFG_329	755.60	Richey, 1989, Table 2, p.42
36	M49er	FFG_330	754.90	Richey, 1989, Table 2, p.42
37	M49er	FFG_331	753.50	Richey, 1989, Table 2, p.42
38	M49er	FFG_332	744.00	Richey, 1989, Table 2, p.42
39	M49er	FFG_333	746.30	Richey, 1989, Table 2, p.42
40	M49er	FFG_334	743.10	Richey, 1989, Table 2, p.42
41	M49er	FFG_335	757.10	Richey, 1989, Table 2, p.42
42	M49er	FFG_336	754.40	Richey, 1989, Table 2, p.42
43	M49er	FFG_337	738.50	Richey, 1989, Table 2, p.42
44	M49er	FFG_338	744.80	Richey, 1989, Table 2, p.42
45	M49er	FFG_339	711.10	Richey, 1989, Table 2, p.42
46	M49er	FFG_340	721.40	Richey, 1989, Table 2, p.42
47	M49er	FFG_342	747.60	Richey, 1989, Table 2, p.43
48	M49er	FFG_344	713.40	Richey, 1989, Table 2, p.43
49	M49er	FFG_345	775.50	Richey, 1989, Table 2, p.43
50	M49er	FFG_347	766.00	Richey, 1989, Table 2, p.43
51	M49er	FFG_348	790.90	Richey, 1989, Table 2, p.43
52	M49er	FFG_349	764.20	Richey, 1989, Table 2, p.43
53	M49er	FFG_350	808.90	Richey, 1989, Table 2, p.43
54	M49er	FFG_351	732.20	Richey, 1989, Table 2, p.43
55	M49er	FFG_352	731.50	Richey, 1989, Table 2, p.43
56	M49er	FFG_353	751.70	Richey, 1989, Table 2, p.43
57	M49er	FFG_354	817.80	Richey, 1989, Table 2, p.43
58	M49er	FFG_361	1011.00	Richey, 1989, Table 2, p.44
59	M49er	FFG_366	960.40	Richey, 1989, Table 2, p.44
60	M49er	FFG_367	975.90	Richey, 1989, Table 2, p.44
61	M49er	FFG_371	1012.90	Richey, 1989, Table 2, p.44
62	M49er	FFG_374	946.40	Richey, 1989, Table 2, p.45
63	M49er	FFG_383	955.30	Richey, 1989, Table 2, p.45
64	M49er	FFG_384	976.00	Richey, 1989, Table 2, p.45
65	M49er	FFG_387	966.60	Richey, 1989, Table 2, p.45
66	M49er	FFG_388	959.20	Richey, 1989, Table 2, p.46
67	M49er	FFG_390	974.40	Richey, 1989, Table 2, p.46
68	M49er	FFG_391	973.50	Richey, 1989, Table 2, p.46
69	M49er	FFG_392	967.80	Richey, 1989, Table 2, p.46
70	M49er	FFG_393	835.60	Richey, 1989, Table 2, p.46
71	M49er	FFG_394	925.90	Richey, 1989, Table 2, p.46
72	M49er	FFG_395	918.40	Richey, 1989, Table 2, p.46
73	M49er	FFG_396	901.60	Richey, 1989, Table 2, p.46
74	M49er	FFG_398	825.70	Richey, 1989, Table 2, p.46
75	M49er	FFG_402	1002.50	Richey, 1989, Table 2, p.46
76	M49er	FFG_403	963.00	Richey, 1989, Table 2, p.47

Table B.2. Elevations of Stratigraphic Layers Near WIPP (Continued)

	Layer	Well ID	Elevation	Source		Layer	Well ID	Elevation	Source
1	M49er	FFG_404	925.70	Richey, 1989, Table 2, p.47	39	M49er	FFG_489	764.60	Richey, 1989, Table 2, p.52
2	M49er	FFG_407	958.30	Richey, 1989, Table 2, p.47	40	M49er	FFG_490	855.60	Richey, 1989, Table 2, p.52
3	M49er	FFG_419	997.00	Richey, 1989, Table 2, p.48	41	M49er	FFG_491	855.90	Richey, 1989, Table 2, p.52
4	M49er	FFG_420	992.70	Richey, 1989, Table 2, p.48	42	M49er	FFG_492	817.50	Richey, 1989, Table 2, p.52
5	M49er	FFG_421	983.60	Richey, 1989, Table 2, p.48	43	M49er	FFG_493	803.60	Richey, 1989, Table 2, p.53
6	M49er	FFG_422	976.60	Richey, 1989, Table 2, p.48	44	M49er	FFG_494	811.30	Richey, 1989, Table 2, p.53
7	M49er	FFG_432	931.80	Richey, 1989, Table 2, p.48	45	M49er	FFG_495	799.40	Richey, 1989, Table 2, p.53
8	M49er	FFG_438	892.60	Richey, 1989, Table 2, p.49	46	M49er	FFG_496	715.40	Richey, 1989, Table 2, p.53
9	M49er	FFG_455	837.60	Richey, 1989, Table 2, p.50	47	M49er	FFG_497	721.50	Richey, 1989, Table 2, p.53
10	M49er	FFG_456	829.00	Richey, 1989, Table 2, p.50	48	M49er	FFG_498	737.00	Richey, 1989, Table 2, p.53
11	M49er	FFG_457	885.10	Richey, 1989, Table 2, p.50	49	M49er	FFG_499	715.40	Richey, 1989, Table 2, p.53
12	M49er	FFG_458	888.20	Richey, 1989, Table 2, p.50	50	M49er	FFG_500	726.00	Richey, 1989, Table 2, p.53
13	M49er	FFG_459	816.60	Richey, 1989, Table 2, p.50	51	M49er	FFG_501	731.50	Richey, 1989, Table 2, p.53
14	M49er	FFG_462	884.10	Richey, 1989, Table 2, p.50	52	M49er	FFG_502	724.80	Richey, 1989, Table 2, p.53
15	M49er	FFG_463	913.50	Richey, 1989, Table 2, p.51	53	M49er	FFG_503	705.40	Richey, 1989, Table 2, p.53
16	M49er	FFG_464	900.40	Richey, 1989, Table 2, p.51	54	M49er	FFG_504	723.60	Richey, 1989, Table 2, p.53
17	M49er	FFG_465	902.80	Richey, 1989, Table 2, p.51	55	M49er	FFG_505	754.70	Richey, 1989, Table 2, p.53
18	M49er	FFG_467	506.20	Richey, 1989, Table 2, p.51	56	M49er	FFG_506	749.20	Richey, 1989, Table 2, p.53
19	M49er	FFG_468	493.50	Richey, 1989, Table 2, p.51	57	M49er	FFG_507	712.80	Richey, 1989, Table 2, p.53
20	M49er	FFG_470	509.60	Richey, 1989, Table 2, p.51	58	M49er	FFG_508	763.30	Richey, 1989, Table 2, p.53
21	M49er	FFG_471	525.80	Richey, 1989, Table 2, p.51	59	M49er	FFG_509	767.80	Richey, 1989, Table 2, p.54
22	M49er	FFG_472	564.20	Richey, 1989, Table 2, p.51	60	M49er	FFG_510	767.30	Richey, 1989, Table 2, p.54
23	M49er	FFG_473	491.60	Richey, 1989, Table 2, p.51	61	M49er	FFG_511	728.20	Richey, 1989, Table 2, p.54
24	M49er	FFG_474	750.70	Richey, 1989, Table 2, p.51	62	M49er	FFG_512	748.30	Richey, 1989, Table 2, p.54
25	M49er	FFG_475	749.70	Richey, 1989, Table 2, p.51	63	M49er	FFG_513	763.00	Richey, 1989, Table 2, p.54
26	M49er	FFG_476	821.80	Richey, 1989, Table 2, p.51	64	M49er	FFG_514	754.70	Richey, 1989, Table 2, p.54
27	M49er	FFG_477	774.50	Richey, 1989, Table 2, p.51	65	M49er	FFG_515	722.60	Richey, 1989, Table 2, p.54
28	M49er	FFG_478	755.60	Richey, 1989, Table 2, p.52	66	M49er	FFG_516	715.90	Richey, 1989, Table 2, p.54
29	M49er	FFG_479	752.50	Richey, 1989, Table 2, p.52	67	M49er	FFG_517	809.30	Richey, 1989, Table 2, p.54
30	M49er	FFG_480	754.40	Richey, 1989, Table 2, p.52	68	M49er	FFG_518	797.90	Richey, 1989, Table 2, p.54
31	M49er	FFG_481	731.80	Richey, 1989, Table 2, p.52	69	M49er	FFG_519	765.70	Richey, 1989, Table 2, p.54
32	M49er	FFG_482	761.40	Richey, 1989, Table 2, p.52	70	M49er	FFG_520	653.00	Richey, 1989, Table 2, p.54
33	M49er	FFG_483	785.10	Richey, 1989, Table 2, p.52	71	M49er	FFG_521	673.30	Richey, 1989, Table 2, p.54
34	M49er	FFG_484	772.20	Richey, 1989, Table 2, p.52	72	M49er	FFG_522	531.70	Richey, 1989, Table 2, p.54
35	M49er	FFG_485	779.40	Richey, 1989, Table 2, p.52	73	M49er	FFG_523	541.30	Richey, 1989, Table 2, p.54
36	M49er	FFG_486	766.30	Richey, 1989, Table 2, p.52	74	M49er	FFG_524	693.10	Richey, 1989, Table 2, p.55
37	M49er	FFG_487	763.90	Richey, 1989, Table 2, p.52	75	M49er	FFG_525	543.30	Richey, 1989, Table 2, p.55
38	M49er	FFG_488	748.00	Richey, 1989, Table 2, p.52	76	M49er	FFG_527	958.90	Richey, 1989, Table 2, p.55

Table B.2. Elevations of Stratigraphic Layers Near WIPP (Continued)

	Layer	Well ID	Elevation	Source
1	M49er	FFG_528	951.60	Richey, 1989, Table 2, p.55
2	M49er	FFG_535	939.70	Richey, 1989, Table 2, p.55
3	M49er	FFG_548	930.60	Richey, 1989, Table 2, p.56
4	M49er	FFG_562	670.60	Richey, 1989, Table 2, p.57
5	M49er	FFG_563	582.50	Richey, 1989, Table 2, p.57
6	M49er	FFG_569	689.20	Richey, 1989, Table 2, p.57
7	M49er	FFG_584	773.20	Richey, 1989, Table 2, p.58
8	M49er	FFG_600	729.10	Richey, 1989, Table 2, p.58
9	M49er	FFG_601	645.60	Richey, 1989, Table 2, p.58
10	M49er	FFG_606	723.00	Richey, 1989, Table 2, p.58
11	M49er	FFG_607	743.10	Richey, 1989, Table 2, p.59
12	M49er	FFG_608	754.60	Richey, 1989, Table 2, p.59
13	M49er	FFG_609	758.30	Richey, 1989, Table 2, p.59
14	M49er	FFG_610	746.70	Richey, 1989, Table 2, p.59
15	M49er	FFG_611	731.80	Richey, 1989, Table 2, p.59
16	M49er	FFG_612	733.40	Richey, 1989, Table 2, p.59
17	M49er	FFG_613	728.50	Richey, 1989, Table 2, p.59
18	M49er	FFG_620	759.80	Richey, 1989, Table 2, p.59
19	M49er	FFG_638	591.70	Richey, 1989, Table 2, p.60
20	M49er	FFG_639	566.30	Richey, 1989, Table 2, p.60
21	M49er	FFG_640	649.10	Richey, 1989, Table 2, p.60
22	M49er	FFG_643	688.90	Richey, 1989, Table 2, p.60
23	M49er	FFG_644	723.50	Richey, 1989, Table 2, p.60
24	M49er	FFG_648	558.40	Richey, 1989, Table 2, p.60
25	M49er	FFG_652	878.70	Richey, 1989, Table 2, p.60
26	M49er	FFG_653	880.00	Richey, 1989, Table 2, p.61
27	M49er	FFG_654	899.50	Richey, 1989, Table 2, p.61
28	M49er	FFG_655	897.30	Richey, 1989, Table 2, p.61
29	M49er	FFG_656	894.30	Richey, 1989, Table 2, p.61
30	M49er	FFG_657	906.20	Richey, 1989, Table 2, p.61
31	M49er	FFG_658	898.20	Richey, 1989, Table 2, p.61
32	M49er	FFG_659	901.90	Richey, 1989, Table 2, p.61
33	M49er	FFG_660	919.20	Richey, 1989, Table 2, p.61
34	M49er	FFG_662	894.60	Richey, 1989, Table 2, p.61
35	M49er	FFG_664	888.20	Richey, 1989, Table 2, p.61
36	M49er	FFG_666	938.10	Richey, 1989, Table 2, p.62
37	M49er	FFG_667	923.30	Richey, 1989, Table 2, p.62
38	M49er	FFG_670	946.10	Richey, 1989, Table 2, p.62
39	M49er	FFG_672	943.70	Richey, 1989, Table 2, p.62
40	M49er	FFG_674	937.00	Richey, 1989, Table 2, p.62
41	M49er	FFG_675	896.00	Richey, 1989, Table 2, p.62
42	M49er	FFG_676	905.00	Richey, 1989, Table 2, p.62
43	M49er	FFG_677	932.40	Richey, 1989, Table 2, p.62
44	M49er	FFG_679	934.80	Richey, 1989, Table 2, p.62
45	M49er	FFG_689	817.20	Richey, 1989, Table 2, p.63
46	M49er	FFG_690	824.80	Richey, 1989, Table 2, p.63
47	M49er	FFG_691	816.30	Richey, 1989, Table 2, p.63
48	M49er	FFG_692	806.20	Richey, 1989, Table 2, p.63
49	M49er	FFG_693	817.70	Richey, 1989, Table 2, p.63
50	M49er	FFG_694	810.10	Richey, 1989, Table 2, p.63
51	M49er	FFG_695	814.10	Richey, 1989, Table 2, p.63
52	M49er	FFG_696	815.90	Richey, 1989, Table 2, p.63
53	M49er	FFG_697	818.10	Richey, 1989, Table 2, p.64
54	M49er	FFG_698	861.40	Richey, 1989, Table 2, p.64
55	M49er	FFG_699	811.10	Richey, 1989, Table 2, p.64
56	M49er	FFG_700	801.40	Richey, 1989, Table 2, p.64
57	M49er	FFG_701	810.60	Richey, 1989, Table 2, p.64
58	M49er	FFG_702	811.70	Richey, 1989, Table 2, p.64
59	M49er	FFG_703	817.20	Richey, 1989, Table 2, p.64
60	M49er	FFG_704	806.20	Richey, 1989, Table 2, p.64
61	M49er	FFG_705	735.50	Richey, 1989, Table 2, p.64
62	M49er	FFG_706	755.00	Richey, 1989, Table 2, p.64
63	M49er	FFG_707	741.00	Richey, 1989, Table 2, p.64
64	M49er	FFG_708	791.60	Richey, 1989, Table 2, p.64
65	M49er	FFG_709	681.50	Richey, 1989, Table 2, p.64
66	M49er	FFG_710	682.50	Richey, 1989, Table 2, p.64
67	M49er	FFG_711	694.40	Richey, 1989, Table 2, p.65
68	M49er	FFG_712	735.60	Richey, 1989, Table 2, p.65
69	M49er	FFG_713	672.50	Richey, 1989, Table 2, p.65
70	M49er	FFG_714	790.30	Richey, 1989, Table 2, p.65
71	M49er	FFG_715	799.70	Richey, 1989, Table 2, p.65
72	M49er	FFG_716	697.90	Richey, 1989, Table 2, p.65
73	M49er	FFG_717	722.50	Richey, 1989, Table 2, p.65
74	M49er	FFG_718	723.50	Richey, 1989, Table 2, p.65
75	M49er	FFG_719	696.70	Richey, 1989, Table 2, p.65
76	M49er	FFG_720	699.60	Richey, 1989, Table 2, p.65

Table B.2. Elevations of Stratigraphic Layers Near WIPP (Continued)

	Layer	Well ID	Elevation	Source
1	M49er	FFG_721	698.00	Richey, 1989, Table 2, p.65
2	M49er	FFG_723	808.20	Richey, 1989, Table 2, p.65
3	M49er	FFG_724	738.90	Richey, 1989, Table 2, p.65
4	M49er	FFG_725	712.30	Richey, 1989, Table 2, p.65
5	M49er	FFG_726	698.90	Richey, 1989, Table 2, p.65
6	M49er	FFG_727	702.90	Richey, 1989, Table 2, p.66
7	M49er	FFG_728	696.40	Richey, 1989, Table 2, p.66
8	M49er	FFG_729	706.60	Richey, 1989, Table 2, p.66
9	M49er	FFG_730	724.80	Richey, 1989, Table 2, p.66
10	M49er	FFG_731	720.70	Richey, 1989, Table 2, p.66
11	M49er	FFG_732	739.50	Richey, 1989, Table 2, p.66
12	M49er	FFG_733	806.50	Richey, 1989, Table 2, p.66
13	M49er	FFG_734	758.60	Richey, 1989, Table 2, p.66
14	M49er	FFG_735	704.10	Richey, 1989, Table 2, p.66
15	M49er	FFG_736	758.70	Richey, 1989, Table 2, p.66
16	M49er	FFG_737	702.60	Richey, 1989, Table 2, p.66
17	M49er	FFG_738	713.80	Richey, 1989, Table 2, p.66
18	M49er	FFG_739	753.90	Richey, 1989, Table 2, p.66
19	M49er	FFG_740	754.70	Richey, 1989, Table 2, p.66
20	M49er	FFG_741	721.20	Richey, 1989, Table 2, p.66
21	M49er	FFG_742	774.50	Richey, 1989, Table 2, p.67
22	M49er	FFG_743	757.20	Richey, 1989, Table 2, p.67
23	M49er	FFG_744	739.70	Richey, 1989, Table 2, p.67
24	M49er	FFG_745	730.30	Richey, 1989, Table 2, p.67
25	M49er	FFG_746	719.80	Richey, 1989, Table 2, p.67
26	M49er	H1	882.70	Mercer, 1983, Table 1
27	M49er	H10C	756.80	Mercer, 1983, Table 1
28	M49er	H2C	890.30	Mercer, 1983, Table 1
29	M49er	H3	880.30	Mercer, 1983, Table 1
30	M49er	H4C	920.20	Mercer, 1983, Table 1
31	M49er	H5C	845.80	Mercer, 1983, Table 1
32	M49er	H6C	890.40	Mercer, 1983, Table 1
33	M49er	H7C	937.60	Mercer, 1983, Table 1
34	M49er	H8C	924.80	Mercer, 1983, Table 1
35	M49er	H9C	899.40	Mercer, 1983, Table 1
36	M49er	P1	910.50	Mercer, 1983, Table 1
37	M49er	P10	860.40	Mercer, 1983, Table 1
38	M49er	P11	840.90	Mercer, 1983, Table 1
39	M49er	P12	887.90	Mercer, 1983, Table 1
40	M49er	P13	889.50	Mercer, 1983, Table 1
41	M49er	P14	906.10	Mercer, 1983, Table 1
42	M49er	P15	938.50	Mercer, 1983, Table 1
43	M49er	P16	915.00	Mercer, 1983, Table 1
44	M49er	P17	900.40	Mercer, 1983, Table 1
45	M49er	P18	868.40	Mercer, 1983, Table 1
46	M49er	P19	849.50	Mercer, 1983, Table 1
47	M49er	P2	850.10	Mercer, 1983, Table 1
48	M49er	P20	845.30	Mercer, 1983, Table 1
49	M49er	P21	845.80	Mercer, 1983, Table 1
50	M49er	P3	888.50	Mercer, 1983, Table 1
51	M49er	P4	864.10	Mercer, 1983, Table 1
52	M49er	P5	868.10	Mercer, 1983, Table 1
53	M49er	P6	913.50	Mercer, 1983, Table 1
54	M49er	P7	920.50	Mercer, 1983, Table 1
55	M49er	P8	898.50	Mercer, 1983, Table 1
56	M49er	P9	868.70	Mercer, 1983, Table 1
57	M49er	REF	874.00	Rechard et al.,1991, Figure 2.2-1
58	M49er	SaltShft	875.54	Bechtel, Inc., 1986, Appendix D
59	M49er	WIPP11	842.10	Mercer, 1983, Table 1
60	M49er	WIPP11	842.20	SNL and USGS, 1982a, Table 2
61	M49er	WIPP12	866.80	SNL and D'Appolonia Consulting, 1983, Table 2
62	M49er	WIPP12	866.90	Mercer, 1983, Table 1
63	M49er	WIPP13	880.20	Mercer, 1983, Table 1
64	M49er	WIPP16	681.20	Mercer, 1983, Table 1
65	M49er	WIPP18	866.60	Mercer, 1983, Table 1
66	M49er	WIPP19	866.90	Mercer, 1983, Table 1
67	M49er	WIPP21	870.80	Mercer, 1983, Table 1
68	M49er	WIPP22	869.50	Mercer, 1983, Table 1
69	M49er	WIPP25	908.60	Mercer, 1983, Table 1
70	M49er	WIPP26	957.70	Mercer, 1983, Table 1
71	M49er	WIPP27	921.70	Mercer, 1983, Table 1
72	M49er	WIPP28	954.70	Mercer, 1983, Table 1
73	M49er	WIPP30	908.00	Mercer, 1983, Table 1
74	M49er	WIPP32	921.40	Mercer, 1983, Table 1
75	M49er	WIPP33	891.60	Mercer, 1983, Table 1
76	M49er	WIPP34	846.10	Mercer, 1983, Table 1

Table B.2. Elevations of Stratigraphic Layers Near WIPP (Continued)

	Layer	Well ID	Elevation	Source
1	M49er	WastShft	875.18	Bechtel, Inc., 1986, Appendix E
2	MB126	AirShft	509.31	Holt and Powers, 1990, Figure 22
3	MB126	AirShft	509.64	Holt and Powers, 1990, Figure 22
4	MB126	DOE1	485.50	U.S. DOE, Sep 1982, Table 2
5	MB126	DOE2	484.90	Mercer et al., 1987, Table 3-2
6	MB126	DOE2	485.40	Mercer et al., 1987, Table 3-2
7	MB126	ERDA9	511.60	SNL and USGS, 1982b, Table 2
8	MB126	ExhtShft	512.54	Bechtel, Inc., 1986, Appendix F
9	MB126	ExhtShft	512.72	Bechtel, Inc., 1986, Appendix F
10	MB126	REF	511.60	Rechard et al.,1991, Figure 2.2-1
11	MB126	SaltShft	514.21	Bechtel, Inc., 1986, Appendix D
12	MB126	SaltShft	514.47	Bechtel, Inc., 1986, Appendix D
13	MB126	WIPP11	513.00	SNL and USGS, 1982a, Table 2
14	MB126	WIPP12	513.80	SNL and D'Appolonia Consulting, 1983, Table 2
15	MB126	WastShft	512.40	Bechtel, Inc., 1986, Appendix E
16	MB126	WastShft	512.75	Bechtel, Inc., 1986, Appendix E
17	MB136	AirShft	412.87	Holt and Powers, 1990, Figure 22
18	MB136	AirShft	417.16	Holt and Powers, 1990, Figure 22
19	MB136	ExhtShft	415.52	Bechtel, Inc., 1986, Appendix F
20	MB136	ExhtShft	418.86	Bechtel, Inc., 1986, Appendix F
21	MB136	SaltShft	418.84	Bechtel, Inc., 1986, Appendix D
22	MB136	SaltShft	421.37	Bechtel, Inc., 1986, Appendix D
23	MB136	WastShft	415.27	Bechtel, Inc., 1986, Appendix E
24	MB136	WastShft	419.66	Bechtel, Inc., 1986, Appendix E
25	MB138	AirShft	393.81	Holt and Powers, 1990, Figure 22
26	MB138	AirShft	393.98	Holt and Powers, 1990, Figure 22
27	MB138	DH207	395.92	Krieg, 1984, Table I
28	MB138	DH207	396.16	Krieg, 1984, Table I
29	MB138	DH211	398.83	Krieg, 1984, Table I
30	MB138	DH211	398.98	Krieg, 1984, Table I
31	MB138	DH215	399.23	Krieg, 1984, Table I
32	MB138	DH215	399.41	Krieg, 1984, Table I
33	MB138	DH219	397.58	Krieg, 1984, Table I
34	MB138	DH219	397.82	Krieg, 1984, Table I
35	MB138	DH223	394.10	Krieg, 1984, Table I
36	MB138	DH223	394.31	Krieg, 1984, Table I
37	MB138	DH227	391.03	Krieg, 1984, Table I
38	MB138	DH227	391.18	Krieg, 1984, Table I
39	MB138	DH77	409.65	Krieg, 1984, Table I
40	MB138	DH77	409.95	Krieg, 1984, Table I
41	MB138	DO201	396.40	Krieg, 1984, Table I
42	MB138	DO201	396.58	Krieg, 1984, Table I
43	MB138	DO203	406.94	Krieg, 1984, Table I
44	MB138	DO203	407.15	Krieg, 1984, Table I
45	MB138	DO205	412.06	Krieg, 1984, Table I
46	MB138	DO205	412.30	Krieg, 1984, Table I
47	MB138	DO45	403.83	Krieg, 1984, Table I
48	MB138	DO45	404.01	Krieg, 1984, Table I
49	MB138	DO52	401.39	Krieg, 1984, Table I
50	MB138	DO52	401.51	Krieg, 1984, Table I
51	MB138	DO56	406.69	Krieg, 1984, Table I
52	MB138	DO56	406.84	Krieg, 1984, Table I
53	MB138	DO63	410.47	Krieg, 1984, Table I
54	MB138	DO63	410.68	Krieg, 1984, Table I
55	MB138	DO67	410.38	Krieg, 1984, Table I
56	MB138	DO67	410.50	Krieg, 1984, Table I
57	MB138	DO88	409.07	Krieg, 1984, Table I
58	MB138	DO88	409.33	Krieg, 1984, Table I
59	MB138	DO91	408.81	Krieg, 1984, Table I
60	MB138	DO91	409.02	Krieg, 1984, Table I
61	MB138	DOE1	368.60	U.S. DOE, Sep 1982, Table 2
62	MB138	DOE2	370.40	Mercer et al., 1987, Table 3-2
63	MB138	ERDA9	396.00	SNL and USGS, 1982b, Table 2
64	MB138	ERDA9	396.40	SNL and USGS, 1982b, Table 2
65	MB138	ExhtShft	396.86	Bechtel, Inc., 1986, Appendix F
66	MB138	ExhtShft	397.03	Bechtel, Inc., 1986, Appendix F
67	MB138	MB139_2	396.15	Krieg, 1984, Table I
68	MB138	MB139_2	396.30	Krieg, 1984, Table I
69	MB138	REF	396.00	Rechard et al.,1991, Figure 2.2-1
70	MB138	REF	396.40	Rechard et al.,1991, Figure 2.2-1
71	MB138	SaltShft	399.79	Bechtel, Inc., 1986, Appendix D
72	MB138	SaltShft	399.80	Bechtel, Inc., 1986, Appendix D
73	MB138	SaltShft	399.76	Krieg, 1984, Table I
74	MB138	SaltShft	399.91	Krieg, 1984, Table I
75	MB138	WIPP11	430.40	SNL and USGS, 1982a, Table 2
76	MB138	WIPP12	411.00	SNL and D'Appolonia Consulting, 1983, Table 2

Table B.2. Elevations of Stratigraphic Layers Near WIPP (Continued)

	Layer	Well ID	Elevation	Source
1	MB138	WastShft	395.89	Bechtel, Inc., 1986, Appendix E
2	MB138	WastShft	396.07	Bechtel, Inc., 1986, Appendix E
3	MB138	WastShft	396.31	Krieg, 1984, Table I
4	MB138	WastShft	396.49	Krieg, 1984, Table I
5	MB139	DH207	377.63	Krieg, 1984, Table I
6	MB139	DH207	378.70	Krieg, 1984, Table I
7	MB139	DH211	380.73	Krieg, 1984, Table I
8	MB139	DH211	381.31	Krieg, 1984, Table I
9	MB139	DH215	381.03	Krieg, 1984, Table I
10	MB139	DH215	382.04	Krieg, 1984, Table I
11	MB139	DH219	379.91	Krieg, 1984, Table I
12	MB139	DH219	380.58	Krieg, 1984, Table I
13	MB139	DH223	376.70	Krieg, 1984, Table I
14	MB139	DH223	377.64	Krieg, 1984, Table I
15	MB139	DH227	373.78	Krieg, 1984, Table I
16	MB139	DH227	374.42	Krieg, 1984, Table I
17	MB139	DH77	392.37	Krieg, 1984, Table I
18	MB139	DH77	393.35	Krieg, 1984, Table I
19	MB139	DO201	378.26	Krieg, 1984, Table I
20	MB139	DO201	379.11	Krieg, 1984, Table I
21	MB139	DO203	389.84	Krieg, 1984, Table I
22	MB139	DO203	390.63	Krieg, 1984, Table I
23	MB139	DO205	394.29	Krieg, 1984, Table I
24	MB139	DO205	394.69	Krieg, 1984, Table I
25	MB139	DO45	385.11	Krieg, 1984, Table I
26	MB139	DO45	386.36	Krieg, 1984, Table I
27	MB139	DO52	383.44	Krieg, 1984, Table I
28	MB139	DO52	384.57	Krieg, 1984, Table I
29	MB139	DO56	388.89	Krieg, 1984, Table I
30	MB139	DO56	389.53	Krieg, 1984, Table I
31	MB139	DO63	392.79	Krieg, 1984, Table I
32	MB139	DO63	393.46	Krieg, 1984, Table I
33	MB139	DO67	393.19	Krieg, 1984, Table I
34	MB139	DO67	394.13	Krieg, 1984, Table I
35	MB139	DO88	392.06	Krieg, 1984, Table I
36	MB139	DO88	392.99	Krieg, 1984, Table I
37	MB139	DO91	391.62	Krieg, 1984, Table I
38	MB139	DO91	392.66	Krieg, 1984, Table I
39	MB139	DOE1	350.40	U.S. DOE, Sep 1982, Table 2
40	MB139	DOE2	339.00	Mercer et al., 1987, Table 3-2
41	MB139	DOE2	340.00	Mercer et al., 1987, Table 3-2
42	MB139	ERDA9	378.10	SNL and USGS, 1982b, Table 2
43	MB139	ERDA9	379.00	SNL and USGS, 1982b, Table 2
44	MB139	MB139_2	377.44	Krieg, 1984, Table I
45	MB139	MB139_2	378.42	Krieg, 1984, Table I
46	MB139	REF	378.10	Rechard et al.,1991, Figure 2.2-1
47	MB139	REF	379.00	Rechard et al.,1991, Figure 2.2-1
48	MB139	SaltShft	381.64	Bechtel, Inc., 1986, Appendix D
49	MB139	SaltShft	382.44	Bechtel, Inc., 1986, Appendix D
50	MB139	SaltShft	381.38	Krieg, 1984, Table I
51	MB139	SaltShft	382.29	Krieg, 1984, Table I
52	MB139	WIPP11	419.10	SNL and USGS, 1982a, Table 2
53	MB139	WIPP12	395.90	SNL and D'Appolonia Consulting, 1983, Table 2
54	MB139	WastShft	377.14	Bechtel, Inc., 1986, Appendix E
55	MB139	WastShft	378.22	Bechtel, Inc., 1986, Appendix E
56	MB139	WastShft	378.04	Krieg, 1984, Table I
57	MB139	WastShft	379.10	Krieg, 1984, Table I
58	Magenta	AEC7	890.30	Mercer, 1983, Table 1
59	Magenta	AEC8	858.70	Mercer, 1983, Table 1
60	Magenta	AirShft	858.82	Holt and Powers, 1990, Figure 22
61	Magenta	B25	858.40	Mercer, 1983, Table 1
62	Magenta	DOE1	838.60	U.S. DOE, Sep 1982, Table 2
63	Magenta	DOE2	829.00	Mercer et al., 1987, Table 3-2
64	Magenta	ERDA10	915.90	Mercer, 1983, Table 1
65	Magenta	ERDA6	897.60	Mercer, 1983, Table 1
66	Magenta	ERDA9	860.40	Mercer, 1983, Table 1
67	Magenta	ERDA9	856.70	SNL and USGS, 1982b, Table 2
68	Magenta	ExhtShft	855.39	Bechtel, Inc., 1986, Appendix F
69	Magenta	FFG_002	667.50	Richey, 1989, Table 2, p.21
70	Magenta	FFG_004	717.80	Richey, 1989, Table 2, p.21
71	Magenta	FFG_005	674.90	Richey, 1989, Table 2, p.21
72	Magenta	FFG_006	670.00	Richey, 1989, Table 2, p.21
73	Magenta	FFG_007	655.90	Richey, 1989, Table 2, p.21
74	Magenta	FFG_009	657.40	Richey, 1989, Table 2, p.21
75	Magenta	FFG_011	664.20	Richey, 1989, Table 2, p.21
76	Magenta	FFG_012	667.80	Richey, 1989, Table 2, p.21

Table B.2. Elevations of Stratigraphic Layers Near WIPP (Continued)

	Layer	Well ID	Elevation	Source
1	Magenta	FFG_013	674.80	Richey, 1989, Table 2, p.21
2	Magenta	FFG_014	721.10	Richey, 1989, Table 2, p.21
3	Magenta	FFG_016	644.90	Richey, 1989, Table 2, p.21
4	Magenta	FFG_017	648.30	Richey, 1989, Table 2, p.22
5	Magenta	FFG_018	652.30	Richey, 1989, Table 2, p.22
6	Magenta	FFG_019	644.70	Richey, 1989, Table 2, p.22
7	Magenta	FFG_020	718.40	Richey, 1989, Table 2, p.22
8	Magenta	FFG_023	654.10	Richey, 1989, Table 2, p.22
9	Magenta	FFG_024	638.80	Richey, 1989, Table 2, p.22
10	Magenta	FFG_025	652.20	Richey, 1989, Table 2, p.22
11	Magenta	FFG_026	649.50	Richey, 1989, Table 2, p.22
12	Magenta	FFG_027	643.10	Richey, 1989, Table 2, p.22
13	Magenta	FFG_028	612.70	Richey, 1989, Table 2, p.22
14	Magenta	FFG_029	599.20	Richey, 1989, Table 2, p.22
15	Magenta	FFG_030	598.30	Richey, 1989, Table 2, p.22
16	Magenta	FFG_031	590.10	Richey, 1989, Table 2, p.22
17	Magenta	FFG_032	592.10	Richey, 1989, Table 2, p.22
18	Magenta	FFG_033	588.30	Richey, 1989, Table 2, p.22
19	Magenta	FFG_034	582.40	Richey, 1989, Table 2, p.23
20	Magenta	FFG_035	572.60	Richey, 1989, Table 2, p.23
21	Magenta	FFG_036	582.20	Richey, 1989, Table 2, p.23
22	Magenta	FFG_037	571.80	Richey, 1989, Table 2, p.23
23	Magenta	FFG_038	559.60	Richey, 1989, Table 2, p.23
24	Magenta	FFG_039	778.80	Richey, 1989, Table 2, p.23
25	Magenta	FFG_040	720.90	Richey, 1989, Table 2, p.23
26	Magenta	FFG_041	780.60	Richey, 1989, Table 2, p.23
27	Magenta	FFG_042	785.40	Richey, 1989, Table 2, p.23
28	Magenta	FFG_043	788.10	Richey, 1989, Table 2, p.23
29	Magenta	FFG_044	741.00	Richey, 1989, Table 2, p.23
30	Magenta	FFG_047	613.90	Richey, 1989, Table 2, p.23
31	Magenta	FFG_048	630.90	Richey, 1989, Table 2, p.23
32	Magenta	FFG_049	620.90	Richey, 1989, Table 2, p.23
33	Magenta	FFG_050	627.60	Richey, 1989, Table 2, p.24
34	Magenta	FFG_051	627.30	Richey, 1989, Table 2, p.24
35	Magenta	FFG_052	630.30	Richey, 1989, Table 2, p.24
36	Magenta	FFG_053	623.30	Richey, 1989, Table 2, p.24
37	Magenta	FFG_054	620.60	Richey, 1989, Table 2, p.24
38	Magenta	FFG_055	621.10	Richey, 1989, Table 2, p.24
39	Magenta	FFG_056	621.80	Richey, 1989, Table 2, p.24
40	Magenta	FFG_057	625.20	Richey, 1989, Table 2, p.24
41	Magenta	FFG_058	623.60	Richey, 1989, Table 2, p.24
42	Magenta	FFG_059	623.60	Richey, 1989, Table 2, p.24
43	Magenta	FFG_060	627.30	Richey, 1989, Table 2, p.24
44	Magenta	FFG_061	626.00	Richey, 1989, Table 2, p.24
45	Magenta	FFG_062	553.20	Richey, 1989, Table 2, p.24
46	Magenta	FFG_063	513.70	Richey, 1989, Table 2, p.24
47	Magenta	FFG_064	538.60	Richey, 1989, Table 2, p.24
48	Magenta	FFG_065	520.60	Richey, 1989, Table 2, p.24
49	Magenta	FFG_066	473.90	Richey, 1989, Table 2, p.24
50	Magenta	FFG_067	516.40	Richey, 1989, Table 2, p.25
51	Magenta	FFG_068	481.90	Richey, 1989, Table 2, p.25
52	Magenta	FFG_069	502.40	Richey, 1989, Table 2, p.25
53	Magenta	FFG_070	532.20	Richey, 1989, Table 2, p.25
54	Magenta	FFG_071	790.70	Richey, 1989, Table 2, p.25
55	Magenta	FFG_072	721.10	Richey, 1989, Table 2, p.25
56	Magenta	FFG_073	699.50	Richey, 1989, Table 2, p.25
57	Magenta	FFG_074	703.30	Richey, 1989, Table 2, p.25
58	Magenta	FFG_075	756.00	Richey, 1989, Table 2, p.25
59	Magenta	FFG_076	818.10	Richey, 1989, Table 2, p.25
60	Magenta	FFG_078	855.20	Richey, 1989, Table 2, p.25
61	Magenta	FFG_079	829.70	Richey, 1989, Table 2, p.25
62	Magenta	FFG_080	808.30	Richey, 1989, Table 2, p.25
63	Magenta	FFG_081	727.90	Richey, 1989, Table 2, p.26
64	Magenta	FFG_082	759.30	Richey, 1989, Table 2, p.26
65	Magenta	FFG_083	674.70	Richey, 1989, Table 2, p.26
66	Magenta	FFG_084	702.20	Richey, 1989, Table 2, p.26
67	Magenta	FFG_085	695.60	Richey, 1989, Table 2, p.26
68	Magenta	FFG_086	705.60	Richey, 1989, Table 2, p.26
69	Magenta	FFG_087	680.00	Richey, 1989, Table 2, p.26
70	Magenta	FFG_088	674.60	Richey, 1989, Table 2, p.26
71	Magenta	FFG_089	656.00	Richey, 1989, Table 2, p.26
72	Magenta	FFG_091	700.40	Richey, 1989, Table 2, p.26
73	Magenta	FFG_092	716.60	Richey, 1989, Table 2, p.26
74	Magenta	FFG_093	718.10	Richey, 1989, Table 2, p.26
75	Magenta	FFG_094	720.20	Richey, 1989, Table 2, p.26
76	Magenta	FFG_095	688.80	Richey, 1989, Table 2, p.26

Table B.2. Elevations of Stratigraphic Layers Near WIPP (Continued)

	Layer	Well ID	Elevation	Source
1	Magenta	FFG_096	671.20	Richey, 1989, Table 2, p.26
2	Magenta	FFG_097	651.70	Richey, 1989, Table 2, p.27
3	Magenta	FFG_098	625.40	Richey, 1989, Table 2, p.27
4	Magenta	FFG_099	620.90	Richey, 1989, Table 2, p.27
5	Magenta	FFG_100	603.90	Richey, 1989, Table 2, p.27
6	Magenta	FFG_101	574.90	Richey, 1989, Table 2, p.27
7	Magenta	FFG_102	593.50	Richey, 1989, Table 2, p.27
8	Magenta	FFG_103	655.40	Richey, 1989, Table 2, p.27
9	Magenta	FFG_104	551.10	Richey, 1989, Table 2, p.27
10	Magenta	FFG_105	909.60	Richey, 1989, Table 2, p.27
11	Magenta	FFG_106	939.70	Richey, 1989, Table 2, p.27
12	Magenta	FFG_107	923.00	Richey, 1989, Table 2, p.27
13	Magenta	FFG_108	918.40	Richey, 1989, Table 2, p.27
14	Magenta	FFG_109	898.90	Richey, 1989, Table 2, p.27
15	Magenta	FFG_110	865.70	Richey, 1989, Table 2, p.27
16	Magenta	FFG_111	871.70	Richey, 1989, Table 2, p.27
17	Magenta	FFG_112	861.00	Richey, 1989, Table 2, p.28
18	Magenta	FFG_113	875.10	Richey, 1989, Table 2, p.28
19	Magenta	FFG_114	905.60	Richey, 1989, Table 2, p.28
20	Magenta	FFG_115	895.50	Richey, 1989, Table 2, p.28
21	Magenta	FFG_116	911.00	Richey, 1989, Table 2, p.28
22	Magenta	FFG_117	911.30	Richey, 1989, Table 2, p.28
23	Magenta	FFG_120	923.00	Richey, 1989, Table 2, p.28
24	Magenta	FFG_121	928.10	Richey, 1989, Table 2, p.28
25	Magenta	FFG_122	926.60	Richey, 1989, Table 2, p.28
26	Magenta	FFG_123	900.60	Richey, 1989, Table 2, p.28
27	Magenta	FFG_124	865.30	Richey, 1989, Table 2, p.28
28	Magenta	FFG_125	890.90	Richey, 1989, Table 2, p.28
29	Magenta	FFG_126	886.20	Richey, 1989, Table 2, p.28
30	Magenta	FFG_127	891.20	Richey, 1989, Table 2, p.28
31	Magenta	FFG_128	926.60	Richey, 1989, Table 2, p.28
32	Magenta	FFG_129	899.40	Richey, 1989, Table 2, p.28
33	Magenta	FFG_130	929.60	Richey, 1989, Table 2, p.28
34	Magenta	FFG_132	935.10	Richey, 1989, Table 2, p.29
35	Magenta	FFG_133	938.10	Richey, 1989, Table 2, p.29
36	Magenta	FFG_134	944.00	Richey, 1989, Table 2, p.29
37	Magenta	FFG_135	917.50	Richey, 1989, Table 2, p.29
38	Magenta	FFG_136	919.10	Richey, 1989, Table 2, p.29
39	Magenta	FFG_137	927.90	Richey, 1989, Table 2, p.29
40	Magenta	FFG_138	880.60	Richey, 1989, Table 2, p.29
41	Magenta	FFG_139	889.70	Richey, 1989, Table 2, p.29
42	Magenta	FFG_140	829.20	Richey, 1989, Table 2, p.29
43	Magenta	FFG_141	854.20	Richey, 1989, Table 2, p.29
44	Magenta	FFG_142	829.40	Richey, 1989, Table 2, p.29
45	Magenta	FFG_143	839.30	Richey, 1989, Table 2, p.29
46	Magenta	FFG_147	897.90	Richey, 1989, Table 2, p.29
47	Magenta	FFG_155	914.10	Richey, 1989, Table 2, p.30
48	Magenta	FFG_157	915.30	Richey, 1989, Table 2, p.30
49	Magenta	FFG_158	937.20	Richey, 1989, Table 2, p.30
50	Magenta	FFG_159	936.70	Richey, 1989, Table 2, p.30
51	Magenta	FFG_160	929.70	Richey, 1989, Table 2, p.30
52	Magenta	FFG_161	936.10	Richey, 1989, Table 2, p.30
53	Magenta	FFG_162	933.30	Richey, 1989, Table 2, p.30
54	Magenta	FFG_163	933.90	Richey, 1989, Table 2, p.30
55	Magenta	FFG_166	936.00	Richey, 1989, Table 2, p.31
56	Magenta	FFG_167	922.10	Richey, 1989, Table 2, p.31
57	Magenta	FFG_168	944.60	Richey, 1989, Table 2, p.31
58	Magenta	FFG_169	957.30	Richey, 1989, Table 2, p.31
59	Magenta	FFG_170	922.90	Richey, 1989, Table 2, p.31
60	Magenta	FFG_171	931.50	Richey, 1989, Table 2, p.31
61	Magenta	FFG_172	937.20	Richey, 1989, Table 2, p.31
62	Magenta	FFG_173	914.10	Richey, 1989, Table 2, p.31
63	Magenta	FFG_180	920.50	Richey, 1989, Table 2, p.31
64	Magenta	FFG_181	951.30	Richey, 1989, Table 2, p.32
65	Magenta	FFG_182	847.60	Richey, 1989, Table 2, p.32
66	Magenta	FFG_184	927.80	Richey, 1989, Table 2, p.32
67	Magenta	FFG_185	934.50	Richey, 1989, Table 2, p.32
68	Magenta	FFG_186	863.80	Richey, 1989, Table 2, p.32
69	Magenta	FFG_188	874.10	Richey, 1989, Table 2, p.32
70	Magenta	FFG_189	902.20	Richey, 1989, Table 2, p.32
71	Magenta	FFG_190	882.40	Richey, 1989, Table 2, p.32
72	Magenta	FFG_191	878.10	Richey, 1989, Table 2, p.32
73	Magenta	FFG_192	815.30	Richey, 1989, Table 2, p.32
74	Magenta	FFG_194	822.10	Richey, 1989, Table 2, p.33
75	Magenta	FFG_195	834.00	Richey, 1989, Table 2, p.33
76	Magenta	FFG_196	876.90	Richey, 1989, Table 2, p.33

Table B.2. Elevations of Stratigraphic Layers Near WIPP (Continued)

	Layer	Well ID	Elevation	Source
1	Magenta	FFG_197	878.10	Richey, 1989, Table 2, p.33
2	Magenta	FFG_198	877.50	Richey, 1989, Table 2, p.33
3	Magenta	FFG_199	867.50	Richey, 1989, Table 2, p.33
4	Magenta	FFG_200	880.90	Richey, 1989, Table 2, p.33
5	Magenta	FFG_201	873.20	Richey, 1989, Table 2, p.33
6	Magenta	FFG_202	816.50	Richey, 1989, Table 2, p.33
7	Magenta	FFG_203	823.00	Richey, 1989, Table 2, p.33
8	Magenta	FFG_204	846.50	Richey, 1989, Table 2, p.33
9	Magenta	FFG_205	860.50	Richey, 1989, Table 2, p.33
10	Magenta	FFG_206	874.50	Richey, 1989, Table 2, p.33
11	Magenta	FFG_207	872.30	Richey, 1989, Table 2, p.33
12	Magenta	FFG_208	882.10	Richey, 1989, Table 2, p.34
13	Magenta	FFG_209	873.20	Richey, 1989, Table 2, p.34
14	Magenta	FFG_210	865.90	Richey, 1989, Table 2, p.34
15	Magenta	FFG_212	852.80	Richey, 1989, Table 2, p.34
16	Magenta	FFG_213	874.50	Richey, 1989, Table 2, p.34
17	Magenta	FFG_214	854.90	Richey, 1989, Table 2, p.34
18	Magenta	FFG_215	831.20	Richey, 1989, Table 2, p.34
19	Magenta	FFG_216	716.80	Richey, 1989, Table 2, p.34
20	Magenta	FFG_217	851.40	Richey, 1989, Table 2, p.34
21	Magenta	FFG_218	844.00	Richey, 1989, Table 2, p.34
22	Magenta	FFG_219	889.70	Richey, 1989, Table 2, p.34
23	Magenta	FFG_220	836.70	Richey, 1989, Table 2, p.34
24	Magenta	FFG_221	796.20	Richey, 1989, Table 2, p.34
25	Magenta	FFG_222	749.80	Richey, 1989, Table 2, p.34
26	Magenta	FFG_224	655.70	Richey, 1989, Table 2, p.35
27	Magenta	FFG_225	662.40	Richey, 1989, Table 2, p.35
28	Magenta	FFG_226	661.00	Richey, 1989, Table 2, p.35
29	Magenta	FFG_228	651.70	Richey, 1989, Table 2, p.35
30	Magenta	FFG_229	679.40	Richey, 1989, Table 2, p.35
31	Magenta	FFG_230	665.10	Richey, 1989, Table 2, p.35
32	Magenta	FFG_231	681.80	Richey, 1989, Table 2, p.35
33	Magenta	FFG_232	695.60	Richey, 1989, Table 2, p.35
34	Magenta	FFG_233	685.80	Richey, 1989, Table 2, p.35
35	Magenta	FFG_234	722.70	Richey, 1989, Table 2, p.35
36	Magenta	FFG_235	698.60	Richey, 1989, Table 2, p.35
37	Magenta	FFG_236	746.40	Richey, 1989, Table 2, p.35
38	Magenta	FFG_237	712.10	Richey, 1989, Table 2, p.35
39	Magenta	FFG_238	691.00	Richey, 1989, Table 2, p.36
40	Magenta	FFG_239	679.10	Richey, 1989, Table 2, p.36
41	Magenta	FFG_240	671.20	Richey, 1989, Table 2, p.36
42	Magenta	FFG_241	666.30	Richey, 1989, Table 2, p.36
43	Magenta	FFG_242	783.10	Richey, 1989, Table 2, p.36
44	Magenta	FFG_243	743.10	Richey, 1989, Table 2, p.36
45	Magenta	FFG_244	780.80	Richey, 1989, Table 2, p.36
46	Magenta	FFG_245	573.00	Richey, 1989, Table 2, p.36
47	Magenta	FFG_246	578.50	Richey, 1989, Table 2, p.36
48	Magenta	FFG_247	563.80	Richey, 1989, Table 2, p.36
49	Magenta	FFG_248	571.20	Richey, 1989, Table 2, p.36
50	Magenta	FFG_249	569.70	Richey, 1989, Table 2, p.36
51	Magenta	FFG_250	651.50	Richey, 1989, Table 2, p.36
52	Magenta	FFG_251	544.90	Richey, 1989, Table 2, p.36
53	Magenta	FFG_252	683.90	Richey, 1989, Table 2, p.36
54	Magenta	FFG_253	639.20	Richey, 1989, Table 2, p.36
55	Magenta	FFG_254	630.00	Richey, 1989, Table 2, p.36
56	Magenta	FFG_255	587.70	Richey, 1989, Table 2, p.37
57	Magenta	FFG_256	535.20	Richey, 1989, Table 2, p.37
58	Magenta	FFG_257	579.40	Richey, 1989, Table 2, p.37
59	Magenta	FFG_258	594.90	Richey, 1989, Table 2, p.37
60	Magenta	FFG_259	561.10	Richey, 1989, Table 2, p.37
61	Magenta	FFG_260	603.80	Richey, 1989, Table 2, p.37
62	Magenta	FFG_261	592.80	Richey, 1989, Table 2, p.37
63	Magenta	FFG_263	526.60	Richey, 1989, Table 2, p.37
64	Magenta	FFG_264	760.50	Richey, 1989, Table 2, p.37
65	Magenta	FFG_265	755.90	Richey, 1989, Table 2, p.37
66	Magenta	FFG_266	736.70	Richey, 1989, Table 2, p.37
67	Magenta	FFG_267	713.50	Richey, 1989, Table 2, p.37
68	Magenta	FFG_268	690.70	Richey, 1989, Table 2, p.37
69	Magenta	FFG_269	702.40	Richey, 1989, Table 2, p.38
70	Magenta	FFG_270	774.50	Richey, 1989, Table 2, p.38
71	Magenta	FFG_271	815.00	Richey, 1989, Table 2, p.38
72	Magenta	FFG_272	822.50	Richey, 1989, Table 2, p.38
73	Magenta	FFG_273	797.40	Richey, 1989, Table 2, p.38
74	Magenta	FFG_274	834.20	Richey, 1989, Table 2, p.38
75	Magenta	FFG_275	840.30	Richey, 1989, Table 2, p.38
76	Magenta	FFG_276	845.20	Richey, 1989, Table 2, p.38

Table B.2. Elevations of Stratigraphic Layers Near WIPP (Continued)

	Layer	Well ID	Elevation	Source
2	Magenta	FFG_277	836.70	Richey, 1989, Table 2, p.38
3	Magenta	FFG_278	845.80	Richey, 1989, Table 2, p.38
4	Magenta	FFG_279	840.90	Richey, 1989, Table 2, p.38
5	Magenta	FFG_280	837.30	Richey, 1989, Table 2, p.38
6	Magenta	FFG_281	814.20	Richey, 1989, Table 2, p.38
7	Magenta	FFG_283	563.90	Richey, 1989, Table 2, p.39
8	Magenta	FFG_284	712.00	Richey, 1989, Table 2, p.39
9	Magenta	FFG_285	741.30	Richey, 1989, Table 2, p.39
10	Magenta	FFG_286	820.20	Richey, 1989, Table 2, p.39
11	Magenta	FFG_287	793.10	Richey, 1989, Table 2, p.39
12	Magenta	FFG_288	744.90	Richey, 1989, Table 2, p.39
13	Magenta	FFG_289	719.90	Richey, 1989, Table 2, p.39
14	Magenta	FFG_290	806.50	Richey, 1989, Table 2, p.39
15	Magenta	FFG_291	742.50	Richey, 1989, Table 2, p.39
16	Magenta	FFG_292	758.40	Richey, 1989, Table 2, p.39
17	Magenta	FFG_293	750.70	Richey, 1989, Table 2, p.39
18	Magenta	FFG_294	572.80	Richey, 1989, Table 2, p.39
19	Magenta	FFG_295	560.20	Richey, 1989, Table 2, p.39
20	Magenta	FFG_297	539.20	Richey, 1989, Table 2, p.39
21	Magenta	FFG_298	552.40	Richey, 1989, Table 2, p.40
22	Magenta	FFG_299	569.10	Richey, 1989, Table 2, p.40
23	Magenta	FFG_300	520.60	Richey, 1989, Table 2, p.40
24	Magenta	FFG_301	491.10	Richey, 1989, Table 2, p.40
25	Magenta	FFG_302	518.50	Richey, 1989, Table 2, p.40
26	Magenta	FFG_303	511.20	Richey, 1989, Table 2, p.40
27	Magenta	FFG_304	517.50	Richey, 1989, Table 2, p.40
28	Magenta	FFG_305	509.30	Richey, 1989, Table 2, p.40
29	Magenta	FFG_306	469.30	Richey, 1989, Table 2, p.40
30	Magenta	FFG_307	493.50	Richey, 1989, Table 2, p.40
31	Magenta	FFG_308	465.70	Richey, 1989, Table 2, p.40
32	Magenta	FFG_309	508.10	Richey, 1989, Table 2, p.40
33	Magenta	FFG_310	539.20	Richey, 1989, Table 2, p.40
34	Magenta	FFG_311	486.50	Richey, 1989, Table 2, p.40
35	Magenta	FFG_312	510.60	Richey, 1989, Table 2, p.40
36	Magenta	FFG_313	915.10	Richey, 1989, Table 2, p.41
37	Magenta	FFG_314	843.10	Richey, 1989, Table 2, p.41
38	Magenta	FFG_315	764.30	Richey, 1989, Table 2, p.41
39	Magenta	FFG_316	747.90	Richey, 1989, Table 2, p.41
40	Magenta	FFG_317	777.00	Richey, 1989, Table 2, p.41
41	Magenta	FFG_318	742.20	Richey, 1989, Table 2, p.41
42	Magenta	FFG_319	751.60	Richey, 1989, Table 2, p.41
43	Magenta	FFG_320	741.30	Richey, 1989, Table 2, p.41
44	Magenta	FFG_321	737.90	Richey, 1989, Table 2, p.41
45	Magenta	FFG_322	733.20	Richey, 1989, Table 2, p.41
46	Magenta	FFG_323	729.50	Richey, 1989, Table 2, p.41
47	Magenta	FFG_324	745.30	Richey, 1989, Table 2, p.41
48	Magenta	FFG_325	800.40	Richey, 1989, Table 2, p.41
49	Magenta	FFG_326	736.10	Richey, 1989, Table 2, p.41
50	Magenta	FFG_327	729.10	Richey, 1989, Table 2, p.42
51	Magenta	FFG_328	734.50	Richey, 1989, Table 2, p.42
52	Magenta	FFG_329	733.90	Richey, 1989, Table 2, p.42
53	Magenta	FFG_330	733.20	Richey, 1989, Table 2, p.42
54	Magenta	FFG_331	728.50	Richey, 1989, Table 2, p.42
55	Magenta	FFG_332	719.30	Richey, 1989, Table 2, p.42
56	Magenta	FFG_333	722.80	Richey, 1989, Table 2, p.42
57	Magenta	FFG_334	718.10	Richey, 1989, Table 2, p.42
58	Magenta	FFG_335	733.70	Richey, 1989, Table 2, p.42
59	Magenta	FFG_336	730.60	Richey, 1989, Table 2, p.42
60	Magenta	FFG_337	713.80	Richey, 1989, Table 2, p.42
61	Magenta	FFG_338	720.70	Richey, 1989, Table 2, p.42
62	Magenta	FFG_339	684.80	Richey, 1989, Table 2, p.42
63	Magenta	FFG_340	694.00	Richey, 1989, Table 2, p.42
64	Magenta	FFG_342	726.90	Richey, 1989, Table 2, p.43
65	Magenta	FFG_344	692.70	Richey, 1989, Table 2, p.43
66	Magenta	FFG_345	752.10	Richey, 1989, Table 2, p.43
67	Magenta	FFG_347	744.70	Richey, 1989, Table 2, p.43
68	Magenta	FFG_348	773.30	Richey, 1989, Table 2, p.43
69	Magenta	FFG_349	742.20	Richey, 1989, Table 2, p.43
70	Magenta	FFG_350	789.10	Richey, 1989, Table 2, p.43
71	Magenta	FFG_351	705.60	Richey, 1989, Table 2, p.43
72	Magenta	FFG_352	705.60	Richey, 1989, Table 2, p.43
73	Magenta	FFG_353	726.70	Richey, 1989, Table 2, p.43
74	Magenta	FFG_354	800.80	Richey, 1989, Table 2, p.43
75	Magenta	FFG_361	986.90	Richey, 1989, Table 2, p.44
76	Magenta	FFG_366	940.60	Richey, 1989, Table 2, p.44
77	Magenta	FFG_367	954.60	Richey, 1989, Table 2, p.44

Table B.2. Elevations of Stratigraphic Layers Near WIPP (Continued)

	Layer	Well ID	Elevation	Source
1	Magenta	FFG_371	997.70	Richey, 1989, Table 2, p.44
2	Magenta	FFG_374	940.90	Richey, 1989, Table 2, p.45
3	Magenta	FFG_383	938.80	Richey, 1989, Table 2, p.45
4	Magenta	FFG_384	945.80	Richey, 1989, Table 2, p.45
5	Magenta	FFG_387	940.30	Richey, 1989, Table 2, p.45
6	Magenta	FFG_388	936.70	Richey, 1989, Table 2, p.46
7	Magenta	FFG_390	954.00	Richey, 1989, Table 2, p.46
8	Magenta	FFG_391	951.50	Richey, 1989, Table 2, p.46
9	Magenta	FFG_392	948.60	Richey, 1989, Table 2, p.46
10	Magenta	FFG_393	816.10	Richey, 1989, Table 2, p.46
11	Magenta	FFG_394	908.60	Richey, 1989, Table 2, p.46
12	Magenta	FFG_395	901.60	Richey, 1989, Table 2, p.46
13	Magenta	FFG_396	884.30	Richey, 1989, Table 2, p.46
14	Magenta	FFG_398	805.60	Richey, 1989, Table 2, p.46
15	Magenta	FFG_402	979.40	Richey, 1989, Table 2, p.46
16	Magenta	FFG_403	941.40	Richey, 1989, Table 2, p.47
17	Magenta	FFG_404	901.60	Richey, 1989, Table 2, p.47
18	Magenta	FFG_407	940.00	Richey, 1989, Table 2, p.47
19	Magenta	FFG_408	913.20	Richey, 1989, Table 2, p.47
20	Magenta	FFG_419	976.60	Richey, 1989, Table 2, p.48
21	Magenta	FFG_420	973.50	Richey, 1989, Table 2, p.48
22	Magenta	FFG_421	960.10	Richey, 1989, Table 2, p.48
23	Magenta	FFG_422	958.30	Richey, 1989, Table 2, p.48
24	Magenta	FFG_432	924.10	Richey, 1989, Table 2, p.48
25	Magenta	FFG_438	874.60	Richey, 1989, Table 2, p.49
26	Magenta	FFG_455	817.50	Richey, 1989, Table 2, p.50
27	Magenta	FFG_456	812.50	Richey, 1989, Table 2, p.50
28	Magenta	FFG_457	868.10	Richey, 1989, Table 2, p.50
29	Magenta	FFG_458	872.60	Richey, 1989, Table 2, p.50
30	Magenta	FFG_459	799.50	Richey, 1989, Table 2, p.50
31	Magenta	FFG_462	865.80	Richey, 1989, Table 2, p.50
32	Magenta	FFG_463	893.10	Richey, 1989, Table 2, p.51
33	Magenta	FFG_464	880.00	Richey, 1989, Table 2, p.51
34	Magenta	FFG_465	883.00	Richey, 1989, Table 2, p.51
35	Magenta	FFG_467	488.20	Richey, 1989, Table 2, p.51
36	Magenta	FFG_468	465.50	Richey, 1989, Table 2, p.51
37	Magenta	FFG_470	484.90	Richey, 1989, Table 2, p.51
38	Magenta	FFG_471	500.50	Richey, 1989, Table 2, p.51
39	Magenta	FFG_472	538.30	Richey, 1989, Table 2, p.51
40	Magenta	FFG_473	468.20	Richey, 1989, Table 2, p.51
41	Magenta	FFG_474	729.40	Richey, 1989, Table 2, p.51
42	Magenta	FFG_475	728.90	Richey, 1989, Table 2, p.51
43	Magenta	FFG_476	805.00	Richey, 1989, Table 2, p.51
44	Magenta	FFG_477	760.80	Richey, 1989, Table 2, p.51
45	Magenta	FFG_478	739.70	Richey, 1989, Table 2, p.52
46	Magenta	FFG_479	736.40	Richey, 1989, Table 2, p.52
47	Magenta	FFG_480	732.50	Richey, 1989, Table 2, p.52
48	Magenta	FFG_481	715.70	Richey, 1989, Table 2, p.52
49	Magenta	FFG_482	744.30	Richey, 1989, Table 2, p.52
50	Magenta	FFG_483	767.80	Richey, 1989, Table 2, p.52
51	Magenta	FFG_484	753.60	Richey, 1989, Table 2, p.52
52	Magenta	FFG_485	762.60	Richey, 1989, Table 2, p.52
53	Magenta	FFG_486	749.50	Richey, 1989, Table 2, p.52
54	Magenta	FFG_487	746.50	Richey, 1989, Table 2, p.52
55	Magenta	FFG_488	731.20	Richey, 1989, Table 2, p.52
56	Magenta	FFG_489	748.40	Richey, 1989, Table 2, p.52
57	Magenta	FFG_490	838.80	Richey, 1989, Table 2, p.52
58	Magenta	FFG_491	836.40	Richey, 1989, Table 2, p.52
59	Magenta	FFG_492	798.60	Richey, 1989, Table 2, p.52
60	Magenta	FFG_493	785.30	Richey, 1989, Table 2, p.53
61	Magenta	FFG_494	792.10	Richey, 1989, Table 2, p.53
62	Magenta	FFG_495	783.00	Richey, 1989, Table 2, p.53
63	Magenta	FFG_496	688.60	Richey, 1989, Table 2, p.53
64	Magenta	FFG_497	701.10	Richey, 1989, Table 2, p.53
65	Magenta	FFG_498	714.10	Richey, 1989, Table 2, p.53
66	Magenta	FFG_499	689.50	Richey, 1989, Table 2, p.53
67	Magenta	FFG_500	704.70	Richey, 1989, Table 2, p.53
68	Magenta	FFG_501	710.10	Richey, 1989, Table 2, p.53
69	Magenta	FFG_502	702.90	Richey, 1989, Table 2, p.53
70	Magenta	FFG_503	684.00	Richey, 1989, Table 2, p.53
71	Magenta	FFG_504	706.00	Richey, 1989, Table 2, p.53
72	Magenta	FFG_505	739.50	Richey, 1989, Table 2, p.53
73	Magenta	FFG_506	730.90	Richey, 1989, Table 2, p.53
74	Magenta	FFG_507	692.40	Richey, 1989, Table 2, p.53
75	Magenta	FFG_508	744.10	Richey, 1989, Table 2, p.53
76	Magenta	FFG_509	745.20	Richey, 1989, Table 2, p.54

Table B.2. Elevations of Stratigraphic Layers Near WIPP (Continued)

	Layer	Well ID	Elevation	Source
1	Magenta	FFG_510	744.80	Richey, 1989, Table 2, p.54
2	Magenta	FFG_511	702.30	Richey, 1989, Table 2, p.54
3	Magenta	FFG_512	720.80	Richey, 1989, Table 2, p.54
4	Magenta	FFG_513	740.70	Richey, 1989, Table 2, p.54
5	Magenta	FFG_514	731.20	Richey, 1989, Table 2, p.54
6	Magenta	FFG_515	697.90	Richey, 1989, Table 2, p.54
7	Magenta	FFG_516	691.30	Richey, 1989, Table 2, p.54
8	Magenta	FFG_517	788.80	Richey, 1989, Table 2, p.54
9	Magenta	FFG_518	778.10	Richey, 1989, Table 2, p.54
10	Magenta	FFG_519	743.70	Richey, 1989, Table 2, p.54
11	Magenta	FFG_520	635.40	Richey, 1989, Table 2, p.54
12	Magenta	FFG_521	655.00	Richey, 1989, Table 2, p.54
13	Magenta	FFG_522	504.30	Richey, 1989, Table 2, p.54
14	Magenta	FFG_523	516.90	Richey, 1989, Table 2, p.54
15	Magenta	FFG_524	675.10	Richey, 1989, Table 2, p.55
16	Magenta	FFG_525	513.70	Richey, 1989, Table 2, p.55
17	Magenta	FFG_527	938.70	Richey, 1989, Table 2, p.55
18	Magenta	FFG_528	934.20	Richey, 1989, Table 2, p.55
19	Magenta	FFG_532	915.60	Richey, 1989, Table 2, p.55
20	Magenta	FFG_535	919.90	Richey, 1989, Table 2, p.55
21	Magenta	FFG_548	914.10	Richey, 1989, Table 2, p.56
22	Magenta	FFG_562	652.30	Richey, 1989, Table 2, p.57
23	Magenta	FFG_563	564.80	Richey, 1989, Table 2, p.57
24	Magenta	FFG_569	670.60	Richey, 1989, Table 2, p.57
25	Magenta	FFG_584	767.70	Richey, 1989, Table 2, p.58
26	Magenta	FFG_600	727.60	Richey, 1989, Table 2, p.58
27	Magenta	FFG_601	623.00	Richey, 1989, Table 2, p.58
28	Magenta	FFG_606	703.50	Richey, 1989, Table 2, p.58
29	Magenta	FFG_607	723.30	Richey, 1989, Table 2, p.59
30	Magenta	FFG_608	731.80	Richey, 1989, Table 2, p.59
31	Magenta	FFG_609	738.80	Richey, 1989, Table 2, p.59
32	Magenta	FFG_610	722.40	Richey, 1989, Table 2, p.59
33	Magenta	FFG_611	707.40	Richey, 1989, Table 2, p.59
34	Magenta	FFG_612	715.70	Richey, 1989, Table 2, p.59
35	Magenta	FFG_613	713.50	Richey, 1989, Table 2, p.59
36	Magenta	FFG_620	738.50	Richey, 1989, Table 2, p.59
37	Magenta	FFG_638	573.10	Richey, 1989, Table 2, p.60
38	Magenta	FFG_639	543.80	Richey, 1989, Table 2, p.60
39	Magenta	FFG_640	630.80	Richey, 1989, Table 2, p.60
40	Magenta	FFG_643	669.70	Richey, 1989, Table 2, p.60
41	Magenta	FFG_644	706.40	Richey, 1989, Table 2, p.60
42	Magenta	FFG_648	541.30	Richey, 1989, Table 2, p.60
43	Magenta	FFG_652	859.80	Richey, 1989, Table 2, p.60
44	Magenta	FFG_653	859.90	Richey, 1989, Table 2, p.61
45	Magenta	FFG_654	880.00	Richey, 1989, Table 2, p.61
46	Magenta	FFG_655	878.10	Richey, 1989, Table 2, p.61
47	Magenta	FFG_656	876.90	Richey, 1989, Table 2, p.61
48	Magenta	FFG_657	889.80	Richey, 1989, Table 2, p.61
49	Magenta	FFG_658	881.80	Richey, 1989, Table 2, p.61
50	Magenta	FFG_659	886.10	Richey, 1989, Table 2, p.61
51	Magenta	FFG_660	901.50	Richey, 1989, Table 2, p.61
52	Magenta	FFG_662	876.30	Richey, 1989, Table 2, p.61
53	Magenta	FFG_664	868.40	Richey, 1989, Table 2, p.61
54	Magenta	FFG_666	920.50	Richey, 1989, Table 2, p.62
55	Magenta	FFG_667	905.60	Richey, 1989, Table 2, p.62
56	Magenta	FFG_670	926.90	Richey, 1989, Table 2, p.62
57	Magenta	FFG_672	925.70	Richey, 1989, Table 2, p.62
58	Magenta	FFG_674	921.70	Richey, 1989, Table 2, p.62
59	Magenta	FFG_675	877.70	Richey, 1989, Table 2, p.62
60	Magenta	FFG_676	891.90	Richey, 1989, Table 2, p.62
61	Magenta	FFG_677	917.80	Richey, 1989, Table 2, p.62
62	Magenta	FFG_679	917.10	Richey, 1989, Table 2, p.62
63	Magenta	FFG_689	799.50	Richey, 1989, Table 2, p.63
64	Magenta	FFG_690	805.00	Richey, 1989, Table 2, p.63
65	Magenta	FFG_691	796.20	Richey, 1989, Table 2, p.63
66	Magenta	FFG_692	786.40	Richey, 1989, Table 2, p.63
67	Magenta	FFG_693	797.00	Richey, 1989, Table 2, p.63
68	Magenta	FFG_694	789.40	Richey, 1989, Table 2, p.63
69	Magenta	FFG_695	794.90	Richey, 1989, Table 2, p.63
70	Magenta	FFG_696	797.00	Richey, 1989, Table 2, p.63
71	Magenta	FFG_697	799.20	Richey, 1989, Table 2, p.64
72	Magenta	FFG_698	841.60	Richey, 1989, Table 2, p.64
73	Magenta	FFG_699	792.80	Richey, 1989, Table 2, p.64
74	Magenta	FFG_700	782.50	Richey, 1989, Table 2, p.64
75	Magenta	FFG_701	788.60	Richey, 1989, Table 2, p.64
76	Magenta	FFG_702	792.80	Richey, 1989, Table 2, p.64

Table B.2. Elevations of Stratigraphic Layers Near WIPP (Continued)

	Layer	Well ID	Elevation	Source
1	Magenta	FFG_703	798.90	Richey, 1989, Table 2, p.64
2	Magenta	FFG_704	785.50	Richey, 1989, Table 2, p.64
3	Magenta	FFG_705	715.60	Richey, 1989, Table 2, p.64
4	Magenta	FFG_706	736.10	Richey, 1989, Table 2, p.64
5	Magenta	FFG_707	720.30	Richey, 1989, Table 2, p.64
6	Magenta	FFG_708	773.30	Richey, 1989, Table 2, p.64
7	Magenta	FFG_709	664.50	Richey, 1989, Table 2, p.64
8	Magenta	FFG_710	665.40	Richey, 1989, Table 2, p.64
9	Magenta	FFG_711	675.20	Richey, 1989, Table 2, p.65
10	Magenta	FFG_712	718.80	Richey, 1989, Table 2, p.65
11	Magenta	FFG_713	655.80	Richey, 1989, Table 2, p.65
12	Magenta	FFG_714	770.20	Richey, 1989, Table 2, p.65
13	Magenta	FFG_715	783.00	Richey, 1989, Table 2, p.65
14	Magenta	FFG_716	680.80	Richey, 1989, Table 2, p.65
15	Magenta	FFG_717	703.30	Richey, 1989, Table 2, p.65
16	Magenta	FFG_718	706.70	Richey, 1989, Table 2, p.65
17	Magenta	FFG_719	679.40	Richey, 1989, Table 2, p.65
18	Magenta	FFG_720	679.10	Richey, 1989, Table 2, p.65
19	Magenta	FFG_721	679.10	Richey, 1989, Table 2, p.65
20	Magenta	FFG_723	791.70	Richey, 1989, Table 2, p.65
21	Magenta	FFG_724	719.10	Richey, 1989, Table 2, p.65
22	Magenta	FFG_725	694.90	Richey, 1989, Table 2, p.65
23	Magenta	FFG_726	682.70	Richey, 1989, Table 2, p.65
24	Magenta	FFG_727	680.00	Richey, 1989, Table 2, p.66
25	Magenta	FFG_728	677.80	Richey, 1989, Table 2, p.66
26	Magenta	FFG_729	688.90	Richey, 1989, Table 2, p.66
27	Magenta	FFG_730	705.60	Richey, 1989, Table 2, p.66
28	Magenta	FFG_731	703.00	Richey, 1989, Table 2, p.66
29	Magenta	FFG_732	720.60	Richey, 1989, Table 2, p.66
30	Magenta	FFG_733	787.60	Richey, 1989, Table 2, p.66
31	Magenta	FFG_734	741.90	Richey, 1989, Table 2, p.66
32	Magenta	FFG_735	684.60	Richey, 1989, Table 2, p.66
33	Magenta	FFG_736	739.10	Richey, 1989, Table 2, p.66
34	Magenta	FFG_737	682.80	Richey, 1989, Table 2, p.66
35	Magenta	FFG_738	697.00	Richey, 1989, Table 2, p.66
36	Magenta	FFG_739	734.40	Richey, 1989, Table 2, p.66
37	Magenta	FFG_740	736.70	Richey, 1989, Table 2, p.66
38	Magenta	FFG_741	702.90	Richey, 1989, Table 2, p.66
39	Magenta	FFG_742	753.70	Richey, 1989, Table 2, p.67
40	Magenta	FFG_743	740.40	Richey, 1989, Table 2, p.67
41	Magenta	FFG_744	722.90	Richey, 1989, Table 2, p.67
42	Magenta	FFG_745	708.90	Richey, 1989, Table 2, p.67
43	Magenta	FFG_746	699.10	Richey, 1989, Table 2, p.67
44	Magenta	H1	864.10	Mercer, 1983, Table 1
45	Magenta	H10C	741.00	Mercer, 1983, Table 1
46	Magenta	H2C	872.60	Mercer, 1983, Table 1
47	Magenta	H3	862.90	Mercer, 1983, Table 1
48	Magenta	H4C	901.30	Mercer, 1983, Table 1
49	Magenta	H5C	828.70	Mercer, 1983, Table 1
50	Magenta	H6C	871.10	Mercer, 1983, Table 1
51	Magenta	H7C	928.40	Mercer, 1983, Table 1
52	Magenta	H8C	904.40	Mercer, 1983, Table 1
53	Magenta	H9C	878.70	Mercer, 1983, Table 1
54	Magenta	P1	890.70	Mercer, 1983, Table 1
55	Magenta	P10	838.80	Mercer, 1983, Table 1
56	Magenta	P11	824.80	Mercer, 1983, Table 1
57	Magenta	P12	870.20	Mercer, 1983, Table 1
58	Magenta	P13	870.20	Mercer, 1983, Table 1
59	Magenta	P14	886.00	Mercer, 1983, Table 1
60	Magenta	P15	919.30	Mercer, 1983, Table 1
61	Magenta	P16	896.70	Mercer, 1983, Table 1
62	Magenta	P17	883.30	Mercer, 1983, Table 1
63	Magenta	P18	845.20	Mercer, 1983, Table 1
64	Magenta	P19	832.40	Mercer, 1983, Table 1
65	Magenta	P2	832.40	Mercer, 1983, Table 1
66	Magenta	P20	827.30	Mercer, 1983, Table 1
67	Magenta	P21	829.30	Mercer, 1983, Table 1
68	Magenta	P3	869.90	Mercer, 1983, Table 1
69	Magenta	P4	847.90	Mercer, 1983, Table 1
70	Magenta	P5	848.90	Mercer, 1983, Table 1
71	Magenta	P6	895.20	Mercer, 1983, Table 1
72	Magenta	P7	901.90	Mercer, 1983, Table 1
73	Magenta	P8	880.50	Mercer, 1983, Table 1
74	Magenta	P9	851.90	Mercer, 1983, Table 1
75	Magenta	REF	856.70	Rechard et al.,1991, Figure 2.2-1
76	Magenta	SaltShft	858.77	Bechtel, Inc., 1986, Appendix D

Table B.2. Elevations of Stratigraphic Layers Near WIPP (Continued)

	Layer	Well ID	Elevation	Source
1	Magenta	WIPP11	822.60	Mercer, 1983, Table 1
2	Magenta	WIPP11	822.70	SNL and USGS, 1982a, Table 2
3	Magenta	WIPP12	847.30	SNL and D'Appolonia Consulting, 1983, Table 2
4	Magenta	WIPP12	848.00	Mercer, 1983, Table 1
5	Magenta	WIPP13	865.90	Mercer, 1983, Table 1
6	Magenta	WIPP16	668.70	Mercer, 1983, Table 1
7	Magenta	WIPP18	848.60	Mercer, 1983, Table 1
8	Magenta	WIPP19	849.20	Mercer, 1983, Table 1
9	Magenta	WIPP21	853.10	Mercer, 1983, Table 1
10	Magenta	WIPP22	852.20	Mercer, 1983, Table 1
11	Magenta	WIPP25	887.30	Mercer, 1983, Table 1
12	Magenta	WIPP26	939.40	Mercer, 1983, Table 1
13	Magenta	WIPP27	914.70	Mercer, 1983, Table 1
14	Magenta	WIPP28	933.30	Mercer, 1983, Table 1
15	Magenta	WIPP30	888.50	Mercer, 1983, Table 1
16	Magenta	WIPP32	915.60	Mercer, 1983, Table 1
17	Magenta	WIPP33	876.00	Mercer, 1983, Table 1
18	Magenta	WIPP34	827.60	Mercer, 1983, Table 1
19	Magenta	WastShft	857.36	Bechtel, Inc., 1986, Appendix E
20	RSResid	AirShft	783.13	Holt and Powers, 1990, Figure 22
21	RSResid	ExhtShft	779.98	Bechtel, Inc., 1986, Appendix F
22	RSResid	SaltShft	780.44	Bechtel, Inc., 1986, Appendix D
23	RSResid	WastShft	781.82	Bechtel, Inc., 1986, Appendix E
24	ReposFlr	AirShft	383.74	Holt and Powers, 1990, Figure 22
25	ReposFlr	ExhtShft	381.61	Bechtel, Inc., 1986, Appendix F
26	ReposFlr	SaltShft	380.08	Bechtel, Inc., 1986, Appendix D
27	ReposFlr	WastShft	380.70	Bechtel, Inc., 1986, Appendix E
28	Salado	AEC7	811.60	Mercer, 1983, Table 1
29	Salado	AEC8	776.40	Mercer, 1983, Table 1
30	Salado	B25	782.20	Mercer, 1983, Table 1
31	Salado	ERDA10	836.10	Mercer, 1983, Table 1
32	Salado	ERDA6	830.60	Mercer, 1983, Table 1
33	Salado	ERDA9	783.60	Mercer, 1983, Table 1
34	Salado	FFG_002	578.80	Richey, 1989, Table 2, p.21
35	Salado	FFG_004	627.90	Richey, 1989, Table 2, p.21
36	Salado	FFG_005	581.90	Richey, 1989, Table 2, p.21
37	Salado	FFG_007	559.00	Richey, 1989, Table 2, p.21
38	Salado	FFG_009	575.10	Richey, 1989, Table 2, p.21
39	Salado	FFG_011	570.30	Richey, 1989, Table 2, p.21
40	Salado	FFG_012	572.10	Richey, 1989, Table 2, p.21
41	Salado	FFG_013	582.50	Richey, 1989, Table 2, p.21
42	Salado	FFG_014	623.00	Richey, 1989, Table 2, p.21
43	Salado	FFG_016	545.00	Richey, 1989, Table 2, p.21
44	Salado	FFG_017	555.30	Richey, 1989, Table 2, p.22
45	Salado	FFG_018	558.40	Richey, 1989, Table 2, p.22
46	Salado	FFG_019	548.90	Richey, 1989, Table 2, p.22
47	Salado	FFG_020	622.40	Richey, 1989, Table 2, p.22
48	Salado	FFG_023	553.50	Richey, 1989, Table 2, p.22
49	Salado	FFG_024	539.20	Richey, 1989, Table 2, p.22
50	Salado	FFG_025	560.40	Richey, 1989, Table 2, p.22
51	Salado	FFG_026	552.60	Richey, 1989, Table 2, p.22
52	Salado	FFG_027	545.60	Richey, 1989, Table 2, p.22
53	Salado	FFG_028	549.60	Richey, 1989, Table 2, p.22
54	Salado	FFG_029	537.90	Richey, 1989, Table 2, p.22
55	Salado	FFG_030	532.80	Richey, 1989, Table 2, p.22
56	Salado	FFG_031	522.40	Richey, 1989, Table 2, p.22
57	Salado	FFG_032	519.00	Richey, 1989, Table 2, p.22
58	Salado	FFG_033	518.80	Richey, 1989, Table 2, p.22
59	Salado	FFG_034	517.80	Richey, 1989, Table 2, p.23
60	Salado	FFG_035	504.90	Richey, 1989, Table 2, p.23
61	Salado	FFG_036	510.30	Richey, 1989, Table 2, p.23
62	Salado	FFG_037	502.90	Richey, 1989, Table 2, p.23
63	Salado	FFG_038	491.90	Richey, 1989, Table 2, p.23
64	Salado	FFG_039	694.40	Richey, 1989, Table 2, p.23
65	Salado	FFG_040	624.90	Richey, 1989, Table 2, p.23
66	Salado	FFG_041	691.90	Richey, 1989, Table 2, p.23
67	Salado	FFG_042	695.20	Richey, 1989, Table 2, p.23
68	Salado	FFG_043	697.00	Richey, 1989, Table 2, p.23
69	Salado	FFG_044	645.60	Richey, 1989, Table 2, p.23
70	Salado	FFG_047	526.10	Richey, 1989, Table 2, p.23
71	Salado	FFG_048	527.60	Richey, 1989, Table 2, p.23
72	Salado	FFG_049	526.70	Richey, 1989, Table 2, p.23
73	Salado	FFG_050	537.40	Richey, 1989, Table 2, p.24
74	Salado	FFG_051	530.90	Richey, 1989, Table 2, p.24
75	Salado	FFG_052	565.70	Richey, 1989, Table 2, p.24
76	Salado	FFG_053	510.50	Richey, 1989, Table 2, p.24

Table B.2. Elevations of Stratigraphic Layers Near WIPP (Continued)

	Layer	Well ID	Elevation	Source
1	Salado	FFG_054	518.80	Richey, 1989, Table 2, p.24
2	Salado	FFG_055	521.20	Richey, 1989, Table 2, p.24
3	Salado	FFG_056	520.90	Richey, 1989, Table 2, p.24
4	Salado	FFG_057	524.60	Richey, 1989, Table 2, p.24
5	Salado	FFG_058	526.70	Richey, 1989, Table 2, p.24
6	Salado	FFG_059	529.70	Richey, 1989, Table 2, p.24
7	Salado	FFG_060	532.80	Richey, 1989, Table 2, p.24
8	Salado	FFG_061	532.50	Richey, 1989, Table 2, p.24
9	Salado	FFG_062	479.20	Richey, 1989, Table 2, p.24
10	Salado	FFG_063	438.40	Richey, 1989, Table 2, p.24
11	Salado	FFG_064	461.20	Richey, 1989, Table 2, p.24
12	Salado	FFG_065	449.60	Richey, 1989, Table 2, p.24
13	Salado	FFG_066	401.70	Richey, 1989, Table 2, p.24
14	Salado	FFG_067	435.90	Richey, 1989, Table 2, p.25
15	Salado	FFG_068	396.50	Richey, 1989, Table 2, p.25
16	Salado	FFG_069	407.90	Richey, 1989, Table 2, p.25
17	Salado	FFG_070	442.00	Richey, 1989, Table 2, p.25
18	Salado	FFG_071	700.20	Richey, 1989, Table 2, p.25
19	Salado	FFG_072	645.80	Richey, 1989, Table 2, p.25
20	Salado	FFG_073	623.30	Richey, 1989, Table 2, p.25
21	Salado	FFG_074	630.70	Richey, 1989, Table 2, p.25
22	Salado	FFG_075	683.40	Richey, 1989, Table 2, p.25
23	Salado	FFG_076	741.90	Richey, 1989, Table 2, p.25
24	Salado	FFG_078	776.90	Richey, 1989, Table 2, p.25
25	Salado	FFG_079	750.40	Richey, 1989, Table 2, p.25
26	Salado	FFG_080	727.50	Richey, 1989, Table 2, p.25
27	Salado	FFG_081	644.40	Richey, 1989, Table 2, p.26
28	Salado	FFG_082	673.00	Richey, 1989, Table 2, p.26
29	Salado	FFG_083	604.60	Richey, 1989, Table 2, p.26
30	Salado	FFG_084	626.00	Richey, 1989, Table 2, p.26
31	Salado	FFG_085	620.90	Richey, 1989, Table 2, p.26
32	Salado	FFG_086	630.30	Richey, 1989, Table 2, p.26
33	Salado	FFG_087	601.30	Richey, 1989, Table 2, p.26
34	Salado	FFG_088	595.30	Richey, 1989, Table 2, p.26
35	Salado	FFG_089	576.70	Richey, 1989, Table 2, p.26
36	Salado	FFG_091	614.20	Richey, 1989, Table 2, p.26
37	Salado	FFG_092	633.70	Richey, 1989, Table 2, p.26
38	Salado	FFG_093	637.70	Richey, 1989, Table 2, p.26
39	Salado	FFG_094	637.00	Richey, 1989, Table 2, p.26
40	Salado	FFG_095	618.70	Richey, 1989, Table 2, p.26
41	Salado	FFG_096	605.00	Richey, 1989, Table 2, p.26
42	Salado	FFG_097	580.60	Richey, 1989, Table 2, p.27
43	Salado	FFG_098	555.90	Richey, 1989, Table 2, p.27
44	Salado	FFG_099	550.20	Richey, 1989, Table 2, p.27
45	Salado	FFG_100	530.40	Richey, 1989, Table 2, p.27
46	Salado	FFG_101	500.20	Richey, 1989, Table 2, p.27
47	Salado	FFG_102	512.40	Richey, 1989, Table 2, p.27
48	Salado	FFG_104	474.30	Richey, 1989, Table 2, p.27
49	Salado	FFG_105	812.90	Richey, 1989, Table 2, p.27
50	Salado	FFG_106	840.70	Richey, 1989, Table 2, p.27
51	Salado	FFG_107	836.10	Richey, 1989, Table 2, p.27
52	Salado	FFG_108	836.10	Richey, 1989, Table 2, p.27
53	Salado	FFG_109	831.80	Richey, 1989, Table 2, p.27
54	Salado	FFG_110	798.60	Richey, 1989, Table 2, p.27
55	Salado	FFG_111	806.20	Richey, 1989, Table 2, p.27
56	Salado	FFG_112	784.80	Richey, 1989, Table 2, p.28
57	Salado	FFG_113	802.20	Richey, 1989, Table 2, p.28
58	Salado	FFG_114	828.80	Richey, 1989, Table 2, p.28
59	Salado	FFG_115	803.50	Richey, 1989, Table 2, p.28
60	Salado	FFG_116	795.20	Richey, 1989, Table 2, p.28
61	Salado	FFG_117	810.80	Richey, 1989, Table 2, p.28
62	Salado	FFG_119	828.20	Richey, 1989, Table 2, p.28
63	Salado	FFG_120	819.30	Richey, 1989, Table 2, p.28
64	Salado	FFG_121	830.60	Richey, 1989, Table 2, p.28
65	Salado	FFG_122	813.80	Richey, 1989, Table 2, p.28
66	Salado	FFG_123	815.30	Richey, 1989, Table 2, p.28
67	Salado	FFG_124	785.50	Richey, 1989, Table 2, p.28
68	Salado	FFG_126	813.00	Richey, 1989, Table 2, p.28
69	Salado	FFG_127	824.10	Richey, 1989, Table 2, p.28
70	Salado	FFG_128	852.60	Richey, 1989, Table 2, p.28
71	Salado	FFG_129	815.60	Richey, 1989, Table 2, p.28
72	Salado	FFG_130	854.90	Richey, 1989, Table 2, p.28
73	Salado	FFG_132	852.80	Richey, 1989, Table 2, p.29
74	Salado	FFG_133	837.60	Richey, 1989, Table 2, p.29
75	Salado	FFG_134	861.70	Richey, 1989, Table 2, p.29
76	Salado	FFG_135	844.00	Richey, 1989, Table 2, p.29

Table B.2. Elevations of Stratigraphic Layers Near WIPP (Continued)

	Layer	Well ID	Elevation	Source
1	Salado	FFG_136	844.40	Richey, 1989, Table 2, p.29
2	Salado	FFG_137	853.20	Richey, 1989, Table 2, p.29
3	Salado	FFG_138	798.30	Richey, 1989, Table 2, p.29
4	Salado	FFG_139	810.10	Richey, 1989, Table 2, p.29
5	Salado	FFG_140	750.00	Richey, 1989, Table 2, p.29
6	Salado	FFG_141	782.90	Richey, 1989, Table 2, p.29
7	Salado	FFG_142	757.80	Richey, 1989, Table 2, p.29
8	Salado	FFG_144	825.10	Richey, 1989, Table 2, p.29
9	Salado	FFG_145	830.60	Richey, 1989, Table 2, p.29
10	Salado	FFG_146	826.00	Richey, 1989, Table 2, p.29
11	Salado	FFG_147	816.30	Richey, 1989, Table 2, p.29
12	Salado	FFG_148	832.10	Richey, 1989, Table 2, p.29
13	Salado	FFG_149	842.10	Richey, 1989, Table 2, p.30
14	Salado	FFG_152	836.70	Richey, 1989, Table 2, p.30
15	Salado	FFG_155	830.90	Richey, 1989, Table 2, p.30
16	Salado	FFG_156	837.60	Richey, 1989, Table 2, p.30
17	Salado	FFG_158	856.80	Richey, 1989, Table 2, p.30
18	Salado	FFG_159	859.60	Richey, 1989, Table 2, p.30
19	Salado	FFG_160	855.60	Richey, 1989, Table 2, p.30
20	Salado	FFG_161	856.80	Richey, 1989, Table 2, p.30
21	Salado	FFG_162	857.70	Richey, 1989, Table 2, p.30
22	Salado	FFG_163	856.20	Richey, 1989, Table 2, p.30
23	Salado	FFG_164	854.70	Richey, 1989, Table 2, p.30
24	Salado	FFG_165	838.80	Richey, 1989, Table 2, p.30
25	Salado	FFG_166	858.30	Richey, 1989, Table 2, p.31
26	Salado	FFG_167	836.70	Richey, 1989, Table 2, p.31
27	Salado	FFG_168	843.10	Richey, 1989, Table 2, p.31
28	Salado	FFG_169	861.30	Richey, 1989, Table 2, p.31
29	Salado	FFG_170	839.10	Richey, 1989, Table 2, p.31
30	Salado	FFG_171	848.00	Richey, 1989, Table 2, p.31
31	Salado	FFG_172	851.90	Richey, 1989, Table 2, p.31
32	Salado	FFG_173	831.50	Richey, 1989, Table 2, p.31
33	Salado	FFG_177	812.60	Richey, 1989, Table 2, p.31
34	Salado	FFG_178	539.20	Richey, 1989, Table 2, p.31
35	Salado	FFG_179	816.80	Richey, 1989, Table 2, p.31
36	Salado	FFG_180	825.10	Richey, 1989, Table 2, p.31
37	Salado	FFG_181	869.00	Richey, 1989, Table 2, p.32
38	Salado	FFG_182	757.10	Richey, 1989, Table 2, p.32
39	Salado	FFG_183	837.30	Richey, 1989, Table 2, p.32
40	Salado	FFG_184	851.60	Richey, 1989, Table 2, p.32
41	Salado	FFG_185	840.00	Richey, 1989, Table 2, p.32
42	Salado	FFG_186	766.30	Richey, 1989, Table 2, p.32
43	Salado	FFG_188	781.20	Richey, 1989, Table 2, p.32
44	Salado	FFG_189	805.00	Richey, 1989, Table 2, p.32
45	Salado	FFG_190	793.40	Richey, 1989, Table 2, p.32
46	Salado	FFG_191	780.00	Richey, 1989, Table 2, p.32
47	Salado	FFG_192	708.00	Richey, 1989, Table 2, p.32
48	Salado	FFG_194	738.80	Richey, 1989, Table 2, p.33
49	Salado	FFG_195	753.50	Richey, 1989, Table 2, p.33
50	Salado	FFG_196	792.50	Richey, 1989, Table 2, p.33
51	Salado	FFG_197	790.10	Richey, 1989, Table 2, p.33
52	Salado	FFG_198	783.90	Richey, 1989, Table 2, p.33
53	Salado	FFG_199	780.60	Richey, 1989, Table 2, p.33
54	Salado	FFG_200	785.20	Richey, 1989, Table 2, p.33
55	Salado	FFG_201	778.70	Richey, 1989, Table 2, p.33
56	Salado	FFG_202	723.60	Richey, 1989, Table 2, p.33
57	Salado	FFG_203	727.60	Richey, 1989, Table 2, p.33
58	Salado	FFG_204	767.20	Richey, 1989, Table 2, p.33
59	Salado	FFG_205	768.50	Richey, 1989, Table 2, p.33
60	Salado	FFG_206	779.40	Richey, 1989, Table 2, p.33
61	Salado	FFG_207	775.70	Richey, 1989, Table 2, p.33
62	Salado	FFG_208	780.30	Richey, 1989, Table 2, p.34
63	Salado	FFG_209	787.30	Richey, 1989, Table 2, p.34
64	Salado	FFG_210	766.00	Richey, 1989, Table 2, p.34
65	Salado	FFG_212	768.40	Richey, 1989, Table 2, p.34
66	Salado	FFG_213	795.30	Richey, 1989, Table 2, p.34
67	Salado	FFG_214	757.70	Richey, 1989, Table 2, p.34
68	Salado	FFG_215	734.60	Richey, 1989, Table 2, p.34
69	Salado	FFG_216	520.60	Richey, 1989, Table 2, p.34
70	Salado	FFG_217	756.30	Richey, 1989, Table 2, p.34
71	Salado	FFG_218	744.00	Richey, 1989, Table 2, p.34
72	Salado	FFG_219	783.30	Richey, 1989, Table 2, p.34
73	Salado	FFG_220	742.20	Richey, 1989, Table 2, p.34
74	Salado	FFG_221	684.90	Richey, 1989, Table 2, p.34
75	Salado	FFG_222	604.50	Richey, 1989, Table 2, p.34
76	Salado	FFG_224	558.10	Richey, 1989, Table 2, p.35

Table B.2. Elevations of Stratigraphic Layers Near WIPP (Continued)

	Layer	Well ID	Elevation	Source
1	Salado	FFG_225	566.30	Richey, 1989, Table 2, p.35
2	Salado	FFG_226	561.90	Richey, 1989, Table 2, p.35
3	Salado	FFG_228	549.30	Richey, 1989, Table 2, p.35
4	Salado	FFG_229	572.10	Richey, 1989, Table 2, p.35
5	Salado	FFG_230	558.40	Richey, 1989, Table 2, p.35
6	Salado	FFG_231	578.20	Richey, 1989, Table 2, p.35
7	Salado	FFG_232	586.10	Richey, 1989, Table 2, p.35
8	Salado	FFG_233	581.90	Richey, 1989, Table 2, p.35
9	Salado	FFG_234	616.30	Richey, 1989, Table 2, p.35
10	Salado	FFG_235	595.90	Richey, 1989, Table 2, p.35
11	Salado	FFG_236	641.90	Richey, 1989, Table 2, p.35
12	Salado	FFG_237	600.80	Richey, 1989, Table 2, p.35
13	Salado	FFG_238	584.30	Richey, 1989, Table 2, p.36
14	Salado	FFG_239	570.50	Richey, 1989, Table 2, p.36
15	Salado	FFG_240	568.80	Richey, 1989, Table 2, p.36
16	Salado	FFG_241	562.70	Richey, 1989, Table 2, p.36
17	Salado	FFG_242	681.30	Richey, 1989, Table 2, p.36
18	Salado	FFG_243	615.10	Richey, 1989, Table 2, p.36
19	Salado	FFG_244	689.30	Richey, 1989, Table 2, p.36
20	Salado	FFG_245	470.60	Richey, 1989, Table 2, p.36
21	Salado	FFG_246	473.10	Richey, 1989, Table 2, p.36
22	Salado	FFG_247	460.10	Richey, 1989, Table 2, p.36
23	Salado	FFG_248	464.50	Richey, 1989, Table 2, p.36
24	Salado	FFG_249	464.20	Richey, 1989, Table 2, p.36
25	Salado	FFG_250	545.50	Richey, 1989, Table 2, p.36
26	Salado	FFG_251	432.20	Richey, 1989, Table 2, p.36
27	Salado	FFG_252	567.50	Richey, 1989, Table 2, p.36
28	Salado	FFG_253	521.90	Richey, 1989, Table 2, p.36
29	Salado	FFG_254	517.80	Richey, 1989, Table 2, p.36
30	Salado	FFG_255	467.30	Richey, 1989, Table 2, p.37
31	Salado	FFG_256	438.90	Richey, 1989, Table 2, p.37
32	Salado	FFG_257	484.00	Richey, 1989, Table 2, p.37
33	Salado	FFG_258	497.70	Richey, 1989, Table 2, p.37
34	Salado	FFG_259	456.80	Richey, 1989, Table 2, p.37
35	Salado	FFG_260	515.10	Richey, 1989, Table 2, p.37
36	Salado	FFG_261	502.60	Richey, 1989, Table 2, p.37
37	Salado	FFG_262	440.50	Richey, 1989, Table 2, p.37
38	Salado	FFG_263	406.80	Richey, 1989, Table 2, p.37
39	Salado	FFG_264	653.50	Richey, 1989, Table 2, p.37
40	Salado	FFG_265	634.60	Richey, 1989, Table 2, p.37
41	Salado	FFG_266	609.60	Richey, 1989, Table 2, p.37
42	Salado	FFG_267	582.70	Richey, 1989, Table 2, p.37
43	Salado	FFG_268	563.30	Richey, 1989, Table 2, p.37
44	Salado	FFG_269	568.30	Richey, 1989, Table 2, p.38
45	Salado	FFG_270	689.40	Richey, 1989, Table 2, p.38
46	Salado	FFG_271	733.30	Richey, 1989, Table 2, p.38
47	Salado	FFG_272	697.20	Richey, 1989, Table 2, p.38
48	Salado	FFG_273	701.70	Richey, 1989, Table 2, p.38
49	Salado	FFG_274	747.40	Richey, 1989, Table 2, p.38
50	Salado	FFG_275	767.20	Richey, 1989, Table 2, p.38
51	Salado	FFG_276	766.20	Richey, 1989, Table 2, p.38
52	Salado	FFG_277	753.50	Richey, 1989, Table 2, p.38
53	Salado	FFG_278	722.40	Richey, 1989, Table 2, p.38
54	Salado	FFG_279	735.70	Richey, 1989, Table 2, p.38
55	Salado	FFG_280	738.20	Richey, 1989, Table 2, p.38
56	Salado	FFG_281	709.30	Richey, 1989, Table 2, p.38
57	Salado	FFG_283	450.50	Richey, 1989, Table 2, p.39
58	Salado	FFG_284	596.20	Richey, 1989, Table 2, p.39
59	Salado	FFG_285	616.00	Richey, 1989, Table 2, p.39
60	Salado	FFG_286	728.70	Richey, 1989, Table 2, p.39
61	Salado	FFG_287	693.10	Richey, 1989, Table 2, p.39
62	Salado	FFG_288	616.90	Richey, 1989, Table 2, p.39
63	Salado	FFG_289	639.10	Richey, 1989, Table 2, p.39
64	Salado	FFG_290	733.40	Richey, 1989, Table 2, p.39
65	Salado	FFG_291	615.10	Richey, 1989, Table 2, p.39
66	Salado	FFG_292	686.70	Richey, 1989, Table 2, p.39
67	Salado	FFG_293	672.40	Richey, 1989, Table 2, p.39
68	Salado	FFG_294	458.20	Richey, 1989, Table 2, p.39
69	Salado	FFG_295	438.90	Richey, 1989, Table 2, p.39
70	Salado	FFG_297	420.30	Richey, 1989, Table 2, p.39
71	Salado	FFG_298	490.00	Richey, 1989, Table 2, p.40
72	Salado	FFG_299	441.40	Richey, 1989, Table 2, p.40
73	Salado	FFG_300	416.90	Richey, 1989, Table 2, p.40
74	Salado	FFG_301	359.40	Richey, 1989, Table 2, p.40
75	Salado	FFG_302	420.30	Richey, 1989, Table 2, p.40
76	Salado	FFG_303	404.80	Richey, 1989, Table 2, p.40

Table B.2. Elevations of Stratigraphic Layers Near WIPP (Continued)

	Layer	Well ID	Elevation	Source		Layer	Well ID	Elevation	Source
1	Salado	FFG_304	399.30	Richey, 1989, Table 2, p.40	39	Salado	FFG_344	622.60	Richey, 1989, Table 2, p.43
2	Salado	FFG_305	399.60	Richey, 1989, Table 2, p.40	40	Salado	FFG_345	628.60	Richey, 1989, Table 2, p.43
3	Salado	FFG_306	361.40	Richey, 1989, Table 2, p.40	41	Salado	FFG_347	655.30	Richey, 1989, Table 2, p.43
4	Salado	FFG_307	383.80	Richey, 1989, Table 2, p.40	42	Salado	FFG_348	686.10	Richey, 1989, Table 2, p.43
5	Salado	FFG_308	323.00	Richey, 1989, Table 2, p.40	43	Salado	FFG_349	678.80	Richey, 1989, Table 2, p.43
6	Salado	FFG_309	388.60	Richey, 1989, Table 2, p.40	44	Salado	FFG_350	712.30	Richey, 1989, Table 2, p.43
7	Salado	FFG_310	430.00	Richey, 1989, Table 2, p.40	45	Salado	FFG_351	571.50	Richey, 1989, Table 2, p.43
8	Salado	FFG_311	387.40	Richey, 1989, Table 2, p.40	46	Salado	FFG_352	573.10	Richey, 1989, Table 2, p.43
9	Salado	FFG_312	384.10	Richey, 1989, Table 2, p.40	47	Salado	FFG_353	598.40	Richey, 1989, Table 2, p.43
10	Salado	FFG_313	832.20	Richey, 1989, Table 2, p.41	48	Salado	FFG_354	722.40	Richey, 1989, Table 2, p.43
11	Salado	FFG_314	734.90	Richey, 1989, Table 2, p.41	49	Salado	FFG_361	905.80	Richey, 1989, Table 2, p.44
12	Salado	FFG_315	650.90	Richey, 1989, Table 2, p.41	50	Salado	FFG_362	841.50	Richey, 1989, Table 2, p.44
13	Salado	FFG_316	624.20	Richey, 1989, Table 2, p.41	51	Salado	FFG_363	881.50	Richey, 1989, Table 2, p.44
14	Salado	FFG_317	693.10	Richey, 1989, Table 2, p.41	52	Salado	FFG_366	863.80	Richey, 1989, Table 2, p.44
15	Salado	FFG_318	666.00	Richey, 1989, Table 2, p.41	53	Salado	FFG_367	876.90	Richey, 1989, Table 2, p.44
16	Salado	FFG_319	662.00	Richey, 1989, Table 2, p.41	54	Salado	FFG_370	919.30	Richey, 1989, Table 2, p.44
17	Salado	FFG_320	616.00	Richey, 1989, Table 2, p.41	55	Salado	FFG_371	919.90	Richey, 1989, Table 2, p.44
18	Salado	FFG_321	612.90	Richey, 1989, Table 2, p.41	56	Salado	FFG_374	855.00	Richey, 1989, Table 2, p.45
19	Salado	FFG_322	616.80	Richey, 1989, Table 2, p.41	57	Salado	FFG_376	896.40	Richey, 1989, Table 2, p.45
20	Salado	FFG_323	626.80	Richey, 1989, Table 2, p.41	58	Salado	FFG_381	875.10	Richey, 1989, Table 2, p.45
21	Salado	FFG_324	653.20	Richey, 1989, Table 2, p.41	59	Salado	FFG_383	867.20	Richey, 1989, Table 2, p.45
22	Salado	FFG_325	713.50	Richey, 1989, Table 2, p.41	60	Salado	FFG_385	856.50	Richey, 1989, Table 2, p.45
23	Salado	FFG_326	657.50	Richey, 1989, Table 2, p.41	61	Salado	FFG_387	862.00	Richey, 1989, Table 2, p.45
24	Salado	FFG_327	645.30	Richey, 1989, Table 2, p.42	62	Salado	FFG_390	863.50	Richey, 1989, Table 2, p.46
25	Salado	FFG_328	620.50	Richey, 1989, Table 2, p.42	63	Salado	FFG_391	868.30	Richey, 1989, Table 2, p.46
26	Salado	FFG_329	613.20	Richey, 1989, Table 2, p.42	64	Salado	FFG_392	863.20	Richey, 1989, Table 2, p.46
27	Salado	FFG_330	611.60	Richey, 1989, Table 2, p.42	65	Salado	FFG_393	752.70	Richey, 1989, Table 2, p.46
28	Salado	FFG_331	602.60	Richey, 1989, Table 2, p.42	66	Salado	FFG_394	846.70	Richey, 1989, Table 2, p.46
29	Salado	FFG_332	587.00	Richey, 1989, Table 2, p.42	67	Salado	FFG_395	842.20	Richey, 1989, Table 2, p.46
30	Salado	FFG_333	598.80	Richey, 1989, Table 2, p.42	68	Salado	FFG_396	787.30	Richey, 1989, Table 2, p.46
31	Salado	FFG_334	589.10	Richey, 1989, Table 2, p.42	69	Salado	FFG_403	846.90	Richey, 1989, Table 2, p.47
32	Salado	FFG_335	607.80	Richey, 1989, Table 2, p.42	70	Salado	FFG_408	827.80	Richey, 1989, Table 2, p.47
33	Salado	FFG_336	603.20	Richey, 1989, Table 2, p.42	71	Salado	FFG_411	789.10	Richey, 1989, Table 2, p.47
34	Salado	FFG_337	584.60	Richey, 1989, Table 2, p.42	72	Salado	FFG_413	835.20	Richey, 1989, Table 2, p.47
35	Salado	FFG_338	589.60	Richey, 1989, Table 2, p.42	73	Salado	FFG_421	879.40	Richey, 1989, Table 2, p.48
36	Salado	FFG_339	553.80	Richey, 1989, Table 2, p.42	74	Salado	FFG_426	856.50	Richey, 1989, Table 2, p.48
37	Salado	FFG_340	559.90	Richey, 1989, Table 2, p.42	75	Salado	FFG_432	837.30	Richey, 1989, Table 2, p.48
38	Salado	FFG_342	651.60	Richey, 1989, Table 2, p.43	76	Salado	FFG_433	816.80	Richey, 1989, Table 2, p.48

Table B.2. Elevations of Stratigraphic Layers Near WIPP (Continued)

	Layer	Well ID	Elevation	Source
1	Salado	FFG_438	797.50	Richey, 1989, Table 2, p.49
2	Salado	FFG_445	827.20	Richey, 1989, Table 2, p.49
3	Salado	FFG_453	726.50	Richey, 1989, Table 2, p.50
4	Salado	FFG_455	723.90	Richey, 1989, Table 2, p.50
5	Salado	FFG_456	730.90	Richey, 1989, Table 2, p.50
6	Salado	FFG_457	784.50	Richey, 1989, Table 2, p.50
7	Salado	FFG_458	785.50	Richey, 1989, Table 2, p.50
8	Salado	FFG_459	717.20	Richey, 1989, Table 2, p.50
9	Salado	FFG_462	781.30	Richey, 1989, Table 2, p.50
10	Salado	FFG_463	811.40	Richey, 1989, Table 2, p.51
11	Salado	FFG_464	787.60	Richey, 1989, Table 2, p.51
12	Salado	FFG_465	783.90	Richey, 1989, Table 2, p.51
13	Salado	FFG_467	380.30	Richey, 1989, Table 2, p.51
14	Salado	FFG_468	322.20	Richey, 1989, Table 2, p.51
15	Salado	FFG_470	360.00	Richey, 1989, Table 2, p.51
16	Salado	FFG_471	372.40	Richey, 1989, Table 2, p.51
17	Salado	FFG_472	439.30	Richey, 1989, Table 2, p.51
18	Salado	FFG_473	339.50	Richey, 1989, Table 2, p.51
19	Salado	FFG_474	634.90	Richey, 1989, Table 2, p.51
20	Salado	FFG_475	637.80	Richey, 1989, Table 2, p.51
21	Salado	FFG_476	711.40	Richey, 1989, Table 2, p.51
22	Salado	FFG_477	679.70	Richey, 1989, Table 2, p.51
23	Salado	FFG_478	655.30	Richey, 1989, Table 2, p.52
24	Salado	FFG_479	661.10	Richey, 1989, Table 2, p.52
25	Salado	FFG_480	641.60	Richey, 1989, Table 2, p.52
26	Salado	FFG_481	635.20	Richey, 1989, Table 2, p.52
27	Salado	FFG_482	665.40	Richey, 1989, Table 2, p.52
28	Salado	FFG_483	690.90	Richey, 1989, Table 2, p.52
29	Salado	FFG_484	672.20	Richey, 1989, Table 2, p.52
30	Salado	FFG_485	682.80	Richey, 1989, Table 2, p.52
31	Salado	FFG_486	668.70	Richey, 1989, Table 2, p.52
32	Salado	FFG_487	669.40	Richey, 1989, Table 2, p.52
33	Salado	FFG_488	648.90	Richey, 1989, Table 2, p.52
34	Salado	FFG_489	663.10	Richey, 1989, Table 2, p.52
35	Salado	FFG_490	765.70	Richey, 1989, Table 2, p.52
36	Salado	FFG_491	752.60	Richey, 1989, Table 2, p.52
37	Salado	FFG_492	720.50	Richey, 1989, Table 2, p.52
38	Salado	FFG_493	709.70	Richey, 1989, Table 2, p.53
39	Salado	FFG_494	713.20	Richey, 1989, Table 2, p.53
40	Salado	FFG_495	696.40	Richey, 1989, Table 2, p.53
41	Salado	FFG_496	555.40	Richey, 1989, Table 2, p.53
42	Salado	FFG_497	601.70	Richey, 1989, Table 2, p.53
43	Salado	FFG_498	589.20	Richey, 1989, Table 2, p.53
44	Salado	FFG_499	549.90	Richey, 1989, Table 2, p.53
45	Salado	FFG_500	582.80	Richey, 1989, Table 2, p.53
46	Salado	FFG_501	625.40	Richey, 1989, Table 2, p.53
47	Salado	FFG_502	567.20	Richey, 1989, Table 2, p.53
48	Salado	FFG_503	573.70	Richey, 1989, Table 2, p.53
49	Salado	FFG_504	618.80	Richey, 1989, Table 2, p.53
50	Salado	FFG_505	650.50	Richey, 1989, Table 2, p.53
51	Salado	FFG_506	649.50	Richey, 1989, Table 2, p.53
52	Salado	FFG_507	549.10	Richey, 1989, Table 2, p.53
53	Salado	FFG_508	628.80	Richey, 1989, Table 2, p.53
54	Salado	FFG_509	616.30	Richey, 1989, Table 2, p.54
55	Salado	FFG_510	615.20	Richey, 1989, Table 2, p.54
56	Salado	FFG_511	570.60	Richey, 1989, Table 2, p.54
57	Salado	FFG_512	576.70	Richey, 1989, Table 2, p.54
58	Salado	FFG_513	606.00	Richey, 1989, Table 2, p.54
59	Salado	FFG_514	577.30	Richey, 1989, Table 2, p.54
60	Salado	FFG_515	556.20	Richey, 1989, Table 2, p.54
61	Salado	FFG_516	545.90	Richey, 1989, Table 2, p.54
62	Salado	FFG_517	732.50	Richey, 1989, Table 2, p.54
63	Salado	FFG_518	720.20	Richey, 1989, Table 2, p.54
64	Salado	FFG_519	659.90	Richey, 1989, Table 2, p.54
65	Salado	FFG_520	542.70	Richey, 1989, Table 2, p.54
66	Salado	FFG_521	604.70	Richey, 1989, Table 2, p.54
67	Salado	FFG_522	382.40	Richey, 1989, Table 2, p.54
68	Salado	FFG_523	388.90	Richey, 1989, Table 2, p.54
69	Salado	FFG_524	561.70	Richey, 1989, Table 2, p.55
70	Salado	FFG_525	388.40	Richey, 1989, Table 2, p.55
71	Salado	FFG_526	911.10	Richey, 1989, Table 2, p.55
72	Salado	FFG_527	871.10	Richey, 1989, Table 2, p.55
73	Salado	FFG_528	864.10	Richey, 1989, Table 2, p.55
74	Salado	FFG_530	930.20	Richey, 1989, Table 2, p.55
75	Salado	FFG_531	855.20	Richey, 1989, Table 2, p.55
76	Salado	FFG_532	838.50	Richey, 1989, Table 2, p.55

Table B.2. Elevations of Stratigraphic Layers Near WIPP (Continued)

	Layer	Well ID	Elevation	Source
1	Salado	FFG_535	850.40	Richey, 1989, Table 2, p.55
2	Salado	FFG_536	853.50	Richey, 1989, Table 2, p.55
3	Salado	FFG_537	840.60	Richey, 1989, Table 2, p.55
4	Salado	FFG_564	557.80	Richey, 1989, Table 2, p.57
5	Salado	FFG_584	690.90	Richey, 1989, Table 2, p.58
6	Salado	FFG_585	643.40	Richey, 1989, Table 2, p.58
7	Salado	FFG_602	743.70	Richey, 1989, Table 2, p.58
8	Salado	FFG_606	603.20	Richey, 1989, Table 2, p.58
9	Salado	FFG_607	624.30	Richey, 1989, Table 2, p.59
10	Salado	FFG_608	593.70	Richey, 1989, Table 2, p.59
11	Salado	FFG_609	586.10	Richey, 1989, Table 2, p.59
12	Salado	FFG_610	588.30	Richey, 1989, Table 2, p.59
13	Salado	FFG_611	579.40	Richey, 1989, Table 2, p.59
14	Salado	FFG_612	624.90	Richey, 1989, Table 2, p.59
15	Salado	FFG_613	621.80	Richey, 1989, Table 2, p.59
16	Salado	FFG_640	519.50	Richey, 1989, Table 2, p.60
17	Salado	FFG_643	576.10	Richey, 1989, Table 2, p.60
18	Salado	FFG_652	786.40	Richey, 1989, Table 2, p.60
19	Salado	FFG_653	788.60	Richey, 1989, Table 2, p.61
20	Salado	FFG_654	812.30	Richey, 1989, Table 2, p.61
21	Salado	FFG_655	812.90	Richey, 1989, Table 2, p.61
22	Salado	FFG_656	808.90	Richey, 1989, Table 2, p.61
23	Salado	FFG_657	830.00	Richey, 1989, Table 2, p.61
24	Salado	FFG_658	816.20	Richey, 1989, Table 2, p.61
25	Salado	FFG_659	821.10	Richey, 1989, Table 2, p.61
26	Salado	FFG_660	845.10	Richey, 1989, Table 2, p.61
27	Salado	FFG_662	810.20	Richey, 1989, Table 2, p.61
28	Salado	FFG_664	794.90	Richey, 1989, Table 2, p.61
29	Salado	FFG_666	860.10	Richey, 1989, Table 2, p.62
30	Salado	FFG_667	845.80	Richey, 1989, Table 2, p.62
31	Salado	FFG_668	905.10	Richey, 1989, Table 2, p.62
32	Salado	FFG_669	890.60	Richey, 1989, Table 2, p.62
33	Salado	FFG_670	876.00	Richey, 1989, Table 2, p.62
34	Salado	FFG_671	873.50	Richey, 1989, Table 2, p.62
35	Salado	FFG_672	868.10	Richey, 1989, Table 2, p.62
36	Salado	FFG_673	870.50	Richey, 1989, Table 2, p.62
37	Salado	FFG_674	860.20	Richey, 1989, Table 2, p.62
38	Salado	FFG_675	819.20	Richey, 1989, Table 2, p.62
39	Salado	FFG_676	831.80	Richey, 1989, Table 2, p.62
40	Salado	FFG_677	857.10	Richey, 1989, Table 2, p.62
41	Salado	FFG_679	861.10	Richey, 1989, Table 2, p.62
42	Salado	FFG_685	825.70	Richey, 1989, Table 2, p.63
43	Salado	FFG_689	718.10	Richey, 1989, Table 2, p.63
44	Salado	FFG_690	718.10	Richey, 1989, Table 2, p.63
45	Salado	FFG_691	711.40	Richey, 1989, Table 2, p.63
46	Salado	FFG_693	712.60	Richey, 1989, Table 2, p.63
47	Salado	FFG_694	680.30	Richey, 1989, Table 2, p.63
48	Salado	FFG_695	702.60	Richey, 1989, Table 2, p.63
49	Salado	FFG_696	703.10	Richey, 1989, Table 2, p.63
50	Salado	FFG_697	699.90	Richey, 1989, Table 2, p.64
51	Salado	FFG_698	734.90	Richey, 1989, Table 2, p.64
52	Salado	FFG_699	691.00	Richey, 1989, Table 2, p.64
53	Salado	FFG_700	682.20	Richey, 1989, Table 2, p.64
54	Salado	FFG_701	686.50	Richey, 1989, Table 2, p.64
55	Salado	FFG_702	693.70	Richey, 1989, Table 2, p.64
56	Salado	FFG_703	716.90	Richey, 1989, Table 2, p.64
57	Salado	FFG_704	686.40	Richey, 1989, Table 2, p.64
58	Salado	FFG_705	610.80	Richey, 1989, Table 2, p.64
59	Salado	FFG_706	637.10	Richey, 1989, Table 2, p.64
60	Salado	FFG_707	616.70	Richey, 1989, Table 2, p.64
61	Salado	FFG_708	669.70	Richey, 1989, Table 2, p.64
62	Salado	FFG_710	579.20	Richey, 1989, Table 2, p.64
63	Salado	FFG_711	570.60	Richey, 1989, Table 2, p.65
64	Salado	FFG_716	553.10	Richey, 1989, Table 2, p.65
65	Salado	FFG_717	621.90	Richey, 1989, Table 2, p.65
66	Salado	FFG_718	612.80	Richey, 1989, Table 2, p.65
67	Salado	FFG_719	571.20	Richey, 1989, Table 2, p.65
68	Salado	FFG_720	570.60	Richey, 1989, Table 2, p.65
69	Salado	FFG_721	594.40	Richey, 1989, Table 2, p.65
70	Salado	FFG_723	712.50	Richey, 1989, Table 2, p.65
71	Salado	FFG_724	633.80	Richey, 1989, Table 2, p.65
72	Salado	FFG_725	610.50	Richey, 1989, Table 2, p.65
73	Salado	FFG_726	589.10	Richey, 1989, Table 2, p.65
74	Salado	FFG_727	575.50	Richey, 1989, Table 2, p.66
75	Salado	FFG_728	590.40	Richey, 1989, Table 2, p.66
76	Salado	FFG_729	595.90	Richey, 1989, Table 2, p.66

Table B.2. Elevations of Stratigraphic Layers Near WIPP (Continued)

	Layer	Well ID	Elevation	Source		Layer	Well ID	Elevation	Source
1	Salado	FFG_730	622.70	Richey, 1989, Table 2, p.66	39	Salado	P20	746.80	Mercer, 1983, Table 1
2	Salado	FFG_731	617.70	Richey, 1989, Table 2, p.66	40	Salado	P21	751.60	Mercer, 1983, Table 1
3	Salado	FFG_733	698.30	Richey, 1989, Table 2, p.66	41	Salado	P3	791.50	Mercer, 1983, Table 1
4	Salado	FFG_734	654.10	Richey, 1989, Table 2, p.66	42	Salado	P4	766.20	Mercer, 1983, Table 1
5	Salado	FFG_735	584.00	Richey, 1989, Table 2, p.66	43	Salado	P5	769.40	Mercer, 1983, Table 1
6	Salado	FFG_736	615.40	Richey, 1989, Table 2, p.66	44	Salado	P6	821.40	Mercer, 1983, Table 1
7	Salado	FFG_737	559.30	Richey, 1989, Table 2, p.66	45	Salado	P7	823.60	Mercer, 1983, Table 1
8	Salado	FFG_738	610.20	Richey, 1989, Table 2, p.66	46	Salado	P8	799.80	Mercer, 1983, Table 1
9	Salado	FFG_739	628.60	Richey, 1989, Table 2, p.66	47	Salado	P9	771.50	Mercer, 1983, Table 1
10	Salado	FFG_740	609.00	Richey, 1989, Table 2, p.66	48	Salado	WIPP11	754.30	Mercer, 1983, Table 1
11	Salado	FFG_741	602.30	Richey, 1989, Table 2, p.66	49	Salado	WIPP12	767.20	Mercer, 1983, Table 1
12	Salado	FFG_742	646.50	Richey, 1989, Table 2, p.67	50	Salado	WIPP13	780.50	Mercer, 1983, Table 1
13	Salado	FFG_743	630.70	Richey, 1989, Table 2, p.67	51	Salado	WIPP18	770.50	Mercer, 1983, Table 1
14	Salado	FFG_744	630.00	Richey, 1989, Table 2, p.67	52	Salado	WIPP19	773.90	Mercer, 1983, Table 1
15	Salado	FFG_745	598.30	Richey, 1989, Table 2, p.67	53	Salado	WIPP21	776.90	Mercer, 1983, Table 1
16	Salado	FFG_746	581.80	Richey, 1989, Table 2, p.67	54	Salado	WIPP22	775.10	Mercer, 1983, Table 1
17	Salado	H1	784.50	Mercer, 1983, Table 1	55	Salado	WIPP25	807.10	Mercer, 1983, Table 1
18	Salado	H10C	666.30	Mercer, 1983, Table 1	56	Salado	WIPP26	866.50	Mercer, 1983, Table 1
19	Salado	H2C	796.70	Mercer, 1983, Table 1	57	Salado	WIPP27	841.50	Mercer, 1983, Table 1
20	Salado	H3	783.10	Mercer, 1983, Table 1	58	Salado	WIPP28	858.40	Mercer, 1983, Table 1
21	Salado	H4C	825.40	Mercer, 1983, Table 1	59	Salado	WIPP29	863.80	Mercer, 1983, Table 1
22	Salado	H5C	751.60	Mercer, 1983, Table 1	60	Salado	WIPP30	816.60	Mercer, 1983, Table 1
23	Salado	H6C	800.70	Mercer, 1983, Table 1	61	Salado	WIPP32	870.80	Mercer, 1983, Table 1
24	Salado	H7C	877.80	Mercer, 1983, Table 1	62	Salado	WIPP33	812.60	Mercer, 1983, Table 1
25	Salado	H8C	823.00	Mercer, 1983, Table 1	63	Salado	WIPP34	749.80	Mercer, 1983, Table 1
26	Salado	H9C	797.00	Mercer, 1983, Table 1	64	Supra_R	AEC7	1113.70	Mercer, 1983, Table 1
27	Salado	P1	813.30	Mercer, 1983, Table 1	65	Supra_R	AEC8	1076.60	Mercer, 1983, Table 1
28	Salado	P10	738.50	Mercer, 1983, Table 1	66	Supra_R	B25	1039.10	Mercer, 1983, Table 1
29	Salado	P11	745.50	Mercer, 1983, Table 1	67	Supra_R	ERDA10	1027.50	Mercer, 1983, Table 1
30	Salado	P12	800.10	Mercer, 1983, Table 1	68	Supra_R	ERDA6	1079.00	Mercer, 1983, Table 1
31	Salado	P13	799.80	Mercer, 1983, Table 1	69	Supra_R	ERDA9	1042.10	Mercer, 1983, Table 1
32	Salado	P14	814.70	Mercer, 1983, Table 1	70	Supra_R	FFG_002	1090.30	Richey, 1989, Table 2, p.21
33	Salado	P15	843.70	Mercer, 1983, Table 1	71	Supra_R	FFG_004	1068.30	Richey, 1989, Table 2, p.21
34	Salado	P16	814.40	Mercer, 1983, Table 1	72	Supra_R	FFG_005	1089.70	Richey, 1989, Table 2, p.21
35	Salado	P17	798.90	Mercer, 1983, Table 1	73	Supra_R	FFG_006	1091.50	Richey, 1989, Table 2, p.21
36	Salado	P18	728.20	Mercer, 1983, Table 1	74	Supra_R	FFG_007	1093.90	Richey, 1989, Table 2, p.21
37	Salado	P19	740.00	Mercer, 1983, Table 1	75	Supra_R	FFG_009	1094.80	Richey, 1989, Table 2, p.21
38	Salado	P2	753.20	Mercer, 1983, Table 1	76	Supra_R	FFG_011	1092.70	Richey, 1989, Table 2, p.21

Table B.2. Elevations of Stratigraphic Layers Near WIPP (Continued)

	Layer	Well ID	Elevation	Source
1	Supra_R	FFG_012	1092.10	Richey, 1989, Table 2, p.21
2	Supra_R	FFG_013	1080.20	Richey, 1989, Table 2, p.21
3	Supra_R	FFG_014	1068.60	Richey, 1989, Table 2, p.21
4	Supra_R	FFG_016	1099.70	Richey, 1989, Table 2, p.21
5	Supra_R	FFG_017	1100.90	Richey, 1989, Table 2, p.22
6	Supra_R	FFG_018	1116.50	Richey, 1989, Table 2, p.22
7	Supra_R	FFG_019	1111.00	Richey, 1989, Table 2, p.22
8	Supra_R	FFG_020	1091.50	Richey, 1989, Table 2, p.22
9	Supra_R	FFG_023	1109.80	Richey, 1989, Table 2, p.22
10	Supra_R	FFG_024	1124.60	Richey, 1989, Table 2, p.22
11	Supra_R	FFG_025	1117.60	Richey, 1989, Table 2, p.22
12	Supra_R	FFG_026	1116.00	Richey, 1989, Table 2, p.22
13	Supra_R	FFG_027	1117.40	Richey, 1989, Table 2, p.22
14	Supra_R	FFG_028	1183.90	Richey, 1989, Table 2, p.22
15	Supra_R	FFG_029	1145.40	Richey, 1989, Table 2, p.22
16	Supra_R	FFG_030	1154.30	Richey, 1989, Table 2, p.22
17	Supra_R	FFG_031	1168.30	Richey, 1989, Table 2, p.22
18	Supra_R	FFG_032	1158.50	Richey, 1989, Table 2, p.22
19	Supra_R	FFG_033	1143.60	Richey, 1989, Table 2, p.22
20	Supra_R	FFG_034	1139.30	Richey, 1989, Table 2, p.23
21	Supra_R	FFG_035	1121.10	Richey, 1989, Table 2, p.23
22	Supra_R	FFG_036	1147.60	Richey, 1989, Table 2, p.23
23	Supra_R	FFG_037	1129.30	Richey, 1989, Table 2, p.23
24	Supra_R	FFG_038	1118.30	Richey, 1989, Table 2, p.23
25	Supra_R	FFG_039	1046.10	Richey, 1989, Table 2, p.23
26	Supra_R	FFG_040	1077.20	Richey, 1989, Table 2, p.23
27	Supra_R	FFG_041	1065.30	Richey, 1989, Table 2, p.23
28	Supra_R	FFG_042	1069.50	Richey, 1989, Table 2, p.23
29	Supra_R	FFG_043	1067.10	Richey, 1989, Table 2, p.23
30	Supra_R	FFG_044	1080.50	Richey, 1989, Table 2, p.23
31	Supra_R	FFG_047	1112.80	Richey, 1989, Table 2, p.23
32	Supra_R	FFG_048	1106.10	Richey, 1989, Table 2, p.23
33	Supra_R	FFG_049	1119.20	Richey, 1989, Table 2, p.23
34	Supra_R	FFG_050	1132.50	Richey, 1989, Table 2, p.24
35	Supra_R	FFG_051	1131.10	Richey, 1989, Table 2, p.24
36	Supra_R	FFG_052	1132.00	Richey, 1989, Table 2, p.24
37	Supra_R	FFG_053	1137.50	Richey, 1989, Table 2, p.24
38	Supra_R	FFG_054	1150.20	Richey, 1989, Table 2, p.24
39	Supra_R	FFG_055	1145.10	Richey, 1989, Table 2, p.24
40	Supra_R	FFG_056	1136.60	Richey, 1989, Table 2, p.24
41	Supra_R	FFG_057	1134.80	Richey, 1989, Table 2, p.24
42	Supra_R	FFG_058	1147.70	Richey, 1989, Table 2, p.24
43	Supra_R	FFG_059	1156.10	Richey, 1989, Table 2, p.24
44	Supra_R	FFG_060	1138.40	Richey, 1989, Table 2, p.24
45	Supra_R	FFG_061	1137.50	Richey, 1989, Table 2, p.24
46	Supra_R	FFG_062	1122.60	Richey, 1989, Table 2, p.24
47	Supra_R	FFG_063	1118.10	Richey, 1989, Table 2, p.24
48	Supra_R	FFG_064	1127.20	Richey, 1989, Table 2, p.24
49	Supra_R	FFG_065	1110.70	Richey, 1989, Table 2, p.24
50	Supra_R	FFG_066	1113.70	Richey, 1989, Table 2, p.24
51	Supra_R	FFG_067	1127.50	Richey, 1989, Table 2, p.25
52	Supra_R	FFG_068	1125.00	Richey, 1989, Table 2, p.25
53	Supra_R	FFG_069	1130.20	Richey, 1989, Table 2, p.25
54	Supra_R	FFG_070	1130.80	Richey, 1989, Table 2, p.25
55	Supra_R	FFG_071	1115.30	Richey, 1989, Table 2, p.25
56	Supra_R	FFG_072	1105.20	Richey, 1989, Table 2, p.25
57	Supra_R	FFG_073	1107.40	Richey, 1989, Table 2, p.25
58	Supra_R	FFG_074	1107.00	Richey, 1989, Table 2, p.25
59	Supra_R	FFG_075	1108.30	Richey, 1989, Table 2, p.25
60	Supra_R	FFG_076	1097.30	Richey, 1989, Table 2, p.25
61	Supra_R	FFG_078	1087.20	Richey, 1989, Table 2, p.25
62	Supra_R	FFG_079	1091.20	Richey, 1989, Table 2, p.25
63	Supra_R	FFG_080	1082.30	Richey, 1989, Table 2, p.25
64	Supra_R	FFG_081	1097.00	Richey, 1989, Table 2, p.26
65	Supra_R	FFG_082	1084.80	Richey, 1989, Table 2, p.26
66	Supra_R	FFG_083	1115.60	Richey, 1989, Table 2, p.26
67	Supra_R	FFG_084	1107.60	Richey, 1989, Table 2, p.26
68	Supra_R	FFG_085	1108.90	Richey, 1989, Table 2, p.26
69	Supra_R	FFG_086	1107.30	Richey, 1989, Table 2, p.26
70	Supra_R	FFG_087	1107.30	Richey, 1989, Table 2, p.26
71	Supra_R	FFG_088	1108.90	Richey, 1989, Table 2, p.26
72	Supra_R	FFG_089	1108.60	Richey, 1989, Table 2, p.26
73	Supra_R	FFG_091	1091.20	Richey, 1989, Table 2, p.26
74	Supra_R	FFG_092	1097.60	Richey, 1989, Table 2, p.26
75	Supra_R	FFG_093	1097.90	Richey, 1989, Table 2, p.26
76	Supra_R	FFG_094	1095.10	Richey, 1989, Table 2, p.26

Table B.2. Elevations of Stratigraphic Layers Near WIPP (Continued)

	Layer	Well ID	Elevation	Source
1	Supra_R	FFG_095	1138.70	Richey, 1989, Table 2, p.26
2	Supra_R	FFG_096	1174.40	Richey, 1989, Table 2, p.26
3	Supra_R	FFG_097	1149.40	Richey, 1989, Table 2, p.27
4	Supra_R	FFG_098	1208.20	Richey, 1989, Table 2, p.27
5	Supra_R	FFG_099	1205.80	Richey, 1989, Table 2, p.27
6	Supra_R	FFG_100	1153.10	Richey, 1989, Table 2, p.27
7	Supra_R	FFG_101	1142.70	Richey, 1989, Table 2, p.27
8	Supra_R	FFG_102	1127.20	Richey, 1989, Table 2, p.27
9	Supra_R	FFG_103	1108.60	Richey, 1989, Table 2, p.27
10	Supra_R	FFG_104	1127.50	Richey, 1989, Table 2, p.27
11	Supra_R	FFG_105	995.20	Richey, 1989, Table 2, p.27
12	Supra_R	FFG_106	981.50	Richey, 1989, Table 2, p.27
13	Supra_R	FFG_107	987.60	Richey, 1989, Table 2, p.27
14	Supra_R	FFG_108	1015.90	Richey, 1989, Table 2, p.27
15	Supra_R	FFG_109	1039.10	Richey, 1989, Table 2, p.27
16	Supra_R	FFG_110	1045.50	Richey, 1989, Table 2, p.27
17	Supra_R	FFG_111	1062.20	Richey, 1989, Table 2, p.27
18	Supra_R	FFG_112	1056.10	Richey, 1989, Table 2, p.28
19	Supra_R	FFG_113	1054.90	Richey, 1989, Table 2, p.28
20	Supra_R	FFG_114	1014.70	Richey, 1989, Table 2, p.28
21	Supra_R	FFG_115	970.50	Richey, 1989, Table 2, p.28
22	Supra_R	FFG_116	972.00	Richey, 1989, Table 2, p.28
23	Supra_R	FFG_117	966.20	Richey, 1989, Table 2, p.28
24	Supra_R	FFG_119	950.10	Richey, 1989, Table 2, p.28
25	Supra_R	FFG_120	956.50	Richey, 1989, Table 2, p.28
26	Supra_R	FFG_121	958.60	Richey, 1989, Table 2, p.28
27	Supra_R	FFG_122	954.00	Richey, 1989, Table 2, p.28
28	Supra_R	FFG_123	961.60	Richey, 1989, Table 2, p.28
29	Supra_R	FFG_124	977.20	Richey, 1989, Table 2, p.28
30	Supra_R	FFG_125	976.20	Richey, 1989, Table 2, p.28
31	Supra_R	FFG_126	1014.20	Richey, 1989, Table 2, p.28
32	Supra_R	FFG_127	1019.20	Richey, 1989, Table 2, p.28
33	Supra_R	FFG_128	994.30	Richey, 1989, Table 2, p.28
34	Supra_R	FFG_129	961.90	Richey, 1989, Table 2, p.28
35	Supra_R	FFG_130	979.90	Richey, 1989, Table 2, p.28
36	Supra_R	FFG_132	1002.20	Richey, 1989, Table 2, p.29
37	Supra_R	FFG_133	993.00	Richey, 1989, Table 2, p.29
38	Supra_R	FFG_134	988.20	Richey, 1989, Table 2, p.29
39	Supra_R	FFG_135	1002.50	Richey, 1989, Table 2, p.29
40	Supra_R	FFG_136	1007.50	Richey, 1989, Table 2, p.29
41	Supra_R	FFG_137	1007.40	Richey, 1989, Table 2, p.29
42	Supra_R	FFG_138	1023.90	Richey, 1989, Table 2, p.29
43	Supra_R	FFG_139	1023.50	Richey, 1989, Table 2, p.29
44	Supra_R	FFG_140	1042.60	Richey, 1989, Table 2, p.29
45	Supra_R	FFG_141	1030.40	Richey, 1989, Table 2, p.29
46	Supra_R	FFG_142	1042.80	Richey, 1989, Table 2, p.29
47	Supra_R	FFG_143	1052.70	Richey, 1989, Table 2, p.29
48	Supra_R	FFG_144	905.00	Richey, 1989, Table 2, p.29
49	Supra_R	FFG_145	905.30	Richey, 1989, Table 2, p.29
50	Supra_R	FFG_146	912.90	Richey, 1989, Table 2, p.29
51	Supra_R	FFG_147	908.30	Richey, 1989, Table 2, p.29
52	Supra_R	FFG_148	907.70	Richey, 1989, Table 2, p.29
53	Supra_R	FFG_149	916.50	Richey, 1989, Table 2, p.30
54	Supra_R	FFG_152	905.30	Richey, 1989, Table 2, p.30
55	Supra_R	FFG_155	918.10	Richey, 1989, Table 2, p.30
56	Supra_R	FFG_156	908.30	Richey, 1989, Table 2, p.30
57	Supra_R	FFG_157	926.00	Richey, 1989, Table 2, p.30
58	Supra_R	FFG_158	941.80	Richey, 1989, Table 2, p.30
59	Supra_R	FFG_159	1001.30	Richey, 1989, Table 2, p.30
60	Supra_R	FFG_160	1002.50	Richey, 1989, Table 2, p.30
61	Supra_R	FFG_161	987.90	Richey, 1989, Table 2, p.30
62	Supra_R	FFG_162	988.80	Richey, 1989, Table 2, p.30
63	Supra_R	FFG_163	988.80	Richey, 1989, Table 2, p.30
64	Supra_R	FFG_164	955.90	Richey, 1989, Table 2, p.30
65	Supra_R	FFG_165	935.70	Richey, 1989, Table 2, p.30
66	Supra_R	FFG_166	993.00	Richey, 1989, Table 2, p.31
67	Supra_R	FFG_167	1019.60	Richey, 1989, Table 2, p.31
68	Supra_R	FFG_168	1001.00	Richey, 1989, Table 2, p.31
69	Supra_R	FFG_169	986.00	Richey, 1989, Table 2, p.31
70	Supra_R	FFG_170	934.80	Richey, 1989, Table 2, p.31
71	Supra_R	FFG_171	956.80	Richey, 1989, Table 2, p.31
72	Supra_R	FFG_172	986.00	Richey, 1989, Table 2, p.31
73	Supra_R	FFG_173	1022.60	Richey, 1989, Table 2, p.31
74	Supra_R	FFG_177	913.20	Richey, 1989, Table 2, p.31
75	Supra_R	FFG_178	888.20	Richey, 1989, Table 2, p.31
76	Supra_R	FFG_179	896.40	Richey, 1989, Table 2, p.31

Table B.2. Elevations of Stratigraphic Layers Near WIPP (Continued)

	Layer	Well ID	Elevation	Source
1	Supra_R	FFG_180	1062.20	Richey, 1989, Table 2, p.31
2	Supra_R	FFG_181	1016.50	Richey, 1989, Table 2, p.32
3	Supra_R	FFG_182	986.00	Richey, 1989, Table 2, p.32
4	Supra_R	FFG_183	1020.50	Richey, 1989, Table 2, p.32
5	Supra_R	FFG_184	1047.90	Richey, 1989, Table 2, p.32
6	Supra_R	FFG_185	1022.60	Richey, 1989, Table 2, p.32
7	Supra_R	FFG_186	1013.50	Richey, 1989, Table 2, p.32
8	Supra_R	FFG_188	979.00	Richey, 1989, Table 2, p.32
9	Supra_R	FFG_189	1046.10	Richey, 1989, Table 2, p.32
10	Supra_R	FFG_190	1037.80	Richey, 1989, Table 2, p.32
11	Supra_R	FFG_191	1041.50	Richey, 1989, Table 2, p.32
12	Supra_R	FFG_192	1031.40	Richey, 1989, Table 2, p.32
13	Supra_R	FFG_194	1075.40	Richey, 1989, Table 2, p.33
14	Supra_R	FFG_195	1059.20	Richey, 1989, Table 2, p.33
15	Supra_R	FFG_196	1042.40	Richey, 1989, Table 2, p.33
16	Supra_R	FFG_197	1034.50	Richey, 1989, Table 2, p.33
17	Supra_R	FFG_198	1031.40	Richey, 1989, Table 2, p.33
18	Supra_R	FFG_199	1038.80	Richey, 1989, Table 2, p.33
19	Supra_R	FFG_200	1040.90	Richey, 1989, Table 2, p.33
20	Supra_R	FFG_201	1074.10	Richey, 1989, Table 2, p.33
21	Supra_R	FFG_202	1075.60	Richey, 1989, Table 2, p.33
22	Supra_R	FFG_203	1071.40	Richey, 1989, Table 2, p.33
23	Supra_R	FFG_204	1096.40	Richey, 1989, Table 2, p.33
24	Supra_R	FFG_205	1082.00	Richey, 1989, Table 2, p.33
25	Supra_R	FFG_206	1067.70	Richey, 1989, Table 2, p.33
26	Supra_R	FFG_207	1072.60	Richey, 1989, Table 2, p.33
27	Supra_R	FFG_208	1060.10	Richey, 1989, Table 2, p.34
28	Supra_R	FFG_209	1074.10	Richey, 1989, Table 2, p.34
29	Supra_R	FFG_210	1066.20	Richey, 1989, Table 2, p.34
30	Supra_R	FFG_212	1078.40	Richey, 1989, Table 2, p.34
31	Supra_R	FFG_213	1051.60	Richey, 1989, Table 2, p.34
32	Supra_R	FFG_214	1061.60	Richey, 1989, Table 2, p.34
33	Supra_R	FFG_215	1041.80	Richey, 1989, Table 2, p.34
34	Supra_R	FFG_216	993.60	Richey, 1989, Table 2, p.34
35	Supra_R	FFG_217	1057.70	Richey, 1989, Table 2, p.34
36	Supra_R	FFG_218	1053.10	Richey, 1989, Table 2, p.34
37	Supra_R	FFG_219	1036.30	Richey, 1989, Table 2, p.34
38	Supra_R	FFG_220	1051.00	Richey, 1989, Table 2, p.34
39	Supra_R	FFG_221	1027.80	Richey, 1989, Table 2, p.34
40	Supra_R	FFG_222	1019.90	Richey, 1989, Table 2, p.34
41	Supra_R	FFG_224	1133.60	Richey, 1989, Table 2, p.35
42	Supra_R	FFG_225	1138.30	Richey, 1989, Table 2, p.35
43	Supra_R	FFG_226	1150.30	Richey, 1989, Table 2, p.35
44	Supra_R	FFG_228	1133.60	Richey, 1989, Table 2, p.35
45	Supra_R	FFG_229	1146.00	Richey, 1989, Table 2, p.35
46	Supra_R	FFG_230	1134.50	Richey, 1989, Table 2, p.35
47	Supra_R	FFG_231	1120.10	Richey, 1989, Table 2, p.35
48	Supra_R	FFG_232	1124.10	Richey, 1989, Table 2, p.35
49	Supra_R	FFG_233	1114.70	Richey, 1989, Table 2, p.35
50	Supra_R	FFG_234	1112.80	Richey, 1989, Table 2, p.35
51	Supra_R	FFG_235	1117.10	Richey, 1989, Table 2, p.35
52	Supra_R	FFG_236	1101.20	Richey, 1989, Table 2, p.35
53	Supra_R	FFG_237	1137.80	Richey, 1989, Table 2, p.35
54	Supra_R	FFG_238	1152.80	Richey, 1989, Table 2, p.36
55	Supra_R	FFG_239	1177.10	Richey, 1989, Table 2, p.36
56	Supra_R	FFG_240	1162.20	Richey, 1989, Table 2, p.36
57	Supra_R	FFG_241	1165.30	Richey, 1989, Table 2, p.36
58	Supra_R	FFG_242	1115.00	Richey, 1989, Table 2, p.36
59	Supra_R	FFG_243	1153.70	Richey, 1989, Table 2, p.36
60	Supra_R	FFG_244	1120.00	Richey, 1989, Table 2, p.36
61	Supra_R	FFG_245	1170.70	Richey, 1989, Table 2, p.36
62	Supra_R	FFG_246	1161.90	Richey, 1989, Table 2, p.36
63	Supra_R	FFG_247	1145.40	Richey, 1989, Table 2, p.36
64	Supra_R	FFG_248	1150.00	Richey, 1989, Table 2, p.36
65	Supra_R	FFG_249	1169.20	Richey, 1989, Table 2, p.36
66	Supra_R	FFG_250	1159.80	Richey, 1989, Table 2, p.36
67	Supra_R	FFG_251	1139.00	Richey, 1989, Table 2, p.36
68	Supra_R	FFG_252	1134.10	Richey, 1989, Table 2, p.36
69	Supra_R	FFG_253	1108.60	Richey, 1989, Table 2, p.36
70	Supra_R	FFG_254	1111.60	Richey, 1989, Table 2, p.36
71	Supra_R	FFG_255	1122.60	Richey, 1989, Table 2, p.37
72	Supra_R	FFG_256	1136.00	Richey, 1989, Table 2, p.37
73	Supra_R	FFG_257	1137.20	Richey, 1989, Table 2, p.37
74	Supra_R	FFG_258	1120.40	Richey, 1989, Table 2, p.37
75	Supra_R	FFG_259	1139.60	Richey, 1989, Table 2, p.37
76	Supra_R	FFG_260	1111.00	Richey, 1989, Table 2, p.37

Table B.2. Elevations of Stratigraphic Layers Near WIPP (Continued)

	Layer	Well ID	Elevation	Source
1	Supra_R	FFG_261	1106.10	Richey, 1989, Table 2, p.37
2	Supra_R	FFG_262	1109.50	Richey, 1989, Table 2, p.37
3	Supra_R	FFG_263	1115.60	Richey, 1989, Table 2, p.37
4	Supra_R	FFG_264	1121.10	Richey, 1989, Table 2, p.37
5	Supra_R	FFG_265	1130.80	Richey, 1989, Table 2, p.37
6	Supra_R	FFG_266	1131.40	Richey, 1989, Table 2, p.37
7	Supra_R	FFG_267	1120.40	Richey, 1989, Table 2, p.37
8	Supra_R	FFG_268	1115.90	Richey, 1989, Table 2, p.37
9	Supra_R	FFG_269	1105.80	Richey, 1989, Table 2, p.38
10	Supra_R	FFG_270	1057.00	Richey, 1989, Table 2, p.38
11	Supra_R	FFG_271	1049.40	Richey, 1989, Table 2, p.38
12	Supra_R	FFG_272	1073.50	Richey, 1989, Table 2, p.38
13	Supra_R	FFG_273	1079.20	Richey, 1989, Table 2, p.38
14	Supra_R	FFG_274	1137.20	Richey, 1989, Table 2, p.38
15	Supra_R	FFG_275	1135.70	Richey, 1989, Table 2, p.38
16	Supra_R	FFG_276	1125.90	Richey, 1989, Table 2, p.38
17	Supra_R	FFG_277	1123.20	Richey, 1989, Table 2, p.38
18	Supra_R	FFG_278	1098.20	Richey, 1989, Table 2, p.38
19	Supra_R	FFG_279	1107.90	Richey, 1989, Table 2, p.38
20	Supra_R	FFG_280	1120.30	Richey, 1989, Table 2, p.38
21	Supra_R	FFG_281	1147.30	Richey, 1989, Table 2, p.38
22	Supra_R	FFG_283	1090.90	Richey, 1989, Table 2, p.39
23	Supra_R	FFG_284	1117.10	Richey, 1989, Table 2, p.39
24	Supra_R	FFG_285	1112.50	Richey, 1989, Table 2, p.39
25	Supra_R	FFG_286	1101.50	Richey, 1989, Table 2, p.39
26	Supra_R	FFG_287	1094.60	Richey, 1989, Table 2, p.39
27	Supra_R	FFG_288	1110.40	Richey, 1989, Table 2, p.39
28	Supra_R	FFG_289	1081.90	Richey, 1989, Table 2, p.39
29	Supra_R	FFG_290	1103.40	Richey, 1989, Table 2, p.39
30	Supra_R	FFG_291	1132.00	Richey, 1989, Table 2, p.39
31	Supra_R	FFG_292	1090.60	Richey, 1989, Table 2, p.39
32	Supra_R	FFG_293	1085.10	Richey, 1989, Table 2, p.39
33	Supra_R	FFG_294	1095.50	Richey, 1989, Table 2, p.39
34	Supra_R	FFG_295	1087.50	Richey, 1989, Table 2, p.39
35	Supra_R	FFG_297	1104.90	Richey, 1989, Table 2, p.39
36	Supra_R	FFG_298	1070.00	Richey, 1989, Table 2, p.40
37	Supra_R	FFG_299	1078.40	Richey, 1989, Table 2, p.40
38	Supra_R	FFG_300	1062.20	Richey, 1989, Table 2, p.40
39	Supra_R	FFG_301	1046.40	Richey, 1989, Table 2, p.40
40	Supra_R	FFG_302	1092.70	Richey, 1989, Table 2, p.40
41	Supra_R	FFG_303	1099.30	Richey, 1989, Table 2, p.40
42	Supra_R	FFG_304	1088.10	Richey, 1989, Table 2, p.40
43	Supra_R	FFG_305	1093.90	Richey, 1989, Table 2, p.40
44	Supra_R	FFG_306	1075.90	Richey, 1989, Table 2, p.40
45	Supra_R	FFG_307	1078.70	Richey, 1989, Table 2, p.40
46	Supra_R	FFG_308	1075.90	Richey, 1989, Table 2, p.40
47	Supra_R	FFG_309	1093.60	Richey, 1989, Table 2, p.40
48	Supra_R	FFG_310	1087.50	Richey, 1989, Table 2, p.40
49	Supra_R	FFG_311	1085.40	Richey, 1989, Table 2, p.40
50	Supra_R	FFG_312	1076.90	Richey, 1989, Table 2, p.40
51	Supra_R	FFG_313	1106.10	Richey, 1989, Table 2, p.41
52	Supra_R	FFG_314	1121.10	Richey, 1989, Table 2, p.41
53	Supra_R	FFG_315	1131.10	Richey, 1989, Table 2, p.41
54	Supra_R	FFG_316	1133.20	Richey, 1989, Table 2, p.41
55	Supra_R	FFG_317	1097.60	Richey, 1989, Table 2, p.41
56	Supra_R	FFG_318	1123.50	Richey, 1989, Table 2, p.41
57	Supra_R	FFG_319	1120.70	Richey, 1989, Table 2, p.41
58	Supra_R	FFG_320	1129.60	Richey, 1989, Table 2, p.41
59	Supra_R	FFG_321	1124.70	Richey, 1989, Table 2, p.41
60	Supra_R	FFG_322	1124.70	Richey, 1989, Table 2, p.41
61	Supra_R	FFG_323	1120.40	Richey, 1989, Table 2, p.41
62	Supra_R	FFG_324	1122.00	Richey, 1989, Table 2, p.41
63	Supra_R	FFG_325	1079.90	Richey, 1989, Table 2, p.41
64	Supra_R	FFG_326	1117.70	Richey, 1989, Table 2, p.41
65	Supra_R	FFG_327	1102.20	Richey, 1989, Table 2, p.42
66	Supra_R	FFG_328	1121.40	Richey, 1989, Table 2, p.42
67	Supra_R	FFG_329	1120.40	Richey, 1989, Table 2, p.42
68	Supra_R	FFG_330	1115.60	Richey, 1989, Table 2, p.42
69	Supra_R	FFG_331	1103.70	Richey, 1989, Table 2, p.42
70	Supra_R	FFG_332	1124.70	Richey, 1989, Table 2, p.42
71	Supra_R	FFG_333	1130.50	Richey, 1989, Table 2, p.42
72	Supra_R	FFG_334	1125.90	Richey, 1989, Table 2, p.42
73	Supra_R	FFG_335	1129.60	Richey, 1989, Table 2, p.42
74	Supra_R	FFG_336	1124.10	Richey, 1989, Table 2, p.42
75	Supra_R	FFG_337	1124.40	Richey, 1989, Table 2, p.42
76	Supra_R	FFG_338	1123.50	Richey, 1989, Table 2, p.42

Table B.2. Elevations of Stratigraphic Layers Near WIPP (Continued)

	Layer	Well ID	Elevation	Source
1	Supra_R	FFG_339	1107.90	Richey, 1989, Table 2, p.42
2	Supra_R	FFG_340	1107.00	Richey, 1989, Table 2, p.42
3	Supra_R	FFG_342	1056.10	Richey, 1989, Table 2, p.43
4	Supra_R	FFG_344	1040.60	Richey, 1989, Table 2, p.43
5	Supra_R	FFG_345	1073.20	Richey, 1989, Table 2, p.43
6	Supra_R	FFG_347	1039.70	Richey, 1989, Table 2, p.43
7	Supra_R	FFG_348	1035.70	Richey, 1989, Table 2, p.43
8	Supra_R	FFG_349	1034.80	Richey, 1989, Table 2, p.43
9	Supra_R	FFG_350	1041.50	Richey, 1989, Table 2, p.43
10	Supra_R	FFG_351	1102.80	Richey, 1989, Table 2, p.43
11	Supra_R	FFG_352	1103.10	Richey, 1989, Table 2, p.43
12	Supra_R	FFG_353	1095.80	Richey, 1989, Table 2, p.43
13	Supra_R	FFG_354	1051.00	Richey, 1989, Table 2, p.43
14	Supra_R	FFG_361	1012.50	Richey, 1989, Table 2, p.44
15	Supra_R	FFG_362	1010.70	Richey, 1989, Table 2, p.44
16	Supra_R	FFG_363	1009.50	Richey, 1989, Table 2, p.44
17	Supra_R	FFG_364	993.60	Richey, 1989, Table 2, p.44
18	Supra_R	FFG_366	1010.40	Richey, 1989, Table 2, p.44
19	Supra_R	FFG_367	1006.40	Richey, 1989, Table 2, p.44
20	Supra_R	FFG_370	1012.90	Richey, 1989, Table 2, p.44
21	Supra_R	FFG_371	1012.90	Richey, 1989, Table 2, p.44
22	Supra_R	FFG_372	1006.40	Richey, 1989, Table 2, p.45
23	Supra_R	FFG_373	998.10	Richey, 1989, Table 2, p.45
24	Supra_R	FFG_374	995.20	Richey, 1989, Table 2, p.45
25	Supra_R	FFG_376	1010.40	Richey, 1989, Table 2, p.45
26	Supra_R	FFG_381	1021.40	Richey, 1989, Table 2, p.45
27	Supra_R	FFG_383	1046.10	Richey, 1989, Table 2, p.45
28	Supra_R	FFG_384	976.00	Richey, 1989, Table 2, p.45
29	Supra_R	FFG_385	990.60	Richey, 1989, Table 2, p.45
30	Supra_R	FFG_387	1019.90	Richey, 1989, Table 2, p.45
31	Supra_R	FFG_388	1019.60	Richey, 1989, Table 2, p.46
32	Supra_R	FFG_389	1008.00	Richey, 1989, Table 2, p.46
33	Supra_R	FFG_390	1022.60	Richey, 1989, Table 2, p.46
34	Supra_R	FFG_391	1025.30	Richey, 1989, Table 2, p.46
35	Supra_R	FFG_392	1019.60	Richey, 1989, Table 2, p.46
36	Supra_R	FFG_393	1061.60	Richey, 1989, Table 2, p.46
37	Supra_R	FFG_394	1050.30	Richey, 1989, Table 2, p.46
38	Supra_R	FFG_395	1059.20	Richey, 1989, Table 2, p.46
39	Supra_R	FFG_396	1090.00	Richey, 1989, Table 2, p.46
40	Supra_R	FFG_398	1011.60	Richey, 1989, Table 2, p.46
41	Supra_R	FFG_399	1001.60	Richey, 1989, Table 2, p.46
42	Supra_R	FFG_401	972.30	Richey, 1989, Table 2, p.46
43	Supra_R	FFG_402	1023.10	Richey, 1989, Table 2, p.46
44	Supra_R	FFG_403	995.20	Richey, 1989, Table 2, p.47
45	Supra_R	FFG_404	976.60	Richey, 1989, Table 2, p.47
46	Supra_R	FFG_407	969.90	Richey, 1989, Table 2, p.47
47	Supra_R	FFG_408	965.00	Richey, 1989, Table 2, p.47
48	Supra_R	FFG_409	970.50	Richey, 1989, Table 2, p.47
49	Supra_R	FFG_411	957.70	Richey, 1989, Table 2, p.47
50	Supra_R	FFG_413	968.70	Richey, 1989, Table 2, p.47
51	Supra_R	FFG_418	1033.90	Richey, 1989, Table 2, p.48
52	Supra_R	FFG_419	1052.50	Richey, 1989, Table 2, p.48
53	Supra_R	FFG_420	1045.10	Richey, 1989, Table 2, p.48
54	Supra_R	FFG_421	1047.00	Richey, 1989, Table 2, p.48
55	Supra_R	FFG_422	1054.30	Richey, 1989, Table 2, p.48
56	Supra_R	FFG_426	996.10	Richey, 1989, Table 2, p.48
57	Supra_R	FFG_432	978.40	Richey, 1989, Table 2, p.48
58	Supra_R	FFG_433	968.00	Richey, 1989, Table 2, p.48
59	Supra_R	FFG_438	1082.20	Richey, 1989, Table 2, p.49
60	Supra_R	FFG_445	960.70	Richey, 1989, Table 2, p.49
61	Supra_R	FFG_453	1049.50	Richey, 1989, Table 2, p.50
62	Supra_R	FFG_455	1061.30	Richey, 1989, Table 2, p.50
63	Supra_R	FFG_456	1063.40	Richey, 1989, Table 2, p.50
64	Supra_R	FFG_457	1023.50	Richey, 1989, Table 2, p.50
65	Supra_R	FFG_458	1025.80	Richey, 1989, Table 2, p.50
66	Supra_R	FFG_459	1070.50	Richey, 1989, Table 2, p.50
67	Supra_R	FFG_462	1032.10	Richey, 1989, Table 2, p.50
68	Supra_R	FFG_463	1021.10	Richey, 1989, Table 2, p.51
69	Supra_R	FFG_464	1035.40	Richey, 1989, Table 2, p.51
70	Supra_R	FFG_465	1031.40	Richey, 1989, Table 2, p.51
71	Supra_R	FFG_467	1025.70	Richey, 1989, Table 2, p.51
72	Supra_R	FFG_468	1064.70	Richey, 1989, Table 2, p.51
73	Supra_R	FFG_470	1067.10	Richey, 1989, Table 2, p.51
74	Supra_R	FFG_471	1036.60	Richey, 1989, Table 2, p.51
75	Supra_R	FFG_472	1032.40	Richey, 1989, Table 2, p.51
76	Supra_R	FFG_473	1060.70	Richey, 1989, Table 2, p.51

Table B.2. Elevations of Stratigraphic Layers Near WIPP (Continued)

	Layer	Well ID	Elevation	Source
1	Supra_R	FFG_474	1100.60	Richey, 1989, Table 2, p.51
2	Supra_R	FFG_475	1103.70	Richey, 1989, Table 2, p.51
3	Supra_R	FFG_476	1090.10	Richey, 1989, Table 2, p.51
4	Supra_R	FFG_477	1102.80	Richey, 1989, Table 2, p.51
5	Supra_R	FFG_478	1104.80	Richey, 1989, Table 2, p.52
6	Supra_R	FFG_479	1106.40	Richey, 1989, Table 2, p.52
7	Supra_R	FFG_480	1096.10	Richey, 1989, Table 2, p.52
8	Supra_R	FFG_481	1090.90	Richey, 1989, Table 2, p.52
9	Supra_R	FFG_482	1103.40	Richey, 1989, Table 2, p.52
10	Supra_R	FFG_483	1094.20	Richey, 1989, Table 2, p.52
11	Supra_R	FFG_484	1095.60	Richey, 1989, Table 2, p.52
12	Supra_R	FFG_485	1096.50	Richey, 1989, Table 2, p.52
13	Supra_R	FFG_486	1097.60	Richey, 1989, Table 2, p.52
14	Supra_R	FFG_487	1097.00	Richey, 1989, Table 2, p.52
15	Supra_R	FFG_488	1088.60	Richey, 1989, Table 2, p.52
16	Supra_R	FFG_489	1086.60	Richey, 1989, Table 2, p.52
17	Supra_R	FFG_490	1072.60	Richey, 1989, Table 2, p.52
18	Supra_R	FFG_491	1077.50	Richey, 1989, Table 2, p.52
19	Supra_R	FFG_492	1067.40	Richey, 1989, Table 2, p.52
20	Supra_R	FFG_493	1069.20	Richey, 1989, Table 2, p.53
21	Supra_R	FFG_494	1069.50	Richey, 1989, Table 2, p.53
22	Supra_R	FFG_495	1072.30	Richey, 1989, Table 2, p.53
23	Supra_R	FFG_496	1108.30	Richey, 1989, Table 2, p.53
24	Supra_R	FFG_497	1090.60	Richey, 1989, Table 2, p.53
25	Supra_R	FFG_498	1104.90	Richey, 1989, Table 2, p.53
26	Supra_R	FFG_499	1091.50	Richey, 1989, Table 2, p.53
27	Supra_R	FFG_500	1091.50	Richey, 1989, Table 2, p.53
28	Supra_R	FFG_501	1075.60	Richey, 1989, Table 2, p.53
29	Supra_R	FFG_502	1092.40	Richey, 1989, Table 2, p.53
30	Supra_R	FFG_503	1064.10	Richey, 1989, Table 2, p.53
31	Supra_R	FFG_504	1070.50	Richey, 1989, Table 2, p.53
32	Supra_R	FFG_505	1077.80	Richey, 1989, Table 2, p.53
33	Supra_R	FFG_506	1069.80	Richey, 1989, Table 2, p.53
34	Supra_R	FFG_507	1051.90	Richey, 1989, Table 2, p.53
35	Supra_R	FFG_508	1051.90	Richey, 1989, Table 2, p.53
36	Supra_R	FFG_509	1066.50	Richey, 1989, Table 2, p.54
37	Supra_R	FFG_510	1080.50	Richey, 1989, Table 2, p.54
38	Supra_R	FFG_511	1102.80	Richey, 1989, Table 2, p.54
39	Supra_R	FFG_512	1073.50	Richey, 1989, Table 2, p.54
40	Supra_R	FFG_513	1061.00	Richey, 1989, Table 2, p.54
41	Supra_R	FFG_514	1060.10	Richey, 1989, Table 2, p.54
42	Supra_R	FFG_515	1082.30	Richey, 1989, Table 2, p.54
43	Supra_R	FFG_516	1075.00	Richey, 1989, Table 2, p.54
44	Supra_R	FFG_517	1053.10	Richey, 1989, Table 2, p.54
45	Supra_R	FFG_518	1036.30	Richey, 1989, Table 2, p.54
46	Supra_R	FFG_519	1033.90	Richey, 1989, Table 2, p.54
47	Supra_R	FFG_520	1030.80	Richey, 1989, Table 2, p.54
48	Supra_R	FFG_521	1028.70	Richey, 1989, Table 2, p.54
49	Supra_R	FFG_522	1055.20	Richey, 1989, Table 2, p.54
50	Supra_R	FFG_523	1041.80	Richey, 1989, Table 2, p.54
51	Supra_R	FFG_524	1024.10	Richey, 1989, Table 2, p.55
52	Supra_R	FFG_525	1047.00	Richey, 1989, Table 2, p.55
53	Supra_R	FFG_526	1033.90	Richey, 1989, Table 2, p.55
54	Supra_R	FFG_527	1031.70	Richey, 1989, Table 2, p.55
55	Supra_R	FFG_528	1023.50	Richey, 1989, Table 2, p.55
56	Supra_R	FFG_530	1016.50	Richey, 1989, Table 2, p.55
57	Supra_R	FFG_531	998.20	Richey, 1989, Table 2, p.55
58	Supra_R	FFG_532	990.30	Richey, 1989, Table 2, p.55
59	Supra_R	FFG_534	1021.10	Richey, 1989, Table 2, p.55
60	Supra_R	FFG_535	995.90	Richey, 1989, Table 2, p.55
61	Supra_R	FFG_536	996.10	Richey, 1989, Table 2, p.55
62	Supra_R	FFG_537	985.40	Richey, 1989, Table 2, p.55
63	Supra_R	FFG_543	997.90	Richey, 1989, Table 2, p.56
64	Supra_R	FFG_548	1047.30	Richey, 1989, Table 2, p.56
65	Supra_R	FFG_552	922.90	Richey, 1989, Table 2, p.56
66	Supra_R	FFG_562	981.50	Richey, 1989, Table 2, p.57
67	Supra_R	FFG_563	969.90	Richey, 1989, Table 2, p.57
68	Supra_R	FFG_564	969.30	Richey, 1989, Table 2, p.57
69	Supra_R	FFG_568	957.10	Richey, 1989, Table 2, p.57
70	Supra_R	FFG_569	952.20	Richey, 1989, Table 2, p.57
71	Supra_R	FFG_584	1006.80	Richey, 1989, Table 2, p.58
72	Supra_R	FFG_585	1025.00	Richey, 1989, Table 2, p.58
73	Supra_R	FFG_600	1003.40	Richey, 1989, Table 2, p.58
74	Supra_R	FFG_601	983.90	Richey, 1989, Table 2, p.58
75	Supra_R	FFG_602	1053.10	Richey, 1989, Table 2, p.58
76	Supra_R	FFG_606	1012.90	Richey, 1989, Table 2, p.58

Table B.2. Elevations of Stratigraphic Layers Near WIPP (Continued)

	Layer	Well ID	Elevation	Source		Layer	Well ID	Elevation	Source
1	Supra_R	FFG_607	1001.30	Richey, 1989, Table 2, p.59	39	Supra_R	FFG_677	1064.40	Richey, 1989, Table 2, p.62
2	Supra_R	FFG_608	1018.60	Richey, 1989, Table 2, p.59	40	Supra_R	FFG_679	1060.70	Richey, 1989, Table 2, p.62
3	Supra_R	FFG_609	1025.30	Richey, 1989, Table 2, p.59	41	Supra_R	FFG_685	1003.50	Richey, 1989, Table 2, p.63
4	Supra_R	FFG_610	1023.20	Richey, 1989, Table 2, p.59	42	Supra_R	FFG_689	1059.20	Richey, 1989, Table 2, p.63
5	Supra_R	FFG_611	1009.20	Richey, 1989, Table 2, p.59	43	Supra_R	FFG_690	1052.20	Richey, 1989, Table 2, p.63
6	Supra_R	FFG_612	977.10	Richey, 1989, Table 2, p.59	44	Supra_R	FFG_691	1052.50	Richey, 1989, Table 2, p.63
7	Supra_R	FFG_613	945.90	Richey, 1989, Table 2, p.59	45	Supra_R	FFG_692	1057.70	Richey, 1989, Table 2, p.63
8	Supra_R	FFG_618	897.00	Richey, 1989, Table 2, p.59	46	Supra_R	FFG_693	1050.60	Richey, 1989, Table 2, p.63
9	Supra_R	FFG_620	909.90	Richey, 1989, Table 2, p.59	47	Supra_R	FFG_694	1042.40	Richey, 1989, Table 2, p.63
10	Supra_R	FFG_621	905.90	Richey, 1989, Table 2, p.59	48	Supra_R	FFG_695	1048.50	Richey, 1989, Table 2, p.63
11	Supra_R	FFG_638	975.40	Richey, 1989, Table 2, p.60	49	Supra_R	FFG_696	1050.60	Richey, 1989, Table 2, p.63
12	Supra_R	FFG_639	961.50	Richey, 1989, Table 2, p.60	50	Supra_R	FFG_697	1045.80	Richey, 1989, Table 2, p.64
13	Supra_R	FFG_640	966.20	Richey, 1989, Table 2, p.60	51	Supra_R	FFG_698	1039.70	Richey, 1989, Table 2, p.64
14	Supra_R	FFG_643	975.40	Richey, 1989, Table 2, p.60	52	Supra_R	FFG_699	1029.60	Richey, 1989, Table 2, p.64
15	Supra_R	FFG_644	936.70	Richey, 1989, Table 2, p.60	53	Supra_R	FFG_700	1027.10	Richey, 1989, Table 2, p.64
16	Supra_R	FFG_648	960.70	Richey, 1989, Table 2, p.60	54	Supra_R	FFG_701	1032.10	Richey, 1989, Table 2, p.64
17	Supra_R	FFG_652	1106.40	Richey, 1989, Table 2, p.60	55	Supra_R	FFG_702	1036.60	Richey, 1989, Table 2, p.64
18	Supra_R	FFG_653	1096.10	Richey, 1989, Table 2, p.61	56	Supra_R	FFG_703	1047.00	Richey, 1989, Table 2, p.64
19	Supra_R	FFG_654	1098.50	Richey, 1989, Table 2, p.61	57	Supra_R	FFG_704	1032.70	Richey, 1989, Table 2, p.64
20	Supra_R	FFG_655	1093.00	Richey, 1989, Table 2, p.61	58	Supra_R	FFG_705	1023.80	Richey, 1989, Table 2, p.64
21	Supra_R	FFG_656	1091.80	Richey, 1989, Table 2, p.61	59	Supra_R	FFG_706	1025.70	Richey, 1989, Table 2, p.64
22	Supra_R	FFG_657	1083.30	Richey, 1989, Table 2, p.61	60	Supra_R	FFG_707	1019.30	Richey, 1989, Table 2, p.64
23	Supra_R	FFG_658	1088.10	Richey, 1989, Table 2, p.61	61	Supra_R	FFG_708	1026.60	Richey, 1989, Table 2, p.64
24	Supra_R	FFG_659	1072.60	Richey, 1989, Table 2, p.61	62	Supra_R	FFG_709	1008.60	Richey, 1989, Table 2, p.64
25	Supra_R	FFG_660	1071.10	Richey, 1989, Table 2, p.61	63	Supra_R	FFG_710	1007.40	Richey, 1989, Table 2, p.64
26	Supra_R	FFG_662	1085.70	Richey, 1989, Table 2, p.61	64	Supra_R	FFG_711	1012.90	Richey, 1989, Table 2, p.65
27	Supra_R	FFG_664	1084.50	Richey, 1989, Table 2, p.61	65	Supra_R	FFG_712	1018.00	Richey, 1989, Table 2, p.65
28	Supra_R	FFG_666	1063.10	Richey, 1989, Table 2, p.62	66	Supra_R	FFG_713	1011.30	Richey, 1989, Table 2, p.65
29	Supra_R	FFG_667	1059.20	Richey, 1989, Table 2, p.62	67	Supra_R	FFG_714	1024.10	Richey, 1989, Table 2, p.65
30	Supra_R	FFG_668	1043.30	Richey, 1989, Table 2, p.62	68	Supra_R	FFG_715	1025.30	Richey, 1989, Table 2, p.65
31	Supra_R	FFG_669	1036.30	Richey, 1989, Table 2, p.62	69	Supra_R	FFG_716	1060.60	Richey, 1989, Table 2, p.65
32	Supra_R	FFG_670	1049.10	Richey, 1989, Table 2, p.62	70	Supra_R	FFG_717	1056.10	Richey, 1989, Table 2, p.65
33	Supra_R	FFG_671	1044.90	Richey, 1989, Table 2, p.62	71	Supra_R	FFG_718	1044.90	Richey, 1989, Table 2, p.65
34	Supra_R	FFG_672	1058.00	Richey, 1989, Table 2, p.62	72	Supra_R	FFG_719	1040.40	Richey, 1989, Table 2, p.65
35	Supra_R	FFG_673	1037.20	Richey, 1989, Table 2, p.62	73	Supra_R	FFG_720	1019.90	Richey, 1989, Table 2, p.65
36	Supra_R	FFG_674	1064.70	Richey, 1989, Table 2, p.62	74	Supra_R	FFG_721	1026.90	Richey, 1989, Table 2, p.65
37	Supra_R	FFG_675	1078.40	Richey, 1989, Table 2, p.62	75	Supra_R	FFG_723	1054.30	Richey, 1989, Table 2, p.65
38	Supra_R	FFG_676	1084.50	Richey, 1989, Table 2, p.62	76	Supra_R	FFG_724	1044.20	Richey, 1989, Table 2, p.65

Table B.2. Elevations of Stratigraphic Layers Near WIPP (Continued)

	Layer	Well ID	Elevation	Source
1	Supra_R	FFG_725	1029.60	Richey, 1989, Table 2, p.65
2	Supra_R	FFG_726	1018.60	Richey, 1989, Table 2, p.65
3	Supra_R	FFG_727	1020.80	Richey, 1989, Table 2, p.66
4	Supra_R	FFG_728	1012.20	Richey, 1989, Table 2, p.66
5	Supra_R	FFG_729	1014.40	Richey, 1989, Table 2, p.66
6	Supra_R	FFG_730	1018.90	Richey, 1989, Table 2, p.66
7	Supra_R	FFG_731	1022.30	Richey, 1989, Table 2, p.66
8	Supra_R	FFG_732	1040.30	Richey, 1989, Table 2, p.66
9	Supra_R	FFG_733	1028.40	Richey, 1989, Table 2, p.66
10	Supra_R	FFG_734	1029.00	Richey, 1989, Table 2, p.66
11	Supra_R	FFG_735	1016.50	Richey, 1989, Table 2, p.66
12	Supra_R	FFG_736	1025.60	Richey, 1989, Table 2, p.66
13	Supra_R	FFG_737	1040.50	Richey, 1989, Table 2, p.66
14	Supra_R	FFG_738	1018.30	Richey, 1989, Table 2, p.66
15	Supra_R	FFG_739	1015.10	Richey, 1989, Table 2, p.66
16	Supra_R	FFG_740	1015.60	Richey, 1989, Table 2, p.66
17	Supra_R	FFG_741	1014.70	Richey, 1989, Table 2, p.66
18	Supra_R	FFG_742	1023.80	Richey, 1989, Table 2, p.67
19	Supra_R	FFG_743	1013.20	Richey, 1989, Table 2, p.67
20	Supra_R	FFG_744	1012.50	Richey, 1989, Table 2, p.67
21	Supra_R	FFG_745	1006.40	Richey, 1989, Table 2, p.67
22	Supra_R	FFG_746	1007.50	Richey, 1989, Table 2, p.67
23	Supra_R	H1	1035.70	Mercer, 1983, Table 1
24	Supra_R	H10C	1123.80	Mercer, 1983, Table 1
25	Supra_R	H2C	1029.60	Mercer, 1983, Table 1
26	Supra_R	H3	1033.30	Mercer, 1983, Table 1
27	Supra_R	H4C	1016.20	Mercer, 1983, Table 1
28	Supra_R	H5C	1068.90	Mercer, 1983, Table 1
29	Supra_R	H6C	1020.50	Mercer, 1983, Table 1
30	Supra_R	H7C	964.10	Mercer, 1983, Table 1
31	Supra_R	H8C	1046.40	Mercer, 1983, Table 1
32	Supra_R	H9C	1038.10	Mercer, 1983, Table 1
33	Supra_R	P1	1019.60	Mercer, 1983, Table 1
34	Supra_R	P10	1069.50	Mercer, 1983, Table 1
35	Supra_R	P11	1068.00	Mercer, 1983, Table 1
36	Supra_R	P12	1028.40	Mercer, 1983, Table 1
37	Supra_R	P13	1019.60	Mercer, 1983, Table 1
38	Supra_R	P14	1024.10	Mercer, 1983, Table 1
39	Supra_R	P15	1008.90	Mercer, 1983, Table 1
40	Supra_R	P16	1011.30	Mercer, 1983, Table 1
41	Supra_R	P17	1016.80	Mercer, 1983, Table 1
42	Supra_R	P18	1059.80	Mercer, 1983, Table 1
43	Supra_R	P19	1080.50	Mercer, 1983, Table 1
44	Supra_R	P2	1060.40	Mercer, 1983, Table 1
45	Supra_R	P20	1083.00	Mercer, 1983, Table 1
46	Supra_R	P21	1069.50	Mercer, 1983, Table 1
47	Supra_R	P3	1031.10	Mercer, 1983, Table 1
48	Supra_R	P4	1049.70	Mercer, 1983, Table 1
49	Supra_R	P5	1058.00	Mercer, 1983, Table 1
50	Supra_R	P6	1022.30	Mercer, 1983, Table 1
51	Supra_R	P7	1015.60	Mercer, 1983, Table 1
52	Supra_R	P8	1017.70	Mercer, 1983, Table 1
53	Supra_R	P9	1040.00	Mercer, 1983, Table 1
54	Supra_R	WIPP11	1044.20	Mercer, 1983, Table 1
55	Supra_R	WIPP12	1058.30	Mercer, 1983, Table 1
56	Supra_R	WIPP13	1037.80	Mercer, 1983, Table 1
57	Supra_R	WIPP15	996.40	Mercer, 1983, Table 1
58	Supra_R	WIPP16	1031.10	Mercer, 1983, Table 1
59	Supra_R	WIPP18	1053.40	Mercer, 1983, Table 1
60	Supra_R	WIPP19	1046.40	Mercer, 1983, Table 1
61	Supra_R	WIPP21	1041.50	Mercer, 1983, Table 1
62	Supra_R	WIPP22	1044.20	Mercer, 1983, Table 1
63	Supra_R	WIPP25	979.30	Mercer, 1983, Table 1
64	Supra_R	WIPP26	960.70	Mercer, 1983, Table 1
65	Supra_R	WIPP27	968.30	Mercer, 1983, Table 1
66	Supra_R	WIPP28	1020.20	Mercer, 1983, Table 1
67	Supra_R	WIPP29	907.40	Mercer, 1983, Table 1
68	Supra_R	WIPP30	1044.90	Mercer, 1983, Table 1
69	Supra_R	WIPP32	921.40	Mercer, 1983, Table 1
70	Supra_R	WIPP33	1012.90	Mercer, 1983, Table 1
71	Supra_R	WIPP34	1046.40	Mercer, 1983, Table 1
72	Tamarisk	AEC7	882.40	Mercer, 1983, Table 1
73	Tamarisk	AEC8	851.70	Mercer, 1983, Table 1
74	Tamarisk	AirShft	850.99	Holt and Powers, 1990, Figure 22
75	Tamarisk	B25	851.00	Mercer, 1983, Table 1
76	Tamarisk	ERDA10	910.20	Mercer, 1983, Table 1

Table B.2. Elevations of Stratigraphic Layers Near WIPP (Continued)

	Layer	Well ID	Elevation	Source
1	Tamarisk	ERDA6	889.70	Mercer, 1983, Table 1
2	Tamarisk	ERDA9	853.10	Mercer, 1983, Table 1
3	Tamarisk	ExhtShft	847.97	Bechtel, Inc., 1986, Appendix F
4	Tamarisk	FFG_002	660.50	Richey, 1989, Table 2, p.21
5	Tamarisk	FFG_004	710.80	Richey, 1989, Table 2, p.21
6	Tamarisk	FFG_005	667.90	Richey, 1989, Table 2, p.21
7	Tamarisk	FFG_006	661.40	Richey, 1989, Table 2, p.21
8	Tamarisk	FFG_007	649.80	Richey, 1989, Table 2, p.21
9	Tamarisk	FFG_009	650.10	Richey, 1989, Table 2, p.21
10	Tamarisk	FFG_011	657.10	Richey, 1989, Table 2, p.21
11	Tamarisk	FFG_012	659.60	Richey, 1989, Table 2, p.21
12	Tamarisk	FFG_013	667.80	Richey, 1989, Table 2, p.21
13	Tamarisk	FFG_014	713.50	Richey, 1989, Table 2, p.21
14	Tamarisk	FFG_016	637.60	Richey, 1989, Table 2, p.21
15	Tamarisk	FFG_017	640.70	Richey, 1989, Table 2, p.22
16	Tamarisk	FFG_018	645.90	Richey, 1989, Table 2, p.22
17	Tamarisk	FFG_019	637.60	Richey, 1989, Table 2, p.22
18	Tamarisk	FFG_020	712.30	Richey, 1989, Table 2, p.22
19	Tamarisk	FFG_023	647.40	Richey, 1989, Table 2, p.22
20	Tamarisk	FFG_024	632.10	Richey, 1989, Table 2, p.22
21	Tamarisk	FFG_025	646.10	Richey, 1989, Table 2, p.22
22	Tamarisk	FFG_026	643.40	Richey, 1989, Table 2, p.22
23	Tamarisk	FFG_027	636.40	Richey, 1989, Table 2, p.22
24	Tamarisk	FFG_028	607.50	Richey, 1989, Table 2, p.22
25	Tamarisk	FFG_029	594.00	Richey, 1989, Table 2, p.22
26	Tamarisk	FFG_030	592.90	Richey, 1989, Table 2, p.22
27	Tamarisk	FFG_031	584.00	Richey, 1989, Table 2, p.22
28	Tamarisk	FFG_032	586.00	Richey, 1989, Table 2, p.22
29	Tamarisk	FFG_033	582.80	Richey, 1989, Table 2, p.22
30	Tamarisk	FFG_034	577.90	Richey, 1989, Table 2, p.23
31	Tamarisk	FFG_035	566.50	Richey, 1989, Table 2, p.23
32	Tamarisk	FFG_036	576.70	Richey, 1989, Table 2, p.23
33	Tamarisk	FFG_037	566.90	Richey, 1989, Table 2, p.23
34	Tamarisk	FFG_038	554.10	Richey, 1989, Table 2, p.23
35	Tamarisk	FFG_039	772.10	Richey, 1989, Table 2, p.23
36	Tamarisk	FFG_040	713.60	Richey, 1989, Table 2, p.23
37	Tamarisk	FFG_041	773.60	Richey, 1989, Table 2, p.23
38	Tamarisk	FFG_042	777.80	Richey, 1989, Table 2, p.23
39	Tamarisk	FFG_043	782.00	Richey, 1989, Table 2, p.23
40	Tamarisk	FFG_044	733.60	Richey, 1989, Table 2, p.23
41	Tamarisk	FFG_047	607.50	Richey, 1989, Table 2, p.23
42	Tamarisk	FFG_048	623.30	Richey, 1989, Table 2, p.23
43	Tamarisk	FFG_049	614.80	Richey, 1989, Table 2, p.23
44	Tamarisk	FFG_050	621.50	Richey, 1989, Table 2, p.24
45	Tamarisk	FFG_051	622.10	Richey, 1989, Table 2, p.24
46	Tamarisk	FFG_052	624.20	Richey, 1989, Table 2, p.24
47	Tamarisk	FFG_053	615.40	Richey, 1989, Table 2, p.24
48	Tamarisk	FFG_054	613.30	Richey, 1989, Table 2, p.24
49	Tamarisk	FFG_055	612.60	Richey, 1989, Table 2, p.24
50	Tamarisk	FFG_056	615.40	Richey, 1989, Table 2, p.24
51	Tamarisk	FFG_057	617.60	Richey, 1989, Table 2, p.24
52	Tamarisk	FFG_058	615.10	Richey, 1989, Table 2, p.24
53	Tamarisk	FFG_059	617.50	Richey, 1989, Table 2, p.24
54	Tamarisk	FFG_060	618.10	Richey, 1989, Table 2, p.24
55	Tamarisk	FFG_061	619.90	Richey, 1989, Table 2, p.24
56	Tamarisk	FFG_062	547.10	Richey, 1989, Table 2, p.24
57	Tamarisk	FFG_063	508.50	Richey, 1989, Table 2, p.24
58	Tamarisk	FFG_064	531.90	Richey, 1989, Table 2, p.24
59	Tamarisk	FFG_065	515.40	Richey, 1989, Table 2, p.24
60	Tamarisk	FFG_066	469.40	Richey, 1989, Table 2, p.24
61	Tamarisk	FFG_067	511.20	Richey, 1989, Table 2, p.25
62	Tamarisk	FFG_068	475.80	Richey, 1989, Table 2, p.25
63	Tamarisk	FFG_069	496.30	Richey, 1989, Table 2, p.25
64	Tamarisk	FFG_070	526.10	Richey, 1989, Table 2, p.25
65	Tamarisk	FFG_071	784.30	Richey, 1989, Table 2, p.25
66	Tamarisk	FFG_072	715.00	Richey, 1989, Table 2, p.25
67	Tamarisk	FFG_073	690.60	Richey, 1989, Table 2, p.25
68	Tamarisk	FFG_074	698.40	Richey, 1989, Table 2, p.25
69	Tamarisk	FFG_075	749.20	Richey, 1989, Table 2, p.25
70	Tamarisk	FFG_076	810.50	Richey, 1989, Table 2, p.25
71	Tamarisk	FFG_078	847.00	Richey, 1989, Table 2, p.25
72	Tamarisk	FFG_079	823.60	Richey, 1989, Table 2, p.25
73	Tamarisk	FFG_080	800.40	Richey, 1989, Table 2, p.25
74	Tamarisk	FFG_081	720.90	Richey, 1989, Table 2, p.26
75	Tamarisk	FFG_082	753.20	Richey, 1989, Table 2, p.26
76	Tamarisk	FFG_083	668.60	Richey, 1989, Table 2, p.26

Table B.2. Elevations of Stratigraphic Layers Near WIPP (Continued)

	Layer	Well ID	Elevation	Source
2	Tamarisk	FFG_084	694.60	Richey, 1989, Table 2, p.26
3	Tamarisk	FFG_085	687.40	Richey, 1989, Table 2, p.26
4	Tamarisk	FFG_086	697.30	Richey, 1989, Table 2, p.26
5	Tamarisk	FFG_087	671.40	Richey, 1989, Table 2, p.26
6	Tamarisk	FFG_088	667.20	Richey, 1989, Table 2, p.26
7	Tamarisk	FFG_089	649.60	Richey, 1989, Table 2, p.26
8	Tamarisk	FFG_091	692.80	Richey, 1989, Table 2, p.26
9	Tamarisk	FFG_092	706.50	Richey, 1989, Table 2, p.26
10	Tamarisk	FFG_093	710.20	Richey, 1989, Table 2, p.26
11	Tamarisk	FFG_094	713.20	Richey, 1989, Table 2, p.26
12	Tamarisk	FFG_095	681.50	Richey, 1989, Table 2, p.26
13	Tamarisk	FFG_096	665.10	Richey, 1989, Table 2, p.26
14	Tamarisk	FFG_097	645.00	Richey, 1989, Table 2, p.27
15	Tamarisk	FFG_098	619.90	Richey, 1989, Table 2, p.27
16	Tamarisk	FFG_099	615.40	Richey, 1989, Table 2, p.27
17	Tamarisk	FFG_100	598.10	Richey, 1989, Table 2, p.27
18	Tamarisk	FFG_101	569.40	Richey, 1989, Table 2, p.27
19	Tamarisk	FFG_102	587.40	Richey, 1989, Table 2, p.27
20	Tamarisk	FFG_103	652.00	Richey, 1989, Table 2, p.27
21	Tamarisk	FFG_104	545.00	Richey, 1989, Table 2, p.27
22	Tamarisk	FFG_105	901.30	Richey, 1989, Table 2, p.27
23	Tamarisk	FFG_106	931.80	Richey, 1989, Table 2, p.27
24	Tamarisk	FFG_107	916.90	Richey, 1989, Table 2, p.27
25	Tamarisk	FFG_108	912.30	Richey, 1989, Table 2, p.27
26	Tamarisk	FFG_109	892.80	Richey, 1989, Table 2, p.27
27	Tamarisk	FFG_110	859.60	Richey, 1989, Table 2, p.27
28	Tamarisk	FFG_111	867.10	Richey, 1989, Table 2, p.27
29	Tamarisk	FFG_112	854.90	Richey, 1989, Table 2, p.28
30	Tamarisk	FFG_113	869.00	Richey, 1989, Table 2, p.28
31	Tamarisk	FFG_114	898.30	Richey, 1989, Table 2, p.28
32	Tamarisk	FFG_115	889.40	Richey, 1989, Table 2, p.28
33	Tamarisk	FFG_116	904.90	Richey, 1989, Table 2, p.28
34	Tamarisk	FFG_117	902.20	Richey, 1989, Table 2, p.28
35	Tamarisk	FFG_119	937.90	Richey, 1989, Table 2, p.28
36	Tamarisk	FFG_120	913.80	Richey, 1989, Table 2, p.28
37	Tamarisk	FFG_121	922.00	Richey, 1989, Table 2, p.28
38	Tamarisk	FFG_122	920.50	Richey, 1989, Table 2, p.28
39	Tamarisk	FFG_123	894.50	Richey, 1989, Table 2, p.28
40	Tamarisk	FFG_124	857.70	Richey, 1989, Table 2, p.28
41	Tamarisk	FFG_125	883.20	Richey, 1989, Table 2, p.28
42	Tamarisk	FFG_126	880.10	Richey, 1989, Table 2, p.28
43	Tamarisk	FFG_127	885.10	Richey, 1989, Table 2, p.28
44	Tamarisk	FFG_128	917.50	Richey, 1989, Table 2, p.28
45	Tamarisk	FFG_129	893.30	Richey, 1989, Table 2, p.28
46	Tamarisk	FFG_130	920.50	Richey, 1989, Table 2, p.28
47	Tamarisk	FFG_132	929.00	Richey, 1989, Table 2, p.29
48	Tamarisk	FFG_133	932.00	Richey, 1989, Table 2, p.29
49	Tamarisk	FFG_134	935.50	Richey, 1989, Table 2, p.29
50	Tamarisk	FFG_135	910.80	Richey, 1989, Table 2, p.29
51	Tamarisk	FFG_136	911.50	Richey, 1989, Table 2, p.29
52	Tamarisk	FFG_137	919.30	Richey, 1989, Table 2, p.29
53	Tamarisk	FFG_138	874.50	Richey, 1989, Table 2, p.29
54	Tamarisk	FFG_139	882.40	Richey, 1989, Table 2, p.29
55	Tamarisk	FFG_140	823.10	Richey, 1989, Table 2, p.29
56	Tamarisk	FFG_141	845.70	Richey, 1989, Table 2, p.29
57	Tamarisk	FFG_142	821.80	Richey, 1989, Table 2, p.29
58	Tamarisk	FFG_143	831.70	Richey, 1989, Table 2, p.29
59	Tamarisk	FFG_144	903.50	Richey, 1989, Table 2, p.29
60	Tamarisk	FFG_145	905.30	Richey, 1989, Table 2, p.29
61	Tamarisk	FFG_146	912.90	Richey, 1989, Table 2, p.29
62	Tamarisk	FFG_147	893.70	Richey, 1989, Table 2, p.29
63	Tamarisk	FFG_148	907.70	Richey, 1989, Table 2, p.29
64	Tamarisk	FFG_149	912.20	Richey, 1989, Table 2, p.30
65	Tamarisk	FFG_155	905.60	Richey, 1989, Table 2, p.30
66	Tamarisk	FFG_157	907.10	Richey, 1989, Table 2, p.30
67	Tamarisk	FFG_158	931.10	Richey, 1989, Table 2, p.30
68	Tamarisk	FFG_159	928.80	Richey, 1989, Table 2, p.30
69	Tamarisk	FFG_160	924.20	Richey, 1989, Table 2, p.30
70	Tamarisk	FFG_161	930.00	Richey, 1989, Table 2, p.30
71	Tamarisk	FFG_162	925.40	Richey, 1989, Table 2, p.30
72	Tamarisk	FFG_163	927.80	Richey, 1989, Table 2, p.30
73	Tamarisk	FFG_164	955.90	Richey, 1989, Table 2, p.30
74	Tamarisk	FFG_165	935.70	Richey, 1989, Table 2, p.30
75	Tamarisk	FFG_166	928.40	Richey, 1989, Table 2, p.31
76	Tamarisk	FFG_167	914.40	Richey, 1989, Table 2, p.31
77	Tamarisk	FFG_168	933.90	Richey, 1989, Table 2, p.31

Table B.2. Elevations of Stratigraphic Layers Near WIPP (Continued)

	Layer	Well ID	Elevation	Source
1	Tamarisk	FFG_169	949.10	Richey, 1989, Table 2, p.31
2	Tamarisk	FFG_170	916.80	Richey, 1989, Table 2, p.31
3	Tamarisk	FFG_171	924.20	Richey, 1989, Table 2, p.31
4	Tamarisk	FFG_172	933.00	Richey, 1989, Table 2, p.31
5	Tamarisk	FFG_173	906.50	Richey, 1989, Table 2, p.31
6	Tamarisk	FFG_180	915.00	Richey, 1989, Table 2, p.31
7	Tamarisk	FFG_181	946.70	Richey, 1989, Table 2, p.32
8	Tamarisk	FFG_182	842.40	Richey, 1989, Table 2, p.32
9	Tamarisk	FFG_183	939.10	Richey, 1989, Table 2, p.32
10	Tamarisk	FFG_184	924.80	Richey, 1989, Table 2, p.32
11	Tamarisk	FFG_185	929.90	Richey, 1989, Table 2, p.32
12	Tamarisk	FFG_186	857.70	Richey, 1989, Table 2, p.32
13	Tamarisk	FFG_188	869.00	Richey, 1989, Table 2, p.32
14	Tamarisk	FFG_189	894.30	Richey, 1989, Table 2, p.32
15	Tamarisk	FFG_190	874.70	Richey, 1989, Table 2, p.32
16	Tamarisk	FFG_191	870.50	Richey, 1989, Table 2, p.32
17	Tamarisk	FFG_192	806.50	Richey, 1989, Table 2, p.32
18	Tamarisk	FFG_194	815.60	Richey, 1989, Table 2, p.33
19	Tamarisk	FFG_195	828.80	Richey, 1989, Table 2, p.33
20	Tamarisk	FFG_196	869.90	Richey, 1989, Table 2, p.33
21	Tamarisk	FFG_197	870.80	Richey, 1989, Table 2, p.33
22	Tamarisk	FFG_198	871.40	Richey, 1989, Table 2, p.33
23	Tamarisk	FFG_199	859.90	Richey, 1989, Table 2, p.33
24	Tamarisk	FFG_200	873.00	Richey, 1989, Table 2, p.33
25	Tamarisk	FFG_201	865.60	Richey, 1989, Table 2, p.33
26	Tamarisk	FFG_202	808.30	Richey, 1989, Table 2, p.33
27	Tamarisk	FFG_203	815.70	Richey, 1989, Table 2, p.33
28	Tamarisk	FFG_204	837.90	Richey, 1989, Table 2, p.33
29	Tamarisk	FFG_205	853.20	Richey, 1989, Table 2, p.33
30	Tamarisk	FFG_206	867.40	Richey, 1989, Table 2, p.33
31	Tamarisk	FFG_207	865.00	Richey, 1989, Table 2, p.33
32	Tamarisk	FFG_208	874.20	Richey, 1989, Table 2, p.34
33	Tamarisk	FFG_209	866.20	Richey, 1989, Table 2, p.34
34	Tamarisk	FFG_210	858.90	Richey, 1989, Table 2, p.34
35	Tamarisk	FFG_212	845.20	Richey, 1989, Table 2, p.34
36	Tamarisk	FFG_213	868.40	Richey, 1989, Table 2, p.34
37	Tamarisk	FFG_214	848.20	Richey, 1989, Table 2, p.34
38	Tamarisk	FFG_215	823.60	Richey, 1989, Table 2, p.34
39	Tamarisk	FFG_216	710.40	Richey, 1989, Table 2, p.34
40	Tamarisk	FFG_217	843.70	Richey, 1989, Table 2, p.34
41	Tamarisk	FFG_218	835.80	Richey, 1989, Table 2, p.34
42	Tamarisk	FFG_219	879.90	Richey, 1989, Table 2, p.34
43	Tamarisk	FFG_220	832.20	Richey, 1989, Table 2, p.34
44	Tamarisk	FFG_221	787.00	Richey, 1989, Table 2, p.34
45	Tamarisk	FFG_222	741.60	Richey, 1989, Table 2, p.34
46	Tamarisk	FFG_224	648.10	Richey, 1989, Table 2, p.35
47	Tamarisk	FFG_225	656.30	Richey, 1989, Table 2, p.35
48	Tamarisk	FFG_226	654.00	Richey, 1989, Table 2, p.35
49	Tamarisk	FFG_228	643.20	Richey, 1989, Table 2, p.35
50	Tamarisk	FFG_229	672.00	Richey, 1989, Table 2, p.35
51	Tamarisk	FFG_230	658.10	Richey, 1989, Table 2, p.35
52	Tamarisk	FFG_231	674.20	Richey, 1989, Table 2, p.35
53	Tamarisk	FFG_232	688.20	Richey, 1989, Table 2, p.35
54	Tamarisk	FFG_233	678.80	Richey, 1989, Table 2, p.35
55	Tamarisk	FFG_234	715.00	Richey, 1989, Table 2, p.35
56	Tamarisk	FFG_235	691.30	Richey, 1989, Table 2, p.35
57	Tamarisk	FFG_236	738.50	Richey, 1989, Table 2, p.35
58	Tamarisk	FFG_237	704.80	Richey, 1989, Table 2, p.35
59	Tamarisk	FFG_238	685.50	Richey, 1989, Table 2, p.36
60	Tamarisk	FFG_239	673.30	Richey, 1989, Table 2, p.36
61	Tamarisk	FFG_240	664.50	Richey, 1989, Table 2, p.36
62	Tamarisk	FFG_241	659.00	Richey, 1989, Table 2, p.36
63	Tamarisk	FFG_242	776.70	Richey, 1989, Table 2, p.36
64	Tamarisk	FFG_243	735.50	Richey, 1989, Table 2, p.36
65	Tamarisk	FFG_244	773.10	Richey, 1989, Table 2, p.36
66	Tamarisk	FFG_245	566.90	Richey, 1989, Table 2, p.36
67	Tamarisk	FFG_246	573.00	Richey, 1989, Table 2, p.36
68	Tamarisk	FFG_247	558.00	Richey, 1989, Table 2, p.36
69	Tamarisk	FFG_248	566.00	Richey, 1989, Table 2, p.36
70	Tamarisk	FFG_249	564.20	Richey, 1989, Table 2, p.36
71	Tamarisk	FFG_250	644.50	Richey, 1989, Table 2, p.36
72	Tamarisk	FFG_251	538.50	Richey, 1989, Table 2, p.36
73	Tamarisk	FFG_252	677.80	Richey, 1989, Table 2, p.36
74	Tamarisk	FFG_253	632.50	Richey, 1989, Table 2, p.36
75	Tamarisk	FFG_254	623.90	Richey, 1989, Table 2, p.36
76	Tamarisk	FFG_255	580.10	Richey, 1989, Table 2, p.37

Table B.2. Elevations of Stratigraphic Layers Near WIPP (Continued)

	Layer	Well ID	Elevation	Source
1	Tamarisk	FFG_256	529.80	Richey, 1989, Table 2, p.37
2	Tamarisk	FFG_257	573.60	Richey, 1989, Table 2, p.37
3	Tamarisk	FFG_258	587.60	Richey, 1989, Table 2, p.37
4	Tamarisk	FFG_259	553.50	Richey, 1989, Table 2, p.37
5	Tamarisk	FFG_260	597.40	Richey, 1989, Table 2, p.37
6	Tamarisk	FFG_261	586.40	Richey, 1989, Table 2, p.37
7	Tamarisk	FFG_262	1109.50	Richey, 1989, Table 2, p.37
8	Tamarisk	FFG_263	521.10	Richey, 1989, Table 2, p.37
9	Tamarisk	FFG_264	753.20	Richey, 1989, Table 2, p.37
10	Tamarisk	FFG_265	749.80	Richey, 1989, Table 2, p.37
11	Tamarisk	FFG_266	730.90	Richey, 1989, Table 2, p.37
12	Tamarisk	FFG_267	708.30	Richey, 1989, Table 2, p.37
13	Tamarisk	FFG_268	684.60	Richey, 1989, Table 2, p.37
14	Tamarisk	FFG_269	696.90	Richey, 1989, Table 2, p.38
15	Tamarisk	FFG_270	769.30	Richey, 1989, Table 2, p.38
16	Tamarisk	FFG_271	808.90	Richey, 1989, Table 2, p.38
17	Tamarisk	FFG_272	816.40	Richey, 1989, Table 2, p.38
18	Tamarisk	FFG_273	790.10	Richey, 1989, Table 2, p.38
19	Tamarisk	FFG_274	827.20	Richey, 1989, Table 2, p.38
20	Tamarisk	FFG_275	834.30	Richey, 1989, Table 2, p.38
21	Tamarisk	FFG_276	837.60	Richey, 1989, Table 2, p.38
22	Tamarisk	FFG_277	829.10	Richey, 1989, Table 2, p.38
23	Tamarisk	FFG_278	838.50	Richey, 1989, Table 2, p.38
24	Tamarisk	FFG_279	833.30	Richey, 1989, Table 2, p.38
25	Tamarisk	FFG_280	830.90	Richey, 1989, Table 2, p.38
26	Tamarisk	FFG_281	807.40	Richey, 1989, Table 2, p.38
27	Tamarisk	FFG_283	558.10	Richey, 1989, Table 2, p.39
28	Tamarisk	FFG_284	705.90	Richey, 1989, Table 2, p.39
29	Tamarisk	FFG_285	734.90	Richey, 1989, Table 2, p.39
30	Tamarisk	FFG_286	814.10	Richey, 1989, Table 2, p.39
31	Tamarisk	FFG_287	786.10	Richey, 1989, Table 2, p.39
32	Tamarisk	FFG_288	738.80	Richey, 1989, Table 2, p.39
33	Tamarisk	FFG_289	713.80	Richey, 1989, Table 2, p.39
34	Tamarisk	FFG_290	799.50	Richey, 1989, Table 2, p.39
35	Tamarisk	FFG_291	736.70	Richey, 1989, Table 2, p.39
36	Tamarisk	FFG_292	752.30	Richey, 1989, Table 2, p.39
37	Tamarisk	FFG_293	744.60	Richey, 1989, Table 2, p.39
38	Tamarisk	FFG_294	567.00	Richey, 1989, Table 2, p.39
39	Tamarisk	FFG_295	554.70	Richey, 1989, Table 2, p.39
40	Tamarisk	FFG_297	532.50	Richey, 1989, Table 2, p.39
41	Tamarisk	FFG_298	546.70	Richey, 1989, Table 2, p.40
42	Tamarisk	FFG_299	564.20	Richey, 1989, Table 2, p.40
43	Tamarisk	FFG_300	515.40	Richey, 1989, Table 2, p.40
44	Tamarisk	FFG_301	485.60	Richey, 1989, Table 2, p.40
45	Tamarisk	FFG_302	514.20	Richey, 1989, Table 2, p.40
46	Tamarisk	FFG_303	505.10	Richey, 1989, Table 2, p.40
47	Tamarisk	FFG_304	512.90	Richey, 1989, Table 2, p.40
48	Tamarisk	FFG_305	503.20	Richey, 1989, Table 2, p.40
49	Tamarisk	FFG_306	465.10	Richey, 1989, Table 2, p.40
50	Tamarisk	FFG_307	488.00	Richey, 1989, Table 2, p.40
51	Tamarisk	FFG_308	460.50	Richey, 1989, Table 2, p.40
52	Tamarisk	FFG_309	503.20	Richey, 1989, Table 2, p.40
53	Tamarisk	FFG_310	534.60	Richey, 1989, Table 2, p.40
54	Tamarisk	FFG_311	481.00	Richey, 1989, Table 2, p.40
55	Tamarisk	FFG_312	504.50	Richey, 1989, Table 2, p.40
56	Tamarisk	FFG_313	908.10	Richey, 1989, Table 2, p.41
57	Tamarisk	FFG_314	836.10	Richey, 1989, Table 2, p.41
58	Tamarisk	FFG_315	758.50	Richey, 1989, Table 2, p.41
59	Tamarisk	FFG_316	742.10	Richey, 1989, Table 2, p.41
60	Tamarisk	FFG_317	772.70	Richey, 1989, Table 2, p.41
61	Tamarisk	FFG_318	734.60	Richey, 1989, Table 2, p.41
62	Tamarisk	FFG_319	745.80	Richey, 1989, Table 2, p.41
63	Tamarisk	FFG_320	735.50	Richey, 1989, Table 2, p.41
64	Tamarisk	FFG_321	732.10	Richey, 1989, Table 2, p.41
65	Tamarisk	FFG_322	727.40	Richey, 1989, Table 2, p.41
66	Tamarisk	FFG_323	723.40	Richey, 1989, Table 2, p.41
67	Tamarisk	FFG_324	738.00	Richey, 1989, Table 2, p.41
68	Tamarisk	FFG_325	793.40	Richey, 1989, Table 2, p.41
69	Tamarisk	FFG_326	729.10	Richey, 1989, Table 2, p.41
70	Tamarisk	FFG_327	723.60	Richey, 1989, Table 2, p.42
71	Tamarisk	FFG_328	728.70	Richey, 1989, Table 2, p.42
72	Tamarisk	FFG_329	728.40	Richey, 1989, Table 2, p.42
73	Tamarisk	FFG_330	728.00	Richey, 1989, Table 2, p.42
74	Tamarisk	FFG_331	722.70	Richey, 1989, Table 2, p.42
75	Tamarisk	FFG_332	713.80	Richey, 1989, Table 2, p.42
76	Tamarisk	FFG_333	717.30	Richey, 1989, Table 2, p.42

Table B.2. Elevations of Stratigraphic Layers Near WIPP (Continued)

	Layer	Well ID	Elevation	Source
1	Tamarisk	FFG_334	712.60	Richey, 1989, Table 2, p.42
2	Tamarisk	FFG_335	724.80	Richey, 1989, Table 2, p.42
3	Tamarisk	FFG_336	725.10	Richey, 1989, Table 2, p.42
4	Tamarisk	FFG_337	708.00	Richey, 1989, Table 2, p.42
5	Tamarisk	FFG_338	715.20	Richey, 1989, Table 2, p.42
6	Tamarisk	FFG_339	680.30	Richey, 1989, Table 2, p.42
7	Tamarisk	FFG_340	688.80	Richey, 1989, Table 2, p.42
8	Tamarisk	FFG_342	720.20	Richey, 1989, Table 2, p.43
9	Tamarisk	FFG_344	685.10	Richey, 1989, Table 2, p.43
10	Tamarisk	FFG_345	746.60	Richey, 1989, Table 2, p.43
11	Tamarisk	FFG_347	736.70	Richey, 1989, Table 2, p.43
12	Tamarisk	FFG_348	768.10	Richey, 1989, Table 2, p.43
13	Tamarisk	FFG_349	738.00	Richey, 1989, Table 2, p.43
14	Tamarisk	FFG_350	783.00	Richey, 1989, Table 2, p.43
15	Tamarisk	FFG_351	701.10	Richey, 1989, Table 2, p.43
16	Tamarisk	FFG_352	699.50	Richey, 1989, Table 2, p.43
17	Tamarisk	FFG_353	721.20	Richey, 1989, Table 2, p.43
18	Tamarisk	FFG_354	795.30	Richey, 1989, Table 2, p.43
19	Tamarisk	FFG_361	982.60	Richey, 1989, Table 2, p.44
20	Tamarisk	FFG_362	956.40	Richey, 1989, Table 2, p.44
21	Tamarisk	FFG_363	972.90	Richey, 1989, Table 2, p.44
22	Tamarisk	FFG_364	942.70	Richey, 1989, Table 2, p.44
23	Tamarisk	FFG_366	933.90	Richey, 1989, Table 2, p.44
24	Tamarisk	FFG_367	948.50	Richey, 1989, Table 2, p.44
25	Tamarisk	FFG_370	1012.90	Richey, 1989, Table 2, p.44
26	Tamarisk	FFG_371	994.60	Richey, 1989, Table 2, p.44
27	Tamarisk	FFG_372	1006.40	Richey, 1989, Table 2, p.45
28	Tamarisk	FFG_373	945.00	Richey, 1989, Table 2, p.45
29	Tamarisk	FFG_374	929.70	Richey, 1989, Table 2, p.45
30	Tamarisk	FFG_376	984.80	Richey, 1989, Table 2, p.45
31	Tamarisk	FFG_381	1021.40	Richey, 1989, Table 2, p.45
32	Tamarisk	FFG_383	931.20	Richey, 1989, Table 2, p.45
33	Tamarisk	FFG_384	937.90	Richey, 1989, Table 2, p.45
34	Tamarisk	FFG_385	922.00	Richey, 1989, Table 2, p.45
35	Tamarisk	FFG_387	934.60	Richey, 1989, Table 2, p.45
36	Tamarisk	FFG_388	929.40	Richey, 1989, Table 2, p.46
37	Tamarisk	FFG_389	976.60	Richey, 1989, Table 2, p.46
38	Tamarisk	FFG_390	945.50	Richey, 1989, Table 2, p.46
39	Tamarisk	FFG_391	944.50	Richey, 1989, Table 2, p.46
40	Tamarisk	FFG_392	941.90	Richey, 1989, Table 2, p.46
41	Tamarisk	FFG_393	810.60	Richey, 1989, Table 2, p.46
42	Tamarisk	FFG_394	903.10	Richey, 1989, Table 2, p.46
43	Tamarisk	FFG_395	895.80	Richey, 1989, Table 2, p.46
44	Tamarisk	FFG_396	877.20	Richey, 1989, Table 2, p.46
45	Tamarisk	FFG_398	798.50	Richey, 1989, Table 2, p.46
46	Tamarisk	FFG_399	838.50	Richey, 1989, Table 2, p.46
47	Tamarisk	FFG_401	874.80	Richey, 1989, Table 2, p.46
48	Tamarisk	FFG_402	972.00	Richey, 1989, Table 2, p.46
49	Tamarisk	FFG_403	935.30	Richey, 1989, Table 2, p.47
50	Tamarisk	FFG_404	897.40	Richey, 1989, Table 2, p.47
51	Tamarisk	FFG_407	932.40	Richey, 1989, Table 2, p.47
52	Tamarisk	FFG_408	908.60	Richey, 1989, Table 2, p.47
53	Tamarisk	FFG_409	970.50	Richey, 1989, Table 2, p.47
54	Tamarisk	FFG_418	983.30	Richey, 1989, Table 2, p.48
55	Tamarisk	FFG_419	969.00	Richey, 1989, Table 2, p.48
56	Tamarisk	FFG_420	964.30	Richey, 1989, Table 2, p.48
57	Tamarisk	FFG_421	955.00	Richey, 1989, Table 2, p.48
58	Tamarisk	FFG_422	946.10	Richey, 1989, Table 2, p.48
59	Tamarisk	FFG_426	962.00	Richey, 1989, Table 2, p.48
60	Tamarisk	FFG_432	918.00	Richey, 1989, Table 2, p.48
61	Tamarisk	FFG_433	920.50	Richey, 1989, Table 2, p.48
62	Tamarisk	FFG_438	866.70	Richey, 1989, Table 2, p.49
63	Tamarisk	FFG_453	862.20	Richey, 1989, Table 2, p.50
64	Tamarisk	FFG_455	810.40	Richey, 1989, Table 2, p.50
65	Tamarisk	FFG_456	805.20	Richey, 1989, Table 2, p.50
66	Tamarisk	FFG_457	861.30	Richey, 1989, Table 2, p.50
67	Tamarisk	FFG_458	862.30	Richey, 1989, Table 2, p.50
68	Tamarisk	FFG_459	791.90	Richey, 1989, Table 2, p.50
69	Tamarisk	FFG_462	857.50	Richey, 1989, Table 2, p.50
70	Tamarisk	FFG_463	886.40	Richey, 1989, Table 2, p.51
71	Tamarisk	FFG_464	872.30	Richey, 1989, Table 2, p.51
72	Tamarisk	FFG_465	875.30	Richey, 1989, Table 2, p.51
73	Tamarisk	FFG_467	483.30	Richey, 1989, Table 2, p.51
74	Tamarisk	FFG_468	460.00	Richey, 1989, Table 2, p.51
75	Tamarisk	FFG_470	480.10	Richey, 1989, Table 2, p.51
76	Tamarisk	FFG_471	495.00	Richey, 1989, Table 2, p.51

Table B.2. Elevations of Stratigraphic Layers Near WIPP (Continued)

	Layer	Well ID	Elevation	Source
1	Tamarisk	FFG_472	532.80	Richey, 1989, Table 2, p.51
2	Tamarisk	FFG_473	463.60	Richey, 1989, Table 2, p.51
3	Tamarisk	FFG_474	723.30	Richey, 1989, Table 2, p.51
4	Tamarisk	FFG_475	723.80	Richey, 1989, Table 2, p.51
5	Tamarisk	FFG_476	797.40	Richey, 1989, Table 2, p.51
6	Tamarisk	FFG_477	751.70	Richey, 1989, Table 2, p.51
7	Tamarisk	FFG_478	733.60	Richey, 1989, Table 2, p.52
8	Tamarisk	FFG_479	730.00	Richey, 1989, Table 2, p.52
9	Tamarisk	FFG_480	726.40	Richey, 1989, Table 2, p.52
10	Tamarisk	FFG_481	709.00	Richey, 1989, Table 2, p.52
11	Tamarisk	FFG_482	738.60	Richey, 1989, Table 2, p.52
12	Tamarisk	FFG_483	761.40	Richey, 1989, Table 2, p.52
13	Tamarisk	FFG_484	748.10	Richey, 1989, Table 2, p.52
14	Tamarisk	FFG_485	756.80	Richey, 1989, Table 2, p.52
15	Tamarisk	FFG_486	743.40	Richey, 1989, Table 2, p.52
16	Tamarisk	FFG_487	740.40	Richey, 1989, Table 2, p.52
17	Tamarisk	FFG_488	726.60	Richey, 1989, Table 2, p.52
18	Tamarisk	FFG_489	742.30	Richey, 1989, Table 2, p.52
19	Tamarisk	FFG_490	832.70	Richey, 1989, Table 2, p.52
20	Tamarisk	FFG_491	830.30	Richey, 1989, Table 2, p.52
21	Tamarisk	FFG_492	792.50	Richey, 1989, Table 2, p.52
22	Tamarisk	FFG_493	779.80	Richey, 1989, Table 2, p.53
23	Tamarisk	FFG_494	786.00	Richey, 1989, Table 2, p.53
24	Tamarisk	FFG_495	777.20	Richey, 1989, Table 2, p.53
25	Tamarisk	FFG_496	684.30	Richey, 1989, Table 2, p.53
26	Tamarisk	FFG_497	695.60	Richey, 1989, Table 2, p.53
27	Tamarisk	FFG_498	708.40	Richey, 1989, Table 2, p.53
28	Tamarisk	FFG_499	684.60	Richey, 1989, Table 2, p.53
29	Tamarisk	FFG_500	698.60	Richey, 1989, Table 2, p.53
30	Tamarisk	FFG_501	704.00	Richey, 1989, Table 2, p.53
31	Tamarisk	FFG_502	697.40	Richey, 1989, Table 2, p.53
32	Tamarisk	FFG_503	679.40	Richey, 1989, Table 2, p.53
33	Tamarisk	FFG_504	699.90	Richey, 1989, Table 2, p.53
34	Tamarisk	FFG_505	734.30	Richey, 1989, Table 2, p.53
35	Tamarisk	FFG_506	725.40	Richey, 1989, Table 2, p.53
36	Tamarisk	FFG_507	688.40	Richey, 1989, Table 2, p.53
37	Tamarisk	FFG_508	738.60	Richey, 1989, Table 2, p.53
38	Tamarisk	FFG_509	739.10	Richey, 1989, Table 2, p.54
39	Tamarisk	FFG_510	738.70	Richey, 1989, Table 2, p.54
40	Tamarisk	FFG_511	696.50	Richey, 1989, Table 2, p.54
41	Tamarisk	FFG_512	714.80	Richey, 1989, Table 2, p.54
42	Tamarisk	FFG_513	734.90	Richey, 1989, Table 2, p.54
43	Tamarisk	FFG_514	726.00	Richey, 1989, Table 2, p.54
44	Tamarisk	FFG_515	692.80	Richey, 1989, Table 2, p.54
45	Tamarisk	FFG_516	685.50	Richey, 1989, Table 2, p.54
46	Tamarisk	FFG_517	783.70	Richey, 1989, Table 2, p.54
47	Tamarisk	FFG_518	772.00	Richey, 1989, Table 2, p.54
48	Tamarisk	FFG_519	740.10	Richey, 1989, Table 2, p.54
49	Tamarisk	FFG_520	631.70	Richey, 1989, Table 2, p.54
50	Tamarisk	FFG_521	650.40	Richey, 1989, Table 2, p.54
51	Tamarisk	FFG_522	499.70	Richey, 1989, Table 2, p.54
52	Tamarisk	FFG_523	509.30	Richey, 1989, Table 2, p.54
53	Tamarisk	FFG_524	670.80	Richey, 1989, Table 2, p.55
54	Tamarisk	FFG_525	508.50	Richey, 1989, Table 2, p.55
55	Tamarisk	FFG_526	973.50	Richey, 1989, Table 2, p.55
56	Tamarisk	FFG_527	933.60	Richey, 1989, Table 2, p.55
57	Tamarisk	FFG_528	926.00	Richey, 1989, Table 2, p.55
58	Tamarisk	FFG_530	1000.30	Richey, 1989, Table 2, p.55
59	Tamarisk	FFG_531	919.30	Richey, 1989, Table 2, p.55
60	Tamarisk	FFG_532	907.10	Richey, 1989, Table 2, p.55
61	Tamarisk	FFG_534	946.40	Richey, 1989, Table 2, p.55
62	Tamarisk	FFG_535	912.80	Richey, 1989, Table 2, p.55
63	Tamarisk	FFG_536	928.40	Richey, 1989, Table 2, p.55
64	Tamarisk	FFG_537	904.60	Richey, 1989, Table 2, p.55
65	Tamarisk	FFG_543	970.90	Richey, 1989, Table 2, p.56
66	Tamarisk	FFG_548	907.70	Richey, 1989, Table 2, p.56
67	Tamarisk	FFG_562	645.30	Richey, 1989, Table 2, p.57
68	Tamarisk	FFG_563	557.50	Richey, 1989, Table 2, p.57
69	Tamarisk	FFG_568	634.60	Richey, 1989, Table 2, p.57
70	Tamarisk	FFG_569	663.20	Richey, 1989, Table 2, p.57
71	Tamarisk	FFG_584	764.30	Richey, 1989, Table 2, p.58
72	Tamarisk	FFG_585	730.90	Richey, 1989, Table 2, p.58
73	Tamarisk	FFG_600	722.10	Richey, 1989, Table 2, p.58
74	Tamarisk	FFG_601	615.70	Richey, 1989, Table 2, p.58
75	Tamarisk	FFG_602	1053.10	Richey, 1989, Table 2, p.58
76	Tamarisk	FFG_606	695.90	Richey, 1989, Table 2, p.58

Table B.2. Elevations of Stratigraphic Layers Near WIPP (Continued)

	Layer	Well ID	Elevation	Source
1	Tamarisk	FFG_607	718.40	Richey, 1989, Table 2, p.59
2	Tamarisk	FFG_608	726.60	Richey, 1989, Table 2, p.59
3	Tamarisk	FFG_609	732.70	Richey, 1989, Table 2, p.59
4	Tamarisk	FFG_610	713.20	Richey, 1989, Table 2, p.59
5	Tamarisk	FFG_611	703.20	Richey, 1989, Table 2, p.59
6	Tamarisk	FFG_612	712.70	Richey, 1989, Table 2, p.59
7	Tamarisk	FFG_613	705.90	Richey, 1989, Table 2, p.59
8	Tamarisk	FFG_618	701.90	Richey, 1989, Table 2, p.59
9	Tamarisk	FFG_638	567.30	Richey, 1989, Table 2, p.60
10	Tamarisk	FFG_639	537.40	Richey, 1989, Table 2, p.60
11	Tamarisk	FFG_640	623.10	Richey, 1989, Table 2, p.60
12	Tamarisk	FFG_643	662.40	Richey, 1989, Table 2, p.60
13	Tamarisk	FFG_644	701.20	Richey, 1989, Table 2, p.60
14	Tamarisk	FFG_648	536.10	Richey, 1989, Table 2, p.60
15	Tamarisk	FFG_652	853.70	Richey, 1989, Table 2, p.60
16	Tamarisk	FFG_653	854.10	Richey, 1989, Table 2, p.61
17	Tamarisk	FFG_654	874.80	Richey, 1989, Table 2, p.61
18	Tamarisk	FFG_655	873.20	Richey, 1989, Table 2, p.61
19	Tamarisk	FFG_656	870.80	Richey, 1989, Table 2, p.61
20	Tamarisk	FFG_657	883.70	Richey, 1989, Table 2, p.61
21	Tamarisk	FFG_658	874.40	Richey, 1989, Table 2, p.61
22	Tamarisk	FFG_659	879.70	Richey, 1989, Table 2, p.61
23	Tamarisk	FFG_660	896.90	Richey, 1989, Table 2, p.61
24	Tamarisk	FFG_662	870.80	Richey, 1989, Table 2, p.61
25	Tamarisk	FFG_664	862.00	Richey, 1989, Table 2, p.61
26	Tamarisk	FFG_666	914.40	Richey, 1989, Table 2, p.62
27	Tamarisk	FFG_667	899.50	Richey, 1989, Table 2, p.62
28	Tamarisk	FFG_668	947.70	Richey, 1989, Table 2, p.62
29	Tamarisk	FFG_669	934.20	Richey, 1989, Table 2, p.62
30	Tamarisk	FFG_670	919.30	Richey, 1989, Table 2, p.62
31	Tamarisk	FFG_671	917.70	Richey, 1989, Table 2, p.62
32	Tamarisk	FFG_672	919.90	Richey, 1989, Table 2, p.62
33	Tamarisk	FFG_673	914.70	Richey, 1989, Table 2, p.62
34	Tamarisk	FFG_674	915.00	Richey, 1989, Table 2, p.62
35	Tamarisk	FFG_675	871.60	Richey, 1989, Table 2, p.62
36	Tamarisk	FFG_676	884.20	Richey, 1989, Table 2, p.62
37	Tamarisk	FFG_677	910.50	Richey, 1989, Table 2, p.62
38	Tamarisk	FFG_679	910.40	Richey, 1989, Table 2, p.62
39	Tamarisk	FFG_689	793.70	Richey, 1989, Table 2, p.63
40	Tamarisk	FFG_690	798.90	Richey, 1989, Table 2, p.63
41	Tamarisk	FFG_691	790.40	Richey, 1989, Table 2, p.63
42	Tamarisk	FFG_692	780.30	Richey, 1989, Table 2, p.63
43	Tamarisk	FFG_693	790.90	Richey, 1989, Table 2, p.63
44	Tamarisk	FFG_694	783.30	Richey, 1989, Table 2, p.63
45	Tamarisk	FFG_695	788.80	Richey, 1989, Table 2, p.63
46	Tamarisk	FFG_696	790.60	Richey, 1989, Table 2, p.63
47	Tamarisk	FFG_697	793.70	Richey, 1989, Table 2, p.64
48	Tamarisk	FFG_698	835.50	Richey, 1989, Table 2, p.64
49	Tamarisk	FFG_699	786.70	Richey, 1989, Table 2, p.64
50	Tamarisk	FFG_700	777.00	Richey, 1989, Table 2, p.64
51	Tamarisk	FFG_701	781.90	Richey, 1989, Table 2, p.64
52	Tamarisk	FFG_702	786.70	Richey, 1989, Table 2, p.64
53	Tamarisk	FFG_703	791.60	Richey, 1989, Table 2, p.64
54	Tamarisk	FFG_704	779.40	Richey, 1989, Table 2, p.64
55	Tamarisk	FFG_705	709.60	Richey, 1989, Table 2, p.64
56	Tamarisk	FFG_706	730.70	Richey, 1989, Table 2, p.64
57	Tamarisk	FFG_707	714.20	Richey, 1989, Table 2, p.64
58	Tamarisk	FFG_708	767.20	Richey, 1989, Table 2, p.64
59	Tamarisk	FFG_709	658.70	Richey, 1989, Table 2, p.64
60	Tamarisk	FFG_710	659.30	Richey, 1989, Table 2, p.64
61	Tamarisk	FFG_711	668.20	Richey, 1989, Table 2, p.65
62	Tamarisk	FFG_712	710.90	Richey, 1989, Table 2, p.65
63	Tamarisk	FFG_713	648.10	Richey, 1989, Table 2, p.65
64	Tamarisk	FFG_714	761.90	Richey, 1989, Table 2, p.65
65	Tamarisk	FFG_715	774.80	Richey, 1989, Table 2, p.65
66	Tamarisk	FFG_716	676.60	Richey, 1989, Table 2, p.65
67	Tamarisk	FFG_717	698.10	Richey, 1989, Table 2, p.65
68	Tamarisk	FFG_718	700.90	Richey, 1989, Table 2, p.65
69	Tamarisk	FFG_719	674.20	Richey, 1989, Table 2, p.65
70	Tamarisk	FFG_720	671.50	Richey, 1989, Table 2, p.65
71	Tamarisk	FFG_721	673.60	Richey, 1989, Table 2, p.65
72	Tamarisk	FFG_723	785.30	Richey, 1989, Table 2, p.65
73	Tamarisk	FFG_724	713.60	Richey, 1989, Table 2, p.65
74	Tamarisk	FFG_725	689.70	Richey, 1989, Table 2, p.65
75	Tamarisk	FFG_726	677.50	Richey, 1989, Table 2, p.65
76	Tamarisk	FFG_727	674.90	Richey, 1989, Table 2, p.66

Table B.2. Elevations of Stratigraphic Layers Near WIPP (Continued)

	Layer	Well ID	Elevation	Source
1	Tamarisk	FFG_728	673.30	Richey, 1989, Table 2, p.66
2	Tamarisk	FFG_729	683.70	Richey, 1989, Table 2, p.66
3	Tamarisk	FFG_730	701.30	Richey, 1989, Table 2, p.66
4	Tamarisk	FFG_731	697.80	Richey, 1989, Table 2, p.66
5	Tamarisk	FFG_732	713.20	Richey, 1989, Table 2, p.66
6	Tamarisk	FFG_733	781.20	Richey, 1989, Table 2, p.66
7	Tamarisk	FFG_734	737.00	Richey, 1989, Table 2, p.66
8	Tamarisk	FFG_735	679.10	Richey, 1989, Table 2, p.66
9	Tamarisk	FFG_736	732.40	Richey, 1989, Table 2, p.66
10	Tamarisk	FFG_737	678.80	Richey, 1989, Table 2, p.66
11	Tamarisk	FFG_738	692.50	Richey, 1989, Table 2, p.66
12	Tamarisk	FFG_739	729.80	Richey, 1989, Table 2, p.66
13	Tamarisk	FFG_740	730.60	Richey, 1989, Table 2, p.66
14	Tamarisk	FFG_741	697.70	Richey, 1989, Table 2, p.66
15	Tamarisk	FFG_742	748.60	Richey, 1989, Table 2, p.67
16	Tamarisk	FFG_743	735.20	Richey, 1989, Table 2, p.67
17	Tamarisk	FFG_744	717.80	Richey, 1989, Table 2, p.67
18	Tamarisk	FFG_745	705.90	Richey, 1989, Table 2, p.67
19	Tamarisk	FFG_746	693.00	Richey, 1989, Table 2, p.67
20	Tamarisk	H1	856.20	Mercer, 1983, Table 1
21	Tamarisk	H10C	733.70	Mercer, 1983, Table 1
22	Tamarisk	H2C	864.10	Mercer, 1983, Table 1
23	Tamarisk	H3	855.30	Mercer, 1983, Table 1
24	Tamarisk	H4C	893.40	Mercer, 1983, Table 1
25	Tamarisk	H5C	821.40	Mercer, 1983, Table 1
26	Tamarisk	H6C	863.80	Mercer, 1983, Table 1
27	Tamarisk	H7C	921.40	Mercer, 1983, Table 1
28	Tamarisk	H8C	897.70	Mercer, 1983, Table 1
29	Tamarisk	H9C	869.20	Mercer, 1983, Table 1
30	Tamarisk	P1	883.00	Mercer, 1983, Table 1
31	Tamarisk	P10	831.50	Mercer, 1983, Table 1
32	Tamarisk	P11	817.10	Mercer, 1983, Table 1
33	Tamarisk	P12	862.90	Mercer, 1983, Table 1
34	Tamarisk	P13	862.90	Mercer, 1983, Table 1
35	Tamarisk	P14	878.70	Mercer, 1983, Table 1
36	Tamarisk	P15	911.10	Mercer, 1983, Table 1
37	Tamarisk	P16	889.10	Mercer, 1983, Table 1
38	Tamarisk	P17	875.70	Mercer, 1983, Table 1
39	Tamarisk	P18	837.30	Mercer, 1983, Table 1
40	Tamarisk	P19	824.80	Mercer, 1983, Table 1
41	Tamarisk	P2	824.80	Mercer, 1983, Table 1
42	Tamarisk	P20	819.00	Mercer, 1983, Table 1
43	Tamarisk	P21	822.00	Mercer, 1983, Table 1
44	Tamarisk	P3	862.50	Mercer, 1983, Table 1
45	Tamarisk	P4	840.60	Mercer, 1983, Table 1
46	Tamarisk	P5	841.30	Mercer, 1983, Table 1
47	Tamarisk	P6	887.30	Mercer, 1983, Table 1
48	Tamarisk	P7	894.30	Mercer, 1983, Table 1
49	Tamarisk	P8	873.20	Mercer, 1983, Table 1
50	Tamarisk	P9	843.70	Mercer, 1983, Table 1
51	Tamarisk	SaltShft	848.11	Bechtel, Inc., 1986, Appendix D
52	Tamarisk	WIPP11	815.60	Mercer, 1983, Table 1
53	Tamarisk	WIPP12	840.40	Mercer, 1983, Table 1
54	Tamarisk	WIPP13	860.10	Mercer, 1983, Table 1
55	Tamarisk	WIPP18	841.30	Mercer, 1983, Table 1
56	Tamarisk	WIPP19	841.60	Mercer, 1983, Table 1
57	Tamarisk	WIPP21	846.10	Mercer, 1983, Table 1
58	Tamarisk	WIPP22	844.90	Mercer, 1983, Table 1
59	Tamarisk	WIPP25	879.30	Mercer, 1983, Table 1
60	Tamarisk	WIPP26	930.50	Mercer, 1983, Table 1
61	Tamarisk	WIPP27	909.20	Mercer, 1983, Table 1
62	Tamarisk	WIPP28	925.70	Mercer, 1983, Table 1
63	Tamarisk	WIPP29	907.40	Mercer, 1983, Table 1
64	Tamarisk	WIPP30	881.20	Mercer, 1983, Table 1
65	Tamarisk	WIPP32	910.40	Mercer, 1983, Table 1
66	Tamarisk	WIPP33	870.30	Mercer, 1983, Table 1
67	Tamarisk	WIPP34	820.50	Mercer, 1983, Table 1
68	Tamarisk	WastShft	849.83	Bechtel, Inc., 1986, Appendix E
69	Tamerisk	DOE1	831.60	TME 3159, Sep 1982, Table 2
70	Tamerisk	DOE2	821.70	Mercer et al., 1987, Table 3-2
71	Tamerisk	ERDA9	849.10	SNL and USGS, 1982b, Table 2
72	Tamerisk	REF	849.10	Rechard et al.,1991, Figure 2.2-1
73	Tamerisk	WIPP11	815.70	SNL and USGS, 1982a, Table 2
74	Tamerisk	WIPP12	840.10	D'Appolonia Consulting, 1983, Table 2
75	U_Member	AirShft	782.57	IT Corporation, 1990, Figure 22
76	U_Member	DOE1	761.00	TME 3159, Sep 1982, Table 2

Table B.2. Elevations of Stratigraphic Layers Near WIPP (Continued)

	Layer	Well ID	Elevation	Source
1	U_Member	DOE2	749.00	Mercer et al., 1987, Table 3-2
2	U_Member	ERDA9	779.70	SNL and USGS, 1982b, Table 2
3	U_Member	ExhtShft	779.82	Bechtel, Inc., 1986, Appendix F
4	U_Member	REF	779.70	Rechard et al.,1991, Figure 2.2-1
5	U_Member	SaltShft	779.83	Bechtel, Inc., 1986, Appendix D
6	U_Member	WIPP11	754.40	SNL and USGS, 1982a, Table 2
7	U_Member	WIPP12	767.40	D'Appolonia Consulting, 1983, Table 2
8	U_Member	WastShft	781.32	Bechtel, Inc., 1986, Appendix E
9	Unnamed	AEC7	840.60	Mercer, 1983, Table 1
10	Unnamed	AEC8	814.80	Mercer, 1983, Table 1
11	Unnamed	AirShft	817.19	IT Corporation, 1990, Figure 22
12	Unnamed	B25	817.20	Mercer, 1983, Table 1
13	Unnamed	DOE1	799.40	TME 3159, Sep 1982, Table 2
14	Unnamed	DOE2	784.10	Mercer et al., 1987, Table 3-2
15	Unnamed	ERDA10	873.90	Mercer, 1983, Table 1
16	Unnamed	ERDA6	855.00	Mercer, 1983, Table 1
17	Unnamed	ERDA9	820.50	Mercer, 1983, Table 1
18	Unnamed	ERDA9	816.40	SNL and USGS, 1982b, Table 2
19	Unnamed	ExhtShft	814.75	Bechtel, Inc., 1986, Appendix F
20	Unnamed	FFG_002	618.10	Richey, 1989, Table 2, p.21
21	Unnamed	FFG_004	659.90	Richey, 1989, Table 2, p.21
22	Unnamed	FFG_005	622.10	Richey, 1989, Table 2, p.21
23	Unnamed	FFG_006	608.10	Richey, 1989, Table 2, p.21
24	Unnamed	FFG_007	593.70	Richey, 1989, Table 2, p.21
25	Unnamed	FFG_009	596.50	Richey, 1989, Table 2, p.21
26	Unnamed	FFG_011	603.50	Richey, 1989, Table 2, p.21
27	Unnamed	FFG_012	606.20	Richey, 1989, Table 2, p.21
28	Unnamed	FFG_013	634.30	Richey, 1989, Table 2, p.21
29	Unnamed	FFG_014	658.90	Richey, 1989, Table 2, p.21
30	Unnamed	FFG_016	579.40	Richey, 1989, Table 2, p.21
31	Unnamed	FFG_017	587.30	Richey, 1989, Table 2, p.22
32	Unnamed	FFG_018	590.70	Richey, 1989, Table 2, p.22
33	Unnamed	FFG_019	580.30	Richey, 1989, Table 2, p.22
34	Unnamed	FFG_020	655.30	Richey, 1989, Table 2, p.22
35	Unnamed	FFG_023	587.70	Richey, 1989, Table 2, p.22
36	Unnamed	FFG_024	571.80	Richey, 1989, Table 2, p.22
37	Unnamed	FFG_025	591.80	Richey, 1989, Table 2, p.22
38	Unnamed	FFG_026	585.50	Richey, 1989, Table 2, p.22
39	Unnamed	FFG_027	578.50	Richey, 1989, Table 2, p.22
40	Unnamed	FFG_028	572.50	Richey, 1989, Table 2, p.22
41	Unnamed	FFG_029	558.10	Richey, 1989, Table 2, p.22
42	Unnamed	FFG_030	557.20	Richey, 1989, Table 2, p.22
43	Unnamed	FFG_031	547.40	Richey, 1989, Table 2, p.22
44	Unnamed	FFG_032	546.10	Richey, 1989, Table 2, p.22
45	Unnamed	FFG_033	542.20	Richey, 1989, Table 2, p.22
46	Unnamed	FFG_034	542.50	Richey, 1989, Table 2, p.23
47	Unnamed	FFG_035	530.90	Richey, 1989, Table 2, p.23
48	Unnamed	FFG_036	535.60	Richey, 1989, Table 2, p.23
49	Unnamed	FFG_037	528.80	Richey, 1989, Table 2, p.23
50	Unnamed	FFG_038	517.50	Richey, 1989, Table 2, p.23
51	Unnamed	FFG_039	725.50	Richey, 1989, Table 2, p.23
52	Unnamed	FFG_040	645.30	Richey, 1989, Table 2, p.23
53	Unnamed	FFG_041	726.40	Richey, 1989, Table 2, p.23
54	Unnamed	FFG_042	730.00	Richey, 1989, Table 2, p.23
55	Unnamed	FFG_043	728.70	Richey, 1989, Table 2, p.23
56	Unnamed	FFG_044	680.90	Richey, 1989, Table 2, p.23
57	Unnamed	FFG_047	556.00	Richey, 1989, Table 2, p.23
58	Unnamed	FFG_048	573.30	Richey, 1989, Table 2, p.23
59	Unnamed	FFG_049	559.60	Richey, 1989, Table 2, p.23
60	Unnamed	FFG_050	574.90	Richey, 1989, Table 2, p.24
61	Unnamed	FFG_051	566.30	Richey, 1989, Table 2, p.24
62	Unnamed	FFG_052	589.80	Richey, 1989, Table 2, p.24
63	Unnamed	FFG_053	555.60	Richey, 1989, Table 2, p.24
64	Unnamed	FFG_054	556.60	Richey, 1989, Table 2, p.24
65	Unnamed	FFG_055	557.80	Richey, 1989, Table 2, p.24
66	Unnamed	FFG_056	556.90	Richey, 1989, Table 2, p.24
67	Unnamed	FFG_057	558.10	Richey, 1989, Table 2, p.24
68	Unnamed	FFG_058	560.80	Richey, 1989, Table 2, p.24
69	Unnamed	FFG_059	564.80	Richey, 1989, Table 2, p.24
70	Unnamed	FFG_060	563.20	Richey, 1989, Table 2, p.24
71	Unnamed	FFG_061	565.10	Richey, 1989, Table 2, p.24
72	Unnamed	FFG_062	507.20	Richey, 1989, Table 2, p.24
73	Unnamed	FFG_063	465.80	Richey, 1989, Table 2, p.24
74	Unnamed	FFG_064	488.90	Richey, 1989, Table 2, p.24
75	Unnamed	FFG_065	464.50	Richey, 1989, Table 2, p.24
76	Unnamed	FFG_066	429.10	Richey, 1989, Table 2, p.24

Table B.2. Elevations of Stratigraphic Layers Near WIPP (Continued)

	Layer	Well ID	Elevation	Source
1	Unnamed	FFG_067	464.00	Richey, 1989, Table 2, p.25
2	Unnamed	FFG_068	424.00	Richey, 1989, Table 2, p.25
3	Unnamed	FFG_069	441.40	Richey, 1989, Table 2, p.25
4	Unnamed	FFG_070	479.10	Richey, 1989, Table 2, p.25
5	Unnamed	FFG_071	748.30	Richey, 1989, Table 2, p.25
6	Unnamed	FFG_072	674.20	Richey, 1989, Table 2, p.25
7	Unnamed	FFG_073	652.20	Richey, 1989, Table 2, p.25
8	Unnamed	FFG_074	660.30	Richey, 1989, Table 2, p.25
9	Unnamed	FFG_075	712.10	Richey, 1989, Table 2, p.25
10	Unnamed	FFG_076	771.50	Richey, 1989, Table 2, p.25
11	Unnamed	FFG_078	807.70	Richey, 1989, Table 2, p.25
12	Unnamed	FFG_079	780.90	Richey, 1989, Table 2, p.25
13	Unnamed	FFG_080	758.30	Richey, 1989, Table 2, p.25
14	Unnamed	FFG_081	674.90	Richey, 1989, Table 2, p.26
15	Unnamed	FFG_082	705.30	Richey, 1989, Table 2, p.26
16	Unnamed	FFG_083	632.00	Richey, 1989, Table 2, p.26
17	Unnamed	FFG_084	654.70	Richey, 1989, Table 2, p.26
18	Unnamed	FFG_085	649.00	Richey, 1989, Table 2, p.26
19	Unnamed	FFG_086	657.40	Richey, 1989, Table 2, p.26
20	Unnamed	FFG_087	630.00	Richey, 1989, Table 2, p.26
21	Unnamed	FFG_088	622.70	Richey, 1989, Table 2, p.26
22	Unnamed	FFG_089	606.60	Richey, 1989, Table 2, p.26
23	Unnamed	FFG_091	643.80	Richey, 1989, Table 2, p.26
24	Unnamed	FFG_092	662.30	Richey, 1989, Table 2, p.26
25	Unnamed	FFG_093	668.10	Richey, 1989, Table 2, p.26
26	Unnamed	FFG_094	666.60	Richey, 1989, Table 2, p.26
27	Unnamed	FFG_095	645.20	Richey, 1989, Table 2, p.26
28	Unnamed	FFG_096	629.40	Richey, 1989, Table 2, p.26
29	Unnamed	FFG_097	608.40	Richey, 1989, Table 2, p.27
30	Unnamed	FFG_098	581.80	Richey, 1989, Table 2, p.27
31	Unnamed	FFG_099	574.60	Richey, 1989, Table 2, p.27
32	Unnamed	FFG_100	558.70	Richey, 1989, Table 2, p.27
33	Unnamed	FFG_101	527.30	Richey, 1989, Table 2, p.27
34	Unnamed	FFG_102	542.90	Richey, 1989, Table 2, p.27
35	Unnamed	FFG_103	601.70	Richey, 1989, Table 2, p.27
36	Unnamed	FFG_104	502.10	Richey, 1989, Table 2, p.27
37	Unnamed	FFG_105	861.40	Richey, 1989, Table 2, p.27
38	Unnamed	FFG_106	894.60	Richey, 1989, Table 2, p.27
39	Unnamed	FFG_107	878.80	Richey, 1989, Table 2, p.27
40	Unnamed	FFG_108	869.60	Richey, 1989, Table 2, p.27
41	Unnamed	FFG_109	856.20	Richey, 1989, Table 2, p.27
42	Unnamed	FFG_110	824.50	Richey, 1989, Table 2, p.27
43	Unnamed	FFG_111	830.60	Richey, 1989, Table 2, p.27
44	Unnamed	FFG_112	816.80	Richey, 1989, Table 2, p.28
45	Unnamed	FFG_113	830.90	Richey, 1989, Table 2, p.28
46	Unnamed	FFG_114	863.20	Richey, 1989, Table 2, p.28
47	Unnamed	FFG_115	848.30	Richey, 1989, Table 2, p.28
48	Unnamed	FFG_116	865.30	Richey, 1989, Table 2, p.28
49	Unnamed	FFG_117	856.50	Richey, 1989, Table 2, p.28
50	Unnamed	FFG_119	864.80	Richey, 1989, Table 2, p.28
51	Unnamed	FFG_120	865.10	Richey, 1989, Table 2, p.28
52	Unnamed	FFG_121	873.30	Richey, 1989, Table 2, p.28
53	Unnamed	FFG_122	868.70	Richey, 1989, Table 2, p.28
54	Unnamed	FFG_123	861.00	Richey, 1989, Table 2, p.28
55	Unnamed	FFG_124	830.90	Richey, 1989, Table 2, p.28
56	Unnamed	FFG_125	842.10	Richey, 1989, Table 2, p.28
57	Unnamed	FFG_126	846.60	Richey, 1989, Table 2, p.28
58	Unnamed	FFG_127	851.60	Richey, 1989, Table 2, p.28
59	Unnamed	FFG_128	877.60	Richey, 1989, Table 2, p.28
60	Unnamed	FFG_129	852.20	Richey, 1989, Table 2, p.28
61	Unnamed	FFG_130	888.50	Richey, 1989, Table 2, p.28
62	Unnamed	FFG_132	890.90	Richey, 1989, Table 2, p.29
63	Unnamed	FFG_133	895.50	Richey, 1989, Table 2, p.29
64	Unnamed	FFG_134	896.80	Richey, 1989, Table 2, p.29
65	Unnamed	FFG_135	875.10	Richey, 1989, Table 2, p.29
66	Unnamed	FFG_136	876.40	Richey, 1989, Table 2, p.29
67	Unnamed	FFG_137	884.60	Richey, 1989, Table 2, p.29
68	Unnamed	FFG_138	834.90	Richey, 1989, Table 2, p.29
69	Unnamed	FFG_139	847.90	Richey, 1989, Table 2, p.29
70	Unnamed	FFG_140	785.00	Richey, 1989, Table 2, p.29
71	Unnamed	FFG_141	812.50	Richey, 1989, Table 2, p.29
72	Unnamed	FFG_142	788.30	Richey, 1989, Table 2, p.29
73	Unnamed	FFG_143	797.30	Richey, 1989, Table 2, p.29
74	Unnamed	FFG_144	883.70	Richey, 1989, Table 2, p.29
75	Unnamed	FFG_145	887.00	Richey, 1989, Table 2, p.29
76	Unnamed	FFG_146	897.70	Richey, 1989, Table 2, p.29

Table B.2. Elevations of Stratigraphic Layers Near WIPP (Continued)

	Layer	Well ID	Elevation	Source
1	Unnamed	FFG_147	875.40	Richey, 1989, Table 2, p.29
2	Unnamed	FFG_148	894.90	Richey, 1989, Table 2, p.29
3	Unnamed	FFG_149	903.10	Richey, 1989, Table 2, p.30
4	Unnamed	FFG_152	893.10	Richey, 1989, Table 2, p.30
5	Unnamed	FFG_155	894.00	Richey, 1989, Table 2, p.30
6	Unnamed	FFG_156	895.50	Richey, 1989, Table 2, p.30
7	Unnamed	FFG_157	898.60	Richey, 1989, Table 2, p.30
8	Unnamed	FFG_158	918.00	Richey, 1989, Table 2, p.30
9	Unnamed	FFG_159	891.60	Richey, 1989, Table 2, p.30
10	Unnamed	FFG_160	886.10	Richey, 1989, Table 2, p.30
11	Unnamed	FFG_161	894.90	Richey, 1989, Table 2, p.30
12	Unnamed	FFG_162	884.60	Richey, 1989, Table 2, p.30
13	Unnamed	FFG_163	888.20	Richey, 1989, Table 2, p.30
14	Unnamed	FFG_164	928.50	Richey, 1989, Table 2, p.30
15	Unnamed	FFG_165	902.20	Richey, 1989, Table 2, p.30
16	Unnamed	FFG_166	891.80	Richey, 1989, Table 2, p.31
17	Unnamed	FFG_167	877.90	Richey, 1989, Table 2, p.31
18	Unnamed	FFG_168	898.90	Richey, 1989, Table 2, p.31
19	Unnamed	FFG_169	909.20	Richey, 1989, Table 2, p.31
20	Unnamed	FFG_170	893.00	Richey, 1989, Table 2, p.31
21	Unnamed	FFG_171	909.30	Richey, 1989, Table 2, p.31
22	Unnamed	FFG_172	906.10	Richey, 1989, Table 2, p.31
23	Unnamed	FFG_173	867.80	Richey, 1989, Table 2, p.31
24	Unnamed	FFG_177	880.00	Richey, 1989, Table 2, p.31
25	Unnamed	FFG_178	711.40	Richey, 1989, Table 2, p.31
26	Unnamed	FFG_179	875.10	Richey, 1989, Table 2, p.31
27	Unnamed	FFG_180	874.70	Richey, 1989, Table 2, p.31
28	Unnamed	FFG_181	922.90	Richey, 1989, Table 2, p.32
29	Unnamed	FFG_182	804.30	Richey, 1989, Table 2, p.32
30	Unnamed	FFG_183	893.40	Richey, 1989, Table 2, p.32
31	Unnamed	FFG_184	883.60	Richey, 1989, Table 2, p.32
32	Unnamed	FFG_185	891.80	Richey, 1989, Table 2, p.32
33	Unnamed	FFG_186	819.30	Richey, 1989, Table 2, p.32
34	Unnamed	FFG_188	837.60	Richey, 1989, Table 2, p.32
35	Unnamed	FFG_189	859.60	Richey, 1989, Table 2, p.32
36	Unnamed	FFG_190	835.10	Richey, 1989, Table 2, p.32
37	Unnamed	FFG_191	839.40	Richey, 1989, Table 2, p.32
38	Unnamed	FFG_192	764.40	Richey, 1989, Table 2, p.32
39	Unnamed	FFG_194	780.60	Richey, 1989, Table 2, p.33
40	Unnamed	FFG_195	792.80	Richey, 1989, Table 2, p.33
41	Unnamed	FFG_196	827.50	Richey, 1989, Table 2, p.33
42	Unnamed	FFG_197	831.20	Richey, 1989, Table 2, p.33
43	Unnamed	FFG_198	831.80	Richey, 1989, Table 2, p.33
44	Unnamed	FFG_199	818.70	Richey, 1989, Table 2, p.33
45	Unnamed	FFG_200	828.10	Richey, 1989, Table 2, p.33
46	Unnamed	FFG_201	830.00	Richey, 1989, Table 2, p.33
47	Unnamed	FFG_202	763.20	Richey, 1989, Table 2, p.33
48	Unnamed	FFG_203	767.50	Richey, 1989, Table 2, p.33
49	Unnamed	FFG_204	805.30	Richey, 1989, Table 2, p.33
50	Unnamed	FFG_205	816.60	Richey, 1989, Table 2, p.33
51	Unnamed	FFG_206	828.10	Richey, 1989, Table 2, p.33
52	Unnamed	FFG_207	826.00	Richey, 1989, Table 2, p.33
53	Unnamed	FFG_208	834.50	Richey, 1989, Table 2, p.34
54	Unnamed	FFG_209	829.70	Richey, 1989, Table 2, p.34
55	Unnamed	FFG_210	818.70	Richey, 1989, Table 2, p.34
56	Unnamed	FFG_212	809.00	Richey, 1989, Table 2, p.34
57	Unnamed	FFG_213	828.80	Richey, 1989, Table 2, p.34
58	Unnamed	FFG_214	808.60	Richey, 1989, Table 2, p.34
59	Unnamed	FFG_215	784.90	Richey, 1989, Table 2, p.34
60	Unnamed	FFG_216	682.70	Richey, 1989, Table 2, p.34
61	Unnamed	FFG_217	805.60	Richey, 1989, Table 2, p.34
62	Unnamed	FFG_218	794.30	Richey, 1989, Table 2, p.34
63	Unnamed	FFG_219	840.30	Richey, 1989, Table 2, p.34
64	Unnamed	FFG_220	789.50	Richey, 1989, Table 2, p.34
65	Unnamed	FFG_221	744.30	Richey, 1989, Table 2, p.34
66	Unnamed	FFG_222	705.00	Richey, 1989, Table 2, p.34
67	Unnamed	FFG_224	590.10	Richey, 1989, Table 2, p.35
68	Unnamed	FFG_225	598.00	Richey, 1989, Table 2, p.35
69	Unnamed	FFG_226	594.80	Richey, 1989, Table 2, p.35
70	Unnamed	FFG_228	580.70	Richey, 1989, Table 2, p.35
71	Unnamed	FFG_229	607.10	Richey, 1989, Table 2, p.35
72	Unnamed	FFG_230	595.00	Richey, 1989, Table 2, p.35
73	Unnamed	FFG_231	613.80	Richey, 1989, Table 2, p.35
74	Unnamed	FFG_232	625.80	Richey, 1989, Table 2, p.35
75	Unnamed	FFG_233	617.90	Richey, 1989, Table 2, p.35
76	Unnamed	FFG_234	653.50	Richey, 1989, Table 2, p.35

Table B.2. Elevations of Stratigraphic Layers Near WIPP (Continued)

	Layer	Well ID	Elevation	Source
1	Unnamed	FFG_235	628.50	Richey, 1989, Table 2, p.35
2	Unnamed	FFG_236	677.20	Richey, 1989, Table 2, p.35
3	Unnamed	FFG_237	634.40	Richey, 1989, Table 2, p.35
4	Unnamed	FFG_238	621.50	Richey, 1989, Table 2, p.36
5	Unnamed	FFG_239	613.50	Richey, 1989, Table 2, p.36
6	Unnamed	FFG_240	602.60	Richey, 1989, Table 2, p.36
7	Unnamed	FFG_241	598.10	Richey, 1989, Table 2, p.36
8	Unnamed	FFG_242	724.20	Richey, 1989, Table 2, p.36
9	Unnamed	FFG_243	659.30	Richey, 1989, Table 2, p.36
10	Unnamed	FFG_244	715.20	Richey, 1989, Table 2, p.36
11	Unnamed	FFG_245	503.50	Richey, 1989, Table 2, p.36
12	Unnamed	FFG_246	508.10	Richey, 1989, Table 2, p.36
13	Unnamed	FFG_247	493.70	Richey, 1989, Table 2, p.36
14	Unnamed	FFG_248	498.30	Richey, 1989, Table 2, p.36
15	Unnamed	FFG_249	498.30	Richey, 1989, Table 2, p.36
16	Unnamed	FFG_250	580.50	Richey, 1989, Table 2, p.36
17	Unnamed	FFG_251	470.00	Richey, 1989, Table 2, p.36
18	Unnamed	FFG_252	612.60	Richey, 1989, Table 2, p.36
19	Unnamed	FFG_253	561.50	Richey, 1989, Table 2, p.36
20	Unnamed	FFG_254	554.70	Richey, 1989, Table 2, p.36
21	Unnamed	FFG_255	506.30	Richey, 1989, Table 2, p.37
22	Unnamed	FFG_256	470.90	Richey, 1989, Table 2, p.37
23	Unnamed	FFG_257	517.20	Richey, 1989, Table 2, p.37
24	Unnamed	FFG_258	536.40	Richey, 1989, Table 2, p.37
25	Unnamed	FFG_259	494.90	Richey, 1989, Table 2, p.37
26	Unnamed	FFG_260	548.90	Richey, 1989, Table 2, p.37
27	Unnamed	FFG_261	537.30	Richey, 1989, Table 2, p.37
28	Unnamed	FFG_262	477.00	Richey, 1989, Table 2, p.37
29	Unnamed	FFG_263	448.50	Richey, 1989, Table 2, p.37
30	Unnamed	FFG_264	696.20	Richey, 1989, Table 2, p.37
31	Unnamed	FFG_265	677.30	Richey, 1989, Table 2, p.37
32	Unnamed	FFG_266	656.80	Richey, 1989, Table 2, p.37
33	Unnamed	FFG_267	632.70	Richey, 1989, Table 2, p.37
34	Unnamed	FFG_268	606.30	Richey, 1989, Table 2, p.37
35	Unnamed	FFG_269	617.60	Richey, 1989, Table 2, p.38
36	Unnamed	FFG_270	721.10	Richey, 1989, Table 2, p.38
37	Unnamed	FFG_271	767.80	Richey, 1989, Table 2, p.38
38	Unnamed	FFG_272	743.90	Richey, 1989, Table 2, p.38
39	Unnamed	FFG_273	745.30	Richey, 1989, Table 2, p.38
40	Unnamed	FFG_274	785.80	Richey, 1989, Table 2, p.38
41	Unnamed	FFG_275	794.60	Richey, 1989, Table 2, p.38
42	Unnamed	FFG_276	795.80	Richey, 1989, Table 2, p.38
43	Unnamed	FFG_277	789.10	Richey, 1989, Table 2, p.38
44	Unnamed	FFG_278	765.40	Richey, 1989, Table 2, p.38
45	Unnamed	FFG_279	767.70	Richey, 1989, Table 2, p.38
46	Unnamed	FFG_280	780.00	Richey, 1989, Table 2, p.38
47	Unnamed	FFG_281	754.40	Richey, 1989, Table 2, p.38
48	Unnamed	FFG_283	489.20	Richey, 1989, Table 2, p.39
49	Unnamed	FFG_284	641.30	Richey, 1989, Table 2, p.39
50	Unnamed	FFG_285	660.50	Richey, 1989, Table 2, p.39
51	Unnamed	FFG_286	766.20	Richey, 1989, Table 2, p.39
52	Unnamed	FFG_287	733.30	Richey, 1989, Table 2, p.39
53	Unnamed	FFG_288	662.60	Richey, 1989, Table 2, p.39
54	Unnamed	FFG_289	673.90	Richey, 1989, Table 2, p.39
55	Unnamed	FFG_290	760.80	Richey, 1989, Table 2, p.39
56	Unnamed	FFG_291	660.80	Richey, 1989, Table 2, p.39
57	Unnamed	FFG_292	717.80	Richey, 1989, Table 2, p.39
58	Unnamed	FFG_293	710.50	Richey, 1989, Table 2, p.39
59	Unnamed	FFG_294	497.50	Richey, 1989, Table 2, p.39
60	Unnamed	FFG_295	480.00	Richey, 1989, Table 2, p.39
61	Unnamed	FFG_297	455.40	Richey, 1989, Table 2, p.39
62	Unnamed	FFG_298	520.40	Richey, 1989, Table 2, p.40
63	Unnamed	FFG_299	489.80	Richey, 1989, Table 2, p.40
64	Unnamed	FFG_300	473.00	Richey, 1989, Table 2, p.40
65	Unnamed	FFG_301	430.40	Richey, 1989, Table 2, p.40
66	Unnamed	FFG_302	436.80	Richey, 1989, Table 2, p.40
67	Unnamed	FFG_303	442.00	Richey, 1989, Table 2, p.40
68	Unnamed	FFG_304	438.90	Richey, 1989, Table 2, p.40
69	Unnamed	FFG_305	434.60	Richey, 1989, Table 2, p.40
70	Unnamed	FFG_306	405.30	Richey, 1989, Table 2, p.40
71	Unnamed	FFG_307	424.30	Richey, 1989, Table 2, p.40
72	Unnamed	FFG_308	367.80	Richey, 1989, Table 2, p.40
73	Unnamed	FFG_309	427.90	Richey, 1989, Table 2, p.40
74	Unnamed	FFG_310	469.10	Richey, 1989, Table 2, p.40
75	Unnamed	FFG_311	420.30	Richey, 1989, Table 2, p.40
76	Unnamed	FFG_312	424.00	Richey, 1989, Table 2, p.40

Table B.2. Elevations of Stratigraphic Layers Near WIPP (Continued)

	Layer	Well ID	Elevation	Source
1	Unnamed	FFG_313	862.00	Richey, 1989, Table 2, p.41
2	Unnamed	FFG_314	781.60	Richey, 1989, Table 2, p.41
3	Unnamed	FFG_315	694.20	Richey, 1989, Table 2, p.41
4	Unnamed	FFG_316	670.20	Richey, 1989, Table 2, p.41
5	Unnamed	FFG_317	725.10	Richey, 1989, Table 2, p.41
6	Unnamed	FFG_318	702.60	Richey, 1989, Table 2, p.41
7	Unnamed	FFG_319	696.40	Richey, 1989, Table 2, p.41
8	Unnamed	FFG_320	662.00	Richey, 1989, Table 2, p.41
9	Unnamed	FFG_321	661.70	Richey, 1989, Table 2, p.41
10	Unnamed	FFG_322	662.20	Richey, 1989, Table 2, p.41
11	Unnamed	FFG_323	667.90	Richey, 1989, Table 2, p.41
12	Unnamed	FFG_324	692.20	Richey, 1989, Table 2, p.41
13	Unnamed	FFG_325	753.20	Richey, 1989, Table 2, p.41
14	Unnamed	FFG_326	698.00	Richey, 1989, Table 2, p.41
15	Unnamed	FFG_327	681.90	Richey, 1989, Table 2, p.42
16	Unnamed	FFG_328	664.70	Richey, 1989, Table 2, p.42
17	Unnamed	FFG_329	661.40	Richey, 1989, Table 2, p.42
18	Unnamed	FFG_330	661.00	Richey, 1989, Table 2, p.42
19	Unnamed	FFG_331	646.80	Richey, 1989, Table 2, p.42
20	Unnamed	FFG_332	632.80	Richey, 1989, Table 2, p.42
21	Unnamed	FFG_333	643.00	Richey, 1989, Table 2, p.42
22	Unnamed	FFG_334	637.00	Richey, 1989, Table 2, p.42
23	Unnamed	FFG_335	655.00	Richey, 1989, Table 2, p.42
24	Unnamed	FFG_336	650.40	Richey, 1989, Table 2, p.42
25	Unnamed	FFG_337	634.30	Richey, 1989, Table 2, p.42
26	Unnamed	FFG_338	639.00	Richey, 1989, Table 2, p.42
27	Unnamed	FFG_339	604.10	Richey, 1989, Table 2, p.42
28	Unnamed	FFG_340	609.30	Richey, 1989, Table 2, p.42
29	Unnamed	FFG_342	676.30	Richey, 1989, Table 2, p.43
30	Unnamed	FFG_344	650.90	Richey, 1989, Table 2, p.43
31	Unnamed	FFG_345	671.30	Richey, 1989, Table 2, p.43
32	Unnamed	FFG_347	692.80	Richey, 1989, Table 2, p.43
33	Unnamed	FFG_348	733.00	Richey, 1989, Table 2, p.43
34	Unnamed	FFG_349	709.30	Richey, 1989, Table 2, p.43
35	Unnamed	FFG_350	739.70	Richey, 1989, Table 2, p.43
36	Unnamed	FFG_351	621.20	Richey, 1989, Table 2, p.43
37	Unnamed	FFG_352	621.80	Richey, 1989, Table 2, p.43
38	Unnamed	FFG_353	644.10	Richey, 1989, Table 2, p.43
39	Unnamed	FFG_354	756.00	Richey, 1989, Table 2, p.43
40	Unnamed	FFG_361	948.50	Richey, 1989, Table 2, p.44
41	Unnamed	FFG_362	911.00	Richey, 1989, Table 2, p.44
42	Unnamed	FFG_363	937.90	Richey, 1989, Table 2, p.44
43	Unnamed	FFG_364	909.80	Richey, 1989, Table 2, p.44
44	Unnamed	FFG_366	904.00	Richey, 1989, Table 2, p.44
45	Unnamed	FFG_367	922.60	Richey, 1989, Table 2, p.44
46	Unnamed	FFG_370	962.60	Richey, 1989, Table 2, p.44
47	Unnamed	FFG_371	958.60	Richey, 1989, Table 2, p.44
48	Unnamed	FFG_372	941.50	Richey, 1989, Table 2, p.45
49	Unnamed	FFG_373	902.00	Richey, 1989, Table 2, p.45
50	Unnamed	FFG_374	902.20	Richey, 1989, Table 2, p.45
51	Unnamed	FFG_376	939.70	Richey, 1989, Table 2, p.45
52	Unnamed	FFG_381	908.60	Richey, 1989, Table 2, p.45
53	Unnamed	FFG_383	902.20	Richey, 1989, Table 2, p.45
54	Unnamed	FFG_384	912.30	Richey, 1989, Table 2, p.45
55	Unnamed	FFG_385	906.80	Richey, 1989, Table 2, p.45
56	Unnamed	FFG_387	901.60	Richey, 1989, Table 2, p.45
57	Unnamed	FFG_388	893.70	Richey, 1989, Table 2, p.46
58	Unnamed	FFG_389	917.50	Richey, 1989, Table 2, p.46
59	Unnamed	FFG_390	913.50	Richey, 1989, Table 2, p.46
60	Unnamed	FFG_391	913.10	Richey, 1989, Table 2, p.46
61	Unnamed	FFG_392	904.40	Richey, 1989, Table 2, p.46
62	Unnamed	FFG_393	781.00	Richey, 1989, Table 2, p.46
63	Unnamed	FFG_394	877.20	Richey, 1989, Table 2, p.46
64	Unnamed	FFG_395	867.50	Richey, 1989, Table 2, p.46
65	Unnamed	FFG_396	847.10	Richey, 1989, Table 2, p.46
66	Unnamed	FFG_398	767.20	Richey, 1989, Table 2, p.46
67	Unnamed	FFG_399	780.60	Richey, 1989, Table 2, p.46
68	Unnamed	FFG_401	833.60	Richey, 1989, Table 2, p.46
69	Unnamed	FFG_402	936.70	Richey, 1989, Table 2, p.46
70	Unnamed	FFG_403	903.30	Richey, 1989, Table 2, p.47
71	Unnamed	FFG_404	867.20	Richey, 1989, Table 2, p.47
72	Unnamed	FFG_407	898.90	Richey, 1989, Table 2, p.47
73	Unnamed	FFG_408	901.00	Richey, 1989, Table 2, p.47
74	Unnamed	FFG_409	932.40	Richey, 1989, Table 2, p.47
75	Unnamed	FFG_411	873.90	Richey, 1989, Table 2, p.47
76	Unnamed	FFG_413	906.20	Richey, 1989, Table 2, p.47

Table B.2. Elevations of Stratigraphic Layers Near WIPP (Continued)

	Layer	Well ID	Elevation	Source
1	Unnamed	FFG_418	923.00	Richey, 1989, Table 2, p.48
2	Unnamed	FFG_419	936.70	Richey, 1989, Table 2, p.48
3	Unnamed	FFG_420	927.80	Richey, 1989, Table 2, p.48
4	Unnamed	FFG_421	913.80	Richey, 1989, Table 2, p.48
5	Unnamed	FFG_422	915.60	Richey, 1989, Table 2, p.48
6	Unnamed	FFG_426	919.30	Richey, 1989, Table 2, p.48
7	Unnamed	FFG_432	876.90	Richey, 1989, Table 2, p.48
8	Unnamed	FFG_433	892.40	Richey, 1989, Table 2, p.48
9	Unnamed	FFG_438	829.80	Richey, 1989, Table 2, p.49
10	Unnamed	FFG_445	911.60	Richey, 1989, Table 2, p.49
11	Unnamed	FFG_453	772.90	Richey, 1989, Table 2, p.50
12	Unnamed	FFG_455	761.40	Richey, 1989, Table 2, p.50
13	Unnamed	FFG_456	769.90	Richey, 1989, Table 2, p.50
14	Unnamed	FFG_457	822.60	Richey, 1989, Table 2, p.50
15	Unnamed	FFG_458	825.10	Richey, 1989, Table 2, p.50
16	Unnamed	FFG_459	752.30	Richey, 1989, Table 2, p.50
17	Unnamed	FFG_462	820.70	Richey, 1989, Table 2, p.50
18	Unnamed	FFG_463	843.70	Richey, 1989, Table 2, p.51
19	Unnamed	FFG_464	833.60	Richey, 1989, Table 2, p.51
20	Unnamed	FFG_465	835.10	Richey, 1989, Table 2, p.51
21	Unnamed	FFG_467	423.00	Richey, 1989, Table 2, p.51
22	Unnamed	FFG_468	373.10	Richey, 1989, Table 2, p.51
23	Unnamed	FFG_470	402.60	Richey, 1989, Table 2, p.51
24	Unnamed	FFG_471	420.60	Richey, 1989, Table 2, p.51
25	Unnamed	FFG_472	495.60	Richey, 1989, Table 2, p.51
26	Unnamed	FFG_473	383.70	Richey, 1989, Table 2, p.51
27	Unnamed	FFG_474	671.70	Richey, 1989, Table 2, p.51
28	Unnamed	FFG_475	677.70	Richey, 1989, Table 2, p.51
29	Unnamed	FFG_476	751.70	Richey, 1989, Table 2, p.51
30	Unnamed	FFG_477	718.80	Richey, 1989, Table 2, p.51
31	Unnamed	FFG_478	694.00	Richey, 1989, Table 2, p.52
32	Unnamed	FFG_479	698.90	Richey, 1989, Table 2, p.52
33	Unnamed	FFG_480	681.30	Richey, 1989, Table 2, p.52
34	Unnamed	FFG_481	674.50	Richey, 1989, Table 2, p.52
35	Unnamed	FFG_482	703.80	Richey, 1989, Table 2, p.52
36	Unnamed	FFG_483	732.70	Richey, 1989, Table 2, p.52
37	Unnamed	FFG_484	720.70	Richey, 1989, Table 2, p.52
38	Unnamed	FFG_485	723.00	Richey, 1989, Table 2, p.52
39	Unnamed	FFG_486	708.40	Richey, 1989, Table 2, p.52
40	Unnamed	FFG_487	706.90	Richey, 1989, Table 2, p.52
41	Unnamed	FFG_488	692.50	Richey, 1989, Table 2, p.52
42	Unnamed	FFG_489	708.80	Richey, 1989, Table 2, p.52
43	Unnamed	FFG_490	801.30	Richey, 1989, Table 2, p.52
44	Unnamed	FFG_491	793.10	Richey, 1989, Table 2, p.52
45	Unnamed	FFG_492	757.10	Richey, 1989, Table 2, p.52
46	Unnamed	FFG_493	743.20	Richey, 1989, Table 2, p.53
47	Unnamed	FFG_494	747.00	Richey, 1989, Table 2, p.53
48	Unnamed	FFG_495	743.10	Richey, 1989, Table 2, p.53
49	Unnamed	FFG_496	604.20	Richey, 1989, Table 2, p.53
50	Unnamed	FFG_497	642.20	Richey, 1989, Table 2, p.53
51	Unnamed	FFG_498	637.60	Richey, 1989, Table 2, p.53
52	Unnamed	FFG_499	603.20	Richey, 1989, Table 2, p.53
53	Unnamed	FFG_500	635.20	Richey, 1989, Table 2, p.53
54	Unnamed	FFG_501	665.60	Richey, 1989, Table 2, p.53
55	Unnamed	FFG_502	630.90	Richey, 1989, Table 2, p.53
56	Unnamed	FFG_503	616.30	Richey, 1989, Table 2, p.53
57	Unnamed	FFG_504	667.60	Richey, 1989, Table 2, p.53
58	Unnamed	FFG_505	696.20	Richey, 1989, Table 2, p.53
59	Unnamed	FFG_506	690.60	Richey, 1989, Table 2, p.53
60	Unnamed	FFG_507	599.40	Richey, 1989, Table 2, p.53
61	Unnamed	FFG_508	680.70	Richey, 1989, Table 2, p.53
62	Unnamed	FFG_509	662.30	Richey, 1989, Table 2, p.54
63	Unnamed	FFG_510	658.80	Richey, 1989, Table 2, p.54
64	Unnamed	FFG_511	619.40	Richey, 1989, Table 2, p.54
65	Unnamed	FFG_512	634.60	Richey, 1989, Table 2, p.54
66	Unnamed	FFG_513	659.30	Richey, 1989, Table 2, p.54
67	Unnamed	FFG_514	637.00	Richey, 1989, Table 2, p.54
68	Unnamed	FFG_515	610.80	Richey, 1989, Table 2, p.54
69	Unnamed	FFG_516	601.60	Richey, 1989, Table 2, p.54
70	Unnamed	FFG_517	750.70	Richey, 1989, Table 2, p.54
71	Unnamed	FFG_518	735.80	Richey, 1989, Table 2, p.54
72	Unnamed	FFG_519	696.50	Richey, 1989, Table 2, p.54
73	Unnamed	FFG_520	585.40	Richey, 1989, Table 2, p.54
74	Unnamed	FFG_521	628.20	Richey, 1989, Table 2, p.54
75	Unnamed	FFG_522	427.50	Richey, 1989, Table 2, p.54
76	Unnamed	FFG_523	443.20	Richey, 1989, Table 2, p.54

Table B.2. Elevations of Stratigraphic Layers Near WIPP (Continued)

	Layer	Well ID	Elevation	Source
1	Unnamed	FFG_524	607.40	Richey, 1989, Table 2, p.55
2	Unnamed	FFG_525	436.60	Richey, 1989, Table 2, p.55
3	Unnamed	FFG_526	943.10	Richey, 1989, Table 2, p.55
4	Unnamed	FFG_527	888.10	Richey, 1989, Table 2, p.55
5	Unnamed	FFG_528	891.50	Richey, 1989, Table 2, p.55
6	Unnamed	FFG_530	957.70	Richey, 1989, Table 2, p.55
7	Unnamed	FFG_531	888.80	Richey, 1989, Table 2, p.55
8	Unnamed	FFG_532	873.00	Richey, 1989, Table 2, p.55
9	Unnamed	FFG_534	883.30	Richey, 1989, Table 2, p.55
10	Unnamed	FFG_535	875.70	Richey, 1989, Table 2, p.55
11	Unnamed	FFG_536	884.50	Richey, 1989, Table 2, p.55
12	Unnamed	FFG_537	872.60	Richey, 1989, Table 2, p.55
13	Unnamed	FFG_543	926.70	Richey, 1989, Table 2, p.56
14	Unnamed	FFG_548	877.20	Richey, 1989, Table 2, p.56
15	Unnamed	FFG_552	722.00	Richey, 1989, Table 2, p.56
16	Unnamed	FFG_562	614.50	Richey, 1989, Table 2, p.57
17	Unnamed	FFG_563	528.20	Richey, 1989, Table 2, p.57
18	Unnamed	FFG_564	663.00	Richey, 1989, Table 2, p.57
19	Unnamed	FFG_568	625.80	Richey, 1989, Table 2, p.57
20	Unnamed	FFG_569	624.20	Richey, 1989, Table 2, p.57
21	Unnamed	FFG_584	736.60	Richey, 1989, Table 2, p.58
22	Unnamed	FFG_585	678.40	Richey, 1989, Table 2, p.58
23	Unnamed	FFG_600	692.50	Richey, 1989, Table 2, p.58
24	Unnamed	FFG_601	572.70	Richey, 1989, Table 2, p.58
25	Unnamed	FFG_602	794.30	Richey, 1989, Table 2, p.58
26	Unnamed	FFG_606	667.60	Richey, 1989, Table 2, p.58
27	Unnamed	FFG_607	671.80	Richey, 1989, Table 2, p.59
28	Unnamed	FFG_608	654.70	Richey, 1989, Table 2, p.59
29	Unnamed	FFG_609	646.70	Richey, 1989, Table 2, p.59
30	Unnamed	FFG_610	640.10	Richey, 1989, Table 2, p.59
31	Unnamed	FFG_611	635.50	Richey, 1989, Table 2, p.59
32	Unnamed	FFG_612	669.70	Richey, 1989, Table 2, p.59
33	Unnamed	FFG_613	668.70	Richey, 1989, Table 2, p.59
34	Unnamed	FFG_618	679.10	Richey, 1989, Table 2, p.59
35	Unnamed	FFG_620	731.20	Richey, 1989, Table 2, p.59
36	Unnamed	FFG_621	695.00	Richey, 1989, Table 2, p.59
37	Unnamed	FFG_638	530.10	Richey, 1989, Table 2, p.60
38	Unnamed	FFG_639	498.40	Richey, 1989, Table 2, p.60
39	Unnamed	FFG_640	586.60	Richey, 1989, Table 2, p.60
40	Unnamed	FFG_643	637.10	Richey, 1989, Table 2, p.60
41	Unnamed	FFG_644	670.50	Richey, 1989, Table 2, p.60
42	Unnamed	FFG_648	500.50	Richey, 1989, Table 2, p.60
43	Unnamed	FFG_652	815.90	Richey, 1989, Table 2, p.60
44	Unnamed	FFG_653	815.70	Richey, 1989, Table 2, p.61
45	Unnamed	FFG_654	839.10	Richey, 1989, Table 2, p.61
46	Unnamed	FFG_655	840.30	Richey, 1989, Table 2, p.61
47	Unnamed	FFG_656	838.50	Richey, 1989, Table 2, p.61
48	Unnamed	FFG_657	856.20	Richey, 1989, Table 2, p.61
49	Unnamed	FFG_658	842.70	Richey, 1989, Table 2, p.61
50	Unnamed	FFG_659	848.60	Richey, 1989, Table 2, p.61
51	Unnamed	FFG_660	866.40	Richey, 1989, Table 2, p.61
52	Unnamed	FFG_662	837.30	Richey, 1989, Table 2, p.61
53	Unnamed	FFG_664	830.90	Richey, 1989, Table 2, p.61
54	Unnamed	FFG_666	883.90	Richey, 1989, Table 2, p.62
55	Unnamed	FFG_667	869.30	Richey, 1989, Table 2, p.62
56	Unnamed	FFG_668	919.40	Richey, 1989, Table 2, p.62
57	Unnamed	FFG_669	905.80	Richey, 1989, Table 2, p.62
58	Unnamed	FFG_670	889.10	Richey, 1989, Table 2, p.62
59	Unnamed	FFG_671	891.20	Richey, 1989, Table 2, p.62
60	Unnamed	FFG_672	889.80	Richey, 1989, Table 2, p.62
61	Unnamed	FFG_673	887.50	Richey, 1989, Table 2, p.62
62	Unnamed	FFG_674	885.50	Richey, 1989, Table 2, p.62
63	Unnamed	FFG_675	844.20	Richey, 1989, Table 2, p.62
64	Unnamed	FFG_676	854.70	Richey, 1989, Table 2, p.62
65	Unnamed	FFG_677	883.30	Richey, 1989, Table 2, p.62
66	Unnamed	FFG_679	883.90	Richey, 1989, Table 2, p.62
67	Unnamed	FFG_685	911.10	Richey, 1989, Table 2, p.63
68	Unnamed	FFG_689	756.80	Richey, 1989, Table 2, p.63
69	Unnamed	FFG_690	760.80	Richey, 1989, Table 2, p.63
70	Unnamed	FFG_691	752.90	Richey, 1989, Table 2, p.63
71	Unnamed	FFG_692	741.60	Richey, 1989, Table 2, p.63
72	Unnamed	FFG_693	753.70	Richey, 1989, Table 2, p.63
73	Unnamed	FFG_694	743.10	Richey, 1989, Table 2, p.63
74	Unnamed	FFG_695	749.20	Richey, 1989, Table 2, p.63
75	Unnamed	FFG_696	751.60	Richey, 1989, Table 2, p.63
76	Unnamed	FFG_697	754.10	Richey, 1989, Table 2, p.64

Table B.2. Elevations of Stratigraphic Layers Near WIPP (Continued)

	Layer	Well ID	Elevation	Source
1	Unnamed	FFG_698	795.30	Richey, 1989, Table 2, p.64
2	Unnamed	FFG_699	749.50	Richey, 1989, Table 2, p.64
3	Unnamed	FFG_700	744.40	Richey, 1989, Table 2, p.64
4	Unnamed	FFG_701	740.80	Richey, 1989, Table 2, p.64
5	Unnamed	FFG_702	747.00	Richey, 1989, Table 2, p.64
6	Unnamed	FFG_703	753.80	Richey, 1989, Table 2, p.64
7	Unnamed	FFG_704	737.30	Richey, 1989, Table 2, p.64
8	Unnamed	FFG_705	671.80	Richey, 1989, Table 2, p.64
9	Unnamed	FFG_706	694.40	Richey, 1989, Table 2, p.64
10	Unnamed	FFG_707	677.00	Richey, 1989, Table 2, p.64
11	Unnamed	FFG_708	728.80	Richey, 1989, Table 2, p.64
12	Unnamed	FFG_709	625.80	Richey, 1989, Table 2, p.64
13	Unnamed	FFG_710	625.20	Richey, 1989, Table 2, p.64
14	Unnamed	FFG_711	626.10	Richey, 1989, Table 2, p.65
15	Unnamed	FFG_712	669.50	Richey, 1989, Table 2, p.65
16	Unnamed	FFG_713	613.70	Richey, 1989, Table 2, p.65
17	Unnamed	FFG_714	725.10	Richey, 1989, Table 2, p.65
18	Unnamed	FFG_715	735.10	Richey, 1989, Table 2, p.65
19	Unnamed	FFG_716	597.30	Richey, 1989, Table 2, p.65
20	Unnamed	FFG_717	665.20	Richey, 1989, Table 2, p.65
21	Unnamed	FFG_718	656.10	Richey, 1989, Table 2, p.65
22	Unnamed	FFG_719	618.70	Richey, 1989, Table 2, p.65
23	Unnamed	FFG_720	614.50	Richey, 1989, Table 2, p.65
24	Unnamed	FFG_721	639.50	Richey, 1989, Table 2, p.65
25	Unnamed	FFG_723	755.10	Richey, 1989, Table 2, p.65
26	Unnamed	FFG_724	678.00	Richey, 1989, Table 2, p.65
27	Unnamed	FFG_725	646.50	Richey, 1989, Table 2, p.65
28	Unnamed	FFG_726	641.00	Richey, 1989, Table 2, p.65
29	Unnamed	FFG_727	630.70	Richey, 1989, Table 2, p.66
30	Unnamed	FFG_728	638.20	Richey, 1989, Table 2, p.66
31	Unnamed	FFG_729	641.00	Richey, 1989, Table 2, p.66
32	Unnamed	FFG_730	665.30	Richey, 1989, Table 2, p.66
33	Unnamed	FFG_731	662.80	Richey, 1989, Table 2, p.66
34	Unnamed	FFG_732	678.20	Richey, 1989, Table 2, p.66
35	Unnamed	FFG_733	741.90	Richey, 1989, Table 2, p.66
36	Unnamed	FFG_734	699.20	Richey, 1989, Table 2, p.66
37	Unnamed	FFG_735	630.30	Richey, 1989, Table 2, p.66
38	Unnamed	FFG_736	667.80	Richey, 1989, Table 2, p.66
39	Unnamed	FFG_737	611.80	Richey, 1989, Table 2, p.66
40	Unnamed	FFG_738	654.40	Richey, 1989, Table 2, p.66
41	Unnamed	FFG_739	683.80	Richey, 1989, Table 2, p.66
42	Unnamed	FFG_740	653.20	Richey, 1989, Table 2, p.66
43	Unnamed	FFG_741	651.10	Richey, 1989, Table 2, p.66
44	Unnamed	FFG_742	690.70	Richey, 1989, Table 2, p.67
45	Unnamed	FFG_743	675.20	Richey, 1989, Table 2, p.67
46	Unnamed	FFG_744	670.80	Richey, 1989, Table 2, p.67
47	Unnamed	FFG_745	650.40	Richey, 1989, Table 2, p.67
48	Unnamed	FFG_746	637.20	Richey, 1989, Table 2, p.67
49	Unnamed	H1	822.60	Mercer, 1983, Table 1
50	Unnamed	H10C	699.80	Mercer, 1983, Table 1
51	Unnamed	H2C	833.00	Mercer, 1983, Table 1
52	Unnamed	H3	821.80	Mercer, 1983, Table 1
53	Unnamed	H4C	858.90	Mercer, 1983, Table 1
54	Unnamed	H5C	787.30	Mercer, 1983, Table 1
55	Unnamed	H6C	829.40	Mercer, 1983, Table 1
56	Unnamed	H7C	880.60	Mercer, 1983, Table 1
57	Unnamed	H8C	859.30	Mercer, 1983, Table 1
58	Unnamed	H9C	831.80	Mercer, 1983, Table 1
59	Unnamed	P1	847.40	Mercer, 1983, Table 1
60	Unnamed	P10	777.80	Mercer, 1983, Table 1
61	Unnamed	P11	782.10	Mercer, 1983, Table 1
62	Unnamed	P12	828.50	Mercer, 1983, Table 1
63	Unnamed	P13	828.50	Mercer, 1983, Table 1
64	Unnamed	P14	842.70	Mercer, 1983, Table 1
65	Unnamed	P15	876.30	Mercer, 1983, Table 1
66	Unnamed	P16	851.90	Mercer, 1983, Table 1
67	Unnamed	P17	839.10	Mercer, 1983, Table 1
68	Unnamed	P18	773.90	Mercer, 1983, Table 1
69	Unnamed	P19	776.60	Mercer, 1983, Table 1
70	Unnamed	P2	791.30	Mercer, 1983, Table 1
71	Unnamed	P20	784.60	Mercer, 1983, Table 1
72	Unnamed	P21	787.90	Mercer, 1983, Table 1
73	Unnamed	P3	828.40	Mercer, 1983, Table 1
74	Unnamed	P4	805.30	Mercer, 1983, Table 1
75	Unnamed	P5	805.90	Mercer, 1983, Table 1
76	Unnamed	P6	851.60	Mercer, 1983, Table 1

Table B.2. Elevations of Stratigraphic Layers Near WIPP (Continued)

	Layer	Well ID	Elevation	Source
1	Unnamed	P7	856.50	Mercer, 1983, Table 1
2	Unnamed	P8	838.50	Mercer, 1983, Table 1
3	Unnamed	P9	809.30	Mercer, 1983, Table 1
4	Unnamed	REF	816.40	Rechard et al.,1991, Figure 2.2-1
5	Unnamed	SaltShft	813.97	Bechtel, Inc., 1986, Appendix D
6	Unnamed	WIPP11	779.90	Mercer, 1983, Table 1
7	Unnamed	WIPP11	780.00	SNL and USGS, 1982a, Table 2
8	Unnamed	WIPP12	803.90	D'Appolonia Consulting, 1983, Table 2
9	Unnamed	WIPP12	803.80	Mercer, 1983, Table 1
10	Unnamed	WIPP13	817.10	Mercer, 1983, Table 1
11	Unnamed	WIPP15	996.40	Mercer, 1983, Table 1
12	Unnamed	WIPP16	672.70	Mercer, 1983, Table 1
13	Unnamed	WIPP18	807.10	Mercer, 1983, Table 1
14	Unnamed	WIPP19	809.60	Mercer, 1983, Table 1
15	Unnamed	WIPP21	812.00	Mercer, 1983, Table 1
16	Unnamed	WIPP22	811.30	Mercer, 1983, Table 1
17	Unnamed	WIPP25	835.40	Mercer, 1983, Table 1
18	Unnamed	WIPP26	897.00	Mercer, 1983, Table 1
19	Unnamed	WIPP27	871.40	Mercer, 1983, Table 1
20	Unnamed	WIPP28	884.30	Mercer, 1983, Table 1
21	Unnamed	WIPP29	894.60	Mercer, 1983, Table 1
22	Unnamed	WIPP30	845.60	Mercer, 1983, Table 1
23	Unnamed	WIPP32	894.00	Mercer, 1983, Table 1
24	Unnamed	WIPP33	836.70	Mercer, 1983, Table 1
25	Unnamed	WIPP34	784.30	Mercer, 1983, Table 1
26	Unnamed	WastShft	817.02	Bechtel, Inc., 1986, Appendix E
27	V_Triste	AirShft	622.89	IT Corporation, 1990, Figure 22
28	V_Triste	AirShft	625.30	IT Corporation, 1990, Figure 22
29	V_Triste	DOE1	604.50	TME 3159, Sep 1982, Table 2
30	V_Triste	DOE1	605.70	TME 3159, Sep 1982, Table 2
31	V_Triste	DOE2	598.10	Mercer et al., 1987, Table 3-2
32	V_Triste	DOE2	600.30	Mercer et al., 1987, Table 3-2
33	V_Triste	ERDA9	625.70	SNL and USGS, 1982b, Table 2
34	V_Triste	ERDA9	627.60	SNL and USGS, 1982b, Table 2
35	V_Triste	ExhtShft	625.11	Bechtel, Inc., 1986, Appendix F
36	V_Triste	ExhtShft	626.66	Bechtel, Inc., 1986, Appendix F
37	V_Triste	REF	625.70	Rechard et al.,1991, Figure 2.2-1
38	V_Triste	REF	627.60	Rechard et al.,1991, Figure 2.2-1
39	V_Triste	SaltShft	627.89	Bechtel, Inc., 1986, Appendix D
40	V_Triste	SaltShft	628.33	Bechtel, Inc., 1986, Appendix D
41	V_Triste	WIPP11	611.20	SNL and USGS, 1982a, Table 2
42	V_Triste	WIPP11	612.70	SNL and USGS, 1982a, Table 2
43	V_Triste	WIPP12	620.80	D'Appolonia Consulting, 1983, Table 2
44	V_Triste	WIPP12	621.70	D'Appolonia Consulting, 1983, Table 2
45				

REFERENCES FOR APPENDIX B

Bechtel, Inc. 1986. *WIPP Design Validation Final Report.* DOE/WIPP-86-010. Prepared for U.S. Department of Energy. San Francisco, CA: Bechtel National, Inc.

Gonzales, M. 1989. *Compilation and Comparison of Test-Hole Location Surveys in the Vicinity of the Waste Isolation Pilot Plant Site.* SAND88-1065. Albuquerque, NM: Sandia National Laboratories.

Holt, R. M. and D. W. Powers. 1990. *Geologic Mapping of the Air Intake Shaft at the Waste Isolation Pilot Plant.* DOE-WIPP 90-051. Carlsbad, NM: U.S. Department of Energy.

Krieg, R. D. 1984. *Reference Stratigraphy and Rock Properties for the Waste Isolation Pilot Plant (WIPP) Project.* SAND83-1908. Albuquerque, NM: Sandia National Laboratories.

Mercer, J. W. 1983. *Geohydrology of the Proposed Waste Isolation Pilot Plant Site, Los Medaños Area, Southeastern New Mexico.* U.S. Geological Survey Water Resources Investigation 83-4016.

Mercer, J. W., R. L. Beauheim, R. P. Snyder, and G. M. Fairer. 1987. *Basic Data Report for Drilling and Hydrologic Testing of Drillhole DOE-2 at the Waste Isolation Pilot Plant (WIPP) Site.* SAND86-0611. Albuquerque, NM: Sandia National Laboratories.

Rechard, R. P., H. J. Iuzzolino, J. S. Rath, R. D. McCurley, and D. K. Rudeen. 1989. *User's Manual for CAMCON: Compliance Assessment Methodology Controller.* SAND88-1496. Albuquerque, NM: Sandia National Laboratories.

Richey, S. F. 1989. *Geologic and Hydrologic Data for the Rustler Formation near the Waste Isolation Pilot Plant, Southeastern New Mexico.* Albuquerque, NM: U.S. Geological Survey Open-File Report 89-32.

SNL (Sandia National Laboratories) and U.S. Geological Survey. 1982a. *Basic Data Report for Drillhole WIPP 11 (Waste Isolation Pilot Plant - WIPP).* SAND79-0272. Albuquerque, NM: Sandia National Laboratories.

SNL (Sandia National Laboratories) and U.S. Geological Survey. 1982b. *Basic Data Report for Drillhole ERDA 9 (Waste Isolation Pilot Plant - WIPP).* SAND79-0270. Albuquerque, NM: Sandia National Laboratories.

SNL (Sandia National Laboratories) and D'Appolonia Consulting Engineers. 1983. *Basic Data Report for Drillhole WIPP 12 (Waste Isolation Pilot Plant - WIPP).* SAND82-2336. Albuquerque, NM: Sandia National Laboratories.

U.S. DOE (Department of Energy). 1982. *Basic Data Report for Borehole DOE-1, Waste Isolation Pilot Plant (WIPP) Project, Southeastern New Mexico.* TME 3159. Albuquerque, NM: Sandia National Laboratories.

NOMENCLATURE

Mathematical Symbols

A	- cross-sectional area (m^2)
A_m	- amplitude scaling factor for precipitation variation
a	- minimum range of distribution
a_R	- factor for Redlich-Kwong-Soave equation of state
$a_0, a_1, a_2 \ldots$	- coefficients of empirical equations
$2B$	- characteristic fracture spacing or block length (m)
B_ℓ, B_g	- formation volume factor (reservoir conditions/standard conditions) for liquid or gas, respectively
b	- maximum range of distribution
b_R	- factor for Redlich-Kwong-Soave equation of state
$2b_f$	- fracture aperature (m)
C	- concentration (kg/m^3)
C_w	- total concentration of water in solution (e.g., brine)
$C_\ell(S_j)$	- ℓth consequence model of scenario set S_j of the performance assessment methodology
$\hat{C}$	- mass fraction (kg/kg)
C°	- solubility (kg chemical/m^3 fluid)
c	- capacitance ($\beta_b + \phi\beta_\ell$) (Pa^{-1})
D_m	- molecular diffusion in porous media matrix ($D^\square \bullet \tau$) (m^2/s)
$D^\square$	- molecular diffusion in pure fluid (m^2/s)
D_L, D_T	- hydrodynamic dispersion $D_m + \alpha_L\overline{V}$ and $D_m + \alpha_T\overline{V}$, respectively ($m^2/s$)

1	D	- hydrodynamic dispersion tensor
2		
3	d	- diameter
4		
5	d_i	- separation distance to grid point i, e.g., separation distance between
6		interpolated point and a nearby point
7		
8	d_s	- distance traveled by solute
9		
10	E	- Young's modulus (Pa)
11		
12	e	- weighting power for inverse-distance interpolation
13		
14	f	- fanning friction factor
15		
16	f_w	- waste unit factor
17		
18	f_c, f_m, f_s	- volume fraction of combustibles, metals/glass, and sludge, respectively
19		
20	f_{rchg}	- recharge factor evaluated from precipitation fluctuation
21		
22	F(x)	- cumulative distribution function, integral of f(x), probability density
23		function of parameter x
24		
25	f(x)	- distribution of x
26		
27	g	- acceleration due to gravity = ~9.8 m/s^2 or 9.80616 - 2.5928 x 10^{-2}
28		$\cos 2\phi_{lat}$ + 6.9 x 10^{-5} $\cos^2 2\phi_{lat}$ - 3.086 x $10^{-6} z_{sur}$ - 1.543 x $10^{-6} \Delta z$, where
29		ϕ_{lat} is the latitude, z_{sur} is the surface elevation in meters, and Δz is the
30		depth in meters below the surface (Helmert's equation) (Weast and Astle,
31		1981, F-78) (9.792 m/s^2 at 1039.06 m [surface] and 9.791 m/s^2 at 351 m
32		[repository level])
33		
34	h	- multiplier factor
35		
36	h^*	- Plank's constant, 6.6262 $\times$ 10^{-34} J • s
37		
38	K	- hydraulic conductivity (m/s)
39		
40	K_d	- distribution (or partition) coefficient (m^3/kg)
41		
42	K_{bulk}	- bulk modulus (E/(3(1-2ν)) (Pa)
43		
44	k^*	- Boltzmann's constant 1.3806 $\times$ 10^{-23} (J/K)
45		
46	k	- permeability (m^2)
47		

$k_{r\ell}, k_{rg}$ - relative liquid and gas permeability, respectively

L_i - release limit for radionuclide i (from *40 CFR 191* Appendix A, Table 1)

M - molecular weight (g/mol)

M_{dc}, M_{dm}, M_{ds} - average mass of combustibles, metals/glass, and sludge, respectively, per drum (kg)

m_A - atomic mass

$\dot{m}_b, \dot{m}_c, \dot{m}_t$ - gas generation rate, biodegradation (mol/kg cellulose/s), corrosion (mol/m^2 surface area steel/s), and total, respectively

N_R - Reynold's number, $\frac{\rho_f v d}{\mu}$

Np - Peclet number, $\overline{V}d_{50}/\tau D^{\square}$, where d_{50} is average particle diameter (length dimension)

N - molarity (mol/ℓ)

n - number of moles

n_g - number of grid points used for interpolation

nR - number of radionuclides released from repository

nS - number of mutually-exclusive release scenario classes

nk - number of sampling vectors from Monte Carlo (LHS) sampling

nV - number of model parameters

P(r>R) - probability of r > R

$P(r>R|S_j)$ - conditional probability of r > R given scenario set S_j occurs

$P(S_j)$ - probability model of scenario set S_j occurring over 10,000 yr

p - pressure (Pa)

p_c - capillary pressure (Pa)

p_{cr} - critical pressure (Pa)

Q - flow rate

$Q_{i,k}$ - predicted cumulative release for radionuclide i for run k (Ci)

$q_{i,k}$ - predicted release at time t for radionuclide i for run k (Ci/s)

Risk - risk, $Risk = \{S_j, P(S_j), R(S_j), j = 1, ..., nS\}$

R_m, R_f - retardation, matrix and fracture, respectively

$R(S_j(\mathbf{x}_k))$ - calculated, summed, EPA normalized releases for Monte Carlo vector k

$$R(S_j(\mathbf{x}_k)) = \sum_{i=1}^{n_r} \frac{Q_{i,k}}{L_i} \quad k = 1, 2, ..., nK$$

R^* - universal gas constant $\left[8.31441 \frac{Pa \bullet m^3}{mol \bullet K}\right]$

r_{rank} - correlation coefficient, actual and rank transform, respectively

r_{vec} - Monte Carlo simulation (vector) ID

$r_{g/\ell}$ - gas (nonwetting phase)/liquid (wetting phase) ratio

$\bar{r}_p, \bar{r}_f$ - average annual precipitation (m/s), present and future, respectively

S_j - scenario class j

S_s - specific storage (γc) (m^{-1})

S_b - bulk storativity $\left(\frac{A \bullet \Delta z \bullet S_s}{\rho g}\right)$ (m^3/Pa)

s - standard deviation, (s^2 is variance)

s_g, s_ℓ - saturation (ratio of gas or liquid volume to total void volume), gas (nonwetting phase) and liquid (wetting phase), respectively (V/V_v)

$s_{gr}, s_{\ell r}$ - residual saturation, gas (nonwetting phase) and liquid (wetting phase), respectively

T_K - transmissivity (m^2/s)

T - temperature (K)

T_{cr} - critical temperature (Pa)

T_r	- reduced temperature (T/T_{cr})
t	- time (s)
$t_{1/2}$	- radionuclide half life (s)
V	- volume (m^3)
V_{cr}	- theoretical volume of gas assuming ideal gas behavior at critical temperature and pressure of the gas
V_d, V_s, V_w	- volume of the drum, solids, and design capacity of the repository, respectively (m^3)
v	- velocity (m/s)
x,y,z	- variable or parameter
$\bar{x}$	- mean or expected value
x_{50},x_{99}	- value of x at 50% (0.50) quantile and 99% (0.99) quantile
Z	- gas compressibility factor
Δz	- thickness
α	- parameter of probability density function
α_R	- factor for Redlich-Kwong-Soave equation of state
α_L, α_T	- dispersivity, longitudinal or transverse, respectively (m)
β_s, β_b, β_ℓ	- material compressibility solid, bulk [$(1 - \phi)\beta_s$], and liquid, respectively (Pa^{-1})
Γ	- strain rate (dv/dy) (s^{-1})
γ	- unit weight (ρg)
ε	- roughness height (m)
ξ_1,ξ_2	- oldroyd viscosity parameter
Θ	- Pleistocene glaciation frequercy (s^{-1})
$\dot{\theta}$	- angular velocity of drill bit (m/s)

λ	- parameter of probability density function
$\Lambda(t)$	- failure rate function for probability model of human intrusion
μ_ℓ, μ_g	- viscosity, liquid or gas, respectively (Pa • s)
ρ_s, ρ_b, ρ_f	- density, solid, bulk, and fluid, respectively (kg/m^3)
τ	- tortuosity $(\ell/\ell_{path})^2$
Φ	- Holocene precipitation fluctuation frequency (s^{-1})
ϕ_{lat}	- latitude
ϕ_m, ϕ_f	- porosity, matrix and fracture (b/[B + b]), respectively
ζ	- skin resistance from materials lining fractures, (b_s/D_s)
v	- molar volume (m^3/mol)
ν	- Poisson's ratio
ω_R	- acentric factor for Redlich-Kwong-Soave equation of state
χ	- mole fraction
η	- Brooks-Corey relative permeability model parameter exponent

Superscripts

*	- physical constants
°	- property at reference conditions
¤	- property in pure fluid
•	- parameter with respect to time (rate)
_	- mean of parameter

Subscripts

g	- gas
ℓ	- liquid

f	- fracture
m	- matrix

Acronyms

ANL-E	- Argonne National Laboratories, East
ASCII	- American Standard Code for Information Interchange
ALGEBRA	- support program for manipulating data in CAMDAT
BLOT	- a mesh and curve plot program for CAMDAT data
BOAST	- Black Oil Applied Simulation Tool; 3-D, 3-phase code for flow-through porous media
BRAGFLO	- Brine And Gas Flow; 2-D, 2-phase code for flow-through porous media
CAM	- Compliance Assessment Methodology
CAMCON	- Compliance Assessment Methodology CONtroller——controller (driver) for compliance evaluations developed for WIPP
CAMDAT	- Compliance Assessment Methodology DATa——computational data base developed for WIPP (modification of GENESIS and EXODUS)
CCDF	- Complementary Cumulative Distribution Function
CCDFPLT	- program to calculate and display complementary cumulative distribution function
CH	- Contact Handled (TRU waste)
DCL	- Digital Equipment Corporation Command Language
DOE	- U.S. Department of Energy
DRZ	- Disturbed Rock Zone
EPA	- U.S. Environmental Protection Agency
EOS	- equation of state
FD	- Finite-Difference numerical analysis
FE	- Finite-Element numerical analysis
Fm	- formation
GENMESH	- rectilinear three-dimensional finite-difference grid generator

HANF	- Hanford Reservation
HLW	- High-Level Waste
HST3D	- a program to simulate heat and solute transport in a three-dimensional groundwater flow system
INEL	- Idaho National Engineering Laboratory
LANL	- Los Alamos National Laboratory
LHS	- Latin Hypercube Sampling (efficient, stratified Monte Carlo sampling)
LLNL	- Lawrence Livermore National Laboratory
MATSET	- a program to insert user-selected parameter or material values into the computational data base
MOUND	- Mound Laboratory
NEFTRAN	- NEtwork Flow and TRANsport code
NRC	- U.S. Nuclear Regulatory Commission
NTS	- Nevada Test Site
ORNL	- Oak Ridge National Laboratory
PCCSRC	- program for calculating partial correlation coefficients (PCC) and standardized regression coefficients (SRC)
PREBOAST	- preprocessor (translator) for input to BOAST
PREBRAG	- preprocessor (translator) for input to BRAGFLO
PREHST	- preprocessor (translator) for input to HST3D
PRELHS	- preprocessor (translator) for input to LHS
PREPCC	- preprocessor (translator) for input to PCC/SRC
PRENEF	- preprocessor (translator) for input to NEFTRAN
PRESTEP	- preprocessor (translator) for input to STEPWISE
PRESUTRA	- preprocessor (translator) for input to SUTRA
PRESWFT	- preprocessor (translator) for input to SWIFT II

POSTBOAST	- postprocessor (translator) of output from BOAST to CAMDAT
POSTBRAG	- postprocessor (translator) of output from BRAGFLO to CAMDAT
POSTHST	- postprocessor (translator) of output from HST3D to CAMDAT
POSTLHS	- postprocessor (translator) of output from LHS to CAMDAT
POSTSUTRA	- postprocessor (translator) of output from SUTRA to CAMDAT
POSTSWFT	- postprocessor (translator) of output from SWIFT II to CAMDAT
QA	- Quality Assurance
RCRA	- Resource, Conservation, and Recovery Act of 1976 (Public Law 94-580) and subsequent amendments (e.g., HSWA——Hazardous and Solid Waste Amendments of 1984)
RFP	- Rocky Flats Plant
RH	- Remote Handled (TRU waste)
SNL	- Sandia National Laboratories, Albuquerque, NM
SRS	- Savannah River Site
STEPWISE	- stepwise regression program with rank regression and predicted error sum of squares criterion
SWIFTII	- Sandia Waste-Isolation, Flow and Transport code for solving transient, three-dimensional, coupled equations for fluid flow, heat transport, brine-miscible displacement, and radionuclide-miscible displacement in porous and fractured media
SUTRA	- Saturated-Unsaturated TRAnsport code
TRACKER	- a support program to estimate the pathway of a particle released in a fluid velocity field
TRU	- Transuranic
WIPP	- Waste Isolation Pilot Plant
40 CFR 191	- Code of Federal Regulations, Title 40, Part 191

CONVERSION TABLES
FOR SI AND COMMON ENGLISH UNITS

Table 1. Base and Derived SI Units

	Quantity	Name	Symbol	Expression in Terms of Other Units	Expression in Terms of SI Base Units
Base SI Units					
	length	meter	m		
	time	second	s		
	mass	kilogram	kg		
	temperature	kelvin	K		
	amount of substance	mole	mol		
	electric current	ampere	A		
SI-Derived Units					
	force	newton	N		$kg \cdot m \cdot s^{-2}$
	pressure, stress	pascal	Pa	N/m^2	$kg \cdot m^{-1} \cdot s^{-2}$
	energy, work, quantity of heat	joule	J	$N \cdot m$	$kg \cdot m^2 \cdot s^{-2}$
	power, radiant flux	watt	W	J/s	$kg \cdot m^2 \cdot s^{-3}$
	electric potential	volt	V	W/A	$kg \cdot m^2 \cdot s^{-3} \cdot A^{-1}$
	electric resistance	ohm	Ω	V/A	$kg \cdot m^2 \cdot s^{-3} \cdot A^{-2}$
	frequency	hertz	Hz		s^{-1}
	activity (of a radionuclide)	bequerel	Bq		s^{-1}
	absorbed dose	gray	Gy	J/kg	$m^2 \cdot s^{-2}$
	quantity of electricity, electric charge	coulomb	C		$A \cdot s$

Table 2. List of Prefixes

Factor	Prefix	Symbol*
10^{12}	tera	T
10^{9}	giga	G
10^{6}	mega	M
10^{3}	kilo	k
10^{2}	hecto	h
10	deka	da
10^{-1}	deci	d
10^{-2}	centi	c
10^{-3}	milli	m
10^{-6}	micro	μ
10^{-9}	nano	n
10^{-12}	pico	p
10^{-15}	femto	f
10^{-18}	atto	a

* Only the symbols T (tera), G (giga), and M (mega) are capitalized. Compound prefixes are not allowed — for example, use nm (*nano*metre) rather than mμm (*millimicro*metre).

Table 3. Length Conversions

	m	cm	Å	in.	ft	mi	nmi
meter (m)	1	*100	*$1x10^{10}$	39.37	3.281	$6.214x10^{-4}$	$5.400x10^{-4}$
centimeter (cm)	*0.01	1	*$1x10^{8}$	0.3937	$3.281x10^{-2}$	$6.214x10^{-6}$	$5.400x10^{-6}$
angstrom (Å)	*$1x10^{-10}$	*$1x10^{-8}$	1	$3.937x10^{-9}$	$3.281x10^{-10}$	$6.214x10^{-14}$	$5.400x10^{-14}$
inch (in.)	*0.0254	*2.54	*$2.54x10^{8}$	1	$8.333x10^{-2}$	$1.578x10^{-5}$	$1.371x10^{-5}$
foot (ft)	*0.3048	*30.48	*$3.048x10^{9}$	*12	1	$1.894x10^{-4}$	$1.646x10^{-4}$
mile (U.S.) (mi)	1609	$1.609x10^{5}$	$1.609x10^{13}$	*$6.336x10^{4}$	*5280	1	0.8690
nautical mile (nmi)	*1852	*$1.852x10^{5}$	*$1.852x10^{13}$	$7.291x10^{4}$	$6.076x10^{3}$	1.151	1

* Exact

Table 4. Area or Permeability

	m^2	ha	$in.^2$	ft^2	ac	mi^2	Darcy	cm^2
square meters (m^2)	1	*$1x10^{-4}$	1550	10.76	$2.471x10^{-4}$	$3.861x10^{-7}$	$1.013x10^{12}$	*$1.000x10^{4}$
hectare (ha)	*$1x10^{4}$	1	$1.550x10^{7}$	$1.076x10^{5}$	2.471	$3.861x10^{-3}$	$1.013x10^{16}$	*$1.000x10^{8}$
square inches ($in.^2$)	$6.452x10^{-4}$	$6.452x10^{-8}$	1	$6.944x10^{-3}$	$1.594x10^{-7}$	$2.491x10^{-10}$	$6.537x10^{8}$	6.452
square feet (ft^2)	$9.290x10^{-2}$	$9.290x10^{-6}$	144	1	$2.296x10^{-5}$	$3.587x10^{-8}$	$9.413x10^{10}$	929
acre (ac)	4047	0.4047	$6.273x10^{6}$	*$4.356x10^{4}$	1	$1.563x10^{-3}$	$4.100x10^{15}$	$4.047x10^{7}$
square miles (mi^2)	$2.590x10^{6}$	2590	$4.015x10^{9}$	$2.788x10^{7}$	*640	1	2.624	$2.590x10^{10}$
darcy (D)	$9.869x10^{-13}$	$9.869x10^{-17}$	$1.530x10^{-9}$	$1.062x10^{-11}$	$2.439x10^{-16}$	$3.811x10^{-19}$	1	$9.864x10^{-9}$
square centimeters (cm^2)	*$1x10^{-4}$	$1x10^{-8}$	0.1550	$1.076x10^{-3}$	$2.471x10^{-8}$	$3.861x10^{-11}$	$1.013x10^{8}$	1

*Exact

Table 5. Volume

	m^3	l	ft^3	yd^3	gal (U.S.)	bbl	drum	std bx	room	panel	disposal	ac•ft	sec•ft•day	bushel
cubic meters (m^3)	1	*1000	35.31	1.308	264.2	6.290	4.803	0.5618	$2.744x10^{-4}$	$2.169x10^{-5}$	$2.293x10^{-6}$	$8.107x10^{-4}$	$4.087x10^{-4}$	28.38
liter (l)	*$1x10^{-3}$	1	$3.531x10^{-2}$	$1.308x10^{-3}$	0.2642	$6.290x10^{-3}$	$4.803x10^{-3}$	$5.618x10^{-4}$	$2.744x10^{-7}$	$2.169x10^{-8}$	$2.293x10^{-9}$	$8.107x10^{-7}$	$4.087x10^{-7}$	$2.838x10^{-2}$
cubic feet (ft^3)	$2.832x10^{-2}$	28.32	1	$3.704x10^{-2}$	7.481	0.1781	0.1360	$1.591x10^{-2}$	$7.770x10^{-6}$	$6.143x10^{-7}$	$6.494x10^{-8}$	$2.296x10^{-5}$	$1.157x10^{-5}$	0.8036
cubic yard (yd^3)	0.7646	7646	*27	1	201.97	4.809	3.672	0.4295	$2.098x10^{-4}$	$1.659x10^{-5}$	$1.753x10^{-6}$	$6.198x10^{-4}$	$3.125x10^{-4}$	21.70
U.S. gallon (gal)	$3.785x10^{-3}$	3.785	0.1337	$4.951x10^{-3}$	1	$2.381x10^{-2}$	$1.818x10^{-2}$	$2.127x10^{-3}$	$1.039x10^{-6}$	$8.212x10^{-8}$	$8.682x10^{-9}$	$3.069x10^{-6}$	$1.547x10^{-6}$	0.1074
barrel (bbl)	0.1590	159	5.615	0.2079	*42	1	0.7636	$8.932x10^{-2}$	$4.363x10^{-5}$	$3.449x10^{-6}$	$3.646x10^{-7}$	$1.289x10^{-4}$	$6.498x10^{-5}$	4.512
drum (55-gal)	0.2082	208.2	7.352	0.2723	*55	1.310	1	0.1170	$5.713x10^{-5}$	$4.556x10^{-6}$	$4.804x10^{-7}$	$1.688x10^{-4}$	$8.510x10^{-5}$	5.908
standard-waste box (std bx)	1.9	1780	62.86	2.328	470.2	1.120	8.550	1	$4.884x10^{-4}$	$3.895x10^{-5}$	$4.107x10^{-6}$	$1.443x10^{-3}$	$7.275x10^{-4}$	50.51
room volume (room)	3644	$3.644x10^{6}$	$1.287x10^{5}$	4767	$9.627x10^{5}$	$2.292x10^{4}$	$1.750x10^{4}$	2047	1	$7.906x10^{-2}$	$8.358x10^{-3}$	2.955	1.490	$1.034x10^{5}$
panel volume (panel)	$4.610x10^{4}$	$4.610x10^{7}$	$1.628x10^{6}$	$6.029x10^{4}$	$1.218x10^{7}$	$2.899x10^{5}$	$2.214x10^{5}$	$2.590x10^{4}$	12.65	1	0.1057	37.37	18.84	$1.308x10^{6}$
disposal area (disposal)	$4.360x10^{5}$	$4.360x10^{8}$	$1.540x10^{7}$	$5.703x10^{5}$	$1.152x10^{8}$	$2.730x10^{5}$	$2.094x10^{6}$	$2.450x10^{5}$	119.6	9.459	1	353.5	178.2	$1.237x10^{7}$
acre•foot (ac•ft)	1233	$1.233x10^{6}$	*43560	1613	$3.259x10^{5}$	7758	5925	6.930	0.3385	$2.699x10^{-2}$	$2.846x10^{-3}$	1	0.5042	$3.500x10^{4}$
second•foot•day (sec•ft•day)	2447	$2.447x10^{6}$	*86400	*3200	$6.463x10^{5}$	$1.539x10^{4}$	$1.175x10^{4}$	1374	0.6713	$5.353x10^{-2}$	$5.645x10^{-3}$	1.983	1	$6.943x10^{4}$
bushel (bu)	$3.524x10^{-2}$	35.24	1.244	$4.609x10^{-2}$	9.309	0.2216	0.1693	$1.980x10^{-2}$	$9.669x10^{-6}$	$7.711x10^{-7}$	$8.131x10^{-8}$	$2.857x10^{-5}$	$1.440x10^{-5}$	1

*Exact

Table 6. Discharge (Volume/Time)

	m^3/s	m^3/yr	l	ft^3/s	ft^3/min	ft^3/day	acre•ft/day	gal/min	gal/day	bbl/day
cubic meters per second (m^3/s)	1	$3.156x10^7$	*1000	35.31	2119	$3.051x10^6$	70.05	$1.585x10^4$	$2.282x10^7$	$5.434x10^5$
cubic meters per year (m^3/yr)	$3.169x10^{-8}$	1	$3.169x10^{-5}$	$1.119x10^{-6}$	$6.714x10^{-5}$	$9.669x10^{-2}$	$2.220x10^{-6}$	$5.023x10^{-4}$	0.7233	$1.722x10^{-2}$
liters per second (l/s)	*$1x10^{-3}$	$3.156x10^4$	1	$3.531x10^{-2}$	2.119	3051	$7.005x10^{-2}$	15.85	$2.282x10^4$	543.4
cubic feet per second (ft^3/s)	$2.832x10^{-2}$	$8.936x10^5$	28.32	1	*60	*$8.640x10^4$	1.983	448.8	$6.463x10^5$	$1.539x10^4$
cubic feet per minute (ft^3/min)	$4.719x10^{-4}$	$1.489x10^4$	0.4719	$1.667x10^{-2}$	1	1440	$3.306x10^{-2}$	7.481	$1.077x10^4$	256.5
cubic feet per day (ft^3/day)	$3.277x10^{-7}$	10.34	$3.277x10^{-4}$	$1.157x10^{-5}$	$6.944x10^{-4}$	1	$2.296x10^{-5}$	$5.195x10^{-3}$	7.481	0.1781
acre•foot per day (acre• ft/day)	$1.428x10^{-2}$	$4.505x10^5$	14.28	0.5042	30.25	$4.356x10^4$	1	226.3	$3.259x10^5$	7758
gallons per minute (gal/min)	$6.309x10^{-5}$	1991	$6.309x10^{-2}$	$2.228x10^{-3}$	0.1337	19.25	$4.419x10^{-3}$	1	1440	34.29
gallons per day (gal/day)	$4.381x10^{-8}$	1.383	$4.381x10^{-5}$	$1.547x10^{-6}$	$9.283x10^{-5}$	0.1337	$3.069x10^{-6}$	$6.944x10^{-4}$	1	$2.381x10^{-2}$
barrels per day (bbl/day)	$1.840x10^{-6}$	58.07	$1.840x10^{-3}$	$6.498x10^{-5}$	$3.899x10^{-3}$	5.615	$1.289x10^{-4}$	$2.917x10^{-2}$	*42	1

*Exact

Table 7. Velocity, Hydraulic Conductivity, Precipitation

	m/s	m/yr	in./yr	cm/yr	km/yr	ft/s	ft/day	mph	knots	gal/(day•ft^2)
meters per second (m/s)	1	3.156×10^{7}	1.242×10^{9}	3.156×10^{9}	3.156×10^{4}	3.281	2.835×10^{5}	2.237	1.944	2.120×10^{6}
meters per year (m/yr)	3.169×10^{-8}	1	39.37	*100	$*1 \times 10^{-3}$	1.040×10^{-7}	8.983×10^{-3}	7.089×10^{-8}	6.160×10^{-8}	6.719×10^{-2}
inches per year (in./yr)	8.049×10^{-10}	$*2.540 \times 10^{-2}$	1	*2.540	$*2.540 \times 10^{-5}$	2.641×10^{-9}	2.282×10^{-4}	1.800×10^{-9}	1.565×10^{-9}	1.707×10^{-3}
cen-timeters per year (cm/yr)	3.169×10^{-10}	$*1 \times 10^{-2}$	0.3937	1	$*1 \times 10^{-5}$	1.040×10^{-9}	8.983×10^{-5}	7.089×10^{-10}	6.160×10^{-10}	6.719×10^{-4}
kilometers per year (km/yr)	3.169×10^{-5}	*1000	3.937×10^{4}	$*1 \times 10^{5}$	1	1.040×10^{-4}	8.983	7.089×10^{-5}	6.160×10^{-5}	67.19
feet per second (ft/s)	*0.3048	9.619×10^{6}	3.787×10^{8}	9.619×10^{8}	9619	1	$*8.640 \times 10^{4}$	0.6818	0.5925	6.463×10^{5}
feet per day (ft/day)	3.528×10^{-6}	111.3	4383	1.113×10^{4}	0.1113	1.157×10^{-5}	1	7.891×10^{-6}	6.857×10^{-6}	7.481
miles per hour (mph)	0.4470	1.411×10^{7}	5.554×10^{8}	1.411×10^{9}	1.411×10^{4}	1.467	1.267×10^{5}	1	0.8690	9.479×10^{5}
knots	0.5144	1.623×10^{7}	6.391×10^{8}	1.623×10^{9}	1.623×10^{4}	1.688	1.458×10^{5}	1.151	1	1.091×10^{6}
gallons per day per square foot (gal/(day•ft^2))	4.716×10^{-7}	14.88	585.9	1488	1.488×10^{-2}	1.547×10^{-6}	0.1337	$.055 \times 10^{-6}$	9.167×10^{-7}	1

*Exact

Table 8. Force

	N	kg-force	dyne	lbf
Newton (N)	1	0.1020	*$1x10^5$	0.2248
kilogram-force (kg-force)	9.807	1	$9.807x10^5$	2.205
dyne	*$1.00x10^{-5}$	$1.020x10^{-6}$	1	$2.248x10^{-6}$
pound force (lbf)	4.448	0.4536	$4.448x10^5$	1

*Exact

Table 9. Pressure and Stress

	Pa	bar	dyne/cm^2	atm	mm Hg	psi	lb/ft^2
pascal (Pa)	1	*$1x10^{-5}$	*10	$9.869x10^{-6}$	$7.501x10^{-3}$	$1.450x10^{-4}$	$2.089x10^{-2}$
bar	*$1x10^5$	1	*$1x10^6$	0.9869	750.1	14.50	2089
dyne per square centimeters (dyne/cm^2)	*0.1	*$1x10^{-6}$	1	$9.869x10^{-7}$	$7.501x10^{-4}$	$1.450x10^{-5}$	$2.089x10^{-3}$
atmosphere (atm)	$1.013x10^5$	1.013	$1.013x10^6$	1	*760	14.70	2116
millimeter of Mercury (mm Hg)	1333	$1.333x10^{-3}$	1333	$1.316x10^{-3}$	1	$1.934x10^{-2}$	2.785
pound per square inch (psi)	698.5	$6.895x10^{-2}$	$6.895x10^4$	$6.805x10^{-2}$	51.71	1	*144
pounds per square foot (lb/ft^2)	47.88	$4.788x10^{-4}$	478.8	$4.725x10^{-4}$	0.3591	$6.944x10^{-3}$	1

*Exact

Table 10. Absolute Viscosity

	Pa•s (kg/(m•s))	cP	lbm/ft/s	slug/(ft•s) lbf • ft/s^2
Pascal-second (Pa•s) (kg/(m•s))	1	*1000	0.6720	2.089x10^{-2}
centipoise (cP)	*1x10^{-3}	1	6.720x10^{-4}	2.089x10^{-5}
pound mass per foot per second (lbm/ft/s)	1.488	1488	1	3.108x10^{-2}
slug per foot per second (slug/(ft•s) or lbf • ft/s^2)	47.88	4.788x10^4	32.17	1

*Exact

Table 11. Mass

	kg	metric tonne	oz	lbm	short ton	long ton	slug
kilogram (kg)	1	*1x10^{-3}	35.27	2.205	1.102x10^{-3}	9.842x10^{-4}	6.852x10^{-2}
metric tonne (t)	*1000	1	3.527x10^4	2205	1.102	0.9842	68.52
avoirdupois ounce (oz)	2.835x10^{-2}	2.835x10^{-5}	1	*0.0625	*3.125x10^{-5}	2.790x10^{-5}	1.943x10^{-3}
pound mass (lbm)	0.4536	4.536x10^{-4}	*16	1	*5.000x10^{-4}	4.464x10^{-4}	3.108x10^{-2}
short ton	907.2	9.072	*32000	*2000	1	0.8927	62.16
long ton	1016	1.016	*35840	*2240	*1.12	1	69.62
slug	14.59	1.459x10^{-2}	514.8	32.17	1.609x10^{-2}	1.436x10^{-2}	1

*Exact

Table 12. Density

	kg/m^3	g/cm^3	lb/ft^3	lb/gal	lb/bbl
kilogram per cubic meters (kg/m^3)	1	$*1x10^{-3}$	$6.243x10^{-2}$	$8.345x10^{-3}$	2.853
grams per cubic centimeters (g/cm^3)	*1000	1	62.43	8.345	350.5
pounds per cubic feet (lb/ft^3)	16.02	$1.602x10^{-2}$	1	0.1337	5.615
pounds per gallon (lb/gal)	119.8	0.1198	7.481	1	*42
pounds per barrel (lb/bbl)	2.853	$2.853x10^{-3}$	0.1781	$2.381x10^{-2}$	1

*Exact

Table 13. Time

	s	min	h	day	yr
mean solar second (s)	1	$1.6667x10^{-2}$	$2.7779x10^{-4}$	$1.15741x10^{-5}$	$3.1689x10^{-8}$
mean solar minute (min)	*60	1	$1.6667x10^{-2}$	$6.9444x10^{-4}$	$1.9013x10^{-6}$
mean solar hour (h)	*3600	*60	1	$4.16667x10^{-2}$	$1.1408x10^{-4}$
mean solar day	$*8.640x10^{4}$	*1440	*24	1	$2.7379x10^{-3}$
tropical time year (yr)	$3.1557x10^{7}$	$5.2595x10^{5}$	8765.8	365.24	1

*Exact

Table 14. Temperature (T)

	K	°C	°R	°F
kelvin (K)	1	K-273.15	K x 9/5	(K-273.15) x 9/5 +32
Celsius (°C)	°C + 273.15	1	(°C + 273.15) x 9/5	°C x 9/5 +32
Rankine (°R)	°R x 5/9	(°R x 5/9) -273.15	1	°R -459.67
Fahrenheit (°F)	(°F + 459.67) x 5/9	(°F - 32) x 5/9	°F + 459.67	1

Table 15. Specific Activity(1)

	Bq	Ci	kg
becquerel (Bq)	1	2.703×10^{-11}	$\frac{\ln^2}{t_{1/2}} \times \frac{6.022 \times 10^{23}}{M} \times \frac{10^3 g}{kg} = \frac{4.174 \times 10^{26}}{t_{1/2} \times M}$
curie (Ci)	*3.7×10^{10}	1	$\frac{1.128 \times 10^{16}}{t_{1/2} \times M}$
kg	$2.396 \times 10^{-27} \times t_{1/2}^{(2)} \times M^{(3)}$	$8.864 \times 10^{-17} \times t_{1/2} \times M$	1

(1) Specific Activity is $\frac{ds_A}{s_A}$; where $s_A = s_{OA} e^{-\lambda t}$; $\frac{\lambda = \ln^2}{t_{1/2}}$

(2) $t_{1/2}$ is half life in seconds

(3) M is gram molecular weight (g/mol)

*Exact

Table 16. Miscellaneous

To convert:	to	Multiply by	Inverse
1. Angular velocity rad/s	rpm	$\frac{30}{\pi} = 9.549$	$\frac{\pi}{30} = 0.1047$
2. Radioactivity			
a. Dose equivalent Sv	rem	100	0.01
b. Absorbed dose Gy (gray) (1J/kg)	rad	100	0.01
c. Activity (1 disintegration/s) becquerel (Bq)	Ci	2.703×10^{-11}	3.7×10^{10}
d. Charge roentgen (R)	c/kg	2.58×10^{-4}	3876

Distribution

FEDERAL AGENCIES

U. S. Department of Energy (4)
Office of Environmental Restoration
and Waste Management
Attn: L. P. Duffy, EM-1
J. E. Lytle, EM-30
S. Schneider, EM-342
C. Frank, EM-50
Washington, DC 20585

U.S. Department of Energy (5)
WIPP Task Force
Attn: M. Frei, EM-34 (2)
G. H. Daly
S. Fucigna
J. Rhoderick
12800 Middlebrook Rd.
Suite 400
Germantown, MD 20874

U.S. Department of Energy (4)
Office of Environment, Safety and
Health
Attn: R. P. Berube, EH-20
C. Borgstrum, EH-25
R. Pelletier, EH-231
K. Taimi, EH-232
Washington, DC 20585

U. S. Department of Energy (4)
WIPP Project Integration Office
Attn: W. J. Arthur III
L. W. Gage
P. J. Higgins
D. A. Olona
P.O. Box 5400
Albuquerque, NM 87115-5400

U. S. Department of Energy (12)
WIPP Project Site Office (Carlsbad)
Attn: A. Hunt (4)
M. McFadden
V. Daub (4)
J. Lippis
K. Hunter
R. Becker
P.O. Box 3090
Carlsbad, NM 88221-3090

U. S. Department of Energy, (5)
Office of Civilian Radioactive Waste
Management
Attn: Deputy Director, RW-2
Associate Director, RW-10
Office of Program
Administration and
Resources Management
Associate Director, RW-20
Office of Facilities
Siting and
Development
Associate Director, RW-30
Office of Systems
Integration and
Regulations
Associate Director, RW-40
Office of External
Relations and Policy
Office of Geologic Repositories
Forrestal Building
Washington, DC 20585

U. S. Department of Energy
Attn: National Atomic Museum Library
Albuquerque Operations Office
P.O. Box 5400
Albuquerque, NM 87185

U. S. Department of Energy
Research & Waste Management Division
Attn: Director
P.O. Box E
Oak Ridge, TN 37831

U. S. Department of Energy (2)
Idaho Operations Office
Fuel Processing and Waste
Management Division
785 DOE Place
Idaho Falls, ID 83402

U.S. Department of Energy
Savannah River Operations Office
Defense Waste Processing
Facility Project Office
Attn: W. D. Pearson
P.O. Box A
Aiken, SC 29802

U.S. Department of Energy (2)
Richland Operations Office
Nuclear Fuel Cycle & Production Division
Attn: R. E. Gerton
825 Jadwin Ave.
P.O. Box 500
Richland, WA 99352

U.S. Department of Energy (3)
Nevada Operations Office
Attn: J. R. Boland
D. Livingston
P. K. Fitzsimmons
2753 S. Highland Drive
Las Vegas, NV 87183-8518

U.S. Department of Energy (2)
Technical Information Center
P.O. Box 62
Oak Ridge, TN 37831

U.S. Department of Energy (2)
Chicago Operations Office
Attn: J. C. Haugen
9800 South Cass Avenue
Argonne, IL 60439

U.S. Department of Energy
Los Alamos Area Office
528 35th Street
Los Alamos, NM 87544

U.S. Department of Energy (3)
Rocky Flats Area Office
Attn: W. C. Rask
G. Huffman
T. Lukow
P.O. Box 928
Golden, CO 80402-0928

U.S. Department of Energy
Dayton Area Office
Attn: R. Grandfield
P.O. Box 66
Miamisburg, OH 45343-0066

U.S. Department of Energy
Attn: E. Young
Room E-178
GAO/RCED/GTN
Washington, DC 20545

U.S. Bureau of Land Management
101 E. Mermod
Carlsbad, NM 88220

U.S. Bureau of Land Management
New Mexico State Office
P.O. Box 1449
Santa Fe, NM 87507

U.S. Environmental Protection Agency (2)
Office of Radiation Protection Programs (ANR-460)
Attn: Richard Guimond (2)
Washington, D.C. 20460

U.S. Nuclear Regulatory Commission
Division of Waste Management
Attn: H. Marson
Mail Stop 4-H-3
Washington, DC 20555

U.S. Nuclear Regulatory Commission (4)
Advisory Committee on Nuclear Waste
Attn: Dade Moeller
Martin J. Steindler
Paul W. Pomeroy
William J. Hinze
7920 Norfolk Avenue
Bethesda, MD 20814

Defense Nuclear Facilities Safety Board
Attn: Dermot Winters
625 Indiana Avenue NW
Suite 700
Washington, DC 20004

Nuclear Waste Technical Review Board (2)
Attn: Dr. Don A. Deere
Dr. Sidney J. S. Parry
Suite 910
1100 Wilson Blvd.
Arlington, VA 22209-2297

Katherine Yuracko
Energy and Science Division
Office of Management and Budget
725 17th Street NW
Washington, DC 20503

U.S. Geological Survey (2)
Water Resources Division
Attn: Cathy Peters
Suite 200
4501 Indian School, NE
Albuquerque, NM 87110

INSTITUTIONAL DISTRIBUTION

NEW MEXICO CONGRESSIONAL DELEGATION:

Jeff Bingaman
U.S. Senate
524 SHOB
Washington, DC 20510

Pete V. Domenici
U.S. Senate
427 SDOB
Washington, DC 20510

Bill Richardson
House of Representatives
332 CHOB
Washington, DC 20510

Steven H. Schiff
House of Representatives
1520 LHOB
Washington, DC 20510

Joe Skeen
House of Representatives
1007 LHOB
Washington, DC 20510

STATE AGENCIES

Environmental Evaluation Group (5)
Attn: Robert Neill
Suite F-2
7007 Wyoming Blvd., N.E.
Albuquerque, NM 87109

New Mexico Bureau of Mines
and Mineral Resources
Socorro, NM 87801

New Mexico Department of Energy &
Minerals
Attn: Librarian
2040 S. Pacheco
Santa Fe, NM 87505

New Mexico Radioactive Task Force (2)
(Governor's WIPP Task Force)
Attn: Anita Lockwood, Chairman
Chris Wentz, Coordinator/Policy
Analyst
2040 Pacheco
Santa Fe, NM 87505

Bob Forrest
Mayor, City of Carlsbad
P.O. Box 1569
Carlsbad, NM 88221

Chuck Bernard
Executive Director
Carlsbad Department of Development
P.O. Box 1090
Carlsbad, NM 88221

Robert M. Hawk (2)
Chairman, Hazardous and Radioactive
Materials Committee
Room 334
State Capitol
Sante Fe, NM 87503

New Mexico Environment Department
Secretary of the Environment
Attn: J. Espinosa (3)
P.O. Box 968
1190 St. Francis Drive
Santa Fe, NM 87503-0968

New Mexico Environment Department
Attn: Pat McCausland
WIPP Project Site Office
P.O. Box 3090
Carlsbad, NM 88221-3090

ADVISORY COMMITTEE ON NUCLEAR FACILITY SAFETY

John F. Ahearne
Executive Director, Sigma Xi
99 Alexander Drive
Research Triangle Park, NC 27709

James E. Martin
109 Observatory Road
Ann Arbor, MI 48109

Dr. Gerald Tape
Assoc. Universities
1717 Massachusetts Ave. NW
Suite 603
Washington, DC 20036

WIPP PANEL OF NATIONAL RESEARCH COUNCIL'S BOARD ON RADIOACTIVE WASTE MANAGEMENT

Charles Fairhurst, Chairman
Department of Civil and
Mineral Engineering
University of Minnesota
500 Pillsbury Dr. SE
Minneapolis, MN 55455-0220

John O. Blomeke
3833 Sandy Shore Drive
Lenoir City, TN 37771-9803

John D. Bredehoeft
Western Region Hydrologist
Water Resources Division
U.S. Geological Survey (M/S 439)
345 Middlefield Road
Menlo Park, CA 94025

Fred M. Ernsberger
1325 NW 10th Avenue
Gainsville, FL 32601

Rodney C. Ewing
Department of Geology
University of New Mexico
200 Yale, NE
Albuquerque, NM 87131

B. John Garrick
Pickard, Lowe & Garrick, Inc.
2260 University Drive
Newport Beach, CA 92660

Leonard F. Konikow
U.S. Geological Survey
431 National Center
Reston, VA 22092

Jeremiah O'Driscoll
505 Valley Hill Drive
Atlanta, GA 30350

Christopher Whipple
Clement International Corp.
160 Spear St.
Suite 1380
San Francisco, CA 94105-1535

National Research Council (3)
Board on Radioactive
Waste Management
RM HA456
Attn: Peter B. Myers, Staff Director (2)
Dr. Geraldine J. Grube
2101 Constitution Avenue
Washington, DC 20418

PERFORMANCE ASSESSMENT PEER REVIEW PANEL

G. Ross Heath
College of Ocean and
Fishery Sciences HN-15
583 Henderson Hall
University of Washington
Seattle, WA 98195

Thomas H. Pigford
Department of Nuclear Engineering
4159 Etcheverry Hall
University of California
Berkeley, CA 94720

Thomas A. Cotton
JK Research Associates, Inc.
4429 Butterworth Place, NW
Washington, DC 20016

Robert J. Budnitz
President, Future Resources
Associates, Inc.
2000 Center Street
Suite 418
Berkeley, CA 94704

C. John Mann
Department of Geology
245 Natural History Bldg.
1301 West Green Street
University of Illinois
Urbana, IL 61801

Frank W. Schwartz
Department of Geology and Mineralogy
The Ohio State University
Scott Hall
1090 Carmack Rd.
Columbus, OH 43210

FUTURE SOCIETIES EXPERT PANEL

Theodore S. Glickman
Resources for the Future
1616 P St., NW
Washington, DC 20036

Norman Rosenberg
Resources for the Future
1616 P St., NW
Washington, DC 20036

Max Singer
The Potomac Organization, Inc.
5400 Greystone St.
Chevy Chase, MD 20815

Maris Vinovskis
Institute for Social Research
Room 4086
University of Michigan
426 Thompson St
Ann Arbor, MI 48109-1045

Gregory Benford
University of California, Irvine
Department of Physics
Irvine, CA 92717

Craig Kirkwood
College of Business Administration
Arizona State University
Tempe, AZ 85287

Harry Otway
Health, Safety, and Envir. Div.
Mail Stop K-491
Los Alamos National Laboratory
Los Alamos, NM 87545

Martin J. Pasqualetti
Department of Geography
Arizona State University
Tempe, AZ 85287-3806

Michael Baram
Bracken and Baram
33 Mount Vernon St.
Boston, MA 02108

Wendell Bell
Department of Sociology
Yale University
1965 Yale Station
New Haven, CT 06520

Bernard L. Cohen
Department of Physics
University of Pittsburgh
Pittsburgh, PA 15260

Ted Gordon
The Futures Group
80 Glastonbury Blvd.
Glastonbury, CT 06033

Duane Chapman
5025 S. Building, Room S5119
The World Bank
1818 H Street NW
Washington, DC 20433

Victor Ferkiss
23 Sage Brush Circle
Corrales, NM 87048

Dan Reicher
Senior Attorney
Natural Resources Defense Council
1350 New York Ave. NW, #300
Washington, DC 20005

Theodore Taylor
P.O. Box 39
3383 Weatherby Rd.
West Clarksville, NY 14786

MARKERS EXPERT PANEL

Dr. Dieter Ast
Department of Materials Science
Bard Hall
Cornell University
Ithaca, NY 14853-1501

Dr. Victor Baker
Department of Geosciences
Building #77, Gould-Simpson Building
University of Arizona
Tucson, AZ 85721

Mr. Michael Brill
President
BOSTI
1479 Hertel Ave.
Buffalo, NY 14216

Dr. Frank Drake
Board of Studies in Astronomy and
Astrophysics
Lick Observatory
University of California, Santa Cruz
Santa Cruz, CA 95064

Dr. Ben Finney
University of Hawaii at Manoa
Department of Anthropology
Porteus Hall 346, 2424 Maile Way
Honolulu, HI 96822

Dr. David Givens
American Anthropological Association
1703 New Hampshire Ave., NW
Washington, D.C. 20009

Dr. Ward Goodenough
Department of Anthropology
University of Pennsylvania
325 University Museum
33rd and Spruce Streets
Philadelphia, PA 19104-6398

Dr. Maureen Kaplan
Eastern Research Group, Inc.
6 Whittemore Street
Arlington, MA 02174

Mr. Jon Lomberg
P.O. Box 207
Honaunau, HI 96726

Dr. Louis Narens
Department of Cognitive Sciences
School of Social Sciences
University of Califorrnia, Irvine
Irvine, CA 92717

Dr. Frederick Newmeyer
Department of Linguistics
GN-40
University of Washington
Seattle, WA 98195

Dr. Woodruff Sullivan
Department of Astonomy
FM-20
University of Washington
Seattle, WA 98195

Dr. Wendell Williams
Materials Science and Engineering
White Building
Case Western Reserve University
Cleveland, OH 44106

NATIONAL LABORATORIES

Argonne National Labs (2)
Attn: A. Smith
D. Tomasko
9700 South Cass, Bldg. 201
Argonne, IL 60439

Battelle Pacific Northwest Laboratories (3)
Attn: R. E. Westerman
S. Bates
H. C. Burkholder
Battelle Boulevard
Richland, WA 99352

Lawrence Livermore National Laboratory
Attn: G. Mackanic
P.O. Box 808, MS L-192
Livermore, CA 94550

Los Alamos National Laboratories
Attn: B. Erdal, CNC-11
P.O. Box 1663
Los Alamos, NM 87544

Los Alamos National Laboratories
Attn: A. Meijer
Mail Stop J514
Los Alamos, NM 87545

Los Alamos National Laboratories (3)
HSE-8
Attn: M. Enoris
L. Soholt
J. Wenzel
P.O. Box 1663
Los Alamos, NM 87544

Los Alamos National Laboratories (2)
HSE-7
Attn: A. Drypolcher
S. Kosciewiscz
P.O. Box 1663
Los Alamos, NM 87544

Oak Ridge National Labs
Martin Marietta Systems, Inc.
Attn: J. Setaro
P.O. Box 2008, Bldg. 3047
Oak Ridge, TN 37831-6019

Savannah River Laboratory (3)
Attn: N. Bibler
M. J. Plodinec
G. G. Wicks
Aiken, SC 29801

Savannah River Plant (2)
Attn: Richard G. Baxter
Building 704-S
K. W. Wierzbicki
Building 703-H
Aiken, SC 29808-0001

CORPORATIONS/MEMBERS OF THE PUBLIC

Benchmark Environmental Corp. (3)
Attn: John Hart
C. Frederickson
K. Lickliter
4501 Indian School Rd., NE
Suite 105
Albuquerque, NM 87110

Deuel and Associates, Inc.
Attn: R. W. Prindle
7208 Jefferson, NE
Albuquerque, NM 87109

Disposal Safety, Inc.
Attn: Benjamin Ross
Suite 314
1660 L Street NW
Washington, DC 20006

Ecodynamics Research Associates (2)
Attn: Pat Roache
Rebecca Blaine
P.O. Box 8172
Albuquerque, NM 87198

E G & G Idaho (3)
1955 Fremont Street
Attn: C. Atwood
C. Hertzler
T. I. Clements
Idaho Falls, ID 83415

Geomatrix
Attn: Kevin Coppersmith
100 Pine Street #1000
San Francisco, CA 94111

Golden Associates, Inc. (3)
Attn: Mark Cunnane
Richard Kossik
Ian Miller
4104 148th Avenue NE
Redmond, WA 98052

In-Situ, Inc. (2)
Attn: S. C. Way
C. McKee
209 Grand Avenue
Laramie, WY 82070

INTERA, Inc.
Attn: A. M. LaVenue
8100 Mountain Road NE
Suite 213
Albuquerque, NM 87110

INTERA, Inc.
Attn: J. F. Pickens
Suite #300
6850 Austin Center Blvd.
Austin, TX 78731

INTERA, Inc.
Attn: Wayne Stensrud
P.O. Box 2123
Carlsbad, NM 88221

INTERA, Inc.
Attn: William Nelson
101 Convention Center Drive
Suite 540
Las Vegas, NV 89109

IT Corporation (2)
Attn: P. Drez
J. Myers
Regional Office - Suite 700
5301 Central Avenue, NE
Albuquerque, NM 87108

IT Corporation
R. J. Eastmond
825 Jadwin Ave.
Richland, WA 99352

MACTEC (2)
Attn: J. A. Thies
D. K. Duncan
8418 Zuni Road SE
Suite 200
Albuquerque, NM 87108

Pacific Northwest Laboratory
Attn: Bill Kennedy
Battelle Blvd.
P.O. Box 999
Richland, WA 99352

RE/SPEC, Inc. (2)
Attn: W. Coons
Suite 300
4775 Indian School NE
Albuquerque, NM 87110

RE/SPEC, Inc.
Attn: J. L. Ratigan
P.O. Box 725
Rapid City, SD 57709

Reynolds Elect/Engr. Co., Inc.
Building 790, Warehouse Row
Attn: E. W. Kendall
P.O. Box 98521
Las Vegas, NV 89193-8521

Roy F. Weston, Inc.
CRWM Tech. Supp. Team
Attn: Clifford J. Noronha
955 L'Enfant Plaza, S.W.
North Building, Eighth Floor
Washington, DC 20024

Science Applications International Corporation
Attn: Howard R. Pratt,
Senior Vice President
10260 Campus Point Drive
San Diego, CA 92121

Science Applications International Corporation (2)
Attn: George Dymmel
Chris G. Pflum
101 Convention Center Dr.
Las Vegas, NV 89109

Science Applications International Corporation (2)
Attn: John Young
Dave Lester
18706 North Creek Parkway
Suite 110
Bothell, WA 98011

Southwest Research Institute
Center for Nuclear Waste Regulatory Analysis (2)
Attn: P. K. Nair
6220 Culebra Road
San Antonio, Texas 78228-0510

Systems, Science, and Software (2)
Attn: E. Peterson
P. Lagus
Box 1620
La Jolla, CA 92038

TASC
Attn: Steven G. Oston
55 Walkers Brook Drive
Reading, MA 01867

Tech. Reps., Inc. (5)
Attn: Janet Chapman
Terry Cameron
Debbie Marchand
John Stikar
Denise Bissell
5000 Marble NE
Suite 222
Albuquerque, NM 87110

Tolan, Beeson, & Associates
Attn: Terry L. Tolan
2320 W. 15th Avenue
Kennewick, WA 99337

TRW Environmental Safety Systems (TESS)
Attn: Ivan Saks
10306 Eaton Place
Suite 300
Fairfax, VA 22030

Westinghouse Electric Corporation (4)
Attn: Library
L. Trego
C. Cox
L. Fitch
R. F. Kehrman
P.O. Box 2078
Carlsbad, NM 88221

Westinghouse Hanford Company
Attn: Don Wood
P.O. Box 1970
Richland, WA 99352

Western Water Consultants
Attn: D. Fritz
1949 Sugarland Drive #134
Sheridan, WY 82801-5720

Western Water Consultants
Attn: P. A. Rechard
P.O. Box 4128
Laramie, WY 82071

Neville Cook
Rock Mechanics Engineering
Mine Engineering Dept.
University of California
Berkeley, CA 94720

Dennis W. Powers
Star Route Box 87
Anthony, TX 79821

Shirley Thieda
P.O. Box 2109, RR1
Bernalillo, NM 87004

Jack Urich
c/o CARD
144 Harvard SE
Albuquerque, NM 87106

UNIVERSITIES

University of California
Mechanical, Aerospace, and
Nuclear Engineering Department (2)
Attn: W. Kastenberg
D. Browne
5532 Boelter Hall
Los Angeles, CA 90024

University of Hawaii at Hilo
Attn: S. Hora
Business Administration
Hilo, HI 96720-4091

University of New Mexico
Geology Department
Attn: Library
Albuquerque, NM 87131

University of New Mexico
Research Administration
Attn: H. Schreyer
102 Scholes Hall
Albuquerque, NM 87131

University of Wyoming
Department of Civil Engineering
Attn: V. R. Hasfurther
Laramie, WY 82071

University of Wyoming
Department of Geology
Attn: J. I. Drever
Laramie, WY 82071

University of Wyoming
Department of Mathematics
Attn: R. E. Ewing
Laramie, WY 82071

LIBRARIES

Thomas Brannigan Library
Attn: Don Dresp, Head Librarian
106 W. Hadley St.
Las Cruces, NM 88001

Hobbs Public Library
Attn: Marcia Lewis, Librarian
509 N. Ship Street
Hobbs, NM 88248

New Mexico State Library
Attn: Norma McCallan
325 Don Gaspar
Santa Fe, NM 87503

New Mexico Tech
Martin Speere Memorial Library
Campus Street
Socorro, NM 87810

New Mexico Junior College
Pannell Library
Attn: Ruth Hill
Lovington Highway
Hobbs, NM 88240

Carlsbad Municipal Library
WIPP Public Reading Room
Attn: Lee Hubbard, Head Librarian
101 S. Halagueno St.
Carlsbad, NM 88220

University of New Mexico
General Library
Government Publications Department
Albuquerque, NM 87131

NEA/PSAC USER'S GROUP

Timo K. Vieno
Technical Research Centre of Finland (VTT)
Nuclear Engineering Laboratory
P.O. Box 169
SF-00181 Helsinki
FINLAND

Alexander Nies (PSAC Chairman)
Gesellschaft für Strahlen- und
Institut für Tieflagerung
Abteilung für Endlagersicherheit
Theodor-Heuss-Strasse 4
D-3300 Braunscheweig
GERMANY

Eduard Hofer
Gesellschaft für Reaktorsicherheit (GRS)
MBH
Forschungsgelände
D-8046 Garching
GERMANY

Takashi Sasahara
Environmental Assessment Laboratory
Department of Environmental Safety Research
Nuclear Safety Research Center,
Tokai Research Establishment, JAERI
Tokai-mura, Naka-gun
Ibaraki-ken
JAPAN

Alejandro Alonso
Cátedra de Tecnología Nuclear
E.T.S. de Ingenieros Industriales
José Gutiérrez Abascal, 2
E-28006 Madrid
SPAIN

Pedro Prado
CIEMAT
Instituto de Tecnología Nuclear
Avenida Complutense, 22
E-28040 Madrid
SPAIN

Miguel Angel Cuñado
ENRESA
Emilio Vargas, 7
E-28043 Madrid
SPAIN

Francisco Javier Elorza
ENRESA
Emilio Vargas, 7
E-28043 Madrid
SPAIN

Nils A. Kjellbert
Swedish Nuclear Fuel and Waste Management Company (SKB)
Box 5864
S-102 48 Stockholm
SWEDEN

Björn Cronhjort
Swedish National Board for Spent Nuclear Fuel (SKN)
Sehlsedtsgatan 9
S-115 28 Stockholm
SWEDEN

Richard A. Klos
Paul-Scherrer Institute (PSI)
CH-5232 Villingen PSI
SWITZERLAND

NAGRA (2)
Attn: Charles McCombie
Fritz Van Dorp
Parkstrasse 23
CH-5401 Baden
SWITZERLAND

Brian G. J. Thompson
Department of the Environment
Her Majesty's Inspectorate of Pollution
Room A5.33, Romney House
43 Marsham Street
London SW1P 2PY
UNITED KINGDOM

INTERA/ECL (2)
Attn: Trevor J. Sumerling
Daniel A. Galson
Chiltern House
45 Station Road
Henley-on-Thames
Oxfordshire RG9 1AT
UNITED KINGDOM

U.S. Nuclear Regulatory Commission (2)
Attn: Richard Codell
Norm Eisenberg
Mail Stop 4-H-3
Washington, D.C. 20555

Paul W. Eslinger
Battelle Pacific Northwest Laboratories (PNL)
P.O. Box 999, MS K2-32
Richland, WA 99352

Andrea Saltelli
Commission of the European Communities
Joint Resarch Centre od Ispra
I-21020 Ispra (Varese)
ITALY

Budhi Sagar
Center for Nuclear Waste Regulatory Analysis (CNWRA)
Southwest Research Institute
P.O. Drawer 28510
6220 Culebra Road
San Antonio, TX 78284

Shaheed Hossain
Division of Nuclear Fuel Cycle and Waste Management
International Atomic Energy Agency
Wagramerstrasse 5
P.O. Box 100
A-1400 Vienna
AUSTRIA

Claudio Pescatore
Division of Radiation Protection and Waste Management
38, Boulevard Suchet
F-75016 Paris
FRANCE

FOREIGN ADDRESSES

Studiecentrum Voor Kernenergie
Centre D'Energie Nucleaire
Attn: A. Bonne
SCK/CEN
Boeretang 200
B-2400 Mol
BELGIUM

Atomic Energy of Canada, Ltd. (3)
Whiteshell Research Estab.
Attn: Michael E. Stevens
Bruce W. Goodwin
Donna Wushke
Pinewa, Manitoba
ROE 1L0
CANADA

Ghislain de Marsily
Lab. Géologie Appliqué
Tour 26, 5 étage
4 Place Jussieu
F-75252 Paris Cedex 05
FRANCE

Jean-Pierre Olivier
OECD Nuclear Energy Agency (2)
38, Boulevard Suchet
F-75016 Paris
FRANCE

D. Alexandre, Deputy Director
ANDRA
31 Rue de la Federation
75015 Paris
FRANCE

Claude Sombret
Centre D'Etudes Nucleaires
De La Vallee Rhone
CEN/VALRHO
S.D.H.A. BP 171
30205 Bagnols-Sur-Ceze
FRANCE

Bundesministerium fur Forschung und Technologie
Postfach 200 706
5300 Bonn 2
GERMANY

Bundesanstalt fur Geowissenschaften und Rohstoffe
Attn: Michael Langer
Postfach 510 153
3000 Hannover 51
GERMANY

Gesellschaft fur Reaktorsicherheit (GRS) mb (2)
Attn: Bruno Baltes
Wolfgang Muller
Schwertnergasse 1
D-5000 Cologne
GERMANY

Hahn-Mietner-Institut fur Kernforschung
Attn: Werner Lutze
Glienicker Strasse 100
100 Berlin 39
GERMANY

Institut fur Tieflagerung (2)
Attn: K. Kuhn
Theodor-Heuss-Strasse 4
D-3300 Braunschweig
GERMANY

Physikalisch-Technische Bundesanstalt
Attn: Peter Brenneke
Postfach 33 45
D-3300 Braunschweig
GERMANY

Shingo Tashiro
Japan Atomic Energy Research Institute
Tokai-Mura, Ibaraki-Ken
319-11
JAPAN

Netherlands Energy Research Foundation
ECN
Attn: L. H. Vons
3 Westerduinweg
P.O. Box 1
1755 ZG Petten
THE NETHERLANDS

Johan Andersson
Statens Kärnkraftinspektion
SKI
Box 27106
S-102 52 Stockholm
SWEDEN

Fred Karlsson
Svensk Karnbransleforsorjning AB
SKB
Box 5864
S-102 48 Stockholm
SWEDEN

Nationale Genossenschaft fur die Lagerung
Radioaktiver Abfalle (NAGRA) (2)
Attn: Stratis Vomvoris
Piet Zuidema
Hardstrasse 73
CH-5430 Wettingen
SWITZERLAND

D. R. Knowles
British Nuclear Fuels, plc
Risley, Warrington, Cheshire WA3 6AS
1002607 UNITED KINGDOM

AEA Technology
Attn: J.H. Rees
D5W/29 Culham Laboratory
Abington
Oxfordshire OX14 3DB
UNITED KINGDOM

AEA Technology
Attn: W. R. Rodwell
O44/A31 Winfrith Technical Centre
Dorchester
Dorset DT2 8DH
UNITED KINGDOM

AEA Technology
Attn: J. E. Tinson
B4244 Harwell Laboratory
Didcot
Oxfordshire OX11 ORA
UNITED KINGDOM

INTERNAL

1 A. Narath
20 O. E. Jones
1510 J. C. Cummings
1511 D. K. Gartling
3151 S. M. Wayland
3200 N. R. Ortiz
6000 D. L. Hartley
6233 J. C. Eichelberger
6300 T. O. Hunter
6301 E. Bonano
6310 T. E. Blejwas, Acting
6313 L. E. Shephard
6312 F. W. Bingham
6313 L. S. Costin
6315 Supervisor
6316 R. P. Sandoval
6320 R. E. Luna, Acting
6340 W. D. Weart
6340 S. Y. Pickering
6341 J. M. Covan
6341 D. P. Garber
6341 R. C. Lincoln
6341 J. Orona*
6341 Sandia WIPP Central Files (250)
6342 D. R. Anderson
6342 B. M. Butcher
6342 D. P. Gallegos
6342 L. S. Gomez
6342 M. Gruebel
6342 R. Guzowski
6342 R. D. Klett
6342 M. G. Marietta
6342 D. Morrison
6342 A. C. Peterson
6342 R. P. Rechard
6342 P. Swift
6342 M. Tierney
6342 K. M. Trauth
6342 B. L. Baker*
6342 J. Bean*
6342 J. Berglund*
6342 W. Beyeler*
6342 T. Blaine*
6342 K. Brinster*
6342 K. Byle*
6342 L. Clements*
6342 J. Garner*
6342 A. Gilkey*
6342 H. Iuzzolino*
6342 J. Logothetis*
6342 R. McCurley*
6342 J. Rath*
6342 D. Rudeen*
6342 J. Sandha*
6342 J. Schreiber*
6342 P. Vaughn*
6343 T. M. Schultheis
6344 R. L. Beauheim
6344 P. B. Davies
6344 S. J. Finley
6344 E. Gorham
6344 C. F. Novak
6344 S. W. Webb
6345 R. Beraun
6345 L. Brush
6345 A. R. Lappin
6345 M. A. Molecke
6346 D. E. Munson
6346 E. J. Nowak
6346 J. R. Tillerson
6347 A. L. Stevens
6400 D. J. McCloskey
6413 J. C. Helton
6415 R. M. Cranwell
6415 C. Leigh
6415 R. L. Iman
6622 M.S.Y. Chu
9300 J. E. Powell
9310 J. D. Plimpton
9325 J. T. McIlmoyle
9325 R. L. Rutter
9330 J. D. Kennedy
8523-2 Central Technical Files
3141 S. A. Landenberger (5)
3145 Document Processing (8) for DOE/OSTI
3151 G. C. Claycomb (3)

*6342/Geo-Centers

☆ U.S. GOVERNMENT PRINTING OFFICE: 1991—673-122/60034

SANDIA REPORT

SAND91—0893/4 • UC—721
Unlimited Release
Printed April 1992

Preliminary Comparison with 40 CFR Part 191, Subpart B for the Waste Isolation Pilot Plant, December 1991

Volume 4: Uncertainty and Sensitivity Analysis Results

J. C. Helton, J. W. Garner, R. P. Rechard, D. K. Rudeen, P. N. Swift

Prepared by
Sandia National Laboratories
Albuquerque, New Mexico 87185 and Livermore, California 94550
for the United States Department of Energy
under Contract DE-AC04-76DP00789

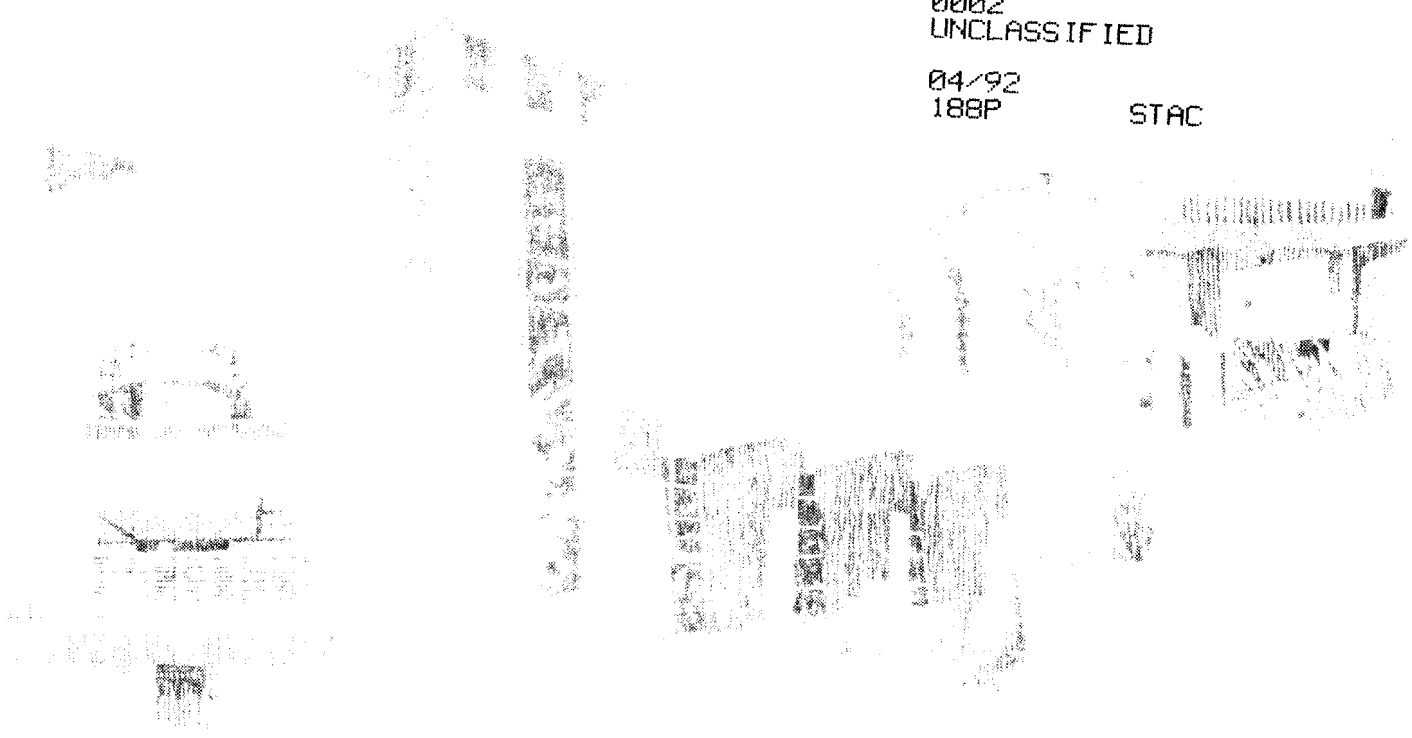

Issued by Sandia National Laboratories, operated for the United States Department of Energy by Sandia Corporation.

Available to DOE and DOE contractors from
Office of Scientific and Technical Information
PO Box 62
Oak Ridge, TN 37831

Prices available from (615) 576-8401, FTS 626-8401

Available to the public from
National Technical Information Service
US Department of Commerce
5285 Port Royal Rd
Springfield, VA 22161

NTIS price codes
Printed copy: A10
Microfiche copy: A01

SAND91-0893/4
Unlimited Release
Printed April 1992

Distribution
Category UC-721

PRELIMINARY COMPARISON WITH 40 CFR PART 191, SUBPART B FOR THE WASTE ISOLATION PILOT PLANT, DECEMBER 1991

VOLUME 4: UNCERTAINTY AND SENSITIVITY ANALYSIS RESULTS

Jon C. Helton[1]
James W. Garner[2], Rob P. Rechard,
David K. Rudeen[3], Peter N. Swift[4]
WIPP Performance Assessment Division
Sandia National Laboratories
Albuquerque, New Mexico 87185

ABSTRACT

The most appropriate conceptual model for performance assessment at the Waste Isolation Pilot Plant (WIPP) is believed to include gas generation due to corrosion and microbial action in the repository and a dual-porosity (matrix and fracture porosity) representation for solute transport in the Culebra Dolomite Member of the Rustler Formation. Under these assumptions, complementary cumulative distribution functions (CCDFs) summarizing radionuclide releases to the accessible environment due to both cuttings removal and groundwater transport fall substantially below the release limits promulgated by the Environmental Protection Agency (EPA). This is the case even when the current estimates of the uncertainty in analysis inputs are incorporated into the performance assessment. The best-estimate performance-assessment results are dominated by cuttings removal. The releases to the accessible environment due to groundwater transport make very small contributions to the total release. The variability in the distribution of CCDFs that must be considered in comparisons with the EPA release limits is dominated by the variable LAMBDA (rate constant in Poisson model for drilling

---

[1] Arizona State University, Department of Mathematics, Tempe, AZ 85287
[2] Applied Physics, Inc., Albuquerque, NM 87109
[3] New Mexico Engineering Research Institute, Albuquerque, NM 87131
[4] Tech Reps, Inc, Albuquerque, NM 87110

intrusions). The variability in releases to the accessible environment due to individual drilling intrusions is dominated by DBDIAM (drill bit diameter). Most of the imprecisely known variables considered in the 1991 WIPP performance assessment relate to radionuclide releases to the accessible environment due to groundwater transport. For a single borehole (i.e., an E2-type scenario), whether or not a release from the repository to the Culebra even occurs is controlled by the variable SALPERM (Salado permeability), with no releases for small values (i.e., $< 5 \times 10^{-21}$ m^2) of this variable. When SALPERM is small, the repository never fills with brine and so there is no flow up an intruding borehole that can transport radionuclides to the Culebra. Further, releases that do reach the Culebra for larger values of SALPERM are small and usually do not reach the accessible environment. A potentially important scenario for the WIPP involves two or more boreholes through the same waste panel, of which at least one penetrates a pressurized brine pocket and at least one does not (i.e., an E1E2-type scenario). For these scenarios, the uncertainty in release to the Culebra is dominated by the variables BHPERM (borehole permeability), BPPRES (brine pocket pressure), and the solubilities for the individual elements (i.e., Am, Np, Pu, Th, U) in the projected radionuclide inventory for the WIPP. Once a release reaches the Culebra, the matrix distribution coefficients for the individual elements are important, with releases to the Culebra often failing to reach the accessible environment over the 10,000-yr period specified in the EPA regulations. To provide additional perspective, the following variants of the 1991 WIPP performance assessment have also been considered: (1) no gas generation in the repository and a dual-porosity transport model in the Culebra; (2) gas generation in the repository and a single-porosity (fracture porosity) transport model in the Culebra; (3) no gas generation in the repository and a single-porosity transport model in the Culebra; (4) gas generation in the repository and a dual-porosity transport model in the Culebra without chemical retardation; and (5) gas generation in the repository, a dual-porosity transport model in the Culebra, and extremes of climatic variation. All of these variations relate to groundwater transport and thus do not affect releases due to cuttings removal, which were found to dominate the results of the 1991 WIPP performance assessment. However, these variations do have the potential to increase the importance of releases due to groundwater transport relative to releases due to cuttings removal.

ACKNOWLEDGMENTS

The WIPP Performance Assessment Division is comprised of both Sandia and contractor employees working as a team to produce these annual preliminary comparisons with EPA regulations, assessments of overall long-term safety of the repository, and interim technical guidance to the program. The on-site team, affiliations, and contributions to the 1991 performance assessment are listed in alphabetical order:

Performance Assessment Division

Name	Affil.	Primary Author of Doc: Sect.	Major Code	Area of Responsibility
R. Anderson	SNL			Division Manager
B. Baker	TEC	V.2:§6.4		SECO2D, Hydrology, Office Manager
J. Bean	UNM	V.2:§4.2.1		BRAGFLO & BOASTII, 2-Phase Flow
J. Berglund	UNM	V.2:Ch.7 Editor V.2	CUTTINGS	Task Ldr., Undisturbed Repository, Cuttings/Cavings/ Engr. Mech.
W. Beyeler	SAI	V.2:§5.3; 6.1;6.3	PANEL GARFIELD	Geostatistics, Analytical Models, CAMCON Systems Codes
K. Brinster	SAI			Geohydrology, Conceptual Models
R. Blaine	ECO			SECO2D & CAMCON Systems Codes
T. Blaine	EPE			Drilling Technology, Exposure Pathways Data
J. Garner	API	V.2:§5.3	PANEL	Source Term, Sens. Anal.
A. Gilkey	UNM			CAMCON Systems Codes
L. Gomez	SNL			Task Ldr., Safety Assessments
M. Gruebel	TRI	V.1:Ch.1,2, 8,9,10		EPA Regulations
R. Guzowski	SAI	V.1:Ch.4		Geology, Scenario Construction
J. Helton	ASU	V.1:Ch.3,4 V.2:Ch.2,3	CCDFPERM	Task Ldr., Uncert./Sens. Anal., Probability Models
H. Iuzzolino	GC	Editor V.3	CCDFPERM	LHS & CAMCON System Codes
R. Klett	SNL			EPA Regulations
P. Knupp	ECO			STAFF2D & SECOTR, Comp. Fluid Dyn.
C. Leigh	SNL		GENII-S	Exposure Pathways
M. Marietta	SNL	Editor (Set)		Dep. Div. Manager, Tech. Coord.
G. de Marsily	UP	V.2:§6.2		Task Ldr., Geostatistics
R. McCurley	UNM	V.2:§4.2.3		SUTRA & CAMCON System Codes
A. Peterson	SNL	Editor V.3		Task Ldr., Inventory
J. Rath	UNM	V.2:§4.2.3		SUTRA, Engr. Mech.
R. Rechard	SNL	Editor V.2 & V.3		Task Ldr., CAMCON, QA, Ref. Data
P. Roache	ECO	V.2:§6.4	SECO	Task Ldr., Comp. Fluid Dyn.
D. Rudeen	UNM	V.2:§4.2.2; 6.5		STAFF2D, Transport
J. Sandha	SAI	Editor V.3		INGRES, PA Data Base
J. Schreiber	SAI	V.2:§4.2.1; 5.2.5 Editor V.3		BRAGFLO & BOASTII, 2-Phase Flow

P. Swift	TRI	V.1:Ch.5,11		Task Ldr., Geology, Climate Var.
M. Tierney	SNL	Editor V.3		Task Ldr., CDF Constr., Probability Models
K. Trauth	SNL			Task Ldr., Expert Panels
P. Vaughn	API	V.2:§5.1; 5.2;5.2.5; App.A	BRAGFLO	Task Ldr., 2-Phase Flow & Waste Panel Chemistry
J. Wormeck	ECO			Comp. Fluid Dyn. & Thermodyn.

The foundation of the annual WIPP performance assessment is the underlying data set and understanding of the important processes in the engineered and natural barrier systems. The SNL Nuclear Waste Technology Department is the primary source of these data and understanding. Assistance with the waste inventory comes from WEC and its contractors. We gratefully acknowledge the support of our departmental and project colleagues. Some individuals have worked closely with the performance assessment team, and we wish to acknowledge their contributions individually:

J. Ball	ReS	Computer System Manager
H. Batchelder	WEC	CH & RH Inventories
R. Beauheim	SNL	Natural Barrier System, Hydrologic Parameters
B. Butcher	SNL	Engineered Barrier System, Unmodified Waste-Form Parameters, Disposal Room Systems Parameters
L. Brush	SNL	Engineered Barrier System, Source Term (Solubility) and Gas Generation Parameters
L. Clements	ReS	Computer System Support
T. Corbet	SNL	Natural Barrier System, Geologic & Hydrologic Parameters, Conceptual Models
P. Davies	SNL	Natural Barrier System, Hydrologic & Transport Parameters, & 2-Phase Flow Mechanistic Modeling
P. Drez	IT	CH & RH Inventories
E. Gorham	SNL	Natural Barrier System, Fluid Flow & Transport Parameters
S. Howarth	SNL	Natural Barrier System, Hydrologic Parameters
R. Kehrman	WEC	CH & RH Waste Characterization
R. Lincoln	SNL	Project Integration
F. Mendenhall	SNL	Engineered Barrier System, Unmodified Waste Form Parameters, Waste Panel Closure (Expansion)
D. Munson	SNL	Reference Stratigraphy, Constitutive Models, Physical & Mechanical Parameters
E. Nowak	SNL	Shaft/Panel Seal Design, Seal Material Properties, Reliability
J. Orona	ReS	Computer System Support
J. Tillerson	SNL	Repository Isolation Systems Parameters
S. Webb	SNL	2-Phase Flow Sensitivity Analysis & Benchmarking

API = Applied Physics Incorporated
ASU = Arizona State University
ECO = Ecodynamics Research Associates
EPE = Epoch Engineering
GC = Geo-Centers Incorporated
IT = International Technology
ReS = ReSpec
SAI = Scientific Applications International Corporation
SNL = Sandia National Laboratories
TEC = Technadyne Engineering Consultants
TRI = Tech Reps, Inc.
UNM = Univ. of New Mexico/New Mexico Engineering Research Institute
UP = University of Paris
WEC = Westinghouse Electric Corporation

Peer Review

Internal/Sandia

T. Corbet	Vol. I, II, III
D. Gallegos	Vol. I, II, III
M. LaVenue	Vol. I, II, III
S. Hora	Vol. I, II, III
M. Marietta	Vol. IV
M. Tierney	Vol. IV

Management/Sandia

W. Weart
T. Hunter

PA Peer Review Panel

R. Heath, Chairman	University of Washington
R. Budnitz	Future Resources Associates, Inc.
T. Cotton	JK Research Associates, Inc.
J. Mann	University of Illinois
T. Pigford	University of California, Berkeley
F. Schwartz	Ohio State University

Department of Energy

R. Becker
J. Rhoderick
P. Higgins

Expert Panels

Futures

M. Baram	Boston University
W. Bell	Yale University
G. Benford	University of California, Irvine
D. Chapman	The World Bank, Cornell University
B. Cohen	University of Pittsburgh
V. Ferkiss	Georgetown University
T. Glickman	Resources for the Future
T. Gordon	Futures Group
C. Kirkwood	Arizona State University
H. Otway	Joint Research Center (Ispra), Los Alamos National Laboratory
M. Pasqualetti	Arizona State University
D. Reicher	Natural Resources Defense Council
N. Rosenberg	Resources for the Future
M. Singer	The Potomac Organization
T. Taylor	Consultant
M. Vinovski	University of Michigan

Source Term

C. Bruton	Lawrence Livermore National Laboratory
I-Ming Chou	U.S. Geological Survey
D. Hobart	Los Alamos National Laboratory
F. Millero	University of Miami

Retardation

R. Dosch	Sandia National Laboratories
C. Novak	Sandia National Laboratories
M. Siegel	Sandia National Laboratories

Geostatistics Expert Group

G. de Marsily, Chairman	University of Paris
R. Bras	Massachusetts Institute of Technology
J. Carrera	Universidad Politecnica de Cataluña
G. Dagan	Tel Aviv University
A. Galli	Ecole des Mines de Paris
A. Gutjahr	New Mexico Institute of Mining and Technology
D. McLaughlin	Massachusetts Institute of Technology
S. Neuman	University of Arizona
Y. Rubin	University of California, Berkeley

Report Preparation (TRI)

Editors:

Volume 1: M. Gruebel (text); S. Laundre-Woerner (illustrations)
Volume 2: D. Scott (text); D. Marchand (illustrations)
Volume 3: J. Chapman (text); D. Pulliam (illustrations)
Volume 4: D. Bissell (text); D. Marchand (illustrations)

D. Rivard, D. Miera, T. Allen, and the Word Processing Department
R. Rohac, R. Andree, and the Illustration and Computer Graphics Departments
S. Tullar and the Production Department

J. Stikar (compilation of PA Peer Review Panel comments)

CONTENTS

FIGURES

TABLES

1. INTRODUCTION

This volume is the fourth in a sequence of reports that document the December 1991 preliminary comparison with 40 CFR 191, Subpart B (the Standard; U.S. EPA, 1985) for the Waste Isolation Pilot Plant (WIPP). The three previous volumes describe the background of the project, the performance-assessment methodology, and the 1991 results (Volume 1); the probability and consequence models used in the calculations (Volume 2); and the reference data base (Volume 3). This volume contains the results of uncertainty and sensitivity analyses conducted using the methodology, modeling system, and data described in the earlier volumes. These analyses provide quantitative and qualitative insights on the relationships between uncertainty in the models and data used in the WIPP performance assessment and the resultant uncertainty in the results of the performance assessment.

Performance assessment for the WIPP is an annual iterative process, with each year's preliminary comparison building on the previous year's until a final defensible comparison with the Standard can be prepared. Results of this preliminary comparison cannot be used to evaluate compliance with the Standard because portions of the modeling system are still under development, data is insufficient in some areas, and the level of confidence in the estimated performance remains uncertain. The current status of the compliance-assessment system is summarized in Chapter 11 of Volume 1. A final evaluation of compliance also cannot be made at this time because the Standard was vacated by a Federal Court of Appeals in 1987, and has not been repromulgated by the Environmental Protection Agency (EPA). By agreement with the State of New Mexico, the Department of Energy (DOE) is evaluating compliance with the Standard as first promulgated until a revised Standard is available (U.S. DOE and State of New Mexico, 1981, as modified).

Uncertainty and sensitivity analysis is an important part of the WIPP performance assessment and contributes to the overall analysis in the following areas: (1) assessment of the uncertainty in performance-assessment results that must be used in comparison with regulatory standards, (2) identification of modeling areas where reductions in uncertainty can significantly improve the confidence that can be placed in performance-assessment results, and (3) verification that the models used within the performance-assessment process are operating properly.

This report is organized as follows. Chapter 2 provides an overview of the structure of the WIPP performance assessment. First, the Kaplan and Garrick ordered-triple representation for risk is introduced as the conceptual model for the overall structure of the WIPP performance assessment. Then, the

definition of scenarios, the determination of scenario probabilities, and the calculation of scenario consequences in the 1991 WIPP performance assessment are described in the context of this representation. The ordered-triple representation for risk facilitates the separation of stochastic and subjective uncertainty and leads naturally to complementary cumulative distribution functions (CCDFs) that are used in comparisons with the EPA Standard for releases to the accessible environment.

Chapter 3 discusses the 45 imprecisely known variables considered in the 1991 WIPP performance assessment and also summarizes the approach to uncertainty and sensitivity analysis being used. Specifically, a Monte Carlo approach to uncertainty/sensitivity involving the following steps is used in the 1991 WIPP performance assessment: (1) develop distributions characterizing the subjective uncertainty in the variables under consideration; (2) generate sample from variables according to their assigned distributions; (3) propagate sample through performance assessment; (4) summarize uncertainty analysis results with means and variances, distribution functions and box plots; and (5) determine sensitivity of performance-assessment results to the sampled variables with scatterplots, regression analysis, partial correlation analysis and possibly other techniques. The distributions assigned to the 45 variables presented in Chapter 2 characterize subjective uncertainty (i.e., a degree of belief as to the value of a fixed but imprecisely known quantity). In contrast, stochastic uncertainty is characterized by the probabilities assigned to the individual scenarios considered in the performance assessment.

At present, the most appropriate physical model for performance assessment at the WIPP is believed to include gas generation due to both corrosion and microbial action in the repository and a dual-porosity representation for radionuclide transport in the Culebra Dolomite Member of the Rustler Formation. This conceptual view was used in the modeling that produced the best-estimate performance-assessment results presented in Chapter 6 of Vol. 1. Chapter 4 of the present volume presents uncertainty and sensitivity analysis results for these modeling assumptions, including results for cuttings removal, groundwater transport, cuttings removal and groundwater transport combined, and the CCDFs that are used in comparisons with the EPA release limits.

In addition to the best-estimate conceptual model involving gas generation in the repository and a dual-porosity transport model in the Culebra, the 1991 WIPP performance assessment also considered the following alternative conceptual models: (1) no gas generation in the repository and a dual-porosity transport model in the Culebra, (2) gas generation in the repository and a single-porosity transport model in the Culebra, (3) no gas generation

in the repository and a single-porosity transport model in the Culebra, (4) gas generation in the repository and dual-porosity transport model without chemical retardation in the Culebra, and (5) climate change with gas generation in the repository and with single- and dual-porosity transport models in the Culebra. Uncertainty and sensitivity analyses for these alternative conceptual models are presented in Chapter 5, including results for groundwater transport, cuttings removal and groundwater transport combined, and the CCDFs that are used in comparison with the EPA release limits.

Chapter 6 contains a concluding discussion that summarizes the uncertainty and sensitivity analysis results and compares the results obtained with the alternative conceptual models.

2. STRUCTURE OF WIPP PERFORMANCE ASSESSMENT

2.1 Conceptual Model

As proposed by Kaplan and Garrick (1981), the outcome of a performance assessment can be represented by a set R of ordered triples of the form

$$R = \{(S_i, pS_i, \mathbf{cS}_i), i=1, \ldots, nS\}, \qquad (2.1\text{-}1)$$

where

S_i = a set of similar occurrences,

pS_i = probability that an occurrence in the set S_i will take place,

$\mathbf{cS}_i$ = a vector of consequences associated with S_i,

nS = number of sets selected for consideration,

and the sets S_i have no occurrences in common (i.e., the S_i are disjoint sets). This representation formally decomposes the outcome of a performance assessment into what can happen (the S_i), how likely things are to happen (the pS_i), and the consequences for each set of occurrences (the $\mathbf{cS}_i$). The S_i are typically referred to as "scenarios" in radioactive waste disposal. Similarly, the pS_i are scenario probabilities, and the vector $\mathbf{cS}_i$ contains environmental releases for individual isotopes, the normalized EPA release summed over all isotopes, and possibly other information associated with scenario S_i. The set R in Eq. 2.1-1 is used as the conceptual model for the WIPP performance assessment.

Although the representation in Eq. 2.1-1 provides a natural conceptual way to view risk, the set R by itself can be difficult to examine. For this reason, the risk results in R are often summarized with complementary cumulative distribution functions (CCDFs). These functions provide a display of the information contained in the probabilities pS_i and the consequences $\mathbf{cS}_i$. With the assumption that a particular consequence result cS in the vector $\mathbf{cS}$ has been ordered so that $cS_i \leq cS_{i+1}$ for i=1, ..., nS, the associated CCDF is shown in Figure 2.1-1. A consequence result of particular interest in performance assessments for radioactive waste disposal is the EPA normalized release to the accessible environment (U.S. EPA, 1985). As indicated in Figure 2.1-1, the EPA places a bound on the CCDF for normalized release to the accessible environment.

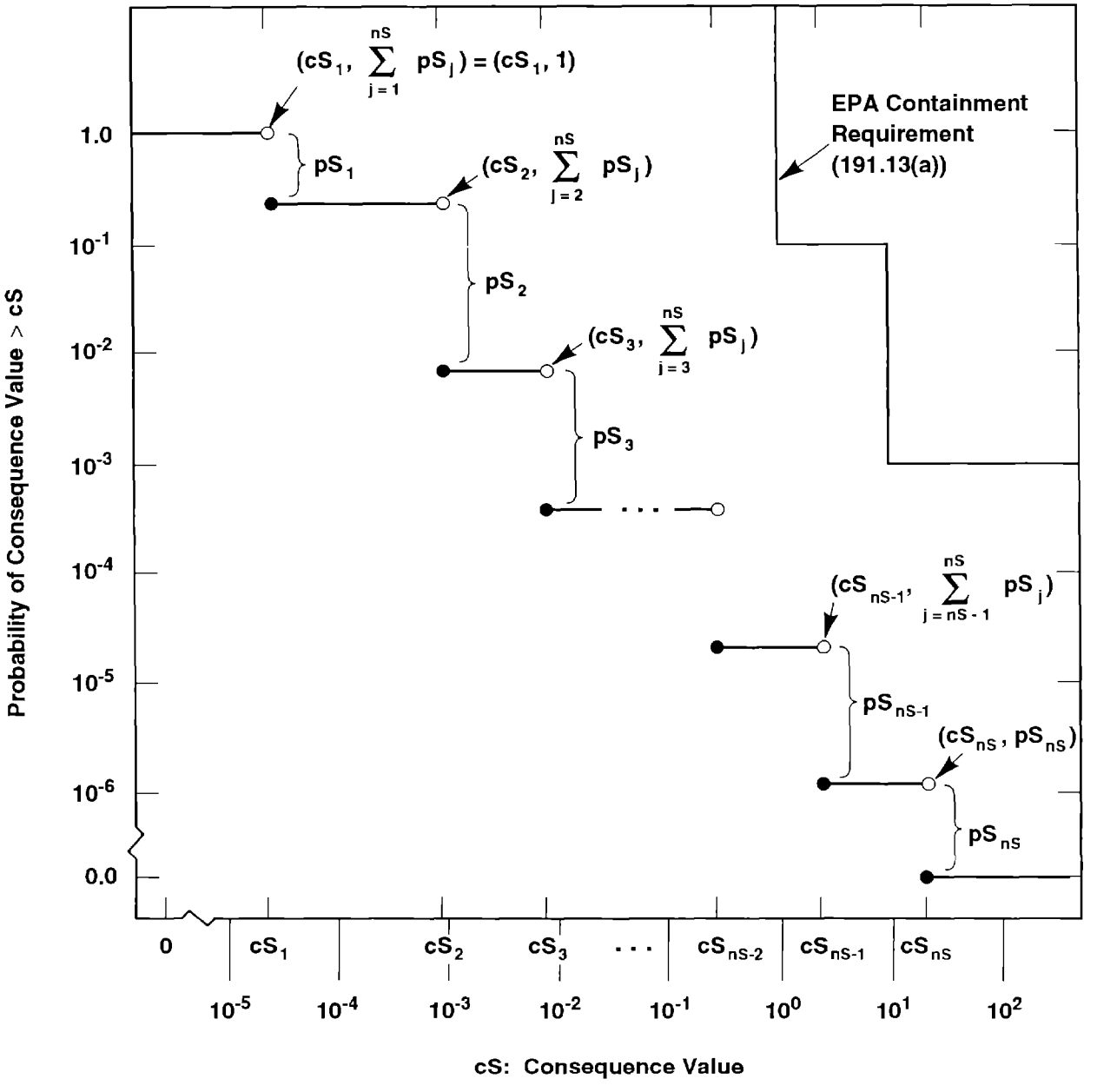

Figure 2.1-1. Estimated Complementary Cumulative Distribution Function (CCDF) for Consequence Result cS (Helton et al., 1991). The open and solid circles at the discontinuities indicate the points included on (solid circles) and excluded from (open circles) the CCDF.

In practice, the outcome of a performance assessment depends on many imprecisely known variables. These imprecisely known variables can be represented by a vector

$$\mathbf{x} = [x_1, x_2, \ldots, x_{nV}], \tag{2.1-2}$$

where each x_j is an imprecisely known input required in the performance assessment and nV is the total number of such inputs. As a result, the set R is actually a function of $\mathbf{x}$:

$$R(\mathbf{x}) = \{[S_i(\mathbf{x}), pS_i(\mathbf{x}), \mathbf{cS}_i(\mathbf{x})], i=1, \ldots, nS(\mathbf{x})\}. \tag{2.1-3}$$

As $\mathbf{x}$ changes, so will $R(\mathbf{x})$ and all summary measures that can be derived from $R(\mathbf{x})$. Thus, rather than a single CCDF for each consequence value contained in $\mathbf{cS}$, there will be a distribution of CCDFs that results from the possible values that $\mathbf{x}$ can take on.

The uncertainty in $\mathbf{x}$ can be characterized by a sequence of probability distributions

$$D_1, D_2, \ldots, D_{nV}, \tag{2.1-4}$$

where D_j is the distribution for the variable x_j contained in $\mathbf{x}$. The definition of these distributions may also be accompanied by the specification of correlations and various restrictions that further define the relations between the x_j. These distributions and other restrictions probabilistically characterize where the appropriate input to use in a performance assessment might fall given that the analysis has been structured so that only one value can be used for each variable.

Once the distributions in Eq. 2.1-4 have been developed, Monte Carlo techniques can be used to determine the uncertainty in $R(\mathbf{x})$ that results from the uncertainty in $\mathbf{x}$. First, a sample

$$\mathbf{x}_k = [x_{k1}, x_{k2}, \ldots, x_{k,nV}], k=1, \ldots, nK, \tag{2.1-5}$$

is generated according to the specified distributions and restrictions, where nK is the size of the sample. The performance assessment is then performed for each sample element $\mathbf{x}_k$, which yields a sequence of risk results of the form

$$R(\mathbf{x}_k) = \{[S_i(\mathbf{x}_k), pS_i(\mathbf{x}_k), \mathbf{cS}_i(\mathbf{x}_k)], i=1, \ldots, nS(\mathbf{x}_k)\} \tag{2.1-6}$$

for k=1, ..., nK. Each set $R(\mathbf{x}_k)$ is the result of one complete performance assessment performed with a set of inputs (i.e., $\mathbf{x}_k$) that the review process producing the distributions in Eq. 2.1-4 concluded was possible. Further, associated with each risk result $R(\mathbf{x}_k)$ in Eq. 2.1-6 is a probability or weight that can be used in making probabilistic statements about the distribution of $R(\mathbf{x})$. When random or Latin hypercube sampling is used, this weight is the reciprocal of the sample size (i.e., 1/nK).

In most performance assessments, CCDFs are the results of greatest interest. For a particular consequence result, a CCDF will be produced for each set $R(\mathbf{x}_k)$ shown in Eq. 2.1-6. This yields a distribution of CCDFs of the form shown in Figure 2.1-2.

An important distinction exists between the uncertainty that gives rise to a single CCDF in Figure 2.1-2 and the uncertainty that gives rise to the distribution of CCDFs in this figure. A single CCDF arises from the fact that a number of different occurrences have a real possibility of taking place. This type of uncertainty is referred to as stochastic variation or uncertainty in this report. A distribution of CCDFs arises from the fact that fixed, but unknown, quantities are needed in the estimation of a CCDF. The development of distributions that characterize what the values for these fixed quantities might be leads to a distribution of CCDFs. In essence, a performance assessment can be viewed as a very complex function that estimates a CCDF. Since there is uncertainty in the values of some of the variables operated on by this function, there will also be uncertainty in the dependent variable produced by this function, where this dependent variable is a CCDF.

Both Kaplan and Garrick (1981) and a recent report by the International Atomic Energy Agency (IAEA, 1989) distinguish between these two types of uncertainty. Specifically, Kaplan and Garrick distinguish between probabilities derived from frequencies and probabilities that characterize degrees of belief. Probabilities derived from frequencies correspond to the probabilities pS_i in Eq. 2.1-1, while probabilities that characterize degrees of belief (i.e., subjective probabilities) correspond to the distributions indicated in Eq. 2.1-4. The IAEA report distinguished between what it calls Type A uncertainty and Type B uncertainty. The IAEA report defines Type A uncertainty to be stochastic variation; as such, this uncertainty corresponds to the frequency-based probability of Kaplan and Garrick and the pS_i of Eq. 2.1-1. Type B uncertainty is defined to be uncertainty that is due to lack of knowledge about fixed quantities; thus, this uncertainty corresponds to the subjective probability of Kaplan and Garrick and the distributions indicated in Equation 2.1-4. This distinction has also been made by other authors, including Vesely and Rasmusen (1984), Paté-Cornell (1986) and Parry (1988).

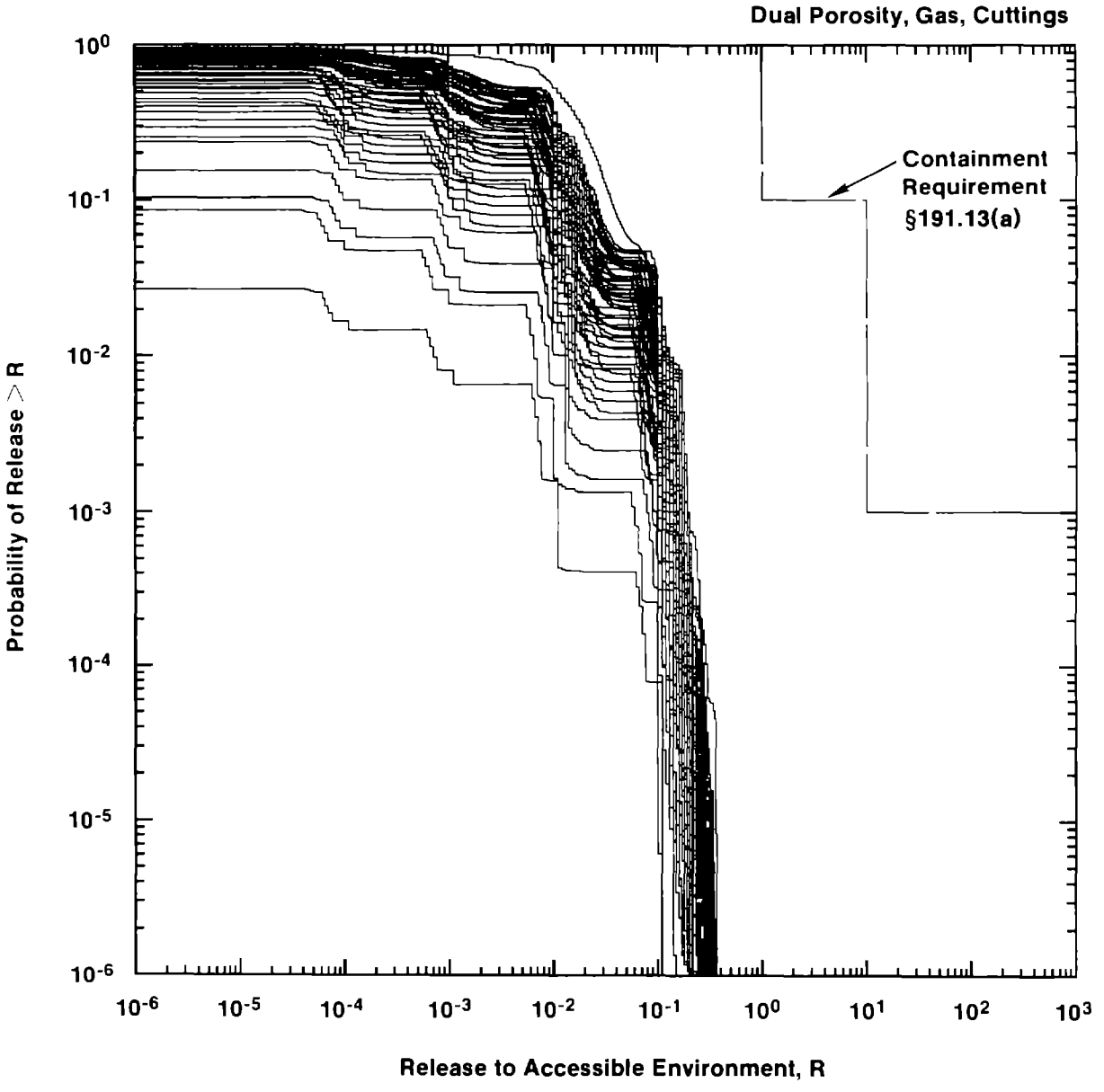

TRI-6342-1293-1

Figure 2.1-2. Distribution of Complementary Cumulative Distribution Functions for Normalized Release to the Accessible Environment Including Both Cuttings Removal and Groundwater Transport with Gas Generation in the Repository and a Dual-Porosity Transport Model in the Culebra Dolomite.

As already indicated, the ordered triple representation shown in Eq. 2.1-1 is used as the conceptual model for the WIPP performance assessment. In consistency with this representation, the scenarios S_i, scenario probabilities pS_i and scenario consequences $\mathbf{cS}_i$ used in the 1991 preliminary WIPP performance assessment are discussed in Sections 2.2, 2.3 and 2.4, respectively. Further, the WIPP performance assessment endeavors to maintain a distinction between stochastic uncertainty and subjective uncertainty. The effect of stochastic uncertainty is represented by the probabilities pS_i discussed in Section 2.4. The characterization of the subjective uncertainty in the inputs to the 1991 WIPP performance assessment is discussed in Section 3. The primary focus of this report is the impact of subjective uncertainties on the outcomes of the 1991 WIPP performance assessment. These impacts will be investigated in Chapters 4 and 5.

2.2 Definition of Scenarios

Scenarios constitute the first element S_i of the ordered triples contained in the set R shown in Eq. 2.1-1 and are obtained by subdividing the set

$$S = \{x: \text{x a single 10,000-yr history beginning at decommissioning of the WIPP}\}. \quad (2.2\text{-}1)$$

Each 10,000-yr history is complete in the sense that it includes a full specification, including time of occurrence, for everything of importance to performance assessment that happens in this time period. In the terminology of Cranwell et al. (1990), each history would contain a characterization for a specific sequence of "naturally occurring and/or human-induced conditions that represent realistic future states of the repository, geologic systems, and ground-water flow systems that could affect the release and transport of radionuclides from the repository to humans."

The WIPP performance assessment uses a two stage procedure for scenario development (Vol. 1, Ch. 4). The purpose of the first stage is to develop a comprehensive set of scenarios that includes all occurrences that might reasonably take place at the WIPP. The result of this stage is a set of scenarios, called summary scenarios, that summarize what might happen at the WIPP. These summary scenarios provide a basis for discussing the future behavior of the WIPP and a starting point for the second stage of the procedure, which is the definition of scenarios at a level of detail that is appropriate for use with the computational models employed in the WIPP performance assessment. The scenarios obtained in this second stage of scenario development are referred to as computational scenarios. The development of summary scenarios is directed at understanding what might happen at the WIPP and answering completeness questions. The development of

computational scenarios is directed at organizing the actual calculations that must be performed to obtain the consequences $\mathbf{cS}_i$ appearing in Eq. 2.1-1, and as a result, must provide a structure that both permits the $\mathbf{cS}_i$ to be calculated at a reasonable cost and holds the amount of aggregation error that enters the analysis to a reasonable level. Here, aggregation error refers to the inevitable loss of resolution that occurs when an infinite number of occurrences (i.e., the elements of S) must be divided into a finite number of sets for analysis (i.e., the subsets S_i of S). The following discussion describes the computational scenarios used in the 1991 WIPP performance assessment.

The development of summary scenarios for the 1991 WIPP performance assessment led to a set S of the form shown in Eq. 2.2-1 in which all credible disruptions were due to drilling intrusions (Vol. 1, Ch. 4). As a result, computational scenarios were defined to provide a systematic coverage of drilling intrusions. Specifically, computational scenarios were defined on the basis of (1) number of drilling intrusions, (2) time of the drilling intrusions, (3) whether or not a single waste panel is penetrated by two or more boreholes, of which at least one penetrates a pressurized brine pocket and at least one does not, and (4) the activity level of the waste penetrated by the boreholes.

The construction of computational scenarios started with the division of the 10,000-yr time period appearing in the EPA regulations into a sequence

$$[t_{i-1}, t_i], \; i = 1, 2, \ldots, nT, \tag{2.2-2}$$

of disjoint time intervals. When the activity levels of the waste are not considered, these time intervals lead to computational scenarios of the form

$$S(\mathbf{n}) = \{x: x \text{ an element of } S \text{ for which exactly n(i) intrusions occur in time interval } [t_{i-1}, t_i] \text{ for i=1, 2, ..., nT}\} \tag{2.2-3}$$

and

$$S^{+-}(t_{i-1},t_i) = \{x: x \text{ an element of } S \text{ for which two or more boreholes penetrate the same waste panel during the time interval } [t_{i-1}, t_i], \text{ with at least one of these boreholes penetrating a pressurized brine pocket and at least one not penetrating a pressurized brine pocket}\}, \tag{2.2-4}$$

where

$$\mathbf{n} = [n(1), n(2), \ldots, n(nT)]. \qquad (2.2\text{-}5)$$

For the 1991 WIPP performance assessment, nT = 5, and each time interval $[t_{i-1}, t_i]$ had a length of 2000 yrs.

When the activity levels of the waste are considered, the preceding time intervals lead to computational scenarios of the form

$$S(\mathbf{l},\mathbf{n}) = \{x: x \text{ an element of } S(\mathbf{n}) \text{ for which the } j^{th} \text{ borehole encounters waste of activity level } \ell(j) \text{ for } j=1, 2, \ldots, nBH, \text{ where nBH is the total number of boreholes associated with a time history in } S(\mathbf{n})\} \qquad (2.2\text{-}6)$$

and

$$S^{+-}(\mathbf{l};t_{i-1},t_i) = \{x: x \text{ an element of } S^{+-}(t_{i-1},t_i) \text{ for which the } j^{th} \text{ borehole encounters waste of activity level } \ell(j) \text{ for } j=1, 2, \ldots, nBH, \text{ where nBH is the total number of boreholes associated with a time history in } S^{+-}(t_{i-1},t_i)\}, \qquad (2.2\text{-}7)$$

where

$$\mathbf{l} = [\ell(1), \ell(2), \ldots, \ell(nBH)] \text{ and } nBH = \sum_{i=1}^{nT} n(i). \qquad (2.2\text{-}8)$$

The computational scenarios $S(\mathbf{l},\mathbf{n})$ and $S^{+-}(\mathbf{l};t_{i-1},t_i)$ were used as the basis for the CCDFs for normalized release to the accessible environment presented in the 1991 WIPP performance assessment (e.g., as shown in Figure 2.1-2).

The definitions of $S^{+-}(t_{i-1},t_i)$ and $S^{+-}(\mathbf{l};t_{i-1},t_i)$ appearing in Eqs. 2.2-4 and 2.2-7 do not use the vector $\mathbf{n}$ designating the time intervals in which drilling intrusions occur that appears in the definitions of $S(\mathbf{n})$ and $S(\mathbf{l},\mathbf{n})$. However, vectors of this form can be incorporated into the definitions of $S^{+-}(t_{i-1},t_i)$ and $S^{+-}(\mathbf{l};t_{i-1},t_i)$. Specifically, let

$$S_i^{+-}(\mathbf{n}) = \{x: x \text{ an element of } S(\mathbf{n}) \text{ for which 2 or more boreholes penetrate the same waste panel during the time interval } [t_{i-1},t_i] \text{ (i.e., } n(i)\geq 2), \text{ with at least one of these boreholes penetrating a pressurized brine pocket and at least one not penetrating a pressurized brine pocket}\}. \qquad (2.2\text{-}9)$$

Then,

$$S^{+-}(t_{i-1},t_i) = \bigcup_{\mathbf{n}\in A(i)} S_i^{+-}(\mathbf{n}), \qquad (2.2\text{-}10)$$

where $\mathbf{n}\in A(i)$ only if $\mathbf{n}$ is a vector of the form defined in Eq. 2.2-5 with $n(i)\geq 2$. The computational scenarios $S_i^{+-}(\mathbf{l},\mathbf{n})$ and $S^{+-}(\mathbf{l};t_{i-1},t_i)$ can be defined analogously for the vector $\mathbf{l}$ indicated in Eq. 2.2-8. In Section 2.3, conservative relations are presented (i.e., Eqs. 2.3-3 and 2.3-4) that bound the probabilities for $S^{+-}(t_{i-1},t_i)$ and $S^{+-}(\mathbf{l};t_{i-1},t_i)$ and are used in the construction of CCDFs of the form appearing in Figure 2.1-2. In Section 2.4, $S^{+-}(t_{i-1},t_i)$ and $S^{+-}(\mathbf{l};t_{i-1},t_i)$, $i = 1, \ldots, nT = 5$, are assigned the groundwater releases (i.e., Eqs. 2.4-13 and 2.4-14) associated with

$$S_1^{+-}(2,0,0,0,0),\ S_2^{+-}(0,2,0,0,0),\ S_3^{+-}(0,0,2,0,0),$$

$$S_4^{+-}(0,0,0,2,0),\ S_5^{+-}(0,0,0,0,2), \qquad (2.2\text{-}11)$$

respectively; these releases are used in the construction of CCDFs of the form appearing in Figure 2.1-2. The subscripts in the preceding notation for $S_1^{+-}(2,0,0,0,0)$ through $S_5^{+-}(0,0,0,0,2)$ are redundant and will be omitted in the remainder of this report.

Additional information on the construction of computational scenarios for the 1991 WIPP performance assessment is available elsewhere (Vol. 2, Ch. 3).

2.3 Determination of Scenario Probabilities

As discussed in Chapters 2 and 3 of Volume 2, probabilities for computational scenarios were determined under the assumption that the occurrence of boreholes through the repository follows a Poisson process with a rate constant λ. The probabilities $pS(\mathbf{n})$ and $pS(\mathbf{l},\mathbf{n})$ for the computational scenarios $S(\mathbf{n})$ and $S(\mathbf{l},\mathbf{n})$ are given by

$$pS(\mathbf{n}) = \left\{\prod_{i=1}^{nT}\left[\frac{\lambda^{n(i)}\left(t_i - t_{i-1}\right)^{n(i)}}{n(i)!}\right]\right\}\exp\left[-\lambda\left(t_{nT} - t_0\right)\right] \qquad (2.3\text{-}1)$$

and

$$pS(\mathbf{l},\mathbf{n}) = \left[\prod_{j=1}^{nBH} pL_{l(j)}\right] pS(\mathbf{n}), \qquad (2.3\text{-}2)$$

where $\mathbf{n}$ and $\mathbf{l}$ are defined in Eqs. 2.2-5 and 2.2-8, respectively, and pL_{ℓ} is the probability that a randomly placed borehole through a waste panel will encounter waste of activity level ℓ. Table 2.3-1 provides an example of probabilities $pS(\mathbf{n})$ calculated as shown in Eq. 2.3-1 with $\lambda = 3.28 \times 10^{-4}$ yr^{-1}, which corresponds to the maximum drilling rate suggested for use by the EPA.

The probabilities $pS^{+-}(t_{i-1},t_i)$ and $pS^{+-}(\mathbf{l};t_{i-1},t_i)$ for the computational scenarios $S^{+-}(t_{i-1},t_i)$ and $S^{+-}(\mathbf{l};t_{i-1},t_i)$ are given by

$$pS^{+-}(t_{i-1},t_i) \triangleq \sum_{\ell=1}^{nP} \left\{1 - \exp[-\alpha(\ell)(t_i-t_{i-1})]\right\} \left\{1 - \exp[-\beta(\ell)(t_i-t_{i-1})]\right\} \tag{2.3-3}$$

and

$$pS^{+-}(\mathbf{l};t_{i-1},t_i) \triangleq \left[\prod_{j=1}^{nBH} pL_{\ell(j)} \right] pS^{+-}(t_{i-1},t_i), \tag{2.3-4}$$

where

$$\alpha(\ell) = [aBP(\ell)]\lambda/aTOT$$

$$\beta(\ell) = [aTOT(\ell) - aBP(\ell)]\lambda/aTOT$$

$aBP(\ell)$ = area (m^2) of pressurized brine pocket under waste panel ℓ,

$aTOT(\ell)$ = total area (m^2) of waste panel ℓ,

aTOT = total area (m^2) of waste panels,

and

nP = number of waste panels.

For the 1991 WIPP performance assessment, $aTOT(\ell)$ and $aBP(\ell)$ were assumed to be the same for all waste panels due to an absence of information on $aBP(\ell)$ for individual panels.

The relations appearing in Eqs. 2.3-1 through 2.3-4 are derived in Volume 2, Chapter 2 of this report under the assumption that drilling intrusions follow a Poisson process (i.e., are random in time and space). The derivations are quite general and include both the stationary (i.e., constant λ) and nonstationary (i.e., time-dependent λ) cases.

TABLE 2.3-1. PROBABILITIES FOR COMPUTATIONAL SCENARIOS INVOLVING MULTIPLE INTRUSIONS OVER 10,000 YRS FOR $\lambda = 3.28 \times 10^{-4}$ YR^{-1}, A 100-YR PERIOD OF ADMINISTRATIVE CONTROL DURING WHICH NO DRILLING INTRUSIONS CAN OCCUR AND 2,000-YR TIME INTERVALS

0 Intrusions
(prob = 3.888E-2)
(cum prob = 3.888E-2)
(# scenarios = 1)

Scenario	Prob
S(0,0,0,0,0)	3.888E-02

1 Intrusion
(prob = 1.263E-1)
(cum prob = 1.651E-1)
(# scenarios = 5)

Scenario	Prob
S(1,0,0,0,0)	2.423E-2
S(0,1,0,0,0)	2.551E-2
S(0,0,1,0,0)	2.551E-2
S(0,0,0,1,0)	2.551E-2
S(0,0,0,0,1)	2.551E-2
	1.263E-1

2 Intrusions
(prob = 2.050E-1)
(cum prob = 3.701E-1)
(# scenarios = 15)

Scenario	Prob
S(2,0,0,0,0)	7.551E-3
S(1,1,0,0,0)	1.590E-2
S(1,0,1,0,0)	1.590E-2
S(1,0,0,1,0)	1.590E-2
S(1,0,0,0,1)	1.590E-2
S(0,2,0,0,0)	8.366E-3
S(0,1,1,0,0)	1.673E-2
S(0,1,0,1,0)	1.673E-2
S(0,1,0,0,1)	1.673E-2
S(0,0,2,0,0)	8.366E-3
S(0,0,1,1,0)	1.673E-2
S(0,0,1,0,1)	1.673E-2
S(0,0,0,2,0)	8.366E-3
S(0,0,0,1,1)	1.673E-2
S(0,0,0,0,2)	8.366E-3
	2.050E-1

3 Intrusions
(prob = 2.219E-1)
(cum prob = 5.920E-1)
(# scenarios = 35)

Scenario	Prob
S(3,0,0,0,0)	1.569E-3
S(2,1,0,0,0)	4.953E-3
S(2,0,1,0,0)	4.953E-3
S(2,0,0,1,0)	4.953E-3
S(2,0,0,0,1)	4.953E-3
S(1,2,0,0,0)	5.214E-3
S(1,1,1,0,0)	1.043E-2
S(1,1,0,1,0)	1.043E-2
S(1,1,0,0,1)	1.043E-2
S(1,0,2,0,0)	5.214E-3
S(1,0,1,1,0)	1.043E-2
S(1,0,1,0,1)	1.043E-2
S(1,0,0,2,0)	5.214E-3
S(1,0,0,1,1)	1.043E-2
S(1,0,0,0,2)	5.214E-3
S(0,3,0,0,0)	1.829E-3
S(0,2,1,0,0)	5.488E-3
S(0,2,0,1,0)	5.488E-3
S(0,2,0,0,1)	5.488E-3
S(0,1,2,0,0)	5.488E-3
S(0,1,1,1,0)	1.098E-2
S(0,1,1,0,1)	1.098E-2
S(0,1,0,2,0)	5.488E-3
S(0,1,0,1,1)	1.098E-2
S(0,1,0,0,2)	5.488E-3
S(0,0,3,0,0)	1.829E-3
S(0,0,2,1,0)	5.488E-3
S(0,0,2,0,1)	5.488E-3
S(0,0,1,2,0)	5.488E-3
S(0,0,1,1,1)	1.098E-2
S(0,0,1,0,2)	5.488E-3
S(0,0,0,3,0)	1.829E-3
S(0,0,0,2,1)	5.488E-3
S(0,0,0,1,2)	5.488E-3
S(0,0,0,0,3)	1.829E-3
	2.219E-1

4 Intrusions
(prob = 1.801E-1)
(cum prob = 7.722E-1)
(# scenarios = 70)

Scenario	Prob
S(4,0,0,0,0)	2.444E-4
S(3,1,0,0,0)	1.029E-3
.	.
.	.
.	.
S(1,1,1,1,0)	6.841E-3
.	.
.	.
.	.
S(0,0,0,1,3)	1.200E-3
S(0,0,0,0,4)	3.000E-4
	1.801E-1

5 Intrusions
(prob = 1.170E-1)
(cum prob = 8.891E-1)
(# scenarios = 126)

6 Intrusions
(prob = 6.331E-2)
(cum prob = 9.525E-1)
(# scenarios = 210)

7 Intrusions
(prob = 2.937E-2)
(cum prob = 9.818E-1)
(# scenarios = 330)

TABLE 2.3-1. PROBABILITIES FOR COMPUTATIONAL SCENARIOS INVOLVING MULTIPLE INTRUSIONS OVER 10,000 YRS FOR $\lambda = 3.28 \times 10^{-4}$ YR^{-1}, A 100-YR PERIOD OF ADMINISTRATIVE CONTROL DURING WHICH NO DRILLING INTRUSIONS CAN OCCUR AND 2,000-YR TIME INTERVALS (concluded)

8 Intrusions (prob = 1.192E-2) (cum prob = 9.937E-1) (# scenarios = 495)	11 Intrusions (prob = 4.123E-4) (cum prob = 9.999E-1) (# scenarios = 1365)	14 Intrusions (prob = 6.464E-6) (cum prob = 1.000E+0) (# scenarios = 3060)
9 Intrusions (prob = 4.301E-3) (cum prob = 9.980E-1) (# scenarios = 715)	12 Intrusions (prob = 1.116E-4) (cum prob = 1.000E+0) (# scenarios = 1820)	15 Intrusions (prob = 1.399E-6) (cum prob = 1.000E+0) (# scenarios = 3876)
10 Intrusions (prob = 1.397E-3) (cum prob = 9.994E-1) (# scenarios = 1001)	13 Intrusions (prob = 2.787E-5) (cum prob = 1.000E+0) (# scenarios = 2380)	

2.4 Calculation of Scenario Consequences

As indicated in Figure 2.4-1, the following five computer models were used to estimate scenario consequences in the 1991 WIPP performance assessment: CUTTINGS, BRAGFLO, PANEL, SECO2D and STAFF2D. Brief descriptions of these models are given in Table 2.4-1. Further, more detailed descriptions of these models and their use in the 1991 WIPP performance assessment are given in Vol. 2 of this report.

As can be seen from Table 2.3-1, there are too many computational scenarios (e.g., $S(\mathbf{n})$ and $S(\mathbf{l},\mathbf{n})$) to perform a detailed calculation for each scenario with the models discussed in Table 2.4-1. For example, 3003 senarios of the form $S(\mathbf{n})$ (i.e., all scenarios involving less than or equal to 10 intrusions) are required to reach a cumulative probability of 0.9994. Construction of a CCDF for comparison against the EPA release limits requires the estimation of cumulative probability through at least the 0.999 level. Thus, depending on the value for the rate constant λ in the Poisson model for drilling intrusions, this may require the inclusion of computational scenarios involving as many as 10 to 12 drilling intrusions, which results in a total of several thousand computational scenarios. Further, this number does not include the effects of different activity levels in the waste. To obtain results for such a large number of computational scenarios, it is necessary

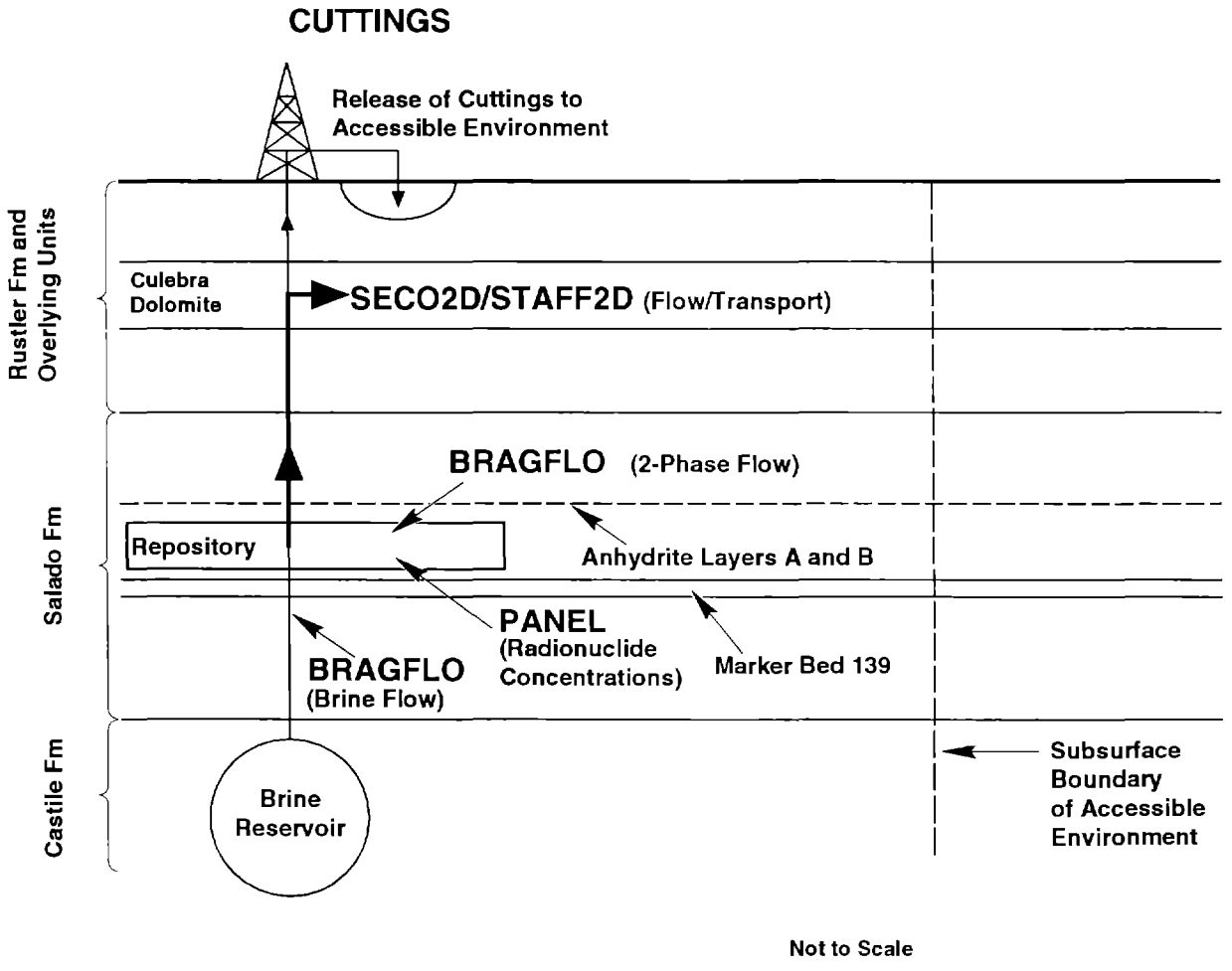

Figure 2.4-1. Models Used in 1991 WIPP Performance Assessment. The names for computer models (i.e., computer codes) are shown in capital letters.

TABLE 2.4-1. SUMMARY OF COMPUTER MODELS USED IN THE 1991 WIPP PERFORMANCE ASSESSMENT

Model	Description
BRAGFLO	Describes the multiphase flow of gas and brine through a porous, heterogenous reservoir. BRAGFLO solves simultaneously the coupled partial differential equations that describe the mass conservation of gas and brine along with appropriate constraint equations, initial conditions, and boundary conditions (Volume 2, Chapter 5 of this report).
CUTTINGS	Calculates the quantity of radioactive material brought to the surface as cuttings and cavings generated by an exploratory drilling operation that penetrates a waste panel (Volume 2, Chapter 7 of this report).
PANEL	Calculates rate of discharge and cumulative discharge of radionuclides from a repository panel through an intrusion borehole. Discharge is a function of fluid flow rate, elemental solubility, and remaining inventory (Volume 2, Chapter 5 of this report).
SECO2D	Calculates single-phase Darcy flow for groundwater-flow problems in two dimensions. The formulation is based on a single partial differential equation for hydraulic head using fully implicit time differencing (Volume 2, Chapter 6 of this report).
STAFF2D	Simulates fluid flow and transport of radionuclides in fractured porous media. STAFF2D is a two-dimensional finite element code (Huyakorn et al., 1989; Volume 2, Chapter 6 of this report).

to plan and implement the overall calculations very carefully. The manner in which this can be done is not unique. The following describes the approach used in the 1991 WIPP performance assessment.

As indicated in Eq. 2.2-2, the 10,000-yr time interval that must be considered in the construction of CCDFs for comparison with the EPA release limits is divided into disjoint subintervals $[t_{i-1}, t_i]$, $i = 1, 2, \ldots, nT$, in the definition of computational scenarios. The following results can be calculated for each time interval:

rC_i = EPA normalized release to the surface environment for cuttings removal due to a single borehole in time interval i with the assumption that the waste is homogeneous (i.e., waste of different activity levels is not present), (2.4-1)

rC_{ij} = EPA normalized release to the surface environment for cuttings removal due to a single borehole in time interval i that penetrates waste of activity level j, (2.4-2)

$rGWl_i$ = EPA normalized release to the accessible environment due to groundwater transport initiated by a single borehole in time interval i (i.e., an E2-type scenario), (2.4-3)

and

$rGW2_i$ = EPA normalized release to the accessible environment due to groundwater transport initiated by two boreholes in the same waste panel in time interval i, of which one penetrates a pressurized brine pocket and one does not (i.e., an E1E2-type scenario), (2.4-4)

with the assumption that the intrusions occur at the midpoints of the time intervals (i.e., at 1000, 3000, 5000, 7000 and 9000 yrs). For the calculation of $rGW1_i$ and $rGW2_i$ in the 1991 WIPP performance assessment, the accessible environment is assumed to begin 5 km from the waste panels (e.g., see Figures 1.5-4, 2.1-1 and 2.1-2 in Vol. 3).

In general, rC_i, rC_{ij} $rGW1_i$ and $rGW2_i$ will be vectors containing a large variety of information; however, for notational simplicity, a vector representation will not be used. For the 1991 WIPP performance assessment, the cuttings release to the accessible environment (i.e., rC_i and rC_{ij}) is determined by the CUTTINGS program, and the groundwater release to the accessible environment (i.e., $rGW1_i$ and $rGW2_i$) is determined through a sequence of linked calculations involving the BRAGFLO, PANEL, SECO2D and STAFF2D programs.

The cuttings releases

$$rC_1,\ rC_2,\ rC_3,\ rC_4,\ rC_5 \tag{2.4-5}$$

correspond to the cuttings releases associated with the computational scenarios

$$S(1,0,0,0,0),\ S(0,1,0,0,0),\ S(0,0,1,0,0),\ S(0,0,0,1,0),\ S(0,0,0,0,1) \tag{2.4-6}$$

under the assumption that all waste is of the same average activity level. Similarly, the groundwater releases

$$rGW1_1,\ rGW1_2,\ rGW1_3,\ rGW1_4,\ rGW1_5 \tag{2.4-7}$$

correspond to the groundwater releases associated with the preceding five scenarios, while

$$rGW2_1,\ rGW2_2,\ rGW2_3,\ rGW2_4,\ rGW2_5 \tag{2.4-8}$$

correspond to the groundwater releases associated with the computational scenarios

$$S^{+-}(2,0,0,0,0),\ S^{+-}(0,2,0,0,0),\ S^{+-}(0,0,2,0,0),\ S^{+-}(0,0,0,2,0),\ S^{+-}(0,0,0,0,2). \quad (2.4\text{-}9)$$

In like manner, rC_{1j} corresponds to the cuttings release associated with the computational scenario $S(j;\ 1,0,0,0,0)$; rC_{2j} corresponds to the cuttings release associated with $S(j;\ 0,1,0,0,0)$, and so on.

The releases rC_i, rC_{ij}, $rGW1_i$ and $rGW2_i$ are used to construct the releases associated with the many individual computational scenarios that are used in the construction of a CCDF for comparison with the EPA release limits. The following assumptions are made:

(1) With the exception of E1E2-type scenarios, no synergistic effects result from multiple boreholes, and thus, the total release for a scenario involving multiple intrusions can be obtained by adding the releases associated with the individual intrusions.

(2) An E1E2-type scenario can only take place when the necessary boreholes occur within the same time interval $[t_{i-1},\ t_i]$.

(3) An E1E2-type scenario involving more than two boreholes will have the same release as an E1E2-type scenario involving exactly two boreholes.

The preceding assumptions are used to construct the releases for individual computational scenarios.

The normalized releases rC_i, rC_{ij} and $rGW1_i$ can be used to construct the EPA normalized releases for the scenarios $S(\mathbf{n})$ and $S(\mathbf{I},\mathbf{n})$. For $S(\mathbf{n})$, the normalized release to the accessible environment, $cS(\mathbf{n})$, can be approximated by

$$cS(\mathbf{n}) = \sum_{j=1}^{nBH} \left(rC_{m(j)} + rGW1_{m(j)}\right), \quad (2.4\text{-}10)$$

where m(j) designates the time interval in which the j^{th} borehole occurs. The vector

$$\mathbf{m} = [m(1),\ m(2),\ \ldots,\ m(nBH)] \quad (2.4\text{-}11)$$

is uniquely determined once the vector **n** appearing in the definition of $S(\mathbf{n})$ is specified. The definition of $S(\mathbf{n})$ in Eq. 2.2-3 contains no information on the activity levels encountered by the individual boreholes, and so $cS(\mathbf{n})$ was constructed with the assumption that all waste is of the same average activity. However, the definition of $S(\mathbf{l},\mathbf{n})$ in Eq. 2.2-6 does contain information on activity levels, and the associated normalized release to the accessible environment, $cS(\mathbf{l},\mathbf{n})$, can be approximated by

$$cS(\mathbf{l},\mathbf{n}) = \sum_{j=1}^{nBH} \left[rC_{m(j),\ell(j)} + rGW1_{m(j)} \right], \tag{2.4-12}$$

which does incorporate the activity levels encountered by the individual boreholes.

For $S^{+-}(t_{i-1},t_i)$, the normalized release to the accessible environment, $cS^{+-}(t_{i-1},t_i)$, can be approximated by

$$cS^{+-}(t_{i-1},t_i) = 2\ rC_i + rGW2_i, \tag{2.4-13}$$

where it is assumed that all waste is of the same average activity for cuttings removal. Similarly, the normalized release $cS^{+-}(\mathbf{l};t_{i-1},t_i)$ for $S^{+-}(\mathbf{l};t_{i-1},t_i)$ can be approximated by

$$cS^{+-}(\mathbf{l};t_{i-1},t_i) = \sum_{j=1}^{2} rC_{i,\ell(j)} + rGW2_i, \tag{2.4-14}$$

which incorporates the activity level of the waste. The approximations for $cS^{+-}(t_{i-1},t_i)$ and $cS^{+-}(\mathbf{l};t_{i-1},t_i)$ in Eqs. 2.4-13 and 2.4-14 are based on exactly two intrusions in the time interval $[t_{i-1},t_i]$. More complicated expressions could be developed to define releases for multiple E1E2-type intrusions. However, due to the low probability of such patterns of intrusion (e.g., compare the probabilities for 2 and ≥2 boreholes in Tables 2-4 and 2-6 of Vol. 2), the use of such expressions would have little impact on the CCDFs used for comparison with the EPA release limits.

The construction process shown in Eqs. 2.4-10 and 2.4-13 to obtain the normalized releases $cS(\mathbf{n})$and $cS^{+-}(t_{i-1},t_i)$ for scenarios $S(\mathbf{n})$ and $S^{+-}(t_{i-1},t_i)$ is illustrated in Table 3-4 of Vol. 3. Further, the construction process shown in Eqs. 2.4-12 and 2.4-14 to obtain normalized releases $cS(\mathbf{l},\mathbf{n})$ and $cS^{+-}(\mathbf{l};t_{i-1},t_i)$ for scenarios $S(\mathbf{l},\mathbf{n})$ and $S^{+-}(\mathbf{l};t_{i-1},t_i)$ is illustrated in Table 3-5 of Vol. 3.

Before continuing, this is a natural place to introduce some additional information on the consequence calculations. Specifically, Table 2.4-2 lists the initial inventory of waste used in the 1991 calculations, Table 2.4-3 lists the decay chains used for transport calculations in the Culebra Dolomite, and Table 2.4-4 lists the activity levels considered in the estimation of cuttings releases. Further, Figure 2.4-2 presents time-dependent inventories expressed in EPA units (i.e., the normalizations used in comparisons with the EPA release limits) used for a single waste panel in the 1991 WIPP performance assessment; the total WIPP inventory is ten times the quantities indicated in this figure. This information will facilitate the interpretation of later uncertainty and sensitivity analysis results.

The cuttings releases used in the 1991 WIPP performance assessment were calculated with the program CUTTINGS for waste of average activity level. Then, the releases for activity levels 1 through 5 shown in Table 2.4-4 were obtained by multiplying the average activity level releases by scale factors of the form

$$SF_{i\ell} = AL_{i\ell}/AL_i, \qquad (2.4\text{-}15)$$

where

$AL_{i\ell}$ = projected radioactivity (Ci/m^2) contained in waste of activity level ℓ at time i, where 1 ~ 1000 yrs, 2 ~ 3000 yrs, 3 ~ 5000 yrs, 4 ~ 7000 yrs and 5 ~ 9000 yrs,

and

AL_i = projected radioactivity (Ci/m^2) contained in waste of average activity at time i.

For example, the scale factor

$$SF_{24} = 184.01/7.9658 = 23.100 \qquad (2.4\text{-}16)$$

is used to convert from a release of average activity at 3000 yrs to a release of activity level 4 at 3000 yrs.

TABLE 2.4-2. POTENTIALLY IMPORTANT RADIONUCLIDES ASSOCIATED WITH INITIAL CONTACT-HANDLED WASTE INVENTORY USED IN CALCULATIONS FOR CUTTINGS REMOVAL AND RELEASE TO CULEBRA DOLOMITE (adapted from Table 3.3-5 of Vol. 3)

Radionuclide	$t_{1/2}$(yr)	Curies	Grams
Pu-238	8.77×10^{1}	9.26×10^{6}	5.41×10^{5}
Pu-239	2.41×10^{4}	8.45×10^{5}	1.36×10^{7}
Pu-240	6.53×10^{3}	1.07×10^{5}	4.69×10^{5}
Pu-242	3.76×10^{5}	2.16×10^{0}	5.50×10^{2}
U-233	1.59×10^{5}	1.037×10^{2}	1.07×10^{4}
U-234	2.44×10^{5}	0	0
U-236	2.34×10^{7}	0	0
Am-241	4.32×10^{2}	1.64×10^{6}	4.79×10^{5}
Np-237	2.14×10^{6}	2.14	3.04×10^{3}
Th-229	7.43×10^{3}	0	0
Th-230	7.70×10^{4}	0	0
Ra-226	1.60×10^{3}	0	0

TABLE 2.4-3. SIMPLIFIED RADIONUCLIDE DECAY CHAINS USED FOR TRANSPORT CALCULATIONS IN THE CULEBRA DOLOMITE (from Ch. 6 of Vol. 2)

(1) Pu-240

(2) Am-241 → Np-237 → U-233

(3) U-234 → Th-230

(4) Pu-239

TABLE 2.4-4. PROJECTED ACTIVITY LEVELS (Ci/m^2) IN THE WIPP DUE TO WASTE THAT IS CURRENTLY STORED AND MAY BE SHIPPED TO THE WIPP (based on Table 3.4-11 of Vol. 3)

Activity Level	Type[a]	Probability[b]	Time (years)					
			0	1000	3000	5000	7000	9000
1	CH	0.40023	3.4833	0.2718	0.1840	0.1688	0.1575	0.1473
2	CH	0.2998	34.8326	2.7177	1.8401	1.6875	1.5748	1.4729
3	CH	0.2242	348.326	27.117	18.401	16.875	15.748	14.729
4	CH	0.0149	3483.26	271.77	184.01	168.75	157.48	147.29
5	RH	0.0588	117.6717	0.1546	0.1212	0.1139	0.1082	0.1030
	Average for CH Waste:		150.7905	11.7648	7.9658	7.3053	6.8174	6.3764

a CH designates contact-handled waste; RH designates remote-handled waste

b Probability that a randomly placed borehole through the waste panels will intersect waste of activity level ℓ, $\ell = 1,2,3,4,5$.

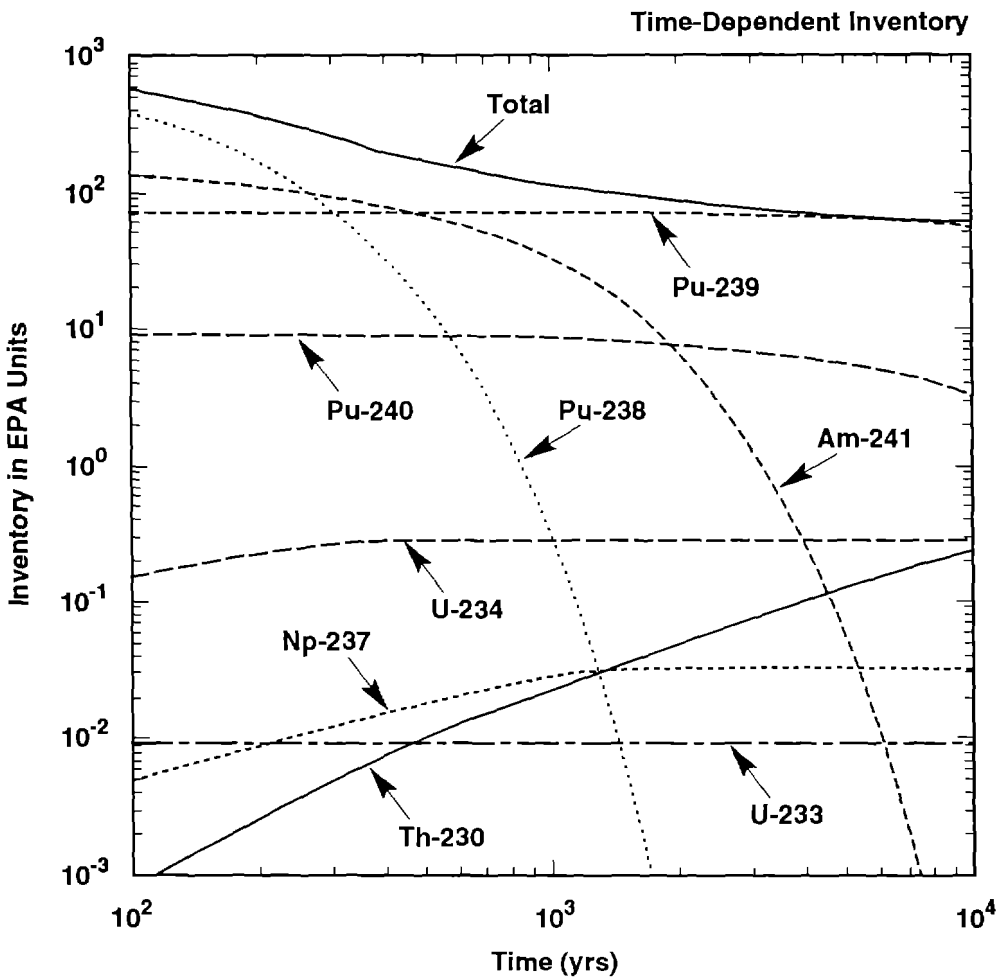

Figure 2.4-2. Time-Dependent Inventory Expressed in EPA Units (i.e., the normalized units used in showing compliance with 40 CFR 191) for a Single Waste Panel. The total WIPP inventory used in the 1991 performance assessment is 10 times the values shown in this figure.

3. UNCERTAIN VARIABLES

The 1991 WIPP performance assessment selected 45 imprecisely known variables for consideration. These variables are listed in Table 3-1 and correspond to the elements x_j, j=1, 2, ..., nV = 45, of the vector **x** shown in Eq. 2.1-2. The distributions indicated in Table 3-1 correspond to the distributions appearing in Eq. 2.1-4 and characterize subjective, or type B, uncertainty.

TABLE 3-1. VARIABLES SAMPLED IN 1991 WIPP PERFORMANCE ASSESSMENT (adapted from Tables 6.0-1, 6.0-2 and 6.0-3 of Vol. 3 of this report)

Variable	Definition
BHPERM	Borehole permeability (k) (m^2). Used in BRAGFLO. Range: 1×10^{-14} to 1×10^{-11}. Median: 3.16×10^{-12}. Distribution: Lognormal. Additional information: Freeze and Cherry, 1979, Table 2-2 (clean sand); Section 4.2.1, Vol. 3. Variable 16 in Latin hypercube sample (LHS).
BPPRES	Initial pressure (p) of pressurized brine pocket in Castile Formation (Pa). Used in BRAGFLO. Range: 1.1×10^7 to 2.1×10^7. Median: 1.26×10^7. Distribution: Piecewise linear. Additional information: Popielak et al., 1983, p. H-52; Lappin et al., 1989, Table 3-19; Section 4.3.1, Vol. 3. Variable 14 in LHS.
BPSTOR	Bulk storativity (S_b) of pressurized brine pocket in Castile Formation (m^3). Used in BRAGFLO. Range: 2×10^{-2} to 2. Median: 2×10^{-1}. Distribution: Lognormal. Additional information: Section 4.3.1, Vol. 3. Variable 15 in LHS.
BPAREAFR	Fraction of waste panel area underlain by a pressurized brine pocket (dimensionless). Used in CCDFPERM in calculation of probability of E1E2-type scenarios. Range: 2.5×10^{-1} to 5.52×10^{-1}. Median: 4×10^{-1}. Distribution: Approximately uniform. Additional information: Section 5.1, Vol. 3. Variable 44 in LHS.
BRSAT	Initial fluid (brine) saturation of waste (dimensionless). Used in BRAGFLO. Range: 0 to 2.76×10^{-1}. Median: 1.38×10^{-1}. Distribution: Uniform. Additional information: Section 3.4.9, Vol. 3. Variable 1 in LHS is uniformly distributed on interval [0,1] and used to select value for BRSAT by preprocessor to BRAGFLO.

TABLE 3-1. VARIABLES SAMPLED IN 1991 WIPP PERFORMANCE ASSESSMENT (adapted from Tables 6.0-1, 6.0-2 and 6.0-3 of Vol. 3 of this report) (continued)

Variable	Definition
CULCLIM	Recharge amplitude factor (A_m) for Culebra (dimensionless). Used in SECO2D. Range: 1 to 1.16. Median: 1.08. Distribution: Uniform. Used in definition of time-dependent heads in Culebra, with the maximum head increasing from the estimated present-day head in the Culebra (i.e., 880 m) for CULCLIM = 1 to a head corresponding to land-surface level (i.e., 1030 m) for CULCLIM = 1.16. Additional information: Section 4.4.3, Vol. 3. Variable 28 in LHS is uniformly distributed on [0,1] and used to select value for CULCLIM by preprocessor to SECO2D. Note: Range of 0 to 0.16 for CULCLIM stated in Section 4.4.3 and Table 6.0-3 of Vol. 3 is incorrect.
CULDISP	Longitudinal dispersivity (α_L) in Culebra (m). Used in STAFF2D. Range : 5×10^1 to 3×10^2. Median: 1×10^2. Distribution: Piecewise uniform. Additional information: Table E-6, Lappin et al., 1989; Section 2.6.2, Vol. 3. Variable 29 in LHS.
CULFRPOR	Fracture porosity (θ_f) in Culebra (dimensionless). Used in STAFF2D and SECO2D. Range: 1×10^{-4} to 1×10^{-2}. Median: 1×10^{-3}. Distribution: Lognormal. Additional information: Tables 1-2 and E-6, Lappin et al. 1989; Section 2.6.4, Vol. 3. Variable 9 in LHS.
CULFRSP	Fracture spacing (2B) in Culebra (m). Used in STAFF2D. Range: 6×10^{-2} to 8. Median: 4×10^{-1} Distribution: Piecewise uniform. Additional information: Memo from Beauheim et al., June 10, 1991, contained in Appendix A, Vol. 3; Section 2.6.4, Vol. 3. Variable 36 in LHS.
CULPOR	Matrix porosity (θ_m) in Culebra (dimensionless). Used in STAFF2D. Range: 9.6×10^{-2} to 2.08×10^{-1}. Median: 1.39×10^{-1}. Distribution: Piecewise uniform. Additional information: Table 4.4, Kelley and Saulnier, 1990; Table E-8, Lappin et al., 1989; Section 2.6.4, Vol. 3. Variable 37 in LHS.
CULTRFLD	Transmissivity field for Culebra. Sixty transmissivity fields consistent with available field data were constructed and ranked with respect to travel time to the accessible environment. CULTRFLD in a pointer variable used to select from these 60 fields, with travel time increasing monotonically with CULTRFLD. Used in STAFF2D and SECO2D. Range: 0 to 1. Distribution: Uniform. Additional information: Sections 6.1 to 6.3, Vol. 2; Section 2.6.9, Vol. 3. Variable 27 in LHS.
DBDIAM	Drill bit diameter (m). Used in CUTTINGS. Range = 2.67×10^{-1} to 4.44×10^{-1}. Median: 3.55×10^{-1}. Distribution: Uniform. Additional information: Section 4.2.2, Vol. 3. Variable 17 in LHS.

TABLE 3-1. VARIABLES SAMPLED IN 1991 WIPP PERFORMANCE ASSESSMENT (adapted from Tables 6.0-1, 6.0-2 and 6.0-3 of Vol. 3 of this report) (continued)

Variable	Definition
EHPH	Index variable used to select the relative areas of the stability regimes for different oxidation states of Np, Pu and U. Used in PANEL in the determination of solubilities. Range: 0 to 1. Median: 0.5. Distribution: Uniform. Additional information: Section 3.3.6, Vol. 3. Variable 18 in LHS.
FKDAM	Fracture distribution coefficient (k_d) for Am in Culebra (m^3/ kg). Used in STAFF2D. Range: 0 to 1×10^3. Median: 9.26×10^1. Distribution: Piecewise uniform. Additional information: Section 2.6.10, Vol. 3. Variable 15 in LHS.
FKDNP	Fracture distribution coefficient (k_d) for Np in Culebra (m^3/kg). Used in STAFF2D. Range: 0 to 1×10^3. Median: 1. Distribution: Piecewise uniform. Additional information: Section 2.6.10, Vol. 3. Variable 16 in LHS.
FKDPU	Fracture distribution coefficient (k_d) for Pu in Culebra (m^3/kg). Used in STAFF2D. Range: 0 to 1×10^3. Median: 2.02×10^2. Distribution: Piecewise uniform. Additional information: Section 2.6.10, Vol. 3. Variable 17 in LHS.
FKDTH	Fracture distribution coefficient (k_d) for Th in Culebra (m^3/kg). Used in STAFF2D. Range: 0 to 1×10^1. Median: 1×10^{-1}. Distribution: Piecewise uniform. Additional information: Section 2.6.10, Vol. 3. Variable 18 in LHS.
FKDU	Fracture distribution coefficient (k_d) for U in Culebra (m^3/kg). Used in STAFF2D. Range: 0 to 1. Median: 7.5×10^{-3}. Distribution: Piecewise uniform. Additional information: Section 2.6.10, Vol. 3. Variable 19 in LHS.
GRCORH	Gas generation rate for corrosion of steel under humid conditions (mol/m^2 surface area steel • s). Used in BRAGFLO. Range: 0 to 5×10^{-1}. Median: 1×10^{-1}. Distribution: Piecewise uniform. Additional information: Memo from Brush, July 8, 1991, contained in Appendix A, Vol.3; Section 3.3.8, Vol. 3. Variable 3 in LHS.
GRCORI	Gas generation rate for corrosion of steel under inundated conditions (mol/m^2 surface area steel • s). Used in BRAGFLO. Range: 0 to 1.3×10^{-8}. Median: 6.3×10^{-9}. Distribution: Piecewise uniform. Additional information: Same as GRCORH. Variable 4 in LHS.
GRMICH	Gas generation rate due to microbial degradation of cellulosics under humid conditions (mol/kg cellulosics • s). Used in BRAGFLO. Range: 0 to 2×10^{-1}. Median: 1×10^{-1}. Distribution: Piecewise uniform. Aditional information: Same as GRCORH. Variable 5 in LHS.

TABLE 3-1. VARIABLES SAMPLED IN 1991 WIPP PERFORMANCE ASSESSMENT (adapted from Tables 6.0-1, 6.0-2 and 6.0-3 of Vol. 3 of this report) (continued)

Variable	Definition
GRMICI	Gas generation rate due to microbial degradation of cellulosics under inundated conditions (mol/kg cellulosics • s). Used in BRAGFLO. Range: 0 to 1.6×10^{-8}. Median: 3.2×10^{-9}. Distribution: Piecewise uniform. Additional information: Same as GRCORH. Variable 6 in LHS.
LAMBDA	Rate constant (λ) in Poisson model for drilling intrusions (s^{-1}). Used in CCDFPERM. Range: 0 to 1.04×10^{-11}. Median: 5.2×10^{-12}. Maximum value corresponds to 30 boreholes per km^2 per 10,000 yr as suggested in 40 CFR 191. Distribution: Uniform. Additional information: Chapters 2 and 3, Vol. 2; Section 5.2, Vol. 3. Variable 43 in LHS.
MBPERM	Permeability (k) in Marker Bed 139 under undisturbed conditions (m^2). Used in BRAGFLO. Range: 6.8×10^{-20} to 9.5×10^{-19}. Median: 7.8×10^{-20}. Distribution: Piecewise uniform with a 0.8 rank correlation with SALPERM. Additional information: Memo from Beauheim, June 14, 1991, contained in Appendix A, Vol. 3; Section 2.4.5, Vol. 3. Variable 12 in LHS.
MBPOR	Porosity (ϕ) in Marker Bed 139 under undisturbed conditions (dimensionless). Used in BRAGFLO. Range: 1×10^{-3} to 3×10^{-2}. Median: 1×10^{-2}. Distribution: Piecewise uniform. Additional information: Section 2.4.7, Vol. 3. Variable 13 in LHS.
MBTHPRES	Threshold displacement pressure (p_t) in Marker Bed 139 (Pa). Used in BRAGFLO. Range: 3×10^3 to 3×10^7. Median: 3×10^5. Distribution: Lognormal. Additional information: Davies, 1991; memo from Davies, June 2, 1991, contained in Appendix A, Vol. 3; Section 2.4.1, Vol. 3. Variable 45 in LHS.
MKDAM	Matrix distribution coefficient (k_d) for AM in Culebra (m^3/kg). Used in STAFF2D. Range: 0 to 1×10^2. Median: 1.86×10^{-1}. Distribution: Piecewise uniform. Additional information: Section 2.6.10, Vol. 3. Variable 38 in LHS.
MKDNP	Matrix distribution coefficient (k_d) for Np in Culebra (m^3/kg). Used in STAFF2D. Range: 0 to 1×10^2. Median: 4.8×10^{-2}. Distribution: Piecewise uniform. Additional information: Section 2.6.10, Vol. 3. Variable 39 in LHS.
MKDPU	Matrix distribution coefficient (k_d) for Pu in Culebra (m^3/kg). Used in STAFF2D. Range: 0 to 1×10^2. Median: 2.61×10^{-1}. Distribution: Piecewise uniform. Additional information: Section 2.6.10, Vol. 3. Variable 40 in LHS.
MKDTH	Matrix distribution coefficient (k_d) for Th in Culebra (m^3/kg). Used in STAFF2D. Range: 0 to 1. Median: 1×10^{-2}. Distribution: Piecewise uniform. Additional information: Section 2.6.10, Vol. 3. Variable 41 in LHS.

TABLE 3-1. VARIABLES SAMPLED IN 1991 WIPP PERFORMANCE ASSESSMENT (adapted from Tables 6.0-1, 6.0-2 and 6.0-3 of Vol. 3 of this report) (continued)

Variable	Definition
MKDU	Matrix distribution coefficient (k_d) for U in Culebra (m^3/kg). Used in STAFF2D. Range: 0 to 1. Median: 2.58×10^{-2}. Distribution: Piecewise uniform. Additional information: Section 2.6.10, Vol. 3. Variable 42 in LHS.
SALPERM	Permeability (k) in Salado (m^2). Used in BRAGFLO. Range: 8.6×10^{-22} to 5.4×10^{-20}. Median: 5.7×10^{-21}. Distribution: Piecewise uniform. Additional information: Memo from Beauheim, June 14, 1991, contained In Appendix A, Vol. 3; Section 2.3.5, Vol. 3. Variable 10 in LHS.
SALPRES	Pressure (p) in Salado (halite and anhydrite components) under undisturbed conditions (Pa). Used in BRAGFLO. Range: 9.3×10^6 to 1.39×10^7. Median: 1.28×10^7. Distribution: Piecewise uniform. Additional information: Memos from Beauheim, June 14, 1991, and Howarth, June 12, 1991, contained in Appendix A, Vol. 3; Section 2.4.6, Vol. 3. Variable 11 in LHS.
SOLAM	Solubility of Am^{+3} in brine (mol/ℓ). Used in PANEL. Range: 5×10^{-14} to 1.4. Median: 1×10^{-9}. Distribution: Piecewise uniform. Additional information: Trauth et al., 1991; Section 3.3.5, Vol. 3. Variable 19 in LHS.
SOLNP4	Solubility of Np^{+4} in brine (mol/ℓ). Used in PANEL. Range: 3×10^{-16} to 2×10^{-5}. Median: 6×10^{-9}. Distribution: Piecewise uniform with 0.99 rank correlation with SOLNP5. For each sample element, value for SOLNP4 is used if EHPH < 0.474/(0.474 + 0.503) = 0.485; otherwise, value for SOLNP4 is used; see Figure 3.3-9, Vol. 3. Additional information: Same as SOLAM. Variable 20 in LHS. Due to the 0.99 rank correlation between SOLNP4 and SOLNP5, the variables SOLNP4 and SOLNP5 are essentially indistinguishable in a rank regression; because of this high correlation, rank regressions presented later in this report use the symbol SOLNP for Np solubility.
SOLNP5	Solubility of Np^{+5} in brine (mol/ℓ). Used in PANEL. Range: 3×10^{-11} to 1.2×10^{-2}. Median: 6×10^{-7}. Distribution: Piecewise uniform with 0.99 rank correlation with SOLNP4. Additional information: Same as SOLAM. Variable 21 in LHS.
SOLPU4	Solubility of Pu^{+4} in brine (mol/ℓ). Used in PANEL. Range: 2×10^{-16} to 4×10^{-6}. Median: 6×10^{-10}. Distribution: Piecewise uniform with 0.99 rank correlation with SOLPU5. For each sample element, value for SOLPU4 is used if EHPH < 0.539/(0.539 + 0.152) = 0.780; otherwise, value for SOLPU5 is used; see Figure 3.3-9, Vol. 3. Additional information: Same as SOLAM. Variable 22 in LHS. Due to the 0.99 rank correlation between SOLPU4 and SOLPU5, the variables SOLPU4 and SOLPU5 are essentially indistinguishable in a rank regression; because of this high correlation, rank regressions presented later in this report use the symbol SOLPU for Pu solubility.

TABLE 3-1. VARIABLES SAMPLED IN 1991 WIPP PERFORMANCE ASSESSMENT (adapted from Tables 6.0-1, 6.0-2 and 6.0-3 of Vol. 3 of this report) (concluded)

Variable	Definition
SOLPU5	Solubility of Pu^{+5} in brine (mol/ℓ). Used in PANEL. Range: 2.5×10^{-17} to 5.5×10^{-4}. Median: 6×10^{-10}. Distribution: Piecewise uniform with 0.99 rank correlation with SOLPU4. Additional information: Same as SOLAM. Variable 23 in LHS.
SOLTH	Solubility of Th in brine (mol/ℓ). Used in PANEL. Range: 5.5×10^{-16} to 2.2×10^{-6}. Median: 1×10^{-10}. Distribution: Piecewise uniform. Additional information: Same as SOLAM. Variable 24 in LHS.
SOLU4	Solubility of U^{+4} in brine (mol/ℓ). Used in PANEL. Range: 1×10^{-15} to 5×10^{-2}. Median: 1×10^{-4}. Distribution: Piecewise uniform with 0.99 rank correlation with SOLU6. For each sample element, value for SOLU4 is used if EHPH < 0.299/(0.299 + .701) = 0.299; otherwise, value for SOLU6 is used; see Figure 3.3-9, Vol. 3. Additional information: Same as SOLAM. Variable 25 in LHS. Due to the 0.99 rank correlation between SOLU4 and SOLU6, the variables SOLU4 and SOLU6 are essentially indistinguishable in a rank regression; because of this high correlation, rank regressions presented later in this report use the symbol SOLU for U solubility.
SOLU6	Solubility of U^{+6} in brine (mol/ℓ). Used in PANEL. Range: 1×10^{-7} to 1. Median: 2×10^{-3}. Distribution: Piecewise uniform with 0.99 rank correlation with SOLU4. Additional information: Same as SOLAM. Variable 26 in LHS.
STOICCOR	Stoichiometric coefficient for corrosion of steel (mol H_2/mol Fe). Used in BRAGFLO. Range: 0 to 1. Median: 5×10^{-1}. Distribution: Uniform. Additional information: Brush and Anderson in Lappin et al., 1989, p. A-6; Section 3.3.8, Vol. 3. Variable 2 in LHS.
STOICMIC	Stoichiometric coefficient for microbial degradation of cellulosics (mol gas/mol CH_2O). Used in BRAGFLO. Range: 0 to 1.67. Median: 8.35×10^{-1}. Distribution: Uniform. Additional information: Brush and Anderson in Lappin et al., 1989, p. A-10; Section 3.3.9, Vol. 3. Variable 9 in LHS.
VMETAL	Fraction of total waste volume that is occupied by IDB (Integrated Data Base) metals and glass waste category (dimensionless). Used in BRAGFLO. Range: 2.76×10^{-1} to 4.76×10^{-1}. Median: 3.76×10^{-1}. Distribution: Normal. Additional information: Section 3.4.1, Vol. 3. Variable 7 in LHS.
VWOOD	Fraction of total waste volume that is occupied by IDB combustible waste category (dimensionless). Used in BRAGFLO. Range: 2.84×10^{-1} to 4.84×10^{-1}. Median: 3.84×10^{-1}. Distribution: Normal. Additional Information: Section 3.4.1, Vol. 3. Variable 8 in LHS.

As discussed in conjunction with Eq. 2.1-5, a Latin hypercube sample (McKay et al., 1979; Iman and Shortencarier, 1984) of size nK = 60 was generated from the variables listed in Table 3-1. The restricted pairing technique developed by Iman and Conover (1982) was used to induce the correlations between variables indicated in Table 3-1 and also to assure that the correlations between other variables were close to zero.

Once the sample indicated in Eq. 2.1-5 was generated from the variables in Table 3-1, the individual sample elements $\mathbf{x}_k$, k=1, ..., 60, were used in the generation of the risk results shown in Eq. 2.1-6. An overview of this process is provided in Sections 2.2, 2.3 and 2.4. In addition to many intermediate results, the final outcome of this process is a distribution of CCDFs of the form shown in Figure 2.1-2.

The analyses leading to the risk results shown in Eq. 2.1-6 were actually repeated a number of times with different modeling assumptions. The specific cases considered are listed in Table 3-2. The first case listed in Table 3-2, gas generation in the repository and a dual-porosity transport model in the Culebra Dolomite, is believed to be the most creditable and is presented as the best-estimate analysis in the 1991 WIPP preliminary performance assessment. The other cases listed in Table 3-2 can be viewed as *ceteris paribus* sensitivity studies that explore various perturbations on this best-estimate analysis.

In addition to the variation between the cases shown in Table 3-2, the sampling-based approach to the treatment of subjective uncertainty also produces uncertainty and sensitivity results for the individual cases. In the following two chapters, box plots and distributions of CCDFs will be used to display the effect of subjective uncertainty on the cases listed in Table 3-2, and the impact of individual variables will be investigated with sensitivity analysis techniques based on scatterplots, regression analysis and partial correlation analysis. Scatterplots will also be used to compare results obtained with the different analysis cases listed in Table 3-2.

Additional information on the uncertainty and sensitivity analysis techniques in use is available elsewhere (Ch. 3, Vol. 1: Helton et al., 1991).

TABLE 3-2. DIFFERENT ANALYSIS CASES SELECTED FOR CONSIDERATION IN THE 1991 WIPP PERFORMANCE ASSESSMENT

Case	Description
1	Gas generation in repository and a dual-porosity (matrix and fracture porosity) transport model in Culebra Dolomite with drilling intrusions occurring at 1000, 3000, 5000, 7000, and 9000 yrs. Considered best-estimate analysis in 1991 WIPP performance assessment. Discussion in Chapter 4.
2	No gas generation in repository and a dual-porosity (matrix and fracture porosity) transport model in Culebra with drilling intrusions occurring at 1000 yrs. The 1991 preliminary comparison is the first one to include a two-phase (brine and gas), Darcy-flow model in the compliance assessment system. Previous deterministic two-phase calculations (Bertram-Howery et al., 1990, Chapter 6) implied that including waste-generated gas would not negatively affect compliance status with the containment requirements when compared to previous comparisons that assumed fully brine-saturated repository conditions. To understand the impact of including new processes associated with waste-generated gas, Case 1 with waste-generated gas is compared with Case 2 without waste-generated gas. Discussion in Section 5.1.
3	Gas generation in repository and a single-porosity (fracture porosity) transport model in Culebra with drilling intrusions occurring at 1000, 3000, 5000, 7000, and 9000 yrs. For fully brine-saturated repository conditions, the 1990 preliminary comparison (Bertram-Howery et al., 1990; Helton et al., 1991) analyzed the importance of a dual-porosity assumption (Reeves et al., 1987) for modeling radionuclide transport. A study to assess the defensibility of this assumption has started. To establish the continuing importance of this work with the new modeling system that includes waste-generated gas, Case 1 with a dual-porosity (matrix and fracture porosity) model for transport is compared with Case 3 with a single-porosity (fracture porosity) model for transport. Discussion in Section 5.2.
4	No gas generation in repository and a single-porosity (fracture porosity) transport model in Culebra with drilling intrusions occurring at 1000 yrs. Included for completeness and to provide an analysis for single-porosity transport that was not complicated by the effects of gas generation. Discussion in Section 5.3.
5	Gas generation in repository and a dual-porosity (matrix and fracture porosity) transport model without chemical retardation in Culebra with drilling intrusions occurring at 1000 yrs. Under agreement with the State of New Mexico (U.S. DOE and State of New Mexico, 1981, as modified, Vol. 1, Appendix B, p. B-14, Comment 14), a case using zero distribution coefficients will continue to be included in these preliminary comparisons until site-specific information becomes available. Case 5 with zero distribution coefficients in a dual-porosity transport model (physical retardation is included) is compared to Case 1 with nonzero distribution coefficients to assess the importance of obtaining a defensible data set for chemical retardation. Discussion in Section 5.4.

TABLE 3-2. DIFFERENT ANALYSIS CASES SELECTED FOR CONSIDERATION IN THE 1991 WIPP PERFORMANCE ASSESSMENT (concluded)

Case	Description
6	Effect of climate change with gas generation in repository and with single- and dual-porosity transport models in the Culebra and intrusions occurring at 1000 yrs. To date, the preliminary comparisons have not addressed the problem of conceptual model uncertainty except for the dual-porosity and waste-generated gas cases. Future comparisons will need to consider alternative conceptual models throughout the modeling system. Case 6 is a first attempt to assess the importance of a simple model (not intended to be a bounding case) for including climate variability through a recharge and infiltration modeling assumption for use with the 2-D confined aquifer conceptual model of the Culebra. Discussion in Section 5.5.

General: The preliminary comparisons are interim analyses to assess the status of compliance and provide annual guidance to the project through uncertainty/sensitivity analyses. The cases included here are intended to help identify and understand important processes in the modeling system for the 1991 guidance.

4. UNCERTAINTY AND SENSITIVITY ANALYSIS RESULTS FOR 1991 PRELIMINARY COMPARISON

At present, the most appropriate conceptual model for performance assessment at the WIPP is believed to include gas generation due to both corrosion and microbial action in the repository and a dual-porosity (matrix and fracture porosity) representation for transport in the Culebra Dolomite Member of the Rustler Formation (i.e., Case 1 in Table 3-2). This conceptual view was used in the modeling that produced the best-estimate performance-assessment results for the WIPP presented in Chapter 6 of Vol. 1. This chapter presents uncertainty and sensitivity analysis results associated with these current best-estimate calculations.

4.1 Uncertainty in CCDFs

The distribution of CCDFs for normalized release to the accessible environment, including both cuttings and cavings removal (hereafter called cuttings removal) and groundwater transport, that results from the imprecisely known variables presented in Chapter 3 is given in Figure 2.1-1. This figure was constructed with a Latin hypercube sample of size 60 generated from the 45 variables in Table 3-1. The construction of each CCDF appearing in Figure 2.1-1 was based on the scenarios, scenario probabilities and scenario consequences described in Sections 2.2, 2.3 and 2.4, respectively. As is the case for all results involving groundwater transport presented in Chapter 4, gas generation is assumed to take place in the repository and a dual-porosity model is used to represent radionuclide transport in the Culebra. The results contained in Figure 2.1-1 are presented in Chapter 6, Vol. 1, of this report as the current best estimate of the CCDFs for comparison with the EPA release limits. As examination of Figure 2.1-1 shows, consideration of gas generation in the repository and a dual-porosity transport model in the Culebra results in all CCDFs being below the EPA release limits.

Although Figure 2.1-1 presents all 60 CCDFs that result for the sample indicated in Eq. 2.1-5, it is rather cluttered and hard to read. A less crowded summary can be obtained by plotting the mean value and selected percentile values for the individual releases appearing on the abscissa. The mean and percentile values are obtained from the exceedance probabilities associated with the individual release values and the weights, or "probabilities" (i.e., 1/60), associated with the individual sample elements. The result of this calculation is shown in Figure 4.1-1 for the mean plus the 10th, 50th (i.e., median) and 90th percentile values. The calculated mean and percentile values are for specific releases on the abscissa of Figure 2.1-1; the curves in Figure 4.1-1 result from connecting these individual

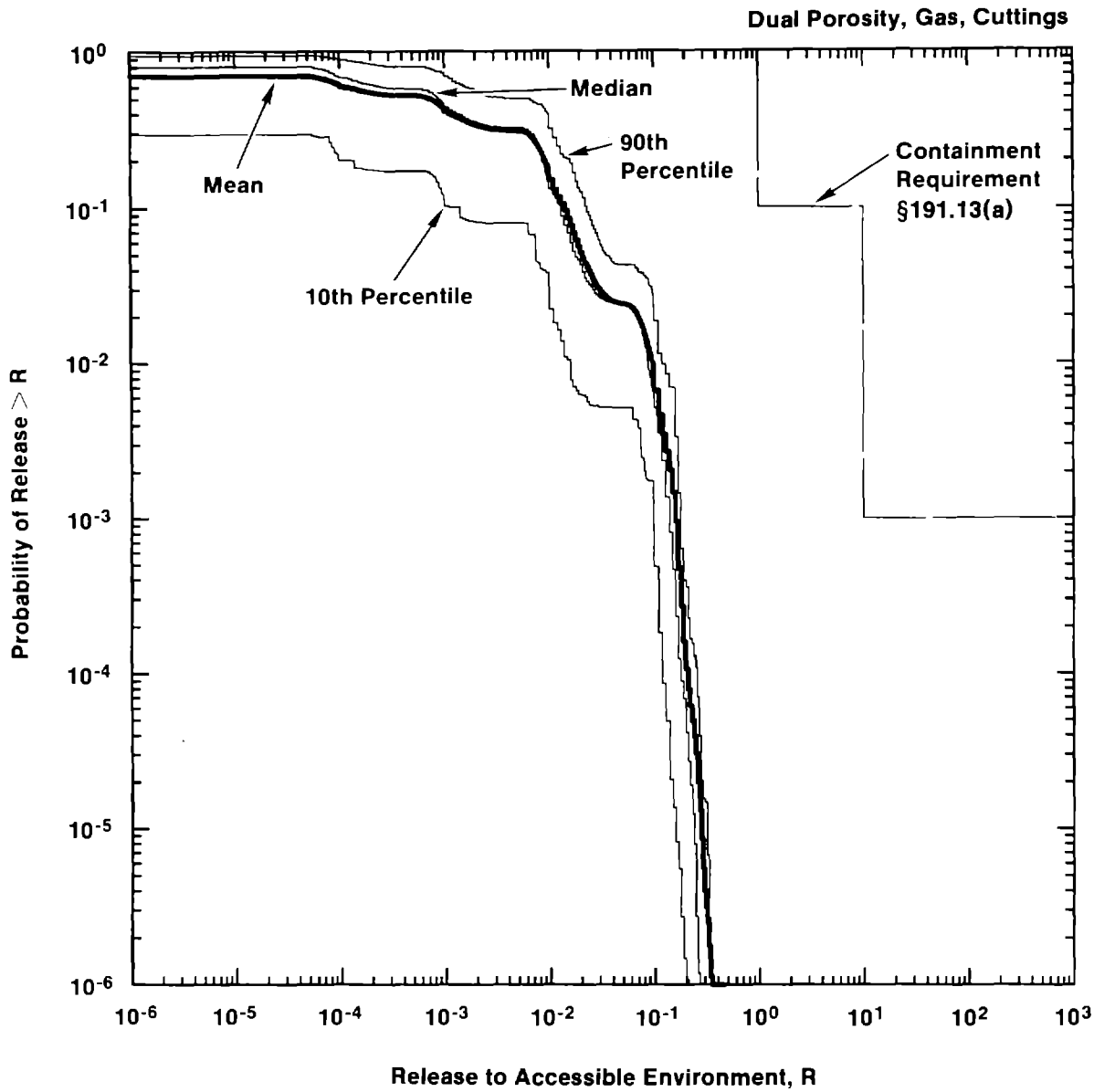

TRI-6342-1294-1

Figure 4.1-1. Mean and Percentile Curves for Distribution of Complementary Cumulative Distribution Functions Shown in Figure 2.1-1 for Normalized Releases to the Accessible Environment Including Both Cuttings Removal and Groundwater Transport with Gas Generation in the Repository and a Dual-Porosity Transport Model in the Culebra Dolomite.

values. The mean and percentile curves appearing in Figure 4.1-1 result from the subjective uncertainty in the variables in Table 3-1, as does the distribution of CCDFs in Figure 2.1-1. In contrast, the individual CCDFs in Figure 2.1-1 provide a representation for stochastic uncertainty.

As indicated in Eqs. 2.4-10 through 2.4-14, the total release to the accessible environment for a given scenario is the sum of a release due to cuttings removal and a release due to groundwater transport. For comparison, Figure 4.1-2 shows the CCDFs that result when only releases due to cuttings removal are considered (upper two frames) and only releases due to groundwater transport are considered (lower two frames). As examination of Figure 4.1-2 shows, releases to the accessible environment are dominated by cuttings removal. The only exception to this occurs for the upper-right CCDF in Figure 2.1-2, which is dominated by the groundwater release. Otherwise, the CCDFs in Figure 2.1-2 are essentially identical to the cuttings-release-only CCDFs in Figure 4.1-2.

As shown in Figure 4.1-2, only 4 groundwater-release-only CCDFs involve normalized releases to the accessible environment that are greater than 10^{-6} at an exceedance probability of 10^{-6}. Further, only 16 CCDFs involve releases that are greater than 10^{-12} at an exceedance probability of 10^{-6}. Thus, the uncertainty characterization and associated modeling for the variables in Table 3-1 lead to limited releases to the accessible environment due to groundwater transport.

The releases associated with the individual release modes (i.e., cuttings removal and groundwater transport) are now considered. Specifically, uncertainty and sensitivity analysis results for cuttings removal are presented in Sections 4.2 and 4.3, followed by similar results for groundwater transport in Sections 4.4 and 4.5. Then, sensitivity analysis results for the CCDFs in Figure 2.1-1 are presented in Section 4.6.

4.2 Uncertainty in Cuttings Removal

The variation in the total normalized release to the accessible environment due to cuttings removal resulting from boreholes intersecting waste of average activity level is shown in Figure 4.2-1 for intrusions occurring at 1000, 3000, 5000, 7000 and 9000 yrs. Specifically, box plots in Figure 4.2-1 show the normalized releases due to cuttings removal (i.e., the rC_i defined in Eq. 2.4-1) for scenarios $S(1,0,0,0,0)$, $S(0,1,0,0,0)$, $S(0,0,1,0,0)$, $S(0,0,0,1,0)$ and $S(0,0,0,0,1)$ as defined in Eq. (2.2-3). Each box plot summarizes the distribution of results obtained with the previously discussed Latin hypercube sample of size 60 from the variables in Table 3-1; thus, each box plot is based on 60 observations.

Cuttings Releases Only

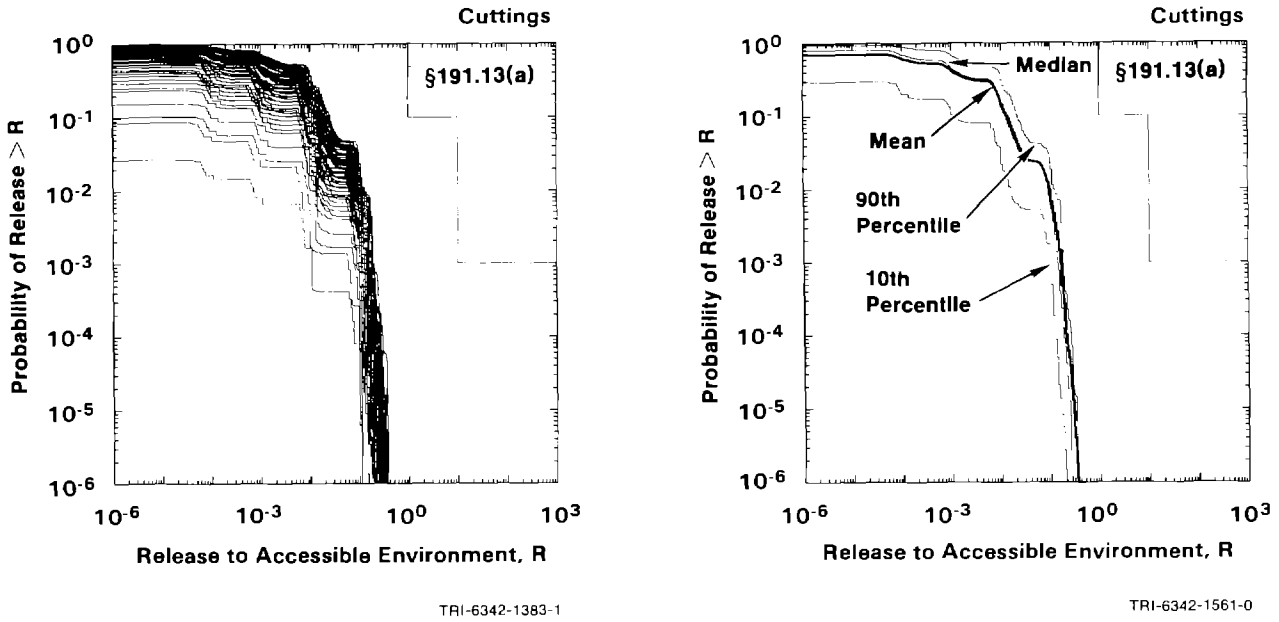

Groundwater Transport Releases Only

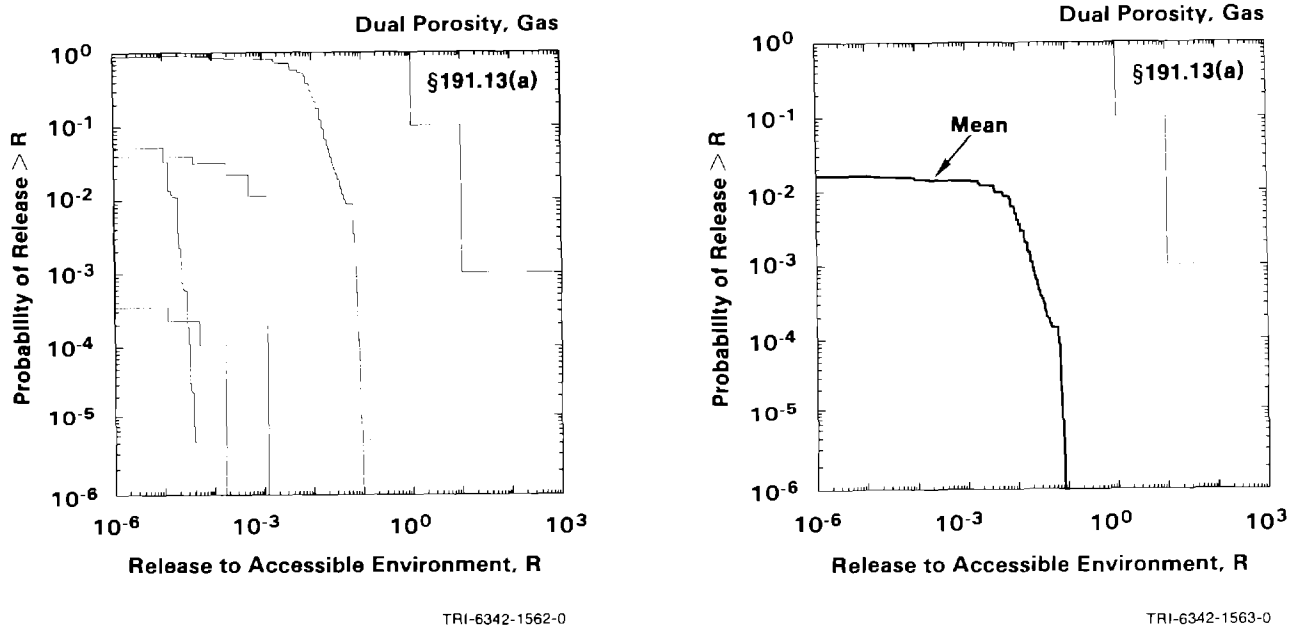

Figure 4.1-2. Comparison of Complementary Cumulative Distribution Functions for Normalized Releases to the Accessible Environment for Cuttings Removal Only (upper two frames) and Groundwater Transport with Gas Generation in the Repository and a Dual-Porosity Transport Model in the Culebra Dolomite (lower two frames).

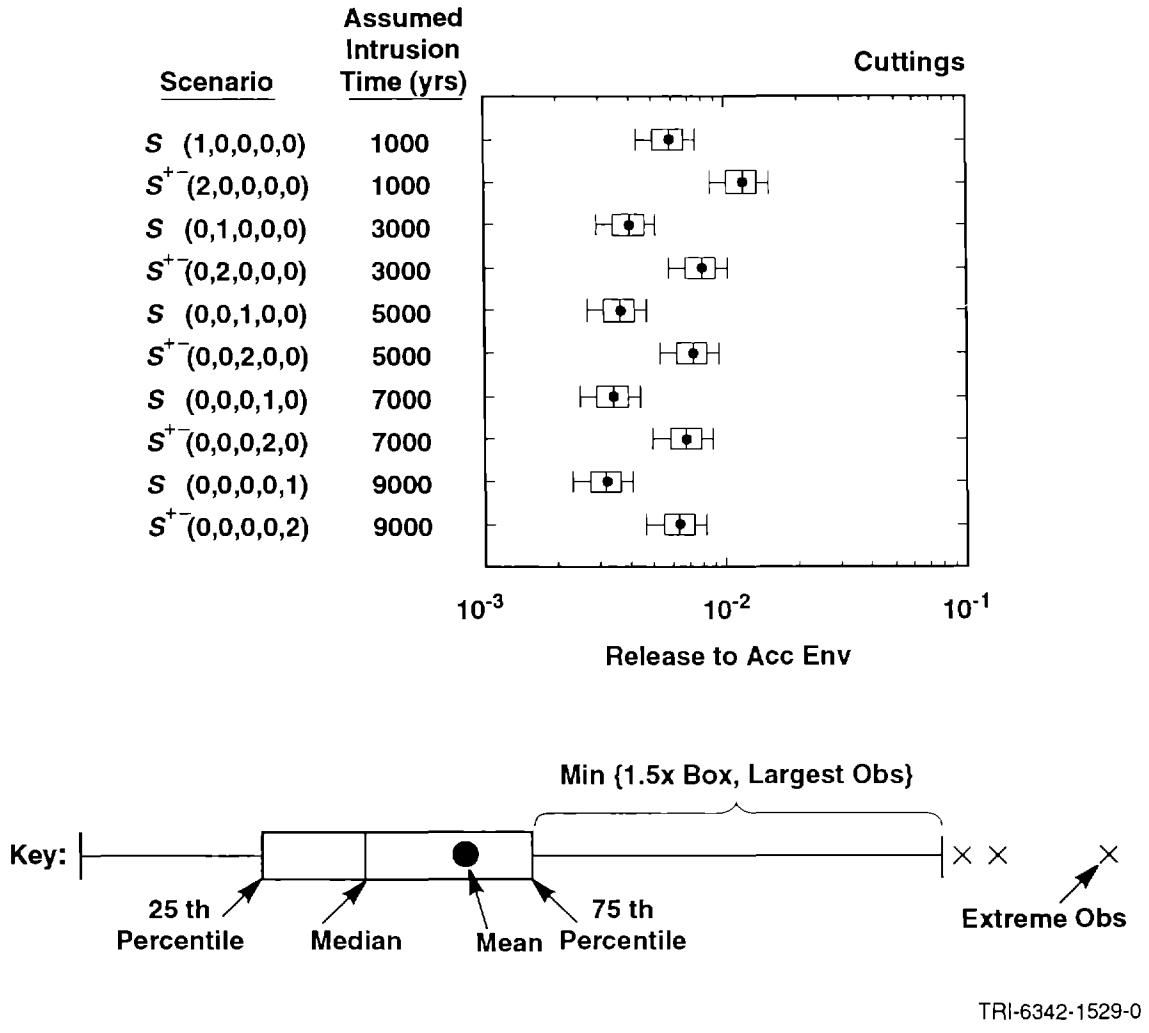

Figure 4.2-1. Total Normalized Release to the Accessible Environment Due to Cuttings Removal from Waste of Average Activity Level.

As a reminder, the endpoints of the boxes in Figure 4.2-1 are formed by the lower and upper quartiles of the data, that is $x_{.25}$ and $x_{.75}$. The vertical line within the box represents the median, $x_{.50}$. The sample mean is identified by the large dot. The bar on the right of the box extends to the minimum of $x_{.75} + 1.5(x_{.75} - x_{.25})$ and the maximum observation. In a similar manner, the bar on the left of the box extends to the maximum of $x_{.25} - 1.5(x_{.75} - x_{.25})$ and the minimum observation. Observations falling outside of these bars are shown with x's. In symmetric distributions, these values would be considered outliers. Extreme values of this type do not appear in Figure 4.2-1 but will be present in most box plots presented in this report. The structure of box plots is illustrated in the key appearing at the bottom of Figure 4.2-1.

All results involving cuttings removal in the 1991 WIPP performance assessment are derived from the total normalized releases for scenarios $S(1,0,0,0,0)$ through $S(0,0,0,0,1)$ summarized in Figure 4.2-1. For comparison and consistency with later figures, Figure 4.2-1 also shows the normalized releases due to cuttings removal (i.e., 2 rC_i) for scenarios $S^{+-}(2,0,0,0,0)$ through $S^{+-}(0,0,0,0,2)$ as defined in Eq. 2.2-9, with the subscript i appearing in the definition of $S_i^{+-}(\mathbf{n})$ in Eq. 2.2-9 omitted due to redundancy. As discussed in conjunction with Eq. 2.4-15, a scale factor is used to convert from releases of waste of average activity level to releases of waste of the five activity levels shown in Table 2.4-4. These scaled releases are then used in the construction of releases due to cuttings removal of waste of different activity levels for scenarios $S(\mathbf{l},\mathbf{n})$ and $S^{+-}(\mathbf{l};t_{i-1},t_i)$ as shown in Eqs. 2.4-12 and 2.4-14, respectively.

As examination of Figure 4.2-1 shows, all of the normalized releases associated with a single borehole and average activity level waste are between 0.001 and 0.01. The largest scale factor defined by Eq. 2.4-15 to convert from an average activity level release to a release of a specified activity level is approximately 23.1, which results for time steps i=1,2,3,4,5 and waste of activity level ℓ=4 (e.g., SF_{24} as shown in Eq. 2.4-16). Thus, a single borehole at the first time step used in the analysis (i.e., 1000 yrs) will not result in a normalized release that exceeds 1, although it is possible that a single borehole into waste of activity level 4 at an earlier time might result in a normalized release greater than 1.

The contribution of individual isotopes to the total normalized release to the accessible environment due to cuttings removal resulting from a single borehole intersecting waste of average activity level is shown in Figure 4.2-2. Only three isotopes contribute to the total release at 1000 yrs:

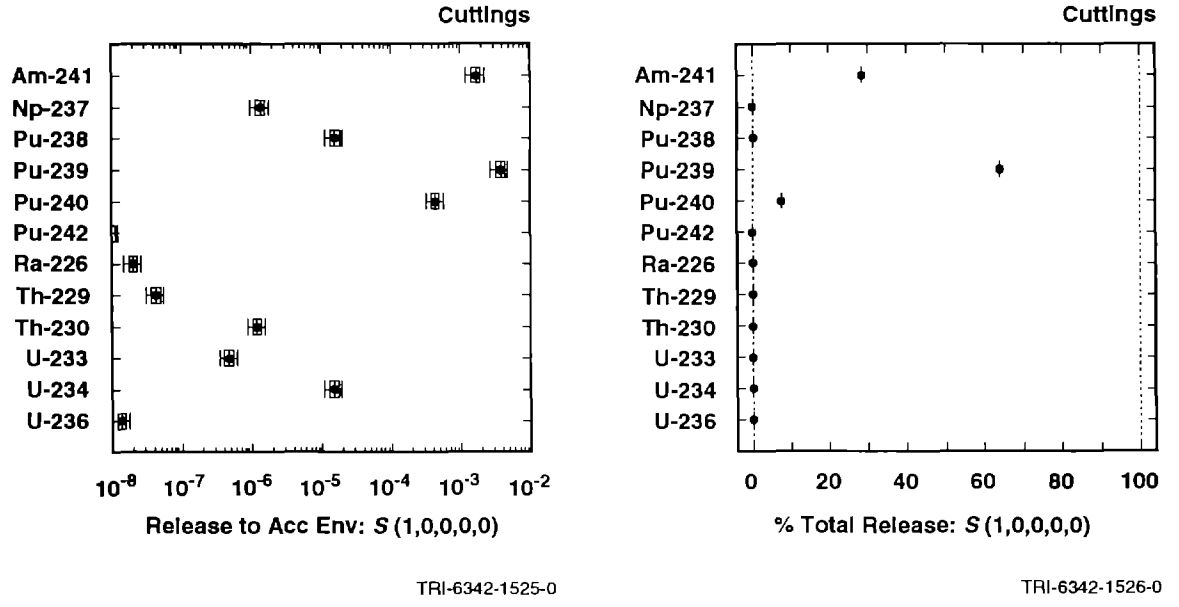

Figure 4.2-2. Normalized Releases to the Accessible Environment for Individual Isotopes and Percent Contribution to the Total Normalized Release for Cuttings Removal Resulting from a Single Borehole Intersecting Waste of Average Activity Level at 1000 Yrs. The results shown in this figure correspond to the releases associated with scenario $S(1,0,0,0,0)$.

Am-241, Pu-239 and Pu-240. No other isotopes make an appreciable contribution to the total release. At later times, the total release is dominated by Pu-239 due to the decay of Am-241, with a small contribution from Pu-240.

4.3 Sensitivity Analysis for Cuttings Removal

Drill bit diameter (DBDIAM) is the only variable in Table 3-1 that affects cuttings removal. This variable is used as an input to the CUTTINGS program, where it is used in the calculation of an eroded or "effective" diameter for the borehole as it passes through the repository. The eroded diameter is the actual determinant of the amount of waste that is removed to the surface.

The relationships between drill bit diameter (DBDIAM), eroded diameter and normalized release to the accessible environment due to cuttings removal are shown in the scatterplots appearing in Figure 4.3-1. Scatterplots present the points (x_k, y_k), $k = 1,2,\ldots, nK$, where x_k and y_k are results associated

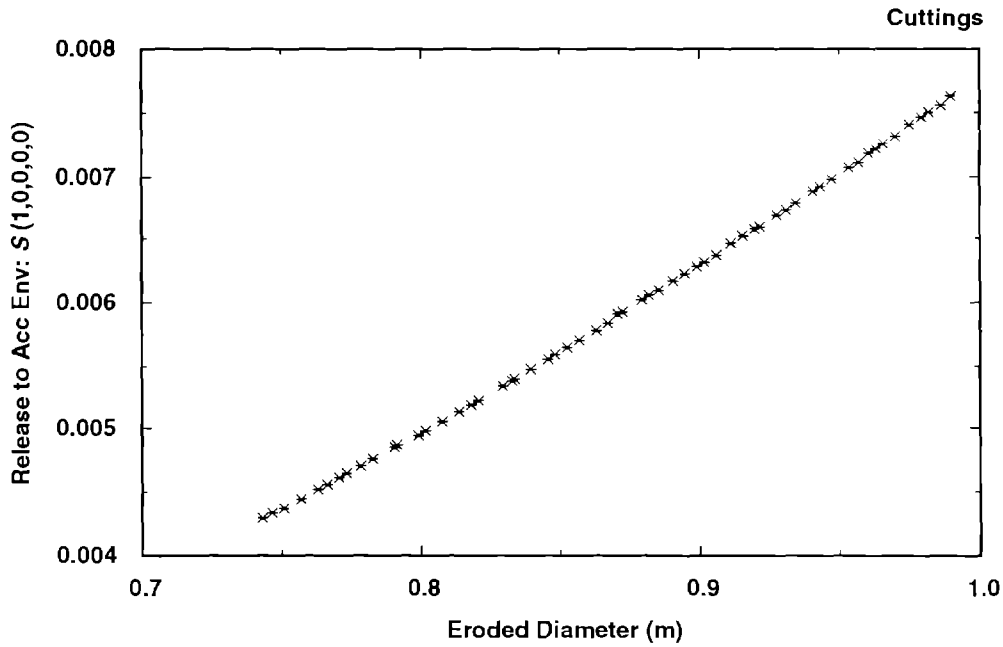

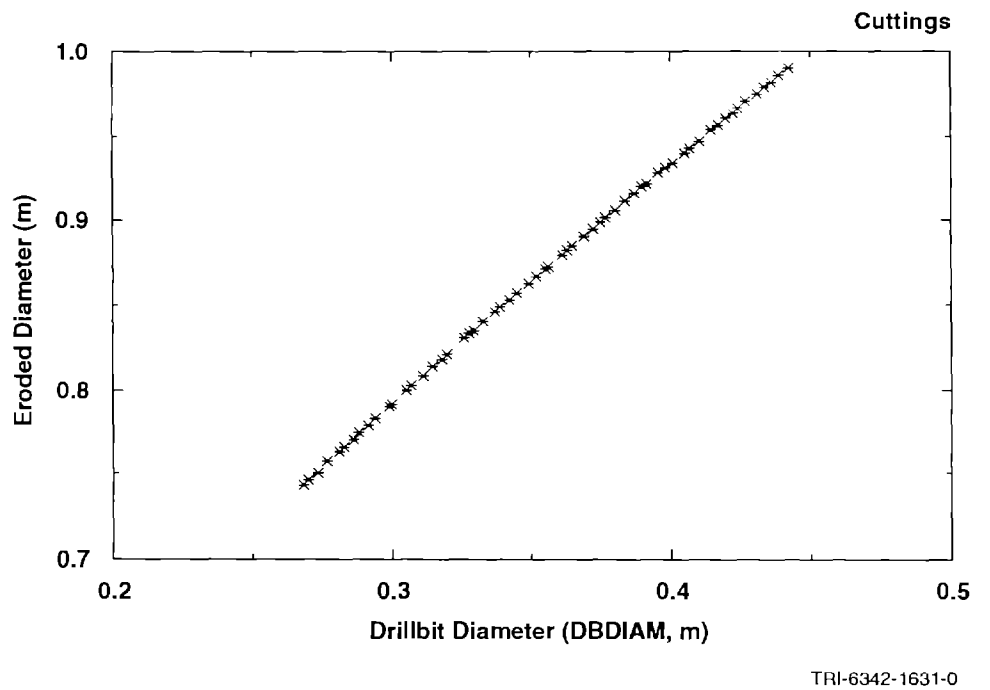

Figure 4.3-1. Scatterplots Displaying Relationships between Drill Bit Diameter (DBDIAM, a sampled variable), Eroded Diameter of Borehole (a calculated variable), and Associated Normalized Cuttings Release to the Accessible Environment (a calculated variable) for Waste of Average Activity Level with Intrusion Occurring at 1000 Yrs (i.e., the release for scenario $S(1,0,0,0,0)$).

with sample element $\mathbf{x}_k$ shown in Eq. 2.1-5 and nK is the sample size. Often, x_k is the value for a particular sampled variable contained in $\mathbf{x}_k$, and y_k is the value for a particular calculated variable contained in one of the vectors $\mathbf{cS}_i(\mathbf{x}_k)$ shown in Eq. 2.1-6. A scatterplot of this type appears in the lower frame of Figure 4.3-1, where x_k corresponds to the value for DBDIAM (drill bit diameter) in $\mathbf{x}_k$ and y_k corresponds to the eroded diameter of the resultant borehole calculated for $\mathbf{x}_k$. In other cases, both x_k and y_k are values calculated for $\mathbf{x}_k$. A scatterplot of this type appears in the upper frame of Figure 4.3-1, where x_k corresponds to the eroded diameter of the resultant borehole calculated for $\mathbf{x}_k$ and y_k corresponds to the normalized release to the accessible environment due to cuttings removal calculated for $\mathbf{x}_k$. Scatterplots facilitate the examination of the results obtained for individual sample elements.

As examination of Figure 4.3-1 shows, release to the accessible environment varies in an almost linear manner with drill bit and eroded borehole diameter. The relationship between normalized release and eroded borehole diameter shown in Figure 4.3-1 is actually quadratic. However, due to the relatively small range for eroded diameter (i.e., approximately 0.75 m to 1.0 m), the relationship is also very close to being linear.

Drill bit diameter provides an excellent example of the choice that must be made in deciding whether a particular variable involves stochastic (i.e., type A) uncertainty or subjective (i.e., type B) uncertainty. Clearly, drill bits of different diameters are used now and also will be used in the future. Thus, the occurrence of boreholes initiated by drill bits of different diameters is a stochastic uncertainty. If this stochastic uncertainty was felt to be important, then drill bit diameter would have to be one of the characteristics used to define the scenarios S_i appearing in Eq. 2.1-1. Further, a probability distribution D_A would have to be developed that described the likelihood that boreholes initiated by drill bits of different sizes would occur. This distribution would be one of the determinants of the probabilities pS_i appearing in Eq. 2.1-1. In contrast, it is also possible to decide that drill bit diameter is not sufficiently important to merit incorporation into the definition of the scenarios S_i, which is equivalent to deciding that the performance assessment can be reasonably carried out with only one value for drill bit diameter. However, given the decision that use of a single appropriately selected drill bit diameter will not compromise the results of the analysis, it may not be clear what this single value should be. In this case, a subjective distribution D_B can be used to characterize where this appropriate value is located. The distributions D_A and D_B are being used to characterize different aspects of the same physical process, and thus will not be the same. For the 1991 WIPP performance assessment, the distribution assigned to drill bit diameter characterizes subjective uncertainty.

4.4 Uncertainty in Groundwater Releases

As discussed in conjunction with Eqs. 2.4-3 and 2.4-4, two types of groundwater releases to the accessible environment are considered in the 1991 WIPP performance assessment: a release initiated by a single borehole (i.e., E2-type scenarios) and a release initiated by two or more boreholes in the same waste panel and time interval, of which at least one penetrates a pressurized brine pocket and at least one does not penetrate a pressurized brine pocket (i.e., E1E2-type scenarios). As already indicated by the groundwater-release-only CCDFs shown in Figure 4.1-2, the releases due to groundwater transport are very small. Additional perspective is provided by Figure 4.4-1, which shows the normalized releases to the accessible environment for scenarios of the E2- and E1E2-type, respectively. Of the 60 sample elements considered in this analysis, only 7 resulted in nonzero releases for an E2-type scenario with intrusion occurring at 1000 yrs (i.e., for $S(1,0,0,0,0)$) and only 15 resulted in nonzero releases for an E1E2-type scenario with intrusion occurring at 1000 yrs (i.e., for $S^{+-}(2,0,0,0,0)$). Further, even the few nonzero releases are small.

The normalized releases shown in Figure 4.4-1 correspond to the releases $rGW1_i$ and $rGW2_i$ shown in Eqs. 2.4-3 and 2.4-4. As shown in Eqs. 2.4-12 and 2.4-14, these releases are used to construct the groundwater releases to the accessible environment for scenarios of the form $S(\mathbf{l},\mathbf{n})$ and $S^{+-}(\mathbf{l};t_{i-1},t_i)$. The best-estimate comparisons with the EPA release limits in the 1991 WIPP performance assessment used the groundwater transport results summarized in Figure 4.4-1.

For additional perspective, Figure 4.4-2 summarizes the normalized releases to the accessible environment and the percent contributions to the total release for individual isotopes for intrusions occurring at 1000 yrs. The percent contributions can only be calculated for the nonzero releases. Specifically, the distributions summarized in Figure 4.4-2 and other similar figures for percent contribution to total release are conditional in the sense that they are based only on the sample elements that have a nonzero total release. As examination of Figure 4.4-2 shows, total release to the accessible environment, when it occurs, is usually dominated by U-234, although there are sample elements in which the release is completely dominated by Np-237, Pu-239 or Th-230. However, the total normalized release is very small in all cases (i.e., always less than 10^{-1} and usually less than 10^{-3}). The releases due to intrusions occurring at later times (i.e., 3000, 5000, 7000, and 9000 yrs) are even smaller than those shown in Figure 4.4-2 due to increased time for decay and decreased time for transport.

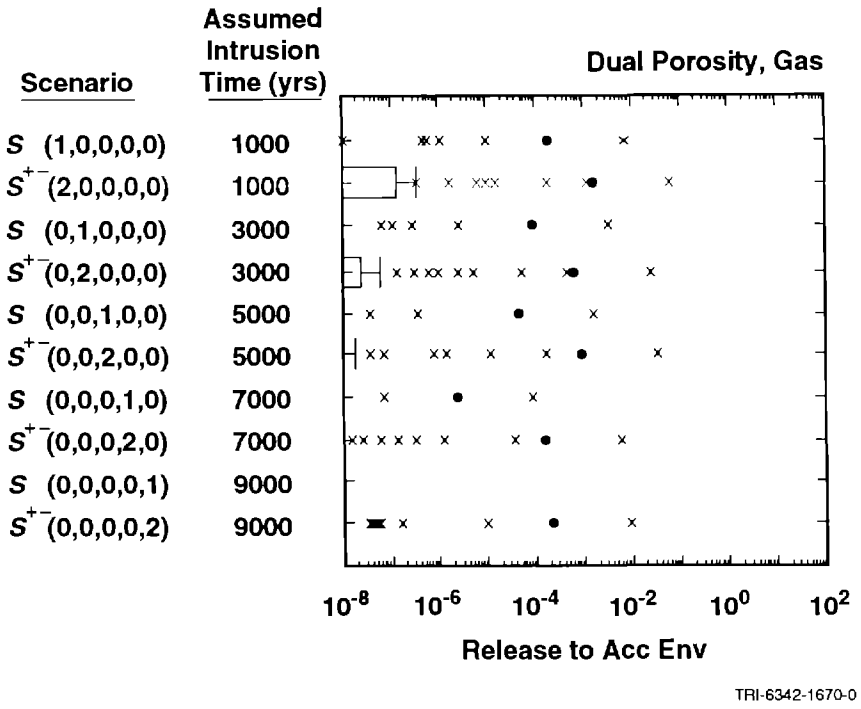

Figure 4.4-1. Total Normalized Release to the Accessible Environment Due to Groundwater Transport with Gas Generation in the Repository and a Dual-Porosity Transport Model in the Culebra Dolomite.

As described in Eqs. 2.4-10 through 2.4-14, the total release to the accessible environment for a scenario is the sum of a cuttings-removal component and a groundwater-transport component. The uncertainty in these individual components is summarized in Figures 4.2-1 and 4.4-1. Total release to the accessible environment, including cuttings removal and groundwater transport, is summarized in Figure 4.4-3. As comparison with Figure 4.2-1 shows, inclusion of releases due to groundwater transport has little effect on the total releases for the individual scenarios.

The large number of zero releases associated with the results shown in Figure 4.4-1 is reassuring with respect to the possible suitability of the WIPP as a disposal facility for transuranic waste. However, these zero releases tend to obscure what is going on in the analysis. Additional insight can be obtained by examining the releases from the repository to the Culebra. The total normalized release to the Culebra as predicted by the PANEL program is shown in Figure 4.4-4. The individual releases summarized in this figure constitute the initial input to the STAFF2D program for radionuclide transport in the Culebra. For the 60 sample elements, 38 result in zero releases to the Culebra due to an E2-type scenario with intrusion occurring at 1000 yrs (i.e., for scenario $S(1,0,0,0,0)$), while only 2 sample elements result in a zero release to the Culebra due to an E1E2-type scenario with intrusion occurring at 1000 yrs (i.e., for scenario $S^{+-}(2,0,0,0,0)$).

Scenario: $S(1,0,0,0,0)$, Assumed Intrusion Time: 1000 yrs

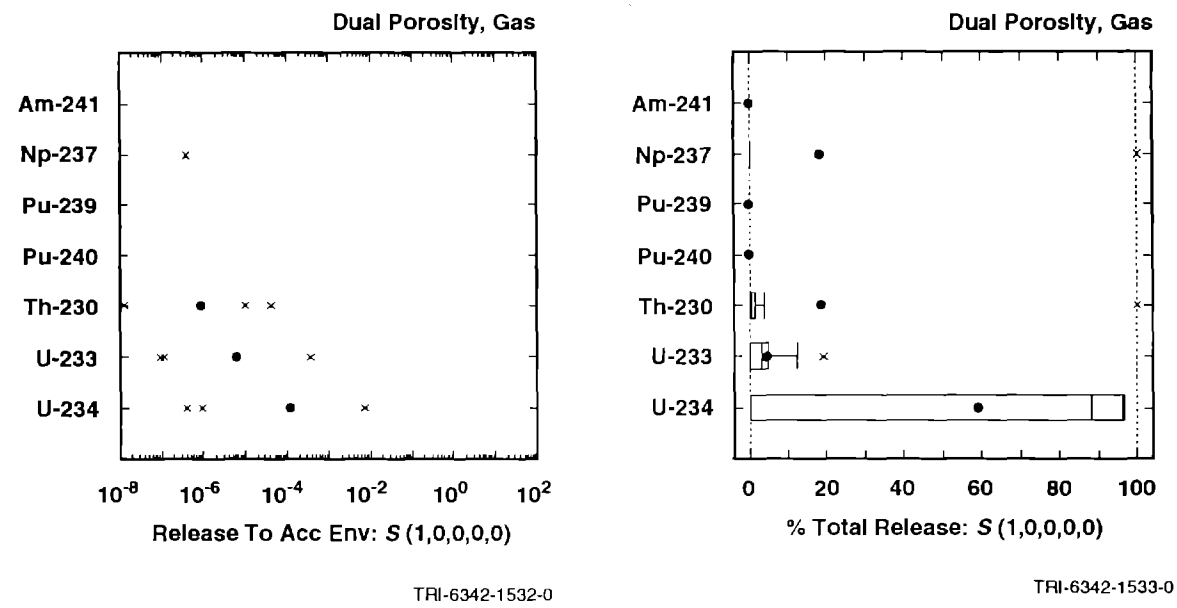

Scenario: $S^{+-}(2,0,0,0,0)$, Assumed Intrusion Time: 1000 yrs

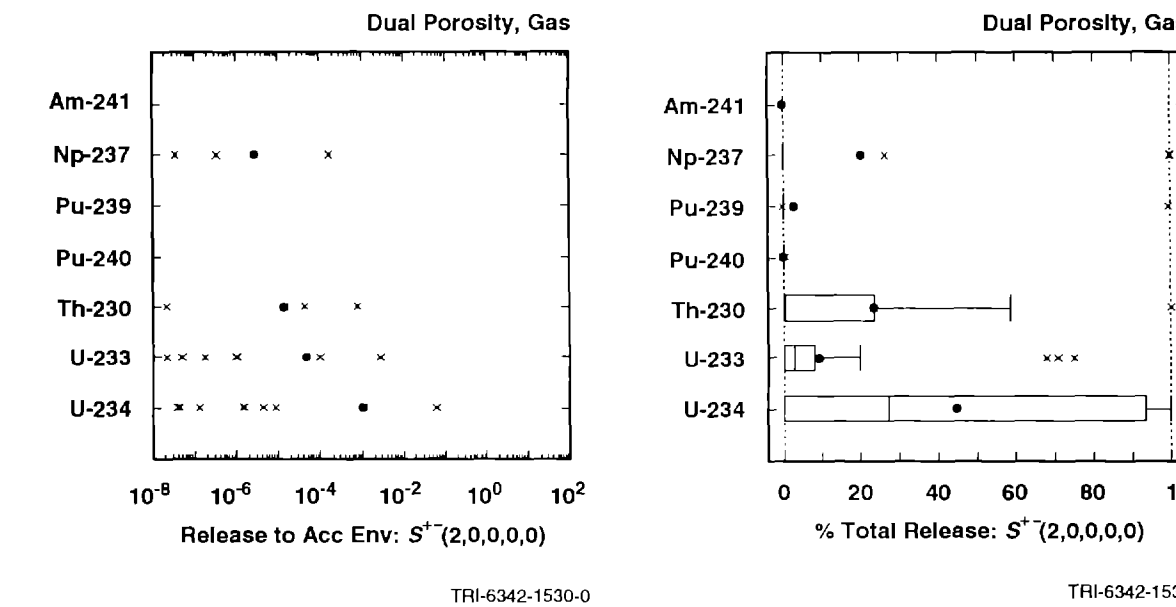

Figure 4.4-2. Normalized Releases for Individual Isotopes to the Accessible Environment Due to Groundwater Transport with Intrusion Occurring at 1000 Yrs, Gas Generation in the Repository and a Dual-Porosity Transport Model in the Culebra Dolomite.

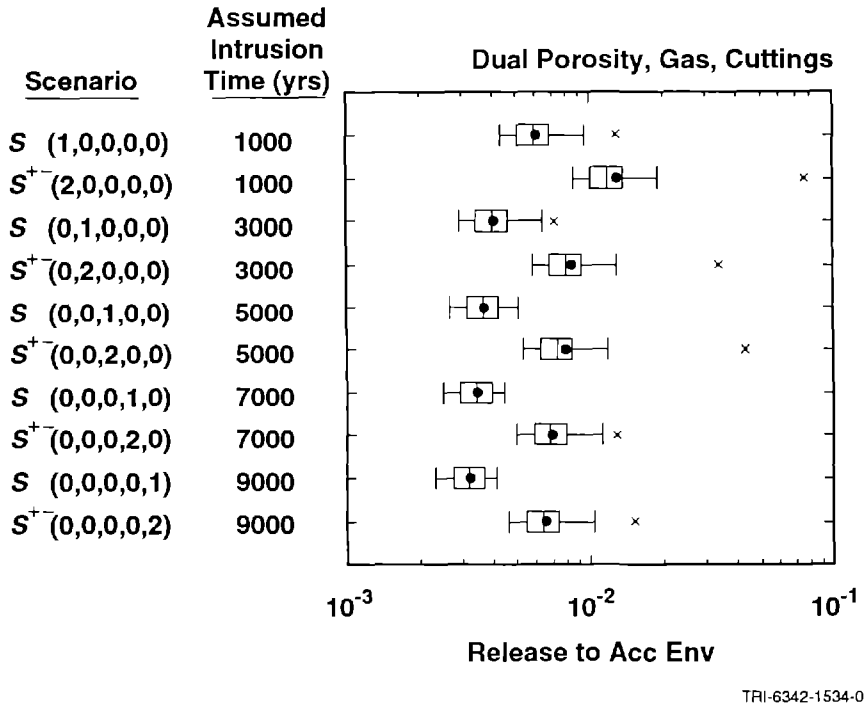

Figure 4.4-3. Total Normalized Release to the Accessible Environment Due to Cuttings Removal and Groundwater Transport with Gas Generation in the Repository and a Dual-Porosity Transport Model in the Culebra Dolomite.

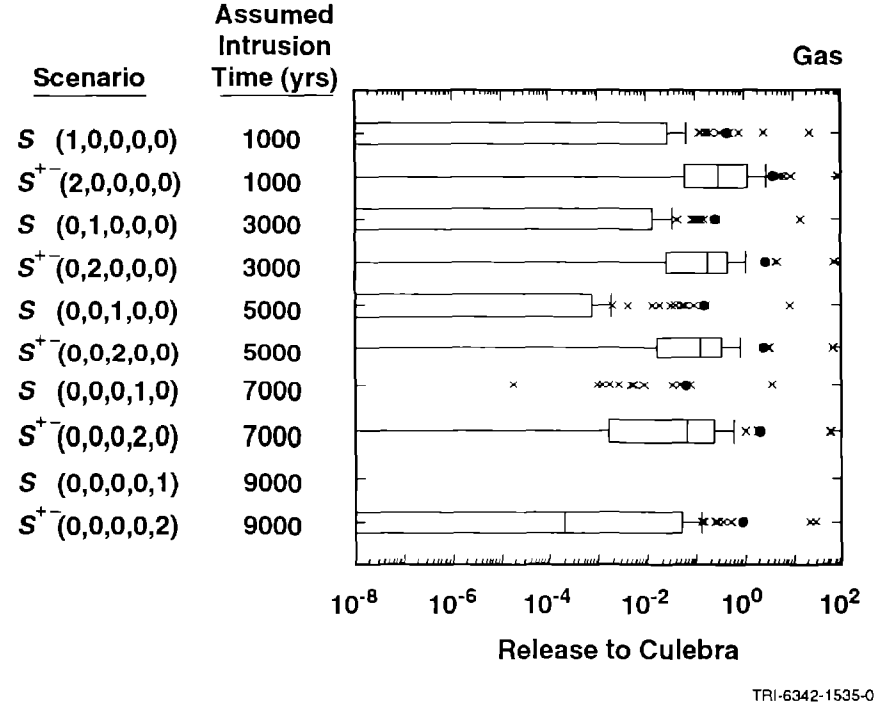

Figure 4.4-4. Total Normalized Release to the Culebra Dolomite as Predicted by the PANEL Program with Gas Generation in the Repository.

Three insights emerge from the information summarized in Figures 4.4-1 and 4.4-4. First, the Culebra appears to provide an effective barrier in reducing groundwater transport releases to the accessible environment. For example, scenario $S(1,0,0,0,0)$ has 22 nonzero releases to the Culebra but only 7 nonzero releases to the accessible environment, and scenario $S^{+-}(2,0,0,0,0)$ has 58 nonzero releases to the Culebra but only 15 nonzero releases to the accessible environment. The extent of this reduction is illustrated for scenario $S^{+-}(2,0,0,0,0)$ by the scatterplot appearing in Figure 4.4-5. Second, even the release to the Culebra for E2-type scenarios is often zero. At present, the probability of E2-type scenarios at the WIPP is estimated to be considerably larger than the probability for E1E2-type scenarios. (e.g., see Chapters 2 and 3 of Vol. 2). Third, the releases to the Culebra may be several orders of magnitude larger for E1E2-type scenarios than for E2-type scenarios. This pattern is illustrated for scenarios $S^{+-}(2,0,0,0,0)$ and $S(1,0,0,0,0)$ by the scatterplot appearing in Figure 4.4-6.

For additional perspective, Figure 4.4-7 summarizes the normalized release to the Culebra for individual isotopes for intrusions occurring at 1000 yrs. As examination of this figure shows, total release into the Culebra tends to be dominated by U-234, although Pu-239 is an important contributor for some sample elements. Further, Am-241 is also an important contributor at 1000 yrs but is unimportant at later times to radioactive decay.

The releases summarized in Figure 4.4-7 are carried into the Culebra by the upward flow of brine from the repository through an intruding borehole. The total brine release to the Culebra is summarized in Figure 4.4-8. The variables that cause the variation in brine flow to the Culebra shown in Figure 4.4-8 are determined in a sensitivity analysis presented in the next section.

4.5 Sensitivity Analysis for Groundwater Releases

Stepwise regression analysis can be used to examine the relationships between the sampled variables listed in Table 3-1 and groundwater releases to the accessible environment. Such analyses can be carried out with the original variables or with these variables transformed in some manner (e.g., logarithms, ranks, ...). The present analysis tried regressions with both the original variables and with their rank-transformed values (Iman and Conover, 1979). The regressions with rank-transformed variables (i.e., rank regressions) generally outperformed the regressions with the original variables.

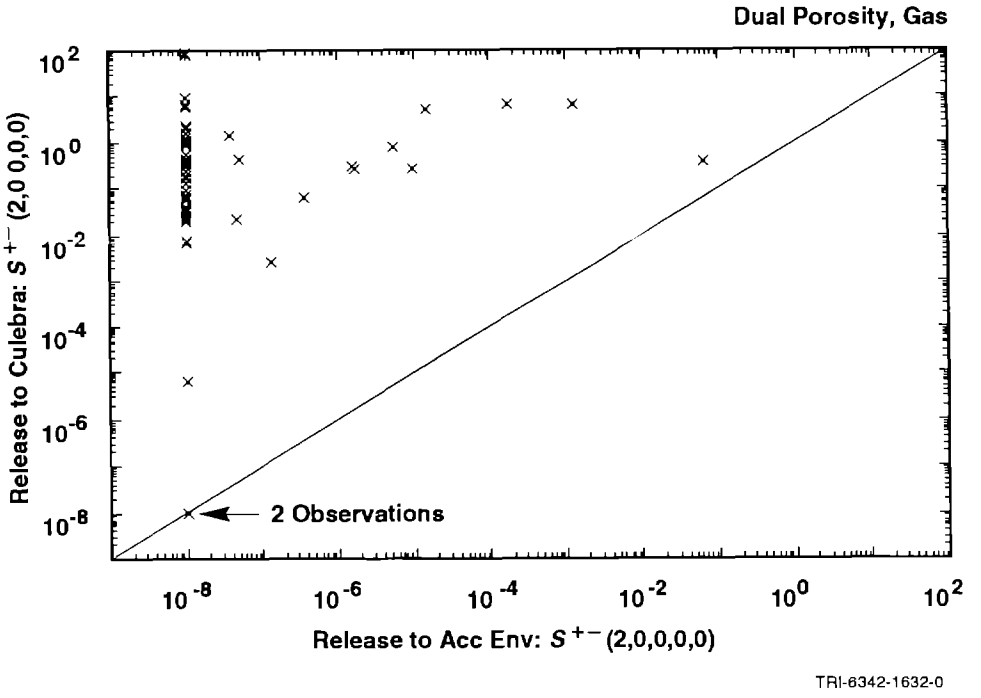

Figure 4.4-5. Scatterplot of Total Normalized Release to the Culebra Dolomite and Total Normalized Release to the Accessible Environment for Scenario S^{+-}(2,0,0,0,0) with Gas Generation in the Repository, a Dual-Porosity Transport Model in the Culebra Dolomite and Intrusion Occurring at 1000 Yrs. For plotting purposes, values less than 10^{-8} are set to 10^{-8}.

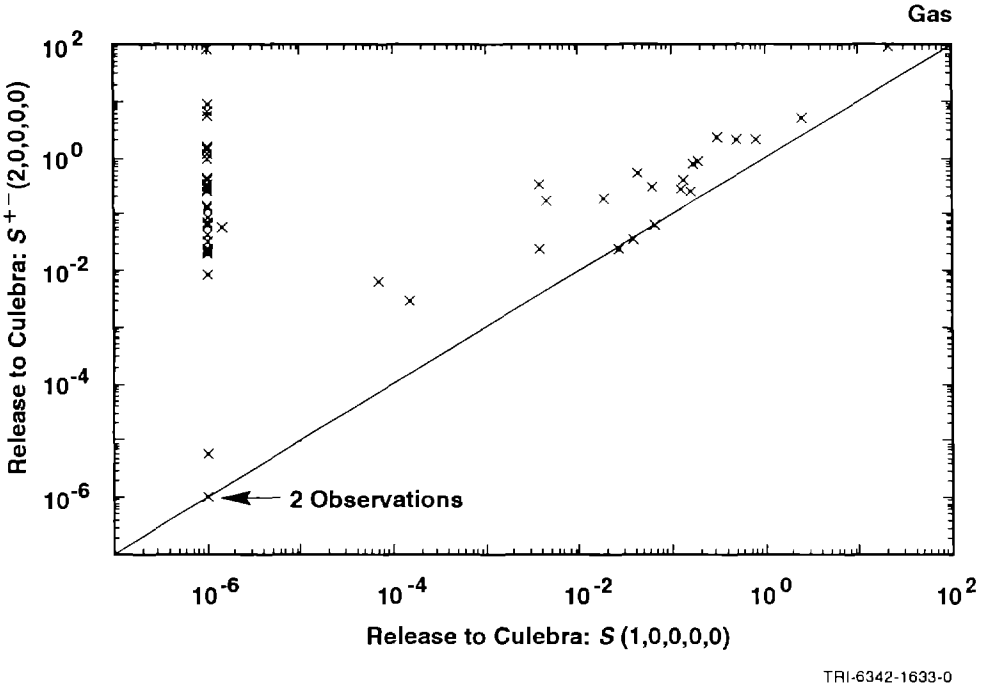

Figure 4.4-6. Scatterplot of Total Normalized Release to the Culebra Dolomite with Gas Generation in the Repository and Intrusion Occurring at 1000 Yrs for Scenarios S(1,0,0,0,0) and S^{+-}(2,0,0,0,0). For plotting purposes, values less than 10^{-6} are set to 10^{-6}.

Scenario: $S(1,0,0,0,0)$, Assumed Intrusion Time: 1000 yrs

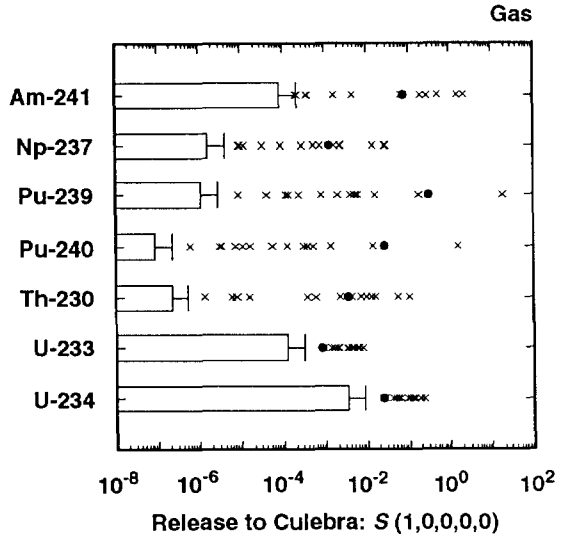

TRI-6342-1536-0

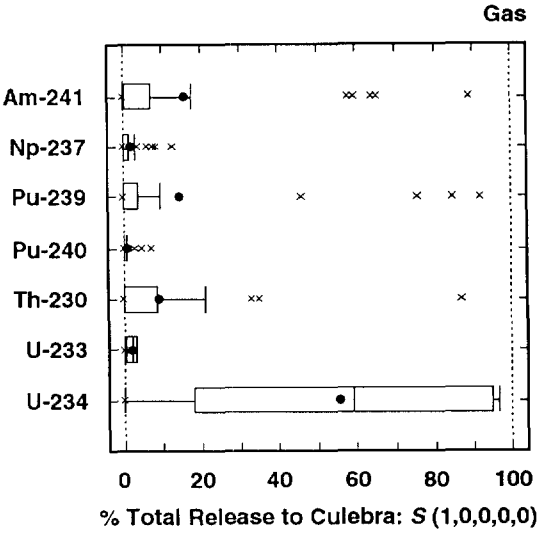

TRI-6342-1537-0

Scenario: $S^{+-}(2,0,0,0,0)$, Assumed Intrusion Time: 1000 yrs

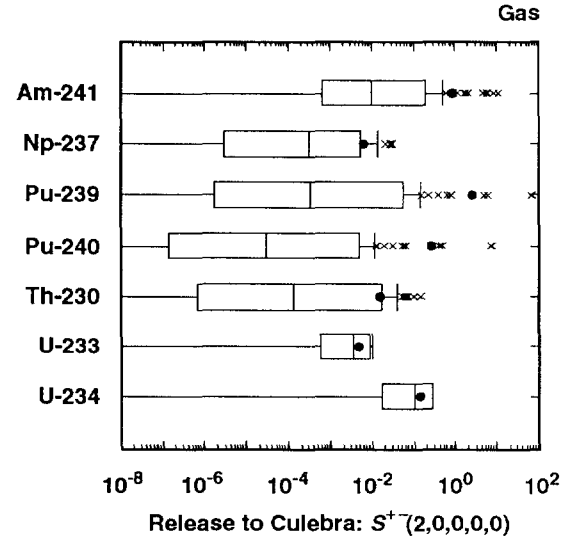

TRI-6342-1538-0

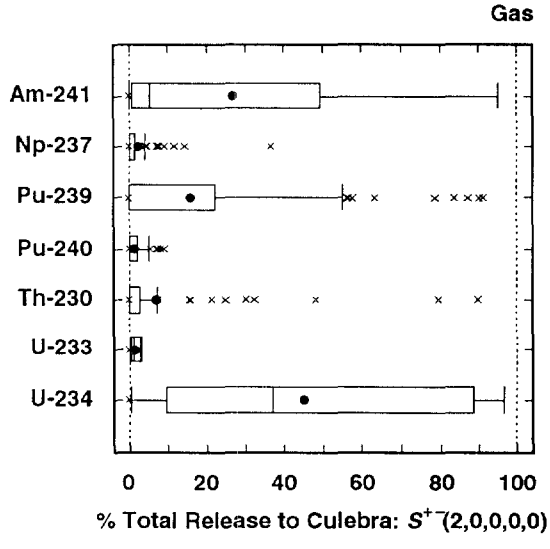

TRI-6342-1539-0

Figure 4.4-7. Normalized Releases for Individual Isotopes to the Culebra Dolomite with Intrusion Occurring at 1000 Yrs and Gas Generation in the Repository.

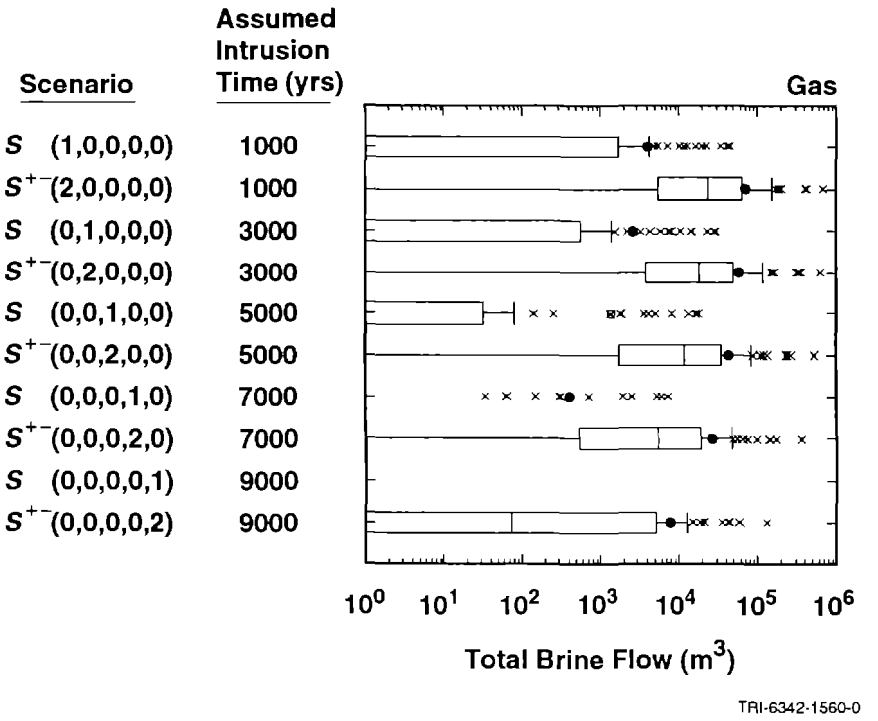

Figure 4.4-8. Total Brine Flow (m^3) from the Repository to the Culebra Dolomite with Gas Generation in the Repository.

Rank regressions for scenario $S(1,0,0,0,0)$ are presented in Table 4.5-1 for release from the repository to the Culebra Dolomite and for groundwater transport one-quarter, one-half and the full distance to the accessible environment. As indicated in Figures 1.5-4, 2.1-1 and 2.1-2 of Vol. 3, the accessible environment is assumed to begin 5 km from the waste panels. The actual dependent variables in the regression analyses are the integrated releases from time of intrusion (i.e., 1000 yrs for scenario $S(1,0,0,0,0)$) to 10,000 yrs. Thus, the dependent variables in the regression analyses summarized in the columns labeled "Release to Culebra", "Quarter Distance", "Half Distance" and "Full Distance" in Table 4.5-1 and other similar tables are integrated radionuclide releases from time of intrusion to 10,000 yrs into the Culebra, through a surface 1.25 km from the repository, through a surface 2.5 km from the repository and through a surface 5 km from the repository, respectively. Further, the column labeled "Variable" lists the variables in the order that they entered the stepwise regression analysis, and the column labeled "R^2" lists the cumulative R^2 value for all variables included in the regression model through the step under consideration. The "+" or "-" appearing in parentheses after the R^2 value designates the sign of the regression coefficient for the variable entering the regression model at the step under consideration. Regression diagnostics (i.e., α-values and the

TABLE 4.5-1. STEPWISE REGRESSION ANALYSES WITH RANK-TRANSFORMED DATA FOR SCENARIO $S(1,0,0,0,0)$ WITH GAS GENERATION IN THE REPOSITORY, A DUAL-POROSITY TRANSPORT MODEL IN THE CULEBRA DOLOMITE AND INTRUSION OCCURRING 1000 YRS AFTER REPOSITORY CLOSURE

	Release to Culebra		Quarter Distance		Half Distance		Full Distance	
Step	Variable	R^2	Variable	R^2	Variable	R^2	Variable	R^2
Dependent Variable: Integrated Discharge Am-241								
1	SALPERM	0.59(+)	--	--	SALPERM	0.14 (+)	--	--
2					FKDAM	0.24 (+)		
3					MKDAM	0.32 (-)		
4					CULFRPOR	0.39 (+)		
Dependent Variable: Integrated Discharge Np-237								
1	SALPERM	0.53(+)	MBPERM	0.20 (+)	SALPERM	0.19 (+)	MBPERM	0.11 (+)
2					MKDNP	0.30 (-)		
Dependent Variable: Integrated Discharge Pu-239								
1	SALPERM	0.56(+)	CULCLIM	0.09 (+)	MBPERM	0.18 (+)	--	--
2					FKDPU	0.27 (+)		
3					VWOOD	0.34 (-)		
Dependent Variable: Integrated Discharge Pu-240								
1	SALPERM	0.56(+)	CULCLIM	0.09 (+)	MBPERM	0.18 (+)	--	--
2					FKDPU	0.27 (+)		
3					VWOOD	0.34 (-)		
Dependent Variable: Integrated Discharge Th-230								
1	SALPERM	0.55(+)	SALPERM	0.48 (+)	SALPERM	0.23 (+)	MKDU	0.20 (-)
2			CULFRPOR	0.57 (+)	MKDU	0.39 (-)	SALPERM	0.34 (+)
3			MKDU	0.65 (-)	CULFRPOR	0.45 (+)	CULCLIM	0.52 (+)
Dependent Variable: Integrated Discharge U-233								
1	SALPERM	0.59(+)	SALPERM	0.32 (+)	SALPERM	0.18 (+)	MKDU	0.17 (-)
2			MKDU	0.46 (-)	MKDU	0.33 (-)	SALPERM	0.32 (+)
3			CULFRPOR	0.56 (+)				
4			CULCLIM	0.61 (+)				

TABLE 4.5-1. STEPWISE REGRESSION ANALYSES WITH RANK-TRANSFORMED DATA FOR SCENARIO $S(1,0,0,0,0)$ WITH GAS GENERATION IN THE REPOSITORY, A DUAL-POROSITY TRANSPORT MODEL IN THE CULEBRA DOLOMITE AND INTRUSION OCCURRING 1000 YRS AFTER REPOSITORY CLOSURE (concluded)

	Release to Culebra		Quarter Distance		Half Distance		Full Distance	
Step	Variable	R^2	Variable	R^2	Variable	R^2	Variable	R^2
Dependent Variable: Integrated Discharge U-234								
1	SALPERM	0.59(+)	SALPERM	0.38 (+)	SALPERM	0.23 (+)	MKDU	0.26 (-)
2			MKDU	0.54 (-)	MKDU	0.43 (-)	SALPERM	0.36 (+)
3			CULFRPOR	0.61 (+)	CULFRPOR	0.51 (+)	CULTRFLD	0.42 (+)
4					CULCLIM	0.57 (+)		
Dependent Variable: EPA Sum for Total Integrated Discharge								
1	SALPERM	0.58(+)	SALPERM	0.51 (+)	SALPERM	0.42 (+)	SALPERM	0.20 (+)
2			CULFRPOR	0.59 (+)	MKDU	0.51 (-)	MKDU	0.32 (-)
3			MKDU	0.64 (-)	CULFRPOR	0.59 (+)	CULCLIM	0.41 (+)
4			CULCLIM	0.69 (+)				
5			MKDAM	0.73 (-)				

PRESS criterion) were used to provide guidance on the variables selected for inclusion in the final regression models. However, the final selection of variables had a significant subjective component, with spurious variables being excluded from the final regression models. The stepwise regression analyses presented in this report were performed with the STEPWISE program (Iman et al., 1980). An overview of the regression-based sensitivity analysis techniques used in the generation of Table 4.5-1 and other similar tables in this report is provided in Section 3.5.2 of Vol. 1, and a more detailed description of these techniques is given in Helton et al. (1991).

As examination of the R^2 values associated with the individual regression analyses in Table 4.5-1 shows, none of the regressions are particularly successful in accounting for the observed variation in either the releases for the individual isotopes or the total EPA normalized release. Specifically, the largest R^2 value in Table 4.5-1 is 0.73 and most R^2 values are considerably smaller. This lack of resolution in the regression models is not surprising given the large number of zero releases associated with the scenario $S(1,0,0,0,0)$.

When thresholds and other complex relationships are present, the examination of scatterplots is often revealing. The scatterplots presented in Figure 4.5-1 for the normalized release of Pu-239 to the Culebra provide an excellent example of the type of information that can sometimes be extracted from scatterplots. As a reminder, the stepwise regression analysis presented in Table 4.5-1 for the release of Pu-239 to the Culebra for scenario $S(1,0,0,0,0)$ selected only the variable SALPERM (Salado permeability) with an R^2 value of 0.56, which indicates that the release is dominated by SALPERM but also that much of the variability in the release is not accounted for. The upper two scatterplots in Figure 4.5-1 provide significantly more insight into what controls the release of Pu-239 to the Culebra.

As shown by the scatterplot appearing in the upper left of Figure 4.5-1, the variable SALPERM acts as a switch for scenario $S(1,0,0,0,0)$ with zero (i.e., $< 10^{-8}$) releases of Pu-239 resulting for SALPERM $< 5 \times 10^{-21}$ m^2, and nonzero releases resulting for SALPERM $> 5 \times 10^{-21}$ m^2. However, given that there is a nonzero release, there is little relationship between SALPERM and the size of the release. As shown by the scatterplot appearing in the upper right of Figure 4.5-1, the size of the nonzero releases is dominated by SOLPU (solubility for Pu).* Thus, SALPERM determines whether or not there is a Pu-239 release to the Culebra, and given that there is a release, SOLPU determines how big the release is. The variable SALPERM acts as a switch for scenario $S(1,0,0,0,0)$ because it determines how long will be required for a waste panel to fill with brine. If the pore space in a waste panel does not fill with brine due to a low value for SALPERM, then there can be no fluid flow to the Culebra and hence no radionuclide release.

For comparison, the lower two frames in Figure 4.5-1 show scatterplots of Pu-239 release to the Culebra versus SALPERM (Salado permeability) and SOLPU (solubility for Pu) for scenario $S^{+-}(2,0,0,0,0)$. As examination of these scatterplots shows, SALPERM has no effect on the Pu-239 release to the

---

* The elements Np, Pu and U were assigned two solubilities (i.e., SOLNP4, SOLNP5, SOLPU4, SOLPU5, SOLU4, SOLU6), with only one solubility being used in each sample element as determined by the variable EHPH (index variable used to select the relative areas of the stability regimes for different oxidation states of Np, Pu and U). All scatterplots involving solubilities presented in this report display the actual solubilities used in the calculation of the releases shown in the plot. Further, the solubilities SOLNP4 and SOLNP5 were sampled with a rank correlation of 0.99, as were the solubilities SOLPU4 and SOLPU5 and also the solubilities SOLU4 and SOLU6. As a result, the variables in the pairs (SOLNP4, SOLNP5), (SOLPU4, SOLPU5) and (SOLU4, SOLU6) are essentially indistinguishable in a regression analysis with rank-transformed data. Therefore, the regression analyses presented in this report use the symbols SOLNP, SOLPU and SOLU to designate the solubility limits for Np, Pu and U.

Scenario: $S(1,0,0,0,0)$, Assumed Intrusion Time: 1000 yrs

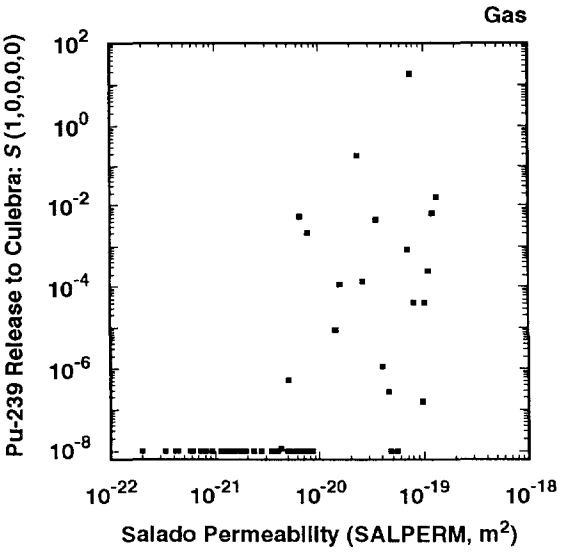

TRI-6342-1583-0

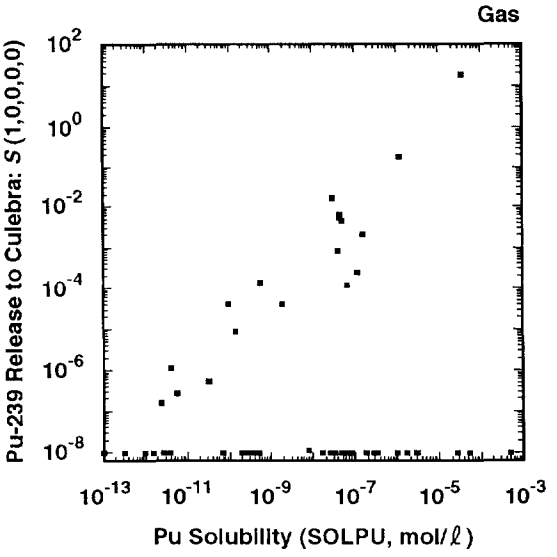

TRI-6342-1584-0

Scenario: $S^{+-}(2,0,0,0,0)$, Assumed Intrusion Time: 1000 yrs

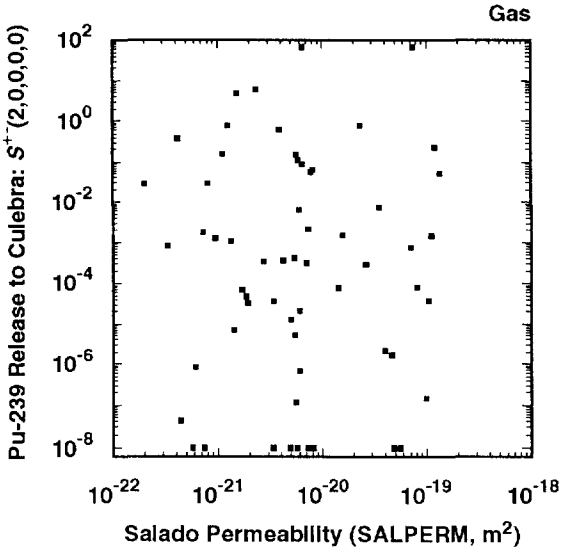

TRI-6342-1585-0

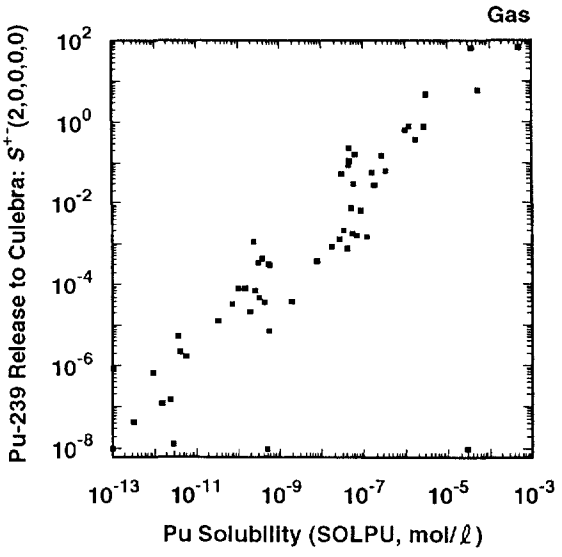

TRI-6342-1586-0

Figure 4.5-1. Scatterplots for Normalized Release of Pu-239 to the Culebra Dolomite with Gas Generation in the Repository and Intrusion Occurring at 1000 Yrs for Variables SALPERM (Salado permeability) and SOLPU (solubility for Pu) and Scenarios $S(1,0,0,0,0)$ and $S^{+-}(2,0,0,0,0)$.

Culebra for scenario $S^{+-}(2,0,0,0,0)$, with the release being dominated by SOLPU. Large brine flows take place through a waste panel for scenario $S^{+-}(2,0,0,0,0,)$ due to the penetration of a pressurized brine pocket, with the result that additional brine inflow that might be influenced by SALPERM is of reduced importance.

Due to its role in determining whether or not the waste panels resaturate, SALPERM (Salado permeability) acts as a switch for all isotopes for scenario $S(1,0,0,0,0)$. Further, the release patterns shown by Pu-239 in Figure 4.5-1 for scenarios $S(1,0,0,0,0)$ and $S^{+-}(2,0,0,0,0)$ are also displayed by Pu-240 and Th-230. A related, but somewhat different, pattern is shown by U-234. As before, SALPERM acts as a switch for scenario $S(1,0,0,0,0)$ but the impact of solubility is reduced due to inventory limits. Scatterplots for BHPERM (borehole permeability) and SOLU (solubility for U) are shown in Figure 4.5-2. The scatterplots for the release of U-234 to the Culebra for scenario $S(1,0,0,0,0)$ show small positive effects for BHPERM and SOLU. However, these effects are not very strong. As a reminder, the numerous zero releases are resulting from the effect of SALPERM as a switch.

Examination of the scatterplots in Figure 4.5-2 for scenario $S^{+-}(2,0,0,0,0)$ gives a clearer view of what is happening. As indicated by the straight lines of points in the two lower scatterplots, many sample elements are resulting in equal releases for scenario $S^{+-}(2,0,0,0,0)$. As shown in Figure 2.4-2, these equal releases correspond to the inventory of U-234 in a single panel. Thus, the release of U-234 for scenario $S^{+-}(2,0,0,0,0)$ is often inventory limited. As the two lower scatterplots in Figure 4.5-2 show, the release of U-234 to the Culebra for scenario $S^{+-}(2,0,0,0,0)$ tends to increase as BHPERM (borehole permeability) and SOLU (solubility for U) increase. However, the larger values assigned to either of these variables result in a complete removal of the U-234 inventory. The indicated effect for BHPERM results because large values for BHPERM lead to large brine flows through the repository and hence a complete removal of U-234 even for the smaller values of SOLU. Similarly, large values of SOLU result in a complete removal of U-234 unless the brine flows are very small (i.e., there are a few sample elements in which a large value for SOLU does not lead to a complete removal of U-234).

The scatterplots shown in Figure 4.5-2 for scenario $S(1,0,0,0,0)$ do not display patterns that are as well-defined as in the scatterplots for scenario $S^{+-}(2,0,0,0,0)$. However, with the insights gained from the scatterplots for scenario $S^{+-}(2,0,0,0,0)$, it is possible to get a better feeling for what is happening for scenario $S(1,0,0,0,0)$. As shown in Figure 4.4-8, the brine

Scenario: $S(1,0,0,0,0)$, Assumed Intrusion Time: 1000 yrs

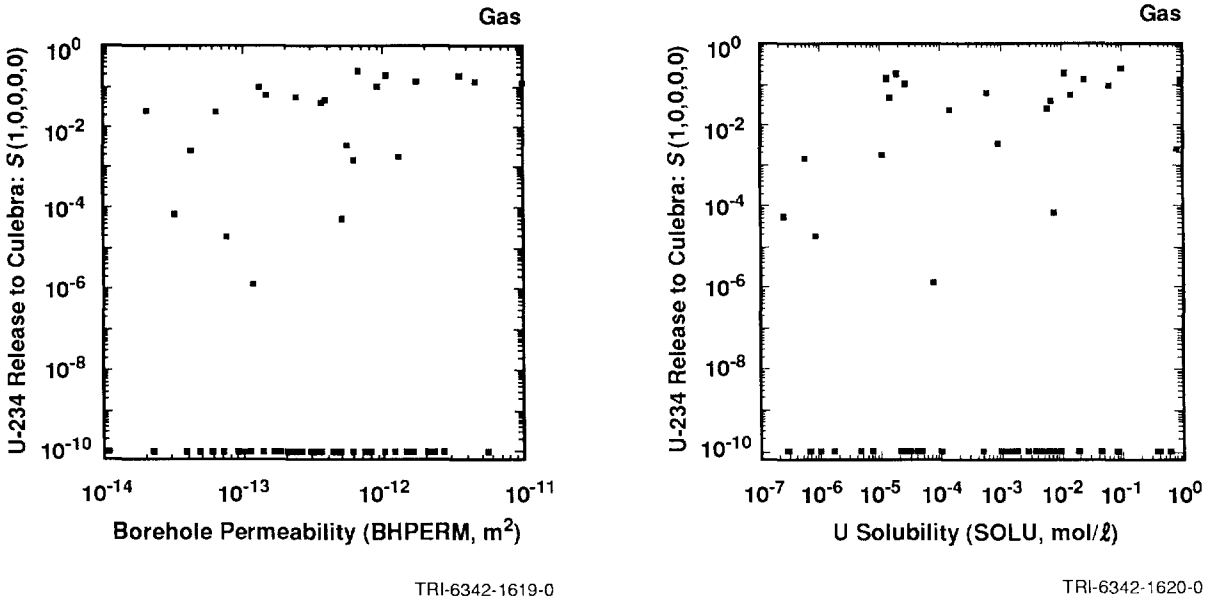

Scenario: $S^{+-}(2,0,0,0,0)$, Assumed Intrusion Time: 1000 yrs

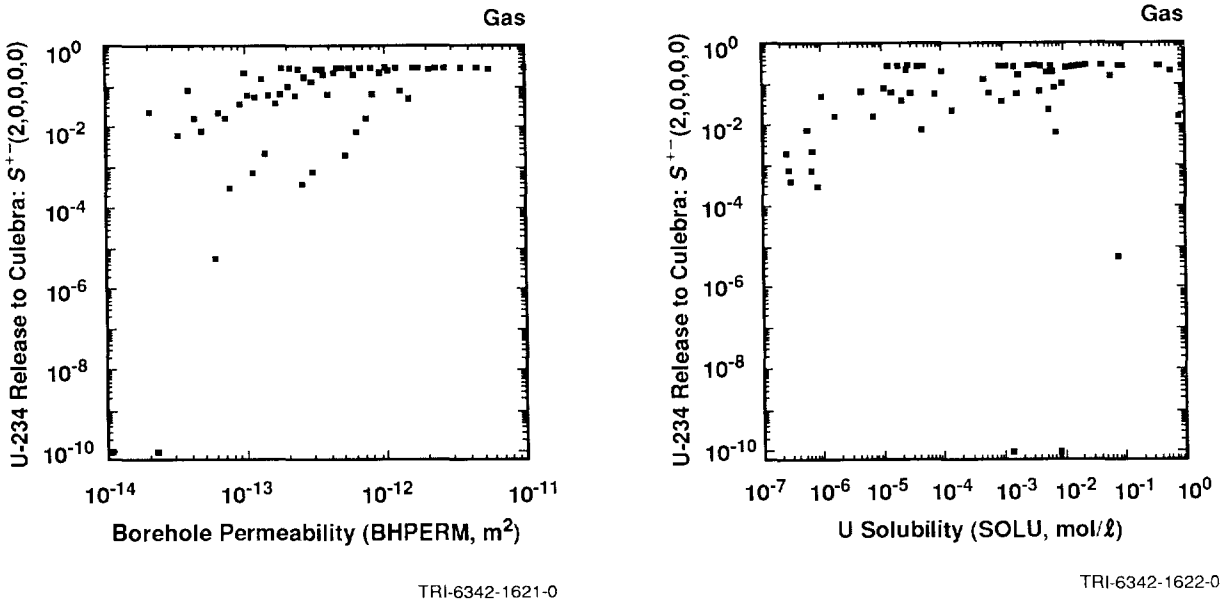

Figure 4.5-2. Scatterplots for Normalized Release of U-234 to the Culebra Dolomite with Gas Generation in the Repository and Intrusion Occurring at 1000 Yrs for Variables BHPERM (borehole permeability) and SOLU (solubility for U) and Scenarios $S(1,0,0,0,0)$ and $S^{+-}(2,0,0,0,0)$.

flows out of the repository are much smaller for scenario $S(1,0,0,0,0)$ than for scenario $S^{+-}(2,0,0,0,0)$. Increasing BHPERM increases this flow and hence tends to increase the release; similarly, increasing SOLU increases the amount of U-234 that can be dissolved and hence tends to increase the size of the release. However, the small size of these flows and their variability due to the effects of other variables such as SALPERM (Salado permeability) and SALPRES (Salado pressure)* produces a more diffuse pattern. Further, the larger values of BHPERM and SOLU for scenario $S(1,0,0,0,0)$ come very close to producing inventory-limited results, although the inventory limits are not quite reached and so the scatterplots for scenario $S(1,0,0,0,0)$ in Figure 4.5-2 do not have the flattened tops displayed by the scatterplots for scenario $S^{+-}(2,0,0,0,0)$.

Scatterplots for the release of Am-241 to the Culebra for BHPERM (borehole permeability) and SOLAM (solubility for Am) are given in Figure 4.5-3 for scenarios $S(1,0,0,0,0)$ and $S^{+-}(2,0,0,0,0)$. The release behavior for Am-241 is similar to that of U-234, although it is complicated by the relatively short half-life (i.e., 432 yrs) of Am-241. For scenario $S(1,0,0,0,0)$, the release to the Culebra tends to increase as BHPERM and SOLAM increase, and many zero releases occur due to the previously discussed role of SALPERM (Salado permeability). However, except for the role of SALPERM as a switch, the relations between the sampled variables and release to the Culebra tend to be rather diffuse for scenario $S(1,0,0,0,0)$.

A somewhat clearer pattern of relationships is shown in Figure 4.5-3 for scenario $S^{+-}(2,0,0,0,0)$. A well-defined relationship between release to the Culebra and BHPERM (borehole permeability) is shown, with the release tending to increase as BHPERM increases. As discussed with respect to U-234, increasing BHPERM increases brine flow through the waste panel and hence release to the Culebra. This effect is particularly important for Am-241 because release to the Culebra is competing with radioactive decay; if Am-241 is not transported to the Culebra relatively early in the 10,000-yr time period that must be considered in the EPA regulations, very little release can occur. The scatterplot for SOLAM (solubility for Am) shows the Am-241 releases to the Culebra increasing as SOLAM increases, with a tendency for the release to level off for larger values of SOLAM (i.e., $> 10^{-7}$ mol/ℓ). As shown in Figure 2.4-2, the inventory of Am-241 in a single waste panel at 1000 yrs is approximately 30 EPA units, which declines rapidly with increasing time due to radioactive decay. The flattening shown in the relationship between release to the Culebra and SOLAM for Am-241, which is bounded above by approximately 10 EPA units, is probably due to inventory

* See Tables 4.5-3 and 5.1-1.

Scenario: $S(1,0,0,0,0)$, Assumed Intrusion Time: 1000 yrs

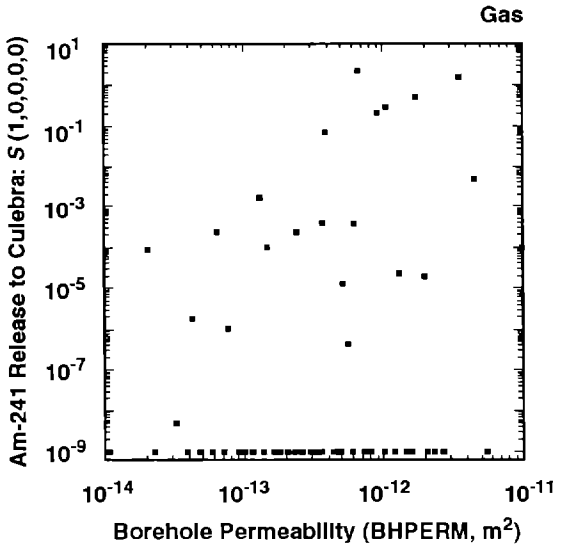

TRI-6342-1684-0

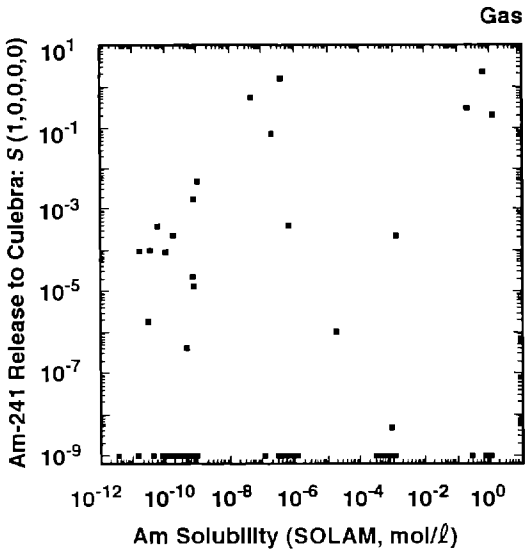

TRI-6342-1685-0

Scenario: $S^{+-}(2,0,0,0,0)$, Assumed Intrusion Time: 1000 yrs

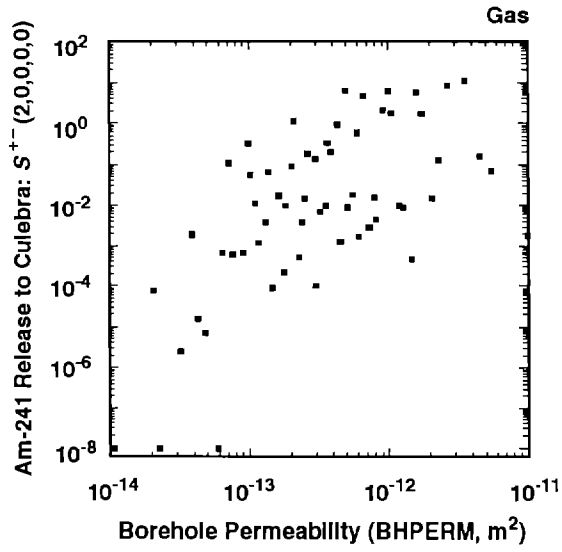

TRI-6342-1686-0

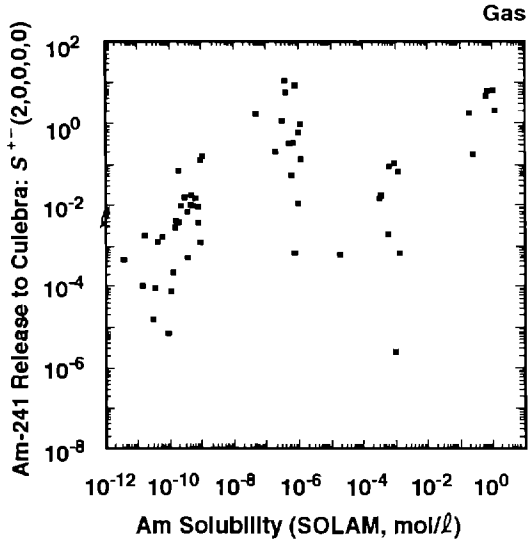

TRI-6342-1687-0

Figure 4.5-3. Scatterplots for Normalized Release of Am-241 to the Culebra Dolomite with Gas Generation In the Repository and Intrusion Occurring at 1000 Yrs for Variables BHPERM (borehole permeability) and SOLAM (solubility for Am) and Scenarios $S(1,0,0,0,0)$ and $S^{+-}(2,0,0,0,0)$.

limitations. The pattern for Am-241 is not as clean as the corresponding pattern shown in Figure 4.5-2 for U-234 due to the strong time dependence of the Am-241 inventory (i.e., compare the time-dependent inventories of Am-241 and U-234 shown in Figure 2.4-2).*

Thus far, the discussion of the sensitivity analysis results in Table 4.5-1 for scenario $S(1,0,0,0,0)$ has focused on the release of individual isotopes to the Culebra. Corresponding releases for scenario $S^{+-}(2,0,0,0,0)$ have also been discussed. Total releases (i.e., summed over all isotopes) to the Culebra and also to the accessible environment for scenario $S(1,0,0,0,0)$ are now considered. As shown by the R^2 values for the regressions for "EPA Sum for Total Integrated Discharge" in Table 4.5-1, the regression models are performing poorly in determining the relationships between the sampled variables and total release, which is not surprising given the complex relationships involving individual isotopes that are shown in Figures 4.5-1 through 4.5-3. Specifically, the final R^2 values for the four regressions are 0.58, 0.73, 0.59 and 0.41. Additional insight on what is causing the variation in total release for scenario $S(1,0,0,0,0)$ can be obtained from the scatterplots in Figure 4.5-4.

The top pair of scatterplots in Figure 4.5-4 is for the total normalized release from the repository to the Culebra. As previously observed for the individual isotopes (e.g., see Figure 4.5-1), SALPERM (Salado permeability) acts as a switch, with a value of approximately 5×10^{-21} m^2 determining whether or not a release to the Culebra will occur. Further, given that a release occurs, its value tends to increase as SALPERM increases. Similarly, releases also tend to increase as BHPERM (borehole permeability) increases, although zero releases are interspersed throughout the range of BHPERM due to the effects of SALPERM. The lower pair of scatterplots in Figure 4.5-4 is for the total normalized release to the accessible environment. As examination of these scatterplots shows, only seven sample elements result in nonzero releases to the accessible environment. Further, these releases tend to increase as BHPERM and SALPERM increase. The large number of zero releases indicated by the scatterplots in Figure 4.5-4 are obscuring (i.e., censoring) the effects of individual variables and, as a result, are leading to regression models with low R^2 values.

---

* The results presented in Figure 4.5-3 are for gas generation in the repository, which does have an effect on the time required to fill the pore space in a waste panel with brine. This effect is more important for isotopes such as Am-241 that have short half-lives than for isotopes with longer half-lives. The effects discussed in this paragraph can be seen more clearly in Figure 5.1-7, which presents the same results but without the assumption of gas generation in the repository.

Scatterplots for Normalized Release to Culebra Dolomite

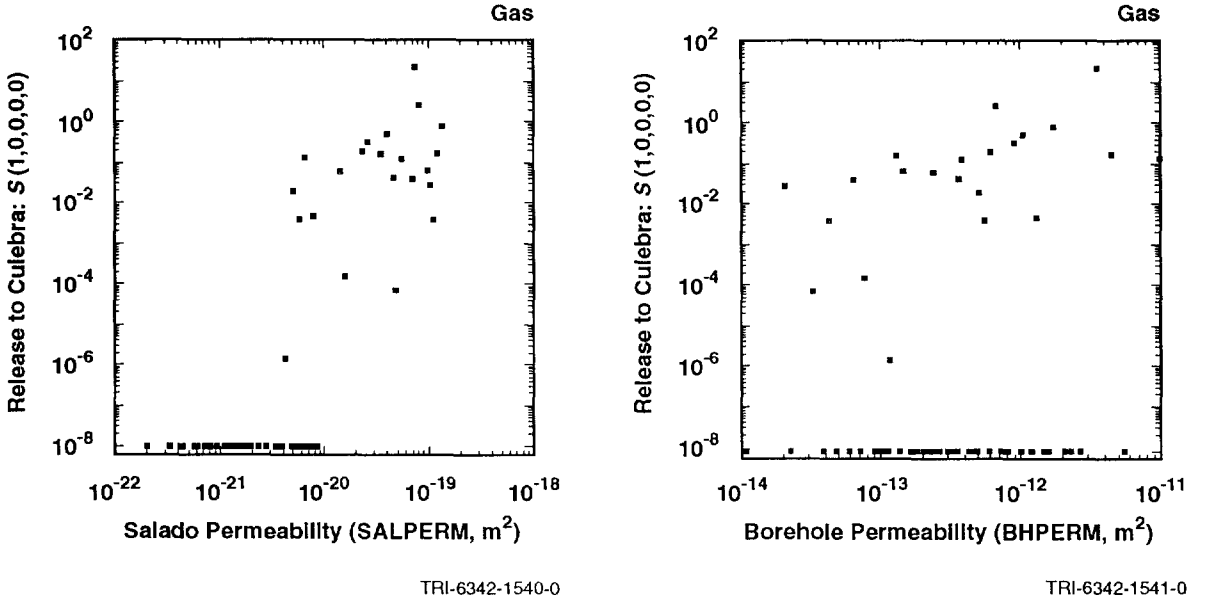

Scatterplots for Normalized Release to Accessible Environment

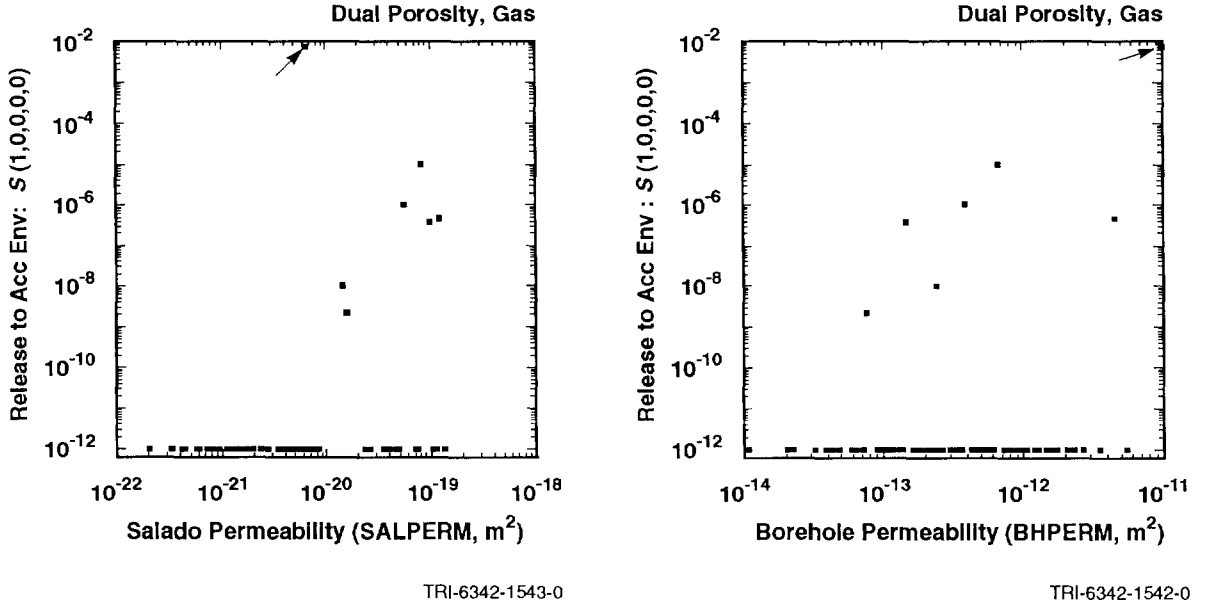

Figure 4.5-4. Scatterplots for Total Normalized Release Associated with Scenario $S(1,0,0,0,0)$ for Groundwater Transport with Gas Generation in the Repository, a Dual-Porosity Transport Model in the Culebra Dolomite and Intrusion Occurring at 1000 Yrs.

Table 4.5-1 also contains analyses for the integrated releases of individual isotopes at one-quarter, one-half and the full distance to the accessible environment. The regressions are very poor, with most analyses leading to final regression models with R^2 values less than 0.5. The reason for this is simple: most of the releases are zero. As already discussed, SALPERM (Salado permeability) causes approximately half the releases to the Culebra to be zero. Further, retardation prevents all isotopes from reaching the accessible environment for most sample elements. The limited releases due to transport within the Culebra as illustrated are Figures 4.4-1, 4.4-2 and 4.5-4.

Rank regressions for scenario $S^{+-}(2,0,0,0,0)$ are presented in Table 4.5-2. The individual regression analyses in Table 4.5-2 generally have higher R^2 values than the corresponding analyses in Table 4.5-1 for scenario $S(1,0,0,0,0)$, which is not surprising given the larger number of nonzero releases for scenario $S^{+-}(2,0,0,0,0)$. As previously discussed in conjunction with Figures 4.5-1 through 4.5-3, the most important variables for release to the Culebra are BHPERM (borehole permeability) and the solubilities for the individual elements (i.e., SOLU, SOLNP, SOLAM, SOLTH and SOLPU). As an example, Figure 4.5-5 contains the scatterplot for BHPERM and total normalized release to the Culebra and shows the well-defined trend between increasing values for BHPERM and increasing releases to the Culebra. After BHPERM and the solubilities, the most important variable is BPPRES (brine pocket pressure).

The matrix distributions coefficients (i.e, MKDU, MKDNP, MKDTH and MKDPU) tend to be the most important variables for integrated release at various points along the transport path in the Culebra. The R^2 values tend to decrease as the length of the transport path increases due to both an increasing number of variables that can affect the results and an increasing number of zero releases. The scatterplots in Figure 4.5-6 for integrated radionuclide transport in the Culebra for one-quarter the distance to the accessible environment provide a graphical representation for what is happening. The top two scatterplots are for Am-241 and Pu-239 versus their matrix distribution coefficients MKDAM and MKDPU. Effectively, all the releases for these two isotopes are zero even though transport is for only one-quarter the distance to the accessible environment (i.e., the largest integrated release values for Am-241 and Pu-239 are less than 10^{-19} and 10^{-9}, respectively). The lower two scatterplots for U-234 are more interesting. The U-234 releases tend to decrease as MKDU (matrix distribution coefficient for U) increases until a switch is reached at a value of approximately 10^{-3} m^3/kg for MKDU, after which the integrated release values for U-234 are zero (i.e., $< 10^{-10}$). Further, given that there is a nonzero release for U-234, this release tends to increase as BHPERM (borehole permeability)

TABLE 4.5-2. STEPWISE REGRESSION ANALYSES WITH RANK-TRANSFORMED DATA FOR SCENARIO S^{+-}(2,0,0,0,0) WITH GAS GENERATION IN THE REPOSITORY, A DUAL-POROSITY TRANSPORT MODEL IN THE CULEBRA DOLOMITE AND INTRUSION OCCURRING 1000 YRS AFTER REPOSITORY CLOSURE

	Release to Culebra		Quarter Distance		Half Distance		Full Distance	
Step	Variable	R^2	Variable	R^2	Variable	R^2	Variable	R^2
Dependent Variable: Integrated Discharge Am-241								
1	SOLAM	0.36 (+)	--	--	--	--	--	--
2	BHPERM	0.74 (+)						
3	BPPRES	0.78 (+)						
Dependent Variable: Integrated Discharge Np-237								
1	SOLNP	0.65 (+)	FKDNP	0.18 (-)	MKDNP	0.55 (-)	MKDNP	0.26 (-)
2	BHPERM	0.78 (+)	MKDNP	0.34 (-)	GRCORI	0.36 (-)		
3	BPPRES	0.82 (+)	BHPERM	0.41 (+)				
4	EHPH	0.85 (+)						
5	GRCORI	0.88 (-)						
Dependent Variable: Integrated Discharge Pu-239								
1	SOLPU	0.74 (+)	MKDPU	0.16 (-)	MKDPU	0.16 (-)	--	--
2	BHPERM	0.85 (+)	FKDPU	0.28 (-)				
3			CULPOR	0.35 (-)				
Dependent Variable: Integrated Discharge Pu-240								
1	SOLPU	0.74 (+)	CULPOR	0.15 (-)	MKDPU	0.17 (-)	--	--
2	BHPERM	0.85 (+)	MKDPU	0.25 (-)				
3			FKDPU	0.35 (-)				
Dependent Variable: Integrated Discharge Th-230								
1	SOLTH	0.69 (+)	MKDU	0.30 (-)	MKDU	0.32 (-)	MKDU	0.35 (-)
2	BHPERM	0.82 (+)	MKDTH	0.45 (-)	MKDTH	0.43 (-)	CULFRSP	0.46 (+)
3			CULFRSP	0.53 (+)	CULFRSP	0.52 (+)	CULCLIM	0.55 (+)
4			DBDIAM	0.58 (+)	CULCLIM	0.58 (+)	MKDTH	0.61 (-)
5			FKDPU	0.63 (-)	FKDPU	0.63 (-)		
6			CULCLIM	0.68 (+)				
7			BHPERM	0.72 (+)				

TABLE 4.5-2. STEPWISE REGRESSION ANALYSES WITH RANK-TRANSFORMED DATA FOR SCENARIO S^{+-}(2,0,0,0,0) WITH GAS GENERATION IN THE REPOSITORY, A DUAL-POROSITY TRANSPORT MODEL IN THE CULEBRA DOLOMITE AND INTRUSION OCCURRING 1000 YRS AFTER REPOSITORY CLOSURE (concluded)

	Release to Culebra		Quarter Distance		Half Distance		Full Distance	
Step	Variable	R^2	Variable	R^2	Variable	R^2	Variable	R^2
Dependent Variable: Integrated Discharge U-233								
1	BHPERM	0.43 (+)	MKDU	0.46 (-)	MKDU	0.48 (-)	MKDU	0.41 (-)
2	SOLU	0.58 (+)	GRCORI	0.53 (-)	SOLNP	0.55 (+)	SOLNP	0.49 (+)
3	BPPRES	0.70 (+)	SOLNP	0.60 (+)	FKDNP	0.60 (-)	FKDNP	0.54 (-)
4	SOLNP	0.74 (-)	BHPERM	0.66 (+)				
5			CULFRSP	0.71 (+)				
6			MKDNP	0.75 (-)				
7			FKDNP	0.77 (-)				
Dependent Variable: Integrated Discharge U-234								
1	BHPERM	0.47 (+)	MKDU	0.62 (-)	MKDU	0.61 (-)	MKDU	0.61 (-)
2	SOLU	0.60 (+)	CULFRSP	0.67 (+)	SOLNP	0.68 (+)	SOLNP	0.68 (+)
3	BPPRES	0.72 (+)	BHPERM	0.71 (+)	CULCLIM	0.71 (+)		
4			CULCLIM	0.74 (+)				
5			EHPH	0.77 (-)				
Dependent Variable: EPA Sum for Total Integrated Discharge								
1	BHPERM	0.46 (+)	MKDU	0.26 (-)	MKDU	0.25 (-)	MKDU	0.24 (-)
2	SOLAM	0.57 (+)	CULFRSP	0.40 (+)	CULFRSP	0.43 (+)	CULFRSP	0.44 (+)
3	BPPRES	0.66 (+)	GRCORI	0.46 (-)	GRCORI	0.49 (-)	GRCORI	0.51 (-)
4	SOLPU	0.69 (+)	BHPERM	0.52 (+)	BHPERM	0.55 (+)	SOLNP	0.58 (+)
5	BPSTOR	0.73 (+)	SOLNP	0.58 (+)	FKDPU	0.60 (-)		
6	SOLU	0.76 (+)	FKDPU	0.63 (-)	MKDNP	0.64 (-)		
7			MKDNP	0.68 (-)	SOLNP	0.68 (+)		
8			FKDNP	0.71 (-)				

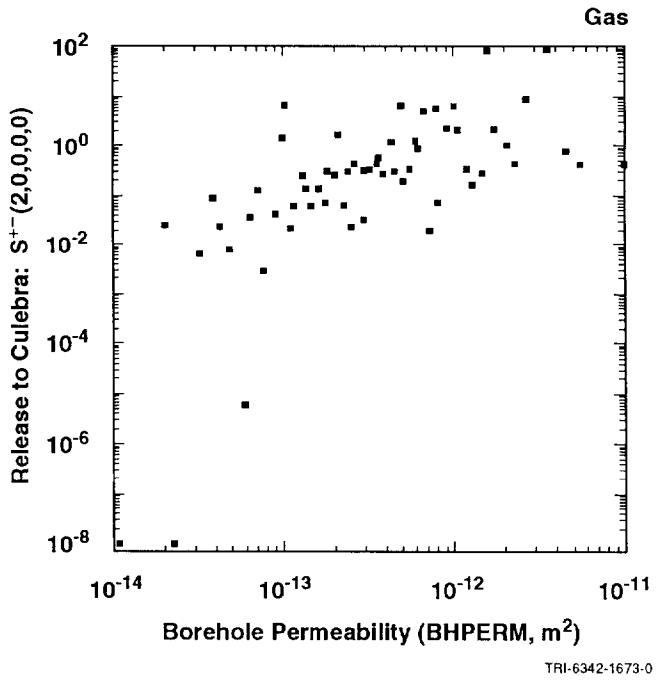

Figure 4.5-5. Scatterplot for Borehole Permeability (BHPERM) versus Total Normalized Release to the Culebra Dolomite for Scenario $S^{+-}(2,0,0,0,0)$ with Gas Generation in the Repository and Intrusion Occurring at 1000 Yrs.

increases. The variable BHPERM is important because it influences both how much U-234 is released to the Culebra and when this release occurs. Specifically, large values for BHPERM result in earlier releases to the Culebra, which allows more time for groundwater transport.

Additional perspective on the variables affecting total release to the accessible environment for scenario $S^{+-}(2,0,0,0,0)$ is provided by the scatterplots appearing in Figure 4.5-7. Of the four variables shown in this figure, only MKDU (matrix distribution coefficient for U) and CULFRSP (Culebra fracture spacing) are selected in the corresponding regression analysis shown in Table 4.5-2 (i.e., the analysis for "EPA Sum for Total Integrated Discharge" at "Full Distance"). As examination of the scatterplots for these variables shows, zero releases tend to be associated with large values of MKDU and the larger releases tend to be associated with the larger values of CULFRSP, which is consistent with the negative regression coefficient determined for MKDU and the positive regression coefficient determined for CULFRSP. The scatterplots for BHPERM (borehole permeability) and CULFRPOR (Culebra fracture porosity) show that both these variables have a positive effect on total release to the accessible environment (i.e., there is a tendency for the release to increase as each of these variables increases). However, neither of these variables is selected

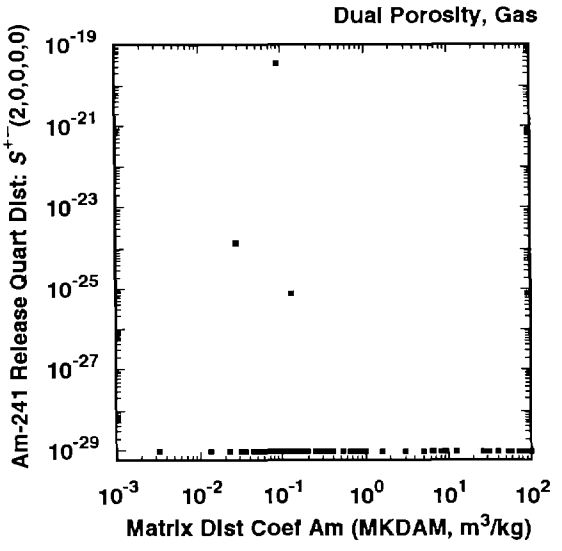

TRI-6342-1624-0

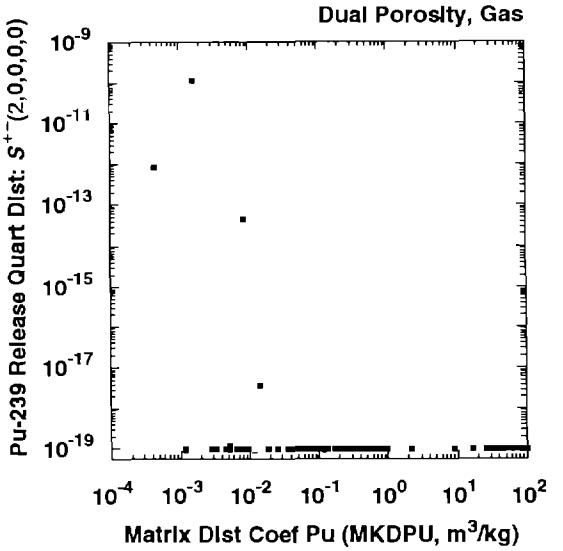

TRI-6342-1625-0

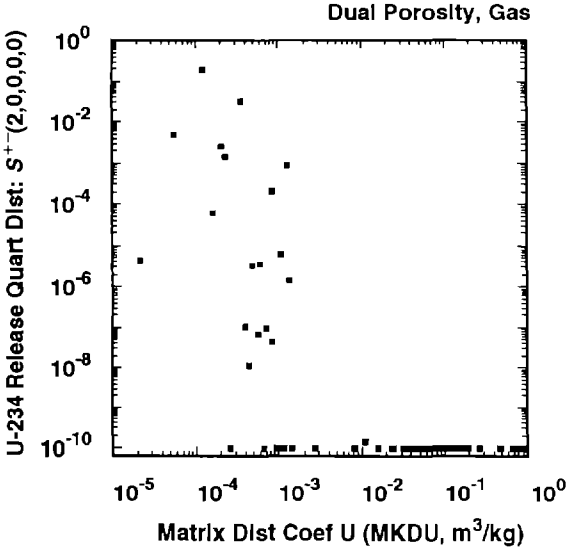

TRI-6342-1626-0

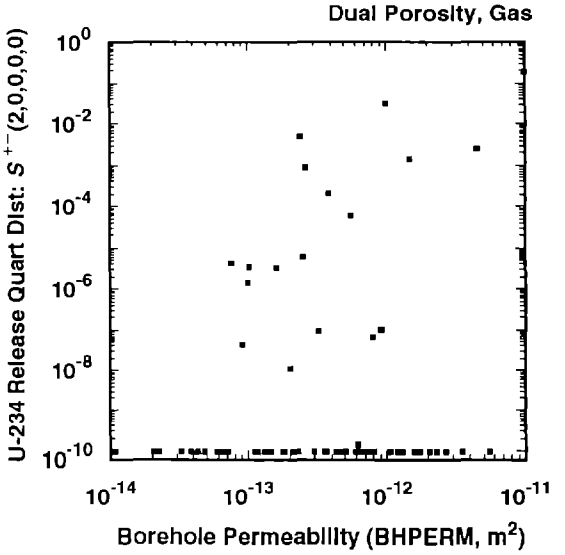

TRI-6342-1627-0

Figure 4.5-6. Scatterplots for Normalized Releases of Individual Isotopes at One-Quarter the Distance to the Accessible Environment for Scenario $S^{+-}(2,0,0,0,0)$ for Groundwater Transport with Gas Generation in the Repository, a Dual-Porosity Transport Model in the Culebra Dolomite and Intrusion Occurring at 1000 Yrs.

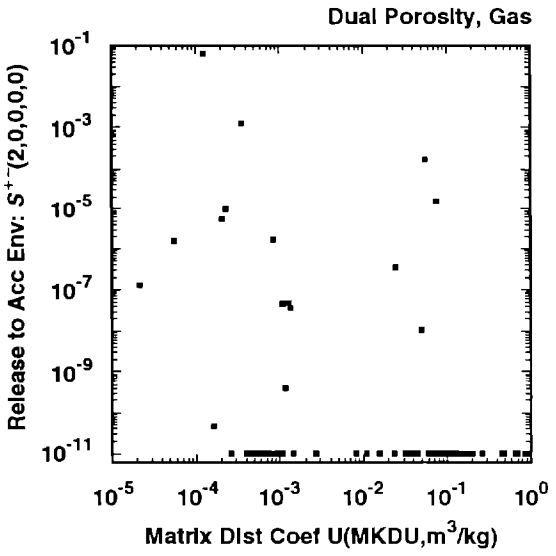

TRI-6342-1544-0

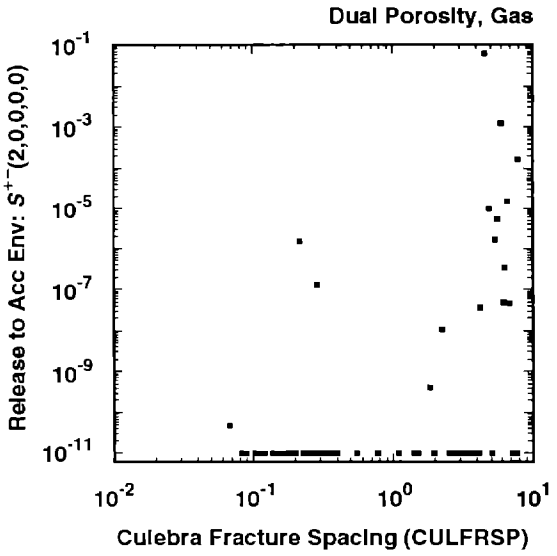

TRI-6342-1545-0

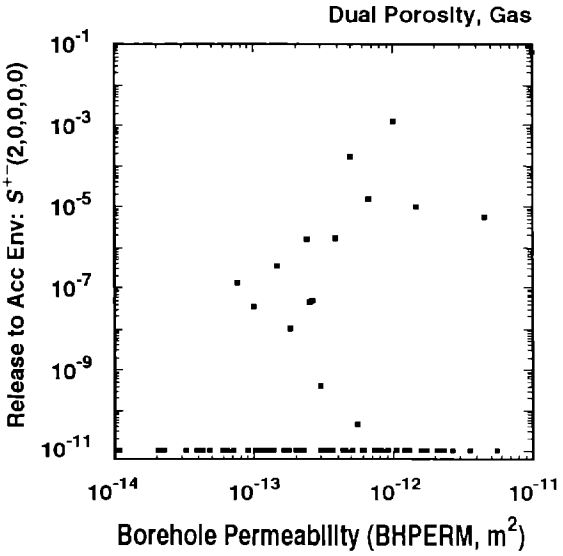

TRI-6342-1546-0

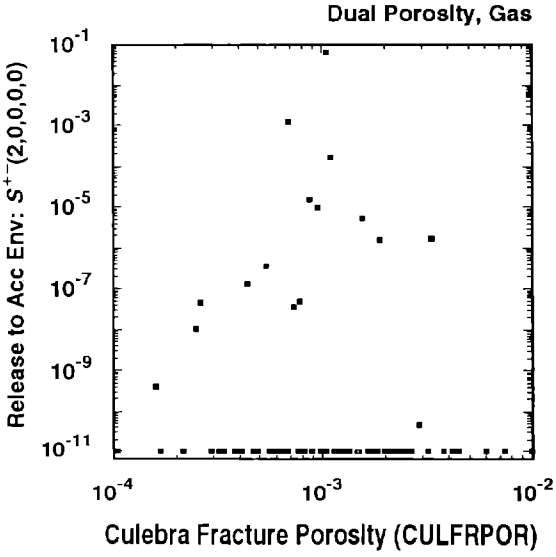

TRI-6342-1547-0

Figure 4.5-7. Scatterplots for Total Normalized Release to the Accessible Environment for Scenario $S^{+-}(2,0,0,0,0)$ for Groundwater Transport with Gas Generation in the Repository, a Dual-Porosity Transport Model in the Culebra Dolomite and Intrusion Occurring at 1000 Yrs.

in the corresponding regression analysis presented in Table 4.5-2 due to the large number of zero releases randomly interspersed over their ranges as a result of the effects of other variables. Thus, total release to the accessible environment for scenario $S^{+-}(2,0,0,0,0)$ provides another example of the fact that, when complex patterns of behavior are present, it is not possible to blindly rely on regression analyses to reveal what is going on. An earlier example of this type of complex behavior was provided by the effect of SALPERM (Salado permeability) on the release to the Culebra for scenario $S(1,0,0,0,0)$.

The sensitivity analysis results in Tables 4.5-1 and 4.5-2 are for groundwater releases to the accessible environment resulting from intrusions occurring at 1000 yrs (i.e., for scenarios $S(1,0,0,0,0)$ and $S^{+-}(2,0,0,0,0)$). Due to the increasing number of zero releases, additional sensitivity analyses for releases to the accessible environment due to intrusions occurring at later times are not particularly revealing. However, due to the larger number of nonzero releases, it is interesting to consider the releases from the repository to the Culebra at additional times.

The total normalized releases to the Culebra due to intrusions occurring at different times are summarized in Figure 4.4-4. Further, the brine flows that carry these releases from the repository to the Culebra are summarized in Figure 4.4-8. Stepwise regression analyses for the brine flows and radionuclide releases summarized in these figures are given in Table 4.5-3. For the E2-type scenarios (i.e., $S(1,0,0,0,0)$, ..., $S(0,0,0,0,1)$), both the brine flows and the normalized releases are dominated by SALPERM (Salado permeability), BHPERM (borehole permeability) and MBPERM (marker bed permeability). For the E1E2-type scenarios (i.e., $S^{+-}(2,0,0,0,0)$ through $S^{+-}(0,0,0,0,2)$), the brine flows are dominated by BHPERM, BPPRES (brine pocket pressure) and DBDIAM (drill bit diameter), and the normalized releases are dominated by BHPERM, BPPRES and solubilities for individual elements (e.g., SOLAM, SOLPU, SOLU). For releases into the Culebra overall, SALPERM is the most important variable for E2-type scenarios, and BHPERM is the most important variable for E1E2-type scenarios.

The elements Np, Pu and U were assigned two solubilities (i.e., SOLNP4, SOLNP5, SOLPU4, SOLPU5, SOLU4 and SOLU6), with only one solubility being used in each sample element as determined by the variable EHPH (index variable used to select the relative areas of the stability regimes for different oxidation states of Np, Pu and U) (Trauth et al., 1991). Specifically, EHPH has a value between 0 and 1 for each sample element. As indicated in Table 3-1 and discussed in more detail in Section 3.5-5 of Vol. 3, solubilities (i.e., SOLNP, SOLPU and SOLU) are then assigned in the following manner for calculations with the PANEL program for each sample element:

TABLE 4.5-3. STEPWISE REGRESSION ANALYSES WITH RANK-TRANSFORMED DATA FOR TOTAL BRINE RELEASE AND TOTAL NORMALIZED RELEASE TO THE CULEBRA DOLOMITE WITH GAS GENERATION IN THE REPOSITORY

	Total Brine		Total Release		Total Brine		Total Release	
Step	Variable	R^2	Variable	R^2	Variable	R^2	Variable	R^2
Time of Intrusion: 1000 yrs								
	Scenario: S(1,0,0,0,0)				Scenario: S^+-(2,0,0,0,0)			
1	SALPERM	0.58(+)	SALPERM	0.58(+)	BHPERM	0.81(+)	BHPERM	0.46(+)
2					BPPRES	0.94(+)	SOLAM	0.57(+)
3					DBDIAM	0.96(+)	BPPRES	0.66(+)
4							SOLPU	0.69(+)
5							BPSTOR	0.73(+)
6							SOLU	0.76(+)
Time of Intrusion: 3000 yrs								
	Scenario: S(0,1,0,0,0)				Scenario: S^+-(0,2,0,0,0)			
1	SALPERM	0.59(+)	SALPERM	0.59(+)	BHPERM	0.81(+)	BHPERM	0.49(+)
2			MBPERM	0.63(+)	BPPRES	0.94(+)	BPPRES	0.62(+)
3					DBDIAM	0.96(+)	SOLPU	0.69(+)
Time of Intrusion: 5000 yrs								
	Scenario: S(0,0,1,0,0)				Scenario: S^+-(0,0,2,0,0)			
1	SALPERM	0.54(+)	SALPERM	0.54(+)	BHPERM	0.82(+)	BHPERM	0.51(+)
2	BHPERM	0.58(+)	BHPERM	0.58(+)	BPPRES	0.94(+)	BPPRES	0.64(+)
3					DBDIAM	0.96(+)	SOLPU	0.70(+)
4							SOLU	0.73(+)
Time of Intrusion: 7000 yrs								
	Scenario: S(0,0,0,1,0)				Scenario: S^+-(0,0,0,2,0)			
1	MBPERM	0.39(+)	MBPERM	0.40(+)	BHPERM	0.83(+)	BHPERM	0.60(+)
2	BHPERM	0.49(+)	BHPERM	0.50(+)	BPPRES	0.92(+)	BPPRES	0.71(+)
3					DBDIAM	0.95(+)	SOLPU	0.75(+)
4							SOLU	0.77(+)
Time of Intrusion: 9000 yrs								
	Scenario: S(0,0,0,0,1)				Scenario: S^+-(0,0,0,0,2)			
1	--	--	--	--	BHPERM	0.78(+)	BHPERM	0.72(+)
2					BPPRES	0.83(+)	BPPRES	0.78(+)
3					DBDIAM	0.85(+)	SOLU	0.80(+)

$$\text{SOLNP} = \begin{cases} \text{SOLNP4 if EHPH} < 0.485 \\ \text{SOLNP5 if EHPH} \geq 0.485, \end{cases}$$

$$\text{SOLPU} = \begin{cases} \text{SOLPU4 if EHPH} < 0.539 \\ \text{SOLPU5 if EHPH} \geq 0.539 \end{cases}$$

and

$$\text{SOLU} = \begin{cases} \text{SOLU4 if EHPH} < 0.299 \\ \text{SOLU6 if EHPH} \geq 0.299. \end{cases}$$

Three scatterplots and one box plot showing the effects of these assignments on release to the Culebra for scenario $S^{+-}(2,0,0,0,0)$ are given in Figure 4.5-8.

The scatterplots are for EHPH (index variable used to select the relative areas of the stability regimes for different oxidation states of Np, Pu and U) versus normalized release of Np, Pu and U to the Culebra. The vertical lines in the scatterplots indicate where the transition from the use of the solubility for one oxidation state to the solubility for the other oxidation state takes place. Although EHPH provides no ordering on the solubilities actually used for a given oxidation state, there should be a general shift in the locations of the points associated with the two oxidation states for a given element if the solubility for one oxidation state tends to produce larger releases than the solubility for the other oxidation state. The three scatterplots give little indication of such a shift. Use of SOLNP5 produces somewhat larger releases for Np than use of SOLNP4, although the effect is not very striking given the large overall variation in release size. Basically, the ranges associated with the individual solubilities are so large and overlap to such an extent that the effects of the different oxidation states are lost. The box plot in Figure 4.5-8 provides a more compact representation of the information contained in the scatterplots and clearly shows the great extent to which the releases predicted with the solubilities for different oxidation states overlap. As indicated in the figure, the number of observations used in the construction of each box plot depends on how many times the corresponding solubility was used in the original sample of size 60 (e.g., 29 observations were used in the construction of the box plot for Np^{+4}).

The distribution of CCDFs for normalized release to the accessible environment due to groundwater transport is shown in the lower left frame of Figure 4.1-2. This is not a particularly interesting distribution as only 4 CCDFs out of a total of 60 are nonzero within the probability and consequence ranges under consideration. For comparison, Figure 4.5-9 shows the

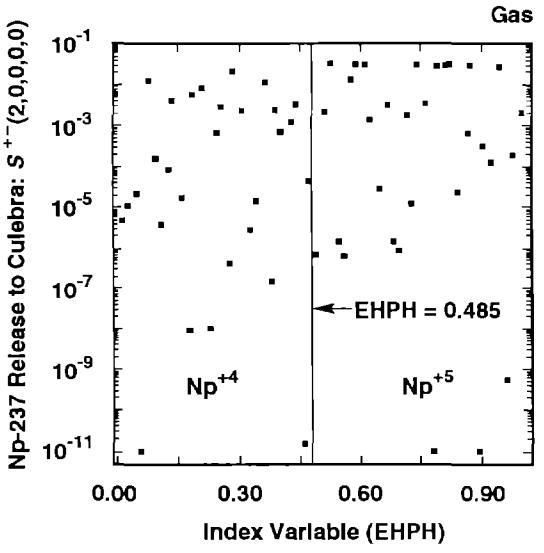

TRI-6342-1611-0

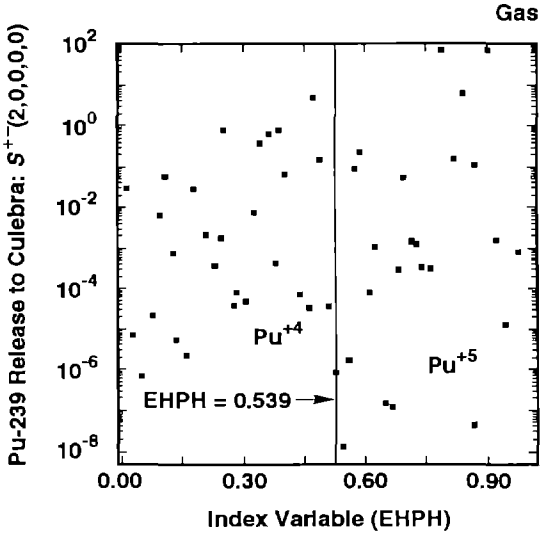

TRI-6342-1612

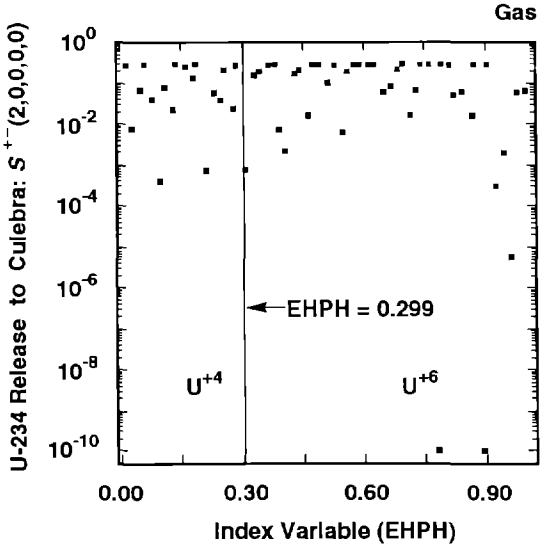

TRI-6342-1613-0

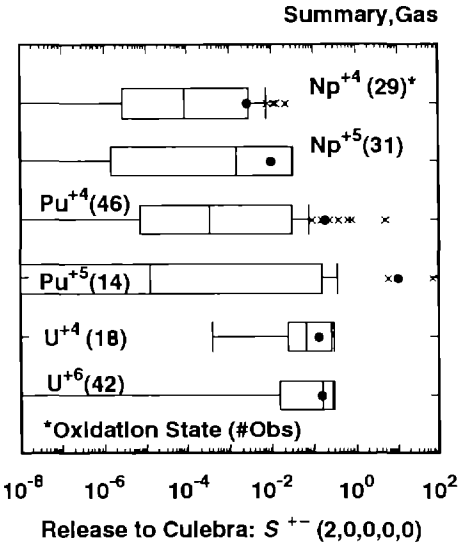

TRI-6342-1614-0

Figure 4.5-8. Effect of Solubilities Determined on the Basis of Oxidation State on the Normalized Releases of Np, Pu and U to the Culebra Dolomite for Scenario S^{+-}(2,0,0,0,0) with Gas Generation in the Repository and Intrusion Occurring at 1000 Yrs.

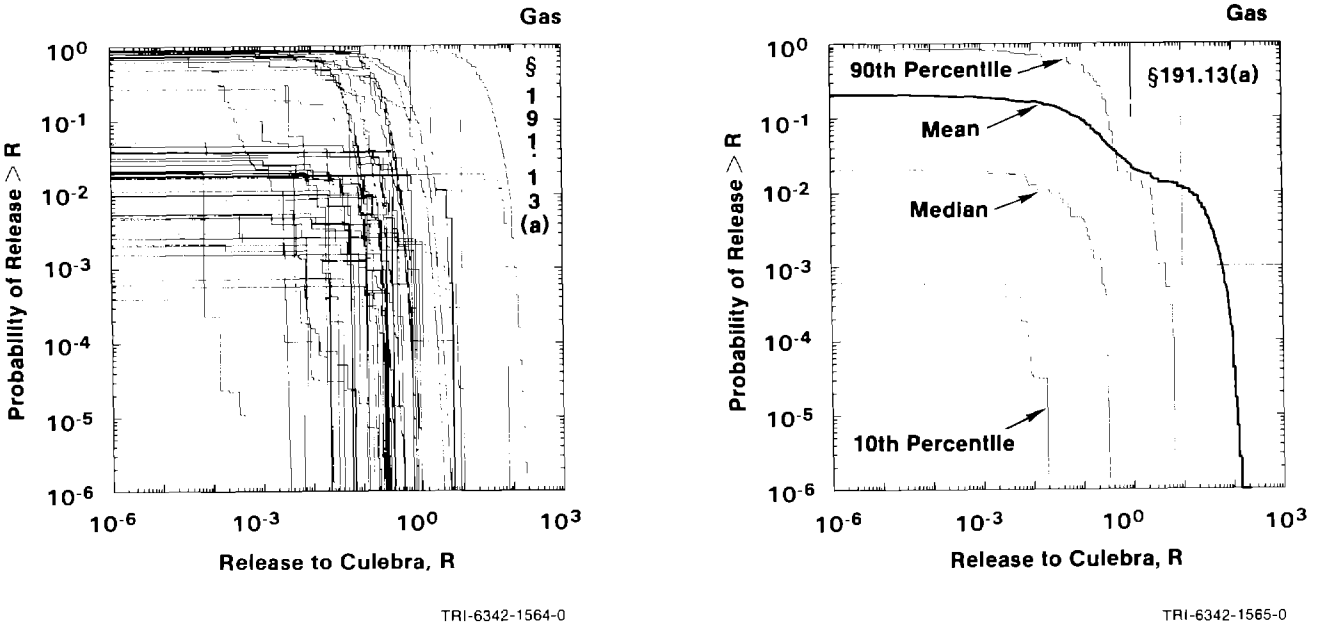

Figure 4.5-9. Distribution of Complementary Cumulative Distribution Functions for Normalized Release to the Culebra Dolomite with Gas Generation in the Repository. The CCDFs in this figure are for release to the Culebra, not release to the accessible environment; the corresponding CCDFs for release to the accessible environment are given in the lower two frames of Figure 4.1-2.

corresponding distribution of CCDFs for normalized release to the Culebra. The CCDFs appearing in Figure 4.5-9 are constructed in the same manner as the CCDFs for release to the accessible environment due to groundwater transport shown in Figure 4.1-2 (see Vol. 2, Chapters 2 and 3) except that releases to the Culebra rather than releases to the accessible environment are used as the consequences associated with the individual scenarios. In contrast to the 4 nonzero CCDFs in Figure 4.1-2 for normalized release to the accessible environment due to groundwater transport, Figure 4.5-9 contains 58 nonzero CCDFs for normalized release to the Culebra. However, only 4 of the CCDFs in Figure 4.5-9 for release to the Culebra cross the EPA release limits. Thus, transport in the Culebra with a dual-porosity model is causing a substantial reduction in radionuclide release to the accessible environment from what is already a small release from the repository.

Distributions of CCDFs of the form shown in Figure 4.5-9 can also be considered in sensitivity studies by performing regression-based analyses for the exceedance probabilities associated with individual release values on the abscissa. Specifically, each value on the abscissa has 60 exceedance probabilities associated with it, where 60 is the sample size being used in

the present analysis. Regression coefficients or partial correlation coefficients can be calculated which relate the variability in the exceedance probabilities associated with a particular release value to the sampled variables listed in Table 3-1. The coefficients calculated in this manner can then be plotted above the corresponding releases. The result of such an analysis for the CCDFs shown in Figure 4.5-9 is presented in Figure 4.5-10. The upper frame contains partial rank correlation coefficients, and the lower frame contains standardized rank regression coefficients. The results obtained for individual values on the abscissa are connected to form the curves displayed in the figure. To control the number of curves, a variable was required to have a partial rank correlation coefficient with an absolute value of at least 0.4 for some release value to be included in the figure. The results appearing in Figure 4.5-10 were calculated with the PCCSRC program (Iman et al., 1985).

As examination of Figure 4.5-10 shows, SALPERM (Salado permeability) and LAMBDA (rate constant in Poisson model for drilling intrusions) are the two most important variables with respect to the exceedance probabilities for small release values, with the values for these probabilities tending to increase as SALPERM and LAMBDA increase. The variables BHPERM (borehole permeability) and SOLPU (solubility of Pu) are less important than SALPERM and LAMBDA for the exceedance probabilities for small release values but become more important for the exceedance probabilities for larger release values, with the values for these probabilities again tending to increase as BHPERM and SOLPU increase.

4.6 Sensitivity Analysis for CCDFs

The most general result of the 1991 WIPP performance assessment is the distribution of CCDFs shown in Figure 2.1-2, which include the releases due to both cuttings removal and groundwater transport to the accessible environment. As discussed in conjunction with Figures 4.5-9 and 4.5-10, a sensitivity analysis can be performed for the CCDFs in Figure 2.1-2 by analyzing the variability associated with the exceedance probabilities for individual normalized releases. The result of this analysis is shown in Figure 4.6-1.

As examination of Figure 4.6-1 shows, the variability of the CCDFs in Figure 2.1-2 is dominated by LAMBDA (rate constant in Poisson model for drilling intrusions) and DBDIAM (drill bit diameter). Of the two variables, LAMBDA is the more important and almost completely dominates the variability in the CCDFs. In particular, the partial rank correlation coefficients and standardized rank regression coefficients shown for LAMBDA in Figure 4.6-1 are very close to one. For perspective, plots of R^2 values for regression

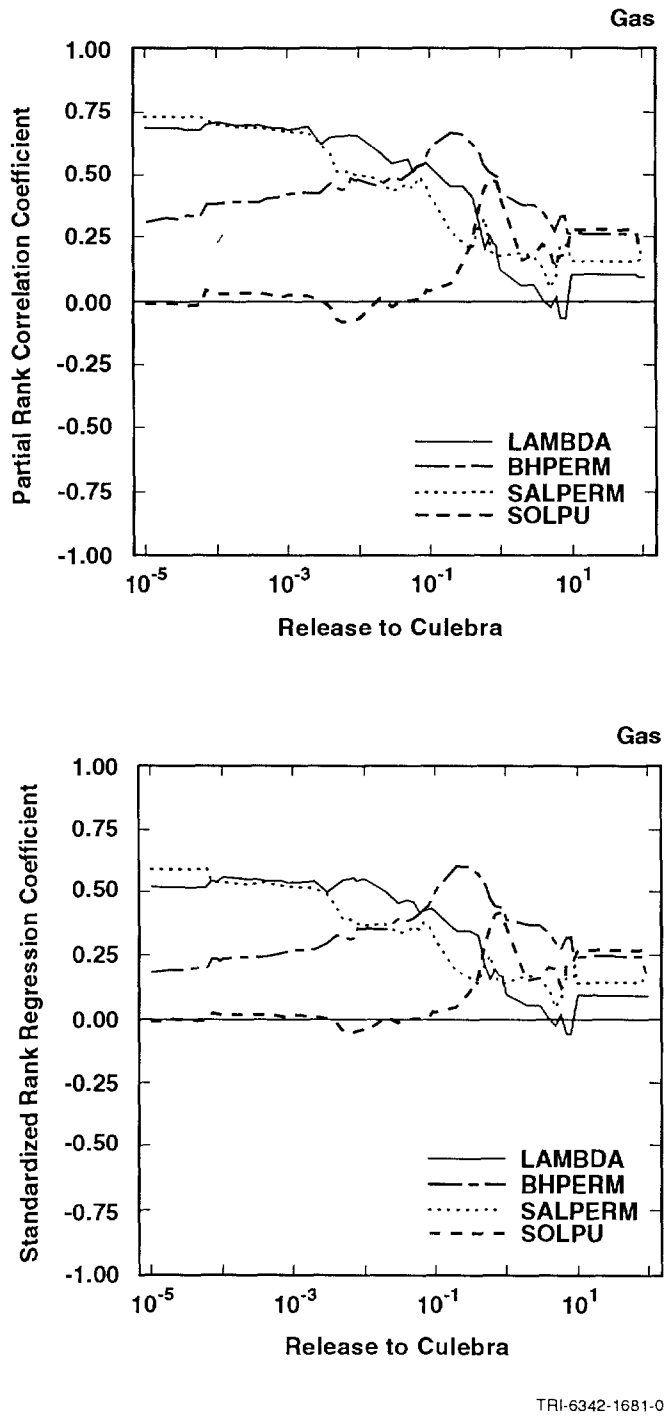

Figure 4.5-10. Partial Rank Correlation Coefficients and Standardized Rank Regression Coefficients for Exceedance Probabilities Associated with the Individual Complementary Cumulative Distribution Functions in Figure 4.5-9 for Normalized Release to the Culebra Dolomite with Gas Generation in the Repository.

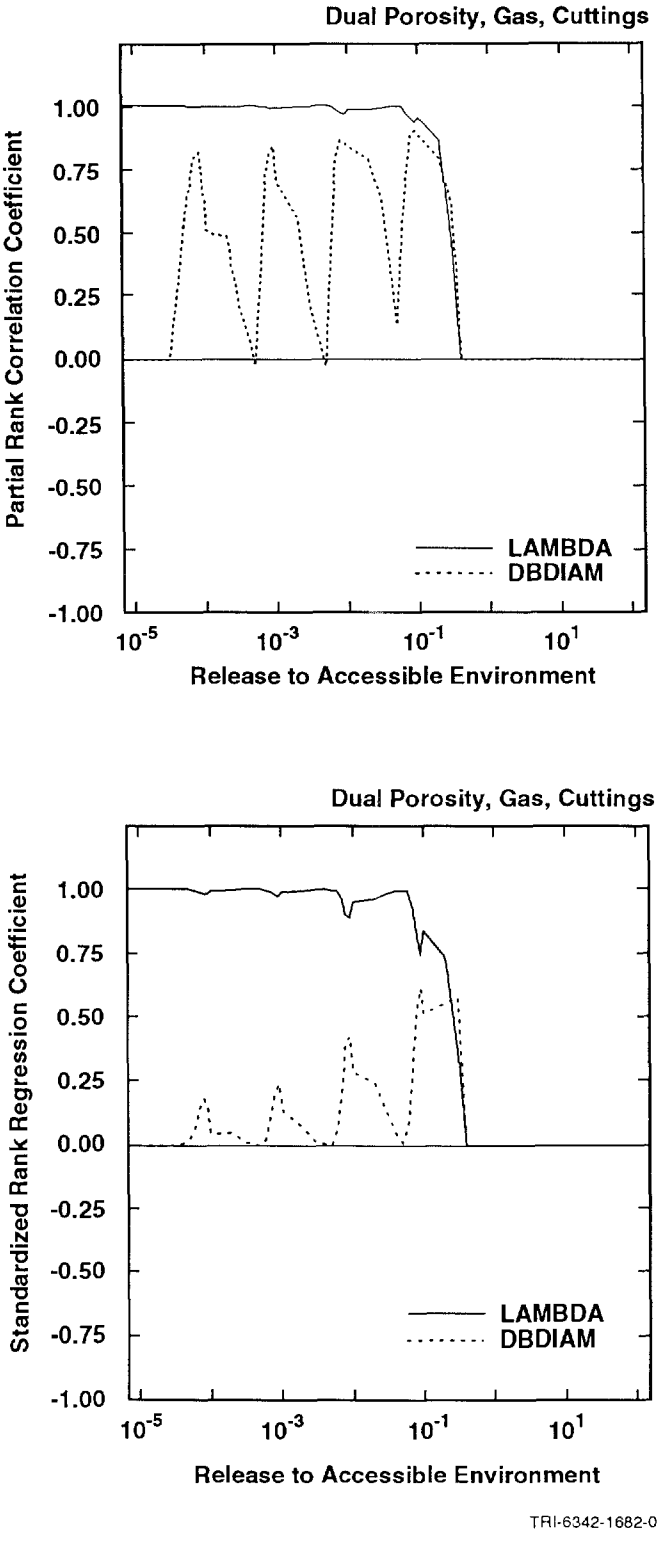

Figure 4.6-1. Partial Rank Correlation Coefficients and Standardized Rank Regression Coefficients for Exceedance Probabilities Associated with Individual Complementary Cumulative Distribution Functions in Figure 2.1-2 for Normalized Release to the Accessible Environment Including Both Cuttings Removal and Groundwater Transport with Gas Generation in the Repository and a Dual-Porosity Transport Model in the Culebra Dolomite.

models using just LAMBDA (upper frame) and both LAMBDA and DBDIAM (lower frame) are shown in Figure 4.6-2. Except for a few downward spikes, the R^2 values for regression models using only LAMBDA are close to one. Further, the downward spikes are substantially reduced and the R^2 values move close to one for regression models using both LAMBDA and DBDIAM.

The spikes involving DBDIAM (drill bit diameter) in Figure 4.6-1 are quite striking and merit additional discussion. These spikes are the result of the discretization of the waste into 5 activity levels as shown in Table 2.4-4 for the calculation of cuttings removal. The effect of this discretization can be seen in the structure of the CCDFs in Figure 2.1-2. As illustrated in Figure 4.6-3, the individual CCDFs in Figure 2.1-2 have 4 plateaus and 4 associated regions of rapid decrease. The first plateau corresponds to no intrusion. The region of rapid decrease between the first and second plateau corresponds to cuttings releases dominated by waste of activity level 1. The second plateau corresponds to a range of releases between releases dominated by activity level 1 and releases dominated by activity level 2. The region of rapid decrease between the second and third plateau corresponds to releases dominated by waste of activity level 2. This pattern continues for the other plateaus. The cuttings release for activity level 5 falls midway between the releases for activity levels 2 and 3 (see Vol. 2, Table 3-3) but does not have a large impact on the structure of the CCDF because the conditional probability of encountering waste of activity level 5 (i.e., 0.0588 as shown in Table 2.4-4) is less than the conditional probability of encountering waste of activity level 3 (i.e., 0.2242). The regions of rapid decrease between plateaus tend to be more stretched out when DBDIAM (drill bit diameter) is large. In particular, DBDIAM affects the location at which the transition from rapid decrease to a plateau occurs but does not affect the height of the plateau, which is determined entirely by LAMBDA (rate constant in Poisson model for drilling intrusions). With respect to Figure 4.6-1, the maximums for DBDIAM are occurring within the regions of rapid descent while the minimums are occurring within the plateaus, which are determined by LAMBDA. The use of more activity levels would eliminate the plateaus and regions of rapid decrease in the CCDFs in Figure 2.1-2 and thus would also eliminate the spikes associated with DBDIAM in Figure 4.6-1. However, although this added resolution would produce smoother CCDFs, it would not cause a significant change in the distribution of CCDFs shown in Figure 2.1-2.

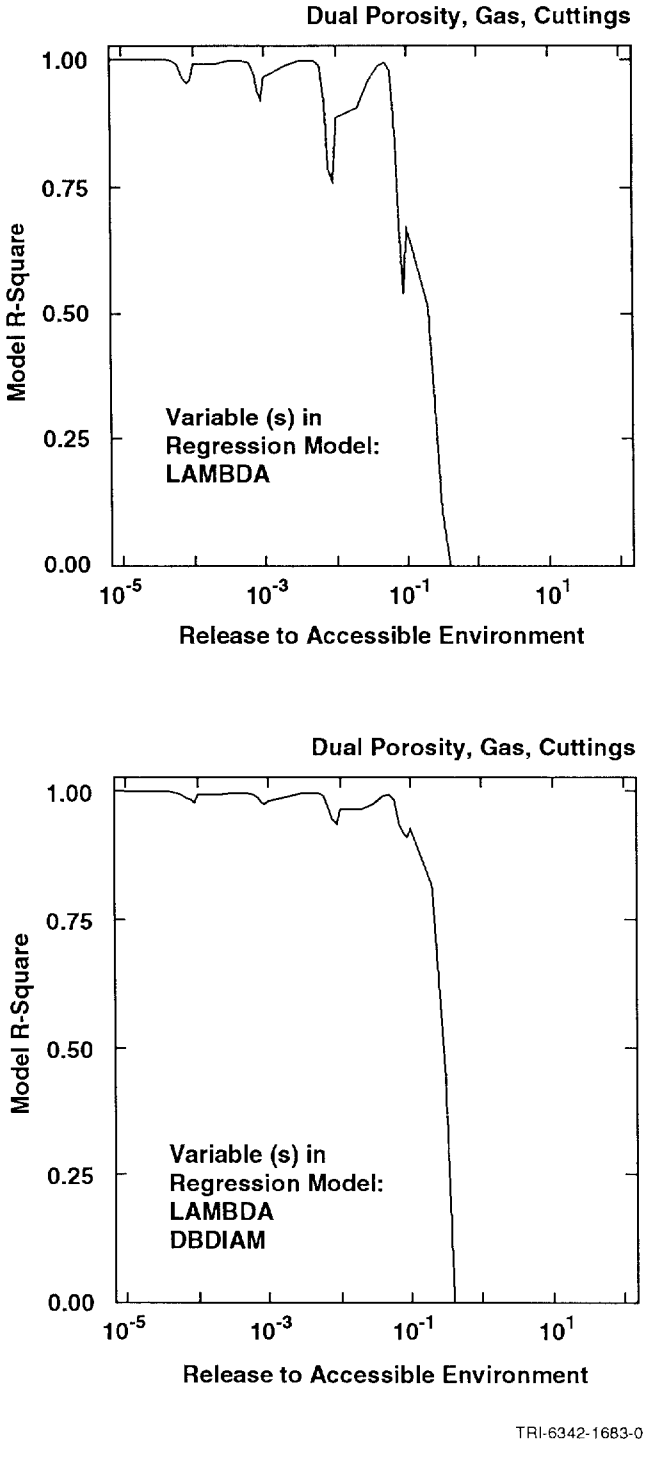

Figure 4.6-2. Coefficient of Determination (R^2 value) in Rank Regression Models for Exceedance Probabilities Associated with Individual Complementary Cumulative Distribution Functions in Figure 2.1-2 for Normalized Release to the Accessible Environment Including Both Cuttings Removal and Groundwater Transport with Gas Generation in the Repository and a Dual-Porosity Transport Model in the Culebra Dolomite.

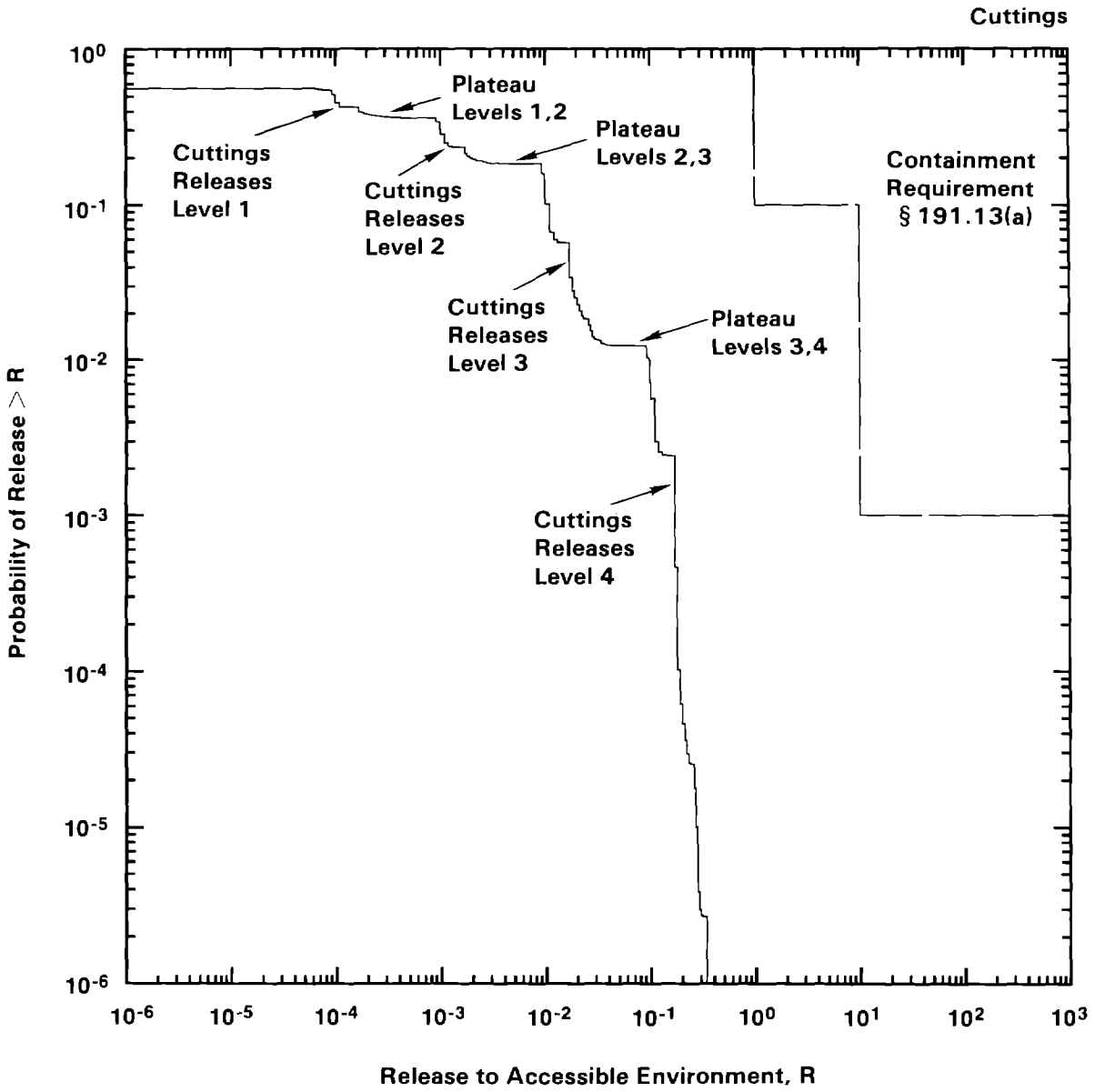

Figure 4.6-3. Structure of Individual Complementary Cumulative Distribution Function in Figure 2.1-2. This figure displays the cuttings release CCDF for sample element 46; the cuttings releases used in the construction of this CCDF are given in Table 3-3 of Vol. 2 of this report.

5. EFFECT OF ALTERNATIVE CONCEPTUAL MODELS

As described in Table 3-2, several alternative conceptual models were considered as part of the 1991 WIPP performance assessment. A summary of the results obtained with these alternative models is presented in this chapter.

5.1 Effect of Waste Generated Gas

The analyses presented in Chapter 4 were performed with the assumption that the production of waste-generated gas would take place due to corrosion and microbial action. The variables GRCORH, GRCORI, GRMICH, GRMICI, STOICCOR, STOICMIC, VMETAL and VWOOD in Table 3-1 relate to the generation of such gas. The presence and impact of waste-generated gas is a topic of considerable interest and uncertainty (Brush, 1990) in the WIPP performance assessment, with 1991 being the first year in which gas generation was incorporated into the annual performance assessment.

To help provide perspective on the impact of gas generation, the analyses presented in Chapter 4 were repeated for scenarios $S(1,0,0,0,0)$ and $S^{+-}(2,0,0,0,0)$ for the same Latin hypercube sample used in Chapter 4 but with an assumption of no gas generation. Results obtained with and without gas generation are compared in Figure 5.1-1, which contains scatterplots for brine flow into the Culebra and total normalized release into the Culebra with and without gas generation for scenarios $S(1,0,0,0,0)$ and $S^{+-}(2,0,0,0,0)$.

As examination of Figure 5.1-1 shows, the presence or absence of gas generation can have a significant impact on radionuclide release to the Culebra. For scenario $S(1,0,0,0,0)$, many sample elements result in no release to the Culebra when gas generation in the repository is assumed to take place. As shown in Figure 4.5-1, the variable SALPERM (Salado permeability) acts as a switch in the presence of gas generation, with no releases to the Culebra occurring for values of SALPERM less than approximately 5×10^{-21} m^2. The removal of gas generation also removes the effect of SALPERM as a switch, which can be seen in the two upper frames in Figure 5.1-1 in the appearance of points indicating nonzero flows and releases above what were zero values for analyses performed with gas generation. Due to the low values for SALPERM, the additional nonzero brine flows into the Culebra in the absence of gas generation are small (see upper left frame in Figure 5.1-1). However, little relationship exists between the size of these brine flows and the actual releases into the Culebra (see upper

Scenario: $S(1,0,0,0,0)$, Assumed Intrusion Time: 1000 yrs

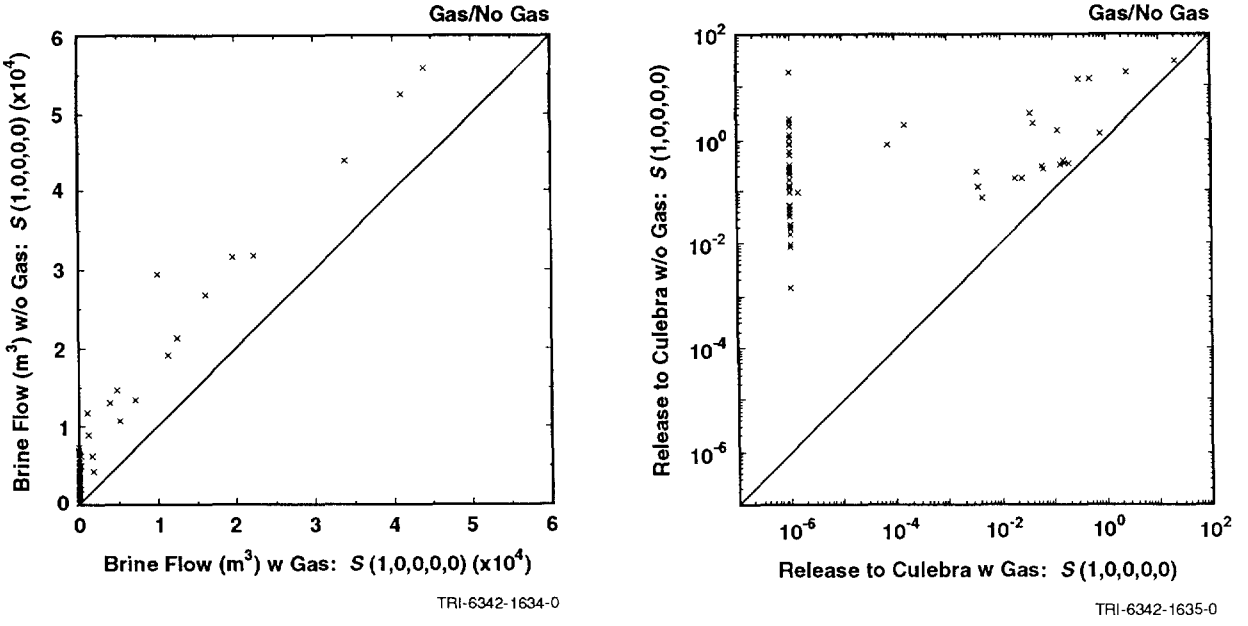

Scenario: $S^{+-}(2,0,0,0,0)$, Assumed Intrusion Time: 1000 yrs

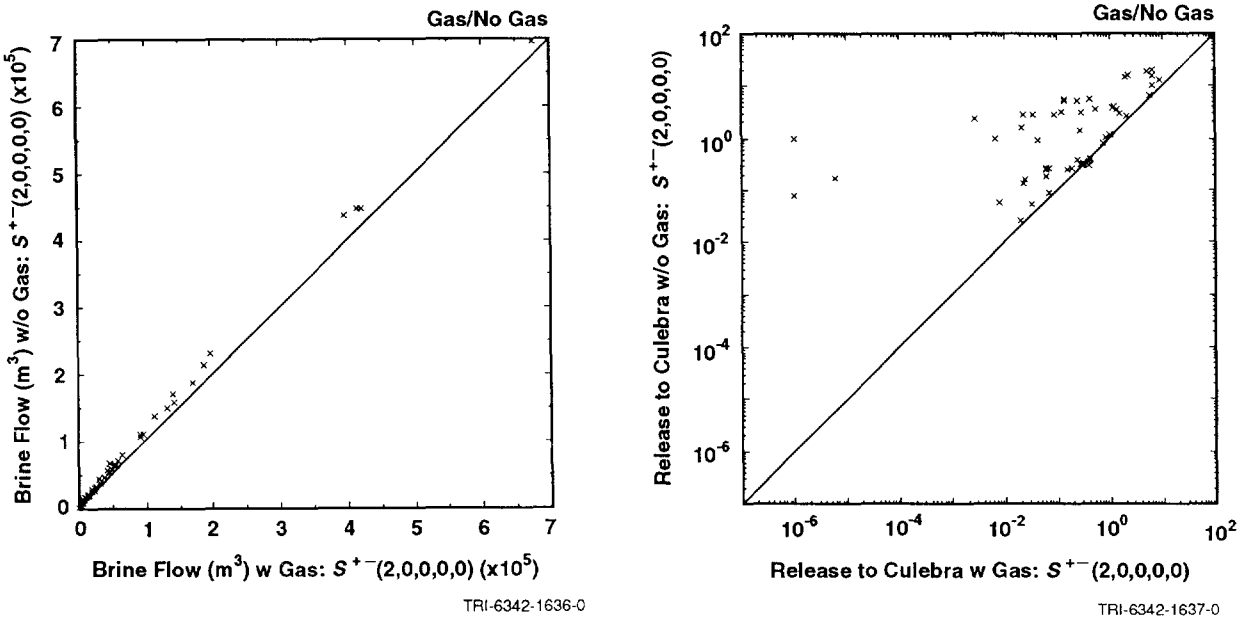

Figure 5.1-1. Scatterplots of Total Brine Flow (m^3) and Total Normalized Release from the Repository to the Culebra Dolomite with and without Gas Generation in the Repository for Scenarios $S(1,0,0,0,0)$ and $S^{+-}(2,0,0,0,0)$ with an Assumed Intrusion Time of 1000 Yrs. For plotting purposes when a logarithmic scale is used, numbers less than 10^{-6} are assigned a value of 10^{-6}.

right frame in Figure 5.1-1). In addition, the nonzero brine flows and radionuclide releases that result for scenario $S(1,0,0,0,0)$ increase in the absence of gas generation, which is indicated by the presence of points above the diagonal lines in the upper two frames of Figure 5.1-1.

For scenario $S^{+-}(2,0,0,0,0)$, the presence or absence of gas generation has little effect on whether or not a release to the Culebra occurs. However, the absence of gas generation does increase the size of the release (see lower right frame in Figure 5.1-1). As most of the brine flow into the Culebra is coming from a pressurized brine pocket in the Castile Formation for the scenario $S^{+-}(2,0,0,0,0)$, gas generation has only a limited effect on this flow (see lower left frame in Figure 5.1-1).

Releases of individual isotopes to the Culebra and to the accessible environment due to groundwater transport are summarized in Figures 5.1-2 and 5.1-3. As examination of these figures shows, transport in the Culebra results in substantial reductions in the releases for the individual isotopes. In particular, Am-241 and Pu-239 are important contributors to the release into the Culebra but make little contribution to the release to the accessible environment.

The radionuclide releases summarized in Figures 5.1-2 and 5.1-3 were calculated with the assumption that no gas generation takes place in the repository. The corresponding results for gas generation in the repository appear in Figures 4.4-7 and 4.4-2, respectively. As already discussed, the releases in Figures 4.4-7 and 4.4-2 tend to be smaller than those in Figures 5.1-2 and 5.1-3 due to the effect that gas generation has on reducing brine inflow to the repository from the Salado Formation.

The CCDFs summarizing groundwater transport releases to the accessible environment for gas generation in the repository and a dual-porosity transport model in the Culebra are given in the lower left frame of Figure 4.1-2. If the no-gas-generation results presented in this section had been calculated for all ten scenarios appearing in Figure 4.4-1, then the equivalent distribution of CCDFs could be obtained for no gas generation, and comparison of the two CCDF distributions would provide an indication of the effect of gas generation on the actual results (i.e., CCDFs) used in comparisons with the EPA release limits. However, to reduce computational costs, the no-gas-generation calculations presented in this section were only performed for scenarios $S(1,0,0,0,0)$ and $S^{+-}(2,0,0,0,0)$. As a result, it is not possible to generate a distribution of CCDFs with the available results for groundwater transport to the accessible environment that is equivalent to the one appearing in Figure 4.1-2.

Scenario: $S(1,0,0,0,0)$, Assumed Intrusion Time: 1000 yrs

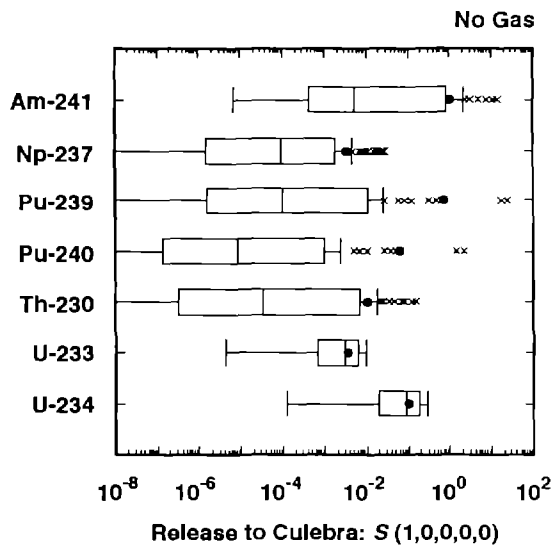

TRI-6342-1548-0

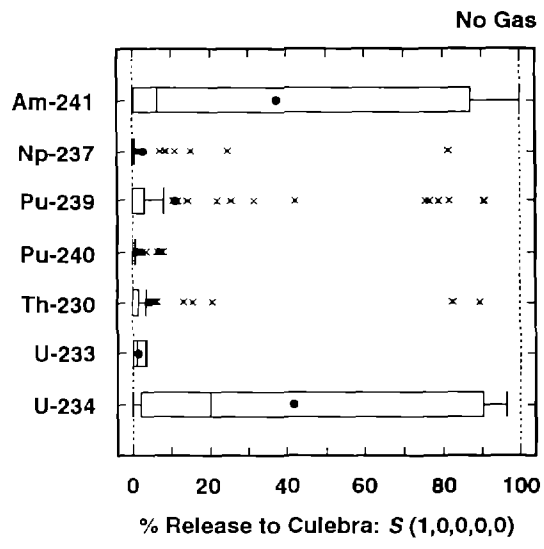

TRI-6342-1549-0

Scenario: $S^{+-}(2,0,0,0,0)$, Assumed Intrusion Time: 1000 yrs

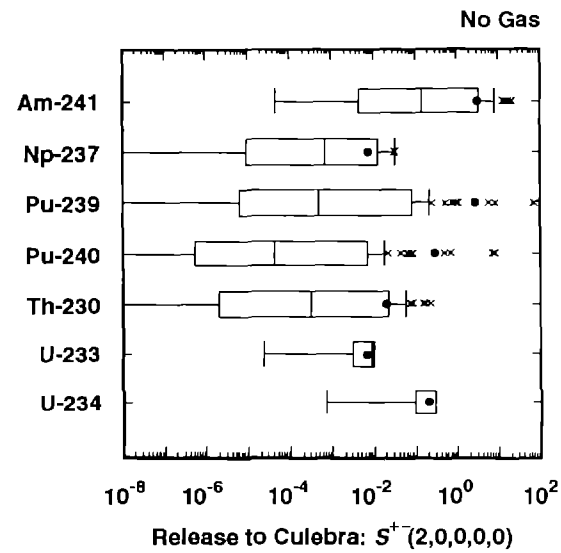

TRI-6342-1550-0

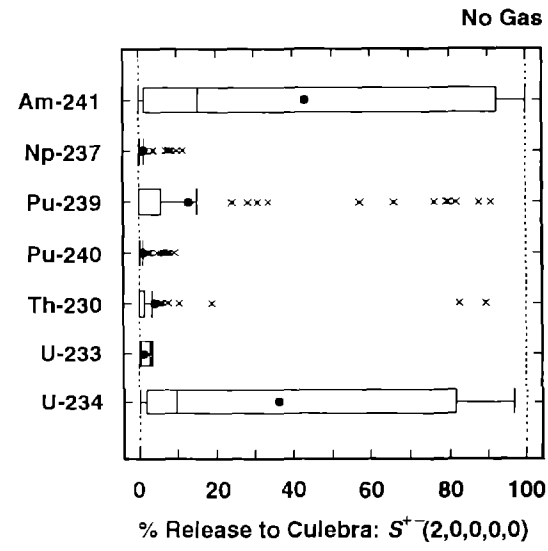

TRI-6342-1551-0

Figure 5.1-2. Normalized Releases for Individual Isotopes into the Culebra Dolomite with Intrusion Occurring at 1000 Yrs and No Gas Generation in the Repository.

Scenario: $S(1,0,0,0,0)$, Assumed Intrusion Time: 1000 yrs

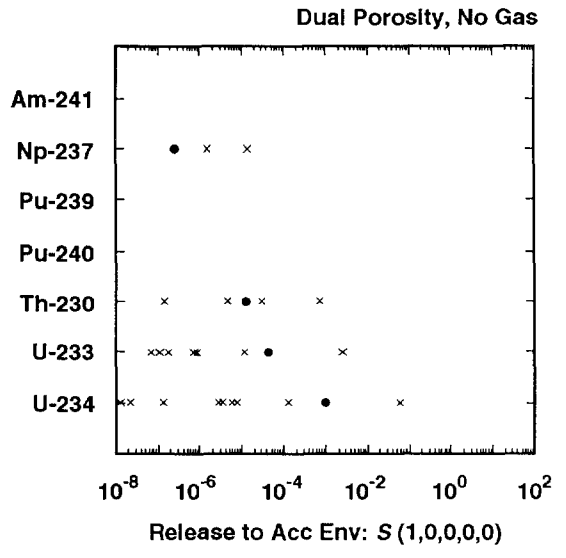

TRI-6342-1552-0

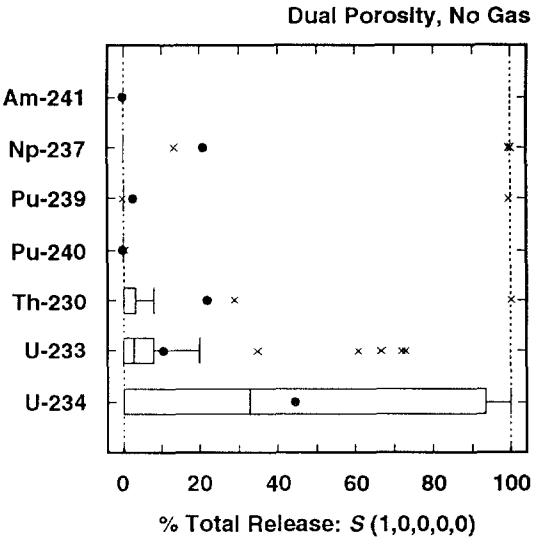

TRI-6342-1553-0

Scenario: $S^{+-}(2,0,0,0,0)$, Assumed Intrusion Time: 1000 yrs

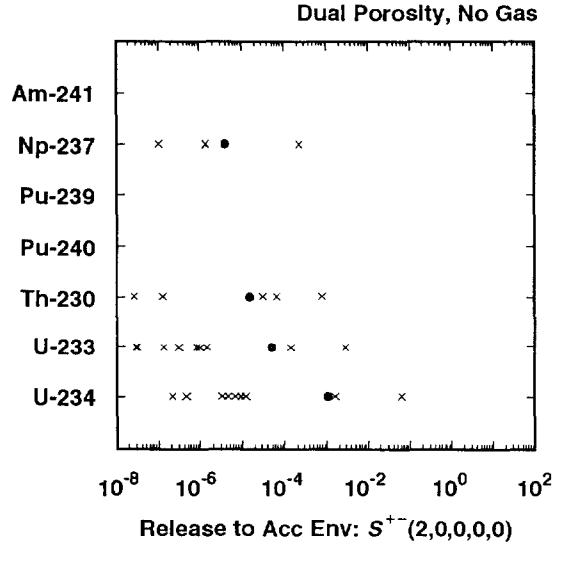

TRI-6342-1554-0

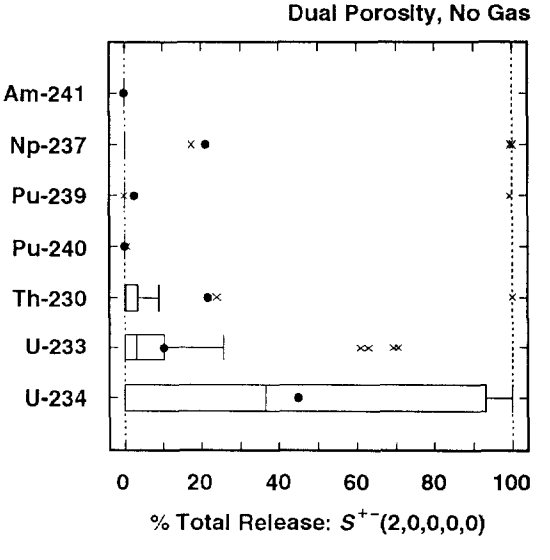

TRI-6342-1555-0

Figure 5.1-3. Normalized Releases for Individual Isotopes to the Accessible Environment Due to Groundwater Transport with Intrusion Occurring at 1000 Yrs, No Gas Generation in the Repository and a Dual-Porosity Transport Model in the Culebra Dolomite.

Another possibility for comparing CCDFs constructed with and without gas generation in the repository is to use only the results for scenarios $S(1,0,0,0,0)$ and $S^{+-}(2,0,0,0,0)$ (i.e., the results for intrusions occurring at 1000 yrs), which is equivalent to assuming that the rate constant λ in the Poisson model for drilling intrusions is equal to zero after 2000 yrs. Such an assumption is actually consistent with recommendations obtained in an external review of potential human disruptions at the WIPP (Hora et al., 1991).

Distributions of CCDFs constructed in this manner for release with and without gas generation in the repository are shown in Figure 5.1-4. As comparison of the results in Figure 5.1-4 shows, both the inclusion and exclusion of gas generation produce distributions of CCDFs that are substantially below the EPA release limits, although the CCDFs obtained without gas generation tend to be somewhat closer to the limits.

As shown in Figure 4.4-1, intrusions occurring after 1000 yrs result in smaller releases than intrusions occurring at 1000 yrs due to increased time for radioactive decay and reduced time for groundwater transport. As a result, consideration of a constant-valued, nonzero λ in the Poison model for drilling intrusions out to 10,000 yrs is unlikely to shift the CCDFs in Figure 5.1-4 up by more than a factor of 5 and an upward shift of 2 is more reasonable. Further, due to the low probability of compounding a large number of independent intrusions in different time intervals, the shift of the CCDFs to the right by more than a factor of 2 or 3 for a constant-valued, nonzero λ out to 10,000 yrs is also unlikely.

Sensitivity analyses for total brine release and total normalized release to the Culebra for scenarios $S(1,0,0,0,0)$ and $S^{+-}(2,0,0,0,0)$ with no gas generation in the repository are presented in Table 5.1-1. For scenario $S(1,0,0,0,0)$, brine release is dominated by SALPERM (Salado permeability), BHPERM (borehole permeability) and SALPRES (Salado pressure), and normalized release is dominated by SOLAM (solubility of Am) and SALPERM. For scenario $S^{+-}(2,0,0,0,0)$, brine release is dominated by BHPERM, BPPRES (brine pocket pressure) and DBDIAM (drill bit diameter), and normalized release is dominated by SOLAM, BHPERM, SOLPU (solubility of Pu) and BPPRES.

The corresponding analyses for brine releases and normalized releases with gas generation are presented in Table 4.5-3 for intrusions occurring at 1000 yrs. For the analyses for scenario $S(1,0,0,0,0)$ with gas generation, the results are dominated by SALPERM (Salado permeability) due to its previously discussed role as a switch. In contrast, additional important variables are identified in the analyses for scenario $S(1,0,0,0,0)$ in Table 5.1-1 because SALPERM does not introduce a discontinuity into the results in the absence

2 With Gas Generation in the Repository

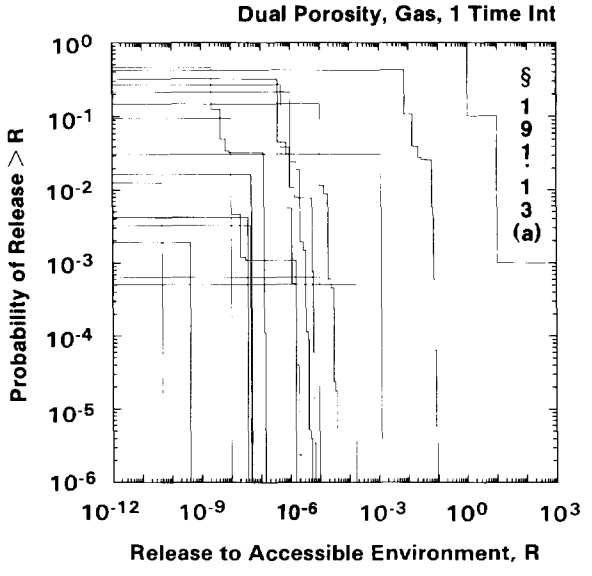

TRI-6342-1567-0

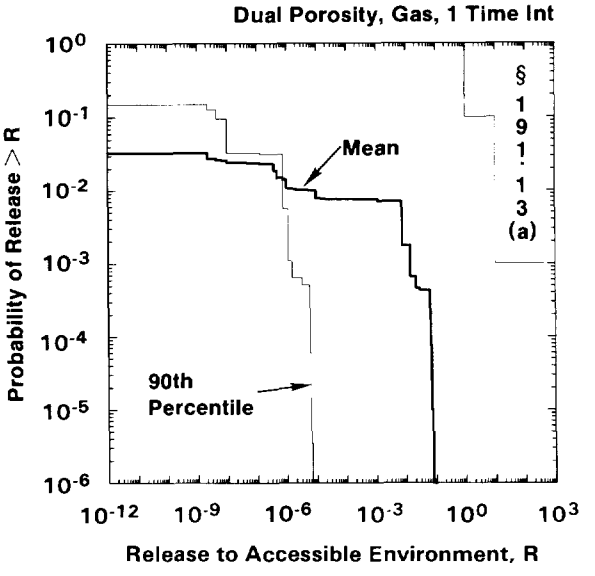

TRI-6342-1568-0

4 Without Gas Generation in the Repository

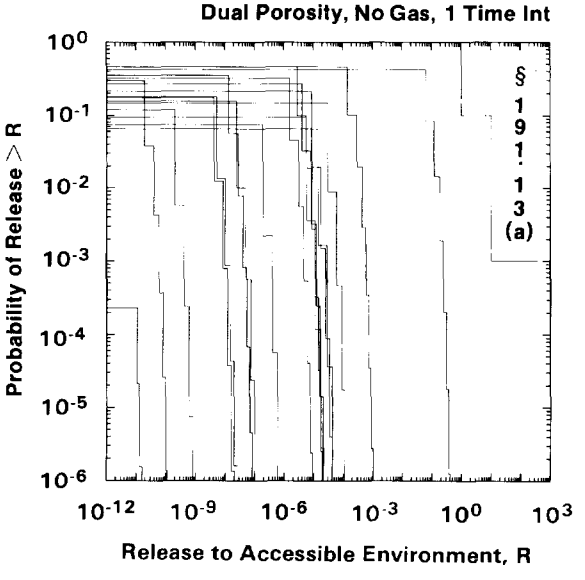

TRI-6342-1569-0

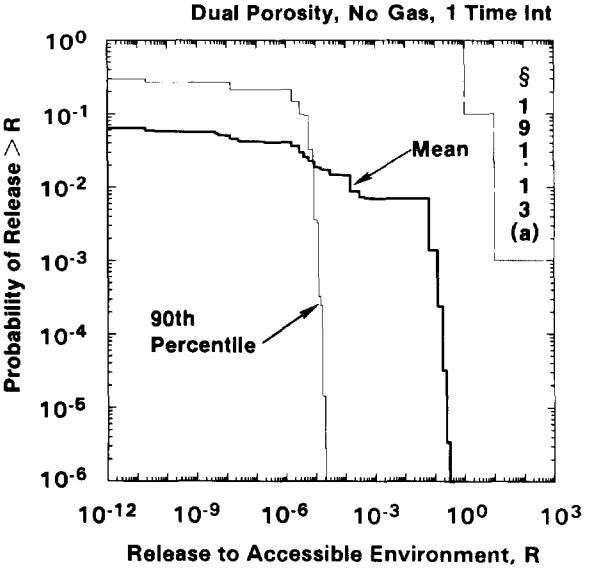

TRI-6342-1570-0

6 Figure 5.1-4. Comparison of Complementary Cumulative Distribution Functions for Normalized
7 Release to the Accessible Environment with Gas Generation in the Repository (upper
8 two frames) and without Gas Generation in the Repository (lower two frames) for a
9 Dual-Porosity Transport Model in the Culebra Dolomite and the Rate Constant λ in the
10 Poisson Model for Drilling Intrusions Equal to Zero After 2000 Yrs.

TABLE 5.1-1. STEPWISE REGRESSION ANALYSES WITH RANK-TRANSFORMED DATA FOR TOTAL BRINE RELEASE AND TOTAL NORMALIZED RELEASE TO THE CULEBRA DOLOMITE WITH NO GAS GENERATION IN THE REPOSITORY AND INTRUSION OCCURRING 1000 YRS AFTER REPOSITORY CLOSURE

	Scenario: $S(1,0,0,0,0)$				Scenario: $S^{+-}(2,0,0,0,0)$			
	Total Brine		Total Release		Total Brine		Total Release	
Step	Variable	R^2	Variable	R^2	Variable	R^2	Variable	R^2
1	SALPERM	0.51(+)	SOLAM	0.42(+)	BHPERM	0.82(+)	SOLAM	0.62(+)
2	BHPERM	0.69(+)	SALPERM	0.65(+)	BPPRES	0.95(+)	BHPERM	0.71(+)
3	SALPRES	0.79(+)			DBDIAM	0.97(+)	SOLPU	0.77(+)
4							BPPRES	0.81(+)

of gas generation. The analyses for scenario $S^{+-}(2,0,0,0,0)$ with and without gas generation are similar. However, there is a reversal in the order of importance of BHPERM (borehole permeability) and SOLAM (solubility of Am) for normalized release to the Culebra, with BHPERM being the most important variable in the presence of gas generation and SOLAM being the most important variable in the absence of gas generation. This switch in order of importance probably results because the presence of gas generation delays the release of material to the Culebra and thus allows more time for the decay of Am-241 before it can be released to the Culebra.

Sensitivity analyses of the groundwater transport results for individual isotopes for scenarios $S(1,0,0,0,0)$ and $S^{+-}(2,0,0,0,0)$ with no gas generation in the repository are presented in Tables 5.1-2 and 5.1-3 for release to the Culebra and for transport one-quarter, one-half and the full distance to the accessible environment. The results presented in these tables are generally similar to those presented in Tables 4.5-1 and 4.5-2 for results obtained with gas generation in the repository, although the analyses for scenario $S(1,0,0,0,0)$ in Table 5.1-2 tend to have larger R^2 values than those in Table 4.5-1 due to the absence of the effect of SALPERM (Salado permeability) as a switch. As shown in Table 5.1-2, the appropriate elemental solubility is the most important variable with respect to the release of each radionuclide to the Culebra, and the appropriate elemental matrix distribution coefficient is the most important variable for the transport of each isotope in the Culebra.

As for the analyses with gas generation in the repository, the examination of scatterplots helps supplement the sensitivity results contained in Tables 5.1-2 and 5.1-3. Scatterplots for the release of Pu-239 to the Culebra without gas generation in the repository are presented in Figure 5.1-5. The top two frames are for scenario $S(1,0,0,0,0)$. As the top left frame shows, SALPERM (Salado permeability) does not act as a switch for releases to the Culebra in the absence of gas generation; for comparison, the corresponding

TABLE 5.1-2. STEPWISE REGRESSION ANALYSES WITH RANK-TRANSFORMED DATA FOR SCENARIO $S(1,0,0,0,0)$ WITH NO GAS GENERATION IN THE REPOSITORY, A DUAL-POROSITY TRANSPORT MODEL IN THE CULEBRA DOLOMITE AND INTRUSION OCCURRING 1000 YRS AFTER REPOSITORY CLOSURE

	Release to Culebra		Quarter Distance		Half Distance		Full Distance	
Step	Variable	R^2	Variable	R^2	Variable	R^2	Variable	R^2
Dependent Variable: Integrated Discharge Am-241								
1	SOLAM	0.81(+)	CULFRSP	0.11 (+)	FKDAM	0.27 (+)	--	--
2	SALPERM	0.90(+)			MKDAM	0.47 (-)		
3	BHPERM	0.92(+)			CULFRPOR	0.53 (+)		
4	SALPRES	0.93(+)						
Dependent Variable: Integrated Discharge Np-237								
1	SOLNP	0.77(+)	FKDNP	0.22 (-)	MKDNP	0.50 (-)	MKDNP	0.26 (-)
2	EHPH	0.86(+)	MKDNP	0.32 (-)			FKDNP	0.37 (-)
3	SALPERM	0.90(+)						
Dependent Variable: Integrated Discharge Pu-239								
1	SOLPU	0.92(+)	MKDPU	0.17 (-)	MKDPU	0.28 (-)	--	--
2	SALPERM	0.94(+)	FKDPU	0.30 (-)	FKDPU	0.37 (+)		
3	BHPERM	0.95(+)			CULFRPOR	0.46 (+)		
4					CULFRSP	0.52 (+)		
Dependent Variable: Integrated Discharge Pu-240								
1	SOLPU	0.91(+)	MKDPU	0.14 (-)	MKDPU	0.19 (-)	--	--
2	SALPERM	0.94(+)	FKDPU	0.24 (-)	FKDPU	0.29 (+)		
3	BHPERM	0.95(+)	CULPOR	0.34 (-)	CULFRSP	0.36 (+)		
4					CULFRPOR	0.43 (+)		
Dependent Variable: Integrated Discharge Th-230								
1	SOLTH	0.94(+)	MKDU	0.42 (-)	MKDU	0.43 (-)	MKDU	0.38 (-)
2	SALPERM	0.96(+)	MKDTH	0.64 (-)	MKDTH	0.58 (-)	CULFRSP	0.49 (+)
3	BHPERM	0.97(+)	CULFRSP	0.72 (+)	CULFRSP	0.68 (+)	MKDTH	0.57 (-)
4	SALPRES	0.97(+)	CULCLIM	0.77 (+)	CULCLIM	0.73 (+)	CULCLIM	0.63 (+)
5			FKDPU	0.80 (-)	FKDPU	0.76 (-)		

TABLE 5.1-2. STEPWISE REGRESSION ANALYSES WITH RANK-TRANSFORMED DATA FOR SCENARIO $S(1,0,0,0,0)$ WITH NO GAS GENERATION IN THE REPOSITORY, A DUAL-POROSITY TRANSPORT MODEL IN THE CULEBRA DOLOMITE AND INTRUSION OCCURRING 1000 YRS AFTER REPOSITORY CLOSURE (concluded)

	Release to Culebra		Quarter Distance		Half Distance		Full Distance	
Step	Variable	R^2	Variable	R^2	Variable	R^2	Variable	R^2
Dependent Variable: Integrated Discharge U-233								
1	SOLU	0.34(+)	MKDU	0.64 (-)	MKDU	0.59 (-)	MKDU	0.47 (-)
2	SALPERM	0.42(+)	SOLNP	0.73 (+)	SOLNP	0.65 (+)	SOLNP	0.54 (+)
3	SALPRES	0.49(+)	CULFRSP	0.79 (+)	FKDNP	0.71 (-)	FKDNP	0.58 (-)
4			FKDNP	0.82 (-)	CULFRSP	0.74 (+)	CULFRSP	0.63 (+)
Dependent Variable: Integrated Discharge U-234								
1	SOLU	0.29(+)	MKDU	0.81 (-)	MKDU	0.72 (-)	MKDU	0.70 (-)
2	SALPERM	0.37(+)	CULFRSP	0.87 (+)	CULFRSP	0.75 (+)		
3	SALPRES	0.43(+)	CULCLIM	0.89 (+)	CULCLIM	0.78 (+)		
Dependent Variable: EPA Sum for Total Integrated Discharge								
1	SOLAM	0.42(+)	MKDU	0.38 (-)	MKDU	0.36 (-)	MKDU	0.29 (-)
2	SALPERM	0.65(+)	CULFRSP	0.54 (+)	CULFRSP	0.54 (+)	CULFRSP	0.48 (+)
3			SOLNP	0.60 (+)	SOLNP	0.61 (+)	SOLNP	0.55 (+)
4			FKDNP	0.65 (-)			FKDNP	0.59 (-)

TABLE 5.1-3. STEPWISE REGRESSION ANALYSES WITH RANK-TRANSFORMED DATA FOR SCENARIO S^{+-}(2,0,0,0,0) WITH NO GAS GENERATION IN THE REPOSITORY, A DUAL-POROSITY TRANSPORT MODEL IN THE CULEBRA DOLOMITE AND INTRUSION OCCURRING 1000 YRS AFTER REPOSITORY CLOSURE

	Release to Culebra		Quarter Distance		Half Distance		Full Distance	
Step	Variable	R^2	Variable	R^2	Variable	R^2	Variable	R^2
Dependent Variable: Integrated Discharge Am-241								
1	SOLAM	0.84(+)	--	--	FKDAM	0.30 (+)	--	--
2	BHPERM	0.93(+)			MKDAM	0.53 (-)		
3	BPPRES	0.94(+)			CULFRPOR	0.58 (+)		
Dependent Variable: Integrated Discharge Np-237								
1	SOLNP	0.77(+)	FKDNP	0.21 (-)	MKDNP	0.50 (-)	MKDNP	0.24 (-)
2	EHPH	0.84(+)	MKDNP	0.35 (-)			FKDNP	0.34 (-)
3	BHPERM	0.88(+)						
4	BPPRES	0.91(+)						
Dependent Variable: Integrated Discharge Pu-239								
1	SOLPU	0.90(+)	MKDPU	0.28 (-)	MKDPU	0.33 (-)	--	--
2	BHPERM	0.94(+)	FKDPU	0.39 (-)	FKDPU	0.41 (+)		
3	BPPRES	0.95(+)			CULFRSP	0.47 (+)		
4	DBDIAM	0.96(+)						
5	EHPH	0.96(+)						
Dependent Variable: Integrated Discharge Pu-240								
1	SOLPU	0.90(+)	MKDPU	0.17 (-)	MKDPU	0.26 (-)	--	--
2	BHPERM	0.94(+)	FKDPU	0.33 (-)	FKDPU	0.36 (+)		
3	BPPRES	0.95(+)						
4	DBDIAM	0.96(+)						
5	EHPH	0.96(+)						
Dependent Variable: Integrated Discharge Th-230								
1	SOLTH	0.90(+)	MKDU	0.40 (-)	MKDU	0.41 (-)	MKDU	0.38 (-)
2	BHPERM	0.95(+)	MKDTH	0.63 (-)	MKDTH	0.58 (-)	CULFRSP	0.50 (+)
3			CULFRSP	0.72 (+)	CULFRSP	0.67 (+)	MKDTH	0.59 (-)
4			CULCLIM	0.78 (+)	CULCLIM	0.74 (+)	CULCLIM	0.65 (+)
5			CULDISP	0.80 (+)	FKDPU	0.76 (-)		
6			FKDPU	0.82 (-)				

TABLE 5.1-3. STEPWISE REGRESSION ANALYSES WITH RANK-TRANSFORMED DATA FOR SCENARIO S^{+-}(2,0,0,0,0) WITH NO GAS GENERATION IN THE REPOSITORY, A DUAL-POROSITY TRANSPORT MODEL IN THE CULEBRA DOLOMITE AND INTRUSION OCCURRING 1000 YRS AFTER REPOSITORY CLOSURE (concluded)

	Release to Culebra		Quarter Distance		Half Distance		Full Distance	
Step	Variable	R^2	Variable	R^2	Variable	R^2	Variable	R^2
Dependent Variable: Integrated Discharge U-233								
1	SOLU	0.25 (+)	MKDU	0.63 (-)	MKDU	0.59 (-)	MKDU	0.48 (-)
2	BHPERM	0.39 (+)	SOLNP	0.71 (+)	SOLNP	0.65 (+)	SOLNP	0.55 (+)
3	SOLNP	0.50 (-)	CULFRSP	0.78 (+)	FKDNP	0.71 (-)	CULFRSP	0.60 (+)
4	BPPRES	0.58 (+)	FKDNP	0.80 (-)	SOLU	0.75 (-)	SOLU	0.65 (-)
					CULFRSP	0.78 (+)	FKDNP	0.69 (-)
Dependent Variable: Integrated Discharge U-234								
1	SOLU	0.20 (+)	MKDU	0.79 (-)	MKDU	0.71 (-)	MKDU	0.70 (-)
2	BHPERM	0.36 (+)	CULFRSP	0.86 (+)	SOLNP	0.77 (+)	SOLNP	0.75 (+)
3			CULCLIM	0.89 (+)	CULFRSP	0.81 (+)	SOLU	0.78 (-)
4					SOLU	0.86 (-)		
Dependent Variable: EPA Sum for Total Integrated Discharge								
1	SOLAM	0.62 (+)	MKDU	0.37 (-)	MKDU	0.36 (-)	MKDU	0.30 (-)
2	BHPERM	0.71 (+)	CULFRSP	0.53 (+)	CULFRSP	0.56 (+)	CULFRSP	0.49 (+)
3	SOLPU	0.77 (+)	SOLNP	0.60 (+)	SOLNP	0.62 (+)	SOLNP	0.56 (+)
4	BPPRES	0.81 (+)	FKDNP	0.65 (-)			FKDNP	0.60 (-)

Scenario: $S(1,0,0,0,0)$, Assumed Intrusion Time: 1000 yrs

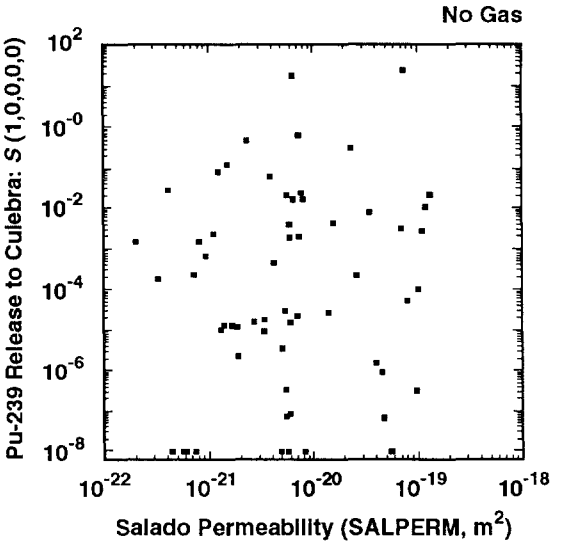

TRI-6342-1607

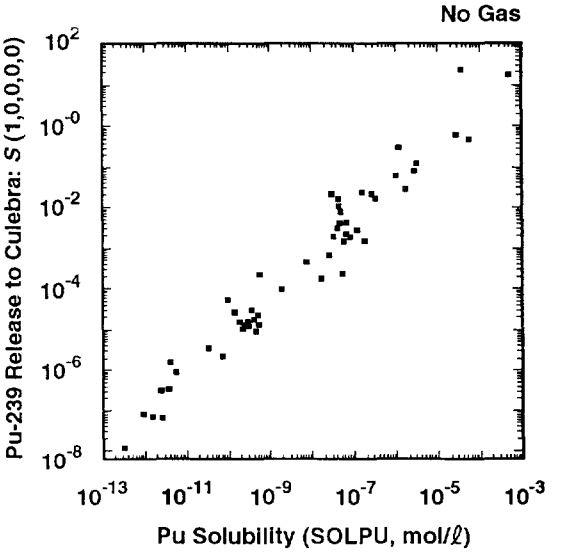

TRI-6342-1608-0

Scenario: $S^{+-}(2,0,0,0,0)$, Assumed Intrusion Time: 1000 yrs

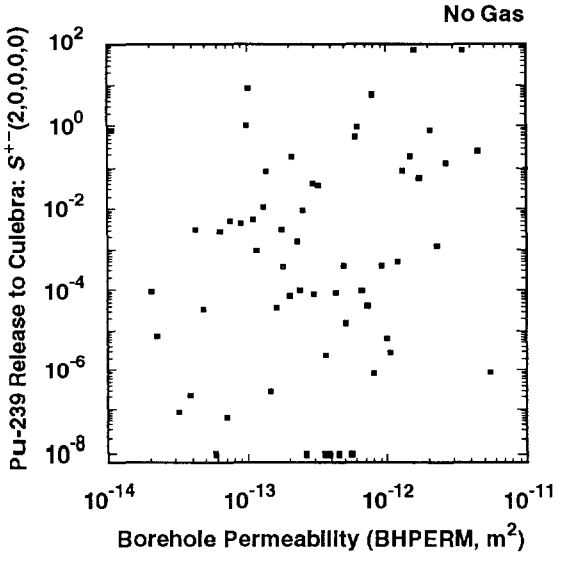

TRI-6342-1609-0

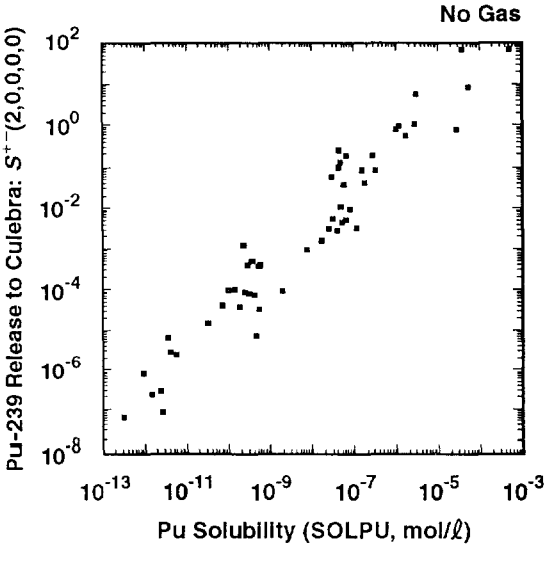

TRI-6342-1610-0

Figure 5.1-5. Scatterplots for Normalized Release of Pu-239 to the Culebra Dolomite without Gas Generation in the Repository for Variables SALPERM (Salado permeability), BHPERM (borehole permeability) and SOLPU (solubility for Pu) and Scenarios $S(1,0,0,0,0)$ and $S^{+-}(2,0,0,0,0)$ with an Assumed Intrusion Time of 1000 Yrs.

scatterplot for gas generation in the repository appears in the upper left frame of Figure 4.5-1 and shows the importance of SALPERM in the presence of gas generation. Rather, as shown in the upper right frame of Figure 5.1-5, the release of Pu-239 to the Culebra for scenario $S(1,0,0,0,0)$ in the absence of gas generation is completely dominated by SOLPU (solubility for Pu). The lower two frames in Figure 4.5-1 are for scenario $S^{+-}(2,0,0,0,0)$. As the right frame shows, the release of Pu-239 to the Culebra for scenario $S^{+-}(2,0,0,0,0)$ is also dominated by SOLPU. The lower left frame is for BHPERM (borehole permeability) and indicates little, if any, visually identifiable relationship between release to the Culebra and BHPERM, although BHPERM is the second variable picked in the regression analysis in Table 5.1-3 for the release of Pu-239 to the Culebra for scenario $S^{+-}(2,0,0,0,0)$. Although BHPERM is an important variable for the release of some isotopes for scenario $S^{+-}(2,0,0,0,0)$ (e.g., see Figure 4.5-2 and 4.5-3 for the gas generation case), its effect is being overwhelmed for Pu-239 by the large range assigned to SOLPU.

Scatterplots for the release of U-234 to the Culebra without gas generation are presented in Figure 5.1-6. The top two frames are for scenario $S(1,0,0,0,0)$. With a little thought, it is easy to understand the pattern shown in the scatterplots contained in these two frames. The upper right frame is for SOLU (solubility for U) and shows the U-234 release to the Culebra initially increasing with SOLU and then flattening off for larger values of SOLU. As shown in Figure 2.4-2, this flattening off corresponds to an inventory-imposed limit (i.e., 0.3 EPA units) on the amount of U-234 available for release to the Culebra. However, there is a great deal of variability in the actual releases associated with the flattened region in the scatterplot for SOLPU due to the effects of SALPERM (Salado permeability), SALPRES (Salado pressure) and BHPERM (borehole permeability). As shown in Table 5.1-1 for scenario $S(1,0,0,0,0)$, increasing each of these variables increases brine flow from the repository to the Culebra and hence tends to increase the U-234 release. However, as shown in the upper left frame in Figure 5.1-1, many of the resultant brine flows are small (i.e., $< 10^4$ m^3), with the result that it is not possible to deplete the U-234 inventory in 10,000 yrs for scenario $S(1,0,0,0,0)$. The scatterplot for SALPERM appears in the upper left frame of Figure 5.1-6. The releases in the scatterplot for SALPERM that are less than 10^{-2} all result from small values for SOLU; when these points are ignored, an increasing relationship between SALPERM and U-234 release to the Culebra can be seen. A similar pattern of relationships involving BHPERM and SOLU can be seen in the two upper scatterplots in Figure 4.5-2 for the release of U-234 for scenario $S(1,0,0,0,0)$ with gas generation in the repository. However, the patterns in Figure 4.5-2 for the gas generation case are much more diffuse due to the many zero releases that result from the interaction of gas generation and SALPERM.

Scenario: S(1,0,0,0,0), Assumed Intrusion Time: 1000 yrs

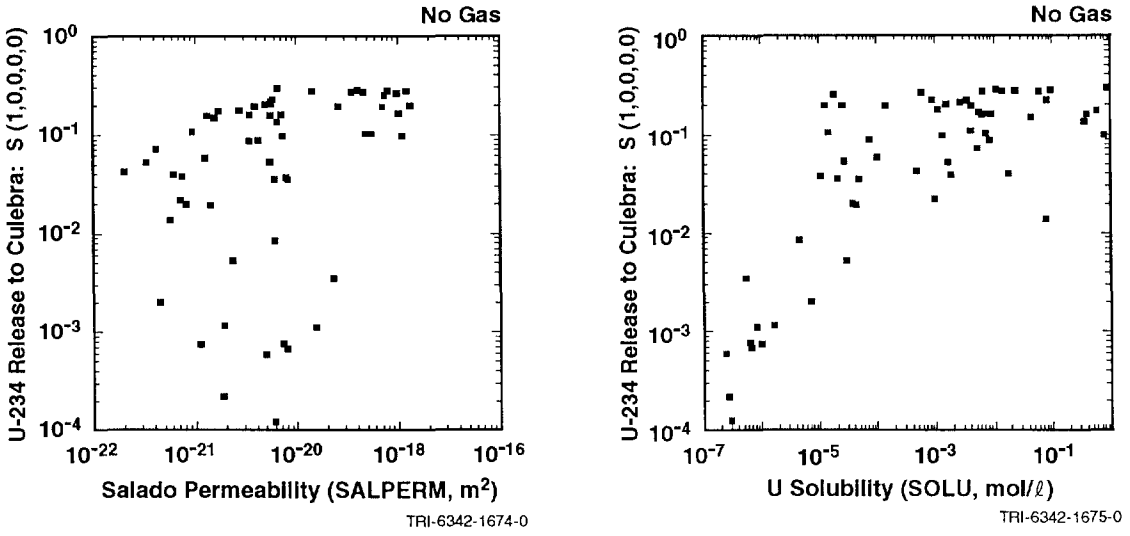

Scenario: S^{+-}(2,0,0,0,0), Assumed Intrusion Time: 1000 yrs

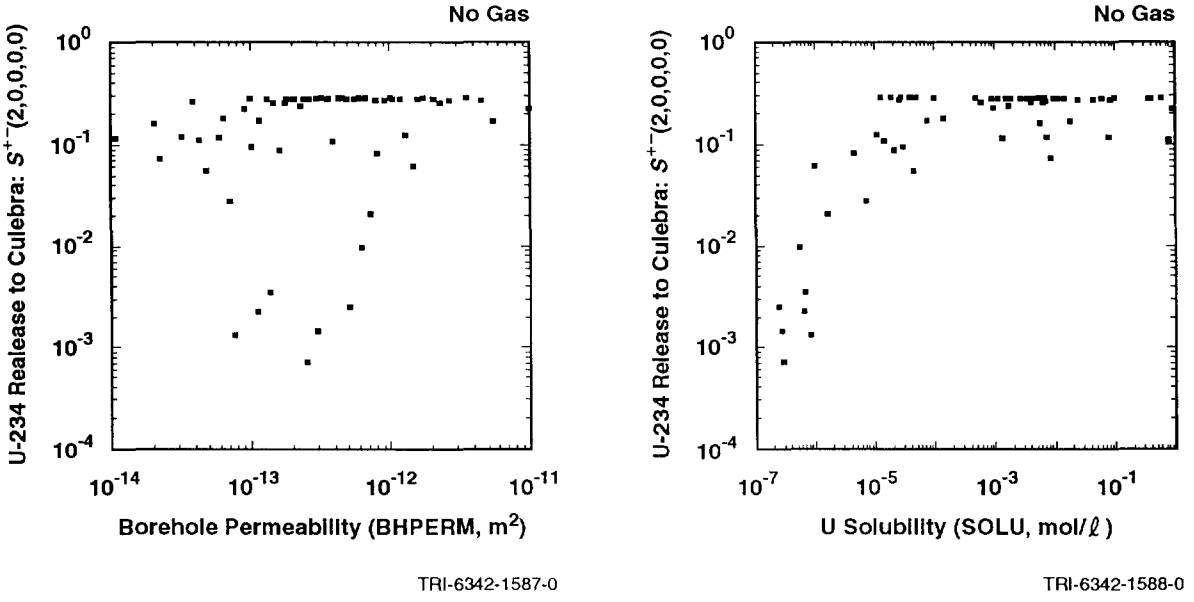

Figure 5.1-6. Scatterplots for Normalized Release of U-234 to the Culebra Dolomite without Gas Generation in the Repository for Variables SALPERM (Salado permeability), BHPERM (borehole permeability) and SOLU (solubility for U) and Scenarios S(1,0,0,0,0) and S^{+-}(2,0,0,0,0) with an Assumed Intrusion Time of 1000 Yrs.

The lower two frames in Figure 5.1-6 are for scenario $S^{+-}(2,0,0,0,0)$. The associated scatterplots show U-234 release to the Culebra increasing with BHPERM (borehole permeability) and SOLU (solubility for U). Further, the effect of an inventory limit on the U-234 release to the Culebra can be clearly seen in the line of equal releases across the top of the two scatterplots. The lower two scatterplots in Figure 5.1-6 for scenario $S^{+-}(2,0,0,0,0)$ show essentially the same pattern as the upper two scatterplots for scenario $S(1,0,0,0,0)$. However, the results for scenario $S^{+-}(2,0,0,0,0)$ are better defined than those for scenario $S(1,0,0,0,0)$ due to the larger brine flows through the panel and into the Culebra. A similar pattern is also shown in Figure 4.5-2 for scenario $S^{+-}(2,0,0,0,0)$ for gas generation in the repository.

Scatterplots for the release of Am-241 to the Culebra without gas generation are presented in Figure 5.1-7. The top two frames are for scenario $S(1,0,0,0,0)$, and the lower two frames are for scenario $S^{+-}(2,0,0,0,0)$. The patterns shown in this figure are similar to those appearing in Figure 5.1-6 for U-234. For both scenarios, the releases initially increase as SOLAM (solubility for Am) increases and then tend to level off for larger values of SOLAM due to inventory limitations. As shown in Figure 2.4-2, the Am-241 inventory in one waste panel at 1000 yrs is approximately 30 EPA units.

Interesting patterns appear in the scatterplots for SALPERM (Salado permeability) and BHPERM (borehole permeability) in Figure 5.1-7 for scenarios $S(1,0,0,0,0)$ and $S^{+-}(2,0,0,0,0)$, respectively. These two scatterplots have two bands that result from the sampling procedure used for SOLAM (solubility for Am). Specifically, the distribution for SOLAM was assumed to be piecewise uniform over several subintervals of a range extending from 5×10^{-14} to 1.4 mol/ℓ, which leads to the clusters of values for SOLAM that can be seen in the two scatterplots involving SOLAM in Figure 5.1-7. The top bands in the scatterplots for SALPERM and BHPERM are associated with the larger values for SOLAM; similarly, the lower bands are associated with the smaller values for SOLAM. If SOLAM had been sampled from a loguniform distribution over the range 5×10^{-14} to 1.4 mol/ℓ, the bands appearing in the scatterplots for SALPERM and BHPERM would be less apparent, although it is possible that they would still be present due to the leveling off of the releases to the Culebra because of inventory limitations. This behavior provides an excellent example of the fact that whether or not a particular variable appears to be important often depends on the ranges assigned to other variables. In this case, SALPERM and BHPERM have well-defined effects when SOLAM is restricted to values below or above the point at which inventory limits are important (i.e., SOLAM $\triangleq 10^{-7}$ mol/ℓ). However, the scatterplots for the two variables would show a much more diffuse pattern if SOLAM had been sampled from a loguniform distribution on the interval $[5 \times 10^{-14}, 1.4]$.

Scenario: S(1,0,0,0,0), Assumed Intrusion Time: 1000 yrs

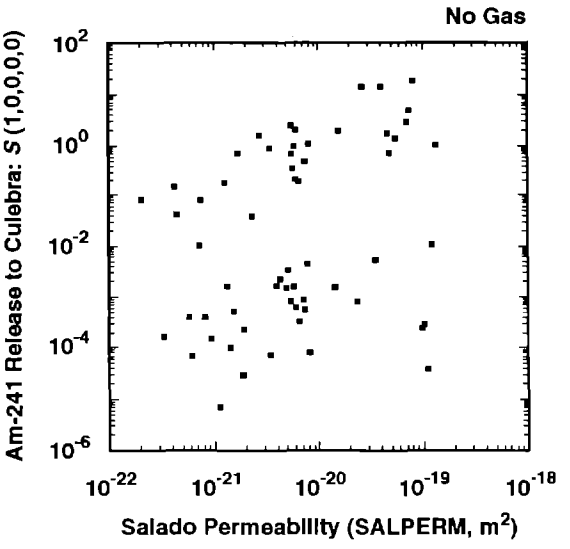

TRI-6342-1589-0

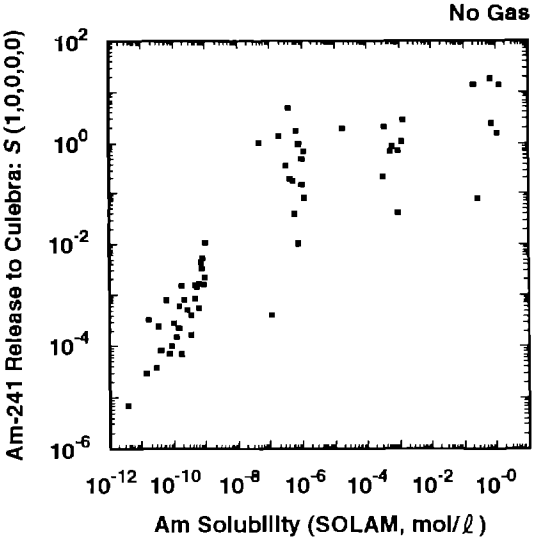

TRI-6342-1590-0

Scenario: S^{+-}(2,0,0,0,0), Assumed Intrusion Time: 1000 yrs

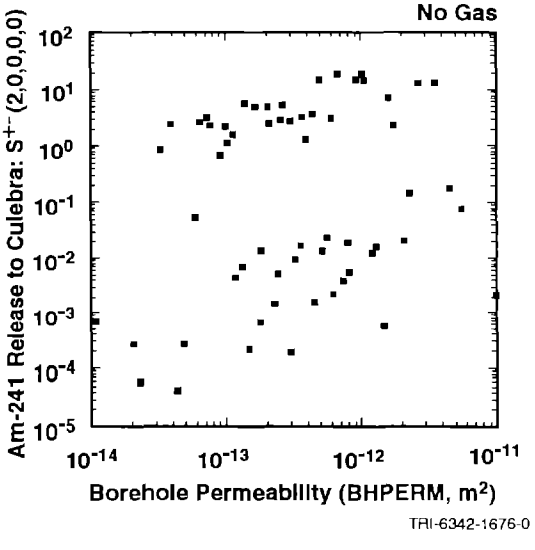

TRI-6342-1676-0

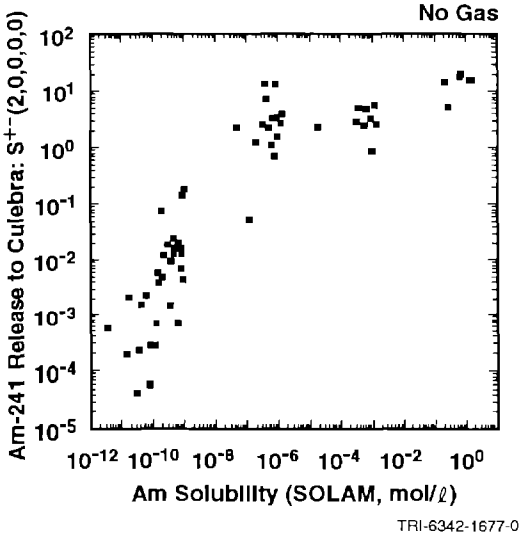

TRI-6342-1677-0

Figure 5.1-7. Scatterplots for Normalized Release of Am-241 to the Culebra Dolomite without Gas Generation in the Repository for Variables SALPERM (Salado permeability), BHPERM (borehole permeability) and SOLAM (solubility for Am) and Scenarios S(1,0,0,0,0) and S^{+-}(2,0,0,0,0) with an Assumed Intrusion Time of 1000 Yrs.

The corresponding scatterplots for Am-241 release to the Culebra with gas generation are shown in Figure 4.5-3. As comparison of the scatterplots in Figures 4.5-3 and 5.1-7 shows, gas generation and no gas generation lead to similar patterns of behavior, although the results shown in Figure 5.1-7 for releases in the absence of gas generation are considerably sharper than those shown in Figure 4.5-3 for releases in the presence of gas generation. In particular, the releases with gas generation shown in Figure 4.5-3 are both smaller and more diffuse than the releases without gas generation shown in Figure 5.1-7 as a result of both less brine inflow to the repository from the Salado Formation and more time for radioactive decay.

The presence or absence of gas generation in the repository only affects release to the Culebra. The groundwater transport analyses for both cases were performed with the same dual porosity transport model in the Culebra and the same sample elements. Thus, the same patterns of behavior shown in Figures 4.5-6 and 4.5-7 for transport in the Culebra with gas generation also hold for transport without gas generation. In particular, as shown by the scatterplot for U-234 in the lower left frame of Figure 4.5-6 for scenario $S^{+-}(2,0,0,0,0)$ and transport one-quarter the distance to the accessible environment, retardation resulting from the matrix distribution coefficients (i.e., MKDAM, MKDNP, MKDPU, MKDTH, MKDU) is very effective in preventing individual isotopes from being transported to the accessible environment. As shown by the upper two frames in Figure 4.5-6, the retardations for Am-241 and Pu-239 effectively cutoff transport in the Culebra with the dual-porosity model.

5.2 Effect of Single-Porosity Transport Model in Culebra Dolomite

Although a dual-porosity transport model is believed to be an appropriate representation for radionuclide transport in the Culebra, the use of a single-porosity transport model has also been proposed (Reeves et al., 1987). To help provide perspective on the impact of a single-porosity rather than a dual-porosity transport model in the Culebra, the analyses presented in Chapter 4 were repeated with a single-porosity transport model.

The CCDFs for groundwater transport to the accessible environment that result from the use of a single-porosity transport model are presented in Figure 5.2-1. The upper left frame displays the CCDFs for the individual sample elements; the corresponding distribution of CCDFs from the analysis with a dual-porosity transport model is shown in the lower left frame of Figure 4.1-2. As comparison of the CCDFs in Figures 5.2-1 and 4.1-2 shows, use of a single-porosity transport model results in considerably larger releases than the use of a dual-porosity transport model.

2 Groundwater Transport Releases Only

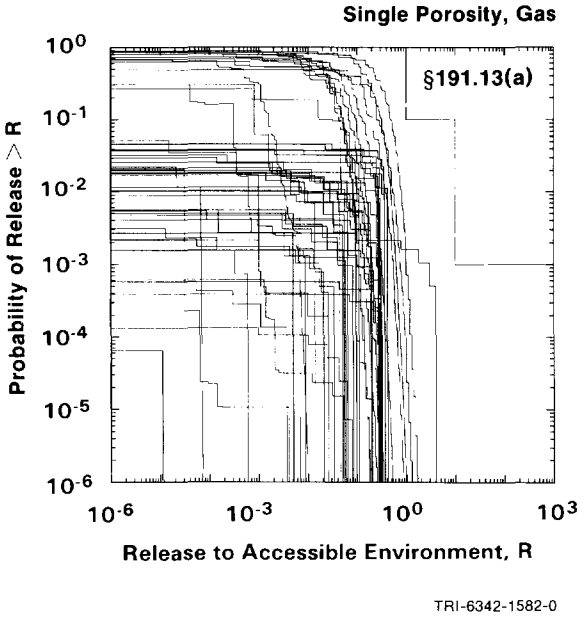

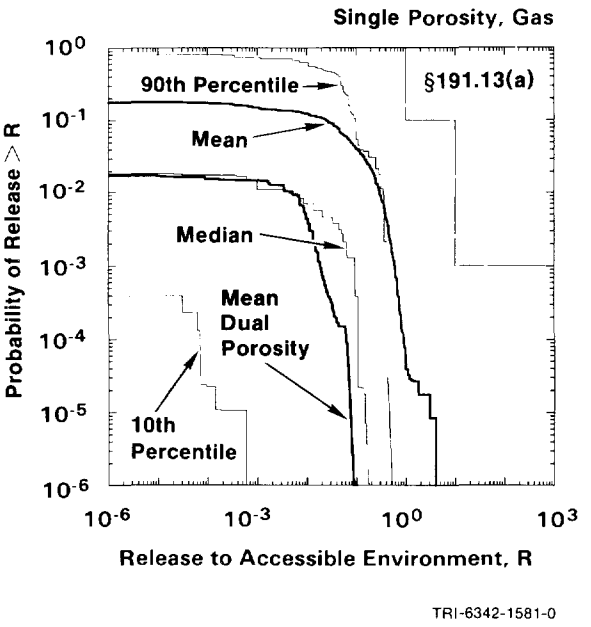

4 Total Release: Groundwater Transport and Cuttings Releases

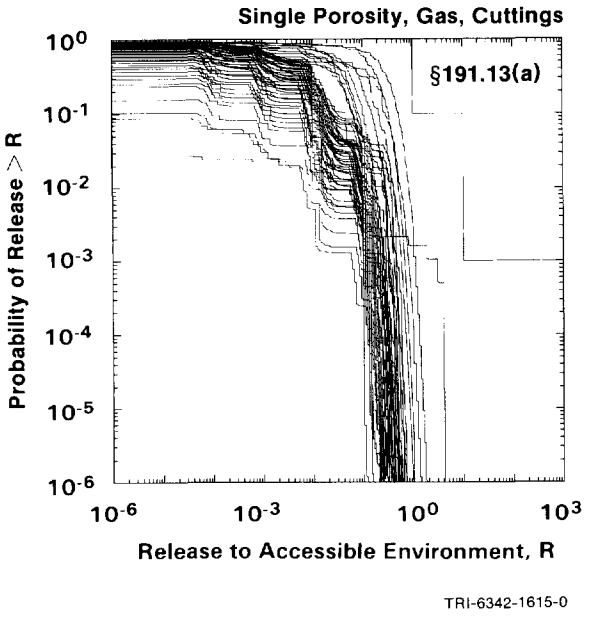

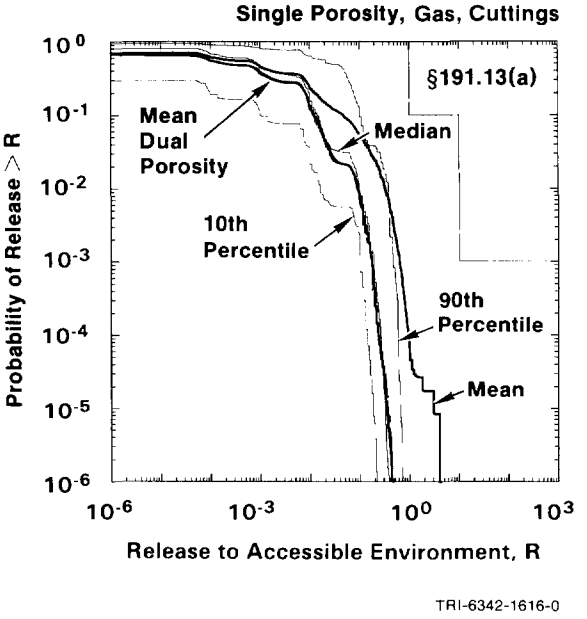

6 Figure 5.2-1. Complementary Cumulative Distribution Functions for Normalized Release to the
7 Accessible Environment for Gas Generation in the Repository and a Single-Porosity
8 Transport Model in the Culebra Dolomite.

The upper right frame in Figure 5.2-1 shows the mean and selected percentile curves for the distribution of CCDFs shown in the upper left frame. The mean CCDF obtained with the dual-porosity transport model is also shown. As comparison of the two mean curves shows, use of the single-porosity model results in a significant increase in the mean CCDF for radionuclide release to the accessible environment. Due to the large variability in the individual CCDFs, the mean CCDFs tend to be dominated by the few larger CCDFs. As a result, simply comparing mean CCDFs probably underestimates the impact of the single-porosity transport model. However, although the single-porosity transport model results in larger releases to the accessible environment than the dual-porosity transport model, none of the individual CCDFs in Figure 5.2-1 cross the EPA release limits.

The two lower frames in Figure 5.2-1 summarize the CCDFs for total release to the accessible environment. As comparison of the results in the upper and lower frames of Figure 5.2-1 shows, release to the accessible environment is still dominated by cuttings removal when the single-porosity transport model is used, although the CCDFs closest to the EPA release limits are determined primarily by groundwater transport releases (i.e., compare the CCDFs closest to the EPA release limits in the upper left and lower left frames of Figure 5.2-1). For comparison, the CCDFs due to cuttings releases only are shown in the upper left frame of Figure 4.1-2. The lower right frame in Figure 5.2-1 contains the mean CCDFs for total release to the accessible environment, including releases due to groundwater transport and cuttings removal, for single- and dual-porosity transport models in the Culebra. As comparison of these two CCDFs shows, the assumption of a single-porosity transport model does cause an upward shift in the mean CCDF.

An alternate comparison of the effects of single-porosity and dual-porosity transport models in the Culebra for scenarios $S(1,0,0,0,0)$ and $S^{+-}(2,0,0,0,0)$ is shown in Figure 5.2-2. As the scatterplots in this figure show, the single-porosity transport model causes the releases associated with the individual sample elements to be shifted upward. For many sample elements, zero releases with the dual-porosity transport model are nonzero releases with the single-porosity transport model. This effect is most pronounced for scenario $S^{+-}(2,0,0,0,0)$. As shown in Figure 4.5-4, the presence of gas generation in the repository results in no releases to the Culebra for many sample elements for scenario $S(1,0,0,0,0)$, with the result that the transport model in use for the Culebra has no effect on the predicted release to the accessible environment for these sample elements.

The total normalized releases to the accessible environment due to groundwater transport with a single-porosity transport model in the Culebra for individual scenarios are summarized in Figure 5.2-3. The corresponding results for the dual-porosity transport model appear in Figure 4.4-1. As

Scenario: $S(1,0,0,0,0)$, Assumed Intrusion Time: 1000 yrs

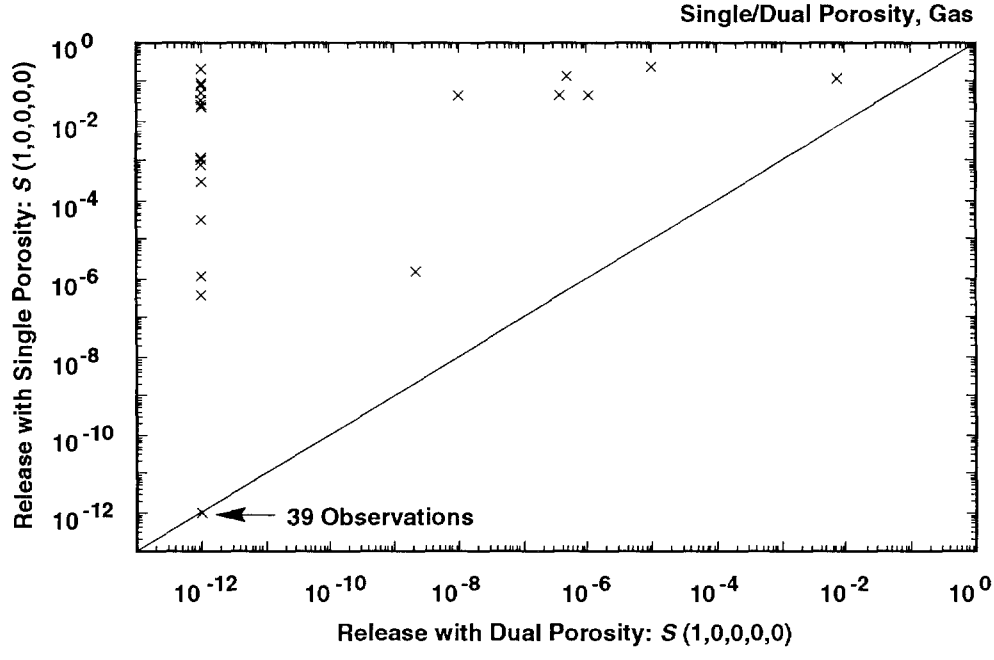

Scenario: $S^{+-}(2,0,0,0,0)$, Assumed Intrusion Time: 1000 yrs

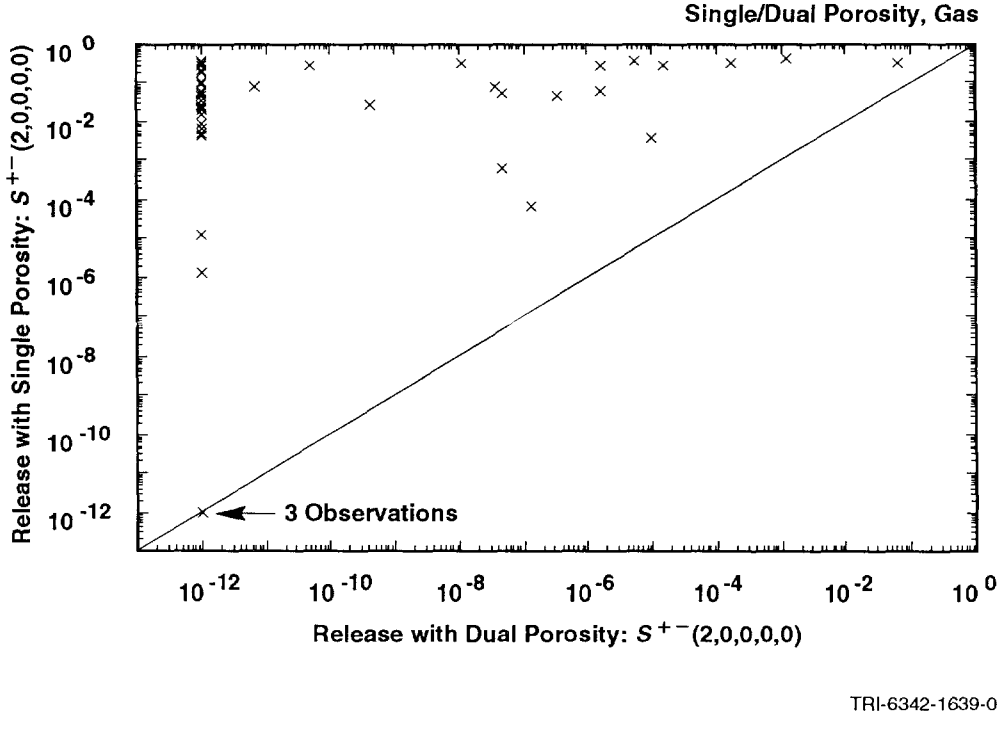

Figure 5.2-2. Scatterplots Comparing Total Normalized Release to the Accessible Environment Due to Groundwater Transport with Gas Generation in the Repository and Intrusion Occurring at 1000 Yrs for Single-Porosity and Dual-Porosity Transport Models in the Culebra Dolomite. For plotting purposes, values less than 10^{-12} are set to 10^{-12}.

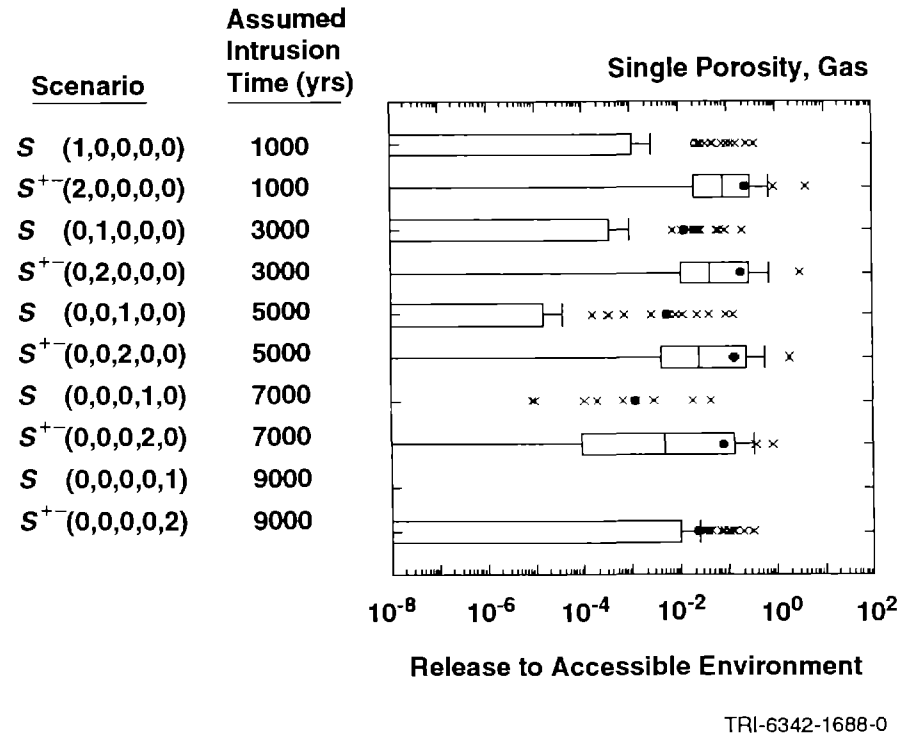

Figure 5.2-3. Total Normalized Release to the Accessible Environment Due to Groundwater Transport with Gas Generation in the Repository and a Single-Porosity Transport Model in the Culebra Dolomite.

already discussed, the releases in Figure 5.2-3 for the single-porosity model are considerably larger than the releases in Figure 4.4-1 for the dual-porosity transport model. The transport model used in the Culebra does not affect cuttings removal. Thus, the cuttings removal results used in the construction of the total releases to the accessible environment are the same regardless of the transport model used in the Culebra. The total releases for individual scenarios due to cuttings removal and groundwater transport with a single-porosity transport model are summarized in Figure 5.2-4. The corresponding results for the dual-porosity transport model are given in Figure 4.4-3. As comparison of Figures 5.2-4 and 4.4-3 shows, total releases to the accessible environment are not completely dominated by cuttings removal when the single-porosity transport model is used, which is the case for the dual-porosity transport model. In particular, the groundwater transport releases for E1E2-type scenarios (i.e., $S^{+-}(2,0,0,0,0)$, ..., $S^{+-}(0,0,0,0,2)$) are often considerably larger than the corresponding releases due to cuttings removal.

Releases of individual isotopes to the Culebra with gas generation in the repository for scenarios $S(1,0,0,0,0)$ and $S^{+-}(2,0,0,0,0)$ are summarized in Figure 4.4-7. The resultant releases to the accessible environment due to groundwater transport with a single-porosity transport model are summarized

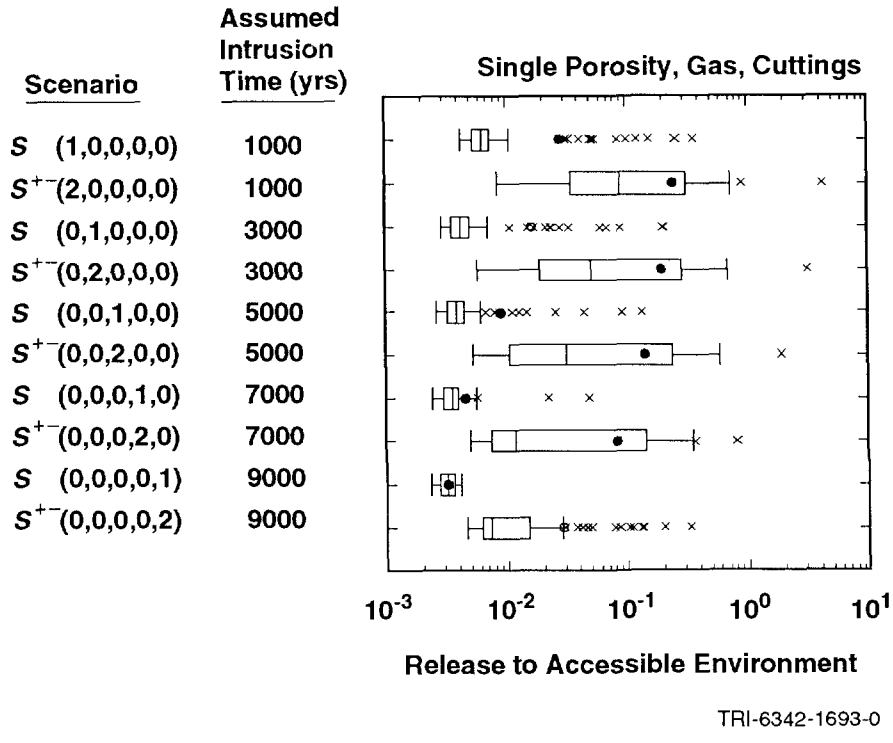

Figure 5.2-4. Total Normalized Release to the Accessible Environment Due to Cuttings Removal and Groundwater Transport with Gas Generation in the Repository and a Single-Porosity Transport Model in the Culebra Dolomite.

in Figure 5.2-5; the corresponding releases for a dual-porosity transport model are summarized in Figure 4.4-2. As already discussed in conjunction with Figures 5.2-1 through 5.2-4, the single-porosity model results in larger total releases to the accessible environment due to groundwater transport than the dual-porosity transport model. As comparison of Figures 4.4-2 and 5.2-5 shows, this pattern also holds for the individual isotopes, with the single-porosity model consistently producing larger releases for the individual isotopes than the dual-porosity transport model.

Sensitivity analyses of the groundwater transport results for individual isotopes for scenarios $S(1,0,0,0,0)$ and $S^{+-}(2,0,0,0,0)$ with gas generation in the repository and a single-porosity transport model in the Culebra are presented in Tables 5.2-1 and 5.2-2 for transport one-quarter, one-half and the full distance to the accessible environment. For convenience, these tables also contain the corresponding sensitivity analysis results for release to the Culebra, although these results have appeared previously in Tables 4.5-1 and 4.5-2.

As discussed in Section 4.5, SALPERM (Salado permeability) acts as switch for scenario $S(1,0,0,0,0)$ that determines whether or not a release from the repository to the Culebra will take place, with the result that the analyses

Scenario: $S(1,0,0,0,0)$, Assumed Intrusion Time: 1000 yrs

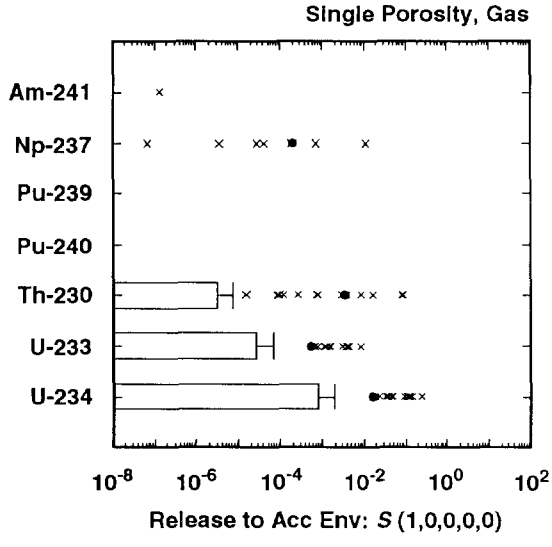

TRI-6342-1654-0

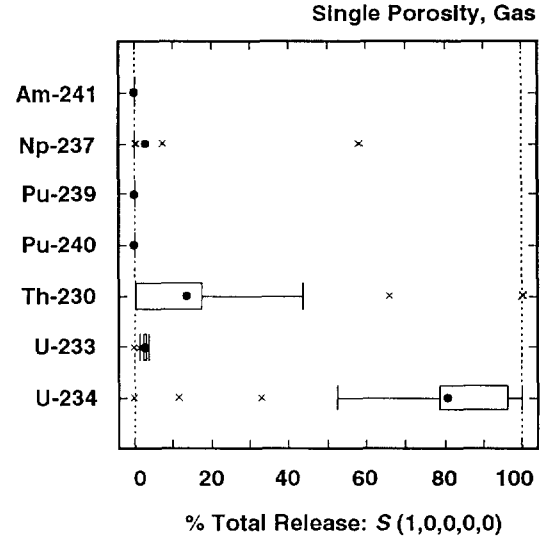

TRI-6342-1655-0

Scenario: $S^{+-}(2,0,0,0,0)$, Assumed Intrusion Time: 1000 yrs

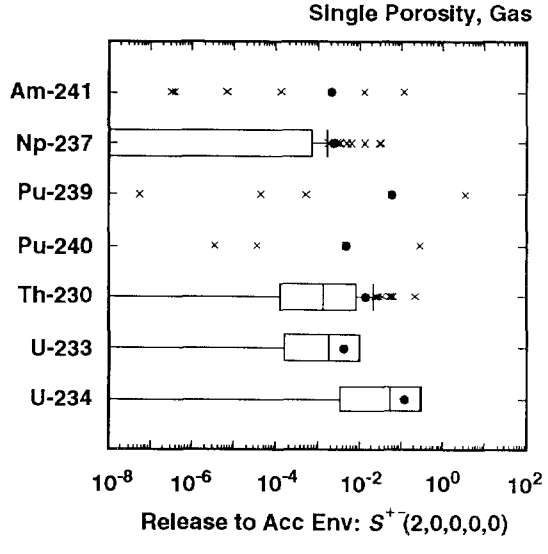

TRI-6342-1656-0

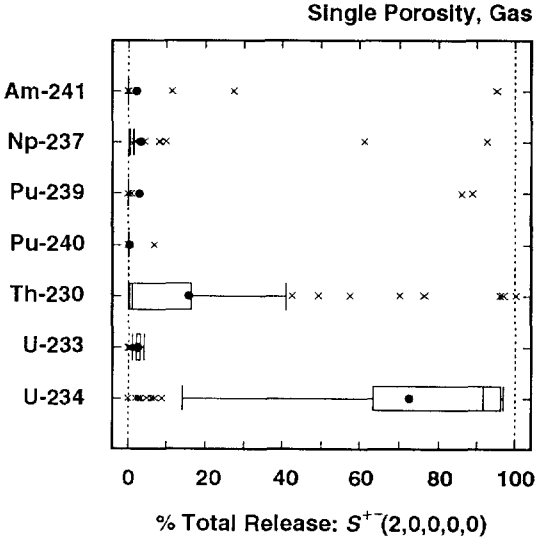

TRI-6342-1657-0

Figure 5.2-5. Normalized Releases for Individual Isotopes to the Accessible Environment Due to Groundwater Transport with Intrusion Occurring at 1000 Yrs, Gas Generation in the Repository and a Single-Porosity Transport Model in the Culebra Dolomite.

TABLE 5.2-1. STEPWISE REGRESSION ANALYSES WITH RANK-TRANSFORMED DATA FOR SCENARIO *S*(1,0,0,0,0) WITH GAS GENERATION IN THE REPOSITORY, A SINGLE-POROSITY TRANSPORT MODEL IN THE CULEBRA DOLOMITE AND INTRUSION OCCURRING 1000 YRS AFTER REPOSITORY CLOSURE

	Release to Culebra*		Quarter Distance		Half Distance		Full Distance	
Step	Variable	R^2	Variable	R^2	Variable	R^2	Variable	R^2
Dependent Variable: Integrated Discharge Am-241								
1	SALPERM	0.59(+)	SALPERM	0.20 (+)	SALPERM	0.55 (+)	SALPERM	0.20 (+)
2			FKDAM	0.35 (-)			FKDAM	0.35 (-)
Dependent Variable: Integrated Discharge Np-237								
1	SALPERM	0.53(+)	MBPERM	0.21 (+)	SALPERM	0.47 (+)	SALPERM	0.24 (+)
2			FKDNP	0.31 (-)				
Dependent Variable: Integrated Discharge Pu-239								
1	SALPERM	0.56(+)	FKDPU	0.16 (-)	SALPERM	0.47 (+)	SALPERM	0.19 (+)
2			SALPERM	0.31 (+)	MBPERM	0.52 (+)	FKDPU	0.27 (-)
Dependent Variable: Integrated Discharge Pu-240								
1	SALPERM	0.56(+)	SALPERM	0.22 (+)	SALPERM	0.53 (+)	SALPERM	0.13 (+)
2			FKDPU	0.38 (-)	MBPERM	0.59 (+)	FKDPU	0.26 (-)
Dependent Variable: Integrated Discharge Th-230								
1	SALPERM	0.55(+)	SALPERM	0.53 (+)	SALPERM	0.53 (+)	SALPERM	0.54 (+)
Dependent Variable: Integrated Discharge U-233								
1	SALPERM	0.59(+)	SALPERM	0.57 (+)	SALPERM	0.56 (+)	SALPERM	0.52 (+)
Dependent Variable: Integrated Discharge U-234								
1	SALPERM	0.59(+)	SALPERM	0.57 (+)	SALPERM	0.56 (+)	SALPERM	0.56 (+)
Dependent Variable: EPA Sum for Total Integrated Discharge								
1	SALPERM	0.58(+)	SALPERM	0.57 (+)	SALPERM	0.57 (+)	SALPERM	0.57 (+)

*Analysis results in this column are the same as those presented in the corresponding column of Table 4.5-1.

TABLE 5.2-2. STEPWISE REGRESSION ANALYSES WITH RANK-TRANSFORMED DATA FOR SCENARIO S^{+-}(2,0,0,0,0) WITH GAS GENERATION IN THE REPOSITORY, A SINGLE-POROSITY TRANSPORT MODEL IN THE CULEBRA DOLOMITE AND INTRUSION OCCURRING 1000 YRS AFTER REPOSITORY CLOSURE

	Release to Culebra*		Quarter Distance		Half Distance		Full Distance	
Step	Variable	R^2	Variable	R^2	Variable	R^2	Variable	R^2
Dependent Variable: Integrated Discharge Am-241								
1	SOLAM	0.36 (+)	FKDAM	0.59 (-)	FKDAM	0.23 (-)	FKDAM	0.38 (-)
2	BHPERM	0.74 (+)	CULFRPOR	0.65 (-)	CULFRPOR	0.44 (-)	CULFRPOR	0.50 (-)
3	BPPRES	0.78 (+)			GRMICH	0.51 (+)		
4					CULFRPOR	0.58 (-)		
Dependent Variable: Integrated Discharge Np-237								
1	SOLNP	0.65 (+)	FKDNP	0.56 (-)	FKDNP	0.49 (-)	FKDNP	0.54 (-)
2	BHPERM	0.78 (+)	SOLNP	0.63 (+)	SOLNP	0.58 (+)	SOLNP	0.64 (+)
3	BPPRES	0.82 (+)	SOLAM	0.68 (+)	SOLAM	0.63 (+)	SOLAM	0.68 (+)
4	EHPH	0.85 (+)	BHPERM	0.72 (+)	BHPERM	0.67 (+)		
5	GRCORI	0.88 (-)						
Dependent Variable: Integrated Discharge Pu-239								
1	SOLPU	0.74 (+)	FKDPU	0.59 (-)	FKDPU	0.24 (-)	FKDPU	0.39 (-)
2	BHPERM	0.85 (+)	CULTRFLD	0.63 (-)				
Variable: Integrated Discharge Pu-240								
1	SOLPU	0.74 (+)	FKDPU	0.63 (-)	FKDPU	0.25 (-)	FKDPU	0.48 (-)
2	BHPERM	0.85 (+)	CULTRFLD	0.67 (-)				
Dependent Variable: Integrated Discharge Th-230								
1	SOLTH	0.69 (+)	FKDTH	0.26 (-)	FKDTH	0.29 (-)	FKDTH	0.33 (-)
2	BHPERM	0.82 (+)	SOLTH	0.37 (+)	BHPERM	0.39 (+)	BHPERM	0.43 (+)
3			BHPERM	0.47 (+)	SOLTH	0.48 (+)	BPPRES	0.52 (+)
4			BPPRES	0.54 (+)	CULFRPOR	0.55 (-)	CULFRPOR	0.58 (-)
5			CULFRPOR	0.61 (-)	BPPRES	0.62 (+)	SOLTH	0.64 (+)
6			DBDIAM	0.67 (+)	DBDIAM	0.68 (+)	DBDIAM	0.69 (+)

*Analysis results in this column are the same as those presented in the corresponding column of Table 4.5-2.

TABLE 5.2-2. STEPWISE REGRESSION ANALYSES WITH RANK-TRANSFORMED DATA FOR SCENARIO S^+-(2,0,0,0,0) WITH GAS GENERATION IN THE REPOSITORY, A SINGLE-POROSITY TRANSPORT MODEL IN THE CULEBRA DOLOMITE AND INTRUSION OCCURRING 1000 YRS AFTER REPOSITORY CLOSURE (concluded)

	Release to Culebra*		Quarter Distance		Half Distance		Full Distance	
Step	Variable	R^2	Variable	R^2	Variable	R^2	Variable	R^2
Dependent Variable: Integrated Discharge U-233								
1	BHPERM	0.43 (+)	BHPERM	0.32 (+)	BHPERM	0.32 (+)	BHPERM	0.30 (+)
2	SOLU	0.58 (+)	BPPRES	0.45 (+)	FKDU	0.45 (-)	FKDU	0.46 (-)
3	BPPRES	0.70 (+)	SOLU	0.57 (+)	SOLU	0.55 (+)	SOLU	0.55 (+)
4	SOLNP	0.74 (-)	FKDU	0.68 (-)	BPPRES	0.65 (+)	BPPRES	0.64 (+)
5			CULFRPOR	0.75 (-)	CULFRPOR	0.71 (-)	CULFRPOR	0.71 (-)
6			CULDISP	0.79 (+)	CULDISP	0.75 (+)	CULDISP	0.74 (+)
Dependent Variable: Integrated Discharge U-234								
1	BHPERM	0.47 (+)	BHPERM	0.31 (+)	BHPERM	0.31 (+)	BHPERM	0.30 (+)
2	SOLU	0.60 (+)	BPPRES	0.44 (+)	FKDU	0.43 (-)	FKDU	0.44 (-)
3	BPPRES	0.72 (+)	SOLU	0.55 (+)	BPPRES	0.53 (+)	SOLU	0.53 (+)
4			FKDU	0.64 (-)	SOLU	0.62 (+)	BPPRES	0.62 (+)
5			CULFRPOR	0.71 (-)	CULFRPOR	0.69 (-)	CULFRPOR	0.69 (-)
6			CULDISP	0.75 (+)	CULDISP	0.73 (+)	CULDISP	0.73 (+)
Dependent Variable: EPA Sum for Total Integrated Discharge								
1	BHPERM	0.46 (+)	BHPERM	0.39 (+)	BHPERM	0.38 (+)	BHPERM	0.37 (+)
2	SOLAM	0.57 (+)	BPPRES	0.54 (+)	BPRES	0.51 (+)	BPPRES	0.50 (+)
3	BPPRES	0.66 (+)	FKDU	0.61 (-)	FKDU	0.58 (-)	FKDU	0.58 (-)
4	SOLPU	0.69 (+)	CULFRPOR	0.68 (-)	CULFRPOR	0.66 (-)	CULFRPOR	0.65 (-)
5	BPSTOR	0.73 (+)	SOLU	0.75 (+)	SOLU	0.73 (+)	SOLU	0.72 (+)
6	SOLU	0.76 (+)	FKDNP	0.80 (-)	FKDNP	0.78 (-)	FKDNP	0.77 (-)
7			BPSTOR	0.82 (+)	CULDISP	0.81 (+)	CULDISP	0.80 (+)
8			CULDISP	0.84 (+)	BPSTOR	0.83 (+)		

*Analysis results in this column are the same as those presented in the corresponding column of Table 4.5-2.

presented in Table 5.2-1 are dominated by SALPERM. Due to the greater number of nonzero releases to the Culebra, the analyses in Table 5.2-2 for scenario $S^{+-}(2,0,0,0,0)$ are considerably more interesting than those in Table 5.2-1 for scenario $S(1,0,0,0,0)$. The variables BHPERM (borehole permeability), BPPRES (brine pocket pressure) and CULFRPOR (Culebra fracture porosity) tend to be important for all isotopes for scenario $S^{+-}(2,0,0,0,0)$. Further, the appropriate solubilities and fracture distribution coefficients are important for the individual isotopes.

Scatterplots for the release of Pu-239, U-234 and Am-241 to the Culebra with gas generation in the repository are given in Figures 4.5-1, 4.5-2 and 4.5-3, respectively, and help provide insights into the regression-based sensitivity analyses for release to the Culebra. Scatterplots can also provide insights on the analyses for transport in the Culebra with a single-porosity model. Scatterplots for the normalized release of Pu-239 and Am-241 to the accessible environment for scenario $S^{+-}(2,0,0,0,0)$ are given in Figure 5.2-6. The top two scatterplots in Figure 5.2-6 are for Pu-239 and show that the release decreases with increasing values for FKDPU (fracture distribution coefficient for Pu) and increases with increasing values for SOLPU (solubility for Pu). However, the releases are small, with only 7 sample elements resulting in release values that exceed 10^{-9}. Thus, even for single-porosity transport, the fracture distribution coefficient FKDPU is leading to retardations that prevent Pu-239 from reaching the accessible environment by groundwater transport.

The stepwise regression analysis presented in Table 5.2-2 for the release of Pu-239 to the accessible environment (i.e., the analysis for "Integrated Discharge Pu-239" at "Full Distance") selected only the variable FKDPU (fracture distribution coefficient for plutonium) with an R^2 value of 0.39, which is not a particularly good regression result. Examination of the two scatterplots in Figure 5.2-6 for Pu-239 provides considerably more information. In particular, these plots show not only the effect of FKDPU but also the effect of SOLPU (solubility for Pu), which was not identified in the regression analysis. This is another example of an analysis in which one variable (i.e., FKDPU) acts as a switch and causes all results to be effectively zero (i.e., $< 10^{-9}$) after a some value for the switch variable (i.e., FKDPU $\triangleq 10^{1}$ m^3/kg). This switch produces a more complex pattern of relationships than can be captured by a simple regression model. It is sometimes possible to design regression models that will represent patterns of this type but the effort requires *a priori* knowledge of the relationships involved.

The lower two scatterplots in Figure 5.2-6 are for Am-241 and show that the release decreases with increasing values for FKDAM (fracture distribution

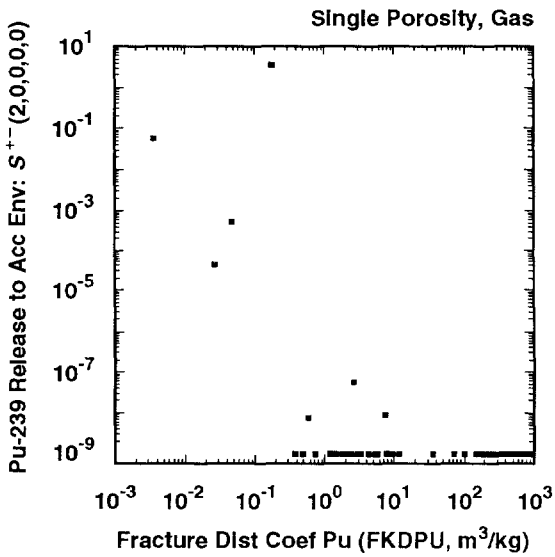

TRI-6342-1603-0

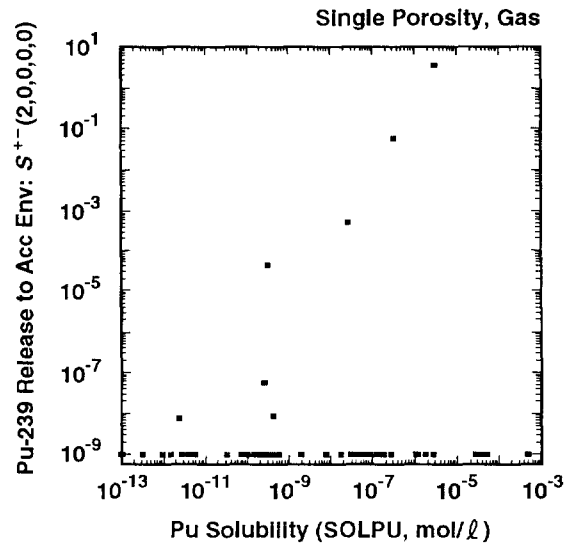

TRI-6342-1604-0

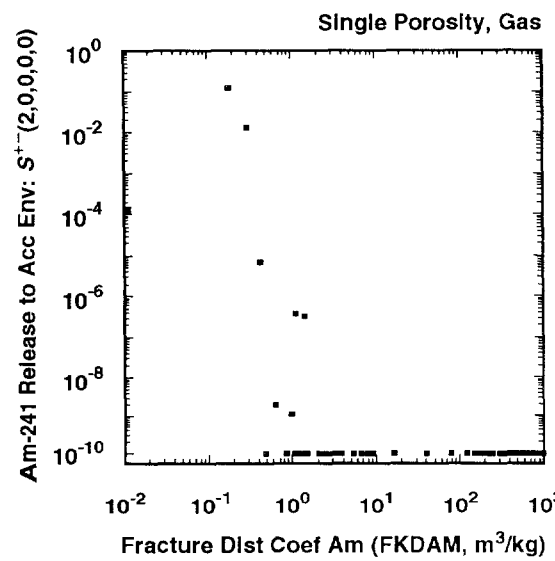

TRI-6342-1605-0

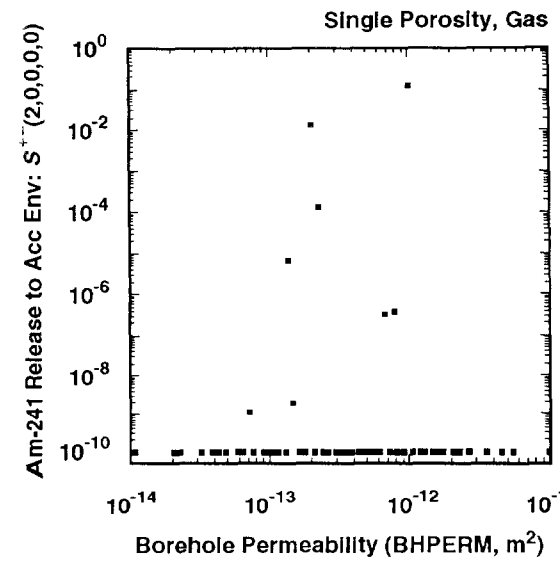

TRI-6342-1606-0

Figure 5.2-6. Scatterplots for Normalized Release of Pu-239 and Am-241 to the Accessible Environment for Scenario $S^{+-}(2,0,0,0,0)$ for Groundwater Transport with Gas Generation in the Repository, a Single-Porosity Transport Model in the Culebra Dolomite and Intrusion Occurring at 1000 Yrs.

coefficient for Am) and increases with increasing values for BHPERM (borehole permeability). The scatterplot for SOLAM (solubility for Am) was not included because the scatterplot for BHPERM showed a stronger relationship. Due to the short half-life of Am-241 (i.e., 432 yr), high values for BHPERM facilitate the release of Am-241 to the Culebra before it is lost due to radioactive decay. As with Pu-239, the two scatterplots in Figure 5.2-6 are more revealing of the factors that control the release of Am-241 to the accessible environment than the corresponding regression analysis in Table 5.2-2.

Scatterplots for the normalized release of U-234 to the accessible environment for scenario $S^{+-}(2,0,0,0,0)$ are given in Figure 5.2-7. The top two scatterplots are for BHPERM (borehole permeability) and SOLU (solubility for U) and show that the release to the accessible environment increases as each of these variables increases. The equal release values appearing at the top of these two scatterplots correspond to the entire inventory of U-234 in a single waste panel (see Figure 2.4-2). Thus, the larger values for BHPERM and SOLU are leading to the release of the entire U-234 inventory to the accessible environment. The lower scatterplot in Figure 5.2-7 is for FKDU (fracture distribution coefficient for U). As examination of this plot shows, the relatively low distribution coefficient values assigned to uranium (i.e., 0 to 1 m^3/kg) result in little retardation, with the result that both BHPERM and SOLU have a more pronounced effect on the U-234 releases to the accessible environment than FKDU. In contrast, the scatterplots in Figure 5.2-6 show more pronounced relationships between FKDPU (fracture distribution coefficient for Pu) and FKDAM (fracture distribution coefficient for Am) and the corresponding releases to the accessible environment for Pu-239 and Am-241 due to the larger values assigned to FKDPU and FKDAM relative to those assigned to FKDU.

Scatterplots similar to those appearing in Figures 5.2-6 and 5.2-7 could also be generated for scenario $S(1,0,0,0,0)$. However, they would be less revealing due to both the smaller releases into the Culebra and the large number of zero releases induced by the role of SALPERM (Salado permeability) in determining whether or not any release into the Culebra will take place.

As indicated by the regressions in Table 5.2-2, there is a negative relationship between CULFRPOR (fracture porosity in Culebra) and integrated discharge in the Culebra. This pattern of decreasing transport with increasing values for CULFRPOR is illustrated by the scatterplot appearing in Figure 5.2-8 for CULFRPOR versus total release to the accessible environment for groundwater transport with a single-porosity model in the Culebra. The negative effect indicated for CULFRPOR in Figure 5.2-8 for single-porosity

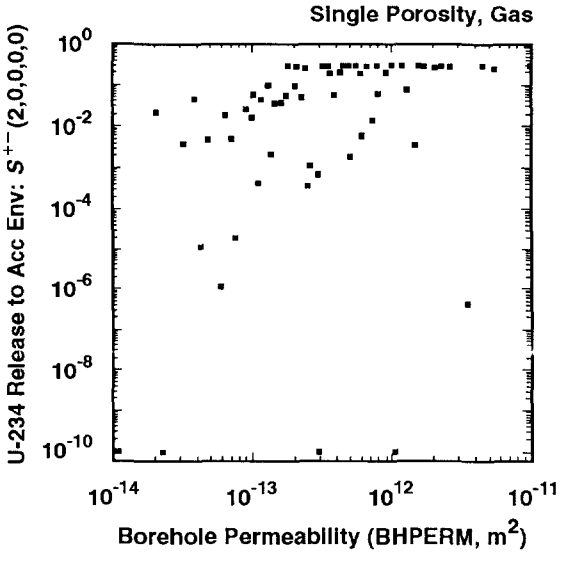

TRI-6342-1591-0

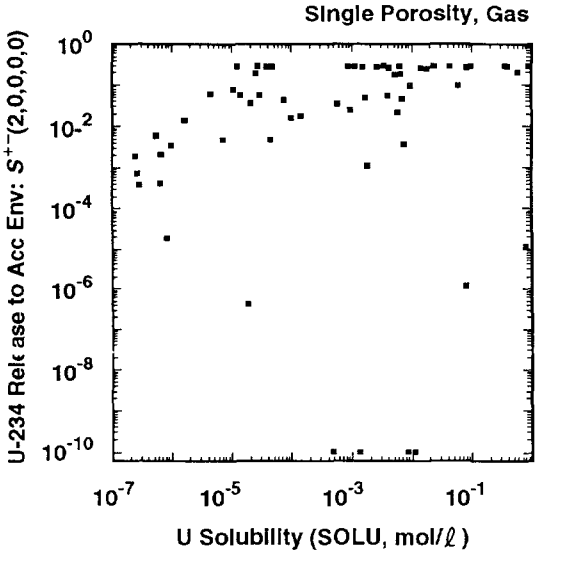

TRI-6342-1592-0

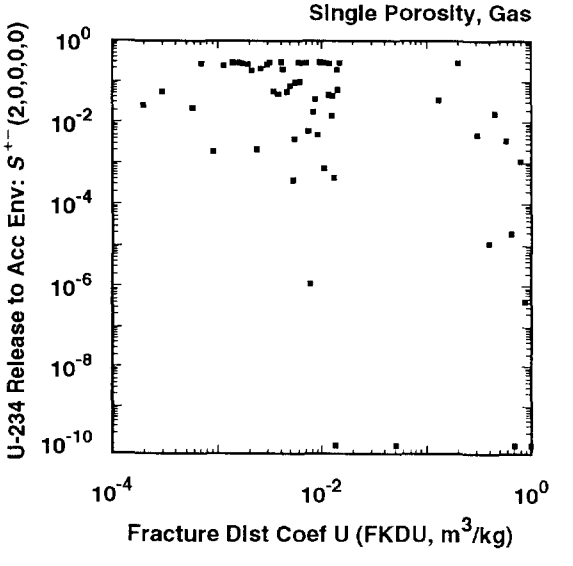

TRI-6342-1593-0

Figure 5.2-7. Scatterplots for Normalized Release of U-234 to the Accessible Environment for Scenario S^{+-}(2,0,0,0,0) for Groundwater Transport with Gas Generation in the Repository, a Single-Porosity Transport Model in the Culebra Dolomite and Intrusion Occurring at 1000 Yrs.

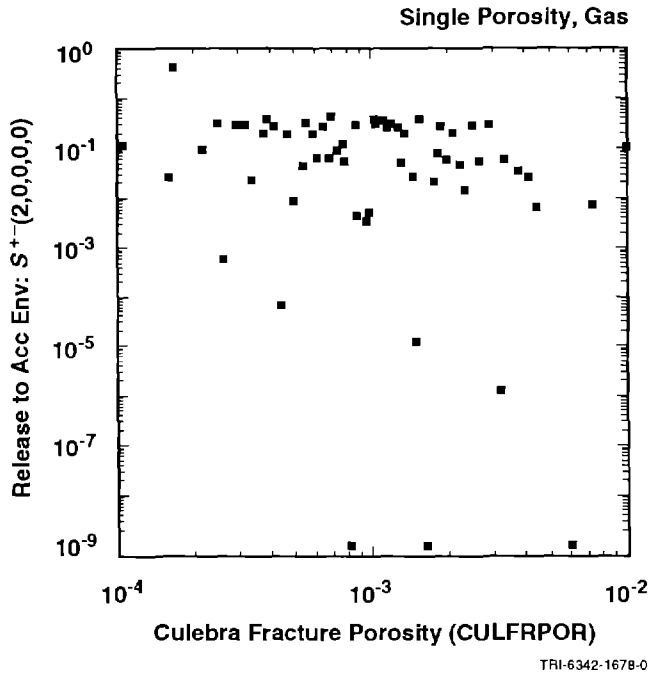

Figure 5.2-8. Scatterplot for Fracture Porosity in Culebra Dolomite (CULFRPOR) versus Total Normalized Release to the Accessible Environment Due to Groundwater Transport for Scenario S^{+-}(2,0,0,0,0) with Gas Generation in the Repository, a Single Porosity Transport Model in the Culebra and Intrusion Occurring at 1000 Yrs.

transport is the reverse of the positive effect indicated for CULFRPOR in Figure 4.5-7 for dual-porosity transport. As shown in these two figures, increasing CULFRPOR decreases release for a single-porosity transport model and causes the reverse effect for a dual-porosity transport model. For the single-porosity transport model, the negative effect of CULFRPOR results because increasing CULFRPOR decreases groundwater velocity, with a resultant decrease in radionuclide transport. The positive effect for the CULFRPOR for the dual-porosity transport model will be explained in Section 5.4 after results for dual-porosity transport without chemical retardation have been presented.

5.3 Effect of No Gas Generation and Single-Porosity Transport Model in Culebra Dolomite

The best estimate analyses presented in Chapter 4 include gas generation in the repository and a dual-porosity transport model in the Culebra. As shown in Sections 5.1 and 5.2, relaxing these assumptions leads to larger releases to the accessible environment due to groundwater transport, although the

total release is not significantly affected due to the dominance of the cuttings releases. For perspective, this section presents the results of analyses performed with no gas generation in the repository and a single-porosity transport model for the Culebra.

Scatterplots comparing releases to the accessible environment with and without gas generation in the repository and with a single-porosity transport model in the Culebra are shown in Figure 5.3-1 for scenarios $S(1,0,0,0,0)$ and $S^{+-}(2,0,0,0,0)$. As examination of this figure shows, no gas generation results in larger releases than those obtained with gas generation. This effect is particularly pronounced for scenario $S(1,0,0,0,0)$ due to the large number of zero releases to the Culebra that occur in the presence of gas generation. As discussed in conjunction with Figure 4.5-1, this effect is due to the role of SALPERM (Salado permeability) as a switch in the presence of gas generation.

The releases to the accessible environment for individual isotopes calculated with no gas generation in the repository and a single-porosity transport model in the Culebra for scenarios $S(1,0,0,0,0)$ and $S^{+-}(2,0,0,0,0)$ are summarized in Figure 5.3-2. The corresponding releases for gas generation in the repository and a dual-porosity transport model in the Culebra are shown in Figure 4.4-2. As is the case for the total release, the releases for the individual isotopes are substantially increased with the assumption of no gas generation and a single-porosity transport model for the Culebra. Even so, the releases for the individual isotopes shown in Figure 5.3-2 tend to be small, with only a few sample elements producing individual isotope releases for scenario $S^{+-}(2,0,0,0,0)$ that exceed 1.

Although the single-porosity transport calculations with gas generation in the repository were performed for intrusions occurring in each of the five time intervals under consideration, the single-porosity transport calculations without gas generation were only performed for intrusions occurring at 1000 yrs. Thus, it is not possible to construct a distribution of CCDFs for single-porosity transport without gas generation in the repository that is equivalent to the distribution shown in Figure 5.2-1 for single-porosity transport with gas generation in the repository. However, as discussed in conjunction with Figure 5.1-4, CCDFs can be constructed for single-porosity transport with and without gas generation under the assumption that the rate constant λ in the Poisson model for drilling intrusions is equal to zero after 2000 yrs. The outcome of this construction is shown in Figure 5.3-3, with the results for gas generation appearing in the two upper frames and the results without gas generation appearing in the two lower frames. When considered in the context of the EPA release limits,

Scenario: $S(1,0,0,0,0)$, Assumed Intrusion Time: 1000 yrs

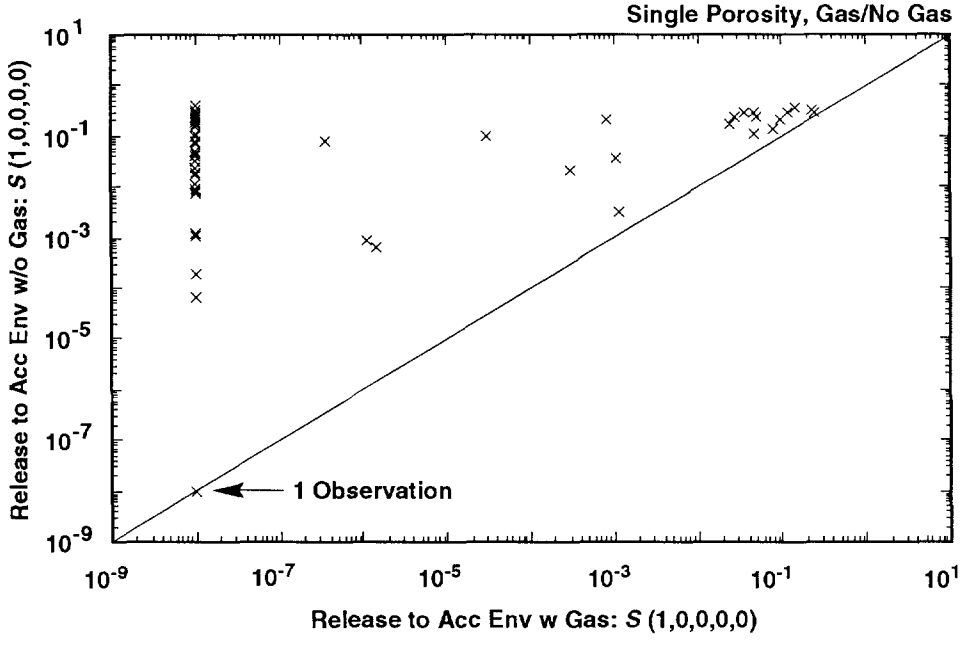

Scenario: $S^{+-}(2,0,0,0,0)$, Assumed Intrusion Time: 1000 yrs

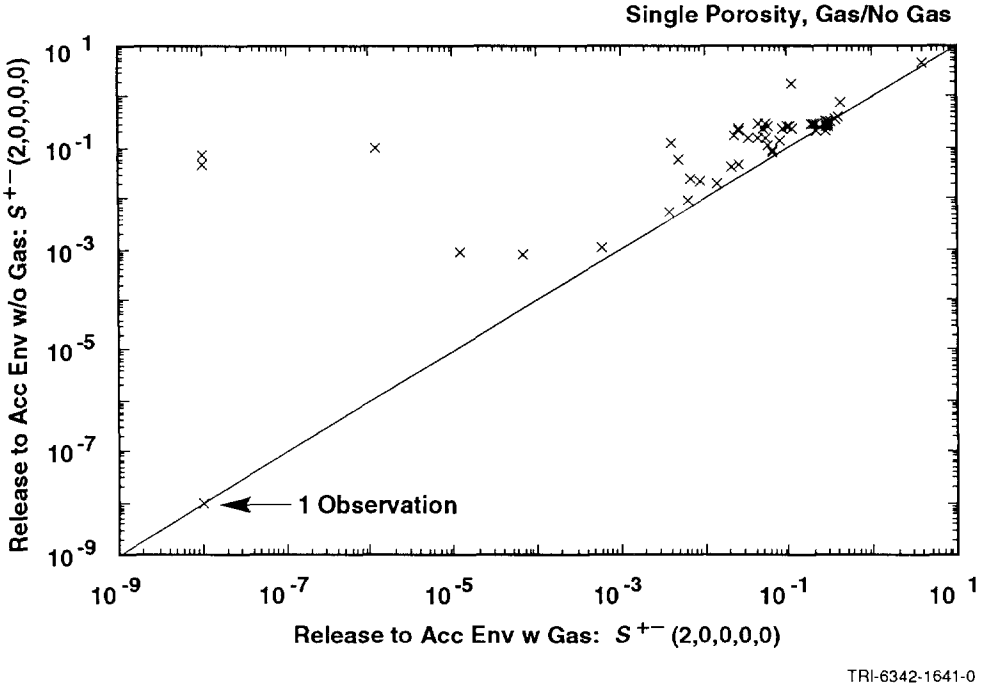

Figure 5.3-1. Scatterplots for Total Normalized Release to the Accessible Environment Due to Groundwater Transport with and without Gas Generation in the Repository for a Single-Porosity Transport Model in the Culebra Dolomite and an Assumed Intrusion Time of 1000 Yrs. For plotting purposes, values less than 10^{-8} are set to 10^{-8}.

Scenario: $S(1,0,0,0,0)$, Assumed Intrusion Time: 1000 yrs

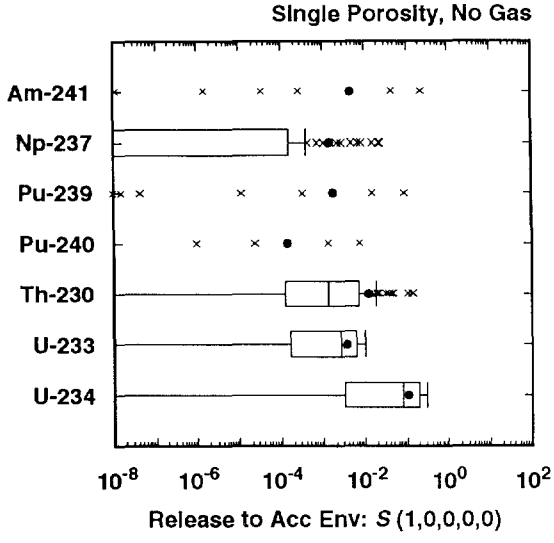

TRI-6342-1650-0

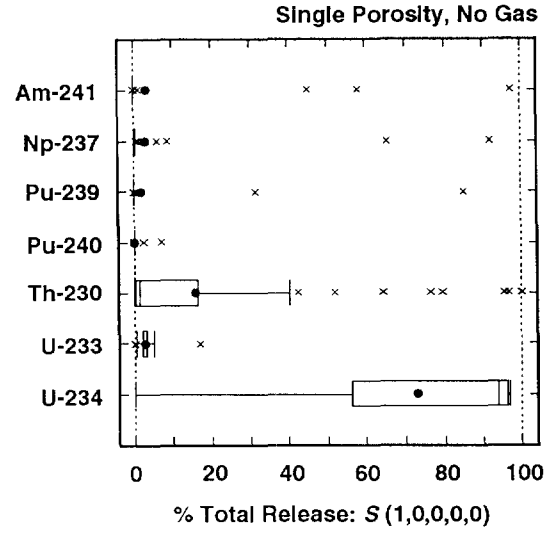

TRI-6342-1651-0

Scenario: $S^{+-}(2,0,0,0,0)$, Assumed Intrusion Time: 1000 yrs

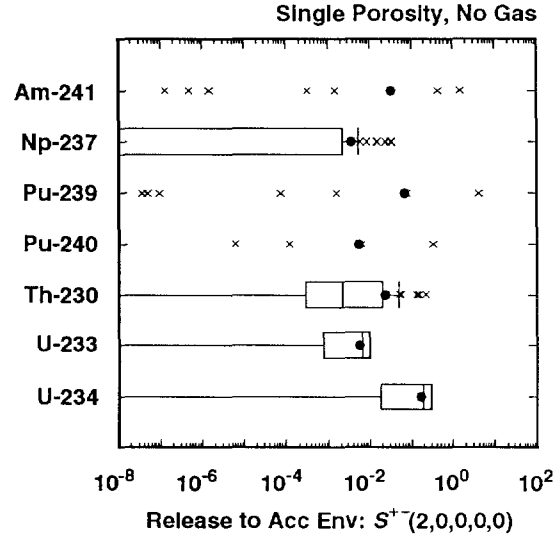

TRI-6342-1652-0

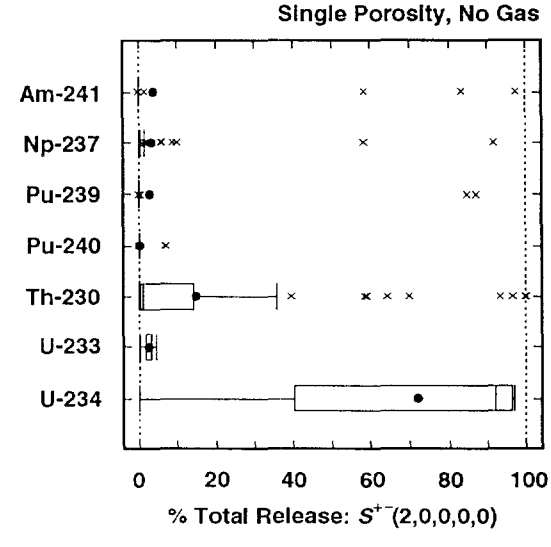

TRI-6342-1653-0

Figure 5.3-2. Normalized Releases for Individual Isotopes to the Accessible Environment Due to Groundwater Transport with Intrusion Occurring at 1000 Yrs, No Gas Generation in the Repository and a Single-Porosity Transport Model in the Culebra Dolomite.

With Gas Generation in the Repository

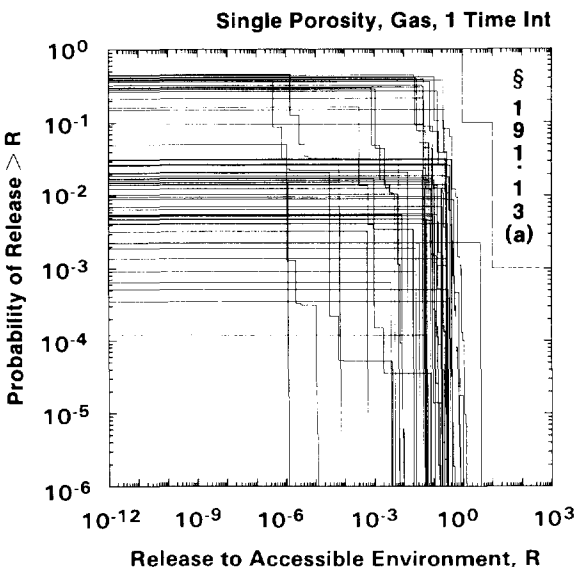

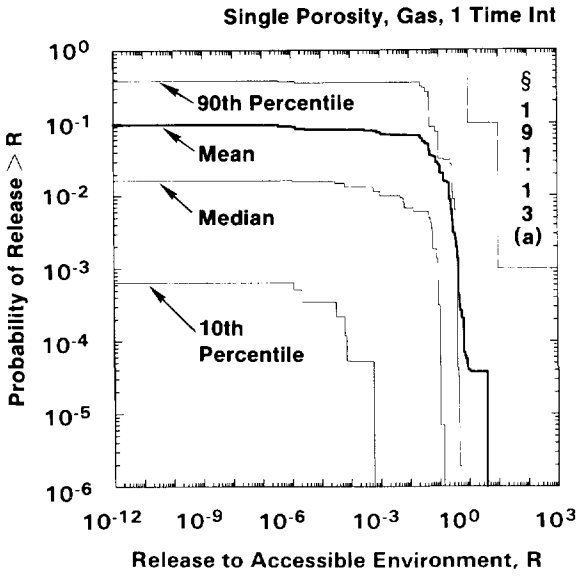

Without Gas Generation in the Repository

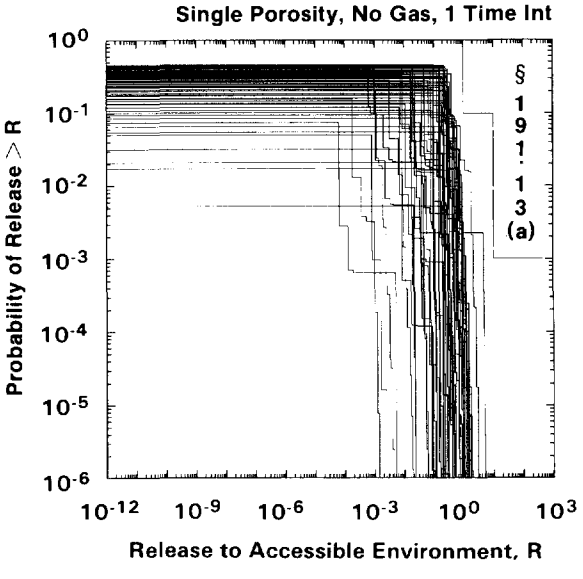

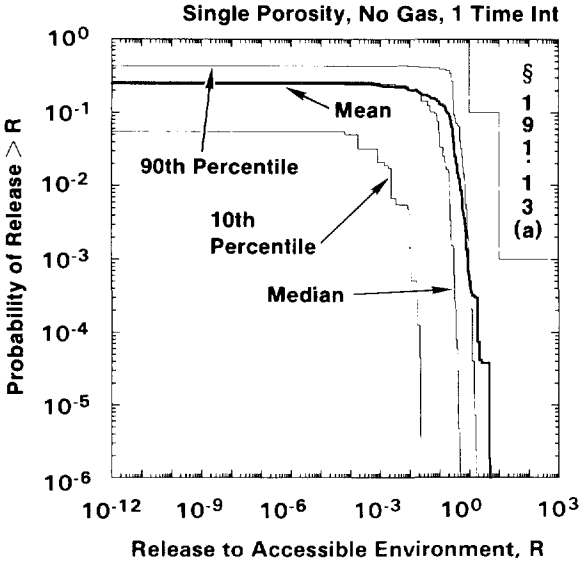

Figure 5.3-3. Comparison of Complementary Cumulative Distribution Functions for Normalized Release to the Accessible Environment with Gas Generation in the Repository (upper two frames) and without Gas Generation in the Repository (lower two frames) for a Single-Porosity Transport Model in the Culebra Dolomite and the Rate Constant λ in the Poisson Model for Drilling Intrusions Equal to Zero After 2000 Yrs.

the assumption of single-porosity transport without gas generation produces CCDFs that are not substantially shifted from those obtained for single-porosity transport with gas generation. Further, all the individual CCDFs fall below the EPA release limits for both cases.

Sensitivity analyses of groundwater transport results for individual isotopes for scenarios $S(1,0,0,0,0)$ and $S^{+-}(2,0,0,0,0)$ with no gas generation in the repository and a single-porosity model in the Culebra are presented in Tables 5.3-1 and 5.3-2. For convenience, these tables also contain the corresponding sensitivity analysis results for release to the Culebra, although these results have appeared previously in Tables 5.1-2 and 5.1-3.

The groundwater transport results in Table 5.3-1 for scenario $S(1,0,0,0,0)$ tend to be dominated by properties of the individual isotopes. In particular, releases at the quarter, half and full distance to the accessible environment tend to increase as the solubilities increase and decrease as the distribution coefficients increase. Increasing SALPERM (Salado permeability) and SALPRES (Salado pressure) also tends to increase the releases for the individual isotopes. This is consistent with the role indicated for these variables in increasing the release of the individual isotopes to the Culebra for scenario $S(1,0,0,0,0)$. Increasing CULFRPOR (Culebra fracture porosity) tends to decrease the release for the individual isotopes by reducing the groundwater flow rate in the Culebra.

The groundwater transport results in Table 5.3-2 for scenario $S^{+-}(2,0,0,0,0)$ are similar to those in Table 5.3-1 for scenario $S(1,0,0,0,0)$. The releases for the individual isotopes tend to be dominated by the appropriate solubilities and distribution coefficients. The variables BPPRES (brine pocket pressure), CULFRPOR (Culebra fracture porosity) and BHPERM (borehole permeability) are often identified in the analyses for the individual isotopes, with the releases increasing as BPPRES and BHPERM increase and decreasing as CULFRPOR increases. The importance indicated for the solubilities BPPRES and BHPERM results from their role in determining release into the Culebra for scenario $S^{+-}(2,0,0,0,0)$.

The sensitivity analysis results obtained for groundwater transport in the Culebra with a single-porosity model in the absence of gas generation are similar to those previously obtained for single-porosity transport with gas generation with the exception that SALPERM (Salado permeability) does not act as a switch for scenario $S(1,0,0,0,0)$. This is not surprising because the absence of gas generation tends to produce larger releases to the Culebra, especially for scenario $S(1,0,0,0,0)$, but the presence or absence of gas generation itself has no effect on the actual transport that takes place in the Culebra. The patterns in the scatterplots for transport in the absence of gas generation for scenarios $S(1,0,0,0,0)$ and $S^{+-}(2,0,0,0,0)$ are similar

TABLE 5.3-1. STEPWISE REGRESSION ANALYSES WITH RANK-TRANSFORMED DATA FOR SCENARIO $S(1,0,0,0,0)$ WITH NO GAS GENERATION IN THE REPOSITORY, A SINGLE-POROSITY TRANSPORT MODEL IN THE CULEBRA DOLOMITE AND INTRUSION OCCURRING 1000 YRS AFTER REPOSITORY CLOSURE

	Release to Culebra*		Quarter Distance		Half Distance		Full Distance	
Step	Variable	R^2	Variable	R^2	Variable	R^2	Variable	R^2
Dependent Variable: Integrated Discharge Am-241								
1	SOLAM	0.81(+)	FKDAM	0.60 (-)	CULFRPOR	0.20 (-)	FKDAM	0.35 (-)
2	SALPERM	0.90(+)	CULFRPOR	0.65 (-)	FKDAM	0.40 (-)	CULFRPOR	0.50 (-)
3	BHPERM	0.92(+)	MBPOR	0.68 (-)	SOLAM	0.52 (+)		
4	SALPRES	0.93(+)			MBPERM	0.57 (+)		
Dependent Variable: Integrated Discharge Np-237								
1	SOLNP	0.77(+)	FKDNP	0.52 (-)	FKDNP	0.47 (-)	FKDNP	0.52 (-)
2	EHPH	0.86(+)	SOLAM	0.60 (+)	SOLAM	0.55 (+)	SOLNP	0.62 (+)
3	SALPERM	0.90(+)	SOLNP	0.65 (+)	SOLNP	0.62 (+)	SOLAM	0.67 (+)
Dependent Variable: Integrated Discharge Pu-239								
1	SOLPU	0.92(+)	FKDPU	0.66 (-)	FKDPU	0.18 (-)	FKDPU	0.40 (-)
2	SALPERM	0.94(+)	CULTRFLD	0.69 (-)				
3	BHPERM	0.95(+)						
Dependent Variable: Integrated Discharge Pu-240								
1	SOLPU	0.91(+)	FKDPU	0.64 (-)	FKDPU	0.20 (-)	FKDPU	0.53 (-)
2	SALPERM	0.94(+)						
3	BHPERM	0.95(+)						
Dependent Variable: Integrated Discharge Th-230								
1	SOLTH	0.94(+)	FKDTH	0.38 (-)	FKDTH	0.42 (-)	FKDTH	0.49 (-)
2	SALPERM	0.96(+)	SOLTH	0.53 (+)	SOLTH	0.54 (+)	SOLTH	0.56 (+)
3	BHPERM	0.97(+)						
4	SALPRES	0.97(+)						
Dependent Variable: Integrated Discharge U-233								
1	SOLU	0.34(+)	SOLU	0.31 (+)	SOLU	0.30 (+)	SOLU	0.25 (+)
2	SALPERM	0.42(+)	FKDU	0.41 (-)	FKDU	0.42 (-)	FKDU	0.40 (-)
3	SALPRES	0.49(+)	SALPERM	0.49 (+)	SALPERM	0.50 (+)	SALPERM	0.49 (+)
4			SALPRES	0.58 (+)	SALPRES	0.58 (+)	SALPRES	0.57 (+)

*Analysis results in this column are the same as those presented in the corresponding column of Table 5.1-2.

TABLE 5.3-1. STEPWISE REGRESSION ANALYSES WITH RANK-TRANSFORMED DATA FOR SCENARIO $S(1,0,0,0,0)$ WITH NO GAS GENERATION IN THE REPOSITORY, A SINGLE-POROSITY TRANSPORT MODEL IN THE CULEBRA DOLOMITE AND INTRUSION OCCURRING 1000 YRS AFTER REPOSITORY CLOSURE (concluded)

	Release to Culebra*		Quarter Distance		Half Distance		Full Distance	
Step	Variable	R^2	Variable	R^2	Variable	R^2	Variable	R^2
Dependent Variable: Integrated Discharge U-234								
1	SOLU	0.29(+)	SOLU	0.32 (+)	SOLU	0.31 (+)	SOLU	0.26 (+)
2	SALPERM	0.37(+)	FKDU	0.41 (-)	FKDU	0.42 (-)	FKDU	0.40 (-)
3	SALPRES	0.43(+)	SALPERM	0.49 (+)	SALPERM	0.50 (+)	SALPERM	0.49 (+)
4			SALPRES	0.57 (+)	SALPRES	0.58 (+)	SALPRES	0.57 (+)
5							SOLU	0.62 (-)
Dependent Variable: EPA Sum for Total Integrated Discharge								
1	SOLAM	0.42(+)	SOLU	0.18 (+)	SOLU	0.20 (+)	SOLU	0.21 (+)
2	SALPERM	0.65(+)	FKDU	0.28 (-)	FKDU	0.31 (-)	FKDU	0.32 (-)
3			SALPERM	0.39 (+)	SALPERM	0.40 (+)	SALPERM	0.42 (+)
4			SALPRES	0.48 (+)	SALPRES	0.49 (+)	SALPRES	0.50 (+)
5			CULFRPOR	0.55 (-)	CULFRPOR	0.56 (-)	CULFRPOR	0.56 (-)
6			FKDPU	0.61 (-)	FKDU	0.62 (-)		

*Analysis results in this column are the same as those presented in the corresponding column of Table 5.1-2.

TABLE 5.3-2. STEPWISE REGRESSION ANALYSES WITH RANK-TRANSFORMED DATA FOR SCENARIO S^{+-}(2,0,0,0,0) WITH NO GAS GENERATION IN THE REPOSITORY, A SINGLE-POROSITY TRANSPORT MODEL IN THE CULEBRA DOLOMITE AND INTRUSION OCCURRING 1000 YRS AFTER REPOSITORY CLOSURE

	Release to Culebra*		Quarter Distance		Half Distance		Full Distance	
Step	Variable	R^2	Variable	R^2	Variable	R^2	Variable	R^2
Dependent Variable: Integrated Discharge Am-241								
1	SOLAM	0.84(+)	FKDAM	0.60 (-)	CULFRPOR	0.21 (-)	FKDAM	0.28 (-)
2	BHPERM	0.93(+)	CULFRPOR	0.65 (-)	FKDAM	0.42 (-)	CULFRPOR	0.47 (-)
3	BPPRES	0.94(+)	MBPOR	0.69 (-)	SOLAM	0.51 (+)	SOLAM	0.52 (+)
4					MBPOR	0.55 (-)		
Dependent Variable: Integrated Discharge Np-237								
1	SOLNP	0.77(+)	FKDNP	0.52 (-)	FKDNP	0.48 (-)	FKDNP	0.51 (-)
2	EHPH	0.84(+)	SOLAM	0.62 (+)	SOLNP	0.57 (+)	SOLNP	0.61 (+)
3	BHPERM	0.88(+)	SOLNP	0.68 (+)	SOLAM	0.63 (+)	SOLAM	0.66 (+)
4	BPPRES	0.91(+)	BHPERM	0.71 (+)				
Dependent Variable: Integrated Discharge Pu-239								
1	SOLPU	0.90(+)	FKDPU	0.59 (-)	FKDPU	0.22 (-)	FKDPU	0.37 (-)
2	BHPERM	0.94(+)	CULTRFLD	0.62 (-)				
3	BPPRES	0.95(+)						
4	BHDIAM	0.96(+)						
5	EHPH	0.96(+)						
Dependent Variable: Integrated Discharge Pu-240								
1	SOLPU	0.90(+)	FKDPU	0.63 (-)	FKDPU	0.21 (-)	FKDPU	0.48 (-)
2	BHPERM	0.94(+)						
3	BPPRES	0.95(+)						
4	BHDIAM	0.96(+)						
5	EHPH	0.96(+)						
Dependent Variable: Integrated Discharge Th-230								
1	SOLTH	0.90(+)	FKDTH	0.36 (-)	FKDTH	0.42 (-)	FKDTH	0.51 (-)
2	BHPERM	0.95(+)	SOLTH	0.54 (+)	SOLTH	0.56 (+)	SOLTH	0.58 (+)
3							BPPRES	0.63 (+)

* Analysis results in this column are the same as those presented in the corresponding column of Table 5.1-3.

TABLE 5.3-2. STEPWISE REGRESSION ANALYSES WITH RANK-TRANSFORMED DATA FOR SCENARIO S^{+-}(2,0,0,0,0) WITH NO GAS GENERATION IN THE REPOSITORY, A SINGLE-POROSITY TRANSPORT MODEL IN THE CULEBRA DOLOMITE AND INTRUSION OCCURRING 1000 YRS AFTER REPOSITORY CLOSURE (concluded)

	Release to Culebra*		Quarter Distance		Half Distance		Full Distance	
Step	Variable	R^2	Variable	R^2	Variable	R^2	Variable	R^2
Dependent Variable: Integrated Discharge U-233								
1	SOLU	0.25 (+)	SOLU	0.24 (+)	SOLU	0.22 (+)	SOLU	0.15 (+)
2	BHPERM	0.39 (+)	FKDU	0.40 (-)	FKDU	0.41 (-)	FKDU	0.30 (-)
3	SOLNP	0.50 (-)	BPPRES	0.48 (+)	BHPERM	0.48 (+)	BPPRES	0.40 (+)
4	BPPRES	0.58 (+)	CULFRPOR	0.56 (-)	BPPRES	0.54 (+)	BHPERM	0.46 (+)
5			BHPERM	0.60 (+)	CULFRPOR	0.59 (-)	CULFRPOR	0.52 (-)
6					CULDISP	0.57 (+)		
Dependent Variable: Integrated Discharge U-234								
1	SOLU	0.20 (+)	SOLU	0.22 (+)	FKDU	0.21 (-)	SOLU	0.15 (+)
2	BHPERM	0.36 (+)	FKDU	0.37 (-)	SOLU	0.40 (+)	FKDU	0.28 (-)
3			BPPRES	0.46 (+)	BPPRES	0.47 (+)	BPPRES	0.40 (+)
4			CULFRPOR	0.52 (-)	BHPERM	0.52 (+)	CULFRPOR	0.47 (-)
5			BHPERM	0.57 (+)	CULFRPOR	0.57 (-)	BHPERM	0.53 (+)
6					CULDISP	0.59 (+)		
Dependent Variable: EPA Sum for Total Integrated Discharge								
1	SOLAM	0.62 (+)	BPPRES	0.13 (+)	SOLU	0.16 (+)	SOLU	0.13 (+)
2	BHPERM	0.71 (+)	FKDU	0.24 (-)	FKDU	0.28 (-)	BPPRES	0.25 (+)
3	SOLPU	0.77 (+)	CULFRPOR	0.34 (-)	BPPRES	0.39 (+)	BHPERM	0.33 (+)
4	BPPRES	0.81 (+)	SOLU	0.44 (+)	BHPERM	0.47 (+)	CULFRPOR	0.41 (-)
5			FKDNP	0.50 (-)	CULFRPOR	0.54 (-)	FKDU	0.48 (-)
6			BHPERM	0.55 (+)	FKDNP	0.59 (-)		
7			SOLAM	0.61 (+)				
8			BPSTOR	0.65 (+)				

* Analysis results in this column are the same as those presented in the corresponding column of Table 5.1-3.

to those appearing in Figures 5.2-6 and 5.2-7 for scenario $S^{+-}(2,0,0,0,0)$ in the presence of gas generation.

5.4 Effect of No Chemical Retardation and Dual-Porosity Transport Model in Culebra Dolomite

As shown in the sensitivity analyses presented in preceding sections, retardation resulting from assumed distribution coefficients (i.e., FKDAM, FKDNP, FKDPU, FKDTH, FKDU, MKDAM, MKDNP, MKDPU, MKDTH, MKDU) for the Culebra Dolomite has an important influence on radionuclide releases to the accessible environment due to groundwater transport. At present, no site-specific observations exist for radionuclide sorption in the Culebra Dolomite, and the distributions characterizing the uncertainty in distribution coefficients were developed through an internal review process at Sandia National Laboratories (SNL) (see Section 2.6.10, Vol. 3, of this report). Due to the indicated importance of distribution coefficients and the absence of site-specific data, the best estimate analyses for the 1991 WIPP performance assessment (i.e., gas generation in the repository and a dual-porosity transport model in the Culebra Dolomite) presented in Chapter 4 were repeated with the distribution coefficients set to zero in each sample element. Under agreement with the State of New Mexico (U.S. DOE and State of New Mexico, 1981, as modified), the effect of zero distribution coefficients will be determined in the annual performance assessments conducted for the WIPP until site-specific information becomes available.

As examination of the scatterplots in Figure 5.4-1 shows, releases to the accessible environment are considerably larger when chemical retardation is assumed to be absent. However, although the releases increase in the absence of chemical retardation, the releases themselves are still relatively small. In particular, only a few sample elements result in normalized releases close to one.

As shown in Figure 4.5-4, approximately half the sample elements for scenario $S(1,0,0,0,0)$ result in no release to the Culebra. For these sample elements, the release to the accessible environment will be zero regardless of the assumptions made with respect to sorption. For scenario $S^{+-}(2,0,0,0,0)$, essentially all sample elements result in releases to the Culebra. As indicated by the points appearing above 10^{-8} in the scatterplot for scenario $S^{+-}(2,0,0,0,0)$ in Figure 5.4-1, many sample elements that produce zero releases in the presence of chemical retardation produce nonzero releases in the absence of chemical retardation. A similar effect can also be seen in the scatterplot for scenario $S(1,0,0,0,0)$ in Figure 5.4-1.

The releases of individual isotopes to the accessible environment on which Figure 5.4-1 is based are shown in Figure 5.4-2. The corresponding release

Scenario: $S(1,0,0,0,0)$, Assumed Intrusion Time: 1000 yrs

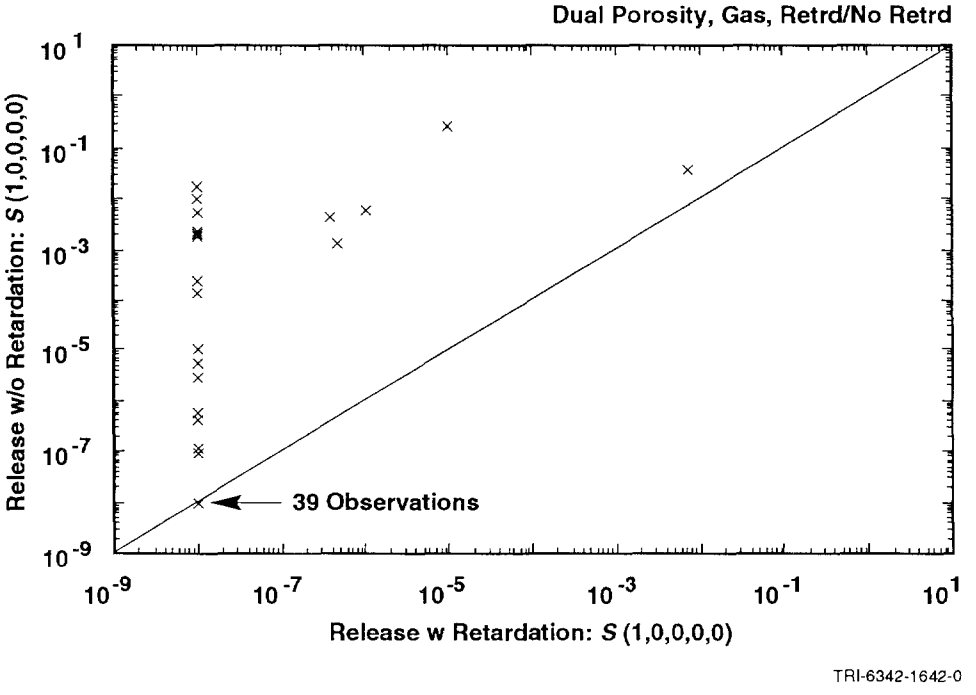

TRI-6342-1642-0

Scenario: $S^{+-}(2,0,0,0,0)$, Assumed Intrusion Time: 1000 yrs

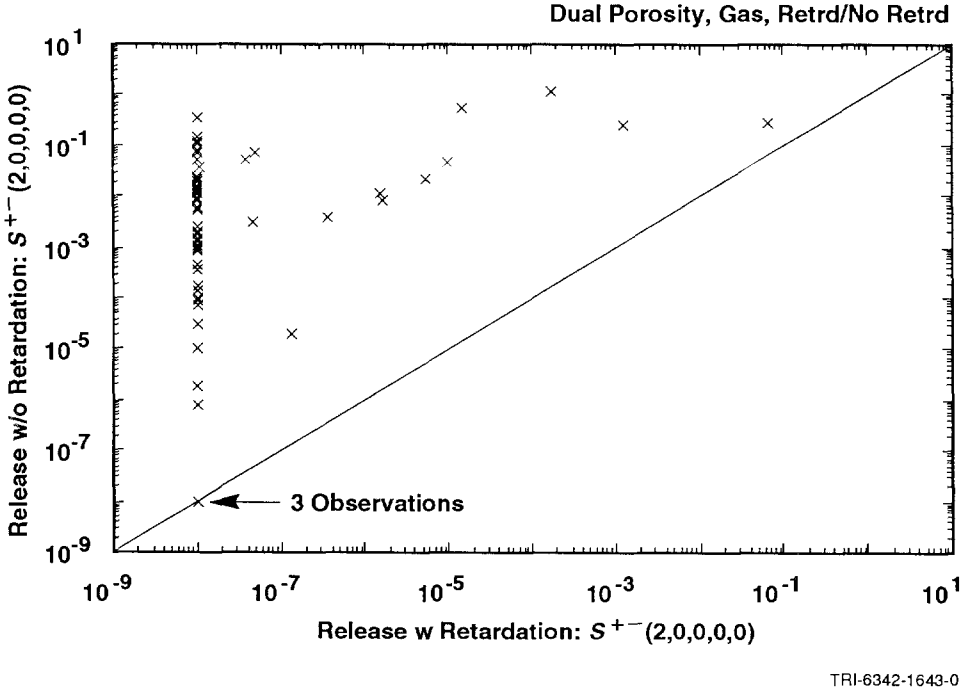

TRI-6342-1643-0

Figure 5.4-1. Scatterplots Comparing Total Normalized Releases to the Accessible Environment Due to Groundwater Transport Calculated by a Dual-Porosity Transport Model with and without Chemical Retardation in the Culebra Dolomite for Gas Generation in the Repository and an Assumed Intrusion Time of 1000 Yrs. For plotting purposes, values less than 10^{-8} are set to 10^{-8}.

Scenario: $S(1,0,0,0,0)$, Assumed Intrusion Time: 1000 yrs

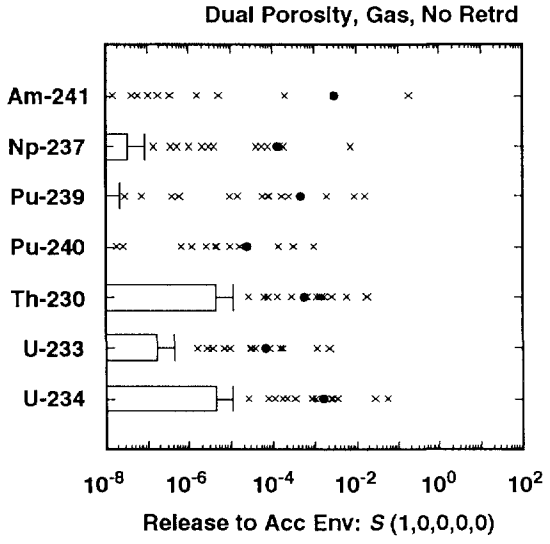

TRI-6342-1556-0

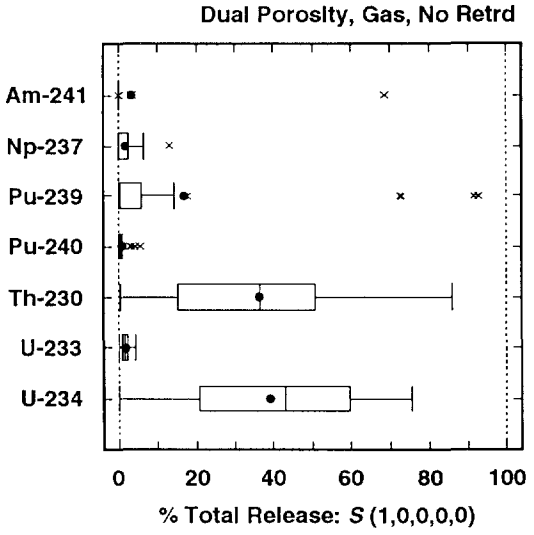

TRI-6342-1557-0

Scenario: $S^{+-}(2,0,0,0,0)$, Assumed Intrusion Time: 1000 yrs

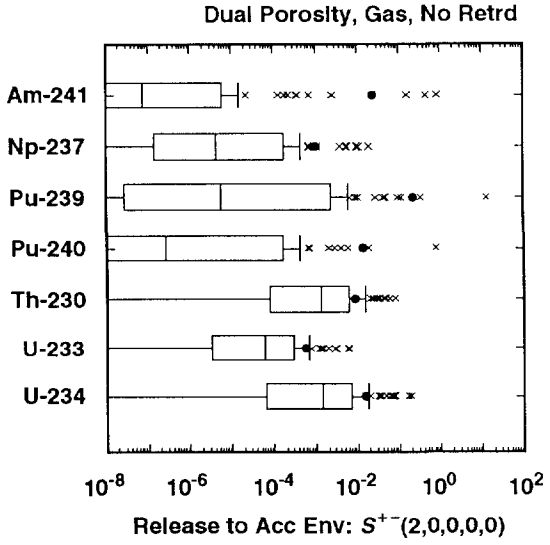

TRI-6342-1558-0

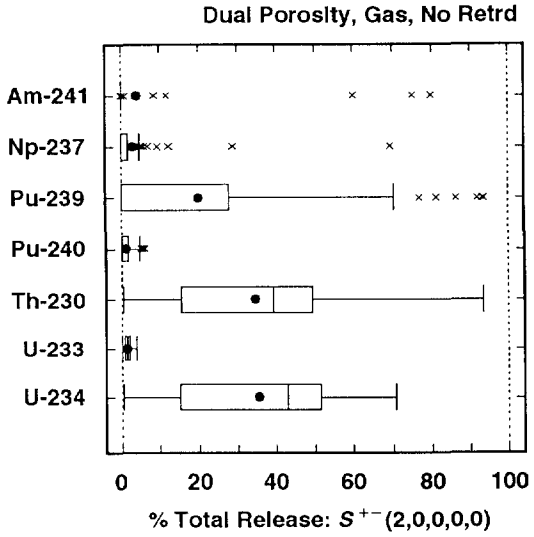

TRI-6342-1559-0

Figure 5.4-2. Normalized Releases for Individual Isotopes to the Accessible Environment Due to Groundwater Transport with Intrusion Occurring at 1000 Yrs, Gas Generation in the Repository and a Dual-Porosity Transport Model without Chemical Retardation in the Culebra Dolomite.

results obtained in the presence of chemical retardation are shown in Figure 4.4-2. As already indicated by the scatterplots appearing in Figure 5.4-1, the releases appearing in Figure 5.4-2 for transport without chemical retardation are considerably larger than those appearing in Figure 4.4-2 for transport with chemical retardation. Further, the major contributors to the total release are also changed. As shown in Figure 4.4-2, U-234 is the major contributor to the total release in the presence of chemical retardation. In contrast, Figure 5.4-2 indicates that Pu-239, Th-230 and U-234 are all important contributors in the absence of chemical retardation; even Am-241 is a dominant contributor for 3 sample elements for scenario $S^{+-}(2,0,0,0,0)$.

As shown in Figure 5.4-1, the assumption of no chemical retardation substantially increases the releases to the accessible environment due to groundwater transport. However, even without chemical retardation, the potential release to the accessible environment over the 10,000-yr period specified in the EPA standard is substantially reduced by groundwater transport in the Culebra. The extent of this reduction is illustrated by the scatterplots appearing in Figure 5.4-3, which show that the releases to the accessible environment due to groundwater transport for many, if not most, sample elements are one or more orders of magnitude less than the original releases to the Culebra.

Transport calculations for no chemical retardation in the Culebra were only performed for intrusions occurring at 1000 yrs (i.e., for scenarios $S(1,0,0,0,0)$ and $S^{+-}(2,0,0,0,0)$). As discussed in conjunction with Figure 5.1-4, these calculations can be used to construct CCDFs for comparison with the EPA release limits under the assumption that the rate constant λ in the Poisson model for drilling intrusions is equal to zero after 2000 yrs. The outcome of this construction is shown in Figure 5.4-4; the corresponding results obtained with retardation in the Culebra appear in the upper two frames of Figure 5.1-4. As comparison of the results in Figures 5.1-4 and 5.4-4 shows, the assumption of no retardation results in CCDFs that are shifted considerably to the right (i.e., closer to the EPA release limits) than the CCDFs obtained with retardation. Even so, only one of the CCDFs obtained without retardation actually crosses the EPA release limits.

Sensitivity analyses of groundwater transport results for individual isotopes for scenarios $S(1,0,0,0,0)$ and $S^{+-}(2,0,0,0,0)$ with gas generation in the repository and a dual-porosity transport model with no chemical retardation in the Culebra are presented in Tables 5.4-1 and 5.4-2. For convenience, these tables also contain the corresponding sensitivity analysis results for release to the Culebra, although these results have appeared previously in Tables 4.5-1 and 4.5-2.

Scenario: S(1,0,0,0,0), Assumed Intrusion Time: 1000 yrs

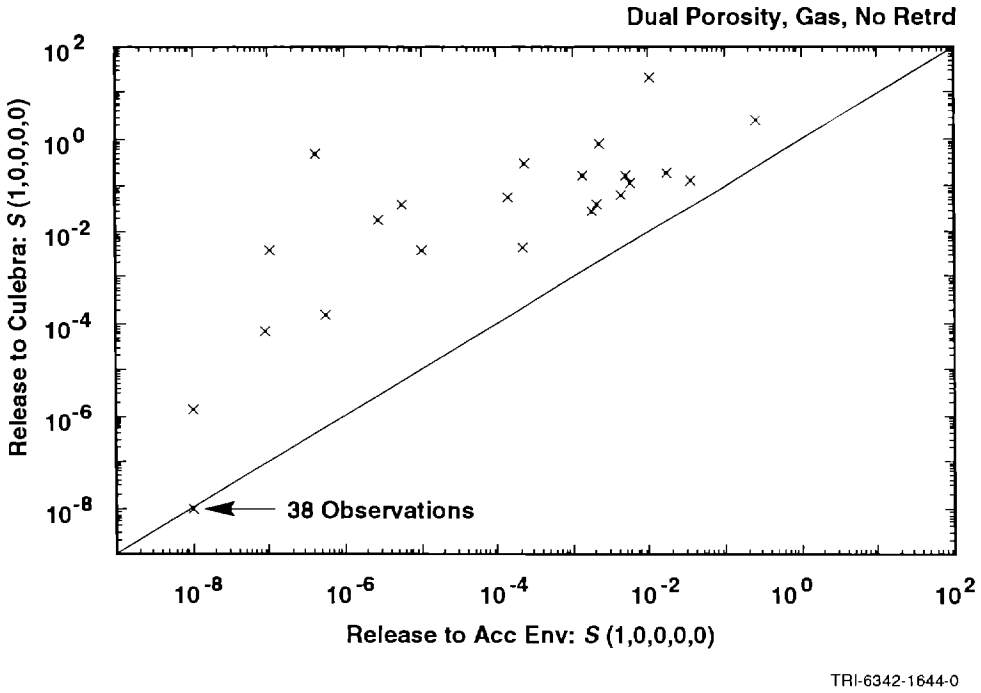

Scenario: S^{+-}(2,0,0,0,0), Assumed Intrusion Time: 1000 yrs

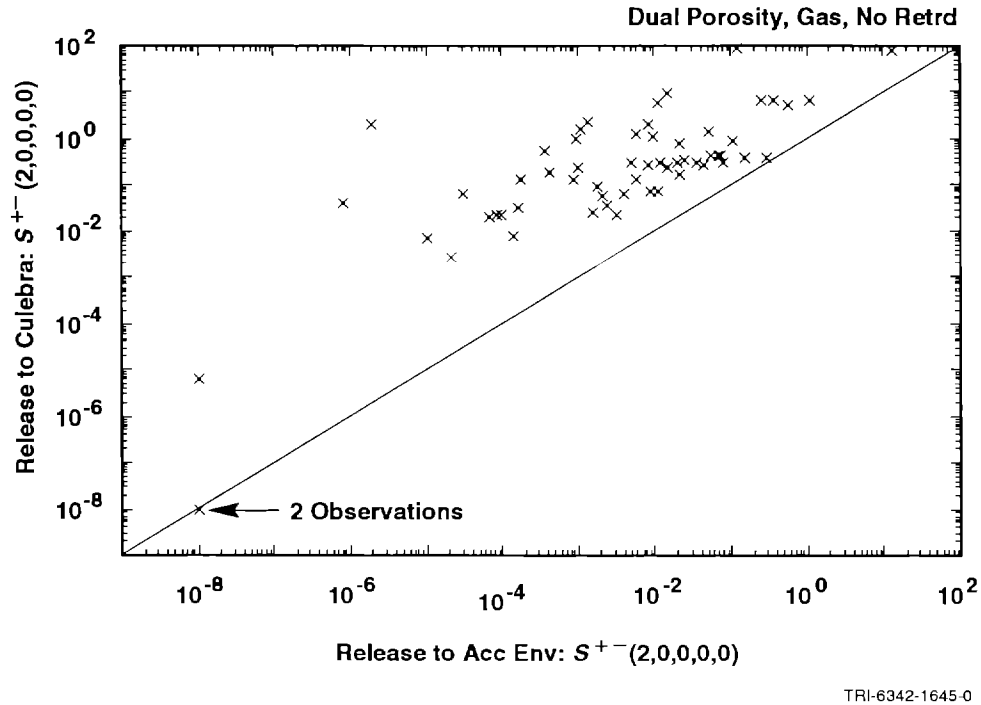

Figure 5.4-3. Scatterplots Comparing Total Normalized Release to the Culebra Dolomite and Total Normalized Release to the Accessible Environment for Scenarios S(1,0,0,0,0) and S^{+-}(2,0,0,0,0) with Gas Generation in the Repository, a Dual-Porosity Transport Model in the Culebra Dolomite, No Chemical Retardation and Intrusion Occurring at 1000 Yrs. For plotting purposes, values less than 10^{-8} are set to 10^{-8}.

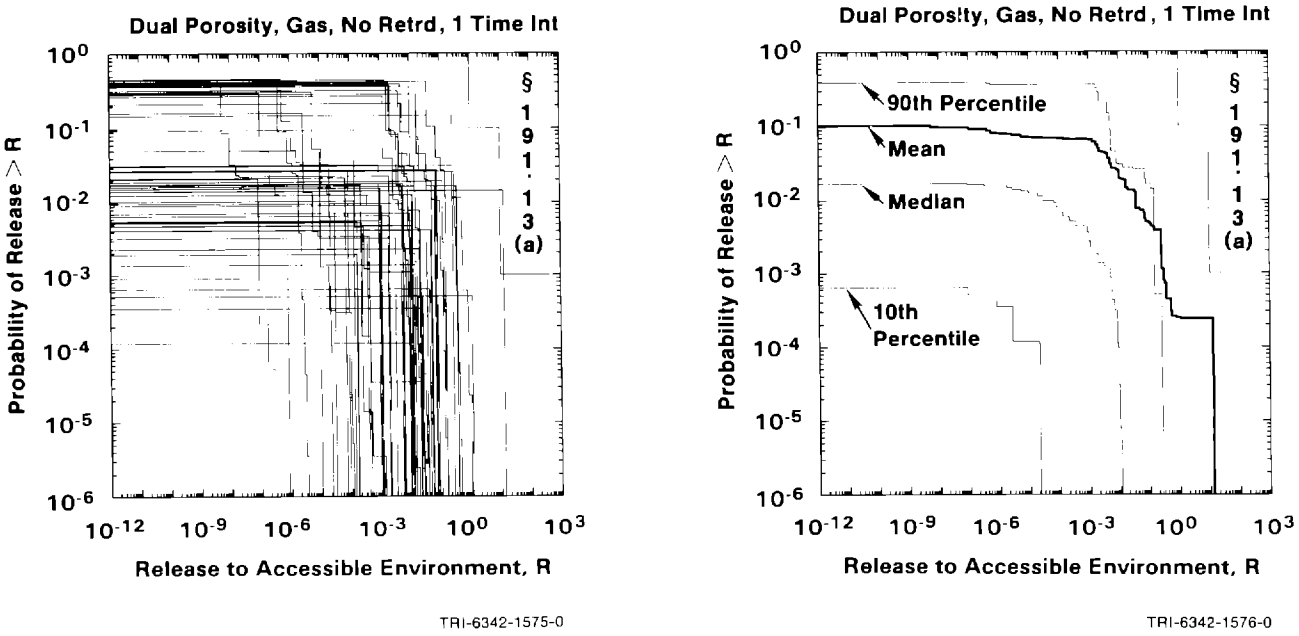

Figure 5.4-4. Complementary Cumulative Distribution Functions for Normalized Release to the Accessible Environment Due to Groundwater Transport for Gas Generation in the Repository, a Dual-Porosity Transport Model in the Culebra Dolomite, No Chemical Retardation and the Rate Constant λ in the Poisson Model for Drilling Intrusions Equal to Zero After 2000 Yrs.

The sensitivity analysis results in Table 5.4-1 for scenario $S(1,0,0,0,0)$ are dominated by SALPERM (Salado permeability). As previously discussed and illustrated by the scatterplots appearing in Figures 4.5-1 and 4.5-4, the importance of SALPERM results from its role as a switch in determining whether or not releases to the Culebra occur. Given that a release to the Culebra occurs, the same factors operate to affect its transport to the accessible environment for scenarios $S(1,0,0,0,0)$ and $S^{+-}(2,0,0,0,0)$. Therefore, as the sensitivity analysis results for scenario $S^{+-}(2,0,0,0,0)$ in Table 5.4-2 are more revealing than those for scenario $S(1,0,0,0,0)$ in Table 5.4-1 due to the absence of SALPERM as a switch, the following discussion will focus on the sensitivity analysis results obtained for $S^{+-}(2,0,0,0,0)$.

The sensitivity analysis results in Table 5.4-2 for scenario $S^{+-}(2,0,0,0,0)$ indicate that the most important variables for integrated transport in the absence of chemical retardation are BHPERM (borehole permeability), BPPRES (brine pocket pressure) and solubilities for the individual elements. These are also the variables that dominate release to the Culebra. However, unlike the analysis results shown in Table 5.4-2 for transport in the Culebra without chemical retardation, the analysis results shown in Table 4.5-2 for transport with chemical retardation are dominated by the distribution

TABLE 5.4-1. STEPWISE REGRESSION ANALYSES WITH RANK-TRANSFORMED DATA FOR SCENARIO $S(1,0,0,0,0)$ WITH GAS GENERATION IN THE REPOSITORY AND A DUAL-POROSITY TRANSPORT MODEL WITH NO CHEMICAL RETARDATION IN THE CULEBRA DOLOMITE

	Release to Culebra*		Quarter Distance		Half Distance		Full Distance	
Step	Variable	R^2	Variable	R^2	Variable	R^2	Variable	R^2
Dependent Variable: Integrated Discharge Am-241								
1	SALPERM	0.59(+)	SALPERM	0.58(+)	SALPERM	0.58(+)	SALPERM	0.57(+)
Dependent Variable: Integrated Discharge Np-237								
1	SALPERM	0.53(+)	MBPERM	0.55(+)	SALPERM	0.56(+)	SALPERM	0.56(+)
Dependent Variable: Integrated Discharge Pu-239								
1	SALPERM	0.56(+)	SALPERM	0.56(+)	SALPERM	0.56(+)	SALPERM	0.55(+)
Dependent Variable: Integrated Discharge Pu-240								
1	SALPERM	0.56(+)	SALPERM	0.56(+)	SALPERM	0.56(+)	SALPERM	0.55(+)
Dependent Variable: Integrated Discharge Th-230								
1	SALPERM	0.55(+)	SALPERM	0.58(+)	SALPERM	0.58(+)	SALPERM	0.58(+)
Dependent Variable: Integrated Discharge U-233								
1	SALPERM	0.59(+)	SALPERM	0.59(+)	SALPERM	0.59(+)	SALPERM	0.58(+)
Dependent Variable: Integrated Discharge U-234								
1	SALPERM	0.59(+)	SALPERM	0.58(+)	SALPERM	0.59(+)	SALPERM	0.59(+)
Dependent Variable: EPA Sum for Total Integrated Discharge								
1	SALPERM	0.58(+)	SALPERM	0.57(+)	SALPERM	0.57(+)	SALPERM	0.57(+)

*Analysis results in this column are the same as those presented in the corresponding column of Table 4.5-1.

TABLE 5.4-2. STEPWISE REGRESSION ANALYSES WITH RANK-TRANSFORMED DATA FOR SCENARIO S^{+}-(2,0,0,0,0) WITH GAS GENERATION IN THE REPOSITORY, A DUAL-POROSITY TRANSPORT MODEL WITH NO CHEMICAL RETARDATION IN THE CULEBRA DOLOMITE AND INTRUSION OCCURRING 1000 YRS AFTER REPOSITORY CLOSURE

	Release to Culebra*		Quarter Distance		Half Distance		Full Distance	
Step	Variable	R^2	Variable	R^2	Variable	R^2	Variable	R^2
Dependent Variable: Integrated Discharge Am-241								
1	SOLAM	0.36 (+)	SOLAM	0.22 (-)	CULFRSP	0.23 (+)	CULFRSP	0.33 (+)
2	BHPERM	0.74 (+)	BHPERM	0.47 (+)	BHPERM	0.39 (+)	CULCLIM	0.52 (+)
3	BPPRES	0.78 (+)	CULCLIM	0.61 (+)	SOLAM	0.55 (+)	SOLAM	0.62 (+)
4			CULFRSP	0.71 (+)	CULCLIM	0.72 (+)	BHPERM	0.72 (+)
5			BPPRES	0.75 (+)	BPPRES	0.75 (+)	BPPRES	0.75 (+)
6					CULTRFLD	0.78 (-)	GRCORI	0.77 (-)
7							CULTRFLD	0.80 (-)
Dependent Variable: Integrated Discharge Np-237								
1	SOLNP	0.65 (+)	SOLNP	0.41 (+)	SOLNP	0.37 (+)	SOLNP	0.34 (+)
2	BHPERM	0.78 (+)	BHPERM	0.65 (+)	BHPERM	0.60 (+)	BHPERM	0.53 (+)
3	BPPRES	0.82 (+)	BPPRES	0.71 (+)	BPPRES	0.66 (+)	CULCLIM	0.62 (+)
4	EHPH	0.85 (+)	EHPH	0.75 (+)	EHPH	0.71 (+)	BPPRES	0.68 (+)
5	GRCORI	0.88 (-)	SOLAM	0.79 (+)	SOLAM	0.75 (+)	CULFRSP	0.73 (+)
6			CULCLIM	0.82 (+)	CULCLIM	0.79 (+)	SOLAM	0.76 (+)
7			GRCORI	0.84 (-)	GRCORI	0.82 (-)	EHPH	0.79 (+)
8							GRCORI	0.81 (-)
Dependent Variable: Integrated Discharge Pu-239								
1	SOLPU	0.74 (+)	SOLPU	0.70 (+)	SOLPU	0.68 (+)	SOLPU	0.63 (+)
2	BHPERM	0.85 (+)	BHPERM	0.82 (+)	BHPERM	0.81 (+)	BHPERM	0.75 (+)
3					CULFRSP	0.83 (+)	CULFRSP	0.80 (+)
4							CULCLIM	0.82 (+)
Dependent Variable: Integrated Discharge Pu-240								
1	SOLPU	0.74 (+)	SOLPU	0.69 (+)	SOLPU	0.68 (+)	SOLPU	0.62 (+)
2	BHPERM	0.85 (+)	BHPERM	0.82 (+)	BHPERM	0.80 (+)	BHPERM	0.74 (+)
3					CULFRSP	0.83 (+)	CULFRSP	0.80 (+)
4							CULCLIM	0.83 (+)

*Analysis results in this column are the same as those presented in the corresponding column of Table 4.5-2.

TABLE 5.4-2. STEPWISE REGRESSION ANALYSES WITH RANK-TRANSFORMED DATA FOR SCENARIO S^{+-}(2,0,0,0,0) WITH GAS GENERATION IN THE REPOSITORY, A DUAL-POROSITY TRANSPORT MODEL WITH NO CHEMICAL RETARDATION IN THE CULEBRA DOLOMITE AND INTRUSION OCCURRING 1000 YRS AFTER REPOSITORY CLOSURE (concluded)

	Release to Culebra*		Quarter Distance		Half Distance		Full Distance	
Step	Variable	R^2	Variable	R^2	Variable	R^2	Variable	R^2
Dependent Variable: Integrated Discharge Th-230								
1	SOLTH	0.69 (+)	BHPERM	0.43 (+)	BHPERM	0.44 (+)	BHPERM	0.31 (+)
2	BHPERM	0.82 (+)	BPPRES	0.60 (+)	BPPRES	0.59 (+)	BPPRES	0.44 (+)
3			SOLU	0.65 (+)	SOLU	0.65 (+)	CULCLIM	0.56 (+)
4			SOLTH	0.69 (+)	CULCLIM	0.69 (+)	CULFRSP	0.62 (+)
5					CULPOR	0.73 (-)	CULPOR	0.68 (-+)
6					SOLTH	0.76 (+)	SOLU	0.73 (+)
Dependent Variable: Integrated Discharge U-233								
1	BHPERM	0.43 (+)	BHPERM	0.43 (+)	BHPERM	0.41 (+)	BHPERM	0.28 (+)
2	SOLU	0.58 (+)	BPPRES	0.58 (+)	BPPRES	0.54 (+)	CULCLIM	0.40 (+)
3	BPPRES	0.70 (+)	SOLU	0.68 (+)	SOLU	0.62 (+)	BPPRES	0.52 (+)
4	SOLNP	0.74 (-)	CULCLIM	0.72 (+)	CULCLIM	0.68 (+)	CULFRSP	0.63 (+)
5					CULPOR	0.72 (-)	SOLU	0.68 (+)
6					CULFRSP	0.76 (+)	CULPOR	0.73 (-)
7							SALPRES	0.75 (+)
Dependent Variable: Integrated Discharge U-234								
1	BHPERM	0.47 (+)	BHPERM	0.43 (+)	BHPERM	0.39 (+)	BHPERM	0.27 (+)
2	SOLU	0.60 (+)	BPPRES	0.56 (+)	BPPRES	0.52 (-)	CULCLIM	0.39 (+)
3	BPPRES	0.72 (+)	SOLU	0.68 (+)	SOLU	0.62 (+)	BPPRES	0.51 (+)
4			CULCLIM	0.72 (+)	CULCLIM	0.68 (+)	CULFRSP	0.59 (+)
5			CULPOR	0.75 (-)	CULPOR	0.73 (-)	CULPOR	0.65 (-)
6					SOLU	0.72 (+)		
Dependent Variable: EPa Sum for Total Integrated Discharge								
1	BHPERM	0.46 (+)	BHPERM	0.47 (+)	BHPERM	0.43 (+)	BHPERM	0.31 (+)
2	SOLAM	0.57 (+)	BPPRES	0.61 (+)	BPPRES	0.58 (+)	CULCLIM	0.46 (+)
3	BPPRES	0.66 (+)	CULCLIM	0.68 (+)	CULCLIM	0.67 (+)	BPPRES	0.60 (+)
4	SOLPU	0.69 (+)	BPSTOR	0.71 (+)			CULFRSP	0.69 (+)
5	BPSTOR	0.73 (+)	CULPOR	0.74 (-)			CULPOR	0.72 (-)
6	SOLU	0.76 (+)	BHDIAM	0.77 (+)				

*Analysis results in this column are the same as those presented in the corresponding column of Table 4.5-2.

coefficients for the individual elements. The effects of the distribution coefficients on the transport results analyzed in Table 4.5-2 are so strong that the effects of other variables that have lesser influence on transport are obscured. As shown in Figure 4.5-6 for transport only one-quarter the distance to the accessible environment, transport is essentially shut off over the 10,000-yr period under consideration due to chemical retardation in the matrix. In contrast, the analyses of transport results obtained without chemical retardation presented in Table 5.4-2 are able to identify the effects of some of these other variables. In particular, integrated releases tend to increase as CULCLIM (recharge amplitude factor for Culebra) and CULFRSP (fracture spacing in Culebra) increase and decrease as CULPOR (matrix porosity in Culebra) increases. However, the most important variables overall in the absence of chemical retardation are those that influence release to the Culebra (i.e., BHPERM, BPPRES and elemental solubilities).

As seen previously, the examination of scatterplots often helps provide perspective on regression-based sensitivity analysis and sometimes reveals relationships that are not apparent in the regression models. Other than the previously identified role of SALPERM (Salado permeability) as a switch for scenario $S(1,0,0,0,0)$, examination of scatterplots for the no-retardation calculations did not reveal any unusual patterns. However, it is still useful to examine a few scatterplots to develop a feeling for the relationships indicated in Table 5.4-2.

Scatterplots for normalized release of Am-241 and Pu-239 to the accessible environment for scenario $S^{+-}(2,0,0,0,0)$ are given in Figure 5.4-5. The scatterplot for Am-241 involves CULFRSP (Culebra fracture spacing), which is the first variable selected in the regression model presented in Table 5.4-2 for release to the accessible environment (i.e., for the "Full Distance" results). The rank-regression model presented in Table 5.4-2 indicates that release increases as CULFRSP increases and that this variable can account for approximately 33% of the variability in the release. This result is consistent with the pattern shown in Figure 5.4-5, where the release tends to increase as CULFRSP increases but with considerable variability around this trend.

The scatterplot for Pu-239 in Figure 5.4-5 involves SOLPU (solubility for Pu), which again is the first variable selected in the regression model presented in Table 5.4-2 for release to the accessible environment. In this case, the rank-regression model involving only SOLPU indicates that release increases as SOLPU increases and that SOLPU can account for approximately 63% of the variability in the release. This increasing relationship between release and SOLPU for Pu-239 can be readily seen in the scatterplot in

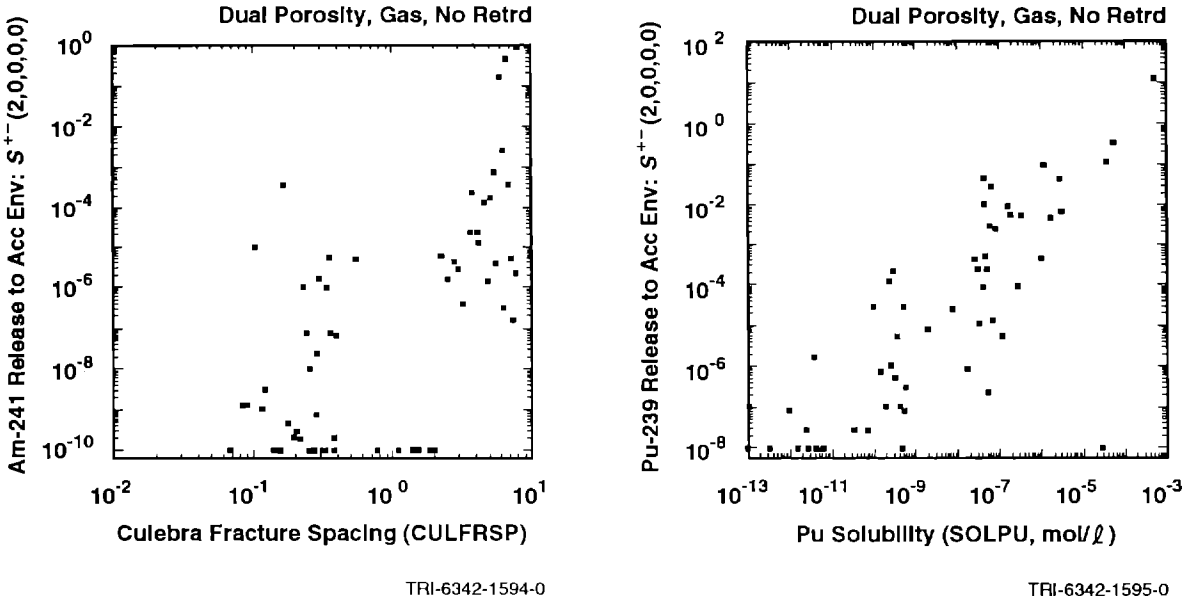

Figure 5.4-5. Scatterplots for Normalized Release of Am-241 and Pu-239 to the Accessible Environment Due to Groundwater Transport for Variables CULFRSP (Culebra fracture spacing) and SOLPU (solubility for Pu) for Scenario S^{+-}(2,0,0,0,0) with Gas Generation in the Repository, a Dual-Porosity Transport Model in the Culebra Dolomite, No Chemical Retardation and Intrusion Occurring at 1000 Yrs.

Figure 5.4-5. Further, as indicated by the R^2 values in the regression models in Table 5.4-2 (i.e., 0.33 for Am-241 and 0.63 for Pu-239), the relationship in the scatterplot for Pu-239 is considerably tighter than the one in the scatterplot for Am-241.

Scatterplots appear in Figure 5.4-6 for the release of U-234 to the accessible environment for scenario S^{+-}(2,0,0,0,0) and the variables BHPERM (borehole permeability), CULCLIM (recharge amplitude factor for Culebra) and SOLU (solubility for U). As shown in Table 5.4-2 for the release of U-234 to the accessible environment, increasing each of these variables tends to increase the release although no single variable dominates. For example, BHPERM is the most influential variable (i.e., is selected first in the stepwise regression analysis with rank-transformed data) but can account for only 27% of the observed variability. This pattern is apparent in the scatterplots in Figure 5.4-6, where release tends to increase with each of BHPERM, CULCLIM and SOLU but with much variability around this increasing trend.

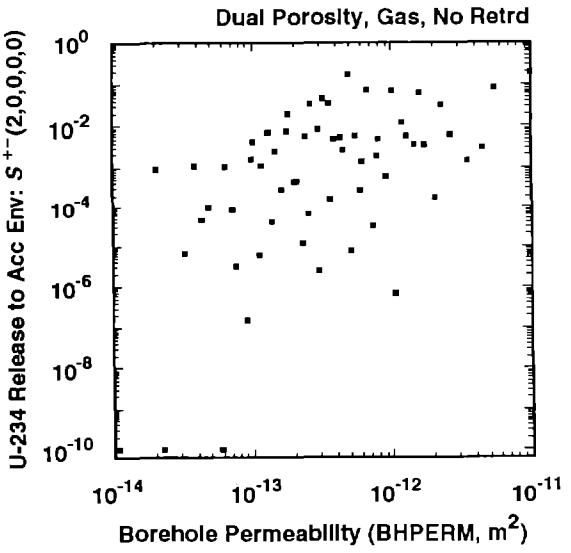

TRI-6342-1596-0

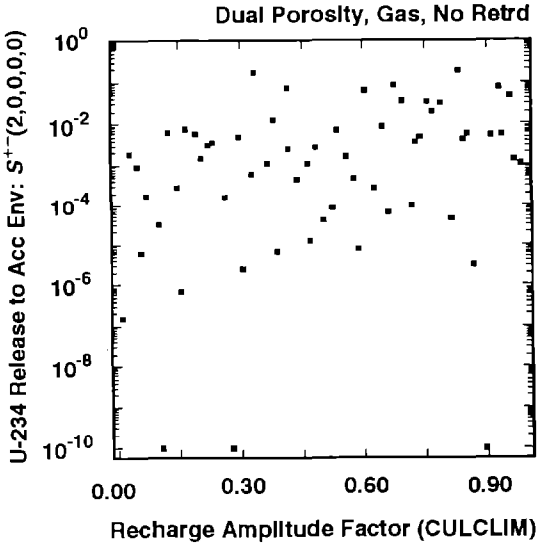

TRI-6342-1598-0

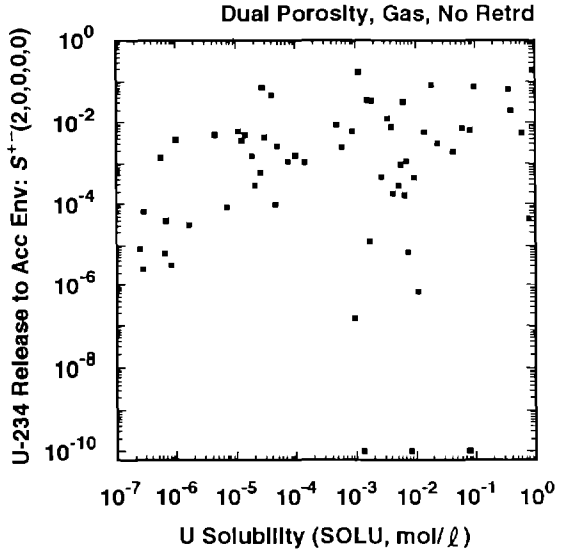

TRI-6342-1597-0

Figure 5.4-6. Scatterplots for Normalized Release of U-234 to the Accessible Environment Due to Groundwater Transport for Variables BHPERM (borehole permeability), CULCLIM (recharge amplitude factor for Culebra) and SOLU (solubility of U) for Scenario $S^{+-}(2,0,0,0,0)$ with Gas Generation in the Repository, A Dual-Porosity Transport Model in the Culebra Dolomite, No Chemical Retardation and Intrusion Occurring at 1000 Yrs.

This is a natural point at which to consider the importance of the variable CULFRPOR (fracture porosity in Culebra). As shown in the scatterplots appearing in Figures 4.5-7 and 5.2-8 for groundwater transport with chemical retardation, increasing CULFRPOR increases groundwater transport when a dual-porosity transport model is used and decreases groundwater transport when a single-porosity transport model is used. Further, CULFRPOR is not identified as being an important variable in the sensitivity analyses presented in Table 5.4-2 for groundwater transport with a dual-porosity transport model and no chemical retardation. The reason for the absence of CULFRPOR from the analyses presented in Table 5.4-2 is easily seen from the scatterplot appearing in Figure 5.4-7, which shows little relationship between CULFRPOR and total release to the accessible environment.

As discussed in Section 5.2, the negative effect of CULFRPOR (fracture porosity in Culebra) on radionuclide release for a single-porosity transport model results from the decrease in groundwater velocity that occurs as CULFRPOR increases. For dual-porosity transport, the presence of a positive effect for CULFRPOR when chemical retardation takes place and the absence of this effect when chemical retardation does not take place suggests that CULFRPOR is involved in the implementation of chemical retardation for the dual-porosity transport model. This is indeed the case, with both CULFRPOR and CULFRSP (Culebra fracture spacing) being involved in the definition of a "skin resistance" that controls radionuclide movement from a fracture to the surrounding matrix for the dual-porosity transport model implemented in STAFF2D (Huyakorn, et al., 1989).

The skin resistance in STAFF2D is defined by

$$\zeta = \left(\frac{b_s}{b_f}\right) \left(\frac{\phi_f B}{(1-\phi_f)\ \tau D^{\alpha}}\right), \qquad (5.4\text{-}1)$$

where

ζ = skin resistance (s/m),

b_s = width of clay lining in fracture (m),

b_f = width of fracture (m),

ϕ_f = fracture porosity (i.e., the sampled variable CULFRPOR in Table 3-1),

B = half the distance between fractures (m) (i.e., one-half the sampled variable CULFRSP in Table 3-1),

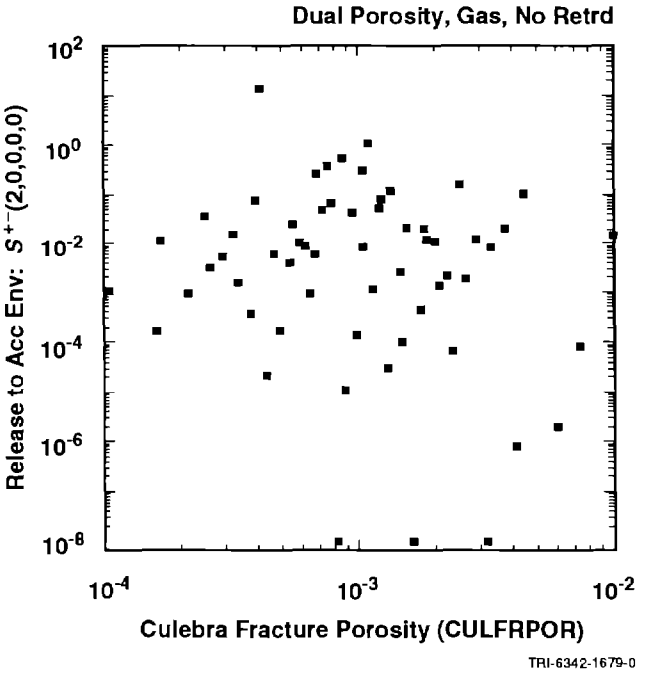

Figure 5.4-7. Scatterplot for Fracture Porosity in Culebra Dolomite (CULFRPOR) versus Total Normalized Release to the Accessible Environment Due to Groundwater Transport for Scenario S^{+-}(2,0,0,0,0) with Gas Generation in the Repository, a Dual-Porosity Transport Model in the Culebra Dolomite, No Chemical Retardation and Intrusion Occurring at 1000 Yrs.

τ = clay tortuosity, which was fixed at 1.2×10^{-2} in the 1991 WIPP performance assessment (Vol. 3, Section 2.6.7)

and

D^{α} = molecular diffusion coefficient (m^2/s), which was fixed at the median elemental values shown in Table 3.3-12, Vol. 3, for the 1991 WIPP performance assessment.

As skin resistance increases, the rate of radionuclide movement from a fracture to the surrounding matrix will decrease.

For the 1991 WIPP performance assessment, the ratio b_s/b_f in Eq. 5.4-1 is assumed to equal 0.1. Further, τ is fixed at 1.2×10^{-2}; D^{α} is fixed for each element at the median value shown in Table 3.3-12, Vol. 3, and $1-\phi_f$ is close to one (i.e., ϕ_f is the sampled variable CULFRPOR shown in Table 3-1, which has a range from 1×10^{-4} to 1×10^{-2}). As a result, the skin resistance ζ is proportional to the product ϕ_f B, which is the product CULFRPOR*CULFRSP/2 in the notation used in this report. Thus, ζ should

increase, with the result that radionuclide transport in the Culebra should also increase, as CULFRPOR and CULFRSP increase, which is exactly the pattern that has been observed (e.g., see the scatterplots for CULFRSP and CULFRPOR in Figure 4.5-7 and the regression analyses in Tables 5.1-2 and 5.1-3). Further, as shown in Figure 5.4-8, a stronger relationship exists between release to the accessible environment and the product CULFRSP*CULFRPOR (i.e., 2 ϕ_f B) than appears in Figure 4.5-7 for either variable by itself.

5.5 Effect of Climate Change

The 1991 WIPP performance assessment used the variable CULCLIM (recharge amplitude factor for Culebra) to study the effects of uncertainty in the future climate in southeastern New Mexico. Specifically, CULCLIM is used in the relationship

$$\frac{h_f(t)}{h_p} = \frac{3A_m + 1}{4} - \frac{A_m - 1}{2}\left(\cos \Theta t + \frac{1}{2}\cos \Phi t - \sin \frac{1}{2}\Phi t\right) \qquad (5.5\text{-}1)$$

to define time-dependent heads in the Culebra, where

$h_f(t)$ = head (m) in Culebra at time t (sec),
h_p = estimate of present-day boundary head in Culebra (e.g., 880 m),
A_m = recharge amplitude factor (dimensionless) for Culebra (i.e., CULCLIM),
Θ = frequency (Hz) for Pleistocene glaciations (i.e., 1.7×10^{-12} Hz),
Φ = frequency (Hz) for second-order climatic fluctuations (i.e., 2×10^{-10} Hz)

and

t = time (sec), with t=0 corresponding to closure of the WIPP.

As discussed in Section 4.4 of Vol. 3, this function is not used to predict future climates, but rather is designed to provide a simple way to examine the influence of possible climatic changes during the next 10,000 yrs. The periodicity of the function is based on approximately 30,000 yrs of paleoclimatic data from southeastern New Mexico and the surrounding region and the global record of Pleistocene glaciations (Swift, in press). The glacial frequency term Θ produces a maximum value of the function $h_f(t)$ at 60,000 yrs, and has little effect during the regulatory period. Most of the introduced variability results from second-order fluctuations controlled by the higher-frequency term Φ. This variability corresponds conceptually to the frequency of nonglacial climatic fluctuations observed in both late Pleistocene and Holocene paleoclimatic data.

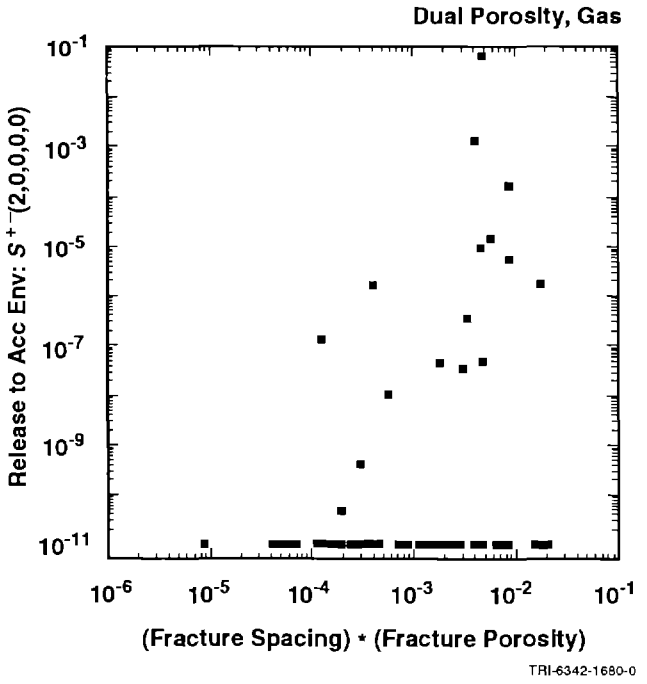

Figure 5.4-8. Scatterplot for Total Normalized Release to the Accessible Environment Due to Groundwater Transport versus the Product of Culebra Fracture Spacing (CULFRSP, m) and Culebra Fracture Porosity (CULFRPOR) (i.e., the product CULFRSP*CULFRPOR) for Scenario S^{+-}(2,0,0,0,0) with Gas Generation in the Repository, a Dual-Porosity Transport Model in the Culebra Dolomite and Intrusion Occurring at 1000 Yrs.

As discussed in Section 6.4.2 of Vol. 2, climatic fluctuations are linked to the groundwater-flow model through the sampled variable CULCLIM (i.e., A_m), which is a scaling factor used to modify hydraulic heads in the Culebra Dolomite along a portion of the northern boundary of the model domain. At its minimum value of 1, CULCLIM results in no change in prescribed boundary heads during the 10,000-yr period. At its maximum value of 1.16, CULCLIM results in boundary heads varying from their estimated present values (e.g., 880 m) to maximum values corresponding to the ground surface (e.g., 1030 m). Intermediate values for CULCLIM result in maximum heads at elevations between their present evaluation and the ground surface.

Considerable interest exists in the effects of climatic variation. Therefore, although the original Latin hypercube sample indicated in Eq. 2.1-5 contained CULCLIM as a variable, analyses for single- and dual-porosity transport in the Culebra with gas generation in the repository and chemical retardation were repeated with CULCLIM set to 1 and to 1.16.

The results of these calculations for total normalized release to the accessible environment are summarized by the scatterplots appearing in Figures 5.5-1 and 5.5-2 for dual- and single-porosity transport, respectively, with the ordinate displaying the results for CULCLIM = 1 and

Scenario: $S(1,0,0,0,0)$, Assumed Intrusion Time: 1000 yrs

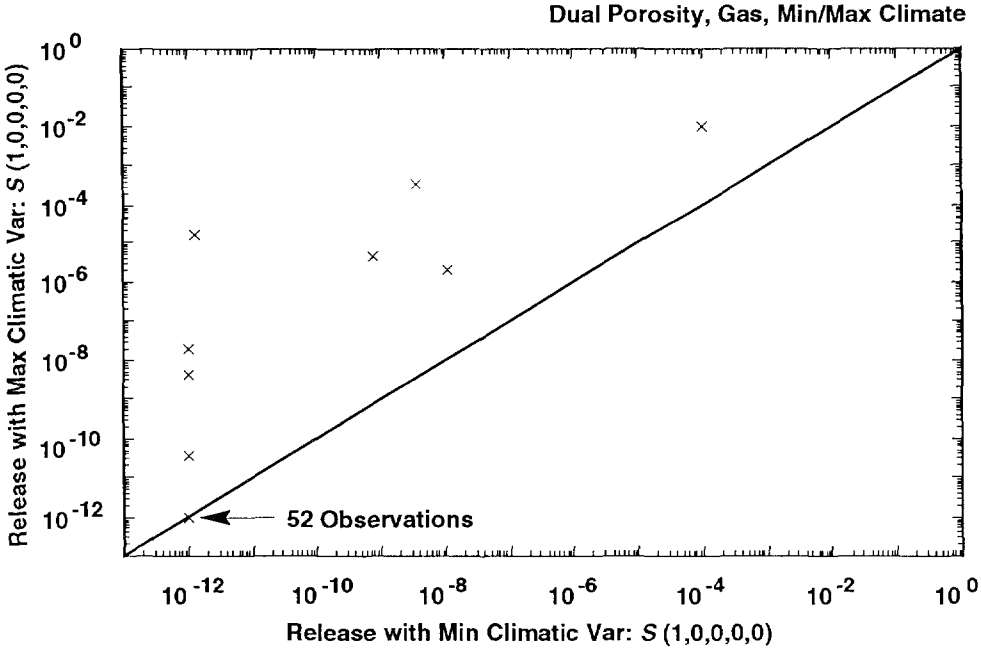

TRI-6342-1646-0

Scenario: $S^{+-}(2,0,0,0,0)$, Assumed Intrusion Time: 1000 yrs

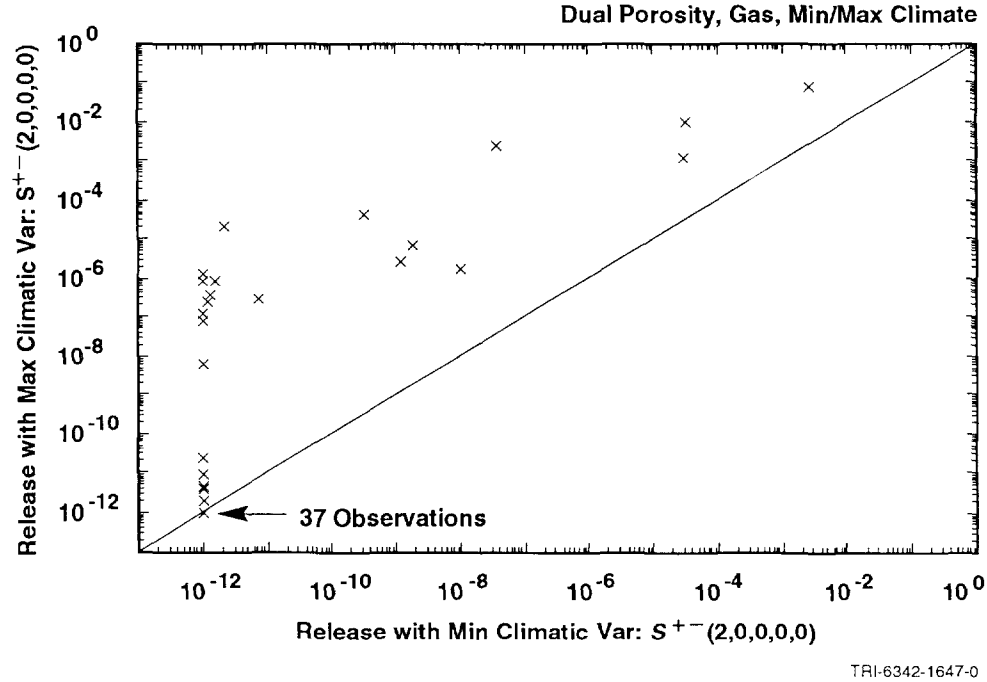

TRI-6342-1647-0

Figure 5.5-1. Scatterplots for Total Normalized Release to the Accessible Environment Due to Groundwater Transport with Minimum (i.e., CULCLIM = 1) and Maximum (i.e., CULCLIM = 1.16) Climatic Variation for Gas Generation in the Repository, a Dual-Porosity Transport Model with Chemical Retardation in the Culebra and Intrusion Occurring at 1000 Yrs. For plotting purposes, values less than 10^{-12} are set to 10^{-12}.

Scenario: $S(1,0,0,0,0)$, Assumed Intrusion Time: 1000 yrs

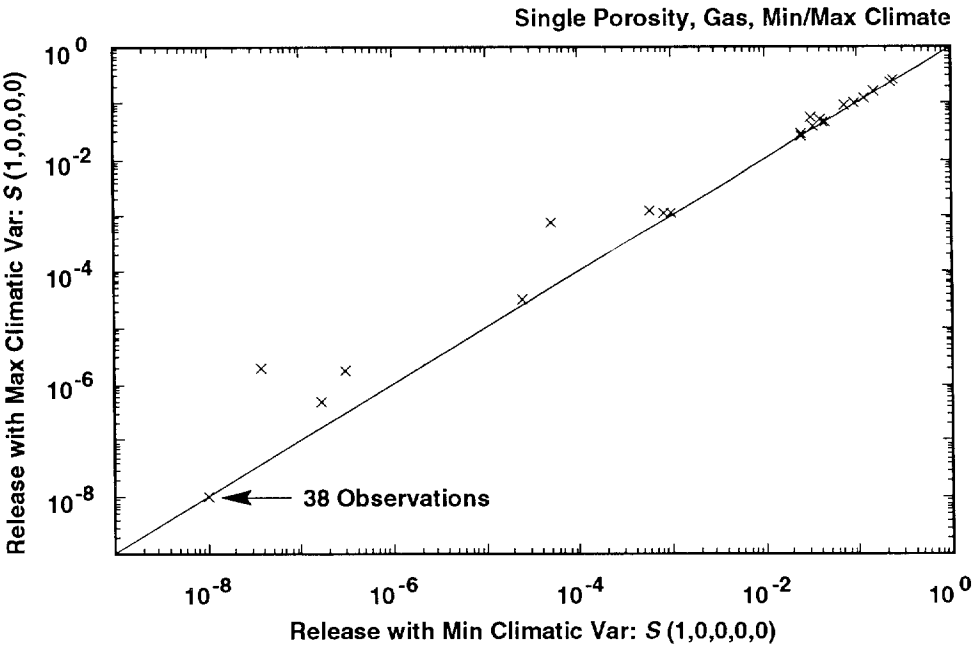

Scenario: $S^{+-}(2,0,0,0,0)$, Assumed Intrusion Time: 1000 yrs

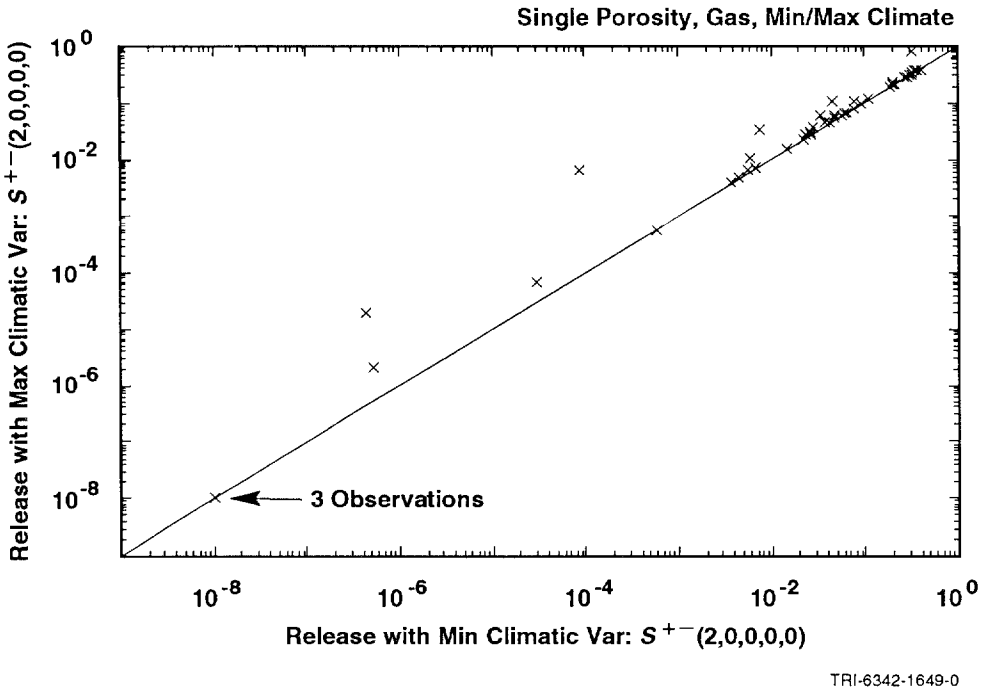

Figure 5.5-2. Scatterplots for Total Normalized Release to the Accessible Environment Due to Groundwater Transport with Minimum (i.e., CULCLIM = 1) and Maximum (i.e., CULCLIM = 1.16) Climatic Variation for Gas Generation in the Repository, a Single-Porosity Transport Model with Chemical Retardation in the Culebra and Intrusion Occurring at 1000 Yrs. For plotting purposes, values less than 10^{-8} are set to 10^{-8}.

the abscissa displaying the results for CULCLIM = 1.16. As shown in Figure 5.5-1, an assumption of increased rainfall, and hence increased head at the northern recharge boundary used for the Culebra, leads to increased releases for the dual-porosity transport model. However, these increased releases are too small to cause a violation of the EPA release limits. In contrast, the results in Figure 5.5-2 show that an assumption of increased rainfall has almost no effect on the releases for the single-porosity transport model.

As shown in Figure 5.5-3, most U-234 releases to the Culebra are transported to the accessible environment within the 10,000-yr time period specified in the EPA standard when a single-porosity transport model is used. The observations shown in Figure 5.5-3 in which this does not occur tend to be those in which uranium has one of its larger distribution coefficient values, in which case the total release is dominated by some other isotope that has a small distribution coefficient value. Thus, the total releases to the accessible environment for single-porosity transport in the Culebra and CULCLIM=1 are dominated by isotopes whose entire release to the Culebra is transported to the accessible environment within the 10,000-yr period in the EPA standard. As a reminder, most releases are dominated by U-234 (see Figure 5.2-5). Thus, although increasing CULCLIM to 1.16 will increase groundwater flow and hence result in earlier releases to the accessible environment, an increased release over 10,000 yrs will not take place. For the dual-porosity transport model, the releases to the accessible environment are substantially less than the releases to the Culebra for all isotopes (e.g., compare the results in Figures 5.1-2 and 5.1-3). In this case, increasing the groundwater flow rate will increase the release to the accessible environment, although the total releases remain small.

Transport calculations for CULCLIM = 1 and CULCLIM = 1.16 were only performed for scenarios $S(1,0,0,0,0)$ and $S^{+-}(2,0,0,0,0)$. As a result, CCDFs for comparison with the EPA release limits using nonzero intrusion probabilities over 10,000 yrs cannot be constructed. However, as already shown in Figures 5.1-4, 5.3-3 and 5.4-3, CCDFs can be constructed for comparison with the EPA release limits under the assumption that the rate constant λ in the Poisson model for drilling intrusions is equal to zero after 2000 yrs. The result of this construction for dual-porosity transport in the Culebra is shown in Figure 5.5-4. As examination of this figure shows, the CCDFs obtained for the maximum recharge case (i.e., CULCLIM = 1.16) are shifted to the right relative to those obtained with present-day recharge (i.e., CULCLIM = 1). However, even for the maximum recharge, the releases due to groundwater transport are substantially smaller than the release due to cuttings removal summarized in the CCDFs shown in Figure 4.1-2. The small effect indicated for CULCLIM in Figure 5.5-4 is consistent with the small effect indicated for

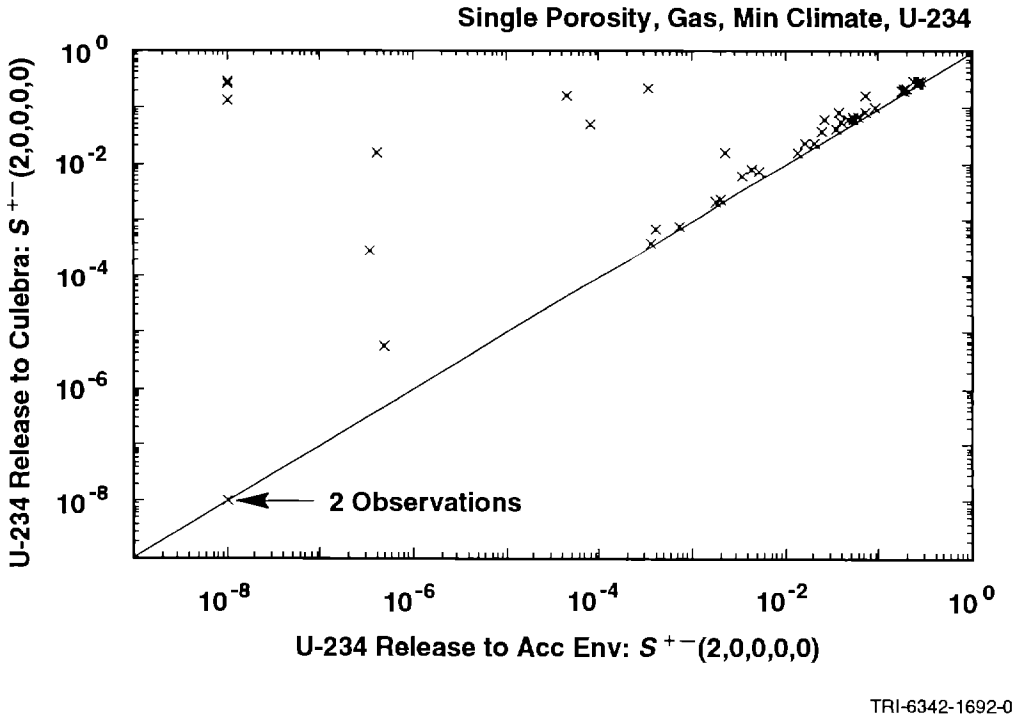

Figure 5.5-3. Scatterplot for Normalized U-234 Release to the Culebra Dolomite versus Normalized U-234 Release to the Accessible Environment Due to Groundwater Transport with Minimum (i.e., CULCLIM = 1) Climatic Variation for Scenario $S^{+-}(2,0,0,0,0)$ with Gas Generation in the Repository, a Single-Porosity Transport Model with Chemical Retardation in the Culebra and Intrusion Occurring at 1000 Yrs. For plotting purposes, values less than 10^{-8} are set to 10^{-8}.

CULCLIM in the scatterplot appearing in Figure 5.4-6 for the release of U-234 to the accessible environment with a dual-porosity transport model and no chemical retardation, where the relative effect of CULCLIM is actually greater than in the analyses presented in this section due to the absence of chemical retardation.

The CCDFs in Figure 5.5-4 are for dual-porosity transport in the Culebra. A similar figure could be generated for single-porosity transport. However, as shown in Figure 5.5-2, the release results for CULCLIM = 1 and CULCLIM = 1.16 are essentially identical when the single-porosity transport model is used, and so the resultant CCDFs would also be the same.

Present-Day Recharge (CULCLIM = 1)

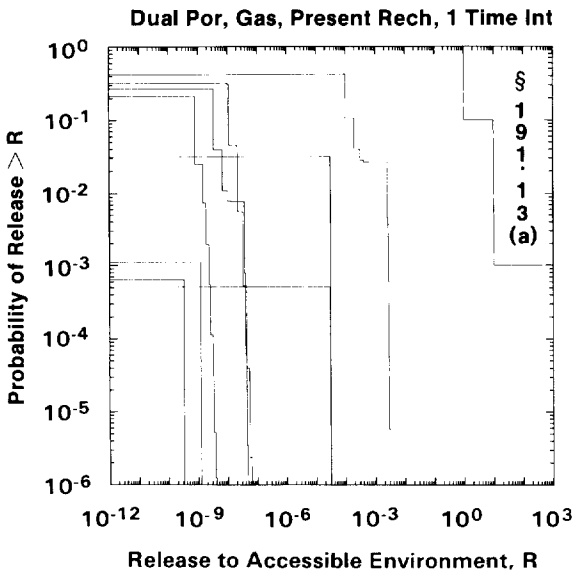

TRI-6342-1571-0

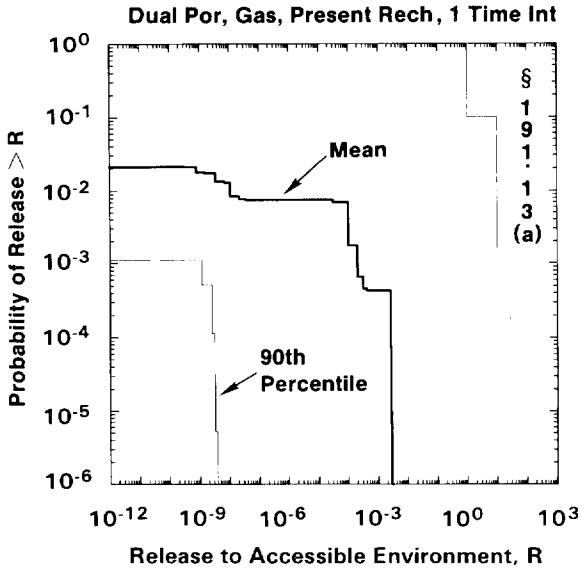

TRI-6342-1572-0

Maximum Recharge (CULCLIM = 1.16)

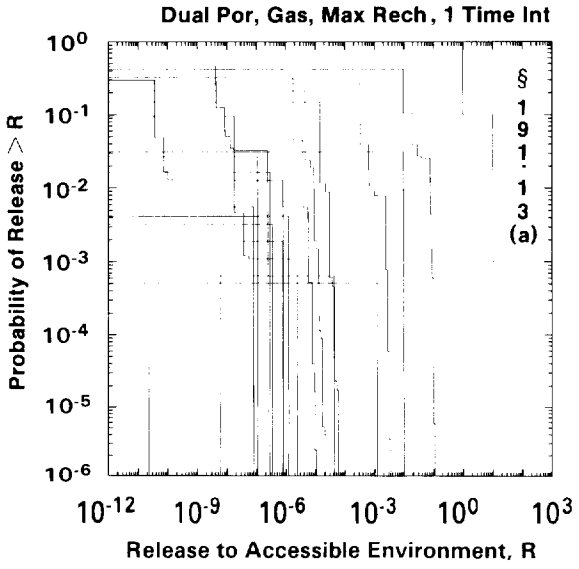

TRI-6342-1573-0

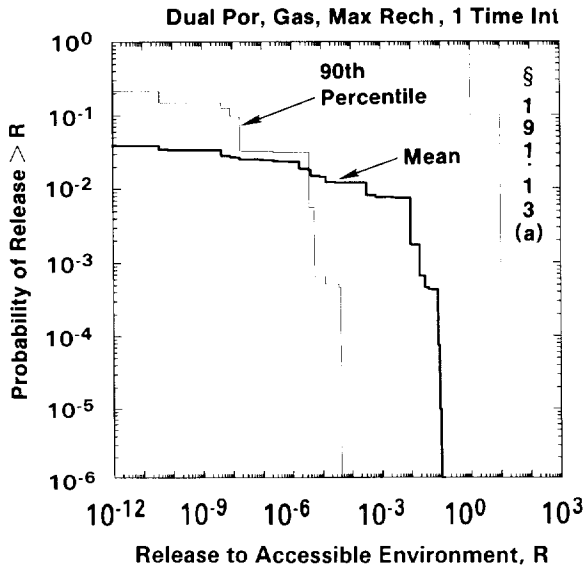

TRI-6342-1574-0

Figure 5.5-4. Comparison of Complementary Cumulative Distribution Functions for Normalized Release to the Accessible Environment with Present-Day Recharge (CULCLIM = 1) and Maximum Recharge (CULCLIM = 1.16) for Gas Generation in the Repository, a Dual-Porosity Transport Model in the Culebra Dolomite and the Rate Constant λ in the Poisson Model for Drilling Intrusions Equal to Zero After 2000 Yrs.

6. DISCUSSION

At present, the most appropriate conceptual model for use in performance assessment at the WIPP is believed to include gas generation due to corrosion and microbial action in the repository and a dual-porosity (matrix and fracture porosity) representation for solute transport in the Culebra Dolomite. Under these assumptions, CCDFs summarizing radionuclide releases to the accessible environment due to both cuttings removal and groundwater transport fall substantially below the release limits promulgated by the EPA. This is the case even when the current estimates of the uncertainty in analysis inputs are incorporated into the performance assessment. Although the results of this analysis offer encouragement with respect to the suitability of the WIPP as a disposal facility for transuranic waste, they should be regarded as preliminary (Table 11-1, Vol. 1).

The best-estimate performance-assessment results indicated in the preceding paragraph are dominated by cuttings removal. The releases to the accessible environment due to groundwater transport make very small contributions to the total release. The variability in the distribution of CCDFs that must be considered in comparisons with the EPA release limits is dominated by the variable LAMBDA (rate constant in Poisson model for drilling intrusions).

The variability in releases to the accessible environment due to individual drilling intrusions was controlled by DBDIAM (drill bit diameter), which was the only imprecisely known variable considered in the model for cuttings removal. If cuttings removal continues to dominate the CCDFs for releases to the accessible environment in future analyses, a more detailed analysis of the variables used in the modeling of cuttings removal should be performed.

Most of the imprecisely known variables considered in the 1991 WIPP performance assessment relate to radionuclide releases to the accessible environment due to groundwater transport. For a single borehole (i.e., an E2-type scenario), whether or not a release from the repository to the Culebra even occurs is controlled by the variable SALPERM (Salado permeability), with no releases for small values (i.e., $< 5 \times 10^{-21}$ m^2) of this variable. When SALPERM is small, the repository never fills with brine and so there is no flow up an intruding borehole that can transport radionuclides to the Culebra. Further, releases that do reach the Culebra for larger values of SALPERM are small and usually do not reach the accessible environment.

A potentially important scenario for the WIPP involves two or more boreholes through the same waste panel, of which at least one penetrates a pressurized brine pocket and at least one does not (i.e., an E1E2-type scenario). For

these scenarios, the uncertainty in release to the Culebra is dominated by the variables BHPERM (borehole permeability), BPPRES (brine pocket pressure), and the solubilities for the individual elements in the projected radionuclide inventory for the WIPP (i.e., Am, Np, Pu, Th, U). Once radionuclides are released to the Culebra, the matrix distribution coefficients for the individual elements are important, with releases to the Culebra often failing to reach the accessible environment over the 10,000-yr period specified in the EPA regulations. As an example, Pu-239 dominates the releases to the accessible environment due to cuttings removal, is an important contributor to the total release to the Culebra, and yet is rarely a significant contributor to the total release to the accessible environment due to groundwater transport as a result of the large distribution coefficients associated with plutonium (e.g., median values for fracture and matrix distribution coefficients are 2.02×10^{2} and 2.61×10^{-1} m^3/kg, respectively). In contrast, U-234 has relatively small distribution coefficient values (e.g., median values for fracture and matrix distribution coefficients for uranium are 7.5×10^{-3} and 2.58×10^{-2} m^3/kg, respectively) and usually dominates the releases to the accessible environment due to groundwater transport.

As indicated by the preceding discussion, a small subset of the 45 variables presented in Table 3-1 dominates the best-estimate results obtained in the 1991 WIPP performance assessment. The most important variable overall is LAMBDA (rate constant in Poisson model for drilling intrusions). As shown in Figure 4.6-1, LAMBDA completely dominates the uncertainty in the CCDFs that must be compared against the EPA release limits. The releases to the accessible environment due to groundwater transport are very small in the best-estimate analyses (i.e., gas generation in the repository and a dual-porosity transport model in the Culebra), with the result that the releases to the accessible environment are dominated by cuttings removal. Although the uncertainty in cuttings removal for individual boreholes is determined by DBDIAM (drill bit diameter) in the 1991 WIPP performance assessment, the variables that determine, or prevent, releases to the accessible environment due to groundwater transport are more important due to the larger quantities of radionuclides that have the potential to be released.

The following variables are important in determining radionuclide releases to the accessible environment due to groundwater transport: solubilities for the individual elements (i.e., SOLAM, SOLNP4, SOLNP5, SOLPU4, SOLPU5, SOLTH, SOLU4, SOLU6), borehole permeability (BHPERM), Salado permeability (SALPERM), and matrix distribution coefficients (i.e., MKDAM, MKDNP, MKDPU, MKDTH, MKDU). It is difficult to put an absolute ranking on the importance of these variables. For example, any one of the following three conditions is sufficient to effectively prevent radionuclide releases to the accessible environment due to groundwater transport: (1) low solubilities, (2) low

borehole permeability, and (3) high matrix distribution coefficients. Further, for intrusions involving a single borehole, low values for Salado permeability prevent releases to the Culebra and hence to the accessible environment. The uncertainty in the WIPP performance assessment results for groundwater transport to the accessible environment would be reduced by better characterizations of the possible values for these variables.

The solubilities and distribution coefficients for the individual elements are not equally important. Due to the large inventory and long half-life of Pu-239 (see Figure 2.4-2), the solubility and distribution coefficient for plutonium are important variables. A similar, but slightly less strong statement, can be made for americium because of the presence of Am-241 in the WIPP inventory. However, the properties of americium are less important than those of plutonium due to the relatively short half-life of Am-241 (i.e., 432 yrs) relative to the 10,000-yr period that must be considered in comparison with EPA release limits. The solubilities and distribution coefficients for neptunium and thorium are relatively unimportant due to the small amounts of Np-237 and Th-230 in the WIPP inventory (see Figure 2.4-2). Uranium presents an intermediate situation. The estimated inventory of U-234 in one waste panel is approximately 0.3 EPA units or, equivalently, 3 EPA units in the entire repository (see Figure 2.4-2). Relatively high solubilities and low distribution coefficients result in U-234 tending to dominate the releases to the accessible environment even though the inventory of Pu-239 in a single waste panel is much higher (i.e., approximately 70 EPA units). Due to large contributions of U-234 to the total normalized release to the accessible environment due to groundwater transport, improvements in the estimates for the solubility and distribution coefficient for uranium could reduce the uncertainty in the total releases due to groundwater transport. In summary and conditional on current estimates of the waste to be disposed of at the WIPP, the most important elements for the characterization of solubilities and distribution coefficients for comparisons with the EPA release limits are plutonium, uranium and americium.

After the preceding variables, the sensitivity analyses for groundwater transport with gas generation in the repository and a dual-porosity transport model in the Culebra identified several other variables that had lesser effects, including CULFRPOR (Culebra fracture porosity), CULFRSP (Culebra fracture spacing), CULCLIM (recharge amplitude factor for Culebra) and several variables related to gas generation. The variable BPPRES (brine pocket pressure) was also selected in analyses for E1E2-type scenarios. Increasing each of CULFRPOR, CULFRSP, CULCLIM and BPPRES tends to increase releases. Increasing gas generation tended to decrease releases, although none of the individual variables related to gas generation appeared to have a large effect. However, SALPERM (Salado permeability) acted as a switch for releases into the Culebra for a single borehole only in the presence of gas

generation. Increasing fracture distribution coefficients (i.e., FKDAM, FKDNP, FKDPU, FKDTH, FKDU) tended to decrease releases due to groundwater transport, although the effects of these distribution coefficients were generally smaller than the effects of the corresponding matrix distribution coefficients. Although solubilities were important, the use of solubilities defined on the basis of oxidation states for neptunium (i.e., SOLNP4 and SOLNP5), plutonium (i.e., SOLPU4 and SOLPU5) and uranium (i.e., SOLU4 and SOLU6) had little effect on the releases from the repository to the Culebra, with both oxidation states for each element producing overlapping releases.

Sensitivity analysis results depend on both the ranges assigned to variables and the impact that incremental changes in these variables have on the predicted variable of interest. As a result, variables with large ranges and/or large incremental effects can obscure the effects of other variables. In analyses such as those presented in this report, sensitivity analysis results are conditional on the characterizations of subjective uncertainty assigned to the input variables selected for consideration. In particular, as the knowledge base for individual variables is improved (i.e., as subjective uncertainty is reduced), these variables may cease to be important contributors to uncertainty in the outcome of a performance assessment and thus be superseded in importance by other previously less important variables. However, with the assumption that new sources of uncertainty are not identified, the overall uncertainty in the results of the analysis should decrease as the uncertainty in important variables is reduced.

Sensitivity analysis results only measure the effects of the sampled variables and thus are conditional on the conceptual models analyzed and on the numerical representations employed for these conceptual models. Therefore, the following variants of the 1991 WIPP performance assessment have also been considered to provide additional perspective on the impact of subjective uncertainty: (1) no gas generation in the repository and a dual-porosity transport model in the Culebra, (2) gas generation in the repository and a single-porosity (fracture porosity) transport model in the Culebra, (3) no gas generation in the repository and a single-porosity transport model in the Culebra, (4) gas generation in the repository and a dual-porosity transport model in the Culebra without chemical retardation, and (5) gas generation in the repository, a dual-porosity transport model in the Culebra, and extremes of climatic variation. All of these variations relate to groundwater transport and thus do not affect releases due to cuttings removal, which were found to dominate the results of the 1991 WIPP performance assessment. However, these variations do have the potential to increase the importance of releases due to groundwater transport relative to releases due to cuttings removal. Further, these variations remove the effects of some of the dominant variables identified in the sensitivity analyses for gas generation in the repository and a dual-porosity transport

model in the Culebra, and thus provide an opportunity to observe the impact of additional variables listed in Table 3-1.

The presence of gas generation was found to reduce releases to the Culebra for an E2-type scenario. When gas generation is present, the variable SALPERM (Salado permeability) acts as a switch that determines whether or not a release to the Culebra will occur. The role of SALPERM as a switch goes away when gas generation is not considered. In this case, the repository is generally brine saturated by the time the first drilling intrusion occurs (i.e., at 1000 yrs in the 1991 WIPP performance assessment) and release to the Culebra is dominated by the solubilities for the individual elements (i.e., Am, Np, Pu, Th, U), with a lesser effect due to SALPERM as a result of its influence on the amount of fluid flowing up the borehole. Sample elements that result in zero releases to the Culebra with gas generation in the repository result in nonzero releases without gas generation. Further, nonzero releases in the presence of gas generation in the repository tend to be larger in the absence of gas generation. The absence of gas generation also results in larger releases to the Culebra for E1E2-type scenarios. Since the absence of gas generation can result in larger releases to the Culebra, it can also lead to larger releases to the accessible environment due to groundwater transport. However, when the dual-porosity transport model is used, many releases to the accessible environment are zero and even the nonzero releases tend to be small (usually substantially less than 0.1). As a result, total releases to the accessible environment due to cuttings removal and groundwater transport are also dominated by cuttings removal when no gas generation in the repository and a dual-porosity transport model in the Culebra are assumed.

The use of a single-porosity rather than a dual-porosity transport model in the Culebra was found to result in substantially larger releases to the accessible environment due to groundwater transport. Specifically, normalized releases are often several orders of magnitude higher when a single-porosity transport model is used, and many zero releases with the dual-porosity transport model are nonzero with the single-porosity transport model. However, despite these increases in groundwater releases, the CCDFs for total releases to the accessible environment constructed with results obtained for gas generation in the repository and a single-porosity transport model in the Culebra are below the EPA release limits, although they are considerably above the corresponding CCDFs constructed with dual-porosity results. Unlike results obtained with the dual-porosity transport model, many of the groundwater releases to the accessible environment obtained with the single-porosity transport model are larger than the corresponding cuttings releases. For comparison, the mean CCDFs for cuttings removal, groundwater transport with a dual-porosity transport model, and groundwater transport with a single-porosity transport model are shown in Figure 6-1.

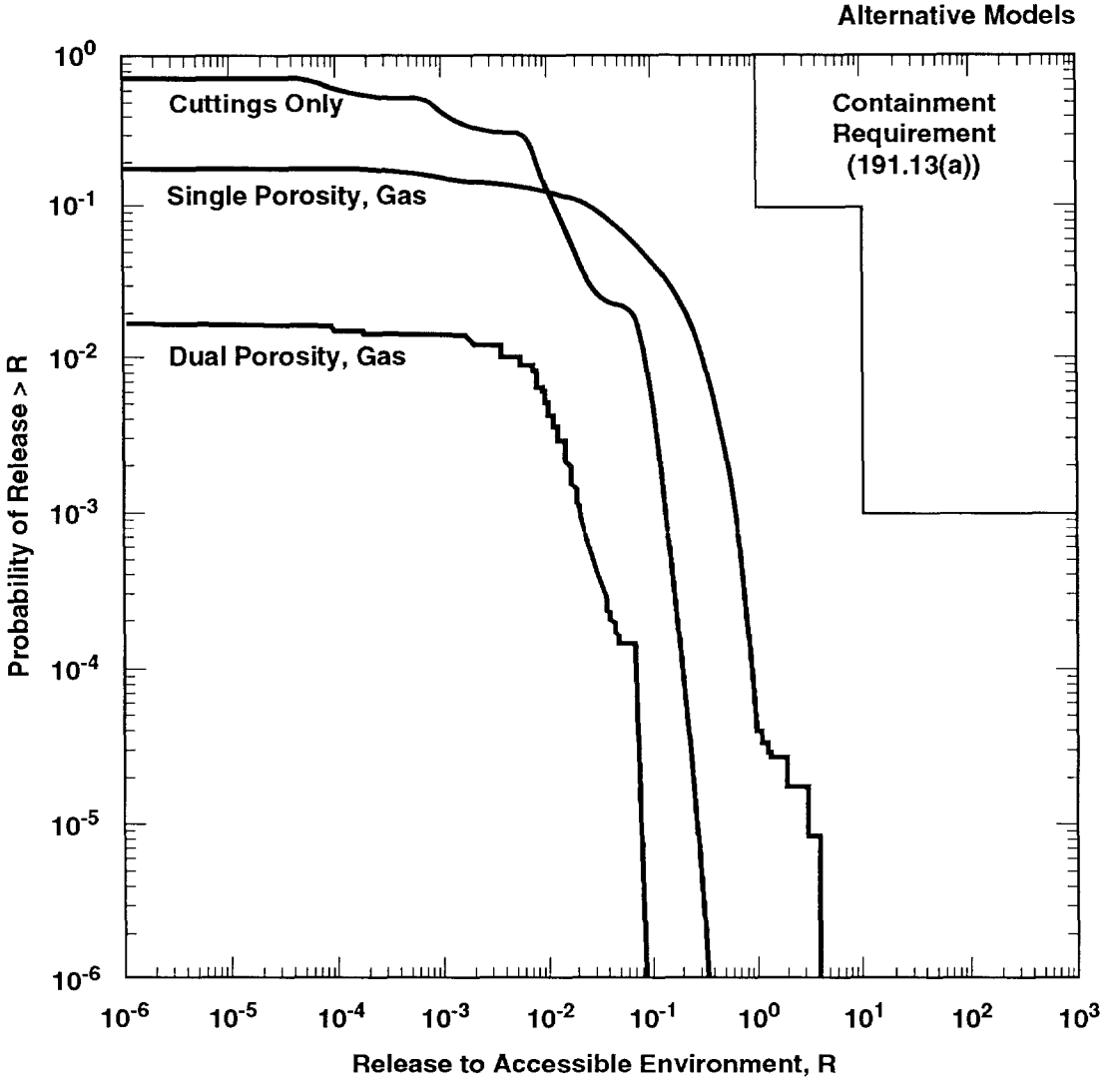

Figure 6-1. Mean Complementary Cumulative Distribution Functions for Normalized Releases to the Accessible Environment for Cuttings Removal, Groundwater Transport with Gas Generation in the Repository and a Dual-Porosity Transport Model in the Culebra Dolomite, and Groundwater Transport with Gas Generation in the Repository and a Single-Porosity Transport Model in the Culebra Dolomite. The distributions of CCDFs on which the mean CCDFs in this figure are based appear in Figures 4.1-2 and 5.2-1.

As already discussed, the absence of gas generation in the repository results in larger releases to the Culebra than the presence of gas generation, and the use of a single-porosity transport model in the Culebra results in larger releases to the accessible environment than the use of a dual-porosity model. Thus, rather unsurprisingly, even larger groundwater-transport releases result for no gas generation in the repository and a single-porosity transport model in the Culebra. The analyses for no gas generation in the repository and a single-porosity transport model in the Culebra were performed for intrusions occurring only at 1000 yrs. Thus, it is not possible to construct the CCDFs used for comparison with the EPA release limits that include intrusions occurring after 1000 yrs. However, given the releases observed for intrusions at 1000 yrs, some of the resultant CCDFs would probably intersect the EPA release limits, although the bulk of the CCDF distribution would be below these limits.

At present, no experimental data are available for the Culebra Dolomite that can be used to estimate radionuclide retardation during transport by flowing groundwater. As a result, there is significant uncertainty in what the appropriate values should be for these quantities. The 1991 WIPP performance assessment considered a range of elemental distribution coefficients developed through an internal review process at SNL (Section 2.3.4, Vol. 3), which in turn lead to retardations for use within the transport calculations. To help provide perspective on the importance of chemical retardation, dual-porosity transport calculations without chemical retardation were performed for the Culebra for intrusions occurring at 1000 yrs and releases into the Culebra predicted with gas generation in the repository. As should be the case, these calculationd lead to larger releases to the accessible environment than were obtained with chemical retardation. However, these releases are still small, with few releases exceeding 0.1 EPA release units and most releases much smaller. The releases predicted for no gas generation in the repository and a single-porosity transport model with chemical retardation in the Culebra are generally larger than the releases predicted for gas generation in the repository and a dual-porosity transport model without chemical retardation in the Culebra. The analyses for gas generation in the repository and a dual-porosity transport model without chemical retardation in the Culebra were performed only for intrusions occurring at 1000 yrs. Thus, with the available results, it is not possible to construct CCDFs for comparison with the EPA release limits that include intrusions occurring after 1000 yrs. However, given the releases observed for intrusions at 1000 yrs, few if any of these CCDFs would intersect the EPA release limits and most of the CCDFs would be considerably below the EPA limits.

Summaries of the releases to the accessible environment obtained under different modeling assumptions are provided in Figures 6-2 and 6-3 for

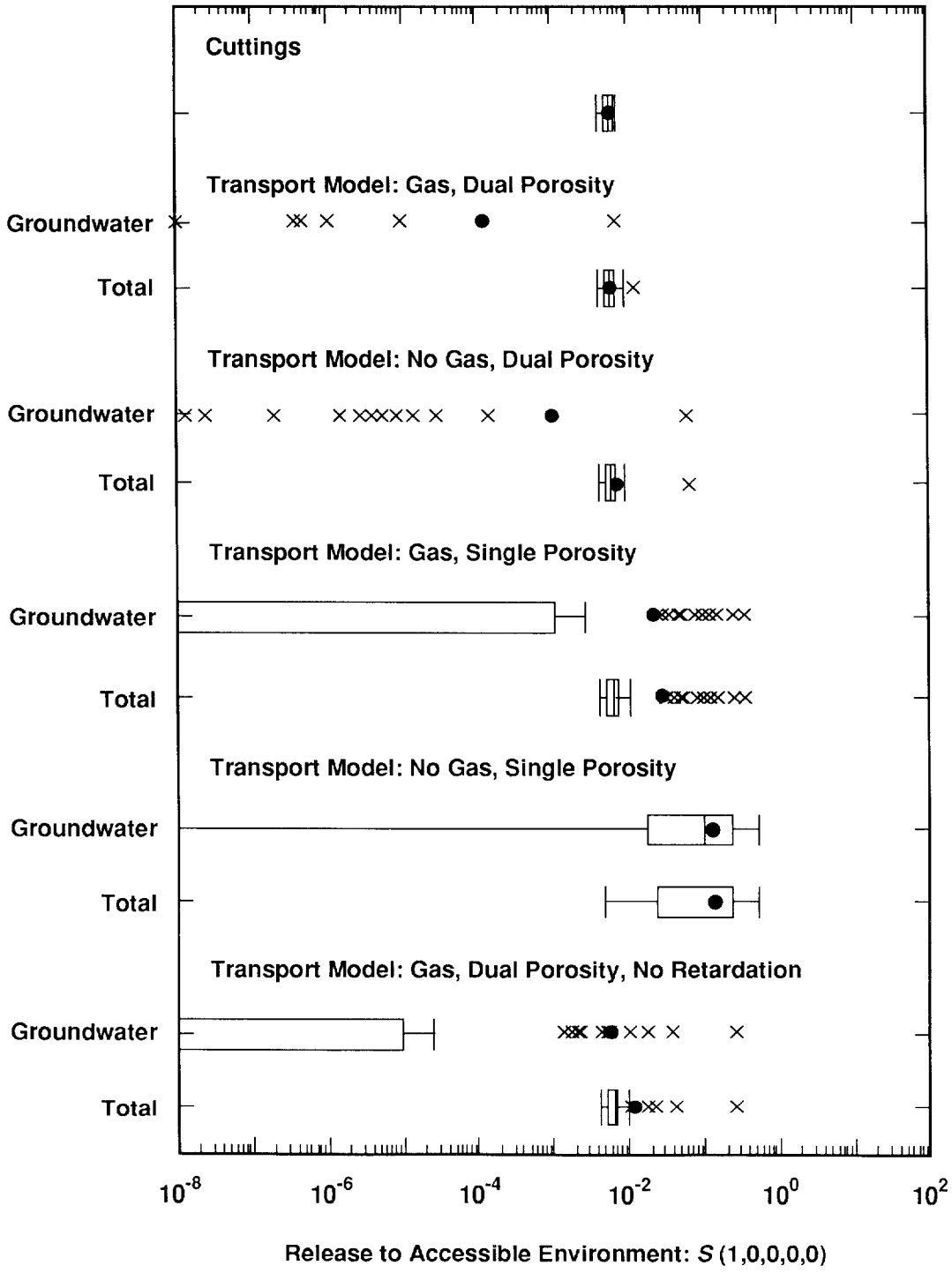

Figure 6-2. Summary of Normalized Releases to the Accessible Environment for E2-type Scenarios with Intrusion Occurring at 1000 Yrs (i.e., for scenario S(1,0,0,0,0)).

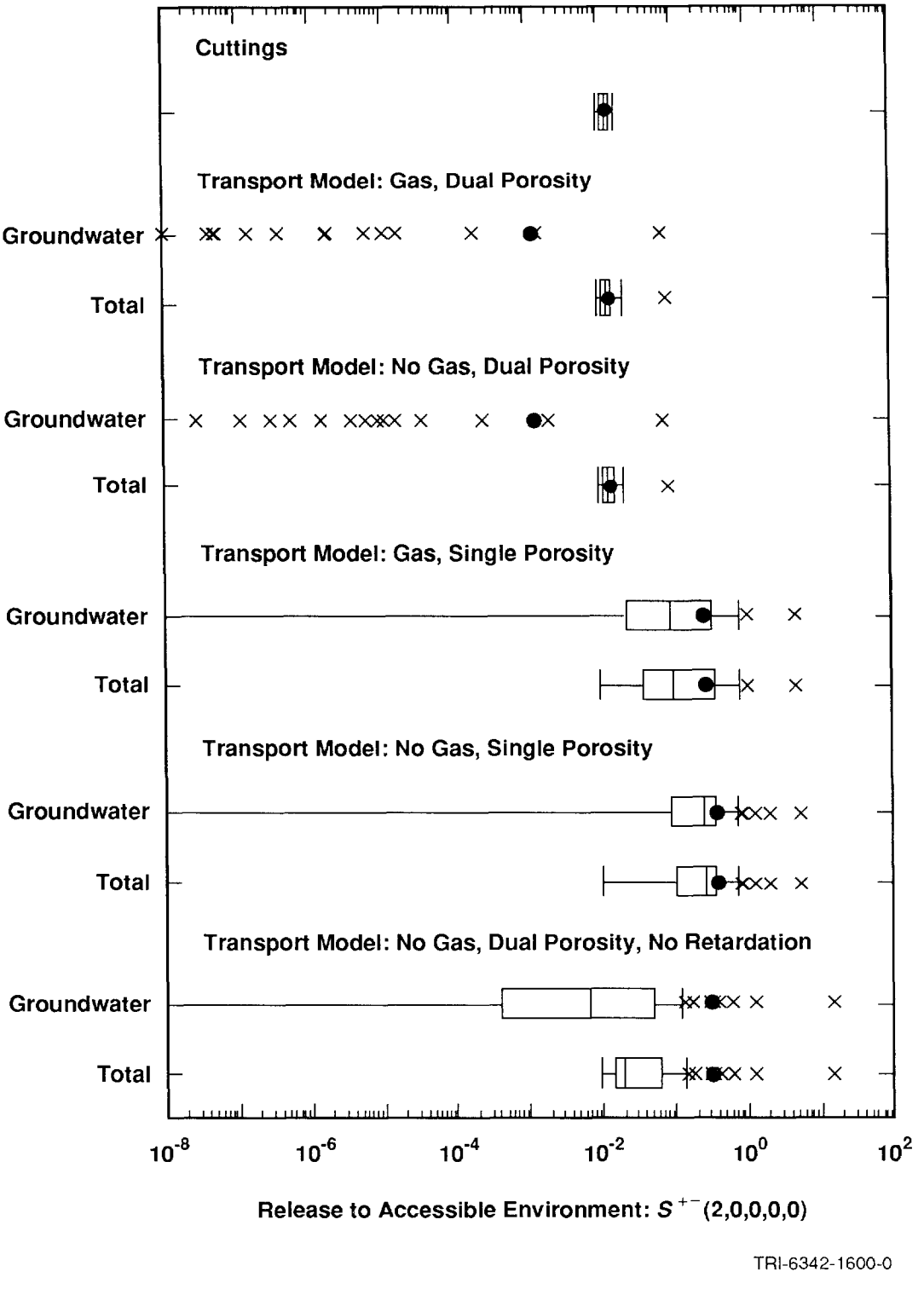

Figure 6-3. Summary of Normalized Releases to the Accessible Environment for E1E2-type Scenarios with Intrusion Occurring at 1000 Yrs (i.e., for scenario $S^{+-}(2,0,0,0,0)$).

E2- and E1E2-type scenarios, respectively, for intrusions occurring at 1000 yrs (i.e., for scenarios $S(1,0,0,0,0)$ and $S^{+-}(2,0,0,0,0)$ in the more explicit notation used in the body of the report). As examination of these figures shows, dual-porosity transport in conjunction with chemical retardation results in releases to the accessible environment that are completely dominated by cuttings removal. Even when dual-porosity transport in conjunction with no chemical retardation is assumed, the median release due to cuttings removal is larger than the median release due to groundwater transport. In contrast, the releases to the accessible environment for single-porosity transport are often larger than the corresponding releases due to cuttings removal.

Mean CCDFs for releases to the accessible environment due to groundwater transport are shown in Figure 6-4 for the various alternative conceptual models considered in the 1991 WIPP performance assessment. For several of the alternative conceptual models, calculations were performed only for intrusions occurring at 1000 yrs. As a result, the CCDFs in Figure 6-4 were constructed with the assumption that the rate constant in the Poisson model for drilling intrusions (i.e., LAMBDA) is equal to zero after 2000 yrs. This assumption is consistent with recommendations made in an expert review of future human intrusions at the WIPP (Hora et al., 1991). As examination of Figure 6-4 shows, all of the alternative conceptual models result in mean CCDFs for release to the accessible environment that are below the EPA release limits, although there is considerable variation in the location of the individual CCDFs.

The final variant on the best-estimate analysis for the 1991 WIPP performance assessment was the consideration of two extremes of climatic variation, with one extreme resulting in boundary heads in the Culebra remaining constant at present-day values (e.g., 880 m) and the other extreme resulting in time-dependent fluctuations in heads along a recharge strip at the northern boundary of the model domain that ranged from present-day values to a maximum value corresponding to the surrounding land surface (e.g., 1030 m). As shown in Figures 6-5 and 6-6, these variations were found to have limited effect on the releases to the accessible environment due to groundwater transport with either a dual-porosity or a single-porosity transport model in the Culebra. However, additional investigations of the effects of uncertainty and variability in future climatic conditions will be performed as alternative conceptual models for regional groundwater recharge and flow are examined (e.g., Beauheim and Holt, 1990). Although climatic fluctuations have little impact on releases calculated using the current conceptual model for recharge, results presented in this report should not be extrapolated to other models for the location and amount of recharge to the Culebra.

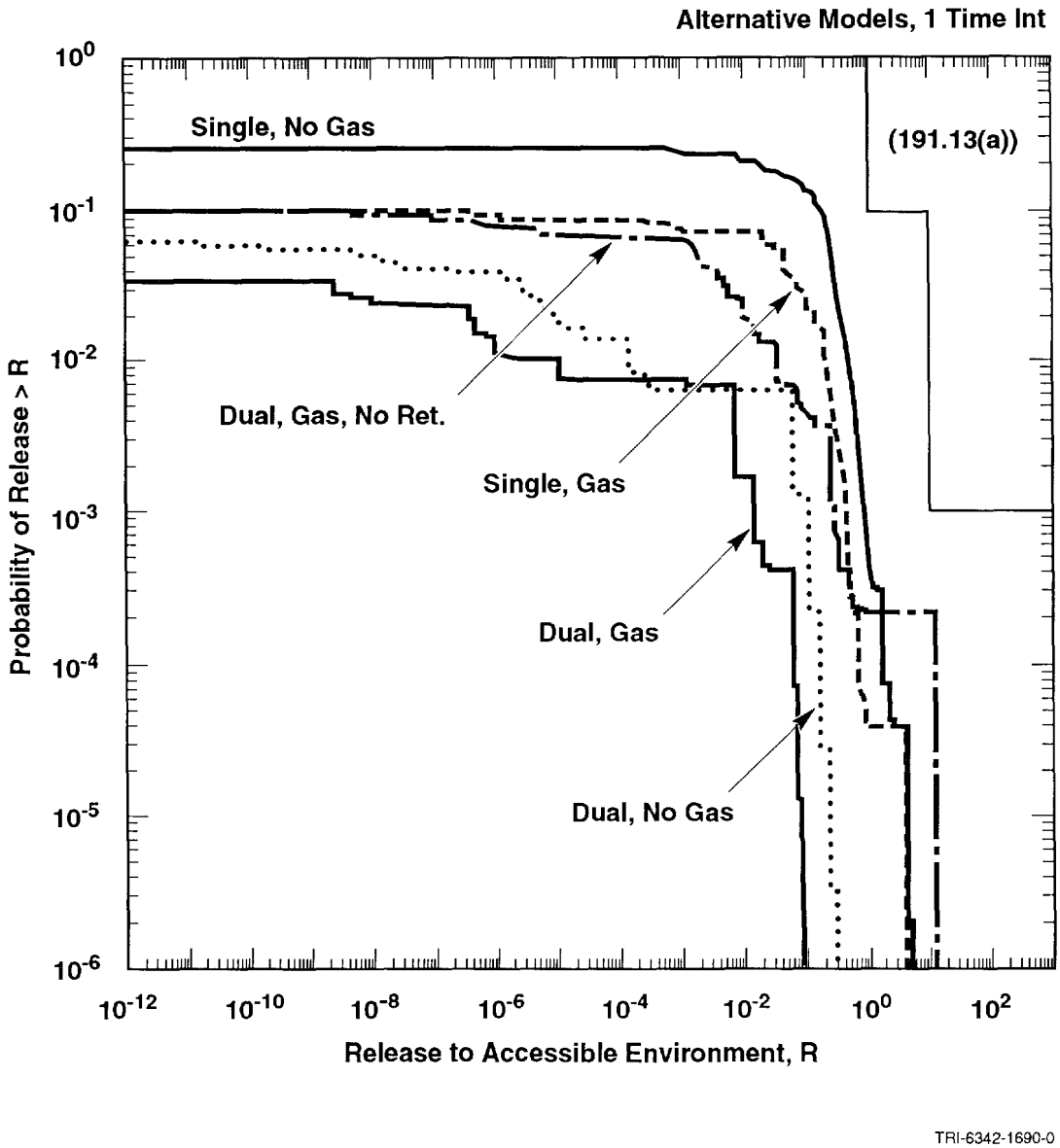

Figure 6-4. Mean Complementary Cumulative Distribution Functions for Normalized Releases to the Accessible Environment Due to Groundwater Transport Obtained with Alternative Conceptual Models and the Rate Constant λ in the Poisson Model for Drilling Intrusions Set to Zero After 2000 Yrs. The distributions of CCDFs on which the mean CCDFs in this figure are based appear in Figures 5.1-4, 5.3-3 and 5.4-4.

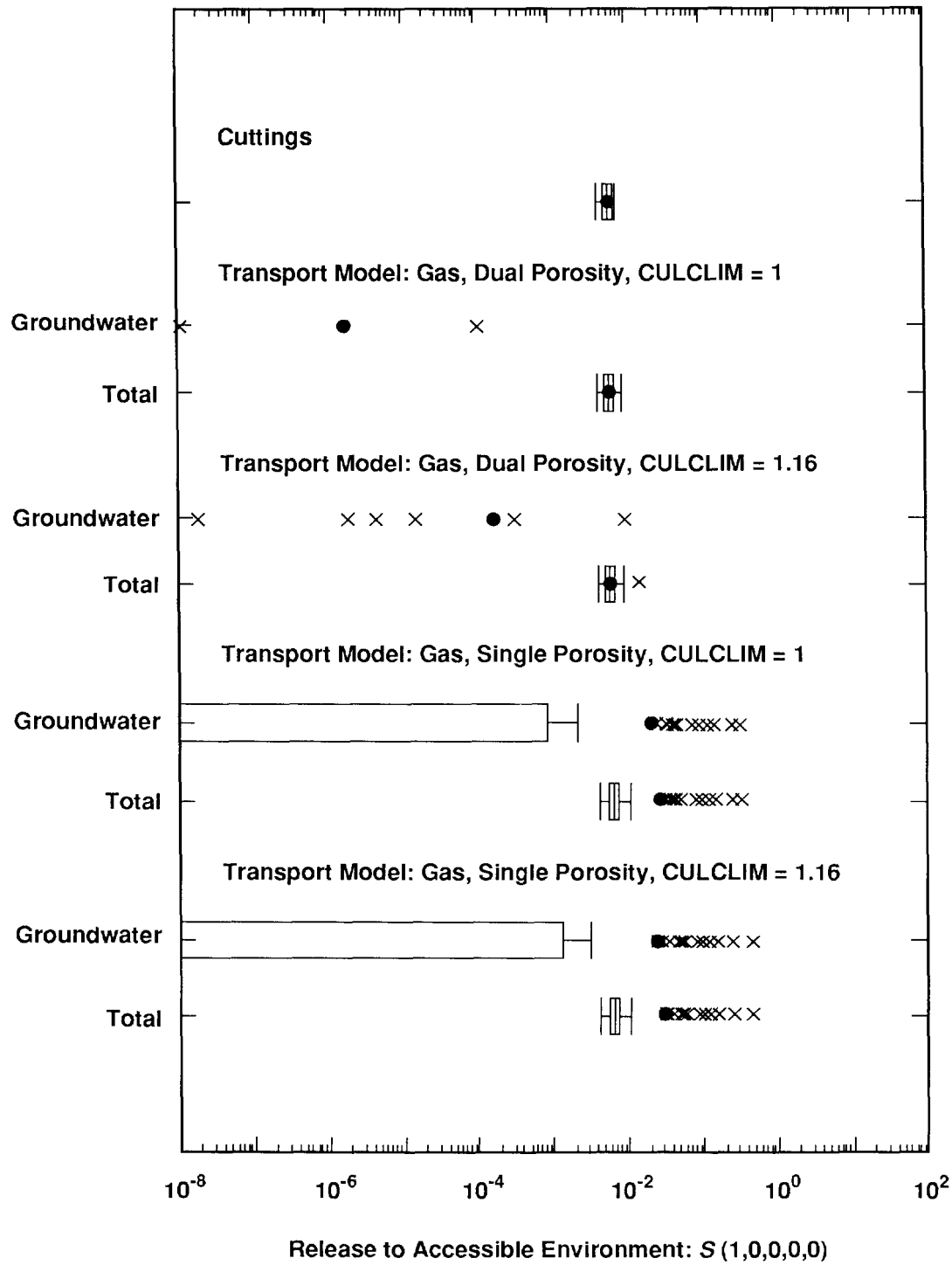

Figure 6-5. Summary of Normalized Releases to the Accessible Environment for Present-Day Recharge (CULCLIM = 1) and Maximum Recharge (CULCLIM = 1.16) of the Culebra Dolomite for E2-type Scenarios with Intrusion Occurring at 1000 Yrs (i.e., for scenario $S(1,0,0,0,0)$).

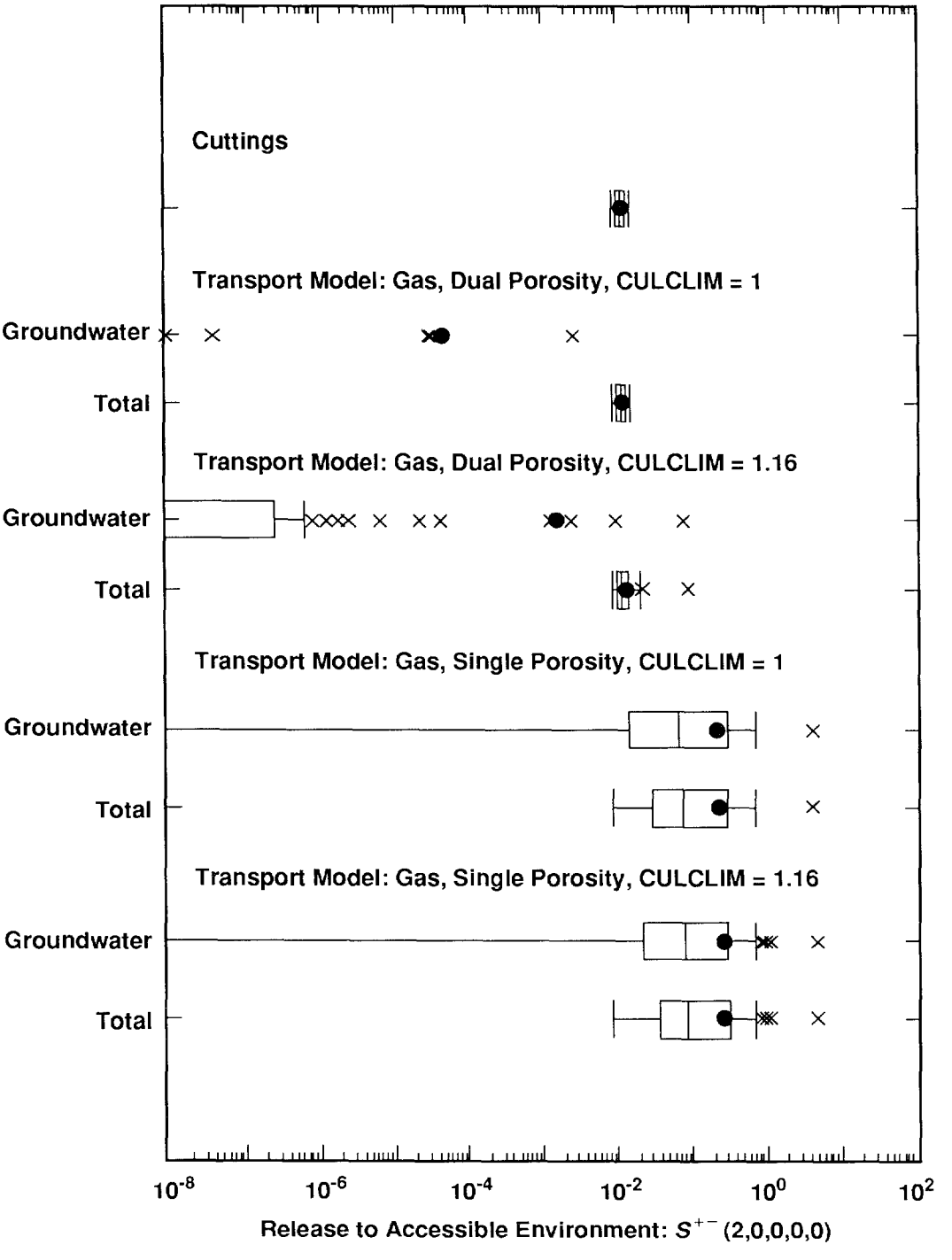

TRI-6342-1602-0

Figure 6-6. Summary of Normalized Releases to the Accessible Environment for Present-Day Recharge (CULCLIM = 1) and Maximum Recharge (CULCLIM = 1.16) of the Culebra Dolomite for E1E2-type Scenarios with Intrusion Occurring at 1000 Yrs (i.e., for scenario S^{+-}(2,0,0,0,0)).

A summary of the relative importance of the 45 imprecisely known variables considered in the 1991 WIPP performance assessment (i.e., the variables listed in Table 3-1) is presented in Table 6-1. As previously discussed, the importance of individual variables is conditional on both the conceptual model in use and the assessed uncertainty in the other variables under consideration. The summary in Table 6-1 is based on results obtained in the analyses for the alternative conceptual models, with special emphasis being placed on the results obtained in the best-estimate analysis (i.e., gas generation in the repository and a dual-porosity transport model in the Culebra). Although this report contains many formal sensitivity analyses, the summary results presented in Table 6-1 are not taken directly from specific analyses but rather are based on an overall impression of the results obtained in many individual sensitivity analyses. Alterations in the ordering of variable importance given in Table 6-1 are possible as variables are added or deleted from consideration, the assessed uncertainty in individual variables is changed, and the conceptual model in use is refined. Further, the selection of a specific conceptual model and its associated numerical implementation for use in the WIPP performance assessment could alter the relative importance of individual variables indicated in Table 6-1. To date the uncertainty associated with plausible alternative conceptual models has not been incorporated into a representation for the overall uncertainty in WIPP performance-assessment results.

Annual performance assessments, including uncertainty and sensitivity analysis, are performed for the WIPP to provide perspective on compliance with the EPA regulations and guidance for additional research to support a final decision on the acceptability or unacceptability of the WIPP as a disposal facility for transuranic waste. The following insights have emerged from these analyses and are providing guidance to current research efforts:

(1) The rate constant in the Poisson model for drilling intrusions (LAMBDA) is a, if not the, dominant determinant of the CCDFs used for comparison with the EPA release limits. An expert review process is being used to develop a better understanding of this important parameter (Hora et al., 1991; Vol. 1, Section 4.3).

(2) Given that a drilling intrusion has occurred, the interplay between Salado permeability and gas generation is an important determinant of both whether or not a release to the Culebra occurs and the size of such a release should it occur. Research programs are underway to study both Salado permeability (Saulnier, 1988 and 1991; Wawersik and Beauheim, 1991) and gas generation in the repository (Brush, 1990).

TABLE 6-1. SUMMARY OF VARIABLE IMPORTANCE IN THE 1991 WIPP PERFORMANCE ASSESSMENT. The summary presented in this table is based on results obtained in the sensitivity analyses associated with the alternative conceptual models, with special emphasis being placed on results obtained in the best-estimate analysis (i.e., gas generation in the repository and a dual-porosity transport model in the Culebra Dolomite), and is conditional on these conceptual models, the numerical implementation of these conceptual models in the WIPP performance assessment, the assessed subjective uncertainty in the 45 variables listed in Table 3-1 and the fixed values used for other variables required in the performance assessment.

IMPORTANT
Borehole permeability (BHPERM)
Culebra fracture porosity (CULFRPOR)
Culebra fracture spacing (CULFRSP)
Drill bit diameter (DBDIAM)
Fracture distribution coefficients (FKDAM, FKDNP, FDKPU, FDKTH, FKDU, with plutonium, americium and uranium being the most important elements)
Matrix distribution coefficients for individual elements (MKDAM, MKDNP, MKDPU, MKDTH, MKDU)
Rate constant in Poisson model for drilling intrusions (LAMBDA)
Salado permeability (SALPERM)
Solubilities for individual elements (SOLAM, SOLNP4, SOLNP5, SOLPU4, SOLPU5, SOLTH, SOLU4, SOLU6)
SMALL EFFECTS OBSERVED
Brine pocket pressure (BPPRES)
Brine pocket storativity (BPSTOR)
Culebra dispersivity (CULDISP)
Culebra porosity (CULPOR)
Culebra transmissivity field (CULTRFLD)
Gas Generation rate for corrosion of steel under inundated conditions (GRCORI). The individual variables related to gas generation (GRCORH, GRCORI, GRMICH, GRMICI, STOICCOR, STOICMIC, VMETAL, VWOOD) had limited identifiable impacts on analysis results. However, the presence or absence of gas generation had an important effect on radionuclide release to the Culebra and on the effect that Salado permeability has on this release.

TABLE 6-1. SUMMARY OF VARIABLE IMPORTANCE IN THE 1991 WIPP PERFORMANCE ASSESSMENT. The summary presented in this table is based on results obtained in the sensitivity analyses associated with the alternative conceptual models, with special emphasis being placed on results obtained in the best-estimate analysis (i.e., gas generation in the repository and a dual-porosity transport model in the Culebra Dolomite), and is conditional on these conceptual models, the numerical implementation of these conceptual models in the WIPP performance assessment, the assessed subjective uncertainty in the 45 variables listed in Table 3-1 and the fixed values used for other variables required in the performance assessment. (concluded)

SMALL EFFECTS OBSERVED (continued)
Index variable used to select relative areas of the stability regimes for different oxidation states of neptunium, plutonium and uranium (EHPH)
Marker Bed 139 permeability (MBPERM, 0.8 rank correlation with Salado permeability)
Recharge amplitude factor for Culebra (CULCLIM)
Salado pressure (SALPRES)
LIMITED OR NO EFFECTS OBSERVED
Fraction of total waste volume that is occupied by IDB (Integrated Data Base) metals and glass waste category (VMETAL)
Fraction of total waste volume that is occupied by IDB combustible waste category (VWOOD)
Fraction of waste panel area underlain by a pressurized brine pocket (BPAREAFR, effect overwhelmed by uncertainty in rate constant in Poisson model for drilling intrusions)
Gas generation rate due to microbial degradation of cellulosics under humid conditions (GRMICH)
Gas generation rate due to microbial degradation of cellulosics under inundated conditions (GRMICI)
Gas generation rate for corrosion of steel under humid conditions (GRCORH)
Initial fluid (brine) saturation of waste (BRSAT)
Marker Bed 139 porosity (MBPOR)
Stoichiometric coefficient for corrosion of steel (STOICCOR)
Stoichiometric coefficient for microbial degradation of cellulosics (STOICMIC)
Threshold displacement pressure in Marker Bed 139 (MBTHPRES)

(3) Elemental solubilities are important determinants of the amounts of radionuclides that can be transported from the repository to the Culebra by brine flowing up an intruding borehole. An experimental program is underway to determine the chemical conditions that could exist in the repository (Brush, 1990) and the solubilities that would exist under such conditions (Brush, 1990; Phillips and Molecke, in review).

(4) Distribution coefficients are important determinants of radionuclide transport in the Culebra. Laboratory experiments with cores removed from the Culebra Dolomite are currently underway to provide estimates of both physical and chemical retardation (Gelbard and Novak, 1992).

(5) The use of a single- or dual-porosity transport model has significant impact on predicted radionuclide transport in the Culebra. Existing information, INTRAVAL evaluations and additional experiments are being utilized to assess the appropriateness of these two models.

(6) In the absence of chemical retardation, the flow patterns in the Culebra can have a significant impact on radionuclide transport to the accessible environment. An extensive effort is underway to estimate the range of transmissivity fields for the Culebra that is consistent with available field data (Vol. 2, Section 6.2).

The following possibilities for additional investigation also arise from the uncertainty and sensitivity analyses performed in support of the 1991 WIPP performance assessment, although they are not being pursued at present:

(1) Cuttings removal is important in the 1991 WIPP performance assessment. The releases associated with drilling intrusions may be increased by processes involving spalling into the borehole. Due to the indicated importance of cuttings removal, processes that could affect these releases need to be considered.

(2) The variable BHPERM (borehole permeability) has a significant impact on the amount of brine that can flow up an intruding borehole and hence on resultant radionuclide releases to the Culebra. Additional investigation of this variable may be appropriate, although difficult due to the dependence of BHPERM on future drilling practices.

(3) The possible existence of pressurized brine pockets in the Castile Formation below the WIPP leads to the scenarios in the current

WIPP performance assessment with the largest releases to the accessible environment. Realistic representation of the extent to which such pockets exist beneath the repository would improve WIPP performance-assessment results.

Now that the 1991 WIPP performance assessment, together with associated uncertainty and sensitivity analyses, has been completed, the following possible improvements to the 1992 performance assessment can be identified:

(1) Use of more resolution in the time at which drilling intrusions occur; in particular, consideration of drilling intrusions at times earlier than 1000 yrs to better incorporate the effects of radioactive decay.

(2) Use of more activity levels in the waste for cuttings removal, possibly in conjunction with a refined activity distribution that takes into account random mixing of waste in the loading of the repository.

(3) Use of separate calculations to determine releases into the Culebra for single boreholes that penetrate pressurized brine pockets (i.e., E1-type scenarios) and single boreholes that do not penetrate pressurized brine pockets (i.e., E2-type scenarios). In the 1991 WIPP performance assessment, these releases were assumed to be the same but this may not be the case in the presence of gas generation in the repository.

(4) Evaluation of direct releases to the surface environment due to brine flow for scenarios that involve penetration of a pressurized brine pocket.

(5) Improved estimation of probabilities for E1E2-type scenarios. At present, these scenarios involve a very specific combination of plug failures in boreholes that is not taken into account in the calculation of their probabilities.

REFERENCES

Beauheim, R. L., and R. M. Holt, 1990. "Hydrogeology of the WIPP Site," in *Geological and Hydrological Studies of Evaporites in the Northern Delaware Basin for the Waste Isolation Pilot Plant (WIPP), New Mexico. Geological Society of America 1990 Annual Meeting Field Trip #14 Guidebook.* Dallas, TX: The Dallas Geological Society. 131-180.

Bertram-Howery, S. G., M. G. Marietta, R. P. Rechard, P. N. Swift, D. R. Anderson, B. L. Baker, J. E. Bean, Jr., W. Beyeler, K. F. Brinster, R. V. Guzowski, J. C. Helton, R. D. McCurley, D. K. Rudeen, J. D. Schreiber, and P. Vaughn. 1990. *Preliminary Comparison with 40 CFR Part 191, Subpart B for the Waste Isolation Pilot Plant, December 1990.* SAND90-2347. Albuquerque, NM: Sandia National Laboratories.

Brush, L. H., 1990. *Test Plan for Laboratory and Modeling Studies of Repository and Radionuclide Chemistry for the Waste Isolation Pilot Plant.* SAND90-0266. Albuquerque, NM: Sandia National Laboratories.

Cranwell, R. M., R. V. Guzowski, J. E. Campbell, and N. R. Ortiz. 1990. *Risk Methodology for Geologic Disposal of Radioactive Waste: Scenario Selection Procedure.* NUREG/CR-1667, SAND80-1429. Albuquerque, NM: Sandia National Laboratories.

Freeze, R. A., and J. A. Cherry. 1979. *Groundwater.* New Jersey: Prentice-Hall, Inc.

Gelbard, F., and C. F. Novak. 1992. "Program Plan to Determine Radionuclide Retardation for the WIPP Site." Copy on file at Waste Management Transportation Library. Albuquerque, NM: Sandia National Laboratories.

Helton, J. C., J. W. Garner, R. D. McCurley, and D. K. Rudeen. 1991. *Sensitivity Analysis Techniques and Results for Performance Assessment at the Waste Isolation Pilot Plant.* SAND90-7103. Albuquerque, NM: Sandia National Laboratories.

Hora, S. C., D. von Winterfeldt, and K. M. Trauth. 1991. *Expert Judgement on Inadvertent Human Intrusion into the Waste Isolation Pilot Plant.* SAND90-3063. Albuquerque, NM: Sandia National Laboratories.

Huyakorn, P. S., H. O. White, Jr., and S. Panday. 1989. *STAFF2D Solute Transport and Fracture Flow in Two Dimensions.* Herndon, VA: Hydrogeologic, Inc.

IAEA (International Atomic Energy Agency). 1989. *Evaluating the Reliability of Predictions Made Using Environmental Transfer Models.* Safety Series Report No. 100. Vienna: International Atomic Energy Agency.

Iman, R. L., and W. J. Conover. 1979. "The Use of the Rank Transform in Regression." *Technometrics* 21: 499-509.

Iman, R. L., and W. J. Conover. 1982. "A Distribution-Free Approach to Inducing Rank Correlation Among Input Variables." *Communications in Statistics,* vol. B11, no. 3: 311-334.

Iman, R. L., and M. J. Shortencarier. 1984. ***A FORTRAN 77 Program and User's Guide for the Generation of Latin Hypercube and Random Samples for Use with Computer Models.*** NUREG/CR-3624, SAND83-2365. Albuquerque, NM: Sandia National Laboratories.

Iman, R. L., J. M. Davenport, E. L. Frost, and M. J. Shortencarier. 1980. ***Stepwise Regression with PRESS and Rank Regression (Program User's Guide).*** SAND79-1472. Albuquerque, NM: Sandia National Laboratories.

Iman, R. L., M. J. Shortencarier, and J. D. Johnson. 1985. ***A FORTRAN 77 Program and User's Guide for the Calculation of Partial Correlation and Standardized Regression Coefficients.*** NUREG/CR-4122, SAND85-0044. Albuquerque, NM: Sandia National Laboratories.

Kaplan, S., and B. J. Garrick. 1981. "On the Quantitative Definition of Risk." ***Risk Analysis*** 1: 11-27.

Kelly, V. A., and G. J. Saulnier, Jr. 1990. ***Core Analysis From the Culebra Dolomite at the Waste Isolation Pilot Plant.*** SAND90-7011. Albuquerque, NM: Sandia National Laboratories.

Lappin, A. R., R. L. Hunter, D. P. Garber, P. B. Davies, R. L. Beauheim, D. J. Borns, L. H. Brush, B. M. Butcher, T. Cauffman, M. S. Y. Chu, L. S. Gomez, R. V. Guzowski, H. J. Iuzzolino, V. Kelley, S. J. Lambert, M. G. Marietta, J. W. Mercer, E. J. Nowak, J. Pickens, R. P. Rechard, M. Reeves, K. L. Robinson, and M. D. Siegel. 1989. ***Systems Analysis, Long-Term Radionuclide Transport, and Dose Assessments, Waste Isolation Pilot Plant (WIPP), Southeastern New Mexico; March 1989.*** SAND89-0462. Albuquerque, NM: Sandia National Laboratories.

McKay, M. D., W. J. Conover, and R. J. Beckman. 1979. "A Comparison of Three Methods for Selecting Values of Input Variables in the Analysis of Output From a Computer Code." ***Technometrics*** vol. 21, no. 2: 239-245.

Parry, G. W. 1988. "On the Meaning of Probability in Probabilistic Safety Assessment." ***Reliability Engineering and System Safety*** **23**: 309-314.

Paté-Cornell, M. E. 1986. "Probability and Uncertainty in Nuclear Safety Decisions." ***Nuclear Engineering and Design*** **93**: 319-327.

Phillips, M. L. F., and M. A. Molecke. In review. ***Technical Requirements for the CH-TRU Waste Source Term Program.*** SAND91-2111. Albuquerque, NM: Sandia National Laboratories.

Popielak, R. S., R. L. Beauheim, S. R. Black, W. E. Coons, C. T. Ellingson, and R. L. Olson. 1983. ***Brine Reservoirs in the Castile Fm., Waste Isolation Pilot Plant (WIPP) Project, Southeastern New Mexico.*** TME-3153. Carlsbad, NM: U.S. Department of Energy.

Reeves, M., V. A. Kelley, and J. S. Pickens. 1987. *Regional Double-Porosity Solute Transport in the Culebra Dolomite: An Analysis of Parameter Sensitivity and Importance at the Waste Isolation Pilot Plant (WIPP) Site.* SAND87-7105. Albuquerque, NM: Sandia National Laboratories.

Saulnier, G. J., Jr. 1988. *Field Operations Plan for Permeability Testing in the WIPP Underground Facility.* Albuquerque, NM: Sandia National Laboratories.

Saulnier, G. J., Jr. 1991. *Field Operations Plan for Permeability Testing in the WIPP Underground Facility, Addendum I.* Albuquerque, NM: Sandia National Laboratories.

Swift, P. N. In press. "Long-Term Climate Variability at the Waste Isolation Pilot Plant, Southeastern New Mexico," to appear in *Environmental Management.*

Trauth, K. M., R. P. Rechard, and S. C. Hora. 1991. "Expert Judgment as Input to Waste Isolation Pilot Plant Performance Assessment Calculations: Probability Distributions of Significant System Parameters" in *Mixed Waste: Proceedings of the First International Symposium, August 26-29, Baltimore, Maryland.* Eds. A. A. Moghissi and G. A. Benda. American Society of Mechanical Engineers, U.S. Department of Energy, U.S. Environmental Protection Agency, and the University of Maryland

U.S. DOE (Department of Energy) and State of New Mexico. 1981, as modified. "Agreement for Consultation and Cooperation" on WIPP by the State of New Mexico and U.S. Department of Energy, modified 11/30/84 and 8/4/87.

U.S. EPA (Environmental Protection Agency). 1985. *Environmental Standards for the Management and Disposal of Spent Nuclear Fuel, High-Level and Transuranic Radioactive Waste; Final Rule,* 40 CFR Part 191, *Federal Register* 50: 38066-38089.

Vesely, W. E. and D. M. Rasmusen. 1984. "Uncertainties in Nuclear Probabilistic Risk Analyses." *Risk Analysis* 4: 313-322.

Wawersik, W. R., and R. L. Beauheim. 1991. *Test Plan--Hydraulic Fracturing and Hydrologic Tests in Marker Beds 139 and 140.* Albuquerque, NM: Sandia National Laboratories.

Distribution

FEDERAL AGENCIES

U. S. Department of Energy (2)
Office of Environmental Restoration
and Waste Management
Attn: L. P. Duffy, EM-1
C. Frank, EM-50
Washington, DC 20585

U.S. Department of Energy (3)
Office of Environmental Restoration
and Waste Management
Attn: M. Frei, EM-34 (Trevion II)
Washington, DC 20585-0002

U.S. Department of Energy
Office of Environmental Restoration
and Waste Management
Attn: J. Lytle, EM-30 (Trevion II)
Washington, DC 20585-0002

U.S. Department of Energy
Office of Environmental Restoration
and Waste Management
Attn: S. Schneider, EM-342
(Trevion II)
Washington, DC 20585-0002

U.S. Department of Energy (3)
WIPP Task Force
Attn: G. H. Daly
S. Fucigna
J. Rhoderick
12800 Middlebrook Rd.
Suite 400
Germantown, MD 20874

U.S. Department of Energy (4)
Office of Environment, Safety and
Health
Attn: R. P. Berube, EH-20
C. Borgstrum, EH-25
R. Pelletier, EH-231
K. Taimi, EH-232
Washington, DC 20585

U. S. Department of Energy (4)
WIPP Project Integration Office
Attn: W. J. Arthur III
L. W. Gage
P. J. Higgins
D. A. Olona
P.O. Box 5400
Albuquerque, NM 87115-5400

U. S. Department of Energy (11)
WIPP Project Site Office (Carlsbad)
Attn: A. Hunt (4)
V. Daub (4)
J. Lippis
K. Hunter
R. Becker
P.O. Box 3090
Carlsbad, NM 88221-3090

U. S. Department of Energy, (5)
Office of Civilian Radioactive Waste
Management
Attn: Deputy Director, RW-2
Associate Director, RW-10
Office of Program
Administration and
Resources Management
Associate Director, RW-20
Office of Facilities
Siting and
Development
Associate Director, RW-30
Office of Systems
Integration and
Regulations
Associate Director, RW-40
Office of External
Relations and Policy
Office of Geologic Repositories
Forrestal Building
Washington, DC 20585

U. S. Department of Energy
Attn: National Atomic Museum Library
Albuquerque Operations Office
P.O. Box 5400
Albuquerque, NM 87185

U. S. Department of Energy
Research & Waste Management Division
Attn: Director
P.O. Box E
Oak Ridge, TN 37831

U. S. Department of Energy (2)
Idaho Operations Office
Fuel Processing and Waste
Management Division
785 DOE Place
Idaho Falls, ID 83402

U.S. Department of Energy
Savannah River Operations Office
Defense Waste Processing
Facility Project Office
Attn: W. D. Pearson
P.O. Box A
Aiken, SC 29802

U.S. Department of Energy (2)
Richland Operations Office
Nuclear Fuel Cycle & Production
Division
Attn: R. E. Gerton
825 Jadwin Ave.
P.O. Box 500
Richland, WA 99352

U.S. Department of Energy (3)
Nevada Operations Office
Attn: J. R. Boland
D. Livingston
P. K. Fitzsimmons
2753 S. Highland Drive
Las Vegas, NV 87183-8518

U.S. Department of Energy (2)
Technical Information Center
P.O. Box 62
Oak Ridge, TN 37831

U.S. Department of Energy (2)
Chicago Operations Office
Attn: J. C. Haugen
9800 South Cass Avenue
Argonne, IL 60439

U.S. Department of Energy
Los Alamos Area Office
528 35th Street
Los Alamos, NM 87544

U.S. Department of Energy (3)
Rocky Flats Area Office
Attn: W. C. Rask
G. Huffman
T. Lukow
P.O. Box 928
Golden, CO 80402-0928

U.S. Department of Energy
Dayton Area Office
Attn: R. Grandfield
P.O. Box 66
Miamisburg, OH 45343-0066

U.S. Department of Energy
Attn: E. Young
Room E-178
GAO/RCED/GTN
Washington, DC 20545

U.S. Bureau of Land Management
101 E. Mermod
Carlsbad, NM 88220

U.S. Bureau of Land Management
New Mexico State Office
P.O. Box 1449
Santa Fe, NM 87507

U.S. Environmental Protection
Agency (2)
Office of Radiation Protection
Programs (ANR-460)
Attn: Richard Guimond (2)
Washington, D.C. 20460

U.S. Nuclear Regulatory Commission
Division of Waste Management
Attn: H. Marson
Mail Stop 4-H-3
Washington, DC 20555

U.S. Nuclear Regulatory Commission
(4)
Advisory Committee on Nuclear Waste
Attn: Dade Moeller
Martin J. Steindler
Paul W. Pomeroy
William J. Hinze
7920 Norfolk Avenue
Bethesda, MD 20814

U.S. Nuclear Regulatory Commission
(2)
Attn: C. Lui
J. Glynn
Mail Stop NLS-372
Washington, DC 20555

U.S. Nuclear Regulatory Commission
Attn: A. Buslik
Mail Stop NLS-377
Washington, DC 20555

Defense Nuclear Facilities Safety
Board
Attn: Dermot Winters
625 Indiana Avenue NW
Suite 700
Washington, DC 20004

Nuclear Waste Technical Review Board
(2)
Attn: Dr. Don A. Deere
Dr. Sidney J. S. Parry
Suite 910
1100 Wilson Blvd.
Arlington, VA 22209-2297

Katherine Yuracko
Energy and Science Division
Office of Management and Budget
725 17th Street NW
Washington, DC 20503

U.S. Geological Survey (2)
Water Resources Division
Attn: Cathy Peters
Suite 200
4501 Indian School, NE
Albuquerque, NM 87110

STATE AGENCIES

Environmental Evaluation Group (5)
Attn: Robert Neill
Suite F-2
7007 Wyoming Blvd., N.E.
Albuquerque, NM 87109

New Mexico Bureau of Mines
and Mineral Resources
Socorro, NM 87801

New Mexico Energy, Minerals and
Natural Resources Department
Attn: Librarian
2040 South Pacheco
Santa Fe, NM 87505

New Mexico Energy, Minerals and
Natural Resources Department
New Mexico Radioactive Task Force (2)
(Governor's WIPP Task Force)
Attn: Anita Lockwood, Chairman
Chris Wentz,
Coordinator/Policy Analyst
2040 South Pacheco
Santa Fe, NM 87505

Bob Forrest
Mayor, City of Carlsbad
P.O. Box 1569
Carlsbad, NM 88221

Chuck Bernard
Executive Director
Carlsbad Department of Development
P.O. Box 1090
Carlsbad, NM 88221

New Mexico Environment Department
Secretary of the Environment
Attn: J. Espinosa (3)
P.O. Box 968
1190 St. Francis Drive
Santa Fe, NM 87503-0968

New Mexico Environment Department
Attn: Pat McCausland
WIPP Project Site Office
P.O. Box 3090
Carlsbad, NM 88221-3090

New Mexico State Engineer's Office
Attn: Dr. Mustafa Chudnoff
P.O. Box 25102
Santa Fe, NM 87504-5102

ADVISORY COMMITTEE ON NUCLEAR FACILITY SAFETY

John F. Ahearne
Executive Director, Sigma Xi
99 Alexander Drive
Research Triangle Park, NC 27709

James E. Martin
109 Observatory Road
Ann Arbor, MI 48109

Dr. Gerald Tape
Assoc. Universities
1717 Massachusetts Ave. NW
Suite 603
Washington, DC 20036

WIPP PANEL OF NATIONAL RESEARCH COUNCIL'S BOARD ON RADIOACTIVE WASTE MANAGEMENT

Charles Fairhurst, Chairman
Department of Civil and
Mineral Engineering
University of Minnesota
500 Pillsbury Dr. SE
Minneapolis, MN 55455-0220

John O. Blomeke
3833 Sandy Shore Drive
Lenoir City, TN 37771-9803

John D. Bredehoeft
Western Region Hydrologist
Water Resources Division
U.S. Geological Survey (M/S 439)
345 Middlefield Road
Menlo Park, CA 94025

Fred M. Ernsberger
1325 NW 10th Avenue
Gainsville, FL 32601

Rodney C. Ewing
Department of Geology
University of New Mexico
200 Yale, NE
Albuquerque, NM 87131

B. John Garrick
4590 MacArthur Blvd., #400
Newport Beach, CA 92660-2027

Leonard F. Konikow
U.S. Geological Survey
431 National Center
Reston, VA 22092

Jeremiah O'Driscoll
505 Valley Hill Drive
Atlanta, GA 30350

Christopher Whipple
Clement International Corp.
160 Spear St.
Suite 1380
San Francisco, CA 94105-1535

National Research Council (3)
Board on Radioactive
Waste Management
RM HA456
Attn: Peter B. Myers, Staff
Director (2)
Dr. Geraldine J. Grube
2101 Constitution Avenue
Washington, DC 20418

PERFORMANCE ASSESSMENT PEER REVIEW PANEL

G. Ross Heath
College of Ocean and
Fishery Sciences HN-15
583 Henderson Hall
University of Washington
Seattle, WA 98195

Thomas H. Pigford
Department of Nuclear Engineering
4159 Etcheverry Hall
University of California
Berkeley, CA 94720

Thomas A. Cotton
JK Research Associates, Inc.
4429 Butterworth Place, NW
Washington, DC 20016

Robert J. Budnitz
President, Future Resources
Associates, Inc.
2000 Center Street
Suite 418
Berkeley, CA 94704

C. John Mann
Department of Geology
245 Natural History Bldg.
1301 West Green Street
University of Illinois
Urbana, IL 61801

Frank W. Schwartz
Department of Geology and Mineralogy
The Ohio State University
Scott Hall
1090 Carmack Rd.
Columbus, OH 43210

NATIONAL LABORATORIES

Argonne National Labs (2)
Attn: A. Smith
D. Tomasko
9700 South Cass, Bldg. 201
Argonne, IL 60439

Battelle Columbus Laboratories (3)
Attn: Paul Baybutt
R. S. Denning
Steve Unwin
505 King Avenue
Columbus, OH 43201

Battelle Northwest
Attn: Pamela Doctor
P.O. Box 999
Richland, WA 99352

Battelle Pacific Northwest Laboratories (3)
Attn: R. E. Westerman
S. Bates
H. C. Burkholder
Battelle Boulevard
Richland, WA 99352

Los Alamos National Laboratory
Attn: B. Erdal, CNC-11
P.O. Box 1663
Los Alamos, NM 87544

Los Alamos National Laboratory
Attn: A. Meijer
Mail Stop J514
Los Alamos, NM 87545

Los Alamos National Laboratory (3)
HSE-8
Attn: M. Enoris
L. Soholt
J. Wenzel
P.O. Box 1663
Los Alamos, NM 87544

Los Alamos National Laboratory (2)
HSE-7
Attn: A. Drypolcher
S. Kosciewiscz
P.O. Box 1663
Los Alamos, NM 87544

Los Alamos National Laboratory (2)
Analysis and Assessment Division, A-1, MS F600
Attn: M. D. McKay
M. A. Meyer
P.O. Box 1663
Los Alamos, NM 87544

Oak Ridge National Laboratory
Computer Sciences
Attn: Darryl Downing
Building 2029, P.O. Box X
Oak Ridge, TN 37830

Oak Ridge National Laboratory (3)
Engineering Physics and Mathematics Division
Attn: E. M. Oblow
Francois G. Pin
Brian A. Worley
P.O. Box X
Oak Ridge, TN 37830

Oak Ridge National Laboratory (2)
Environmental Sciences Division
Attn: Steve Bartell
R. H. Gardner
P.O. Box X
Oak Ridge, TN 37830

Oak Ridge National Laboratory (2)
Health and Safety Research Division
Attn: David G. Kocher
F. O. Hoffman
P.O. Box X
Oak Ridge, TN 37830

Oak Ridge National Laboratory
Martin Marietta Systems, Inc.
Attn: J. Setaro
P.O. Box 2008, Bldg. 3047
Oak Ridge, TN 37831-6019

Savannah River Laboratory (3)
Attn: N. Bibler
M. J. Plodinec
G. G. Wicks
Aiken, SC 29801

Savannah River Plant (2)
Attn: Richard G. Baxter
Building 704-S
K. W. Wierzbicki
Building 703-H
Aiken, SC 29808-0001

CORPORATIONS/MEMBERS OF THE PUBLIC

Benchmark Environmental Corp. (3)
Attn: John Hart
C. Frederickson
K. Lickliter
4501 Indian School Rd., NE
Suite 105
Albuquerque, NM 87110

Deuel and Associates, Inc.
Attn: R. W. Prindle
7208 Jefferson, NE
Albuquerque, NM 87109

Disposal Safety, Inc.
Attn: Benjamin Ross
Suite 314
1660 L Street NW
Washington, DC 20006

Ecodynamics Research Associates (2)
Attn: Pat Roache
Rebecca Blaine
P.O. Box 8172
Albuquerque, NM 87198

E G & G Idaho (3)
1955 Fremont Street
Attn: C. Atwood
C. Hertzler
T. I. Clements
Idaho Falls, ID 83415

Geomatrix
Attn: Kevin Coppersmith
100 Pine Street #1000
San Francisco, CA 94111

Golden Associates, Inc. (3)
Attn: Mark Cunnane
Richard Kossik
Ian Miller
4104 148th Avenue NE
Redmond, WA 98052

In-Situ, Inc. (2)
Attn: S. C. Way
C. McKee
209 Grand Avenue
Laramie, WY 82070

INTERA, Inc.
Attn: A. M. LaVenue
8100 Mountain Road NE
Suite 213
Albuquerque, NM 87110

INTERA, Inc.
Attn: J. F. Pickens
Suite #300
6850 Austin Center Blvd.
Austin, TX 78731

INTERA, Inc.
Attn: Wayne Stensrud
P.O. Box 2123
Carlsbad, NM 88221

INTERA, Inc.
Attn: William Nelson
101 Convention Center Drive
Suite 540
Las Vegas, NV 89109

IT Corporation (2)
Attn: P. Drez
J. Myers
Regional Office - Suite 700
5301 Central Avenue, NE
Albuquerque, NM 87108

MACTEC (2)
Attn: J. A. Thies
D. K. Duncan
8418 Zuni Road SE
Suite 200
Albuquerque, NM 87108

Pacific Northwest Laboratory
Attn: Bill Kennedy
Battelle Blvd.
P.O. Box 999
Richland, WA 99352

RE/SPEC, Inc. (2)
Attn: W. Coons
Suite 300
4775 Indian School NE
Albuquerque, NM 87110

RE/SPEC, Inc.
Attn: J. L. Ratigan
P.O. Box 725
Rapid City, SD 57709

Reynolds Elect/Engr. Co., Inc.
Building 790, Warehouse Row
Attn: E. W. Kendall
P.O. Box 98521
Las Vegas, NV 89193-8521

Roy F. Weston, Inc.
CRWM Tech. Supp. Team
Attn: Clifford J. Noronha
955 L'Enfant Plaza, S.W.
North Building, Eighth Floor
Washington, DC 20024

Science Applications International Corporation
Attn: Howard R. Pratt,
Senior Vice President
10260 Campus Point Drive
San Diego, CA 92121

Science Applications International Corporation (2)
Attn: George Dymmel
Chris G. Pflum
101 Convention Center Dr.
Las Vegas, NV 89109

Science Applications International Corporation (2)
Attn: John Young
Dave Lester
18706 North Creek Parkway
Suite 110
Bothell, WA 98011

Science Applications International Corporation
Attn: David C. Aldrich
1710 Goodridge Drive
P.O. Box 1303
McLean, VA 22102

Science Applications International Corporation
Attn: Mark D. Otis
P.O. Box 50697
101 S. Park Ave.
Idaho Falls, ID 83405

Southwest Research Institute
Center for Nuclear Waste Regulatory Analysis (2)
Attn: P. K. Nair
6220 Culebra Road
San Antonio, Texas 78228-0510

W. K. Summers
The City of Albuquerque
Public Works Department
Utility Planning Division
P.O. Box 1293
Albuquerque, NM 87103

Systems, Science, and Software (2)
Attn: E. Peterson
P. Lagus
Box 1620
La Jolla, CA 92038

TASC
Attn: Steven G. Oston
55 Walkers Brook Drive
Reading, MA 01867

Tech. Reps., Inc. (6)
Attn: Janet Chapman
Debbie Marchand
John Stikar
Denise Bissell
Dan Scott
5000 Marble NE
Suite 222
Albuquerque, NM 87110

Tolan, Beeson, & Associates
Attn: Terry L. Tolan
2320 W. 15th Avenue
Kennewick, WA 99337

TRW Environmental Safety Systems (TESS)
Attn: Ivan Saks
10306 Eaton Place
Suite 300
Fairfax, VA 22030

Westinghouse Electric Corporation (4)
Attn: Library
L. Trego
C. Cox
L. Fitch
R. F. Kehrman
P.O. Box 2078
Carlsbad, NM 88221

Westinghouse Hanford Company
Attn: Don Wood
P.O. Box 1970
Richland, WA 99352

Western Water Consultants
Attn: D. Fritz
1949 Sugarland Drive #134
Sheridan, WY 82801-5720

Western Water Consultants
Attn: P. A. Rechard
P.O. Box 4128
Laramie, WY 82071

D. G. Cacuci
Dept. of Nuclear Engineering
University of Illinois
103 South Goodwin Avenue
Urbana, IL 61801-2984

W. J. Conover
College of Business Administration
Texas Tech University
Lubbock, TX 79409

Neville Cook
Rock Mechanics Engineering
Mine Engineering Dept.
University of California
Berkeley, CA 94720

John Evans
Harvard School of Public Health
665 Huntington Avenue
Boston, MA 02115

F. E. Haskin
Dept. of Chemical & Nuclear Engr.
University of New Mexico
Albuquerque, NM 87131

Max Henrion
Dept. of Engineering and Public Policy
Carnegie-Mellon University
Pittsburgh, PA 15213

Carl Irwin
Department of Mathematics
West Virginia University
Morgantown, WV 26505

Stan Kaplan
Pickard, Lowe and Garrick, Inc.
2260 University Drive
Newport Beach, CA 92660

Thomas B. Kirchner
Natural Resource Ecology Lab
Colorado State University
Fort Collins, CO 85023

Greg McRae
Dept. of Chemical Engineering
Carnegie-Mellon University
Pittsburgh, PA 15213

M. Granger Morgan
Dept. of Engineering and Public Policy
Carnegie-Mellon University
Pittsburgh, PA 15213

Dennis W. Powers
Star Route Box 87
Anthony, TX 79821

H. Rabitz
Department of Chemistry
Princeton University
Princeton, NJ 08544

K. H. Reckhow
School of Forestry and Environmental Studies
Duke University
Durham, NC 27706

S. K. Seaholm
University of Minnesota
Div. of Health Computer Science
Box 511 UMHC
420 Delaware St., SE
Minneapolis, MN 55455

Shirley Thieda
P.O. Box 2109, RR1
Bernalillo, NM 87004

Jack Urich
c/o CARD
144 Harvard SE
Albuquerque, NM 87106

F. Ward Whicker
Dept. of Radiology and Radiation Biology
Colorado State University
Fort Collins, CO 80523

UNIVERSITIES

University of California
Mechanical, Aerospace, and Nuclear Engineering Department (3)
Attn: W. Kastenberg
D. Browne
G. Apostolakis
5532 Boelter Hall
Los Angeles, CA 90024

University of Hawaii at Hilo
Attn: S. Hora
Business Administration
Hilo, HI 96720-4091

University of New Mexico
Geology Department
Attn: Library
Albuquerque, NM 87131

University of New Mexico
Research Administration
Attn: H. Schreyer
102 Scholes Hall
Albuquerque, NM 87131

University of Wyoming
Department of Civil Engineering
Attn: V. R. Hasfurther
Laramie, WY 82071

University of Wyoming
Department of Geology
Attn: J. I. Drever
Laramie, WY 82071

University of Wyoming
Department of Mathematics
Attn: R. E. Ewing
Laramie, WY 82071

LIBRARIES

Thomas Brannigan Library
Attn: Don Dresp, Head Librarian
106 W. Hadley St.
Las Cruces, NM 88001

Hobbs Public Library
Attn: Marcia Lewis, Librarian
509 N. Ship Street
Hobbs, NM 88248

New Mexico State Library
Attn: Norma McCallan
325 Don Gaspar
Santa Fe, NM 87503

New Mexico Tech
Martin Speere Memorial Library
Campus Street
Socorro, NM 87810

New Mexico Junior College
Pannell Library
Attn: Ruth Hill
Lovington Highway
Hobbs, NM 88240

Carlsbad Municipal Library
WIPP Public Reading Room
Attn: Lee Hubbard, Head Librarian
101 S. Halagueno St.
Carlsbad, NM 88220

University of New Mexico
General Library
Government Publications Department
Albuquerque, NM 87131

NEA/PERFORMANCE ASSESSMENT ADVISORY GROUP (PAAC)

P. Duerden
ANSTO
Lucas Heights Research Laboratories
Private Mail Bag No. 1
Menai, NSW 2234
AUSTRAILIA

Gordon S. Linsley
Division of Nuclear Fuel Cycle and Waste Management
International Atomic Energy Agency
P.O. Box 100
A-1400 Vienna
AUSTRIA

Nicolo Cadelli
Commission of the European Communities
200, Rue de la Loi
B-1049 Brussels
BELGIUM

R. Heremans
Organisme National des Déchets Radioactifs et des Matiéres Fissiles
ONDRAF
Place Madou 1, Boitec 24/25
B-1030 Brussels
BELGIUM

J. Marivoet
Centre d'Etudes de l'Energie Nucléaire
CEN/SCK
Boeretang 200
B-2400 Mol
BELGIUM

P. Conlon
Waste Management Division
Atomic Energy Control Board (AECB)
P.O. Box 1046
Ottawa, Canada KIP 559
CANADA

A. G. Wikjord
Manager, Environmental and Safety Assessment Branch
Atomic Energy of Canada Limited (AECL)
Whiteshell Nuclear Research Establishment
Pinawa, Manitoba ROE 1LO
CANADA

Jukka-Pekka Salo
Teollisuuden Voima Oy (TVO)
Fredrikinkatu 51-53 B
SF-00100 Helsinki
FINLAND

Timo Vieno
Technical Research Centre of Finland (VTT)
Nuclear Energy Laboratory
P.O. Box 208
SF-02151 Espoo
FINLAND

Timo Äikäs
Teollisuuden Voima Oy (TVO)
Fredrikinkatu 51-53 B
SF-00100 Helsinki
FINLAND

M. Claude Ringeard
Division de la Sécurité et de la Protection de l'Environment (DSPE)
Commissariat á l'Energie Atomique
Agence Nationale pour la Gestion des Déchets Radioactifs (ANDRA)
Route du Panorama Robert Schuman
B. P. No. 38
F-92266 Fontenay-aux-Roses Cedex
FRANCE

Gérald Ouzounian
Agence Nationale pour la Gestion des Déchets Radioactifs (ANDRA)
Route du Panorama Robert Schuman
B. P. No. 38
F-92266 Fontenay-aux-Roses Cedex
FRANCE

Claudio Pescatore
Division of Radiation Protection and Waste Management
OECD Nuclear Energy Agency
38, Boulevard Suchet
F-75016 Paris
FRANCE

M. Dominique Greneche
Commissariat á l'Energie Atomique
IPSN/DAS/SASICC/SAED
B. P. No. 6
F-92265 Fontenay-aux-Roses Cedex
FRANCE

Robert Fabriol
Bureau de Recherches géologiques et miniéres (BRGM)
B. P. 6009
45060 Orléans Cedex 2
FRANCE

P. Bogorinski
Gesellschaft für Reaktorsicherheit (GRS) mbH
Schwertnergasse 1
D-5000 Köln 1
GERMANY

R. Storck
GSF - Institut für Tieflagerung
Theodor-Heuss-Strabe 4
D-3300 Braunschweig
GERMANY

Ferrucio Gera
ISMES S.p.A
Via del Crociferi 44
I-00187 Roma
ITALY

Hideo Matsuzuru
Head, Environmental Assessment Laboratory
Dept. of Environmental Safety Research
Nuclear Safety Research Center
Tokai Research Establishment, JAERI
Tokai-mura, Naka-gun
Ibaraki-ken
JAPAN

Hiroyuki Umeki
Isolation System Research Program
Radioactive Waste Management Project
Power Reactor and Nuclear Fuel Development Corporation (PNC)
1-9-13, Akasaka
Minato-ku
Tokyo 107
JAPAN

P. Carboneras Martinez
ENRESA
Calle Emilio Vargas 7
R-28043 Madrid
SPAIN

Tönis Papp
Swedish Nuclear Fuel and Waste Management Co.
Box 5864
S 102 48 Stockholm
SWEDEN

Conny Hägg
Swedish Radiation Protection Institute (SSI)
Box 60204
S-104 01 Stockholm
SWEDEN

J. Hadermann
Paul Scherrer Institute
Waste Management Programme
CH-5232 Villigen PSI
SWITZERLAND

J. Vigfusson
USK- Swiss Nuclear Safety
Inspectorate
Federal Office of Energy
CH-5303 Würenlingen
SWITZERLAND

D. E. Billington
Departmental Manager - Assessment
Studies
Radwaste Disposal R&D Division
AEA Decommissioning & Radwaste
Harwell Laboratory, B60
Didcot Oxfordshire OX11 ORA
UNITED KINGDOM

P. Grimwood
Waste Management Unit
BNFL
Sellafield
Seascale, Cumbria CA20 1PG
UNITED KINGDOM

Alan J. Hooper
UK Nirex Ltd
Curie Avenue
Harwell, Didcot
Oxfordshire, OX11 ORH
UNITED KINGDOM

Jerry M. Boak
Yucca Mountain Project Office
U.S. Department of Energy
P.O. Box 98608
Las Vegas, NV 89193
UNITED STATES

Seth M. Coplan (Chairman)
U.S. Nuclear Regulatory Commission
Division of High-Level Waste
Management
Mail Stop 4-H-3
Washington, DC 20555
UNITED STATES

A. E. Van Luik
Intera/M&O
The Valley Bank Center
101 Convention Center Dr.
Las Vegas, NV 89109
UNITED STATES

NEA/PSAG USER'S GROUP

Alexander Nies (PSAC Chairman)
Gesellschaft für Strahlen- und
Institut für Tieflagerung
Abteilung für Endlagersicherheit
Theodor-Heuss-Strasse 4
D-3300 Braunscheweig
GERMANY

Eduard Hofer
Gesellschaft für Reaktorsicherheit
(GRS) MBH
Forschungsgelände
D-8046 Garching
GERMANY

Takashi Sasahara
Environmental Assessment Laboratory
Department of Environmental Safety
Research
Nuclear Safety Research Center,
Tokai Research Establishment, JAERI
Tokai-mura, Naka-gun
Ibaraki-ken
JAPAN

Alejandro Alonso
Cátedra de Tecnología Nuclear
E.T.S. de Ingenieros Industriales
José Gutiérrez Abascal, 2
E-28006 Madrid
SPAIN

Pedro Prado
CIEMAT
Instituto de Tecnología Nuclear
Avenida Complutense, 22
E-28040 Madrid
SPAIN

Miguel Angel Cuñado
ENRESA
Emilio Vargas, 7
E-28043 Madrid
SPAIN

Francisco Javier Elorza
ENRESA
Emilio Vargas, 7
E-28043 Madrid
SPAIN

Nils A. Kjellbert
Swedish Nuclear Fuel and Waste
Management Company (SKB)
Box 5864
S-102 48 Stockholm
SWEDEN

Björn Cronhjort
Swedish National Board for Spent
Nuclear Fuel (SKN)
Sehlsedtsgatan 9
S-115 28 Stockholm
SWEDEN

Richard A. Klos
Paul-Scherrer Institute (PSI)
CH-5232 Villingen PSI
SWITZERLAND

NAGRA (2)
Attn: Charles McCombie
Fritz Van Dorp
Parkstrasse 23
CH-5401 Baden
SWITZERLAND

Daniel A. Galson
Intera Information Technologies
Park View House, 14B Burton Street
Melton Mowbray
Leicestershire, LEI3, 1AE
UNITED KINGDOM

Brian G. J. Thompson
Department of the Environment
Her Majesty's Inspectorate of
Pollution
Room A5.33, Romney House
43 Marsham Street
London SW1P 2PY
UNITED KINGDOM

INTERA/ECL
Attn: Trevor J. Sumerling
Chiltern House
45 Station Road
Henley-on-Thames
Oxfordshire RG9 1AT
UNITED KINGDOM

U.S. Nuclear Regulatory Commission
(2)
Attn: Richard Codell
Norm Eisenberg
Mail Stop 4-H-3
Washington, D.C. 20555

Paul W. Eslinger
Battelle Pacific Northwest
Laboratories (PNL)
P.O. Box 999, MS K2-32
Richland, WA 99352

Andrea Saltelli
Commission of the European
Communities
Joint Resarch Centre od Ispra
I-21020 Ispra (Varese)
ITALY

Budhi Sagar
Center for Nuclear Waste Regulatory
Analysis (CNWRA)
Southwest Research Institute
P.O. Drawer 28510
6220 Culebra Road
San Antonio, TX 78284

Shaheed Hossain
Division of Nuclear Fuel Cycle and
Waste Management
International Atomic Energy Agency
Wagramerstrasse 5
P.O. Box 100
A-1400 Vienna
AUSTRIA

Claudio Pescatore
Division of Radiation Protection and
Waste Management
38, Boulevard Suchet
F-75016 Paris
FRANCE

GEOSTATISTICS EXPERT WORKING GROUP (GXG)

Rafael L. Bras
R.L. Bras Consulting Engineers
44 Percy Road
Lexington, MA 02173

Jesus Carrera
Universidad Politecnica de Cataluña
E.T.S.I. Caminos
Jordi, Girona 31
E-08034 Barcelona
SPAIN

Gedeon Dagan
Department of Fluid Mechanics and Heat Transfer
Tel Aviv University
P.O. Box 39040
Ramat Aviv, Tel Aviv 69978
ISRAEL

Ghislain de Marsily (GXG Chairman)
University Pierre et Marie Curie
Laboratorie de Geologie Applique
4, Place Jussieu - T.26 - 5^{e} etage
75252 Paris Cedex 05
FRANCE

Alain Galli
Centre de Geostatistique
Ecole des Mines de Paris
35 rue St. Honore
77035 Fontainebleau
FRANCE

Steve Gorelick
Department of Applied Earth Sciences
Stanford University
Stanford, CA 94305-2225

Peter Grindrod
Intera Information Technologies Ltd.
Chiltern House, 45 Station Road
Henley-on-Thames
Oxfordshire, RG9 1AT
UNITED KINGDOM

Alan Gutjahr
Department of Mathematics
New Mexico Institute of Mining and Technology
Socorro, NM 87801

C. Peter Jackson
Harwell Laboratory
Theoretical Studies Department
Radwaste Disposal Division
Bldg. 424.4
Oxfordshire Didcot Oxon OX11 ORA
UNITED KINDGOM

Peter Kitanidis
60 Peter Coutts Circle
Stanford, CA 94305

Ray Mackay
Department of Civil Engineering
University of Newcastle Upon Tyne
Newcastle Upon Tyne NE1 7RU
UNITED KINGDOM

Dennis McLaughlin
Parsons Laboratory
Room 48-209
Department of Civil Engineering
Massachusetts Institute of Technology
Cambridge, MA 02139

Shlomo P. Neuman
College of Engineering and Mines
Department of Hydrology and Water Resources
University of Arizona
Tucson, AZ 85721

Christian Ravenne
Geology and Geochemistry Division
Institut Francais du Pétrole
1 & 4, av. de Bois-Préau BP311
92506 Rueil Malmaison Cedex
FRANCE

Yorim Rubin
Department of Civil Engineering
University of California, Berkeley
Berkeley, CA 94720

FOREIGN ADDRESSES

Radiation Protection Program CEC
Attn: G. Neale Kelly
Rue de la Loi, 200
B-1049 Bruxelles
BELGIUM

Radiation Protection Program CEC
Attn: Jaak Sinnaeve
Rue de la Loi, 200
B-1049 Bruxelles
BELGIUM

Studiecentrum Voor Kernenergie
Centre D'Energie Nucleaire
Attn: A. Bonne
SCK/CEN
Boeretang 200
B-2400 Mol
BELGIUM

Atomic Energy of Canada, Ltd. (3)
Whiteshell Research Estab.
Attn: Michael E. Stevens
Bruce W. Goodwin
Donna Wushke
Pinewa, Manitoba
ROE 1LO
CANADA

National Water Research Institute
Attn: E. Halfon
Canada Centre for Inland Waters
Burlington, Ontario
CANADA

Esko Peltonen
Industrial Power Company Ltd.
TVO
Fredrikinkatu 51-53
SF-00100 Helsinki 10
FINLAND

Jean-Pierre Olivier
OECD Nuclear Energy Agency (2)
38, Boulevard Suchet
F-75016 Paris
FRANCE

D. Alexandre, Deputy Director
ANDRA
31 Rue de la Federation
75015 Paris
FRANCE

Claude Sombret
Centre D'Etudes Nucleaires
De La Vallee Rhone
CEN/VALRHO
S.D.H.A. BP 171
30205 Bagnols-Sur-Ceze
FRANCE

BGA/ISH/ZBD
Attn: Anton Bayer
P.O. Box 1108
D-8042 Neuherberg
GERMANY

Bundesministerium fur Forschung und Technologie
Postfach 200 706
5300 Bonn 2
GERMANY

Bundesanstalt fur Geowissenschaften und Rohstoffe
Attn: Michael Langer
Postfach 510 153
3000 Hannover 51
GERMANY

Gesellschaft fur Reaktorsicherheit
Attn: Bernard Krzykacz
D-8046 Garching
GERMANY

Gesellschaft fur Reaktorsicherheit (GRS) mb (2)
Attn: Bruno Baltes
Wolfgang Muller
Schwertnergasse 1
D-5000 Cologne
GERMANY

Hahn-Mietner-Institut fur Kernforschung
Attn: Werner Lutze
Glienicker Strasse 100
100 Berlin 39
GERMANY

Institut fur Tieflagerung (2)
Attn: K. Kuhn
Theodor-Heuss-Strasse 4
D-3300 Braunschweig
GERMANY

Kernforschungszentrum Karlsruhe/INR
Attn: Joachim Ehrhardt
Postfach 3640
D-7500 Karlsruhe 1
GERMANY

Kernforschungszentrum Karlsruhe/INR
Attn: Friedmar Fischer
Postfach 3640
D-7500 Karlsruhe 1
GERMANY

Physikalisch-Technische Bundesanstalt
Attn: Peter Brenneke
Postfach 33 45
D-3300 Braunschweig
GERMANY

Japan Atomic Energy Research Institute
Department of Reactor Safety Research
Attn: T. Ishigami
Tokai-mura, Naka-gun, Ibaraki-ken
319-11
JAPAN

Shingo Tashiro
Japan Atomic Energy Research Institute
Tokai-Mura, Ibaraki-Ken
319-11
JAPAN

Catholic University Brabant
Attn: J. P. C. Kleijnen
Tilburg
THE NETHERLANDS

Delft University of Technology
Dept. of Mathematics
Attn: Roger Cooke
Julianalaan 132
Delft
THE NETHERLANDS

Netherlands Energy Research Foundation
ECN
Attn: L. H. Vons
3 Westerduinweg
P.O. Box 1
1755 ZG Petten
THE NETHERLANDS

Johan Andersson
Swedish Nuclear Power Inspectorate
Statens Kärnkraftinspektion (SKI)
Box 27106
S-102 52 Stockholm
SWEDEN

Fred Karlsson
Svensk Karnbransleforsorjning AB
SKB
Box 5864
S-102 48 Stockholm
SWEDEN

Abtielung fur die Sicherheit der Kernanlagen
Attn: S. Chakraborty
Eidgenossisches Amt fur Energiewirtschaft
CH-5303
Wurenlingen
SWITZERLAND

Nationale Genossenschaft fur die Lagerung Radioaktiver Abfalle (NAGRA) (2)
Attn: Stratis Vomvoris
Piet Zuidema
Hardstrasse 73
CH-5430 Wettingen
SWITZERLAND

D. R. Knowles
British Nuclear Fuels, plc
Risley, Warrington, Cheshire WA3 6AS
1002607 UNITED KINGDOM

AEA Technology
Attn: J.H. Rees
D5W/29 Culham Laboratory
Abington
Oxfordshire OX14 3DB
UNITED KINGDOM

AEA Technology
Attn: W. R. Rodwell
044/A31 Winfrith Technical Centre
Dorchester
Dorset DT2 8DH
UNITED KINGDOM

AEA Technology
Attn: J. E. Tinson
B4244 Harwell Laboratory
Didcot
Oxfordshire OX11 ORA
UNITED KINGDOM

The University of Reading
Department of Statistics
Attn: Derek J. Pike
Whiteknights
Reading RG6 2AN
UNITED KINGDOM

National Radiological Protection
Board
Attn: M. Crick
Chilton, Didcot
Oxon OX11 ORQ
UNITED KINGDOM

National Radiological Protection
Board
Attn: Marion Hill
Chilton, Didcot
Oxon OX11 ORQ
UNITED KINGDOM

National Radiological Protection
Board
Attn: J. A. Jones
Chilton, Didcot
Oxon OX11 ORQ
UNITED KINGDOM

United Kingdom Atomic Energy
Authority
Attn: William Nixon
Safety & Reliability Directorate
Wigshaw Lane
Culcheth
Warrington WA3 4NE
UNITED KINGDOM

INTERNAL

1 A. Narath
20 O. E. Jones
1502 J. C. Cummings
1511 D. K. Gartling
3151 S. M. Wayland
6000 D. L. Hartley
6119 R. L. Beauheim
6119 P. B. Davies
6119 E. D. Gorham
6119 C. F. Novak
6119 S. W. Webb
6121 D. E. Munson
6121 E. J. Nowak
6121 J. R. Tillerson
6233 J. C. Eichelberger
6300 D. E. Miller
6301 E. J. Bonano
6302 T. E. Blejwas, Acting
6303 S. Y. Pickering
6303 W. D. Weart
6312 F. W. Bingham
6313 Supervisor
6313 L. S. Costin
6315 Supervisor
6316 R. P. Sandoval
6320 R. E. Luna, Acting
6341 J. M. Covan
6341 D. P. Garber
6341 A. L. Stevens
6341 J. Orona*
6341 Sandia WIPP Central Files (250)
6342 D. R. Anderson
6342 S. Bertram-Howery
6342 B. M. Butcher
6342 D. P. Gallegos
6342 L. S. Gomez
6342 M. Gruebel
6342 R. Guzowski
6342 R. D. Klett
6342 M. G. Marietta
6342 A. C. Peterson
6342 R. P. Rechard
6342 P. Swift
6342 M. Tierney
6342 K. M. Trauth
6342 B. L. Baker*
6342 J. Bean*
6342 J. Berglund*
6342 W. Beyeler*
6342 T. Blaine*
6342 K. Brinster*
6342 K. Byle*
6342 L. Clements*
6342 J. Garner*
6342 A. Gilkey*
6342 H. Iuzzolino*
6342 J. Logothetis*
6342 R. McCurley*
6342 J. Rath*
6342 D. Rudeen*
6342 J. Sandha*
6342 J. Schreiber*
6342 P. Vaughn*
6343 T. M. Schultheis
6345 R. Beraun
6345 L. Brush
6345 R. C. Lincoln
6345 F. T. Mendenhall
6345 M. A. Molecke
6347 Supervisor
6347 D. R. Schafer
6400 D. J. McCloskey
6400 N. R. Ortiz
6411 R. J. Breeding
6412 A. L. Camp
6412 S. E. Dingman
6412 A. C. Payne
6413 F. T. Harper
6413 J. C. Helton (20)
6413 J. L. Sprung
6416 D. A. Zimmerman
6419 M. P. Bohn
6453 L. F. Restrepo
6613 J. E. Campbell
6613 R. M. Cranwell
6613 R. L. Iman
6613 C. Leigh
6622 M.S.Y. Chu
9300 J. E. Powell
9330 J. D. Kennedy
8523-2 Central Technical Files
3141 S. A. Landenberger (5)
3145 Document Processing (8) for DOE/OSTI
3151 G. C. Claycomb (3)

*6342/Geo-Centers

U.S. GOVERNMENT PRINTING OFFICE: 1992—673-122/60127